Advances in Photosynthesis and Respiration
Volume 22

Photosystem II

The Light-Driven Water:Plastoquinone Oxidoreductase

$$2\,H_2O + 2\,PQ \xrightarrow{h\nu} 2\,PQH_2 + O_2$$

Edited by
Thomas J. Wydrzynski and Kimiyuki Satoh
Assistant Editor
Joel A. Freeman

Springer

Photosystem II

Advances in Photosynthesis and Respiration

VOLUME 22

The scope of our series, beginning with volume 11, reflects the concept that photosynthesis and respiration are intertwined with respect to both the protein complexes involved and to the entire bioenergetic machinery of all life. *Advances in Photosynthesis and Respiration* is a book series that provides a comprehensive and state-of-the-art account of research in photosynthesis and respiration. Photosynthesis is the process by which higher plants, algae, and certain species of bacteria transform and store solar energy in the form of energy-rich organic molecules. These compounds are in turn used as the energy source for all growth and reproduction in these and almost all other organisms. As such, virtually all life on the planet ultimately depends on photosynthetic energy conversion. Respiration, which occurs in mitochondrial and bacterial membranes, utilizes energy present in organic molecules to fuel a wide range of metabolic reactions critical for cell growth and development. In addition, many photosynthetic organisms engage in energetically wasteful photorespiration that begins in the chloroplast with an oxygenation reaction catalyzed by the same enzyme responsible for capturing carbon dioxide in photosynthesis. This series of books spans topics from physics to agronomy and medicine, from femtosecond processes to season long production, from the photophysics of reaction centers, through the electrochemistry of intermediate electron transfer, to the physiology of whole orgamisms, and from X-ray christallography of proteins to the morphology or organelles and intact organisms. The goal of the series is to offer beginning researchers, advanced undergraduate students, graduate students, and even research specialists, a comprehensive, up-to-date picture of the remarkable advances across the full scope of research on photosynthesis, respiration and related processes.

The titles published in this series are listed at the end of this volume and those of forthcoming volumes on the back cover.

Photosystem II

The Light-Driven Water:Plastoquinone Oxidoreductase

Edited by

Thomas J. Wydrzynski
The Australian National University,
Canberra, Australia

and

Kimiyuki Satoh
Okayama University,
Okayama, Japan

Assistant Editor

Joel A. Freeman

Springer

A C.I.P. Catalogue record for this book is available from the Library of Congress.

ISBN-10 1-4020-4249-3 (HB)
ISBN-13 978-1-4020-4249-2 (HB)
ISBN-10 1-4020-4254-X (e-book)
ISBN-13 978-1-4020-4254-6 (e-book)

Published by Springer,
P.O. Box 17, 3300 AA Dordrecht, The Netherlands.

www.springeronline.com

Front Cover Image. An underwater scene of *Vallisneria* sp. from Ewans Ponds conservation area, V South Australia. Note the stream of oxygen gas bubbles being produced by Photosystem II. Photograph was taken by Warwick Hillier.

The camera ready text was prepared by Lawrence A. Orr, Center for the Study of Early Events in Photosynthesis, Arizona State University, Tempe, Arizon 85287-1604, U.S.A.

Printed on acid-free paper

Printed in the Netherlands.

From the Series Editor

Advances in Photosynthesis and Respiration

Volume 22, Photosystem II: The Light-Driven Water:Plastoquinone Oxidoreductase

I am delighted to announce the publication, in *Advances in Photosynthesis and Respiration* (AIPH) Series, of *Photosystem II: The Light-Driven Water: Plastoquinone Oxidoreductase,* a book covering the central role of the oxygen-evolving system for life on earth; it deals with both the structure and the function of this unique process. Two distinguished authorities have edited this volume: Thomas J. Wydrzynski of Australia and Kimiyuki Satoh of Japan. Some of the earlier volumes have included descriptions of Photosystem II: Volume 4 (*Oxygenic Photosynthesis: The Light Reactions*, edited by Donald R. Ort and Charles F. Yocum); Volume 10 (*Photosynthesis: Photobiochemistry and Photobiophysics*, authored by Bacon Ke); and Volume 19 (*Chlorophyll a Fluorescence: A Signature of Photosynthesis*, edited by George C. Papageorgiou and Govindjee) . The current volume follows the 21 volumes listed below.

Published Volumes (1994–2005)

- *Volume 1*: *Molecular Biology of Cyanobacteria* (28 Chapters; 881 pages; 1994; edited by Donald A. Bryant, from USA; ISBN: 0-7923-3222-9);
- *Volume 2: Anoxygenic Photosynthetic Bacteria* (62 Chapters; 1331 pages; 1995; edited by Robert E. Blankenship, Michael T. Madigan and Carl E. Bauer, from USA; ISBN: 0-7923-3682-8);
- *Volume 3: Biophysical Techniques in Photosynthesis* (24 Chapters; 411 pages; 1996; edited by the late Jan Amesz and the late Arnold J. Hoff, from The Netherlands; ISBN: 0-7923-3642-9);
- *Volume 4: Oxygenic Photosynthesis: The Light Reactions* (34 Chapters; 682 pages; 1996; edited by Donald R. Ort and Charles F. Yocum, from USA; ISBN: 0-7923-3683-6);
- *Volume 5: Photosynthesis and the Environment* (20 Chapters; 491 pages; 1996; edited by Neil R. Baker, from UK; ISBN: 0-7923-4316-6);
- *Volume 6: Lipids in Photosynthesis: Structure, Function and Genetics* (15 Chapters; 321 pages; 1998; edited by Paul-André Siegenthaler and Norio Murata, from Switzerland and Japan; ISBN: 0-7923-5173-8);
- *Volume 7: The Molecular Biology of Chloroplasts and Mitochondria in Chlamydomonas* (36 Chapters; 733 pages; 1998; edited by Jean David Rochaix, Michel Goldschmidt-Clermont and Sabeeha Merchant, from Switzerland and USA; ISBN: 0-7923-5174-6);
- *Volume 8: The Photochemistry of Carotenoids* (20 Chapters; 399 pages; 1999; edited by Harry A. Frank, Andrew J. Young, George Britton and Richard J. Cogdell, from USA and UK; ISBN: 0-7923-5942-9);
- *Volume 9: Photosynthesis: Physiology and Metabolism* (24 Chapters; 624 pages; 2000; edited by Richard C. Leegood, Thomas D. Sharkey and Susanne von Caemmerer, from UK, USA and Australia; ISBN: 0-7923-6143-1);
- *Volume 10: Photosynthesis: Photobiochemistry and Photobiophysics* (36 Chapters; 763 pages; 2001; authored by Bacon Ke, from USA; ISBN: 0-7923-6334-5);
- *Volume 11: Regulation of Photosynthesis* (32 Chapters; 613 pages; 2001; edited by Eva-Mari Aro and Bertil Andersson, from Finland and Sweden; ISBN: 0-7923-6336-1);
- *Volume 12: Photosynthetic Nitrogen Assimilation and Associated Carbon and Respiratory Metabolism* (16 Chapters; 284 pages; 2002; edited by Christine Foyer and Graham Noctor, from UK and France);
- *Volume 13: Light Harvesting Antennas* (17 Chapters; 513 pages; 2003; edited by Beverley Green and William Parson, from Canada and USA; ISBN: 0-7923-6335-3);
- *Volume 14: Photosynthesis in Algae* (19 Chapters; 479 pages; 2003; edited by Anthony Larkum,

Susan Douglas and John Raven, from Australia, Canada and UK; ISBN: 0-7923-6333-7);

- *Volume 15: Respiration in Archaea and Bacteria: Diversity of Prokaryotic Electron Transport Carriers* (13 Chapters; 326 pages; 2004; edited by Davide Zannoni, from Italy; ISBN: 1-4020-2001-5);
- *Volume 16: Respiration in Archaea and Bacteria 2: Diversity of Prokaryotic Respiratory Systems* (13 chapters; 310 pages; 2004; edited by Davide Zannoni, from Italy; ISBN: 1-4020-2002-3);
- *Volume 17: Plant Mitochondria: From Genome to Function* (14 Chapters; 325 pages; 2004; edited by David A. Day, A. Harvey Millar and James Whelan, from Australia; ISBN: 1-4020-2339-5);
- *Volume 18: Plant Respiration: From Cell to Ecosystem* (13 Chapters; 250 pages; 2005; edited by Hans Lambers, and Miquel Ribas-Carbo from Australia and Spain; ; ISBN: 1-4020-3588-8)
- *Volume 19: Chlorophyll a Fluorescence: A Signature of Photosynthesis* (31 Chapters; 817 pages; 2004; edited by George C. Papageorgiou and Govindjee, from Greece and USA; ISBN: 1-4020-3217-X);
- *Volume 20: Discoveries in Photosynthesis* (111 Chapters; 1262 + xxx pages; 2005; edited by Govindjee, J. Thomas Beatty, Howard Gest and John F. Allen, from USA, Canada and Sweden (& UK) ; ISBN: 1-4020-3323-0); and
- *Volume 21: Photoprotection, Photoinhibition, Gene Regulation, and Environment* (21 Chapters; ~500 pages; 2005; edited by Barbara Demmig-Adams, William W. Adams III and Autar K. Mattoo, all from USA; ISBN:1-4020-3564-0)

For a description of the scope of the AIPH Series, see the back cover of this book. Further information on these books and ordering instructions can be found at <http://www.springeronline.com> under the Book Series 'Advances in Photosynthesis and Respiration.' Special discounts are available for members of the International Society of Photosynthesis Research, ISPR (<http://www.photosynthesisresearch.org>). To ensure your discount, please order through Noeline. Gibson@springer-sbm.com.

Photosystem II: The Light-Driven Water:Plastoquinone Oxidoreductase

Photosystem II is truly an unprecedented discovery of evolution; one couldn't have modeled it 30–40 years ago despite all the advances in chemistry, physics and biology. It consists of a light-harvesting unit (antenna) and a reaction center unit that operates at an unusually high redox potential; it is this latter unique characteristic that allows it to oxidize water to oxygen at its 'oxygen-evolving complex.' A book on this unique system has been edited by two outstanding authorities in the area of the structure and the function of the oxygen-evolving Photosystem II: Thomas J. Wydrzynski (of the Research School of Biological Sciences, The Australian National University, Canberra, Australia) and Kimiyuki Satoh (of the Department of Biology, Okayama University, Okayama, Japan).

Respiring organisms, including humans, on this planet depend on the oxygen that green plants generate through Photosystem II. Thus, this book is a very important addition to the already published books in the AIPH Series. It essentially addresses water first as a source of the electrons that are necessary for the reductive syntheses of organic matter, and then as a source of molecular oxygen that is necessary for the energy producing catabolic oxidations, including respiration.

During the last decade, or so, dramatic advances have been made in elucidating the structure of Photosystem II to near atomic scale with the X-ray crystallography, and in relating it to its biophysical, biochemical and molecular biological properties. Thirty-four chapters, authored by 75 internationally acknowledged experts, summarize this extraordinary scientific progress, covering areas that range from the capture of fleeting photons, their conversion into chemical energy (oxidation-reduction), to the dynamic regulatory processes that sustain and optimize the photosynthetic oxidation of water. A discussion is also provided on the beginnings of Photosystem II and photosynthesis more than 3 billion years ago (in the Archaean Era) and on its eventful evolution to the present day diversity of microbial and higher plants. Lastly, the design of artificial (biomimetic) Photosystems II is also discussed. Who knows, one day these systems may serve the needs of humanity either on Earth, or on some distant outpost in space.

The book is designed to be used by graduate students, beginning researchers and advanced undergraduate students in the areas of plant sciences, microbiology, cell and molecular biology, biochemistry, biophysics, bioenergetics and chemistry, as well as those in agriculture and biotechnology.

This book is appropriately dedicated to a pioneer in the field Gerald T. Babcock (the dedication is authored by Charles F. Yocum, Robert Blankenship and Shelagh Ferguson-Miller, all of USA). Kimiyuki Satoh (Japan), Thomas J. Wydrzynski (Australia) and Govindjee (USA) provide an *Introduction* to Photosystem II and the chapters in this volume (*Chapter 1*). It is followed by five chapters that deal with the *Protein Constituents of Photosystem II*: Beverley Green (Canada) and Elisabeth Gantt (USA) discuss the distal and extrinsic antenna (*Chapter 2*); Julian Eaton-Rye (New Zealand) and Cindy Putnam-Evans (USA) summarize our understanding of the CP 47 and CP43 core antenna components (*Chapter 3*); Peter Nixon (UK), Mary Sarcina (UK) and Bruce Diner (USA) provide an account of the D1 and D2 core proteins (*Chapter 4*). This is followed by *Chapter 5*, by Terry Bricker (USA) and Robert Burnap (USA) on the oxygen enhancing extrinsic proteins, and *Chapter 6*, by Leeann Thornton (USA), Johnna Roose (USA), Himadri Pakrasi (USA) and Masahiko Ikeuchi (Japan) on the low molecular weight components.

The next nine chapters focus on the *Organization of the Functional Sites in Photosystem II*: Gernot Renger and Alfred Holzwarth (both of Germany) discuss the primary electron transfer (*Chapter 7*); Vasili Petrouleas (Greece) and Anthony Crofts (USA) summarize information on the quinone-iron acceptor complex (*Chapter* 8); Bruce Diner and David Britt (both of USA) discuss the redox active tyrosines Y_Z and Y_D (*Chapter* 9); Vittal Yachandra (USA) summarizes the current understanding about the organization of the manganese ions of the manganese cluster of the O_2-evolving complex (*Chapter* 10); Richard Debus (USA) summarizes what is known about protein ligands of the manganese cluster (*Chapter 11*); Karin Åhrling (Australia), Ronald Pace (Australia) and Michael Evans (UK) provide information on spectroscopic observations and their implications on structural and functional details of catalytic manganese cluster (*Chapter 12*); Hans van Gorkom (The Netherlands) and Charles Yocum (USA) discuss the roles of Calcium and Chloride ions (*Chapter 13*); Jack van Rensen (The Netherlands) and Vyacheslav Klimov (Russia) address the unique role of bicarbonate on the acceptor side and the donor side of Photosystem II reaction center (*Chapter 14*); and Peter Faller, Christian Fufezan and William Rutherford (all of France) examine the secondary electron transfer pathways around the Photosystem II reaction center (*Chapter 15*).

Subsequently, in the next six chapters, the focus shifts to the *Structural Basis for Photosystem II*: Takumi Noguchi (Japan) and Catherine Berthomieu (France) analyze the molecular structure of the intermediates of the system, using information obtained from vibrational spectroscopy (*Chapter 16*); Robert Bittl (Germany) and Asako Kawamori (Japan) summarize the configuration of the electron transport intermediates of Photosystem II, as obtained by electron paramagnetic resonance spectroscopy (*Chapter 17*); Ben Hankamer (Australia), James Barber (UK) and Jon Nield (UK) describe the structure of the core/antenna holocomplex as visualized by electron microscopy (*Chapter 18*); Horst Witt (Germany) discusses the first three-dimensional structure of Photosystem II obtained by X-ray crystallography and other biophysical methods (*Chapter 19*); Jian-Ren Shen and Nobuo Kamiya (both of Japan) discuss this structure, using also X-ray crystallography (*Chapter 20*); and James Barber and So Iwata (both of UK) discuss a somewhat refined structure, and its implications to the function of Photosystem II (*Chapter 21*).

These chapters on the structure are followed by four chapters on *Molecular Dynamics of Photosystem II*: Laura Barter (UK), David Klug (UK) and Rienk van Grondelle (The Netherlands) summarize our understanding about excitation energy trapping and its equilibration (*Chapter 22*); Barry Pogson (Australia), Heather Rissler (Australia) and Harry Frank (USA) elaborate the role of carotenoids in energy quenching (*Chapter 23*); Vladimir Shinkarev (USA) discusses the pattern and the analyses of the O_2 evolution in a train of light flashes (*Chapter 24*); and Warwick Hillier (Australia) and Johannes Messinger (Germany) present an overview on the mechanism of water oxidation (*Chapter 25*).

This is followed by a discussion of *Assembly and Biodynamics of Photosystem II* in four chapters: Charles Dismukes, Gennady Ananyev and Richard Watt (all of USA) discuss the photoassembly of the catalytic manganese cluster (*Chapter 26*); Wah Soon Chow (Australia) and Eva-Mari Aro (Finland) summarize our understanding of photoinactivation and mechanisms of recovery (*Chapter 27*); Kenichi Yamaguchi (USA), Stephen Mayfield (USA) and Mamoru Sugita (Japan) present a current picture of transcriptional and translational regulation of gene expression (*Chapter 28*); and Steven Theg and Lan-Xin Shi (both of USA) discuss transport and post-translational processing in biosynthesis and homeostatis (*Chapter 29*).

This is followed by a discussion of the *Comparison of Photosystem II with Other Natural/Artificial Systems* in four chapters: Charles Dismukes and Robert Blankenship (both of USA) describe the origins and the evolution of oxygenic photosynthesis (*Chapter 30*); Gary Brudvig (USA) and Mårten Wikström present mechanistic comparisons between Photosystem II and Cytochrome *c* oxidase (*Chapter 31*); Lázló Kálmán (Hungary), JoAnn Williams (USA) and James Allen (USA) summarize research on mimicking the properties of Photosystem II in purple bacterial reaction centers (*Chapter 32*); Brian Gibney (USA) and Cecilia Tommos (Sweden) discuss de novo protein design in respiration and photosynthesis (*Chapter 33*); and Ann Magnuson, Stenbjörn Styring and Leif Hammarström (all of Sweden) end this book with an understanding of Photosystem II through artificial photosynthesis.

A Bit of History: First Clear Evidence of the Series Scheme, and the Naming of System 2 (Now Photosystem II) by Louis N.M. Duysens, Jan Amesz and B. M. Kamp in 1961

A recently published time-line on oxygenic photosynthesis covers many aspects of the history of 'Photosystem II' (see Govindjee and D. Krogmann (2004) Discoveries in oxygenic photosynthesis (1727–2003): A perspective. Photosynth Res 80: 15–57). Chapter 1 of this book by K. Satoh, T.J. Wydrzynski and Govindjee includes a historical account of Photosystem II (for references, see this chapter). In a paper, published on May 6, 1961, Louis N.M. Duysens, Jan Amesz and B.M. Kamp (Two photochemical systems in photosynthesis. Nature 190: 510-511) used for the first time the name 'System 2' for the photosystem responsible for the action spectrum of chlorophyll *a* fluorescence; it was the system that was suggested to oxidize water to oxygen, and reduce cytochrome. 'System 1', on the other hand, oxidized cytochrome, and reduced pyridine nucleotide. Duysens and colleagues added first red light (680 nm light; absorbed mainly by chlorophyll) and observed oxidation of a cytochrome in a red alga *Porphyridium cruentum*, and then they added green light (562 nm; absorbed mainly in phycoerythrin) and observed reduction of this oxidized cytochrome. Addition of the herbicide DCMU eliminated the reduction of cytochrome by green light, but not its oxidation by red light. This antagonistic effect of light 1 and 2 on cytochrome provided not only the evidence for the series scheme of photosynthesis, but was the first paper to call the system that oxidized water and reduced cytochrome as 'System 2' (currently, Photosystem II), whereas the other system that oxidized cytochrome as 'System 1' (currently, Photosystem I). In this seminal paper, Duysens and colleagues had recognized not only their own work, but that of Robert Emerson (with Marcia Brody), Eugene Rabinowitch (with Emerson, and with Rajni Govindjee and Jan B. Thomas), C. Stacy French (with V.K. Young, and with Jack Myers), Norman Bishop, and Leo Vernon (with L.P. Zaugg). Since in sunlight both systems are excited simultaneously and begin to function almost simultaneously, it is not a question of which starts first. The naming of the system is thus arbitrary.

Future AIPH Books

The readers of the current series are encouraged to watch for the publication of the forthcoming books (not necessarily arranged in the order of future appearance):

- *The Structure and Function of Plastids* (Editors: Robert Wise and J. Kenneth Hoober; expected to contain 27 Chapters and ~775 pages; ISBN: 1-4020-4060-1);
- *Biochemistry, Biophysics and Biological Functions of Chlorophylls* (Editors: Bernhard Grimm, Robert J. Porra, Wolfhart Rüdiger and Hugo Scheer);
- *Photosystem I: The Light-Driven Plastocyanin: Ferredoxin Oxidoreductase* (Editor: John Golbeck);
- *Biophysical Techniques II* (Editors : Thijs J. Aartsma and Jörg Matysik);
- *Photosynthesis: A Comprehensive Treatise; Biochemistry, Biophysics Physiology and Molecular Biology, Part 1* (Editors: Julian Eaton-Rye and Baishnab Tripathy); and
- *Photosynthesis: A Comprehensive Treatise; Biochemistry, Biophysics Physiology and Molecular Biology, Part 2* (Editors: Baishnab Tripathy and Julian Eaton-Rye).

In addition to these contracted books, we are already in touch with prospective Editors for the following books:

- Molecular Biology of Cyanobacteria II
- Protonation and ATP Synthases
- Genomics and Proteomics

- Protein Complexes of Respiration and Photosynthesis
- Sulfur Metabolism in Photosynthetic Systems
- Molecular Biology of Stress in Plants
- Global Aspects of Photosynthesis and Respiration (2 volumes)
- Artificial Photosynthesis.

Readers are encouraged to send their suggestions for future volumes (topics, names of future editors, and of future authors) to me by E-mail (gov@uiuc.edu) or fax (1-217-244-7246).

In view of the interdisciplinary character of research in photosynthesis and respiration, it is my earnest hope that this series of books will be used in educating students and researchers not only in Plant Sciences, Molecular and Cell Biology, Integrative Biology, Biotechnology, Agricultural Sciences, Microbiology, Biochemistry, and Biophysics, but also in Bioengineering, Chemistry, and Physics.

Acknowledgments

I take this opportunity to thank Thomas J. Wydrzynski and Kimiyuki Satoh for their outstanding and painstaking editorial work. We are grateful to them for (personally) subsidizing 8 of the 16 color plates in this volume. I thank all the 75 authors of volume 22: without their authoritative chapters, there would be no such volume. I thank Jacco Flipsen and Noeline Gibson (both of Springer) for their friendly working relationship with us that led to the production of this book. I thank Jeff Haas (Director of Information Technology, Life Sciences, University of Illinois at Urbana-Champaign, UIUC) and Evan DeLucia (Head, Department of Plant Biology, UIUC) for their support. My family (my wife Rajni Govindjee; our daughter Anita, her husband Morten Christiansen, and our grand-daughter Sunita; our son Sanjay, his wife Marilyn, and our grandsons Arjun and Rajiv) has been very supportive during the preparation of this book.

I am grateful to George Papageorgiou for his suggestions to improve this Editorial.

Special thanks go to Larry Orr for his wonderful work in typesetting this book. His constant advise to the editors and his outstanding interactions with all those involved in in this book are a source of inspiration to all of us.

August 1, 2005

Govindjee
Series Editor, *Advances in Photosynthesis and Respiration*
University of Illinois at Urbana-Champaign,
Department of Plant Biology
Urbana, IL 61801-3707, USA
E-mail: gov@uiuc.edu
URL: http://www.life.uiuc.edu/govindjee

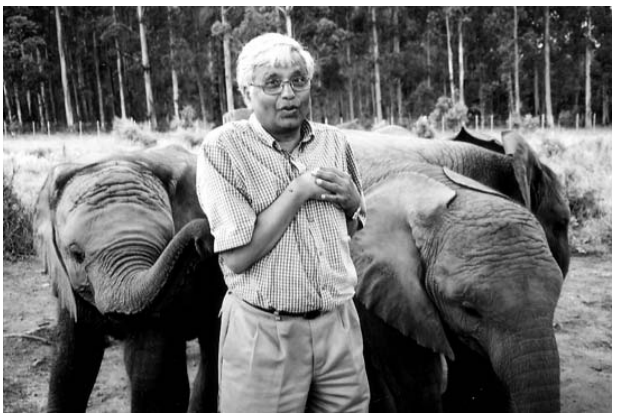

Govindjee in South Africa, 2005

Govindjee**,** born in 1932, has been Professor Emeritus of Biochemistry, Biophysics and Plant Biology at the University of Illinois at Urbana-Champaign (UIUC), Illinois, USA, since 1999. He received his B.Sc. (Chemistry and Biology) and M.Sc. (Botany: Plant Physiology) from the University of Allahabad, India, in 1952 and 1954, respectively. He earned his Ph.D. in Biophysics from the UIUC in 1960, working first with Robert Emerson and then with Eugene Rabinowitch. He served on the faculty of the University of Allahabad from 1954–1956; and the UIUC from 1961–1999. His honors include: Fellow of the American Association of Advancement of Science (AAAS); Fellow of the National Academy of Sciences (India); Distinguished Lecturer of the School of Life Sciences at UIUC (1976) ; President of the American Society for Photobiology (1980–1981); Fulbright Senior Lecturer (1996–1997); and Honorary President of the 2004 International Photosynthesis Congress (Montreal, Canada). Govindjee's research interests have been, since 1960, on the function of Photosystem (PS) II even before it was called as such. Most of his work has been collaborative, but due to lack of space, the names of his collaborators are not mentioned here; they are available on his web page (http://www.life.uiuc.edu/govindjee). He discovered that, in addition to auxiliary pigments, a short-wavelength form of Chlorophyll (Chl) *a* is present in what is now called PS II (1960); discovery of the two-light two-pigment system effect in Chl *a* fluorescence (1960); Emerson Enhancement Effect in NADP reduction in chloroplasts (1963,1964). Together with his graduate students, he discovered a 693–696 nm emission band when photosynthesis was saturated or blocked; made the first measurements on the temperature dependence, down to 4K, of Chl *a* fluorescence; provided explanation for the fluorescence transient curve in terms of a traffic jam of electrons on the acceptor side of PS I, as well as in terms of non-Q_A-related changes. Again, with several graduate students, he focused on the role and the site of bicarbonate ions on PS II, particularly on its acceptor side: a role of bicarbonate on the protonation at the Q_B site was suggested. His other major contributions have been the first picosecond measurements on the primary charge separation in PS II, and the theory of 'thermoluminescence from PS II'. It is worth mentioning that George C. Papageorgiou, and Thomas J. Wydrzynski, editor of volume 19 and this volume, respectively, had worked with Govindjee for their doctorate degrees at the UIUC. His current interests are: (1) Imaging and regulation of lifetime of Chl *a* fluorescence in single algal or cyanobacterial cells; (2) History of photosynthesis research; and (3) Photosynthesis education. He is a member of the American Society of Plant Biology, American Society for Photobiology, Biophysical Society of America, and the International Society of Photosynthesis Research (ISPR). For further information, see his web page at: (http://www.life.uiuc.edu/govindjee). He can be reached by e-mail at gov@life.uiuc.edu.

Contents

Part III: Organization of Functional Sites in Photosystem II

Preface

Photosystem II: The Light-Driven Water:Plastoquinone Oxidoreductase is the 22nd volume in the *Advances in Photosynthesis and Respiration* (AIPH) series (Series Editor, Govindjee) published by Springer (formerly Kluwer Academic Publishers). Photosystem II (PS II) is the heart of oxygenic photosynthesis, catalyzing the oxidation of water to molecular oxygen. Many volumes in the AIPH series have dealt with the biophysics, biochemistry and molecular biology of PS II but always within the framework of a much broader picture. In Volume 4, *Oxygenic Photosynthesis: The Light Reactions*, PS II was discussed along with Photosystem I and thylakoid structure while in Volume 10, *Photosynthesis: Photobiochemistry and Photobiophysics*, PS II was included with discussions on bacterial photosynthesis. In other volumes such as Volume 5, *Photosynthesis and the Environment*, the role of PS II in stress response and photo-inhibition was discussed; in Volume 13, *Light Harvesting Antennas*, the various light harvesting pigment-proteins of PS II are documented; and in Volume 19, *Chlorophyll a Fluorescence: A Signature of Photosynthesis*, the use of PS II chlorophyll fluorescence as a molecular probe was taken to a global scale. The present volume is unique in the AIPH series in that it covers all aspects of the biophysics, biochemistry and molecular biology of PS II, making it the most comprehensive text to be published on this subject to date. A companion volume on *Photosystem I* is currently being edited by John Golbeck.

All aerobic organisms on earth, whether plant, animal or microbial, depend on the function of PS II to maintain the atmospheric O_2 that sustains life. The strongest oxidant known in biology is created within PS II by visible light and is used to oxidize water as the ultimate source of electrons for the carbon-fixing reactions (i.e., the Calvin-Benson-Bassham cycle). The carbon-fixing reactions store chemical energy in the form of organic food stuff and as consequence, molecular oxygen is released as a by-product. Several other books (Volumes 15, 16, 17, 18) in the AIPH series cover the equally important, reverse process of photosynthesis, i.e., respiration, in which molecular oxygen is reduced to water by metabolically burning the organic food stuff releasing the stored chemical energy to power all other life processes.

PS II is an extremely complex enzyme that catalyzes a series of reaction events, from the capture and transfer of light energy (occurring on the femtosecond or the 10^{-15} s time scale) to the efficient conversion of excitation energy into the chemical energy of a stabilized charge separation and the transfer of electrons from water to plastoquinone (occurring on a millisecond or the 10^{-3} s time scale). In recent years there has been a dramatic surge in our knowledge of the molecular organization, dynamics, and reaction paths of PS II. In particular, the overall atomic structure of PS II has been successfully elucidated by X-ray crystallographic analysis, down to a 3.2–3.5 Å resolution. This last accomplishment is no trivial feat considering the subunit complexity and molecular size of the PS II core complex (molecular mass ~260,000 kDa). Simultaneously, the biophysics and molecular biology of PS II has also been greatly advanced. Thus, the time was ripe for a comprehensive book dedicated to PS II to appear in the literature and to summarize our current knowledge as a basis for future research and for the application of the unique PS II chemistry in biotechnology and renewable energy schemes.

To begin the book, we provide a special perspective dedicated to the late Gerald (Jerry) T. Babcock as one of the truly outstanding pioneers in PS II research. His untimely death in 2000 occurred just as he was advocating a new proposal for the mechanism of water oxidation. As the readers of this book will soon realize, many of Jerry's ideas continue to provide the underlying basis of current thinking. The following 34 chapters in the book were written by authors who were invited as leading experts in their respective fields of PS II research. Many chapters are jointly authored by experts from different parts of the world so as to provide the reader with the most in depth perspective on each topic. A total of 75 authors from 13 countries have contributed to the book, representing major centers of PS II research in Europe, North America, Asia and Australia and making this book a truly international effort. The book is divided into six distinct parts which are summarized as follows:

Part I, *A Perspective of Photosystem II Research*, provides an introduction to PS II, correlating our current knowledge of PS II with important historical developments in photosynthesis research. The structural and functional properties of PS II that

are discussed in detail in the following chapters are outlined and put into the perspective of PS II as a functional unit in the broader framework of oxygenic photosynthesis. The future of PS II research and its role in biotechnological applications are also summarized.

Part II, *Protein Constituents of Photosystem II*, is devoted to a comprehensive description of the protein subunit composition of PS II, focusing on the known function(s) of each component. Emphasis is placed on the diverse distal and extrinsic antenna pigment-proteins involved in the light-harvesting function of PS II found across the many different classes of photosynthetic organisms; the CP43 and CP47 proximal antenna pigment-proteins, which are universal components of PSII that channel the excitation energy in the light-harvesting array to the photochemical reaction center; the intrinsic D1 and D2 subunits, which form the reaction core and harbor the primary photo-reactants and the electron carriers that catalyze the oxidation of water and the reduction of plastoquinone; the O_2-enhancing extrinsic proteins of the thylakoid membrane, which are important for optimizing molecular oxygen production by PS II; and the identification and proposed structure and function of minor protein components contained in the PS II complexes from cyanobacteria, algae and higher plants.

Part III, *Organization of the Functional Sites in Photosystem II*, discusses in depth the arrangement and properties of the electron transfer components in PS II. These functional components include the reaction center P680, chlorophyll-pheophytin complex that forms the site of primary charge separation in the PS II; the Q_A and Q_B iron-quinone acceptor complex that links the one-electron reactions at the reaction center with the two-electron reduction of plastoquinone; the Y_Z redox-active tyrosine that mediates a proton-coupled electron transfer from the manganese-calcium (Mn_4Ca) cluster to the reaction center and the symmetrical Y_D redox-active tyrosine that interacts with the PS II donor side; the catalytic Mn_4Ca cluster that sequentially accumulates oxidizing equivalents from the reaction center and catalyzes the production of molecular O_2 from water; and the side-path electron donors chlorophyll Z, cytochrome b_{559} and β-carotene, which provide alternate electron transfer routes for the dissipation of excess energy in PS II. Emphasis is also given in this section to the function of the calcium and chloride in the O_2-producing reactions and the role of bicarbonate in electron transfer on both the donor and acceptor sides of the PS II reaction center.

Part IV, *Structural Basis for Photosystem II*, provides the latest information on the atomic and molecular structure of PS II in both prokaryotic and eukaryotic photosynthetic organisms. A range of biophysical techniques are employed in the structural studies, which include the molecular analysis of the PS II functional sites by vibrational spectroscopy (e.g. Fourier transform infrared or FTIR spectroscopy) and electron paramagnetic resonance (EPR) spectroscopy; the determination of the subunit organization in PS II core and antenna holocomplexes by electron cryomicroscopy; and the resolution of atomic structure of the PS II core complex from thermophilic species of cyanobacteria by X-ray crystallography down to 3.5–3.8 Å.

Part V, *Molecular Dynamics of Photosystem II*, provides detailed accounts of the molecular events that define the role of PS II function in oxygenic photosynthesis. These include an analysis of the energy trapping and equilibration with the PS II reaction center; the special role of carotenoid pigments in the quenching of the excess energy absorbed by PS II; the unique flash-induced oscillatory processes in PS II that are characteristic in promoting electron transfer from water to plastoquinone; and the ultimate question of how the oxidation of water takes place to produce molecular oxygen without the formation of highly reactive oxygen radical intermediates.

Part VI, *Assembly and Biodynamics of Photosystem II*, is devoted to discussions of the unique biodynamic processes that sustain PS II function in vivo. Topics include the special process for the light-induced assembly of the catalytic Mn_4Ca cluster; the mechanisms of recovery from the light-induced inactivation of PS II, in particular, the special damage and repair cycle of the D1 protein; transcriptional and translational regulation during PS II gene expression; and the transport and post-translational processing in PS II protein biosynthesis.

Part VII, *Comparison of Photosystem II with Other Natural/Artificial Systems*, addresses the role of PS II with respect to life on earth in general and more specifically to applications in biotechnology. The peculiar lack of diversity in the structural/functional organization of the catalytic site for water oxidation in PSII of present-day photosynthetic organisms is central to the role PS II has had in the evolution of life. Similarly, a comparison between PS II and the cytochrome *c* oxidase enzyme, which catalyzes the

reverse reaction by reducing O_2 to water, reveals very little mechanistic commonality, implying that the appearance of PS II was a unique, one-time event in the history of the earth. Finally, attempts to mimic PS II reactions in natural bacterial reaction centers, synthetic proteins, and bioinorganic complexes stand unique in the construction and application of artificial photosynthesis.

Throughout the conceptualization, refinement and final realization of this book, we have many people to thank. First of all we wish to sincerely thank all of the authors. Their patience, fortitude and willingness to provide in depth accounts covering all aspects of PS II structure and function have made this book a truly outstanding addition to the scientific literature.

Likewise, without the expert advice of the many outside reviewers, a book of this scope would not have been possible. In this capacity, we sincerely thank: Jan M. Anderson, The Australian National University; Lars Eric Andreasson, University of Gothenburg; Terry M. Bricker, Louisiana State University; Gary W. Brudvig, Yale University; Wah-Soon (Fred) Chow, The Australian National University; Richard Debus, University of California at Riverside; Bruce Diner, E.I. du Pont de Nemours & Company; Julian Eaton-Rye, University of Otago; Graham Flemming, University of California at Berkeley; Govindjee, University of Illinois at Urbana-Champaign; Sam Hay, The Australian National University; Warwick Hillier, The Australian National University; Vaughan Hurry, University of Umeå; Wolfgang Junge; University of Osnabrück; Hiroyuki Koike, University of Hyogo; Johannes Messinger, Max Planck Institute for Bioinorganic Chemistry; Mamoru Mimuro, Kyoto University; Melvin Y. Okamura, University of California at San Diego; Takaaki Ono, Institute of Physical and Chemical Research; Ronald J. Pace, The Australian National University; Jean-David Rochaix, University of Geneva; Michael Seibert; National Renewable Energy Laboratory; Jian-Ren Shen, Okayama University; Michael R. Wasilewski, Northwestern University; Vittal K. Yachandra, Lawrence Berkeley National Laboratory.

We also wish to thank those who were critical for finalizing the book for publication. In this regard we sincerely thank Joel Freeman for his expert assistance in the editing of the book. Without his help the final stages would have taken a lot longer to come to fruition. And we offer a very special thanks to the person who was most crucial in bringing this book to the publication stage, Larry Orr. Through our many mistakes we caused many problems for Larry, and we wish to express our sincere appreciation of his perseverance, expert assistance and unlimited guidance in bringing this book to print. In terms of the practical aspects in publishing the book we thank the staff at Springer, in particular Jacco Flipsen and Noeline Gibson.

Last but not least we give our very special thanks to Govindjee. He has provided generous advice and encouragement to us and to the authors over the several years from the inception of this project to its final outcome. As the AIPH Series Editor, Govindjee has promoted the most comprehensive set of books on photosynthesis yet to appear, covering subjects from the historical perspectives of photosynthesis to its relationship with respiration and the functioning of the biosphere. Govindjee has provided a treatise for our time comparable to the Eugene I. Rabinowich treatise on Photosynthesis of 50 years ago.

Finally, TW thanks all those in the Photobioenergetics Group for their understanding and support during this project, in particular to Sam Hay, Brett Wallace, Adele Williamson, Iain McConnell and Brendon Conlan. A special thanks from TW goes to Warwick Hillier, for being an outstanding scientific colleague and a good mate over the years. KS thanks his wife (Tamiko Satoh) for her support.

August 1, 2005

Thomas J. Wydrzynski
The Australian National University,
Canberra,Australia
Email: tom.wydrzynski@anu.edu.au

Kimiyuki Satoh
Okayama University, Okayama, Japan
Email: kimiyuki@cc.okayama-u.ac.jp

Thomas John Wydrzynski

Thomas J. Wydrzynski was born in 1947 in Saint Louis, Missouri, and is currently a Senior Fellow in the Research School of Biological Sciences (RSBS) at the Australian National University (ANU), Canberra, Australia. He completed his PhD (Plant Physiology) in 1977 at the University of Illinois at Urbana-Champaign (UIUC) under the supervision of Govindjee. For his PhD thesis research he was the first to apply solvent water proton nuclear magnetic resonance (NMR) relaxation measurements as a dynamic probe of the functional manganese in Photosystem II in situ. Also, while he was a PhD student, he provided the first clear experimental evidence, in 1975, for a site of bicarbonate action on the electron acceptor site in Photosystem II. He was awarded a National Science Foundation (NSF) Energy-Related Postdoctoral Research Fellowship in 1976 and worked with Kenneth Sauer at the Lawrence Berkeley National Laboratory from 1977 to 1979, where he obtained some of the first experimental evidence to indicate that the functional manganese changes oxidation state during O_2 production. He then joined industry and worked from 1980 to 1984 in the Biotechnology Division, Corporate Research, Standard Oil Company Indiana in Chicago (now a part of the British Petroleum (BP) Corporation). Subsequently, he re-joined academia and received research fellowships from the Alexander von Humboldt Foundation, Germany (1985), the Science and Technology Agency, Japan (1985), the Wennergren Foundation, Sweden (1986), the Nordiska Forseningsradet (NFR), Sweden (1987), and the Deutscheforschungsgemeinschaft (DFG), Germany (1989). Over this period in his career he worked with Gernot Renger at the Max-Volmer Institute for Physical and Biophysical Chemistry, Technical University Berlin, Germany; Tore Vänngård in the Department of Biochemistry and Biophysics, Chalmers University, Göteborg, Sweden; and Yorinao Inoue in the Solar Energy Research Group, the RIKEN Institute of Physical and Chemical Research, Saitama, Japan. During this time he pursued the idea that the controlled access of solvent water through the protein superstructure to the catalytic site was critical not only for maintaining the stability of the functional manganese but also in O-O bond formation during O_2 production. In 1991 he joined the Research School of Biological Science (RSBS) at The Australian National University in Canberra and during 1998-2001 became the first Head of the newly created Photobioenergetics Group. At the RSBS he embarked on some of his most significant work by developing with his PhD students the first rapid (millisecond time range) mass spectrometric methods of oxygen isotopic exchange for monitoring the substrate water directly at the catalytic site in Photosystem II. The binding properties of the substrate water as determined by these measurements are critical for the chemical mechanism of O_2 formation. In 2000, he set up a research program on the design and synthesis of photo-active proteins in which the first artificial, quinone-based photosynthetic reaction center was engineered from a natural cytochrome protein. The overall goal of these studies is to establish the practical experimental principles for the future development of artificial systems for light energy conversion processes. In 2002, he set up another research program under a Human Frontier Scientific Program grant to study the evolutionary chemistry of oxygenic photosynthesis in present-day organisms from extreme and unusual environments and the possible role of bicarbonate as an alternative substrate for O_2 production. With respect to other professional activities, he was chair of the organizing committees for the *Robertson Symposium on Chlorophyll Fluorescence* in 1994 and the *22nd Annual Meeting of the Australian Society for Biophysics* in 1998, co-chair for two symposia at the *12th International Photosynthesis Congress* in 2001, and was on the organizing committee and co-editor for the special symposium *From Biophysics to Molecular Biology: A Path in the Research of Photosystem II* in 2004.

Kimiyuki Satoh

Kimiyuki Satoh is an Emeritus Professor at the Okayama University in Japan. He received his undergraduate degree from Okayama University and obtained his Ph.D. (Doctor of Science) from the University of Tokyo in 1972 in Biochemistry and Biophysics. He started his work on photosynthesis under the guidance of Professor Hirosi Huzisige of Okayama University. At that time, he contributed to the identification of ferredoxin-dependent nitrite reductase in chloroplasts, and was involved in the analysis of photoinactivation of photochemical activities in chloroplasts. From 1975 to 1977, he was a postdoctoral fellow in the laboratory of Professor Warren Butler at the University of California at San Diego, La Jolla, California. Here, he initiated work on the biochemical separation of chlorophyll protein complexes aiming to identify the pigment-protein complexes responsible for each one of the three fluorescence emission bands (F685; F696 and F735), observed at 77 K. Through this study, he became deeply involved in the biochemical study of Photosystem II (PS II) and succeeded in purifying the PS II core complex from spinach by introducing isoelectric focusing. He then worked in the laboratories of J. Philip Thornber at the University of California at Los Angeles, and of Charles Arntzen at the Plant Research Laboratory at Michigan Sate University, East Lansing, Michigan. There, he identified the polypeptide composition of the purified PS II core complex. In collaboration with Arntzen's research group, he demonstrated that the PS II core complex contains two polypeptides of apparent molecular masses of about 30 kDa, which eventually were identified as the D1 and D2 proteins. In 1982, he became Professor of Plant Physiology at the Okayama University, where he continued his work on the PS II core complex. One of the successes in his laboratory was the isolation of an O_2-evolving PS II core complex, which was the first demonstration that O_2 evolution could take place in the isolated protein-pigment complex. A major achievement from his laboratory at the Okayama University was the isolation of the D1-D2-cytochrome b_{559} complex. This study established that the site of primary charge separation in the PS II is located in the complex that contains D1 and D2 proteins, the proteins that are homologous to the L and M subunits of the purple bacterial reaction center. He then purified the carboxy-terminal processing protease for the D1 precursor protein from spinach and extensively analyzed the enzymatic process. From 1992 to 1997, he served as an Adjunct Professor in the National Institute for Basic Biology at Okazaki. Since then, he has been engaged in the random mutagenesis of the D1 protein from the cyanobacterium *Synechocystis* sp. PCC 6803 with the goal of obtaining photo-tolerant mutants and mutants deficient in autotrophy for use in detailed structure/function analyses of the PS II reaction center. Kimiyuki Satoh has served as the President of the Japanese Society of Plant Physiologists (2002–2003) and as the Secretary of the International Society of Photosynthesis Research (2001–2004).

Joel Freeman

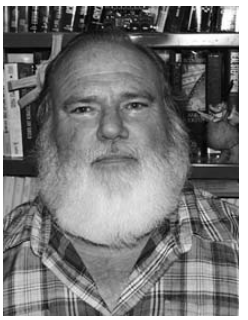

Larry Orr

Joel Freeman, born in 1978, was the technical officer for the Photobioenergetics Group in the Research School of Biological Sciences at the Australian National University (2002–2005). He completed his Bachelor of Aquaculture with honours in 2001 from The University of Tasmania. During this period, he was granted membership in the Golden Key National Honour Society (1998) and placed on the Dean's Roll of Excellence (1998-2000). He then joined the Photobioenergetics Group where he has developed a protocol for the extraction of the functional manganese and calcium from Photosystem II and has since worked on projects including spectroscopic studies of Photosystem II in chlorophyll *d*-containing *Acaryochloris marina*, hydrogen production mechanism in microalgae and its industrial potential and the evolutionary biology of oxygenic photosynthesis, in particular, the role of bicarbonate in Photosystem II steady-state electron transport in *Spirulina maxima*. Joel now works as a policy and technical officer with Plant Programs at the Australian Quarantine and Inspection Service. He assists in the development and implementation of operational standards and procedures for the importation of grains, seeds and nursery stock into Australia.

Larry Orr was born in 1947 and raised in a traveling carnival until his family settled down in northern Wisconsin. Years later he graduated from Arizona State University (ASU) with a BA in English (literature, not grammar). Like most Liberal Arts majors, he worked at a variety of odd jobs until he landed a position in 1983 as Administrative Coordinator for the NSF office in McMurdo, Antarctica. There he became very interested in working with the scientists that came to 'The Ice' from all over the world and, using one of his odd skills learned as a pizza parlor manager, produced the most famous pizza parties on the continent. After leaving the Antarctic program, he was hired for a similar position with the ASU Center for the Study of Early Events in Photosynthesis in 1988. No pizzas were needed there, but other past job skills proved useful: writing, photography, purchasing, proof-reading, office administration, editing, word processing and typesetting. Still at the Photosynthesis Center, he is interested in science education, especially photosynthesis, for the general public. Larry has played a key role in the success of the AIPH (Advances in Photosynthesis and Respiration) Series since its inception in 1994. He has guided, with humor, the Editors as well as the authors in 'staying on track.' Together with Govindjee, Larry has produced one of the most used web articles on 'Photosynthesis and the Web.' It is available at http://photoscience.la.asu.edu/photosyn/photoweb/; as well as at http://www.life.uiuc.edu/govindjee/photoweb/. It is currently undergoing revision; thus, readers are welcome to send suggestions to larry.orr@asu.edu and gov@life.uiuc.edu.

Author Index

Color Plates

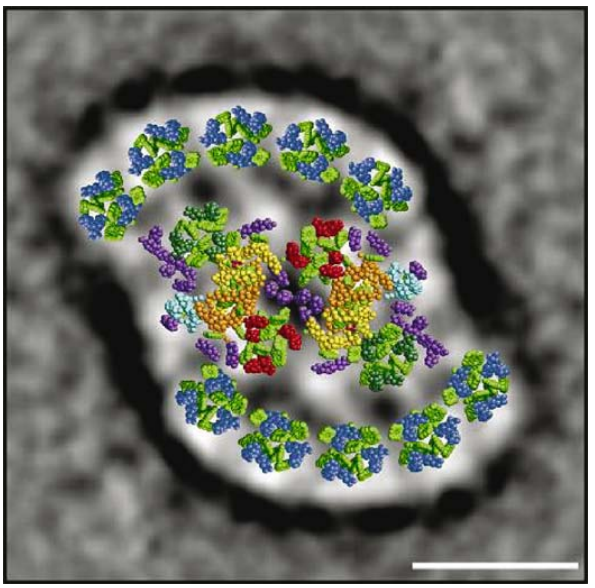

Fig. 1. Prochloron PS II dimer surrounded by 10 prochlorophyte Chl *a/b* (Pcb) monomers. Color code: green, Chl *a* or Chl *b*; blue, transmembrane helices; yellow, D1; orange, D2; dark green, CP43; red, CP47; purple, low molecular weight subunits; cyan, cytochrome b_{559}. Scale bar, 100 Å. Courtesy of J. Barber. See Chapter 2, p. 31.

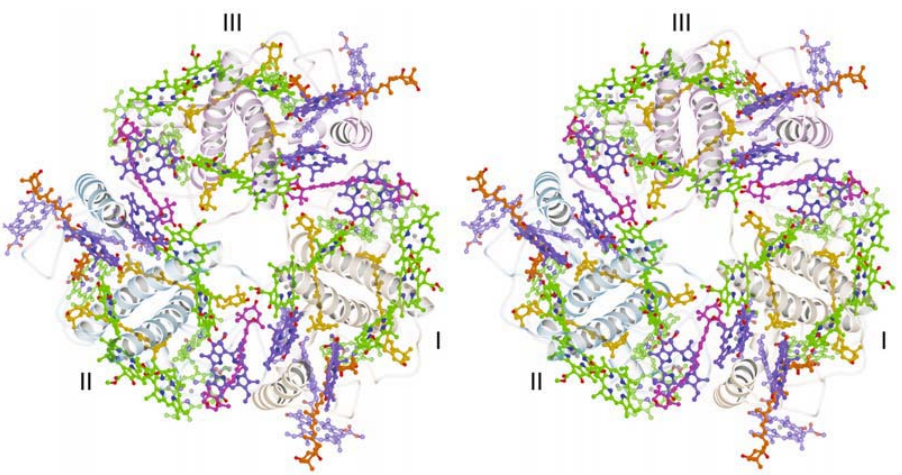

Fig. 2. Stereogram of LHCII trimer (individual monomers indicated by I, II and III) viewed from the stromal side, showing positions of Chls and carotenoids. Color code green, Chl *a*; blue, Chl *b*; orange, neoxanthin; magenta, xanthophyll-cycle carotenoids;grey ribbons, helices. Courtesy of W. Chang. See Chapter 2, p. 35.

T. Wydrzynski and K. Satoh (eds): Photosystem II: The Light-Driven Water:Plastoquinone Oxidoreductase, pp. CP1–CP16.

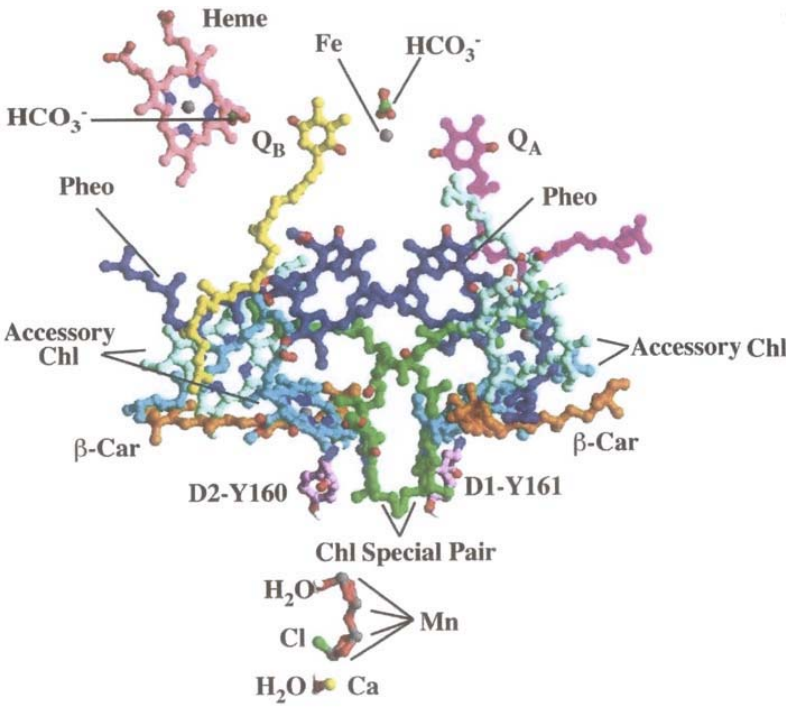

Fig. 1. The modeled cofactors in the PS II reaction center. Adapted from Van Rensen (2002) and originally from Xiong et al. (1998a). See Chapter 14, p. 334.

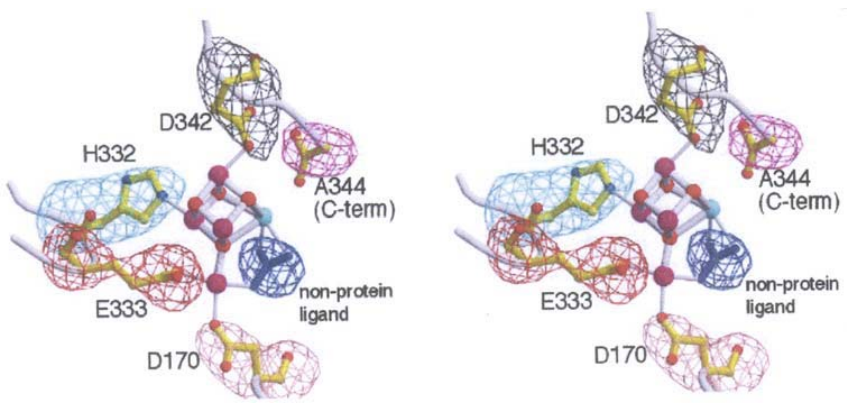

Fig. 2. Stereoviews of electron density maps for part of the water-oxidizing complex; a putative non-protein ligand (modeled as bicarbonate) is shown in blue. Reproduced with permission from Ferreira et al. (2004). See Chapter 14, p 342.

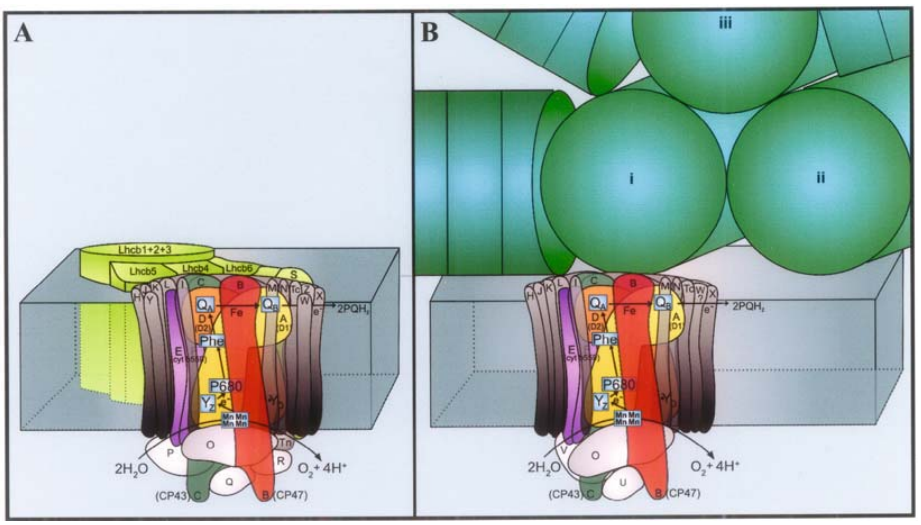

Fig. 1. Cartoons of PS II and its associated light-harvesting components (A) of higher plants and green algae and (B) of cyanobacteria, emphasizing subunit composition and primary and secondary electron transfer steps that occur in the reaction center D1 and D2 proteins. In the case of the higher plants and green algae (A) note that the secondary antenna is made up of Chl *a/b* binding Lhcb proteins, intrinsic to the membrane, while in (B), the cyanobacterial PS II is serviced by a large extrinsic, soluble phycobiliprotein mass on its stromal side. Also note, when comparing the two systems, the compositional differences present for the lumenally bound extrinsic subunits of the OEC. See Chapter 18, p 412.

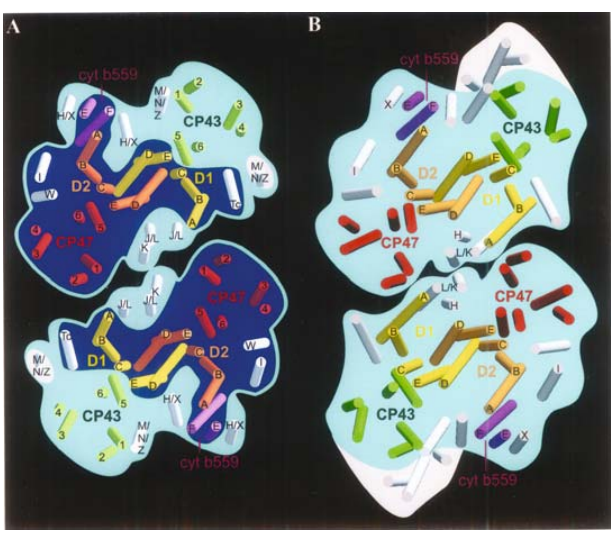

Fig. 2. Comparison of the PS II core dimer of (A) spinach (Hankamer et al., 2001b) and (B) S. elongatus (Zouni et al., 2001), and respective assignments of the low molecular weight (LMW) single transmembrane helical subunits. The dark blue region in (A) shows the helix organization of the spinach CP47-RC subcomplex (Rhee et al., 1998), which had to be modified, two transmembrane helices adjacent to helix B of the D1 and D2 proteins being removed. The remaining cyan regions contain the additional transmembrane helices of CP43 and other LMW core dimer subunits. Color code: red, CP47; green, CP43; yellow, D1; orange, D2; purple, Cyt b_{559}; white, LMW subunits. See Chapter 18, p. 415.

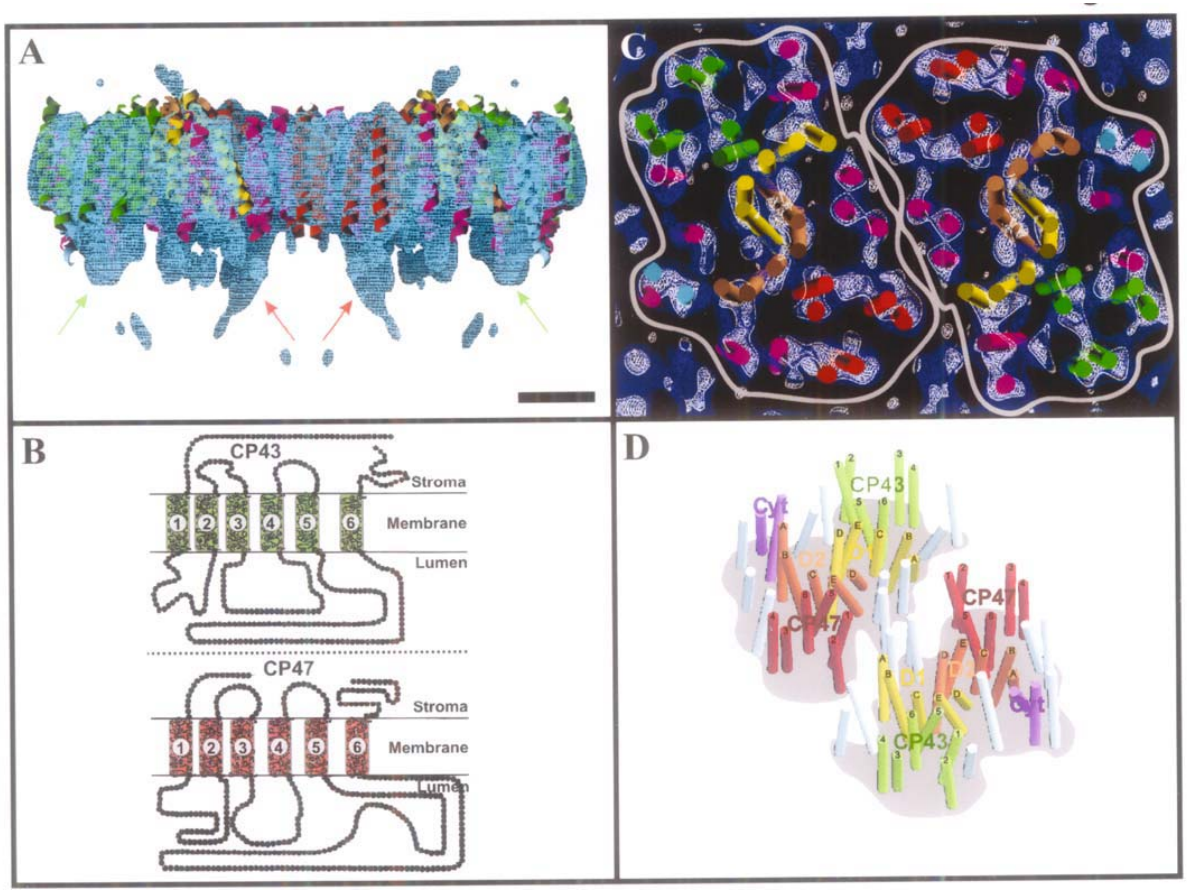

Fig. 1 (A) Side view of the 3D map of the spinach PS II core dimer, stromal side uppermost, emphasizing the transmembrane region and lumenal extensions assigned to the loops joining helices 5 and 6 of CP47 (red arrows) and CP43 (green arrows) (Hankamer et al., 2001b). Color code as for panel (C) below. (B) Predicted folding from hydropathy analyses of CP43 and CP47 (Hankamer et al., 2001b). (C) Transmembrane view of a section of the 3D map of the spinach PS II core dimer (Hankamer et al., 2001b). The map is sampled at ~1 Å and is displayed as chicken-wire contours, with compensation for high-resolution fade out (white contours, temperature factor –1000, 1.5 σ) and with no compensation (blue contours, 1.3 σ). Fitted transmembrane helices color code: yellow, D1; orange, D2; red, CP47; green, CP43; cyan, α- and β-subunits of Cyt *b*559; magenta, LMW subunits. (D) An oblique view of the 3D structural model of the spinach PS II core dimer from electron crystallography. Color code as for panel (C) above, except: purple, α- and β-subunits of Cyt b_{559}; white, LMW subunits (Hankamer et al., 2001a). Bar for panels (A) and (C) represents 2.5 nm. See Chapter 18, p. 413.

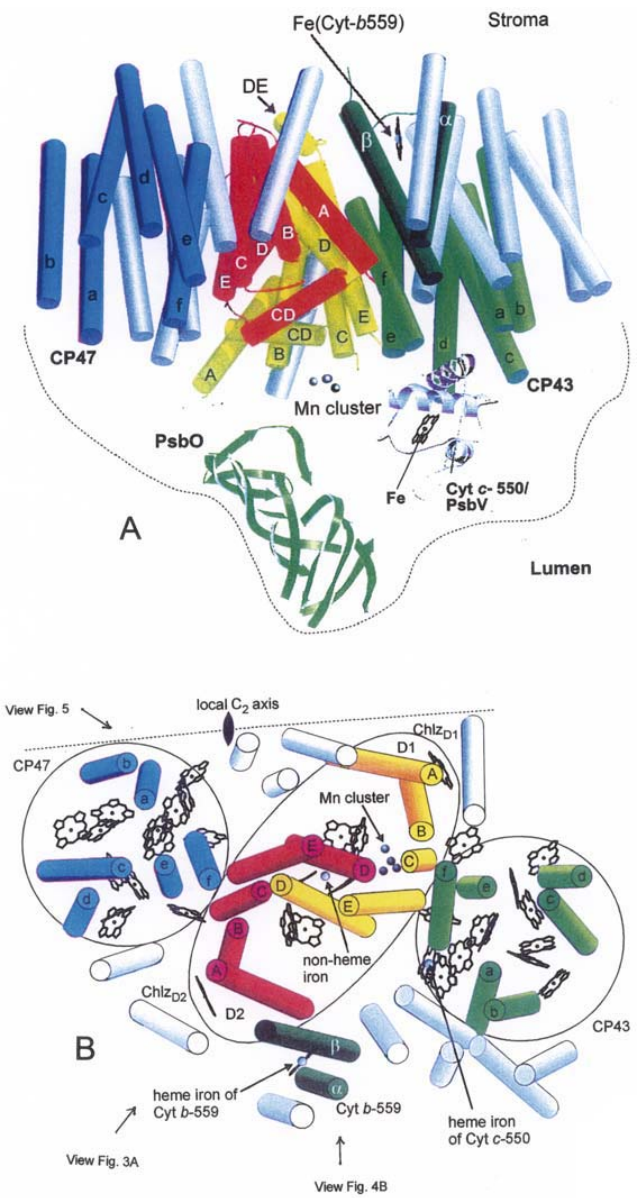

Fig. 1. Structure of the monomeric part of PS II with assignment of helices, cofactors and subunits at 3.8 Å resolution adapted from Zouni et al. (2001a). (A) Side view of PS II monomer along the long axis of D2/D1 subunits with slightly tilted membrane plane. The five transmembrane helices of subunit D1/D2 are indicated in red and yellow. The six transmembrane helices of the antenna subunit CP47/CP43 are colored dark blue and green. The twelve transmembrane helices of eight small subunits are light-blue and have not been assigned here. The α and β helices of Cyt b_{559} are dark green. The extrinsic subunit PsbO (33 kDa) is shown as a β-sheet structure and Cyt c_{550} (17 kDa) as helical model. The Mn cluster within the membrane is located close to the domain of the extrinsic subunits. For clarity the Chl cofactors and others have been omitted. (B) The structure in (A) with view direction from the stromal side onto the membrane plane. The local c_2-axis at the interface between the two monomeric parts of the dimer are indicated as well as the view direction of Color Plate 6, Fig. 1A. See Chapter 19, p. 433.

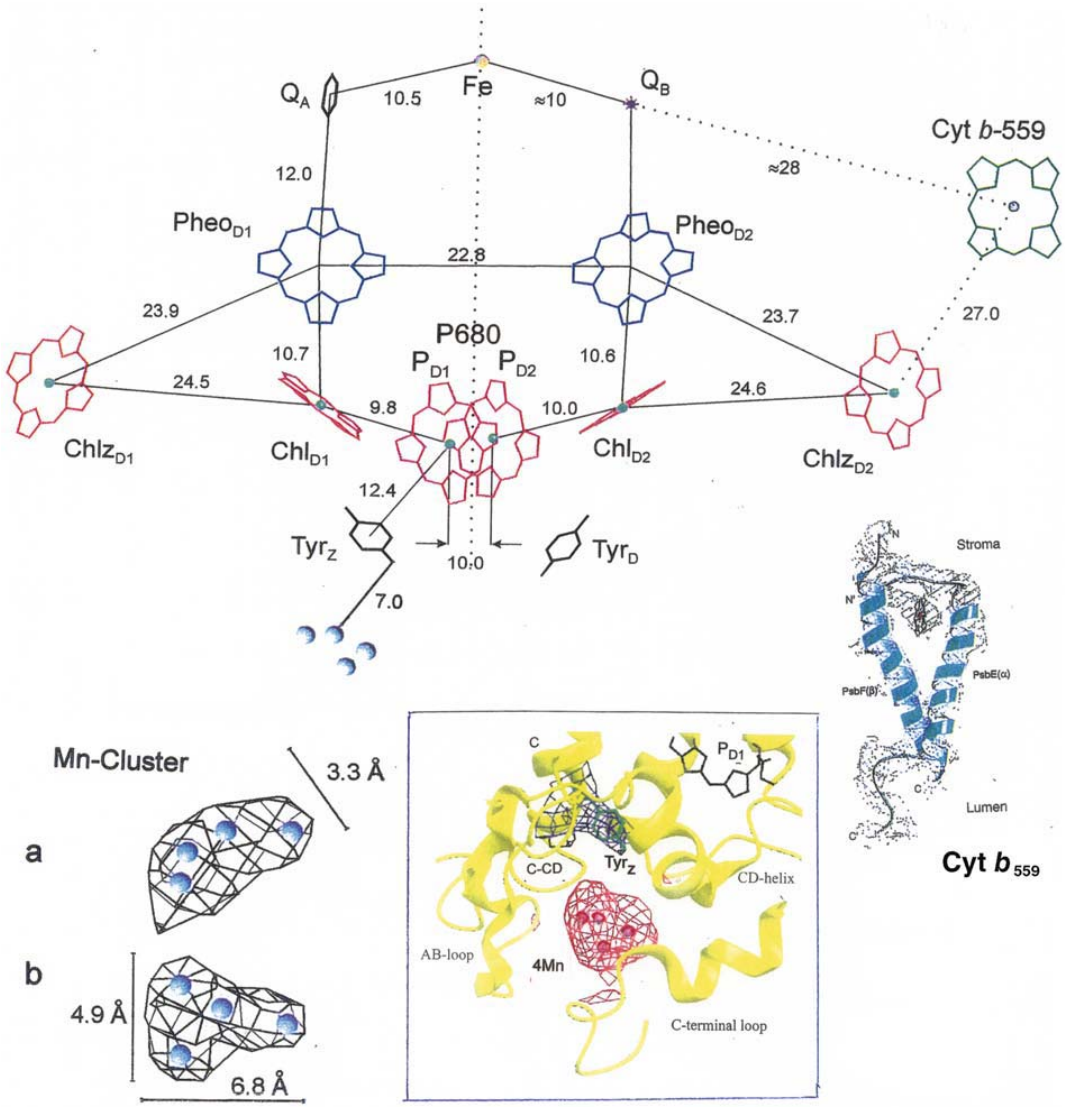

Fig. 1. Top: Arrangement of cofactors of the electron transport chain (ETC) located in subunit D1/D2 at 3.8 Å resolution (view direction as indicated in Color Plate 5, Fig. 1B and along the membrane plane). The center-to-center distances (Å) are indicated as well as the dotted pseudo-c_2 axis which is parallel to the local c_2 axis. The symmetry of the ETC is broken with the location of the Cyt b_{559} towards the stromal side and the Mn cluster towards the lumenal side. See also the close up view of Cyt b_{559} along the membrane plane. Bottom left: (a) Mn cluster with view along the membrane plane; its long axis points towards the lumen tilted ~23° against the plane; (b) view from the lumen onto the plane; Bottom right: Mn cluster surrounded by helices and loops of subunit D1 at 3.6 Å resolution. The position of P_{D1} of P680 and Y_Z of the ETC are indicated. Density of the Mn cluster contoured at 2.0 σ and of Y_Z at 0.7 σ (Zouni et al., 2001a,b). See Chapter 19, p. 437.

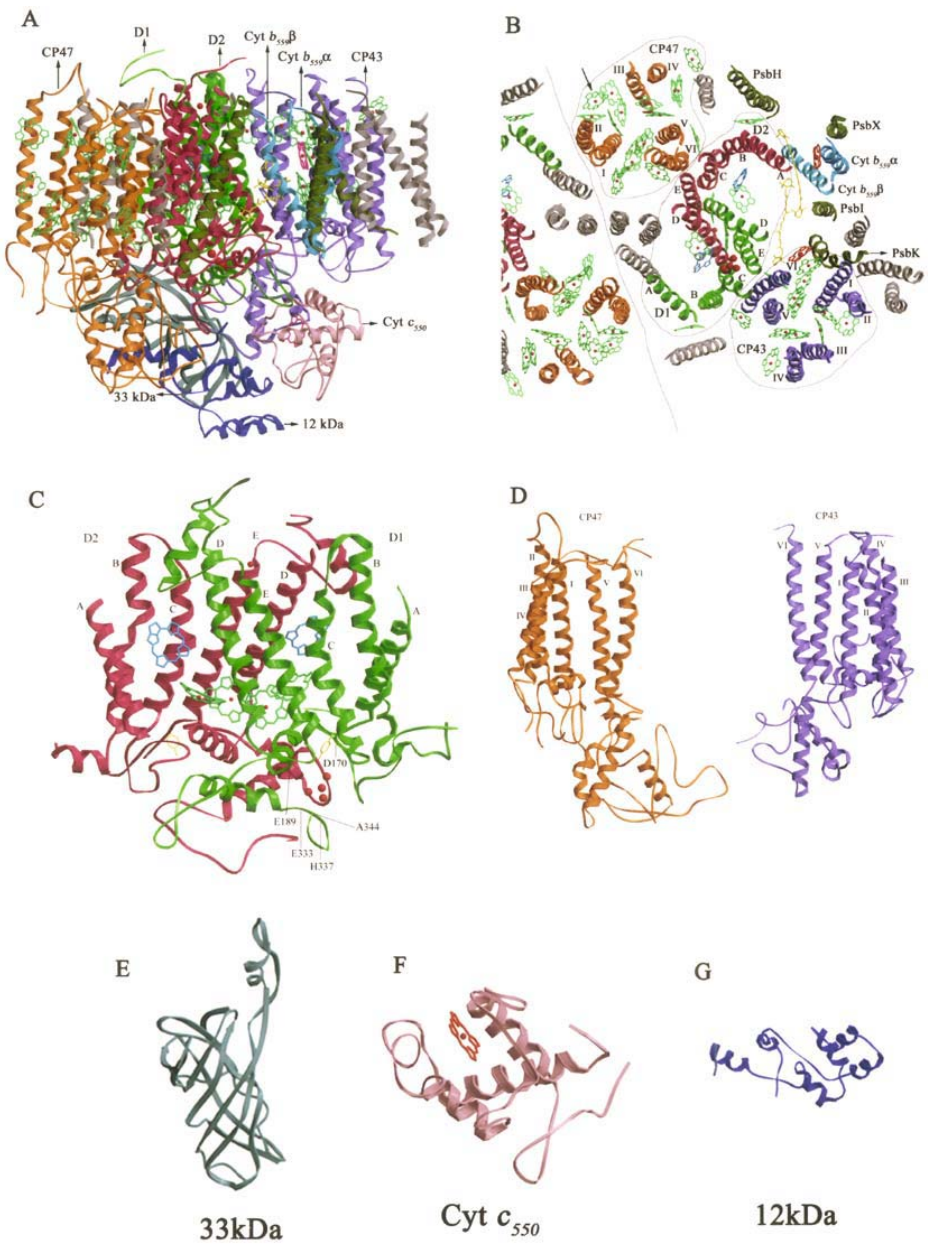

Fig. 1. Crystal structure of PS II from *T. vulcanus*. (A) Side view of one PS II monomer. (B), Top view of the transmembrane region from the lumenal side of one PS II monomer, together with part of a neighboring PS II monomer showing the formation of a PS II dimer in the crystal. Trans membrane helices (TMHs) of D1/D2 subunits are numbered A-E, and TMHs of CP47/CP43 are numbered I-VI. An arrow in (B) indicates one additional Chl found in CP47 of *T. vulcanus's* structure but not in *T. elongatus's* structure. (C) Structures of D1/D2 subunits. Four Chls and two Pheos are shown, together with Y_Z, Y_D and the Mn-cluster. Residues possibly providing ligands to the Mn-cluster are labeled. (D) Structures of CP47, CP43 subunits. (E) Structure of the 33kDa protein; (F) Structure of Cyt c_{550}. (G) Structure of the 12kDa protein. See Chapter 20, p. 455.

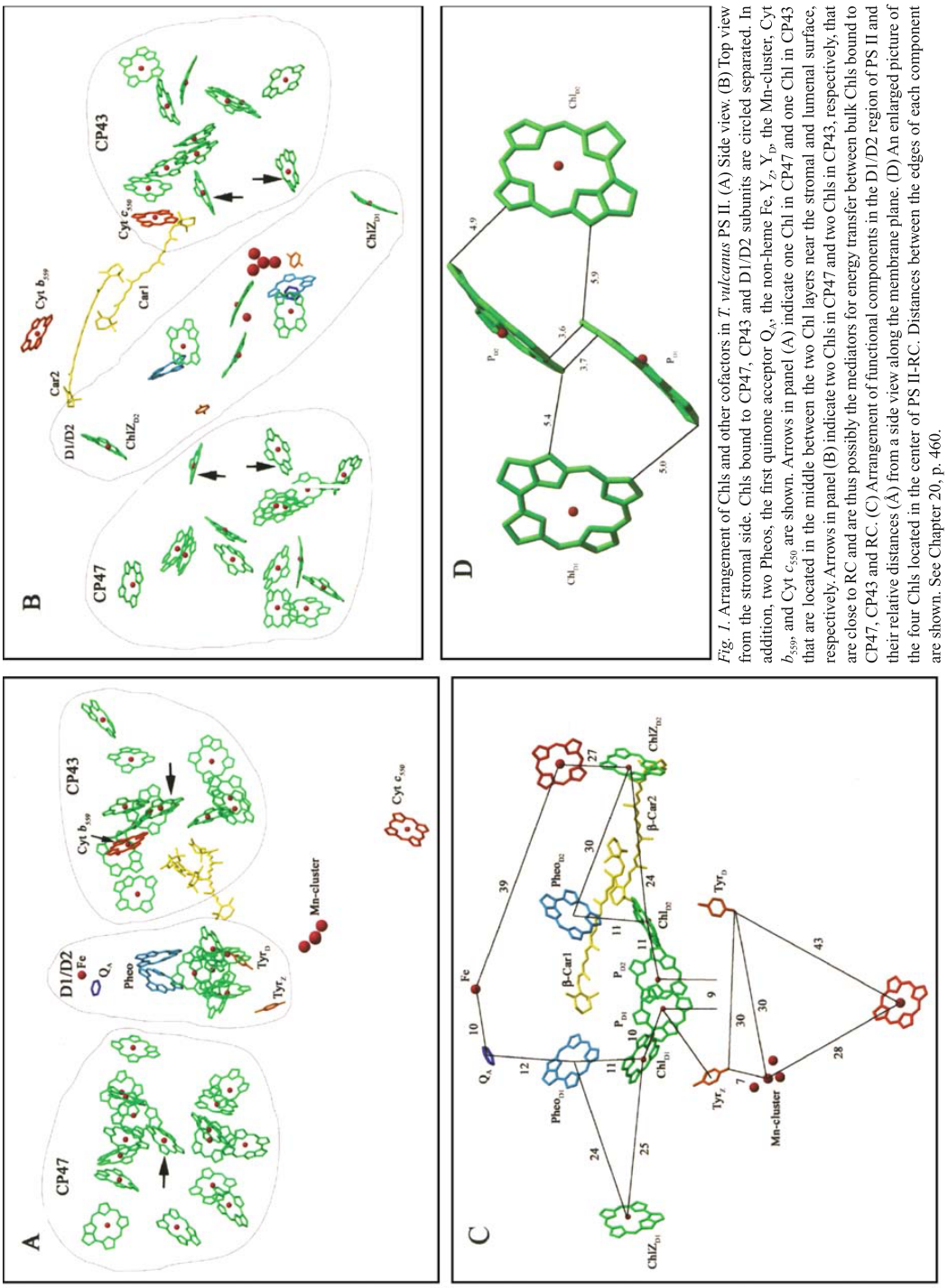

Fig. 1. Arrangement of Chls and other cofactors in *T. vulcanus* PS II. (A) Side view. (B) Top view from the stromal side. Chls bound to CP47, CP43 and D1/D2 subunits are circled separated. In addition, two Pheos, the first quinone acceptor Q_A, the non-heme Fe, Y_Z, Y_D, the Mn-cluster, Cyt b_{559}, and Cyt c_{550} are shown. Arrows in panel (A) indicate one Chl in CP47 and one Chl in CP43 that are located in the middle between the two Chl layers near the stromal and lumenal surface, respectively. Arrows in panel (B) indicate two Chls in CP47 and two Chls in CP43, respectively, that are close to RC and are thus possibly the mediators for energy transfer between bulk Chls bound to CP47, CP43 and RC. (C) Arrangement of functional components in the D1/D2 region of PS II and their relative distances (Å) from a side view along the membrane plane. (D) An enlarged picture of the four Chls located in the center of PS II-RC. Distances between the edges of each component are shown. See Chapter 20, p. 460.

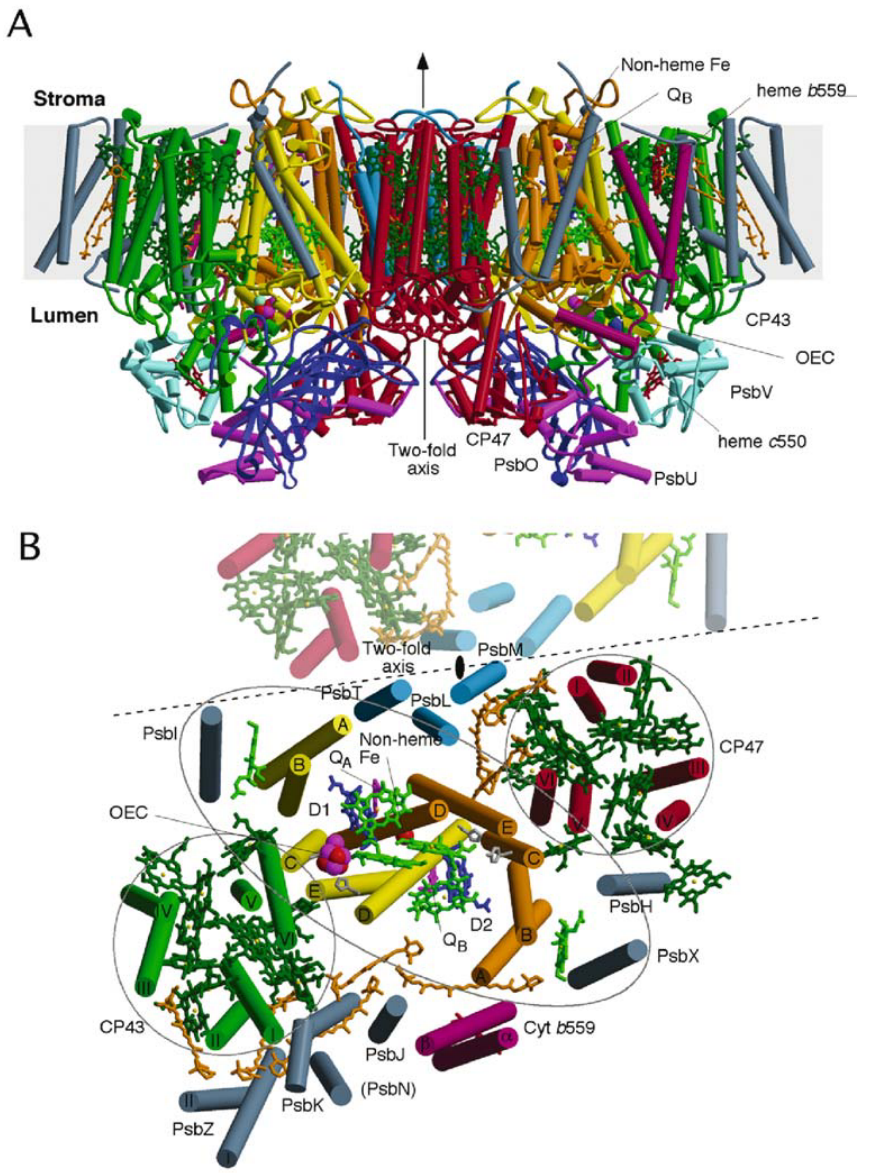

Fig. 1. Overall structure of PS II. (A) View of the PS II dimer perpendicular to the membrane normal. Helices are represented as cylinders with D1 in yellow, D2 in orange, CP47 in red, CP43 in green, Cyt *b*559 in wine red, PsbL, PsbM, and PsbT in medium blue, and PsbH, PsbI, PsbJ, PsbK, PsbX, PsbZ and the putative PsbN in grey. The extrinsic proteins are PsbO in blue, PsbU in magenta, and PsbV in cyan. Chlorophylls of the D1/D2 reaction center are light green, pheophytins are blue, chlorophylls of the antenna complexes are dark green, β-carotenes are orange, hemes and non-heme Fe are red, Q_A and Q_B are magenta. The oxygen evolving center (OEC) is shown as the red (oxygen atoms), magenta (Mn ions) and cyan (Ca^{2+}) balls. (B) View of the PS II monomer along the membrane normal from the lumenal side. A part of the other monomer in the dimer is shown to emphasize the region of monomer/monomer interaction along the dotted line. The pseudo-two-fold axis perpendicular to the membrane plane passing through the non-heme Fe relates the transmembrane helices of the D1/D2 heterodimer, the low molecular weight subunits, PsbI and PsbX and CP43 and CP47 as emphasized by the black lines encircling these subunits. Color coding is the same as in (A). See Chapter 21, p. 473.

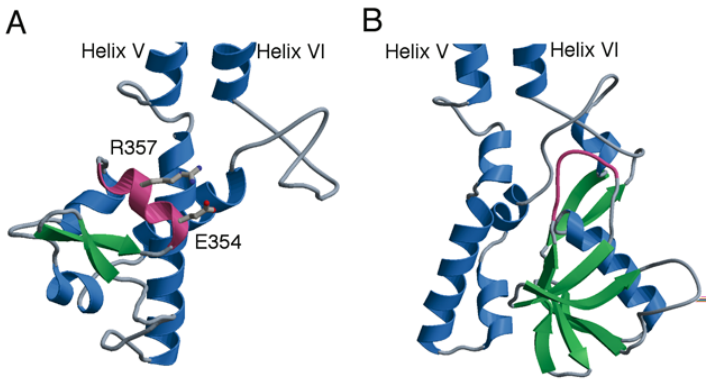

Fig. 1. Structure of the large extrinsic domains of (A) CP43 and (B) CP47. The membrane extrinsic domain of CP43 contains two long (residues 305 to 325; 385 to 399) and two short α-helices (residues 363 to 370; 376 to 383), a 2 strand β-sheet (residues 340 to 344; 348 to 352) and a 3/10 helix (residues 353 to 359). The 3/10 helix, composed of GGETMRFWD (residues 352 to 360) is fully conserved in all CP43 sequences and contains residues involved in water oxidation at the OEC (Glu354 and Arg357), is shown in pink. The lumenal domain of CP47 contains two long (residues 280 to 294; 413 to 427) and four short helices (residues 271 to 278; 297 to 305; 306 to 314; 328 to 335), and a four-stranded (residues 343 to 347; 352 to 354; 398 to 403; 407 to 412), a three-stranded (residues 355 to 357; 369 to 372; 376 to 381) and a two-stranded β-sheet (residues 336 to 338; 430 to 433). The conserved FFETFSVLV sequence (residues 362 to 370), forms a hydrophobic environment around Y_D (D2-Tyr160). See Chapter 21, p. 475.

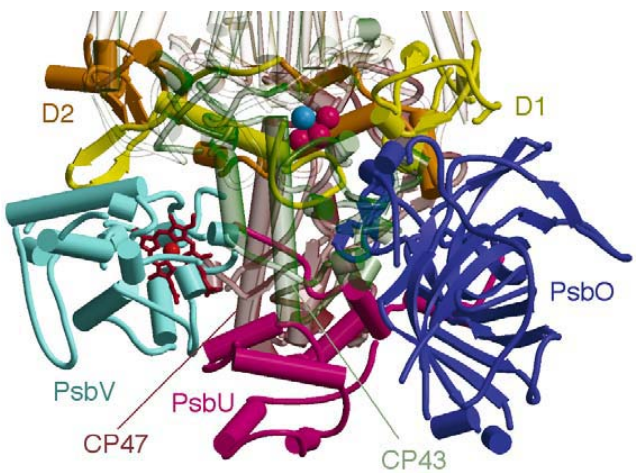

Fig. 2. A view of the lumenal surface showing the extrinsic proteins PsbO, PsbU and PsbV, the large extrinsic loops of CP47 and CP43 and the lumenal portions of the D1 and D2 proteins. Together these polypeptides form a 'protein-cap' over the OEC. See Chapter 21, p. 476.

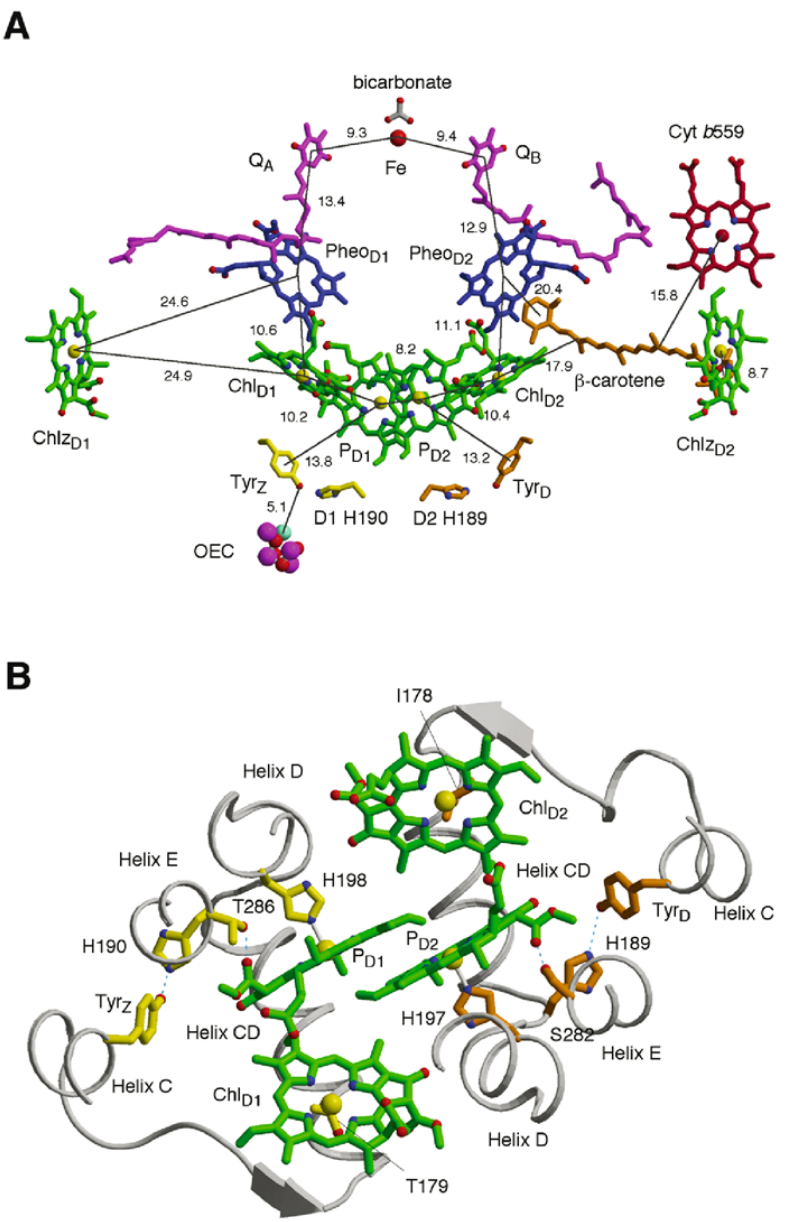

Fig. 1. Cofactors involved in electron transfer. (A) Electron transfer cofactors shown perpendicular to the internal pseudo-two-fold. The phytyl tails of the chlorophylls and pheophytins have been removed for clarity. The side chains of Y_Z (D1-Tyr161) and D1-His190 are shown in yellow and Y_D (D2-Tyr160) and D2-His189 in orange. The four chlorophylls comprising P680 are in direct van der Waals contact, and other electron transfer distances are given in Å. (B) The P680 dimer of chlorophylls (P_{D1} and P_{D2}) and accessory chlorophylls (Chl_{D1} and Chl_{D2}). The protein main chain is depicted in light grey while the side chain bonds and carbon atoms follow the coloring of the protein subunits (yellow, D1; orange, D2). The histidine ligands, D1-His 198 and D2-His 197, are shown as well as the redox active Y_Z-D1-His 190 and Y_D-D2-His 189 pairs. The view is down the pseudo-two-fold axis from the stromal side. See Chapter 21, p. 477.

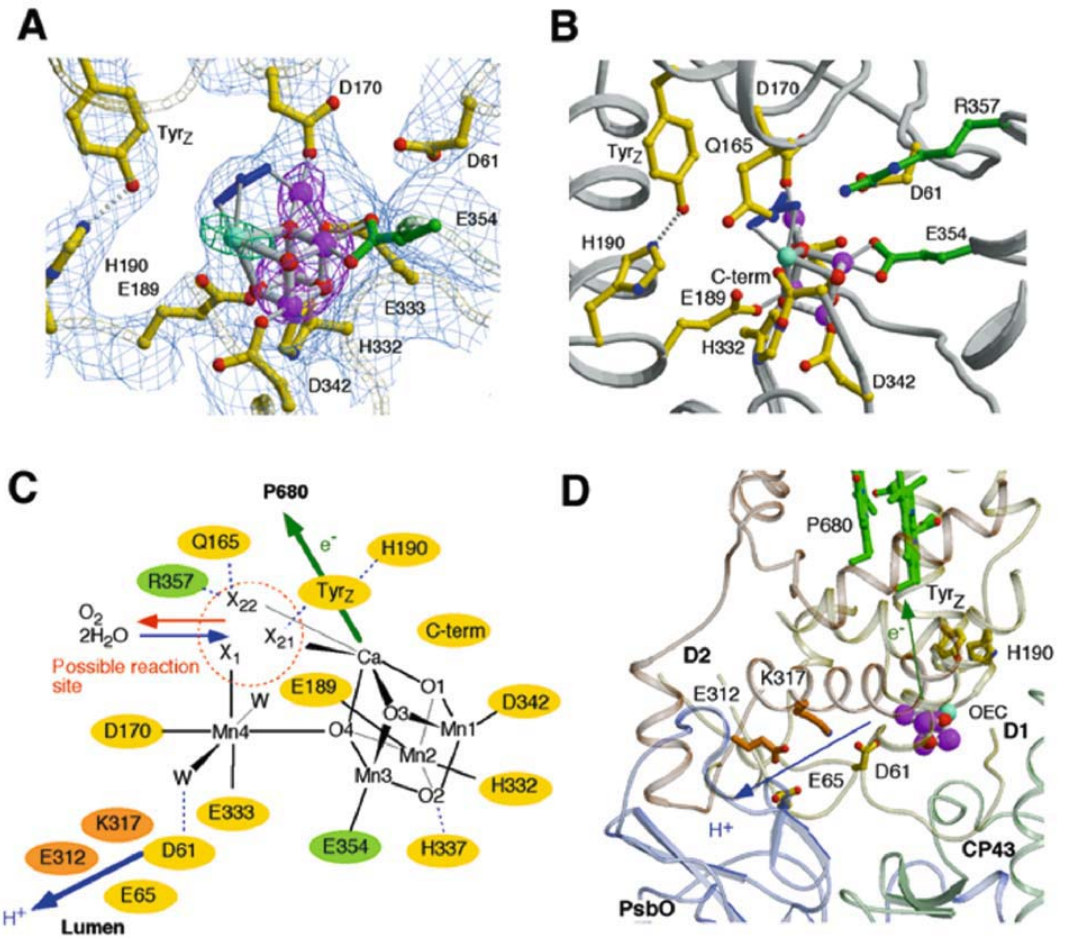

Fig. 1. The oxygen evolving center (OEC). (A) View of the OEC with side chain ligands and possible catalytically important side chain residues. Mn ions, Ca^{2+} and oxygen atoms are shown in magenta, cyan and red, respectively. One unidentified non-protein ligand to the OEC is colored in blue. Protein main chain is depicted in light grey while the side chain bonds and carbon atoms follow the color coding of the protein subunits (yellow, D1; green, CP43). σ_A weighted $2|F_o| - |F_c|$ density is shown as a light blue wire mesh contoured at 1.5σ. Anomalous difference Fourier maps at 1.89340 Å (Mn edge, contoured at 10σ.) and 2.25430 Å (highlights Ca^{2+}, contoured at 7σ) wavelengths are shown in magenta and blue-green, respectively. (B) The same as (A) but with a rotation around the y-axis of 40° and without electron density and anomalous difference maps. (C) Schematic view of the OEC. Residues in D1, D2 and CP43 subunits are shown in yellow, orange and green, respectively. X_1, X_{21} and X_{22} are possible substrate water binding positions to Mn_4 (X_1) and to Ca^{2+} (X_{21} and X_{22}) identified from the position of the non-protein ligand and coordination pattern of Mn and Ca^{2+} ions. Possible water molecules, which are not visible at the current resolution, are indicated as W. (D) Hydrophilic pathway between the active site and lumen (blue arrow). The residue coloring is the same as in (B). See Chapter 21, p. 480.

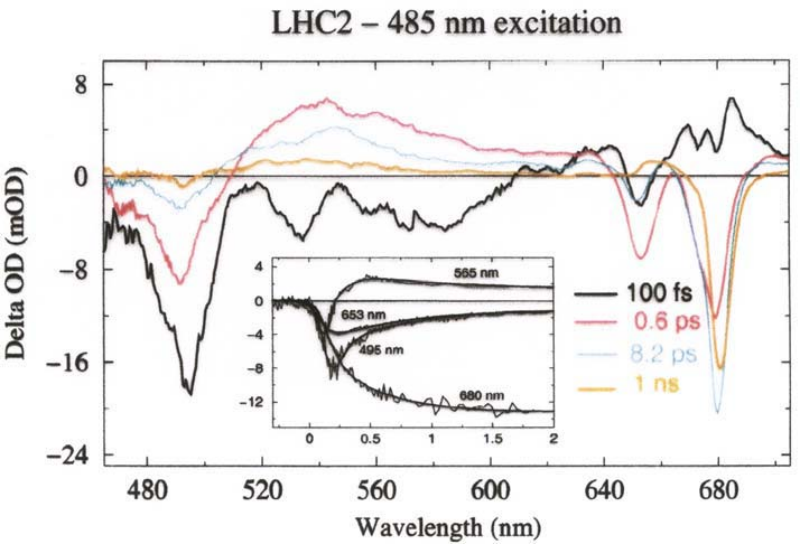

Fig. 1. Spectral evolution in LHCII at 77K following excitation with a 100fs laser pulse at 485nm. The experimental spectra as a function of delay time were analyzed with a linear scheme A->B->C->D->A with increasing decay times to visualize the spectral evolution in the system and the resulting Species Associated Difference Spectra (SADS) have been plotted. (black), lifetime 100 fs; (red), lifetime 0.6 ps; (blue), lifetime 8.2 ps; (yellow), lifetime 1ns. The insert shows the experimental kinetics at some selected wavelengths including the fits based on this model adapted from Gradinaru et al. (2000). See Chapter 22, p. 495.

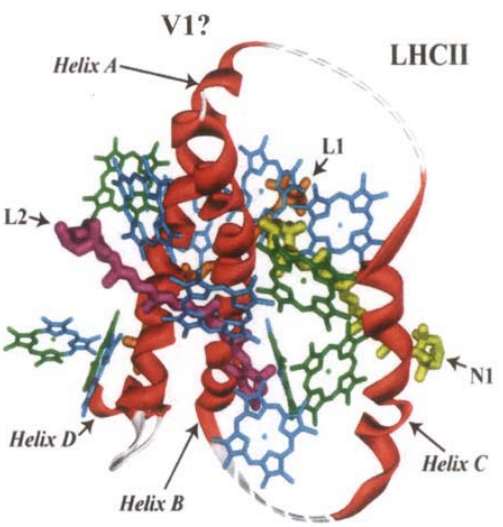

Fig. 2. Carotenoids and LHCIIb assembly. Specificity of each binding site is indicated (L, lutein; V, violaxanthin; N, neoxanthin; Z, zeaxanthin). An LHCIIb monomer binds approximately 7 Chl *a* molecules (blue) and 5 Chl *b* molecules (green) (Kühlbrandt, et al., 1994; Bassi and Caffarri 2000). In an LHCIIb monomer, the L1 site is occupied by lutein (orange), while the L2 site is typically occupied by either lutein or violaxanthin (purple). The N1 site is specific for binding neoxanthin (yellow). Violaxanthin is proposed to bind loosely to the V1 site and is inter-exchangeable with zeaxanthin during the xanthophyll cycle (Caffarri et al, 2001). Adapted from Croce et al., (1999) and Bassi and Caffarri (2000). See Chapter 23, p. 521.

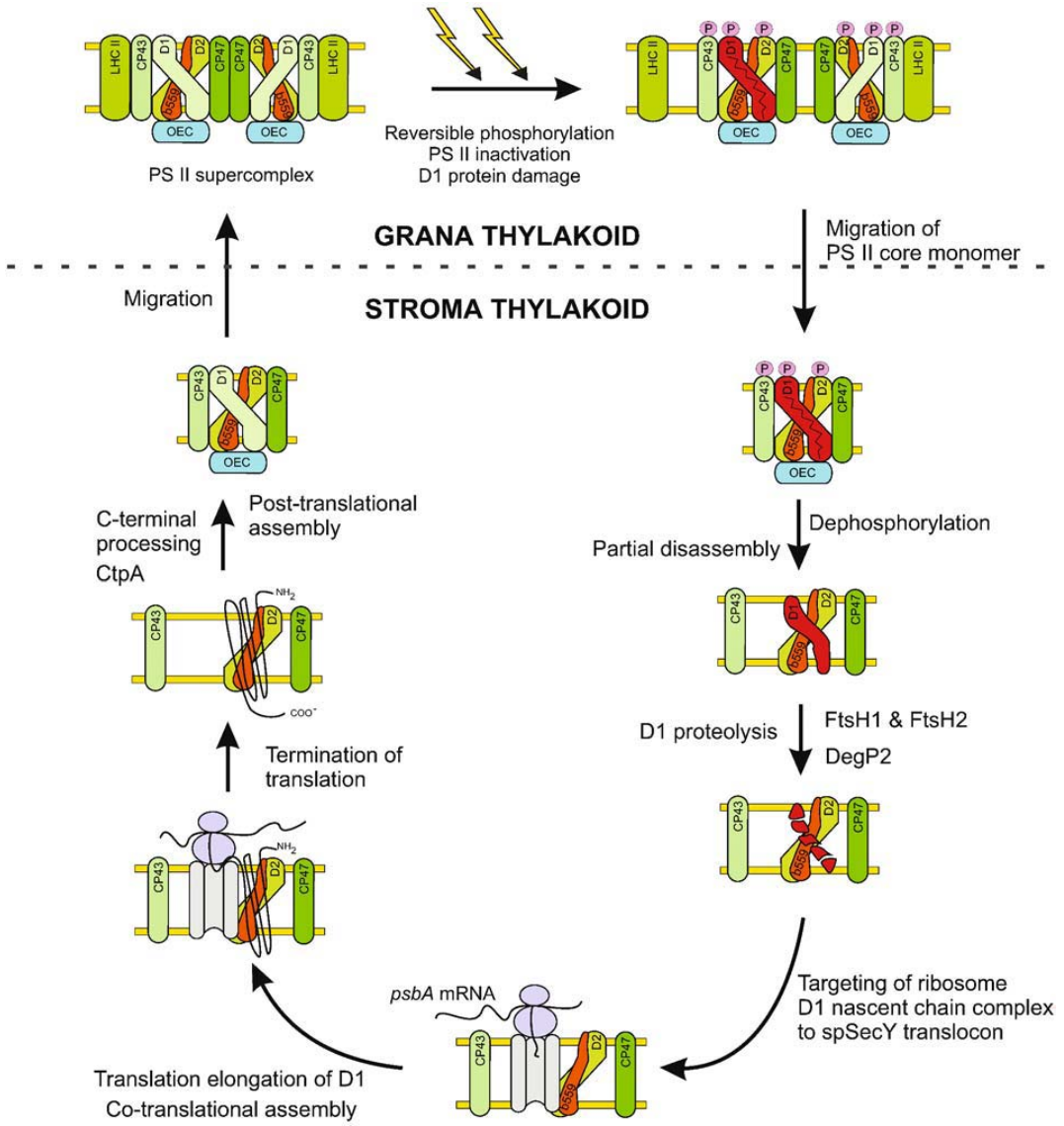

Fig. 1. Photoinhibition-repair cycle of the PS II complexes. See Chapter 27, p. 642, text for details.

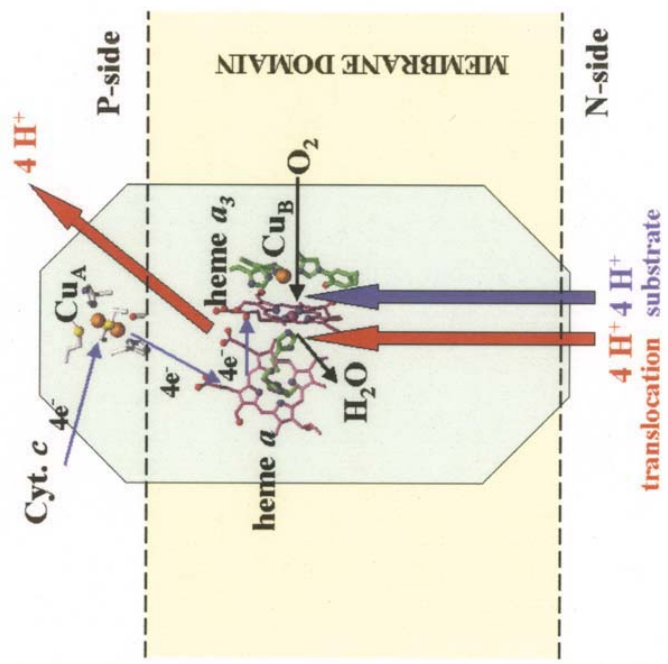

Fig. 2. Overall function of CcO. Heme groups are shown in purple and copper ions in orange. The histidine ligands of the heme groups and of Cu_B are shown in green, as is the tyrosine residue in the binuclear site that is covalently bonded to one of the histidine ligands of Cu_B. The blue arrows depict how the chemistry of O_2 reduction to water (by electron and proton transfer) is oriented with respect to the positively charged P-side and negatively charged N-side of the membrane. Red arrows depict proton translocation. The program VMD was used for the molecular graphics (Humphrey et al., 1996). See Chapter 31, p. 702.

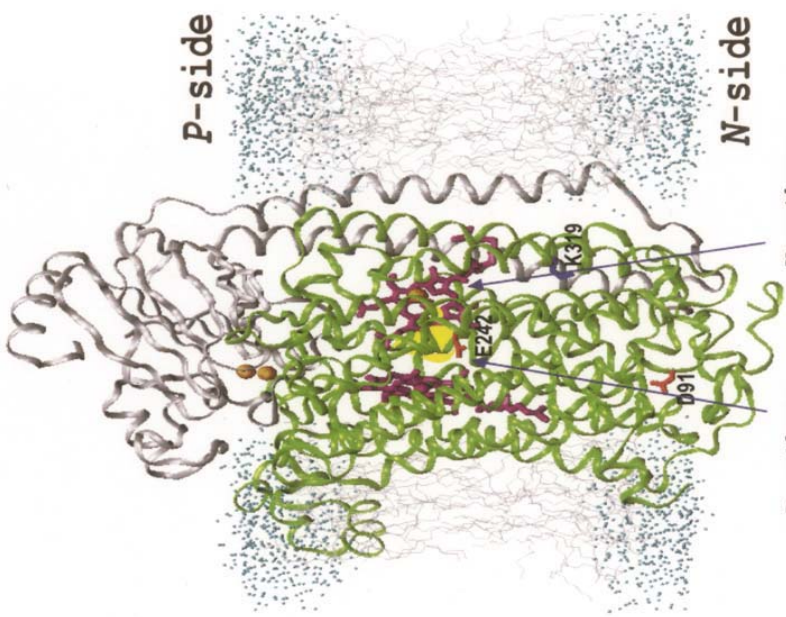

Fig. 1. Rhodobacter sphaeroides CcO (Svensson-Ek et al., 2002) in a model membrane. Two subunits are shown in different colors: I, green; II, grey. The redox centers are marked with hemes in purple and coppers orange. The structure is drawn from 1M56.pdb and a model membrane, by the program MOLSCRIPT (Kraulis, 1991). The proton transfer pathways D and K are roughly outlined, as are the key proton transfer residues Asp91, Glu242 and K319 (numbering according to the bovine heart enzyme). A hydrophobic cavity between Glu242 and heme a_3 (yellow) may transiently contain a number of water molecules. See Chapter 31, p. 700.

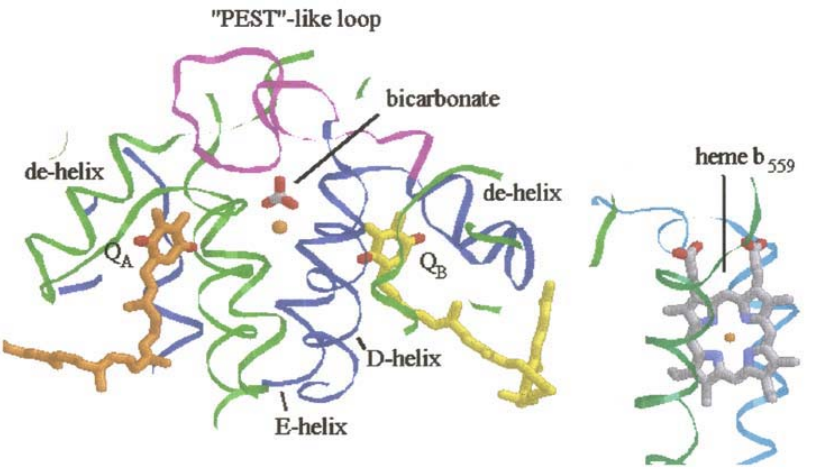

Fig. 1. Photosystem II viewed from the side to show the topology of the acceptor side. Coordinates were taken from the structure by Ferreira et al. (2004) (PDB ID 1s5l), by abstraction of a monomer of the main functional subunits and chromophores. The D1 subunit is in blue (with the 'PEST'-like loop in magenta), D2 in green, shown by ribbons. Prosthetic groups are shown as stick models, with C-atoms of Q_A in orange, Q_B in yellow, and bicarbonate and heme b_{559} in gray, other atoms in CPK-colors. Other structural features discussed in the text are indicated. See Chapter 8, p, 187.

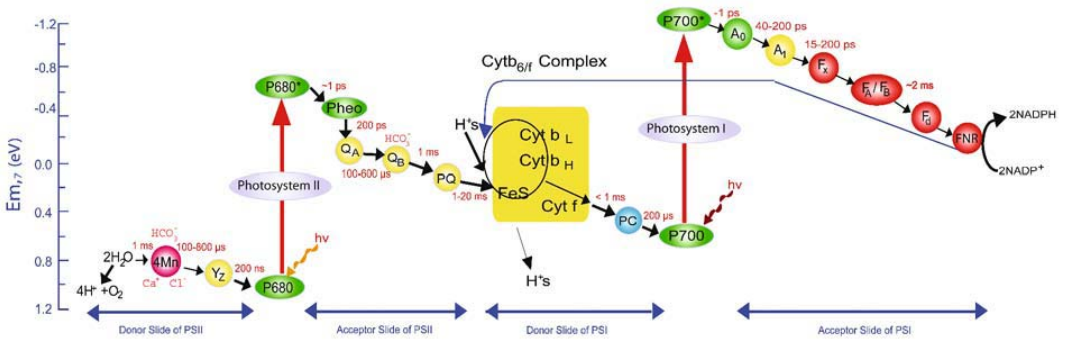

Fig. 2. The Z-scheme of oxygenic photosynthesis for electron transfer from water to nicotinamide adenine dinucleotide phosphate (NADP) modified from Fig. 4 of Govindjee (2004). From left to right: Mn stands for Mn cluster; Y_z, for tyrosine-161 on the D1 protein; P680, for the primary electron donor of PS II; Pheo, for pheophytin; Q_A, for the first plastoquinone electron acceptor of PS II; Q_B, for the second plastoquinone electron acceptor of PS II; PQ, for the plastoquinone pool; Cyt b_L and Cyt b_H, for low and high potential cytochrome b_6; Cyt b_6f, for cytochrome b_6f complex; Cyt *f*, for cytochrome *f*; FeS, for Rieske iron sulfur; PC, for plastocyanin; P700, for the primary electron donor for PS I; A_0, for a monomer Chl; A_1, for vitamin K; F_X, F_A and F_B, for iron sulfur centers 'x', 'A' and 'B,' respectively; and F_d, for ferredoxin. Also shown are the approximate half-times for most of the reactions, the existence of the 'Q'-cycle, the cyclic reaction around PS I, and the possible sites for calcium, chloride and bicarbonate ions in PS II. See Chapter 1, p. 13.

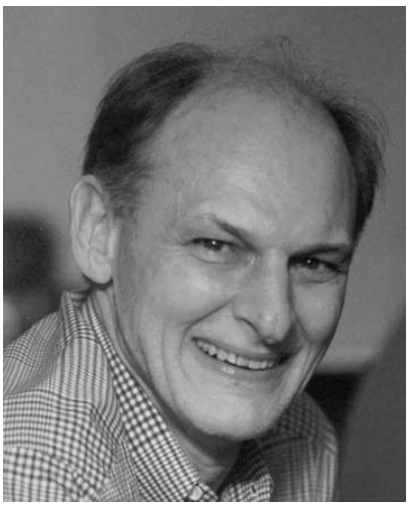

Gerald T. Babcock
(1946–2000)

Dedication/Perspective: A tribute to Jerry Babcock

The assembly and publication of a book covering all aspects of Photosystem II (PS II), including analogies between this enzyme system and cytochrome oxidase, would have thrilled and delighted Jerry. If one looks at the contents of this volume, it takes very little time to discover a number of chapters (for example 7, 9–13, 16, 17, 25 and 31) where Jerry would have been a leading choice as an author. A cursory inspection of the citations at the end of many more of these chapters will turn up his name as a contributor of important results to our understanding of mechanistic and structural aspects of PS II and cytochrome oxidase. It is this breadth of impact of Jerry's research that makes this book such a fitting tribute to our colleague, who had even more to contribute, when his untimely death ended an outstanding scientific career. *Photosystem II: The Light Driven Water:Plastoquinone Oxidoreductase* stands as a lasting tribute to the life and work of Jerry Babcock, and it is our honor and privilege to dedicate it to his memory.

An obituary of Jerry appeared in *Photosynthesis Research* [68: 89–94 (2001)]. We have expanded on material from that paper for this dedication to enlarge on some aspects of Jerry's life so that readers, including his many friends and colleagues, may gain some larger sense of the scope of Jerry's many activities, and the impression he made on people throughout his life.

Jerry's impact on science was signaled by a number of events that were held in his honor after his death. The first of these, organized by Les Dutton, was a symposium entitled 'Et:pcet:HAT:pt[1]: 40 Years of Tunneling in Biology' that was held at the Johnson Research Foundation of the University of Pennsylvania in May, 2001. The second symposium, organized by one of us (SF-M) and John McCracken at Michigan State University, was held in June, 2001 and focused on research topics that Jerry addressed in his lifetime. The third symposium was a satellite conference featuring talks on photosynthetic electron transfer held at Couran Cove, Australia, organized by Karin Åhrling and Ron Pace, preceding the International Photosynthesis Congress held in Brisbane in August of 2001. A fourth event, a symposium organized by Gernot Renger and Tom Wydrzynski, was held as part of the International Photosynthesis Congress and featured talks on PS II and the O_2-evolving reaction. In addition, a special lecture, 'The G.T. Babcock Memorial Lecture,' was designated at the International

[1]Electron transfer: proton coupled electron transfer: Hydrogen Atom Transfer: proton transfer

T. Wydrzynski and K. Satoh (eds): Photosystem II: The Light-Driven Water:Plastoquinone Oxidoreductase, pp. 1–10.

Congress of Bioinorganic Chemistry in Florence (Italy) in 2001 and given by one of us (SF-M) on electron transport in cytochrome *c* oxidase. A special issue of *Biochimica et Biophysica Acta* [1655: 1–413 (2004)], edited by Peter Brzezinski, Cecelia Tommos and Anders Ehrenberg, was dedicated to Jerry.

Jerry Babcock was the firstborn son of Emelda (Mel) and Frank Babcock. He was born on February 9, 1946, in Minneapolis, Minnesota, and received his primary and secondary school education there. He also began his athletic career as a basketball player in the Minneapolis school system. Jerry enrolled at Creighton University, Omaha, Nebraska, for his undergraduate education. He received his B.S. degree with honors in Chemistry, and he was also a member of the varsity basketball team, playing on a National Collegiate Athletic Association scholarship. Paul Michael, a former classmate at Creighton, remembers Jerry's undergraduate days, and in doing so also explains for us Jerry's later fascination with, and competition in, pick up basketball games at many Gordon Research Conferences. Paul T. Michael (of Arlington, Virginia) writes:

'We both graduated from Creighton in early summer of 1968 and Jerry — who practically everyone called 'Babs' — began a rapid ascent in academia that ultimately led him to the Michigan State University academic community. If I remember correctly, Babs obtained his advanced degrees from U. Cal-Berkeley and did 'post doc' work at Rice University before he arrived in East Lansing. But it must be understood that Babs was a Creighton University 'Bluejay' long before he became a Michigan State University 'Spartan.' That distinction is important. Being a Bluejay meant Babs had the chance to be an athlete and play at the highest level of competition in college basketball at that time. Like many Jesuit schools, Creighton takes its basketball seriously and it had some of the most competitive schedules in the nation during Babs' college days.

'Babs started his athletic career at Creighton as a walk-on for a Freshman basketball team that included 8 athletic scholarship players. He then made the varsity team his sophomore year, also as a walk-on, and played in a number of games. He made the varsity again in his junior year, as a walk-on, but his playing time increased substantially. As a senior, Babs made the varsity once again. But that year he was a Bluejay basketball player who had an athletic scholarship and started in every game, save one due to illness.

'Babs had arrived. Everyone knew that his intelligence was extraordinary. But in his senior year, he became a full-fledged 'jock.' That image might be difficult to accept or comprehend for someone who only came to know Babs when he was an adult, especially in an academic environment. But I am positive that Babs was as happy and thrilled with his athletic accomplishments at Creighton as he was with his academic achievements. He persevered and earned an athletic scholarship by honing his skills and talents. He started his senior year and played against some of the best college players in the 20th century. Those with a working knowledge of basketball will appreciate the fact that Babs went, to use a cliche, toe-to-toe with the likes of Elvin Hayes and Bob Lanier (both of whom are in the NBA's Hall of Fame). In fact, I have a vivid memory of Babs in a confrontation during a road game towards the end of our senior year. Babs was standing, roughly speaking, nose (his) to belly-button (belonging to 6' 11", 285 lb., size 22 EEE sneaker, Bob Lanier of St. Bonaventure) and shouting at the owner of the belly-button in question (a person whose size was blotting out the overhead lighting in Babs' immediate personal space) to shut up and go to Hades.

'There is no doubt that Babs' intelligence was overwhelming. He would have attained a perfect 4.0 grade average for his entire college career had it not been for the B+ in a mandatory ROTC course one semester. But I know he was just as proud of two other numbers he posted in that period: 5.0 and 5.9. Those were his averages in his senior year, this brainy guy from St. Louis Park, Minnesota who had big dreams, in points (5.0) and rebounds (5.9) over a full varsity basketball season as a starter against players who would later earn their living in professional basketball. Another thing is worth mentioning about his year as a 'formal' jock at Creighton. I believe all of his friends in East Lansing would have enjoyed seeing Babs blush, turning bright red on the court in the final home game of his senior year when the student body began to chant 'Jerry, Jerry, Jerry' towards the end of the game in recognition of what Babs had achieved as an athlete.

'Two final thoughts may help to flesh out the person I am attempting to describe. About 7 or 8 weeks before our graduation in 1968, Babs showed me a letter he had received from the Dallas Cowboys professional football team. While Dallas typically had great teams in those years, it also had the reputation of having the most complicated, complex system of plays and

formations used in the National Football League. For that reason, Dallas sought individuals who were great athletes and, if possible, also had shown a level of academic achievement not usually associated with college athletes. It was rumored that Dallas maintained a database (on a computer, no less) by which it kept tabs on intelligent athletes who might have potential, even if they were not football players. That was the purpose of the letter Babs received. The Dallas Cowboys had invited him to a special camp early that summer for the proverbial tryout, even though Babs had not played football since high school. As I recall, the letter indicated the Cowboys thought he might have some potential as a tight end, since he was about 6' 4" and weighed a little over 200 lbs. Those who knew him may recall that he also had very large hands with long fingers, even for someone of his size. If you think about it, Babs might have ended up playing with Roger Staubach. We urged him to accept the invitation, but he just chuckled and said he had other things in life to pursue.'

After graduation from Creighton, Jerry joined Kenneth Sauer's group at the University of California at Berkeley as a Ph.D. student in 1968. Berkeley was then, as now, a center for the application of biophysical techniques to problems in photosynthesis. These were exciting years for progress in understanding the mechanism of photosynthetic O_2 evolution, with the flashing light experiments of Pierre Joliot and Bessel Kok that established the period four pattern of O_2 release. Jerry took this area as his thesis topic and continued researching it for his entire scientific career. Along with Charles Weiss, a postdoc in the Sauer group, he built a Joliot-style oxygen electrode that was a complex marvel of pumps, hoses and a hodge-podge of electronics salvaged from other uses. It was not pretty but it worked remarkably well. This 'make it work' philosophy was characteristic of Jerry and his approach to science. Soon Jerry supplemented his work with the oxygen electrode with studies on EPR signals associated with photosynthesis. Barry Commoner had first observed these signals some years earlier and the laboratory of Melvin Calvin had done some work on them in photosynthetic bacteria, but Jerry was the first at Berkeley to study Signal II, which was associated with PS II. Its sluggish kinetics initially suggested that it was not a mainstream electron carrier and therefore didn't receive much attention. Under Ken's guidance, Jerry undertook a systematic investigation of the 'Signal II' species, and showed that there was, in fact, more than one contributing radical component in the signal (Babcock and Sauer, 1975). By a variety of treatments that affected O_2 evolution, Jerry was able to show that the kinetic behaviors of these signals coincided with the presence or absence of a functional O_2-evolving reaction. Out of these investigations emerged the first systematic nomenclature for these important PSII redox intermediates: Signal IIs, the dark-stable form of the signal, Signal IIf, the EPR signal from a second species detected upon inhibition of water oxidation, and lastly, Signal IIvf, a very rapidly decaying species associated with the fully functional O_2-evolving reaction. It was on the basis of work by Jerry and one of us (RB) that Ken Sauer's group was able to position the Signal IIf/IIvf species as a redox intermediate between the O_2-evolving reaction and the primary electron donor, P680, of PS II (Blankenship et al., 1975). But the molecular identity of Signal II (later renamed 'Z') was still elusive. Some experiments indicated that it might be a quinone, but the data were not very convincing. Jerry would return to this question later in his independent scientific career.

In the autumn of 2000, a note was found in the drawer of the desk that Jerry occupied from 1968–1972 in the Calvin laboratory. It is clearly written in Jerry's handwriting and reads:

'It is very important to have a long range goal; once this is realized the steps necessary toward its attainment become logical progressions and not arbitrary plunges into the void.'

We have not been able to determine if Jerry was the author of this quote or if he found it somewhere else, but it typifies his thoughtful approach to science.

During the time that Jerry was a graduate student, he was the natural leader, both scientifically and socially, of the Sauer group, which consisted of a substantial number of students, postdocs and other visitors who came and went. Among the most memorable recurring events were the abalone diving expeditions that took place with some regularity on the Northern California coast near Salt Point. To get to the abalone it was necessary to free dive to a significant depth in cold and invariably murky waters in the presence of thick stands of giant kelp. After reaching the bottom, you had to swim around and find an abalone, measure it with a gauge to determine if it was of legal size and then pry it off the rock with a metal bar akin to a tire iron. If the abalone sensed its impending fate it would clamp down firmly on the rock and become almost impossible to remove. Jerry was the master of this very challenging activ-

ity. He could routinely stay down much longer than anyone else, despite his heavy smoking habit, (which can lead to significant amounts of CO-hemoglobin in the blood). He also had the knack to pop the abalone off the rocks quickly and easily. Sometimes he would surface with two or three in his arms from a single dive! After the diving expedition, the abalone would be brought back to Berkeley and that evening a huge pot luck abalone feed would take place, with pounded, breaded and fried abalone as center stage, but with a wide range of other dishes provided by other guests.

One of us (RB) was a student in the Sauer group at that time, beginning studies two years after Jerry arrived. It is often customary to have a more senior graduate student serve as an informal mentor for new students. Jerry served that role for RB and they spent many hours together doing experiments and discussing both the details of the work and general aspects of science and its relation to society.

After Jerry received his Ph.D. in 1973, he spent a year as a post-doctoral fellow in the Sauer group. In 1974, he joined Graham Palmer's laboratory at Rice University where he began research on cytochrome oxidase that was to later become a major part of his independent scientific career. His weekdays were spent learning about cytochrome oxidase, with fellow postdoc Larry Vickery, resulting in several ground breaking (and still often quoted) papers on the electronic properties of the heme centers of cytochrome oxidase (Babcock et al., 1976, 1978; Tweedle et al., 1978). During this time he augmented his experimental expertise with techniques such as resonance Raman spectroscopy that would be critical to the success of his later research. It is less widely known that many weekends (when Graham was out of town) were spent flashing thylakoid membrane suspensions that were quickly transferred into an EPR cryostat in search of paramagnetic signals that Jerry believed would be associated with the S_2 state of the Kok-Joliot Cycle. It remained for G.C. (Chuck) Dismukes and Yona Siderer to find this elusive signal (Dismukes and Siderer, 1980), the well-known S_2 multiline signal of Photosystem II.

Canoeing was a favorite mode of relaxation for Jerry, as many of his former students and post-docs will testify. At Rice, Jerry organized several memorable outings. However, in one case he neglected to call ahead to check on the water level in the east fork of the San Jacinto River, and members of the Palmer group ended up carrying their canoes some distance down a dry riverbed to the point where they were to be picked up.

Jerry was recruited by the Chemistry Department at Michigan State University (MSU), where he joined the faculty as an assistant professor in 1976, and where he spent the rest of his career. He was promoted to associate professor with tenure in 1980 and to full professor in 1984; from 1990 to 1998, he was chair of the Chemistry Department. In 1997, he received the highest honor his university can bestow, the title of University Distinguished Professor. When he arrived at MSU, Jerry set about establishing a first-rate facility for the application of physical methods to the characterization of cytochrome oxidase and photosynthetic systems. He began the process of recruiting a research group of enthusiastic graduate students and initiated a number of innovative research projects that continued to the end of his career. In his first work on cytochrome oxidase, he collaborated with Irving Salmeen (Ford Motor Company) and Chris Chang (at MSU) to carry out a series of resonance Raman studies on oxidase and model heme compounds (Salmeen et al., 1978; Babcock and Chang, 1979; Babcock and Salmeen, 1979). These and subsequent studies were critical to defining the complex vibrational spectrum of the enzyme, knowledge that would be key to later incisive investigations of the mechanism of oxygen reduction and the nature of the metal ligands. A particularly important contribution from model studies (Ward et al., 1983) and spectral analysis of oxidase (Callahan and Babcock, 1983) was one of the first explicit molecular models of how a redox reaction could be linked to proton pumping in cytochrome oxidase (Babcock and Callahan, 1983). During a sabbatical with Bill Woodruff in Austin, Texas, the first time-resolved resonance Raman studies on cytochrome oxidase were carried out (Babcock et al., 1984, 1985). This began a 15-year intensive effort to pin down the elusive oxygen intermediates of the cytochrome oxidase reaction, an effort that would require pushing resonance Raman spectroscopy to its limits.

With the oxidase experiments up and running, Jerry returned to investigations of the Signal II species associated with Photosystem II that involved his first graduate students in this area (Christine Yerkes, Demetrios Ghanotakis) and a post-doctoral fellow, Patrick O'Malley. The focus of this research was to extend the characterization of the EPR signal (Yerkes

and Babcock, 1981; Ghanotakis et al., 1982), and to discover its molecular origins. In the first of these experiments, a search was made for model compounds that would simulate the EPR spectrum of Signal II, by now called 'Z'. This approach identified quinone radicals as promising candidates (O'Malley and Babcock, 1984a), but the spectroscopic data from these compounds was never entirely satisfactory, and the plastoquinone content of Photosystem II preparations was insufficient to account for the presence of Q_A, Q_B, and the two additional quinones needed for the two EPR signals comprising the different Signal II species. The alternate approach was to apply isotopic labeling techniques and assess the results using EPR. The first experiments by Bridgette Barry, who was a joint post-doc with Jerry and Lee McIntosh, explored incorporation of deuterated tyrosine into cells of *Synechocystis* PCC 6803; the EPR properties of 'Z' were dramatically modified (altered lineshape, narrowed linewidth), a result showing that 'Z' was in fact a tyrosine radical (Barry and Babcock, 1987). This key result was quickly followed by the site-directed mutagenesis experiments, in collaboration with Rick Debus and Lee McIntosh, which identified the redox active tyrosines of PS II as Tyr161 of D1 and Tyr160 of D2 (Debus et al., 1988a, 1988b). These seminal findings prompted one last revision of the nomenclature for these important redox constituents of PS II, to Y_Z and Y_D.

Other work on PS II derived from a collaboration with one of the authors (CY), who spent a sabbatical year in the Babcock lab. They had had an informal collaboration over the preceding years, but the inability to get EPR time in Ann Arbor cemented their scientific and personal relationships for the foreseeable future. Jerry was the ideal host, but there were some strains along the way. While house sitting during a Babcock foray to Egypt after the 1980 Photosynthesis Congress in Greece, two family cats passed away, sequentially. The actual cause turned out to be a feline distemper virus rampant in East Lansing at the time, but until this was proven to be the case, the new sabbatical visitor in the Babcock lab was introduced to one and all as the 'cat killer'. The hallmark of interactions with Jerry was an easy-going give- and- take in which ideas were floated, demolished, refined and refloated, until experiments got done, or the 'refloat' element in the cycle expired. Although the basic elements for the PS II preparation now known as 'BBY' (short for Berthold Babcock Yocum) had been completed while CY was a post-doc at Cornell, publication had been deferred owing to a general attitude of disbelief about the possibility of isolating active PS II among the senior people in the photosynthesis field. Jerry's complaints about the difficulties of making EPR measurements on $Y_D^{\bullet}$ and $Y_Z^{\bullet}$ in the presence of a very large signal from $P700^+$ accelerated the publication process. By coupling a revised biochemical methodology with some EPR measurements that revealed the orientation of $Y_D^{\bullet}$ in the new preparation, Berthold et al. (1981) managed to get the paper accepted in FEBS Letters. Jerry's only misgiving about this joint effort was that no one cited it for the EPR results. On the other hand, he had an ongoing fascination with the citation 'hits' the paper garnered (it's about 1300 at this point), and we had a small party on the occasion of citation 'hit' 1000.

Quantification of the Mn content of PS II and characterization of its inhibitor sensitivity (Yocum et al., 1981) were other early results of our collaboration. Longer term interactions between the Babcock and Yocum groups were central to the discovery that Ca^{2+} was an essential cofactor for water oxidation (Ghanotakis et al., 1984a,b) and to the isolation and characterization of stable PS II reaction center preparations that resulted in a reevaluation of the pigment content of the reaction center (Ghanotakis et al., 1989). Jerry's generosity was a key element in this work, as was mutual respect for one another's points of view. Instrument time could always be found, no matter how pressing other research projects might be, and he never demanded to be added to a paper as an author on the basis of use of one of his instruments. This was true of his interactions with all of his colleagues and collaborators.

Other research by Jerry's group in this period examined the spectroscopic properties of Photosystem I (PS I). Prior research had established that the reaction center was comprised of a chlorophyll *a* dimer, but that in $P700^+$ the unpaired spin was localized predominantly on a single chlorophyll molecule (O'Malley and Babcock, 1984b). A sabbatical visit to Leiden University (The Netherlands) in 1983 brought Jerry to the Biophysics Department of the Huygens Laboratory, where he worked with Arnold Hoff (1939–2002) to apply electron spin echo techniques to a study of Signal II (de Groot et al., 1986), and with Hans van Gorkom's group (Dekker et al., 1984) on UV absorbance changes associated with the S-states.

The oxidase research evolved to a point where Jerry

and his graduate student, Costas Varotsis, had refined the technology to detect the oxygen intermediates in the energy transducing oxygen reduction reaction of cytochrome oxidase (Varotsis et al., 1989). Time-resolved resonance Raman was a powerful but challenging methodology demanding large quantities of enzyme and yielding very low signal to noise. Nevertheless, Jerry and Costas (famous for making 50 heart preparations of bovine cytochrome oxidase) were able to resolve and identify the transient vibrational modes for oxygen bound to reduced heme a_3 and the ferryl-oxo intermediate after the oxygen was cleaved (Varotsis and Babcock, 1990; Varotsis et al., 1990, 1993). A predicted peroxy intermediate was frustratingly undetectable, a fact that became more understandable in terms of the theory that Jerry and his collaborators developed in the last few years before his death, suggesting a concerted, four electron reduction of the oxygen (Proshlyakov et al., 1998, 2000) involving formation of a tyrosine radical at the active site.

The power of resonance Raman spectroscopy and all of the groundwork done by Jerry and coworkers in identifying many of the vibrational modes in oxidase allowed him to play a key role in the analysis of mutant forms of a bacterial oxidase from *Rhodobacter sphaeroides*, in collaboration with one of us (SF-M), Robert Gennis and their colleagues. These studies identified the ligands of the metal centers in the enzyme (Shapleigh et al., 1992), and gave an amazingly accurate model of their arrangement in the active site (Calhoun et al., 1993; Hosler et al., 1993) several years before the crystal structure was obtained. Jerry's continued active involvement in Raman and EPR studies of mutant forms of cytochrome *c* oxidase, until the time of his death, was crucial to the characterization and understanding of many altered forms of oxidase, leading to new insights into the mechanism of electron and proton transfer (Fetter et al., 1995; Qian et al., 1997). The detailed EPR analysis of the manganese-substituted Mg site in oxidase, carried out by Jerry and colleagues in collaboration with SF-M and Jon Hosler (Espe et al., 1995; Hosler et al., 1995) continues to provide a powerful tool for understanding the structure and function of this region of oxidase above the hemes where protons and water exit (Florens et al., 1999, 2001). Over this period of nearly 15 years of collaboration between Jerry and SF-M, regular joint group meetings were held, which usually left either the chemistry students or the biochemistry students somewhat bemused. However, Jerry's skillful tutoring in spectroscopy and diplomatic 'rephrasing' of information invariably led to considerable enlightenment and was a constant joy to behold.

Jerry's continuing interest in the chemistry and function of tyrosine radicals gradually evolved into a rethinking of the possible roles of these species in the mechanism of photosynthetic oxygen evolution. A difficulty with conventional models for cycling of the S-states is that if one assumes that the mechanism involves sequential oxidations of the Mn cluster, two problems are encountered. First, metal-centered oxidations would, in theory, produce a potentially damaging accumulation of positive charges within the water-oxidizing site, and second, the final step of the cycle ($S_3 \rightarrow S_4 \rightarrow S_0$) might require formation of a Mn^{5+} species; generation of this oxidation state is generally believed to be beyond the capabilities of biological redox systems. As Jerry viewed this problem, the latter issue could be resolved if the S_4 state involved the combination of S_3 and the neutral tyrosine radical, $Y_Z^{\bullet}$. If this were so, it would involve $Y_Z^{\bullet}$ directly in H_2O oxidation chemistry. The former difficulty, ameliorating possible damage to PS II stability from the accumulation of excessive positive charge, could be accomplished if the chemical mechanism for H_2O oxidation were reformulated to avoid charge buildup on the Mn cluster. Jerry, his post-docs (Curt Hoganson, Kurt Warnecke), and his collaborators (Bruce Diner, John McCracken, Cecelia Tommos) devised a theoretical mechanism (Babcock, 1995; Hoganson et al., 1995; Hoganson and Babcock, 1997; Babcock et al., 1997; Blomberg et al., 1997; Lydakis-Simantiris et al., 1997; Tommos et al., 1998; Tommos and Babcock, 2000) for oxygen evolution in which Mn-bound H_2O was oxidized by $Y_Z^{\bullet}$ via an H-atom abstraction reaction. This reformulation of electron transfer on the oxidizing side of PS II would require that the Mn cluster and Y_Z be in relatively close proximity to one another to facilitate the H-atom transfer reaction. Pulsed magnetic resonance measurements on modified forms of PS II that accumulate the $S_2 Y_Z^{\bullet}$ state (Lakshmi et al., 1998) have placed the tyrosine within 7–8 Å of the Mn cluster, as would be required for a functioning H-atom abstraction mechanism. This distance is supported by the solution of the PS II crystal structure (Zouni et al., 2001; Kamiya and Shen, 2003; Ferreira et al., 2004), where a Mn-Y_Z separation of about 7 Å is

proposed. The 'charge-neutral' model has stimulated new debates about the mechanism of H_2O oxidation, and is now being tested in a number of laboratories around the world.

The neutral radical proposal illustrates how Jerry's wide-ranging interests meshed with his ability to draw together information from a number of fields in order to synthesize new ideas and models for fundamental processes in electron transfer systems. In addition to his research on reaction centers and cytochrome oxidase, Jerry also collaborated on a number of problems in related systems, such as myeloperoxidase, green heme protein, ribonucleotide reductase, hydroxylamine oxidoreductase, galactose oxidase, DNA Photolyase and guanylate cyclase. His collaborators in this work included A. Ehrenberg, A. Hooper, M. Marletta, A. Sancar, B.-M. Sjöberg, J. Stubbe, R. Wever and J. Whittaker. Members of the Babcock group who worked on these and closely related projects include Guert Deinum, Rene Floris, Matt Gardner, Yvonne Gindt, Tony Oertling, Hans Schelvis, Steve Siebold, and Esther Vollenbroek, among others. Near the end of his life, he began another new research initiative, which employed Fourier transform infrared spectroscopy to characterize the PS II S-states (Hillier and Babcock, 2001).

Jerry received a number of awards and honors in the course of his career. Among them was a Distinguished Faculty Award from Michigan State University (1989), a visiting professorship at the Collège de France (1990), the Philips Lecture at Haverford College (1990), a Sigma Xi Senior Research Award (1995), a Michigan Academic Governing Board Award (1999), and the Charles F. Kettering Award for excellence in photosynthesis research, presented by the American Society of Plant Physiologists in 2000. He was sought after as a member of federal advisory panels, and served in this capacity for a number of agencies, including USDA (United States Department of Agriculture), NIH (National Institutes of Health, USA), and DOE (Department of Energy, USA). He was a member of several editorial boards, including Photochemistry and Photobiology, Annual Reviews of Physical Chemistry, Biochimica Biophysica Acta - Reviews on Bioenergetics, Biochemistry, and Journal of Biological Chemistry. He chaired the 1985 Gordon Research Conference on Physicochemical Aspects of Photosynthesis and was chair-elect of a forthcoming Gordon Conference on Radicals. He was an invited speaker at numerous regional, national and international meetings. It was not uncommon for Jerry to prepare the overheads for these talks the night before, in longhand, and many of us remember his posters at various meetings, which were often hand written, on brown paper that was in many instances derived from grocery bags.

Although these professional activities consumed an enormous amount of time, Jerry was able to mentor 33 graduate students, and 33 post-doctoral fellows. The research expertise of these students was divided about equally between photosynthetic and cytochrome oxidase research projects. He was also a gifted teacher in the classroom, something that was easily deduced from listening to one of Jerry's symposium presentations. It is significant that even when he had been promoted to the top faculty ranks he continued to teach a course in introductory chemistry.

When we look back on Jerry's professional career, there are several themes that emerge. The first of these is Jerry's success as a teacher. He was superb in the classroom, but he also had a real love for imparting clear explanations of his research, and of the techniques that he used, to his peers. For example, he could explain the basics of EPR to biochemists, and even to molecular biologists. The second theme was an unending quest for a complete understanding of the fundamental chemistry involved in all of the systems that he studied. He was most demanding of himself in this arena, and one can see in his papers a steady progression towards the basic working principles of cytochrome oxidase and Photosystem II. A third theme is Jerry's unusual capacity to draw together people working in very different areas, and to focus them on a particular goal. His collaborative work with Maarten Wikstrom, Lee McIntosh, Bruce Diner, Bill Woodruff, Per Siegbahn and Margareta Blomberg, Harry Gray, Mike Marletta, Dave Britt, Ron Wever, William Smith, Les Dutton, the authors of this 'dedication,' and many others testifies not only to the breadth of his interests, but also to his personal skills in drawing a diverse group of people into common enterprises. We would be remiss as historians if we did not point out here that the atmosphere and menu at Dagwood's Bar and Grill in Lansing was a critical factor in lubricating many of Jerry's collaborations.

Jerry Babcock's life now seems like a 'brief candle' to those of us who had the privilege to interact closely with him. Death has interrupted a career that was at one and the same time in a mature phase, allowing us all to benefit from his wisdom, keen insight and broad-

based knowledge, and yet still moving in exciting new directions that were only beginning to bear fruit. We have cited only a small portion of Jerry's output in this 'dedication.' He authored or coauthored 253 papers and reviews on his research, and we will never know how much further Jerry's ever-inquiring mind and innovation would have taken him. What we do know is that our fields of research profited immensely from Jerry's exceptional gifts, and that we are all far richer for the time that we had with him.

Acknowledgments

Peter Brzezinski generously provided the photograph of Jerry we have used here and in the *Photosynthesis Research* obituary. We thank Ms. Vada O'Donnell, Jerry's last secretary, for her work in collecting material that was assembled for a memorial booklet distributed at the Michigan State University symposium held in his honor. We have used material from that publication in writing this chapter. We are grateful to Prof. J. N. Siedow (Duke University) for his recollections and assistance, and we thank Paul Michael for permission to use his reminiscence of Jerry. It is inevitable, given both space limitations and the wide range of Jerry's interests and collaborations, that we have not been able to mention everyone who was part of his scientific career. We apologize for these omissions.

References

Babcock GT (1995) Photosystem II as a metallo-radical enzyme. In: Mathis P (ed) Photosynthesis: From Light to Biosphere, Vol II, pp 209–215. Kluwer Academic Publishers, Dordrecht

Babcock GT and Callahan PM (1983) Redox-linked hydrogen bond strength changes in cytochrome *a*: Implications for the cytochrome oxidase proton pump. Biochemistry 22: 2314–2319

Babcock GT and Chang CK (1979) Oxygen binding to ferrous heme *a* and a synthetic analog. FEBS Lett 97: 358–362

Babcock GT and Salmeen I (1979) Resonance Raman spectra and optical properties of oxidized cytochrome oxidase. Biochemistry 18: 2493–2498

Babcock GT and Sauer K (1975) The rapid component of electron paramagnetic resonance signal II: A candidate for the physiological donor to Photosystem II in spinach chloroplasts. Biochim Biophys Acta 376: 329–344

Babcock GT, Vickery LE and Palmer G (1976) The electronic state of heme in cytochrome oxidase. I. Magnetic circular dichroism of the isolated enzyme and its derivatives. J Biol Chem 251: 7907–7919

Babcock GT, Vickery LE and Palmer G (1978) The electronic state of heme in cytochrome oxidase. II. Redox potential interaction and heme iron spin state behavior observed during reductive titrations. J Biol Chem 253: 2400–2411

Babcock GT, Jean JM, Johnston LN, Palmer G and Woodruff WH (1984) Time-resolved resonance Raman spectroscopy of transient species formed during the oxidation of cytochrome oxidase by dioxygen. J Am Chem Soc 106: 8305–8306

Babcock GT, Jean JM, Johnston LN, Palmer G and Woodruff WH (1985) Flow-flash time-resolved resonance Raman spectroscopy of the oxidation of reduced and of mixed valence cytochrome oxidase by dioxygen. J Inorg Biochem 23: 243–251

Babcock GT, Espe M, Hoganson CW, Lydakis-Simantiris N, McCracken J, Shi W, Styring S, Tommos C and Warncke K (1997) Tyrosyl radicals in enzyme catalysis: Some properties and a focus on photosynthetic water oxidation. Acta Chem Scand 51: 533–540

Barry BA and Babcock GT (1987) Tyrosine radicals are involved in the photosynthetic oxygen-evolving system. Proc Natl Acad Sci USA 84: 7099–7103

Berthold DA, Babcock GT and Yocum CF (1981) A highly resolved, oxygen-evolving Photosystem II preparation from spinach thylakoid membranes: EPR and electron transport properties. FEBS Lett 134: 231–234

Blankenship RE, Babcock GT, Warden JT and Sauer K (1975) Observation of a new EPR transient in chloroplasts that may reflect the electron donor to Photosystem II at room temperature. FEBS Lett 51: 287–293

Blomberg MRA, Siegbahn PEM, Styring S, Babcock GT, Åkermark B and Korall P (1997) A quantum chemical study of hydrogen abstraction from manganese coordinated water by a tyrosyl radical: A model for water oxidation in Photosystem II. J Am Chem Soc 119: 8285–8292

Calhoun MW, Thomas JW, Hill JJ, Hosler JP, Shapleigh JP, Tecklenberg MMJ, Ferguson-Miller S, Babcock GT, Alben JO and Gennis RB (1993) Identity of the axial ligand of the high spin heme in cytochrome oxidase: Spectroscopic characterization of mutants in the *bo*-type oxidase of *Escherichia coli* and the aa_3-type oxidase of *Rhodobacter sphaeroides*. Biochemistry 32: 10905–10911

Callahan PM and Babcock GT (1983) The origin of the cytochrome *a* absorption red-shift: A pH dependent interaction between its heme *a* formyl and protein in cytochrome oxidase. Biochemistry 22: 452–461

Debus RJ, Barry BA, Babcock GT and McIntosh L (1988a) Site-directed mutagenesis identifies a tyrosine radical involved in the photosynthetic oxygen evolving system. Proc Natl Acad Sci USA 85: 427–430

Debus RJ, Barry BA, Sithole I, Babcock GT and McIntosh L (1988b) Directed mutagenesis indicates that the donor to P_{680}^{+} in Photosystem II is Tyr-161 of the D1 polypeptide. Biochemistry 27: 9071–9074

DeGroot A, Plijter JJ, Evelo R, Babcock GT and Hoff AJ (1986) The influence of the oxidation state of the oxygen-evolving complex of Photosystem II on the spin-lattice relaxation time of signal II as determined by electron spin echo spectroscopy. Biochim Biophys Acta 848: 8–15

Dekker JP, Ghanotakis DF, Plijter JJ, van Gorkom HJ and Babcock GT (1984) Kinetics of the oxygen-evolving complex in salt-washed Photosystem II preparations. Biochim Biophys Acta 767: 515–523

Dismukes GC and Siderer Y (1980) Intermediates of a polynuclear manganese center involved in photosynthetic oxidation of water. Proc Natl Acad Sci USA 78: 274–278

Espe M, Hosler J, Ferguson-Miller S, Babcock GT and McCracken J (1995) A CW- and pulsed-EPR characterization of the Mn^{2+} binding site in *Rhodobacter sphaeroides* cytochrome *c* oxidase. Biochemistry 34: 7593–7602

Fetter J, Qian J, Shapleigh J, Thomas J, Garcia-Horsman A, Schmidt E, Hosler J, Babcock GT, Gennis R and Ferguson-Miller S (1995) Possible proton relay pathways in cytochrome *c* oxidase. Proc Natl Acad Sci USA 92: 1604–1608

Florens L, Hoganson C, McCracken J, Fetter J, Mills D, Babcock GT and Ferguson-Miller S (1999) The role of magnesium and its associated water channel in activity and regulation of cytochrome *c* oxidase, In: Peschek G, Loeffelhardt W and Schmetterer G (eds) The Phototropic Prokaryotes, pp 329–339. Kluwer Academic/Plenum Press, Dordrecht

Florens L, Schmidt B, McCracken J, and Ferguson-Miller S (2001) Fast deuterium access to the buried magnesium/manganese site in cytochrome *c* oxidase. Biochemistry 40:7491–7497

Ghanotakis DF, Yerkes CT and Babcock GT (1982) The role of ADRY reagents in destabilizing high-potential oxidizing equivalents generated in chloroplast Photosystem II. Biochim Biophys Acta 682: 21–31

Ghanotakis DF, Babcock GT and Yocum CF (1984a) Calcium reconstitutes high rates of oxygen evolution in polypeptide depleted Photosystem II preparations. FEBS Lett 167: 127–130

Ghanotakis DF, Topper JN, Babcock GT and Yocum CF (1984b) Water-soluble 17 and 23 kDa polypeptides restore oxygen evolution activity by creating a high-affinity site for Ca^{2+} on the oxidizing side of Photosystem II. FEBS Lett 170: 169–173

Ghanotakis DF, de Paula JC, Demetriou DM, Bowlby NR, Petersen J, Babcock GT and Yocum CF (1989) Isolation and characterization of the 47 kDa protein and the D1-D2-cytochrome *b*-559 complex. Biochim. Biophys. Acta 974: 44–53

Hillier W and Babcock GT (2001) S-state dependent FTIR difference spectra for the Photosystem II oxygen-evolving complex. Biochemistry 40: 1503–1509

Hoganson CW and Babcock GT (1997) A metalloradical mechanism for the generation of oxygen from water in photosynthesis. Science 277: 1953–1956

Hoganson CW, Lydakis-Simantiris N, Tang X-S, Tommos C, Warncke K, Babcock GT, Diner BA, McCracken J and Styring S (1995) A hydrogen-atom abstraction model for the function of Y_Z in photosynthetic oxygen evolution. Photosynth Res 46: 177–184

Hosler JP, Ferguson-Miller S, Calhoun MW, Thomas JW, Hill J, Lemieux L, Ma J, Georgiou J, Fetter J, Shapleigh J, Tecklenburg MMJ, Babcock GT and Gennis RB (1993) Insight into active-site structure and function of cytochrome oxidase by analysis of site-directed mutants of bacterial cytochrome aa_3 and cytochrome b_o. J Bioenerg Biomembr 25: 121–136

Hosler J, Espe M, Zhen Y, Babcock GT and Ferguson-Miller S (1995) Analysis of site-directed mutants locates a non-redox active metal near the active site of cytochrome *c* oxidase in *Rhodobacter sphaeroides*. Biochemistry 34: 7586–7592

Lakshmi KV, Easton SS, Eaton GR, Frank HA and Brudvig GW (1998) Analysis of dipolar and exchange interactions between manganese and tyrosine Z in the $S_2Y_Z^*$ state of acetate-inhibited Photosystem II via EPR spectral simulations at X- and Q-bands. J Phys Chem B 102: 8327–8325

Lydakis-Simantiris N, Ghanotakis DF and Babcock GT (1997) Kinetic isotope effects on the reduction of the Y_Z radical in oxygen-evolving and tris-washed Photosystem II membranes by time-resolved EPR. Biochim Biophys Acta 1322: 129–140

O'Malley PJ and Babcock GT (1984a) EPR Properties of immobilized quinone cation radicals and the molecular origin of signal II in spinach chloroplasts. Biochim Biophys Acta 765: 370–379

O'Malley PJ and Babcock GT (1984b) ENDOR evidence supporting a monomeric nature for P_{700}^+ in spinach chloroplasts. Proc Natl Acad Sci USA 81: 1098–1101

Proshlyakov DA, Pressler MA and Babcock GT (1998) Dioxygen activation and bond cleavage by mixed-valence cytochrome *c* oxidase. Proc Natl Acad Sci USA 95: 8020–8025

Proshlyakov DA, Pressler MA, DeMaso C, Leykam JF, DeWitt DL and Babcock GT (2000) Oxygen activation and reduction in respiration: Involvement of redox-active tyrosine 244. Science 290: 1588–1591

Qian J, Shi W, Pressler M, Hoganson C, Mills D, Babcock GT, and Ferguson-Miller S (1997) Aspartate-407 in *Rhodobacter sphaeroides* cytochrome *c* oxidase is not required for proton pumping or manganese binding. Biochemistry 36: 2539–2543

Salmeen I, Rimai L and Babcock GT (1978) Raman spectra of heme *a*, cytochrome oxidase-ligand complexes, and alkaline denatured oxidase. Biochemistry 17: 800–806

Shapleigh JP, Hosler JP, Tecklenburg MMJ, Kim Y, Babcock GT, Gennis RB and Ferguson-Miller S (1992) Definition of the catalytic sites of cytochrome oxidase: The specific ligands of heme *a* and the binuclear metal center. Proc Natl Acad Sci USA 89: 4786–4790

Tommos C and Babcock GT (2000) Proton and hydrogen atom currents in photosynthetic water oxidation. Biochim Biophys Acta 1458: 199–219

Tommos C, Hoganson CW, Di Valentin N, Lydakis-Simantiris L, Dorlet P, Westphal K, Chu HA, McCracken J and Babcock GT (1998) Manganese and tyrosyl radical function in photosynthetic oxygen evolution. Curr Opin Chem Biol 2: 244–252

Tweedle MF, Wilson LJ, Garcia-Iniguez L, Babcock GT and Palmer G (1978) Electronic state of heme in cytochrome oxidase. III. The magnetic susceptibility of beef heart cytochrome oxidase and some of its derivatives from 7–200 K. Direct evidence for an anti-ferromagnetically coupled Fe(III)/Cu(II) pair. J Biol Chem 253: 8065–8071

Varotsis C and Babcock GT (1990) Appearance of the ν (Fe^{IV}=O) vibration from a ferryl-oxo intermediate in the cytochrome oxidase/dioxygen reaction. Biochemistry 29: 7357–7362

Varotsis C, Woodruff WH and Babcock GT (1989) Time-resolved resonance Raman detection of ν (Fe-O) in an early intermediate in the reduction of dioxygen by cytochrome oxidase. J Am Chem Soc 111: 6439–6440; 112, 1297

Varotsis C, Woodruff WH and Babcock GT (1990) Direct detection of a dioxygen adduct of cytochrome a_3 in the mixed valence cytochrome oxidase/dioxygen reaction. J Biol Chem 265: 11131–11136

Varotsis C, Zhang Y, Appelman EH and Babcock GT (1993) Resolution of the reaction sequence during the reduction of O_2 by cytochrome-oxidase. Proc Natl Acad Sci USA 90: 237–241

Ward B, Callahan PM, Young R, Babcock GT and Chang CK (1983) Red-shifts in the optical spectra of porphyrin Schiff's

bases upon protonation. J Am Chem Soc 105: 634–636
Yerkes CT and Babcock GT (1981) Photosystem II oxidation of charged electron donors: Surface charge effects. Biochim Biophys Acta 590: 360–372
Yocum CF, Yerkes CT, Blankenship RE, Sharp RR and Babcock GT (1981) Stoichiometry, inhibitor sensitivity, and organization of manganese associated with photosynthetic oxygen evolution. Proc Natl Acad Sci USA 78: 7507–7511
Zouni A, Witt HT, Kern J, Fromme P, Krauss N, Saenger W and Orth P (2001) Crystal structure of Photosystem II from *Synechococcus elongatus* at 3.8 Å resolution. Nature 409: 739–743

Charles F. Yocum*
Departments of Molecular, Cellular and Developmental Biology and Chemistry
University of Michigan, Ann Arbor, MI 48109, U.S.A.

Robert E. Blankenship
Department of Chemistry and Biochemistry
Arizona State University
Tempe, AZ 85287, U.S.A.

Shelagh Ferguson-Miller
Department of Biochemistry
Michigan State University
East Lansing, MI 48824, U.S.A.

* Author for correspondence, email: cyocum@umich.edu

Chapter 1

Introduction to Photosystem II

Kimiyuki Satoh*
Department of Biology, Okayama University, Okayama 700-8530, Japan

Thomas J. Wydrzynski*
Photobioenergetics Group, Research School of Biological Sciences, The Australian National University, Canberra ACT 0200, Australia

Govindjee
Department of Biochemistry and of Plant Biology, and Center of Biophysics and Computational Biology, University of Illinois at Urbana-Champaign, Urbana, IL 61801-3707, U.S.A.

Summary

This chapter briefly traces some of the early studies and key findings which have led to our current perception and understanding of Photosystem II, the water:plastoquinone oxidoreductase in oxygenic photosynthesis. Starting with the discovery of oxygen and the idea of two photosystems, the progressive identification of the unique structural and functional aspects of Photosystem II are outlined and related to the corresponding chapters in the book. The aim is to integrate the detailed descriptions in the various chapters in the context of the structure and function of Photosystem II as a whole. The chapter ends with a brief perspective for the future study and application of Photosystem II research.

*Authors for correspondence, email: kimiyuki@cc.okayama-u.ac.jp; tom.wydrzynski@anu.edu.au

T. Wydrzynski and K. Satoh (eds): Photosystem II: The Light-Driven Water:Plastoquinone Oxidoreductase, pp. 11–22.

I. Discovery of Oxygen and O_2 Production by Plants

The ability of plants to generate oxygen was first described by Joseph Priestley (1733-1804) and published in his book entitled *Experiments and Observations on Different Kinds of Air* (1772). In this study, Priestley observed the phenomenon in which mint plants revealed a 'power to restore the air which had been injured by the burning of candles.' This 'special power' of plants was described in the scientific terms of those days as the ability to change 'phlogisticated air' into 'dephlogisticated air.' In retrospect, this observation was the first scientific recognition of the functioning in plants of the water/plastoquinone oxido-reductase, i.e., Photosystem II (PS II), the focus of this book. However, the precise chemical mechanism and biological machinery responsible for this process were far beyond the scientific understanding at that time. During the same period, the presence of a distinct component or element in the atmosphere was discovered and later named by Antoine Laurent Lavoisier (1743–1794) as 'oxygen' (Lavoisier, 1789; also see Karl Wilhelm Scheele, 1781, who had called it 'fire air'). It was later recognized that oxygen was equivalent to 'dephlogisticated air' and it is now widely accepted that the bulk of the life-sustaining oxygen in the atmosphere today arose from the functioning of PS II since its appearance during the evolution of life on earth.

The requirement of light, carbon dioxide and water in the overall process, as well as the coupling between O_2 production and organic matter synthesis, were subsequently recognized; the energetic meaning of this unique physiological process, called 'photosynthesis,' was established by Julius Robert Mayer (1814–1878; see Mayer, 1845). Chlorophyll (Chl) was identified as the major light absorber for driving the process (Timiriazeff, 1874) and by the beginning of the 20th century overall photosynthesis was described simply as follows:

$$CO_2 + H_2O \xrightarrow[\text{Chl}]{h\nu} [CH_2O] + O_2 \quad (1)$$

where, $[CH_2O]$ represents a unit of organic material (i.e., sugar). In this formulation, the source of O_2 could be either the carbon dioxide or the water. However, Robin Hill (1937) quite elegantly demonstrated that O_2 production could be decoupled from organic synthesis in isolated chloroplast fragments by using an inorganic oxidant, such as potassium ferricyanide, as a terminal electron acceptor (for a historical review, see Govindjee and Krogmann, 2004).

II. Conceptual Development of Photosystem II

In the early part of the 20th century, Robert Emerson and William Arnold (1932a,b) demonstrated that several hundred Chl molecules worked together to produce one O_2 molecule. This led Hans Gaffron and Kurt Wohl (1936) to propose the concept of the 'photosynthetic unit' as a network assembly of Chl molecules which functioned to supply excitation energy to a photochemical catalytic center that powers photosynthesis. Following the concept of the photosynthetic unit, Emerson and Lewis (1943) demonstrated that far red light (>700nm) gives a poorer quantum yield of O_2 production than red light. This phenomenon was called the 'red drop.' However, the decline in the quantum yield could be avoided if supplementary light absorbed by an 'accessory pigment' of shorter wavelength was added to the far-red light. This phenomenon is known as the 'Emerson enhancement effect' (Emerson et al., 1957; Emerson and Rabinowitch, 1960; Govindjee and Rabinowitch, 1960; Myers and French, 1960) and led to the concept for the existence of two light reactions and two pigment systems in oxygenic photosynthesis. The implication that the two light reactions and two pigment systems act together in a series was proposed by Robin Hill and Fay Bendall (1960) as part of a working hypothesis to explain the role of cytochromes (Cyt) in photosynthetic electron transport (for a review, see Duysens, 1989). Subsequently, the involvement of a short-wavelength reaction and a long-wavelength reaction in oxygenic photosynthesis was demonstrated by light-induced absorbance changes and electron transport studies (Kok, 1959; Duysens et al., 1961; Losada et al., 1961;

Abbreviations: BRC – bacterial reaction center; Car – carotene; Chl Z – redox active Chl of PS II; Chl – chlorophyll; Cyt – cytochrome; D1, D2 – RC core subunits of PS II; LHCP – light harvesting Chl *a/b* protein of PS II; OEC – oxygen evolving complex; P680 – primary electron donor of PS II; Pheo – pheophytin; PQ – plastoquinone; PS II – Photosystem II; Q_A – primary PQ acceptor; Q_B – secondary PQ acceptor; RC – reaction center; S_n – states of the water oxidizing complex for n = 0, 1, 2, 3, or 4; Y_D – redox-active tyrosine on D2 protein; Y_Z – redox active tyrosine on D1 protein

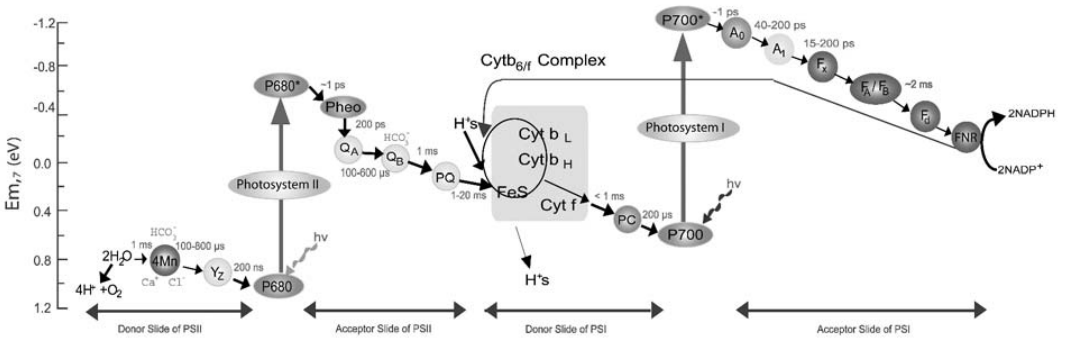

Fig. 1. The Z-scheme of oxygenic photosynthesis for electron transfer from water to nicotinamide adenine dinucleotide phosphate (NADP) modified from Fig. 4 of Govindjee (2004). From left to right: Mn stands for Mn cluster; Y_z, for tyrosine-161 on the D1 protein; P680, for the primary electron donor of PS II; Pheo, for pheophytin; Q_A, for the first plastoquinone electron acceptor of PS II; Q_B, for the second plastoquinone electron acceptor of PS II; PQ, for the plastoquinone pool; Cyt b_L and Cyt b_H, for low and high potential cytochrome b_6; Cyt b_6f, for cytochrome b_6f complex; Cyt *f*, for cytochrome *f*; FeS, for Rieske iron sulfur; PC, for plastocyanin; P700, for the primary electron donor for PS I; A_0, for a monomer Chl; A_1, for vitamin K; F_x, F_A and F_B, for iron sulfur centers 'x', 'A' and 'B,' respectively; and F_d, for ferredoxin. Also shown are the approximate half-times for most of the reactions, the existence of the 'Q'-cycle, the cyclic reaction around PS I, and the possible sites for calcium, chloride and bicarbonate ions in PS II. See Color Plate 16, Fig. 2.

Witt et al., 1961). Thus the hypothesis of Hill and Bendall, called the 'zigzag model' or 'Z-scheme,' was experimentally substantiated and the names 'Photosystem I' (light reaction 1) and 'Photosystem II' (light reaction 2) were proposed (Duysens et al., 1961). A current picture of the Z-scheme is illustrated in Fig. 1. Here, PS II is shown as the functional unit transferring electrons from water to the plastoquinone (PQ) acceptor, that in turn, donates electrons via the Cyt b_6f complex to Photosystem I. Thus, the PS II functional unit operating in O_2 evolving organisms is called the 'water/plastoquinone oxido-reductase.' For earlier detailed discussions of overall oxygenic photosynthesis, see Ort and Yocum (1996) and Ke (2001)

III. O_2 Production — Phenomenology

The oxidation of water to molecular oxygen requires the extraction of four electrons and four protons (H^+s) from two H_2O molecules (Fig. 1). Using algal suspensions, Pierre Joliot et al. (1969) provided dramatic experimental evidence to show that O_2 is released through a cyclical period-four reaction. These researchers observed that for dark-adapted algae, excited by a train of single-turnover light flashes, very little (or no) O_2 is produced after the 1st and 2nd flashes in the sequence while the maximum O_2 is produced after the 3rd flash. Thereafter, progressively smaller peaks in the O_2 yield occur after the 7th and 11th flashes, following a basic periodicity of four, until the oscillations damp out to a steady-state level after the third or the fourth cycle. Figure 2, *top*, shows a typical trace of O_2 flash yield measurements from a spinach thylakoid sample while Fig. 2, *bottom left*, shows a plot of the data. The periodicity of four can readily be explained by the chemistry of water oxidation, but the maximal O_2 yield on the 3rd flash and the damped oscillations indicate(s) a much higher level of complexity in the mechanism (for a review, see Whitmarsh and Govindjee, 2002).

Based on the results of Joliot et al. (1969) and their own, Bessel Kok et al. (1970) developed an elegant kinetic model to account for the O_2 flash yield pattern by PS II. In this model, a special oxidizable component is proposed to cycle through a series of five intermediate states, termed the S_n states (where n = 0, 1, 2, 3, or 4), before reacting with water to produce O_2. Each S_n state differs from the previous S_{n-1} state by the accumulation of one oxidizing equivalent until S_4 is reached, at which point O_2 is released and the S_0 state is regenerated. To account for the peak yield after the 3rd flash and the damping in the oscillations, the following additional assumptions were made for a macroscopic population of O_2-evolving centers: (i) the S_1 state is stable in the dark; (ii) the S_2 and S_3 states eventually deactivate to the S_1 state if not advanced by another incoming photon (as indicated by the dashed arrows in Fig. 2, *bottom right*); (iii) upon reaching

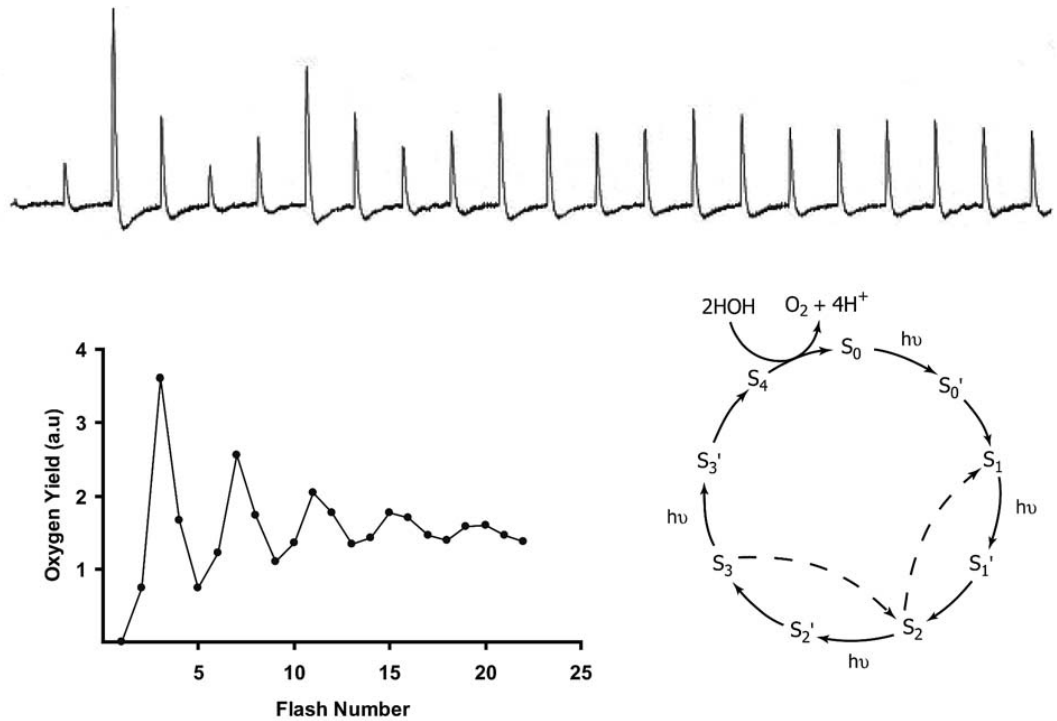

Fig. 2. (*Top*): Typical traces of O_2 flash yield measurements from a spinach thylakoid sample as a function of flash number. (*Bottom left)*: Oxygen yield as a function of flash numbers showing the periodicity of four and the first maximum at the 3rd flash (Joliot et al., 1969). (*Bottom right):* A simplified S-state model where the subscripts under 'S' reflect the positive charges; and the 'S' states with primes indicate the states formed after a light reaction (cf. Kok et al., 1970). Figure modified from Wydrzynski (1977).

the S_4 state, O_2 is released through an instantaneous dark reaction; (iv) after flash activation there is a finite time before an S_n state can be advanced by another incoming photon (as indicated by the $S_n \rightarrow S_n' \rightarrow S_{n+1}$ transitions in Fig. 2, *bottom right*); and (v) there is a certain small probability for a double hit (i.e., where an O_2-evolving center advances two S-states during a given light flash; a double hit thus depends on the flash duration) or a miss (i.e., where an O_2-evolving center fails to advance to the next higher S_{n+1} state during a given flash) to occur after an activating light flash. With these assumptions, the model can readily explain the observed O_2 flash yield pattern. This insightful model is illustrated in Fig. 2, *bottom right*, and has guided the research on the operation of the electron transfer pathways and the mechanism of O_2 production in PS II for more than 35 years. Flash-induced O_2 release and other oscillatory processes in the PS II are discussed in detail by Shinkarev (Chapter 24) while the implications of the oscillatory reactions in the water oxidation chemistry are discussed by Hillier and Messinger (Chapter 25). A historical account of the discovery of the period four flash pattern in O_2 production is given by Joliot (2003).

IV. Isolation of the Chemical Entity—Structural Organization of Photosystem II

A. Core Complex

Willstätter and Stoll (1913) provided the chemical identification of Chl, and Smith (1938) showed the association of Chl with proteins in vivo. Thus, various procedures were attempted for the direct isolation of the functional pigment-protein complexes from photosynthetic tissues or from isolated chloroplasts in order to identify the minimum unit capable of

photosynthesis (Thomas et al., 1953). A remarkable achievement in this experimental approach was made by Keith Boardman and Jan Anderson (1964) who were able to separate digitonin-solubilized spinach chloroplasts into two fractions that were each enriched in one of the two Photosystems according to the Z-scheme, i.e., PS I (lighter fraction) and PS II (heavier fraction). In this isolation procedure, PS II activity was associated with the membrane fraction enriched in Chl *b*, which is now known to contain the grana of chloroplast thylakoid membranes (see Anderson, 2002). Refined preparations of this membrane fraction, e.g., the so-called BBY particles (Berthold et al., 1981), retain full O_2-evolving activity and have been used extensively in the analysis of PS II structure and function.

Upon the introduction of polyacrylamide gel electrophoresis (PAGE) under partially denaturing conditions (i.e., the so-called green gels) (Ogawa et al., 1966; Thornber et al., 1966; Ogawa, 2003), a special pigment-protein complex of the PS II could be isolated that had no photochemical activity. This pigment-protein complex became known as the 'light-harvesting Chl *a*/*b* protein' or LHCP (Thornber and Highkin, 1974; Thornber, 1975), that functions as the distal antenna of PS II in green plants. Current information on the structure and function of the distal and extrinsic antenna complexes of the PS II from a variety of oxygenic photosynthetic organisms is summarized by Green and Gantt (Chapter 2).

During the early 1980s, a variety of methods using non-ionic detergents, e.g., sugar based detergents, were found to be effective in isolating pigment-protein complexes with PS II activity from a diverse range of cyanobacteria, green algae and higher plants (Satoh and Butler, 1978; Satoh, 1985, 2003). Through these studies, the 'PS II core complex' was firmly established as a definitive chemical entity. The early core complexes were found to consist of 6 major polypeptide components, i.e., CP47 and CP43, which are the Chl *a*-containing pigment-proteins that constitute the proximal or core antenna of PS II (for details, see Chapter 3, Eaton-Rye and Putman-Evans); the D1 and D2 proteins, which constitute the catalytic core (for details, see Chapter 4, Nixon et al.), and the Cyt b_{559}, (α and β subunits) which is possibly involved as a side path electron carrier (for details, see Chapter 6, Thornton et al.; Chapter 15, Faller et al.). In addition to the major subunits, refined preparations were found to contain several low molecular weight components as well (Kashino et al., 2002; Chapter 6, Thornton et al.).

During the early investigations, isolated core complexes consisting mainly of the major polypeptide components did not exhibit any O_2-evolving activity. However, later studies (Tang and Satoh, 1985) showed that core complexes which retain an additional major polypeptide corresponding to the 33 kDa extrinsic protein (or *psb*O gene product) are capable of producing O_2. Thus, the water/plastoquinone oxido-reductase was identified as the minimal core complex plus the 33 kDa extrinsic protein.

The 33 kDa extrinsic protein was first isolated by Kuwabara and Murata (1979) from spinach chloroplast fragments and could be released from the inverted thylakoid membranes by various salt wash and chaotropic treatments (Åkerlund and Jansson, 1981; Yamamoto et al., 1981). The loss of the protein correlated with a loss in the O_2-evolving activity. The first successful reconstitution assays to analyze the role of proteins bound to the luminal surface were achieved by Åkerland (1981). In addition to the 33 kDa extrinsic protein, two other extrinsic proteins (i.e., the *psb*P and *psb*Q gene products or the so-called 23 kDa and 16 kDa extrinsic proteins, respectively) were identified in optimizing the O_2-evolving activity in these studies with higher plants. Further details on the structure and function of the oxygen enhancing extrinsic proteins are presented by Bricker and Burnap (Chapter 5).

B. The Total Picture

In subsequent investigations of PS II, many additional small, membrane-spanning polypeptides have been identified, though many of their functions still remain to be determined (for details, see Chapter 6, Thornton et al.). It is now known that PS II contains as many as 28 different protein components in vivo, although some of these protein components may be restricted only to cyanobacterial species while others only to eukaryotic species. Cryoelectron and X-ray crystallography have recently greatly facilitated the structural elucidation of PS II, from the level of the in vivo macroscopic organization of the polypeptide components to the high resolution molecular structure of the antenna pigments and electron transfer cofactors (Hankamer et al., 1999; Zouni et al., 2001; Kamiya and Shen, 2003; Biesiadka et al. 2004; Ferreira et al., 2004). The current overall static view of PS II is presented in several chapters of this book. Structural analysis by electron cryo-microscopy of

cyanobacterial and higher plant PS II is summarized by Hankamer et al. (Chapter 18); the first X-ray crystallographic analysis of PS II complexes from *Thermosynechococcus elongatus* (a thermophilic cyanobacterium isolated by Sakae Katoh from the Beppu hot spring in Japan; Yamaoka et al., 1978), in combination with various biophysical analyses, is summarized by Witt (Chapter 19); the crystallization and the 3D structure at 3.7 Å resolution of PS II complexes from *T. vulcanus* are discussed by Shen and Kamiya (Chapter 20); and the refined, higher resolution 3.5 Å structure and its implications for the PS II complexes from *T. elongatus* are presented by Barber and Iwata (Chapter 21). In addition, the immediate chemical environment and the contribution of the protein backbone and side chains to the various functional sites in PS II, as determined by the powerful tool of Fourier transform infrared (FTIR) difference spectroscopy, are discussed by Noguchi and Berthomieu (Chapter 16). Finally, information on the orientation and through-space interactions among the various electron transfer cofactors in PS II, as determined by electron paramagnetic resonance (EPR) spectroscopy, are summarized by Bittl and Kawamori (Chapter 17).

V. Functional Sites — Catalytic Role of Photosystem II

A. Primary Photochemistry

The establishment of the core complex as a chemical entity made it possible to analyze in detail the structure and function of PS II. A long standing question had been on which PS II protein subunit is the site of primary charge separation located. Since isolated core complexes can contain up to 50 Chl per PS II unit, both antenna and reaction center (RC) pigments are present. In early studies, several lines of evidence seemed to suggest that CP47 was the site of the primary charge separation (Nakatani et al., 1984; for a review, see Satoh, 1985) and so at that time it was often referred to as the 'P680 apo-protein' (for a review, see Satoh, 2003). However, it was also suggested that the D1 and D2 proteins were the site of the primary charge separation, since these proteins were found to have some sequence homology with the L and M subunits of the purple bacterial reaction center (BRC) (Michel and Deisenhofer, 1985; Trebst, 1986). Subsequently, Osamu Nanba and Kimiyuki Satoh (1987) succeeded in isolating a sub-core complex consisting of the D1 and D2 proteins, the α and β subunits of Cyt b_{559}, and the *psb*I gene product. This complex had a minimal pigment composition and contained 6 (or 5) Chl *a*, 2 pheophytin (Pheo) *a* and 2 β-carotenes (β-Cars). Since this complex was found to be photochemically active in the primary charge separation (Danielius et al., 1987; Okamura et al., 1987; Takahashi et al., 1987), the stage was set to focus on the structural and molecular analysis of the D1 and D2 proteins as the RC subunits (for reviews, see Evans, 1987; Satoh, 1988, 2003; Chapter 4, Nixon et al.).

The photoactive pigment in PS II, originally labeled as Chl a_{II}, was first identified in digitonin-treated spinach thylakoids by the light-induced difference spectrum with maximum absorbance changes at 430 and 680 nm (Döring et al., 1969; Chapter 7, Renger and Holzwarth; Chapter 19, Witt). These absorbance changes were initially taken to indicate that it was a 'sensitizer,' but soon thereafter were interpreted to be due to the photo-oxidation of a special Chl molecule in the PSII RC serving as the primary electron donor. Hence Chl a_{II} became generally referred to as P680 (Floyd et al., 1971). In comparison with the BRC, P680 was sometimes considered to be a 'special pair' (van Mieghem et al., 1991). With the advancement in biophysical methods of analysis and 3D crystallographic determinations of the PS II core (Zouni et al., 2001; Kamiya and Shen, 2003; Ferreira et al., 2004; Chapter 19, Witt; Chapter 20, Shen and Kamiya; Chapter 21, Barber and Iwata), P680 is now interpreted as a specially organized, multimeric pigment complex (Chapter 7, Renger and Holzwarth) that confers the unique properties needed to promote the main path electron transfer from water to plastoquinone (PQ) as well as the side path electron transfer around the redox-active Chl (Chl Z), Cyt b_{559} and β-Car that is involved in the dissipation of excess oxidizing power (Chapter 15, Faller et al.). Thus, light energy initially trapped in the distal (Chapter 2, Green and Gantt) and/or the proximal (Chapter 3, Eaton-Rye and Putman-Evans) antenna components is directed to the core RC where it activates the primary electron donor P680 (for details, see Chapter 22, Barter et al.). Since $P680^+$ is the strongest known oxidant in biology, it can be highly destructive to PS II if it is not rapidly deactivated through the O_2-evolving reactions. This photo-destruction was initially recognized when it was discovered that the D1 protein, which binds P680, is the most rapidly turning-over protein in

PS II (Ellis, 1977). As a result, oxygenic organisms have developed various mechanisms to quench excess energy (discussed in Chapter 23, Pogson et al.), particularly under conditions of stress, and to repair damaged PS II components (discussed in Chapter 27, Chow and Aro).

B. Charge Stabilization

The beauty of photosynthetic RCs is that once the primary charge separation takes place, it is rapidly stabilized by secondary electron transfer which considerably reduces the probability for back reaction. Hence, the quantum yield for the primary charge separation in photosynthetic RCs approaches unity. In PS II, after excitation, the electron initially localized on the primary acceptor Pheo (Klimov et al., 1977), located in the P680 complex, is rapidly transferred to the first metastable acceptor termed Q_A. This acceptor was determined to be a specially bound PQ molecule based on its difference absorption spectrum (Stiehl and Witt, 1968). Earlier, Duysens and Sweers (1963) had proposed the existence of 'Q' on the PS II acceptor side that acted as a quencher of Chl *a* fluorescence which was later identified as Q_A (for details, see Papageorgiou and Govindjee, 2004). Q_A serves only as a single electron carrier and transfers the electron to a second bound PQ molecule termed Q_B. In contrast to Q_A, Q_B can accept two electrons. Upon being doubly reduced Q_B becomes protonated and the resulting plastoquinol is released from the binding site and is replaced by another molecule from the PQ pool within the membrane. Thus, Q_B acts as a two-electron gate revealing binary oscillations in the electron transfer on the acceptor side of PS II. The functioning of a two-electron gate was first discovered in the PS II by Bouges-Bocquet (1973) and by Velthuys and Amesz (1974) and later confirmed in the BRC (Vermeglio, 2002).

Closely associated with the Q_A and Q_B electron acceptors is a non-heme iron ion. A unique role of bicarbonate at the acceptor side of PS II, particularly on the two-electron gate, was discovered by Govindjee et al. (1976) (van Rensen et al., 1999; Chapter 14, van Rensen and Klimov) and may involve the non-heme iron. Details on the structure and function of the quinone-iron acceptor complex are provided by Petrouleas and Crofts (Chapter 8).

On the donor side of PS II, the oxidation of water to molecular oxygen is catalyzed through the strong oxidizing power generated by $P680^+$. As discussed above, one O_2 molecule is released after every four turnovers of P680. The question had been as to how the oxidizing power is transferred from $P680^+$ to the oxygen evolving complex (OEC). Initially it was determined that the first electron donor to $P680^+$ was located on the D1/ D2 heterodimer by selective iodo-labeling of the polypeptides in core complexes (Takahashi et al., 1986). The isotopic labeling experiments established the functioning of the tyrosine radical observed as the EPR signal IIf (vf) on the donor side of PS II (Barry and Babcock, 1987). Subsequently, Debus et al. (1988) provided the first, direct molecular biological evidence that the first donor to $P680^+$ is tyrosine-161 residue (termed Y_Z) on the D1 protein in *Synechocystis* sp. PCC 6803 (Chapter 9, Diner and Britt; Chapter 11, Debus). However, PS II was known to contain another redox-active tyrosine (termed Y_D) located in a homologous position to Y_Z on the D2 protein. In contrast to Y_Z, which is directly involved in the O_2-evolving reactions, Y_D does not participate in the main path of electron transfer from water to PQ. However, it does interact in the dark redox equilibrium of the early S states. Details on the structure and function of the redox-active tyrosines in PS II are discussed by Diner and Britt (Chapter 9).

C. Water Oxidation

One of the largely unresolved problems in PS II research is the molecular mechanism by which O_2 is produced (Renger, 2003). Upon promulgation of the S-state hypothesis in the early 1970s, the quest began to identify the chemical nature of the 'charge accumulating' intermediate. Since Mn can take on a number of stable oxidation states and was localized in PS II (Cheniae and Martin, 1966), it was long suspected that Mn is directly involved in the O_2-evolving reactions. Early EPR studies revealed an inverse relationship between the O_2-evolving activity and the appearance of the room-temperature, 6-line EPR signal characteristic of aqueous Mn^{2+} ions after treatments which inactivated the O_2-evolving activity by releasing bound Mn (Lozier et al., 1971; Blankenship and Sauer, 1974). In addition, there were early indications from nuclear magnetic resonance (NMR) proton relaxation rate measurements that bound Mn changes oxidation state during the O_2-evolving reactions (Wydrzynski et al., 1976; Sharp, 1992; Wydrzynski, 2004). However, first direct measurements of the intact, bound Mn in PS II could not be made until the discovery of the low-temperature (e.g.,

~10 K), S_2-state Mn multi-line EPR signal (Dismukes and Siderer, 1981) and the first applications of Mn X-ray absorption spectroscopy (XAS) (Kirby et al., 1981a,b).

With the discovery of the low-temperature, S_2-state Mn multi-line EPR signal, and later of the Mn EPR signal arising from the S_1 state (Åhrling et al., 1997; Messinger et al., 1997), the functional Mn could be probed in situ. Starting in the 1980s and continuing until the present, a vast library of EPR measurements have accumulated under conditions which variously perturbed the Mn center. It became clear very early that several Mn ions interacted magnetically to give rise to these EPR signals, though it was controversial as to whether it involved 2 or 4 Mn ions (Chapter 12, Åhrling et al.). The 3D crystal structures of PS II clearly show a cluster of 4 Mn ions at the catalytic site (Chapter 19, Witt; Chapter 20, Shen and Kamiya; Chapter 21, Barber and Iwata) but do not reveal the oxidation states nor how the 4 Mn ions interact with one another.

Another technique that provides information on the immediate chemical environment around the functional Mn as well as on the possible Mn oxidation states in non-crystalline samples of PS II is Mn X-ray absorption spectroscopy (XAS). Like the EPR, studies using this technique began in the 1980s and continue today. In conjunction with Mn EPR measurements, the Mn XAS measurements provide support and verification of the interpretations of the 3D crystallographic structure of the Mn functional site. Details on the results from the Mn XAS measurements of PS II are summarized by Yachandra (Chapter 10).

Crucial to the functional organization of the Mn site, as well as of the other electron transfer cofactors, is the role of protein environment, in particular as to which amino acid residues provide ligands. Information on this aspect has been obtained through the use of site-directed mutants of PS II proteins in conjunction with the various types of spectroscopic analysis (i.e., FTIR, EPR, XAS). It appears that most of the ligands to the Mn cluster are provided by the D1 protein, although the recent refined 3D crystallographic structure of PS II indicates that one ligand is provided by the CP43 protein (Chapter 21, Barber and Iwata). However, it is important to point out that not all ligands to the four Mn ions in the cluster have as yet been accounted for. The latest information on the protein environment of the catalytic Mn cluster is presented by Debus (Chapter 11).

Despite the wealth of structural information on the Mn cluster, very little is still known about the exact mechanism by which molecular oxygen is formed. With four Mn ions involved at the catalytic site as well as one or more redox-active amino acid residues (e.g., Y_Z and possibly a histidine), any number of reaction paths may take place. In addition, calcium and chloride cofactors are known to be intimately involved (Chapter 13, van Gorkom and Yocum). Important questions for understanding the correct reaction path are: (i) at which step in the catalytic sequence do the two substrate water molecules bind; and (ii) how does the O-O bond form. In the past it has been experimentally difficult to get information on these questions, mainly because of the difficulty to distinguish the substrate water from the solvent water. However, the substrate water can be probed by oxygen isotope exchange measurements using mass spectrometry. Early ^{18}O isotope labeling studies established that water is the ultimate source of the O_2 produced during photosynthesis (Ruben et al., 1941). In other oxygen isotope exchange measurements (Radmer and Ollinger, 1980, 1986; Bader et al., 1983) a similar conclusion was made though the binding of the two substrate water molecules could not be determined. In more recent measurements, however, the kinetic resolution of the isotopic exchange was greatly improved in which the binding of the two substrates could be separately distinguished (Messiniger et al., 1995; Hillier et al., 1998). The results from this experimental approach revealed for the first time that one substrate water molecule is bound to the catalytic site throughout the S-state cycle while the second substrate water molecule is bound in at least the S_2 and S_3 states, and that the O-O bond forms during the last step of the reaction sequence (Hillier and Wydrzynski, 2000). These observations therefore place limits on the types of reaction paths that may be possible in the formation of O_2 during photosynthesis (Hillier and Wydrzynski, 2001). A detailed summary of the mechanism for the oxidation of water by PS II is given by Hillier and Messinger (Chapter 25).

VI. Future Perspectives

A. Structure and Biodynamics

Success in the X-ray crystallographic analysis (Zouni et al., 2001; Kamiya and Shen, 2003; Ferreira et al.,

2004) has had a great impact on what we currently know about the molecular structure and function of PS II. However, higher resolution structures will be needed in the future to fully understand the molecular details of catalytic components and to determine the exact mechanism of water oxidation. In particular, crystallographic analysis of PS II from higher plants and mutated cyanobacteria will be needed.

Of equal importance to the structural analysis is an understanding of the biodynamics of PS II function of which much less is currently known. For example, important clues on the mechanism of water oxidation can be gleaned from understanding the photo-assembly process of the catalytic Mn cluster. The current status of knowledge on this aspect is discussed by Dismukes et al. (Chapter 26). Likewise, the damage-repair cycle hypothesis proposed by Kyle et al. (1984) has not yet been substantiated, although considerable evidence has accumulated (for the latest details, see Chapter 27, Chow and Aro). Other aspects of PS II biodyanmics include transcriptional and translational regulation in the biosynthesis and homeostasis of PS II components (Chapter 28, Yamaguchi et al.) and the transport and post-translational processing events (Chapter 29, Theg and Shi), including, e.g., the carboxy-terminal processing of D1 precursor protein (Yamamoto and Satoh, 1999). In all future studies in these aspects of PS II, the application of comprehensive molecular biological techniques will be essential.

B. Origin, Evolution and Artificial O_2 Producing Systems

Trying to understand the origin and evolution of PS II that may have taken place 2–3 billion years ago is not only a matter of general interest to biologists but is a useful approach to understand the unique structural and functional properties of PS II as they exist today. However, although there are significant variations in the light-harvesting components (Chapter 2, Green and Gantt) and in the minor protein components (Chapter 6, Thornton et al.) of PS II among the cyanobacteria, algae and higher plants, there doesn't seem to be much variation in the PS II RC and the water oxidizing catalytic site itself — the organization and operation of the catalytic site appears to be the same in all organisms studied thus far. This unusual aspect of PS II (since most enzymes show variations characteristic of divergent or convergent evolution) is touched upon by Dismukes and Blankenship (Chapter 30, Dismukes and Blankenship). Nevertheless, the authors of this Chapter do promote some interesting arguments to suggest that bicarbonate ions may have served as an immediate substrate for the production of O_2 in the distant past, in light of the fact that the CO_2 level of the atmosphere at that time was considerably higher than it is today and the finding that there is an apparent bicarbonate requirement for the reactions on the donor side of P680 (Stemler, 2002; Chapter 14, van Rensen and Kimov). The likelihood of this hypothesis may be ascertained in the future by studies of ancient representatives of cyanobacteria present today (e.g., species from *Gleobacter* or from stromatolites) and of cyanobacteria living in extreme environments (e.g., *Arthrospira* strains living in African soda lakes). Still other approaches to try to understand the place of PS II in the evolution of life is to make mechanistic and structural comparisons between PS II and cytochrome *c* oxidase, which catalyzes the reverse reaction of reducing O_2 to water (for details, see Chapter 31, Brudvig and Wikström) and to modify natural bacterial reaction centers to have unique PS II properties through protein engineering (for details, see Chapter 32, Kálmán et al.).

Although there is considerable research yet to be done in order to understand all of the intricacies of PS II, there is now enough knowledge of the structure and function, as discussed in this book, to mimic PS II reactions for future efficient energy conversion processes through protein engineering (for details, see Chapter 33, Gibney and Tommos) and bio-inorganic chemistry (for details, see Chapter 34, Magnuson et al.). Therefore, for young scientists interested in understanding one of Nature's most unique enzymes, the future research of PS II remains an exciting challenge.

Acknowledgments

We thank Joel Freeman for his unlimited help in preparing this chapter and Rumana Tayyab for her help in drawing Fig. 1.

References

Åhrling KA, Peterson S and Styring S (1997) An oscillating manganese electron paramagnetic resonance signal from the S_0 state of the oxygen evolving complex in Photosystem II. Biochemistry 36: 13148–13152

Anderson JM (2002) Changing concepts about the distribution of Photosystems I and II between grana-appressed and stroma-exposed thylakoid membranes. Photosynth Res 73: 157–164

Åkerlund HE (1981) Partial reconstitution of the photosynthetic water splitting in inside out thylakoid vesicles. In: Akoyunoglou G (ed) Proceedings 5th International Congress on Photosynthesis, Vol 2, pp 465–472. Balaban International Science Service, Philadelphia

Åkerlund HE and Jansson C (1981) Localization of a 34,000 and a 23,000 Mr polypeptide to the luminal side of the thylakoid membrane. FEBS Lett 124: 229–232

Bader KP, Thibault P and Schmid GH (1983) A study on oxygen evolution and on the S-state distribution in thylakoid preparations of the filamentous blue-green alga *Oscillatoria chalybea*. Z Naturforsch 38c: 778–792

Barry BA and Babcock GT (1987) Tyrosine radicals are involved in the photosynthetic oxygen-evolving system. Proc Natl Acad Sci USA 84: 7099–7103

Berthold DA, Babcock GT and Yocum JF (1981) A highly resolved, oxygen-evolving Photosystem II preparation from spinach thylakoid membranes. FEBS Lett 134: 231–234

Biesiadka J, Bernhard L, Kern J, Irrgang K-D and Zouni A (2004) Crystal structure of cyanobacterial Photosystem II at 3.2 Å resolution: A closer look at the Mn-cluster. Phys Chem Chem Phys 6:4733–4736

Blankenship RE and Sauer K (1974) Manganese in photosynthetic oxygen evolution. I. Electron paramagnetic resonance study of the environment of manganese in tris-washed chloroplasts. Biochim Biophys Acta 357: 252–266

Boardman NK and Anderson JM (1964) Isolation from spinach chloroplasts of particles containing different proportions of chlorophyll *a* and chlorophyll *b* and their possible role in the light reactions of photosynthesis. Nature 293: 166–167

Bouges-Bocquet B (1973) Electron transfer between the two photosystems in spinach chloroplasts. Biochim Biophys Acta 314: 250–256

Cheniae GM and Martin IF (1966) Studies on the function of manganese in photosynthesis. Brookhaven Symposium in Biology 19: 409–417

Danielius RV, Satoh K, van Kan PJM, Plijter JJ, Nuijs AM and van Gorkom HJ (1987) The primary reaction of Photosystem II in the D1-D2-cytochrome *b*559 complex. FEBS Lett 213: 241–244

Debus RJ, Barry BA, Sithole I, Babcock GT and McIntosh L (1988) Directed mutagenesis indicates that the donor to P_{680}^{+} in Photosystem II is tyrosine-161 of the D1 polypeptide. Biochemistry 27: 9071–9074

Dismukes GC and Siderer Y (1981) Intermediates of a polynuclear manganese cluster involved in the photosynthetic oxidation of water. Proc Natl Acad Sci USA 78: 274–278

Döring G, Stiehl HH and Witt HT (1969) A second chlorophyll reaction in the electron transport chain of photosynthesis — registered by the repetitive excitation technique. Z Naturforsch 22b: 639–644

Duysens LNM (1989) The discovery of the two photosystems. A personal account. Photosynth Res 21:61–80

Duysens LNM and Sweers HE (1963) Mechanism of two photochemical reactions in algae as studied by means of fluorescence. In: Japanese Society of Plant Physiologists (ed) Studies on Microalgae and Photosynthetic Bacteria, pp 353–372. Univ Tokyo Press, Tokyo

Duysens LNM, Amesz J and Kamp BM (1961) Two photochemical systems in photosynthesis. Nature 190: 510–511

Ellis RJ (1977) Protein synthesis by isolated chloroplasts. Biochim Biophys Acta 463: 185–215

Emerson R and Arnold W (1932a) A separation of the reactions in photosynthesis by means of intermittent light. J Gen Physiol 15: 391–420

Emerson R and Arnold W (1932b) The photochemical reaction in photosynthesis. J Gen Physiol 16: 191–205

Emerson R and Lewis CM (1943) The dependence of the quantum yield of *Chlorella* photosynthesis on the wavelength of light. Am J Bot 30: 165–178

Emerson R and Rabinowitch E (1960) Red drop and the role of auxiliary pigments in photosynthesis. Plant Physiol 35: 477–485

Emerson R, Chalmers RV and Cederstrand CN (1957) Some factors influencing the long wave limit of photosynthesis. Proc Natl Acad Sci USA 43: 133–143

Evans MCW (1987) Plant reaction centre defined. Nature 327:284–285

Ferreira KN, Iverson TM, Maghlaoui K, Barber J and Iwata S (2004) Architecture of the photosynthetic oxygen-evolving center. Science 303: 1831–1837

Floyd RA, Chance B and DeVault D (1971) Low temperature photo-induced reactions in green leaves and chloroplasts. Biochim Biophys Acta 226: 103–112

Gaffron H and Wohl K (1936) Zur Theorie der Assimilation. Naturwissenschaften 24: 81-90; 103-107

Govindjee (2004) Chlorophyll *a* fluorescence: A bit of basics and history. In: Papageorgiou GC and Govindjee (eds) Chlorophyll *a* Fluorescence: A Signature of Photosynthesis, pp 1–42. Springer, Dordrecht

Govindjee and Krogmann D (2004) Discoveries in oxygenic photosynthesis (1727–2003): A perspective. Photosynth Res 80: 15–57

Govindjee and Rabinowitch E (1960) Two forms of chlorophyll *a* with distinct photochemical functions. Science 132: 159–159

Govindjee, Pulles MPJ, Govindjee R, van Gorkom HJ and Duysens LNM (1976) Inhibition of the reoxidation of the secondary electron acceptor of Photosystem II by bicarbonate depletion. Biochim Biophys Acta 449: 602–605

Hankamer B, Morris EP and Barber J (1999) Revealing the structure of the oxygen-evolving core dimmer of Photosystem II by cryoelectron crystallography. Nat Struct Biol 6: 560–564

Hill R (1937) Oxygen evolution by isolated chloroplasts. Nature 139: 881–882

Hill R and Bendall F (1960) Function of the cytochrome components in chloroplasts: A working hypothesis. Nature 186: 136–137

Hillier W and Wydrzynski T (2000) The affinities for the two substrate water binding sites in the O_2 evolving complex of Photosystem II vary independently during S-state turnover. Biochemistry 39: 4399–4405

Hillier W and Wydrzynski T (2001) Oxygen ligand exchange at metal sites — implications for the O_2 evolving mechanism of Photosystem II. Biochim Biophys Acta 1503: 197–209

Hillier W, Messinger J and Wydrzynski T (1998) Kinetic resolution and temperature dependence of the $H_2{}^{18}O/H_2{}^{16}O$ exchange rates for the two substrate water molecules in the S_3 state of the photosynthetic water oxidation complex. Biochemistry

37: 16908–16914
Joliot P (2003) Period-four oscillations of the flash-induced oxygen formation in photosynthesis. Photosynth Res 76: 65–72
Joliot P, Barbieri G and Chabaud R (1969) Un nouveaux modele des centres photochimiques du système II. Photochem Photobiol 10: 309–329
Kamiya N and Shen JR (2003) Crystal structure of oxygen-evolving Photosystem II from *Thermosynechococcus vulcanus* at 3.7-Å resolution. Proc Natl Acad Sci USA 100: 98–103
Kashino Y, Lauber WM, Carroll JA, Wang Q, Whitmarsh J, Satoh K and Pakrasi HB (2002) Proteomic analysis of a highly active Photosystem II preparation from the *Synechocystis* sp. PCC 6803 reveals the presence of novel polypeptides. Biochemistry 41: 8004–8012
Ke B (2001) Photosynthesis: Photobiochemistry and Photobiophysics. Kluwer Academic Publishers, Dordrecht
Kirby JA, Goodin DB, Wydrzynski T, Robertson AS and Klein MP (1981a) State of manganese in the photosynthetic apparatus. 1. Extended X-ray absorption fine structure studies on chloroplast and di-μ-oxo-bridged dimanganese model compounds. J Am Chem Soc 103: 5529–5537
Kirby JA, Goodin DB, Wydrzynski T, Robertson AS and Klein MP (1981b) State of manganese in the photosynthetic apparatus 2. X-ray absorption edge studies of manganese in photosynthetic membranes. J Am Chem Soc 103: 5537–5542
Klimov VV, Klevanik AV, Shuvalov VA and Krasnovsky AA (1977) Reduction of pheophytin in the primary light reaction of Photosystem II. FEBS Lett 82: 183–186
Kok B (1959) Light-induced absorption changes in photosynthetic organisms. II. A split-beam difference spectrophotometer. Plant Physiol 34: 184–192
Kok B, Forbush B and McGloin M (1970) Cooperation of charges in photosynthetic O_2 evolution. 1. Photochem Photobiol 11: 457–475
Kuwabara T and Murata N (1979) Purification and characterization of 33 kilodalton protein of spinach chloroplasts. Biochim Biophys Acta 581: 228–236
Kyle DJ, Ohad I and Arntzen CJ (1984) Membrane protein damage and repair, selective loss of a quinine protein function in chloroplast membrane. Proc Natl Acad Sci USA 81: 4070–4074
Lavoisier AL (1789) Traité élémentaire de chimie. Chez Cuchet, librarie, Rue et Hôtel Serpente, Academie Royal des Sciences, Paris
Losada M, Whatley FR and Arnon D (1961) Separation of two light reactions in non-cyclic phosphorylation of green plants. Nature 190: 606–610
Lozier R, Baginsky M and Butler WL (1971) Inhibition of electron transport in chloroplasts by chaotrophic agents and the use of manganese as an electron donor to Photosystem II. Photochem Photobiol 14: 323–328
Mayer JR (1845) Die organische Bewegung in ihrem Zussamenhag mit dem Stoffwechsel: Ein Beitrag zur Naturkunde. Verlag der C. Drechsler'schen Buchhandlung, Heilbronn
Messinger J, Badger M and Wydrzynski T (1995) Detection of one slowly exchanging substrate water molecule in the S_3 state of Photosystem II. Proc Natl Acad Sci USA 92: 3209–3213
Messinger J, Nugent JHA and Evans MCW (1997) Detection on an EPR multiline signal for the S_0^- state in Photosystem II. Biochemistry 36: 11015–11060
Michel H and Deisenhofer J (1985) X-Ray diffraction studies on crystalline bacterial photosynthetic reaction center: A progress report and conclusions on the structure of Photosystem II reaction centers. In: Staehelin LA and Arntzen CJ (eds) Encyclopedia of Plant Physiology; New Series Photosynthesis, Vol III, pp 371–381. Springer-Verlag, Berlin
Myers J and French CS (1960) Evidences from action spectra for a specific participation of chlorophyll *b* in photosynthesis. J Gen Physiol 43: 723–736
Nakatani H, Ke B, Dolan E and Arntzen CJ (l984) Identity of the Photosystem II reaction center polypeptide. Biochim Biophys Acta 765: 347–352
Nanba O and Satoh K (1987) Isolation of a Photosystem II reaction center consisting of D-1 and D-2 polypeptides and cytochrome *b*-559. Proc Natl Acad Sci USA 84: 109–112
Ogawa T (2003) Physical separation of chlorophyll-protein complexes. Photosynth Res 76: 227–232
Ogawa T, Obata F and Shibata K (1966) Two pigment proteins in spinach chloroplasts. Biochim Biophys Acta 112: 223–234
Okamura MY, Satoh K, Issacson RA and Feher G (1987) Evidence of the primary charge separation in the D1/D2 complex of Photosystem II from spinach: EPR of the triplet state. In Biggins J (ed) Progress in Photosynthesis Research. Vol 1, pp 379–381. Martinus Nijhoff, Boston
Ort DR and Yocum CF (eds) (1996) Oxygenic Photosynthesis: The Light Reactions. Kluwer Academic Publishers, Dordrecht
Papageorgiou G and Govindjee (eds) (2004) Chlorophyll *a* Fluorescence: A Signature of Photosynthesis. Springer, Dordrecht
Priestley J (1772) Observations on different kinds of air. Phil Trans R Soc London 62: 147–264
Radmer R and Ollinger O (1980) Isotopic composition of the photosynthetic O_2 flash yields in the presence of $H_2{}^{18}O$ and $HC^{18}O_3^-$. FEBS Lett 110: 57–61
Radmer R and Ollinger O (1986) Do the higher oxidation states of the photosynthetic O_2-evolving system contain bound H_2O? FEBS Lett 195: 285–289
Renger G (2003) Apparatus and mechanism of photosynthetic oxygen evolution: A personal perspective. Photosynth Res 76: 269– 288
Ruben S, Randall M, Kamen MD and Hyde JJ (1941) Heavy O (^{18}O) as tracer in study of Photosynthesis. J Am Chem Soc 63: 877–880
Satoh K (1985) Protein-pigments and Photosystem II reaction center. Photochem Photobiol 42: 845–853
Satoh K (1988) Reality of P-680 chlorophyll protein-Identification of the site of primary photochemistry in oxygenic photosynthesis. Physiol Plant 72: 209–212
Satoh K (2003) The identification of the Photosystem II reaction center: A personal story. Photosynth Res 76: 233–240
Satoh K and Butler WL (1978) Low temperature spectral properties of subchloroplast fractions purified from spinach. Plant Physiol 61: 373–379
Scheele CW (1781) Traite chimique de l'air et du feu. Rue et Hôtel Serpente, Academie Royale des Sciences, Paris
Sharp RR (1992) Proton NMR relaxation due to the photosynthetic oxygen evolving center. In: Pecoraro VL (ed) Manganese Redox Enzymes, pp 177–196. VCH Publishers Inc, New York
Smith EL (1938) Solutions of chlorophyll-protein compounds (phyllochlorins) extracted from spinach. Science 88: 170–172
Stemler AJ (2002) The bicarbonate effect, oxygen evolution, and

the shadow of Otto Warburg. Photosynth Res 73: 185–192
Stiehl HH and Witt HT (1968) Die kurzezeitigen ultravioletten Differenzspektren bei der Photosynthese. Z Naturforschg 23b: 220-224
Takahashi Y, Takahashi M and Satoh K (1986) Identification of the site of iodide photooxidation in the Photosystem II reaction center complex. FEBS Lett 208: 347–351
Takahashi Y, Hansson Ö, Mathis P and Satoh K (1987) Primary radical pair in the Photosystem II reaction center. Biochim Biophys Acta 893: 49–59
Tang X-S and Satoh K (1985) The oxygen-evolving Photosystem II core complex. FEBS Lett 179: 60–64
Thomas JB, Blaauw OH and Duysens LNM (1953) On the relation between size and photochemical activity of fragments of spinach grana. Biochim Biophys Acta 10: 230–240
Thornber JP (1975) Chlorophyll-proteins: Light-harvesting and reaction center components of plants. Ann Rev Plant Physiol 26: 127–158
Thornber JP and Highkin HR (1974) Composition of the photosynthetic apparatus of normal barley leaves and a mutant lacking chlorophyll b. Eur J Biochem 41: 109–116
Thornber JP, Smith CA and Bailey JL (1966) Partial characterization of two chlorophyll-protein complexes isolated from spinach-beet chloroplasts. Biochem J 100: 14p–15p
Timiriazeff CA (1874) Sur l'action de la lumiere dans la decomposition de l'acide carbonique par la granule de chlorophylle. International Botanical Congress, Firenze, Italy, May, pp 108-117.
Trebst A (1986) The topology of the plastoquinone and herbicide binding peptides of Photosystem II in the thylakoid membrane. Z Naturforsch 41c: 240–245
Van Mieghem FJE, Satoh K and Rutherford AW (1991) A chlorophyll tilted 30° relative to the membrane in the Photosystem II reaction centre. Biochim Biophys Acta 1058: 375–378
van Rensen JJS, Xu C and Govindjee (1999) Role of bicarbonate in Photosystem II, the water-plastoquinone oxido-reductase of plant photosynthesis. Physiol Plant 105: 585–592
Velthuys BR and Amesz J (1974) Charge accumulation at the reducing side of system 2 of photosynthesis. Biochim Biophys Acta 325:138–148
Vermeglio A (2002) The two-electron gate in photosynthetic bacteria. Photosynth Res 73: 83–86
Whitmarsh J and Govindjee (2002) Photosystem II. Encyclopedia of Life Sciences. McMillan Publishers Ltd, Nature Publishing Group, London, UK (http://www.els.net)
Willstätter R and Stoll A (1913) Untersuchungen über Chlorophyll. Justus Springer, Berlin (English translation by Schertz FM and Merz AR, Science Printing Press, Lancaster, Pennsylvania, 1928)
Witt HT, Müller A and Rumberg B (1961) Experimental evidence for the mechanism of photosynthesis. Nature 191: 194–195
Wydrzynski T (1977) The role of manganese in photosynthetic oxygen evolution. PhD thesis. University of Illinois at Urbana-Champaign, Illinois
Wydrzynski T (2004) Early indications for manganese oxidation state changes during photosynthetic oxygen production: A personal account. Photosynth Res 80: 125–135
Wydrzynski T, Zumbulyadis N, Schmidt PG, Gutowsky HS and Govindjee (1976) Proton relaxation and charge accumulation during oxygen evolution in photosynthesis. Proc Natl Acad Sci USA 73: 1196–1198
Yamamoto Y and Satoh K (1999) The carboxy-terminal processing of precursor D1 protein of Photosystem II reaction center by a nuclear-encoded protease (CtpA). In: Argyroudi-Akoyunoglou JH and Senger H (eds) The Chloroplast: From Molecular Biology to Biotechnology, pp 271–276. Kluwer Academic Publishers, Dordrecht
Yamamoto Y, Doi M, Tamura N and Nishimura M (1981) Release of polypeptides from highly active O_2-evolving Photosystem-2 preparation by Tris treatment. FEBS Lett 133: 265–268
Yamaoka T, Satoh K and Katoh S (1978) Photosynthetic activities of a thermophilic blue-green alga. Plant Cell Physiol 19: 943–954
Zouni A, Witt HT, Kern J, Fromme P, Krauss N, Saenger W and Orth P (2001) Crystal structure of Photosystem II from *Synechococcus elongatus* at 3.8 Å resolution. Nature 409: 739–743

Chapter 2

Distal and Extrinsic Photosystem II Antennas

Beverley R. Green*
Botany Department, University of British Columbia, Vancouver, B.C. V6T 1Z4, Canada

Elisabeth Gantt
Cell Biology and Molecular Genetics, University of Maryland, College Park, MD 20742, U.S.A.

Summary

The distal and extrinsic light-harvesting antennas of Photosystem II (PS II) provide the capability to match electron flow through Photosystem I thus allowing for regulated responses to environmental changes. In this chapter we provide a concise up-to-date description of these antenna complexes and discuss what is known about their function. The cyanobacteria and red algal PS II antennas are phycobiliproteins organized into complex membrane-extrinsic structures called phycobilisomes. A small group of cyanobacteria lack phycobilisomes and instead use the membrane-intrinsic prochlorophyte chlorophyll (Chl) *a/b* proteins. PS II of eukaryotes is

*Author for correspondence, email: brgreen@interchange.ubc.ca

T. Wydrzynski and K. Satoh (eds): Photosystem II: The Light-Driven Water:Plastoquinone Oxidoreductase, pp. 23–44.

primarily served by members of the light-harvesting complex (LHC) superfamily which has become widely diversified into Chl *a/b* and Chl *a/c* antennas. As members of the LHC superfamily, cryptophyte algae also have novel phycobilins in the thylakoid lumen, and dinoflagellate algae have a unique peridinin-Chl *a* protein. Atomic resolution structures of these two antennas and the major plant LHC are opening up a new era in understanding energy transfer.

I. Introduction

Light-harvesting antennas are the pigment-protein complexes that serve to absorb light energy and transfer it to the photosynthetic reaction centers of Photosystem I (PS I) and Photosystem II (PS II). The core antennas are the antennas that bind only chlorophyll (Chl) *a* and are most intimately associated with the photosystems. PS I has a combined core antenna-reaction center, where about 90 additional Chl *a* molecules are bound to the same two membrane-intrinsic proteins (PsaA and PsaB) as the reaction center chromophores. An interesting exception is the PS I core antenna of *Acaryochloris* with 180 Chl *d* per 1 Chl *a* (Hu et al., 1998). In contrast, PS II has two separate Chl *a*-proteins, CP47 and CP43, that bind only 16 and 14 Chl *a* respectively (Table 1). The core Chl *a* antennas are discussed in Chapter 3 (Eaton-Rye and Putnam-Evans).

The fact that the PS II core antennas bind only one-third the number of Chls as the PS I core means that PS II requires additional light-harvesting capacity in order to maintain linear electron flow. The distal and extrinsic antennas provide that capacity. The 'distal' antenna complexes are defined as those that are membrane-bound but not part of the core antenna, and the 'extrinsic' antennas are those that are attached to the surface of the thylakoid membrane (Green and Durnford, 1996). Both kinds of antenna are regulated qualitatively and quantitatively in response to physiological status and environmental signals. This provides the flexibility required for acclimation to different light, temperature and nutrient regimes, as well as to short-term changes in the redox state of the electron transport chain.

In spite of the great variety of light-harvesting antennas, only three major types of light-absorbing chromophores and only four protein families are employed in all the antennas of PS II (Table 1). Open-chain tetrapyrroles called phycobilins are attached to members of the phycobiliprotein family: they are generally found in complex membrane-extrinsic structures called phycobilisomes (PBS). Several groups of cyanobacteria lack PBSs but have a unique membrane-bound Chl *a/b* antenna using proteins related to the core antenna. The chloroplasts of photosynthetic eukaryotes employ members of the light-harvesting complex (LHC) superfamily, which bind Chl *b* or *c* in addition to Chl *a* and have three trans-membrane helices. Members of this well-studied family transfer energy to either or both photosystems, and have an important role in photoprotection as well as light-gathering. The peridinin-Chl *a* antenna is unique to dinoflagellates; because the carotenoid peridinin rather than Chl plays the major role in light-harvesting, it is being extensively studied as a model system in energy transfer (Ilagan et al., 2004).

Many aspects of light-harvesting antennas were extensively covered in a recent book in this same series (Green and Parson, 2003), and in individual chapters in two other books (Frank et al., 1999; Larkum et al., 2003). This chapter is restricted to the antennas of PS II, and our aim is to provide a concise introduction and update of material in the above volumes.

Abbreviations: B-PE, R-PE – phycoerythrin of red algae (Bangiophycean, Rhodophycean); Chl – chlorophyll; CP24, CP26, CP29 – minor internal Chl *a/b* antennas that connect the external antennas with the PS II core; CP43, CP47 – antennas of the PS II core complex; FCP – fucoxanthin-Chl *a/c* protein; IsiA – Chl *a* protein induced by Fe limitation (CP43′); LHC – member of light-harvesting complex superfamily; LHCII – major LHC antenna of PS II in higher plants; PBS – phycobilisome; Pcb – prochlorophyte Chl *a/b* protein; PS I, PS II – Photosystem I, Photosystem II; PsaA, PsaB – PS I reaction center-core antenna proteins; RC1, RC2 – reaction centers of PS I, PS II; RP-HPLC – reversed-phase high performance liquid chromatography; SDS-PAGE – sodium dodecyl sulfate-polyacrylamide gel electrophoresis

II. Phycobiliproteins and Phycobilisomes

A. Phycobiliprotein Types

Phycobiliproteins are the predominant antenna pigments in cyanobacteria, rhodophytes, glaucophytes, and in many cryptophytes. They are water soluble pigments that are readily released upon cell breakage and produce vibrant blue- or orange to red-colored solutions. Chemically, the chromophores are linear

Table 1. Light-harvesting antennas of Photosystem II

Family	Chromophores	Where found	Organization/Location
Core complex			
Core antennas CP43, CP47	Chl *a*, β-carotene	All oxygenic organisms	Part of PS II core
Prochlorophyte Chl *a/b* proteins	Chl *a, b*	Only in 3 genera of cyanobacteria (prochlorophytes)	Thylakoid membrane
Phycobiliprotein	Phycobilins	Cyanobacteria, glaucophytes, rhodophytes, cryptophytes	Phycobilisomes, stromal side of thylakoid membrane, except cryptophytes
LHC (light-harvesting complex) superfamily	Chl *a* plus one or more of *b, c1, c2, c3*; variety of carotenoids	Chloroplasts, except glaucophytes (none), rhodophytes (PS I only)	Thylakoid membrane
Peridinin-Chl *a* protein	Chl *a*, peridinin	Dinoflagellates only	Trimers in thylakoid lumen

tetrapyrroles that are covalently bound to the apoprotein by thioether linkages to one or two rings (rings A/D) (MacColl and Guard-Friar, 1987; Mimuro and Kikuchi, 2003; Scheer, 2003). The effectiveness of phycobiliproteins as antennas was proven in the 1950s by elegant action spectra done largely by Haxo and co-workers; they are beautifully illustrated in a compilation by Haxo (1960). It is now well established that the energy absorbed by the antenna pigments is transferred between them and finally to reaction centers by the Förster-type exchange mechanism (Mimuro and Kikuchi, 2003; Parson and Nagarajan, 2003). This mechanism requires an overlap of the wavelength functions and occurs efficiently when the donating and accepting chromophores are within about 20Å and no more than 100Å apart. Maximal transfer efficiency is assured by close packing of chromophores on the phycobiliproteins at one level, and furthered by the close association of phycobiliproteins to one another.

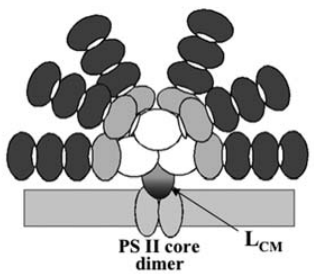

Fig. 1. Diagram of a generic phycobilisome linked through the L_{CM} (core to membrane linker) to a dimeric PS II complex. Each PS II monomer has a PS II reaction center (RC2) and CP47 and CP43 core antennas (not shown). The outer phycoerythrin (PE, dark gray) is connected via phycocyanin (PC, light gray) to the allophycocyanin core (APC, white circles) , with linker polypeptides (small ovals) assuring correct phycobiliprotein stacking. Excitation energy transfer from phycoerythrin to Chl is seen by the decrease in fluorescence maxima of participating pigments.

1. Phycobiliprotein Characteristics in Cyanobacteria and Red Algae

Allophycocyanin and phycocyanin are the two principal types of phycobiliproteins that occur in all cyanobacteria, glaucophytes and red algae which have phycobilisomes as light harvesting antennas (Figs. 1, 2A). Phycoerythrin is the third principal phycobiliprotein type. Within cells these pigments exist as aggregates of the α and β subunits. An α and β combination is often referred to as a 'monomer' and larger ones as 'trimers' or 'hexamers,' but the terminology can be rather arcane for the general reader and thus quotes are used. In solution phycobiliproteins tend to be more stable as aggregates of 3α+3β , or as 6α+6β . The most stable are the large aggregates of phycoerythrins (designated as B-bangiophycean and R-rhodophycean) which often consist of a combination of 6α, 6β , and 1γ subunits with a total molecular mass of about 260,000 kDa. Allophycocyanins have the fewest chromophores with 12 per 'hexamer' (1 each per α and β subunit), and they only have phycocyanobilin chromophores. Phycocyanobilin is also the common chromophore of phycocyanins, but more chromophores (1 per α

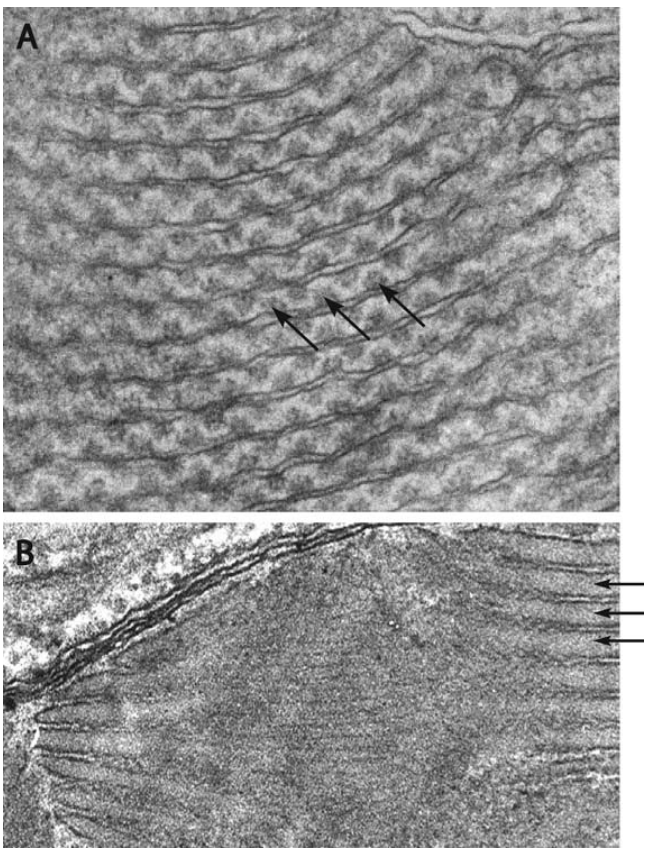

Fig. 2. Localization of phycobiliproteins: A. Hemispherically shaped phycobilisomes (arrows) attached to the stromal side of thylakoids in a red alga (*Porphyridium cruentum*). The localization is the same in cyanobacteria although the phycobilisomes are usually hemidiscoidally shaped. B. In cryptophytes (*Chroomonas*) the phycobiliproteins are concentrated in the thylakoid lumen (arrows) in an apparently highly ordered manner.

subunit and 2 per β subunit) are bound than in allophycocyanins. Some phycocyanin apoproteins may also bind other chromophores, i.e., phycobiliviolin (as in phycoerythrocyanin) or phycoerythrobilin (as in R-phycocyanin). Phycoeryrthrins bind many phycoerythrobilin chromophores, and often also phycourobilins , with a total of 24 or more per 'hexamer' (6α, 6β , 1γ) (Toole and Allnutt, 2003). Because of their high chromogenicity, individual phycobiliproteins have found uses as fluorescent cytological markers in animal cell analysis. Also, PBSs of some red algae are highly useful for biomedical cytology since they contain spectrally distinct absorbing and fluorescing chromophores and a large number of chromophores (Toole and Allnutt, 2003).

From the crystal structures of the principal types of phycobiliproteins one can see that they follow the same folding pattern, a typical 'globin fold' (see summary in Mimuro and Kikuchi, 2003). The arrangement of the α and β subunits is such that 3 'monomers' form a 'trimer' around a central cavity with the chromophores arranged on the outer rim of the 'trimer,' except in allophycocyanin where the chromophores on the β subunit face into the cavity. An extensive comparison of phycobiliprotein sequences suggests that they are derived from two evolutionary lines that originated from a common ancestor (Apt et al., 1995a). Several residues are of critical importance for chromophore attachments and for folding of the proteins. Present in almost all phycobiliproteins is the

Cys at residue 84 (or 88) which is a chromophore binding site in α and β subunits, Arg90 and Asp91 which are important for maintaining the proper chromophore orientation, and Gly118 (or 114), which is necessary for the proper charge interaction between helices that probably interact with linker polypeptides. Additional chromophore binding residues in phycoerythrins and phycocyanins are Cys155 (or 140) (Apt et al., 1995a; Mimuro and Kikuchi, 2003).

2. Cryptophyte Phycobiliproteins

Cryptophyte phycobiliproteins are similar to those in cyanobacteria and rhodophytes in having phycoerythrin- and phycocyanobilin-type chromophores but with a variety of unique bilin isomers including 15,16 dihydrobiliverdin, mesobiliverdin, bilin-618 and bilin–584, some of which are related to phytochrome bilin (Glazer and Wedemayer, 1995; Wedemayer et al., 1996). Any one species has only phycocyanin or phycoerythrin, but never both, and no allophycocyanin has been reported. However, the phycobiliproteins are organized as $(\alpha_1\beta)(\alpha_2\beta)$ 'heterodimers' (Wilk et al., 1999); the α_1 and α_2 subunits are not identical. They are tightly packed in the thylakoid lumen (Fig. 2B) rather than organized into complex phycobilisomes on the stromal side (Fig. 2A) (Gantt et al., 1971; Ludwig and Gibbs, 1989). The close packing presumably orients the chromophores for maximal energy transfer. One reason for this structural difference is that the α subunits are not closely related to the α subunits of cyanobacteria or red algae: they appear to have been recruited from some other source, possibly from a linker protein (Apt et al., 1995a; Reuter et al., 1999). However, the β subunits of cryptophyte phycocyanin or phycoerythrin do share substantial sequence relatedness with those of their cyanobacterial/rhodophyte equivalents (Apt et al., 1995a). The structure of the PE545 phycobiliprotein heterodimer has been solved to 1.63Å resolution by X-ray crystallography (Wilk et al., 1999) and is discussed in some detail in MacPherson and Hiller (2003). Evolutionarily the cryptophyte chloroplast is believed to have originated by the secondary acquisition of a red algal chloroplast, with partial support from a similarity between the β subunits.

The functional contribution of phycobiliproteins as antenna pigments in cryptophytes is as well accepted as in cyanobacteria and rhodophytes. Most cryptophytes are certainly capable of photoautotrophic growth, but it is not clear to what extent they are capable of mixo- or even heterotrophic growth, especially since non-photosynthetic cryptophytes are by no means rare. *Chroomonas* sp. grown under photoautotrophic growth conditions exhibited an increase in Chl and phycocyanin content under low light, typical of a phototroph, but was also able to utilize glycerol as carbon source (Gantt, 1980). Upon exciting phycoerythrin Bruce et al. (1986) found fluorescence emission at both 688 nm and 725 nm (at 77K) in whole cells. This, plus a very low phycoerythrin emission suggests that energy is transferred to both reaction centers. When Lichtlé et al. (1987) characterized the photosystem particles from *Cryptomonas*, they established that phycoerythrin was associated with a functionally active PS II particle, but not with PS I. Macpherson and Hiller (2003) reviewed spectroscopic studies and concluded that the phycobilins preferentially transfer energy to PS II rather than PS I, but whether it goes via the Chl *a/c* complex is not clear. More studies combining biochemical fractionation with spectroscopy, using a broader selection of cryptophyte species, are clearly in order.

3. Prochlorophyte Phycobiliproteins

Phycoerythrin has been found in several low light strains of *Prochlorococcus marinus*, one of the 'green cyanobacteria' or prochlorophytes that have a Chl *a/b* antenna and do not have PBSs (Hess et al., 1996; Ting et al., 2001; Partensky and Garczarek, 2003). The phycoerythrin has phycoerythrobilin and phycourobilin and has three apoprotein types (α, β, and γ), i.e., it is compositionally similar to that in higher red algae. Genes for phycocyanin and allophycocyanin are absent from the genomes of either strain (Dufresne et al., 2003; Partensky and Garczarek, 2003). Because these basal phycobiliproteins are absent, it is not surprising that PBSs have not been found. Presumably the phycoerythrin-containing strains could benefit under low light by being able to harvest the blue and green light absorbing regions, provided that the energy absorbed is functionally transferred to a reaction center. However, the spectral overlap of phycoerythrin with Chl *a* is poor and thus any transfer would be quite inefficient. Even though the spectral overlap with Chl *b* is slightly better, action spectral measurements and fractionation studies are required to assess the contribution of phycoerythrin to photosynthesis.

B. Phycobilisomes

1. Structure

The phycobilisome (PBS) can be viewed as an exquisitely engineered antenna that acts as an energy transfer funnel to PS II (Fig.1). The close packing of 'trimers' and 'hexamers' of various types of chromophores allows for their interaction with only the most minimal loss of energy. Whether in simple or complex PBS, the chromophores are oriented for maximal absorption and transfer of energy from higher to lower energy states and between chromophores (recently reviewed by Mimuro and Kikuchi, 2003; Toole and Allnutt, 2003). Specific linker polypeptides are involved in facilitating an optimized phycobiliprotein to phycobiliprotein arrangement, resulting in the PBS. The role, type and location of rod and core linker polypeptides, though fascinating, is beyond the generally interested reader but are reviewed by Apt et al. (1995a), Mimuro and Kikuchi (2003) and Toole and Allnutt (2003). In cryptophytes the phycobiliproteins are not organized in PBSs but are packed into the thylakoid lumen (Fig. 2B).

The simplest phycobilisome type is a simple rod, with allophycocyanin as a base on the thylakoid membrane and a phycocyanin rod extending distally into the stroma (e.g., *Gloeobacter*). More typical are PBSs in many cyanobacteria where a multimeric allophycocyanin center is surrounded by phycocyanin rods. Phycoerythrin may be added distally in cyanobacteria that adapt to red or green light, a phenomenon referred to as complementary chromatic adaptation, summarized in an excellent recent review by Grossman et al. (2003). Although the most complex PBSs occur in red algae, they are variations on the same theme represented by the generic PBS model in Fig. 1. Spectrally, the red algal phycobiliproteins are similar to those in cyanobacteria (Gantt et al., 2003; Mimuro and Kikuchi, 2003). Energy transfer between phycobiliproteins occurs within picoseconds, and transfer to Chl occurs within nanoseconds as has been determined in whole cells and in isolated PBSs (Mimuro and Kikuchi, 2003). A tight energetic coupling is verifiable by the very low fluorescence emission from the individual phycobiliprotein types.

2. Acclimation to Light and Nutrient Status

Acclimation of red algae to changes in light intensity and light quality were recently reviewed by Gantt et al. (2003). It should be noted that complementary chromatic 'adaptation' to red or green light, as studied in cyanobacteria such as *Fremyella* (excellently reviewed by Grossman et al., 2003) has never been credibly proven in any red alga. More commonly, nutrient limitation effects, especially nitrogen deficiency account for changes in the phycobiliprotein ratios in the red algae.

In cyanobacteria, *Synechocystis* sp. PCC 6803 has become a model system for determining the global changes of nutrient stress and light stress. With most of the genes being available for microarray analysis, Hihara et al. (2001) followed the changes from low light to high light (20 to 300 μmol photons m^{-2} sec^{-1}). They generally found that PS I and PS II genes were down regulated, but the response of PBS-related genes varied. Whereas the allophycocyanin genes were initially down regulated, they recovered, unlike phycocyanin genes. They suggest that phycocyanin as the peripheral phycobiliprotein is more strictly regulated than allophycocyanin. Furthermore, the down regulation of phycobiliprotein and PS I and PS II transcripts was noted to result from the impairment of the inorganic carbon uptake mechanism (Wang et al., 2004). Another analysis on the same cyanobacterium examined the response to iron deficiency (Singh et al., 2003). PBS gene transcripts declined when cells were transferred to the deficient conditions, but apparently the phycobiliprotein and Chl content remained at a level sufficient to continue in the photosynthetic state. Although such analyses provide a global view, follow-up physiological and biochemical studies are needed for each species. For example, in examining the effect of nitrate and sulfur limitation on phycobiliprotein synthesis in *Synechocystis*, Richaud et al. (2001) did not obtain the expected PBS degradation and chlorosis predicted from previous studies on *Synechococcus.* Clearly differences in regulation, or signaling, are suggested from their results.

3. Association with Photosystem II: Energy Distribution and Dissipation

That PBS are structurally and functionally associated with PS II in rhodophytes and cyanobacteria has been demonstrated by isolation of PBS/PS II particles with PS II activity as shown by O_2 evolution and reduction of electron acceptors (Gantt et al., 1988, 2003). Although at this time there is no direct evidence for a direct physical coupling of PBSs to PS I, as verified by isolation of functional complexes, it is certainly a possibility. State I and state II change measurements

and the suggestion that PBSs are mobile while PS II units are not, have been interpreted as evidence for a PBS-PS I association (Joshua and Mullineaux, 2005). A shuttling of PBS between PS II and PS I would be an attractive mechanism to avoid photoinhibition.

Photoinhibition and its attendant photodamage are a problem when the energy of light absorbed by the antenna systems cannot be utilized or otherwise dissipated (Chapters 23, Pogson et al.; 27, Chow and Aro). One might expect red algae and cyanobacteria, which have low light compensation points, to be more sensitive to photoinhibition. Furthermore, they do not have a highly varied carotenoid composition nor do they have an obvious xanthophyll cycle, which could play a role in minimizing damage from over-excitation. On the contrary, rhodophytes and cyanobacteria have been shown to be rather resistant to photodamage from high light and to have rapid recovery times after high light exposure (Gantt et al., 2003). Classic manifestations of photoinhibition, such as that in higher plants involving light-dependent phosphorylation of PS II, have not been clearly demonstrated in phycobilisome-containing organisms (Biggins et al., 1983; McConnell et al., 2002; Gantt et al., 2003).

In green plants an excitation transfer connection between PS II and PS I (state change) can be brought about by phosphorylation of LHCII polypeptides and their migration to PS I (Chapter 27, Chow and Aro). With the apparent lack of LHCII polypeptides in red algae and their complete absence in cyanobacteria, this mechanism of preventing damage from over-excitation of RC2 is not likely. State changes in green plants, as measured by a decrease in PS II fluorescence, occur relatively slowly, with durations of minutes. In algae with PBSs the apparent state changes are orders of magnitude faster, and the increase of PS I fluorescence appears to be independent of the quenching in PS II fluorescence (Bruce et al., 1986; Delphin et al., 1998).

What alternatives exist in PBS-containing organisms to dissipate energy and prevent photoinhibition, if the energy is not redistributed at the level of reaction centers? Dissipation through fluorescence or thermal conversion are recognized alternatives, but direct evidence is still lacking. From whole cell fluorescence studies in cyanobacteria, Sarcina et al. (2001) favor the hypothesis that over-excitation from excess PBS energy to RC2 is prevented by the physical detachment of the PBS and their movement to and attachment to RC1. With their fluorescence assay, using whole cells, they have examined a number of cyanobacteria and they characterize all of them as having mobile PBSs. According to their interpretation, the RC2 centers are stationary but the PBSs are mobile and their mobility is limited by their size. If this is true, why is it possible to isolate active PBS-PS II particles, but not PBS-PS I particles?

A compelling set of experiments was performed that critically addressed the state I and II transitions in the unicellular red alga *Rhodella violacea* and elucidated critical factors that resolve apparent inconsistencies (Delphin et al., 1998). These experiments showed that inhibition of protein phosphorylation did not influence the state transitions, thus supporting previous findings (Biggins et al.,1983). They further demonstrated that the PS II quenched fluorescence state results from the ΔpH across the membrane and not from the reduction of the plastoquinone pool. Even very low intensities of green light (state II light), absorbed only by PBS antenna of PS II, were sufficient for inducing the ΔpH. The PS II fluorescence quenching was relaxed upon uncoupling the ΔpH gradient and by activation of ATPase; hence it was proposed that the quenching relaxation is related to the utilization of the ΔpH by ATP synthase (Delphin et al., 1998). The collective results make clear that substantial differences exist between red algae and green plants in the distribution of excitation energy. Recently McConnell et al. (2002) came up with a combined model of regulated excitation energy distribution in cyanobacteria which encompasses an explanation for various results and interpretations. Their model allows a significant portion of excitation energy to be transferred from PBSs directly to the reaction center chromophores of PS II. Distribution to PS I would only require a small movement of PS I with regard to the PBS-PS II complex. Whereas the observations by Delphin were not discussed by McConnell et al. (2002), it seems quite probable that changes in the ΔpH may be involved in bringing about conformational changes of membrane proteins and hence some energy redistribution.

If *Acaryochloris*, a Chl *d*-containing prokaryote that tends to form ectosymbiotic relationships (Murakami et al., 2004), represents a primitive state, it is an interesting example from an evolutionary standpoint. Hu et al. (1999) found that phycocyanin and allophycocyanin are present in this organism but it does not have cyanobacterial-type PBS structure. Upon fractionating *Acaryochloris* thylakoids, Hu et al. (1999) found allophycocyanin and phycocyanin associated with the PS II particles, but not with PS I

particles, suggesting structural attachment to PS II reaction centers only. Studies thus far have shown relatively low 'phycobilisome' densities in *Acaryochloris*, but this could be different in free-living cells where dependence on photosynthesis is greater.

III. Prochlorophyte Antennas and the IsiA Proteins

In most cyanobacteria, PS II is dependent on PBSs for the acquisition of absorbed light energy, as explained above. However, there are three unrelated genera of cyanobacteria (*Prochlorococcus*, *Prochloron* and *Prochlorothrix*) that have lost their PBSs (reviewed in Matthijs et al., 1995; Ting et al., 2002). Instead, they employ membrane-intrinsic Chl *a/b* antennas. All the prochlorophyte Chl *a/b* antenna proteins (Pcbs) are related to each other and are part of the same protein family as the CP43 and CP47 apoproteins of the PS II core (Laroche et al., 1996; van der Staay et al., 1998; reviewed in Green, 2003). There is no sequence relatedness between these Chl *a/b* proteins and the Chl *a/b* proteins of higher plants and green algae. The Chl *d*-containing *Acaryochloris* (Section II.A.3) has Chl *d*-binding antenna proteins that belong to the same gene family, probably acquired by lateral gene transfer (Chen et al., 2005).

Extensive biochemical studies on the Chl *a/b* antenna of *Prochlorothrix* (van der Staay et al., 1992) and the high light-adapted Med4 strain of *Prochlorococcus* (Garczarek et al., 1998) suggested that it was associated primarily with PS II. However, other evidence pointed to a PS I association (Post et al., 1993). It was recently discovered that in the moderate low-light-adapted MIT9313 strain of *Prochlorococcus*, the Pcb subunits are associated with PS II under normal growth conditions. Rather than encircling the PS II dimer, the Pcbs form 5-membered arcs on either side (Bibby et al., 2003a). A similar organization has been found in the third prochlorophyte, *Prochloron didemni* (Bibby et al., 2003b) (Fig. 3). This is a completely novel organization for any PS II antenna. In both cases, spectroscopic analysis supports the transfer of excitation energy from the Chl *a/b* antenna to PS II.

However, in the very low light-adapted SS120 strain of *Prochlorococcus,* 18 Pcb Chl *a/b* proteins were found to form a ring around the PS I trimer (Bibby et al., 2001a). In the case of *Prochlorococcus* MIT9313, the Pcb subunits found around the PS II dimer are encoded by the *pcbA* gene, which is constitutively expressed. The PS I/PS II dilemma was solved when it was discovered that under conditions of Fe limitation the *pcbB* gene is also expressed and the PcbB-Chl *a/b* proteins form an 18-membered ring around the PS I trimer, helping to compensate for a decrease in the total number of PS I units (Bibby et al., 2003a). The Pcbs that associate with PS II do not seem to be induced by Fe deprivation (Bibby et al., 2003a). The location of the Chl *a/b* antenna proteins thus appears to depend on the species and on the environment where it is found.

Prochlorococcus predominates in the tropical and subtropical oceans, which tend to be poor in nitrogen and iron (Ting et al., 2002). There is no red light and limited green light at depths of 100–200 m where low-light-adapted *Prochlorococcus* strains predominate. Consistent with the antenna role, the number of *pcb* genes within the *Prochlorococcus* genus is related to the light environment of the ecotype: there are eight genes in the very low-light-adapted strain SS120, two in the moderately low-light-adapted strain MIT9313 and only one in the high-light-adapted strain MED4 (LaRoche et al., 1996; Garczarek et al., 2000, 2001).

The significance of the iron connection is that iron is often the limiting nutrient in ocean waters (Ting et al., 2002). Transfer of cyanobacteria to Fe limited conditions causes decreased synthesis of PBSs and reaction centers, and induces the synthesis of a Chl *a*-binding protein called IsiA (Burnap et al., 1993; Sandström et al., 2002), another member of the core complex family (Green, 2003). IsiA forms a ring of 18 monomers around PS I (Bibby et al., 2001b; Boekema et al., 2001), closely resembling the ring of 18 Pcb monomers around PS I in *Prochlorococcus*. This addition substantially increases its antenna size and thereby compensates for the decreased number of PS I centers (Bibby et al., 2001a; Boekema et al., 2001). The fact that IsiA (also called CP43´) appears to be associated only with PS I is puzzling in view of several lines of evidence that suggest it functions to protect PS II from excess light energy, i.e., photooxidative damage (Park et al., 1999; Ivanov et al., 2000; Sandström et al., 2001, 2002). However, it has recently been shown that under prolonged iron deprivation, there is an excess of free IsiA, which could function to shield PS II from excess light (Yeremenko et al., 2004).

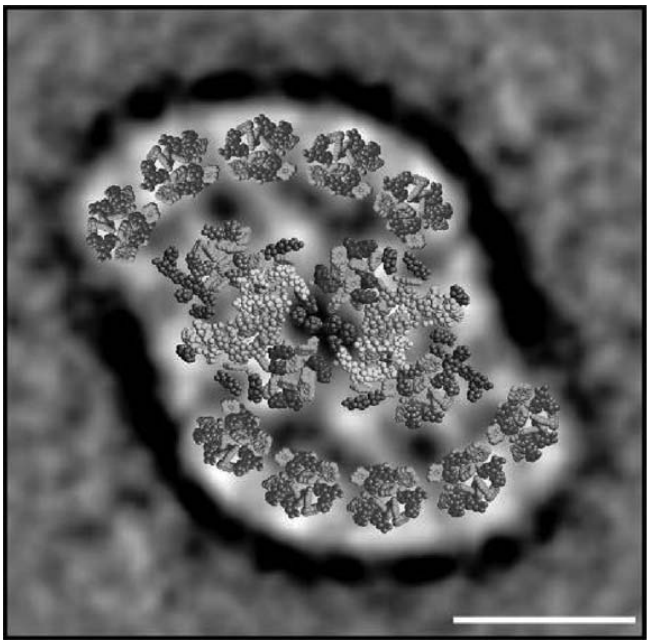

Fig. 3. Prochloron PS II dimer (center) with five prochlorophyte Chl *a/b* (Pcb) monomers in an arc above, and five monomers below. Light gray squares, Chl *a* or Chl *b*; Other atoms belong to trans-membrane helices. Scale bar, 100 Å. (Courtesy of J. Barber). See Color Plate 1, Fig. 1.

IV. The LHC Superfamily of Chloroplasts

A. Overview

The predominant light-harvesting antennas of eukaryotes (chloroplasts) are members of the light-harvesting comples (LHC) superfamily. The Chl *a/b*-binding proteins of the 'green line' (plants and green algae) have been the most extensively studied, particularly those members that are associated with PS II (Green and Durnford, 1996; Paulsen, 1997; Bassi et al., 1997; Jansson, 1999; Bassi and Caffarri, 2000; van Amerongen and Dekker, 2003). A large group of ecologically important algae have Chl *a/c*-binding proteins that are clearly related to the Chl *a/b* proteins of the green line, but it is not clear whether any of these Chl-proteins are specifically associated with PS II, or whether they all transfer excitation energy to both photosystems. Members of the family in red algae bind only Chl *a* and are associated only with PS I, so they will not be discussed further (but see Gantt et al., 2003). This section will therefore concentrate on the Chl *a/b* antennas of higher plants and green algae, since it is this group whose relationship to PS II is best understood..

Members of this family are also involved in energy dissipation and photoprotection (Chapter 23, Pogson et al.). The antenna proteins, particularly LHCII, are able to dissipate energy directly by fluorescence but also by thermal dissipation with the assistance of carotenoids, particularly the xanthophylls. In higher plants, the PsbS protein plays an important role in this energy dissipation (Chapter 23, Pogson et al.). A group of proteins called the Elips (originally 'early light-induced proteins') plays a role in photoprotection. In fact, the LHC superfamily may have originated as photoprotective proteins dealing with excess excitation energy, and only later diversified so some members function to absorb light in low-light environments (Green and Pichersky, 1994; Green and Kühlbrandt, 1995).

B. The Chlorophyll a/b Family of Higher Plants and Green Algae

1. The Chlorophyll a/b Protein Complexes

The Chl *a/b*-proteins of PS II are listed in Table 2 (as reviewed earlier by Green and Durnford, 1996; Bassi et al., 1997). The native form of LHCII, the major complex, is a trimer. In the thylakoid membrane, there are a number of trimers per PS II, some closely and some more loosely associated with PS II core dimers. When the higher plant LHCII is dissociated, three polypeptides can be resolved by sodium dodecyl sulfate-polyacrylamide gel electrophoresis (SDS-PAGE) or reversed-phase high performance liquid chromatography (RP-HPLC). Lhcb1 and Lhcb2 are very similar in sequence, and are present in approximately 3:1 ratio. Lhcb3 is shorter, and is a minor component. Analysis of purified LHCII trimers showed 12–14 Chls/polypeptide and a Chl *a/b* ratio of 1.3–1.4. Each monomer also binds two molecules of lutein, one of neoxanthin and a sub-stoichiometric amount of violaxanthin (reviewed in Morosinotto et al., 2003).

CP26 and CP29 contain one polypeptide each (Lhcb5 and Lhcb4 respectively) and are considered 'core' Chl *a/b* proteins, being situated between LHCII trimers and PS II core (see below). The component CP24 (Lhcb6) is also considered to be part of the 'core' of PS II, but its role has not been determined. Even when isolated by the same methods as the LHCII trimer, the minor complexes CP29 and CP26 contain fewer Chls per polypeptide and have higher Chl *a/b* ratios than LHCII trimers (Table 2). In addition, they appear to bind only one lutein and one other xanthophyll per polypeptide. It is not clear whether this difference in pigment binding is due to lower stability of monomeric complexes compared to trimeric ones, or whether these proteins simply have fewer binding sites. CP24 is difficult to work with as it is rather unstable; reconstituted CP24 binds 10 Chls and 2 carotenoids (Pagano et al., 1998).

There are some differences between green algae and higher plants. *Chlamydomonas reinhardtii* has CP29 and CP26 homologs but lacks a CP24 homolog (Teramoto et al., 2001; Elrad and Grossman, 2004; Minagawa and Takahashi, 2004). Furthermore, the many closely related polypeptides that make up the major LHCII cannot be assigned to Lhcb1, Lhcb2 and Lhcb3 categories; this suggests that the diversification of LHCII polypeptides happened after the chlorophyte and streptophyte lineages diverged (Green and Durnford, 1996; Stauber et al., 2003; Elrad and Grossman, 2004; Minagawa and Takahashi, 2004).

2. Three-Dimensional Structure of LHCII

The structure of purified pea LHCII, consisting of trimers containing the Lhcb1 and Lhcb2 proteins, was first solved to 3.4 Å resolution by electron crystallography (Kühlbrandt et al., 1994). It showed that each polypeptide chain had three membrane-spanning helices, with a small amphipathic alpha-helix at the C-terminus (Helix D in Fig. 4). The first (B) and third (A) helices, which share substantial sequence similarity, are related by a local two-fold axis and connected by reciprocal cross-bridges linking Arg on one helix and Glu on the other. Two carotenoid molecules (assigned to lutein) were located in the grooves on either side of the paired helices, cross-bracing them. At this level of resolution, each carotenoid head-group appeared to be in close proximity to 2 or 3 Chls, and to be protected by one of the loops conserved in all members of the Chl *a/b* family (Kühlbrandt et al., 1994; Green and Kühlbrandt, 1995). The 13 Chls were arrayed in two layers corresponding to the two galactolipid leaflets of the membrane. At this resolution, it was not possible to distinguish between Chl *a* and Chl *b*, since they differ only by a methyl or formyl at one position (Fig. 5). Based on intermolecular distances, 7 molecules were tentatively assigned to Chl *a* and 6 to Chl *b* (Kühlbrandt et al., 1994).

The structure of the spinach LHCII trimer has recently been determined at 2.72Å resolution by X-ray crystallography, using a novel crystallization method (Liu et al., 2004). The new structure confirms that the protein has three membrane-spanning helices, cross-braced by two lutein molecules (Figs. 4, 6, and color Plate X). In addition to the small helix D on the lumenal surface, another small helix (E) is in the corresponding position on the other side of the two-fold axis relating the first and third helices. As suggested from reconstitution and mutagenesis experiments (Rogl and Kühlbrandt, 1999; Croce et al., 1999a), a neoxanthin is between the crossed helices (B, A) and the middle helix (C) (Fig. 4). All three of these carotenoids are close enough to Chls to transfer energy to them. The fourth carotenoid-binding site is a crevice between monomer units, which is occupied by violaxanthin and other xanthophyll-cycle carotenoids (Fig. 6). The relatively exposed position of this carotenoid may account for the substoichiometric amounts

Table 2: Chlorophyll *a/b* antennas of plant and green algal Photosystem II

Chl-protein complex (preparation)	Polypeptides	Chl *a*/ polypeptide	Chl *b*/ polypeptide	Carotenoids*	Ref.
LHCII (crystal)	Lhcb1, Lhcb2	8	6	2 Lut, 1 Nx, 1 X	(a)
LHCII (crystal)	Lhcb1, Lhcb2	7	5	2 Lut	(b)
LHCII (biochemical)	Lhcb1, Lhcb2, Lhcb3	7–8	5–6	2 Lut, 0.5 Nx, 1 Vx	(c)
		7	5.5	2 Lut, 1 Nx, 0.4 Vx	(d)
		7	5	1.7 Lut, 1 Nx, 0.3 Vx	(e)
		8	6	1.8 Lut, 0.9 Nx, 0.2Vx	(f)
CP29 (biochemical)	Lhcb4	6	2	1 Lut, 0.5 Nx, 0.6 Vx	(g)
				1.3 Lut, 0.4 Nx, 0.6 Vx	(h)
CP26 (biochemical)	Lhcb5	6	3	1 X, 0.5 Nx, 0.5 Vx	(i)
				1.2 Lut, 0.4 Nx, 0.4 Vx	(h)
CP24 (biochemical)	Lhcb6	6	4	1 Lut, 1 Vx	(i)

*Lut, lutein; Nx, neoxanthin; Vx, violaxanthin; X, xanthophyll cycle carotenoid. (a) Liu et al. (2004); (b) Kühlbrandt et al. (1994); (c) Nussberger et al. (1993); (d) Rogl and Kühlbrandt (1999); (e) Remelli et al. (1999); (f) Peterman et al. (1997); (g) Bassi et al. (1999); (h) Das and Frank (2002); (i) Bassi et al. (1997).

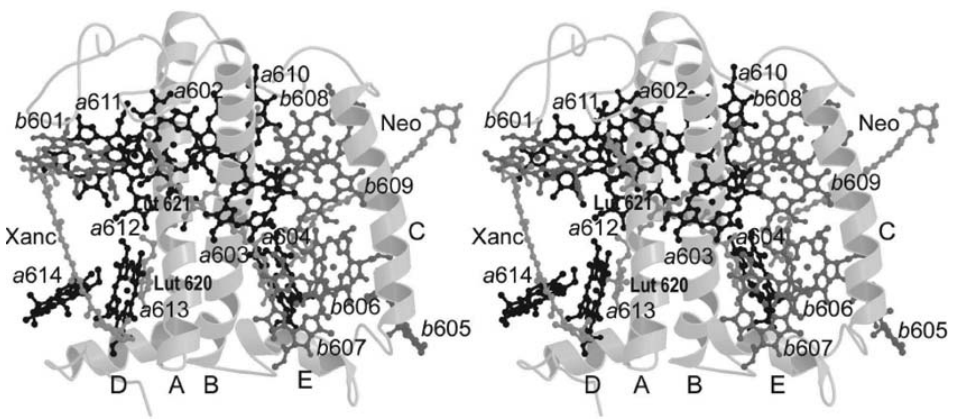

Fig. 4. Stereogram of LHCII monomer, numbered according to Liu et al. (2004) (Table 3). Black, Chl *a*; grey, Chl *b*; light grey, carotenoids; ribbons, α-helices. (Courtesy of W.R. Chang and Z.F. Liu).

found in most purified complexes (Table 2).

The new structure has 14 Chl molecules which can be clearly identified as 8 Chl *a* and 6 Chl *b*. Three of the porphyrin rings tentatively assigned to Chl *a* or *b* in the 1994 structure have been reassigned, and two new Chls have been resolved, bound between monomer units in the trimer (Fig.6). Because a large number of studies since 1994 have used the Chl numbering of the Kühlbrandt et al. (1994) paper, the Chl designations of both models are listed in Table 3. Most of the formyl groups of Chl *b* are H-bonded, in contrast to the methyl groups of Chl *a* which appear to be in hydrophobic environments, but it is not known whether these small differences are enough to determine binding specificity. There are extensive hydrophobic interactions between monomer units, involving not only the protein, the xanthophyll-cycle carotenoid and several Chls, but also the single phosphatidylglycerol molecule that is an integral part of the structure and is known to

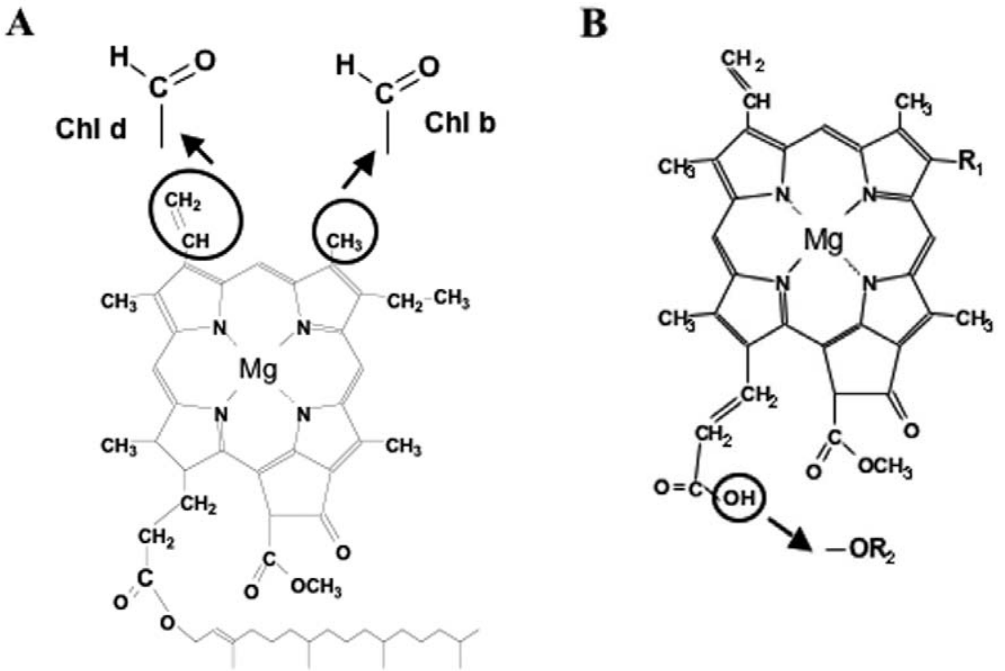

Fig. 5. Chlorophyll structures. A. Chl *a* with modifications giving Chl *d* and Chl *b* (circled). The phytyl sidechain is not to scale. B. Chl c_1 (R_1 = -CH_2CH_3) and c_2 (R_1 = -CH=CH_2). A new non-polar form is esterified with monogalactosyldiacylglycerol (circle, R_2) at the 17^3 position (Garrido et al., 2000).

be essential for trimerization (Hobe et al., 1994; Nussberger et al., 1994).

3. Molecular Biological Approaches: Native and Recombinant Complexes

In the decade between the publication of the two LHCII structure models, there were a large number of studies aimed at determining the positions of the pigments more precisely. They were made possible by the discovery that LHCII could be reconstituted from purified pigments and polypeptides synthesized in *E. coli,* and that the reconstituted pigment-protein complexes had crystal structures and spectroscopic properties almost indistinguishable from the native complexes (Hobe et al., 1994; Peterman et al., 1997; reviewed by Paulsen, 1997). As a result, it was possible to make site-directed and deletion mutants, and to detect a motif required for trimerization of LHCII (Hobe et al., 1995). The CP29 protein (Lhcb4) has also been used extensively in renaturation studies, probably due to its relative stability as a monomer (Pascal et al., 2001).

In general, recombinant Chl-protein complexes bind as much Chl as native complexes isolated from detergent fractionated membranes. However, the pigment ratios of the recombinant complexes depend strongly on the mixture of pigments presented to the renaturing protein (Meyer and Wilhelm, 1993; Paulsen, 1997). For example, it is possible to reconstitute LHCII (actually the Lhcb1 protein) with little or no Chl *a* (Kleima et al., 1999), and CP29 can fold correctly with a variety of Chl *a/b* ratios (Giuffra et al., 1997). There is also considerable flexibility in carotenoid binding (Croce et al., 1999b; Hobe et al., 2000).

One of the first studies showed that site b3 (a614) on helix D was probably a Chl *a* binding site (Rogl and Kühlbrandt, 1999); this was confirmed in the 2004 structure (Liu et al., 2004). However, a number of studies suggested that this site and several others could bind both Chls *a* and *b* and generally bound a mixture of them in vitro (Bassi et al., 1999; Remelli et al., 1999; Yang et al., 1999). This was disputed on spectroscopic grounds by Rogl et al. (2002), and no evidence for mixed sites was found in the new LHCII

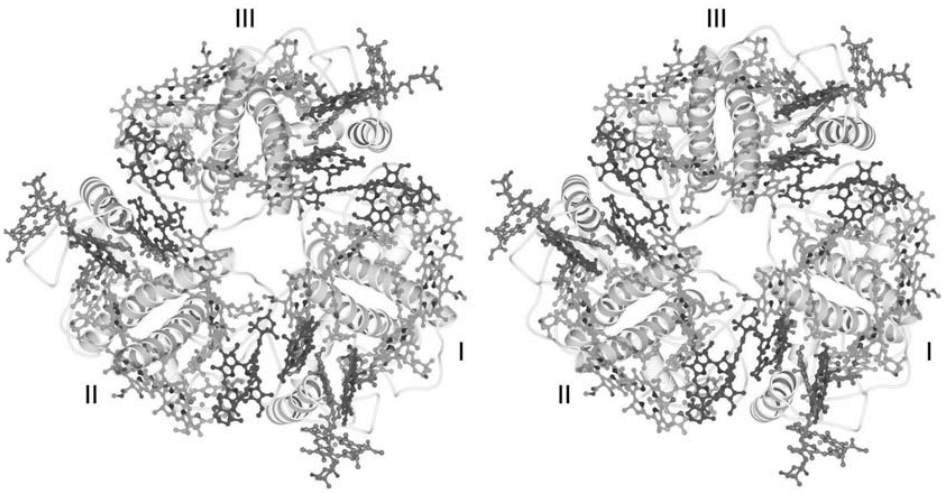

Fig. 6. Stereogram of LHCII trimer viewed from stromal side, showing positions of Chls and carotenoids. Dark Grey, Chl *a*; light grey, Chl *b*; ribbons: α-helices. (Courtesy of W.R. Chang and Z.F. Liu). See Color Plate 1, Fig. 2.

Table 3. Labels and positions of pigments in crystal structures of LHCII

Kühlbrandt et al. (1994)	Liu et al. (2004)	Residue bound, Helix (helix number)
Chl *a*1	Chl *a* 610	Glu180, Helix A (3)
Chl *a*2	Chl *a* 612	Asn183, Helix A (3)
Chl *a*3	Chl *a* 613	Gln197, Helix A (3)
Chl *a*4	Chl *a* 602	Glu65, Helix B (1)
Chl *a*5	Chl *a* 603	His68, Helix B (1)
Chl *a*6	Chl *a* 604	---, Helix B (1)
Chl *a*7	Chl *b* 607	Gln131, Helix C (2) (H_2O)
Chl *b*1	Chl *b* 608	C-A loop (H_2O)
Chl *b*2	Chl *a* 611	---, Helix A (3)
Chl *b*3	Chl *a* 614	His212, Helix D
Chl *b*5	Chl *b* 609	Glu139, Helix C (2)
Chl *b*6	Chl *b* 606	---, Helix C (2)
----	Chl *b* 601	Tyr24
----	Chl *b* 605	Val119, B-C loop

structure (Liu et al., 2004). The site-directed mutants did correctly support the binding of Chl *b* in sites *b*5 (*b*609) and *b*6 (*b*606), and their interaction with neoxanthin in the neighborhood of Helix C (Remelli et al., 1999; Croce et al., 1999a).

So far as the other Chl-proteins are concerned, it seems to be generally agreed that there are 8 highly conserved Chl binding sites in all light-harvesting members of the LHC superfamily, including the red algal proteins that bind only Chl *a* and are associated only with PS I (Grabowski et al., 2001). In LHCII, four of these sites correspond to *a*1 (*a*610),

*a*2 (*a*612), *a*4 (*a*602), and *a*5 (*a*603), where the Chls are ligated through the central Mg^{++} by side-chains on Helices B and A (first and third trans-membrane helices). The other sites are *b*5 (*b*609) and *b*6 (*b*606) which involve a Glu and a Gln on Helix C, site *a*3 (*a*603) at the end of Helix B and site *b*3 (now *a*614) on the small lumenal Helix D. This would account very nicely for the 6 Chl *a* and 2 Chl *b* of native and reconstituted CP29. However, studies on reconstituted CP29 suggested that sites *a*3 (*a*613), *b*3 (*a*614), *b*5 (*b*609) and *b*6 (*b*606) had mixed occupancy in that complex (Bassi et al., 1999; Simonetto et al., 1999), and similar studies proposed that the additional Chl of CP26 was in a site corresponding to *b*2 (*a*611) (Croce et al., 2002). Whether the mixed binding sites are found in vivo, and how closely the minor complexes mirror the structure of LHCII are open questions.

4. Organization of Chlorophyll a/b Antennas in the Thylakoid Membrane

We now have a general idea of how the Chl *a/b* antennas are organized around the PS II core in the thylakoid membrane, largely based on electron microscopy of negative stained preparations with advanced image-processing (Boekema et al., 1995, 1999a, b, 2000; Nield et al., 2000a, b; reviewed by van Amerongen and Dekker, 2003; Dekker and Boekema, 2004). It was aided by the LHCII structure (Kühlbrandt et al.,1994), which was used to model the minor complexes because of their sequence relatedness (Green and Pichersky, 1994), and more recently by the X-ray crystallographic structures of cyanobacterial PS II cores (Zouni et al., 2001; Kamiya and Shen, 2003; Ferreira et al., 2004; Chapters 19–21). Figure 7 shows the PS II core dimer outlined in the center, surrounded by the three minor complexes CP29, CP26 and CP24. The position of CP26 is based on its cross-linking to CP43 (Harrer et al., 1998), selective extraction (Boekema et al., 1999b), and its absence in an *Arabidopsis Lhcb5* antisense line (Yakushevska et al., 2003). The position of CP29 was deduced on the basis of cross-linking and selective extraction (Harrer et al., 1998; Miao et al., 1998; Boekema et al., 1999b, 2000). CP24 is placed next to CP29 by elimination, and because *Lhcb4* antisense plants are deficient in both of them (Andersson et al., 2001).

Most PS II preparations that retain the antennas bind two types of LHCII trimers, which have been named 'S' and 'M' for strongly and moderately bound (Boekema et al., 1999a). Particles with additional 'L' (loose) trimers associated with them are also found; presumably these correspond to LHCII units that move in the plane of the membrane during state transitions and transfer excitation energy to PS I. The implications of PS II super-complex organization for energy transfer are discussed in detail by van Amerongen and Dekker (2003).

Antisense plants have provided some surprises. *Arabidopsis* plants carrying an anti-*Lhcb2* construct were severely depleted in both the major LHCII polypeptides, but had no decrease in photosynthetic activity or in grana stacking despite the lack of LHCII trimers (Andersson et al., 2003; Ruban et al., 2003). What they did have was an excess of Lhcb5 (CP26) which formed trimers with a small amount of the minor Lhcb3 protein, and associated with PS II cores in a manner almost indistinguishable from the LHCII trimers in Fig. 7. This demonstrates yet again the adaptability of the LHC superfamily (Green, 2001), at least under controlled growth conditions. However, neither these plants nor antisense lines for other Chl *a/b* proteins produced as many seeds as the wild-type *Arabidopsis* under field conditions (Andersson et al., 2003; Ganetag et al., 2004).

5. Energy Transfer Studies on Chlorophyll a/b Proteins

Progressive improvements in isolation of native complexes and reconstitution of defined complexes have permitted faster and better energy transfer studies, reviewed by van Amerongen and Dekker (2003). In view of the new LHCII structure (Liu et al., 2004), some time for reflection will be needed in order to interpret biophysical results in its light. We have therefore decided not to attempt to cover the work of the last few years, but to direct the reader's attention to some relevant papers, for example Croce et al. (2003), Gradinaru et al. (2003), Ma et al. (2003), Palacios et al. (2003), Rogl et al. (2002, 2003), Olszowka et al. (2004) and Novoderezhkin et al. (2004). Readers should also consult recent issues of Journal of Physical Chemistry B, Biochemistry, Journal of Biological Chemistry, Journal of Molecular Biology and Photosynthesis Research for the latest insights.

C. Antennas of Algae with Chlorophyll c

1. The Chlorophyll a/c Proteins

All the algae that have the Chls *c* (*c1*, *c2* or *c3*) rather than Chl *b* as accessory pigment are believed to have

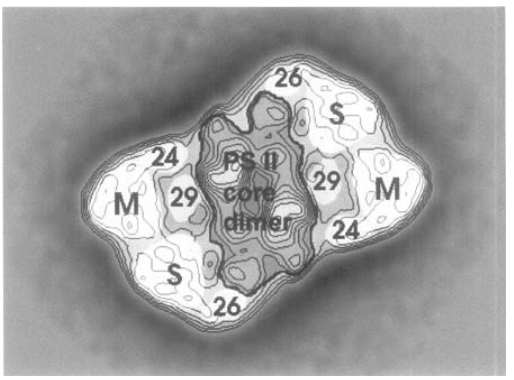

Fig. 7. PS II core dimer (outlined) flanked by minor Chl *a/b* complexes CP29 (29), CP26 (26) and CP24 (24), strongly bound (S) and moderately strongly bound (M) LHCII trimers. Image from electron microscopy and image processing of purified PS II particles from *Arabidopsis thaliana* (Yakushevska et al., 2003) and earlier work cited therein (courtesy of E. Boekema).

originated by secondary endosymbiosis involving a non-photosynthetic eukaryote host and a red algal intracellular symbiont (Gibbs, 1981; Cavalier-Smith, 2000; MacFadden 1999, 2001; Green et al., 2003). All that remains of the endosymbiont are the plastid(s) plus many nuclear genes that were transferred from the endosymbiont nucleus to the host nucleus during establishment of the endosymbiotic relationship. The algae with Chl *c* include the heterokonts, haptophytes, cryptophytes and dinoflagellates. These are not small exotic groups, as one might think from reading most plant physiology textbooks. In fact, they dominate the marine environment and account for as much as 25% of the CO_2 fixed on a global scale (Field et al., 1998). These algae have membrane-intrinsic light-harvesting antennas that bind one of the Chls *c* (Fig. 5B) as well as Chl *a* and a variety of carotenoids (Green and Durnford, 1996; Caron et al., 2001). Their polypeptides are members of the LHC superfamily, i.e., they are related to the Chl *a/b* proteins of the 'green line' and the PS I-associated antennas of red algae, which bind only Chl *a* (Durnford et al., 1999; Deane et al., 2000).

The Chl *a/c* protein complexes in heterokonts and haptophytes are frequently referred to as fucoxanthin-Chl *a/c* complexes (FCPs) because fucoxanthin is the predominant carotenoid. The haptophytes are distinguished by a substantial fraction of 19-acyloxy derivatives of fucoxanthin. Minor amounts of other carotenoids such as vaucheriaxanthin and heteroxanthin may be specific to certain heterokont genera. Cryptophytes have alloxanthin and crocoxanthin in their LHCs, and dinoflagellates have peridinin (Hiller, 1999). In addition, the Chl *a/c* proteins bind the xanthophylls involved in non-photochemical quenching: violaxanthin and/or diadinoxanthin, and their de-epoxidized derivatives zeaxanthin, antheraxanthin and diadinoxanthin.

Values for Chl *a/c* ratios of purified Chl-protein complexes are generally 4–5, higher than the Chl *a/b* ratio in plants (Hiller, 1999; Caron et al., 2001; Macpherson and Hiller, 2003). The number of carotenoid molecules per polypeptide varies with the species and the preparation method but appears to be equal to or greater than the number of Chls per polypeptide. A FCP from *Laminaria* purified by iso-electric focusing had 6 Chl *a*, 2 Chl *c* and 8 fucoxanthin (Pascal et al., 1998). Resonance Raman spectroscopy indicated that at least some of the Chl *a* were bound at positions analogous to those of LHCII. Given the lack of sequence conservation between Chl *a/b* and Chl *a/c* proteins in the region of the second helix (Helix C), the Chl *c* could be associated with this helix (similarly to Chl *b* in LHCII), possibly bound to conserved Gln and Glu residues. Some of the carotenoids could be arranged around this helix as in LHCII trimers. The two major FCPs of the diatom *Cyclotella* can be isolated as trimers (Büchel, 2003), so by analogy with tobacco LHCII there could be room for additional carotenoids and Chls between the monomer units.

2. Thylakoid Organization and Energy Transfer

Phylogenetic analysis shows that the Chl *a/b* branch of the family diverged from the line leading to the Chl *a/c* proteins before the former separated into PS II and PS I-associated complexes (Green and Durnford, 1996; Durnford et al., 1999). This means that we cannot expect to find Chl-proteins analogous to the minor Chl *a/b* protein complexes, i.e., CP29, CP26 and CP24. There is no evidence for specific association of any of the Chl *a/c* proteins with PS II; in fact thin sections immuno-labeled with an anti-FCP antibody showed that the FCPs were uniformly distributed in appressed and non-appressed thylakoids (Lichtlé et al., 1992a, b; Pyszniak and Gibbs, 1992). There are no grana stacks in these algae as there are in higher plants.

Most of the Chl *a/c* genes that have been sequenced appear to be members of families with numerous almost-identical sequences (Bhaya and

Grossman, 1993; Apt et al., 1995b; De Martino et al., 2000). However, some of the Chl *a/c* sequences of the diatoms *Cyclotella* and *Thalassiosira* and the raphidophyte *Heterosigma* are more divergent, and branch with the red algal and cryptophyte PS I-associated LHCs on phylogenetic trees (Durnford et al., 1999; Eppard and Rhiel, 1998; Eppard et al., 2000; Green, 2003; Armbrust et al., 2004). This suggests that there may be members of the family that are preferentially associated with PS I. There is some suggestive biochemical evidence for association of FCPs with PS I (Büchel and Wilhelm, 1993; Bathke et al., 1999; Büchel, 2003).

Spectroscopic data suggests that most of the FCPs transfer energy to both photosystems (Macpherson and Hiller, 2003). Research on energy transfer up to the beginning of 2003 was reviewed by MacPherson and Hiller (2003), and earlier work was reviewed by Hiller (1999) with an emphasis on carotenoids.

3. The Peridinin-Chlorophyll a Protein of Dinoflagellates

In addition to the Chl *a/c* proteins, two groups of chromophyte algae have unique extrinsic antenna complexes. The cryptophytes have phycobiliproteins with unique α subunits, which are not organized into phycobilisomes and are packed into the thylakoid lumen (Fig. 2B; Section II.A.2; Hiller, 1999; Macpherson and Hiller, 2003). The dinoflagellates have a completely novel antenna, the peridinin-Chl *a* protein, organized as trimers in the thylakoid lumen. Neither the protein sequence nor its fold is related to anything else in the databanks. Its distinguishing characteristic is that it binds more carotenoid than Chl. The major form has 8 peridins to 2 Chl *a* and the minor ('high salt') form has 6 peridinins to 2 Chl *a* (Sharples et al., 1996). The protein forms a boat-like structure with alpha-helices as the ribs; four peridinins are clustered around each Chl *a* (Hofmann et al., 1996; Hiller, 1999; Macpherson and Hiller, 2003).

The availability of the high resolution structure (2.0Å) of the major form trimer and the fact that the carotenoids play a very prominent role in light-harvesting, means that this protein is a model system for studying carotenoid-protein and carotenoid-Chl interactions. Chl-Chl energy transfer is also important, both within and between monomers. Spectroscopic studies up to 2002 were reviewed by Macpherson and Hiller (2003). Recent studies have extended the analysis to the minor ('high-salt') form (Ilagan et al., 2004) and to a detailed model of the carotenoid energy states in the major form (Shima et al., 2003). However, there is no definitive evidence for association of the trimer with either photosystem (Macpherson and Hiller, 2003).

D. Photoprotection and the LHC Family

As well as harnessing light energy, photosynthetic organisms need mechanisms to cope with its deleterious effects. In order to avoid damage from free radicals and active oxygen species, excess energy must be dissipated in one of three ways: by increased electron flow (if electron acceptors are available), as fluorescence from the antenna complexes, or by thermal deactivation, which is referred to as non-photochemical quenching (Bassi and Caffarri, 2000; Morosinotto et al., 2003; Krause and Jahns, 2003; Holt et al., 2004; reviewed in Chapter 23, Pogson et al.). Xanthophyll carotenoids are essential for non-photochemical quenching, and in green plants and green algae they appear to be bound to PS II-associated members of the LHC family. In the green line, the xanthophyll violaxanthin is de-epoxidized to zeaxanthin in two steps (via antheraxanthin) a process activated by the decrease in lumenal pH resulting from increased electron flow down the photosynthetic electron transport chain. In contrast, most heterokont algae have the carotenoid diadinoxanthin, which undergoes a one-step de-epoxidation to diatoxanthin (Lohr and Willhelm, 1999). The increase in de-epoxidized xanthophylls leads to an increase in thermal dissipation mediated by the carotenoids. In higher plants, the four-helix PsbS protein has been shown to play a crucial role in non-photochemical quenching (Li et al., 2000, 2002, 2004; Bergantino et al., 2003). There is also evidence that conformational changes in the Chl *a/b* proteins themselves, as well as the migration of a fraction of the LHCII population between grana and stroma, are also involved in non-photochemical quenching (Krause and Jahns, 2003).

The marine environment inhabited by diatoms (the best-studied of the Chl *a/c* algae) is characterized by large and often rapid fluctuations in light intensity due to water movements as well as cloud cover. Acclimation to high light is faster than in plants (Lavaud et al., 2002a, 2004) and the non-photochemical quenching is proportional to the amount of diatoxanthin produced (Lavaud et al., 2002a). It does not involve movement of Chl-proteins in the plane of the membrane, since

there is no lateral segregation in Chl *a/c* algae. Both violaxanthin and diadinoxanthin cycles can operate at the same time (Lohr and Wilhelm, 1999). Exposure to high light intensity over a period of more than a few hours causes an increase in the xanthophyll pool size, but any photoinhibition appears to be rapidly reversible (Ting and Owens, 1994). Chlororespiration may increase the proton gradient in the dark (Ting and Owens, 1993; Jakob et al., 1999; Dijkman and Kroon, 2002), but could also be providing a run-off pathway to O_2 in the light (Lavaud et al., 2002b).

In higher plants and green algae, there are several members of the LHC superfamily that bind little or no Chl and appear to function only in photoprotection (Green and Kühlbrandt, 1995; Montané and Kloppstech, 2000; Heddad and Adamska, 2002). The three-helix Elips and two-helix Seps are induced in response to high light, and are believed to play a role in photoprotection (Heddad and Adamska, 2000; Hutin et al., 2003). However, no genes encoding PsbS or any of these proteins have been found in the genome of the diatom *Thalassiosira pseudonana* (Armbrust et al., 2004). This suggests that although the xanthophyll cycles play an important role in the Chl *a/c* line, the molecular mechanisms of non-photochemical quenching are not the same as in the Chl *a/b* line.

Acknowledgments

We would like to thank Drs. Wenrui Chang, Zhenfeng Liu, Egbert Boekema and James Barber for their generous gifts of figures.

References

Andersson J, Walters RG, Horton P and Jansson S (2001) Antisense inhibition of the photosynthetic antenna proteins CP29 and CP26: Implications for the mechanism of protective energy dissipation. Plant Cell 13: 1193–1204

Andersson J, Wentworth M, Walters RG, Howard CA, Ruban AV, Horton P and Jansson S (2003) Absence of the Lhcb1 and Lhcb2 proteins of the light-harvesting complex of Photosystem II-effects on photosynthesis, grana stacking and fitness. Plant J 35: 350–361

Apt KE, Collier JL and Grossman AR (1995a) Evolution of the phycobiliproteins. J Mol Biol 248: 79–96

Apt KE, Clendennen SK, Powers DA and Grossman AR (1995b) The gene family encoding the fucoxanthin chlorophyll proteins from the brown alga *Macrocystis pyrifera*. Mol Gen Gen 246: 455–464

Armbrust EV, Berges JA, Bowler C, Green BR, Martinez D, Putnam NH, Zhou S, Allen AE, Apt KE, Bechner M, Brzezinski MA, Chaal BK, Chiovitti A, Davis AK, Demarest MS, Detter JC, Glavina T, Goodstein D, Hadi MZ, Hellsten U, Hildebrand M, Jenkins BD, Jurka J, Kapitonov VV, Kröger N, Lau WWY, Lane TW, Larimer FW, Lippmeier JC, Lucas S, Medina M, Montsant A, Obornik M, Parker MS, Palenik B, Pazour GJ, Richardson PM, Rynearson TA, Saito MA, Schwartz DC, Thamatrakoln K, Valentin K, Vardi A, Wilkerson FP and Rokhsar DS (2004) The genome of the diatom *Thalassiosira pseudonana*: Ecology, evolution, and metabolism. Science 306: 79–86

Bassi R and Caffarri S (2000) Lhc proteins and the regulation of photosynthetic light harvesting function by xanthophylls. Photosynth Res 64: 243–256

Bassi R, Sandonà D and Croce R (1997) Novel aspects of chlorophyll *a/b*-binding proteins. Physiol Plant 100: 769–779

Bassi R, Croce R, Cugini D and Sandonà D (1999) Mutational analysis of a higher plant antenna protein provides identification of chromophores bound into multiple sites. Proc Natl Acad Sci USA 96: 10056–10061

Bathke L, Rhiel E, Krumbein WE and Marquardt J (1999) Biochemical and immunochemical investigations on the light-harvesting system of the cryptophyte *Rhodomonas* sp.: Evidence for a Photosystem I specific antenna. Plant Biol 1: 516–523

Bergantino E, Segalla A, Brunetta A, Teardo E, Rigoni F, Giacometti GM and Szabò I (2003) Lihgt- and pH-dependent structural changes in the PsbS subunit of Photosystem II. Proc Natl Acad Sci USA 100: 15265–15270

Bhaya D and Grossman AR (1993) Characterization of gene clusters encoding the fucoxanthin chlorophyll proteins of the diatom *Phaeodactylum tricornutum*. Nucleic Acids Res 21: 4458–4466

Bibby TS, Nield J, Partensky F and Barber J (2001a) Antenna ring around Photosystem I. Nature 413:590

Bibby TS, Nield J and Barber J (2001b) A Photosystem II-like protein, induced under iron-stress, forms an antenna ring around the Photosystem I trimer in cyanobacteria. Nature 412: 743–745

Bibby TS, Mary I, Nield J, Partensky F and Barber J (2003a) Low-light-adapted *Prochlorococcus* species possess specific antennae for each photosystem. Nature 424: 1051–1054

Bibby TS, Nield J, Chen M, Larkum AWD and Barber J (2003b) Structure of a Photosystem II supercomplex isolated from *Prochloron didemni* retaining its chlorophyll *a/b* light-harvesting system. Proc Natl Acad Sci USA 100: 9050–9054

Biggins J, Campbell CL and Bruce D (1983) Mechanism of the light state transition in photosynthesis II. Analysis of phosphorylated polypeptides in the red alga *Porphyridium cruentum*. Biochim Biophys Acta 767: 138–144

Boekema EJ, Hankamer B, Bald D, Kruip J, Nield J, Boonstra AF, Barber J and Rögner M (1995) Supramolecular structure of the Photosystem II complex from green plants and cyanobacteria. Proc Natl Acad Sci USA 92: 175–179

Boekema EJ, van Roon H, Calkoen F, Bassi R and Dekker JP (1999a) Multiple types of association of Photosystem II and its light-harvesting antenna in partially solubilized Photosystem II membranes. Biochemistry 38: 2233–2239

Boekema EJ, van Roon H, van Breemen JFL and Dekker JP (1999b) Supramolecular organization of Photosystem II and its light-harvesting antenna in partially solubilized Photosystem II membranes. Eur J Biochem 266: 444–452

Boekema EJ, van Breemen JFL, van Roon H and Dekker JP (2000) Conformational changes in Photosystem II supercom-

plexes upon removal of extrinsic subunits. Biochemistry 39: 12907–12915

Boekema EJ, Hifney A, Yakushevska AE, Piotrowski M, Keegstra W, Berry S, Michel K-P, Pistorius EK and Kruip J (2001) A giant chlorophyll-protein complex induced by iron deficiency in cyanobacteria. Nature 412: 745–748

Bruce D, Biggins J, Steiner T and Thewalt M (1986) Excitation energy transfer in the cryptophytes. Fluorescence excitation spectra and picosecond time-resolved emission spectra of intact algae at 77 K. Photochem Photobiol 44: 519–525

Büchel C (2003) Fucoxanthin-chlorophyll proteins in diatoms: 18 and 19 kDa subunits assemble into different oligomeric states. Biochemistry 42: 13027–13034

Büchel C and Wilhelm C (1993) Isolation and characterization of a Photosystem I-associated antenna (LHC I) and a Photosystem I-core complex from the chlorophyll *c*-containing alga *Pleurochloris meiringensis* (Xanthophyceae) J Photochem Photobiol B 20: 87–93

Burnap RL, Troyan T and Sherman LA (1993) The highly abundant chlorophyll-protein complex of iron-deficient *Synechococcus* sp. PCC7942 (CP43′) is encoded by the *isi*A gene. Plant Physiol. 103: 893–902

Caron L, Douady D, de Martino A and Quinet M (2001) Light harvesting in brown algae. Cahiers de Biologie Marine 42: 109–124

Cavalier-Smith T (2000) Membrane heredity and early chloroplast evolution. Trends Plant Sci 5: 174–182

Chen M, Hiller RG, Howe CJ and Larkum AWD (2005) Unique origin and lateral transfer of prokaryotic chlorophyll-*b* and chlorophyll-*d* light-harvesting systems. Mol Biol Evol 22: 21–28.

Croce R, Remelli R, Varotto C, Breton J and Bassi R (1999a) The neoxanthin binding site of the major light harvesting complex (LHCII) from higher plants. FEBS Lett 456: 1–6

Croce R, Weiss S and Bassi R (1999b) Carotenoid-binding sites of the major light-harvesting complex II of higher plants. J Biol Chem 42: 29613–29623

Croce R, Canino G, Ros F and Bassi R (2002) Chromophore organization in the higher-plant Photosystem II antenna proteins CP26. Biochemistry 41: 7334–7343

Croce R, Muller MG, Bassi R and Holzwarth AR (2003) Chlorophyll *b* to chlorophyll *a* energy transfer kinetics in the CP29 antenna complex: A comparative femtosecond absorption study between native and reconstituted proteins. Biophys J 84: 2508–2516

Das SK and Frank HA (2002) Pigment compositions, spectral properties, and energy transfer efficiencies between the xanthophylls and chlorophylls in the major and minor pigment-protein complexes of Photosystem II. Biochemistry 41: 13087–13095

Deane JA, Fraunholz M, Su V, Maier U-G, Martin W, Durnford DG and McFadden GI (2000) Evidence for nucleomorph to host nucleus gene transfer: Light-harvesting complex proteins from cryptomonads and chlorarachniophytes. Protist 151: 239–252

Delphin E, Duval J-C, Etienne A-L and Kirilovsky D (1998) ΔpH-dependent Photosystem II fluorescence quenching induced by saturating, multiturnover pulses in red algae. Plant Physiol 118: 103–113

De Martino A, Douady D, Quinet-Szely M, Rousseau B, Crépineau F, Apt K and Caron L (2000) The light-harvesting antenna of brown algae. Highly homologus proteins encoded by a multigene family. Eur J Biochem 267: 5540–5549

Dijkman NA and Kroon BMA (2002) Indications for chlororespiration in relation to light regime in the marine diatom *Thalassiosira weissflogii*. J Photochem Photobiol B 66: 179–187

Dufresne A, Salanoubat M, Partensky F, Artiguenave F, Axmann IM, Barbe V, Duprat S, Galperin MY, Koonin EV, Le Gall F, Makarova KS, Ostrowski M, Oztas S, Robert C, Rogozin IB, Scanlan DJ, Tandeau de Marsac N, Weissenbach J, Wincker P, Wolf YI and Hess WR (2003) Genome sequence of the cyanobacterium *Prochlorococcus marinus* SS120, a nearly minimal oxyphototrophic genome. Proc Natl Acad Sci. 100: 10020–10025

Durnford DG, Deane JA, Tan S, McFadden GI, Gantt E and Green BR (1999) A phylogenetic assessment of the eukaryotic light-harvesting antenna proteins, with implications for plastid evolution. J Mol Evol 48: 59–68

Elrad D and Grossman AR (2004) A genome's-eye view of the light-harvesting polypeptides of *Chlamydomonas reinhardtii*. Curr Genet 45: 61–75

Eppard M and Rhiel E (1998) The genes encoding light-harvesting subunits of *Cyclotella cryptica* (Bacillariophyceae) constitute a complex and heterogeneous family. Mol Gen Genet 260: 335–345

Eppard M, Krumbein WE, von Haeseler A and Rhiel E (2000) Characterization of fcp4 and fcp12, two additional genes encoding light harvesting proteins of *Cyclotella cryptica* (Bacillariophyceae) and phylogenetic analysis of this complex gene family. Plant Biol 2: 283–289

Ferreira KN, Iverson TM, Maghlaoui K, Barber J and Iwata S (2004) Architecture of the photosynthetic oxygen-evolving center. Science 303: 1831–1838

Field CB, Behrenfeld MJ, Randerson JT and Falkowski P (1998) Primary production of the biosphere: Integrating terrestrial and oceanic components. Science 281: 237–240

Frank HA, Young AJ, Britton G and Cogdell RJ (eds) (1999) Photochemistry of Carotenoids. Kluwer Academic Publishers, Dordrecht

Ganetag U, Kühlheim C, Andersson J and Jansson S (2004) Is each light-harvesting complex protein important for plant fitness? Plant Physiol 134: 502–509

Gantt E (1980) Photosynthetic cryptophytes. In: Cox ER (ed) Phytoflagellates, pp 381–405. Elsevier/North-Holland, Amsterdam

Gantt E, Edwards MR and Provasoli L (1971) Chloroplast structure of the Cryptophyceae: Evidence for phycobiliproteins within intrathylakoidal spaces. J Cell Biol 48: 280–290

Gantt E, Clement-Metral JD and Chereskin BM (1988) Photosystem II-phycobilisome complex preparations. In: Packer L and Glazer AN (eds) Methods in Enzymology: Cyanobacteria Vol 167, 287–290. Academic Press, San Diego

Gantt E, Grabowski B and Cunningham FX (2003) Antenna systems of red algae: phycobilisomes with Photosystem II and chlorophyll complexes with Photosystem I. In: Green BR and Parson WW (eds) Light-Harvesting Antennas in Photosynthesis, pp 307–322 . Kluwer Academic Publishers, Dordrecht

Garczarek L, van der Staay GWM, Thomas JC and Partensky F (1998) Isolation and characterization of Photosystem I from two strains of the marine oxychlorobacterium *Prochlorococcus*. Photosynth Res 56: 131–141

Garczarek L, Hess WR, Holtzendorff J, van der Staay GWM and

Partensky F (2000) Multiplication of antenna genes as a major adaptation to low light in a marine prokaryote. Proc Natl Acad Sci 97: 4098–4101

Garczarek L, van der Staay GWM, Hess WR, Le Gall F and Partensky F (2001) Expression and phylogeny of the multiple antenna genes of the low-light adapted strain *Prochlorococcus marinus* SS120 (Oxyphotobacteria). Plant Mol Biol 46: 683–693

Garrido JL, Otero J, Maestro MA and Zapata M (2000) The main nonpolar chlorophyll *c* from *Emiliana huxleyi* (Prymnesiophyceae) is a chlorophyll c_2-monogalactosyldiacylglyceride ester: A mass spectrometry study. J Phycol 36: 497–505

Gibbs SP (1981) The chloroplasts of some algal groups may have evolved from endosymbiotic eukaryotic algae. Ann NY Acad Sci 361: 193–208

Giuffra E, Zucchelli G, Sandonà D, Croce R, Cugini D, Garlaschi FM, Bassi R and Jennings RC (1997) Analysis of some optical properties of a native and reconstituted Photosystem II antenna complex, CP29—pigment binding sites can be occupied by chlorophyll *a* or chlorophyll *b* and determine spectral forms. Biochemistry 36: 12984–12993

Glazer AN and Wedemayer GJ (1995) Cryptomonad biliproteins—an evolutionary perspective. Photosynth Res 46: 93–105

Grabowski B, Cunningham FX Jr and Gantt E (2001) Chlorophyll and carotenoid binding in a simple red algal light-harvesting complex crosses phylogenetic lines. Proc Natl Acad Sci USA 98: 2911–2916

Gradinaru CC, van Grondelle R and van Amerongen H (2003) Selective interaction between xanthophylls and chlorophylls in LHCII probed by femtosecond transient absorption spectroscopy. J Phys Chem B 107: 3938–3943

Green BR (2001) Was 'molecular opportunism' a factor in the evolution of different photosynthetic light-harvesting pigment systems? Proc Natl Acad Sci USA 98: 2119–2121

Green BR (2003) The evolution of light-harvesting antennas. In: Green BR and Parson WW (eds) Light-Harvesting Antennas in Photosynthesis, pp 129–168. Kluwer Academic Publishers, Dordrecht

Green BR and Durnford DG (1996) The chlorophyll-carotenoid proteins of oxygenic photosynthesis. Annu Rev Plant Physiol Plant Mol Biol 47: 685–714

Green BR and Kühlbrandt W (1995) Sequence conservation of light-harvesting and stress-response proteins in relation to the three-dimensional molecular structure of LHCII. Photosynth Res 44:139–148

Green BR and Parson WW (eds) (2003) Light-Harvesting Antennas in Photosynthesis. Kluwer Academic Publishers, Dordrecht

Green BR and Pichersky E (1994) Hypothesis for the evolution of three-helix Chl *a/b* and Chl *a/c* light-harvesting antenna proteins from two-helix and four-helix ancestors. Photosynth Res 39: 149–162

Green BR, Anderson JM and Parson WW (2003) Photosynthetic membranes and their light-harvesting antennas. In: Green BR and Parson WW (eds) Light-Harvesting Antennas in Photosynthesis, pp 1–28. Kluwer Academic Publishers, Dordrecht

Grossman AR, van Wassenbergen LG and Kehoe D (2003) Environmental regulation of phycobilisome biosynthesis. In: Green BR and Parson WW (eds) Light-Harvesting Antennas in Photosynthesis, pp 471–494. Kluwer Academic Publishers, Dordrecht

Harrer R, Bassi R, Testi MG and Schäfer C (1998) Nearest-neighbor analysis of a Photosystem II complex from *Marchantia polymorpha* L. (liverwort), which contains reaction center and antenna proteins. Eur J Biochem 255: 196–205

Haxo FT (1960) The wavelength dependence of photosynthesis and the role of accessory pigments. In: Allen MB (ed) Comparative Biochemistry of Photoreactive Systems, pp 339–360. Academic Press, New York and London

Heddad M and Adamska I (2002) The evolution of light stress proteins in photosynthetic organisms. Comp Funct Genomics 3: 504–510

Hess WR, Parentsky F, van der Staay GW, Garcia-Fernandez JM, Börner T and Vaulot D (1996) Coexistence of phycoerythrin and a chlorophyll *a/b* antennae in a marine prokaryote. Proc Natl Acad Sci USA 93: 11126–11130

Hihara Y, Kamei A, Kanehisa M, Kaplan A and Ikeuchi M (2001) DNA microarray analysis of cyanobacterial gene expression during acclimation to high light. Plant Cell 13: 793–806

Hiller RG (1999) Carotenoids as components of the light-harvesting proteins of eukaryotic algae. In: Frank HA, Young AJ, Britton G and Cogdell RJ (eds) Photochemistry of Carotenoids, pp 81–98. Kluwer Academic Publishers, Dordrecht

Hobe S, Prytulla S, Kühlbrandt W and Paulsen H (1994) Trimerization and crystallization of reconstituted light-harvesting chlorophyll *a/b* complex. EMBO J 13: 3423–3429

Hobe S, Förster R, Klinger J and Paulsen H (1995) N-proximal sequence motif in light-harvesting chlorophyll *a/b*-binding protein is essential for the trimerization of light-harvesting chlorophyll *a/b* complex. Biochemistry 34: 10224–10228

Hobe S, Niemeier H, Bender A and Paulsen H (2000) Carotenoid binding sites in LHCIIb—Relative affinities towards major xanthophylls of higher plants. Eur J Biochem 267: 616–624

Hofmann E, Wrench PM, Sharples FP, Hiller RG, Welte W and Diederichs K (1996) Structural basis of light harvesting by carotenoids: Peridinin-chlorophyll-protein from *Amphidinium carterae.* Science 272: 1788–1791

Holt NE, Fleming GR and Niyogi KK (2004) Toward an understanding of the mechanism of nonphotochemical quenching in green plants. Biochemistry 43: 8281–8289

Hu Q, Miyashita H, Miyashita H, Iwasaki I, Kurano N, Miyachi S, Iwaki M and Itoh S (1998) A Photosystem I reaction center driven by chlorophyll *d* in oxygenic photosynthesis. Proc Natl Acad Sci USA 95: 13319–13323

Hu Q, Marquardt J, Iwasaki I, Miyashita H, Kurano N, Mörschel E and Miyachi S (1999) Molecular structure, localization and function of biliproteins in the chlorophyll *a/d* containing oxygenic photosynthetic prokaryote *Acaryochloris marina*. Biochim Biophys Acta 1412: 250–261

Hutin C, Nussaume L, Moise N, Moya I, Kloppstech K and Havaux M (2003) Early light-induced proteins protect *Arabidopsis* from photooxidative stress. Proc Natl Acad Sci USA 100: 4921–4926

Ilagan RP, Shima S, Melkozernov A, Lin S, Blankenship RE, Sharples FP, Hiller RG, Birge RR and Frank HA (2004) Spectroscopic properties of the main-form and high-salt peridinin-chlorophyll *a* proteins from *Amphidinium carterae.* Biochemistry 43: 1478–1487

Ivanov AG, Park Y-I, Miskiewicz E, Raven JA, Huner NPA and Öquist G (2000) Iron stress restricts photosynthetic intersystem electron transport in *Synechococcus* sp. PCC 7942. FEBS Lett 485: 173–177

Jakob T, Goss R and Wilhelm C (1999) Activation of diadinoxanthin de-epoxidase due to a chlororespiratory proton gradient in the dark in the diatom *Phaeodactylum tricornutum*. Plant Biology 1: 76–82

Jansson S (1999) A guide to the Lhc genes and their relatives in *Arabidopsis*. Trends Plant Sci 4: 236–240

Joshua S and Mullineaux CW (2005) Phycobilisome diffusion is required for light-state transitions in cyanobacteria. Plant Physiology 135: 2112–2119

Kamiya N and Shen J-R (2003) Crystal structure of oxygen-evolving Photosystem II from *Thermosynechococcus vulcanus* at 3.7Å resolution. Proc Natl Acad Sci USA 100: 98–103

Kleima FJ, Hobe S, Calkoen F, Urbanus ML, Peterman EJG, van Grondelle R, Paulsen H and van Amerongen H (1999) Decreasing the chlorophyll *a/b* ratio in reconstituted LHCII: Structural and functional consequences. Biochemistry 38: 6587–6596

Krause GH and Jahns P (2003) Pulse amplitude modulated chlorophyll fluorometry and is application in plant science. In: Green BR and Parson WW (eds) Light-Harvesting Antennas in Photosynthesis, pp 353–372. Kluwer Academic Publishers, Dordrecht

Kühlbrandt W, Wang DN and Fujiyoshi Y (1994) Atomic model of plant light-harvesting complex by electron crystallography. Nature 367:614–621

Larkum WD, Douglas SE and Raven JA (eds) (2003) Photosynthesis in Algae. Kluwer Academic Publishers, Dordrecht

LaRoche J, van der Staay GWM, Partensky F, Ducret A, Aebersold R, Li R, Golden SS, Hiller RG, Wrench PM Larkum AWD and Green BR (1996) Independent evolution of the prochlorophyte and green plant chlorophyll *a/b* light-harvesting proteins. Proc Natl Acad Sci US 93: 15244–14248

Lavaud J, Rousseau B, van Gorkom HJ and Etienne A-L (2002a) Influence of the diadinoxanthin pool size on photoprotection in the marine planktonic diatom *Phaeodactylum tricornutum*. Plant Physiol 129: 1398–1406

Lavaud J, van Gorkom HJ and Etienne A-L (2002b) Photosystem II electron transfer cycle and chlororespiration in planktonic diatoms. Photosynth Res 74: 51–59

Lavaud J, Rousseau B and Etienne A-L (2004) General features of photoprotection by energy dissipation in planktonic diatoms (Bacillariophyceae). J Phycol 40: 130–137

Li XP, Björkman O, Shih C, Grossman AR, Rosenquist M, Jansson S and Niyogi KK (2000) A pigment-binding protein essential for regulation of photosynthetic light harvesting. Nature 403: 391–395

Li XP, Müller-Moulé P, Gilmore AM and Niyogi KK (2002) PsbS-dependent enhancement of feedback de-excitation protects Photosystem II from photoinhibition. Proc Natl Acad Sci USA 99: 15222–15227

Li XP, Gilmore AM, Caffarri S, Bassi R, Golan T, Kramer D and Niyogi KK (2004) Regulation of photosynthetic light harvesting involves intrathylakoid lumen pH sensing by the PsbS protein. J Biol Chem 279: 22866–22874

Lichtlé C, Duval JC and Lemoine Y (1987) Comparative biochemical, functional and ultrastructural studies of photosystem particles from a Cryptophycea: *Cryptomonas rufescence*; isolation of an active phycoerythrin particle. Biochim Biophys Acta 894: 76–90

Lichtlé C, McKay RML and Gibbs SP (1992a) Immunogold localization of Photosystem I and Photosystem II light-harvesting complexes in cryptomonad chloroplasts. Biol Cell 74: 187–194

Lichtlé C, Spilar A and Duval JC (1992b) Immunogold localization of light-harvesting and Photosystem I complexes in the thylakoids of *Fucus serratus* (Phaeophyceae). Protoplasma 166: 99–106

Liu ZF, Yan HC, Wang KB, Kuang TY, Zhang JP, Gul LL, An XM and Chang WR (2004) Crystal structure of spinach major light-harvesting complex at 2.72 Å resolution. Nature 428: 287–292

Lohr M and Wilhelm C (1999) Algae displaying the diadinoxanthn cycle also possess the violaxanthin cycle. Proc Natl Acad Sci USA 96: 8784–8789

Ludwig M and Gibbs SP (1989) Localization of phycoerythrin at the lumenal surface of the thylakoid membrane in *Rhodomonas lens*. J Cell Biol 108: 875–884

Ma YZ, Holt NE, Li XP, Niyogi KK and Fleming GR (2003) Evidence for direct carotenoid involvement in the regulation of photosynthetic light harvesting. Proc Natl Acad Sci USA 100: 4377–4382

MacColl R and Guard-Friar D (1987) Phycobiliproteins. CRC Press, Boca Raton

Macpherson AN and Hiller RG (2003) Light-harvesting systems in chlorophyll *c*-containing algae. In: Green BR and Parson WW (eds) Light-Harvesting Antennas in Photosynthesis, pp. 323–352. Kluwer Academic Publishers, Dordrecht

Matthijs HCP, van der Staay GWM and Mur LR (1995) Prochlorophytes: The 'other' cyanobacteria? In: Bryant DA (ed) The Molecular Biology of Cyanobacteria, pp 49–64. Kluwer Academic Publishers, Dordrecht

McConnell MD, McConnell RK, Sergej V and Bruce D (2002) Regulation of the distribution of chlorophyll and phycobilins-absorbed excitation energy in cyanobacteria. A structure-based model for the light state transition. Plant Physiol. 130: 1202–1212

McFadden GI (1999) Endosymbiosis and evolution of the plant cell. Curr Opinion Plant Biol 2: 513–519

McFadden GI (2001) Primary and secondary endosymbiosis and the origin of plastids. J Phycol 37: 951–959

Meyer M and Wilhelm C (1993) Reconstitution of light-harvesting complexes from *Chlorella fusca* (Chlorophyceae) and *Mantoniella squamata* (Prasinophyceae). Z Naturforsch 48c: 461–473

Miao JH, Irrgang KD, Salnikow J, Franke P and Vater J (1998) Close vicinity of Lhcb1 and Lhcb4 in Photosystem II—Membrane fragments as verified by chemical cross-linking. Eur J Biochem 257: 586–591

Mimuro M and Kikuchi H (2003) Antenna systems and energy transfer in cyanophyta and rhodophyta. In: Green BR and Parson WW (eds) Light-Harvesting Antennas in Photosynthesis, pp 281–306. Kluwer Academic Publishers, Dordrecht

Minagawa J and Takahashi Y (2004) Structure, function and assembly of Photosystem II and its light-harvesting proteins. Photosynth Res 82: 241–263

Montané MH and Kloppstech K (2000) The family of light-harvesting-related proteins (LHCs, ELIPs, HLIPs): Was the harvesting of light their primary function? Gene 258: 1–8

Morosinotto T, Caffarri S, Dall'Osto L and Bassi R (2003) Mechanistic aspects of the xanthophyll dynamics in higher plant thylakoids. Physiol Plant 119: 347–354

Murakami A, Miyashita H, Iseki M, Adachi K and Mimuro M (2004) Chlorophyll *d* in an epiphytic cyanobacterium of red

algae. Science 303: 1633
Nield J, Funk C and Barber J (2000a) Supermolecular structure of Photosystem II and location of the PsbS protein. Phil Trans Roy Soc Lond B 355: 1337–1344
Nield J, Orlova EV, Morris EP, Gowen B, van Heel M and Barber J (2000b) 3D map of the plant Photosystem II supercomplex obtained by cryoelectron microscopy and single particle analysis. Nat Struct Biol 7: 44–47
Novoderezhkin VI, Palacios MA, van Amerongen H and van Grondelle R (2004) Energy-transfer dynamics in the LHCII complex of higher plants: Modified redfield approach. J Phys Chem B 108: 10363–10375
Nussberger S, Dorr K, Wang DN, Kühlbrandt W (1993) Lipid-protein interactions in crystals of plant light-harvesting complex. J Mol Biol 234: 347–356
Nussberger S, Dekker JP, Kühlbrandt W, van Bolhuis BM, van Grondelle R and van Amerongen H (1994) Spectroscopic characterization of three different monomeric forms of the main chlorophyll *a/b* binding protein from chloroplast membranes. Biochemistry 33: 14775–14783
Olszowka D, Krawczyk S and Maksymiec W (2004) A study of molecular interactions in light-harvesting complexes LHCIIb, CP29, CP26 and CP24 by Stark effect spectroscopy. Biochim Biophys Acta 1657: 61–70
Pagano A, Cinque G and Bassi R (1998) In vitro reconstitution of the recombinant Photosystem II light-harvesting complex CP24 and its spectroscopic characterization. J Biol Chem 273: 17154–17165
Palacios MA, Frese RN, Gradinaru CC, van Stokkum IHM, Premvardhan LL, Horton P, Ruban AV, van Grondelle R and van Amerongen H (2003) Stark spectroscopy of the light-harvesting complex II indifferent oligomerisation states. Biochim Biophys Acta 1605: 83–95
Parson WW and Nagarajan V (2003) Optical spectroscopy in photosynthetic antennas. In: Green BR and Parson WW (eds) Light-Harvesting Antennas in Photosynthesis, pp 84–127. Kluwer Academic Publishers, Dordrecht
Partensky F and Garczarek L (2003) The photosynthetic apparatus of green oxyphotobacteria. In: Larkum WD, Douglas SE and Raven JA (eds) Photosynthesis in Algae, pp 29–62. Kluwer Academic Publishers, Dordrecht
Park Y-I, Sandström S, Gustafsson P and Öquist G (1999) Expression of the isiA gene is essential for the survival of the cyanobacterium *Synechococcus*. sp. PCC7942 by protecting Photosystem II from excess light under iron limitation. Mol Microbiol 32: 123–129
Pascal AA, Caron L, Rousseau B, Lapouge K, Duval JC and Robert B (1998) Resonance Raman spectroscopy of a light-harvesting proteins from the brown alga *Laminaria saccharina*. Biochemistry 37: 2450–2457
Pascal A, Gastaldella M, Ceoldo S, Bassi R, Robert B (2001) Pigment conformation and pigment-protein interactions in the reconstituted Lhcb4 antenna protein. FEBS Lett 492: 54–57
Paulsen H (1997) Pigment ligation to proteins of the photosynthetic apparatus in higher plants. Physiol Plant 100: 760–768
Peterman EJG, Gradinaru CC, Calkoen F, Borst JC, van Grondelle R and van Amerongen H (1997) Xanthophylls in light-harvesting complex II of higher plants: Light harvesting and triplet quenching. Biochemistry 36: 12208–12215
Post AF, Ohad I, Warner KM and Bullerjahn GS (1993) Energy distribution between photosystems I and II in the photosynthetic prokaryote *Prochlorothrix hollandica* involves a chlorophyll *a/b* antenna which associates with Photosystem I. Biochim Biophys Acta 1144: 374–384
Pyszniak AM and Gibbs SP (1992) Immunochemical localization of Photosystem I and the fucoxanthin-chlorophyll *a/c* light-harvesting complex in the diatom, *Phaeodactylum tricornutum*. Protoplasma 189: 208–217
Remelli R, Varotto C, Sandonà D, Croce R and Bassi R (1999) Chlorophyll binding to monomeric light-harvesting complex. A mutation analysis of chromophore-binding residues. J Biol Chem 274: 33510–33521
Reuter W, Wiegand G, Huber R and Than M (1999) Structural analysis and 2.2Å of orthorhombic crystals presents the asymmetry of the allophycocyanin-linker complex, AP.LC7.8, from the phycobilisomes of *Mastigocladus laminosus*. Proc Natl Acad Sci USA 96: 1364–1368
Richaud C, Zabulon G, Joder A and Thomas J-C (2001) Nitrogen or sulfur starvation differentially affects phycobilisome degradation and expression of the nblA gene in *Synechocystis* strain PCC 6803. J Bacteriol 183: 2989–2994
Rogl H and Kühlbrandt W (1999) Mutant trimers of light-harvesting complex II exhibit altered pigment content and spectroscopic features. Biochemistry 38: 16214–16222
Rogl H, Schödel R, Lokstein H, Kühlbrandt W and Schubert A (2002) Assignment of spectral substructures to pigment-binding sites in higher plant light-harvesting complex LHC-II. Biochemistry 41: 2281–2287
Rogl H, Kühlbrandt W and Barth A (2003) Light-induced changes in the chemical bond structure of light-harvesting complex II probed by FTIR spectroscopy. Biochemistry 42: 10223–10228
Ruban AV, Wentworth M, Yakushevska AE, Andersson J, Lee PJ, Keegstra W, Dekker JP, Boekema EJ, Jansson S and Horton P (2003) Plants lacking the main light-harvesting complex retain Photosystem II macro-organization. Nature 421: 648–652
Sandström S, Park Y-I, Öquist G and Gustafsson P (2001) CP43´, the *isi*A gene product, functions as an excitation energy dissipater in the cyanobacterium *Synechococcus* sp. PCC 7942. Photochem Photobiol 74: 431–437
Sandström S Ivanov AG, Park Y-I , Öquist G and Gustafsson P (2002) Iron stress responses in the cyanobacterium *Synechococcus* sp. PCC7942. Physiol Plant 116: 255–263
Sarcina M, Tobin MJ and Mullineaux CW (2001) Diffusion of phycobilisomes on the thylakoid membranes of the cyanobacterium *Synechococcus* 7942. Effects of phycobilisome size, temperature, and membrane lipid composition. J Biol Chem 276: 46830–46834
Scheer H (2003) The pigments. In: Green BR and Parson WW (eds) Light-Harvesting Antennas in Photosynthesis, pp 29–81. Kluwer Academic Publishers, Dordrecht
Sharples FP, Wrench PM, Ou K and Hiller RG (1996) Two distinct forms of the peridinin-chlorophyll *a*-protein from *Amphidinium carterae*. Biochim Biophys Acta 1276: 117–123
Shima S, Ilagan RP, Gillespie N, Sommer BJ, Hiller RG, Sharples FP, Frank HA and Birge RR (2003) Two-photon and fluorescence spectroscopy and the effect of environment on the photochemical properties of peridinin in solution and in the peridinin-chlorophyll-protein from *Amphidinium carterae*. J Phys Chem A 107: 8052–8066
Simonetto R, Crimi M, Sandonà D, Croce R, Cinque G, Breton J and Bassi R (1999) Orientation of chlorophyll transition

moments in the higher-plant light-harvesting complex CP29. Biochemistry 38: 12974–12983

Singh AK, McIntyre LM and Sherman LA (2003) Microarray analysis of the genome-wide response to iron deficiency and iron reconstitution in the cyanobacterium *Synechocystis* sp. PCC 6803. Plant Physiol 132: 1825–1839

Stauber EJ, Fink A, Markert C, Kruse O, Johanningmeier U and Hippler M (2003) Proteomics of *Chlamydomonas reinhardtii* light-harvesting proteins. Euk Cell 2: 978–994

Teramoto H, Ono T and Minagawa J (2001) Identification of *Lhcb* gene family encoding the light-harvesting chlorophyll-*a/b* proteins of Photosystem II in *Chlamydomonas reinhardtii*. Plant Cell Physiol 42:849–856

Ting CS and Owens TG (1993) Photochemical and nonphotochemical fluorescence quenching processes in the diatom *Phaeodactylum tricornutum*. Plant Physiol 101: 1323–1330

Ting CS and Owens TG (1994) The effects of excess irradiance on photosynthesis in the marine diatom *Phaeodactylum tricornutum*. Plant Physiol 106: 763–770

Ting CS, Rocap G, King J and Chisholm SW (2001) Phycobiliprotein genes of the marine photosynthetic prokaryote *Prochlorococcus*: Evidence for rapid evolution of genetic heterogeneity. Microbiology 147: 3171–3182

Ting CS, Rocap G, King J and Chisholm SW (2002) Cyanobacterial photosynthesis in the oceans: The origins and significance of divergent light-harvesting strategies. Trends Microbiol 10: 134–142

Toole CA and Allnutt FCT (2003) Red, cryptomonad and glaucocystophyte algal phycobiliproteins. In: Larkum WD, Douglas SE and Raven JA (eds) Photosynthesis in Algae, pp 305–334. Kluwer Academic Publishers, Dordrecht

van Amerongen H and Dekker JP (2003) Light-harvesting in Photosystem II. In: Green BR and Parson WW (eds) Light-Harvesting Antennas in Photosynthesis, pp 219–251. Kluwer Academic Publishers, Dordrecht

van der Staay GWM, Brouwer A, Baard RL, van Mourik F and Matthijs HCP (1992) Separation of photosystems I and II from the oxychlorobacterium (prochlorophyte) *Prochlorothrix hollandica* and association of Chl *b* binding antennae with PS II. Biochim Biophys Acta 975: 317–324

van der Staay GWM, Yurkova N and Green BR (1998) The 38 kDa chlorophyll *a/b* protein of the prokaryote *Prochlorothrix hollandica* is encoded by a divergent *pcb* gene. Plant Mol Biol 36: 709–716

Wang H-L, Postier BL, and Burnap RL (2004) Alterations in global patterns of gene expression in *Synechocystis* sp. PCC 6803 in response to inorganic carbon limitation and the inactivation of *ndhR*, a LysR family regulator. J Biol Chem, 279: 5739–5751

Wedemayer G, Kidd D and Glazer AN (1996) Cryptopomonad biliproteins: Bilin types and location. Photosynth Res 48: 163–170

Wilk KE, Harrop SJ, Jankova L, Edler D, Keenan G, Sharples F, Hiller RG and Curmi PMG (1999) Evolution of a light-harvesting protein by addition of new subunits and rearrangement of conserved elements: Crystal structure of a cryptophyte phycoerythrin at 1.63Å resolution. Proc Natl Acad Sci USA 96: 8901–8906

Yakushevska AE, Keegstra W, Boekema EJ, Dekker JP, Andersson J, Jansson S, Ruban AV and Horton P (2003) The structure of Photosystem II in *Arabidopsis*: Localization of the CP26 and CP29 antenna complexes. Biochemistry 42: 604–613

Yang C, Kosemund K, Cornet C and Paulsen H (1999) Exchange of pigment-binding amino acids in light-harvesting chlorophyll *a/b* protein. Biochemistry 38: 16205–16213

Yeremenko N, Kouřil R, Ihalainen JA, D'Haene S, van Oosterwijk N, Andrizhiyevskaya EG, Keegstra W, Dekker HL, Hagemann M, Boekema EJ, Matthijs HCP and Dekker JP (2004) Supramolecular organization and dual function of the IsiA chlorophyll-binding protein in cyanobacteria. Biochemistry 43: 10308–10313

Zouni A, Will H-T, Kern J, Fromme P, Krauss N, Saenger W and Orth P (2001) Crystal structure of Photosystem II from *Synechococcus elongatus* at 3.8 Å resolution. Nature 409: 739–743

Chapter 3

The CP47 and CP43 Core Antenna Components

Julian J. Eaton-Rye*
Department of Biochemistry, University of Otago, P.O. Box 56, Dunedin, New Zealand

Cindy Putnam-Evans
Department of Biology, East Carolina University, Greenville, NC 27858, U.S.A.

Summary

The CP47 and CP43 subunits of Photosystem II bind chlorophyll *a* and belong to a family of (bacterio)chlorophyll-binding proteins that serve as core antenna polypeptides in both anoxygenic and oxygenic photosynthesis. Uniquely, both of these proteins possess extended hydrophilic domains that contribute to the environment of the oxygen-evolving complex. Structural studies have shown that these polypeptides are associated with both intrinsic components of the reaction center and with the extrinsic proteins that enhance O_2 evolution under physiological conditions. The biochemical, spectroscopic and molecular techniques that have been used to define these interactions, as well as the functional domains within these proteins, are presented and encompass studies performed on photosynthetic eukaryotes and cyanobacteria.

*Author for correspondence, email: julian.eaton-rye@stonebow.otago.ac.nz

T. Wydrzynski and K. Satoh (eds): Photosystem II: The Light-Driven Water:Plastoquinone Oxidoreductase, pp. 45–70.

I. Introduction

The chlorophyll *a*-binding proteins CP47 (chlorophyll protein with an apparent molecular mass of 47 kDa) and CP43 (chlorophyll protein with an apparent molecular mass of 43 kDa) are encoded by the *psbB* and *psbC* genes, respectively, and serve as the proximal antenna of Photosystem II (PS II). Both polypeptides possess six transmembrane helices that are arranged in pairs to form a trimer of dimers. These membrane-spanning domains provide ligands for the antenna pigment molecules and this structural motif is also found in the N-terminal helices of the Photosystem I (PS I) reaction center proteins PsaA and PsaB as well as the corresponding helices in the homodimeric reaction centers from the *Chlorobiaceae* and *Heliobacteriaceae* (Amesz, 1995; Feiler and Hauska, 1995; Jordan et al., 2001). Recognition of the structural similarities between these chlorophyll-binding proteins has provided support for the concept that all reaction centers are derived from a common ancestor (Rhee et al., 1998; Schubert et al., 1998).

The primary sequences of CP47 and CP43, from a range of oxygenic photosynthetic organisms, are presented in Figs. 1 and 2 together with their domain organization. Both topological and structural studies have established that the N- and C-termini are found on the stromal side (or cytosolic side in cyanobacteria) of the thylakoid membrane (Sayre and Wrobel-Boerner, 1994; Rhee et al., 1998; Zouni et al., 2001; Kamiya and Shen, 2003; Ferriera et al., 2004; Chapters 19–21). In both polypeptides the six-helix bundle forming the trimer-of-dimers motif is formed by helices I and II, helices III and IV and helices V and VI, with the helices connected via five hydrophilic loops denoted as A–E. In both cases loop E is large comprising ~190 amino acids in CP47 and ~130 residues in CP43. These domains contribute to the protein environment of the oxygen-evolving complex (OEC) of the photosystem and correspond to masses of ~22 and 15 kDa, respectively (Figs. 1 and 2).

Within the PS II dimer CP47 is found on the D2 side, and CP43 on the D1 side, of each monomeric reaction center thus positioning CP43 on the outside of the dimeric complex. The original isolation of these polypeptides found that CP43 was more easily purified from isolated PS II complexes while the removal of CP47 required treatment with $LiClO_4$ and high concentrations of dodecyl maltoside (Ghanotakis et al., 1989). Initial work was performed in spinach and the nomenclature for these proteins arose from apparent molecular masses based on polyacrylamide gel electrophoresis (PAGE). Using 77 K low-temperature fluorescence spectroscopy on excised bands obtained from PAGE, the characteristic 695 nm emission was shown to arise from CP47 and the emission at 685 nm from CP43 (Nakatani et al., 1984). Since CP47 gave rise to the long-wavelength emission it was initially hypothesized that CP47 contained the PS II reaction center; however, the recognition of the homology between the D1 and D2 polypeptides and the L and M subunits of the *Rhodopseudomonas viridis* reaction

Abbreviations: apcE – gene encoding the phycobilisome anchor protein; CP – chlorophyll protein; CPa1 – chlorophyll *a*-binding protein CP47; CPa2 – chlorophyll *a*-binding protein CP43; D1 and D2 – reaction center core subunits; DTSP – dithiobis(succi nimidyl)propionate; EDC – 1-ethyl-3-(3-dimethylaminopropyl) carbodiimide; FAC2 – Monoclonal antibody recognizing an epitope between Pro-360 and Ser-391 in CP47; L and M – bacterial photosynthetic reaction center core subunits; NHS-biotin – N-hydroxysuccinimide biotin; OEC – oxygen-evolving complex; *orf62* – chloroplast open reading frame 62; P680 – primary electron donor of Photosystem II; PAGE – polyacrylamide gel electrophoresis; *petB* and *petD* – genes for subunits of the cytochrome b_6f complex; PsaA – Photosystem I reaction center core subunit; PsaB – Photosystem I reaction center core subunit; *psbx* – genes for Photosystem II proteins where x = *A,B,C,D,H,I, K,N,O,P,Q,T,U,V*; Psbx – Photosystem II protein subunits where x = B,C,O,N,U,V; PS I – Photosystem I; PS II – Photosystem II; Q_A – primary plastoquinone acceptor; Q_B – secondary plastoquinone acceptor; SDS – sodium dodecyl sulfate; Sn – state of the water-oxidizing complex for n = 0,1,2,3, or 4; *trnG* – chloroplast gene for tRNA-Gly; Y_D – redox active tyrosine on D2; Y_Z – redox active tyrosine on D1

Fig. 1 (opposite). Alignment of protein sequences for the chlorophyll *a*-binding protein CP47 (PsbB). Consensus sequences for: 102 green plants (GP); 5 green algae (GA); 4 chlorophyll *a*/*c*-containing organisms (AC); 3 red algae (RA), and 10 cyanobacteria (CY). Uppercase indicates amino acids conserved in all sequences; lowercase indicates the amino acids most frequently present. In the case of GP lowercase was only used at positions where more than one sequence carried a substitution. A majority consensus sequence at all positions is also shown (CON). The sequences for *Euglena gracilis* and *Prochlorothrix hollandica* were not incorporated. The domain structure of CP47 is indicated by the solid black line, with I to VI representing membrane-spanning domains and A to E hydrophilic interconnecting loops. The N- and C- termini are exposed to the stromal side of the membrane (or the cytosolic side in cyanobacteria) and loops A, C and E project into the lumenal compartment. Additional domains shown are: (1) regions cross-linked by EDC to the PsbO protein (grey lines); (2) region cross-linked by DTSP to the PsbO protein (black round dots); (3) antigenic determinant for the monoclonal antibody FAC2 (black square dots); and (4) regions shielded from NHS-biotin modification by the PsbO protein (grey dashed line). The black arrow indicates a lysylendopeptidase C cleavage site which prevents reconstitution of the PsbO protein and inhibits O_2 evolution. The calculated molecular mass of CP47 is ~56 kDa.

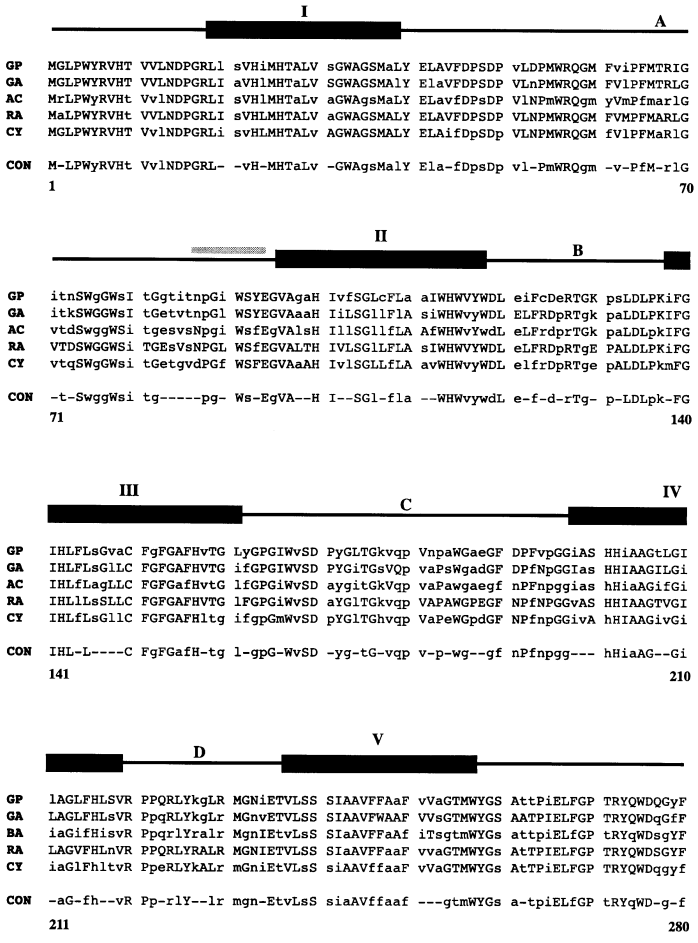
I
A
GP MGLPWYRVHT VVLNDPGRLl sVHiMHTALV sGWAGSMaLY ELAVFDPSDP vLDPMWRQGM FviPFMTRIG
GA MGLPWYRVHT VVLNDPGRLI aVHlMHTaLV SGWAGSMAlY ElaVFDPSDP VLnPMWRQGM FVlPFMTRLG
AC MrLPWyRVHt VvlNDPGRLI sVHlMHTaLv aGWAgsMaLY ELavfDPsDP VlNPmWRQgm yVmPfmarlG
RA MaLPWYRVHt VVLNDPGRLI sVHLMHTALV aGWAGSMALY ELAVFDPSDP VLNPMWRQGM FVMPFMARLG
CY MGLPWYRVHT VvlNDPGRLi svHLMHTALv AGWAGSMALY ELAifDpSDp VLNPMWRQGM fVlPFMaRlG
CON M-LPWyRVHt VvlNDPGRL- -vH-MHTaLv -GWAgsMalY Ela-fDpsDp vl-PmWRQgm -v-PfM-rlG
1 70
II
B
GP itnSWgGWsI tGgtitnpGi WSYEGVAgaH IvfSGLcFLa aIWHWVYWDL eiFcDeRTGK psLDLPKiFG
GA itkSWGGWsI tGetvtnpGl WSYEGVAaaH IiLSGllFlA siWHWvyWDL ELFRDpRTgk paLDLPKIFG
AC vtdSwggWSi tgesvsNpgi WsfEgVAlsH IllSGllfLA AfWHWvYwdL eLFrdprTGk paLDLpkIFG
RA VTDSWGGWSi TGEsVsNPGL WSfEGVALTH IVLSGlLFLA sIWHWVYWDL eLFRDpRTgE PALDLPKiFG
CY vtqSWgGWsi tGetgvdPGf WSFEGVAaAH IvlSGLLfLA avWHWvyWDL elfrDpRTge pALDLPkmFG
CON -t-SwggWsi tg-----pg- Ws-EgVA--H I--SGl-fla --WHWvywdL e-f-d-rTg- p-LDLpk-FG
71 140
III
C
IV
GP IHLFLsGvaC FgFGAFHvTG LyGPGIWvSD PyGLTGkvqp VnpaWGaeGF DPFvpGGiAS HHiAAGtLGI
GA IHLFLsGllC FGFGAFHVTG ifGPGIWVSD PYGiTGsVQp vaPsWgadGF DPfNpGGIas HHIAAGILGi
AC IHLfLagLLC FGFGAfHvtG lfGPGiWvSD aygitGkVqp vaPawgaegf nPFnpggias hHiaAGifGi
RA IHLlLsSLLC FGFGAFHVTG lFGPGiWvSD aYGlTGkvqp VAPAWGPEGF NPfNPGGvAS HHIAAGTVGI
CY IHLfLsGllC FGFGAFHltg ifgpGmWvSD pYGlTGhvqp VaPeWGpdGF NPfnpGGivA hHIAAGivGi
CON IHL-L----C FgFGafH-tg l-gpG-WvSD -yg-tG-vqp v-p-wg--gf nPfnpgg--- hHiaAG--Gi
141 210
D
V
GP lAGLFHLSVR PPQRLYkgLR MGNiETVLSS SIAAVFFaaF vVaGTMWYGS AttPiELFGP TRYQWDQGyF
GA LAGLFHLsVR PpqRLYkgLr MGnvETVLSS SIAAVFWAAF VVsGTMWYGS AATPIELFGP TRYQWDqGfF
BA iaGifHisvR PpqrlYralr MgnIEtvLsS SIaAVFFaAf iTsgtmWYGs attpiELfGP tRYqWDsgYF
RA LAGVFHLnVR PPQRLYRALR MGNIETVLSS SIaAVFFaaF vvaGTMWYGs AtTPIELFGP TRYQWDSGYF
CY iaGlFhltvR PpeRLYkALr mGniEtVLsS siAAVffaaF vVaGTMWYGs AtTPiELFGP TRYQWDqgyf
CON -aG-fh--vR Pp-rlY--lr mgn-EtvLsS siaAVffaaf ---gtmWYGs a-tpiELfGP tRYqWD-g-f
211 280
Loop E
GP QQEIyRrvga glaenlSlSE aWsKIPeKLA FYDYIGNNPA KGGLFRAGsM DnGDGIAvGW LGHpiFrDKe
GA qqEIekRVqa slaeGaslSe AWskIPEKLa FYDYIGNNPA KGGLFRaCAM nsGDGIAvGW LGHavFkdke
AC qqeIErrVet slaeglslse awseiPdKLa fYDYiGnNPA KGGLFRaGPm nKGDGiaeaW lGhpvFqdke
RA QQEiEkRVea nlsqGaslsE AWSkIPDKLA FYDYIGNNPA KGGLFRAGPM NKGDGiAeAW LGHpVFQDKe
CY qqEInRRVqt alaqGatlee AwssIPEKLA FYDYvGNsPA KGGLFRtGpm nkGDGiaqsW lGHpvFkdke
CON qqei--rv-- -l-----l-e aws-iP-KLa fYDY-Gn-PA KGGLFR---m --GDGia--W lGh--F-dke
281 350
GP GrELFVRRMP TFFETFPVVL vDgdGiVrAD vPFRRaESKY SVEQVGVtVe FYGGeLngvs ysDPatVKKY
GA GrELFVRRMP tFFETFPVvL lDkdGiVRAD vPFRRaESKY SIEQVGVsVt FYGGELDGvt FnDPaTVKKY
AC greLtVRRmP aFFETFPViL vDkdGiiRAD IpFRRaeSkY SiEQvgVtvt fyGGklnGqt lndaptVKky
RA GrELtVRRMP AFFEtFPvIL VDKDGIiRAD IPFRRAESKY SIEQVGVTcs FYGGKlNgQs FnDAasVKkY
CY GreLeVRRlP nFFEtFPvil tdkdGvVrAD IPfRRaEsKy SfEqtGvtvs fyGGdlngqt ftdpadVKky
CON greL-VRR-P -FFEtFPv-l -d-dG--rAD -pfRRaesky S-Eq-gv--- fyGG-l-g-- --d---VKky
351 420
VI
GP ARRaQLGEIF ElDRATLKSD GVFRSSPRGW FTFGHAtFAL lFFfGHIWHG aRTLFRDvFA GIDPdLDaqv
GA ARrAQLGeiF EFDRatLqSD GVFRsSPRGW FTFgHlcFAL LFFFGHIWHG aRTiFRDVFa GIDpDlddQV
AC ARKaQlGeif eFDrttlesD GVFRsSpRGW YtFgHanfal lFFfGHLWHg gRtlFrdvft Gigaevteqv
RA ARKAQlGEVF EFDRttLdSD GVFRsSPRGW FTFgHANFAL lFFFGHLWHG sRTiFRDVFA GIGAEVTEQV
CY ArkAqlGEiF eFDrETlnSD GvFRtSpRgW FTfgHavFaL LFfFGHiWHg aRTlfrDvFa Gidpdleeqv
CON ArkaqlGe-f e-Dr-tl-sD GvFR-SpRgW -tfgH--fal lFffGH-WHg -Rt-frdvf- Gi------qv
421 490
GP EFGaFQKlGD PTTrrQvv
GA EFGafqKLGD tstrrqav
AC EfGafqKLGD rsTkkqgav
RA EFGvFQKvGD rstKKQgav
CY EfGlfqKlGD ksTRrkeav
CON EfG-fqK-GD --t------
491 509

I
Loop E
A
II
B
III
C
VI
IV
D
V
GP vETLFNGTla LagRDQETTG FAWWAGNARL INLSGKLLGA HVaHAGLiVF WAGAMNLFEV AHFvPEKPMY
GA vETLFNGTiL vgGRDQEaTG FAWWAGNARL INLSGKLLGA HVAHAGLiVF WAGAMNLFEV aHFvPEKPMY
AC Mk+++++++ ++gRtlegsr fAWWSGNaRl InlSGKLLGA HvaHaGLiVF WaGamtLFEv aHfvpekPly
RA vetpfNn+++ vgGrsIESTG FAWWSGNARL INlSGKLLGA HVAHAGliVF WTGAMTLFEv aHfvPeKPLY
CY mvTLSn+++++ ++gRDqeStG FAWWSGNARL INLSGKLLGA HVAHAGLiVF WaGAMtLFEv aHfvpeKPmy
CON ---------- ---r--e--- faWW-GNaRl InlSGKLLGA HvaHaGliVF W-Gam-LFEv aHfvpekp-y
1 70
GP NNTaYPSEFY GPTGPEASQA QAFTFLVRDQ RLGAnvGSAQ GPTGLGKYLM RSPTGEviFG GETMRFWDLR
GA NnTaYPSEFY GPTGPEASQa QaFTFLVRDQ RLGANvaSaQ GPTGLGKYLM RSPtGEIIFG GETMRFWDFR
AC NnTaYPSEfy gPtGpEASQs QaFTFLVRDQ rLGakvasaq GPTgLgKYLM RSPsGEiIfG GETmRFWslr
RA NNTaYPSEFY GPTgpEASQA QAFTFLVRDQ RLGaNvASaQ GPTGLGKYLM RSPtGEiIfG GETMRFWDLR
CY NNTaYPSEFy GPTgaEASQa QafTFLvRDQ rlGANvgSAq GPTGLGKYLM RSPtGEIIfG GETMRFWDFr
CON NnTaYPSEFy gPtg-EASQ- QaFtFLvRDQ rlGa-v-saq GPTgLgKYLM RSP-GE-IfG GETmRFW--r
281 350
GP APWLEPLRGP NGLDLsrLkk DIQPWQERRS AEYMTHAPLG SLNSVGGVAT EINAVNYVSP RSWLaTSHFV
GA aPWlEPLRGP NGLDLnKLKn DIQPWQERRs AEYMTHAPLG SLNSVGGVAT EINAVNfVSP RSWLatSHFv
AC apWveplRgp nGlDlnKlkn DIQsWQERRA AeyMTHAPlG sLNSVGGvaT EiNsvNYVSP RSWLtssHwf
RA APWlEPLRgp NGLDLNKlKN DIQPWQERRA AEYMTHAPLG SlNSVGGVAT EINSvNYVSP RSWLTPSHFf
CY GPwlEPLEGP NGLdLdKlkN DIQPWQaRRA AeYMTHAPlg SlNSVGGvaT eiNsfNyVsp RaWLatshFv
CON -pw-epl-gp nGld----kn DIQ-WQ-RR- AeyMTHAPlg slNSVGGvaT eiN--N-Vsp R-WL--sH--
351 420
GP EQGLILLPHL ATLGWGVGPG GEviDTFPYF VSGVLHLISS AVLGFGGIYH alLGPETLEE sfPFFGYvWK
GA EQGLILLPHL AtLGyGVGPG GEVIDTfPYF VSGVLHLISS AVLGFGGVYH sliGPETLEE SfPFFGYvWK
AC eQGfIllphL atiGyyvGpg geIidtypyF vvgVlHLiss avlgfGGiYH slfGperLEE s+++FgydWr
RA EQGmILIPHL ATLGWGVgPg GEIvdTfPYF vvGVlHLiSS AVLGFGGiYH s1iGPdeLEe SfpFFGYDWR
CY EQGIIllphl ATlGwGVGpg GEViDtFPyF VVGVlHLISS AVLGiGGiYH AvRGPEcLEe YSsFFgyDWk
CON eQG-Illphl at-g-gvgpg ge--dt-pyF v-gVlHliss avlg-gG--LEe ----Fgy-W-
71 140
GP DraKMTTILG IHLILLGiGa FLlVlKAlyF GGvYDFTWAPG GGDVRkITNl TLsPsviFGy lLkSPFGGBG
GA DKNKMTtLIG iHLiLlGiGA wLLVwKAMyf GGvYDFTWAPG GGDVRvItnP TtspavIFgY l1kSPFGGeG
AC DrnrmTtiG aHLvllGlas llvlvkAlyl gGlYDFwapG GGDvRli+++ tlnpvigGy l1kaPfGgdG
RA DKNKMTTILG IHLiLLGIGA FLLVIKAlFi gGvYDFTWAPG GGDvRfisNP TLNPavIFgY lLKSPFGGdG
CY DKNgMTnIiG yHLilLGcGa lLlVfKAmFf GGvYDFTWAPG GGDVRvItNP TLnPavIFGY l1ksPFGGeG
CON D-n-mT-I-G -HL-llG--a -llv-k---- gG-YDtwapG GGDvR-I--- t--p-vi-gy l1k-pfGg-G
141 210
GP WIvSVDdLED iIGGHvWlGs iClGGiWHI LTKPFAWaRR AfVWSGEAYL SVSLgAlsvF GFiACCFVWF
GA WIcSVDNmED iIGGHiWIGt lcIfGGIWHI lTKPwaWARR AFVWSGEAYL SYSLGAIavA GfiACCfsWF
AC WivSVNNmED ivGGHiwvGl YciIGGlWHi ltKPfawavR gfvwSgEAYL sYSLvalslm gfiAavYsWY
RA WIvsVNNMED lIGGHiWIGv iCiaGGIWHI lTKPFaWARR AFVWSGEAYL SYSLgALslM GfiAaqyaWY
CY WivsVnnmED iiGGHIwigl icIsGGiWHi lTkPFgWarR AfiWsGEAYL SYSLGALSlM gfIAscfvWf
CON Wi-sV---ED --GGH-w-g- -ci-GgiwHi ltkP--Wa-R -f-wsgEAYL sYSL-al--- gfiA----Wf
211 280

center by Trebst (1986) together with the purification of a photochemically active PS II core complex by Nanba and Satoh (1987) firmly positioned the reaction center on the D1 and D2 proteins (Michel and Deisenhofer, 1988).

As proximal or core antenna pigment proteins CP47 and CP43 are able to absorb light directly and also to be coupled to three different classes of peripheral antenna systems. These are the phycobilisomes found in the cyanobacteria and red algae, the chlorophyll *a*/*c*-binding proteins that are characteristic of the brown algae, and the chlorophyll *a/b*-binding proteins of green algae and other plants (Chapter 2, Green and Gantt). In addition the composition of the lumenal proteins that form part of the protein environment of the catalytic site for water splitting are different in these taxa. All organisms that utilize chlorophyll *a/b*-binding proteins have the *psbO*, *psbP* and *psbQ* gene products while the remaining organisms have PsbO and two proteins encoded by *psbV* and *psbU* (Chapter 5). However, a further 24 kDa protein is associated with PS II in the red alga *Cyanidium caldarium* and has been shown to be related to PsbQ (Enami et al., 1998, 2000; Ohta et al., 2003). Similarly proteins with homology to PsbP and PsbQ are also encoded in cyanobacterial genomes and may be functionally associated with the OEC (Kashino et al., 2002; De Las Rivas et al., 2004; Thornton et al., 2004; Summerfield et al., 2005). Since CP47 and CP43 may have specific interactions with different antenna and lumenal proteins the consensus sequences for the different oxygenic photoautotrophs are compared in Figs. 1 and 2. In both proteins the largest variation is observed within chlorophyll *a*/*c*-containing organisms; however, inspection of all sequences in Figs. 1 and 2 reveals that considerable conservation is found. Frequently at positions where differences are observed the alternative residues present possess similar biochemical properties and a summary of the classes of amino acids found at these positions is provided in Bricker and Frankel (2002).

In early literature CP47 and CP43 are also referred to as CPa1 and CPa2 (Bricker 1990). They are also referred to as PsbB and PsbC, and occasionally PS II-B and PS II-C. Both proteins are absolutely required for water splitting and plastoquinone reduction by the photosystem. This chapter will survey the literature pertaining to the structure and function of these polypeptides with an emphasis on recent biochemical and mutagenesis studies directed at understanding the contributions these polypeptides make to PS II activity. The reader is also referred to additional reviews that provide in-depth information on these proteins (Bricker 1990; Barber et al., 2000; Bricker and Frankel, 2002).

Fig. 2 (opposite). Alignment of protein sequences for the chlorophyll *a*-binding protein CP43 (PsbC). Consensus sequences for: 54 green plants (GP); 6 green algae (GA); 5 chlorophyll *a*/*c*-containing organisms (AC); 4 red algae (RA), and 8 cyanobacteria (CY). Uppercase indicates amino acids conserved in all sequences: lowercase indicates the amino acids most frequently present. The positions of variable insertions or deletions are shown with the plus symbol (+). In the case of GP lowercase was only used at positions where more than one sequence carried a substitution. A majority consensus sequence at all positions is also shown (CON). The sequences for *Euglena gracilis* and *Prochlorothrix hollandica* were not incorporated. The domain structure of CP43 is indicated by the solid black line, with I to VI representing membrane-spanning domains and A to E hydrophilic interconnecting loops. The N- and C- termini are exposed to the stromal side of the membrane (or the cytosolic side in cyanobacteria) and loops A, C and E project into the lumenal compartment. The black arrow indicates a trypsin cleavage site which prevents reconstitution of the PsbO protein and inhibits O_2 evolution. *Synechocystis* sp. PCC 6803 possesses a one amino acid deletion at position 7 which must be taken into account when identifying the position of mutations from this organism. The calculated molecular mass of CP43 is ~50 kDa.

II. The *psbB* and *psbC* Genes

A. Operon Arrangement

In chloroplasts of land plants the *psbB* gene is present in the *psbB-psbT-psbH-petB-petD* operon and *psbC* is co-transcribed with *psbD*. The *psbB-psbT-psbH-petB-petD* operon is unusual in that it encodes proteins for both PS II and the cytochrome b_6f complex and is thus a model for the study of differential expression of genes coding for components of two complexes (Tanaka et al., 1987; Barkan 1988; Kohchi et al., 1988; Westhoff and Herrmann, 1988; Hird et al., 1991). In this operon genes are co-transcribed from a single prokaryotic-like promoter and then processed into oligocistronic and monocistronic mRNAs (Westhoff and Herrmann, 1988; Dixit et al., 1999). Additionally, the gene encoding PsbN is located on the complimentary strand between *psbT* and *psbH*.

In other photosynthetic eukaryotes this gene cluster, although present, is organized in varied arrangements (Keller et al., 1989; Johnson and Schmidt, 1993; Reith and Munholland, 1993; Hong et al., 1995); while in cyanobacteria *psbB* has been found by itself

or with *psbT* (Mayes and Barber, 1991; Kaneko et al., 1996). As a consequence, the pentacistronic operon found in land plants has been suggested to support the monophyletic origin of plastids (Douglas, 1994). Additionally, the *psbB* gene has been used in phylogenetic studies with cyanobacteria and plants (Urbach et al., 1998; Summerfield et al., 2001; Soltis et al., 2002).

Likewise, the *psbD-psbC* operon found in cyanobacteria and land plants also supports a monophyletic origin of plastids and variation in the *psbC* region has been used for phylogenetic studies (Douglas, 1994; Ziegenhagen and Fladung, 1997). The operon is found in plastids of rhodophytes and chromophytes but not in all green algae (Maid and Zetsche, 1992; Kowallick, 1993; Maul et al., 2002). In barley where the *psbD-psbC* operon is found as part of a complex region that includes *psbK*, *psbI*, *orf62* and *trnG*, expression results in multiple mRNAs of different sizes under the control of at least three different promoters (Sexton et al., 1990a,b; Christopher and Hoffer, 1998; Kim et al., 1999). In contrast, *psbC* is not co-transcribed with *psbD* in *Chlamydomonas reinhardtii* and translation control utilizes nuclear-encoded *cis*-elements interacting with sequences in the un-translated 5′ region of the *psbC* mRNA (Zerges et al., 1997, 2003). However, in cyanobacteria the translational start codon is upstream of the end of the *psbD* gene and evidence suggests that dicistronic and monocistronic mRNAs are obtained although monocistronic message for *psbC* has not been observed in all cases (Golden and Stearns, 1988; Carpenter et al., 1990; Gingrich et al., 1990; Yu and Vermaas, 1990). The CP43 sequences presented in Fig. 2 are based on the cyanobacterial start site.

B. Gene Deletions and Inactivation

Deletion or interruption of the *psbB* gene in cyanobacteria resulted in the virtual loss of the major PS II reaction center components from the thylakoid membranes giving rise to obligate photoheterotrophic strains (Vermaas et al., 1987, 1988; Eaton-Rye and Vermaas, 1991). However, the D1 protein has been detected in *psbB* deletion strains demonstrating that D1 can be present in thylakoid membranes that lack assembled PS II reaction centers (Vermaas et al., 1996; Clarke and Eaton-Rye, 2000).

Studies utilizing deletion, chemical, and site-directed mutagenesis of *psbC* also point to a role for CP43 in PS II assembly and the O_2-evolving process. Following nitrosoguanidine mutagenesis Dzelzkalns and Bogorad (l988) recovered a *Synechocystis* sp. PCC 6803 mutant containing a deletion within *psbC.* This mutant was unable to grow photoautotrophically or to evolve O_2. In experiments that identified GUG as the start codon in the *psbC* gene of *Synechocystis* sp. PCC 6803, Carpenter et al. (1990) constructed two mutations within the GUG start codon resulting in strains that lacked CP43 in thylakoid membranes and failed to grow photoautotrophically. Earlier Vermaas et al. (1988) produced a mutant in *Synechocystis* sp. PCC 6803 in which *psbC* had been inactivated; this strain was devoid of O_2-evolving activity and immunoblots demonstrated the absence of CP43, although the PS II core proteins D1, D2 and CP47 were present, albeit at significantly reduced amounts. Similar results were observed in four separate mutants in *Chlamydomonas reinhardtii* which failed to accumulate CP43 in their thylakoids due to impaired synthesis or stability of the *psbC* gene products (Rochaix et al., 1989). Rögner et al. (1991) constructed *Synechocystis* sp. PCC 6803 mutants where either the entire *psbD1-C* operon was deleted or a single base substitution was introduced into the *psbC* start codon. Photosystem II core complexes were isolated from both mutants, though they assembled to approximately 10% of the level found in wild type. However, these core complexes were able to carry out light-driven electron transfer from the redox-active tyrosine Y_z (Chapter 9) to the primary plastoquinone acceptor Q_A (Chapter 8). Thus, deletion or interruption of *psbC* produces mutants lacking CP43 but containing other core PS II proteins at reduced levels. These mutants demonstrated an ability to carry out limited light-driven electron transport but were unable to evolve O_2 or grow photoautotrophically.

III. Overview of Energy Transfer and Chlorophyll Binding

Biochemical studies with spinach preparations have identified approximately 15 bound chlorophyll *a* and 2–3 β-carotenes in both CP47 and CP43 (Barbato et al., 1991; Zheleva et al., 1998). Modeling of putative His ligands for chlorophyll in CP47 has been carried out for spinach in conjunction with an 8 Å map for the transmembrane regions of CP47 and CP43, derived from cryo-electron crystallography, and the homology between these proteins and the six

N-terminal helices of PsaA and PsaB of PS I (Rhee et al., 1997, 1998; Hankamer, et al., 1999; Barber et al., 1999; Chapter 18, Hankamer et al.). This work indicated that His-23, His-26, His-114, His-157 and His-216 in CP47 are potential chlorophyll ligands whereas the other His residues appeared to be too far from the remaining densities attributed to chlorophyll molecules (Barber et al., 2000). In addition since the number of chlorophylls exceeds the number of His residues in both CP47 and CP43 other amino acids are expected to serve in this role.

More precise information on the number and position of chlorophylls within CP47 and CP43 has been provided by the crystal structures obtained from *Thermosynechococcus elongatus* and *Thermosynechococcus vulcanus* at 3.8 and 3.7 Å, respectively (Zouni et al., 2001; Kamiya and Shen, 2003). An interesting observation to emerge from a comparison between these two cyanobacterial PS II structures is that an additional chlorophyll was observed in CP47 of *T. vulcanus* and CP43 both gained and lost a chlorophyll. This gave a total of 17 chlorophylls in CP47 and 13 in CP43; however, the electron densities of the additional chlorophylls in the *T. vulcanus* structure are weak and may not in fact represent porphyrins (J.-R. Shen, personal communication). This interpretation is supported by the more recent 3.5 Å X-ray structure from *T. elongatus* (Ferreira et al., 2004; PDB 1S5L). The data obtained by Ferreira et al. (2004) identified 16 and 14 chlorophylls bound to CP47 and CP43, respectively (Fig 3).

When examining CP47 and CP43 it is clear that the pigments are generally organized in two tiers near the stromal and lumenal sides of the membrane as previously observed in the corresponding core antenna region of PsaA and PsaB (Schubert et al., 1998; Barber et al., 2000; Vasil'ev et al., 2001; de Weerd et al., 2002a). A model based on the 3.8 Å structure of *T. elongatus* by Zouni et al. (2001) is consistent with energy transfer to the reaction center principally being through a chlorophyll on the stromal side of the membrane in both proteins (de Weerd et al., 2002a). Vasil'ev et al. (2001) had also reached a similar conclusion using a refinement of the *T. elongatus* structure that yielded two additional

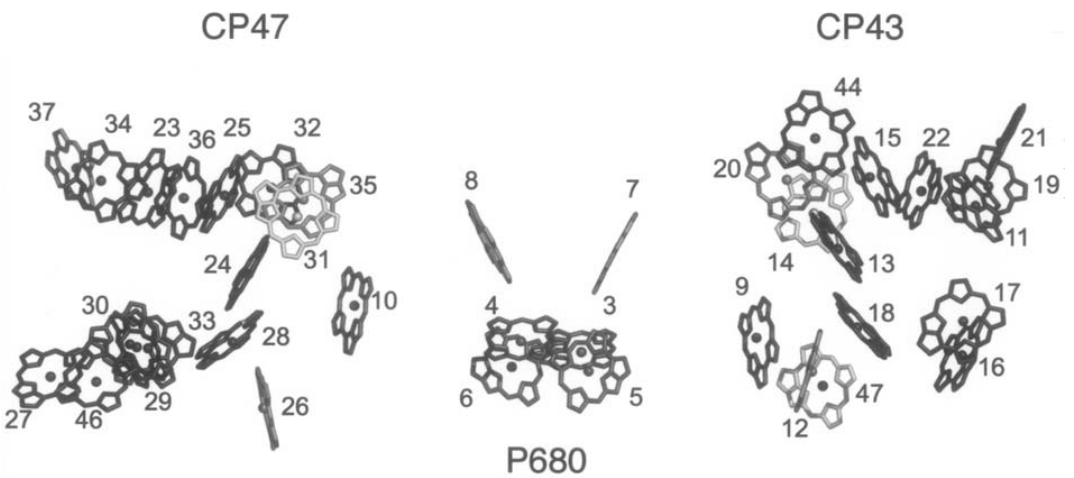

Fig. 3. Assignment of chlorophyll *a* molecules in the core antenna proteins of PS II. The porphyrin assignments shown are from the 3.5 Å data obtained for PS II crystals from *Thermosynechococcus elongatus* by Ferreira and co-workers (2004; PDB 1S5L). The view is perpendicular to the membrane normal. Porphyrin assignments 7 and 8 represent the pheophytins associated with D1 and D2, respectively. Chlorophylls 9 and 10 are the accessory chlorophylls of D1 and D2, respectively. The four chlorophylls comprising P680 are 3–6. The histidyl ligands for the antenna chlorophylls of CP47 and CP43 are summarized below with the corresponding chlorophyll shown in parentheses. CP47: His-9 (32); His-23 (25); His-26 (24); His-100 (30); His-114 (37); His-142 (34); His-157 (27); His-201 (33); His-202 (29); His-216 (23) His-455 (28); His-466 (31) and His-469 (35). CP43: His-41 (15); His-44 (13); His-106 (17); His-120 (21); His-152 (19); His-225 (16); His-239 (11); His-418 (18); His-429 (14) and His-432 (20). The His numbering is the same as that used in Figs. 1 and 2. Chlorophyll 44 in CP43 is ligated by Asn-39. For details on other putative non-histidyl ligands and the association of β-carotene molecules with CP47 and CP43, see Chapter 21.

chlorophylls in CP47, one on each side of the membrane, and a further chlorophyll on the stromal side of CP43. Using the numbering in Fig. 3, the putative chlorophylls most efficiently transferring energy to the reaction center are 31 in CP47 and 14 in CP43 with weaker contributions from chlorophylls 35 and 26 in CP47 and 12 and 20 in CP43 (Vasil'ev et al., 2001; Ferreira et al., 2004).

A conclusion reached from limited coupling between antenna and reaction center pigments is that the rate of energy transfer to the reaction center is slow when compared to the rate of charge separation. Moreover, a physical separation between chromophores with antenna and electron transfer functions appears to be a general property as this has also been observed in bacterial and PS I reaction centers (Visscher et al., 1989; Krauß et al., 1996; Hu et al., 1998; Vasil'ev et al., 2001). In contrast, excitation energy transfer within CP47 and CP43 is rapid with typically sub-picosecond transfer rates between pigments within a tier and rates between the stromal and lumenal pigments not exceeding a few picoseconds (Groot et al., 1999; Vasil'ev et al. 2001; de Weerd et al., 2002a).

The characteristic absorbance at 690 nm that is associated with CP47 arises from a single oscillator with the strength of approximately one chlorophyll oriented at a large angle with the plane of the thylakoid membrane (van Dorssen et al., 1987a,b; deWeerd et al., 2002a,b). Using the numbering of Ferreira et al. (2004) in Fig. 3, this species has been assigned to chlorophyll 37 by modeling and is located furthest from chlorophyll 31. Therefore, this would tend to slow down energy transfer to the reaction center, although at room temperature this effect is expected to be small (Vasil'ev et al., 2001; de Weerd et al., 2002b). However, the dimeric structure of PS II suggests that CP47-CP47 interactions may be important in the super-complex and therefore energy transfer between neighboring CP47 complexes may be possible utilizing an energy transfer pathway involving the long wavelength absorbing chlorophyll. In cyanobacteria a structural-based role for CP47 regarding the redistribution of excitation energy has been proposed in the light state-transition responsible for the balancing of absorbed excitation energy between the two photosystems. Assuming that the transfer of energy absorbed by chlorophyll is independent of that absorbed by the phycobilisomes, energy absorbed by chlorophyll could be transferred to PS I via the core antenna when the absorption cross section of PS I is increased. Although either of the proximal antenna proteins could fulfill this function, the presence of the 690 nm absorption favors CP47 in this role (McConnell et al., 2002).

A. Mutagenesis Studies of Putative Chlorophyll-Binding Ligands

Although CP47 and CP43 share <20% sequence identity, hydrophobicity plots of both proteins place 11 or 12 His residues in CP47 and 10 His residues in CP43 in membrane-spanning regions. As shown in Figs. 1 and 2, these residues are found on either side of the membrane and are typically spaced by 2, 13 or 14 amino acids (Vermaas et al., 1987; Bricker, 1990). Histidine imidazoles were initially identified as ligands to the central Mg^{2+} of bacteriochlorophyll in purple bacteria (Deisenhofer et al., 1985; Tronrud et al., 1986; McDermott et al., 1995) and light-harvesting complex II in plants (Kühlbrandt et al., 1994). These observations, taken together with the recognition that chlorophyll molecules were found in layers on either side of thylakoid membranes in light-harvesting complex II and the core antenna of PS I, resulted in the conserved His residues in CP47 and CP43 being investigated for a similar role in PS II (Eaton-Rye and Vermaas, 1992; Shen et al., 1993; Shen and Vermaas, 1994; Manna and Vermaas, 1997).

The initial experiments in both CP47 and CP43 replaced His with either Gln or Asn as residues that might provide axial ligands, while Tyr was chosen as it was not expected to coordinate the Mg^{2+} (Eaton-Rye and Vermaas, 1992; Shen et al., 1993; Shen and Vermaas, 1994; Manna and Vermaas, 1997). Interestingly, it has now been shown that Tyr coordinates a chlorophyll in PsaB, while the expectation that His residues serve as chlorophyll ligands in CP47 and CP43 was further strengthened by the fact that 65 chlorophylls out of 90 are coordinated by His imidazoles in the cyanobacterial PS I reaction center (Jordan et al., 2001).

1. Mutagenesis of Histidine Residues in CP47

The number of His residues in the first pair of helices in CP47 has been the subject of debate. There are five conserved His residues between the N-terminus and the start of loop B that connects helix II with helix III. In helix II the predicted folding models of CP47 place His-100 on the lumenal side of the

membrane and hence His-114 on the stromal side. In helix I hydropathy analyses position His-23 and 26 on the stromal or cytosolic side; however, the N-terminal hydrophilic domain of the protein contains a His residue at position 9, which if positioned in the membrane would retain the spacing of 14 residues and place His-23 and His-26 on the lumenal side. Vermaas (1993) was the first to point out that the charges on the surrounding amino acids would cancel in a helical domain and therefore charge would not be a constraint if His-9 was in the membrane-spanning domain. Experimentally His-9 has been substituted with Tyr in a PS I-minus/*apcE*-minus strain of *Synechocystis* sp. PCC 6803 which lacks both PS I and assembled phycobilisomes (Shen and Vermaas, 1994). The phenotype of the H9Y mutant (where His-9 has been mutated to Tyr) was similar to that observed for the H26Y strain with both mutants exhibiting an approximately 20% drop in active PS II centers. It should be noted that throughout this chapter the single letter amino acid code is used to identify mutants carrying amino acid substitutions.

The assignment of putative histidyl ligands to chlorophyll, based on the 3.5 Å PS II structure from *T. elongatus* (PDB 1S5L), is summarized in the legend of Fig. 3. At this resolution His-9 is the axial ligand to chlorophyll 32, His-23 to chlorophyll 25 and His-26 to chlorophyll 24. Chlorophyll 24 is located in the middle of the membrane and has been suggested to participate in energy transfer between the upper and lower tiers of antenna chlorophylls (Ferreira et al., 2004). Thus, although His-9 is a chlorophyll ligand, His-23 remains associated with the cytosolic side of the membrane.

Experimentally substituting Tyr at His-23, His-100 and His-114 produced mutants with impaired PS II assembly and reduced rates of O_2 evolution. Asparagine was introduced at these positions and significantly restored O_2 evolution suggesting that Asn was able to act as a chlorophyll ligand, thereby supporting the notion that these residues are involved in the coordination of the Mg^{2+} (Fig. 3). The most striking result in this series of mutagenesis experiments was obtained when His-100 and His-114 were replaced by Gln which is also known to act as a chlorophyll ligand (Kühlbrandt et al., 1994; Jordan et al., 2001). Uniquely, the H114Q mutant displayed a 2 or 3 nm blue shift of the 695 nm fluorescence emission. Based on this observation and modeling studies, His-114 has been proposed to be the ligand to the chlorophyll giving rise to the 690 nm absorption of the low-temperature trap in CP47 (Shen and Vermaas, 1994; Vasil'ev et al., 2001; de Weerd et al., 2002b). However, chlorophyll 24 has also been suggested as a candidate for the long-wavelength absorbing species in CP47 and chlorophyll 13 in CP43 has been suggested to have a similar role (Ferreira et al., 2004).

Tyrosine and Asn substitutions have also been introduced at the His residues in helices III and IV. The introduction of Tyr at His-157 and His-201 did not create severe restrictions on photoautotrophic growth and His-201 is in fact not conserved in all organisms although the alternative residue is Asn in each example. In contrast, the H202Y and H216Y mutants exhibited impaired O_2 evolution that was largely reversed in the H216N strain. Taken together the results from the substitutions at His residues in helices I-IV imply that putative pigment-protein interactions are not all functionally equivalent. However, double and triple mutants involving His residues in different helices as well as the within a single helix were generally additive (Shen et al., 1993; Shen and Vermaas, 1994).

Since a number of mutants exhibited impaired antenna function based on the light intensities required to saturate O_2 evolution, as well as altered fluorescence decay kinetics, the hypothesis was put forward that replacing His with Tyr may result in pheophytination of chlorophyll and impaired trapping and excitation energy transfer in such mutants (Shen et al., 1993; Shen and Vermaas, 1994; de Weerd et al., 2002b). This interpretation was supported by the 77 K fluorescence excitation spectra monitoring the 695 nm emission. In the His to Tyr mutants increases in the 413 nm and 531 nm absorption regions were observed which coincide with absorption maxima of pheophytin (Shen and Vermaas, 1994). Whether-or-not chlorophylls are converted to pheophytin via the loss of Mg^{2+} in these mutants or pheophytin is incorporated instead of a chlorophyll in the biogenesis of the complex is not known. Moreover, the possibility that certain mutants actually lose pigment binding cannot be discounted since there is a significant destabilization of PS II in the H23Y and H114Y mutants that is not observed in the H26Y, H157Y and H216Y strains.

There are no His residues in helix V; however, this does not preclude this transmembrane domain from a role in providing axial ligands for antenna pigments. In *T. elongatus* eight chlorophylls on PsaA are coordinated by Gln (2), the carbonyl backbone (1) and water (5) and ten chlorophylls on PsaB are

coordinated by Gln (1), Asp (1), Tyr (1) and water (7) (Jordan et al., 2001). To initially investigate the function of the three conserved His residues in helix VI each residue was replaced by Gln yielding the three mutants H455Q, H466Q and H469Q (Eaton-Rye and Vermaas, 1992). Both the H455Q and H466Q mutants assembled functional PS II centers at similar levels to the wild type. Subsequently, the additional mutants H455T, H455Y, and a double mutant F430L/H469Q were constructed that were not photoautotrophic (Wu et al., 1999). This series of experiments is consistent with His-455 and His-466 performing a role in chlorophyll binding and His-466 has been identified as the apparent ligand to chlorophyll 31, the putative species most efficiently transferring energy to the reaction center (Vasil'ev et al., 2001; Ferreira et al., 2004). At His-469 Gln was unable to replace His and the number of assembled PS II centers in the H469Q mutant fell to approximately 20% of the wild type, although the centers present retained the capacity for O_2 evolution (Eaton-Rye and Vermaas, 1992; Huang et al., 2001). These results suggest that His-469 may perform a role associated with the stability of PS II. Additionally, the introduction of Pro, Lys and Tyr residues at this position resulted in obligate photoheterotrophic strains and PS II centers did not assemble in these cells (Wu et al., 1999; Huang et al., 2001). Interestingly, an intergenic suppressor has been obtained that restores significant rates of O_2 evolution, photoautotrophic growth and assembly of PS II to these mutants. However, the gene responsible for the suppression has not yet been identified (Huang et al., 2001).

2. Mutagenesis of Histidine Residues in CP43

The investigation of His residues in CP43 has been less extensive. However, Gln and Tyr substitutions have been introduced at three positions from helices I and II that correspond to His-23, His-100 and His-114 in CP47. The resulting CP43 mutants: H105Q, H119Q and H119Y were photoautotrophic, whereas the strains H40Q, H40Y and H105Y were obligate photoheterotrophs (Manna and Vermaas, 1997). These experiments were conducted in *Synechocystis* sp. PCC 6803 which possesses a one amino acid deletion at position 7 when compared to plant sequences (see Fig. 2). The results obtained in the H105Q and H105Y cells are consistent with His-105 acting as a chlorophyll ligand. In this study His-119 was effectively substituted by Tyr as well as Gln. This residue corresponds to His-114 in CP47, which is the putative ligand for the low energy chlorophyll giving rise to the 690 nm absorption band, and suggests that these corresponding residues are not functional homologues. Ferreira et al. (2004) have assigned His-105 as the ligand for chlorophyll 17 and His-119 as the ligand for chlorophyll 21 (Fig. 3). However, of the three residues investigated substitutions at His-40, the putative ligand for chlorophyll 15, produced the most interesting results as the H40Q mutant was still able to evolve O_2 even though it was unable to support photoautotrophic growth. Surprisingly, this mutant exhibited impaired oxidation of Q_A^- by the secondary plastoquinone acceptor Q_B and showed increased charge recombination between Q_A^- and the donor side of PS II, suggesting an increased steady-state level of the oxidized primary donor $P680^+$ in this strain (Manna and Vermaas, 1997). The assignment of the histidyl ligands for the CP43 chlorophylls is summarized in the legend of Fig. 3.

IV. The Hydrophilic Domains of CP47 and CP43

Before the structural data demonstrated the arrangement of CP47 and CP43 in the thylakoid membrane, the topology had been established for CP43 by Sayre and Wrobel-Boerner (1994) who utilized antipeptide antibodies against the extrinsic loops A, C, D and E and the N- and C-termini. After limited trypsin hydrolysis and peptide mapping of thylakoid membranes, they concluded that CP43 contained six membrane-spanning helices, that the N- and C-termini were stromally exposed and that the extrinsic loops A, C and E were exposed to the lumen. This result supported the hypothesis for the domain organization of CP47 and CP43 based on an earlier analysis of hydropathy plots (Vermaas et al., 1987; Bricker, 1990).

The similarity between the chlorophyll *a*-binding proteins of PS I and PS II is most prominent in the membrane-spanning domains of the trimer-of-dimers motif whereas the hydrophilic domains connecting the transmembrane helices have diverged to reflect the specific roles these proteins play in the photosystems (Schubert et al., 1998; Barber et al., 1999). In PS II, hydrophilic and membrane-spanning domains of CP47 and CP43 as well as those of D1 and D2 are similar between plants, algae and cyanobacteria and the *psbA* gene from the higher plant *Poa annua*, encoding D1, has been successfully expressed in

the cyanobacterium *Synechocystis* sp. PCC 6803 resulting in fully functional PS II complexes (Nixon et al., 1991). However, the *psbB* and *psbC* genes from spinach cannot substitute for their cyanobacterial counterparts. To identify domains that could be exchanged between spinach and cyanobacterial core antenna proteins, Carpenter et al. (1993) generated chimeric spinach/cyanobacterial CP43 mutants in *Synechocystis* sp. PCC 6803 and found that an obligate photoheterotroph was produced when most of the *psbC* gene was of spinach origin. However, transformation with a plasmid containing the 3′, 50% of *psbC* from the cyanobacterium restored photoautotrophic growth to chimeric mutants. In contrast similar *psbB* chimeric strains indicated that only amino acid residues 97 to 229 of CP47 need be of cyanobacterial origin (Vermaas et al., 1996). This region includes loops B, C and part of loop D.

The available structural data for the arrangement of PS II super-complexes that contain both peripheral and core antenna proteins from green plants and cyanobacteria suggest the possibility that the extrinsic proteins of PS II, that are found associated with the lumenal face of the photosystem, may play a structural role. Thus, in addition to their ability to enhance O_2 evolution at physiological calcium and chloride concentrations, they may stabilize PS II in a manner that is specific to the structural constraints imposed by the different organization of the peripheral antenna proteins. Therefore, in addition to functionally important interactions between the core antenna proteins and different types of peripheral antenna systems, the lumenal domains of CP47 and CP43 may have specific protein-protein interactions in different types of photosynthetic organisms. The function of the hydrophilic domains has been investigated through oligonucleotide-directed mutagenesis studies in *Synechocystis* sp. PCC 6803 and by biochemical investigations that have been performed in large part using spinach.

A. Mutagenesis of Hydrophilic Domains of CP47 in Synechocystis sp. PCC 6803

Extensive mutagenesis studies, summarized in Fig. 4, have been directed at understanding the roles of the hydrophilic domains joining the membrane-spanning helices in CP47 and the C-terminal region. However, the system designed for introducing mutations into the first 95 amino acids has only been utilized in investigating the role of His-9, His-23 and His-26 as discussed above (Shen and Vermaas, 1994). In contrast loops, B-E and the C-terminus have been probed by the introduction of short deletions designed to create a map identifying important regions while circumventing the impracticality of mutating all of the residues found in these domains (Eaton-Rye and Vermaas, 1991; Haag et al., 1993; Morgan et al., 1998; Clarke and Eaton-Rye, 2000; Clarke et al., 2002).

Four strains were created with deletions in loop B that extends from Asp-119 to Lys-137. The mutants Δ(D119-L122) and Δ(D134-K137) (where this nomenclature indicates deletions from Asp-119 to Leu-122 and Asp-134 and Lys-137, respectively) were obligate photoheterotrophs and only appeared to have low-levels of assembled PS II centers. In contrast, strains carrying deletions in the middle of loop B remained photoautotrophic. Loop D spans helices IV and V (from Arg-220 to Thr-236) and it is noteworthy that the corresponding loops in PsaA and PsaB contain an extra helix that is absent in CP47. All deletions introduced into loop D produced obligate photoheterotrophic strains and it is possible that these mutants prevent the correct insertion of CP47 into the membrane (Clarke et al., 2002). Interestingly, all of the deletions that have been introduced into the C-terminal domain remain photoautotrophic. However, the Δ(S471-T473) mutant was found to have slowed rates of Q_A^- oxidation and thus exhibited a similar disruption of electron flow between Q_A and Q_B as observed in chimeric cyanobacterial/spinach CP47 strains (Vermaas et al., 1996). A further unexpected phenotype was the generation of protein adducts that were recognized by a D1-specific antibody (Clarke et al., 2002). In the 3.7 Å PS II structure from *T. vulcanus*, and the 3.5 Å structure from *T. elongatus*, the C-terminal amino acids in the vicinity of Arg-476 to Gly-481 of CP47 are close to Glu-226 to Gly-236 of the DE loop of the D1 protein. The current data suggests that deletions, particularly those closest to the C-terminus of CP47, can facilitate the formation of protein aggregates including D1 (Clarke et al., 2002). In addition, both PS II structures position residues at the N-terminus of CP47 in close proximity to this region of the DE loop although any functional significance of these putative protein-protein interactions requires experimental clarification.

Short deletions of between three and five amino acids have also been introduced into loop C by Clarke and Eaton-Rye (2000). Loop C in CP47 is approximately half the length observed for the corresponding domain in PsaA and PsaB and it

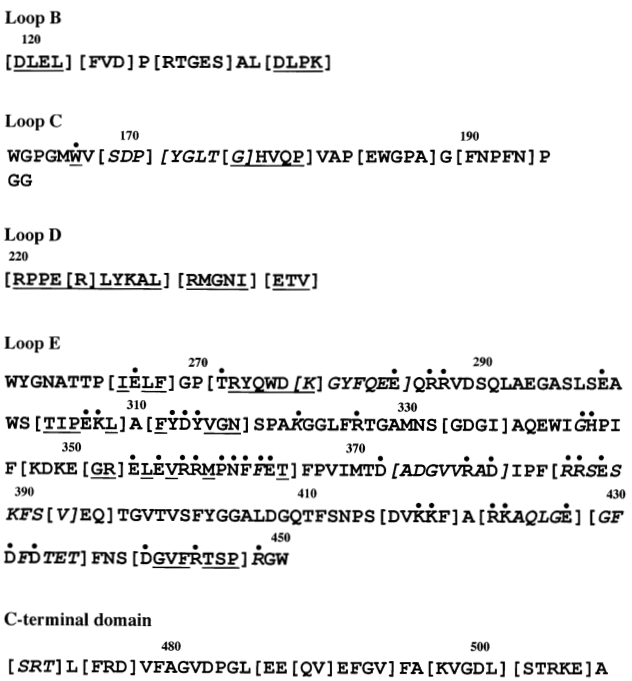

Fig. 4. Summary of mutations introduced into hydrophilic loops of CP47 in *Synechocystis* sp. PCC 6803. Deletions are indicated by square brackets and individual amino acids that have been mutated are indicated by a black dot above the residue. Deletions or point mutations creating strains that are unaffected or mildly affected are shown in normal font; moderately affected strains are shown in italics, and introduced mutations that resulted in obligate photoheterotrophic strains are underlined. The underlining or italic font for deletions containing point mutations have been modified to indicate the phenotype of the point mutations.

is 14 residues shorter than loop C in CP43. All of the deletions introduced into loop C resulted in a significant destabilization of PS II with the deletion between Gly-176 and Pro-180 producing an obligate photoheterotrophic strain and the deletions in the mutants Δ(S169-P171) and Δ(Y172-G176) reduced the level of PS II to <20% of that found in the control. The two remaining mutants, Δ(E184-A188) and Δ(F190-N194), were photoautotrophic even though the number of photosystems was reduced and they exhibited an increased susceptibility to photoinactivation. The Δ(E184-A188) strain was also unable to grow under chloride-limiting conditions, which suggests that loop C may contribute to the polypeptide structure that is required for chloride retention in the photosystem (Bricker and Frankel, 1998).

To explore the role of loop C within the lumenally exposed protein environment associated with the OEC, both the Δ(E184-A188) and Δ(F190-N194) strains were characterized in the absence of the PsbO, PsbU and PsbV proteins. In all cases PS II activity was further destabilized with the Δ(E184-A188) mutant being more impaired than the Δ(F190-N194) strain and the order of importance for the removal of the extrinsic proteins was found to be ΔPsbV ≥ ΔPsbO >ΔPsbU. In the available structural models of PS II the PsbV protein is in contact with loop E of CP43; therefore the sensitivity of CP47 mutants to the removal of PsbV cannot be explained in structural terms at the current resolution of the crystallographic data. In the case of loop C two mutants have also been introduced at Trp-167. The W167R strain was unable to grow photoautotrophically whereas the W167S cells exhibited a reduced rate of both photoautotrophic growth and O_2 evolution. Moreover, an enhanced rate of photoinactivation was observed in both mutants (Elanskaya et al., 1994; Wu et al., 1996).

The domain that clearly distinguishes both CP47 and CP43 from the additional chlorophyll-binding proteins that possess the trimer-of-dimers motif

is loop E (see Figs. 1 and 2). Loop E of CP47 is positioned such that a large portion is exposed directly to the lumenal compartment. The structural data indicate that this domain is not in direct contact with the D1 protein and is therefore not expected to provide any ligands to the Mn of the catalytic site (Kamiya and Shen, 2003; Ferreira et al., 2004). To probe for the function of this region fifteen scanning segment-deletions have been introduced; one of these, from Gly-351 to Thr-365, deleted 15 amino acids and it is likely that the obligate photoheterotrophic phenotype of the corresponding mutant resulted from a structural perturbation (Eaton-Rye and Vermaas, 1991). In Fig. 4 the remaining fourteen deletions are shown and these produced mutants carrying deletions of between 3 and 8 amino acids (Eaton-Rye and Vermaas, 1991; Haag et al., 1993; Morgan et al., 1998). Five of these resulted in obligate photoheterotrophic strains with impaired PS II assembly; however, this phenotype appeared to depend on the location of the deletion rather than the length. Deletions in the first 60 amino acids of the loop were not tolerated and the mutant Δ(D440-P447), carrying a deletion adjacent to the start of the last transmembrane domain, was also an obligate photoheterotroph (Haag et al., 1993). The deletions in loop E were originally designed to include Glu and Asp amino acids and the objective was to establish if specific residues within a deletion were responsible for the observed phenotypes. The charged residues within the deletions in the non-photoautotrophic strains were each subsequently investigated by Putnam-Evans et al. (1996a,b). In this work all strains obtained were found to be photoautotrophic and it was suggested that the phenotype of the original deletion strains arose from the structural perturbation introduced by the deletion (Putnam-Evans et al. 1996a; Bricker and Frankel, 2002).

Putnam-Evans et al. (1992, 1996b) also mutated all conserved charged residues between Glu-364 and Arg-444 in loop E. These experiments produced innocuous mutations at all positions except the basic residues Arg-384 and Arg-385. In Fig. 1 it can be seen that positive residues are conserved at these positions in all species examined. Amino acid substitutions at this location created mutants exhibiting a reduction in O_2-evolving capability, an alteration in the quantum yield for O_2 evolution, a slowing in the rise time of O_2 release during the $S_3 \rightarrow [S_4] \rightarrow S_0$ transition (for a discussion of the S-states, see Chapter 24) and an increase in the S_2 decay lifetime (Putnam-Evans and Bricker 1992; Putnam-Evans et al., 1996b). Relative to wild type, the severity of the phenotype following the introduction of mutations at these sites was: RR384,385EE > RR384,385GG > R384G > R385G. In addition, PsbO was found to exhibit weakened binding in the RR384,385EE and RR384,385GG strains which accelerated the $t_{1/2}$ for dark inactivation of PS II from 44 h in wild type to 9 h in the RR384,385EE mutant and an intermediate $t_{1/2}$ of 22 h in the RR384,385GG strain (Qian et al., 1997). In addition, deletion of the *psbO* gene in the RR384,385EE mutant was found to have little effect suggesting that the mutations in the RR384,385EE strain, and removal of the PsbO protein, affect similar parameters associated with the reaction mechanism for O_2 evolution and that Arg-384 and Arg-385 form one of the binding sites for the PsbO polypeptide (Bricker and Frankel, 2002).

Additional site-directed mutagenesis experiments targeting basic amino acids in loop E have revealed that mutations introduced at Lys-321 and Arg-448 alter the chloride-requirement for photoautotrophic growth (Putnam-Evans and Bricker, 1994, 1997). The K321G mutant failed to assemble PS II centers under chloride-limiting conditions and in normal BG-11 only 60% of PS II was present; additionally the rate of photoinactivation was increased three-fold when compared to wild type at high light intensities (Putnam-Evans and Bricker, 1997). Earlier, the mutant R448G had been shown to prevent the assembly of PS II under chloride-limiting conditions (Putnam-Evans and Bricker, 1994). Using a random mutagenesis approach the additional mutants R448K, R448Q, R448S and R448W were obtained and the strain R448D was subsequently produced (Wu et al., 1999; Bricker et al., 2001; Bricker and Frankel, 2002). Both the R448D and R448W mutants were obligate photoheterotrophs although R448Q cells exhibited higher rates of O_2 evolution than the R448K strain suggesting that charge was not the only factor governing the requirement for Arg at this position. Interestingly, when the R448S mutant was grown in normal BG-11 medium and then placed in chloride-limiting conditions, the O_2-evolving activity was lost at the same rate as wild type ($t_{½}$ = 16–17 min). However, when the chloride step down was reversed by the addition of 5 mM chloride, the recovery of O_2-evolving activity was retarded by approximately six-fold in the R448S strain when compared with the control. Bricker et al. (2001) therefore suggested that mutations at Arg-448 introduce a defect in the

low affinity, rapidly exchanging chloride-binding site described by Lindberg and Andreasson (1996). Additional details of strains carrying mutations at Arg-448 are discussed in Bricker and Frankel (2002).

B. Biochemical Studies Directed at Lumenal Domains of CP47

A well-established interaction exists between the PsbO protein and CP47 and this is also discussed in Chapter 5. An early series of experiments utilizing alkaline Tris-washed PS II membranes, obtained from spinach, induced a conformational change associated with loop E of CP47 (Bricker and Frankel, 1987). This treatment removed the PsbO, PsbP and PsbQ proteins along with all four of the manganese associated with the O_2-evolving site; this led to the exposure of an epitope between Pro-360 and Ser-391 that was recognized by FAC2, a specific monoclonal antibody (Bricker and Frankel, 1987; Frankel and Bricker, 1989). Also, in PS II membranes it has been shown that the C-terminal portion of loop E can be cross-linked to the N-terminal amino acids of PsbO by 1-ethyl-3-(3-dimethylaminopropyl)carbodiimide (EDC) (Bricker et al., 1988; Enami et al., 1991; Odom and Bricker, 1992). This reagent cross-links amino groups to carboxylic acids that are in van der Waals contact (Hackett and Strittmatter, 1984). Peptide mapping of the cross-linked complex obtained with EDC revealed that the domain between Glu-364 and Asp-440 was cross-linked to the first 76 amino acids of PsbO (Odom and Bricker, 1992).

Earlier it had been demonstrated that the reagent dithiobis(succinimidyl)propionate (DTSP) also cross-linked these two proteins and that this involved the region Lys-418 to Lys-438 on CP47 (Enami et al., 1987; Bricker et al., 1988; Queirolo, 1992; Bricker and Frankel, 2002). In complimentary studies it has been shown that the reagent N-hydrosuccinimidobiotin labels amino groups on CP47 when PsbO has been removed (Frankel and Bricker, 1990). Subsequent peptide-mapping studies identified two biotinylated domains: these were Lys-304 to Lys-321 and Lys-389 to Lys-419 in loop E from spinach CP47 (Frankel and Bricker, 1992). The PsbO protein also shields CP47 from proteolytic digestion by trypsin and lysoendopeptidase C (Bricker and Frankel, 1987; Hayashi et al., 1993). The experiments with lysoendopeptidase C also found that O_2-evolving activity and the ability of the PsbO protein to rebind to PS II decreased in parallel with the proteolytic cleavage at Lys-389 in loop E (Hayashi et al., 1993). These results therefore indicated that the region of loop E in the vicinity of Lys-389 was important for PsbO binding and O_2-evolving activity (Seidler, 1996). The results of the protein cross-linking experiments, biotinylation studies and peptidase studies are summarized in Fig. 1.

Post-translational modification of specific amino acids in the vicinity of the OEC has been reported that produced activated carbonyl groups capable of forming covalent adducts with amines (Ouellette et al., 1998; Anderson et al., 2000). Labeling of these groups has provided evidence for quinone cofactors located on D1, D2 and CP47. Since labeling did not occur in the presence of the PsbP and PsbQ proteins, and the absence of PsbO and manganese favored labeling, it has been suggested that the putative quinone cofactors are located in a sterically restricted domain. While it has been postulated that such modified amino acids associated with the O_2-evolving site of PS II could play a functional role in water splitting, the location of these cofactors has not yet been mapped on to any of the labeled proteins (Ouellette et al., 1998; Anderson et al., 2000). However, evidence for post-translational modification of Asp-348 in spinach CP47 resulting in the generation of an aspartyl aldehyde has been obtained (Anderson et al., 2004).

Loop A of CP47 has also been shown to cross-link to PsbO with EDC therefore indicating that Loop A is in van der Waals contact with a domain on PsbO (Ohta et al., 1995). These studies, using spinach PS II-enriched membranes, indicate that Asp-87 or Glu-94 in loop A interact with PsbO in the vicinity of Lys-60, Lys-66, Lys-76 and/or Lys-130. Intriguingly, the available PS II structural data supports this conclusion and further indicates that each PsbO protein in the dimer may bind to Loop E of one reaction center monomer and loops A and E of the opposite monomer. This therefore suggests that protein interactions between lumenal subunits of the two reaction centers of the dimeric PS II holoenzyme are important in optimizing the protein environment surrounding the site of water splitting.

C. The Removal of the Extrinsic Proteins in CP47 Mutants

The interpretation of the phenotypes observed in the segment-deletion mutants within hydrophilic domains of CP47 is difficult since it is hard to distinguish between a phenotype arising from the removal of an

important residue or a more indirect structural change (Putnam-Evans et al., 1996a; Bricker and Frankel, 2002). Functional complementation of the loop E obligate photoheterotrophic strain Δ(D440-P447) using combinatorial mutants found that restoration of the wild-type length was sufficient to support photoautotrophic growth while none of the amino acid residues within the deletion were indispensable (Tichy and Vermaas, 1998). Several of the photoautotrophic strains obtained by these authors however did exhibit an altered chloride requirement and therefore residues between Asp-440 and Pro-447 appear to play a similar role in chloride binding as ascribed to the Arg-448 mutants examined by Bricker et al. (2001).

A different approach was taken by Morgan et al. (1998) who selected two loop E deletion mutants that had remained photoautotrophic. These deletions were chosen to act as probes for the effect of the removal PsbO, PsbV or PsbU on otherwise innocuous mutations within loop E. These studies targeted both the domain between Glu-364 and Asp-440 that had been shown to cross-link to N-terminus of PsbO (Odom and Bricker, 1992) and the epitope recognized by FAC2 (Bricker and Frankel, 1987; Frankel and Bricker, 1989). The two deletion mutants selected were Δ(R384-V392) which is located within the FAC2 epitope and Δ(G429-T436), which is at the C-terminal end of the loop E domain that cross-links to the N-terminus of PsbO.

The removal of PsbO, PsbU or PsbV in the Δ(G429-T436) strain resulted in <20% of PS II centers assembling and none of these mutants remained photoautotrophic. Thus, removal of the extrinsic proteins had an additional effect to that introduced by deletion of Gly-429 to Thr-436. In contrast, the Δ(R384-V392):ΔPsbO and Δ(R384-V392):ΔPsbU strains remained photoautotrophic and thus behaved in a similar fashion to the RR384,385EE mutant indicating that removal of PsbO has a similar effect on O_2 evolution to the creation of the RR384,385EE and Δ(R384-V392) strains (Eaton-Rye and Vermaas, 1991; Putnam-Evan et al., 1996b; Morgan et al., 1998). It has also been shown that the Δ(A373-D380) mutant as well as the Δ(R384-V392), RR384,385EE and RR384,385GG strains all exhibit weakened binding of PsbO (Gleiter et al., 1994; Qian et al., 1997). Interestingly, the Δ(R384-V392):ΔPsbV mutant assembled approximately 37% of the control level of PS II centers but these were inactive and the strain was an obligate photoheterotroph (Morgan et al., 1998). Thus, although PsbV is associated with loop E of CP43, it appears to play an important role in stabilizing PS II in both the Δ(R384-V392) and Δ(G429-T436) mutants; in these examples it is possible that PsbV confers stabilization through PsbU as this protein is seen to be in contact with PsbO and PsbV in the 3.7 Å, and 3.5 Å, resolution structures (Kamiya and Shen, 2003; Ferreira et al., 2004).

It has also been shown that removal of PsbO in wild type and the RR384,385EE mutant increases the quantum yield of photoactivation in hydroxylamine-treated PS II (Burnap et al., 1996; Qian et al., 1997). In contrast, the quantum yield of photoactivation in the Δ(R384-V392) mutant as well as the Δ(A373-D380) strain was considerably reduced when compared to wild type (Gleiter et al., 1995; Morgan et al., 1998). While the experimental conditions in these studies are not directly comparable, the results suggest that other residues in the vicinity of Ala-373 to Val-392, or other residues perturbed as a result of the two deletions influence the photoactivation process. An in-depth discussion of this point is provided in Bricker and Frankel (2002).

As discussed earlier (Section IV.A.), the introduction of mutations at conserved charged amino acids between Glu-364 and Asp-440 demonstrated that only substitutions at Arg-384 and Arg-385 in *Synechocystis* sp. PCC 6803 produced impaired phenotypes. In contrast when otherwise innocuous mutations at Glu-364 were investigated in the absence of the extrinsic proteins unexpected results were obtained. The mutants E364G:ΔPsbV and E364Q:ΔPsbV were not photoautotrophic and assembled less than 20% of the wild-type level of PS II; however, the phenotypes of the E364G and E364Q strains were both similar to wild type (Morgan et al., 1998). In contrast, mutants at Asp-431 and Asp-433 lacking PsbV were found to have phenotypes similar to the photoautotrophic ΔPsbV control strain even though charged residues at these positions are highly conserved (Eaton-Rye and Shand, 2001). Therefore, Glu-364 appears to play an important role in the assembly or operation of PS II that is unmasked upon removal of PsbV. It is therefore interesting that Ferreira et al. (2004) have identified the adjacent Phe-362 and Phe-363 residues as part of a conserved motif (FFESFPVIL in *T. elongatus* (Fig. 1)) from which Phe-362 and Phe-363 contribute to the hydrophobic environment in the vicinity of the redox active Y_D from the D2 protein. This location corresponds to the equivalent position of the metal cluster of the OEC on D1 (Chapter 9).

An equally intriguing observation has been

the discovery that the E364Q:ΔPsbV, Δ(R384-V392):ΔPsbV and Δ(R384-V392):ΔPsbO:ΔPsbU strains are all unable to grow photoautotrophically in BG-11 media at pH 7.5 but have their photoautotrophic growth restored when grown at pH 10.0 (Eaton-Rye et al., 2003). In contrast, the F363R, Δ(G429-T436) and Δ(E184-A188) mutants, which exhibit photoautotrophic growth, albeit with an altered requirement for chloride, become obligate photoheterotrophs upon removal of PsbV at both pH 7.5 and pH 10.0 (Clarke and Eaton-Rye, 1999, 2000; Eaton-Rye et al., 2003). The specificity of this pH dependence points to a mechanism for the acclimation of PS II activity in response to the external pH that may provide novel information on the operation of PS II during environmental conditions that result in pH variation.

D. Mutagenesis of Loop E in CP43 in Synechocystis sp. PCC 6803

Mutagenesis techniques have also been utilized to study the role of the large extrinsic loop E of CP43 in PS II assembly and function. Kuhn and Vermaas (1993) produced a set of eight deletion mutants in *Synechocystis* sp. PCC 6803 in which 7–11 codons were deleted within the region of *psbC* encoding loop E. The deleted segments spanned Gln-298 to Ala-386, which comprise approximately 70% of this domain and are shown in Fig. 5. Significantly, all deletion mutants failed to grow photoautotrophically and none exhibited detectable O_2-evolving activity. This result is striking in comparison to the similar experiments with *psbB* in which only a subset of the deletions produced in loop E of CP47 resulted in strains that exhibited impaired photoautotrophic growth or PS II activity (Eaton-Rye and Vermaas, 1991; Haag et al., 1993; Morgan et al., 1998). The presence of CP43 in the thylakoids of these mutants ranged from almost wild-type levels in one strain to no detectable CP43 in several mutants. The levels of the other PS II core proteins D1, D2 and CP47 were also decreased in all mutants, with the effect being most pronounced for D2. These observations were similar to those seen in mutants in which the entire *psbC* gene had been deleted or inactivated. Only one of the eight deletion strains assembled any functional centers as assessed by PS II-specific herbicide-binding studies employing [^{14}C]-diuron. Additionally, fluorescence emission spectra supported the lack of functional assembly of the PS II complex.

Given the severe phenotype of the deletion mutants, site-directed mutagenesis was used to alter specific amino acid residues within loop E of CP43 in an effort to identify residues that are critical for PS II function and that may interact directly with the O_2-evolving site. The numbering of residues in CP43 is problematic beyond the discrepancy introduced by the deletion of a single amino acid in the *Synechocystis* sp. PCC 6803 sequence. The original proposal for the start codon by Alt et al. (1984) was 36 bases up-stream of the subsequently identified position in cyanobacteria (Chisholm and Williams, 1988; Golden and Stearns, 1988; Carpenter et al., 1990). The N-terminus of the protein has also been shown to undergo post-translational modifications including an endoproteolytic cleavage between Glu-2 and Thr-3 (Ikeuchi et al., 1987; Michel et al., 1988). Therefore, in certain cases Thr-3 in Fig. 2 is regarded as the start of the protein (e.g., Knoepfle et al., 1999; Barber et al., 2000). In the following discussion the numbering in the original papers is given together with identification of the equivalent residues in Figs. 2 and 5.

Five amino acid substitutions within the large extrinsic loop in *Synechocystis* sp. PCC 6803 have been constructed that show defects associated with the OEC. Mutagenesis of Arg-305 and Arg-342 to Ser resulted in mutants showing impaired PS II activity (Knoepfle et al., 1999). The R305S mutant (see Arg-307 in Fig. 5) grew photoautotrophically

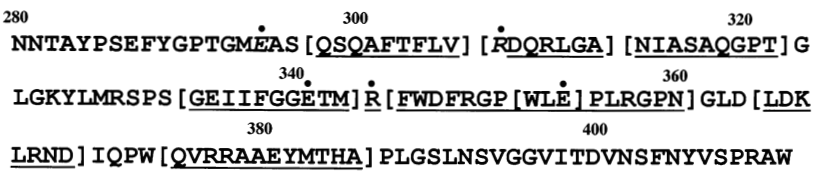

Fig. 5. Summary of mutations introduced into loop E of CP43 in *Synechocystis* sp. PCC 6803. Deletions or point mutations creating strains that are unaffected or mildly affected are shown in normal font; moderately affected strains are shown in italics, and introduced mutations that resulted in obligate photoheterotrophic strains are underlined.

and accumulated normal quantities of CP43, D1, CP47 and the PsbO protein but it evolved O_2 to only 70% of control rates at saturating light intensities. In agreement, chlorophyll fluorescence yield measurements indicated that this mutant assembled approximately 70% of the PS II centers found in the control strain. The R342S mutant (see Arg-344 in Fig. 5) failed to grow photoautotrophically and exhibited no capacity for O_2 evolution, except when grown photoheterotrophically in media containing both glucose and diuron. Under these conditions O_2-evolving activity was observed in the R342S mutant at a level of approximately 10% of the control rate. The apparent protective effect of diuron may have resulted from a reduction of damaging oxidizing-side radicals in the presence of this PS II inhibitor (Chu et al., 1995; Wu et al., 1996). Isolated thylakoid membranes from this mutant also accumulated normal amounts of PS II core proteins. Variable chlorophyll fluorescence yield measurements for the R342S mutant, however, indicated that it assembled a severely reduced number of PS II centers able to oxidize water, and these centers showed an extreme sensitivity to photoinactivation. Both strains exhibited an increase (2.5- and 8-fold for R305S and R342S, respectively) in fluorescence rise times using water as an electron donor, indicative of a slowing of electron transport from the OEC to Y_z. These data confirmed that the R305S and R342S mutations each produced a defect associated with the OEC of PS II. The R305S mutant additionally showed further impairment of PS II activity when grown in chloride-depleted media. This effect may be explained in part by the loss of PsbV (Section IV.E.3).

Based on the PS II minus phenotype of the R342S mutant (numbering system used by Knoepfle et al., 1999) and the fact that CP43 is in contact with D1, Arg-342 has been proposed as a potential ligand to the manganese cluster (Debus, 2000). Earlier work (Enami et al., 1997) showed that this residue, corresponding to Arg-345 in Fig. 2, was cleaved by trypsin in the absence of PsbO and thus was presumed to be at or near a binding site for the PsbO protein (Section IV.E.2). However, the R342S mutant is more severely impaired than mutants lacking PsbO, and thus the phenotype of this mutant could not be explained by an alteration in PsbO binding alone. The recent structural model for PS II provided by Ferreira et al. (2004) indicates that the OEC contains a cubane Mn_3CaO_4 cluster linked to a fourth Mn by a mono-μ-oxo bridge and at 3.5 Å resolution the putative ligands for the cluster have been assigned (Chapter 21). Significantly, Arg-345 (Fig. 2) is associated with a non-protein ligand to the fourth Mn ion and is suggested to form a hydrogen bond to the substrate water during the reaction cycle. Therefore, the results obtained with the R342S mutant (Knoepfle et al., 1999) provide experimental support for the direct participation of CP43 in water splitting.

Rosenberg et al. (1999) constructed three mutants in *Synechocystis* sp. PCC 6803 where Glu residues in the large extrinsic loop were altered to Gln. The E293Q strain (see Glu-295 in Fig. 5) exhibited normal photoautotrophic growth and accumulated normal quantities of the CP43, CP47, D1 and PsbO proteins. However, this mutant evolved O_2 to only 56% of control rates at saturating light intensities and variable chlorophyll fluorescence yield measurements indicated that this strain assembled approximately 60% of the functional PS II centers found in the control. The E339Q mutant (see Glu-341 in Fig. 5) grew photoautotrophically but at a severely reduced rate. Both immunological analysis and variable chlorophyll fluorescence yield experiments indicated that the E339Q strain assembled a normal complement of PS II centers. However, less than one-half of the centers could support electron transfer from water to Q_A and the mutant evolved O_2 at 20% of the rate found in the control. Both E293Q and E339Q strains exhibited an increased sensitivity to photoinactivation. These results show that the mutations in the E293Q and E339Q cells also produced defects associated with the OEC. Moreover, the model by Ferriera et al. (2004), based on their 3.5 Å X-ray crystal structure shows that Glu-354 of CP43 ligates the third Mn in the cubane cluster (this is Glu-339 in the numbering system of Rosenberg et al. (1999) and Glu-341 in Fig. 5; the numbering given for this residue in Ferriera et al. (2004) assumes the Met start of CP43 to be 12 residues up-stream of the start shown in Fig. 2). Thus, two residues within the CP43 large extrinsic loop, Glu-341 and Arg-344 in Fig. 5, appear to be involved in water splitting.

The E352Q mutant (see Glu-354 in Fig. 5) exhibited the most severe phenotype of all mutants constructed. This mutant failed to grow photoautotrophically and exhibited no capacity for O_2 evolution under any conditions. Measurements of the variable chlorophyll fluorescence yield indicated that this mutant assembled no functional PS II centers. Immunological analysis of isolated thylakoid membranes from the E352Q strain revealed a complete absence of any detectable CP43 and reduced levels of both the D1

and PsbO proteins. The Glu to Gln mutation in the E352Q strain appears to affect the stability of the PS II complex.

There is little information on the role, structurally or otherwise, of the lumenally exposed loops A and C in CP43. The *Synechocystis* sp. PCC 6803 mutant characterized by Dzelzkalns and Bogorad (l988), which lacked any PS II activity, was found to result from a deletion in *psbC* that corresponds to a deletion of amino acids 190–257 in Fig. 2. Loop C approximately spans amino acids 171–220, and thus more than half of Loop C is missing in this mutant together with all of transmembrane helix IV and all but three amino acids of loop D which is located on the cytosolic side. Therefore, it is likely that the phenotype of this mutant resulted from a gross perturbation of the native structure.

E. Interaction of CP43 with Other Photosystem II Subunits

1. Interaction of CP43 with D1

Given the intimate association of CP43 and D1 now confirmed by X-ray crystallography (Zouni et al., 2000; Kamiya and Shen, 2003; Ferreira et al., 2004; Chapters 19–21), there is little information based on biochemical studies that demonstrates a direct interaction of these two proteins. Mori and Yamamoto (1992) showed that D1, CP43 and CP47 were lost during Tris-treatment under low-light illumination (20 μmol photons · m^{-2} sec^{-1}) in spinach PS II membranes. They speculated that this loss was a consequence of donor-side photoinhibition, since it could be prevented by the addition of exogenous electron donors to PS II. No degradation products of either D1 or CP43 were directly observed. In an expanded study, this same loss of D1, CP43 and CP47 was observed both in PS II membranes and in isolated PS II complexes subjected to the same treatment (Mori et al., 1995). In both preparations high molecular mass polypeptides were detected by SDS/urea PAGE and immunoblotting, and these cross-reacted with antibodies against D1 and antibodies generated against either CP43 or CP47. Thus, the loss of CP43 could partially be attributed to the formation of a cross-linked product between CP43 and D1 (Mori et al., 1995). Similar results were obtained with Tris-treated PS II membranes subjected to illumination at very high light intensities (5000 μmol photons · m^{-2} sec^{-1}) (Yamamoto and Akasaka, 1995). In these experiments three degradation products of CP43 were observed, as well as high molecular weight cross-linked products containing D1. In reconstitution experiments, the presence of the PsbO protein appeared to inhibit both the degradation of CP43 and the appearance of cross-linked products. This suggests that a lumenal domain on CP43 forms at least one site susceptible to proteolytic attack. Currently, the exact sites of cross-linking between CP43 and D1 are unknown.

Given the well-known role of D1 in turnover of the photosystem under photoinhibitory conditions (reviewed in Yamamoto, 2001; Chapter 27, Chow and Aro), the above data also infer a role for CP43 in this process by virtue of its close association with D1. Early work indicated that D1 turnover during photoinhibition occurred via proteolytic degradation (Aro et al., 1990; Virgin et al., 1990). Studies using various classes of protease inhibitors demonstrated that a serine-type protease was responsible for the turnover of D1 (Virgin et al., 1991; Virgin et al., 1992) and that this protease was tightly associated with the PS II complex (Virgin et al., 1990; Aro et al., 1993). Some evidence points to CP43 acting as a serine protease capable of degrading D1 during photoinhibition (Giacometti et al., 1992; Salter et al., 1992). Using spinach PS II core preparations, Salter et al. (1992) demonstrated that CP43 could be covalently labeled with the serine protease inhibitor [^{14}C]-diisopropyl fluorophosphate. Photoinactivation-induced cleavage of D1, which occurred in the region between transmembrane helices D and E on a stroma-exposed site, was inhibited by this labeling of CP43. The radiolabeled serine in CP43 was not identified; however, since cleavage of D1 occurs in the exposed region, the labeled serine by necessity has to occur on the stromal surface of CP43.

Degradation of D1 and D2 under photoinhibitory conditions has been reported in isolated PS II reaction center complexes containing D1, D2, the α and β subunits of cytochrome b_{559}, and the *psbI* gene product, but lacking CP43 (Shipton and Barber, 1991). It was suggested that degradation of D1 occurs through an autoproteolytic mechanism. This argues against CP43 acting as a serine protease. However, the presence of contaminating amounts of CP43 or some other protease was not addressed. Additionally, Virgin et al. (1991) showed that only 60% inhibition of D1 degradation occurred in the presence of diisopropylfluorophosphate suggesting that other proteases and/or mechanisms appear to exist that are

involved in the process of D1 turnover (reviewed in Yamamoto, 2001).

2. Interaction of CP43 with PsbO

Early biochemical evidence by Isogai et al. (1985) supported the hypothesis that the lumen-exposed loops of CP43 provided sites of interaction between CP43 and components of the OEC. These authors showed that CP43 could be cleaved by trypsin in spinach PS II membranes following removal of the PsbO protein by washing with $CaCl_2$. The extent of degradation of CP43 was directly correlated with the extent of removal of PsbO and the authors concluded that these data demonstrated a direct interaction between PsbO and CP43. However, the exact site(s) of cleavage within CP43 were not identified. Enami et al. (1997) mapped the trypsin cleavage sites and showed that Arg-26 (Arg-14 in Fig. 2), located on the stromal side of the membrane, was cleaved in NaCl-washed spinach PS II membranes that lack the PsbP and PsbQ extrinsic proteins. However, upon removal of PsbO two additional residues, Arg-357 (Arg-345 in Fig.2) and Lys-457 (Lys-445 in Fig.2), were cleaved. One of these residues, Arg-357, lies within the large extrinsic loop E. In addition to cleavage of CP43, cleavage at Arg-59 of the α-subunit of cytochrome b_{559} was also observed. In reconstitution experiments the ability of PsbO to rebind to trypsinized $CaCl_2$-washed membranes decreased with increasing trypsin concentration; indicating that either a domain around Arg-357, within loop E, and/or a domain close to Arg-59 in cytochrome b_{559}, was required for binding. It should be noted that the fragment Gly-458 to Asn-473 (corresponding to Gly-446 to the C-terminus in Fig. 2), is found in the stroma and is therefore highly unlikely to be involved in the binding of PsbO. The authors speculated that removal of PsbO causes a conformational change within CP43 that allows Lys-457 to be accessible to trypsin. These data collectively indicate that PsbO is closely associated with CP43. These results are also consistent with the current structural models of PS II in which CP43 appears to be in contact with the PsbO, PsbU and PsbV proteins.

3. Interaction of CP43 with PsbV

The mutation in the R305S strain (that corresponds to a mutation at Arg-307 in Fig. 5) was introduced into the large extrinsic loop of CP43 from *Synechocystis* sp. PCC 6803 and resulted in a strain that grew photoautotrophically and exhibited approximately 70% of the O_2-evolving activity of wild type (Knoepfle et al., 1999). However, PS II activity in this mutant was dramatically decreased when it was grown in media depleted of chloride (Young et al., 2002; Section IV.D). Under chloride-limiting conditions, this mutant failed to grow photoautotrophically and it evolved O_2 to only approximately 20% of the control. The mutant also showed an enhanced susceptibility to photoinactivation. Additionally, stabilization of the S_2 state of the OEC was observed for the mutant under chloride-limiting conditions.

The observed phenotype of this mutant is similar to that observed when *psbV*, the gene encoding cytochrome c_{550}, has been deleted (Shen et al., 1995a,b). The *psbV* deletion mutant does not grow photoautotrophically under chloride-limiting conditions (or, for that matter, under calcium-limiting conditions), and exhibits an enhanced susceptibility to photoinactivation and a stabilization of the S_2 state (Morgan et al., 1998; Shen et al., 1998). To study the possible effects of the mutation on PS II assembly, the PS II complexes of both mutant and control strains grown in chloride-depleted media were isolated utilizing a six-residue His-tag located on the 3′ terminus of the CP47 protein (Bricker et al., 1998, 2002). Immunoblots of the isolated PS II core particles demonstrated that for control and R305S cells there was no detectable loss of the CP43, CP47, D1 and PsbO proteins. The PS II particles were also probed for the presence of PsbV. Reduced minus oxidized difference spectra of control PS II particles showed an asymmetric peak with a maximum absorbance at 559 nm and a pronounced shoulder at about 550 nm. These peaks arise from cytochrome b_{559} and PsbV, respectively (Kashino et al., 2002). The PS II particles from the R305S mutant, however, showed a highly symmetrical peak with no apparent shoulder at 550 nm and an absorption maximum of 559.5 nm, indicating that the particles contained little or no PsbV. Staining of cytochromes using a chemiluminescent substrate showed no detectable PsbV present in the PS II particle preparation; however, PsbV was present in whole cell extracts from the mutant at levels comparable to those observed for the control, indicating that the protein was synthesized but failed to be incorporated into the PS II complex. Thus, it appears that replacement of Arg-305 (Arg-307 in Fig. 5) by Ser prevents the strong association of PsbV with PS II indicating this residue may form part of the

binding domain. Inspection of the 3.5 Å structure from *T. elongatus* suggests that Arg-307 in Fig. 5 may form a hydrogen bond with Asn-49 from PsbV. Interestingly, an Asp to Asn mutation at the adjacent residue in *Synechocystis* sp. PCC 6803 also results in a mutant showing an altered dependency on chloride (C. Putnam-Evans, unpublished).

F. Covalent Modifications of Hydrophilic Domains of CP43

Anderson et al. (2002) used tandem mass spectrometry to map post-translational modifications occurring in the large extrinsic loop of CP43. Specifically, these modifications were mapped to a conserved peptide, APWLEPLR within the large extrinsic loop between Ala-351 and Arg-358 in Fig. 2. Within this peptide, the indole side chain of Trp-353 was shown to be post-translationally modified such that it exhibited mass shifts of +4, +16 and +18. The +4 modification was identified as kynurenine, and the +16 and +18 modifications were identified as oxindolylalanine and hydroxyindole derivatives, respectively. Kynurenine and the oxindolylalanine derivatives have been reported in other proteins; however, the hydroxyindole modification appears to be unique. The authors speculated that these modifications are caused by reactive oxygen species generated during the catalytic cycle and/or under conditions in which normal PS II function has been disrupted. Since both the modified and unmodified peptides were observed, indicating a transient accumulation, these modifications may act as a signal for turnover of the photosystem.

The stromally exposed N-terminus of CP43 is also post-translationally modified. N-terminal sequence data for spinach CP43 shows that the first residue of the mature protein is N-acetyl-phosphothreonine (Michel et al., l988; Vener et al., 2001). The two N-terminal residues of the primary translation product (Met and Glu) are removed post-translationally and Thr at position 3 is both acetylated and phosphorylated. This phosphorylated Thr is oriented to the stromal side of the thylakoid (Michel et al., l988). The cyanobacterial *psbC* gene encodes a protein in which a Thr residue located at position 3 is also conserved (Chisholm and Williams, l988). However, phosphorylation of CP43 has not been demonstrated in cyanobacteria. In higher plants, light activates the reversible, redox-dependent phosphorylation of many thylakoid proteins including the PS II proteins D1, D2, PsbH, and CP43 (Vener et al., 1998). Reversible phosphorylation of PS II proteins plays a role in the control of PS II turnover, though the exact role of phospho-CP43 is not clear. In both spinach and *Arabidopsis*, PS II proteins (including CP43) have been shown to undergo rapid dephosphorylation in response to certain stress conditions, such as elevated temperature or high light irradiance (Elich et al., 1993; Rokka et al., 2000; Vener et al., 2001). In spinach, this dephosphorylation is catalyzed by a thylakoid phosphatase that is activated by the heat-induced release of a membrane associated peptidyl-prolyl cis-trans isomerase, TLP40 (Rokka et al., 2000). The TLP40 polypeptide acts as a regulatory subunit of the phosphatase. During turnover of the photosystem, it is known that the D1 protein is not subject to proteolysis until dephosphorylated. Whether or not this is also true for CP43 and the other phosphorylated PS II proteins is unclear.

V. Conclusions

Both CP47 and CP43 represent single gene products with multiple functions within PS II. The presence of the six-helix trimer-of-dimers motif is evidence for their evolution from an ancestral reaction center and modification of their hydrophilic domains, particularly their respective large lumenal domains connecting helices V and VI, is related to establishing the protein environment required for the assembly and function of the catalytic site for water splitting. The available data also point to critical roles for these proteins in the assembly and turnover of the photosystem. As structural studies refine the current model for PS II the rational design of experiments to identify essential protein-protein and protein-cofactor interactions will progress. The past twenty years has witnessed considerable progress and frequently unexpected developments regarding the roles of both of these core antenna polypeptides. The identification of the 695 nm fluorescence emission with CP47 led to a proposal that this subunit contained the PS II reaction center and isolated reaction center cores lacking CP43 have resulted in complexes able to evolve O_2 (Büchel et al., 1999). However, O_2 evolution from these CP43-less photosystems was not shown to exhibit the classical period-of-four O_2 release associated with the S-states of PS II (Bricker and Frankel, 2002). In contrast, the current images of PS II reveal the proximity of CP43 to D1 and indicate that loop E of CP43 participates in ligation of the Mn cluster at the active site. As is the

case with other areas of PS II research the impending development of a high-resolution structure of PS II holds the key for a rapid advance in understanding the biology and function of CP47 and CP43 and a full appreciation of their essential roles in oxygenic photosynthesis.

Acknowledgments

Support for the preparation of this chapter was provided by a grant from the New Zealand Marsden Fund (UOO309) to JJE-R and a National Science Foundation grant (MCB-9982981) to CP-E The authors thank Bronwyn Carlisle for the preparation of Fig. 3 and Dr Tina Summerfield for a critical reading of the text.

References

Alt J, Morris J, Westhoff P and Herrman RG (1984) Nucleotide sequence of the clustered genes for the 44 kd chlorophyll *a* apoprotein and the '32 kd'-like protein of the Photosystem II reaction center in the spinach plastid chromosome. Curr Genet 8: 597–606

Amesz J (1995) The antenna-reaction center complex of heliobacteria. In: Blankenship RE, Madigan MT and Bauer CE (eds) Anoxygenic Photosynthetic Bacteria, pp 687–697. Kluwer Academic Publishers, Dordrecht

Anderson LB, Ouellette AJA and Barry BA (2000) Probing the structure of Photosystem II with amines and phenylhydrazine. J Biol Chem 275: 4920–4927

Anderson LB, Maderia M, Ouellette AJA, Putnam-Evans C, Higgins LA, Krick T, MacCoss MJ, Lim H, Yates III JR and Barry BA (2002) Posttranslational modifications in the CP43 subunit of Photosystem II. Proc Natl Acad Sci USA 99: 14676–14681

Anderson LB, Ouellette AJA, Eaton-Rye J, Maderia M, MacCoss MJ, Yates III JR and Barry BA (2004) Evidence for a post-translational modification, aspartyl aldehyde, in a photosynthetic membrane protein. J Am Chem Soc 126: 8399–8405

Aro EM, Hundal T, Carlberg I and Andersson B (1990) In vitro studies on light-induced inhibition of photosystem-II and D1-protein degradation at low-temperatures. Biochim Biophys Acta 1019: 269–275

Aro E-M, Virgin I and Andersson B (1993) Photoinhibition of Photosystem II. Inactivation, protein damage and turnover. Biochim Biophys Acta 1143: 113–134

Barbarto R, Race HL, Friso G and Barber J (1991) Chlorophyll levels in the pigment-binding proteins of Photosystem II. A study based on the chlorophyll to cytochrome ratio in different Photosystem II preparations. FEBS Lett 286: 86–90

Barber J, Nield J, Morris EP and Hankamer B (1999) Subunit positioning in Photosystem II revisited. Trends Biochem Sci 24: 43–45

Barber J, Morris E and Büchel C (2000) Revealing the structure of the Photosystem II chlorophyll-binding proteins, CP43 and CP47. Biochim Biophys Acta 1459: 239–247

Barkan A (1988) Proteins encoded by a chloroplast transcription unit are each translated from both monocistronic and polycistronic mRNAs. EMBO J 7: 2637–2644

Bricker TM (1990) The structure and function of CPa-1 and CPa-2 in Photosystem II. Photosynth Res 24: 1–13

Bricker TM and Frankel LK (1987) Use of a monoclonal antibody in structural investigations of the 49-kDa polypeptide of Photosystem II. Arch Biochem Biophys 256: 295–301

Bricker TM and Frankel LK (1998) The structure and function of the 33 kDa extrinsic protein of Photosystem II. A critical review. Photosynth Res 56: 157–173

Bricker TM and Frankel LK (2002) The structure and function of CP47 and CP43 in Photosystem II. Photosynth Res 72: 131–146

Bricker TM, Odom WR and Queirolo CB (1988) Close association of the 33 kDa extrinsic protein with the apoprotein of CPa1 in Photosystem II. FEBS Lett 231: 111–117

Bricker TM, Morvant J, Masri N, Sutton HM and Frankel LK (1998) Isolation of a highly active Photosystem II preparation from *Synechocystis* 6803 using a histidine-tagged mutant of CP 47. Biochim Biophys Acta 1409: 50–57

Bricker TM, Lowrance J, Sutton H and Frankel LK (2001) Alterations of the oxygen-evolving apparatus in a ^{448}Arg → ^{448}S mutant in the CP47 protein of Photosystem II under normal and low chloride conditions. Biochemistry 40: 11483–11489

Bricker TM, Young A, Frankel LK and Putnam-Evans C (2002) Introduction of the ^{305}Arg → ^{305}Ser mutation in the large extrinsic loop E of the CP43 protein of *Synechocystis* sp. PCC 6803 leads to the loss of cytochrome *c*550 binding to Photosystem II. Biochim Biophys Acta 1556: 92–96

Büchel C, Barber J, Ananyev G, Eshaghi S, Watt R and Dismukes C (1999) Photoassembly of the manganese cluster and oxygen evolution from monomeric and dimeric CP47 reaction center Photosystem II complexes. Proc Natl Acad Sci USA 96: 14288–14293

Burnap RL, Qian M and Pierce C (1996) The manganese-stabilizing protein of Photosystem II modifies the in vivo deactivation and photoactivation kinetics of the H_2O oxidation complex in *Synechocystis* sp. PCC6803. Biochemistry 35: 874–882

Carpenter SD, Charite J, Eggers B and Vermaas WFJ (1990) The *psb*C start codon in *Synechocystis* sp. PCC 6803. FEBS Lett 260: 135–137

Carpenter SD, Ohad I and Vermaas WFJ (1993) Analysis of chimeric spinach/cyanobacterial CP43 mutants of *Synechocystis* sp. PCC 6803: The chlorophyll-protein CP43 affects the water-splitting system of Photosystem II. Biochim Biophys Acta 1144: 204–212

Chisholm D and Williams JGK (1988) Nucleotide sequence of psbC, the gene encoding the CP-43 chlorophyll *a*-binding protein of Photosystem II, in the cyanobacterium *Synechocystis* 6803. Plant Mol Biol 10: 293–301

Christopher DA and Hoffer PH (1998) DET1 represses a chloroplast blue light-responsive promoter in a developmental and tissue-specific manner in *Arabidopsis thaliana*. Plant J 14: 1–11

Chu HA, Nguyen AP and Debus RJ (1995) Amino acid residues that influence the binding of manganese or calcium to Photosystem II. 1. The lumenal interhelical domains of the D1

polypeptide. Biochemistry 34: 5839–5858
Clarke SM and Eaton-Rye JJ (1999) Mutation of Phe-363 in the Photosystem II protein CP47 impairs photoautotrophic growth, alters the chloride requirement, and prevents photosynthesis in the absence of either PS II-O or PS II-V in *Synechocystis* sp. PCC 6803. Biochemistry 38: 2707–2715
Clarke SM and Eaton-Rye JJ (2000) Amino acid deletions in loop C of the chlorophyll *a*-binding protein CP47 alter the chloride requirement and/or prevent the assembly of Photosystem II. Plant Mol Biol 44: 591–601
Clarke SM, Funk C, Hendry GS, Shand JA, Wydrzynski T and Eaton-Rye JJ (2002) Amino acid deletions in the cytosolic domains of the chlorophyll *a*-binding protein CP47 slow Q_A^- oxidation and/or prevent the assembly of Photosystem II. Plant Mol Biol 50: 563–572
Debus RJ (2000) The polypeptides of Photosystem II and their influence on mangano-tyrosyl based oxygen evolution. In: Sigel A and Sigel H (eds) Metal Ions in Biological Systems, Vol 37, pp 657–711. Marcel Dekker, New York
Deisenhofer J, Epp O, Sinning I and Michel H (1995) Crystallographic refinement at 2.3 Å resolution and refined model of the photosynthetic reaction center from *Rhodopseudomonas viridis*. J Mol Biol 246: 429–457
De las Rivas J, Balsera M and Barber J (2004) Evolution of oxygenic photosynthesis: Genome-wide analysis of the OEC extrinsic proteins. Trends Plant Sci 9: 18–25
de Weerd FL, van Stokkum IHM, van Amerongen H, Dekker JP and van Grondelle R (2002a) Pathways for energy transfer in the core light-harvesting complexes CP43 and CP47 of Photosystem II. Biophys J 82: 1586–1597
de Weerd FL, Palacios MA, Andrizhiyevskaya EG, Dekker JP and van Grondelle R (2002b) Identifying the lowest electronic states of the chlorophylls in the CP47 core antenna protein of Photosystem II. Biochemistry 41: 15224–15233
Dixit R, Trivedi PK, Nath P and Sane PV (1999) Organization and post-transcriptional processing of the *psb*B operon from chloroplasts of *Populus deltoides*. Curr Genet 36: 165–172
Douglas SE (1994) Chloroplast origins and evolution. In: Bryant DA (ed) Molecular Biology of the Cyanobacteria, pp 91–118. Kluwer Academic Publishers, Dordrecht
Dzelzkalns VA and Bogorad L (1988) Molecular analysis of a mutant defective in photosynthetic oxygen evolution and isolation of a complementing clone by a novel screening procedure. EMBO J 7: 333–338
Eaton-Rye JJ and Shand JA (2001) Mutations between Gly-429 and Thr-436 in loop E of the chlorophyll *a*-binding protein CP47 characterized in the presence or absence of the membrane-extrinsic proteins of the water-oxidizing complex of Photosystem II. In: PS2001 Proceedings: 12th International Congress on Photosynthesis, S13-004, CSIRO Publishing, Melbourne (CD-ROM)
Eaton-Rye JJ and Vermaas WFJ (1991) Oligonucleotide-directed mutagenesis of *psb*B, the gene encoding CP47, employing a deletion strain of the cyanobacterium *Synechocystis* sp. PCC 6803. Plant Mol Biol 17: 1165–1177
Eaton-Rye JJ and Vermaas WFJ (1992) Characterization of a histidine to glutamine substitution at residue 469 in CP47 of Photosystem II. In: Murata N (ed) Research in Photosynthesis, Vol I, pp 239–242. Kluwer Academic Publishers, Dordrecht
Eaton-Rye JJ, Shand JA and Nicoll WS (2003) pH-dependent photoautotrophic growth of specific Photosystem II mutants lacking lumenal extrinsic polypeptides in *Synechocystis* PCC 6803. FEBS Lett 543: 148–153
Elanskaya IV, Allakhverdiev SI, Boichenko VA, Klimov V, Demeter S, Timofeev KN and Shestakov SV (1994) Photochemical characterization of cyanobacterium *Synechocystis* sp. PCC 6803 mutants with impaired Photosystem II proteins. Biochemistry (Moscow) 59: 929–934
Elich TD, Edelman M, and Matoo AK (1993) Dephosphorylation of Photosystem II core proteins is light-regulated in vivo. EMBO J 12:4857–4862
Enami I, Satoh K and Katoh S (1987) Crosslinking between the 33 kDa extrinsic protein and the 47 kDa chlorophyll-carrying protein of the PS II reaction center core complex. FEBS Lett 226: 161–165
Enami I, Kaneko M, Kitamura N, Koike H, Sonoike K, Inoue Y and Katoh S (1991) Total immobilization of the extrinsic 33 kDa protein in spinach Photosystem II membrane preparations. Protein stoichiometry and stabilization of oxygen evolution. Biochim Biophys Acta 1060: 224–232
Enami I, Tohri A, Kamo M, Ohta H and Shen J-R (1997) Identification of domains on the 43 kDa chlorophyll-carrying protein (CP43) that are shielded from tryptic attack by binding of the extrinsic 33 kDa protein with Photosystem II complex. Biochim Biophys Acta 1320: 17–26
Enami I, Kikuchi S, Fukuda T, Ohta H and Shen J-R (1998) Binding and functional properties of four extrinsic proteins of Photosystem II from a red alga, *Cyanidium caldarium*, as studied by release-reconstitution experiments. Biochemistry 37: 2787–2793
Enami I, Yoshihara S, Tohri A, Okumura A, Ohta H and Shen J-R (2000) Cross-reconstitution of various extrinsic proteins and Photosystem II complexes from cyanobacteria, red algae and higher plants. Plant Cell Physiol 41: 1354–1364
Feiler U and Hauska G (1995) The reaction center from green sulphur bacteria. In: Blankenship RE, Madigan MT and Bauer CE (eds) Anoxygenic Photosynthetic Bacteria, pp 665–685. Kluwer Academic Publishers, Dordrecht
Ferreira KN, Iverson TM, Maghlaoui K, Barber J and Iwata S (2004) Architecture of the photosynthetic oxygen-evolving center. Science 303: 1831–1838
Frankel LK and Bricker TM (1989) Epitope mapping of the monoclonal antibody FAC2 on the apoprotein of CPa-1 in Photosystem II. FEBS Lett 257: 279–282
Frankel LK and Bricker TM (1990) Interaction of CPa-1 with components involved with water oxidation in Photosystem II: Mapping of NHS-biotinylation sites and the epitope of the monoclonal antibody FAC2 to the large extrinsic loop region of CPa-1. In: Baltscheffsky M (ed) Current Research in Photosynthesis Vol I, pp 639–642. Kluwer Academic Publishers, Dordrecht
Frankel LK and Bricker TM (1992) Interaction of CPa-1 with the manganese-stabilizing protein of Photosystem II: Identification of domains on CPa-1 which are shielded from *N*-hydroxysuccinimide biotinylation by the manganese-stabilizing protein. Biochemistry 31: 11059–11064
Ghanotakis DF, de Paula JC, Demetriou DM, Bowlby NR, Peterson J, Babcock GT and Yocum CF (1989) Isolation and characterization of the 47 kDa protein and the D1-D2-cytochrome *b*-559 complex. Biochim Biophys Acta 974: 44–53
Giacometti GM, Barbato R, Friso G, Frizzo A and Rigoni F (1992) Photosystem II degradation pathways after photoin-

hibition of isolated thylakoids. In: Murata N (ed) Research in Photosynthesis, Vol IV, pp 505–508 Kluwer Academic Publishers, Dordrecht

Gingrich JC, Gasparich GE, Sauer K and Bryant DA (1990) Nucleotide sequence and expression of the two genes encoding D2 protein and the single gene encoding the CP43 protein of Photosystem II in the cyanobacterium *Synechococcus* sp. PCC 7002. Photosynth Res 24: 137–150

Gleiter HM, Haag E, Shen J-R, Eaton-Rye JJ, Inoue Y and Vermaas WFJ (1994) Functional characterization of mutant strains of the cyanobacterium *Synechocystis* sp. PCC 6803 lacking short domains within the large, lumen-exposed loop of the chlorophyll protein CP47 in Photosystem II. Biochemistry 33: 12063–12071

Gleiter HM, Haag E, Shen J-R, Eaton-Rye JJ, Seeliger AG, Inoue Y, Vermaas WFJ and Renger G (1995) Involvement of the CP47 protein in stabilization and photoactivation of a functional water-oxidizing complex in the cyanobacterium *Synechocystis* sp. PCC 6803. Biochemistry 34: 6847–6856

Golden SS and Stearns GW (1988) Nucleotide sequence and transcript analysis of three Photosystem II genes from the cyanobacterium *Synechococcus* sp. PCC7942. Gene 67: 85–96

Groot M-L, Frese RN, de Weerd FL, Bromek K, Pettersson Å, Perterman EJG, van Stockkum IHM, van Grondelle R and Dekker JP (1999) Spectroscopic properties of the CP43 core antenna protein of Photosystem II. Biophys J 77: 3328–3340

Haag E, Eaton-Rye JJ, Renger G and Vermaas WFJ (1993) Functionally important domains of the large hydrophilic loop of CP47 as probed by oligonucleotide-directed mutagenesis in *Synechocystis* sp. PCC 6803. Biochemistry 32: 4444–4454

Hackett CS and Strittmatter P (1984) Covalent cross-linking of the active sites of vesicle-bound cytochrome b_5 and NADH-cytochrome b_5 reductase. J Biol Chem 259: 3275–3282

Hankamer B, Morris EP and Barber J (1999) Revealing the structure of the oxygen-evolving core dimer of Photosystem II by cryoelectron crystallography. Nat Struct Biol 6: 560–564

Hayashi H, Fujimura Y, Mohanty PS and Murata N (1993) The role of CP47 in the evolution of oxygen and the binding of the extrinsic 33-kDa protein to the core complex of Photosystem II as determined by limited proteolysis. Photosynth Res 36: 35–42

Hird SM, Webber AN, Wilson RJ, Dyer TA and Gray JC (1991) Differential expression of the psbB and psbH genes encoding the 47 kDa chlorophyll *a*-protein and the 10 kDa phosphoprotein of Photosystem II during chloroplast development in wheat. Curr Genet 19: 199–206

Hong L, Stevenson JK, Roth WB and Hallick RB (1995) Euglena gracilis chloroplast psbB, psbT, psbH and psbN gene cluster: Regulation of psbB-psbT pre-mRNA processing. Mol Gen Genet 247: 180–188

Hu X, Damjanovic A, Ritz T and Schulten K (1998) Architecture and mechanism of the light-harvesting apparatus of purple bacteria. Proc Natl Acad Sci USA 95: 5935–5941

Huang IY, Lynch DP and Eaton-Rye JJ (2001) Mutagenesis of histidine–469 in the Photosystem II chlorophyll *a*-binding protein CP47 in Synechocystis sp. PCC 6803. In: PS2001 Proceedings: 12th International Congress on Photosynthesis, S22-028, CSIRO Publishing, Melbourne (CD-ROM)

Ikeuchi M, Plumley FG, Inoue Y and Schmidt GW (1987) Phosphorylation of Photosystem II components, CP43 apoprotein, D1, D2, and 10 to 11 kilodalton protein in chloroplast thylakoids of higher plants. Plant Physiol 85: 638–642

Isogai Y, Yamamoto Y and Nishimura M (1985) Association of the 33-kDa polypeptide with the 43-kDa component in Photosystem II particles. FEBS Lett 187: 240–244

Johnson CH and Schmidt GW (1993) The *psbB* gene cluster of the *Chlamydomonas reinhardtii* chloroplast: sequence and transcriptional analyses of *psbN* and *psbH*. Plant Mol Biol 22: 645–658

Jordan P, Fromme P, Witt HT, Klukas O, Saenger W and Krauß N (2001) Three-dimensional structure of cyanobacterial Photosystem I at 2.5 Å resolution. Nature 411: 909–917

Kamiya N and Shen J-R (2003) Crystal structure of oxygen-evolving Photosystem II from *Thermosynechococcus vulcanus* at 3.7-Å resolution. Proc Natl Acad Sci USA 100: 98–103

Kaneko T, Sato S, Kotani H, Tanaka A, Asamizu E, Nakamura Y, Miyajima N, Hirosawa M, Sugiura M, Sasamoto S, Kimura T, Hosouchi T, Matsuno A, Muraki A, Nakazaki N, Naruo K, Okumura S, Shimpo S, Takeuchi C, Wada T, Watanabe A, Yamada M, Yasuda M, Tabata S (1996) Sequence analysis of the genome of the unicellular cyanobacterium *Synechocystis* sp. Strain PCC 6803. II. Sequence determination of the entire genome and assignment of potential protein-coding regions. DNA Res 3: 109–136

Kashino Y, Lauber WM, Carroll JA, Wang Q, Whitmarsh J, Satoh K and Pakrasi HB (2002) Proteomic analysis of a highly active Photosystem II preparation from the cyanobacterium *Synechocystis* sp. PCC 6803 reveals the presence of novel polypeptides. Biochemistry 41: 8004–8012

Keller M, Weil JH and Nair CKK (1989) Nucleotide sequence of the psbB gene of *Euglena gracilis.* Plant Mol Biol 13: 723–725

Kim M, Thum KE, Morishige DT and Mullet JE (1999) Detailed architecture of the barley chloroplast *psbD-psbC* blue light-responsive promoter. J Biol Chem 274: 4684–4692

Knoepfle N, Bricker TM and Putnam-Evans C (1999) Site-directed mutagenesis of basic arginine residues 305 and 342 in the CP 43 protein of Photosystem II affects oxygen-evolving activity in *Synechocystis* 6803. Biochemistry 38: 1582–1588

Kohchi T, Yoshida T, Komano T and Ohyama K (1988) Divergent mRNA transcription in the chloroplast *psbB* operon. EMBO J 7: 885–891

Kowallik KV (1993) Origin and evolution of plastids from chlorophyll $a+c$-containing algae: Suggested ancestral relationships to red and green algal plastids. In: Lewin RA (ed) Origin of Plastids: Symbiogenesis, Prochlorophytes and the Origin of Chloroplasts, pp 223–263. Chapman and Hall, New York

Krauß N, Schubert W-D, Klukas O, Fromme P, Witt HT and Saenger W (1996) Photosystem I at 4 Å resolution represents the first structural model of a joint photosynthetic reaction centre and core antenna system. Nat Struct Biol 3: 965–973

Kuhn MG, and Vermaas WFJ (1993) Deletion mutations in a long hydrophilic loop in the Photosystem II chlorophyll-binding protein CP43 in the cyanobacterium *Synechocystis* sp. PCC 6803. Plant Mol Biol 23: 123–133

Kühlbrandt W, Wang DN and Fujiyoshi Y (1994) Atomic model of plant light-harvesting complex by electron crystallography. Nature 367: 614–621

Lindberg K and Andréasson L-E (1996) A one-site, two-state model for the binding of anions in Photosystem II. Biochem-

istry 35: 14259–14267
Maid U and Zetsche K (1992) A 16 kb small single-copy region separates the plastid DNA inverted repeat of the unicellular red alga *Cyanidium caldarium*: Physical mapping of the IR-flanking regions and nucleotide sequences of the *psbD-psbC*, *rps16*, 5S rRNA and *rpl21* genes. Plant Mol Biol 19: 1001–1010
Manna P and Vermaas W (1997) Mutational studies on conserved histidine residues in the chlorophyll-binding protein CP43 of Photosystem II. Eur J Biochem 247: 666–672
Maul JE, Lilly JW, Cui L, dePamphilis CW, Miller W, Harris EH and Stern DB (2002) The *Chlamydomonas reinhardtii* plastid chromosome: Islands of genes in a sea of repeats. Plant Cell 14: 2659–2679
Mayes SR and Barber J (1991) Primary structure of the *psbN-psbH-petC-petA* gene cluster of the cyanobacterium *Synechocystis* PCC 6803. Plant Mol Biol 17: 289–293
McConnell MD, Koop R, Vasil'ev S and Bruce D (2002) Regulation of the distribution of chlorophyll and phycobilin-absorbed excitation energy in cyanobacteria. A structure-based model for the light state transition. Plant Physiol 130: 1201–1212
McDermott G, Prince SM, Freer AA, Hawthornthwaite-Lawless AM, Papiz MZ, Cogdell RJ and Isaacs NW (1995) Crystal structure of an integral membrane light-harvesting complex from photosynthetic bacteria. Nature 374: 517–521
Michel H and Deisenhofer J (1988) Relevance of the photosynthetic reaction center from purple bacteria to the structure of Photosystem II. Biochemistry 27: 1–7
Michel H, Hunt DF, Shabanowitz J and Bennett J (1988) Tandem mass spectrometry reveals that three Photosystem II proteins of spinach chloroplasts contain *N*-acetyl-*O*-phosphothreonine at their NH_2 termini. J Biol Chem 263: 1123–1130
Morgan TR, Shand JA, Clarke SM and Eaton-Rye JJ (1998) Specific requirements for cytochrome *c*-550 and the manganese-stabilizing protein in photoautotrophic strains of *Synechocystis* sp. PCC 6803 with mutations in the domain Gly-351 to Thr-436 of the chlorophyll-binding protein CP47. Biochemistry 37: 14437–14449
Mori H and Yamamoto Y (1992) Deletion of antenna chlorophyll-*a*-binding proteins CP43 and CP47 by tris-treatment of PS II membranes in weak light: Evidence for a photo-degradative effect on the PS II components other than the reaction center-binding proteins. Biochim Biophys Acta 1100: 293–298
Mori H, Yamashita Y, Akasaka T and Yamamoto Y (1995) Further characterization of the loss of antenna chlorophyll-binding protein CP43 from Photosystem II during donor-side photoinhibition. Biochim Biophys Acta 1228: 37–42
Nakatani HY, Ke B, Dolan E and Arntzen CJ (1984) Identity of the Photosystem II reaction center polypeptide. Biochim Biophys Acta 765: 347–352
Nanba O and Satoh K (1987) Isolation of a Photosystem II reaction center consisting of D-1 and D-2 polypeptides and cytochrome *b*-559. Proc Natl Acad Sci USA 84: 109–112
Nixon PJ, Rögner M and Diner BA (1991) Expression of a higher plant *psbA* gene in *Synechocystis* 6803 yields a functional hybrid Photosystem II reaction center complex. Plant Cell 3: 383–395
Odom WR and Bricker TM (1992) Interaction of CPa-1 with the manganese-stabilizing protein of Photosystem II: Identification of domains cross-linked by 1-ethyl-3-[3-(dimethylamino)propyl]carbodiimide. Biochemistry 31: 5616–5620
Ohta H, Yoshida N, Sano M, Hirano M, Nakazato K and Enami I (1995) Evidence for electrostatic interaction of the loop A on CP 47 with the extrinsic 33 kDa protein. In: Mathis P (ed) Photosynthesis: From Light to Biosphere, Vol II, pp 361–364. Kluwer Academic Publishers, Dordrecht
Ohta H, Suzuki T, Ueno M, Okumura A, Yoshihara S, Shen J-R and Enami I (2003) Extrinsic proteins of Photosystem II. An intermediate member of the PsbQ protein family in red algal PS II. Eur J Biochem 270: 4156–4163
Ouellette AJA, Anderson LB and Barry BA (1998) Amine binding and oxidation at the catalytic site for photosynthetic water oxidation. Proc Natl Acad Sci USA 95: 2204–2209
Putnam-Evans C and Bricker TM (1992) Site-directed mutagenesis of the CPa-1 protein of Photosystem II: Alteration of the basic residue pair ^{384,385}R to ^{384,385}G leads to a defect associated with the oxygen-evolving complex. Biochemistry 31: 11482–11488
Putnam-Evans C and Bricker TM (1994) Site-directed mutagenesis of the CP47 protein of Photosystem II: Alteration of the basic residue ^{448}R to ^{448}G prevents the assembly of functional Photosystem II centers under chloride-limiting conditions. Biochemistry 33: 10770–10776
Putnam-Evans C and Bricker TM (1997) Site-directed mutagenesis of the basic residues ^{321}K to ^{321}G in the CP 47 protein of Photosystem II alters the chloride requirement for growth and oxygen-evolving activity in *Synechocystis* 6803. Plant Mol Biol 34: 455–463
Putnam-Evans C, Wu J and BrickerTM (1996a) Site-directed mutagenesis of the CP 47 protein of Photosystem II: Alteration of conserved charged residues which lie within lethal deletions of the large extrinsic loop E. Plant Mol Biol 32: 1191–1195
Putnam-Evans C, Burnap R, Wu J, Whitmarsh J and Bricker TM (1996b) Site-directed mutagenesis of the CP 47 protein of Photosystem II: Alteration of conserved charged residues in the domain ^{364}E-^{444}R. Biochemistry 35: 4046–4053
Qian M, Al-Khaldi SF, Putnam-Evans C, Bricker TM and Burnap RL (1997) Photoassembly of the Photosystem II $(Mn)_4$cluster in site-directed mutants impaired in the binding of the manganese-stabilizing protein. Biochemistry 36: 15244–15252
Queirolo C (1992) Assemblage of spinach Photosystem II proteins: CPa-1 and MSP interactions. Ph.D. Dissertation, Louisiana State University, Baton Rouge
Reith M and Munholland J (1993) A high-resolution gene map of the chloroplast genome of the red alga *Porphyra purpurea*. Plant Cell 5: 465–475
Rhee K-H, Morris EP, Zheleva D, Hankamer B, Kühlbrandt W and Barber J (1997) Two-dimensional structure of plant Photosystem II at 8-Å resolution. Nature 389: 522–526
Rhee K-H, Morris EP, Barber J and Kühlbrandt W (1998) Three-dimensional structure of the plant Photosystem II reaction center at 8 Å resolution. Nature 396: 283–286
Rochaix JD, Kuchka M, Mayfield S, Schirmer-Rahire M, Girard-Bascou J and Bennoun P (1989) Nuclear and chloroplast mutations affect the synthesis or stability of the chloroplast *psb*C gene product in *Chlamydomonas reinhardtii.* EMBO J 8: 1013–1021
Rögner M, Chisholm DA and Diner BA (1991) Site-directed mutagenesis of the *psb*C gene of Photosystem II: Isolation and functional characterization of CP43-less Photosystem II core complexes. Biochemistry 30: 5387–5395
Rokka A, Aro EM, Herrmann RG, Andersson B and Vener AV (2000) Dephosphorylation of Photosystem II reaction center

proteins in plant photosynthetic membranes as an immediate response to abrupt elevation of temperature. Plant Physiol 123:1525–1535

Rosenberg C, Christian J, Bricker TM and Putnam-Evans C (1999) Site-directed mutagenesis of glutamate residues in the large extrinsic loop of the Photosystem II protein CP 43 affects oxygen-evolving activity and PS II assembly. Biochemistry 38: 15994–16000

Salter AH, Virgin I, Hagman A and Andersson B (1992) On the molecular mechanism of light-induced D1 protein degradation in Photosystem II core particles. Biochemistry 31: 3990–3998

Sayre RT and Wrobel-Boerner EA (1994) Molecular topology of the Photosystem II chlorophyll *a*-binding protein, CP43: Topology of a thylakoid membrane protein. Photosynth Res 40: 11–19

Schubert WD, Klukas O, Saenger W, Witt HT, Fromme P and Krauß N (1998) A common ancestor for oxygenic and anoxygenic photosynthetic systems: A comparison based on the structural model of Photosystem I. J Mol Biol 280: 297–314

Seidler A (1996) The extrinsic polypeptides of Photosystem II. Biochim Biophys Acta 1277: 35–60

Sexton TB, Christopher DA and Mullet JE (1990a) Light-induced switch in barley *psbD-psbC* promoter utilization: A novel mechanism regulating chloroplast gene expression. EMBO J 9: 4485–4494

Sexton TB, Jones JT and Mullet JE (1990b) Sequence and transcriptional analysis of the barley ctDNA region upstream of *psb*D-*psb*C encoding *trn*K(UUU), *rps*16, *trn*Q(UUG), *psb*K, *psb*I, and *trn*S(GCU). Curr Genet 17: 445–454

Shen G and Vermaas WFJ (1994) Mutation of chlorophyll ligands in the chlorophyll-binding CP47 protein as studied in a *Synechocystis* sp. PCC 6803 Photosystem I-less background. Biochemistry 33: 7379–7388

Shen G, Eaton-Rye JJ and Vermaas WFJ (1993) Mutation of histidine residues in CP47 leads to destabilization of the Photosystem II complex and to impairment of light energy transfer. Biochemistry 32: 5109–5115

Shen J-R, Burnap RL and Inoue Y (1995a) An independent role of cytochrome *c*-550 in cyanobacterial Photosystem II as revealed by double-deletion mutagenesis of the *psb*O and *psb*V genes in *Synechocystis* sp. PCC 6803. Biochemistry 34: 12661–12668

Shen J-R, Vermaas W and Inoue Y (1995b) The role of cytochrome *c*-550 as studied through reverse genetics and mutant characterization in *Synechocystis* sp. PCC 6803. J Biol Chem 270: 6901–6907

Shen J-R, Qian M, Inoue Y and Burnap RL (1998) Functional characterization of *Synechocystis* sp. PCC 6803 Δ*psb*U and Δ*psb*V mutants reveals important roles of cytochrome *c*-550 in cyanobacterial oxygen evolution. Biochemistry 37: 1551–1558

Shipton CA and Barber J (1991) Photoinduced degradation of the D1 polypeptide in isolated reaction centers of Photosystem II: Evidence for an autoproteolytic process triggered by the oxidizing side of the photosystem. Proc Natl Acad Sci USA 88: 6691–6695

Soltis, DE, Soltis PS and Zanis ML (2002) Phylogeny of seed plants based on evidence from eight genes. Am J Bot 89: 1670–1681

Summerfield TC, Galloway DJ and Eaton-Rye JJ (2001) The use of *psbB* for the identification of cyanobacterial lichen symbionts. In: PS2001Proceedings: 12th International Congress on Photosynthesis, S3-041, CSIRO Publishing, Melbourne (CD-ROM)

Summerfield TC, Shand JA, Bentley FK and Eaton-Rye JJ (2005) PsbQ (Sll1638) in *Synechocystis* sp. PCC 6803 is required for Photosystem II activity in specific mutants and in nutrient-limiting conditions. Biochemistry 44: 805–815

Tanaka M, Obokata J, Chunwongse J, Shinozaki K and Sugiura M (1987) Rapid splicing and stepwise processing of a transcript from the *psbB* operon in tobacco chloroplasts: Determination of the intron sites in *petB* and *petD*. Mol Gen Genet 209: 427–431

Thornton LE, Ohkawa H, Roose JL, Kashino Y, Keren N and Pakrasi HB (2004) Homologs of plant PsbP and PsbQ proteins are necessary for regulation of Photosystem II activity in the cyanobacterium *Synechocystis* 6803. Plant Cell 16: 2164–2175

Tichy M and Vermaas W (1998) Functional analysis of combinatorial mutants altered in a conserved region in loop E of the CP47 protein in *Synechocystis* sp. PCC 6803. Biochemistry 37: 1523–1531

Trebst A (1986) The topology of the plastoquinone and herbicide binding peptides of Photosystem II in the thylakoid membrane. Z Naturforsch 41c: 240–245

Tronrud DE, Schmidt MF and Matthews BW (1986) Structure and X-ray amino acid sequence of a bacteriochlorophyll *a* protein from *Prosthecochloris aestuarii* refined at 1.9 Å resolution. J Mol Biol 188: 443–454

Urbach E, Scanlan DJ, Distel DL, Waterbury JB and Chisholm SW (1998) Rapid diversification of marine picophytoplankton with dissimilar light-harvesting structures inferred from sequences of *Prochlorococcus* and *Synechococcus* (Cyanobacteria). J Mol Evol 46: 188–201

van Dorssen RJ, Breton J, Plijter JJ, Satoh K and van Gorkom HJ (1987a) Spectroscopic properties of the reaction center and of the 47 kDa protein of Photosystem II. Biochim Biophys Acta 893: 267–274

van Dorssen RJ, Plijter JJ, Dekker JP, den Ouden A, Amesz J and van Gorkom HJ (1987b) Spectroscopic properties of chloroplast grana membranes and of the core of Photosystem II. Biochim Biophys Acta 890: 134–143

Vasil'ev S, Orth P, Zouni A, Owens TG and Bruce D (2001) Excited-state dynamics in Photosystem II: Insights from the X-ray crystal structure. Proc Natl Acad Sci USA 98: 8602–8607

Vener AV, Ohad I and Andersson B (1998) Protein phosphorylation and redox sensing in chloroplast thylakoids. Curr Opin Plant Biol 1: 217–223

Vener AV, Harms A, Sussman M and Vierstra RD (2001) Mass spectrometric resolution of reversible protein phosphorylation in photosynthetic membranes of *Arabidopsis thaliana*. J Biol Chem 276: 6959–6966

Vermaas W (1993) Molecular-biological approaches to analyze Photosystem II structure and function. Ann Rev Plant Physiol Plant Mol Biol 44: 457–481

Vermaas WFJ, Williams JGK and Arntzen CJ (1987) Sequencing and modification of *psbB*, the gene encoding the CP47 protein of Photosystem II, in the cyanobacterium *Synechocystis* 6803. Plant Mol Biol 8: 317–326

Vermaas WFJ, Ikeuchi M and Inoue Y (1988) Protein composition of the Photosystem II core complex in genetically engineered mutants of the cyanobacterium *Synechocystis* sp. PCC 6803.

Photosynth Res 17: 97–113

Vermaas, WFJ, Shen G and Ohad I (1996) Chimeric CP47 mutants of the cyanobacterium *Synechocystis* sp. PCC 6803 carrying spinach sequences: Construction and function. Photosynth Res 48: 147–162

Virgin I, Ghanotakis DF and Andersson B (1990) Light-induced D1-protein degradation in isolated Photosystem II core complexes. FEBS Lett 269: 45–48

Virgin I, Salter AH, Ghanotakis DF and Andersson B (1991) Light-induced D1 protein degradation is catalyzed by a serine-type protease. FEBS Lett 287: 125–128

Virgin I, Salter AH, Hagman A, Vass I, Styring S and Andersson B (1992) Molecular mechanisms behind light-induced inhibition of Photosystem II electron transport and degradation of reaction center polypeptides. Biochim Biophys Acta 1101: 139–142

Visscher KJ, Bergstöm H, Sundström V, Hunter CN and van Grondelle R (1989) Temperature-dependence of energy-transfer from the long wavelength antenna BChl-896 to the reaction center in *Rhodospirillum-rubrum*, *Rhodobacter-sphaeroides* (WT and M21 mutant) from 77 to 177K, studied by picosecond absorption-spectroscopy. Photosynth Res 22: 211–217

Westhoff P and Herrmann RG (1988) Complex RNA maturation in chloroplasts. The *psbB* operon from spinach. Eur J Biochem 171: 551–564

Wu J, Putnam-Evans C and Bricker TM (1996) Site-directed mutagenesis of the CP 47 protein of Photosystem II: ^{167}W in the lumenally exposed loop C is required for Photosystem II assembly and stability. Plant Mol Biol 32: 537–542

Wu J, Masri N, Lee W, Frankel LK and Bricker TM (1999) Random mutagenesis in the large extrinsic loop E and transmembrane α-helix VI of the CP 47 protein of Photosystem II. Plant Mol Biol 39: 381–386

Yamamoto Y (2001) Quality control of Photosystem II. Plant Cell Physiol 42: 121–128

Yamamoto Y and Akasaka T (1995) Degradation of antenna chlorophyll-binding protein CP43 during photoinhibition of Photosystem II. Biochemistry 34: 9038–9045

Young A, McChargue M, Frankel LK, Bricker TM and Putnam-Evans C (2002) Alterations of the oxygen-evolving apparatus induced by a ^{305}Arg → ^{305}Ser mutation in the CP43 protein of Photosystem II from *Synechocystis* sp. PCC 6803 under chloride-limiting conditions. Biochemistry 41: 15747–15753

Yu J and Vermaas WFJ (1990) Transcript levels and synthesis of Photosystem II components in cyanobacterial mutants with inactivated Photosystem II genes. Plant Cell 2: 315–322

Zerges W, Girard-Bascou J and Rochaix J-D (1997) Translation of the chloroplast *psbC* mRNA is controlled by interactions between its 5′ leader and the nuclear loci *TBC1* and *TBC3* in *Chlamydomonas reinhardtii*. Mol Cell Biol 17: 3440–3448

Zerges W, Auchincloss AH and Rochaix J-D (2003) Multiple translational control sequences in the 5′ leader of the chloroplast *psbC* mRNA interact with nuclear gene products in *Chlamydomonas reinhardtii*. Genetics 163: 895–904

Zheleva D, Sharma J, Panico M, Morris HR and Barber J (1998) Isolation and characterization of monomeric and dimeric CP47-reaction center Photosystem II complexes. J Biol Chem 273: 16122–16127

Ziegenhagen B and Fladung M (1997) Variation in the *psbC* gene region of gymnosperms and angiosperms as detected by a single restriction site polymorphism. Theor Appl Genet 94: 1065–1071

Zouni A, Witt H-T, Kern J, Fromme P, Krauß N, Saenger W and Orth P (2001) Crystal structure of Photosystem II from *Synechococcus elongatus* at 3.8 Å resolution. Nature 409: 739–743

Chapter 4

The D1 and D2 Core Proteins

Peter J. Nixon*
Wolfson Biochemistry Building, Division of Biology, Imperial College London, South Kensington Campus, London SW7 2AZ, U.K.

Mary Sarcina
Department of Biology, University College London, Darwin Building, Gower Street, London WC1E 6BT, U.K.

Bruce A. Diner
Central Research and Development, Experimental Station, E. I. du Pont de Nemours & Co. Inc., Wilmington, DE 19880-0173, U.S.A.

*Author for correspondence, email: p.nixon@imperial.ac.uk

T. Wydrzynski and K. Satoh (eds): Photosystem II: The Light-Driven Water:Plastoquinone Oxidoreductase, pp. 71–93.

Summary

In 1977, Chua and Gillham (J Cell Biology 74: 441–452) reported for the first time the existence of two chloroplast-encoded proteins within the thylakoid membrane of the green alga *Chlamydomonas reinhardtii*, which they termed D-1 and D-2. The D1 and D2 proteins are now recognized as the Photosystem II reaction center polypeptides with a key role in binding all of the co-factors involved in photosynthetic water oxidation. In this chapter we summarize some of the biochemical and mutagenesis data that has been instrumental in shaping this view of the D1 and D2 proteins.

I. Introduction

Although the Photosystem II (PS II) complex — i.e., water-plastoquinone oxidoreductase, is composed of over twenty-five subunits, the important light-induced electron transfer reactions occur within a heterodimer composed of the D1 and D2 polypeptides (D1/D2). Recent structural studies have now identified the positions of the Chl and Pheo pigments within D1/D2 and, importantly, the location of the Mn-Ca metal cluster which catalyses photosynthetic water oxidation (Zouni et al., 2001; Kamiya and Shen, 2003; Biesiadka et al., 2004; Ferreira et al., 2004). Perhaps one of the most reassuring aspects of the structural studies has been how much had been correctly predicted in advance. In this chapter, we describe the background that led to the emergence of D1 and D2 as the PS II reaction center (RC) subunits, plus the key mutagenesis and biochemical experiments that identified the likely binding sites for the various pigments and redox-active components within the D1 and D2 heterodimer.

Abbreviations: BRC – reaction center from purple non-sulfur photosynthetic bacteria; B_A/B_B – PS II chlorophylls in similar position to the two accessory BChls of the BRC; BChl – bacteriochlorophyll; BPheo – bacteriopheophytin; C-terminal – carboxyl-terminal; Chl – chlorophyll; Chl Z_{D1} –peripheral Chl in the PS II RC, ligated by D1-His118; Chl Z_{D2} – peripheral Chl in the PS II RC, ligated by D2-His117; Cyt – cytochrome; ENDOR – electron nuclear double resonance; EPR – electron paramagnetic resonance; ESEEM – electron spin-echo envelope modulation; FTIR – Fourier transform infrared ; P – special pair of BChl in the BRC; P680 – historical term for the primary electron donor within PS II; P_A/P_B – chlorophylls in PS II in similar position to the special pair of BChl of BRC; $Pheo_A/Pheo_B$ – pheophytin *a* molecules in PS II in similar position to the BPheo molecules of the BRC; Q_A – primary quinone electron acceptor; Q_B – secondary quinone electron acceptor; RC – reaction center; S_2 – Mn cluster that has accumulated two of the four oxidizing equivalents needed for water oxidation; SDS-PAGE – sodium dodecyl sulfate-polyacrylamide gel electrophoresis; Y_D – redox-active tyrosine, D2-Tyr160; Y_Z – redox-active tyrosine, D1-Tyr161, which acts as the immediate oxidant of the Mn cluster

II. Identification of the D1 and D2 Proteins

A. Terminology

The D1 and D2 nomenclature was first used in studies aimed at identifying those thylakoid proteins that were synthesized by the chloroplast of the green alga *Chlamydomonas reinhardtii* (Chua and Gillham, 1977). Cells were pulse-labeled with [^{14}C]-acetate in the presence of an inhibitor of cytoplasmic protein synthesis, and the radiolabeled thylakoid proteins separated by denaturing polyacrylamide gel electrophoresis. Two broad areas of radioactivity were identified by autoradiography and termed 'diffuse band-1' (D-1) and 'diffuse band-2' (D-2). In these experiments, D-1 possessed an apparent molecular mass of about 34 kDa and D-2 appeared to be 30 kDa. Although D-1 and D-2 might have been composed of a number of different co-migrating polypeptides, the notation D1 and D2 (sometimes D_1 and D_2) has been subsequently used to describe the *psbA* and *psbD* gene products, respectively, in all oxygenic photosynthetic organisms.

B. Linking the psbA Gene to Its Gene Product in the Thylakoid Membrane

1. The Rapidly-Turning-Over 32-kDa Protein

Early studies on the synthesis of thylakoid membrane proteins in isolated chloroplasts of higher plants revealed that a major product was a protein of apparent molecular mass 32 kDa (Bottomley et al., 1974; Eaglesham and Ellis, 1974). Given that it did not seem to correspond to an abundant polypeptide, this particular protein appeared to be undergoing rapid synthesis and degradation within the membrane — hence its name. The gene encoding this protein, now termed *psbA*, was mapped onto the chloroplast genome by a number of different groups and the first sequences, from spinach and tobacco, were published in 1982 (Zurawski et al., 1982).

2. The 32-kDa Herbicide-Binding Protein

A large number of herbicides block photosynthetic electron flow on the acceptor side of PS II. Through the use of the radiolabeled photoaffinity herbicide, azido-[^{14}C]-atrazine, Pfister and co-workers showed that a 32-kDa protein was a target (Pfister et al., 1981). By proteolytic fingerprinting this particular tagged protein and the 32-kDa rapidly-turning-over protein, it was concluded that they were one and the same (Steinback et al., 1981). Confirmation that *psbA* encoded the herbicide-binding protein came with the identification of a mutation, Ser264Gly, in the *psbA* gene product of a spontaneous atrazine-resistant biotype of *Amaranthus hybridus* (Hirschberg and McIntosh, 1983). This same mutation has now been found in a variety of herbicide-resistant photosynthetic organisms (for a review, see Oettmeier, 1999).

3. The Q_B-Binding Protein

Several lines of evidence (for a review, see Kyle, 1985) have indicated that the binding site for herbicides in PS II was coincident with, or near to, the binding site for the secondary quinone electron acceptor, Q_B, which takes part in the binary gate mechanism for the transmission of electrons into the plastoquinone pool (Bouges-Bocquet, 1973; Velthuys and Amesz 1974). These included the influence of the Q_B redox state on the affinity of PS II for herbicides (Velthuys, 1981), EPR studies (Rutherford et al., 1984), inhibition of herbicide binding using plastoquinone analogues (Vermaas et al., 1983; Oettmeier et al., 1984) and slowing of Q_B reduction in atrazine-resistant plants (Bowes et al., 1980). Together these data led to the idea that D1, encoded by *psbA*, was the Q_B-binding protein of PS II, as well as a target for several classes of herbicide (for a review, see Oettmeier, 1999).

C. The Link Between the psbD Gene and Its Gene Product

The *psbD* gene was located first on the chloroplast genome of *C. reinhardtii* using a combination of antibodies raised against proteins in the D2 region of denaturing gels and an *E. coli*-based transcription-translation of cloned chloroplast DNA fragments (Rochaix, 1981). The sequence was first published in 1984 (Rochaix et al., 1984) and later in an amended form (Erickson et al., 1986). Using this gene, *psbD* was subsequently isolated from a variety of chloroplasts (Alt et al., 1984; Holschuh et al., 1984; Rasmussen et al., 1984) and cyanobacterial sources (Williams and Chisholm, 1987). The identification of the *psbD* gene product in thylakoids was initially uncertain, especially for higher plants, because of the lack of specific antibodies. For *C. reinhardtii,* D2 was identified indirectly on the basis of radioactive labeling of thylakoid proteins and concluded to be a component of the PS II core complex (Delepelaire, 1984). Confirmation that the *psbA* and *psbD* gene products were indeed components of the PS II complex from higher plants came with the use of specific antibodies raised to the gene products expressed in *E. coli* (Nixon et al., 1986).

III. The Primary Structures of D1 and D2

D1 is synthesized as a precursor protein in higher plants (Grebanier et al., 1978) with, unusually, a carboxyl-terminal (C-terminal) extension (Marder et al., 1984). With the apparent exception of *Euglena gracilis* (Karabin et al., 1984) and some species of dinoflagellates (Yamamoto et al., 2001), the presence of a C-terminal extension for D1 appears ubiquitous. Protein sequencing of mature D1 from spinach (M Takahashi et al., 1988; Y Takahashi et al., 1990), the green alga *C. reinhardtii* (B. A. Diner, personal communication) and the cyanobacterium *Synechocystis* 6803 (Nixon et al., 1992a) has confirmed that in all cases the C-terminal residue of mature D1 is Ala344 so that 9, 8 and 16 amino-acid residues are removed,

respectively, from their precursor molecules. In contrast, D2 is not C-terminally processed (Y. Takahashi et al., 1990).

In spinach, the initiating N-formylmethionine residue of both D1 and D2 is removed leaving Thr2 at the N-terminus, which is acetylated. These Thr residues can also be phosphorylated in both D1 and D2 (Michel et al., 1988). The physiological significance for D1 and D2 phosphorylation in higher plants remains unclear although evidence points to a role in regulating their degradation (Koivuniemi et al., 1995). D1 has also been suggested to be palmitoylated in higher plants (Mattoo and Edelman, 1987) but the site of attachment and physiological importance remain obscure. For cyanobacteria, D1 and D2 do not appear to be phosphorylated, whereas in the green alga *C. reinhardtii* there are reports that D2, but not D1, is phosphorylated (Delepelaire, 1983, 1984; de Vitry et al., 1991). Bands assigned to the phosphorylated (D2.1) and non-phosphorylated forms (D2.2) of D2 have been resolved by SDS-PAGE conducted in the presence of 8 M urea (Delepelaire, 1983, 1984). The phosphorylation site in D2.1 has yet to be identified.

The molecular masses for D1 and D2, determined by mass spectrometry, are approximately 38.0 kDa and 39.5 kDa, respectively, as predicted from the gene sequences (Sharma et al., 1997). However, upon SDS-PAGE analysis they usually migrate with apparent sizes of between 30–34 kDa (Satoh et al., 1983), depending on the electrophoretic conditions, most notably the concentration of urea in the gel. In the absence of urea, D1 migrates as two immunodetectable bands (at 34 and 30 kDa), the faster of which is likely to be a more compact structural 'conformer' (Taylor et al., 1988). D2 migrates between these two D1 bands (Nixon et al., 1986; Sayre et al., 1986). Inclusion of urea at concentrations greater than 6M causes the two D1 bands to collapse to a single band of apparent size 30 kDa, so that D2 now migrates slower than D1. Before the availability of specific antisera, the aberrant electrophoretic migration of D1 and D2 together with their poor staining by Coomassie blue, led to much confusion concerning their identification. It is even possible that the radiolabeled bands first assigned to D1 and D2 in non-urea containing polyacrylamide gels (Chua and Gillham, 1977) actually represent the two different electrophoretic conformers of D1 (Nixon, 1988).

IV. Identification of the D1 and D2 Proteins as the Photosystem II Reaction Center Subunits

A. Interpretations of Sequence Similarities

DNA sequencing studies revealed early on that the *psbA* and *psbD* gene products shared some sequence similarity and possessed similar hydropathy profiles, suggestive of an evolutionary relatedness (Rochaix et al., 1984). While the overall sequence identity between the two was relatively unimpressive (27% in *C. reinhardtii*), there were regions of high sequence identity approaching 60% (Rochaix et al., 1984). In concurrent work, it was realized that the L and M subunits of the RC of purple non-sulfur photosynthetic bacteria (hereafter called the BRC) also showed significant regions of sequence similarity to D1 and D2 (Williams et al., 1983, 1984; Youvan et al., 1984). In the absence of detailed structural information, the significance of these similarities was unclear. Based on what was known about D1 and PS II at the time, it was suggested that the areas of similarity were related to a function in quinone binding (Hearst and Sauer, 1984; Rochaix et al., 1984).

A major step in understanding the structure of PS II came paradoxically with the elucidation of the structure of the BRC from *Rhodopseudomonas viridis* (Deisenhofer et al., 1985). The previously observed areas of strong sequence similarity between D1/D2 and the L/M subunits were in regions of the BRC involved in binding the special pair of BChl molecules, and not quinone as first thought. Other key residues such as the four His residues involved in ligating the non-heme iron on the acceptor side of the BRC were also found in D1 and D2. Consequently it was quickly realized from these studies that D1 and D2 were most likely the RC subunits of PS II (Michel and Deisenhofer, 1986) fulfilling roles analogous to L/M of the BRC. Other key residues in L/M were conserved in D1/D2 so that folding models could be drawn for D1/D2 in the absence of direct experimental data (Trebst, 1986; Barber, 1987a; Michel and Deisenhofer, 1988). At that time the dogma in the literature, based on a variety of biochemical evidence, was that CP47, encoded by *psbB*, was the PS II RC subunit (Camm and Green, 1983; Nakatani et al., 1984; de Vitry et al., 1984; Satoh, 1986). However with hindsight it is now clear that D1 and D2 were either present in the active PS II preparations but

had escaped detection or that inappropriate assays for PS II RC activity were used.

B. Isolation of Photosystem II Reaction Center Complexes

The first direct experimental support for the D1/D2 RC model of PS II came with the isolation by Nanba and Satoh (1987) from spinach of the so-called PS II RC complex, sometimes referred to as the 'D1/D2/Cyt b_{559}' complex. Although this preparation did not contain Mn, lacked a fully functional secondary electron donor, Y_Z, and had lost the two quinone electron acceptors, Q_A and Q_B, it still retained the ability to perform light-induced charge separation indicative of the formation of the primary radical pair, $P680^+$ $Pheo^-$ (Danielius et al., 1987; Y. Takahashi et al., 1987). As the complex lacked CP47, this result suggested that D1 and D2 bound P680 and the redox-active Pheo. Other features to support the presence of P680 and the Pheo electron acceptor within this complex were the abilities to generate a spin-polarized chlorophyll triplet state (Rutherford et al., 1981; Okamura et al., 1987) associated with charge recombination of the radical pair and to photoaccumulate either reduced Pheo in the presence of dithionite (Nanba and Satoh, 1987), or oxidized chlorophyll, possibly $P680^+$, upon addition of silicomolybdate (Barber et al., 1987). For a review of the isolated PS II RC see Satoh (1993).

Analysis of the PS II RC complex by SDS-PAGE and Coomassie-blue staining revealed two bands with approximate sizes of 30 kDa plus a further fainter staining band at about 60 kDa. The CP47 and CP43 apopolypeptides were both undetectable (Nanba and Satoh, 1987). Vital immunochemical experiments later confirmed the two 30-kDa bands as the D1 and D2 subunits and the 60-kDa band as either a mixture of D1 and D2 homodimers (Satoh et al., 1987) or a D1/D2 heterodimer (Marder et al., 1987). Also present within this preparation were the low molecular mass α and β subunits of cytochrome b_{559}, which could be detected spectroscopically (Nanba and Satoh, 1987), and the PsbI subunit, also encoded by the chloroplast genome (Ikeuchi and Inoue, 1988a; Webber et al., 1989). The nuclear-encoded PsbW subunit was found later in some preparations of the D1/D2/Cyt b_{559} complex (Lorković et al., 1995), but its absence in other preparations suggests a location on the periphery of the D1/D2/Cyt b_{559} complex (Alizadeh et al., 1999). Important confirmation that D1 and D2 bound the Chl and Pheo molecules of the RC came with the isolation and analysis of a D1/D2 complex depleted of Cyt b_{559} and PsbI (Tang et al., 1990).

D1/D2/Cyt b_{559} complexes have now been isolated from *C. reinhardtii* (Alizadeh et al., 1995), and *Synechocystis* 6803 (Giorgi et al., 1996), so it is clear that the subunit structure of the PS II RC is conserved across the whole range of oxygenic organisms. Radio-labeling studies (Alizadeh et al., 1999) and determination of the ratio of amino acids (Satoh, 1993) have further indicated that the five subunits are present in equimolar amounts.

C. Folding Models of the D1/D2 Heterodimer

Based on hydropathy plots, D1 was originally proposed to consist of seven transmembrane helices (Rao et al., 1983), rather than the five predicted by Michel and Deisenhofer (1986). Experiments involving the binding of site-specific D1 antibodies to inside-out and right-side-out thylakoid vesicles, and trypsin accessibility to D1, provided early support for a five transmembrane helix model for D1 (Sayre et al., 1986).

In the absence of detailed structural information, a number of computer-based models were developed for the D1/D2 heterodimer using the structure of the BRC as a template (Svensson et al., 1990; Ruffle et al., 1992; Svensson et al., 1996; Xiong et al., 1998). In all models there are two branches, A and B, of chlorins spanning the membrane (Fig. 1). Based on the nomenclature developed for the BRC, the 2 Chls analogous to the special pair of BChl molecules are designated in this chapter as P_A and P_B, the 2 Chls analogous to the accessory BChl molecules are designated B_A and B_B (these Chls are termed Chl_{D1} and Chl_{D2} in Chapters 19–21), and the 2 pheophytins are designated $Pheo_A$ and $Pheo_B$. Midway between the primary (Q_A) and secondary (Q_B) quinone electron acceptors is a non-heme iron atom (Fe). Two additional chlorophylls (Chl Z_{D1} and Chl Z_{D2}) found in PS II, but not the BRC, are included in Fig. 1 (Xiong et al., 1998).

Superficially the computer-generated models are very similar, although there are significant differences with regard to the amino-acid residues lining the co-factor binding sites (reviewed in Xiong et al., 1998). Nevertheless these models are consistent with early structural data obtained by EPR such as the orientations of $Pheo_A$ and Q_A (Dorlet et al., 2000) and distances estimated from the spin-lattice relaxation of paragmagnetic species: 39.5 ± 2.5 Å for Fe(II)-

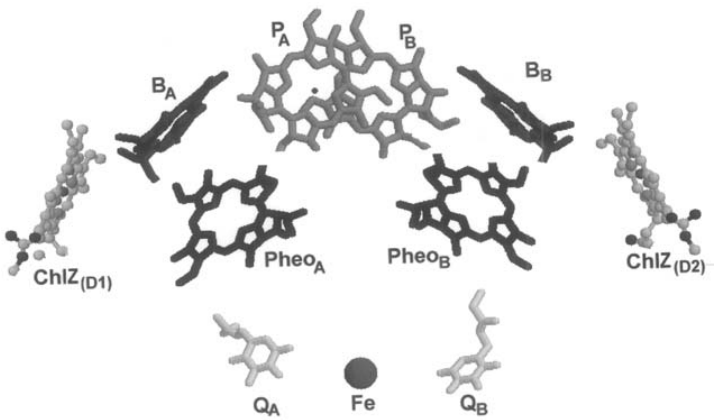

Fig. 1. Nomenclature and model of the transmembrane arrangement of the pigment, quinone and non-heme cofactors within the D1/D2 heterodimer, based on a close analogy to the BRC. The P_A/P_B and B_A/B_B Chl molecules within PS II occupy similar (but not identical) positions to the special-pair and accessory BChl molecules, respectively, of the BRC. $Pheo_A$ and $Pheo_B$ are equivalent to the two BPheo molecules of the BRC. Q_A is the primary quinone electron acceptor, Q_B the secondary quinone electron acceptor, and Fe the non-heme iron atom. In the BRC, electron transfer proceeds down the 'A' branch from P_A/P_B via B_A to $BPheo_A$ then Q_A and finally to Q_B. In PS II there are two extra Chls termed Chl $Z_{(D1)}$ and Chl $Z_{(D2)}$, ligated by D1-His118 and D2-His117, respectively.

Chl Z^+ (Koulougliotis et al., 1994), 37 ± 5 Å for both Fe(II)-$Y_D^{\bullet}$ and Fe(II)-$Y_Z^{\bullet}$ (Koulougliotis et al., 1995) and 20 ± 4.2 Å for Fe(II)-$Pheo_A^-$ (Deligiannakis and Rutherford, 1996). The close structural similarity between the acceptor sides of PS II and the BRC, suggested by these and other early studies, has now been conclusively shown in recent X-ray crystallographic studies (Zouni et al., 2001; Kamiya and Shen, 2003; Biasiadka et al., 2004; Ferreira et al., 2004).

Figure 2 displays folding models for D1 and D2 based on those of Svensson et al. (1996). Highlighted are key residues predicted from sequence comparisons to be involved in binding various cofactors within PS II. Unfortunately the lack of sequence similarity between D1/D2 and L/M in the extrinsic loops connecting the transmembrane helices has limited the ability of the computer-based structural models to provide clear guidance as the structure of the lumenal regions and hence the possible site of the Mn cluster.

V. Mutagenesis of the D1 and D2 Proteins

Two model organisms have been widely used for the mutagenesis of D1 and D2: the cyanobacterium *Synechocystis* sp. PCC 6803 (reviewed by Nixon et al., 1992b; Vermaas, 1993; Debus 2001; Diner 2001) and the green alga *Chlamydomonas reinhardtii* (reviewed by Ruffle and Sayre, 1998). The ability of a D1 protein from a chloroplast to be successfully integrated into a cyanobacterial PS II complex, without loss of O_2-evolving activity (Nixon et al., 1991), suggests that the mechanism of water oxidation by PS II is highly conserved throughout nature. In general, mutagenesis experiments have provided strong support for the general arrangement of pigments shown in Fig. 1 and have provided crucial information on the location of the redox-active components within PS II including the Mn cluster. In the following sections we will discuss some of the key mutants. Unless indicated otherwise, the numbering of residues comes from the *Synechocystis* sequences. For further details, see Chapters 9 (Diner and Britt) and 11 (Debus).

A. Mutations Affecting the Donor Side

1. Tyrosines Y_Z and Y_D

The first demonstration of the power and usefulness of mutagenesis studies for PS II came with the identification of the tyrosine electron donors, Y_Z and Y_D. In the early literature these electron donors are sometimes called Z and D, respectively. Z lies on the electron transfer pathway connecting the Mn cluster to $P680^+$ whereas D is on a side-path. In their oxidized states they give rise to EPR signals of similar shape, the so-called Signal II, but show different kinetics

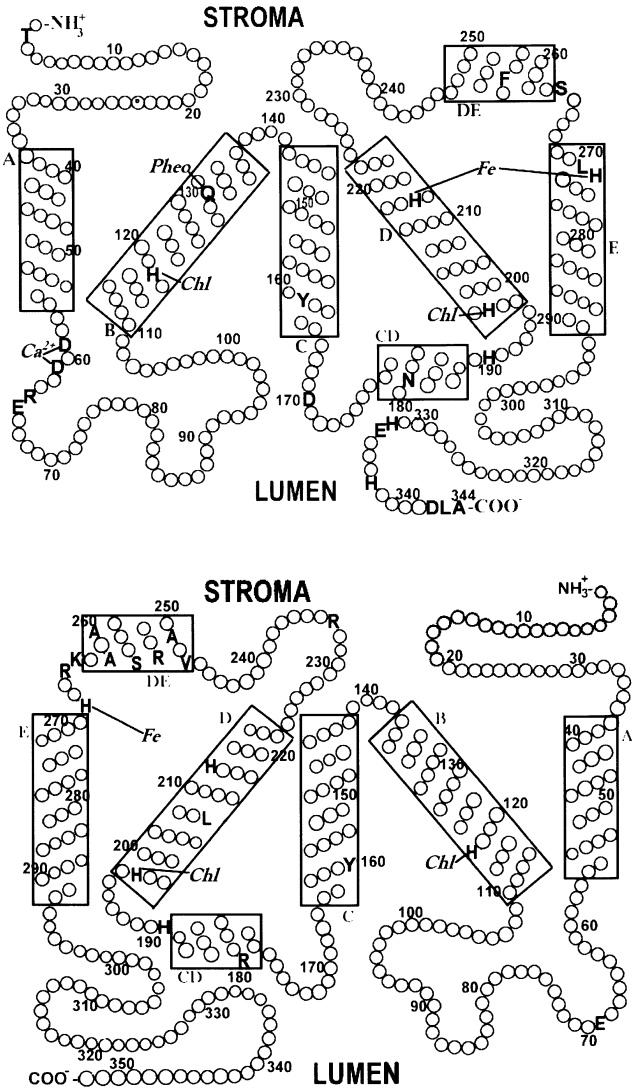

Fig. 2. Folding models for the D1 (top) and D2 (bottom) subunitsof *Synechocystis* 6803 based on ones drawn by Svensson et al. (1996). Each subunit consists of five (A-E) transmembrane helices and two (CD and DE) helices that lie parallel to the membrane. Amino-acid residues that are discussed in the text are indicated by the one-letter code. Possible amino-acid ligands to P_A, P_B, Chl Z_{D1}, Chl $Z_{D2,}$ $Pheo_A$, $Pheo_B$, and Fe are indicated.

of formation and decay: oxidation of Z gives rise to Signal II_{vf} (very fast) in intact PS II or Signal II_f (fast) in samples lacking a Mn cluster (Blankenship et al., 1975). Signal II_s (slow) (Babcock and Sauer, 1973) is an extremely stable signal and is associated with oxidation of D. On the basis of the hyperfine structure of Signal II and its simulation using model compounds, together with other arguments, early work suggested that Z might be a plastosemiquinone cation (PQH_2^+) (O'Malley et al., 1984). However, PS II complexes with fully functional Z and Q_A only contain sufficient extractable plastoquinone to

account for the single Q_A molecule (de Vitry et al., 1986). A resolution to the chemical identity of D, and by extrapolation Z, came with a beautiful series of experiments by Barry and Babcock in which they showed that Signal II_s became narrower when PS II incorporated deuterated tyrosine but not deuterated plastoquinone, so implicating tyrosine as the origin of D (Barry and Babcock, 1987). A similar analysis of isolated PS II complexes containing deuterated tyrosine later confirmed Z to be also a tyrosine residue (Boerner and Barry, 1993). Radio-iodination experiments in which $^{125}I^-$ is activated by PS II-mediated oxidation prior to modification of protein side chains, suggested that D1 and D2 contained Z and D, respectively (Y. Takahashi et al., 1986; Ikeuchi and Inoue, 1987). Folding models predicted the presence of two symmetrically placed Tyr residues, D1-Tyr161 and D2-Tyr160, in the region of iodination (Ikeuchi and Inoue, 1988b; Y. Takahashi and Satoh, 1989). Mutation of D2-Tyr160 to Phe in *Synechocystis* 6803 caused loss of the dark stable Signal II associated with D (Debus et al., 1988a; Vermaas et al., 1988) but still allowed assembly of an O_2-evolving PS II complex. Mutation in *Synechocystis* 6803 of the symmetrical tyrosine in D1 to either Phe (Debus et al., 1988b; Metz et al., 1989), or Trp, His, Cys and Met (Nixon et al., 1992b), all produced strains that were incapable of photosynthetic water oxidation. Analysis of manganese-depleted core complexes isolated from these mutants by EPR and optical spectroscopy further demonstrated that the lesion in electron transfer was at the level of donor Z (Metz et al., 1989). So far no other residue appears to be oxidized when placed at this position. Together these data led to the attribution of D1-Tyr161 and D2-Tyr160 as donors Y_Z and Y_D, respectively. It is now recognized that when oxidized, Y_Z and Y_D form the neutral radical species, $Y_Z^{\bullet}$ and $Y_D^{\bullet}$, and not the cationic species sometimes cited in the literature (reviewed by Diner, 2001; Chapter 9, Dinner and Britt).

2. D1-His190 and D2-His189

A variety of EPR evidence has indicated that $Y_Z^{\bullet}$ and $Y_D^{\bullet}$ are H-bonded (reviewed by Diner, 2001). ENDOR (Tang et al., 1993, Campbell et al., 1997), high-field EPR (Un et al., 1996) and FTIR (Hienerwadel et al., 1997) experiments, using a D2-His189 mutant of *Synechocystis* 6803, strongly support the presence of a H-bond between $Y_D^{\bullet}$ and D2-His189. The situation regarding the role of D1-His190 appeared more complicated with ^{15}N pulsed-ENDOR not favoring a direct H-bond between $Y_Z^{\bullet}$ and D1-His190 (Campbell, 1999). These experimental results are consistent with several of the computer-generated models, which have suggested that D2-His189 might H-bond to the phenolic oxygen of $Y_D^{\bullet}$, but that D1-His190 is too far away to H-bond to $Y_Z^{\bullet}$ (reviewed by Xiong et al., 1998).

All mutants created at D1-His190 in *Synechocystis* 6803 (Diner et al., 1991a; Nixon et al., 1992b; Nixon and Diner, 1994; Chu et al., 1995a; Diner and Nixon, 1998; Hays et al., 1998; 1999) and *C. reinhardtii* (Roffey et al., 1994) are unable to evolve O_2 apart from Lys and Arg substitutions at approximately 13% of wild type rates (Chu et al., 1995a; Hays et al., 1998). The oxidation of Y_Z is dramatically slowed by greater than 200-fold in mutants such as D1-His190Gln and Asp (Diner et al., 1991a; Diner and Nixon, 1998; Hays et al., 1998) but can be partially restored through the addition of small organic bases such as imidazole (Hays et al., 1998). Similarly the rate of re-reduction of $Y_Z^{\bullet}$ in manganese-depleted PS II complexes, through charge recombination, is also much slower and likewise can be accelerated through addition of small bases (Hays et al., 1998). Together these data support a model in which D1-His190 acts as a general acid/base catalyzing the protonation/abstraction of the phenolic proton of Y_Z during its proton-coupled reduction/oxidation (Hayes et al., 1998). Unless Y_Z is able to be deprotonated, its oxidation is blocked. There is still debate as to whether D1-His190 forms a direct H-bond to Y_Z or is linked indirectly through other proton-carriers. See Chapter 9, Diner and Britt, for a more detailed account.

3. Mutants Affecting the Binding and Function of the Manganese Cluster

Based on folding models for D1 and D2, residues exposed to the lumen have been subjected to site-directed mutagenesis (for reviews, see Diner, 2001; and Debus, 2001). The chief targets for mutagenesis were carboxylates and histidine residues, both of which are excellent candidates for ligating metal ions. Some early support for a role for His in ligating the cluster came from chemical modification experiments (Tamura et al., 1989). Pulsed EPR experiments have since unambiguously confirmed this proposal (Tang et al., 1994). The participation of histidine and carboxylate residues in Mn binding in PS II has also been suggested on the basis of non-competitive inhi-

bition experiments between exogenous Mn^{2+} and the artificial electron donor to PS II, diphenylcarbazide (Seibert et al., 1989; Preston and Seibert, 1991).

One of the surprises of the brute-force mutagenesis approach was how difficult it was to knock out the assembly of a functional Mn cluster (Pakrasi and Vermaas 1992; Nixon et al., 1992b). In part this may reflect the ability of alternate ligands such as water and chloride to substitute for a missing proteinaceous ligand. Nevertheless, this observation strengthened the significance of residues at which mutation specifically blocked Mn assembly.

a. The LF-1 Mutant of Scenedesmus obliquus

One of the first and most important mutants affecting the assembly of the Mn cluster in PS II was the LF-1 (low fluorescence –1) mutant of *Scenedesmus obliquus*, which was generated through X-ray mutagenesis (Metz and Bishop, 1980). Originally identified in chlorophyll-fluorescence based screens as low-fluorescent, the LF-1 was consistent with an impairment on the donor side of PS II. Biochemical studies indicated that the PS II could accumulate and retain electron transfer activity across the membrane but was unable to assemble a functional Mn cluster, with only 1–2 Mn bound to each PS II center (Metz and Bishop, 1980; Metz et al., 1980). A polypeptide of apparent molecular mass 34 kDa in the wild type showed a shift to an apparent molecular mass of 36 kDa in LF-1. No other differences in the electrophoretograms were detected, so the 34-kDa subunit was suggested to be involved in binding Mn (Metz et al., 1980). Originally thought to be a modified form of the 33-kDa extrinsic protein involved in stabilizing of the Mn cluster (Bishop, 1983) or possibly D2 (Metz and Seibert, 1984), the 36-kDa polypeptide is now known to be precursor D1 (Metz et al., 1986; Taylor et al., 1988; Diner et al., 1988). The phenotype of LF-1 results from a single base deletion and a consequent frameshift in the coding region for CtpA, the D1 processing protease (Trost et al., 1997), which is needed to remove the C-terminal extension. That the inability to assemble the Mn cluster was due to a block in D1 maturation, rather than some other target for the processing protease, was confirmed through the construction of the D1-S345P mutant of *Synechocystis* 6803 which was unable to process precursor D1 because of a modified cleavage site. The phenotype of this mutant was essentially identical to that of LF-1 (Nixon et al., 1992a).

Overall the LF-1 mutant provided the first mutagenesis evidence to indicate a role for D1 in the assembly of the Mn cluster, not just in Q_B binding. However, it still remains unclear to what extent the C-terminal extension causes indirect structural perturbations on the lumenal side of PS II.

b. D1-Asp170

This was the first amino acid residue to be identified as important for assembly of a functional Mn cluster (Nixon and Diner, 1990). Mutants created at this residue in either *Synechocystis* 6803 (Nixon and Diner, 1992; Boerner et al., 1992) or *C. reinhardtii* (Whitelegge et al., 1995) were to varying degrees able to accumulate active PS II. Retention of a residue that was capable of ligation to a metal allowed the assembly of a cluster whereas substitution with a non-ligand such as Ala showed no O_2 evolution but was still able to assemble an otherwise functional PS II complex with regard to electron transfer from Y_Z to Q_B (Nixon and Diner, 1992). Mutations at Asp170 also affected the ability of detergent-solubilized PS II complexes, with the Mn cluster removed, to bind and oxidize Mn^{2+} to Mn^{3+} at a high-affinity site within PS II (Diner and Nixon, 1992; Nixon and Diner, 1992). This high-affinity site, implicated first by EPR (Hoganson et al., 1989), is probably identical to the binding site for the first Mn ion in the natural light-driven process of photoactivation that assembles the functional Mn cluster (Radmer and Cheniae, 1977). More recent evidence to support the idea that Asp170 acts as a ligand to the Mn (III) has come from parallel mode EPR measurements (Campbell et al., 2000). The structural model of PS II from Imperial College London has now confirmed a role for Asp170 in ligating one of the Mn ions of the intact cluster (Ferreira et al., 2004). Somewhat surprisingly mutants D1-Asp170Val, Leu and Ile are able to assemble a functional cluster in a fraction of the centers despite the presence of a non-ligand at this position (Chu et al., 1995a). Presumably an alternative ligand is operating in these mutants.

c. His332, Glu333, His337, Asp342 in the Carboxyl-Terminal Region of D1

Mutation of a number of residues in the C-terminal region of D1 specifically compromised the ability to assemble a functional Mn cluster (Nixon et al., 1992a; Nixon and Diner, 1994; Chu et al., 1995b). In the case

of some, but not all, of the mutants created at D1-His332, D1-Glu333 and D1-Asp342 O_2 evolution is blocked (Nixon et al., 1992b; Nixon and Diner, 1994; Chu et al., 1995b), consistent with their roles as Mn ligands (Ferreira et al., 2004). Those substitutions that allow assembly of a Mn cluster have the potential to act as ligands. Many of the mutants constructed in this region of D1, such as at D1-His337, allow O_2 evolution but the activity is readily photoinhibited (Nixon et al., 1992b; Chu et al., 1995b). The most detailed analysis so far of mutants in this region of D1 has come from an ESEEM study of PS II complexes isolated from a D1-His332Glu mutant of *Synechocystis* 6803, in which the Mn cluster assembles but is unable to pass beyond the S_2 state (Debus et al., 2001). Since this residue is now known to be a ligand to the Mn cluster (Ferreira et al., 2004), these results highlight the importance of appropriate ligation for controlling the redox properties of the cluster. Of importance was the finding that the high-affinity Mn^{2+}-binding site characterized in isolated PS II complexes is largely preserved in C-terminal mutants lacking a functional cluster (Nixon et al., 1992a,b; Nixon and Diner, 1994). This feature distinguishes the C-terminal D1 mutants from those at D1-Asp170.

d. The Carboxyl-Terminal Residue at Ala-344

In some of the first mutagenesis studies on D1 in *Synechocystis* 6803, the effect of deleting progressively larger portions of the C-terminus was examined (Nixon et al., 1992a). Removal of the C-terminal extension, so that only the mature form of D1 was synthesized, did not block assembly of functional PS II. This important finding, which holds also for the green alga *C. reinhardtii* (Lers et al., 1992; Schrader and Johanningmeier, 1992), showed that the C-terminal extension was not required for integration of D1 into the thylakoid membrane, a possibility that had been suggested in early studies on D1 maturation (Marder et al., 1984). Removal of an additional residue, leaving D1-Leu343 as the C-terminal residue, allowed the assembly of PS II complexes competent in the oxidation of Y_Z but blocked the formation of an active Mn cluster. Deletion of additional residues further reduced the ability to accumulate PS II centers, all of which were inactive for O_2 evolution (Nixon et al., 1992a). These results therefore highlighted the functional importance of the C-terminal residue for the Mn cluster. A number of residues (Gly, Met, Ser, Val, Tyr, Lys) could substitute for Ala-344 without blocking totally the assembly of the Mn cluster. Therefore it was suggested that it was the free carboxyl group that was important for functionality (Nixon et al., 1992a).

e. Other Residues Affecting the Manganese Cluster

A number of D1 mutants have been characterized that retain oxygen-evolving ability but show modified properties. Amongst these are mutants created at D1-Asp59, D1-Asp61 and D1-Glu65, in the lumenal loop connecting helices A and B. These residues had been speculated for some time to be involved in binding metal ions, either Mn or Ca^{2+}. A role for D1-Asp59 and D1-Asp61 in binding Ca^{2+} was given impetus with the finding that photoautotrophic growth of mutants constructed at these sites was sensitive to the depletion of Ca^{2+} from the growth medium (Nixon and Diner, 1994; Chu et al., 1995a). More detailed analyses of mutants at these positions are consistent with an important role for these residues in stabilizing intermediates formed during the assembly of the Mn cluster, possibly through the binding of a calcium ion, although this has yet to be probed directly (Qian et al., 1999). In addition, mutants at these residues show slower production of O_2 indicative of a slower cycling through the higher S-state transitions (Hundelt et al., 1998; Qian et al., 1999).

Besides D1-Asp59 and D1-Asp61, the photoautotrophic growth of mutants at D1-Glu333 and D1-Asp342 in the C-terminal region are also sensitive to the depletion of Ca^{2+} (Nixon and Diner, 1994; Chu et al., 1995a) or chloride (Nixon and Diner, 1994) from the growth medium. These phenotypes are also observed with many D2 mutants (Keilty et al., 2001) and mutants lacking extrinsic proteins of PS II (summarized in Li and Burnap, 2001). Ca^{2+} and chloride play a role in the function of the Mn cluster, suggesting direct or indirect effects of all these mutations on their normal binding within PS II or in the case of chloride, a possible role as a replacement ligand to the cluster. One indirect effect of mutating these, and other residues such as D1-Arg64, might be to prevent correct binding of the extrinsic proteins to the lumenal side of PS II (Li and Burnap, 2001).

Another feature of many D1 mutants, including mutants constructed at the C-terminus of D1, as well as the D2-Glu69Gln mutant (Vermaas et al., 1990), is the enhanced sensitivity to light-induced inactivation of O_2 evolution by mutant cells. There are many

possible causes for such a phenotype including the damaging effects of relatively long-lived highly oxidizing species within PS II, the production of reactive oxygen species at the modified Mn clusters (Chu et al., 1995b) and effects on the D1 repair cycle (Dalla Chiesa et al., 1996). Thus enhanced sensitivity to photoinhibition is in itself not compelling evidence for a role for that residue in binding Mn. For more details see Chapter 11, Debus.

f. Model for Location and Assembly of the Manganese Cluster Based on Mutagenesis Data

On the basis of the mutagenesis data, Diner et al., (1991a) proposed a simple structural model for the location of the Mn cluster within D1 (Fig. 3). In order to bring all the crucial residues identified by mutagenesis into a compact cluster that could ligate the Mn cluster, the C-terminal region of D1 had to be folded back so that it was present close to D1-Asp170. The location of Asp170 only 9 residues away from D1-Tyr161, the oxidant of the cluster, also suggested that the Mn cluster was located close to Y_Z; indeed estimates from computer modeling studies placed Asp170 6–7 Å from Y_Z (e.g., Svenson et al., 1996). At the time of the proposal of the model in Fig. 3, EPR data suggested that the Mn cluster was greater than 10 Å from Y_Z (Hoganson and Babcock, 1988) and, in other work, possibly up to 32 Å away (Un et al., 1994). Such distances led to the exclusion of Asp170 as a ligand in early computer models (Svensson et al., 1990). However more recent EPR analyses have indicated a much smaller distance (7–9 Å) between the Mn cluster and Y_Z (Dorlet et al., 1998; Peloquin et al., 1998; Lakshmi et al., 1999). The proposed location of the Mn cluster in Fig. 3 also agrees very well with the structural models determined by X-ray crystallography (Kamiya and Shen, 2003; Biesiadka et al., 2004; Ferreira et al., 2004).

The mutagenesis data have also allowed a model to be proposed for the coupling of D1 processing to the assembly of the Mn cluster (Diner et al., 1991a; Nixon et al., 1992a). In this model, the first Mn ion is proposed to bind at a high-affinity site of which D1-Asp170 is an important component. It is this Mn ion that is oxidized first by PS II in photoactivation. In order to complete the assembly of the cluster, removal of the C-terminal extension is required. At the same time this cleavage reaction would reveal

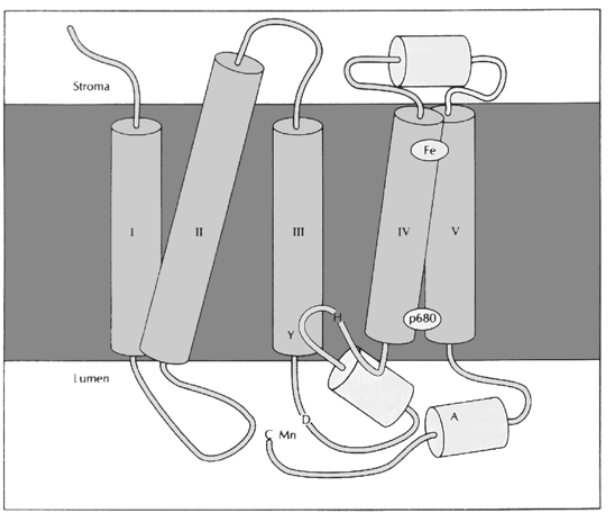

Fig. 3. The folding model of D1 proposed by Diner et al. (1991a), showing the location of the Mn cluster (Mn) within PS II based on the analysis of site-directed mutants of *Synechocystis* 6803. The five transmembrane helices of D1 are labeled here as I-V. The cluster was proposed to be coordinated by D1-Asp170 (D) and by residues within the C-terminal region of D1, including the C-terminus itself (C). Also shown are Yz (Y), the oxidant of the Mn cluster, which is thought to be close to D1-H190 (H), as well as P680 (p680) and the non-haem iron (Fe). A possible amphiphilic helix (helix A) was suggested to bring the C-terminal residues towards D1-Asp170 (D). Reprinted with permission from Elsevier Science.

the carboxy terminus at D1-Ala344, which might act as a ligand to the cluster, perhaps following a substantial conformational change to bring the C-terminus close to D1-Asp170. The involvement of the free C-terminus in ligating Mn (or Ca^{2+}) explains nicely why processing is required for assembly of a functional Mn cluster.

The presence of the C-terminal extension provides a selective advantage to cells growing in mixed culture compared to those without (Ivleva et al. 2000). However it remains unclear what advantage the extension conveys. One possibility is that removal of the extension is coupled to the stepwise assembly of the most stable and active cluster. In its absence, there might be an increased chance that inappropriate ligands are used so that although active clusters might still assemble, there is a greater likelihood of forming poorer functioning clusters with a greater propensity for causing damage to PS II. Alternatively, the C-terminal extension might play a role in optimizing the assembly of PS II in the PS II repair cycle. While the model in Fig. 3 emphasized an exclusive role for D1 in binding the Mn cluster, it was always recognized that other PS II subunits might participate, as eventually revealed in the structural model from Imperial College (Ferreira et al., 2004).

4. D1-His198 and D2-His197

The histidines that coordinate the two members of the special pair found in the L and M subunits of the BRC are conserved in PS II at D1-His198 and D2-His197. This naturally led to a model in which these latter residues also ligated the chlorophyll molecules, P_A and P_B, respectively, (Fig. 1) in a broadly similar way to that found in the BRC, although there had to be some structural distortion to explain the absence of strong excitonic coupling between the two Chls (Durrant et al., 1995). However, the presence of P_A and P_B in PS II was not immediately accepted because of the significant redox and spectral differences observed between PS II and the BRC. For instance, because $P680^+$ is much more oxidizing than the bacterial equivalent, van Gorkom and Schelvis (1993) pointed out that P_B as well as B_B might not be retained in PS II to avoid unwanted oxidation of Chl. Also models were suggested in which P_A was rotated from perpendicular to the membrane plane to 30 degrees (Noguchi et al., 1993) so as to accommodate EPR data on the orientation of the chlorophyll molecule carrying the $P680^T$ state (van Mieghem et al., 1991).

Early mutagenesis studies indicated that D1-His198 and D2-His197 were indeed important since replacement by leucine (Nixon et al., 1992b) and tyrosine (Vermaas et al., 1987), respectively, led to loss of PS II from the membrane. More recently a number of mutations have been made at these positions that allowed assembly of functional PS II complexes. These mutants have subsequently proved to be an invaluable resource in addressing questions regarding the nature of P680 (Diner et al., 2001) and the energetics of primary charge separation (Merry et al., 1998).

In the most detailed work so far on these mutants, Diner et al. (2001) have applied optical and EPR spectroscopies to examine the $P680^+$ and $P680^T$ states in core complexes isolated from mutants of *Synechocystis* 6803 constructed at either D1-His198 or D2-His197. Mutation of D1-His198 caused both shifts in the $P680^+$–P680-absorbance difference spectrum and appreciable modulation of the $P680^+$/P680 redox couple. Mutation of D2-His197 had less dramatic effects on these parameters. The triplet-minus-singlet optical difference spectrum for P680 was in contrast unchanged in all mutants. These results therefore support a model in which following charge separation the chlorophyll cation (usually called $P680^+$) is stabilized primarily on P_A (ligated by D1-His198) and to a lesser degree (approx 20%) on P_B (ligated by D2-His197). Results obtained with the above mutants and other data in the literature also support the idea that charge separation is initiated mainly from the singlet excited state of the accessory chlorophyll, B_A*, and that the P680 triplet state is stabilized at low temperature mainly on B_A and not P_A (Noguchi et al., 1998; Sarcina et al., 1998). At first sight, such a scheme for PS II primary photochemistry is in sharp contrast with that for the BRC where the BChl singlet, cation and triplet states are located on the special pair of BChls (P). However, a major rethinking of this dogma suggests that there are multiple pathways for stable charge separation in the BRC including charge separation from B_A* not just P* (van Brederode and van Grondelle, 1999; Dekker and van Grondelle, 2000). PS II differs from the BRC in that the excited singlet states are much closer in energy in the former resulting in extensive delocalization of the excited state of the RC within a multimer of pigments rather than localized to the special pair (Durrant et al., 1995). At low temperature (4K) the excited state energy in PS II is exclusively localized on B_A implying that charge separation at

this temperature must be occurring from B_A^* (Diner et al., 2001; Diner and Rappaport, 2002).

5. D1-His118 and D2-His117

Initial measurements of the pigment stoichiometry of the D1/D2/Cyt b_{559} complex isolated by Nanba and Satoh (1987) suggested a ratio of about 5 Chl per 2 Pheo molecules. For the BRC, there are 4 BChl molecules and 2 BPheo. Hence it was anticipated by analogy that the pigment stoichiometry for the D1/D2/Cyt b_{559} complex would in fact be 4 Chl/2 Pheo (Barber, 1987b). However, following suggestions that this was so (e.g., Barber et al., 1987; Aured et al., 1994; Chang et al., 1994; Pueyo et al., 1995), a consensus has now emerged in favor of a ratio of 6 Chl per 2 Pheo for the most stable form of the PS II RC (Gounaris et al., 1990; Kobayashi et al., 1990; Eijckelhoff and Dekker, 1995). Thus, the D1/D2/Cyt b_{559} complex contains 2 additional Chls compared with the BRC. Important confirmation that it was the D1/D2 heterodimer that bound these 2 extra Chl came with the isolation of a D1/D2 complex (Tang et al., 1990).

The possible ligands for these two 'extra' Chl molecules focused on two symmetrically related His residues, D1-His118 and D2-His117, not conserved in the BRC, which are predicted to lie in the second transmembrane helix of D1 and D2, respectively (Michel and Deisenhofer, 1988). Computer modeling studies placed these Chls on the exterior of the D1/D2 heterodimer in a position to interact with the neighboring CP47 and CP43 subunits and to act possibly as linker Chls connecting the pigments in CP47 and CP43 to those involved in primary photochemistry in D1 and D2 (Ruffle et al., 1992). Measurements of energy transfer within the isolated PS II RC indeed suggested two populations of pigments: A peripheral pool, which shows a relatively slow rate of energy transfer to P680 (Schelvis et al., 1994), possibly bound to D1-His118 and D2-His117, and an inner core of pigments that shows rapid equilibration of excitation energy (Durrant et al., 1992).

Mutation of D2-His117 to residues that could potentially coordinate Chl (Cys, Met, Asn and Thr) still allowed photoautotrophic growth in *Synechocystis* 6803, whereas other substitutions impaired accumulation of PS II to varying degrees (Pakrasi and Vermaas, 1992; Lince and Vermaas, 1998; Stewart et al., 1998). Fluorescence studies on the D2-His118Thr mutant suggested that energy transfer into the PS II RC was slowed, consistent with a role in binding Chl (Lince and Vermaas, 1998; Vasil'ev and Bruce, 2000). A comparison by EPR, near-infrared absorbance and resonance Raman spectroscopies of PS II complexes isolated from *Synechocystis* 6803 mutants D2-His117Gln and its counterpart, D1-His118Gln, (Stewart et al., 1998) led to the conclusion that D1-His118, and not D2-His117, was the axial ligand to Chl Z, a photooxidizable Chl molecule that had been identified earlier in PS II from higher plants (de Paula et al., 1985). The possible physiological role of Chl Z in protection form photoinhibition and its mode of oxidation and reduction are described in detail in Chapter 15 (Faller and Rutherford) of this volume. Based on symmetry arguments Stewart et al (1998) further suggested that D2-His117 also acted as an axial ligand to Chl but that this Chl, termed Chl D, was redox-inactive. The Chl Z and Chl D nomenclature is an extension of that used to describe the two redox-active tyrosines in PS II–Y_Z and Y_D.

The PS II structure determined to a resolution of 3.8 Å by Zouni and co-workers confirmed the presence of two Chls, termed Chl Z_{D1} and Chl Z_{D2}, within the predicted vicinity of D1-His118 and D2-His117, respectively (Zouni et al., 2001). One of the interesting features of this PS II structure was the finding that Cyt b_{559} was located on the D2 side of the complex (Zouni et al., 2001). This meant that Cyt b_{559}, suggested initially to be the direct reductant of Chl Z^+ (Thompson and Brudvig, 1988) was in fact closer to Chl D than Chl Z. Had Chl Z been misassigned so that D2-His117 rather than D1-His118 was the true ligand? The possibility that the Chl bound to D2-His117 could be redox-active has received recent experimental support from studies of D2-His117Asn/Gln and D1-His118Gln mutants of *C. reinhardtii* (Ruffle et al., 2001; Wang et al., 2002). The EPR spectrum assigned to Chl Z^+ obtained from PS II RCs isolated from the D2-His117Asn mutant was broadened compared to the wild type and the D1-His118Gln mutant, which both showed similar spectra. This broadening has been interpreted in terms of a possible rotation of the Chl (Wang et al., 2002). Mutation of both D1-His118 and D2-His117 in *C. reinhardtii* altered energy transfer into the PS II RC consistent with modification to peripheral Chls of the RC. These results are in apparent contradiction to the conclusions made by Stewart et al. (1998). A possible reconciliation of these data has recently emerged from comparative studies on the identity of the photooxidizable accessory Chls in PS II from *Synechocystis* 6803 and spinach (Tracewell et al., 2001).

For *Synechocystis* 6803 it appears that only Chl Z (Chl Z_{D1}) is photooxidized whereas in spinach, and hence possibly *C. reinhardtii*, both Chl Z and Chl D (Chl Z_{D2}) can be photooxidized. This contrasts with early studies where only one of the accessory Chls was thought to be photooxidizable in the plant system (de Paula et al., 1985). Given the current uncertainty it seems prudent to adopt the nomenclature Chl Z_{D1} and Chl Z_{D2} to describe these two Chl species rather than Chl Z and Chl D.

B. Mutations Affecting the Acceptor Side

1. The Pheophytins

It has long been established that Pheo is reduced during primary charge separation in PS II (Klimov et al., 1977). Pigment analysis of the PS II RC supported the presence of 2 Pheo per RC. Based on the analogy with the BRC the two Pheo would be on separate branches of co-factors in the RC, with the Pheo bound to D1 on the active branch. Sequence comparisons indicated that the C9-keto group of each Pheo would be positioned so that $Pheo_A$ could form a H-bond to residue 130 of D1 and $Pheo_B$ to residue 130 of D2 (Michel and Deisenhofer, 1988). Interestingly the residue at D1-130 is not totally conserved within PS II–for the majority of organisms it is a glutamic acid whereas for *Synechocystis* 6803 it is a glutamine. Early ENDOR (Lubitz et al., 1989), resonance Raman (Moenne-Loccoz et al., 1990) and FTIR experiments (Nabedryk et al., 1990) all suggested the presence of a H-bond to the photoactive Pheo in plants. Confirmation that residue 130 of D1 plays an important role in the optical properties of a redox-active Pheo came with the analysis of PS II RCs isolated from mutants D1-Gln130Glu and D1-Gln130Leu constructed in *Synechocystis* 6803 (Giorgi et al., 1996). The Q_x transition was shifted from 541.5 nm in the wild type to 540 nm in the D1-Gln130Leu mutant and to 544nm in the D1-Gln130Glu mutant. In plants, where residue D1-130 is naturally a Glu, the Q_x transition is already at 544 nm. The degree of the red shift in the mutants correlates with the probable strength of the H-bond to this residue, a similar behavior to that found in the equivalent mutants in the BRC at L-104 (Bylina et al., 1988). Since only 1 of the 2 Pheo in the PS II RC is photoactive (Nanba and Satoh, 1987), these data also provided compelling evidence to support the assumption that it was the D1-bound Pheo that was redox-active and that electron proceeded predominantly down the A-branch as in the BRC. This conclusion has been recently reinforced from analysis of PS II RCs in which the D1-bound Pheo was replaced by a 13-OH-Pheo derivative (Germano et al 2001). FTIR analysis of mutant *Synechocystis* 6803 PS II RCs (P. J. Nixon and J. Breton, unpublished) have confirmed the presence of a H-bond between residue 130 and the C9-keto group. This conclusion is also supported by a recent high field EPR study of PS II RCs isolated from D1-Glu130His, Gln and Leu mutants of *C. reinhardtii* (Dorlet et al., 2001). Overall these data provided important experimental support to the idea that the location and orientation of the redox-active Pheo is conserved between PS II and the BRC.

Besides identifying the location of pigment molecules within PS II through the effects of mutation on the optical, redox or vibrational properties of the molecule, it is possible to create mutants in which a different type of pigment molecule is inserted into the site. In BRCs, when an imidazole ligand is supplied in the correct region of the BPheo pocket, a BChl is inserted instead, presumably because the central Mg^{2+} is stabilized (Kirmaier et al., 1991). Based on sequence comparisons, the analogous mutants have now been constructed in PS II. The D2-Leu209His mutant of *Synechocystis* 6803 (DA Force and BA Diner, unpublished data) replaces the redox-active Pheo with a Chl, the result of which is that primary charge separation occurs with a reduced quantum yield. Mutant D1-Leu210His stabilizes insertion of a Chl for the redox-inactive Pheo (DA Force and BA Diner, unpublished data). This latter mutant is very important, as it has provided the first mutagenesis data in favor of a strong structural similarity between PS II and the BRC with regard to the redox-inactive Pheo molecule. A strong similarity between PS II and the BRC in terms of the orientation, not just the location, of the two Pheo molecules, is also suggested from recent spectroscopic experiments on isolated PS II RCs containing a 13-OH-Pheo derivative (Germano et al., 2001, 2002).

2. The Accessory Chlorophylls B_A and B_B

The His residues that act as axial ligands to the accessory BChls in the BRC are not conserved in D1 and D2 (Michel and Deisenhofer, 1988). This feature raised the possibility of quite dramatic differences to the BRC in this part of PS II. The identification of accessory molecules in the first structures of PS II

was vital evidence that this was not the case (Rhee et al., 1998). Presumably there are alternative ligands to these Chl in PS II such as water molecules, for which there is precedence (Hofmann et al., 1996), the protein backbone or perhaps a different type of amino-acid side chain. Inspection of the CD helices in D1 and D2 has identified two potential ligands: D2-Arg180 and D1-Asn181. Mutation of D2-Arg180 in *Synechocystis* 6803 has not provided definitive evidence concerning a role as a Chl ligand although there were clear effects on Y_D (Manna et al., 1998).

3. The Iron-Quinone Complex

A variety of early biophysical evidence suggested a close analogy between PS II and the BRC with regard the acceptor side of the complex (reviewed by Diner et al., 1991b). Both contain a tightly bound quinone, Q_A, which acts as a 1-electron carrier (Q_A/Q_A^-) and a second quinone, Q_B, which is reduced by Q_A^- to first the semiquinone anion, Q_B^-, and, following a second turnover of the RC, to the quinol. Following protonation the quinol, Q_BH_2, is released from the Q_B-binding site (Bouges-Bocquet, 1973; Velthuys and Amesz, 1974; Chapter 8, Petrouleas and Crofts). For the BRC, the binding sites for Q_A and Q_B are located in the M and L subunits, respectively. By analogy the equivalent sites in PS II would be in D2 and D1. For the BRC, the non-heme iron located between Q_A and Q_B is ligated by 4 His residues plus a glutamate, at position 232 in the M subunit of *Rhodopseudomonas viridis* (Deisenhofer et al., 1985). In PS II there is no obvious homologue to this Glu residue. Instead FTIR experiments indicate that bicarbonate acts as a bidentate ligand to the iron (Hienerwadel and Berthomieu, 1995). The bicarbonate ligand can be displaced competitively by a collection of ligands which include NO and carboxylate anions, resulting in a modest slowing of the reaction $Q_A^- Q_B \rightarrow Q_AQ_B^-$ and a marked slowing of the reaction $Q_A^- Q_B^- \rightarrow Q_AQ_BH_2$ (Diner and Petrouleas, 1990; Petrouleas et al., 1994). These observations and earlier bicarbonate depletion experiments have led to the conclusion that bicarbonate is involved in protonation reactions coupled to the formation of Q_B^- (Eaton-Rye and Govindjee, 1988) and of Q_BH^- (van Rensen et al., 1988) (reviewed in Diner et al., 1991b). Extensive mutagenesis experiments have also been directed at identifying residues that might be important for bicarbonate binding. Mutation of D2-Lys264 and D2-Arg265, which lie close to D2-His268 impair bicarbonate binding (Diner et al., 1991a). Two other residues, D2-Arg233 and D2-Arg251, have a weaker effect on bicarbonate binding (Cao et al., 1991).

Photosystem II differs from BRCs in that the non-heme iron is redox-active. First identified as Q_{400}, the iron shows reversible oxidation/reduction with a reduction potential of 400 mV at pH 7 (Diner and Petrouleas, 1987). The 4 His residues that ligate the iron in the BRC are conserved in D1 and D2 at D1-His215, D1-His272, D2-His214 and D2-His268. The effect of mutating these residues in PS II has not been fully explored although initial reports suggest, perhaps surprisingly, that replacement of D2-His268 by Gln (Vermaas et al., 1994) and of D1-His215 by Leu (Nixon et al., 1992b) leads to the accumulation of PS II centers but with a much lower quantum yield of Q_A reduction.

Computer generated models for PS II have identified a number of D2 residues that could line the Q_A-binding pocket, including D2-Ala249, Ser254, Ala258, Ala260 and His268 (e.g., Ruffle et al., 1992). Mutagenesis studies have now confirmed the importance of these residues for PS II function (Vermaas et al., 1994; Ermakova-Gerdes and Vermaas, 1998; Ermakova-Gerdes et al., 2001). An interesting property of these mutants, such as the D2-Val247Met, Ala249Thr double mutant (Ermakova-Gerdes and Vermaas, 1998) and the D2-His268Gln mutant (Vermaas et al., 1994) is the apparent ease of loss of Q_A from its binding site and the ability to reconstitute with artificial quinones. D2-Trp253 has attracted attention because it is in an analogous position to residue M-Trp250 of *Rp. viridis*, which lies between Q_A and $BPheo_A$, and which is required for retention of Q_A (Coleman and Youvan, 1990). In the D2-Trp253Phe mutant, Q_A^- is destabilized, consistent with a close location for this residue (Vermaas, 1993).

Analysis by ESEEM of PS II centers isolated from wild type *Synechocystis* 6803 and mutant D2-Ala260Gly, in which ^{15}N had been incorporated, has provided overwhelming experimental support for a weak H-bond between an oxygen of Q_A and the peptide nitrogen of D2-Ala260 (Peloquin et al., 1999). Such an interaction is predicted from structural models based on the BRC (Diner et al., 1991b). Another, stronger H-bond exists between Q_A^- and an unidentified peptide nitrogen. However, evidence for a predicted H-bond between Q_A^- and D2-His215, thought to ligate the non-heme iron, based on structural homology with the BRCs, is not apparent in the ESEEM spectra (Peloquin et al., 1999; but see

Deligiannakis et al., 1999). The inability to see this interaction does not necessarily mean that it does not exist, as the magnetic coupling may be extremely weak and may depend on the pH and the coordination of the non-heme iron. Thus, while there is significant structural conservation between the Q_A-binding sites of PS II and the BRC, the strength of the H-bonds to Q_A^- is likely to depend on subtle differences in the position of the H-bonding residues and on the interaction of D2-His215 with the non-heme iron.

The Q_B-binding pocket within PS II is formed from residues present in transmembrane helices D and E of D1 and the stromal DE loop connecting them (Fig. 2). The predicted DE loop in D1 is 17 amino-acid residues longer than that found in the L subunit. Mutagenesis has indicated that PS II can tolerate dramatic changes in the length and sequence of this loop although there are deleterious effects on Q_B function (Kless et al., 1994; Nixon et al., 1995).

Sequence alignments between D1 and the L subunit indicate only 9 out of 77 residues to be identical in the region from D1-Phe206 to D1-Gly282. Of the conserved residues, residue D1-His215 is the equivalent to L-His190 of *Rp. viridis*, which H-bonds to Q_B and ligates the non-heme iron. D1-Ser264 appears to be homologous to L-Ser223 of the BRC, since mutation of both gives rise to herbicide resistance (Oettmeier, 1999). L-Ser223 plays a role in the protonation of Q_B^- to Q_BH (Paddock et al., 1990) and might be involved in stabilizing the binding of Q_BH^- in the Q_B site (Lancaster and Michel, 1997). Replacement of D1-Ser264 by Gly reduces the affinity for Q_B but has little effect on the protonation of the quinol in PS II (Taoka and Crofts, 1990) indicating other pathways for protonation, such as via D1-His252, which was suggested early on to have a role in the protonation of Q_B^- and Q_BH^- (H. Robinson and A.R. Crofts, personal communication). In support of this view, a recent report (Lupínková et al., 2002) shows a dramatic effect of mutating this site on the rate of oxidation of Q_A^-. Other residues identified by mutagenesis as important for Q_B binding are D1-Phe255 and D1-Leu271 (Ohad and Hirschberg, 1992). For further details see Chapter 8, Petrouleas and Crofts.

PS II is a known target for a number of different classes of herbicides, including the triazines and ureas. Herbicide resistance is afforded by mutation of any one of 16 amino-acid residues within D1, in a region extending from D1-Phe211 to D1-Leu275 (reviewed by Oettmeier, 1998). According to the structural models for D1, these mutations cluster within a defined region of D1 (Erickson et al., 1989). The binding pocket for the herbicides in PS II overlaps with that for Q_B so that many, but not all, herbicide-resistant mutants also affect the binding of Q_B and modulate its redox properties (Ohad and Hirschberg, 1992).

VI. Concluding Remarks

The study of D1 and D2 mutants has proved to be a remarkably successful approach to probe the link between PS II structure and function. Not only has it provided ample evidence to support the close analogies between PS II and the BRC with respect to the electron acceptor sides of both complexes, but it has also identified several residues in D1, which could not have been predicted by comparison to BRCs, that play key roles in photosynthetic water-oxidation. The importance of D1-Asp170 for assembly of the Mn cluster led to the suggestion that the Mn cluster was close to the CD loop of D1 (Nixon and Diner, 1992). Mutagenesis experiments also identified residues within the C-terminal region of D1 that were important for assembly of the Mn cluster. The emerging structural models of PS II have confirmed that these regions of D1 are indeed involved in ligating the Mn cluster (Zouni et al., 2001; Kamiya and Shen, 2003; Biesiadka et al., 2004; Ferreira et al., 2004). Now that a detailed structural model for PS II is available, with side-chain information (Ferreira et al., 2004), there will be tremendous interest in the construction and analysis of new mutants (and possibly the reassessment of previously constructed ones). To this end, it would be highly beneficial to develop a thermophilic cyanobacterium, such as *Thermosynechococcus elongatus*, as a suitable model system to combine mutagenesis and spectroscopic experiments with structural studies.

Acknowledgments

The authors gratefully acknowledge the financial support of the Royal Society and the BBSRC (to PJN and MS) and a grant from the NRICGP/USDA program (to BAD, grant no. 2001-35318–111270).

References

Alizadeh S, Nixon PJ, Telfer A and Barber J (1995) Isolation and characterisation of the photosystem two reaction centre complex from a double mutant of *Chlamydomonas reinhardtii*. Photosynth Res 43: 165–171

Alizadeh S, Morais F, Barber J and Nixon PJ (1999) Isotopic labelling of the polypeptide subunits of the isolated Photosystem II reaction-centre complex of *Chlamydomonas reinhardtii* suggests an αβ heterodimeric structure for cytochrome *b*-559. J Photochem Photobiol 48: 148–153

Alt J, Morris J, Westhoff P and Herrmann RG (1984) Nucleotide sequence of the clustered genes for the 44 kd chlorophyll *a* apoprotein and the '32 kd'-like protein of Photosystem II reaction center in the spinach plastid chromosome. Current Genet 8: 597–606

Aured M, Moliner E, Alfonso M, Yruela I, Toon SP, Seibert M and Picorel R (1994) Pigment stoichiometry of the Photosystem II reaction center from higher plants. Biochim Biophys Acta 1187: 187–190

Babcock GT and Sauer K (1973) Electron paramagnetic resonance signal II in spinach chloroplasts. I. Kinetic analysis for untreated chloroplasts. Biochim Biophys Acta 325: 483–503

Barber J (1987a) Rethinking the structure of the Photosystem two reaction centre. Trends Biochem Sci 12: 123 –124

Barber J (1987b) Photosynthetic reaction centres: A common link. Trends Biochem Sci 12: 321–326

Barber J, Chapman DJ and Telfer A (1987) Characterisation of a PS II reaction centre isolated from the chloroplasts of *Pisum sativum*. FEBS Lett 220: 67–73

Barry BA and Babcock GT (1987) Tyrosine radicals are involved in the photosynthetic oxygen-evolving system. Proc Natl Acad Sci USA 84: 7099–7103

Biesiadka J, Lull B, Kern J, Irrang K-D and Zouni A (2004) Crystal structure of cyanobacterial Photosystem II at 3.2 Å resolution: A closer look at the Mn-cluster. Phys Chem Chem Phys 6: 4733–4736

Bishop NI (1983) Identification of Photosystem II-thylakoid proteins through mutational analysis with *Chlamydomonas* and *Scenedesmus* phenotypes. In: Inoue Y, Crofts AR, Govindjee, Murata N, Renger G and Satoh K (eds) The Oxygen evolving System, pp 177–187. Academic Press, London

Blankenship RE, Babcock GT, Warden JT and Sauer K (1975) Observation of a new EPR transient in chloroplasts that may reflect the electron donor to Photosystem II at room temperature. FEBS Lett 51: 287–293

Boerner RJ and Barry BA (1993) Isotopic labelling and EPR spectroscopy show that a tyrosine residue is the terminal electron donor, Z, in manganese-depleted Photosystem II preparations. J Biol Chem 268: 17151–17154

Boerner RJ, Nguyen AP, Barry BA and Debus RJ (1992) Evidence from directed mutagenesis that aspartate 170 of the D1 polypeptide influences the assembly and/or stability of the manganese cluster in the photosynthetic water-splitting complex. Biochemistry 31: 6660–6672

Bottomley W, Spencer D and Whitfeld PR (1974) Protein synthesis in isolated spinach chloroplasts: Comparison of light-driven and ATP-driven synthesis. Arch Biochem Biophys 164: 106–117

Bowes J, Crofts AR and Arnzen CJ (1980) Redox properties on the reducing side of Photosystem II in chloroplasts with altered herbicide binding properties. Biochim Biophys Acta 200: 303–308

Bouges-Bocquet B (1973) Electron transfer between the two photosystems in spinach chloroplasts. Biochim Biophys Acta 314: 235–254

Bylina EJ, Kirmaier C, McDowell L, Holten D and Youvan DC (1988) Influence of an amino-acid residue on the optical properties and electron transfer dynamics of a photosynthetic reaction centre complex. Nature 336: 182–184

Camm EL and Green BR (1983) Relationship between the two chlorophyll *a*-protein complexes and the photosystem two reaction center. Biochim Biophys Acta 724: 291–293

Campbell KA (1999) Continuous wave and puslsed EPR studies of Photosystem II and N-containing complexes. Thesis, Chemistry Department, University of California, Davis

Campbell KA, Peloquin JM, Diner BA, Tang X-S, Chisholm DA, Britt RD (1997) The tau-nitrogen of D2 histidine 189 is the hydrogen bond donor to the tyrosine radical $Y_D^{\bullet}$ of Photosystem II. J Am Chem Soc 119: 4787–4788

Campbell KA, Force DA, Nixon PJ, Dole F, Diner BA and Britt RD (2000) Dual-mode EPR detects the initial intermediate in photoassembly of the Photosystem II Mn cluster: The influence of amino acid residue 170 of the D1 polypeptide on Mn coordination. J Am Chem Soc 122: 3754–3761

Cao J, Vermaas WFJ and Govindjee (1991) Arginine residues in the D2 polypeptide may stabilize bicarbonate binding in Photosystem II of *Synechocystis* sp. PCC 6803. Biochim Biophys Acta 1059: 171–180

Chang H-C, Jankowiak R, Reddy NRS, Yocum CF, Picorel R, Seibert M and Small GJ (1994) On the question of the chlorophyll *a* content of the Photosystem II reaction center. J Phys Chem 98: 7725–7735

Chua N-H and Gillham NW (1977) The sites of synthesis of the principal thylakoid membrane polypeptides in *Chlamydomonas reinhardtii*. J Cell Biol 74: 441–452

Chu H-A, Nguyen AP and Debus RJ (1995a) Amino acid residues that influence the binding of manganese or calcium to Photosystem II. 1. The lumenal interhelical domains of the D1 polypeptide. Biochemistry 34: 5839–5858

Chu H-A, Nguyen AP and Debus RJ (1995b) Amino acid residues that influence the binding of manganese or calcium to Photosystem II. 2. The carboxy-terminal domain of the D1 polypeptide. Biochemistry 34: 5859–5882

Coleman WJ and Youvan DC (1990) Spectroscopic analysis of genetically modified photosynthetic reaction centers. Annu Rev Biophys Biophys Chem 19: 333–367

Dalla Chiesa M, Deák Z, Vass I, Barber J and Nixon PJ (1996) The lumenal loop connecting transmembrane helices I and II of the D1 polypeptide is important for assembly of the photosystem two complex. Photosynth Res 50: 79–91

Danielius RV, Satoh K, van Kan PJM, Plijter JJ, Nuijs AM and van Gorkom HJ (1987) The primary reaction of Photosystem II in the D1-D2-cytochrome *b*-559 complex. FEBS Lett 213: 241–244

Debus RJ (2001) Amino acid residues that modulate the properties of tyrosine Y_Z and the manganese cluster in the water oxidizing complex of Photosystem II. Biochim Biophys Acta 1503: 164–186

Debus RJ, Barry BA, Babcock GT and McIntosh L (1988a) Site-directed mutagenesis identifies a tyrosine radical involved in the photosynthetic oxygen-evolving system. Proc Natl Acad

Sci USA 85: 427–430

Debus RJ, Barry BA, Sithole I, Babcock GT and McIntosh L (1988b) Directed mutagenesis indicates that the donor to P_{680}^+ in Photosystem II is tyrosine-161 of the D1 polypeptide. Biochemistry 27: 9071–9074

Debus RJ, Campbell KA, Gregor W, Li Z-L, Burnap RL and Britt RD (2001) Does histidine 332 of the D1 polypeptide ligate the manganese cluster in Photosystem II? An electron spin echo envelope modulation study. Biochemistry 40: 3690–3699

Deisenhofer J, Epp O, Miki K, Huber R and Michel H (1985) Structure of the protein subunits in the photosynthetic reaction centre of *Rhodopseudomonas viridis* at 3Å resolution. Nature 318: 618–624

Dekker JP and van Grondelle R (2000) Primary charge separation in Photosystem II. Photosynth Res 63: 195–208

Delepelaire P (1983) Characterisation of additional thylakoid membrane polypeptides synthesized inside the chloroplast in *Chlamydomonas reinhardtii*. Photobiochem Photobiophys 6: 279–291

Delepelaire P (1984) Partial characterisation of the biosynthesis and integration of the Photosystem II reaction centre in the thylakoid membrane of *Chlamydomonas reinhardtii*. EMBO J 3: 701–706

Deligiannakis Y and Rutherford AW (1996) Spin-lattice relaxation of the pheophytin, $Pheo^-$, radical of Photosystem II. Biochemistry 35: 11239–11246

Deligiannakis Y, Hanley J and Rutherford AW (1999) 1D- and 2D-ESEEM study of the semiquinone radical Q_A^- of Photosystem II. J Am Chem Soc 121: 7653–7664

de Paula JC, Innes JB and Brudvig GW (1985) Electron transfer in Photosystem II at cryogenic temperatures. Biochemistry 24: 8114–8120

de Vitry C, Wollman F-A and Delepelaire P (1984) Function of the polypeptides of the Photosystem II reaction center in *Chlamydomonas reinhardtii*. Localization of the primary reactants. Biochim Biophys Acta 767: 415–422

de Vitry C, Carles C and Diner BA (1986) Quantitation of plastoquinone-9 in Photosystem II reaction center particles. FEBS Lett 196: 203–206

de Vitry C, Diner BA and Popot J-L (1991) Photosystem II particles from *Chlamydomonas reinhardtii*. J. Biol Chem 266:16614–16621

Diner BA (2001) Amino acid residues involved in the coordination and assembly of the manganese cluster of Photosystem II. Proton-coupled electron transport of the redox-active tyrosines and its relationship to water oxidation. Biochim Biophys Acta 1503: 147–163

Diner BA and Nixon PJ (1992) The rate of reduction of oxidized redox-active tyrosine, Z^+, by exogenous Mn^{2+} is slowed in a site-directed mutant, at aspartate 170 of polypeptide D1 of Photosystem II, inactive for photosynthetic oxygen evolution. Biochim Biophys Acta 1101: 134–138

Diner BA and Nixon PJ (1998) Evidence for D1-His190 as the proton acceptor implicated in the oxidation of redox-active tyrosine Y_Z of PS II. In: Garab G (ed) Photosynthesis: Mechanisms and Effects, Vol II, pp 1177–1180. Kluwer Academic Publishers, Dordrecht

Diner BA and Petrouleas V (1987) Q_{400}, the non-heme iron of the Photosystem II iron-quinone complex. A spectroscopic probe of quinone and inhibitor binding to the reaction center. Biochim Biophys Acta 895: 107–125

Diner BA and Petrouleas V (1990) Formation by NO of nitrosyl adducts of redox components of the Photosystem II reaction center. II. Evidence that HCO_3^-/CO_2 binds to the acceptor-side non-heme iron. Biochim Biophys Acta 1015: 141–149

Diner BA and Rappaport F (2002) Structure, dynamics, and energetics of the primary photochemistry of Photosystem II of oxygenic photosynthesis. Annu Rev Plant Biol 53: 551–580

Diner BA, Ries DF, Cohen BN and Metz JG (1988) COOH-terminal processing of polypeptide D1 of the Photosystem II reaction center of *Scenedesmus obliquus* is necessary for the assembly of the oxygen-evolving complex. J Biol Chem 263: 8972–8980

Diner BA, Nixon PJ and Farchaus JW (1991a) Site-directed mutagenesis of photosynthetic reaction centers. Curr Opin Struct Biol 1: 546–554

Diner BA, Petrouleas V and Wendoloski JJ (1991b) The iron-quinone electron-acceptor complex of Photosystem II. Physiol Plant 81: 423–436

Diner BA, Schlodder E, Nixon PJ, Coleman WJ, Rappaport F, Lavergne J, Vermaas WFJ and Chisholm DA (2001) Site-directed mutations at D1-His198 and D2-His197 of Photosystem II in *Synechocystis* PCC 6803: Sites of primary charge separation and cation and triplet stabilisation. Biochemistry 40: 9265–9281

Dorlet P, Valentin MD, Babcock GT, McCracken JL (1998) Interaction of $Y_Z^\bullet$ with its environment in acetate-treated Photosystem II membranes and reaction center cores. J Phys Chem B 102: 8239–8247

Dorlet P, Rutherford AW and Un S (2000) Orientation of the tyrosyl D, pheophytin anion, and semiquinone $Q_A\bullet$ radicals in Photosystem II determined by high-field electron paramagnetic resonance. Biochemistry 39: 7826–7834

Dorlet P, Xiong L, Sayre RT and Un S (2001) High field EPR study of the pheophytin anion radical in wild type and D1-E130 mutants of Photosystem II in *Chlamydomonas reinhardtii*. J Biol Chem 276: 22313–22316

Durrant JR, Hastings G, Joseph DM, Barber J, Porter G and Klug DR (1992) Subpicosecond equilibration of excitation energy in isolated Photosystem II reaction centers. Proc Natl Acad Sci USA 89: 11632–11636

Durrant JR, Klug DR, Kwa SLS, van Grondelle R, Porter G and Dekker JP (1995) A multimer model for P680, the primary electron donor of Photosystem II. Proc Natl Acad Sci USA 92: 4798–4802

Eaglesham ARJ and Ellis RJ (1974) Protein synthesis in chloroplasts. II. Light-driven synthesis of membrane proteins by isolated pea chloroplasts. Biochim Biophys Acta 335: 396–407

Eaton-Rye JJ and Govindjee (1988) Electron transfer through the quinone acceptor complex of Photosystem II after one or two actinic flashes in bicarbonate-depleted spinach thylakoid membranes. Biochim Biophys Acta 935: 248–257

Eijckelhoff C and Dekker JP (1995) Determination of the pigment stoichiometry of the photochemical reaction center of Photosystem II. Biochim Biophys Acta 1231: 21–28

Erickson JM, Rahire M, Malnoe P, Girard-Bascou J, Pierre Y, Bennoun P and Rochaix J-D (1986) Lack of the D2 protein in a *Chlamydomonas reinhardtii psbD* mutant affects PS II stability and D1 expression. EMBO J 5: 1745–1754

Erickson JM, Pfister K, Rahire M, Togasaki RK, Mets L and Rochaix J-D (1989) Molecular and biophysical analysis of herbicide-resistant mutants of *Chlamydomonas reinhardtii*:

structure-function relationships of the Photosystem II D1 polypeptide. Plant Cell 1: 361–371

Ermakova-Gerdes S and Vermaas W (1998) Mobility of the primary electron-accepting plastoquinone Q_A of Photosystem II in a *Synechocystis* sp. PCC 6803 carrying mutations in the D2 protein. Biochemistry 37: 11569–11578

Ermakova-Gerdes S, Yu Z and Vermaas W (2001) Targeted random mutagenesis to identify functionally important residues in the D2 protein of Photosystem II in *Synechocystis* sp. strain PCC 6803. J Bacteriol 183: 145–154

Ferreira KN, Iverson TM, Maghlaoui K, Barber J and Iwata S (2004) Architecture of the photosynthetic oxygen-evolving center. Science 303: 1831–1838

Germano M, Shkuropatov AY, Permentier H, de Wijn R, Hoff AJ, Shuvalov VA and van Gorkom HJ (2001) Pigment organisation and their interactions in reaction centers of Photosystem II: Optical spectroscopy at 6K of reaction centers with modified pheophytin composition. Biochemistry 40: 11472–11482

Germano M, Pascal A, Shkuropatov AY, Robert B, Hoff AJ and van Gorkom HJ (2002) Pheophytin-protein interactions in Photosystem II studied by resonance Raman spectroscopy of modified reaction centers. Biochemistry 41: 11449–11455

Giorgi LB, Nixon PJ, Merry SAP, Joseph DM, Durrant JR, De Las Rivas J, Barber J, Porter G and Klug DR (1996) Comparison of primary charge separation in the Photosystem II reaction centre complex isolated from wild type and D1-130 mutants of the cyanobacterium *Synechocystis* PCC 6803. J Biol Chem 271: 2093–2101

Gounaris K, Chapman DJ, Booth P, Crystall B, Giorgi LB, Klug DR, Porter G and Barber J (1990) Comparison of the D1/D2/cytochrome *b*559 reaction centre complex of photosystem two isolated by two different methods. FEBS Lett 265: 88–92

Grebanier AE, Coen DM, Rich A and Bogorad L (1978) Membrane proteins synthesised but not processed by isolated maize chloroplasts. J Cell Biol 78: 734–746

Hays A-MA, Vassiliev IR, Golbeck JH and Debus RJ (1998) Role of D1-His190 in the proton-coupled electron transfer reactions in Photosystem II: A chemical complementation study. Biochemistry 37: 11352–11365

Hays A-MA, Vassiliev IR, Golbeck JH and Debus RJ (1999) Role of D1-His190 in the proton-coupled oxidation of tyrosine Y_Z in manganese-depleted Photosystem II. Biochemistry 38: 11851–11865

Hearst JE and Sauer K (1984) Protein sequence homologies between portions of the L and M subunits of reaction centers of *Rhodopseudomonas capsulata* and the Q_B-protein of chloroplast thylakoid membranes: A proposed relation to quinone-binding sites. Z Naturforsch 39c: 421–424

Hienerwadel R and Berthomieu C (1995) Bicarbonate-binding to the non-haem iron of Photosystem II investigated by Fourier transform infrared difference spectroscopy and ^{13}C-labeled bicarbonate. Biochemistry 34: 16288–16297

Hienerwadel R, Boussac A, Breton J, Diner BA and Berthomieu C (1997) Fourier transform infrared difference spectroscopy of Photosystem II tyrosine D using site-directed mutagenesis and specific isotope labeling. Biochemistry 36: 14712–14723

Hirschberg J and McIntosh L (1983) Molecular basis of herbicide resistance in *Amaranthus hybridus*. Science 222:1346–1349

Hofmann E, Wrench PM, Sharples FP, Hiller RG, Welte W and Diederichs K (1996) Structural basis of light harvesting by carotenoids: Peridinin-chlorophyll-protein from *Amphidinium carterae*. Science 272: 1788–1791

Hoganson CW and Babcock GT (1988) Electron-transfer events near the reaction center in O_2-evolving Photosystem II preparations. Biochemistry 27: 5848–5855

Hoganson CW, Ghanotakis DF, Babcock GT and Yocum CF (1989) Mn^{2+} reduces Y_z^+ in manganese-depleted Photosystem II preparations. Photosynth Res 22: 285–293

Holschuh K, Bottomley W and Whitfeld PR (1984) Structure of the spinach chloroplast genes for the D2 and 44 kd reaction-centre proteins of Photosystem II and for $tRNA_{Ser}$ (UGA). Nucl Acids Res 12: 8819–8834

Hundelt M, Hays A-M A, Debus RJ and Junge W (1998) Oxygenic Photosystem II: The mutation D1-D61N in *Synechocystis* sp. PCC 6803 retards S-state transitions without affecting electron transfer from Y_Z to P_{680}^+. Biochemistry 37: 14450–14456

Ikeuchi M and Inoue Y (1987) Specific ^{125}I labeling of D1 (herbicide-binding protein). An indication that D1 functions on both the donor and acceptor sides of Photosystem II. FEBS Lett 210: 71–76

Ikeuchi M and Inoue Y (1988a) A new Photosystem II reaction center component (4.8 kDa protein) encoded by chloroplast genome. FEBS Lett 241: 99–104

Ikeuchi M and Inoue Y (1988b) Partial characterization of the iodination site in D1 protein of manganese-retaining and manganese-depleted Photosystem II membranes. Plant Cell Physiol 29: 695–705

Ivleva NB, Shestakov SV and Pakrasi HB (2000) The carboxyl-terminal extension of the precursor D1 protein of Photosystem II is required for optimal photosynthetic performance of the cyanobacterium *Synechocystis* sp. PCC 6803. Plant Physiol 124: 1403–1411

Kamiya N and Shen J-R (2003) Crystal structure of oxygen-evolving Photosystem II from *Thermosynechococcus vulcanus* at 3.7-Å resolution. Proc Natl Acad Sci USA 100: 98–103

Karabin GD, Farley M and Hallick RB (1984) Chloroplast gene for Mr 32000 polypeptide of Photosystem II in *Euglena gracilis* is interrupted by four introns with conserved boundary sequences. Nucl Acids Res 12: 5801–5812

Keilty AT, Vavilin DV and Vermaas WFJ (2001) Functional analysis of combinatorial mutants with changes in the C-terminus of the CD loop of the D2 protein in Photosystem II of *Synechocystis* sp. PCC 6803. Biochemistry 40: 4131–4139

Kirmaier C, Gaul D, DeBey R, Holten D and Schenck CC (1991) Charge separation in a reaction center incorporating bacteriochlorophyll for photoactive bacteriopheophytin. Science 251: 922–927

Kless H, Oren-Shamir M, Malkin S, McIntosh L and Edelman M (1994) The D-E region of the D1 protein is involved in multiple quinone and herbicide interactions in Photosystem II. Biochemistry 33: 10501–10507

Klimov VV, Klevanik AV, Shuvalov VA and Krasnovsky AA (1977) Reduction of pheophytin in the primary light reaction of Photosystem II. FEBS Lett 82: 183–186

Kobayashi M, Maeda H, Watanabe T, Nakane H and Satoh K (1990) Chlorophyll *a* and β-carotene content in the D_1/D_2/cytochrome *b*-559 reaction center complex from spinach. FEBS Lett 260: 138–140

Koivuniemi A, Aro EM and Andersson B (1995) Degradation of D1- and D2-proteins of Photosystem II in higher plants is regulated by reversible phosphorylation. Biochemistry 34: 16022–16029

Koulougliotis D, Innes JB and Brudvig GW (1994) Location of chlorophyll$_Z$ in Photosystem II. Biochemistry 33: 11814–11822

Koulougliotis D, Tang X-S, Diner BA and Brudvig GW (1995) Spectroscopic evidence for the symmetric location of tyrosines D and Z in Photosystem II. Biochemistry 34: 2850–2856

Kyle DJ (1985) The 32000 Dalton Q_B protein of Photosystem II. Photochem Photobiol 41: 107–116

Lakshmi KV, Eaton SS, Eaton GR and Brudvig GW (1999) Orientation of the tetranuclear manganese cluster and tyrosine Z in the O_2-evolving complex of Photosystem II: An EPR study of the $S_2Y_Z^{\bullet}$ state in oriented acetate-inhibited Photosystem II membranes. Biochemistry 38: 12758–12767

Lancaster CRD and Michel H (1997) The coupling of light-induced electron transfer and proton uptake as derived from crystal structures of reaction centres from *Rhodopseudomonas viridis* modified at the binding site of the secondary quinone, Q_B. Structure 5: 1339–1359

Lers A, Heifetz PB, Boynton JE, Gillham NW and Osmond CB (1992) The carboxyl-terminal extension of the D1 protein of Photosystem II is not required for optimal photosynthetic performance under CO_2- and light-saturated growth conditions. J Biol Chem 267: 17494–17497

Li Z-L and Burnap RL (2001) Mutations of arginine 64 within the putative Ca^{2+}-binding lumenal interhelical a-b loop of Photosystem II D1 protein disrupt binding of the manganese stabilizing protein and cytochrome c_{550} in *Synechocystis* sp. PCC6803. Biochemistry 40: 10350–10359

Lince MT and Vermaas W (1998) Association of His117 in the D2 protein of Photosystem II with a chlorophyll that affects excitation-energy transfer efficiency to the reaction center. Eur J Biochem 256: 595–602

Lorković ZJ, Schröder WP, Pakrasi HB, Irrgang K-D, Herrmann RG and Oelmüller R (1995) Molecular characterization of PsbW, a nuclear-encoded component of the Photosystem II reaction center complex in spinach. Proc Natl Acad Sci USA 92: 8930–8934

Lubitz W, Isaacson RA, Okamura MY, Abresch EC, Plato M and Feher G (1989) ENDOR studies of the intermediate electron acceptor radical anion $I^{\bullet-}$ in Photosystem II reaction centers. Biochim Biophys Acta 977: 227–232

Lupínková L, Metz JG, Diner BA, Vass I and Komenda J (2002) Histidine residue 252 of the Photosystem II polypeptide is involved in a light-induced cross-linking of the polypeptide with the α subunit of cytochrome *b*-559: study of a site-directed mutant of *Synechocystis* PCC 6803. Biochim Biophys Acta 1554: 192–201

Manna P, LoBrutto R, Eijckelhoff C, Dekker JP and Vermaas W (1998) Role of Arg180 of the D2 protein in Photosystem II structure and function. Eur J Biochem 251: 142–154

Marder JB, Goloubinoff P and Edelman M (1984) Molecular architecture of the rapidly metabolised 32-kilodalton protein of Photosystem II. Indications for COOH-terminal processing of a chloroplast membrane polypeptide. J Biol Chem 259: 3900–3908

Marder JB, Chapman DJ, Telfer A, Nixon PJ and Barber J (1987) Identification of *psbA* and *psbD* gene products, D1 and D2, as reaction centre proteins of photosystem two. Plant Mol Biol 9: 325–333

Matoo AK and Edelman M (1987) Intramembrane translocation and posttranslational palmitoylation of the chloroplast 32-kDa herbicide-binding protein. Proc Natl Acad Sci USA 84: 1497–1501

Merry SAP, Nixon PJ, Barter LMC, Schilstra M, Porter G, Barber J, Durrant JR and Klug DR (1998) Modulation of quantum yield of primary radical formation in Photosystem II by site-directed mutagenesis affecting radical cations and anions. Biochemistry 37: 17439–17447

Metz JG and Bishop NI (1980) Identification of a chloroplast membrane polypeptide associated with the oxidising side of Photosystem II by the use of select low-fluorescent mutants of *Scenedesmus*. Biochem Biophys Res Commun 94: 560–566

Metz JG and Seibert M (1984) Presence in Photosystem II core complexes of a 34-kilodalton polypeptide required for water photolysis. Plant Physiol 76: 829–832

Metz JG, Wong J and Bishop NI (1980) Changes in electrophoretic mobility of a chloroplast membrane polypeptide associated with the loss of the oxidising side of Photosystem II in low fluorescent mutants of *Scenedesmus*. FEBS Lett 114: 61–66

Metz JG, Pakrasi HB, Seibert M and Arntzen CJ (1986) Evidence for a dual function of the herbicide-binding D1 protein in Photosystem II. FEBS Lett 205: 269–274

Metz JG, Nixon PJ, Rögner M, Brudvig GW and Diner BA (1989) Directed alteration of the D1 polypeptide of Photosystem II: Evidence that tyrosine-161 is the redox component, Z, connecting the oxygen-evolving complex to the primary electron donor, P680. Biochemistry 28: 6960–6969

Michel H and Deisenhofer J (1986) X-ray diffraction studies on a crystalline bacterial photosynthetic reaction center: A progress report and conclusions on the structure of Photosystem II reaction centers. In: Staehelin LA and Arntzen CJ (eds) Photosynthesis III. Photosynthetic Membranes and Light Harvesting Systems, pp 371–381. Springer-Verlag, Berlin

Michel H and Deisenhofer J (1988) Relevance of the photosynthetic reaction center from purple bacteria to the structure of Photosystem II. Biochemistry 27: 1–7

Michel H, Hunt DF, Shabanowitz J and Bennett J (1988) Tandem mass spectrometry reveals that three Photosystem II proteins of spinach chloroplasts contain N-acetyl-O-phosphothreonine at their NH_2 termini. J Biol Chem 263: 1123–1130

Moenne-Loccoz P, Robert B and Lutz M (1990) Structure of the primary reactants in Photosystem II: Resonance Raman studies of D1D2 particles. In: Baltscheffsky M (ed) Current Research in Photosynthesis, Vol I, pp 423–426. Kluwer Academic Publishers, Dordrecht

Nabedryk E, Andrianambinintsoa S, Berger G, Leonhard M, Mäntele W and Breton J (1990) Characterisation of bonding interactions of the intermediary electron acceptor in the reaction center of Photosystem II by FTIR spectroscopy. Biochim Biophys Acta 1016: 49–54

Nakatani HY, Ke B, Dolan E and Arntzen CJ (1984) Identity of the Photosystem II reaction centre polypeptide. Biochim Biophys Acta 765: 347–352

Nanba O and Satoh K (1987) Isolation of a Photosystem II reaction center consisting of D-1 and D-2 polypeptides and cytochrome *b*-559. Proc Natl Acad Sci USA 84, 109–112

Nixon PJ (1988) An investigation of the *psbA* and *psbD* gene products of higher plants. PhD Thesis, University London.

Nixon PJ and Diner BA (1990) Protein coordination of the photosynthetic oxygen-evolving complex, a quaternary electron counter. In: Pedersen PC and Onarel B (eds) Proceedings of the Twelfth International Conference of the IEEE Engineer-

ing in Medicine and Biology Society, Vol 12, pp 1732–1734. IEEE, Piscataway

Nixon PJ and Diner BA (1992) Aspartate 170 of the Photosystem II reaction center polypeptide D1 is involved in the assembly of the oxygen-evolving manganese cluster. Biochemistry 31: 942–948

Nixon PJ, Dyer TA, Barber J and Hunter CN (1986) Immunological evidence for the presence of the D1 and D2 proteins in PS II cores of higher plants. FEBS Lett. 209: 83–86

Nixon PJ, Rögner M and Diner BA (1991) Expression of a higher plant *psbA* gene in *Synechocystis* 6803 yields a functional hybrid Photosystem II reaction center complex. Plant Cell 3: 383–395

Nixon PJ, Trost JT and Diner BA (1992a) Role of the carboxy terminus of polypeptide D1 in the assembly of a functional water-oxidizing manganese cluster in Photosystem II of the cyanobacterium *Synechocystis* sp. PCC 6803: Assembly requires a free carboxyl group at C-terminal position 344. Biochemistry 31: 10859–10871

Nixon PJ, Chisholm DA and Diner BA (1992b) Isolation and functional analysis of random and site-directed mutants of Photosystem II. In: Shewry PR and Gutteridge S (eds) Plant Protein Engineering, pp 93–141. Cambridge University Press, Cambridge.

Nixon PJ and Diner BA (1994) Analysis of water-oxidation mutants constructed in the cyanobacterium *Synechocystis* sp. PCC 6803. Biochem Soc Trans 22: 338–343.

Nixon PJ, Komenda J, Barber J, Deak Z, Vass I and Diner BA (1995) Deletion of the PEST-like region of photosystem two modifies the Q_B-binding pocket but does not prevent rapid turnover of D1. J Biol Chem 270: 14919–14927

Noguchi T, Inoue Y and Satoh K (1993) FT-IR studies on the triplet state of P_{680} in the Photosystem II reaction center: Triplet equilibrium within a chlorophyll dimer. Biochemistry 32: 7186–7195

Noguchi T, Tomo T and Inoue Y (1998) Fourier transform infrared study of the cation radical of P680 in the Photosystem II reaction center: Evidence for charge delocalization on the chlorophyll dimer. Biochemistry 37: 13614–13625

Oettmeier W (1999) Herbicide resistance and supersensitivity in Photosystem II. Cell Mol Life Sci 55: 1255–1277

Oettmeier W, Soll H-J and Neumann E (1984) Herbicide and plastoquinone binding to Photosystem II. Z Naturforsch 39c: 393–396

Ohad N and Hirschberg J (1992) Mutations in the D1 subunit of Photosystem II distinguish between quinone and herbicide binding sites. Plant Cell 4: 273–282

Okamura MY, Satoh K, Isaacson RA and Feher G (1987) Evidence of the primary charge separation in the D1/D2 complex of Photosystem II from spinach: EPR of the triplet state. In: Biggins J (ed) Progress in Photosynthesis Research, Vol 1, pp 379–381. Martinus Nijhoff Publishers, Dordrecht

O'Malley PJ, Babcock GT and Prince RC (1984) The cationic plastoquinone radical of the chloroplast water splitting complex. Hyperfine splitting from a single methyl group determines the EPR spectral shape of signal II. Biochim Biophys Acta 766: 283–288

Paddock ML, McPherson PH, Feher G and Okamura MY (1990) Pathway of proton transfer in bacterial reaction centers: Replacement of serine-L223 by alanine inhibits electron and proton transfers associated with the reduction of quinone to dihydroquinone. Proc Natl Acad Sci USA 87: 6803–6807

Pakrasi HB and Vermaas WFJ (1992) Protein engineering of Photosystem II. In: Barber J (ed) The Photosystems: Structure, Function and Molecular Biology, pp 231–257. Elsevier Science Publishers, Amsterdam

Peloquin JM, Campbell KA and Britt RD (1998) Mn-55 pulsed ENDOR demonstrates that the Photosystem II 'split' EPR signal arises from a magnetically-coupled mangano-tyrosyl complex. J Am Chem Soc 120: 6840–6841

Peloquin JM, Tang X-S, Diner BA and Britt RD (1999) An electron spin-echo envelope modulation (ESEEM) study of the Q_A binding pocket of PS II reaction centers from spinach and *Synechocystis*. Biochemistry 38: 2057–2067

Petrouleas V, Deligiannakis Y and Diner BA (1994) Binding of carboxylate anions at the non-heme Fe(II) of PS II. II. Competition with bicarbonate and effects on the Q_A/Q_B electron transfer rate. Biochim. Biophys. Acta 1188: 271–277

Pfister K, Steinback KE, Gardner G and Arntzen CJ (1981) Photoaffinity labelling of a herbicide receptor protein in chloroplast membranes. Proc Natl Acad Sci USA 78: 981–985

Preston C and Seibert M (1991) The carboxyl modifier 1-ethyl-3-[3-(dimethylamino)propyl]carbodiimide (EDC) inhibits half of the high-affinity Mn-binding site in Photosystem II membrane fragments. Biochemistry 30: 9615–9624

Pueyo JJ, Moliner E, Seibert M and Picorel R (1995) Pigment content of D1-D2-cytochrome *b*559 reaction centre preparations after removal of CP47 contamination: An immunological study. Biochemistry 34: 15214–15218

Qian M, Dao L, Debus RJ and Burnap RL (1999) Impact of mutations within the putative Ca^{2+}-binding lumenal interhelical a–b loop of the Photosystem II D1 protein on the kinetics of photoactivation and H_2O-oxidation in *Synechocystis* sp. PCC6803. Biochemistry 38: 6070–6081

Radmer R and Cheniae GM (1977) Mechanisms of oxygen evolution. In: Barber J (ed) Primary Processes of Photosynthesis, Vol 2, pp 301–348. Elsevier, Amsterdam

Rasmussen OF, Bookjans G, Stummann BM and Henningsen KW (1984) Localisation and nucleotide sequence of the gene for the membrane polypeptide D2 from pea chloroplast DNA. Plant Mol Biol 3: 191–199

Rao JKM, Hargrove PA and Argos P (1983) Will the seven helix bundle be a common structure for integral membrane proteins? FEBS Lett 156: 165 –169

Rhee K-H, Morris EP, Barber J and Kühlbrandt W (1998) Three-dimensional structure of the plant Photosystem II reaction centre at 8 Å resolution. Nature 396: 283–286

Rochaix J-D (1981) Organisation, function and expression of the chloroplast DNA of *Chlamydomonas reinhardtii*. Experientia 37: 323–332

Rochaix J-D, Dron M, Rahire M and Malnoe P (1984) Sequence homology between the 32 K Dalton and the D2 chloroplast membrane polypeptides of *Chlamydomonas reinhardtii*. Plant Mol Biol 3: 363–370

Roffey RA, van Wijk KJ, Sayre RT and Styring S (1994) Spectroscopic characterization of tyrosine-Z in histidine 190 mutants of the D1 protein in Photosystem II (PS II) in *Chlamydomonas reinhardtii*. J Biol Chem 269: 5115–5121

Ruffle SV and Sayre RT (1998) Functional analysis of Photosystem II. In: Rochaix J-D, Goldschmidt-Clermont M and Merchant S (eds) Advances in Photosynthesis, Vol 7, The molecular biology of chloroplasts and mitochondria in *Chlamydomonas*,

pp 287–322. Kluwer Academic Publishers, Dordrecht
Ruffle SV, Donnelly D, Blundell TL and Nugent JHA (1992) A three-dimensional model of the Photosystem II reaction centre of *Pisum sativum*. Photosynth Res 34: 287–300
Ruffle SV, Wang J, Johnston HG, Gustafson TL, Hutchison RS, Minagawa J, Crofts A and Sayre RT (2001) Photosystem II peripheral accessory chlorophyll mutants in *Chlamydomonas reinhardtii*. Biochemical characterization and sensitivity to photo-inhibition. Plant Physiol 127: 633–644
Rutherford AW, Paterson DR, Mullet JE (1981) A light-induced spin-polarized triplet detected by EPR in Photosystem II reaction centers. Biochim. Biophys. Acta 635: 205–214
Rutherford AW, Zimmerman JL and Mathis P (1984) EPR of PS II interactions, herbicide effects and a new signal. In: Sybesma C (ed) Advances in Photosynthesis Research, Vol I, pp 445–448. Martinus Nijhoff/Dr W Junk Publishers, The Hague
Sarcina M, Diner BA, Breton J and Nixon PJ (1998) FTIR studies on the P680 cation and triplet states in WT and mutant PS II reaction centres of *Synechocystis* 6803. In: Garab G (ed) Photosynthesis: Mechanisms and Effects, Vol II, pp 1053–1056. Kluwer Academic Publishers, Dordrecht
Satoh K (1986) Photosystem II particles largely depleted in the two intrinsic polypeptides in the 30 kDa region from *Synechococcus* sp. Identification of a subunit which carries the Photosystem II reaction centre. FEBS Lett 204: 357–362
Satoh K (1993) Isolation and properties of the Photosystem II reaction center. In The Photosynthetic Reaction Center, Vol 1, pp289–318. Academic Press Inc., San Diego, USA.
Satoh K, Nakatani HY, Steinback KE, Watson J and Arntzen CJ (1983) Polypeptide composition of a Photosystem II core complex: Presence of a herbicide-binding protein. Biochim Biophys Acta 724: 142–150
Satoh K, Fujii Y, Aoshima T and Tado T (1987) Immunological identification of the polypeptide bands in the SDS-polyacrylamide gel electrophoresis of Photosystem II preparations. FEBS Lett 216: 7–10
Sayre RT, Andersson B and Bogorad L (1986) The topology of a membrane protein: The orientation of the 32 kd Qb-binding chloroplast thylakoid membrane protein. Cell 47: 601–608
Schelvis JPM, van Noort PI, Aartsma TJ and van Gorkom HJ (1994) Energy transfer, charge separation and pigment arrangement in the reaction center of Photosystem II. Biochim Biophys Acta 1184: 242–250
Schrader S and Johanningmeier U (1992) The carboxy-terminal extension of the D1-precursor protein is dispensable for a functional Photosystem II complex in *Chlamydomonas reinhardtii*. Plant Mol Biol 19: 251–256
Seibert M, Tamura N, and Inoue Y (1989) Lack of photoactivation capacity in Scenedesmus obliquus LF-1 results from loss of half the high-affinity manganese-binding site. Relationship to the unprocessed D1 protein. Biochim Biophys Acta 974: 185–191
Sharma J, Panico M, Barber J and Morris HR (1997) Purification and determination of intact molecular mass by electrospray ionisation mass spectrometry of the Photosystem II reaction center subunits. J Biol Chem 272: 33153–33157
Steinback KE, McIntosh L, Bogorad L and Arntzen CJ (1981) Identification of the triazine receptor protein as a chloroplast gene product. Proc Natl Acad Sci USA 78: 7463–7467
Stewart DH, Cua A, Chisholm DA, Diner BA, Bocian DF and Brudvig GW (1998) Identification of histidine 118 in the D1 polypeptide of Photosystem II as the axial ligand to chlorophyll Z. Biochemistry 37: 10040–10046
Svensson B, Vass I, Cedergren E and Styring S (1990) Structure of donor side components in Photosystem II predicted by computer modelling. EMBO J 9: 2051–2059
Svensson B, Etchebest C, Tuffery P, van Kan P, Smith J and Styring S (1996) A model for the Photosystem II reaction center core including the structure of the primary donor P_{680}. Biochemistry 35: 14486–14502
Takahashi Y and Satoh K (1989) Identification of the photochemically iodinated amino-acid residue on the D1-protein in the Photosystem II core complex by peptide mapping analysis. Biochim Biophys Acta 973: 138–146
Takahashi Y, Takahashi M and Satoh K (1986) Identification of the site of iodide photooxidation in the Photosystem II reaction center complex. FEBS Lett 208: 347–351
Takahashi Y, Hansson Ö, Mathis P and Satoh K (1987) Primary radical pair in the Photosystem II reaction centre. Biochim Biophys Acta 893: 49–59
Takahashi M, Shiraishi T and Asada K (1988) COOH-terminal residues of D1 and 44kDa CP-a2 at spinach PS II core complex. FEBS Lett 240: 6–8
Takahashi Y, Nakane H, Kojima H and Satoh K (1990) Chromatographic purification and determination of the carboxy-terminal sequences of Photosystem II reaction center proteins, D1 and D2. Plant Cell Physiol 31: 273–280
Tamura N, Ikeuchi M and Inoue Y (1989) Assignment of histidine residues in D1 protein as possible ligands for functional manganese in photosynthetic water-oxidizing complex. Biochim Biophys Acta 973: 281–289
Tang X-S, Fushimi K and Satoh K (1990) D1-D2 complex of the Photosystem II reaction center from spinach. Isolation and partial characterisation. FEBS Lett 273: 257–260
Tang X-S, Chisholm DA, Dismukes GC, Brudvig GW and Diner BA (1993) Spectroscopic evidence from site-directed mutants of *Synechocystis* PCC6803 in favor of a close interaction between histidine 189 and redox-active tyrosine 160, both of polypeptide D2 of the Photosystem II reaction center. Biochemistry 32: 13742–13748
Tang X-S, Diner BA, Larsen BS, Gilchrist Jr ML, Lorrigan GA and Britt RD (1994) Identification of histidine at the catalytic site of the photosynthetic oxygen-evolving complex. Proc Natl Acad Sci USA 91: 704–708
Taoka S and Crofts AR (1990) Two-electron gate in triazine resistant and susceptible *Amaranthus hybridus*. In: Baltscheffsky M (ed) Current Research in Photosynthesis, Vol I, pp 547–550. Kluwer Academic Publishers, Dordrecht
Taylor MA, Nixon PJ, Todd CM, Barber J and Bowyer JR (1988) Characterisation of the D1 protein in a Photosystem II mutant (LF-1) of *Scenedesmus obliquus* blocked on the oxidising side. Evidence supporting non-processing of D1 as the cause of the lesion. FEBS Lett 235: 109–116
Thompson LK and Brudvig GW (1988) Cytochrome *b*-559 may function to protect Photosystem II from photoinhibition. Biochemistry 27: 6653–6658
Tracewell CA, Cua A, Stewart DH, Bocian DF and Brudvig GW (2001) Characterization of carotenoid and chlorophyll photooxidation in Photosystem II. Biochemistry 40: 193–203
Trebst A (1986) The topology of the plastoquinone and herbicide binding peptides of Photosystem II in the thylakoid membrane. Z Naturforsch 41c: 240–245

Trost JT, Chisholm DA, Jordan DB and Diner BA (1997) The D1 C-terminal processing protease of Photosystem II from *Scenedesmus obliquus*. J Biol Chem 272: 20348–20356

Un S, Brunel L-C, Brill TM, Zimmermann J-L and Rutherford AW (1994) Angular orientation of the stable tyrosyl radical within photosystem two by high-field 245-GHz electron paramagnetic resonance. Proc Natl Acad Sci USA 91: 5262–5266

Un S, Tang X-S, Diner BA (1996) 245 GHz High-Field EPR Study of Tyrosine-D$^{\bullet}$ and Tyrosine-Z$^{\bullet}$ in mutants of Photosystem II. Biochemistry 35: 679–684

van Brederode ME and van Grondelle R (1999) New and unexpected routes for ultrafast electron transfer in photosynthetic reaction centers. FEBS Lett 455: 1–7

van Gorkom HJ and Schelvis JPM (1993) Kok's oxygen clock: What makes it tick? The structure of P680 and consequences of its oxidizing power. Photosynth Res 38: 297–301

van Miegham FJE, Satoh K and Rutherford AW (1991) A chlorophyll tilted 30° relative to the membrane in the Photosystem II reaction centre. Biochim Biophys Acta 1058: 379–385

van Rensen JJS, Tonk TJM and de Bruijn SM (1988) Involvement of bicarbonate in the protonation of the secondary quinone electron acceptor of Photosystem II via the non-heme iron of the quinone-iron acceptor complex. FEBS Lett 226: 347–351

Vasil'ev S and Bruce D (2000) Picosecond time-resolved fluorescence studies on excitation energy transfer in a histidine 117 mutant of the D2 protein of Photosystem II in *Synechocystis* 6803. Biochemistry 39: 14211–14218

Velthuys BR (1981) Electron-dependent competition between plastoquinone and inhibitors for binding to Photosystem II. FEBS Lett 126: 277–281

Velthuys BR and Amesz J (1974) Charge accumulation at the reducing side of system 2 of photosynthesis. Biochim Biophys Acta 333: 85–94

Vermaas W (1993) Molecular-biological approaches to analyze Photosystem II structure and function. Annu Rev Plant Phys Mol Biol 44: 457–481

Vermaas WFJ, Arntzen CJ, Gu L-Q and Yu C-A (1983) Interaction of herbicides and azidoquinones at the Photosystem II binding site in the thylakoid membrane. Biochim Biophys Acta 723: 266–275

Vermaas WFJ, Williams JGK and Arntzen CJ (1987) Site-directed mutations of two histidine residues in the D2 protein inactivate and destabilise Photosystem II in the cyanobacterium *Synechocystis* 6803. Z Naturforsch 42c: 762–768

Vermaas WFJ, Rutherford AW and Hansson Ö (1988) Site-directed mutagenesis in Photosystem II of the cycanobacterium *Synechocystis* sp. PCC 6803: donor D is a tyrosine residue in the D2 protein. Proc Natl Acad Sci USA 85: 8477–8481

Vermaas W, Charité J and Shen G (1990) Glu-69 of the D2 protein in Photosystem II is a potential ligand to Mn involved in photosynthetic oxygen evolution. Biochemistry 29: 5325–5332

Vermaas W, Vass I, Eggers B and Styring S (1994) Mutation of a putative ligand to the non-haem iron in Photosystem II: Implications for Q_A reactivity, electron transfer, and herbicide binding. Biochim Biophys Acta 1184: 263–272

Wang J, Gosztola D, Ruffle SV, Hemann C, Seibert M, Wasielewski MR, Hille R, Gustafson TL Johnston HG, Gustafson TL and Sayre RT (2002) Functional asymmetry of Photosystem II D1 and D2 peripheral chlorophyll mutants of *Chlamydomonas reinhardtii*. Proc Natl Acad Sci USA 99: 4091–4096

Webber AN, Packman L, Chapman DJ, Barber J and Gray JC (1989) A fifth encoded-encoded polypeptide is present in the Photosystem II reaction centre complex. FEBS Lett 242: 259–262

Whitelegge JP, Koo D, Diner BA, Domian I and Erickson JM (1995) Assembly of the Photosystem II oxygen-evolving complex is inhibited in *psbA* site-directed mutants of *Chlamydomonas reinhardtii*. Aspartate 170 of the D1 polypeptide. J Biol Chem 270: 225–235

Williams JG and Chisholm DA (1987) Nucleotide sequences of both *psbD* genes from the cyanobacterium *Synechocystis* 6803. In Biggins J (ed) Progress in Photosynthesis Research, pp 809–812. Martinus Nijhoff Publishers, Dordrecht

Williams JC, Steiner LA, Ogden RC, Simon MI and Feher G (1983) Primary structure of the M subunit of the reaction centre from *Rhodopseudomonas sphaeroides*. Proc Natl Acad Sci USA 80: 6505–6509

Williams JC, Steiner LA, Feher G and Simon MI (1984) Primary structure of the L subunit of the reaction centre from *Rhodopseudomonas sphaeroides*. Proc Natl Acad Sci USA 81: 7303–7307

Xiong J, Subramaniam S and Govindjee (1998) A knowledge-based three dimensional model of the Photosystem II reaction center of *Chlamydomonas reinhardtii*. Photosynth Res 56: 229–254

Yamamoto Y, Inagaki N, Satoh F and Satoh K (2001) Some aspects of carboxyl-terminal processing of precursor D1 protein of Photosystem II. In: PS2001 Proceedings, S5-023, CSIRO Publishing, Australia

Youvan DC, Bylina EJ, Alberti M, Begusch H and Hearst JE (1984) Nucleotide and deduced polypeptide sequences of the photosynthetic reaction-center, B870 antenna, and flanking polypeptides from *R. capsulata*. Cell 37: 949–957

Zouni A, Witt H-T, Kern J, Fromme P, Krauß N, Saenger W and Orth P (2001) Crystal structure of Photosystem II from *Synechococcus elongatus* at 3.8Å resolution. Nature 409: 739–743

Zurawski G, Bohnert HJ, Whitfeld PR and Bottomley W (1982) Nucleotide sequence of the gene for the M_r 32,000 thylakoid membrane protein from *Spinacia oleracea* and *Nicotiana debneyi* predicts a totally conserved primary translation product of M_r 38,950. Proc Natl Acad Sci USA 79: 7699–7703

Chapter 5

The Extrinsic Proteins of Photosystem II

Terry M. Bricker*
Biochemistry and Molecular Biology Section, Department of Biological Sciences, Louisiana State University, Baton Rouge, LA 70803, U.S.A.

Robert L. Burnap
Department of Microbiology and Molecular Genetics, Oklahoma State University, Stillwater, OK 74078, U.S.A.

Summary

In this chapter the structure and function of the extrinsic proteins of Photosystem II (PS II) are examined. Higher plants and green algae contain the 33 kDa manganese-stabilizing protein and the 24 kDa and the 16 kDa extrinsic proteins while the cyanobacteria contain the same manganese-stabilizing protein, cytochrome c_{550}, and the 12 kDa extrinsic protein. These proteins serve as enhancers of O_2 evolution, optimizing PS II activity at physiological calcium and chloride concentrations. They shield the manganese cluster from exogenous reductants and reactants in the surrounding aqueous phase. A number of molecular, biochemical, and structural studies

*Author for correspondence, email: btbric@lsu.edu

T. Wydrzynski and K. Satoh (eds): Photosystem II: The Light-Driven Water:Plastoquinone Oxidoreductase, pp. 95–120.

have been used to probe the structures and functions of these proteins within the photosystem. We will discuss the proposed functional roles for these components, their structure (as deduced from biochemical and X-ray crystallographic studies) and the location of their proposed binding domains within the PS II complex.

I. Introduction

In higher plants and cyanobacteria at least six intrinsic proteins appear to be required for O_2 evolution (Murata et al., 1984; Burnap and Sherman, 1991; Bricker, 1992). These are CP47, CP43, the D1 protein, the D2 protein, and the α and β subunits of cytochrome b_{559}. (see Chapters 3, 4 and 6 for details on these components). Insertional inactivation or deletion of the genes for these components results in the complete loss of O_2 evolution activity. Additionally, a number of low molecular mass components appear to be associated with Photosystem II (PS II) (Ikeuchi et al., 1989; Chapter 6), although the functions of these proteins remain obscure. While PS II complexes containing only these components can evolve O_2, they do so at very low rates (about 25% of control), are extremely susceptible to photoinactivation, and require high, non-physiological levels of calcium and chloride (Murata et al., 1984; Bricker, 1992).

In higher plants, three extrinsic proteins, with apparent molecular masses of 33 kDa (the manganese-stabilizing protein or MSP), 24 kDa and 16 kDa are required for maximal rates of O_2 evolution at physiological inorganic cofactor concentrations. These proteins are encoded by the *psb*O, *psb*P, and *psb*Q genes, respectively. They were originally identified in inverted PS II thylakoid vesicles (Akerlund et al., 1982) and PS II membrane fragments (Kuwabara and Murata, 1983). In some organisms, it appears that each of these genes is represented by a small multigene family. In cyanobacteria, only the MSP is present (however, see Chapter 6 and the discussion below on possible psbP and psbQ homologues in cyanobacteria), with the functions of the 24 kDa and 16 kDa proteins appearing to be provided by cytochrome (Cyt) c_{550} (encoded by *psb*V) and a 12 kDa protein (encoded by *psb*U) (Shen and Inoue, 1993a,b). These components apparently interact with intrinsic membrane proteins and each other to yield fully functional O_2-evolving complexes. Of these extrinsic proteins, the MSP appears to play a central role in the stabilization of the manganese cluster and is essential for efficient and stable O_2 evolution. The 24 kDa and 16 kDa proteins and their cyanobacterial counterparts, Cyt c_{550} and the 12 kDa protein, appear to be required for optimal rates of O_2 evolution at physiological calcium and chloride concentrations. In this chapter we will summarize the information available concerning the structures and functions of the extrinsic proteins of PS II.

Abbreviations:CD – circular dichroism; C-terminal – carboxy-terminal; Cyt – cytochrome; DTSP – dithiobis(succinimidyl propionate); EDC – 1-ethyl-3-(3-dimethylaminopropyl) carbodiimide; EPR – electron paramagnetic resonance; EXAFS – extended X-ray absorption fine structure; FTIR – Fourier transform infrared; GME – glycine methylester; kDa – kiloDalton; LDAO – lauryldimethylamine oxide; $(Mn)_4$ – catalytic manganese cluster; MSP – manganese-stabilizing protein; NHS – N-hydroxysuccinimide; N-terminal – amino-terminal; PS II – Photosystem II; S_n – states of the O_2-evolving cycle, n = 0, 1, 2, 3, or 4; TL – thermoluminescence

II. The 33 kDa Manganese-Stabilizing Protein (PsbO)

A. Structure

A sequence alignment for the mature manganese stabilizing protein (MSP) is shown in Fig. 1. The amino acid sequence is relatively highly conserved, with 43% of the residues being either completely conserved or conservatively replaced across the 22 proteins for which derived amino acid sequence information is available. Interestingly, all of the cyanobacterial sequences examined exhibit a 9 or 10 amino acid residue N-terminal truncation with respect to the spinach sequence and most exhibit an eight amino acid insertion between residues Pro138-Glu139 of the spinach sequence. The presence of these conserved features in the cyanobacterial sequences is of unknown consequence (however, see below).

The mature MSP from spinach contains 247 amino acid residues and possesses a calculated mass of 26.53 kDa (Oh-Oka et al., 1986). The MSP does not appear to be post-translationally modified (other than the removal of its transit sequences), since MALDI (matrix assisted laser desorption/ionization) mass spectrometry measurements yield a molecular mass very similar to the predicted value (Zubrzycki et al., 1998). This protein migrates anomalously dur-

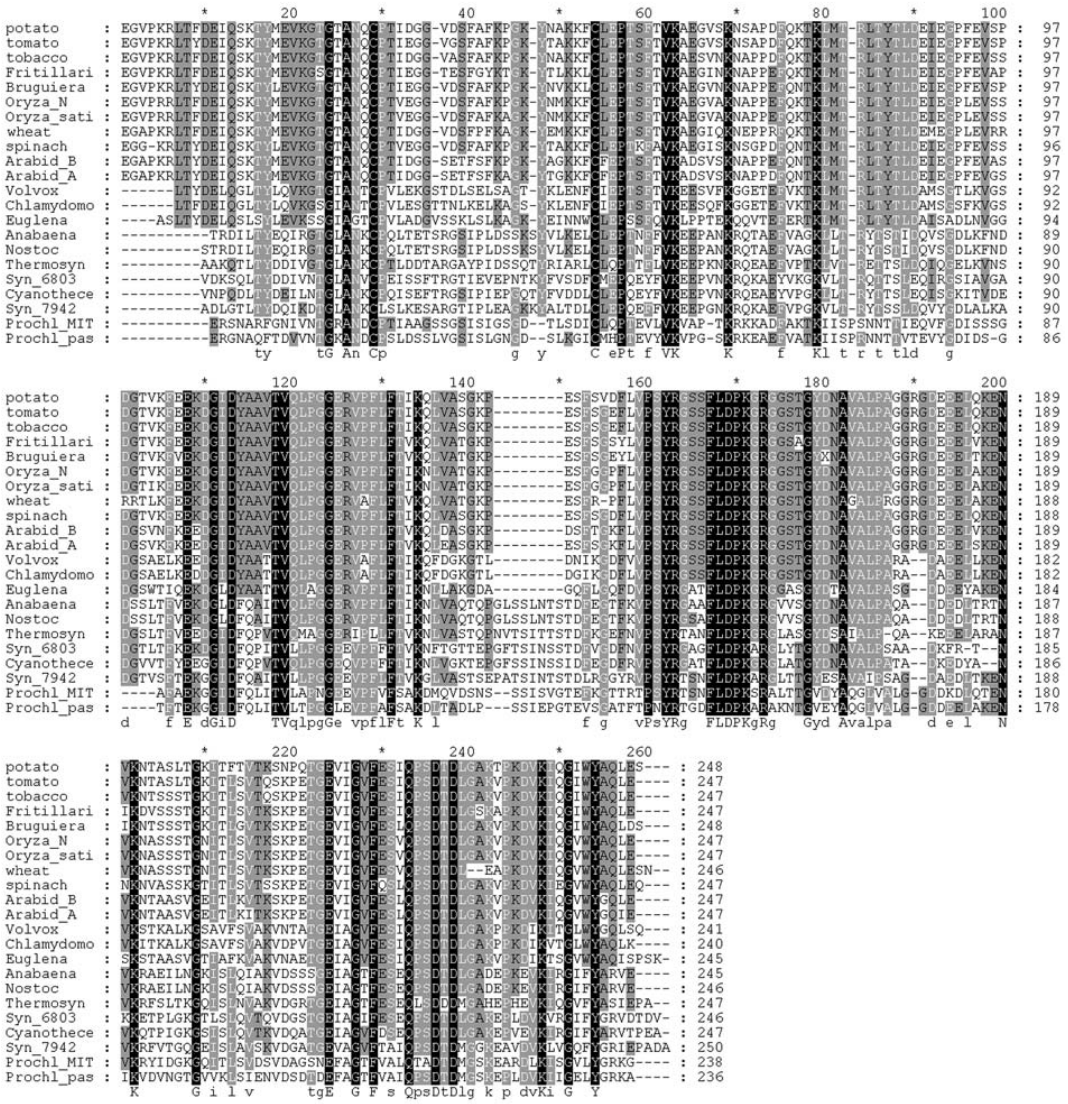

Fig. 1. Alignment of the amino acid sequences of phyletically diverse 33 kDa manganese-stabilizing proteins (PsbO). The alignments were calculated using ClustalW implemented at the Biology Workbench at San Diego Supercomputer facility. The Gonnet series weight matrix was used with the following parameter settings: gap open penalty, 10.00; gap extension penalty, 0.10; % identity for delay, 30; residue-specific gap penalties, on; penalize end gaps, on; hydrophilic gap penalties, on; gap separation distance, 0; hydrophilic residue, GPSNDQEKR. The figure was rendered using GeneDoc programs.

ing SDS-PAGE and gel filtration, yielding apparent masses of 33 and 41 kDa, respectively (Lydakis-Simantiris et al., 1999b). Additionally, dynamic light-scattering experiments, analytical ultracentrifugation (Zubrzycki et al., 1998), and small angle X-ray scattering (Svensson et al., 2002) indicate that the MSP exhibits an extended structure in solution with an axial ratio of 4-5:1.

No successful X-ray crystallographic studies have been reported for isolated MSP, although Anati and

Adir (2000) have reported observing microcrystals of the protein and have argued that these consisted of dimers. However, these crystals were too small to perform structural analysis. Within the crystal structures of PS II from *Synechococcus elongatus* and *Thermosynechococcus vulcanus* (Zouni et al., 2001; Kamiya and Shen, 2003; Biesiadka et al., 2004; Ferreira et al., 2004; Chapters 19–21), an electron density has been identified which was hypothesized to arise from the MSP. About 80% of the MSP has been modeled as polyalanine (Kamiya and Shen, 2003), forming a cylindrical structure (20 Å × 45 Å) which is rich in β-sheet structure (see below).

A variety of low resolution biochemical and biophysical studies have been performed on the MSP. These include far-UV CD measurements, FTIR studies, and site-specific labeling and mapping experiments. These investigations have yielded interesting and, in large measure, complementary results. Far-UV secondary structure determinations (Xu et al., 1994; Shutova et al., 1997) have revealed that the extrinsic MSP contains a high proportion of β-sheet (~35%) and a relatively low proportion of α-helical structure (~8%). Most FTIR studies (Ahmed et al., 1995; H. Zhang et al., 1995; L.-X. Zhang et al., 1996 1996) also indicate a high proportion of β-sheet (36–50%) with varying amounts of reported α-helical structure (2–20%). Several structural models based on these low resolution studies have been proposed (Bricker and Frankel, 1998; Pazos et al., 2001; for a more detailed discussion of the secondary and tertiary structure of the MSP in solution, see Popelkova et al., 2003a). Hutchison et al. (1998) have reported isotope-editing experiments in which ^{12}C-labeled PS II membranes were reconstituted with ^{13}C-labeled MSP. Upon binding of the labeled MSP to PS II, a substantial increase in β-sheet content and a decrease in random and/or turn structure were observed.

B. Interactions of the Manganese-Stabilizing Protein within Photosystem II

The interaction of the MSP with other PS II proteins is quite strong. Miyao and Murata (1989) determined a single K_d of 12 nM for MSP binding to PS II membranes. Leuschner and Bricker (1996) observed two MSPs per PS II in higher plants (see below), which exhibited K_d of 2.4 and 1.5 nM, respectively. In both of these studies, rebinding was performed in the presence of high chloride concentrations (>100 mM) in order to maintain the manganese cluster in an intact and functional state. Consequently, the actual K_d may be much lower.

Several site-specific chemical labeling studies have been performed to probe the interactions of the MSP with PS II (Frankel and Bricker, 1995; Seidler, 1996a; Miura et al., 1997; Frankel et al., 1999). In these studies, the MSP was modified with reagents which specifically label individual amino acid residues. Comparison of the distribution of the modified residues present was then performed after labeling of the MSP either in association with the intrinsic components of PS II or in solution. Frankel and Bricker (1995) used N-hydrosuccinimidobiotin to selectively label lysyl residues under these two conditions. Four domains (Glu1-Lys4, Lys20, Lys101-Lys105, and Lys159-Lys186) of the MSP were labeled *only* when the protein was free in solution. This indicates that these domains are shielded when the MSP is interacting with PS II. Miura et al. (1997) utilized a number of amino group modification reagents in a similar series of experiments. These results, in large measure, were very congruent to those outlined above (Frankel and Bricker, 1995).

Miura et al. (1997) also modified the aspartyl and glutamyl residues on the MSP with glycine methyl ester (GME) in a 1-ethyl-3-(3-dimethylaminopropyl) carbodiimide (EDC)-catalyzed reaction. This resulted in the modification of more than eight carboxylate residues. After modification, they found that at a GME-labeled MSP to PS II reaction center ratio of 5:1, the modified protein could still bind to PS II and fully reconstitute O_2 evolution activity. They concluded that carboxylate residues on the MSP did not participate in the binding of the MSP to PS II. Other investigators, however, have come to opposite conclusions. Seidler (1996a) examined the role of carboxylates on the MSP in the binding of this component to PS II. Differential activation of the carboxylates on the MSP and on the intrinsic proteins of PS II was performed using EDC and sulfo-NHS (N-hydroxy succinimide). These studies indicated that all of the carboxyl groups involved in crosslink formation were present on the MSP. Frankel et al. (1999) demonstrated that MSP which had been labeled in solution with GME-EDC under conditions very similar to those utilized by Miura et al. (1997) exhibited very poor binding (and O_2 evolution reconstitution) at low GME-labeled MSP to PS II reaction center ratios. The modified protein exhibited highly sigmoidal binding and O_2 evolution reactivation kinetics. The locations of the differentially modified

carboxylate residues were mapped by protease digestion and mass spectrometry. These studies indicated that GME-EDC modification(s) within the domains Asp157-Asp168 and/or Glu212-Gln247 (C-terminus) are responsible for the binding kinetics observed for the chemically modified MSP.

It should finally be noted that chemical modification of Trp241 of the MSP with N-bromosuccinimide leads to a greatly decreased affinity of the modified protein to PS II and a loss of the ability of the modified protein to reconstitute O_2 evolution (Yu et al., 2001). Far-UV CD measurements indicated that modification of this residue led to a loss of solution structure of the protein, with the changes being very similar to those observed after mutagenic truncation of the C-terminus (Lydakis-Simantiris et al., 1999a; see below).

C. Residues of the Manganese-Stabilizing Protein Required for Binding

Eaton-Rye and Murata (1989) demonstrated that the 16-18 N-terminal amino acid residues of the MSP were required for the binding of this protein to PS II. Chymotrypsin or V8 protease was used to remove the N-terminal 16 to 18 amino acid residues, respectively, from the MSP. These proteolytically modified proteins could not bind to MSP-depleted PS II membranes. They reported that far-UV CD analysis indicated that no major structural changes occurred in the MSP after protease treatment. These results are consistent with results indicating that an N-terminal domain of the MSP is not NHS-biotinylated when this protein is associated with PS II (Frankel and Bricker, 1995) and that the N-terminal domain is crosslinked to CP47 with EDC (Odom and Bricker, 1992).

Two experimental systems have been used to introduce site-directed mutations into the DNA encoding the extrinsic MSP in an attempt to identify residues that are required for either binding to PS II or function. First, mutations have been introduced into the cloned *psbO* gene (Seidler et al., 1992; Betts et al., 1996a; Motoki et al., 2002). The modified MSP was then expressed in an *E. coli* expression system, the protein purified and refolded, and then extrinsic protein-depleted PS II was reconstituted with the purified altered protein. Second, mutations were introduced into the *psbO* gene of *Synechocystis* 6803 (Burnap et al., 1994). The phenotypic consequences of these mutations were evaluated in vivo although some in vitro studies have been performed. In the following discussion, the spinach amino acid numbers will be used for both systems.

Seidler et al. (1992, 1996b) identified two residues in spinach which, when modified, appear to lower the affinity of the MSP for PS II. Alteration of Asp109 to a lysyl residue yields a modified protein that exhibits a 10-fold lower affinity for PS II. Alteration of this residue to Asn109, however, results in a modified protein with normal binding characteristics. Alteration of Asp157 to either Asn157 or Lys157 yields a protein with decreased binding affinity. A similar mutation was introduced in *Synechocystis* by Burnap et al. (1994). Modification of Asp168 to Ala168 in spinach yields a modified protein with extremely sigmoidal binding characteristics (C. F. Yocum, personal communication), which can, nevertheless, almost fully reconstitute O_2 evolution activity. Other modifications near the C-terminus also appear to profoundly affect binding and activity. The replacement of Val235 with Ala235 yields a modified protein which exhibits a defect in the ability to bind to PS II membranes and reconstitute O_2 evolution activity at 4 °C (Betts et al., 1996b). At room temperature the binding characteristics of this altered protein appear normal. In competition rebinding experiments with this altered protein and wild-type protein, the binding of the wild-type protein is highly preferred (Betts et al., 1997). Interestingly, if modified protein is first bound to PS II membranes and then wild-type protein is added in an attempt to displace the modified component, only half of the altered protein is removed (see below). The requirement of an intact C-terminus of the MSP has been probed by deletion mutagenesis (Betts et al., 1998). Removal of the C-terminal dipeptide did not affect binding or function of the protein while removal of the C-terminal tripeptide seriously weakened binding of the protein and resulted in poor reconstitution of O_2 evolution activity. Deletion of the C-terminal tetrapeptide resulted in a protein that could neither bind nor reconstitute activity. Within this domain, it appears the Leu245 may be the most critical residue. Certainly, replacement of this single residue with glutamate results in a disturbed phenotype nearly as severe as the C-terminal tripeptide deletion (Lydakis-Simantiris et al., 1999a).

As noted previously, the N-terminus of the MSP has been implicated in binding to PS II (Eaton-Rye and Murata, 1989; Odom and Bricker, 1992). Controversy exists concerning the roles of residues near the N-terminus in binding of the MSP to PS II. In spinach, Seidler et al. (1996a) reported that alteration of Asp9 to either Asn9 or Lys9 results in proteins which exhibit phenotypes that are indistinguishable from that of wild-type (Seidler and Rutherford, 1996).

They also argued that, because the acidic residue at position 10 is not conserved, being replaced by glutamine in *Anabaena* and *Synechococcus* (Borthakur and Haselkorn, 1989; Miura et al., 1993), then it isn't involved in binding and/or function. However, in the *Synechocystis* system, alteration of Asp9 to Lys9 and alteration of Asp10 to His10, Arg10, Asn10, or Ser10 all resulted in significant changes in the phenotype of cell lines that contain these mutations (Qian et al., 1997). All of these mutants exhibited a 20–30% decrease in O_2 evolution rates and a decrease in binding strength of the MSP to PS II. This indicates that all or most of the PS II centers present contain the modified MSP but that it is less tightly bound. After the hydroxylamine extraction of manganese, the Asp10Ser and Asp10His mutants exhibited a photoactivation rate intermediate between the rates for wild-type and the Δ*psb*O strain.

Recently, site-directed mutagenesis has been used to introduce short N-terminal deletions into the spinach protein (Popelkova et al., 2002a). The deletion of the three N-terminal amino acid residues results in a protein that is fully competent in the reconstitution of O_2 evolution activity. The deletion of the N-terminal ten amino acid residues, however, yields a protein that exhibits a marked decrease in its ability to reconstitute O_2 evolution. Additionally, only one copy of this modified protein can bind to the photosystem (in these studies two copies of wild-type protein are observed to bind). Further results indicated that N-terminal deletions involving the domain Thr15-Glu18 essentially completely abolished the binding of MSP to PS II (Popelkova et al., 2002b). Thus, two N-terminal binding domains were identified in these studies. Deletion of the first, Lys4-Glu10, abolishes the binding of one copy of the MSP to PS II while the second, Thr15-Glu18, abolishes the binding of the second copy. Further studies have indicated that the threonyl residues located in these two domains (Thr7 and Thr15) are critical in determining the specificity of these interactions (Popelkova et al., 2003b). Interestingly, cyanobacterial MSP sequences typically exhibit sequence truncation at their N-termini (Fig. 1) and only possess one of these identified MSP binding domains. It has been speculated that the absence of one of these binding domains in cyanobacteria results in these organisms possessing only one MSP per PS II (Popelkova et al., 2002b).

The roles of the conserved cysteinyl residues (Cys28 and Cys51) have also been examined by site-directed mutagenesis. Early biochemical studies indicated that these residues formed a disulfide bond and that this interaction was required for the interaction of the MSP with PS II (Tanaka and Wada, 1988). Later studies in spinach, however, demonstrated the double mutant CC28,51AA (Cys28Ala, Cys51Ala) exhibited essentially normal binding and fully reconstituted O_2-evolving activity (Betts et al., 1996a). This shows conclusively that the disulfide bridge is not required for binding or activity.

D. Evidence for Binding to CP47

Considerable biochemical evidence is available demonstrating the interaction of CP47 with the MSP. CP47 is a large (508 amino acid) intrinsic membrane component of PS II. It is a chlorophyll *a*-binding protein which contains six transmembrane helixes and a large (190 amino acid) lumenally exposed loop, termed loop E (Bricker, 1990; Bricker and Frankel, 2002; Chapter 3, Eaton-Rye and Putnam-Evans).

Limited proteolysis studies performed both in the presence and absence of the MSP indicate the MSP shields CP47 from tryptic attack (Bricker and Frankel, 1987). Hayashi et al. (1993) showed that both the O_2-evolving capacity and MSP binding capacity of endoproteinase Lys-C-treated PS II decreased in parallel with cleavage at Lys389 on CP47. These authors concluded that the region of CP47 in the vicinity of Lys389 was necessary for the binding of the MSP and the maintenance of O_2 evolution by extrinsic protein-depleted PS II.

A variety of protein crosslinkers are capable of crosslinking CP47 to the MSP in spinach PS II membranes. These include dithio*bis*(succinimidyl propionate) (DTSP) (Enami et al., 1987; Bricker et al., 1988), 2-iminothiolane (E. Camm, personal communication) and the water-soluble carbodiimide EDC (Bricker et al., 1988; Enami et al., 1991). EDC is particularly interesting because it crosslinks amino groups to carboxyl groups which are in van der Waals contact (Hackett and Strittmatter, 1984). Proteins crosslinked by this reagent are assumed to be interacting via a salt bridge. Odom and Bricker (1992) have mapped the domains on both the MSP and CP47 that are crosslinked with EDC. The domain Glu364-Asp440 of CP47 is crosslinked to the N-terminal domain (Glu1-Lys76) of the MSP. Seidler (1996a) has argued, based on mutagenesis studies, that the most likely residue on CP47 to participate in the production of this crosslinked product is Lys389. It has also been shown that EDC generates crosslinks

between the lumenally exposed loop A of CP47 and the MSP (Ohta et al., 1995). In addition to these intermolecular crosslinks, intramolecular crosslinks have been documented within the MSP (Bricker et al., 1988; Ohta et al., 1995; Seidler, 1996a).

In addition to these crosslinking studies, it has been demonstrated that the MSP shields lysyl residues located on CP47 from labeling with the amino group-modifying reagent NHS-biotin (Frankel and Bricker, 1990; Ishikawa et al., 2002). Treatments that remove the MSP from spinach PS II membranes allow the specific labeling of CP47 with this reagent. Two domains, Lys304-Lys321 and Lys389-Lys419, both of which lie in the large extrinsic loop E of CP47, are the only regions biotinylated on this protein (Frankel and Bricker, 1992). Recently, Ishikawa et al. (2002) demonstrated that NHS labeling of CP47 in Tris-washed PS II core complexes prevents efficient reconstitution of the MSP to PS II. The labeled residues were not identified in this study, however, the labeling conditions were similar to those described previously (Frankel and Bricker, 1990).

If CP47 is involved in the binding of the MSP, which residues are involved? We hypothesize that a number of points of interaction exist between CP47 (and possibly other PS II components, see below) and the MSP. The cooperation of these interactions yields the extremely strong observed binding of the MSP to PS II. Site-directed mutagenesis experiments have focused on producing alterations in the large extrinsic loop E of CP47. Gleiter et al. (1994) examined a number of photoautotrophic mutant strains of *Synechocystis* that carried short deletions in the extrinsic loop E (Eaton-Rye and Vermaas, 1991; Haag et al., 1993). They found that the mutants Δ(Ala373-Asp380) and Δ(Arg384-Val392) exhibited a marked decrease in the ability to bind the MSP. Site-directed mutagenesis results by Putnam-Evans and Bricker (1992) demonstrated that the residues Arg384 and Arg385 were important for maintaining high rates of O_2 evolution. Interestingly, PS II particles isolated from the RR384,385GG mutant did not contain bound MSP (C Putnam-Evans and TM Bricker, unpublished observations). Subsequently, Putnam-Evans et al. (1996) showed that the only conserved charged residues in the domain Glu364-Arg444 whose alteration influenced O_2 evolution activity were Arg384 and Arg385. The most seriously affected mutant examined, RR384,385EE, exhibited a phenotype very similar (but not identical, see below) to that exhibited by Δ*psbO* strains. This included a 60% reduction in the O_2 evolution rate, an increase in the S_2 lifetime and a retarded $S_3 \rightarrow [S_4] \rightarrow S_0$ transition. Qian et al. (1997) have demonstrated that the thylakoids of this mutant bind the MSP extremely poorly. Additionally, they found that deletion of the *psbO* gene in this strain (yielding the mutant RR384,385EE/-MSP) had little additional effect on the phenotype of this mutant. This indicates that both the RR384,385EE mutation and the deletion of the *psbO* gene affect the same processes. The most dramatic difference between the RR384,385EE mutant and the Δ*psbO* strain is the observed rates of dark inactivation in these mutants. Wild-type *Synechocystis* exhibits a $t_{½}$ for dark inactivation of 44 hrs. The Δ*psbO* strain dark inactivates very rapidly, exhibiting a $t_{½}$ of about 0.4 hrs while RR384,385EE exhibits an intermediate rate of 9 hours. The triple mutant RR384,385EE/-MSP had a dark inactivation rate which was identical to that observed in the Δ*psbO* strain. This may indicate that the mechanism of dark inactivation is distinct from those processes that affect the S_2 lifetime and $S_3 \rightarrow [S_4] \rightarrow S_0$ transition in these mutants. We believe that these results indicate that the arginyl residues located at positions 384 and 385 in the large extrinsic loop E of CP47 form a major binding domain of the MSP to PS II. In the absence of these interactions the MSP is only weakly bound to PS II and is only partially functional.

E. Evidence for Binding to Other Components

A number of other PS II components have been suggested to be involved in the binding of the MSP to PS II. It should be noted that none of these other hypothesized interactions have been supported by the same weight of evidence which has been provided for the CP47-MSP interaction. Nevertheless, it remains very possible that other components are involved in the PS II-MSP interaction.

The chlorophyll-protein CP43 is structurally very similar to CP47. Both proteins appear to contain six transmembrane helixes and to possess large, lumenally exposed domains between the fifth and sixth helixes (Bricker, 1990; Chapter 3, Eaton-Rye and Putnam-Evans). Isogai et al. (1985) reported that upon removal of the MSP, CP43 became much more accessible to trypsin. Enami et al. (1997) have extended these studies. They reported that removal of the MSP followed by trypsin treatment resulted in cleavage of CP43 at Arg357. This pattern of cleavage is remarkably similar to that observed to

occur at Lys389 in CP47 (Hayashi et al., 1993). Additionally, the α-subunit of Cyt b_{559} was cleaved at Arg59. Reconstitution experiments indicated that the rebinding of the MSP to trypsin-treated PS II membranes decreased in parallel with the observed cleavage of CP43 and Cyt b_{559}. Possible residues of CP43 that may be involved in binding the MSP have not yet been identified.

The D1 and D2 proteins of PS II have also been implicated in binding of the MSP. Site-directed mutations at position Arg64 in the D1 protein appear to disrupt binding of the MSP (and to a lesser extent Cyt c_{550}) (Li and Burnap, 2001). The mutant Arg64Glu, altered in the putative calcium-binding A-B loop, exhibited very similar defects to those observed in Δ*psbO* mutants. Thylakoids isolated from this mutant exhibited an 80% loss of bound MSP. These results indicate that either Arg64 (or residues in its vicinity) contributes to the formation of a binding domain for the MSP or that conformational changes in the A-B loop induced by this mutation disrupt a distant binding site.

In the PS II crystal structure from *Thermosynechococcus* (Kamiya and Shen, 2003), the MSP appears to interact with CP47 and CP43 and perhaps other intrinsic components of the photosystem. These findings are consistent with the large body of biochemical data described above. The residues on CP47 and CP43 which are involved in the interaction, however, cannot be identified at this time. Additionally, the residues on the MSP required for its interaction with the intrinsic components of the photosystem cannot be determined from the current crystal structure.

F. The Stoichiometry of the Manganese-Stabilizing Protein

There is considerable controversy concerning the stoichiometry of the MSP within PS II. Early studies indicated that there were one to three copies of the MSP per PS II reaction center (Andersson et al., 1984; Murata et al., 1984; Millner et al., 1987) . Murata et al. (1984) and Enami et al. (1991) reported a stoichiometry of one MSP per PS II. A number of low resolution electron microscopy studies (Boekema et al., 1995a; Holzenburg et al., 1996; Hasler et al., 1997) and the cyanobacterial crystal structures (Zouni et al., 2001; Kamiya and Shen, 2003; Biesiadka et al., 2004; Ferreira et al., 2004; Chapters 19–21) are interpreted as indicating one copy of the MSP per PS II reaction center. This is the most commonly accepted value.

Nevertheless, significant biochemical evidence indicates that there are two copies of this protein within PS II, at least in higher plants (Yamamoto et al., 1987; Xu and Bricker, 1992; Seidler, 1994; Leuschner and Bricker, 1996; Betts et al., 1997; for a more complete discussion, see Bricker and Frankel, 1998). The recent observation that two binding determinants for PS II exist on the MSP and that one of these is lacking in the cyanobacterial sequences (Popelkova et al., 2002b) may help explain the apparent contradiction which exists between the higher plant biochemical experiments and the cyanobacterial crystal structures (Zouni et al., 2001; Kamiya and Shen, 2003; Biesiadka et al., 2004; Ferreira et al., 2004; Chapters 19–21). It has been suggested that in higher plants, one copy of the MSP may play a regulatory role while the second copy may be structural (Betts et al., 1997).

G. The Function of the Manganese-Stabilizing Protein

The term 'manganese-stabilizing protein' was applied to the 33 kDa extrinsic component based on the observation that removal of this component from PS II leads to a destabilization of the manganese cluster at low, physiological chloride concentrations. Under these conditions, two of the four manganese become paramagnetically uncoupled (Mavankal et al., 1986) and are eventually lost to the bulk media (Miyao and Murata, 1984b; Ono and Inoue, 1984). In the presence of high chloride concentrations (>100 mM) the manganese cluster remains intact and oxygen can be evolved in the absence of the MSP (Miyao and Murata, 1984b; Bricker, 1992) but at significantly lower rates (20–40% of control).

Earlier studies examined the possibility that the MSP was involved in the ligation of either manganese or calcium at the active site of PS II. Abramowicz and Dismukes (1984), for instance, reported that extracted MSP contained bound manganese. Other studies, however, clearly demonstrated that the MSP could be essentially completely removed with the manganese cluster remaining intact and O_2 evolution proceeding at a significant (albeit lower) rate (Miyao and Murata, 1984b; Kuwabara et al., 1985; Bricker, 1992). Additionally, EXAFS experiments performed on PS II membranes depleted of the MSP indicated that essentially no change occurred in the structure of the manganese cluster upon removal of this com-

ponent (Cole et al., 1986). It should be noted that these studies do not preclude the possibility that the MSP provides one or a few terminal ligands to the manganese cluster, with these ligands being replaced by water or hydroxide upon removal of the protein.

Mutants lacking the MSP cannot grow at low calcium (Philbrick et al., 1991) or chloride (Engels et al., 1994) concentrations. Early studies suggested that the MSP was involved in calcium binding at the active site of PS II (Coleman and Govindjee, 1987; Wales et al., 1989; Webber and Gray, 1989). A number of more recent studies, however, indicate that the MSP is not directly involved in calcium binding (see Seidler, 1996b, for an in-depth discussion). Seidler and Rutherford (1996), for instance, demonstrated that in the absence of the MSP, the high affinity binding site for calcium associated with the O_2-evolving site persists. These studies do not, however, eliminate the possibility that the MSP may provide one or a few ligands to calcium. These ligands could hypothetically be replaced by water or hydroxide upon the removal of the MSP.

Functionally, what parameters of the O_2-evolving process are affected by the biochemical or genetic removal of the MSP? Miyao et al. (1987) performed flash O_2 yield measurements on MSP-depleted PS II membranes. These indicated that the S_2 lifetime in 33 kDa-depleted samples was increased five-fold and that the lifetime of the S_3 state was also increased. Additionally, the $S_2 \rightarrow S_3$ transition was inhibited and the $S_3 \rightarrow [S_4] \rightarrow S_0$ transition was retarded two- to three-fold. Ono and Inoue (1985), using thermoluminescence as a probe for S-state transitions, observed that MSP depletion inhibited the $S_3 \rightarrow [S_4] \rightarrow S_0$ transition. The S_2 multiline signal has also been examined in MSP depleted samples (Miller et al., 1987; Styring et al., 1987). The intensity of the S_2 multiline signal decreased. Miller et al. (1987) found no significant decrease in the shape of the multiline signal while Styring et al. (1987) reported a significant shape change of this signal, particularly at low field values. Interpretation of these spectra was complicated, however, by the relatively low signal intensity of the multiline signal, the presence of the $g_y = 2.26$ signal arising from low potential Cyt b_{559} and the presence of hexa-aquomanganese.

Similar results were obtained upon examination of the Δ*psb*O mutants. Burnap and Sherman (1991) demonstrated that this strain could grow photoautotrophically in standard BG-11 media, although it evolved O_2 at a significantly lower rate than wild type. These strains, however, cannot grow photoautotrophically at low calcium (Philbrick et al., 1991) and chloride concentrations (Engels et al., 1994). Flash O_2 yield measurements on the Δ*psb*O mutant showed an increased stabilization of the S_2 and S_3 states and that the $S_3 \rightarrow [S_4] \rightarrow S_0$ transition was slowed at least five-fold (Burnap et al., 1992). A parallel retardation in the rate of Y_z reduction was also observed (Razeghifard et al., 1997). Thermoluminescence (TL) measurements also indicated a higher stability of the S_2 and S_3 states (Burnap et al., 1992; Vass et al., 1992).

It is possible that the MSP may participate more directly in the water-oxidizing process (Hutchinson et al., 1999). PS II membranes were reconstituted with uniformly ^{13}C-labeled MSP in an isotope editing experiment. FTIR was then used to monitor changes in the protonation state of the MSP during S state turnover. During the $S_1 \rightarrow S_2$ transition, spectra were obtained which were consistent with the deprotonation of the MSP. The proton acceptor did not appear to reside on the protein. These results suggest that the MSP may serve to stabilize the charged S_2 transition state.

Interestingly, the oxidation state of the manganese cluster appears to modify the structure of bound MSP (Hong et al., 2001). Treatment of PS II membranes with 100 μM hydroxylamine leads to the reduction of the manganese cluster which, however, remains intact, and the exposure of tryptic sites on the MSP. Trypsin treatment of reduced samples leads to the rapid digestion of the MSP, which is normally quite resistant to trypsin attack when associated with the PS II reaction center (in the presence of an oxidized manganese cluster).

III. The 24 kDa and 16 kDa Proteins (PsbP and PsbQ) in Higher Plants

A. Structures of the 24 kDa and 16 kDa Proteins

In higher plants, the 24 kDa (also termed 23 kDa) and 16 kDa (also termed 17 or 18 kDa) proteins appear to be involved in modulation of the calcium and chloride requirements for O_2 evolution. These proteins are encoded by the *psbP* and *psbQ* nuclear genes, which encode proteins with predicted molecular masses of 20.2 kDa and 16.5 kDa (in spinach), respectively (Jansen et al., 1987). Significantly, fewer biochemical and molecular studies have been performed on these

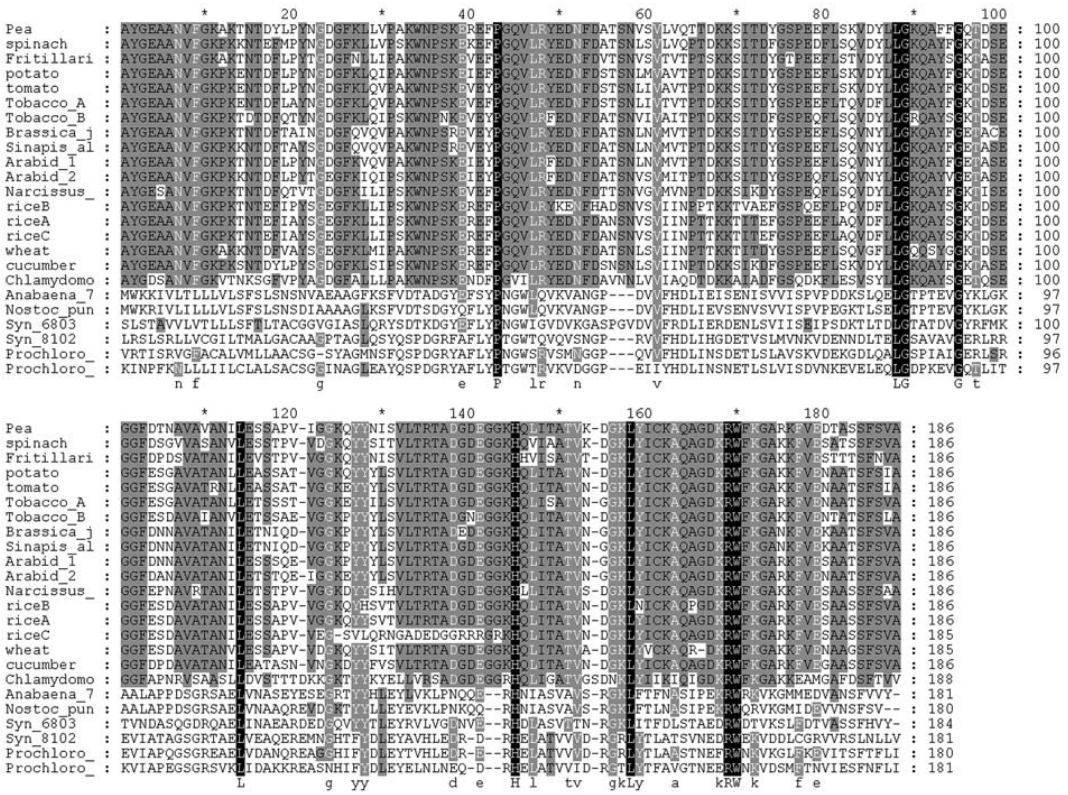

Fig. 2. Alignment of the amino acid sequences of phyletically diverse extrinsic 24 kDa protein (PsbP). Apparent homologs from cyanobacteria are included (bottom sequences). The alignments were performed as described in the legend of Fig. 1.

components than on the MSP. Sequence alignments for these proteins are found in Figs. 2 and 3. As is the case for the MSP, the structure of these proteins has been probed by CD and FTIR. The 24 kDa protein contains a low proportion of α-helix (5%) and high proportion of β-sheet (37%) and random/turn (58%) secondary structure (Zhang et al., 1998). Recent progress in the crystallization of the 24 kDa protein may provide more detailed structural information in the near future (Ifuku et al., 2003).

The 16 kDa component is estimated to contain significantly higher amounts of α-helical structure (30–60%) than observed for the MSP and 24 kDa proteins and lower amounts of β-sheet (7-28%) (Zhang et al., 1999; Balsera et al., 2003). Recently, the crystal structure of this protein has been determined at a resolution of 1.95 Å (Calderone et al., 2003). The protein is a four-helix bundle which is consistent with the high amount of α-helical structure previously observed (Zhang et al., 1999; Balsera et al., 2003). Unfortunately, the N-terminal 37 amino acid residues of the protein are not observed in the current structure. It is unclear if this domain is unordered or if it has been lost due to proteolysis.

The 24 kDa and 16 kDa components can be removed from PS II by treatment with 1 M NaCl (Akerlund et al., 1982) while the 16 kDa can be removed specifically by treatment with 500 mM NaCl and 20% methanol (Yamamoto and Kubota, 1987). Removal of these proteins appears to introduce alterations in the structure of the PS II complex. Image analysis of PS II supercomplexes from higher plants (which retain the light-harvesting antennae of the photosystem) from which these components were removed by NaCl-washing, indicates that CP29 moves 1.2 nm towards the central core of the PS II complex (Boekema et

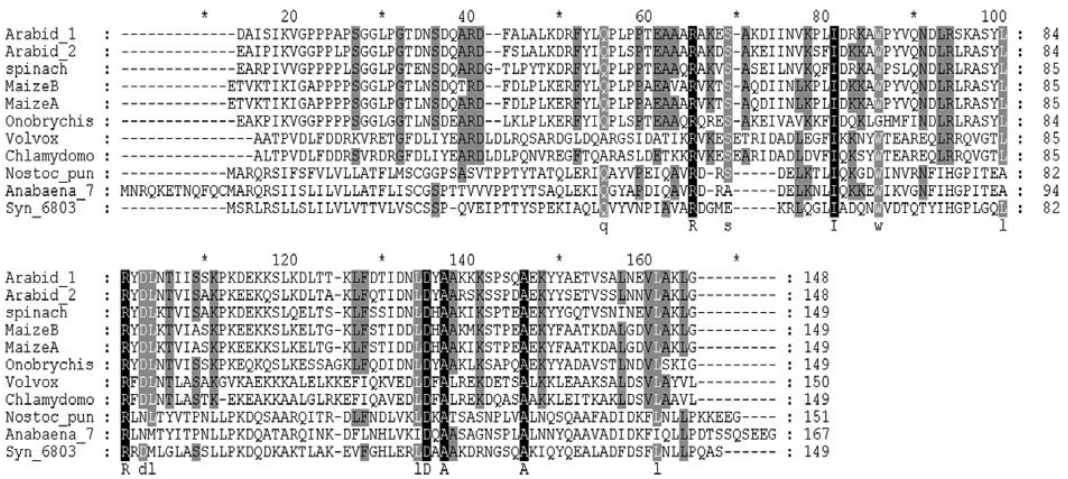

Fig. 3. Alignment of the amino acid sequences of phyletically diverse extrinsic 16 kDa protein (PsbQ). Apparent homologs from cyanobacteria are included (bottom sequences). The alignments were performed as described in the legend of Fig. 1.

al., 2000). Alterations in the structure/function of the core proteins of the PS II complex may also be affected by the removal of these extrinsic proteins. Atrazine-binding at the Q_B site, which is located on the D1 protein and exposed at the stromal surface of the PS II, is markedly increased in the absence of the 24 kDa and 16 kDa proteins (Rashid and Carpentier, 1990). This may indicate that removal of these components from the lumenal face of the complex induces transmembrane alterations in the structure of the Q_B-binding site. It should be noted, however, that it is unclear in this and the previous study if the alterations observed are due to the release of the 24 kDa and 16 kDa components per se, or due to the concomitant disruption of the high affinity calcium- and chloride-binding sites induced by the release of the proteins (see below).

The binding sites on the intrinsic membrane proteins for the 24 kDa and 16 kDa proteins to PS II have not been identified, nor have the residues on the 24 kDa and 16 kDa components which are required for these protein-protein associations with PS II been mapped. It should be noted that three-dimensional crystals of higher plant PS II uniformly diffract X-rays poorly, yielding resolutions of >6 Å (Adir, 1999). While the crystal structure of cyanobacterial PS II is obviously quite important for our understanding of the photosystem, it is of little utility in identifying the binding domains of the 24 kDa and 16 kDa proteins in higher plants, since the 24 kDa and 16 kDa proteins have no recognizable homology with their apparent cyanobacterial counterparts (Cyt c_{550} and the 12 kDa protein). Low resolution studies have been performed by electron diffraction on two-dimensional crystals of higher plant PS II or by electron microscopic imaging of detergent solubilized PS II particles followed by signal averaging (Boekema et al., 1995b; Holzenburg et al., 1996; Morris et al., 1997; Stoylova et al., 1997; Boekema et al., 1998; Boekema et al., 2000; Nield et al., 2000; Chapter 18, Hankamer et al.). A number of these studies have identified areas of electron or image density, which have been assigned to the 24 kDa and 16 kDa proteins. These regions are exposed at the lumenal face of the PS II complex. The 24 kDa and 16 kDa proteins appear to be positioned over the CP43/D1 side of the heterodimer (with the MSP being positioned over the D2/CP47 side).

In reconstitution experiments with PS II membranes preparations, the MSP appeared to be required for the binding of the 24 kDa protein and the 24 kDa protein appeared to be required for the binding of the 16 kDa protein (Andersson et al., 1984; Kavelaki and Ghanotakis, 1991). However, differential extraction experiments using either a butanol-water phase separation system (Yamamoto et al., 1987) or Hg^{+2} (Bernier and Carpentier, 1995) indicated that the MSP could be removed from PS II preparations without the concomitant extraction of the 24 kDa

and 16 kDa proteins. It is possible that the MSP is required for binding of the 24 kDa component but that upon binding, conformational changes occur within the intrinsic components of PS II which allow the selective removal of the MSP and retention of the 24 kDa and 16 kDa proteins. In any event, the MSP, 24 kDa and 16 kDa proteins must be in close proximity; crosslinking experiments performed with homobifunctional crosslinkers (6–11 Å span) indicated that the MSP is within 11 Å of the 24 kDa protein and that the 24 kDa protein is within 11 Å of the 16 kDa component. (Enami et al., 1990). Additionally, in cross-reconstitution experiments, salt-washed spinach PS II membranes which had been reconstituted with either cyanobacterial or red algal MSP could only partially rebind spinach 24 kDa protein and could bind no spinach 16 kDa protein. This indicates that there are structural determinants present on the spinach MSP which are required for the binding of the 24 kDa and 16 kDa proteins and which are absent in the cyanobacterial and red algal proteins (Enami et al., 2000). Chemical modification experiments (Bricker and Frankel, 2003) indicated that carboxylate groups on the MSP were required for efficient binding of the 24 kDa protein to PS II. The most likely residues involved in these interactions were the residues Glu1, Glu32, Glu139 and/or Glu187, which are not conserved in cyanobacterial MSP.

The residues present on the 24 kDa and 16 kDa proteins that are required for their binding to PS II have not been rigorously identified. Limited proteolysis of the 24 kDa protein indicated that removal of the eight N-terminal residues (Ala1-Phe8) of this component somewhat lowered its binding affinity to PS II (twice the amount of protein was required to saturate binding) but did not affect its ability to support O_2 evolution or cofactor sequestration (Miyao et al., 1988). Removal of the N-terminal thirteen residues (Glu1-Leu13) from the 16 kDa protein, however, essentially abolished binding of this component to the photosystem (Kuwabara et al., 1986). These residues are not resolved in the current crystal structure of this component (Calderone et al., 2003). The residues on the intrinsic proteins required for the binding of the 24 kDa and 16 kDa components have not been identified. The same is true for possible residues on the MSP required for 24 kDa protein binding and possible residues on the 24 kDa protein required for 16 kDa protein binding.

B. Functions of the 24 kDa and 16 kDa Proteins

Removal of the 24 kDa and 16 kDa proteins by NaCl treatment results in a marked loss of O_2 evolution activity (to about 25% of control). Much of the lost activity can be restored by reconstitution of the extracted protein(s) to protein-depleted PS II (Akerlund et al., 1982; Miyao and Murata, 1983), but only if the reconstitution is performed in the presence of calcium and chloride (Ghanotakis et al., 1984b; Ghanotakis et al., 1985). Reconstitution of the 24 kDa and 16 kDa components in the absence of these inorganic cofactors does not result in the restoration of O_2 evolution. It should be noted that high, non-physiological concentrations of calcium and chloride can support high rates of O_2 evolution activity even in the absence of the 24 kDa and 16 kDa proteins (Ghanotakis et al., 1984a; Miyao and Murata, 1984a; Nakatani, 1984; Chapter 13, van Gorkom and Yocum). Inhibition of O_2-evolving activity by extraction of the 24 kDa and 16 kDa proteins is accelerated in the light. This appears to be due to differential binding affinities for both calcium (Boussac and Rutherford, 1988; Adelroth et al., 1995) and chloride (Wincencjusz et al., 1998; Wincencjusz et al., 1999), which are S-state dependent. The binding affinity of PS II for calcium is similar in the presence and absence of the 24 kDa and 16 kDa proteins (Adelroth et al., 1995). However, the rate of binding of calcium to PS II was enhanced in the absence of these two components, as was the rate of dissociation of the cofactor from the PS II complex. These results indicate that the 24 kDa and 16 kDa proteins modulate the k_{on} and k_{off} rate constants for calcium but do not significantly alter its K_d. The 24 kDa and 16 kDa also appear to act as a diffusional barrier for chloride (Wincencjusz et al., 1998).

Depletion of the 24 kDa and 16 kDa proteins markedly increases the accessibility of the manganese cluster to exogenous reductants (Ghanotakis et al., 1984c). In intact PS II membranes, hydroquinone does not inhibit O_2 evolution where hydroxylamine inhibits O_2 evolution activity with an I_{50} of about 1 mM. In NaCl-treated samples, however, hydroquinone exhibits an I_{50} of about 100 μM and the I_{50} for hydroxylamine is about 50 μM. These results demonstrate that the 24 kDa and 16 kDa proteins shield the manganese cluster from bulky exogenous reductants. While small reductants can access the manganese cluster in the presence of the 24 kDa and 16 kDa

proteins, their access is greatly facilitated by the removal of these extrinsic components. Removal of these components may directly influence the structure of the manganese cluster. TL studies appear to indicate that the $S_2Q_A^-$ state is more stable in calcium-depleted PS II preparations lacking the 24 kDa protein (Ono et al., 1992; Homann and Madabusi, 1993) (for an alternative viewpoint, however, see Johnsson et al., 1994). Whether this is due to modifications of the environment of the manganese cluster or to alterations in the Q_A site (via transmembrane effects) is unclear. It was, nevertheless, hypothesized that the observed differential stability was due to an alteration of the conformational state of the manganese cluster. The S_1-state parallel polarization 'multiline' EPR signal from spinach PS II preparations can also be observed after removal of these components (Campbell et al., 1998a). This signal had previously been observed only in cyanobacterial samples (Campbell et al., 1998b). The authors hypothesized that the removal of the 24 kDa and 16 kDa proteins may directly alter the magnetic properties of the manganese cluster or, alternatively, removal of these components may effect the interaction of calcium and/or chloride with the manganese cluster in the S_1 state. These results seem to indicate a close interaction between the manganese cluster and the 24 kDa and 17 kDa proteins.

C. Putative Homologues of PsbP and PsbQ in Cyanobacteria

BLASTP searches of cyanobacterial genomic databases with spinach 24 kDa and 16 kDa protein sequences identify a number of genes which encode proteins that are similar to these higher plant components. For example, the *Nostoc* gene *all*3076 and the *Synechocystis* gene *sll*1418 encode proteins that share a 25–30% identity (40–50% similarity) with the 24 kDa protein, while the *Synechocystis sll*1638 gene encodes a protein with a 27% identity (51% similarity) to the 16 kDa protein. What (if any) roles these putative proteins play in the function, assembly or stability of cyanobacterial PS II is yet to be determined. Interestingly, a recent proteomic study of cyanobacterial PS II (Kashino et al., 2002) identified 31 proteins which were associated with a highly purified His-tagged PS II preparation (Bricker et al., 1998). All of the known cyanobacterial PS II proteins (except PsbN) were identified in this study (Chapter 6, Chandler et al.). The PsbQ homologue (Sll1638 protein) was also found to be associated with this PS II preparation.

IV. Multiple Expressed Genes of the Extrinsic Proteins in Higher Plants

It should be noted that two different *psbO* genes (*psbO*-1 and *psbO*-2) are expressed in *Arabidopsis* under normal growth conditions, yielding two different MSPs (MSP-1 and MSP-2, respectively). These have been identified on two-dimensional IEF-SDS PAGE gels of lumenally localized proteins (Kieselbach et al., 2000; Schubert et al., 2002). A high fluorescence mutant was identified in which a stop codon had been introduced at amino acid residue 74 of the mature protein (Gln74 → Stop) in the *psbO-1* gene, which led to the loss of this component (Murakami et al., 2002). The mutant plants compensated for this defect by accumulating an increased amount of the MSP-2 protein. The mutant exhibited a lower F_v/F_m, lower rates of O_2 evolution and slow growth. Two hypotheses could explain this result. If a single MSP is associated with each PS II reaction center, then two populations of PS II would exist in *Arabidopsis* thylakoids, one containing MSP-1, which is capable of high rates of electron transport and exhibits a high F_v/F_m, and a second population containing MSP-2, which exhibits the mutant characteristics. It is unclear what advantage the plant would accrue from such an arrangement. Alternatively, if two copies of MSP were associated with the PS II reaction center (see above), one each of MSP-1 and MSP-2, one copy could play a primarily functional role (MSP-1) and the second could play primarily a structural role (MSP-2) as previously hypothesized (Betts et al., 1997). In the absence of a functional MSP-1, PS II reaction centers containing two copies of MSP-2 would uniformly exhibit the mutant phenotype. Further study is obviously required on this interesting mutant to differentiate between these (or other) hypotheses.

Multiple expressed genes (*psbQ-1* and *psbQ-2*) for the 16 kDa protein have also been observed in *Arabidopsis* by two-dimensional electrophoresis of lumenal extracts (Schubert et al., 2002) and a putative gene encoding a second 24 kDa protein (*psbP-2*) has been identified by genomic analysis. The PsbP-2 protein does not appear to be expressed under normal growth conditions and its possible expression under stress conditions has not been examined. Additionally, numerous expressed proteins whose genes exhibit high similarity to the 24 kDa and 16 kDa proteins have been observed in *Arabidopsis* and spinach lumenal extracts (Schubert et al., 2002). Possible functions for these proteins in PS II have not been determined.

V. Cytochrome c_{550} (PsbV) in Cyanobacteria

A. Identification of Cytochrome c_{550} as a Component of Photosystem II

The presence of a low potential (E_m ~ –250 mV) *c*-type cytochrome in cyanobacteria has been known since the 1960s (Holten and Meyers, 1963) and is variously designated as Cyt c_{550} (or c_{549}) according to its alpha absorbance band peak position. Cyt c_{550} has a molecular mass of approximately 16,000 and, as is typical of c-type cytochromes, binds its heme moiety via thioether linkages to a pair of cysteine residues. The protein was originally suggested to have a role in hydrogen metabolism based upon its mid-point potential and the fact that the cytochrome appears to accumulate most abundantly in algal mats, which are often characterized by semi-anaerobic conditions and thus, where reductive dissimilatory metabolism may be important for algal survival (Ho et al., 1979; Krogmann, 1991). The association of Cyt c_{550} with the PS II complex was, however, not clarified until more recently (Shen et al., 1992; Shen and Inoue, 1993a,b). Interestingly, Cyt c_{550} was already evident in the first highly active PS II preparation, which was obtained by LDAO solubilization of thylakoids from the thermophilic cyanobacterium *Phormidium laminosum* (Stewart and Bendall, 1978, 1979, 1980, 1981). The cytochrome in this early preparation was found to be difficult to remove from the thylakoid membranes and exhibited approximately the same fold enrichment during the purification of the PS II particles as the Cyt b_{559} (Stewart and Bendall, 1981). However, it was not until Shen characterized a highly purified PS II preparation from *Thermosynechococcus vulcanus* (Shen et al., 1992) and deleted the gene from *Synechocystis* sp. PCC 6803 that the presence of Cyt c_{550} was finally determined to be a component of the PS II of cyanobacteria (Shen et al., 1995a,b). This conclusion has been verified in material used to obtain the PS II crystal structures obtained recently from cyanobacteria (Zouni et al., 2001; Kamiya and Shen, 2003; Biesiadka et al., 2004; Ferreira et al., 2004; Chapters 19–21). Nevertheless, current evidence does not preclude the possibility that the cytochrome is bifunctional with a subpopulation of the total cellular population of the molecule functioning outside the lumenal domain of PS II (Krogmann, 1991). Indeed, this possibility was already suggested during the initial molecular genetic characterization of the *Synechocystis* sp. PCC 6803 cytochrome (Kang et al., 1994). An alignment of the known cyanobacterial sequences is shown in Fig. 4.

B. Structure of Cytochrome c_{550}

The structures of Cyt c_{550} from two species of cyanobacteria, *Synechocystis* sp. PCC 6803 and *Arthrospira maxima*, have been solved to atomic resolutions of 1.21 and 2.3 Å, respectively (Frazao et al., 2001; Sawaya et al., 2001). Cyt c_{550} exhibits bis-histidyl axial coordination of the heme Fe which may account, in part, for its low midpoint potential of E_m= –250 mV (Holten and Meyers, 1963; Navarro et al., 1995; Vrettos et al., 2001) The imidazole rings of the opposing histidines lie approximately in the same plane, which is consistent with the EPR characteristics that suggest that the planes of the imidazole rings adopt an unstrained, parallel orientation (Vrettos et al., 2001). As discussed below, additional factors besides the bis-histidyl coordination likely contribute, however, to the low midpoint potential measured in Cyt c_{550}. Curiously, the heme group in the published structures is not in a ruffled conformation characteristic of c-type cytochromes and predicted based upon analysis of Raman spectra (Vrettos et al., 2001). The ruffled conformation is anticipated due to distortion caused by steric hindrance imposed by the thioether linkages with the cysteines within the highly conserved Cys-X-X-Cys-His heme-binding motif characteristic of *c*-type cytochromes. It is not clear whether the absence of ruffling is a modeling oversight or a genuine feature of the low potential cytochromes. The polypeptide chain of the cytochrome exhibits a fold involving four α helices that largely envelops the heme and is typical of Class I, c-type cytochromes. This point was illustrated in the crystallographic study of Sawaya et al. (2001), which also presents the paralogous structure of the *Arthrospira maxima* cytochrome c_6 that serves as an electron donor to Photosystem I. The α-carbon backbones of the Cyt c_{550} and Cyt c_6 from *Arthrospira maxima* are superimposable, with a root mean square deviation of only 0.7 Å, despite low overall sequence identity (32%). Interestingly, the structural and sequence homology is not distributed uniformly across the two paralogs. First, Cyt c_{550} is a considerably longer polypeptide, having 130 amino acids versus the 89 amino acids of Cyt c_6. To a large measure this is due to the considerably longer N-terminus (~22 amino acids longer) of the mature Cyt c_{550}. This longer N-terminus, absent in Cyt c_6, adopts an

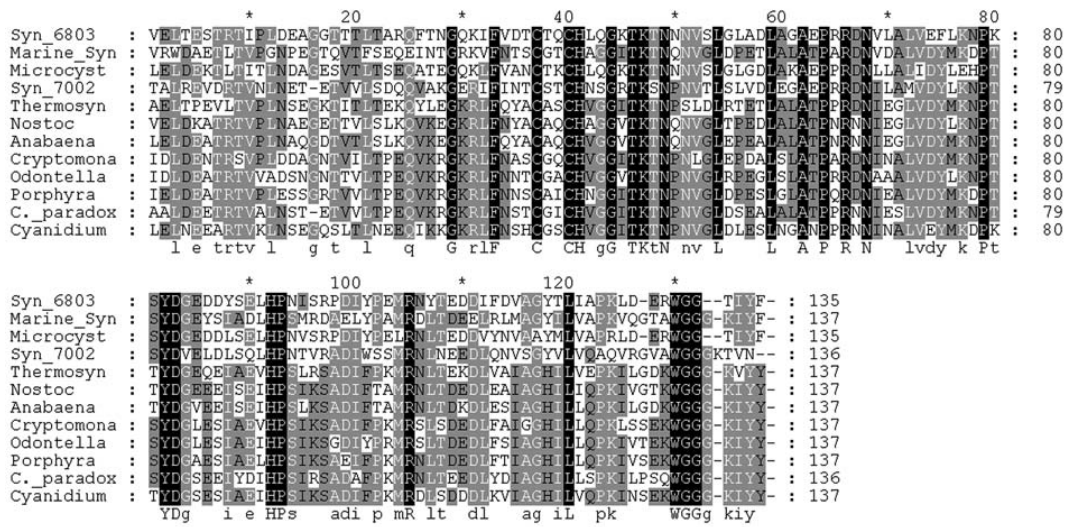

Fig. 4. Alignment of the amino acid sequences of cytochrome c_{550} (PsbV). The alignments were performed as described in the legend of Fig. 1.

antiparallel β sheet configuration with an intervening hairpin structure connecting the two strands of the sheet. Following the unique N-terminus, he Cyt c_{550} and Cyt c_6 have very similar folds up to and including the conserved Cys-x-x-Cys-His heme- binding sequence motif that forms the thioether attachments and histidyl fifth iron ligand. Beyond this region of high sequence and structural similarity between Cyt c_{550} and Cyt c_6 and towards the C-terminus, the similarity decreases dramatically, perhaps indicating a frame-shift type mutation eventually led to the replacement of the methionine by histidine at the sixth ligand position of the heme. Obviously, analogous arguments could be made if one assumes that low potential cytochrome evolutionarily predates the high potential cytochrome. However, this scenario seems less likely given the broader distribution of the high potential cytochromes. A clue to the evolution of the low potential cytochrome may lie in the tandem arrangement of Cyt c_{550} and Cyt c_6 in the genomes of *Thermosynechococcus* and *Anabaena* sp. PCC7120. Tandem chromosomal arrangements of homologous genes are generally thought to be the result of gene duplication and subsequent divergence events.

As mentioned, the bis-histidyl coordination of the heme iron at least partly accounts for the low potential of Cyt c_{550}. This is consistent with the observation that b-type cytochromes and several tetraheme c-type cytochromes have relatively negative midpoint potentials (~+100 to –250 mV) and exhibit bis-histidyl coordination of the heme. The imino moiety at the ε nitrogen of the histidyl at the sixth ligand position contributes to the negativity of the midpoint by offering more electron density to the coordinated iron in comparison to a sixth position sulfur ligand of methionine, as is typically found in higher potential *c*-type cytochromes (typically E_m = +200–350 mV). On the other hand, other factors contribute to the tuning of the midpoint potential. Solvent exposure of the heme, especially to the propionates, is thought to have a role in modulating the midpoint potential with increasing exposure correlated with downshifting the potential. A more negative midpoint potential due to increased solvent exposure of the heme moiety is deduced by analysis of trends of midpoint potential versus heme exposure across different species of cytochrome, the effect of mutations excluding or including solvent from the heme-binding pocket, and the effect of protein unfolding of *c*-type cytochromes. Consistent with these analyses, calculation of solvent exposure of the hemes of *Arthrospira* c_{550} and c_6 gives exposure values of 9.7% versus 6.3% of their surface areas, respectively (Sawaya et al., 2001). Interestingly, when the redox potential of Cyt c_{550} was measured while the molecule was adsorbed to a graphite electrode surface, an E_m of –108 mV was obtained and

the authors suggested that the approximately 150 mV more positive value compared to previous solution measurements was due to the exclusion of solvent from the interface between adsorbed cytochrome and the electrode surface. Comparative inspection of the 3-D structures reveals that the heme and the axial ligand are accessible to water in the c_{550} structure, but not the Cyt c_6 structure. This raises the possibility that the protonation state of the histidine (His92) could control the redox potential, but this remains unexplored. Additionally, this hypothetical protonation could facilitate the dissociation of ligand and allow reaction with alternate ligands at this sixth Fe coordination position. However, displacement of the histidyl ligand by cyanide is not observed (Vrettos et al., 2001), even under a wide range of ambient pHs (R. L. Burnap, unpublished); therefore dissociation of the histidyl ligand appears unlikely. Other factors influencing the midpoint potential include hydrogen bonding to the heme and its ligands as well as more global charge density distributions of the heme environment. For example, the heme propionate D groups are hydrogen bonded to the amide backbone in Cyt c_{550}, offering little or no electron density compensation upon reduction of the heme, whereas the propionate D in Cyt c_6 is hydrogen bonded to a pair of lysines, which could stabilize the addition of the electron to the heme occurring upon reduction of the cytochrome.

C. Binding and Stoichiometry of Cytochrome c_{550}

A single Cyt c_{550} molecule is modeled within the cyanobacterial PS II crystal structures (Zouni et al., 2001; Kamiya and Shen, 2003; Biesiadka et al., 2004; Ferreira et al., 2004; Chapters 19–21). This assignment was made on the basis of density resembling the characteristic *c*-type cytochrome folding of α-helices around an apparent porphyrin. The cytochrome is situated laterally to the region of density assigned to MSP relative to the axis, perpendicular to the membrane plane. The heme Fe of Cyt c_{550} is approx. 26 Å from the center of electron density assigned to the Mn cluster. Based upon the position of the defined helices, the heme edge exposed in the isolated cytochrome appears to be oriented towards the $(Mn)_4$ cluster. However, the crystallographic structure is presently not at sufficient resolution to determine the composition of the intervening region.

Although biochemical analysis of the binding and stoichiometry of Cyt c_{550} is sparse, some information is available. The binding of one Cyt c_{550} per PS II monomer was estimated from titration curves (Shen et al., 1992; Shen and Inoue, 1993a), which is in agreement with estimates of cytochrome *c* content (taking into account Cyt b_{559}) (Tang et al., 1993; Reifler et al., 1998; Lakshmi et al., 2002), and the crystal structure analysis mentioned above. In contrast, a model containing two Cyt c_{550} per PS II monomer was proposed based upon considerations of the isolated cytochrome and its dimeric packing in the crystals used to define its high resolution structure when dissociated from PS II (Sawaya et al., 2001). However, the two Cyt c_{550} per PS II monomer model seems less likely given the above considerations and recent results indicating that the cytochrome exists as a monomer in solution (Lakshmi et al., 2002), not a dimer as supposed by the authors of the two Cyt c_{550} per PS II monomer model (Sawaya et al., 2001). The binding of Cyt c_{550} shows a dependence upon the presence of MSP, although the dependence on MSP binding appears to be stronger in the red alga *Cyanidium caldarium* (Enami et al., 1998) compared to the cyanobacterium *Thermosynechococcus* (Shen and Inoue, 1993a). Despite these apparent binding differences, the ability of Cyt c_{550} to promote the reconstitution of O_2 evolution following removal of the extrinsic PS II proteins was, however, found to be strictly dependent upon the presence of MSP in PS II from both of these organisms (Shen and Inoue, 1993a; Enami et al., 1998). Chemical crosslinking using EDC followed by gel electrophoresis and immunoblot analysis led to the identification of three major crosslinked products that contained: Cyt c_{550} and PsbU; Cyt c_{550}, PsbU, and MSP; Cyt c_{550}, PsbU, and D2 (Han et al., 1994). On the basis of these results, it was concluded that Cyt c_{550} is in physical contact with the other two extrinsic proteins. Since the binding of Cyt c_{550} had been previously assessed to bind independently of MSP (Shen and Inoue, 1993a), the authors also concluded that the D2 protein forms a direct binding site for the cytochrome. With the important caveat that the lumenally exposed portions of the intrinsic PS II polypeptides remain largely unresolved, this conclusion is supported by the recent PS II crystal structures which places Cyt c_{550} near the D2 protein and in contact with MSP and PsbU (Zouni et al., 2001; Kamiya and Shen, 2003; Biesiadka et al., 2004; Ferreira et al., 2004; Chapters 19–21).

Inspection of the available crystal structures sug-

gests that an additional contact with the lumenal portion of CP43 may exist. In this regard, recent examination of *Synechocystis* PS II particles bearing the mutation Arg305Ser in loop E of CP43 has demonstrated that the binding of Cyt c_{550}, but not MSP, is perturbed. This observation was taken as evidence that CP43 forms part of the Cyt c_{550} binding site (Bricker et al., 2002). It is worth mentioning that the failure of the EDC crosslinking to identify a Cyt c_{550}-CP43 product may reflect the absence of carboxylate-primary amino groups at the proposed binding interface or the solvent inaccessibility of such contacts if they indeed exist. An analogous experiment in which isolated *Synechocystis* thylakoids containing mutations in the loop E of CP47 caused a weakened binding of MSP but little loss in the binding of Cyt c_{550} (R. L. Burnap, unpublished). Summing up, these results collectively support the hypothesis that MSP and Cyt c_{550} occupy independent, perhaps adjacent, binding sites on the intrinsic portion of the PS II complex and that the structural interactions between these two extrinsic proteins are relatively weak.

Structural alignment of the atomic resolution of Cyt c_{550} structure, with the more poorly resolved cytochrome modeled within the PS II crystal structure, suggests several interesting features of the Cyt c_{550}. Analysis of the spatial distribution of conserved and mutable residues in Cyt c_{550} reveals, not unexpectedly, that residues predicted to be at the interface between Cyt c_{550} and its binding site on the intrinsic portion of PS II are the most highly conserved. The strictly conserved Arg105 (*Synechocystis* numbering) appears oriented towards the intrinsic portion of the PS II complex and thus is a candidate for participating in an ionic binding interaction. Both the amino and carboxy termini protrude and are predicted to be oriented towards the intrinsic portion of the complex. The C-terminal position is occupied by phenylalanine or the conservative replacement, tyrosine.

D. Function of Cytochrome c_{550}

Despite its low E_m, Cyt c_{550} is intimately associated with the water-oxidation complex, which operates at potentials greater than +1000 mV. There is no evidence that Cyt c_{550} participates in the redox events of the water oxidation reaction. Indeed, current evidence weighs heavily against such a participation in water oxidation enzymology. Neither biochemical nor genetic removal of Cyt c_{550} results in the abolition of water oxidation activity (Shen and Inoue, 1993b; Enami et al., 1995; Shen et al., 1995a,b; Enami et al., 1998). Removal of Cyt c_{550} does affect the kinetics of the S-state transitions and the dark stability of the S_2 and S_3 states, but O_2 evolution persists and exhibits its characteristic period four oscillations under flash illumination (Shen et al., 1998). Genetic removal of Cyt c_{550} results in a pronounced destabilization of the entire PS II complex (⅓ normal accumulation) (Shen et al., 1995b; Shen et al., 1998). Destabilization of the PS II complex is a general phenotype shared by a variety of mutations in different PS II proteins (Vermaas et al., 1988)) and thus it is difficult to ascribe a particular functional significance to this feature. Furthermore, it is important to note that when maximal whole cell O_2 evolution rates in the deletion mutant are normalized to the reduced PS II content, then the maximal PS II turnover appears largely unaffected (Shen et al., 1995a). This fits with the observation that O_2 release during the $S_3 \rightarrow S_4 \rightarrow S_0$ transition, measured polarographically under flash illumination, is only slightly retarded (Shen et al., 1998). Therefore, it is highly unlikely that Cyt c_{550} is directly involved in the redox events of S-state cycling during the process of water oxidation. On the other hand, binding Cyt c_{550} is important for the stability of the $(Mn)_4$ and appears to modulate its structure and reactivity in a manner not unlike the 24 kDa protein. The presence of Cyt c_{550} is correlated with the ability to form the g = 4.1 EPR signal of the $(Mn)_4$ poised in the S_2 state in *Synechocystis* PS II particles (Lakshmi et al., 2002). Material depleted of Cyt c_{550} lost the ability to form the signal and reconstitution with purified Cyt c_{550} led to a partial restoration of the signal. The g = 4.1 signal has been proposed to form at the expense of the multiline signal and the interconversion between the two signals is thought to result from alterations in the exchange couplings within the $(Mn)_4$ (de Paula et al., 1986; Boussac et al., 1998). The yield of the g = 4.1 signal depends inversely upon the chloride binding (Ono et al., 1986; Lindberg and Andreasson, 1996) and directly upon the binding of the 24 kDa and 16 kDa proteins in higher plant PS II preparations (de Paula et al., 1986). The similar effects of stabilization of the g = 4.1 signal by the binding of Cyt c_{550} to the cyanobacterial PS II and the 24 kDa and 16 kDa proteins in plant PS II led to the conclusion that the 24 kDa protein is functionally homologous to Cyt c_{550} (Lakshmi et al., 2002). Whether other functional properties of the 24 kDa protein are mirrored by Cyt c_{550} remains largely unresolved. As discussed above, the 24 kDa protein is generally agreed to control access

of calcium to its binding site near the $(Mn)_4$. It is not clear whether Cyt c_{550} exerts a similar control over the accessibility of calcium in cyanobacterial and red algal PS II. Nevertheless, there are some indications that the functional homologies extend beyond stabilization of the g = 4.1 signal. Biochemical depletion-reconstitution studies with *Cyanidium* demonstrated that removal of Cyt c_{550} and PsbU makes O_2 evolution strongly dependent upon calcium and chloride, as is found with higher plant PS II-depleted of the 24 and 16 kDa proteins. However, it is worth noting that the level of total reconstitution in this system rarely exceeds 65%, so that mitigation by these ions of damage to PS II may complicate the analysis. Better levels (~80%) of restoration of initial O_2 evolution activity are obtained using the thermophilic cyanobacterium *Thermosynechoccus vulcanus* (Shen and Inoue, 1993b). Using this system, it was concluded that calcium alone cannot substitute for Cyt c_{550}, which differs from the ability of calcium to restore activity lost upon removal of the 24 kDa and 16 kDa proteins of plant PS II (Shen and Inoue, 1993b). Careful studies using Chelex-treated buffers to examine the calcium dependence of water oxidation in a manner allowing kinetic discrimination of high affinity calcium binding sites remain, however, to be performed with cyanobacterial and red algal preparations. Therefore, it is not yet possible to make thorough comparisons with experiments testing the effects of the 24 kDa protein on calcium binding in higher plant preparations. Deletion of Cyt c_{550} in *Synechocystis* increases the demand for both calcium and chloride in the culture medium for PS II-dependent growth, which has been taken as evidence that Cyt c_{550} modulates either the affinity or accessibility of the PS II sites for the inorganic cofactors (Shen et al., 1998). TL measurements reveal an upshift in the TL peak for the $S_2Q_A^-$ and $S_2Q_B^-$ charge recombinations upon removal of calcium in higher plant PS II, indicating an alteration in the redox properties of the $(Mn)_4$ upon calcium depletion (Ono and Inoue, 1988; Ono and Inoue, 1989b; Ono and Inoue, 1989a; Ono and Inoue, 1990; Ono et al., 1992). This upshift in the TL peaks, however, is only observed in the presence of the 24 kDa protein (Ono et al., 1992). An upshift in the TL peak for the $S_2Q_A^-$ and $S_2Q_B^-$ charge recombinations is also observed in the Cyt c_{550} deletion mutant (Shen et al., 1998). These results are consistent with the proposition that Cyt c_{550} modulates the binding of calcium in cyanobacterial PS II. Again it is important to note that similar observations have been made with the MSP deletion mutant and therefore it is difficult to exclude a more generalized effect due to the absence of extrinsic proteins per se.

Besides affecting the calcium and chloride$^-$ requirements, Cyt c_{550} appears to modify the stability of the $(Mn)_4$. The absence of Cyt c_{550} due to genetic deletion causes a dramatic in vivo destabilization of the O_2 evolution activity in the dark and an increased susceptibility to photoinhibition. Both of these characteristics are shared by deletion mutants lacking MSP (Burnap and Sherman, 1991; Mayes et al., 1991; Bricker, 1992). While susceptibility to photoinhibition may be a general property shared by many donor-side mutants (Vermaas et al. 1990; Mayes et al., 1991), the instability of O_2 evolution activity in the dark is not but has been associated with mutants that lack MSP or are severely impaired in MSP binding (Engels et al., 1994; Burnap et al., 1995; Gleiter et al., 1995; Burnap et al., 1996). The O_2 evolution activity lost in the dark is readily restored by re-illumination under weak light. The kinetics of activity restoration resemble the kinetics of photoactivation (Cheniae and Martin, 1971; Engels et al., 1994; Burnap et al., 1995), suggesting that the loss of activity is due to the disassembly of the $(Mn)_4$ and the restoration of activity is due to the light-driven assembly of metals into the apoprotein (Shen et al., 1998). A function in stabilization of the water oxidation complex is also indicated by experiments showing that biochemical removal and reconstitution of Cyt c_{550} in *Synechococcus* sp. PCC 7002 thylakoids results in a lower temperature threshold for the inactivation of O_2 evolution by heat treatment (Nishiyama et al., 1994). Clearly, Cyt c_{550} is important for maintaining the structural integrity of the water oxidation complex and in doing so, it appears to modulate the activity of the catalytic activity of the $(Mn)_4$. What is not clear is whether or not it may have additional functions that would involve the heme moiety of the protein. It is possible that Cyt c_{550} is merely an evolutionary vestige of a previously operating donor-side electron transfer pathway that no longer operates in the contemporary water oxidizing photosystem. However, it is difficult to rationalize the retention of the heme moiety though the eons and in so many taxonomic groups.

VI. The PsbU Protein in Cyanobacteria

As with Cyt c_{550}, the PsbU protein was already evident in early PS II core particle preparations obtained

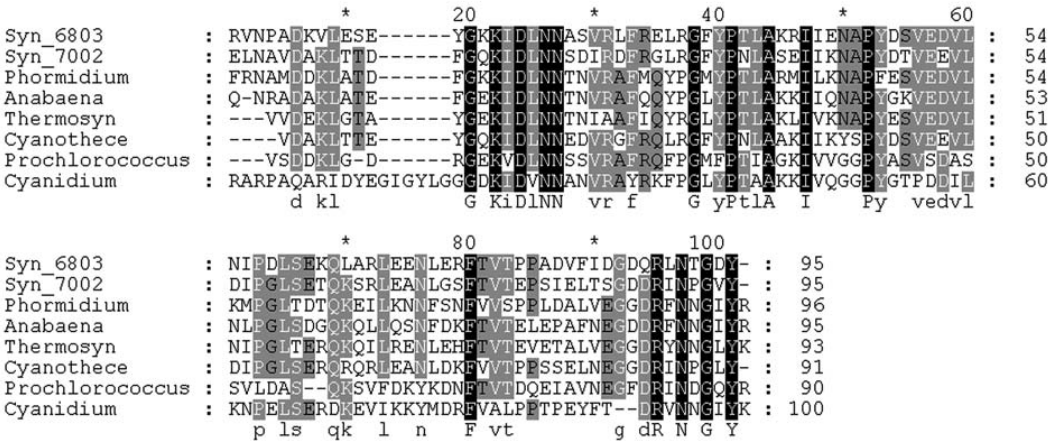

Fig. 5. Alignment of the amino acid sequences of the 12 kDa protein (PsbU). The alignments were performed as described in the legend of Fig. 1.

from thermophilic cyanobacteria. However, unlike the cytochrome, a specific function in the retention of water oxidation activity was realized for PsbU during these early investigations (Stewart and Bendall, 1981; Stewart et al., 1985a,b). Specifically, it was noticed that O_2-evolving activity was diminished upon the loss of PsbU (so-called 12 kDa or 9 kDa protein depending upon the species) and that the retention of activity and PsbU depended upon the inclusion of high concentrations of glycerol in the isolation buffers (Stewart et al., 1985a,b).

Compared to the other PS II extrinsic proteins, information on the binding and function of PsbU is sparse. The most recent PS II crystal structure models (Kamiya and Shen, 2003) and earlier models based upon electron microscopic examination of polypeptide-depleted and reconstituted PS II particles have placed PsbU in a structurally bridging position between MSP and Cyt c_{550} (Kuhl et al., 1999; Nield et al., 2000). A contact with both MSP and cytochrome c_{550} is also indicated by the EDC crosslinking experiments mentioned above (Han et al., 1994) and thus support the crystal structure assignment. This assessment is also consistent with the observation from biochemical depletion-reconstitution experiments showing that the binding of PsbU completely depends upon the presence of both MSP and Cyt c_{550} (Shen and Inoue, 1993a,b; Enami et al., 1998, 2000). As with the other extrinsic proteins, PsbU influences the demand for PS II calcium and chloride. In *Cyanidium caldarium*, a thermophilic, acidophilic red alga, the PsbU protein functions to minimize the calcium and chloride requirements of the water oxidation reaction. As with Cyt c_{550}, biochemical depletion-reconstitution studies with *Synechococcus* sp. PCC7002, demonstrated that PsbU is required for maximal stabilization of the water oxidation complex against heat inactivation (Nishiyama et al., 1997, 1999). PsbU from *Cyanidium* has been heterologously expressed in *E. coli* and shown to reconstitute activity of polypeptide-depleted PS II core complexes to a similar extent as the native protein (Ohta et al., 1999). An alignment of the known cyanobacterial sequences is shown in Fig. 5.

VII. Conclusions

Despite considerable progress in our understanding of the functional and structural attributes of the extrinsic proteins of PS II, it is clear that significant questions remain unanswered. The mechanisms by which these proteins facilitate O_2 evolution at physiological cofactor concentrations remain to be determined. While an understanding of the basic structural organization of the cyanobacterial extrinsic subunits appears to be near at hand (Zouni et al., 2001; Kamiya and Shen, 2003; Biesiadka et al., 2004; Ferreira et al., 2004; Chapters 19–21), the organization of the higher plant extrinsic subunits remains largely speculative. Additionally, the ongoing debate concerning the

stoichiometry of the MSP in cyanobacterial *vs.* higher plant PS II remains unresolved. A rationale for the presence of the low potential Cyt c_{550} in the cyanobacterial photosystem is also lacking. The possible roles and functions of the *psbP* and *psbQ* homologues in the cyanobacteria are only beginning to be explored. Finally, the role (if any) of the observed heterogeneity of the extrinsic subunits of higher plant PS II has yet to be determined. There is undoubtedly much work that needs to be done.

Acknowledgments

This work was supported by grants from the National Science Foundation to TMB and RLB and by a grant from the Department of Energy to T.M.B. Special thanks to Ms. Laurie K. Frankel for her critical reading of this chapter and her many helpful suggestions.

References

Abramowicz DA and Dismukes GC (1984) Manganese proteins isolated from spinach thylakoid membranes and their role in O_2 evolution. II. A binuclear manganese-containing 34 kDa protein, a probable component of the water dehydrogenase system. Biochim Biophys Acta 765: 318–328

Adelroth P, Lindberg K and Andreasson L-E (1995) Studies of Ca^{+2} binding in spinach Photosystem II using $^{45}Ca^{+2}$. Biochemistry 34: 9021–9027

Adir N (1999) Crystallization of the oxygen-evolving reaction centre of Photosystem II in nine different detergent mixtures. Acta Crystal 55: 891–894

Ahmed A, Tajmir-Riahi HA and Carpentier R (1995) A quantitative secondary structure analysis of the 33 kDa extrinsic protein of Photosystem II by FTIR spectroscopy. FEBS Lett 363: 65–68

Akerlund H-E, Jansson C and Andersson B (1982) Reconstitution of photosynthetic water splitting in inside-out thylakoid vesicles and identification of a participating polypeptide. Biochim Biophys Acta 681: 1–10

Anati R and Adir N (2000) Crystallization of dimers of the manganese-stabilizing protein of Photosystem II. Photosynth Res 64: 167–177

Andersson B, Larsson C, Jansson C, Ljungberg U and Akerlund H-E (1984) Immunological studies on the organization of proteins in photosynthetic oxygen evolution. Biochim Biophys Acta 766: 21–26

Balsera M, Arellano JB, Gutierrez JR, Heredia P, Revuelta JL and De Las Rivas J (2003) Structural analysis of the psbQ protein of Photosystem II by Fourier transform infrared and circular dichroic spectroscopy and by bioinformatic methods. Biochemistry 42: 1000–1007

Bernier M and Carpentier R (1995) The action of mercury on the binding of the extrinsic polypeptides associated with the water oxidizing complex of Photosystem II. FEBS Lett 360: 251–254

Betts S, Ross JR, Hall KU, Pichersky E and Yocum CF (1996a) Functional reconstitution of Photosystem II with recombinant manganese-stabilizing proteins containing mutations that remove the disulfide bridge. Biochim Biophys Acta 1274: 135–142

Betts SD, Ross JR, Pichersky E and Yocum CF (1996b) Cold-sensitive assembly of a mutant manganese-stabilizing protein caused by a val to ala replacement. Biochemistry 35: 6302–6307

Betts SD, Ross JR, Pichersky E and Yocum CF (1997) Mutation Val235Ala weakens binding of the 33-kDa manganese stabilizing protein of Photosystem II to one of two sites. Biochemistry 36: 4047–4053

Betts SD, Lydakis-Simantiris N, Ross JR and Yocum CF (1998) The carboxyl-terminal tripeptide of the manganese-stabilizing protein is required for quantitative assembly into Photosystem II and for high rates of oxygen evolution activity. Biochemistry 37: 14230–14236

Biesiadke J, Loll B, Kern J, Irrgang K-D and Zouni A (2004) Crystal structure of cyanobacterial Photosystem II at 3.2 Å resolution: A closer look at the Mn-cluster. Phys Chem Chem Phys 6: 4733–4736

Boekema EJ, Hankamer B, Bald D, Kruip J, Nield J, Boonstra AF, Barber J and Rogner M (1995a) Supramolecular structure of the Photosystem II complex from green plants and cyanobacteria. Proc Natl Acad Sci USA 92: 175–179

Boekema EJ, Hankamer B, Bald D, Kruip J, Nield J, Boonstra AF, Barber J and Rogner M (1995b) Supramolecular structure of the Photosystem II complex from green plants and cyanobacteria. Proc Natl Acad Sci USA 92: 175–179

Boekema EJ, Nield J, Hankamer B and Barber J (1998) Localization of the 23-kDa subunit of the oxygen-evolving complex of Photosystem II by electron microscopy. Eur J Biochem 252: 268–276

Boekema EJ, van Breeman JFL, van Roon H and Dekker JP (2000) Conformational changes in Photosystem II supercomplexes upon removal of extrinsic subunits. Biochemistry 39: 12907–12915

Borthakur D and Haselkorn R (1989) Nucleotide sequence of the gene encoding the 33 kDa water oxidizing polypeptide in *Anabaena* sp. strain PCC 7120 and its expression in *E. coli*. Plant Mol Biol 13: 427–439

Boussac A and Rutherford AW (1988) Nature of the inhibition of the oxygen-evolving enzyme of Photosystem II induced by NaCl washing and reversed by the addition of Ca^{+2} or Sr^{+2}. FEBS Lett 236: 432–436

Boussac A, Kuhl H, Un S, Rogner M and Rutherford AW (1998) Effect of near-infrared light on the S_2-state of the manganese complex of Photosystem II from *Synechococcus elongatus*. Biochemistry 37: 8995–9000

Bricker TM (1990) The structure and function of CPa-1 and CPa-2 in Photosystem II. Photosynth Res 24: 1–13

Bricker TM (1992) Oxygen evolution in the absence of the 33 kDa manganese-stabilizing protein. Biochemistry 31: 4623–4628

Bricker TM and Frankel LK (1987) Use of a monoclonal antibody in structural investigations of the 49 kDa polypeptide of Photosystem II. Arch Biochem Biophys 256: 295–301

Bricker TM and Frankel LK (1998) The structure and function of the 33 kDa extrinsic protein of Photosystem II. A critical review. Photosynth Res 56: 157–173

Bricker TM and Frankel LK (2002) The structure and function of CP47 and CP43 in Photosystem II. Photosynth Res 72: 131–146

Bricker TM and Frankel LK (2003) Carboxylate groups on the manganese-stabilizing protein are required for efficient binding of the 24 kDa protein to Photosystem II. Biochemistry 42: 2056–2061

Bricker TM, Odom WR and Queirolo CB (1988) Close association of the 33 kDa extrinsic protein with the apoprotein of CPa-1 in Photosystem II. FEBS Lett 231: 111–117

Bricker TM, Morvant J, Masri N, Sutton H and Frankel LK (1998) Isolation of a highly active Photosystem II preparation from *Synechocystis* 6803 using a histidine-tagged mutant of CP 47. Biochim Biophys Acta 1409: 50–57

Bricker TM, Young A, Frankel LK and Putnam-Evans C (2002) Introduction of the ^{305}Arg to ^{305}Ser mutation in the large extrinsic loop E of the CP43 protein of *Synechocystis* sp. PCC6803 leads to the loss of cytochrome c_{550} binding to Photosystem II. Biochim Biophys Acta 1556: 92–96

Burnap RL and Sherman LA (1991) Deletion mutagenesis in *Synechocystis* sp. PCC 6803 indicates that the Mn-stabilizing protein of Photosystem II is not essential for oxygen evolution. Biochemistry 30: 440–446

Burnap RL, Shen J-R, Jursinic PA, Inoue Y and Sherman LA (1992) Oxygen yield and thermoluminescence characteristics of a cyanobacterium lacking the manganese-stabilizing protein of Photosystem II. Biochemistry 31: 7404–7410

Burnap RL, Qian M, Shen J-R, Inoue Y and Sherman LA (1994) Role of disulfide linkage and putative intermolecular binding residues in the stability and binding of the extrinsic manganese-stabilizing proteins to the Photosystem II reaction center. Biochemistry 33: 13712–13718

Burnap RL, Qian M, Al-Khaldi S and Pierce C (1995) Photoactivation and S-state cycling kinetics in Photosystem II mutants in *Synechocystis* sp. PCC6803. In: Mathis P (ed) Photosynthesis: From Light to Biosphere, Vol II, pp 443–446. Kluwer Academic Publishers, Dordrecht

Burnap RL, Qian M and Pierce C (1996) The manganese-stabilizing protein of Photosystem II modifies the in vivo deactivation and photoactivation kinetics of the H_2O oxidation complex in *Synechocystis* sp. PCC6803. Biochemistry 35: 874–882

Calderone V, Trabucco M, Vujicic A, Battistutta R, Giacometti GM, Andreucci F, Barbato R and Zanotti G (2003) Crystal structure of the PsbQ protein of Photosystem II from higher plants. EMBO Reports 4: 900–905

Campbell KA, Gregor W, Pham DP, Peloquin JM, Debus RJ and Britt RD (1998a) The 23 and 17 kDa proteins of Photosystem II modulate the magnetic properties of the S_1-state manganese cluster. Biochemistry 37: 5039–5045

Campbell KA, Peloquin JM, Pham DP, Debus RJ and Britt RD (1998b) Parallel polarization EPR detection of an S_{-1}-state 'multiline' EPR signal in Photosystem II particles from *Synechocystis* sp. PCC 6803. J Am Chem Soc 120: 447–448

Cheniae GM and Martin IF (1971) Effects of hydroxylamine on Photosystem II. I. Factors affecting the decay of O_2 evolution. Plant Physiol 47: 568–575

Cole J, Boska M Blough NV and Sauer K (1986) Reversible and irreversible effects of alkaline pH on Photosystem II electron-transfer reactions. Biochim Biophys Acta 848: 41–47

Coleman WJ and Govindjee (1987) A model for the mechanism of chloride activation of oxygen evolution in Photosystem II. Photosynth Res 13: 199–223

de Paula JC, Li PM, Miller AF, Wu BW and Brudvig GW (1986) Effect of the 17- and 23-kilodalton polypeptides, calcium, and chloride on electron transfer in Photosystem II. Biochemistry 25: 6487–6494

Eaton-Rye JJ and Murata N (1989) Evidence that the amino-terminus of the 33 kDa extrinsic protein is required for binding to the Photosystem II complex. Biochim Biophys Acta 977: 219–226

Eaton-Rye JJ and Vermaas WFJ (1991) Oligonucleotide-directed mutagenesis of *psb*B, the gene encoding CP 47, employing a deletion strain of the cyanobacterium *Synechocystis* sp. PCC 6803. Plant Mol Biol 17: 1165–1177

Enami I, Satoh K and Katoh S (1987) Crosslinking between the 33 kDa extrinsic protein and the 47 kDa chlorophyll-carrying protein of the PS II reaction center core complex. FEBS Lett 226: 161–165

Enami I, Mochizuki Y, Takahashi S, Kakuno T, Horio T, Satoh K and Katoh S (1990) Evidence from crosslinking for the nearest neighbor relationships among the three extrinsic proteins of spinach Photosystem II complexes that are associated with oxygen evolution. Plant Cell Physiol 31: 725–729

Enami I, Kaneko M, Kitamura N, Koike H, Sonoike K, Inoue Y and Katoh S (1991) Total immobilization of the extrinsic 33 kDa protein in spinach Photosystem II membrane preparations. Protein stoichiometry and stabilization of oxygen evolution. Biochim Biophys Acta 1060: 224–232

Enami I, Murayama H, Ohta H, Kamo M, Nakazato K and Shen JR (1995) Isolation and characterization of a Photosystem II complex from the red alga *Cyanidium caldarium*: Association of cytochrome c_{550} and a 12 kDa protein with the complex. Biochim Biophys Acta 1232: 208–216

Enami I, Tohri A, Kamo M, Ohta H and Shen J-R (1997) Identification of domains on the 43 kDa chlorophyll-carrying protein (CP 43) that are shielded from tryptic attack by binding of the extrinsic 33 kDa protein with Photosystem II complex. Biochim Biophys Acta 1320: 17–26

Enami I, Kikuchi S, Fukuda T, Ohta H and Shen JR (1998) Binding and functional properties of four extrinsic proteins of Photosystem II from a red alga, *Cyanidium caldarium*, as studied by release-reconstitution experiments. Biochemistry 37: 2787–2793

Enami I, Yoshihara S, Tohri A, Okumura A, Ohta H and Shen JR (2000) Cross-reconstitution of various extrinsic proteins and Photosystem II complexes from cyanobacteria, red algae and higher plants. Plant Cell Physiol 41: 1354–1364

Engels DH, Lott A, Schmid GH and Pistorius EK (1994) Inactivation of the water oxidizing enzyme in manganese stabilizing protein-free mutant cells of the cyanobacterium *Synechococcus* PCC 7942 and *Synechocystis* PCC6803 during dark incubation and conditions leading to photoinactivation. Photosynth Res 42: 227–244

Ferreira KN, Iverson TM, Maghlaovi K, Barber J and Iwata S (2004) Architecture of the photosynthetic oxygen-evolving center. Science 303: 1831–1838

Frankel LK and Bricker TM (1990) Mapping of NHS-biotinylation sites and the epitope of the monoclonal antibody FAC2 on the apoprotein of CPa-1. In: Baltscheffsky M (ed) Current Research in Photosynthesis, Vol I, pp 639–642. Kluwer Academic Publishers, Dordrecht

Frankel LK and Bricker TM (1992) Interaction of CPa-1 with the

manganese-stabilizing protein of photosystem II: Identification of domains on CPa-1 which are shielded from N-hydroxysuccinimide biotinylation by the manganese-stabilizing protein. Biochemistry 31: 11059–11063

Frankel L and Bricker TM (1995) Interaction of the 33-kDa extrinsic protein with Photosystem II: Identification of domains on the 33-kDa protein that are shielded from NHS—biotinylation by Photosystem II. Biochemistry 34: 7492–7497

Frankel LK, Cruz JA and Bricker TM (1999) Carboxylate groups on the manganese-stabilizing protein are required for its efficient binding to Photosystem II. Biochemistry 38: 14275–14278

Frazao C, Enguita FJ, Coelho R, Sheldrick GM, Navarro JA, Hervas M, De la Rosa MA and Corrondo MA (2001) Crystal structure of low-potential cytochrome c_{549} from *Synechocystis* sp. PCC 6803 at 1.21 Å resolution. J Biol Inorg Chem 6: 324–332

Ghanotakis DF, Babcock GT and Yocum CF (1984a) Calcium reconstitutes high rates of oxygen evolution in polypeptide depleted Photosystem II preparations. FEBS Lett 167: 127–130

Ghanotakis DF, Topper JN, Babcock GT and Yocum CF (1984b) Water-soluble 17-kDa and 23-kDa polypeptides restore oxygen evolution activity by creating a high-affinity biding-site for Ca^{2+} on the oxidizing side of Photosystem II. FEBS Lett. 170: 169–173

Ghanotakis DF, Topper JN and Yocum CF (1984c) Structural organization of the oxidizing side of Photosystem II: Exogenous reductants reduce and destroy the Mn-complex in Photosystem II membranes depleted of the 17 and 23 kDa polypeptides. Biochim Biophys Acta 767: 524–531

Ghanotakis DF, Babcock GT and Yocum CF (1985) On the role of water-soluble polypeptides (17, 23 kDa) calcium and chloride in photosynthetic oxygen evolution. FEBS Lett 192: 1–3

Frazao C, Enguita FJ, Coelho R, Sheldrick GM, Navarro JA, Hervas M, De la Rosa MA and Corrondo MA (2001) Crystal structure of low-potential cytochrome c_{549} from *Synechocystis* sp. PCC 6803 at 1.21 Å resolution. J. Biol Inorg Chem 6: 324–332

Gleiter HM, Haag E, Shen J-R, Eaton-Rye JJ, Inoue Y and Vermaas WFJ (1994) Functional characterization of mutant strains of the cyanobacterium *Synechocystis* PCC 6803 lacking short domains within the large, lumen-exposed loop of the chlorophyll protein CP47 in Photosystem II. Biochemistry 33: 12063–12071

Gleiter HM, Haag E, Shen J-R, Eaton-Rye JJ, Seeliger AG, Inoue Y, Vermaas WFJ and Renger G (1995) Involvement of the CP47 protein in stabilization and photoactivation of a functional water-oxidizing complex in the cyanobacterium *Synechocystis* sp. PCC 6803. Biochemistry 34: 6847–6856

Haag E, Eaton-Rye JJ, Renger G and Vermaas WFJ (1993) Functionally important domains of the large hydrophilic loop of CP 47 as probed by oligonucleotide-directed mutagenesis in *Synechocystis* sp. PCC 6803. Biochemistry 32: 4444–4454

Hackett CS and Strittmatter P (1984) Covalent crosslinking of the active sites of vesicle-bound cytochrome b_5 and NADH cytochrome b_5 reductase. J Biol Chem 259: 3275–3282

Han K-C, Shen J-R, Ikeuchi M and Inoue Y (1994) Chemical crosslinking studies of extrinsic proteins in cyanobacterial Photosystem II. FEBS Lett 355: 121–124

Hasler L, Ghanotakis D, Fedtke B, Spyridaki A, Miller M, Muller SA, Engle A and Tsotis G (1997) Structural analysis of Photosystem II: Comparative studies of cyanobacterial and higher plant Photosystem II complexes. J Struct Biol 119: 273–283

Hayashi H, Fujimura Y, Mohanty PS and Murata N (1993) The role of CP 47 in the evolution of oxygen and the binding of the extrinsic 33-kDa protein to the core complex of Photosystem II as determined by limited proteolysis. Photosynth Res 36: 35–42

Ho KK, Ulrich EL, Krogmann DW and Gomez-Lojero C (1979) Isolation of photosynthetic catalysts from cyanobacteria. Biochim Biophys Acta 545: 236–248

Holten RW and Meyers J (1963) Cytochromes of a blue-green algae: Extraction of a *c*-type with a strongly negative redox potential. Science 142: 234–235

Holzenburg A, Flint TD, Shepard FH and Ford RC (1996) Photosystem II: Mapping the locations of the oxygen evolution-enhancing subunits by electron microscopy. Micron 27: 121–127

Homann PH and Madabusi LM (1993) Modification of the thermoluminescence properties of Ca^{+2}-depleted Photosystem II membranes by the 23 kDa extrinsic polypeptide and by oligocarboxylic acids. Photosynth Res 35: 29-39

Hong SK, Pawlikowski SA, Van der Meulen KA and Yocum CF (2001) The oxidation state of the Photosystem II manganese cluster influences the structure of the manganese-stabilizing protein. Biochim Biophys Acta 1504: 262–274

Hutchison R, Betts SD, Yocum CF and Barry BA (1998) Conformational changes in the extrinsic manganese-stabilizing protein upon binding to the Photosystem II reaction center: An isotope editing and FTIR study. Biochemistry 37: 5643–5653

Hutchinson RS, Steenhuis JJ, Yocum CF, Razeghifard MR and Barry BB (1999) Deprotonation of the 33-kDa, extrinsic, manganese-stabilizing subunit accompanies photooxidation of the manganese in Photosystem II. J. Biol. Chem. 274: 31987–31995

Ifuku K, Nakatsu T, Kato H and Sato F (2003) Crystallization and preliminary crystallographic studies on the extrinsic 23 kDa protein in the oxygen-evolving complex of Photosystem II. Acta Crystal D 59: 1462–1463

Ikeuchi M, Koike H and Inoue Y (1989) N-terminal sequencing of Photosystem II low-molecular-mass proteins. 5 and 3.1 kDa components of the O_2-evolving core complex from higher plants. FEBS Lett 242: 263–269

Ishikawa Y, Yamamoto Y, Otsubo M, Theg SM and Tamura N (2002) Chemical modification of amine groups on PS II protein(s) retards photoassembly of the photosynthetic water-oxidizing complex. Biochemistry 41: 1972–1980

Isogai Y, Yamamoto Y and Nishimura M (1985) Association of the 33 kDa polypeptide with the 43 kDa component in Photosystem II particles. FEBS Lett 187: 240–244

Jansen T, Rother C, Steppuhn J, Reinke H, Beyreuther K, Jansson C, Andersson B and Herrmann RG (1987) Nucleotide sequence of cDNA clones encoding the complete 23 kDa and 16 kDa precursor proteins associated with the oxygen-evolving complex from spinach. FEBS Lett 216: 234–240

Johnsson GN, Boussac A and Rutherford AW (1994) The origin of 40–50 °C thermoluminescence bands in Photosystem II. Biochim Biophys Acta 1184: 85–92

Kamiya N and Shen J-R (2003) Crystal structure of oxygen-evolving Photosystem II from *Thermosynechococcus vulcanus* at 3.7 Ångstrom resolution. Proc Natl Sci Acad USA 100: 98–103

Kang C, Chitinis PR, Smith S and Krogmann DW (1994) Cloning and sequence analysis of the gene encoding the low

potential cytochrome *c* of *Synechocystis* PCC 6803. FEBS Letters 344: 5–9

Kashino Y, Lauber WM, Carroll JA, Wang Q, Whitmarsh J, Satoh K and Pakrasi HB (2002) Proteomic analysis of a highly active Photosystem II preparation from the cyanobacterium *Synechocystis* sp. PCC 6803 reveals the presence of novel polypeptides. Biochemistry 41: 8004–8012

Kavelaki K and Ghanotakis DF (1991) Effect of the manganese complex on the binding of the extrinsic proteins (17 kDa, 23 kDa and 33 kDa) of photosystem. Photosynth Res 29: 149–155

Kieselbach T, Bystedt M, Hynds P, Robinson C and Schroder WP (2000) A peroxidase homologue and novel plastocyanin located by proteomics to the *Arabidopsis* chloroplast thylakoid lumen. FEBS Lett 480: 271–276

Krogmann DW (1991) The low potential cytochrome *c* of cyanobacteria and algae. Biochim Biophys Acta 1058: 35–37

Kuhl H, Rogner M, Van Breemen JF and Boekema EJ (1999) Localization of cyanobacterial Photosystem II donor-side subunits by electron microscopy and the supramolecular organization of Photosystem II in the thylakoid membrane. Eur J Biochem 266: 453–459

Kuwabara T and Murata N (1983) Characterization of 33-kilodalton, 24-kilodalton and 18-kilodalton proteins in the photosynthetic oxygen-evolving system of spinach. In: Inoue Y, Crofts AR, Govindjee, Murata N, Renger G and Satoh K (eds) The Oxygen-Evolving System of Photosynthesis, pp 223–228. Academic Press, Tokyo

Kuwabara T, Miyao M, Murata T and Murata N (1985) The function of the 33 kDa protein in the oxygen evolution system studied by reconstitution experiments. Biochim Biophys Acta 806:283–289

Kuwabara T, Murata T, Miyao M and Murata N (1986) Partial degradation of the 18 kDa of the photosynthetic oxygen-evolving complex: A study of a binding site. Biochim Biophys Acta 850: 146–155

Lakshmi KV, Reifler MJ, Chisholm DA, Wang JY, Diner BA and Brudvig GW (2002) Correlation of the cytochrome c_{550} content of cyanobacterial Photosystem II with the EPR properties of the oxygen-evolving complex. Photosynth Res72 (2): 175–189

Leuschner C and Bricker TM (1996) Interaction of the 33 kDa extrinsic protein with Photosystem II: Rebinding of the 33 kDa extrinsic protein to Photosystem II membranes which contain four, two, or zero manganese per Photosystem II reaction center. Biochemistry 35: 4551–4557

Li ZL and Burnap RL (2001) Mutations of arginine 64 within the putative calcium-binding interhelical a-b loop of the Photosystem II D1 protein disrupt binding of the manganese-stabilizing protein and cytochrome c_{550} in *Synechocystis* sp. PCC6803. Biochemistry 40: 10350–10359

Lindberg K and Andreasson L-E (1996) A one-site, two-state model for the binding of anions in Photosystem II. Biochemistry 35: 14259–14267

Lydakis-Simantiris N, Betts SD and Yocum CF (1999a) Leucine 245 is a critical residue for folding and function of the manganese-stabilizing protein of Photosystem II. Biochemistry 38: 15528–15535

Lydakis-Simantiris N, Hutchison RS, Betts SD, Barry BA and Yocum CF (1999b) Manganese stabilizing protein of Photosystem II is a thermostable, natively unfolded polypeptide. Biochemistry 38: 404–414

Mayes SR, Cook KM, Self SJ, Zhang Z and Barber J (1991) Deletion of the gene encoding the Photosystem II 33 kDa protein from *Synechocystis* sp PCC 6803 does not inactivate water-splitting but increases vulnerability to photoinhibition. Biochim Biophys Acta 1060: 1–12

Mavankal G, McCain DC and Bricker TM (1986) Effects of chloride on paramagnetic coupling of manganese in calcium chloride-washed Photosystem II preparations. FEBS Lett 202: 235-239

Miller AF, De Paula JC and Brudvig GW (1987) Formation of the S_2-state and structure of the manganese complex in Photosystem II lacking the extrinsic 33 kDa polypeptide. Photosynth Res 12: 205–218

Millner PA, Gogel G and Barber J (1987) Investigation of the spatial relationships between photosystem 2 polypeptides by reversible crosslinking and diagonal electrophoresis. Photosynth Res 13: 185–198

Miura K, Shimazu T, Motoki A, Kani S, Hirano M and Katoh S (1993) Nucleotide sequence of the Mn-stabilizing protein gene of the thermophilic cyanobacterium *Synechococcus elongatus*. Biochim Biophys Acta 1172: 357–360

Miura T, Shen J-R, Takahashi S, Kamo M, Nakamura E, Ohta H, Kamei A, Inoue Y, Domae N, Takio K, Nakazato K, Inoue Y and Enami I (1997) Identification of domains on the extrinsic 33-kDa protein possibly involved in electrostatic interaction with Photosystem II complex by means of chemical modification. J Biol Chem 272: 3788–3798

Miyao M and Murata N (1983) Partial disintegration and reconstitution of the photosynthetic oxygen evolution complex. Biochim Biophys Acta 725: 87–93

Miyao M and Murata N (1984a) Calcium-ions can be substituted for the 24 kDa polypeptide in photosynthetic oxygen evolution. FEBS Lett 168: 118–120

Miyao M and Murata N (1984b) Role of the 33 kDa polypeptide in preserving Mn in photosynthetic oxygen-evolution. FEBS Lett 170: 350–354.

Miyao M and Murata N (1989) The mode of binding of three extrinsic proteins of 33 kDa, 23 kDa and 18 kDa in the Photosystem II complex of spinach. Biochim Biophys Acta 977: 315–321

Miyao M, Murata M, Lavorel J, Maison-Petri B, Boussac A and Etienne A-L (1987) Effects of the 33 kDa protein on the S-state transitions in photosynthetic oxygen evolution. Biochim Biophys Acta 890: 151–159

Miyao M, Fujimura Y and Murata N (1988) Partial degradation of the extrinsic 23 kDa protein of the Photosystem II complex of spinach. Biochim Biophys Acta 936: 465–474

Morris EP, Hankamer B, Zheleva D, Friso G and Barber J (1997) The three-dimensional structure of a Photosystem II core complex determined by electron crystallography. Structure 5: 837–849

Motoki A, Usui M, Shimazu T, Hirano M and Katoh S (2002) A domain of the Mn-stabilizing protein from *Synechococcus elongatus* involved in functional binding to Photosystem II. J Biol Chem 277: 14747-14756

Murakami R, Ifuku K, Takabayashi A, Shikanai T, Endo T and Sato F (2002) Characterization of an *Arabidopsis thaliana* mutant with impaired *psb*O, one of two genes encoding extrinsic 33-kDa proteins in Photosystem II. FEBS Lett 523: 138–142

Murata N, Miyao M, Omata T, Matsunami H and Kuwabara T (1984) Stoichiometry of components in the photosynthetic oxygen evolution system of Photosystem II particles prepared

with Triton X-100 from spinach chloroplast. Biochim Biophys Acta 765: 363–369

Navarro JA, Hervas M, De la Cerda B and De la Rosa MA (1995) Purification and physicochemical properties of the low potential cytochrome C_{549} from the cyanobacterium *Synechocystis* sp. PCC 6803. Arch Biochem Biophys 3186: 46–52

Nakatani HY (1984) Photosynthetic oxygen evolution does not require the participation of polypeptides of 16 and 24 kDa. Biochem Biophys Res Comm 120: 299–304

Nield J, Orlova EV, Morris EP, Gowen B, van Heel M and Barber J (2000) 3D map of the plant Photosystem II supercomplex obtained by cryoelectron microscopy and single particle analysis. Nat Struct Biol 7: 44–47

Nield J, Kruse O, Ruprecht J, da Fonseca P, Buchel C and Barber J (2000) Three-dimensional structure of *Chlamydomonas reinhardtii* and *Synechococcus elongatus* Photosystem II complexes allows for comparison of their oxygen-evolving complex organization. J Biol Chem 275: 27940–27946

Nishiyama Y, Hayashi H, Watanabe T and Murata N (1994) Photosynthetic oxygen evolution is stabilized by cytochrome c_{550} against heat inactivation in *Synechococcus* sp PCC 7002. Plant Physiol 105: 1313–1319

Nishiyama Y, Los DA, Hayashi H and Murata N (1997) Thermal protection of the oxygen-evolving machinery by PsbU, an extrinsic protein of Photosystem II, in *Synechococcus* species PCC 7002. Plant Physiol 115: 1473–1480

Nishiyama Y, Los DA and Murata N (1999) PsbU, a protein associated with Photosystem II, is required for the acquisition of cellular thermotolerance in *Synechococcus* species PCC 7002. Plant Physiol 120: 301–308

Odom WR and Bricker TM (1992) Interaction of CPa-1 with the manganese-stabilizing protein of Photosystem II: Identification of domains crosslinked by 1-ethyl-3-[3-(dimethylamino) propyl]carbodiimide. Biochemistry 31: 5616–5620

Oh-Oka H, Tanaka S, Wada K, Kuwabara T and Murata N (1986) Complete amino acid sequence of 33 kDa protein isolated from spinach Photosystem II particles. FEBS Lett 197: 63–66

Ohta H, Yoshida N, Sano M, Hirano M, Nakazato K and Enami I (1995) Evidence for electrostatic interaction of the loop A on CP 47 with the extrinsic 33 kDa protein. In: Mathis P (ed) Photosynthesis: From Light to Biosphere, Vol II, pp 361–364. Kluwer Academic Publishers, Dordrecht

Ohta H, Okumura A, Okuyama S, Akiyama A, Iwai M, Yoshihara S, Shen JR, Kamo M and Enami I (1999) Cloning, expression of the *psb*U gene, and functional studies of the recombinant 12-kDa protein of Photosystem II from a red alga *Cyanidium caldarium*. Biochem Biophys Res Comm 260: 245–50

Ono T and Inoue Y (1984) Ca^{+2}-dependant restoration of O_2-evolving activity in $CaCl_2$-washed PS II particles depleted of 33, 24, and 16 kDa polypeptides. FEBS Lett 168: 281–286

Ono T and Inoue Y (1985) S-state turnover in the O_2-evolving system of $CaCl_2$-washed Photosystem II particles depleted of three peripheral proteins as measured by thermoluminescence. Removal of 33 kDa protein inhibits S_3 to S_4 transition. Biochim Biophys Acta 806: 331–340

Ono TA and Inoue Y (1988) Discrete extraction of the calcium atom functional for oxygen evolution in higher plant Photosystem II by a simple low pH treatment. FEBS Lett 227: 147–152

Ono TA and Inoue Y (1989a) Removal of calcium by pH 3.0 treatment inhibits S_2 to S_3 transition in photosynthetic oxygen evolution system. Biochim Biophys Acta 973: 443–449

Ono TA and Inoue Y (1989b) Roles of calcium ion in oxygen evolution in higher plant Photosystem II: Effects of replacement of calcium ion site by other cations. Arch Biochem Biophys 275: 440–448

Ono TA and Inoue Y (1990) Abnormal redox reactions in the photosynthetic O_2-evolving centers in NaCl/EDTA-washed PS II. A dark-stable EPR multiline signal and an unknown positive charge accumulator. Biochim Biophys Acta 1020: 269–277

Ono T, Zimmerman JL, Inoue Y and Rutherford AW (1986) EPR evidence for a modified S-state transition in chloride-depleted Photosystem II. Biochim Biophys Acta 851: 193–201

Ono T, Izawa S and Inoue Y (1992) Structural and functional modulation of the manganese cluster in Ca^{+2}-depleted Photosystem II by binding of the 24 kDa extrinsic protein. Biochemistry 31: 7648–7655

Pazos F, Heredia P, Valencia A and de las Rivas J (2001) Threading structural model of the manganese-stabilizing protein PsbO reveals presence of two possible beta-sandwich domains. Proteins 45: 372–381

Philbrick JB, Diner BA and Zilinskas BA (1991) Construction and characterization of cyanobacterial mutants lacking the manganese-stabilizing protein of Photosystem II. J Biol Chem 266: 13370–13376

Popelkova H, Im MM, D'Auria J, Betts SD, Lydakis-Simantiris N and Yocum CF (2002a) N-terminus of the Photosystem II manganese-stabilizing protein: Effects of sequence elongation and truncation. Biochemistry 41: 2702–2711

Popelkova H, Im MM and Yocum CF (2002b) N-terminal truncations of manganese stabilizing protein identify two amino acid sequences required for binding of the eukaryotic protein to Photosystem II and reveal the absence of one binding-related sequence in cyanobacteria. Biochemistry 41: 10038–10045

Popelkova H, Wyman A and Yocum CF (2003a) Amino acid sequences and solution structures of manganese-stabilizing protein that affects reconstitution of Photosystem II activity. Photosynth Res 77: 21–34

Popelkova H, Im MM and Yocum CF (2003b) Binding of manganese-stabilizing protein to Photosystem II: Identification of essential N-terminal threonine residues and domains that prevent nonspecific binding. Biochemistry 42: 6193–6200

Putnam-Evans C and Bricker TM (1992) Site-directed mutagenesis of the CPa-1 protein of Photosystem II: Alteration of the basic residue pair ^{384,385}R to ^{384,385}G leads to a defect associated with the oxygen-evolving complex. Biochemistry 31: 11482–11488

Putnam-Evans C, Wu J, Burnap R, Whitmarsh J and Bricker TM (1996) Site-directed mutagenesis of the CP 47 protein of Photosystem II: Alteration of conserved charged residues in the domain ^{364}E-^{444}R. Biochemistry 35: 4046–4053

Qian M, Al-Khaldi S, Putnam-Evans C, Bricker TM and Burnap RL (1997) Photoassembly of the Photosystem II $(Mn)_4$ cluster in site-directed mutants impaired in the binding of the manganese stabilizing protein. Biochemistry 36: 15244–15252

Rashid A and Carpentier R (1990) The 16 and 23 kDa extrinsic polypeptides and the associated Ca^{2+} and Cl^- modify atrazine interaction with the Photosystem II core complex. Photosynth Res 24: 221–227

Razeghifard MR, Wydrzynski T, Pace RJ and Burnap RL (1997) Y_z reduction kinetics in the absence of the manganese-stabilizing protein of Photosystem II. Biochemistry 36: 14474–14478

Reifler MJ, Chisholm DA, Wang J, Diner BA and Brudvig GW (1998) Engineering and rapid purification of histidine-tagged Photosystem II from *Synechocystis* PCC 6803. In: Garab G (ed) Photosynthesis: Mechanisms and Effects, Vol II, pp 1189–1192. Kluwer Academic Publishers, Dordrecht

Sawaya MR, Krogmann DW, Serag A, Ho, Yeates TO and Kerfeld CA (2001) Structures of cytochrome c_{549} and cytochrome c_6 from the cyanobacterium *Arthrospira maxima*. Biochemistry 40: 9215–9225

Schubert M, Petersson U-A, Hass BJ, Funk C and Schroder WP (2002) Proteome map of the chloroplast lumen of *Arabidopsis thaliana*. J Biol Chem 277: 8354–8365

Seidler A (1994) Introduction of a histidine tail at the N-terminus of a secretory protein expressed in *E. coli*. Protein Engineering 7: 1277–1280

Seidler A (1996a) Intermolecular and intramolecular interactions of the 33 kDa protein of Photosystem II. Eur J Biochem 242: 485–490

Seidler A (1996b) The extrinsic polypeptides of Photosystem II. Biochim Biophys Acta 1277: 35–60

Seidler A and Rutherford AW (1996) The role of the extrinsic 33 kDa protein in Ca^{2+} binding in Photosystem II. Biochemistry 35: 12104–121010

Seidler A, Roll K and Michel H (1992) Characterization of the 33 kDa protein of the oxygen-evolving complex of higher plants by site-directed mutagenesis. In: Murata N (ed) Research in Photosynthesis, Vol II, pp 409–412. Kluwer Academic Press, Dordrecht

Seidler A, Rutherford AW and Michel H (1996a) The extrinsic 33 kDa protein of Photosystem II: Improved expression plasmids and progress in mutational analysis. In: Mathis P (ed) Photosynthesis: From Light to Biosphere, Vol II, pp 259–263. Kluwer Academic Press, Dordrecht

Seidler A, Rutherford AW and Michel H (1996b) On the role of the N terminus of the extrinsic 33 kDa protein of Photosystem II. Plant Mol Biol 31: 183-188

Shen G, Eaton-Rye JJ and Vermaas WFJ (1993) Mutation of histidine residues in CP 47 leads to a destabilization of the Photosystem II complex and to impairment of light energy transfer. Biochemistry 32: 5109–5115

Shen J-R and Inoue Y (1993a) Cellular localization of cytochrome c_{550}: Its specific association with cyanobacterial Photosystem II. J Biol Chem 268: 20408–20413

Shen J-R and Inoue Y (1993b) Binding and functional properties of two new extrinsic components, cytochrome c_{550} and a 12 kDa protein in cyanobacterial Photosystem II. Biochemistry 32: 1825–1832

Shen J-R, Ikeuchi M and Inoue Y (1992) Stoichiometric association of extrinsic cytochrome c_{550} and the 12 kDa protein with a highly purified oxygen-evolving PS II core complex from *Synechococcus vulcanus*. FEBS Lett 301: 145–149

Shen J-R, Burnap RL and Inoue Y (1995a) An independent role of cytochrome c_{550} in cyanobacterial Photosystem II as revealed by double-deletion mutagenesis of the *psb*O and *psb*V genes in *Synechocystis* sp. PCC 6803. Biochemistry 34: 12661–12668

Shen J-R, Vermaas WFJ and Inoue Y (1995b) The role of cytochrome c_{550} as studied through reverse genetics and mutant characterization in *Synechocystis* sp. PCC 6803. J Biol Chem 270: 6901–6907

Shen J-R, Qian M, Inoue Y and Burnap RL (1998) Functional characterization of *Synechocystis* sp. PCC 6803 Δ*psb*U and Δ*psb*V mutants reveals important roles of cytochrome c_{550} in cyanobacterial oxygen evolution. Biochemistry 37: 1551–1558

Shutova T, Irrgang K-D, Shubin V, Klimov VV and Renger G (1997) Analysis of pH-induced structural changes of the isolated extrinsic 33 kilodalton protein of Photosystem II. Biochemistry 36: 6350–6358

Stewart A and Bendall D (1978) Preparation of active fractions enriched in Photosystem I and Photosystem II from the thermophilic blue-green alga *Phormidium laminosum*. Biochem Soc Trans 6: 1040–1041

Stewart A and Bendall D (1979) Properties of oxygen-evolving photosystem-II particles from *Phormidium laminosum*, a thermophillic blue-green alga. Biochem J 194: 877–887

Stewart A and Bendall D (1980) Photosynthetic electron transport in a cell-free preparation from the thermophilic blue-green alga *Phormidium laminosum*. Biochem J 188: 351–61

Stewart A and Bendall D (1981) Properties of oxygen-evolving Photosystem-II particles from *Phormidium laminosum*, a thermophilic blue-green alga. Biochem J 194: 877–887

Stewart AC, Ljungberg U, Aukerlund H- and Anderson B (1985a) Studies on the polypeptide composition of the cyanobacterial oxygen-evolving complex. Biochim Biophys Acta 808: 353–362

Stewart AC, Siczkowski M and Ljungberg U (1985b) Glycerol stabilizes oxygen evolution and maintains binding of a 9 kDa polypeptide in Photosystem II particles from the cyanobacterium *Phormidium laminosum.* FEBS Lett 193: 175–179

Stoylova SS, Flint TD, Ford RC and Holzenburg A (1997) Projection structure of Photosystem II in vivo determined by cryo-electron crystallography. Micron 28: 439–446

Styring S, Miyao M and Rutherford AW (1987) Formation and flash-dependent oscillation of the S_2-state multiline EPR signal in an oxygen-evolving Photosystem II preparation lacking the three extrinsic proteins in the oxygen-evolving system. Biochim Biophys Acta 767: 32–38

Svensson B, Tiede DM and Barry BA (2002) Small-angle X-ray scattering studies of the manganese-stabilizing protein in Photosystem II. J Phys Chem B 106 :8485–8488

Tanaka S and Wada K (1988) The status of cysteine residues in the 33 kDa protein of spinach Photosystem II complexes. Photosynth Res 17: 255–266

Tang XS, Chisholm DA, Dismukes GC, Brudvig GW and Diner BA (1993) Spectroscopic evidence from site directed mutants of *Synechocystis* PCC6803 in favor of a close interaction between histidine 189 and redox active tyrosine 160, both of polypeptide D2 of the Photosystem II reaction center. Biochemistry 32: 13742–13748

Vass I, Cool KM, Zsuzsanra D, Mayes SR and Barber J (1992) Thermoluminescence and flash oxygen characterization of the IC2 deletion mutant of *Synechocystis* sp. PCC6803 lacking the Photosystem II 33 kda protein. Biochim Biophys Acta 1102: 195–201

Vermaas WFJ, Ikeuchi M and Inoue Y (1988) Protein composition of the Photosystem II core complex in genetically engineered mutants of the cyanobacterium *Synechocystis* PCC 6803. Photosynth Res 17: 97–113

Vermaas WFJ, Charite J and Shen G (1990) Glu-69 of the D2 Protein in Photosystem II is a potential ligand to Mn involved in photosynthetic oxygen evolution. Biochemistry 29: 5325–5332

Vrettos JS, Reifler MJ, Kievit O, Lakshmi KV, de Paula JC and Brudvig GW (2001) Factors that determine the unusually low reduction potential of cytochrome c_{550} in cyanobacterial Photosystem II. J Biol Inorg Chem 6: 708–716.

Wales R, Newman BJ, Pappin D and Gray JC (1989) The extrinsic 33 kDa protein of the oxygen-evolving complex of Photosystem II is a putative calcium-binding protein and is encoded by a multi-gene family in pea. Plant Mol Biol 12: 439–451

Webber AN and Gray JC (1989) Detection of calcium binding by Photosystem II polypeptides immobilized onto nitrocellulose membranes. FEBS Lett 249: 79–82

Wincencjusz H, Yocum CF and van Gorkom HJ (1998) S-state dependence of chloride binding affinities and exchange dynamics in the intact and polypeptide depleted O_2 evolving complex of Photosystem II. Biochemistry 37: 8595–8604

Wincencjusz H, Yocum CF and van Gorkom HJ (1999) Activating anions that replace chloride in the oxygen-evolving complex of Photosystem II slow the kinetics of the terminal step in water oxidation and destabilize the S_2 and S_3 states. Biochemistry 38: 3719–3725

Xu Q and Bricker TM (1992) Structural organization of proteins on the oxidizing side of Photosystem II: Two molecules of the 33 kDa manganese-stabilizing protein per reaction center. J Biol Chem 267: 25816–25821

Xu Q, Nelson J and Bricker TM (1994) Secondary structure of the 33 kDa, extrinsic protein of Photosystem II: A far-UV circular dichroism study. Biochim Biophys Acta 1188: 427–431

Yamamoto Y and Kubota F (1987) Specific release of the extrinsic 18-kDa protein from spinach Photosystem II particles by the treatment with NaCl and methanol and its application for large scale purification of the three extrinsic proteins of Photosystem II without chromatography. Biochim Biophys Acta 893: 579–583

Yamamoto Y, Nakayama S, Cohn CL and Krogmann DW (1987) Highly efficient purification of the 33-, 24-, and 18-kDa proteins in spinach Photosystem II by butanol/water phase partitioning and high-performance liquid chromatography. Arch Biochem Biophys 255: 156–161

Yu Y, Li R, Xu CH, Ruan KC, Shen YK and Govindjee (2001) N-bromosuccinimide modification of tryptophan 241 at the c-terminus of the manganese-stabilizing protein of plant Photosystem II influences its structure and function. Physiol Plant 111: 108–115

Zhang H, Fischer G and Wydrzynski T (1995) An FTIR study of calcium interactions in Photosystem II. In: Mathis P (ed) Photosynthesis: From Light to Biosphere, Vol II, pp 447–450. Kluwer Academic Press, Dordrecht

Zhang H, Ishikawa Y, Yamamoto Y and Carpentier R (1998) Secondary structure and thermal stability of the extrinsic 23 kDa protein of Photosystem II studied by Fourier transform infrared spectroscopy. FEBS Lett 426: 347–351

Zhang H, Yamamoto Y, Ishikawa Y and Carpentier R (1999) Characterization of the secondary structure and thermostability of the extrinsic 16 kilodalton protein of spinach Photosystem II by Fourier transform infrared spectroscopy. J Mol Struct 513: 127–132

Zhang L-X, Liang H-G, Wang J, Li WR and Yu TZ (1996) Fluorescence and Fourier-transform infrared spectroscopic studies on the role of disulfide bond in the calcium binding in the 33 kDa protein of Photosystem II. Photosynth Res 48: 379–384

Zouni A, Witt H-T, Kern J, Fromme P, Krauss N, Saenger W and Orth P (2001) Crystal structure of Photosystem II from *Synechococcus elongatus* at 3.8Å resolution. Nature 409: 739–743

Zubrzycki IZ, Frankel LK, Russo PS and Bricker TM (1998) Hydrodynamic studies on the manganese-stabilizing protein of Photosystem II. Biochemistry 37: 13553–13558

Chapter 6

The Low Molecular Weight Proteins of Photosystem II

Leeann E. Thornton, Johnna L. Roose and Himadri B. Pakrasi*
Department of Biology, Washington University, Box 1137, Saint Louis, MO 63130, U.S.A.

Masahiko Ikeuchi
Department of Life Sciences (Biology), University of Tokyo, Komaba 3-8-1, Meguro, Tokyo 153-8902, Japan

Summary

Photosystem II (PS II) has a complex arrangement of membrane spanning and soluble subunits responsible for its unique role in oxygenic photosynthesis. Advances in several areas of biology have contributed significantly to our understanding of individual subunits and the PS II complex as a whole. In recent years, the genome sequences of several plants and many cyanobacteria have been completed allowing for comparisons of their genes. This information, along with previous biochemical evidence, has strengthened the conclusion that the

*Author for correspondence, email: pakrasi@wustl.edu

T. Wydrzynski and K. Satoh (eds): Photosystem II: The Light-Driven Water:Plastoquinone Oxidoreductase, pp. 121–137.

PS II protein components are highly conserved, from the primitive cyanobacterium *Gloeobacter violaceus* PCC 7421 to the vascular plant *Arabidopsis thaliana*. Advances in purification of PS II samples and protein identification have confirmed the presence of several novel proteins and provide new tools for the analysis of PS II in various mutants and under different growth conditions. Recent structural studies have also contributed tremendously to our understanding of the organization of PS II subunits and cofactors. The combination of genomic, proteomic, and structural studies will continue to be a source of new insights into the assembly, regulation and function of PS II. This chapter highlights the contributions of such studies to our understanding of the numerous low molecular weight PS II components.

I. Introduction

Photosystem II (PS II) is a large protein complex consisting of at least 20 subunits that contribute to optimal charge separation and O_2 evolution. PS II is made up of many subunits that are highly conserved in all the organisms from which it has been isolated. The complexity of PS II is conserved between the primitive single-membrane system of *Gloeobacter violaceus* PCC 7421 and the intricately structured thylakoid membranes of chloroplasts. Despite its bulk, PS II is still assembled frequently in photosynthetic organisms because it has a very high turnover rate. PS II is the target of extensive photodamage requiring rapid removal of its damaged subunits and reassembly of new ones. Understanding PS II as a whole requires examining the complex on many different levels from ultrastructure to the function of individual components in a number of photosynthetic organisms.

Recently, great advances have been made towards determining the structural components of PS II. Innovative technologies in protein purification and crystallization, recent developments in genome sequence annotation, and the implementation of high throughput proteome analysis have shed new light on the big picture of PS II, both for its form and its functions. Zouni and coworkers achieved 3.8 Å resolution crystal structure of PS II from *Thermosynechococcus elongatus* BP-1, which provides an arrangement for many of the membrane-spanning helixes (Zouni et al., 2001; Chapter 19, Witt). PS II from another cyanobacterium, *Thermosynechococcus vulcanus*, was crystallized to 3.7 Å resolution, with a similar subunit arrangement as was seen in the Zouni study (Kamiya and Shen, 2003; Chaptere 20, Shen and Kamiya). A second structure was determined for PS II from *T. elongatus* at 3.5 Å resolution with different assignments for some of the small membrane spanning subunits (Ferreira et al, 2004; Chapter 21, Barber and Iwata). Continued efforts in purification and crystallization of PS II will shed further light on the variability in the arrangement of subunits between organisms and also under different growth conditions (Biesiadka et al., 2004.

Progress in the field of genomics has allowed broad comparisons of the PS II subunits found in cyanobacteria and plants based on predicted amino acid sequence similarities. Table 1 shows the list of PS II genes, which were obtained from the complete sets of open reading frames of *Synechocystis* sp. PCC 6803 (Kaneko et al., 1996), *Anabaena* sp. PCC 7120 (Kaneko et al., 2001), *T. elongatus* (Nakamura et al., 2002), *Prochlorococcus marinus* MED4 (Rocap et al., 2003), *Prochlorococcus marinus* MIT9391 (Rocap et al., 2003), *G. violaceus* (Nakamura et al., 2003b) and *Synechococcus* sp. WH8102 (Palenik et al., 2003), or extracted from nucleotide sequences of the complete or incomplete genome data of *Nostoc punctiforme* ATCC 29133, *Trichodesmium erythraeum*, and *Arabidopsis thaliana*. Inclusion of *Arabidopsis* in this comparison mostly among cyanobacteria allows comparison of several additional PS II subunits, because plants have acquired genes that appear not to be present in cyanobacteria. On the other hand, some cyanobacteria have PS II genes that are not present in other cyanobacteria. For example, *G. violaceus* lacks *psbY, psbZ*, *psb27* and the second copy of *psbD*, in spite of its relatively large genome size (4.6 Mb). Phylogenetic analysis of 16S rRNA indicates that *G. violaceus* is one of the most anciently

Abbreviations: Cyt – cytochrome; DCBQ – 2,6-dichloro-*p*-benzoquinone; His-tag – histidine tag; HP and LP – high and low redox potential, respectively; LHCII – light harvesting complex associated with PS II; MALDI/MS – matrix assisted laser desorption ionization/mass spectrometry; ORF – open reading frame; P680 – primary electron donor in PS II; PQ – plastoquinone; PS I and PS II – Photosystem I and II, respectively; Q_A – the primary quinone acceptor of PS II on the D2 subunit; Q_B – the secondary quinone acceptor of PS II on the D1 subunit; Sec – secretion; TGIR – The Institute for Genomic Reseach

branched species among cyanobacteria. If so, the gene composition of *G. violaceus* may suggest that the ancestral PS II consisted of a simpler subunit composition. Alternatively, components, which are missing in *G. violaceus*, may be related to the development of the thylakoid membrane system, since it is the only organism that lacks thylakoids. Another anomalous organism is *P. marinus* MED 4, which lacks *psbU* and *psbV* since *P. marinus* MIT 9313, a close relative, retains both of them. *P. marinus* MED 4 is known to be a high-light adapted ecotype with multiple *hlip* and photolyase genes (Hess et al., 2001). Such adaptation may be coupled with the absence of two extrinsic proteins in PS II.

The inclusion of *Arabidopsis* in Table 1 reveals the changes that have taken place in PS II genes during the evolution from cyanobacteria to chloroplasts. Many of the PS II components are encoded by single copy genes in the chloroplast. There are also PS II genes in the plant nuclear genome that encode subunits not found in cyanobacteria (PsbW, PsbR, PsbS, and $PsbT_N$), and presumably not necessary for a free-living photosynthetic organism. Furthermore, there are plant PS II proteins (PsbP and PsbQ) whose functional role has been examined thoroughly, whereas the function of homologs in cyanobacteria remains an open question. Table 1 is an example of the type of information that can be gathered from genomic analysis of PS II-containing organisms. Such information is useful for establishing the different components used in PS II activity in various model organisms.

Studies on the biochemical composition of PS II are providing correlations between the structure and genetic data from various organisms. Comprehensive analysis of a highly active, histidine (His)-tag purified PS II from *Synechocystis* 6803 using the latest protein identification technologies revealed a number of PS II subunits that had never been seen in such a purified protein complex (Kashino et al., 2002a). A similar study in *T. vulcanus* (Kashino et al., 2002b) revealed that the protein make up of PS II in the two organisms is very similar, with only a few subtle variations, such as a different apparent molecular weight of the cytochrome (Cyt) b_{559} large subunit. Irrgang et al. (2001) examined PS II core components from both *T. elongatus* and spinach to show that there are expected differences in some of the subunit components, but the behavior of the complexes in forming monomers and dimers is essentially the same.

In this chapter, we will discuss the low molecular weight protein subunits of PS II with respect to the new discoveries that contribute to a better overall understanding of the function of the entire protein complex. Most of the proteins discussed are less than 10 kDa, but a few are between 10 and 13 kDa. This group includes the heme-binding heterodimer, Cyt b_{559}, whose function has been a subject of intense debate for almost thirty years (Chapter 15, Faller and Rutherford). The majority of the proteins covered in this chapter consists of single helix, membrane-spanning proteins that are usually organized peripherally to the large integral proteins. Many of these proteins are not essential for PS II activity, but they appear to be important in regulation or biogenesis. PS II also has small soluble, extrinsic proteins, associated with either the stromal/cytoplasmic or lumenal surface of PS II. The small extrinsic proteins discussed here do not have a known role in oxygen evolution activity as do the larger extrinsic proteins described in Chapter 5 (Bricker and Burnap). Most of the small PS II subunits found in cyanobacteria are also present in plants and encoded by genes in the chloroplast genome.

II. Membrane Spanning Subunits

A. PsbE/F — Cytochrome b_{559}

This enigmatic member of the PS II complex is a heme-linked heterodimer of the single membrane spanning proteins, PsbE and PsbF. Cyt b_{559} was first biochemically characterized by Garewal and Wasserman (1974b), who developed an efficient Triton-based purification method. Using this purification method (Garewal and Wasserman, 1974a), Cyt b_{559} was isolated and sequenced (Herrmann et al., 1984; Widger et al., 1985). The protein contains one α subunit, PsbE, and one β subunit, PsbF, each of which contributes one histidine residue to coordinate a single heme to give its unique two-chain structure. PsbE is 9 kDa and PsbF is 4 kDa and the proteins are 83 and 39 amino acids, respectively.

In most PS II-containing bacteria, the proteins are encoded by the *psbEFLJ* operon. The gene, *psbF*, was actually found because its ribosome-binding region overlaps the stop codon for *psbE* (Herrmann et al., 1984). Genetic analysis of Cyt b_{559} in *Synechocystis* 6803 (Pakrasi et al., 1988, 1990, 1991) and *Chlamydomonas reinhardtii* (Morais et al., 1998, 2001) indicated that it is required for PS II activity but may not be involved in primary electron transport. A recent study of tobacco chloroplast mutants indicated

Table 1. List of Photosystem II genes in representative genomes

Photosystem II gene	*Synechocystis* sp. PCC 6803	*Anabaena* sp. PCC 7120	*N. punctiforme* ATCC 29133	*Trichodesmium erythraeum*	*T. elongatus* BP-1	*P.marinus* MED4	*P.marinus* MIT9313	*G.violaceus* PCC 7421	*Synechococcus* sp. WH8102	*Arabidopsis thaliana*
psbA: D1 reaction center protein	*slr1311* *sll1867* *slr1181*	*all3572* *alr3727* *alr4592* *alr4866* *alr3742*	4 genes	yes	*tlr1843* *tlr1844* *tlr1477*	*PMM0223*	*PMT0419* *PMT1532*	*gll3144* *glr0779* *glr1706* *glr2322* *glr2656*	*SYNW0983* *SYNW1470* *SYNW1919* *SYNW2151*	chloroplast
psbB: CP47 chlorophyll-binding protein	*slr0906*	*all0138*	yes	yes	*tlr1530*	*PMM0315*	*PMT1665*	*glr2999*	*SYNW1982*	chloroplast
psbC: CP43 chlorophyll-binding protein	*sll0851*	*alr4291*	yes	yes	*tlr1631*	*PMM1158*	*PMT1180*	*glr2324*	*SYNW0676*	chloroplast
psbD: D2 reaction center protein	*sll0849* *slr0927*	*alr4290* *alr4548*	yes	yes	*tlr1630* *tlr0455*	*PMM1157*	*PMT1179*	*glr2323*	*SYNW0677* *SYNW2232*	chloroplast
psbE: cytochrome b559 large subunit	*ssr3451*	*asr3845*	yes	yes	*tsr1541*	*PMM0297*	*PMT1896*	*gsr0856*	*SYNW0204*	chloroplast
psbF: cytochrome b559 small subunit	*smr0006*	*asr3846*	yes	yes	*tsr1542*	*PMM0298*	*PMT1897*	*gsr0857*	*SYNW0203*	chloroplast
psbH: small membrane-spanning protein	*ssl2598*	*asl0846*	yes	yes	*tsl1386*	*PMM0251*	*PMT1837*	*gsr3002*	*SYNW0269*	chloroplast
psbI: small membrane-spanning protein	*sml0001*	*asr1277*	yes	yes	*tsr1074*	*PMM0253*	*PMT1840*	*gsl3634*	*SYNW0266*	chloroplast
psbJ: small membrane-spanning protein	*smr0008*	*asr3848*	yes	yes	*tsr1544*	*PMM0300*	*PMT1899*	*gsr0859*	*SYNW0201*	chloroplast
psbK: small membrane-spanning protein	*sml0005*	*asl0885*	yes	yes	*tsl0176*	*PMM0272*	*PMT1863*	*gsr2807*	*SYNW0243*	chloroplast
psbL: small membrane-spanning protein	*smr0007*	*asr3847*	yes	yes	*tsr1543*	*PMM0299*	*PMT1898*	*gsr0858*	*SYNW0202*	chloroplast
psbM: small membrane-spanning protein	*sml0003*	*asl0883*	yes	yes	*tsl2052*	*PMM0317*	*PMT1663*	*gsl2997*	*SYNW1980*	chloroplast
psbO: manganese-stabilizing protein	*sll0427*	*all3854*	yes	yes	*tll0444*	*PMM0228*	*PMT1800*	*glr3691*	*SYNW0303*	At5g66570 At3g50820
psbP: 23 kDa extrinsic protein	*sll1418*	*all3076*	yes	yes	*tlr2075*	*PMM1098*	*PMT1078*	*gll1440*	*SYNW0927*	At1g06680 At1g76450 At1g77090 At2g28605 At2g30790 At2g39470 At3g55330 At3g56650 At4g15510 At5g11450
psbQ: 16 kDa extrinsic protein	*sll1638*	*all1355*	yes	yes	*tll2057*	no	no	no	*SYNW2505*	At4g21280 At4g05180 At3g01440
psbR: 10 kDa extrinsic protein	no	no	no	no	no	no	no	no	no	At1g79040
psbS: light harvesting complex regulator	no	no	no	no	no	no	no	no	no	At1g44575
psbTc: small membrane-spanning protein	*smr0001*	*asl0137*	yes	yes	*tsr1531*	*PMM0314*	*PMT1666*	*gsr3000*	*SYNW1983*	chloroplast
psbTn: extrinsic protein	no	no	no	no	no	no	no	no	no	At3g21050 At1g51400
psbU: 12 kDa extrinsic protein	*sll1194*	*alr1216*	yes	yes	*tll2409*	no	*PMT0178*	*gll2873*	*SYNW2192*	no
psbV: cytochrome c550	*sll0258*	*all0259*	yes	2 genes	*tll1285* *tll1284*	no	*PMT1427*	*gll2337* *gll2338*	*SYNW1537*	no
psbW: small membrane-spanning protein	no	no	no	no	no	no	no	no	no	At2g30570
psbX: small membrane-spanning protein	*sml0002*	*asr0941*	yes	yes	*tsr2013*	*PMM0062*	*PMT1590*	*gsr1874*	*SYNW0334*	At2g06520
psbY: small membrane-spanning protein	*sml0007*	*asr1025*	yes	yes	*tsl0836*	*PMM1117*	*PMT1048*	no	*SYNW0898*	At1g67740
psbZ: small membrane-spanning protein	*sll1281*	*asr3992*	yes	yes	*tsr1967*	*PMM1644*	*PMT0080*	no	*SYNW0081*	chloroplast
psb27: 11 kDa extrinsic protein	*slr1645*	*all1258*	yes	yes	*tll2464*	*PMM0507*	*PMT1260*	no	*SYNW1772*	At1g03600 At1g05385
psb28: 13kD extrinsic protein	*sll1398*	*all0801* *all1082*	yes	yes	*tlr0493*	*PMM0926*	*PMT0604*	gsl0928	*SYNW1065*	At4g28660

that PsbE and PsbF are each required for the stable insertion of the other, and without these proteins, the D1 subunit is not stable (Swiatek et al., 2003). Further supporting the connection between D1 stability and Cyt b_{559} is evidence from Lupinkova et al. (2002) indicating that *Synechocystis* 6803 D1 His252 is required for adduct formation with the N-terminal serine of Cyt b_{559} under damaging conditions.

Historically, one of the dilemmas in understanding the structure of Cyt b_{559} was the orientation of the subunits relative to each other and the thylakoid membrane. It was postulated that the Cyt has an $\alpha_2\beta_2$ topology with the β subunit C-terminus in the stroma and the associated heme closer to the lumen (McNamara et al., 1997). With the publication of the PS II crystal structure from *T. elongatus*, it seems that the debate is finally resolved in favor of a parallel heterodimer with the N-termini of both subunits in the stroma (Zouni et al., 2001).

Another controversy that is still unresolved regards the number of cytochrome heterodimers per PS II center. One of the major difficulties involves purifying the PS II center without disturbing the cytochromes bound to the system. In two recent studies using purified PS II with a poly-histidine tagged CP47 there are different ratios of Cyt b_{559} to PS II centers. Lakshmi and colleagues (Lakshmi et al., 2002) found 1.1 Cyt b_{559} hemes in a his-tagged PS II preparation, while Kashino et al. (2002a) found 1.9 hemes per PS II. The current crystal structure indicates that there is one Cyt b_{559} per PS II (Ferreira et al, 2004), so whether one is removed more easily or the extinction coefficient of a single heme is variable remains an open question.

An attribute of Cyt b_{559} that makes it unique as well as difficult to understand is its changing midpoint potential. The two predominant forms are the high potential (HP) and low potential (LP) with their redox midpoint at 370–435 mV and 0–80 mV, respectively. An interesting correlation between Cyt b_{559} and the O_2 evolution activity of PS II can be drawn from the contribution of electrons from the manganese cluster in forcing a shift from LP to HP cytochrome (Mizusawa et al., 1997). In this study, PS II complexes were depleted of Mn, which abolished O_2 evolution activity and caused the HP cytochrome to convert to LP. Mizusawa et al. (1997) showed that during photoactivation conditions, electron donation from the Mn cluster was sufficient to convert LP cytochrome to HP. Furthermore, this study linked the interconversion between cytochrome redox forms to Q_A^- oxidation.

An early hypothesis for the role of Cyt b_{559} in PS II was that it cycled extra electrons around the reaction center to release excess energy. A study in spinach chloroplasts revealed that oxidation of Cyt b_{559} in the presence of water oxidation inhibitors could be considered physiologically relevant under conditions when the water-splitting machinery cannot keep up with the oxidation capacity of the chlorophyll (Heber et al., 1979). It has been proposed that Cyt b_{559} is photooxidized by P680 through Chl Z (a fluorescence quencher) to protect the water oxidation complex from damage when excess energy is absorbed (Thompson and Brudvig, 1988). The cytochrome can be re-reduced by Q_B under some conditions, supporting the idea for its involvement in an electron path alternative to the water oxidation path (Buser et al., 1992). Even though the b_{559} heme is relatively far away from the Q_B site for direct electron transfer (Zouni et al., 2001; Kamiya and Shen, 2003; Ferreira et al, 2004; Chapters 19–21), recent evidence by Lupinkova and colleagues (Lupinkova et al., 2002) suggests that the link between the N-terminal serine of Cyt b_{559} and His252 on D1 could allow for an electron tunnel from Q_B to the Cyt b_{559} heme.

Another model for the function of Cyt b_{559} allowing for photoprotection and encompassing the changing midpoint potential has been called a molecular switch mechanism. Evidence supporting a single electron redox protection mechanism in PS II (Nedbal et al., 1992; Barber and De Las Rivas, 1993; Poulson et al., 1995) suggests that under increasing light intensity the LP form of Cyt b_{559} accumulates as an alternate path for electrons from P680 through pheophytin. As evidenced in (Poulson et al., 1995) the slow photochemistry of Cyt b_{559} in vivo is justified by the

Table 1, Legend. 'Yes' means the presence of a specified gene, which is confirmed by BLAST search but is not yet annotated as an ORF. Nucleotide and deduced sequence data were downloaded from the web (Nakamura et al., 2002). Complete names for the organisms included in the table are: *Synechocystis* sp. PCC 6803; *Anabaena* sp. PCC 7120; *Nostoc punctiforme* ATCC 29133; *Trichodesmium erythraeum*; *Thermosynechococcus elongatus* BP-1; *Prochlorococcus marinus* MED4; *Prochlorococcus marinus* MIT9313; *Gloeobacter violaceus* PCC 7421; *Synechococcus* sp. WH8102; and *Arabidopsis thaliana*. *Arabidopsis* genes were identified by searching the *Arabidopsis* genome with *Synechocystis* 6803 PS II genes, where applicable. The nomenclature for the nuclear genes refers to locus numbers as published in the The Institute for Genomic Research *Arabidopsis* database (2002). Nomenclature for cyanobacterial genes is as the ORFs are annotated in Cyanobase (Nakamura et al., 2003a). The table was updated Dec. 12, 2003, so annotations are current as of that date.

slow build up of reducing equivalents on the acceptor side during illumination. In this model, the acceptor side of PS II is oxidized by LP Cyt b_{559} and the HP form reduces the donor side. A major difference between this model and the Chl Z quenching model is that it is best applied under limited photo-stress as opposed to constant illumination.

Both models incorporate Cyt b_{559} into PS II activity as part of an alternate electron pathway. It appears evident that Cyt b_{559} is not required for water oxidation, even though it is important in the function of PS II under physiological conditions. A recent study by Morais et al. (2001) used mutations in the heme-binding site of Cyt b_{559} in *C. reinhardtii* to show that redox activity of the cytochrome is not necessary for O_2 evolution from PS II. The authors mention in the discussion that there could be a very low level of heme binding in vivo which would allow for the small number of assembled PS II centers in their mutant (Morais et al., 2001). It is unclear if there is normal PS II activity in the complete absence of a Cyt b_{559} heme. Much progress has been made towards speculating the role of Cyt b_{559} in PS II, which allows for grand debates. Further studies are required to determine how the presence of Cyt b_{559} and its redox contributions influence the activity of PS II (for more details see Chapter 12, Ahrling et al.).

B. PsbH

The PsbH subunit has a molecular weight in the range of 6–10 kDa. It was identified in PS II preparations from higher plants (spinach and wheat), the green alga *C. reinhardtii*, and the cyanobacterium *T. vulcanus* by N-terminal sequencing (Hird et al., 1986; Michel and Bennett, 1987; Dedner et al., 1988; Koike et al., 1989). The *psbH* gene was identified based on sequence homology in *Synechocystis* 6803 (Abdel-Mawgood and Dilley, 1990) and more recently PsbH was identified as a protein in *Synechocystis* 6803 thylakoids by MALDI/MS analysis (Abdel-Mawgood and Dilley, 1990; Szabo et al., 2001; Kashino et al., 2002a). Using a mutant with a His-tag at the N-terminus of the PsbH protein, Buchel et al. (2001) investigated the location of the PsbH protein in *C. reinhardtii* PS II by gold labeling the protein using a Ni-NTA linker. Their results indicate a position close to the two transmembrane helices of Cyt b_{559}. Although they were unable to identify cross-linked products between PsbH and Cyt b_{559}, PsbH did cross-link to PsbX, which has been shown to be close to Cyt b_{559}. More recently, PsbH was assigned to a helix adjacent to PsbX in the PS II structure (Ferreira et al, 2004).

The *psbH* gene is co-transcribed with the Cyt b_6f complex genes *petC* and *petA* in higher plants, but is monocistronic in *Synechocystis* 6803 (Mayes et al., 1993). In *C. reinhardtii*, the *psbB, psbT* and *psbH* genes are located in the same gene cluster; however, deletion mutagenesis showed that *psbB/T* and *psbH* are transcribed separately since disruption at either locus had no effect on the other (Summer et al., 1997). A similar *psbB/T/H* cluster is also found in some cyanobacteria such as *G. violaceus*, suggesting that the cluster may reflect an ancient gene arrangement.

In spinach and *C. reinhardtii,* PsbH undergoes light dependent phosphorylation at a threonine residue (position 2 or 3 in the mature peptide depending on the species) on the stromal side of the thylakoid membrane, which is usually followed by a region of basic amino acids (Dedner et al., 1988; Michel and Bennett, 1987). Recent mass spectroscopic analyses of higher plant thylakoid proteins have identified two phosphorylation sites on PsbH. In *Arabidopsis,* PsbH is phosphorylated at Thr2 and Thr4 (Vener et al., 2001). Gomez et al. (2002) also found direct evidence for a second phosphorylation site on PsbH from spinach and pea. In their MS analysis, two 80 Da adducts on PsbH were identified, corresponding to a doubly phosphorylated PsbH peptide. Additionally, they observed two 32 Da adducts associated with the doubly phosphorylated PsbH peptide, which they hypothesize is the result of oxidative modification.

Sundby et al. (1989) reported that sodium bicarbonate has a negative effect on the phosphorylation of PsbH in spinach and that depletion of endogenous bicarbonate stimulated phosphorylation of PsbH. To account for the observed competition between bicarbonate and phosphorylation, they suggest that basic amino acids may provide a binding site for the bicarbonate anion.

Cyanobacterial PsbH does not have the conserved threonine residue that serves as the phosphorylation site in photosynthetic eukaryotes. However, PsbH from *Synechocystis* 6803 is phosphorylated in vitro. *Synechocystis* 6803 PsbH contains a threonine residue at position 5, but there has been no direct evidence for its phosphorylation. Phosphorylation was light independent, but was inhibited by oxidizing conditions. When PS II membranes from plants were subjected to high light stress, PsbH was degraded (Race and Gounaris, 1993).

Deletion of *psbH* in *Synechocystis* 6803 results

in a mutant capable of photoautotrophic growth at a reduced rate. O_2 evolution, fluorescence, and thermoluminescence measurements indicate that electron flow from Q_A to Q_B is impaired (Mayes et al., 1993). It was concluded that PsbH is not required for cyanobacterial PS II assembly and function in vivo, but the polypeptide probably optimizes electron flow by interacting with the Q_B site on the D1 protein. In further analysis of the *psbH* deletion mutant, Komenda and colleagues (Komenda et al., 2002) also found weakened attachment of CP47 to the D1-D2 heterodimers as well as weakened binding of bicarbonate to the acceptor side of PS II.

Quite a different phenotype was observed in the *C. reinhardtii* mutant lacking PsbH (O'Connor et al., 1998; Summer et al., 1997). Although PS II core proteins are translated and inserted into the thylakoid membrane as in wild type cells, PS II centers do not accumulate. The PS II deficiency is also observed in dark grown cells suggesting the effect is not due to photoinhibition. Therefore, PsbH plays an important role in PS II assembly and stability in *C. reinhardtii*. Interestingly, O'Connor et al. (1998) also found that the site-directed mutant Thr3Ala of PsbH in *C. reinhardtii*, which eliminates the identified phosphorylation site, has a phenotype identical to wild type. A slight, but consistent decrease is O_2 evolution activity was observed in Thr3Ala compared to wild type. This may result from a slight structural change in PsbH upon phosphorylation that effects activity. Also, it is likely that another phosphorylation site exists in the *C. reinhardtii* protein since two phosphorylation sites were identified in higher plant PsbH.

In summary, the PsbH protein functions differently in PS II of cyanobacteria and that of photosynthetic eukaryotes as evidenced by the different mutant phenotypes. While there is some destabilization of cyanobacterial PS II in the absence of PsbH, the protein is absolutely required for PS II assembly and stability in *C. reinhardtii*. The observed impairment of Q_A to Q_B electron flow in the *Synechocystis* 6803 *psbH* mutant may in fact be due to slight structural changes in PS II. Phosphorylation of PsbH is probably a regulatory mechanism for electron flow within PS II or PS II turnover upon photoinhibition. Either situation is likely to differ between cyanobacteria and higher plants, so differences in phosphorylation are expected.

C. PsbI

The *psbI* gene in the chloroplasts of higher plants and the genome of cyanobacteria encodes a 4.8 kDa protein, 36–39 residues in length depending on the species. It was identified as an intrinsic PS II reaction center component in spinach, and N-terminal sequence data revealed it to be encoded by a chloroplast gene (Ikeuchi and Inoue, 1988). PsbI was later found in PS II reaction center preparations from *T. vulcanus* (Ikeuchi et al., 1989a). Crosslinking studies showed that the N-terminal domain of PsbI from spinach is in close contact with the D2 protein and the α subunit of Cyt b_{559} (Tomo et al., 1993). In contrast, PS II structural analysis has placed PsbI near the dimer interface, which is closer to D1 and CP43 than D2 and Cyt b_{559} (Ferreira et al, 2004).

A *C. reinhardtii psbI* deletion mutant is capable of photoautotrophic growth under low light conditions, but not high light conditions. The amount of assembled PS II centers and O_2 evolution activity is 10–20% that of wild type as determined by variable fluorescence yield and steady state O_2 evolution activities. Unlike other PS II-deficient mutants, the high light sensitivity of the *psbI* deletion mutant persisted when the mutant was grown on medium containing acetate (Kunstner et al., 1995). Thus in *C. reinhardtii*, PsbI is required for both assembly and function of PS II.

A different phenotype was observed for the *Synechocystis* 6803 *psbI* deletion mutant. The cyanobacterial mutant had a loss of only 25–30% PS II activity compared to the wild type. Other PS II proteins accumulated to wild type levels with no significant destabilization of PS II centers, and the *Synechocystis* 6803 mutant is only slightly more light sensitive than the wild type (Ikeuchi et al., 1995b). The conclusion from the *Synechocystis* 6803 mutant indicates that PsbI is not absolutely required for PS II assembly and function in cyanobacteria, but optimizes PS II activity.

PS II centers have not been isolated for further biochemical analysis from either of the mutants described above. Because of their more stable PS II centers, the thermophilic cyanobacterium *T. elongatus* represents a better system for isolating mutant PS II centers for more detailed biochemical analyses. Katoh and Ikeuchi (2001a) created such a *psbI* deletion mutant and found the isolated PS II centers to be exclusively monomeric. The mutant also had decreased light harvesting efficiency. These results demonstrate that PsbI plays a major structural role in PS II dimer assembly and the functional assembly of the antenna complex, but is not required for PS II function in vitro.

D. PsbJ

The PsbJ subunit is encoded by the *psbJ* gene, a member of the *psbEFLJ* operon that is conserved in most oxygenic photosynthetic organisms. The *psbJ* gene was determined to be the second open reading frame closely downstream of the genes encoding the subunits of Cyt b_{559}, and was given its name because of a presumed association with PS II (Cushman et al., 1988). The protein encoded by *psbJ* in *Synechocystis* 6803 was determined to be localized in the thylakoid membrane and have a role in PS II activity (Lind et al., 1993). PsbJ is predicted to be 4.1 kDa and is 40 amino acids long with 9 amino acid-long N/C-terminal extensions flanking a single membrane spanning helix. Even though PsbJ was predicted to be part of PS II for many years, it was first seen in an isolated PS II preparation in a recent study by Kashino et al. (2002a). More recently, it has been identified to be a component of the crystallized PS II complex (Ferreira et al, 2004).

Mutations in *psbJ* have been made in both *Synechocystis* 6803 (Lind et al., 1993) and tobacco (Hager et al., 2002; Regel et al., 2001), which showed that PsbJ is required for photoautotrophic growth in tobacco but not in *Synechocystis* 6803. A major difference in PS II activity between cyanobacterial and tobacco Δ*psbJ* mutants is that the electron flow from Q_A^- to Q_B is slowed by only 40% in the *Synechocystis* 6803 mutant and by almost two orders of magnitude in the tobacco mutant (Regel et al., 2001). Single flash O_2 evolution experiments in both *Synechocystis* 6803 and tobacco indicated that PsbJ is required for the stability of the S_n-states of the Mn cluster in the O_2 evolution apparatus (Regel et al., 2001). In the *Synechocystis* 6803 *psbJ* mutant, the decay of the S_3 state via back electron flow from the acceptor side is twenty times faster than in wild type cells (Regel et al., 2001). In tobacco, young Δ*psbJ* leaves have slightly impaired PS II driven photochemistry while mature leaves are severely damaged (Hager et al., 2002), suggesting that light-induced photodamage is accumulated in the absence of PsbJ. The damage accumulated in mature Δ*psbJ* tobacco leaves includes the loss of oxygen enhancer (OE) proteins, but this appears to be a general result of the damage and not directly resulting from the absence of PsbJ since those proteins are properly assembled in younger leaves. Like many of the other small subunits of PS II, it is unclear what the exact role of PsbJ is in the complex.

E. PsbK

The *psbK* gene encodes a 3.9–4.2 kDa polypeptide predicted to contain a single transmembrane region with its N-terminal domain in the thylakoid lumen. In spinach, the translation product has 98 residues, but the mature protein is only 37 amino acids in length. PsbK was first identified as a chloroplast-encoded spinach PS II component (Murata et al., 1988). The cyanobacterial PsbK subunit was first identified in *T. vulcanus* PS II preparations (Koike et al., 1989). Later, *psbK* identification and cloning in *Synechocystis* 6803 revealed a gene coding for a 45 residue mature protein with a short 8 amino acid presequence that is cleaved upon insertion into the thylakoid membrane (Ikeuchi et al., 1991). De Vitry et al. (1991) reported detectable amounts of PsbK in *C. reinhardtii* PS II core complexes. PsbK was later found in the dimer form of CP43-depleted PS II from spinach indicating a tighter association with the PS II core complex than originally reported (Rhee et al., 1998). In contrast, it was reported that PsbK present in PS II core complexes from *C. reinhardtii* is specifically bound to CP43 (Sugimoto and Takahashi, 2001). Interestingly, the PsbK helix is closely associated with CP43 in the cyanobacterial PS II crystal structure (Ferreira et al, 2004).

Because PsbK remains bound to PS II after removal of LHCII, but is not present in the PS II reaction center core, it was concluded that PsbK was not essential for PS II activity (Murata et al., 1988). However, PsbK inactivation in *C. reinhardtii* chloroplasts results in mutants that are unable to accumulate normal amounts of PS II and cannot grow photoautotrophically. Growth rates returned to wild-type levels on acetate-containing medium. Pulse labeling experiments confirmed a PS II destabilization in the mutant rather than a reduction in polypeptide synthesis. This phenotype suggests that the PsbK protein is necessary for PS II stabilization in vivo (Takahashi et al., 1994).

psbK deletion mutants in the cyanobacterium *Synechocystis* 6803 grow photoautotrophically at a two-fold reduced rate and have slightly reduced PS II activity compared to the wild type. These results demonstrate that PsbK is not essential for PS II activity in prokaryotic cells. PsbK may have other functions in cyanobacteria because addition of glucose to the medium does not fully restore wild-type growth rates as observed in other PS II deficient mutants (Ikeuchi et al., 1991).

A detailed biochemical analysis of the PS II centers in these mutants was not possible, but recently a deletion mutant in the thermophilic bacterium *T. elongatus,* afforded such a study (Katoh and Ikeuchi, 2001a). The mutant phenotype was similar to that observed for the *Synechocystis* 6803 mutant. Cells were capable of photoautotrophic growth at slightly, but reproducibly slower rates under various temperature conditions. The O_2 evolution activity of the PsbK-depleted PS II particles was comparable to the wild type at low concentrations of DCBQ. At higher DCBQ concentrations, PsbK-depleted PS II particles had a lower O_2 evolution activity (Katoh and Ikeuchi, 2001a). A similar acceptor dependency was also observed for PsbX in the same organism (Katoh and Ikeuchi, 2001b).

F. PsbL

Another member of the *psbEFLJ* operon is the gene encoding the small PS II subunit, PsbL. It is predicted to be 38 amino acids long with a single membrane spanning helix and a 17-amino acid soluble N-terminal extension. The PsbL helix is located near the dimer interface with PsbT and PsbM in cyanobacteria (Ferreira et al, 2004). A *Synechocystis* 6803 Δ*psbL* mutant lacks a functional PS II complex (Anbudurai and Pakrasi, 1993; Kitamura et al., 1994; Ozawa et al., 1997) while the tobacco mutant retains residual PS II activity (Swiatek et al., 2003). Tobacco Δ*psbL* cannot grow photoautotrophically and is hypersensitive to light (Swiatek et al., 2003). Additionally, the PsbJ subunit is lost in the tobacco Δ*psbL* mutant, but PsbJ does not seem to be required for the presence of PsbL (Swiatek et al., 2003).

In vitro reconstitution of hydrophobic components in a partially disintegrated PS II complex has only been successful for PsbL protein (Nagatsuka et al., 1991). When PQ-depleted PS II partial complex consisting of CP47/D1/D2/PsbI/PsbW was reconstituted with PQ and PsbL, functional Q_A activity was restored. Such reconstitution is specifically dependent on the addition of PsbL (Kitamura et al., 1994). Further analysis using recombinant PsbL showed that the C-terminal part of PsbL is crucial for recovering the Q_A electron transfer activity in the reconstituted complexes (Ozawa et al., 1997). These studies suggest that PsbL is necessary for electron transfer from Q_A.

G. PsbM

The PsbM subunit was originally identified by N-terminal sequencing as a 4.7 kDa protein in PS II preparations from *T. vulcanus* isolated in the presence of Triton X-100 and urea. It was found to be homologous to ORF34 from tobacco and liverwort chloroplast DNA and was predicted to have a single transmembrane segment (Ikeuchi et al., 1989b). The PsbM protein was also identified in PS II particles from *C. reinhardtii* (de Vitry et al., 1991). Analysis of *Synechocystis* 6803 PS II by Kashino et al. (2002a) confirmed the presence of the PsbM protein for the first time in that organism. The PsbM helix was also seen in the *T. elongatus* PS II crystal structure (Ferreira et al, 2004). Recently, *psbM* disruption mutant was created in *T. elongatus* but no clear phenotype was detected (C. Aoyama, M. Iwai, M. Ikeuchi, personal communication). Although it is associated with PS II from all model organisms studied, no functions have been hypothesized for PsbM.

H. PsbN

Based on a partial N-terminal sequence of a 4.7 kDa polypeptide in isolated PS II preparation from *T. vulcanus*, Ikeuchi et al. (1989b) named it the PsbN protein. The *psbN* gene is present in cyanobacteria as well as the chloroplast genomes of a number of plants and algae. Zouni et al. (2001) have stated that the crystallized PS II complex from *T. elongatus* has the PsbN protein, although the primary data supporting this statement has not been published yet. Subsequently, a helix near PsbK was tentatively named PsbN in the most recent PS II crystal structure (Ferreira et al, 2004). In contrast, Kashino et al. (2002b) have shown that the original assignment of the PsbN protein in *T. vulcanus* was incorrect, and this protein is actually $PsbT_c$ (see below). Therefore, the presence of PsbN in PS II remains ambiguous.

I. PsbS

The integral PS II subunit, PsbS, is a 22 kDa protein found in plants and not in cyanobacteria. PsbS was originally found as a coprecipitant in an antibody pull down experiment with PsbO and PsbP from spinach thylakoids (Ljungberg et al., 1984a). It has amino acid sequence homology to chlorophyll *a*/*b* binding proteins that make up the light harvesting complex (LHC) (Wedel et al., 1992). Most LHC proteins have

three membrane spanning domains, but PsbS has four such spans. Even though PsbS is suggested to bind chlorophyll (Funk et al., 1995), it was recently shown to have a very weak affinity for pigments (Dominici et al., 2002). An *Arabidopsis* mutant deficient in PS II nonphotochemical quenching, npq4, was cloned and mapped to the *psbS* locus (Li et al., 2000). Further analysis of this mutant revealed that PsbS deficient plants had normal quantum yield of electron transport and normal O_2 evolution, but decreased non-photochemical quenching when exposed to high light (Li et al., 2000). Other studies on the transcript levels of *psbS* indicate that it may play a role in the greening process of hypocotyls and is probably regulated by the phytochrome system (Adamska et al., 1996). PsbS does not appear to have a direct role in the activity of PS II, and will be discussed further for its role in pigment association in Chapter 23 (Pogson et al.).

J. $PsbT_c$

In the early 1990s, two PS II proteins were almost simultaneously named PsbT. Among them, the first one is encoded by the *ycf8* ORF in the chloroplast genomes of plants and *C. reinhardtii*, and is hence, referred to as the $PsbT_c$. This gene is usually located downstream of the *psbB* gene for the CP47 protein. $PsbT_c$ is a ~4 kDa intrinsic membrane protein, with a single predicted membrane-span. This protein is also present in cyanobacterial PS II (Kashino et al., 2002a).

The *psbT*$_c$ (*smr0001*) gene has been inactivated in *Synechocystis* 6803 (H. Katoh and M. Ikeuchi, personal communication), but the mutant has not been functionally characterized. *psbT*$_c$ was also inactivated in *T. elongatus* causing a decrease in the dimer form of PS II, but little defect was detected in the O_2 evolving activity of the complex or in photoautotrophic growth rate (Iwai et al., 2001). Interestingly, the most recent PS II structural model shows $PsbT_c$ at the dimer interface, consistent with a proposed role in dimerization (Ferreira et al, 2004). A *psbT*$_c$ inactivation mutant strain of *C. reinhardtii* has been studied in considerable detail (Monod et al., 1994; Ohnishi and Takahashi, 2001). This mutant grows well under moderate light intensities, but dies under high light. Moreover, the rates of photo-inactivation as well as photo-degradation of the PS II complex in this mutant are similar to those in the wild-type strain. In contrast, the recovery of photo-damaged PS II is significantly slower in this mutant. Radioactive pulse-chase analysis showed that the absence of $PsbT_c$ does not affect the rate of synthesis of major PS II proteins, such as D1, D2, CP47 and CP43, suggesting that $PsbT_c$ is involved in a post-translational step during the repair of PS II. Biochemical fractionation of *C. reinhardtii* thylakoid membranes has shown that $PsbT_c$ cofractionates with the D1/D2 heterodimer complex that is depleted of CP47 and CP43. Based on these data, it has been suggested: that (i) $PsbT_c$ is closely associated with D1, and (ii) $PsbT_c$ may act as a scaffold for the replacement of photo-inactivated D1.

K. $PsbT_N$

The second PsbT protein is a ~5 k Da hydrophilic protein (Ikeuchi et al., 1989c; Kapazoglou et al., 1995). The gene for this protein is localized in the nuclear genome of plants, and has recently been named the *PsbT*$_N$ gene. The precursor form of this protein has a relatively long bipartite transit peptide that localizes the mature protein in the thylakoid lumen. Hence, $PsbT_N$ is a lumenal extrinsic protein in higher plant PS II. Homologs of this protein have not been found in cyanobacteria (Table 1). The function of the protein in PS II is currently unknown.

L. PsbW

PsbW is a nuclear-encoded 4.6–6kDa protein associated with PS II particles in photosynthetic eukaryotes. It was first identified in spinach and was predicted to be an integral membrane protein with a single transmembrane domain. Its topology in the membrane is the opposite of most PS II membrane proteins as it has a lumenal N-terminus (Irrgang et al., 1995). Recently *psbW* has been characterized in the green algae *C. reinhardtii* as well. The gene codes for a protein of 115 residues containing a bipartite transit peptide of 59 residues and a 56 residue mature protein (Iwai et al., 2001). The *psbW* gene is absent from the *Synechocystis* 6803 genome and all other prokaryotes examined. (Note: In the *Synechocystis* 6803 database, *psb28* is mistakenly annotated as *psbW*. See below.)

Studies by Lorkovic et al. (1995) on spinach PsbW revealed a gene that codes for a 54 residue mature protein with an 83 residue bipartite presequence. The mRNA levels were upregulated ten-fold by light, but the transcript and the protein were also detectable in etiolated seedlings. Further characterization in spin-

ach found that 80% of the PsbW protein localizes to the grana region of the thylakoids. PsbW is located close to the D1-D2 heterodimer based on its presence in reaction center preparations (Shi and Schroder, 1997). Using the blue-native gel electrophoresis system to separate PS II monomers and dimers from pea thylakoids, Thidholm et al. (2002) found PsbW exclusively associated with dimeric PS II. They also reported that PsbW is directly assembled into PS II dimers in a process dependent on its negatively charged N-terminus. These experimental data are contradictory to the previous evidence that PsbW is closely associated with the D1-D2 heterodimer. Further evidence is needed to explain how PsbW could be associated with the PS II dimer interface and be tightly bound to D1-D2 at the same time.

An *Arabidopsis* antisense mutant of PsbW with a >96% decrease in *psbW* transcript was generated by Shi et al. (2000). The mutant contained no dimeric PS II supercomplex, but retained normal electron transfer properties. O_2 evolution activity was decreased by 50% due to the disappearance of up to 40% of the D1 and D2 proteins. The amounts of other PS II proteins were also affected to differing degrees. In a more detailed investigation of the PsbW antisense mutant (Thidholm et al., 2001), quantum yield measurements after periods of light stress showed the antisense plants to be much more sensitive to photoinhibition than wild type plants. Thus, lack of PsbW results in less stable PS II dimers. Based on this phenotype, the conclusion is that PsbW is required for PS II dimer formation and PS II stability in higher plants.

PsbW also undergoes light induced proteolysis in a process similar to that described for the D1 protein. Although PsbW contains a number of serines and threonines, it is not phosphorylated under conditions that lead to the phosphorylation of other PS II proteins. Despite its lack of phosphorylation, it is protected from degradation under conditions when other PS II proteins are phosphorylated. These results support the conclusion that the PsbW protein becomes susceptible to proteolysis when PS II is destabilized as a result of D1 photodamage (Hagman et al., 1997).

M. PsbX

PsbX, a nuclear-encoded, 4.1 kDa membrane protein associated with PS II, was first identified in spinach (Ikeuchi et al., 1989c). The PsbX protein has been characterized in plants and cyanobacteria by biochemical and genetic analysis. In plants, it cross-links to Cyt b_{559}; however, it is not present in isolated PS II reaction centers (Shi et al., 1999). In cyanobacterial PS II structures, PsbX has been assigned to the helix that lies closest to the Cyt b_{559} helices (Ferreira et al, 2004; Kamiya and Shen, 2003). The PsbX mRNA levels were also found to be tightly light regulated such that no mRNA is detectable in the dark (Shi et al., 1999).

The deletion of *psbX* in the cyanobacterium *Synechocystis* 6803 did not affect growth rate, electron transport, or water oxidation, but the number of functionally active PS II centers was only 30% of wild type. PsbX mRNAs were observed under various light conditions suggesting that the transcripts are not as tightly light-regulated in cyanobacteria compared to higher plants (Funk, 2000). A PsbX deletion mutant in the thermophilic cyanobacterium *T. elongatus* also had a photoautotrophic phenotype, but showed a growth defect under low CO_2 conditions. The mutant had a lower O_2 evolution activity in the presence of high concentrations of artificial quinone acceptors compared to wild type, suggesting the PsbX protein is involved in quinone turnover at the Q_B site (Katoh and Ikeuchi, 2001b).

Like the PsbW subunit, the PsbX protein is inserted into the membrane by a mechanism independent of the previously characterized translocation machineries despite the presence of a bipartite transit peptide (Kim et al., 1996). Tissier and colleagues (Tissier et al., 2002) reported that the C-terminal acidic residues are essential for the maturation of PsbX. A single Glu to Val substitution at position 5 prevents proper insertion in to the membrane. Processing is partially restored by the hydrophilic residue Asn, implying that this domain is important for cleavage. Substitution of the C-terminal Glu residues with Val causes the cleavage site to be buried in the membrane, but insertion is not affected. These results suggest that there are stringent requirements on the peptide sequence of PsbX for insertion into the membrane and cleavage by the thylakoid processing protease, even though the mechanism of insertion is not defined.

N. PsbY

The small PS II subunit, PsbY, was first identified as a component of spinach and tobacco PS II preparations by Gau et al. (1995). It is a 4–5 kDa, single membrane-spanning protein with a 14–15 amino acid C-terminal soluble domain. In spinach and

Arabidopsis psbY encodes a 20–23 kDa precursor protein with a bipartite signal peptide targeting it to the chloroplast thylakoid membrane (Gau et al., 1998; Mant and Robinson, 1998). The precursor protein contains four hydrophobic regions, two of which resemble the signal peptides preceding the PsbW and PsbX mature protein sequence that is used for Sec-independent insertion into the thylakoid membrane (Thompson et al., 1999). Initial activity studies of PsbY concluded that it was a manganese requiring L-arginine metabolizing enzyme suspected to be important to the function of the manganese cluster in the O_2 evolution center of PS II (Gau et al., 1995). A *Synechocystis* 6803 mutant in *psbY* was able to grow normally under photoautotrophic conditions and had normal rates of PS II O_2 evolution, indicating that it is not essential for photosynthesis and is not an important manganese ligand in the O_2-evolving center (Meetam et al., 1999). PsbY was found to be part of a purified PS II complex from *Synechocystis* 6803 (Kashino et al., 2002a), but was not identified in the most recent PS II crystal structure (Ferreira et al, 2004). The functional role of PsbY in PS II remains to be determined.

O. PsbZ

PsbZ is a relatively new addition to the group of proteins known to be part of PS II. Encoding PsbZ is a gene that was located in many chloroplast genomes and was named *ycf 9* for hypothetical chloroplast open reading frame. The gene usually encodes a protein of about 62 amino acids with a predicted molecular mass of 6.5 kDa. It is predicted to have two membrane spanning domains but is most likely cleaved by a lumenal peptidase between the membrane spanning regions.

The brief history of this open reading frame was summed up in a recent review (Eckardt, 2001), which discussed the difficulty in determining the function of the protein because of the lack of homoplasmic mutants in chloroplasts. One of the first tobacco Δ*psbZ* mutants did not exhibit a phenotype in normal growth conditions, but the authors found that the protein was associated with the light-harvesting complex of PS II (Ruf et al., 2000). Two more papers published almost concurrently examined tobacco Δ*psbZ* mutants with different interpretations of the function of PsbZ. The mutant studied by Baena-Ganzales et al. (2001) still contained at least 5% of the wild-type gene, which could have produced a sufficient amount of the wild-type protein to influence the phenotype of the mutant. This study found that the rate of PS II O_2 evolution was unchanged in the Δ*psbZ* mutant and the rate of electron flow from PS II to PS I was enhanced, and suggested that PsbZ is involved in regulating electron transport depending on the prevailing conditions. The second Δ*psbZ* paper published almost simultaneously as the above study examined transplastomic knockouts in both tobacco and *C. reinhardtii* and concluded that PsbZ is necessary for the stability of the PS II-LHCII super complex (Swiatek et al., 2001). Because two organisms were examined and complementary experiments were performed in each, the Swiatek study conclusively supports a role for PsbZ that was suggested in the other manuscripts. The work by Swiatek et al. (2001) indicates that as a connection between PS II and LHCII, PsbZ helps mediate nonphotochemical quenching when PS II is exposed to light exceeding the water oxidation capacity of PS II, either in higher than normal light intensities or in low temperatures. In the cyanobacterial PS II structure, the two PsbZ helices are located on the perimeter of the dimer near CP43 (Ferreira et al, 2004). Thus, an analogous location in plant PS II would be consistent with PsbZ coordinating light harvesting protein association. More evidence is required to determine the mode of coordination of PsbZ between PS II and LHCII in plants. The mechanism of PsbZ activity is yet to be discovered.

III. Extrinsic Subunits

A. PsbR

PsbR is a 10 kDa extrinsic protein found only in plants and identified as a soluble protein released from spinach PS II preparations (Ljungberg et al., 1984b). Antisense potato plants were generated containing 1–3% of the normal PsbR protein levels to determine if the protein were necessary for PS II activity, but there was no decrease in either PS II accumulation or growth rate (Stockhaus et al., 1990). So far, analysis of this protein has not indicated a functional role in water oxidation.

B. Psb27

The Psb27 subunit was originally identified from the N-terminal sequence of a ~11 kDa polypeptide component of a purified PS II preparation from

Synechocystis 6803 (Ikeuchi et al., 1995a). This protein was originally named PsbZ. As discussed above, a distinctly different and smaller PS II protein is now called PsbZ (Swiatek et al., 2001). According to a recent nomenclature, the 11 kDa protein of PS II has been named Psb27 (Kashino et al., 2002a).

The Psb27 polypeptide in *Synechocystis* 6803 has one predicted membrane-spanning domain followed by a cleavage site for signal peptidase II. Thus, the Psb27 protein is expected to be a lumen-localized extrinsic protein of PS II. The Arabidopsis homologs (At1g03600 and At1g05385) of Psb27 were found in a proteomics study of the thylakoid lumen (Peltier et al., 2002). Although it is associated with PS II from many model organisms (Table 1), this protein was not identified in the cyanobacterial PS II crystal structure (Ferreira et al, 2004). Furthermore, no mutant has been described for this subunit, and no function has been hypothesized.

C. Psb28

The Psb28 subunit was originally identified from the N-terminal sequence of a ~13 kDa polypeptide component of a purified PS II preparation from *Synechocystis* 6803 (Ikeuchi et al., 1995a). This protein was originally named Psb13. A homologue of this protein is the deduced product of *ycf79*, an open reading frame in the chloroplast genome of *Porphyra*. Finally, the protein was also named PsbW. According to a recently published nomenclature, Psb13 has been renamed Psb28, and a different and smaller PS II protein is called PsbW (see above) (Kashino et al., 2002a).

The Psb28 protein is predicted to have no hydrophobic membrane-spanning domain and to be localized in the stroma/cytoplasm. If this prediction is correct, Psb28 is the only known extrinsic stromal/cytoplasmic protein in PS II. There was no unassigned density in the recently published PS II crystal structure that could be attributed to Psb28 on the stromal surface of PS II (Ferreira et al, 2004).

A knockout mutation of the *psb28* gene in *Synechocystis* 6803 results in reduced growth rate under photosynthetic conditions when calcium and chloride is not added to the growth medium (H. Katoh and M. Ikeuchi, personal communication). Future detailed studies of this interesting mutant strain may unravel the functional role of the Psb28 protein in PS II.

IV. Conclusion

Clearly, there is still much to be learned about the role of each subunit and how it contributes to the activity of the PS II complex. There are 18 small proteins discussed in this chapter, and there are possibly more polypeptides in various organisms that are important to PS II function. PS II is an extremely complex enzyme, which evolved before the intricate membrane systems found in most photosynthetic organisms were developed, suggesting that the task of light-induced water oxidation was not a small hurdle to jump. Functional studies, biochemical analyses, and structural arrangements from multiple photosynthetic organisms are necessary for understanding how all of the individual units of PS II work together in unique intricacy.

Acknowledgments

The preparation of this chapter was supported by funding from the National Science Foundation, Department of Energy and United States Department of Agriculture. LET and JLR were supported by graduate student fellowships from the National Science Foundation.

References

Abdel-Mawgood AL and Dilley RA (1990) Cloning and nucleotide sequence of the psbH gene from cyanobacterium *Synechocystis* 6803. Plant Mol Biol 14: 445–446

Adamska I, Funk C, Renger G and Andersson B (1996) Developmental regulation of the PsbS gene expression in spinach seedlings: The role of phytochrome. Plant Mol Biol 31: 793–802

Anbudurai PR and Pakrasi HB (1993) Mutational analysis of the PsbL protein of Photosystem II in the cyanobacterium *Synechocystis* sp. PCC 6803. Z Naturforsch 48c: 267–274

Baena-Gonzalez E, Gray JC, Tyystjarvi E, Aro EM and Maenpaa P (2001) Abnormal regulation of photosynthetic electron transport in a chloroplast *ycf9* inactivation mutant. J Biol Chem 276: 20795–20802

Barber J and De Las Rivas J (1993) A functional model for the role of cytochrome *b*559 in the protection against donor and acceptor side photoinhibition. Proc Natl Acad Sci USA 90: 10942–10946

Biesiadka J, Loll B, Kern J, Irrgang K-D and Zouni A (2004) Crystal structure of cyanobacterial Photosystem II at 3.2 Å resolution: A closer look at the Mn-cluster. Phys Chem Chem Phys 6: 4733–4736

Buchel C, Morris E, Orlova E and Barber J (2001) Localisation of the PsbH subunit in Photosystem II: A new approach using

labelling of His-tags with a Ni(2+)-NTA gold cluster and single particle analysis. J Mol Biol 312: 371–379

Buser CA, Diner BA and Brudvig GW (1992) Photooxidation of cytochrome *b*559 in oxygen-evolving Photosystem II. Biochemistry 31: 11449–11459

Cushman JC, Christopher DA, Little MC, Hallick RB and Price CA (1988) Organization of the *psbE*, *psbF*, *orf38*, and *orf42* gene loci on the *Euglena gracilis* chloroplast genome. Curr Genet 13: 173–180

de Vitry C, Diner BA and Popo JL (1991) Photosystem II particles from *Chlamydomonas reinhardtii*. Purification, molecular weight, small subunit composition, and protein phosphorylation. J Biol Chem 266: 16614–16621

Dedner N, Meyer HE, Ashton C and Wildner GF (1988) N-Terminal sequence-analysis of the 8 Kda protein in *Chlamydomonas reinhardii*—localization of the phosphothreonine. FEBS Lett 236: 77–82

DOE Joint Genome Institute (2002) JGI Programs: Microbial Genomics. http://www.jgi.doe.gov/JGI_microbial/html/index.html (August 28, 2002)

Dominici P, Caffarri S, Armenante F, Ceoldo S, Crimi M and Bassi R (2002) Biochemical properties of the PsbS Subunit of Photosystem II either purified from chloroplast or recombinant. J Biol Chem 277: 22750–22758

Eckardt NA (2001) A role for PsbZ in the core complex of Photosystem II. Plant Cell 13: 1245–1248

Ferreira KN, Iverson TM, Maghlaoui K, Barber J and Iwata S (2004) Architecture of the photosynthetic oxygen-evolving center. Science 303: 1831–1838

Funk C (2000) Functional analysis of the PsbX protein by deletion of the corresponding gene in *Synechocystis* sp. PCC 6803. Plant Mol Biol 44: 815–827

Funk C, Schroder WP, Napiwotzki A, Tjus SE, Renger G and Andersson B (1995) The PS II-S protein of higher plants: A new type of pigment-binding protein. Biochemistry 34: 11133–11141

Garewal HS and Wasserman AR (1974a) Triton X-100-4 M urea as an extraction medium for membrane proteins. I. Purification of chloroplast cytochrome *b*559. Biochemistry 13: 4063–4071

Garewal HS and Wasserman AR (1974b) Triton X-100-4 M urea as an extraction medium for membrane proteins. II. Molecular properties of pure cytochrome *b*559: A lipoprotein containing small polypeptide chains and a limited lipid composition. Biochemistry 13: 4072–4079

Gau AE, Thole HH and Pistorius EK (1995) Isolation and partial characterization of a manganese requiring L-Arginine metabolizing enzyme being present in Photosystem II complexes of spinach and tobacco. Z Naturforsch 50c: 638–651

Gau AE, Thole HH, Sokolenko A, Altschmied L, Hermann RG and Pistorius EK (1998) PsbY, a novel manganese-binding, low-molecular-mass protein associated with Photosystem II. Mol Gen Genet 260: 56–68

Gomez SM, Nishio JN, Faull KF and Whitelegge JP (2002) The chloroplast grana proteome defined by intact mass measurements from liquid chromatography mass spectrometry. Mol Cell Proteomics 1: 46–59

Hager M, Hermann M, Biehler K, Krieger-Liszkay A and Bock R (2002) Lack of the small plastid-encoded PsbJ polypeptide results in a defective water-splitting apparatus of Photosystem II, reduced Photosystem I levels, and hypersensitivity to light. J Biol Chem 277: 14031–14039

Hagman A, Shi LX, Rintamaki E, Andersson B and Schroder WP (1997) The nuclear-encoded PsbW protein subunit of Photosystem II undergoes light-induced proteolysis. Biochemistry 36: 12666–12671

Heber U, Kirk MR and Boardman NK (1979) Photoreactions of cytochrome *b*-559 and cyclic electron flow in Photosystem II of intact chloroplasts. Biochim Biophys Acta 546: 292–306

Herrmann RG, Alt J, Schiller B, Widger WR and Cramer WA (1984) Nucleotide sequence of the gene for apocytochrome b-559 on the spinach plastid chromosome: Implications for the structure of the membrane protein. FEBS Lett 176: 239–244

Hess WR, Rocap G, Ting CS, Larimer F, Stilwagen S, Lamerdin J and Chisholm SW (2001) The photosynthetic apparatus of *Prochlorococcus*: Insights through comparative genomics. Photosynth Res 70: 53–71

Hird SM, Dyer TA and Gray JC (1986) The gene for the 10kDa phosphoprotein of Photosystem II is located in chloroplast DNA. FEBS Lett 209: 181–186

Ikeuchi M and Inoue Y (1988) A new Photosystem II reaction center component (4.8 kDa protein) encoded by chloroplast genome. FEBS Lett 241: 99–104

Ikeuchi M, Koike H and Inoue Y (1989a) Identification of *psbI* and *psbL* gene products in cyanobacterial Photosystem II reaction center preparation. FEBS Lett 251: 155–160

Ikeuchi M, Koike H and Inoue Y (1989b) N-terminal sequencing of low-molecular-mass components in cyanobacterial Photosystem II core complex. Two components correspond to unidentified open reading frames of plant chloroplast DNA. FEBS Lett 253: 178–182

Ikeuchi M, Takio K and Inoue Y (1989c) N-terminal sequencing of Photosystem II low-molecular-mass proteins. 5 and 4.1 kDa components of the O2-evolving core complex from higher plants. FEBS Lett 242: 263–269

Ikeuchi M, Eggers B, Shen GZ, Webber A, Yu JJ, Hirano A, Inoue Y and Vermaas W (1991) Cloning of the *psb*K gene from *Synechocystis* sp. PCC 6803 and characterization of Photosystem II in mutants lacking PS II-K. J Biol Chem 266: 11111–11115.

Ikeuchi M, Inoue Y and Vermaas W (1995a) Characterization of Photosystem II subunits from the cyanobacterium *Synechocystis* sp. PCC 6803. In Mathis P (ed) Photosynthesis: From Light to Biosphere, pp 297–300. Kluwer Academic Publishers, Dordrecht

Ikeuchi M, Shukla VK, Pakrasi HB and Inoue Y (1995b) Directed inactivation of the *psbI* gene does not affect Photosystem II in the cyanobacterium *Synechocystis* sp. PCC 6803. Mol Gen Genet 249: 622–628

Irrgang KD, Shi LX, Funk C and Schroder WP (1995) A nuclear-encoded subunit of the Photosystem II reaction center. J Biol Chem 270: 17588–17593

Irrgang KD, Georgalis Y, Franke P, Behlke J, Saenger W and Zouni A (2001) Structural comparison of oxygen-evolving Photosystem II core complexes from *Synechococcus elongatus* and *Spinacia oleracea*. In: PS2001 Proceedings: 12th International Congress on Photosynthesis, S5-028. CSIRO Publishing, Melbourne (CD-ROM)

Iwai M, Katoh H and Ikeuchi M (2001) Functional analysis of PS II-T protein of Photosystem II complex from the thermophilic cyanobacterium, *Thermosynechococcus* (formerly *Synechococcus*) *elongatus* BP-1. In: PS2001 Proceedings: 12th International Congress on Photosynthesis, S22-031. CSIRO

Publishing, Melbourne (CD-ROM)
Kamiya N and Shen J-R (2003) Crystal structure of oxygen-evolving Photosystem II from *Thermosynechococcus vulcanus* at 3.7 Å resolution. Proc Natl Acad Sci USA 100: 98–103
Kaneko T, Sato S, Kotani H, Tanaka A, Asamizu E, Nakamura Y, Miyajima N, Hirosawa M, Sugiura M, Sasamoto S, Kimura T, Hosouchi T, Matsuno A, Muraki A, Nakazaki N, Naruo K, Okumura S, Shimpo S, Takeuchi C, Wada T, Watanabe A, Yamada M, Yasuda M and Tabata S (1996) Sequence analysis of the genome of the unicellular cyanobacterium *Synechocystis* sp. strain PCC6803. II. Sequence determination of the entire genome and assignment of potential protein-coding regions. DNA Res 3: 109–136
Kaneko T, Nakamura Y, Wolk CP, Kuritz T, Sasamoto S, Watanabe A, Iriguchi M, Ishikawa A, Kawashima K, Kimura T, Kishida Y, Kohara M, Matsumoto M, Matsuno A, Muraki A, Nakazaki N, Shimpo S, Sugimoto M, Takazawa M, Yamada M, Yasuda M and Tabata S (2001) Complete genomic sequence of the filamentous nitrogen-fixing cyanobacterium *Anabaena* sp. strain PCC 7120. DNA Res 8: 205–213; 227–253
Kapazoglou A, Sagliocco F and Dure L, 3rd (1995) PS II-T, a new nuclear encoded lumenal protein from Photosystem II. Targeting and processing in isolated chloroplasts. J Biol Chem 270: 12197–12202
Kashino Y, Lauber WM, Carroll JA, Wang Q, Whitmarsh J, Satoh K and Pakrasi HB (2002a) Proteomic analysis of a highly active Photosystem II preparation from the cyanobacterium *Synechocystis* sp. PCC 6803 reveals the presence of novel polypeptides. Biochemistry 41: 8004–8012
Kashino Y, Koike H, Yoshio M, Egashira H, Ikeuchi M, Pakrasi HB and Satoh K (2002b) Low-molecular-mass polypeptide components of a Photosystem II preparation from the thermophilic cyanobacterium *Thermosynechococcus vulcanus*. Plant Cell Physiol 43: 1366–1373
Katoh H and Ikeuchi M (2001a) Characterization of PS II-I or PS II-K protein-depleted Photosystem II from *Thermosynechococcus elongatus* strain BP-1. PS II-I protein plays an essential role in dimerization of Photosystem II. In: PS2001 Proceedings: 12th International Congress on Photosynthesis, S5-050. CSIRO Publishing, Melbourne (CD-ROM)
Katoh H and Ikeuchi M (2001b) Targeted disruption of *psbX* and biochemical characterization of Photosystem II complex in the thermophilic cyanobacterium *Synechococcus elongatus*. Plant Cell Physiol 42: 179–188
Kim SJ, Robinson D and Robinson C (1996) An *Arabidopsis thaliana* cDNA encoding PS II-X, a 4.1 kDa component of Photosystem II: A bipartite presequence mediates SecA/delta pH-independent targeting into thylakoids. FEBS Lett 390: 175–178
Kitamura K, Ozawa S, Shiina T and Toyoshima Y (1994) L protein, encoded by *psbL*, restores normal functioning of the primary quinone acceptor, QA, in isolated D1/D2/CP47/Cytb-559/I Photosystem II reaction center core complex. FEBS Lett 354: 113–116
Koike H, Mamada K, Ikeuchi M and Inoue Y (1989) Low-molecular-mass proteins in cyanobacterial Photosystem II: identification of *psbH* and *psbK* gene products by N-terminal sequencing. FEBS Lett 244: 391–396
Komenda J, Lupinkova L and Kopecky J (2002) Absence of the *psbH* gene product destabilizes Photosystem II complex and bicarbonate binding on its acceptor side in *Synechocystis* PCC 6803. Eur J Biochem 269: 610–619
Kunstner P, Guardiola A, Takahashi Y and Rochaix JD (1995) A mutant strain of *Chlamydomonas reinhardtii* lacking the chloroplast Photosystem II psbI gene grows photoautotrophically. J Biol Chem 270: 9651–9654
Lakshmi KV, Reifler MJ, Chisholm DA, Wang JY, Diner BA and Brudvig GW (2002) Correlation of the cytochrome *c*550 content of cyanobacterial Photosystem II with the EPR properties of the oxygen-evolving complex. Photosynth Res 72: 175–189
Li XP, Bjorkman O, Shih C, Grossman AR, Rosenqvist M, Jansson S and Niyogi KK (2000) A pigment-binding protein essential for regulation of photosynthetic light harvesting. Nature 403: 391–395
Lind LK, Shukla VK, Nyhus KJ and Pakrasi HB (1993) Genetic and immunological analyses of the cyanobacterium *Synechocystis* sp. PCC 6803 show that the protein encoded by the *psbJ* gene regulates the number of Photosystem II centers in thylakoid membranes. J Biol Chem 268: 1575–1579
Ljungberg U, Akerlund HE, Larsson UK and Andersson B (1984a) Identification of polypeptides associated with the 23 and 33 kDa proteins of photosynthetic oxygen evolution. Biochim Biophys Acta 767: 145–152
Ljungberg U, Akerlund HE and Andersson B (1984b) The release of a 10-kDa polypeptide from everted Photosystem II thylakoid membranes by alkaline Tris. FEBS Lett 175: 255–258
Lorkovic ZJ, Schroder WP, Pakrasi HB, Irrgang KD, Herrmann RG and Oelmüller R (1995) Molecular characterization of PsbW, a nuclear-encoded component of the Photosystem II reaction center complex in spinach. Proc Natl Acad Sci USA 92: 8930–8934
Lupinkova L, Metz J, Diner B, Vass I and Komenda J (2002) Histidine residue 252 of the Photosystem II D1 polypeptide is involved in a light-induced cross-linking of the polypeptide with the alpha subunit of cytochrome *b*-559: Study of a site-directed mutant of *Synechocystis* PCC 6803. Biochim Biophys Acta 1554: 192
Mant A and Robinson C (1998) An *Arabidopsis* cDNA encodes an apparent polyprotein of two non-identical thylakoid membrane proteins that are associated with Photosystem II and homologous to algal *ycf32* open reading frames. FEBS Lett 423: 183–188
Mayes SR, Dubbs JM, Vass I, Hideg E, Nagy L and Barber J (1993) Further characterization of the *psbH* locus of *Synechocystis* sp PCC 6803 — inactivation of *psbH* impairs Q(a) to Q(B) electron-transport in photosystem-2. Biochemistry 32: 1454–1465
McNamara VP, Sutterwala FS, Pakrasi HB and Whitmarsh J (1997) Structural model of cytochrome *b*559 in Photosystem II based on a mutant with genetically fused subunits. Proc Natl Acad Sci USA 94: 14173–14178
Meetam M, Keren N, Ohad I and Pakrasi HB (1999) The PsbY protein is not essential for oxygenic photosynthesis in the cyanobacterium *Synechocystis* sp. PCC 6803. Plant Physiol 121: 1267–1272
Michel HP and Bennett J (1987) Identification of the phosphorylation site of an 8.3 kDa protein from Photosystem II of spinach. FEBS Lett 212: 102–108
Mizusawa N, Miyao M and Yamashita T (1997) Restoration of the high-potential form of cytochrome *b*-559 by electron transport reactions through Photosystem II in tris-treated Photosystem II. Biochim Biophys Acta 1318: 145–158

Monod C, Takahashi Y, Goldschmidt-Clermont M and Rochaix JD (1994) The chloroplast *ycf8* open reading frame encodes a Photosystem II polypeptide which maintains photosynthetic activity under adverse growth conditions. Embo J 13: 2747–2754

Morais F, Barber J and Nixon PJ (1998) The chloroplast-encoded alpha subunit of cytochrome *b*-559 is required for assembly of the photosystem two complex in both the light and the dark in *Chlamydomonas reinhardtii*. J Biol Chem 273: 29315–29320

Morais F, Kuhn K, Stewart DH, Barber J, Brudvig GW and Nixon PJ (2001) Photosynthetic water oxidation in cytochrome *b*(559) mutants containing a disrupted heme-binding pocket. J Biol Chem 276: 31986–31993

Murata N, Miyao M, Hayashida N, Hidaka T and Sugiura M (1988) Identification of a new gene in the chloroplast genome encoding a low-molecular-mass polypeptide of Photosystem II complex. FEBS Lett 235: 391–396

Nagatsuka T, Fukuhara S, Akabori K and Toyoshima Y (1991) Disintegration and reconstitution of Photosystem II reaction center core complex. II. Possible involvement of low-molecular-mass proteins in the functioning of Q_A in the PS II reaction center. Biochim Biophys Acta 1057: 223–231

Nakamura Y, Kaneko T, Sato S, Ikeuchi M, Katoh H, Sasamoto S, Watanabe A, Iriguchi M, Kawashima K, Kimura T, Kishida Y, Kiyokawa C, Kohara M, Matsumoto M, Matsuno A, Nakazaki N, Shinpo S, Sugimoto M, Takeuchi C, Yamada M and S. T (2002) Complete genome structure of the thermophilic cyanobacterium *Thermosynechococcus elongatus* BP-1. DNA Res 9: 123–130

Nakamura Y, Hirosawa M, Kaneko T and Tabata S (2003a) Cyanobase. http://www.kazusa.or.jp/cyanobase/ (Dec. 12, 2003)

Nakamura Y, Kaneko T, Sato S, Mimuro M, Miyashita H, Tsuchiya T, Sasamoto S, Watanabe A, Kawashima K, Kishida Y, Kiyokawa C, Kohara M, Matsumoto M, Matsuno A, Nakazaki N, Shimpo S, Takeuchi C, Yamada M and Tabata S (2003b) Complete genome structure of *Gloeobacter violaceus* PCC 7421, a cyanobacterium that lacks thylakoids. DNA Res 10: 137–145

Nedbal L, Samson G and Whitmarsh J (1992) Redox state of a one-electron component controls the rate of photoinhibition of Photosystem II. Proc Natl Acad Sci USA 89: 7929–7933

O'Connor HE, Ruffle SV, Cain AJ, Deak Z, Vass I, Nugent JH and Purton S (1998) The 9-kDa phosphoprotein of Photosystem II. Generation and characterisation of *Chlamydomonas* mutants lacking PS II-H and a site-directed mutant lacking the phosphorylation site. Biochim Biophys Acta 1364: 63–72

Ohnishi N and Takahashi Y (2001) PsbT polypeptide is required for efficient repair of photodamaged Photosystem II reaction center. J Biol Chem 276: 33798–33804

Ozawa S, Kobayashi T, Sugiyama R, Hoshida H, Shiina T and Toyoshima Y (1997) Role of PS II-L protein (*psbL* gene product) on the electron transfer in Photosystem II complex. 1. Over-production of wild-type and mutant versions of PS II-L protein and reconstitution into the PS II core complex. Plant Mol Biol 34: 151–161

Pakrasi HB, Williams JG and Arntzen CJ (1988) Targeted mutagenesis of the *psbE* and *psbF* genes blocks photosynthetic electron transport: Evidence for a functional role of cytochrome *b*559 in Photosystem II. EMBO J 7: 325–332

Pakrasi HB, Nyhus KJ and Granok H (1990) Targeted deletion mutagenesis of the beta subunit of cytochrome b559 protein destabilizes the reaction center of Photosystem II. Z Naturforsch 45c: 423–429

Pakrasi HB, De Ciechi P and Whitmarsh J (1991) Site directed mutagenesis of the heme axial ligands of cytochrome *b*559 affects the stability of the Photosystem II complex. EMBO J 10: 1619–1627

Palenik B, Brahamsha B, Larimer FW, Land M, Hauser L, Chain P, Lamerdin J, Regala W, Allen EE, McCarren J, Paulsen I, Dufresne A, Partensky F, Webb EA and Waterbury J (2003) The genome of a motile marine *Synechococcus*. Nature 424: 1037–1042

Peltier JB, Emanuelsson O, Kalume DE, Ytterberg J, Friso G, Rudella A, Liberles DA, Soderberg L, Roepstorff P, von Heijne G and van Wijk KJ (2002) Central functions of the lumenal and peripheral thylakoid proteome of *Arabidopsis* determined by experimentation and genome-wide prediction. Plant Cell 14: 211–236

Poulson M, Samson G and Whitmarsh J (1995) Evidence that cytochrome *b*559 protects Photosystem II against photoinhibition. Biochemistry 34: 10932–10938

Race HL and Gounaris K (1993) Identification of the *psbH* gene product as a 6 kDa phosphoprotein in the cyanobacterium *Synechocystis* 6803. FEBS Lett 323: 35–39

Regel RE, Ivleva NB, Zer H, Meurer J, Shestakov SV, Herrmann RG, Pakrasi HB and Ohad I (2001) Deregulation of electron flow within Photosystem II in the absence of the PsbJ protein. J Biol Chem 276: 41473–41478

Rhee KH, Morris EP, Barber J and Kühlbrandt W (1998) Three-dimensional structure of the plant Photosystem II reaction centre at 8 Å resolution. Nature 396: 283–286

Rocap G, Larimer FW, Lamerdin J, Malfatti S, Chain P, Ahlgren NA, Arellano A, Coleman M, Hauser L, Hess WR, Johnson ZI, Land M, Lindell D, Post AF, Regala W, Shah M, Shaw SL, Steglich C, Sullivan MB, Ting CS, Tolonen A, Webb EA, Zinser ER and Chisholm SW (2003) Genome divergence in two *Prochlorococcus* ecotypes reflects oceanic niche differentiation. Nature 424: 1042–1047

Ruf S, Biehler K and Bock R (2000) A small chloroplast-encoded protein as a novel architectural component of the light-harvesting antenna. J Cell Biol 149: 369–378

Shi LX and Schroder WP (1997) Compositional and topological studies of the PsbW protein in spinach thylakoid membrane. Photosynth Research 53: 45–53

Shi LX, Kim SJ, Marchant A, Robinson C and Schroder WP (1999) Characterisation of the PsbX protein from Photosystem II and light regulation of its gene expression in higher plants. Plant Mol Biol 40: 737–744

Shi LX, Lorkovic ZJ, Oelmüller R and Schroder WP (2000) The low molecular mass PsbW protein is involved in the stabilization of the dimeric Photosystem II complex in *Arabidopsis thaliana*. J Biol Chem 275: 37945–37950

Stockhaus J, Hofer M, Renger G, Westhoff P, Wydrzynski T and Willmitzer L (1990) Anti-sense RNA efficiently inhibits formation of the 10 kd polypeptide of Photosystem II in transgenic potato plants: analysis of the role of the 10 kd protein. EMBO J 9: 3013–3021

Sugimoto I and Takahashi Y (2001) Localization of a small chloroplast-encoded polypeptide PsbK in Photosystem II core complexes. In: PS2001 Proceedings: 12th International Congress on Photosynthesis, S5-033. CSIRO Publishing, Melbourne (CD-ROM)

Summer EJ, Schmid VH, Bruns BU and Schmidt GW (1997) Requirement for the H phosphoprotein in Photosystem II of *Chlamydomonas reinhardtii*. Plant Physiol 113: 1359–1368

Sundby C, Larsson UK and Henrysson T (1989) Effects of bicarbonate on thylakoid protein phosphorylation. Biochim Biophys Acta 975: 277–282

Swiatek M, Kuras R, Sokolenko A, Higgs D, Olive J, Cinque G, Muller B, Eichacker LA, Stern DB, Bassi R, Herrmann RG and Wollman FA (2001) The chloroplast gene *ycf9* encodes a Photosystem II (PS II) core subunit, PsbZ, that participates in PS II supramolecular architecture. Plant Cell 13: 1347–1367

Swiatek M, Regel RE, Meurer J, Wanner G, Pakrasi HB, Ohad I and Herrmann RG (2003) Effects of selective inactivation of individual genes for low molecular mass subunits of the Photosystem II assembly by chloroplast transformation: The *psbEFLJ* operon in *Nicotiana tabacum*. Mol Gen Genet 268: 699–710

Szabo I, Seraglia R, Rigoni F, Traldi P and Giacometti GM (2001) Determination of Photosystem II subunits by matrix-assisted laser desorption/ionization mass spectrometry. J Biol Chem 276: 13784–13790

Takahashi Y, Matsumoto H, Goldschmidt-Clermont M and Rochaix JD (1994) Directed disruption of the *Chlamydomonas* chloroplast *psbK* gene destabilizes the Photosystem II reaction center complex. Plant Mol Biol 24: 779–788

The Institute for Genomic Research (2002) TIGR Database-*Arabidopsis thaliana*. http://www.tigr.org/tdb/e2kl/ath1/ath1.shtml. (Aug. 28, 2002)

Thidholm E, Shi LX, Lindstrom V, Funk C and Schroder WP (2001) The PsbW protein; Its location and involvement in photoinhibition. In: PS2001 Proceedings: 12th International Congress on Photosynthesis, S5-026. CSIRO Publishing, Melbourne (CD-ROM)

Thidholm E, Lindstrom V, Tissier C, Robinson C, Schroder WP and Funk C (2002) Novel approach reveals localisation and assembly pathway of the PsbS and PsbW proteins into the Photosystem II dimer. FEBS Lett 513: 217–222

Thompson LK and Brudvig GW (1988) Cytochrome *b*-559 may function to protect Photosystem II from photoinhibition. Biochemistry 27: 6653–6658

Thompson SJ, Robinson C and Mant A (1999) Dual signal peptides mediate the signal recognition particle/Sec-independent insertion of a thylakoid membrane polyprotein, PsbY. J Biol Chem 274: 4059–4066

Tissier C, Woolhead CA and Robinson C (2002) Unique structural determinants in the signal peptides of 'spontaneously' inserting thylakoid membrane proteins. Eur J Biochem 269: 3131–3141

Tomo T, Enami I and Satoh K (1993) Orientation and nearest neighbor analysis of *psbI* gene product in the Photosystem II reaction center complex using bifunctional cross-linkers. FEBS Lett 323: 15–18

Vener AV, Harms A, Sussman MR and Vierstra RD (2001) Mass spectrometric resolution of reversible protein phosphorylation in photosynthetic membranes of *Arabidopsis thaliana*. J Biol Chem 276: 6959–6966

Wedel N, Klein R, Ljungberg U, Andersson B and Herrmann RG (1992) The single-copy gene psbS codes for a phylogenetically intriguing 22 kDa polypeptide of Photosystem II. FEBS Lett 314: 61–66

Widger WR, Cramer WA, Hermodson M and Herrmann RG (1985) Evidence for a hetero-oligomeric structure of the chloroplast cytochrome *b*-559. FEBS Lett 191: 186–190

Zouni A, Witt HT, Kern J, Fromme P, Krauss N, Saenger W and Orth P (2001) Crystal structure of Photosystem II from *Synechococcus elongatus* at 3.8 A resolution. Nature 409: 739–743

Chapter 7

Primary Electron Transfer

Gernot Renger*
Max-Volmer-Laboratorium für Biophysikalische Chemie, Institut für Chemie, Technische Universität Berlin, Straße des 17. Juni 135, D-10623 Berlin, Germany

Alfred R. Holzwarth
Max-Planck-Institut für Bioanorganische Chemie, Stiftstraße 34 - 36, D-45413 Mülheim an der Ruhr, Postfach, Germany

*Author for correspondence, email: renger@pc-109ws.chem.tu-berlin.de

T. Wydrzynski and K. Satoh (eds): Photosystem II: The Light-Driven Water:Plastoquinone Oxidoreductase, pp. 139–175.

Summary

This chapter reviews our current state of knowledge on the primary electron transfer in Photosystem II (PS II). Properties of chlorophyll (Chl) *a* in solution and the basic features of pigment-pigment and pigment-protein interactions as well as the principles underlying excitation energy transfer and electron transfer are briefly outlined. Using this description as a starting point, and based on recent information available for the spatial arrangement of the cofactors, the general features of light-induced charge separation in PS II are presented. Special attention is given to the unique properties of the photoactive pigment P680, which consists of a special multimeric pigment complex of the form $(\text{Chl } a)_4\ (\text{Pheo})_x$ with x = 0, 1 or 2. The possible electronic structures of ^{1}P680*, ^{3}P680 and $P680^{+\bullet}$ as well as the underlying features that establish the extraordinarily high oxidizing power of $P680^{+\bullet}$ are discussed. Evidence is presented that in the first electron transfer event a 'monomeric' type Chl *a* within the multichromophoric P680 transfers an electron from its excited singlet state to an associated pheophytin (Pheo) *a* molecule which acts as the primary electron acceptor. This event is followed by rapid spin redistribution, leading to predominant localization of the electron hole on a Chl *a* in P680 designated as P_{D1}, which is part of a 'dimeric' structural motif termed $P_{D1}P_{D2}$ and is in close proximity to the redox-active tyrosine Y_Z. The process leading to the formation of the radical ion pair $P680^{+\bullet}$ $Pheo^{-\bullet}$ comprises a cascade of radical pair states of decreasing energy through a sequence of relaxation reactions with the protein environment. The role of the protein environment in the primary charge separation process is emphasized.

I. Introduction

The essential processes of photosynthetic water cleavage take place in a multimeric pigment-protein complex referred to as Photosystem II (PS II), which acts as a water:plastoquinone oxidoreductase. This complex contains more than 20 subunits and is anisotropically incorporated into the thylakoid membrane. The overall process comprises three types of reaction sequences (for reviews, see G. Renger, 1999, 2003):

$$P_{RC}Acc_1Acc_2 \xrightarrow{h\nu} {}^1P_{RC} * Acc_1Acc_2 \rightarrow P_{RC}^{+\bullet}Acc_1^{-\bullet}Acc_2 \rightarrow P_{RC}^{+\bullet}Acc_1Acc_2^{-\bullet} \quad (1)$$

$$4\oplus + 2H_2O \rightarrow O_2 + 4H^+_{Lumen} \quad (2)$$

$$4\ominus + 4H^+_{Stroma} + 2PQ \rightarrow 2PQH_2 \quad (3)$$

where P_{RC} symbolizes the photoactive pigment in the reaction center (RC) that leads by electron ejection from its lowest excited singlet state to formation of the primary cation-anion radical pair $P_{RC}^{+\bullet}Acc_1^{-\bullet}$, which is stabilized by rapid electron transfer from the reduced primary acceptor $Acc_1^{-\bullet}$ to the secondary acceptor Acc_2; the symbols $\oplus$ and $\ominus$ are used for the redox equivalents that give rise to oxidative water cleavage (sequence (2)) and plastoquinol formation (sequence (3)), respectively; H^+_{Lumen} and H^+_{Stroma} represent the proton release into the lumen and uptake from the stroma, respectively, of the thylakoid membrane. All cofactors that catalyze reaction sequences (1)–(3) are incorporated into a supramolecular protein complex consisting of the D1 and D2 polypeptides (Chapter 4, Nixon et al.). According to recent structural data (Chapters 18–21) binding of (some) cofactors for sequence (2) involves at least one additional polypeptide. This chapter describes the nature, functional properties and geometrical arrangement of the cofactors that are involved in reaction sequence (1). Details for reaction sequence (2) are described in Chapters 9–12 and 25 and reaction sequence (3) is described in Chapter 8.

Abbreviations: (B)Chl – (bacterio)chlorophyll; (B)Pheo – (bacterio)pheophytin; BRC – bacterial reaction center; D1/D2/Cyt b_{559} – minimum PS II complex containing cofactors of primary charge separation of PS II; EET – excited state energy transfer; ET – electron transfer; FCWD – Franck-Condon weighted density of states; NHI – nonheme iron; LH – light harvesting; P – special pair; P680 – primary electron donor in PS II; P700 – primary electron donor in PS I; PS – photosystem; Q_A – primary plastoquinone acceptor; Q_B – secondary plastoquinone acceptor: RC – reaction center; WT – wild type

II. Cofactors of Stable Charge Separation in Photosystem II

The nature of the cofactors for stable charge separation in PS II, P_{RC}, Acc_1 and Acc_2, were identified by measuring light induced absorption difference spec-

tra that characterize the turnover of each individual component (Ke, 2004). Figure 1 summarizes the original data used to identify the chemical species that constitute P_{RC}, Acc_1 and Acc_2. Figure 1A shows the difference spectrum of flash induced absorption changes measured in digitonin-treated spinach thylakoids. These data reflect the spectral characteristics of the turnover of the photoactive pigment P_{RC} of PS II (Döring et al., 1969). Based on this feature, P_{RC} was identified as a special chlorophyll (Chl) *a*, now generally referred to as P680. At nearly the same time, the acceptor component Acc_2 could be assigned to a specially bound plastoquinone (Q_A), as illustrated by the difference spectrum for $Q_A^{-\bullet}/Q_A$ in Fig. 1C (Stiehl, 1969; see also Stiehl and Witt, 1969). Later, pheophytin *a* (Pheo) was found to act as the electron acceptor Acc_1 for the primary charge separation in PS II (Klimov et al., 1977). The difference spectrum for $Pheo^-/Pheo$ is depicted in Fig. 1B. Based on this knowledge, the overall reaction pattern of stable charge separation according to sequence (1) can be more specifically formulated by the following sequence:

$$P680PheoQ_A \overset{h\nu}{\rightleftharpoons} {}^1P680^*PheoQ_A \overset{k_{PC}}{\underset{k_{-1}}{\rightleftharpoons}} P680^{+\bullet}Pheo^{-\bullet}Q_A \overset{k_{stab}}{\underset{k_{-2}}{\rightleftharpoons}} P680^{+\bullet}PheoQ_A^{-\bullet} \qquad (4)$$

where the rate constants k_{PC} and k_{stab} describe primary charge separation and its stabilization, respectively; and k_{-1} and k_{-2} are the rate constants of the corresponding back reactions.

Although the basic principles of the photosynthetic RCs are very similar and highly conserved throughout evolution, the photoactive pigment P680 of PS II is unique. The cation radical $P680^{+\bullet}$ formed as a result of the primary charge separation is one of the strongest oxidants in biology and the energetic prerequisite for the oxidation of water to molecular oxygen. With an estimated reduction potential of +1.1 to +1.26 V (Jursinic and Govindjee, 1977; Klimov et al., 1979; Rappaport et al., 2002), $P680^{+\bullet}$ exceeds the oxidizing power of the cation radicals in all other natural photosynthetic reaction centers by at least 0.5 V. The underlying molecular mechanism for the unusual redox properties of P680 is still not satisfactorily clarified and remains a challenge for current and future research activities (Section IV.D.2).

This particular feature, as well as the energetic behavior and kinetics of the reaction pattern, depends on the specific structural arrangement of the components within the protein matrix, which tunes the energetics and reaction coordinates of the cofactors. Advancement in our understanding of the functional and structural role of the protein matrix in light-induced charge separation was only achieved after the development of isolation procedures for RCs preparations with a minimum content of proteins and cofactors while retaining full functional activity. The first milestone in this line of research came almost 40 years ago with the isolation of reaction centers from anoxygenic purple bacteria (Reed and Clayton,

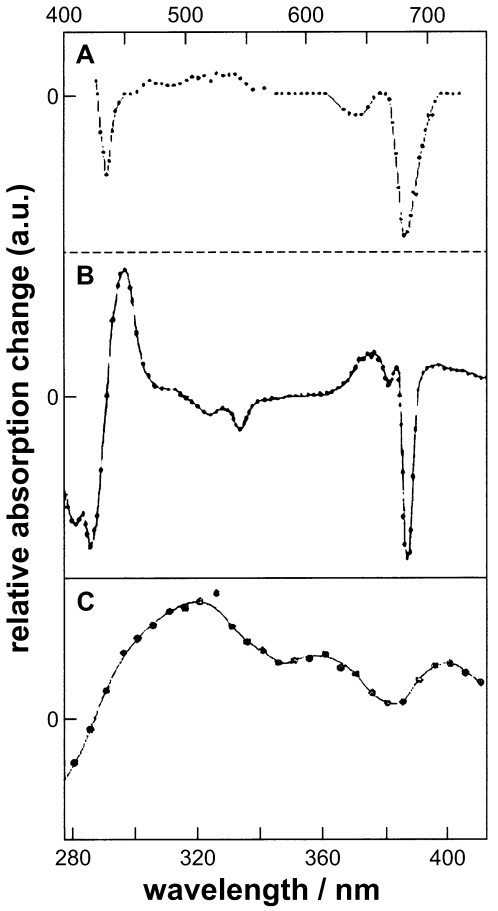

Fig. 1. Difference absorption spectra of $P_{680}^{+\bullet}/P_{680}$ (A), $Pheo^{-\bullet}/Pheo$ (B) and $Q_A^{-\bullet}/Q_A$ (C). The spectra were redrawn from data published in Döring et al. (1969), Klimov et al. (1977) and Stiehl (1969), respectively. Top wavelength scale refers to panel A and B, the bottom scale to panel C

1968). A similar achievement for PS II was only reached about 20 years later when a minimal preparation had been developed that could perform the primary radical pair formation $P680^{+\bullet}Pheo^{-\bullet}$(Nanba and Satoh, 1987).

A comparison with the well-characterized RCs from purple bacteria (BRCs) led to the conclusion that the cofactors of reaction sequence (1) in PS II are incorporated into the heterodimeric protein matrix of the D1 and D2 polypeptides (Michel and Deisenhofer, 1988). Thorough pigment analyses revealed that D1/D2/Cyt b_{559} preparations contain about 6 Chl *a* per 2 Pheo *a* (Kobayashi et al., 1990; Eickelhoff et al., 1996; Zheleva et al., 1996; Kurreck et al., 1997a); however, non-stoichiometric ratios from 6–8 Chls per 2 Pheo are often obtained (Konermann and Holzwarth, 1996). In addition to the chlorin pigments these preparations also contain two spectrally distinct β-carotene molecules (Kobayashi et al., 1990). In order to unravel the properties of such a multipigment arrangement, it is necessary to analyze in detail the interactions among the pigments and their coupling to the protein matrix. Before describing our current state of knowledge on the energetics and functional properties of the PS II RC, a brief summary of general pigment-pigment and pigment-protein interactions is presented.

III. Photophysical Properties of Pigment Protein Complexes

The spectral and functional properties of pigments bound into a protein matrix are essentially dependent on three parameters: (i) the chemical nature of the pigment; (ii) the strength of the pigment-pigment coupling; and (iii) the mode of pigment-protein interaction.

A. Chlorophyll and Pheophytin

The structure of Chl *a* and its spectral properties in dilute solutions of nucleophilic and/or polar solvents, where dimerization or higher aggregation does not occur, are summarized in Fig. 2. Chl *a* and Pheo *a* are both characterized by a carbon skeleton that contains: (i) a five ring chlorin with a conjugated π-electron system (symbolized by thick-lined bonds); and (ii) an extended hydrophobic phytyl chain that is connected via an ester bond with the propionate of ring IV. Chl *a* contains Mg^{2+} as the central atom complexed by the tetrapyrrole ring, whereas Pheo *a* is the free base without a central metal ion. The absorption spectra of monomeric Chl *a* exhibit strong bands in the red and blue (Soret-band) spectral regions due to spin- and symmetry-allowed electronic transitions. In addition, symmetry-forbidden nπ* transitions with much lower oscillator strength (a factor 10–100 smaller as compared to the ππ* transitions) are present due to the central pyrrolic nitrogen and the 13^1 keto oxygen of ring V with occupied nonbonding orbitals. The relative positions of the energy levels of ππ* and nn* transitions depend strongly on the polarity of the environment (Petke et al., 1978).

The transition from the ground (S_0) to the first excited singlet state (S_1) is located in the red spectral range and polarized in the y-direction of the molecular axis system (Fig. 2, bottom right side). Accordingly, it is symbolized by Q_y in Platt's notation. The second excited singlet state (S_2) giving rise to the Q_x transition is comparatively weak and its energetics resembles that of the vibronically excited Q_y (1,0) transition. Actually, the relative position of Q_x (0,0) and Q_y (1,0) depends strongly on the solvent properties. The strong absorption in the blue region (Soret band) arises from transitions into higher excited singlet states and is predominantly polarized in the x-direction (B_x transition) (for a review, see Scheer, 1991). The higher excited singlet states rapidly relax within a few picoseconds down to the lowest electronically and vibronically excited state ^{1}Chl *a** (S_1). In dilute (1μM) solutions without aggregation, ^{1}Chl *a** has a lifetime of 5.5 ± 0.3 ns (Vasilev et al., 1997). This value is the result of essentially two decay pathways with rate constants $k_{rad} \approx 6.5 \cdot 10^7\ s^{-1}$ and $k_{ISC} \approx 1.3 \cdot 10^8\ s^{-1}$ for radiative emission and intersystem crossing into the triplet state (T_1), respectively (Parker and Joyce, 1967). Dissipation of excitation via radiationless transition from ^{1}Chl *a** into the ground state Chl *a* is virtually negligible for monomeric Chl *a* in protic solvents but becomes dominant in Chl *a* aggregates.

Due to the very fast internal conversion processes (sub-ps to ps time domain) from higher excited singlet states, the reaction properties of electronically excited Chl *a* are almost exclusively determined by the behavior of the S_1 state. Accordingly, regardless of the excitation wavelength, radiative emission gives rise to a characteristic red fluorescence (the radiative emission from higher excited singlet states in the blue is weaker by several orders of magnitude and difficult to detect, see Leupold et al., 2002). As a consequence,

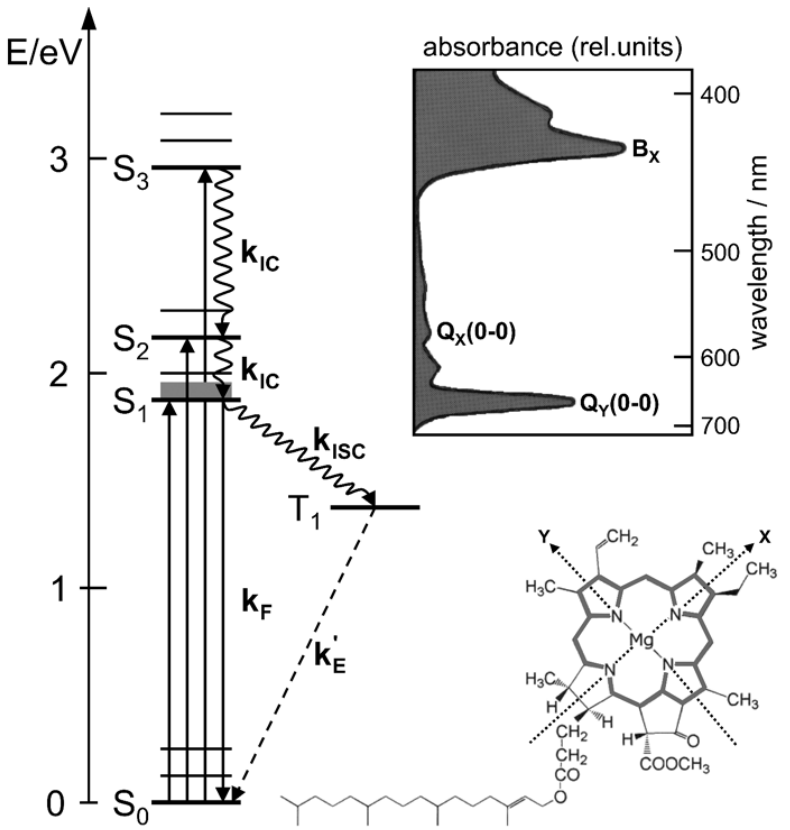

Fig. 2. Energy level diagram (left side), molecular structure (bottom, right side), and absorption spectrum of Chl *a* in ethanol (taken from Petke et al., 1979) (top, right side). The conjugated π-electron system is symbolized by the thick grey lines in the molecular structure. Energy levels of electronically excited states are characterized by thick and vibrational states of the molecules by thin bars. Phonons with their much smaller energy differences form a quasi-continuum symbolized by grey area (only S_1 is considered). Rate constants k_F k_E', k_{IC} and k_{ISC} symbolize fluorescence, phosphorescence, interval conversion and intersystem crossing, respectively. For simplicity, only 0–0 transitions are explicitly shown, and radiationless transitions to the ground state are omitted (this process is negligible for dilute Chl *a* solutions, see text).

all useful natural photochemical reactions start from ^{1}Chl *a** (S_1). The lowest triplet state ^{3}Chl *a* formed via intersystem crossing from ^{1}Chl *a** (S_1) plays an important role for photochemical reactions of Chl *a* in solution (because of its much longer lifetime in the ms-range) but is not involved in formation of the primary radical pair $P680^{+\bullet}Pheo^{-\bullet}$(Section V.A). In contrast, however, ^{3}Chl triggers undesirable side reactions that nature tries to minimize. The population of ^{3}Chl *a* in photosynthetic organisms gives rise to deleterious reactions due to the sensitized generation of highly reactive singlet oxygen $^1\Delta_g O_2$. Therefore, suitable mechanisms are required to protect the apparatus from rapid photodamage under aerobic conditions (Section VI.B).

The coordination of the central Mg^{2+} of Chl is unsaturated. As a consequence, Chls form complexes with nucleophilic ligands and with each other, due to the electron donating properties of the carboxylic groups and the electron accepting properties of the central Mg^{2+} ion (Norris et al., 1974). In the absence of suitable ligands from the solvent molecules, Chls self-aggregate, often through the action of small amounts of water and/or liganding functions of their

own side chains. The type of complex formed depends on the nature of the solvent. In general, apolar solvents favor the formation of large Chl aggregates (often employing an equivalent of one or two water molecules as a bridging structure). On the other hand, in polar nucleophilic and/or hydrogen-bonding solvents complexation occurs between monomeric Chl and the solvent nucleophile. Alternatively, oligomeric adducts are formed, comprising again bifunctional polar liquids (e.g., H_2O) as a bridge. The role of the functional groups of Chls and the charge of detergent molecules for aggregation in micellar solution has been summarized in Agostiano et al. (2002). Self-aggregation of pigments in photosynthetic organisms is a dominating factor only for the formation of the chlorosomes that act as antenna systems in green bacteria. In this case, bacteriochlorophyll (BChl) *c*, *d* or *e* molecules undergo supramolecular self-organization via an internal hydroxy group (Balaban et al., 2000) where proteins do not play any structural role. In other antenna systems and all RCs the (B)Chls are noncovalently bound to proteins. This gives rise to special coordination with amino acid residues and axial ligand(s). Information on the type of coordination can be obtained from modern spectroscopic techniques like resonance Raman or FTIR spectroscopy. Chl *a* in both solvents and in proteins is typically pentacoordinated (for reviews, see Mäntele, 1996; Robert, 1996). This is fully supported by the recent high resolution X-ray structure of PS I (Fromme et al., 2001). Interestingly, the pentacoordination depends on the stereoisomery of the ligation at asymmetric C-atoms of the chlorin ring. Studies on model systems reveal that the binding of the fifth ligand is favored from the side of the macrocycle where the methoxycarbonyl moiety of ring V protrudes (Oba and Tamiaki, 2002). In PS I of thermophilic cyanobacteria 82 Chls out of the total amount of 96 Chls are pentacoordinated from the 'anti' side with respect to the stereoisomery of the phytylester at the proprionate of ring IV (Balaban et al., 2002).

The redox properties of Chl *a* and Pheo *a* have been thoroughly analyzed in solution by cyclic voltammetry (Watanabe and Kobayashi, 1991). Monomeric Chl *a* in solution is characterized by standard redox potentials versus normal hydrogen electrode (NHE) of about +0.85V and about –0.95V for its one-electron oxidation and reduction, respectively. The corresponding values for Pheo *a* in solution are about +1.3 V and about –0.65 V, respectively. It is interesting to note that Chl $a^{+\bullet}$ in solution exhibits markedly lower oxidation power than $P680^{+\bullet}$ and that aggregate formation in solution leads to even less oxidizing cation radicals. These findings illustrate that the protein environment plays a key role in establishing the special pigment complex P680 with its strongly oxidizing species $P680^{+\bullet}$ (Section IV.D.2).

A functionally important structural parameter is the planarity of the chlorin ring. Studies with conformationally designed non-planar molecules revealed that distortions of ring planarity gives rise to significant changes in the optical and redox properties (for a review, see Fajer, 2000). According to theoretical calculations these distortions lead to a destabilization of the highest occupied molecular orbital (HOMO) with little effect on the lowest unoccupied molecular orbital (LUMO) (Senge et al., 2000).

B. Pigment-Pigment Interactions

The strength of the pigment-pigment interaction depends on the interpigment distance, mutual orientation and the nature of the intervening medium. Accordingly, different features emerge, depending on the mode and strength of coupling between the pigments. For the sake of simplicity the general features of the reaction behavior will be illustrated for a system consisting of only two interacting pigments. In the electronic ground state, the interaction between two pigments (H_{12}) gives rise to an energy shift of the ensemble due to the van der Waals interaction. A more complex pattern arises when the pigment ensemble is electronically excited. The properties in this case are described by a Hamiltonian of the type:

$$\mathbf{H} = \mathbf{H}_1 + \mathbf{H}_2 + \mathbf{H}_{12} \qquad (5)$$

where $\mathbf{H}_i$ (i = 1,2) are the Hamiltonians of the separated pigments 1 and 2 without interaction and having eigenfunctions $\varphi^0_{i,k}$ (i=1.2) with k = g or e, which describes the ground (g) and electronically excited (e) state(s), respectively; and $\mathbf{H}_{12}$ is the interaction operator.

Depending on the nature of $\mathbf{H}_{12}$ the interaction can give rise to two basically different reaction types. This is illustrated in Fig. 3 on the basis of a simple (HOMO/LUMO) analysis for the two identical pigments P_1 and P_2. The two types of reactions are: (i) excited state energy transfer (EET); and (ii) electron transfer (ET) from one pigment to the other. These are the types of processes taking place in the primary

reaction sequences in photosynthetic antennae and in RCs in general, as will be outlined in Section IV. When the strength of electronic coupling (V_{12}) is weak compared to the electron-vibrational coupling, the rate constant of the corresponding reactions can be calculated by quantum mechanical perturbation theory within the framework of Fermi's Golden Rule:

$$k_{12} = \frac{2\pi}{\hbar}|V_{12}|^2 \times \text{FCWI} \qquad (6)$$

where V_{12} is the matrix element of electronic coupling between the initial (i) state ($^1P_1^*P_2$) and the final (f) state ($P_1^!P_2^*$ or $P_1^{+\bullet}P_2^{-\bullet}$) in Fig. 3 and FCWD is the Franck-Condon weighted density of states. The value of V_{12} is given by $\langle\psi_f|\mathbf{H}_{12}|\psi_i\rangle$, in which ψ_i and ψ_f are the wave functions of the initial ($^1P_1^*P_2$) and final ($P_1^!P_2^*$ or $^1P_1^{+\bullet}P_2^{-\bullet}$) states, respectively.

1. Excited State Energy Transfer

In the case of excitation energy transfer (EET) two limiting domains can be distinguished: weak and strong coupling, where V_{12} is much smaller or larger, respectively, compared to the Franck-Condon width of the optical transitions of the individual pigments (Section III.B.2).

a. Weak Coupling (Förster-Type Energy Transfer)

In the limiting case of very weak coupling, the electronic structure of the participating pigments remains virtually unaffected and the excited state is localized on one of the pigments and transferred from the donor (D) to the acceptor (A) pigment via an incoherent hopping type process. An evaluation of scheme (1) within the framework of the point-dipole approximation (where the center-to-center distance between the pigments is large as compared with the pigment dimension; Davydov, 1962) leads to the widely used Förster equation for the rate of pairwise EET (Förster, 1965):

$$k_{EET}^{\text{Förster}} = \frac{A \cdot \kappa^2}{n^4 R^6} \frac{1}{\tau_0} \int F_D(\nu)\varepsilon_A(\nu)\frac{d\nu}{\nu^4} \qquad (7)$$

where A is a constant; n is the refractive index of the medium; κ^2 is a factor describing the mutual orientation of the transition dipole moments of the donor and acceptor pigment ($0 \le \kappa^2 \le 4$); R is the distance between the donor (D) and acceptor (A) point transition dipole moments; τ_0 is the radiative lifetime of the excited state of the donor; $F_D(\nu)$ and $\varepsilon_A(\nu)$ are the spectral distributions of the normalized donor emission and acceptor absorption, respectively.

The Förster type EET according to Eq. (7) provides only a pertinent description if, in addition to the validity of the point dipole approximation, the pig-

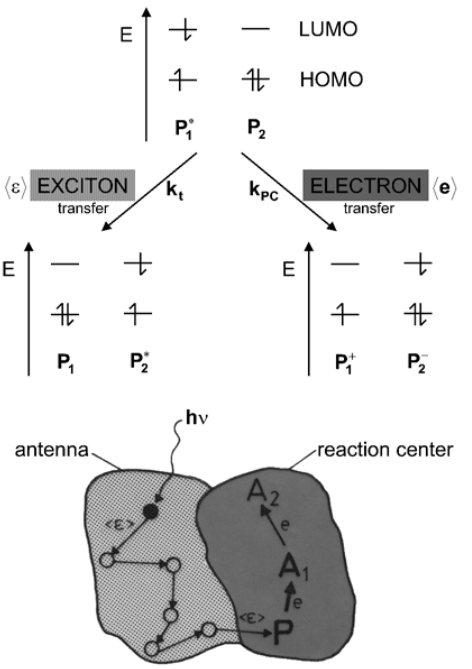

Fig. 3. Electronic coupling between two pigment molecules, P_1 and P_2, of the same orbital structure. The interaction can either lead to excited state (exciton†, symbolized by ‹ε›) (left side) or electron (right side) transfer from pigment molecule P_1 in its lowest excited singlet state (P_1^*) to pigment molecule P_2 in the electronic ground state. For simplicity, only the highest occupied molecular orbital (HOMO) and lowest unoccupied molecular orbital (LUMO) are shown. The lower part shows a schematic representation of the processes in the antenna system and reaction center (corresponding back reactions are omitted), where P is the photochemical pigment and A_1, A_2 the primary, secondary acceptor, respectively.

† In photosynthesis research the word 'exciton' is used as an operational term to describe an excited electronic state that resides on more than one pigment in a group of molecules during its lifetime (Pearlstein, 1982).

ment-pigment coupling is weak enough to ensure that the individual properties of the donor (lifetime and lineshape of fluorescence) and acceptor (lineshape of absorption), including oscillator strengths, are not perturbed. However, in the case of static disorder, it is difficult to obtain the homogeneous line shapes $F_D(\nu)$ and $\varepsilon_A(\nu)$ in Eq. (7). Furthermore, apart from the necessity of having structural information for obtaining κ^2, the use of correct values for the refractive index (n) in biological systems is also important (Knox and van Amerongen, 2002). In the case of more than two pigment molecules within a pigment protein complex, the pattern becomes even more complex if aggregates of strongly coupled pigments are formed (for an extension of the Förster theory to the EET dynamics between aggregates, see Sumi, 1999; Scholes et al., 2001).

In addition to Förster type EET, which originates from Coulombic interaction between the transition dipole moments without exchange of electrons between the interacting pigments, the overlap of electronic wavefunctions at close distance also gives rise to an electron exchange. In this case the electron from the LUMO of P_1^* (see Fig. 3) is transferred to the LUMO of P_2 and simultaneously an electron of opposite spin from the HOMO of P_2 to the HOMO of P_1^*. The net result is the same as for the Förster type EET, but the mechanism is quite different. As a consequence, another type of EET, referred to as the Dexter mechanism (Dexter, 1953), emerges with a rate constant given by:

$$k_{ET}^{Dexter} = \frac{2\pi}{\hbar}\left|V_{DA}^{exch}\right|^2 \int F_D(\nu)\varepsilon_A(\nu)\,d\nu \qquad (8)$$

where V_{DA}^{exch} is the electronic matrix element for the exchange interaction between donor (D) and acceptor (A) that decays exponentially with distance R between D and A; $F_D(\nu)$ and $\varepsilon_A(\nu)$ are the same parameters as in Eq. (7). The contribution of exchange processes to overall singlet-singlet EET is comparatively small for (B)Chls in photosynthetic organisms. Even for the strongly coupled pigments in the bacterial antenna complex LH2, values of only 10–15% were reported in a theoretical study (Tretiak et al., 2000). However they play a key role for triplet state energy transfer from ^{3}(B)Chl to carotenoids in photosynthetic organism (section VI B).

b. Strong Coupling (Exciton Concept)

In the case of strong coupling, delocalized excited states exist that can be described as a linear combination of locally excited states. For a dimer of two pigments P_1 and P_2 one obtains:

$$\psi_g = \psi^\circ_{1,g}\psi^\circ_{2,g} \text{ and } \psi_e = c_1\psi^\circ_{1,e}\psi^\circ_{2,g} + c_2\psi^\circ_{1,g}\psi^\circ_{2,e} \qquad (9)$$

where $\psi^\circ_{i,g}$ and $\psi^\circ_{i,e}$ are the exact normalized wavefunctions of the noninteracting (superscript 0) pigments (i = 1,2) of the ground (g) and first excited (e) states; and c_1 and c_2 are constants. The energy difference between the excited and ground state of the dimer is given by:

$$\Delta E^*_{dimer} = \langle\psi_e|\mathbf{H}|\psi_e\rangle - \langle\psi_g|\mathbf{H}|\psi_g\rangle \qquad (10)$$

The evaluation for a homodimer with the Hamiltonian $\mathbf{H} = \mathbf{H}_1 + \mathbf{H}_2 + \mathbf{H}_{12}$, leads to the expression:

$$\Delta E^*_{homodimer} = \Delta E^*_{monomer} + \Delta W \pm \varepsilon_{exciton} \qquad (11)$$

where $\Delta E^*_{monomer} = \varepsilon_e - \varepsilon_g$ (ε_g and ε_e are the electronic energies of the separated monomeric pigment molecules with $\varepsilon_g = \varepsilon_{1,g} = \varepsilon_{2,g}$ and $\varepsilon_e = \varepsilon_{1,e} = \varepsilon_{2,e}$); $\Delta W = \langle\psi^\circ_{1,e}\psi^\circ_{2,g}|\mathbf{H}_{12}|\psi^\circ_{1,e}\psi^\circ_{2,g}\rangle - \langle\psi^\circ_{1,g}\psi^\circ_{2,g}|\mathbf{H}_{12}|\psi^\circ_{1,g}\psi^\circ_{2,g}\rangle$ is the difference of the van der Waals energies of the interacting pigments in the excited and ground state of the dimer, respectively; and the term $\varepsilon_{exciton} = \langle\psi^\circ_{1,e}\psi^\circ_{2,g}|\mathbf{H}_{12}|\psi^\circ_{1,g}\psi^\circ_{2,e}\rangle$ is referred to as exciton interaction energy.

As a consequence of Eq.(11), instead of a single transition $\Delta E^*_{monomer}$ in the noninteracting monomers, two different transitions emerge for the excitonically coupled pigments in the homodimer with an energy gap of $2\varepsilon_{exciton}$. This feature is schematically shown in Fig. 4. The extent of exciton splitting and the oscillator strength of both transitions ($\Delta E^*(+) = \Delta E^*_{monomer} + \Delta W + \varepsilon_{exciton}$ and $\Delta E^*(-) = \Delta E^*_{monomer} + \Delta W - \varepsilon_{exciton}$) depend on the distance between the pigments R, the oscillator strengths of the optical transition of the isolated monomers and the mutual orientation of the transition dipole moments within the dimer (Hochstrasser and Kasha, 1964). The excitation energy in this case is delocalized over the two pigments, which act as a kind of supermolecule.

If the two pigments in the dimer differ in their transition energies ΔE^*_i (i = 1,2) by $\Delta\Delta E^*$ (either due to different chemical nature — e.g., a Chl *a*/Chl *b* heterodimer, or to environmental differences), the

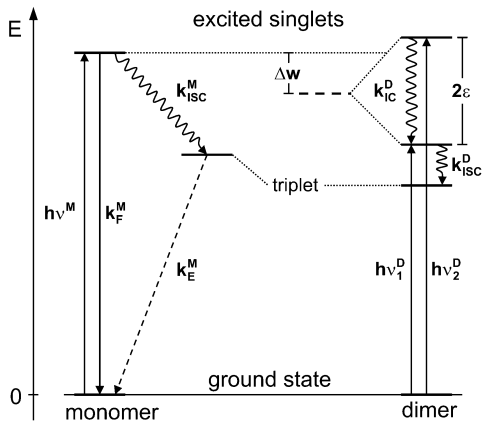

Fig. 4. Electronic energy level diagram of a monomer and a strongly coupled homodimer. Rate constants k_F, k_F, k_{IC}, and k_{ISC} represent processes of fluorescence, phosphorescence, intersystem crossing and internal conversion, respectively, in the monomer (M) and dimer (D). k^D_{IC} is the rate constant for internal conversion from high to low energy exciton level(s). For simplicity, the ground state energy of the monomer and dimer are set at equal levels and the pathways of k^D_F and k^D_E are not shown. Likewise, the radiationless decay of the monomer (its contribution to the overall decay of the lowest excited singlet state is negligible for dilute solutions of monomeric Chl *a*, see Section III. A) and the vanishingly small splitting of the triplet state in the dimer (Schmidt and Reinecker, 1985) are omitted. The oscillator strength of the two transitions in the dimer ($h\nu^D_1$ and $h\nu^D_2$) depends on the strength and mutual orientation of the transition dipole moments of the two individual pigment molecules forming the dimer (for details, see Hochstrasser and Kashha, 1964).

two exciton transitions $\Delta E^*(+)$ and $\Delta E^*(-)$ are given by:

$$\Delta E^*(\pm) = \frac{1}{2}\left(\Delta E^*_{monomer,1} + \Delta E^*_{monomer,2} + 2\Delta W \pm \sqrt{\left(\Delta\Delta E^*\right)^2 + 4\varepsilon^2_{exciton}}\right) \quad (12)$$

The exciton states are described by normalized wavefunctions $\psi_{dimer,c}(\pm)$, where $c_1 = \sin\alpha$ and $c_2 = \cos\alpha$ in Eq. (9) with:

$$\tan\alpha = \frac{\Delta\Delta E^* \pm \sqrt{\left(\Delta\Delta E^*\right)^2 + 4\left(\varepsilon_{excition}\right)^2}}{2\varepsilon_{excition}} \quad (13)$$

An inspection of Eqs. (11) and (12) reveals that significant excitonic effects on the spectral properties of the dimer can only be observed if $\Delta\Delta E^*$ is small compared with $\varepsilon_{exciton}$. On the other hand, if $\Delta\Delta E^* >> \varepsilon_{exciton}$ is satisfied, the two pigments retain their individual, nonperturbed optical properties. In actual pigment protein complexes containing more than two strongly coupled pigments, a more complicated pattern of exciton states emerges (Pearlstein, 1991; Tretiak et al., 2000). Additionally, the above exciton description assumes only a two-state system, whereas inclusion of higher excited states and charge transfer (CT) states would further complicate the picture. This treatment would ultimately be necessary to fully describe excitonic effects on transient absorption spectra (T. Renger and May, 1997).

So far only the electronic wavefunctions have been explicitly considered. The overall properties of a pigment molecule, however, are described by $\psi_{i,k}(\vec{r},\vec{R})$, where $\vec{r}$ and $\vec{R}$ are the coordinates of electrons and nuclei, respectively. In most cases, the Born-Oppenheimer approximation can be used:

$$\psi^\circ_{ik}(\vec{r},\vec{R}) \approx \psi^\circ_{ik}(\vec{r})Q^\circ_{ikv}(\vec{R}) \quad (14)$$

where i and k describe the pigment number and electronic excitation state, respectively; and v symbolizes the state of nuclear vibrations. As a consequence of the Born-Oppenheimer approximation, the electronic transition dipole moment can be treated as independent of coordinates $\vec{R}$ and the effect of nuclear motions is given by the Franck-Condon (FC) factor:

$$\left|\langle Q_{iev}(\vec{R})|Q_{igv}(\vec{R})\rangle\right|^2 \quad (15)$$

The complexity of the system is nicely illustrated for Chl *a* in glassy diether at low temperatures. In this 'simple' case, 37 vibrational modes in the range of 263–1530 cm^{-1} were shown to contribute to the FC factor (Avarmaa and Rebane, 1985). In pigment-protein complexes, the protein matrix modulates the spectral and reactive properties. Attempts have been reported to describe the bandshape of Chl *a* absorption at room temperature in glasses and a protein matrix (Zucchelli et al., 2002; Section III.C).

Based on these generalized considerations within a simplified framework, it is obvious that the detailed description and understanding of the optical and EET properties of protein systems containing several pigments is a highly complex and challenging task. Attempts at theoretical descriptions of a coupled multi-pigment protein complex with its environment have been reported by T. Renger and Marcus (2002a). A suitable theory would greatly benefit the interpre-

tation of the spectral properties of photosynthetic multi-chromophore proteins.

2. Electron Transfer

Electron transfer (ET) reactions between molecules take place via vibrationally coupled electron tunneling. Regardless of the electronic state (ground or excited state) of the redox partners, the rate constant of the reaction can be obtained by using Fermi's Golden Rule (Eq. (6)). The initial (i) and final (f) states include a multidimensional system of vibrations comprising both the redox groups and their environment. It has been the remarkable achievement of the theory by R.A. Marcus (Marcus and Sutin, 1985) to project a reaction pathway onto parabolic free energy curves of states i and f. This concept is illustrated in Fig. 5. Depending on the strength of electronic coupling between D and A, two limiting cases can be distinguished: (i) strong coupling; and (ii) weak coupling. In the case of strong coupling, a marked energy splitting emerges at the crossing of the potential curves for states i and f (Fig. 5, right side) and, as a consequence, the ET occurs within the same potential curve of the nuclei — i.e., the process is adiabatic. On the other hand, if the coupling is rather weak, the splitting is so small that the ET process involves a crossover between the potential curves for states i and f — i.e., the process is non-adiabatic (Fig. 5, left side).

For the vast majority of ET reactions in biological systems, which is actually 'long range' electron transfer, the nonadiabatic approximation turns out to be sufficiently satisfied (Moser and Dutton, 1996). Huppmann et al. (2003) showed that even the fastest ET reactions of the light induced charge separation in the reaction centers of anoxygenic purple bacteria are nonadiabatic at room temperature and a transition to the adiabatic regime occurs only at rather low nonphysiological temperatures. Within the framework of Fermi's Golden Rule (Eq. (6)), the rate constant of nonadiabatic ET can be obtained by quantum mechanical calculations of the matrix element $|V_{fi}|^2$ of electronic coupling between states i (DA or $^1D^*A$

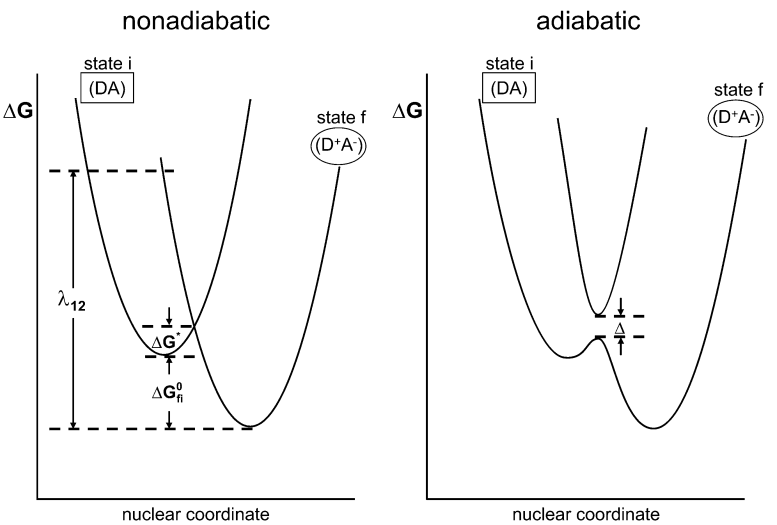

Fig. 5. Coupling of electron tunneling and nuclear motion in redox reactions. The ordinate represents the energy of the nuclei of the whole system – i.e., donor plus acceptor plus surrounding. The multidimensional energy hypersurface is extremely simplified by using a one-dimensional harmonic potential. The abscissa describes the nuclear geometry for the initial (DA) and the final (D^+A^-) state of the whole system (different geometries of the initial and final state are symbolized by a square and oval, respectively). Left side: non-adiabatic electron transfer—i.e., the process occurs in the vicinity of the crossover of the potential curves of the initial (i) and final (f) states with a comparatively low transmission coefficient. Right side: adiabatic electron transfer — i.e., strong coupling leads to splitting of the energy (its magnitude is symbolized by Δ) near the crossover nuclear geometry so that the initial state (DA) proceeds to the final state (D^+A^-) within the same potential surface.

in the case of photoreactions) and f ($D^{+\bullet}A^{-\bullet}$) and using various approaches for determining the factor FCWD of Eq. (6). The magnitude of $|V_{fi}|^2$ depends on the overlap of the wavefunctions and therefore exponentially decreases with increasing distances between the interacting redox groups:

$$|V_{fi}(R_{DA})|^2 = |V_{fi}(0)|^2 \exp(-\beta R_{DA}) \quad (16)$$

where R_{DA} is the edge to edge distance between D and A and β is a constant. For many biological systems, including BRCs, the logarithm of the rate constant, $\log k_{ET}$, was found to be linearly dependent on R_{DA} with a slope of about 1.4 $Å^{-1}$ (the actual value depends on the packing density of atoms in the protein environment connecting D and A (Page et al., 1999; Kawatsu et al., 2001).

The most widely used procedure for obtaining an expression of the FCWD factor is the Marcus theory (Marcus and Sutin, 1985), which is based on a classical treatment of nuclear motion. As a result, the following expression emerges:

$$k_{fi}^{ET} = \frac{2\pi}{\hbar}|V_{fi}|^2 \left(4\pi\lambda_{fi}k_B T\right)^{-\frac{1}{2}} \times \exp\left[-\frac{\left(\Delta G_{fi}^{\circ} + \lambda_{fi}\right)^2}{4\lambda_{fi}k_B T}\right] \quad (17)$$

where k_B is the Boltzmann constant; ΔG_{fi}° and λ_{fi} are the standard Gibb's energy gap and the reorganization energy, respectively, between states f and i.

The Marcus theory with a 'classical' reorganization energy parameter λ_{fi}^{cl} that describes the changes in the vibrational modes of the redox groups themselves and their microenvironment (e.g., solvent polarization) can be only successfully applied when the dominating vibrations are thermally activated. If this condition is not satisfied (e.g., at low temperatures), the FCWD factor has to be calculated by quantum mechanical treatment of the vibrations. This is especially important for the interpretation of low temperature data where ET can be associated to a significant extent with nuclear tunneling (for analysis of BRCs, see Warshel et al., 1989; D. Xu and Schulten, 1994; Vos et al., 2000).

It should be mentioned that the Marcus concept of intersecting parabolas with the activated state at the crossing point has to be modified when nonlinear solute-solvent coupling is present — e.g., when the electronic polarizability varies significantly between states i and f (for further discussion, see Small et al., 2003).

C. Pigment-Protein Interactions

In the visible spectral range, coupling of electronic states of the pigments with those of the proteins can be neglected (matrix isolated pigments) and only the interaction with the nuclear motions of the protein (phonons) have to be considered. In the case of electronic transitions, the coupling with the intramolecular vibrations of the pigment molecule has to be extended by the interaction with the vibrational modes of the matrix. Low-frequency ($\nu < 150$ cm^{-1}) intermolecular modes (phonons) of pigment-protein complexes play an important role in mediating EET and ET processes in photosynthetic units (for a review, see O. Kühn et al., 1997).

The coupling strength and the average frequency of the modes can be obtained from low temperature line narrowing spectroscopy (fluorescence line narrowing and hole burning) (Peterman et al., 1997; Pieper et al., 1999). Complementary information is gathered from measurements of inelastic neutron scattering (Pieper et al., 2004). In addition to the general phenomenon of electron-phonon coupling, the specific properties of the protein matrix have to be taken into account. Essentially two phenomena are of relevance: (i) the different type of ligation of Chls; and (ii) energetic differences due to variations of conformational states of the protein in the microenvironment of the pigments. The former effect has been analyzed by quantum mechanical molecular orbital (MO) calculations of Chl molecules using various amino acid residues as ligands. Variations of the Q_y transition energies of almost 500 cm^{-1} were found for Chl *a* (Gudowska-Nowak et al., 1990; Nishigaki et al., 2001). Therefore, the nature of the ligand significantly modulates the optical properties. The second effect gives rise to inhomogeneous line broadening (static disorder), if the fluctuations of conformation are comparatively slow. This is typical for a protein environment.

It is clear that the protein matrix and its dynamics, which cover wide domains in time ($<10^{-12}$ to 10^3 s) and space (local, large-scale, or collective), are most relevant modulators of the kinetics and energetics of EET and ET processes (for a review, see Karplus and McCammon, 1983). Since proteins do not possess a unique state of minimum Gibbs energy like glasses,

they attain a large number of conformational substates separated by energy barriers of different height and width. These characteristics can lead to complex temperature dependencies of the kinetics due to the variety of activation energies for transitions between conformational substates. As a result, ET reactions cannot simply be described by a single discrete rate constant k_{ET} but only by an average parameter $k_{ET,ave}$ that is given by:

$$\log k_{ET,ave} = \int f(k_{ET}) \log k_{ET} \, d \log k_{ET} \qquad (18)$$

where $f(k_{ET})$ is a distribution function of rate constants for individual conformational states. ET reactions exhibit complex nonexponential kinetics when $f(k_{ET})$ significantly deviates from a δ function and the rate of transition between conformational sub-states is slow compared with $k_{ET,ave}$. This effect is illustrated for the recombination rate at low temperature between $P^{+\bullet}$ and $Q_A^{-\bullet}$ in BRCs (McMahon et al., 1998). An analogous effect on the protein dynamics can be achieved at room temperature when isolated BRCs are embedded into solid trehalose/water glasses of high viscosity (Palazzo et al., 2002).

IV. Nature and Properties of P680 and Pheo

A deeper understanding of the nature and the properties of the cofactors requires a thorough knowledge of their arrangement and mode of coordination within the D1/D2 heterodimeric protein matrix. The current knowledge on the structural arrangement will be briefly summarized before discussing implications on the properties of P680 and Pheo. Further structural details are given in Chapters 18–21.

A. Arrangement of the Cofactors within the D1/D2 Heterodimer

The X-ray crystal structure of functionally fully competent PS II core complexes from the thermophilic cyanobacteria *Thermosynechococcus elongatus* and *T. vulcanus* has been reported at a resolution of 3.7–3.8 Å (Zouni et al., 2001; Vasil'ev et al., 2001; Kamiya and Shen, 2003) and recently improved to 3.5 Å (Ferreira et al. 2004) and further to 3.2 Å (Biesiadka et al., 2004) for *T. elongatus*. Figure 6 shows the arrangement of the Chl *a* and Pheo *a* molecules and the cofactors Q_A, Y_Z and the tetranuclear manganese cluster of the water oxidizing complex (WOC) together with the non heme iron (NHI) center

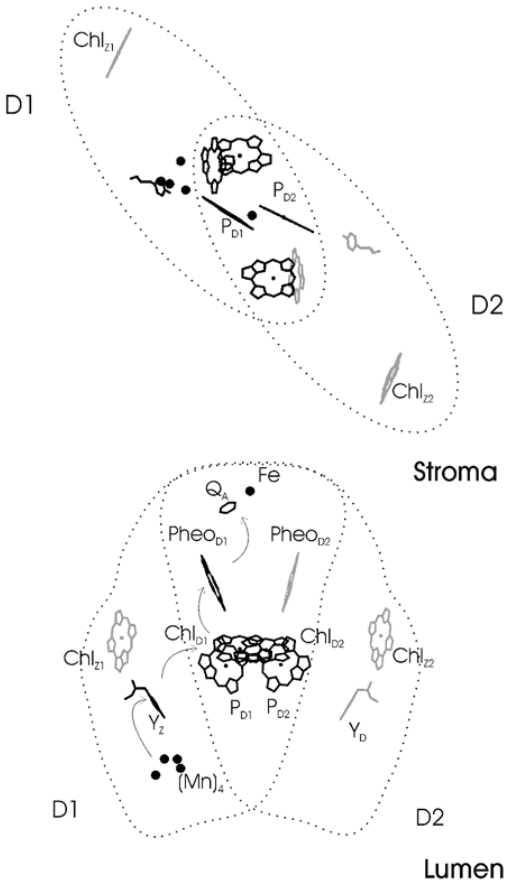

Fig. 6. Top view (upper part) and side view (bottom part) of the structural array of the cofactors of PSII within the heterodimer of polypeptides D1 and D2. Chl_{D1}, Chl_{D2}, P_{D1} and P_{D2} are the four Chl *a* and $Pheo_{D1}$ and $Pheo_{D2}$ the two Pheo *a* molecules of the reaction center pigment core (RC-PC); Chl_{A1} and Chl_{A2}, the distal Chl *a* molecules; Q_A, plastoquinone acceptor; $(Mn)_4$, the tetranuclear manganese cluster of the water oxidizing complex; and Fe, the non heme iron center. For the sake of better illustration, the cofactors of the active branch of P680 (Chl_{D1} and P_{D1}) and $Pheo_{D1}$ are marked by bold black symbols while the other components are marked in grey. The dimensions of polypeptides D1 and D2 are symbolized by dotted contour lines. The data was kindly provided by Jan Kern. See text for details.

near Q_A. The arrangement of the chlorin rings readily reveals that there are two types of Chl *a* molecules: (i) a core of four closely interacting pigments referred to as $(Chl\ a)_4$; and (ii) two Chl *a* molecules at the periphery that are spatially well separated from $(Chl\ a)_4$ with the shortest center to center distances of about 24.5 Å (Zouni et al., 2001). Information on

the putative orientation of the two β-carotenes are presented in Kamiya and Shen (2003) and Ferreira et al. (2004).

Based on the large distance, the two well-separated Chl *a* molecules, designated as peripheral chlorophylls Chl_{Z1} and Chl_{Z2}, can be ignored as these species do not substantially contribute to pigment-pigment interaction (the widely used symbols Chl_D and Chl_Z for the peripheral Chls are replaced here because the assignment to Chl_{Z2} and Chl_{Z1} in Fig. 6 is still not clear) (Wang et al., 2002). Interestingly, corresponding peripheral BChl molecules are not present in the BRCs, where only four BChls and two BPheos are bound to the L and M heterodimer (Deisenhofer and Michel, 1993). Therefore, it seems likely that Chl_{Z1} and Chl_{Z2} are of special functional relevance in PS II. This idea was confirmed by studies on mutants of *Chlamydomonas reinhardtii* where the axial histidine ligands His118 of D1 (Chl_{Z1}) and His117 of D2 (Chl_{Z2}) were replaced with other amino acid residues (Ruffle et al., 2001). Although Chl_{Z1} and Chl_{Z2} were also suggested to be constituents of the EET pathway form CP43 and CP47 to the tetrameric $(Chl\ a)_4$ (Johnston et al., 2000), model calculations based on the new structural information revealed that Chl_{Z1} and Chl_{Z2} play only a very minor role compared with the direct EET from Chls of CP43 and CP47 to the reaction center pigment core (RC-PC) that consists of $(Chl\ a)_4Pheo_x$ (Section IV.B) (Vasiliev et al., 2001, 2004). In D1/D2/Cyt b_{559} preparations, Chl_{Z1} and Chl_{Z2} affect the EET to the RC-PC in different ways as deduced from a kinetic analysis of Pheo bleaching in the Q_y band at different excitation wavelengths (Wang et al., 2002). The peripheral Chl(s) is (are) inferred to play a critical role in protection to light stress (Schweitzer et al., 1998; Lince and Vermaas, 1998). It is interesting to note that the equivalent amino-acid replacements at D1-His118 and D2-His117 do not result in the same phenotype (Ruffle et al., 2001). An independent line of evidence for heterogeneity in Chl_{Z1} and Chl_{Z2} properties is the finding that only one Chl is removed when D1/D2/Cyt b_{559} samples are prepared by using metal affinity chromatography (Vacha et al., 1995). The mechanistic implications of the functional asymmetry of Chl_{Z1} and Chl_{Z2} must be analyzed in future studies.

B. Structural Comparisons Between P680, P700 and the Bacterial Special Pair

In the first published X-ray crystal struture at 3.8 Å resolution (Zouni et al., 2001), the nearest neighbor center-to-center distances between the four Chl *a* molecules within the tetramer $(Chl\ a)_4$ complex were reported to be almost identical at 10.0 ± 0.2 Å while the corresponding distances between the nearest neighbor Chl *a* and Pheo *a* are only slightly longer (~10.6 Å). Therefore excitonic coupling between the six pigments needs to be considered. Based on a simplified model for the site energies of the pigments and their vibrational couplings, a theoretical study reported values in the range of about 50 cm^{-1} to 140 cm^{-1} for the excitonic coupling between each of the P_{D1}, P_{D2} and the two other Chl *a* molecules in the $(Chl\ a)_4$ complex and between Chl_{D1} – $Pheo_{D1}$ and Chl_{D2} – $Pheo_{D2}$ (T. Renger and Marcus, 2002b). The couplings of the six pigments give rise to a redistribution of the oscillator strength towards the lower energy exciton states. Similar coupling strengths were reported in another study (Barter et al., 2003). The new PS II structure at 3.2 Å resolution (Biesiadka et al., 2004) has been used for a theoretical analysis of the spectral properties. The results obtained basically confirm the excitonic couplings of the six pigments but the values of the coupling strengths, covering a range of about 30–160 cm^{-1}, differ from the earlier report (Raszewski et al., 2005). Another spectroscopic study including theoretical calculations led to the conclusion that $Pheo_{D2}$ is probably decoupled and that a pentamer model with five excitonically coupled chlorins (i.e., P_{D1}, P_{D2}, Chl_{D1}, Chl_{D2} and $Pheo_{D1}$) may be a more realistic description (Jankoviak et al., 2002). The situation becomes even more puzzling as circular dichroism (CD) measurements seem to indicate that neither of the two Pheos is excitonically coupled with the $(Chl\ a)_4$ unit (Vacha et al., 2002). These conclusions are not in agreement with the recent high level calculations (Raszewski et al., 2005). The CD spectral data were obtained with preparations that may have had different degrees of intactness and as a consequence modified modes of excitonic coupling. Studies using intact PS II preparations with high O_2 evolution capacity were also interpreted in favour of the conclusion that the Pheos are not excitonically coupled with $(Chl\ a)_4$ (Peterson-Arsköld, 2003). In summary, the currently available data seems to indicate that the four Chls P_{D1}, P_{D2}, Chl_{D1} and Chl_{D2} are excitonically coupled while the extent of pheophytin interaction remains a controversial issue. In contrast, it is generally agreed that the excited states of the peripheral pigments Chl_{Z1} and Chl_{Z2} are highly localized and unaffected in their Q_y transition energies by exciton coupling (T. Renger and Marcus, 2002b; Raszewski et al., 2005).

The above-mentioned findings support earlier proposals that P680 is a multimeric pigment complex (Tetenkin et al., 1989, Durrant et al., 1995, Prokhorenko and Holzwarth, 2000). In general, the pigment arrangement of (Chl *a*)$_4$ and the two Pheos resembles that of the four BChls and two BPheos within the BRCs (Deisenhofer and Michel, 1993). In these organisms the photoactive pigment P is known to be a strongly excitonically coupled special pair (Knapp et al., 1985). However, in spite of the basically similar pigment organization significant structural differences exist between (Chl *a*)$_4$ in PS II and the photoactive special pair P of both anoxygenic bacteria and P700 of PS I. The most striking difference is the center-to-center distance between P_{D1} and P_{D2} in PS II (Zouni et al., 2001; Kamiya and Shen, 2003; Biesiadka et al., 2004; Feirreira et al. 2004), which is longer than the corresponding values for the two BChls in the special pair P (7.6 Å) (Michel and Deisenhofer, 1988) and for the heterodimeric P700 (6.3 Å) (Fromme et al., 2001). The P700 consists of Chl *a* and its 13^2 epimer Chl *a´* (in Chl *a´* the positions of –H and –COOCH$_3$ at the asymmetric C-atom (13^2) of ring V are exchanged, see Fig. 2). 13^2 epimers are a general feature of PS I-type RCs in anoxygenic and oxygenic photosynthesic organisms (for a review, see Akiyama et al., 2002). Although the physiological significance of 13^2 epimers in the photoactive pigment is not yet clear, the description as a special pair is a reasonable approximation for P700, but appears to be less appropriate for P680. To support this idea, P680 can be compared with P of the BRCs. The shorter distance and higher oscillator strength of BChls in the BRCs leads to large excitonic splitting within the special pair P (500–1000 cm^{-1}) (Knapp et al., 1985), markedly exceeding the values calculated for the presumed Chl *a* dimer in P680. When taking into account the value of the shorter distance between P_{D1} and P_{D2} reported by Biesiadka et al. (2004) and Ferreira et al. (2004), the calculated excitonic coupling of about 160 cm^{-1} (Raszewski et al., 2005) still remains smaller than that of the special pair P in BRCs. As a consequence of this difference, there is a marked red shift of the transition into the lower energy exciton state ΔE^* (-) (Section III.B.1.b) of P in anoxygenic bacteria (compared with the absorption bands of the two monomeric BChl molecules in the BRC and in the antenna) that is absent in PS II. Accordingly, the absorption band of P680 is highly congested and strongly overlaps with the Q_y transitions of antenna Chl *a* molecules. Consequently, P680 acts as a very shallow trap for excitation energy (Holzwarth, 1989; G. Renger, 1992). Furthermore, the lowest excited singlet state is not localized on the elusive dimer P_{D1}-P_{D2}. This idea is supported by theoretical calculations based on the PS II structure at 3.2 Å resolution (Raszewski et al., 2005). It therefore appears more reasonable to assign P680 to a (Chl *a*)$_4$(Pheo *a*)$_x$ unit with x = 0, 1 or 2 (vide supra) and to consider ^{1}P680*, ^{3}P680 and P680$^{+\bullet}$ as states with specific electronic configurations of this entity. For the sake of simplicity, the pigment unit (Chl *a*)$_4$(Pheo *a*)$_x$ will be designated as reaction center pigment compex (RC-PC). The molecular orbital (MO) schemes of ^{1}(RC-PC)*, ^{3}(RC-PC) and (RC-PC)$^{+\bullet}$ depend not only on pigment couplings but also on the mode of pigment-protein interaction within the (RC-PC). Our current state of knowledge is limited by both the restricted structural resolution (Zouni et al., 2001; Kamiya and Shen, 2003; Biesiadka et al., 2004; Ferreira et al. 2004) and by the lack of sufficiently detailed spectral information. It is still a matter of debate as to what extent the experimental data from D1/D2/Cyt b_{559} preparations reflect the true properties of P680. Comparative magnetic cicular dichroism (MCD) measurements of intact PS II core complexes and D1/D2/Cyt b_{559} preparations revealed significant differences between the two sample types (Smith et al., 2002), confirming earlier studies based on measurements of difference absorption spectra (Hillmann et al.,1995). In this respect the often used designation of D1/D2/Cyt b_{559} preparations as PS II-RCs is highly misleading when compared with the well-defined isolated BRCs. The D1/D2/Cyt b_{559} preparations not only lack components of the PS II acceptor side, including NHI (Kurreck et al., 1997b), but are also unable to oxidize the tyrosine residues Y_Z and Y_D (Telfer et al., 2002; Chapter 9). Furthermore, in marked contrast to BRCs, PS II is characterized by an extraordinary subunit composition (Shi and Schröder, 2004) that has remained virtually invariant during evolution from cyanobacteria to higher plants (Raymond and Blankenship, 2004). Nevertheless, recent data seem to indicate that the intrinsic primary electron transfer rates leading to P680$^{+\bullet}$Pheo$^{-\bullet}$ formation in isolated D1/D2/Cyt b_{559} complexes are not seriously affected compared to their values in intact PS II (A.R. Holzwarth, unpublished results).

In summary, any assignment of P680 to a single Chl *a* molecule or a 'special pair' analogous to P in BRC or P700 in PS I is inadequate and misleading. Xiong et al. (2004) presented in a study on a *C.*

reinhardtii mutant, where $Pheo_{D2}$ of the 'inactive branch' is replaced by Chl *a*, clear evidence for the interdependence of the six pigments in (RC-PC). They found that PS II complexes isolated from this D1-Leu210His mutant were virtually unable to evolve O_2 (< 4% of the wild type (WT) control) and to photoaccumulate $Q_A^{-\bullet}$. On the other hand, the kinetics of primary charge separation are not substantially altered in D1/D2/Cyt b_{559} preparations from this mutant. These results were interpreted by the assumption that the distribution of the excited state energy in ^{1}(RC-PC)* of the D1-Leu210His mutant differs from that of the WT, thus leading to dissipative decay via fluorescence at the expense of charge separation (Xiong et al., 2004).

C. The Electronic State $^1P680^*$ and the Lowest Triplet State $^3P680$

Several attempts have been made to unravel the nature of the lowest excited singlet state ($^1P680^*$) and the lowest triplet state ($^3P680$) of P680. Modification of the coordination of the central Mg^{2+} of the Chl *a* molecules P_{D1} and P_{D2} is one promising approach to avoid problems from the use of D1/D2/Cyt b_{559} preparations and the overlapping spectral properties due to excitonic coupling (Section IV.B). Based on FTIR measurements (Noguchi et al., 1998) in both P_{D1} and P_{D2} the Mg^{2+} central atoms are most likely pentacoordinated with His-residues (D1-His198 and D2-His197, respectively, in *Synechocystis* sp. PCC 6803) as axial ligands (Merry et al., 1998). Replacement of the D1-His198 and D2-His197 by Gln and Ala leads to the assembly of functionally competent PS II complexes whereas replacement with the larger Leu is disastrous and prevents any detectable assembly of stable PS II complexes (Diner et al., 2001). Since both Ala and Leu residues do not coordinate to Mg^{2+} of Chl *a*, the drastically different properties are explained by replacement of the His ligand by a water molecule in the case of the Ala mutant but not in the Leu mutant due to size exclusion (Diner and Rappaport, 2002). A thorough spectral analysis of whole cells and of mangenese depleted PS II core complexes isolated from these mutants in comparison with the corresponding WT samples led to the conclusion that within the RC-PC, the Q_y transition with the lowest energy is localized preferentially on Chl_{D1} and is characterized by a peak position of 684 nm at 5 K and 681–682 nm at 80 K (Hillmann et al., 1995). In contrast, the Q_y transition of the native P_{D1} has been determined to be at 672.5 nm (Diner et al., 2001). Alternatively these spectral features have been interpreted as exciton bands of the P_{D1}-P_{D2}-dimer (Smith et al., 2002). Taking into account the values calculated for dipole-dipole coupling within the ^{1}(RC-PC)* the above mentioned assignment of the Q_y-transitions at 672.5 and 681–684 nm of P_{D1} and Chl_{D1}, respectively, would imply that significant heterogeneity among the four Chl *a* molecules may exist due to differences in their microenvironment. With respect to the assignments, it is important to note that both site heterogeneity and excitonic coupling contribute to the experimental spectra (T. Renger and Marcus, 2002b; Raszewski et al., 2005).

If the energy difference caused by disorder is large compared with excitonic coupling, the excitation becomes localized on individual pigments, as illustrated for the simplest case of a dimeric unit (Eq. (12)). At physiological temperatures, thermal energy (kT) is comparable to the spectral differences between Chl *a* molecules caused by the heterogeneity in the ^{1}(RC-PC)*. Thus, the excited state is expected to be delocalized via rapid equilibration in the subpicosecond time domain (Müller et al., 1996). At very low temperatures, however, the excitation is likely to be trapped in an exciton state with a large contribution of $Chla_{D1}$ (Prokhorenko and Holzwarth, 2000) and the primary step of charge separation appears to take place from $^1Chl^*_{D1}$ to Pheo (Section V). Analysis by Jankowiak et al. (2002) led to the conclusion that a distribution of different states with lowest excitation energy exists within the macroscopic ensemble depending on the nature of the PS II sample. Another interesting implication of the multimer model is the possible mixing of singlet and radical pair states. As a consequence, the ^{1}(RC-PC)* singlet states comprise some degree of charge transfer character (Barter et al., 2003). Calculations based on the new PS II structure (Biesiadka et al., 2004) suggest that the lowest exciton state of ^{1}(RC-PC)* is dominated by Chl_{D1} (Raszewski, 2005)

A different situation arises for the triplet state. In this case, the excitonic splitting is drastically smaller because the transitions are spin-forbidden according to first order perturbation theory (Schmidt and Reinecker, 1985). Therefore, this effect is negligibly small and can be ignored. The localization of the triplet state was first obtained from orientation studies. Van Mieghem and Rutherford (1993) showed that the plane of the chlorin ring where the triplet resides markedly differs from the normal of the thylakoid

membrane. This geometry is drastically different from the parallel orientation with the membrane normal of ^{3}P in BRCs (Tiede and Dutton, 1981) and raised questions on the origin of triplet formation in PS II and the possibility of migration within the Chl *a* ensemble. The latter process was shown to indeed take place and the energy gap for triplet delocalization was estimated to be of the order of 10 meV (Noguchi et al., 1998). Studies using *Synechocystis* mutants and isolated D1/D2/Cyt b_{559} complexes led to the conclusion that at temperatures below liquid nitrogen temperature, the triplet state is localized at Chl_{D1} and that it becomes delocalized at higher temperatures (Kamlowski et al., 1996; Diner et al., 2001). This conclusion is suported by a theoretical analysis (Raszewski et al., 2005).

D. The Cation Radical P680$^{+\bullet}$

The unusually high oxidizing power of $P680^{+\bullet}$ is the energetic prerequisite for oxidative water cleavage. For an understanding of this unique property several questions need to be addressed: (i) how is the cation formed and where is the hole predominantly located; (ii) how is electron transfer from Y_Z to $P680^{+\bullet}$ efficiently achieved and how are dissipative side reactions minimized; (iii) what are the mechanisms to destabilize $P680^{+\bullet}$ as compared to Chl $a^{+\bullet}$ in solution; and (iv) what is the role of pigment-protein interactions in tuning the energetic and kinetic properties?

With our current state of knowledge, a straightforward answer to these questions cannot be given because P680 can attain different electronic configurations, depending on temperature, detergent content, allosteric effects with other protein subunits within the PS II core complex, among other factors. At present the system is far too complex for a complete quantum mechanical and molecular dynamics treatment. Thus the following sections summarize our fragmentary knowledge in an attempt to address the above questions.

1. Electron Ejection from ^{1}P680* and Distribution of the Hole within P680$^{+\bullet}$

Coherent photon echo spectroscopy is a suitable method that can detect the first step of excitation or electron transfer from the initially excited pigment molecule. Application of this technique to D1/D2/Cyt b_{559} preparations at 1.3 K revealed that an electron from $^1Chl^*_{D1}$ is transferred to $Pheo_{D1}$ forming the primary radical pair $Chl^{+\bullet}_{D1}Pheo^{-\bullet}_{D1}$ (Prokhorenko and Holzwarth, 2000). At present, this data is the only direct experimental evidence for $^1Chl^*_{D1}$ acting as the primary electron donor. No corresponding experimental results are available for higher temperatures or intact PS II complexes. The initial location of the hole on $Chl^{+\bullet}_{D1}$ is supported by theoretical analysis (Raszewski et al., 2005) and by results obtained using incoherent spectroscopic techniques on WT and mutant PS II particles from *Synechocystis* (Diner et al., 2001). For structural reasons, however, the position of $^1Chl^*_{D1}$ is not favorable for an efficient transfer of the oxidizing redox equivalent to Y_Z and the WOC (see Fig. 6). A more suitable location would be P_{D1}. It is therefore assumed that $Chl^{+\bullet}_{D1}$ rapidly oxidizes P_{D1} leading to the radical pair $P^{+\bullet}_{D1}Pheo^{-\bullet}_{D1}$ and the charge separation is inferred to be a two step process (Prokhorenko and Holzwarth, 2000; Section V.A). The lifetime of $P680^{+\bullet}$ can be as long as several hundreds of microseconds (Haveman and Mathis, 1976; G. Renger and Wolf, 1976). The long lifetime raises the question as to where the hole is located within $P680^{+\bullet}$. The participation of Pheos can be excluded for energetic reasons (its reduction potential is +1.3 V in solution, Section III.A) and of Chl_{Z1} and Chl_{Z2} for kinetic reasons (the large distances between these species and the RC-PC pigments result in rather slow electron transfer reactions, see Sections III. B.2 and IV.A).

Electron nuclear double resonance (ENDOR) spectroscopy can be used to determine spin density distributions (Lubitz and Lendzian, 1996). One of the most important results using this technique is the finding that in BRCs, the sharing of the electron hole between the two BChls of the special pair depends not only on the species but also on the type of detergent used for sample preparation (Müh et al., 1997). Analogous ENDOR measurements of D1/D2/Cyt b_{559} preparations reveal an 80% probability that the hole is localized to one specific Chl *a*, most likely P_{D1} (Rigby et al., 1994). This result, however, should be considered with caution in the light of the possible problems in using D1/D2/Cyt b_{559} preparations (vide supra). Strictly speaking, sound experimental evidence is lacking for the distribution probability of the hole within $P680^{+\bullet}$. However, for physiological reasons (i.e., the highly efficient oxidation of Y_Z) it seems likely that in PS II samples, with an intact WOC, the hole is located with a high probability on P_{D1}. This conclusion is supported by comparative measurements in WT and mutants of *Synechocystis*,

where the axial P_{D1} ligand D1-His198 is replaced by Glu (Diner et al., 2001; Diner and Rappaport, 2002). The preferential probability of localization on P_{D1} is expected to originate from an asymmetric protein environment as was previously discussed for the asymmetry of the redox properties of manganese within the tetranulear cluster of the WOC (G. Renger, 1987). An electrical potential gradient of the order of 50 mV/nm around the RC-PC unit would be sufficient for a rather pronounced localization of the hole on P_{D1} at room temperature (at lower temperatures the effect is even stronger). The existence of strong local electrostatic fields near $P680^{+\bullet}$ have been inferred from measurements of light induced ^{13}C NMR signals in D1/D2/Cyt b_{559}preparations. The data obtained were interpreted by an asymmetric spin density distribution within the chlorin ring system of $P680^{+\bullet}$ that is markedly different from the symmetric distribution in $P^{+\bullet}$ of purple bacteria. A protonation of the keto group at ring V is discussed as one possibility of generating the strong local electric field that is responsible for the shift of the spin density to ring III of the Chl *a* moiety within $P680^{+\bullet}$ (Matysik et al., 2000). It was suggested that the asymmetry within the $P_{D1} - P_{D2}$ pair probably arises from the positive charge of the proton trapped in the environment of Y_D^{ox}. The role of Y_D as a positive charge generator in a hydrophobic environment and its key function for spin distribution in $P680^{+\bullet}$ has been summarized in a review by Rutherford and Faller (2004).

2. Possible Factors for the High Oxidizing Power of $P680^{+\bullet}$

Based on the earlier structure model of Zouni et al. (2001) the 'large' distance of about 10 Å between the chlorophylls P_{D1} and P_{D2} was considered as a prerequisite in establishing a strongly oxidizing Chl $a^{+\bullet}$ species. Consequently, the key event in the evolution of the O_2-evolving PS II is proposed to be a mutation of the protein that resulted in the separation of the two pigments in the 'special chlorophyll pair' (Rutherford and Faller, 2003). New information on the PS II structure, however, reveals that the distance between P_{D1} and P_{D2} is shorter (Biesiadka et al., 2004; Ferreira et al., 2004) than originally reported (Zouni et al., 2001). Therefore, the hypothesis of Rutherford and Faller (2003) appears to be less attractive. Apart from this particular point there exists little doubt that the redox properties of the Chl *a* molecules within the RC-PC unit are essentially determined by the binding environment of the D1/D2 heterodimer (including the binding domains for cationic cofactors and the protein-protein interactions with other subunits in the PS II complex). For example, systematic studies have shown that the pigment-protein interactions modulate the reduction potential of the special pair P in BRCs (Chapter 32, Kálmán et al.). The reduction potential was found to depend strongly on the hydrogen bonding to the BChl carbonyl groups. Additional hydrogen bonds to these carbonyl groups, introduced by genetic engineering, causes an incremental increase of about 85 mV per bond while a decrease is obtained after removal of the single hydrogen-bond existing in the WT. Likewise, a correlation was found between the increase of the redox potential of $P/P^{+\bullet}$ and the strength of the hydrogen bond to the C_{13}^1 keto carbonyl group of ring V of the BChl molecules at the P_M position of the special pair (Ivancich et al., 1998). Furthermore, the influence of an additional negative charge in the protein matrix on the decrease of the reduction potential due to stabilization of $P^{+\bullet}$ has been illustrated by replacing particular residues (Asn → Asp) at an average distance of 13 Å to the atoms of the conjugated π electron system of P. It was shown that the insertion of an additional negative charge gives rise to a shift of –45 up to –75 mV (depending on the position) and that the effect of two negative charges is additive (Williams et al., 2001).

Spiedel et al. (2002) analyzed the role of charge-dipole interactions in mutants of His168 in the L- and Phe197 in the M-subunit (these residues are in contact with ring I of each of the two BChls in P). The E_m-value could be modulated within a range of 250 mV with a strong correlation between ΔE_m and the dipole strength. An important feature emerging from a detailed analysis of electrostatic interactions in RCs, isolated from different mutants of *Rb. sphaeroides*, is the conclusion that the effects of ionizable amino acid residues on the properties of P are strongly screened by counter ions (Johnson et al., 2003). Slight upshifts of E_m by 30–50 mV are also induced by addition of solvents like glycerol or dimethylsulfoxide (DMSO) to suspensions of BRCs (Paschenko et al., 2003).

When taking into account these findings, hydrogen bonding appears to be an attractive mechanism for modulating the reduction potential of P680. However, this possibility is of limited potential for Chl *a* because this molecule lacks the acetyl group at ring I (it is replaced by a vinyl group, see Fig. 2) that was shown to be important for affecting the redox potential

of $P/P^{+\bullet}$ in BRCs. Therefore, the insertion of positive charges (amino acid residues or inert cations — e.g., Ca^{2+}) into the heterodimeric D1/D2 protein matrix of PS II seems to be a more relevant 'tool' to destabilize the radical state $P680^{+\bullet}$. In line with this idea, the positive charge of Y_D^{ox} is assumed to enhance the oxidizing power of $P680^{+\bullet}$ (Diner and Rappaport, 2002). However, the effect on E_m is comparatively small as deduced from kinetic studies on $P680^{+\bullet}$ reduction by Y_Z in the nanosecond time domain (Jeans et al., 2002) and the major role of Y_D^{ox} appears to be the modulation of spin distribution within $P680^{+\bullet}$ (Section IV.D.1) rather than a significant contribution to its unique oxidizing power. A comparative study using PS II core complexes from *Synechocystis* WT and a mutant, where tyrosine Y_D was replaced by phenylalamine, confirms that the effect of Y_D^{ox} on the E_m is very small (≤10 mV) (Diner et al., 2004).

Alternative possibilities for tuning the midpoint potential are the prevention of 'puckering' of the chlorin ring (Barkigia and Fajer, 1993; Fajer, 2000, 2004), and/or 'frozen protein conformations' that block relaxation of the protein environment in response to formation of the positive charge at $P680^{+\bullet}$ (Mulkidjanian, 1999). The latter suggestion seems to be at variance with the finding of a substantial relaxation of the free energy of the radical pair after charge separation on the nanosecond time scale (Section V.C.2.b). Fletcher and Therien (2002) showed that the cofacial porphyrin motif can be largely modified in its electronic structure and redox properties. This 'tool' of tuning the π-π interaction between macrocycles could be also considered for tailoring the redox properties of P680.

Another important factor that has so far escaped detailed analysis is the role of lipids. The structural arrangement was resolved for three lipid molecules in the BRC from *Rb. sphaeroides*. Based on these results it was concluded that lipid-cofactor interactions may have a significant energetic effect and contribute to functional differences between the active and inactive branch (Camara-Artigas et al., 2002). Rinyu et al. (2004) found that the negatively charged cardiolipin causes a shift of 30–40 mV towards more negative values of the midpoint potentials of Q_A in BRCs. Charged lipids could also be used to modulate the redox properties and hole distribution within the $(Chl\ a)_4$ unit of P680. This question remains to be answered.

A very interesting result was obtained by global treatment of environmental effects. Density functional calculations revealed that the reduction potential of Chl $a^{+\bullet}$ reaches values of >+1.3 V within a hydrophobic environment of a dielectric constant of about 2 (Hasegawa and Noguchi, 2005). Based on new PS II structures (Ferreira et al., 2004; Biesiadka et al., 2004) the E_m values of the six Chls bound to the D1/D2 heterodimer were calculated by using an electrostatic continuum model (Ishikita et al., 2005). Values in the range of +1.1 to +1.3 V were obtained for P_{D1}, P_{D2}, Chl_{D1} and Chl_{D2} while those of Chl_{Z1} and Chl_{Z2} were much lower (about 0.9V) and not far from the E_m value of Chl *a* in solution (Section III.A). This study shows that the essential contributions to the drastic E_m upshift of the (RC-PC) Chls originate from the D1/D2 protein matrix (about 80% of the total effect) and only to a minor extent from the other subunits. Specific hydrogen bonds are inferred to be not essential. The different values obtained on the basis of the structure models of Ferreira et al. (2004) and Biesiadka et al. (2004) reveal that resolutions of 3.5 and 3.2 Å, respectively, are not sufficient for detailed calculations. Furthermore, the reported data of Ishikita et al. (2005) imply that the hole of $P680^{+\bullet}$ should be trapped at Chl_{D1} at low temperatures. This prediction raises questions on the pathway of ET from Y_Z to $P680^{+\bullet}$, in particular with respect to the experimental findings of aY_Z^{ox} formation at 7 K in about 50% of the PS II core complexes of *T. elongatus* (Zhang et al., 2004). Accordingly, further studies are required to resolve the details of the redox tuning of the Chls in (RC-PC). Regardless of these details it is clear that the nature of the protein matrix is the key factor for the unusually high oxidizing power of $P680^{+\bullet}$. Furthermore, the distance to the other Chls with lower E_m values in the PS II complex (e.g., Chl_{Z1} and Chl_{Z2}) and to the carotenoids must be large enough to prevent undesired dissipative and destructive side reactions.

Dynamic structural changes of the protein environment can lead to time dependent variations of the local charge distribution, thus affecting the energetics and kinetics of charge separation. The relevance of this important phenomenon will be outlined in Section V.C.

Until recently P680 has been envisaged as a Chl *a* complex. However, with the discovery of O_2-evolving cyanobacteria containing mainly Chl *d* (*Acaryochloris marina*) and the finding that the photoactive pigment of PS I is a special Chl *d* dimer in these species (Akiyama et al., 2002), questions arise as to the nature of the corresponding photoac-

tive pigment(s) in PS II of this species. Mimuro et al. (2004) suggest that in these organisms PS II still contains P680 with Chl *a* as essential constituent but the experimental evidence for this conclusion is limited. Further studies are required to clarify this very important point. In this respect it is interesting to mention that mutants of *Synechocystis* have been constructed by genetic engineering where Chl *a* and Pheo *a* are partly replaced by Chl *b* and Pheo *b* in the PS II core (Vavilin et al., 2003). These findings show that Chl *a* and Pheo *a* are not necessarily the only chlorin molecules that can constitute a functionally competent PSII with intact WOC activity.

E. The Anion Radical Pheo$^{-\bullet}$

In contrast to the modification of the properties of Chl *a* in order to achieve the unique photoactive complex P680 (Section IV.D), the Pheo *a* molecules in PS II are much less affected. The midpoint potential E_m of Pheo/Pheo$^{-\bullet}$ in PS II was determined to be –610 mV (Klimov et al., 1979). This value is almost the same as that of Pheo *a* in solution (Section III. A). However, when taking into account electrostatic effects due to the presence of $Q_A^{-\bullet}$ during the redox titration, the actual 'working potential' of Pheo/Pheo$^{-\bullet}$ is expected to be shifted towards less negative values. Experimental studies reveal that this effect is about 85 mV (Gibasiewicz et al., 2001) so that an E_m value of about –525 mV seems to be more realistic for functional complexes with an oxidized Q_A.

PS II contains two Pheo molecules (see Fig. 6) in analogy to the two BPheos in BRCs. Accordingly, for an understanding of the characteristics of the two Pheo species in PS II it is most suitable to use as a guide the well-resolved properties of the corresponding BPheos in BRCs. A spectacular finding in terms of function is that in spite of an almost symmetric arrangement of the cofactors, the charge separation in the BRC is a unidirectional process involving only $BChl_A$, $BPheo_A$ and Q_A (Bylina et al., 1988; Michel-Beyerle et al., 1988; Zinth and Kaiser, 1993). A switch of the electron transfer pathway into the other direction can only be achieved if the protein matrix is specifically modified by genetic engineering. Mutants with BRCs of reversed 'sidedness' of the ET-pathway leading to significant $P^{+\bullet}Q_B^{-\bullet}$ formation have been generated (Laible et al., 2003; Wakeham et al., 2003). In analogy to the wild-type BRC, the two Pheo *a* molecules in PS II are assumed to be functionally heterogeneous — i.e., only one ($Pheo_{D1}$) participates in the formation of $P680^{+\bullet}Pheo^{-\bullet}$. It is interesting to note that in PS II the functional branching not only comprises the steps leading to $P680^{+\bullet}Q_A^{-\bullet}$ formation and subsequent PQ reduction at the Q_B site but also the pathway for water oxidation via Y_Z in the D1 polypeptide D1 exhibits a striking 'sidedness.'

The functional differences of the two BPheos are reflected in their spectral properties. In the visible/near infrared (VIS/NIR) region of BRCs, the Q_y transition of the 'active' $BPheo_A$ at about 760 nm is red shifted by almost 10 nm relative to $BPheo_B$ (Robert et al., 1985). Likewise, the peak positions in the Q_x region exhibit a similar difference with 530 nm and 540 nm for $BPheo_B$ and $BPheo_A$, respectively. Studies on spectral properties of Pheo in PS II, mainly analyzed in D1/D2/Cyt b_{559} samples, gave conflicting results (Mimuro et al., 1995; Konermann and Holzwarth, 1996; Shkurapatov et al., 1997; Yruela et al. 2002). Apart from the ambiguities due to the sample type, a further complication emerges from the fact that the spectra of samples with photoaccumulated Pheo$^{-\bullet}$ are influenced by both a change of the excitonic interactions and the electrochromic effect of the negatively charged Pheo$^{-\bullet}$ on the (RC-PC) pigments. A reliable estimation of the spectral effects due to excitonic interaction requires calculations on the basis of detailed information on the geometrical arrangement of the pigments, in particular the mutual orientation of the transition dipole moments (Raszewski et al., 2005) Experimental data for more native PSII complexes has been obtained by using samples isolated from *Synechocystis* WT and mutant cells. These preparations contain Q_A and the electrochromic effect of the negative charge of $Q_A^{-\bullet}$ in its reduced semiquinone form (Section V.C.2.) on $Pheo_{D1}$ provides a specific fingerprint for its spectral identification. In these samples λ_{max} values of 685.6 and 669.3 nm were measured at 77 K for the 'active' and 'inactive' Pheo, respectively (Stewart et al., 2000). These values, however, have to be corrected for effects due to excitonic interactions. Based on measurements of optical spectra at 1.7 K, values of 685 nm and 685.8 nm were obtained for $Pheo_{D1}$ in O_2-evolving PS II core complexes and PS II membrane fragments from spinach, respectively, while a slightly shorter wavelength of 683.0 nm was reported for $Pheo_{D1}$ in O_2-evolving PS II core complexes from *Synechocystis* (Peterson-Arsköld et al., 2003). Two conclusions emerge from the data: (i) the Q_y peak of the active Pheo in PS II exhibits a similar red shift

relative to that of the inactive Pheo as observed in BRCs (vide supra); and (ii) D1/D2/Cyt b_{559} preparations may be of limited value for detailed spectral analyses (see Section IV.B). For the Q_x-region, data were reported for the 'active' Pheo in isolated D1/D2/Cyt b_{559} preparations from different organisms. The difference spectra for $Pheo_{D1}^{-\bullet}$ formation were found to be slightly red shifted by 2–3 nm in plant material (peak around 544 nm) compared with samples from cyanobacteria (Giorgi et al., 1996). Comparative measurements of time-resolved absorption changes of PS II preparations from WT *C. reinhardtii* and a mutant, where $Pheo_{D2}$ is replaced by Chl *a*, reveal that the red shifted absorption band in the Q_x region (543.5 nm) belongs to $Pheo_{D1}$ of the 'active' branch (Xiong et al., 2004).

A well-resolved characteristic of $BPheo_A$ is the hydrogen bonding of its ring V keto group by Glu104 of the L-subunit of BRCs (Feher et al., 1988; Michel and Deisenhofer, 1988). An analogous feature was found for the 'active' Pheo in PSII where the hydrogen bond was assumed to be formed between the ring V keto group and the corresponding Glu130 of polypeptide D1 (Lubitz et al., 1989; Moënne-Loccoz et al., 1989; Nabedryk et al., 1990). Direct experimental evidence for this assignment was obtained from high field EPR studies of $Pheo_{D1}^{-\bullet}$ in *C. reinhardtii* mutants where Glu 130 is replaced by His, Gln or Leu (Dorlet et al., 2001). Optical difference spectra of $Pheo^{-\bullet}$/Pheo are also affected by changes of the hydrogen bond. Giorgi et al., (1996) found that the peak position in the Q_X-region shifts by 2–3 nm in D1/D2/Cyt b_{559} preparations isolated from *Synechocystis* mutants, where Gln130 is changed to Glu or Leu (in contrast to plants, the WT cells contain Gln at position 130 instead of Glu).

Based on high field EPR studies, Dorlet et al. (2001) inferred that the differences in g-values between $BPheo_A^{-\bullet}$ in *R. viridis* and $Pheo_{D1}^{-\bullet}$ in PS II from spinach are predominantly due to structural differences between the two types of reaction centers. The striking feature of a conserved hydrogen bond raises a question on its possible functional relevance. A comparison of the ENDOR-spectra of $Pheo^{-\bullet}$ in solution with that of the photoaccumulated species in D1/D2/Cyt b_{559} preparations led to the conclusion that the protein matrix exerts constraints that lead to structural changes of the Pheo, most likely a rotation of the vinyl group (Lubitz et al., 1989). These authors speculated that this change could give rise to an optimal electron transfer rate via orbital overlap. On the other hand, replacement by site directed mutagenesis of Glu104 in the L-subunit in purple bacteria was shown to exert only minor effects on the kinetics of the ET steps leading to $P^{+\bullet}Q_A^{-\bullet}$ formation (Bylina et al., 1988). Analogous experiments cannot be performed in D1/D2/Cyt b_{559} preparations due to the lack of Q_A. The results reported so far for $P680^{+\bullet}Pheo^{-\bullet}$ formation indicate that the detected 20–30 ps kinetics are not changed in the samples isolated from the above mentioned mutants of *Synechocystis* where D1-Gln130 is replaced by Glu or Leu (Giorgi et al., 1996). In contrast to the virtual invariance of the (20–30 ps) kinetics to changes in the hydrogen bonding to the keto group of ring V, the midpoint potential of Pheo varies as deduced from $P680^{+\bullet}Pheo^{-\bullet}$ recombination rates. Merry et al. (1998) concluded that replacement of D1-Gln130 by Glu causes an upshift by about +30 mV, whereas Leu gives rise to a downshift by about –75 mV. Although these changes are comparatively small, they could be of relevance for the pathway of $P680^{+\bullet}Q_A^{-\bullet}$ recombination and the probability of $^3P680$ formation (Section VI.A). This raises a question on the evolutionary advantage of the replacement of Gln130 in PS II of cyanobacteria by Glu in plants because an upshift of the midpoint potential of Pheo is expected to enhance the probability of dangerous $^3P680$ formation (providing that the midpoint potential of $Q_A^{-\bullet}/Q_A$ is the same as in cyanobacteria). Since detailed information on this point is lacking, it appears premature to speculate on the reason for the exchange of Gln/Glu during evolution.

V. Kinetics and Energetics of Charge Separation

The light-induced charge separation in PS II via overall reaction sequence Eq. (4) comprises basically two steps: (i) formation of the radical ion pair $P680^{+\bullet}Pheo^{-\bullet}$; and (ii) stabilization of the primary charge separation by rapid electron transfer from $Pheo^{-\bullet}$ to Q_A. The unique properties of PS II are connected with the first step. Since P680 acts as a shallow trap and due to the nature of $(Chl\ a)_4\ Pheo_X$ (Section IV.B), the overall kinetics of $P680^{+\bullet}Pheo^{-\bullet}$ formation are complex.

A. Mechanism and Kinetics of Formation of the Radical Ion Pair P680$^{+\bullet}$ Pheo$^{-\bullet}$

The kinetics of $P680^{+\bullet}$ $Pheo^{-\bullet}$ formation comprise different equilibration steps between the electronically excited antenna Chls and P680, $^1P680^*$ and $P680^{+\bullet}$ $Pheo^{-\bullet}$, and the molecules within the $(Chl\ a)_4$ unit. Depending on the kinetics of these processes, two limiting cases can arise for the overall reaction: (i) an EET-limited process, or (ii) a trapping-limited process (Chapter 22, Barter et al.).

The 'exciton-radical pair equilibrium' model was developed by Holzwarth and coworkers, based on the assumption of rapid excited state equilibration (Schatz et al., 1987, 1988; Holzwarth, 1989). According to this model, the overall reaction is trapping-limited. As a consequence, the measured rate constant for $P680^{+\bullet}$ $Pheo^{-\bullet}$ formation , k_{PC}^{trap}, can be expressed as the product of the intrinsic rate constant k_{PC}^{int} and a constant K_{eq}^* that summarizes all EET equilibration steps between excited singlet states within the antenna and at P680 — i.e., K_{eq}^* is the population probability of $^1P680^*$ provided that the equilibration is sufficiently fast. Based on this model, the rate constant k_{PC}^{trap} is expected to depend on the 'spectrally weighted' antenna size that is a temperature dependent number due to the thermal population of states (G. Renger et al., 1995). This general conclusion was basically confirmed by measurements of excited state trapping monitored via fluorescence lifetime measurements in samples with functionally competent PS II complexes of different antenna size (Schatz et al., 1988; Roelofs et al., 1992; G. Renger et al., 1995; Trissl and Lavergne, 1995). As a result of these studies, the intrinsic rate constant was estimated to be about $(3\ ps)^{-1}$ at room temperature. This value exhibits a striking similarity with the corresponding molecular rate constant for the formation of $P^{+\bullet}BPheo_A^{-\bullet}$ in the BRCs (Zinth and Kaiser, 1993). It is a reflection of the close structural and functional similarities of the charge separation in the BRCs and PS II (Michel and Deisenhofer, 1988). However, in the case of purple bacteria, the spectral properties of P (Section IV.B) and the isolation of *intact* RCs permit a straightforward analysis of the kinetics. These conditions are not satisfied for PS II. In order to minimize the effects due to the equilibration processes between antenna and P680, numerous experiments were performed with D1/D2/Cyt b_{559} preparations. Apart from still unresolved questions on this sample type (Section IV.B), the data of different research groups led to seemingly conflicting conclusions on k_{PC}^{int}. Values ranging from about $(3\ ps)^{-1}$ up to $(20\ ps)^{-1}$ at room temperature were reported (Wasielewski et al., 1989; Klug et al., 1995; Müller et al., 1996; Greenfield et al., 1997; Giorgi et al., 1996; Seibert and Wasielewski, 2003), whereas at low temperatures even markedly higher rate constants were obtained by some authors (Tang et al., 1991; Groot et al., 1997).

The idea of a trapping-limited process in intact PS II cores has been questioned. Based on structural data of the pigment arrangement in PS II, the overall reaction of photochemical light capture in PS II was inferred to be limited by EET of the order of 100 ps between the antenna and the RC (Vasiliev et al., 2001). Similarly, a much larger value for k_{PC}^{int} of $\geq(700\ fs)^{-1}$ was also obtained from this analysis. Based on transient absorption and time resolved fluorescence spectroscopy the trapping has recently been inferred to be neither diffusion- nor trapping-limited in CP47-D1/D2 particles but somewhere in between (Andrizhiyevskaya et al., 2004). In vivo the PS II core is coupled with proximal and peripheral antenna complexes. Van Amerongen and Dekker (2003) concluded that a straightforward distinction between trap and exciton diffusion limited trapping cannot be made for PS II in native thylakoid membranes. The thylakoid structure and organization of the antenna systems in various organisms can affect the overall trapping in various ways, also depending on environmental conditions.

In a detailed study using coherent photon echo spectroscopy at 1.3 K and D1/D2/Cyt b_{559} preparations as the sample material, the charge separation leading to $P680^{+\bullet}Pheo^{-\bullet}$ formation was inferred to occur via a two-step electron transfer after fast EET equilibration within the ^{1}(RC-PC)* unit. The data are interpreted by the following scheme (Prokhorenko and Holzwarth, 2000):

$$
\begin{array}{l}
[^1(RC-PC)^*]_{initial} \\
100\text{–}500\ fs \Big\Uparrow \\
[^1(RC-PC)^*]_{equil} \\
\qquad k_{PC,1}^{int} \Big\Uparrow \\
[Chl_{D1}^{+\bullet}\ P_{D1}\ P_{D2}\ Chl_{D2}]\ Pheo_{D1}^{-\bullet} \\
\qquad k_{PC,2}^{int} \Big\Uparrow \\
[Chl_{D1}\ P_{D1}^{+\bullet}\ P_{D2}\ Chl_{D2}]\ Pheo_{D1}^{-\bullet}
\end{array}
\qquad (19)
$$

where $[^1(RC-PC)^*]_{initial}$ describes the initial formation of an electronically excited singlet state in the unit and $[^1(RC-PC)^*]_{equil}$ is the excited singlet state population reached after rapid excited state equilibration. The values of the rate constants $k^{int}_{PC,1}$ and $k^{int}_{PC,2}$ are about $(1.5\ ps)^{-1}$ and $(25\ ps)^{-1}$, respectively, at 1.3 K. They are most likely somewhat different at room temperature, which could not be tested using the same methodology. It is important, however, to note that the experimentally observed rates, in contrast to the described intrinsic rates k^{int}, are highly dispersive due to the variable mixing of the exciton states into the wavefunctions of the electron donor and acceptor and sample inhomogeneities. Thus, the long-standing discussion of a specific electron transfer rate in PS II RCs becomes meaningless. The observable electron transfer rates (at least at low temperature) span a range of 1–2 orders of magnitude, despite a single intrinsic electron transfer rate. Each RC has its own electron transfer rate, depending on the specific nuclear arrangement and coupling between pigment and protein (Prokhorenko and Holzwarth, 2000). This conclusion is confirmed by low temperature hole burning experiments on D1/D2/Cyt b_{559} preparation containing five Chls (Riley et al., 2004). At higher temperatures this picture will be further modified by additional time-dependent effects due to nuclear motion of the protein. At present, it is not clear as to what extent the kinetics of primary charge separation are dispersive at room temperature.

Regardless of the exact numbers for the rate constants, the scheme including a fast intrinsic hole transfer seems to reflect the general pattern of primary charge separation in PS II. This conclusion is supported by two different lines of experimental evidence: (i) spectroscopic studies at different temperatures on PS II core complexes from *Synechococcus* mutants where the His-ligands of P_{D1} (D1-His 198) and P_{D2} (D2-His 197) are replaced by different residues (Glu, Gln, Asn, Ala, Thr, Cys, Lys, Val) (Diner et al., 2001); and (ii) measurements of absorption changes with femtosecond time resolution at 77 K, using D1/D2/Cyt b_{559} preparations where the 'inactive' Pheo was substituted by 13′-deoxy-13^1-hydroxypheophytin (Germano et al., 2004). Accordingly, the formation of $P680^{+\bullet}Pheo^{-\bullet}$ in PS II can be summarized as:

$$^1(RC-PC)^*_{initial} \xleftrightarrow{\langle\varepsilon\rangle} {}^1(RC-PC)^*_{equil} \xleftrightarrow{k^{int}_{PC,1}} (P680)^{+\bullet}_1 Pheo^{-\bullet} \xleftrightarrow{k^{int}_{PC,2}} (P680)^{+\bullet}_2 Pheo^{-\bullet} \qquad (20)$$

with (RC-PC), $(P680)^{+\bullet}_1 Pheo^{-\bullet}$, and $(P680)^{+\bullet}_2 Pheo^{-\bullet}$ symbolizing $[(Chl\text{-}a)_4Pheo_x]$, $[Chl_{D1}{}^{+\bullet}P_{D1}P_{D2}Chl_{D1}]$ $Pheo^{-\bullet}_{D1}$, and $[Chl_{D1}P^{+\bullet}_{D1}P_{D2}Chl_{D2}]Pheo^{-\bullet}_{D1}$, respectively, and ‹ε› a singlet exciton (see footnote Section III. B.1.a).

A comparison of this scheme for PS II with the reaction pattern of $P^{+\bullet}$ $BPheo^{-\bullet}$ formation in purple bacteria reveals striking mechanistic differences with respect to the role of Chl_{D1} and $BChl_A$ that are located at equivalent positions within the six pigment cores of both types of organisms. In the former case, Chl_{D1} is assumed to be the photoactive constituent – i.e., the electron is transferred from $^1Chl^*_{D1}$ to Pheo *a* followed by re-reduction of $Chl^{+\bullet}_{D1}$ with P_{D1} as donor, while in the latter case, $BChl_A$ serves as electron acceptor for $^1P^*$ and $BChl^{-\bullet}_A$ becomes rapidly reoxidized by BPheo. Furthermore, the decay of $BChl^{-\bullet}_A$ is faster than the rate of its formation (Zinth and Kaiser, 1993), whereas $Chl^{+\bullet}_{D1}$ is inferred to be comparatively long-lived relative to its formation, at least at low temperatures (Prokhorenko and Holzwarth, 2000).

The peculiarities of charge separation in PS II satisfy the energetic constraints for the generation of a strongly oxidizing species by dissociation of the singlet exciton into a radical ion pair at the dimeric unit $Chl_{D1}Pheo_{D1,}$ leading to $Chl^{+\bullet}_{D1}Pheo^{-\bullet}_{D1}$. The alternative of a $P^{+\bullet}_{D1}$ $Chl^{-\bullet}_{D1}$ radical pair formation in the primary step of charge separation (Diner et al., 2001) appears to be highly unlikely. A comparison of the energetics for one-electron reduction of Chl *a* and Pheo *a* (Section III.A) readily shows that a $P^{+\bullet}_{D1}$ $Chl^{-\bullet}_{D1}$ pair with a strongly oxidizing cation radical is much less favorable at an exciton energy of about 1.8 eV, unless the energetics of $Chl^{-\bullet}_{D1}$ anion radical formation are not unconventionally and strongly modulated by the protein environment.

Until now, considerations on the mechanism of the primary charge separation in photosynthetic reaction centers have been restricted to the chlorins. Recent studies on nuclear wave packet motion between the potential surfaces of states $^1P^*$ and $P^{+\bullet}BChl^{-\bullet}_A$ in BRCs, however, suggest that a bridging water molecule between one BChl moiety of the special pair (P_B) and the monomeric $BChl_A$ might be involved in the pathway of the primary electron transfer step (Yakovlev et al., 2002). This is an attractive idea that should be taken into account in future considerations on charge separation in PS II.

B. Mechanism and Kinetics of Formation of the Radical Ion Pair $P680^{+\bullet}Q_A^{-\bullet}$

The light induced charge separation product $P680^{+\bullet}Pheo^{-\bullet}$ must be 'stabilized' by rapid electron transfer from $Pheo_{D1}^{-\bullet}$ to Q_A (Fig. 6) in order to minimize the dissipative recombination of the radical ion pair $P680^{+\bullet}$ $Pheo^{-\bullet}$ (Section VI.A). The kinetics of the 'stabilization' reaction have been resolved by measurements of flash-induced absorption changes that are characteristic for transient populations of $Pheo^{-\bullet}$ and $Q_A^{-\bullet}$ (Fig. 1). $Pheo_{D1}^{-\bullet}$ reoxidation (Nuijs et al., 1986; Schatz et al., 1987, 1988) and $Q_A^{-\bullet}$ formation (Eckert et al., 1988; Bernarding et al., 1994) exhibit virtually the same kinetics with lifetimes of about 300 ps. Analysis of the fluorescence decay kinetics within the framework of the 'exciton-radical pair equilibrium' model (Roelofs et al., 1992; Vasil'ev et al., 1996) and curve fitting of photovoltage measurements (Leibl et al., 1989) led to comparable values of 300–500 ps. Interestingly, a rate constant of about $(300\ ps)^{-1}$ differs only slightly from the corresponding value of about $(200\ ps)^{-1}$ for the electron transfer from $BPheo_A^{-\bullet}$ to Q_A in BRCs (Zinth and Kaiser, 1993). This is another reflection of the close similarity between the acceptor side of PS II and BRCs (Section V.B). Differences between the two types of RCs, however, exist in terms of the effects owing to replacement of exchangeable protons by deuterons and the removal of the NHI (Fig. 6). The kinetic H/D effect is more pronounced in BRCs (Paschenko et al., 2003) than in PS II membrane fragments (Vasil'ev et al., 1996). A gentle extraction of the NHI (MacMillan et al., 1995; Kurreck et al., 1996) is virtually without effect on the rate of $Pheo_{D1}^{-\bullet}$ reoxidation by Q_A (Bernarding et al., 1994) and the properties of $Q_A^{-\bullet}$ in PS II (Noguchi et al., 1999), while the corresponding ET step from $BPheo_A^{-\bullet}$ to Q_A in BRCs becomes retarded by a factor of about 20. On the other hand, the kinetics remain unaffected when NHI-depleted BRCs are additionally deprived of the H-subunit (Liu et al., 1991). This illustrates both the differences between PS II and BRCs and the regulatory role of protein subunits that do not contain cofactors. Another important difference between BRCs and PS II is the mode of axial coordination of the NHI. In addition to the four His ligands in the two types of organisms, the NHI of BRCs is coordinated by a Glu residue (Deisenhofer and Michel, 1993) while in PS II the equivalent site is most likely occupied by bicarbonate (Ferreira et al., 2004). As a consequence, the PS II is characterized by a striking bicarbonate effect that is missing in BRCs (van Rensen et al., 1999; Chapter 14, van Rensen and Klimov).

The electron transfer from $Pheo_{D1}^{-\bullet}$ to Q_A is the essential step in order to achieve a charge separation that is sufficiently stable to provide the driving force for the reaction sequences summarized by Eqs. (2) and (3). Therefore, only PS II complexes containing Q_A in their oxidized form are functionally competent for efficient trapping of electronically excited states in form of a useful electrochemical potential difference. Accordingly, this functionally competent state is referred to as 'open' reaction center, while PS II is 'closed' when lacking Q_A or containing reduced plastoquinone in form of the semiquinone $Q_A^{-\bullet}$ or the double reduced quinol Q_AH_2. As a consequence, Q_A acts as photochemical quencher of Chl *a* fluorescence (Duysens and Sweers, 1963). This property is the basis of widely used fluorometric methods for non-invasive monitoring of the functional state of photosynthetic apparatus (Papageorgiou and Govindjee, 2004). The properties of Q_A are described in detail in Chapter 8 (Petrouleas and Crofts).

C. Energetics of $P680^{+\bullet}$ $Q_A^{-\bullet}$ Formation and Protein Relaxation Processes

A thorough analysis of the photosynthetic organisms as converters of light into Gibbs energy has to be performed within the framework of irreversible thermodynamics (Bell and Gudkov, 1992; for a review, see Walz, 1997). This challenging problem should not to be confused with analysis of the energetics for charge separation within the RCs (Parson, 1978). The former topic is beyond the scope of this chapter and therefore only the latter one will be addressed.

1. Energies of the Initial ($^1P680^*$) and 'Final' ($P680^{+\bullet}$ $Q_A^{-\bullet}$) States

The energetics of each process is determined by the initial and the 'final' states. The initial state of 'stable' charge separation in PS II is the lowest electronically excited singlet state formed at P680 after photon absorption and subsequent rapid radiationless equilibration via vibrational relaxation. The Q_y transition at 680 nm corresponds with an energy of 1.83 eV. The rapid distribution of the excited state between the energetic levels available by a bed of pigments with virtually isoenergetic Q_y transitions (at room temperature the energy differences among the Chl *a* molecules are

comparable with kT) gives rise to an entropy term $k_B \ln W$, where k_B is the Boltzmann constant and W is the thermodynamic probability. In the simplest case of an array of identical pigment molecules with negligibly small exciton splitting but connected via rapid incoherent Förster-type EET (Section III. B1.a), the value of W corresponds to the number of pigments N_{Chl}. In reality, however, the levels are not isoenergetic in the PS II antenna and W is smaller than N_{Chl}. Effects due to different site energies can be expressed to a first approximation by using an 'effective pigment number' (G. Renger et al., 1995). The decrease of the Gibbs energy that arises from excited state equilibration in PS II with an antenna size of $N_{Chl} \approx 250$ is estimated to be about –120 meV (Gibasiewicz et al., 2001). However, as discussed by Krishtalik (1986), the configurational rather than the Gibbs energy is the key parameter for the energetics of charge separation. The configurational energy of $^1P680^*/P680$ is 1.83 eV.

The 'final' state $P680^{+\bullet}\ Q_A^{-\bullet}$ is less well defined because the free energy of the redox couples $P680/P680^{+\bullet}$ and $Q_A^{-\bullet}/Q_A$ depends not only on the chemical nature of the cofactors but also on effects due to the protein environment (Eq. (21), Section V.C.4). In principle, reduction potentials are thermodynamic parameters that are defined by equilibrium conditions. However, the state $P680^{+\bullet}\ Q_A^{-\bullet}$ does not attain a true equilibrium and even the values of the thermodynamically well-defined redox potentials are not precisely known for $P680/P680^{+\bullet}$ and $Q_A^{-\bullet}/Q_A$. So far, no straightforward redox titrations could be performed for $P680/P680^{+\bullet}$ and only estimations of +1.12 V up to +1.26 V are reported for this system (Jursinic and Govindjee, 1977; Klimov et al., 1979; Rappaport et al., 2002). In contrast, numerous redox titration experiments have been performed over the last three decades to determine the redox potential of $Q_A^{-\bullet}/Q_A$. A collection of data gathered from these studies shows a clustering of the value around –300 mV, –100 mV, 0 mV and +50 to +100 mV (for illustration, see Fig. 1 in Krieger et al., 1995). Some of these large variations can be explained by the finding that the reduction potential depends on the functional integrity of the WOC (Krieger et al., 1995). For a rough estimation, a value of about –100 mV seems to be a reasonable assumption. In this case, a free energy content of about 1.2 eV is obtained for the radical pair $P680^{+\bullet}\ Q_A^{-\bullet}$. On the basis of these estimates, the efficiency of the 'useful' charge separation in PS II is calculated to be about 67%. This number is rather large compared with the efficiency of charge separation in anoxygenic purple bacteria that is reported to be about 35% in *Rhodobacter sphaeroides* for the $P870^{+\bullet}\ Q_A^{-\bullet}$ radical pair (Warncke and Dutton, 1993). The difference between the two organisms is almost entirely due to the necessity of developing a strongly oxidizing species $P680^{+\bullet}$ as an energetic prerequisite for water oxidation.

2. Effects of the Protein Environment

The process of charge separation takes place with cofactors that are embedded into a tailored protein matrix. The formation of different states of the reaction sequence gives rise to response of the protein matrix in a time dependent manner. Any charge density redistribution within the cofactor(s) due to population of a particular state necessarily leads to changes in the interaction with the atoms of other cofactors and the protein environment. The general principles of conformational adaptation induced by spatial shift of charges (e.g., electron and proton movement) and the implications to biological processes have been outlined earlier by Christophorov et al. (2000). At this stage, only the states will be discussed that are relevant for charge separation by leading to $P680^{+\bullet}\ Pheo^{-\bullet}$ formation.

Based on the scheme of Eq. (20), a thorough calculation of the energetics requires detailed information on the electronic configuration of the different states and their interaction with the environment. An indispensable — but not sufficient — prerequisite for a straightforward analysis is the knowledge of a high-resolution structure of the whole system. This condition is not satisfied at present for PS II with a crystal structure of 3.2–3.8 Å resolution (Zouni et al., 2001; Kamiya and Shen, 2003; Biesiadka et al., 2004; Ferreira et al., 2004) and therefore only some rough estimations can be presented. To illustrate the complexity of the problem, information on the functionally and structurally much better characterized BRCs will be used for comparison.

3. Energetics and Relaxation Processes During the Lifetime of $^1P680^*$

In general, the dipole moment and nuclear configuration of electronically excited pigments differ from those of the ground state and therefore relaxation processes through the environment are induced. Furthermore, charge transfer states can be populated

in coupled pigments like the special pair in BRCs (Haran et al., 1996; H. Xu et al., 2002) and probably also in the multimeric ^{1}(RC-PC)* of PS II (Barter et al., 2003; Raszewski et al., 2005). The relaxation processes within the excited state $^1P^*$ were found to be ultrafast (Haran et al., 1996; Yakovlev et al., 2002). In PS II the initially formed excited state ^{1}(RC-PC)* equilibrates in the sub-ps time domain (Durrant et al., 1992; Müller et al., 1996) that is most likely followed by a response of the protein matrix. The energetics of this very fast environmental response is expected to be in the range of tens of meV but precise values are unknown (Paschenko et al., 2003)

4. Energetics and Relaxation Processes During the Lifetime of $P680^{+\bullet}$ $Pheo^{-\bullet}$

As outlined in Section V.A, the radical pair $P680^{+\bullet}Pheo^{-\bullet}$ can attain two different states, $P680_1^{+\bullet}$ $Pheo^-$ and $P680_2^{+\bullet}Pheo^{-\bullet}$, that are distinguished by their mode of hole localization. If one accepts the scheme proposed (Prokhorenko and Holzwarth, 2000), and summarized by Eq. (19), an energetic gap of about 50 meV would be sufficient to assure that the spin density of the cation radical is predominantly located at P_{D1} (Section IV.D.1).

Apart from this particular nature of the states of $P680^{+\bullet}$ the dissociation of an exciton (see footnotte in Section III.B.1.a) into a cation-anion radical pair inherently leads to generation of spatially separated electrical charges. A general method for the calculation of the Gibbs energy of radical pair formation $P^{+\bullet}Pheo^{-\bullet}$ in BRCs (ΔG°_{RP}) has been presented by Parson et al. (1990). In analogy to this approach, the expression for ΔG°_{RP} of $P680^{+\bullet}Pheo^{-\bullet}$ is given by the sum of several contributions:

$$\Delta G^\circ_{RP} = I_{P680} - A_{Pheo} + \Delta E^\circ_{RP} + \Delta E_{RP,\mu} + \Delta E_{ind,\mu} + \Delta G_{bulk} \quad (21)$$

where the sum of the first two parameters, the ionization potential of P680, I_{P680}, and the electron affinity of Pheo, A_{Pheo}, is the energy of formation of the individual radicals ($P680^{+\bullet}$ and $Pheo^{-\bullet}$) in the vacuum at infinite large separation; and the sum of the last four terms gives the ΔG of the electrostatic interaction. ΔE°_{RP} is the change of electrostatic energy when the radicals are put together at equilibrium distance; $\Delta E_{RP,\mu}$ is the interaction energy of the charges of the radical pair with the charge of each atom μ of the protein matrix, bound solvent water molecules and other cofactors; $\Delta E_{ind,\mu}$ is the induced dipole interaction due to polarization of atoms μ; and ΔG_{bulk} is the contribution due to interaction with the bulk solution.

An inspection of Eq. (21) shows that ΔG°_{RP} is a time dependent quantity because the last three parameters are functions of the nuclear coordinates of atoms μ of the protein matrix and the solvent molecules that vary with time due to relaxation processes. As a consequence, multiphasic kinetics emerge (vide infra). In principle, calculations on the basis of Eq. (21) can be performed by using quantum mechanical methods in combination with molecular dynamics simulations. To achieve detailed and reliable information with this approach is a great scientific challenge. It is clear that at present this goal cannot be reached for PS II partly because of our rather limited knowledge on the static structure of this complex (Section IV.A and Chapters 19–21) coupled with the complex nature of PS II. On the other hand, for BRCs sufficient data is available for successful attempts to calculate ΔG°_{RP}.

Based on the static crystallographic structure, values of about –90 meV were calculated for the energy gap between $^1P^*$ and the radical pair $P^{+\bullet}BPheo_A^{-\bullet}$ and about –200 meV for the subsequent relaxation (Parson et al., 1990). These values have to be compared with estimates gathered from experimental results of delayed fluorescence that lead to corresponding $\Delta G°$-values of –170 meV and –80 meV (Woodbury et al., 1986; Ogrodnik et al., 1988). A rather satisfying correspondence exists for the overall $\Delta G°$ between $^1P^*$ and the 'relaxed' radical pair $P^{+\bullet}BPheo_A^{-\bullet}$. However, the results obtained for the energetics of the relaxation processes exhibit striking differences.. To rationalize the discrepancies, possible limitations of theoretical and experimental approaches have to be taken into consideration. Theoretical calculations are based on the structure derived from X-ray diffraction pattern analyses that are not precise enough as shown by a combined quantum mechanical/molecular mechanical method proposed for refinement of the cofactor geometry (Hunter et al., 1999). Furthermore, calculation on the role of nuclear motions for the electron transfer reaction are mainly based on spin-boson (dispersed-polaron) models (for a recent detailed study on the primary ET steps in BRC, see Parson and Warshel, 2004, and references therein). Therefore, the data obtained critically depend on the reliability of the underlying model. On the other hand, the relevance of values based on delayed fluorescence measurements are restricted by the limitations in the

inherent time scale of the experiment. In this case the time scale is longer than the charge recombination step, which in turn is substantially longer than the charge separation step. Furthermore, in BRCs the primary charge separation generates the radical pair $P^{+\bullet}BChl_A^{-\bullet}$ that subsequently leads via a very fast reaction to $P^{+\bullet}BPheo^{-\bullet}$. The ΔG value for this reaction was shown to be much smaller with values of tens of meV (Huppmann et al., 2002). Limitations of the time resolution are less critical for data gathered from prompt fluorescence (Müller et al., 1995). Variations of the ΔG°_{RP} values could also originate from the use of different sample material. It remains to be clarified as to what extent the chromatophore membrane affects the energetics of the relaxation processes in the BRCs.

Apart from the problems in obtaining precise data on the energetics of relaxation processes, another way to discuss this topic appears to provide interesting conclusions. For an optimal electron transfer rate, the reorganization energy needs to match the free energy gap (see Eq. (17)). The free energy loss due to nuclear rearrangement on the ultrafast time scale of the initial electron transfer step must be very small, both due to the limited nuclear relaxation rates and the low polarity environment. Thus, an ultrafast rate for the primary photosynthetic electron transfer step can only be achieved if the free energy loss is very small. Accordingly, the actual free energy difference between the excited state and the initial unrelaxed radical pair may be a rather narrow gap. This idea is supported by early experiments, which show a seemingly contradictory result — i.e., upon lowering of the temperature the free energy loss approaches a limit of close to zero (Woodbury and Parson, 1984).

Compared with the studies on BRCs, substantially less information is available for PS II. Values of about –150 mV were gathered from analyses of fluorescence decay kinetics of intact PS II core complexes (Vasil'ev et al., 1996). Time-resolved photovoltage measurements with unstacked PS II membrane fragments and data evaluation within the framework of the exciton radical pair equilibrium model lead to a very similar ΔG°_{RP} value of about –160 meV. This energy gap was shown to be markedly diminished (by about 85 meV) by the negative charge on $Q_A^{-\bullet}$ whereas formation of Q_AH_2 leads to marginal effects at most (Gibasievicz et al., 2001). The influence of the negative charge of $Q_A^{-\bullet}$ on the properties of $Pheo_{D1}^{-\bullet}$ also gives rise to a pronounced electrochromic bandshift that is well known as C550 reflecting the population of the $Q_A^{-\bullet}$ redox state (van Gorkom, 1974).

Based on fluorescence quantum yield and lifetime measurements of D1/D2/Cyt b_{559} preparations, a ΔG° value of –110 meV at 277 K was obtained for the energy gap between $^1(RC-core)^*$ and $(P680^{+\bullet}Pheo^{-\bullet})_{relaxed}$ while from the 1.5 ns lifetime component a ΔG°_{RP} of –70 meV was estimated (Booth et al., 1990). A detailed low temperature study of charge recombination fluorescence and radical pair relaxation revealed that five different relaxation steps can be distinguished with increasing gaps of free energy (Konermann et al., 1997). The difference of free energy between the excited state $^1P680^*$ and the first radical pair RP_1 (ΔG°_1) was shown to be only –1.5 meV at 77K and the total energy drop (ΔG°_{total}) between $^1P680^*$ and the 'relaxed' radical pair was about 46 meV within the available time scale of measurement. An analogous analysis was performed at room temperature by using His-tagged PS II core complexes from *Synechocystis* with high O_2 evolving capacity (Vasil'ev et al. 2002). In perfect agreement with the results of Konerman et al. (1997), relaxation steps within a ladder of radical pair states were inferred to take place but with a total $\Delta G°$ of –167 mV (this value nicely fits with earlier data, vide supra). The quantitative ΔG^{o} difference between the two reports is not surprising because sample material and temperature were different. The key point of these studies is the clear demonstration of the importance of protein relaxation modes for the stabilization of the radical pair. At low temperature these relaxation processes are substantially slower due to the decreased mobility of the protein. Of central relevance is the demonstration that the radical pair energetics is characterized by a sequential relaxation via a series of radical pairs, and not by sample heterogeneity with a population distribution of reaction centers characterized by inherently different free energy gaps (Konermann et al., 1997; Vasil'ev et al., 2002). The apparent discrepancy between free energy gaps of the initial and final state of the radical pair at room and low temperatures originates from the largely different protein conformational relaxation rates at the different temperature. Thus, it is difficult to mark the initial radical pair state and determine its free energy at room temperature. Regardless of this problem, the results suggest that the initial free energy gap is likely to be small and not strongly dependent on temperature. This supports the notion that charge separation in PS II (most likely in all RCs) comprises a rather small initial Gibbs energy gap (perhaps only a few meV) in order to obtain the high rates of electron

transfer according to Marcus theory in a medium of low polarity (vide supra). This leaves the initial radical pair 'vulnerable' for charge recombination. Thus, a fundamental function of the protein is to provide rapid and efficient relaxation channels to lower the free energy gap once the radical pair is formed in order to prevent back reactions. It is attractive to hypothesize that probably the protein environment around the reaction center has been optimized during evolution to fulfill this active role.

The model of a sequential radical pair relaxation after charge separation can be generalized in a scheme where the thermodynamic parameters become time-dependent (Peloquin et al., 1994; Holzwarth and Müller, 1996). This behavior is fundamentally different from static distributions of free energy differences. It reflects the essential time-dependent role of protein conformational relaxation in stabilizing the intermediate radical pair states. A clear illustration of this principle is presented in a study on time-resolved fluorescence in chromatophores from anoxygenic purple bacteria (Müller et al., 1995). Data gathered over a wide range of temperatures (10–295 K), and from mutants where the redox potential of $P/P^{+\cdot}$ is shifted by up to 350 mV, are well described by a sequence of relaxations of the radical pair $P^{+\cdot}BPheo^{-\cdot}$, including three different states (Katiliene et al., 2003). In summary, proteins play an active role in supporting charge separation by providing efficient relaxation channels that span a wide time domain from picoseconds up to nanoseconds and perhaps extending into the microsecond range.

5. Energetics and Turnover of $P680^{+\cdot}$ $Q_A^{-\cdot}$

The radical pair $P680^{+\cdot}$ $Q_A^{-\cdot}$ is sufficiently stable to permit efficient $P680^{+\cdot}$ reduction by Y_Z followed by oxidation of the WOC. For a continuous turnover, PS II has to be reopened by oxidation of $Q_A^{-\cdot}$. This is achieved by stepwise electron transfer to another plastoquinone molecule, Q_B, that transiently binds to a special pocket (i.e., the Q_B site, see Chapter 8, Petrouleas and Crofts). There exist several lines of evidence that the electron transfer step from $Q_A^{-\cdot}$ to Q_B requires structural flexibility of the protein matrix. X-ray crystallography studies of reaction centers from the purple bacterium *Rb. sphaeroides* led to the proposal that, compared to the position of Q_B in the dark-adapted state, the ubiquinone head group is displaced by about 5 Å and rotated by 180° around the isoprenoid side chain when the samples are illuminated (Stowell et al., 1997). This pronounced structural change was suggested to limit the rate of $Q_A^{-\cdot}$ reoxidation by Q_B. However, this idea has been questioned (Q. Xu et al., 2002) and seems to be obsolete according to step-scan FTIR-measurements (Remy and Gerwert, 2003) and time resolved X-ray crystallography analysis (Baxter et al., 2004). With respect to the corresponding reaction in PS II, indirect lines of evidence show that the formation of $Q_B^{-\cdot}$ in PS II also strongly depends on the conformational flexibility of the protein (G. Renger et al., 1993; Garbers et al., 1998; Reifarth and G. Renger, 1998; P. Kühn et al., 2005). Bulk water molecules play a key role as 'plasticizers' as illustrated in PS II membrane fragments of different extent of dehydration (Kaminskaya et al., 2003; P. Kühn et al., 2005). The nature of the structural triggering of Q_A^- reoxidation remains to be clarified for both the BRC and PS II.

After stepwise electron reduction with $Q_A^{-\cdot}$ as reductant, PQH_2 is released from the Q_B-site and becomes replaced by another molecule from the plastoquinone pool (Crofts and Wraight, 1983; Chapter 8, Petrouleas and Crofts). For a high efficiency of this process, the reduction potential of $Q_A^{-\cdot}$ has to be sufficiently low. In PS II complexes with intact WOC, a value of about –100 mV seems to be reasonable (Section V.C.1). However, a significant upshift of the reduction potential by about 150 mV was found in systems lacking the WOC (Krieger et al., 1995). As a consequence, the driving force for $Q_B(Q_B^{-\cdot})$ reduction by $Q_A^{-\cdot}$ is drastically diminished and a large fraction of PS II centers becomes 'closed.' This energetic shift is assumed to be of physiological relevance for newly synthesized PS II complexes that do not contain a functionally competent WOC (Strasser and Sironval, 1972). In this case, the back reaction between $P680^{+\cdot}$ and $Q_A^{-\cdot}$ is assumed to protect against destructive action by the strongly oxidizing $P680^{+\cdot}$ radical (G. Renger and Wolff, 1976). Of the different pathways for the back reaction (Section VI) one leads to $^3P680$ which acts as sensitizer for singlet oxygen formation. A shift of the reduction potential of $Q_A^{-\cdot}$ towards a more positive value diminishes the probability of $^3P680$ formation and therefore leads to further protection of PS II complexes without WOC to rapid photodegradation (Krieger-Liszkay and Rutherford, 1998).

VI. Forward, Back and Side Reactions of Radical Ion Pair $P680^{+\bullet}\ Q_A^{-\bullet}$

In Sections V.A and V.B the kinetics of the forward reactions leading to $P680^{+\bullet}\ Q_A^{-\bullet}$ were described. However, all of these steps can be reversed. Furthermore, the population of states like $^3P680$ or the extent of competing reactions (e.g., oxidation of components like Chl_Z, Car, Cyt b_{559}, see Chapter 15, Faller et al.) depend on the functional state of the PS II complex.

A. $P680^{+\bullet}\ Q_A^{-\bullet}$ Recombination and $^3P680$ Formation

The lifetime of the radical pair $P680^{+\bullet}\ Q_A^{-\bullet}$ is limited by the tunneling rate of the direct electron transfer that leads to $P680Q_A$ in its ground state. The rate constant of this reaction depends on $\Delta G°$, λ and the edge-to-edge distance $R_{P680\text{-}Q}$(Eq. (17)). The distance between the spin density centers of the radicals $P680^{+\bullet}$ and $Q_A^{-\bullet}$ have been determined by using pulsed EPR spectroscopy and a value of 27.4 Å was obtained (Zech et al., 1997). Based on these findings and recent crystal structure data (Zouni et al. 2001; Kamiya and Shen, 2003; Biesiadka et al., 2004; Ferreira et al., 2004), a realistic edge-to-edge distance of about 20 Å can be derived (see also Fig. 6). Within the framework of the empirical rate constant-distance relationship (Moser and Dutton, 1996) a rate constant of the order of $(5\ ms)^{-1}$ is obtained that represents the maximum value for the case of $-\Delta G^\circ = \lambda$. The actual value of the maximum rate constant depends on the precise values of the distance and of parameter β (Eq. (16)). An estimation of about $(5\ ms)^{-1}$ corresponds with a reported experimental value of $(2.5\ ms)^{-1}$ (Reinman and Mathis, 1981). In systems lacking a functionally competent WOC the oxidized component Y_Z^{ox} is slowly re-reduced. If $P680^{+\bullet}$ cannot be reduced by Y_Z, it recombines with $Q_A^{-\bullet}$ with a dominating kinetics of 150–200 μs (Haveman and Mathis, 1976; G. Renger and Wolff, 1976). This reaction is about one order of magnitude faster than the direct electron transfer from $Q_A^{-\bullet}$ to $P680^{+\bullet}$. Therefore, a 100–200 μs kinetics indicate that, in this case, the dominating pathway of the recombination reaction between $P680^{+\bullet}$ and $Q_A^{-\bullet}$ is the thermally activated uphill reversal of the forward reaction leading to intermediary population of state $P680^{+\bullet}\ Pheo^{-\bullet}$. The lifetime of 150–200 μs is not markedly affected by the redox state of Y_Z, is virtually independent of pH in $5 \le pH \le 8$ and is invariant to replacement of exchangeable protons by deuterons (Christen et al., 1997). Based on an analysis of the H/D exchange effect on the probability of misses in the period four oscillation pattern of flash induced O_2 evolution (Christen et al., 1999) it was also inferred that for PS II complexes with intact WOC (at least in plants) the 150–200 μs kinetics dominate the pathway of $P680^{+\bullet}\ Q_A^{-\bullet}$ recombination via the reverse of the forward reaction, with $P680^{+\bullet}\ Pheo^{-\bullet}$ as intermediate. The contribution of the indirect pathway via $P680^{+\bullet}\ Pheo^{-\bullet}$ has been estimated to be almost 80% of the total recombination of $P680^{+\bullet}\ Q_A^{-\bullet}$ in WT cells of *Synechocystis* (Rappaport et al., 2002). This route that also dominates the recombination reaction in WT cells of the green algae *C. reinhardtii* (Cuni et al., 2004) can lead to significant population of the triplet state $^3P680$. A fluorometric study on leaves from *Arabidopsis thaliana* with modified lipid content revealed that the extent of the recombination reaction increases in mutants lacking the lipid digalactosyldiacylglycerol (Steffen et al., 2005). This finding indicates that specific lipids are of functional/structural relevance for PS II.

B. $P680^{+\bullet}\ Pheo^{-\bullet}$ Recombination

The charge separation from the electronically excited singlet state $^1P680^*$ preserves the spin multiplicity and generates a singlet state radical pair $^1[P680^{+\bullet}\ Pheo^{-\bullet}]$. The two states equilibrate (via an exciton-radical pair equilibrium, Section V.A) but the total population of these states rapidly decays due to competing reactions. Under physiological conditions, the most efficient reaction is the reoxidation of $Pheo^{-\bullet}$ by Q_A via a 300 ps kinetics (Section V.B). However, in PS II complexes either deprived of Q_A or with Q_A in a nonfunctional reduced state, the most efficient reaction channel is blocked and $^1[P680^{+\bullet}\ Pheo^{-\bullet}]$ decays via alternative pathways. In this case the lifetime of $^1[P680^{+\bullet}\ Pheo^{-\bullet}]$ is significantly lengthened. Recombination times of the order of 50 ns were obtained for $P680^{+\bullet}\ Pheo^{-\bullet}$ in D1/D2/Cyt b_{559} preparations (Danielus et al., 1987; Takahashi et al., 1987; Kurreck et al., 1997a). These samples lack Q_A. In PS II complexes closed by formation of $Q_A^{-\bullet}$ the recombination time is significantly shorter (Eckert et al., 1987; Schatz et al., 1987,1988; Leibl et al., 1989; Roelofs and Holzwarth, 1990). Essentially three reaction pathways of $P680^{+\bullet}\ Pheo^{-\bullet}$ decay have to be taken into consideration: (i) back reaction to the electronically excited singlet state $^1P680^*$ followed by radiative emission

and nonradiative dissipation; (ii) spin dephasing in $^1[P680^{+\bullet}\ Q_A^{-\bullet}]$ under formation of the triplet radical pair $^3[P680^{+\bullet}\ Q_A^{-\bullet}]$ and subsequent recombination into the triplet state $^3P680$; and (iii) direct recombination of $^1[P680^{+\bullet}\ Pheo^{-\bullet}]^*$ into the ground state.

Among these competing pathways only the $^3P680$ formation (Section IV.C) is of physiological relevance because Chl triplets give rise to singlet oxygen ($^1\Delta_gO_2$) via the sensitized reaction:

$$^3Chl + {}^3\Sigma_gO_2 \rightarrow {}^1Chl(S_0) + {}^1\Delta_gO_2 \qquad (22)$$

The species $^1\Delta_gO_2$ is very reactive and leads to oxidative degradation reactions.

It is still a matter of discussion as to what extent the nature of a 'closed' PS II by either lacking Q_A or population of states $Q_A^{-\bullet}$ (or QH_2), affect the extent of $^3P680$ formation. This problem will not be discussed here (however, see Diner et al., 2001). Chlorophyll triplets in the antenna are most efficiently quenched by rapid transfer to Car with a rate that is much faster than ^3Chl formation (Schödel et al., 1998). In contrast, in the case of $^3P680$ this process is inefficient due to the required large distances between P680 and Car (Section IV.D.2) and the physiologically relevant role of the two β-carotenes in the D1/D2 heterodimer is predominantly the quenching of $^1\Delta_gO_2$ generated via population of $^3P680$ (Telfer, 2002). In addition, the β-carotenes also participate as electron shuttles in protective electron transport pathways in the PS II core when the normal function of water cleavage is disturbed (Telfer 2002, Vasil'ev et al. 2003). Direct measurements of the electronic decay constant of carotenoid polyenes ($\beta = 0.22$ Å^{-1}, see Section III. B.2, Eq. (16)) (He et al., 2005) support the idea that β-carotene acts as an 'electronic wire.' The implication of $^3P680$ formation for photodamage are beyond the scope of this chapter and will not be discussed here (however, see Krieger-Liszkay and Rutherford, 1998; Chapters 23, Pogson et al. and 27, Chow and Aro).

C. Reduction of P680$^{+\bullet}$

The efficient exploitation of the radical pair $P680^{+\bullet}\ Q_A^{-\bullet}$ as the driving force for water cleavage can be only achieved by fast electron transfer from Y_Z to $P680^{+\bullet}$. In systems with intact WOC the kinetics of this reaction are surprisingly complex with at least three components with rate constants of $(20–30\ ns)^{-1}$, about $(300\ ns)^{-1}$ and tens of microseconds (Schilstra et al., 1998; Christen et al., 1999). As in the case of light-induced charge separation (Section V.C.2) these multiphasic kinetics are possibly a reflection of the effect of protein relaxation on electron transfer reaction in biological systems (Cherepanov et al., 2001; G. Renger, 2001, 2004; P. Kühn et al., 2005). For further details of the properties and reactivity of Y_Z see Chapter 9.

VII. Concluding Remarks and Future Perspectives

In this chapter the principles of EET and ET have been summarized describing our current knowledge on the energetics, kinetics and mechanism of light-induced charge separation in PS II. The similarities in the general functional and structural organization of this process with the RCs of anoxygenic (non-oxygen evolving) purple bacteria are outlined. On the other hand, striking differences emerge from the indispensable prerequisite of generating electron holes of sufficiently strong oxidizing power to permit water oxidation. Therefore, the understanding of the nature and the properties of the photoactive component P680 is of central relevance. The most important conclusion is the idea that P680 is not a single chromophore or special pair but a multimeric pigment complex with the surrounding protein that forms an integral and decisive part for its functional properties. Thus, the regulation of electron transfer processes by protein dynamics is of fundamental relevance for a deeper understanding of structure-function relations not only in photosynthetic reaction centers but biological systems in general. The distinction between cofactors and protein matrix (apoprotein) appears to be a futile concept for a deeper understanding. As a consequence, it seems more appropriate to consider enzymes in general and the Photosystems in particular as specially tailored molecular machines (G. Renger, 2004). This conclusion is clearly illustrated by the dramatic evolutionary jump that occurred within a rather narrow geologic time window in the transition from the RCs of anoxygenic bacteria to the oxygen evolving PS II. As a result, compared with the BRCs, the complexity of PS II drastically increased as reflected by the number of at least 18 (and possibly more than 25) distinct subunits with only minor changes at all levels of PS II development from cyanobacteria to higher plants (Raymond and Blankenship, 2004). The unraveling of the principles of functional 'giant' molecules and their interaction

with regulatory subunits is a great and fascinating challenge for future research.

Acknowledgments

We would like to thank T. Noguchi for providing unpublished results on calculations of the redox potential of P680/P680$^+$, J. Kern for Fig. 6, T. Renger for helpful discussion, P. Kühn for preparing the electronic versions of Figures 1–5 and Govindjee and T. Wydrzynski for critical reading of the manuscript and invaluable help in improving the language.

References

Agostiano A, Catucci L, Colafemmina G and Scheer H (2002) Role of functional groups and surfactant charge in regulating chlorophyll aggregation in micellar solutions. J Phys Chem 106: 1446–1454

Akiyama M, Miyashita H, Kise H, Watanabe T, Mimuro M, Miyachi S and Kobayashi M (2002) Quest for minor but key chlorophyll molecules in photosynthetic reaction centers—unusual pigment composition in the reaction centers of the chlorophyll *d*-dominated cyanobacterium *Acaryochloris marina*. Photosynth Res 74: 97–107

Andrizhiyevskaya EG, Frolov D, van Grondelle R and Dekker JP (2004) On the role of the CP47 core antenna in the energy transfer and trapping dynamics of Photosystem II. Phys Chem Chem Phys 6: 4810–4819

Avarmaa RA and Rebane KK (1985) High-resolution optical spectra of chlorophyll molecules. Spectrochim Acta 41A: 1365–1380

Balaban TS, Leitich J, Holzwarth AR and Schaffner K (2000) Autocatalyzed self-aggregation of (31R)-[Et,Et]bacteriochlorophyll cf molecules in nonpolar solvents. Analysis of the kinetics. J Phys Chem B 104: 1362–1372

Balaban TS, Fromme P, Holzwarth AR, Krauß N and Prokhorenko VI (2002) Relevance of the diastereotopic ligation of magnesium atoms of chlorophylls in Photosystem I. Biochim Biophys Acta 1556: 197–207

Barkigia KM and Fajer J (1993) Models of photosynthetic chromophores: Molecular structures of chlorins and bacteriochlorins. In: Deisenhofer J and Norris JR (eds) The Photosynthetic Reaction Center, Vol II, pp 513–539. Academic Press, New York

Barter LMC, Durrant JR and Klug DR (2003) A quantitative structure-function relationship for the Photosystem II reaction center: Supermolecular behaviour in natural photosynthesis Proc Natl Acad Sci USA 100: 946–951

Baxter RHG, Ponomarenko N, Srajer V, Pahl R, Moffat K and Norris JR (2004) Time-resolved crystallographic studies of light-induced structural changes in the photosynthetic reaction center. Proc Natl Acad Sci USA 101: 5982–5987

Bell LN and Gudkov ND (1992) Thermodynamics of light energy conversion. In: Barber J (ed) Topics in Photosynthesis, The Photosystems: Structure, Function and Molecular Biology, pp 17–43. Kluwer Academic Publishers, Dordrecht

Bernarding J, Eckert HJ, Eichler HJ, Napiwotzki A and Renger G (1994) Kinetic studies on the stabilisation of the primary radical pair P680$^+$Pheo$^-$ in different Photosystem II preparations from higher plants. Photochem Photobiol 59: 566–573

Biesiadka J, Loll B, Kern J, Irrgang K-D and Zouni A (2004) Crystal structure of cyanobacterial Photosystem II at 3.2 Å resolution: A closer look at the Mn-cluster. Phys Chem Chem Phys 6: 4733–4736

Booth PJ, Crystall B, Giorgi LB, Barber J, Klug DR and Porter G (1990) Thermodynamic properties of D1/D2/cytochrome *b*-559 reaction centres investigated by time-resolved fluorescence measurements. Biochim Biophys Acta 1016: 141–152

Bylina EJ, Kirmaier C, McDowell L, Holten D and Youvan DC (1988) Influence of an amino-acid residue on the optical properties and electron transfer dynamics of a photosynthetic reaction centre complex. Nature 336: 182–184

Camara-Artigas A, Brune D and Allen JP (2002) Interactions between lipids and bacterial reaction centers determined by protein crystallography. Proc Natl Acad Sci USA 99: 11055–11060

Cherepanov DA, Krishtalik LI and Mulkidjanian AY (2001) Photosynthetic electron transfer controlled by protein relaxation: Analysis by Langevin stochastic approach. Biophys J 80: 1033–1049

Christen G, Karge M, Eckert HJ and Renger G (1997) The role of protonation steps in electron transfer reactions in Tris-treated PS II membrane fragments. Photosynthetica 33: 529–539

Christen G, Seeliger A and Renger G (1999) P^+_{680} reduction kinetics and redox transition probability of the water oxidising complex as a function of pH and H/D isotope exchange in spinach thylakoids. Biochemistry 38: 6082–6092

Christophorov LN, Holzwarth AR, Kharkyanen VN and van Mourik F (2000) Structure-function self-organization in nonequilibrium macromolecular systems. Chem Phys 256: 45–60

Crofts AR and Wraight CA (1983) The electrochemical domain of photosynthesis. Biochim Biophys Acta 726: 149–185

Cuni A, Xiong L, Sayre R, Rappaport F and Lavergne J (2004) Modification of the pheophytin midpoint potential in Photosystem II: Modulation of the quantum yield of charge separation and of charge recombination pathways. Chem Phys Phys Chem 6: 4825–4831

Danielius RV, Satoh K, van Kan PJM, Plijter JJ, Nuijs AM and van Gorkom HJ (1987) The primary reaction of Photosystem II in the D1-D2-cytochrome *b*-559 complex. FEBS Lett 213: 241–244

Davydov AS (1962) Theory of Molecular Excitons. McGraw-Hill, New York

Deisenhofer J and Michel H (1993) Three-dimensional structure of the reaction center of *Rhodopseudomonas viridis*. In: Deisenhofer J and Norris JR (eds) The Photosynthetic Reaction Center, Vol II, pp 541–558. Academic Press, New York

Dexter DI (1953) A theory of sensitised luminescence in solids. J Chem Phys 21: 836–850

Diner BA and Rappaport F (2002) Structure, dynamics, and energetics of the primary photochemistry of Photosystem II of oxygenic photosynthesis. Annu Rev Plant Biol 53: 551–580

Diner BA, Schlodder E, Nixon PJ, Coleman WJ, Rappaport F, Lavergne J, Vermaas WFJ and Chisholm DA (2001) Site-directed mutations at D1-His198 and D2-His197 of Photosystem II in *Synechocystis* PCC 6803: Sites of primary charge

separation and cation triplet stabilization. Biochemistry 40: 9265–9281

Diner BA, Bautista JA, Nixon PJ, Berthomieu C, Hienerwadel R, Britt RD, Vermaas WFJ and Chisholm DA (2004) Coordination of proton and electron transfer form the redox-active tyrosine, Y_Z, of Photosystem II and examination of the electrostatic influence of oxidized tyrosine, Y_D (H^+). Phys Chem Chem Phys 6: 4844–4850

Döring G, Renger G, Vater J and Witt HT (1969) Properties of the photoactive chlorophyll aII in photosynthesis. Z Naturforsch 24b: 1139–1143

Dorlet P, Xiong L, Sayre RT and Un S (2001) High field EPR study of the pheophytin anion radical in wild type and D1-E130 mutants of Photosystem II in *Chlamydomonas reinhardtii*. J Biol Chem 276: 22313–22316

Durrant JR, Hastings G, Joseph DM, Barber J, Porter G and Klug DR (1992) Subpicosecond equilibration of excitation energy in isolated Photosystem II reaction centers. Proc Natl Acad Sci USA 89: 11632–1163

Durrant JR, Klug DR, Kwa SLS, van Grondelle RV, Porter G and Dekker JP (1995) A multimer model for P680, the primary electron donor of Photosystem II. Proc Natl Acad Sci USA 92: 4798–4802

Duysens LMN and Sweers HE (1963) Mechanism of two photochemical reactions in algae as studied by means of fluorescence. In: Takamiya A and Shibata K (eds) Studies on Microalgae and Photosynthetic Bacteria, pp 353–372. Univ Tokyo Press, Tokyo

Eckert HJ, Renger G, Bernarding J, Faust P, Eichler HJ and Salk J (1987) Examination of fluorescence lifetime and radical pair decay in PS II membrane fragments from spinach. Biochim Biophys Acta 893: 208–218

Eckert HJ, Wiese N, Bernarding J, Eichler HJ and Renger G (1988) Analysis of the electron transfer from $Pheo^-$ to Q_A in PS II membrane fragments from spinach by time resolved 325 nm absorption changes in the picosecond domain. FEBS Lett 240: 153–158

Eijckelhoff C, van Roon H, Groot ML, van Grondelle R and Dekker JP (1996) Purification and spectroscopic characterization of Photosystem II reaction center complexes isolated with or without Triton X-100. Biochemistry 35: 12864–12872

Fajer J (2000) Structural effects in chemistry and biology. J Porphyrins Phthalocyanines 4: 382–385

Fajer J (2004) Chlorophyll chemistry before and after crystals of photosynthetic reaction centers. Photosynth Res 80: 165–172

Feher G, Isaacson RA, Okamura MY and Lubitz W (1988) ENDOR of exchangeable protons of the reduced intermediate acceptor in reaction centers from *Rhodobacter Sphaeroides* R-26 In: Breton J and Vermeglio A (eds) The Photosynthetic Bacterial Reaction Center: Structure and Dynamics, pp 229–235. Plenum Press, New York

Ferreira K, Iverson TM, Maghlouni K, Barber J and Iwata S (2004) Architecture of the photosynthetic oxygen-evolving center. Science 303: 1831–1838

Fletcher JT and Therien MJ (2002) Extreme electronic modulation of the cofacial porphyrin structural motif. J Am Chem Soc 124: 4298–4311

Förster Th (1965) Delocalized excitation and excitation transfer. In: Sinanoglu O (ed) Modern Quantum Chemistry Vol III, pp 93–137. Academic Press, New York

Fromme P, Jordan P and Krauß N (2001) Structure of Photosystem I. Biochim Biophys Acta 1507: 5–31

Garbers A, Kurreck J, Reifarth F, Renger G and Parak F (1998) Correlation between protein flexibility and electron transfer from Q_A^- to Q_B in PS II membrane fragments from spinach. Biochemistry 37: 11399–11404

Germano M, Gradinaru CC, Shkuropatov AY, van Stokkum IHM, Shuvalov VA, Dekker JP, van Grondelle R and van Gorkom HJ (2004) Energy and electron transfer in Photosystem II reaction centers with modified pheophytin composition. Biophys J 86: 1664–1672

Gibasiewicz K, Dobek A, Breton J and Leibl W (2001) Modulation of primary radical pair kinetics and energetics in Photosystem II by the redox state of the quinone electron acceptor Q_A. Biophys J 80: 1617–1630

Giorgi LB, Nixon PJ, Merry SAP, Joseph DM, Durrant JR, De Las Rivas J, Barber J, Porter G and Klug DR (1996) Comparison of primary charge separation in the Photosystem II reaction center complex isolated from wild-type and D1-130 mutants of the cyanobacterium *Synechocystis* PCC 6803. J Biol Chem 271: 2093–2101

Greenfield SR, Seibert M, Govindjee and Wasielewski MRJ (1997) Direct measurement of the effective rate constant for primary charge separation in isolated Photosystem II reaction centers. J Phys Chem B 101: 2251–2255

Groot M-L, van Mourik F, Eijckelhoff C, van Stokkum IHM, Dekker JP and van Grondelle R (1997) Charge separation in the reaction center of Photosystem II studied as a function of temperature. Proc Natl Acad Sci USA 94: 4389–4394

Gudowska-Nowak E, Newton MD and Fajer J (1990) Conformational and environmental effects on bacteriochlorophyll optical spectra: Correlations of calculated spectra with structural results. J Phys Chem 94:5795–5801

Haran G, Wynne K, Moser CC, Dutton PL and Hochstrasser RM (1996) Femtosecond infrared studies of photosynthetic reaction centers: New charge transfer bands and ultrafast energy redistribution. In: Barbara PF, Fujimoto JG, Knox WH and Zinth Z (eds) Ultrafast Phenomena X, pp 326–327. Springer Verlag, Berlin

Hasegawa K and Noguchi T (2005) Density functional theory calculations on the dielectric-constant dependence of the oxidation potential of chlorophyll: Implication for the high potential of P680 in Photosystem II. Biochemistry 44: 8865–8872

Haveman J and Mathis P (1976) Flash-induced absorption changes of the primary donor of Photosystem II at 820 nm in chloroplasts inhibited by low pH or Tris-treatment. Biochim Biophys Acta 440: 346–355

He J, Chen F, Li J, Sankey OF, Terazono Y, Herrero Ch, Gust D, Moore TA, Moore AL and Lindsay SM (2004) Electronic decay constant of carotenoid polyenes from single-molecule measurements. J Am Chem Soc 127: 1384–1385

Hillmann B, Brettel K, van Mieghem FJE, Kamlowski A, Rutherford AW and Schlodder E (1995) Charge recombination in Photosystem II. 2. Transient absorbance difference spectra and their temperature dependence. Biochemistry 34: 4814–4827

Hochstrasser RM and Kasha M (1964) Application of the exciton model to mononuclear lamellar systems. Photochem Photobiol 3: 317–331

Holzwarth AR (1989) Applications of ultrafast laser spectroscopy for the study of biological systems. Quart Rev Biophys

22: 239–326
Holzwarth AR and Müller MG (1996) Energetics and kinetics of radical pairs in reaction centers from *Rhodobacter sphaeroides*. A femtosecond transient absorption study. Biochemistry 35:11820–11831
Hunter CN, Hughes JM, Reimer JR and Hush NS (1999) Modelling the bacterial photosynthetic reaction center. 2. A combined quantum mechanical/molecular mechanical study of the structure of the cofactors in the reaction centers of purple bacteria. J Phys Chem B 103: 4906–4915
Huppman P, Arlt T, Penzkofer H, Schmidt S, Bibikova M, Dohse B, Oesterhelt D, Wachtveitl J and Zinth W (2002) Kinetics, energetics and electronic coupling of the primary electron transfer reactions in mutated reaction centers of *Blastochloris viridis*. Biophys J 82: 3186–3197
Huppman P, Spörlein, S, Bibikova M, Oesterhelt D, Wachtveitl J and Zinth W (2003) Electron transfer in reaction centers of *Blastochloris viridis*: Photosynthetic reactions approximating the adiabatic regime. J Phys Chem A 107: 8302–8309
Ishikita H, Loll B, Biesiadka J, Saenger W, and Knapp E-W (2005) Redox potentials of chlorophylls in the Photosystem II reaction center. Biochemistry 44: 4118–4124
Ivancich A, Arltz K, Williams JC, Allen JP, Mattioli TA (1998) Effects of hydrogen bonds on the redox potential and electronic structure of the bacterial primary electron donor. Biochemistry 37: 11812–11820
Jankowiak R, Hayes JM and Small GJ (2002) An excitonic pentamer model for the core Q_y states of the isolated Photosystem II reaction center. J Phys Chem B 106: 8803–8814
Jankowiak R, Rätsep M, Hayes J, Zazubovich V, Picorel R, Seibert M and Small GJ (2003) Primary charge-separation rate at 5 K in isolated Photosystem II reaction centers containing five and six chlorophyll *a* molecules. J Phys Chem B 107: 2068–2074
Jeans C, Schilstra MJ, Ray N, Husain S, Minagawa J, Nugent JHA and Klug DR (2002) Replacement of tyrosine D with phenylalanine affects the normal proton transfer pathways for the reduction of $P680^+$ in oxygen-evolving Photosystem II particles from *Chlamydomonas*. Biochemistry 41: 15754–15761
Johnson ET, Nagarajan V, Zazubovich V, Riley K, Small GJ and Parson WW (2003) Effects of ionisable residues on the absorption spectrum and initial electron-transfer kinetics in the photosynthetic reaction center of *Rhodobacter sphaeroides*. Biochemistry 42: 13673–13683
Johnston H, Wang J, Ruffle SV, Sayre RT and Gustafson TL (2000) Fluorescence decay kinetics of wild type D2-H117N mutant Photosystem II reaction centers isolated from *Chlamydomonas reinhardtii*. J Phys Chem B 104: 4777–4781
Jursinic P and Govindjee (1977) Temperature dependence of delayed light emission in the 6–340 microsecond range after a single flash in chloroplasts. Photochem Photobiol 26: 617–628
Kaminskaya O, Renger G and Shuvalov VA (2003) Effect of dehydration on light induced reactions in Photosystem II: Evidence for the presence of two functionally different Cytochromes *b*559. Biochemistry 42: 8119–8132
Kamiya N and Shen J-R (2003) Crystal structure of oxygen-evolving Photosystem II from *Thermosynechococcus vulcanus* at 3.7-Å resolution. Proc Natl Acad Sci USA 100: 98–103
Kamlowski A, Frankemöller L, Van der Est A, Stehlik D and Holzwarth AR (1996) Evidence for delocalization of the triplet state ^{3}P680 in the D1/D2/Cyt b_{559}-complex of Photosystem II. Ber Bunsenges Phys Chem 100: 2045–2051
Karplus M and McCammon JM (1983) Dynamics of proteins: Elements and function. Annu Rev Biochem 52: 263–300
Katiliene Z, Katilius E and Woodbury NW (2003) Energy trapping and detrapping in reaction center mutants from *Rhodobacter sphaeroides*. Biophys 84: 3240–3251
Kawatsu T, Kakitani T and Yamato T (2001) Worm model for electron tunneling in proteins: Consolidation of the pathway model and the Dutton plot. J Phys Chem B 105: 4424–4435
Ke B (2001) Photosynthesis: Photobiochemistry and Photobiophysics. Kluwer Academic Publishers, Dordrecht
Klimov VV, Klevanik AV, Shuvalov VA and Krasnovsky AA (1977) Reduction of pheophytin in the primary light reaction of Photosystem II. FEBS Lett 82: 183–186
Klimov VV, Allakhverdiev SI, Demeter S and Krasnovsky AA (1979) Photoreduction of pheophytin in Photosystem II of chloroplasts as a function of redox potential of the medium. Dokl Akad Nauk SSSR 249: 227–230
Klug DR, Rech T, Josef DM, Barber J, Durrant JR an Porter G (1995) Primary processes in isolated Photosystem II reaction centers probed by magic angle transient absorption spectroscopy. Chem Phys 194: 433–442
Knapp EW, Fischer SF, Zinth W, Sander M, Kaiser W, Deisenhofer J and Michel H (1985) Analysis of optical spectra from single crystals of *Rhodopseudomonas viridis* reaction centers. Proc Natl Acad Sci USA 82: 8463–8467
Knox RS and van Amerongen H (2002) Refractive index dependence of the Förster resonance excitation transfer rate. J Phys Chem B 106: 5289–5293
Kobayashi M, Maeda H, Watanabe T, Nakane H and Satoh K (1990) Chlorophyll *a* and β-carotene content in the D1/D2/cytochrome b_{559} reaction center complex from spinach. FEBS Lett 260: 138–140
Konermann L and Holzwarth AR (1996) Analysis of the absorption spectrum of Photosystem II reaction centers: Temperature dependence, pigment assignment and inhomogeneous broadening. Biochemistry 35: 829–842
Konermann L, Gatzen G and Holzwarth AR (1997) Primary processes and structure of the Photosystem II reaction center. V. Modeling of the fluorescence kinetics of the D1-D2-Cyt-*b*559 complex at 77K. J Phys Chem B 101: 2933–2944
Krieger-Liszkay A and Rutherford AW (1998) Influence of herbicide binding on the redox potential of the quinone acceptor in Photosystem II: Relevance to photodamage and phytotoxicity. Biochemistry: 37: 17339–17344
Krieger A, Rutherford AW and Johnson GN (1995) On the determination of the redox midpoint potential of the primary quinone acceptor, Q_A, in Photosystem II. Biochim Biophys Acta 1229: 193–201
Krishtalik LI (1986) Energetics of multielectron reactions. Photosynthetic oxygen evolution. Biochim Biophys Acta 849: 162–171
Kühn O, Renger T, May V, Voigt J, Pullerits T and Sundström V (1997) Exciton-vibrational coupling in photosynthetic antenna complexes: theory meets experiment. Trends Photochem Photobiol 4: 213–256
Kühn P, Eckert H-J, Eichler H-J and Renger G (2004) Analysis of the $P680^{+\cdot}$ reduction pattern and its temperature dependence in oxygen evolving PS II core complexes from thermophilic cyanobacteria and higher plants. Phys Chem Chem Phys 6: 4838–4843

Kühn P, Pieper J, Kaminskaya O, Eckert H-J, Lechner R, Shuvalov V and Renger G (2005) Reaction pattern of Photosystem II: Oxidative water cleavage and protein flexibility. Photosynth Res 84: 317–323

Kurreck J, Garbers A, Reifarth F, Andréasson LE, Parak F and Renger G (1996) Isolation and properties of PS II membrane fragments depleted of the non heme iron center. FEBS Lett 381: 53–57

Kurreck J, Liu B, Napiwotzki A, Sellin S, Eckert HJ, Eichler HJ and Renger G (1997a) Stoichiometry of pigments and radical pair formation under saturating pulse excitation in D1/D2/Cyt *b*559 preparations. Biochim Biophys Acta 1318: 307–315

Kurreck J, Garbers A, Parak F and Renger G (1997b) Highly purified D1/ D2/ Cyt b_{559} preparations from spinach do not contain the non heme iron center. FEBS Lett 403: 283–286

Laible PD, Kirmaier C, Udawatte CSM, Hofman SJ, Holten D and Hanson DK (2003) Quinone reduction via secondary b-branch electron transfer in mutant bacterial reaction centers. Biochemistry 42: 1718–1730

Leibl W, Breton J, Deprez J and Trissl HW (1989) Photoelectronic study on the kinetics of trapping and charge stabilization in oriented PS II membranes. Photosynth Res 22: 257–275

Leupold D, Teuchner K, Ehlert J, Irrgang KD, Renger G and Lokstein H (2002) Two-photon excited fluorescence from higher electronic states of chlorophylls in photosynthetic antenna complexes: A new approach to investigate spectral heterogeneity ('chlorophyll forms') Biophys J 82: 1580–1585

Lince MT and Vermaas W (1998) Association of His117 in the D2 protein of Photosystem II with a chlorophyll that affects excitation: Energy transfer efficiency to the reaction center. Eur J Biochem 256: 595–602

Liu B, van Kan PJM and Hoff AJ (1991) Influence of the H-subunit and Fe^{2+} on electron transport from I^- to Q_A in Fe^{2+} free and/or H-free reaction centers from *Rhodobacter sphaeroides* R-26. FEBS Lett 289: 23–28

Lubitz W and Lendzian F (1996) ENDOR Spectroscopy In: Amesz J and Hoff AJ (eds) Biophysical Techniques in Photosynthesis, pp 255–275. Kluwer Academic Publishers, Dordrecht

Lubitz W, Isaacson RA, Okamura MY, Abresch EC, Plato M and Feher G (1989) ENDOR studies of the intermediate electron acceptor radical anion $I^{-\bullet}$ in Photosystem II reaction centers. Biochim Biophys Acta 977: 227–232

MacMillan F, Lendzian F, Renger G and Lubitz W (1995) EPR and ENDOR investigation of the primary electron acceptor radical anion Q_A^- in iron-depleted Photosystem II membrane fragments. Biochemistry 34: 8144–8156

Mäntele W (1996) Infrared and Fourier-transformed infrared spectroscopy. In: Amesz J and Hoff AJ (eds) Biophysical Techniques in Photosynthesis, pp 137–157. Kluwer Academic Publishers, Dordrecht

Marcus RA and Sutin N (1985) Electron transport in chemistry and biology. Biochem Biophys Acta 811: 265–322

Matysik J, Gast AP, van Gorkom HJ and de Groot HJM (2000) Photochemically induced nuclear spin polarization in reaction centers of Photosystem II observed by ^{13}C-solid-state NMR reveals a strongly asymmetric electronic structure of the $P_{680}^{+\bullet}$ primary donor chlorophyll. Proc Natl Acad Sci USA 97: 9865–9870

McMahon BH, Muller JD, Wraight CA and Nienhaus GU (1998) Electron transfer and protein dynamics in the photosynthetic reaction center. Biophys J 74: 2567–2587

Merry SAP, Nixon PJ, Barter LMC, Schilstra M, Porter G, Barber J, Durrant JR and Klug DR (1998) Modulation of quantum yield of primary radical pair formation in Photosystem II by site-directed mutagenesis affecting radical cations and anions. Biochemistry 37: 17439–17447

Michel H and Deisenhofer J (1988) Relevance of the photosynthetic reaction center from purple bacteria to the structure of Photosystem II. Biochemistry 27:1–7

Michel-Beyerle ME, Plato M, Deisenhofer J, Michel H, Bixon M and Jortner J (1988) Unidirectionality of charge separation in reaction centers of photosynthetic bacteria. Biochim Biophys Acta 932:52–70

Mimuro M, Tomo T, Nishimura Y, Yamazaki I and Satoh K (1995) Identification of a photochemically inactive pheophytin molecule in the spinach D1-D2-Cyt *b*559 complex. Biochim Biophys Acta 1232: 81–88

Mimuro M, Akimoto S, Gotoh T, Yokono M, Akiyama M, Tsuchiya T, Miyashita H, Kobayashi M and Yamazaki I (2004) Identification of the primary electron donor in PS II of the Chl *d*-dominated cyanobacterium *Acaryochloris marina*. FEBS Lett 556: 95–98

Moënne-Loccoz R, Robert B and Lutz M (1989) A resonance Raman characterization of the primary electron acceptor in Photosystem II. Biochemistry 28: 3641–3645

Moser CC and Dutton PC (1996) Outline of theory of protein electron transfer. In: Bendall DS (ed) Protein Electron Transfer, pp 1–21. BIOS Scientific Publishers, Oxford

Müh F, Rautter J and Lubitz W (1996) Two distinct conformations of the primary electron donor in reaction centers from *Rhodobacter sphaeroides* revealed by ENDOR/TRIPLE Spectroscopy. Biochemistry 36: 4155–4162

Mulkidjanian A (1999) Photosystem II of green plants: On the possible role of retarded protonic relaxation in water oxidation. Biochim Biophys Acta 1410: 1–6

Müller MG, Dorra D, Holzwarth AR, Gad'on N and Drews G (1995) Time-dependent radical pair relaxation in chromatophores of an antenna-free mutant from *Rhodobacter capsulatus*. In: Mathis P (ed) Photosynthesis: From Light to Biosphere. Vol 1, pp 595–598. Kluwer Academic Publishers, Dordrecht

Müller MG, Hucke M, Reus M and Holzwarth AR (1996) Primary processes and structure of the Photosystem II reaction center: IV. Low intensity femtosecond transient absorption spectra of D1-D2 reaction centers. J Phys Chem 100: 9527–9536

Nabedryk E, Andrianambinintsoa S, Berger G, Leonhard M, Mäntele W and Breton J (1990) Characterization of bonding interactions of the intermediary electron acceptor in the reaction center of Photosystem II by FTIR spectroscopy. Biochim Biophys Acta 1016: 49–54

Nanba O and Satoh K (1987) Isolation of a Photosystem II reaction center consisting of D1 and D2 polypeptides and cytochrome b559. Proc Natl Acad Sci USA 84: 109–112

Nishigaki A, Ohshima S, Nakayama K, Okada M and Nagashima U (2001) Application of molecular orbital calculations to interpret the chlorophyll spectral forms in pea Photosystem II. Photochem Photobiol 73: 245–248

Noguchi T, Tomo T and Inoue Y (1998) Fourier transform infrared study of the cation radical of P680 in the Photosystem II reaction center: Evidence for charge delocalization on the chlorophyll dimer. Biochemistry 37: 13614–13625

Noguchi T, Kurreck J, Inoue Y and Renger G (1999) Comparative FTIR analysis of the microenvironment of Q_A^- in cyanide and

high pH treated and 'iron depleted' PS II membrane fragments. Biochemistry 38: 4846–4852

Norris JR, Scheer H and Katz JJ (1974) Models of antenna and reaction center chlorophylls. Ann NY Acad Sci 244: 260

Nuijs AM, van Gorkom HJ, Plijter JJ and Duysens LNM (1986) Primary-charge separation and excitation of chlorophyll *a* in Photosystem II particles from spinach as studied by picosecond absorbance-difference spectroscopy. Biochim Biophys Acta 848: 167–175

Oba T and Tamiaki H (2002) Which side of the π-macrocycle plane of (bacterio)chlorophylls is favored for binding the fifth ligand? Photosynth Res 74: 1–10

Ogrodnik A, Volk M, Letterer R, Feick R and Michel-Beyerle ME (1988) Determination of free energies in reaction centers of *Rb. sphaeroides*. Biochim Biophys Acta 936: 361–371

Page CC, Moser CC, Chen X and Dutton PL (1999) Natural engineering principles of electron tunneling in biological oxidation-reduction. Nature 402: 47–52

Palazzo G, Mallardi A, Hochkoeppler A, Cordone L and Venturoli G (2002) Electron transfer kinetics in photosynthetic reaction centers embedded in trehalose glasses: Trapping of conformational substates at room temperature. Biophys J 82: 558–568

Papageorgiou GC and Govindjee (eds) (2004) Chlorophyll *a* Fluorescence: A Signature of Photosynthesis. Springer, Berlin

Parker CA and Joyce TA (1967) Delayed fluorescence and some properties of the chlorophyll triplets. Photochem Photobiol 6: 395–406

Parson WW (1978) Thermodynamics of the primary reactions of photosynthesis. Photochem Photobiol 28: 389–393

Parson WW and Warshel (2004) A density-matrix model of photosynthetic electron transfer with microscopically estimated vibrational relaxation times. Chem Phys 296: 201–216

Parson WW, Chu ZT and Warshel A (1990) Electrostatic control of charge separation in bacterial photosynthesis. Biochim Biophys Acta 1017: 251–272

Paschenko VZ, Gorokhov VV, Knox PP, Krasilnikov PM, Redlin H, Renger G and Rubin AB (2003) Energetics and mechanisms of high efficiency of charge separation and electrons transfer processes in *Rhodobacter sphaeroides* reaction centers. Bioelectrochemistry 61: 73–84

Pearlstein RM (1982) Chlorophyll singlet exciton. In: Govindjee (ed) Photosynthesis 1, Energy Conversion by Plants and Bacteria, pp 293–330. Academic Press, New York

Pearlstein RM (1991) Theoretical interpretation of antenna spectra. In: Scheer H (ed) Chlorophylls, pp 1047–1078. CRC Press, New York

Peloquin JM, Williams JC, Lin X, Alden RG, Taguchi AKW, Allen JP and Woodbury NW (1994) Time-dependent thermodynamics during early transfer in reaction centers from *Rhodobacter sphaeroides*. Biochemistry 33: 8089–8100

Peterman EJG, Pullerits T, van Grondelle R and Van Amerongen H (1997) Electron-phonon coupling and vibronic fine structure of light-harvesting complex II of green plants; Temperature dependent absorption and high-resolution fluorescence spectroscopy. J Phys Chem B 101: 4448–4457

Peterson-Arsköld S, Masters VM, Prince BJ, Smith PJ, Pace RJ and Krausz E (2003) Optical Spectra of Synechocystis and Spinach Photosystem II Preparations at 1.7 K: Identification of the D1-Pheophytin Energies and Stark Shifts: J Am Chem Soc 125

Petke JD, Maggiora GM, Shipman L and Christoffersen RE (1979) Stereoelectronic properties of photosynthetic and related systems-V. *Ab initio* configuration interaction calculation on the ground and lower excited singlet and triplet states of ethyl chlorophyllide *a* and ethyl pheophorbide *a*. Photochem Photobiol 30: 203–223

Pieper J, Voigt J, Renger G and Small GJ (1999) Analysis of phonon structure in line-narrowed optical spectra. Chem Phys Lett 310: 296–302

Pieper J, Irrgang K-D, Renger G and Lechner RE (2004) Density of vibrational states of solubilized LHC II complexes of green plants studied by inelastic neutron scattering. J Phys Chem B 108: 10556–10565

Prokhorenko VI and Holzwarth AR (2000) Primary processes and structure of the Photosystem II reaction center: A photon echo study. J Phys Chem B 104: 11563–11578

Rappaport F, Guergova-Kuras M, Nixon PJ, Diner BA and Lavergne J (2002) Kinetics and pathways of charge recombination in Photosystem II. Biochemistry 41: 8518–8527

Raszewski G, Saenger W and Renger T (2005) Theory of optical spectra of Photosystem II reaction centers: Location of the triplet state and the identity of the primary electron donor. Biophys J 88: 986–998

Raymond J and Blankenship RE (2004) The evolutionary development of the protein complement of Photosystem 2. Biochim Biophys Acta 1655: 133–139

Reed DW and Clayton RK (1968) Isolation of a reaction center fraction from *Rhodopseudomonas sphaeroides*. Biochem Biophys Res Commun 30: 471–475

Reifarth F and Renger G (1998) Indirect evidence for structural changes coupled with Q_B^- formation in Photosystem II. FEBS Lett 428: 123–126

Remy A and Gerwert K (2003) Coupling of light-induced electron transfer to proton uptake in photosynthesis. Nature Struct Biol 10: 637–644

Reinman S and Mathis P (1981) Influence of temperature on Photosystem II electron transfer reactions. Biochim Biophys Acta 635: 249–258

Renger G (1987) Mechanistic aspects of photosynthetic water cleavage. Photosynthetica 21: 203–224

Renger G (1992) Energy transfer and trapping in Photosystem II. In: Barber J (ed) Topics in Photosynthesis, The Photosystems: Structure, Function and Molecular Biology, pp 45–99. Elsevier, Amsterdam

Renger G (1999) Molecular mechanism of water oxidation. In: Singhal GS, Renger G, Govindjee, Irrgang, KD and Sopory SK (eds) Concepts in Photobiology: Photosynthesis and Photomorphogenesis, pp 292–329. Kluwer Academic Publishers, Dordrecht and Narosa Publishing Co., Delhi

Renger G (2001) Photosynthetic water oxidation to molecular oxygen: Apparatus and mechanism. Biochim Biophys Acta 1503: 210–228

Renger G (2003) Apparatus and mechanism of photosynthetic oxygen evolution: A personal perspective. Photosynth Res 76: 269–288

Renger G (2004) Coupling of electron and proton transfer in oxidative water cleavage in photosynthesis. Biochim. Biophys. Acta

Renger T and Marcus RA (2002a) On the relation of protein dynamics and exciton relaxation in pigment-protein complexes: An estimation of the spectral density and a theory for the cal-

culation of optical spectra. J Chem Phys 22: 9997–10019
Renger T and Marcus RA (2002b) Photophysical properties of PS-2 reaction centers and a discrepancy in exciton relaxation times. J Phys Chem B 106: 1809–1819
Renger T and May V (1997) Multiple exciton effects in molecular aggregates: Application to a photosynthetic antenna complex. Phys Rev Lett 78: 3406–34
Renger G and Wolff Ch (1976) The existence of a high photochemical turnover rate at the reaction centers of system II in Tris-washed chloroplasts. Biochim Biophys Acta 423: 610–614
Renger G, Gleiter HM, Haag E and Reifarth F (1993) Photosystem II: thermodynamics and kinetics of electron transport from Q_A^- to Q_B (Q_B^-) and deleterious effects of copper (II). Z Naturforsch 48c: 234–240
Renger G, Eckert HJ, Bergmann A, Bernarding J, Liu B, Napiwotzki A, Reifarth F and Eichler JH (1995) Fluorescence and spectroscopic studies on exciton trapping and electron transfer in Photosystem II of higher plants. Austr J Plant Physiol 22: 167–181
Rigby SEJ, Nugent JHA and O'Malley PJ (1994) ENDOR and special triple resonance studies of chlorophyll cation radicals in Photosystem II. Biochemistry 33: 10043–1050
Riley K, Jankowiak, R, Rätsep M, Small GJ and Zazubovich V (2004) Evidence for highly dispersive primary charge separation kinetics and gross heterogeneity in the isolated PS II reaction center of green plants. J Phys Chem 108: 10346–10356
Rinyu L, Marin EW, Takahashi E, Maroti P and Wraight CA (2003) Modulation of the free energy of the primary quinone acceptor (Q_A) in reaction centers from *Rhodobacter sphaeroides*: Contributions from the protein and protein-lipid (cardiolipin) interactions. Biochim Biophys Acta 1655: 93–101
Robert B (1996) Resonance Raman studies in photosynthesis—chlorophyll and carotenoid molecules. In: Amesz J and Hoff AJ (eds) Biophysical Techniques in Photosynthesis, pp 161–174. Kluwer Academic Publishers, Dordrecht
Robert B, Lutz M and Tiede DM (1985) Selective photochemical reduction of either of the two bacteriopheophytins in reaction centers of *Rps. sphaeroides* R-26. FEBS Lett 2439: 326–330
Roelofs TA and Holzwarth AR (1990) In search of a putative long-lived relaxed radical pair state in closed Photosystem II. Kinetic modeling of picosecond fluorescence data. Biophys J 57: 1141–1153
Roelofs TA, Lee CH and Holzwarth AR (1992) Global target analysis of picosecond chlorophyll fluorescence kinetics from pea chloroplasts. Biophys J 61: 1147–1163
Ruffle SV, Wang J, Johnston HG, Gustafson TL, Hutchison RS, Minagawa J, Crofts A and Sayre RT (2001) Photosystem II peripheral accessory chlorophyll mutants in *Chlamydomonas reinhardtii*. Biochemical characterization and sensitivity to photo-inhibition. Plant Physiol 127: 633–644
Rutherford AW and Faller P (2003) Photosystem II: Evolutionary perspectives. Phil. Trans R Soc Lond B 358: 245–253
Rutherford AW and Faller P (2004) The stable tyroxyl radical in Photosystem II: Why D? Biochim Biophys Acta 1655: 222–230
Schatz GH, Brock H and Holzwarth AR (1987) Picosecond kinetics of fluorescence and absorbance changes in Photosystem II particles excited by low photon density. Proc Natl Acad Sci USA 84: 8414–8418
Schatz GH, Brock H and Holzwarth AR (1988) Kinetic and energetic model for the primary processes in Photosystem II. Biophys J 54: 397–405
Scheer H (ed) (1991) Chlorophylls. CRC Press, Boca Raton
Schilstra MJ, Rappaport F, Nugent JHA, Barnett CJ and Klug DR (1998) Proton/hydrogen transfer affects the S-state-dependent microsecond phases of $P680^+$ reduction during water splitting. Biochemistry 37: 3974–3981
Schmidt U and Reineker P (1985) Triplet excitons in molecular pairs. Mol Phys 55: 77–95
Schödel R, Irrgang KD, Voigt J and Renger G (1998) Rate of carotenoid triplet formation in solubilized light-harvesting complex II (LHCII) from spinach. Biophys J 75: 3143–3153
Scholes GD, Jordanides XJ and Fleming GR (2001) Adapting the Förster theory of energy transfer for modeling dynamics in aggregated molecular assemblies. J Phys Chem B 105: 1640–1651
Schweitzer RH, Melkozernov AN, Blankenship RE and Brudvig GW (1998) Time-resolved fluorescence measurements of Photosystem II: The effect of quenching by oxidized chlorophyll Z. J Phys Chem B 102: 8320–8326
Seibert M and Wasielewski M (2003) The isolated Photosystem II reaction center: First attempts to directly measure the kinetics of primary charge separation. Photosynth Res 76: 263–268
Senge MO, Renner MW, Kalisch WW and Fajer J (2000) J Chem Soc, Dalton Trans: 381
Shi L-X and Schröder WP (2004) The low molecular mass subunits of the photosynthetic supracomplex, photosystem II. Biochim Biophys Acta 1608: 75–96
Shkuropatov AY, Khatypov RA, Volshchukova TS, Shkuropatova VA, Owens TG and Shuvalov VA (1997) Spectral and photochemical properties of borohydride-treated D1-D2-cytochrome *b*-559 complex of Photosystem II. FEBS Lett 420: 171–174
Small DW, Matyushov DV and Voth GA (2003) The theory of electron transfer reactions: What may be missing? J Am Chem Soc 125: 7470–7478
Smith PJ, Peterson S, Masters VM, Wydrzynski T, Styring S, Krausz E and Pace RJ (2002) Magneto-optical measurements of the pigments in fully active Photosystem II core complexes from plants. Biochemistry 41: 1981–1989
Spiedel D, Jones MR and Robert B (2002) Tuning of the redox potential of the primary electron donor in reaction centres of purple bacteria: Effects of amino acid polarity and position. FEBS Lett 527: 171–175
Steffen R, Kelly AA, Huyer PJ, Dörmann P and Renger G (2005) Investigations on the reaction pattern of Photosystem II in leaves from *Arabidopsis thaliana* wild type plants and mutants with genetically modified lipid content: II. Galactolipid deficiency. Biochemistry 44: 3134–3142
Stewart DH, Nixon PJ, Diner BA and Brudvig GW (2000) Assignment of the Q_y absorbance bands of Photosystem II chromophores by low-temperature optical spectroscopy of wild-type and mutant reaction centers. Biochemistry 39: 14583–14594
Stiehl HH (1969) Untersuchungen periodisch angeregter Absorptionsänderungen im Reaktionszentrum II der Photosynthese. PhD Thesis. Technische Universität, Berlin
Stiehl HH and Witt HT (1969) Quantitative treatment of the function of plastoquinone in photosynthesis. Z Naturforsch 24b: 1588–1598
Stowell MHB, Phillips TM, Rees DC, Soltis SM, Abresch E and Feher G (1997) Light-induced structural changes in photosynthetic reaction center: Implications for mechanism of electron-proton transfer. Science 276: 812–816

Strasser RJ and Sironval C (1972) Induction of Photosystem II activity in flashed leaves. FEBS Lett 28: 56–60

Sumi H (1999) Theory on rates of excitation-energy transfer between molecular aggregates through distributed transition dipoles with application to the antenna system in bacterial photosynthesis. J Phys Chem 103: 252–260

Takahashi Y, Hansson Ö, Mathis P and Satoh K (1987) Primary radical pair in the Photosystem II reaction center. Biochim Biophys Acta 893: 49–59

Tang D, Jankowiak R, Seibert M and Small GJ (1991) Effects of detergent on the excited state structure and relaxation dynamics of the Photosystem II reaction center: A high resolution hole burning study. Photosynth Res 27: 19–29

Telfer A (2002) What is β-carotene doing in the Photosystem II reaction centre? Phil Tans R Soc Lond B 357: 1431–1440

Tetenkin VL, Gulyaev BA, Seibert M and Rubin AB (1989) Spectral properties of stabilized D1/D2/cytochrome *b*-559 Photosystem II reaction center complex. FEBS Lett 250: 459–463

Tiede DM and Dutton PL (1981) Orientation of the primary quinone of bacterial photosynthetic reaction centers contained in chromatophore and reconstituted membranes. Biochim Biophys Acta 637: 278–290

Tretiak S, Middleton C, Chernyak V and Mukamel S (2000) Exciton Hamiltonian for the bacteriochlorophyll system in the LH2 antenna complex of purple bacteria. J Phys Chem B 104: 4519–4528

Trissl HW and Lavergne J (1995) Fluorescence induction from Photosystem II: Analytical equations for the yields of photochemistry and fluorescence derived from analysis of a model including exciton-radical pair equilibrium and restricted energy transfer between photosynthetic units. Austral J Plant Physiol 22: 183–193

Vacha F, Josephs DM, Durrant JR, Telfer A, Klug DR, Porter G and Barber J (1995) Photochemistry and spectroscopy of a five-chlorophyll reaction center of Photosystem II isolated by using a Cu affinity column. Proc Natl Acad Sci USA 92: 2929–2933

Vacha F, Durchan M and Siffel P (2002) Excitonic interactions in the reaction centre of Photosystem II studied by using circular dichroism. Biochim Biophys Acta 1554: 147–152

van Amerongen H, Dekker JP (2003) Light-Harvesting in Photosystem II. In: Green BR, Parson WW (eds) Light-Harvesting Antennas in Photosynthesis, pp 219–251. Kluwer Academic Publishers, Dordrecht

van Gorkom HJ (1974) Identification of the reduced primary electron acceptor of Photosystem II as a bound semiquinone anion. Biochim Biophys Acta 347: 439–442

van Mieghem FJE and Rutherford AW (1993) Comparative spectroscopy of photosystem-II and purple bacterial reaction centres. Biochem Soc Trans 21: 986–991

van Rensen JJS, Xu C and Govindjee (1999) Role of bicarbonate in the Photosystem II, the water-plastoquinone oxido-reductase of plant photosynthesis. Physiol Plantarum 105: 585–592

Vasil'ev S, Bergmann A, Redlin H, Eichler H.-J and. Renger G (1996) On the role of exchangeable hydrogen bonds for the kinetics of P^{+}_{680} Q^{-}_{A} formation and P^{+}_{680} $Pheo^{-\cdot}$ recombination in Photosystem II. Biochim Biophys Acta 1276: 35–44

Vasil'ev S, Schrötter T, Bergmann A, Irrgang KD, Eichler HJ and Renger G (1997) Cryoprotectant-induced quenching of chlorophyll a fluorescence from LHC II in vitro: Time resolved fluorescence and steady state spectroscopic studies. Photosynthetica 33: 553–561

Vasil'ev S, Orth P, Zouni A, Owens TG and Diner B (2001) Excited-state dynamics in Photosystem II: insights from the X-ray crystal structure. Proc Natl Acad Sci USA 98: 8602–8607

Vasil'ev S, Lee C-I, Brudvig GW and Bruce D (2002) Structure-based kinetic modeling of excited-state transfer and trapping in histidine-tagged Photosystem II core complexes from *Synechocystis*. Biochemistry 41: 12236–12243

Vasil'ev S, Brudvig GW and Bruce D (2003) The X-ray structure of Photosystem II reveals a novel electron transport pathway between P680, cytochrome b_{559} and the energy-quenching cation, Chl_{Z}^{+}. FEBS Letters 543: 159–163

Vasil'ev S, Shen J-R, Kamiya N and Bruce D (2004) The orientations of core antenna chlorophylls in Photosystem II are optimized to maximize the quantum yield of photosynthesis. FEBS Lett 561: 111–116

Vavilin D, Xu H, Lin S and Vermaas W (2002) Energy and Electron Transfer in Photosystem II of a Chlorophyll *b*-Containing *Synechocystis sp*. PCC 6803 Mutant. Biochemistry 42: 1731–1746

Vos MH, Rischel C, Jones MR and Martin JL (2000) Electrochromic detection of a coherent component in the formation of the charge pair $P^{+}HL^{-}$ in bacterial reaction centers. Biochemistry 39: 8353–8361

Wakeham MC, Goodwin MG, McKibbin C and Jones MR (2003) Photo-accumulation of the $P^{+}Q_{B}$ radical pair state in purple bacterial reaction centres that lack the Q_{A} ubiquinone. FEBS Lett 540: 234–240

Walz D (1997) Nonequilibrium thermodynamics applied to energy conversion in biological systems. In: Gräber P and Milazzo G (eds) Bioenergetics, pp 1–56. Birkhäuser Verlag, Basel

Wang J, Gosztola D, Ruffle SV, Hemann C, Seibert M, Wasielewski MR, Hille R, Gustafson TL and Sayre RT (2002) Functional asymmetry of Photosystem II D1 and D2 peripheral chlorophyll mutants of *Chlamydomonas reinhardtii*. Proc Natl Acad Sci USA 99: 4091–4096

Warncke K and Dutton PS (1993) Influence of Q_{A} site redox cofactor structure on equilibrium binding, in situ electrochemistry, and electron-transfer performance in the photosynthetic reaction center protein. Biochemistry 32: 4769–4779

Warshel A, Chu ZT and Parson WW (1989) Dispersed polaron simulations of electron transfer in photosynthetic reaction centers. Science 24: 112–116

Wasielewski MR, Johnson DG, Seibert M and Govindjee (1989) Determination of the primary charge separation rate in isolated Photosystem II reaction centers with 500 fs time resolution. Proc Natl Acad Sci USA 86: 524–528

Watanabe T and Kobayashi M (1991) Electrochemistry of chlorophylls. In: Scheer H (ed) Chlorophylls, pp 287–315. CRC Press, Boca Raton

Williams JC, Haffa ALM, McCulley JL, Woodbury NW and Allen JP (2001) Electrostatic interactions between charged amino acid residues and the bacteriochlorophyll dimer in reaction centers from *Rhodobacter sphaeroides*. Biochemistry 40: 15403–15407

Woodbury NW and Parson WW (1984) Nanosecond fluorescence from isolated photosynthetic reaction centers of *Rhodopseudomonas sphaeroides*. Biochim Biophys Acta 767:345–361

Woodbury NW, Parson WW, Gunner MR, Prince RC and Dutton PL (1986) Radical-pair energetics and decay mechanisms in

reaction centers containing anthraquinones, naphtoquinones or benzoquinones in place of ubiquinone. Biochim Biophys Acta 851: 6–22

Xiong L, Seibert M, Gusev AV, Wasielewski MR, Hemann C, Hille CR and Sayre RT (2004) Substitution of a chlorophyll into the inactive branch pheophytin-binding site impairs charge separation in Photosystem II. J Phys Chem 108: 16904–16911

Xu D and Schulten K (1994) Coupling of protein motion to electron transfer in a photosynthetic reaction center: Investigating the low temperature behaviour in the framework of the spin-boson model. Chem Phys 182: 91–117

Xu H, Zhang R-B, Ma S-H, Qu Z-W, Zhang X-K and Zhang Q-Y (2002) Theoretical studies on the mechanism of primary electron transfer in the photosynthetic reaction center of *Rhodobacter sphaeroides*. Photosynth Res 74: 11–36

Xu Q, Baciou L, Sebban P and Gunner MR (2002) Exploring the energy landscape for Q_A^- to Q_B electron transfer in bacterial photosynthetic reaction centers: effect of substrate position and tail length on the conformational gating step. Biochemistry 41: 10021–10025

Yakovlev AG, Shkuropatov AY and Shuvalov VA (2002) Nuclear wave packet motion between P* and $P^+B_A^-$ potential surfaces with a subsequent electron transfer to H_A in bacterial reaction centers at 90 K. Electron transfer pathway. Biochemistry 41: 2667–2674

Yruela I, Torrado E, Roncel M and Picorel R (2001) Light-induced absorption spectra of the D1-D2-cytochrome *b*559 complex of Photosystem II: Effect of methyl viologen concentration. Photosynth Res 67: 199–206

Zech SG, Kurreck J, Eckert HJ, Renger G, Lubitz W and Bittl R (1997) Pulsed EPR measurement of the distance between P^+_{680} and Q_A^- in Photosystem II. FEBS Lett 414: 454–456

Zhang C, Boussac A and Rutherford A W (2004) Low-temperature electron transfer in Photosystem II: A tyrosyl radical and semiquinone charge pair. Biochemistry 43: 13787–13795

Zheleva D, Hankamer B and Barber J (1996) Heterogeneity and pigment composition of isolated Photosystem II reaction centers. Biochemistry 35: 15074–15079

Zinth W and Kaiser W (1993) Time-resolved spectroscopy of the primary electron transfer in reaction centers of Rhodobacter sphaeroides and *Rhodopseudomonas viridis*. In: Deisenhofer J and Norris JR (eds) The Photosynthetic Reaction Center, Vol II, pp 71–88. Academic Press, San Diego

Zouni A, Witt HT, Kern J, Fromme P, Krauß N, Saenger W and Orth P (2001) Crystal structure of Photosystem II from *Synechococcus elongatus* at 3.8 Å resolution. Nature 409: 739–743

Zucchelli G, Jennings RC, Garlaschi FM, Cinque G, Bassi R and Cremonesi O (2002) The calculated in vitro and in vivo chlorophyll-a absorption bandshape. Biophys J 82: 378–390

Chapter 8

The Iron-Quinone Acceptor Complex

Vasili Petrouleas[1]
Institute of Materials Science, NCSR 'Demokritos', 153 10 Aghia Paraskevi Attikis, Greece

Antony R. Crofts[2]
Department of Biochemistry, 419 Roger Adams Lab, 600 S. Mathews Avenue, and Center for Biophysics and Computational Biology, University of Illinois at Urbana-Champaign, Urbana, IL 61801, U.S.A.

Both authors welcome correspondence, email: [1] vpetr@ims.demokritos.gr; [2] a-crofts@life.uiuc.edu

T. Wydrzynski and K. Satoh (eds): Photosystem II: The Light-Driven Water:Plastoquinone Oxidoreductase, pp. 177–206.

Summary

The flux of reducing equivalents out of Photosystem II (PS II) occurs through the two-electron gate function catalyzed by the iron-quinone complex on the acceptor side. The mechanism of the two-electron gate has been studied more completely in bacterial reaction centers, where an understanding of function has benefited from a structural context. However, the two-electron gate was discovered in green plants, and a large body of work had suggested that the mechanism and main structural features are similar in the two systems, and this is now confirmed by structures. In PS II a number of additional properties are found, which result from the redox activity of the non-heme iron of the acceptor complex, and from the lability of its ligands. Pending structures for PS II at a higher resolution, much of the discussion on the molecular architecture had borrowed the structural context from the bacterial homologue. One theme in this chapter is the justification for this borrowing that comes from the application of spectroscopic approaches to the PS II acceptor complex. This has been especially successful in studies of the Q_A-site semiquinone, the magnetic interaction between the semiquinone formed at the site and the iron, and the interaction of external ligands with the iron. A second theme, reflecting the poor stability of the semiquinone of the Q_B-site in isolated PS II preparations, is the use of indirect approaches, including kinetic studies and structural modeling, to understand the structure-function interface. The crystallographic structures now available provide a gratifying validation of these alternative approaches.

I. Introduction

The flux of reducing equivalents out of Photosystem II (PS II) occurs through the two-electron gate function catalyzed by the iron-quinone complex on the acceptor side. The complex consists of two plastoquinone molecules, Q_A and Q_B, separated by a non-heme iron(II) ion, and the protein milieu that houses these redox centers. The two quinones operate as sequential electron acceptors, Q_A being a one- and Q_B a two-electron acceptor. Electron transfer rates between the two quinones are of the order of a few tenths of a millisecond, but these vary depending on the treatment. Speculation about the spatial organization of the iron-quinone complex had been derived mainly from spectroscopic studies and protein-sequence comparisons with the bacterial reaction center (BRC) from *Rhodopseudomonas viridis* and *Rhodobacter sphaeroides*, now validated by crystallographic structures (see Fig. 1 for an overview). In the present chapter we avoid repeating topics that were extensively covered in earlier reviews (Crofts and Wraight, 1983; Rich and Moss, 1987; Diner et al., 1991; Diner and Babcock, 1996). Emphasis is rather given to selected aspects of the iron-quinone complex, the progress that has been made in recent years, and topics/views which were not adequately covered in the earlier reviews.

Abbreviations: Atrazine – 6-chloro-n-ethyl-N′-(1-methylethyl)-1,3,5-triazine-2,4-diamine; BQ – benzoquinone; BRC – bacterial reaction center; Chl – chlorophyll; Cyt – cytochrome; D1, D2 – reaction center core subunits of PS II; DCBQ – 2,5-Dichloro-*p*-BQ; DCMU – 3(3,4-dichlorophenyl)-1,1-dimethylurea; I. S. – isomer shift; NR – neutral red; *o*-phenanthroline – 1,10-phenanthroline; *p*-BQ – 1,4-benzoquinone; PDB – protein data bank; P-p-BQ – Phenyl-*p*-BQ; PQ – plastoquinone; PS II – Photosystem II; Q_A, Q_B, – primary and secondary PQ acceptors of PS II; QSAR – Quantitative Structure Activity Relationship; UQ – ubiquinone

II. Probing the Iron-Quinone Complex Through the Iron Site

A. General

The iron located between the two quinones has strong spectral and structural similarities to the general class (not often recognized as such) of non-heme mononuclear-iron centers found in oxygen-activating enzymes with diverse catalytic functions, including

oxidations, mono- and di-oxygenations, and hydrations (Michel and Deisenhofer, 1988; Anderson et al., 1989; Diner et al., 1991; Lipscomb and Orville, 1992; Que et al., 1996; Feher and Okamura, 1999). Characteristic of this type of iron center is the flexibility of the iron coordination. The coordination number varies between 3 and 6 with the most common ligands being nitrogens (histidine-imidazole), and oxygens (carboxylate, phenolate, water). The variation in the ligand donor set modulates to a great extent the redox potential of the iron between extreme limits. A different number of labile ligands can be found in each case and this is linked to the specific catalytic function of the iron. Characteristic is the reversible binding of small molecules like nitric oxide and cyanide (Lipscomb and Orville, 1992; Orville and Lipscomb, 1997). Hegg and Que (1997) comparing the structures of a number of different enzymes catalyzing diverse reactions noted that, the common coordination feature in this type of iron centers is a 2-His-1-carboxylate facial triad. The occupation of the three remaining coordination sites by additional endogenous protein residues and/or exogenous ligands (e.g., substrate molecules) tunes to a great extent the properties of the metal center (Hegg and Que, 1997; Que, 2000). The iron of the BRC has perhaps the most inert coordination with 4 His plus a fixed glutamate bidentate ligand (Deisenhofer et al., 1985; Allen et al., 1988) and a high E_m (Beijer and Rutherford, 1987; Diner and Petrouleas, 1987b). Based on extensive spectroscopic and sequence homologies (Rutherford, 1987; Michel and Deisenhofer, 1988; reviewed in Diner et al., 1991), the iron of PS II is also assumed to be coordinated by four histidines, two from each of the two protein subunits D1 and D2. Compared to the BRC, there are important differences in the fifth and sixth coordination positions. At least one of these positions is occupied by bicarbonate in PS II (Diner and Petrouleas, 1990). According to FTIR studies, bicarbonate binds as a bidentate ligand in the reduced state of the iron (Fe^{2+}), and monodentate in the oxidized state (Hienerwadel and Berthomieu, 1995). The iron of PS II has at least two labile ligands and is redox active, as detailed below. These properties differentiate it from its bacterial counterpart, and suggest a more rich physiological function. The lability of the bicarbonate ligand probably explains certain heterogeneities associated with the iron-quinone complex.

B. Ligand Exchange Reactions and Effects on the Q_A/Q_B Electron Transfer Rate

In PS II, unlike the BRC where no lability of ligands has been reported, a number of molecules can bind reversibly at the non-heme iron site often in competition with bicarbonate, resulting in most cases in deceleration of the electron transfer.

1. Nitric Oxide

A direct demonstration of exogenous ligand binding to the iron has been provided by treatment with nitric oxide, which gives rise to a pronounced EPR signal at $g = 4.0$, characteristic of an iron-nitrosyl complex with $S = 3/2$ (Petrouleas and Diner, 1990). This is accompanied by an at least tenfold decrease of the electron transfer rate between Q_A and Q_B from the second saturating flash excitation onward (Diner and Petrouleas, 1990). The effects of NO are reversed by the addition of approximately 10 mM bicarbonate (Diner and Petrouleas, 1990). This suggests that bicarbonate is a labile ligand to the iron, confirming earlier predictions (Michel and Deisenhofer, 1988; van Rensen et al., 1988). Orientation studies of the $g = 4$ signal imply that NO, and by extrapolation one of the oxygens of bicarbonate, occupy a position homologous to one of the glutamate oxygens of the purple bacteria (Deligiannakis et al., 1992). Formate, an anion which also competes with bicarbonate (see below), binds simultaneously with NO, as it does not decrease the Fe^{2+}-NO signal but it changes somewhat its rombicity (Diner and Petrouleas, 1990). Direct evidence for the simultaneous binding of NO and another anion to the iron, has been provided by the observation of pronounced superhyperfine structure on the $g = 4$ signal from the fluoride nucleus, under the simultaneous presence of NO and F^- (Sanakis et al., 1999). NO and F^- have been suggested to bind cis to each other in a hexa-coordinate arrangement (Sanakis et al., 1999). It is reasonable to assume that NO and formate bind in a similar fashion. Experiments with oriented membranes (J. Hanley and V. Petrouleas, unpublished) show that the orientation of the $g = 4$ signal principal axes does not change (except for an interconversion of the x and y axis) in the presence of fluoride. This and the fact that the added anions do not alter significantly the spin Hamiltonian parameters of the Fe^{2+}-NO $S = 3/2$ configuration strongly suggests that the iron-NO complex in the absence of exogenous anions is also hexa-coordinate.

It is possible that at the initial stages of bicarbonate displacement, bicarbonate binds simultaneously with NO as a monodentate ligand. Full displacement of bicarbonate (and replacement, for example, by water) is probably facilitated by the reduction of Q_A^-, as the experiment described below suggests. This would offer a possible explanation of the observation mentioned above, that the NO-induced deceleration of the electron transfer develops fully from the second flash and onward (Diner and Petrouleas, 1990). It could also explain the small modification (small increase in rombicity) of the Fe^{2+}-NO EPR signal following the first illumination/dark-adaptation cycle in a series of cycles effecting successive electron transfers among the quinones (Petrouleas and Diner, 1990).

Recently a new mode of transient binding of NO to the iron has been reported. The affinity for this mode of binding is enhanced by the reduction of Q_A (Goussias et al., 2002). The new transient state is trapped at –30 °C and is characterized by EPR signals with *g* values of 2.016 in the presence of NO alone or 2.027 and 1.976 in the simultaneous presence of NO and CN^-. An important implication of the results is a trans influence of Q_A reduction on the bicarbonate ligation to the iron. This is transmitted presumably via hydrogen-bonding (H-bonding) of Q_A with an imidazole ligand to the iron. In the absence of CN^-, NO has been concluded to bind in a 5-coordinate geometry, under these conditions.

Prolonged incubation with NO appears to result in a dinitrosyl-iron species (Goussias et al., 2002). Reduction by free NO explains probably the appearance of weak EPR signals in dark-adapted material very similar to a synthetic $Fe(NO)_2$(imidazole) species, but full evolution of the signal is effected by illumination. Presumably Q_A^- reduces the dinitrosyl complex under these conditions.

The proposed iron coordination in the presence of NO and the various anions is summarized in Scheme 1.

2. Cyanide

Cyanide, binds stepwise (Koulougliotis et al., 1993; Sanakis et al., 1994). With an approximate K_d of 10-20 μM, it eliminates the $g = 4.0$ signal induced

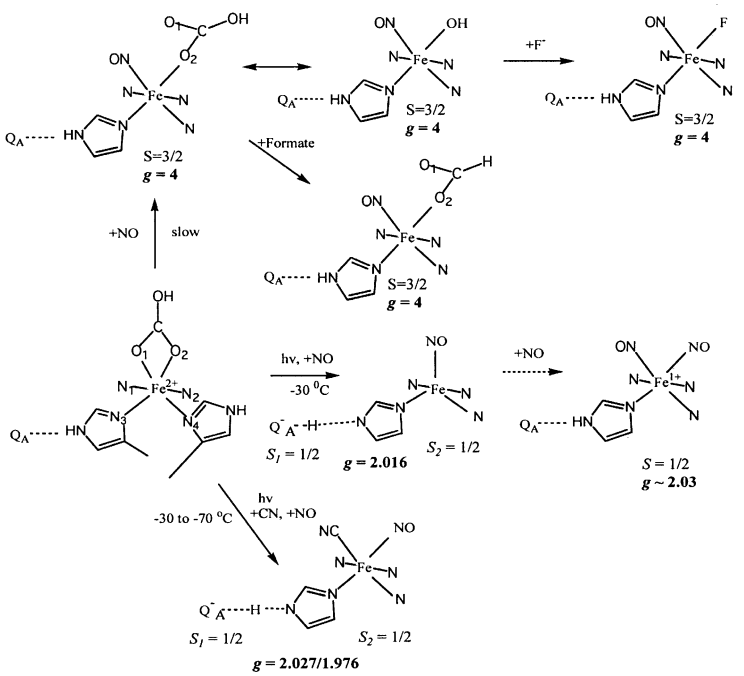

Scheme 1. Suggested modes of NO binding to the iron.

by NO. At higher concentrations, K_d 0.1-0.2 mM, CN^- causes a shift of the $Q_A^-Fe^{2+}$ signal to $g = 1.98$ and modifies the split-pheophytin signal (Sanakis and Petrouleas, 1995), and with an approximate K_d of 1.2 mM it converts the iron to low spin ($S = 0$) (Sanakis et al., 1994). The cyanide experiments imply that up to three sites at (or near) the non-heme iron are accessible to exogenous ligands. The data do not provide direct evidence that all cyanides bind as iron ligands, since binding in the vicinity of the iron could explain some of the effects. It is expected, however, that conversion of the iron ion to its low spin form would require the binding of more than one CN^- ligand. This is corroborated by FTIR studies, which reveal at least two CN^- bands in the Q_A^-/Q_A spectra (Noguchi et al., 1999a). The effects of cyanide can be reversed by prolonged storage in a cyanide free medium at pH 6 (Sanakis et al., 1994).

3. Carboxylate Anions

Apart from NO and cyanide, a number of carboxylate anions appear to bind at the non-heme iron in apparent competition with bicarbonate. Formate (in particular) and acetate have been studied extensively in the past as competitive inhibitors of bicarbonate (Robinson et al., 1984; Stemler and Murphy, 1985; Eaton-Rye and Govindjee, 1988). The extension of the studies to a series of carboxylate anions (e.g., glycolate, glyoxylate, oxalate and lactate) (Deligiannakis et al., 1994; Petrouleas et al., 1994) has yielded important new insights onto the mode of action of the carboxylate ligands to the iron. The anions compete with NO for binding to the iron (Deligiannakis et al., 1994) implying that they bind as bidentate ligands. Formate, the smallest of the carboxylate anions appears to be the only exception, binding simultaneously with NO (see Section II.B.1). Difference (Fe^{2+}/Fe^{3+}) FTIR spectroscopy with ^{12}C- and $^{13}C_1$-labeled lactate indicates that this anion binds through one carboxylate oxygen and the hydroxyl group in both oxidation states of the iron (Berthomieu and Hienerwadel, 2001). Glycolate, an anion that has a similar effect with lactate on the Fe^{3+} EPR spectra (Deligiannakis et al., 1994) and on significantly lowering the midpoint potential of the iron (discussed below), is inferred to bind in a similar fashion (Berthomieu and Hienerwadel, 2001).

4. Effects of the Iron Ligation on the Q_A/Q_B Electron Transfer Rate

Of all the molecules that bind at the iron site bicarbonate appears to be unique (with the possible exception of cyanide, whose effects on the electron transfer rate are not fully understood, Koulougliotis et al., 1993) in supporting an undiminished electron flow in the iron-quinone complex. Replacement with formate is well known to induce a pronounced slowing of the electron transfer rate; a three- to four-fold slowing on the first flash, and a ≥tenfold slowing on subsequent flashes (Robinson et al., 1984; Snel and van Rensen, 1984; Eaton-Rye and Govindjee, 1988). NO has a similar effect (Diner and Petrouleas, 1990). Among the various carboxylate anions examined, glycolate has a similar pronounced effect and notably it exerts its effects at a concentration at least 3-fold lower than that of formate with a K_m of 0.5–0.7 mM at pH 6.3 (Petrouleas et al., 1994). Glyoxylate and oxalate induce less pronounced effects (Petrouleas et al., 1994). It has been suggested that bicarbonate plays a role in the protonation of Q_B (Stemler and Murphy, 1985; van Rensen et al., 1988; Diner et al., 1991). The parallel effects of the various anions on the midpoint potential (and its pH dependence) of the iron (see below), the $Q_A^-Fe^{2+}$ EPR signals (see below), and the Q_A/Q_B electron transfer rate, could be explained if we assume that, binding of the anions to the iron modifies the pK_a of a nearby group(s) involved in the protonation of Q_B (Nugent et al., 1988; Deligiannakis et al., 1994; Petrouleas et al., 1994). Insights are offered by FTIR studies, which indicate a hydrogen-bond network from the non-heme iron toward the Q_B pocket involving bicarbonate and D1- His215 (Berthomieu and Hienerwadel, 2001). Independent support of these suggestions comes from the counter effect that Q_A reduction has on the bicarbonate ligation (detected by the use of NO) transmitted via the H-bonding of D2-His 215 to Q_A^- (Goussias et al., 2002; see Scheme 1). The symmetric shape and binding of the bicarbonate molecule, the pK_a of its protonatable groups together with its size could be critical factors in the support of its proposed role. When bicarbonate is exchanged by other molecules, e.g.. NO, an alternative slow proton pathway may function. As however, according to scheme 1, bicarbonate may still remain bound as a monodentate ligand until after the reduction of Q_A by a first flash in a flash series, the protonation-limited slowing of the electron transfer appears after the second flash. It is possible that certain anions whose effect on the electron transfer rate is moderate (e.g., glyoxylate), can substitute in part for bicarbonate or affect the pK_a values of protonatable groups along the proton translocation pathway.

C. Redox Properties of the Iron

The interesting redox properties of the iron have been reviewed extensively in the past (Diner and Petrouleas, 1987b). Briefly, the Fe^{3+}/Fe^{2+} couple has been identified as the Q_{400} electron acceptor (Ikegami and Katoh, 1973) with a midpoint potential of about 400 mV at pH 7 that varies by approximately –60 mV per pH unit between pH 5.3 and 8.5 (Bowes et al., 1979a; Petrouleas and Diner, 1986). This potential is rather high for participation of the iron in electron transfer reactions. Once the iron is oxidized, however, Q_A^- reduces it rapidly ($t_{½}$ = 7 μs at pH 6.5, reviewed in Diner and Petrouleas, 1987b). On the other hand a number of exogenous quinones (e.g. *p*-BQ, P-*p*-BQ, and DCBQ) acting through the Q_B site can oxidize the iron, once reduced by Q_A^- to the semiquinone form (Zimmermann and Rutherford, 1986; Petrouleas and Diner, 1987a,b). The carboxylate anions that compete with bicarbonate for binding at the iron modify significantly the redox properties of the iron (Deligiannakis et al., 1994). Glycolate and lactate lower the midpoint potential to 340 mV and make it pH-independent, while oxalate, malate and formate induce midpoint potentials higher than 500 mV in the pH range 6.1 to 7.5. Glyoxylate and pyruvate have intermediate effects. The effect of these anions has being attributed to the shift of the pK_a of an ionizable group that is responsible for the pH dependence of the midpoint potential of the iron. Molecules that bind at the Q_B site (DCMU, *o*-phenanthroline, atrazine, P-p-BQ) appear to raise to a variable extent the midpoint potential of the iron. Oxidation of the iron, on the other hand, lowers the affinity for binding at the Q_B site (Wraight, 1985).

D. Spin States of the Iron and the Semiquinone-Iron Magnetic Interactions

The iron can attain a variety of spin states following a number of reversible treatments.

S = 5/2, obtained in the Fe^{3+} state. The EPR spectra are characterized by resonances at g = 8.15, 5.63, 3.51 (Petrouleas and Diner, 1986) assigned to a system with parameters, D = 2–3 K, E/D = 0.11 (Diner and Petrouleas, 1987b; Aasa et al., 1989). Binding of exogenous molecules at the Q_B site reduces the E/D value resulting in some cases in axial spectra (Itoh et al., 1986; Diner and Petrouleas, 1987a,b). Orientation studies indicate that the g_y axis runs along the homologous direction of the bacterial twofold symmetry axis (Deligiannakis et al., 1992). The g_z axis is inferred to lie along the N-Fe-N direction defined by the nitrogen ligands from the histidines not participating in the binding of the two quinones. Photoreducible high-spin iron signals initially attributed to heme iron have been now assigned to the non-heme iron of the acceptor side (Nugent, 2001). Carboxylate molecules bound on the iron exert small effects on the D parameter but some of the anions induce resonances at g = 4.3 corresponding to D = 0.7 K and E/D = 0.315 (Deligiannakis et al., 1994). No evidence for the trapping of the intermediate $Q_A^-Fe^{3+}$ has been presented. It is possible, however, that the light-induced decrease of the Fe^{3+} signal at 77 K and lower temperatures (Diner and Petrouleas, 1987b; Nugent, 2001) may be due to the alteration of the Fe^{3+} signal by the magnetic interaction with Q_A^- rather than the reduction of the Fe^{3+}, which may be limited by the uptake of a proton.

S = 2, natural state (Fe^{2+}) in the majority of centers. No EPR signals have been reported for this integer-spin state, but Mossbauer spectroscopy has provided valuable information (reviewed in Debrunner, 1996). Useful insights have been provided by comparison with a series of synthetic model compounds (Boinnard et al., 1990; Garge et al., 1990; Rakotonandrasana et al., 1991; Martinez Lorente et al., 1995). The Mossbauer spectra in BBY preparations are heterogenous containing at least two components assigned to the non-heme iron with a common isomer shift of 1.19 mm/s and quadrupole splittings 2.07 mm/s (comp.1), and 2.99 (comp. 2) (Petrouleas et al., 1992). Component 2 appears to be the dominant one in most preparations (Petrouleas et al., 1992; Picorel et al., 1994; Garbers et al., 1998). In preparations from *Chlamydomonas reinhardtii* a single component with a similar isomer shift but an average quadrupole splitting was observed (Petrouleas and Diner, 1982). The isomer shift in all cases indicates octahedral coordination with oxygens or nitrogen ligands, as was originally suggested for the homologous iron in *R. sphaeroides* R-26 (Debrunner et al., 1975; Boso et al., 1981). Treatment with formate converts all of the absorption area to a component 1 type spectrum (Diner and Petrouleas, 1987b; Semin et al., 1990; Petrouleas et al., 1992). In the reduced state, the primary quinone, Boinnard et al., 1990; (S=½), interacts magnetically with the non-heme iron (S = 2). This results in a severe broadening of the EPR spectrum of the semiquinone and the appearance of heterogenous features in the g 1.6 – 1.9 region of the EPR spectra

(Nugent et al., 1981; Rutherford and Zimmermann, 1984; Nugent et al., 1992) with pronounced anisotropy (Rutherford, 1985). Notable is the pH dependent equilibrium between the '1.9' and the '1.84' form of the $Q_A^-Fe^{2+}$ signal (Rutherford and Zimmermann, 1984) and the dramatic enhancement by formate of the g = 1.84 form of the $Q_A^-Fe^{2+}$ signal (Vermaas and Rutherford, 1984). A correlation appears to exist between component 1 in the Mossbauer spectra, the g = 1.84 form and the non-oxidizable configuration of the iron (Petrouleas et al., 1992; Deligiannakis et al., 1994). The smaller quadrupole splitting value of component 1 (Petrouleas et al., 1992), as well as of the bacterial Fe^{2+} (Debrunner et al., 1975; Boso et al., 1981), has been assigned to a radial expansion of the 3d electrons of the iron, an effect that would stabilize the Fe^{2+} oxidation state, as observed experimentally. Apart from formate a number of carboxylate anions substituting for bicarbonate appear to support either the '1.9' or the '1.84' configuration (Deligiannakis et al., 1994). The pH-dependent heterogeneity in the presence of bicarbonate alone and the changes induced by the various carboxylate anions have been attributed to the shift of the pK_a of a critical ionizable group (Deligiannakis et al., 1994), possibly His D1-215 (Berthomieu and Hienerwadel, 2001). Cyanide at moderate concentrations induces an entirely new $Q_A^-Fe^{2+}$ EPR signal with pronounced intensity at g = 1.98 (Koulougliotis et al., 1993). The shift of the signal close to g = 2.0 must be due primarily to changes in the zero-field splitting of the iron(II) .

EPR signals in the g = 1.8 to 1.9 region have been also reported for the $Q_B^-Fe^{2+}$ state (Heathcote and Rutherford, 1987; Hubbard et al., 1989). A prominent EPR signal at g = 1.66 has been detected from the state $Q_A^-Fe^{2+}Q_B^-$ (Hallahan et al., 1991).

S = 3/2, obtained by the binding of NO to the iron. The EPR spectra are characterized by a prominent derivative at g = 4, indicative of axial symmetry with a small rhombicity (Petrouleas and Diner, 1990). The respective spin Hamiltonian parameters are, D = 10 ± 2 cm^{-1} and E/D = 0.013 and these change slightly following the simultaneous binding of formate (Diner and Petrouleas, 1990) or fluoride (Sanakis et al., 1999). In the presence of fluoride the parameters become D = 8 cm^{-1} and E/D = 0.025, as determined by the simulation of the EPR spectra at two different microwave frequencies, X and Q band (Sanakis et al., 1999). Studies of oriented spinach membranes treated with NO show that g_x lies on the membrane plane while g_y is oriented at 30° and g_z at 60° with respect to the membrane plane (Deligiannakis et al., 1992). A similar axes orientation is observed in the simultaneous presence of F^- (Hanley and Petrouleas, unpublished). The simultaneous binding of NO and fluoride to the iron induces prominent hyperfine splitting of the g = 4 resonance from the fluoride nucleus (I = ½). Following reduction of Q_A the system of the two half-integer interacting spins (½ for the semiquinone and 3/2 for the iron-NO complex) does not have detectable resonances at X-band frequencies but it has resonances at Q band. In the simultaneous presence of fluoride, however, prominent resonances with components in perpendicular and parallel mode EPR at X- and Q-band frequencies are observed. The system of the two half-integer interacting spins has been successfully simulated with an antiferromagnetic-coupling constant of 0.5 cm^{-1} in the presence, and 1.3 cm^{-1} in the absence of F^- (Sanakis et al., 1999). No isotopic effect (^{14}NO-Fe vs ^{15}NO-Fe) could be detected in the CW EPR and ESEEM spectra, indicating that the spin density on the nitrogen nucleus of NO is very small (Deligiannakis et al., 1998). The coupling to three or four imidazole nitrogens could be detected by the application of the Hyscore spectroscopy, yielding the first spectroscopic evidence supporting histidine ligation to the iron (Deligiannakis et al., 1998).

S = ½, obtained under variable conditions. These conditions are: (i) chemical oxidation of the iron in the presence of high concentrations of cyanide (2 or 3 cyanide ions bound on the iron) (Sanakis and Petrouleas, 1995). The EPR spectra are characterized in this case by weak resonances at g_x = 2.60 and g_y = 2.33. (ii) binding of NO or NO and CN in the presence of the reduced Q_A at –30 °C (Goussias et al., 2002). New $Q_A^-Fe^{2+}$ EPR signals appear in this case at 2.016, presence of NO alone, or 2.027, 1.976 in the simultaneous presence of NO and CN^- and unlike all other signals from the complex (with the exception of the free semiquinone signal) the signals saturate at very low microwave power. Electron Spin Echo Envelope Modulation (ESEEM) experiments show the existence of two protein ^{14}N nuclei coupled to electron spin. These two nitrogens have been detected consistently in the environment of the semiquinone Q_A^- in a number of PS II preparations. The signals can be simulated with the assumption of a S = ½ state of the iron-NO(CN) complex interacting with the semiquinone radical with aniferromagnetic J values in the range 0.025 t0 0.05 cm^{-1} (Goussias et al., 2002). (iii) binding of two NO molecules on the iron. One-

electron reduction of this dinitrosyl species yields a half integer configuration characterized by *g* values of 2.05, 2.03, 2.01 (Goussias et al., 2002).

S = 0, diamagnetic state of the iron. This state is obtained in the presence of high concentrations of cyanide (2 or 3 cyanide ions bound on the iron) and is characterized by Mossbauer spectra with isomer shift = 0.26 mm/s and quadrupole splitting = 0.36 mm/s (Sanakis et al., 1994). The conversion of the iron to a diamagnetic form has allowed the observation and study of the unperturbed semiquinone radical at *g* = 2.045 (see below). Mossbauer experiments in a PS^- mutant from *C. reinhardtii* (Burda et al., 2003) indicated that the non-heme iron in these preparations occurs naturally in a low spin form.

The free semiquinone, Q_A^-, radical. Apart from the reversible conversion of the iron to *S* = 0 by cyanide (Sanakis et al., 1994), Q_A^- can be decoupled from the iron by treatments extending an original method of Klimov et al. (1980), including trypsinization (Macmillan et al., 1990) or replacement of the iron with the diamagnetic Zn^{2+} (Astashkin et al., 1995) (the binding of Zn^{2+} has not been demonstrated under these conditions), or by treatment of core complexes from *Synechocystis* with high concentrations of phosphate on the hydroxyapatite column (Tang et al., 1995), or by a high pH treatment (Deligiannakis et al., 1997). Probably all these treatments (except for the cyanide treatment) result in removal of the iron (Kurreck et al., 1996; Deligiannakis et al., 1999). The decoupled Q_A^- is characterized at X-band EPR by a 9.5 G wide derivative at *g* = 2.0045 (Sanakis et al., 1994) with resolved anisotropy at Q-band EPR and an unusually large g_{xx} component indicating weaker hydrogen bonds compared with plastosemiquinone in solution and possible π-interaction with aromatic amino acid residues (MacMillan et al., 1995a). The application of ^{1}H-ENDOR spectroscopy (MacMillan et al., 1995b; Rigby et al., 1995; Zheng and Dismukes, 1996) has provided useful information about the orientation of the hydrogen bonds and has indicated an asymmetry in the H-bonding. ESEEM spectroscopy detected coupling of the semiquinone electron spin to protein nitrogens (Astashkin et al., 1995; Deligiannakis et al., 1995, 1997; MacMillan et al., 1995a; Tang et al., 1995; Astashkin et al., 1998; Deligiannakis et al., 1999). These studies have been extended to intact preparations in which the iron is in its high-spin form (Peloquin et al., 1999). Apart from variations attributed to the effects of the different treatments and the pH, the experiments agree generally on the presence of two interacting nitrogen nuclei. These have been assigned to D1-Ala261 and D1-His215 (Astashkin et al., 1995; Deligiannakis et al., 1997), but this is contested by Peloquin et al. (1999) based on site directed mutagenesis and earlier His-labeling studies (Tang et al., 1995). It is generally agreed however that H-bonding between D1-His215 and Q_A^- exists (although its spectroscopic signature is not agreed upon), as suggested by FTIR studies (Noguchi, 1999a,b), too, and by analogy with the arrangement in the photosynthetic bacteria (Spoyalov et al., 1996). This H-bonding serves presumably as a conduit for the magnetic interaction between Q_A^- and the iron.

E. On the Role of the Iron

The iron is located midway between the two quinones, but its direct participation in the electron transfer reactions has not been demonstrated. Actually, the use in the iron-quinone complex of a type of iron that is not generally employed in electron transfer reactions, but rather in catalytic reactions, suggests that the iron could serve alternate roles. It cannot be a mere coincidence that PS II, a photochemical center that performs one of the most crucial and at the same time potentially harmful (through its byproducts) reactions (the splitting of water), would employ a reactive and redox active conformation of this type of iron. Of the rather extensive list of proposed roles of the iron (reviewed in Diner and Petrouleas, 1987b; Diner et al., 1991), we will concentrate on a few likely functions.

A minimal role. The similar organization and function of the acceptor side of the reaction centers of the bacteria and PS II, despite the gross differences in the donor side organization and function, suggests that the iron plays an essential role common to both systems. It is reasonably assumed that the iron is an important structural element around which the reaction center is organized (Diner et al., 1991). Furthermore, the role of the iron in stabilizing the semiquinone form of Q_A has been demonstrated (Dutton et al., 1978).

Regulation of the electron transfer rate on the acceptor side. The lability of the iron ligands in non-heme (non-iron-sulfur) proteins is associated with specific catalytic reactions. In PS II this property is associated with at least one function, the unusual regulation of the electron transfer rate known as the bicarbonate effect, (Chapter 14, van Rensen and Klimov). The presence of bicarbonate as a ligand to

the iron is essential for the undiminished electron flow between the two quinones. The physiological need for such a control mechanism has been stressed earlier (Diner et al., 1991), and can be outlined briefly as follows. In cases of low CO_2/HCO_3^- stromal concentrations, bicarbonate would dissociate from the iron resulting in a diminished electron transfer rate by PS II and accordingly lower O_2 production, reducing the wasteful reaction of RuBP with excess O_2 (photorespiration). An attractive extension of this idea has considered glycolate, a product of photorespiration and an efficient competitor of bicarbonate, as being involved in a feedback mechanism under these conditions (Petrouleas et al., 1994). It has been noted however, that the binding of glycolate is poor at the physiological high pH of the stromal side. The possibility however, that the relative affinity of bicarbonate and glycolate for the iron site changes during illumination, remains to be tested. Of interest in this respect are the recent experiments with NO implying that the binding affinity of bicarbonate is significantly reduced in the Q_A^- state (Goussias et al., 2002).

Protective functions. The function of the iron-quinone complex in a potentially O_2-rich environment renders it susceptible to damage by the reaction with active oxygen species. Such species could be produced at the donor side or via interaction of O_2 with the reduced quinones (Cleland and Grace, 1999; Nugent, 2001). The iron has accordingly been proposed to have a protective role, acting as an oxidase or a catalase (Diner and Petrouleas, 1987b) or as a weak superoxide dismutase (Nugent, 2001). From a different perspective, the binding of superoxide to a metal center, most likely the non-heme iron, to form a peroxide intermediate has been proposed recently as an important pathway in $OH^{\bullet}$ production during photodamage (Pospisil et al., 2004). It is notable that the iron has all the properties that could support a catalytic role. It has labile ligands, it is redox active, has direct access to the electron transfer chain (Q_A^- reduces Fe^{3+} with a $t_{½} = 7$ μs at pH 6.5, reviewed in Diner and Petrouleas, 1987b), and is properly located between the two quinones.

In summary, while the iron in both BRC and PS II is an essential structural element of the electron-transport chain, in PS II it also has a catalytic role. It is notable that the location of the iron would couple a catalytic function to photochemical electron transfer. This is a rare combination not found in other proteins employing this type of iron.

III. Organization of the Quinone Binding Sites: The Two-Electron Gate

A. Structural Models of the Quinone Sites

Neither of the earlier crystallographic structures of PS II available at the time of writing (Zouni et al., 2001 (PDB ID 1fe1); Kamiya and Shen, 2003 (PDB ID 1izl)) was at a resolution that allowed detailed discussion, and neither showed a Q_B-site occupant (Chapters 19, Witt; and 20, Shen and Kamiya). This likely reflected both a weaker occupancy of the Q_B-site than of the Q_A-site, and also some loss of structural integrity on detergent extraction, so that the isolated protein had an even lower occupancy than in situ. Based on the homology in sequence between D1, D2, and L, M subunit pairs, and the common physicochemical and biochemical properties of the acceptor side, several groups had modeled structures for the PS II site, using the reaction centers from *Rps. viridis* and *Rb. sphaeroides* as a template (Crofts et al., 1987; Bowyer et al., 1990; Ruffle et al., 1992; Xiong et al., 1998a). For the Q_A-site, much spectroscopic evidence is available to support the validity of these models, as discussed above, but no detailed spectroscopic information of a similar quality is available for the Q_B site. As a consequence, discussion of the structure-function interface has had to depend on indirect methods for information about the molecular architecture. The BRC-based models served as a valuable aid for understanding the binding of plastoquinone and inhibitors to the Q_B-site of PS II, and although the earlier PS II structures were at a relatively low resolution, they did show a conformation around the putative Q_B pocket similar to that expected from the models. Since submission of this review, a more complete structure has become available (Ferreira et al., 2004; PDB ID 1s5l; Chapter 21, Barber and Iwata) that contains both Q_A and Q_B quinones (Fig. 1), and in which side chain coordinates have been modeled. The structure shows a configuration of the acceptor side similar in essentials to that modeled in the late 1980s (Crofts et al., 1987) (Fig. 2), although rotamers chosen for side chains in the earlier model were in some cases inappropriate. The configuration consists of the carboxyl-terminal end of the **D**-helix, followed by a loop (the 'PEST'-like loop, with no homology in the bacterial structure) connecting to a transverse **de**-helix, which is connected by a sharp turn and an extended loop to the amino-terminal end of **E**-helix. These spans frame

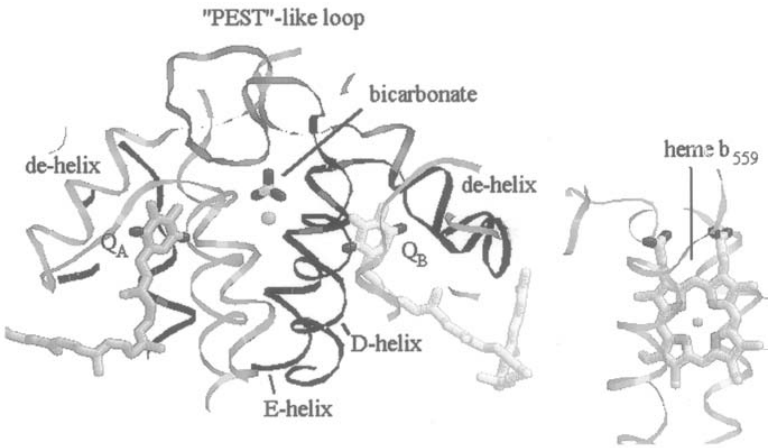

Fig. 1. Photosystem II viewed from the side to show the topology of the acceptor side. Coordinates were taken from the structure by Ferreira et al. (2004) (PDB ID 1s5l), by abstraction of a monomer of the main functional subunits and chromophores. The D1 subunit (with the 'PEST'-like loop) and D2 are shown by ribbons. Prosthetic groups are shown as stick models, comprising the C-atoms of Q_A, Q_B, and bicarbonate and heme b_{559}. Other structural features discussed in the text are indicated. See Color Plate 16, Fig. 1.

the Q_B binding pocket. The helical ends of **D** and **E** were expected to contain the conserved Fe ligands, D1-His 215 and D1-His272, now identified as such in the Ferreira et al. (2004) structure.

In BRCs, the H-bonding of the quinone at the Q_B-site, and the mechanistic implications, are still somewhat controversial. Interpretation of earlier structures was likely confused by partial occupancy, and by contributions to the electron densities from water, and from quinone in two different positions (Lancaster and Michel, 1997; Stowell et al., 1997). In more recent studies with *Rb. sphaeroides*, structures of the dark-adapted reaction center show most of the quinone displaced about 5 Å out of the pocket (Stowell et al., 1997; Fritzsch et al., 1998; Kuglstatter et al., 2001). On illumination, the quinone rotates and moves so that the Q_B-pocket is fully occupied, likely by a reduced form (Stowell et al., 1997). The functional significance of the quinone displacement seen in these crystallographic structures has been challenged by Breton and colleagues on the basis if FTIR spectra that favor a proximal position for the active quinone, similar to that observed for the semiquinone (Breton et al., 2002; Nabedryk et al., 2003). Studies of the temperature dependence of electron transfer from Q_A^- to Q_B in spinach chloroplasts, combined with measurements of protein flexibility through Mossbauer spectroscopy of ^{57}Fe-enriched material have shown an inhibition that correlates with decreased flexibility (Garbers et al., 1998; Reifarth and Renger, 1998). This was interpreted as showing a similar need for structural reorientation of the headgroup of plastoquinone in the Q_B-pocket of PS II. However, in view of the FTIR evidence, this interpretation should be regarded as tentative. In the BRC, the bonding of the reduced form after illumination was similar to that originally suggested in the *Rps. viridis* structures (1prc and 2prc; Deisenhofer et al., 1995; Lancaster and Michel, 1999), including H-bonds with the L-subunit to His190 (an Fe-ligand), backbone -NH groups from Ile224 and Gly225, and to -OH of Ser223. The latter was also H-bonded to Asn(Asp)213. When ubiquinone is displaced by 1,3,5-triazine (7prc), the herbicide binds through similar H-bonds to the two backbone -NH groups and to -OH of Ser223 and also to -OH of Tyr222 (Lancaster and Michel, 1999). The H-bonding distances suggest that the serine bond is no stronger with triazine (2.93 Å) than with the UQ-2 (2.79 Å).

In BRCs, extensive kinetic, mutational and computational studies have provided a comprehensive picture of the mechanism of electron and proton transfer (reviewed by Okamura et al., 2000; Wraight, 2004), but in the structural context of the proteolipid/detergent micelle. In PS II, kinetic characterization of mutant strains modified in the D1 subunit, and comparison of the patterns of inhibitor sensitivity, provided some validation of the structural models, as

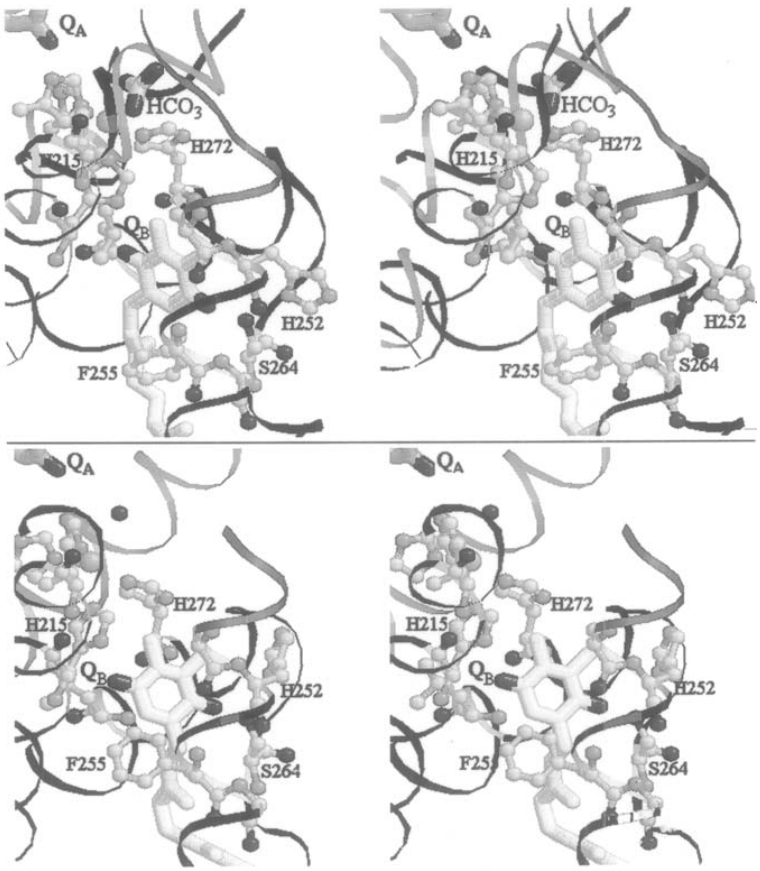

Fig. 2. The Q_B-site structure compared to the model. The structure is from PDB ID 1s5l (Ferriera et al., 2004) viewed looking down into the Q_B-site from the N-phase. The model is that from Crofts et al. (1987), with refinement by H. H. Robinson, C. Yerkes and A. R. Crofts (unpublished) viewed from a similar perspective. Residues referred to in the text are highlighted.

will be discussed at greater length below. In an early model of the PS II Q_B-pocket based on the *Rps. viridis* structure as a template (Fig. 2), we assumed that plastoquinone and atrazine bound to the residues of the D1-subunit shown by alignment to be homologous to L-subunit residues, e.g., His215 (*His190*), Asn266 (*Gly225*), and possibly Ser264 (*Ser223*) (bacterial residues in italics), through H-bonds in the Q_B-site (*A. hybridus* sequence), with additional groups of interest His252 (*Asp (Asn)213*), Phe265 (*Phe216*) (Crofts et al., 1987). The choice of -NH backbone H-bonds was somewhat arbitrary, since, although the putative serine ligand (Ser264/*Ser223*) is well conserved, D1 has an extra residue between Ser264 and His272 (the other Fe ligand) compared to the L-subunit. The figure shows the putative liganding residues, several others modified in strains with herbicide resistance (see below), and His252, suggested to be the residue responsible for binding a proton to stabilize Q_B^- in the site (Crofts et al., 1987; Bowyer et al., 1990). More recent models had suggested additional features that are absent from the bacterial template, including potential sites for bicarbonate binding (Ruffle et al., 1992; Xiong et al., 1998a). The bi-dentate liganding of the Fe by bicarbonate suggested in the latter model is well supported by EPR and FTIR studies. These features are now all confirmed in the Ferreira et al. (2004) structure.

B. Mechanism of the Two-Electron Gate

1. Kinetic Models of the Two-Electron Gate

Although the Q_B-site has been recalcitrant to exploration by molecular spectroscopy, a major advantage of studies of the two-electron gate in oxygenic systems has been the ability to follow the kinetics of electron transfer in intact membrane preparations through use of the change in fluorescence yield. As the closed reaction center reopens, the high fluorescence yield associated with reduction of Q_A^- evolves to a low fluorescence state with kinetics reflecting the electron transfer to the Q_B-site occupant (Joliot, 1974; Bowes and Crofts, 1980). Because the reaction center communicates with the plastoquinone pool in the native configuration, the rates measured depend not only on the rate constants for electron transfer, but also on the occupant of the Q_B-site (quinone or semiquinone), and on the kinetics of exchange of Q and QH_2 with the pool. Recognition of the contribution of these exchange processes to the kinetics made it possible to obtain detailed kinetic parameters describing both the electron transfer and the interaction with the quinone pool (Robinson and Crofts, 1983).

The commonly accepted model is the two-electron gate proposed by Bouges-Bocquet (1973) and Velthyus (1974, 1981) for PS II, and by Wraight (1981) for BRCs, in which quinone and quinol forms freely exchange at the Q_B-site, and the semiquinone form generated after one flash is non-exchangeable. However, we should note that there are dissenting views (Kashino et al., 1996). Kinetic models for the reactions of the two-electron gate in BRCs and chloroplasts have been extensively reviewed (Crofts and Wraight, 1983; Shinkarev and Wraight, 1993; Okamura et al., 2000; Wraight, 2004).

In an early model for green plants, based on experiments with pea thylakoid membranes, Robinson and Crofts (1983) recognized explicitly the relatively weak binding of plastoquinone, required to account for the biphasic nature of the electron transfer following a single flash from the dark-adapted state. The slower phase was attributed to the second-order process of reduction of quinone from the pool (Scheme 2). A similar model has recently been used to measure the deuterium isotope effect on the rates of the separate electron transfers (de Wijn and van Gorkom, 2001). In the earlier model, the pH dependence of the apparent equilibrium constant for sharing an electron between primary and secondary quinones, K_{app}, was accounted for by postulating a single residue close to the Q_B-site whose pK was changed when Q_B was reduced to form the semiquinone anion (Robinson and Crofts, 1983, 1987; Crofts et al., 1984). With modification, this model also accounted well for the kinetics and thermodynamics of inhibitor binding at the Q_B-site (Taoka and Crofts, 1987; Taoka, 1989) of electron transfer in susceptible and resistant *Amaranthus hybridus* biotypes (Bowes et al., 1980; Taoka, 1989;

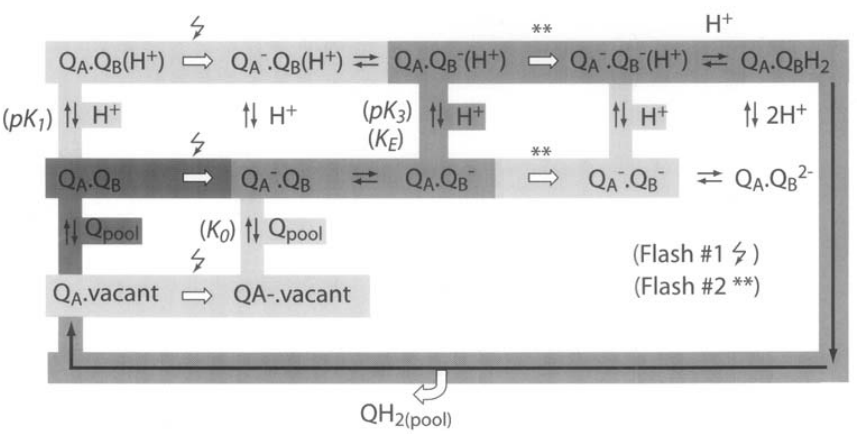

Scheme 2. The kinetic model discussed. Under physiological conditions, most centers start in the dark-gray box, and progress through the mid-gray path. The remainder start in the light-gray box, and rejoin the mid-gray pathway after the second-order binding of PQ from the pool. See text for details.

Taoka and Crofts, 1990), and in herbicide resistant mutants of *C. reinhardtii* (Crofts et al., 1993). Since this more complete model has been described only briefly (Taoka and Crofts, 1990), we will summarize its main points here.

The biphasic kinetics in the 10 ms range were assumed to reflect two distinct populations of PS II. Reaction centers after long dark adaptation have either a secondary quinone bound at the Q_B-site (Q_AQ_B), or a vacant Q_B-site (Q_A.vacant), as shown in Scheme 2. An actinic flash produces either Q_A^-.vacant, or $Q_A^-Q_B$. Both Q_A^-.vacant and $Q_A^-Q_B$ are closed centers, with the same high fluorescence yield. At time >50 μs after the flash, when reactions on the donor side have reached equilibrium, the fluorescence yield reflects the electrons remaining on Q_A^-. In centers initially in the Q_AQ_B state, the electron is transferred to Q_B in a first-order process, generating $Q_AQ_B^-$ (with low fluorescence), with a half time of approximately 150 to 200 μs. Since the electron on Q_A can be transferred to Q_B only when a plastoquinone is present at the Q_B-site, electron transfer in centers initially with a vacant site must first involve a binding of quinone in a second-order process, and then transfer of the electron, with a slower kinetics reflecting the convolution of the binding and electron transfer reactions. Both phases are well fitted by exponential decay curves. Since the more rapid phase accounted for more than half those centers which transfer an electron within 10 ms, and the quinone pool was oxidized under our conditions, the minor fraction of initially vacant centers would become occupied from a pool of plastoquinone in greater than five-fold excess over the reaction center. Reaction from this pool would therefore follow pseudo-first-order kinetics.

Rate constants for electron transfer and binding reactions can be calculated from the kinetic curves for the two separate electron transfers observed after one or two actinic flashes given to preparations starting in a defined initial state (usually with all centers having an oxidized Q_B, following prolonged dark-adaptation). Analysis of the decay kinetics after the first flash can be greatly simplified by making use of the following explicit assumptions derived from the model outlined above: (i) the ratio of the amplitude of the fast component to that of the slow component in the decay kinetics following an actinic flash is equal to the ratio of the fraction of reaction centers initially in the Q_AQ_B state over that in the Q_A.vacant state; (ii) under our experimental conditions, the binding of a plastoquinone to the vacant site is a pseudo-first order reaction; (iii) the dissociation constant of a plastoquinone from its binding site following an actinic flash (from $Q_A^-Q_B$) is the same as that in the dark (from Q_AQ_B).

Solution of the standard rate equations gives Eqs. (1) and (2) for the observed rate constant r_1 and r_2. The apparent equilibrium constant for sharing an electron between quinones Q_A and Q_B is K_{app}, defined in Eq. (3). The dissociation constant, K_0, of plastoquinone from the Q_B-site, is the ratio of the on- and off-rate constants (k_{AV}, k_{VA}) (Eq. (4)). K_E is the equilibrium constant for the electron transfer reaction, with forward and reverse rate constants k_{AB} and k_{BA}. The equilibrium constants are related through Eqs. (3) and (4) (see below for further discussion).

$$r_1 + r_2 = k_{VA}(1 + K_0) + k_{BA}\{1 + K_{app}(1 + K_0)\} \quad (1)$$

$$r_1 r_2 = k_{VA}k_{BA}(1 + K_0)\,(1 + K_{app}) \quad (2)$$

$$K_{app} = \frac{\left[Q_AQ_B^-\right]}{\left[Q_A^- \cdot vac\right] + \left[Q_A^- \cdot Q_B\right]} = \frac{\dfrac{k_{AB}}{k_{BA}}}{\left(1 + \dfrac{A_0}{B_0}\right)} = \frac{K_E}{(1 + K_0)} \quad (3)$$

$$K_0 = \frac{A_0}{B_0} = \frac{k_{AV}}{k_{VA}} = \frac{\left[Q_A \cdot vac\right]}{\left[Q_AQ_B\right]} \quad (4)$$

In these equations, species in square brackets represent fractions of the reaction centers in a particular state as indicated in the bracket. States $Q_A.vac$ and $Q_A^-.vac$ represent centers with a vacant Q_B-site, with the Q_A oxidized and reduced respectively. Variables r_1 and r_2 are the measured rate constants for the slow and fast phases of electron transfer derived directly from the biphasic decay kinetics of Q_A^- by fitting the kinetic curves with two exponential components and a residual. The Q_A^- kinetics are obtained from the fluorescence curves after the latter have been corrected for the non-linear relation between fluorescence yield and concentration of Q_A^-. Variables A_0 and B_0 are the amplitudes of the slow and fast components of the biphasic decay kinetics, again obtained directly from kinetic analysis of the data.

Using the above equations, the four rate-constants k_{AV}, k_{VA}, k_{AB} and k_{BA} (defined in Table 1) can be deter-

Table 1. Physico-chemical constants for the reactions of the two-electron gate following an actinic flash

Constant	Reaction	Wild type	S264G	Notes
A. pK values				(1)
pK_1	$Q_AQ_B\,(H^+) \leftrightarrows Q_AQ_B + H^+$	6.2	6.2	
pK_2	$Q_A.vac\,(H^+) \leftrightarrows Q_A.vac + H^+$	6.9	6.2	
pK_3	$Q_AQ_B^-\,(H^+) \leftrightarrows Q_AQ_B^- + H^+$	8.1	7.0	
B. Equilibrium (K) or rate (k) constants				
$K_{O,\,pK}$	$Q_A^-Q_B \leftrightarrows Q_A^-\,(+\,Q_{pool})$	0.12 ± 0.02	0.57 ± 0.06	(2,3)
K_E	$Q_A^-Q_B \leftrightarrows Q_AQ_B^-$	3.1 ± 0.7	4.7 ± 0.8	
k_{VA}	$Q_A^-\,(+\,Q_{pool}) \rightarrow Q_A^-Q_B$	500	650	(2,4)
k'_{VA}	$Q_A^-(H^+)\,(+\,Q_{pool}) \rightarrow Q_A^-Q_B(H^+)$	500	650	(2,4)
k_{AV}	$Q_A^-Q_B \rightarrow Q_A^-\,(+\,Q_{pool})$	60	370	(2,4)
k'_{AV}	$Q_A^-Q_B(H^+) \rightarrow Q_A^-(\,H^+)(+\,Q_{pool})$	300	3,370	(2,4)
k_{AB}	$Q_A^-Q_B \rightarrow Q_AQ_B^-$	3,000	10,000	(5,6)
k'_{AB}	$Q_A^-Q_B(H^+) \rightarrow Q_AQ_B^-(\,H^+)$	3,000	10,000	(5,6)
k_{BA}	$Q_AQ_B^- \rightarrow Q_A^-Q_B$	987	2,200	(5,6)
k'_{BA}	$Q_AQ_B^-(H^+) \rightarrow Q_A^-Q_B(H^+)$	12	340	(5,6)

Notes. (1) It is assumed that values for pK_1 and pK_2, and the fraction of vacant reaction centers in the dark (determined by K_O), are the same after dark adaptation as those following an actinic flash. (2) Although these reactions involve the quinone pool, constants shown are based on the pseudo-first-order process, with $[Q_{pool}]$ assumed to be 1. (3) The true value can be obtained from $K'_O = K_O\,[PQ]_{pool}$; we have previously estimated $[PQ]_{pool}$ = 5 mM under oxidizing conditions (Crofts et al., 1984). (4) Rate constants k_{ij} are for reaction at pH above pK_2. Rate constants k'_{ij} are for reaction at pH below pK_1. (5) Rate constants k_{ij} are for reaction at pH above pK_3. Rate constants k'_{ij} are for reaction at pH below pK_1. (6) The difference between rate constants k and k′ does not reflect a change in the rate constant for the electron transfer process (since K_E is independent of pH), but a change in concentration of substrate for the backreaction, $[Q_AQ_B^-]$, associated with pK_3.

mined from four measured parameters; the fast and slow apparent rate constants; the fraction of vacant (or Q_B-bound) reaction centers (both determined from the corrected decay kinetics); and the apparent equilibrium constant, K_{app}. This last variable is the only term not obtained directly from the kinetic experiments. In fluorescence experiments, it can be measured from the ratio of back-reactions from Q_A^- or from $Q_AQ_B^-$. The former can be measured from the decay of Q_A^-, measured through fluorescence yield, or spectrophotometry, following illumination by a saturating flash in the presence of DCMU; the latter from loss of the binary pattern when the fluorescence yield decay was monitored at ~200 μs following a series of flashes (Robinson and Crofts, 1983, 1987), or through the $S_2 \rightarrow S_1$ deactivation on the donor side. The equilibrium constant can also be determined through thermoluminescence from the temperatures for Q and B components (Rutherford et al., 1982).

Another feature of importance in fitting theoretical curves to the experimental results was the fraction of centers in which the decay of fluorescence occurs in the seconds time range, attributed to non-functional centers. This fraction was often higher in mutant strains than in the native strain, but we do not have a ready explanation for this in the framework of our model. Inhomogeneities in the population of PS II that give rise to differences in kinetic behavior as assayed by fluorescence have been discussed extensively elsewhere (Govindjee, 1990; Joliot et al., 1992; Lavergne et al., 1992), and are outside the scope of this review.

2. The pH Dependence of the Apparent Equilibrium Constant, K_{app}

Measurement of K_{app} as a function of pH showed a dependence over the range 5.5–8.0, indicating that the

$Q_AQ_B^-$ state was stabilized by uptake of a H^+ (Robinson and Crofts, 1984). The curve could be well fit by assuming that a single group underwent a pK change from ~6 (pK_1) to ~8 (pK_3) due to the Coulombic effect experienced by the group on formation of a semiquinone anion on reduction of Q_B. Similar studies of the pH dependence of rate and equilibrium constants in a herbicide resistant strain of *A. hybridus* showed that the pH dependence changed on mutation of D1-Ser264 to glycine (Taoka and Crofts, 1990; Crofts et al., 1993). Part of the change could be attributed to a change in K_0; in the wild biotype, the fraction of the reaction centers with a vacant Q_B-site was found to vary with pH, but this dependence was lost in the mutant strain. The pH dependence for binding could be characterized by two pKs, given in Eq. (5).

$$K_0 = \frac{[Q_A \cdot vac]_{tot}}{[Q_AQ_B]_{tot}} = \frac{[Q_A \cdot vac] + [Q_A \cdot vac(H^+)]}{[Q_AQ_B] + [Q_AQ_B(H^+)]} = \frac{[Q_A \cdot vac]_{pK_2}}{[Q_AQ_B]_{pK_1}} \frac{\left(1 + \frac{[H^+]}{K_2^d}\right)}{\left(1 + \frac{[H^+]}{K_1^d}\right)} \quad (5)$$

where K_0 is the value of the dissociation constant measured at a particular value of pH. The terms $[Q_A.vac]_{pK}$ and $[Q_AQ_B]_{pK}$ are the fractional concentrations of vacant and Q_B occupied centers at pH above pK_2 (assumed to be the higher pK value), and K^d_1 and K^d_2 are the acid dissociation constants of $Q_AQ_B(H^+)$ and $Q_A.vac(H^+)$, respectively. With the simplifying assumptions given above, Eq. (5) expresses the pH dependence of K_0 and hence of A_O/B_O (Eq. (4)). The factor $[Q_A.vac]_{pK}/[Q_AQ_B]_{pK}$ gives $K_{0,pK}$, the dissociation constant above pK_2. The results (summarized in Table 1) show that in the physiological range, plastoquinone binds more tightly at the Q_B-site in the susceptible than in the resistant strain. This raises interesting mechanistic questions to be discussed further below.

3. Estimation of the Rate Constants for the Reactions Including the Protonated Species, and Proton-Uptake at the Q_B-site

The rate constants for reactions involving both protonated and unprotonated species can be calculated from three pKs and the rate constants obtained from kinetic experiments. The parameters can be expressed in terms of these pKs, and following the same rationale as above, the following equations can be used in analysis of the kinetic data:

$$K_{app} = \frac{K_E}{(1 + K_0)} \frac{\left(1 + \frac{[H^+]}{K_3}\right)}{\left(1 + \frac{[H^+]}{K_1}\right)} \quad (6)$$

from which

$$\frac{k_{AB}}{k_{BA}} = K_E \frac{\left(1 + \frac{[H^+]}{K_3}\right)}{\left(1 + \frac{[H^+]}{K_1}\right)} \quad (7)$$

Parameters for K_0 can be obtained through Eq. (5).

Table 1 compares values obtained with susceptible and resistant biotypes. The values of the on-rate constants for quinone binding were similar for both biotypes, in the range from 500 to 650 s^{-1}, and in each case were pH independent. In the resistant biotype, the rate constants for unbinding of quinone were the same from the protonated and deprotonated sites. In the susceptible biotype, the off-rate constant at pH values above pK_2 (i.e., from the deprotonated site) is 6 times smaller than in the resistant strain, and about 5 times smaller than that from the protonated site. As a consequence, in the pH range above pK_2 (the likely physiological range) the susceptible strain binds quinone about 4-5 times more strongly than the resistant strain; in the susceptible strain, a quinone can reach both the protonated and the deprotonated binding species at the same frequency, but it leaves the protonated site 5 times more frequently than the deprotonated site. Below pK_1, both strains show about the same affinity for quinone.

Direct measurement of the kinetics of the two-electron gate from the proton uptake associated with the reduction of the Q_B species in chloroplasts is complicated by a number of problems: (*i*) delays due to exchange with buffering groups in the membrane, and the tortuous pathway through the appressed regions of the grana stacks to the bulk phase (Polle and Junge, 1986); and (*ii*) the indirect coupling

through protonation of protein side-chains, which leads to uptake of a proton on each flash, although the semiquinone is anionic (Fowler, 1977; Saphon and Crofts, 1977; Hope and Morland, 1979; Hope and Matthews, 1983; Robinson and Crofts, 1984; Crofts et al, 1987). Detailed discussion of these difficulties is beyond the scope of this review, but the interested reader is referred to a paper by Haumann and Junge (1994), who measured rates corresponding more closely to the electron transfer rates by using neutral red (NR) as an indicator. Interestingly, the proton uptake was slower on the first flash (760 μs for H^+-uptake compared to150 μs for the electron transfer) than on the second flash (300 μs compared to 620 μs for the electron transfer). This was interpreted as showing that transfer of the second electron depended on protonation of the $Q_A^-Q_B^-$ state, as suggested in bacterial reaction centers (Wraight, 1979).

4. The Second Order Rate Constant for Binding of Plastoquinone

The turn-over time of the two-electron gate can be measured from the reduction of the plastoquinone pool on strong illumination, which takes about 20 ms (Stiehl and Witt, 1968). With about 10 quinone molecules/PS II in the pool, this represents about 2 ms for the transfer of each pair of electrons, including all binding and unbinding reactions. A similar value was found from the rate of generation of the species able to accept a proton, with half time of 0.8 ms (Hope and Matthews, 1983). In experiments in which the reopening time was studied by varying the delay time between the second and third flashes of a series, the Q_B-site was able to evolve from the $Q_A^-Q_B^-$ state, formed immediately after a second flash from the dark-adapted state, to Q_AQ_B state, detected by the characteristic rapid kinetics, with half time of 0.6 ms (Robinson and Crofts, 1987). The overall process involved electron transfer, unbinding of QH_2 and binding of Q, so the observed halftime must reflect a convolution of times for these partial processes, each of which was less. The pseudo-first order rate constants for binding of quinone derived from the kinetics after the first flash (k_{VA}) involved only a fraction of centers - those with a vacant binding site. When adjusted to compensate for this fraction, the approximate half times for binding of quinone are 0.4 and 0.8 ms for the susceptible and the resistant biotype, respectively, in good agreement with earlier values. The second-order rate constant for the binding of quinone can be found by using these values and an estimated concentration for plastoquinone in the membrane. Assuming these to be 5 mM in the susceptible and 4 mM in the resistant strains, the second order rate constants (referred to concentrations in the membrane) are found to be $1 \times 10^5\ M^{-1}s^{-1}$ and $2 \times 10^5\ M^{-1}s^{-1}$, respectively. The dissociation constant for plastoquinone with respect to membrane concentration, $K'_0 = K_0[Q_{pool}]$, is then 0.6×10^{-3} M in the susceptible and 2.28×10^{-3} M in the resistant strain (see Table 1, and legend).

5. The Pathway for Electron Transfer in Susceptible and Resistant Biotypes

In the physiological pH range (e.g. pH 7–8), the distribution of states is rather different in the susceptible and resistant biotypes, so that the pathway for electron transfer shows different characteristics. In the susceptible strain, most centers (80-90%) have the Q_B-site occupied, and electron transfer occurs from $Q_A^-Q_B$ with the forward rate constant of $3 \times 10^3\ s^{-1}$, and terminates either on $Q_AQ_B^-$ (with 20%) or on $Q_AQ_B^-(H^+)$ (with 80%). In the resistant biotype, only about two thirds of the Q_B-sites are initially occupied; in these centers, electron transfer occurs from $Q_A^-Q_B$ with the rate constant of $10^4\ s^{-1}$; in the remaining centers, electron transfer occurs through the second-order route following binding of plastoquinone. The reaction comes to equilibrium with a substantial fraction of centers still in the Q_A^- state; of those centers undergoing successful forward electron transfer, the electron was distributed with ⅔ on $Q_AQ_B^-$ and ⅓ on $Q_AQ_B^-(H^+)$.

6. Role of D1-Ser264 in the Mechanism of the Q_B-Site

The mechanism discussed above was developed in the context of experiments with wild-type and herbicide resistant strains of *A. hybridis*. The resistant strain followed the general trend for atrazine tolerant mutants of higher plants where Ser264 is replaced by glycine (Hirschberg and McIntosh, 1983; Goloubinoff et al., 1984; Bettini et al., 1987; Taoka and Crofts, 1990; Sunby et al., 1993). In contrast, in *C. reinhardtii* (Erickson et al., 1984) and cyanobacteria (Golden and Haselkorn, 1985; Ajlani et al., 1989a, b) the common substitution is by alanine. More recently, a resistant mutant of *Euglena* was described that carries a substitution of the homologous Ser265 to

threonine (Aiach et al., 1992). This repeated loss of Ser264 is highly significant, indicating that it might play an important role in herbicide binding. Trebst (1986) and Bowyer et al. (1991) suggested that Ser264 contributes to the binding of inhibitors of the urea-atrazine family to the Q_B site by H-bonding of its side chain hydroxyl group to the NH group in the herbicide molecule, in analogy with the observed H-bonding of the herbicide terbutryne to Ser223 in the L subunit of bacterial reaction centers (Michel et al., 1986). Another study (Tietjen et al., 1991) proposed that Ser264 would stabilize the structure of the Q_B site by H-bonding to His252. This histidine residue could also be involved in binding of the proton that stabilizes the semiquinone Q_B^- in the pocket (Crofts et al., 1987).

The change of Ser264 to glycine in the resistant strain was associated with a change in affinity for atrazine of about 3300-fold, but of only about 10-fold for plastoquinone. The resistivity for atrazine represents a change in binding free-energy of 20.3 kJ.mol^{-1}, in the range expected for a buried H-bond, but for plastoquinone, the 10-fold change in binding represents only 5.65 kJ.mol^{-1}. The differential change in affinity may be understood in terms of the model discussed above if one or both of the two back-bone H-bonds are ligands for plastoquinone, but the serine -OH forms only a weak H-bond. Conversely, the serine -OH forms a strong H-bond for the herbicide.

Perhaps the most intriguing aspect of the studies of Taoka and Crofts (1990) was that the mechanistic phenotype of the resistant strain differed from the susceptible strain through pK changes. Since serine does not have a pK in the physiological range, this suggests that the loss of Ser264 involves also a loss of interaction with a dissociable group. In our sequence alignment, His252 occupied the same position relative to a conserved phenylalanine (255 in D1, 216 in *Rps. viridis* L-subunit) as L-Asn(Asp)213 in the BRCs, and was naturally positioned in the model to form a H-bonded with Ser264. These interactions might facilitate a proton relay mechanism by which proton(s) could be transferred to the Q_B-site on reduction by a second electron. The results could then be explained by a fractional contribution of the Ser264 -OH to quinone binding, modulated by a sharing of the H-bond with His252. The structural speculations underlying this mechanistic model have been validated by the Ferreria et al. (2004) structure (Chapter 21, Barber and Iwata), and these authors also suggested a similar involvement of His252 in interactions with Ser 264 in stabilization of the SQ. Details of the functional relation of the structure to the pKs identified in this work remain to be determined. However, results from mutagenesis of His252 in *C. reinhardtii* (S. Padden and A. Crofts, unpublished, and see below) support a model of this sort.

C. Binding of Inhibitors and Exogenous Quinones at the Q_B-Site

The studies summarized above have strongly suggested that Q_B is relatively weakly bound. This is also apparent from the ease with which it can be displaced by exogenous electron acceptors and various inhibitors (Velthuys, 1976; Bowes and Crofts, 1981a; Velthuys, 1982; Crofts and Wraight, 1983; Lavergne, 1982a; Taoka et al., 1983; Bowyer et al., 1991). This occurs in several steps, involving electron transfer back to Q_A followed by dissociation of quinone, to generate an intermediate Q_A^-.vacant state that is the substrate for binding. In the case of inhibitor binding, the result is an inhibitor-induced reduction involving the reactions:

$$\overset{\text{Inhibitor}}{Q_AQ_B^- \leftrightarrows Q_A^-Q_B \leftrightarrows Q_A^-\{\text{vacant}\} \leftrightarrows Q_A^-\text{Inhibitor}} \quad (8)$$

Exogenous quinones can follow a similar reaction path, with an additional step of electron transfer from Q_A^-, to generate a foreign semiquinone at the site (Lavergne, 1982b; Taoka et al., 1983; Zimmermann and Rutherford, 1986; Petrouleas and Diner, 1987). The mechanism of loss of the Q_B^- species is thought to involve displacement of the oxidized form (Q_B) present in a fraction of centers as a result of the relatively small equilibrium constant favoring electron transfer from $Q_A^-Q_B$ to $Q_AQ_B^-$. If the exogenous reagent is an electron acceptor (for example, benzoquinone), the semiquinone is generated. If the semiquinone has a high enough potential, it can accept an electron from the non-heme Fe, to generate the oxidized form:

$$\begin{aligned} &\overset{Q_{ex}}{Q_A.Fe.Q_B^- \leftrightarrows Q_A^-.Fe.Q_B \leftrightarrows Q_A^-\{\text{vacant}\} \leftrightarrows} \\ &Q_A.Fe.Q_{ex}^- \leftrightarrows Q_A.Fe^+.Q_{ex}^{2-} \end{aligned} \quad (9)$$

A consequence of the reaction pathway leading to inhibitor-induced reduction of Q_A is that the titer of inhibitor is higher for binding to the $Q_AQ_B^-$ state than to the Q_AQ_B state (Lavergne, 1982c; Taoka and Crofts, 1987). A second consequence is that inhibitor binding is pH dependent.

Taoka and Crofts (1987) investigated kinetic aspect of inhibitor binding to the oxidized and 1-electron reduced states of the Q_B-site, and measures on and off rate constants as a function of pH for several different inhibitors (DCMU, atrazine, *o*-phenanthroline, and two cyanoacrylate derivatives 964S and 965, Huppatz and Phillips, 1984, which differ by stereo rotation about one C-atom), as summarized below:

(i) Binding of inhibitors to the oxidized state of the secondary quinone site was essentially pH independent.

(ii) Binding to the one-electron reduced state was slower, and strongly pH dependent.

(iii) For all the inhibitors studied, both the difference in rate, and the pH dependence, could be accounted for in terms of a simple hypothesis. They reflect the lowered concentration of the open sites at which the inhibitor binds, associated with formation of a stable semiquinone at the site. The concentration of open sites was described by the set of equilibrium constants determining the distribution of an electron between primary and secondary quinone acceptors discussed above.

(iv) When these factors were accounted for, the second-order rate constants for inhibitor binding were found to be constant with pH, and close to those for binding to oxidized centers, assuming that the reaction partner was the vacant quinone binding site in either state, and that the binding constant for plastoquinone from the pool was the same for oxidized and one-electron reduced centers.

(v) Second-order rate constants for binding and unbinding of each of the inhibitors with respect to concentration in the membrane phase were determined by taking account of the partition coefficients between aqueous and membrane phase. DCMU and the two cyanoacrylates showed similar values for binding rate constant ($2–8 \times 10^4\ M^{-1}.s^{-1}$), close to the value estimated for plastoquinone binding ($\sim 10^5\ M^{-1}s^{-1}$, see above), but *o*-phenanthroline was slower (about $0.4 \times 10^4\ M^{-1}.s^{-1}$). DCMU and 964S are effective inhibitors because of their very slow unbinding ($<0.02\ s^{-1}$), but 965R is an ineffective inhibitor because of its rapid unbinding ($2–3\ s^{-1}$). The bulky *o*-phenanthroline is a poor inhibitor both because of its slower rate of binding, and relatively high rate of unbinding ($0.3\ s^{-1}$).

Several of these conclusions are of more general interest to wider studies of binding from the lipid phase, since it is likely that similar sites in other quinone processing enzymes will show similar characteristics. Inhibitor binding follows a pattern familiar from studies of soluble enzymes, except that the relevant concentration term is that for the membrane phase. The conclusions are also of interest with respect to studies of inhibitor binding using the conventional Quantitative Structure Activity Relationship (QSAR) approach (for a comprehensive view, see Huppatz, 1996; and articles in Yoshida et al., 1993), since they indicate clearly the parameters that underlie some of the fitting variables used to quantify differential aspects of inhibitor binding.

D. Structural and Mechanistic Information from Mutagenesis Studies

1. Herbicide Resistant Strains of Chlamydomonas and Cyanobacteria

Herbicide resistance was originally found in higher plants (see Moreland, 1993, for historical review; Draber et al., 1991; Oettmeier, 1992, 1999), and these continue to provide interesting new strains (Alfonso et al., 1996); however, most recent work on herbicide resistance has been in algae or cyanobacteria, which are more amenable to genetic manipulation. Erickson et al. (1984, 1989) and Galloway et al. (1984) studied mutations in the D1-subunit in *C. reinhardtii* generated by selection for herbicide resistance, and these have also been investigated in greater detail in other labs (Baroli, 1992; Govindjee et al., 1992; Draber et al., 1993; Crofts et al., 1993; Oettmeier et al, 1993; Tietjen et al., 1993). These studies have covered detailed measurements of inhibitor resistance for a wide range of inhibitors, kinetic analysis, and use of QSAR and computational modeling to predict from the differential inhibitor sensitivities structural features associated with differential binding.

In a detailed kinetic study, following the protocols outlined above, Baroli and colleagues (Baroli, 1993; Crofts et al., 1994) were able to deconvolute the contributions of rate constants and equilibrium constants for plastoquinone binding and electron transfer to the overall process. Two mutations in D1, Ser264Ala and Ala251Val, led to a marked slowing of kinetics for reduction of plastoquinone to the bound semiquinone. In Ser264Ala, the second electron transfer was also slower, but was normal in Ala251Val. In mutant

Gly256Asp, the electron transfer kinetics were normal after the first flash, but slowed after the second. In mutants Leu275Phe, Val219Ile, and Phe255Tyr, the electron transfer kinetics after both flashes were similar to those in wild type. Among the amino acid substitutions in D1 covered by these studies, two clear groups could be established:

(i) Mutations that confer herbicide resistance, but had no marked effect on the electron transfer between the plastoquinone acceptors of PS II. These mutations are Val219Ile, Phe255Tyr, Leu275Phe and Gly256Asp (Table 2). In the case of Gly256Asp, the normal kinetic parameters observed were in contrast to a slowed electron transfer reported from earlier work (Erickson et al., 1989; Govindjee et al., 1992). However, the earlier experiments were performed using averaging, with a short dark period between actinic flashes. When the experiment was performed under uncoupled conditions and with a longer dark interval, electron transfer on the first flash was similar to wild type, but that after a second flash was inhibited. It seems likely that the slowed kinetics previously reported reflected a dominant contribution from a mixed population of states, with the inhibited 1-electron reduced state dominating, and possibly some slowing due to reduction of the plastoquinone pool. The slowed electron transfer on the second flash may have reflected an interference of the aspartate side chain with proton processing associated with the second electron transfer.

(ii) Mutations that confer herbicide resistance and considerably modify the electron transfer between the plastoquinone acceptors, as with Ser264Ala and Ala251Val. In general, the Ser264Ala mutation showed in exaggerated form the characteristics of the Ser264Gly mutation in high plants. Only a slight change in the apparent equilibrium constant for electron transfer was observed. The slow electron transfer in this mutant was due to a high dissociation constant for plastoquinone rather than a change in K_{app}. This supports the suggestion that Ser264, besides being involved in the binding of inhibitors, also plays an important role in plastoquinone binding. The high value of K_0 comes from an increased fraction of centers in the state Q_A.vacant in the dark. Also, both the on- and off- rate constants for binding and dissociation of plastoquinone are increased in this mutant. In centers in the Q_AQ_B state, however, the electron transfer reaction proceeds 3.5 times more rapidly than in wild type. Assuming structural homology with the bacterial reaction center, the loss of the –OH on Ser264 might be expected to result in a weaker binding, or binding to an alternative site, at the end of the pocket distal from the Fe in these mutant strains as discussed above. Since reaction centers are strongly dependent on distance, the more rapid rate for the bound quinone might reflect a shorter bonding distance to the N of D1-His215, which provides a H-bond to the other quinone — C=O at the proximal end of the binding pocket for electron transfer reactions. In effect, the mutations may 'push' the plastoquinone molecules closer together, allowing for a faster electron transfer.

The structural basis for differential inhibitor resistance has been explored in detailed QSAR studies using the mutant strains tested against a wide range of substituted triazines and triazinones (Tietjen et al., 1993) and 4-nitro-6-alhylphenols (Draber et al., 1993). Complementary studies at some of these sites have explored a wider range of mutations (Forster et al., 1997; Lardans et al., 1997; Johanningmeier et al., 2000) that extend the database for discussion of structure-function relationships.

2. Specific Mutagenesis of Herbicide Resistance Sites in Synechocystis

Following earlier work on spontaneous mutants selected for herbicide resistance (Robinson et al., 1987), a similar set of mutants showing various degrees of herbicide resistance have also been generated in *Synechocystis* sp. PCC 6714, both as single mutants, and with combinations of changes at the individual sites (Astier et al., 1986, 1993; Etienne et al., 1990). These showed interesting variations in selectivity for different herbicides compared to the results for *Chlamydomonas* and higher plants.

*3. Combinatorial Mutagenesis of a Conserved Span of the **de** Loop*

Vermaas and colleagues (Vermaas et al., 1989; Kless et al., 1993; Kless and Vermaas, 1995) used combinatorial mutagenesis to explore the role substantial spans between helices **D** and **E** of D1 and D2. In the Kless et al. (1993) study, spans from the loop

starting at the end of helix **D** of D2 were replaced by residues from the equivalent span in D1. Interestingly, the mutant strains retained function with relatively minor changes, but these include changes in herbicide binding or stability of the semiquinones at both sites, as measured from glow curves, indicating perhaps that although the span contributes little to either catalytic site, there are pleotrophic effects over a larger volume. This is in line with the structural data. In the Kless and Vermaas (1995) study, the role of four conserved residues (Tyr254, Phe255, Gly257, Arg257) in the putative **de**-helix of the D1 subunit of the *Synechocystis* sp. PCC 6803 was explored. 25 mutants with functional PS II were isolated, all of which showed different codon combinations at positions 254 to 257. None of the conserved residues was found to be mandatory for PS II function. However, 24 of the functional mutants contained Tyr or Phe at position 254 while at the other three positions many different amino acid combinations could be functionally accommodated. Most of the PS II properties were similar in the mutants compared to wild type. Noticeable modifications in the mutants concerned the semiquinone equilibrium on electron transfer between Q_A and Q_B, and the affinity of PS II inhibitors. The authors concluded that, even though many different combinations of amino acids in positions 254 to 257 may satisfy the primary function, complex requirements need to be combined for optimized performance. Most functional sequences maintained an amphipathic arrangement, assuming a helical conformation. In their alignment, Tyr254 was proposed to be functionally analogous to Phe216 of the L subunit in purple bacteria, and they suggested that Tyr254 faced the Q_B binding pocket to allow a contribution to binding of Q_B. The alternative candidate for the residue functionally equivalent to Phe216 is Phe255, as suggested in the Crofts et al. (1987) model, and this is the configuration shown in the Ferreira et al. (2004) structure (Chapter 21, Barber and Iwata). The rotation of the helical axis by ~100° brings the polar face of the helix to the aqueous interface, positioning His252 for interaction with Ser264.

4. Specific Mutagenesis of D1-His252 Shows an Important Role in H^+-Processing

Diner et al. (1991) briefly reported a mutation of His252 in the **de**-helix of the Q_B-site (His252Leu) of *C. reinhardtii*, studied in collaboration with Peter Nixon, which showed an inhibited electron transfer to Q_B. S. Padden and A. Crofts (unpublished) have constructed a more extensive series of mutants at this site (His252Asp, Lys, Asn and Gln) in order to test the role in stabilization of the semiquinone and proton delivery. Only the His252Asp mutant was able to grow photosynthetically. Cells evolved O_2 at rates 40–60% those observed in cells with wild-type D1 protein, and showed rapid electron transfer to the Q_B-site for both odd and even flashes. However, the rate on the first flash was slower than that on the second, reversing the pattern of the binary oscillation in the fluorescence yield measured at ~200 μs after each of a series of flashes. Both His252Asn and His252Gln showed some rapid electron transfer from Q_A^- to Q_B following the first actinic flash after dark-adaptation, but with a reduced yield. Both were severely inhibited on the second flash. His252Lys was severely inhibited even after the first flash. Thermoluminescence studies after illumination with 1 saturating flash immediately before freezing showed glow-curves for all strains in which the peak was shifted to higher temperatures. From this we conclude than even in the strongly inhibited His252Lys strain, some electron transfer to Q_B occurred.

The pattern of dependence of electron transfer rate on flash number observed at pH 7.0 with His252Asp was similar to that seen in wild-type at pH above the pK at 8.0 for the Q_B^- state. This suggests that in His252Asp, a pK shift similar to that in wild-type might be occurring, but starting with a pK in the dark lower than that in wild-type, as might be expected for the more acidic aspartate side chain. The rapid electron transfer after the first flash observed with strains His252Gln and His252Asn shows that reduction of Q_B was not dependent on delivery of a proton to the site through this pathway. The strongly inhibited rate after the second flash can be readily interpreted as showing that transfer of the second electron has to wait for binding of the first proton (Wraight, 1979), dependent on a dissociable group at this site. The behavior of these mutant strains supports the suggestion of a role for His252 in proton delivery to the Q_B-site. We are currently investigating the pH dependence of rates and equilibrium constants for the electron transfer from Q_A^- to Q_B in these strains to further test this hypothesis.

5. Excision of Residues from the PEST Sequence of the **de**-*Loop*

The span leading from the top of helix **D** to the **de** he-

lix contains a sequence called the 'PEST-like' region (Greenberg et al., 1987), which has been suggested as a likely site for proteolysis in the turnover of D1 associated with photoprotection. Nixon at al. (1995) deleted a substantial span (residues 226-233) in this region, and showed that the resultant strain was able to grow photosynthetically, with light-saturated rates similar to wild type. Remarkably, electron transfer on the acceptor side was still rapid, despite excision of this substantial section of the **de**-loop, and the likely structural consequences. Not surprisingly, the properties of the site were modified, and measurements using thermoluminescence and fluorescence yield kinetic changes showed that Q_B^- was destabilized relative to Q_A^-. Measurements of D1 turnover showed an enhanced turnover in the deletion strain indicating that the PEST sequence was not required. Similar deletion studies have been reported by Mulo et al. (1997, 1998), in which excision of span 225-239 resulted in an autotrophic strain with a functional but modified Q_B-site, and with a similar susceptibility to photoinhibition to wild type. Excision of spans 225-249 or 240-249 gave heterotrophic strains with modified Q_B-pockets, severely inhibited electron transfer, and impaired recovery from photoinhibition. The authors concluded that no specific sequence in the **de**-loop was essential for D1 polypeptide degradation. The Ferreira et al. (2004) structure shows that the loop between 225 and 249 is well removed from the Q_B-site, consistent with the lack of effect on two-electron gate function shown by these results.

6. Mutagenesis to Explore the Bicarbonate Effect

Govindjee and colleagues have used specific mutagenesis in *Synechocystis* and *Chlamydomonas* to test the hypothesis that arginine residues in the neighborhood of the quinone binding sites might serve as ligands to bicarbonate. Mutation of D1-Arg269 to glycine led to substantial changes in stability of the complex, 17-fold change in rate of electron transfer from Q_A^- to Q_B, loss of thermoluminescence peaks, but not to any change in formate/bicarbonate binding as judged from the $Q_A^-.Fe^{2+}$ EPR signal (Hutchison et al., 1996; Xiong et al., 1997). Mutation at Arg257 (Xiong et al., 1998b) to glutamate (Arg257Glu) or methionine (Arg257Met) were able to function with near normal kinetics of electron transfer between the Q_A and Q_B sites, but with a somewhat reduced equilibrium constant for the forward reaction. Interestingly, both mutations led to greatly reduced sensitivity to inhibition by incubation with formate, which displaced bicarbonate in native strains. Several of single and double mutants in the **de**-helix and the loop around Ser264 in *Synechocystis* PCC 6714 showed similar differential effects on formate sensitivity (Vernotte et al., 1995 or 1993). Since the bicarbonate effect is normally studied through the formate effect (Blubaugh and Govindjee, 1988; van Rensen et al., 1999; van Rensen, 2002), conclusions about the role of any of these residues in binding of bicarbonate must remain tentative.

E. Effects of Occupation of the Q_B-site on the E_m for Q_A and on the Equilibrium Constants in the Two-Electron Gate

Many reports have been published showing changes in E_m of the Q_A/Q_A^- couple on addition of inhibitors that bind to the Q_B-site, both in BRCs and PS II. Although most workers had assumed that any effects with DCMU were small, recent work has suggested that this might not be the case (Krieger-Liszkay and Rutherford, 1998). For example, the E_m for Q_A/Q_A^- is shifted from –70 to –30 mV by DCMU, and to –130 mV in the presence of bromoxynil. An interesting discussion of these effects in the light of the sensitivity to photo-oxidative damage has recently been published (Rutherford and Krieger-Liszkay, 2001, 2002; Fufezan et al., 2002). It should be noted that values for K_{app} calculated using the kinetic approach above depend on the assumption that the E_m value of the Q_A couple is the same whether the Q_B-site is occupied by DCMU or by the $Q_B/Q_B^{\cdot -}$ couple; the potential of Q_A in the absence of inhibitor as always measured with QH_2 in the site. A change in E_m for the Q_A/Q_A^- couple changes the probability for population of different intermediate states, and should therefore affect the back reaction rate measured. It is not clear how large an effect this would be compared to that arising from occupancy by Q_B, but the K_{app} values measured from the ratio of back reaction rates will likely have to be corrected. In addition, estimation of the E_m for the $Q_B/Q_B^{\cdot -}$ couple from the equilibrium constant depends directly on the value assumed for E_m Q_A/Q_A^-. In a recent study, Rappaport et al. (2002) measured the back reaction rates from Q_A^- to P^+ in strains in which the free-energy gap between Q_A and the intermediate pheophytin acceptor (Pheo) of the photochemical reaction was varied. Their analysis has called into question the commonly assumed values

for midpoint potentials of the Q_A/Q_A^-, Pheo/Pheo$^-$, and P^+/P couples. These recent developments will open this area to further revision, and perhaps some reinterpretation of earlier work.

Although Q_A acts as a single electron acceptor under physiological conditions, double reduction is possible under extreme reducing conditions (see van Mieghem et al, 1989, for a reinterpretation of the observations of Evans et al., 1985). Diner and Babcock (1996) present a critical discussion of the related literature.

F. Role of the Q_B-Site in Back-Reactions to the S-States

1. Back Reaction from Q_B^- to the S_2-State

The back reaction after a single flash from the dark-adapted state ($S_2Q_B^-$ back reaction) can be assayed by fluorescence measurements, as discussed at length in the context of the kinetic model above. The reaction has also been studied extensively through relaxation of the S_2-state, and through delayed fluorescence, thermoluminescence, and electroluminescence (Bowes and Crofts, 1979; van Gorkom, 1996; Vass and Govindjee, 1996; de Wijn et al., 2001). The overall reaction is close to stoichiometric in yield, but energy levels strongly affect the path, especially the fraction of centers decaying through pathways populating the excited state. Since the rate observed through fluorescence yield experiments and S_2-state deactivation are similar, and since the equilibrium constant calculated as above, and from thermoluminescence, are similar, a back reaction via Q_A^- and pheophytin is generally assumed, generating a small fraction of intermediate states with sufficient energy to populate the singlet level to give delayed fluorescence or thermoluminescence (Crofts et al., 1971; Bowes and Crofts, 1981b; Rutherford et al., 1982; Demeter et al., 1993; Johnson et al., 1994; Krieger et al., 1998).

2. Back Reaction from QH_2 to the S_3-State—A Possible Role for Cytochrome b_{559}

The relaxation of the S_3-state generated by two-flash excitation from the dark-adapted state, as measured by O_2 yield, shows kinetics similar to that of the S_2 relaxation (Diner, 1977). However, in this case, the source of electrons is not obvious. The acceptor side complex evolves to the initial state (Q_AQ_B or Q_A.vacant) within 4 ms after two flashes, leaving the two reducing equivalents as QH_2 in the pool (Robinson and Crofts, 1987). The E_m of the pool is ~100 mV, so the probability of re-population of the reduced acceptor complex would be low (from the values above, at neutral pH, K_{eq} for the reaction $Q_A.Q_B + QH_2 \leftrightarrows Q_A^-Q_B^- + Q + 2H^+$ is $\sim 10^{-3}$). Moreover, Diner (1977) found that the rate of the back reaction after two flashes ($Q_B^{2-}S_3 \rightarrow Q_B^-S_2$) was only weakly dependent on the degree of reduction of the quinone pool, suggesting that this is not the pathway. An alternative source of electrons would be from the endogenous reductants (carotenoids, ancillary Chls, Cyt b_{559}) that are known to donate to $P680^+$ when the Mn-complex is disrupted. Since the equilibrium constants between P680 and the relevant S-state transitions are relatively small, this reductant pool would also be available to reduce the S_2 and S_3 states. However, no accumulation of the oxidized forms of these reductants is observed when the S-state system is intact (Diner, 1998). If they are involved, a pathway for their reduction from an additional pool must therefore be postulated. The obvious source is the quinone pool, and indeed, a DCMU-sensitive pathway for reduction of Cyt b_{559} has been demonstrated (Buser et al., 1992), and a plastoquinol oxidase activity involving Cyt b_{559} has been suggested (Kruk and Strzalka, 2001; Bondarava et al., 2003). From the inhibitor sensitivity, this must involve the Q_B-site. The structures currently available allow calculation of possible rate constants in putative steps. These show that the heme of Cyt b_{559} is ~24 Å from the expected position of Q_B. With a driving force of 250 mV, and a value for λ of 0.75 V, a rate constant of ~0.53 s^{-1}, assuming 100% occupancy, can be calculated using the Moser et al. (1995) equations. This is in line with measured values for rates of deactivation, and a plausible occupancy. The most likely acceptor would be the ancillary Chl of D2, liganded by His117, since mutation of the ligand leads to loss of Chl photooxidation (Chl Z^+) (Ruffle et al., 2001). The edge-to-edge distance between heme b_{559} and this Chl is ~21.5 Å; with a driving force of ~400 mV, and any reasonable value for λ, this step would not be rate-limiting. In this simple scenario, electrons for reduction of both the S-states could follow the same pathway through Cyt b_{559}, since the Q_B^- would be a better substrate than QH_2 for reduction of Q_A.

An alternative and in some ways more attractive mechanism, using a similar reaction pathway, is for the Q_B-site to catalyze an 'oxidant-induced reduction' reaction:

$$QH_2 + \text{Cyt } b_{559} + Q_A \leftrightarrows Q + \text{Cyt } b^-_{559} + Q_A^- + 2H^+ \quad (10)$$

The reaction would proceed via an intermediate $Q_AQ_B^-$ state, in which the semiquinone would be sufficiently reducing to force the second electron onto Q_A (the overall equilibrium constant would be ~10^3), thus providing parallel pathways for the two electrons, one of which would return via Cyt b_{559} and Chl Z, and the other via Q_A^- and the normal S_2 deactivation pathway.

$$S_3 + Chl_Z \rightarrow S_2 + Chl_Z^+ \quad (11)$$

$$Chl_Z^+ + \text{Cyt } b^-_{559} \rightarrow Chl_Z + \text{Cyt } b_{559}$$

$$QH_2 + \text{Cyt } b_{559} + Q_A \leftrightarrows \text{Cyt } b^-_{559} + Q_AQ_B^- + 2H^+$$

$$Q_AQ_B^- \leftrightarrows Q_A^-Q_B \leftrightarrows Q_A^- + Q$$

$$S_2 + Q_A^- \rightarrow S_1 + Q_A$$

$$S_3 + QH_2 \rightarrow S_1 + Q + 2H^+$$

Discrimination between these two possibilities might not be easy, since in both cases, deactivation of the S_3-state would involve electron transfer from plastoquinol to S_3 via Cyt b_{559}. However, an involvement of both Cyt b_{559} and the ancillary D2 Chl, Chl_Z, could be readily tested by observation of the S_3 decay kinetics in mutant strains with the ligands to these two groups modified (Morais et al., 2001; Ruffle et al., 2001).

A role for interaction between the Q_B-site and Cyt b_{559} in the protein processing consequent on photodamage is suggested by an interesting study of a covalent bond formed between b_{559} and D1 through His252 (Lupinkova et al., 2002).

Deactivation of the higher S-states by the back reaction plays an obvious role in removal of potentially harmful oxidants. Less obvious is the fact that this also removes potentially harmful reductants, – Q_A^- has a reducing potential in the range to generate superoxide by reduction of O_2, and even the Q_B/Q_B^- couple reacts with O_2 at a low rate, as seen in the slowed kinetics for oxidation under anaerobic conditions when the back reaction is prevented by hydroxylamine (H. H. Robinson and A. R. Crofts, unpublished). Ohad and colleagues (Keren et al., 1997) have examined the inactivation of PS II under flash illumination at a repetition rate in the range of the lifetime of the Q_A^- and Q_B^- states back reacting with S_2 or S_3. Inactivation, or D1 degradation, showed a dependence on the interval between flashes, with half-maximal effects at ~50 s (compared to $t_{½}$ ~7 s for the back reaction from Q_A^-) in the presence of DCMU, and ~150 s (compared to the back reaction time from Q_B^- with $t_{½}$ ~ 35 s). The inactivation was much less under anaerobic conditions, showing a requirement for O_2. The authors interpreted the data as showing a mechanism in which the back reaction generates damaging oxygen radicals through involvement of the Chl triplet. However, it seems possible that a direct reduction of O_2 by the reduced acceptor quinones might provide an alternative mechanism. These topics are discussed in greater detail elsewhere in this volume.

IV. Conclusions

The structural information from spectroscopy, specific mutagenesis, kinetic studies and modeling has been remarkably successful in predicting specific structural features relating to the mechanism of the two-electron gate, now revealed by crystallographic studies. This success may be viewed as validating these approaches, but also provides some confidence in the kinetic models, and the conclusions drawn from them. With more detailed structures, the scope for future work in which the molecular architecture of the two-electron gate is explored through a combination of these approaches holds the promise of a detailed understanding of the reactions on the acceptor side of PS II.

Acknowledgments

VP acknowledges insightful discussions with Drs N. Ioannidis and Y. Sanakis. Research support for the lab of VP was provided through the European Community programs ERBFMRXCT980214, and ERBFMRXCT980174. ARC acknowledges earlier support from Department of Energy and United States Department of Agriculture that covered the research work discussed in the second part, the major contributions of Dr. Howie Robinson and Shinichi Taoka to development of the kinetic models discussed, and more recent useful discussions with Dr. Vlad Shinkarev.

References

Aasa R, Andreasson L-E, Styring S and Vanngard T (1989) The nature of the Fe(III) EPR signal from the acceptor-side iron in Photosystem II. FEBS Lett 243: 156–160

Aiach A, Ohmann E, Bodner U and Johanningmeier U (1992) A herbicide resistant *Euglena* mutant carrying a Ser to Thr substitution of position 265 in the D1 protein of Photosystem II. Z Naturforsch 47c: 245–248

Ajlani G, Kirilovsky D, Picaud M and Astier C (1989a) Molecular analysis of *psbA* mutations responsible for various herbicide resistance phenotypes in *Synechocystis* 6714. Plant Mol Biol 13: 469–480

Ajlani G, Meyer I, Vemotte C and Astier C (1989b) Mutation in phenol-type herbicide resistance maps within the *psbA* gene in *Synechocystis* 6714. FEBS Lett 246: 207– 210

Alfonso M, Pueyo JJ, Gaddour K, Etienne AL, Kirilovsky D and Picorel R (1996) Induced new mutation of D1 serine-268 in soybean photosynthetic cell cultures produced atrazine resistance, increased stability of $S_2Q_B^-$ and S_3Q_B states, and increased sensitivity to light stress. Plant Physiol 112: 1499–1508

Allen JP, Feher G, Yeates TO, Komiya H and Rees DC (1988) Structure of the reaction center from *Rhodobacter sphaeroides* R-26: Protein-cofactor (quinones and Fe^{2+}) interactions. Proc Natl Acad Sci USA 85: 8487–8491

Anderson BF, Baker HM, Norris GE, Rice DW and Baker EN (1989) Structure of human lactoferrin: Crystallographic structure analysis and refinement at 2.8 Å resolution. J Mol Biol 209: 711–734

Astashkin AY, Kawamori A, Kodera Y, Kuroiwa S and Akabori K (1995) An electron spin echo envelope modulation study of the primary acceptor quinone in Zn-substituted plant Photosystem II. J Chem Phys 102: 5583–5588

Astashkin AV, Hara H, Kuroiwa S, Kawamori A and Akabori K (1998) A comparative electron spin echo envelope modulation study of the primary electron acceptor quinone in Zn-substituted and cyanide-treated preparations of Photosystem II. J Chem Phys 108: 10143–10151.

Astier C, Meyer I, Vernotte C and Etienne A-L (1986) Photosystem II electron transfer in highly herbicide resistant mutants of *Synechocystis* 6714. FEBS Lett 207: 234–238

Astier C, Perewoska I, Picaud M, Kirilovsky D and Vernotte C (1993) Structural analysis of the Q_B pocket of the D1 subunit of Photosystem II in *Synechocystis* PCC6714 and 6803. Z Naturforsch 43c: 199–204

Baroli I (1992) The two-electron gate of Photosystem II in wild type and herbicide-resistant mutants of *C. reinhardtii.* MSc Thesis, University of Illinois

Beijer C and Rutherford AW (1987) The iron-quinone acceptor complex in *Rhodospirillum rubrum* chromatophores studied by EPR. Biochim Biophys Acta 890: 169–178

Berthomieu C and Hienerwadel R (2001) Iron coordination in Photosystem II: Interaction between bicarbonate and the Q_B pocket studied by Fourier transform infrared spectroscopy. Biochemistry 40: 4044–4052

Bettini P, McNally S, Sevignac M, Darmency H, Gasquez J and Dron M (1987) Atrazine resistance in *Chenopodium album*: Low and high levels of resistance to the herbicide are related to the same chloroplast PSBA gene mutation. Plant Physiol 84: 1442–1446

Blubaugh D and Govindjee (1988) The molecular mechanism of the bicarbonate effect at the plastoquinone reductase site of photosynthesis. Photosynth Res 19: 85–128

Boinnard D, Cassoux P, Petrouleas V, Savariault JM and Tuchagues JP (1990) Iron(II) complexes of 2,2′-biimidazole and 2,2′-bibenzimidazole as models of the photosynthetic mononuclear non-heme ferrous sites. Synthesis, molecular and crystal structure, and Mossbauer and magnetic studies. Inorg Chem 29: 4114–4122

Bondarava N, De Pascalis L, Al-Babili S, Goussias C, Golecki JR, Beyer P, Bock R and Krieger-Liszkay A (2003) Evidence that Cyt b_{559} mediates the oxidation of reduced plastoquinone in the dark. J Biol Chem 278:13554–13560

Boso B, Debrunner P, Okamura MY and Feher G (1981) Mossbauer spectroscopy studies of photosynthetic reaction centers from *Rhodopseudomonas sphaeroides* R-26. Biochim Biophys Acta 638: 173–177

Bouges-Bocquet B (1973) Electron transfer between the two photosystems in spinach chloroplasts. Biocheim Biophys Acta 314: 250–256

Bowes JM and Crofts AR (1980) Binary oscillations in the rate of reoxidation of the primary acceptor of Photosystem II. Biochim Biophys Acta 590: 373–384

Bowes JM and Crofts AR (1981a) Effect of DBMIB on the secondary electron acceptor B of Photosystem II. Arch Biochem Biophys 209: 682–686

Bowes JM and Crofts AR (1981b) The role of pH and membrane potential in the reactions of Photosystem II as measured by effects on delayed fluorescence. Biochim Biophys Acta 637: 464–472

Bowes JM, Crofts AR and Itoh S (1979a) A high potential acceptor for photosystern II. Biochim Biophys Acta 547: 327–335

Bowes JM, Crofts AR and Itoh S (1979b) Effects of pH on reactions on the donor side of Photosystem II. Biochim Biophys Acta 547: 336–346

Bowes JM, Crofts AR and Arntzen CJ (1980) Redox reactions on the reducing side of Photosystem II in chloroplasts with altered herbicide binding properties. Arch Biochem Biophys 200: 303–308

Bowyer J, Hilton M, Whitelegge J, Jewess P, Camilleri P, Crofts AR and Robinson HH (1990) Molecular modelling studies on the binding of phenylurea inhibitors to the D1 protein of Photosystem II. Z Naturforsch 45c: 379–387

Bowyer JR, Camilleri P and Vermaas WFJ (1991) Photosystem II and its interaction with herbicides. In: Baker NR and Percival MP (eds) Topics in Photosynthesis, Vol 10, Herbicides, pp 27–85. Elsevier Science Publishers BV, Amsterdam

Breton J, Boullais C, Mioskowski C, Sebban P, Baciou L and Nabedryk E (2002) Vibrational spectroscopy favors a unique Q_B binding site at the proximal position in wild-type reaction centers and in the Pro-l209 → Tyr mutant from *Rhodobacter sphaeroides*. Biochemistry 41: 12921–12927

Burda K, Kruk J, Borgstadt R, Stanek J, Strzalka K, Schmid GH and Kruse O (2003) Mossbauer studies of the non-heme iron and cytochrome b_{559} in a *Chlamydomonas reinhardtii* PS I^- mutant and their interactions with α-tocopherol quinone. FEBS Lett 535: 159–165

Buser CA, Diner BA and Brudvig GW (1992) Photooxidation of cytochrome *b*-559 in oxygen-evolving Photosystem II. Biochemistry 31: 11449–11459

Cleland RE and Grace SC (1999) Voltammetric detection of

superoxide production by Photosystem II. FEBS Lett 457: 348–352

Crofts AR and Wraight CA (1983) The electrochemical domain of photosynthesis. Biochim Biophys Acta 726: 149–185

Crofts AR, Wraight CA and Fleischman DE (1971) Energy conservation in the photochemical reactions of photosynthesis and its relation to delayed fluorescence. FEBS Lett 15: 89–100

Crofts AR, Robinson HH and Snozzi M (1984) Reactions of quinols at catalytic sites; a diffusional role in H-transfer. In: Sybesma C (ed) Advances in Photosynthesis Research, Vol I, pp 461–468. Martinus Nijhoff/Dr W Junk, The Hague

Crofts AR, Robinson HH, Andrews K, Van Doren S and Berry E (1987) Catalytic sites for reduction and oxidation of quinones. In: Papa S, Chance B and Ernster L (eds) Cytochrome Systems: Molecular Biology and Bioenergetics, pp 617–624. Plenum Publ Corp, New York

Crofts AR, Baroli I, Kramer D and Taoka S (1993) Kinetics of electron transfer between Q_A and Q_B in wild-type and herbicide-resistant mutants of *C. reinhardtii*. Z Naturforsch 48c: 259–266

de Wijn R and van Gorkom HJ (2001) Kinetics of electron transfer from Q_A to Q_B in Photosystem II. Biochemistry 40: 11912–11922

de Wijn R, Schrama T and van Gorkom HJ (2001) Secondary stabilization reactions and proton-coupled electron transport in Photosystem II investigated by electroluminescence and fluorescence spectroscopy. Biochemistry 40: 5821–5834

Debrunner, PG (1996) Mossbauer spectroscopy. In: Amesz J and Hoff J (eds) Biophysical Techniques in Photosynthesis, pp 355–373. Kluwer Academic Publishers, Dordrecht

Debrunner PG, Schulz CE, Feher G and Okamura MY (1975) Mossbauer study of reaction centers from *R. sphaeroides*. Biophys J 15: 226a.

Deisenhofer J and Michel H (1989) The photosynthetic reaction center from the purple bacterium *Rhodopseudomonas viridis.* Science 245: 1463–1473

Deisenhofer J, Epp O, Miki K, Huber R and Michel H (1985) Structure of the protein subunits in the photosynthetic reaction centre of *Rhodopseudomonas viridis* at 3 Å resolution. Nature 318: 618–624

Deisenhofer J, Epp O, Sinning I and Michel H (1995) Crystallographic refinement at 2.3-angstrom resolution and refined model of the photosynthetic reaction centre from *Rhodopseudomonas viridis*. J Mol Biol 246: 429–457

Deligiannakis Y, Tsekos N, Petrouleas V and Diner BA (1992) Orientation dependence of the Fe^{2+}-NO and Fe^{3+} EPR signal associated with the non-heme iron of Photosystem II. Biochim Biophys Acta 1140: 163–168

Deligiannakis Y, Petrouleas V and Diner BA (1994) Binding of carboxylate anions at the non-heme Fe(II) of PS II. I Effects on the $Q_A^-Fe^{2+}$ and Q_AFe^{3+} EPR spectra and the redox properties of the iron. Biochim Biophys Acta 1188: 260–270

Deligiannakis Y, Boussac A and Rutherford AW (1995) ESEEM study of the plastoquinone anion radical ($Q_A^{\bullet-}$) in ^{14}N- and ^{15}N-labeled Photosystem II treated with CN^-. Biochemistry 34: 16030–16038

Deligiannakis Y, Jegerschold C and Rutherford AW (1997) EPR and ESEEM study of the plastoquinone anion radical Q_A^- in Photosystem II treated at high pH. Chem Phys Lett 270: 564–572

Deligiannakis Y, Ioannidis N and Petrouleas V (1998) lD- and 2D-ESEEM study of the [Fe-NO](S=3/2) complex of PS II. In Garab G (ed): Photosynthesis: Mechanisms and Effects, Vol II, pp 1117–1120. Kluwer Academic Publishers, Dordrecht

Deligiannakis Y, Hanley, J and Rutherford AW (1999) lD- and 2D-ESEEM study of the semiquinone radical Q_A^- of Photosystem II. J Am Chem Soc 121: 7653–7664

Demeter S, Goussias Ch, Bemat G, Kovacs L and Petrouleas V (1993), Participation of the g = 1.9 and g = 1.82 EPR forms of the semiquinone-iron complex, $Q_A^-Fe^{2+}$ of Photosystem II in the generation of the Q and C thermoluminescence bands, respectively. FEBS Lett 336: 352–356

Diner BA (1977) Dependence of the deactivation reactions of Photosystem II on the redox state of the plastoquinone pool A, varied under anaerobic conditions. Equilibria on the acceptor side of Photosystem II. Biochim Biophys Acta 460: 247–258

Diner BA (1998) Application of spectroscopic techniques to the study of Photosystem II mutations engineered in *Synechocystis* and *Chlamydomonas*. Method Enzymol 297: 337–360

Diner BA and Babcock GT (1996) Structure, dynamics, and energy conversion efficiency in Photosystem II. In: Ort DR and Yocum CF (eds) Oxygenic Photosynthesis: The Light Reactions, pp 213–247. Kluwer Academic Publishers, Dordrecht

Diner BA and Petrouleas V (1987a) Light-induced oxidation of the acceptor-side Fe(lI) of Photosystem II by exogenous quinones acting through the Q_B binding site. II. Blockage by inhibitors and their effects on the Fe(III) EPR spectra. Biochim Biophys Acta 893: 138–148

Diner BA and Petrouleas V (1987b) Q_{400}, the non-heme iron of the Photosystem II iron-quinone complex. A spectroscopic probe of quinone and inhibitor binding to the reaction center. Biochim Biophys Acta 895: 107–125

Diner BA and Petrouleas V (1990) Formation by NO of nitrosyl adducts of redox components of the Photosystem II reaction center. II. Evidence that HCO_3^-/CO_2 binds to the acceptor-side non-heme iron. Biochim Biophys Acta 1015: 141–149

Diner BA, Petrouleas V and Wendoloski JJ (1991) The iron-quinone electron-acceptor complex of Photosystem II. Physiol Plant 81: 423–436

Draber W, Tietjen K, Kluth JF and Trebst A (1991) Herbicides in photosynthesis research. Angew Chem Int Ed Engl 30: 1621–1633

Draber W, Hilp U, Likusa H, Schindler M. and Trebst A (1993) Inhibition of photosynthesis by 4-nitro-6-alkyl-phenols: Structure-activity studies in wild-type and five mutants of *Chlamydomonas reinhardtii* thylakoids. Z Naturforsch 43c: 213–223

Dutton PL, Prince RC and Tiede DM (1978) The reaction center of photosynthetic bacteria. Photochem Photobiol 28: 939–949

Eaton-Rye JJ and Govindjee (1988) Electron transfer through the quinone acceptor complex of photosystern II after one or two actinic flashes in bicarbonate-depleted spinach thylakoid membranes. Biochim Biophys Acta 935: 248–257

Erickson JM, Rahire M, Bennoun P, Delepelaire P, Diner B and Rochaix JD (1984) Herbicide resistance in *Chlamydomonas reinhardtii* results from a mutation in the chloroplast gene for the 32 kDa protein of PS II. Proc Natl Acad Sci USA 81: 3617–3621

Erickson JM, Pfister K, Rahire M, Togasaki R, Mets L and Rochaix J-D (1989) Molecular and biophysical analysis of herbicide-resistant mutants of *Chlamydomonas reinhardtii:* Structure-function relationship of the photosystern II Dl polypeptide.

Plant Cell l: 361–371.
Etienne A-L, Ducruet J-M, Ajlani G and Vernotte C (1990) Comparative studies on electron transfer in Photosystem II of herbicide-resistant mutants from different organisms. Biochim Biophys Acta 1015: 435–440
Evans MCW, Atkinson YE and Ford RC (1985) Redox characterization of the photosystern II electron acceptors. Evidence for two electron carriers between pheophytin and Q. Biochim Biophys Acta 806: 247–254
Feher G and Okamura MY (1999) The primary and secondary acceptors in bacterial photosynthesis. Appl Magn Reson 16: 63–100
Ferreira KN, Iverson TM, Maghlaoui K, Barber J and Iwata S (2004) Architecture of the Photosynthetic Oxygen-Evolving Center. Science 303: 1831-1838
Forster B, Heifetz PB, Lardans A, Boynton JE, Gillham NW (1997) Herbicide resistance and growth of D1 Ala(251) mutants in *Chlamydomonas*. Z Naturforsch 52c: 9–10
Fowler CF (1977) Proton translocation in chloroplasts and its relationship to electron transport between the photosystems. Biochim Biophys Acta 459: 351–363
Fritzsch G, Kampmann L, Kapaun G and Michel H (1998) Water clusters in the reaction centre of *Rhodobacter sphaeroides*. Photosynth Res 55: 1–6.
Fufezan C, Rutherford AW and Krieger-Liszkay A (2002) Singlet oxygen production in herbicide-treated Photosystem II. FEBS Lett. 532: 407–410
Galloway R and Mets LJ (1984) Atrazine, bromacil and diuron resistance in *Chlamydomonas*. A single non-mendelian genetic locus controls the structure of the thylakoid binding site. Plant Physiol 74: 469–474
Garbers A, Reifarth F, Kurreck J, Renger G and Parak F (1998) Correlation between protein flexibility and electron transfer from Q_A^- to Q_B in PS II membrane fragments from spinach. Biochemistry 37: 11399–11404
Garge P, Chikate R, Padhye S, Savariault JM, de Loth P and Tuchagues J-P (1990) Iron(II) complexes of ortho-functionalized para-naphtoquinones. 2. Crystal and molecular structure of bis(aquo)bis(lawsone)iron(II) and intermolecular magnetic exchange interactions in bis(3-aminolawsone)iron(II). Inorg Chem 29: 3315–3320
Golden SS and Haselkorn R (1985) Mutation to herbicide resistance maps within the *psb*A gene of *Anacystis nidulans* R2. Science 229: 1104–1107
Goussias CH, Deligiannakis Y, Sanakis Y, Ioannidis N and Petrouleas V (2002) Probing subtle coordination changes in the iron- quinone complex of Photosystem II during electron transfer, by the use of NO. Biochemistry 41: 15212–152233
Govindjee (1990) Photosystem II heterogeneity: The acceptor side. Photosynth Res 25: 151-160
Govindjee, Eggenberg P, Pfister K and Stasser RJ (1992) Chlorophyll *a* fluorescence decay in herbicide-resistant D1 mutants of *Chlamydomonas reinhardtii* and the formate effect. Biochim Biophys Acta 1101: 353–358
Greenberg BM, Gaba V, Mattoo AK and Edelman M (1987) Identification of a primary in vivo degradation product of the rapidly-turning-over 32-kD protein of Photosystem II. EMBO J 6: 2865–2869
Hallahan BJ, Ruffle SV, Bowden SJ and Nugent JHA (1991) Identification and characterisation of EPR signals involving Q_B semiquinone in plant Photosystem II. Biochim Biophys Acta 1059: 181–188
Haumann M and Junge W (1994) The rates of proton uptake and electron transfer at the reducing side of Photosystem II in thylakoids. FEBS Lett 347: 45–50
Heathcote P and Rutherford AW (1987) An E.P.R. signal arising from Q_B^-Fe in *Chromatium vinosum* strain D. In: Biggins J (ed) Progress in Photosynthesis Research, Vol I, pp 201–204. Martinus Nijhoff Publisher, Dordrecht
Hegg EL and Que L Jr (1997) The 2-His-1-carboxylate facial triad. An emerging structural motif in mononuclear non-heme iron(II) enzymes. Eur J Biochem 250: 625–629
Hienerwadel R and Berthomieu C (1995) Bicarbonate binding to the non-heme iron of Photosystem II investigated by Fourier transform infrared difference spectroscopy and ^{13}C-labeled bicarbonate. Biochemistry 34: 16288–16297
Hirschberg J and McIntosh L (1983) Molecular basis of herbicide resistance in *Amaranthus hybridus*. Science 222:1346–1349
Hope AB and Matthews DB (1983) Further studies on proton translocations in chloroplasts after single-turnover flashes: 1. Proton uptake. Aust J Plant Physiol 10: 363–372
Hope A and Morland A (1979) Proton Translocation in isolated spinach chloroplasts after single-turnover actinic flashes. Aust J Plant Physiol 6: 289–304
Hubbard JAM, Corrie AR, Nugent JHA and Evans MCW (1989) Properties of the Photosystem II electron acceptor complex of *Phormidium laminosum*. Biochim Biophys Acta 977: 91–96
Huppatz JL (1996) Quantifying the inhibitor-target site interactions of Photosystem II herbicides. Weed Science 44: 743-748
Huppatz JL and Phillips JN (1984) Cyanoacrylate inhibitors of the Hill reaction. III. Stereochemical and electronic aspects of inhibitor binding. Z Naturforsch 39c: 617–622
Hutchison RS, Xiong J, Sayre RT and Govindjee (1996) Construction and characterization of a Photosystem II D1 mutant (arginine-269-glycine) of *Chlamydomonas reinhardtii*. Biochim Biophys Acta 1277: 83–92
Ikegami and Katoh S (1973) Studies on chlorophyll fluorescence in chloroplasts II. Effect of ferricyanide on the induction of fluorescence in the presence of 3-(3,4-dichlorophenyl)-1,1-dimethylurea. Plant Cell Physiol 14: 829–836
Itoh S, Tang XS and Satoh K (1986) Interaction of the high spin Fe atom in the photosystern II reaction center with the quinones Q_A and Q_B in purified oxygen-evolving PS II reaction center complex and in PS II particles. FEBS Lett 205: 275–281
Johanningmeier U, Sopp G, Brauner M, Altenfeld U, Orawski G, Oettmeier W (2000) Herbicide resistance and supersensitivity in Ala(250) or Ala(251) mutants of the D1 protein in *Chlamydomonas reinhardtii*. Pesticide Biochem Physiol 66: 9–19
Johnson GN, Boussac A and Rutherford AW (1994) The origin of 40–50 °C thermoluminescence bands in Photosystem II. Biochim Biophys Acta 1184: 85–92
Joliot P (1974) Effect of low temperature (–30 to –60 °C) on the reoxidation of the Photosystem II primary electron transfer in the presence and absence of 3(3,4-dichlorophenyl)-1,1-dimethylurea. Biochim. Biophys. Acta 357: 439–448
Joliot P, Lavergne J and Beal D (1992) Plastoquinone compartmentation in chloroplasts: I. Evidence for domains with different rates of photo-reduction. Biochim Biophys Acta 1101: 1–12
Kaminskaya, OP, Drachev LA, Konstantinov AA, Semenov AY and Skulachev VP (1986) Electrogenic reduction of the secondary quinone acceptor in chromatophores of *Rhodospirillum rubrum:*

Rapid kinetic measurements. FEBS Lett 202: 224–228
Kamiya N and Shen JR (2003) Crystal structure of oxygen-evolving Photosystem II from T*hermosynechococcus vulcanus* at 3.7-Å resolution. Proc Natl Acad Sci USA 100: 98–103
Kashino Y, Yamashita M, Okamoto Y, Koike H and Satoh K (1996) Mechanisms of electron flow through the Q_B site in Photosystem II. 3. Effects of the presence of membrane structure on the redox reactions at the Q_B site. Plant Cell Physiol 37: 976–982
Keren N, Berg A, Vankan PJM, Levanon H and Ohad I (1997) Mechanism of Photosystem II photoinactivation and D1 protein degradation at low light — the role of back electron flow. Proc Natl Acad Sci USA 94: 1579–1584
Kless H and Vermaas WFJ (1995) Many combinations of amino acid sequences in a conserved region of the D1 protein satisfy Photosystem II function. J Mol Biol 246: 120–131
Kless H Oren-Shamir M, Ohad I, Edelman M and Vermaas WFJ (1993) Protein modifications in the D2 protein of Photosystem II affect properties of the Q_B/herbicide binding environment. Z Naturforsch 43c: 170–184
Klimov VV, Dolan E, Shaw ER and Ke B (1980) Interaction between the intermediary electron acceptor (pheophytin) and a possible plastoquinone-iron complex in Photosystem II reaction centers. Proc Natl Acad Sci USA 77: 7227–7231
Koulougliotis D, Kostopoulos T, Petrouleas V and Diner BA (1993) Evidence for CN-binding at the PS II non-heme Fe^{2+}. Effects on the EPR signal for Q_AFe^{2+} and on Q_A/Q_B electron transfer. Biochim Biophys Acta 1141: 275–282
Krieger A, Rutherford AW and Jegerschold C (1998) Thermoluminescence measurements on chloride-depleted and calcium-depleted Photosystem II. Biochim Biophys Acta 1364: 46–54
Krieger-Liszkay A and Rutherford AW (1998) Influence of herbicide binding on the redox potential of the quinone acceptor in Photosystem II: Relevance to photodamage and phytotoxicity. Biochemistry 37: 17339-17344
Kruk J and Strzalka K (2002) Redox changes of cytochrome b_{559} in the presence of plastoquinones. J Biol Chem 276: 86-91
Kuglstatter A, Ermler U, Michel H, Baciou L and Fritzsch G (2001) X-ray structure analyses of photosynthetic reaction center variants from *Rhodobacter sphaeroides*: Structural changes induced by point mutations at position L209 modulate electron and proton transfer. Biochemistry 40: 4253–4260
Kurreck J, Garbers A, Reifarth F, Andreasson L-E, Parak F, Renger G (1996) Isolation and properties of PS II membrane fragments depleted of the non heme iron center. FEBS Letters 381: 53–57
Lancaster CRD and Michel H (1997) The coupling of light-induced electron transfer and proton uptake as derived from crystal structures of reaction centres from *Rhodopseudomonas viridis* modified at the binding site of the secondary quinone, Q_B. Structure 5: 1339–1359
Lancaster CRD and Michel H (1999) Refined structures of reaction centres from *Rhodopseudomonas viridi*s in complexes with the herbicide atrazine and two chiral atrazine derivatives also lead to a new model of the bound carotenoid. J Mol Biol 286: 883–898
Lardans A, Gillham NW, Boynton JE (1997) Site-directed mutations at residue 251 of the Photosystem II D1 protein of *Chlamydomonas* that result in a nonphotosynthetic phenotype and impair D1 synthesis and accumulation. J Biol Chem 272: 210–216
Lavergne J (1982a) Interaction of exogenous benzoquinone with Photosystem II in chloroplasts: The semiquinone form acts as a dichlorophenyldimethylurea-insensitive secondary acceptor. Biochim Biophys Acta 679: 12–18
Lavergne J (1982b) Mode of action of 3-(3,4-dichlorophenyl)-1,1-dimethylurea: Evidence that the inhibitor competes with plastoquinone for binding to a common site on the acceptor side of Photosystem II. Biochim Biophys Acta 682: 345–353
Lavergne J (1982c) Two types of primary acceptors in chloroplast Photosystem II: I. Different recombination properties. Photobiochem Photobiophys 3: 257–271
Lavergne J, Bouchaud JP and Joliot, P. (1992) Plastoquinone compartmentation in chloroplasts: II. Theoretical aspects. Biochim Biophys Acta 1101: 13–22
Lipscomb JD and Orville AM (1992) Mechanistic aspects of dihydroxybenzoate dioxygenases. In: Sigel H and Sigel A (eds) Metal Ions in Biological Systems, Vol 28, pp 243–298. Marcel Dekker Inc, New York
Lupinkova L, Metz JG, Diner BA, Vass I and Komenda J (2002) Histidine residue 252 of the Photosystem II D1 polypeptide is involved in a light-induced cross-linking of the polypeptide with the alpha subunit of cytochrome *b*-559: Study of a site-directed mutant of *Synechocystis* PCC 6803. Biochim Biophys Acta 1554: 192–201
MacMillan F, Gleiter H, Renger G, Lubitz W (1990) EPR/ ENDOR studies of plastoquinone anion radical in Photosystem II ($Q_A^{\cdot}$) and in organic solvents. In: Baltscheffsky M (ed) Current Research in Photosynthesis, Vol I, pp 531–534. Kluwer Academic Publishers, Dordrecht
MacMillan F, Kurreck I, Adir N, Lendzian F, Kass H, Reifarth F, Renger G and Lubitz W (1995a) EPR, ENDOR and ESEEM investigation of the electron acceptor radical anion $Q_A^{-\bullet}$ in photo system II (PS II) reaction centres. In Mathis P (ed) Photosynthesis: From Light to Biosphere, Vol I, pp 659–662. Kluwer Academic Publishers, Dordrecht
MacMillan F, Lendzian F, Renger G and Lubitz W (1995b) EPR and ENDOR investigation of the primary electron acceptor radical anion $Q_A^{\bullet -}$ in iron-depleted Photosystem II membrane fragments. Biochemistry 34: 8144–8156
Lorente MA, Dahan F, Sanakis Y, Petrouleas V, Bousseksou A and Tuchagues JP (1995) New ferrous complexes based on the 2,2´-biimidazole ligand: Structural, Mossbauer and Magnetic properties. Inorg. Chem. 34: 5346–5357
Michel H and Deisenhofer J (1988) Relevance of the photosynthetic reaction center from purple bacteria to the structure of Photosystem II. Biochemistry 27: 1–7
Michel H, Epp 0 and Deisenhofer J (1986) Pigment-protein interactions in the photosynthetic reaction centre from *Rhodopseudomonas viridis.* EMBO J 5: 2445–2451
Morais F, Kuhn K, Stewart DH, Barber J, Brudvig GW and Nixon PJ (2001) Photosynthetic water oxidation in cytochrome b_{559} mutants containing a disrupted heme-binding pocket. J Biol Chem 276: 31986–31993
Moreland DE (1993) Research on biochemistry of herbicides: An historical overview. Z. Naturforsch. 48c: 121–132
Moser CC, Page CC, Farid R and Dutton PL (1995) Biological electron transfer. J Bioenerg Biomemb 27: 263–274
Mulo P, Tyystjarvi T, Tyystjarvi E, Govindjee, Maenpaa P and Aro EM (1997) Mutagenesis of the d-e loop of Photosystem II reaction centre protein D1 — function and assembly of Photosystem II. Plant Mol Biol 33: 1059–1071

Mulo P, Laakso S, Maenpaa P and Aro EM (1998) Stepwise photoinhibition of Photosystem II – studies with *Synechocystis* species PCC 6803 mutants with a modified de loop of the reaction center polypeptide D1. Plant Physiol 117: 483–490

Nabedryk E, Breton J, Sebban P and Baciou L (2003) Quinone (Q_B) binding site and protein structural changes in photosynthetic reaction center mutants at Pro-L209 revealed by vibrational spectroscopy. Biochemistry 42: 5819–5827

Nixon PJ, Komenda J, Barber J, Deak Z, Vass I and Diner BA (1995) Deletion of the PEST-like region of Photosystem II modifies the Q_B-binding pocket but does not prevent rapid turnover of D1. J Biol Chem 270: 14919–4927

Noguchi T, Kurreck J, Inoue Y and Renger G (1999a). Comparative FTIR analysis of the microenvironment of $Q_A^{-\bullet}$ in cyanide-treated, high pH-treated and iron-depleted Photosystem II membrane fragments. Biochemistry 38: 4846–4852

Noguchi T, Inoue Y, and Tang X-S (1999b). Hydrogen bonding interaction between the primary quinone acceptor Q_A and a histidine side chain in Photosystem II as revealed by Fourier transform infrared spectroscopy. Biochemistry 38: 399–403

Nugent JHA (2001) Photoreducible high spin iron electron paramagnetic resonance signals in dark-adapted Photosystem II: Are they oxidised non-haem iron formed from interaction of oxygen with PS II electron acceptors? Biochim Biophys Acta 1504: 288–298

Nugent IHA, Diner BA and Evans MCW (1981) Direct detection of the electron acceptor of Photosystem 11. FEBS Lett 124: 241–244

Nugent JHA, Corrie AR, Demetriou C, Evans MCW and Lockett CJ (1988) Bicarbonate binding and the properties of Photosystem II electron acceptors. FEBS Lett 235: 71–75

Nugent JHA, Doetschman DC and Maclachlan DJ (1992) Characterization of the multiple EPR line shapes of iron-semiquinones in photosystem 2. Biochemistry 31: 2935–2941

Oettmeier W (1992) Herbicides of Photosystem II. In Barber J (ed) Topics in Photosynthesis Vol. 11: The Photosystems: Structure, Function and Molecular Biology, pp 349–408. Elsevier Science Publishers BV, Amsterdam

Oettmeier W (1999) Herbicide resistance and supersensitivity in Photosystem II. Cell Mol Life Sci 55: 1255–1277

Oettmeier W, Masson K, Kloos R and Reil E (1993) On the orientation of Photosystem II inhibitors in the Q_B-binding niche: Acridones, xanthones and quinones. Z Naturforsch 43c: 146–151

Okamura MY, Paddock ML, Graige MS and Feher G (2000) Proton and electron transfer in bacterial reaction centers. Biochim Biophys Acta 1458: 148–163

Orville AM and Lipscomb JD (1997) Cyanide and nitric oxide binding to reduced protocatechuate 3,4-dioxygenase: Insight into the basis for order-dependent ligand binding by intradiol catecholic dioxygenases. Biochemistry 36: 14044–14055

Peloquin JM, Tang X-S, Diner BA and Britt RD (1999) An electron spin-echo envelope modulation (ESEEM) study of the Q_A binding pocket of PS II reaction centers from spinach and *Synechocystis*. Biochemistry 38: 2057–2067

Petrouleas V and Diner BA (1982) Investigation of the iron components in Photosystem II by Mossbauer spectroscopy. FEBS Lett 147: 11–114

Petrouleas V and Diner BA (1986) Identification of Q_{400}, a high-potential electron acceptor of Photosystem II, with the iron of the quinone-iron acceptor complex. Biochim Biophys Acta 849: 264–275

Petrouleas V and Diner BA (1987) Light-induced oxidation of the acceptor-side Fe(II) of Photosystem II by exogenous quinones acting through the Q_B binding site. I. Quinones, kinetics and pH-dependence. Biochim Biophys Acta 893: 126–137

Petrouleas V and Diner BA (1990) Formation by NO of nitrosyl adducts of redox components of the Photosystem II reaction center. I. NO binds to the acceptor-side non-heme iron. Biochim Biophys Acta 1015: 131–140

Petrouleas V, Sanakis Y, Deligiannakis Y, Diner BA (1992) The non-heme Fe(II) of PS II: (1) Binding of new carboxylate anions, (2) Study of two Mossbauer components. In: Murata N (ed) Research in Photosynthesis, Vol II, 119–122. Kluwer Academic Publishers, Dordrecht

Petrouleas V, Deligiannakis Y, and Diner BA (1994) Binding of carboxylate anions at the non-heme Fe(II) of PS II. II. Competition with bicarbonate and effects on the Q_A/Q_B electron transfer rate. Biochim Biophys Acta 1188: 271–277

Picorel R, Williamson DL, Yruela I and Seibert M (1994) The state of iron in the oxygen-evolving core complex of the cyanobacterium *Phormidium laminosum:* Mossbauer spectroscopy. Biochim Biophys Acta 1184: 171–177

Polle A and Junge W (1986) The slow rise of the flash-light-induced alkalization by Photosystem II of the suspending medium of thylakoids is reversibly related to thylakoid stacking. Biochim Biophys Acta 848: 257—264

Pospisil P, Arato A, Krieger-Liszkay A and Rutherford AW (2004) Hydroxyl Radical Generation by Photosystem II. Biochemistry 43: 6783–6792

Que L Jr (2000) One motif — many different reactions. Nature Struct Biol 7: 182–184

Que L Jr and Raymond YNH (1996) Dioxygen activation by enzymes with mononuclear non-heme iron active sites. Chem Rev: 96, 2607–2624

Rakotonandrasana A, Boinnard D, Savariault JM, Tuchagues JP, Petrouleas V, Cartier C and Verdaguer M (1991) Iron(II) complexes with polydentate Schiff base ligands as models of the photosynthetic mononuclear non-heme ferrous sites. Synthesis, characterization, molecular crystal structure, EXAFS and XANES studies, Mossbauer spectroscopy and magnetic properties. Inorg Chim Acta 180: 19–31

Rappaport F, Guergova-Kuras M, Nixon PJ, Diner BA and Lavergne J (2002) Kinetics and pathways of charge recombination in Photosystem II. Biochemistry 41: 8518–8527

Reifarth F and Renger G (1998) Indirect evidence for structural changes coupled with $Q_B^{\bullet -}$ formation in Photosystem II. FEBS Lett 428: 123–126

Rigby SEJ, Heathcote P, Evans MCW and Nugent JHA (1995) ENDOR and special TRIPLE resonance spectroscopy of $Q_A^{\bullet -}$ of photosystem 2. Biochemistry 34: 12075-12081

Robinson HH and Crofts AR (1983) Kinetics of the oxidation-reduction reactions of the Photosystem II quinone acceptor complex, and the pathway for deactivation. FEBS Lett 153: 221–226

Robinson HH and Crofts AR (1984) Kinetics of proton uptake and the oxidation-reduction reactions of the quinone acceptor complex of Photosystem II from pea chloroplasts. In: Sybesma C (ed) Advances in Photosynthesis Research, Vol 1, pp 477–480. Martinus Nijhoff/ Dr W Junk Publishers, The Hague

Robinson, HH and Crofts AR (1987) Kinetics of the changes in oxidation-reduction states of the acceptors and donors of

Photosystem II in pea thylakoids measured by flash fluorescence. In Biggins J (ed) Progress in Photosynthesis Research, Vol 2, pp 429–432. Martinus Nijhoff / Dr W Junk Publishers, The Hague

Robinson HH, Eaton-Rye JJ, van Rensen JJS and Govindjee (1984) The effects of bicarbonate depletion and formate incubation on the kinetics of oxidation-reduction reactions of the Photosystem II quinone acceptor complex. Z Naturforsch 39c: 382–385

Robinson HH, Golden S, Brusslan J and Haselkorn R (1987) Functioning of Photosystem II in mutant strains of the cyanobacterium *Anacystis nidulans* R2. In: Biggins J (ed) Progress in Photosynthesis Research, Vol IV, pp 825–828. Matinus Nijhoff Publishers, Dordrecht

Ruffle SV, Donnelly D, Blundell TL and Nugent JHA (1992) A three-dimensional model of the Photosystem II reaction centre of *Pisum sativum*. Photosynth Res 34: 287–300

Ruffle SV, Wang J, Johnston HG, Gustafson TL, Hutchison RS, Minagawa J, Crofts AR and Sayre RT (2001). Photosystem II peripheral accessory chlorophyll mutants in *Chlamydomonas reinhardti*i. Biochemical characterization and sensitivity to photo-inhibition. Plant Physiol 127: 633–644

Rutherford AW (1985) Orientation of EPR signals arising from components in Photosystem II membranes. Biochim Biophys Acta 807: 189–201

Rutherford AW (1987) How close is the analogy between the reaction centre of PS II and that of purple bacteria? 2. The electron acceptor side. In: Biggins J (ed) Progress in Photosynthesis Research, Vol 1, pp 277–283. Martinus Nijhoff Publishers, Dordrecht

Rutherford AW and Krieger-Liszkay A (2001) Herbicide-induced oxidative stress in Photosystem II. Trends Biol Sci 26: 648–653

Rutherford AW and Krieger-Liszkay A (2002) Singlet oxygen production in herbicide-treated Photosystem II. FEBS Lett 532: 407–-410

Rutherford AW and Zimmermann J-L (1984) A new EPR signal attributed to the primary plastoquinone acceptor in Photosystem II. Biochim Biophys Acta 767: 168–175

Rutherford AW, Crofts AR and Inoue Y (1982) Thermoluminescence as a probe of Photosystem II photochemistry; the origin of the flash induced glow peaks. Biochim Biophys Acta 682: 457–465

Sanakis Y and Petrouleas V (1995) Cyanide binding at the non heme iron of PS II and effects on certain EPR signals. In Mathis P (ed) Photosynthesis: From Light to Biosphere, Vol I, pp 823–826. Kluwer Academic Publishers, Dordrecht

Sanakis Y, Petrouleas V, and Diner BA (1994) Cyanide binding at the non-heme Fe^{2+} of the iron-quinone complex of Photosystem II: At high concentrations cyanide converts the Fe^{2+} from high ($S = 2$) to low ($S = 0$) spin. Biochemistry 33: 9922–9928

Sanakis Y, Petasis D, Petrouleas V and Hendrich M (1999) Simultaneous binding of fluoride and NO to the nonheme iron of Photosystem II: Quantitative EPR evidence for a weak exchange interaction between the semiquinone Q_A^- and the iron-nitrosyl complex. J Am Chem Soc 121: 9155–9164

Saphon S and Crofts AR (1977) The H^+/e ratio in chloroplasts is 2. Possible errors in its determination. Z Naturforsch 32c: 810–816

Semin BK, Loviagina ER, Aleksandrov AY, Kaurov YN and Novakova AA (1990) Effect of formate on Mossbauer parameters of the non-heme iron of PS II particles of cyanobacteria. FEBS Lett 270: 184–186

Shinkarev V and Wraight CA (1993) Electron and proton transfer in the acceptor quinone complex of reaction centers of photosynthetic bacteria. In Deisenhofer J (ed) The Photosynthetic Reaction Center, Vol 1, pp 193–255. Academic Press, New York

Snel JFH and van Rensen JJS (1984) Reevaluation of the role of bicarbonate and formate in the regulation of photosynthetic electron flow in broken chloroplasts. Plant Physiol 75: 146–150

Spoyalov AP, Hulsebosch RJ, Shochat S, Gast P, Hoff AJ (1996) Evidence that Ala M260 is hydrogen-bonded to the reduced primary acceptor quinone $Q_A^{\bullet-}$ in reaction centers of *Rb. sphaeroides*. Chem Phys Lett 263: 715–720

Stemler A and Murphy J (1983) Determination of the binding constant of $H^{14}CO_3^-$ to the Photosystem II complex in maize chloroplasts: Effects of inhibitors and light. Photochem Photobiol 38:101–707

Stemler A and Murphy JB (1985) Bicarbonate-reversible and irreversible inhibition of Photosystem II by monovalent anions. Plant Physiol 77: 974–977

Stiehl HH and Witt HT (1969) Quantitative treatment of the function of plastoquinone in photosynthesis. Z Naturforsch 24c: 1588–1598

Stowell MHB, McPhillips TM, Rees DC, Soltis SM, Abresch E and Feher G (1997) Light-induced structural changes in photosynthetic reaction center — implications for mechanism of electron-proton transfer. Science 276: 812–816

Sundby C, Chow WS and Anderson JM (1993) Effects on Photosystem I1 function, photoinhibition, and plant performance of the spontaneous mutation of serine 264 in the Photosystem I1 reaction center D1 protein in triazine-resistant *Brassica napus* L. Plant Physiol 103: 105–113

Tang X-S, Peloquin JM, Lorigan GA, Britt RD and Diner BA (1995) The binding environment of the reduced primary quinone electron acceptor Q_A of PS II. In: Mathis P (ed) Photosynthesis: From Light to Biosphere, Vol I, pp 775–778. Kluwer Academic Publishers, Dordrecht

Taoka S (1989) Kinetics of electron transfer and binding of inhibitors in the two-electron gate of chloroplasts. PhD Thesis, University of Illinois at Urbana-Champaign

Taoka S and Crofts AR (1987) Competition of Inhibitors with the secondary quinone in dark-adapted thylakoid membranes. In: Biggins J (ed) Progress in Photosynthesis Research Vol 2, pp 425–428, Martinus Nijhoff / Dr W Junk Publishers, The Hague

Taoka S and Crofts AR (1990) Two-electron gate in triazine resistant and susceptible *Amaranthus hybridus*. In: Baltscheffsky M (ed) Current Research in Photosynthesis, Vol I, pp 547–550. Kluwer Academic Publishers, Dordrecht

Taoka S, Robinson HH and Crofts AR (1983) Kinetics of the reactions of the two-electron gate of Photosystem II: Studies on the competition between plastoquinone and inhibitors. In Inoue Y, Crofts AR, Govindjee, Murata N, Renger G and Satoh K (eds) The Oxygen Evolving System of Photosynthesis, pp 369–381. Academic Press, Tokyo

Tietjen KG, Draber W, Goossens J, Jansen JR, Kluth JF, Schindler M, Wroblowsky H-J, Hilp U and Trebst A (1993) Binding of triazines in the Q_B-binding niche of Photosystem II. Z Naturforsch 48c: 205–212

Trebst A (1986) The topology of the plastoquinone and herbicide

binding peptides of Photosystem II in the thylakoid membrane. Z Naturforsch 41c: 240–245

van Gorkom HJ (1996) Electroluminescence. Photosynth Res 48: 107–116

van Mieghem F, Nitschke W, Mathis P and Rutherford AW (1989) The influence of the quinone-iron electron acceptor complex on the reaction centre photochemistry of Photosystem II. Biochim Biophys Acta 977: 207–214

van Rensen JJS (2002) Role of bicarbonate at the acceptor side of Photosystem II. Photosynth Res 73: 185–192

van Rensen JJS, Tonk WJM and de Bruijn SM (1988) Involvement of bicarbonate in the protonation of the secondary quinone electron acceptor of Photosystem II via the non-haem iron of the quinone iron acceptor complex. FEBS Lett 226: 347–351

van Rensen JJS, Xu CH and Govindjee (1999) Role of bicarbonate in Photosystem II, the water-plastoquinone oxidoreductase of plant photosynthesis. Physiol Plant 105: 585–592

Vass I and Govindjee (1996) Thermoluminescence from the photosynthetic apparatus. Photosynth Res 48: 117–126

Velthuys BR (1976) Charge accumulation and recombination in system 2 of photosynthesis. PhD Thesis, Rijksuniversiteit te Leiden

Velthuys BR (1981) Electron-dependent competition between plastoquinone and inhibitors for binding to Photosystem II. FEBS Lett 126: 277–281

Velthuys BR (1982) The function of plastoquinone in electron transfer. In: Trumpower BL (ed) Function of Quinones in Energy-Conserving Systems, pp 401–408. Academic Press, New York

Velthuys BR and Amesz J (1974) Charge accumulation at the reducing side of system 2 of photosynthesis. Biochm Biophys Acta 325: 138–148

Vermaas WFJ and Rutherford AW (1984) EPR measurements on the effects of bicarbonate and triazine resistance in the acceptor side of Photosystem II. FEBS Lett 175: 243–248

Vermaas WFJ, Renger G and Arntzen CJ (1989) Herbicide/quinone interactions in photosystem 11. Z Naturforsch 139c: 368–373

Vernotte C, Briantais JM, Astier C, Govindjee (1993) Differential effects of formate in single and double mutants of D1 in *Synechocystis* PCC 6714. Biochim Biophys Acta 1229: 296–301

Wraight CA (1979) Electron acceptors of bacterial photosynthetic reaction centers. Biochim Biophys Acta 548: 309–327

Wraight CA (1981) Oxidation-reduction physical chemistry of the acceptor quinone complex in bacterial photosynthetic reaction centers: Evidence for a new model of herbicide activity. Isr J Chem 21: 348–354

Wraight CA (1985) Modulation of herbicide-binding by the redox state of Q_{400}, an endogenous component of Photosystem II. Biochim Biophys Acta 809: 320–330

Wraight CA (2004) Proton and electron transfer in the acceptor quinone complex of photosynthetic reaction centers from *Rhodobacter sphaeroides.* Frontiers in Biosciences 9: 309–337

Xiong J, Hutchison RS, Sayre RT, Govindjee (1997) Modification of the Photosystem II acceptor side function in a D1 mutant (arginine-269-glycine) of *Chlamydomonas reinhardtii*. Biochim Biophys Acta 1322: 60–76

Xiong J, Subramaniam S and Govindjee (1998a) A knowledge based 3-D model of the Photosystem II reaction center of *Chlamydomonas reinhardtii*. Photosynthesis Research 56: 229–254

Xiong J, Minagawa J, Crofts A, Govindjee (1998b) Loss of inhibition by formate in newly constructed Photosystem II D1 mutants, D1-R257E and D1-R257M, of *Chlamydomonas reinhardtii*. Biochim Biophys Acta 1365: 473–491

Yoshida S, Oettmeier W and Boger P (1993) Proceedings of International Workshop on Chloroplast Metabolism and its Inhibition by Herbicides, Saitama, Japan, 1992. Z Naturforsch 48c: 119–405

Zheng M, and Dismukes GC (1996) The Conformation of the isoprenyl chain relative to the semiquinone head in the primary electron acceptor (Q_A) of higher plant PS II (plastosemiquinone) differs from that in bacterial reaction centers (ubisemiquinone or menasemiquinone) by ca. 90°. Biochemistry 35: 8955–8963

Zimmermann J-L and Rutherford AW (1986) Photoreductant-induced oxidation of Fe^{2+} in the electron acceptor complex of Photosystem II. Biochim Biophys Acta 851: 416–423

Zouni A, Witt H-T, Kern J, Fromme P, Krauß N, Saenger W and Orth P (2001) Crystal structure of Photosystem II from *Synechococcus elongatus* at 3.8 Å resolution. Nature 409: 739–743

Chapter 9

The Redox-Active Tyrosines Y_Z and Y_D

Bruce A. Diner*
Central Research and Development, Experimental Station,
E. I. du Pont de Nemours & Co., Wilmington, DE 19880-0173 U.S.A.

R. David Britt
Department of Chemistry, University of California at Davis, Davis, CA 95616, U.S.A.

Summary

Photosystem II (PS II) contains two redox-active tyrosines, Y_D and Y_Z, located in homologous locations in the reaction center polypeptides D2 and D1, respectively. These are the best characterized of the enzymatic reactions that involve tyrosyl radical formation. The reasons for this extensive knowledge include the ability in PS II to measure tyrosine oxidation and reduction with nanosecond time resolution from liquid helium to room temperature and in preparations that have been modified by site-directed mutagenesis. The abundance and purity of PS II preparations and the recent ability to crystallize them also allows the application of a wide variety of spectroscopic techniques to the characterization of the redox-active tyrosines. This chapter describes the discovery of these redox components, the kinetics, energetics and mechanism of their oxidation and reduction and detailed information on their spectroscopic characteristics with a particular emphasis

*Author for correspondence, email: Bruce.A.Diner@usa.dupont.com

T. Wydrzynski and K. Satoh (eds): Photosystem II: The Light-Driven Water:Plastoquinone Oxidoreductase, pp. 207–233.

on magnetic resonance methods. The close interaction of tyrosine Y_Z with the oxygen-evolving complex has implicated Y_Z directly in the mechanism of water oxidation. The role of this tyrosine in this mechanism has been the source of a great deal of debate and interest in recent years, heightened by the improving resolution of the PS II crystal structure.

I. Introduction

Tyrosyl radicals have now been described as intermediates in numerous enzymatic reactions. A partial list includes ribonucleotide reductase, prostaglandin synthase, galactose oxidase, cytochrome oxidase as well as Photosystem II (PS II) (Stubbe and van der Donk, 1998). The latter has the advantage of being triggered by light, which allows the kinetics of tyrosine oxidation to be followed on the nanosecond time scale and over a wide range of temperatures from 4 to 300 K. In addition, the ability to readily observe in PS II reversible oxidation-reduction reactions of tyrosine with excellent signal/noise using a wide variety of spectroscopic techniques has provided detailed information on the mechanism and energetics of this process. This chapter will provide an overview of what we have learned about the tyrosyl radicals of PS II.

Commoner et al. (1956) first reported the observation in tobacco chloroplasts of a light-induced electron paramagnetic resonance (EPR) signal that came to be known as Signal II. There was little indication at the time of the chemical nature of the radical, though its greater linewidth (16–19 G) and its hyperfine structure distinguished it from Signal I, a chlorophyll cation radical that arises from the oxidized primary donor of Photosystem I (PS I) ($P700^+$) (Weaver, 1962). In extensive studies of Signal II, Babcock, Blankenship and Sauer (Babcock and Sauer, 1973a,b, 1975a,b,c; Blankenship et al., 1975a,b; Babcock et al., 1976) were able to distinguish three kinetic components, all of which showed similar EPR spectra. These were called Signal IIs, f and vf (for slow, fast and very fast, respectively) and were shown to arise from PS II as indicated by their induction by red light (as opposed to the far-red sensitized PS I) in spinach chloroplasts and their sensitivity to the state of the oxygen-evolving complex (OEC) and under certain conditions to DCMU, an herbicide inhibitor of PS II. Signal IIs was generated from the S_2 and S_3 states of the OEC with a rise time of ~1s at room temperature and was sensitive to OEC inactivation (Babcock and Sauer, 1973a). Signal IIs had a lifetime measured on the hours time scale. Signal IIf, observed upon inactivation of the OEC (e.g., by Tris wash) (Babcock and Sauer, 1975b), had a rise time initially shown to be <500 μs and a lifetime of close to 100 ms, resulting from charge recombination with reduced acceptor, Q_A^-, in the presence of DCMU. The Signal IIf lifetime was shown to depend upon the presence, accessibility and reduction potential of exogenous donors. Blankenship et al. (1975b) showed by EPR that the precursor, responsible for Signal IIf, was a direct donor to $P680^+$ with a risetime for oxidation consistent with the $\tau = 35$ μs reported by Gläser et al. (1974) for $P680^+$ reduction using optical methods. A direct comparison of the rise of Signal IIf and the decay of $P680^+$ and their respective pH dependencies confirmed this conclusion (Boska et al., 1983). With better time resolution, a signal (Signal IIvf), with similar line shape and amplitude to Signal IIf, could be observed using EPR in the presence of the OEC with a rise time of <100 μs (Blankenship et al., 1975b) and a decay time of ≤1 ms that depended on the S-state of the OEC (Babcock et al., 1976). The redox component(s) responsible for Signal IIf and vf had similar EPR (Hoganson and Babcock, 1988) and optical difference spectra (Gerken et al., 1988) and were therefore likely one and the same species, the risetime and lifetime of which depended on the presence of the OEC. The marked influence of the OEC on the power saturation characteristics of Signal IIf (vf) (Warden et al., 1976; Yocum and Babcock, 1981) also implied that the species responsible for this signal was located in close proximity to the Mn cluster. Much

Abbreviations: CEP – concerted electron/proton transfer; CW – continuous wave as opposed to pulsed mode; DCMU – 3-(3,4-dichlorophenyl)-1,1-dimethylurea; ENDOR – electron nuclear double resonance; EPR – electron paramagnetic resonance; ESEEM – electron spin echo envelope modulation; ESE-ENDOR – pulsed electron spin envelope ENDOR; ETPT – electron transfer followed by proton transfer; FTIR – Fourier transform infrared; HAT – hydrogen atom transfer; OEC – oxygen evolving complex; P680 – PS II primary electron donor chlorophyll complex; PS I – Photosystem I; PS II – Photosystem II; PTET – proton transfer followed by electron transfer; Signal II – EPR signal attributed to $Y_D^\bullet$ (Signal IIs) and $Y_Z^\bullet$ (Signal IIf and vf); Sn – states of the water oxidizing complex for n = 0, 1, 2, 3 or 4; WT – wild type; Y_D (D) – redox-active tyrosine on the D2 protein (D2-Tyr160); Y_Z (Z) – redox-active tyrosine on the D1 protein (D1-Tyr161)

more accurate estimates of the distance between the two have been obtained more recently (Peloquin et al., 1998; Lakshmi et al., 1999), based on the weak dipolar coupling observed between the two under conditions that generate the S_3-split signal (Boussac et al., 1990a; Hallahan et al., 1992; MacLachlan and Nugent, 1993)(see below).

The donors responsible for Signal IIs and IIf (vf) became known as donors D and Z, respectively. The similarity in their EPR spectra implied that they arose from the same chemical species.

II. Chemical Nature of Signal II

The first attempts at establishing the chemical nature of these donors were described in a paper by Kohl and Wood (1969), who reported that lipid extraction and reconstitution of chloroplast fragments with perdeuterated plastoquinone modified the EPR spectrum of Signal II. The conclusion that a plastoquinone free radical contributed to Signal II influenced the thinking of subsequent work which included EPR studies of model quinoid radicals (Kohl et al., 1969; Hales and Das Gupta, 1981; Ghanotakis et al., 1983; O'Malley and Babcock, 1984), theoretical arguments for a particular localization of the electron spin density of quinoid radicals that could explain the hyperfine structure of the EPR and electron nuclear double resonance (ENDOR) spectra of Signal II (O'Malley et al., 1984), and observed similarities between the optical spectra for Z^+/Z and those known for quinoid radicals (Dekker et al., 1984a,b; Diner and De Vitry, 1984). While neutral or cationic plastoquinone radicals remained the favored assignment based on spectroscopic data, there remained some doubt in that the plastoquinone content of isolated PS II core complexes (~1.2 per reaction center (De Vitry et al., 1986)) was insufficient to account for the presence of Q_A, Z and D. The ultimate proof that D was in reality a tyrosine was provided in a key paper by Barry and Babcock (1987) who showed that labeling of *Synechocystis* sp. PCC 6803 with perdeuterated tyrosine resulted in the loss of the hyperfine structure of Signal IIs. As no label was incorporated into plastoquinone, it was clear that Signal IIs was a tyrosine free radical. The similarity in the EPR spectra of oxidized D and Z implied that both were tyrosyl radicals, with the g_{iso}-value of 2.0046 in both cases consistent with the formation of the neutral ($D^{\bullet}$ and $Z^{\bullet}$) rather than the cation radical ($D^{+\bullet}$ and $Z^{+\bullet}$). The tyrosine assignment was further strengthened by the observations of Ikeuchi and Inoue (1988) and of Takahashi and Satoh (1989) of a light-induced iodination of D1-Tyr161. The latter authors as well as Debus et al. (1988a) and Vermaas et al. (1988) remarked on the presence of homologous tyrosines at D1-161 and D2-160 of the D1 and D2 polypeptides, respectively. These were located at the lumenal side of the third transmembrane helix of both polypeptides in regions of considerable homology. Site directed replacement of D2-Tyr160 with phenylalanine (Debus et al., 1988a; Vermaas et al., 1988) resulted in the loss of $D^{\bullet}$. An analogous replacement at D1-Tyr161 (Debus et al., 1988b; Metz et al., 1989) resulted in the loss of $Z^{\bullet}$. The optical absorbance changes associated with Z oxidation (Dekker et al., 1984b; Diner and De Vitry, 1984; Gerken et al., 1988) were shown to bear a strong resemblance to those associated with tyrosine oxidation in water (Bent and Hayon, 1975). A strong case had thus been established in favor of the conclusion that both $D^{\bullet}$ and $Z^{\bullet}$ were tyrosyl radicals. The loss of the EPR hyperfine structure (see below) of $Z^{\bullet}$ in WT (Boerner and Barry, 1993) and in D-less (Tang et al., 1996a) PS II core complexes containing perdeuterated tyrosine sealed the assignment. The ability to observe photoautotrophic growth, albeit impaired, in the case of the D2-Tyr160Phe (D) mutation and none for the D1-Tyr161Phe (Z) mutation, where O_2 activity was completely lost, favored the location of Z and not D as the intermediate redox component between $P680^+$ and the OEC, consistent with the dependence of the formation and decay kinetics of $Z^{\bullet}$ on the oxidation state of the OEC. With the clear identification of both Z and D with tyrosine, they have come to be called Y_Z and Y_D, respectively, Y being the letter symbol for tyrosine. The earlier observations of an alteration in EPR Signal II upon reconstitution with deuterated plastoquinone (Kohl and Wood, 1969) remain unexplained but may have been a consequence of structural changes associated with the reconstitution procedure that resulted in the loss or broadening of the radical hyperfine structure. Another example of the loss of the hyperfine structure of Y_D was found by Boussac and Etienne (1984) in their redox titration of this species.

A. Electronic Structure

EPR spectroscopy has been extensively used to characterize the electronic structure of tyrosine radicals, including $Y_D^{\bullet}$ and $Y_Z^{\bullet}$. Figure 1 shows the X-band EPR

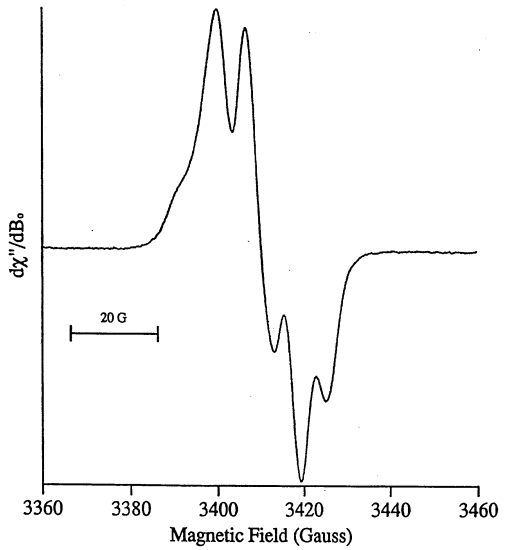

Fig. 1. X-band continuous wave (CW) EPR signal of $Y_D^{\bullet}$ ($T \leq 20$ K) in a spinach PS II-enriched (BBY) preparation (Berthold et al., 1981).

spectrum of $Y_D^{\bullet}$ from spinach. This fairly complex lineshape results from an interplay of *g*-anisotropy with comparable hyperfine interactions with several strongly coupled protons.

Various advanced EPR methods have been useful for probing further spectroscopic details of the two PS II tyrosine radicals, and for comparing these to tyrosine radicals in other enzymes. For example, high frequency/field EPR ($\nu \geq 94$ GHz) provides a very useful spectroscopic handle for these tyrosine radicals, in that by going to high field the *g*-anisotropy is greatly increased, allowing resolution of the three principal *g*-matrix components (Gulin et al., 1992; Un et al., 1994, 1996; Farrar et al., 1997; Dorlet et al., 2000; Hofbauer et al., 2001; Chapter 17, Bittl and Kawamori). Specifically, at high frequency/field, the 'powder pattern' features associated with the three *g*-values are split well beyond the spectral breadth introduced by the field-independent hyperfine terms. This is shown in Fig. 2. The g_y (≈ 2.0045) and g_z (≈ 2.0021) values for tyrosine radicals are relatively insensitive to environmental effects, but the g_x component, which is aligned along the C-O bond axis, varies appreciably (≈ 2.0064 to 2.0090) for different protein environments, and the precise value is often taken as a measure of the degree of hydrogen bonding (Section V). Because the orientation of the *g*-axes is

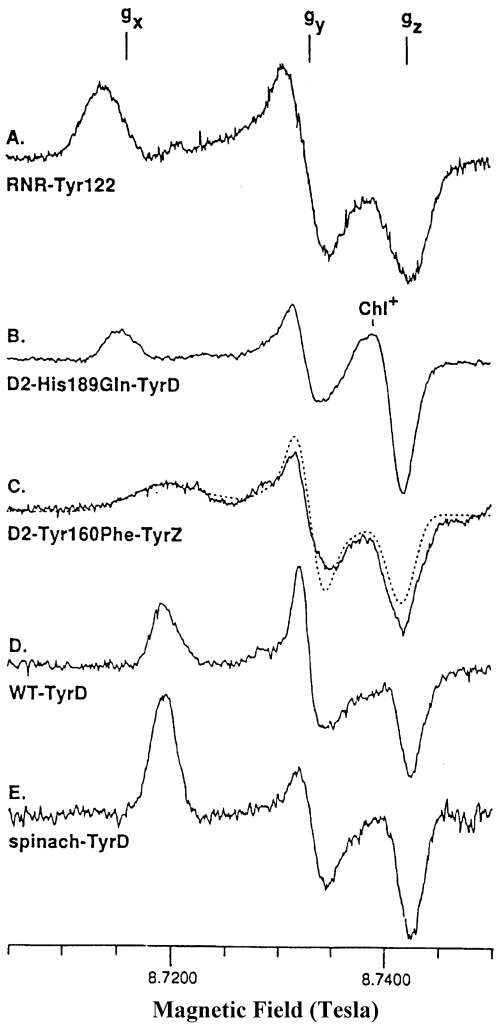

Fig. 2. High field (245 GHz) EPR signals at 4K of (A) $Tyr_{122}^{\bullet}$ of *E. coli* ribonucleotide reductase, $g_x = 2.00868$; (B) $Y_D^{\bullet}$ in Mn-depleted PS II core complexes from the mutant D2-His189Gln of *Synechocystis,* $g_x = 2.00832$; (C) $Y_Z^{\bullet}$ measured in Mn-depleted PS II core complexes from the *Synechocystis* Y_D-less mutant, D2-Tyr160Phe. Dotted line – calculated spectrum for $Y_Z^{\bullet}$ assuming a g_x-value of 2.0075 (additional details provided in Un et al., 1966), $g_x = 2.0075$; (D) $Y_D^{\bullet}$ in Mn-depleted PS II core complexes from WT *Synechocystis*, $g_x = 2.00740$ and (E) $Y_D^{\bullet}$ in spinach PS II-enriched membranes, $g_x = 2.00737$. From Un et al. (1996).

known relative to the tyrosine ring molecular axes, recent high field studies of $Y_D^{\bullet}$ using oriented PS II membranes (Dorlet et al., 2000) or PS II single crystals (Hofbauer et al., 2001) provide detailed in-

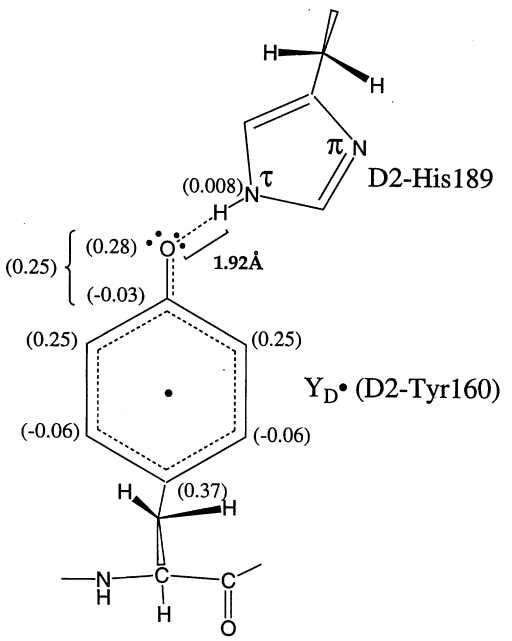

Fig. 3. Spin density distribution for $Y_D^{\bullet}$ (D2-Tyr160) hydrogen bonded to D2-His189.

formation about the orientation of the phenoxyl ring of the $Y_D^{\bullet}$ radical relative to the membrane normal and the PS II crystalline axes. The phenoxyl ring is tilted about 26° from the membrane normal.

A precise measurement of hyperfine couplings, with magnetic nuclei at natural abundance (^{1}H) or specifically introduced (^{2}H, ^{13}C, ^{17}O) into the $Y_D^{\bullet}$ and $Y_Z^{\bullet}$ tyrosine radicals, provides a direct measure of their distributions of unpaired spin density. A summary of the spin densities is illustrated in Fig. 3. A comparison with parallel experimental results on other protein tyrosine radicals, as well as on tyrosine radicals generated by UV-irradiation in frozen solution (Hulsebosch et al., 1997), can be made. For example, the ^{17}O hyperfine interaction can be directly observed from the EPR spectrum of $Y_D^{\bullet}$ of *Synechocystis* PS II incorporating ^{17}O-labelled tyrosine (Dole et al., 1997). From this measurement, the spin density on the oxygen of the $Y_D^{\bullet}$ radical was determined to be 0.28, which is close to that determined by similar ^{17}O-labelling of the R2-Y_{122} tyrosine of ribonucleotide reductase (Hoganson et al., 1996) and of the neutral tyrosine radical in frozen solution (Hulsebosch et al., 1997). Historically, most of the data leading to spin density assignments within the phenoxyl rings of the two tyrosines have come from proton ENDOR (Hoganson and Babcock, 1992; Rigby et al., 1994; Gilchrist et al., 1995; Tommos et al., 1995) and deuteron electron spin echo envelope modulation (ESEEM) experiments (Warncke et al., 1994; Tommos et al., 1995). For example, Fig. 4 shows pulsed proton ENDOR for $Y_D^{\bullet}$ from spinach, along with ENDOR simulations for the different coupled protons and their sum (Gilchrist et al., 1995). Good hyperfine values also come from high frequency EPR simulations (Dorlet et al., 2000), particularly from the single crystal data (Hofbauer et al., 2001). The most specific assignments of matching hyperfine features to specific hydrogens come from specific deuteron labeling studies (Warncke et al., 1994; Tommos et al., 1995). It is straightforward to relate the hydrogen hyperfine values to the spin densities of the carbons to which they are bound (McConnell, 1956; McConnell and Chesnut, 1958). At least in a broad sense, the spin densities around the phenoxyl ring are relatively invariant over various tyrosine radicals, including $Y_D^{\bullet}$ and $Y_Z^{\bullet}$ from different organisms. As seen in Figs. 3 and 4, large couplings are observed for the 3 and 5 ring hydrogens (see Fig. 4 for the nomenclature), and on the order of 25% of the spin density is on each of the adjacent carbons. In contrast, small couplings are observed to the 2 and 6 ring hydrogens, and the spin densities of their adjacent carbons are only about –0.06 each. The C1 carbon does not have a directly bonding hydrogen, but its large spin density (≈ 0.32–0.38) projects on the two protons of the adjacent β-methylene carbon in an angular dependent ($\alpha\cos^2\theta$) fashion (inset of Fig. 4), and thus a measurement of the two hyperfine couplings for these two protons can determine the angles θ_1 and θ_2, where $\theta_2 = 120° - \theta_1$. For example, for spinach $Y_D^{\bullet}$, the β-methylene proton ENDOR (Fig. 4) leads to an assignment of these angles to be approximately 47° and 73°. These angles, which designate the ring orientation, vary appreciably among various protein tyrosine radicals, including $Y_D^{\bullet}$ and $Y_Z^{\bullet}$, and are also species-dependent. Because at least one of the two β-methylene protons is usually one of the strongest coupled to the electron spin of the radical, the CW EPR lineshapes are strongly modulated by these angles as well. Of particular note is a recent EPR study from the Hoff laboratory (Nieuwenhuis et al., 1998), which employed enantioselective deuteration of the β-methylene group hydrogens of tyrosine incorporated into *Synechocystis* PS II. For *Synecho-*

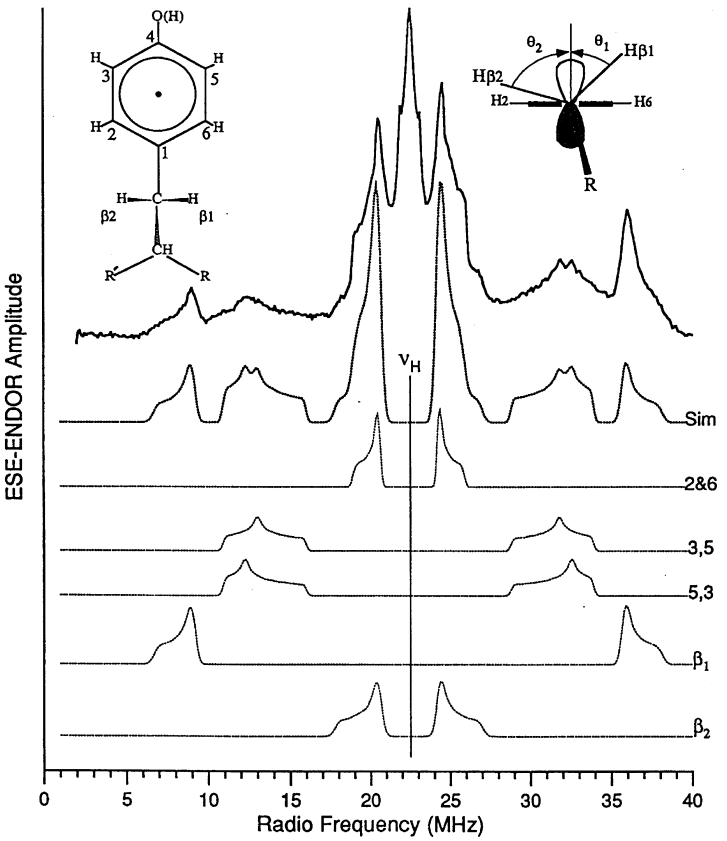

Fig. 4. Simulation of pulsed proton ENDOR (ESE-ENDOR) for $Y_D^{\bullet}$ from spinach, along with ENDOR simulations for the different coupled protons and their sum. From Gilchrist et al. (1995).

cystis, $Y_D^{\bullet}$, the prochiral H_R hydrogen has the largest hyperfine coupling (smallest dihedral angle), which is contrary to the stronger H_S coupling observed for a tyrosine radical in frozen solution. This observation was taken as strong evidence for a constrained environment of the $Y_D^{\bullet}$ tyrosine radical, consistent with a tight distribution of the dihedral angle for $Y_D^{\bullet}$, reported earlier from analysis of deuteron ESEEM (Warncke et al., 1994). In contrast, ESEEM of ^{2}H-labelled $Y_Z^{\bullet}$ of Mn-depleted *Synechocystis* PS II shows appreciable disorder in the dihedral angle (Tommos et al., 1995; Warncke et al., 1995).

B. Mn-$Y_Z^{\bullet}$ Interaction

A major source of knowledge about the interaction of the Y_Z tyrosine with the catalytic Mn cluster has been the EPR spectroscopy of an interesting radical signal observed in inhibited PS II samples. For example, calcium depletion of PS II particles by NaCl/EGTA-washing (Boussac and Rutherford, 1988; Boussac et al., 1989; 1990a) or low pH citrate treatment (Ono and Inoue, 1988; 1989) eliminates oxygen-evolving activity. In such Ca^{2+}-depleted PS II particles, illumination at a temperature of 273 K leads to the formation of a broad (130–180 G full width at half maximum) $g = 2$ EPR signal with an unusual 'split' lineshape. Other treatments that block O_2 evolution, such as acetate or fluoride incubation, lead to similar signals upon such illumination, although the signal widths vary appreciably depending on the details of the treatment and the resulting extrinsic polypeptide composition (Baumgarten et al., 1990; Andreasson and Lindberg, 1992; Boussac et al., 1992; Hallahan

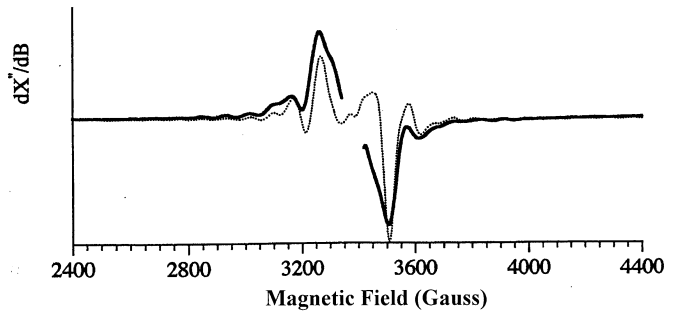

Fig. 5. CW-EPR 'illuminated minus annealed' difference spectrum of the split EPR signal in acetate-treated spinach PS II membranes. The solid lines represent experimental data and the dotted lines numerical simulations. The experimental and simulation details are provided in Peloquin et al. (1988).

et al., 1992; MacLachlan and Nugent, 1993). Figure 5 shows the CW EPR spectrum of the split signal formed by acetate incubation. The flash dependence of the split signal amplitude in Ca^{2+}-depleted samples demonstrates that it originates from a donor-side configuration formally equivalent to the S_3 state (Boussac et al., 1990a). Also, UV absorption changes associated with the formation of the split signal were interpreted as favoring an oxidized histidine as the origin for this signal, with the unusual breadth attributed to a magnetic coupling with the Mn cluster (Boussac et al., 1990a). The histidine assignment was initially supported by Fourier transform infrared (FTIR) difference spectra correlated with radical formation (Berthomieu and Boussac, 1995), but later re-evaluated in support of $Y_Z^{\bullet}$ as the organic radical, the appearance of which coincided with the split signal (Berthomieu et al., 1998). An alternate origin for the split signal was also put forward by Hallahan et al. (1992), whose CW EPR experiments were interpreted to favor $Y_Z^{\bullet}$ as the radical component of the broad spectrum.

Gilchrist et al. (1995) used pulsed EPR spectroscopy to address the molecular origin of the split signal in Ca^{2+}-depleted PS II. In this ESE-ENDOR study, the proton ENDOR spectrum of the split signal was shown to closely match the spectra of biological tyrosine radicals such as $Y_D^{\bullet}$ (see Fig. 4). Figure 6 shows the comparison of the ^1H ENDOR of the split signal from Ca^{2+}-depleted spinach PS II with the $Y_Z^{\bullet}$ signal trapped in a Y_D-less (D2-Tyr160Phe) *Synechocystis* mutant (Britt et al., 1995). The spectral match is quite good, providing strong support for a $Y_Z^{\bullet}$ assignment for the origin of the split signal. The detailed assignment of the different proton resonances can be made

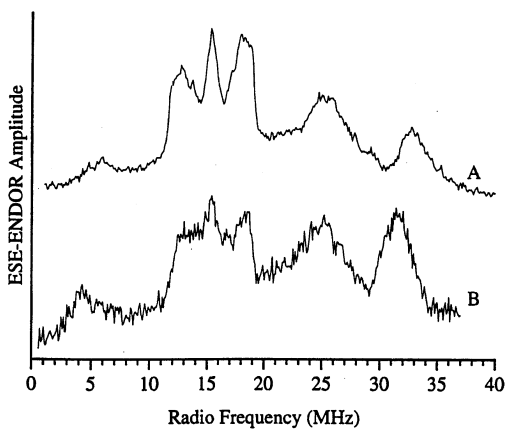

Fig. 6. ESE-ENDOR spectra in the proton resonance regions for (A) $Y_Z^{\bullet}$ in Mn-depleted PS II particles of the *Synechocystis* Y_D-less mutant D2-Tyr160Phe. (B) Split signal trapped in Ca^{2+}-depleted spinach PS II-enriched membranes. From Britt et al. (1995).

by comparison with the $Y_D^{\bullet}$ ENDOR spectrum shown earlier (Fig. 4), with weakly coupled protons at the 2 and 6 positions, more strongly coupled 3 and 5 position protons, and a strongly coupled β-methylene proton. As described earlier, the frequencies of the β-methylene proton couplings provide an accurate measurement of the phenoxy ring orientation relative to the β-methylene group CH bond angles, and from their similar frequencies we can infer that the corresponding angles are quite similar (within ≈ 2°) for *Synechocystis* $Y_Z^{\bullet}$ and $Y_Z^{\bullet}$ trapped in the Ca^{2+}-depleted split signal form (Britt et al., 1995). Tang et al. (1996b) used the ESEEM pulsed EPR experiment along with *Synechocystis* PS II particles grown al-

ternatively with deuterated (d_7) or natural abundance tyrosine to show that the ratio of the ESEEM spectra of the split EPR signal generated in deuterated vs. natural abundance samples showed similar features to those found for the $Y_D^{\bullet}$ tyrosine, and of the sort previously reported for $Y_D^{\bullet}$ by Warncke et al. (1994). This work was taken as very direct evidence that the split signal arises from a tyrosine radical, presumably $Y_Z^{\bullet}$. Peloquin et al. (1998) also used high frequency ESE-ENDOR to observe the ^{55}Mn transitions of the split signal, an important observation to conclusively show that the S_2-state Mn cluster is the other spin partner to the $Y_Z^{\bullet}$ radical.

Given this $Y_Z^{\bullet}$-S_2-state assignment, one can simulate the EPR (Dorlet et al., 1998; Lakshmi et al., 1998; Peloquin et al., 1998) and ESE-ENDOR (Peloquin et al., 1998) spectra to extract magnetic coupling parameters, and to model a distance between the Mn cluster and the $Y_Z^{\bullet}$ radical. The estimated distance range has varied in different papers from different groups. For example, Gilchrist et al. (1995) used a dipolar approximation for the interspin coupling and extracted a 4.5 Å distance. More recently Dorlet et al. (1998) and Lakshmi et al. (1999) provided excellent split signal EPR simulations with dominant exchange interactions. Peloquin et al. (1998) used a common set of exchange and dipolar couplings to simulate both the acetate-treated PS II split signal EPR and ^{55}Mn ENDOR spectra. The EPR simulation (dotted line) is shown along with the experimental trace in Fig. 5. The distance between the C4 tyrosine carbon and the nearest Mn of the cluster was estimated to be between 8.6 and 11.5 Å in this study. The recent 3.5 Å resolution X-ray structure of PS II (Ferreira et al., 2004) shows a 5.1 Å distance between the tyrosine oxygen and the Ca^{2+} of the OEC, somewhat longer to the cluster Mn and consistent with the previous EPR- and ENDOR- derived distances (Dorlet et al., 1998; Lakshmi et al., 1998; Peloquin et al., 1998).

Evidence for a short Mn cluster-$Y_Z^{\bullet}$ distance provided a major line of evidence for mechanistic models involving $Y_Z^{\bullet}$ directly in water oxidation through a coupling of electron and proton transfer (Gilchrist et al., 1995; Hoganson et al., 1995; Hoganson and Babcock, 1997). It is interesting that a number of treatments (Cl-depletion, Ca^{2+}-depletion and acetate treatment) all block the $S_2 \rightarrow S_3$-state transition, resulting in a trappable S_2-$Y_Z^{\bullet}$ configuration. It is likely that there is a common origin of this induced lesion in the Kok cycle. Vrettos et al. (2001) have argued that disruption of H-bonding between $Y_Z^{\bullet}$ and the Mn cluster, possibly through the loss of a substrate Mn-bound water could disrupt this S-state transition. In this context, it is interesting to note the recent ESEEM results on acetate-treated PS II which shows that acetate binding results in a dehydration of the Mn cluster (Clemens et al., 2002).

III. Protonation States of the Oxidized and Reduced Forms of Tyrosine

Having established that there are two redox active tyrosines in PS II, the question remains as to the nature of the initial state of the tyrosine (tyrosine or tyrosinate) and the final state of the oxidation product (neutral or cation radical).

A. Reduced Tyrosine

Candeias et al. (1998) compared the optical difference spectra of Tyr$^{\bullet}$/Tyr in pulse radiolysis experiments at pH 7.8 and 12 to those reported in the literature for $Y_Z^{\bullet}/Y_Z$ and $Y_D^{\bullet}/Y_D$ and concluded that both of these tyrosines were always in the tyrosinate form in situ with or without the presence of the Mn cluster. The reference difference spectra reported by Candeias et al. (1998) differ, however, markedly from those reported using UV flash photolysis by Bent and Hayon (1975) at pH 7.5 (protonated tyrosine) which much more closely resemble the biological spectra. Haumann et al. (1999) have suggested the presence of a tyrosinate in Mn-intact PS II at physiological pH based on optical difference spectra and on the rapid electron transfer limited rate for the oxidation of Y_Z by $P680^+$ at physiological pH (see below). These spectra required, however, substantial correction for the presence of Q_A^-, and were compared to what were erroneously attributed to absolute in vitro spectra (Rappaport and Lavergne, 2001). Hienerwadel et al. (1996, 1997) compared the $Y_D^{\bullet}/Y_D$ FTIR difference spectrum to that of cresol$^{\bullet}$/cresol. Negative signals (arising from Y_D) in Mn-depleted PS II core complexes at 1615 and 1513–1510 cm^{-1} were attributed to the ν8(CC) and to the ν19(CC) ring modes of the side chain of Y_D, respectively. These modes would be expected to be located at 1600 and 1499 cm^{-1}, respectively, if Y_D were in the tyrosinate form. In addition, a negative signal at 1252 cm^{-1} was attributed to the δ(COH) mode of Y_D. Similar signals were observed by Noguchi et al. (1997) in the presence of the Mn cluster. These observations

argue that Y_D is protonated at pH 6 in the presence and absence of the Mn cluster. Negative FTIR signals at 1618 and 1521 cm^{-1} for the ν8(CC) and to ν19(CC) ring modes, respectively, of the side chain of Y_Z and at 1255 cm^{-1} for the δ(COH) mode in the $Y_Z^{\bullet}/Y_Z$ difference spectrum were likewise attributed to the protonated form of Y_Z at pH 6 in Mn-depleted PS II core complexes (Berthomieu et al., 1998). The observation of similar signals (1521 and 1254 cm^{-1}) for a tyrosine coupled to the oxidation of the OEC (S_2/S_1) in PS II core complexes containing an intact Mn cluster (Noguchi et al., 1997) might indicate that Y_Z is in the protonated state at pH 6.0 in this case as well. This assignment, however, assumes that the tyrosine that is sensitive to the oxidation of the OEC is Y_Z. Thus, the FTIR measurements in the absence of the Mn cluster argue strongly that the reduced tyrosines, Y_D and Y_Z, are both protonated at physiological pHs. A similar case can be made for Y_D in the presence of the OEC. However, the case for protonated Y_Z in the presence of the OEC is weaker and needs to be re-examined. It remains unclear why there are differences between the model tyrosine spectra of Candeias et al. (1998) and Bent and Hayon (1975). The latter spectra, however, support the conclusion arrived at by FTIR. Westphal et al. (2000) have argued that the $Tyr^{\bullet}/Tyr^{-}$ reduction potential of 0.68 V measured in water is likely to be lowered to 0.26 V in situ for $Y_Z^{\bullet}/Y_Z^{-}$ because of the electrostatic penalty associated with the formation of the tyrosinate in a medium of low dielectric. This penalty would make $Y_Z^{\bullet}$ a poor oxidant, with a reduction potential that is inconsistent with that of 0.9–1.0 V, necessary to drive the oxidation of H_2O to O_2. This thermodynamic argument therefore lends further support for the likelihood of a protonated state for Y_Z and Y_D.

B. Oxidized Tyrosine

Two possibilities then exist for the product of tyrosine oxidation, the neutral radical where there is deprotonation of the phenolic-OH accompanying electron transfer or the protonated radical in the absence of deprotonation. The zero crossing point (g_{iso}-value) ranges from 2.0032 for the protonated radical to 2.0044 for the neutral radical (Dixon and Murphy, 1976). Barry and Babcock (1987) pointed out that as the g_{iso} value of $Y_Z^{\bullet}$ and $Y_D^{\bullet}$ is 2.0046 it is likely that $Y_Z^{\bullet}$ and $Y_D^{\bullet}$ are both neutral radicals. FTIR measurements have shown that the Y_D and Y_Z phenolic protons are exchangeable upon replacement of H_2O with D_2O (Hienerwadel et al., 1997; Berthomieu et al., 1998). The replacement of the exchangeable proton with a deuteron is also observable in the ENDOR and ESEEM spectra of $Y_D^{\bullet}$ and $Y_Z^{\bullet}$ (Rodriguez et al., 1987; Evelo et al., 1989; Tang et al., 1993, 1996a,b; Diner et al., 1998; Tommos et al., 1998) and by kinetic means making use of a kinetic isotope effect (see below). The strength of the dipolar hyperfine coupling (3.5–3.7 MHz) and the virtual absence of an isotropic hyperfine component for the exchangeable proton in $Y_D^{\bullet}$ (Rodriguez et al., 1987; Evelo et al., 1989; Hoganson and Babcock, 1992; Rigby et al., 1994) and $Y_Z^{\bullet}$ (Force et al., 1995; Tommos et al., 1995; Tang et al., 1996a) indicates these to be hydrogen bonded neutral tyrosyl radicals. Furthermore, the site-directed replacement of the phenolic proton acceptor, D2-His189 (see below) with a glutamine (Tang et al., 1993), resulted in the complete loss of the hyperfine coupling to $Y_D^{\bullet}$ due to the exchangeable proton. These observations all support the formation of the neutral radical upon oxidation of both Y_Z and Y_D, an observation that is consistent with the extremely acidic pKa of –2 reported for the cation radical (Dixon and Murphy, 1976). The redox properties of tyrosine also argue for the formation of the neutral radical. The formation of the cation radical $TyrOH - e^{-} \rightarrow TyrOH^{+\bullet}$ is thermodynamically rather unfavorable (Harriman, 1987; Tommos et al., 1999). Using literature values for the pKa of the oxidized (–2) (Dixon and Murphy, 1976) and reduced (10.3) (Harriman, 1987), (9.9) (Tommos et al., 1999) forms of tyrosine and the measured reduction potential of $TyrO^{\bullet}/TyrO^{-}$ ($E_{>pKared}$ = 0.72 V vs. NHE, (Harriman, 1987), 0.65 V (Tommos et al., 1999)), one can calculate from the thermodynamic cycle that the reduction potential for the redox couple $TyrOH^{+\bullet}$/TyrOH should be 1.35–1.45 V (Diner, 2001). That the reduction potential of $P680^{+}$ is estimated to be $E'_{P^{+}/P} = 1.12$ V (Klimov and Krasnovskii, 1981) means that the oxidation of tyrosine to the cation radical by the oxidized primary donor would be highly unfavorable and inconsistent with measured equilibrium constant, $K_{zp} >> 1$ (where $K_{zp} = Y_Z^{\bullet}(H^{+})P680/Y_ZP680^{+}$, see below). The term $Y_Z^{\bullet}(H^{+})$ is meant to indicate that the phenolic proton released upon formation of the neutral radical remains bound to the reaction center, but not to $Y_Z^{\bullet}$ (for at least the first few hundred microseconds). The above calculation is based on the aqueous solution properties of tyrosine. The oxidation to the cation radical is likely to be even more unfavorable in a medium of low dielectric (Tommos et al., 1999).

The above discussion thus favors the loss of the phenolic proton upon oxidation to form the neutral radical for both Y_Z and Y_D, (TyrOH – e^- → TyrO$^\bullet$ + H^+)

IV. Localization of Y_Z and Y_D

Two groups (Debus et al., 1988a; Vermaas et al., 1988) constructed site-directed mutations in *Synechocystis* at D2-160, replacing the tyrosine with a phenylalanine (D2-Tyr160Phe). The mutation resulted in the complete loss of the EPR signal arising from Y_D despite the presence of wild type (WT) levels of PS II reaction centers. While able to grow photoautotrophically, the mutant did so at a rate 3–4 times slower than WT. The construction of the site-directed mutation at D2-160 was followed shortly thereafter by the corresponding mutation, D1-Tyr161Phe (Debus et al., 1988b; Metz et al., 1989). This mutation resulted in the loss of the EPR signal arising from $Y_Z^\bullet$. It also slowed the reduction of $P680^+$ to the millisecond time range in PS II core complexes where reduction occurred via charge recombination with Q_A^-. This observation implied the loss of rapid electron donation to $P680^+$, a characteristic of Y_Z. This mutant was unable to grow photoautotrophically, consistent with the loss of the redox component linking $P680^+$ to the OEC. Saturation-recovery EPR measurements placed $Y_Z^\bullet$ and $Y_D^\bullet$ equidistant from the non-heme iron of the reaction center at a distance of 37 ±5 Å (Koulougliotis et al., 1995). This distance was consistent with predictions for the location of D1-Tyr161 and D2-Tyr160 (homologous to L-Arg135 and M-Arg165 of *Rhodobacter sphaeroides*) based on a mapping of PS II (Ruffle et al., 1992; Svensson et al., 1996; Xiong et al., 1998) onto the three dimensional structure of the bacterial reaction centers (Allen et al., 1986; Michel and Deisenhofer, 1988; El-Kabbani et al., 1991). The location of these tyrosines has now been confirmed by the X-ray crystallographic structure of PS II core complexes from the thermophilic *Synechococcus elongatus* (now *Thermosynechococcus elongatus*) (Zouni et al., 2001; Kamiya and Shen, 2003; Ferreira et al., 2004; Chapters 19–21).

V. The Proton Acceptor and Hydrogen-Bonding

As pointed out above, the oxidation of both Y_Z and Y_D in the presence and absence of the Mn cluster occurs with the liberation of a proton. There has been a growing appreciation in recent years of the importance of Y_Z deprotonation, upon oxidation, for the mechanism of water oxidation. Y_Z oxidation/deprotonation allows this tyrosine to be a direct participant in the mechanism of water oxidation, both as an electron sink for the oxidation of the Mn cluster and as a proton sink for the protons of the coordinated substrate water molecules (Gilchrist et al., 1995; Hoganson et al., 1995; Britt, 1996a; Tommos and Babcock, 1998; Westphal et al., 2000; Cukier, 2004). Support for this view has come from a number of sources: (i) the proposal by Krishtalik (1986, 1990) for the coupling of water oxidation to the protonation of a base whose pKa is redox state dependent; (ii) the solution pKa of ~10 for the phenolic-OH of tyrosine and of –2 for the cation radical; (iii) the physical proximity of Y_Z to the Mn cluster based on spin coupling (Boussac et al., 1990a; Hallahan et al., 1992; Gilchrist et al., 1995; Tang et al., 1996b; Dorlet et al., 1998; Lakshmi et al., 1998; Peloquin et al., 1998); (iv) suggested hydrogen-bonded contact between Y_Z and the Mn cluster based on the sensitivity of Y_Z vibrational modes to the S-state (Noguchi et al., 1997) and of the spin state of the Mn cluster to the redox state of Y_Z (Szalai et al., 1998); and (v) the suggested exothermicity of H$^\bullet$ transfer associated with the breaking of the O–H bond of H_2O or $–OH^-$, bound to Mn, and the formation of an O-H bond in tyrosine (Lind et al., 1990; Bordwell and Cheng, 1991; Gardner and Mayer, 1995; Pecoraro et al., 1998). Consequently, how proton-coupled electron transfer occurs in PS II is of critical importance for the understanding of donor-side electron transfer in this photosystem. As we will see below, the proton-coupled electron transfer occurs most rapidly between a hydrogen-bonded proton donor/acceptor pair. The experimental observations leading to the identification of the proton acceptor to the redox active tyrosines will be explored in the paragraphs that follow.

A. Spectroscopic Techniques

Three independent spectroscopic techniques (ENDOR and ESEEM, high field EPR and FTIR) have indicated that the two redox-active tyrosines are hydrogen bonded in their radical states, most likely by the protonated base that serves in its deprotonated form as the immediate proton acceptor upon oxidation (Babcock et al., 1989). The first of these

experiments, CW and pulsed ENDOR and ESEEM, provide the most direct probe of H-bonding for tyrosine radicals (Britt, 1996b). In general, these experiments can probe for the presence of magnetic nuclei in the vicinity of a paramagnetic molecule. Specifically, this can be a proton or deuteron introduced into the exchangeable H-bond hydrogen site, and hyperfine coupled to the unpaired electron spin delocalized onto the tyrosine ring (see Section II.A). These techniques have all indicated the presence of a proton hyperfine interaction that is sensitive to $^2H/^1H$ exchange (Rodriguez et al., 1987; Evelo et al., 1989; Tang et al., 1993; Force et al., 1995; Tang et al., 1996a; Diner et al., 1998). High field EPR can resolve the g_x component of the tyrosyl radical anisotropic g-tensor. The value of this component is quite sensitive to the orientation and strength of a hydrogen bond to the phenolic oxygen of the radical and has been used to characterize hydrogen bonding to several tyrosyl radicals (Un et al., 1996). FTIR can detect a ν(CO) vibrational mode, the value of which is a sensitive measure of the hydrogen bonding strength to the phenolic oxygen of the tyrosyl radical. Values between 1497 and 1512 cm^{-1} have been observed for the PS II tyrosyl radicals in the WT and in non-hydrogen bonding mutants (Hienerwadel et al., 1997; Berthomieu et al., 1998). An important advantage of this technique is that it can also be used to characterize hydrogen bonding in the reduced state of the tyrosine (e.g., δ(COH) bending mode, see below).

We have had good success in observing deuterons exchanged into the two PS II tyrosine sites using pulsed ^2H ENDOR (Force et al., 1995). ^2H ENDOR (and ESEEM) offers the advantage that the exchanged

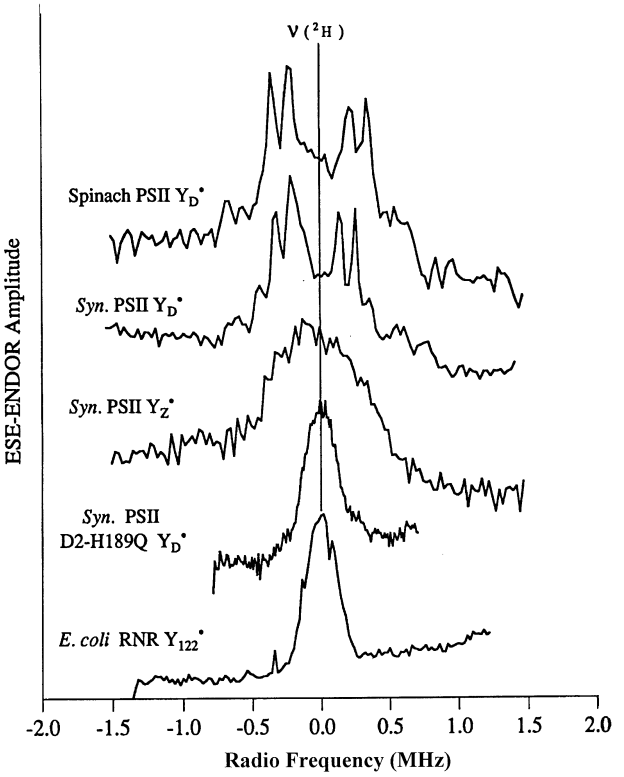

Fig. 7. Mims ^2H pulsed ENDOR (ESE-ENDOR) for (starting from the top) $Y_D^•$ in PS II enriched membranes from spinach, $Y_D^•$ in Mn-depleted *Synechocystis* PS II core complexes, $Y_Z^•$ in Mn-depleted *Synechocystis* PS II core complexes from the Y_D-less (D2-Tyr160Phe) mutant, $Y_D^•$ in Mn-depleted *Synechocystis* PS II core complexes from the D2-His189Gln mutant and $Y_{122}^•$ in *E. coli* ribonucleotide reductase. Adapted from Force et al. (1995).

hydrogens are observed directly, rather than as a subtraction between two spectra obtained before and after exchange. The top two traces of Fig. 7 show the ^{2}H ENDOR for $Y_D^{\bullet}$ in spinach and *Synechocystis* PS II preparations. These $Y_D^{\bullet}$ H-bonding signatures are rather similar. The highly resolved features arise from dipolar hyperfine coupling and from the electric quadrupolar coupling of the spin $I = 1$ ^{2}H nucleus. From the through-space dipolar coupling and the spin density on the tyrosine oxygen (0.28 ± 0.001) measured from PS II incorporating ^{17}O-labeled tyrosine, one can estimate a distance of 1.9 Å between the deuteron and the $Y_D^{\bullet}$ tyrosine oxygen (Dole et al., 1997) (Fig. 3).

It was pointed out by Debus et al. (1988a) that there exist in the homologous D1 and D2 polypeptides a pair of conserved histidines, D1-His190 and D2-His189, that are likely located not far from the redox active tyrosines. This suggestion was reinforced by efforts at what is largely molecular replacement type modeling of the PS II reaction center (Ruffle et al., 1992; Svensson et al., 1996; Xiong et al., 1998). The above-mentioned spectroscopic techniques as well as measurements of the rates of electron transfer to $P680^+$ have implicated these histidines as either the hydrogen bonding partners or as likely proton acceptors upon tyrosine oxidation or both.

B. Y_D

The spectroscopic evidence for hydrogen bonding between Y_D (and $Y_D^{\bullet}$) and D2-His189 is quite strong. Site-directed mutations at D2-His189 result in some cases in a perturbation of the X-band EPR spectrum of $Y_D^{\bullet}$ (Tang et al., 1993; Tommos et al., 1993). While not directly due to the loss of a hydrogen bond, these changes probably result from alterations in the orientation of the β-methylene protons relative to the p_z orbital of the C1 carbon of the aromatic ring, altering the hyperfine coupling of these protons to the electronic spin. The most structurally conservative (least perturbed X-band EPR spectrum) of these site-directed changes, D2-His189Gln, resulted in the loss of a ^{2}H/^{1}H exchangeable proton hyperfine component at 3.5 MHz (Tang et al., 1993). Consistent with this observation, is the loss, in the ^{2}H ESE-ENDOR of $Y_D^{\bullet}$ in the PS II core complex of this mutant (Fig. 7, second trace from bottom), of the deuteron coupling assigned to the hydrogen bond. This spectrum is identical to that of the tyrosyl radical of *E. coli* ribonucleotide reductase (Fig. 7, bottom trace) which is known to lack a hydrogen bond (Bender et al., 1989; Un et al., 1996). This same mutation resulted in the displacement of the g_x component of the anisotropic g-tensor of $Y_D^{\bullet}$ from 2.00740 in the WT to 2.00832 in the D2-His189Gln mutant, only slightly lower than that observed in the non-hydrogen bonded tyrosyl radical of *E. coli* ribonucleotide reductase (2.00868) (Fig. 2) (Bender et al., 1989; Nordlund et al., 1990; Un et al., 1996).

The position of the FTIR-detected ν(CO) mode of a tyrosine radical is upshifted upon increasing strength of hydrogen bonding. FTIR spectra indicate the displacement of the ν(CO) mode of $Y_D^{\bullet}$ from 1503 in the WT to 1497 cm^{-1} in the D2-His189Gln mutant (Hienerwadel et al., 1997). The latter is also very close to the ν(CO) signal observed at 1498 cm^{-1} for the non-hydrogen bonded tyrosyl radical of *E. coli* ribonucleotide reductase by resonance Raman spectroscopy (Backes et al., 1989). All of these observations indicate that the replacement of D2-His189 by Gln results in the loss of the hydrogen bond to the phenolic oxygen in $Y_D^{\bullet}$. Based on the ν(CC) and ν(CO) stretch modes and the δ(COH) bending mode detected by FTIR (Hienerwadel et al., 1997), it appears that Y_D in the mutant remains a hydrogen bond donor, not to histidine as in the WT but to the carbonyl oxygen of the glutamine side chain.

The identity of the specific H-bond donor(s) can be interrogated by ENDOR methods as well. For example, Fig. 8 shows a series of ^{15}N ESE-ENDOR experiments targeting the $Y_D^{\bullet}$ tyrosine in *Synechocystis* PS II preparations incorporating different ^{15}N labelings (Campbell et al., 1997). Trace (a) shows the ^{15}N ESE-ENDOR for a globally ^{15}N labeled WT sample. A pair of features is split symmetrically about the ~1.5 MHz ^{15}N Larmor frequency due to non-zero hyperfine interactions with one or more ^{15}N nuclei. Trace (b) shows the ESE-ENDOR for a sample ^{15}N-labelled at only the histidine nitrogen sidechain positions. In this case we observe a pair of sharp isotropic lines split by 0.8 MHz about the ^{15}N Larmor frequency. These peaks are not observed when only the histidine π-nitrogen is labeled (trace (c)), indicating that a histidine τ-nitrogen is the hydrogen bond donor (Fig. 3). Figure 8 (trace d) shows the ^{15}N ESE-ENDOR of a globally ^{15}N-labelled sample from mutant D2-His189Gln. In this case, the isotropic histidine peaks are gone, directly demonstrating that D2-His189 is indeed the hydrogen bond donor. Thus we have a very clear description of hydrogen bonding for the *Synechocystis* $Y_D^{\bullet}$ tyrosine radical, with a strong hydrogen bond

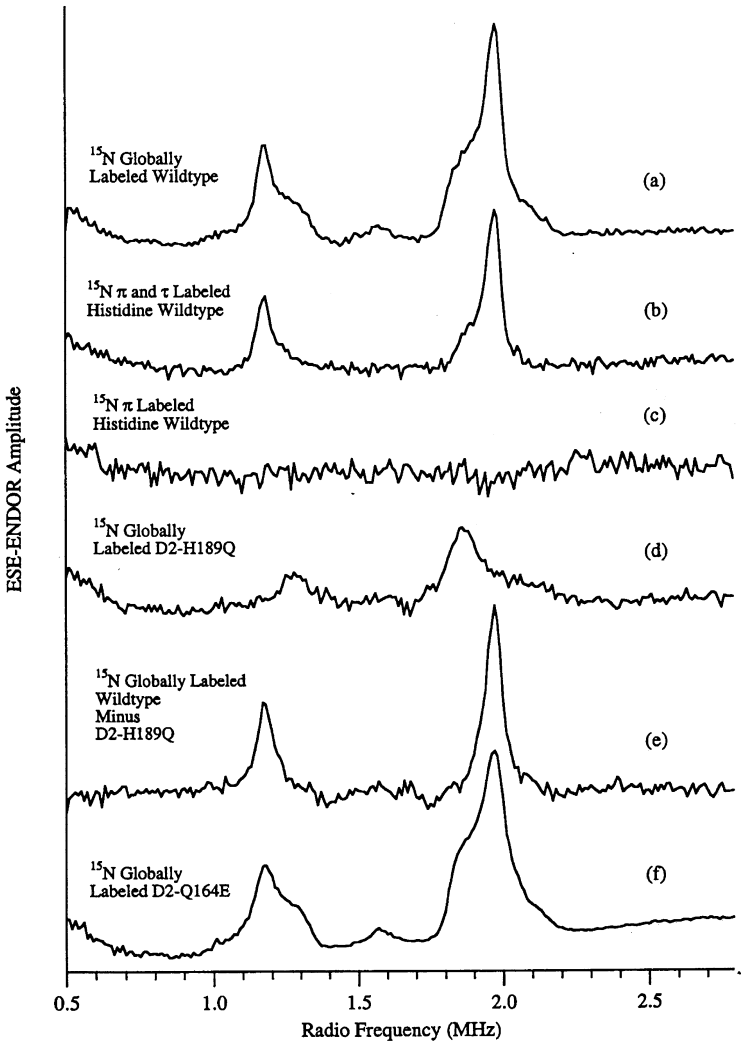

Fig. 8. Mims ^{15}N pulsed ENDOR (ESE-ENDOR) for Mn-depleted PS II core complexes from *Synechocystis* prepared from (a) WT globally labeled with ^{15}N ($Na^{15}NO_3$); (b) a histidine-tolerant strain of WT labeled with ^{15}N-histidine (π- and τ-nitrogens labeled with ^{15}N); (c) a histidine-tolerant strain of WT labeled with ^{15}N-histidine (π-nitrogen labeled with ^{15}N); (d) the D2-His198Gln mutant globally labeled with ^{15}N; (e) the difference (a) – (d); (f) the D2-Gln164Glu mutant globally labeled with ^{15}N. From Campbell et al. (1997).

donated by the τ-nitrogen of the D2-His189 residue (Fig. 3). This assignment has been confirmed in a recently published X-ray crystal structure of PS II (Ferreira et al., 2004).

Using ^{15}N-labelled tyrosine, we have assigned the broad remnant features in the D2-His189Gln mutant ^{15}N ENDOR spectrum to the peptide nitrogen of the $Y_D^{\bullet}$ tyrosine (K.A. Campbell, R.D. Britt and B.A. Diner, personal communication). Remarkably, a subtraction of the D2-His189Gln mutant ^{15}N ENDOR spectrum from the corresponding wild type spectrum gives a difference spectrum (trace (e)) virtually indistinguishable from the histidine labeled spectrum (trace (b)).

While ^{1}H ENDOR (Tang et al., 1993), high field EPR (Un et al., 1996) and FTIR (Berthomieu et al.,

1998) all indicate the loss of a $^2H/^1H$ exchangeable $Y_D^{\bullet}$ hydrogen bonded proton in the D2-His189Gln mutant *Synechocystis* PS II core complexes, simulations of three-pulse time domain ESEEM studies appear more consistent with two equal strength deuteron bonds to $Y_D^{\bullet}$ (470 kHz) in the exchanged centers (Diner et al., 1998). These observations would then imply that the mutation results in the loss of two nearly equivalent hydrogen bonds only one of which can come from D2-His189. What the source of the second hydrogen bond is and why it would be lost upon mutation at D2-189 are unclear. ESEEM studies in spinach BBY membranes (Berthold et al., 1981) similar to those performed in *Synechocystis*, indicate however only a single deuteron bond to $Y_D^{\bullet}$ (Diner et al., 1998).

C. Y_Z

The characterization of the proton acceptor to Y_Z has been more complicated than for Y_D. Because $Y_Z^{\bullet}$ is rapidly (≤1 ms) rereduced by *S*-state turnover, it is not possible to trap the $Y_Z^{\bullet}$ radical in uninhibited, intact PS II preparations. However, we can use pulsed EPR to study the $Y_Z^{\bullet}$ environment in Mn-depleted preparations, where the $Y_Z^{\bullet}$ re-reduction is slowed. The center trace of Fig. 7 shows the ^2H ESE-ENDOR for $Y_Z^{\bullet}$ in such a sample (Force et al., 1995). One observes that the overall width of the ^2H ENDOR feature is about the same as for the hydrogen-bonded $Y_D^{\bullet}$ radicals, but the resolution of sharp features is completely absent. The large ^2H ENDOR linewidth is in sharp contrast to the case for Y_D in mutant D2-His189Gln and for the tyrosyl $Y_{122}^{\bullet}$ radical from *E. coli* ribonucleotide reductase (bottom two traces of Fig. 7), tyrosine radicals which, as mentioned above, are not hydrogen bonded. We interpret the $Y_Z^{\bullet}$ ESE-ENDOR linewidth as support for hydrogen bonding for the $Y_Z^{\bullet}$ radical, but the lack of resolved spectral features indicates disorder in the hyperfine and/or quadrupolar couplings, which may indicate appreciable structural disorder in the site.

High field (245 GHz) EPR shows the g_x component of the anisotropic g-tensor for $Y_Z^{\bullet}$ to be broadened but close in value (2.00750) to that of $Y_D^{\bullet}$ (2.00740) (Fig. 2). These g_x values are in contrast to what is observed for $Y_D^{\bullet}$ in the D2-His189Gln mutant (2.00832) and *E. coli* ribonucleotide reductase (2.00868), neither of which are hydrogen bonded. CW ENDOR (Tang et al., 1996a) measurements also reflect disorder in the hydrogen bonding of $Y_Z^{\bullet}$. The disorder in the hydrogen bonding of $Y_Z^{\bullet}$ is likely a reflection of the ESEEM detected (Tommos et al., 1995; Warncke et al., 1995) conformational disorder that this radical shows in the bond angles between the tyrosine ring plane and the tyrosyl β-methylene C-H bonds in Mn-depleted PS II. $Y_Z^{\bullet}$, with a ν(CO) mode at 1512 cm^{-1} is even more strongly hydrogen bonded than $Y_D^{\bullet}$ where this mode is 1503 cm^{-1} (Berthomieu et al., 1998).

Three-pulse ESEEM measurements of $Y_Z^{\bullet}$ $^2H/^1H$ exchanged Mn-depeleted PS II core complexes show two dipolar coupled deuterons (Diner et al., 1998). A good fit to the time domain $^2H/^1H$ ratioed spectra could be obtained with either two equivalently coupled deuterons (407 kHz) or with two dissimilar deuterons (552 and 283 kHz). Most likely there is a distribution of multiple deuterons as in the case of spinach BBY membranes which was simulated by one strongly coupled and several weakly coupled deuterons (Tommos et al., 1998).

As pointed out above, there is present in the D1-polypeptide a histidine (D1-His190) in a location homologous to that of D2-His189. Detailed measurements of the pH-dependence of the rate and of a deuterium isotope effect on Y_Z oxidation in Mn-depleted WT PS II centers (Ahlbrink et al., 1998; Diner et al., 1998; Hays et al., 1998, 1999) indicated that at pH ≤7.5 the rate of Y_Z oxidation by $P680^+$ was limited by proton (or $H^{\bullet}$) transfer (but see below). That D1-His190 acts as a proton acceptor for Y_Z, similar to the role of D2-His189 in the oxidation of Y_D, is indicated by a marked slowing of the rate of oxidation of Y_Z by $P680^+$ upon site-directed replacement of D1-His189 by other residues (Diner et al., 1991; Kramer et al., 1994; Nixon and Diner, 1994; Roffey et al., 1994a,b; Chu et al., 1995; Diner and Nixon, 1998; Hays et al., 1998, 1999; Mamedov et al., 1998). The slowing of the kinetics in these mutants could be in part reversed by chemical rescue, the pH dependence of which depends on the pKa of the added exogenous organic bases (e.g., imidazole, ethanolamine) (Hays et al., 1998, 1999). These observations imply that histidine is the endogenous base in wild type PS II centers. FTIR spectra of $Y_Z^{\bullet}/Y_Z$ (Berthomieu et al., 1998) and $Y_D^{\bullet}/Y_D$ (Hienerwadel et al., 1996) show features similar to tyrosine in the presence of methyl imidazole, ν_{7a}(CO) at 1271–1279 cm^{-1} and δ(COH) at 1250–1255 cm^{-1} (Hienerwadel et al., 1996) that were attributed to Y_Z and Y_D hydrogen bonded to a histidine side chain. Enhancement of a feature at 1232–33 cm^{-1} arising from the ν_{8a}(CC) mode of tyrosine was suggested to reflect hydrogen bonding of $Y_Z^{\bullet}$ and $Y_D^{\bullet}$ by histidine. Furthermore, loss

of features at 1107 cm^{-1} and 1095 cm^{-1} upon Y_Z and Y_D oxidation, respectively, have been attributed to C-N stretch modes of histidine.

While the above observations imply a close interaction between Y_Z and D1-His190, ^{15}N ESE-ENDOR spectra of $Y_Z^{\bullet}$ in Mn-depleted PS II core complexes show no evidence of isotropically coupled histidine nitrogen (Campbell, 1999) as observed above for Y_D (Campbell et al., 1997). Figure 9 focuses on the ^{15}N ENDOR spectra for $Y_Z^{\bullet}$ of Mn-depleted *Synechocystis* PS II preparations (Campbell, 1999). Traces (a) and (b) respectively show the illuminated ($Y_Z^{\bullet}$ + $Y_D^{\bullet}$ trapped) and the dark ($Y_D^{\bullet}$ only) ^{15}N ENDOR spectra for globally ^{15}N-labelled, Mn depleted *Synechocystis* PS II. Trace (c) shows the difference spectrum, which should correspond to the ^{15}N ENDOR spectrum of $Y_Z^{\bullet}$. This difference spectrum is very similar to the $Y_Z^{\bullet}$ ^{15}N ENDOR spectrum obtain in an illuminated $Y_Z^{\bullet}$-trapped, Y_D-less mutant (D2-Tyr160Phe) sample (trace (d)). In neither $Y_Z^{\bullet}$ spectrum do we observe the sharp isotropically-coupled ^{15}N peaks of the sort assigned to the hydrogen-bonded D2-His189 partnered with $Y_D^{\bullet}$ (Fig. 8, trace (e)). The observed broad ^{15}N ENDOR features appear to closely match the tyrosine peptide nitrogen peaks in the $Y_D^{\bullet}$ spectra (Fig. 8, trace (d)). ^{15}N-histidine specifically-labeled wild type PS II preparations reveal no ^{15}N ENDOR or ESEEM features (data not shown) produced upon

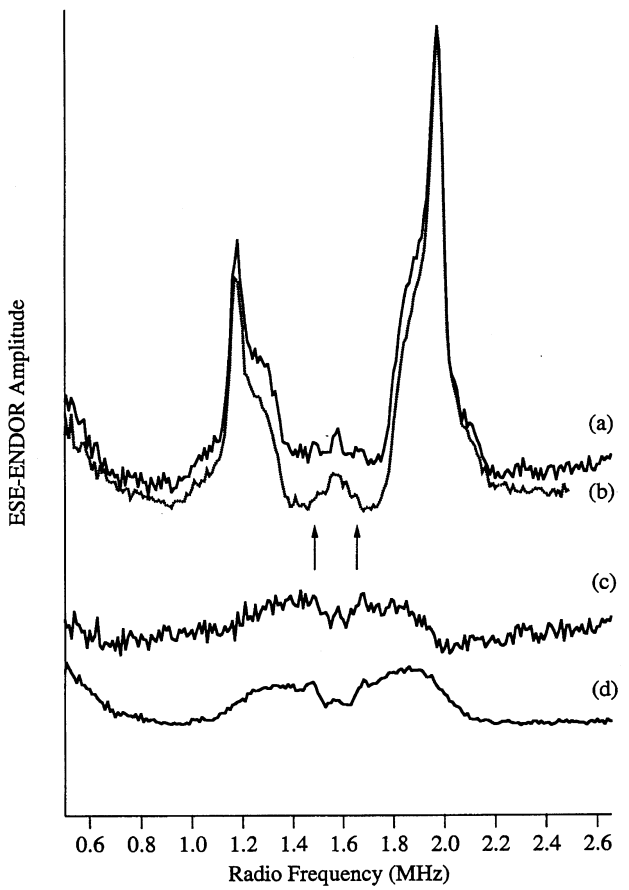

Fig. 9. ^{15}N pulsed ENDOR (ESE-ENDOR) spectra measured in Mn-depleted PS II core complexes from globally ^{15}N-labelled *Synechocystis*. (a) shows $Y_Z^{\bullet}$ + $Y_D^{\bullet}$ trapped; (b) only $Y_D^{\bullet}$ trapped; (c) (a) – (b) which corresponds to the ^{15}N ENDOR spectrum of $Y_Z^{\bullet}$; (d) $Y_Z^{\bullet}$ in complexes from the globally ^{15}N-labelled Y_D-less (D2-Tyr160Phe) mutant. Adapted from Campbell (1999).

illumination and trapping of $Y_Z^{\bullet}$, including the small 0.2 MHz-separated features shown by the arrows in Fig. 9. Thus, we have been unable to identify any histidine hyperfine couplings that would support a $Y_Z^{\bullet}$-D1-His190 hydrogen-bonding interaction comparable to the $Y_D^{\bullet}$-D2-His189 case. It is certainly possible that such an interaction is disrupted by the Mn depletion step needed to trap the magnetically-isolated $Y_Z^{\bullet}$ radical, although as noted above, even following Mn depletion there are dramatic reductions in the $Y_Z^{\bullet}$ oxidation rates in D1-His190 mutants compared to WT. This observation has been taken as evidence that D1-His190 is the direct proton acceptor in this proton-coupled electron transfer reaction. Indeed, in the most highly resolved X-ray crystal structure of PS II (Ferreira et al., 2004), $Y_Z^{\bullet}$ is reported to be directly H-bonded to D1-His190. Although the data described above do not relate directly to the Mn intact case, they suggest the possibility that D1-His190 might not be directly hydrogen bonded to $Y_Z^{\bullet}$ in Mn-depleted PS II. That D1-His190 is necessary for rapid oxidation of Y_Z at room temperature, even in the Mn-depleted samples, could imply an intermediate hydrogen bonded chain between Y_Z and D1-His190, a gated interaction between $Y_Z^{\bullet}$ and D1-His190, or a disconnect between the two at the low temperature of the ESE-ENDOR experiments. However, a recent density functional theoretical analysis (M. Brynda, personal communication) of the Tyr$^{\bullet}$-His H-bonded pair indicates that the strength of the isotropic ^{15}N His-coupling depends on the relative orientations of the Tyr and His ring planes. For certain orientations this coupling is lost completely. Thus, we should not rule out the possibility that $Y_Z^{\bullet}$ may indeed be directly H-bonded by D1-His190 in the Mn-depleted case, but that the direct H-bonding may in some cases be more difficult to detect by ^{15}N ESE-ENDOR.

VI. Kinetics of Y_Z Oxidation and Reduction

A. Intact Mn Cluster

The rate of oxidation of Y_Z by $P680^+$ in PS II core complexes containing an intact Mn cluster is multiphasic, with major submicrosecond components ($t_{½}$) of 20–60 ns for states S_0 and S_1 and 50 and 250–300 ns for the states S_2 and S_3, respectively (Mauzerall and Malley, 1971; Brettel et al., 1984; Schlodder et al., 1984; Meyer et al., 1989; Karge et al., 1996; Haumann et al., 1997; Ahlbrink et al., 1998; Schilstra et al., 1998). The slowing in states S_2/S_3 relative to S_0/S_1 has been attributed to the accumulation of a positive charge on the Mn cluster (and a lowering of the $Y_ZP680^+ \rightleftharpoons Y_Z^{\bullet}(H^+)P680$ equilibrium constant, K_{zp}, Brettel et al., 1984), resulting from a lack of proton release on the $S_1 \rightarrow S_2$ transition of the OEC (Fowler, 1977; Saphon and Crofts, 1977; Rappaport and Lavergne, 1991; Lavergne and Junge, 1993) or to a structural change associated with the formation of S_2 (Christen and Renger, 1999). The equilibrium constants K_{zp} in the submicrosecond time domain (29 for S_0 and S_1, 2 for S_2 and S_3 (Brettel et al., 1984)), increase upon relaxation at longer times (Bouges-Bocquet, 1980; Schlodder et al., 1985; Shinkarev and Wraight, 1993) but remain lower in the S_2 and S_3 states. Thus there are components of Y_Z oxidation in the microsecond range (1–150 μs) that oscillate with period four, the most marked of which are in the S_2 and S_3 states, as shown by indirect measurements of the dequenching of the fluorescence yield in the microsecond time range (Christen et al., 1999; Delosme and Joliot, 2002) and by direct measurements of $P680^+$ reduction (Schlodder et al., 1985; Schilstra et al., 1998; Christen and Renger, 1999). These low equilibrium constants result in kinetic components associated with $Y_Z^{\bullet}$ reduction by the Mn cluster (see below) to be visible in the kinetics of reduction of $P680^+$ (Schlodder et al., 1985). $P^+Q_A^-$ charge recombination and the non-negligible equilibrium concentrations of $P680^+$ and Q_A^-, particularly upon excitation in the S_2 and S_3 states, account for the misses observed in the progression of the Kok-Joliot cycle of the OEC (Schlodder et al., 1985; Shinkarev and Wraight, 1993).

The submicrosecond components for the oxidation of Y_Z in each S state show only a weak pH dependence (Christen et al., 1999), very small deuterium isotope effects (≤1.1), and small activation energies (~10 kJ/mol) (Eckert and Renger, 1988)). Components in the 1–30 μs time range are most enhanced by the replacement of H_2O with D_2O in the S_0 and less so in the S_3 state (Schilstra et al., 1998). Christen and Renger (1999) observed the enhancement of a 2 μs component in the S_0 and S_1 states, less so in the S_2 and S_3 state upon H/D exchange. They reported that slower components (35 and 150 μs) are more affected in the S_2 and S_3 states than in S_0 and S_1. A consequence of the slowing of $P680^+$ reduction by solvent replacement is an enhanced charge recombination between Q_A^- and $P680^+$, resulting in an increase in the miss parameter, α, of the Kok-Joliot cycle (Christen and Renger, 1999). The microsecond kinetic components

thus appear to be coupled to internal proton movement as proton release to the bulk phase takes longer, occurring in 85–100 μs (Ahlbrink et al., 1998; Schilstra et al., 1998; Christen and Renger, 1999). In a contrary opinion, however, Tommos and Babcock (2000) have suggested that 'domino deprotonation' could reach the bulk phase rapidly enough to account for the microsecond phases. Rappaport and Lavergne (2001) have provided a detailed comparison of these models and their corresponding energetics. They point out the significant influence of the electrostatic interaction between Y_ZO^- and $HisH^+$ and possibly of $P680^+$ itself on the formation of tyrosinate in a proton first mechanism for the oxidation of Y_Z. They caution, however, that one generally assumes that the PS II centers are participating in a homogeneous process where there is no intrinsic heterogeneity between the centers to account for the multiphasic kinetic relaxation, an assumption that may not be correct.

The rate of reduction of Y_Z by the intact Mn cluster shows a marked dependence on S state, with lifetimes of <3 to 250 μs reported for $S_0 \rightarrow S_1$, 30–140 μs for $S_1 \rightarrow S_2$, 100–600 μs for $S_2 \rightarrow S_3$ and 1–4.5 ms for $S_3 \rightarrow S_0$ (Rappaport et al., 1994; Diner and Babcock, 1996; Razeghifard et al., 1997, and references therein). These rates show the following deuterium kinetic isotope effects and activation energies (in parentheses) –1.3 (5 kJ/mol) for $S_0 \rightarrow S_1$; 1.2–1.3 (14.6 kJ/mol) for $S_1 \rightarrow S_2$; 2.1–2.4 (35 kJ/mol) for $S_2 \rightarrow S_3$; and 1.4 (37.5 kJ/mol) for $S_3 \rightarrow S_4 \rightarrow S_0$ (Haumann et al., 1997; Karge et al., 1997; Westphal et al., 2000). Of the S-state transitions, $S_2 \rightarrow S_3$ shows the most marked pH dependence (Rappaport et al., 1994; Haumann et al., 1997) (factor of 2 between pH 8 (120 μs) and 5.2 (250 μs)) and isotope effect on both the rate and the activation energy (45 kJ/mol in D_2O) implying that this step is the one most limited by proton transfer.

B. Mn-Depleted

Upon loss of the Mn cluster, the rate of Y_Z oxidation by $P680^+$ is markedly slowed, despite the large increase in the K_{zp} equilibrium constant for $Y_ZP680^+ = Y_Z^{\bullet}(H^+)P680$ (18–600 for the pH range 5–8.5) (Yerkes et al., 1983; Buser et al., 1990). Conjeaud and Mathis (1980) reported rates ranging from 2 μs at pH 9 to 44 μs at pH 4. This rate was examined in more detail by a number of workers using PS II core complexes from pea (Ahlbrink et al., 1998) and from *Synechocystis* (Diner et al., 1998; Hays et al., 1999) and shown to be multiphasic with the data fit by up to four components ranging from τ= 320 ns to 140 μs (Hays et al., 1999). The fastest components reported by Ahlbrink et al. (1998) and Hays et al. (1999) (τ = 1.4 μs and 320 ns, respectively) showed pH-independent rates, the amplitudes of which were pH-dependent (pKas of 7.0 and 7.5, respectively). A similar pKa was detected indirectly by Mamedov et al. (1998) through measurements of fluorescence induction in Mn-depleted thylakoids of *Chlamydomonas*. Diner et al. (1998), with microsecond time resolution, but using a mutant lacking Y_D (D2-Tyr160Phe), and fitting the data with two rate constants (allowed to vary with pH) plus an offset, found a slightly higher pKa of 8.3. Ahlbrink et al. (1998) and Hays et al. (1999) assumed that one or more of the component reaction rates were pH-independent with the component amplitudes pH-dependent. Ahlbrink (1998) and Diner et al. (1998) assumed as in the earlier work of Conjeaud and Mathis (1980), that the microsecond component rates were pH-dependent. These reflect slow and fast proton equilibration, respectively, with respect to the rate of electron transfer and are not easy to distinguish (for discussion, see Rappaport and Lavergne, 2001). All three groups also examined the effect of H/D exchange on the rate of Y_Z oxidation and as a function of pH. Isotope effects of between 2.5 and 3.6 were reported for components dominating at pH≤7.0 Both Ahlbrink et al. (1998) and Diner et al. (1998) found that the deuterium isotope disappeared at pH>9 ($k_H/k_D \leq 1.1$) while the fastest 320 ns component of Hays et al.(1999), which contributes ≥80% in this pH range, was reported to still show an isotope effect of k_H/k_D=1.7. Ahlbrink et al. (1998) also reported an activation energy of 0.30 eV for the major slow kinetic component with a pH-dependent $t_{½}$ of 24 μs at pH 5. A fast kinetic component with a largely pH independent $t_{½}$ of 1 μs that dominates above pH 9 has an activation energy of 0.15 eV. Two possible models (Fig. 10) for the behavior in the absence of the Mn cluster (Ahlbrink et al., 1998) attribute the pKas mentioned above to either that of the proton acceptor (e.g., D1-His190, imidazolium$^+$/imidazole) or to Y_Z itself (TyrOH/TyrO$^-$). In both models, $Y_Z^{\bullet}$ is the neutral radical. In the first case, the proton acceptor, His, above its pKa is H-bonded by Y_Z and allows rapid deprotonation of Y_Z coupled to its oxidation. The phenolic proton transfer to the proton acceptor is fast and Y_Z oxidation is electron transfer limited. Below the pKa, Y_Z cannot deprotonate to $HisH^+$, which is already protonated, forcing the proton transfer to a

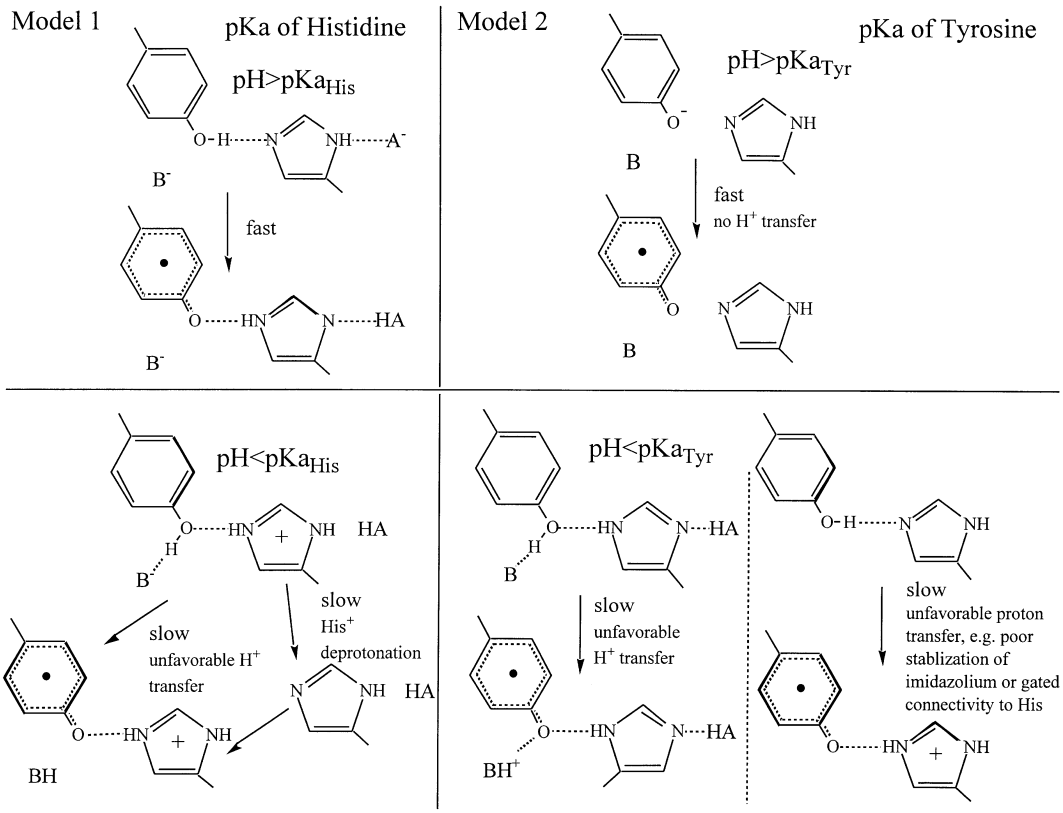

Fig. 10. Two possible models for the oxidation of Y_Z by $P680^+$ in the absence of the Mn cluster. See text for details.

less favorable (lower pKa or more distant) acceptor, B^-, or to His following the deprotonation of $HisH^+$. The rate is slower, with a higher activation energy and pH-dependent, possibly through a choice of several less favorable or secondary proton acceptors. In the Mn-intact centers the pKa of the proton acceptor would be <4.5 while in the Mn-depleted centers the pKa would be 7.0. In the second case, the formation of the tyrosinate above the pKa results in oxidation via pure electron transfer as no proton transfer is necessary. Below the pKa, the tyrosine must give up its proton to the acceptor, resulting in a deuterium isotope effect and an elevated activation energy. In this model the pKa of Y_Z/Y_Z^- would be <4.5 in Mn-intact centers and 7.0 in Mn-depleted centers. The major slow, pH-dependent component observed below the pKa in the Mn-depleted centers could arise from the lower pKa values of the secondary proton acceptors, hydrogen bonded to the primary proton acceptor. One major difficulty with this model is the pKa≤4.5 for the Mn-intact centers. This is unusually low for a tyrosine, the pKa of which in aqueous solution is normally 10. However, the presence of nearby Mn or Ca^{2+} could potentially lower the tyrosine pKa. A number of authors have argued that Y_Z is in the tyrosinate state in Mn-intact centers (Candeias et al., 1998; Haumann et al., 1999).

Hays et al. (1999) have shown that in Mn-depleted PS II core complexes of the D1-His190Ala mutant, kinetic components for Y_Z oxidation $t_{½}$<2.5 μs constitute <20% of the oxidation of Y_Z at pH ≤9.0. However, at pH>9.0 a new rapid component ($t_{½}$<2.5 μs) appears with an approximate pKa of 10.3, which these authors attribute to that of Y_Z/Y_Z^-. The addition of the bases imidazole and ethanolamine to core complexes of this mutant, introduces rapid kinetic components ($t_{½}$<2.5 μs) with pKas of 6.9 and 9.5, respectively. Each of these pKas corresponds to the pKa of the respective

base in aqueous solution. The interpretation of Hays et al. (1999) for these observations is that the pKa that governs the appearance of the rapid component for Y_Z oxidation is that of the base which acts as the proton acceptor to Y_Z, D1-His190 in the WT and the exogenous bases in the D1-His190Ala mutant, consistent with Model 1 above.

As mentioned above, ESE-ENDOR spectra of ^{15}N-labeled Mn depleted PS II cores showed evidence for an isotropically coupled histidine nitrogen in the case of $Y_D^{\bullet}$ indicative of a direct H-bond between $Y_D^{\bullet}$ and D2-His189 (Campbell et al., 1997). No such coupling is observed for $Y_Z^{\bullet}$ in Mn-depleted PS II cores, implying that Y_Z and D1-His190 are not directly H-bonded. These may be linked by a hydrogen bonded chain (Hays et al., 1999) to explain the dependence of the rate of Y_Z oxidation on D1-His190. Alternatively, the two may be linked intermittently at room temperature (gated mechanism) (Diner et al., 1998) such that D1-His190 facilitates Y_Z deprotonation but where the state frozen in at the low temperature of the ESE-ENDOR measurement shows no substantial presence of a linkage between the two.

VII. Kinetics of Y_D Oxidation and Reduction and Comparison

Given that Y_D is located in a position symmetric with respect to Y_Z in the reaction center and that Y_D forms a well-defined hydrogen bond to D2-His190, it is surprising that Y_D does not show, under physiological conditions, as rapid electron transfer to $P680^+$. The importance of Y_D to the function of PS II is, however, demonstrated by its role in the assembly of the Mn cluster (Ananyev et al., 2002) and the impairment of photosynthetic growth (Vermaas et al., 1988) in the D2-Tyr160Phe mutant. A global kinetic study of electron transfer in PS II (Buser et al., 1990) attributed a $t_{½}$ of 10–20 ms to the oxidation of Y_D by $P680^+$ between pH 5 and 7.5. Recently, the oxidation of Y_D was re-examined in a Y_Z-less mutant of *Synechocystis* (D1-Tyr161Phe). Faller et al. (2001) found that a fast component of Y_D oxidation ($t_{½}$ = 190 ns) appeared with increasing pH, showing a pKa of 7.7. This pKa agrees with that proposed by Vass and Styring (1991) for the pH-dependence of the rate of oxidation of Y_D by the S_2 state (pKa=7.3–7.5). Faller et al. (2002) also found a similar pKa (7.6) for the oxidation of Y_D at cryogenic temperatures (5–15 K). This ability to oxidize Y_D at low temperature contrasts with the oxidation of Y_Z which can no longer occur at ≤180° C in Mn-depleted PS II (Kuehne and Brudvig, 2002). As above for Y_Z, two models for the origin of the pKa were proposed, involving either the His^+/His or the Y_D/Y_D^- acid-base couples (Faller et al., 2002). In the first case, the $Y_D^{\bullet}$-His^+ couple would carry a positive charge on the D2-His189 unless the distal proton of the imidazole ring were transferred to a secondary proton acceptor. O'Malley (1998) has made predictions from hybrid density functional calculations of phenolic H-bond distances and relative spin densities on the phenolic oxygen, the C4 ring carbon and the H-bonded τ-imidazole nitrogen. These parameters differ for the imidazole and the imidazolium H-bonded to the Tyr$^{\bullet}$. Those measured for $Y_D^{\bullet}$ (Fig. 3) lie between the two, but closer to the neutral imidazole, implying the presence of a secondary proton acceptor in H-bonded contact with the π-imidazole nitrogen of D2-His189 able to at least partially dissipate the charge on the imidazole by proton transfer (Diner, 2001).

A number of questions still remain unanswered. Why is the oxidation of Y_Z so much faster in the Mn-intact versus the Mn-depleted centers, despite the increase in the driving force of the reaction following loss of the OEC? Why, below the pKa, the rate of oxidation of Y_Z is so much faster than that of Y_D, despite the larger driving force for the latter? Why is the reduction potential of $Y_D^{\bullet}/Y_D$ so much less than that of $Y_Z^{\bullet}/Y_Z$ in Mn-intact and Mn-depleted centers?

The slowing of the oxidation of Y_Z upon depletion of Mn could be the consequence of the loss of a well-structured hydrogen bonded link between Y_Z and D1-His190 (Westphal et al., 2000). The latest X-ray crystal structure of PS II from *Thermosynechococcus elongatus* (Ferreira et al., 2004) places D1-His190 close to Y_Z in the Mn-intact centers. The inability to detect an isotropically coupled His τ-nitrogen in the ESE-ENDOR spectrum of $Y_Z^{\bullet}$ in Mn-depleted PS II cores (Campbell, 1999) and the disorder in the hydrogen bonding to the phenol oxygen (Force et al., 1995) and in the orientation of the ring of $Y_Z^{\bullet}$ (Tommos et al., 1995; Warncke et al., 1995), both of which contrast with Y_D (Hoganson and Babcock, 1992), could explain the slowing of Y_Z oxidation by an impairment of proton transfer. Babcock et al. (1997) have proposed that the reason for the slow oxidation of Y_D relative to Y_Z might have to do with a larger reorganization energy associated with the retention of the phenolic proton close by $Y_D^{\bullet}$. While this proposal was invoked to support the release of the phenolic proton of Y_Z

to the bulk phase, it is possible that the greater polarizablity of the environment of Y_Z facilitates the stabilization of a retained plus charge. The ability to observe such a large stimulation in rate associated with the oxidation of Y_D at alkaline pH (Faller et al., 2001) might also reflect an increased hydrophilicity (polarizability) in the environment of this tyrosine as the pH increases. The reduction potential of $Y_Z^{\bullet}/Y_Z$ at ~ 1 V (Diner and Babcock, 1996) is close to what one would expect for tyrosine in aqueous solution. What remains a puzzle is why the reduction potential of $Y_D^{\bullet}/Y_D$ is so low (0.72–0.76 V) (Boussac and Etienne, 1984; Vass and Styring, 1991). Placing the tyrosine in a hydrophobic environment would be expected to exert the opposite effect on reduction potential (Tommos et al., 1999).

VIII. Mechanisms for Y_Z Oxidation and Reduction

A. Oxidation

There are three possible mechanisms by which the oxidation of tyrosine might occur to produce the neutral radical (Diner et al., 1998; Rappaport and Lavergne, 2001; Sjödin et al., 2002). These are: (i) electron transfer producing $TyrOH^{+\bullet}$ followed by proton transfer (ETPT); (ii) proton transfer producing $TyrO^-$ followed by electron transfer (PTET); and (iii) concerted electron and proton transfer (CEP) with both reactions occurring simultaneously, through a common transition state. These reactions have recently been discussed in an interesting comparison between a tyrosine-linked photoactive $Ru(II)(bpy)_3$ complex and PS II (Sjödin et al., 2000; Sjödin et al., 2002). These authors conclude that the oxidation of Y_Z is via the CEP mechanism in Mn-depleted PS II as well. Their arguments are that below the pKa of (7.0–8.3) ETPT would not show the observed pH dependence of the slow kinetic phases and that PTET would not show a pH dependence at all because the rate of proton transfer in the tyrosine-proton acceptor pair (e.g., D1-His190) would be expected to be pH independent. They conclude, furthermore, that the deuterium isotope effect, an elevated reorganization energy (1.4 eV), and an elevated pH-dependent activation energy all point to a CEP mechanism for PS II as in the case of the synthetic ruthenium complex, even though, in the latter case, the phenolic proton is transferred to water. The pH-dependence of the rate is rationalized by its influence on ΔG^0(–60 meV/ΔpH unit) due to the pH-dependence of the reduction potential of $Y_Z^{\bullet}/Y_Z$ (Harriman, 1987; Tommos et al., 1999). Diner et al. (2001) have varied the reduction potential, E′, of $P680^+$/P680 by introducing site-directed mutations at position D1-198 and D2-197, replacing the WT histidine at these positions with other residues in Mn-depleted PS II core complexes. A variation in reduction potential of ~110 mV relative to WT, at pH 5.7, modulates the rate of oxidation of Y_Z by $P680^+$ by a factor of 3 (Diner et al., 2001, 2004), from 31 ± 1 ms^{-1} at –82 mV to 92 ± 25 ms^{-1} at +27 mV, both potentials relative to WT (47 ± 7 ms^{-1})[1]. Figure 11 shows a similar dependence of the rate of Y_Z oxidation by $P680^+$ on the change in ΔG^0 (the difference in reduction potential between redox couples $Y_Z^{\bullet}/Y_Z$ and $P680^+$/P680), varied by these two independent means. Shown are the same pH-dependent phase measured in the tens of microsecond range by Diner et al. (2001) and by Ahlbrink et al. (1998). The effect of pH on what Ahlbrink and co-workers observe as a 'slow phase' of the rate of Y_Z oxidation is equivalent to the k_2 kinetic phase of Hays et al. (1999). The dependence of the rate on ΔG^0 over four pH units indicates that $-\Delta G^0 << \lambda$, consistent with the reorganization energy (λ) of 1.4 eV that Sjödin et al. (2002) deduce from the temperature dependence of the rate. A similar slope to that observed by varying the pH is observed for the dependence of the rate of $P680^+$ reduction on $\delta\Delta G^0$ (by varying the reduction potential of $P680^+$/ P680) where $\delta\Delta G^0 = -F\delta E'$ and $\delta E' = E'_{mut} - E'_{WT}$. While not an absolute proof, this agreement is consistent with a CEP mechanism in which the rate depends on the driving force of the overall reaction (Sjödin et al., 2002; Diner et al., 2004).

B. Reduction

ETPT, PTET, CEP and hydrogen-atom transfer (HAT) mechanisms have also been compared (Westphal et al., 2000; Cukier, 2004) for the reduction of $Y_Z^{\bullet}$ by the Mn cluster in the intact system. In the HAT mechanism, a hydrogen atom is transferred to $Y_Z^{\bullet}$ from a water bound to the Mn cluster. These authors have argued that the formation of charged intermediates, $Y_Z^-Mn^+(H_2O)$ and $Y_Z^{+\bullet}Mn(OH^-)$ results in an electrostatic penalty arising from the creation of charged

[1] Note that in Table 4 of ref. (Diner et al., 2001) a typographical error left out the m in ms^{-1} for the rate constant k_1.

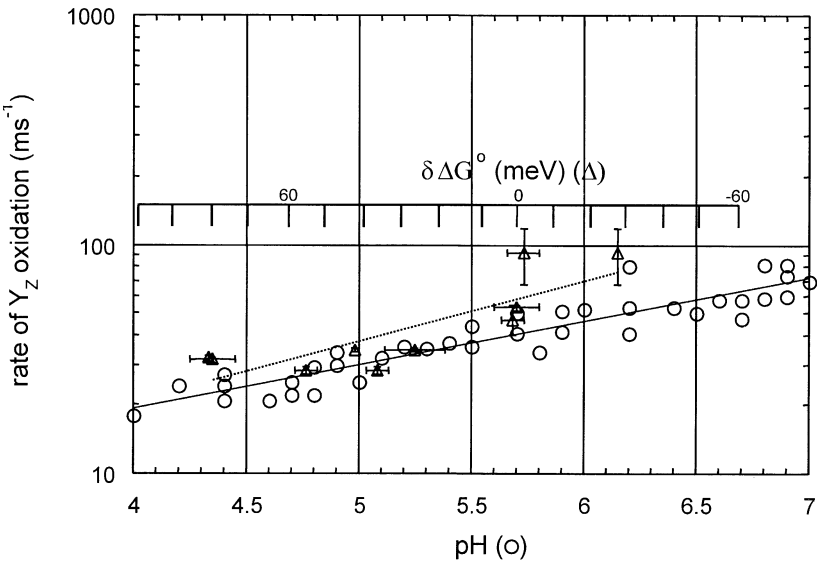

Fig. 11. Dependence of the rate of Y_Z oxidation by $P680^+$ on the change in the driving force (ΔG^0) of the reaction. $\delta\Delta G^0$ is the change in the difference in reduction potential between redox couples $Y_Z^{\cdot}/Y_Z$ and $P680^+/P680$) by changing E´ of $P680^+/P680$ through site-directed mutation or by changing the pH which modifies the reduction potential of $Y_Z^{\cdot}/Y_Z$ ($\delta\Delta G^0 = -60$ meV/ΔpH unit). The rates shown correspond to the same pH-dependent kinetic phase measured by Diner et al. (2001, 2004) (△) and by Ahlbrink et al. (1998) (○).

species in a low dielectric environment. In the ETPT case, the free energy of formation of $Y_Z^{-}Mn^{+}(H_2O)$ (15.7 kcal/mol for S_0-S_1 and higher for the other S-state transitions) leads to a predicted activation energy considerably higher than what is measured experimentally (≤9 kcal/mol) (Karge et al., 1997; Westphal et al., 2000). Likewise the formation of $Y_Z^{+\cdot}Mn(OH^{-})$ for PTET with a ΔpKa of ≥9 for the protonation of $Y_Z^{\cdot}$ predicts a ΔG of 12 kcal/mol and as much as 23 kcal/mol including the electrostatic penalty. These estimates are also far greater than the measured activation energies for the S-state transitions. Cukier, Babcock and coworkers (Westphal et al., 2000, Cukier, 2004) consider the HAT model (an adiabatic process where the electron donor and acceptor are strongly coupled) to be the most likely for $Y_Z^{\cdot}$ reduction by the Mn cluster. Small Franck-Condon factors associated with this model are consistent with the small Arrhenius pre-exponential factors that have been seen for S-state oxidation. Hydrogen-atom transfer would also be consistent with the modest kinetic isotope effects and microsecond rates of electron transfer, far slower than the ns or faster rates predicted for non-adiabatic electron tunneling (Page et al., 1999; Tommos and Babcock, 2000).

The most recent X-ray structure of PS II (Ferreira et al., 2004) shows Y_Z to be in close proximity to a putative water molecule, X_{21}, coordinating the Ca^{2+} of the OEC. Were X_{21} to be the second substrate water molecule poised for nucleophilic attack onto an oxygen intermediate bound to Mn_4, then it is possible that in the final step of the S-state cycle $Y_Z^{\cdot}$ participates in a HAT mechanism involving X_{21}. This mechanism, however, seems less likely in the earlier S-state transitions where the first substrate water, X_1, is far from $Y_Z^{\cdot}$. The mobility described above for Y_Z could be consistent with the need for this tyrosine to hydrogen bond with D1-His190 early in the S-state cycle and with X_{21} late in the cycle.

IX. Concluding Remarks

Probably one of the most anxiously awaited results in the photosynthesis community is a high resolution X-ray structure of the PS II reaction center and in particular that of the Mn cluster. As evidence points to a more intimate role of Y_Z in the mechanism of water oxidation, the position, orientation and hydrogen bonding partners of this tyrosine will be

critical to our understanding of the process of water oxidation. While considerable progress has already been made, we expect that with further refinement of the PS II structure, there will be a firmer structural basis within which the kinetic and thermodynamic characteristics of tyrosine oxidation and reduction can be interpreted to better understand the coupling of electron and proton transfer for both tyrosines. A high resolution structure should also help to identify the proton acceptor for Y_Z in the intact system, the pathways by which protons are expelled to the thylakoid lumen from the Mn cluster or from Y_Z or both and the reasons for the large difference in reduction potential of Y_Z and Y_D.

Acknowledgments

The authors gratefully acknowledge the support of the United States Department of Agriculture (NRI/CGP award no. 2003-35318-13589) to BAD and of the National Science Foundation (MCB-9513648) and the NIH (GM48242) to RDB The authors have greatly benefited from discussions over the years with Drs. Gerald T. Babcock, Catherine Berthomieu, Kristy A. Campbell, Richard J. Debus, Peter Faller, Leif Hammarström, Rainer Hienerwadel, Melvin Okamura, Mark Paddock and Fabrice Rappaport regarding the ins and outs of coupled electron and proton transfer of the redox active tyrosines of PS II. This paper is contribution #8442 of the Central Research and Development Department, E. I. du Pont de Nemours & Co.

References

Ahlbrink R, Haumann M, Cherepanov D, Boegershausen O, Mulkidjanian A and Junge W (1998) Function of tyrosine Z in water oxidation by Photosystem II: Electrostatical promotor instead of hydrogen abstractor. Biochemistry 37: 1131–1142

Allen JP, Feher G, Yeates TO, Rees DC, Deisenhofer J, Michel H and Huber R (1986) Structural homology of reaction centers from *Rhodopseudomonas sphaeroides* and *Rhodopseudomonas viridis* as determined by X-ray diffraction. Proc Natl Acad Sci U SA 83: 8589–8593

Ananyev GM, Sakiyan I, Diner BA and Dismukes GC (2002) A functional role for tyrosine-D in assembly of the inorganic core of the water oxidase complex of Photosystem II and the kinetics of water oxidation. Biochemistry 41: 974–980

Andreasson LE and Lindberg K (1992) The inhibition of photosynthetic oxygen evolution by ammonia probed by EPR. Biochim Biophys Acta 1100: 177–183

Babcock GT and Sauer K (1973a) Electron paramagnetic resonance signal II in spinach chloroplasts. I. Kinetic analysis for untreated chloroplasts. Biochim Biophys Acta 325: 483–503

Babcock GT and Sauer K (1973b) Electron paramagnetic resonance signal II in spinach chloroplasts. II. Alternative spectral forms and inhibitor effects on kinetics of signal II in flashing light. Biochim Biophys Acta 325: 504–519

Babcock GT and Sauer K (1975a) Rapid component of electron paramagnetic resonance signal II. Candidate for the physiological donor to Photosystem II in spinach chloroplasts. Biochim Biophys Acta 376: 329–344

Babcock GT and Sauer K (1975b) Rapid, light-induced transient in electron paramagnetic resonance signal II activated upon inhibition of photosynthetic oxygen evolution. Biochim Biophys Acta 376: 315–328

Babcock GT and Sauer K (1975c) Two electron donation sites for exogenous reductants in chloroplast Photosystem II. Biochim Biophys Acta 396: 48–62

Babcock GT, Blankenship RE and Sauer K (1976) Reaction kinetics for positive charge accumulation on the water side of chloroplast Photosystem II. FEBS Lett 61: 286–289

Babcock GT, Barry BA, Debus RJ, Hoganson CW, Atamian M, McIntosh L, Sithole I and Yocum CF (1989) Water oxidation in Photosystem II: From radical chemistry to multielectron chemistry. Biochemistry 28: 9557–9565

Babcock GT, Espe M, Hoganson C, Lydakis-Simantiris N, McCracken J, Shi W, Styring S, Tommos C and Warncke K (1997) Tyrosyl radicals in enzyme catalysis: some properties and a focus on photosynthetic water oxidation. Acta Chem Scand 51: 533–540

Backes G, Sahlin M, Sjoberg BM, Loehr TM and Sanders-Loehr J (1989) Resonance Raman spectroscopy of ribonucleotide reductase. Evidence for a deprotonated tyrosyl radical and photochemistry of the binuclear iron center. Biochemistry 28: 1923–1929

Barry BA and Babcock GT (1987) Tyrosine radicals are involved in the photosynthetic oxygen-evolving system. Proc Natl Acad Sci USA 84: 7099–7103

Baumgarten M, Philo JS and Dismukes GC (1990) Mechanism of photoinhibition of photosynthetic water oxidation by chloride depletion and fluoride substitution: Oxidation of a protein residue. Biochemistry 29: 10814–10822

Bender CJ, Sahlin M, Babcock GT, Barry BA, Chandrashekar TK, Salowe SP, Stubbe J, Lindström B, Petersson L, Ehrenberg A and Sjöberg B-M (1989) An ENDOR study of the tyrosyl free radical in ribonucleotide reductase from *Escherichia coli*. J Am Chem Soc 111: 8076–8083

Bent DV and Hayon E (1975) Excited state chemistry of aromatic amino acids and related peptides. I. Tyrosine. J Am Chem Soc 97: 2599–2606

Berthold DA, Babcock GT and Yocum CF (1981) A highly resolved, oxygen-evolving Photosystem II preparation from spinach thylakoid membranes. EPR and electron-transport properties. FEBS Lett 134: 231–234

Berthomieu C and Boussac A (1995) Histidine oxidation in the S2 to S3 transition probed by FTIR difference spectroscopy in the Ca^{2+}-depleted Photosystem II: Comparison with histidine radicals generated by UV irradiation. Biochemistry 34: 1541–1548

Berthomieu C, Hienerwadel R, Boussac A, Breton J and Diner BA (1998) Hydrogen bonding of redox-active tyrosine Z

of Photosystem II probed by FTIR difference spectroscopy. Biochemistry 37: 10547−10554

Blankenship RE, Babcock GT and Sauer K (1975a) Kinetic study of oxygen evolution parameters in tris-washed, reactivated chloroplasts. Biochim Biophys Acta 387: 165−175

Blankenship RE, Babcock GT, Warden JT and Sauer K (1975b) Observation of a new EPR transient in chloroplasts that may reflect the electron donor to Photosystem II at room temperature. FEBS Lett 51: 287−293

Boerner RJ and Barry BA (1993) Isotopic labeling and EPR spectroscopy show that a tyrosine residue is the terminal electron donor, Z, in manganese-depleted Photosystem II preparations. J Biol Chem 268: 17151−17154

Bordwell FG and Cheng J (1991) Substituent effects on the stabilities of phenoxyl radicals and the acidities of phenoxyl radical cations. J Am Chem Soc 113: 1736−1743

Boska M, Sauer K, Buttner W and Babcock GT (1983) Similarity of EPR signal IIf rise and P-680$^+$ decay kinetics in Tris-washed chloroplast Photosystem II preparations as a function of pH. Biochim Biophys Acta 722: 327−330

Bouges-Bocquet B (1980) Kinetic models for the electron donors of Photosystem II of photosynthesis. Biochim Biophys Acta 594: 85−103

Boussac A and Etienne AL (1984) Midpoint potential of signal II (slow) in Tris-washed Photosystem II particles. Biochim Biophys Acta 766: 576−581

Boussac A and Rutherford AW (1988) Nature of the inhibition of the oxygen-evolving enzyme of Photosystem II induced by sodium chloride washing and reversed by the addition of calcium(2+) or strontium(2+). Biochemistry 27: 3476−3483

Boussac A, Zimmermann JL and Rutherford AW (1989) EPR signals from modified charge accumulation states of the oxygen-evolving enzyme in calcium-deficient Photosystem II. Biochemistry 28: 8984−8989

Boussac A, Zimmermann JL, Rutherford AW and Lavergne J (1990a) Histidine oxidation in the oxygen-evolving photosystem-II enzyme. Nature 347: 303−306

Boussac A, Zimmermann JL and Rutherford AW (1990b) Factors influencing the formation of modified S2 EPR signal and the S3 EPR signal in calcium-depleted Photosystem II. FEBS Lett 277: 69−74

Boussac A, Sétif P and Rutherford AW (1992) Inhibition of tyrosine Z photooxidation after formation of the S3-state in calcium-depleted and chloride-depleted photosystem-II. Biochemistry 31: 1224−1234

Brettel K, Schlodder E and Witt HT (1984) Nanosecond reduction kinetics of photooxidized chlorophyll-aII (P-680) in single flashes as a probe for the electron pathway, proton-release and charge accumulation in the oxygen-evolving complex. Biochim Biophys Acta 766: 403−415

Britt RD (1996a) Oxygen evolution. In: Ort DR and Yocum CF (eds) Oxygenic Photosynthesis: The Light Reactions, pp 137−164. Kluwer Academic Publishers, Dordrecht

Britt RD (1996b) Electron spin echo methods in photosynthesis research. In: Hoff AJ and Amesz J (eds) Biophysical Techniques in Photosynthesis, pp 235−253. Kluwer Academic Publishers, Dordrecht

Britt RD, Randall DW, Ball JA, Gilchrist ML, Jr., Force DA, Sturgeon BE, Lorigan GA, Tang X-S, Diner BA, Klein MP, Chan MK and Armstrong WH (1995) Electron spin echo-ENDOR studies of the tyrosine radicals and the manganese cluster of Photosystem II. In: Mathis P (ed) Photosynthesis: From Light to Biosphere, Vol 2, pp 223−228. Kluwer Academic Publishers, Dordrecht

Buser CA, Thompson LK, Diner BA and Brudvig GW (1990) Electron-transfer reactions in manganese-depleted Photosystem II. Biochemistry 29: 8977−8985

Campbell KA (1999) CW and pulsed EPR studies of Photosystem II and Mn-containing complexes. Thesis, University of California, Davis

Campbell KA, Peloquin JM, Diner BA, Tang X-S, Chisholm DA and Britt RD (1997) The tau-nitrogen of D2 histidine 189 is the hydrogen bond donor to the tyrosine radical YD$^\bullet$ of Photosystem II. J Am Chem Soc 119: 4787−4788

Candeias LP, Turconi S and Nugent JHA (1998) Tyrosine YZ and YD of Photosystem II. Comparison of optical spectra to those of tyrosine oxidized by pulsed radiolysis. Biochim Biophys Acta 1363: 1−5

Christen G and Renger G (1999) The role of hydrogen bonds for the multiphasic P680$^{+\bullet}$ reduction by YZ in Photosystem II with intact oxygen evolution capacity. Analysis of kinetic H/D isotope exchange effects. Biochemistry 38: 2068−2077

Christen G, Seeliger A and Renger G (1999) P680$^{+\bullet}$ reduction kinetics and redox transition probability of the water oxidizing complex as a function of pH and H/D isotope exchange in spinach thylakoids. Biochemistry 38: 6082−6092

Chu HA, Nguyen AP and Debus RJ (1995) Amino acid residues that influence the binding of manganese or calcium to Photosystem II. 1. The lumenal interhelical domains of the D1 polypeptide. Biochemistry 34: 5839−5858

Clemens KL, Force DA and Britt RD (2002) Acetate binding at the Photosystem II oxygen evolving complex: An S2-state multiline signal ESEEM study. J Am Chem Soc 124: 10921−10933

Commoner B, Heise JJ and Townsend J (1956) Light-induced paramagnetism in chloroplasts. Proc Natl Acad Sci USA 42: 710−718

Conjeaud H and Mathis P (1980) The effects of pH on the reductions kinetics of P-680 in Tris-treated chloroplasts. Biochim Biophys Acta 590: 353−359

Cukier RI (2004) Theory and simulation of proton-coupled electron transfer, hydrogen-atom transfer, and proton translocation in proteins. Biochim Biophys Acta 1655: 37−44

De Vitry C, Carles C and Diner BA (1986) Quantitation of plastoquinone-9 in Photosystem II reaction center particles. Chemical identification of the primary quinone, electron acceptor Q_A. FEBS Lett 196: 203−206

Debus RJ, Barry BA, Babcock GT and McIntosh L (1988a) Site-directed mutagenesis identifies a tyrosine radical involved in the photosynthetic oxygen-evolving system. Proc Natl Acad Sci USA 85: 427−430

Debus RJ, Barry BA, Sithole I, Babcock GT and McIntosh L (1988b) Directed mutagenesis indicates that the donor to P^+_{680} in Photosystem II is tyrosine-161 of the D1 polypeptide. Biochemistry 27: 9071−9074

Dekker JP, Brok M and Van Gorkom HJ (1984a) Absorbance changes of Z^+, the component responsible for EPR signal II fast in Tris-treated Photosystem II particles. In: Sybesma C (ed) Advances in Photosynthesis Research, Vol 1, pp 171−174. Martinus Nijhoff/Dr. W. Junk Publishers, The Hague

Dekker JP, Van Gorkom HJ, Brok M and Ouwehand L (1984b) Optical characterization of Photosystem II electron donors. Biochim Biophys Acta 764: 301−309

Delosme R and Joliot P (2002) Period four oscillations in chlorophyll *a* fluorescence. Photosynth Res 73: 165–168

Diner BA (2001) Amino acid residues involved in the coordination and assembly of the manganese cluster of Photosystem II. Proton-coupled electron transport of the redox-active tyrosines and its relationship to water oxidation. Biochim Biophys Acta 1503: 147–163

Diner BA and Babcock GT (1996) Structure, dynamics, and energy conversion efficiency in Photosystem II. In: Ort DR and Yocum CF (eds) Oxygenic Photosynthesis: The Light Reactions, pp 213–247. Kluwer Academic Publishers, Dordrecht

Diner BA and de Vitry C (1984) Optical spectrum and kinetics of the secondary electron donor, Z, of Photosystem II. In: Sybesma C (ed) Advances in Photosynthesis Research, Vol 1, pp 407–411. Martinus Nijhoff/Dr. W. Junk Publishers, The Hague

Diner BA and Nixon PJ (1998) Evidence for D1-His190 as the proton acceptor implicated in the oxidation of redox-active tyrosine Y_Z of PS II. In: Garab G (ed) Photosynthesis: Mechanism and Effects, Vol II, pp 1177–1180. Kluwer Academic Publishers, Dordrecht

Diner BA, Nixon PJ and Farchaus JW (1991) Site-directed mutagenesis of photosynthetic reaction centers. Curr Opin Struct Biol 1: 546–554

Diner BA, Force DA, Randall DW and Britt RD (1998) Hydrogen bonding, solvent exchange, and coupled proton and electron transfer in the oxidation and reduction of redox-active tyrosine Y_Z in Mn-depleted core complexes of Photosystem II. Biochemistry 37: 17931–17943

Diner BA, Schlodder E, Nixon PJ, Coleman WJ, Rappaport F, Lavergne J, Vermaas WFJ and Chisholm D (2001) Site-directed mutations at D1-His198 and D2-His197 of Photosystem II in *Synechocystis* PCC 6803: Sites of primary charge separation and cation and triplet stabilization. Biochemistry 40: 9265–9281

Diner BA, Bautista JA, Nixon PJ, Berthomieu C, Hienerwadel R, Britt RD, Vermaas WFJ and Chisholm DA (2004) Coordination of proton and electron transfer from the redox-active tyrosine, Y_Z, of Photosystem II and examination of the electrostatic influence of oxidized tyrosine, $Y_D^{\bullet}$ (H^+) Phys Chem Chem Phys 6: 4844–4850

Dixon WT and Murphy D (1976) Determination of the acidity constants of some phenol radical cations by means of electron spin resonance. J Chem Soc, Faraday Trans 2 72: 1221–1230

Dole F, Diner BA, Hoganson CW, Babcock GT and Britt RD (1997) Determination of the electron spin density on the phenolic oxygen of the tyrosyl radical of Photosystem II. J Am Chem Soc 119: 11540–11541

Dorlet P, Valentin MD, Babcock GT and McCracken JL (1998) Interaction of $Y_Z^{\bullet}$ with its environment in acetate-treated Photosystem II membranes and reaction center cores. J Phys Chem B 102: 8239–8247

Dorlet P, Rutherford AW and Un S (2000) Orientation of the tyrosyl D, pheophytin anion, and semiquinone $Q_A^{\bullet-}$ radicals in Photosystem II determined by high-field electron paramagnetic resonance. Biochemistry 39: 7826–7834

Eckert HJ and Renger G (1988) Temperature dependence of P680+ reduction in oxygen-evolving PS II membrane fragments at different redox states Si of the water oxidizing system. FEBS Lett 236: 425–431

El-Kabbani O, Chang CH, Tiede D, Norris J and Schiffer M (1991) Comparison of reaction centers from *Rhodobacter sphaeroides* and *Rhodopseudomonas viridis*: Overall architecture and protein-pigment interactions. Biochemistry 30: 5361–5369

Evelo RG, Hoff AJ, Dikanov SA and Tyryshkin AM (1989) An ESEEM study of the oxidized electron donor of plant Photosystem II: Evidence that $D^{\bullet}$ is a neutral tyrosine radical. Chem Phys Lett 161: 479–484

Faller P, Debus RJ, Brettel K, Sugiura M, Rutherford AW and Boussac A (2001) Rapid formation of the stable tyrosyl radical in Photosystem II. Proc Natl Acad Sci USA 98: 14368–14373

Faller P, Rutherford AW and Debus RJ (2002) Tyrosine D oxidation at cryogenic temperature in Photosystem II. Biochemistry 41: 12914–12920

Farrar CT, Gerfen GJ, Griffin RG, Force DA and Britt RD (1997) Electronic structure of the Y_D tyrosyl radical in Photosystem II: A high-frequency electron paramagnetic resonance spectroscopic and density functional theoretical study. J Phys Chem B 101: 6634–6641

Ferreira KN, Iverson TM, Maghlauoui K, Barber J and Iwata S (2004) Architecture of the photosynthetic oxygen-evolving center. Science 303: 1831–1838

Force DA, Randall DW, Britt RD, Tang X-S and Diner BA (1995) ^{2}H ESE-ENDOR study of hydrogen bonding to the tyrosine radicals $Y_D^{\bullet}$ and $Y_Z^{\bullet}$ of Photosystem II. J Am Chem Soc 117: 12643–12644

Fowler CF (1977) Proton evolution from Photosystem II. Stoichiometry and mechanistic considerations. Biochim Biophys Acta 462: 414–421

Gardner KA and Mayer JM (1995) Understanding C-H bond oxidations: $H^{\bullet}$ and H^- transfer in the oxidation of toluene by permanganate. Science 269: 1849–1851

Gerken S, Brettel K, Schlodder E and Witt HT (1988) Optical characterization of the immediate electron donor to chlorophyll aII^+ in oxygen-evolving Photosystem II complexes. Tyrosine as possible electron carrier between chlorophyll aII and the water-oxidizing manganese complex. FEBS Lett 237: 69–75

Ghanotakis DF, O'Malley PJ, Babcock GT and Yocum CF (1983) Structure and inhibition of components on the oxidizing side of Photosystem II. In: Inoue Y, Crofts AR, Govindjee, Murata N, Renger G and Satoh K (eds) Oxygen Evolving System of Photosynthesis, pp 91–101. Academic Press, Tokyo

Gilchrist ML, Jr., Ball JA, Randall DW and Britt RD (1995) Proximity of the manganese cluster of Photosystem II to the redox-active tyrosine Y_Z. Proc Natl Acad Sci USA 92: 9545–9549

Glaser M, Wolff C, Buchwald HE and Witt HT (1974) On the photoactive chlorophyll reaction in system II of photosynthesis. Detection of a fast and large component. FEBS Lett 42: 81–85

Gulin VI, Dikanov SA, Tsvetkov YD, Evelo RG and Hoff AJ (1992) Very high frequency (135 GHz) EPR of the oxidized primary donor of the photosynthetic bacteria *Rb. sphaeroides* R-26 and *Rps. viridis* and of YD. (signal II) of plant Photosystem II. Pure Appl Chem 64: 903–906

Hales BJ and Das Gupta A (1981) Supposition of the origin of signal II from random and oriented chloroplasts. Biochim Biophys Acta 637: 303–311

Hallahan BJ, Nugent JHA, Warden JT and Evans MCW (1992) Investigation of the origin of the 'S3' EPR signal from the oxygen-evolving complex of Photosystem 2: The role of tyrosine Z. Biochemistry 31: 4562–4573

Harriman A (1987) Further comments on the redox potentials of tryptophan and tyrosine. J Phys Chem 91: 6102–6104

Haumann M, Bogershausen O, Cherepanov D, Ahlbrink R and Junge W (1997) Photosynthetic oxygen evolution: H/D isotope effects and the coupling between electron and proton transfer during the redox reactions at the oxidizing side of Photosystem II. Photosynth Res 51: 193–208

Haumann M, Mulkidjanian A and Junge W (1999) Tyrosine-Z in oxygen-evolving Photosystem II: A hydrogen-bonded tyrosinate. Biochemistry 38: 1258–1267

Hays AM, Vassiliev IR, Golbeck JH and Debus RJ (1998) Role of D1-His190 in proton-coupled electron transfer reactions in Photosystem II: A chemical complementation study. Biochemistry 37: 11352–11365

Hays AM, Vassiliev IR, Golbeck JH and Debus RJ (1999) Role of D1-His190 in the proton-coupled oxidation of tyrosine Y_Z in manganese-depleted Photosystem II. Biochemistry 38: 11851–11865

Hienerwadel R, Boussac A, Breton J and Berthomieu C (1996) Fourier transform infrared difference study of tyrosineD oxidation and plastoquinone Q_A reduction in Photosystem II. Biochemistry 35: 15447–15460

Hienerwadel R, Boussac A, Breton J, Diner B and Berthomieu C (1997) Fourier transform infrared difference spectroscopy of Photosystem II tyrosine D using site-directed mutagenesis and specific isotope labeling. Biochemistry 36: 14712–14723

Hofbauer W, Zouni A, Bittl R, Kern J, Orth P, Lendzian F, Fromme P, Witt HT and Lubitz W (2001) Photosystem II single crystals studied by EPR spectroscopy at 94 GHz: The tyrosine radical $Y_D^{\bullet}$. Proc Natl Acad Sci USA 98: 6623–6628

Hoganson CW and Babcock GT (1988) Electron-transfer events near the reaction center in oxygen-evolving Photosystem II preparations. Biochemistry 27: 5848–5855

Hoganson CW and Babcock GT (1992) Protein-tyrosyl radical interactions in Photosystem II studied by electron spin resonance and electron nuclear double resonance spectroscopy: comparison with ribonucleotide reductase and in vitro tyrosine. Biochemistry 31: 11874–11880

Hoganson CW and Babcock GT (1997) A metalloradical mechanism for the generation of oxygen from water in photosynthesis. Science 277: 1953–1956

Hoganson CW, Lydakis-Simantiris N, Tang X-S, Tommos C, Warncke K, Babcock GT, Diner BA, McCracken J and Styring S (1995) A hydrogen-atom abstraction model for the function of Yz in photosynthetic oxygen evolution. Photosynth Res 46: 177–184

Hoganson CW, Sahlin M, Sjoeberg B-M and Babcock GT (1996) Electron magnetic resonance of the tyrosyl radical in ribonucleotide reductase from *Escherichia coli*. J Am Chem Soc 118: 4672–4679

Hulsebosch RJ, van den Brink JS, Nieuwenhuis SAM, Gast P, Raap J, Lugtenberg J and Hoff AJ (1997) Electronic structure of the neutral tyrosine radical in frozen solution. Selective ^{2}H-, ^{13}C-, and ^{17}O-isotope labeling and EPR spectroscopy at 9 and 35 GHz. J Am Chem Soc 119: 8685–8694

Ikeuchi M and Inoue Y (1988) Partial characterization of the iodination site in D1 protein of manganese-retaining and manganese-depleted Photosystem II membranes. Plant Cell Physiol 29: 695–705

Kamiya N and Shen J-R (2003) Crystal structure of oxygen-evolving Photosystem II from *Thermosynechococcus vulcanus* at 3.7 Å resolution. Proc Natl Acad Sci USA 100: 98–103

Karge M, Irrgang KD, Sellin S, Feinaeugle R, Liu B, Eckert HJ, Eichler HJ and Renger G (1996) Effects of hydrogen/deuterium exchange on photosynthetic water cleavage in PS II core complexes from spinach. FEBS Lett 378: 140–144

Karge M, Irrgang K-D and Renger G (1997) Analysis of the reaction coordinate of photosynthetic water oxidation by kinetic measurements of 355 nm absorption changes at different temperatures in Photosystem II preparations suspended in either H_2O or D_2O. Biochemistry 36: 8904–8913

Klimov VV and Krasnovskii AA (1981) Pheophytin as the primary electron acceptor in Photosystem 2 reaction centers. Photosynthetica 15: 592–609

Kohl DH and Wood PM (1969) Molecular identity of ESR signal II observed in photosynthetic systems: The effect of heptane extraction and reconstitution with plastoquinone and deuterated plastoquinone. Plant Physiol 44: 1439–1445

Kohl DH, Wright JR and Weissman M (1969) Electron spin resonance studies of free radicals derived from plastoquinone, alph.- and gamma-tocopherol and their relations to free radicals observed in photosynthetic materials. Biochim Biophys Acta 180: 536–544

Koulougliotis D, Tang X-S, Diner BA and Brudvig GW (1995) Spectroscopic evidence for the symmetric location of tyrosines D and Z in Photosystem II. Biochemistry 34, 2850–2856

Kramer DM, Roffey RA, Govindjee and Sayre RT (1994) The AT thermoluminescence band from *Chlamydomonas reinhardtii* and the effects of mutagenesis of histidine residues on the donor side of the Photosystem II D1 polypeptide. Biochim Biophys Acta 1185: 228–237

Krishtalik LI (1986) Energetics of multielectron reactions. Photosynthetic oxygen evolution. Biochim Biophys Acta 849: 162–171

Krishtalik LI (1990) Activation energy of photosynthetic oxygen evolution: An attempt at theoretical analysis. Bioelectrochem Bioenerg 23: 249–263

Kuehne H and Brudvig GW (2002) Proton-coupled electron transfer involving tyrosine Z in Photosystem II. J Phys Chem B 106: 8189–8196

Lakshmi KV, Eaton SS, Eaton GR, Frank HA and Brudvig GW (1998) Analysis of dipolar and exchange Interactions between manganese and tyrosine Z in the $S2Y_Z^{\bullet}$ state of acetate-inhibited Photosystem II via EPR spectral simulations at X- and Q-bands. J Phys Chem B 102: 8327–8335

Lakshmi KV, Eaton SS, Eaton GR and Brudvig GW (1999) Orientation of the tetranuclear manganese cluster and tyrosine Z in the O_2-evolving complex of Photosystem II: An EPR study of the $S2Y_Z^{\bullet}$ State in oriented acetate-inhibited Photosystem II membranes. Biochemistry 38: 12758–12767

Lavergne J and Junge W (1993) Proton release during the redox cycle of the water oxidase. Photosynth Res 38: 279–296

Lind J, Shen X, Eriksen TE and Merenyi G (1990) The one-electron reduction potential of 4-substituted phenoxyl radicals in water. J Am Chem Soc 112: 479–482

MacLachlan DJ and Nugent JHA (1993) Investigation of the S3 electron paramagnetic resonance signal from the oxygen-evolving complex of Photosystem II: Effect of inhibition of oxygen evolution by acetate. Biochemistry 32: 9772–9780

Mamedov F, Sayre RT and Styring S (1998) Involvement of histidine 190 on the D1 protein in electron/proton transfer reactions on the donor side of Photosystem II. Biochemistry 37: 14245–14256

Mauzerall D and Malley M (1971) Light-induced increase in

fluorescence yield in *Chlorella* is complete in 60 nanoseconds. Photochem Photobiol 14: 225–227

McConnell HM (1956) Indirect hyperfine interactions in the paramagnetic resonance spectra of aromatic free radicals. J Chem Phys 24: 764–766

McConnell HM and Chesnut DB (1958) Theory of isotropic hyperfine interactions in p-electron radicals. J Chem Phys 28: 107–117

Metz JG, Nixon PJ, Rogner M, Brudvig GW and Diner BA (1989) Directed alteration of the D1 polypeptide of Photosystem II: Evidence that tyrosine-161 is the redox component, Z, connecting the oxygen-evolving complex to the primary electron donor, P680. Biochemistry 28: 6960–6969

Meyer B, Schlodder E, Dekker JP and Witt HT (1989) Oxygen evolution and Chl aII+ (P-680+) nanosecond reduction kinetics in single flashes as a function of pH. Biochim Biophys Acta 974: 36–43

Michel H and Deisenhofer J (1988) Relevance of the photosynthetic reaction center from purple bacteria to the structure of Photosystem II. Biochemistry 27: 1–7

Nieuwenhuis SAM, Hulsebosch RJ, Raap J, Gast P, Lugtenburg J and Hoff AJ (1998) Structure of the Y_D tyrosine radical in Photosystem II. Determination of the orientation of the phenoxyl ring by enantioselective deuteration of the methylene group. J Am Chem Soc 120: 829–830

Nixon PJ and Diner BA (1994) Analysis of water-oxidation mutants constructured in the cyanobacterium *Synechocystis* sp. PCC 6803. Biochem Soc Trans 22: 338–343

Noguchi T, Inoue Y and Tang X-S (1997) Structural coupling between the oxygen-evolving Mn cluster and a tyrosine residue in Photosystem II as revealed by Fourier transform infrared spectroscopy. Biochemistry 36: 14705–14711

Nordlund P, Sjoeberg BM and Eklund H (1990) Three-dimensional structure of the free radical protein of ribonucleotide reductase. Nature 345: 593–598

O'Malley PJ (1998) Hybrid density functional studies of the oxidation of phenol-imidazole hydrogen-bonded complexes: A model for tyrosine oxidation in oxygenic photosynthesis. J Am Chem Soc 120: 11732–11737

O'Malley PJ and Babcock GT (1984) EPR properties of immobilized quinone cation radicals and the molecular origin of signal II in spinach chloroplasts. Biochim Biophys Acta 765: 370–379

O'Malley PJ, Babcock GT and Prince RC (1984) The cationic plastoquinone radical of the chloroplast water splitting complex. Hyperfine splitting from a single methyl group determines the EPR spectral shape of signal II. Biochim Biophys Acta 766: 283–288

Ono T and Inoue Y (1988) Discrete extraction of the calcium atom functional for oxygen evolution in higher plant Photosystem II by a simple low pH treatment. FEBS Lett 227: 147–152

Ono T and Inoue Y (1989) Removal of calcium by pH 3.0 treatment inhibits S2 to S3 transition in the photosynthetic oxygen evolution system. Biochim Biophys Acta 973: 443–449

Page CC, Moser CC, Chen X and Dutton PL (1999) Natural engineering principles of electron tunnelling in biological oxidation-reduction. Nature 402: 47–52

Pecoraro VL, Baldwin MJ, Caudle MT, Hsieh W-Y and Law NA (1998) A proposal for water oxidation in Photosystem II. Pure Appl Chem 70: 925–929

Peloquin JM, Campbell KA and Britt RD (1998) ^{55}Mn pulsed ENDOR demonstrates that the Photosystem II 'split' EPR signal arises from a magnetically-coupled mangano-tyrosyl complex. J Am Chem Soc 120: 6840–6841

Rappaport F and Lavergne J (1991) Proton release during successive oxidation steps of the photosynthetic water oxidation process: Stoichiometries and pH dependence. Biochemistry 30: 10004–10012

Rappaport F and Lavergne J (2001) Coupling of electron and proton transfer in the photosynthetic water oxidase. Biochim Biophys Acta 1503: 246–259

Rappaport F, Blanchard-Desce M and Lavergne J (1994) Kinetics of electron transfer and electrochromic change during the redox transitions of the photosynthetic oxygen-evolving complex. Biochim Biophys Acta 1184: 178–192

Razeghifard MR, Klughammer C and Pace RJ (1997) Electron paramagnetic resonance kinetic studies of the S states in spinach thylakoids. Biochemistry 36: 86–92

Rigby SEJ, Nugent JHA and O'Malley PJ (1994) The dark stable tyrosine radical of Photosystem 2 studied in three species using ENDOR and EPR spectroscopies. Biochemistry 33: 1734–1742

Rodriguez ID, Chandrashekar TK and Babcock GT (1987) ENDOR characterization of water/deuterium oxide exchange in the D^+Z^+ radical in photosynthesis. In: Biggins J (ed) Progress in Photosynthesis, Vol 1, pp 471–474. Martinus Nijhoff Publishers, Dordrecht

Roffey RA, Kramer DM, Govindjee and Sayre RT (1994a) Lumenal side histidine mutations in the D1 protein of Photosystem II affect donor side electron transfer in *Chlamydomonas reinhardtii*. Biochim Biophys Acta 1185: 257–270

Roffey RA, van Wijk KJ, Sayre RT and Styring S (1994b) Spectroscopic characterization of tyrosine-Z in histidine 190 mutants of the D1 protein in Photosystem II (PS II) in *Chlamydomonas reinhardtii*. Implication for the structural model of the donor side of PS II. J Biol Chem 269: 5115–5121

Ruffle SV, Donnelly D, Blundell TL and Nugent JHA (1992) A three-dimensional model of the Photosystem II reaction center of *Pisum sativum*. Photosynth Res 34: 287–300

Saphon S and Crofts AR (1977) Protolytic reactions in Photosystem II: A new model for the release of protons accompanying the photooxidation of water. Z Naturforsch 32C: 617–626

Schilstra MJ, Rappaport F, Nugent JHA, Barnett CJ and Klug DR (1998) Proton/hydrogen transfer affects the S-state-dependent microsecond phases of $P680^+$ reduction during water splitting. Biochemistry 37: 3974–3981

Schlodder E, Brettel K, Schatz GH and Witt HT (1984) Analysis of the Chl-aII^+ reduction kinetics with nanosecond time resolution in oxygen-evolving Photosystem II particles from *Synechococcus* at 680 and 824 nm. Biochim Biophys Acta 765: 178–185

Schlodder E, Brettel K and Witt HT (1985) Relation between microsecond reduction kinetics of photooxidized chlorophyll aII (P-680) and photosynthetic water oxidation. Biochim Biophys Acta 808: 123–131

Shinkarev VP and Wraight CA (1993) Oxygen evolution in photosynthesis: From unicycle to bicycle. Proc Natl Acad Sci USA 90: 1834–1838

Sjödin M, Styring S, Kermark B, Sun L and Hammarström L (2000) Proton-coupled electron transfer from tyrosine in a

tyrosine-ruthenium-tris-bipyridine complex: Comparison with tyrosine Z oxidation in Photosystem II. J Am Chem Soc 122: 3932–3936

Sjödin M, Styring S, Akermark B, Sun L and Hammarström L (2002) The mechanism for proton-coupled electron transfer from tyrosine in a model complex and comparisons with Y_Z oxidation in Photosystem II. Phil Trans Royal Soc London, B 357: 1471–1479

Stubbe J and van der Donk WA (1998) Protein radicals in enzyme catalysis. Chem Rev 98: 705–762

Svensson B, Etchebest C, Tuffery P, Kan Pv, Smith J and Styring S (1996) A model for the Photosystem II reaction center core including the structure of the primary donor P680. Biochemistry 35: 14486–14502

Szalai VA, Kuhne H, Lakshmi KV and Brudvig GW (1998) Characterization of the interaction between manganese and tyrosine Z in acetate-inhibited Photosystem II. Biochemistry 37: 13594–13603.

Takahashi Y and Satoh K (1989) Identification of the photochemically iodinated amino acid residue on D1-protein in the Photosystem II core complex by peptide mapping analysis. Biochim Biophys Acta 973: 138–146

Tang XS, Chisholm DA, Dismukes GC, Brudvig GW and Diner BA (1993) Spectroscopic evidence from site-directed mutants of *Synechocystis* PCC6803 in favor of a close interaction between histidine 189 and redox-active tyrosine 160, both of polypeptide D2 of the Photosystem II reaction center. Biochemistry 32: 13742–13748

Tang X-S, Randall DW, Force DA, Diner BA and Britt RD (1996b) Manganese-tyrosine interaction in the Photosystem II oxygen-evolving complex. J Am Chem Soc 118: 7638–7639

Tang X-S, Zheng M, Chisholm DA, Dismukes GC and Diner BA (1996a) Investigation of the differences in the local protein environments surrounding tyrosine radicals $Y_Z^{\bullet}$ and $Y_D^{\bullet}$ in Photosystem II using wild-type and the D2-Tyr160Phe mutant of *Synechocystis* 6803. Biochemistry 35: 1475–1484

Tommos C and Babcock GT (1998) Oxygen production in nature: A light-driven metalloradical enzyme process. Acc Chem Res 31: 18–25

Tommos C and Babcock GT (2000) Proton and hydrogen currents in photosynthetic water oxidation. Biochim Biophys Acta 1458: 199–219

Tommos C, Davidsson L, Svensson B, Madsen C, Vermaas W and Styring S (1993) Modified EPR spectra of the tyrosine D radical in Photosystem II in site-directed mutants of *Synechocystis* sp. PCC 6803: Identification of side chains in the immediate vicinity of tyrosine D on the D2 protein. Biochemistry 32: 5436–5441

Tommos C, Tang X-S, Warncke K, Hoganson CW, Styring S, McCracken J, Diner BA and Babcock GT (1995) Spin-density distribution, conformation, and hydrogen bonding of the redox-active tyrosine Y_Z in Photosystem II from multiple-electron magnetic-resonance spectroscopies: Implications for photosynthetic oxygen evolution. J Am Chem Soc 117: 10325–10335

Tommos C, McCracken J, Styring S and Babcock GT (1998) Stepwise disintegration of the photosynthetic oxygen-evolving complex. J Am Chem Soc 120: 10441–10452

Tommos C, Skalicky JJ, Pilloud DL, Wand AJ and Dutton PL (1999) De novo proteins as models of radical enzymes. Biochemistry 38: 9495–9507

Un S, Brunel L-C, Brill TM, Zimmermann J-L and Rutherford AW (1994) Angular orientation of the stable tyrosyl radical within Photosystem II by high-field 245-GHz electron paramagnetic resonance. Proc Natl Acad Sc USA 91: 5267–5271

Un S, Tang X-S and Diner BA (1996) 245 GHz high-field EPR study of tyrosine-$D^{\bullet}$ and tyrosine-$Z^{\bullet}$ in mutants of Photosystem II. Biochemistry 35: 679–684

Vass I and Styring S (1991) pH-Dependent charge equilibria between tyrosine-D and the S states in Photosystem II. Estimation of relative midpoint redox potentials. Biochemistry 30: 830–839

Vermaas WFJ, Rutherford AW and Hansson O (1988) Site-directed mutagenesis in Photosystem II of the cyanobacterium *Synechocystis* sp. PCC 6803: Donor D is a tyrosine residue in the D2 protein. Proc Natl Acad Sci USA 85: 8477–8481

Vrettos JS, Limburg J and Brudvig GW (2001) Mechanism of photosynthetic water oxidation: Combining biophysical studies of Photosystem II with inorganic model chemistry. Biochim Biophys Acta 1503: 229–245

Warden JT, Blankenship RE and Sauer K (1976) A flash photolysis ESR study of Photosystem II. Signal IIvf, the physiological donor to $P\text{-}680^{+}$. Biochim Biophys Acta 423: 462–478

Warncke K, McCracken J and Babcock GT (1994) Structure of the Y_D tyrosine radical in Photosystem II as revealed by ^2H Electron Spin Echo Envelope Modulation (ESEEM) spectroscopic analysis of hydrogen hyperfine interactions. J Am Chem Soc 116: 7332–7340

Warncke K, Tang X-S, Tommos C, Babcock GT, Diner BA and McCracken J (1995) Static side chain conformational distribution in the Y_Z tyrosine radical in manganese-depleted, Y_D- Photosystem II. In: Mathis P (ed) Photosynthesis: From Light to Biosphere, Vol 1, pp 711–714. Kluwer Academic Publishers, Dordrecht

Weaver EC (1962) Possible interpretation of the slow-decaying EPR signal in algal suspensions. Arch Biochem Biophys 99: 193–196

Westphal KL, Tommos C, Cukier RI and Babcock GT (2000) Concerted hydrogen-atom abstraction in photosynthetic water oxidation. Curr Opin Plant Biol 3: 236–242

Xiong J, Subramanian S and Govindjee (1998) A knowledge-based three dimensional model of the Photosystem II reaction center of *Chlamydomonas reinhardtii*. Photosynth Res 56: 229–254

Yerkes CT, Babcock GT and Crofts AR (1983) A tris-induced change in the midpoint potential of Z, the donor to Photosystem II, as determined by the kinetics of the back reaction. FEBS Lett 158: 359–363

Yocum CF and Babcock GT (1981) Amine-induced inhibition of photosynthetic oxygen evolution. A correlation between the microwave power saturation properties of signal IIf and Photosystem II-associated manganese. FEBS Lett 130: 99–102

Zouni A, Witt H-T, Kern J, Fromme P, Krauss N, Saenger W and Orth P (2001) Crystal structure of Photosystem II from *Synechococcus elongatus* at 3.8 Å resolution. Nature 409: 739–743

Chapter 10

The Catalytic Manganese Cluster: Organization of the Metal Ions

Vittal K. Yachandra*
Melvin Calvin Laboratory, Physical Biosciences Division, Lawrence Berkeley National Laboratory, Berkeley, CA 94720, U.S.A.

Summary

The light-induced oxidation of water to O_2 is catalyzed by a four-manganese atom cluster associated with Photosystem II (PS II). This chapter summarizes ongoing investigations of the oxidation state, the structure and the associated cofactors calcium and chloride of the catalytic Mn cluster using X-ray and electron paramagnetic resonance (EPR) spectroscopy. Manganese K-edge X-ray spectroscopy, Kβ X-ray emission spectroscopy (XES), and extended X-ray absorption fine structure (EXAFS) studies have not only determined the oxida-

*Email: VKYachandra@LBL.gov

T. Wydrzynski and K. Satoh (eds): Photosystem II: The Light-Driven Water:Plastoquinone Oxidoreductase, pp. 235–260.

tion states and structural features, but also changes that occur in oxidation state of the Mn cluster and in its structural organization during the accumulation of oxidizing equivalents leading to O_2 formation. Combining X-ray spectroscopy information with X-ray diffraction studies, and consistent with the available EPR data, we have succeeded in limiting the range of likely structures of the Mn cluster. EXAFS studies at the strontium and calcium K-edges have provided evidence that the catalytic center is a Mn/Ca heteronuclear complex. Based on the X-ray spectroscopy data, models for the structure and a mechanism for O_2 evolution are presented.

I. Introduction

Most of the O_2 in the atmosphere that supports life on earth is generated by plants, algae, and cyanobacteria by the photo-induced oxidation of water to dioxygen:

$$2H_2O \rightarrow O_2 + 4e^- + 4H^+ \quad (1)$$

This reaction is catalyzed by a manganese/calcium complex (Mn_4Ca), which sequentially stores four oxidizing equivalents (i.e. the S_n states, where n = 0 – 4) that are used to oxidize two molecules of water to molecular oxygen (Kok et al., 1970; for a review, see Joliot, 2003). The Mn complex is part of the multiprotein Photosystem II (PS II) assembly (Chapters 3–6), which contains the reaction center involved in photosynthetic charge separation (Chapter 7) and an antenna complex of chlorophyll molecules (Chapter 2). The assembly also contains cytochrome b_{559} (Chapter 15) and a Fe-quinone electron acceptor complex (Chapter 8).

X-ray absorption spectroscopy (XAS) (Sauer et al., 1992; Robblee et al., 2001) and electron paramagnetic resonance (EPR) (Dismukes and Siderer, 1981; Messinger et al., 1997b; Britt et al., 2000) studies have emerged as the primary methods to provide structural and chemical information about the oxygen evolving complex (OEC) and devise a working model for its Mn cluster. XAS has been used to examine the structural environment of metal ions in many proteins (Cramer, 1988; Yachandra, 1995). The energy of the incoming X-ray photons and of the outgoing fluorescence is specific to the Mn atom; hence, other metals or the protein matrix normally co-purified with the OEC in a PS II preparation do not interfere. Element-specificity and applicability to non-crystalline samples have made X-ray spectroscopy a useful technique for probing the structure of the Mn complex in the complicated environment of PS II, which has many components such as non-heme iron, cytochrome, chlorophylls that interfere with other techniques. The structural studies can also be performed on crystals, or on frozen solutions and several of the S state intermediates mentioned above have been stabilized as frozen solutions and studied by X-ray spectroscopy. The different regions of the X-ray spectrum provide complementary information: X-ray absorption near edge spectroscopy (XANES) yield information about the oxidation states and site symmetry of the absorbing atom while extended X-ray absorption fine structure (EXAFS) is sensitive to distances, numbers, and atomic number of atoms around the absorbing atom. The more recently used technique of X-ray emission spectroscopy (XES) has also provided information regarding the identity of the oxidation states of Mn complex in the various S-states and the changes accompanying the S-state advance.

Critical questions related to the process of photosynthetic water oxidation are: (i) What are the oxidation state(s) and structural changes in the Mn complex as the OEC proceeds through the S-state cycle? and (ii) What is the mechanism by which four electrons are removed from two water molecules by the Mn complex to produce an O_2 molecule? Electron paramagnetic resonance (EPR) and X-ray spectroscopy studies and the interplay between these two methods have provided significant insights into the structure and the mechanism of the OEC. This chapter focuses on the application of X-ray spectroscopic techniques to resolve structural questions regarding the Mn cluster in the OEC, with emphasis on the results from our laboratory. Many excellent reviews are available for comprehensive surveys of the Mn complex and the OEC, EPR, and XAS literature (Debus, 1992; Rutherford et al., 1992; Britt, 1996;

Abbreviations: Chl – chlorophyll; <E> – 1st-moment value; EPR – electron paramagnetic resonance; EXAFS – extended X-ray absorption fine structure; FT – Fourier transform; IPE – inflection point energy; MLS – multiline EPR signal; Mn_4 – catalytic manganese cluster; OEC – oxygen evolving complex; PS II – Photosystem II; S_n – states of the OEC for n = 0, 1, 2, 3, or 4; XANES – X-ray absorption near edge spectroscopy; XAS – X-ray absorption spectroscopy; XES – X-ray emission spectroscopy; Y_D^{ox} – oxidized form of the redox active tyrosine on D2; $Y_Z^{\bullet}$ – oxidized form of the redox active tyrosine on D1

Yachandra et al., 1996, 2002; Penner-Hahn, 1998; Robblee et al., 2001).

II. Oxidation States of the Manganese

Two key questions for the understanding of photosynthetic water oxidation are: (i) do all four oxidizing equivalents necessary to oxidize water to O_2 accumulate on the four Mn ions of the OEC, or do some ligand-centered oxidations take place before the formation and release of O_2 during the $S_3 \rightarrow [S_4] \rightarrow S_0$ transition; and (ii) what are the oxidation state assignments for the Mn during S-state advancement. X-ray absorption and emission spectroscopy of Mn, along with EPR have provided answers to these two pivotal questions.

A. Manganese X-Ray Absorption Near Edge Spectroscopy (XANES)

X-ray absorption near-edge spectroscopy (XANES) is the most well-known of the X-ray techniques and has been extensively used to investigate the oxidation states of redox-active metals in metalloprotein active sites. XANES results from the excitation of a 1s electron (K-shell) to a higher, bound orbital (Fig. 1, *Left*). The higher the oxidation state of the metal, the more positive the overall charge of the atom, and higher energy is required to excite an electron out of an orbital (Shulman et al., 1976). The first formally allowed electric dipole transition is the 1s→4p transition. Due to the size of the 4p orbital, it overlaps with p-orbitals of the ligands, either through σ or π bonding. Consequently, this transition is sensitive to the oxidation state and the ligand environment of the metal. For certain symmetries around the metal, the formally electric-dipole forbidden 1s→3d transition can be observed (arrow points to it in Fig. 1, *Middle* which is expanded in the inset), occurring at a lower energy than the main edge transitions (Roe et al., 1984). This transition is due to mixing of metal 3d and 4p orbitals, and gives information about the ligand as well as about the oxidation state and symmetry of the metal complex (Westre et al., 1997). To increase the sensitivity of XANES, absorption is detected as an excitation spectrum by measuring the Kα fluorescence (2p to 1s) of the Mn atoms (Jaklevic et al., 1977).

The pioneering application of Mn XANES to PS II was performed by Kirby et al. (1981) on chloroplasts and Goodin et al. (1984) on PS II preparations in the early 1980s. These studies, although extremely difficult because of the low Mn concentration, showed that the Mn K-edge from the S_2 state is shifted to higher energy relative to the Mn K-edge from the S_1 state. Dramatic improvements in detector technology and cryostat cooling capabilities have made XANES experiments practical using concentrated PS II preparations (McDermott et al., 1988; Guiles et al., 1990a; DeRose et al., 1994), and the collection of XANES spectra from dilute, single-flash saturable PS II samples is now achievable. Three different groups have investigated the oxidation states of Mn for the S_0, S_1, S_2, and S_3 states using XANES on single-flash saturable PS II samples. Based on shifts in the absorption edge, or lack thereof, Roelofs et al. (1996) proposed that Mn is oxidized during the $S_0 \rightarrow S_1$ and $S_1 \rightarrow S_2$ transitions, but is not oxidized during the $S_2 \rightarrow S_3$ transition. In contrast, Ono et al. (1992) and Iuzzolino et al. (1998) interpret their XANES results to indicate that Mn is oxidized during each S-state transition, although Ono et al. (1992) reported no independent S-state determination for their samples and Iuzzolino et al. (1998) had significant S-state inhomogeneity in their samples. However, improved XANES data for S-state transitions, have shown a Mn K-edge shift of only 0.4 eV for the S_2 to S_3 transition (Ono et al., 1994). The results of Roelofs et al (1996) indicating the absence of Mn centered oxidation during the S_2 to S_3 transition has been reproduced by Messinger et al. (2001) using both XANES (Fig. 1, *Middle* and *Right*) and Mn XES studies (see below).

B. Manganese Kβ X-Ray Emission Spectroscopy (XES)

The recent studies by Messinger et al. (2001) have combined EPR, XANES and XES studies to address the questions of oxidation state assignments and changes during the S state cycle. In contrast to XANES, Kβ XES detects the X-ray emission from the relaxation of a 3p electron to a 1s hole, which is created by excitation of a 1s electron into the continuum (Fig. 2, *Left*). In a simplified model, two final states exist due to a constructive ($K\beta_{1,3}$) or destructive ($K\beta'$) spin-exchange interaction between the unpaired electrons in the 3p and 3d orbitals (Tsutsumi et al., 1976). The magnitude of the exchange interaction depends on the number of unpaired electrons in the 3d orbital. In the high spin case, increasing the oxidation state of the metal decreases the number of

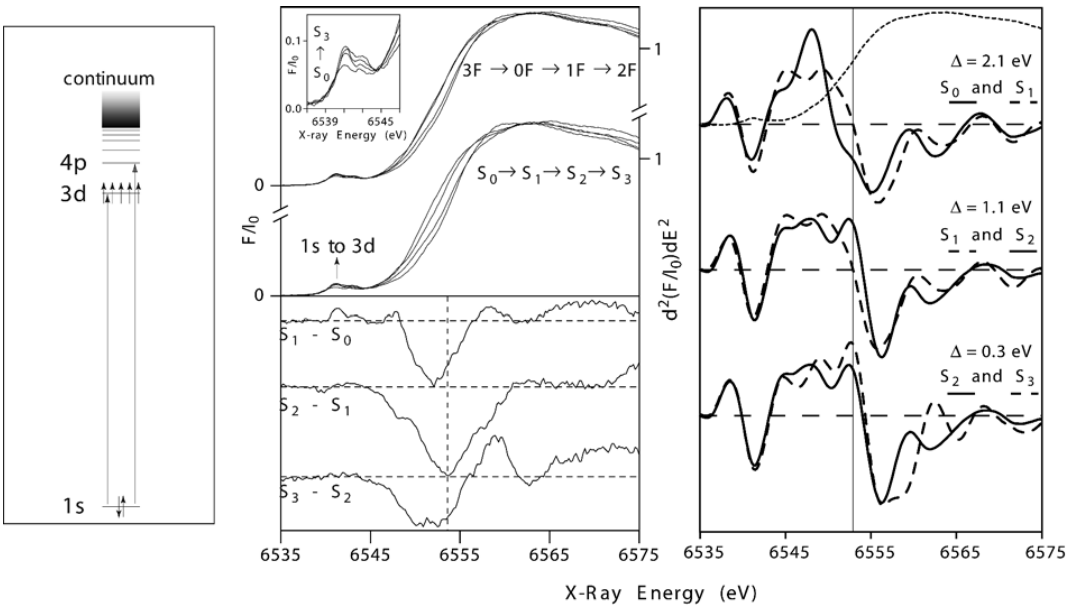

Fig. 1. Left. A schematic diagram for the excitation and emission processes involved in Mn XANES. The weak 1s to 3d transition is dipole-forbidden and the principal transition is from 1s to a molecular orbital with p character. To enhance sensitivity, the X-ray absorption spectra are collected as excitation spectra using Mn Kα (2p to 1s) fluorescence detection. *Middle Top*. Mn K-edge XANES spectra of flash-illuminated PS II samples. Pure S-state spectra (bottom) were obtained from the flash spectra (top) by deconvolution using multiline EPR spectra. The pre-edge region (principally a 1s → 3d transition) for the $S_0 - S_3$ states is shown in the inset. The inflection point energy (IPE) changes from S_0 to S_1 and S_1 to S_2 transitions are substantial but are much smaller for the S_2 to S_3 transition. *Middle Bottom*. S-state Mn XANES difference spectra show that each transition is unique. The horizontal dashed lines show the zero value for each difference spectrum. Adapted from Messinger et al. (2001) and Visser et al. (2001). *Right.* Second derivatives of the normalized, pure S-state Mn K-edge spectra of the Mn-cluster of PS II. For clarity a vertical dashed line has been drawn at the inflection point energy (IPE) of the S_1-state. The change in IPE (Δ in eV) for each S-state advance is given at the right shows the significant shifts for the S_0 to S_1 and S_1 to S_2 transitions but is much smaller for the S_2 to S_3 transition indicating that a Mn centered oxidation is unlikely for the S_2 to S_3 transition. For reference, the K-edge spectrum of the S_1-state is plotted as well (dashed line). Adapted from Messinger et al. (2001).

unpaired 3d electrons; concomitantly, the spin exchange interaction decreases. Accordingly, the $K\beta_{1,3}$ transition shifts to a higher and the Kβ′ transition shifts to a lower energy (Peng et al., 1994). Compared to the 4p orbitals, the 3p orbitals have less overlap with the ligand orbitals, because they are smaller and more buried within the electronic shells. Therefore, Kβ XES is less sensitive to the ligand environment compared to XANES. The $K\beta_{1,3}$ transition is better resolved than the Kβ′ transition due to a difference in relaxation processes. Hence, the $K\beta_{1,3}$ transition is used as a indicator of the oxidation state of the metal. A more accurate view on Kβ XES requires the ligand-field multiplet formalism. This indicates that there is some dependence of the ligand environment on Kβ XES spectra.

Shown in Fig. 2, *Middle*, and inset are the Kβ emission spectra of $Mn(IV)O_2$, $Mn_2(III)O_3$, and Mn(II)O, which illustrate the features of Kβ emission spectra and their sensitivity to the oxidation states of Mn. As the oxidation state of Mn increases from Mn(II) to Mn(III) to Mn(IV), fewer unpaired 3d valence electrons are available to interact with the 3p hole; thus, the magnitude of the 3p – 3d exchange interaction becomes smaller, leading to a decrease in the Kβ′ – $K\beta_{1,3}$ splitting. The consequence is that, if one focuses only on the more intense $K\beta_{1,3}$ emission peak, it shifts to lower energy as Mn is oxidized. Whereas the Kβ emission spectrum is sensitive to oxidation state through a 3p – 3d exchange interaction, the technique of XANES spectroscopy is sensitive to oxidation state through a different mechanism: core-hole shielding effects. This is why, upon Mn oxidation, $K\beta_{1,3}$ emission spectra shift to lower energy, while XANES

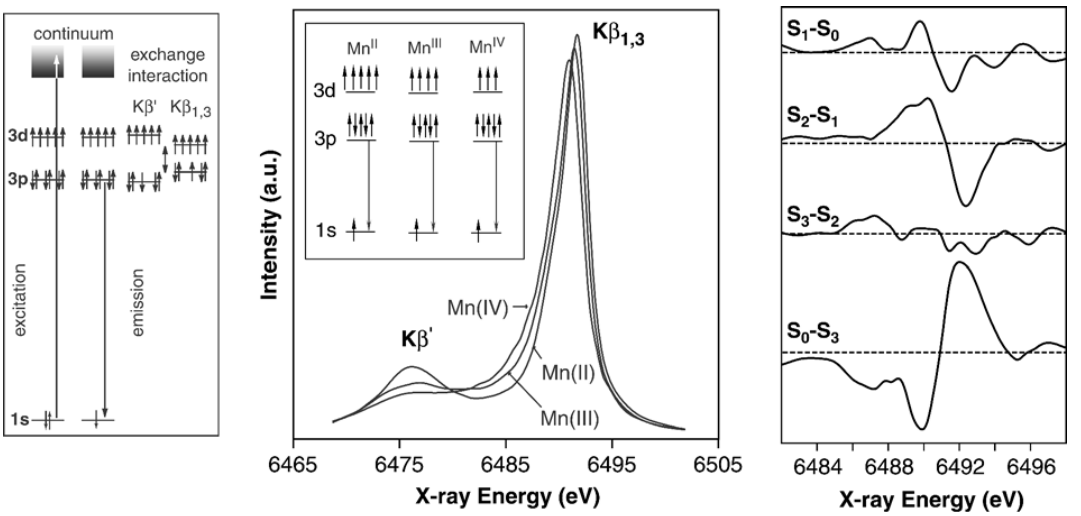

Fig. 2. Kβ spectra of Mn(II), (III) and (IV) oxides. *Left.* Energy level diagram showing the absorption (1s to continuum) and emission processes (3p to 1s) involved in Kβ Mn XES. In a simplified model, two final spin states exist with either a constructive ($K\beta_{1,3}$) or destructive (Kβ') spin exchange interaction between the unpaired 3p and 3d electrons. The magnitude of the interaction depends on the number of unpaired 3d electrons, which is related to the oxidation state of the metal. Adapted from Messinger et al. (2001) and Visser et al. (2001). *Middle.* Changes in the Kβ spectrum due to Mn oxidation. The inset shows a pictorial representation of the Kβ fluorescence transition for each of the oxides. Kβ XES arises from the emission of a 3p electron to 1s hole, which is formed following X-ray absorption. *Right.* The S_1-S_0, S_2-S_1, S_3-S_2 and S_0-S_3 difference high resolution Mn X-ray Kβ-emission spectra. The derivative shapes indicate shifts in the energy of the spectra between the S_0 and S_1, and S_1 and S_2 spectra, indicating oxidations of Mn. The S_3-S_2 difference spectra demonstrates the similarity of the spectra, suggesting that this advance does not involve a Mn centered oxidation. Adapted from Messinger et al. (2001).

spectra shift to higher energy.

Using a 1st-moment analysis, the position of the main $K\beta_{1,3}$ peak has been calculated for each S-state. Based on the shifts, or lack thereof, of the 1st moments (<E>), it was concluded that Mn is oxidized during the S_0 to S_1 and S_1 to S_2 but not oxidized during the S_2 to S_3 transition. The results (shown as difference spectra in Fig. 2, *Right*) show a shift in energy between the S_0 and S_1 state spectra and between the S_1 and S_2 state spectra and seen in the derivative-shaped difference spectra. However, there is very little change between the S_2 and S_3 states, as seen in the difference spectrum (Messinger et al., 2001).

C. Oxidation State Changes During S-State Transitions

Besides determining whether Mn is oxidized or not during the S-state transitions, both XANES and XES also allow one to assign the oxidation states of the Mn atoms. This is often done by comparison to Mn model compounds.

1. S_1 to S_2 Transition

Mn K-edge XANES spectra (Fig. 1, *Middle* and *Right*) and the $K\beta_{1,3}$ emission spectra (Fig. 2, *Right*) indicate the presence of Mn oxidation from $Mn_4(III_2,IV_2)$ to $Mn_4(III,IV_3)$ during the S_1 to S_2 transition (Roelofs et al., 1996; Messinger et al., 2001), where the S_2 state is characterized by the multiline (MLS) or the g=4.1 EPR signal (Cole et al., 1987). This conclusion is corroborated by several other spectroscopic studies (Saygin and Witt, 1987; Kretschmann et al., 1988; Styring and Rutherford, 1988; Evelo et al., 1989; Dekker, 1992; Sharp, 1992) and is also confirmed by EPR spectroscopic measurements. S_2-state EPR multiline signal simulations (Hasegawa et al., 1998; Hasegawa et al., 1999) and ^{55}Mn ENDOR spectroscopy on the S_2 state (Peloquin et al., 2000) are most consistent with the oxidation states of $Mn_4(III,IV_3)$; however, other simulations (Zheng and Dismukes, 1996) prefer oxidation states of $Mn_4(III_3,IV)$ in the S_2 state.

If the S_2 state is proposed to be either in the

$Mn_4(III,IV_3)$ or the $Mn_4(III_3,IV)$ oxidation states, then the oxidation states of Mn in the S_1 state must be either $Mn_4(III_2,IV_2)$ or $Mn_4(III_4)$, which are both one-electron reductions from the oxidation-state proposals for the S_2 state. Although the oxidation state of $Mn_4(III_4)$ for the S_1 state has been suggested by a few groups (Zheng and Dismukes, 1996; Kuzek and Pace, 2001; Chapter 12, Ahrling et al.), the XANES spectrum or its 2nd derivative of the S_1 state (Figs. 1 *Middle* and *Right*) shows that its edge shape is unlike the edge shape observed for Mn(III) complexes. When the XANES spectrum of the S_1 state, or its 2nd-derivative, is fit using Mn(III) and Mn(IV) model compounds, it cannot be fit well using only Mn(III) model compounds (Riggs et al., 1992; Yachandra et al., 1993). Furthermore, inspection of the only available set of tetranuclear Mn complexes with all O ligation, four distorted $Mn_4(III_3,IV)$ cubanes, shows XANES inflection point energy (IPE) values at ~6551 eV for these complexes (Cinco et al., 1999) consistent with the S_0-state XANES IPE of 6550.8 eV and lower than the S_1-state XANES IPE of 6552.9 eV. These results are consistent with the conclusion that the oxidation states of Mn in the S_1 state are $Mn_4(III_2,IV_2)$, not $Mn_4(III_4)$.

An oxidation-state assignment of $Mn_4(III_2,IV_2)$ is also consistent with recent Kβ XES experiments on the S_1 state. In fitting the $K\beta_{1,3}$ emission spectrum for the S_1 state, Bergmann et al. (1998) found that the best fit to the experimental data was obtained using equal amounts of the $K\beta_{1,3}$ emission spectra from Mn(III) and Mn(IV) model compounds; the fit was significantly worse if only Mn(III) or only Mn(IV) was used for the fit (Bergmann et al., 1998). It is therefore most likely that the oxidation states for Mn are $Mn_4(III_2,IV_2)$ in the S_1 state and $Mn_4(III,IV_3)$ in the S_2 state.

2. S_0 to S_1 Transition

The Mn K-edge XANES spectra for the S_0 to S_1 transition, displayed in Fig. 1, *Middle*, and the 2nd derivatives (Fig. 1, *Right*) show a clear shift of 2.1 eV (as determined by the 2nd-derivative IPE values) in the XANES edge position. In addition, the S_1/S_0 Kβ XES difference spectrum, shown in Fig. 2, *Right*, is derivative-shaped, which is indicative of Mn oxidation during this transition. Because the S_1 state has Mn oxidation states of $Mn_4(III_2,IV_2)$, as detailed above, the changes in the X-ray spectroscopic data could be due to either a Mn(II) to Mn(III) oxidation or a Mn(III) to Mn(IV) oxidation.

The finding that the S_1-S_0 XANES difference spectrum (Fig. 1, *Middle*) is somewhat different from the S_2-S_1 difference spectrum suggests that the S_0 to S_1 transition most likely reflects a Mn(II) to Mn(III) oxidation. The shape of the XANES edge is different for the S_0-state and S_1-state spectra; this is shown in part by the peak at 6548 eV in the 2nd derivative of the S_0-state XANES spectrum (Fig. 1, *Right*). This is suggestive of the presence of Mn(II), based on comparison to the 2nd derivatives of Mn(II)-containing model compounds. The significantly larger shift in the 2nd-derivative IPE values for the S_0 to S_1 transition compared to the S_1 to S_2 transition is also indicative for a Mn(II) to Mn(III) oxidation. This is based on the finding that, for homologous sets of model compounds, the shifts in the IPE value for Mn(II) to Mn(III) oxidations are usually larger than those seen for Mn(III) to Mn(IV) oxidations.

Other spectroscopic studies (Saygin and Witt, 1987; Kretschmann et al., 1988; Styring and Rutherford, 1988; Evelo et al., 1989; Guiles et al., 1990a; Dekker, 1992; Sharp, 1992; Messinger et al., 1997a,b; Åhrling et al., 1998) concur that Mn oxidation occurs during the S_0 to S_1 transition. The greater spectral width of the S_0-state EPR multiline signal compared to the S_2-state EPR multiline signal has been attributed to the presence of Mn(II) in the S_0 state (Messinger et al., 1997a,b; Åhrling et al., 1998), which suggests a Mn(II) to Mn(III) oxidation for the S_0 to S_1 transition. The presence of Mn(II) in the S_0 state may also explain why Y_D^{ox} can oxidize the S_0 state to the S_1 state, but not the S_1 state to the S_2 state.

The Kβ XES and XANES difference spectra, in addition to other spectroscopic data are consistent with the assignment of the S_0 to S_1 transition as a Mn(II) to Mn(III) oxidation. Therefore, the oxidation states of Mn in the S_0 state are proposed to be $Mn_4(II,III,IV_2)$, which change upon Mn oxidation to $Mn_4(III_2,IV_2)$ in the S_1 state, although the oxidation states of $Mn_4(III_3,IV)$ for the S_0 state cannot be unequivocally excluded.

3. S_2 to S_3 Transition

The most controversial S-state transition has been the S_2 to S_3 transition. Most debate has focused on whether this transition is a Mn-centered (Ono et al., 1992; Iuzzolino et al., 1998) or ligand-centered (Guiles et al., 1990b; Roelofs et al., 1996; Messinger et al., 2001) oxidation. In addition, a redox isomerism

between Mn and ligands has been proposed for the S_3 state (Renger, 1997). If Mn were to be oxidized during the S_2 to S_3 transition, the oxidation would have to be a Mn(III) to Mn(IV) transition. A Mn(IV) to Mn(V) transition is unlikely to occur with Mn(III) still present in the complex given the proposed reactivity of the Mn(V) ion. Moreover, Mn(V) has a very distinctive Mn XANES spectrum that has not been observed in PS II preparations (V. Yachandra, unpublished). Thus, it would be expected that the XANES and Kβ XES difference spectra, as well as the observed shifts in the XANES IPE values and the Kβ emission spectra 1st-moment values, <E>, would be essentially identical to the S_1 to S_2 transition, where a Mn(III) to Mn(IV) oxidation also occurs. However, as described below, the spectroscopic results for the S_2 to S_3 transition are completely different from those of the S_1 to S_2 transition.

The XANES results from Fig. 1 provide strong support for a ligand-based oxidation of the OEC occurring during the S_2 to S_3 transition, based on the small (0.3 eV) shift in the XANES 2nd-derivative IPE values. The fact that the S_3-S_2 XANES difference spectrum is significantly different from the S_2-S_1 difference spectrum (Fig. 1, *Middle*) is inconsistent with a Mn(III) to Mn(IV) oxidation occurring during the S_2 to S_3 transition. Instead, the S_3-S_2 XANES difference spectrum shows how the shape of the XANES edge changes between the S_2 and S_3 states, which is consistent with a ligand-based oxidation.

Therefore, based on the XANES data, it is reasonable to suggest that, a ligand radical is formed in the S_3 state in lieu of Mn oxidation; this will be denoted by $Mn_4(III,IV_3)^{\cdot}$. This interpretation is reinforced by the Kβ emission spectra and especially, the Kβ XES difference spectra from Fig. 2, *Right*. The difference spectra show that the derivative-shaped difference spectrum that is expected if Mn is oxidized, as in the S_0 to S_1 and S_1 to S_2 transitions, is absent in the S_2 to S_3 transition. In addition, the <E> value of 6490.157 eV for the S_3 state argues against Mn oxidation during the S_2 to S_3 transition, because it is inconsistent with a $Mn_4(IV_4)$ oxidation state, which is required for the S_3 state if Mn is oxidized during the S_2 to S_3 transition. Comparison of the S_3-state <E> value to the <E> values from 18 different monomeric, dimeric, trimeric, and tetrameric Mn(IV) model compounds with different ligands, including Cl^-, shows that the S_3-state <E> value is higher than the <E> value for any of the Mn(IV) compounds studied. It is difficult to explain this result unless Mn(III) is still present in the S_3 state, which means that, based on the $Mn_4(III,IV_3)$ redox states derived for the S_2 state, a Mn-based oxidation cannot occur during the S_2 to S_3 transition. The EXAFS studies from the S_2 state described below also support this assignment.

D. Summary of Oxidation State Assignments

The Mn K-edge energy and shape do not depend solely on the oxidation state of the Mn atoms, but also on the ligand environment. This is caused by mixing of the ligand and the Mn atomic orbitals. It is possible that a change in structure and ligand environment will influence the main-edge energy and shape. Therefore, care must be exercised when correlating the Mn K-edge energies to Mn oxidation states without taking into account the nature of the ligand environment. This is especially a problem when sets of compounds with different ligand structures, different nuclearities, and different analysis methods to determine edge positions are used to infer oxidation-state information about biological systems, such as in Kuzek and Pace (2001) and Carrell et al. (2002). However, numerous studies have shown that there is a clear correlation between Mn oxidation state and Mn K-edge energy if the ligand environment stays the same, i.e. the IPE shifts to a higher energy upon oxidation within sets of homologous compounds.

A detailed XANES and XES study by Visser et al. (2001) of homologous di-μ-oxo and mono-μ-oxo bridged binuclear compounds in different oxidation states shows that in contrast to Mn K-edge XANES, Kβ XES spectra show much less dependence on ligand environment. The shifts in XES spectra are the same for a Mn(III) to Mn(IV) oxidation, irrespective of whether the Mn is part of a di- or mono-μ-oxo bridged structure (Visser et al., 2001). We have also completed a XES study of homologous sets of tri- and tetranuclear Mn compounds in different oxidation states and we have found that the XES spectra are much less dependent on the ligation or structure and are primarily dependent on the oxidation state of Mn (V. Yachandra, unpublished).

Considering both the limitations and strengths of the two methods of XANES and XES, by comparison with numerous Mn models and the knowledge from EXAFS data (see below), we have proposed the oxidation states shown in Fig. 3. Figure 3 summarizes the Kβ XES and XANES flash patterns from our most recent and in our opinion the most comprehensive study that leads to the conclusions about Mn oxidation

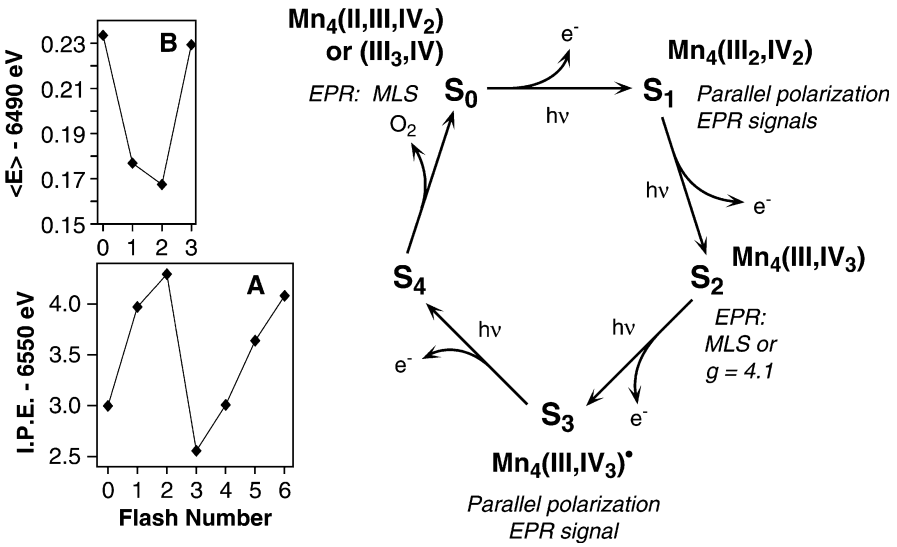

Fig. 3. Left. (A) Inflection-point energy (IPE) in eV of the Mn K-edge of PS II membranes as a function of the number of applied flashes. (B) The first moments of the Mn Kβ emission spectra (<E>) as a function of flash number. The Mn K-edge shifts to higher energy as Mn is oxidized. The first moment of the Mn Kβ fluorescence shifts to lower energy as Mn is oxidized. The complementary and mutually reinforcing results provide a strong case for Mn oxidation during the S_0 to S_1 and S_1 to S_2 advances but no Mn-centered oxidation at the S_2 to S_3 advance. *Right*. The S-state scheme for O_2 evolution and the oxidation states that are consistent with the EPR signals and the X-ray absorption and emission spectroscopy results. Adapted from Messinger et al. (2001).

states. Both spectroscopies show a clear shift in the spectra to higher energy for XANES spectroscopy and lower energy for Kβ XES between the samples given 0 and 1 flashes indicating the presence of Mn oxidation during the S_1 to S_2 transition. The small change between samples given 1 and 2 flashes in both spectroscopies provides strong support for the S_2 to S_3 transition proceeding without a Mn-based oxidation. On the next transition, $S_3 \rightarrow [S_4] \rightarrow S_0$, O_2 is released, shifting the position of the spectra of samples given 3 flashes to lower energy for XANES spectroscopy and higher energy for Kβ XES. These flash patterns are explained by the proposed oxidation states of the Mn cluster in the S_0, S_1, S_2, and S_3 states, as shown. These oxidation states are: S_0: $Mn_4(II,III,IV_2)$ or $Mn_4(III_3,IV)$, S_1: $Mn_4(III_2,IV_2)$, S_2: $Mn_4(III,IV_3)$, S_3: $Mn_4(III,IV_3)^{\bullet}$, where the superscript dot represents an oxidation that is not Mn centered.

III. Structure of the Manganese Cluster

Extended X-ray absorption fine structure (EXAFS) spectra at the Mn K-edge results from the modulation of the absorption cross section by the constructive and destructive interference of the 1s photoelectron wave with that backscattered from neighboring atoms (Sayers et al., 1971). The EXAFS modulations can be theoretically modeled to derive exquisitely detailed information about the distance from Mn to neighboring atoms to ~4 Å, often to an accuracy as precise as 0.015 Å (Yachandra, 1995). However, determination of the number of such interactions is susceptible to many uncertainties and can often be as large as 25%. The EXAFS approach has been used to determine the distances from Mn and identify the backscattering atoms of the Mn cluster present in the OEC. It is not possible to distinguish between O or N. But it is often facile to distinguish between light atoms such as N, or O, which are potential ligand atoms and backscattering from a heavier atom such as Mn or Ca that would only be present in a multi- or hetero-nuclear Mn complex. To interpret the results in terms of the coordination environment of the Mn, it has been necessary to examine a number of inorganic complexes of known structure, generously provided to us by our collaborators (Guiles et al., 1990a; DeRose et al., 1994; Cinco et al., 1999). The EXAFS

spectrum is usually presented as a Fourier transform (FT), which is similar to a radial distribution function with each Fourier peak representing shells of neighboring atoms from the absorbing atom. Dichroism resulting from oriented membranes can be used to derive information about the vectorial direction of the particular interaction. A typical Fourier transform from an S_1 state is shown in Fig. 4, *Top* (Yachandra et al., 1993; DeRose et al., 1994) and from oriented PS II membranes in the S_1 state in Fig 4, *Bottom* (Mukerji et al., 1994). Three distinct Fourier peaks are resolved in Fig. 4, *Top*, and dichroism is evident in all of the peaks in Fig. 4, *Bottom*.

On the basis of the latest findings, we conclude that each Mn is surrounded by a first coordination shell of O or N atoms at ~1.8 to ~2.1 Å (Fourier peak I), a set of Mn atoms at ~2.7 Å (Fourier peak II) and additional Mn and Ca at ~3.3 Å (Fourier peak III). Using model-compound data, it was straightforward to assign the two or three 2.7 to 2.8 Å Mn-Mn vectors to di-μ-oxo or hydroxo bridges between pairs of Mn atoms and the 3.3 Å Mn-Mn vector to one or two mono-μ-oxo bridged or similar longer interactions (Kirby et al., 1981; Yachandra et al., 1986, 1987; McDermott et al., 1988; George et al., 1989; Penner-Hahn et al., 1990; MacLachlan et al., 1992; DeRose et al., 1994; Mukerji et al., 1994; Kusunoki et al., 1995; Robblee et al., 2001). Furthermore, studies using Sr to replace Ca and, subsequently, direct measurements using Ca EXAFS, show unambiguously the presence of one or two 3.4 Å Mn-Ca vectors where the bridging motif could also be mono-μ-carboxylato or mono-μ-hydroxo (see below). The use of vector terminology to describe these interatomic interactions is particularly appropriate because of the direction information available from dichroism measurements on oriented samples. Furthermore, analysis of the EXAFS leads to the conclusion that the di- or mono-μ-oxo bridged Mn and Ca vectors are not co-linear; that is any three metal atoms in the cluster cannot be linear.

On the basis of such data many topological tetranuclear Mn structures (**A** through **K**) compatible with the observed EXAFS data have been presented (DeRose et al., 1994) (Fig. 5). These models have been described in detail (DeRose et al., 1994; Robblee et al., 2001). However, until recently only one of those options, **A**, was widely used as a working model, although options **E**, **F** and **G** (the nomenclature was initially introduced in DeRose et al. (1994)) have been shown to be preferred on the basis of EPR and ENDOR simulations (Hasegawa et al., 1999; Peloquin and Britt, 2001). Some of the structures, **A** through **K**, are less likely. Structure **C** and variations consisting of two isolated di-μ-oxo Mn–Mn moieties are preferred by Pace and co-workers based on their EPR simulations (Smith and Pace, 1996) but **C** is not widely accepted on the basis of EPR simulations by other groups (Boussac and Rutherford, 2000; Britt et al., 2000; Peloquin et al., 2000) or EXAFS data (Latimer et al., 1998). It is also physically impossible

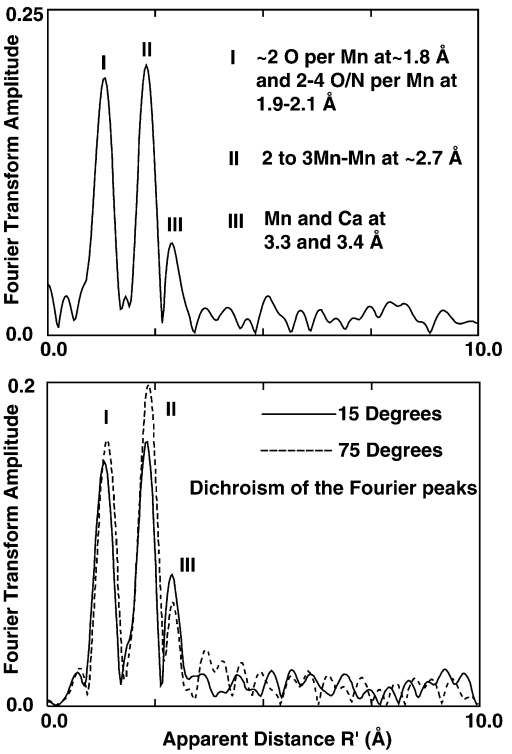

Fig. 4. Typical Fourier transform of the EXAFS spectrum from a S_1 state sample from an isotropic sample (*Top*) and oriented sample (*Bottom*). The three main Fourier peaks labeled I, II and III are assigned to ~ 2 O ligand atoms per Mn at 1.8 Å and 2-4 N/O ligand atoms per Mn at 1.9–2.1 Å (Fourier peak I), 2-3 Mn-Mn interactions at ~2.7 Å (Fourier peak II), and Mn and Ca at 3.3 and 3.4 Å (Fourier peak III), respectively. The dichroism of the Fourier peaks I, II and III is clear and can be used to determine the orientation of the vectors in the PS II membrane. Fourier peak II, that has been assigned to Mn-Mn interactions at ~2.7 Å, is maximal when the e-vector of the X-rays is parallel to the membrane plane (the angle on the figure is between the membrane normal and the X-ray e-vector.). Adapted from Yachandra et al. (1993), DeRose et al. (1994) and Mukerji et al. (1994).

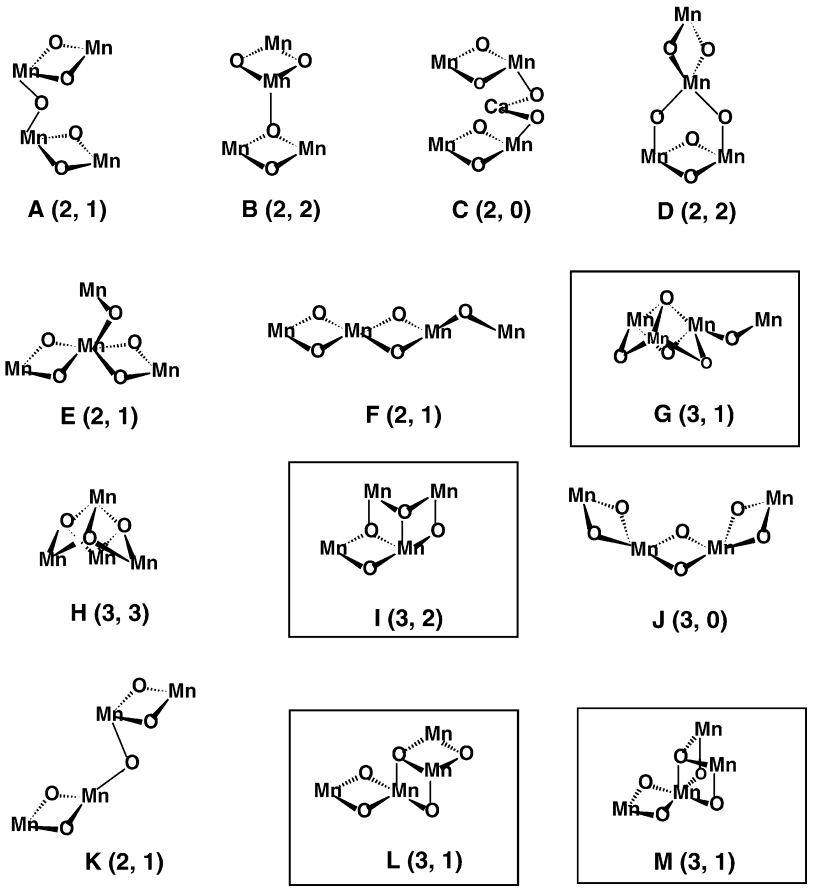

Fig. 5. Topological models for the Mn complex identified as compatible with the EXAFS data by DeRose et al. (1994) and Robblee at al. (2002). The numbers in parenthesis are the number of short 2.7 to 2.8 Å Mn-Mn vectors and long 3.3 to 3.4 Å Mn-Mn vectors. The options **G**, **I**, **L** and **M** all have 3 short 2.7 to 2.8 Å Mn-Mn vectors and are in better agreement with the X-ray diffraction studies; options **E**, **F** and **G** have been identified as compatible with EPR and ENDOR data. Option **G** or a topological isomer seems to be the best model by all presently available criteria; X-ray diffraction, EXAFS and EPR.

with four Mn atoms to obtain three Mn–Mn distances (see below) at 2.7 – 2.85 Å with two separated di-μ-oxo Mn–Mn moieties. Structure **H**, with three 3.3 Å Mn–Mn distances is unlikely, as shown by the EXAFS spectra from a similar set of complexes – a series of distorted cubanes (Cinco et al., 1999). The more likely candidates were considered to be **A**, **E**, **F**, **G** or **K** on the basis of EXAFS and EPR data; only **G** contained three Mn-Mn distances at ~2.7 Å, while the others had two such interactions.

A. Heterogeneity in the Mn-Mn Distances and Structural Implications

As mentioned above determining the number of Mn-backscattering atoms can be difficult. The number of the Mn-Mn 2.7 and 3.3 Å vectors (shown in parenthesis in Fig. 5) are especially important in this endeavor as these data directly lead or preclude certain arrangements of the Mn atoms that comprise the Mn cluster. The distance of the Mn-Mn vectors (at ~2.7 and 3.3 Å) is particularly important because it is easily the most reliably determinable parameter from the Mn EXAFS spectra of PS II. It is informative to focus on

Table 1. Curve-fitting results for Fourier peak at ~2.7 Å that is characteristic of oxo-bridged Mn moieties from the S-states

S-state	References	R_1 (Å)	R_2 (Å)	N_1	N_2	N_1:N_2
S_0^* state	Table III from Guiles et al. (1990a)	2.69	2.87	1.0	0.5	2:1
S_2 (g = 4.1) state	Table 4B from Liang et al. (1994)	2.72	2.85	0.76	0.44	1.7:1
NH_3-inhibited S_2 state	Table 1 from Dau et al. (1995)	2.71	2.86	0.75	0.5	1.5:1
F^--inhibited S_2 state	Table 2 from DeRose et al. (1995)	2.71	2.85	0.8	0.4	2:1
S_3 state	Table 1B from Liang et al. (2000)	2.82	2.95	0.7	0.4	1.8:1
S_0 state	Table 3 from Robblee et al. (2002)	2.72	2.86	1.05	0.46	2.3:1
S_0 state	Table 4 from Robblee et al. (2002)	2.72	2.85	1.02	0.51	2:1

N_1 and N_2 are the number of Mn-Mn interactions, normalized to one Mn in the Mn_4 complex, at the two distances R_1 and R_2, respectively. An N of 1 translates to two Mn-Mn distances and a N of 0.5 translates to 1 Mn-Mn distance at the corresponding distance. The N_1:N_2 ratio of 2:1 in the ~2.7 and ~2.8 Å Mn-Mn distances shows there are a total of 3 such short Mn-Mn distances in the OEC.

the ~2.7 Å Mn-Mn distance. When only one Mn-Mn 2.7 Å distance can be derived from the data as in the case of the S_1 and S_2 states, then one is constrained by the uncertainty in the number of such interactions that is inherent to the EXAFS methodology; it is at present two or three such Mn-Mn interactions. However, when the distance degeneracy is lifted and there are two resolvable 2.7 or 2.8 Å Mn-Mn distances then one can determine the number of such vectors to a much higher accuracy because one can only have an integral number of each of such interactions.

Interestingly, when we examined states that exhibited such heterogeneity in the 2.7 Å Mn-Mn distances, it became quite clear that there was distinct preference for the existence of three such Mn-Mn vectors as described below (summarized in Table 1). Figure 6, *Left* shows the Fourier transforms (FT) of the k^3-weighted EXAFS data from the S_0 and S_1 states. The Fourier peak II was isolated and fit to the EXAFS equation with one or two distances for the S_0 and S_1 states. Figure 6, *Right* shows the best fits to two Mn-Mn distances for the S_0 state as a function of the number of each of the Mn-Mn interactions. The contour plot graphically illustrates that the global minimum at two Mn-Mn interactions at ~2.7 Å and one Mn-Mn interaction at ~2.85 Å is very well defined (Robblee et al., 2002).

We have re-examined the data from the S_0* (S_0 state induced by NH_2OH incubation), the g=4.1 S_2, the NH_3- or F^-inhibited S_2, and the S_3 states, where we have shown that there is distance heterogeneity in the Mn-Mn vectors. The results of this re-examination are given in Table 1, which show that none of the S-states that exhibit distance heterogeneity are best fit by an equal N value for both Mn–Mn shells; the fit results from these S-states are in fact more consistent with a 2:1 N_1:N_2 ratio, where N_1 corresponds to the shorter distance. In each case, the ratio of the number of the two Mn-Mn interactions was ~2:1. This leads us to think that there may be three Mn interactions at ~2.7 Å in the Mn cluster in its native state, one of which is perturbed in the S_0, F^-- and NH_3-inhibited S_2 and the g=4.1 S_2 states, and all three are perturbed in the S_3 state.

On the basis of these re-evaluations of the results from the S_0 state and earlier data, it is important to consider the options that include three di-μ-oxo bridged moieties in the Mn cluster. Figure 5 shows several such options, **G**, **I**, and **J**, that were proposed earlier, and two newer options, **L** and **M**, among several others that can be conceived. Options **J** and **I** are less likely structures because **J** lacks a Mn-Mn interaction at 3.3 Å, and **I** has two such interactions. The EXAFS data from an inorganic compound (Auger et al., 1990) with the motif in option **J** is very different from that obtained from a PS II sample (V. Yachandra, unpublished). Options **G**, **L** and **M** all have three di-μ-oxo bridges and one mono-μ-oxo bridge; that is three 2.7 Å and one 3.3 Å Mn-Mn interactions. Options **L** and **M** are also similar to the structure proposed on the basis of density functional theory calculations although Ca is not included in **L**

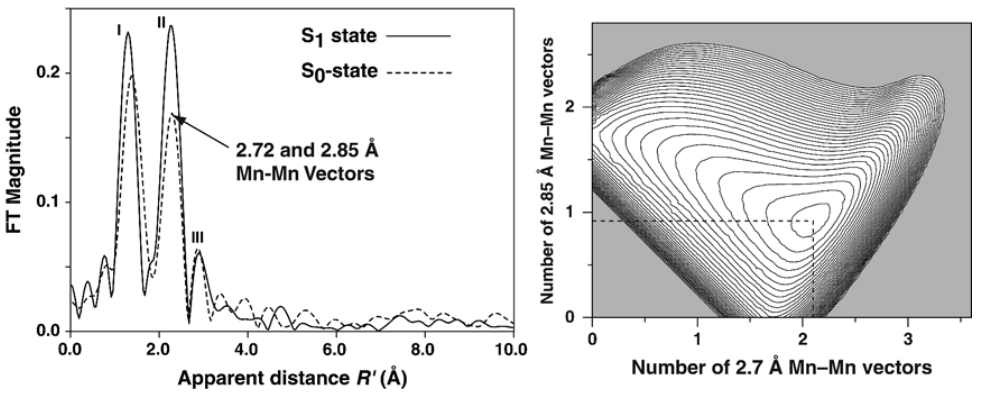

Fig. 6. Left. Fourier transforms of the S_0 (dashed line) and S_1 state (solid line) of the Mn-EXAFS spectra. The main Fourier peaks are labeled I, II and III. There are clear differences in amplitude and position of these peaks between the S_0 and S_1 states. The peak labeled II is from Mn-Mn interactions at ~2.7 Å, and in the S_0 state this vector is best fit to two distances at 2.72 and 2.85 Å. *Right.* The contour plot shows the fit-quality-parameter ε^2 for the S_0 state plotted versus the number of the two Mn-Mn interactions. The dashed lines shows the distinct minimum at one Mn-Mn vector at 2.85 Å and two Mn-Mn vectors at 2.7 Å. Adapted from (Robblee et al., 2002).

and **M** and is an integral part of the Siegbahn model (Siegbahn, 2000).

In addition to the constraints imposed by considering the EXAFS and EPR data, a preliminary structure of the OEC has been recently reported based on X-ray crystallographic data from PS II (Zouni et al., 2001; Kamiya and Shen, 2003; Ferreira et al., 2004; Chapters 19–21) and a further criterion for narrowing the choice of favored cluster geometries comes from these X-ray crystallography data of PS II. These data are most consistent with an OEC that is asymmetric and shaped somewhat like a 'Y'. The arrangement of the Mn atoms has been described as pear-shaped (an elongated ellipsoid) with all four Mn lying approximately in the same plane. Presently, **G**, **L** and **M** are qualitatively in agreement with the asymmetry seen in the electron density of the Mn cluster (Zouni et al., 2001) and should be considered as possibilities for a topological model of the OEC based on the insights developed from the EXAFS spectroscopy results, with option **G** being the best in terms of being compatible with the most criteria; electron density, EPR, and EXAFS. However, as confirmed by Mn and Sr EXAFS studies (Latimer et al., 1995; Cinco et al., 1998) the OEC is most accurately described as a Mn/Ca heteronuclear cluster; therefore, Ca should be incorporated into each of the proposed structures so that 1–2 Mn–Ca vectors exist which are oriented close to the membrane normal (Ferreira et al., 2004; Chapter 21).

B. S-State Transitions and Structural Changes

Although EXAFS studies may not be able to uniquely identify the structure of the Mn complex, they are invaluable in understanding the changes in structure, if any, that might be occurring during the S-state transitions. As noted above, EXAFS is exquisitely sensitive to distances of neighboring atoms from Mn and hence can provide an unique window into how the Mn cluster changes as it proceeds through the catalytic cycle, as summarized in Fig. 7. These changes in structure provide a rationale for testing various mechanisms that have been proposed as described below.

1. S_1 to S_2 (MLS) Transition

EXAFS studies of the S_1 state and the S_2 state characterized by the multiline EPR signal revealed that the Mn–Mn distances are essentially the same: ~2.7 Å and 3.3 Å in both states. This distance is consistent with those found in numerous studies of di- and mono-μ-oxo-bridged and Mn_2(III,IV) and Mn_2(IV,IV) complexes. Oxidation of a mono- or di-μ-oxo bridged Mn motif from (III,III) to (III,IV) or from (III,IV) to (IV,IV) has minimal effect on the Mn-Mn separation in many inorganic models (Wieghardt, 1989; Pecoraro, 1992; Pecoraro and Hsieh, 2000).

Interestingly, EXAFS studies on oriented PS II in the S_1 and S_2 states show that there maybe heterogeneity in the 2.7 Å vector, a contention that is supported

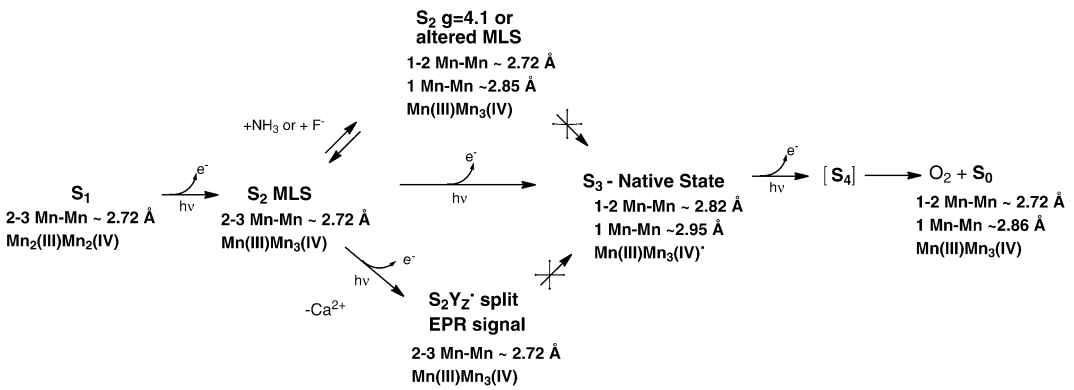

Fig. 7. Summary of the changes in oxidation states and Mn–Mn distances at 2.7 to 3.0 Å in the native S_1, native S_2, modified S_2, S_3' ($S_2Y_Z^{\bullet}$), native S_3 and S_0 states of PS II as determined by Mn EXAFS.

by related studies on modified S_2 states. This Mn-Mn vector has been determined to be at an average angle of ~60° to the membrane normal (Mukerji et al., 1994; Dau et al., 1995).

2. S_1 to S_2 (g=4.1) Transition

The inequivalence of the di-μ-oxo bridged Mn units becomes more evident in the S_2 state that is prepared by illumination at 130 K and characterized by the *g*=4.1 EPR signal (Liang et al., 1994). Similar results were obtained with NH_3-treated and annealed S_2 state samples (Dau et al., 1995) and in F^--treated samples (DeRose et al., 1995). The scheme in Fig. 7 shows that there are paths from the MLS S_2 state that lead to two states: the S_2-*g*=4.1 state inhibited by NH_3/F^- or the $S_2Y_Z^{\bullet}$ states; neither of these states can proceed to the physiologically relevant S_3 state. These states are depicted in Fig. 7 as branching away from the normal pathway leading to the S_3 state by photon absorption. However, the S_2-*g*=4.1 state generated by 820 nm illumination at 130 K (Boussac et al., 1996) can proceed to an S_3 state (Zimmermann and Rutherford, 1986). In the modified S_2 states, one of the Mn-Mn distances increases to ~2.85 Å, whereas there is very little change in the other one or two 2.7 Å or the 3.3 Å Mn-Mn distance. With the degeneracy of the 2.7 Å lifted, it has been possible by studying the dichroism of the Fourier peak, to assign the relative orientation of the 2.7 and 2.85 Å vectors (Dau et al., 1995), which are oriented at 55° and 67° respectively to the membrane normal.

The NH_3-treated and F^--treated samples cannot advance beyond the modified S_2 state ($S_2Y_Z^{\bullet}$ state). It is likely that F^- or NH_3 prevent the oxidation of a ligand atom, thereby blocking structural changes from occurring that are necessary for the formation of the S_3 state, and thus inhibiting O_2 evolution activity. In the case of NH_3, it is probably due to an amido-group (NH_2^-) replacement of the oxo-bridge involved in oxidation. The modification of the MLS spectra upon addition of NH_3 (Beck et al., 1986) and ESEEM studies using $^{14}NH_3$ and $^{15}NH_3$ demonstrated that NH_3 becomes a ligand of Mn (Britt et al., 1989). The asymmetry parameter derived from ESEEM results suggested that the amido group is likely to be a bridging ligand (Britt et al., 1989). It is probable that the oxo-bridge that is displaced by NH_3 is oxidized during the S_2 to S_3 transition (see next section).

3. S_2 to S_3 Transition

Earlier XAS data from the S_3 state samples produced by a cryogenic double-turnover method indicated increased disorder in the peak at 2.7 Å; that a structural change that involved the lengthening of the Mn-Mn distance was occurring between the S_2 and S_3 states and was absent during the S_1 to S_2 state transition (Guiles et al., 1990b). More recent detailed analysis of data from native S_3 state samples created under physiological conditions with saturating actinic flash illumination show there is a significant change in the 2.7 Å Mn-Mn distances that characterize the di-μ-oxo bridged Mn-Mn; with an increase in the short Mn-Mn distances from 2.7 Å to ~2.8 and ~3.0 Å (Liang et al., 2000).

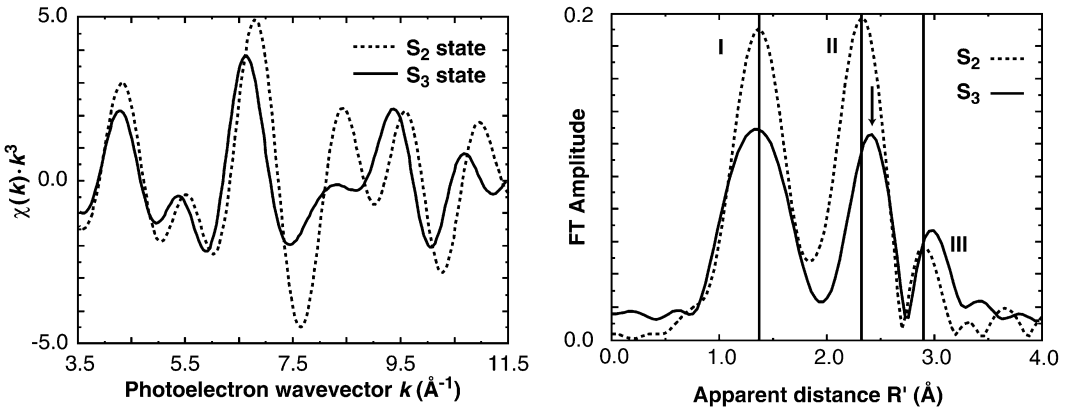

Fig. 8. Left. Fourier-filtered *k*-space EXAFS data from S_2 (dashed line) and S_3 (solid line) state of PS II samples. The differences in phase, frequency and amplitudes between the raw S_2 and S_3 state EXAFS spectra are very obvious in these spectra. *Right.* Fourier transform power spectra of S_2 (dashed line) and S_3 (solid line) states of PS II. The major Fourier peaks are labeled I, II and III. The spectra are clearly different between the S_2 and S_3 states. There is a reduction in amplitude in all three peaks in the S_3 state compared to the S_2 state. More importantly, peaks II and III are at a greater apparent distance R' for the S_3 state compared to the S_2 state as shown.

The perturbation in the Mn-Mn distances is different from that observed in the modified S_2 states. Each of the altered S_2 states gives a fit that is consistent with the alteration of one of the Mn-Mn distances from ~2.72 to 2.85 Å. Unlike the modified S_2 states, the position of Fourier peak II from the native S_3 state clearly shifts to a longer distance in the FTs (Fig. 8) with one or two Mn-Mn distances of 2.82 Å and one Mn-Mn distance of 2.95 Å (Liang et al., 2000). These results underscore the point that during the S_2 to S_3 transition under physiological conditions, *all* of the di-μ-oxo-bridged Mn-Mn units undergo structural changes that lead to an increase in the Mn-Mn distances. A change in the Mn-Mn distance from 2.7 to 3.0 Å was also observed in samples that had been depleted of Ca by NaCl treatment (MacLachlan et al., 1994). The best fits for the Mn-O/N shell shorter Mn-O distance is characteristic of Mn-O bridging distances and it increases from 1.80 Å in the S_2 state to 1.86 Å in the S_3 state. This is a significant change, and it provides additional evidence for the involvement of the bridging oxygen atoms during the S_2 to S_3 transition.

The results from isotropic S_3 samples are supported by polarized EXAFS studies on oriented PS II in the native S_3 state. The data confirm that the two Mn-Mn vectors units are not equivalent. The polarized EXAFS data are different from those observed in the S_2 state (Mukerji et al., 1994; Dau et al., 1995). Fourier peak II of S_3 is dichroic and is readily resolved to Mn-Mn distances of ~2.8 Å and ~3.0 Å, each with its own distinct projection on the membrane normal (Fernandez et al., 1998). Schiller et al. (1998) have reported results on the oriented S_3 state, showing an increase in the amplitude of Fourier peak II that is interpreted as an increase in the number of 2.7 Å Mn-Mn interactions in the S_3 state. However, a closer examination of their FTs indicates that Fourier peak II occurs at a longer distance and is broader compared to that in the S_2 state.

In the S_3 state it is seen that Fourier peak III at ~3.3 Å occurs at a greater apparent distance than that of the S_2 state indicating a lengthening of the two Mn-Mn distances or the Mn-Mn and Mn-Ca distances compared to the S_2 state by 0.04-0.2 Å.

Significant changes are observed in the Mn-Mn distances in the S_3 state compared to the S_1 and the S_2 states (Fig. 8). These changes in Mn-Mn distances are interpreted as consequences of the onset of substrate water oxidation in the S_3 state. Mn-centered oxidation is evident during the S_0 to S_1 and S_1 to S_2 transitions. During the S_2 to S_3 transition, we propose that the changes in Mn-Mn distances are the result of ligand or water oxidation, leading to the formation of an oxyl radical intermediate formed at a bridging or terminal position. The reaction of the oxyl radical with OH^-, H_2O, or an oxo group during the subsequent S-state conversion is proposed to lead to the formation of the O-O bond (Chapter 25).

4. S_2 to S_3' ($S_2Y_Z^{\bullet}$) Transition

The other unproductive state generated from the S_2-MLS state is denoted in Fig. 7 as the S_3' state or $S_2Y_Z^{\bullet}$ state generated in Ca-depleted samples. The Ca-depleted samples are inactive in O_2 evolution, while a broad $g = 2$ EPR signal has been observed in such samples. The $g = 2$ broadened EPR signal has been confirmed to arise from the tyrosine Y_Z radical (Gilchrist et al., 1995; Peloquin et al., 1998) and it is proposed that the signal is broadened by interaction with the spin on the Mn cluster (Lakshmi et al., 1998).

EXAFS analysis from Ca-depleted S_3' state samples ($S_2Y_Z^{\bullet}$) (Latimer et al., 1998) shows that Fourier peak II (Mn-Mn distance of ~2.7 Å) in the FT of S_3' state samples ($S_2Y_Z^{\bullet}$) was invariant relative to that of the native S_2 state sample. The EXAFS fits showed that the ~2.7 Å Mn-Mn distances did not lengthen as observed in the native S_3 state samples and are essentially unchanged from those of the native S_2 state. This finding is surprising because the Mn K-edges from these Ca-depleted samples showed a behavior similar to the native PS II in that little or no shift was observed in the S_2' to S_3' (or $S_2Y_Z^{\bullet}$) transition. This difference between the native S_3 and Ca-depleted S_3' states indicate that the core di-μ-oxo-bridged structure is probably dissimilar in the native S_3 and the S_3' ($S_2Y_Z^{\bullet}$) states, with the structure in the $S_2Y_Z^{\bullet}$ state resembling the native S_2 state structure. It is intriguing how the transfer of one electron from the Mn cluster onto Y_Z result in major changes in the Mn-Mn distances as is observed in the native S_3 state. The roles of the Y_Z and the Mn cluster in the process of water oxidation are clearly delineated by the comparison of the S_3 and the S_3' (or $S_2Y_Z^{\bullet}$) states. Instead of the Mn cluster just providing a scaffolding for water oxidation, this comparison shows that the structural change in the Mn cluster initiated by the transfer of an electron from the Mn cluster to Y_z during the S_2 to S_3 transition might provide the trigger to the chemistry of the formation of the O-O bond, via the formation of a ligand radical. The results show that the Mn cluster is involved in a much more intimate manner in the catalysis than just providing the framework. The implications to the mechanism are significant (Chapter 25).

In Ca-depleted systems the tyrosine Y_Z radical is stabilized and the oxidation of the Mn-OEC and the concomitant changes in Mn-Mn distances are prevented. In the S_3 state, with Ca present, the oxidation equivalent resides on the Mn cluster leading to profound changes in the Mn-Mn distances. Thus, Ca is proposed to play a crucial role in controlling the redox potential and thus the course of the mechanism of water oxidation.

5. S_0 to S_1 Transition

Early EXAFS experiments by Guiles et al. (1990a) with the S_0 state used chemical treatments to get around the problem of low concentrations. However, the S_0 state generated in this manner was designated as S_0^* to emphasize that it is generated through chemical treatment and is thus not a native S-state. Although hampered by a low signal-to-noise ratio and the uncertainty about the relationship between the chemically generated S_0^* state and the native S_0 state, those experiments provided the first evidence from EXAFS that heterogeneity may exist in the 2.7 Å Mn–Mn distances in the S_0 state in the form of a reduced amplitude of Fourier peak II in the S_0^* state relative to that in the S_1 state.

Riggs-Gelasco et al. (1996a) examined reduced S states of the OEC generated by treatment with NH_2OH or hydroquinone and observed a decrease in the amplitude of the 2.7 Å Mn–Mn Fourier peak. This was interpreted as a reduction in the number of Mn–Mn vectors instead of the appearance of distance heterogeneity.

Recent EXAFS experiments by Robblee et al. (2002) show that, in the S_0 state, heterogeneity most likely exists in the 2.7 Å Mn–Mn distances with one or two Mn-Mn distances at 2.72 Å and one Mn-Mn distance at 2.85Å (as described above, see Fig. 6), which can be explained through the protonation of a di-μ-oxo-bridged Mn–Mn moiety and/or the presence of Mn(II) (Chapter 25). The presence of distance heterogeneity in the S_0 state has been exploited in the curve-fitting procedure, whose results are suggestive of the possibility that three di-μ-oxo-bridged Mn–Mn moieties may exist in the OEC instead of the two di-μ-oxo-bridged Mn–Mn moieties that are widely used in proposed structural models for the OEC (see above).

IV. Structural Role of the Calcium Cofactor

Along with Mn and Cl^-, Ca is an essential cofactor in O_2 evolution (Debus, 1992; Chapter 13, van Gorkom and Yocum). Depleting this cofactor suppresses

OEC activity, which can be restored (up to 90%) by replenishing with Ca^{2+}. Partial reactivation (up to 40%) results from addition of Sr^{2+} to Ca-depleted PS II membranes (Ghanotakis et al., 1984; Boussac and Rutherford, 1988b) and no other metal ions can restore activity, making this requirement highly specific for Ca or Sr (Ghanotakis et al., 1985; Ono and Inoue, 1989).

Although Sr^{2+} replenishes the Ca-depleted centers to a similar extent as added Ca^{2+}, the slower kinetics of the OEC turnover yields an overall lower steady-state rate (Boussac and Rutherford, 1988a) (40%) at saturating light intensities. Substitution of Ca with Sr also alters the EPR multiline signal (MLS) from the S_2 state, giving narrower hyperfine splitting and different intensity patterns (Boussac and Rutherford, 1988b; Sivaraja et al., 1989). Most researchers addressing the stoichiometry of the Ca cofactor in PS II now conclude that functional water oxidase activity requires one essential Ca^{2+}, which can be removed by low-pH/citrate or 1.2 M NaCl wash (Cammarata and Cheniae, 1987; Katoh et al., 1987; Ono and Inoue, 1988; Shen et al., 1988; Adelroth et al., 1995). In higher plants, another more tightly bound Ca is associated with the light-harvesting complex (LHC II) and requires harsher treatments for its removal (Han and Katoh, 1993; Chen et al., 1995).

A. Manganese Extended X-Ray Absorption Fine Structure (EXAFS) and Calcium

Several investigations have involved removal of Ca and substitution of various metals into this binding site, followed by EXAFS studies on the Mn cluster. One set of experiments using Mn EXAFS on Sr-reactivated PS II membranes was interpreted to indicate a 3.4–3.5 Å distance between the Ca (Sr) and the Mn cluster (Latimer et al., 1995). This conclusion was based on the observation of increased amplitude in Fourier peak III at 3.3 Å upon replacement of Ca with Sr, a heavier atom and better X-ray scatterer. Analysis of EXAFS spectra from purified PS II membrane preparations indicated a Mn–Ca interaction at slightly longer distance (MacLachlan et al., 1992) (~3.6-3.7 Å). Ca depletion by NaCl-washing of PS II membranes removed the 16 and 23 kDa extrinsic proteins and led to a reduced amplitude for this 3.6 Å feature and because of the lower X-ray scattering ability of Na, this result was interpreted as possible Na^{+} substitution for Ca^{2+} at this distance (MacLachlan et al., 1994). Another Mn EXAFS study (Riggs-Gelasco et al., 1996b) did not detect any changes in the Fourier peak at 3.3 Å when Ca was replaced with Sr^{2+} or Dy^{3+} in PS II reaction center complexes lacking the 16 and 23 kDa extrinsic polypeptides; however, it was proposed that Ca might be linked via a hydrogen bond to the oxo ligand of the Mn cluster.

B. Strontium Extended X-Ray Absorption Fine Structure (EXAFS) and Calcium

1. Isotropic Samples

The most common approach, as described above (Latimer et al., 1995; Riggs-Gelasco et al., 1996b), was to substitute other metals (such as Sr) for Ca and then use Mn EXAFS to detect changes in the cluster. Isolating the Mn-Ca or Sr component of the EXAFS spectrum from the combined EXAFS from all Mn-ligand and Mn-Mn interactions can be difficult. The reverse experiment where one probes for backscattering from Mn using Ca or Sr EXAFS (Ca/Sr cofactor point-of-view for nearby Mn) is an elegant alternative and is more definitive than Mn EXAFS results. Such studies on both isotropic and oriented PS II membranes have yielded unequivocal evidence for the proximity of Ca to the Mn cluster (see below).

Several factors favor Sr as the better cofactor for XAS study. First, the X-ray energies involved (16 keV for the K-edge) are more penetrating and not attenuated by air. The higher X-ray absorption cross-section and fluorescence yield of Sr also make the experiment practicable. The Sr EXAFS-based experiment requires PS II samples with Sr substituted for Ca while maintaining O_2-evolving activity and a stoichiometry of 1 Sr per PS II, to focus on the functional cofactor binding site. Along with reactivated Sr-PS II, an inactivated sample can be prepared by treating with hydroxylamine (NH_2OH) to disrupt the Mn cluster and suppress water oxidase activity (Tamura and Cheniae, 1985).

By using Sr EXAFS on isotropic Sr-reactivated PS II membranes, the proximity of Sr (and implicitly Ca) to within 3.5 Å of the Mn cluster (Cinco et al., 1998) has been confirmed. The finding was based on the presence of a second Fourier peak (peak II, Fig. 9, *Top*) in the Sr EXAFS from functional samples, a peak that is absent from inactive, hydroxylamine-treated PS II. This Fourier peak was found to fit best to two Mn at ~3.5 Å rather than lighter atoms (C, O, P, S, Cl). Both types of samples share similar first coordination shells of oxygen (Peak I, Fig. 9, *Top*).

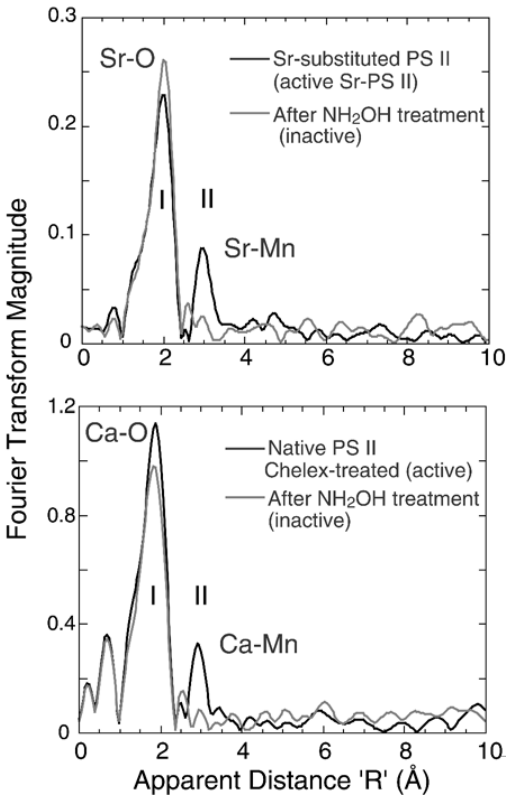

Fig. 9. Top. Fourier transforms of Sr EXAFS for intact and inactive Sr-substituted PS II samples (Chelex-treated). The dominant Fourier Peak I is due to ligating oxygens in the first coordination sphere and is common to both samples. The two Sr-PS II samples differ mainly at the '*R*' = 3.0 Å region, where the intact samples exhibit Fourier Peak II. Disruption of the Mn cluster in NH_2OH-treated sample leads to the absence of Peak II. *Bottom.* Fourier transform of Ca EXAFS from Chelex-treated, layered samples with 2 Ca/PS II with O_2-evolving activity and an S_2 EPR multiline signal. The FTs show the presence of a second Fourier peak in the 2Ca/PS II sample that fits to Ca-Mn that is absent in the control sample where the Mn complex has been disrupted with NH_2OH.

2. Oriented Samples

The technique of using Sr EXAFS has been extended to using polarized Sr EXAFS on layered Sr-substituted samples, to provide important angle information. Polarized EXAFS involves collecting spectra for different incident angles (θ) between the membrane normal of the layered sample and the X-ray electric field vector. Dichroism in the EXAFS can occur, depending on how the particular absorber–backscatterer (A–B) vector is aligned with the electric field. Through analysis of the dichroism, the average orientation (ϕ) of this A–B vector relative to the membrane normal, and the average number of scatterers per absorbing atom (N_{iso}) can be extracted. Constraints on the structural model are then imposed by these parameters.

Sr-substituted PS II samples made by a process of Ca depletion, Sr^{2+} reactivation, and Chelex treatment to remove excess Sr were layered onto flat Mylar films to produce oriented samples (Mukerji et al., 1994; Dau et al., 1995). The Fourier transforms from the polarized Sr EXAFS showed extreme dichroism in Fourier peak II (Fig. 10, *Left*). Nonlinear least-squares regression analysis produced the solid curve shown in Fig. 10, *Right* as the best fit of the 15 data points (angles from six separate samples) and the result translates to 1–2 Sr–Mn vectors with an average angle of 0° or 23° for the average relative angle between the Sr–Mn vectors and the membrane normal depending on the method of analysis.

3. Orientation of the Manganese Complex

The orientation data from the Sr EXAFS experiments can be combined with the dichroism data from Mn EXAFS data to calculate the orientation of the 3.3 Å Mn–Mn vector. The Fourier peak in the Mn EXAFS which contains the Mn–Mn (3.3 Å) and Mn–Ca (3.4 Å) contributions, is dichroic, with an average angle of 43 ± 10° with respect to the membrane normal (Mukerji et al., 1994). By including the Mn-Ca vector at 23°, an angle of ~62° for the 3.3 Å Mn–Mn vector can be calculated. Previous polarized Mn EXAFS experiments on PS II have shown angles of 55° and 67° for the 2.7 Å Mn–Mn vectors (Mukerji et al., 1994; Dau et al., 1995). Thus it follows that all Mn–Mn vectors lie at roughly the same angle (~61°) with respect to the membrane normal, but are not restricted to being collinear, because the PS II membranes are ordered in one dimension only. The electron density from the X-ray diffraction studies (Zouni et al., 2001) are in agreement with such an assignment; the plane containing the Mn electron density is at ~67° to the membrane normal.

C. Calcium Extended X-Ray Absorption Fine Structure (EXAFS)

In a complementary and definitive experiment, Ca K-edge EXAFS studies have been used to probe the

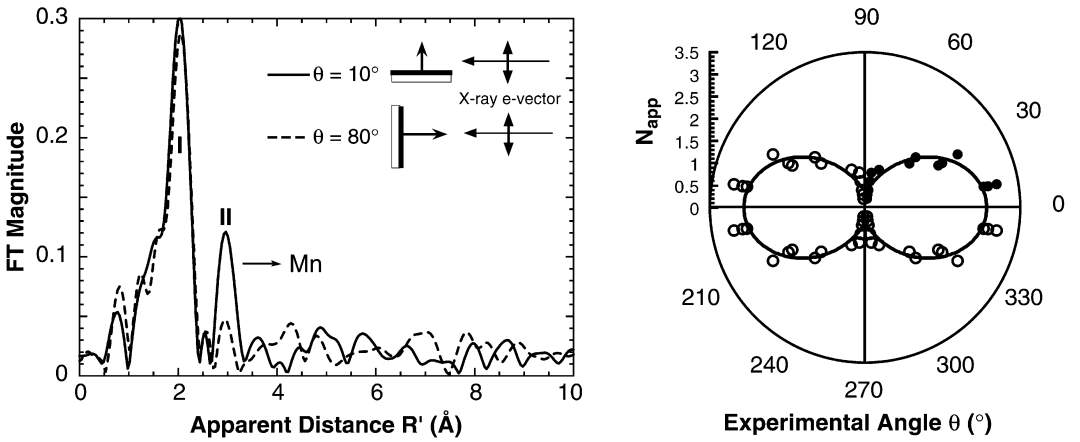

Fig. 10. Left. Fourier transforms of Sr-EXAFS from oriented Sr-PS II samples at two angles (θ). The dichroism is most readily apparent in Fourier peak II (R′ = 3.0 Å) which is assigned to backscattering from Mn. *Right.* The polar plot shows N_{exp} (filled circles) plotted vs. the angle of detection, θ. The solid line is the best fit from which we obtain N_{iso} (number of Mn neighbors to Sr is ~2) and φ (~23°), the angle the Mn-Sr vector makes with the membrane normal.

binding site of the native cofactor for any nearby Mn, within ~ 4 Å. The use of Ca EXAFS spectroscopy has produced results essentially congruent with those found by other independent methods: Sr EXAFS on Sr-reactivated PS II (Cinco et al., 1998) and Mn EXAFS on similar samples (Latimer et al., 1995), but it focuses on the native cofactor and avoids the treatments involving Ca depletion and Sr substitution. Like the earlier Sr EXAFS, the Ca EXAFS study has focused on the Ca cofactor of PS II (poised in the S_1 state). This technique is a more sensitive and direct probe of the Ca binding site in PS II and the Ca EXAFS experiment directly probed the Ca cofactor in as close to a native system as possible.

The FT of the Ca EXAFS is shown in Fig. 9, *Bottom* and the spectra are remarkably similar to the Fourier transforms of the earlier Sr EXAFS study with Sr substituted for Ca. The first (largest) Fourier peak corresponds to the coordinating oxygen atoms closest to Ca. In contrast to the control (NH_2OH-treated) sample, the Chelex-treated PS II shows a second Fourier peak. When Fourier peak II is isolated and simulated with possible scattering atoms, it corresponded best to Mn at 3.4 Å, rather than to light atom (C, O or Cl) neighbors. These results were consistent with the earlier Sr EXAFS studies.

The results are summarized in a motif shown in Fig. 11 and this motif depicts the Ca linked to two Mn by single-O bridges, which can be supplied by protein residues or water. Only single-oxygen bridges (not bidentate bridges) can provide the required 3.4 Å distance indicated by the Ca EXAFS fitting. This bridge may be derived from carboxylate ligands (aspartate or glutamate protein residues), protein backbone carboxyl, water or hydroxide.

Because significant information about Mn–Mn and Mn–Ca vector angles is now available, topological models previously discussed can be refined to include the presence of Ca and account for the dichroism data (Fig. 11). We have chosen to modify two options: option **F** (from Fig. 5) where the two di-μ-oxo motifs are formed using a common Mn atom and the mono-μ-oxo motif is placed at the end of the trinuclear unit, and option **G** can be thought of as at the corners of the base of a trigonal pyramid, with an O atom at the apex and three additional O atoms forming bridges pairwise among the Mn atoms below the base with the fourth Mn linked to one of the corner Mn atoms by a single O-atom bridge. Option **F** has two 2.7 to 2.8 Å Mn-Mn vectors while **G** has three such vectors. These structures are consistent with simulations of EPR and ENDOR data and also qualitatively in agreement with the reported electron density of the Mn cluster, especially the first option for **G** with Ca.

It has been speculated that Ca controls substrate water binding to the catalytic Mn site (Chen et al., 1995) and recent mechanisms have suggested the

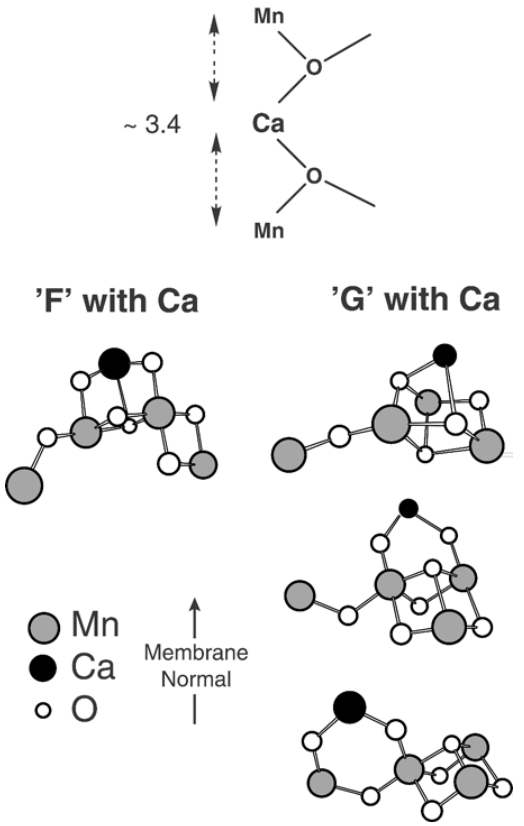

Fig. 11. Top. Model of Ca-binding site of the oxygen-evolving complex in PS II. From the results of the Ca EXAFS studies on PS II, the Ca cofactor is linked by two single-O bridges to two Mn. The oxygens can be provided by water, hydroxyl or protein residues (carboxylate, phenolate). Other ligands to Ca are not shown. The arrangement shown here is not unique as other placements of the two Mn around the Ca are conceivable (Cinco et al., 2002). *Bottom.* Refined models for the active site of the OEC in PS II. These models combine the finding from oriented Sr-substituted PS II samples with previous results from Mn EXAFS on oriented PS II samples. These are derived from core structures that have been described in earlier studies and the models presented here are based on options **F** and **G** from Fig. 5 (**F** with Ca is a variation on a model originally proposed by Siegbahn, 2000).

crucial involvement of the cofactor (Ananyev and Dismukes, 1997; Renger, 1997; Limburg et al., 1999; Siegbahn, 2000). The results Mn EXAFS, Sr EXAFS and Ca EXAFS are mutually consistent and converge toward the conclusion that the Ca cofactor is intimately structurally linked with the Mn cluster in PS II. Taken together, the three methods offer compelling evidence that the catalytic center of photosynthetic O_2 evolution is a heteronuclear Mn_4Ca cluster (for further details, see Chapter 21, Barber and Iwata).

V. Structural Role of the Chloride Cofactor

Despite a multitude of spectroscopic studies, definitive structural evidence for Mn-Cl ligation has not yet been reported. There is one functional Cl^- per PS II unit (Lindberg and Andréasson, 1996; Olesen and Andréasson, 2003), but it is unclear whether chloride is a ligand to one of the Mn atoms in any of the S-states (Lindberg et al., 1990). Steady-state kinetic studies indicate the presence of a halide binding site on the Mn complex (Sandusky and Yocum, 1986; Yocum, 1992; Lindberg and Andréasson, 1996) and activity is inhibited by some compounds which compete with the Cl^- binding site, such as fluoride (Sandusky and Yocum, 1986), primary amines (Sandusky and Yocum, 1986) and acetate (Clemens et al., 2002). Ono et al. (1986) have shown that Cl^- depleted PS II particles in the S_2 state do not have the usual multiline EPR signal but rather have a signal at g=4.1, signifying that an alternative S_2 state is formed. A similar EPR signal is observed on treatment with F^-. It was found that when the OEC is in this alternative state, it can no longer advance to higher S-states. However, the EPR multiline signal is restored following illumination and subsequent addition of Cl^-. Recent studies indicate that the presence of the Cl^- is necessary only for the S_2 to S_3 and S_3 to S_0 transitions of the OEC, while the earlier steps of the cycle can proceed in its absence (Wincencjusz et al., 1997, 1998). These studies indicate that Cl^- is closely associated with the structure of the OEC and the mechanism of O_2 evolution, but its detailed role is as yet unclear.

F^- perturbation of the Mn–Mn distances by treatment with F^- is one of the most direct structural data available that implies halide as a ligand of Mn. XAS studies of F^- inhibited samples show that one of the two 2.7 Å Mn–Mn distances is increased to ~2.8 Å, which is suggestive of F^- binding to the Mn cluster (DeRose et al., 1995). The recent ESEEM results from acetate treated PS II samples (Clemens et al., 2002) also provide the most direct spectroscopic evidence to date for the presence of a chloride ligand to Mn.

There is evidence from EXAFS studies with oriented S_3 state samples indicating the presence of Mn-Cl ligation in the S_3 state (Fernandez et al., 1998). EXAFS results from isotropic samples in the S_3 state have shown that there is considerable change

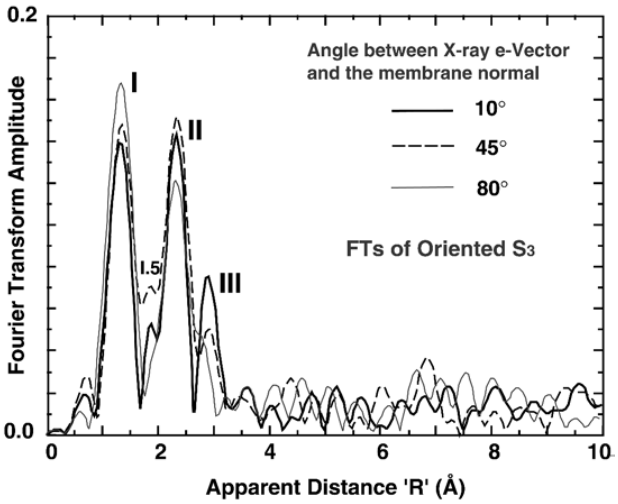

Fig. 12. The Fourier transform of an oriented S_3 sample. The Mn-Mn vectors represented by Fourier peaks labeled II and III are dichroic. Interestingly, a Fourier peak labeled 1.5 is discernible that is not observed in other S-states and it fits best to Cl, indicating the possible presence of a Cl ligand to Mn at a distance of 2.2 Å (Fernandez et al., 1998) in the S_3 state.

in the Mn–Mn distances as the system advances from the S_2 to the S_3 state (Liang et al., 2000). The two 2.7 Å Mn–Mn distances in the S_2 state increase to ~2.8 and ~3.0 Å in the S_3 state. With the aim of determining the relative orientation of the 2.8 and 2.9–3.0 Å Mn–Mn vectors, we initiated XAS studies of oriented S_3 state samples. The FT in Fig. 12 shows that the two Mn–Mn vectors are dichroic. Interestingly, maybe because of the lengthening of the Mn–Mn vectors, a new Fourier peak is observed between the first and second Fourier peaks, labeled 1.5 in Fig. 12. Comparing this FT with that of a Mn binuclear complex with one Cl^- as a terminal ligand to a Mn atom shows that the peak corresponding to Cl backscattering in the model complex is found at approximately the same apparent distance as the new Fourier peak in the PS II samples (Fernandez et al., 1998). In other model compounds, the amplitude of this peak increases as the ratio of Cl/Mn increases and the peak is absent when Cl^- is not present as a ligand. In the S_3 state sample, this peak does not fit to lower Z atoms such as C, N, or O. The fit is significantly better for Cl backscattering at ~2.2 Å. The fits for the model compound are very similar. Dichroism studies on S_3 state samples show that the Fourier peak is larger at the 10° orientation compared to the 80° orientation, which suggests that the Mn–Cl vector is more parallel to the membrane normal.

VI. Mechanism of Water Oxidation and O_2 Evolution

The mechanisms for water oxidation and oxygen evolution that have been proposed can be broadly divided into four categories in which the character of the oxygen atoms that ultimately form dioxygen is different. In these four groups the oxygen atoms come from: two terminal oxygens bound to two separate Mn atoms, one terminal oxygen and one oxygen not bound to the Mn cluster, one terminal and one bridging oxygen, or two μ-oxo bridges. Each of these mechanisms involves distinctly different Mn–O bonds formed and broken during the catalytic cycle (see Chapter 25 for details).

The contribution of X-ray studies to the mechanism of O_2 evolution is in resolving whether an oxygen atom derived from a bridging position in the Mn cluster is involved in the ultimate formation of dioxygen and in the determination of whether Mn centered oxidation occurs during each stage of the S-state transitions. Our X-ray spectra are strongly supportive of Mn cluster oxidation during the $S_0 \rightarrow S_1$ and $S_1 \rightarrow S_2$ transitions, they do not support a similar Mn-centered oxidation during $S_2 \rightarrow S_3$. Furthermore, EXAFS analyses show clear evidence of non-degeneracy in the three 2.7 Å vector lengths in S_0 and S_3, but not in S_1 and S_2, and shows significant structural change

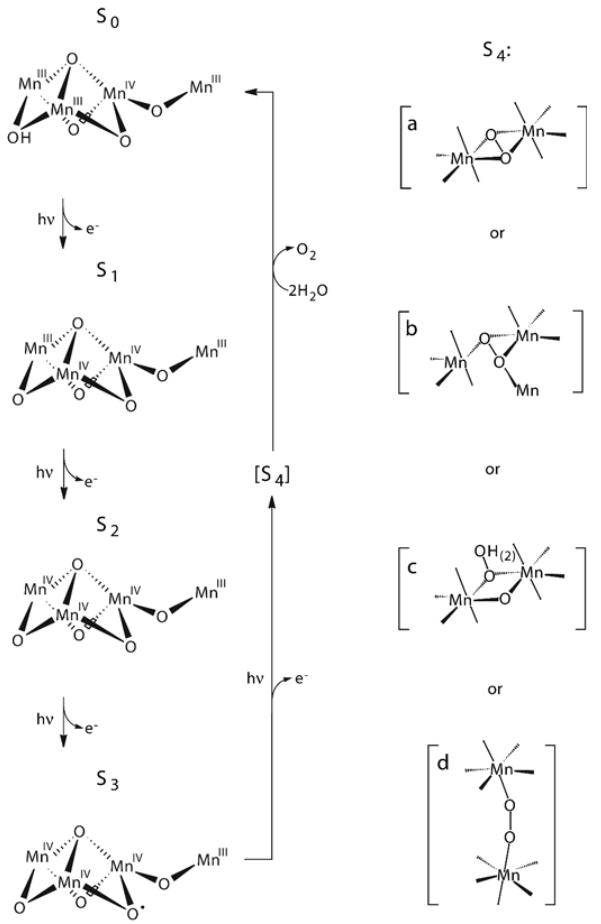

Fig. 13. Summary of changes in Mn oxidation states and Mn-Mn distances during photosynthetic water oxidation using option **G** in Fig. 5. In the $S_1 \rightarrow S_2$ transition, one Mn(III) is oxidized to Mn(IV), and the Mn–Mn distances do not change. During the $S_2 \rightarrow S_3$ transition, the oxidizing equivalent is localized on the μ-oxo bridge, which triggers the increase in Mn–Mn distances. In the $S_3 \rightarrow [S_4] \rightarrow S_0$ transition, a short-lived peroxo intermediate might be formed in the S_4 state. (a), (b), (c) and (d) are 4 mechanisms for O-O bond formation in the S_4 state. Mechanisms (a), (b) and (c) are where one or two bridging O atoms are directly involved in O-O bond formation; a motif that is consistent with XAS data. Mechanism (d) would require localization of an oxidizing equivalent on an oxo bridge that later exchanges or rearranges to a terminal O ligand before O-O bond formation. During the $S_0 \rightarrow S_1$ transition, a Mn(II) → Mn(III) oxidation or a Mn(III) to Mn(IV) concurrent with a deprotonation of a hydroxy to an oxo causing the decrease of the Mn–Mn distance is indicated. For clarity, Y_Z, the cofactors Ca^{2+} and Cl^-, and terminal Mn ligands are not shown. Mn–Mn distances were determined by EXAFS spectroscopy. As mentioned in DeRose et al. (1994), Cinco et al. (2002) and Robblee et al. (2002) other possible topological models exist for the OEC; similar mechanisms that can be proposed for each of the alternative topological models should be considered equally viable.

during the S_2 to S_3 transition that is not accompanied by a Mn-centered oxidation. The X-ray spectroscopy evidence supports the involvement of a bridging O atom in the mechanism of the formation of the O-O bond. These observations must be considered in any postulation of mechanistic aspects of the successive steps in water oxidation.

Our proposed mechanism (illustrated in Fig. 13 using the proposed model **G**) where the O-O bond is formed between one critical bridging oxygen and another oxygen atom derived from a bridging/terminal oxygen ligand or an exogenous oxygen also

avoids the formation of the O–O bond until the most oxidized state (S_4) is reached (Fig. 13, (a), (b), (c)). All four options for the S_4 state generate O_2 which is derived from inequivalent oxygen atoms in the S_3 state, as shown by $^{16}O/^{18}O$ water-exchange measurements on the S_3 state (Messinger et al., 1995; Hillier et al., 1998). In addition, a recent $H_2{}^{16}O/H_2{}^{18}O$ FTIR experiment has shown the presence of an exchangeable di-μ-oxo-bridge in the S_1 and S_2 states (Chu et al., 2000). This mechanism precludes the formation and release of peroxide or other oxidation products of water in the earlier S-states, thus preventing the system from 'short circuiting' and avoiding the risk of damaging the polypeptides of PS II.

Acknowledgments

This work was supported by the National Institutes of Health grant (GM 55302) and by the Director, Office of Science, Office of Basic Energy Sciences, Division of Energy Biosciences, United States Department of Energy under contract DE-AC03-76SF00098. I am grateful to every one of the very talented and motivated graduate students and postdocs, and many sabbatical visitors to the Calvin Lab that I have had the privilege to work with on the oxygen evolving complex over the last two decades and more; each and every one of them can recognize some aspect of the work presented here that they were responsible for and that has contributed to the present understanding of the Mn cluster in the OEC. Specifically, the contributions to the research presented in this article by Roehl Cinco, John Robblee, Johannes Messinger, Henk Visser, Uwe Bergmann, Pieter Glatzel, Carmen Fernandez, Elodie Anxolabéhère-Mallart, Shelly Pizarro, Karen McFarlane, Junko Yano, Steve Cramer and Ken Sauer is gratefully acknowledged. Mel Klein's profound influence and contributions to the EPR and X-ray spectroscopy research pervades the work presented in this chapter. I extend my thanks to our collaborators Profs. W. H. Armstrong, G. W. Brudvig, G. Christou, T. Collins, J.-J. Girerd, R. N. Mukherjee, V. L. Pecoraro and K. Wieghardt who have generously provided all the inorganic Mn compounds that has made all the difference in analyzing the data from PS II. Synchrotron radiation facilities were provided by the Stanford Synchrotron Radiation Laboratory (SSRL) and the Advanced Photon Source (APS), both supported by the United States Department of Energy and the National Institutes of Health.

References

Adelroth P, Lindberg K and Andréasson LE (1995) Studies of Ca^{2+} binding in spinach Photosystem II using $^{45}Ca^{2+}$. Biochemistry 34: 9021–9027

Åhrling KA, Peterson S and Styring S (1998) The S_0 state EPR signal from the Mn cluster in Photosystem II arises from an isolated S=½ ground state. Biochemistry 37: 8115–8120

Ananyev GM and Dismukes GC (1997) Calcium induces binding and formation of a spin-coupled dimanganese (II, II) center in the apo-water oxidation complex of Photosystem II as precursor to the functional tetra-Mn/Ca cluster. Biochemistry 36: 11342–11350

Auger N, Girerd J-J, Corbella M, Gleizes A and Zimmermann J-L (1990) Synthesis, structure, and magnetic properties of the stable triangular $[Mn(IV)_3O_4]^{4+}$ core. J Am Chem Soc 112: 448–450

Beck WF, Depaula JC and Brudvig GW (1986) Ammonia binds to the manganese site of the O_2-evolving complex of Photosystem-II in the S_2 state. J Am Chem Soc 108: 4018–4022

Bergmann U, Grush MM, Horne CR, DeMarois P, Penner-Hahn JE, Yocum CF, Wright DW, Dubé CE, Armstrong WH, Christou G, Eppley HJ and Cramer SP (1998) Characterization of the Mn oxidation states in Photosystem II by Kβ X-ray fluorescence spectroscopy. J Phys Chem B 102: 8350–8352

Boussac A and Rutherford AW (1988a) S-state formation after Ca^{2+} depletion in the Photosystem II oxygen-evolving complex. Chem Script 28A: 123–126

Boussac A and Rutherford AW (1988b) Nature of the inhibition of the oxygen-evolving enzyme of Photosystem II induced by NaCl washing and reversed by the addition of Ca^{2+} or Sr^{2+}. Biochemistry 27: 3476–3483

Boussac A and Rutherford AW (2000) Comparative study of the g=4.1 EPR signals in the S_2 state of Photosystem II. Biochim Biophys Acta 1457: 145–156

Boussac A, Girerd J-J and Rutherford AW (1996) Conversion of the spin state of the manganese complex in Photosystem II induced by near-infrared light. Biochemistry 35: 6984–6989

Britt RD (1996) Oxygen evolution. In: Ort DR and Yocum CF (eds) Oxygenic Photosynthesis: The Light Reactions, pp 137–164. Kluwer Academic Publishers, Dordrecht

Britt RD, Zimmermann J-L, Sauer K and Klein MP (1989) Ammonia binds to the catalytic manganese of the oxygen-evolving complex of Photosystem II. Evidence by electron spin-echo envelope modulation spectroscopy. J Am Chem Soc 111: 3522–3532

Britt RD, Peloquin JM and Campbell KA (2000) Pulsed and parallel-polarization EPR characterization of the Photosystem II oxygen-evolving complex. Ann Rev Biophys Biomol Struct 29: 463–495

Cammarata KV and Cheniae GM (1987) Studies on 17, 24 kDa depleted Photosystem II membranes. Plant Physiol 84: 587–595

Carrell TG, Tyryshkin AM and Dismukes GC (2002) An evaluation of structural models for the photosynthetic water-oxidizing complex derived from spectroscopic and X-ray diffraction signatures. J Biol Inorg Chem 7: 2–22

Chen C, Kazimir J and Cheniae GM (1995) Calcium modulates the photoassembly of Photosystem II $(Mn)_4$-clusters by preventing ligation of nonfunctional high-valency states of manganese. Biochemistry 34: 13511–13526

Chu H-A, Sackett H and Babcock GT (2000) Identification of

a Mn-O-Mn cluster vibrational mode of the oxygen-evolving complex in Photosystem II by low-frequency FTIR spectroscopy. Biochemistry 39: 14371–14376

Cinco RM, Robblee JH, Rompel A, Fernandez C, Yachandra VK, Sauer K and Klein MP (1998) Strontium EXAFS reveals the proximity of calcium to the manganese cluster of oxygen-evolving Photosystem II. J Phys Chem B 102: 8248–8256

Cinco RM, Rompel A, Visser H, Aromí G, Christou G, Sauer K, Klein MP and Yachandra VK (1999) Comparison of the manganese cluster in oxygen-evolving Photosystem II with distorted cubane manganese compounds through X-ray absorption spectroscopy. Inorg Chem 38: 5988–5998

Cinco RM, Holman KLM, Robblee JH, Yano J, Pizarro SA, Bellacchio E, Sauer K and Yachandra VK (2002) Calcium EXAFS establishes the Mn-Ca cluster in the oxygen-evolving complex of Photosystem II. Biochemistry 41: 12928–12933

Clemens KL, Force DA and Britt RD (2002) Acetate binding at the Photosystem II oxygen evolving complex: An S_2-state multiline signal ESEEM study. J Am Chem Soc 124: 10921–10933

Cole J, Yachandra VK, Guiles RD, McDermott AE, Britt RD, Dexheimer SL, Sauer K and Klein MP (1987) Assignment of the g = 4.1 EPR signal to manganese in the S_2 state of the photosynthetic oxygen-evolving complex: An X-ray absorption edge spectroscopy study. Biochim Biophys Acta 890: 395–398

Cramer SP (1988) Biochemical application of X-ray absorption spectroscopy. In: Koningsberger DC and Prins R (eds) X-Ray Absorption: Principles, Applications, Techniques of EXAFS, SEXAFS and XANES, pp 327–320. John Wiley & Sons, New York

Dau H, Andrews JC, Roelofs TA, Latimer MJ, Liang W, Yachandra VK, Sauer K and Klein MP (1995) Structural consequences of ammonia binding to the manganese cluster of the photosynthetic oxygen-evolving complex: An X-ray absorption study of isotropic and oriented Photosystem II particles. Biochemistry 34: 5274–5287

Debus RJ (1992) The manganese and calcium ions of photosynthetic oxygen evolution. Biochim Biophys Acta 1102: 269–352

Dekker JP (1992) Optical studies on the oxygen-evolving complex of Photosystem II. In: Pecoraro VL (ed) Manganese Redox Enzymes, pp 85–103. VCH Publishers, New York

DeRose VJ, Mukerji I, Latimer MJ, Yachandra VK, Sauer K and Klein MP (1994) Comparison of the manganese oxygen-evolving complex in Photosystem II of spinach and *Synechococcus* sp. with multinuclear manganese model compounds by X-ray absorption spectroscopy. J Am Chem Soc 116: 5239–5249

DeRose VJ, Latimer MJ, Zimmermann J-L, Mukerji I, Yachandra VK, Sauer K and Klein MP (1995) Fluoride substitution in the Mn cluster from Photosystem II: EPR and X-ray absorption spectroscopy studies. Chem Phys 194: 443–459

Dismukes GC and Siderer Y (1981) Intermediates of a polynuclear manganese cluster involved in photosynthetic oxidation of water. Proc Natl Acad Sci USA 78: 274–278

Evelo RG, Styring S, Rutherford AW and Hoff AJ (1989) EPR relaxation measurements of Photosystem-II reaction centers — influence of S-state oxidation and temperature. Biochim Biophys Acta 973: 428–442

Fernandez C, Cinco RM, Robblee JH, Messinger J, Pizarro SA, Sauer K, Klein MP and Yachandra VK (1998) Calcium and chloride cofactors of the oxygen evolving complex — X-ray absorption spectroscopy evidence for a Mn/Ca/Cl heteronuclear cluster. In: Garab G (ed) Photosynthesis: Mechanisms and Effects, Vol II, pp 1399–1402. Kluwer Academic Publishers, Dordrecht

Ferreira K, Iverson TM, Mughlouni K, Barber J and Iwata S (2004) Architecture of the photosynthetic oxygen-evolving center. Science 303: 1831–1838

George GN, Prince RC and Cramer SP (1989) The manganese site of the photosynthetic water-splitting enzyme. Science 243: 789–791

Ghanotakis DF, Babcock GT and Yocum CF (1984) Calcium reconstitutes high rates of oxygen evolution in polypeptide depleted Photosystem II preparations. FEBS Lett 167: 127–130

Ghanotakis DF, Babcock GT and Yocum CF (1985) Structure of the oxygen-evolving complex of Photosystem II: Calcium and lanthanum compete for sites on the oxidizing side of Photosystem II which control the binding of water-soluble polypeptides and regulate the activity of the manganese complex. Biochim Biophys Acta 809: 173–180

Gilchrist ML, Jr., Ball JA, Randall DW and Britt RD (1995) Proximity of the manganese cluster of Photosystem II to the redox-active tyrosine Y_z. Proc Natl Acad Sci USA 92: 9545–9549

Goodin DB, Yachandra VK, Britt RD, Sauer K and Klein MP (1984) The state of manganese in the photosynthetic apparatus. 3. Light-induced changes in X-ray absorption (K-edge) energies of manganese in photosynthetic membranes. Biochim Biophys Acta 767: 209–216

Guiles RD, Yachandra VK, McDermott AE, Cole JL, Dexheimer SL, Britt RD, Sauer K and Klein MP (1990a) The S_0 state of Photosystem II induced by hydroxylamine: Differences between the structure of the manganese complex in the S_0 and S_1 states determined by X-ray absorption spectroscopy. Biochemistry 29: 486–496

Guiles RD, Zimmermann JL, McDermott AE, Yachandra VK, Cole JL, Dexheimer SL, Britt RD, Wieghardt K, Bossek U, Sauer K and Klein MP (1990b) The S_3 state of Photosystem II: Differences between the structure of the manganese complex in the S_2 and S_3 states determined by X-ray absorption-spectroscopy. Biochemistry 29: 471–485

Han K-C and Katoh S (1993) Different localization of two Ca^{2+} in spinach oxygen-evolving Photosystem II membranes. Evidence for involvement of only one Ca^{2+} in oxygen evolution. Plant Cell Physiol 34: 585–593

Hasegawa K, Kusunoki M, Inoue Y and Ono T-A (1998) Simulation of S_2-state multiline EPR signal in oriented Photosystem II membranes: Structural implications for the manganese cluster in an oxygen-evolving complex. Biochemistry 37: 9457–9465

Hasegawa K, Ono T-A, Inoue Y and Kusunoki M (1999) Spin-exchange interactions in the S_2-state manganese tetramer in photosynthetic oxygen-evolving complex deduced from g=2 multiline EPR signal. Chem Phys Lett 300: 9–19

Hillier W, Messinger J and Wydrzynski T (1998) Kinetic determination of the fast exchanging substrate water molecule in the S_3 state of Photosystem II. Biochemistry 37: 16908–16914

Iuzzolino L, Dittmer J, Dörner W, Meyer-Klaucke W and Dau H (1998) X-ray absorption spectroscopy on layered Photosystem II membrane particles suggests manganese-centered oxidation of the oxygen-evolving complex for the S_0-S_1, S_1-S_2, and S_2-S_3 transitions of the water oxidation cycle. Biochemistry 37: 17112–17119

Jaklevic J, Kirby JA, Klein MP, Robertson AS, Brown GS and

Eisenberger P (1977) Fluorescence detection of EXAFS: Sensitivity enhancement for dilute species and thin films. Solid State Commun 23: 679–682

Joliot P (2003) Period-four oscillations of the flash-induced oxygen formation in photosynthesis. Photosynth Res 76: 65–72

Kamiya N and Shen JR (2003) Crystal structure of oxygen-evolving Photosystem II from *Thermosynechococcus vulcanus* at 3.7 Å resolution. Proc Natl Acad Sci USA 100: 98–103

Katoh S, Satoh K, Ohno T, Chen J-R and Kashino Y (1987) Numbers of calcium ions associated with oxygen evolving Photosystem II preparations with different affinities. In: Biggins J (ed) Progress in Photosynthesis Research, Vol I, pp 625–628. Martinus Nijhoff Publishers, Dordrecht

Kirby JA, Robertson AS, Smith JP, Thompson AC, Cooper SR and Klein MP (1981) State of manganese in the photosynthetic apparatus. 1. Extended X-ray absorption fine structure studies on chloroplasts and di-μ-oxo-bridged dimanganese model compounds. J Am Chem Soc 103: 5529–5537

Kok B, Forbush B and McGloin M (1970) Cooperation of charges in photosynthetic oxygen evolution. I. A linear four step mechanism. Photochem Photobiol 11: 457–475

Kretschmann H, Dekker JP, Saygin Ö and Witt HT (1988) An agreement on the quaternary oscillation of ultraviolet absorption changes accompanying the water splitting in isolated Photosystem II complexes from the cyanobacterium *Synechococcus* sp. Biochim Biophys Acta 932: 358–361

Kusunoki M, Takano T, Ono T, Noguchi T, Yamaguchi Y, Oyanagi H and Inoue Y (1995) Advanced EXAFS studies of the S_1 state manganese cluster in plant Photosystem II. In: Mathis P (ed) Photosynthesis: From Light to Biosphere, Vol II, pp 251–254. Kluwer Academic Publishers, Dordrecht

Kuzek D and Pace RJ (2001) Probing the Mn oxidation states in the OEC Insights from spectroscopic, computational and kinetic data. Biochim Biophys Acta 1503: 123–137

Lakshmi KV, Eaton SS, Eaton GR, Frank HA and Brudvig GW (1998) Analysis of dipolar and exchange interactions between manganese and tyrosine Z in the $S_2Y_Z^{\bullet}$ state of acetate-inhibited Photosystem II via EPR spectral simulations at X- and Q-bands. J Phys Chem B 102: 8327–8335

Latimer MJ, DeRose VJ, Mukerji I, Yachandra VK, Sauer K and Klein MP (1995) Evidence for the proximity of calcium to the manganese cluster of Photosystem II: Determination by X-ray absorption spectroscopy. Biochemistry 34: 10898–10909

Latimer MJ, DeRose VJ, Yachandra VK, Sauer K and Klein MP (1998) Structural effects of calcium depletion on the manganese cluster of Photosystem II: Determination by X-ray absorption spectroscopy. J Phys Chem B 102: 8257–8265

Liang W, Latimer MJ, Dau H, Roelofs TA, Yachandra VK, Sauer K and Klein MP (1994) Correlation between structure and magnetic spin state of the manganese cluster in the oxygen-evolving complex of Photosystem II in the S_2 state: Determination by X-ray absorption spectroscopy. Biochemistry 33: 4923–4932

Liang W, Roelofs TA, Cinco RM, Rompel A, Latimer MJ, Yu WO, Sauer K, Klein MP and Yachandra VK (2000) Structural change of the Mn cluster during the $S_2 \rightarrow S_3$ state transition of the oxygen-evolving complex of Photosystem II. Does it reflect the onset of water/substrate oxidation? Determination by Mn X-ray absorption spectroscopy. J Am Chem Soc 122: 3399–3412

Limburg J, Szalai VA and Brudvig GW (1999) A mechanistic and structural model for the formation and reactivity of a Mn^{v}=O species in photosynthetic water oxidation. J Chem Soc, Dalton Trans 1353–1361

Lindberg K and Andréasson LE (1996) A one-site, two-state model for the binding of anions in Photosystem II. Biochemistry 35: 14259–14267

Lindberg K, Wydrzynski T, Vänngård T and Andréasson L-E (1990) Slow release of chloride from ^{36}Cl-labeled Photosystem II membranes. FEBS Lett 264: 153–155

MacLachlan DJ, Hallahan BJ, Ruffle SV, Nugent JHA, Evans MCW, Strange RW and Hasnain SS (1992) An EXAFS study of the manganese oxygen-evolving complex in purified Photosystem II membrane fractions. The S_1 and S_2 states. Biochem J 285: 569–576

MacLachlan DJ, Nugent JHA, Bratt PJ and Evans MCW (1994) The effects of calcium depletion on the O_2-evolving complex in spinach PS II: The S_1^*, S_2^* and S_3^* states and the role of the 17 kDa and 23 kDa extrinsic polypeptides. Biochim Biophys Acta 1186: 186–200

McDermott AE, Yachandra VK, Guiles RD, Cole JL, Dexheimer SL, Britt RD, Sauer K and Klein MP (1988) Characterization of the manganese O_2-evolving complex and the iron-quinone acceptor complex in Photosystem II from a thermophilic cyanobacterium by electron paramagnetic resonance and X-ray absorption spectroscopy. Biochemistry 27: 4021–4031

Messinger J, Badger M and Wydrzynski T (1995) Detection of *one* slowly exchanging substrate water molecule in the S_3 state of Photosystem II. Proc Natl Acad Sci USA 92: 3209–3213

Messinger J, Nugent JHA and Evans MCW (1997a) Detection of an EPR multiline signal for the S_0^* state in Photosystem II. Biochemistry 36: 11055–11060

Messinger J, Robblee J, Yu WO, Sauer K, Yachandra VK and Klein MP (1997b) The S_0 state of the oxygen-evolving complex in Photosystem II is paramagnetic: Detection of an EPR multiline signal. J Am Chem Soc 119: 11349–11350

Messinger J, Robblee JH, Bergmann U, Fernandez C, Glatzel P, Visser H, Cinco RM, McFarlane KL, Bellacchio E, Pizarro SA, Cramer SP, Sauer K, Klein MP and Yachandra VK (2001) Absence of Mn-centered oxidation in the $S_2 \rightarrow S_3$ transition: Implications for the mechanism of photosynthetic water oxidation. J Am Chem Soc 123: 7804–7820

Mukerji I, Andrews JC, DeRose VJ, Latimer MJ, Yachandra VK, Sauer K and Klein MP (1994) Orientation of the oxygen-evolving manganese complex in a Photosystem II membrane preparation: An X-ray absorption spectroscopy study. Biochemistry 33: 9712–9721

Olesen K and Andréasson LE (2003) The function of the chloride ion in photosynthetic oxygen evolution. Biochemistry 42: 2025–2035

Ono T-A and Inoue Y (1988) Discrete extraction of the Ca atom functional for O_2 evolution in higher plant Photosystem II by a simple low pH treatment. FEBS Lett 227: 147–152

Ono T-A and Inoue Y (1989) Roles of Ca^{2+} in O_2 evolution in higher plant Photosystem II: Effects of replacement of Ca^{2+} site by other cations. Arch Biochem Biophys 275: 440–448

Ono T-A, Zimmermann JL, Inoue Y and Rutherford AW (1986) EPR evidence for a modified S-state transition in chloride-depleted Photosystem II. Biochim Biophys Acta 851: 193–201

Ono T-A, Noguchi T, Inoue Y, Kusunoki M, Matsushita T and Oyanagi H (1992) X-ray detection of the period-four cycling of the manganese cluster in photosynthetic water oxidizing enzyme. Science 258: 1335–1337

Ono T-A, Noguchi T, Inoue Y, Kusunoki M, Yamaguchi H and Oyanagi H (1994) Study of the intermediate S-states for water oxidation in the normal and Ca-depleted photosynthetic oxygen-evolving enzyme by means of flash-induced X-ray absorption near edge structure spectroscopy. Biochem Soc Trans 22: 331-335

Pecoraro VL (ed) (1992) Manganese Redox Enzymes. VCH Publishers, New York

Pecoraro VL and Hsieh W-Y (2000) The use of model complexes to elucidate the structure and function of manganese redox enzymes. In: Sigel A and Sigel H (eds) Manganese and Its Role in Biological Processes, pp 429–504. Marcel Dekker Inc., New York

Peloquin JM and Britt RD (2001) EPR/ENDOR characterization of the physical and electronic structure of the OEC Mn cluster. Biochim Biophys Acta 1503: 96–111

Peloquin JM, Campbell KA and Britt RD (1998) ^{55}Mn pulsed ENDOR demonstrates that the Photosystem II 'split' EPR signal arises from a magnetically-coupled mangano-tyrosyl complex. J Am Chem Soc 120: 6840–6841

Peloquin JM, Campbell KA, Randall DW, Evanchik MA, Pecoraro VL, Armstrong WH and Britt RD (2000) ^{55}Mn ENDOR of the S_2-state multiline EPR signal of Photosystem II: Implications on the structure of the tetranuclear cluster. J Am Chem Soc 122: 10926–10942

Peng G, de Groot FMF, Hämäläinen K, Moore JA, Wang X, Grush MM, Hastings JB, Siddons DP, Armstrong WH, Mullins OC and Cramer SP (1994) High-resolution manganese X-ray fluorescence spectroscopy. Oxidation-state and spin-state sensitivity. J Am Chem Soc 116: 2914–2920

Penner-Hahn JE (1998) Structural characterization of the Mn site in the photosynthetic oxygen-evolving complex. Struct Bond 90: 1–36

Penner-Hahn JE, Fronko RM, Pecoraro VL, Yocum CF, Betts SD and Bowlby NR (1990) Structural characterization of the manganese sites in the photosynthetic oxygen-evolving complex using X-ray absorption- spectroscopy. J Am Chem Soc 112: 2549–2557

Renger G (1997) Mechanistic and structural aspects of photosynthetic water oxidation. Physiol Plant 100: 828–841

Riggs PJ, Yocum CF, Penner-Hahn JE and Mei R (1992) Reduced derivatives of the manganese cluster in the photosynthetic oxygen-evolving complex. J Am Chem Soc 114: 10650–10651

Riggs-Gelasco PJ, Mei R, Yocum CF and Penner-Hahn JE (1996a) Reduced derivatives of the Mn cluster in the oxygen-evolving complex of Photosystem II: An EXAFS study. J Am Chem Soc 118: 2387–2399

Riggs-Gelasco PJ, Mei R, Ghanotakis DF, Yocum CF and Penner-Hahn JE (1996b) X-ray absorption spectroscopy of calcium-substituted derivatives of the oxygen-evolving complex of Photosystem II. J Am Chem Soc 118: 2400–2410

Robblee JH, Cinco RM and Yachandra VK (2001) X-ray spectroscopy-based structure of the Mn cluster and mechanism of photosynthetic oxygen evolution. Biochim Biophys Acta 1503: 7–23

Robblee JH, Messinger J, Cinco RM, McFarlane KL, Fernandez C, Pizarro SA, Sauer K and Yachandra VK (2002) The Mn cluster in the S_0 state of the oxygen-evolving complex of Photosystem II studied by EXAFS spectroscopy: Are there three di-μ-oxo-bridged Mn_2 moieties in the tetranuclear Mn complex? J Am Chem Soc 124: 7459–7471

Roe AL, Schneider DJ, Mayer RJ, Pyrz JW, Widom J and Que L, Jr (1984) X-ray absorption spectroscopy of iron-tyrosinate proteins. J Am Chem Soc 106: 1676–1681

Roelofs TA, Liang W, Latimer MJ, Cinco RM, Rompel A, Andrews JC, Sauer K, Yachandra VK and Klein M (1996) Oxidation states of the manganese cluster during the flash-induced S-state cycle of the photosynthetic oxygen-evolving complex. Proc Natl Acad Sci USA 93: 3335–3340

Rutherford AW, Zimmermann J-L and Boussac A (1992) Oxygen evolution. In: Barber J (ed) The Photosystems: Structure, Function, and Molecular Biology, pp 179–229. Elsevier Science Publishers BV, Amsterdam

Sandusky PO and Yocum CF (1986) The chloride requirement for photosynthetic oxygen evolution: Factors affecting nucleophilic displacement of chloride from the oxygen-evolving complex. Biochim Biophys Acta 849: 85–93

Sauer K, Yachandra VK, Britt RD and Klein MP (1992) The photosynthetic water oxidation complex studied by EPR and X-ray absorption spectroscopy. In: Pecoraro VL (ed) Manganese Redox Enzymes, pp 141–175. VCH Publishers, New York

Sayers DE, Stern EA and Lytle F (1971) New technique for investigating noncrystalline structures. Fourier analysis of the extended X-ray-absorption fine structure. Phys Rev Lett 27: 1204–1207

Saygin Ö and Witt HT (1987) Optical characterization of intermediates in the water-splitting enzyme system of photosynthesis—possible states and configurations of manganese and water. Biochim Biophys Acta 893: 452–469

Schiller H, Dittmer J, Iuzzolino L, Dörner W, Meyer-Klaucke W, Solé VA, Nolting H-F and Dau H (1998) Structure and orientation of the oxygen-evolving manganese complex of green algae and higher plants investigated by X-ray absorption linear dichroism spectroscopy on oriented Photosystem II membrane particles. Biochemistry: 37: 7340–7350

Sharp RR (1992) Proton NMR relaxation due to the photosynthetic oxygen-evolving center. In: Pecoraro VL (ed) Manganese Redox Enzymes, pp 177–196. VCH Publishers, New York

Shen J-R, Satoh K and Katoh S (1988) Calcium content of oxygen-evolving Photosystem II preparations from higher plants. Effects of NaCl treatment. Biochim Biophys Acta 933: 358–364

Shulman RG, Yafet Y, Eisenberger P and Blumberg WE (1976) Observation and interpretation of X-ray absorption edges in iron compounds and proteins. Proc Natl Acad Sci USA 73: 1384–1388

Siegbahn PEM (2000) Theoretical models for the oxygen radical mechanism of water oxidation and of the water oxidizing complex of Photosystem II. Inorg Chem 39: 2923–2935

Sivaraja M, Tso J and Dismukes GC (1989) A calcium-specific site influences the structure and activity of the manganese cluster responsible for photosynthetic water oxidation. Biochemistry 28: 9459–9464

Smith PJ and Pace RJ (1996) Evidence for two forms of the g=4.1 signal in the S_2 state of Photosystem II. Two magnetically isolated manganese dimers. Biochim Biophys Acta 1275: 213–220

Styring SA and Rutherford AW (1988) The microwave power saturation of S_{IIslow} varies with the redox state of the oxygen-evolving complex in Photosystem II. Biochemistry 27: 4915–4923

Tamura N and Cheniae G (1985) Effects of Photosystem-II extrinsic proteins on microstructure of the oxygen-evolving

complex and its reactivity to water analogs. Biochim Biophys Acta 809: 245–259

Tsutsumi K, Nakamori H and Ichikawa K (1976) X-ray manganese Kβ emission spectra of manganese oxides and manganates. Phys Rev B 13: 929–933

Visser H, Anxolabéhère-Mallart E, Bergman U, Glatzel P, Robblee JH, Cramer SP, Girerd J-J, Sauer K, Klein MP and Yachandra VK (2001) Mn K-edge XANES and Kβ XES studies of two Mn-oxo binuclear complexes. Investigation of three different oxidation states relevant to the oxygen-evolving complex of Photosystem II. J Am Chem Soc 123: 7031–7039

Westre TE, Kennepohl P, DeWitt JG, Hedman B, Hodgson KO and Solomon EI (1997) A multiplet analysis of Fe K-edge 1s to 3d pre-edge features of iron complexes. J Am Chem Soc 119: 6297–6314

Wieghardt K (1989) The active centers in manganese-containing metalloproteins and inorganic model complexes. Angew Chem Int Ed Engl 28: 1153–1172

Wincencjusz H, van Gorkom HJ and Yocum CF (1997) The photosynthetic oxygen evolving complex requires chloride for its redox state S_2 to S_3 and S_3 to S_0 transitions but not for S_0 to S_1 or S_1 to S_2 transitions. Biochemistry 36: 3663–3670

Wincencjusz H, Yocum CF and van Gorkom HJ (1998) S-state dependence of chloride binding affinities and exchange dynamics in the intact and polypeptide-depleted O_2 evolving complex of Photosystem II. Biochemistry 37: 8595–8604

Yachandra VK (1995) X-ray absorption spectroscopy and applications in structural biology. In: Sauer K (ed) Methods of Enzymology, Vol 246, pp 638–675. Academic Press, San Diego

Yachandra VK (2002) Structure of the manganese complex in Photosystem II: Insights from X-ray spectroscopy. Phil Trans R Soc London B 357: 1347–1357

Yachandra VK, Guiles RD, McDermott A, Britt RD, Dexheimer SL, Sauer K and Klein MP (1986) The state of manganese in the photosynthetic apparatus. 4. Structure of the manganese complex in Photosystem II studied using EXAFS spectroscopy. The S_1 state of the oxygen-evolving Photosystem II complex from spinach. Biochim Biophys Acta 850: 324–332

Yachandra VK, Guiles RD, McDermott AE, Cole JL, Britt RD, Dexheimer SL, Sauer K and Klein MP (1987) Comparison of the structure of the manganese complex in the S_1 and S_2 states of the photosynthetic O_2-evolving complex: An X-ray absorption spectroscopy study. Biochemistry 26: 5974–5981

Yachandra VK, DeRose VJ, Latimer MJ, Mukerji I, Sauer K and Klein MP (1993) Where plants make oxygen: A structural model for the photosynthetic oxygen-evolving manganese cluster. Science 260: 675–679

Yachandra VK, Sauer K and Klein MP (1996) Manganese cluster in photosynthesis: Where plants oxidize water to dioxygen. Chem Rev 96: 2927–2950

Yocum CF (1992) The calcium and chloride requirements for photosynthetic water oxidation. In: Pecoraro VL (ed) Manganese Redox Enzymes, pp 71–84. VCH Publishers, New York

Zheng M and Dismukes GC (1996) Orbital configuration of the valence electrons, ligand field symmetry, and manganese oxidation states of the photosynthetic water oxidizing complex: Analysis of the S_2 state multiline EPR signals. Inorg Chem 35: 3307–3319

Zimmermann JL and Rutherford AW (1986) Electron paramagnetic resonance properties of the S_2 state of the oxygen-evolving complex of Photosystem II. Biochemistry 25: 4609–4615

Zouni A, Witt HT, Kern J, Fromme P, Krauss N, Saenger W and Orth P (2001) Crystal structure of Photosystem II from *Synechococcus elongatus* at 3.8 Å resolution. Nature 409: 739–743

Chapter 11

The Catalytic Manganese Cluster: Protein Ligation

Richard J. Debus*
Department of Biochemistry, University of California-Riverside, Riverside, CA 92521-0129, U.S.A.

Summary

Water oxidation in Photosystem II (PS II) takes place under severe constraints. Because little surplus free energy is available, the midpoint potential of the $(Mn)_4$ cluster must be tightly controlled to prevent it from increasing substantially as oxidizing equivalents are accumulated. In addition, the release of toxic, highly reactive intermediates of water oxidation must be minimized. To operate under these constraints, the reactivity of the $(Mn)_4$-Ca^{2+}-Y_Z complex is carefully controlled by its protein environment. This chapter describes the site-directed mutagenesis studies that have been undertaken to identify the amino acid residues that are responsible for this control. These residues include those that ligate the Mn and Ca^{2+} ions and those that influence the electron and proton transfer reactions of Y_Z and the $(Mn)_4$-Ca^{2+} metal cluster. Most characterizations relied initially on non-invasive methods that were conducted in vivo. With improved methods for purifying PS II, characterizations increasingly involve newer developments in magnetic resonance, vibrational, and optical absorption spectroscopy. On the basis of the mutagenesis studies that are described in this chapter, possible ligands of the

*Email: richard.debus@ucr.edu

T. Wydrzynski and K. Satoh (eds): Photosystem II: The Light-Driven Water:Plastoquinone Oxidoreductase, pp. 261–284.

$(Mn)_4$ cluster were proposed to include D1-Asp170, D1-His332, D1-Glu333, D1-His337 and D1-Asp342, plus the carboxyl-terminus of the D1 polypeptide at D1-Ala344. Possible ligands of the Ca^{2+} ion were proposed to include D1-Asp59, D1-Asp61 and D1-Asp342. In addition, D1-Glu189 was proposed to participate in a network of hydrogen bonds that facilitates electron transfer from the $(Mn)_4$ cluster to $Y_Z^{\bullet}$ during the higher S state transitions and D1-His190 was proposed to serve as the proton acceptor for Y_Z. The recent 3.2 Å and 3.5 Å X-ray crystallographic structural models of PS II support some of these proposals, but conflict with others, most notably the ligation of Ca^{2+} and the roles of D1-Glu189 and, in the 3.5 Å structural model, the role of the carboxyl-terminus of the D1 polypeptide. Two surprising aspects of the structural models are that one Mn ion is ligated by both D1-Asp170 and D1-Glu333 and another is ligated by both D1-Glu189 and D1-His332. The properties of the D1-Asp170 and D1-Glu333 mutants differ markedly, as do the properties of the D1-Glu189 and D1-His332 mutants. The main points of agreement and disagreement between the mutagenesis studies and the recent X-ray crystallographic structural models are discussed.

I. Introduction

The O_2-evolving complex (OEC) in Photosystem II (PS II) consists of the $(Mn)_4$ cluster, Y_Z, and a Ca^{2+} ion. Attempts to identify the locations of the $(Mn)_4$ cluster and Y_Z began in earnest after Kimiyuki Satoh and coworkers discovered that the D1/D2 heterodimer is the site of charge separation between P680 and Pheo (Nanba and Satoh, 1987; Okamura et al., 1987). This seminal discovery, coupled with the discovery that $Y_D^{\bullet}$ is a tyrosine radical (Barry and Babcock, 1987), led immediately to the identification of Y_D as Tyr160 of the D2 polypeptide (Debus et al., 1988a; Vermaas et al., 1988) and Y_Z as Tyr161 of the D1 polypeptide (Debus et al., 1988b; Metz et al., 1989) [*Synechocystis* numbering is used here and throughout]. Parallels between the D1/D2 heterodimer in PS II and the L/M heterodimer in the bacterial reaction center (BRC) (Trebst, 1986; Michel and Deisenhofer, 1988) led to the general belief that the $(Mn)_4$ cluster would be located in the lumenal domains of the D1 and D2 polypeptides. As soon as appropriate deletion strains for efficiently introducing site-directed mutations into the D1 and D2 polypeptides of *Synechocystis* sp. PCC 6803 were constructed (Debus et al., 1990; Vermaas et al., 1990; Nixon et al., 1992b), all conserved Asp, Glu, His, and Tyr residues in the lumenal domains of the D1 polypeptide and all conserved Asp, Glu, His, Asn, and Gln residues in the lumenal domains of the D2 polypeptide were targeted (for early reviews, see Diner et al., 1991; Nixon et al., 1992a; Pakrasi and Vermaas, 1992; Debus, 1992). Systems for introducing mutations into the D1 polypeptide of *Chlamydomonas reinhardtii* (Roffey et al., 1991; Minagawa and Crofts, 1994; Whitelegge et al., 1995) were developed shortly thereafter. All of the mutagenesis studies of PS II have been performed with the cyanobacterium, *Synechocystis* sp. PCC 6803 and the green alga, *Chlamydomonas reinhardtii*.

Some of the initial characterizations of site-directed mutants focused on Asp170 of the D1 polypeptide because this residue is located only 9 residues from Y_Z (Boerner et al., 1992; Diner and Nixon, 1992; Nixon and Diner, 1992). These initial characterizations showed that this residue is crucial for the assembly or stability of the $(Mn)_4$ cluster (Boerner et al., 1992; Nixon and Diner, 1992) and serves as a component of a high-affinity Mn(II) binding site (Diner and Nixon, 1992; Nixon and Diner, 1992). The extension of these studies to other positions in the D1 polypeptide was often frustrated by the instability of the $(Mn)_4$ cluster in many mutants. Accordingly, a great deal of effort was directed at characterizing mutants by non-invasive methods in vivo. These methods relied primarily on measuring changes in the yield of chlorophyll *a* fluorescence that were caused by single flashes, multiple flashes, or short periods of continuous illumination given in the presence or absence of DCMU (Nixon and Diner, 1992; Nixon et al., 1992b; Chu et al., 1994a; Diner, 1998). The characterization of the D1-Asp170 mutants by these methods provided the basis for extending these methods to other residues and a number of compendia were published (Nixon and Diner, 1994; Chu et al.,

Abbreviations: BRC – bacterial reaction center; Chl *a* – chlorophyll *a*; Cyt c_{550} – cytochrome c_{550}; D1/D2 – reaction center core subunits; DCMU – 3-(3,4-dichlorophenyl)-1,1-dimethylurea; EDTA – ethylenediaminetetraacetic acid; ENDOR – electron nuclear double resonance; EPR – electron paramagnetic resonance; ESEEM – electron spin echo envelope modulation; EXAFS – extended X-ray absorption fine structure; FTIR – Fourier transform infrared; OEC – oxygen evolving complex; P680 – primary electron donor of PS II; PS II – Photosystem II; Q_A – primary plastoquinone acceptor of PS II; S_n – states of the OEC for n = 0, 1, 2, 3, or 4; UV – ultraviolet; Vis – visible; XANES – X-ray absorption near edge structure.; Y_D – redox active tyrosine on D2; Y_Z – redox active tyrosine on D1

1995a,b). The development of improved methods of purifying PS II particles from *Synechocystis* sp. PCC 6803 with conventional chromatography (Tang and Diner, 1994) and with metal ion affinity chromatography (Bricker et al., 1998; Reifler et al., 1998) has facilitated the biophysical characterization of increasing numbers of mutants with magnetic resonance (EPR, ENDOR, ESEEM), vibrational (FTIR), and UV/Vis optical absorption spectroscopies.

Meanwhile, in parallel to the mutagenesis studies, numerous chemical modification studies were providing evidence that the $(Mn)_4$ cluster is coordinated by both carboxylate and histidine residues (Tamura et al., 1989; Seibert et al., 1989; Preston and Seibert, 1991a,b; Blubaugh and Cheniae, 1992; Magnuson and Andréasson, 1997; Tamura et al., 1997; Ghirardi et al., 1998a,b). On the basis of combined chemical modification and protease digestion studies, specific residues (D1-His337 and D2-His339) were proposed as ligands to the $(Mn)_4$ cluster (Preston and Seibert, 1991a; Ghirardi et al., 1998b). Magnetic resonance studies were also being performed and, on the basis of ESEEM (DeRose et al., 1991; Zimmermann et al., 1993) and ENDOR (Tang et al., 1993a) analyses, it was concluded that the $(Mn)_4$ cluster is ligated by at least one nitrogen atom. Subsequent ESEEM studies, conducted with [^{15}N]histidine-labeled PS II particles, refined this conclusion to show that the $(Mn)_4$ cluster is ligated by at least one histidine residue (Tang et al., 1994) and that this residue coordinates the $(Mn)_4$ cluster with its $\varepsilon 2$ (τ) nitrogen (Gilchrist, 1996). Additional evidence for coordination by histidine was provided by an FTIR study of [^{15}N]histidine-labeled PS II particles (Noguchi et al., 1999).

On the basis of the site-directed mutagenesis and biochemical studies that had been conducted by late 2003, most or all of the amino acid residues that ligate the $(Mn)_4$ cluster were expected to be contributed by the D1 polypeptide (Fig. 1). The recent 3.2 Å and 3.5 Å X-ray crystallographic structural models of PS II (Biesiadka et al., 2004; Ferreira et al., 2004; Chapter 21, Barber and Iwata) have confirmed this expectation, showing that the $(Mn)_4$ cluster is surrounded mostly by residues form the D1 polypeptide, but also by some residues from CP43. In the 3.5 Å structural model, only one Mn ligand, CP43-Glu354, is provided by a polypeptide other than D1. Accordingly, this chapter focuses on the extensive mutagenesis studies that have been directed at the lumenal domains of the D1 polypeptide and describes the few mutagenesis studies that have been directed at the large lumenal loop of CP43. For earlier reviews on this subject, see Debus (2001) and Diner (2001).

II. The D1 Polypeptide

A. The Loop Connecting Helices A and B

The loop connecting helices A and B contains six conserved carboxylate residues, three conserved tyrosine residues, and one conserved histidine residue. These are Asp59, Asp61, Glu65, Tyr73, His92, Tyr94, Glu98, Asp103, Glu104, and Tyr107. The mutations Tyr73Phe, Tyr94Phe, Glu98Gln, Glu98Asp, Asp103Asn Asp103Glu, Glu104Gln, Glu104Asp, and Tyr107Phe caused no discernible alterations to either photoautotrophic growth or O_2 evolution (Chu

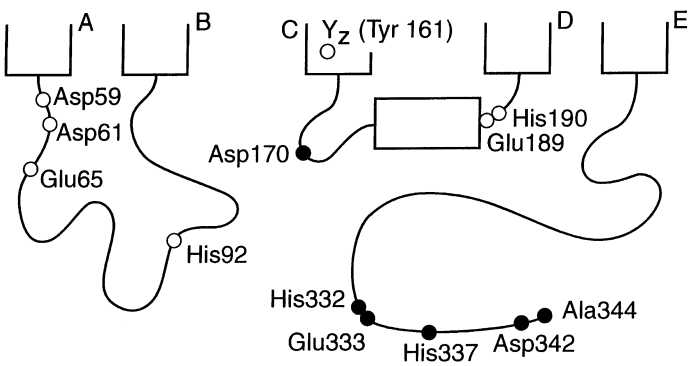

Fig. 1. Schematic folding pattern of the lumenal domains of the D1 polypeptide. Amino acid residues that have been found to influence the properties of the $(Mn)_4$ cluster or Y_Z are indicated. Residues that were identified as possible ligands of the $(Mn)_4$ cluster by site-directed mutagenesis studies are indicated by filled circles. Modified from Debus (2001).

et al., 1995a). Consequently, it was concluded that neither Tyr73, Tyr94, Glu98, Asp103, Glu104, nor Tyr107 are crucial to the mechanism of O_2 evolution (Chu et al., 1995a). In contrast, most of the mutations that were constructed at Asp59, Asp61, Glu65, and His92 were deleterious to O_2 evolution, at least to some extent (Nixon et al., 1992a; Nixon and Diner, 1994; Chu et al., 1995a), and have been investigated further. The conserved residue Arg64 has also been targeted (Li and Burnap, 2001).

1. Aspartate 59 and Aspartate 61

All mutatations have been constructed in *Synechocystis* sp. PCC 6803 (Nixon et al., 1992a; Nixon and Diner, 1994; Chu et al., 1995a). Aspartate 59 has been changed to Glu, Asn, and Val. Aspartate 61 has been changed to Glu, Asn, Ala, and Val. The Asp59Glu, Asp59Asn, and Asp61Glu mutants are strongly photoautotrophic; the others are weakly so. The OECs in the Asp59Glu and Asp61Glu mutants are relatively unimpaired: Asp59Glu and Asp61Glu cells contain only ~60% and ~80% the PS II content of wild-type cells, respectively, but evolve O_2 at ~60% the rate of wild-type cells. The OECs in the other mutants are considerably more impaired: Asp59Asn, Asp61Asn, and Asp61Ala cells contain 60–100% the PS II content of wild-type cells, but evolve O_2 at only 20–30% the rate of wild-type cells. The OECs in the Asp59Val and Asp61Val mutants are even more impaired. The Asp59Asn and Asp61Glu mutants exhibit O_2 flash-yields that have normal period-four oscillations (Qian et al., 1999). However, Asp59Asn, Asp61Asn, and Asp61Ala cells lose O_2-evolving activity rapidly when illuminated with saturating light (Chu et al., 1995a).

On the basis of Chl *a* fluorescence analyses that were conducted with intact cells, it was concluded that essentially all of the PS II reaction centers in the Asp59 and Asp61 mutants contain intact, photooxidizable $(Mn)_4$ clusters in vivo (Chu et al., 1995a). Therefore, it was concluded that neither Asp59 nor Asp61 is likely to ligate the assembled $(Mn)_4$ cluster. This conclusion agrees with the recent 3.2 Å and 3.5 Å X-ray crystallographic structural models (Biesiadka et al., 2004; Ferreira et al., 2004; Chapter 21, Barbe and Iwata). However, the rate of O_2 release is slowed dramatically in Asp61Asn and Asp61Ala cells (10-fold in Asp61Asn cells and 8-fold in Asp61Ala cells) (Hundelt et al., 1998a) and is slowed to lesser extents in Asp61Glu and Asp59Asn thylakoid membranes (Qian et al., 1999). Subsequent analyses of Asp61Asn PS II particles showed that the $S_1 \rightarrow S_2$ and $S_2 \rightarrow S_3$ transitions are slowed approximately 2-fold and that the $S_3 \rightarrow S_0$ transition is slowed 10-fold (Hundelt et al., 1998a,b) in this mutant. The $S_3 \rightarrow S_0$ transition is also slowed in Asp59Asn and Asp61Glu thylakoid membranes, but to lesser extents. The lifetimes of the S_2 and S_3 states are shortened in Asp59Asn and Asp61Glu thylakoid membranes (Qian et al., 1999), suggesting that both the S_2/S_1 and S_3/S_2 midpoint potentials are increased in these mutants. Slight increases in the S_2/S_1 midpoint potential were also suggested on the basis of Chl *a* fluorescence analyses of intact cells (Chu et al., 1995a). The rate of electron transfer from Y_Z to $P680^{\bullet+}$ is unchanged in at least the Asp61Asn mutant (Hundelt et al., 1998a).

The PS II reaction centers in Asp59Asn and Asp61Ala cells appear to have substantially diminished affinities for Ca^{2+}. Neither mutant grew photoautotrophically when Ca^{2+} was omitted from the growth medium and neither Sr^{2+}, nor Mg^{2+}, nor Na^+ would substitute (Chu et al., 1995a). When Asp59Asn and Asp61Ala cells were propagated photoheterotrophically in the absence of Ca^{2+}, little or no O_2 evolution was observed, the rate of electron transfer from Y_Z to $P680^{\bullet+}$ slowed dramatically [as is observed in PS II preparations that have been rigorously depleted of Ca^{2+} ions (Satoh and Katoh, 1985; Boussac et al., 1992)], and PS II became very sensitive to light-induced damage (Chu et al., 1995a). On the basis of these results, it was proposed that Asp59 and Asp61 influence the binding of Ca^{2+} and may form part of a Ca^{2+} binding site (Chu et al., 1995a). Subsequently, it was proposed that binding Ca^{2+} to this site promotes a repositioning of the *C*-terminal domain of the D1 polypeptide during the light-driven assembly (photoactivation) of the $(Mn)_4$ cluster (Chen et al., 1995; Chapter 26). In apparent support of this proposal, at least one unstable photoactivation assembly intermediate is destabilized dramatically in Asp59Asn and Asp61Glu cells (Qian et al., 1999). Nevertheless, neither residue ligates Ca^{2+} in the recent 3.2 Å and3.5 Å X-ray crystallographic structural models (Biesiadka et al., 2004; Ferreira et al., 2004; Chapter 20). Therefore, mutations at Asp59 and Asp61 must cause structural changes that weaken the affinity for Ca^{2+} for a distant site. Similar mutation-induced weakening of the affinity of PS II for Ca^{2+} has been observed at Arg64 (below) and in the *C*-terminal domain of the D1 polypeptide (Section II.C).

2. Arginine 64

The Arg64Glu, Arg64Gln, and Arg64Val mutations have been constructed in *Synechocystis* sp. PCC 6803 (Li and Burnap, 2001). All three mutants are photoautotrophic. The Arg64Glu and Arg64Gln mutants have decreased PS II contents and light-saturated rates of O_2 evolution compared to wild-type cells, and lose O_2-evolving activity rapidly in darkness. All three mutants exhibit O_2 flash-yields that have normal period-four oscillations. In the Arg64Glu and Arg64Gln mutants, the oscillations are characterized by larger miss parameters and the rate of O_2 release is slowed three to five-fold. On the basis of Chl *a* fluorescence analyses, it was concluded that the S_2/S_1 midpoint potential of the $(Mn)_4$ cluster is decreased slightly in Arg64Glu and Arg64Gln cells. Paradoxically, the lifetime of the S_2 state, as measured with O_2 flash yields, decreased considerably in Arg65Glu thylakoid membranes and decreased slightly in Arg64Gln thylakoid membranes. It was suggested that the accelerated decay of the S_2 state in the latter measurements is caused by accelerated electron transfer from Y_D to the S_2 state of the $(Mn)_4$ cluster (Li and Burnap, 2001).

The PS II reaction centers in the Arg64Glu and Arg64Gln mutants appear to have substantially diminished affinities for Ca^{2+}. Neither mutant grew photoautotrophically when Ca^{2+} was replaced by Na^+ in the growth medium (Li and Burnap, 2001). The quantum yield for the light-driven assembly of the $(Mn)_4$ cluster is higher in Arg64Glu than in wild-type cells, although at least one unstable photoactivation assembly intermediate is destabilized, as was observed previously in Asp59Asn and Asp61Glu cells (Section II.A.1).

The Arg64Glu mutation greatly destabilizes the binding of the extrinsic 33 kDa polypeptide and, to a lesser extent, destabilizes the binding of Cyt c_{550}. It was suggested that Arg64 forms a salt-bridge to the extrinsic 33 kDa polypeptide or that the Arg64Glu mutation, and to a lesser extent, the Arg64Gln mutation, cause structural alterations that interfere with the binding of the extrinsic polypeptides and Ca^{2+} to PS II (Li and Burnap, 2001). In the recent X-ray crystallographic structural models, several residues of the extrinsic 33 kDa polypeptide are located very close to D1-Arg64 (Biesiadka et al., 2004; Ferreira et al., 2004; Chapter 21, Barber and Iwata).

3. Glutamate 65

The Glu65Asp, Glu65Gln, Glu65Ala, and Glu65Leu mutations have been constructed in *Synechocystis* sp. PCC 6803 (Nixon et al., 1992a; Nixon and Diner, 1994; Chu et al., 1995a). All four mutants are photoautotrophic, although only Glu65Asp is strongly so. The OEC in the Glu65Asp mutant is essentially unimpaired: Glu65Asp cells contain ~90% the PS II content of wild-type cells and evolve O_2 at ~90% the rate of wild-type cells. The OECs in the other mutants are considerably more impaired: cells of these mutants contain 90–100% the PS II content of wild-type cells, but evolve O_2 at only 10–20% the rate of wild-type cells.

On the basis of Chl *a* fluorescence analyses that were conducted with intact cells, it was concluded that essentially all of the PS II reaction centers in the Glu65 mutants contain intact, photooxidizable $(Mn)_4$ clusters in vivo (Chu et al., 1995a). Therefore, it was concluded that Glu65 is unlikely to ligate the $(Mn)_4$ cluster. This conclusion agrees with the recent X-ray crystallographic structural models (Biesiadka et al, 2004; Ferreira et al., 2004; Chapter 20). It was also concluded that the S_2/S_1 midpoint potential of the $(Mn)_4$ cluster is slightly increased in Glu65Leu cells (Nixon et al., 1992a) and that electron transfer from $Q_A^{\bullet -}$ to Q_B is slowed slightly in Glu65Gln and Glu65Ala cells (Chu et al., 1995a).

The Glu65Asp, Glu65Gln, and Glu65Ala mutants grew photoautotrophically when Ca^{2+} was omitted from the growth medium. Therefore, it was concluded that Glu65 has little or no influence on the binding of Ca^{2+} (Chu et al., 1995a).

4. Histidine 92

The His92Leu, His92Gln, and His92Asn mutations have been constructed in *Synechocystis* sp. PCC 6803 (Nixon et al., 1992a; Chu et al., 1995a; R.J. Debus, unpublished). All three mutants are photoautotrophic and exhibit only slightly impaired light-saturated rates of O_2 evolution. On the basis of Chl *a* fluorescence analyses that were conducted with intact cells, it was concluded that essentially all PS II reaction centers in all three mutants contain intact, photooxidizable $(Mn)_4$ clusters in vivo (Chu et al., 1995a; R.J. Debus, unpublished). Therefore, it was concluded that His92 is unlikely to ligate the assembled $(Mn)_4$ cluster.

The His92Leu mutant grows photoautotrophically at normal rates when Ca^{2+} is replaced by Sr^{2+},

grows at a much slower rate when Ca^{2+} is replaced by Mg^{2+}, but fails to grow photoautotrophically when Ca^{2+} is replaced by Na^{+} (Chu et al., 1995a). When propagated photoheterotrophically in media having Na^{+} substituted for Ca^{2+}, His92Leu cells exhibit low rates of O_2 evolution (< 5% compared to wild-type) and somewhat altered Chl *a* fluorescence properties suggestive of a decreased S_2/S_1 midpoint potential (Chu et al., 1995a). However, the cells show no unusual light-sensitivity. It was concluded that the His92Leu mutation introduces structural perturbations that weaken the affinity of PS II for Ca^{2+} ions (Chu et al., 1995a), but that this affinity is weakened to a much lesser extent than in Asp59Asn and Asp61Ala cells.

B. The Loop Connecting Helices C and D

The loop connecting helices C and D contains two conserved carboxylate residues and one conserved histidine residue. These are Asp170, Glu189, and His190. These residues have been targeted extensively because of the close proximity (in sequence) of Asp170 to Y_Z (Tyr161) and because early modeling studies had predicted that His190 would interact with Y_Z (Debus et al., 1988a; Svensson et al., 1990). Other residues that have been targeted in this loop are Gln165, Phe186, Gln187, Asn191, and His195.

1. Aspartate 170

All possible mutations except Asp170Pro have been constructed in *Synechocystis* sp. PCC 6803 (Boerner et al., 1992; Diner and Nixon, 1992; Nixon and Diner, 1992; Chu et al., 1994a, 1995a; R.J. Debus, unpublished). The Asp170Val mutant has also been obtained as a spontaneous pseudorevertant of Asp170Ala cells (Chu et al., 1995a). The Asp170His, Asp170Asn, Asp170Thr, and Asp170Pro mutations have been constructed in *Chlamydomonas reinhardtii* (Whitelegge et al., 1995). The Asp170Glu mutant is photoautotrophic and evolves O_2 at ~60% the rate of wild-type cells. The Asp170His and Asp170Val mutants are weakly photoautotrophic and evolve O_2 at ~50% and ~40% the rate of wild-type cells, respectively. Photoautotrophic growth is abolished in all other mutants. Most of the mutants have PS II contents that are similar to that of wild-type cells. Only the Asp170Phe, Asp170Trp, and Asp170Pro mutants contain sharply diminished PS II contents.

Among the non-photoautotrophic mutants, O_2 evolution is abolished in Asp170Ser, Asp170Thr, Asp170Ala, Asp170Gly, Asp170Tyr, and Asp170Pro cells, nearly abolished in Asp170Asn and Asp170Trp cells, and diminished substantially in all others. The Asp170Asn mutant assembles $(Mn)_4$ clusters in only ~5% of PS II reaction centers. The Asp170Ala, Asp170Ser, and Asp170Thr mutants assemble no $(Mn)_4$ clusters in in vivo.

In those Asp170 mutants that evolve O_2, the assembled $(Mn)_4$ clusters appear to function normally, exhibiting O_2 flash-yields that have normal period-four oscillations. However, most exhibit slightly decreased S_2/S_1 midpoint potentials and longer S_2 state lifetimes. The mutants that evolve O_2 do not lose this activity rapidly during illumination with saturating light, unlike some of the mutants that have been constructed at Asp59 and Asp61 (Section II.A.1) or in the *C*-terminal domain (Section II.C). On the basis of Chl *a* fluorescence analyses that were conducted with intact cells, it was also concluded that, in the O_2-evolving mutants, significant percentages of PS II reaction centers lack $(Mn)_4$ clusters in vivo. This percentage was estimated to be 20–25% in Asp170Glu cells, ~50% in Asp170His and Asp170Val cells, and ~60% in Asp170Leu, Asp170Ile, and Asp170Arg cells. In these mutants, the $(Mn)_4$ cluster was proposed to be unstable or to be assembled inefficiently. A recent EPR/ESEEM study has shown that the S_1 state and S_2 state multiline EPR signals of Asp170His PS II particles closely resemble those of wild-type PS II particles (Debus et al., 2003). These similarities support the conclusion of earlier studies (Nixon and Diner, 1992; Chu et al., 1994a; Whitelegge et al., 1995), that those $(Mn)_4$ clusters that are assembled in Asp170His cells function normally. The amplitudes of the S_1 and S_2 state multiline EPR signals in Asp170His PS II particles correlate with the lower O_2-evolving activity of Asp170His cells and PS II particles (40–60% compared to wild-type), showing that inefficient assembly of the $(Mn)_4$ cluster, not instability, is the reason that fewer $(Mn)_4$ clusters are present in Asp170His cells (Debus et al., 2003).

On the basis of Chl *a* fluorescence measurements, it was concluded that the rate of electron transfer from Y_Z to $P680^{\bullet+}$ is slowed slightly in most of the Asp170 mutants, although not in Asp170His cells and to only a small extent in Asp170Val cells (Chu et al., 1994a, 1995a). Furthermore, the $Y_Z^{\bullet}/Y_Z$ midpoint potential appeared to be increased in Asp170Ser and Asp170Ala cells (Nixon and Diner, 1992; Chu et al., 1995a). Because of the proximity of Asp170 to

Y_Z (Tyr161 of the D1 polypeptide), such mutation-induced alterations to the environment of Y_Z might not be unexpected.

The high-affinity Mn(II) binding site that is present in Mn-depleted wild-type PS II particles is eliminated in at least the Asp170Asn, Asp170Ala, and Asp170Ser mutants (Nixon and Diner, 1992; Diner and Nixon, 1992). In these mutants, the K_M for binding and oxidzing Mn(II) ions is increased 50- to 60-fold. When Mn-depleted wild-type PS II particles are illuminated in the presence of Mn(II) ions, $Y_Z^{\bullet}$ oxidizes Mn(II) to Mn(III) and a parallel polarization EPR signal of the Mn(III) ion is observed (Campbell et al., 2000). This signal shows hyperfine structure that is consistent with either an elongated six-coordinate octahedral Mn(III) geometry or a five-coordinate square-pyramidal Mn(III) geometry. In Mn-depleted Asp170Glu and Asp170His PS II particles, $Y_Z^{\bullet}$ is also capable of oxidizing Mn(II) ions (Nixon and Diner, 1992; Diner and Nixon, 1992; Campbell et al., 2000). However, a different Mn(III) EPR signal is observed in Asp170His PS II particles, and no Mn(III) EPR signal is observed in Asp170Glu PS II particles (Campbell et al., 2000). Instead, the illuminated Asp170Glu PS II particles exhibit a perpendicular polarization EPR signal that is suggestive of Mn(IV). These results show that Asp170 forms part of the binding site for the first Mn(II) ion that is photooxidized during the light-driven assembly (photoactivation) of the Mn cluster and that the residue that is present at this position influences the coordination environment and redox properties of the photooxidized Mn(II) ion (Chapter 26).

If Asp170 ligates the first Mn(II) ion that is photooxidized during photoactivation of the Mn cluster, it would seem logical that this residue would also ligate the assembled $(Mn)_4$ cluster. Indeed, most studies of Asp170 mutants have suggested this possibility. However, in apparent contradiction to this supposition, Asp170Val cells are photoautotrophic and Asp170Leu and Asp170Ile cells evolve O_2 at ~20% the rate of wild-type cells (Chu et al., 1995a). Neither Val, nor Leu, nor Ile would be expected to ligate Mn. One explanation is that Asp170, although required for the efficient photooxidation of the first Mn ion that is ligated during assembly of the $(Mn)_4$ cluster, does not remain as a ligand to the *assembled* $(Mn)_4$ cluster. However, if Asp170 does not ligate the assembled $(Mn)_4$ cluster, it is difficult to explain why replacement of this residue with Asn is more deleterious to O_2 evolution than replacement with Val, Leu, or Ile. To resolve this paradox, it was proposed that Val, Leu, and Ile, being bulky and hydrophobic, cause structural perturbations that permit the missing carboxylate moiety to be replaced by another residue, a peptide carbonyl group, or a water molecule (Chu et al., 1995a). Compensatory, mutation-induced structural rearrangements have been observed in other systems (Chu et al., 1995a).

Recently, FTIR and ESEEM studies were performed to determine if Asp170 ligates the $(Mn)_4$ cluster and, if so, if it ligates the Mn ion that undergoes oxidation during the $S_0 \rightarrow S_1$, $S_1 \rightarrow S_2$, or $S_2 \rightarrow S_3$ transitions. Both studies were conducted with Asp170His PS II particles.

In one FTIR study (Chu et al., 2001), a low frequency vibrational mode that appears at ~606 cm^{-1} in the S_2 state in wild-type PS II particles shifted to ~612 cm^{-1} in Asp170His PS II particles (Fig. 2, bottom panel). Because this mode had been assigned previously to a Mn-O-Mn structural unit (Chu et al., 2000), the shift of this mode in Asp170His PS II particles shows that Asp170 is structurally coupled to the $(Mn)_4$ cluster. This FTIR study also showed that the Asp170His mutation produces no significant alterations in the mid-frequency region (1800 – 1200 cm^{-1}) of the S_2-*minus*-S_1 FTIR difference spectrum (Fig. 2, top panel). The lack of such alterations shows that the carboxylate stretching modes of Asp170 are not changed during the $S_1 \rightarrow S_2$ transition[1].

A more recent FTIR study has shown that the Asp170His mutation does not significantly alter the mid-frequency regions of *any* of the $S_0 \rightarrow S_1$, $S_1 \rightarrow S_2$, or $S_2 \rightarrow S_3$ FTIR difference spectra (Debus et al., 2005). Therefore, *none* of these S state transitions significantly alters the carboxylate stretching modes of Asp170. Because Asp170 ligates the $(Mn)_4$ cluster in both the recent 3.2 Å and 3.5 Å X-ray crystallographic structural models (Biesiadka et al., 2004; Ferreira et al., 2004; Chapter 21, Barber and Iwata), the simplest explanation for the FTIR data is that the Mn ion that is ligated by Asp170 does not increase its charge or oxidation state during the $S_0 \rightarrow S_1$, $S_1 \rightarrow S_2$, or $S_2 \rightarrow S_3$ transitions. This conclusion has profound

[1]The authors of an earlier FTIR study of Asp170Glu PS II particles concluded that carboxylate stretching modes of Asp170 are changed significantly during the $S_1 \rightarrow S_2$ transition in wild-type PS II particles (Steenhuis et al., 1999). However, the FTIR difference spectra that are reported in Steenhuis et al. (1999) are unlike the S_2-*minus*-S_1 FTIR difference spectra that have been reported by any other laboratory and are undoubtedly dominated by artifacts (Chu et al., 2004).

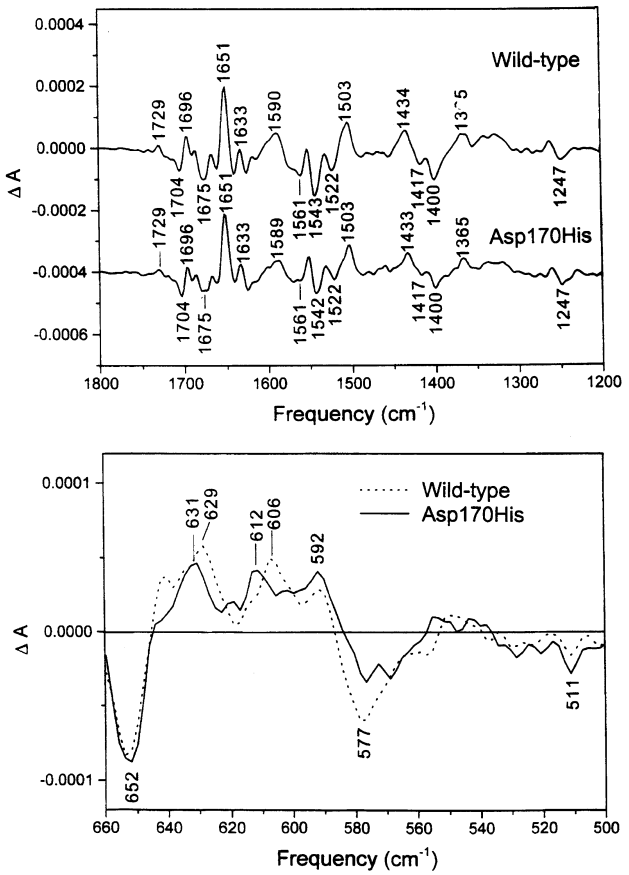

Fig. 2. The S_2-*minus*-S_1 FTIR difference spectra of wild-type and D1-Asp170His PS II particles in the mid-frequency (top panel) and low-frequency (bottom panel) regions of the spectrum. Note the similarity of the wild-type and Asp170His spectra in the mid-frequency region (top panel). Note also that, in the low frequency region of the spectrum (bottom panel), a mode at ~606 cm^{-1} in the wild-type PS II particles shifts to ~612 cm^{-1} in the Asp170His PS II particles. This mode has been assigned to a Mn-O-Mn structural unit in the $(Mn)_4$ cluster. In the lower panel, the amplitude of the Asp170His spectrum has been multiplied by a factor of 1.4 to facilitate comparison. Modified from Chu et al. (2001). More rrecent FTIR data show that the Asp170His mutation causes no significant changes to the S_1-*minus*-S_0, S_2-*minus*-S_1, or S_3-*minus*-S_2 FTIR difference spectra in the mid-frequency region (Debus et al., 2005a).

implications for the mechanism of water oxidation. The proximity of Asp170 to Y_Z, to the Ca ion, and to a putative proton transfer pathway leading to the protein exterior in the 3.5 Å X-ray crystallographic strutural model (Ferreira et al, 2004; Chapter 21, Barber and Iwata), has led to the idea that Asp170 ligates the most catalytically active Mn ion in the $(Mn)_4$ cluster. Recent mechanistic proposals that are based on the 3.5 Å structural model postulate that this Mn ion undergoes oxidation during one or more of the $S_0 \rightarrow S_1$, $S_1 \rightarrow S_2$, or $S_2 \rightarrow S_3$ transitions (McEvoy and Brudvig, 2004; Messinger, 2004; Lundberg and Siegbahn, 2004). In contrast, the FTIR data imply that either (1) the oxidation of this Mn ion occurs only during the transitory $S_3 \rightarrow S_4$ transition, or (2) the oxidation increments and O_2 formation chemistry that occur during the catalytic cycle involve only the remaining $(Mn)_3$ portion of the $(Mn)_4$ cluster.

In the ESEEM study (Debus et al., 2003), the two-pulse ESEEM spectrum of the 9.2 GHz S_2 state multiline EPR signal of Asp170His PS II particles was shown to resemble that of wild-type PS II particles. In particular, no additional histidyl nitrogen modulation appeared at 4–5 MHz and no significant new

modulation was observed. The explanation of these data that was favored by the authors of the ESEEM study is that both Asp170 and His170 ligate the $(Mn)_4$ cluster, but the additional nitrogen hyperfine coupling in the Asp170His mutant is too strong or anisotropic to be detected in the ESEEM analysis (Debus et al., 2003). There is ample precedent for such a scenario from studies of model compounds and metalloenzymes (Debus et al., 2003). In particular, nitrogen atoms that are bound axially to the Mn(III) ion in di-μ_2-oxo-bridged Mn(III)Mn(IV) model compounds have strong hyperfine couplings that escape detection in ESEEM analyses (Randall, 1997). In contrast, nitrogen atoms that are bound to the Mn(IV) ion are detected easily. Once the structure of the $(Mn)_4$ cluster is known accurately, analyses of relevant $(Mn)_4$ model compounds may show if the inability to detect additional histidyl nitrogen modulation in Asp170His PS II particles with a 9 GHz ESEEM analysis provides a clue about the valence of the Mn ion that is ligated by Asp170.

The Asp170His mutant grew photoautotrophically when Ca^{2+} was omitted from the growth medium and its light-saturated rate of O_2 evolution decreased only slightly (Chu et al., 1995a). In addition, the Chl *a* fluorescence properties of Asp170His and Asp170Ala cells that had been propagated photoheterotrophically in media having Na^+ substituted for Ca^{2+} were altered only slightly (Chu et al., 1995a). On the basis of these results, it was concluded that Asp170 has little or no influence on the binding of Ca^{2+} (Chu et al., 1995a).

In the recent 3.2 Å and 3.5 Å X-ray crystallograpic structural models, Asp170 is identified as ligating the same Mn ion as Glu333 (Biesiadka et al., 2004; Ferreira et al., 2004; Chapter 21, Barber and Iwata). Ligation of the same Mn ion by Asp170 and Glu333 is surprising because the Asp170 and Glu333 mutants exhibit very different properties (Section II.C.2).

2. Glutamate 189

All possible mutations except Glu189Pro and Glu189Trp have been constructed in *Synechocystis* sp. PCC 6803 (Chu et al., 1995a; Debus et al., 2000a). The Glu189Gln, Glu189Asp, and Glu189Leu mutations have also been constructed in *Chlamydomonas reinhardtii* (Svensson et al., 1998). The Glu189Gln, Glu189Lys, Glu189Arg, Glu189Leu, and Glu189Ile mutants are photoautotrophic. The OECs in these mutants are relatively unimpaired: Glu189Gln, Glu189Lys, and Glu189Arg cells contain 70–100% the PS II content of wild-type cells and evolve O_2 at 70–80% the rate of wild-type cells, while Glu189Leu and Glu189Ile cells contain ~60% the PS II content of wild-type cells and evolve O_2 at 40–60% the rate of wild-type cells. All other Glu189 mutants are non-photoautotrophic. None of the non-photoautotrophic mutants evolves O_2 to a significant extent (Chu et al., 1995a; Debus et al., 2000a). The non-photoautotrophic mutants contain ≥ 90% the PS II content of wild-type cells, except for the Glu189Val, Glu189Cys, Glu189Tyr, and Glu189Phe mutants. The latter contain 50–70% the PS II content of wild-type cells.

On the basis of Chl *a* fluorescence analyses that were conducted with intact cells, it was concluded that, in all of the Glu189 mutants, significant percentages of PS II reaction centers lack photooxidizable $(Mn)_4$ clusters in vivo. These percentages were estimated to be 10–20% in Glu189Gln, Glu189Lys, Glu189Arg, Glu189Ile, Glu189Asp, Glu189Asn cells, 20–30% in Glu189Leu, Glu189His, Glu189Gly, Glu189Val, and Glu189Cys cells, 30–50% in Glu189Ser and Glu189Phe cells, and 50–70% in Glu189Ala, Glu189Thr, Glu189Met, and Glu189Tyr cells (Chu et al., 1995a; Debus et al., 2000a; R.J. Debus, unpublished). It was also concluded that S_2/S_1 midpoint potential is relatively unchanged in most of the Glu189 mutants, but that the $S_2 \rightarrow S_3$ or $S_3 \rightarrow S_0$ transition is slowed dramatically in the non-photoautotrophic mutants. Intact Glu189Gln PS II particles exhibit normal S_1 and S_2 mutiline EPR signals (Debus et al., 2000a) and exhibit an S_2-*minus*-S_1 FTIR difference spectrum that resembles that of wild-type PS II particles (R.J. Debus, unpublished)[2].

Intact Glu189Gln PS II particles show normal kinetics of O_2 release and a normal rate of electron transfer from the $(Mn)_4$ cluster to $Y_Z^{\bullet}$ during the $S_3 \rightarrow S_0$ transition (Clausen et al., 2001). Intact Glu189Gln, Glu189Lys, and Glu189Arg PS II particles also exhibit normal rates of electron transfer from the $(Mn)_4$ cluster to $Y_Z^{\bullet}$ during the $S_1 \rightarrow S_2$ and $S_2 \rightarrow S_3$

[2]There is a report that the $Y_Z^{\bullet}$-*minus*-Y_Z FTIR difference spectrum of Mn-depleted Glu189Gln PS II particles shows alterations that can be attributed to the loss of a Glu residue or to the appearance of an additional Asp or Glu residue in the environment of Y_Z in the mutant (Pujols-Ayala and Barry, 2002). However, the wild-type and mutant spectra that are reported in Pujols-Ayala and Barry (2002) are unlike that of $Y_Z^{\bullet}$-*minus*-Y_Z (Berthomieu et al., 1998) and appear to be dominated by the spectral features of $Q_A^{\bullet-}$-*minus*-Q_A (Berthomieu and Hienerwadel, 2005; Chapter 16, Noguchi and Berthomieu).

transitions (Clausen et al., 2001). Finally, the rate of electron transfer from Y_Z to $P680^{\bullet+}$ is normal in intact Glu189Gln, Glu189Lys, and Glu189Arg PS II particles and the rate of charge recombination between $Q_A^{\bullet-}$ and $P680^{\bullet+}$ is normal in Mn-depleted Glu189Gln PS II particles (Clausen et al., 2001).

In contrast, PS II particles that are isolated from the non-photoautotrophic mutants (e.g., Glu189Asp, Glu189Asn, Glu189His, Glu189Gly, and Glu189Ser) exhibit no S_1 or S_2 state multiline EPR signals and are unable to advance beyond an altered $S_2Y_Z^{\bullet}$ state, as shown by the accumulation of narrow $S_2Y_Z^{\bullet}$ EPR signals under multiple turnover conditions (Debus et al., 2000a). Also, the quantum yield for oxidizing the S_1 state $(Mn)_4$ cluster is very low in Glu189Gly and Glu189Ser PS II particles, corresponding to a ≥1400-fold slowing of the rate of Mn oxidation by $Y_Z^{\bullet}$. Charge recombination between $Q_A^{\bullet-}$ and $Y_Z^{\bullet}$ is accelerated in the non-photoautotrophic Glu189 mutants, showing that the mutations alter the redox properties of Y_Z in addition to those of the Mn cluster (Debus et al., 2000a).

Because of the near-native characteristics of the Glu189Gln, Glu189Lys, Glu189Arg mutants, and because only 10–20% of the PS II reaction centers in Glu189 mutants having substitutions as diverse as Gln, Lys, Arg, Asp, and Asn lack photooxidizable Mn ions in vivo, it was proposed that Glu189 does not ligate the assembled $(Mn)_4$ cluster (Chu et al., 1995a; Debus et al., 2000a; Debus, 2001). Instead, Glu189 was proposed to participate in a network of hydrogen bonds that facilitates electron transfer from the $(Mn)_4$ cluster to $Y_Z^{\bullet}$ during the higher S state transitions (Debus et al., 2000a; Debus, 2001). This network is believed to be disrupted by inhibitory treatments (e.g., the addition of acetate or ammonia or the depletion of Ca^{2+} or Cl^-) that prevent advancement beyond the $S_2Y_Z^{\bullet}$ state (Szalai and Brudvig, 1996; Tommos and Babcock, 2000; Vrettos et al., 2001; Vrettos and Brudvig, 2002) and was proposed to be similarly disrupted in the non-photoautotrophic Glu189 mutants (Debus et al., 2000a; Debus, 2001). To account for the near-native characteristics of the Glu189Gln, Glu189Lys, and Glu189Arg mutants, it was proposed that the network of hydrogen bonds involving Glu189 is maintained by Gln because of its hydrogen bonding characteristics and by Lys and Arg because of their flexibility and hydrogen bonding characteristics (Chu et al., 1995a; Debus et al., 2000a; Debus, 2001). To account for the photoautotrophic nature of the Glu189Leu and Glu189Ile mutants, it was proposed that the relative bulk and hydrophobicity of Leu and Ile cause structural perturbations that permit the missing Glu189 carboxylate moiety to be replaced by another residue or by a water molecule (Chu et al., 1995a).

In the recent 3.2 Å and 3.5 Å X-ray crystallographic structural models, Glu189 is identified as a ligand of the $(Mn)_4$ cluster (Biesiadka et al., 2004; Ferreira et al., 2004; Chapter 21, Barber and Iwata). Reconciling the many mutagenesis studies of this residue with the crystallographic structural models will require further study. In the crystallographic structural models, Glu189 is identified as ligating the same Mn ion as His332. Ligation of the same Mn ion by Glu189 and His332 is surprising because the Glu189 and His332 mutants exhibit very different properties (Section II.C.1).

The Glu189Gln mutant grew photoautotrophically, but at a slightly slower rate, when Ca^{2+} ions were omitted from the growth medium (Chu et al., 1995a). Under these conditions, the O_2-evolving activity and PS II content of Glu189Gln cells were diminished slightly, but the mutant's Chl *a* fluorescence characteristics were unchanged. The fluorescence properties of Glu189Asp cells were also unchanged when these cells were propagated photoheterotrophically in media having Na^+ substituted for Ca^{2+} (Chu et al., 1995a). Consequently, it was concluded that Glu189 has little or no influence on the binding of Ca^{2+} (Chu et al., 1995a).

3. Histidine 190

All possible mutations except His190Ile, His190Met, His190Pro, and His190Trp have been constructed in *Synechocystis* sp. PCC 6803 (Diner et al., 1991; Nixon et al., 1992a; Nixon and Diner, 1994; Chu et al., 1995a; Hays et al., 1998; Diner and Nixon, 1998). The His190Phe, His190Tyr, and His190Arg mutations have also been constructed in *Chlamydomonas reinhardtii* (Roffey et al., 1994a,b; Kramer et al., 1994; Svensson et al., 1998). All of the mutations abolish photoautotrophic growth. All of the mutations except His190Lys and His190Arg abolish O_2 evolution. The His190Lys and His190Arg mutants evolve O_2 at only ~13% the rate of wild-type cells (Chu et al., 1995a; Hays et al., 1998). This O_2-evolving activity is lost rapidly during illumination with saturating light (Chu et al., 1995a). On the basis of Chl *a* fluorescence measurements that were conducted with intact cells, it was estimated that essentially no

PS II reaction centers in His190Gln, His190Asn, His190Leu, and His190Tyr cells and only ~30% of the PS II reaction centers in His190Arg cells contain photooxidizable Mn ions in vivo (Chu et al., 1995a). The PS II contents of most of the His190 mutants are similar to that of wild-type cells. The exceptions are His190Leu, His190Tyr, and His190Phe cells. These contain ~60% the PS II content of wild-type cells.

Although His190 was once considered to be a possible ligand of the $(Mn)_4$ cluster, it clearly plays a pivotal role in Y_Z function. Electron transfer from Y_Z to $P680^{\bullet+}$ is severely disrupted in all of the His190 mutants (Diner et al., 1991; Nixon et al., 1992a; Kramer et al., 1994; Nixon and Diner, 1994; Roffey et al., 1994a; Chu et al., 1995a; Diner and Nixon, 1998; Hays et al., 1998, 1999; Mamedov et al., 1998; R.J. Debus, unpublished). In purified His190 mutant PS II particles, the rate of electron from Y_Z to $P680^{\bullet+}$ is slowed more than 1000-fold at neutral pH values (Diner and Nixon, 1998; Hays et al., 1998, 1999). This rate is accelerated dramatically in the presence of small organic bases (e.g., 5–100 mM imidazole) (Hays et al., 1998, 1999) or at elevated pH values (i.e., at pH > 9) (Mamedov et al., 1998; Hays et al., 1999). The efficiency of Y_Z oxidation exhibits an apparent pK_A value of ~10.3 in His190Ala PS II particles (Hays et al., 1999). This apparent pK_A value decreases in the presence small organic bases, becoming the same as the solution pK_A value of the added base. Because the disruption of Y_Z oxidation is partly restored in the presence of small organic bases and at elevated pH values, it was concluded that the oxidation of Y_Z requires its deprotonation and that His190 serves as the proton acceptor[3].

The value of ~10.3 was assigned to the pK_A of Y_Z in the absence of the His190 imidazole moiety (Hays et al., 1999). In the recent 3.2 Å and 3.5 Å X-ray crystallographic structural models, His190 is identified as forming a hydrogen bond with Y_Z (Biesiadka et al., 2004; Ferreira et al., 2004; Chapter 21, Barber and Iwata).

[3]It has been argued that His190 does *not* serve as the proton acceptor for Y_Z because a light-*minus*-dark FTIR difference spectra that was attributed to $Y_Z^{\bullet}$-minus-Y_Z in His190Gln PS II particles resembled the spectrum that was attributed to $Y_Z^{\bullet}$-minus-Y_Z in wild-type PS II particles (Bernard et al., 1995; Pujols-Ayala and Barry, 2002). However, the wild-type and mutant spectra that are reported in Bernard et al. (1995) and Pujols-Ayala and Barry (2002) are unlike the spectrum of $Y_Z^{\bullet}$-*minus*-Y_Z (Berthomieu et al., 1998) and appear to be dominated by the spectral features of $Q_A^{\bullet-}$-*minus*-Q_A (Berthomieu and Hienerwadel, 2005; Chapter 16, Noguchi and Berthomieu).

Because the rate of electron transfer from Y_Z to $P680^{\bullet+}$ is slowed dramatically in the His190 mutants, the flash-induced yield of $Y_Z^{\bullet}$ is low [e.g., 30–38% in His190Gln PS II particles (Diner and Nixon, 1998; Pujols-Ayala and Barry, 2002) and 10–15% in His190Phe and His190Tyr PS II membranes (Roffey et al., 1994b)]. However, under continuous illumination, $Y_Z^{\bullet}$ can be photoaccumulated to the same yield as in wild-type PS II preparations, at least in His190Gln, His190Glu, and His190Asp PS II preparations (Tang et al., 1993b; Bernard et al., 1995; Pujols-Ayala and Barry, 2002).

In all of the His190 mutants that have been examined, the reduction of $Y_Z^{\bullet}$ is also slowed dramatically (Mamedov et al., 1998; Hays et al., 1998). This reduction is accelerated substantially by the addition of small organic bases (e.g., 0.5 to 5 mM imidazole) (Hays et al., 1998). On the basis of these observations, it was concluded that the hydroxyl proton of Y_Z remains bound to His190 during the lifetime of $Y_Z^{\bullet}$ and that the reprotonation of $Y_Z^{\bullet}$ is required for its reduction (Hays et al., 1998).

4. Glutamine 165, Phenylalanine 186, Glutamine 187, Asparagine 191 and Histidine 195

The Gln165Glu, Gln165Ala, Gln187Glu, and Gln187Ala mutations have been constructed in *Synechocystis* sp. PCC 6803 (R.J. Debus, unpublished). All four mutants are photoautotrophic but have not been studied further. On the basis of the recent 3.5 Å X-ray crystallographic structural model of PS II, Gln165 has been suggested to provide hydrogen bonds that help stabilize intermediates in O=O bond formation (Ferreira et al., 2004; Chapter 21, Barber and Iwata). The Asn161Ala, Asn161Leu, and Asn161Asp mutations have been constructed in *Chlamydomonas reinhardtii* (Svensson et al., 1998). All three mutants are photoautotrophic but show an apparent decrease in the S_2/S_1 midpoint potential (Svensson et al., 1998). The Phe186Leu, Phe186Ser, Phe186Ala, Phe186Tyr, and Phe186Trp mutations have been constructed in *Synechocystis* sp. PCC 6803 (Wiklund et al., 2001). None of the mutants is photoautotrophic except Phe186Leu. The non-photoautotrophic mutants show little or no O_2-evolving activity (Wiklund et al., 2001). The Phe186Leu mutant evolves O_2 at ~70% of the rate of wild-type cells (Wiklund et al., 2001) but its O_2 flash yields show no period-four oscillations (Funk et al., 2001).

The His195Leu mutation has been constructed in

Synechocystis sp. PCC 6803 (Nixon et al., 1992a) and grows photoautotrophically. The His195Asn, His195Asp, and His195Tyr mutations have been constructed in *Chlamydomonas reinhardtii* (Roffey et al., 1991; Roffey et al., 1994a). These mutants grow autotrophically, although the growth and O_2 evolving rates of His195Asp and His195Tyr cells are lower than that of wild-type cells (Roffey et al., 1994a). On the basis of Chl *a* fluorescence measurements that were conducted with intact and Mn-depleted thylakoid membranes, it was concluded that the $Y_Z^{\bullet}/Y_Z$ midpoint potential is increased substantially in the H195D mutant (Roffey et al., 1994a).

C. The Carboxyl-Terminal Domain

The *C*-terminal domain of the D1 polypeptide contains five conserved carboxylate residues and two conserved histidine residues. Each has been targeted. The following mutations, each constructed in *Synechocystis* sp. PCC 6803, caused no discernable alterations to either photoautotrophic growth or O_2 evolution: Asp308Asn, Asp308Ala, Asp319Glu, Asp319Asn, Asp319Ala, Glu329Asp, Glu329Gln (Nixon et al., 1992a; Chu et al., 1995b). Consequently, it was concluded that neither Asp308, nor Asp319, nor Glu329 is crucial to the mechanism of photosynthetic water oxidation (Chu et al., 1995b). No further investigations of these residues have been undertaken. In contrast, all of the mutations that have been constructed at His332, Glu333, His337, and Asp342 are deleterious to O_2 evolution. None of these residues appears to ligate the first Mn(II) ion that is bound during the light-driven assembly of the $(Mn)_4$ cluster (Nixon and Diner, 1994; Chapter 26, Dismukes et al.), but all four influence the assembly or stability of the $(Mn)_4$ cluster and all four influence the binding of Ca^{2+} to PS II. Also, many of the His332, Glu333, His337, and Asp342 mutants are extremely sensitive to light and many of the mutations that have been constructed at these positions appear to interfere with the binding of the extrinsic 33 kDa polypeptide. In addition to these four residues, the conserved residue Arg334 and the *C*-terminus of the D1 polypeptide at Ala344 have been targeted.

1. Histidine 332

The His332Glu, His332Gln, His332Asp, His332Asn, His332Lys, His332Arg, His332Leu, His332Tyr, His332Ser, and His332Gly mutations have been constructed in *Synechocystis* sp. PCC 6803 (Nixon and Diner, 1994; Chu et al., 1995b; Diner, 2001). None are photoautotrophic. Only the His332Gln and His332Ser mutants evolve O_2, and at only 10–15% the rate of wild-type cells. Both mutants lose O_2-evolving activity rapidly when illuminated with saturating light. The PS II contents of His332Glu and His332Asp cells are similar to that of wild-type cells, whereas the PS II contents of the other mutants are 50–80% compared to wild-type cells, except the His332Leu and His332Tyr mutants, whose PS II contents are only 30–40% compared to wild-type cells (Chu et al., 1995b). A photoautotrophic suppressor mutant has been isolated from His332Gly cells (Diner, 2001). However, this suppressor mutant retains the His332Gly mutation and the compensating mutation is not in the D1 polypeptide.

On the basis of Chl *a* fluorescence analyses that were conducted with intact cells, it was concluded that one or more of the S state transitions is slowed substantially in the His332Glu, His332Asp, and His332Lys mutants and to lesser extents in all of the other mutants except His332Gln (Chu et al., 1995b). It was also concluded that S_2/S_1 midpoint potential is essentially unchanged in His332Gln and His332Ser cells, is slightly decreased in His332Asp cells, and is substantially decreased in His332Glu, His332Asn, and His332Lys cells (Chu et al., 1995b). In the His332Arg, His332Leu, and His332Tyr mutants, charge recombination between $Q_A^{\bullet-}$ and the donor side of PS II is especially slow and has been speculated to occur between $Q_A^{\bullet-}$ and a single Mn(III) ion (Chu et al., 1995b). The kinetics of charge recombination in these mutants resemble those of cells that lack the extrinsic 33 kDa polypeptide (Chu et al., 1994a). Consequently, it was proposed that these His332 mutants interfere with the normal binding of the extrinsic 33 kDa polypeptide to PS II (Chu et al., 1994b, 1995b).

The rate of electron transfer from $Q_A^{\bullet-}$ to Q_B is slowed considerably in many His332 mutants and the $Y_Z^{\bullet}/Y_Z$ midpoint potential appears to be increased in His332Glu, His332Asp, His332Asn, and His332Lys cells (Chu et al., 1995b). On the other hand, electron transfer from Y_Z to $P680^{\bullet+}$ appears to proceed normally in all of the His332 mutants.

In all of the His332 mutants except His332Glu and His332Asp, substantial percentages of PS II reaction centers lack photooxidizable Mn ions in vivo (Chu et al., 1995b). These percentages vary from 15–20% in His332Gln and His332Lys cells to ~40%

in His332Asn cells. Therefore, it was concluded that His332 influences the assembly or stability of the $(Mn)_4$ cluster. However, the high-affinity Mn-binding site that was identified in the Asp170 mutants remains intact (Nixon and Diner, 1994). Several His332 mutants (e.g., His332Ser, His332Lys, His332Arg, His332Leu, and His332Tyr) are extremely sensitive to light-induced damage. Because cells that assemble no $(Mn)_4$ clusters in vivo (e.g., cells of the mutants Asp170Ala and Asp170Ser) are not particularly sensitive to light, it was proposed that the extreme light-sensitivity of the His332 mutants is caused by the release of toxic, activated oxygen species from perturbed $(Mn)_4$ clusters (Chu et al., 1995b).

Intact His332Glu PS II particles exhibit an altered S_2 state multiline EPR signal that has more hyperfine lines and narrower splittings than the S_2 state multiline EPR signal that is observed in wild-type PS II preparations (Debus et al., 2000b). However, the quantum yield for oxidizing the S_1 state $(Mn)_4$ cluster is very low, corresponding to an 8,000-fold slowing of the rate of electron transfer from the $(Mn)_4$ cluster to $Y_Z^{\bullet}$. In addition, the temperature threshold for forming the S_2 state is approximately 100 K higher than in wild-type PS II preparations. Furthermore, His332Glu PS II preparations are unable to advance beyond an altered $S_2Y_Z^{\bullet}$ state, as shown by the accumulation of a narrow $S_2Y_Z^{\bullet}$ EPR signal under multiple turnover conditions. Charge recombination between $Q_A^{\bullet -}$ and $Y_Z^{\bullet}$ is also accelerated, showing that the His332Glu mutation alters the redox properties of Y_Z in addition to those of the Mn cluster. These results are consistent with His332 being close to the $(Mn)_4$ cluster and participating in a network of hydrogen bonds that facilitates electron transfer from the $(Mn)_4$ cluster to $Y_Z^{\bullet}$ during the higher S state transitions (Debus et al., 2000b).

An ESEEM study of His332Glu PS II particles was undertaken to address whether or not His332 ligates the assembled $(Mn)_4$ cluster (Debus et al., 2001). This study revealed that the nitrogen modulation that is observed near 5 MHz in the two-pulse ESEEM spectrum of the S_2 state multiline EPR signal of wild-type PS II particles is diminished substantially in His332Glu PS II particles (Fig. 3) (Debus et al., 2001). Because this modulation arises from magnetic coupling between the $(Mn)_4$ cluster and 1–2 histidyl ligands (Tang et al., 1994; Gilchrist, Jr., 1996), its diminished amplitude in His332Glu PS II particles provides strong evidence that His332 ligates the $(Mn)_4$ cluster. The diminished nitrogen

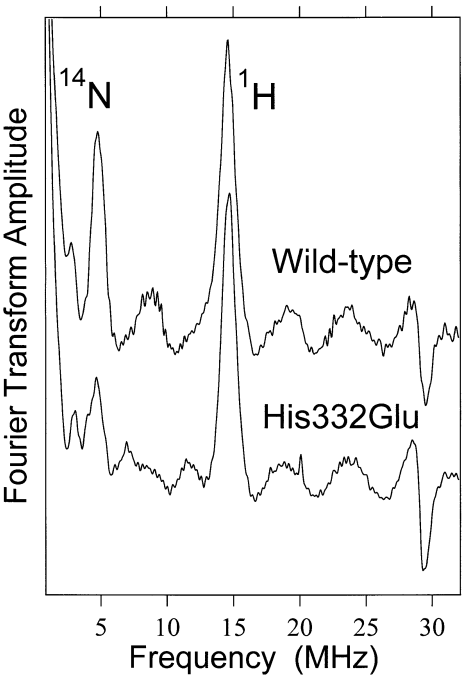

Fig. 3. Two-pulse time domain ESEEM spectra of the 9.2 GHz S_2 state multiline EPR signals in wild-type and His332Glu PS II particles. In the spectrum of the wild-type PS II particles, the 4.8 MHz feature corresponds to nitrogen modulation from at least one histidyl ligand of the $(Mn)_4$ cluster. Note that the amplitude of this feature is sharply diminished in His332Glu PS II particles, consistent with the ligation of the $(Mn)_4$ cluster by His332. The features at ~14.5 and ~29 GHz correspond to protons that are weakly coupled to the electron spin of the $(Mn)_4$ cluster. Modified from Debus et al. (2001).

modulation amplitude could represent either the loss of the ligating His332 ε2 (τ) nitrogen, decreasing the coordination number of one Mn ion from six to five, or the replacement of the ligating nitrogen with an oxygen from glutamate or with an oxygen from another residue, peptide group, or water molecule (Debus et al., 2001).

Ligation of the $(Mn)_4$ cluster by His332 is the simplest and most straight-forward explanation for the diminished histidyl nitrogen modulation in the His332Glu mutant. In support of this explanation, His332 was identified as a ligand of the $(Mn)_4$ cluster in the recent 3.2 Å and 3.5 Å X-ray crystallographic structural models (Biesiadka et al., 2004; Ferreira et al., 2004; Chapter 21, Barber and Iwata).

The PS II reaction centers in the His332 mutants

appear to have substantially diminished affinities for Ca^{2+}. When His332Gln, His332Glu, His332Asp, His332Asn or His332Leu cells were propagated photoheterotrophically in media containing Na^+ substituted for Ca^{2+}, the rate of electron transfer from Y_Z to $P680^{\bullet+}$ slowed dramatically, as is observed in Asp59Asn and Asp61Ala cells that have been propagated under the same conditions (Section II.A.1) and in PS II preparations that have been rigorously depleted of Ca^{2+} ions (Satoh and Katoh, 1985; Boussac et al., 1992). Because histidine is unlikely to ligate Ca^{2+}, it was proposed that the diminished affinity for Ca^{2+} ions was an indirect consequence of the His332 mutations (Chu et al., 1995b).

In the recent 3.2 Å and 3.5 Å X-ray crystallographic structural models of PS II, His332 was identified as a ligand of the same Mn ion that is ligated by Glu189 (Biesiadka et al, 2004: Ferreira et al., 2004; Chapter 21, Barber and Iwata). It is surprising that Glu189 and His332 would ligate the same Mn ion because the Glu189 and His332 mutants exhibit very different properties. Several of the His332 mutants are very sensitive to light-induced damage, whereas none of the Glu189 mutants are particularly sensitive to light. Furthermore, mutations of His332 substantially decrease the affinity of PS II for Ca^{2+}, whereas mutations of Glu189 do not.

2. Glutamate 333

The Glu333Gln, Glu333Asp, Glu333Asn, Glu333His, Glu333Ala, and Glu333Tyr mutations have been constructed in *Synechocystis* sp. PCC 6803 (Nixon et al., 1992a; Nixon and Diner, 1994; Chu et al., 1995b). Only the Glu333Gln mutant is photoautotrophic. This mutant evolves O_2 at ~36% the rate of wild-type cells. This O_2-evolving activity is lost rapidly during illumination with saturating light. The PS II contents of the mutants are 65–90% for Glu333Gln cells, ~60% for Glu333Asp, Glu333His, and Glu333Tyr cells, and 40–50% for Glu333Asn and Glu333Ala cells compared to wild-type cells (Chu et al., 1995b). On the basis of Chl *a* fluorescence analyses that were conducted with intact cells, it was concluded that the S_2/S_1 midpoint potential is essentially unchanged in the Glu333Gln and Glu333Asp mutants, but is slightly decreased in the Glu333Asn and Glu333His mutants (Chu et al., 1995b). In Glu333Ala and Glu333Tyr cells, charge recombination between $Q_A^{\bullet-}$ and the donor side of PS II is especially slow and has been speculated to occur between $Q_A^{\bullet-}$ and a single Mn(III) ion (Chu et al., 1995b). The kinetics of charge recombination in these mutants resemble those of cells that lack the extrinsic 33 kDa polypeptide (Chu et al., 1994a). Consequently, it was proposed that, like some of the His332 mutants (Section II.C.1), some of the Glu333 mutants interfere with normal binding of the extrinsic 33 kDa polypeptide to PS II (Chu et al., 1994b, 1995b). The rate of electron transfer from $Q_A^{\bullet-}$ to Q_B is slowed considerably in Glu333Asp and Glu333His cells and the $Y_Z^{\bullet}/Y_Z$ midpoint potential appears to be increased slightly in Glu333Asp cells (Chu et al., 1995b). On the other hand, electron transfer from Y_Z to $P680^{\bullet+}$ appears to proceed normally in all of the Glu333 mutants.

In all of the Glu333 mutants, substantial percentages of PS II reaction centers lack photooxidizable Mn ions in vivo (Chu et al., 1995b). These percentages range from ~25% and ~40% in Glu333Gln and Glu333Asp cells, respectively, to ~60% in Glu333Tyr cells. Therefore, it was concluded that Glu333 influences the assembly or stability of the $(Mn)_4$ cluster. However, the high-affinity Mn-binding site that was identified in the Asp170 mutants remains intact (Nixon and Diner, 1994). All of the Glu333 mutants are extremely sensitive to light-induced damage. Because cells that assemble no $(Mn)_4$ clusters in vivo (e.g., cells of the mutants Asp170Ala and Asp170Ser) are not particularly sensitive to light, it was proposed that the extreme light sensitivity of the light-sensitive Glu333 mutants is caused by the release of toxic, activated oxygen species from perturbed $(Mn)_4$ clusters (Chu et al., 1995b).

Because the Glu333Gln cells evolve O_2 and because Gln can functionally replace His as a ligand to Fe in cytochrome *c* peroxidase (Choudhury et al., 1994), it was proposed that Glu333 is a possible ligand of the $(Mn)_4$ cluster (Chu et al., 1995b). As an alternative possibility, it was also suggested that Glu333 may participate in a network of hydrogen bonds that can be maintained, in part, by Gln (Chu et al., 1995b). In the recent 3.2 Å and 3.5 Å X-ray crystallographic structural models (Biesiadka et al., 2004; Ferreira et al., 2004; Chapter 21, Barber and Iwata), Glu333 is identified as a ligand of the $(Mn)_4$ cluster

The PS II reaction centers in the Glu333 mutants appear to have substantially diminished affinities for Ca^{2+}. When Glu333Gln or Glu333Asp cells were propagated photoheterotrophically in media containing Na^+ substituted for Ca^{2+}, the rate of electron transfer from Y_Z to $P680^{\bullet+}$ slowed dramatically, as was observed for several His332 mutants (Section II.C.1)

and in PS II preparations that have been rigorously depleted of Ca^{2+} ions (Satoh and Katoh, 1985; Boussac et al., 1992). It was argued that the diminished affinity for Ca^{2+} ions is an indirect consequence of the Glu333 mutations (Chu et al., 1995b).

In the recent 3.2 Å and 3.5 Å X-ray crystallographic structural models, Glu333 was identified as a ligand of the same Mn ion that is ligated by Asp170 (Biesiadka et al., 2004; Ferreira et al., 2004; Chapter 21, Barber and Iwata). Like the situation with Glu189 and His332, it is surprising that Asp170 and Glu333 would ligate the same Min ion because the Asp170 and Glu333 mutants exhibit such different properties. Several of the Asp170 mutants eliminate the high-affinity binding site for the first Mn(II) ion that is oxidized during photoactivation of the $(Mn)_4$ cluster, whereas the Glu333 mutations reportedly do not. All of the Glu333 mutants are highly sensitive to light-induced damage, whereas none of the Asp170 mutants are particularly sensitive to light. Mutations of Glu333 substantially decrease the affinity of PS II for Ca^{2+}, whereas mutations of Asp170 do not.

3. Arginine 334

The Arg334Glu and Arg334Val mutants have been constructed in *Synechocystis* sp. PCC 6803 (Li and Burnap, 2002). Both mutants are photoautotrophic. The O_2-evolving activities of Arg334Glu and Arg334Val cells are ~70% and ~38% compared to that of wild-type cells, respectively, and the PS II contents of Arg334Glu and Arg334Val cells are ~70% and ~90%, respectively, compared to wild-type cells. Both mutants exhibit O_2 flash-yields that have period-four oscillations, but the oscillations are more strongly damped and are characterized by higher miss parameters and altered initial S state distributions. The rate of O_2 release is slowed dramatically in Arg334Glu and Arg334Val cells (~5-fold in Arg334Glu and ~15-fold in Arg334Val) and thylakoid membranes (Li and Burnap, 2002). Indeed, the rate of O_2 release in Arg334Val cells is the slowest that has ever been measured in any mutant or biochemically altered preparation. The Arg334Glu and Arg334Val thylakoid membranes also showed a dramatically increased lifetime for the S_2 state, as measured by O_2 flash yields, but showed a slightly destabilized lifetime for the S_3 state (Li and Burnap, 2002). Paradoxically, the S_2/S_1 midpoint potential in the mutants appeared to be essentially unchanged from that in wild-type cells, as estimated from the kinetics of charge recombination between $Q_A^{\bullet-}$ and the S_2 state. Because the decay of the S_2 state in the O_2 flash yield measurements corresponds to charge recombination from $Q_B^{\bullet-}$ rather than from $Q_A^{\bullet-}$, it was suggested that the stability of the of the S_2 state might be time-dependent, with the $(Mn)_4$ cluster slowly rearranging to form a more stable configuration once the S_2 state is achieved (Li and Burnap, 2002).

4. Histidine 337

The His337Arg, His337Glu, His337Gln, His337Asp, His337Asn, His337Leu, His337Val, His337Tyr, His337Phe, His337Ser, His337Thr, and His337Gly mutations have been constructed in *Synechocystis* sp. PCC 6803 (Nixon et al., 1992a; Nixon and Diner, 1994; Chu et al., 1995b; R.J. Debus, unpublished). The His337Phe mutant has also been obtained as spontaneous pseudorevertant of His337Val cells (Chu et al., 1995b). The His337Arg, His337Gln, His337Asn, and His337Phe mutants are photoautotrophic, although His337Gln, His337Asn, and His337Phe cells are only weakly photoautotrophic. The His337Arg, His337Phe, His337Gln, His337Asn, His337Glu, His337Leu, and His337Asp mutants evolve O_2 at ~50%, ~40%, ~40%, ~20%, ~20%, ~12%, and ~5% the rate of wild-type cells, respectively (Chu et al., 1995b). However, in His337Glu, His337Asp, His337Asn, and His337Leu cells, this O_2-evolving activity is lost rapidly during illumination with saturating light. The PS II contents of the mutants are 80–100% for His337Arg and His337Phe cells, 50–70% for His337Glu, His337Gln, His337Asp, His337Asn, and His337Leu cells, and ~40% for His337Val and His337Tyr cells compared to wild-type cells (Chu et al., 1995b). The His337Leu mutant loses its O_2-evolving activity rapidly in darkness.

On the basis of Chl *a* fluorescence analyses that were conducted with intact cells, it was concluded that the S_2/S_1 midpoint potential is essentially unchanged in His337Phe and His337Leu cells, slightly increased in His337Arg cells, and slightly decreased in His337Gln, His337Asn, and His337Glu cells (Chu et al., 1995b). In His337Asp, His337Val, and His337Tyr cells, charge recombination between $Q_A^{\bullet-}$ and the donor side of PS II is especially slow and has been speculated to occur between $Q_A^{\bullet-}$ and a single Mn(III) ion (Chu et al., 1995b). The kinetics of charge recombination in these mutants resemble those of cells that lack the extrinsic 33 kDa polypeptide (Chu et al., 1994a). Consequently, it was proposed that some

of the His337 mutants interfere with the normal binding of the extrinsic 33 kDa polypeptide to PS II (Chu et al., 1994b, 1995b). The $Y_Z^{\bullet}/Y_Z$ midpoint potential appears to be increased substantially in His337Phe and His337Leu cells. The rate of electron transfer from $Q_A^{\bullet-}$ to Q_B is slowed considerably in most of the His337 mutants, whereas electron transfer from Y_Z to $P_{680}^{\bullet+}$ appears to proceed normally in all of the His337 mutants (Chu et al., 1995b).

In all of the His337 mutants, substantial percentages of PS II reaction centers lack photooxidizable Mn ions in vivo (Chu et al., 1995b). These percentages were 10–15% in His337Phe cells, 20–30% in His337Gln, His337Glu, His337Asn, His337Val, His337Leu, and His337Tyr cells, 30–40% in His337Arg cells, and 40–50% in His337Asp cells. Therefore, it was concluded that His337 influences the assembly or stability of the $(Mn)_4$ cluster. Several of the His337 mutants are extremely sensitive to light-induced damage. Because cells that assemble no $(Mn)_4$ clusters in vivo (e.g., cells of the mutants Asp170Ala and Asp170Ser) are not particularly sensitive to light, it was proposed that the extreme light-sensitivity of the light-sensitive His337 mutants is caused by the release of toxic, activated oxygen species from perturbed $(Mn)_4$ clusters (Chu et al., 1995b).

The $(Mn)_4$ clusters in His337Val cells are severely perturbed, whereas those in His337Leu cells evolve O_2, and those in His337Phe cells support photoautotrophic growth (Chu et al., 1995b). To explain the curious observation that progressively larger hydrophobic residues cause progressively fewer perturbations, the bulky Leu and Phe residues were proposed to cause structural perturbations that permit the missing imidazole moiety of His337 to be replaced by another residue, a peptide carbonyl group, or a water molecule (Chu et al., 1995b).

Because of the behavior of the His337Arg and His337Gln mutants, it was proposed that His337 either ligates the $(Mn)_4$ cluster or serves as a crucial hydrogen bond donor (Chu et al., 1995b). The recent 3.5 Å X-ray crystallographic structural model (Ferreira et al., 2004; Chapter 21, Barber and Iwata) is more consistent with the latter proposal. In this model, His337 forms a hydrogen bond to a μ_3-oxo bridge that connects three Mn ions.

The PS II reaction centers in the His337 mutants appear to have substantially diminished affinities for Ca^{2+}. When His337Gln and His337Asn cells were propagated photoheterotrophically in media containing Na^+ substituted for Ca^{2+}, the rate of electron transfer from Y_Z to $P680^{\bullet+}$ slowed dramatically, as was observed for several His332 and Glu333 mutants (Sections II.C.1 and II.C.2) and in PS II preparations that have been rigorously depleted of Ca^{2+} ions (Satoh and Katoh, 1985; Boussac et al., 1992). It was proposed that the apparently diminished affinity for Ca^{2+} ions is an indirect consequence of the His337 mutations (Chu et al., 1995b).

5. Aspartate 342

The Asp342Glu, Asp342Asn, Asp342His, Asp342Ala, and Asp342Val mutations have been constructed in *Synechocystis* sp. PCC 6803 (Nixon and Diner, 1994; Chu et al., 1995b). Only the Asp342Glu mutant is photoautotrophic. The Asp342Glu, Asp342Asn, and Asp342His mutants evolve O_2, but at only ~20%, ~33%, and ~6% of the rate of wild-type cells, respectively (Chu et al., 1995b). The PS II contents of the mutants are ~90% for Asp342Glu cells, ~60% for Asp342Asn, and 30–50% for Asp342Asn and Asp342Ala cells compared to wild-type cells. These characteristics are not caused by a failure to post-translationally cleave the *C*-terminal extension of the D1 polypeptide's precursor form because the same characteristics were obtained in double mutants that also contained a stop codon in place of Ser345 (Chu et al., 1995b). The O_2-evolving activity of the Asp342 mutants is lost rapidly during illumination with saturating light. The Asp342Glu mutant loses O_2-evolving activity in darkness, but at a slower rate than His337Leu cells (Chu et al., 1995b) (Section III.C.4).

On the basis of Chl *a* fluorescence analyses that were conducted with intact cells, it was concluded that the S_2/S_1 midpoint potential is unchanged in Asp342Asn cells but is slightly increased in Asp342Glu cells (Chu et al., 1995b). In Asp342His and Asp342Ala cells, charge recombination between $Q_A^{\bullet-}$ and the donor side of PS II is especially slow and has been speculated to occur between $Q_A^{\bullet-}$ and a single Mn(III) ion (Chu et al., 1995b). The kinetics of charge recombination in these mutants resemble those of cells that lack the extrinsic 33 kDa polypeptide (Chu et al., 1994a). Consequently, it was proposed that some of the Asp342 mutants interfere with the normal binding of the extrinsic 33 kDa polypeptide to PS II (Chu et al., 1994a; Chu et al., 1995b). The rate of electron transfer from $Q_A^{\bullet-}$ to Q_B is slowed considerably in Asp342Asn, Asp342His, and Asp342Ala cells and the $Y_Z^{\bullet}/Y_Z$ midpoint potential

appears to be increased substantially in Asp342Asn cells. On the other hand, electron transfer from Y_Z to $P680^{\bullet+}$ appears to proceed normally in all of the Asp342 mutants (Chu et al., 1995b).

In all of the Asp342 mutants, substantial percentages of PS II centers lack photooxidizable Mn ions in vivo (Chu et al., 1995b). These percentages were 20–30% in Asp342Glu cells, 30–40% in Asp342Asn cells, 40–50% in Asp342His cells, and ~20% in Asp342Ala cells. Therefore, it was concluded that Asp342 influences the assembly or stability of the $(Mn)_4$ cluster. However, the high-affinity Mn-binding site that was identified in the Asp170 mutants remains intact (Nixon and Diner, 1994). The Asp342Asn and Asp342His mutants are extremely sensitive to light-induced damage. Because cells that assemble no $(Mn)_4$ clusters in vivo (e.g., cells of the mutants Asp170Ala and Asp170Ser) are not particularly light-sensitive, it was proposed that the extreme light-sensitivity of the light-sensitive Asp342 mutants is caused by the release of toxic, activated oxygen species from perturbed $(Mn)_4$ clusters (Chu et al., 1995b).

Because Asp342Glu and Asp342Asn cells evolve O_2 and because Asn can replace Asp as a ligand to Fe in cytochrome *bo* ubiquinol oxidase (Calhoun et al., 1993), it was proposed that Asp342 is a possible ligand of the $(Mn)_4$ cluster (Chu et al., 1995b). As an alternative possibility, it was also suggested that Asp342 may serve a structural role, such as optimally positioning a histidyl ligand of the $(Mn)_4$ cluster (Chu et al., 1995b). In the recent 3.5 Å X-ray crystallographic structural model of PS II, Asp342 is identified as a ligand of the $(Mn)_4$ cluster (Ferreira et al., 2004; Chapter 21, Barber and Iwata).

The PS II reaction centers in the Asp342 mutants appear to have substantially diminished affinities for Ca^{2+}. When Asp342Glu and Asp342Asn cells were propagated photoheterotrophically in media containing Na^+ substituted for Ca^{2+}, the rate of electron transfer from Y_Z to $P680^{\bullet+}$ slowed dramatically, as was observed for several His332, Glu333, and His337 mutants (Sections II.C.1, II.C.2, and II.C.4) and in PS II preparations that have been rigorously depleted of Ca^{2+} ions (Satoh and Katoh, 1985; Boussac et al., 1992). It was proposed that Asp342 may form part of a Ca^{2+} binding site, possibly as a bridging ligand between Mn and Ca^{2+} (Chu et al., 1995b). As an alternative possibility, it was also suggested that diminished affinity for Ca^{2+} ions may be an indirect consequence of the Asp342 mutations. In the recent 3.5 Å X-ray crystallographic structural model of PS II, Asp342 is identified as a ligand of Mn but not of Ca^{2+} (Ferreira et al., 2004; Chapter 21, Barber and Iwata).

6. The Carboxyl-Terminus at Alanine 344

In most organisms, the D1 polypeptide is synthesized with an extension of 8–16 residues on its *C*-terminus. This extension is post-translationally cleaved so that the mature D1 polypeptide has Ala344 as its *C*-terminal residue (Takahashi et al., 1988, 1990; Nixon et al., 1992b). The Ala344Gly, Ala344Ser, Ala344Met, Ala344Val, Ala344Tyr, Ala344Lys, Ala344Asn, Ala344Asp and Ala344stop mutants have been constructed in *Synechocystis* sp. PCC 6803 (Nixon et al., 1992b; Chu et al., 1994b; Chu et al., 2004; Mizusawa et al., 2004a,b) and the Ala344Ser mutant has been constructed in *Chlamydomonas reinhardtii* (Hatano-Iwasaki et al., 2001). In addition, the Leu343Phe and Leu343Phe/Ala344Ser mutants have been constructed in *Chlamydomonas reinhardtii* (Hatano-Iwasaki et al., 2001). All of the Ala344 mutants are photoautotrophic except for Ala344Tyr, Ala344Lys, and A344stop. The latter mutant has a truncated *C*-terminus and assembles no $(Mn)_4$ clusters (Nixon et al., 1992b). However, the high-affinity Mn-binding site that was identified in the Asp170 mutants remains intact (Nixon et al., 1992b). The Ala344Gly, Ala344Ser, Ala344Val, Ala344Asn and Ala344Asp mutants evolve O_2 at 50–90%, 75%, 90%, 60% and 40% the rate of wild-type cells, respectively, whereas the Ala344Lys and Ala344Tyr mutants evolve O_2 at ~10% and ~20% the rate of wild-type cells, respectively. The Leu343Phe mutant is photoautotrophic, but the Leu343Phe/Ala344Ser double mutant is non-photoautotrophic, evolves O_2 at only 20–30% the rate of wild-type cells, and contains assembled $(Mn)_4$ clusters that appear to be heterogeneous (Hatano-Iwasaki et al., 2001). The Ala344Gly, Ala344Asp and Ala344Asn mutants fail to grow photoautotrophically in high light. All three of these mutations increase the fraction of PS II reaction centers that exhibit the g = 4.1 EPR signal and all three perturb the symmetric carboxylate streching mode of least one carboxylate residue, but not the C-terminal carboxylate of Ala344 (Mizusawa et al, 2004a,b). The Ala344Gly mutant shifts seveal bands in the low-frequency (670–350 cm^{-1}) S_2-*minus*-S_1 FTIR difference spectrum, including the putative Mn-O-Mn S_2 state mode at 606 cm^{-1} (Mizusawa et al., 2004a). The latter result shows that the Ala344Gly mutation perturbs the structure of the $(Mn)_4$ core.

On the basis of a study of D1 mutants having

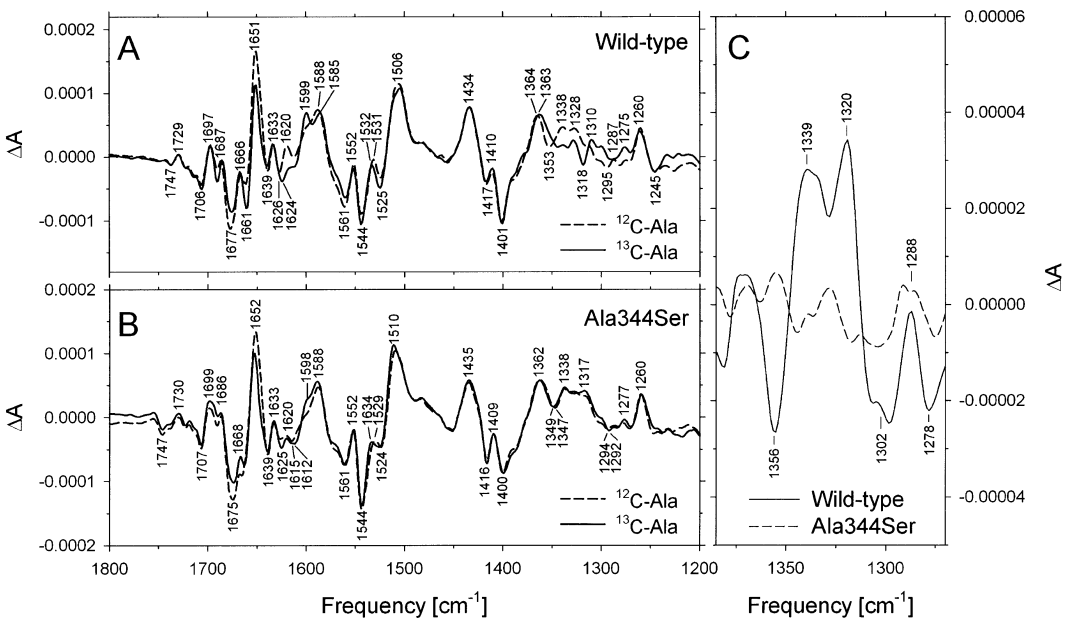

Fig. 4. Comparison of the mid-frequency (1800 – 1200 cm^{-1}) S_2-*minus*-S_1 FTIR difference spectra of (A) wild-type and (B) D1-Ala344Ser PS II particles purified from *Synechocystis* cells that had been propagated in the presence of unlabeled (^{12}C) alanine (dashed lines) or [1-^{13}C]alanine (solid lines). Note that the incorporation of [1-^{13}C]alanine alters features in the symmetric carboxylate stretching region (1450–1300 cm^{-1}) of the spectrum of the wild-type PS II particles, but not in spectrum of the Ala344Ser PS II particles. Panel (C) shows the double difference spectra, ^{12}C-*minus*-^{13}C, of the wild-type (solid line) and Ala344Ser (dashed line) PS II particles that were obtained by subtracting the S_2-*minus*-S_1 FTIR difference spectra of the [1-^{13}C]alanine-labeled PS II particles from the S_2-*minus*-S_1 FTIR difference spectra of the unlabeled PS II particles. Only the region from 1385–1270 cm^{-1} is shown. These data are consistent with a single S_1 state mode at ~1356 cm^{-1} in the wild-type PS II particles shifting to ~1339 cm^{-1} or ~1320 cm^{-1} after the incorporation of [1-^{13}C]alanine, and with a single S_2 state mode at ~1320 cm^{-1} or ~1339 cm^{-1} shifting to ~1302 cm^{-1}. These modes can be assigned to the α-COO^- group of Ala344. Modified from Chu et al. (2004). Similar data were presented recently by Kimura et al. (2005).

truncated or unprocessed *C*-terminii (e.g., Ala344stop and Ser345Pro, respectively), it was proposed that the *C*-terminus of the D1 polypeptide at Ala344 ligates the assembled $(Mn)_4$ cluster (Nixon et al., 1992b). To test this hypothesis, an isotope-edited FTIR study was undertaken to determine if the *C*-terminus of the D1 polypeptide ligates the $(Mn)_4$ cluster and, if so, if it ligates the Mn ion that undergoes oxidation during the $S_1 \rightarrow S_2$ transition (Chu et al., 2004). In this study, PS II particles were purified from wild-type, Ala344Gly, and Ala344Ser cells of *Synechocystis* sp. PCC 6803 that had been propagated in the presence of [1-^{13}C]alanine or unlabeled (^{12}C) alanine. The S_2-*minus*-S_1 FTIR difference spectra revealed that one symmetric carboxylate stretching mode was shifted by [1-^{13}C]alanine-labeling in wild-type PS II particles but not in Ala344Gly or Ala344Ser PS II particles (Fig. 4). Because the *C*-terminal α-COO^- group of Ala344 is the only carboxylate group that can be labeled in the wild-type PS II particles but not in the mutant PS II particles (because it is no longer provided by alanine in the mutants), the [1-^{13}C]alanine-sensitive carboxylate mode in the wild-type PS II particles could be assigned to the α-COO^- group of Ala344. This mode appears at ~1356 cm^{-1} in the S_1 state and at ~1339 cm^{-1} or ~1320 cm^{-1} in the S_2 state. These are downshifts of ~58 cm^{-1} in the S_1 state and either ~75 or ~94 cm^{-1} in the S_2 state compared to the frequency of this mode in free ionic carboxylate groups in solution. These downshifts are consistent with unidentate ligation of a metal ion by the α-COO^- group of Ala344. Indeed, it is difficult to imagine a mechanism that could cause a 58–94 cm^{-1} downshift of a symmetric carboxylate stretching mode other than unidentate ligation of a metal ion. The shifts are incompatible with protonation of a carboxylate group and there is no precedent for a hydrogen bonding interaction causing such a large

downshift of a symmetric carboxylate stretching mode. Furthermore, overnight exchange of ^2H_2O for ^1H_2O caused no significant alterations in this region of the S_2-*minus*-S_1 FTIR difference spectrum (Noguchi et al., 1995; Noguchi and Sugiura, 2002).

The removal of Ca^{2+} from PS II does not substantially alter the symmetric carboxylate stretching region of the S_2-*minus*-S_1 FTIR difference spectrum (Kimura and Ono, 2001). Furthermore, the biosynthetic replacement of Ca with Sr does not shift the symmetric carboxylate stretching mode of the α-COO^- group of Ala 344, whereas it does shift the symmetric carboxylate stretching modes of 3–4 other carboxylate groups (Strickler et al., 2005). Therefore, it was concluded that the α-COO^- group of Ala344 ligates Mn and not Ca^{2+}. The further downshift of the symmetric carboxylate stretching mode of this group in response to the $S_1 \rightarrow S_2$ transition (from ~1356 cm^{-1} to either ~1339 cm^{-1} or ~1320 cm^{-1}) is consistent with the α-COO^- group of Ala344 ligating a Mn ion whose charge increases during the $S_1 \rightarrow S_2$ transition. Accordingly, it was proposed that the α-COO^- group of Ala344 ligates the Mn ion that undergoes oxidation during the $S_1 \rightarrow S_2$ transition (Chu et al., 2004), although this proposal assumed that the extra oxidizing equivalent of the S_2 state is localized primarily on a single Mn(IV) ion that is produced during the $S_1 \rightarrow S_2$ transition. Recently, it has been argued that the electron that is removed from the $(Mn)_4$ cluster during the $S_1 \rightarrow S_2$ transition originates from a strongly delocalized orbital (Glatzel et al., 2004). If so, then the extra positve charge that is created during this transition is spread over multiple Mn ions. The downshift of the symmetric carboxylate strecthing mode of the α-COO^- group of Ala344 that occurs during the $S_1 \rightarrow S_2$ transition (Chu et al., 2004; Kimura et al., 2005) has recently been shown to be reversed during the $S_3 \rightarrow S_0$ transition (Kimura et al, 2005; R.J. Debus, unpublished). Also, [1-^{13}C]alanine labeling of wild-type PS II particles slightly perturbs bands between 640 and 610 cm^{-1} in the low-frequency S_2-*minus*-S_1 FTIR difference spectrum (Kimura et al., 2005). The altered bands were attributed to bending modes of the metal-ligated α-COO^- group of Ala344.

In the recent 3.5 Å X-ray crystallographic structural model (Ferreira et al., 2004; Chapter 21, Barber and Iwata), the α-COO^- group of Ala344 does not ligate any metal ion, in clear disagreement with interpretations of the FTIR data. Further study will be required to ascertain the cause of this disagreement.

III. The CP43 Polypeptide

The large hydrophilic loop of CP43 interacts with the D1 polypeptide and may be required for the efficient assembly and stability of the $(Mn)_4$ cluster (Bricker and Frankel, 2002). The importance of specific domains in this loop has been probed in *Synechocystis* sp. PCC 6803 by segment deletion (Kuhn and Vermaas, 1993) and site-directed (Knoepfle et al., 1999; Rosenberg et al., 1999; Young et al., 2002; Bricker et al., 2002) mutagenesis. Photoautotrophic growth and O_2 evolution are abolished in all of the deletion mutants (Kuhn and Vermaas, 1993). The Glu293Gln, Arg305Ser, Glu339Gln, Arg342Ser, and Glu352Gln mutants have been reported[4].

The Glu293Gln mutant is photoautotrophic. These cells exhibit slightly diminished rates of O_2 evolution compared to wild-type cells, and are somewhat sensitive to light-induced damage (Rosenberg et al., 1999).

The Arg305Ser mutant is photoautotrophic and evolves O_2 at 60–70% the rate of wild-type cells (Knoepfle et al., 1999). The PS II content of Arg305Ser cells is 70–80% compared to wild-type cells. The Arg305Ser mutant is moderately sensitive to light-induced damage (Knoepfle et al., 1999). The lifetime the S_2 state is increased in this mutant (Young et al., 2002) and, on the basis of Chl *a* fluorescence measurements that were conducted with intact cells, it was concluded that electron transfer from the $(Mn)_4$ cluster to $Y_Z^{\bullet}$ is slightly retarded (Knoepfle et al., 1999). The Arg305Ser mutation also weakens the binding of Cyt c_{550} to PS II (Bricker et al., 2002). The Arg305Ser mutant is very sensitive to the depletion of Cl^- ions from the growth medium. When propagated in Cl^--depleted media, Arg305Ser cells are only very weakly photoautotrophic, their O_2 evolving activity decreases to ~20% compared to that of wild-type cells, and their PS II content diminishes significantly.

[4]Multiple numbering systems are in use for CP43 (Bricker and Frankel, 2002). The residues Glu293, Arg305, Glu339, Arg342 and Glu352 that have been described in the mutagenesis studies correspond to Glu308, Arg320, Glu354, Arg357, and Glu367, respectively, in the recent 3.5 Å X-ray crystallographic structural model (Ferreira et al., 2004; Chapter 21, Barber and Iwata). The numbering system that was used in the mutagenesis studies is used in this chapter. The different numbering systems arise because *psbC* (the gene encoding CP43) has an unusual start codon, because CP43 is post-translationally processed at its amino terminus, and because, in *Synechocystis* sp. PCC 6803, there is a deletion of one residue at position 7 compared to the amino acid sequences of CP43 in other organisms.

Furthermore, the light-sensitivity of the mutant cells increased (Young et al., 2002).

The Glu339Gln mutant is very weakly photoautotrophic and evolves O_2 at ~20% the rate of wild-type cells. However, its PS II content is about the same as wild-type cells. This mutant is also somewhat sensitive to light-induced damage (Rosenberg et al., 1999). On the basis of these observations, Glu339 has been suggested to be required for the assembly or stability of the $(Mn)_4$ cluster (Bricker and Frankel, 2002). In the recent 3.5 Å X-ray crystallographic structural model, this residue ligates a Mn ion with both of its carboxylate oxygen atoms (Ferreira et al., 2004; Chapter 21, Barber and Iwata).

The Arg342Ser mutant is non-photoautotrophic and evolves O_2 at ~20% the rate of wild-type cells (Knoepfle et al., 1999). The PS II content of Arg342Ser cells is 60–70% compared to wild-type cells. This mutant is so sensitive to light-induced damage that O_2 evolution can only be detected when cells are propagated photoheterotrophically in media containing DCMU (Knoepfle et al., 1999). On the basis of Chl *a* fluorescence measurements that were conducted with intact cells, it was concluded that electron transfer from the $(Mn)_4$ cluster to $Y_Z^{\bullet}$ is slowed dramatically in this mutant (Knoepfle et al., 1999). On the basis of the recent 3.5 Å X-ray crystallographic structural model, this residue has been proposed to provide hydrogen bonds that stabilize intermediates that are associated with O=O bond formation (Ferreira et al., 2004; Chapter 21, Barber and Iwata).

The Glu352Gln mutant is non-photoautotrophic and appears to be unable to assemble stable PS II centers (Rosenberg et al., 1999).

IV. Concluding Remarks

In this chapter, I have described the site-directed mutagenesis studies that have been undertaken to characterize the nature of the water oxidizing site in PS II. The recent 3.2 Å and 3.5 Å crystallographic structural models, and future structures determined under conditions that minimize radiation damage to the $(Mn)_4$ cluster, with increasingly higher resolution, and in different S states, will greatly magnify the power of site-directed mutagenesis. With structural ambiguities increasingly eliminated, mutational studies will focus on functional and mechanistic questions. The power of mutational studies conducted in the light of solid structural information is demonstrated by recent studies of bacteriorhodopsin (Luecke and Lanyi, 2003; Edmonds and Luecke, 2004; Lanyi, 2004), BRCs (Paddock et al., 2003; Wraight, 2004), cytochrome *c* oxidase (Brzezinski and Larsson, 2003; Mills and Ferguson-Miller, 2003; Gennis, 2004; Wikström, 2005), and the cytochrome bc_1 complexes (Crofts, 2004; Smith et al., 2004). In all of these systems, site-directed mutagenesis has provided spectacular new insights because of the availability of high resolution X-ray structures. The next 10 years will be an exciting time to pursue the secrets of PS II.

Acknowledgments

The author is grateful for support from the National Science Foundation (MCB 0111065) and the National Institutes of Health (GM 66136).

References

Barry BA and Babcock GT (1987) Tyrosine radicals are involved in the photosynthetic oxygen-evolving system. Proc Natl Acad Sci USA 84: 7099–7103

Bernard MT, MacDonald GM, Nguyen AP, Debus RJ and Barry BA (1995) A difference infrared study of hydrogen bonding to the Z$^{\bullet}$ tyrosyl radical of Photosystem II. J Biol Chem 270: 1589–1594

Berthomieu C and Hienerwadel R (2005) Vibrational spectroscopy to study the properties of redox-active tyrosines in Photosystem II and other proteins. Biochim Biophys Acta 1707: 51–66

Berthomieu C, Hienerwadel R, Boussac A, Breton J and Diner BA (1998). Hydrogen-bonding of redox-active tyrosine Z of Photosystem II probed by FTIR difference spectroscopy. Biochemistry 37: 10547–10554

Biesiadka J, Loll B, Kern J, Irrgang KD and Zouni A (2005) Crystal structure of Photosystem II at 3.2 Å resolution: A closer look at the Mn-cluster. Phys Chem Chem Phys 6: 4733–4736

Blubaugh DJ and Cheniae GM (1992) Photoassembly of the Photosystem II manganese cluster. In: Murata N (ed) Research in Photosynthesis, Vol II, pp 361–364. Kluwer Academic Publishers, Dordrecht

Boerner RJ, Nguyen AP, Barry BA and Debus RJ (1992) Evidence from directed mutagenesis that aspartate 170 of the D1 polypeptide influences the assembly of the manganese cluster in the photosynthetic water-splitting complex. Biochemistry 31: 6660–6672

Boussac A., Sétif P and Rutherford AW (1992) Inhibition of tyrosine Z photooxidation after formation of the S_3-state in Ca^{2+}-depleted and Cl^-depleted Photosystem II. Biochemistry 31: 1224–1234

Bricker TM and Frankel LK (2002) The structure and function of CP47 and CP43 in Photosystem II. Photosynth Res 72: 131–146

Bricker TM, Morvant J, Masri N, Sutton HM and Frankel, LK (1998) Isolation of a highly active Photosystem II preparation from *Synechocystis* 6803 using a histidine-tagged mutant of CP 47. Biochim Biophys Acta 1409: 50–57

Bricker TM, Young A, Frankel LK and Putnam-Evans C (2002) Introduction of the ^{305}Arg → ^{305}Ser mutation in the large extrinsic loop E of the CP43 protein of *Synechocystis* sp PCC 6803 leads to the loss of cytochrome c_{550} binding to Photosystem II. Biochim Biophys Acta 1556: 92–96

Brzezski P and Larsson G (2003) Redox-driven proton pumping by heme-copper oxidases. Biochim Biophys Acta 1605: 1–13

Calhoun MW, Lemieux LJ, Thomas JW, Hill JJ, Chepuri Goswitz V, Alben JO and Gennis RB (1993) Spectroscopic characterization of mutants supports the assignment of histidine-419 as the axial ligand of heme *o* in the binuclear center of the cytochrome *bo* ubiquinol oxidase from *Escherichia coli*. Biochemistry 32: 13254–13261

Campbell KA, Force DA, Nixon PJ, Dole F, Diner BA and Britt RD (2000). Dual-mode EPR detects the initial intermediate in photoassembly of the Photosystem II Mn cluster: The influence of amino acid residue 170 of the D1 polypeptide on Mn coordination. J Am Chem Soc 122: 3754–3761

Chen C, Kazimir J and Cheniae GM (1995) Calcium modulates the photoassembly of Photosystem II $(Mn)_4$-clusters by preventing ligation of nonfunctional high-valency states of manganese. Biochemistry 34: 13511–13526

Choudhury K, Sundaramoorthy M, Hickman A, Yonetani T, Woehl E, Dunn MF and Poulos TL (1994) Role of the proximal ligand in peroxidase catalysis: Crystallographic, kinetic, and spectral studies of cytochrome *c* peroxidase proximal ligand mutants. J Biol Chem 269: 20239–20249

Chu H-A, Nguyen AP and Debus RJ (1994a) Site-Directed Photosystem II mutants with perturbed oxygen evolving properties: 1. Instability or inefficient assembly of the manganese cluster in vivo. Biochemistry 33: 6137–6149

Chu H-A, Nguyen AP and Debus RJ (1994b) Site-directed Photosystem II mutants with perturbed oxygen evolving properties. 2. Increased binding or photooxidation of manganese in the absence of the extrinsic 33-kDa polypeptide in vivo. Biochemistry 33: 6150–6157

Chu H-A, Nguyen AP and Debus RJ (1995a) Amino acid residues that influence the binding of manganese or calcium to Photosystem II. 1. The lumenal inter-helical domains of the D1 polypeptide. Biochemistry 34: 5839–5858

Chu H-A, Nguyen AP and Debus RJ (1995b) Amino acid residues that influence the binding of manganese or calcium to Photosystem II. 2. The Carboxyl-terminal domain of the D1 polypeptide. Biochemistry 34: 5859–5882

Chu H-A, Sackett H and Babcock GT (2000). Identification of a Mn-O-Mn cluster vibrational mode of the oxygen-evolving complex in Photosystem II by low-frequency FTIR spectroscopy. Biochemistry 39: 14371–14376

Chu H-A, Debus RJ and Babcock GT (2001) D1-Asp170 is structurally coupled to the oxygen evolving complex in Photosystem II as revealed by light-induced Fourier transform infrared difference spectroscopy. Biochemistry 40: 2312–2316

Chu H-A, Hillier W and Debus RJ (2004). Evidence that the *C*-terminus of the D1 polypeptide of Photosystem II is ligated to the manganese ion that undergoes oxidation during the S_1 to S_2 Transition: An isotope edited FTIR study. Biochemistry 43: 3152–3166

Clausen K, Winkler S, Hays A-MA, Hundelt M, Debus,RJ and Junge W (2001) Photosynthetic water oxidation in *Synechocystis* sp PCC6803: Mutations D1-E189K, R and Q are without influence on electron transfer at the donor side of Photosystem II. Biochim Biophys Acta 1506: 224–235

Crofts AR (2004) The cytochrome bc_1 complex: Function in the context of structure. Annu Rev Physiol 66: 689–733

Debus RJ (1992) The manganese and calcium ions of photosynthetic oxygen evolution. Biochim Biophys Acta 1102: 269–352

Debus RJ (2001) Amino acid residues that modulate the properties of tyrosine Y_Z and the manganese cluster in the water oxidizing complex of Photosystem II. Biochim Biophys Acta 1503: 164–186

Debus RJ, Barry BA, Babcock GT and McIntosh L (1988a). Site-directed mutagenesis identifies a tyrosine radical involved in the photosynthetic oxygen-evolving system. Proc Natl Acad Sci USA 85: 427–430

Debus RJ, Barry BA, Sithole I, Babcock GT and McIntosh L (1988b) Directed mutagenesis indicates that the donor to P_{680}^+ in Photosystem II is tyrosine-161 of the D1 polypeptide. Biochemistry 27: 9071–9074

Debus RJ, Nguyen AP and Conway AB (1990) Identification of ligands to manganese and calcium in Photosystem II by site-directed mutagenesis. In: Baltscheffsky M (ed) Current Research in Photosynthesis, Vol I, pp 829–832. Kluwer Academic Publishers, Dordrecht

Debus RJ, Campbell KA, Pham DP, Hays A-MA and Britt RD (2000a) Glutamate 189 of the D1 polypeptide modulates the magnetic and redox properties of the manganese cluster and tyrosine Y_Z in Photosystem II. Biochemistry 39: 6275–6287

Debus RJ, Campbell KA, Peloquin JM, Pham DP and Britt RD (2000b) Histidine 332 of the D1 polypeptide modulates the magnetic and redox properties of the manganese cluster and tyrosine Y_Z in Photosystem II. Biochemistry 39: 470–478

Debus RJ, Campbell KA, Gregor W, Li Z-L, Burnap RL and Britt RD (2001) Does histidine 332 of the D1 polypeptide ligate the manganese cluster in Photosystem II? An electron spin echo envelope modulation study. Biochemistry 40: 3690–3699

Debus RJ, Aznar C, Campbell KA, Gregor W, Diner BA and Britt RD (2003) Does aspartate 170 of the D1 polypeptide ligate the manganese cluster in Photosystem II? An EPR and ESEEM study. Biochemistry 42: 10600–10608

Debus RJ, Strickler MA, Walker LM and Hillier W (2005) No evidence from FTIR difference spectroscopy that aspartate-170 of the D1 polypeptide ligates a manganese ion that undergoes oxidation during the S_0 to S_1, S_1 to S_2, or S_2 to S_3 transtitions in Photosystem II. Biochemistry 44: 1367–1374

DeRose VJ, Yachandra VK, McDermott AE, Britt RD, Sauer K and Klein MP (1991) Nitrogen ligation to manganese in the photosynthetic oxygen-evolving complex: Continuous-wave and pulsed EPR studies of Photosystem II particles containing ^{14}N or ^{15}N. Biochemistry 30: 1335–1341

Diner BA (1998) Application of spectroscopic techniques to the study of Photosystem II mutations engineered in *Synechocystis* and *Chlamydomonas*. Methods Enzymol 297: 337–360

Diner, BA (2001) Amino acid residues involved in the coordination and assembly of the manganese cluster of Photosystem II. Proton-coupled electron transport of the redox-active tyrosines and its relationship to water oxidation. Biochim Biophys Acta 1503: 147–163

Diner BA and Nixon PJ (1992) The rate of reduction of oxidized redox-active tyrosine, Z+, by exogenous Mn^{2+} is slowed in a site-directed mutant, at Aspartate 170 of polypeptide D1 of Photosystem II, inactive for photosynthetic oxygen evolution. Biochim Biophys Acta 1101: 134–138

Diner BA and Nixon PJ (1998) Evidence for D1-His190 as the proton acceptor implicated in the oxidation of redox-active tyrosine Y_Z of PS II. In: Garab G (ed) Photosynthesis: Mechanisms and Effects, Vol II, pp 1177–1180, Kluwer Academic Publishers, Dordrecht

Diner BA, Nixon PJ and Farchaus JW (1991) Site-directed mutagenesis of photosynthetic reaction centers. Curr Opin Struct Biol 1: 546–554

Edmonds BW and Luecke H (2004) Atomic resolution structures and the mechanism of ion pumping in bacteriorhodopsin. Front Biosci 9: 1556–1566

Ferreira KN, Iverson TM, Maghlaoui K, Barber J and Iwata I (2004) Architecture of the photosynthetic oxygen-evolving center. Science 303:1831–1838

Funk C, Wiklund R, Schröder WP and Jansson C (2001) D1´ centers are less efficient than normal Photosystem II centers. FEBS Lett 505: 113–117

Gennis RB (2004) Coupled proton and electron transfer reactions in cytochrome oxidase. Front Biosci 9: 581–591

Ghirardi ML, Lutton TW and Seibert M (1998a) Effects of carboxyl amino acid modification on the properties of the high-affinity, manganese-binding site in Photosystem II. Biochemistry 37: 13559–13566

Ghirardi ML, Preston C and Seibert M (1998b) Use of a novel histidyl modifier to probe for residues on tris-treated Photosystem II membrane fragments that may bind functional manganese. Biochemistry 37: 13567–13574

Gilchrist ML, Jr (1996) Pulsed electron paramagnetic resonance investigation of photosynthetic oxygen evolution. PhD Dissertation. University of California at Davis

Glatzel P, Bergmann U, Yano J, Visser H, Roblee JH, Gu W, de Groot FMF, Christou G, Pecoraro VL, Cramer SP and Yachandra VK (2004) The electronic structure of Mn in oxides, coordination complexes, and the oxygen-evolving complex of Photosystem II studied by resonant inelastic X-ray scattering. J Am Chem Soc 126: 9946–9959

Hatano-Iwasaki A, Minagawa J, Inoue Y. and Takahashi Y (2001) Two functionally distinct manganese clusters formed by introducing a mutation in the carboxyl terminus of a Photosystem II reaction center polypeptide, D1, of the green alga *Chlamydomonas reinhardtii*. Biochim Biophys Acta 1504: 299–310

Hays A-MA, Vassiliev IR, Golbeck JH and Debus RJ (1998) Role of D1-His190 in proton-coupled electron transfer reactions in Photosystem II: A chemical complementation study. Biochemistry 37: 11352–11365

Hays A-MA, Vassiliev IR, Golbeck JH and Debus RJ (1999) Role of D1-His190 in the proton-coupled oxidation of tyrosine Y_Z in Mn-depleted Photosystem II. Biochemistry 38: 11851–11865

Hundelt M, Hays A-MA, Debus RJ and Junge W (1998a) Oxygenic Photosystem II: The mutation D1-D61N in *Synechocystis* sp. PCC 6803 retards S-State transitions without affecting electron transfer from Y_Z to P_{680}^+. Biochemistry 37: 14450–14456

Hundelt M, Hays A-MA, Debus RJ and Junge W (1998b). The mutation D1-D61N in PS II of *Synechocystis*: Retardation of ET from OEC $\rightarrow Y_Z^{ox}$ and no effect on $Y_Z \rightarrow P_{680}^+$. In: Garab G (ed) Photosynthesis: Mechanisms and Effects, Vol II, pp 1387–1390. Kluwer Academic Publishers, Dordrecht

Kimura Y and Ono T-A (2001) Chelator-induced disappearance of carboxylate stretching vibrational modes in S_2/S_1 FTIR spectrum in oxygen-evolving complex of Photosystem II. Biochemistry 40: 14061–14068

Kimura Y, Mizusawa N, Yamanari T, Ishii A and Ono T-A (2005) Structural changes of D1 C-terminal α-carboxylate during S-state cycling of photosynthetic oxygen evolution. J Biol Chem 280: 2078–2083

Knoepfle N, Bricker TM and Putnam-Evans,C (1999) Site-directed mutagenesis of basic arginine residues 305 and 342 in the CP 43 protein of Photosystem II affects oxygen-evolving activity in *Synechocystis* 6803. Biochemistry 38: 1582–1588

Kramer DM, Roffey RA, Govindjee and Sayre RT (1994) The A_T thermoluminescence band from *Chlamydomonas reinhardtii* and the effects of mutagenesis of histidine residues on the donor side of the Photosystem II D1 polypeptide. Biochim Biophys Acta 1185: 228–237

Kuhn MG and Vermaas WFJ (1993) Deletion mutations in a long hydrophilic loop in the Photosystem II chlorophyll-binding protein CP43 in the cyanobacterium *Synechocystis* sp. PCC 6803. Plant Mol Biol 23: 123–133

Lanyi JK (2004) Bacteriorhodopsin. Annu Rev Physiol 66: 665–688

Li Z-L and Burnap RL (2001). Mutations of arginine 64 within the putative Ca^{2+}-binding lumenal interhelical a-b loop of the Photosystem II D1 protein disrupt binding of the manganese stabilizing protein and cytochrome c_{550} in *Synechocystis* sp PCC6803 Biochemistry 40: 10350–10359

Li Z-L and Burnap RL (2002) Mutations of basic arginine residue 334 in the D1 protein of Photosystem II lead to unusual S_2 state properties in *Synechocystis* sp PCC 6803. Photosynth Res 72: 191–201

Luecke H and Lanyi JK (2003) Structural clues to the mechanism of ion pumping in bacteriorhodopsin. Adv Protein Chem 63: 111–130

Lundberg M and Siegbahn PEM (2004) Theoretical investigations of structure and mechanism of the oxygen-evolving complex in PS II. Phys Chem Chem Phys 6: 4772–4780

Magnuson A and Andréasson L-E (1997) Different manganese binding sites in Photosystem II probed by selective chemical modification of histidyl and carboxylic acid residues. Biochemistry 36: 3254–3261

Mamedov F, Sayre RT and Styring S (1998) Involvement of histidine 190 on the D1 protein in electron/proton transfer reactions on the donor side of Photosystem II. Biochemistry 37: 14245–14256

McEvoy JP and Brudvig GW (2004) Structure-based mechanism of photosynthetic water oxidation. Phys Chem Chem Phys 6: 4754–4763

Messinger J (2004) Evaluation of different mechanistic proposals for water oxidation in photosynthesis on the basis of Mn_4O_2Ca structures for the catalytic site snd spectroscopic data. Phys Chem Chem Phys 6: 4764–4771

Metz JG, Nixon PJ, Rögner M, Brudvig GW and Diner BA (1989) Directed alteration of the D1 polypeptide of Photosystem II: Evidence that tyrosine-161 is the redox component, Z, connecting the oxygen-evolving complex to the primary electron donor, P680. Biochemistry 28: 6960–6969

Michel H and Deisenhofer J (1988) Relevance of the photosyn-

thetic reaction center from purple bacteria to the structure of Photosystem II. Biochemistry 27: 1–7

Mills DA and Ferguson-Miller S (2003) Understanding the mechanism of proton movement linked to oxygen reduction in cytochrome *c* oxidase: Lessens from other proteins. FEBS Lett 545: 47–51

Minagawa J and Crofts AR (1994) A robust protocol for site-directed mutagenesis of the D1 protein in *Chlamydomonas reinhardtii*: A PCR-spliced *psbA* gene in a plasmid conferring spectinomycin resistance was introduced into a *psbA* deletion strain. Photosynth Res 42: 121–131

Mizusawa N, Kimura Y, Ishii A, Yamanari T, Nakazawa S, Teramoto H and Ono T-A (2004a) Impact of replacement of D1 C-terminal alanine with glycine on structure and function of photosynthetic oxygen-evolving complex. J Biol Chem 279: 29622–29627

Mizusawa N, Yamanari T, Kimura Y, Ishii A, Nakazawa S and Ono T-A (2004b) Changes in the functional and structural properties of the Mn cluster induced by replacing the side group of the C-terminus of the D1 protein of Photosystem II. Biochemistry 43: 14644–14652

Nanba O and Satoh Ki (1987) Isolation of a Photosystem II reaction center consisting of D-1 and D-2 polypeptides and cytochrome *b*-559. Proc Natl Acad Sci USA 84: 109–112

Nixon PJ and Diner BA (1992) Aspartate 170 of the Photosystem II reaction center polypeptide D1 is involved in the assembly of the oxygen-evolving manganese cluster. Biochemistry 31: 942–948

Nixon PJ and Diner BA (1994) Analysis of water-oxidation mutants constructed in the cyanobacterium *Synechocystis* sp. PCC 6803. Biochem Soc Trans 22: 338–343

Nixon PJ, Chisholm DA and Diner BA (1992a) Isolation and functional analysis of random and site-directed mutants of Photosystem II. In: Shewry P and Gutteridge S (eds) Plant Protein Engineering, pp 93–141. Cambridge University Press, Cambridge

Nixon PJ, Trost JT and Diner BA (1992b) Role of the carboxyl terminus of polypeptide D1 in the assembly of a functional water-oxidizing manganese cluster in Photosystem II of the cyanobacterium *Synechocystis* sp. PCC 6803: Assembly requires a free carboxyl group at *C*-terminal position 344. Biochemistry 31: 10859–10871

Noguchi T and Sugiura M (2002) FTIR detection of water reactions during the flash-induced S-state cycle of the photosynthetic water-oxidizing complex. Biochemistry 41: 15706–15712

Noguchi T, Ono T-A and Inoue Y (1995) A carboxylate ligand interacting with water in the oxygen-evolving center of Photosystem II as revealed by Fourier transform infrared spectroscopy. Biochim Biophys Acta 1232: 59–66

Noguchi T, Inoue Y and Tang X-S (1999) Structure of a histidine ligand in the photosynthetic oxygen-evolving complex as studied by light-induced Fourier transform infrared spectroscopy. Biochemistry 38: 10187–10195

Okamura MY, Satoh Ki, Isaacson RA and Feher G (1987) Evidence of the primary charge separation in the D1/D2 complex of Photosystem II from spinach: EPR of the triplet state. In: Biggins J. (ed) Progress in Photosynthesis Research, Vol I, pp 379–381, Martinus Nijhoff Publishers, Dordrecht

Padock ML, Feher G and Okamura MY (2003) Proton transfer pathways and mechanism in bacterial reaction centers. FEBS Lett 555: 45–50

Pakrasi HB and Vermaas WFJ (1992) Protein engineering of Photosystem II. In: Barber J. (ed) The Photosystems: Structure, Function and Molecular Biology, pp 231–257, Elsevier Science Publishers BV, Amsterdam

Preston C and Seibert M (1991a) Protease treatments of Photosystem II membrane fragments reveal that there are four separate high-affinity Mn-binding sites. Biochemistry 30: 9625–9633

Preston C and Seibert M (1991b) The carboxyl modifier 1-ethyl-3-[3-(dimethylamino)propyl] carboddimide (EDC) inhibits half of the high-affinity Mn-binding site in Photosystem II membrane fragments. Biochemistry 30: 9615–9624

Pujols-Ayala I and Barry BA (2002) Histidine 190-D1 and glutamate 189-D1 provide structural stabilization in Photosystem II. Biochemistry 41: 11456–11465

Qian M, Dao L, Debus RJ and Burnap RL (1999). Impact of mutations within the putative Ca^{2+}-binding lumenal interhelical a-b loop of the Photosystem II D1 protein on the kinetics of photoactivation and H_2O-oxidation in *Synechocystis* sp. PCC 6803. Biochemistry 38: 6070–6081

Randall DW (1997) Pulsed EPR studies of tyrosine radicals and manganese complexes: Insights into photosynthetic water oxidation. PhD Dissertation. University of California at Davis

Reifler MJ., Chisholm DA, Wang J, Diner BA and Brudvig GW (1998) Engineering and rapid purification of histidine-tagged Photosystem II from *Synechocystis* PCC 6803. In: Garab G (ed) Photosynthesis, Mechanisms and Effects, Vol II, pp 1189–1192. Kluwer Academic Publishers, Dordrecht

Roffey RA, Golbeck JH, Hille CR and Sayre RT (1991) Photosynthetic electron transport in genetically altered Photosystem II reaction centers of chloroplasts. Proc Natl Acad Sci USA 88: 9122–9126

Roffey RA, Kramer DM, Govindjee and Sayre RT (1994a) Lumenal side histidine mutations in the D1 protein of Photosystem II affect donor side electron transfer in *Chlamydomonas reinhardtii*. Biochim Biophys Acta 1185: 257–270

Roffey RA, van Wijk KJ, Sayre RT and Styring S (1994b) Spectroscopic characterization of tyrosine-Z in histidine 190 mutants of the D1 protein in Photosystem II (PS II) in *Chlamydomonas reinhardtii*: Implications for the structural model of the donor side of PS II. J Biol Chem 269: 5115–5121

Rosenberg C, Christian J, Bricker TM and Putnam-Evans C (1999) Site-directed mutagenesis of glutamate residues in the large extrinsic loop of the Photosystem II protein CP 43 affects oxygen-evolving activity and PS II assembly. Biochemistry 38: 15994–16000

Satoh Ka and Katoh S (1985) A functional site of Ca^{2+} in the oxygen-evolving Photosystem II preparation from *Synechococcus* sp. FEBS Lett 190: 199–203

Seibert M, Tamura N and Inoue Y (1989) Lack of photoactivation capacity in *Scenedesmus obliquus* LF-1 results from loss of half the high-affinity manganese-binding site: Relationship to the unprocessed D1 protein. Biochim Biophys Acta 974: 185-191

Smith JL, Zhang H, Yan J, Kurisu G and Cramer WA (2004) Cytochrome *bc* complexes: A common core of structure and function surrounded by diversity in the outlying provinces. Curr Opin Struct Biol 14: 432–439

Steenhuis JJ, Hutchison RS and Barry BA (1999) Alterations in carboxylate ligation at the active site of Photosystem II. J Biol Chem 274: 14609–14616

Strickler MA, Welker LM, Hillier W and Debus RJ (2005)

Evidence from biosynthetically incorporated strontium and FTIR difference spectroscopy that the C-terminus of the D1 polypeptide of Photosystem II does not ligate calcium. Biochemistry 44: 8571–8577

Svensson B, Minagawa J and Crofts AR (1998) Characterization of Photosystem II donor-side mutants in *Chlamydomonas reinhardtii*. In: Garab G (ed) Photosynthesis: Mechanisms and Effects, Vol II, pp 1451–1454. Kluwer Academic Publishers, Dordrecht

Svensson B. Vass I, Cedergren E and Styring S (1990) Structure of donor side components in Photosystem II predicted by computer modelling. EMBO J. 9: 2051–2059

Szalai VA and Brudvig GW (1996) Reversible binding of nitric oxide to tyrosyl radicals in Photosystem II. Nitric oxide quenches formation of the S_3 EPR signal species in acetate-inhibited Photosystem II. Biochemistry 35: 15080–15087

Takahashi M-A, Shiraishi T and Asada K (1988) COOH-terminal residues of D1 and the 44 kDa CPa-2 spinach Photosystem II core complex. FEBS Lett 240: 6–8

Takahashi Y, Nakane H, Kojima H and Satoh Ki (1990) Chromatographic purification and determination of the carboxyl-terminal sequences of Photosystem II reaction center proteins, D1 and D2. Plant Cell Physiol 31: 273–280

Tamura N, Ikeuchi M and Inoue Y (1989) Assignment of histidine residues in the D1 protein as possible ligands for functional manganese in the photosynthetic water-oxidizing complex. Biochim Biophys Acta 973: 281–289

Tamura N, Noda K, Wakamatsu K, Kamachi H, Inoue H and Wada K (1997). Involvement of carboxyl groups of the PS II reaction center proteins in photoactivation of the apo-water-oxidizing complex. Plant Cell Physiol 38: 578–585

Tang, X-S and Diner, BA (1994) Biochemical and spectroscopic characterization of a new oxygen-evolving Photosystem II core complex from the cyanobacterium *Synechocystis* sp. PCC 6803. Biochemistry 33: 4594–4603

Tang X-S, Sivaraja M and Dismukes GC (1993a) Protein and substrate coordination to the manganese cluster in the photosynthetic water oxidizing complex: ^{15}N and ^{1}H ENDOR spectroscopy of the S_2 state multiline signal in the thermophilic cyanobacterium *Synechococcus elongatus*. J Am Chem Soc 115: 2382–2389

Tang X-S, Chisholm DA, Dismukes GC, Brudvig GW and Diner BA (1993b) Spectroscopic evidence from site-directed mutants of *Synechocystis* PCC 6803 in favor of a close interaction between histidine 189 and redox-active tyrosine 160, both of polypeptide D2 of the Photosystem II reaction center. Biochemistry 32: 13742–13748

Tang X-S, Diner BA, Larsen BS, Gilchrist ML, Jr, Lorigan GA and Britt RD (1994) Identification of histidine at the catalytic site of the photosynthetic oxygen-evolving complex. Proc Natl Acad Sci USA 91: 704–708

Tommos C and Babcock GT (2000) Proton and hydrogen currents in photosynthetic water oxidation. Biochim Biophys Acta 1458: 199–219

Trebst A (1986) The topology of the plastoquinone and herbicide binding peptides of Photosystem II in the thylakoid membrane. Z Naturforsch 41c: 240–245

Vermaas WFJ, Rutherford AW and Hansson Ö (1988) Site-directed mutagenesis in Photosystem II of the cyanobacterium *Synechocystis sp.* PCC 6803: Donor D is a tyrosine residue in the D2 protein. Proc Natl Acad Sci USA 85: 8477–8481

Vermaas WFJ, Charité J and Eggers B (1990) System for site-directed mutagenesis in the *psbDI/C* operon of *Synechocystis* sp. PCC 6803. In: Baltscheffsky M (ed) Current Research in Photosynthesis, Vol I, pp 231–238. Kluwer Academic Publishers, Dordrecht

Vrettos JS and Brudvig GW (2002) Water oxidation chemistry of Photosystem II. Phil Trans R Soc Lond B 357: 1395–1405

Vrettos JS, Limburg J and Brudvig GW (2001) Mechanism of photosynthetic water oxidation: Combining biophysical studies of Photosystem II with inorganic model chemistry. Biochim Biophys Acta 1503: 229–245

Whitelegge JP, Koo D, Diner BA, Domian I and Erickson JM (1995) Assembly of the Photosystem II oxygen-evolving complex is inhibited in *psb*A site-directed mutants of *Chlamydomonas reinhardtii*. J Biol Chem 270: 225–235

Wiklund R, Salih GF, Mäenpää P and Jansson C (2001) Engineering of the protein environment around the redox-active TyrZ in Photosystem II—the role of F186 and P162 in the D1 protein of *Synechocystis* 6803. Eur J Biochem 268: 5356–5364

Wikström M (2005) Cytochrome *c* oxidase: 25 years of the elusive proton pump. Biochim Biophys Acta 1655: 241–47

Wraight CA (2004) Proton and electron transfer in the acceptor quinone complex of photosynthetic reaction centers from *Rhodobacter sphaeroides*. Frontiers in Biosciences 9: 309–337

Young A, McChargue M, Frankel LK, Bricker TM and Putnam-Evans C (2002) Alterations of the oxygen-evolving apparatus induced by a $^{305}Arg \rightarrow {}^{305}Ser$ mutation in the CP43 protein of Photosystem II from *Synechocystis* sp PCC 6803 under chloride-limiting conditions. Biochemistry 41: 15747–15753

Zimmermann J-L, Boussac A and Rutherford AW (1993) The manganese center of oxygen-evolving and Ca^{2+}-depleted Photosystem II: A pulsed EPR spectroscopy study. Biochemistry 32: 4831–4841

Chapter 12

The Catalytic Manganese Cluster: Implications from Spectroscopy

Karin A. Åhrling[1] and Ronald J. Pace*[2]
[1]*Research School of Biological Sciences and* [2]*Department of Chemistry, Faculty of Science, The Australian National University, Canberra, ACT 0200, Australia*

Michael C. W. Evans
Department of Biology, University College London, Gower Street, London WC1E 6BT, U.K.

Summary

Recent spectroscopic studies on the water oxidizing complex (WOC) of Photosystem II are discussed in terms of the possible nature and structures for the Mn containing catalytic site. Emphasis is given to the various electron paramagnetic resonance techniques which have been increasingly employed, as well as examination of complementary data from optical and X-ray absorption spectroscopies. All of the quasi-stable intermediate states of the catalytic turnover cycle of the WOC (S_0 to S_3) are now accessible spectroscopically. We show that the available data may be rationalized by a scheme in which the 'active,' catalytically cycling component of the water oxidizing site contains a pair of coupled, oxo bridged Mn ions, closely associated with a Ca ion. The structure of the active Mn site resembles the structure of the dinuclear Mn catalase. During functional turnover, oxidizing equivalents are stored both in Mn ions and ligand groups and one Mn ion has a unique, low symmetry ligand environment.

*Author for correspondence, email: Ron.Pace@anu.edu.au

T. Wydrzynski and K. Satoh (eds): Photosystem II: The Light-Driven Water:Plastoquinone Oxidoreductase, pp. 285–305.

I. Introduction

Understanding the structure and mechanism of the Mn containing water oxidation center in Photosystem II (PS II) remains one of the last great challenges in bioenergetics. Fundamental questions remain concerning how and where the four oxidizing equivalents necessary to effect the oxidation of two water molecules to molecular oxygen are stored, the chemical nature of the substrate site and the precise events attending the critical O–O bond formation step.

The water oxidizing complex (WOC) contains four Mn ions and at least one Ca ion (Chapters 10, 13 and 25). O_2 is produced by a four step catalytic process involving up to five kinetically identifiable intermediate states, the S_n states (n = 0 – 4). For each S state advance (Chapter 24, Shinkarev) an electron is withdrawn and an oxidizing equivalent is generated and stored within the WOC. Some of these electrons come from Mn centers, whose mean oxidation state is above +2. Two conclusions concerning the structure and the chemistry of the water oxidizing site are currently not disputed: (i) The four Mn ions are all magnetically coupled, at least pair wise, by μ-oxo and possibly μ-carboxylato bridges (Yachandra et al., 1993; Chapter 10), with a characteristic Mn-Mn separation of 2.7–2.8Å in the pairs for the lower S states. (ii) Substrate water is able to freely exchange with the catalytic site up to the S_3 state (Messinger et al., 1995; Chapter 25). Water oxidation thus occurs in a concerted four electron reaction during the $S_3 \rightarrow S_0$ transition.

Spectroscopic approaches have sought to define models of the Mn catalytic site structure and determine what is oxidized and when, during the redox accumulation phase of the S cycle. Most information has come from X-ray absorption, optical and electron paramagnetic resonance (EPR) spectroscopies—with strong reliance on comparisons with data from model compounds. Such studies are now complemented by X-ray crystallographic analysis of the PS II complex isolated from thermophilic bacteria (Chapters 19–21). The early work relied principally on optical absorption spectroscopy, but following the discovery of Mn derived EPR signals from the S_2 state of the WOC in the early 1980s, the EPR technique has dominated. Although detailed discussion of X-ray absorption spectroscopies, as applied to the WOC, is given elsewhere (Chapter 10, Yachandra), we briefly discuss results relevant to the oxidation states of the Mn atoms within the catalytic site.

In this chapter we seek to distil a spectroscopically consistent model of the WOC. Results obtained from PS II containing fully intact, functionally competent Mn centers are principally used, although extensive studies exist on inhibited, co-factor depleted forms of the enzyme (Debus, 1992).

Abbreviations: Chl – chlorophyll; CW – continuous wave; Cyt c_{550} – cytochrome c_{550}; EG – ethylene glycol; ENDOR – electron nuclear double resonance; EPR – electron paramagnetic resonance; ESEEM – electron spin echo envelope modulation; EtOH – ethanol; EXAFS – extended X-ray absorption fine structure; HOMO – highest occupied molecular orbital; LUMO – lowest unoccupied molecular orbital; MeOH – methanol; MLS – multiline signal; NIR – near infrared; NQR – nuclear quadrupole resonance; pp – peak to peak; PS II – Photosystem II; S_n – states of the water oxidizing complex for n=0,1,2,3 or 4; WOC – water oxidizing complex; XANES – X-ray absorption near edge spectroscopy

II. S-State Spectroscopy

All S states (except S_4) are now able to be studied by the three general types of spectroscopy outlined above, although those states with an odd number of unpaired electrons (the Kramers states, S_0 and S_2) are more accessible to EPR. We do not address in detail PS II studies involving over-reduced ('negative' S state) centers (Messinger et al., 1997c), although these have clear relevance for possible Mn site structures and are briefly examined in that light.

A. S_1 State

This is the dark stable state of the WOC, and at sufficiently low temperature the Mn center(s) becomes diamagnetic for long dark adapted samples (Koulougliotis et al., 1992). The Mn cluster thus has even net spin and since S_1 contains no Mn(II) (Kuzek and Pace, 2001), the only plausible possibilities for the Mn oxidation states are $Mn(III)_4$ or $(Mn(III)_2Mn(IV)_2)$ (Chapter 10, Yachandra). Mn X-ray absorption near edge spectroscopy (XANES) has been extensively applied by several groups to determine the mean Mn oxidation level of the WOC, particularly for the S_1 state. Most data exist for the K edge, which exhibits an approximately three-fold greater variation with metal oxidation state than the L_β edge (Bergmann et al., 1998). Two points are important: (i) There is no theoretically rigorous way to precisely define the absorption edge energy position—most commonly the inflection point (2nd derivative zero crossing) or

energy at half height is used, but alternative methods of analysis have been proposed (Dau et al., 2001); (ii) The edge energy depends on the ligand environment of the metal center, as well as its formal oxidation state. The model compound calibration set should thus contain compounds as close as possible, chemically and structurally, to the protein metal centers being examined.

At present, the Mn K edge energies assigned to particular S states appear variable. In Fig. 1 we summarize the available data from four research groups for functional PS II undergoing at least one S-state advancement from S_1. This includes four independent data sets for complete S state cycling by flash turnover and a number of examples of $S_1 \rightarrow S_2$ conversion by continuous low temperature illumination. It is immediately evident that the incremental changes in edge energy with S state advancement are generally consistent between data sets, especially when averaged estimates from inflection and half height measures (where available) are used, but the absolute K edge energy of the S_1 state varies from 6551.5 to 6553 eV. This variation is well outside the limits of experimental/calibration uncertainty (Yachandra et al., 1996) for the technique and occurs when the same analysis methods, by the same groups are applied to different samples. It presumably reflects a real variation in the apparent redox level of the Mn in the functional dark-adapted state. From published XANES data the above S_1 state edges correspond to mean Mn oxidation levels of (III) and (III-IV) respectively (Kuzek and Pace, 2001). The simplest interpretation of these observations is that one pair of Mn is able to exist in the $Mn(III)_2$ or $Mn(IV)_2$ oxidation levels, while the other undergoes at least one catalytic turnover cycle (starting from S_1 $Mn(III)_2$), i.e., the four Mn are organized as two weakly interacting pairs. This was also the conclusion drawn from EXAFS and XANES studies of the controlled reduction of Mn in PS II by exogenous reductants, (Riggs-Gelasco et al., 1996). Factors determining the oxidation state of the putative 'spectator' pair are not yet clear, but appear to involve sample condition and cryoprotectant-dilute samples (~5 mg/ml Chl) and/or glycerol cryoprotectant favor lower edge energies while concentrated (thin) samples and/or sucrose cryoprotectant give higher values.

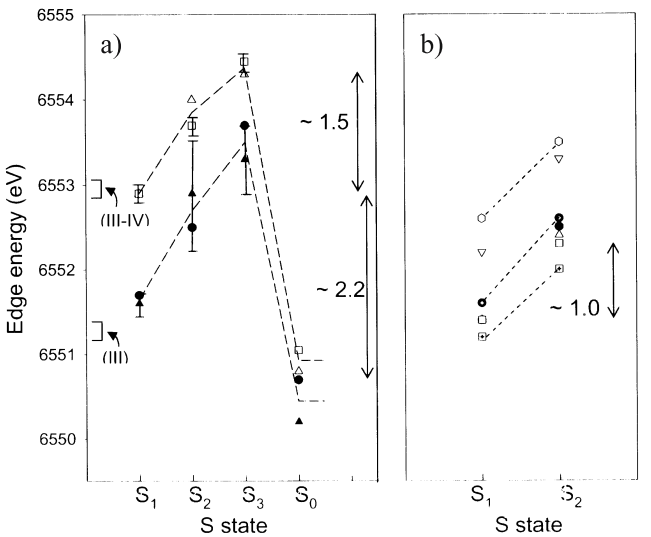

Fig. 1. Plot of Mn XANES K edge energies (inflection points, energies at half height) for S states in functional plant PS II. a) Deconvoluted results for all S states from multiple flash turnover series. Data points: ▲ (Roelofs et al., 1996), □ (Iuzzolino et al., 1998); ● (Ono, et al., 1992); △ (Messinger, et al., (2001). Dashed curves are trend lines through data sets commencing with approximately same S_1 edge energies. Differences between inflection and half height measures are greater for S_2 , S_3 in Roelofs et al. (1996)) than in Iuzzolino et al. (1998) (variation bars). b) Single turnover data (plant and cyanobacterial PS II) from continuous low temperature illumination advancement (inflection) (McDermott, et al., 1988; Sauer, et al., 1988; Guiles, et al., 1990; MacLachlan, et al., 1992, 1994; Liang, et al., 1994; Dau, et al., 1995).

1. Electron Paramagnetic Resonance

It is established that the total spin of the Mn center(s) in the S_1 state is even, with the metals anti-ferromagnetically coupled to give a diamagnetic (S=0) ground state (Koulougliotis et al., 1992). If the coupling is weak enough, then integer spin states (S = 1, 2 etc.) may become thermally accessible at cryogenic temperatures (< ~50 K). Integer spin systems are often most visible with parallel polarization EPR. Two such signals have now been seen in the S_1 state of PS II from higher plants and cyanobacteria, following the initial discovery of one form in plants (Dexheimer et al., 1990). Both forms are seen at low field (g ~5–12). One is broad and featureless and seen in intact higher plant PS II, while the other is clearly hyperfine structured. This structured S_1 signal is seen in cyanobacterial PS II and in spinach PS II lacking the 17 and 23 kDa extrinsic peptides (Peloquin and Britt, 2001). Since the latter are absent from cyanobacteria, whose PS II core preparations often loose the Cyt c_{550} extrinsic protein during column purification, the structured signal probably comes from centers that are somewhat solvent exposed. However the number of resolved hyperfine lines indicates that a center with at least two coupled Mn is involved.

Figure 2 shows the temperature dependence of the S_1 signals over the range ~2–10 K. Signal intensity is not absolute in these studies and the relative scales from Yamauchi et al. (1997) and Peloquin and Britt (2001) have been arbitrarily matched at $T^{-1} = 0.25$. Both signals plausibly arise from excited states similarly elevated above the ground diamagnetic state. The plant signal has been modeled as the S=1 state from a near axial, weakly antiferromagnetically coupled system with exchange parameter, $J = -0.87$ cm^{-1} . The effective zero field parameters of the S=1 state are $D = \pm 0.14$ cm^{-1} and $E/D = -0.11$ (Yamauchi et al., 1997). The orientation of the molecular z (i.e., D) axis is close to the membrane plane. The hyperfine pattern from the structured signal has been preliminarily modeled as arising from an S=2, Mn tetramer (Peloquin and Britt, 2001).

Yamauchi et al. (1997) have shown that the presence of small alcohols methanol (MeOH), ethylene glycol (EG), but not glycerol, suppress the S=1 signal, while still permitting functional turnover to the S_2 state and beyond. From EPR (Kawamori et al., 1989; see below), both MeOH and EG can penetrate near to the Mn site(s) in S_2 and so presumably in S_1. These molecules most likely influence the S=1 signal by

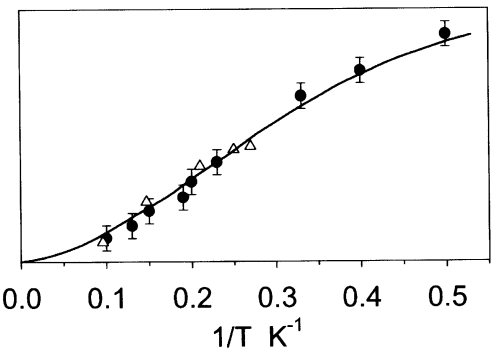

Fig. 2. Temperature dependence of the S_1 signals from a) ● (Yamauchi et al., 1997) and b) Δ (Peloquin and Britt, 2001). The arbitrary signal intensity scales of the original data have been matched at 1/T = 0.25 (see text). Curve is a fit to the exchange model in Yamauchi et al. (1997).

modulating the magnitude of the net antiferromagnetic coupling in a Mn cluster responsible for the signal (see below). This coupling must be small ($|J|$ < ~10 cm^{-1}) for the signal to be easily visible.

The weak, variable net antiferromagnetism in S_1 is probably not related to the apparent S_1 oxidation state variability discussed above, as the S=1 signal is observable in conditions nominally favoring either possibility for the Mn redox states in S_1. Because high-valent (III-IV or IV-IV) oxo-bridged Mn pairs with oxygen ligands and inter-metal separations of 2.7–2.8 Å (as seen in the S_1 state) appear always to be strongly antiferromagnetically coupled (Law et al., 2000), the S=1 signal implies linearly coupled structures (chain like), with one pair (III_2 or IV_2) strongly coupled silent and the other (always III_2), being weakly to moderately antiferromagnetically coupled. This is quite possible for III-III pairs (Manchandra et al., 1995) and then the two Mn dimers would need to be weakly or negligibly coupled between themselves.

B. S_2 State

This state is the most spectroscopically studied of the Kok cycle intermediates. Because there is an edge shift (Fig. 1) on $S_1 \rightarrow S_2$ turnover and S_2 has readily visible Kramers state EPR signals (multiline and g ~4.1 signals), it is generally supposed that a single Mn center oxidation occurs (i.e., Mn(III) → Mn(IV)). However ligand as well as metal center changes may alter the Mn K edge position (Kuzek and Pace, 2001;

Carell et al., 2002). The first spectroscopic technique used to probe the S state dependence of the Mn oxidation levels in PS II was UV-visible absorption spectroscopy (for a review, see Debus, 1992). The reported $S_1 \rightarrow S_2$ difference spectra are consistent and summarized in Kuzek and Pace (2001). Model compound spectra for single Mn(III) → Mn(IV) transitions in well characterized oxo-bridged model Mn compounds (including Mn catalase), however, are all qualitatively opposite to the $S_1 \rightarrow S_2$ difference spectrum. Rather, the $S_1 \rightarrow S_2$ difference strongly suggests histidine radical formation (oxidation of a deprotonated imidazolate anion side chain). Since one histidine is observed as a ligand to Mn in the multiline EPR signal of the S_2 state (see S_2 EPR, below), this suggests that a histidine ligand to Mn III, rather than Mn itself, is oxidized on going from S_1 to S_2 in these studies. Ligand oxidation is further supported by the observation and characterization of a near infra-red (NIR) absorption difference band in PS II core complexes (spinach) associated with the physiological $S_1 \rightarrow S_2$ transition (Baxter et al., 1999). The band shape closely matches the action spectrum for NIR induced multiline → g ~4.1 transition (see below) within the formal S_2 state (Boussac et al., 1996). The band is very weak, but its intensity and position are totally consistent with it being the 'Jahn Teller' d–d transition within the split e_g levels of Mn(III) (Kuzek and Pace, 2001). Since S_1 contains no Mn(II), the band is present in a Mn(III) ion that does not undergo oxidation, but rather alters its *ligand environment* on forming the S_2 multiline state. This alteration presumably 'tunes' the e_g level split to bring the band into view (i.e., between ~750–1000 nm). In total, these data argue against Mn oxidation occurring on the $S_1 \rightarrow S_2$ transition (see also $S_0 \rightarrow S_1$, below).

1. Electron Paramagnetic Resonance

Although the optical data do not support Mn oxidation on $S_1 \rightarrow S_2$ advance, the reader may now suspect that things are rarely that simple in PS II. The optical studies are carried out on dilute samples, undergoing multiple flash induced turnover under conditions typically used for O_2 activity assays. Cryoprotectants and reagents such as ethanol (EtOH), EG and MeOH are normally absent. The latter are frequently used in EPR because they enhance or stabilize certain Mn derived signals, particularly in the S_2 state, while not obviously inhibiting functional turnover (particularly MeOH, which is non inhibitory up to several molar). Moreover, in optical turnover experiments, the first flash (i.e., first $S_1 \rightarrow S_2$ advance in a series) data are usually ignored, as the results are often 'anomalous' (Rappaport et al., 1994, and references therein). This is difficult with XANES or EPR studies, which work with concentrated samples and limited turnover efficiencies.

a. Multiline Signal

The 'canonical' Mn-derived signal from the S_2 state is the hyperfine structured 'multiline' signal (MLS), first seen in 1981 (Dismukes and Siderer, 1981). This bears a general resemblance to the spin 1/2 signals seen in mixed-valence (III-IV or III-II) oxo-bridged Mn dimers, but contains more lines (~18–20) and 'superhyperfine' structure than typically seen in model dimer compounds. Its total reliably detectable width is ~172 mT, with small, variable features possibly extending beyond this. Data, from various sources, however suggest that the MLS, as conventionally generated for EPR study, is not always a homogeneous species (de Paula and Brudvig, 1985; Boussac, 1997; Evans et al., 2000; Lorigan and Britt, 2000). It appears to consist of two signal types, a 'broad' and 'narrow' form, first inferred by Boussac from NIR turnover effects on the multiline signal (Boussac, 1997). Recent work isolates the spectral shapes of these two signals and identifies some, at least, of the factors influencing their generation (Åhrling et al., 2004).

Figure 3a shows a comparison of MLSs generated by 200 K illumination, with approximately 3% MeOH or EtOH in the buffer medium, taken under similar conditions. In both cases little or no g ~4 species is present (see below), indicating that most centers are in the MLS form of S_2. Although generally similar, there are numerous differences between the spectra. The +MeOH spectrum has more intensity in the central regions, particularly downfield, while the peak intensities and substructure resolution near the edges are very similar for the two spectra. This suggests a 'second' component may be present in the +MeOH spectrum, which is spectrally narrower than the +ETOH 'broad' MLS, but with similar hyperfine peak spacing (~9 mT). This narrow component decays on sample storage at 77 K much more quickly than the broad component, which is typically stable for months (Evans et al., 2000). Figure 3b shows the narrow MLS obtained by subtracting the residual spectrum of a 77 K stored +MeOH sample from that

of the same freshly prepared (by one flash turnover) sample (Åhrling et al., 2004). This corresponds to at least 50 % of the total initial MLS intensity, with an apparent g value of ~1.90. Remarkably, both forms turn over efficiently by single flash advancement, but only the broad form is present by the 5th flash (Fig. 3d). At some point in the first turnover cycle, centers convert from a capacity to display the narrow to broad S_2 forms. However, Styring and coworkers have previously shown (Åhrling et al., 1997) that the MeOH promoted S_0 state signal (see below) is present out to 8 flashes in a turnover series, so that MeOH effects on S_2 are largely uncoupled from those on S_0. It now seems that single turnover (from dark S_1) in the presence of approximately 1M EtOH generates a broad MLS in essentially pure form, while MeOH gives a mixture, typically containing about 50% of the narrow form. In the absence of alcohols, mixtures seem favored, based on spectral shapes (see examples in Smith et al., 1993, and Fig. 3g).

There is a significant difference between multiline signals (broad or narrow) formed in the presence of MeOH and those formed in its absence. The latter are sensitive, in varying degree, to NIR induced conversion to higher spin states (see below), while the +MeOH MLS is totally resistant (Boussac, 1997). MeOH thus induces effects additional to those determining the balance of broad/narrow MLS forms, even the broad form in the presence of MeOH is NIR insensitive and spectrally distinct (Fig. 3a).

Britt and coworkers have performed pulsed Mn electron nuclear double resonance (ENDOR) on the MLS (Randall et al., 1995; Peloquin et al., 1998, 2000). They noted significant differences between the ENDOR from samples with and without EtOH (Peloquin et al., 1998). Figures 3e and g show their data for MeOH and EtOH containing samples. The +EtOH spectra (Fig. 3e) are of low intensity and display a number of approximately equally spaced (ca. 15–20 MHz) features. They resemble ENDOR from Mn(III) centers in model dimer (III–IV) complexes, but at half the mean frequency. The pattern arises from an interaction of quadrupolar and anisotropic hyperfine parameters characteristic of Mn(III) ions. The non-EtOH spectra (no additions, +MeOH) spectra are quite different, generally sharper, more intense, but again concentrated mainly in the 80–150 MHz region. The latter is typical of Mn(IV) (spin 3/2) centers in strongly coupled (III-IV) dimers, but the frequency spread is greater. The ENDOR envelope variation with observation field position (Fig. 3g) suggests orientation selection from centers with Mn hyperfine anisotropy at all contributing ENDOR frequencies. Figure 3f shows that good overall simulations of the total MLS as frequently observed are possible using tetrameric models (Peloquin et al., 2000) with Mn in the (III)-$(IV)_3$ oxidation state and most couplings nearly isotropic (Zheng and Dismukes, 1996). The ENDOR and variable NIR turnover suggest that Mn oxidation can occur on the $S_1 \rightarrow S_2$ transition, particularly under limited turnover conditions and in the presence of MeOH. When oxidation occurs, susceptibility to NIR turnover is lost, implying the oxidized Mn is that ion responsible for the NIR d-d band discussed above (when Mn(III).

A large body of magnetic resonance data now exists for the S_2 MLS, including multi-frequency EPR (Åhrling and Pace, 1995) and Mn-ligand ENDOR. This should be sufficient to fully define the spin Hamiltonian for the ML center, including the number of Mn effectively contributing. In practice, this is complicated by the now evident non homogeneity of the MLS and the different experimental conditions under which measurements have been performed.

Four groups have performed detailed simulation analyses on the MLS (Åhrling and Pace, 1995; Zheng and Dismukes, 1996; Hasegawa et al., 1998; Peloquin et al., 2000). The last three assumed tetrameric Mn models and the first a dimer model. The tetramer models differ in detail but all require four roughly equivalent Mn hyperfine constants ~180–250 MHz. The Mn clusters have different exchange connectivities, but couplings are tuned to give individual ion hyperfine projections mostly near unit magnitude. (Hasegawa et al., 1998). This results in multiline patterns which fit the observed (+MeOH) X-band spectrum well over most of its width. Typically, more peaks are predicted than reliably observed, with the simulations extending with low intensity beyond the experimental spectral width. However, these simulations are all reasonably consistent with the ^{55}Mn ENDOR in Fig 3, and predict no ENDOR transitions above ~160 MHz.

The first and so far only multi-frequency simulation study of the MLS (4, 9 and 35 GHz (Åhrling and Pace, 1995)), assumed a mixed valence dimer model for the Mn cluster with unusual, anisotropic hyperfine parameters for both the formal Mn(III) and (IV) centers. The nuclear quadrupole interactions (>60MHz) needed to model the highly structured S band (+EtOH) spectrum (Haddy et al., 1989) are much larger than seen in model compounds and do

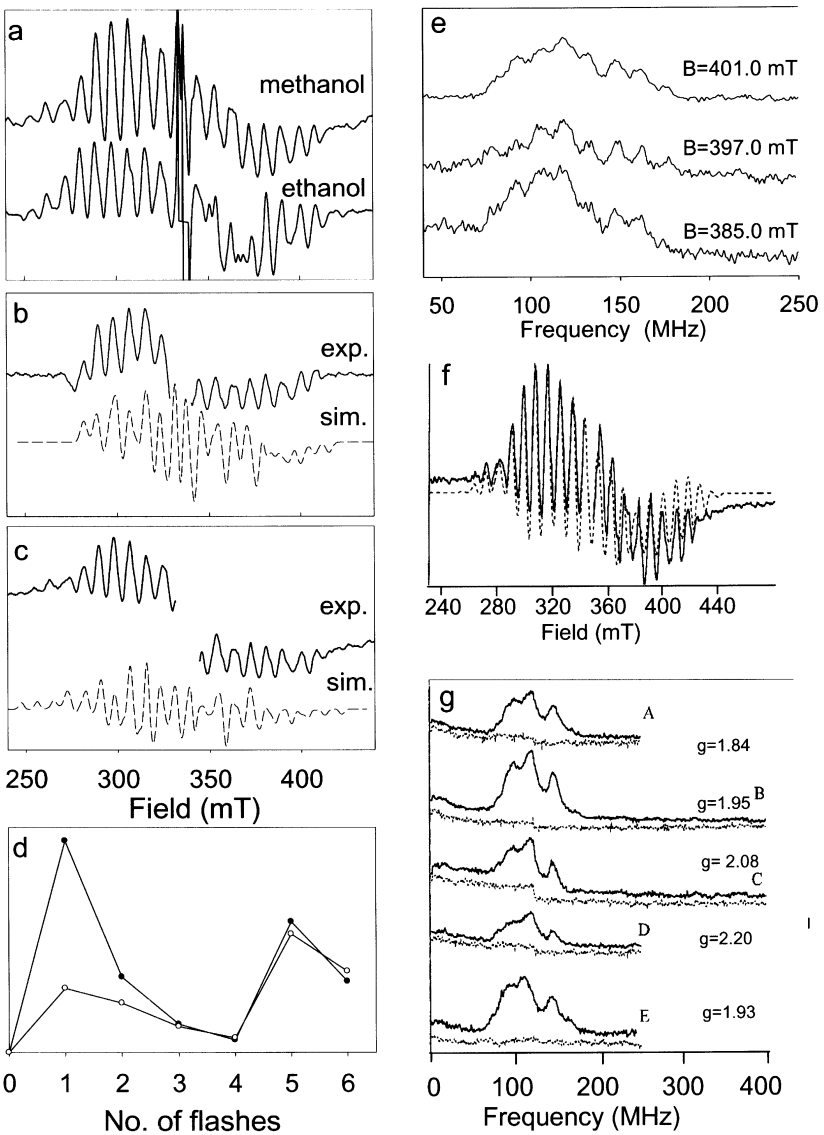

Fig. 3. a) X-band EPR spectra of the MLS generated by 200K illumination with green light of PS II membranes in the presence of approximately 1M EtOH, or MeOH in buffer medium. Spectra have similar total intensities (instrument, sample conditions as in Åhrling et al., 1998b). b) Narrow MLS (solid) in PS II membranes (difference between MLS of freshly prepared single flash (20 °C) turnover sample and same sample stored for 12 weeks at 77K). Buffer with 1M MeOH, instrument, sample conditions as above, with microwave frequency at 9.43 GHz. Dashed line is simulation using parameter values from Table 1. c) Broad MLS in presence of MeOH (solid, from Åhrling et al., 2004) and simulation (dashed), using parameter values from Table 1. d) Laser flash turnover pattern of total MLS intensity for sample as in b) (procedure as in Åhrling et al. (1998a)). Solid points are MLS intensities in samples cryogenically frozen within approximately 3 sec of flash turnover generation and stored at 77 K for < 5 hours. Open points are same samples after long storage (above). e) and g) Davies ^{55}Mn ESE ENDOR of PS II particles in the S_2 state, reproduced from Randall et al. (1995) and Peloquin et al. (2000), respectively. See original references for instrument conditions. Buffer with e) ~1.2 M EtOH, g) as indicated. g positions in the absorption signal envelopes for ENDOR recording as indicated. f) Simulation of MLS in presence of MeOH using tetramer model (Peloquin et al., 2000), assuming Mn (III)-(IV)$_3$. The parameters in Table 1 predict ENDOR transitions in the ranges ~70 – 130 MHz for the MnIV ion. Transitions for the MnIII ion in the broad form are predicted from ~290–350 MHz.

not reproduce either type of observed Mn ENDOR spectrum (Peloquin et al., 2000). However, the narrow MLS in Fig. 3b has significant intensity over a width of only ~120 mT. This is typical of Mn (III-IV) dimers (Schafer et al., 1998) and could not arise from a magnetic tetramer unless some Mn centers had small (<140 MHz) effective hyperfine couplings, which are not seen in ENDOR. Moreover, it is likely that lower S state multiline signals (see S_0 below) arise from systems that are effectively Mn dimers. Even a tetrameric Mn cluster, with oxidation states III_3IV or IV_3III, has a range of exchange coupling conditions giving a spin 1/2 ground state with hyperfine contributions from only two (III-IV) ions, the other two being anti-ferromagnetically coupled 'silent' (Carell et al., 2002). The Mn cluster geometries (Chapters 19–21) from crystal structures are insufficiently resolved at present to determine if this is likely. In principle Mn ENDOR can resolve the question, as a dimer model of the broad MLS predicts ENDOR frequencies above ~260 MHz (for the Mn(III). Only two groups have reported such studies (on +MeOH samples). One group (Peloquin et al., 2000) sees no such high frequency transitions reproducibly and the other does (Kammel, 2003). Dimer simulations of the broad and narrow MLS are shown in Fig. 3b and c, with parameters listed in Table 1. The high frequency ENDOR measurements are technically demanding and clearly further study is desirable. The CW multiline spectra in Peloquin et al. (2000) suggest that a roughly equal mixture of broad and narrow forms were present in this work.

b. g = 4.1 Signal

This is the other extensively studied EPR signal from the S_2 intermediate of the OEC . It appears as a near symmetrical, Gaussian derivative-shaped feature at S- and X-band, crossing around g = 4.1–4.2 (Fig. 4), but exhibiting partially resolved fine structure splitting at higher frequencies (Åhrling et al., 1998b). The signal is observed routinely in higher plant photosystem preparations, but it is unclear whether the same species is seen in cyanobacterial PS II (see below), The plant signal clearly derives from Mn-containing centers, as Mn hyperfine structure has been resolved on it (Kim et al., 1990; Smith et al., 1993) and the signal undergoes S state cycling (Zimmerman and Rutherford, 1986).

There appear to be two distinct types of Mn-derived g = 4.1 signals in plants, which are spectroscopically quite similar at X-band, but distinguishable at Q-band (Smith et al., 1993). They have qualitatively different temperature dependences and so must arise from Mn clusters with different internal couplings. One behaves quantitatively as the first excited, spin 3/2 state of the Mn center giving rise the spin 1/2 MLS state (Smith and Pace, 1996a) and is always seen in the presence of the latter. For this excited state to be visible, the net anti-ferromagnetic coupling in the center must be weak (J ~2–3 cm^{-1}). While we generate this species, others have found difficulty in doing so. Both g = 4.1 types seem to be present in some earlier studies (Zimmerman and Rutherford, 1984). This appears to mirror the situation in S_1, where the conditions giving rise to the comparably weak coupling in the parallel polarization signal are not straightforwardly reproduced. The matter is still under investigation.

The second and most readily generated g = 4.1 species, first reported in 1984 (Casey and Sauer, 1984) is a ground state (Smith and Pace, 1996a) and may appear alone or in the presence of the MLS. From the beginning, it was recognised that the phenomenology of the signal's low temperature (~140 K) illumination formation and higher temperature (~200 K) dark inter-conversion to the MLS, suggested it was an 'intermediate' redox species between the primary charge separating components of PS II and the MLS site. Boussac and Rutherford (1996) showed that the reverse process, MLS to g = 4.1 inter-conversion, could be stimulated by low temperature (~140 K) near infrared (NIR) illumination of PS II centers in the MLS, S_2 state (Boussac et al., 1996). The action spectrum for this process coincides closely with a very weak absorption band in a Mn(III) center within the physiological (after several turnovers) S_2 state (Kuzek and Pace, 2001).

The excited state g = 4.1 species is almost certainly a near axial spin 3/2 center, from its field position, shape and temperature dependence relative to signals identifiable as the associated spin 1/2 and 5/2 states. It has been successfully modeled as such from oriented membrane spectra (Åhrling et al., 1998b). The spin state of the ground state species is less clear. It has been modeled at several frequencies as a near axial spin 3/2 center (Åhrling et al., 1998b), and as a rhombic spin 5/2 center (Haddy et al., 1992). Low temperature magnetization measurements (Horner et al., 1998) suggested a spin 5/2 assignment. These experiments require the absolute concentrations of all relevant paramagnetic centers in PS II to be reliably

Table 1. Catalytic Mn-dimer oxidation states, EPR parameters [1]

S state EPR signal	Mn A Oxidation State	[2] A_x, A_y, A_z (A_{iso}) [3] [q_x, q_y, q_z]	Mn B Oxidation State	[2] A_x, A_y, A_z (A_{iso}) [3] [q_x, q_y, q_z]	[9] g_x, g_y, g_z
S_0 (MeOH)	II	[4] 268, 276, 247 (264)	III	[4] 251, 340, 172 (254) [–10.8, +7.2, +3.6]	1.96, 1.98, 2.03
S_0 (NO)	III	[5] 214, 214, 111 (180)	II	[5](267)	1.97, 1.97, 2.01
S_2 (broad MLS)	III	[6] 294, 360, 104 (252)	IV	[6] 115, 253, 230 (199) [+6.2, –0.2, –6.0]	1.99, 2.00, 2.01
S_2 (narrow MLS)	III	[6] 177, 175, 253 (203)	IV	[6] 115, 241, 201 (186)	1.93, 1.94, 1.93
S_1 parallel polarization Plant [7]	III		III		D = ± 0.14 E/D = –0.11 g = 2.0
S_3 parallel polarization [8]	III		III (IV) plus oxidized bridge oxo		D = ± 0.435 E/D = –0.317 g = 2.0

[1] Hyperfine and quadrupole parameters in MHz. Fine structure D parameters (S_1, S_3) in cm^{-1}. [2] Mn intrinsic ion hyperfine constant magnitudes. Absolute signs are negative in all cases. [3] Mn quadrupole hyperfine constants, where determined. [4] Assumed strong coupling dimer (Bencini and Gatteschi, 1990). $A_{(A)}$ (true ion)=3/7 $A_{(A)}$ (fit), $A_{(B)}$ (true ion)= –3/4 $A_{(B)}$ (fit). [5] Intermediate coupling dimer, (Sarrou et al., 1998). [6] Assumed strong coupling dimer. $A_{(A)}$ (true ion) = 1/2 $A_{(A)}$ (fit), $A_{(B)}$ (true ion) = – $A_{(B)}$ (fit). [7] Plant g ~4.8 parallel polarization signal (Mino and Kawamori, 2001). Assumed spin state, S=1. [8] Plant g ~8,12 rhombic parallel polarization signal (Mino and Kawamori, 2001). Assumed spin state, S=1. [9] g-tensor value.

known. The NIR induced MLS ↔ g 4.1 inter-conversion protocol however allows a simple, minimally inferential determination to be made.

Figure 4 shows a difference spectrum (NIR illuminated – S_2 state MLSS_2) for the NIR induced MLS to g = 4.1 conversion in spinach PS II core complexes (Smith et al., 2002). Here the g = 4.1 signal appears as a positive feature, while the MLS component is negative, corresponding to the loss of this signal. Assuming only that the NIR induced conversion is one to one on centers, then the relative integrated intensities of the g = 4.1 and multiline EPR signals will determine the spin state of the g = 4.1 signal, as the MLS is known to arise from a spin 1/2 center. Following Hansson et al. (1987), the signal intensity ratios are:

$$\frac{[\text{g4 INTENSITY}]}{[\text{MLS INTENSITY}]} = \frac{0.50.\left(g_{\perp}^2 + g_{II}^2\right)}{4.g_{4\,app}.g_{2\,app}} = 0.32 \text{ for spin } 3/2 \qquad (1)$$

$$= \frac{\left(g_{4.3}\right)^2}{3.g_{4\,app}.g_{2\,app}} = 0.75 \text{ for spin } 5/2 \qquad (2)$$

Here $g_{2\,app}$ is the MLS g value, taken as 2.00, $g_{4\,app}$ is the apparent g value of the g ~4 signal , taken as 4.1. In Eq (1) the parallel and perpendicular g tensor components are taken as 2.0 and 4.1 respectively for the $m_s = \pm 1/2$ doublet of the axial 3/2 state (~50% of intensity in g ~4 region (Hansson et al., 1987)). In Eq. (2), $g_{4.3}$, which determines the transition probability of the quasi-isotropic center doublet of the rhombic 5/2 state, is taken as 4.3. This is still true at X-band, to good approximation, for a system with the fine structure parameters used to model the g = 4.1 signal in (Haddy et al., 1992; Smith and Pace, 1996a). In Eqs. (1) and (2), the doublet sublevels of the spin systems are assumed equally populated at an observation temperature ~10 K, consistent with the fine structure parameter values used in modeling the signals. Determining the intensity ratios by direct signal integration or the Gaussian envelope approximation (see Fig. 4), the ratio, for several sample types/condition, is 0.27 ± 0.03. This strongly suggests that the ground state, like the excited state g = 4 species, is a near axial spin 3/2 center.

Both characterizations of the S_1 parallel polarization signal (Dexheimer and Klein, 1992; Yamauchi et al., 1997) in plant PS II indicate that loss of the

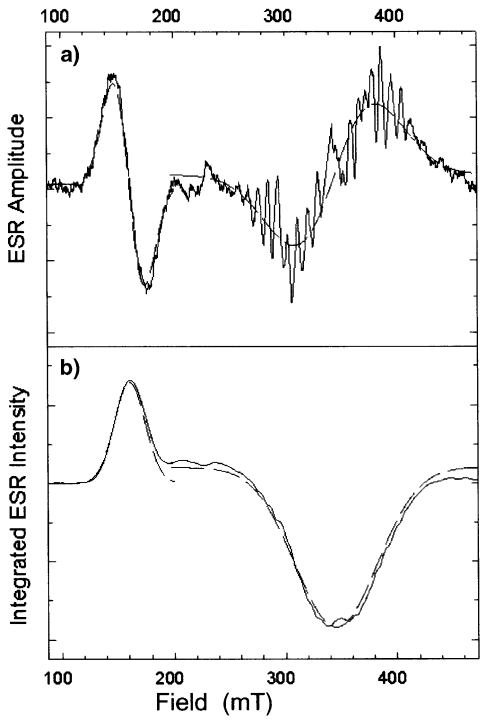

Fig. 4. a) Ground state g=4.1 species generated by low temperature (140–150 K) NIR illumination turnover from the MLS S_2 state, in spinach PS II core complexes (see references in Smith et al., 2002 for conditions etc.). In these difference spectra, the NIR generated g = 4.1 signal is positive while the lost MLS appears negative. b) First integrals (absorption) of the derivative signal intensities of the g= 4.1 an MLS regions from a), as well as mean Gaussian approximations for the MLS and g~4 signals (dashed). The g=4.1/ MLS integrated signal intensity ratio from integration of b) or Gaussian fits is 0.26 ± 0.03.Turnover conditions in a) are such that negligible high g species are formed.

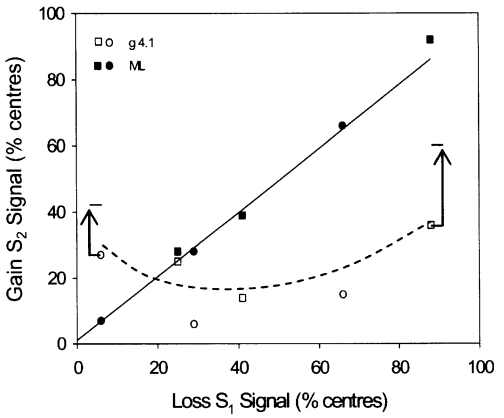

Fig. 5. Plot of the correlation between S_2 state signal formation, by various means, and loss of the g ~4.7 S_1 parallel polarisation signal in PS II membrane particles from plants. Data from Dexheimer and Klein (1992), ○,● and Yamauchi et al. (1997) ■, □ have been combined and scaled to the same initial dark state S_1 signal amplitude (assumed 100% of centres) and same slope of linear fit through the respective MLS data points (see original references). Per center scaling of MLS and g = 4.1 signal amplitudes in both cases is from the original data (see text). Comparisons of the peak height signal quantitations used in these studies with 'one for one' NIR turnover spectra (as in Fig. 4) suggest that the g = 4.1 fractional intensities in Fig. 5 are underestimated by 30-60 % (bars).

S=1 signal on $S_1 \rightarrow S_2$ advance, correlates only with the formation of the MLS, not the ground state g = 4.1 signal. In Fig. 5 we have combined results from both sources to show the fractional increase in S_2 signals (MLS and g = 4.1) per center with loss of S_1 signal. The original (arbitrary scale) data have been normalized assuming the maximum (dark state) S_1 signal corresponds to 100% of centers and that the dark annealing, 200K g = 4.1 → MLS inter-conversion (as performed), is one to one on centers in each case. Comparisons with the spectra in Fig. 4 (NIR inter-conversion at lower temperature) suggests that the latter assumption probably underestimates the g ~4 center population by a factor of ~1.3 – 1.6, i.e., some g ~4 centers simply recombine to S_1 on annealing. Nonetheless, Fig. 5 clearly demonstrates that the S_1 parallel polarization centers convert only to the MLS form on turnover and that the g = 4.1 signal may be simultaneously present in a substantial fraction (25 to 50 %) of centers that contain either the S_1 parallel polarization *or* S_2 MLS. That the g = 4.1 and MLSs arise from magnetically unconnected centers is the obvious conclusion, as was in fact originally (Dexheimer and Klein, 1992) and more recently (Mino and Kawamori, 2001) drawn.

From the above, we assign the ground g = 4.1 signal to a state of the 'spectator' Mn pair, discussed earlier. We have shown (Åhrling et al., 1998b) that a three center system, consisting of two Mn (III_2 or IV_2) bridged by an oxidizable ligand can generate such a spin 3/2 state and proposed that the ligand is the redox active intermediate, tyrosine Y_Z (Kuzek and Pace, 2001). This system also exhibits a spin 1/2 excited state, with radical like appearance, under suitable

sample conditions (glycerol or EG as cryoprotectant (Smith and Pace, 1996b), but not sucrose (Boussac and Rutherford, 2000). For the spin 1/2 signal to be visible, the anti-ferromagnetic exchange couplings in the cluster must be sufficiently weak. We speculate that this may be related to the apparent oxidation state lability of the spectator Mn pair discussed above.

c. High g Signals

Two classes of 'high g' (i.e., $g_{apparent} > 4$) signals have been identified in the S_2 state of functional PS II. The first is generated by NIR (or IR containing) illumination of MLS state samples, at temperatures below 200 K. These high g signals (g ~9–5), are seen in both higher plant and cyanobacterial photosystems. In plants (where first observed), the signals are formed in competition with the g = 4.1 signal, and are progressively favored as the NIR illumination temperature drops below 100 K (Boussac et al., 1998). In cyanobacteria, the high g species appear to be the only types systematically seen and at present no signals closely resembling the 'classical' g = 4.1 spectrum from plants have been reported from cyanobacterial PS II by inter-conversion from MLS centers. The high g signals are variable in shape and field position, show a complex temperature dependence (indicating that they arise from more than one EPR transition) and almost certainly derive from systems of total (non integral) spin ≥ 5/2. They have been interpreted to arise from higher spin states of the catalytic Mn cluster in PS II (Boussac et al., 1998).

The second class of high g signal (Smith and Pace, 1996a) is clearly identified with the MLS and excited state g = 4.1 species. The field position (g ~6) and temperature dependence indicate that it arises from the next highest (spin 5/2) state in that quasi-axial, weakly coupled manifold (Åhrling et al., 1998b). Unlike the cases described above, the signal clearly derives from Mn centers and exhibits partially resolved Mn hyperfine structure (min. spacing ~4 mT). It is co-generated with the MLS and excited state g ~4 species by 200 K $S_1 \rightarrow S_2$ turnover in sucrose cryoprotected spinach PS II. It is currently unknown if the signal forms in cyanobacterial preparations.

The picture to this point of the S_2 state spectroscopy appears nothing if not complex. We suggest that a pattern may be evident however:

(i) Either ligand or Mn center oxidation may occur in the functional S_2-state. Ligand (His^+) oxidation is probably the physiological form and gives rise to the MLS type susceptible to NIR induced turnover. Whether metal or ligand oxidization is favored depends on turnover conditions, small alcohol (MeOH) concentrations.

(ii) NIR turnover probably involves excitation of a d–d transition in the Mn(III) to which the His^+ ligand is co-ordinated (see Section III) If this leads to meta-stable metal → ligand electron transfer, the resulting [Mn(IV) – His] configuration may here result in a slightly higher effective redox potential for the MLS Mn dimer (see Fig. 8). This could induce electron transfer into the MLS cluster, reducing it and oxidizing other lower potential centers within the photosystem (e.g., acceptor non-heme iron, Cyt b_{559} and the proposed (Y_Z – Mn) cluster).

(iii) The putative (Y_Z – Mn) cluster may exist only in eukaryotic PS II (higher plants etc., see Section III). NIR induced signals from this center (i.e., the ground g = 4.1 species) would then be seen only in plants. Additional transfer from other centers (e.g., non-heme iron) may also occur, leading to EPR signals corresponding to oxidized forms of the latter.

(iv) At present the NIR induced high g signals show no resolved Mn hyperfine, unlike the MLS and g = 4.1 signals. In some instances (e.g., Fig. 5 in Boussac et al., 1998), the signals are quite narrow (~20 mT pp width), so that special circumstances, such as involvement with radicals or particular coupling schemes would need to operate if they were Mn related. It is also quite possible (V. Petrouleas, personal communication) that the apparently narrow shape of the proposed spin 7/2 species, first seen by Nugent and coworkers (Nugent et al., 1997; Sanakis et al., 2001) is distorted by background subtraction effects. The high g signals are generally much more variable in shape than the known Mn derived species. We suggest that in some cases at least, they arise from the oxidized form of the acceptor non-heme iron, which is a low symmetry spin 5/2 center. Its spectral shape is variable (Miller and Brudvig, 1991) and it is easily formed in cyanobacterial PS II.

d. Ligand Electron Spin Echo Envelope Modulation and Electron Nuclear Double Resonance Spectroscopy in the S_2 State

Pulsed EPR spectroscopy (particularly ESEEM) has been extensively applied to study nuclear interactions with the Mn catalytic site. These arise from the individual Mn centers themselves, from protein supplied ligands, co-factors, and exogenous molecules including substrate water. Pulsed experiments are generally more selective and informative than earlier studies of 'superhyperfine' couplings from labeled species (with ^{15}N, ^{17}O etc.) using CW X-band EPR (reviewed in Debus, 1992). However, because of magnetization relaxation limitations, the only Mn signals amenable to study are those with net spin 1/2 or weakly interacting spin 1/2 centers. To date this has meant the S_2 state MLSs and S_3 'split' signal in practice (see Chapter 10).

Britt et al. (1989) pioneered the use of pulsed EPR in PS II study. They have observed ^{14}N coupling to the MLS from a single histidine (Tang et al., 1994), in two pulse ESEEM studies (Fig. 6a). This coupling, which behaves very similarly in plant and cyanobacterial PS II centers, is notable in that low frequency, single quantum nuclear quadrupole resonance (NQR) transitions are not seen and that ^{15}N substitution (Fig. 6b) leads to total loss of nitrogen modulation. This is in contrast to the case for NH_3 interaction with the MLS center (Britt et al., 1989), where low frequency ^{14}N and ^{15}N resonances are readily detected. The latter behavior is typical for 'conventional' metal–N ligand interaction, while the former is characteristic of very strong, axially anisotropic N nuclear hyperfine coupling. Comparison with the computational results of McCracken et al. (1992) indicate that the MLS N-hyperfine coupling tensor is of order; $A_\perp$ approximately –4–5 MHz and $A_{II} > 10$ MHz. This would suggest a π spin density approaching 10% on one histidine nitrogen (Carrington and McLachlan, 1967), consistent with ring oxidation.

An obvious application of pulsed EPR spectroscopy in PS II is to detect labeled substrate water interaction with the Mn catalytic site. This has not proved straightforward. Line broadening of the S_2 MLS CW spectrum in samples extensively incubated in partially (~40%) ^{17}O labeled H_2O, gave the first estimates of ^{17}O hyperfine couplings (Hansson et al., 1986). When the corresponding ESEEM experiment was first performed (Turconi et al., 1997), no significant specific interaction of the labeled water and the MLS Mn center was observed. Subsequently, in a similar study of ^2H_2O binding to the MLS center (Evans et al., 2000), it was found that only the central region of the MLS spectrum gave detectable ^2H ESEEM modulations and that their intensity decayed faster on 77 K sample storage than the total MLS intensity (Fig. 6c,d). Re-illumination at 200 K regenerated the original MLS intensity and ^2H ESEEM signals. This behavior clearly echoes the general shape and differential storage stability of the broad and narrow MLS forms discussed above. It was then realized that the 1997 study on $H_2{}^{17}O$ binding involved samples that had been stored for some time on liquid N_2, following illumination to S_2. These still possessed substantial MLS intensity. Recently Evans et al. (2004) have re-examined the matter with freshly illuminated samples. Figure 6e shows that ^{17}O modulations are

Fig. 6. Fourier transformed (frequency domain) ESEEM spectra of the nuclear interactions of various species (indicated in boxes) with the Mn center in PS II, detected by electron spin echo spectroscopy at various positions on the relevant MLS EPR absorption envelope. See original references for samples/conditions. a) Two pulse spectra from *Synechosystis* with biochemically incorporated ^{14}N or ^{15}N histidine (Tang et al., 1994). Intense modulations at low frequencies (~2–6 Mhz) are seen for ^{14}N but not ^{15}N nuclei. This is characteristic of strong, axial hyperfine coupling of the nitrogens to the electron spin (see text). b) MLS envelope positions and c) Three pulse ^2H modulation spectra for ^2H_2O treated PS II membranes (Evans et al., 2000) The spectra were acquired at the indicated field positions from freshly illuminated samples. Traces 1 and 6 are multiplied by 10. d) Differential decay of the total ^2H modulation (▲) and MLS intensity (△) on storage at 77 K for samples in b,c. The region over which significant ^2H modulation is seen corresponds to the general narrow MLS shape from Fig. 3b and the intensity of the ^2H coupled MLS component is again ~ 50 % of the initial total (cf. Fig. 3d). e) Three pulse light minus dark ^{17}O modulation ratio-ed spectra for $H_2{}^{17}O$ and $H_2{}^{16}O$ treated and freshly illuminated PS II membranes (as in Evans et al., 2004). The single and multiple quantum branch transitions are indicated. The hyperfine interaction is near isotropic (a_{ISO} ~4.5-5) and the quadrupole term (e^2Qq/h) is > 6 MHz. f) Three pulse ^1H modulation spectra for ^1H MeOH treated PS II membranes (as in Åhrling et al., 2004). Spectra from field positions across the MLS envelope (as in b) were aligned at a common ^1H Larmor frequency (16.2 MHz) and averaged (smearing out non proton couplings). Three quasi-isotropic proton couplings are indicated. Width of the intense low frequency peak is due partly to overlapping, distributed N resonances from lower field spectra. g) Three pulse $^2H/^1H$ time domain divided spectra for $^2H_3$ and $^1H_3$ MeOH treated PS II membranes (Force et al., 1998; Evans et al., 1999), aligned at common Larmor frequency (2.48MHz). Data from Evans et al. (1999) are ^2H Larmor aligned and averaged, analogous to f. For freshly illuminated samples, the intensity distribution of the ^2H modulations from $[^2H]_3$ MeOH across the MLS envelope, as seen in Evans et al. (1999), is very similar to that for ^2H_2O (as in c). Magnitudes of the larger ^2H couplings expected from the ^1H couplings in f are indicated.

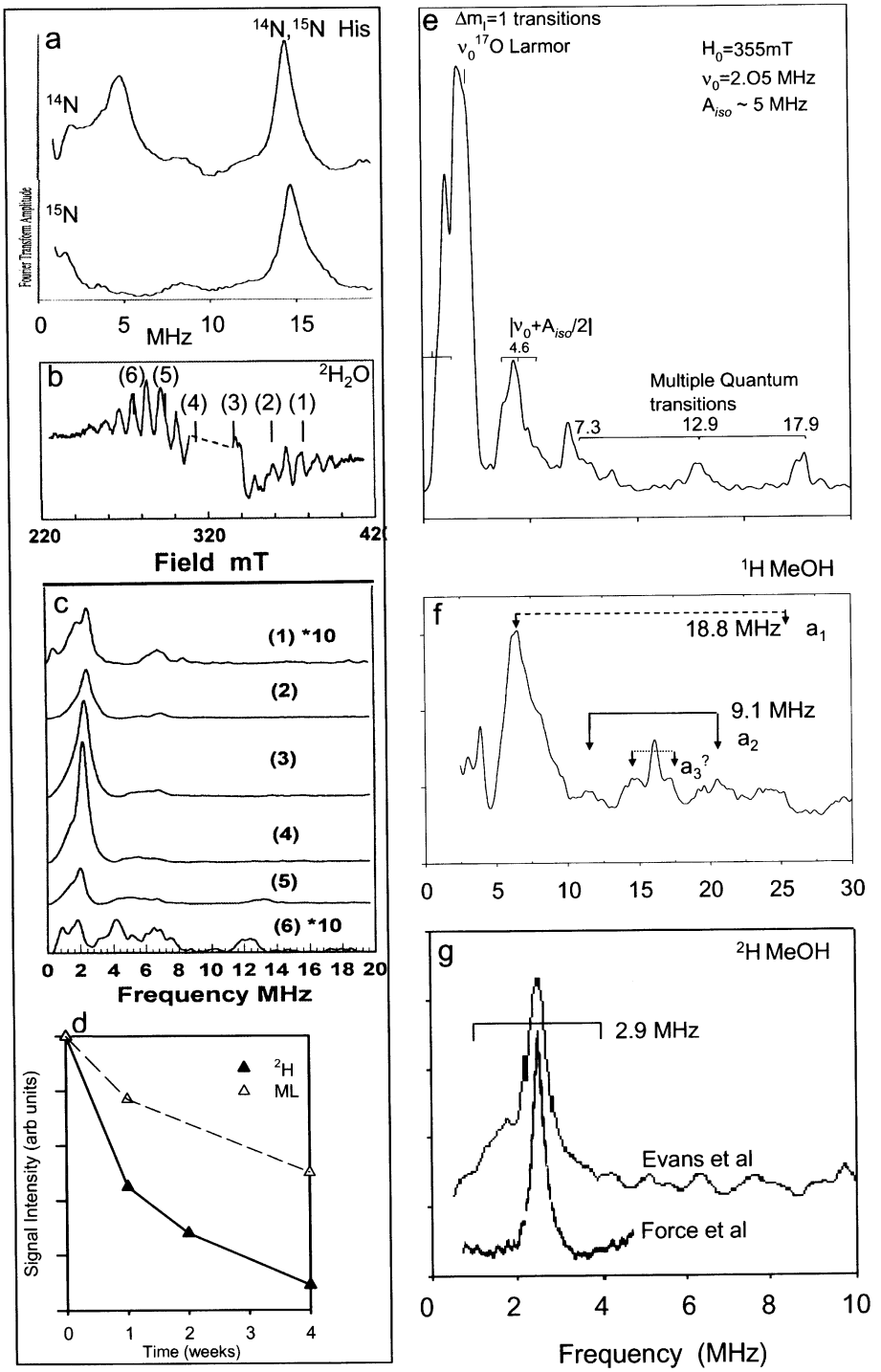
a
^{14}N,^{15}N His
^{14}N
^{15}N
Fourier Transform Amplitude
0 5 MHz 10 15
b
(6) (5) (4) (3) (2) (1)
$^{2}H_2O$
220 320 42
Field mT
c
(1) *10
(2)
(3)
(4)
(5)
(6) *10
0 2 4 6 8 10 12 14 16 18 20
Frequency MHz
d
^{2}H
ML
Signal Intensity (arb units)
0 1 2 3 4
Time (weeks)
e
Δm_I=1 transitions
ν_0 ^{17}O Larmor
H_0=355mT
ν_0=2.O5 MHz
A_{iso} ~ 5 MHz
$|\nu_0+A_{iso}/2|$
4.6
Multiple Quantum transitions
7.3 12.9 17.9
^{1}H MeOH
f
18.8 MHz a_1
9.1 MHz
a_2
a_3?
0 5 10 15 20 25 30
g
^{2}H MeOH
2.9 MHz
Evans et al
Force et al
0 2 4 6 8 10
Frequency (MHz)

now clearly visible near the center of the MLS pattern in the S_2 state. ^{17}O possesses a spin 5/2 nucleus, with a larger quadrupole moment than ^{14}N. The frequency domain spectrum in Fig 6e shows well resolved high frequency overtone resonances, consistent with strong ^{17}O coupling to the Mn cluster. The ^{17}O quadrupole term and the internal orientation of the quadrupole tensor axes, relative to the hyperfine tensor, are very similar to the case of water binding axially to the heme iron in P450 (Thomann et al., 1995). The apparent hyperfine coupling term (a_{iso} ~5 MHz) however, is approximately twice that inferred for the water bound to the Fe^{3+} center in P450 (2.6 MHz). This would be consistent with the actual a_{iso} term being essentially the same as in the P450 binding, but with the water bound to a quasi–axial Mn(III) ion in the narrow form MLS dimer, for which the nuclear hyperfine projection constant is 2.

Although not present physiologically, MeOH and other small alcohols interact with the Mn cluster in mechanistically interesting ways. MeOH interaction has been examined with both the methyl $[^2H]_3$ and normal $[^1H]_3$ species (Force et al., 1998; Evans et al., 1999) at concentrations which have no influence on catalytic water splitting activity. The picture that emerges is remarkably similar to that for water binding. Strong coupling to the methyl hydrogens/deuterons is seen only on a 'fast decaying', narrow component of the MLS spectrum. Figure 6f shows data (freshly illuminated) for ^1H methanol interaction with the MLS center (Åhrling et al., 2004). At field positions near the center of the MLS pattern, ESEEM modulation frequencies symmetrically spaced about the proton Larmor value are evident, as well as low frequency (< 5 MHz) contributions from N (cf. Fig. 6a). That the former derive from proton couplings is confirmed by 'averaging' the Fourier transformed ESEEM spectra taken across the MLS pattern (Fig. 6b), all aligned at a common proton Larmor frequency (Fig. 6f). This causes resonances not originating from protons to 'smear out' while proton peaks add. The data indicate three quasi-isotropic couplings of approximately 19, 9 and <3 MHz respectively. At present the numbers of protons contributing to each coupling are not known, but the couplings are absent from the ESEEM of corresponding $[^2H]_3$ methyl MeOH treated samples. Figurre 6g shows methanol $^2H/^1H$ difference spectra, averaged at the deuteron Larmor alignment. The peak shape is consistent with strong methyl deuteron couplings (2.9, 1.4 and < 0.5 MHz) expected from the above proton couplings. These couplings are much larger than the weak interactions seen in nominally comparable experiments by Force et al. (1998), who surveyed a range of deuterated alcohols. Their data, reproduced in Fig. 6g, are consistent with approximately 4Å point dipole interaction distances between the deuterons and the Mn center electron spin. A similar result was obtained for $[^2H]_6$ EtOH. Both alcohols appeared to exhibit very similar specific binding (K_D ~80 mM) to site(s) clearly near the MLS center. Examination of the CW multiline patterns in Force et al. suggest that the broad MLS was dominant in their samples (see discussion in Åhrling et al., 2004).

Large proton couplings that are readily resolved in ESEEM are generally 'isotropic' contact terms, or nearly so. Commonly these arise when methyl or methylene protons are β positioned relative to a group with π electron spin density. Then the coupling magnitude depends sensitively on the dihedral angle between the C–H bond and π axis direction (Carrington and McLachlan, 1967). Interpreting the (three) strong MeOH couplings in these terms, suggests significant p orbital spin density on the methanol O bound in the narrow MLS center (see Section III). This would require direct Mn-O ligation, possibly of the deprotonated methoxide species (Fig. 8B). However, this binding site is almost certainly *not* the substrate water site inferred above in the same MLS center type, as MeOH is non-inhibitory at the concentrations of these studies and both narrow and broad center forms turn over fully, at least once, in the presence of MeOH (Fig. 3d).

Two other small molecule species whose interactions with the MLS center have been studied by pulsed EPR are NH_3 (Britt et al., 1989) and halides (Cl^- and Br^-) (Boussac, 1995). Ammonia is mildly inhibitory and binds directly to the MLS center. Small anions have long been known to interact with the OEC and stimulate catalytic function (Debus, 1992). However Cl^- and Br^- do not directly ligate Mn in the S_2 MLS center (Boussac, 1995). Their mode of action remains as yet somewhat unclear.

CW ENDOR has been used to study ^1H and ^{15}N interaction with the MLS center (Kawamori et al., 1989; Tang et al., 1993; Fiege et al., 1996). The ^1H results are generally consistent, 1–2 exchangeable protons with mainly dipolar coupling to the Mn spins (~2.5–4 Å distant). Tang et al. (1993) see no evidence of direct water co-ordination to the Mn, while Fiege et al. (1996) suggest one Mn bound water molecule in S_2. The differences arise principally from the spin

coupling models used to interpret the results. ^{15}N couplings of approximately 1 and 4 MHz are seen for globally N-substituted *S. elongatus* (Tang et al., 1993). Since large, anisotropic ^{15}N couplings would not easily be seen in the CW experiment, while small (i.e., < 5 MHz) couplings should have been detectable in the ^{15}N labeled histidine ESEEM (above), the couplings seen by CW ENDOR are probably not due to the ring nitrogens of the Mn_B histidine ligand (see Section III). Presumably they are due to more distant, perhaps peptide nitrogens.

C. S_3 State

On the $S_2 \rightarrow S_3$ transition, the non integral spin EPR signals from S_2 are lost, requiring oxidation of some component in the Mn center(s). Either ligand or Mn oxidation have been suggested from Mn XANES shift results (Roelofs et al., 1996; Iuzzolino et al., 1998). Figure 1 suggests that the Mn edge shift on $S_2 \rightarrow S_3$ is probably the least for any S state turnover. Additionally, EXAFS data show that the Mn cluster undergoes a significant structural change on going to S_3, which is not seen on the transition to S_2. The alteration consists mainly of: (i) an increase of ~0.2–0.3Å, in the Mn–Mn separation of one of the bridged Mn dimers (Yachandra et al., 1996), or (ii) this plus an increase in first shell O ligation to Mn (Dau et al., 2001). Such a change would be unprecedented for Mn(III) → Mn(IV) oxidation in a dimer. It could however represent oxidation of a bridging species, probably an oxo group. The apparent ligation state change seen by Dau and coworkers is interesting and we return to this below.

Recently a parallel polarization signal from the functional S_3 state in plant and cyanobacterial PS II has been observed, by both flash turnover and continuous illumination (approximately 240K), (Matsukawa et al., 1999; Boussac et al., 2000; Ioannidis and Petrouleas, 2000; Ioannidis et al., 2002) . The signal also has components visible in transverse mode. Matsukawa et al. (1999) have studied oriented samples and the temperature dependence of these signals (compare S_1 signals (Fig. 2)). The spectra have been simulated as a near rhombic S=1 center, with fine structure parameters $D = \pm 0.44$ cm^{-1} and $E/D = -0.32$, in a weakly anti-ferromagnetically coupled system ($J = -1.20$ cm^{-1}). Such weak coupling is consistent with interruption of anti-ferromagnetic exchange pathways by bridge oxidation. MeOH (but not EtOH) suppresses the parallel polarization signals, consistent with this molecule increasing the net anti-ferromagnetic interaction in the cycling Mn cluster, in all S states, without inhibiting catalytic function (see also S_0 below).

D. S_0 State

The large Mn XANES edge shift (see Fig. 1) on the $S_0 \rightarrow S_1$ transition, coupled with the appearance of the characteristic Mn(II) 'nose' in the edge shape of the S_0 state (Dau et al., 2001), indicates Mn(II) → Mn(III) oxidation on this step. The $S_0 \rightarrow S_1$ UV-visible difference spectrum is also quantitatively consistent with this (Kuzek and Pace, 2001).

The discovery of a broad, hyperfine structured, spin 1/2 multiline type signal in S_0 suggests the presence of Mn(II) in a coupled center which is minimally a Mn(II) – Mn(III) dimer (i.e., spin 5/2–spin 2). This signal, first produced by chemical reduction of S_1 (Messinger et al., 1997a) and flash turnover to S_0 (Åhrling et al., 1997) in plants, has recently been observed by flash turnover in cyanobacteria (Boussac et al., 2000). It is generated in the presence of MeOH, where it is clearly a ground state (Åhrling et al., 1998a). A possible interpretation is that the cycling Mn center of the native S_0 intermediate has net ferromagnetic coupling, making it high spin (≥ 9/2) and difficult to detect by EPR. MeOH switches the coupling to net anti-ferromagnetic, consistent with its behavior in other S states.

Figure 7 shows the S_0 signal generated by flash turnover in plant PS II. It is over 200 mT wide, with approximately 20 resolved peaks. Shown also is a simulation of the spectrum as a Mn(II) – Mn(III) dimer in the strong exchange limit (Åhrling and Pace, 2004). The simulation parameters are given in Table 1. Notably, the unusually rhombic Mn(III) hyperfine terms are similar to those of the Mn(IV) in the broad MLS simulation. The Mn(II) parameters are nearly isotropic (expected for a d^5 ion), with the same quasi axial symmetry as the Mn(III) ion in the broad MLS simulation. A complete identification of all the redox states in the catalytic Mn dimer is then suggested (Table 1). However, alternative explanations of the S_0 signal have been proposed (Messinger et al., 1997b; Kusunoki, 2001).

One other dimer spin 1/2 EPR signal is observable in the functional OEC. This is a multiline species produced by treatment of PS II with NO, which develops after sample incubation (>1 hour) at approximately 240 K (Goussias et al., 1997). The X-band EPR spec-

trum and simulation parameters (Table 1) are very similar to those of the dinuclear Mn catalase enzyme in the weakly coupled Mn(II) – Mn(III) state (Sarrou et al., 1998). Studies on oriented samples (Hanley et al., 2000) show that the parallel (z) direction of the system is close to the membrane plane normal. Flash turnover from the NO MLS state restores normal oxygen generation function, with an initial retardation of three flashes, suggesting a modified, formal S_{-2} state (Messinger et al., 1997c). However no uncoupled Mn(II) ('six line Mn') is visible by EPR. In a XANES monitored study of controlled chemical reduction of Mn in PS II, Penner-Hahn and coworkers showed (Riggs-Gelasco et al., 1996) that reduction below a Mn edge energy of approximately 6550 eV caused irreversible turnover inhibition with Mn mobilization, or appearance of bound but uncoupled Mn(II) (six line), depending on reductant conditions. A 'Mn reduced' S_{-2} state would have an edge energy 2–3 eV below that of S_0, i.e., approximately 6548 eV, see Fig. 1). Together, these data suggest that the Mn oxidation level in the NO MLS state is not below a formal S_0 level and that the II – III dimer configuration is a variant of that discussed above for the native S_0 state. Since the OEC catalytic site normally holds two substrate molecules and is proton accessible, the following redox couples are relevant:

$$NO_{(g)} + H_2O \leftrightharpoons HNO_2 + H^+ + e^-$$
$$E_0(\text{pH } 7) \text{ –0.56 V} \qquad (1)$$

$$(H)NO_2 + H_2O \leftrightharpoons NO_3^- + 3H^+ + 2e^-$$
$$E_0(\text{pH } 7) \sim +0.2 \text{ V} \qquad (2)$$

Reaction (1) should be able to reduce S_1 centers to S_0 in the dark. If the resulting NO_2^- remains bound to Mn during removal of excess NO, Reaction (2) could subsequently occur during flash turnover, proceeding through an 'S_2' like state on the second flash (probably seen by Schansker et al. (2002)) and resulting in a net *3* electron retardation. The bimolecular oxidations in reactions (1) and (2), each involving one water molecule and a small oxo species, clearly evoke the water oxidation reaction for which the catalytic site is actually designed.

III. A Spectroscopic Model for the Catalytic Site

We have proposed a model of the Mn organization involving two magnetically isolated, bridged dimers, separated by a distance sufficient to allow fast (~10^6 s^{-1}) electron transfer (Kuzek and Pace, 2001). One dimer is the principal redox accumulator and presumably contains the substrate site. The Mn–metal interaction at ~3.3 –3.5Å, seen in the Mn EXAFS of PS II (Chapter 10, Yachandra) is then due to Mn–Ca interaction. Ca is a known component of the OEC and necessary for catalytic water oxidation. Ca may be functionally replaced by Sr and ~2 Mn are within 3.5Å of the Sr center. Rutherford et al. (1992) and Limburg et al. (1999) have proposed that Ca binds at least one water molecule and activates it for nucleophilic attack by the other substrate molecule. Moreover, mechanistic modeling (Limburg et al., 1999) suggests that only two Mn may actively participate in the water oxidation process.

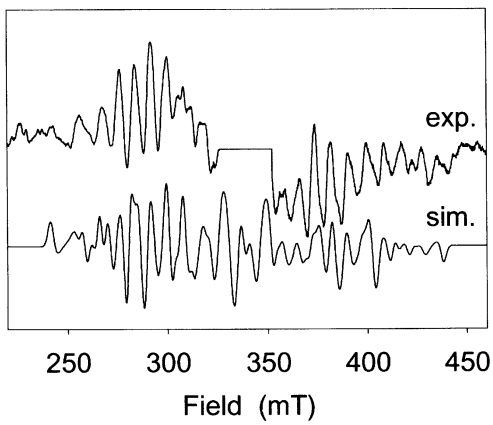

Fig. 7. (Top) Experimental S_0 state signal formed by flash turnover of plant PS II membrane samples containing approximately 1 M MeOH (from Åhrling et al., 1997). (Bottom) Simulated spectrum using a strong exchange dimer model and parameter values from Table 1.

The current X-ray structural data on the cyanobacterial PS II core complex (Chapters 19–21) suggest compact electron density envelopes (of somewhat different shapes) and unknown S state(s) for the metals in the catalytic site. Highly purified preparations of cyanobacterial PS II may not however retain all of the Mn contained within comparably purified plant core preparations The plant preparations lack totally the 17 and 23 kDa proteins, but still retain approximately 5 Mn per reaction center in total, display very high activity and all the expected spectroscopic properties (Smith et al., 2002). Therefore, we suggest a model for the catalytic Mn-Ca cluster, assumed

common to all PS II, illustrated in Fig. 8. This is a 'minimum' structure suggested by spectroscopy and based on the Mn dimer-ligand model first proposed in Åhrling and Pace (1995), now incorporating Ca. The Mn component has numerous features in common with the dinuclear catalytic site in Mn catalase (Barynin et al., 2001) and could be viewed as 'catalase plus Ca' (Åhrling and Pace, 2004). The three metal centers form an 'incomplete cubane.' In the most recent x-ray structures from Ferreira et al. (2004) and Biesiadka et al. (2004), features similar to this are evident. Ca shares a μ_3 oxo bridge with the two Mn, consistent with the above EXAFS results. The molecular axis orientation is from EPR modeling of S_2 state signals (Åhrling et al., 1998b) (z axis approximately in membrane plane, as for the S_1 state *D* tensor, see above).

In Fig. 8, the two Mn spin centers are labeled A and B. Mn_A has oxidation state II in the normal (+MeOH) S_0 state and is Mn III thereafter. In the 'broad and narrow MLS' S_2 configurations, Mn_A is approximately 5 and 6 co-ordinate respectively, with opposite Jahn-Teller and hyperfine asymmetries (Fig. 8B). A water (hydroxide) molecule is 'tightly' bound axially in the narrow form, giving rise to the strong ^{17}O ESEEM, while MeOH, probably always equatorially bound when directly ligated (i.e., approximately in the μ oxo plane), now undergoes σ bonding into the half occupied $d_{x^2-y^2}$ orbital on $Mn_{(A)}$, resulting in significant π spin density on the O. Three strong β proton couplings result at He temperatures, where methyl rotation is frozen out. We suspect that MeOH displaces a protein ligand when binding (Fig. 8A) and it is the only alcohol small enough to do this. In

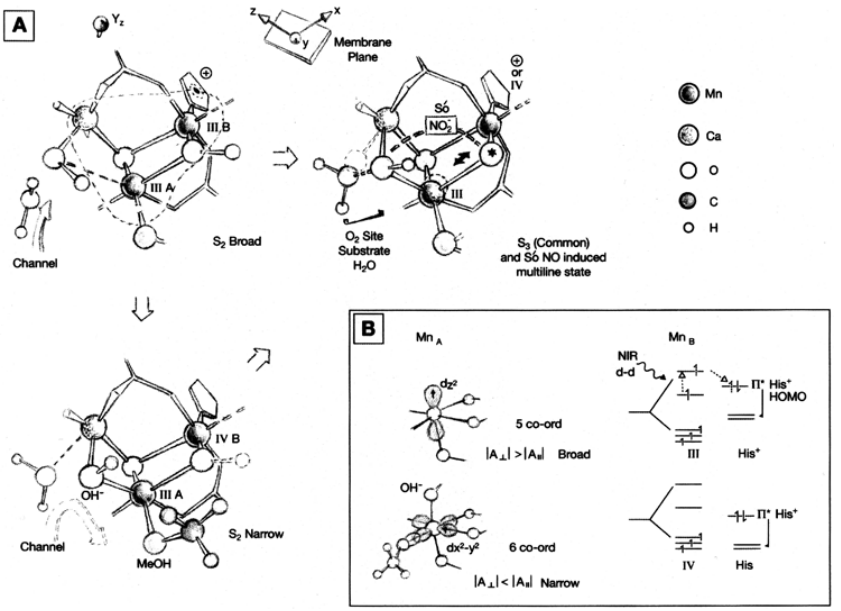

Fig. 8. A. Molecular model of the Mn –Ca water oxidizing site in PS II, suggested by a range of spectroscopic modelling and structural data. Configuration of the Mn dimer is quite similar to that in di-nuclear Mn catalase (Barynin et al., 2001). The dashed envelope in S_2 broad corresponds reasonably with the catalytic site metal electron density volume in the ~4Å X-ray diffraction pattern of cyanobacterial PS II (Zouni et al., 2001). One substrate water (or OH^-) bridges weakly between Ca and Mn_A in the S_2 broad form and strongly ligates Mn_A axially in the S_2 narrow and common S_3 forms. Indicated in the latter is the suggested location of NO_2^- binding in the NO (S_0) state (see text). MeOH (or MeO^-) binding is presumed to occur by displacement of a protein ligand as shown (S_2 narrow). The oxidizable histidine ligand to Mn_B is probably D1 His332. B. Distinct electron configurations that the Mn_A and Mn_B spin centres may each take in S_2. Both types of quasi–axial e_g orbital occupancy occur with Mn_A (3+ oxidation state). Mn_B has III or IV formal oxidation state, depending on whether the lower e_g level (~d_{z^2}) in the III state lies above or below the HOMO of the His ring ligand. This is possibly determined by the extent of σ donation into Mn_B by the bridge oxo's, which would modulate the metal d orbital energies, relative to the His ligand energy levels (roughly invariant). Bridge mediated 'redox communication' between the Mn could be mechanistically relevant. The NIR induced III → IV conversion on Mn_B occurs by way of a d–d transition and charge transfer to His^+, as shown.

the S_3 state, bridge oxidation is presumed to result in displacement of Mn_A (as shown) and the metal is probably now always 6 co-ordinate. Thus depending on the balance of forms in S_2, one will (Dau et al., 2001), or will not (Yachandra et al., 1996), detect a change (increase) in the Mn-O first shell interactions with EXAFS, along with an increase in the Mn–Mn separation in one dimer.

Mn_B exists in a very unusual environment, a reflection perhaps of the demanding chemistry which the catalytic site performs. Because Mn_B operates at a 'higher' mean redox level than $Mn(III)_A$ (III in S_0, III or IV in both S_2 and S_3), it is probably 6 co-ordinate, but with low ligand symmetry. The oxidizable histidine which ligates Mn_B is probably His332. The MLS spectrum of the partially functional D1- His332Glu mutant in *Synechocystis* 6803 (Debus et al., 2001) is quite similar to the NH_3 MLS, suggesting similar Mn parameters, so that Mn_B is in the (IV) state in these cases (the NH_3 multiline is totally resistant to NIR turnover (Boussac et al., 1996)). Ligation along the rhombic quadrupole direction (dashed) must be unique. It is probably not an oxo or nitrogen species, but unlikely to be Cl^- either. The matter is currently under study. Under physiological turnover, Mn_B maintains a constant oxidation state of (III). However for reasons not yet clear, electron removal from either the filled HOMO level of the His ring, or the singly occupied d_{z^2} level of Mn_B is favored (lower potential) on the first transition to S_2 (Kuzek and Pace, 2001). In the first case (normal, Fig. 8B), NIR excitation of the d-d transition in the e_g levels can lead to spin allowed metal to ligand charge transfer, producing the meta-stable (higher redox potential in these circumstances) Mn(IV) species. This tends to spontaneous reduction by electron transfer from the environment, mostly by back reaction from the His presumably. Whenever an electron comes from elsewhere, however, (other Mn cluster, acceptor iron, etc.) the system meta-stably accumulates the S_1 (no MLS)-oxidized donor form. This appears to be totally consistent with the NIR turnover phenomenology and explains observations such as the NIR effect on the S_3 state, where 'split' type signals are seen (Boussac et al., 2000; Ioannidis and Petrouleas, 2000), i.e., the S_2–Y_z(ox) state (see also Chapter 10). When Mn_B is already in the (IV) state (narrow, NH_3 MLS types), no NIR turnover is of course possible.

It is unknown which bridge oxygen is oxidized in S_3, but the μ_2 group (O* in Fig. 8A) seems more likely. The S_3 configuration may in fact resemble the NO S_0 state. Even $Mn(III)_2$ catalase is believed to possess a labile bridge oxo, which on displacement yields a weakly coupled μ oxo, μ carboxylato pair (Michaud-Soret et al., 1998). If an analogous bridge displacement is in fact the cold annealing re-arrangement necessary for the NO MLS to form (i.e., following reaction 1) above), then the NO_2^- could bind as a bidentate approximately as indicated in Fig. 8A. The former bridge (O*) would then be displaced onto Mn_B. Probably, the redox states are $Mn(II)_B$ and $Mn(III)_A$, with the NO_2^- tightly bound and the Jahn-Teller axis roughly along the Mn_A–O* direction in Fig. 8A (i.e., nearly along the membrane normal (Hanley et al., 2000)).

References

Åhrling KA and Pace RJ (1995) Simulation of the S_2 state multiline electron paramagnetic resonance signal of Photosystem II: A multifrequency approach. Biophys J 68: 2081–2090

Åhrling KA and Pace RJ (2004) Water oxidation in PS II-H atom abstraction revisited. Biochim Biophys Acta 1655: 172–178

Åhrling KA, Peterson S and Styring S (1997) An oscillating manganese electron paramagnetic resonance signal from the S_0 state of the oxygen evolving complex in Photosystem II. Biochemistry 36: 13148–13152

Åhrling KA, Peterson S and Styring S (1998a) The S_0 state EPR signal from the Manganese Cluster in Photosystem II arises from an isolated S=1/2 ground state. Biochemistry 37: 8115–8120

Åhrling KA, Smith PJ and Pace RJ (1998b) Nature of the Mn centers in Photosystem II. Modeling and behavior of the g=4 resonances and related signals. J Am Chem Soc 120: 13202–13214

Åhrling KA, Evans MCW, Nugent JHA and Pace RJ (2004) The two forms of the S_2 state multiline signal in Photosystem II: Effect of methanol and ethanol. Biochim Biophys Acta 1656: 66–77

Barynin VV, Whittaker MM, Antonyuk SV, Lamzin VS, Harrison PM, Artymiuk PJ and Whittaker JW (2001) Crystal structure of manganese catalase from *Lactobacillus plantarium.* Structure 9: 725–738

Baxter R, Krausz E, Wydrzynski T and Pace RJ (1999) Identification of the near-infrared absorption band from the Mn cluster of Photosystem II. J Am Chem Soc 121: 9451–9452

Bencini A and Gatteschi D (1990) Electron Paramagnetic Resonance of Exchange Coupled Systems. Springer-Verlag, Berlin

Bergmann U, Grush MM, Horne CR, DeMarois P, Penner-Hahn JE, Yocum CF, Wright DW, Dube CE, Armstrong WH, Christou G, Eppley HJ and Cramer SP (1998) Characterisation of the Mn oxidation states in Photosystem II by Kb X-ray fluorescence spectroscopy. J Phys Chem B 102: 8350–8352

Biesiadka J, Loll B, Kern J, Irrgang K-D and Zouni A (2004) Crystal structure of cyanobacterial Photosystem II at 3.2 Å resolution: A closer look at the Mn-cluster. Phys Chem Chem

Phys 6: 4733–4736
Boussac A (1995) Exchange of chloride by bromide in the manganese Photosystem II complex studied by cw- and pulsed-EPR. Chem Phys 194: 409–418
Boussac A (1997) Inhomogeneity of the EPR multiline signal from the S_2-state of the Photosystem II oxygen evolving enzyme. J Bioinorg Chem 2: 580–585
Boussac A and Rutherford AW (2000) Comparative study of the g=4.1 EPR signals in the S_2 state of Photosystem II. Biochim Biophys Acta 1457: 145–156
Boussac A, Girerd J-J and Rutherford AW (1996) Conversion of the spin state of the manganese complex in Photosystem II induced by near-infrared light. Biochemistry 35: 6984–6989
Boussac A, Un S, Horner O and Rutherford AW (1998) High-spin states (S>5/2) of the Photosystem II manganese complex. Biochemistry 37: 4001–4007
Boussac A, Sugiura M, Inoue Y and Rutherford AW (2000) EPR study of the oxygen evolving complex in His-tagged Photosystem II f rom the cyanobacterium *Synechococcus elongatus.* Biochemistry 39: 13788–13799
Britt RD, Zimmermann J-L, Sauer K and Klein MP (1989) Ammonia binds to the catalytic Mn of the oxygen-evolving complex of Photosystem II: Evidence by electron spin-echo envelope modulation spectroscopy. J Am Chem Soc 111: 3522–3532
Carell TG, Tyryshkin AM and Dismukes GC (2002) An evaluation of structural models for the photosynthetic water-oxidizing complex derived from spectroscopic and X-ray diffraction signatures. J Biol Inorg Chem 7: 2–22
Carrington A and McLachlan AD (1967) Introduction to Magnetic Resonance — With Applications to Chemistry and Chemical Physics. Harper & Row, London
Casey JL and Sauer K (1984) EPRDetection of a cryogenically photogenerated intermediate in photosynthetic oxygen evolution. Biochim Biophys Acta 767: 21–28
Dau H, Andrews JC, Roelofs TA, Latimer MJ, Liang W, Yachandra VK, Sauer K and Klein MP (1995) Structural consequences of ammonia binding to the manganese center of the photosynthetic oxygen-evolving comples: An X-ray absorption spectroscopy study of isotropic and oriented Photosystem II particles. Biochemistry 34: 5274–5287
Dau H, Iuzzolino L and Dittmer J (2001) The tetra-manganese complex of Photosystem II during its redox cycle — X-ray absorption results and mechanistic implications. Biochim Biophys Acta 1503: 24–39
de Paula JC and Brudvig GW (1985) Magnetic properties of manganese in the photosynthetic O_2-evolving complex. J Am Chem Soc 107: 2643–2648
Debus RJ (1992) The manganese and calcium ions of photosynthetic oxygen evolution. Biochim Biophys Acta 1102: 269–352
Debus RJ, Campbell KA, Gregor W, Li Z-L, Burnap RL and Britt RD (2001) Does histidine 332 of the D1 polypeptide ligate the manganese cluster in Photosystem II? An electron spin echo envelope modulation study. Biochemistry 40: 3690–3699
Dexheimer SL and Klein MP (1992) Detection of a paramagnetic intermediate in the photosynthetic oxygen-evolving complex. J Am Chem Soc 114: 2821–2826
Dexheimer SL, Sauer K and Klein MP (1990) Parallel polarisation EPR studies of the oxygen-evolving complex of Photosystem II. In: Baltscheffsky M (ed) Current Research in Photosynthesis, Vol 1, pp 761–764. Kluwer Academic Publishers, Dordrecht
Dismukes GC and Siderer Y (1981) Intermediates of a polynuclear manganese center involved in photosynthetic oxidation of water. Proc Natl. Acad Sci USA 78: 274–278
Evans MCW, Gourovskaya K and Nugent JHA (1999) Investigation of the interaction of the water oxidising manganese complex of Photosystem II with the aqueous solvent environment. FEBS Lett 450: 285–288
Evans MCW, Rich AM and Nugent JHA (2000) Evidence for the presence of a component of the Mn complex of the Photosystem II reaction center which is exposed to water in the S_2 state of the water oxidation complex. FEBS Lett 477: 113–117
Evans MCW, Nugent JHA, Ball RJ, Muhiuddin IP and Pace RJ (2004) Evidence for a direct Mn-O ligand in water binding to the S_2 state of the photosynthetic water oxidation complex. Biochemistry 43: 989–994
Ferreira KN, Iverson TM, Maghlaoui K, Barber J and Iwata S (2004) Architecture of the photosynthetic oxygen-evolving center. Science 303: 1831–1837
Fiege R, Zweygart W, Bittl R, Adir N, Renger G and Lubitz W (1996) EPR and ENDOR studies of the water oxidizing complex of Photosystem II. Photosynth Res 48: 227–237
Force D A, Randall DW, Lorigan GA, Clemens KL and Britt RD (1998) ESEEM studies of alcohol binding to the manganese cluster of the oxygen evolving complex of Photosystem II. J Am Chem Soc 120: 13321–13333
Goussias C, Ioannidis N and Petrouleas V (1997) Low-temperature interactions of NO with the S_1 and S_2 state of the water-oxidizing complex of Photosystem II. A novel Mn-multiline EPR signal derived from the S_1 state. Biochemistry 36: 9261–9266
Guiles RD, Yachandra VK, McDermott AE, Cole JL, Dexheimer SL, Britt RD, Sauer K and Klein MP (1990) The S_0 state of Photosystem II induced by hydroxylamine: Differences between the structure of the manganese complex in the S_0 and S_1 states determined by X-ray absorption spectroscopy. Biochemistry 29: 486–496
Haddy A, Aasa R and Andreasson L-E (1989) S-Band EPR studies of the S_2-state multiline signal from the photosynthetic oxygen-evolving complex. Biochemistry 28: 6954–6959
Haddy A, Dunham WR, Sands RH and Aasa R (1992) Multi-frequency EPR investigation into the origin of the S_2-state signal at g=4 of the O_2-evolving complex. Biochim Biophys Acta 1099: 25–34
Hanley J, Sarrou J and Petrouleas V (2000) Orientation of the Mn(II)-Mn(III) dimer which results from the reduction of the oxygen-evolving complex of Photosystem II by NO: An EPR study. Biochemistry 39: 15441–15445
Hansson O, Andreasson L-E and Vänngård T (1986) Oxygen from water is coordinated to manganese in the S_2 state of Photosystem II. FEBS Lett 195: 151–154
Hansson O, Aasa R and Vänngård T (1987) The origin of the multiline and g=4.1 electron paramagnetic resonance signals from the oxygen-evolving system of Photosystem II. Biophys J 51: 825–832
Hasegawa K, Kusunoki M, Inoue Y and Ono T-A (1998) Simulation of the S_2-state multiline EPR signal in oriented Photosystem II membranes: Structural implications for the manganese cluster in an oxygen-evolving complex. Biochemistry 37: 9457–9465
Horner O, Riviere EGB, Un S, Rutherford AW, Girerd J-J and Boussac A (1998) SQUID magnetization study of the infrared-induced spin transition in the S_2 state of Photosystem II: Spin

value associated with the g=4.1 EPR signal. J Am Chem Soc 120: 7924–7928

Ioannidis N and Petrouleas V (2000) Electron Paramagnetic Resonance signals from the S_3 state of the oxygen-evolving complex. A broadened Radical signal induced by low-temperature near-infrared light illumination. Biochemistry 39: 5246–5254

Ioannidis N, Nugent JHA and Petrouleas V (2002) Intermediates of the S_3 state of the oxygen-evolving complex of Photosystem II. Biochemistry 41: 9589–9600

Iuzzolino L, Dittmer J, Dörner W, Meyer-Klaucke W and Dau H (1998) X-ray absorption spectroscopy of layered Photosystem II membrane particles suggests manganese centered oxidation of the oxygen-evolving complex for the S_o-S_1,S_1-S_2, and S_2-S_3 transitions of the water oxidation cycle. Biochemistry 37: 17112–17119

Kammel M (2003) Cofactors on the donor side of Photosystem II investigated with EPR techniques. PhD Thesis. Faculty of Mathematics and Science, Technical University, Berlin.

Kawamori A, Inui T, Ono T-A and Inoue Y (1989) ENDOR study on the position of hydrogens close to the manganese cluster in S_2 state of Photosystem II. FEBS Lett 254: 291–224

Kim D H, Britt RD, Klein MP and Sauer K (1990) The g=4.1 EPR signal of the S_2 of the photosynthetic oxygen-evolving complex arises from a multinuclear Mn cluster. J Am Chem Soc 112: 9389–9391

Koulougliotis D, Hirsh DJ and Brudvig GW (1992) The O_2-evolving center of Photosystem Ii is diamagnetic in the S_1 resting state. J Am Chem Soc 114: 8322–8323

Kusunoki M (2001) Simulation of the 'S_0-state' EPR signal from the Mn cluster in Photosystem II. Evidence for a piece of a thermally accessible O_2-binding state. In: PS2001: Proceedings of 12th International Congress on Photosynthesis, CSIRO Publishing, Melbourne (CD-ROM)

Kuzek D and Pace RJ (2001) Probing the Mn oxidation states in the OEC. Insights from spectroscopic, computational and kinetic data. Biochim Biophys Acta 1503: 123–137

Law N A, Kampf JW and Pecoraro VL (2000) A magneto-structural correlation between the Heisenberg constant, J and the Mn-O-Mn angle in [MnIV[m-O)]$_2$ dimers. Inorg Chim Acta 297: 252–264

Liang W, Latimer MJ, Dau H, Roelofs TA, Yachandra VK, Sauer K and Klein MP (1994) Correlation between structure and magnetic spin state of the manganese cluster in the oxygen-evolving complex of Photosystem II in the S_2 state: Determination by X-ray absorption spectroscopy. Biochemistry 33: 4923–4932

Limburg J, Szalai VA and Brudvig GW (1999) A mechanistic and structural model for the formation and reactivity of a MnV=O species in photosynthetic water oxidation. J Chem Soc, Dalton Trans 1353–1361

Lorigan GA and Britt RD (2000) Electron spin-lattice relaxation studies of different forms of the S_2 state multiline EPR signal of the Photosystem II oxygen-evolving complex. Photosynth Res 66: 189–198

MacLachlan DJ, Hallahan B J, Ruffle SV, Nugent JHA, Evans MCW, Strange RW and Hasnain SS (1992) An EXAFS study of the manganese O_2-evolving complex in purified Photosystem II membrane fractions. Biochem J 285: 569–576

MacLachlan DJ, Nugent JHA and Evans MCW (1994) A XANES study of the manganese complex of inhibited PS II membranes indicates manganese redox changes between the modified S_1,S_2 and S_3 states. Biochim Biophys Acta 1185: 103–111

Manchandra R, Brudvig GW and Crabtree RH (1995) High-valent oxomanganese clusters: Structural and mechanistic work relevant to the oxygen-evolving center in Photosystem II. Coord Chem Rev 144: 1–38

Matsukawa T, Mino H, Yoneda D and Kawamori A (1999) Dual-mode EPR study of new signals from the S_3-state of the oxygen-evolving complex in Photosystem II. Biochemistry 38: 4072–4077

McCracken J, Peisach J, Cote CE, McGuirl MA and Dooley DM (1992) Pulsed EPR studies of the semiquinone state of copper-containing amine oxidases. J Am Chem Soc 114: 3715–3720

McDermott AE, Yachandra VK, Guiles RD, Cole JL, Dexheimer SL, Britt RD, Sauer K and Klein MP (1988) Characterization of the manganese O_2-evolving complex and the iron-quinone acceptor complex in Photosystem II from a thermophilic cyanobacterium by electron paramagnetic resonance and X-ray absorption spectroscopy. Biochemistry 27: 4021–4031

Messinger J, Badger M and Wydrzynski T (1995) Detection of *one* slowly exchanging substrate water molecule in the S_3 state of Photosystem II. Proc Natl Acad Sci USA 92: 3209–3213

Messinger J, Nugent JHA and Evans MCW (1997a) Detection of an EPR multiline signal for the S_0* state in Photosystem II. Biochemistry 36: 11055–11060.

Messinger J, Robblee J, Yu W O, Sauer K, Yachandra VK and Klein MP (1997b) The S_0 state of the oxygen evolving complex in Photosystem II is paramagnetic: Detection of an EPR multiline signal. J Am Chem Soc 119: 11349–11350

Messinger J, Seaton G, Wydrzynski T, Wacker U and Renger R (1997c) S_{-3} state of the water oxidase in Photosystem II. Biochemistry 36: 6862–6873

Messinger J, Robblee J H, Bergmann U, Fernandez C, Glatzel PSI, Hanssum B, Renger G, Cramer SP, Sauer K and Yachandra VK (2001) Manganese oxidation states in Photosystem II. In: PS2001: Proceedings of 12th International Congress on Photosynthesis. CSIRO Publishing, Melbourne (CD-ROM)

Michaud-Soret I, Jacquameet L, Debaecker-Petit N, Le Pape L, Barynin VV and Latour J-M (1998) The existence of two oxidised Mn(III)Mn(III) forms of *Thermus thermophilus* manganese catalase. Inorg Chem 37: 3874–3876

Miller A-F and Brudvig GW (1991) A guide to electron paramagnetic resonance spectroscopy of Photosystem II membranes. Biochim Biophys Acta 1056: 1–18

Mino H and Kawamori A (2001) EPR studies of the water oxidizing complex in the S_1 and the higher S states: the Mn cluster and Yz radical. Biochim Biophys Acta 1503: 112–122

Nugent JHA, Turconi S and Evans MCW (1997) EPR investigation of water oxidizing Photosystem II: Detection of new EPR signals at cryogenic temperatures. Biochemistry 36: 7086–7096

Ono T, Noguchi T, Inoue Y, Kusunoki M, Matsushita T and Oyanagi H (1992) X-ray detection of the period-four cycling of the manganese cluster in photosynthetic water oxidizing enzyme. Science 258: 1335–1337

Peloquin JM and Britt RD (2001) EPR/ENDOR characterization of the physical and electronic structure of the OEC Mn cluster. Biochim Biophys Acta 1503: 96–111

Peloquin JM, Campbell KA and Britt DR (1998) ^{55}Mn pulsed ENDOR demonstrates that the Photosystem II 'split' EPR signal arises from a magnetically-coupled mangano-tyrosyl complex. J Am Chem Soc 120: 6850–6841

Peloquin JM, Campbell KA, Randall DW, Evanchik MA, Pecoraro VL, Armstrong WH and Britt DR (2000) ^{55}Mn pulsed

ENDOR of the S_2-state multiline EPR signal of Photosystem II: Implications on the structure of the tetranuclear Mn cluster. J Am Chem Soc 122: 10926–10942

Randall DW, Sturgeon BE, Ball J A, Lorigan GA, Chan MK, Klein MP, Armstrong WH and Britt RD (1995) Mn ESE-ENDOR of a mixed valence Mn(III)Mn(IV) complex: Comparison with the Mn cluster of the photosynthetic oxygen evolving complex. J Am Chem Soc 117: 11780–11789

Rappaport F, Blanchard-Desce M and Lavergne J (1994) Kinetics of electron transfer and electrochemical change during the redox transitions of the photosynthetic oxygen-evolving complex. Biochim Biophys Acta 1184: 178–192

Riggs-Gelasco PJ, Mei R, Yocum CF and Penner-Hahn JE (1996) Reduced derivatives of the Mn cluster in the oxygen evolving complex of Photosystem II: An EXAFS study. J Am Chem Soc 118: 2387–2399

Roelofs TA, Lian W, Latimer MJ, Cinco R M, Rompel A, Andrews JC, Sauer K, Yachandra VK and Klein MP (1996) Oxidation states of the manganese cluster during the flash-induced S-strate cycle of the photosynthetic oxygen-evolving complex. Proc Natl Acad Sci USA 93: 3335–3340

Rutherford AW, Zimmermann JL and Boussac A (1992) Oxygen evolution. In: Barber J (ed) The Photosystems: Structure, Function and Molecular Biology, Vol 11, pp 179–229. Elsevier, Amsterdam

Sanakis Y, Ioannidis N, Sioros G and Petrouleas V (2001) A novel S=7/2 configuration of the Mn cluster of Photosystem II. J Am Chem Soc 123: 10766–10767

Sarrou J, Ioannidis N, Deligiannakis Y and Petrouleas V (1998) AMn(II)-Mn(III) EPR signal arises from the interaction of NO with the S_1 state of the water-oxidizing complex of Photosystem II. Biochemistry 37: 3581–33587

Sauer K, Guiles RD, McDermott A, Cole JL, Yachandra VK, Zimmermann JL, Klein MP, Dexheimer SL and Britt RD (1988) Spectroscopic studies of manganese involvement in photosynthetic oxygen evolution. Chemica Scripta 28A: 87–91

Schafer K-O, Bittl R, Zweygart W, Lendzian F, Haselhorst G, Weyhermuller T, Wieghardt K and Lubitz W (1998) Electronic structure of antiferromagnetically coupled dinuclear manganese (MnIII-MnIV) complexes studies by magnetic resonance techniques. J Am Chem Soc 120: 13104–13120

Schansker G, Goussias C, Petrouleas V and Rutherford AW (2002) Reduction of the Mn cluster of the water-oxidizing enzyme by nitric oxide: Formation of an S–2 state. Biochemistry 41: 3057–3064

Smith PJ and Pace RJ (1996a) Evidence for two forms of the g=4.1 signal in the S_2 of Photosystem II. Two magnetically isolated manganese dimers? Biochim Biophys Acta 1275: 213–220

Smith PJ and Pace RJ (1996b) Evidence for two forms of the g=4.1 signal in Photosystem II of higher plants. Two magnetically isolated manganese dimers? Appl Mag Res 11: 443–460

Smith PJ, Åhrling KA and Pace RJ (1993) Nature of the S_2 state electron paramagnetic resonance signals from the oxygen evolving complex of Photosystem II: Q-band and oriented X-band studies. J Chem Soc, Faraday Trans 89: 2863–2868

Smith PJ, Peterson S, Masters VM, Wydrzynski T, Styring S, Krausz E and Pace RJ (2002) Magneto-optical measurements of the pigments in fully active Photosystem II core complexes from plants. Biochemistry 41: 1981–1989

Tang X-S, Sivaraja M and Dismukes GC (1993) Protein and substrate coordination to the manganese cluster in the photosynthetic water oxidizing complex: ^{15}N and ^{1}H ENDOR spectroscopy of the S_2 state multiline signal in the thermophilic cyanobacterium *Synechococcus elongatus*. J Am Chem Soc 115: 2382–2389

Tang X-S, Diner BA, Larsen B S, Gilchrist JML, Lorigan GA and Britt RD (1994) Identification of histidine at the catalytic site of the photosynthetic oxygen-evolving complex. Proc Natl Acad Sci USA 91: 704–708

Thomann H, Bernardo M, Goldfarb D, Kroneck PMN and Ullrich V (1995) Evidence for water binding to the Fe center in cytochrome P450cam obtained by ^{17}O electron spin echo envelope modulation spectroscopy. J Am Chem Soc 117: 8243–8251

Turconi S, MacLachlan DJ, Bratt PJ, Nugent JHA and Evans MCW (1997) Analysis of the interaction of water with the manganese cluster of Photosystem II using isotopically labeled water. Biochemistry 36: 879–885

Yachandra VK, DeRose V J, Latimer MJ, Mukerji I, Sauer K and Klein MP (1993) Where plants make oxygen: A structural model for the photosynthetic oxygen-evolving manganese cluster. Science 260: 675–679

Yachandra VK, Sauer K and Klein MP (1996) Manganese cluster in photosynthesis: Where plants oxidise water to dioxygen. Chem Rev 96: 2927–2950

Yamauchi T, Mino H, Matsukawa T, Kawamori A and Ono T (1997) Parallel polarization electron paramagnetic resonance studies of the S_1-state manganese cluster in the photosynthetic oxygen evolving system. Biochemistry 36: 7520–7526

Zheng M and Dismukes GC (1996) Orbital configuration of the valence electrons, ligand field symmetry and manganese oxidation states of the photosynthetic water oxidizing complex: Analysis of the S_2 state multiline EPR signals. Inorg Chem 35: 3307–3319

Zimmerman J and Rutherford AW (1984) EPR studies of the oxygen-evolving enzyme of Photosystem II. Biochim Biophys Acta 767: 160–167

Zimmerman J-L and Rutherford AW (1986) Electron Paramagnetic Resonance Properties of the S_2 State of the Oxygen-Evolving Complex of Photosystem II. Biochemistry 25: 4609–4615.

Zouni A, Witt HT, Kern J, Fromme P, Krauss N, Saenger W and Orth P (2001) Crystal structure of Photosystem II from *Synechococcus elongatus* at 3.8Å resolution. Nature 409: 739–743

Chapter 13

The Calcium and Chloride Cofactors

Hans J. van Gorkom*
Department of Biophysics, Huygens Laboratory, Leiden University, P.O. Box 9504, 2300 RA Leiden, The Netherlands

Charles F. Yocum
Department of Molecular, Cellular and Developmental Biology and Department of Chemistry, University of Michigan, Ann Arbor, MI 48109-1048, U.S.A.

*Author for correspondence, email: vangorkom@biophys.leidenuniv.nl

T. Wydrzynski and K. Satoh (eds): Photosystem II: The Light-Driven Water:Plastoquinone Oxidoreductase, pp. 307–327.

Summary

Single atoms of Ca^{2+} and Cl^- are closely associated with the tetranuclear Mn cluster of Photosystem II (PS II). Extraction of either cofactor blocks advancement of the S-state cycle beyond S_2. In the case of Cl^- depletion, this modification has been proposed to result from replacement of the anion as a Mn ligand. This would cause a decrease of the potential, and thereby localization of the Mn(IV) state on the Mn to which Cl^- was bound. The implications of this hypothesis, and of the notion that the ligand replacing Cl^- in the modified S_2 state is most likely hydroxyl (OH^-), are discussed and found to provide a plausible explanation for apparently conflicting reports in the literature. The location of Ca^{2+} with respect to the Mn cluster is less certain. Although the metal is positioned so as to interfere with the attack of a small ligand, such as hydroxylamine (NH_2OH), on the Mn cluster, the distance between Ca^{2+} and atoms of the Mn cluster is not resolved at the present time. Calcium can be shown to reinforce the stability of Mn ligation by PS II. However, its role in water oxidation must extend beyond structural effects to account for the block in electron transfer at S_2 observed in Ca^{2+}-depleted PS II, and the upward shift in the minimum temperature at which the transition from S_1 to S_2 occurs. The inactivation of PS II caused by replacement of Ca^{2+} with lanthanides suggests that it functions as a site for binding of water molecules destined for oxidation at the Mn site in PS II.

I. Introduction

The cycling of the redox intermediates, or S-states (Chapter 24, Shinkarev), of the O_2-evolving reaction of Photosystem II (PS II) is the key to oxidation of H_2O. This redox cycle requires not only the presence of four atoms of Mn (Chapters 10, Yachandra, and 26 Dismukes et al.), at least two of which undergo oxidation on the S-state transitions from S_0 to S_3, but also Ca^{2+} and Cl^-. As far as can be determined at the present time, these cofactors are necessary for S-state advancement from S_2 to S_3, and for Cl^- it is known that the anion is also required for the S_3 to S_0 transition. In contrast to the Mn atoms in PS II, which are strongly ligated, release of Ca^{2+} and Cl^- can be readily achieved by procedures that affect binding of small (23, 17 kDa) extrinsic polypeptides to PS II (Chapter 5, Bricker and Burnap). In this chapter we review the current state of knowledge about the roles of Ca^{2+} and Cl^- as essential cofactors in the Mn catalyzed reactions of water oxidation by PS II.

The earliest work to establish a function for Cl^- as an essential cofactor for photosynthetic electron transfer was complicated by a lack of highly purified PS II preparations. In early experiments, it could be shown that plants grown on a Cl^--free hydroponic medium appeared to be robust. Nevertheless, chloroplasts isolated from these plants showed a strong dependence on certain added anions (Cl^-, $Br^- > NO_3^- > I^-$; no activity was observed with F^-, PO_4^{3-}, or SO_4^{2-}) for O_2 production (Arnon and Whatley, 1949). When improved analytical techniques revealed the presence of small amounts of Cl^- in 'Cl^- free' water, the dependence of photosynthetic electron transfer on Cl^- was rediscovered in the 1960's (Bove et al., 1963). By applying selective inhibition procedures to PS II in chloroplasts, it was later shown that Cl^- acted at a site on the electron donor side of the light reaction (Izawa et al., 1969). Subsequent research has reinforced the hypothesis that Cl^- is a cofactor of the oxygen-evolving complex (OEC), and has provided a number of insights concerning its mode of action in the mechanism of water oxidation.

The involvement of Ca^{2+} in the O_2 evolving reaction was discovered well after Cl^- had been identified as an essential cofactor. Some experiments with cyanobacteria suggested that Ca^{2+} might be required for PS II electron transfer (Becker and Brand, 1982), but the complexity of this experimental system did not lend itself to detailed investigations on the possible role of Ca^{2+} in PS II-catalyzed electron transfer reactions. Experiments to characterize the roles of the extrinsic polypeptides of isolated spinach PS II led to the definitive discovery that Ca^{2+} is required for O_2 evolution. Removal of these proteins inhibited O_2 evolution (Ghanotakis et al., 1984a; Miyao and Murata, 1984), but activity was not recovered

Abbreviations: EDTA – ethylenediaminetetraacetate; EGTA – ethyleneglycol bis (beta-aminoethyl ether)-N,N,N′,N′-tetraacetate; EXAFS – extended X-ray absorption fine structure; Mn_4 – manganese cluster ligated to PS II in unspecified oxidation states; OEC – oxygen-evolving complex; PS II – Photosystem II; S_n – oxidation state of the OEC (n = 0 to 4); XANES – X-ray absorption near edge structure; Y_Z – a redox active tyrosine residue located on the D1 protein of the PS II reaction center that serves as the electron donor to the photoactive chlorophyll

when the polypeptides were rebound (Ghanotakis et al., 1984b). Attempts to discover the origin of this observation resulted in the demonstration that Ca^{2+} was necessary for water oxidation.

The extrinsic proteins appear to regulate binding of Ca^{2+} and Cl^-, but both ions are able to stimulate O_2 evolution in the absence of the polypeptides. Although successive dissociation of the 17 kDa, 23 kDa, and 33 kDa extrinsic proteins from PS II may lead to a sequential release of the Cl^-, Ca^{2+}, and Mn cofactors, respectively, this appears to be merely because the less tightly bound cofactors are lost first. There is no evidence for direct binding of the cofactors to the extrinsic proteins. Instead, current evidence favors ligation of Mn and Ca^{2+} to the D1 reaction center polypeptide, possibly with additional ligands from a lumenal loop of the core antenna proteins CP47 or CP43. The location of the tetranuclear Mn cluster in PS II is clear from the recently resolved crystal structures (Zouni et al., 2001; Kamiya and Shen, 2003; Ferreira et al., 2004; Chapters 19–21), but the exact location of the Ca^{2+} and Cl^- ions remains unclear. Most evidence suggests a close association with the Mn cluster.

II. Chloride

A. Chloride in Biological Systems

Chloride is the most abundant halide found in living systems. For example, human plasma is about 100 mM Cl^-, and concentrations as high as 0.5 M have been reported in the vacuoles of some marine algae. The most common role of the ion is to act as a source of negative charge in the formation of membrane potentials, in particular in the nervous system, or as a counter ion that is co-transported along with H^+. A number of Cl^--specific channels are found in biological membranes as a consequence of the ion's role in electrical potentials (Li and Weinman, 2002). There are some examples of enzymes where Cl^- functions as a cofactor, or as a substrate, but these instances are comparatively rare when compared to the case of Ca^{2+} and its interactions with a variety of proteins, which is discussed later. In the case of some, but not all, α-amylases the anion is required for activity. In those enzymes where it is required, Cl^- is known to be ligated by positively charged arginine guanidinium groups, where it interacts with carboxyl groups to change their pKa values (Brayer et al., 1995; Feller et al., 1996). Interestingly, all α- amylases also contain at least one bound Ca^{2+} atom. The haloperoxidases are a class of enzymes that utilize Cl^-, Br^-, or I^- as substrates. These enzymes are capable of catalyzing an array of reactions in which the products can be halogenated organic compounds or proteins, HOCl, or Cl_2 (Metzler, 2001). Myeloperoxidase is also capable of producing HOCl, which in turn reacts with H_2O_2 to generate reactive O_2 species that are used to kill bacteria. The mechanism proposed for chloroperoxidase involves Cl^- attack on the compound I form of the enzyme, -Fe(IV)=O, to produce an Fe-hypochlorite intermediate (Fe(III)-O Cl) (Metzler, 2001). Finally, under some conditions, Cl^- is bound as a bridging ligand between heme a and Cu_B of oxidized cytochrome oxidase (Fabian et al., 2001). The halide is not considered to be necessary for the mechanism of O_2 reduction by oxidase, however; its binding kinetics are too slow relative to the turnover rate of the enzyme.

B. Chloride in Photosystem II

None of the roles of Cl^- in biochemistry seems to provide a helpful analogy to its function in the OEC of PS II, which continues to be the subject of active experimentation. The maximum rate of light-induced O_2 evolution is reversibly decreased by a variety of conditions used to deplete Cl^- from the OEC. Intact thylakoids are susceptible to depletion by simple washing procedures using Cl^- free buffers. More efficient extraction is obtained if the wash step is carried out at alkaline pH, in the presence of an uncoupler that allows the lumenal pH to equilibrate with the pH of the external milieu (Kelly and Izawa, 1978; Theg and Homann, 1982). A similar approach can be used with intact PS II preparations, but recourse to an uncoupler is not required in this case. Nearly 100% dependence of activity on added Cl^- can be achieved in PS II preparations lacking the smaller extrinsic polypeptides (Miyao and Murata, 1985). The S_0 to S_1 and S_1 to S_2 transitions can still take place, but the S_2 state, and also the S_3 state if it is formed prior to Cl^- depletion, are unable to perform further transitions (Wincencjusz et al., 1997). A subsequent charge separation will only oxidize Y_Z (Gilchrist et al., 1995; Haumann et al., 1996; Szalai and Brudvig, 1996; Wincencjusz et al., 1997). If $Y_Z^{\bullet}$ is not reduced by charge recombination, then the next charge separation produces $P680^+$ (Itoh et al., 1984; Theg et al., 1984; Lübbers et al., 1993). Little is known about the

modified S_3 state, because it can be produced only by Cl^- depletion in that state. The modified S_2 state, in contrast, accumulates on illumination and has been extensively studied, especially by EPR (Rutherford et al., 1992; Britt, 1996). The multiline signal of the Mn cluster in S_2 is suppressed and the g = 4.1 signal increases in intensity (Casey and Sauer, 1984; Britt, 1996), indicating a modified electronic configuration of the Mn cluster. [See Britt (1996) and Chapters 10 (Yachandra) and 12 (Ahrling et al.) for comprehensive discussions of EPR multiline signals]. Thermoluminescence and charge recombination kinetics indicate a decreased potential of the modified S_2 state (Ono et al., 1986; Vass et al., 1987).

All of this suggests an essential and specific role of Cl^- in regulating the redox chemistry of the Mn cluster. On the other hand, it has been reported that all PS II centers remain active if Cl^- is removed from intact PS II by prolonged dialysis under conditions that avoid dissociation of the extrinsic proteins. In that case the rate of O_2 evolution saturates at a lower light intensity and reaches a substantially lower maximum than does the light-saturated rate obtained in the presence of Cl^- (Lindberg and Andréasson, 1996). It has even been suggested that the Cl^- dependence of O_2 evolution may be a consequence caused by the treatments used to remove the anion (Wydrzynski et al., 1990), but this assertion is clearly at odds with, for instance, the observation that substituting NO_3^- for Cl^- slows the S_3 to S_0 transition in untreated PS II to an extent similar to what is observed in extrinsic polypeptide-depleted PS II (Wincencjusz et al., 1998). Nevertheless, the question of whether O_2 evolution can occur, even if only transiently, in the absence of Cl^- may have important consequences, as will be detailed below.

C. The Chloride Binding Site

1. Stoichiometry

Nearly all studies on the role of Cl^- in PS II have relied on the dependence of O_2 evolution in anion-depleted preparations on added Cl^- to determine the extent of depletion of the anion, owing to the difficulties associated with direct detection of Cl^-. Theg and Homann (1982) carried out the first studies employing $^{36}Cl^-$ for direct quantification of the bound ion, and found variable amounts of Cl^- bound to intact thylakoid membranes (1-5 Cl^-/300 Chl). The stoichiometry question was revisited later by Lindberg and Andréasson (Lindberg et al., 1990), who used an isolated PS II preparation and ^{36}Cl to investigate the kinetics and stoichiometry of binding. A binding stoichiometry of somewhat less than one Cl^- per PS II was found, with an apparent dissociation constant, K_d (free Cl^- concentration yielding 50 % occupancy of the binding site), of 20 μM and a release time of about one hour. Since a similar time was minimally required for binding (at high Cl^- concentration), it was concluded that both on and off rates are limited by the same conformational change of the protein, temporarily allowing access to the site (Lindberg et al., 1993). Later it was found, however, that the properties of the binding site change in the absence of Cl^-: the K_d increased to 0.5 mM and the exchange time decreased to seconds (Lindberg and Andréasson, 1996). The binding site can slowly revert to its high-affinity, slow-exchange state, but only if the low-affinity site is occupied by Cl^-, or an anion that can functionally substitute for it, and if the PS II structure is intact, i.e., no loss of the extrinsic polypeptides has occurred. The capacity to recover the high-affinity state is lost upon prolonged exposure to Cl^--free medium and upon dissociation of one or more of the extrinsic polypeptides. The even lower Cl^- affinity and the faster exchange time detected in polypeptide-depleted preparations is attributed to this modification. The essential Cl^- cofactor in such material is generally believed to function, albeit with modified binding characteristics, at the same site quantified by Lindberg et al., as 1 per PS II in intact preparations.

2. Exchange Kinetics and Binding Affinity

While the long retention time in intact PS II is an essential factor that allowed investigators to quantify $^{36}Cl^-$ binding, it is also a serious impediment to most other studies on the role of Cl^-. Many hours of dialysis in nearly Cl^--free medium are required to remove the anion from intact PS II, and even then only a partial dependence of light-induced O_2 evolution on added Cl^- is observed. The light-saturated rate is lower in the absence of Cl^- than in its presence, but the effect seems to disappear at the lowest light intensities (Lindberg and Andréasson, 1996) and may not be directly related to the function of Cl^- in the binding site (Wincencjusz et al., 1999).

PS II preparations that will evolve O_2 at high rates in the presence of Cl^-, but show little or no activity in its absence, can be obtained by employing condi-

tions that cause dissociation of the 17 and 23 kDa extrinsic polypeptides from PS II, such as incubation with 25 mM SO_4^{2-} (which does not bind to the Cl^- site) at pH 7.5 (Sandusky et al., 1983). In the absence of the extrinsic polypeptides Cl^- can be replaced in seconds, but in intact PS II Cl^- replacement by a competing anion can also be much faster than its release in a medium without Cl^- or competing anions (Wincencjusz et al., 1998). Apparently in this case the binding site equilibrates rapidly only with a small sequestered domain, isolated from the bulk medium by the extrinsic polypeptides. The exchange rate depends on the probability that a competing anion is present in the domain and can be greatly accelerated by adding a large excess of the anion.

The extrinsic polypeptides seem to impose a passive diffusion barrier, without modifying the characteristics of the Cl^- binding site itself. The common notion that O_2 evolution in the absence of the polypeptides requires much higher Cl^- concentrations than in their presence (Homann, 1988a) was found to be due instead to a low Cl^- binding affinity in the higher S-states formed upon illumination (Wincencjusz et al., 1998). In the presence of the polypeptides, however, Cl^- release is too slow to be detected on the usual timescale of O_2 evolution measurements. In the dark-adapted state the OEC is largely in S_1, for which Wincencjusz et al. (1998) found K_d values, in polypeptide-depleted PS II, slightly below those reported for steady state O_2 evolution by intact PS II (Homann, 1988b), while those in high S-states were at least an order of magnitude higher.

3. Specificity

A limited group of anions (Br^-, NO_3^-, NO_2^-, and I^-) can substitute functionally for Cl^-. The activating anions differ in the maximum light-saturated rate of O_2 evolution they can support (decreasing in the order $Cl^- \approx Br^- >> NO_3^- > NO_2^- > I^-$), in both intact PS II and in PS II preparations depleted of the extrinsic polypeptides, but these differences may be unrelated to their effect on the Cl^- binding site. Extrapolated to low light intensity or measured in a series of single-turnover flashes, these differences vanish. In this case, different rates may still be observed as a result of the reduced lifetime of the higher S-states in the presence of an electron donor like iodide, which was shown to be unrelated to the anion at the Cl^- binding site (Rashid and Homann, 1992; Wincencjusz et al., 1999). Otherwise, S-state turnover in the O_2 evolving complex appears to be equally efficient with any of the activating anions in the binding site (Wincencjusz et al., 1999), and according to Lindberg and Andréasson (1996), even without any added activator in intact PS II. The only kinetic difference that can definitely be attributed to the anion bound at the Cl^- binding site is in the time constant of the S_3 to S_0 transition, which is increased, especially by NO_3^- (Sinclair, 1984; Wincencjusz et al., 1998). The maximum effect is less than a factor of 4, however, and does not seem to decrease the efficiency of O_2 evolution in a flash series. This phenomenon is of interest because the anion must presumably be closely associated with the site of water oxidation in order to affect the rate-limiting step of this reaction.

Competitive inhibitors of Cl^- action in PS II include the monovalent anions F^-, OH^-, and CH_3COO^-, as well as N_3^-, which seems to inhibit selectively at low pH (Haddy et al., 1999), and a range of primary amines (NH_3, methylamine, *t*-butylamine, Tris, aminoethylpropanediol). These inhibitors are useful research tools, but in vivo only OH^- is likely to ever approach inhibitory concentrations in the thylakoid lumen. The loss of Cl^- from PS II is strongly pH dependent, leading to a pronounced Cl^- dependence of O_2 evolution at high pH in isolated PS II, and, in intact thylakoids, in the presence of an uncoupler (Homann 1988b). The pH dependence of the extent of Cl^- binding to PS II has an apparent pK_a near 7.5 (Lindberg et al., 1993), which may be attributed to competitive binding of OH^- at the Cl^- site. A dissociation constant lower than 1 μM would make OH^- by far the most tightly bound species and, as will be argued below, its affinity for the Cl^- binding site could be much higher still in the S_2 and S_3 states.

4. Location

The essential Cl^- ion is probably bound to Mn or is located in close proximity to the metal. Since the activators and competitive inhibitors are all Lewis bases and their binding to the OEC presumably involves a Lewis acid as the reaction partner, higher oxidation states of Mn were proposed to be the site of Cl^- ligation (Sandusky and Yocum, 1984). Spectroscopic evidence for Cl^- ligation to Mn is still lacking, however. The closest results are those of Clemens et al. (2002), who report that deuterated acetate bound to the Cl^- site is so close in proximity to Mn that it is probably a ligand. Also, the narrowing of the g = 4.1 EPR signal by the competitive inhibitors has

been interpreted to indicate Mn ligation (Haddy et al., 1992). A contrary conclusion was presented by Hasegawa et al. (2002), who concluded from FTIR difference spectroscopy that NO_3^-, when substituting for Cl^-, is not metal-ligated but close enough to Mn for its N-O vibrations to be modified by the S_1 to S_2 transition.

Other components of PS II that might be involved in regulating the properties of the Cl^- binding site are the Ca^{2+} ion and amino acid residues of the D1 and CP47 proteins. Mutations in the large extrinsic 'E' loop of CP47 in *Synechocystis* PCC 6803 have been reported which have a clear effect on Cl^- binding to PS II (Putnam-Evans and Bricker, 1994, 1997; Morgan et al., 1998; Tichy and Vermaas, 1998; Clarke and Eaton-Rye, 1999; Chapter 3, Eaton-Rye and Putnam-Evans). A common feature of the phenotypes of all of these mutants is that in Cl^--depleted photoautotrophic medium, they grow either very slowly, or not at all. Assays of O_2 evolution in Cl^- sufficient medium produces activity, showing that this phenotype is at least partially reversible. The extrinsic 33 kDa manganese stabilizing protein appears to be present in many of these mutants. However, a primary site of interaction between PS II and manganese stabilizing protein resides in the region(s) of the CP47 'E' loop that have been altered by mutagenesis. It is therefore probable that a defect in binding of manganese stabilizing protein to PS II in these mutants creates a 'leak' with respect to Cl^- retention. There is no evidence available at the present time to suggest that any of the amino acids altered by mutation participate directly in Cl^- binding.

D. The Functional Role of Chloride

1. Earlier Models

The current state of knowledge concerning the role of Cl^- in the O_2 evolving reaction presents an unsettled view of the function of the anion. Quantification by means of $^{36}Cl^-$ assays, which show the anion to be present in active preparations at a stoichiometry of about 1/PS II reaction center, indicate that bulk anion effects on the stability of polypeptides of PS II, for example, cannot explain the Cl^- requirement of O_2 evolution. Results obtained with thylakoids from Cl^--deficient plants, from thylakoids washed in Cl^--free media, and from mutant cyanobacteria would indicate that the ion is an essential constituent of the OEC. Although apparently conflicting results on the ability of intact PS II to function without Cl^- have been reported, there is no disagreement that the system is dependent on the presence of Cl^- for activity after extraction of the 23 and 17 kDa polypeptides. In the absence of the anion, the S_2 and S_3 states appear to be modified such that further S-state advance is impossible and subsequent charge separations are lost by back reactions. A fully satisfactory explanation for these observations has yet to appear.

In view of the evidence for a close association of Cl^- with the Mn cluster, most models proposed for the role of Cl^- involve regulation of the potential or reactivity of the Mn atom or atoms to which the Cl^- ion is supposed to be bound. As a bridging ligand between two Mn atoms, Cl^- would facilitate valence rearrangement within the cluster (Sandusky and Yocum, 1984). The distance between neighboring Mn atoms is at most 3.3 Å, however, and the observed effect of Cl^- depletion (a block of electron transfer beyond S_2) does not appear to reflect a modest kinetic limitation. Models envisaging an alternating ligation to Mn in high S-states and to Ca^{2+} in low S-states (Tommos et al., 1998), or the prevention of premature binding and oxidation of H_2O (Rutherford, 1989), are not consistent with the S-state dependent effects of Cl^- depletion. Although recent models proposed for the Mn cluster and H_2O oxidation include Cl^- as a Mn ligand (Yachandra et al., 1993; Pecoraro et al., 1998; Vrettos et al., 2001a; Chapter 10, Yachandra), these models do not provide an explicit accounting of the observed effects of Cl^- depletion.

2. Proximal and Distal Manganese

Soft ligands like Cl^- would make the Mn to which the anion is ligated a stronger oxidant than would a harder oxo ligand. To explain why such an effect might be needed for the S_2 to S_3 transition to occur, this reaction has been proposed to proceed via transient oxidation of an Mn (III) proximal to Y_Z, which is blocked in the Cl^- depleted S_2 state because this 'gateway' Mn is already in the Mn(IV) state (Baumgarten et al., 1990, Wincencjusz et al., 1997). The EPR spectrum of the modified S_2 state, showing a large g = 4.1 signal but no g=2 multiline, is generally attributed to a modified valence distribution in the cluster, and the notion of a compulsory transient oxidation of a Mn(III) proximal to Y_Z on the S_2 to S_3 transition seems compatible with the geometry of the Mn cluster, which is suggested to form a monomer-trimer arrangement, based on inspection of the X-ray structure. Unfortunately,

the implied valence distributions in the normal and modified S_2 states are not consistent with the Mn oxidation states predicted recently by Peloquin et al. (2000) in a model based on EPR and ENDOR data. This model predicts that the 'dangler'— presumably proximal — Mn is a Mn(IV) state in both cases. The 'proximal' and 'distal' Mn would have to correspond to the second and third Mn in the dangler model, respectively. Perhaps the Mn-tyrosine distance is not the main reason why distal Mn(III) cannot be oxidized by $Y_Z^{\bullet}$ in the presence of proximal Mn(IV).

Since Cl^- would be bound to a Mn(III) in S_2 as well as in S_1, its weaker binding in S_2 cannot be attributed directly to ligand crowding around the much smaller Mn(IV), as proposed earlier (Wincencjusz et al., 1998). Instead, the lower Cl^- binding affinity would simply reflect the 80 mV stabilization of the S_2 state by Cl^- depletion estimated on the basis of its charge recombination characteristics (Ono et al., 1986, Vass et al., 1987). The effect of Cl^- depletion on the potential of the proximal Mn would be a decrease by 80 mV, plus the unknown potential difference between the proximal and distal Mn ions in the presence of Cl^-, because in this model the recombination is now with proximal Mn(IV) whereas charge recombination of normal S_2 takes place with the distal Mn(IV). This difference may be small, however, because both the g = 4.1 and the g=2 multiline signals are normally seen in the S_2 state, and the midpoint potential of the proximal Mn must be lower than that of Y_Z if oxidation of proximal Mn by $Y_Z^{\bullet}$ is to occur on the S_2 to S_3 transition. In order to explain why Cl^- depletion in the S_3 state blocks the S_3 to S_0 transition (Wincencjusz et al., 1997), one might assume that the redox potential of the proximal Mn(IV) is lowered to a point where it is ineffective in catalyzing water oxidation.

3. OH^- Binding in the S_2 State

A decrease of the potential of the proximal Mn by Cl^- depletion is expected if the anion is replaced by a harder ligand that is not impeded by ligand crowding, and that binds more strongly to Mn(IV) than to Mn(III), due to the larger ligand field stabilization energy of Mn(IV). In contrast to Cl^-, NO_3^-, and possibly to all activating anions, all competitive inhibitors seem to bind to the Cl^- site preferentially in the higher S-states (Velthuys, 1975; Sandusky and Yocum, 1986), but only OH^- is physiologically relevant. The effects of Cl^- depletion therefore suggest that a key function of the Cl^- ion in PS II is to exclude OH^- from the binding site.

This new insight not only accounts for the S-state dependent effects of Cl^- depletion, but also suggests a satisfactory explanation for the most puzzling observations reported in the literature on Cl^- effects in PS II. The pH dependence of Cl^- binding in S_1 shows a steep decline around pH 7.5, or 0.3 μM OH^- (Lindberg et al., 1993). A much higher OH^- binding affinity in S_2 than in S_1 may explain why Cl^- depletion causes a pH decrease on the S_1 to S_2 transition in PS II core particles (lacking the extrinsic 23 and 17 kDa polypeptides) at pH 6 (Haumann et al., 1996), which might reflect the binding of an OH^-.

In intact PS II the presence of the extrinsic polypeptides prevents rapid exchange at the Cl^- binding site, as indicated by the observation that O_2 evolution measurements on intact PS II reflect the Cl^- affinity before illumination, in the S_1 state (Wincencjusz et al., 1998). For the same reason, O_2 evolution measurements on Cl^- depleted intact PS II might reflect the OH^- binding affinity in the dark-adapted state and show activity at pH < 7.5, if it is not the absence of Cl^- but the presence of OH^- that inhibits PS II. Indeed, Izawa et al. (1969) reported an 80% decrease of the quantum efficiency of O_2 evolution in the absence of Cl^- at pH 8 and a 50% decrease at pH 7.5, and Lindberg and Andréasson (1996) found no decrease at all at pH 6.3. The latter authors insist that any residual Cl^- in these measurements was far below its K_d; if correct, it would appear that O_2 evolution under conditions of lowered turnover does not require the Cl^- ion as long as OH^- has no access to the Cl^- binding site.

Conversely, intact but inactive PS II, initially containing OH^- trapped at the binding site, may be expected to result from Cl^- depletion by a 10-30 s exposure to pH 10 (Homann, 1985). Van Vliet and Rutherford (1996) reported that in the absence of Cl^- such samples are indeed inactive at pH 6.3 and produce only the modified S_2 state upon illumination. A significant reactivation of O_2 evolution was observed if, before measurement at pH 6.3, the pH 10-shocked sample was stirred under dim light for 10-20 minutes at pH 7.3 in the presence of 25 mM F^-. This reactivation is more easily explained by OH^- release, followed by rebinding of Cl^- if present, than by binding of the well-known inhibitor F^-, whose concentration must have been non-saturating. One might speculate that a more complete recovery of O_2 evolution would be observed under better conditions for OH^- release (a longer incubation, at lower pH, in

the dark, and in the absence of F^-).

4. Consequences of Chloride Loss on the Chemistry of Manganese Oxidation

If H_2O oxidation can indeed occur temporarily without Cl^- in its binding site, with no other obvious change than a lower maximum rate, the Mn cluster cannot be too drastically disturbed by its absence. The coordination number of the Mn(III) in the S_2 state is actually not yet clear and could be either 6 or 5 (Zheng and Dismukes, 1996; Peloquin et al., 2000). Perhaps the possibility should be considered that the proximal Mn(III) becomes 5-coordinate in the absence of Cl^- and the ligand and structural rearrangements required to shift it to 6-coordinate on oxidation of S_2 to S_3 is what limits the turnover rate in such samples. The necessity to avoid a rate limitation on the donor side of PS II, which would cause rapid photo-oxidative destruction of the PS II reaction center, makes Cl^- an essential cofactor of photosynthetic O_2 evolution, regardless of the ability of the extrinsic polypeptides to delay inactivation by OH^-. The Cl^- dissociation constant in S_3 might not be much lower than the Cl^- concentration in the thylakoid lumen (Wincencjusz et al., 1998). If so, then PS II appears to be designed to lose the Cl^- ion relatively easily, which might play a functional role in stress responses or in reaction center disassembly after photoinhibition. Whatever its mechanism proves to be, the essential role of the Cl^- ion in PS II requires a more detailed and comprehensive explanation than is currently available.

III. Calcium

A. Calcium in Biological Systems

Calcium enjoys a unique prominence among metals with respect to its diversity of biological functions. A divalent alkaline earth metal, Ca^{2+}, with an ionic radius of about 1 Å, is redox inert. The most common coordination numbers of the metal are six and seven, although complexes containing eight-coordinate Ca^{2+} have been observed (Kretsinger and Nelson, 1976). The calcium salts of some bases (Cl^-, Br^-, I^-, NO_3^-) are water-soluble; other, harder bases (F^-, PO_4^{3-}, SO_4^{2-}) form salts that are highly insoluble owing to the relatively high lattice energies of these compounds. As a consequence, it is not surprising that calcium phosphate is a major component of tissues like bone and teeth.

At a more subtle level, an important function of Ca^{2+} in biology is to participate as a critical component of intracellular and intercellular signaling pathways. One of the best known of these systems is that involving the calmodulins, a family of proteins that bind Ca^{2+} with high affinity ($K_d = 10^{-7} – 10^{-6}$ M), and in this metallated form then bind to enzymes to regulate their activity. A classic example is that of glycogen phosphorylase kinase, which is activated by phosphorylation of regulatory subunits, as well as by binding of Ca^{2+} to a calmodulin, which is one of the regulatory subunits of the enzyme. Other proteins that bind Ca^{2+} with exceptionally high affinities include the troponins, calbindins, and parvalbumins (Kretsinger and Nelson, 1976; Strynadka and James, 1989; Lewit-Bentley and Rety, 2000). In all cases these proteins possess one or more Ca^{2+} binding domains comprised of a well-conserved motif of amino acid side chains that donate oxo, carboxylato, or carbonyl group ligands to the metal, and where the structure of the metal binding domain is comprised of a 'helix-loop-helix (HLH)', or EF Hand motif named after a convenient means of visualizing the tertiary structure of the domain (Kretsinger and Nelson, 1976). The motif contains a sequence of 12 amino acids in the pattern: +X * +Y * +Z * *-Y -X * * -Z. Residues +/– X, Y and Z are amino acids that donate ligands to Ca^{2+}; the intervening * residues do not supply ligands. These proteins, as a group, are designed to bind or release Ca^{2+} in a cellular milieu where the metal concentration may fluctuate by less than 1–2 μM. Investigations into the structures of these EF Hand sites reveals that in addition to oxo ligands from amino acid side chains, protein-bound Ca^{2+} can also ligate one or two H_2O molecules in some cases. A key feature of these proteins is a rearrangement of protein tertiary structure induced by Ca^{2+} binding.

The calcium cofactor proteins comprise another family in which the metal is required for activity. In contrast to the HLH/EF Hand family, the Ca^{2+} cofactor proteins have limited amino acid sequence identity in their binding sites. The metal is usually bound with a lower affinity than in the case of the HLH proteins (Kd's in the range of 10^{-5} to 10^{-3} M) (Kretsinger and Nelson, 1976). In contrast to the HLH Ca^{2+} binding domain, which is contained in a relatively compact, continuous sequence of amino acids, the cofactor protein binding sites utilize amino acid ligands that are more widely spaced in the protein's primary amino

acid sequence. This fundamental difference in the placement of ligating residues may also account, in part, for the somewhat lower affinity of Ca^{2+} for binding sites in a number of these proteins. Evidence for the structural importance of Ca^{2+} is readily apparent with the Ca^{2+} cofactor proteins, which include lipases, nucleases, proteases, and concanavalin A (a lectin). For example, thermolysin acquires thermostability upon binding of Ca^{2+}, and trypsin is more active when Ca^{2+} occupies its binding site in this protease; the generalization for Ca^{2+} function in this group of proteins is that metal binding contributes to stabilization of protein tertiary structure. Table 1 provides a brief summary of Ca^{2+} binding sequences, and of the Ca^{2+} affinities for these sites.

The ability of alternate metals to occupy Ca^{2+} binding sites has proven to be a useful tool in probing the structure of Ca^{2+} binding sites. The lanthanides have been used extensively to probe Ca^{2+} sites, on account of the fluorescence of species like Eu^{3+} or Tb^{3+}; binding of these metals to Ca^{2+} sites generates a large enhancement of fluorescence emission. Paramagnetic lanthanides have also been used as probes (Martin and Richardson, 1979). These metals possess ionic radii similar to that of Ca^{2+}, but have +3, rather than +2 charges. In many cases, lanthanides do not destroy the activity of the protein in question; however, in some cases inhibition is observed, and in these instances, Ca^{2+} is a component of the active site of the enzyme (Kretsinger and Nelson, 1976; Martin and Richardson, 1979), rather than a structural component. Strontium will replace Ca^{2+}, and Cd^{2+} is also able to occupy Ca^{2+} binding sites. ^{113}Cd-NMR has been used to probe Ca^{2+} binding sites. Competition occurs between Ca^{2+} and Mg^{2+} or Mn^{2+}, and alkali metals (Na^+, K^+) will also occupy Ca^{2+} binding sites, with a preference for Na^+ (Kretsinger and Nelson, 1976) owing to the similarity of its ionic radius to that of Ca^{2+}.

B. The Calcium Binding Site in Photosystem II

1. Extrinsic Photosystem II Polypeptides and Calcium Binding

The site of Ca^{2+} action within the PS II electron transport chain can be shown to reside on the oxidizing side; addition of Ca^{2+} to extrinsic polypeptide depleted PS II restored O_2 evolution and also accelerated the half-time for reduction of $Y_Z^{\cdot}$ after a flash. Other metals (Na^+, K^+, Mg^{2+}, Ba^{2+}) that were tested for activity reconstitution were ineffective, save for Sr^{2+}, which restored activity to about one half the level obtained in the presence of Ca^{2+} (Ghanotakis et al., 1984a). The early experiments that examined the topography of the Ca^{2+} binding site utilized PS II samples that had first been depleted of Ca^{2+}, and to which the extrinsic 23 and 17 kDa polypeptides were then rebound. When

Table 1. Ca^{2+} binding sequences in cofactor proteins and in HLH/EF Hand proteins. All sequences are aligned on the first coordinating residue for purposes of comparison. Single-letter amino acid designations are used for the ligating residues; intervening residues are designated by (x). Residues marked with * provide bidendate ligands to the metal, residues marked with # in Concanavalin A ligate both Ca^{2+} and Mn^{2+}, and underlined residues contribute peptide-bond carbonyl ligands to the metal. Data taken from Kretsinger and Nelson (1976), Strynadka and James (1989) and Yocum (1991).

Protein	Sequence	Number of H_20	K_d Ca^{2+} (μM)
Phospholipase A2	Y(x)G(x)G(xxxxxxxxxxxxxxxx)E*	2	250
Staphylococcal Nuclease	D(x)D(xxxxxxxxxxxxxxxxx)DT(x)E	1	1,000
Trypsin	E(x)N(xx)V(xxxx)E	2	400
Concanavalin A	D*#(x)Y(x)N(xxxxx)D#	2	300
Thermolysin (site 2)	D*(x)D(x)Q	3	< 1
Parvalbumin (CD site)	D(x)D(x)S(x)E(x)E(xx)E*	0	0.2
Parvalbumin (EF site)	D(x)D(x)D(x)K(x)G(xx)E	1	0.2
Calmodulin (loop 3)	D(x)D(x)N(x)Y(x)S(xx)E	1	6
MCBP[1] (EF site)	D(x)D*(x)D(x) K(xxxx)E*	1	0.1

[1]Muscle Ca^{2+} Binding Protein

Ca^{2+} was added to the reconstituted sample and the appearance of O_2 evolution activity was tracked, it was found that about an hour was required for activity recovery to reach a maximum (Ghanotakis et al., 1984b). This contrasted with the result obtained by mixing Ca^{2+} with polypeptide-depleted PS II samples, where activity was restored immediately. These results were interpreted to indicate that the 23 and 17 kDa polypeptides formed part of a structure that facilitated Ca^{2+} retention by PS II. Neither of these extrinsic proteins has been shown to bind Ca^{2+}. There is a report that the 33 kDa manganese stabilizing protein does bind Ca^{2+} (Wales et al., 1989; Webber and Gray, 1989), but this is probably due to adventitious binding of Ca^{2+} due to the acidic pI (5.2) of the protein. Ädelroth eet al. (1995) reported that upon removal of the 33 kDa extrinsic protein, Ca^{2+} binding was substantially weakened, and interpreted the result to indicate that loss of this extrinsic subunit of PS II might remove a barrier between the Ca^{2+} binding site and the external medium. In agreement with Tamura and Cheniae (1988), Ädelroth et al. also showed that upon removal of Mn along with all extrinsic polypeptides, a further loss of Ca^{2+} binding could be observed. Since there are no firm data to link any of the extrinsic polypeptides to Ca^{2+} binding, current hypotheses and models concerning the location of the Ca^{2+} binding site in PS II do not invoke a role for any of these proteins as donors of ligands to the metal.

An alternate method for Ca^{2+} depletion of PS II, exposure to low pH (3) in a citrate buffer, releases the metal with minimal release of the extrinsic 23 and 17 kDa polypeptides (Ono and Inoue, 1988). In some respects, this form of Ca^{2+}-depleted PS II resembles the Ca^{2+}-depleted, polypeptide-reconstituted material described above. Maximal reincorporation of Ca^{2+} required long incubation times, and addition of a chelator (EDTA or EGTA) after reconstitution had little effect on activity. This would indicate that Ca^{2+} rebinds to a site that is not accessible to EDTA when the extrinsic polypeptides are present. Analyses of the consequences of pH 3 exposure, and of the structure of the Ca^{2+}-depleted enzyme, indicate that low pH can affect binding of the extrinsic polypeptides to PS II (Shen and Inoue, 1991), and reveal modest structural alterations to the structure of PS II. For example, a small reductant (NH_2OH) gains access to the Mn cluster in the OEC more rapidly after Ca^{2+} extraction (Sivaraja et al., 1989; Vander Meulen et al., 2002), even though the extrinsic 23 and 17 kDa polypeptides are still present in the preparation.

Since none of the extrinsic proteins can be shown to retain tightly bound Ca^{2+}, searches for the location of the Ca^{2+} binding site of the OEC have focused on the lumenal domains of the D1 and D2 intrinsic proteins of the PS II reaction center (Debus, 1992, 2001; Chapter 11, Debus). These polypeptides, D1 in particular, are the subject of intense scrutiny with respect to their potential roles in Mn binding in PS II. Acidic amino acid residues (Glu, Asp) are prime candidates for such a role in Mn ligation, and these same residues could, in theory, be used as ligands for Ca^{2+}. Extensive mutagenesis experiments using *Synechocyctis* 6803 have identified several residues in the lumenal, interhelical a-b loop of D1 (Chu et al., 1995a, 1995b; Qian et al., 1999), as well as residues at the C-terminus of the protein, as potential ligands to Ca^{2+}. The 3.7-3.8 Å crystal structure of PS II has located the electron density of the Mn cluster (Zouni et al., 2001; Kamiya and Shen, 2003). Ferreira et al. (2004) have placed Ca^{2+} in close association with the Mn cluster (see Chapter 21, Barber and Iwata). Although one cannot completely rule out the possibility that the 33 kDa extrinsic manganese stabilizing protein plays a role in Ca^{2+} binding, the best evidence now available points to ligation by amino acid residues in the interhelical loop domains of D1. Because the D1 protein is also involved in ligation of cofactors on the reducing side, its transmembrane α-helices could, in theory, transmit a perturbation on the oxidizing side to the reducing side of PS II. This phenomenon might account for the reported effects of Ca^{2+} depletion on electron acceptor kinetics. Electron transfer from Q_A^- to Q_B is inhibited (Dekker et al., 1984; Andréasson et al., 1995) and the midpoint potential of Q_A is increased by more than 100 mV (Krieger et al., 1993). A physiological role of the latter effect in protection against photoinhibition has been proposed (Krieger and Rutherford, 1997). However, at the present time there is no evidence that potentially photoinhibitory conditions might induce a sufficient decrease of the Ca^{2+} binding affinity (K_d = 60 μM) and release time (80 h) for loss of Ca^{2+} from PS II to occur.

2. Stoichiometry and Binding Affinity

Calcium's ubiquitous distribution in biological systems, combined with its appearance as a contaminant in nearly all buffers, glassware, and even in relatively pure water, creates a problem in quantifying the contents of the metal in PS II. Early determinations of

Ca^{2+} concentrations in PS II preparations produced estimates of up to ca. 170 Ca^{2+}/PS II reaction center, almost all of which was associated with binding sites outside the OEC (e.g., starch granules). Even after inactivation of PS II by high salt exposure, the resulting preparations still contained ca. 100 Ca^{2+}/PS II. Modifications in the biochemical methods used to extract Ca^{2+} from PS II, along with use of plants (rice, wheat) other than market spinach as sources of thylakoid membranes, yielded preparations in which lower Ca^{2+} stoichiometries were obtained (1–3 Ca^{2+}/PS II) (Cammarata and Cheniae, 1987; Shen et al., 1988a,b). In a systematic study using PS II preparations from spinach and rice, as well as more highly purified 'core' material, it could be shown that there were two bound Ca^{2+} atoms in PS II, one of which was readily extractable, and whose loss affected O_2 evolution activity (Shen et al., 1988a). The second Ca^{2+} atom was presumed to be tightly bound to the light harvesting chlorophyll *a/b* protein (LHCII) of the antenna system, based on its loss from the 'core' preparation, and on the finding of a single Ca^{2+} atom in PS II preparations from a chlorophyll *b*-less mutant of rice, which lacks LHCII (Han and Katoh, 1993). Some of these results were problematic; it was shown in one case (Shen et al., 1988b) that release of extrinsic polypeptides inhibited O_2 evolution, but under these conditions there was no detectable loss of Ca^{2+} from the enzyme. The function of the second tightly bound Ca^{2+} atom in PS II has not been clarified. Its binding site is presumably associated with an antenna protein of which only one copy per PS II is present. Other investigations have found multiple (>2) sites for Ca^{2+} binding in isolated spinach PS II preparations (Grove and Brudvig, 1998), but the nature and location of these sites have not been characterized in detail.

Another extensive analysis of Ca^{2+} binding in PS II was carried out using spinach plants grown on $^{45}Ca^{2+}$ (Ädelroth et al., 1995). It was found that isolated PS II contained about 1.5 Ca^{2+}/PS II center, and that the loss, and restoration of about 1 Ca^{2+}/PS II correlated with inhibition and reconstitution of O_2 evolution activity in these preparations. Combined with the analyses in Han and Katoh (1993), the $^{45}Ca^{2+}$ binding data provide strong support for the presence of a single Ca^{2+} atom in the OEC. At least one, and possibly more, Ca^{2+} ions are also bound to PS II membranes (BBY-type preparations). One of these binding sites resides in the antenna protein ensemble; other binding sites have not been identified, nor is it clear that these sites have any function in PS II.

Measurements of the affinity of Ca^{2+} for its site of action in PS II have utilized various preparations of the enzyme, and have been carried out under illumination in the steady state, as well as under static conditions in darkness. The results of these experiments have been mixed, in that a variety of values have been obtained, and the origins of the diversity in measured affinities is not entirely clear. A summary of selected results is given in Table 2. As a general rule, Ca^{2+} affinities (K_M values derived from steady state activity assays, or K_d values obtained by measurements of Ca^{2+} binding under static conditions) in the literature can be divided into two groups, those falling into the low to medium μM range, and those in the mM range. Furthermore, values in both concentration ranges have been reported for the same PS II preparation, in darkness and in light. Steady-state assays of reactivation of the OEC by Ca^{2+} have given K_M values in the low (7–50 μM) to medium (100-500 μM) range, and in the high ($\geq$ 1 mM) range as well. Dark incubation with $^{45}Ca^{2+}$ produced values of K_d for Ca^{2+} of 26 μM and 0.5 mM for polypeptide-depleted PS II, and of 60 μM and 1.7 mM for citrate-treated PS II (the extrinsic polypeptides are retained after this extraction method). Activity recovered in the latter preparation was insensitive to EGTA, but optimal activity in the polypeptide-depleted preparation required addition of Ca^{2+} to the assay buffer (Ädelroth et al., 1995).

In all preparations of PS II examined to date, a high-affinity binding site for Ca^{2+} can be detected in dark-adapted, as well as in illuminated samples. The range of values (K_M or K_d) is approximately 10–70 μM, and is relatively insensitive to the presence or absence of the 23 and 17 kDa polypeptides, provided long incubation times are used when restoring Ca^{2+} to the sample (Ädelroth et al.,1995). In the absence of the 23and 17 kDa polypeptides, however, divalent metal chelators (EDTA or EGTA) inhibit the activity of illuminated Ca^{2+} reconstituted samples. This result indicates that even if S_1 can bind Ca^{2+} with high affinity, binding of the metal in the higher S-states is weaker in the absence of the extrinsic polypeptides (Boussac and Rutherford, 1988a). Thus, one function of these proteins would seem to be to prevent rapid dissociation of the metal from its binding site, as proposed by Ädelroth et al. (1995). The second, lower affinity Ca^{2+} binding site reported by a number of investigators (see Table 2) has K_M or K_d values that can exceed 1 mM. Analysis of K_M and V_{MAX} values in a preparation containing two or more activities is not straightforward (when transforming data to

Table 2. Representative determinations of Ca^{2+} binding affinities in PS II

Preparation	Extrinsics Released	Measurement Condition	K_M (μM)	K_d	References
Salt-Washed PS II	23, 17 kDa	Steady-State	70, 2000	–	a
Salt-Washed PS II	(23, 17 kDa)*	Steady-State	200, 460	–	a
Salt-Washed-pH 5 PS II	23, 17 kDa	Steady-State	10, 120	–	b
Salt-Washed-pH5 PS II	23, 17 kDa	Static	–	70	c
Salt-Washed PS II	23, 17 kDa	Static	–	26, 500	d
Citrate-Treated PS II	No	Static	–	60, 1700	d
Citrate-Treated PS II	No	Steady-State	800		e

*Han and Katoh (1995) used 0.5 M NaCl in this series of experiments, and reported that under this condition extraction of the 23 and 17 kDa polypeptides is incomplete. References: [a] Han and Katoh, 1995; [b] Chen and Cheniae, 1995; [c] Vrettos et al., 2001a; [d] Ädelroth et al., 1995; [e] Vander Meulen et al., 2002.

Lineweaver-Burk or Eadie-Hofstee plots, the overlapping activities 'contaminate' one another), so exact determinations of K_M values can be quite difficult. If there is a generalization to be derived from the multiple activities associated with Ca^{2+} reconstitution of PS II activity, it would be that the lowest affinity sites seem to be associated with the smallest fraction of PS II centers.

It is probable that the method of Ca^{2+} extraction can affect the apparent affinity for Ca^{2+} in PS II. For example, incomplete release of the extrinsic polypeptides, in particular retention of the 23 kDa subunit (Miyao and Murata, 1986), which has been closely linked to Ca^{2+} binding in PS II, would result in retention of a fraction of centers that can rebind Ca^{2+} with high affinity. Likewise, exposure to the high salt concentrations needed to release the polypeptides and Ca^{2+} may create subtle changes in the structure of the Ca^{2+} site that affect rebinding of the ion.

If one takes the highest affinities measured for the Ca^{2+} site in the OEC (< 100 μM, and as low as 10- 20 μM), then on the basis of data from other Ca^{2+} binding proteins, the PS II affinity values would suggest that this site is not a member of a common HLH/EF-hand family, where K_d values for Ca^{2+} are on the order of 1 μM. EF-Hand like motifs have not been detected among the primary sequences of any of the PS II polypeptides (Yocum, 1991). One cannot, however, rule out the existence of a novel binding sequence derived from protein-protein interactions among the subunits of PS II, in particular D1 and D2, or a combination of interactions of one or both of these intrinsic subunits and one of the extrinsic subunits. Alternatively, a Ca^{2+} cofactor protein-type site may be present, and this could easily escape detection by amino acid sequence analysis owing to the lack of strong sequence conservation among these Ca^{2+} binding sites.

3. Metal-Metal Competition at the Calcium Site

Following the approaches that have been productively used to analyze other biological Ca^{2+} binding sites, a number of groups have explored the ability of other metals to displace Ca^{2+} from its binding site. The only metal to replace Ca^{2+} with retention of OEC function is Sr^{2+}, albeit a lower (ca. 50% of the activity obtained with Ca^{2+} is restored) level (Ghanotakis et al., 1984a; Boussac and Rutherford, 1988b). A wide range of mono-, di-, and trivalent metals has been used to replace Ca^{2+}, without restoration of O_2 evolution activity. A list of these metals is given in Table 3. Several points emerge from a consideration of the results summarized in this table. First, the Ca^{2+} site shows a preference for metals with ionic radii of ca. 1 Å. In the alkaline earth series, the order of activity is narrowly restricted to Ca^{2+} and Sr^{2+}; Mg^{2+} is likely to be too small to form stable complexes in the site, as evidenced by the estimated K_d value, and Ba^{2+} is apparently too large to be accommodated in the site. Second, ionic ligation is likely to dominate over more covalent bonding interactions. Cadmium occupies the site with a reasonable affinity, but is inef-

Table 3. Metal ion effects on Ca^{2+}-activated O_2 evolution

Metal	Ionic Radius (Å)	Coordination Number	Effect on O_2 Evolution Activity	K_i^* or K_d^+ (mM)
Ca^{2+}	0.99	6–8	(Activator)	–
Sr^{2+}	1.13	6–8	(Activator)	–
Ba^{2+}	1.35	6–8	Weak Inhibitor	–
Mg^{2+}	0.65	6	No Effect	2.84^+
Ni^{2+}	0.69	4–6	Weak Inhibitor	1.70^+
Mn^{2+}	0.80	6	Weak Inhibitor	–
Cd^{2+}	1.03	6–8	Competitive Inhibitor	0.30^*, 0.144^+
La^{3+}	1.04	7–9	Competitive Inhibitor	0.05^*
Dy^{3+}	0.91	7–9	Competitive Inhibitor	0.12^+
Na^+	0.98	4–7	Competitive Inhibitor[1]	5, $>100^+$
K^+	1.33	6–8	Competitive Inhibitor	$3–8^+$
Cs^+	1.65	6–8	Competitive Inhibitor	$8–10^+$

[1]Na^+ inhibition includes a small non-competitive contribution whose origin is unknown at present.

fective in restoring activity; this may be due in part to a shift in ligation to include nitrogen donors (the imidazole group of His, for example) in place of some of the oxygen ligands normally employed to ligate Ca^{2+}. Third, the site responds to lanthanide binding in a manner similar to that of Ca^{2+} cofactor proteins in which Ca^{2+} is a component of the active site of the enzyme, rather than just a structural element.

Some issues remain to be clarified in these investigations. For example, three groups have produced widely differing findings with respect to the binding/inhibition induced by the alkali metals. One group finds no binding by Na^+, K^+, or Cs^+ (Vrettos et al., 2001b), whereas the other two groups (Waggoner et al., 1989; Ono et al., 2001) report competition between K^+ or Cs^+ for the Ca^{2+} site, but differ with respect to inhibition by Na^+, the monovalent cation whose ionic radius is closest to that of Ca^{2+}. This discrepancy deserves further attention. Monovalent metals should, in theory, compete for the PS II Ca^{2+} site (Kretsinger and Nelson, 1976). Some of the difficulties with respect to monovalent cations may be due to differences in the extent to which the Cl^- concentration is controlled in various experiments, or to subtle differences in the methods used for Ca^{2+} extraction. However, there is, at present, no clear resolution of the issue of why there are failures to observe any interaction by Na^+ and other monovalent ions with the Ca^{2+} site. It is equally difficult to explain how K^+ (1.33 Å) is able to compete more effectively for the PS II Ca^{2+} site than is Na^+ (0.98 Å) (Ono et al., 2001).

C. Calcium and the S-State Cycle

The manifestation of Ca^{2+} depletion in the steady state is loss of O_2 evolution activity. Research to pin down the precise nature of the lesion in the S-state cycle has relied heavily on EPR spectroscopy, with additional information coming from thermoluminescence measurements. In the case of EPR, an important method for following S-state advancements has been to monitor the formation of the S_2 state by the appearance (or lack of) the signals observed at cryogenic temperatures. Continuous illumination of intact PS II preparations at 200 K, which limits PS II to a single turnover, or flash illumination at >273 K produces the g=2, S = ½ multiline signal, which is attributed to a $Mn(III)/Mn(IV)_3$ oxidation state of the Mn cluster that gives rise to >16 hyperfine lines with a line spacing of about 88 G (Chapters 10, Yachandra and 15, Faller and Rutherford). Modifications of Cl^- content by addition of F^- or a lowered illumination temperature (ca 160 K) will produce the g=4.1 signal, also associated with S_2. A number of phenomena have been reported, which relate to the Ca^{2+} status of PS II:

(i) Substitution of Sr^{2+} for Ca^{2+} in PS II samples depleted of the 23 and 17 kDa polypeptides modifies the multiline signal (narrowed line spacings), and, surprisingly, the g=4.1 form of S_2 is observed as well (Boussac and Rutherford, 1988b). Appearance of this latter signal contrasts with the case of polypeptide-depleted PS II samples supplemented with Ca^{2+}, where the normal multiline signal is

observed, and the g=4.1 signal is absent (Ghanotakis et al., 1987). The origin of the Sr^{2+}-induced modification in the paramagnetic behavior of S_2 is not well understood.

(ii) In the absence of Ca^{2+}, 200 K illumination fails to produce the multiline signal (Ghanotakis et al., 1987). Illumination at a higher temperature (ca. 270 K) in the absence of Ca^{2+} does generate the signal, however (Ono and Inoue, 1990b), so Ca^{2+} binding lowers the threshold temperature for Mn oxidation by $Y_Z^{\bullet}$ in PS II.

(iii) Long term illumination of PS II in high salt and EGTA, or illumination in the presence of high salt followed immediately by addition of EDTA, both at room temperature, results in formation of a modified multiline signal (Boussac et al., 1989; Ono and Inoue, 1990a) characterized by a greater number (26) of hyperfine lines with narrowed spacings (55G). This abnormal form of the S_2 multiline signal is also characterized by an unusual stability, manifested by an extended half life (ca. 5 min with Ca^{2+} or Sr^{2+} added after illumination (Boussac et al., 1989), up to several hours with no addition (Ono and Inoue, 1990a)).

(iv) Illumination at 0 °C of PS II samples trapped in the Ca^{2+}-depleted, modified S_2 state causes a disappearance of the altered multiline signal and the appearance of a ca. 140-180 G wide 'split' EPR signal (Boussac and Rutherford, 1992). Although originally believed to arise from a histidine radical (Boussac et al., 1990), later pulsed EPR experiments have definitively assigned this signal to the state $S_2Y_Z^{\bullet}$ (Tang et al., 1996). From this result, it is apparent that S-state advancements coupled to Mn oxidation cannot proceed beyond S_2 in the absence of Ca^{2+}, at least when chelators (EDTA, EGTA) are present in the PS II sample.

Studies have also been carried out on the modified S_2 state after Ca^{2+} depletion using the technique of thermoluminescence. This method provides information on charge-separated states in PS II by reporting changes in the temperatures at which recombination occurs in samples subjected to illumination and freezing. Heating such samples produce light emission at characteristic temperatures for states such as S_2/Q_A^- or S_2/Q_B^-. The most recent such investigation (Ono et al., 2001) shows that the S_2/Q_A^- light emission peak from Ca^{2+} depleted and monovalent cation reconstituted PS II shifts from about 8 °C with Ca^{2+} bound, to 38 °C when K^+, Rb^+ or Cs^+ are present. With added Na^+, the emission temperature is 10 °C and with Li^+, it drops to 2 °C. The authors conclude on the basis of the appearance of the high temperature thermoluminescence band with K^+, Rb^+ and Cs^+ that the redox potential of S_2 has decreased to a lower value. Accompanying experiments to detect the S_2 multiline signal showed a correlation between the absence of the EPR signal and the presence in the Ca^{2+} site of K^+, Rb^+ or Cs^+ (Ono et al., 2001). The signal, diminished in intensity, is present when Na^+ or Li^+ are added to a Ca^{2+} depleted sample. These data are interpreted to indicate that for the S_1 to S_2 transition, occupancy of the Ca^{2+} site by a metal that competes strongly for the site blocks formation of the multiline signal, even though it can be shown by thermoluminescence that charge separation has occurred.

Effects of Sr^{2+} on the S-state cycle have also been examined by monitoring the kinetics associated with $Y_Z^{\bullet}$ reduction (Westphal et al., 2000). In polypeptide depleted samples where Sr^{2+} was substituted for Ca^{2+}, it was found that the S_3 to S_0 transition was slowed, from about 5 ms to 18 ms. The lower S-state transitions were also slowed (from 200 to 900 μs for S_1 to S_2, and from 450 to 1300 μs for S_2 to S_3). The authors ascribe these kinetic defects to an introduction of a disturbance in interactions between the Mn cluster and substrate H_2O, which in turn affect H-atom abstraction reactions associated with the mechanism of water oxidation.

D. Interactions between Calcium and the Manganese Cluster

1. Spectroscopic Investigations

Techniques for probing the structure and oxidation states of the PS II Mn cluster have included X-ray absorption and magnetic resonance spectroscopies, augmented by biochemical probing of the Ca^{2+} and Mn sites in PS II. Extended X-ray absorption fine structure, or EXAFS, is useful for determining distances between scattering atoms. In the case of the OEC, the technique has been applied extensively to characterization of the Mn cluster (Chapter 10). Three shells of scattering atoms surrounding the Mn atoms of the OEC have been detected, one at ca. 1.85 Å arising from O or N ligands to the Mn, one at 2.7 Å, which is ascribed to a Mn-Mn distance, and lastly, a

3.3 Å distance. This long distance has been assigned to Mn alone (Riggs-Gelasco et al., 1996a); substitutions of lanthanides, Sr^{2+} or Cd^{2+} in the Ca^{2+} site, or Ca^{2+} depletion itself, had no effect on the 3.3 Å scatterer. Another investigation concluded that the 3.3 Å species represents a combination of scattering from Mn and Ca^{2+} (Latimer et al., 1995). Later experiments have not clarified the discrepancy between these results. Strontium EXAFS, which should detect backscattering from metal ligands as well as from any nearby Mn atoms, is interpreted to indicate that there is a Sr^{2+}-Mn distance of about 3.5 Å in the OEC (Cinco et al., 1998), but the samples giving this result do not exhibit a Sr^{2+}-modified multiline signal. A more recent report from the same group has employed Ca^{2+} EXAFS on PS II samples containing 2 Ca^{2+} / PS II (Cinco et al., 2002). The results are interpreted as being consistent with a Ca^{2+}-Mn interaction at about 3.5 Å. In both the Sr^{2+} and Ca^{2+} EXAFS investigations, addition of NH_2OH to remove the Mn cluster results in a loss of the 3.5 Å scattering component. Consequences of Mn release for functional Ca^{2+} binding have not yet been considered, although it has been shown that in the absence of a functional Mn cluster, Ca^{2+} binding to the OEC cannot be detected (see below).

Lanthanum EXAFS (L-edge measurements) to probe the environment of La^{3+} bound to PS II detects a scatterer at 3.5 Å, which is assigned to carbon atoms, and another scatterer detected at 4.49 Å is assigned to a La-Mn interaction (W.J. Chen and Ta 2001). While these samples have been thoroughly Ca^{2+} depleted, no data are given on the number of bound La^{3+} ions per PS II reaction center, so the distances reported here may include scattering from La^{3+} atoms bound to sites that are not related to the Mn cluster. In theory, ^{113}Cd substitution for Ca^{2+} can provide an important probe that can be utilized by NMR. The strategy has been employed in a solid-state NMR experiment (Matysik et al., 2000), where it was found that Cd^{2+} occupies a symmetric site where the metal is coordinated by six or eight ligands. The signal exhibits an intensity maximum at about –60 °C, and declines in intensity on either side of this temperature. One explanation advanced by the authors for the temperature dependency is that the Cd^{2+} in the Ca^{2+} site is located close enough to the Mn cluster to be affected by the paramagnetism from that site in S_1 (Campbell et al., 1998), which manifests itself upon sample cooling.

Calcium binding and effects of S-state advancement on Ca^{2+} ligands have also been examined by Fourier transform infrared spectroscopy (FTIR) (Chapter 13, van Gorkom and Yocum). Using the differences between difference spectra (S_2 to S_1) of samples of Ca^{2+}-sufficient and Ca^{2+}-depleted PS II, it was observed that negative bands at 1560 and 1403 cm^{-1} and positive bands at 1587 and 1364 cm^{-1} were lost upon Ca^{2+} extraction (Noguchi et al., 1995). These bands were assigned to stretching modes of a carboxylate group (from Asp, Glu, or a C-terminal amino acid). Additional probing with ^{15}N-labeled spinach PS II showed that the stretching modes are shifted by 100-200 cm^{-1}, which was interpreted as evidence for a bridging ligation function of the carboxylate group. Kimura and Ono (2001) interpreted their FTIR results with EGTA and EDTA to suggest that these chelators can replace a carboxylate group ligated to Mn in PS II samples depleted of Ca^{2+}. A series of later FTIR experiments (Kimura et al., 2002) characterized double difference spectra of samples in which Ca^{2+} was replaced by Sr^{2+}, Ba^{2+}, or monovalent ions (Na^+, K^+, Rb^+, or Cs^+). Using the 1404 cm^{-1} FTIR band as an indicator of carboxylate ligation, it was shown that the larger monovalent ions (K^+, Rb^+, or Cs^+) and Ba^{2+} abolished this band. Shifts in amide I frequencies, and the appearance of new bands in these samples (which were reversed by Ca^{2+} addition) were interpreted as evidence for perturbations in structure of the OEC, as well as in a hydrogen bonding network that is proposed to be required in the chemical mechanism for H_2O oxidation. Further refinements of these results can be achieved by isotopic labeling of carboxy amino acids, and the outcomes of such experiments would be useful in a better understanding of changes in Ca^{2+} ligation that may occur during the cycle of Mn redox reactions in the S-state cycle.

2. Photoassembly of the Manganese Cluster and S-State Turnovers

Calcium plays a critical role in the mechanism of photoactivation, which is the process by which Mn^{2+} is ligated by the OEC, photooxidized, and assembled into functional tetranuclear clusters (Chapter 26). A number of publications deal with the interactions between Ca^{2+} and Mn binding sites during assembly of the Mn cluster (Tamura and Cheniae, 1986; Tamura et al., 1989; Miller and Brudvig, 1989, 1990; Blubaugh and Cheniae, 1992; C.G. Chen and Cheniae, 1993, 1995; Ananyev and Dismukes, 1997; Ananyev et al., 1999; Büchel et al., 1999). To summarize briefly the results of a number of reconstitution experiments, it has been established that reassembly of the Mn

cluster can occur in the absence of any of the extrinsic polypeptides. Calcium is necessary, however, for assembly of the Mn cluster. How this occurs is not apparent, given the observations that in the absence of a functional Mn cluster, high affinity Ca^{2+} binding to PS II cannot be observed (Tamura and Cheniae 1988; Ädelroth et al., 1995). A further complication is apparent from experiments showing that Ca^{2+} and Mn^{2+} can compete for one another's binding sites in PS II (Miller and Brudvig 1989; Miller and Brudvig 1990; Booth et al., 1996). Nevertheless, a simple model for the role of Ca^{2+} in photoactivation has evolved that assigns a dual function to the metal (C.G. Chen et al., 1995). First, Ca^{2+} is necessary as a structural element to promote Mn binding to its functional sites in the OEC. Second, the presence of Ca^{2+} during the photoactivation process prevents nonproductive binding of Mn in 3+ or 4+ oxidation states.

Another Mn-Ca^{2+} interaction has been revealed in experiments where illumination of PS II samples in the presence of high salt was shown to accelerate the extraction of polypeptides and Ca^{2+} during inhibition of O_2 evolution activity (Miyao and Murata, 1986). The catalytic effect of light in promoting inactivation of the OEC was explored in more detail using PS II samples subjected to short light flashes (Boussac and Rutherford, 1988a). Following a flash sequence, the intact enzyme was mixed with high salt, incubated, and then assayed for activity. Relative to the S_1 state, Ca^{2+} release from S_2 was enhanced, but even more inactivation was observed when an S_3 -poised sample was exposed to high salt. Simple interpretations of this result are not easy to come by. Protonation of metal ligands during S-state turnovers has been suggested as a contributing factor (Boussac and Rutherford, 1988a). Alternatively, accelerated Ca^{2+} release in higher S-states might arise from electrostatic factors (charge repulsion between accumulated Mn (IV) species and Ca^{2+}, for example). Finally, if Ca^{2+} were ligated by carboxylate groups that bridge to Mn atoms, as in concanavalin A, an increase of positive charge on a Mn atom could weaken Ca^{2+} binding by the other carboxyl oxygen atom and lead to the metal's release upon formation of S_2 or S_3.

3. Biochemical Probing

Biochemical experiments have also been conducted to probe the nature of the relationship between Ca^{2+} binding and the Mn cluster. Reductants attack the cluster, producing Mn^{2+}, which is released from the OEC. The structural integrity of the OEC, as well as the presence or absence of Ca^{2+} and Cl^- affects the extent to which a given reductant can access the Mn cluster and generate Mn^{2+} (Mei and Yocum, 1991, 1992, 1993). Addition of Ca^{2+} to a PS II preparation lacking the 23 and 17 kDa polypeptides slows the rate at which NH_2OH inactivates the OEC. In the case of the large reductant hydroquinone, Ca^{2+} appears to block reduction of the cluster. However, XANES, EXAFS and EPR experiments show that under these conditions the reductant has generated a pair of EPR active hexaquo Mn^{2+} ions, detectable at room temperature, that are inaccessible to release by EDTA (Mei and Yocum 1991, 1992; Riggs-Gelasco et al., 1996b). The resulting oxidation state of Mn in the OEC is predicted to be Mn(IV)/Mn(IV)/Mn(II)/Mn(II) (Riggs et al., 1992). The unusual stability of this reduced derivative of the OEC is proposed to be due to a structural contribution from Ca^{2+} at its binding site that stabilizes the ligation environment of the Mn cluster. Addition of NH_2OH to such a sample produces a rapid decay of activity, and release of Mn^{2+} into solution (Mei and Yocum, 1992), presumably because of NH_2OH attack on the Mn (IV) atoms remaining in the OEC.

E. Models for a Catalytic Role of Calcium in the Oxygen-Evolving Complex

Models for Ca^{2+} function in the OEC, other than in a structural capacity, include proposals in which the metal acts as a binding site for Cl^-, for H_2O, or for both. A complete review of possible models for the mechanism by which Mn oxidizes H_2O is given in Chapter 25. For purposes of this chapter, we will consider only the proposals for Ca^{2+} participation in the reaction, without discussing individual models in detail. One model hypothesizes that Cl^- binds to Ca^{2+} in S_1, and shifts to an Mn atom upon formation of S_2 (Tommos et al., 1998); this model is now considered to be unlikely (C. Hoganson, personal communication). An alternate model proposes that Ca^{2+} and an Mn atom jointly form the binding site for the Cl^- atom in PS II (Vrettos et al., 2001a). This formulation is consistent with proposals that Cl^- is ligated to Mn in the OEC, and also positions the Ca^{2+} atom in relatively close proximity to a Mn atom, although the authors make no predictions about Mn-Ca distances in the model. Valid alternate models would include those in which Ca^{2+} occupies a site without ligated Cl^-.

The prevalence of H_2O molecules bound to Ca^{2+}

atoms in the Ca^{2+} cofactor proteins as well as in other complexes of the metal would support the proposal that Ca^{2+} is the site for ligation of substrate H_2O molecules (Rutherford, 1989; Yocum, 1991; Pecoraro et al., 1998; Vrettos et al., 2001a). A function in substrate binding is consistent with the inhibitory nature of lanthanide substitution into the Ca^{2+} site in PS II. Vrettos et al. (2001b), in their investigation of metal ion substitutions for Ca^{2+} in PS II made the observation that the catalytically active ions (Ca^{2+}, Sr^{2+}) with respect to H_2O oxidation were also the strongest Lewis acids. In agreement with a proposal by Riggs-Gelasco and co-workers (1996a), they hypothesized that Lewis acidity of the occupant of the Ca^{2+} site would affect the acidity of a bound H_2O. Vrettos and co-workers (2001a) propose that the consequence of this would be to make the Ca^{2+}-bound H_2O a better attacking nucleophile in a reaction with a Mn^{V}=O intermediate, formed in S_4. This would produce the O-O bond, and lead to formation of O_2. Like other models for the mechanism of H_2O oxidation, this proposal is still in its speculative stages. It does, however, utilize known properties of the Ca^{2+} site, as well as the ligand preferences of Ca^{2+} in proposing a mechanism for substrate binding and utilization that is supported by the data of Hendry and Wydrzynski (2003), whose water exchange data suggest that at least one substrate molecule may interact with Ca^{2+} in PS II. For further details, see Ferreiro et al. (2004) and Chapter 21 (Barber and Iwata)

IV. Concluding Remarks

Chloride and Ca^{2+} are essential for S-state advances beyond S_2, and Cl^- is required for the S_3 to S_0 transition. The mechanistic details concerning how these ions affect redox reactions in the OEC are still a matter of speculation. In the case of Ca^{2+}, the results from a number of experiments characterizing the inhibited activity of PS II after substitution of lanthanides for Ca^{2+} are consistent with the presence of Ca^{2+} in the active site of the O_2 evolving reaction. This conclusion must be qualified by the provision that results from other Ca^{2+} binding proteins, which are not redox active, may not prove to be relevant to the case of the involvement of Ca^{2+} in the redox reactions catalyzed by PS II. Should Ca^{2+} prove to be a component of the O_2-evolving apparatus, then the most logical role for the metal would be to function as a binding site for substrate H_2O or OH^-. Essential details to support such a hypothesis will likely come from improvements in the resolution of PS II crystal structures, to the point where Mn-Ca distances and coordinating ligands can be discerned with certainty. For Cl^-, there appear to be no useful analogies that can be drawn from other systems that require this anion. As in the case of Ca^{2+}, the exact details of Cl^- function in the O_2 evolving reaction are still obscure. If Cl^- is a ligand to Mn, as indirect evidence indicates, the observed effects of Cl^- depletion may be rationalized on the basis of a decrease in the redox potential of the Mn to which the anion is bound, when it is replaced by an alternate ligand, for example OH^-. Maintaining a high redox potential of a particular Mn atom may be the only role of Cl^- in PS II. There is currently no evidence to suggest that it plays a more dynamic role (for example in ligand-metal rearrangements) in the S-state cycle, or that it participates directly in the chemistry associated with H_2O oxidation, although this possibility cannot be definitively excluded at the present time. Although progress has been made in understanding the roles of Ca^{2+} and Cl^- in the OEC, there is obviously a need for further experimentation on these cofactors. The advent of PS II crystal structures, coupled with explorations of the Mn cluster by magnetic resonance techniques will be of great value in understanding the structural context in which Ca^{2+} and Cl^- function. Coupling of this information with the results of new experiments on the dynamics of the interactions of these cofactors with the Mn cluster should greatly improve our understanding of the process of H_2O oxidation and of electron transfer within PS II.

Acknowledgments

The authors' research on the roles of Ca^{2+} and Cl^- in PS II has received generous support from the Netherlands Organization for the Advancement of Research (N.W.O.) (HJvG) and from the United States Department of Agriculture Competitive Research Grants Program and the National Science Foundation (CFY).

References

Ädelroth P, Lindberg K and Andréasson LE (1995) Studies of Ca^{2+} binding in spinach Photosystem II using $^{45}Ca^{2+}$. Biochemistry 34: 9021–9027

Ananyev GM and Dismukes GC (1997) Calcium induces binding

and formation of a spin-coupled dimanganese(II,II) center in the apo-water oxidation complex of Photosystem II as precursor to the functional tetra-Mn/Ca cluster. Biochemistry 36: 11342–11350

Ananyev GM, Murphy A, Abe Y and Dismukes GC (1999) Remarkable affinity and selectivity for Cs^+ and uranyl (UO_2^{2+}) binding to the manganese site of the apo-water oxidation complex of Photosystem II. Biochemistry 38: 7200–7209

Andréasson LE, Vass I and Styring S (1995) Ca^{2+} depletion modifies the electron-transfer on both donor and acceptor sides in Photosystem II from spinach. Biochim Biophys Acta 1230: 155–164

Arnon DI and Whatley FR (1949) Is chloride a coenzyme of photosynthesis? Science 110: 554–556

Baumgarten M, Philo JS and Dismukes GC (1990) Mechanism of photoinhibition of photosynthetic water oxidation by chloride depletion and fluoride substitution: Oxidation of a protein residue. Biochemistry 29: 10814–10822

Becker DW and Brand JJ (1982) An in vivo requirement for calcium in Photosystem II of *Anacystis nidulans*. Biochem Biophys Res Commun 109: 1134–1139

Blubaugh DJ and Cheniae GM (1992) Photoassembly of the PS2 Mn/Ca cluster. Photosynth Res 34: 147–147

Booth PJ, Rutherford AW and Boussac A (1996) Location of the calcium binding site in Photosystem II: A Mn^{2+} substitution study. Biochim Biophys Acta 1277: 127–134

Boussac A and Rutherford AW (1988a) Ca^{2+} Binding to the oxygen evolving enzyme varies with the redox state of the Mn cluster. FEBS Lett 236: 432–436

Boussac A and Rutherford AW (1988b) Nature of the inhibition of the oxygen-evolving enzyme of Photosystem II induced by NaCl washing and reversed by the addition of Ca^{2+} or Sr^{2+}. Biochemistry 27: 3476–3483

Boussac A and Rutherford AW (1992) The origin of the split S_3 EPR signal in Ca^{2+}-depleted Photosystem II-histidine versus tyrosine. Biochemistry 31: 7441–7445

Boussac A, Zimmermann JL and Rutherford AW (1989) EPR signals from modified charge accumulation states of the oxygen evolving enzyme in Ca^{2+}-deficient Photosystem II. Biochemistry 28: 8984–8989

Boussac A, Zimmermann JL, Rutherford AW and Lavergne J (1990) Histidine oxidation in the oxygen-evolving Photosystem II enzyme. Nature 347: 303–306

Bove JM, Bove C, Whatley FR and Arnon DI (1963) Chloride requirement for oxygen evolution in photosynthesis. Z Naturforsch 18b: 683–688

Brayer GD, Luo YG and Withers SG (1995) The structure of human pancreatic alpha-amylase at 1.8 Å resolution and comparisons with related enzymes. Protein Sci 4: 1730–1742

Britt RD (1996) Oxygen evolution. In: Ort DR and Yocum CF (eds) Oxygenic Photosynthesis: The Light Reactions, pp 137–164. Kluwer Academic Publishers, Dordrecht

Büchel C, Barber J, Ananyev G, Eshaghi S, Watt R and Dismukes GC (1999) Photoassembly of the manganese cluster and oxygen evolution from monomeric and dimeric CP47 reaction center Photosystem II complexes. Proc Natl Acad Sci USA 96: 14288–14293

Cammarata KV and Cheniae GM (1987) Studies on 17, 24 Kd depleted Photosystem II membranes. 1 Evidences for high and low affinity calcium sites in 17, 24 kD depleted PS II membranes from wheat versus spinach. Plant Physiol 84: 587–595

Campbell KA, Gregor W, Pham DP, Peloquin JM, Debus RJ and Britt RD (1998) The 23 and 17 kDa extrinsic proteins of Photosystem II modulate the magnetic properties of the S-1-state manganese cluster. Biochemistry 37: 5039–5045

Casey JL and Sauer K (1984) EPR detection of a cryogenically photogenerated intermediate in photosynthetic oxygen evolution. Biochim Biophys Acta 767: 21–28

Chen CG and Cheniae GM (1993) The photoassembly of active O_2-evolving Mn clusters by 17/23 kDa-less NH_2OH-PS II is modulated by Ca^{2+}. Plant Physiol 102: 144

Chen CG and Cheniae GM (1995) High affinity binding of the Ca^{2+} essential for O_2 evolution is dependent on the existence of the Mn-cluster but it independent of the extrinsic proteins. In Mathis P (ed) Photosynthesis: From Light to Biosphere, Vol II, pp 329–332. Kluwer Academic Publishers, Dordrecht

Chen CG, Kazimir J and Cheniae GM (1995) Calcium modulates the photoassembly of Photosystem II (Mn)(4)-clusters by preventing ligation of nonfunctional high-valency states of manganese. Biochemistry 34: 13511–13526

Chen WJ and Ta Y (2001) The EXAFS study on the local structure of lanthanum in spinach PS II. Biol Trace Elem Res 82: 231–237

Chu HA, Nguyen AP and Debus RJ (1995a) Amino acid residues that influence the binding of manganese or calcium to Photosystem II. 1 The lumenal interhelical domains of the D1 polypeptide. Biochemistry 34: 5839–5858

Chu HA, Nguyen AP and Debus RJ (1995b) Amino acid residues that influence the binding of manganese or calcium to Photosystem II. 2 The carboxy-terminal domain of the D1 polypeptide. Biochemistry 34: 5859–5882

Cinco RM, Robblee JH, Rompel A, Fernandez C, Yachandra VK, Sauer K and Klein MP (1998) Strontium EXAFS reveals the proximity of calcium to the manganese cluster of oxygen-evolving Photosystem II. J Phys Chem B 102: 8248–8256

Cinco RM, Holman KLM, Robblee JH, Yano J, Pizarro SA, Bellacchio E, Sauer K and Yachandra VK (2002) Calcium EXAFS establishes the Mn-Ca cluster in the oxygen-evolving complex of Photosystem II. Biochemistry 41: 12928–12933

Clarke SM and Eaton-Rye JJ (1999) Mutation of Phe-363 in the Photosystem II protein CP47 impairs photoautotrophic growth, alters the chloride requirement, and prevents photosynthesis in the absence of either PS II-O or PS II-V in *Synechocystis* sp. PCC 6803. Biochemistry 38: 2707–2715

Clemens KL, Force DA and Britt RD (2002) Acetate binding at the Photosystem II oxygen evolving complex: An S_2-state multiline signal ESEEM study. J Am Chem Soc 124: 10921–10933

Debus RJ (1992) The manganese and calcium ions of photosynthetic oxygen evolution. Biochim Biophys Acta 1102: 269–352

Debus RJ (2001) Amino acid residues that modulate the properties of tyrosine Y_Z and the manganese cluster in the water oxidizing complex of Photosystem II. Biochim Biophys Acta 1503: 164–186

Dekker JP, Ghanotakis DF, Plijter JJ, van Gorkom HJ and Babcock GT (1984) Kinetics of the oxygen-evolving complex in salt-washed Photosystem II preparations. Biochim Biophys Acta 767: 515–523

Fabian M, Skultety L, Brunel C and Palmer G (2001) Cyanide stimulated dissociation from the catalytic center of oxidized cytochrome *c* oxidase. Biochemistry 40: 6061–6069

Feller G, LeBussy O, Houssier C and Gerday C (1996) Structural

and functional aspects of chloride binding to *Alteromonas haloplanctis* α-amylase. J Biol Chem 271: 23836–23841

Ferreira K, Iverson TM, Mughlouni K, Barber J and Iwata S (2004) Architecture of the photosynthetic oxygen-evolving center. Science 303: 1831–1838

Ghanotakis DF, Babcock GT and Yocum CF (1984a) Calcium reconstitutes high rates of oxygen evolution in polypeptide depleted Photosystem II preparations. FEBS Lett 167: 127–130

Ghanotakis DF, Topper JN, Babcock GT and Yocum CF (1984b) Water-soluble 17-Kda and 23-kDa polypeptides restore oxygen evolution activity by creating a high-affinity binding site for Ca^{2+} on the oxidizing side of Photosystem II. FEBS Lett 170: 169–173

Ghanotakis DF, Demetriou DM and Yocum CF (1987) Isolation and characterization of an oxygen-evolving Photosystem II reaction center core preparation and a 28 kDa Chl-*a* binding protein. Biochim Biophys Acta 891: 15–21

Gilchrist ML, Ball JA, Randall DW and Britt RD (1995) Proximity of the manganese cluster of Photosystem II to the redox active tyrosine Y_Z. Proc Natl Acad Sci USA 92: 9545–9549

Grove GN and Brudvig GW (1998) Calcium binding studies of Photosystem II using a calcium-selective electrode. Biochemistry 37: 1532–1539

Haddy A, Dunham WR, Sands RH and Aasa R (1992) Multifrequency EPR investigations into the S_2-state signal at g = 4.1 of the O_2 evolving complex. Biochim Biophys Acta 1099: 25–34

Haddy A, Hatchell JA, Kimel RA and Thomas R (1999) Azide as a competitor of chloride in oxygen evolution by Photosystem II. Biochemistry 38: 6104–6110

Han K and Katoh S (1993) Different localization of 2 Ca^{2+} in spinach oxygen-evolving Photosystem II membranes—Evidence for involvement of only one Ca^{2+} in oxygen revolution. Plant Cell Physiol. 34: 585–593

Han KC and Katoh S (1995) Different binding affinity sites of Ca^{2+} for reactivation of oxygen evolution in NaCl-washed Photosystem II membranes represent differently modified states of a single binding site. Biochim Biophys Acta 1232: 230–236

Hasegawa K, Kimura Y and Ono T (2002) Chloride cofactor in the photosynthetic oxygen-evolving complex studied by Fourier transform infrared spectroscopy. Biochemistry 41: 13839–13850

Haumann M, Drevenstedt W, Hundelt M and Junge W (1996) Chloride depletion of Photosystem II of green plants exposes amino acid redox cofactor of water oxidation. Biochim Biophys Acta 1273: 237–250

Hendry G, and Wydrzynski T (2003) $^{18}O_2$ isotope exchange measurements reveal that calcium is involved in the binding of one substrate water molecule to the oxygen-evolving complex in Photosystem II. Biochemistry 42: 6209–6217.

Homann PH (1985) The association of functional anions with the oxygen-evolving center of chloroplasts. Biochim Biophys Acta 809: 311–319

Homann PH (1988a) Chloride relations of photosystem-II membrane preparations depleted of, and resupplied with, their 17-kDa and 23-kDa extrinsic polypeptides. Photosynth Res 15: 205–220

Homann PH (1988b) The chloride and calcium requirements of photosynthetic water oxidation: Effects of pH. Biochim Biophys Acta 934: 1–13

Itoh S, Yerkes CT, Koike H, Robinson HH and Crofts AR (1984) Effects of chloride depletion on electron donation from the water-oxidizing complex to the Photosystem II reaction center as measured by the microsecond rise of chlorophyll fluorescence in isolated pea chloroplasts. Biochim Biophys Acta 766: 612–622

Izawa S, Heath RL and Hind G (1969) Role of chloride ion in photosynthesis.3. Effect of artificial electron donors upon electron transport. Biochim Biophys Acta 180: 388–398

Kimura Y, Hasegawa K and Ono T (2002) Characteristic changes of the S_2/S_1 difference FTIR spectrum induced by Ca^{2+} depletion and metal cation substitution in the photosynthetic oxygen-evolving complex. Biochemistry 41: 5844–5853

Kamiya N and Shen J-R (2003) Crystal structure of oxygen-evolving Photosystem II from *Thermosynechococcus vulcanus* at 3.7-Å resolution. Proc Natl Acad Sci USA 100: 98–103

Kelley PM and Izawa S (1978) The role of chloride in Photosystem II. I. Effects of chloride ion on Photosystem II electron transport and on hydroxylamine inhibition. Biochim Biophys Acta 502: 198–210

Kimura, Y and Ono, TA (2001) Chelator-induced disappearance of carboxylate stretching vibrational modes in S_2/S_1 FTIR spectrum in oxygen-evolving complex of Photosystem II. Biochemistry 40: 14061-14068

Kretsinger RH and Nelson DJ (1976) Calcium in biological systems. Coord Chem Rev 18: 29–124

Krieger A and Rutherford AW (1997) Comparison of chloride-depleted and calcium-depleted PS II: The midpoint potential of Q_A and susceptibility to photodamage. Biochim Biophys Acta 1319: 91–98

Krieger A, Weis E and Demeter S (1993) Low-pH-induced Ca^{2+} ion release in the water-splitting system is accompanied by a shift in the midpoint redox potential of the primary quinone acceptor Q_A. Biochim Biophys Acta 1144: 411–418

Latimer MJ, Derose VJ, Mukerji I, Yachandra VK, Sauer K and Klein, MP (1995) Evidence for the proximity of calcium to the manganese cluster of Photosystem II—determination by X-ray absorption spectroscopy. Biochemistry 34: 10898–10909

Lewit-Bentley A and Rety S (2000) EF-hand calcium-binding proteins. Curr Opin Struct Biol 10: 637–643

Li X and Weinman SA (2002) Chloride channels and hepatocellular function: Prospects for molecular identification. Annu Rev Physiol 64: 609–633.

Lindberg K and Andréasson L-E (1996) A one-site, two-state model for the binding of anions in Photosystem II. Biochemistry 35: 14259–14267

Lindberg K, Wydrzynski T, Vänngård T and Andréasson L-E (1990) Slow release of chloride from ^{36}Cl-labeled Photosystem II membranes. FEBS Lett 264: 153–155

Lindberg K, Vänngård T and Andréasson L-E (1993) Studies of the slowly exchanging chloride in Photosystem II of higher plants. Photosynth Res 38: 401–408

Lübbers K, Drevenstedt W and Junge W (1993) Chloride depletion of photosynthetic water oxidase. FEBS Lett 336: 304–308

Martin RB and Richardson FS (1979) Lanthanides as probes for calcium in biological systems. Q Rev Biophys 12: 181–209

Matysik J, Alia, Nachtegaal G, van Gorkom HJ, Hoff AJ and de Groot HJM (2000) Exploring the calcium-binding site in Photosystem II membranes by solid-state Cd^{113} NMR. Biochemistry 39: 6751–6755

Mei R and Yocum CF (1991) Calcium retards NH_2OH inhibition

of O_2 evolution activity by stabilization of Mn^{2+} binding to Photosystem II. Biochemistry 30: 7836–7842

Mei R and Yocum CF (1992) Comparative properties of hydroquinone and hydroxylamine reduction of the Ca^{2+}-stabilized O_2-evolving complex of Photosystem II — Reductant-dependent Mn^{2+} formation and activity inhibition. Biochemistry 31: 8449–8454

Mei R and Yocum C (1993) Characterization of inhibitory effects of NH_2OH and its N-methyl derivatives on the O_2-evolving complex of Photosystem II. Photosynth Res 38: 449–453

Metzler D (2001) Biochemistry: The Chemical Reactions of Living Cells, Vol 1. Harcourt Academic Press, San Diego

Miller AF and Brudvig GW (1989) Manganese and calcium requirements for reconstitution of oxygen-evolution activity in manganese-depleted Photosystem II membranes. Biochemistry 28: 8181–8190

Miller AF and Brudvig GW (1990) Electron transfer events leading to reconstitution of oxygen evolution activity in manganese-depleted Photosystem II membranes. Biochemistry 29: 1385–1392

Miyao M and Murata N (1984) Calcium ions can be substituted for the 24-kDa polypeptide in photosynthetic oxygen evolution. FEBS Lett 168: 118–120

Miyao, M and Murata, N (1985) The Cl^- effect on photosynthetic oxygen evolution—interaction of Cl^- with 18-kDa, 24-kDa and 33-kDa proteins. FEBS Lett 180: 303–308

Miyao M and Murata N (1986) Light-dependent inactivation of photosynthetic oxygen evolution during NaCl treatment of Photosystem II particles—the role of the 24-kDa protein. Photosynth Res 10: 489–496

Morgan TR, Shand JA, Clarke SM and Eaton-Rye JJ (1998) Specific requirements for cytochrome *c*-550 and the manganese-stabilizing protein in photoautotrophic strains of *Synechocystis* sp. PCC 6803 with mutations in the domain Gly-351 to Thr-436 of the chlorophyll-binding protein CP47. Biochemistry 37: 14437–14449

Noguchi T, Ono T and Inoue Y (1995) Direct detection of a carboxylate bridge between Mn and Ca^{2+} in the photosynthetic oxygen-evolving center by means of Fourier-transform infrared spectroscopy. Biochim Biophys Acta 1228: 189–200

Ono T and Inoue Y (1988) Discrete extraction of the Ca atom functional for O_2 evolution in higher plant Photosystem II by a simple low pH treatment. FEBS Lett 227: 147–152

Ono T and Inoue Y (1990a) Abnormal redox reactions in photosynthetic O_2-evolving centers in NaCl/EDTA-washed PS II— a dark-stable EPR multiline signal and an unknown positive charge accumulator. Biochim Biophys Acta 1020: 269–277

Ono TA and Inoue Y (1990b) A marked upshift in threshold temperature for the S_1 to S_2 transition induced by low pH treatment of PS II membranes. Biochim Biophys Acta 1015: 373–377

Ono T, Zimmermann JL, Inoue Y and Rutherford AW (1986) EPR evidence for a modified S-transition in chloride-depleted Photosystem II. Biochim Biophys Acta 851: 193–201

Ono T, Rompel A, Mino H and Chiba N (2001) Ca^{2+} function in photosynthetic oxygen evolution studied by alkali metal cations substitution. Biophys J 81: 1831–1840

Pecoraro VL, Baldwin MJ, Caudle MT, Hsieh WY and Law NA (1998) A proposal for water oxidation in Photosystem II. Pure Appl Chem 70: 925–929

Peloquin JM, Campbell KA, Randall DW, Evanchik MA, Pecoraro VL, Armstrong WA and Britt RD (2000) ^{55}Mn ENDOR of the S_2 state mutliline signal of Photosystem II: Implications on the structure of the tetranuclear Mn cluster. J Am Chem Soc 122: 10926–10942

Putnam-Evans C and Bricker TM (1994) Site-directed mutagenesis of the CP47 protein of Photosystem II—alteration of the basic residue ^{448}R to 448G prevents the assembly of functional Photosystem II centers under chloride-limiting conditions. Biochemistry 33: 10770–10776

Putnam-Evans C and Bricker TM (1997) Site-directed mutagenesis of the basic residues K-321 to (321)G in the CP 47 protein of Photosystem II alters the chloride requirement for growth and oxygen-evolving activity in *Synechocystis* 6803. Plant Mol Biol 34: 455–463

Qian M, Dao LA, Debus RJ and Burnap RL (1999) Impact of mutations within the putative Ca^{2+}-binding lumenal interhelical a-b loop of the Photosystem II D1 protein on the kinetics of photoactivation and H_2O oxidation in *Synechocystis* sp PCC6803. Biochemistry 38: 6070–6081

Rashid A and Homann PH (1992) Properties of iodide-activated photosynthetic water-oxidizing complexes. Biochim Biophys Acta 1101: 303–310

Riggs PJ, Mei R, Yocum CF and Penner-Hahn JE (1992) Reduced derivatives of the manganese cluster in the photosynthetic oxygen-evolving complex. J Am Chem Soc 114: 10650–10651

Riggs-Gelasco PJ, Mei R, Ghanotakis DF, Yocum CF and Penner-Hahn JE (1996a) X-ray absorption spectroscopy of calcium-substituted derivatives of the oxygen-evolving complex of Photosystem II. J Am Chem Soc 118: 2400–2410

Riggs-Gelasco PJ, Mei R, Yocum CF and Penner-Hahn JE (1996b) Reduced derivatives of the Mn cluster in the oxygen-evolving complex of Photosystem II: An EXAFS study. J Am Chem Soc 118: 2387–2399

Rutherford AW (1989) Photosystem II, the water-splitting enzyme. Trends Biochem Sci 14: 227–232

Rutherford AW, Zimmermann JL and Boussac A (1992) Oxygen evolution. In: Barber J (ed) The Photosystems: Structure, Function and Molecular Biology, pp 179–229. Elsevier Science Publishers, New York

Sandusky PO and Yocum CF (1984) The chloride requirement for photosynthetic oxygen evolution; analysis of the effects of chloride and other anions on amine inhibition of the oxygen-evolving complex. Biochim Biophys Acta 766: 603–611

Sandusky PO and Yocum CF (1986) The chloride requirement for photosynthetic oxygen evolution: factors affecting nucleophilic displacement of chloride from the oxygen-evolving complex. Biochim Biophys Acta 849: 85–93

Sandusky PO, Selvius DeRoo CL, Hicks DB, Yocum CF, Ghanotakis DF and Babcock GT (1983) Electron transport activity and polypeptide composition in the isolated Photosystem II complex. In: Inoue Y, Crofts AR, Govindjee, Murata N, Renger G and Satoh K (eds) The Oxygen Evolving System of Photosynthesis, pp 189–199. Academic Press, Tokyo

Shen JR and Inoue Y (1991) Low pH-induced dissociation of 3 extrinsic proteins fro O_2 evolving Photosystem II. Plant Cell Physiol. 32: 453–457.

Shen JR, Satoh K and Katoh S (1988a) Isolation of an oxygen-evolving Photosystem II preparation containing only one atom of calcium from a chlorophyll *b* deficient mutant of rice. Biochim Biophys Acta 936: 386–394

Shen JR, Satoh K and Katoh S (1988b) Calcium content of oxygen-evolving Photosystem II preparations from higher

plants—Effects of NaCl treatment. Biochim Biophys Acta 933: 358–364

Sinclair J (1984) The influence of anions on oxygen evolution by isolated chloroplasts. Biochim Biophys Acta 764: 247–252

Sivaraja M, Tso J and Dismukes GC (1989) A calcium-specific site influences the structure and activity of the manganese cluster responsible for photosynthetic water oxidation. Biochemistry 28: 9459–9464

Strynadka NCJ and James MNG (1989) Crystal-structures of the helix-loop-helix calcium-binding proteins. Annu Rev Biochem 58: 951–998

Szalai VA and Brudvig GW (1996) Reversible binding of nitric oxide to tyrosyl radicals in Photosystem II. Nitric oxide quenches formation of the S_3 EPR signal species in acetate-inhibited Photosystem II. Biochemistry 35: 15080–15087

Tamura N and Cheniae GM (1986) Requirements for the photoligation of Mn^{2+} in PS II membranes and the expression of water-oxidizing activity of the polynuclear Mn-catalyst. FEBS Lett 200: 231–236

Tamura N and Cheniae GM (1988) Photoactivation of the water oxidizing complex: The mechanism and general consequences to photosystem 2. In: Stevens ES and Bryant DA (eds) Light-Energy Transduction in Photosynthesis: Higher Plant and Bacterial Models, pp 227–242. American Society for Plant Physiology, Rockville

Tamura N, Inoue Y and Cheniae GM (1989) Photoactivation of the water-oxidizing complex in Photosystem II membranes depleted of Mn, Ca and extrinsic proteins. 2 Studies on the functions of Ca^{2+}. Biochim Biophys Acta 976: 173–181

Tang XS, Randall DW, Force DA, Diner BA and Britt RD (1996) Manganese-tyrosine interaction in the Photosystem II oxygen-evolving complex. J Am Chem Soc 118: 7638–7639

Theg SN and Homann PH (1982) Light-, pH-, and uncoupler-dependent association of chloride with chloroplast thylakoids. Biochim Biophys Acta 679: 221–234

Theg SN, Jursinic PA and Homann PH (1984) Studies on the mechanism of chloride action in photosynthetic water oxidation. Biochim Biophys Acta 766: 636–646

Tichy M and Vermaas W (1998) Functional analysis of combinatorial mutants altered in a conserved region in loop E of the CP47 protein in *Synechocystis* sp. PCC 6803. Biochemistry 37: 1523–1531

Tommos C, Hoganson CW, Di Valentin M, Lydakis-Simantiris N, Dorlet P, Westphal K, Chu HA, McCracken J and Babcock GT (1998) Manganese and tyrosyl radical function in photosynthetic oxygen evolution. Curr Opin Chem Biol 2: 244–252

Vander Meulen KA, Hobson A and Yocum CF (2002) Calcium depletion modifies the structure of the Photosystem II O_2-evolving complex. Biochemistry 41: 958–966

Van Vliet P and Rutherford AW (1996) Properties of chloride-depleted oxygen-evolving complex of Photosystem II studied by electron paramagnetic resonance. Biochemistry 35: 1829–1839

Vass I, Ono TA and Inoue Y (1987) Stability and oscillation properties of thermoluminescent charge pairs in the O_2-evolving system depleted of Cl^- or the 33 kDa extrinsic protein. Biochim Biophys Acta 892: 224–235

Velthuys BR (1975) Binding of the inhibitor NH_3 to the oxygen evolving apparatus of spinach chloroplasts. Biochim Biophys Acta 396: 392–401

Vrettos JS, Limburg J and Brudvig GW (2001a) Mechanism of photosynthetic water oxidation: Combining biophysical studies of Photosystem II with inorganic model chemistry. Biochim Biophys Acta 1503: 229–245

Vrettos JS, Stone DA and Brudvig GW (2001b) Quantifying the ion selectivity of the Ca^{2+} site in Photosystem II: Evidence for direct involvement of Ca^{2+} in O_2 formation. Biochemistry 40: 7937–7945

Waggoner CM, Pecoraro V and Yocum CF (1989) Monovalent cations (Na^+, K^+, Cs^+) inhibit calcium activation of photosynthetic oxygen evolution. FEBS Lett 244: 237–240

Wales R, Newman BJ, Pappin D and Gray JC (1989) The extrinsic 33 kDa polypeptide of the oxygen-evolving complex of Photosystem II is a putative calcium-binding protein and is encoded by a multi-gene family in pea. Plant Mol Biol 12: 439–451

Webber AN and Gray JC (1989) Detection of calcium binding by Photosystem II polypeptides immobilized onto nitrocellulose membrane. FEBS Lett 249: 79–82

Westphal KL, Lydakis-Simantiris N, Cukier RI and Babcock GT (2000) Effects of Sr^{2+} substitution on the reduction rates of Y_Z in PS II membranes—Evidence for concerted hydrogen-atom transfer in oxygen evolution. Biochemistry 39: 16220–16229

Wincencjusz H, van Gorkom HJ and Yocum CF (1997) The photosynthetic oxygen evolving complex requires chloride for its redox state $S_2 \rightarrow S_3$ and $S_3 \rightarrow S_0$ transitions but not for $S_0 \rightarrow S_1$ or $S_1 \rightarrow S_2$ transitions. Biochemistry 36: 3663–3670

Wincencjusz H, Yocum CF and van Gorkom HJ (1998) S-state dependence of chloride binding affinity and exchange dynamics in the intact and polypeptide-depleted O_2 evolving complex of Photosystem II. Biochemistry 37: 8595–8604

Wincencjusz H, Yocum CF and van Gorkom HJ (1999) Activating anions that replace Cl^- in the O_2-evolving complex of Photosystem II slow the kinetics of the terminal step in water oxidation and destabilize the S_2 and S_3 states. Biochemistry 38: 3719–3725

Wydrzynski T, Baumgart F, Macmillan F and Renger G (1990) Is there a direct cofactor requirement in the oxygen-evolving reactions of Photosystem II? Photosynth Res 25: 59–72

Yachandra VK, DeRose VJ, Latimer MJ, Mukerji I, Sauer K and Klein MP (1993) Where plants make oxygen: A structural model for the photosynthetic oxygen-evolving manganese cluster. Science 260: 675–679

Yocum CF (1991) Calcium activation of photosynthetic water oxidation. Biochim Biophys Acta 1059: 1–15

Zheng M and Dismukes GC (1996) Orbital configuration of the valence electrons, ligand field symmetry, and manganese oxidation states of the photosynthetic water oxidizing complex: Analysis of the S_2 state multiline EPR signals. Inorg Chem 35: 3307–3319

Zouni A, Witt HT, Kern J, Fromme P, Krauss N, Saenger W and Orth P (2001) Crystal structure of Photosystem II from *Synechococcus elongatus* at 3.8 Ångstrom resolution. Nature 409: 739–743

Chapter 14

Bicarbonate Interactions

Jack J. S. van Rensen*
Graduate School of Experimental Plant Sciences, Wageningen University, Laboratory of Plant Physiology, Arboretumlaan 4, 6703 BD Wageningen, The Netherlands

Vyacheslav V. Klimov
Institute of Basic Biological Problems, Russian Academy of Sciences, Pushchino, Moscow Region 142290 Russia

*Author for correspondence, email: Jack.VanRensen@WUR.nl

T. Wydrzynski and K. Satoh (eds): Photosystem II: The Light-Driven Water:Plastoquinone Oxidoreductase, pp. 329–345.

Summary

Photosystem II (PS II) is the location for the antagonistic interactions between bicarbonate and monovalent anions such as formate. Incubation of PS II-containing samples with formate results in the inhibition of electron flow activity, which can be restored only by addition of bicarbonate. This bicarbonate effect exists on both the acceptor as well as on the donor side of PS II. The bicarbonate interaction on the acceptor side is located between the primary and secondary quinones and can be demonstrated in intact cells or leaves as well as in isolated thylakoid or core preparations. At physiological pH, bicarbonate is suggested to ligate to the non-heme iron between the D1 and D2 proteins and form hydrogen bonds to several amino acids of the D1 and D2 proteins. On the one hand, bicarbonate may stabilize, through conformational means, the reaction center proteins by protonation of certain amino acids near the secondary quinone electron acceptor; while on the other hand, it may play a significant role in the assembly and functioning of the water-oxidizing complex. A probable functional role in vivo is that it controls PS II electron flow in order to cope with stress conditions leading to, for instance, photoinhibition or thermoinactivation.

I. Introduction

Carbon dioxide is required for photosynthesis. It is fixed by ribulose 1,5-bisphosphate carboxylase and further reduced to carbohydrate. However, CO_2 is also involved in the photosynthetic electron transport of plants, algae and cyanobacteria. Warburg and Krippahl (1958) first discovered that CO_2 accelerated the production of O_2 upon irradiation of isolated chloroplasts in the presence of an electron acceptor such as ferricyanide. This phenomenon was experimentally difficult to reproduce until Stemler and Govindjee (1973), extending the work of Good (1963), described a method whereby reproducible and large increases in the rate of the Hill reaction in isolated chloroplasts were observed upon addition of bicarbonate to CO_2-depleted samples. The method depends on depletion of the chloroplasts from CO_2 by flushing the suspension in the dark with nitrogen gas, while the chloroplasts are suspended in a medium of a pH between 5.5 and 6.0, and containing high anion (usually formate) concentration. Because of the low pH, the equilibrium of bicarbonate/CO_2 is directed to CO_2 which as a gas is flushed away with the nitrogen. The electron flow rate is then measured in the CO_2-depleted samples at a pH of usually 6.5. The very low rate can be stimulated by the addition of bicarbonate. Carbon dioxide is the diffusing species, while bicarbonate is the binding species. Because the stimulation is induced by addition of bicarbonate, the phenomenon is named the bicarbonate effect. The bicarbonate effect is illustrated in Fig. 1. The electron transport rate is recorded as O_2 evolution. The Hill reaction rate is very low after 30 min of CO_2 depletion (and is usually zero after 60 min of depletion); it is strongly recovered after incubation during 60–90 s in the dark with bicarbonate. Movement of the negatively charged formate ion is hindered by the negatively charged surface of the thylakoid membrane. Because the negative charge is less in darkness compared with light condition, the depletion (using formate) and recovery is better when performed in darkness (Vermaas and Van Rensen, 1981; Van Rensen et al., 1984).

The action of bicarbonate is located in the Photosystem II (PS II) core complex (Chapters 3–6). This protein complex carries out photochemical reactions, including the primary charge separation and the subsequent electron transfer from water to plastoquinone. At the expense of light energy, water is split, and O_2 and plastoquinol are formed (Fig. 2). The central core of PS II consists of the D1 and D2 proteins where all the redox active components are embedded. These components include a tetra-manganese cluster (Chapter 10), two tyrosine residues (Chapter 9), six chlorophyll (Chl) *a* molecules and two pheophytins (Pheo) (Chapter 7), the plastoquinones Q_A and Q_B, and a non-heme iron (Chapter 8) that does not directly participate in electron transfer, but is vital for the transfer process.

Abbreviations: Chl – chlorophyll; DCBQ – 2,5-dichloro-benzoquinone; DCMU – 3-(3,4-dichlorophenyl)-1,1-dimethylurea; DCPIP – 2,6-dichlorophenolindophenol; DPC – 1,5-diphenylcarbazide; EPR – electron paramagnetic resonance; FTIR – Fourier transform infrared; P_{680} – the primary electron donor of PS II; Pheo – the pheophytin primary electron acceptor of PS II; PQ – plastoquinone; PS I, PS II – Photosystem I, Photosystem II; Q_A – primary plastoquinone electron acceptor of PS II; Q_B – secondary plastoquinone electron acceptor of PS II; WOC – water-oxidizing complex; Y_Z – redox active tyrosine on D1

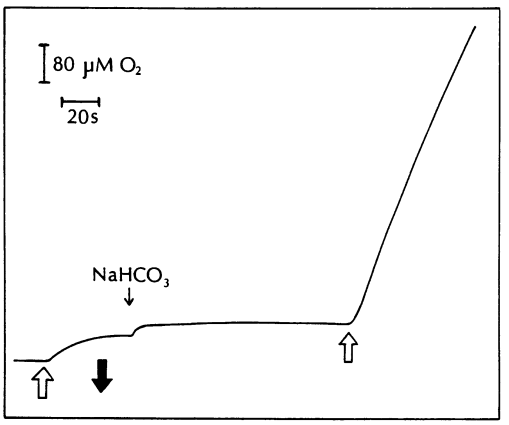

Fig. 1. Recording of the Hill reaction in chloroplasts depleted of CO_2 during 30 min, before and after addition of 10 mM $NaHCO_3$. Arrows upwards: light on; arrow downwards: light off. The depletion medium contained 0.3 M sorbitol, 25 mM sodium formate, 20 mM sodium phosphate (pH 5.8), 10 mM NaCl and 5 mM $MgCl_2$. The depletion was performed in the dark, while the chloroplast thylakoids were flushed with nitrogen gas. The reaction medium had the same composition as the depletion medium, except that sodium phosphate was at 50 mM (pH 6.5); further additions were 0.5 mM ferricyanide, 5 mM NH_4Cl and chloroplasts equivalent to 25 μg Chl ml^{-1}.

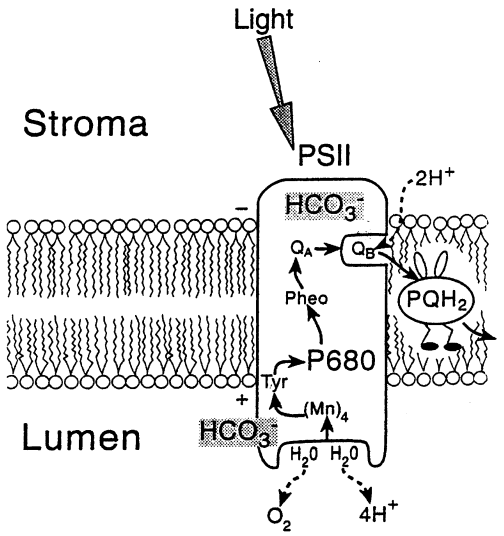

Fig.2. A scheme for PS II. The PS II oxidizes water to oxygen, reduces a plastoquinone molecule and releases protons in the lumen of the thylakoid membrane. Location of bicarbonate effects are highlighted by showing it at two places: on the acceptor as well as on the donor side. (From Van Rensen et al., 1999)

Bicarbonate affects PS II on the acceptor as well as at the donor side, which are located towards the stromal and the lumenal sides of the thylakoid, respectively. There are many reviews on the effects of bicarbonate on PS II, including Govindjee and Van Rensen (1978), Blubaugh and Govindjee (1988a), Diner et al. (1991), Van Rensen (1992), Govindjee and Van Rensen (1993), Klimov and Baranov (2001) and Van Rensen (2002).

II. Bicarbonate Requirement on the Electron Acceptor Side of Photosystem II

The discoverer of the bicarbonate effect, Otto Warburg, was convinced that his finding was proof of his theory that CO_2 was involved in the liberation of O_2 by the photosynthetic process. If the evolved O_2 should originate from CO_2 , the effect of bicarbonate on the Hill reaction must be located on the oxidizing (water) side of PS II. Although Alan Stemler (for review, see Stemler, 1982) always has been convinced that there was an effect of bicarbonate on the donor side, few were persuaded by the evidence. By the mid 1970s it was found that bicarbonate has an effect on the acceptor side of PS II (Wydrzynski and Govindjee, 1975). It appeared that this effect was much more easy to reproduce and since then, most attention was on this acceptor side effect. However, more recent research from the group of Vyacheslav Klimov has been able to demonstrate also an effect of bicarbonate on the donor side.

A. Evidence for Bicarbonate Effects on the Acceptor Side

The first proof that bicarbonate has an effect on electron flow on the acceptor side of PS II came from studies on fluorescence induction. Further fluorescence studies, measurements of the effect of bicarbonate on different parts of the electron transport chain, and interaction studies with herbicides affecting PS II indicated clearly an effect of bicarbonate on the acceptor side of PS II.

1. Fluorescence Studies

The first indication for an effect of bicarbonate on the reducing side of PS II was obtained by Wydrzynski and Govindjee (1975), who measured

Chl *a* fluorescence induction kinetics in chloroplasts after CO_2 depletion. The variable Chl *a* fluorescence monitors the redox state of Q_A, in which oxidized Q_A is a quencher of fluorescence whereas Q_A^- is not. Therefore, a rapid accumulation of Q_A^- due to an inhibition of electron transport beyond Q_A is easily detected by fluorescence induction measurements. CO_2 depletion causes a fast increase in the variable fluorescence yield, similar but not identical to that observed in normal chloroplasts in the presence of the herbicide DCMU (Wydrzynski and Govindjee, 1975). DCMU blocks the reoxidation of Q_A^- by the secondary quinone acceptor Q_B.

On the other hand, the decay of the Chl *a* fluorescence yield after a saturating flash monitors the re-oxidation of Q_A^-. The half-time of the Q_A^- re-oxidation is increased upon CO_2 depletion (Jursinic et al., 1976), indicating that the re-oxidation of Q_A^- is inhibited. Detailed information about the effect of CO_2 depletion was obtained by measuring the decay of the Chl *a* fluorescence yield after various numbers of short saturating flashes. By this technique the following events can be monitored, where after an uneven number of flashes:

$$Q_AQ_B \xrightarrow{hv} Q_A^-Q_B \leftrightarrow Q_AQ_B^-$$

and after an even number of flashes:

$$Q_AQ_B^- \xrightarrow{hv} Q_A^-Q_B^- \leftrightarrow Q_AQ_B^{2-}$$

Subsequently, Q_B^{2-} becomes protonated and exchanges with the PQ pool, i.e.

$$Q_AQ_B^{2-} + 2H^+ + PQ \leftrightarrow Q_AQ_B + PQH_2$$

Govindjee et al. (1976) found no differences in the decay of the fluorescence yield after various number of flashes in control and in CO_2-depleted chloroplasts, to which bicarbonate was added. In CO_2-depleted chloroplasts, however, they found little effect on the decay after one or two flashes, but a very large slowing down of the decay after three or more flashes. Later studies (Robinson et al., 1984) showed that in CO_2-depleted chloroplasts the Q_A^- decay after 1 flash is about five-fold slower than in control chloroplasts, and after 3 or more flashes 36-fold slower. Although the absolute values of the rates of Q_A^- decay in this type of experiment depend on the conditions of the experiment, there is a small inhibition of CO_2 depletion on the Q_A^- reoxidation by Q_B or by Q_B^-, and a very large inhibition of the protonation of Q_B^{2-} and/or exchange of Q_BH_2 with the PQ pool. In CO_2-depleted chloroplasts three electrons can be stored leading to $Q_A^-Q_B^{2-}$.

2. Electron Transport Chain Measurements

The site of inhibition of CO_2 depletion was also determined by studying its effect on various parts of the electron transport chain (Khanna et al., 1977). There was no effect of CO_2 depletion on electron transport from reduced diaminodurene to methyl viologen, indicating the absence of an effect on PS I-dependent electron transport. A large bicarbonate effect was demonstrated on the electron flow from water to oxidized diaminodurene in the presence of dibromothymoquinone (DBMIB), indicating an effect before the PQ pool. Since there was no effect of bicarbonate on electron transport in trypsin-treated chloroplasts in which ferricyanide accepts electrons directly at the Q_A site (Van Rensen and Vermaas, 1981), it was concluded that the bicarbonate effect is located between Q_A and the PQ pool.

3. Interaction with Herbicides

The localization of the bicarbonate effect between Q_A and the PQ pool was further substantiated from the interaction of bicarbonate (or formate) with PS II-inhibiting herbicides. Van Rensen and coworkers (Van Rensen, 1982) studied the interaction of bicarbonate and herbicides through their effects on electron transport in isolated chloroplasts. By adding various concentrations of bicarbonate to CO_2-depleted chloroplasts various rates of restoration of Hill reaction were obtained. It was demonstrated that the system thylakoid membrane versus bicarbonate has the Michaelis-Menten kinetics and can be treated like a system enzyme versus substrate. From double reciprocal plots of the rate of the Hill reaction as a function of the bicarbonate concentration the apparent dissociation constant (K_d) of the thylakoid-bicarbonate complex could be calculated. When 100 mM formate is present in the reaction medium, the apparent K_d is about 1 mM bicarbonate. The K_d for bicarbonate depends on the presence of both formate and of herbicides. After Stemler and Murphy (1983) determined a K_d of about 80 μM, Snel and Van Rensen (1984) confirmed that, in the presence of low concentrations of

formate the apparent K_d decreases, approaching 80 μM $NaHCO_3$ in the absence of formate. In the presence of urea, triazine or phenol-type herbicides the K_d for bicarbonate increases by at least 2-fold. Thus, these herbicides decrease the apparent affinity of the thylakoid membrane for bicarbonate.

The involvement of the D1 protein in the bicarbonate effect was also indicated from studies using herbicide-resistant mutants. Khanna et al. (1981) observed an increased dissociation constant for bicarbonate in thylakoids of triazine-resistant *Amaranthus hybridus*, in which the D1 protein has a change of serine for glycine at position 264. While the dissociation constant was 1 mM in the sensitive thylakoids, it was about 2 mM in the resistant ones, i.e., the affinity for bicarbonate was lower in the resistant membranes.

B. The Bicarbonate Binding Niche

The binding environment of bicarbonate has been studied by several methods including the use of mutants of algae and cyanobacteria being resistant to PS II-inhibiting herbicides and cyanobacteria mutated in the D1 or D2 proteins, obtained by site-directed mutagenesis. Komenda et al. (2002) reported the involvement of the *psbH* gene product in bicarbonate binding. Research, mainly by Govindjee's group, led to the conclusion that there are two binding sites of bicarbonate at the acceptor side (Blubaugh and Govindjee, 1988b; Xiong et al., 1996).

1. Binding at the Non-Heme Iron

Vermaas and Rutherford (1984) demonstrated that formate addition to thylakoids increases the amplitude of the g = 1.82 EPR signal of $Q_A^-Fe^{2+}$ 10-times. A formate/bicarbonate effect was clearly demonstrated by measurements of EPR spectra of the $Q_A^-FeQ_B$ complex with and without bicarbonate (Bowden et al., 1991). The Mössbauer spectrum of Fe is affected significantly by formate and is returned to its original on re-addition of bicarbonate, indicating the Fe is a key element in the binding of the formate that is displaced by bicarbonate (Diner and Petrouleas, 1987; Semin et al., 1990; Chapter 8, Petrouleas and Crofts). A Fourier transform infrared (FTIR) difference spectroscopy study using ^{13}C-labeled bicarbonate has established that bicarbonate is a bidentate ligand of the non-heme iron (Hienerwadel and Berthomieu, 1995). Examining the effects of a number of carboxylate anions on the EPR signals associated with the non-heme iron, Petrouleas et al. (1994) observed that glycolate, glyoxylate and oxylate compete with NO, formate and bicarbonate for binding to the iron (Chapter 8, Petrouleas and Crofts). It appears that many monovalent anions are able to bind as dissociable ligands to the non-heme iron of PS II.

Both in PS II and in purple bacteria, a non-heme iron is located between Q_A and Q_B. In the bacterial reaction center (and also in PS II), the non-heme iron is almost equidistant to the primary and secondary quinone electron acceptors. Four histidines from the polypeptides L and M and a bidentate glutamate provide the six ligands to the iron. On the basis that only reaction centers of PS II, not those of photosynthetic bacteria, show the bicarbonate effect, Michel and Deisenhofer (1988) and Van Rensen et al. (1988) suggested that glutamate 232 of the M subunit fulfills the role of bicarbonate in *Rhodopseudomonas viridis*. Since M-Glu232 forms a ligand to iron, bicarbonate was suggested to form a bidentate ligand to the iron in PS II. In addition to the bicarbonate, the non-heme iron is liganded by the four histidines, D1-His215, D1-His272, D2-His214, and D2-His268. The binding site for bicarbonate at the non-heme iron was modeled by Xiong et al. (1996). The residues that form the binding pocket are positively charged and hydrophobic. They may include D1-Leu233, D1-Val219, D2-Asn230, D2-Thr231, D2-Phe232, D2-Arg233, D2-Ala234, D2-Pro237 and D2-Lys264. The hydroxyl oxygen of the bicarbonate is separated from the main-chain hydrogen of D2-Arg233 by 4.8 Å. However, D2-Lys264 appeared to be the most likely candidate to interact directly with the bicarbonate ion. Recently, the structure of PS II at 3.5 Å of the cyanobacterium *Thermosynechococcus elongatus* was reported (Ferreira et al., 2004). In their PS II structure, the non-heme Fe is associated with an electron density which is sufficient to accommodate the bicarbonate anion. Close to this non-protein density are D1-Tyr246 and D2-Lys264, positioned and oriented such that they could stabilize the bicarbonate by hydrogen bonding. In Fig. 3, a model of the bicarbonate binding niche is presented.

2. Binding at the Q_B Site

Characterization of a number of Q_B mutants that are also herbicide-resistant implicated that the Q_B binding niche is involved in the binding of bicarbonate (Cao

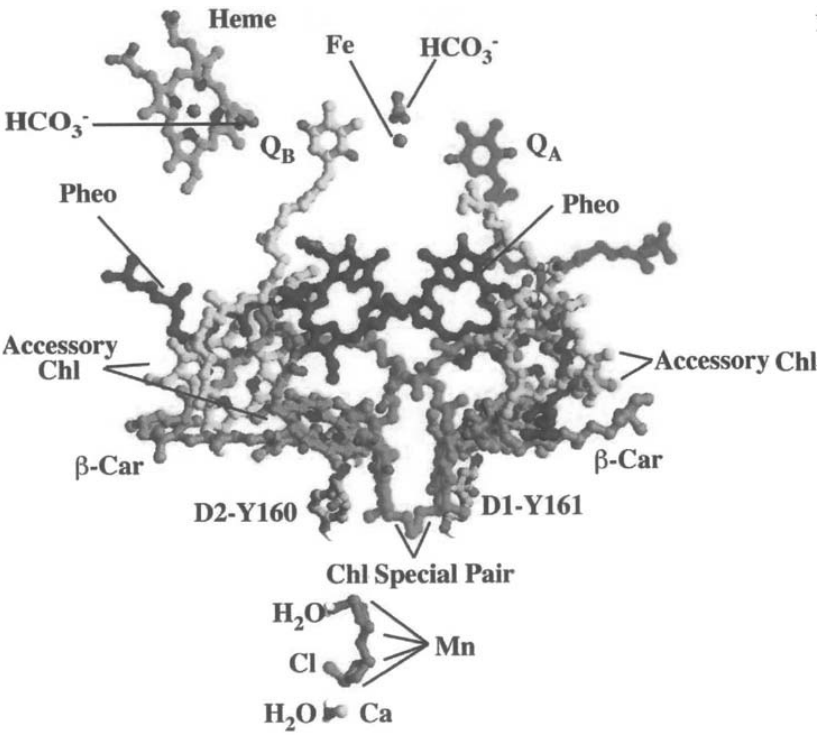

Fig. 3. The modeled cofactors in the PS II reaction center (modified from Van Rensen, 2002; originally from Xiong et al., 1998a). See Color Plate 2, Fig. 1.

et al., 1992; Mäenpää et al., 1995; Vernotte et al., 1995). The tested residues involved were: D1-Phe211, D1-Val219, D1-Glu242, D1-Glu243, D1-Glu244, D1-Ala251, D1-Phe255, D1-Gly256, D1-Ser264, D1-Asn266 and D1-Leu275. Because anionic bicarbonate/formate is very probably the active species involved, it may be expected that the binding would be electrostatic in nature and therefore positively charged amino acid residues are likely to participate in anion binding. While the Q_B binding pocket is composed of the residues including D1-Met214, D1-Leu218, D1-Ala251, D1-Phe255 and D1-Leu271 (Ferreira et al., 2004), only three positively charged D1 residues, D1-His252, D1-Arg257 and D1-Arg269, are found near the Q_B binding niche. Sequence analysis of the D1 protein indicates that D1-Arg257 is closer to the Q_B binding niche than D1-Arg269, making it a more likely residue to be involved in the protonation of Q_B. This residue is thought to be located on the stromal side between the putative transmembrane helices D and E of D1 and may be located within or close to the D1-de helix. Xiong et al. (1998b) constructed two site-directed mutants, D1-Arg257Glu and D1-Arg257Met. The characterization of these two mutants lead to the conclusion that D1-Arg257 with its positively charged side chain is important for the binding of formate and also, in all likelihood, bicarbonate. In Fig. 3, also the binding at the Q_B site is illustrated.

C. Possible Functional Roles of Bicarbonate on the Acceptor Side

1. Protonation of Reduced Q_B

Because absence of bicarbonate most drastically slows down the reduction of Q_B by Q_A^- after the second actinic flash, and the pKa of $H_2O + CO_2 / HCO_3^- + H^+$ is about 6.3, it has been proposed several times that bicarbonate is involved in the protonation of Q_B^{2-}. Formate is not able to function in such a way, because the pK_a of formate is 3.8. Evidence for such a function

was presented by Van Rensen et al. (1988), Eaton-Rye and Govindjee (1988) and Xu et al. (1991). Xiong et al. (1996) modeled a bicarbonate and a water molecule in the Q_B binding niche and proposed a hypothesis to explain the mechanism of Q_B protonation mediated by bicarbonate and water. The bicarbonate, stabilized by D1-Arg257, would donate a proton to Q_B^{2-} through the intermediate D1-His252, and a water molecule would donate another proton to Q_B^{2-}. Based on the discovery of a water transport channel in the bacterial reaction center, an analogous channel for transporting water and bicarbonate may be proposed in the PS II model. The putative channel is primarily positively charged near Q_B, and the non-heme iron.

2. Stabilization of Tertiary Structure

Because bicarbonate is liganded to the non-heme iron, an additional role of bicarbonate may be to serve to stabilize the Q_A-Fe-Q_B structure. Upon the removal of bicarbonate, the distance between Q_A and Q_B may be altered, slowing down the rate of the Q_A^- to Q_B electron transfer, although a larger effect is in the protonation of reduced Q_B ($Q_A^- \rightarrow Q_B^-$; $Q_B^{2-} + 2\ H^+ \rightarrow Q_BH_2$).

3. In Vivo Requirement

The current knowledge of the bicarbonate effect is almost exclusively based on experiments carried out with isolated thylakoid membranes. The observation of a bicarbonate effect in vivo is difficult to distinguish, due to the obvious requirement for CO_2 in the Calvin cycle. Garab et al. (1983) demonstrated the effects of bicarbonate on the energization of thylakoid membrane in leaves. Mende and Wiessner (1985) concluded that in intact cells of the green algae *Chlamydobotrys stellata* both sides of PS II are affected in the absence of bicarbonate. Chlorophyll fluorescence experiments in leaves under a very low photosynthesis and the measurements of electron flow independent of carbon assimilation (leaf discs infiltrated with methyl viologen, acting as a terminal electron acceptor instead of CO_2) have suggested that CO_2 (bicarbonate) modifies the redox state of the quinone electron acceptors of PS II in vivo independently of carbon assimilation and thereby acts as a cofactor for efficient PS II electron flow in the leaf (Ireland et al., 1987).

What advantage is there for PS II reaction centers to have, unlike their bacterial counterparts (Shopes et al., 1989; Wang et al., 1992), a reversible ligand to the non-heme iron? One likely possibility is a regulatory one, in which binding of bicarbonate to PS II regulates the flow of electrons through PS II. Snel and Van Rensen (1984) proposed a link with photorespiration, and Diner et al. (1991) suggested a relation with photoinhibition.

Snel and Van Rensen (1984) indicated that formate is a metabolite related with photorespiration. Glyoxylate, which is an intermediate in photorespiration, may be oxidized by H_2O_2 forming formate. Under highly respiratory conditions, e.g., high irradiance and high O_2/CO_2 ratio, high rates of glyoxylate and hydrogen peroxide formation may be expected, resulting in high rates of decarboxylation of glyoxylate, yielding high concentrations of formate. Thus, there is a pathway from photosynthetically produced O_2 to formate, which inhibits linear electron flow. Such a pathway may be regarded as a negative feedback mechanism involved in the regulation of linear electron flow.

Under conditions that photosynthesis can proceed well, enough bicarbonate is probably bound to PS II, in order for PS II to function normally. However, under stress conditions (e.g., drought, high light intensity, high temperature) the stomata may close, which leads to a decrease in internal CO_2 concentration resulting in a lowered bicarbonate concentration that may limit the activity of PS II. It has been suggested several times that bicarbonate may be involved in the process of photoinhibition (Diner et al., 1991; Sundby et al., 1992; Gong et al., 1993; Schansker and Van Rensen, 1993; Mäenpää et al., 1995; Vass et al., 1995; Klimov et al., 1997a). As photoinhibition occurs at high light intensity, the acceptor side of PS II becomes highly reduced. This reduced state is related to a decreased affinity of PS II for bicarbonate (Van Rensen et al., 1988). This may lead to the diffusion from its binding site at the non-heme iron, resulting in an impaired rate of electron transfer from Q_A^- to Q_B or to Q_B^-. Finally the reaction center may become overreduced. Because the area of PS II is 'rich' in oxygen, photooxidation involving reactive oxygen species may occur, leading to the degradation of the D1 protein. Komenda et al. (2002) reported that in *Synechocystis* PCC 6803 the binding of bicarbonate to the PS II acceptor side was weakened if the PsbH protein was not present. Absence of this *psbH* gene product led, in addition, to increased oxidative stress in PS II, causing a higher sensitivity to photoinhibition.

III. Bicarbonate Requirement on the Electron Donor Side of Photosystem II

Interpretation of the stimulating effect of bicarbonate on PS II activities has been controversial. In the earlier 1970s the site of bicarbonate action was thought to be in the water-oxidizing complex (WOC) (Stemler and Govindjee, 1973), and a model including bicarbonate as a mediator for the photosynthetic water oxidation had been suggested (Metzner, 1978; Stemler, 1980). This model, however, seemed to be in contradiction with the results of isotopic experiments (Radmer and Ollinger, 1980).

It was shown that bicarbonate depletion may affect both the electron acceptor and the donor sides of PS II (Mende and Wiessner, 1985). On the other hand, El-Shintinawy and Govindjee (1990) found that bicarbonate has two sites of action: the first accelerates the electron flow beyond Q_A, and the other stimulates it between the secondary electron donor, Y_Z, and Q_A (the site between the primary electron acceptor, Pheo, and Q_A was speculated for the latter case). So, the idea of a bicarbonate requirement for the acceptor side of PS II began to dominate (for a detailed discussion, see Stemler, 2002).

However, strong evidence for bicarbonate requirement for the WOC of PS II recently has been provided (for a review, see Klimov and Baranov, 2001). The following approaches were used in those experiments for removing bicarbonate from PS II preparations to reveal and augment the bicarbonate effects: (i) replacement of bicarbonate in its possible binding site(s) by the anion formate; (ii) a 100–1000 dilution (and washing in some cases) of concentrated (2–5 mg Chl ml^{-1}) PS II preparations into the medium depleted of endogenous bicarbonate by means of both flushing with CO_2-depleted air and/or boiling; (iii) a shift of the medium pH to a value lower than the pK for H_2CO_3 dissociation (pH 6.4).

A. Effects in Untreated O_2-Evolving Membrane Fragments

It was clearly demonstrated that formate induces bicarbonate-reversible inhibition of electron transfer in both the electron acceptor and donor sides of PS II (Klimov et al., 1995a,b, 1997b; Wincencjusz et al., 1996; Allakhverdiev et al., 1997). Upon the addition of formate at concentration of 5 mM or higher, a typical bicarbonate effect on the acceptor side of PS II (as described earlier in the classical work by Wydrzynski and Govindjee (1975)) was revealed by means of measurements of Chl fluorescence (Klimov et al., 1995a,b). The initial level of fluorescence (F_0) as well as the sum F_0 plus photoinduced change of Chl fluorescence yield (ΔF) was increased while the addition of bicarbonate reversed the effects. The effect of formate was similar to that induced by 1 μM DCMU and it was related to the blocking of electron transfer between Q_A and Q_B, due to removal of bicarbonate with binding of formate to the non-heme Fe (Wydrzynski and Govindjee, 1975; Diner and Petrouleas, 1990).

In contrast, at 100–1000 times lower concentrations, formate induced a decrease (reversed by addition of bicarbonate) of the ΔF without changing the F_0 level (Fig. 4A) which is characteristic of reversible inhibition of electron transfer on the donor side of PS II. Similar effects of the ΔF inhibition and its subsequent reactivation with bicarbonate without a change in F_0 was observed upon placing a PS II preparation into a medium depleted of CO_2 (compare 1 and 2 in Fig. 4A) which demonstrated that in both cases the inhibition of electron transfer on the donor side of PS II was related to removal of bicarbonate from its binding site.

The effects on the donor side of PS II observed upon either partial removal of bicarbonate or the addition of 10–100 μM formate were also revealed under the conditions when the known bicarbonate-dependent step of electron transfer between Q_A and Q_B was not operable (Klimov et al., 1995a). Photoaccumulation of the long-lived state of PS II reaction center with the reduced primary electron acceptor, $Pheo^-$, (that occurs due to competition of electron donation to the RC with charge recombination in the ion-radical pair [P_{680}^+ $Pheo^-$]) is observed after pre-reduction of Q_A and Q_B (Klimov et al., 1977). It was shown (Klimov et al., 1995a) that the rate of photoaccumulation of $Pheo^-$ was considerably inhibited by bicarbonate depletion or addition of formate and the photoreaction was restored with bicarbonate. Similarly, photoaccumulation of the oxidized primary electron donor, P_{680}^+, in the presence of SiMo (taking electrons from Pheo and, probably, from Q_A, i.e., before the electron transfer between Q_A and Q_B) also depended on the presence of formate and bicarbonate in the medium (Klimov et al., 1995a).

Flash-induced absorbance changes at 295 nm oscillating with period of four due to accumulation of charges in the WOC of PS II preparations were sufficiently inhibited upon the addition of formate at

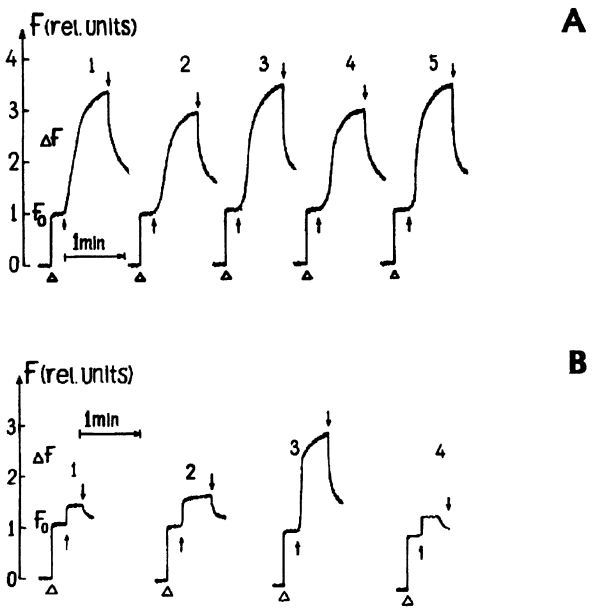

Fig. 4. Effect of the removal and re-addition of bicarbonate on photoinduced changes of Chl fluorescence yield (ΔF*)* related to photoreduction of Q_A in PS II membrane fragments (DT-20). (A) untreated DT-20: (1) in the medium non-depleted of bicarbonate; (2) after depletion of bicarbonate in the medium by a 60-min flushing with CO_2-free air; (3) '2' plus 6 mM $NaHCO_3$; (4) after the addition of 10μM $NaHCO_2$ to sample '1'; (5) '4' plus 6 mM $NaHCO_3$. (B) Tris-treated (Mn-depleted) DT-20: (1) in the bicarbonate-depleted medium with no additions; (2) after the addition of 0.2 μM $MnCl_2$; (3) after the addition of 0.2 μM $MnCl_2$ plus 5 mM $NaHCO_3$; (4) after the addition of 5 mM $NaHCO_3$. The medium contains 50 mM MES-NaOH buffer, pH 6.2 and 35 mM NaCl; 10 μg Chl ml^{-1}; Δ, switching on the measuring light (480 nm, 0.15 W m^{-2}) ↑ and ↓ actinic light (λ> 600 nm, 100 W m^{-2}) on and off, respectively. For details, see Klimov et al. (1995b).

concentration of 10–100 μM and they were restored with bicarbonate (Wincencjusz et al., 1996). In the same range of formate concentration a considerable suppression of photoreduction of DCBQ from water was observed while in the presence of tetraphenylboron, which replaces water as the electron donor to PS II reaction center, inhibition of photoreduction of exogenous quinones took place only at formate concentration higher than 10 mM. These results strongly support the conclusion that formate inhibits photochemical reactions of PS II due to its binding to two independent sites. One of them (with a higher formate binding) is associated with the WOC since it is revealed only when the WOC is operable while the other one (with a 1000 times lower formate binding) inhibits the electron transfer on the acceptor side of PS II (Klimov et al., 1995a,b, 1997b; Wincencjusz et al., 1996).

The importance of bicarbonate for both functional and structural manifestation of the WOC was convincingly shown using EPR-measurements (Klimov et al., 1997b; Hulsebosch et al., 1998). The light-induced EPR Signal II related to photooxidation of the secondary electron donor of PS II, Y_Z, was activated upon the addition of 100 μM formate that was consistent with the idea that formate inhibits the electron donation from the WOC to Y_Z^+, while photooxidation of Y_Z was not impaired. Elimination of the formate effect with bicarbonate suggests that the electron donation to Y_Z^+ is bicarbonate-dependent. This conclusion was strongly supported by the kinetic measurements of the flash-induced EPR Signal II: in the presence of 100 μM formate, the reduction of Y_Z^+ from the WOC was greatly slowed down and it occurred largely by back reaction with reduced electron acceptors. Bicarbonate was shown to prevent the loss of the fast electron donation from the WOC to Y_Z^+ (Klimov et al., 1997b).

The functional modification of the WOC with formate was accompanied by considerable structural re-arrangements in the Mn-cluster that led to the release of one or two free Mn^{2+}-atoms per PS II reac-

tion center as revealed by the appearance of the 6-line EPR signal of Mn^{2+} (Klimov et al., 1997b). Protective effect of bicarbonate against the formate-induced modifications of the WOC suggested that formate might act by replacing bicarbonate that is essential for Mn binding. The data on bicarbonate-reversible loss of the S_2 multiline EPR signal upon removal of bicarbonate from spinach PS II particles by means of washing in CO_2 free medium (Hulsebosch et al., 1998) are in line with the conclusion. Similar effects of formate on EPR signals of PS II preparations were reported (Feyziev et al., 2000), and Stemler and Lavergne (1997) have shown that formate modifies the S_1-state of the WOC so that it becomes reducible to the S_0-state.

An attempt to find direct evidence for possible ligation of bicarbonate to WOC components was made in a work using Fourier transform infrared spectroscopy (FTIR) (Yruela et al., 1998). It was shown that the light-induced FTIR difference spectrum originating from the donor side of PS II was considerably modified upon washing a PS II preparation with the medium depleted of bicarbonate: the main negative bands at 1560, 1541, 1522 and 1507 cm^{-1} and positive bands at 1589 and 1365 cm^{-1} disappeared upon bicarbonate removal and they were partially restored by bicarbonate addition. Similar ^{13}C-bicarbonate labeling FTIR measurements led to the conclusion that the negative band at 1560 cm^{-1} and positive bands at 1589 cm^{-1} and 1365 cm^{-1} could be assigned to COO^- stretching modes from bicarbonate. The first two bands corresponded to asymmetric stretching modes [$U_{as}(COO^-)$] while the latter one could be ascribed to symmetric stretching mode [$U_s(COO^-)$] of bicarbonate. The results were consistent with the suggestion that bicarbonate could be a ligand to the WOC. A disadvantage of those experiments was that they were done under continuous illumination. Similar measurements of flash-induced FTIR spectrum are needed in order to assign them to specific S-state transitions and to reveal possible ligation of bicarbonate to the Mn-cluster.

B. Stimulating Effects during Reconstitution of the Water-Oxidizing Complex

Bicarbonate requirement for the donor side of PS II was especially evident during reconstitution of the Mn-cluster of the WOC in Mn-depleted PS II preparations (apo-WOC-PS II) (Klimov et al., 1995a,b, 1997b; Allakhverdiev et al., 1997; Baranov et al., 2000, 2004). An efficient restoration of electron donation from the added Mn^{2+} to the PS II reaction center (lost due to removal of Mn) could be reached only in the presence of bicarbonate in the medium (Klimov et al., 1995a,b, 1997b). That effect of bicarbonate was clearly shown for reactivation of photoinduced ΔF (Fig. 4B), photoreduction of DCPIP and photooxidation of P_{680} (Klimov et al., 1995a,b). It was important that the bicarbonate requirement was not revealed if Mn^{2+} was substituted for other exogenous electron donors (NH_2OH, diphenylcarbazide) (Klimov et al., 1995a,b). The data clearly demonstrated that the observed stimulatory effects of bicarbonate were associated with reconstitution of a Mn center rather than with the electron transfer on the acceptor side of PS II.

The increased restoration of PS II activities with Mn^{2+} in the presence of bicarbonate was accompanied by an increased functional binding of Mn^{2+} to PS II which was revealed in the experiments on removal of the added Mn^{2+} from PS II membranes by centrifugation and suspension of the pellet in a medium freed of Mn^{2+} or by the addition of EDTA (Klimov et al., 1995a,b). In both cases the effect of bicarbonate leading to an increased binding of Mn^{2+} was especially clear when the experiments were done under illumination.

It was shown that the formation of bicarbonate complexes with Mn^{2+} considerably changed the redox properties of the metal: redox potential of its oxidation was shifted from +1.2 V (aqua ion Mn^{2+}) to +0.92 V for $Mn^{2+}(HCO_3^-)^+$ and to +0.63 V for $Mn^{2+}(HCO_3^-)_2$ (Kozlov et al., 1997) which, of course, is important for redox interaction of Mn^{2+} with apo-WOC-PS II.

Measurements of flash-induced EPR Signal II demonstrated that bicarbonate is probably not needed for photooxidation of Y_Z in Mn-depleted PS II while the fast electron donation to Y_Z^+ from the added Mn^{2+} requires bicarbonate (Klimov et al., 1997b). The fast phase of re-reduction of Y_Z^+ (characteristic of the functionally competent WOC) could be restored only upon joint addition of bicarbonate and Mn^{2+} (and it was not seen if one of the two was absent).

Bicarbonate was also required for structural rearrangements of Mn^{2+} leading to the formation of a functionally active Mn-center in the apo-WOC-PS II (Klimov et al., 1997b). The characteristic 6-line EPR signal of added Mn^{2+} (2–4 Mn per one PS II reaction center) was diminished upon illumination (evidently due to photooxidation of Mn^{2+} to Mn^{3+}). However, the signal completely recovered if bicarbonate was not

added to the medium. Upon the addition of bicarbonate, a part of the signal was eliminated already in the dark and it practically disappeared upon illumination and, what was especially important, the signal did not recover after the actinic light was switched off. So, the EPR-silent (at room temperature) form of manganese (which is also characteristic of manganese in the WOC) became more stable in the presence of bicarbonate.

The conclusion on creation of a functionally (and structurally) competent form of the WOC in the presence of bicarbonate was strongly supported by the appearance of the characteristic, period four, oscillations of the flash-induced absorbance changes at 295 nm after photoactivation of apo-WOC-PS II in the presence of both Mn^{2+} and bicarbonate (Klimov et al., 1997b). In the absence of bicarbonate, the oscillations were not restored. Besides, the S_2-multiline EPR signal also could be restored in those samples only if Mn^{2+} was added jointly with bicarbonate (Hulsebosch et al., 1998).

What was most important, bicarbonate was required for photoreactivation of the WOC competent in O_2 evolution. In Mn-depleted PS II preparation, photoactivation of both photoinduced ΔF and O_2 evolution with added Mn^{2+} was very low if the experiments were done in bicarbonate-depleted medium while both of the activities were considerably restored if the photoactivation was done after the addition of bicarbonate (Allakhverdiev et al., 1997). The bicarbonate requirement could be revealed without a special procedure for bicarbonate depletion if the pH of the medium used for photoactivation was shifted to pH 6 – pH 5.5 (lower than the pK for H_2CO_3 dissociation) leading to a sufficient lowering of HCO_3^- concentration in the medium. (A similar stimulatory effect of bicarbonate on O_2 evolution was observed in an untreated O_2-evolving PS II preparation (Allakhverdiev et al., 1997)). From 2 to 4 Mn per PS II reaction center was enough for maximum photoactivation of the O_2-evolving function if the photoactivation was performed in the presence of bicarbonate.

From the analysis of the concentration dependence of the stimulating effects of bicarbonate it was found that the dissociation constant (K_d) for bicarbonate bound to the WOC is equal to 20–34 μM (Allakhverdiev et al., 1997). In addition, a K_d lower than 10 μM was found although its correct value was not determined.

Much progress has been made in investigation of the mechanism of photoactivation of the WOC in Mn-depleted PS II preparations due to new experimental developments which have enabled kinetic resolution of the first three intermediates formed during assembly of the inorganic core of the WOC (Zaltsman et al., 1997; Chapter 26). The first light-dependent step can be related to the formation of $Mn^{III}(OH)_2^+$-WOC-PS II intermediate, whose concentration defined the yield of the process of the WOC assembly. Using this photoactivation approach it was shown (Baranov et al., 2000) that at pH 6.0 bicarbonate considerably (1.2–3 times) accelerated photoreassembly of the WOC from apo-WOC-PS II when Mn^{2+} is added in stoichiometrically between 2 and 4 Mn per PS II reaction center at a concentration of Ca^{2+} equal to 8 mM. Nearly 50% of the bicarbonate effect was observed at 15–25 μM of added bicarbonate at pH 6.0 that corresponded to ~10 μM of HCO_3^- and was close to the concentration of added Mn^{2+}. Analysis of the data suggested that bicarbonate stimulated the first light-dependent step of apo-WOC-PS II photoactivation increasing, probably, the quantity of the first intermediate through the formation of $Mn^{III}(OH)(HCO_3)^+$ -WOC-PS II intermediate (Baranov et al., 2000). When using 10–50-fold higher concentrations of Mn^{2+} and Ca^{2+}, bicarbonate addition causes a 300% stimulation of the rate and a 50% increase in yield of photoassembled O_2-evolving PS II centers revealing a new lower affinity site for bicarbonate interaction in the WOC (Baranov et al., 2004).

C. Stabilizing Effects during Photo- and Thermo-Inactivation

Experiments on PS II photoinhibition in CO_2/bicarbonate-depleted samples provided contradictory results. There are data showing that in thylakoids bicarbonate protects the PS II machinery against photoinhibition (Sundby, 1990; Sundby et al., 1992). According to other publications, depletion of bicarbonate in thylakoid membranes (by formate treatment (Sundby, 1990; Sundby et al., 1992)) or in green algae (using bicarbonate-depleted medium (Demeter et al., 1995)) resulted in a lower susceptibility of PS II to photoinhibition that was consistent with the idea of blocking the electron transfer between Q_A and Q_B in bicarbonate-depleted samples since similar protection against photoinhibition was reached upon DCMU addition.

It has been shown that in PS II membranes, the rate of photoinhibition of PS II activities (photoinduced

ΔF and photoreduction of DCPIP) in the medium depleted of CO_2/bicarbonate was considerably decreased upon addition of 5 mM $NaHCO_3$ (Klimov et al., 1997a). A similar protecting effect was revealed when 100 μM $MnCl_2$ was added instead of bicarbonate. In PS II membrane fragments depleted of Mn, the photoinhibition led to irreversible loss of the capability of PS II to be reactivated by Mn^{2+}, and the rate of photoinhibition was decreased by a factor of 2 or 5 if the preillumination was done in the presence of 0.2 μM $MnCl_2$ (4 Mn per PS II reaction center) added alone or in combination with 5 mM $NaHCO_3$, respectively. A similar protective effect of bicarbonate was also revealed in the dark, during thermoinactivation of O_2-evolving PS II preparations at 40 °C: the rate of thermoinactivation was decreased by a factor 3 if bicarbonate was added to the medium (Klimov et al., 1997a). The stabilizing effect of bicarbonate was also observed in thylakoid membranes from *Synechococcus* sp. PCC 7002 treated with 0.1% Triton X-100, and in unbroken spinach chloroplasts (Klimov et al., 2003). Besides, bicarbonate protected the WOC against inactivation induced by pre-incubation of PS II membrane fragments (25° C) and thylakoids (40° C) at low pH (5.0–5.5) in non-bicarbonate-depleted medium (Klimov et al., 2003). The results are consistent with the idea that bicarbonate is an essential component of the WOC, and it is required for both functioning and stability of the Mn-containing enzyme.

D. Possible Functional Roles of Bicarbonate on the Donor Side

The following explanations of the bicarbonate requirement for the donor side of PS II have been suggested.

1. Bicarbonate as an Electron Donor to the Water-Oxidizing Complex

Bicarbonate may serve as an electron donor (alternative to water or as a way of involvement of water molecules in the oxidative reactions) to the Mn-containing WOC (Klimov et al., 1995a,b). The possible involvement of bicarbonate in the chemistry of photosynthetic O_2 evolution was developed earlier (Metzner, 1978; Stemler, 1980). However, it was not confirmed by experiments on O_2-evolution in the presence of $HC^{18}O_3^-$ or $H_2{}^{18}O$ that showed that oxygen atoms from $HC^{18}O_3^-$ were evidently not included in O_2 molecules evolved in PS II (Radmer and Ollinger, 1980). On the other hand, carbonic anhydrase activity of PS II has been revealed (Stemler, 1986, 1997) and it considerably increased upon isolation of the O_2-evolving core complexes from PS II membrane fragments (Moskvin et al., 1998, 2003). Besides, a novel carbonic anhydrase associated with PS II has been discovered in *Chlamydomonas reinhardtii* (Park et al., 1999). Recently, it has been shown that this carbonic anhydrase is very important for both activity and stability of the WOC (Villarejo et al., 2002) though participation of this carbonic anhydrase in providing an ample supply of CO_2 for Rubisco is also considered (Park et al., 1999; Hanson et al., 2003). One can suggest that due to multiple exchange of HCO_3^-/CO_2 species on the carbonic anhydrase enzymatic center, the labeled ^{18}O could "leak" to water (concentration of which is a few orders higher than that of added bicarbonate) that could be responsible for the lack of $^{18}O_2$-evolution from $HC^{18}O_3^-$ (Stemler, 1982; Klimov et al., 1995b). Most of the data on restoration of electron transfer with bicarbonate in apo-WOC-PS II in the presence of Mn^{2+} and the absence of the reactivation in the absence of Mn^{2+} do not contradict the idea about direct oxidation of bicarbonate with Mn-containing WOC.

2. Bicarbonate as a Transient Ligand during the Assembly of the Mn Cluster

Bicarbonate is required only for the process of assembly of the functionally competent WOC from the cofactor-depleted apo-WOC-PS II centers (appearing as a result of disassembling of the WOC under stress conditions or when newly synthesized). There are many possible ways of bicarbonate involvement in photoactivation of the WOC (Klimov et al., 1995a,b). Photooxidation of Mn^{2+} to Mn^{3+} (as an important step of the WOC photoactivation) is facilitated upon formation of complexes $Mn(HCO_3)^+$ and $Mn(HCO_3)_2$ due to either lowering the redox potential of Mn^{2+} oxidation (Kozlov et al., 1997) or the decrease (or loss) of positive charge(s) that is favorable for the accessibility of Mn^{2+} to its specific binding site(s) (Klimov et al., 1995b). According to Baranov et al. (2000), during photoactivation bicarbonate may: (i) act as an integral cofactor within the WOC (possible ligand to the first Mn); (ii) act as a Bronsted base to accelerate proton release during formation of either the dark precursor (apo-WOC-$Mn(OH)^+$) or IM_1 (apo-WOC-$Mn(OH)_2^+$); (iii) directly deliver one or

more hydroxide ions during formation of the latter two species (with release of CO_2); (iv) act as a membrane soluble anion which electrostatically elevates the local concentration of Mn^{2+} in PS II.

Comparative studies of electrochemical and functional properties of complexes of Mn^{2+} and Mn^{3+} with bicarbonate and other carboxylates (formate and acetate) show that the unique capability of bicarbonate to initiate the assembly of the tetramanganese cluster of the WOC from Mn^{2+} and apo-WOC-PS II can be attributed to formation of electroneutral, easily oxidizable, oligomeric Mn-bicarbonate complexes that serve as building blocks for the WOC (Y.N. Kozlov and V.V. Klimov, unpublished). It is suggested that due to this property bicarbonate might have been critical to the evolution of the first O_2-evolving cyanobacteria from a non-oxygenic bacterial precursor in the Archean period (>2.2 BYA) (Dismukes et al., 2001).

3. Bicarbonate Activation Through Binding to Other Components

Bicarbonate increases the Mn^{2+} binding (Klimov et al., 1995a,b), the formation of the Mn-cluster capable of water oxidation (Allakhverdiev et al., 1997; Baranov et al., 2000, 2004) and stabilizes the WOC (Klimov et al., 1997a, 2003) indirectly, though its binding to other PS II components that is important for structural/functional organization of the whole PS II complex and, in particular, for functional binding of Mn. Govindjee et al. (1997) suggested that bicarbonate bound to the acceptor side is required for PS II activity both on the acceptor and the donor sides. The non-heme Fe, the known binding site for bicarbonate (Diner and Petrouleas, 1990), evidently can not be responsible for the bicarbonate effects on the WOC since the effects are induced by formate concentrations which are approximately 1000 times lower than those required for bicarbonate removal from the acceptor side of PS II (Klimov et al.,1995a,1995b, 1997b;Wincencjusz et al., 1996).

4. Bicarbonate as an Integral Cofactor in the Water-Oxidizing Complex

Bicarbonate may be an integral cofactor of the WOC. It can be involved in direct ligation of the Mn atoms that is important for the assembly of the functionally competent Mn-cluster or for modulation of its redox capabilities. Reactivation of O_2-evolution along with reactivation of electron donation to the PS II reaction center in Mn-depleted PS II preparations (Allakhverdiev et al., 1997; Klimov et al., 1997b; Baranov et al., 2000, 2004) shows that bicarbonate is required for reconstitution of the WOC rather than only for reactivation of the electron flow (if $Mn(HCO_3)_2$ would be just a good electron donor for PS II). Data on the increased functional binding of Mn^{2+} in the presence of bicarbonate (Klimov et al., 1995a,b), the release of Mn^{2+} from the WOC in the presence of formate (Klimov et al., 1997b) and the protecting effect of bicarbonate against thermal disassembly of the WOC (Klimov et al., 1997a, 2003) confirm the idea that bicarbonate participates in the assembling of the Mn-cluster.

One can suggest that some of the carboxyl group(s) taking part in the formation of Mn-containing WOC (Yachandra et al., 1993; Noguchi et al., 1995) belong to bicarbonate rather than to amino-acid residues. The results of FTIR measurements are consistent with the idea that bicarbonate may act as a bridging ligand between the redox-active Mn and Ca^{2+} within the WOC (Yruela et al., 1998) although more reliable experiments dealing with difference absorption FTIR spectra of specific S-transitions of the WOC are needed. In a recent publication on X-ray structure of the PS II core complex from *Thermosynechococcus elongatus* (Ferreira et al., 2004), a bicarbonate molecule is tentatively included as non-protein ligand at the WOC because this molecule can be readily accommodated into the density and fulfils the coordination chemistry of Mn and Ca^{2+} ions (Fig. 5).

IV. Conclusions

It is well established that bicarbonate stimulates electron transfer between the primary and secondary electron acceptors, Q_A and Q_B, in formate-inhibited PS II. The non-heme Fe between Q_A and Q_B plays an essential role in the bicarbonate binding. A second binding site on the acceptor side of PS II is an arginine in the D1 protein, D1-Arg257. It is suggested that the role of bicarbonate action at the acceptor side is to stabilize the reaction center proteins of PS II, and, to act in the protonation of the reduced secondary quinone electron acceptor of PS II, Q_B.

Strong evidence of a bicarbonate requirement for the WOC, both O_2-evolving and assembling from apo-WOC and Mn^{2+}, of PS II preparations has been presented in a number of publications. The following explanations for the involvement of bicarbonate in

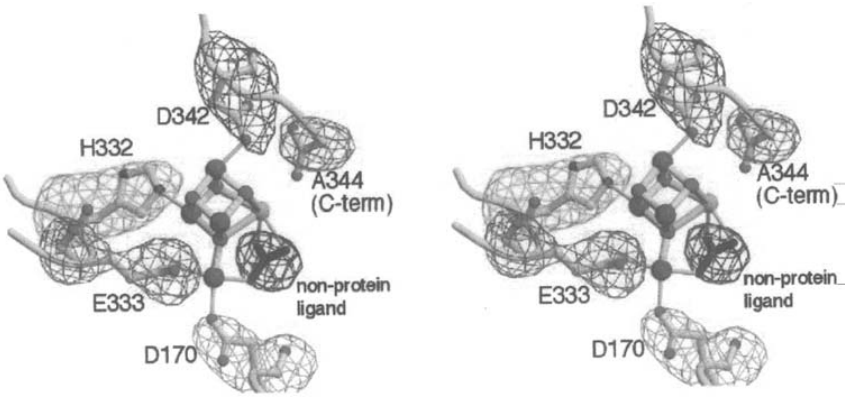

Fig. 5. Stereoviews of electron density maps for part of the water-oxidizing complex; a putative non-protein ligand (modeled as bicarbonate) is shown. Reproduced with permission from Ferreira et al. (2004). See Color Plate 2, Fig. 2.

the events on the donor side of PS II are considered: (i) bicarbonate serves as an electron donor (alternative to water or as a way of involvement of water molecules in the oxidative reactions) to the Mn-containing O_2-center; (ii) bicarbonate facilitates assembly of the WOC from apo-WOC and Mn^{2+} due to formation of the complexes $Mn(HCO_3)^+$ and $Mn(HCO_3)_2$ leading to an easier oxidation of Mn^{2+} with PS II; (iii) the WOC is stabilized by bicarbonate through its binding to other components of PS II; (iv) bicarbonate is an integral component of the WOC essential for its function and stability; it may be considered as a direct ligand to the Mn-cluster.

While it is clear that there are effects of bicarbonate on the acceptor as well as on the donor side in PS II, much more research is needed to clear the roles of this important anion. It may be expected that more detailed experiments become possible when the structure of this water-plastoquinone oxido-reductase becomes known in more detail.

Acknowledgments

VVK is thankful to the Human Frontiers Science Program (Grant RGP0029) and to the program Physical Chemistry Biology Russian Academy of Sciences for financial support.

References

Allakhverdiev S, Yruela I, Picorel R and Klimov V (1997) Bicarbonate is an essential constituent of the water-oxidizing complex of Photosystem II. Proc Natl Acad Sci USA 94: 5050–5054

Baranov SV, Ananyev GM, Klimov VV and Dismukes GC (2000) Bicarbonate accelerates assembly of the inorganic core of the water-oxidizing complex in manganese-depleted Photosystem II: A proposed biogeochemical role for atmospheric carbon dioxide in oxygenic photosynthesis. Biochemistry 39: 6060–6065

Baranov SV, Tyryshkin AM, Katz D, Dismukes GC, Ananyev GM, Klimov VV (2004) Bicarbonate is a native cofactor for assembly of the manganese cluster of the photosynthetic water oxidizing complex. Kinetics of reconstitution of O_2 evolution by photoactivation. Biochemistry 43: 2070–2079

Blubaugh DJ and Govindjee (1988a) The molecular mechanism of the bicarbonate effect at the plastoquinone reductase site of photosynthesis. Photosynth Res 19: 85–128

Blubaugh DJ and Govindjee (1988b) Kinetics of the bicarbonate effect and the number of bicarbonate binding sites in thylakoid membranes. Biochim Biophys Acta 936: 208–214

Bowden SJ, Hallahan BJ, Ruffle SV, Evans MCW and Nugent JHA (1991) Preparation and characterization of Photosystem II core particles with and without bound bicarbonate. Biochim Biophys Acta 1060: 89–96

Cao J, Ohad N, Hirschberg J, Xiong J and Govindjee (1992) Binding affinity of bicarbonate and formate in herbicide-resistant D1 mutants of *Synechocystis* sp PCC-7942. Photosynth Res 34: 397–408

Demeter S, Janda T, Kovacs L, Mende D and Wiessner W (1995) Effects of in vivo CO_2-depletion on electron transport and photoinhibition in the green algae, *Chlamydobotrys stellata* and *Chlamydomonas reinhardtii*. Biochim Biophys Acta 1229: 166–167

Diner BA and Petrouleas V (1987) Q_{400}, the non-heme iron of the Photosystem II iron-quinone complex. A spectroscopic probe of quinone and inhibitor binding to the reaction center. Biochim Biophys Acta 895: 107–125

Diner BA and Petrouleas V (1990) Formation by NO of nitrosyl adducts of redox components of the Photosystem II reaction center. II. Evidence that HCO_3^-/CO_2 binds to the acceptor side

non-heme iron. Biochim Biophys Acta 1015: 141–149
Diner BA, Petrouleas V and Wendoloski JJ (1991) The iron-quinone electron-acceptor complex of Photosystem II. Physiol Plant 81: 423–436
Dismukes GC, Klimov VV, Baranov SV, Kozlov YuN, DasGupta J and Tyryshkin A (2001) The origin of atmospheric oxygen on earth: The innovation of oxygenic photosynthesis. Proc Natl Acad Sci USA 98: 2170–2175
Eaton-Rye JJ and Govindjee (1988) Electron transfer through the quinone acceptor complex of Photosystem II after one or two actinic flashes in bicarbonate-depleted spinach thylakoid membranes. Biochim Biophys Acta 935: 248–257
El-Shintinawy F and Govindjee (1990) Bicarbonate effect in leaf discs from spinach. Photosynth Res 24: 189–200
Ferreira KN, Iverson TM, Maghlaoui K, Barber J and Iwata S (2004) Architecture of the photosynthetic oxygen-evolving center. Science 303: 1782–1784
Feyziev YM, Yoneda D, Yoshii T, Katsuta N, Kawamori A and Watanabe Y (2000) Formate-induced inhibition of the water-oxidizing complex of Photosystem II studied by EPR. Biochemistry 39: 3848–3855
Garab G, Sanchez Burgos AA, Zimányi L and Faludi-Dániel (1983) Effect of CO_2 on the energization of thylakoids in leaves of higher plants. FEBS Lett 154: 323–327
Gong H, Nilsen S and Allen JF (1993) Photoinhibition of photosynthesis in vivo - involvement of multiple sites in a photodamage process under CO_2-free and O_2-free conditions. Biochim Biophys Acta 1142: 115–122
Good NE (1963) Carbon dioxide and the Hill reaction. Plant Physiol 38: 298–304
Govindjee and Van Rensen JJS (1978) Bicarbonate effects on the electron flow in isolated broken chloroplasts. Biochim Biophys Acta 505: 183–213
Govindjee and Van Rensen JJS (1993) Photosystem II reaction center and bicarbonate. In: Deisenhofer J and Norris JR (eds) The Photosynthetic Reaction Center, Vol I, pp 357–388. Academic Press, New York
Govindjee, Pulles MJP, Govindjee R, Van Gorkom, HJ and Duysens LNM (1976) Inhibition of the reoxidation of the secondary electron acceptor of Photosystem II by bicarbonate depletion. Biochim Biophys Acta 449: 602–605
Govindjee, Xu C and van Rensen JJS (1997) On the requirement of bound bicarbonate for Photosystem II. Z Naturforsch 52c: 24–32
Hanson DT, Franklin LA, Samuelsson G and Badger MR (2003) The *Chlamydomonas reinhardtii cia3* mutant lacking a thylakoid lumen-localized carbonic anhydrase is limited by CO_2 supply to rubisco and not Photosystem II function in vivo. Plant Physiology 132: 2267–2275
Hienerwadel R and Berthomieu C (1995) Bicarbonate binding to the non-heme iron of Photosystem II investigated by Fourier transform infrared difference spectroscopy and ^{13}C-labeled bicarbonate. Biochemistry 34: 16288–16297
Hulsebosch RJ, Allakhverdiev SI, Klimov VV, Picorel R and Hoff AJ (1998) Effect of bicarbonate on the S_2 multiline EPR signal of the oxygen-evolving complex in Photosystem II membrane fragments. FEBS Lett 424: 146–148
Ireland CR, Baker NR and Long SP (1987) Evidence for a physiological role of CO_2 in the regulation of photosynthetic electron transport in intact leaves. Biochim Biophys Acta 893: 434–443
Jursinic P, Warden J and Govindjee (1976) A major site of bicarbonate effect in system II reaction: Evidence from ESR Signal II_{vf}, fast fluorescence yield changes and delayed light emission. Biochim Biophys Acta 440: 322–330
Khanna R, Govindjee and Wydrzynski T (1977) Site of bicarbonate effect in Hill reaction. Evidence from the use of artificial electron acceptors and donors. Biochim Biophys Acta 462: 208–214
Khanna R, Pfister K, Keresztes A, Van Rensen JJS and Govindjee (1981) Evidence for a close spatial location of the binding sites for CO_2 and for Photosystem II inhibitors. Biochim Biophys Acta 634: 105–116
Klimov VV and Baranov SV (2001) Bicarbonate requirement for the water-oxidizing complex of Photosystem II. Biochim Biophys Acta 1503: 187–196
Klimov VV, Klevanik AV, Shuvalov VA and Krasnovsky AA (1977) Reduction of pheophytin in the primary light reaction of photosystem 2. FEBS Lett 82: 183–186
Klimov VV, Allakhverdiev SI, Baranov SV and Feyziev YaM (1995a) Effects of bicarbonate and formate on the donor side of Photosystem II. Photosynth Res 46: 219–225
Klimov VV, Allakhverdiev SI, Feyziev YaM and Baranov SV (1995b) Bicarbonate requirement for the donor side of Photosystem II. FEBS Lett 363: 251–255
Klimov VV, Baranov S and Allakhverdiev S (1997a) Bicarbonate protects the donor side of Photosystem II against photoinhibition and thermoinactivation. FEBS Lett 418: 243–246
Klimov VV, Hulsebosch R, Allakhverdiev S, Wincencjusz H, van Gorkom H and Hoff A (1997b) Bicarbonate may be required for ligation of manganese in the oxygen evolving complex of Photosystem II. Biochemistry 36: 16277–16281
Klimov VV, Allakhverdiev SI, Nishiyama Y, Khorobrykh AA and Murata N (2003) Stabilization of the oxygen-evolving complex of Photosystem II by bicarbonate and glycinebetaine in thylakoid and subthylakoid preparations. Functional Plant Biology 30: 797–803
Komenda J, Lupinkova, L and Kopecky J (2002) Absence of the *psbH* gene product destabilizes Photosystem II complex and bicarbonate binding on its acceptor side in *Synechocystis* PCC 6803. Eur J Biochem 269: 610–619
Kozlov YN, Kazakova AA and Klimov VV (1997) Changes in the redox potential and catalase activity of Mn^{2+} ions during formation Mn-bicarbonate complexes. Membr Cell Biol 7: 115–120
Mäenpää P, Miranda T, Tyystjärvi E, Tyystjärvi T, Govindjee, Ducruet JM, Etiene AL and Kirilovski D (1995) A mutation in the D-de loop of D1 modifies the stability of the S_2Q_A and S_2Q_B states in Photosystem II. Plant Physiol 107: 187–197
Mende D and Wiessner W (1985) Bicarbonate in vivo requirement of Photosystem II in the green alga *Chlamydobotrys stellata*. J Plant Physiol 118: 259–266
Metzner H (1978) Oxygen evolution as energetic problem. In: Metzner H (ed) Photosynthetic Oxygen Evolution, pp 59–76. Academic Press, London
Michel H and Deisenhofer J (1988) Relevance of the photosynthetic reaction center from purple bacteria to the structure of Photosystem II. Biochemistry 27: 1–7
Moskvin OV, Razguliaeva AYu, Shutova TV, Khristin MS, Ivanov BN and Klimov VV (1998) Carbonic anhydrase activity of different Photosystem II preparation. In: Garab G (ed) Photosynthesis: Mechanisms and Effects, pp 1201–1204. Kluwer

Academic Publishers, Dordrecht
Moskvin OV, Shutova TV, Khristin MS, Ignatova LK, Villarejo A, Ivanov BN, Samuelsson G and Klimov VV (2003) Carbonic anhydrase activities in pea thylakoids. A Photosystem II core complex associated carbonic anhydrase. Photosynth Res 79: 93–100
Noguchi T, Ono T and Inoue Y (1995) A carboxylate ligand interacting with water in the oxygen-evolving center of Photosystem II as revealed by Fourier transform infrared spectroscopy. Biochim Biophys Acta 1228: 189–200
Park Y-Il, Karlsson J, Rojdestvenski I, Pronina N, Klimov V, Oquist G and Samuelsson G (1999) Role of a novel Photosystem II-associated carbonic anhydrase in photosynthetic carbon assimilation in *Chlamydomonas reinhardtii*. FEBS Lett 444: 102–105
Petrouleas V, Deligiannakis Y and Diner BA (1994) Binding of carboxylate anions at the non-heme Fe(II) of PS II. 2. Competition with bicarbonate and effects on the Q_A/Q_B electron transfer rate. Biochim Biophys Acta 1188: 271–277
Robinson HH, Eaton-Rye JJ, Van Rensen JJS and Govindjee (1984) The effects of bicarbonate depletion and formate incubation on the kinetics of oxidation-reduction reactions of the Photosystem II quinone acceptor complex. Z Naturforsch 39c: 382–385
Radmer R and Ollinger O (1980) Isotopic composition of photosynthetic O_2 flash yield in the presence of $H_2{}^{18}O$ and $HC^{18}O_3^-$. FEBS Lett 110: 57–61
Schansker G and Van Rensen JJS (1993) Characterization of the complex interaction between the electron acceptor silicomolybdate and Photosystem II. Photosynth Res 37: 165–175
Semin BK, Loviagina ER, Aleksandrov AY, Kaurov YN and Novakova AA (1990) Effect of formate on Mössbauer parameters of the non-heme iron of PS II particles of cyanobacteria. FEBS Lett 270: 184–186
Shopes RJ, Blubaugh D, Wraight C and Govindjee (1989) Absence of a bicarbonate-depletion effect in electron transfer between quinones and reaction centers of *Rhodobacter sphaeroides*. Biochim Biophys Acta 974: 114–118
Snel JFH and Van Rensen JJS (1984) Reevaluation of the role of bicarbonate and formate in the regulation of photosynthetic electron flow in broken chloroplasts. Plant Physiol 75: 146–150
Stemler AJ (1980) Inhibition of Photosystem II by formate: possible evidence for direct role of bicarbonate in photosynthetic oxygen evolution. Biochim Biophys Acta 593: 103–112
Stemler AJ (1982) The functional role of bicarbonate in photosynthetic light reaction II. In: Govindjee (ed) Photosynthesis, Development, Carbon Metabolism and Plant Productivity, Vol II, pp 513–538. Academic Press, New York
Stemler A (1986) Carbonic anhydrase associated with thylakoids and Photosystem II particles from maize. Biochim Biophys Acta 850: 97–107
Stemler A (1997) The case for chloroplast thylakoid carbonic anhydrase. Physiol Plant 99: 348–353
Stemler AJ (2002) The bicarbonate effect, oxygen evolution, and the shadow of Otto Warburg. Photosynth Res: 177–183
Stemler AJ and Govindjee (1973) Bicarbonate ion as a critical factor in photosynthetic oxygen evolution. Plant Physiol 52: 119–123
Stemler AJ and Murphy JB (1983) Determination of the binding constant of $H^{14}CO_3^-$ to the Photosystem II complex in maize chloroplasts: Effects of inhibitors and light. Photochem Photobiol 38: 701–707
Stemler A and Lavergne J (1997) Evidence that formate destabilizes the S_1 state of the oxygen-evolving mechanism in Photosystem II. Photosynth Res 51: 83–92
Sundby C (1990) Bicarbonate effects on photo-inhibition. Including an explanation for the sensitivity to photo-inhibition under anaerobic conditions. FEBS Lett 274: 77–81
Sundby C, Mattsson M and Schiött T (1992) Effects of bicarbonate and oxygen concentration on photoinhibition of thylakoid membranes. Photosynth Res 34: 263–270
Van Rensen JJS (1982) Molecular mechanisms of herbicide action near Photosystem II. Physiol Plant 54: 515–521
Van Rensen JJS (1992) The role of bicarbonate in the activity of Photosystem 2. Photosynthetica 27: 311–321
Van Rensen JJS (2002) Role of bicarbonate at the acceptor side of Photosystem II. Photosynth Res 73: 185–192
Van Rensen JJS and Vermaas WFJ (1981) Action of bicarbonate and Photosystem II inhibiting herbicides on electron transport in pea grana and in thylakoids of a blue-green alga. Physiol Plant 51: 106–110
Van Rensen JJS, Hobé JH, Werner RM and Snel JFH (1984) Reactivation of electron transport in CO_2-depleted chloroplasts by bicarbonate is influenced by thylakoid surface potential. In: Sybesma C (ed) Advances in Photosynthesis Research, Vol I, pp 613–616. Martinus Nijhoff/Dr W Junk Publishers, The Hague
Van Rensen JJS, Tonk WJM and De Bruijn SM (1988) Involvement of bicarbonate in the protonation of the secondary quinone electron acceptor of Photosystem II via the non-heme iron of the quinone-iron acceptor complex. FEBS Lett 226: 347–351
Van Rensen JJS, Xu C and Govindjee (1999) Role of bicarbonate in Photosystem II, the water-plastoquinone oxido-reductase of plant photosynthesis. Physiol Plant 105: 585–592
Vass I, Sanakis Y, Spetea C and Petrouleas V (1995) Effects of photoinhibition on the $Q_A^-Fe^{2+}$ complex of Photosystem II studied by EPR and Mössbauer spectroscopy. Biochemistry 34: 4434–4440
Vermaas WFJ and Van Rensen JJS (1981) Mechanism of bicarbonate action on photosynthetic electron transport in broken chloroplasts. Biochim Biophys Acta 636:168–174
Vermaas WFJ and Rutherford AW (1984) EPR measurements on the effects of bicarbonate and triazine resistance on the acceptor side of Photosystem II. FEBS Lett 175: 243–248
Vernotte C, Briantais JM, Astier C and Govindjee (1995) Differential effects of formate in single and double mutants of D1 in *Synechocystis* sp. PCC 6714. Biochim Biophys Acta 1229: 296–301
Villarejo A, Shutova T, Moskvin O, Forssen M, Klimov V and Samuelsson G (2002) A Photosystem II-associated carbonic anhydrase regulates the efficiency of photosynthetic oxygen evolution. EMBO J 21: 1930–1938
Wang X, Cao J, Maroti P, Stilz HU, Finkele U, Lauterwasse C, Zinth W, Oesterhelt D, Govindjee and Wraight C (1992) Is bicarbonate in Photosystem II the equivalent of the glutamate ligand to the iron atom in bacterial reaction centers? Biochim Biophys Acta 1100: 1–8
Warburg O and Krippahl G (1958) Hill-reaktionen. Z Naturforsch 13b: 509–514
Wincencjusz H, Allakhverdiev SI, Klimov VV and van Gorkom HJ (1996) Bicarbonate-reversible formate inhibition at the donor side of Photosystem II. Biochim Biophys Acta 1273: 1–3

Wydrzynski T and Govindjee (1975) A new site of bicarbonate effect in Photosystem II of photosynthesis: Evidence from Chl fluorescence transients in spinach chloroplasts. Biochim Biophys Acta 387: 403–408

Xiong J, Subramaniam S and Govindjee (1996) Modeling of the D1/D2 proteins and cofactors of the Photosystem II reaction center: Implications for herbicide and bicarbonate binding. Protein Sci 5: 2054–2073

Xiong J, Subramaniam S and Govindjee (1998a) A knowledge-based three dimensional model of the Photosystem II reaction center of *Chlamydomonas reinhardtii*. Photosynth Res 56: 229–254

Xiong J, Minagawa J, Crofts A and Govindjee (1998b) Loss of inhibition by formate in newly constructed Photosystem II D1 mutants, D1-R257E and D1-R257M, of *Chlamydomonas reinhardtii.* Biochim Biophys Acta 1365: 473–491

Xu C, Taoka S, Crofts AR and Govindjee (1991) Kinetic characteristics of formate/formic acid binding at the plastoquinone reductase site in spinach thylakoids. Biochim Biophys Acta 1098: 32–40

Yachandra VK, DeRose VJ, Latimer MJ, Mukerji I, Sauer K and Klein MP (1993) Where plants make oxygen: A structural model for the photosynthetic oxygen-evolving manganese cluster. Science 260: 675–679

Yruela I, Allakhverdiev SI, Ibarra JV and Klimov VV (1998) Bicarbonate binding to the water-oxidizing complex in the Photosystem II. A Fourier transform infrared spectroscopy study. FEBS Lett 425: 396–400

Zaltsman L, Bruntrager E, Ananyev G and Dismukes GC (1997) A quantitative kinetic model for photo-assembly of the photosynthetic water oxidase from its inorganic constituents: requirements for manganese and calcium in the kinetically resolved steps. Biochemistry 36: 8914–8922

Chapter 15

Side-Path Electron Donors: Cytochrome b_{559}, Chlorophyll Z and β-Carotene

Peter Faller*, Christian Fufezan and A. William Rutherford*
Service de Bioénergétique, Département de Biologie Joliot-Curie, CNRS URA 2096, CEA Saclay, F-91191 Gif-sur-Yvette, France

*Authors for correspondence, email: faller@lcc-toulouse.fr; [2]rutherford@dsvidf.cea.fr

T. Wydrzynski and K. Satoh (eds): Photosystem II: The Light-Driven Water:Plastoquinone Oxidoreductase, pp. 347–365.

Summary

β-Carotene (Car), cytochrome (Cyt) b_{559} and a monomeric chlorophyll (Chl) designated as chlorophyll Z, all undergo oxidation in Photosystem (PS) II under some illumination conditions. These components are not part of the direct electron transfer that leads to water oxidation and plastoquinone reduction and are thus designated 'side-path electron donors.' Under the usual conditions of PS II function, the quantum yield for the oxidation of these components is low; however, under certain experimental conditions, particularly low temperatures, the dominant reactions can be those involving the side-path donors. Car is a branch point in the side-path electron donation, being oxidized by P^+ (the kinetically competent Chl cation radical), and reduced by Cyt $b_{559,}$ which is itself reduced by electrons from the pool of plastoquinol, possibly through the Q_B site. This all occurs on the D2-side of the reaction center. When the Cyt b_{559} is pre-oxidized, Car^+ is reduced by Chl Z. There are two candidates for Chl Z, the more obvious candidate on the D2 side and the less straightforward candidate on D1 side of the reaction center. The side-pathway is usually rationalized as a photoprotective cycle aimed at removing long-lived P^+ and thus limiting oxidative damage. Based on the low quantum yields, we consider this unlikely. Instead we suggest that the side-path constitutes a photoprotective cycle in which the aim is to reduce the Car cation, rather than P^+, returning the carotene cation to its unoxidized state, preventing adventitious reactions and allowing it to play its a role as a singlet O_2 quencher in the heart of PS II.

I. Introduction

Photosystem II (PS II) is a photochemical enzyme that uses light to drive the reduction of plastoquinone and the oxidation of water. The structure and function of PS II has been extensively reviewed (Goussias et al., 2002; Rappaport and Diner, 2002; Chapters 18–21). Several components have been shown to be oxidized in PS II other than the components directly associated with water oxidation. Cytochrome b_{559} (Cyt b_{559}), a chlorophyll Z (Chl Z), β-carotene (Car) have all been reported as 'side-path' electron donors in PS II. Understanding the side-path donors, their nature, structure, position, how they work and their significance to PS II function are all important for several reasons. First, these species may play roles in the regulation and protection of the reaction center (RC) under physiologically relevant conditions. Second, they constitute a significant proportion of the cofactors in PS II that cannot be ignored in structural terms and they may have as yet undetermined functional roles. Last, and of particular importance, a precise understanding of when and where the reactions of the side-path donors contribute to PS II electron transfer allows them to be clearly distinguished from the processes directly involved in enzyme function, and their influence on the kinetics of enzyme function to be fully understood.

Here we review the side-path electron donor pathway that involves Cyt b_{559}, Chl Z and Car. We deal with some structural aspects of Chl Z and Car, but Cyt b_{559} is only discussed in respect to its involvement in the alternative electron pathway, other aspects are covered elsewhere (Stewart and Brudvig, 1998; Chapter 16, Noguchi and Berthomieu).

Abbreviations: BRC – bacterial reaction center; Car – redox active β-carotene; Car_{D2} – β-carotene associated with D2; $Car_{D2\text{-}43}$ – β-carotene associated with both D2 and CP43; Chl Z – side-path redox-active Chl; Chl – chlorophyll; Chl_{D1}, Chl_{D2} – monomeric Chls that are bound to D1 and D2, respectively; Cyt b_{559} – cytochrome b_{559}; D1, D2 – reaction center core proteins; ENDOR – electron nuclear double resonance; EPR – electron paramagnetic resonance; ESEEM – electron spin echo envelope modulation; FTIR – Fourier transform infrared; HYSCORE – hyperfine sublevel correlation spectroscopy; OEC – oxygen evolving complex; P – central cluster of Chls that comprise the primary electron donor; $P_{D1}P_{D2}$ – two monomeric Chls associated with D1 and D2, respectively, that are counterparts to the special pair Chls in the BRC; PS II – Photosystem II; Q_A, Q_B, – primary and secondary plastoquinone electron acceptors; Y_Z, Y_D – redox-active tyrosines bound to D1 and D2, respectively

II. Location of Accessory Electron Donors

A scheme of the structure of PS II is shown in Fig. 1. This is based on the refined 3.5 Å X-ray diffraction crystal structure (Zouni et al., 2001; Kamiya and Shen, 2003; Ferreira et al., 2004) but is similar in most respects to earlier models that were based on the structure of the purple bacterial reaction center (BRC), comparative spectroscopy, sequence analysis

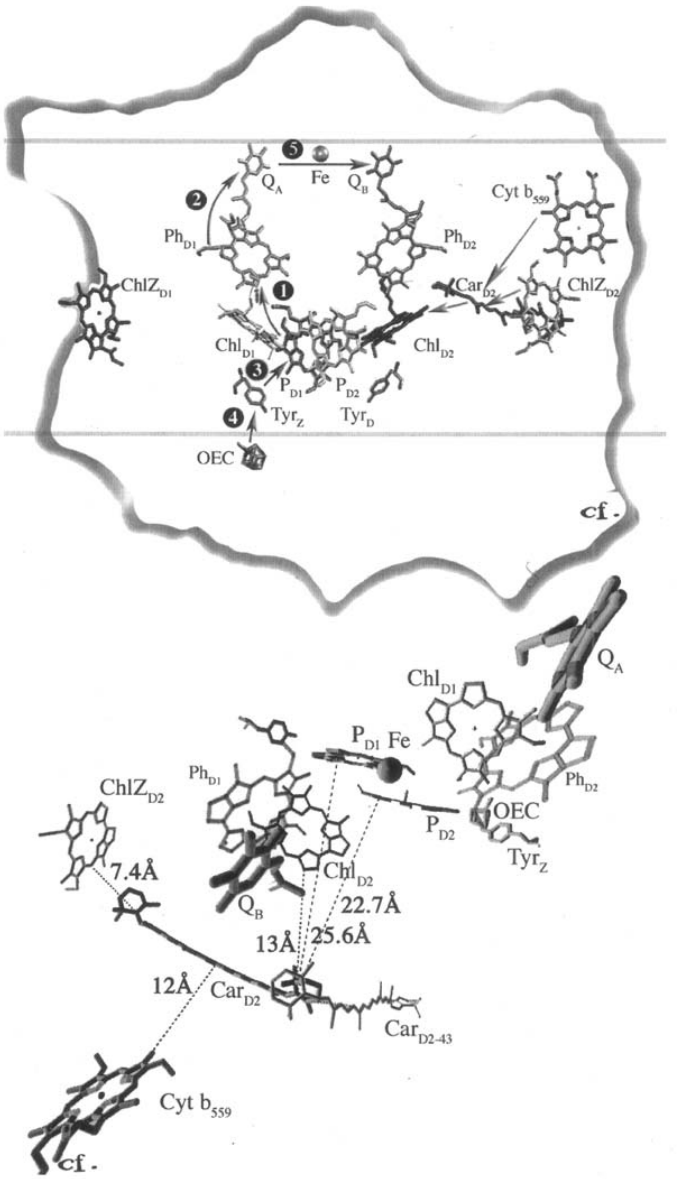

Fig. 1. The upper part shows a structural model of the PS II reaction center showing the arrangement of the cofactors. The electron transfer chain resulting in water oxidation and plastoquinone reduction is marked by numbered arrows. The numbers indicate the order in which the reactions take place. The electron transfer chain from the side-path donors is marked with unnumbered arrows. The cofactors are labeled with abbreviations that are defined in the text but are supposed to be as evident as possible. The boundary of the D1/D2/Cyt b_{559} complex is given as is the approximate position of the membrane. The model is drawn based on the current crystal structure (Ferreira et al., 2004). The lower part shows a view of PS II from above (non-heme iron side) showing the positioning of the carotenes Car_{D2} and Car_{D2-43}, Chl Z_{D2} and Cyt b_{559} relative to the central Chls of PS II. The vectors shown are the shortest distances between Car_{D2} its potential electron transfer partners (including P_{D1} P_{D2} and Chl_{D2}) measured edge to edge from the conjugated parts of the molecules (data from the coordinates from Ferreira et al., 2004).

and folding models, biochemical work, electron diffraction and spectroscopic structural measurements (Rutherford and Faller, 2001).

A. Cytochrome b_{559}

From the early days, the fact that Cyt b_{559} was oxidized at cryogenic temperatures led to the idea that it must be integral to the core of the reaction center (Knaff and Arnon, 1969). This idea was confirmed when the smallest isolated complex that was still capable of charge separation was found to contain only the D1, D2 and Cyt b_{559} (Nanba and Satoh, 1987). From the crystal structure, Cyt b_{559} is located adjacent to the D2 subunit (Zouni et al., 2001).

The number of Cyt b_{559} per PS II has been debated for many years (Stewart and Brudvig, 1998). The first crystal structure of PS II from cyanobacteria showed the presence of only one Cyt b_{559} (Zouni et al., 2001). One might have expected this to end the debate. However, Zouni et al. (2001) raised the possibility that a second cytochrome could have been lost during the preparation. The symmetry-related location on the D1-side indeed contains two *trans*-membrane helices like those of the cytochrome but there is no heme. However we consider that the loss of the putative second heme may well have occurred during the evolution rather than the isolation of PS II (for further discussion, see Stewart and Brudvig, 1998; Chapter 16, Noguchi and Berthomieu).

B. Chlorophyll Z

The smallest PS II reaction center preparation contains six Chls, two pheophytins, two β-carotenes and one heme. One or two of the Chls and a β-carotene can be lost when harsher isolation procedures are used (Satoh, 1996). This stoichiometry differs from that in the BRC, which contains four bacterio-Chls (BChls) rather than six. An obvious explanation was that the two additional and easily lost Chls in PS II corresponded to the Chl Z and its symmetrical counterpart that were predicted to be bound to D1-His118 and D2-His117 on the periphery of the complex (Ruffle et al., 1992).

Other evidence for the location of the Chl Z (and its symmetrical counterpart) came from EPR relaxation studies that placed Chl $Z^{+\bullet}$ at a distance of 39.5 Å from the non-heme Fe, a distance that corresponded well to the predicted position of D1-His118 and D2-His117 in the folding model (Koulougliotis et al., 1994). Further strong evidence came from site-directed mutagenesis on the D1-His118 and D2-His117, the supposed ligands of Chl Z_{D1} and Chl Z_{D2}, respectively. These mutants showed changes attributable to Chl Z as measured by resonance Raman (Stewart et al., 1998) and fluorescence quenching (Wang et al., 2002). Given this information, densities attributable to Chl Z were pointed out in both D1 and D2 in the crystallographic models (Zouni et al., 2001). The question of whether the oxidizable Chl Z corresponds to Chl Z_{D1} or Chl Z_{D2} is discussed below.

C. β-Carotene

The observations that carotenoid could be oxidized at liquid helium temperature (Schenck et al., 1982; Hanley et al., 1999) indicated that it must be in the heart of the RC. The isolated D1/D2/Cyt b_{559} complex indeed contained two Car molecules (Satoh, 1996) and these could be oxidized upon illumination under some circumstances (Telfer et al., 1991; Telfer, 2002).

While the first crystal structure of PS II at 3.8 Å assigned densities to the other cofactors as predicted from earlier work, no densities were assigned to the carotenoids (Zouni et al., 2001). The second structure by Kamiya and Shen (2003) at 3.7 Å assigned some density to the carotenoids, placing two Car molecules on D2. Shen revised this model, making the *cis* Car into all *trans*, extending one Car so that it approached the Chl Z_{D2} (Shen and Kamiya, 2003). The first refined crystal structure at 3.5 Å supported this position for the one β-carotene (see Fig. 1) but the second was less closely associated with D2 (Ferreira et al., 2004).

The Car most closely associated with D2 (Car_{D2}) lies approximately parallel to the membrane plane along the outside surface of the D2 and approaches the Chl Z_{D2} (see Fig. 1). As it crosses over the D2 surface, it runs along the interface between D2, the J-subunit and the β-subunit of Cyt b_{559} (Chapter 6, Thornton et al.). One of the head groups of Car_{D2} gets very close (nearest aromatic edge to edge 7.4 Å) to Chl Z_{D2}, while the other head group is only 3.8 Å from the second carotenoid. This Car, which is approximately perpendicular to the membrane plane (and to the Car_{D2}), runs from D2 to the CP43 subunit, and is thus designated here $Car_{D2\text{-}43}$. In addition to its proximity to Car_{D2}, the $Car_{D2\text{-}43}$ runs down the outside of D2, approaching only a few amino acids (notably those of the J, K and D1 subunits), and reaching the

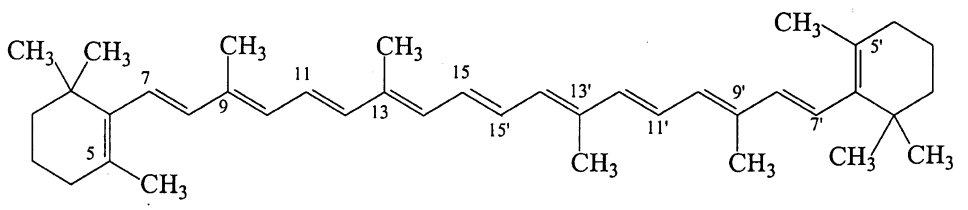

Fig. 2. Chemical structure of β-carotene.

lumenal side antenna Chls of CP43. Intriguingly, on the way it rubs up against the isoprene tails of the Chl_{D2} and Q_B near the surface of D2. It also approaches (to within 8.7 Å) a third carotenoid that is mainly associated with the K subunit (see Ferreira et al., 2004).

Seven carotenoids were modeled into the crystal structure of PS II, which fits reasonably well to the estimated number based on extraction of pigments from the complex (J. Barber, personal communication; however, see Tracewell et al. (2001b) who reported more than twice this number in *Synechocystis*). In addition to the three carotenoids mentioned above, the remaining four are arranged in two pairs, one pair on the outer surface of CP43 and another in a similar location on CP47, both well away from potential side-path action. It seems quite possible that the two Car molecules associated with the isolated D1/D2/Cyt b_{559} correspond to the Car_{D2} and $Car_{D2\text{-}43}$, described above, with the Car_{D2} being held in place by the cytochrome subunit and $Car_{D2\text{-}43}$ being attached to the first Car but more loosely bound to the exterior of D1/D2.

The location of the Car_{D2} in the crystal structure (Fig. 1) corresponds in general terms to the predictions for the redox active carotenoid from spectroscopic work, in that it is located between the central pigments, the Cyt b_{559} and the Chl Z (Hanley et al., 1999). Other more specific suggestions based on spectroscopy appear less successful: (i) The electron spin echo modulation (ESEEM) identification of a close interaction between $Car^{+\bullet}$ and a tryptophan nitrogen nucleus led Deligiannakis et al. (2000) to identify a group of conserved tryptophans in D2 as the likely site for the Car. The crystal structure shows that these tryptophans do not constitute the site (Ferreira et al., 2004). Indeed there are no appropriately located tryptophans close to either Car_{D2} or $Car_{D2\text{-}43}$ in the structure. An alternative candidate for the nitrogen coupling is not yet clear; however, the close association with the Chl Z_{D2} raises the possibility that a tetrapyrrol nitrogen could be involved. (ii) The dipolar 38 Å distance from the non-heme iron to $Car^{+\bullet}$ deduced from a saturation recovery method (Lakshmi et al., 2003) corresponds poorly with the crystal structure. Considerations of the spin distribution led the authors to place the $Car^{+\bullet}$ on the luminal side of the reaction center with the nearest part of the molecule at 38 Å: far from the actual location (the nearest part of the $Car^{+\bullet}$ to the Fe is 28 Å). The discrepancy could be due to an unexpected localization of the spin on the $Car^{+\bullet}$ or to technical problems such overlap from the Chl $Z^{+\bullet}$ signals (see also the next paragraph). (iii) Tracewell and Brudvig (2003) observed the apparent influence of the redox state of Y_D on the absorption spectrum of the $Car^{+\bullet}$. This was attributed to an electrostatic effect of $Y_D^{\bullet}(H^+)$on the closer of the two carotenoids. The proximity of the Car to the Y_D and the model deduced from that work fits poorly with the crystal structure. However the effect is worth reinvestigating in the light of the new structural model.

The current crystal structure contradicts models in which the two Car molecules were positioned symmetrically in both D1 and D2 (Faller et al., 2001a; Tracewell et al., 2001a,b; Lakshmi et al., 2003; Telfer, 2002). In these cases the models were not based on spectroscopic evidence for a D1 side Car, but rather on the extension of the cofactor symmetry in the reaction center. In fact, for carotenoids, the BRC, which has provided the basis for models of PS II for decades, did not exhibit such symmetry for the location of the carotenoid (Michel and Deisenhofer, 1988), and the current crystal structure of PS II is like the BRC in that respect (Ferreira et al., 2004).

Having listed the apparent mismatches between the crystal structure and the spectroscopic models, it is worth making the following points. The crystal structure has a resolution of 3.5 Å and precedence indicates that at this resolution carotenoids are among the more difficult cofactors to fit due to their similarities with isoprene tails and lipids. Thus, some

changes in the precise location of the carotenoids might be expected as the crystal structure improves. Secondly, the structure raises the possibility that electron transfer between adjacent carotenoids could allow the cation to migrate out away from D2 into the peripheral antenna under some conditions. This could mean that the spectroscopists are measuring a carotene cation different from $Car_{D2}^{+\bullet}$, at least under some experimental conditions.

III. Spectroscopic Studies

A. β-Carotene

1. Neutral Carotenes

Spectroscopic and biochemical analyses showed that two Car molecules were present in the D1/D2/Cyt b_{559} complex. There is still some debate concerning their *cis* or *trans* configuration (Telfer, 2002). Isolation studies gave conflicting results (Bialek-Bylka et al., 1995; Yruela et al., 1998). The majority of the spectroscopic studies assumed that both are in the *trans* configuration (Tracewell et al., 2001b; Telfer, 2002). The recent crystallographic model of Kamiya and Shen (2003) suggested that one of the Cars was in a *cis* conformation, but this model was later revised to both being all-*trans* (Shen, 2003). The refined crystal structure shows only one (all *trans*) β-carotene (Car_{D2}) within D1/D2 and that is located in D2 (Ferreira et al., 2004). A second (all *trans*) β-carotene runs from D2 to CP43 (Car_{D2-43}) and approaches (3.8 Å) the Car_{D2}. We suggested above that the second Car co-isolated with D1/D2/Cyt b_{559} complexes could be Car_{D2-43}, stuck to the outside of the complex.

Linear dichroism measurements on D1/D2/Cyt b_{559} complex preparations showed a positive and a negative peak that was interpreted either as arising from excitonic interactions between the two Car molecules (i.e., proximity) or reflecting the presence of two distinct Car molecules (Van Dorssen et al., 1987a; Renge et al., 1996; Germano et al., 2001; for recent reviews see Tracewell et al., 2001b; Telfer, 2002). The most recent data is interpreted as a two strongly coupled carotenoids (Frese et al., 2003). Similarly several studies indicate a different orientation of the dipole moment of the two transitions, indicating a different orientation for the two neutral carotenoids (van Dorssen et al., 1987b; Breton et al., 1988; Kwa et al., 1992; Tomo et al., 1997). The carotenoid with absorption transitions at 507/473/443nm is nearly parallel to the membrane while the 489/458/429nm carotenoid is closer to 45° to the membrane but approximately perpendicular to the other carotenoid. These data appear to be consistent with the idea that the two β-carotenes in D1/D2/Cyt b_{559} complexes correspond to Car_{D2} and Car_{D2-43} in the most recent crystal structure, at least within the limits of the resolution of that model. The Car moleucles are close enough to be coupled and they appear to be all-*trans* and oriented at approximately right angles to each other (Ferreira et al., 2004). The Car with absorption transitions at 507/473/443nm (Car_{507}) would then correspond to the Car_{D2}, while the 489/458/429nm carotene (Car_{489}) would correspond to Car_{D2-43}. The latter is expected to be more exposed to solvent and detergent, so is more likely to exhibit variability its spectroscopic and chemical properties in isolated D1/D2/Cyt b_{559} complexes.

2. Electronic Absorption of the β-Carotene Cation Radical

The $Car^{+\bullet}$ in PS II shows a strong absorbance band at about 990 nm in spinach and *Synechocystis* with an extinction coefficient of about 160,000 (Hanley et al. 1999, Tracewell et al., 2001a). A shoulder around 880 nm was also assigned to $Car^{+\bullet}$ (Faller et al., 2001a; Tracewell et al., 2001a). The position at 990 nm is typical for β-carotene cation radical as reported in in vitro experiments (Mathis and Vermeglio, 1972; Dawe and Land, 1975; Moore et al., 1984; Edge et al., 2000). It is also distinct from the doubly oxidized β-carotene cation that absorbs at around 800 nm (Jeevarajan et al., 1996a). Tracewell et al. (2003) deconvoluted the $Car^{+\bullet}$ spectrum in a range of experimental conditions and concluded that two different $Car^{+\bullet}$ species exist. Given the most recent model where two Car molecules are in close proximity and a third is fairly close (Ferreira et al., 2004), it seems possible that the two spectra represent different environments that perturb the charge distribution over the two or more carotenoids under different experimental conditions.

3. Electron Magnetic Resonance Studies

The $Car^{+\bullet}$ shows an X-band electron paramagnetic resonance (EPR) signal at g = 2.0025 ± 0.0001 and line-width about 10.5 ±1 G (Hanley et al., 1999; Faller et al., 2001a). These values are similar to $Car^{+\bullet}$ generated in vitro and typical for organic radicals

in general (Grant et al., 1988). Faller et al. (2000) and Lakshmi et al. (2000) measured high field EPR of $Car^{+\bullet}$ in PS II in spinach and *Synechocystis*, respectively. The g-values reported agreed quite well (spinach/*Synechocystis*:g_x 2.00322/35, g_y 2.00252/1, g_z 2000211/27). These g-values are clearly distinct from the g-values obtained from the canthaxanthin cation radical (a carotenoid having two ketogroups at position 4, see Fig. 2), generated in vitro (on silica-alumina surface). The $Car^{+\bullet}$ in PS II has a rhombic g-tensor, while the g-value of the canthaxanthin cation radical on the silica-alumina surface is axial (Konovalova et al., 1999). The origin of this difference is not clear yet, but the different environment between the protein matrix and the silica-alumina surface could be responsible, rather than the influence of the two keto groups (Faller et al., 2000; see below). Indeed it is possible that the carotenoid on the silica-alumina surface has undergone significant chemical changes.

ESEEM and hyperfine sublevel correlation spectroscopy (HYSCORE) measurements were interpreted as showing that $Car^{+\bullet}$ in PS II interacts with an indol nitrogen from a tryptophan in its vicinity (Deligiannakis et al., 2000). The Car_{D2} in the recent crystal structure (Ferreira et al., 2004) does not approach any such tryptophan. How can this be explained? Three possibilities arise: (i) The assignment could be wrong (perhaps the pyrrol nitrogen of the neighboring Chl Z_{D2} is responsible for the ^{14}N couplings). (ii) As a result of electron transfer, the cation could be on a different carotenoid, however, a preliminary hunt shows that the more peripheral carotenoids do not approach any tryptophan groups either; the nearest appears to be Trp271 of D1 at around 6 Å. (iii) The crystal structure at the level of the carotene may be wrong or, as they say in the trade: 'it may yet undergo further refinement.'

The β-carotene cation radical generated on silica-alumina showed an interaction with an Al nucleus (Konovalova et al., 2001). The ENDOR measurement of $Car^{+\bullet}$ in PS II showed the largest hyperfine splitting in the range of ~8 MHz suggesting that the spin is delocalized over the Car molecule. Comparable hyperfine splittings were obtained from β-carotene cation radical formed by oxidation with iodine in organic solvent (Faller et al., 2001). These observed hyperfine splitting values were confirmed recently by a density functional theory study of Himo (2001). This study suggested a spin delocalization over the entire π-conjugated system including the double bonds in the head groups (see Fig. 2).

Electron nuclear double spin (ENDOR) measurement of the β-carotene cation radical and two other carotenoid radical cations (canthaxantincation radical and 8′-apo-β-caroten-8′-al) on a silica alumina solid supports exhibited high hyperfine splitting values of about 13 MHz (Jeevarajan et al., 1993). Based on semi-empirical INDO-type calculations, this was assigned to the methyl groups at position 13 and 13′ (see Fig. 2). This indicated a higher spin concentration in the middle of the molecule compared to the measurement mentioned above. These differences could again be due to interaction with the support (Faller et al., 2000; Himo, 2001) or to different conformations (Konovalova et al., 2001)

4. Vibrational Spectroscopy

Fourier transform infrared (FTIR) spectroscopy of β-carotene cation radical in PS II and organic solvents (oxidized by iodine) was reported by Noguchi et al. (1994). Bands at 1465, 1441, 1148, 992 and 966 cm^{-1} were assigned to $Car^{+\bullet}$ in PS II, which were partly comparable to the β-carotene cation radical in organic solvents (1479, 1151 and 1001 cm^{-1}). The authors pointed out that the structure of β-carotene cation radical in PS II and organic solvents differ somewhat, but no details or possible reason was given or discussed.

Raman measurements of $Car^{+\bullet}$ in D1/D2/Cyt b_{559} complexes and PS II membranes have been reported (Pascal et al., 1999; Vrettos et al., 1999; Telfer et al., 2003). The most intense bands were very similar in the different studies and were located around 1001, 1154, 1484 and 1525 cm^{-1}. The spectra of $Car^{+\bullet}$ in D1/D2/Cyt b_{559} complexes and PS II membranes were in agreement with a slightly twisted all-*trans* conformation of the $Car^{+\bullet}$(A. Pascal, personal communication). The most recent study attributed vibrational bands at 1485 and 1525 cm^{-1} to the Car_{507} and bands at 1491 and 1537 cm^{-1} to a Car_{489} cation (Telfer et al., 2003). Based on the orientation data described above and the crystal structure (Ferreira et al., 2004), we might assign these to the Car_{D2} (Car_{507}) and the $Car_{D2\text{-}43}$ (Car_{489}) in the crystal structure. The legitimacy of these assignments will be tested by future refinements of the crystal structure.

Jeevarajan et al. (1996b) reported that the extent of the downshift of the v1 frequency (around 1530 cm^{-1}) in going from neutral carotenoids to the radical cation depends on the length of the conjugated chain.

By applying this hypothesis to the $Car^{+\bullet}$ in D1/D2/Cyt b_{559} complex, a more localized spin distribution, i.e., not over the entire conjugated chain, was suggested (Pascal et al., 1999). However, this was contradicted by the EPR measurements as well as the density functional theory study (Faller et al., 2000, 2001b; Himo, 2002).

The resonance Raman spectrum of $Car^{+\bullet}$ in intact (water oxidizing) and Mn-depleted PS II showed no significant differences. In contrast, minor differences were observed when it was compared to $Car^{+\bullet}$ in D1/D2/Cyt b_{559} preparations indicating that latter preparation affects the structure pigments (A. Pascal, personal communication). This fits with the crystal structure which shows that the carotenes are predicted to be exposed in D1/D2/Cyt b_{559} preparations.

B. The Active Chlorophyll Z Cation Radical

The realization that $Car^{+\bullet}$ can accumulate in the majority of the centers by illumination at temperatures lower than 77K raised questions about many earlier studies done under such conditions where it had been assumed that only Chl $Z^{+\bullet}$ was present. It seems likely that such studies would have been at least contaminated with $Car^{+\bullet}$ (see above and Hanley at al., 1999; Vrettos et al., 1999). This holds in particular for (X-band) EPR studies where $Car^{+\bullet}$ and $Chl^{+\bullet}$ show almost identical spectra (see below) but this may also have been a problem in other kinds of spectroscopic studies.

1. Electron Magnetic Resonance Studies

Chl $Z^{+\bullet}$ shows an X-band EPR signal at g=2.0025 ±0.0001 and a line width of about 10.5 ±1 G (Visser et al., 1977; DePaula et al., 1985; Hanley et al., 1999). These values are similar to $Car^{+\bullet}$ generated in PS II and therefore virtually indistinguishable. They were distinguished originally by matching optical absorption studies (Hanley et al., 1999); and subsequently by using more sophisticated EPR methods. High-field EPR of Chl $Z^{+\bullet}$ was measured in spinach and *Synechocystis*: (MacMillan et al., 1998; Faller et al., 2000; Lakshmi et al., 2000). The two studies of spinach PS II showed essentially identical g-values (e.g., g_x 2.00308, g_y 2.00253, g_z 2.00216), whereas Chl $Z^{+\bullet}$ from *S. lividus* exhibited a higher g-anisotropy (g_x-g_z = 11.0) and a very low g_z value (g_x 2.00312, g_y 2.00263, g_z 2.00202). This remains unexplained. The spectrum of Chl $Z^{+\bullet}$ at high field is also somewhat different from $Chl^{+\bullet}$ generated in organic solvent, probably reflecting the different environment (Bratt et al., 2000; Un et al., 2001).

ESEEM was measured on Chl $Z^{+\bullet}$ by Deligannakis et al. (2000) and a spectrum dominated by features originating from the pyrol ^{14}N nuclei were reported. Also ENDOR measurements of Chl $Z^{+\bullet}$ revealed similar hyperfine couplings to those seen for $Chl^{+\bullet}$ in organic solvents (Lubitz, 1991; Rigby et al., 1994; Faller et al., 2001b). In the pulsed ENDOR study of Chl $Z^{+\bullet}$, two hyperfine couplings at 10.8 and 14.9 MHz were detected and assigned to the β-H at position 17 and 18 (Fig. 3). In contrast, $Chl^{+\bullet}$ in organic solvent exhibited only one broad hyperfine coupling at 12.5MHz. Hence it appears that the protein imposes a distinct conformation, leading to two distinct and resolved hyperfine couplings in Chl $Z^{+\bullet}$ (Faller et al., 2001b).

2. Vibrational Spectroscopy

FTIR difference spectrum of Chl $Z^{+\bullet}$/Chl Z exhibited positive bands at around 1747 and 1714 cm^{-1}, which were assigned to the carboxy C=O and keto C=O, respectively (Fig. 3) (Noguchi et al., 1994; Noguchi and Inoue, 1995). Again the spectrum was similar to $Chl^{+\bullet}$/Chl in organic solvent. Resonance Raman on Chl $Z^{+\bullet}$ was reported by Cua et al. (1998). Since the illumination was given at 30K it seems likely that some $Car^{+\bullet}$ was also formed and probably contributed significantly to the spectrum (the $Car^{+\bullet}$ electronic absorption spectrum tales down to the absorption of Chl $Z^{+\bullet}$). It seems that most of the bands detected in the $Car^{+\bullet}$ spectrum were also present in the Chl $Z^{+\bullet}$ spectrum. Also the most prominent band around 1480 cm^{-1} of Chl $Z^{+\bullet}$ has a corresponding band in $Car^{+\bullet}$, i.e., at 1484 cm^{-1}, which is also one of the most intense bands (Vrettos et al., 1999; Pascal et al., 1999; Telfer et al., 2003). This is supported by FTIR, where both, Chl $Z^{+\bullet}$ and $Car^{+\bullet}$, exhibited a band around 1480 cm^{-1}. Thus, the designation of the band around 1480 cm^{-1} as a benchmark for Chl $Z^{+\bullet}$ (Tracewell et al., 2001a) is questionable (Telfer et al., 2003).

3. Orientation

Information concerning the angular orientation of Chl $Z^{+\bullet}$ with respect to the membrane has been obtained from one-dimensional oriented PS II membranes by high-field EPR measurements (Faller et al., 2000). Assuming a similar orientation of the g-tensor in

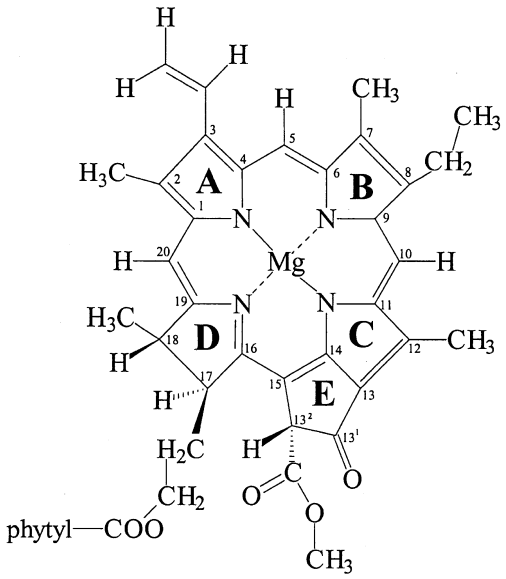

Fig. 3. Chemical structure of chlorophyll *a*.

Chl $Z^{+\bullet}$ as for BChl $a^{+\bullet}$, the ring plane of the Chl $Z^{+\bullet}$ was found to be oriented perpendicular to the membrane plane. This is consistent with the orientation of both Chls assigned to Chl Z_{D1} and Chl Z_{D2} in the current model from crystallography shown in Fig. 1 (Zouni et al., 2001; Ferreira et al., 2003).

IV. Electron Transfer Pathways

A. The Mainline Electron Transfer Pathway

A few hundred picoseconds after the absorption of a photon by PS II the radical pair formed consists $P^{+\bullet}/Q_A^{-\bullet}$ (electron transfer reactions shown as arrows 1 and 2 in Fig. 1), where $P^{+\bullet}$ is a Chl cation radical located on one or the other (through a redox equilibration) of the two Chl monomers (P_{D1} and P_{D2}) and $Q_A^{-\bullet}$ is a plastosemiquinone (reviewed in Rappaport and Diner 2002; Chapter 7, Renger and Holzwarth). Tyrosine 161 of D1 (Y_Z) acts as an electron donor to $P_{D1}^{+\bullet}$ (arrow 3 in Fig. 1) and the $Y_Z^{+\bullet}$ oxidizes the Mn cluster in the first step of the redox cycle required for water oxidation (arrow 4 in Fig. 1). In the majority of centers donation from Y_Z to P_{D1} is rapid and efficient in out-competing the charge recombination reaction $P^{+\bullet}/Q_A^{-\bullet}$ to PQ_A. In some centers Y_Z donation is slower, reflecting heterogeneities, perhaps associated with pKs on groups affecting, for example, the de-protonation of the tyrosine, the location of the $P^{+\bullet}$ cation and the redox potentials of these cofactors. On each state in the enzyme cycle the rates of donation vary depending on accumulated charges, movements of charged species (protons, and possibly Cl^-) and structural changes. As a result $P^{+\bullet}$ is relatively long-lived in a statistical fraction of center during enzyme function. In centers where the OEC is dysfunctional or absent (e.g., prior to or during assembly of the Mn cluster) then long-lived $P^{+\bullet}$ is expected to occur on the majority of charge separations.

When electron donation to $P^{+\bullet}$ is slow, and consequently $P^{+\bullet}$ long-lived, the back-reaction from $Q_A^{-\bullet}$ will occur (200 μs^{-1} ms) (for a review, see Rappaport and Diner, 2002). This reaction will be in competition with electron transfer from $Q_A^{-\bullet}$ to Q_B (or $Q_B^{-\bullet}$) (arrow 5 in Fig. 1). Thus in some centers the lifetime of P^+ could be significantly longer than the $P^{+\bullet}/Q_A^{-\bullet}$ radical pair recombination lifetime. Prior to photoactivation Q_A has a higher potential and this decreases the efficiency $Q_A^{-\bullet}$ to Q_B electron transfer and may limit the long-lived $P^{+\bullet}$ as well as affecting the charge recombination route (Johnson et al., 1995).

$P^{+\bullet}$ is the most oxidizing species in PS II with an estimated potential of around 1.1 V or higher (Rappaport and Diner, 2002; Rutherford and Faller, 2002). It is potentially capable of oxidizing cofactors or amino acid side chains in its vicinity other than the those directly involved in the water-plastoquinone oxidoreductase activity. The side-path electron donations (arrows from the right in Fig. 1) are generally considered to function as redox quenchers of $P^{+\bullet}$, limiting unwanted and potentially damaging side-reactions. Given the high yields of water oxidation, the yields of oxidation of the side-path donors are expected to be very low; however, the yields are liable to increase under any of the conditions where the lifetime of $P^{+\bullet}$ increases.

B. Side-Path Electron Donors: Historical Summary

The oxidation of Cyt b_{559} upon illumination has been known and studied for many years (Stewart and Brudvig, 1998). In intact PS II this occurs in the majority of the centers with a low quantum yield when illumination is given at 77K or below. In some centers a high quantum yield electron donation probably from Y_Z, can take place, forming the $Y_Z^{+\bullet}$ $Q_A^{-\bullet}$ state,

at least when in the S_0 and S_1 states (Nugent et al., 2002; Zhang and Styring, 2003; C. Zhang and A.W. Rutherford, unpublished). At temperatures where the Mn oxidation can take place (around 200K or higher, depending on the S-state), Cyt b_{559} oxidation is greatly out competed (Mathis and Vermeglio, 1975; DePaula et al., 1985). At physiological temperatures a small fraction of the cytochrome seems to go oxidized through the redox equilibration of the oxidizing equivalent in the S_2 and S_3 redox states of the OEC (Buser et al., 1992).

If Cyt b_{559} is preoxidized, Chl $Z^{+\bullet}$ is generated instead with similar yields (Visser et al., 1977; Thompson and Brudvig, 1988). This turns out to be the most common situation in PS II preparations where the electron donor side is modified, damaged or where the Mn complex is absent. The redox potential of the cytochrome is extremely sensitive to mistreatment and shifts from the (usually) native high potential form to the low potential form resulting in the oxidation of the heme under ambient redox conditions (Stewart and Brudvig, 1998). However, when the Cyt b_{559} is reduced in Mn-depleted PS II it can be oxidized with a low quantum yield upon illumination at all temperatures below that where Y_Z donation is inhibited (lower than around –30 °C) (Faller et al., 2001a).

Carotenoid cation photogeneration was observed first when lipophilic redox reagents were added to PS II (Velthuys, 1981; Schenck et al., 1982) but early on it was recognized that the presence of these chemicals was not required under some conditions (Schenck et al., 1982). For many years its sub-stoichiometry and the involvement of the lipophilic anion in most studies, cast carotenoid oxidation as a merely interesting chemical quirk and a redox role for carotenoid in PS II chemistry was rarely considered. This view changed in recent years and it is now thought that β-carotene acts as an electron donor to $P^{+\bullet}$ and is reduced by the Chl Z and Cyt b_{559} (Hanley et al., 1999). In what follows we deal with some of the data and arguments that have contributed to the current understanding of the electron transfer pathway involving Cyt b_{559}, Chl Z and Car.

C. The Alternate Electron Transfer Pathway

The pathway of the alternative donors was addressed by Thompson and Brudvig (1988), considering only Cyt b_{559} and Chl Z, since at that time Car was not recognized as a relevant player. In this work the ability of either Cyt b_{559} or Chl Z to compete with the electron donation of the Mn-cluster/Y_Z was measured. It was assumed that Mn-cluster/Y_Z donation rate gradually decelerated upon lowering the temperature and hence at a given temperature the side-path donors start to compete with the Mn-cluster/Y_Z donation, eventually becoming the dominant donors. This implies that at the temperature where 50% of the side-path donor and 50% Mn-cluster/Y_Z were oxidized upon illumination, the donation rates by the two competing pathways are equal. This experiment was done by: (i) measuring photo-generation of oxidized Cyt b_{559} (i.e., with Cyt b_{559} reduced prior to illumination); and (ii) measuring photo-generation of Chl $Z^{+\bullet}$ (i.e., when Cyt b_{559} was oxidized prior to illumination). It was found that Cyt b_{559} oxidation and Chl Z oxidation showed identical temperature dependencies; thus, it was concluded that the electron donation reaction competing with Y_Z and Mn oxidation was identical for the oxidation of Cyt b_{559} and for Chl Z. The simplest explanation for these observations was a linear electron donation pathway Cyt $b_{559} \rightarrow$ Chl Z $\rightarrow P^{+\bullet}$ (Thompson and Brudvig, 1988).

More recent data indicate that the kinetic model behind these experiments should be revised. Flash kinetic studies by E. Schlodder and H. Derr (personal communication) showed that Y_Z electron donation does not gradually slow down allowing the side-path donors to take over. In fact Y_Z electron donation to $P^{+\bullet}$ only decelerated from a rate of $t_{½}$ = 20 ns at 300 K to $t_{½}$ = 4.2 µs at 150 K. The slower Y_Z electron donation to $P^{+\bullet}$ ($t_{½}$ = 4.2µs) is gradually replaced by the 2ms phase of the $P^{+\bullet}/Q_A^{-\bullet}$ recombination as the temperature is lowered. The rate of oxidation of the side-path donors ($t_{½}$ 20 ms, depending on temperature) remains much slower than this and occurs with a low quantum yield (Hillmann and Schlodder, 1997; Faller et al., 2001a; R. Edge, P. Faller and A.W. Rutherford, unpublished).

A re-interpretation of the Thompson and Brudvig experiment is as follows: The point where Y_Z and the side-pathway become oxidized to an equal extent is not due to a direct competition between two donors with similar rates. Rather, it is due to a cooling-induced heterogeneity of the centers, where in half of the centers Y_Z is oxidized with $t_{½}$ = 4.2 µs while in the other half Y_Z oxidation does not take place and $P^{+\bullet}/Q_A^{-\bullet}$, recombination occurs instead ($t_{½} \sim$ 2 ms). In these centers the continuous illumination results in the photo-accumulation of oxidized electron donors of the side-path with a low quantum yield.

This situation may be complicated further if in

some centers Y_Z donation remains rapid (Nugent et al., 2002; Zhang and Styring, 2003; Zhang et al., 2004) and if in other centers the 'switching off' of Y_Z donation occurs in stages as the temperature is lowered, allowing a low quantum yield donation from Y_Z, in competition with the side-path donors prior to switching off altogether as the temperature is lowered.

The discovery that formation of $Car^{+\bullet}$ upon illumination at low temperature in greater yields than was previously reported, raised the question of where the Car fits in the electron side-pathway and a range of possibilities were considered (Hillman and Schlodder, 1997; Hanley et al., 1999; Vrettos et al., 1999). The observation of Hanley et al. (1999) that the near stoichiometric formation of $Car^{+\bullet}$ upon illumination at 20K was replaced by Chl $Z^{+\bullet}$ when warmed in the dark to temperatures above 77K, led to the suggestion that the following pathway was present:

$$\text{Chl Z} \rightarrow \text{Car} \rightarrow P^{+\bullet}$$

Further support for this arrangement came from the observation that $Car^{+\bullet}/Q_A^{-\bullet}$ recombination could occur at low temperature in competition with the electron donation reaction from Chl Z (Hanley et al., 1999). Similarly Tracewell et al. (2001a) also showed that the recombination of $Car^{+\bullet}/Q_A^{-\bullet}$ was faster than Chl $Z^{+\bullet}/Q_A^{-\bullet}$. Both observations imply a closer localization of Car than Chl Z relative to P.

Hanley et al. (1999) showed that Cyt b_{559} could be oxidized at 20K despite the fact that Chl Z → Car donation was blocked at this temperature in the majority of centers. This led them to favor a branched pathway over the simple linear pathway:

$$\begin{array}{l} \text{Cyt } b_{559} \rightarrow \text{Car} \rightarrow P^{+\bullet} \\ \qquad\qquad\quad \uparrow \\ \qquad\qquad\quad \text{Chl Z} \end{array}$$

It is important to note that while this contradicted the earlier model of Thompson and Brudvig (1988), it did not contradict their data nor their primary conclusion, i.e., that Cyt b_{559} oxidation and Chl Z oxidation were both dependant on the same electron donation reaction to P^+, a reaction that was favored as electron donation from Y_Z was inhibited by lowering the temperature.

Subsequent studies on electron donation rates and yields of the alternative donors also favored this so-called branched pathway and specifically argued against other possible pathways that had been raised earlier (Faller et al., 2001a). The branched pathway (Hanley et al., 1999) was later corroborated by the X-ray crystallographic model (Zouni et al., 2001), which indicated that the edge-to-edge distances between either cofactor (Cyt b_{559} and Chl Z) to the central Chls was more than 35 Å and 25 Å, respectively. Even the shorter Chl Z distance allows only a slow electron transfer rate (~1 s^{-1} according to Page et al., 1999), nearly three orders of magnitude slower than the observed rates. Furthermore the distance between the Cyt b_{559} and the Chl Z was found to be about 24 Å, indicating that direct electron transfer between the cofactors would be very slow. Thus, the Car as an intermediate in the electron transfer as proposed in the branched pathway (Hanley et al., 1999), is required to explain the electron donation rates from Cyt b_{559} and Chl Z to $P^{+\bullet}$. The recent assignment of density to Car in D2 in the crystallographic model supports the branched pathway (Kamya and Shen, 2003; Ferreira et al., 2004; see section III and Figs. 1a and b).

The estimated $t_{½}$ for Car oxidation of 1–2 ms at room temperature (Telfer et al., 1991; R. Edge, P. Faller and A.W. Rutherford, unpublished) is faster than the maximal rate for the 22.7Å distance (i.e., $t_{½}$ = 29 ms, based on Page et al., 1999) between Car and the cation-bearing Chl P_{D1} (note the 25.6 Å distance between Car_{D2} to P_{D2}) (Ferreira et al., 2004; Fig. 2). It thus seems likely that donation occurs via an intermediate cofactor with Chl_{D2} being the likely candidate. The shortest distance between the Car_{D2} and the Chl_{D2} is around 13.1 Å, a distance that would allow a maximum electron transfer rate with a half-time of around 50 nanoseconds (Page et al., 1999). Thus even a very small fraction of the cation on the Chl_{D2}, through an equilibrium with the P Chls, would allow the appropriate kinetics of Car oxidation. Fig. 1 then shows Car_{D2} donating to $P^{+\bullet}$ via Chl_{D2} as the most likely pathway.

The shortest distance between Cyt b_{559} and Car_{D2} is 12 Å units, this corresponds to a maximum rate in the tens of nanoseconds time-scale (Page et al., 1999), in accordance with Cyt b_{559} oxidation being rate-limited by Car_{D2} oxidation (Faller et al., 2001a). Even with the Car_{D2} being closer to both the $Car_{D2\text{-}43}$ and to the Chl Z_{D2} than the Cyt b_{559}, the much lower potential of the cytochrome ensures that it out-competes $Car_{D2\text{-}43}$ and Chl Z as the final location of positive charge-equivalent.

The oxidized Cyt b_{559} can be reduced by electrons from the electron acceptor side. The rate for this reaction is very slow in PS II membranes, being pH-dependent and occurring in the time-scale of many seconds (Buser et al., 1992). In thylakoids, however, in which Q_B functions normally, the rate appears faster ($t_{½}$ = 100 ms) (Whitmarsh and Cramer, 1977). The reaction is inhibited by DCMU and this and the pH dependence of the reaction led Buser et al. (1992) to suggest that electron donor to the oxidized cytochrome is Q_BH_2. In this way the side path connects to the main-line of electron transfer completing a cycle that short-circuits normal electron transfer.

The Q_B head group is 26 Å units from the Cyt b_{559}. This corresponds to a maximal donation rate of around 2.7s much slower than the 100ms rate seen in chloroplasts. There are several possible explanations for this, among which are the following: (i) The electron donation in chloroplasts may not be from Q_BH_2 but from by PQH_2 directly from the membrane side. Indeed the crystal structure shows that the heme is relatively exposed to the membrane. (ii) Another possibility is that electron donation from Q_BH_2 does not occur from the Q_B site but a position closer to the heme as it leaves the site. If we assume that the hydroquinone backs out the way quinone came in, then the position of isoprene chain may represent an entry/exit channel. The quinone's tail gets to within 12 Å of the heme on its way to an obvious channel that connects to the membrane. At this position the Q_BH_2 donation to the heme would be a much more kinetically favorable reaction. The observation that that DCMU inhibits Cyt b_{559} reduction at a lower concentrations than Q_B reduction, implies that these reactions occurs at different sites, an observation that fits with both of the potential explanations discussed here.

D. Side-Path Donors: Which Side of the Reaction Center?

The arguments associated with this question are complex and have swung back and forth as new observations were made. The key observations in favor of the involvement of D1 are as follows: (i) A change in the ligand to Chl Z_{D1} results in a spectroscopic change associated with side-path donation while no such effect was seen when Chl Z_{D2} was mutated (Stewart et al., 1998). (ii) EPR measurements give a distance from Q_A to Chl Z that is compatible only with Chl Z being on the D1 side (Kawamori et al., 2002). The key observations in favor of the involvement of the D2 side are as follows: (i) A change in the ligand to Chl Z_{D2} results in spectroscopic changes associated with side path donation (Wang et al., 2003). (ii) EPR distance measurements from $Y_D^{\bullet}$ to Chl Z indicate that Chl Z is on the D2 side (Shigemori et al., 1998). (iii)The Cyt b_{559} is only on the D2-side (Zouni et al., 2001). (iv) The carotene is only on the D2 side (Kamiya and Shen, 2003; Ferreira et al., 2004).

The early debate between the proponents of either the D1-side or the D2-side was tilted strongly in the direction of D2, when the crystal structure showed that Cyt b_{559} was on the D2 side. The proponents of the D1-side then favored a 'both sides' model, putting their faith in a symmetrical reaction center, and encouraged by spectroscopic features that could be interpreted indicating two Chl Zs and two Car cations (Tracewell et al., 2001a,b; Telfer et al., 2003; Tracewell and Brudvig, 2003). The idea was put forward that symmetrical carotenoids could be present, allowing the positive charge to equilibrate between both carotenoids and both Chl Zs (Tracewell et al., 2001a,b; Tracewell and Brudvig, 2003). The absence of a D1 Car contradicts this model (Kamiya and Shen, 2003; Ferreira et al., 2004).

A novel solution was proposed to explain the involvement of Chl Z_{D1} when faced with the absence of a D1 Car. An electron transfer link was suggested through a series of Chls in CP 43, allowing the $Car_{D2}^{+\bullet}$ to oxidize the Chl Z_{D1} (Vasil'ev et al., 2003). This 'long-way-around' model was based on the poorly resolved crystal structure by Kamya and Shen (2003). In this model two carotenoids were proposed in D2, neither of which approached Chl Z_{D2}; thus it was implied that Chl Z_{D2} was not involved in the side-path. This model had a short life-time since Shen (2003) began revising his model of the carotenoids in 2003, only to be overtaken by a refined crystal structure (Ferreira et al., 2004). The 'long-way-around' model was dealt something of a double whammy by the following features of this structural model: (i) The Car_{D2} is close to Chl Z_{D2} making it rather likely that Chl Z_{D2} is involved in side-path electron transfer reactions. (ii) Even though an updated 'long way around' model can be defined (in which the Car_{D2} to $Car_{D2\text{-}43}$ gap is 3.8 Å, $Car_{D2\text{-}43}$ connects to the lumenal-side layer of CP43 Chls, and the CP43 Chls are, as expected for antenna pigments, in relatively close contact), the key CP43 Chl in the structure of Kamiya and Shen (2003), the Chl that triggered the original 'long way around' model, is absent in the structure of Ferreira

et al. (2004), leaving the nearest CP43 Chl to Chl Z_{D1} at a distance of 13 Å. These arguments do not argue strongly against the 'long way around' model nor the involvement of Chl Z_{D1}, they just make it less attractive.

Overall, the experimental data argue strongly for a D2-side path involving Car_{D2} as a donor to $P^{+\bullet}$, followed by electron donation from Cyt b_{559} to the $Car^{+\bullet}$ and finally slow electron donation from Q_BH_2 or PQH_2 to oxidized Cyt b_{559}. The involvement of Chl Z is much less clear. The proximity of Chl Z_{D2} to Car_{D2} indicates that electron transfer would be rapid, fitting with reports of partial Chl $Z^{+\bullet}$ formation at very low temperatures. The localization of the charge on Chl Z at higher temperatures indicates a lower redox potential than Car, but this may be more marked in isolated complexes, in which the peripheral position of both the Chl Z molecules and the carotenes could make them susceptible to solvent or detergent induced changes. A redox role for Chl Z_{D2} seems likely. The involvement of Chl Z_{D1}, is less clear and further experiments are required to determine the nature of its involvement in side path electron transfer.

V. Function of the Alternative Electron Transfer Pathway

A. A Protective Cycle for Redox Quenching of the Primary Electron Donor Cation

Many different functions for Cyt b_{559} have been suggested and these are dealt with in some detail elsewhere (Stewart and Brudvig, 1998). Here however we shall only discuss those associated with the function of the electron transfer side-pathway. Perhaps the most commonly held view for the existence of the side pathway focuses on the perceived necessity to provide electrons to $P^{+\bullet}$ in order to prevent it doing oxidative damage to the surrounding protein and neighboring chromophores. The idea is that whenever $P^{+\bullet}$ is sufficiently long-lived, the side-path can donate and thereby prevent unspecific oxidation reactions in the reaction center. This idea was proposed when the simple linear Cyt b_{559} to Chl Z to P pathway was considered to exist (Thompson and Brudvig, 1988) but it remains as valid for the more recently proposed branched pathway with Car as the branch point (Hanley et al., 1999). This begs the question whether this pathway can donate efficiently enough to provide an advantage to the organism.

The big question then is this: What is the rate of electron donation from Car to $P^{+\bullet}$ at room temperature? In D1/D2/Cyt b_{559} particles this rate was measured as the formation of the $Car^{+\bullet}$ at 980 nm and was found to be around 1 ms (Telfer et al., 1991). In more intact systems the measured rates vary but what is seen at all temperatures measured is that the yield for $Car^{+\bullet}$ formation is small and its apparent rate is the same as the lifetime of P^+ (R. Edge, P. Faller, K. Brettel, W. Leibl and A.W. Rutherford, unpublished). This implies that the real rate is significantly slower than the apparent rate. We attempted to optimize the rate and yield of $Car^{+\bullet}$ formation by removal of the Mn cluster, and then slowing the Y_Z donation rate by lowering the pH. Under these conditions the $P^{+\bullet}$ decay rate is dominated by slow Y_Z donation to $P^{+\bullet}$ or by $P^{+\bullet}/Q_A^{-\bullet}$ recombination. Even under these conditions the yield of $Car^{+\bullet}$ formation was low and its rate was equivalent to $P^{+\bullet}$decay. This suggests that the donation rate is slow even compared to $P^+/{}^{\bullet}Q_A^{-\bullet}$ recombination (200 μs) and from the yield of $Car^{+\bullet}$ formation we could estimate the rate to be in the region of 2 ms, similar to that reported in D1/D2/Cyt b_{559} particles (Telfer et al., 1991). We must conclude that even under the most extreme conditions, the efficiency of electron donation from the side pathway is low. These results indicate that the side-path can play at best a minor photoprotective role by electron donation to $P^{+\bullet}$. This conclusion based on work done at physiological temperature is backed up by the low temperature studies. The original work from de Paula et al. (1985) and Thompson and Brudvig (1988) that led to the suggestion that the side-path competed effectively with Y_Z donation as the temperature was lowered, led to the expectation that the two donation rates were similar at the cross-over temperature (approx 140K). As discussed above, this now appears to be incorrect and even at this temperature electron donation is slow (Schlodder and Derr, 2000; P. Faller and A.W. Rutherford, unpublished), competing poorly with the $P^{+\bullet}/Q_A^{-\bullet}$ reaction and the side-path is oxidized as a result of low quantum yield photo-accumulation.

The room temperature studies on Car were done under conditions where the Cyt b_{559} was pre-oxidized. Such studies starting with it in its reduced form, and measuring its yield per flash should reflect the efficiency of the side-path electron donation to $P^{+\bullet}$. Using this approach Buser et al. (1992) showed low yields in both intact and Mn-depleted PS II. Furthermore the rate of Cyt b_{559} oxidation was found to be close to that of lifetime of the final radical pair: $S_2Q_A^{-\bullet}$ and

$Y_Z^{\bullet}Q_A^{-\bullet}$ respectively. This is interpreted as showing that Cyt b_{559} reduction occurs as a result of an equilibrium between all the potential electron donors. Thus, the rate of electron donation from the side-pathway must be very slow even when the Cyt b_{559} is reduced prior to illumination.

There are no direct measurements of Chl Z formation in the literature. This is because absorption changes associated with its oxidation overlap with those of $P^{+\bullet}$, and while $P^{+\bullet}$ is formed with a quantum yield of 1, that of Chl Z is expected to be around two orders of magnitude smaller at most.

Hillman and Schlodder (1997) studied the $P^{+\bullet}$ formation and decay at low temperature in Mn-depleted PS II. The chemistry is dominated by $P^{+\bullet}/Q_A^{-\bullet}$ recombination but every time the side pathway donates an electron, $Q_A^{-\bullet}$ is trapped and the size of the $P^{+\bullet}$ signal is decreased on the subsequent flash. Measurement of the flash-induced decrease in the $P^{+\bullet}$ signal provides a measure of the yield and therefore the rate of electron donation from the side-pathway ($t_{½}$ of ~15 ms for Cyt b_{559} and 25 ms for Car donation to $P^{+\bullet}$ (Faller et al., 2001a).

Despite the very large optical change arising from $Car^{+\bullet}$, it has not been detected as a kinetic intermediate in oxidized Cyt b_{559} formation. It thus appears that electron donation from Cyt b_{559} to $Car^{+\bullet}$ is much faster than electron donation from Car to $P^{+\bullet}$. The current crystallographic model corresponds with this situation, with a much closer distance between Cyt b_{559} and Car_{D2} (12 Å) compared to Car to $P^{+\bullet}$(23 Å) (n.b., above we argued for a route, $Car_{D2} \rightarrow Chl_{D2} \rightarrow P$, where the distance for the first step is 13.1 Å and where the location of the cation on Chl_{D2} occurs through an equilibrium which greatly favors $P^{+\bullet}$), resulting in much faster electron transfer between Cyt b_{559} and Car_{D2}.

For the Chl $Z \rightarrow Car^{+\bullet}$ electron transfer, no data are yet available. The new crystal structure model with Car_{D2} approaching Chl Z_{D2} to a distance of 7.4 Å (Ferreira et al., 2004) indicates that electron transfer from Chl Z_{D2} to $Car_{D2}^{+\bullet}$ could in principle be rapid (tens of ps). So here again electron donation from Car to $P^{+\bullet}$ is the rate limiting step in the side-pathway. Furthermore, as we argued above, any involvement from Chl Z_{D1}, should it occur, is likely to be even slower that the rate of Car_{D2} oxidation by $P^{+\bullet}$. All of the above data indicate that electron donation from the side-path is too slow and inefficient to act as a significant protective pathway.

B. A Redox Mechanism for the Generation of a Fluorescence Quencher

A second mechanism has been proposed based on the fact that Chl $Z^{+\bullet}$ is a very effective quencher of PS II (Schweitzer and Brudvig, 1997). This arises from the broad absorption of Chl cation in the near infra-red, with a broad maximum around 820 nm. The idea is that the side pathway donates electrons at a low efficiency to $P^{+\bullet}$ and under most circumstances the electron comes from Cyt b_{559} which is in turn reduced slowly by PQH_2, perhaps through the Q_B site. However under certain conditions, (such as under conditions of stress), the side-path electron donation to $P^{+\bullet}$ outruns Cyt b_{559}^{ox} reduction. This could result from inefficiencies in the normal electron donation pathway (during photo-activation or inhibition of the Mn cluster) or whenever Cyt b_{559}^{ox} reduction is slow or does not occur (e.g., due to a shift to a low potential redox form). This would result in formation of the Chl $Z^{+\bullet}$. The quenching could dissipate energy and thus would help protect the reaction center from photodamage. One might expect that the lifetime of the Chl $Z^{+\bullet}$ quencher would be limited by an electron from the quinone complex arriving on the pre-oxidized Cyt b_{559}.

Again this basic idea of Chl $Z^{+\bullet}$ acting as a protective quencher was suggested when the linear Cyt $b_{559} \rightarrow$ Chl $Z \rightarrow P^{+\bullet}$ pathway was under consideration, however the realization that Car is involved as a branch point did not change the validity of the idea. The additional possibility exists that the $Car^{+\bullet}$ itself may also be a quencher (Hanley et al., 1999) and indeed may contribute to the quenching effect attributed to Chl $Z^{+\bullet}$, especially if their potentials are relatively close. The main question concerning the validity of this model is whether Chl $Z^{+\bullet}$ has a lifetime that is long enough at room temperature to allow it to play a useful quenching role. There have been several reports of quenching states generated in PS II under various (mainly detrimentally strong light) conditions. It remains possible that these correspond to long-lived Chl $Z^{+\bullet}$ states. The specific link between such states and Chl $Z^{+\bullet}$ has yet to be demonstrated however.

It is worth pointing out that a role for Chl $Z^{+\bullet}$ as a protective fluorescence quencher would correspond to situation in which the redox potential of the Chl was significantly lower than the neighboring species (particularly the carotene and other Chls). In this way the charge would localize on the Chl Z and not wander around the reaction center leading to

potentially undesirable chemistry. Thus we consider that this role is not particularly compatible with the equal potential equilibrium model recently proposed by Tracewell et al. (2003).

C. A New Perspective: A Protective Cycle for Redox Quenching of the β-Carotene Cation Radical

Photodamage can occur due to the formation of triplet Chl (^{3}Chl) either from excited Chl singlet through inter-system crossing or through radical pair recombination (Rutherford and Krieger-Liskay, 2001; Chapters 23 and 27) . The latter mechanism occurs within photosynthetic reaction centers. ^{3}Chl reacts readily with O_2 generating singlet oxygen, $^1O_2$, a very potent oxidant that can kill the organism. The protection provided by the carotenoids is achieved through a close association between the carotenoids and Chl which leads to a quenching of the Chl triplet. Moreover, carotenoids are also known to quench singlet oxygen directly (Cogdell and Frank, 1987; Chapters 23 and 27).

Radical pair recombination Chl triplet is thought to be an important source of photodamage in PS II (Rutherford and Krieger-Liskay, 2001; Chapter 27, Chow and Aro). In BRCs a carotenoid is located close to the primary electron donor, $P^{+\bullet}$, on the inactive branch of the reaction center, the equivalent of the D2-side in PS II, and quenches the Chl triplet generated by radical pair recombination (Cogdell and Frank, 1987).

While an equivalent role for carotenoid sounds like a particularly good idea in PS II, especially since it is by its nature in an O_2-rich environment and its Chl triplet state is at a higher energy and thus even more ready to generate singlet oxygen, there is no evidence that the carotenoid is able to quench Chl triplet either in D1/D2/Cyt b_{559} particles (Takahashi et al., 1987) or in more intact PS II (Hillmann et al., 1995; Van Mieghem et al., 1995). A likely explanation for this is that, unlike $P^{+\bullet}$ in the BRC, $P^{+\bullet}$ in PS II is so oxidizing that it would be able to oxidize carotenoid in competition with the Y_Z thus decreasing the efficiency of water oxidation (Telfer, 2002). On the other hand, there is indirect evidence that the β-carotenes in PS II do play a role in scavenging singlet oxygen (Telfer et al., 1994).

Thinking along these lines it is possible to rationalize the existence of the side-path electron transfer chain. It is simply a result of two features of PS II: (i) the very high redox potential of $P^{+\bullet}$, which means that any near by component will be oxidized; and (ii) the requirement for carotenoid to be at the center of the reaction center so that it can play a protective role as a singlet oxygen quencher. The Car thus occupies a compromise position: it is close enough to the core Chls to allow singlet oxygen to be quenched close to its site of generation but at this distance it cannot avoid a very low quantum yield of oxidation by $P^{+\bullet}$. Thus we see that the donation pathway from Cyt b_{559} is there to remove the highly oxidative $Car^{+\bullet}$ in order to prevent non-specific damage and to return it to its active, $^1O_2$ quenching form. The reduction of Cyt b_{559} with electrons from the reducing side of PS II restores it to its reduced form, primed to quench $Car^{+\bullet}$ whenever it is generated with a low quantum yield. This then fits with the idea that electron transfer is much more efficient from Cyt b_{559} to $Car^{+\bullet}$ than for Car to $P^{+\bullet}$. Because of the large number of photochemical events occurring in PS II and the periods in the lifetime of the enzyme when water oxidation does not occur (e.g., prior to assembly of the Mn cluster), Car oxidation is predicted to be inevitable.

The redox quenching role for Cyt b_{559} could be its main function. However, the variable redox potential of the cytochrome remains unexplained. One can dip into the many suggestions in the literature (reviewed in Stewart and Brudvig, 1998) looking for an explanation but that suggested by Schweitzer and Brudvig (1997), i.e., that the cytochrome redox state controls the production of the fluorescence quencher Chl $Z^{+\bullet}$, as described above, is the most appropriate for the present discussion since it relates to the side-path electron donors. This aspect of the function of the side-path can be painlessly incorporated into our new model. However it is not yet clear if Chl $Z^{+\bullet}$ acts as a quencher under physiologically relevant conditions. Most studies indicate that it is short-lived but there is little information about the fate of Chl $Z^{+\bullet}$ and its reaction partners[1].

[1] The first observations of $Car^{+\bullet}$ formation in PS II were made when a range of chemicals reagents were added to the sample. These chemicals fall under the definition of 'ADRY' reagents as defined by Renger (1973) in that they accelerate the deactivation of the OEC and include FCCP, ANT2P, tetraphenol boron and phenolic herbicides. While their function is not wholly clear, extending earlier thinking (Renger, 1973; Ghanotakis et al., 1982) in the context of the side-pathway, we consider that they work as high potential electron donors to any species within the lipophilic environment that has a potential high enough to oxidize the ADRY reagent. Potentially this could include the Mn cluster in the S_2 and S_3 state, the tyrosyl radicals and P^+. It seems that after donating an electron to PS II, the oxidized ADRY reagent remains rapidly diffusible in the lipophilic environment. When it encounters an

VII. Conclusions

The side pathway of electron donors in PS II is made up of a branched pathway in which the Car on D2 donates to $P^{+\bullet}$ and the $Car^{+\bullet}$ formed is rapidly reduced by Cyt b_{559}, or by Chl Z should the cytochrome be pre-oxidized. The electron donation from Car to $P^{+\bullet}$ is slow and works at a very low quantum yield. It is suggested that this reaction has evolved to be as slow as possible in order to minimize competition with water oxidation. The fact that it occurs at all may be due to the need for Car to be in the heart of the reaction center, close to the source of singlet O_2 generation (i.e., the radical pair recombination Chl triplet). The quenching of singlet O_2 is proposed to be the principal role of Car but in fulfilling this role it is inevitably at risk of being oxidized by $P^{+\bullet}$. When this rare but inevitable event occurs it is the role of the Cyt b_{559} to return $Car^{+\bullet}$ to its active unoxidized form, at the same time preventing potentially damaging reactions caused by $Car^{+\bullet}$. The cycle is completed when the oxidized Cyt b_{559} is reduced by electrons from the plastoquinone pool, possibly through the Q_B site.

Thus we suggest that the side-pathway of electron transfer in PS II plays a protective role aimed at maintaining Car in its active, unoxidized form. The role of Chl Z may be to act as a fluorescence quencher and hence energy trap, when oxidized by $Car^{+\bullet}$, a reaction that only occurs when Cyt b_{559} is already oxidized. The redox state of the Cyt b_{559} thus would regulate this quencher. Many questions remain, particularly the identity of Chl Z and the role of Chl Z on the D1 side, and the possibilities remain open that the cation equilibrates between Car_{D2} and Chl Z_{D2}, between Car_{D2} and the $Car_{D2\text{-}43}$, and between Car_{D2} and Chl Z_{D1} via $Car_{D2\text{-}43}$ and a several Chls of CP43 . Doubtless, some of these ambiguities will be resolved with further experimentation focusing on identifying the carotenoids and Chls that bear the cation under different conditions.

oxidizable species it extracts an electron from it returning to its active state as a donor ready to donate to another reaction center, hence the ability of these reagents to work in sub-stoichiometric concentrations. In this model Cyt b_{559} can be oxidized by ADRY reagents, possibly due to the reagent itself being oxidized by $Y_D^{+\bullet}$ in a dark-adapted system. Carotenoid cations are much less stable so their formation is observed only transiently immediately after the flash illumination. It seems quite possible that carotenoids other than those in the D2 part of the reaction center are oxidized when lipophilic anions are present in the sample. Indeed we have observed that the amplitude of carotenoid cation generated per flash at room temperature in the presence of tetraphenol boron is found to be smaller in PS II preparations with smaller antenna implying that the oxidized reagent is able to react with carotenoids in the antenna (R. Edge and A.W. Rutherford, unpublished).

Acknowledgments

We thank Drs. Tony Mattioli, Sun Un, Ruth Edge, Charilaos Goussias, Anabella Ivancich, Yiannis Deligiannakis, Jonathan Hanley, Alain Boussac, Klaus Brettel, Paul Mathis, Andy Pascal and Bruno Robert (CEA Saclay), Anja Liszkay (University of Freiburg, Germany), Fabrice Rappaport (IBPC, Paris) Richard J. Debus (UC Riverside), Thorsten Maly, Fraser MacMillan (University of Frankfurt), Gary Brudvig (Yale), Alison Telfer (London) and Bruce Diner (DuPont) for helpful discussion. P.F. was supported by a grant from the Swiss National Science Foundation and C.F. was a Marie Curie Training Site studentship supported by the EU.

References

Bialek-Bylka GE, Tomo T, Satoh K and Koyama Y (1995) 15-*cis*-beta-carotene found in the reaction center of spinach Photosystem II. FEBS Lett 363 : 137–140

Bratt PJ, Poluektov, OG, Thurnauer MC, Krzystek J, Brunel L-C, Schrier J, Hsiao Y-W, Zerner M and Angerhofer A (2000) The *g*-factor anisotropy of plant chlorophyll a^+. J Phys Chem B 104: 6973–6977

Breton J, Duranton J and Satoh K (1988) Orientation of pigments in the reaction center and the core antenna of Photosystem II. In: Scheer H and Schneider S (eds) Photosynthetic Light-Harvesting Systems: Organization and Function, pp 375–386. Walter de Gruyter, Berlin

Buser CA, Diner BA and Brudvig GW (1992) Photooxidation of cytochrome *b*559 in oxygen-evolving Photosystem II. Biochemistry 31:11449–11459

Cogdell RJ and Frank HA (1987) How carotenoids function in photosynthetic bacteria? Biochim Biophys Acta 895: 63–79

Cua A, Stewart DH, Brudvig GW and Bocian DF (1998) Selective resonance Raman scattering from chlorophyll Z in Photosystem II via excitation into near-infrared absorption band of the cation. J Am Chem Soc 120: 4532–4533

Dawe EA and Land EJ (1975) Radical ions derived from photosynthetic polyenes. J Chem Soc Faraday Trans 1, 71 : 2162–2169

De Paula JC, Innes JB and Brudvig GW (1985) Electron transfer in Photosystem II at cryogenic temperatures. Biochemistry 24: 8114–8120

Deligiannakis Y, Hanley J and Rutherford AW (2000) Carotenoid oxidation in Photosystem II: 1D and 2D ESEEM study. J Am Chem Soc 122: 400–401

Diner BA, Schlodder E, Nixon PJ, Coleman WJ, Rappaport F, Lavergne J, Vermaas WFJ and Chrisholm DA (2001) Site-di-

rected mutations at D1-His198 and D2-His197 of Photosystem II in *Synechocystis* PCC 6803: Sites of primary charge separation and cation and triplet stabilization. Biochemistry 40: 9265–9281

Edge R, Land EJ, McGarvey DJ, Burke M and Truscott TG (2000) The reduction potential of the β-carotene+/β-carotene couple in an aqueous micro-heterogeneous environment. FEBS Lett 471:125–127

Faller P, Rutherford AW and Un S (2000) High-field EPR study of carotenoid and the angular orientation of chlorophyll-z in Photosystem II. J Phys Chem B 104: 10960–10963

Faller P, Pascal A and Rutherford AW (2001a) β-Carotene redox-reaction in Photosystem II: Electron transfer pathway. Biochemistry 40: 6431–6440

Faller P, Maly T, Rutherford AW and MacMillan F (2001b) Chlorophyll and carotenoid radicals in Photosystem II studied by pulsed ENDOR. Biochemistry 40: 320–326

Ferreira KN, Iverson TM, Maghlaoui K, Barber J and Iwata S (2004) The architecture of the oxygen evolving enzyme. Science 303: 1831–1838

Frese RN, Germano M, de Weerd FL, van Stokkum, AY, Shuvalov VA, van Gorkom HJ and Dekker JP (2003) Electric field effects on the chlorophylls, pheophytins and beta carotenes in the reaction centre of Photosystem II. Biochemistry 42: 9205–9213

Germano M, Shkuropatov AJ, Permentier H, de Wijn R, Hoff AJ, Shuvalov VA and van Gorkom HJ (2001) Pigment organization and their interactions in reaction centers of Photosystem II: Optical spectroscopy at 6 K of reaction centers with modified pheophytin composition. Biochemistry 40: 11472–11482

Ghanotakis D.F., Yerkes, C.T. and Babcock G. T. (1982) The role of reagents accelerating the deactivation reactions of the water splitting enzyme. Biochim Biophys Acta 682: 21–31

Grant JL, Kramer VJ, Ding R and Kispert LD (1988) Carotenoid cation radicals: electrochemical, optical, and EPR study. J Am Chem Soc 110: 2151–2157

Goussias H, Boussac A and Rutherford AW (2002) Photosystem II and photosynthetic oxidation of water: An overview. Philos Trans Roy Soc Lond B Biol Sci 357: 1369–1381

Hanley J, Deligiannakis Y, Pascal A, Faller P and Rutherford AW (1999) Carotenoid oxidation in Photosystem II. Biochemistry 38: 8189–8195

Hillmann B and Schlodder E (1997) Electron transfer reactions in Photosystem II core complexes from *Synechococcus* at low temperature-difference spectrum of P680+Qa-/p680 Qa at 77K. Biochim Biophys Acta 1231: 76–88

Hillmann B, Brettel K, van Mieghem F, Kamlowski A, Rutherford AW and Schlodder E (1995) Charge recombination reactions in Photosystem II. 2. Transient absorbance difference spectra and their temperature dependence. Biochemistry 34 : 4814–4827

Himo F (2001) Density functional theory study of the β-carotene radical cation. J Phys Chem A 105: 7933–7937

Jeevarajan AS, Kispert L D and Piekara-Sady L (1993) An ENDOR study of carotenoid cation radicals on silica-alumina solid supports. Chem Phys Lett 209: 269–274

Jeevarajan JA, Wei CC, Jeevarajan AS and Kispert LD (1996a) Optical absorption spectra of dications of carotenoids. J Phys Chem 100: 5637–5641

Jeevarajan AS, Kispert LD, Chumanov G, Zhou C and Cotton TM (1996a) Resonance Raman study of carotenoid cation radicals. Chem Phys Lett 259: 515–522

Johnson G, Rutherford AW and Krieger A (1995) A change in the midpoint potential of QA in Photosystem II associated with photo-acrtivation of oxygen evolution. Biochim Biophys Acta 1229: 202–207

Kamiya N and Shen JR (2003) Crystal structure of oxygen-evolving Photosystem II from *Thermosynechococcus vulcanus* at 3.7-Å resolution. Proc Natl Acad Sci USA 100: 98–103

Kawamori A, Katsuta N and Hara H (2002) Structural analysis of three-spin systems of Photosystem II by PELDOR. Appl Magn Reson 23: 557–569

Konovalova TA, Krzystek J, Bratt PJ, van Tol J, Brunel L-C and Kispert LD (1999) 95–670 GHz EPR studies of canthaxanthin radical cation stabilized on a silica-alumina surface. J Phys Chem B 103: 5782–5786

Konovalova TA, Dikanov SA, Bowman MK and Kispert LD (2001) Detection of anisotropic hyperfine components of chemically prepared carotenoid radical cations: 1D and 2D ESEEM and pulsed ENDOR study. J Phys Chem B 105: 8361–8368

Koulougliotis D, Innes JB and Brudvig GW (1994) Localization of chlorophyll z in Photosystem II. Biochemistry 33:11814–11822

Knaff DB and Arnon DI (1969) Light-induced oxidation of a chloroplast *b*-type cytochrome at –189 °C. Proc Natl Acad Sci USA 63: 963–969

Kwa SLS, Newell WR, van Grondelle R and Dekker JP (1992) The reaction center of Photosystem II studied by polarized fluorescence spectroscopy. Biochim Biophys Acta 1099: 193–202

Lakshmi KV, Reifler MJ, Brudvig GW, Poluektov OG, Wagner AM and Thurnauer MC (2000) High-field EPR study of carotenoid and chlorophyll cation radicals in Photosystem II. J Phys Chem B 104: 10445–10448

Lakshmi KV, Poluektov OG, Reifler MJ, Wagner AM, Thurnauer MC and Brudvig GW (2003) Pulsed high frequency EPR study on the location of carotenoid and chlorophyll cation radicals in Photosystem II. J Am Chem Soc 125: 5005–5014

Lubitz W (1991) EPR and ENDOR studies of chlorophyll cation and anion radicals. In: Scheer H (ed) Chlorophylls, pp 903–944. CRC Press, Boca Raton

MacMillan F, Rohrer M, Krzystek J, Brunel L-C and Rutherford AW (1998) A high-field/high frequency EPR characterization of the primary donor (P^+) in bacterial and plant photosynthetic reaction centers. In: Garab G (ed) Photosynthesis: Mechanism and Effects, Vol 2, pp 715–718. Kluwer Academic Publishers, Dordrecht

Mathis P and Vermeglio A (1972) Transient forms of carotenoids. Triplet state and radical cation. Photochem Photobiol 15 : 157–164

Mathis P and Vermeglio A (1975) Chlorophyll radical cation in Photosystem II of chloroplasts. Millisecond decay at low temperature. Biochim Biophys Acta 369 : 371–381

Michel H and Deisenhofer J (1988) Relevance of the photosynthetic reaction center from purple bacteria to the structure of Photosystem II. Biochemistry 27: 1–7

Moore TA, Gust D, Mathis P, Mialocq J-C, Chachaty C, Bensasson RV, Land EJ, Doizi D, Liddell PA, Lehman WR, Nemethy GA and Moore AL (1984) Photo-driven charge separation in a carotenoporphyrinquinone triad. Nature 307: 630–632

Nanba O and Satoh K (1987) Isolation of a Photosystem II reaction center consisting of D-1 and D2 polypeptides and cytochrome *b*-559. Proc Natl Acad Sci USA 84: 109–112

Noguchi T and Inoue Y (1995) Molecular interactions of the redox-active accessory chlorophyll on the electron donor side

of Photosystem II as studied by Fourier transform infrared spectroscopy. FEBS Lett 370: 241–244

Noguchi T, Mitsuka T and Inoue Y (1994) Fourier transform infrared spectrum of the radical cation of β-carotene photoinduced in Photosystem II. FEBS Lett 356: 179–182

Nugent JHA, Muhiuddin IP and Evans MCW (2002) Electron transfer from the water oxidizing complex at cryogenic temperatures. Biochemistry 41: 4117–4126

Page CC, Moser CC, Chen X and Dutton PL (1999) Natural engineering principles of electron tunneling in biological oxidation-reduction. Nature 402: 47–52

Pascal A, Telfer A, Barber J and Robert B (1999) Fourier-transform resonance Raman spectra of cation carotenoid in Photosystem II reaction centres. FEBS Lett 453: 11–14

Rappaport F and Diner BA (2002) Structure, dynamics, and energetics of the primary photochemistry of Photosystem II of oxygenic photosynthesis. Annu Rev Plant Biol 53 : 551–580

Renge I, van Grondelle R and Dekker JP (1996) Matrix and temperature effects on absorption spectra of β-carotene and pheophytin in solution and in green plant Photosystem II. J Photochem Photobiol A 96: 109–121

Renger G (1973) Studies on the mechanism of destabilization of the positive charges trapped in the photosynthetic water splitting enzyme system Y by a deactivation-accelerating agent. Biochim Biophys Acta 314: 390–402 314

Rhee K-H (1998) Three-dimensional structure of Photosystem II reaction center by electron cryo-microscopy. PhD Thesis. Univ Heidelberg, Heidelberg

Rigby SEJ, Nugent JHA and O'Malley PJ (1994) ENDOR and special triple resonance studies of chlorophyll cation radicals in photosystem 2. Biochemistry 33: 10043–10050

Ruffle SV, Donnelly D, Blundell T and Nugent JHA (1992) A three-dimensional model of the Photosystem II reaction center of *Pisum sativum.* Photosynth Res 34: 287–300

Rutherford AW and Faller P (2001) The heart of Photosystem II in glorious 3D. Trends Biochem Sci 26: 341–344

Rutherford AW and Faller P (2002) Photosystem II: evolutionary perspectives. Philos Trans Roy Soc Lond B Biol Sci 358: 245–253

Rutherford AW and Krieger-Liskay A (2001) Herbicide induced oxidative stress in Photosystem II. Trends Biochem Sci 26: 648–653

Satoh K (1996) Introduction to the Photosystem II reaction center — Isolation and biochemical and biophysical characterization. In: Ort DR and Yocum CF (eds) Oxygenic Photosynthesis: The Light Reactions, pp 193- 211. Kluwer Academic Publishers, Dordrecht

Schenck CC, Diner B, Mathis P and Satoh K (1982) Flash-induced carotenoid radical formation in Photosystem II. Biochim Biophys Acta 680: 216–227

Schweitzer RH and Brudvig GW (1997) Fluorescence quenching by chlorophyll cations in Photosystem II. Biochemistry 36: 11351–11359

Shen JR and Kamiya N (2003) Functions of carotenoids and other pigments in Photosystem II from a structural point of view. (Abstract 425) European Photobiological Society Meeting, Vienna

Shigemori K, Hara H, Kawamori A and Akabori K (1998) Determination of distances from tyrosine D to QA and chlorophyll Z in Photosystem II studied by '2+1' pulsed EPR. Biochim Biophys Acta 1363: 187–198

Stewart DH and Brudvig GW (1998) Cytochrome *b*559 of Photosystem II. Biochim Biophys Acta 1367: 63–87

Stewart DH, Cua A, Chisholm DA, Diner BA, Bocian DF, Brudvig GW (1998) Identification of histidine 118 in the D1 polypeptide of Photosystem II as the axial ligand to chlorophyll Z. Biochemistry 37:10040–10046

Takahashi Y, Hansson O, Mathis P and Satoh K (1987) Primary radical pair in the Photosystem II reaction center. Biochim Biophys Acta 893: 49–59

Telfer A (2002) What is β-carotene doing in the photosystem two reaction centre? Philos Trans Roy Soc Lond B 357:1431–1439

Telfer A, De Las Rivas J and Barber J (1991) β-Carotene within the isolated Photosystem II reaction centre: photooxidation and irreversible bleaching of this chromophore by oxidized P680. Biochim Biophys Acta 1060: 106 –114

Telfer A, Dhami S, Bishop SM, Phillips D and Barber J (1994) β-Carotene quenches singlet oxygen formed by isolated Photosystem II reaction centers. Biochemistry 33: 14469–14474

Telfer A, Frolov D, Barber J, Robert B and Pascal A (2003) Oxidation of the two beta-carotene molecules in the Photosystem II reaction center. Biochemistry 42:1008–1015

Thompson LK and Brudvig GW (1988) Cytochrome *b*-559 may function to protect Photosystem II from photoinhibition. Biochemistry 27:6653–6658

Tomo T, Mimuro M, Iwaki M, Kobayashi M, Itoh S and Satoh K (1997) Topology of pigments in the isolated Photosystem II reaction center studied by selective extraction. Biochim Biophys Acta 1321: 21–30

Tracewell CA and Brudvig GW (2003) Two redox active beta-carotene molecules in Photosystem II. Biochemistry 42: 9127–9136

Tracewell CA, Cua A, Stewart D, Bocian DF and Brudvig GW (2001a) Characterization of carotenoid and chlorophyll photooxidation in Photosystem II. Biochemistry 40: 193–203

Tracewell CA, Vrettos JS, Bautista JA, Frank HA and Brudvig GW (2001b) Carotenoid photooxidation in Photosystem II. Arch Biochem Biophys 365:61–69

Un S, Dorlet P and Rutherford AW (2001) A high-field EPR tour of radicals in Photosystem I and II. Appl Magn Reson 21: 341–361

Van Dorssen RJ, Breton J, Plijter JJ, Satoh K, van Gorkom HJ and Amesz J (1987a) Spectrocopical properties of the reaction center and of the 47kDa chlorophyll protein of Photosystem II. Biochim Biophys Acta 893: 267–274

Van Dorssen RJ, Plijter JJ, Dekker JP, den Ouden A, Amesz J. and van Gorkom HJ (1987b) Spectroscopic properties of chloroplast grana membranes and the core of Photosystem II. Biochim Biophys Acta 890: 134–143

Van Mieghem F, Brettel K, Hillmann B, Kamlowski A, Rutherford AW and Schlodder E (1995) Charge recombination reactions in Photosystem II. I. Yields, recombination pathways, and kinetics of the primary pair. Biochemistry 34: 4798–4813

Vasil'ev S, Brudvig GW and Bruce D (2003) The X-ray structure of Photosystem II reveals a novel electron transport pathway between P680, cytochrome *b*559 and the energy-quenching cation, ChlZ+. FEBS Lett 543 : 159–163

Velthuys BR (1981) Carotenoid and cytochrome *b*559 reactions in Photosystem II in the presence of tetraphenylboron. FEBS Lett 126: 272–276

Visser JWM, Rijgersberg CP and Gast P (1977) Photooxidation

of chlorophyll in spinach chloroplasts between 10K and 180K. Biochim Biophys Acta 460: 36–46

Vrettos JS, Stewart DH, dePaula JC and Brudvig GW (1999) Low-temperature optical and resonance Raman of carotenoid cation radical in Photosystem II. J Phys Chem B 103: 6403–6406

Wang J, Gosztola D, Ruffle SV, Hemann C, Seibert M, Wasielewski MR, Hille R, Gustafson TL and Sayre RT (2002) Functional asymmetry of Photosystem II D1 and D2 peripheral chlorophyll mutants of *Chlamydomonas reinhardtii*. Proc Natl Acad Sci USA 99: 4091–4096

Whitmarsh J and Cramer WA (1977) Kinetics of the photoreduction of cytochrome *b*-559 by Photosystem II. Biochim Biophys Acta 460: 280–289

Yurela I, Tomas R, Sanjuan ML, Torrado E, Aured M and Picorel R (1998) The configuration of β-carotene in the Photosystem II reaction center. Photochem Photobiol 68: 729–737

Zhang C and Styring S (2003) Formation of split electron paramagnetic resonance signals in Photosystem II suggests that Tyrosine Z can be photoxidised at 5K in the S_0 and S_1 states of the oxygen evolving complex. Biochemistry 42: 8066–8076

Zhang C, Boussac A and Rutherford AW (2004) Low-temperature electron transfer in Photosystem II: A tyrosyl radical and semiquinone charge pair. Biochemistry 43: 13787–13795

Zouni A, Witt HT, Kern J, Fromme P, Krauss N, Saenger W and Orth P (2001) Crystal structure of Photosystem II from *Synechococcus elongatus* at 3.8 Å resolution. Nature 409: 739–743

Chapter 16

Molecular Analysis by Vibrational Spectroscopy

Takumi Noguchi*
Institute of Materials Science, University of Tsukuba, Tsukuba, Ibaraki 305-8573, Japan

Catherine Berthomieu*
CEA/Cadarache, DSV DEVM, Laboratoire de Bioénergétique Cellulaire, UMR 6191 CNRS-CEA-Aix-Marseille II CEA 1000, Bât. 156, F-13108 Saint-Paul-lez-Durance, Cedex, France

Summary

Vibrational spectroscopy, which includes infrared and Raman spectroscopies, provides structural information of molecules by detecting molecular vibrations based on chemical bonds and interactions. These methods have been applied to the study of various cofactors in Photosystem II. In particular, light-induced Fourier transform infrared (FTIR) difference spectroscopy has proven to be a powerful method to reveal detailed structures of the binding sites of cofactors including protein moieties and water molecules. Information available by FTIR difference spectroscopy includes hydrogen bonding and protonation state of chemical groups, which play an essential role in proton transfer and also in controlling redox reactions, but are often not available by X-ray crystallography. The FTIR investigations cover all the redox cofactors of Photosystem II in both the main and peripheral electron-transfer pathways, i.e., the manganese-cluster, the redox-active tyrosines Y_Z and Y_D, the primary donor P680, the primary acceptor pheophytin, the quinone acceptors Q_A and Q_B, the non-heme iron, cytochrome b_{559}, chlorophyll Z, and β-carotene. This article reviews how the structures and reactions of these cofactors have been studied using mainly FTIR spectroscopy with the assistance of Raman spectroscopy.

*Authors for correspondence, email: T. Noguchi, tnoguchi@ims.tsukuba.ac.jp; C. Berthomieu, catherine.berthomieu@cea.fr

T. Wydrzynski and K. Satoh (eds): Photosystem II: The Light-Driven Water:Plastoquinone Oxidoreductase, pp. 367–387.

I. Introduction

Vibrational spectroscopy, which mainly indicates infrared (IR) absorption and Raman spectroscopies, is one of standard methods to study molecular structures. It detects molecular vibrations and hence provides the information of molecular structures based on the positions and strengths of chemical bonds and interactions. Such type of molecular structure differs from that obtained by X-ray crystallography, which provides three-dimensional positions of atoms. Since chemical reactions are consecutive processes of rearrangements of chemical bonds and interactions, vibrational spectroscopy is adopted for the investigation of reaction mechanisms. In addition, vibrational spectroscopy is particularly well suited for the detection of hydrogen-bonds (H-bonds) and (de)protonation reactions both of the protein and cofactors, which often play a crucial role in enzymatic reactions, whereas it is not easy to determine the positions of protons by X-ray crystallography. Thus, X-rays crystallography and vibrational spectroscopy are complementary methods. The whole structure of a protein and the relative positions of amino acid residues are determined by X-ray crystallography, while structural details including H-bonds and protonation status of chemical groups at the active site are analyzed by vibrational spectroscopy, both in the enzyme resting state and during the reaction.

Raman spectroscopy has been applied to photosynthetic pigments in vivo and in vitro for more than 30 years (Lutz, 1984). Utilizing resonance Raman effect, the Raman spectra of pigments can be selectively obtained in proteins by adjusting an excitation wavelength to the electronic transition of the pigment. However, application of resonance Raman spectroscopy to the redox cofactors in Photosystem II (PS II) has been rather limited. Indeed, Raman scattering from the large number of chlorophyll and carotenoid molecules present in membrane fragments and core complexes that keep the full function of electron transfer, overwhelms that from a target molecule. The Fourier transform (FT)-Raman technique, which uses near-infrared light for excitation, can be used to selectively detect radical species of chlorophyll (Chl) and carotenoid that show specific electronic absorption bands in the near-infrared region. Another unique technique is surface-enhanced Raman scattering (SERS) spectroscopy, which detects enhanced Raman scattering from the molecules in close distance to an electrode surface.

Infrared (IR) spectroscopy has been a popular method for studying photosynthetic proteins during the last 15 years, in part thanks to the development of Fourier transform infrared (FTIR) spectrometers. With a dispersive-type IR spectrometer, IR application was mostly limited to the study of the secondary structures of whole proteins using the amide I bands arising from the C=O stretches of the polypeptide backbone. The Fourier transform method provides a very precise definition of the wavenumber axis of spectra, which makes FTIR spectroscopy a method reproducible and suitable for detecting small spectral changes. Also Fourier transform (FT) spectrometers are more sensitive and absorption differences in the range of 10^{-5} absorption units can be detected. Thus, by recording reaction-induced infrared absorption changes, FTIR difference spectra corresponding to slight structural reorganization at the reacted active site can be obtained, which give structural information at the molecular level, even in a large protein like PS II complexes. One of the merits of FTIR spectroscopy is that it provides information not only concerning the cofactor but also concerning surrounding protein moieties and water molecules, whereas resonance Raman spectroscopy provides more specific information of the cofactor itself. In the last years, FTIR has been used in the PS II study by an increasing number of laboratories, and has become one of the major methods to study the redox cofactors of PS II in complement to magnetic techniques such as EPR, ENDOR and ESEEM.

This chapter focuses on the application of IR and Raman spectroscopies to the structures and reactions of redox cofactors in PS II. We should note that these spectroscopies have also been applied to the study of whole protein conformation of PS II proteins and to the interactions of Chl molecules in antenna complexes, which we could not include in this review

Abbreviations: BRC – bacterial reaction center; Car – carotene; Chl Z – redox-active chlorophyll; Chl – chlorophyll; Chl_T – chlorophyll triplet; DCMU – 3-(3,4-dichlorophenyl)-1,1-dimethylurea; ENDOR – electron nuclear double resonance; EPR – electron paramagnetic resonance; ESEEM – electron spin echo envelope modulation; FTIR – Fourier transform infrared; FT-Raman – Fourier transform Raman; IR – infrared; OEC – oxygen-evolving complex; P680 – primary electron donor; Pheo – pheophytin; PS II – Photosystem II; Q_A – primary quinone acceptor; Q_B – secondary quinone acceptor; SERDS – shifted-excitation Raman difference spectroscopy; SERS – surface-enhanced Raman scattering; S_n – states of the water oxidizing complex for n = 0, 1, 2, 3, or 4; WT – wild-type; Y_D – redox-active tyrosine on the D2 protein; Y_Z – redox-active tyrosine on the D1 protein

because of space limitation. Also, readers are recommended to refer to previous reviews for details in the technical aspects of FTIR and Raman spectroscopies and applications to other photosynthetic systems (Lutz, 1984; Lutz and Mäntele, 1991; Mäntele, 1995; Nabedryk, 1996).

II. Light-Induced Fourier Transform Infrared (FTIR) Difference Technique

In this section, we briefly describe the light-induced FTIR difference technique, which is the major method used so far for the vibrational spectroscopic study of PS II, and stress the important practical aspects of this technique. Since electron transfer in PS II is initiated by light absorption, FTIR spectra of the reacting cofactors can be obtained as light-induced difference spectra. Although PS II contains many pigment and metal cofactors, the FTIR spectrum of a target cofactor can be selectively measured by carefully choosing experimental conditions such as material (e.g., PS II membranes, isolated reaction center complexes, Mn-depleted PS II), temperature, continuous or flash illumination, duration of data acquisition after illumination, etc. to stabilize solely one intermediary state during spectrum acquisition. Since charge separation in PS II always induces redox reactions on both the electron donor and acceptor sides, a light-induced difference spectrum may reveal structural changes from both sides. Thus, for selective detection of a single cofactor, an artificial electron acceptor or donor is included in the sample system to abstract an electron or a hole out of the protein. An ideal artificial electron donor or acceptor should not exhibit IR bands in the region of absorption of the protein and cofactor. The ferricyanide/ferrocyanide redox couple is a good example of such an artificial electron donor/acceptor system. Another point to care for is to eliminate heating effect possibly consecutive to sample illumination. Since IR spectra are quite sensitive to a subtle temperature change, strong or long illumination often leads to artifacts in the obtained light-induced difference spectra (Onoda et al., 2000). Also, a long delay between the two absorption spectra recorded before and after sample illumination may lead in drifts of the base line. The same can be observed for long spectral acquisition, depending on the stability of the used FTIR spectrometer. Finally, even slight changes of the water vapor content in the spectrometer gives spectra contaminated with the IR rotation modes of water.

Thus, the first step in an FTIR study is to define experimental conditions to record pure spectra corresponding to the formation of only one intermediary state with no spectral artifacts. The second step, which is also common in Raman studies, is to assign the bands to specific vibrating groups or normal modes, and then interpret the observed frequency in terms of structure and interactions with the environment. This approach implies the comparison with spectra of model compounds in different buffers, the use of specific isotope labeling and the comparison of wild type (WT) and proteins altered by site-directed mutagenesis. Normal mode analysis of cofactors and amino acid side groups is also significant in this approach.

III. Cofactors on the Electron Donor Side

A. P680 and the Triplet State of Chlorophyll

The primary donor Chl of PS II, P680, has an extremely high redox potential of ~1.1 V in order to accomplish oxidation of water in the oxygen-evolving complex (OEC) (Chapter 7). This specific property of P680 should be achieved by its geometrical and electronic structure, molecular interactions with surrounding protein moieties, and the electrostatic environment around P680, but the exact reason for this high potential of P680 remains unclear. FTIR spectroscopy can be a powerful tool to address this question. It is noted here that we restrict the term 'P680' to the Chls that possess a hole immediately after charge separation and then oxidize Y_Z. The Chl(s) that initiates charge separation, can be an excitonically coupled multimer (Durrant et al., 1995) or another Chl molecule (Diner et al., 2001).

The excited triplet state of Chl generated by charge recombination of the radical pair in PS II has been thought to be located on P680 for a long time, and hence has been termed ^{3}P680. This idea was based on the observation that the Q_y bleach upon triplet formation was found at about 680 nm (e.g., den Blanken et al., 1983), and on the analogy to bacterial reaction center (BRC) (when triplet transfer to carotenoid is absent) and Photosystem I, in which the triplet state resides on the primary donor (Budil and Thurnauer, 1991). Based on this view, a triplet-minus-singlet

FTIR spectrum was first measured as '^{3}P680/P680' using the D1-D2-Cyt b_{559} complex (Noguchi et al., 1993a) (Fig. 1a). The spectrum showed prominent negative and positive peaks at 1669 and 1627 cm^{-1} assignable to the keto C=O stretches of the ground singlet and excited triplet states of Chl, respectively. The position of the major C=O bleach upon triplet formation was basically consistent with the value of 1672 cm^{-1} obtained in the resonance Raman study by Moënne-Loccoz et al. (1990). The large downshift of the keto C=O stretching frequency upon triplet formation was also exhibited in the triplet/singlet FTIR spectra of isolated Chl *a* in organic solutions (Noguchi et al., 1993a). In addition to this major band pair, a minor band pair was found at 1707 and 1659 cm^{-1} as keto C=O vibrations of singlet and triplet Chl, respectively. The intensity ratio of the minor pair to the major one increased as the temperature was raised and hence it was concluded that the triplet state is in a thermal equilibrium between two Chl molecules. The energy gap between the two triplet Chls was estimated to be 8.4 ± 0.7 meV (Noguchi et al., 1993a). This value was basically in agreement with that of 12–13 meV estimated from the temperature dependence on the EPR spectra of the triplet state (Kamlowski et al., 1996; Bosch et al. 1996). The peak frequencies of 1669 and 1707 cm^{-1} indicate that the former keto C=O is engaged in H-bonding, whereas the latter is in a highly hydrophobic environment. In addition, a differential signal was observed at 1716/1723 cm^{-1} that can be assigned to the carbomethoxy C=O stretches of triplet/singlet Chl with H-bonding interaction (Noguchi et al., 1993a).

FTIR difference spectra upon cation formation of P680 (P680$^+$/P680) was measured using the D1-D2-Cyt b_{559} complex in the presence of silicomolybdate (Breton et al., 1997a) or ferricyanide (Noguchi et al., 1998) as an electron acceptor. Comparable spectra were observed irrespective of the acceptor species. The P680$^+$/P680 spectrum (Fig. 1b) showed negative peaks at 1704 and 1679 cm^{-1} and positive peaks at 1729 and 1711 cm^{-1} [negative peaks at 1701 and 1681 cm^{-1} and positive peaks at 1724 and 1710 cm^{-1} in the spectrum by Breton et al. (1997a)], which are the candidates for the keto C=O vibrations of P680 (for negative peaks) and P680$^+$ (for positive peaks). However, no negative peak was found at 1669 cm^{-1}, where the major negative band was located in the triplet/singlet spectrum (Fig. 1a). From this observation, it was concluded that the major population of the triplet state is on a Chl molecule different from P680

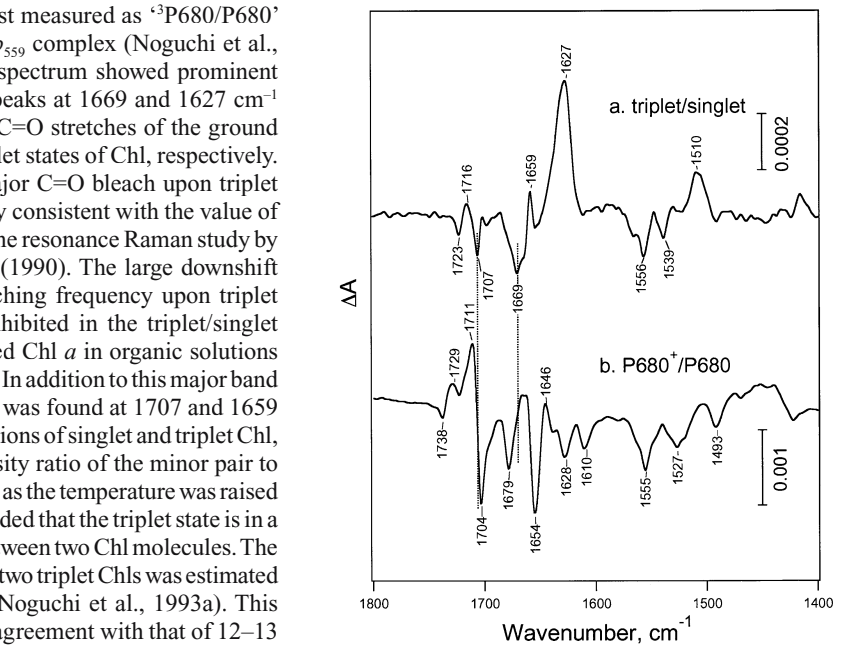

Fig. 1. Light-induced FTIR difference spectra of the D1-D2-Cyt b_{559} complexes upon formation of the excited triplet state of chlorophyll (a) and of the cation radical of P680 (b). See Noguchi et al. (1993a, 1998) for details.

that possesses a positive charge (Breton et al., 1997a; Noguchi et al., 1998, 2001; Sarcina et al., 1998). The minor population of the triplet state can be on P680, because the peak position at 1707 cm^{-1} in the triplet/singlet spectrum is basically in agreement with that of the major peak at 1704 cm^{-1} in the P680$^+$/P680 spectrum (The slight difference in frequency can be explained by the differential shape of the 1711/1704 cm^{-1} bands in P680$^+$/P680) (Noguchi et al., 1998). Thus, the two band pairs in the triplet/singlet FTIR spectrum were reinterpreted as a triplet equilibrium between a monomeric Chl (designated as Chl_T) and P680. From the intensity ratio of keto C=O bands and extrapolation of its temperature dependence, about 86% and more than 70% of the triplet population were estimated to be localized on Chl_T at 80 and 293 K, respectively (Noguchi et al., 1993a, 1998, 2001). Time-resolved IR measurements showed that triplet formation on Chl_T is quite fast and the time constant of the $^3Chl_T$ formation (τ ~57 ns) roughly agreed with that of the P680$^+$Phe$^-$ recombination (Noguchi et al., 2001). Thus, two alternative mechanisms of

triplet formation were proposed: (i) $^3Chl_T$ is directly formed from the $P680^+Phe^-$ radical pair by charge recombination at Chl_T; and (ii) $^3P680$ is once formed and then the triplet is transferred to Chl_T with a time constant much smaller than 50 ns.

Another characteristic of the $P680^+/P680$ spectrum is a broad positive band centered at 1940 cm^{-1} (Noguchi et al., 1998; Breton, 2001), which was reminiscent of broad mid-IR electronic bands of primary donor cations in purple bacteria (Breton et al., 1992), green bacteria (Nabedryk et al., 1996; Noguchi et al., 1996), heliobacteria (Nabedryk et al., 1996; Noguchi et al., 1997a), and Photosystem I (Breton et al., 1999a). The presence of this electronic band is direct evidence for charge delocalization over Chl molecules (Breton et al., 1992). The X-ray crystal structure of PS II recently showed that the arrangement of the special pair and two adjacent accessory Chls are basically conserved between the bacterial reaction center and PS II (Zouni et al., 2001; Kamiya and Shen; 2003, Ferreira et al. 2004; Chapters 19–21). Thus, P680 is most probably the Chl dimer corresponding to the bacterial P, and hence a hole is delocalized over these two Chl molecules. The rather small mid-IR electronic band of $P680^+$ compared with that of bacterial P^+ (Noguchi et al., 1998; Breton, 2001; Breton et al., 1992), suggesting weaker electronic coupling between the two Chl molecules, is consistent with larger separation of the dimer in PS II (8.2–10 Å) compared with that in purple bacteria (7.6 Å) (Zouni et al., 2001; Kamiya and Shen, 2003, Ferreira et al. 2004). Chl_T is probably a monomeric Chl in the D1 subunit corresponding to the accessory bacteriochlorophyll (B_L) in BRC (Noguchi et al., 2001; Diner et al., 2001; Noguchi, 2002). This assignment explains the nearly parallel orientation of the triplet Chl observed by EPR spectroscopy (Van Mieghem et al., 1991), the time-resolved IR data of rapid $^3Chl_T$ formation in favor of the mechanism of direct charge recombination on Chl_T (Noguchi et al., 2001), and the phenomena of rapid triplet quenching in the presence of Q_A^- (Van Mieghem et al., 1995).

B. The Redox-Active Tyrosines Y_Z and Y_D

In PS II, two tyrosine of the polypeptides D1 (D1-Tyr161, Y_Z) and D2 (D2-Tyr160, Y_D) form radicals with very different properties. Y_D forms a dark stable radical, the function of which is debated (Rutherford et al., 2004), while Y_Z is directly involved in electron transfer to the OEC and possibly participates directly to the proton or hydrogen atom abstraction from the substrate water at the Mn-cluster (Tommos and Babcock, 1998). The two radicals differ in redox potential, accessibility to exogenous reductants, stability, and proximity to OEC (for a review, see Diner, 2001; Chapter 9, Diner and Britt). The structural factors and interactions of the two radicals that explain their different properties have been addressed by different spectroscopic methods, including (high-field) EPR, ENDOR, ESEEM and kinetic approaches. In WT PS II, $Y_D^\bullet$ is H-bonded to the side chain of D2-His189, while a radical free of H-bond is observed in the D2-His189Gln mutant (Tang et al., 1993; Campbell et al., 1997). $Y_Z^\bullet$ is also H-bonded, but in Mn-depleted PS II, the properties of this H-bond differ from that formed by $Y_D^\bullet$ and the H-bond donor(s) is (are) yet to be identified (Diner, 2001). Hydrogen bond to D1-His190 is observed in the new three-dimensional structure resolved for the PS II of *T. elongatus* (Ferreira et al., 2004; Chapter 21, Barber and Iwata).

The structure and interactions of the two tyrosine radicals have been investigated using FTIR spectroscopy. FTIR difference spectra corresponding solely to $Y_D^\bullet/Y_D$ and $Y_Z^\bullet/Y_Z$ were obtained in Mn-depleted PS II from spinach as well as from *Synechocystis* sp. 6803 (Hienerwadel et al., 1995, 1996, 1997; Berthomieu et al., 1998a; Noguchi et al., 1997b; Chu et al., 2000c, 2004). The $Y_D^\bullet/Y_D$ spectra reported by the four above mentioned independent research groups all agree, while different spectra are proposed by the group of B.A. Barry (MacDonald et al., 1993; Kim and Barry, 1998; Kim et al., 1998). This discrepancy concerns actually not only spectra assigned to $Y_D^\bullet/Y_D$ or $Y_Z^\bullet/Y_Z$, but also to S_2/S_1 and Q_A^-/Q_A (Steenhuis and Barry, 1997; Steenhuis et al., 1999; MacDonald et al., 1993). Artifacts during spectra acquisition and miss-assignment of spectra are the main problems at the origin of these discrepancies, between the results of B.A. Barry and colleagues and those obtained by the rest of the FTIR community on PS II. This has been precisely discussed earlier (Hienerwadel et al. 1996; Onoda et al. 2000, and Chu et al., 2004). In particular FTIR spectra assigned to Q_A^-/Q_A by all other research groups (Berthomieu et al., 1990, 1992a; Noguchi et al., 1992, 1999c,d; Araga et al., 1993; Zhang et al., 1997; Chu et al., 1999; Kimura and Ono, 2001; Remy et al., 2004) are surprisingly assigned either to $Y_D^\bullet/Y_D$ or $Y_Z^\bullet/Y_Z$ (MacDonald et al., 1993; Kim and Barry, 1998; Kim et al., 1998) or even Chl^+/Chl (MacDonald et al., 1995). Hereafter, these spectra will not be further discussed.

The IR modes of the tyrosine residues in the reduced and radical state were identified by comparison of spectra recorded with PS II core preparations from *Synechocystis* sp. 6803 grown in presence of unlabeled or $^{13}C_6$-, $^{13}C_1$-, or $^{2}H_4$-labeled Tyr (Hienerwadel et al., 1997; Noguchi et al., 1997b; Berthomieu et al., 1998a). The frequencies of these modes were analyzed by comparison with IR spectra recorded with model compounds. The IR spectra of the phenoxyl, p-methyl phenoxyl, and tyrosine radicals generated by UV photochemistry at 40 K are dominated by a mode at 1503–1515 cm^{-1} assigned to the ν(C-O) IR mode, since it is sensitive to $^{13}C_1$-labeling of tyrosine and ^{18}O-labeling of phenol (Berthomieu and Boussac, 1995a; Hienerwadel et al., 1996; Berthomieu et al., 1998b; see also Capuccio et al., 2002). The IR data are in agreement with several resonance Raman data obtained for these radicals, notably for ^{17}O-labeled phenoxyl radical (Mukherjee et al., 1995 and references therein).

In PS II, the frequency of the ν(C-O) IR mode was shown to be sensitive to the interactions formed by the tyrosyl radical. In the D2-His189Gln mutant, where $Y_D^{\bullet}$ is not H-bonded, the ν(C-O) mode of $Y_D^{\bullet}$ is observed at 1497 cm^{-1}, a frequency very close to that identified by resonance Raman (RR) spectroscopy for the tyrosyl radical of ribonucleotide reductase, (1498 cm^{-1}) for which the structure shows that there is no H-bond (Backes et al., 1989). Formation of a H-bond to $Y_D^{\bullet}$ in WT PS II induces an upshift of this IR mode by + 6 cm^{-1} to 1503 cm^{-1} (Hienerwadel et al., 1997; Noguchi et al., 1997b). The frequency identified for $Y_Z^{\bullet}$, at 1512 cm^{-1} thus indicates that $Y_Z^{\bullet}$ also forms a H-bond in PS II, possibly stronger than that formed by $Y_D^{\bullet}$, and/or with an other proton acceptor (Fig. 2) (Berthomieu et al., 1998a,b; Hienerwadel et al., 1998).

The upshift of the ν(C-O) mode upon H-bond formation or exposure to a polar environment for phenoxyl or tyrosyl radicals is confirmed by recent IR data for phenoxyl radicals obtained in argon matrix (i.e., deprived from H-bonds) at cryogenic temperature (Spanget-Larsen et al., 2001). In these conditions, the ν(C-O) IR mode appears at 1481 cm^{-1}, i.e., at 20 cm^{-1} below the frequency observed for radicals formed in frozen solutions. The differ-

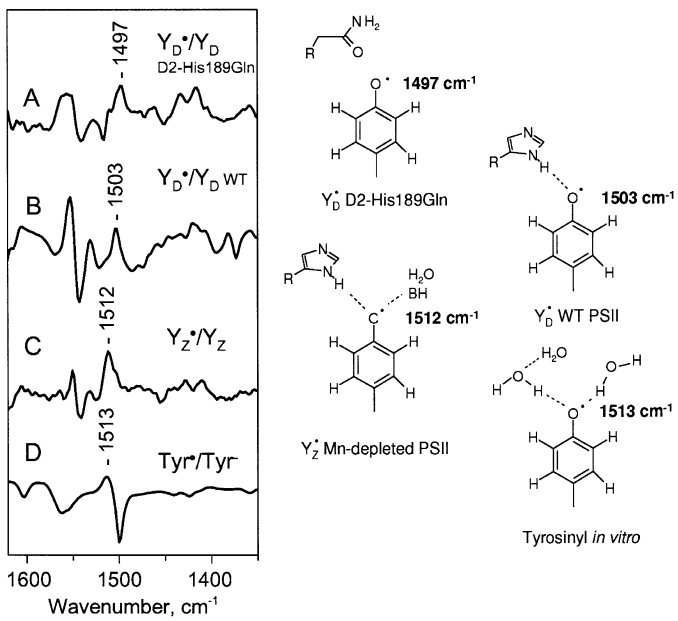

Fig. 2. FTIR difference spectra in the absorption region of the ν(C-O) mode of tyrosine radicals. From top to bottom, $Y_D^{\bullet}/Y_D$ in the D2-His189Gln mutant, $Y_D^{\bullet}/Y_D$ in WT PS II and $Y_Z^{\bullet}/Y_Z$ in Mn-depleted PS II from the D2-Tyr160Phe mutant of *Synechocystis* sp. PCC 6803, and $Tyr^{\bullet}/Tyr^{-}$ spectrum obtained by UV-photochemistry at 40 K in borate buffer at pH 12 (left). Molecular interactions proposed for $Y_D^{\bullet}$ and $Y_Z^{\bullet}$ in these systems (right), (Berthomieu et al., 1998; Hienerwadel et al., 1998).

ence is assigned to the polarized state of water, which would increase the quinoid character of the C-O bond of the radical, so as to specific interactions between phenoxyl radicals and water.

The normal modes of tyrosyl or phenoxyl radicals have been described by functional density methods (Mukherjee et al., 1995; Qin and Wheeler, 1995a,b). Comparison of experimental and computed isotopic shifts on these modes showed that a correct description can be achieved using these techniques (Mukherjee et al., 1995; Qin and Wheeler, 1995a; Nwobi et al., 1997). Recently, modeling of an H-bond between the phenoxyl radical and one or two water molecules or a Na^+ concluded to a significant upshift of the vibrational frequency of the ν(C-O) (+29 and +69 cm^{-1}, respectively, O'Malley, 2000). The H-bond to imidazole or imidazolium side chains also lead to calculated mode frequencies very close to those observed for $Y_D^{\bullet}$ and $Y_Z^{\bullet}$ in PS II (O'Malley, 2002). Other calculations propose a more complex situation, with an upshift of the ν(C-O) mode frequency upon H-bonding of phenoxyl radicals for H-bonds with $O_{\circ\circ\circ}H$ distances down to 1.65 Å. For H-bond with shorter $O_{\circ\circ\circ}H$ distances, a frequency downshift of the ν(C-O) mode would occur, due to repulsive Coulombic interactions between the phenoxyl and the hydrogen atom (Ivancich et al., 1999). These calculations would explain the low frequency of 1488–1484 cm^{-1} proposed by RR spectroscopy for the ν(C-O) mode for the tyrosyl radical of beef liver catalase. For this enzyme, the H-bond was deduced from the g-value of the radical obtained by high-field EPR (Ivancich et al., 1999).

These calculations predict the same g_x value for phenoxyl radicals forming different types of H-bonding interaction, with one or two water molecules, or with a carboxylate at different distances from the radical (Ivancich et al., 1999). Indeed for $Y_D^{\bullet}$ and $Y_Z^{\bullet}$, the same g_x value is observed, while different frequencies of the IR ν(C-O) mode are obtained (Un et al., 2001). ESEEM or ENDOR data also reflect differences in the number and distribution of H-bonds for the two radicals (Diner, 2001). In conclusion, high field EPR magnetic (ENDOR, ESEEM) and vibrational spectroscopies are complementary for the detailed analysis of the interactions formed by the radical and its environment. Other experimental values should be obtained in mutants, for which the structure is known to precisely correlate spectroscopic properties, structure and environments.

For reduced Y_Z and Y_D, the ν_{8a}(CC), ν_{19}(CC) ring stretching modes have been identified, at frequencies typical for neutral tyrosine (Hienerwadel et al. 1997; Noguchi et al., 1997b; Berthomieu et al., 1998a). Also, two modes are observed, at 1279 and 1255 cm^{-1} for Y_Z and at 1275 and 1250 cm^{-1} for Y_D, which have been assigned to the ν_{7a}(CO) and δ(COH) IR modes. This assignment was made by comparison with IR spectra of p-methyl-phenol recorded in different solvents. The frequency and relative intensity of these two modes are characteristic of the interactions formed by p-methyl-phenol and its environment (Hienerwadel et al., 1997). In PS II, the band pattern observed for Y_D and Y_Z allows to conclude that both tyrosine are neutral and in H-bonding interaction with the imidazole side chain of a histidine (Hienerwadel et al., 1997; Berthomieu et al., 1998a). Recent normal mode determination for p-methyl-phenol imidazole complexes, using density functional calculations, is in total agreement with these experimental data (O'Malley, 2002).

The $S_2Y^{\bullet}/S_2Y$ FTIR spectrum, corresponding probably to the formation of the Y_Z radical by illumination at 0 °C in Ca^{2+}-depleted PS II membranes of PS II (Tang et al., 1996) was obtained with ^{14}N and ^{15}N labeled PS II membranes (Berthomieu and Boussac, 1995b). This spectrum presents large analogy with the $Y_Z^{\bullet}/Y_Z$ FTIR difference spectrum recorded on Mn-depleted PS II from spinach or *Synechocystis* sp. PCC 6803 (Berthomieu et al., 1998a). In particular, the ν(C-O) mode of $Y_Z^{\bullet}$ appears at the same frequency in both spectra. However signals sensitive to ^{15}N labeling are present only in the $S_2Y^{\bullet}/S_2Y$ spectrum, which are similar to bands of the 4-MeImH$^{\bullet}$/4-MeImH_2^+ spectrum obtained at pH 6 by UV-photochemistry at 40 K (Berthomieu and Boussac, 1995a,b). This suggests the contribution from histidine IR modes in the $S_2Y_Z^{\bullet}/S_2Y_Z$ spectrum recorded with Ca^{2+}-depleted PS II. These IR modes may be due to D1-His190 in the vicinity of Y_Z.

C. The Oxygen Evolving Complex

The oxygen evolving complex (OEC) has a structural core called the Mn-cluster, which consists of four Mn ions and one Ca ion. The structure of the Mn cluster and its protein ligands were modeled by X-ray crystallography at 3.5–3.8 Å resolution (Zouni et al., 2001; Kamiya and Shen, 2003; Ferreira et al., 2004; Chapters 19–21), but a conclusive view has not been obtained yet. In the OEC, two water molecules are oxidized and molecular oxygen and four protons

are produced. The O_2-evolving reaction proceeds through a light-driven cycle of five intermediates, the S_i states (i = 0–4) (Chapter 25). The S_1 state is most dark stable, and each S state except for the S_4 state is advanced to the next state by flash illumination. Molecular oxygen is released upon flash illumination on the S_3 state via the unstable S_4 state.

The FTIR spectrum of the OEC was first obtained as a difference spectrum upon the $S_1 \rightarrow S_2$ transition in the frequency region of 1800–1000 cm^{-1} (Noguchi et al. 1992, 1993b, 1995a,b). Single flash illumination on dark-adapted PS II membranes at 250 K produces the S_2 state, which is stabilized for more than several minutes at this temperature. On the electron acceptor side, an electron is abstracted out of the protein by an exogenous electron acceptor, ferricyanide. Ferricyanide and its reduced form, ferrocyanide, do not show bands in the region above 1000 cm^{-1} except for the CN stretching bands at 2115 and 2037 cm^{-1}, respectively, which can be a good indicator of advancement of electron-transfer reactions. In the PS II membranes from spinach, however, ferricyanide pre-oxidizes the non-heme iron, which then becomes an endogenous electron acceptor and gives FTIR signals as an Fe^{2+}/Fe^{3+} difference (Section IV.C). To prevent this non-heme iron oxidation, the redox potential of the medium was lowered by adding ferrocyanide at the ferrocyanide/ferricyanide ratio of 9 (Noguchi and Inoue, 1995a). Under these conditions, the flash-induced S_2/S_1 difference spectrum without acceptor-side signals was obtained (Noguchi et al., 1995a,b). A virtually identical S_2/S_1 spectrum can also be obtained by subtracting the Q_A^-/Q_A spectrum from the $S_2Q_A^-/S_1Q_A$ spectrum in the presence of 3-(3,4-dichlorophenyl)-1,1-dimethylurea (DCMU) (Noguchi et al., 1995a). Comparable S_2/S_1 and $S_2Q_A^-/S_1Q_A$ spectra have been reported in several laboratories (Noguchi et al., 1993b, 1995a,b; Zhang et al., 1998; Chu et al., 1999, 2001b; Kimura and Ono, 2001; Remy et al., 2004). In addition, Zhang et al. (1998) measured an $S_2Q_B^-/S_1Q_B$ spectrum using the rapid-scan time-resolved method at room temperature.

The frequency region of 1800–1000 cm^{-1} in the S_2/S_1 difference spectrum exhibits the bands of amino acid side groups and polypeptide main chains coupled to the Mn-cluster. Several prominent peaks were observed in the symmetric (1450–1300 cm^{-1}) and asymmetric (1600–1500 cm^{-1}) stretching regions of carboxylate groups (Noguchi et al., 1995a,b). These bands downshifted upon uniform ^{13}C labeling of PS II, whereas the bands in the symmetric COO^- region were unchanged upon ^{15}N labeling (some bands in the asymmetric COO^- region changed upon ^{15}N labeling because of the superimposing amide II bands; see below), being consistent with the assignment to the COO^- vibrations (Noguchi et al., 1995a, 1999a; Noguchi and Sugiura, 2003; Kimura et al., 2003). The presence of several carboxylate bands in the S_2/S_1 spectrum strongly suggests that ligands to the Mn-cluster contain carboxylate groups of Asp, Glu, or the *C*-terminus, in agreement with the prediction from site-directed mutagenesis (Debus, 1992; Chapter 11).

Prominent peaks were also observed in the region of amide I bands (1700–1600 cm^{-1}) arising from the C=O stretches of backbone amides (Noguchi and Sugiura, 2003). The presence of amide I bands indicates that some changes in protein conformations take place upon S_2 formation. The peak frequencies ranging over the amide I region suggest that the protein moiety of the OEC includes various types of secondary structures (Noguchi et al., 1995a). Uniform ^{15}N labeling shifted down some bands around 1550 cm^{-1}, suggesting the presence of the amide II bands (NH bend + CN stretch) coupled to the amide I bands (Noguchi et al., 1995a; Noguchi and Sugiura, 2003; Kimura et al., 2003).

Ca^{2+} and Cl^- ions play an essential role in O_2 evolution and are thought to be located in the close vicinity of the Mn-cluster (Debus, 1992; Britt, 1996; Chapter 13). In the S_2/S_1 spectra, Ca^{2+} depletion (with EDTA and K^+, see below) led to disappearance of the positive/negative band pairs at 1364/1403 and 1587/1560 cm^{-1} attributable to the symmetric and asymmetric COO^- stretches, respectively, concomitant with reduced intensities in the amide I region (Noguchi et al, 1995a). This observation indicated that there is a carboxylate group closely related to Ca^{2+}, which drastically changes its structure upon $S_1 \rightarrow S_2$ transition. From the empirical relationship between the coordination type of carboxylate and the frequency difference between the symmetric and asymmetric vibrations ($\Delta\nu$) (Deacon and Phillips, 1980; Nakamoto, 1997), the large $\Delta\nu$ change from 157 to 223 cm^{-1} upon S_2 formation was interpreted as due to the structural change from bridging bidentate to unidentate coordination (Noguchi et al., 1995a). Thus, Noguchi et al. (1995a) proposed that the carboxylate group bridges the Mn and Ca ions in the S_1 state, and the coordination to Ca is disrupted upon S_2 formation. In contrast, Smith et al. (1997) suggested from the FTIR data of various manganese

carboxylate complexes that the general criteria for the coordination type based on the $\Delta\nu$ value do not hold over the range of Mn oxidation levels. Kimura and Ono (2001, 2003) recently claimed that Ca^{2+} depletion itself does not affect the COO^- bands, but besides Ca^{2+} depletion, the presence of chelators such as EDTA is necessary to eliminate the bands. In addition, Kimura et al. (2002) showed that replacement of Ca^{2+} ion with K^+, Rb^+, Cs^+, and Ba^{2+}, which have ionic radii larger than Ca^{2+}, also diminishes the same COO^- bands. They proposed that the chelator replaces the original carboxylate ligand and interacts with the Mn-cluster, and the metal substitution disrupts the hydrogen bond network around the Mn-cluster. However, no bands of the chelators were newly observed, and the relationship between the chelator interaction and metal substitution giving the same effect on the carboxylate bands is unclear. Thus, the experimental results as well as their interpretations are still controversial. Further studies are necessary to elucidate the structure and its change of the carboxylate group relevant to Ca^{2+}.

Upon Cl^- depletion, strong features in the amide I region of the S_2/S_1 spectra were mostly suppressed (Noguchi et al., 1995c) concomitant with decrease in the intensities of symmetric COO^- bands (Hasegawa et al., 2002a). The normal COO^- features were restored by addition of Br^-, I^- and NO_3^-, which can function in the Cl^- site (Hasegawa et al., 2002a). The stretching vibrations of NO_3^- in the S_2/S_1 spectra of NO_3^--substituted PS II preparations were identified around 1400 cm^{-1} using $^{15}NO_3^-$ and $N^{18}O_3^-$ (Hasegawa et al., 2002a, 2004). From comparison of the observed NO_3^- frequencies with those of metal-bound NO_3^-, it was suggested that NO_3^- in the Cl^- site is coupled to the Mn-cluster but not as a direct ligand.

The effect of H/D exchange on the protein bands of the S_2/S_1 spectrum was studied, and it was found that an asymmetric COO^- band upshifted by 18 cm^{-1} from 1561 to 1579 cm^{-1} (Noguchi et al., 1995b). FTIR measurements of model carboxylate compounds that have different types of H-bonding interactions with water molecules, showed that a large upshift by ~20 cm^{-1} upon H/D exchange reflects strong H-bonding of a carboxylate group with a water ligand to a metal ion (Noguchi et al., 1995b). The upshift of an asymmetric COO^- frequency by coupling with water was also reproduced by theoretical calculation (Fischer and Wydrzynski, 2001). Taken together, it has been suggested that there is a carboxylate ligand H-bonded to substrate water coordinated to the Mn ion (Noguchi et al., 1995b).

Chu et al. (2001a, 2004) incorporated L-[1-^{13}C]alanine into the PS II particles of *Synechocystis* PCC 6803 and measured the S_2/S_1 FTIR spectra. Symmetric COO^- bands at ~1356 cm^{-1} in the S_1 state and at ~1339 or ~ 1320 cm^{-1} in the S_2 state downshifted upon L-[1-^{13}C]alanine labeling. These signals arise from the α-COO^- groups of D1-Ala344, because the shifts were not observed in D1-Ala344Gly and D1-Ala344Ser PS II particles. It was proposed that the *C*-terminal α-COO^- groups of D1-Ala344 ligates the Mn ion that undergoes an oxidation during the $S_1 \rightarrow S_2$ transition (Chu et al., 2004), being consistent with the results of mutagenesis (Nixon et al., 1992) and X-ray crystallography (Kamiya and Shen, 2003) (but see Ferreira et al., 2004; Chapter 21, Barber and Iwata).

IR spectra of an imidazole side group show a characteristic C-N stretching band around 1100 cm^{-1} (Hasegawa et al., 2000, 2002b). In this frequency region of the S_2/S_1 spectrum, relatively small negative peak was observed at 1113–1114 cm^{-1} in spinach PS II membranes and PS II core complexes from *Synechocystis* PCC 6803. This band downshifted by 7 cm^{-1} upon both global ^{15}N labeling of spinach and ^{15}N labeling of histidine side chains of the *Synechocystis* cores. Thus, this band was definitely assigned to a histidine side chain, which is probably a ligand to the Mn-cluster (Noguchi et al., 1999b), being consistent with the results in the ESEEM and ENDOR studies (DeRose et al., 1991; Tang et al., 1994). There is a correlation between the protonation forms of an imidazole group and the frequency and N-deuteration shift of the C-N stretching band around 1100 cm^{-1} (Noguchi et al., 1999b; Hasegawa et al., 2000, 2002b). On the basis of this correlation, it was indicated that the histidine side chain detected in the S_2/S_1 spectrum is protonated at the Nπ site, and hence probably coordinated to the Mn ion at the Nτ site. In addition, several small peaks were observed in the 2850–2500 cm^{-1} region of the S_2/S_1 spectrum, which downshifted upon global ^{15}N labeling and selective [^{15}N]His labeling. These peaks are attributed to Fermi resonance between the H-bonded NH stretching mode and the overtones and combinations of imidazole vibrations. Hence, the presence of these Fermi resonance peaks indicates that the NH group of this histidine is H-bonded (Noguchi et al., 1999b).

The tyrosine bands in the S_2/S_1 spectrum were identified at 1254 and 1521 cm^{-1}, which downshifted by 25 and 15 cm^{-1} upon [ring-4-^{13}C]tyrosine labeling of *Synechocystis* cores and were assigned to the COH [the original assignment was the CO stretch but the

band may include a significant contribution from the COH bend (Berthomieu et al., 1998a)] and ring C=C vibrations, respectively (Noguchi et al., 1997b). The COH band position at 1254 cm^{-1} was basically in agreement with that of the $Y_Z^{\bullet}/Y_Z$ spectrum at 1255 cm^{-1} (Berthomieu et al., 1998a) but a little higher than that of $Y_D^{\bullet}/Y_D$ spectrum at 1250–1251 cm^{-1} (Hienerwadel et al., 1997; Noguchi et al., 1997b) in *Synechocystis* core complexes. From these observations together with the close proximity of Y_Z to the Mn-cluster (Gilchrist et al., 1995; Zouni et al., 2001), it was suggested that Y_Z is structurally coupled to the Mn-cluster via H-bonds.

Water shows strong OH stretching bands in the high frequency region of 3800–3000 cm^{-1}. The S_2/S_1 spectrum in the weakly H-bonded OH region (3800–3500 cm^{-1}) was obtained escaping from absorption saturation by bulk water using the core complexes from *Thermosynechococcus elongatus* at 250 K (Noguchi and Sugiura, 2000). Positive and negative bands were observed at 3618 and 3585 cm^{-1}, respectively, and both bands exhibited downshifts by 12 cm^{-1} upon replacement of $H_2{}^{16}O$ by $H_2{}^{18}O$. Upon D_2O substitution, the 3618/3585 cm^{-1} bands largely downshifted to 2681/2652 cm^{-1}. From these observations, these bands were assigned to the weakly H-bonded O-H stretching vibrations of a water molecule, which is a substrate or an active water molecule coupled to the Mn-cluster. The upshift by 33 cm^{-1} upon S_2 formation indicates that the H-bonding of the water O-H in the S_1 state becomes weaker in the S_2 state. The intramolecular coupling with the other O-H vibration of the water molecule, which was estimated by decoupling experiments using a H_2O/D_2O (1:1) mixture, indicated that this water has a considerably asymmetric H-bonding structure and this asymmetry becomes more prominent upon S_2 formation. This view was also confirmed by the theoretical calculation of the coupling strength of water vibrations (Fischer and Wydrzynski, 2001).

The lower frequency region under 1000 cm^{-1} yields Mn-ligand vibrations and hence provides direct structural information about the coordination sphere of the Mn-cluster. Chu et al. (1999; 2000a,b; 2001b,c) obtained S_2/S_1 spectra in the lower-frequency region of 1000–350 cm^{-1} by overcoming technical difficulties by using partially dehydrated samples, a custom-built band-bass filter (Hawkins et al., 1998), appropriate materials for windows and a beam splitter, and low-frequency sensitive detectors. They found that the bands at 606/625 cm^{-1} (S_2/S_1) downshifted by about 10 cm^{-1} upon ^{18}O substitution and thus assigned these bands to the Mn-O-Mn vibrations (Chu et al., 2000b). It was also shown that the 606 cm^{-1} band was upshifted to 618 cm^{-1} by Sr^{2+} substitution but not affected by ^{44}Ca substitution. From this observation, they suggested that Ca^{2+} communicates with, but is not integral to, the manganese core (Chu et al., 2000b). Furthermore, Chu et al. (2001b) measured the S_2/S_1 spectrum of the PS II particles from the D1-Asp170His mutant of *Synechocystis* PCC 6803 and showed that there was no appreciable change in the mid-IR region but the 606 cm^{-1} band shifted to 612 cm^{-1} in the mutant. This result indicates that D1-Asp170 is structurally coupled to the Mn-O-Mn structure. Recently, Kimura et al. (2003) examined the low-frequency S_2/S_1 bands using uniformly ^{15}N- or ^{13}C-labeled core complexes, and suggested that most of the low-frequency bands are derived from the coupling between the Mn-cluster and the protein.

Resonance Raman spectroscopy should also be informative on the core structure of the Mn-cluster, but strong Raman scattering from Chl and carotenoid molecules has been hampering detection of Raman scattering from the Mn-cluster by a conventional resonance Raman technique. Seibert and Cotton (1985) applied SERS spectroscopy to the OEC and observed a band at 225 cm^{-1} in PS II membranes depleted of the three extrinsic proteins. Although the exact origin was uncertain, they suggested that this signal is related to the presence of functional Mn on the surface of PS II membranes lacking the 33 kDa extrinsic protein (Seibert and Cotton, 1985; Seibert et al., 1988). Cua et al. (2000) measured resonance Raman spectra of the Mn-cluster with 820-nm excitation using the technique of shifted-excitation Raman difference spectroscopy (SERDS). They found several low-frequency bands attributable to the Mn-ligand vibrations in the S_1 state. Four bands at 500–300 cm^{-1} downshifted in D_2O, and hence were assigned to the $Mn\text{-}OH_2$ or Mn-OH vibrations.

Aiming at better understanding of the low-frequency vibrational spectra of the Mn-cluster, FTIR or Raman measurements of various oxo-bridged Mn complexes with different Mn oxidation states were performed and the bands were assigned by isotopic substitution and normal mode analyses (Albela et al., 2001; Visser et al., 2002; Cua et al., 2003).

To date, most of the FTIR studies on the OEC have been performed on the $S_1 \rightarrow S_2$ transition, the first flash-induced transition in dark-adapted samples. However, to investigate the molecular mechanism

of O_2 evolution, it is essential to measure the FTIR spectra of higher S-state transitions. Chu et al. (2000c) obtained an S_3/S_2 difference spectrum in the 1800–1200 cm^{-1} region by subtracting a one-flash spectrum (S_2/S_1) from a two-flash spectrum (S_3/S_2 + S_2/S_1) measured at 250 K, and showed significantly different bond rearrangement in the OEC upon the $S_2 \rightarrow S_3$ transition compared to the $S_1 \rightarrow S_2$ transition. The same measurement was applied to the lower frequency region (650–350 cm^{-1}), showing that the band at ~621 cm^{-1} arises from the Mn-O-Mn vibration in the S_3 state (Chu et al., 2001d). On the other hand, Hillier and Babcock (2001) and Noguchi and Sugiura (2001) independently measured FTIR difference spectra of all the flash-induced S-state transitions ($S_1 \rightarrow S_2$, $S_2 \rightarrow S_3$, $S_3 \rightarrow S_0$ and $S_0 \rightarrow S_1$) in the 1800–1200 cm^{-1} region by subjecting samples to a series of flashes. The former group used PS II membranes from spinach and the measurement was performed at 265 K, while the latter used PS II core complexes from *T. elongatus* at 10 °C. Despite different conditions, comparable spectra were obtained by the two groups. Flash-induced spectra during the S-state cycle measured using moderately hydrated core complexes from *S. elongatus* are presented in Fig. 3 (Noguchi and Sugiura, 2002a). The 1st, 2nd, 3rd, and 4th-flash spectra virtually represent the S_2/S_1, S_3/S_2, S_0/S_3 and S_1/S_0 difference spectra, respectively, because: (i) the 1st to 4th-flash spectra showed considerably different spectral features; (ii) the 5th, 6th, 7th, and 8th-flash spectra were similar to the 1st, 2nd, 3rd, and 4th-flash spectra, respectively; and (iii) the intensities of prominent peaks showed clear period-four oscillation patterns (Noguchi and Sugiura, 2001, 2002a). Similarly to the S_2/S_1 spectrum, other S-state spectra showed prominent bands in the symmetric and asymmetric COO^- stretching regions as well as in the amide I region (Noguchi and Sugiura, 2003), suggesting that carboxylate groups are deeply involved in the O_2-evolving reaction. In the 3rd and 4th-flash spectra,bands are observed at the similar frequencies to the bands in the 1st and 2nd-flash spectra with opposite signs (Fig. 3). This observation indicates that the reactions and structural changes in the protein moieties in the $S_1 \rightarrow S_2 \rightarrow S_3$ transitions are reversed in the $S_3 \rightarrow S_0 \rightarrow S_1$ transitions. The similar S-state measurement was extended to the water OH(D) region using moderately hydrated (or deuterated) PS II core complexes, and the reactions of water molecules during the S-state cycle were directly monitored by FTIR (Noguchi and Sugiura, 2002b).

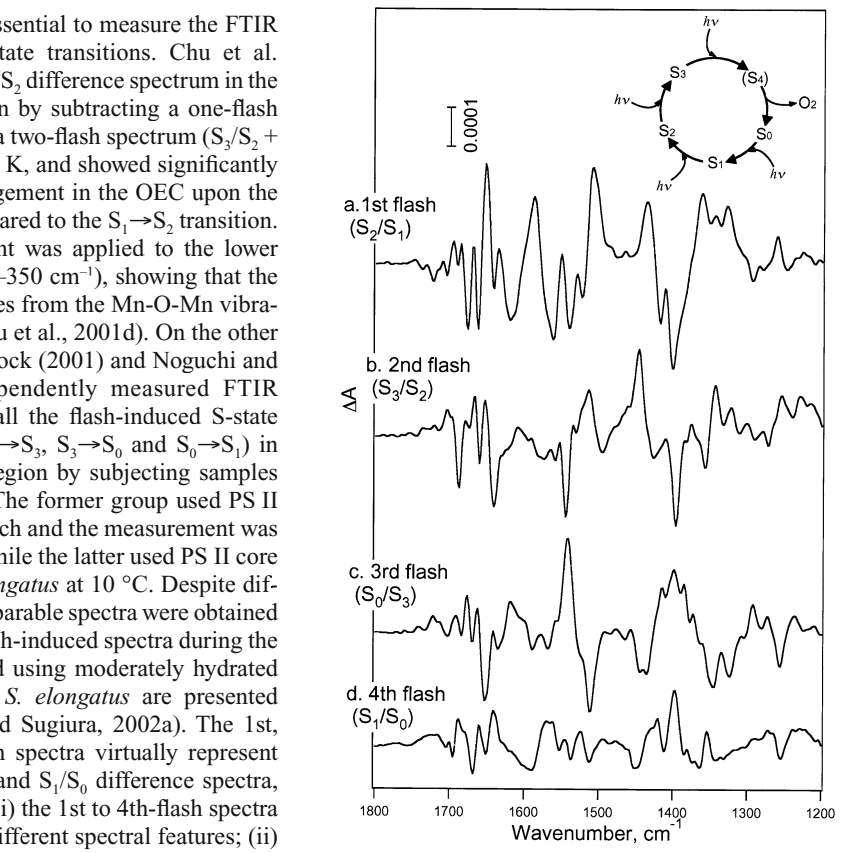

Fig. 3. Flash-induced FTIR difference spectra of the PS II core complexes from *Synechococcus elongatus* during the S-state cycle of O_2-evolving machinary (Noguchi and Sugiura, 2002a). Difference spectra upon the 1st (a), 2nd (b), 3rd (c) and 4th (d) flashes reveal structural changes in the $S_1 \rightarrow S_2$, $S_2 \rightarrow S_3$, $S_3 \rightarrow S_0$ and $S_0 \rightarrow S_1$ transitions, respectively.

IV. Cofactors on the Electron-Acceptor Side

A. Pheophytin

The first FTIR difference spectrum recorded with PS II was that corresponding to the photoreduction of the intermediary electron acceptor pheophytin ($Pheo^-$/Pheo spectrum; Tavitian et al., 1986). The $Pheo^-$ was stabilized under continuous illumination at –40 °C on PS II-enriched membranes in presence of dithionite (Tavitian et al., 1986). Very large similarities were observed between this $Pheo^-$/Pheo spectrum and the spectrum recorded upon bacteriopheophytin (H_A) reduction in the BRC (Nabedryk et al., 1986). FTIR difference spectra obtained by spectroelectro-

chemistry of pheophytin and pyropheophytin in a cell designed for UV-Vis and infrared measurements, showed that in tetrahydrofuran, the 10a-ester C=O and 9-keto groups of neutral pheophytin, at 1743 and 1706 cm^{-1}, are downshifted to 1728 and 1656 cm^{-1} upon anion formation (Nabedryk et al., 1990). Very similar results were reported upon spectroelectrochemistry of bacteriopheophytin *b* in solution (Mäntele et al., 1987). In PS II, three IR signals are observed at 1739, 1721 and 1677 cm^{-1} for neutral Pheo. The signal at 1677 cm^{-1} is assigned to the 9-keto ν(C=O) mode. The low frequency of this mode for Pheo in PS II as compared to pheophytin in tetrahydrofuran is explained by a strong H-bond formed with the side chain of D1-Glu130, stronger than that formed in *Rps. viridis* BRC, where the 9-keto C=O of H_A is H-bonded to L-Glu104 (Nabedryk et al., 1990; Breton et al., 1999b). The two signals at 1739 and 1721 cm^{-1}, first proposed to account for D1-Glu130 side chain and for the 10a-ester ν(C=O) Pheo modes, respectively (Nabedryk et al., 1990) have been reinterpreted in light of recent data obtained with WT and mutants in the BRC of *Rps. viridis* (Breton et al., 1999b), as corresponding to the 10a-ester C=O mode of two populations of Pheo. Indeed in bacterial RC, it was shown that the 10a-ester C=O mode of H_A occupies discrete conformations that appear to depend on the precise interaction of the cofactor with the protein, and possibly the presence or absence of the H-bond between L-Glu104 and the 9-keto C=O (Breton et al., 1999b). The same heterogeneity in 10a-ester C=O environment is proposed for the Pheo of PS II (Dejonghe et al., 1998).

B. The Quinone Acceptors Q_A and Q_B

The FTIR spectrum corresponding solely to Q_A^-/Q_A was obtained using Mn-depleted PS II enriched membranes in presence of hydroxylamine as electron donor to $P680^+$ and DCMU, to prevent electron transfer to the secondary quinone acceptor Q_B (Berthomieu et al., 1990). Spectra with higher signal to noise ratio where then obtained adding phenazine methosulfate to re-oxidize Q_A^- in presence of DCMU (Fig.4) (Berthomieu et al., 1992a; Hienerwadel et al., 1996). In these conditions, EPR control experiments showed that Q_A^- is generated with high yield by illumination, while no radical from the electron donor side of PS II (Y_Z or Chl) is detected (Hienerwadel et al., 1996). By comparison with the infrared absorption

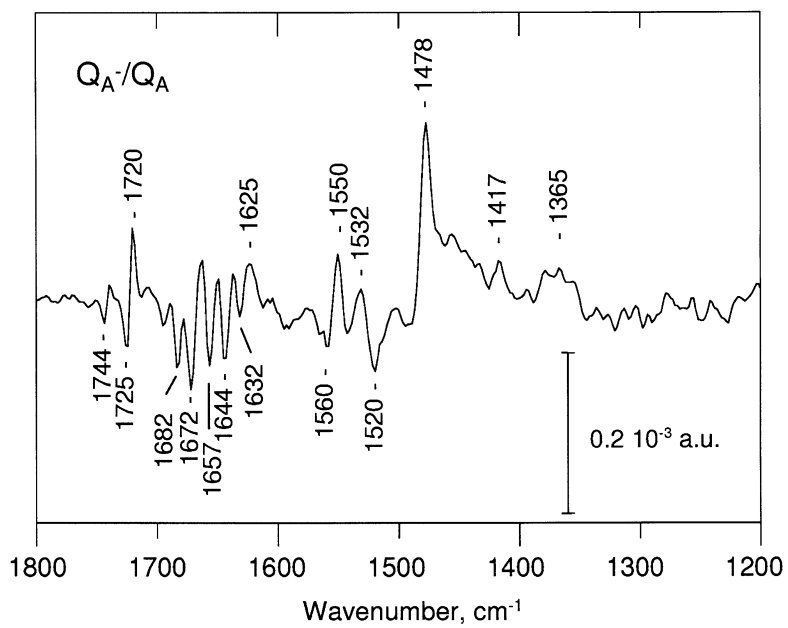

Fig. 4. Q_A^-/Q_A FTIR difference spectrum recorded with Mn-depleted PS II enriched membranes (Berthomieu et al., 1992a).

of plastoquinone-9 or with Q^{-}•/Q FTIR difference spectra recorded by spectroelectrochemistry of the ubiquinone model compound (Bauscher et al., 1990), a positive band at 1478 cm^{-1} in the Q_A^-/Q_A spectrum was proposed to account for the ν(C⇢O) mode of the semiquinone anion Q_A^-, and two bands at 1645 and/or 1630 cm^{-1} to the neutral quinone ν(C=O) mode(s) (Berthomieu et al., 1990). Accordingly, these signals are not modified in Q_A^-/Q_A spectra recorded with ^{15}N-labeled PS II-enriched membranes (Berthomieu et al. 1992a; Hienerwadel et al., 1996). The Q_A^-/Q_A spectrum extended to the low frequency region (1000–600 cm^{-1}) shows other IR signals tentatively assigned to neutral plastoquinone Q_A and the semiquinone Q_A^- (Chu et al., 1999). In particular, a difference band at 754/750 cm^{-1} in the Q_A^-/Q_A spectrum could correspond to a Q_A ring stretch/bend mode, predicted by normal mode calculations, at 759 cm^{-1} for neutral PQ_9 and at 754 cm^{-1} for the semiquinone anion (Chu et al., 1999).

The Q_A^-/Q_A fingerprint spectrum, was used to analyze the effect of lipids and of small PS II subunits on the level of Q_A reconstitution in PS II core complexes (Araga et al., 1993). Very similar Q_A^-/Q_A spectra have been obtained in several laboratories and with PS II from plants and from the cyanobacterium *Synechocystis sp*. 6803 (Araga et al., 1993; Dejonghe et al., 1998; Noguchi et al., 1992; Chu et al., 1999; Zhang et al., 1997; Remy et al. 2004). In particular, Zhang et al. (1997) obtained the Q_A^-/Q_A spectrum, using time-resolved FTIR spectroscopy and confirmed the assignment of the band at 1479 cm^{-1} to the semiquinone state by comparison of its DCMU-sensitive decay kinetic, which follows the Q_A^- decay measured by the Chl *a* fluorescence kinetics.

The semiquinone band at 1479 cm^{-1} is insensitive to the depletion of the non heme iron at pH 6.5, while cyanide binding at the iron or high pH treatment, leading to the binding of hydroxyl anion on the iron induce a frequency downshift by 4 and 2 cm^{-1} of this mode, respectively (Noguchi et al., 1999c). The two latter treatments are proposed to break a H-bonding interaction between Q_A^- and D2-His215, a ligand of the iron. Other changes in the Q_A^-/Q_A FTIR spectrum upon cyanide or hydroxyl binding to the non heme iron, correspond to IR modes of the protein backbone and side chains. In particular, modes of the histidine ligand(s) of the iron were identified in the Q_A^-/Q_A-FTIR spectrum using [^{15}N]His-labeled PS II core complexes from *Synechocystis* sp.6803 (Noguchi et al., 1999d). A ^{15}N-sensitive mode at 1179 cm^{-1} appears well above the 1151 cm^{-1} frequency of the His model 4(5)-methylimidazole in solution, indicative of a H-bonded His. In contrast to the prediction from the X-ray crystallographic structure of the BRC, no IR signals from tryptophan could be detected upon tryptophan labeling in the Q_A^-/Q_A spectrum in PS II. The predicted π - π interaction is not strong enough to influence the vibrations of the indole ring of tryptophan upon Q_A reduction (Noguchi et al., 1999d).

Finally, differential signals centered at 1741 and 1721 cm^{-1} in the Q_A^-/Q_A spectrum, are assigned to the electrostatic response of the 10a-ester C=O mode of Pheo upon Q_A^- formation, by comparison with data obtained with WT and mutants of the BRC (Berthomieu et al., 1990; Dejonghe et al., 1998; Breton et al., 1997b; Breton et al., 1999b).

Very limited information is available at present concerning the IR modes of Q_B in PS II. There is no pure Q_B^-/Q_B FTIR difference spectrum available for PS II. The $S_2Q_B^-/S_1Q_B$ spectrum obtained by time-resolved FTIR spectroscopy of intact PS II-enriched membranes shows an intense positive band at 1480 cm^{-1} (Zhang et al., 1998). This band was assigned to Q_B^- based on its decay kinetics. By analogy with the IR absorption of Q_A^- of PS II and of Q_B^- in BRCs (Breton et al., 1991), Zhang et al. (1998) tentatively assigned the 1480 cm^{-1} band to the ν(C⇢O) mode of the semiquinone anion Q_B^-.

C. The Non Heme Iron

In PS II, the non heme iron located on the C_2-symmetry axis, between the two electron acceptor quinones Q_A and Q_B (Chapter 8) has a midpoint potential of 400 mV at pH 7 which presents a pH dependence of –60 mV/pH unit, showing that its oxidation is accompanied by the deprotonation of a residue in its vicinity. In place of the glutamate providing the 5th and 6th ligands of the iron in BRC, an exchangeable bicarbonate molecule was shown to bind to the iron in PS II (Petrouleas and Diner, 1990; Chapter 14). This bicarbonate is necessary for the reduction and protonation of $Q_B^-(H)$ into the quinol Q_BH_2 (Diner et al., 1991; Govindjee and van Rensen, 1993) and could play a regulatory role in the function of PS II.

In Mn-depleted PS II, the non heme iron is oxidized in the dark by ferricyanide. After light-induced charge separation, Fe^{3+} is reduced by electron transfer from the semiquinone anion Q_A^- and the Fe^{2+} state has a half time of 20 s. At the electron donor side, $Y_Z^{\bullet}$ is reduced within 2 s after the flash (Hienerwadel et

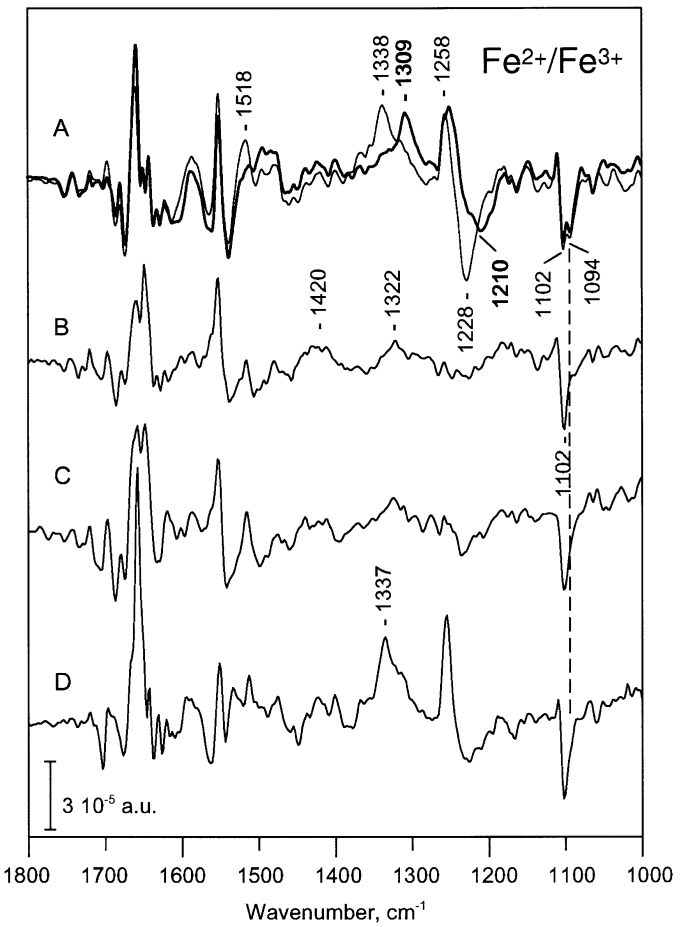

Fig. 5. Fe^{2+}/Fe^{3+} FTIR difference spectra recorded in presence of (A) ^{12}C- (thin line) and ^{13}C-bicarbonate (bold line), (B) glycolate, (C) glyoxalate, and (D) bicarbonate and o-phenanthroline (Hienerwadel and Berthomieu, 1995; Berthomieu and Hienerwadel, 2001).

al., 1993; Hienerwadel and Berthomieu, 1995a). The Fe^{2+}/Fe^{3+} spectrum (Fig. 5), recorded on Mn-depleted PS II membranes in presence of ferricyanide, 2 s after flash illumination shows band shifts and intensity changes of IR modes from ligands and neighboring residues of the non heme iron (Hienerwadel et al., 1993; Hienerwadel and Berthomieu, 1995a). Titration of the S_2Fe^{2+}/S_1Fe^{3+} FTIR spectra as function of the potential of the sample, controlled by different relative concentrations of ferricyanide and ferrocyanide, showed that the IR changes associated to the non heme iron titrate with the expected pH dependent midpoint potential (Noguchi and Inoue, 1995a).

In the Fe^{2+}/Fe^{3+} spectrum, the bicarbonate $\nu_{as}(COO^-)$ and $\nu_s(COO^-)$ IR modes were identified by comparison of FTIR difference spectra recorded in the presence of ^{12}C and ^{13}C bicarbonate (Fig. 5A) (Hienerwadel and Berthomieu, 1995a). For carboxylate anions ligands of a metal, the frequency difference between these two modes is correlated to the mode of binding to the metal (Deacon and Phillips, 1980). The small frequency difference (192 cm^{-1}) between the $\nu_{as}(COO^-)$ and $\nu_s(COO^-)$ modes at 1530 ± 10 and 1338 cm^{-1} for bicarbonate in the Fe^{2+}-state, as compared to H-bonded ionic bicarbonate, strongly indicates that bicarbonate is a bidentate ligand of Fe^{2+} (Hienerwadel and Berthomieu, 1995a). The strong up- and downshifts of the ν_{as} and ν_s (COO^-) modes

of bicarbonate upon iron oxidation (1658 ± 20 cm^{-1} and 1228 cm^{-1}, respectively) result in a frequency difference of 430 ± 20 cm^{-1} that is not only explained by the increased charge on the iron, but indicates that bicarbonate is a monodentate ligand of the oxidized iron. The sensitivity of the ν_s(CO) mode of bicarbonate to $^1H/^2H$ exchange in both the Fe^{2+} and Fe^{3+} states and the presence in the Fe^{2+} state of a δ(COH) mode at 1258 cm^{-1} confirm that bicarbonate and not carbonate is the iron ligand and further exhibits H-bond(s) with the protein. The ^{13}C isotope-sensitive modes of bicarbonate are not affected by ^{15}N labeling of the PS II membranes, excluding that formation of a carbamate occurs in PS II. The recent three-dimensional structure of PS II obtained on *T. elongatus* also concludes that bicarbonate is a bidentate ligand of Fe^{2+} (Ferreira et al. 2004; Chapter 21, Barber and Iwata).

^{15}N sensitive signals at 1111/1102 and 1094 cm^{-1} are assigned to side-chain modes from histidine ligands of the iron. From comparison with an IR study on protoporphyrin IX- (methyl)-imidazole models at different pH (Berthomieu et al., 1992b), it was proposed that the signal at 1094 cm^{-1} corresponds to a histidine ligand that deprotonates upon iron oxidation. This His signal is absent in Fe^{2+}/Fe^{3+} spectra recorded with PS II membranes with glycolate, lactate and glyoxylate (Fig. 5B-C) (Hienerwadel et al., 1995b; Berthomieu and Hienerwadel, 2001). This signal is also absent in spectra recorded with PS II membranes with o-phenanthroline, an inhibitor of Q_B fixation expected to interact with the His ligand of the iron and located at the Q_B binding pocket (D1-His215) (Fig. 5D) (Hienerwadel and Berthomieu, 1995b; Berthomieu and Hienerwadel, 2001). Thus it is proposed that this D1-His215, ligand of the iron and in contact with the Q_B pocket is responsible for the signal at 1094 cm^{-1}, and deprotonates upon iron oxidation. Bicarbonate regulates the properties of this histidine. A broad positive continuum, maximum at ≈2550 cm^{-1}, is observed in the presence of bicarbonate, but absent with o-phenanthroline or modified in samples containing lactate, glycolate, and glyoxylate. This continuum is interpreted as the existence of an interaction of bicarbonate and D1-His215 with a H-bond network from the non heme iron toward the Q_B pocket (Berthomieu and Hienerwadel, 2001). The regulation mechanism of PS II by bicarbonate (for a review, see Govindjee and van Rensen, 1993) could be due to the regulation by bicarbonate of the properties of D1-His215 and of protonatable residues implicated in the protonation mechanisms of Q_B(H).

V. Cofactors in Secondary Electron-Transfer Pathways

Cytochrome b_{559} (Cyt b_{559}), Chl Z and β-carotene (Car) form a side path to reduce $P680^+$ in the electron transfer reactions in PS II. This side path becomes active when electron transfer from the Mn-cluster via Y_Z is blocked by Mn depletion or by decreasing the temperature. Electron transfer pathways between P680 and these three species are still under debate (Vrettos et al., 1999; Faller et al., 2001; Chapter 15, Faller et al.). This peripheral electron transfer is postulated to play a protective role against photoinhibition (Stewart and Brudvig, 1998; Tracewell et al., 2001a).

A. Cytochrome b_{559}

In intact PS II, most of the Cyt b_{559} is in a high potential (HP) form, with E_m = 370 mV, which is readily converted in intermediary (IP) or low (LP) potential form, with E_m = 60–200 mV by various treatments that alter the membrane structure and/or damage the OEC (Roncel et al., 2001; reviewed in Steward and Brudvig, 1998). The molecular origin of the differences between the two HP and LP forms, was investigated by FTIR difference spectroscopy (Berthomieu et al., 1992b). First, the IR modes sensitive to the oxidation state of *b*-type cytochromes were analyzed by the spectro-electrochemistry of isolated Cyt b_{559} and of protoporphyrin IX-(methyl)imidazole model compounds (Berthomieu et al., 1992b). It was shown that modes from both the heme, the histidine ligands and the protein contribute to the electrochemically induced red -*minus*- ox (or ox -*minus*- red) FTIR difference spectra of Cyt b_{559}. In particular, a difference band at 1660/1652 cm^{-1} was assigned to a structural change at the level of a peptide carbonyl upon Cyt b_{559} oxidation in PS II enriched membranes. This difference band is tentatively assigned to an interaction between peptide carbonyls of the transmembrane α-helices and the histidine ligands of the iron. This signal is twice larger upon oxidation of Cyt b_{559} HP than for Cyt b_{559} LP. This difference suggests that one of the histidines to peptide H-bonds no longer exists for Cyt b_{559} LP. Other spectral differences, at 1700 cm^{-1} and 1530–1510 cm^{-1} in the FTIR spectra recorded upon photooxidation of HP and LP Cyt b_{559} show that the mechanisms of heme oxidation in vivo implies different molecular processes for the two forms HP and LP.

EPR data on Cyt b_{559} LP and HP as well as resonance Raman data (Desbois and Lutz, 1992) and the measurement of the pH dependence of the Cyt b_{559} midpoint potential in presence or absence of the histidine modifier diethylpyrocarbonate (Roncel et al., 2001) also suggest that a structural change at (or deprotonation of) a histidine ligand is linked to the change in midpoint potential of Cyt b_{559}

B. Chlorophyll Z and β-Carotene

Chl Z is proposed to be a Chl attached to D1-His118 (Stewart et al., 1998) or D2-His117 (Ruffle et al., 1998), while two carotenes (Car) molecules in the PS II RC was modeled to be located on the D2 side in the X-ray crystal structure (Kamiya and Shen, 2003). Continuous illumination on PS II samples at cryogenic temperatures in the presence of ferricyanide, which pre-oxidizes Cyt b_{559}, accumulates the cation radicals of Chl Z and Car. The Car cation is photo-produced to higher extent at lower temperatures (Schenck et al., 1982; Noguchi et al., 1994; Hanley et al., 1999). An FTIR spectrum representing solely a Chl Z^+/Chl Z difference was measured using Mn-depleted PS II membranes in the presence of ferricyanide and silicomolybdate at 210 K (Noguchi and Inoue, 1995b). The spectrum showed a prominent positive/negative bands at 1714/1684 cm^{-1}, which were assigned to the keto C=O stretches of cation/neutral species of Chl Z. The keto C=O position of 1684 cm^{-1} of Chl Z indicates that this C=O group is H-bonded or in a highly polar environment. Carbomethoxy C=O bands were observed at 1747/1736 cm^{-1}, indicative of a slightly polar environment. The band pattern of the macrocycle C=C stretching vibrations showed that Chl Z has a 5-coordinate structure.

A resonance Raman spectrum of Chl Z^+ was measured by Cua et al. (1998) using the SERDS method with 820-nm excitation. The band pattern of the SERDS spectrum of Chl Z^+ was significantly altered in the D1-His118Gln mutant of *Synechocystis* PCC 6803, whereas that in D2-His117Gln remained identical to the wild-type, and hence it was proposed that D1-His118 is the axial ligand to Chl Z (Stewart et al., 1998). This idea, however, was in disagreement with the suggestion by Ruffle et al. (1998) that D2-His117 is the ligand to the redox-active Chl based on the mutants on D2-His117 in *Chlamydomonas reinhardtii*. These contradictory views were reconciled by the possibility of alternate electron-donation pathways on the D1 and D2 sides (Tracewell et al., 2001b).

A light-induced FTIR spectrum upon the formation of Car cation was measured using PS II membranes at 80 K (Noguchi et al., 1994). In the spectrum obtained as a mixture of the $Car^+Q_A^-$/$CarQ_A$ and Chl $Z^+Q_A^-$/Chl ZQ_A differences, strong positive bands assignable to the Car cation were observed at 1465–1440, 1148, and 992 cm^{-1}. Also, resonance FT-Raman spectra of Car cation in PS II reaction center and Mn-depleted core complexes were obtained with 1064-nm excitation, showing peaks at 1527–1525, 1485–1484, 1154–1149, and 1003–1001 cm^{-1} (Pascal et al., 1999; Vrettos et al., 1999). Resonance Raman measurements by several different excitation wavelengths showed that both Car molecules in the PS II reaction center complex are oxidized and they exhibit different vibrational properties (Telfer et al., 2003).

Acknowledgments

This work was supported by a Grant-in-Aid for Scientific Research (No. 14540607) from the MEXT of Japan (to TN). CB acknowledges the contribution of Alain Boussac, Jacques Breton, Bruce Diner, Rainer Hienerwadel and Eliane Nabedryk to the work described here.

References

Albela B, Chottard G and Girerd JJ (2001) Biomimetic approach to the oxygen evolving center: resonance Raman investigation of a manganese μ-oxo dimer in three oxidation states. J Biol Inorg Chem 6: 430–434

Araga C, Akabori K, Sasaki J, Maeda A, Shiina T and Toyoshima Y (1993) Functional reconstitution of the primary quinone acceptor, Q_A, in the Photosystem II core complexes. Biochim Biophys Acta 1142: 36–42

Backes G, Sahlin M, Sjöberg B-M, Loehr TM and Sanders-Loehr J (1989) Resonance Raman spectroscopy of ribonucleotide reductase. Evidence for a deprotonated tyrosyl radical and photochemistry of the binuclear iron center. Biochemistry 28: 1923–1929

Bauscher M, Nabedryk E, Bagley K, Breton J and Mäntele W (1990) Investigation of models for photosynthetic electron acceptors. Infrared spectroelectrochemistry of ubiquinone and its anion. FEBS Lett 261: 191–195

Berthomieu C and Boussac A (1995a) FTIR and EPR study of radicals of aromatic amino acids, 4-methylimidazole and phenol generated by UV-irradiation. Biospectroscopy 1: 187–206

Berthomieu C and Boussac A (1995b) Histidine oxidation in

the S_2 to S_3 transition probed by FTIR difference spectroscopy in the Ca^{2+}-depleted Photosystem II: Comparison with histidine radicals generated by UV-irradiation. Biochemistry 34: 1541–1548

Berthomieu C and Hienerwadel R (2001) Iron coordination in Photosystem II: Interaction between bicarbonate and the Q_B pocket studied by Fourier transform infrared spectroscopy. Biochemistry 40: 4044–4052

Berthomieu C, Nabedryk E, Mäntele W and Breton J (1990) Characterization by FTIR spectroscopy of the photoreduction of the primary quinone acceptor Q_A in Photosystem II. FEBS Lett 269: 363–367

Berthomieu C, Nabedryk E, Breton J and Boussac A (1992a) Further characterization of Q_A photoreduction using ^{15}N-labeled PS II membranes. In: Murata N (ed) Research in Photosynthesis, Vol II, pp 53–56. Kluwer Academic Publishers, Dordrecht

Berthomieu C, Boussac A, Mäntele W, Breton J and Nabedryk E (1992b) Molecular changes following oxidoreduction of cytochrome *b*559 characterized by Fourier transform infrared spectroscopy and electron paramagnetic resonance: Photooxidation in Photosystem II and electrochemistry of isolated cytochrome b559 and iron protoporphyrin IX-bisimidazole model compounds. Biochemistry 31: 11460–11471

Berthomieu C, Hienerwadel R, Boussac A, Breton J and Diner BA (1998a) Hydrogen bonding of redox-active tyrosine Z of Photosystem II probed by FTIR difference spectroscopy. Biochemistry 37: 10547–10554

Berthomieu C, Boullais C, Neumann J-M and Boussac A (1998b) Effect of ^{13}C, ^{18}O, and ^{2}H labeling on the infrared modes of UV-induced phenoxyl radicals. Biochim Biophys Acta 1365: 112–116

Bosch MK, Proskuryakov II, Gast P and Hoff AJ (1996) Time-resolved EPR study of the primary donor triplet in D1-D2-cyt*b*559 complexes of Photosystem II: Temperature dependence of spin-lattice relaxation. J Phys Chem 100: 2384–2390

Breton J (2001) Fourier transform infrared spectroscopy of primary electron donors in type I photosynthetic reaction centers. Biochim Biophys Acta 1507: 180–193

Breton J, Berthomieu C, Thibodeau D and Nabedryk E (1991) Probing the secondary quinone (Q_B) environment in photosynthetic bacterial reaction centers by light-induced FTIR difference spectroscopy. FEBS Lett 288: 109–113

Breton J, Nabedryk E and Parson WW (1992) A new infrared electronic transition of the oxidized primary electron donor in bacterial reaction centers: A way to assess resonance interactions between the bacteriochlorophylls. Biochemistry 31: 7503–7510

Breton J, Hienerwadel R and Nabedryk E (1997a) FTIR difference spectrum of the photooxidation of the primary electron donor of Photosystem II. In: Carmona P, Navarro R and Hernanz A (eds) Spectroscopy of Biological Molecules: Modern Trends, pp 101–102. Kluwer Academic Publishers, Dordrecht

Breton J, Nabedryk E, Allen JP and Williams JC (1997b) Electrostatic influence of Q_A reduction on the IR vibrational mode of the 10a-ester C=O of H_A demonstrated by mutations at residues Glu L104 and Trp L100 in reaction centers from *Rhodobacter sphaeroides*. Biochemistry 36: 4515–4525

Breton J, Nabedryk E and Leibl W (1999a) FTIR study of the primary electron donor of Photosystem I (P700) revealing delocalization of the charge in $P700^+$ and localization of the triplet character in $^3P700$. Biochemistry 38: 11585–11592

Breton J, Bibikova M, Oesterhelt D and Nabedryk E (1999b) Conformational heterogeneity of the bacteriopheophytin electron acceptor H_A in reaction centers from *Rhodopseudomonas viridis* revealed by Fourier transform infrared spectroscopy and site-directed mutagenesis. Biochemistry 38: 11541–11552

Britt RD (1996) Oxygen evolution. In: Ort DR and Yocum CF (eds) Oxygenic Photosynthesis: The Light Reactions, pp 137–164. Kluwer Academic Publishers, Dordrecht

Budil DE and Thurnauer MC (1991) The chlorophyll triplet state as a probe of structure and function in photosynthesis. Biochim Biophys Acta 1057: 1–41

Campbell KA, Peloquin OM, Diner BA, Tang X-S, Chrisholm DA and Britt RD (1997) The nitrogen of D2 histidine 189 is the hydrogen bond donor to the tyrosine radical Y_D of Photosystem II. J Am Chem Soc 119: 4787–4788

Cappuccio JA, Ayala I, Elliott GI, Szundi I, Lewis J, Konopelski JP, Barry BA and Einarsdottir O (2002) Modeling the active site of cytochrome oxidase: Synthesis and characterization of a cross-linked histidine-phenol. J Am Chem Soc 124: 1750–1760

Chu H-A, Gardner MT, O'Brien JP and Babcock GT (1999) Low-frequency Fourier transform infrared spectroscopy of the oxygen-evolving and quinone acceptor complexes in Photosystem II. Biochemistry 38: 4533–4541

Chu H-A, Gardner MT, Hillier W and Babcock GT (2000a) Low-frequency Fourier transform infrared spectroscopy of the oxygen-evolving complex in Photosystem II. Photosynth Res 66: 57–63

Chu H-A, Sackett H and Babcock GT (2000b) Identification of a Mn-O-Mn cluster vibrational mode of the oxygen-evolving complex in Photosystem II by low-frequency FTIR spectroscopy. Biochemistry 39: 14371–14376

Chu H-A, Hillier W, Law NA, Sackett H, Haymond S and Babcock GT (2000c) Light-induced FTIR difference spectroscopy of the S_2-to-S_3 state transition of the oxygen-evolving complex in Photosystem II. Biochim Biophys Acta 1459: 528–532

Chu H-A, Babcock GT and Debus RJ (2001a) Possible ligation of the Mn cluster in Photosystem II by the carboxyl-terminus of the D1 polypeptide: An FTIR study. In: PS2001 Proceedings: 12th International Congress on Photosynthesis, S13-026. CSIRO Publishing, Melbourne (CD-ROM)

Chu H-A, Debus RJ and Babcock GT (2001b) D1-Asp170 is structurally coupled to the oxygen-evolving complex in Photosystem II as revealed by light-induced Fourier transform infrared difference spectroscopy. Biochemistry 40: 2312–2316

Chu H-A, Hillier W, Law NA and Babcock GT (2001c) Vibrational spectroscopy of the oxygen-evolving complex and of manganese model compounds. Biochim Biophys Acta 1503: 69–82

Chu H-A, Hillier W, Law NA and Babcock GT (2001d) Identification of a possible Mn-O-Mn cluster vibrational mode of the S_3 state in the oxygen-evolving complex of Photosystem II by low-frequency FTIR difference spectroscopy. In: PS2001 Proceedings: 12th International Congress on Photosynthesis, S13-027. CSIRO Publishing, Melbourne (CD-ROM)

Chu H-A, Hillier W, and Debus RJ (2004) Evidence that the C-terminus of the D1 polypeptide of Photosystem II is ligated to the manganese ion that undergoes oxidation during the S_1 to S_2 transition: An isotope-edited FTIR study. Biochemistry 43: 3152–3166

Cua A, Stewart DH, Brudvig GW and Bocian DF (1998) Selective resonance Raman scattering from chlorophyll Z in

Photosystem II via excitation into the near-infrared absorption band of the cation. J Am Chem Soc 120: 4532–4533

Cua A, Stewart DH, Reifler MJ, Brudvig GW and Bocian DF (2000) Low-frequency resonance Raman characterization of the oxygen-evolving complex of Photosystem II. J Am Chem Soc 122: 2069–2077

Cua A, Vrettos JS, de Paula JC, Brudvig GW and Bocian DF (2003) Raman spectra and normal coordinate analyses of low-frequency vibrations of oxo-bridged manganese complexes. J Biol Inorg Chem 8: 439–451

Deacon GB and Phillips RJ (1980) Relationships between the carbon-oxygen stretching frequencies of carboxylato complexes and the type of carboxylate coordination. Coord Chem Rev 33: 227–250

Debus RJ (1992) The manganese and calcium ions of photosynthetic oxygen evolution. Biochim Biophys Acta 1102: 269–352

Dejonghe D, Andrianambinintsoa S, Berger G and Breton J (1998) Light-induced FTIR difference spectroscopy of Q_A photoreduction in Photosystem II core particles. In: Garab G (ed) Photosynthesis: Mechanisms and Effects, Vol. 2, pp 1121–1124. Kluwer Academic Publishers, Dordrecht

Den Blanken HJ, Hoff AJ, Jongenelis APJM and Diner BA (1983) High-resolution triplet-minus-singlet absorption difference spectrum of Photosystem II particles. FEBS Lett 157: 21–27

DeRose VJ, Yachandra VK, McDermott AE, Britt RD, Sauer K and Klein MP (1991) Nitrogen ligation to manganese in the photosynthetic oxygen-evolving complex: Continuous-wave and pulsed EPR studies of Photosystem II particles containing ^{14}N and ^{15}N. Biochemistry 30: 1335–1341

Desbois A and Lutz M (1992) Redox control of proton transfer in membrane b-type cytochromes: An absorption and resonance Raman study on bis(imidazole)and bis(imidazolate) model complexes of iron-protoporphyrin. Eur Biophys J 20: 321–335

Diner BA (2001) Amino acid residues involved in the coordination and assembly of the manganese cluster of Photosystem II. Proton-coupled electron transport of the redox-active tyrosines and its relationship to water oxidation. Biochim Biophys Acta 1503: 147–163

Diner BA, Petrouleas V and Wendoloski JJ (1991) The iron-quinone electron-acceptor complex of Photosystem II. Physiol Plant 81: 423–436

Diner BA, Schlodder E, Nixon PJ, Coleman WJ, Rappaport F, Lavergne J, Vermaas WFJ and Chisholm DA (2001) Site-directed mutants at D1-His198 and D2-His197 of Photosystem II in *Synechocystis* PCC 6803: Sites of primary charge separation and cation and triplet stabilization. Biochemistry 40: 9265–9281

Durrant JR, Klug DR, Kwa SLS, van Grondelle R, Porter G and Dekker JP (1995) A multimer model for P680, the primary electron donor of Photosystem II. Proc Natl Acad Sci USA 92: 4798–4802

Faller P, Pascal A and Rutherford AW (2001) β-carotene redox reactions in Photosystem II: Electron transfer pathway. Biochemistry 40: 6431–6440

Ferreira KN, Iverson TM, Maghlaoui K, Barber J and Iwata S (2004) Architecture of the photosynthetic oxygen-evolving center. Science 303: 1831–1838

Fischer G and Wydrzynski T (2001) Isotope effects in FTIR difference spectra of the photosynthetic oxygen-evolving catalytic site determined by *ab initio* calculations on model compounds. J Phys Chem B 105: 12894–12901

Gilchrist ML, Ball JA, Randall DW and Britt RD (1995) Proximity of the manganese cluster of Photosystem II to the redox-active tyrosine Y_Z. Proc Natl Acad Sci USA 92: 9594–9549

Govindjee and Van Rensen JJS (1993) Photosystem II reaction center and bicarbonate. In: Deisenhofer J and Norris JR (eds) The Photosynthetic Reaction Center, Vol I, pp 357–389. Academic Press, San Diego

Hanley J, Deligiannakis Y, Pascal A, Faller P and Rutherford AW (1999) Carotenoid oxidation in Photosystem II. Biochemistry 38: 8189–8195

Hasegawa K, Ono T and Noguchi T (2000) Vibrational spectra and *ab initio* DFT calculations of 4-methylimidazole and its different protonation forms: Infrared and Raman markers of the protonation state of a histidine side chain. J Phys Chem B 104: 4253–4265

Hasegawa K, Kimura Y and Ono T (2002a) Chloride cofactor in the photosynthetic oxygen-evolving complex studied by Fourier transform infrared spectroscopy. Biochemistry 41: 13839–13850

Hasegawa K, Ono T and Noguchi T (2002b) *Ab initio* DFT calculations and vibrational analysis of zinc-bound 4-methylimidazole as a model of a histidine ligand in metalloenzymes. J Phys Chem A 106: 3377–3390

Hasegawa K, Kimura Y and Ono T (2004) Oxidation of the Mn cluster induces structural changes of NO_3^- functionally bound to the Cl^- site in the oxygen-evolving complex of Photosystem II. Biophys J 86: 1042–1050

Hawkins GJ, Hunneman R, Gardner MT and Babcock GT (1998) An ultra-wide passband (5–30 μm) filter for FTIR studies of Photosystem II. Infrared Phys Technol 39: 297–306

Hienerwadel R and Berthomieu C (1995a) Bicarbonate binding to the non-heme iron of Photosystem II investigated by FTIR difference spectroscopy and ^{13}C-labeled bicarbonate. Biochemistry 34: 16288–16297

Hienerwadel R and Berthomieu C (1995b) FTIR study of the non-heme iron binding site in Photosystem II: Bicarbonate ^{13}C-labeling and exchange by glycolate. In: Mathis P (ed) Photosynthesis: From Light to Biosphere, Vol I, pp 743–746. Kluwer Academic Publishers, Dordrecht

Hienerwadel R, Boussac A and Berthomieu C (1993) Photoreduction of the non heme iron in Photosystem II studied by FTIR difference spectroscopy. In: Theophanides T, Anastassopoulou J and Fotopoulos N (eds) Fifth International Conference on the Spectroscopy of Biological Molecules, pp 317–318. Kluwer Academic Publishers, Dordrecht

Hienerwadel R, Boussac A, Breton J and Berthomieu C (1995) Tyrosine D radical in Photosystem II investigated by FTIR difference spectroscopy. In: Merlin JC (ed) Spectroscopy of Biological Molecules, pp 193–196. Kluwer Academic Publishers, Dordrecht

Hienerwadel R, Boussac A, Breton J and Berthomieu C (1996) Fourier transform infrared difference study of $Tyrosine_D$ oxidation and plastoquinone Q_A reduction in Photosystem II. Biochemistry 35: 15447–15460

Hienerwadel R, Boussac A, Breton J, Diner BA and Berthomieu C (1997) Fourier transform infrared difference spectroscopy of Photosystem II tyrosine D using site-directed mutagenesis and

specific isotope labeling. Biochemistry 36: 14712–14723
Hienerwadel R, Boussac A, Breton J, Diner BA and Berthomieu C (1998) FTIR study of TyrD and TyrZ: hydrogen bonding interactions. In Garab G (ed) Photosynthesis: Mechanisms and Effects, Vol II, pp 1185–1188. Kluwer Academic Publishers, Dordrecht
Hillier W and Babcock GT (2001) S-state dependent Fourier transform infrared difference spectra for the Photosystem II oxygen evolving complex. Biochemistry 40, 1503–1509
Ivancich A, Mattioli TA and Un S (1999) Effect of protein microenvironment on tyrosyl radicals. A high-field (285 GHz) EPR, resonance Raman, and hybrid density functional study. J Am Chem Soc 121: 5743–5753
Kamiya N and Shen JR (2003) Crystal structure of oxygen-evolving Photosystem II from *Thermosynechococcus vulcanus* at 3.7-Å resolution. Proc. Natl. Acad. Sci. USA 100: 98–103
Kamlowski A, Frankemöller L, van der Est A, Stehlik D and Holzwarth AR (1996) Evidence for delocalization of the triplet state $^3P_{680}$ in the $D_1D_2cytb_{559}$-complex of Photosystem II. Ber Bunsen Phys Chem 100: 2045–2051
Kim S and Barry BA (1998) The protein environment surrounding tyrosyl radicals D• and Z• in Photosystem II: A difference Fourier-transform infrared spectroscopic study. Biophys J 74: 2588–2600
Kim S, Ayala II, Steenhuis JJ, Gonzalez ET and Barry BA (1998) Infrared spectroscopic identification of the C-O stretching vibration associated with the tyrosyl Z• and D• radicals in Photosystem II. Biochim Biophys Acta 1364: 337–360
Kimura Y and Ono T (2001) Chelator-induced disappearance of carboxylate stretching vibrational modes in S_2/S_1 FTIR spectrum in oxygen-evolving complex of Photosystem II. Biochemistry 40: 14061–14068
Kimura Y and Ono T (2003) Functional and structural study on chelator-induced suppression of S_2/S_1 FTIR spectrum in photosynthetic oxygen-evolving complex. J Inorg Biochem 97: 231–239
Kimura Y, Hasegawa K and Ono T (2002) Characteristic changes of the S_2/S_1 difference FTIR spectrum induced by Ca^{2+} depletion and metal cation substitution in the photosynthetic oxygen-evolving complex. Biochemistry 41: 5844–5853
Kimura Y, Mizusawa N, Ishii A, Yamanari T and Ono T (2003) Changes of low-frequency vibrational modes induced by universal ^{15}N- and ^{13}C-isotope labeling in S_2/S_1 FTIR difference spectrum of oxygen-evolving complex. Biochemistry 42: 13170–13177
Lutz M (1984) Resonance Raman studies in photosynthesis. In: Clark RJH and Hester RE (eds) Advances in Infrared and Raman Spectroscopy, Vol 11, pp 211–300. John Wiley & Sons, New York
Lutz M and Mäntele W (1991) Vibrational spectroscopy of chlorophylls. In: Scheer H (ed) Chlorophylls, pp 855–902. CRC Press, Boca Raton
MacDonald GM, Bixby KA and Barry BA (1993) A difference Fourier transform infrared study of two redox-active tyrosine residues in Photosystem II. Proc Natl Acad Sci USA 90: 11024–11028
MacDonald GM, Steenhuis JJ and Barry BA (1995) A difference Fourier transform infrared spectroscopic study of chlorophyll oxidation in hydroxylamine-treated Photosystem II. J Biol Chem 270: 8420–8428
Mäntele W(1995) Infrared vibrational spectroscopy of reaction centers. In: Blankenship RE, Madigan MT and Bauer CE (eds) Anoxygenic Photosynthetic Bacteria, pp 627–647. Kluwer Academic Publishers, Dordrecht
Mäntele W, Wollenweber A, Nabedryk E, Breton J, Rashwan F, Heinze J and Kreutz W (1987) Fourier-transform infrared (FTIR) spectroelectrochemistry of bacteriochlorophylls. In: Biggins J (ed) Progress in Photosynthesis Research, Vol I, pp 329–332. Martinus Nijhoff, Dordrecht.
Moënne-Loccoz P, Robert B and Lutz M (1990) Structure of the primary reactants in Photosystem II: Resonance Raman studies of D1D2 particles. In: Baltscheffsky (ed) Current Research in Photosynthesis, Vol I, pp 423–426. Kluwer Academic Publishers, Dordrecht
Mukherjee A, McGlashen ML and Spiro TG (1995) Ultraviolet resonance Raman spectroscopy and general valence force field analysis of phenolate and phenoxyl radica. J Phys Chem 99: 4918–4922
Nabedryk E (1996) Light-induced Fourier transform infrared difference spectroscopy of the primary electron donor in photosynthetic reaction enters. In: Mantsch HH and Chapman D (eds) Infrared Spectroscopy of Biomolecules, pp 39–81. John Wiley & Sons, New York
Nabedryk E, Mäntele W, Tavitian BA and Breton J (1986) Light-induced Fourier transform infrared spectroscopic investigations of the intermediary electron acceptor reduction in bacterial photosynthesis. Photochem Photobiol 43: 461–465
Nabedryk E, Andrianambinintsoa S, Berger G, Leonhard M, Mäntele W and Breton J (1990) Characterization of bonding interactions of the intermediary electron acceptor in the reaction center of Photosystem II by FTIR spectroscopy. Biochim Biophys Acta 1016: 49–54
Nabedryk E, Leibl W and Breton J (1996) FTIR spectroscopy of primary donor photooxidation in Photosystem I, *Heliobacillus mobilis*, and *Chlorobium limicola*. Comparison with purple bacteria. Photosynth Res 48: 301–308
Nakamoto K (1997) Infrared and Raman Spectra of Inorganic and Coordination Compounds (5th ed.), John Wiley & Sons, New York
Nixon PJ, Trost JT and Diner BA (1992) Role of the carboxy terminus of polypeptide D1 in the assembly of a functional water-oxidizing manganese cluster in Photosystem II of the cyanobacterium *Synechocystis* sp. PCC 6803: Assembly requires a free carboxyl group at C-terminal position 344. Biochemistry 31:10859–10871
Noguchi T (2002) Dual role of triplet localization on the accessory chlorophyll in the Photosystem II reaction center: Photoprotection and photodamage of the D1 protein. Plant Cell Physiol. 43: 1112–1116
Noguchi T and Inoue Y (1995a) Identification of FTIR signals from the non-heme iron in Photosystem II. J Biochem 118: 9–12
Noguchi T and Inoue Y (1995b) Molecular interactions of the redox-active accessory chlorophyll on the electron-donor side of Photosystem II as studied by Fourier transform infrared spectroscopy. FEBS Lett 370: 241–244
Noguchi T and Sugiura M (2000) Structure of an active water molecule in the water oxidizing complex of Photosystem II as studied by FTIR spectroscopy. Biochemistry 39: 10943–10949
Noguchi T and Sugiura M (2001) Flash-induced Fourier transform infrared detection of the structural changes during the S-state cycle of the oxygen-evolving complex in Photosystem II. Biochemistry 40: 1497–1502

Noguchi T and Sugiura M (2002a) Flash-induced FTIR difference spectra of the water oxidizing complex in moderately hydrated Photosystem II core films: Effect of hydration extent on S-state transitions. Biochemistry 41: 2322–2330

Noguchi T and Sugiura M (2002b) FTIR detection of water reactions during the flash-induced S-state cycle of the photosynthetic water oxidizing complex. Biochemistry 41: 15706–15712

Noguchi T and Sugiura M (2003) Analysis of flash-induced FTIR difference spectra of the S-state cycle in the photosynthetic water-oxidizing complex by uniform ^{15}N and ^{13}C isotope labeling. Biochemistry 42: 6035–6042

Noguchi T, Ono T and Inoue Y (1992) Detection of structural changes upon S_1-to-S_2 transition in the oxygen-evolving manganese cluster in Photosystem II by light-induced Fourier transform infrared difference spectroscopy. Biochemistry 31: 5953–5956

Noguchi T, Inoue Y and Satoh K (1993a) FT-IR studies on the triplet state of P680 in the Photosystem II reaction center: Triplet equilibrium within a chlorophyll dimer. Biochemistry 32: 7186–7195

Noguchi T, Ono T and Inoue Y (1993b) Temperature dependence of the $S_1 \rightarrow S_2$ transition in the oxygen-evolving complex of Photosystem II studied by FT-IR spectroscopy. Biochim Biophys Acta 1143: 333–336

Noguchi T, Mitsuka T and Inoue Y (1994) Fourier transform infrared spectrum of the radical cation of β-carotene photoinduced in Photosystem II. FEBS Lett 356: 179–182

Noguchi T, Ono T and Inoue Y (1995a) Direct detection of a carboxylate bridge between Mn and Ca^{2+} in the photosynthetic oxygen-evolving center by means of Fourier transform infrared spectroscopy. Biochim Biophys Acta 1228: 189–200

Noguchi T, Ono T and Inoue Y (1995b) A carboxylate ligand interacting with water in the oxygen-evolving center of Photosystem II as revealed by Fourier transform infrared spectroscopy. Biochim Biophys Acta 1232: 59–66

Noguchi T, Ono T and Inoue Y (1995c) FTIR studies on the structure and reactions of the oxygen-evolving center in Photosystem II. In: Mathis P (ed) Photosynthesis: From Light to Biosphere, Vol II, pp 235–240. Kluwer Academic Publishers, Dordrecht

Noguchi T, Kusumoto N, Inoue Y and Sakurai H (1996) Electronic and vibrational structure of the radical cation of P840 in the putative homodimeric reaction center from *Chlorobium tepidum* as studied by FTIR spectroscopy. Biochemistry 35: 15428–15435

Noguchi T, Fukami Y, Oh-oka H and Inoue Y (1997a) Fourier transform infrared study on the primary donor P798 of *Heliobacterium modesticaldum*: Cysteine S-H coupled to P798 and molecular interactions of carbonyl groups. Biochemistry 36: 12329–12336

Noguchi T, Inoue Y and Tang X-S (1997b) Structural coupling between the oxygen-evolving Mn cluster and a tyrosine residue in Photosystem II as revealed by Fourier transform infrared spectroscopy. Biochemistry 36: 14705–14711

Noguchi T, Tomo T and Inoue Y (1998) Fourier transform infrared study of the cation radical of P680 in the Photosystem II reaction center: Evidence for charge delocalization on the chlorophyll dimer. Biochemistry 37: 13614–13625

Noguchi T, Sugiura M and Inoue Y (1999a) FTIR studies on the amino-acid ligands of the photosynthetic oxygen-evolving Mn-cluster. In: Itoh K and Tasumi M (eds) Fourier Transform Spectroscopy, pp 459–460. Waseda University Press, Tokyo

Noguchi T, Inoue Y and Tang X-S (1999b) Structure of a histidine ligand in the photosynthetic oxygen-evolving complex as studied by light-induced Fourier transform infrared difference spectroscopy. Biochemistry 38: 10187–10195

Noguchi T, Kurreck J, Inoue Y and Renger G (1999c) Comparative FTIR analysis of the microenvironment of Q_A^- in cyanide-treated, high pH-treated and iron-depleted Photosystem II membrane fragments. Biochemistry 38: 4846–4852

Noguchi T, Inoue Y and Tang X-S (1999d) Hydrogen bonding interaction between the primary quinone acceptor Q_A and a histidine side chain in Photosystem II as revealed by Fourier transform infrared spectroscopy. Biochemistry 38: 399–403

Noguchi T, Tomo T and Kato C (2001) Triplet formation on a monomeric chlorophyll in the Photosystem II reaction center as studied by time-resolved infrared spectroscopy. Biochemistry 40: 2176–2185

Nwobi O, Higgins J, Zhou X and Liu R (1997) Density functional calculation of phenoxyl radical and phenolate anion: An examination of the performance of DFT methods. Chem Phys Lett 272: 155–161

O'Malley PJ (2000) Density-functional studies of phenoxyl-Na^+ ion complexes: Implication for tyrosyl free radical interaction in vitro. Chem Phys Lett 325: 69–72

O'Malley PJ (2002) Density functional calculations modelling tyrosine oxidation in oxygenic photosynthetic electron transfer. Biochim Biophys Acta 1553: 212–217

Onoda K, Mino H, Inoue Y and Noguchi T (2000) An FTIR study on the structure of the oxygen-evolving Mn-cluster of Photosystem II in different spin forms of the S_2 state. Photosynth Res 63: 47–57

Pascal A, Telfer A, Barber J and Robert B (1999) Fourier-transform resonance Raman spectra of cation carotenoid in Photosystem II reaction centers. FEBS Lett 453: 11–14

Petrouleas V and Diner BA (1990) Formation by NO of nitrosyl adducts of redox components of the Photosystem II reaction center. I. NO binds to the acceptor-side non-heme iron. Biochim Biophys Acta 1015: 131–140

Qin Y and Wheeler RA (1995a) Similarities and differences between phenoxyl and tyrosine phenoxyl radical structures, vibrational frequencies and spin densities. J Am Chem Soc 117: 6083–6092

Qin Y and Wheeler RA (1995b) Density-functional methods give accurate vibrational frequencies and spin densities for phenoxyl radical. J Phys Chem 102: 1689–1698

Remy A, Niklas J, Kuhl H, Kellers P, Schott T, Rogner M and Gerwert K (2004) FTIR spectroscopy shows structural similarities between photosystems II from cyanobacteria and spinach. Eur J Biochem 271: 563–567

Roncel M, Ortega JM and Losada M (2001) Factors determining the special redox properties of photosynthetic cytochrome b559. Eur J Biochem 268: 4961–4968

Ruffle S, Hutchison R and Sayre RT (1998) Mutagenesis of the symmetry related H117 residue in the Photosystem II D2 protein of *Chlamydomonas*: Implications for energy transfer from accessory chlorophylls. In: Garab G (ed) Photosynthesis: Mechanisms and Effects, Vol II, pp 1013–1016. Kluwer Academic Publishers, Dordrecht

Rutherford, A W, Boussac A and Faller P (2004) The stable tyrosyl radical in Photosystem II: Why D? Biochim Biophys Acta 1655: 222–230

Sarcina M, Breton J, Nabedryk E, Diner BA and Nixon PJ (1998) FTIR studies on the P680 cation and triplet states in WT and mutant PS II reaction centers of *Synechocystis* 6803. In: Garab G (ed) Photosynthesis: Mechanisms and Effects, Vol I, pp 1053–1056. Kluwer Academic Publishers, Dordrecht

Schenck CC, Diner B, Mathis P and Satoh K (1982) Flash-induced carotenoid radical cation formation in Photosystem II. Biochim Biophys Acta 680: 216–227

Seibert M and Cotton TM (1985) A surface-enhanced Raman signal associated with functional manganese in oxygen-evolving Photosystem II membranes. FEBS Lett 182: 34–38

Seibert M, Cotton TM and Metz JG (1988) Surface-enhanced Raman scattering spectroscopy: Probing the lumenal surface of Photosystem II membranes for evidence of manganese. Biochim Biophys Acta 934: 235–246

Smith JC, Gonzalez-Vergara E and Vincent JB (1997) Detection of structural changes upon oxidation in multinuclear Mn-oxo-carboxylate assemblies by Fourier transform infrared spectroscopy: relationship to Photosystem II. Inorg Chim Acta 255: 99–103

Spanget-Larsen J, Gil M, Gorski A, Blake DM, Waluk J and Radziszewski JG (2001) Vibrations of the phenoxyl radical. J Am Chem Soc 123: 11253–11261

Stewart DH and Brudvig GW (1998) Cytochrome b_{559} of Photosystem II. Biochim Biophys Acta 1367: 63–87

Steenhuis JJ and Barry BA (1997) Protein and ligand environments of the S2 state in photosynthetic oxygen evolution: A difference FT-IR study. J Phys Chem B 101:6652–6660

Steenhuis JJ, Hutchison RS and Barry BA (1999) Alterations in carboxylate ligation at the active site of Photosystem II. J Biol Chem 274: 14609–14616

Stewart DH, Cua A, Chisholm DA, Diner BA, Bocian DF and Brudvig GW (1998) Identification of histidine 118 in the D1 polypeptide of Photosystem II as the axial ligand to chlorophyll Z. Biochemisty 37: 10040–10046

Tang X-S, Chrisholm DA, Dismukes GC, Brudwig GW and Diner BA (1993) Spectroscopic evidence from site-directed mutants of *Synechocystis* PCC6803 in favor of a close interaction between histidine 189 and redox-active tyrosine 160, both of polypeptide D2 of the Photosystem II reaction center. Biochemistry 32: 13742–13748

Tang X-S, Diner BA, Larsen BS, Gilchrist ML, Lorigan GA and Britt RD (1994) Identification of histidine at the catalytic site of the photosynthetic oxygen-evolving complex. Proc Natl Acad Sci USA 91: 704–708

Tang X–S, Randall DW, Force DA, Diner BA and Britt RD (1996) Manganese-tyrosine interactions in the Photosystem II oxygen evolving complex. J Am Chem Soc 118: 7638–7639

Tavitian BA, Nabedryk E, Mäntele W and Breton J (1986) Light-induced Fourier transform infrared spectroscopic investigations of primary reactions in Photosystem I and Photosystem II. FEBS Lett 201: 151–157

Telfer A, Frolov D, Barber J, Robert B and Pascal A (2003) Oxidation of the two β-carotene molecules in the Photosystem II reaction center. Biochemistry 42: 1008–1015

Tommos C and Babcock GT (1998) Oxygen production in nature: A light-driven metalloradical enzyme process. Acc Chem Res 31: 18–25

Tracewell CA, Vrettos JS, Bautista JA, Frank HA and Brudvig GW (2001a) Carotenoid photooxidation in Photosystem II. Arch Biochem Biophys 385: 61–69

Tracewell CA, Cua A, Stewart DH, Bocian DF and Brudvig GW (2001b) Characterization of carotenoid and chlorophyll photooxidation in Photosystem II. Biochemistry 40: 193–203

Un S, Gerez C, Elleingand E and Fontecave M (2001) Sensitivity of tyrosyl radical g-values to changes in protein structure: A high-field EPR study of mutants of ribonucleotide reductase. J Am Chem Soc 123: 3048–3054

Van Mieghem FJE, Satoh K and Rutherford AW (1991) A chlorophyll tilted 30° relative to the membrane in the Photosystem II reaction centre. Biochim Biophys Acta 1058: 379–385

Van Mieghem F, Brettle K, Hillmann B, Kamlowski A, Rutherford AW and Schlodder E (1995) Charge recombination reactions in Photosystem II. 1. Yields, recombination pathways, and kinetics of the primary pair. Biochemistry 34: 4798–4813

Visser H, Dube CE, Armstrong WH, Sauer K and Yachandra VK (2002) FTIR spectra and normal-mode analysis of a tetranuclear manganese adamantane-like complex in two electrochemically prepared oxidation states: Relevance to the oxygen-evolving complex of Photosystem II. J Am Chem Soc 124: 11008–11017

Vrettos JS, Stewart DH, de Paula JC and Brudvig GW (1999) Low-temperature optical and resonance Raman spectra of a carotenoid cation radical in Photosystem II. J Phys Chem B 103: 6403–6406

Zhang H, Razeghifard MR, Fischer G and Wydrzynski T (1997) A time-resolved FTIR difference study of the plastoquinone Q_A and redox-active tyrosine Y_Z interactions in Photosystem II. Biochemistry 36: 11762–11768

Zhang H, Fischer G and Wydrzynski T (1998) Room-temperature vibrational difference spectrum for $S_2Q_B^-/S_1Q_B$ of Photosystem II determined by time-resolved Fourier transform infrared spectroscopy. Biochemistry 37: 5511–5517

Zouni A, Witt HT, Kern J, Fromme P, Krauß N, Saenger W and Orth P (2001) Crystal structure of Photosystem II from *Synechococcus elongatus* at 3.8 Å resolution. Nature 409: 739–743

Chapter 17

Configuration of Electron Transfer Components Studied by EPR Spectroscopy

Robert Bittl*
Fachbereich Physik, Freie Universität Berlin, Arnimallee 14, D-14195 Berlin, Germany

Asako Kawamori*
School of Science and Technology, Kwansei Gakuin University, Gakuen 2-1, Sanda 669-1337, Japan

Summary

Orientations and relative positions of paramagnetic intermediates in protein complexes of Photosystem (PS) II can be studied by electron paramagnetic resonance (EPR) spectroscopy. The EPR spectroscopic approaches and results on components of the electron transfer chain in PS II are presented. Where possible the data from EPR spectroscopy are compared to structural data from X-ray analysis. This comparison shows that the EPR-derived orientations and distances between the redox partners in PS II are in general corroborated by the recent X-ray crystallographic models. Furthermore, specific experiments that complement information available from crystallography are discussed.

*Authors for correspondence, email: Robert.Bittl@Physik.FU-Berlin.DE; kawamori@ksc.kwansei.ac.jp

T. Wydrzynski and K. Satoh (eds): Photosystem II: The Light-Driven Water:Plastoquinone Oxidoreductase, pp. 389–402.

I. Introduction

A rather detailed picture of the arrangement of cofactor molecules in Photosystem (PS) II has been available from spectroscopy prior to the structural models based on electron microscopy (Rhee et al., 1998; Chapter 18, Hankamer et al.) and X-ray crystallography (Zouni et al., 2001; Kamiya and Shen, 2003; Ferreira et al., 2004; Chapters 19–21). This picture was based partly on the similarity of spectroscopic results obtained for PS II with those for the purple bacterial reaction center (BRC). A close similarity between the BRC and PS II has been early accepted for the acceptor side (Rutherford, 1985). In contrast, the extent of analogy between the BRC and PS II at the donor side has been controversial for a long time. Rutherford and Acker (1986) speculated that the analogy might include the primary donor, even though apparently contradictory spectroscopic results had been observed. Michel and Deisenhofer (1988) have used biochemical and genetic similarities between the two representatives of Type II reaction centers (with a quinone as terminal electron acceptor as opposed to Type I reaction centers which have a terminal iron-sulfur cluster) to invoke the BRC structure as a relevant model for PS II. A structural model for PS II based on these similarities has been discussed for example by Rutherford (1989). EPR spectroscopy has provided quantitative data supporting this general picture and in addition showed specific differences between the core of PS II and BRC. In this chapter we will briefly introduce the spectroscopic concepts, the early EPR results that formed part of the basis for the hypothesis of a structural similarity between the two representatives of Type II reaction centers and describe more recent quantitative results on the configuration of components of the electron transfer chain in PS II.

Abbreviations: BChl – bacteriochlorophyll; Bpheo – bacteriopheophytin; BRC – purple bacterial reaction center; Chl – chlorophyll; CW – continuous wave; Cyt – cytochrome; D1 – 32 kDa polypeptide of the reaction center core of PS II; D2 – 34 kDa polypeptide of the reaction center core of PS II; ENDOR – electron-nuclear double resonance; EPR – electron paramagnetic resonance; ESE – electron spin echo; ESEEM – electron spin echo envelope modulation; OOP-ESEEM – out-of-phase ESEEM; P680 – primary electron donor in PS II; ^{3}P680 – triplet state of P680; PELDOR – pulsed electron electron double resonance; Pheo – pheophytin; PS I, PS II – Photosystem I, Photosystem II; Q_A – primary quinone acceptor in BRC and PS II; WOC – water oxidizing complex; Y_D – redox active tyrosine residue in D2; Y_Z – redox active tyrosine residue in D1

II. Spectroscopic Background

A. Orientation Information

The orientation of a paramagnetic molecule in a protein can be determined by EPR spectroscopy based on the anisotropy of the Zeeman interaction caused by the anisotropy of the *g*-factor or of the electron-nuclear hyperfine coupling of a paramagnetic state of the molecule. The prerequisites for using this method are: (i) the assignment of the principal axes of the anisotropic magnetic interaction (*g*-factor or hyperfine coupling) with the molecular axes of the cofactor must be known; (ii) oriented samples must be available; and (iii) the anisotropy of the *g*-factor or of the hyperfine coupling must be resolved in the EPR spectra of oriented samples. Orientation-dependent spectra have to be recorded as a function of a relative angle between the external magnetic field and the oriented sample. Dependent on the anisotropic magnetic interaction studied, this can involve standard continuous-wave (CW)-EPR, CW-electron-nuclear double resonance (ENDOR) or pulsed techniques.

Requirement (i) is very often fulfilled, in particular for hyperfine couplings where a close correlation between bond directions and the directions of principal hyperfine axes is established. For a large number of cofactor molecules at least one of the principal *g*-axes is known with respect to the molecular frame.

Ideal systems to satisfy requirement (ii) are protein single crystals. However, single crystals of membrane proteins are difficult to grow and are still scarce. Instead of three-dimensionally ordered single crystals one-dimensionally ordered oriented membranes were often used to study anisotropic magnetic interactions in PS II (Rutherford, 1985). With these one-dimensionally ordered samples, it is impossible to fully determine the orientation of a cofactor molecule within a protein; however, it yields orientation information relative to a specific axis, in general the membrane normal.

With regard to requirement (iii), the anisotropy of hyperfine interactions has only rarely been used to determine cofactor orientations in PS II. In contrast, the *g*-anisotropy has been the major source for this information. Thereby, the advantage of high-field/high-frequency EPR has recently been utilized to achieve the necessary spectral resolution when requirement (iii) is not met at standard fields/frequencies (9 GHz, X-band EPR).

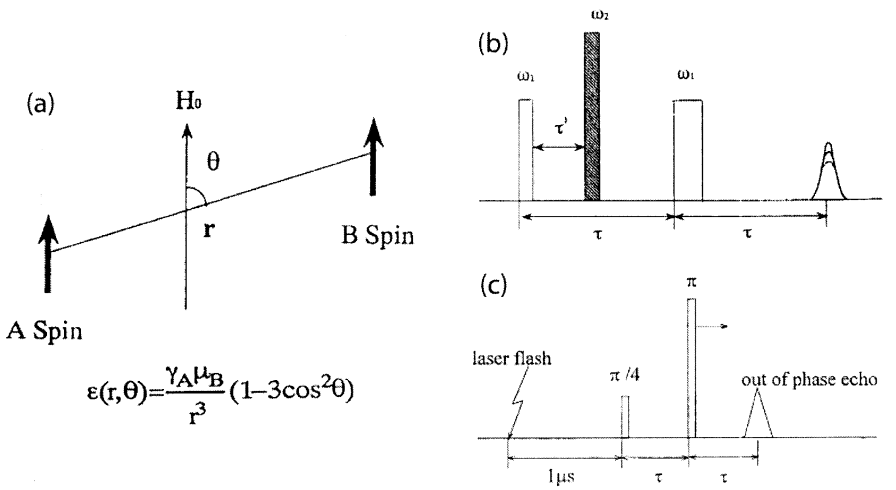

Fig. 1. (a) Dipolar interaction between a pair of paramagnetic species A and B. (b) Pulse sequence for PELDOR on stationary species. (c) Pulse sequence for OOP-ESEEM on spin polarized species.

B. Distance Information

The principle of distance determinations between cofactor molecules by EPR is based on the dipolar interaction between two unpaired spins A and B on paramagnetic states of cofactor molecules (see Fig. 1a). This interaction is described by:

$$D_{AB} = \mu_A\mu_B(3\cos^2\theta - 1)/r^3 \qquad (1)$$

where r is the distance between the unpaired spins and θ is the angle between the axis connecting the two spins and the magnetic field. μ_A and μ_B are the magnetic moments of the interacting spins. In a non-oriented sample, the angle θ assumes all possible values and consequently a powder distribution of dipolar interactions occurs. From such a powder distribution, the principal values (for θ = 0° and θ = 90°) can be extracted in most cases. The obtained principal values of the dipolar coupling can be translated by Eq. (1) into the distance r. In a system with delocalized unpaired electron spins, this distance is the $1/r^3$ weighted average distance of spin densities and will in general slightly deviate from the distance between the molecular centers as obtained by crystallography.

The dipolar interaction between two spins can be observed by different EPR experiments dependent on the magnitude of this interaction, i.e., the distance r and the types of paramagnetic species involved. If one of the two spins shows very fast relaxation, the dipolar interaction between the two spins manifests itself as relaxation enhancement of the second spin. This effect can be observed by measuring a relaxation time of the second spin in presence or absence of the fast relaxing spin.

In the case of moderate relaxation times of both spins, several methods for a direct measurement of the dipolar coupling have been proposed. For short distances r and consequently large dipolar interaction, the EPR spectra show a characteristic line splitting from which the dipolar interaction parameters can be deduced. For distances larger than about 15 Å, the dipolar interaction usually is smaller than the EPR line width and, therefore, unresolved in the EPR spectrum. Nevertheless, using pulsed EPR techniques, it is possible to measure the dipolar coupling directly. When the EPR spectra of the two species are separated by a few mT, pulsed electron-electron double resonance (PELDOR) can be applied. The method was introduced by Milov et al. (1984) to investigate the distributions of spin labels in polymer materials and uses a Hahn-echo sequence with an additional third microwave pulse of different microwave frequency between the two pulses of the Hahn-echo sequence. The pulse sequence is depicted in Fig. 1b. The first and the third pulses with frequency ω_1 are on resonance with spins A and give a spin echo signal of the A spins. The second pulse of frequency ω_2 is on resonance with spins B and inverts the B spins.

This results in a change in the local field at the site of the A spins. The effect of the change of the local field introduces an intensity modulation of the A spin echo dependent on the position of the pulse of frequency ω_2 within the echo sequence. The frequency of the intensity change is proportional to the dipolar interaction parameter D_{AB}. The same pulse sequence can be applied if the spectra of the two spins overlap; however, with $\omega_1 = \omega_2$, it is then called '2+1' sequence (Kurshev et al., 1989).

For the spin-polarized radical pairs with overlapping EPR spectra occurring in photosynthetic reaction centers after laser excitation, the dipolar interaction can be measured by a conventional two-pulse Hahn-echo sequence as shown in a theoretical study (Salikhov et al., 1992). The induced spin echo signal is out-of-phase compared to the (in-phase) signal from a spin system in thermal equilibrium and is modulated as a function of the inter-pulse delay with a frequency proportional to the dipolar coupling. The pulse sequence for this 'out-of-phase' electron spin echo envelope modulation (OOP-ESEEM) is shown in Fig. 1c, and has been first applied to BRC (Dzuba et al., 1995). The Fourier transformation of the echo modulation gives a typical dipolar interaction spectrum from which the distance *r* can be derived. For a description of the method and its application to PS I see, e.g., a review by Bittl and Zech (2001).

III. Orientation of Cofactor Molecules

A. Heme Species

Early spectroscopic works investigating the orientation of cofactors in PS II used oriented chloroplasts. Several publications (Bergström and Vänngård, 1982; Crowder et al., 1982; Hootkins and Bearden, 1983) reported the dependence of the EPR signal of Cyt b_{559} on the orientation between the external magnetic field and the chloroplast membranes. An alignment of the Cyt b_{559} heme plane perpendicular to the chloroplast membrane was found. These EPR data were consistent with an earlier optical dichroism study (Vermeglio et al., 1980). Rutherford (1985) investigated the orientation dependence of several EPR signals in oriented PS II containing membrane fragments. He showed that the Cyt b_{559} EPR signal showed the same orientation dependence as that in chloroplasts indicating that the heme plane of Cyt b_{559} is oriented perpendicular to the photosynthetic membrane. The strong and easily observable orientation dependence of the Cyt b_{559} has since been often used for judging the quality of the ordering of PS II complexes in specific samples.

B. Radicals

The first orientation study on a radical species in PS II was reported on Signal IIs (O'Malley et al., 1984), now known as the oxidized tyrosine radical $Y_D^{ox\bullet}$ (Barry and Babcock, 1987). Even though Signal IIs was then still assigned to a quinone cation, the basic structural information given by O'Malley et al. (1984) and independently by Rutherford (1985) is correct (see below), i.e., the ring plane of the species giving rise to Signal IIs is approximately perpendicular to the photosynthetic membrane.

While these early studies mainly used standard X-band (9 GHz) EPR spectroscopy, more recent studies have made use of the high sensitivity and spectral resolution of high-field/high-frequency EPR. The high spectral resolution allows the selective investigation of individual cofactor radicals even in the presence of a superposition of several radical species. This is due to their slightly different *g*-values which can be resolved in high-field/high-frequency EPR. The anion of the pheophytin in the D1 subunit, $Pheo_{D1}$, and of the primary quinone acceptor Q_A have been investigated by high-frequency (285 GHz) EPR (Dorlet et al., 2000) using PS II from spinach. For Q_A in PS II a very similar orientation of the quinone ring normal with respect to the membrane normal has been determined as for Q_A in the BRC, as well as for the acceptor quinone A_1 in PS I. However, the orientation of the O–O axes of the quinones differ in the three systems. While the O–O axis lies almost in the membrane plane in the BRC, it is slightly more inclined in PS II. In contrast, in PS I this axis lies nearly perpendicular to the membrane plane. This orientation information is based on the knowledge of the orientation of the ***g***-tensor in the molecular frame. For quinone molecules this is well established and in the case of PS I, the EPR-derived angles (MacMillan et al., 1997; Kamlowski et al., 1998) are in good agreement with the X-ray structure at 2.5 Å resolution (Jordan et al., 2001). For PS II such a comparison of the data from Dorlet et al. (2000) is not yet possible due to the limited resolution of the present X-ray models at 3.8 Å (Zouni et al., 2001), 3.7 Å (Kamiya and Shen, 2003), and 3.5 Å (Ferreira et al., 2004).

For the pheophytin anion $Pheo_{D1}$ in PS II again a

very similar orientation of the ring plane with respect to the membrane plane to that of the bacteriopheophytin (Bpheo) H_A in the BRC has been found (Dorlet et al., 2000). A unique assignment of the in-plane ring orientation was not possible since in the case of the Pheo anion the orientation of the in-plane ***g***-tensor components in the molecule, which is necessary, is not yet independently known.

However, assuming an identical in-plane orientation of $Pheo_{D1}$ to the orientation of the Bpheo in the BRC resulted in a reasonable assignment of the ***g***-tensor orientation for the Pheo anion. Therefore, a conserved orientation of the pheophytins in BRC and PS II is very likely.

The study by Dorlet et al. (2000) also presented information regarding a redox active amino acid residue tyrosine Y_D in PS II without a counterpart in the BRC. Two of the three Euler angles describing the molecular orientation within the protein have been determined using the known orientation of the ***g***-tensor in a tyrosyl radical. The ring plane of $Y_D^{ox\bullet}$ has been found to be inclined by 64° with respect to the membrane plane, and the C–O axis makes an angle of 72° with the intersection of the membrane plane and the tyrosine ring plane. As examples of the orientation dependence of the EPR signals at high-field/high-frequency, the $Q_A^{-\bullet}$ and $Y_D^{ox\bullet}$ spectra from Dorlet et al. (2000) are reproduced in Fig. 2.

A high-frequency (94 GHz) study using the recently available single crystals of PS II from the cyanobacteria *Synechococcus elongatus* gave similar results for $Y_D^{ox\bullet}$ (Fig. 3; see Hofbauer et al., 2001). Virtually identical values were found for the angle between the molecular axis along the C–O bond of the tyrosyl radical and the membrane normal. The angle between the normal of the phenoxyl ring plane and the normal of the membrane shows a discrepancy of 10° between these two experiments. In the single crystal study, the third Euler angle that is necessary to completely specify the orientation of the molecule in the protein could also be determined.

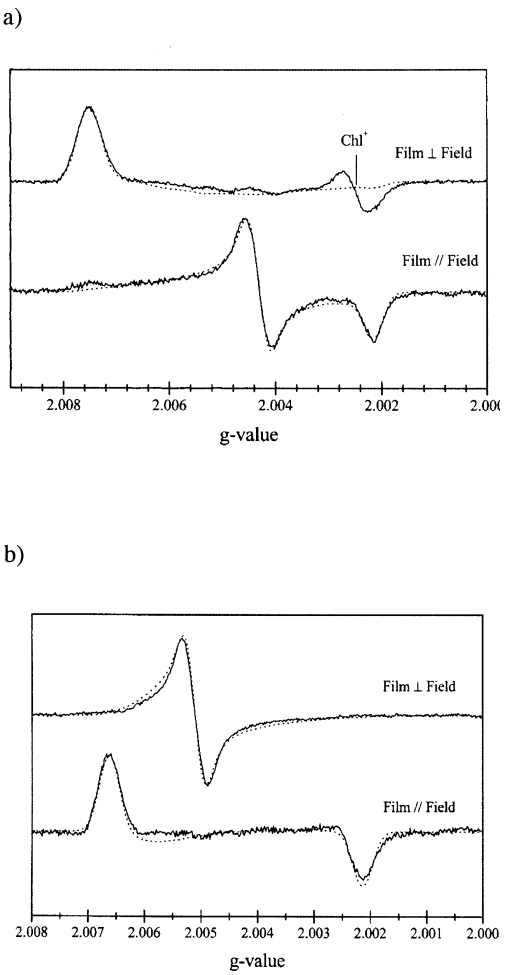

Fig. 2. High-field/high-frequency (285 GHz) EPR spectra of $Y_D^{ox\bullet}$ (a) and $Q_A^{-\bullet}$ (b) in oriented PS II preparations (© American Chemical Society; reprinted with permission from Dorlet et al., 2000).

C. Triplet State

An interesting case with clear differences between PS II and BRC is the triplet state arising from recombination of the radical pair state $P680^{+\bullet}Pheo_{D1}^{-\bullet}$ when electron transfer from the pheophytin to the quinone acceptor Q_A is blocked. The orientation dependence of the triplet EPR signal has been measured for BRC in oriented chromatophore membranes (Hales and Gupta, 1979; Tiede and Dutton, 1981) and in single crystals (Gast et al., 1983). The spectra are consistent with an orientation of the plane of the triplet carrying species perpendicular to the membrane plane, i.e., consistent with the two BChl molecules of the 'special pair' with ring planes perpendicular to the membrane. The assignment of the triplet principal axes to molecular axes in these studies was based on in vitro magneto-photoselection experiments (Thurnauer and Norris, 1977) showing that the triplet zero-field splitting *Z* axis is perpendicular to the ring

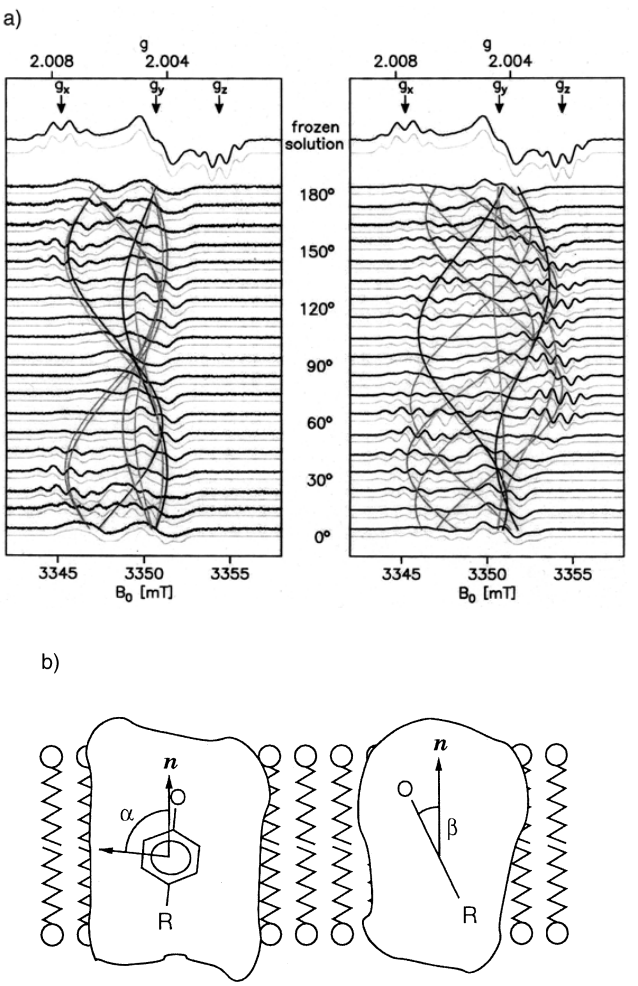

Fig. 3. (a) W-band (94 GHz) EPR spectra of $Y_D^{ox\bullet}$ in frozen solution and in a single crystal of PS II core complexes from *S. elongatus*. (Left) Crystal rotated approximately about the crystallographic a axis. (Right) Arbitrary rotation axis. Dim shaded lines show simulations and curved lines indicate the calculated angular dependence of the effective *g* value of $Y_D^{ox\bullet}$ residues in the unit cell. (b) Orientation of the phenoxyl group of Y_D in PS II from *S. elongatus* with respect to the membrane normal (parallel to the C2 symmetry axis) as derived from the single-crystal EPR spectra. The angle $\alpha = 84°$ is between the g_y direction and the membrane normal **n**; $\beta = 2$□° is the phenoxyl ring plane with respect to **n**. (Reproduced from Hofbauer et al.□ 2□□)□□

plane of BChl. For oriented PS II membrane fragments, Rutherford (1985) and Rutherford and Acker (1986) found an alignment of this zero-field splitting axis approximately perpendicular to the membrane plane, i.e., perpendicular to that seen in BRC. This result has initially been interpreted as evidence for the primary donor P680 in PS II being oriented differently compared to that in BRC (Rutherford and Acker, 1986).

The study on the orientation dependence of the recombination triplet state in PS II (^{3}P680) has later been improved (van Mieghem et al., 1991) by increasing the observable triplet signal intensity in CW-EPR by double reduction of Q_A. The improved signal-to-noise ratio of the spectra allowed a more precise evaluation of the angle between the triplet principal *Z* axis and the membrane normal, and a value of 30° has been given. The assignment of the triplet axis to

a molecular axis was based on the assumption that the triplet is localized on one individual Chl in PS II. This assumption originates from the similarity of the zero-field splitting parameter *D* of ^{3}P680 with that of monomeric Chl, and data from optical spectroscopy (for references, see van Mieghem et al., 1991). Additional evidence for the localization of ^{3}P680 on a monomeric Chl at low temperatures has been provided later by time-resolved ENDOR spectroscopy (Lendzian et al., 2003). For ^{3}P680, no reduction of hyperfine couplings compared to monomeric Chl has been observed, while in BRC the ENDOR data (Lendzian et al., 1998) showed a reduction of hyperfine couplings consistent with a delocalization of the ^{3}P865 triplet state over both halves of the 'special pair.' Transient EPR studies (Kamlowski et al., 1996; Bosch et al., 1996) on ^{3}P680 are also consistent with a localization of the triplet state on a monomeric Chl at low temperatures. All available data supports the assumption of van Mieghem et al. (1991), and justify their conclusion that ^{3}P680 is located on a Chl with a ring plane inclined 30° with respect to the membrane plane. This result was the first evidence for a Chl molecule in the PS II reaction center with a ring plane oriented similar to the 'accessory' BChls, B_A and B_B in the BRC.

Based on their result for the recombination triplet state in PS II, van Mieghem et al. (1991) discussed a model of PS II in which P680 is a Chl analogous to the monomeric 'accessory' BChl in the BRC. It was argued that this orientation of ^{3}P680 seems to present strong evidence for fundamentally different structures of the primary donor region in PS II compared to BRC (van Mieghem et al., 1991) and several alternative models for the primary donor of PS II have been suggested (Noguchi et al., 1993). However, Rutherford and Acker (1986) had already questioned earlier the assignment of the recombination triplet ^{3}P680 with the primary donor P680 and formulated an 'escape clause' for the 'believers in the bacterial analogy' of PS II stating that ^{3}P680 might be located on a Chl analogous to the 'accessory' BChl in BRC, while nevertheless a 'special pair' analog donor P680 could exist. Now, indeed, mounting evidence is available that the triplet carrying species ^{3}P680 and the oxidized species $P680^{+\bullet}$ are located on different molecules (see below). Recently, the orientation of ^{3}P680 has been investigated in a single crystal transient EPR study (Kammel et al., 2003). This study corroborated the alignment of the triplet axes with respect to the membrane normal given by van Mieghem et al. (1991), and provided the complete set of Euler angles to fully specify the orientation of the triplet within PS II. Due to the parallel alignment of the D1/D2-pseudo C_2 symmetry axis with the C_2 symmetry axis for the two PS II monomers forming the PS II dimers present in the single crystals, an experimental assignment of the triplet state to one of the two 'accessory' Chls, either Chl_{D1} or Chl_{D2}, was impossible. A determination of the distance of the triplet-carrying species from another cofactor of the electron transfer chain, e.g., Q_A, by EPR as demonstrated in the BRC (Borovykh et al., 2002) will be able to remove this ambiguity.

IV. Distances Between Cofactor Molecules

A. Short-Lived Radical Pairs

Distance information on short-lived radical pairs in PS II has been obtained by the out-of-phase (OOP) ESEEM method, that was first applied to BRC with known distance between the cofactors of the radical-pair state $P865^{+\bullet}Q_A^{-\bullet}$ (Dzuba et al., 1995). In PS II, two groups almost simultaneously investigated the photo-induced charge-separated state $P680^{+\bullet}Q_A^{-\bullet}$ (Zech et al., 1997; Hara et al., 1997). In the study of Zech et al. (1997), this state has been investigated near room temperature in aqueous PS II suspensions. This is one of the very few ESEEM studies on biological samples at physiological temperatures. On the other hand, Hara et al. (1997) reported a low-temperature study. In the former work, PS II membrane preparations (BBY particles) depleted of the non-heme iron and in the latter samples with Zn^{2+} substituted for the non-heme Fe^{2+} were used to achieve a magnetic decoupling of the reduced quinone acceptor from the non-heme iron. Within their error margins of about 0.4 Å, both studies gave identical distances of 27.4 and 27.2 Å, respectively, between the unpaired electron spins on $P680^{+\bullet}$ and $Q_A^{-\bullet}$ (Fig. 4). In addition frozen solutions of D1/D2/Cyt b_{559}complexes complemented with exogeneous quinones were studied by Hara et al. (1997). The observation of a radical pair state with an identical distance as that of $P680^{+\bullet}Q_A^{-\bullet}$ suggests that benzoquinone can be reconstituted into the Q_A binding site in D1/D2/Cyt b_{559} complexes. This low temperature study has been extended to oriented membranes of spinach PS II (Yoshii et al., 1999a) (see Fig. 4). An angle of about 21° between the axis connecting $P680^{+\bullet}Q_A^{-\bullet}$ and the membrane normal was

found, which is similar to the corresponding angle for $P865^{+\bullet}Q_A^{-\bullet}$ in the structure of *Rhodobacter sphaeroides* (Allen et al., 1987).

The use of aqueous solutions at physiological temperatures by Zech et al. (1997) allowed the observation of the electron transfer from the redox-active tryosine Y_Z to the oxidized $P680^{+\bullet}$. A lower limit of 32 Å could be given for the distance between the unpaired electrons in the state $Y_Z^{ox\bullet}Q_A^{-\bullet}$. Using a theoretical analysis of the OOP-ESEEM experiment under the condition of an electron transfer process (Jeschke and Bittl, 1998), this study was extended using high pH to decouple the non-heme iron from the $Q_A^{-\bullet}$ and to accelerate the Y_Z to $P680^{+\bullet}$ electron transfer after removal of the water-oxidizing complex (WOC). The distance between $Y_Z^{ox\bullet}$ and $Q_A^{-\bullet}$ was determined as (35 ± 1) Å (Zech et al., 1999). The X-ray crystallographic models of PS II (Zouni et al., 2001; Kamiya and Shen, 2003; Ferreira et al., 2004) are in very good agreement with this distance. Almost the same distance (34 ± 1) Å was later obtained for the trapped non-polarized radical pair $Y_Z^{+\bullet}Q_A^{-\bullet}$ by PELDOR in a Y_D-less mutant of *Chlamydomonas reinhardtii* (Kawamori et al., 2002).

The 27 Å distance between $P680^{+\bullet}$ and $Q_A^{-\bullet}$ is about 1 Å shorter than the distance between the primary donor $P^{+\bullet}$ and $Q_A^{-\bullet}$ in the BRC (>28 Å) (Dzuba et al., 1995; Bittl and Zech, 1997) and about 2 Å longer than the distance between $P700^{+\bullet}$ and $A_1^{-\bullet}$ in PS I (25.4 Å) (Zech et al., 1996; Dzuba et al., 1997) measured by the same technique. The 27 Å distance in PS II is consistent with the oxidized species $P680^{+\bullet}$ being located on the 'special pair' analogues P_{D1} and/or P_{D2} in the X-ray structural models of PS II. This is in agreement with the findings in an optical study on mutant PS II with exchanged axial ligands of P_{D1} and P_{D2} (Diner et al., 2001). In this study, the major contribution to $P680^{+\bullet}$ has been assigned to P_{D1} with a minor temperature and preparation dependent contribution of oxidized P_{D2}.

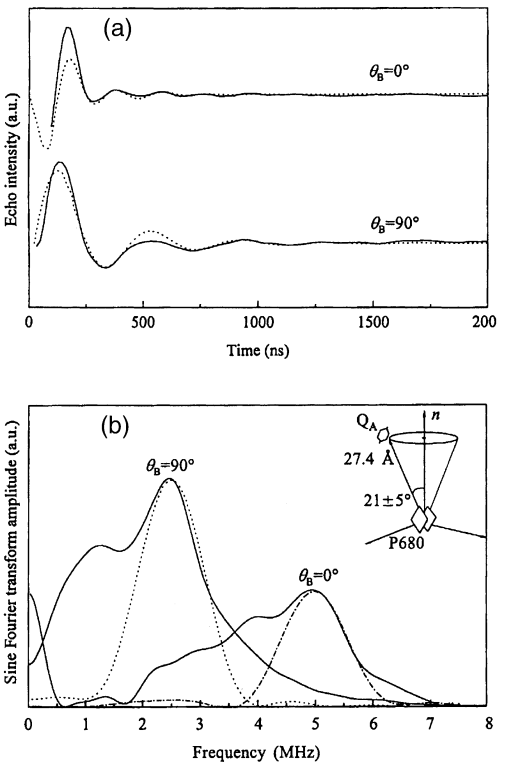

Fig. 4. Angular variation of $P680^{+\bullet}$-$Q_A^{-\bullet}$ OOP-ESEEM (adapted from Yoshii et al., 1999a). (a) OOP-ESEEM spectra observed in oriented Zn-substituted PS II core particles at the field directions $\theta_B = 0°$ (top) and 90° (bottom). (b) Sine Fourier transformation of the time domain spectra obtained from (a). Solid curves show the experimental data observed at 80 K at the orientation of $\theta_B = 0°$ and 90°. The dotted and broken lines show the simulated curves with parameters derived from (a). The inset shows the geometry of P680 and Q_A relative to the membrane normal.

B. Trapped Two-Spin Systems

Since the oxidized tyrosine radical $Y_D^{ox\bullet}$ is present in various types of PS II preparations and gives a well characterized EPR signal, most distances between components of the electron transfer chain in PS II measured by EPR were determined for pairs of radicals with $Y_D^{ox\bullet}$ as one of the partners. A second radical species can be trapped in addition to $Y_D^{ox\bullet}$, depending on the specific treatment of a PS II preparation. For example, after Tris treatment to eliminate the WOC, $Y_Z^{ox\bullet}$ can be trapped by illumination at 253 K. The EPR spectra of pairs of radicals involving $Y_D^{ox\bullet}$ and another organic component of the electron transfer chain overlap, therefore the dipolar spin–spin coupling is usually observed by the '2+1' method.

1. $Y_D^{ox\bullet}$–$Y_Z^{ox\bullet}$

The first study using the '2+1' pulse sequence in PS II was performed for the radical pair $Y_D^{ox\bullet}$–$Y_Z^{ox\bullet}$ by Astashkin et al. (1994) and a distance of 29.5 ± 0.5 Å between the unpaired electrons was determined. The same distance has later been corroborated in a

study using different preparations of Ca-depleted PS II (Hara et al., 1996). The dependence of the time profile of the '2+1' pulse sequence on the magnetic-field direction was observed in oriented membranes of Tris-treated PS II and an angle between the membrane normal and the line connecting $Y_D^{ox\bullet}$ and $Y_Z^{ox\bullet}$ was found to be (80° ± 2)° or (100° ± 2)° (Astashkin et al., 1998), as shown in Fig. 5. Again, the present X-ray model of PS II (Zouni et al., 2001) agrees well with the EPR data.

2. $Y_D^{ox\bullet}$–Chl $Z^{+\bullet}$

So far, the molecular species corresponding to Chl Z, which is a part of an alternative electron transfer pathway from Cyt b_{559} to P680 (Thomson and Brudvig, 1988; Chapter 15, Faller et al.), has not yet been unambiguously identified. Stewart and co-workers (1998) suggested that Chl Z is located in the D1 protein. According to this suggestion Chl Z should be close to $Y_Z^{ox\bullet}$.

The radical pair $Y_D^{ox\bullet}$–Chl $Z^{+\bullet}$ can be prepared by 200 K illumination of Tris-treated PS II. The distance between the unpaired spins and angle between their connecting axis and the membrane normal are 29.5 ± 0.5Å and 50°, respectively, measured in non-oriented (Shigemori et al., 1998) and oriented membranes (Tonaka et al., 2000). In contrast no PELDOR signal could be observed for the pair $Y_Z^{ox\bullet}$–Chl $Z^{+\bullet}$ in an Y_D-less mutant of *C. reinhardtii,* suggesting more than 50 Å for the distance between them (Kawamori et al., 2002). These two results suggest that the active Chl Z defined by de Paula and co-workers (1985) as the donor to $P680^{+\bullet}$ is situated on the D2 protein. However, the possibility that Chl Z may reside on the D1 protein cannot be completely excluded. First, the oxidation of Chl Z might have been inhibited when Y_Z was oxidized, and second a carotenoid might have been trapped in these experiments (Hanley et al., 1999; Faller et al., 2001).

3. $Y_D^{ox\bullet}$–Mn Cluster

A PELDOR study on the Mn cluster in the S_2-state and the $Y_D^{ox\bullet}$ radical in oriented membranes of O_2 evolving PS II revealed the distance and the orientation of the axis connecting $Y_D^{ox\bullet}$ and the Mn cluster with respect to the membrane normal to be 27.3 ± 0.5 Å and 70° or 110°, respectively (Astashkin et al., 1998). This distance is in agreement with earlier data obtained by selective hole-burning (Kodera et al., 1994) and

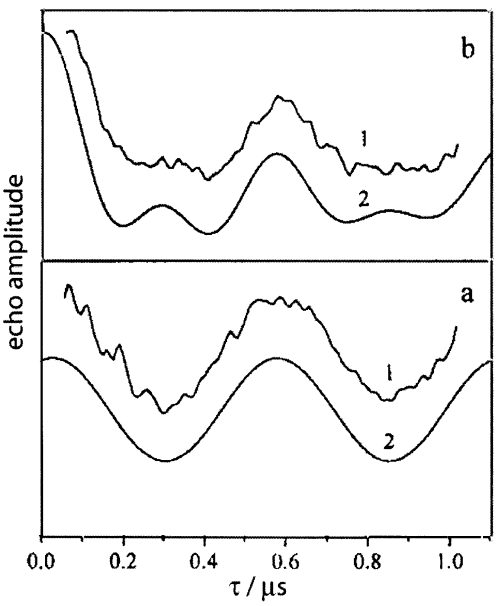

Fig. 5. Dependence of '2+1' time profiles for the spin pair $Y_D^{ox\bullet}$–$Y_Z^{ox\bullet}$ on the sample orientation with respect to the magnetic field (a) 0° and (b) 90° between the membrane normal and the field direction. (1) Experimental traces (2) simulations for a distance of 29.5 Å and the vector Y_Z–Y_D inclined 80° from the membrane normal ***n***. Adapted from Astashkin et al. (1998)

that observed by PELDOR on Ca^{2+}-depleted PS II (Hara et al., 1996).

Recently, PELDOR was applied to $Y_D^{ox\bullet}$ and the Mn cluster in the S_0-state in a PS II preparation reduced with NH_2OH (Arao et al., 2002). A distance between the spins of 34 ± 1 Å was found (as shown in Fig. 6). This value is remarkably larger than the value for the S_2-state. This has been attributed to a movement of the spin center induced by oxidation from the S_0 to the S_2 state (Arao et al., 2002). However, the difference of 7 Å for the distances for the S_0 and S_2 states from Y_D seems to be too large in view of the size of the Mn cluster observed by X-ray crystallography (Zouni et al., 2001; Kamiya and Shen, 2003; Ferreira et al., 2004). An alternative explanation has recently been given in a PELDOR study involving a multi-nuclear iron-sulfur cluster (Elsässer et al., 2002). This study showed that in a case like the tetra-manganese cluster of the WOC the application of the point-dipole approximation for the effective S = ½ spin of the cluster yields, in general, the wrong results. Explicit consideration of the spin coupling in the metal cluster is therefore necessary to obtain correct distance data

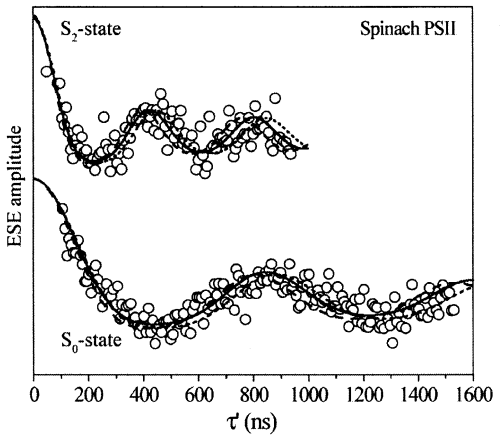

Fig. 6. PELDOR signals for the Mn cluster in the S_2-state and S_0-state. The paramagnetic partner is $Y_D^{ox\bullet}$. The full lines show simulations for the distances 27 Å and 34 Å, respectively, in a point-dipole approximation. The dashed lines show the different simulations with ± 0.5 Å deviations.

from the measured dipolar interaction. The distances between Y_D and the individual Mn ions differ in all three crystallographic models by about 3 Å. Since the spin coupling coefficients for the Mn ions have positive as well as negative signs, the effective dipolar distance can show much larger variations than the 3 Å distance difference for the ions. The different measured dipolar interactions in the S_0 and S_2 states are, therefore, most likely due to changed contributions of the individual Mn-ions to the effective spin in the different redox states of the WOC.

4. $Y_D^{ox\bullet}$–Cyt b_{559}

The EPR signal of oxidized Cyt b_{559} in PS II extends over a wide magnetic field range depending on the orientation of the magnetic field relative to the ***g***-tensor from $g_z = 2.9$ to $g_x = 1.5$ (as reviewed in Stewart and Brudvig, 1998). In the analysis of PELDOR involving Cyt b_{559} as one of the paramagnetic species angular selection effects have to be considered. For measurements at $g \approx 2$, which corresponds approximately to the g_y position, an alignment of the field in the observed centers parallel to the membrane normal with minor contributions from the other orientations has been assumed (Kuroiwa et al., 2000). This assumption is based on the orientation of the g_y axis assumed to be along the membrane normal (Rutherford, 1985). The measurement of the Cyt b_{559}^{+}–Q_A^{-} pair in non-oriented and oriented membranes, an approximate value of the distance of 40 Å and an orientation of 78° between the connecting axis and the membrane normal were obtained (Kuroiwa et al., 2000). These values can be considered to be qualitatively consistent with the X-ray data (Zouni et al., 2001).

5. $Y_D^{ox\bullet}$–Fe^{2+}(Non-Heme Iron)

The distance between $Y_D^{ox\bullet}$ and the non-heme Fe^{2+} has been determined indirectly based on the relaxation enhancement that $Y_D^{ox\bullet}$ experiences due to the presence of the non-heme iron. The relaxation effect of the non-heme Fe^{2+} on $Y_D^{ox\bullet}$ is only observable in the PS II without Mn cluster, since the Mn cluster in O_2-evolving PS II is strongly affecting $Y_D^{ox\bullet}$. A variety of different techniques yielded distances of about 40 Å — temperature dependence of T_1: 38 ± 5 Å (Hirsh et al., 1992); low temperature saturation behavior in high-frequency EPR: 40 Å (Un et al., 1994); selective hole burning: 42 ± 2 Å (Kodera et al., 1994; Hara and Kawamori, 1997). The distance of 40 Å between $Y_D^{\bullet}$ and the non-heme Fe^{2+} is consistent with the distance of 39 Å between $Y_D^{ox\bullet}$ and $Q_A^{\bullet}$ as obtained directly by the '2+1' method (Shigemori et al., 1998; Yoshii et al., 1999b).

6. $P680^{+\bullet}$/$Y_Z^{ox\bullet}$–Mn Cluster

Several distance determinations between the Mn cluster and $P680^{+\bullet}$ or $Y_Z^{ox\bullet}$ have been attempted by EPR. However, as has been discussed above for the case of the distances obtained between $Y_D^{ox\bullet}$ and the Mn cluster in the S_0 and S_2 states, these data have to be considered with caution. They have all been based on the point-dipole approximation, that is very critical in the case of a multinuclear metal complex (see above).

In a temperature-dependent relaxation study, a distance between the Mn cluster (in the S_2-state) and $P680^{+\bullet}$ of 21–25 Å has been given (Kodera et al., 1992). This distance is larger than the 18 Å distance found in the X-ray models of PS II (Zouni et al., 2001; Kamiya and Shen, 2003; Ferreira et al., 2004).

Contradictory data have been reported for the distance between the Mn cluster and Y_Z in the range between 3.5 Å to 20 Å, e.g., 4.5 Å (Tang et al., 1996), 7–9 Å (Peloquin and Britt, 2001), 8.6–11.5 Å (Peloquin et al., 1998), 15 Å (Kodera et al., 1995). Additional references are listed in Lakshmi et al. (1998). Within this broad range, the distance of about

7 Å found in the X-ray models is included. Several problems are the likely origins for the discrepancy in the EPR data and have been discussed by Dorlet et al. (1999). The distance determination relies on the interpretation of the approximately 200 G wide so called 'split signal' which is observed in inhibited PS II preparations. Initially the 'split signal' was found in Ca-depleted samples (Boussac et al., 1989). Later similar signals with varying splitting were observed in Cl-depleted (Baumgarten et al., 1990) and acetate-treated (MacLachlan and Nugent, 1993) samples. The 'split signal' has been assigned to a coupling between S_2 and $Y_Z^{ox\bullet}$ (Tang et al., 1996). However, another interpretation of the 'split signal' (Mino and Kawamori, 2001) exists, where a dipolar coupling between $Y_Z^{ox\bullet}$ and an unknown radical was suggested. Presently, the question regarding the origin of the 'split signal' is not fully resolved and therefore structural conclusions based on measurements involving the 'split signal' have to be considered with care. Even after an agreement about the origin of the 'split signal' will be achieved, critical points remain regarding the interpretation of spin couplings in terms of distances. This is evident from the different signs for the spin coupling between the Mn cluster and $Y_Z^{ox\bullet}$ in Ca-depleted compared to acetate treated samples observed in high-frequency EPR (Dorlet et al., 1999). Dorlet et al. (1999) gave two alternative explanations for this fact, among which changed contributions of the individual ions due to alterations in the electronic structure of the cluster seem to be the most likely source of the difference.

The complex magnetic structure of the Mn cluster and the drastic simplification in the data analysis based on point-dipoles is very likely also the reason why the angle of 75° between the Mn–Y_Z interspin vector and the thylakoid membrane deduced from EPR measurements on oriented samples deviates strongly from the present X-ray models (Zouni et al, 2001; Kamiya and Shen, 2003; Ferreira et al., 2004), where the Mn–Y_Z vector is almost parallel to the membrane normal.

The same reason can be considered as the origin for the discrepancy between the couplings with $Y_Z^{ox\bullet}$ measured for the Mn cluster in the S_1 and S_2 states. The distance of about 15 Å between the Mn cluster and $Y_Z^{ox\bullet}$ has been derived from experiments with the Mn cluster in the S_1-state in Ca^{2+}-depleted PS II (Kodera et al., 1995). This distance is longer than all distances recently reported for the Mn cluster in the S_2-state. The apparent discrepancy again is probably due to deficiencies in the analysis of the distance from measured spin-spin couplings in the case of a multinuclear metal center as discussed above for the Mn–$Y_D^{ox\bullet}$ distances. The contributions of the individual Mn ions to the total spin of the cluster will strongly depend on the oxidation state of the cluster. Therefore, rather different couplings between the Mn cluster and a second spin can be expected as a function of the oxidation state. This in turn leads in general to wrong distance data when using the point-spin approximation for data analysis as shown for a [3Fe-4S] cluster (Elsässer et al., 2002).

V. Concluding Remarks

The examples of EPR derived structural information on the arrangement of components of the electron transfer chain in PS II and their comparison to structural data now available from X-ray crystallography shows that in general the EPR data obtained prior to X-ray analysis are corroborated by later X-ray data. One important conclusion can be drawn for orientation information obtained by EPR on oriented membrane fragments. This method relies on a relatively simple approach to achieve partially ordered samples. The quality of the data obtained from oriented membranes has been demonstrated by single-crystal EPR studies performed on two paramagnetic states in PS II, the stationary $Y_D^{ox\bullet}$ radical and the short-lived triplet state ^{3}P680. In both cases, good to excellent agreement between the single-crystal studies and the experiments on oriented membranes has been found.

For distance data between paramagnetic intermediates of PS II, excellent agreement between X-ray and EPR data is in particular found for pulse-EPR studies on organic radical pair species. Table 1 compares the EPR-derived distances with X-ray distances, where the present resolution of the X-ray structure allows such comparison. The examples shown here for PS II will certainly be reference cases for EPR structure investigations on proteins and protein complexes, where other methods of structural investigations are difficult or impossible. However, EPR studies will remain of interest even after a successful global structure analysis, e.g., by X-ray crystallography, as is obvious for PS II. In general an assignment of functional states to cofactors in a protein is impossible on the basis of a structural model alone. A unique assignment, e.g., of ^{3}P680 and Chl Z in PS II, certainly can be achieved by additional EPR spectroscopic studies.

Table 1. Distances between components of the electron transfer chain in PS II and angles of their connection axis with respect to the membrane normal **n**

Paramagnetic Pair	Distance/Å	(X-ray)*	Angles (°) from **n** axis	Method
P680–Q_A	27.4 ± 0.3[1]	(26_{D1}, 28_{D2})	21 ± 5[2]	OOP-ESEEM
Y_D–Q_A	38.5 ± 0.8[3]	(40)	28 ± 5[4]	'2+1'
Y_Z–Q_A	34 ± 1[5]	(34.2)		OOP-ESEEM, ELDOR
Y_D–Y_Z	29.5 ± 0.5[6]	(29.2)	80 ± 2[7]	'2+1'
Y_D–Chl Z	29.4 ± 0.5[3]	(26.8_{D2})	50 ± 5[8]	'2+1'
Y_D–Mn_4 (S_2)	27.1 ± 0.2[9]	(30.3)	70 ± 2[7]	PELDOR
Y_D–Mn_4 (S_0)	34 ± 0.5	(30.3)		PELDOR
Q_A–Cyt b_{559}	40 ± 3[10]	(47.8)	78 ± 5[10]	PELDOR
Y_D–non-heme Fe	38–42[11]	(37.6)		Selective hole burning, T_1 and saturation

[1] Zech et al. (1997); Hara et al. (1997) [2] Yoshii et al. (1999a) [3] Shigemori et al. (1998) [4] Yoshii et al. (1999b) [5] Zech et al. (1999); Kawamori et al. (2001) [6] Astashkin et al. (1994) [7] Astashkin et al. (1998) [8] Tonaka et al. (2000) [9] Hara et al. (1996) [10] Kuroiwa et al. (2000) [11] Hara and Kawamori (1997); Hirsh et al. (1992); Un et al. (1994). * The distances were calculated from the PDB entry 1FE1 (Zouni et al., 2001) for averages over (representative) atom positions except for Y_D and Y_Z where the C_ζ atom has been used.

So far the EPR-derived structural data for the Mn cluster relative to other components of the electron transfer chain in PS II have to be considered with care. The complex magnetic structure of the Mn cluster renders distance determinations based on the spin-spin interaction of the cluster with a second paramagnetic species difficult. However, on the basis of the X-ray structure existing EPR data involving the Mn cluster can now be better interpreted and new EPR experiments can be designed to gain insight into the magnetic and geometric structure of the Mn cluster and their changes during the S-state cycle.

Acknowledgments

This work was supported by Deutsche Forschungsgemeinschaft (Sfb 498, TP C5), and by Grant-in-Aid for Scientific Research (No. 3640412) from Japan Society of Promotion of Sciences.

References

Allen JP, Feher G, Yeates TO and Rees DC (1987) Structure of the reaction center from *Rhodobacter sphaeroides* R-26: The cofactors. Proc Natl Acad Sci USA 84: 5730–5734

Arao S, Yamada S, Kawamori A, Shen J-R, Ionnidis N and Petrouleas V (2002) EPR studies of manganese spin centers in the even number oxidation states of water oxidizing complex of Photosystem II. In: Kawamori A, Yamaguchi J and Ohta H (eds) EPR in the 21st Century: Basics and Applications to Material, Life and Earth Sciences, pp 466-470. Elsevier Science BV, Amsterdam

Astashkin AV, Kodera Y and Kawamokri A (1994) Distance between tyrosine Z^+ and D^+ in plant Photosystem II as determined by pulsed EPR. Biochim Biophys Acta 1187: 89–93

Astashkin AV, Hara H and Kawamori A (1998) The pulsed electron-electron double resonance and '2+1' electron spin echo study of the oriented oxygen-evolving and Mn-depleted preparations of Photosystem II. J Chem Phys 108: 3805–3812

Barry BA and Babcock GT (1987) Tyrosine radicals are involved in the photosynthetic oxygen-evolving system. Proc Natl Acad Sci USA 84: 7099–7103

Baumgarten M, Philo JS, Dismukes GC, (1990) Mecahnism of photoinhibition of photosynthetic water oxidation by chloride depletion and fluoride substitution: Oxidation of a protein residue. Biochemistry 29: 10814–10822

Bergström J and Vänngård T (1982) Electron-paramagnetic-resonance signals and orientation of cytochromes in the spinach chloroplast thylakoid membrane. Biochim Biophys Acta 682: 452–456

Bittl R and Zech SG (1997) Pulsed EPR study of spin coupled radical pairs in photosynthetic reaction centers: Measurement of the distance between $P_{700}^{+\bullet}$ and $A_1^{-\bullet}$ in Photosystem I and between $P_{865}^{+\bullet}$ and $Q_A^{-\bullet}$ in bacterial reaction centers. J Phys Chem B 101: 1429–1436

Bittl R and Zech SG (2001) Pulsed EPR on short-lived intermediates in Photosystem I. Biochim Biophys Acta 1507: 194–211

Borovykh IV, Kulik LV, Dzuba SA and Hoff AJ (2002) Out-of-Phase Stimulated Spin-Echo Appearing in the Evolution of Spin-Correlated Photosynthetic Triplet-Radical Pairs. J Phys Chem B 106: 12066–12071

Bosch M, Proskuryakov II, Gast P and Hoff AJ (1996) Time-resolved EPR study of the primary donor triplet in D1-D2 cyt *b*559 complexes of Photosystem II: Temperature dependence of spin-lattice relaxation, J Phys Chem 100: 2384–2390

Boussac A, Zimmermann JL and Rutherford AW (1989) EPR signals from modified charge accumulation states of the oxygen-evolving enzyme in calcium-deficient Photosystem II. Biochemistry 28: 8984–8989

Crowder MS, Prince RC and Bearden AJ (1982) Orientation of membrane-bound cytochromes in chloroplasts, detected by low-temperature electron-paramagnetic-resonance spectroscopy. FEBS Lett 144: 204–208

de Paula JC, Innes JM and Brudvig GW (1985) Electron transfer in Photosystem II at cryogenic temperature. Biochemistry 24: 8114–8120

Diner BA, Schlodder E, Nixon PJ, Coleman WJ, Rappaport F, Lavergne J, Vermaas WFJ and Chisholm DA (2001) Site-directed mutations at D1-His198 and D2-His197 of Photosystem II in *Synechocystis* PCC 6803: Sites of primary charge separation and cation and triplet stabilization. Biochemistry 40: 9265–9281

Dorlet PA, Bussac A, Rutherford AW and Un S (1999) Multifrequency high-field EPR study of the interaction between the tyrosyl Z radical and the manganese cluster in plant Photosystem II. J Phys Chem B 103: 10945–10954

Dorlet PA, Rutherford AW and Un S (2000) Orientation of the tyrosyl D, pheophytin anion, and semiquinone Q_A^- radicals in Photosystem II determined by high-field electron paramagnetic resonance. Biochemistry 39: 7826–7834

Dzuba SA, Gast P and Hoff AJ (1995) ESEEM study of spin–spin interactions in spin–polarized P^+Q_A pairs in the photosynthetic purple bacterium *Rhodobacter sphaeroides* R26. Chem Phys Lett 236: 595–602

Dzuba SA, Hara H, Kawamori A, Iwaki M, Itoh S and Tsvetkov YD (1997) Electron spin echo of spin-polarized radical pairs in the intact and quinone-reconstituted plant Photosystem I reaction centers. Chem Phys Lett 264: 238–244

Elsässer C, Brecht M and Bittl R (2002) Pulsed electron-electron double resonance on multinuclear metal cluster: Assignment of spin projection factors based on the dipole interaction. J Am Chem Soc 124: 12606–12611

Faller P, Maly T, Rutherford AW and MacMillan F (2001) Chlorophyll and carotenoid radicals in Photosystem II studied by pulsed ENDOR. Biochemistry 40: 320-326

Ferreira KN, Iverson TM, Maghlauoi K, Barber J, and Iwata S (2004) Architecture of the photosynthetic oxygen-evolving center. Science 303: 1831–1838

Gast P, Wasielewski MR, Schiffer M and Norris JR (1983) Orientation of the primary donor in single crystals of *Rhodopseudomonas viridis* reaction centres. Nature 305: 451–452

Hales BJ and Gupta AD (1979) Orientation of the bacteriochlorophyll triplet and the primary ubiquinone acceptor of *Rhodospirillum rubrum* in membrane multipliers determined by ESR spectroscopy (I). Biochim Biophys Acta 548: 276–286

Hanley J, Deligiannakis Y, Pascal A, Faller P and Rutherford AW (1999) Carotenoid oxidation in Photosystem II. Biochemistry 38: 8189–8195

Hara H and Kawamori A (1997) A selective hole burning method applied to determine distances between paramagnetic species in photosystems. Appl Magn Reson 13: 241–257

Hara H, Kawamori A, Astashkin AV and Ono T (1996) The distances from tyrosine D to redox-active components on the donor side of Photosystem II determined by pulsed electron-electron double resonance. Biochim Biophys Acta 1276: 140–146

Hara H, Dzuba SA, Kawamori A, Akabori K, Tomo T, Satoh K, Iwaki M and Itoh S (1997) The distance between P680 and Q_A in Photosystem II determined by ESEEM spectroscopy. Biochim Biophys Acta 1322: 77–85

Hirsh DJ, Beck WF, Innes JB and Brudvig GW (1992) Using saturation-recovery EPR to measure distances in proteins. Biochemistry 31: 532–541

Hofbauer W, Zouni A, Bittl R, Kern J, Orth P, Lendzian F, Fromme P, Witt HT and Lubitz W (2001) Photosystem II single crystals studied by high frequency EPR spectroscopy at 94 GHz: the tyrosine radical Y_D. Proc Natl Acad Sci USA 98: 6623–6628

Hootkins R and Bearden A (1983) The orientation of the magnetic axes of membrane-bound iron-sulfur clusters and a Cyt b_{559} in the green halophilic alga *Dunaliella parva*. Biochim Biophys Acta 723: 16–29

Jeschke G and Bittl R (1998) Electron spin echo envelope modulation by electronic spin-spin interactions in radical pairs undergoing electron transfer. Chem Phys Lett 294: 323–331

Jordan P, Fromme O, Witt HT, Klukas O, Saenger W and Krauß N (2001) Three-dimensional structure of cyanobacterial Photosystem I at 2.5 Å resolution. Nature 411: 909–917

Kamlowski A, van der Est A, Holzwarth A and Stehlik D (1996) Evidence for delocalization of the triplet state $^3P_{680}$ in the D1D2cyt b559-complex of Photosystem II. Ber Bunsenges Phys Chem 100: 2045–2051

Kamlowski A, Altenberg-Greulich B, van der Est A, Zech SG, Bittl R, Fromme P, Lubitz W and Stehlik D (1998) The quinone acceptor A_1 in Photosystem I: Binding site, and comparison to Q_A in purple bacterial reaction centers. J Phys Chem B 102: 8278–8287

Kamiya N and Shen JR (2003) Crystal structure of oxygen-evolving Photosystem II from *Thermosynechoccus vulcanus* at 3.7-Å resolution. Proc Natl Acad Sci USA 100: 98–103

Kammel M, Kern J, Lubitz W and Bittl R (2003) Photosystem II single crystals studied by transient EPR: The light-induced triplet state. Biochim Biophys Acta 1605: 47–54

Kawamori A, Katsuta N, Mino H, Ishii A, Minagawa J and Ono T (2002) Position of Q_A and Chl_Z relative to tyrosine Y_Z and Y_D in Photosystem II studied by pulsed EPR. J Biol Phys 28: 413–426

Kodera Y. Takura K and Kawamori A (1992) Distance of P680 from the manganese complex in Photosystem II studied by time resolved EPR. Biochim Biophys Acta 1101: 23–32

Kodera Y, Dzuba SA, Hara H and Kawamori A (1994) Distances from tyrosine D^+ to the manganese cluster and the acceptor iron in Photosystem II by selective hole burning in EPR spectra. Biochim Biophys Acta 1186: 91–99

Kodera Y, Hara H, Astashkin AV, Kawamori A and Ono T (1995) EPR study of trapped tyrosine Z^+ in Ca-depleted Photosystem II. Biochim Biophys Acta 1232: 43–51

Kuroiwa S, Tonaka M, Kawamori A and Akabori K (2000) The position of cytochrome b_{559} relative to Q_A in Photosystem II studied by electron-electron double resonance (ELDOR). Biochim Biophys Acta 1460: 330–337

Kurshev VV, Raitsmiring AM and Tsvetkov YD (1989) Selection of dipolar interaction by the '2+1' pulse train in ESE, J Magn Reson 81: 441–454

Lakshmi K, Eaton SS, Eaton GR, Frank HA and Brudvig GW (1998) Analysis of dipolar and exchange interactions between manganese and tyrosine Z in the $S_2Y_Z^\bullet$ state of acetate-inhibited Photosystem II via EPR spectral simulations. J Phys Chem B

102: 8327–8335
Lakshmi K, Eaton SS, Eaton GR and Brudvig GW (1999) Orientation of the tetranuclear manganese cluster and tyrosine Z in the O_2-evolving complex of Photosystem II: An EPR study of the $S_2Y_Z^{\bullet}$ state in oriented acetate-inhibited Photosystem II membranes. Biochemistry 38: 12758–12767
Lendzian F, Bittl R and Lubitz W (1998) Pulsed ENDOR of the photoexcited triplet states of bacteriochlorophyll *a* and of the primary donor P_{865} in reaction centers of *Rhodobacter sphaeroides* R-26. Photosynth Res 55: 189–197
Lendzian F, Bittl R, Telfer A and Lubitz W (2003) Hyperfine structure of the photoexcited triplet state ^{3}P680 in plant PS II reaction centers as determined by pulse ENDOR spectroscopy. Biochim Biophys Acta 1605: 35–46
MacLachlan DJ and Nugent JHA (1993) Investigation of the S3 electron paramagnetic resonance signal from the oxygen-evolving complex of Photosystem II: Effect of inhibition of oxygen evolution by acetate. Biochemistry 32: 9772–9780
MacMillan F, Hanley J, van der Weerd L, Knüpling M, Un S and Rutherford AW (1997) The orientation of the phylloquinone electron acceptor anion radical in Photosystem I. Biochemistry 36: 9297–9303
Michel H and Deisenhofer J (1988) Relevance of the photosynthetic reaction center from purple bacteria to the structure of Photosystem II. Biochemistry 27: 1–7
Milov AD, Ponomarev AB, and Tsvetkov YD (1984) Electron electron double resonance in electron spin echo: Model biradical systems and the sensitized photolysis of decalin, Chem Phys Lett 110: 67–72
Mino H and Kawamori A (2001) EPR Studies of the water oxidizing complex in the S_1 and the higher S state: The manganese cluster and Y_Z radical. Biochim Biophys Acta 1503:112–122
Noguchi T, Inoue Y and Satoh K (1993) FT-IR studies on the triplet state of P680 in the Photosystem II reaction center triplet equilibrium within a chlorophyll dimmer. Biochemistry 32: 7186–7195
O'Malley PJ, Babcock GT and Prince RC (1984) The cationic plastoquinone of the chloroplast water splitting complex: Hyperfine splitting from a single methyl group determines the EPR spectral shape of Signal II. Biochim Biophys Acta 766: 283–288
Peloquin JM and Britt RD (2001) EPR/ENDOR characterization of the physical and electronic structure of the OEC Mn cluster. Biochim Biophys Acta 1503: 96–111
Peloquin JM, Campbell KA and Britt RD (1998) ^{55}Mn Pulsed ENDOR Demonstrates That the Photosystem II 'Split' EPR Signal Arises from a Magnetically Coupled Mangano-Tyrosyl Complex. J Am Chem Soc 120: 6840–6841
Rhee KH, Morris EP, Barber J and Kühlbrandt W (1998) Three-dimensional structure of Photosystem II reaction center at 8 Å resolution. Nature 396: 283–286
Rutherford AW (1985) Orientation of EPR signals arising from components of Photosystem II membranes. Biochim Biophys Acta 807: 189–201
Rutherford AW (1989) Photosystem II, the water splitting enzyme. TIBS 14: 227–232
Rutherford AW and Acker S (1986) Orientation of the primary donor in isolated Photosystem II reaction centers studied by electron paramagnetic resonance. Biophys J 49: 101–102
Salikhov KM, Kandrashkin YE and Salikhov AK (1992) Peculiarities of free induction and primary spin echo signals for spin-correlated radical pairs. Appl Magn Reson 3: 199–216
Shigemori K, Hara H, Kawamori A and Akabori K (1998) Determination of distances from tyrosine D to Q_A and chlorophyll Z in Photosystem II studied by '2+1' pulsed EPR. Biochim Biophys Acta 1363: 187–198
Stewart DH and Brudvig GW (1998) Cytochrome b_{559} of Photosystem II. Biochim Biophys Acta 1367: 63–87
Stewart DH, Cua A, Chisholm DA, Diner BA, Bocian DF and Brudvig GW(1998) Identification of histidine 118 in the D1 polypeptide of Photosystem II as the axial ligand to chlorophyll Z. Biochemistry 37: 10040–10046
Tang X-S, Randall DW, Force DA, Diner BA and Britt RD (1996) Manganese–tyrosin interaction in the Photosystem II oxygen-evolving complex. J Am Chem Soc 118: 7638–7639
Thomson LK and Brudvig GW (1988) Cytochrome b_{559} may function to protect Photosystem II from photoinhibition. Biochemistry 27: 6653–6658
Thurnauer MC and Norris JR (1977) The ordering of the zero field spin sublevels in the chlorophylls. A magnetophotoselection study. Chem Phys Lett 47: 100–105
Tiede DM and Dutton PL (1981) Orientation of the primary quinone of bacterial photosynthetic reaction centers contained in chromatophore and reconstituted membrane. Biochim Biophys Acta 637: 278–290
Tonaka M, Kawamori A, Hara H and Astashkin AV (2000) Three-dimensional structures of electron transfer components in Photosystem II: '2+1' ESE of chlorophyll Z and tyrosine D. Appl Magn Reson 19: 141–150
Un S, Brunel L-C, Brill TM, Zimmermann J-L and Rutherford AW (1994) Angular orientation of the stable tyrosyl radical within Photosystem II by high-field 245-GHz electron paramagnetic resonance. Proc Natl Acad Sci USA 91: 5262–5266
Van Mieghem FJE, Satoh K and Rutherford AW (1991) A chlorophyll tilted 30° relative to the membrane in Photosystem II reaction centre. Biochim Biophys Acta 1058: 379–385
Vermeglio A, Breton J, Barouch Y and Clayton R (1980) Orientation of the hemes of high-potential cytochromes relative to photosynthetic membranes, as shown by the linear dichroism of oriented preparations. Biochim Biophys Acta 593: 299–311
Yoshii T, Hara H, Kawamori A, Akabori K, Iwaki M and Itoh S (1999a) ESEEM study of the location of spin polarized chlorophyll-quinone radical pair in membrane-oriented spinach Photosystem I and II complexes. Appl Magn Reson 16: 565–580
Yoshii T, Kawamori A, Tonaka M and Akabori K (1999b) Relative positions of electron transfer components in Photosystem II studied '2+1' pulsed electron paramagnetic resonance: Y_D and Q_A. Biochim Biophys Acta 1313: 43–49
Zech SG, Kurreck J, Eckert H-J, Renger G, Lubitz W and Bittl R (1997) Pulsed EPR measurement of the distance between $P_{680}^{+\bullet}$ and $Q_A^{-\bullet}$ in Photosystem II. FEBS Lett 414: 454–256
Zech SG, Kurreck J, Renger G, Lubitz W and Bittl R (1999) Determination of the distance between $Y_Z^{ox\bullet}$ and $Q_A^{-\bullet}$ in Photosystem II by pulsed EPR spectroscopy on light-induced radical pairs. FEBS Lett 442: 79–82
Zouni A, Witt HT, Kern J, Fromme P, Krauß N, Saenger W and Orth P (2001) Crystal structure of Photosystem II from *Synechococcus elongatus* at 3.8 Å resolution. Nature 409: 739–743

Chapter 18

Structural Analysis of the Photosystem II Core/Antenna Holocomplex by Electron Microscopy

Ben Hankamer*
Institute of Molecular Bioscience, University of Queensland, St. Lucia, QLD 4072, Australia

James Barber and Jon Nield
Wolfson Laboratories, Department of Biological Sciences, Imperial College London, SW7 2AZ, U.K.

*Author for correspondence, email: b.hankamer@imb.uq.edu.au

T. Wydrzynski and K. Satoh (eds): Photosystem II: The Light-Driven Water:Plastoquinone Oxidoreductase, pp. 403–424.

Summary

Electron microscopy has contributed greatly to the structural biology of Photosystem II (PS II) in higher plants and green algae from the level of its in vivo organization, within the thylakoid membrane, through to the determination of the structure of light-harvesting complex II (LHCII) at 3.4 Å. Freeze-fracture and freeze-etch techniques provided the first visualization of PS II and its antenna systems in vivo. Subsequently a range of PS II and PS II-antenna, super- and mega-complexes were purified from thylakoid membranes using mild detergent solubilization and these were structurally characterized by single particle analysis. In particular these studies showed the structural linkage between the PS II core and a range of bound macromolecular light-harvesting antennae, as well as the overall shape of the extrinsic oxygen-evolving complex. Electron crystallography extended the resolution range, revealing the positioning of PS II subunits and the transmembrane helix organization of both PS II and antenna proteins. This technique also identified many of the chlorin cofactors in the reaction center proteins of D1 and D2, and also in the inner antenna, CP47, and outer antenna of LHCII. Future work will involve obtaining more highly resolved structures of supercomplexes and megacomplexes, using electron cryo-microscopy and including structural information emerging from X-ray and electron crystallography, with the view to gaining a near atomic resolution model of higher plant/green algal PS II as it exists in the native thylakoid membrane.

I. Introduction

In recent years, electron cryo-microscopy (cryo-EM) has developed rapidly in the areas of tomography, single particle analysis and electron crystallography. Cryo-EM tomography has advanced to the stage where a series of tilt images of individual frozen hydrated samples can be used to calculate a 3D reconstruction of organelles and whole cells to a resolution of 5–30 nm. At this resolution individual macromolecular assemblies can be identified, revealing their location, size and shape. This opens up the exciting prospect of being able to fit higher resolution structures, determined by single particle analysis, electron or X-ray crystallography, into the molecular footprints identified within these 3D reconstructions of organelles and whole cells. This combinatorial approach will provide unique insights into the organization and dynamics of macromolecular assemblies, such as Photosystem II (PS II) and its antenna system in vivo.

Single particle analysis lies between cryo-EM tomography and electron crystallography, calculating medium resolution 3D structures of isolated complexes that are randomly oriented in vitreous ice. It is particularly suited to the analysis of large, labile, symmetric macromolecular assemblies, being used in the determination of supermolecular structures of PS II and its antenna system, including the light-harvesting complex (LHCII) system, which have not yet yielded high quality 2D or 3D crystals. 3D reconstructions with a resolution of 7.5–30 Å are now routinely being determined and this range is being extended through a whole array of innovations.

High-resolution electron cryo-crystallography requires large and well-ordered 2D crystals. This approach has to date yielded the highest resolution 3D reconstructions determined by any cryo-EM technique. It is particularly suited for membrane proteins and has yielded structures of LHCII and the PS II core of higher plants.

This chapter summarizes the advances made in cryo-EM techniques and the structural data they have yielded for PS II and its antenna system with a particular focus on higher plants. Such studies are stepping-stones on the road to opening up the fascinating and dynamic 3D world of the in vivo chloroplast.

Abbreviations: 1D – one-dimensional; 2D – two-dimensional; 3D – three-dimensional; CCF – cross-correlation function; Chl – chlorophyll; CP43 – Chl *a*-containing protein with apparent molecular mass of 43kDa; CP47 – Chl *a*-containing protein with apparent molecular mass of 47kDa; Cryo-EM – electron cryo-microscopy; CTF – contrast transfer function; Cyt – cytochrome; Dpi – dots per square inch; EM – electron microscopy; FEG – field-emission gun; FSC – Fourier shell correlation; LHCII – light-harvesting complex of PS II; MSA – multivariate statistical analysis; NMR – nuclear magnetic resonance; OEC – oxygen-evolving complex; PCTF – phase contrast transfer function; PS II – Photosystem II; SNR – signal-to-noise ratio; TEM – transmission electron microscopy; TMH – transmembrane helix

II. Electron Cryo-Microscopy Techniques

Electron cryo-microscopy (cryo-EM) techniques involving the analysis of vitrified samples have revolutionized the structural analysis of macromolecular assemblies, allowing for medium resolution (7.5–30 Å) structures to be achieved from single particle images, and better than 5 Å from electron crystallography of 2D crystals. These techniques complement those structures visualized at lower resolutions by negative staining (Chen et al., 1998; Dubochet et al., 1988). The challenge of cryo-EM is to greatly increase the attainable resolution of the specimen under study, through careful preparation and imaging, in order to minimize electron-beam damage and maximize image contrast.

A. Specimen Preparation

Biological specimens are extremely sensitive to electron beam damage. Their atoms typically scatter electrons weakly, giving rise to low contrast (Chen et al., 1998) and high noise (Dubochet et al., 1988). In order to achieve higher contrast, negative staining techniques have been developed over considerable time, which are easy to implement, but impose some limitations. The main disadvantages are: (i) negative staining accentuates surface features at the expense of internal detail as the stain molecules do not penetrate past the surface of the protein. This imposes a resolution limit of 15–20 Å (Kiselev et al., 1990; Hoenger and Aebi, 1996). (ii) Stain artifacts can cause the variable flattening of the 3D structure by dehydration. Still, negative stain is valid for probing an unknown sample, often for initial 2D/3D structural impressions of the specimen, prior to images taken of vitrified samples that do contain information to atomic resolution. In the latter approach, with the samples embedded in vitreous ice, the molecules remain hydrated under conditions that resemble the native environment more closely.

B. High-Resolution Imaging

In order to produce high quality cryo-EM images using transmission electron microscopy (TEM) several requirements need to be fulfilled. The specimen stage, termed here a cryo-stage, must be mechanically stable, reducing drift during imaging and preventing the accumulation of electric charge, vibrations, stray magnetic fields and heat. The stage can be cooled by either liquid nitrogen or liquid helium (Dubochet et al., 1988; Fujiyoshi, 1998). The sample on the EM grid should be imaged under minimal electron dose conditions to reduce damage by the electron beam. Ideally, the region to be imaged consists of the biological sample embedded in a thin film of vitreous ice, which is suspended across a hole in the carbon foil. The sample is initially viewed at high magnification (150,000×), but on an area of carbon film slightly away from the ice hole, such that the electron beam is at a low dose and does not interact too harshly with the sample and cause irradiation damage – i.e., imaging is performed blind and the image quality only assessed after the film is developed. Phase contrast is then introduced by defocusing the microscope to ~1–2 μm underfocus. Exposures are typically made at ~50,000×, the beam only now interacting with the area to be imaged at high dose. The magnification at which the images are taken, accelerating voltage, total electron dose, and defocus can all be varied depending on the desired resolution. It should be noted that even the most advanced TEM optics are of poor quality in terms of astigmatism, spherical aberration, lens-current fluctuations and chromatic aberration, which can all be quantified in terms of the contrast transfer function (CTF) and corrected for to a certain extent. Another important development is that of the field-emission gun (FEG) (Stowell et al., 1998). A FEG-equipped EM uses very high electric fields to release electrons from a fine tungsten tip (Reimer, 1997). This increases the spatial and temporal coherence of the electron source, boosting the contrast transfer at high resolutions when compared to the standard thermionic emission gun.

Once TEM images of the highest quality are achieved, a range of analytical techniques can be applied depending upon whether the sample has been imaged for single particle analysis, electron crystallography or tomography.

C. Single Particle Analysis

Single particle analysis started developing after the demonstration that a 3D object imaged in an electron beam gave corresponding 2D projection images dependent on its orientation (DeRosier and Klug, 1968). If the angle for each of these 2D projections can be determined, a 3D structure of the molecule may be calculated by projecting the 2D images back along their projection angles, a technique known as back-projection (Radermacher, 1988). Electron

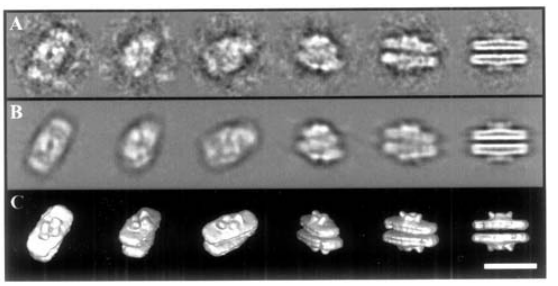

Fig. 1. 3D single particle analysis of the LHCII-PS II supercomplex (Nield et al., 2000c). (A) Selection of typical class averages used for the 3D reconstruction. (B) Reprojections of the 3D map in identical orientations with the corresponding class averages. (C) Surface representation of the final 3D map viewed in the same orientation as the class averages. Bar represents 30 nm.

micrographs of biological molecules are intrinsically noisy and exhibit low intrinsic contrast. Single particle averaging techniques significantly enhance the signal-to-noise ratio (SNR) present within the original images; in turn increasing the limits of resolution and interpretability (see Fig. 1). Now widely used for many structural biology-based problems, single particle averaging (or analysis), cryo- and negative stain-EM, have all recently been reviewed in depth (Orlova, 2000; Saibil, 2000a,b; van Heel et al., 2000; Ruprecht and Nield, 2001; Henderson, 2004). In this section we only briefly introduce the reader to the main steps involved.

1. Interactive Particle Selection and Band-Pass Filtering

First the electron micrographs are digitized by a high fidelity densitometer measured to be at least 2000 dpi, and are then corrected for the CTF (Reimer, 1997). A data set of at least several thousand particles is obtained from the micrographs by picking all discernible particles not overlapping or in close contact with other particles (Harauz et al., 1988). The single particle images are floated out into pixel boxes whose size is just enough to enclose the single particle images and remove as much background as possible. In order to suppress the extreme high and low spatial frequencies present within the images, certain band-pass filters can be applied. It is necessary to do this as very low spatial frequencies can cause fluctuations in the average density, for example the amount and uniformity of the staining, whereas in very high spatial frequencies the SNR is much smaller (Harauz et al., 1988). This can directly affect the success of the further alignment steps as the correlation functions used can emphasize certain spatial frequencies (van Heel et al., 1992). The spatial frequencies are only suppressed, so one can restore them after an initial 3D model has been reconstructed. This is especially important for the high spatial frequencies, which include desired high-resolution information.

2. Reference-Free Alignment and Multivariate Statistical Analysis

The first alignment step is reference-free alignment, which functions to center each particle within its pixel box through a series of translational shifts by using cross-correlation functions (CCFs) (Frank, 1980; Reimer, 1997). All processing is evaluated in Fourier space, taking advantage of the convolution theorem, which enables calculations to be processed many times faster in the computing environment. The reference-free alignment step is iterated several times until a good alignment is achieved while the data set is prevented from being biased towards any particular reference at an early stage in the analysis (Dube et al., 1993; Schatz et al., 1995). Multivariate statistical analysis (MSA), a form of correspondence analysis, is then used to identify the main components of variation within any given set of images, placing each image into a group of similar molecular images of similar rotational orientations. The mechanism of MSA reflects a form of data compression, greatly increasing the speed of the image processing, reducing the effects of noise, and may provide useful information about conformational flexibility or substrate binding (Saibil, 2000b).

3. Classification and Multi-Reference Alignment

In the Imagic-5 program suite, the hierarchical ascendant classification algorithm is used to generate a specified number of classes (van Heel and Stoffler-Meilicke, 1985). The algorithm starts with as many classes as there are images. It then merges the classes that are most similar, where if the resulting increase in total intra-class variance is minimal, each of these classes are then averaged to produce class averages (see Fig. 1A). These class averages have a higher SNR than the raw images and are more easily interpreted. Having produced initial class averages, some are used as references to search through and align the entire data set, generating improved class averages. In this multi-reference alignment (Schatz et al., 1995), each image is translationally and now also rotationally aligned using cross-correlation functions. After a number of iterative cycles much improved class averages are achieved.

4. Angular Reconstitution and 3D Reconstruction

Once improved class averages are achieved, the construction of a 3D model commences. The projection direction of each average, relative to the others, must first be understood (Euler angles). This assumes that all the 2D averages were imaged from identical 3D structures. Imagic-5 employs the angular reconstitution technique, based on the common line projection theorem (van Heel, 1987). An initial 3D reconstruction is calculated by back-projecting the class averages along their assigned Euler angles (Radermacher, 1988). The 3D reconstruction is then reprojected along the Euler angle directions assigned to the class averages (see Fig. 1B). This provides a means to compare how well their corresponding class averages fit to the 3D model (compare Fig. 1B with the class averages of Fig. 1A). Poor quality class averages, perhaps deriving from particles that became damaged prior to imaging (see heterogeneous populations section below), can be identified and removed from the dataset. The remaining class averages are then back-projected once more to produce a more reliable 3D model (see Fig. 1C). Refinement is possible by using the reprojected images from the latest 3D model as references in a new multi-reference alignment. After the 3D model shows no further improvement from iterative refinements, an estimation of the resolution is made by measuring the Fourier shell correlation (FSC) (Orlova et al., 1997; van Heel, 1986). Final presentation of the model is usually by surface-rendering the 3D map, or showing a series of its cross-sections, revealing internal density distribution.

Single particle analysis is able to deal with heterogeneous populations of molecules (van Heel et al., 2000; Ruprecht and Nield, 2001) and in the study of protein complexes that undergo conformational flexibility (Saibil, 2000b). MSA and classification allow a heterogeneous population to be sorted into classes of similar molecules, generating more homogeneous sub-populations for independent analysis, a form of 'computational purification.' This relatively novel application has been used in PS II studies to reveal different conformations of subunit binding (Nield et al., 2000a,c, 2002), and its use will increase as heterogeneous populations of molecules are very difficult to study by X-ray or electron crystallography. Indeed, use of this methodology has facilitated the study of PS II complexes in the recently discovered cyanobacterial organisms *Prochloron didemni* and *Prochlorococcus marinus*. This has revealed that a transmembrane light harvesting protein, Pcb, which is similar in structurre to CP43, binds to PS II reaction centers in a stochiometry of 5 or 4:1, respectively (Bibby et al., 2003a,b).

The best resolutions published to date using single particle analysis are 7.4 Å for the hepatitis B core protein (Böttcher et al., 1997) and 7.5 Å for the 70S ribosome (Matadeen et al., 1999), although 15–25 Å is more usual. Currently the resolution limit is imposed by factors including beam-damage, specimen movement, astigmatism, beam-induced specimen charging, aberrations, beam drift, and the inability to correct for the CTF perfectly. Assuming that image quality is not limiting in terms of the above parameters, an increase in the size of the single particle data set will increase the resolution of retrieved structural detail, suggesting that initially the low signal to noise ratio of cryo-electron micrographs is also a factor (Orlova, 2000). Typically, data sets of 20,000+ particles have proved necessary for the reconstruction of non-symmetric particles to intermediate resolution. In addition, it has been shown that one can exploit any molecular symmetry present to decrease the number of images needed for a given resolution (DeRosier and Klug, 1968; Chiu et al., 1999). Except for the computing power available, there is no upper limit to the size of molecule that can be studied by single-

particle analysis, a significant advantage compared to NMR spectroscopy, although a minimum size of 100 kDa has been suggested due to the requirements of molecular alignment (Henderson, 1995, 2004).

D. Electron Crystallography

In parallel with single particle analysis, electron cryo-crystallography has made rapid advances in recent years, to the point that it is now a viable alternative to X-ray crystallography, for high-resolution structure determination of membrane proteins. Indeed to date electron and X-ray crystallography are the only techniques, which have yielded structures of membrane proteins at, or approaching, atomic resolution.

Most membrane protein structures have been solved by the X-ray approach, although a large number of diverse membrane proteins are now at an advanced stage in their structure determination by electron crystallography. For example, the structure of bacteriorhodopsin has been solved with a resolution of 3.0 Å in the X-Y plane (Henderson et al., 1990; Mitsuoka et al., 1999) with those of LHCII (3.4 Å) (Kühlbrandt et al., 1994), aquaporin (3.8 Å) (Murata et al., 2000) and the cytoskeletal protein tubulin (3.7 Å) (Nogales et al., 1998). Furthermore as electron micrographs contain both amplitude and phase information, thus avoiding the phase problem of X-ray crystallography, a large number of important intermediate resolution structures such as those of the acetyl-choline receptor (4.6 Å) (Miyazawa et al., 1999, 2003), halorhodopsin (5.9 Å) (Kunji et al., 2000), Ca^{2+}-ATPase (6Å) (Xu et al., 2002), glutathione transferase (6 Å) (Schmidt-Krey et al., 2000), GlpF (6.9 Å) (Stahlberg et al., 2000), PS II (7–10 Å) and the NhaA Na^{+}/H^{+} antiporter (7.0 Å) (Williams, 2000) are being solved. These provide valuable information at the level of subunit, α-helix and, in some cases, β-sheet organization.

In contrast to X-ray crystallography, which requires well ordered 3D crystals for atomic resolution structure determination, electron cryo-crystallography requires high quality 2D crystals, which can be produced using either the bilayer or monolayer approach.

1. Bilayer Crystallization

Perhaps the simplest way of producing 2D crystals is by using the bilayer approach (Kühlbrandt, 1992; Hasler et al., 1998; Auer et al., 1999; Levy et al., 1999; Lebeau et al., 2001). Essentially 2D bilayer crystals are produced from purified and detergent-solubilized membrane proteins that are mixed with specifically selected lipids (Fig. 2A). This protein:lipid:detergent blend is depleted of detergent in a controlled manner (Fig. 2B-D) by dilution, dialysis or the addition of detergent-adsorbing beads (Bio Beads). During the initial stages of detergent removal 'rod-like' structures (Fig. 2B) are often observed (Hasler et al., 1998), and are thought to be part of the micelle-bilayer transition stage prior to crystal formation. In the case of PS II, further detergent depletion forces lipid:protein:detergent micelles to fuse along the second axis of the hydrophobic plane (Fig. 2C), giving protein-packed lipid bilayers and 2D crystal nuclei (Fig. 2C). These subsequently grow into 2D crystals (Fig. 2D).

2. Monolayer Crystallization

As its name suggests, this novel technique (Levy et al., 1999) uses a flat lipid monolayer as a template to produce 2D crystals of membrane proteins. The monolayer lipid mixture used is doped with functionalized lipids such as Ni-chelating or charged lipids for the crystallization of His-tagged or charged proteins, respectively. The method involves dispensing a monolayer-forming lipid mixture, dissolved in chloroform, on to the flat surface of a buffer droplet contained in a special crystallization well. Next, detergent solubilized His-tagged membrane proteins, supplemented with bilayer-forming lipids, are injected into the buffer below the monolayer via a side port. On incubation these His-tagged proteins bind to the Ni-chelating lipids in the monolayer. The 2D crystallization process is then induced by the addition of detergent-binding beads (Bio-Beads) via the injection port. As the proteins and bilayer-forming lipids are depleted of detergent, the membrane spanning regions of the membrane proteins begin to incorporate into a lipid bilayer. In the case of FhuA and F_0F_1-ATP synthase, 2D crystal patches were observed 1–2 days after detergent removal (Levy et al., 1999).

3. Electron Crystallographic Analysis

High quality 2D crystals are imaged in vitreous ice at tilt angles ranging between ± 70°, in angular tilt increments selected to attain the desired resolution. The negatives are then digitized using a precision scanner (see above) and the structural informa-

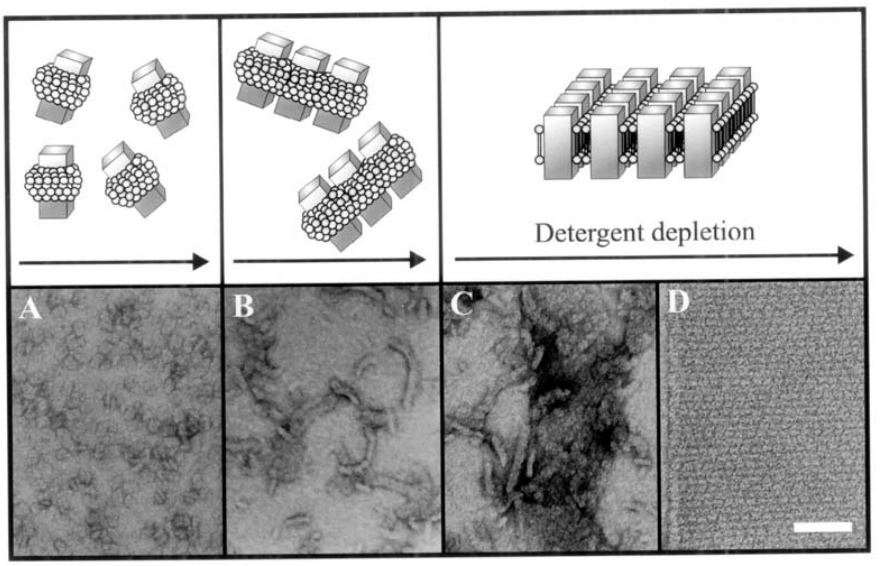

Fig. 2. The process of 2D crystal formation. Solubilized membrane proteins (A) aggregate into 'rod-like' structures (B), crystal nuclei (C) and finally form 2D crystals (D), the process captured by electron microscopy. Above is a diagrammatic version. Bar represents 100 nm.

tion contained in each tilt image is extracted using electron crystallographic approaches. These include filtering out noise unrelated to the crystal lattice and correcting for defects in the flatness and order of the crystal lattice itself (Henderson et al., 1986). The refined tilt images are then merged to generate a 3D reconstruction.

4. Advantages and Limitations of Electron Crystallography

Both the 2D monolayer and 2D bilayer approaches have the advantage over X-ray techniques given that the membrane protein of interest is embedded in a lipid bilayer in a near native environment. Under these conditions the membrane spanning domains of labile (non-rigid) membrane proteins are compressed through the lateral pressure of the lipid bilayer, aiding their stabilization. In theory, 2D crystals are also easier to grow as molecular arrangement is only required in two rather than three dimensions. In addition the electron micrographs of these crystals contain amplitude and phase information, thereby avoiding the lack of phase or 'phase problem' of X-ray crystallography, and allow structural information to be gained from small crystals and crystallization intermediates, the latter allowing for crystallization strategy development. The monolayer technique builds upon these advantages by favoring the formation of large flat bilayer sheet crystal types that are well suited for high-resolution studies. A number of factors can however limit the rate of high-resolution structure determination. Particularly important will be the development of streamlined approaches for high-resolution crystal production. In this respect the functionalized monolayer surface, used as a template in monolayer crystallization, has considerable potential. Other improvements that will benefit high-resolution electron crystallography are the use of new types of EM grids and support films that keep the 2D crystals as flat as possible (Vonck, 2000). The use of single particle techniques may also aid the recovery of high resolution data as the unit cells within a crystal can be classified prior to averaging rather than being subjected to global averaging (Sherman et al., 1998).

E. Electron Cryo-Tomography

In recent years great advances have been made in electron cryo-tomography allowing 3D reconstruction of individual organelles and whole cells to be deter-

mined using variations of the techniques employed for single particle analysis and electron crystallography (Baumeister et al., 1999). The adaptations being implemented address the issues of increased particle size (e.g., whole organelles vs. protein complexes) and the fact that individual organelles and cells do not have identical 3D structures, being fluid and dynamic in nature. Furthermore the technique has been developed to deal with specimens of ~0.25 to 2.0 μm thickness, by using TEMs capable of generating accelerating voltages greater than 400 kV (It should be noted that for single particle analysis or electron crystallography ~120–300 kV voltages are used). The word tomography itself defines that one freedom of rotation is fixed. In practice this means that the specimen being imaged is held in a fixed X-Y orientation while tilting the cryo-stage ± 70° in small increments e.g., 2°, in a manner similar to that employed for electron crystallography. As in the case of single particle analysis and given that these tilt angles are set by the user, back-projections of the tilt images can be made to generate a 3D reconstruction. Here the resolution-limiting factor is usually the precision with which such alignments can be made and the number of tilt images that can be taken of a single object before beam damage compromises the data.

Recent electron tomographic reconstructions have been made in the range 50–70 Å of mitochondria (Deng et al., 1999; Mannella et al., 1998; Perkins et al., 1997; Perkins et al., 1998) and a whole cell of the archaebacterium *Pyrodictium abyssi* (Baumeister et al., 1999). Recent improvements in the technique that have involved embedding the specimen in vitreous ice after plunging in liquid ethane, have aided the recovery of even higher resolution data, such as for *Neurospora* mitochondria (Nicastro et al., 2000). In addition, advanced single particle techniques for precise angular assignment and X-Y drift will help to improve resolution limits still further.

F. Summary

From the above, it can be seen that for a successful multi-disciplinary structural approach, X-ray and electron crystallographies and NMR spectroscopy would be chosen for studies involving individual molecules or small complexes, and single particle analysis employed for the study of larger complexes, present in different functional states or undergoing conformational flexibility. For organelles or whole cells, electron cryo-tomography can provide structural information at reasonably high-resolution. Subsequently, when available, previously determined smaller X-ray structures can be modeled into the larger single particle derived structural frameworks. Indeed this has been achieved over recent years in the field of PS II structural biology, extracting a wealth of new detail for the localization of the many light-harvesting components and co-factors that make up LHCII-PS II complexes, culminating in well-defined 3D structures containing over 50 subunits and having molecular mass in excess of a mega-Dalton.

In the following section we describe how this detail has emerged and how we might now start to use this information in understanding the multitude of in vivo processes that rely on such structure/function relationships.

III. Structure of Higher Plant Photosystem II and Its Antenna System

PS II is a multisubunit pigment-protein complex located within the thylakoid membrane of plants, algae and cyanobacteria and drives the highly oxidizing water splitting reaction. This reaction splits water into molecular oxygen, protons and electrons, thereby sustaining an aerobic atmosphere on Earth and providing the reducing equivalents required for carbon fixation on a global scale. The solar energy required to drive this highly oxidizing reaction is captured by specialized pigment-protein antenna systems, designed to transfer excitation energy efficiently to photochemically active reaction center (RC). Though similar in function, these antenna systems form a diverse range of structures, with those of higher plants and green algae being located in the thylakoid membrane, while those of most classes of cyanobacteria are bound extrinsically to the stromal surface of PS II. Cyanobacterial and higher plant PS II also differ in the lumenal extrinsic proteins associated with the oxygen-evolving complex (OEC) and in their complement of low molecular subunits. This section reviews the structural information obtained for the higher plant system, predominantly derived from single particle analysis and electron crystallography. To aid this process a brief review of PS II subunits is presented.

A. Subunits

1. The Core Complex

The PS II core complexes of higher plants, green algae and cyanobacteria all consist of over 20 subunits (Barber et al., 1997; Hankamer et al., 2001a; Barber, 2003). All of the redox active cofactors involved in the water photolysis reaction are bound to the reaction center proteins, D1 and D2 (Diner and Babcock, 1996; Chapter 4, Nixon et al.). Associated with these two proteins are the chlorophyll (Chl) *a*-binding inner-antenna proteins, CP43 and CP47 (Chapter 3, Eaton-Rye and Putnam-Evans), that have prominent lumenally-exposed protein loops, and the extrinsic lumenally bound proteins of the OEC (Chapter 5, Bricker and Burnap). The OEC provides an optimal micro-environment for the functioning of a four manganese atom cluster that catalyzes water oxidation. In higher plants and green algae, the OEC extrinsic proteins consist of the 33 kDa (PsbO), 23 kDa (PsbP) and 17 kDa (PsbQ) protein subunits, where PsbP and PsbQ are generally thought to be replaced by 9 kDa PsbU and 13 kDa PsbV (Cyt *c*550) proteins in cyanobacteria. In addition to PsbO, PsbP and PsbQ proteins, higher plants and green algae are reported to bind two other extrinsic proteins (PsbR and $PsbT_n$) on the lumenal surface (Barber et al., 1997). Over and above these subunits, the PS II core complexes of higher plants, green algae and cyanobacteria contain a large number of low molecular weight (LMW) intrinsic proteins (Table 1), including the α- and β-subunits of Cyt b_{559}.

Table1. Low molecular weight proteins of Photosystem II

Protein	Subunit	Mass (kDa)
PsbE (c)	α-Cyt b_{559}	9.255 (S)
PsbF (c)	β-Cyt b_{559}	4.409 (S)
PsbH (c)	H protein	7.697 (S)
PsbI (c)	I protein	4.195 (S)
PsbJ (c)	J protein	4.116 (S)
PsbK (c)	K protein	4.283 (S)
PsbL (c)	L protein	4.366 (S)
PsbM (c)	M protein	3.755 (P)
PsbN (c)	N protein	4.722 (T)
$PsbT_c$(c)	T_c protein	3.849 (S)
$PsbT_n$(n)	T_n protein	3.171 (A)
PsbW (n)	W protein	5.928 (S)
PsbX (n)	X protein	4.225 (S)
PsbY (n)	Y protein (A1)	4.673 (S)
PsbZ (c)	Z protein	6.541 (S)

These genes encode 15 low molecular mass PSII proteins of 10 kDa or less. The molecular masses of the mature proteins were calculated from the protein sequences reported in the SWISS-PROT data base using the MacBioSpec program (Sciex Corp., Thornhill, Ontario, Canada). The abbreviations given in brackets after the molecular masses denote the organism for which the subunit mass is given, as follows; *Arabidopsis* (A), pea (P), spinach (S) or tobacco (T).

2. The Antenna System

In higher plants the PS II core complex is linked to an outer antenna system (Fig. 3A) (Chapter 2, Green and Gantt) consisting of six different, but related, membrane proteins (Lhcb1-6) (Green and Durnford, 1996) all of which bind Chl *a*, Chl *b* and carotenoids (Liu et al., 2004). Similar Chl *a*/*b*-binding proteins also make up the outer antennae of green algae, although the number of different types is often larger, e.g., as in *Chlamydomonas*. The structures of two of the higher plant proteins, Lhcb1 and 2, which form a heterotrimer, were determined at a resolution of 3.4 Å by electron crystallography (Kühlbrandt et al., 1994). Each monomer was found to have three transmembrane helices and one surface helix. Seven Chl *a*, six Chl *b* and two carotenoid molecules were also identified in each monomer. Based on this structural information and the sequence homology between the six Lhcb proteins the remaining four are also predicted to have three transmembrane helices and to ligate pigments in a similar way. Another PS II protein, PsbS shares considerable homology with the Lhcb proteins, except that it is predicted to have four transmembrane helices (Green and Durnford, 1996). In the case of cyanobacteria a soluble, extrinsic, phycobilisome antenna system dwarfs the PS II core dimer in size and binds to it on the stromal side, one allophycocyanin core subunit binding to the dimer of the complex (Fig. 3B). The allophycocyanin core (ALC) usually, but not always, consists of three rods lying across the surface of the membrane. From the ALC, rods of phycocyanin radiate out, although in red algae, which also have phycobilisomes, other phycobilins such as phycoerythrin are present. Information on the structure of these water-soluble phycobiliproteins has been derived by X-ray crystallography (Brejc et al., 1995; Adir et al., 2001; Nield et al., 2003) while EM has contributed to our understanding of how

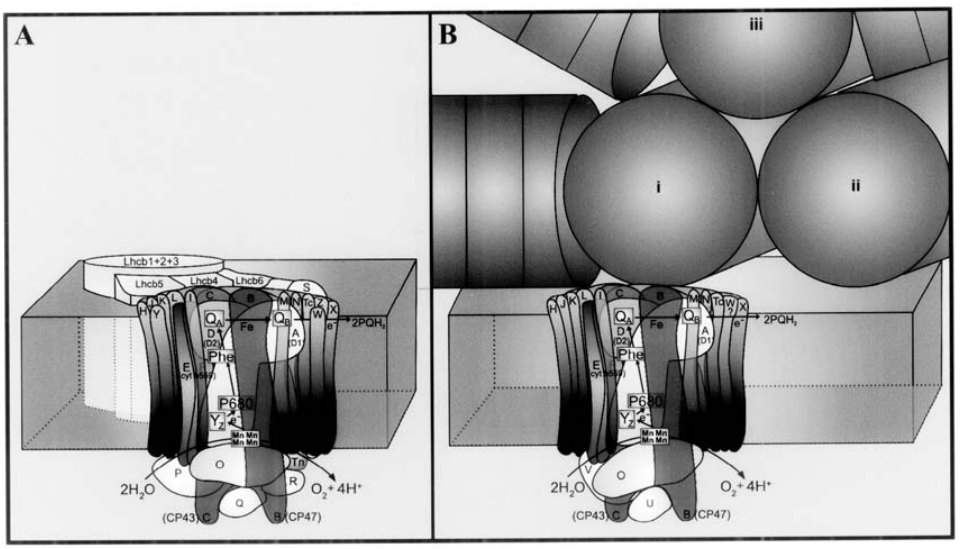

Fig. 3. Cartoons of PS II and its associated light-harvesting components (A) of higher plants and green algae and (B) of cyanobacteria, emphasizing subunit composition and primary and secondary electron transfer steps that occur in the reaction center D1 and D2 proteins. In the case of the higher plants and green algae (A) note that the secondary antenna is made up of Chl *a/b* binding Lhcb proteins, intrinsic to the membrane, while in (B), the cyanobacterial PS II is serviced by a large extrinsic, soluble phycobiliprotein mass on its stromal side. Also note, when comparing the two systems, the compositional differences present for the lumenally bound extrinsic subunits of the OEC. See Color Plate 3, Fig. 1.

they associate to form phycobiliproteins (Morschel and Schatz, 1987; Ducret et al., 1998; da Fonseca et al., 2002).

B. The Core Dimer Structure

Most of the structural details of the higher plant PS II core complex have been determined by electron crystallography, although 3D crystals have been reported (Fotinou et al., 1993; Adir, 1999). However, X-ray structures of a cyanobacterial PS II core complex have now been published (Zouni et al., 2001; Kamiya and Shen, 2003; Ferreira et al., 2004) that allow for comparisons with the higher plant complex to be made. For spinach, two distinct PS II preparations have been isolated that have yielded 2D crystals. The first is a monomeric RC-CP47 subcomplex (dark grey region Fig. 5) (Rhee et al., 1997, 1998), the second an oxygen evolving core complex (Morris et al., 1997; Hankamer et al., 1999, 2001b). The oxygen evolving PS II core complex is a dimer with each monomer component consisting of the D1 and D2 reaction center (RC) subunits, the inner antenna Chl binding proteins, CP47, CP43 and the extrinsic 33 kDa proteins, as well as a number of small membrane proteins, including the α- and β-subunits of Cyt b_{559} (Hankamer et al., 1997b). Electron microscope images of such crystals have yielded a 3D map in negative stain (Morris et al., 1997), a cryo-projection map (Hankamer et al., 1999) and later a 3D structure at a resolution of 10 Å resolution parallel to the membrane plane, again using vitrified samples of non-stained crystals (Hankamer et al., 2001b).

1. The Major Polypeptide Subunits

The side view of the 3D map (Fig. 4A and Fig. 1A of Color Plate 4) of the PS II spinach core dimer (Hankamer et al., 2001b) emphasizes the transmembrane region of the complex (containing fitted helices) and the extensive protrusion of density from the lumenal surface. The two large lumenal domains are thought to correspond to the location of the large lumenal loops of CP43 and CP47 (Fig. 4B and Fig. 1B of Color Plate 4). The positions of the transmembrane helices of the intrinsic PS II subunits (Fig. 4C and Fig. 1C of Color Plate 4) are derived from consideration of the distribution of density within the membrane

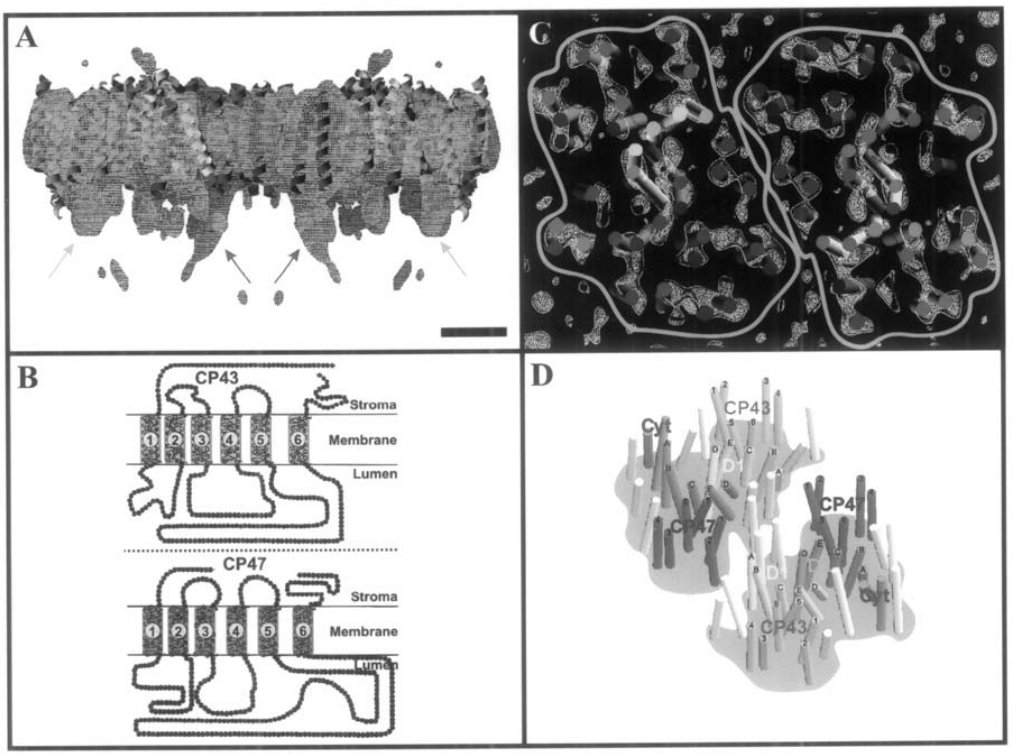

Fig. 4. (A) Side view of the 3D map of the spinach PS II core dimer, stromal side uppermost, emphasizing the transmembrane region and lumenal extensions assigned to the loops joining helices 5 and 6 of CP47 (innermost arrows) and CP43 (outermost arrows) (Hankamer et al., 2001b). (B) Predicted folding from hydropathy analyses of CP43 and CP47 (Hankamer et al., 2001b). (C) Transmembrane view of a section of the 3D map of the spinach PS II core dimer (Hankamer et al., 2001b). The map is sampled at ~1 Å and is displayed as chicken-wire contours, with compensation for high-resolution fade out (outer black contours, temperature factor –1000, 1.5 σ) and with no compensation (inner white contours, 1.3 σ). (D) An oblique view of the 3D structural model of the spinach PS II core dimer from electron crystallography. Bar for panels A and C represents 2.5 nm. See Color Plate 4, Fig. 1.

region. In each case the densities correspond either to individual or pairs of transmembrane helices that can be traced through the membrane plane. The assignment of helices to particular subunits relies in part on comparison with earlier electron crystallographic data obtained from the spinach PS II subcomplex containing the D1/D2 proteins and CP47 (Rhee et al., 1998). Thus the five yellow and five orange transmembrane helices within each monomer have been assigned to the D1 and D2 proteins, respectively. As noted previously their arrangement around a local pseudo-2D fold axis is remarkably similar to that of the L and M subunits of the reaction center of purple bacteria (Deisenhofer et al., 1984). All the transmembrane helices of the D1/D2 heterodimer are accommodated within the density of the map when no compensation is made for high resolution fade out at a threshold of 1.3 σ (blue contours). The positions of the transmembrane helices are better resolved when the high-resolution components of the data are accentuated using a threshold of 1.5 σ (white contours). The six helices colored red, adjacent to the D2 proteins and close to the monomer-monomer interface, belong to CP47. Additional density within the six helical cluster can be attributed to Chl molecules previously identified within the CP47 domain (Rhee et al., 1998). An equivalent set of densities was found adjacent to the D1 protein, and is related to those of the transmembrane helices of CP47 by the local two-fold pseudo-axis of the D1/D2 heterodimer.

These densities accommodate three pairs of helices assigned to CP43 (colored green). As in the case of CP47, additional density within the rings of helices is assumed to be due to bound Chl molecules. The assignment of the CP43 transmembrane helices was suggested previously based on a 2D projection map (Hankamer et al., 1999), but this is now supported by the 3D map in which the densities can be traced across the membrane. Two additional helices, colored cyan, are attributed to the α- and β-subunits of Cyt b_{559} (Rhee, 2001; Zouni et al., 2001; Kamiya and Shen, 2003; Kargul et al., 2003; Ferreira et al., 2004). The remaining transmembrane helices, colored in magenta, belong to the LMW subunits of PS II and will be discussed below.

The numbering of the helices of the D1 and D2 proteins in Fig. 4D and Fig. 1D of Color Plate 4 is based on a direct comparison with the structures of the L and M subunits of purple bacterial reaction center, with which they have a high degree of homology. The numbering of the six transmembrane helices of the CP43 and CP47 is based on structural analogies with the 6 amino-terminal (N-terminal) transmembrane helices of the Photosystem I (PS I) reaction center proteins PsaA and PsaB (Jordan et al., 2001). As shown in Color Plate 4, Fig. 1B, transmembrane helices 5 and 6 of CP43 and CP47 are linked by large lumenal loops consisting of 150 and 200 amino acid residues, respectively. In Color Plate 4, Fig. 1A, green and red arrows are used to indicate significant density protruding from the lumenal surface. Based on the helix assignment shown, it was concluded from the surface topography of the map that these lumenal protrusions are located above the helix pairs assigned to 5 and 6 of CP43 (in green) and CP47 (in red). This conclusion is therefore consistent with the existence of the large loops and the assignment of helices 5 and 6 of CP43 and CP47 in our structural model.

2. Extrinsic Lumenal Proteins

Closely associated with the PS II reaction center D1, D2, CP47 and CP43 proteins are the extrinsic lumenally bound proteins of the OEC. As mentioned above, the OEC extrinsic proteins consist of PsbO, PsbP and PsbQ proteins in higher plants and green algae, with PsbP and PsbQ being replaced by PsbU and PsbV in cyanobacteria. Two other minor extrinsic proteins have also been identified as being bound on the lumenal surface, PsbR and $PsbT_n$ (Barber et al., 1997; Barber, 2003), whose function is as yet unknown. The PsbO protein has generally been accepted as holding a major role in optimizing OEC function and thus water oxidation. In the EM-derived 3D map of Hankamer et al. (2001b), insufficient density was found to accommodate the PsbO protein despite evidence from SDS-PAGE gels that this protein was present in the samples used for electron microscopy (Hankamer et al., 1999). However, studies using single particle analysis, cryo-EM and various biochemical treatments to sequentially wash off the extrinsic proteins, have revealed significant density protruding into the lumen. These 3D difference cryo-EM maps, resolved in the 17–26 Å range, for higher plant LHCII-PS II supercomplexes (Nield et al., 2002) were interpreted as containing one copy of the PsbO per reaction center. Another 2D study involving negatively stained top views supported this as the most likely outcome (Boekema et al., 2000b). Both studies were able to relate the positions of the 33 kDa protein to the underlying intrinsic membrane proteins through 3D and 2D modeling studies, respectively. The more recent X-ray derived maps at 3.5 to 3.8 Å resolution (Zouni et al., 2001; Kamiya and Shen, 2003; Ferreira et al., 2004) also support one PsbO per reaction center in cyanobacterial systems. Investigations into the positional relationships between PsbO and PsbP / PsbQ, or PsbU/PsbV in cyanobacteria, will undoubtedly provide intriguing insights into the evolutionary development of the OEC and the mechanisms necessary for efficient water oxidation (De Las Rivas et al., 2004).

3. The Minor Polypeptide Subunits

In addition to the 22 helices of the major subunits a further 12 transmembrane helices assigned to low molecular weight subunits were identified in the PS II core dimer map (Hankamer et al., 2001a,b). For clarity these have been numbered from i-xii in Fig. 5 and compared with those present in the previously determined CP47-RC subcomplex (Rhee et al., 1998). The helices identified in the CP47-RC subcomplex map are contained in the dark blue region regions shown in Fig. 5A ;and Fig. 2A of Color Plate 3.

It should be noted that the two helices previously assigned immediately adjacent to the B-helices of the D1 and D2 proteins in the map of CP47-RC subcomplex (Rhee et al., 1998), have not been included. It is highly likely that the densities in these regions are due to Chl molecules ligated to D1-His198 and D2-His198 rather than to transmembrane helices

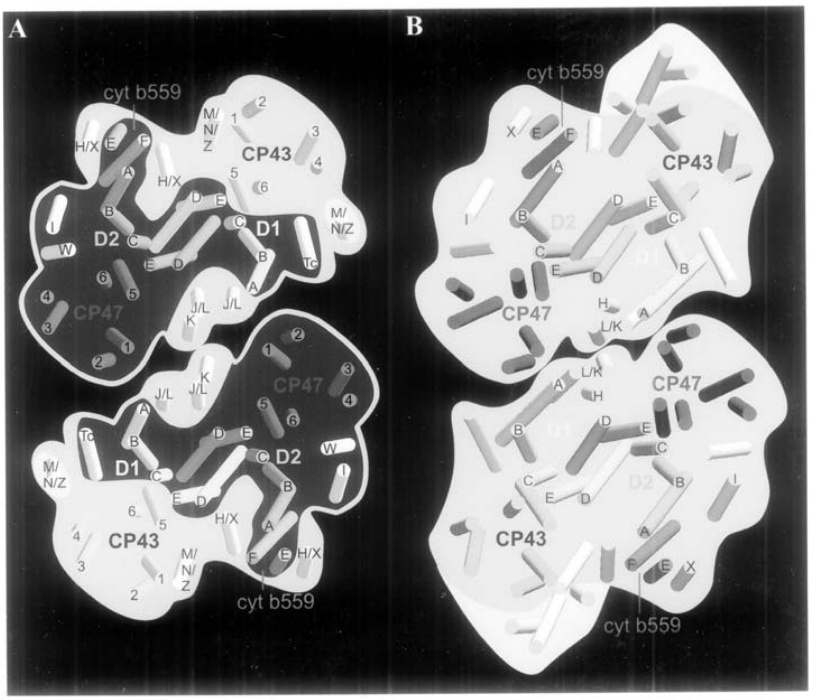

Fig. 5. Comparison of the PS II core dimer of (A) spinach (Hankamer et al., 2001b) and (B) *S. elongatus* (Zouni et al., 2001), and respective assignments of the low-molecular weight single transmembrane helical subunits. The dark grey region in (A) shows the helix organization of the spinach CP47-RC subcomplex (Rhee et al., 1998), which had to be modified, two transmembrane helices adjacent to helix B of the D1 and D2 proteins being removed. The remaining light grey regions contain the additional transmembrane helices of CP43 and other low-molecular weight core dimer subunits. See Color Plate 3, Fig. 2**.**

(Hankamer et al., 2001b). The revised number of LMW subunits in the CP47-RC subcomplex is consistent with mass spectrometry data and N-terminal sequencing analyses of an isolated and monomeric form of this CP47-RC subcomplex, which identified the five LMW proteins; PsbE, PsbF, PsbI, $PsbT_c$ and PsbW (Zheleva et al., 1998).

PsbE and PsbF, the α- and β-subunits of Cyt b_{559}, respectively, have been unambiguously identified in cyanobacterial X-ray structures (Ferreira et al., 2004). Based on their location in the cyanobacterial structures and on previous studies (Rhee, 2001), the two purple helices (Color Plate 3, Fig. 2A) were assigned to PsbE and PsbF as shown. With two of the five LMW protein helices of the CP47-RC subcomplex accounted for, the three remaining LMW proteins, PsbI, $PsbT_c$ and PsbW, can be attributed to the gray helices in the dark blue domain of Color Plate 3, Fig. 2A. The PsbI protein has been shown to cross-link both with the D2 protein and Cyt b_{559}, suggesting that it is on the D2 rather than the D1 side of the reaction center (Tomo et al., 1993). Furthermore, the PsbI protein is tightly associated with the isolated D1/D2 heterodimer while PsbW and $PsbT_c$ are less so (Irrgang et al., 1995; Webber et al., 1989). Consequently we tentatively assigned PsbI to the gray helix, closest to the D2 protein and Cyt b_{559}. Based on this assignment and on the report that PsbW can also be cross-linked to the α-subunit of Cyt b_{559} (PsbE) (Büchel et al., 2001) as well as co-purifying with the D1/D2/Cyt b_{559} RC complex (Irrgang et al., 1995), the second gray helix on the D2 side has been tentatively designated as PsbW. By elimination, $PsbT_c$ can therefore be assigned to the last gray helix in the CP47-RC subcomplex located adjacent to helices A and B of the D1 protein (see Color Plate 3, Fig. 2A).

In addition to the five LMW proteins within the

CP47-RC subcomplex, seven other LMW proteins have been attributed to membrane spanning densities identified in the higher plant PS II core dimer (Color Plate 4, Fig. 1). These additional LMW proteins are indicated as gray rods within the cyan domain of Color Plate 3, Fig. 2A. Of these seven proteins, four have been identified in our spinach dimer core complex by N-terminal sequencing and mass spectrometry; PsbH, PsbL, PsbK, and PsbX. PsbL and PsbK were also previously found in a dimeric, but not monomeric, forms of the spinach CP47 RC complex (Zheleva et al., 1998). This suggests that PsbL and PsbK are likely to be located in the central cyan regions at the interface between the two CP47-RC subcomplexes within the dimeric structure (Color Plate 4, Fig. 1). They may therefore account for two of the three transmembrane helices in this central linker region. In this context it is interesting to note that the pseudo-two-fold symmetry axis which relates the D1 and D2 proteins as well as CP47 and CP43, also approximately relates PsbE and PsbF with two of the gray helices in this central domain found adjacent to helix A of the D1 protein. Furthermore, in most organisms the PsbE, PsbF, PsbJ and PsbL are all coded for by a single chloroplast operon and expressed on a tetracistronic message. This suggests the intriguing possibility that the helix pair roughly symmetrically related to PsbE and PsbF consists of PsbJ and PsbL. Also as noted in Table 1, PsbJ and PsbL have highly conserved amino acid sequences. Consequently these two helices have been labeled J/L placing PsbK closest to the contact point of the PS II core dimer (Color Plate 3, Fig. 2A).

The two remaining LMW proteins that have been identified in the higher plant PS II core dimer are PsbH and PsbX. Recently the PsbH protein was shown to cross-link with the PsbE subunit of Cyt b_{559} in PS II core dimers isolated from the green alga *C. reinhardtii* (Büchel et al., 2001). Using a combination of gold labeling and single particle analysis, it was confirmed that the PsbH subunit was localized to a position close to Cyt b_{559}. As the PsbX subunit has been shown to be cross-linked with PsbH (Büchel et al., 2001) as well as with PsbE (Shi et al., 1999; Büchel et al., 2001) it is suggested that the two helices close to PsbE and PsbF are either PsbX or PsbH. This leaves two unassigned transmembrane helices in the cyan regions of the PS II core dimer. The first of these is adjacent to the helix that we have assigned to $PsbT_c$, with the second located close to helices 1 and 2 of CP43. The remaining three possible gene products that have been suggested to be part of the hydrophobic core of the PS II complex are PsbM, PsbN and PsbZ. Indeed, there is evidence that PsbZ is located close to CP43 (Swiatek et al., 2001). Therefore these helices have tentatively been assigned to M, N or Z as shown in Color Plate 3, Fig. 2A. In cyanobacteria, a cluster of transmembrane helices is observed adjacent to CP43 (Zouni et al., 2001; Kamiya and Shen, 2003; Ferreria et al., 2004), which are absent in the spinach dimer. These may function to link the phycobilisome antenna system of the cyanobacterium to the PS II core dimer. Another possibility is that they confer thermostability, demonstrated by *S. elongatus* PS II being able to grow at 70 °C.

It should be noted that in light of the recent, more highly resolved X-ray structure of Ferreira et al (2004), comparisons regarding the assignment and possible functions of LMW proteins in higher plands need to be rerconsidered (Chapter 21, Barber and Iwata).

C. Evolutionary Implications

The higher plant and cyanobacterial PS II core complexes are both dimeric and the organization of the transmembrane helices of the major subunits, D1, D2, CP43 and CP47 are very similar (Color Plate 3, Fig. 2). The existence of such conserved features amongst these species reinforces the view that the PS II of higher plants and cyanobacteria have a common evolutionary origin. A comparison of the two structures also provides strong evidence that the dimeric nature of the core is the main physiological form of PS II both of higher plants and cyanobacteria. The similarities of the two structures are also carried through to the level of the LMW subunits. The position of Cyt b_{559} and two adjacent small subunits appear to be conserved, as are the cluster of three helices (J, K and L) at the interface between the two monomers (Color Plate 3, Fig. 2A). Transmembrane helices denoted I, Tc and W are also found in both structures. The differences are that in cyanobacterial PS II, a helix putatively assigned as M/N does not appear to be present, but instead an additional cluster of three helices exists, sitting between Cyt b_{559} and helices 1 and 2 of CP43, where only one helix was identified in the higher plant complex. It is possible that these differences relate to the intrinsic versus extrinsic nature of the light-harvesting systems of the two types of photosynthetic organisms, which we discuss below.

D. The Outer Antenna System

A variety of LHCII-PS II complexes exist, whose function is to form an excitonically coupled pigment network in order to capture light energy and transfer it to the PS II RC (Boekema et al., 1995, 1999b). In higher plants the first such high-order complex to be isolated was a LHCII-PS II supercomplex from spinach (Hankamer et al., 1997b) and a similar complex was subsequently purified from the green alga *Chlamydomonas reinhardtii* (Nield et al., 2000b). Both structures were determined at intermediate resolution by single particle analysis and showed considerable homology (Nield et al., 2000b,c), measuring ~330 × 165 × 110 Å. LHCII-PS II super- and mega- complexes isolated from liverwort (*Marchantia polymorpha*) were also structurally similar (Harrer, 2003). The PS II oxygen-evolving core dimer forms the central region of the supercomplex, flanked by two clusters of the Chl *a*/*b* binding subunits Lhcb1, 2, 4, 5 (Hankamer et al., 1997b; Nield et al., 2000c). Each cluster was found to be composed of a LHCII trimer (Lhcb1 and 2) at its outermost tip, which appears to be structurally and excitonically coupled to the PS II core dimer via Lhcb proteins 4 and 5 monomers, also known as CP29 and CP26, respectively. Lhcb4 and 5, together with another Lhcb component, Lhcb6 (sometimes known as CP24), are thought to facilitate the binding of additional LHCII trimers, probably containing Lhcb3 as well as Lhcb1 and Lhcb2, to the edge of the supercomplex, leading to the possibility of still higher order structures being formed (Boekema et al., 2000a).

To further investigate subunit positioning, the transmembrane helical organization of the higher plant core dimer derived from electron crystallography has been modeled into a 17 Å 3D map of the spinach LHCII-PS II supercomplex obtained by single particle analysis (Nield et al., 2000a). This reconstruction also included the Lhcb components, which can be modeled as helices based on the electron crystallographic structure of LHCII (Kühlbrandt et al., 1994). The modeling revealed such details as two LMW membrane proteins, adjacent to helix B of the D1 protein, and appearing to form a link to the LHCII trimer. To be noted is that in cyanobacteria one of these helices is not present (see Color Plate 3, Fig. 2). In this case, the inference has been that over and above a purely structural role it is possible that this additional LMW subunit mediates excitation energy transfer from the outer light-harvesting antenna directly to the reaction center.

Boekema et al. (1999a,b) have performed several studies attempting to search for complexes larger than that currently defined as the LHCII-PS II supercomplex. Their approach has been to subject PS II membranes to partial detergent treatment, analyzing the solubilized membrane patches by single particle analysis, and computationally purifying the dataset. This has shown that LHCII can bind in three ways, strong (S), moderate (M) and loose (L) in three different forms of PS II 'megacomplex'. More recent work has classified images of crystalline arrays of PS II from spinach granal membranes, indicating that crystalline regions contain predominantly LHCII-PS II supercomplexes, and that the megacomplexes may be relegated to non-crystalline areas (Boekema et al., 2000a). As mentioned above, PsbS, shares considerable homology with the Lhcb proteins, except that it is predicted to have four transmembrane helices (Green and Durnford, 1996), and it is likely to be present in these larger, megacomplexes since it is not present in the isolated LHCII-PS II supercomplex (Nield et al., 2000a). The most significant conclusion from all this work is the heterogeneous nature of the associations between PS II and LHCII. It has been proposed that the formation of these different complexes may allow PS II to react to light and stress conditions by providing different routes of excitation energy transfer (Boekema et al., 1999b).

The typical inherent heterogeneity of higher plant/green algal systems does add another dimension of difficulty for structural studies, which has been overcome to a certain degree by 'computer purification' single particle analysis methods, as in relating the position of the OEC extrinsic proteins (Nield et al., 2002). These have shown that by classifying PS II complexes on the amount of peripheral proteins they contain, deductions about how the subunits fit together can be made, and this is also likely to prove a valuable methodology for structural investigations into photosystem and light-harvesting dynamics.

IV. Organization and Dynamics of Higher Plant Photosystem II and Its Antenna In Vivo

The thylakoids of higher plants (Fig. 6A) and to a lesser extent, green algae (Fig. 6B), form intricately arranged 3D membrane networks, segregated into stacked granal and unstacked stromal lamellae. This is

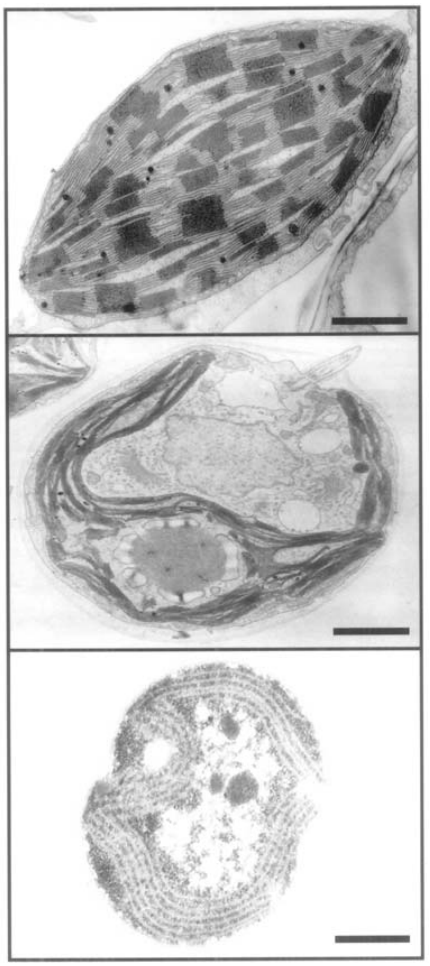

Fig. 6. Typical cross-sections of thylakoid membranes from (A) higher plants, bar represents 1 μm, (B) green algae, bar represents 10 μm, and (C) cyanobacteria, bar represents 10 μm.

in contrast to most cyanobacteria in which the membranes are unstacked (Fig. 6C). It is widely reported that PS II, PS I and ATP synthase in higher plants are spatially separated within these two compartments. PSI and ATP synthase are predominately located in the stroma lamellae while active PS II is present in abundance within the grana (Andersson and Anderson, 1980; Barber, 1980, 1982), with Cyt $b_{6}f$ complex found in both (Albertsson, 1995). However this is a rather static picture of a highly dynamic membrane system. During chloroplast maturation, for example, extensive cubic phase lipid membrane networks observed in etioplasts are converted to the intricate lamellar membrane systems of the grana and stroma lamellae. This process is accompanied by protein synthesis, insertion and segregation to arrive at the mature protein distributions described above. Even in the mature system specific outer light-harvesting antenna Lhcb proteins shuttle between PS II in the grana and PS I in the stroma to optimize electron transport through the two photosystems (Kruse, 2001). Furthermore, the D1 exchange process is reported to involve extensive migration of damaged and repaired CP47-RC subcomplexes between the grana and the stroma lamellae (Zhang and Aro, 2002; Barbato et al., 1992). To develop a picture of the dynamics of PS II and its antenna system in vivo, this section focuses on EM studies of PS II and its antenna system within the native thylakoid membrane.

A. Freeze-Etch and Freeze-Fracture Techniques

Freeze-etch and freeze-fracture microscopy are well suited for imaging the surfaces of membranes and their embedded components. In the freeze-etch process, excess surface water is evaporated from flash frozen membranes under vacuum (typically –100 °C), to reveal the surface contours of the embedded membrane proteins. Subsequent platinum shadowing can further enhance visualization. In contrast, the freeze-fracture process is used to study the structure of membrane embedded components of native membranes. To achieve this, flash frozen thylakoid membranes are cleaved along the internal hydrophobic plane of a bilayer prior to imaging. In such a manner, the thylakoid membrane ultrastructure has been studied extensively for a large number of organisms, including barley, spinach, maize, lettuce, soy bean, *Portulaca*, *Alocasia* and pea (Hankamer et al., 1997a).

A number of reviews in the literature have remarked upon similarities in membrane protein distribution (Miller, 1981; Albertsson, 1995; Hankamer et al., 1997a). In each case a range of membrane protein complexes differing in size and shape were detected and named according to the surfaces in which they were located, as defined by freeze-etch terminology developed by Staehelin (Staehelin, 1976, 1986). Here ESs, PSs, ESu or PSu refer to the endoplasmic (E) and protoplasmic (P) surfaces (S) of stacked (s) and unstacked (u) freeze-etched thylakoid membranes. The corresponding freeze-fracture (F) planes are

referred to as EFs, PFs, EFu and PFu. The constituent components of these particles were in many cases identified by the analysis of mutant membranes. For example, comparison of PSI deficient mutant thylakoid membranes showed that this photosystem formed part of the large PFu particles. Localization of complexes in the stacked and unstacked thylakoid membranes was further facilitated by antibody labeling (Olive and Vallon, 1991).

B. Localization in the Thylakoid Membrane

Through the use of freeze-etch and freeze-fracture techniques, comparative studies of wild type and PS II deficient mutants of tobacco have shown that the thylakoid membranes of the latter to be depleted of ESs and EFs particles, normally located in the grana (Miller and Cushman, 1978). From these results it was concluded that such ESs/EFs particles correspond to the extrinsic and internal parts of PS II respectively. Support for this conclusion came from parallel studies of PS II deficient barley mutants (*xantha*-b12, *viridis*-c12, *viridis*-e64 and *viridis*-zd69), whose granal membranes were also greatly depleted of EFs particles (Simpson, 1978; Staehelin, 1986). The antenna proteins were located using Lhcb protein deficient mutants (e.g. barley mutants *xantha*-l35 and *viridis*-k23 and *chlorina*-f2) and by comparing thylakoid membranes from light and dark grown plants, the latter being depleted in these antenna proteins (Miller et al., 1976; Armond and Arntzen, 1977; Simpson et al., 1978; Simpson, 1979). Freeze-etch images of Lhcb protein depleted membranes also showed the ESs particles to be smaller. Together these results suggested that the PFs particles contained the Lhcb antenna proteins and that they were closely associated with PS II (EFs and ESs) particles in native membranes.

The close association of PS II and Lhcb proteins was characterized in more detail by the analysis of 2D crystalline arrays of ESs complexes (Miller, 1981; Seibert et al., 1987; Simpson, 1979). An image of such an array (Fig. 7) shows a section of the freeze-etch surface (ESs surface) and a part of the protoplasmic fracture face (PFs surface). The Lhcb proteins (PFs particles in the PFs fracture face) have been shown to fit in register into the grooves between the PS II complexes (ESs particles in the freeze-etched ESs surface) thereby providing strong evidence for the existence of supercomplexes of PS II and its light-harvesting antenna system (Hankamer et al., 1997b).

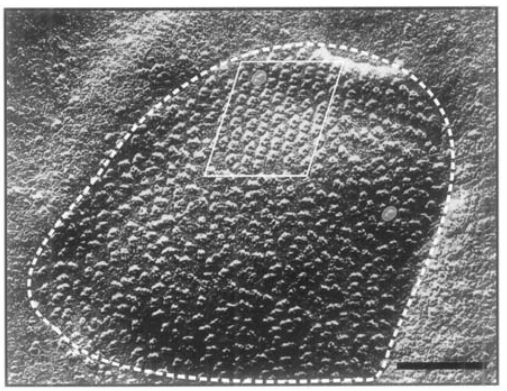

Fig. 7. A lumenal surface of stacked spinach thylakoids revealed by freeze-etching, delineated by a white dashed line, showing the ESs particles attributed to PS II (Seibert et al., 1987). Prior to freeze-etching, the preparation was biochemically washed to remove the OEC extrinsic proteins, which revealed each particle, typically 20 nm in length, to have underlying dimeric features as emphasized here by 2 gray circles. A native 2D array is also shown within a solid white line. Bar represents 100 nm.

C. Heterogeneity—2D Arrays and Randomly Oriented Supercomplexes

The ESs and EFs particles, which contain PS II, are not evenly distributed within the thylakoid membrane. Freeze-etch and freeze-fracture studies have shown that ESs and EFs particles respectively, can be organized into 2D arrays (see Fig. 7) or be more randomly dispersed within the grana. PS II-like particles are also observed in the stroma lamellae. It has been calculated that 85% of PS II particles are located in the granal stacks, which are often referred to as PS IIα. The remaining 15% of PS II complexes are located in the stroma and are termed PS IIβ (Albertsson, 1995; Andersson and Anderson, 1980). PS IIα complexes have approximately twice the antenna size of the PS IIβ complexes (Anderson and Melis, 1983) and are more efficient at reducing ferricyanide and duroquinone (Henrysson and Sundby, 1990). The PS IIα complexes are also more abundant and active than PS IIβ and have yielded most of the available structural data.

The PS IIα population in the grana can itself be divided into subpopulations of differing antenna size (Albertsson et al., 1990) which is consistent with the recent work of Boekema and colleagues (Boekema et al., 1999a,b). Interestingly, freeze-etch studies have shown that some ESs particles within the grana form

2D arrays, while others are more randomly dispersed, forming at least two sub-populations (Simpson, 1979; Seibert et al., 1987). Several publications provide the dimensions of arrayed ESs particles. Wild type ESs arrays in barley are reported to have unit cell dimensions of 175 × 247 Å, 180 × 225 Å and 180 × 240 Å (Seibert et al., 1987), while those of desaturase mutants of *Arabidopsis thaliana* are 190 × 230 Å and 180 × 230 Å (Tsvetkova et al., 1995). More recently, (Boekema et al., 2000a) identified two different lattice types in ordered 2D arrays of LHCII-PS II complexes isolated from spinach thylakoids by mild detergent solubilization. Two types of arrays appeared to reflect the in vivo organization of PS II and its antenna. These were identified to have row spacings of 263 Å and 230 Å respectively. The small-spaced crystals were reported to be less common but more highly ordered. (Boekema et al., 2000) developed a nomenclature in which the PS II core (C), strongly (S), medium (M) and loosely (L) bound LHCII are denoted by the letters in brackets. The crystals with row spacings of 230 Å appear to correspond with the C_2S_2 LHCII-PS II complexes first reported in (Boekema et al., 1995) and which consist of a central core dimer flanked by two sets of strongly bound LHCII (Nield et al., 2000c). The more widely spaced crystalline arrays appear to contain C_2S_2M LHCII-PS II complexes which in addition to the C_2S_2 components appear to bind an additional LHCII trimer and CP24 (Lhcb6) subunit.

The abundance of 2D arrays of LHCII-PS II complexes in native membranes of higher plants suggests that they play an important functional role in vivo. As the complexes in these arrays are in close contact with one another, it is quite possible that the pigments that they bind are able to form an excitonically coupled network within the bilayer plane. The observation that a large number of the Chl molecules in LHCII and PS II are located towards the surface of the membrane-spanning domain and that 2D arrays of LHCII-PS II complex in adjacent granal membranes appear able to interlock structurally, opens up the possibility that these ordered macromolecular assemblies could transfer energy between adjacent membranes and therefore act as 3D excitonically coupled systems.

Under high light conditions PS II is susceptible to photodamage, which ultimately requires the D1 protein to be exchanged (Barber and Andersson, 1992). By excitonically coupling the antenna and reaction centers of PS II in this way, excess excitation energy at one point could be dissipated throughout the network and ultimately passed on to one of the non-excited reaction centers, thereby providing a greater degree of photoprotection than that afforded to non-arrayed complexes.

The unit cell dimensions of typical 2D arrays of LHCII-PS II supercomplexes are only large enough to accommodate approximately 100–140 Chl molecules per reaction center (Hankamer et al., 1997b), although it is estimated that the Chl:RC ratio in the grana membrane is about 250:1 (Lam et al., 1983). The additional Chls, which are probably associated with LHCII, must be accounted for. In this context it should be noted that the ratio of 250:1 is an average value and that the freeze etch images of (Seibert et al., 1987) clearly show that the grana contain a large proportion of non arrayed ESs particles. It is quite possible therefore that the non-arrayed PS II particles are associated with much larger antenna systems, or that a substantial pool of LHCII not associated with PS II exists in these parts of the grana, thus accounting for an overall average of ~250 Chl:RC. One possibility is that non-arrayed ESs particles with large antenna systems may be adapted to exciton trapping under low light conditions, with the arrayed particles providing a degree of photoprotection under high light conditions through a coupled Chl network. This general idea is supported by the fact that PS II complexes binding Lhcb1-6 can be isolated from detergent-solubilized PS II enriched granal membranes by sucrose density gradient centrifugation (Hankamer et al., 1997b). The non-arrayed ESs particles may also include a proportion of PS II subcomplexes containing damaged D1 which are in the processes of migrating to and from the stromal lamellae during the D1 repair cycle (Barbato et al., 1992; Zhang and Aro, 2002).

V. Future Prospects and Concluding Remarks

Although as yet there are no high-resolution X-ray structures of PS II from higher plants or green algae, this information will ultimately materialize. However, it will still be necessary to understand the structural information obtained in terms of PS II function within the thylakoid membrane and establish how the Chl *a/b* light harvesting systems couple to the PS II reaction center core and how, indeed, adjacent PS II megacomplexes associate with each other. All this will need to be understood against a backdrop

of PS II dynamics, including structural changes that occur during biogenesis, D1 turnover, state transitions, non-photochemical quenching and adaptation to different environmental conditions such as light intensities. Electron cryo-tomography, coupled with even higher resolution electron microscopy, as well as X-ray crystallography, will be able to address these challenges. The continuing efforts to obtain a higher resolution 3D structure of the LHCII-PS II supercomplex using single particle analysis and electron crystallography are a step towards the ultimate goal of describing not only how PS II of plants and green algae oxidize water, but also how they regulate this key reaction over a range of different environmental conditions.

Acknowledgments

We wish to thank the Biotechnology and Biological Sciences Research Council (BBSRC) for financial support. JN also acknowledges the Royal Society for supporting him as a University Research Fellow.

References

Adir N (1999) Crystallization of the oxygen-evolving reaction centre of Photosystem II in nine different detergent mixtures. Acta Crystallogr D Biol Crystallogr 55 (Pt 4): 891–894

Adir N, Dobrovetsky Y and Lerner N (2001) Structure of c-phycocyanin from the thermophilic cyanobacterium *Synechococcus vulcanus* at 2.5 Å: Structural implications for thermal stability in phycobilisome assembly. J Mol Biol 313: 71–81

Albertsson PA (1995) The structure and function of the chloroplast photosynthetic membrane — a model for the domain organization. Photosynth Res 46: 141–149

Albertsson PA, Yu SG and Larsson UK (1990) Heterogeneity in Photosystem II. Evidence from fluorescence and gel electrophoresis experiments. Biochim Biophys Acta 1016: 137–140

Anderson JM and Melis A (1983) Localization of different photosystems in separate regions of chloroplast membranes. Proc Natl Acad Sci USA 80: 745–749

Andersson B and Anderson JM (1980) Lateral heterogeneity in the distribution of chlorophyll-protein complexes of the thylakoid membranes of spinach chloroplasts. Biochim Biophys Acta 593: 427–440

Armond P, A. and Arntzen CJ (1977) Localization and characterization of PS II in grana and stroma lamellae. Plant Physiol 59: 398–404

Auer M, Scarborough GA and Kühlbrandt W (1999) Surface crystallisation of the plasma membrane H^+-ATPase on a carbon support film for electron crystallography. J Mol Biol 287: 961–968

Barbato R, Friso G, Rigoni F, Dalla Vecchia F and Giacometti GM (1992) Structural changes and lateral redistribution of Photosystem II during donor side photoinhibition of thylakoids. J Cell Biol 119: 325–335

Barber J (1980) An explanation for the relationship between salt-induced thylakoid stacking and the fluorescence changes associated with changes in spill-over energy from Photosystem II to Photosystem I. FEBS Lett 118: 1–10

Barber J (1982) Influence of surface charges on thylakoid structure and function. Ann Rev Plant Physiol 33: 261–295

Barber J (2003) Photosystem II: the engine of life. Q Rev Biophys 36: 71–89

Barber J and Andersson B (1992) Too much of a good thing: Light can be bad for photosynthesis. Trends Biochem Sci 17: 61–66

Barber J, Nield J, Morris EP, Zheleva D and Hankamer B (1997) The structure, function and dynamics of Photosystem two. Physiologia Plantarum 100: 817–827

Baumeister W, Grimm R and Walz J (1999) Electron tomography of molecules and cells. Trends Cell Biol 9: 81–85

Bibby TS, Mary I, Nield J, Partensky F and Barber J (2003a) Low-light-adapted *Prochlorococcus* species possess specific antennae for each photosystem. Nature 424: 1051–1054

Bibby TS, Nield J, Chen M, Larkum AW and Barber J (2003b) Structure of a Photosystem II supercomplex isolated from *Prochloron didemni* retaining its chlorophyll *a/b* light-harvesting system. Proc Natl Acad Sci USA 100: 9050–9054

Boekema EJ, Hankamer B, Bald D, Kruip J, Nield J, Boonstra AF, Barber J and Rögner M (1995) Supramolecular structure of the Photosystem II complex from green plants and cyanobacteria. Proc Natl Acad Sci USA 92: 175–179

Boekema EJ, van Roon H, Calkoen F, Bassi R and Dekker JP (1999a) Multiple types of association of Photosystem II and its light-harvesting antenna in partially solubilized Photosystem II membranes. Biochemistry 38: 2233–2239

Boekema EJ, Van Roon H, Van Breemen JF and Dekker JP (1999b) Supramolecular organization of Photosystem II and its light-harvesting antenna in partially solubilized Photosystem II membranes. Eur J Biochem 266: 444–452

Boekema EJ, van Breemen JF, van Roon H and Dekker JP (2000a) Arrangement of Photosystem II supercomplexes in crystalline macrodomains within the thylakoid membrane of green plant chloroplasts. J Mol Biol 301: 1123–1133

Boekema EJ, van Breemen JF, van Roon H and Dekker JP (2000b) Conformational changes in Photosystem II supercomplexes upon removal of extrinsic subunits. Biochemistry 39: 12907–12915

Böttcher B, Wynne SA and Crowther RA (1997) Determination of the fold of the core protein of hepatitis B virus by electron cryomicroscopy. Nature 386: 88–91

Brejc K, Ficner R, Huber R and Steinbacher S (1995) Isolation, crystallization, crystal structure analysis and refinement of allophycocyanin from the cyanobacterium *Spirulina platensis* at 2.3 Å resolution. J Mol Biol 249: 424–440

Büchel C, Morris E, Orlova E and Barber J (2001) Localisation of the PsbH subunit in Photosystem II: A new approach using labelling of His-tags with a $Ni^{(2+)}$-NTA gold cluster and single particle analysis. J Mol Biol 312: 371–379

Chen S, Roseman AM and Saibil HR (1998) Electron microscopy of chaperonins. Methods Enzymol 290: 242–253

Chiu W, McGough A, Sherman MB and Schmid MF (1999) High-resolution electron cryomicroscopy of macromolecular assemblies. Trends Cell Biol 9: 154–159

da Fonseca P, Morris EP, Hankamer B and Barber J (2002) Electron crystallographic study of Photosystem II of the cyanobacterium *Synechococcus elongatus*. Biochemistry 41: 5163–5167

De Las Rivas J, Balsera M and Barber J (2004) Evolution of oxygenic photosynthesis: Genome-wide analysis of the OEC extrinsic proteins. Trends Plant Sci 9: 18–25

Deisenhofer J, Epp O, Miki K, Huber R and Michel H (1984) X-ray structure analysis of a membrane protein complex. Electron density map at 3 Å resolution and a model of the chromophores of the photosynthetic reaction center from *Rhodopseudomonas viridis*. J Mol Biol 180: 385–398

Deng Y, Marko M, Buttle KF, Leith A, Mieczkowski M and Mannella CA (1999) Cubic membrane structure in amoeba (*Chaos carolinensis*) mitochondria determined by electron microscopic tomography. J Struct Biol 127: 231–239

DeRosier DJ and Klug A (1968) Reconstruction of three dimensional structures from electron micrographs. Nature 217: 130–134

Diner BA and Babcock GT (1996) Structure, Dynamics and Energy Conversion Efficiency in Photosystem II. In: Ort DR and Yocum CF (eds) Oxygenic Photosynthesis: The Light Reactions, pp 213–247. Kluwer Academic, Dordrecht

Dube P, Tavares P, Lurz R and van Heel M (1993) The portal protein of bacteriophage SPP1: A DNA pump with 13-fold symmetry. EMBO J 12: 1303–1309

Dubochet J, Adrian M, Chang JJ, Homo JC, Lepault J, McDowall AW and Schultz P (1988) Cryo-electron microscopy of vitrified specimens. Q Rev Biophys 21: 129–228

Ducret A, Muller SA, Goldie KN, Hefti A, Sidler WA, Zuber H and Engel A (1998) Reconstitution, characterisation and mass analysis of the pentacylindrical allophycocyanin core complex from the cyanobacterium *Anabaena* sp. PCC 7120. J Mol Biol 278: 369–388

Ferreira KN, Iverson TM, Maghlaoui K, Barber J and Iwata S (2004) Architecture of the photosynthetic oxygen-evolving coneter. Science 303: 1831–1838

Fotinou C, Kokkinidis M, Fritzsch G, Haase W, Michel H and Ghanotakis DF (1993) Characterization of a Photosystem-II core and its 3-D crystals. Photosynth Res 37: 41–48

Frank J (1980) The role of correlation techniques in computer image processing. In: Hawkes PW, Computer Processing of Electron Microscope Images, 187–222. Springer, Berlin

Fujiyoshi Y (1998) The structural study of membrane proteins by electron crystallography. Adv Biophys 35: 25–80

Green BR and Durnford DG (1996) The chlorophyll-carotenoid proteins of oxygenic photosynthesis. Ann Rev Plant Physiol 47: 685–714

Hankamer B, Barber J and Boekema EJ (1997a) Structure and Membrane Organization of Photosystem II From Green Plants. Annu Rev Plant Physiol Plant Molec Biol 48: 641–672

Hankamer B, Nield J, Zheleva D, Boekema E, Jansson S and Barber J (1997b) Isolation and biochemical characterisation of monomeric and dimeric Photosystem II complexes from spinach and their relevance to the organisation of Photosystem II in vivo. Eur J Biochem 243: 422–429

Hankamer B, Morris EP and Barber J (1999) Revealing the structure of the oxygen-evolving core dimer of Photosystem II by cryoelectron crystallography. Nat Struct Biol 6: 560–564

Hankamer B, Morris E, Nield J, Carne A and Barber J (2001a) Subunit positioning and transmembrane helix organisation in the core dimer of Photosystem II. FEBS Lett 504: 142–151

Hankamer B, Morris E, Nield J, Gerle C and Barber J (2001b) Three-dimensional structure of the Photosystem II core dimer of higher plants determined by electron microscopy. J Struct Biol 135: 262–269

Harauz G, Boekema E and van Heel M (1988) Statistical image analysis of electron micrographs of ribosomal subunits. Methods Enzymol 164: 35–49

Harrer R (2003) Associations between light-harvesting complexes and Photosystem II from *Marchantia polymorpha L.* determined by two- and three-dimensional electron microscopy. Photosynth Res 75: 249–258

Hasler L, Heymann JB, Engel A, Kistler J and Walz T (1998) 2D crystallization of membrane proteins: Rationales and examples. J Struct Biol 121: 162–171

Henderson R (1995) The potential and limitations of neutrons, electrons and X-rays for atomic resolution microscopy of unstained biological molecules. Q Rev Biophys 28: 171–193

Henderson R (2004) Realizing the potential of electron cryomicroscopy. Q Rev Biophys 33: 3–13

Henderson R, Baldwin JM, Downing KH, Lepault J and Zemlin F (1986) Structure of the purple membrane from *Halobacterium halobium* — recording, measurement and evaluation of electron micrographs at 3.5 Å resolution. Ultramicroscopy 19: 147–178

Henderson R, Baldwin JM, Ceska TA, Zemlin F, Beckmann E and Downing KH (1990) Model for the structure of bacteriorhodopsin based on high-resolution electron cryo-microscopy. J Mol Biol 213: 899–929

Henrysson T and Sundby C (1990) Characterisation of Photosystem II in stroma thylakoid membranes. Photosynth Res 25:

Hoenger A and Aebi U (1996) 3-D Reconstructions from ice-embedded and negatively stained biomacromolecular assemblies: A critical comparison. J Struct Biol 117: 99–116

Irrgang KD, Shi LX, Funk C and Schroder WP (1995) A nuclear-encoded subunit of the Photosystem II reaction center. J Biol Chem 270: 17588–17593

Jordan P, Fromme P, Witt HT, Klukas O, Saenger W and Krauss N (2001) Three-dimensional structure of cyanobacterial Photosystem I at 2.5 Å resolution. Nature 411: 909–917

Kamiya N and Shen JR (2003) Crystal structure of oxygen-evolving Photosystem II from *Thermosynechococcus vulcanus* at 3.7-Å resolution. Proc Natl Acad Sci USA 100: 98–103

Kargul J, Nield J and Barber J (2003) Three-dimensional reconstruction of a light-harvesting complex I-Photosystem I (LHCI-PS I) supercomplex from the green alga *Chlamydomonas reinhardtii*. J Biol Chem 278: 16135–16141

Kiselev NA, Sherman MB and Tsuprun VL (1990) Negative staining of proteins. Electron Microsc Rev 3: 43–72

Kruse O (2001) Light-induced short-term adaptation mechanisms under redox control in the PS II-LHCII supercomplex: LHC II state transitions and PS II repair cycle. Naturwissenschaften 88: 284–292

Kühlbrandt W (1992) Two-dimensional crystallization of membrane proteins. Q Rev Biophys 25: 1–49

Kühlbrandt W, Wang DN and Fujiyoshi Y (1994) Atomic model of plant light-harvesting complex by electron crystallography. Nature 367: 614–621

Kunji ER, von Gronau S, Oesterhelt D and Henderson R (2000) The three-dimensional structure of halorhodopsin to 5 Å by electron crystallography: A new unbending procedure for two-dimensional crystals by using a global reference structure. Proc

Natl Acad Sci USA 97: 4637–4642
Lam E, Baltimore B, Ortiz W, Chollar S, Melis A and Malkin R (1983) Characterization of a resolved oxygen-evolving photosystem-II preparation from spinach thylakoids. Biochim Biophys Acta 724: 201–211
Lebeau L, Lach F, Venien-Bryan C, Renault A, Dietrich J, Jahn T, Palmgren MG, Kühlbrandt W and Mioskowski C (2001) Two-dimensional crystallization of a membrane protein on a detergent-resistant lipid monolayer. J Mol Biol 308: 639–647
Levy D, Mosser G, Lambert O, Moeck GS, Bald D and Rigaud JL (1999) Two-dimensional crystallization on lipid layer: A successful approach for membrane proteins. J Struct Biol 127: 44–52
Liu Z, Yan H, Wang K, Kuang TY, Zhang J, Gul L, An X and Chang WR (2004) Crystal structure of spinach major light-harvesting complex at 2.72 Å resolution. Nature 428: 728–292
Mannella CA, Buttle K, Rath BK and Marko M (1998) Electron microscopic tomography of rat-liver mitochondria and their interaction with the endoplasmic reticulum. Biofactors 8: 225–228
Matadeen R, Patwardhan A, Gowen B, Orlova EV, Pape T, Cuff M, Mueller F, Brimacombe R and van Heel M (1999) The *Escherichia coli* large ribosomal subunit at 7.5 Å resolution. Structure Fold Des 7: 1575–1583
Miller K, R. (1981) Freeze-etching studies of photosynthetic membranes. In: Griffith JD (ed) Electron Microscopy in Biology, Vol 1, pp 1–30. Wiley-Interscience, New York
Miller KR, Miller GJ and McIntyre KR (1976) The light-harvesting chlorophyll-protein complex of Photosystem II. Its location in the photosynthetic membrane. J Cell Biol 71: 624–638
Miller KR and Cushman RA (1978) A chloroplast membrane lacking Photosystem II. Biochim Biophys Acta 546: 481–499
Mitsuoka K, Hirai T, Murata K, Miyazawa A, Kidera A, Kimura Y and Fujiyoshi Y (1999) The structure of bacteriorhodopsin at 3.0 Å resolution based on electron crystallography: Implication of the charge distribution. J Mol Biol 286: 861–882
Miyazawa A, Fujiyoshi Y, Stowell M and Unwin N (1999) Nicotinic acetylcholine receptor at 4.6 Å resolution: Transverse tunnels in the channel wall. J Mol Biol 288: 765–786
Miyazawa A, Fujiyoshi Y and Unwin N (2003) Structure and gating mechanism of the acetylcholine receptor pore. Nature 424: 949–955
Morris EP, Hankamer B, Zheleva D, Friso G and Barber J (1997) The three-dimensional structure of a Photosystem II core complex determined by electron crystallography. Structure 5: 837–849
Morschel EF and Schatz GH (1987) Correlation of Photosystem II complexes with exoplasmic freeze-fracture particles of cyanobacterium *Synechococcus* sp. Planta 172: 145–154
Murata K, Mitsuoka K, Hirai T, Walz T, Agre P, Heymann JB, Engel A and Fujiyoshi Y (2000) Structural determinants of water permeation through aquaporin-1. Nature 407: 599–605
Nicastro D, Frangakis AS, Typke D and Baumeister W (2000) Cryo-electron tomography of neurospora mitochondria. J Struct Biol 129: 48–56
Nield J, Funk C and Barber J (2000a) Supermolecular structure of Photosystem II and location of the PsbS protein. Philos Trans R Soc Lond B Biol Sci 355: 1337–1344
Nield J, Kruse O, Ruprecht J, da Fonseca P, Büchel C and Barber J (2000b) Three-dimensional structure of *Chlamydomonas reinhardtii* and *Synechococcus elongatus* Photosystem II complexes allows for comparison of their oxygen-evolving complex organization. J Biol Chem 275: 27940–27946
Nield J, Orlova EV, Morris EP, Gowen B, van Heel M and Barber J (2000c) 3D map of the plant Photosystem II supercomplex obtained by cryoelectron microscopy and single particle analysis. Nat Struct Biol 7: 44–47
Nield J, Balsera M, De Las Rivas J and Barber J (2002) Three-dimensional electron cryo-microscopy study of the extrinsic domains of the oxygen-evolving complex of spinach: Assignment of the PsbO protein. J Biol Chem 277: 15006–15012
Nield J, Rizkallah PJ, Barber J and Chayen NE (2003) The 1.45A three-dimensional structure of C-phycocyanin from the thermophilic cyanobacterium *Synechococcus elongatus*. J Struct Biol 141: 149–155
Nogales E, Wolf SG and Downing KH (1998) Structure of the alpha beta tubulin dimer by electron crystallography. Nature 391: 199–203
Olive J and Vallon O (1991) Structural organization of the thylakoid membrane: Freeze-fracture and immunocytochemical analysis. J Electron Microsc Tech 18: 360–374
Orlova EV (2000) Structural analysis of non-crystalline macromolecules: The ribosome. Acta Crystallogr D Biol Crystallogr 56 (Pt 10): 1253–1258
Orlova EV, Dube P, Harris JR, Beckman E, Zemlin F, Markl J and van Heel M (1997) Structure of keyhole limpet hemocyanin type 1 (KLH1) at 15 Å resolution by electron cryomicroscopy and angular reconstitution. J Mol Biol 271: 417–437
Perkins G, Renken C, Martone ME, Young SJ, Ellisman M and Frey T (1997) Electron tomography of neuronal mitochondria: Three-dimensional structure and organization of cristae and membrane contacts. J Struct Biol 119: 260–272
Perkins GA, Song JY, Tarsa L, Deerinck TJ, Ellisman MH and Frey TG (1998) Electron tomography of mitochondria from brown adipocytes reveals crista junctions. J Bioenerg Biomembr 30: 431–442
Radermacher M (1988) Three-dimensional reconstruction of single particles from random and nonrandom tilt series. J Electron Microsc Tech 9: 359–394
Reimer L (1997) Transmission Electron Microscopy: Physics of Image Formation and Microanalysis, Fourth edition. Springer Series in Optical Sciences, Vol 36. Springer, Berlin
Rhee KH (2001) Photosystem II: The solid structural era. Annu Rev Biophys Biomol Struct 30: 307–328
Rhee KH, Morris EP, Barber J and Kühlbrandt W (1998) Three-dimensional structure of the plant Photosystem II reaction centre at 8 Å resolution. Nature 396: 283–286
Ruprecht J and Nield J (2001) Determining the structure of biological macromolecules by transmission electron microscopy, single particle analysis and 3D reconstruction. Prog Biophys Mol Biol 75: 121–164
Saibil HR (2000a) Macromolecular structure determination by cryo-electron microscopy. Acta Crystallogr D Biol Crystallogr 56 (Pt 10): 1215–1222
Saibil HR (2000b) Conformational changes studied by cryo-electron microscopy. Nat Struct Biol 7: 711–714
Schatz M, Orlova EV, Dube P, Jager J and van Heel M (1995) Structure of *Lumbricus terrestris* hemoglobin at 30 Å resolution determined using angular reconstitution. J Struct Biol 114: 28–40
Schmidt-Krey I, Mitsuoka K, Hirai T, Murata K, Cheng Y, Fujiyoshi Y, Morgenstern R and Hebert H (2000) The three-

dimensional map of microsomal glutathione transferase 1 at 6 Å resolution. EMBO J 19: 6311–6316

Seibert M, DeWit M and Staehelin LA (1987) Structural localization of the O_2-evolving apparatus to multimeric (tetrameric) particles on the lumenal surface of freeze-etched photosynthetic membranes. J Cell Biol 105: 2257–2265

Sherman MB, Soejima T, Chiu W and van Heel M (1998) Multivariate analysis of single unit cells in electron crystallography. Ultramicroscopy 74: 179–199

Shi LX, Kim SJ, Marchant A, Robinson C and Schroder WP (1999) Characterisation of the PsbX protein from Photosystem II and light regulation of its gene expression in higher plants. Plant Mol Biol 40: 737–744

Simpson DJ (1978) Freeze-fracture studies on barley plastid membranes II. Wild-type chloroplast. Carlsberg Res Commun 43: 365–389

Simpson DJ (1979) Freeze-fracture studies on barley plastid membranes. III. Location of the light harvesting chlorophyll-protein. Carlsberg Res Commun 44: 305–336

Simpson DJ, Lindberg Moller B and Hoyer-Hansen G (1978) Freeze-fracture structure and polypeptide composition of thylakoids of wild type and mutant barley plastids. In: Akoyunoglou G ed) Chloroplast Development, pp 507–512. Elsevier/North-Holland Biomedical Press, Amsterdam

Staehelin LA (1976) Reversible particle movements associated with unstacking and restacking of chloroplast membranes in vitro. J Cell Biol 71: 136–158

Staehelin LA (1986) Chloroplast structure and supramolecular organization of photosynthetic membranes. In: Staehelin LA (ed) Photosynthesis III, Photosynthetic Membranes and Light Harvesting Systems, pp 1–84. Springer, Berlin

Stahlberg H, Braun T, de Groot B, Philippsen A, Borgnia MJ, Agre P, Kühlbrandt W and Engel A (2000) The 6.9-Å structure of GlpF: A basis for homology modeling of the glycerol channel from *Escherichia coli*. J Struct Biol 132: 133–141

Stowell MH, Miyazawa A and Unwin N (1998) Macromolecular structure determination by electron microscopy: New advances and recent results. Curr Opin Struct Biol 8: 595–600

Swiatek M, Kuras R, Sokolenko A, Higgs D, Olive J, Cinque G, Muller B, Eichacker LA, Stern DB, Bassi R, Herrmann RG and Wollman FA (2001) The chloroplast gene *ycf9* encodes a Photosystem II (PS II) core subunit, PsbZ, that participates in PS II supramolecular architecture. Plant Cell 13: 1347–1367

Tomo T, Enami I and Satoh K (1993) Orientation and nearest neighbor analysis of psbI gene product in the Photosystem II reaction center complex using bifunctional cross-linkers. FEBS Lett 323: 15–18

Tsvetkova NM, Apostolova EL, Brain APR, Williams WP and Quinn PJ (1995) Factors influencing PS II particle array formation in *Arabidopsis thaliana* chloroplasts and the relationship of such arrays to the thermostability of PS II. Biochim Biophys Acta 1228: 201–210

van Heel M (1986) Resolution criteria for three dimensional reconstruction. Optik 73: 119–122

van Heel M and Stoffler-Meilicke M (1985) Characteristic views of *E. coli* and *B. stearothermophilus* 30S ribosomal subunits in the electron microscope. EMBO J 4: 2389–2395

van Heel M (1987) Angular reconstitution: A posteriori assignment of projection directions for 3D reconstruction. Ultramicroscopy 21: 111–124

van Heel M, Schatz M and Orlova E (1992) Correlation functions revisited. Ultramicroscopy 46: 307–316

van Heel M, Gowen B, Matadeen R, Orlova EV, Finn R, Pape T, Cohen D, Stark H, Schmidt R, Schatz M and Patwardhan A (2000) Single-particle electron cryo-microscopy: Towards atomic resolution. Q Rev Biophys 33: 307–369

Vonck J (2000) Parameters affecting specimen flatness of two-dimensional crystals for electron crystallography. Ultramicroscopy 85: 123–129

Webber AN, Packman LC, Chapman DJ, Barber J and Gray JC (1989) The 5th chloroplast-encoded polypeptide is present in the photosystem-II reaction center complex. FEBS Lett 242: 259–262

Williams KA (2000) Three-dimensional structure of the ion-coupled transport protein NhaA. Nature 403: 112–115

Xu C, Rice WJ, He W and Stokes DL (2002) A structural model for the catalytic cycle of Ca(2+)-ATPase. J Mol Biol 316: 201–211

Zhang L and Aro E (2002) Synthesis, membrane insertion and assembly of the chloroplast-encoded polypeptide is present in the photosystem-II reaction center complex. FEBS Lett 512: 13–18

Zheleva D, Sharma J, Panico M, Morris HR and Barber J (1998) Isolation and characterization of monomeric and dimeric CP47-reaction center Photosystem II complexes. J Biol Chem 273: 16122–16127

Zouni A, Witt HT, Kern J, Fromme P, Krauss N, Saenger W and Orth P (2001) Crystal structure of Photosystem II from *Synechococcus elongatus* at 3.8 Ångstrom resolution. Nature 739–743

Chapter 19

Photosystem II: Structural Elements, the First 3D Crystal Structure and Functional Implications

Horst T. Witt*
Max-Volmer-Laboratorium für Biophysikalische Chemie und Biochemie, Technische Universität Berlin, Strasse des 17. Juni 135, D-10623 Berlin, Germany

Summary

In the first part of this chapter structural elements of Photosystem II (PS II) and their functional behavior which have been elucidated primarily through special spectroscopic techniques are described. A transmembrane charge separation was identified as the primary act of light-energy conversion. The chlorophyll-containing P680 complex was discovered as the electron donor of PS II at the lumenal side of the membrane while the bound plastoquinone Q_A was discovered as the first stable electron acceptor and localized at the stromal side of the membrane. This membrane-spanning chlorophyll/quinone couple represents the PS II reaction center (RC)

*Author for correspondence, email: horst.witt@tu-berlin.de

T. Wydrzynski and K. Satoh (eds): Photosystem II: The Light-Driven Water:Plastoquinone Oxidoreductase, pp. 425–447.

that drives water oxidation. This couple also provides a model for the RC of Photosystem I (PS I) and of other photosystems which drive different redox reactions. Two intermediate chlorin molecules located between the chlorophyll/quinone couple were found to function in the path of fast electron transfer from P680 across the membrane to Q_A while a pool of plastoquinones was found to function in a transmembrane path for electrons from reduced Q_A to PS I and for protons from the stroma to the membrane lumen. Primary electron donors located at the membrane base of PS II and PS I were found to be organized as chlorophyll pairs. Electron microscopy identified PS II as a dimer and PS I as a trimer. Based on the sequence homologies between PS II, PS I and the bacterial RC, predictions were made on the helical structure of the PS II complex. The preceding results served as the essential basis for the analysis and interpretation of the 3D crystal structures of PS I and PS II. In the second part of this chapter, the first PS II crystals capable of water oxidation are described. Based on the X-ray structure analysis of these crystals at 3.6 – 3.8 Å resolution, the framework of PS II, the architecture of the antenna system, the electron transfer chain, and the manganese cluster are discussed. The manganese environment is considered in terms of the more recent structure at 3.2 Å resolution. In the third part, functional events are described, especially changes in manganese valences, deprotonations, and the water states which were followed spectroscopically during the quaternary cycling of the water-oxidizing complex and which are summarized in a functional model. Finally, the implication of the high oxidation potential of the PS II RC is discussed as well as the functional cooperation between the dimeric electron donor P680, the monomeric electron donor chlorophyll D1 and the pheophytin D1 within the electron transfer chain.

I. Introduction

The very basis of life on our planet is oxygenic photosynthesis, which absorbs light energy of the sun and converts it into biochemical energy that is used to release oxygen from water into the biosphere. This process is driven by the cooperation of two different light-activated, pigment/protein complexes, Photosystem I (PS I) and Photosystem II (PS II), working in series within the functional membranes of plants, algae and cyanobacteria. In PS II the oxidation of water results in the release of O_2, protons and electrons. The electrons are trapped by a specially bound plastoquinone Q_A forming the first stable reductant. Subsequently, the electrons from PS II are transferred via intermediates energetically further up to a state sufficient to reduce $NADP^+$ to NADPH in PS I. This process is coupled with the formation of a proton gradient across the membrane that drives the formation of ATP. With NADPH and ATP, absorbed CO_2 is reduced to energy-rich carbohydrates.

The reactive components of this 'light driven engine of life' are present in relatively low concentrations; changes during their reaction, e.g., followed optically, are mostly very short-lived and buried in noise. A major breakthrough was made in the 1960s with the introduction of *repetitive* light-pulse spectroscopy (Witt, 1967; Rüppel and Witt, 1969). With this method the signal/noise ratio of the measurements was increased 100-fold, whereby the time resolution could be extended to the ns range. The optical difference spectra observed with this technique during the turnover of photosynthesis gave evidence regarding the nature of the chemical and physical constituents of the photosystems and their reaction sequences. In this way, more than ten components and their behavior, were elucidated at the Max-Volmer-Institute: the dimeric chlorophyll (Chl) *a* complex P700; the Chl *a* complex P680; the specially bound plastoquinone Q_A; the pool of plastoquinones; the catalytic manganese cluster; the redox-active tyrosine; Chl and carotenoid triplet states; and localized and delocalized electrochromic changes which indicate various electric events (for overviews, see Witt, 1971, 1979, 1996; Ke, 2001; for a historical personal perspective, see Witt, 2004). These spectroscopic results have been, together with the X-ray structure analysis, the basis for the characterization of the RCs of PS II and PS I.

Abbreviations: BChl – bacteriochlorophyll; BPheo – bacteriopheophytin; BRC – purple bacterial reaction center; Car – carotene; Chl – chlorophyll; CP43/ CP47 – subunits of the PS II inner antenna system; Cyt – cytochrome; D1/D2 – subunits of the PS II reaction center; ENDOR – electron nuclear double resonance; EPR – electron paramagnetic resonance; ETC – electron transfer chain; EXAFS – extended X-ray absorption fine structure; P680/P700 – primary electron donors of PS II/PS I, respectively; $P_{D1/D2}$ – Chl coordinated by D1/D2 histidines 198/197, respectively; Pheo – pheophytin; PS I/PS II – Photosystem I/Photosystem II; Q – plastoquinone of the pool; Q_A – stable primary plastoquinone acceptor of PS II; Q_B – secondary plastoquinone acceptor of PS II; RC – reaction center; S_n – states of the water-oxidizing complex n = 0,1,2,3,4; TMH – transmembrane α-helix; WOC – water-oxidizing complex; Y_Z/Y_D – redox-active tyrosines 161/160 of the D1/D2 subunits, respectively; Y_Z^{ox} – notation for ($Y_Z^{\bullet}$ … H^+His190)

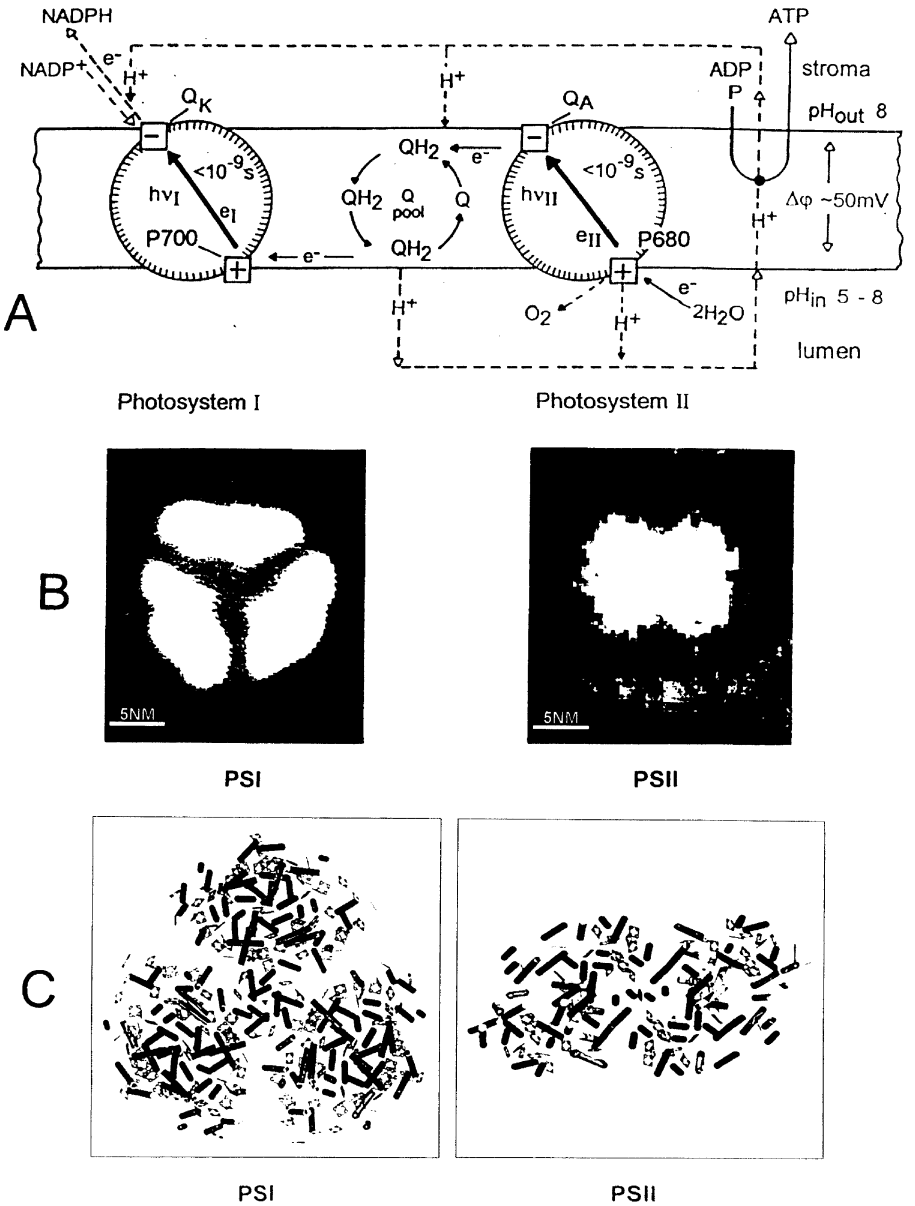

Fig. 1. (A) Spatial organization of the electron donors and acceptors of PS I and PS II in the functional membrane based on spectroscopic analysis in the 1960s (Schliephake et al., 1968). Pathways of electrons and protons and subsequent reactions of water oxidation, $NADP^+$ reduction and ATP formation are indicated. (B) Size and shape of the isolated core of PS I and PS II as trimer and dimer, respectively, based on electron microscopic image analysis (20 Å resolution) (Boekema et al., 1987; Rögner et al., 1987). PS I view onto the membrane plane and PS II approximately along the membrane plane. (C) Organization of the helices and chlorophylls of the trimers of PS I (Schubert et al., 1997) and dimers of PS II (Witt, 2004) with view from the stroma onto the membrane plane based on X-ray structure analysis at 4 Å and 3.8 Å resolution, respectively.

II. Transmembrane Charge Separation Events as Primary Acts of Light Energy Conversion and Spatial Organization of the Electron Donors and Acceptors — Analysis by a Molecular Voltmeter

Up to the 1960s the occurrence of a light-induced primary electron transfer vectorially across a functional membrane had not been considered. However, by following spectroscopic events, it became evident in those years that besides the *energetic* coupling between PS I and PS II, the primary events also included a structural coupling of two photo-induced charge separations across the membrane (Fig. 1A).

Some of the identified difference spectra named in Section I are outstanding in having a characteristic asymmetrical shape at different wavelengths, indicating the formation of an electric field (Junge and Witt, 1968; Emrich et al., 1969; Schmidt et al., 1971, 1972). The spectra are caused by a shift of absorption bands induced by the interaction of an electric field created in the membrane with the electronic energy levels of membrane pigments. These 'electrochromic band shifts' have been used as a *molecular multimeter* signaling — without time restriction — voltages, currents and formation of charges in the membrane (Witt, 1971, 1979).

Details obtained by this method became visible through the following observations: (i) the lifetime of the field-indicating signal in question is shortened with increasing transmembrane permeability, e.g., in the presence of ionophores, indicating a transmembrane direction of the field (Junge and Witt, 1968). (ii) The rise time of the electron from the primary donors to the acceptors (Witt and Wolff, 1970) corresponds to the time for the formation of the transmembrane electrical fields (Wolff et al., 1969). This indicates that the vectorial charge separation across the membrane is a primary *act*. (iii) When one photosystem is blocked, the field amplitude is halved, indicating that transmembrane charge separation occurs in PS I as well as in PS II (Schliephake et al., 1968). (iv) The polarity of the field (positive at membrane inside) gives evidence that the two primary donors (P680 and P700, see below) are located at the lumenal side and the two electron acceptors (quinones Q_A and Q_K, see below) at the stromal side (Fig. 1A). These observations thus indicated that the absorbed light energy is converted into a transmembrane charge-separated state with two reducing and two oxidizing species on opposite sides of the membrane side. The energy of this charged *membrane battery* is thus used for water oxidation, $NADP^+$ reduction and proton-driven phosphorylation. The products of these reactons are used for reduction of CO_2 to energy-rich biochemical compounds and for providing the biosphere with oxygen.

III. The Primary Electron Donor Chlorophyll P680 and Its Stable Electron Acceptor Plastoquinone Q_A — The Engine Driving Water Oxidation

A special Chl *a*, named Chl-a_{II}, later designated as P680, was discovered as the primary electron donor in PS II (Döring et al., 1967, 1968a, 1969). It was elucidated by the analysis of a flash-induced spectrum with changes at 435 and 682 nm. P680 is a Chl *a* complex with outstanding features. Its cationic radical $P680^{+\cdot}$ has one of the highest redox potentials found in nature (~1.2 V) and is thereby capable of oxidizing water through the catalytic Mn-center of PS II (Section XII).

A specially bound plastoquinone molecule, Q_A (formerly named X-320), was identified in single turnover flashes by a spectrum with maximal changes in the UV at 270 and 320 nm (Stiehl and Witt, 1968). This spectrum resembles one that appears when plastosemiquinone is produced in vitro. This assignment was also supported by the kinetic behavior: the decay time of the difference spectrum Q_A^-–Q_A coincides with the rise time of the spectrum of a plastohydroquinone (Stiehl and Witt, 1969) (see below), showing to be its precursor, i.e., a plastosemiquinone. Later, the spectrum of Q_A was refined (van Gorkom, 1974) and assigned definitively (Gerken et al., 1989). Q_A is tightly bound to the D2 protein of PS II and can be reduced only to a semiquinone. The kinetics of Q_A reduction indicate that Q_A is the stable primary acceptor of the electron released from the excited P680 and is, according to Section II, located at the stromal membrane side with P680 at the lumenal side.

Thus, the reaction center (RC) of PS II became evident as the transmembrane-spanning redox couple P680-Q_A, functioning in the light-induced transmembrane charge separation P680-Q_A → $P680^{+\cdot}$-Q_A^- (Fig. 1A). The cationic radical $P680^{+\cdot}$ subsequently extracts, via the redox-active tyrosine Y_Z, four electrons from the water-oxidizing Mn cluster after four, sequential light-induced turnovers. Thereafter one O_2 is released from two substrate H_2O

molecules at the Mn-cluster (for details see Section XI). Q_A^- reduces — via a secondary plastoquinone Q_B — molecules of the plastoquinone pool (named Q) to plastohydroquinone (Section VI). Q_A^- is stable for some hundred μs before its electron is transferred via Q_B to the pool. Recombination with $P680^{+\bullet}$ does not take place because the latter extracts an electron already within 20–260 ns from Y_Z (see below).

IV. The Membrane-Spanning Chlorophyll/Quinone Couple as a Reaction Center Model for Different Photosystems

The features of PS II evaluated in the late 1960s (Section III) have given us the first information on the organization of a photosynthetic RC in the form of a membrane-spanning chlorophyll/plastoquinone couple. Years later, the characteristics of the PS II RC were shown to be valid also for other RCs. In the anoxygenic purple bacterium *Rhodopseudomonas sphaeroides*, a ubiquinone, Q_U, acts as the stabilizing electron acceptor of the primary donor P870 (Clayton and Straley, 1970; Slooten, 1972). A transmembrane charge separation was also shown by an electrochromic band shift (Jackson and Crofts, 1969). The RC of purple bacteria (BRC) as a membrane-spanning chlorophyll/quinone couple was later confirmed by X-ray structure analysis (Deisenhofer et al., 1985). In the green filamentous bacteria, a menaquinone, Q_M, was discovered as the stable electron acceptor of the primary donor P885 (Vasmel and Amesz, 1983). It remains to be demonstrated whether a napthoquinone, Q_N, acts as an electron acceptor of the primary donors P840 and P800 in the green sulfur- and heliobacteria, respectively. In PS I, a phylloquinone, Q_K, was shown to be the stable acceptor of the primary donor P700 (Brettel et al., 1986; Malkin, 1986). A transmembrane charge separation between P700 and Q_K was also measured in PS I (Schliephake et al., 1968). This chlorophyll/quinone couple was later directly elucidated by X-ray structure analysis of PS I (Schubert et al., 1997).

V. Two Chlorins between the Chlorophyll/Quinone Couple as a Fast Path for Electrons Crossing the Membrane

It was shown that two chlorins function between the chlorophyll/quinone couple as transient electron carriers: in PS II these chlorins are a Chl *a* (Section X) and a Pheo (Klimov and Krasnovskii, 1981); in PS I, they are two Chls *a* (Jordan et al., 2001), and in the BRC, a BChl (Deisenhofer et al., 1985) and a BPheo (Shuvalov et al., 1976). The presence of these two chlorins *inter alia* is important for a fast electron transfer from the excited primary donor to the quinones. In this way the deactivation of the excited state into the ground state is low and the effectiveness of light conversion is kept high. This is obviously realized through electron transfer along the π-electron system of the two neighboring chlorins, acting as a molecular wire, via electron tunneling; this takes place on a ps to 100 ps time scale. For the BRC this mechanism has been evaluated in detail (Kuhn, 1986).

VI. The Plastoquinone Pool as the Pathway for Transfer of Electrons from Q_A to Photosystem I and of Protons from the Outer Aqueous Phase to the Membrane Lumen

In contrast to Q_A, which appears in a single turnover flash as a semiquinone (Section III), a new spectrum assigned to plastohydroquinone was discovered in longer flashes or in a train of single turnover flashes. This spectrum corresponds to one that appears when plastoquinone A is reduced in vitro in methanol (Stiehl and Witt, 1968, 1969). The optical change in vivo disappears after extraction of the quinone but reappears after reconstitution with prepared plastoquinone. The maximal absorption changes in vivo indicate that a pool with a capacity of 5–10 Q molecules is located between PS I and PS II in the lipid bilayer of the membrane. The stepwise reduction of Q molecules of the pool by the bound Q_A^- via Q_B causes Q^{2-} formation and proton uptake at the stromal side of the membrane. QH_2 diffuses within the membrane until it reaches a binding site at the lumenal side, where it is finally reoxidized and deprotonated via a soluble Cyt c_6 (or a plastocyanin) by the oxidized P700 of PS I. The catalytic function of the membrane-intrinsic Cyt b_6f complex operating between QH_2 and Cyt c_6 became evident later (Hauska et al., 1996)[1]. A stoichiometric coupling of 1:1:1 between stromal H^+ uptake, trans-

[1] The Cyt b_6f complex channels one electron of QH_2, via 2Fe-2S, Cyt *f* and a soluble electron carrier Cyt c_6 (or plastocyanin), towards the oxidized P700, and the the second electron, via Cyt b_6, back to a Q of the pool for a subsequent reduction.

membrane electron transfer and lumenal H^+ release was measured in the absence of a so-called 'Q cycle' (Tiemann et al., 1979). In this way it became clear that the Q pool acts structurally as a transmembrane bridge for electron transfer between PS II and PS I which is coupled with proton translocation between the outer and inner aqueous membrane phases that drives phosphorylation of ADP (Fig. 1A).

The Q reduction occurs after one Q of the pool has transiently docked to a binding site B on protein subunit D1, where it is then named 'Q_B.' A special Q_B molecule does not exist. After receiving two electrons through two turns of Q_A^- and uptake of two protons from the medium, the fully reduced form of Q_B is released into the pool and replaced by a new, oxidized Q from the pool, allowing a subsequent cycle of reduction and release (Bouges-Bocquet, 1973; Velthuys and Amesz, 1974).

VII. Primary Electron Donors Organized as Chlorophyll Pairs

In PS I a pigment with absorption changes at 700 nm was discovered by Kok (1956). Changes observed later at 438 nm (Kok, 1961; Witt et al., 1961) indicated that P700 is a special Chl *a.* The difference spectrum of its oxidation ($P700^{+\bullet}$–P700), inducible also at 125K (Witt et al., 1961) and with a risetime <20 ns (Witt and Wolff, 1970), identified P700 as the primary electron donor of PS I. Besides the band at 700 nm, another one was observed at 682 nm; this double band was explained by an excitonic coupling between two pigments and it was concluded that the primary electron donor P700 might be a Chl dimer (Döring et al., 1968b). A dimeric structure was also suggested later from EPR studies of P700 and named 'special pair' (Norris et al., 1971). The idea of a dimeric donor became important because it called for proof whether such a structure is characteristic also for primary donors of other RCs in photosynthesis. And, indeed, this became successively evident in the following years for different photosystems (see below). With respect to PS I, direct evidence for the proposal of a P700 dimer became available by X-ray structure analysis (Witt et al., 1992; Krauß et al., 1993; Käß et al., 2001). The refined PS I structure at 2.5 Å resolution even shows that one of the two Chls is a C13[2] epimer of Chl *a* (Jordan et al., 2001), that is, P700 is a heterodimer.

With the X-ray structure determination of crystals of the BRC (Deisenhofer et al., 1985), it was also shown that in these anoxygenic bacteria the primary donor P870 is a dimer of BChl *a*. With the X-ray structure analysis of PS II crystals (Section X) it became evident that P680 is a dimer of Chl *a*. The distances between the two Chls within the pairs are, however, different, varying from interacting dimers to more like monomeric coupled Chls, with corresponding different properties (see Section XII).

VIII. Identification of Photosystem II as a Dimer and Photosystem I as a Trimer

An essential further step towards an improved structural analysis of PS I and PS II was realized in the 1980s by the use of thermophilic cyanobacteria. These organisms are prokaryotes capable of water oxidation and possibly the most ancient species capable of water cleavage. Grown in large reactors, high yields of protein became available, allowing extensive screening for optimizing the isolation, purification and crystallization of the photosystems (Schatz and Witt, 1984a,b; Rögner et al., 1987; Dekker et al., 1988). Based on these improvements, highly purified RCs of PS I and PS II isolated from *Thermosynechococcus elongatus* became the essential prerequisite for revealing the closer structural organization of the two photosystems[2].

First information on the supramolecular structure of the photosystems was obtained in 1987 by electron microscopy at ~20 Å resolution using the highly purified PS I and PS II core complexes from *T. elongatus*. Structures were visualized by averaging the aligned images of single complexes with a digitizing camera. PS I complexes showed a trimeric organization, each trimer having a diameter of 190 Å and a width of 60 Å (Boekema et al., 1987); the structure resembles a clover leaf (Fig. 1B). Each monomeric subunit within the trimer represents a functional PS I unit (Rögner et al., 1990). PS II shows a dimeric structure with dimensions of about 170 × 135 × 55 Å (Rögner et al., 1987; Dekker et al., 1988) (Fig. 1B). Years later this 'electron microscopic image analysis' of single particles was applied to other complexes of PS II (Kuhl et al., 1999; Nield et al., 2000; Chapter 18, Hankamer et al.).

[2]Following these results, other groups used the cyanobacterial material for crystallization (see Chapters 20, Shen and Kamiya, and 21, Barber and Iwata.

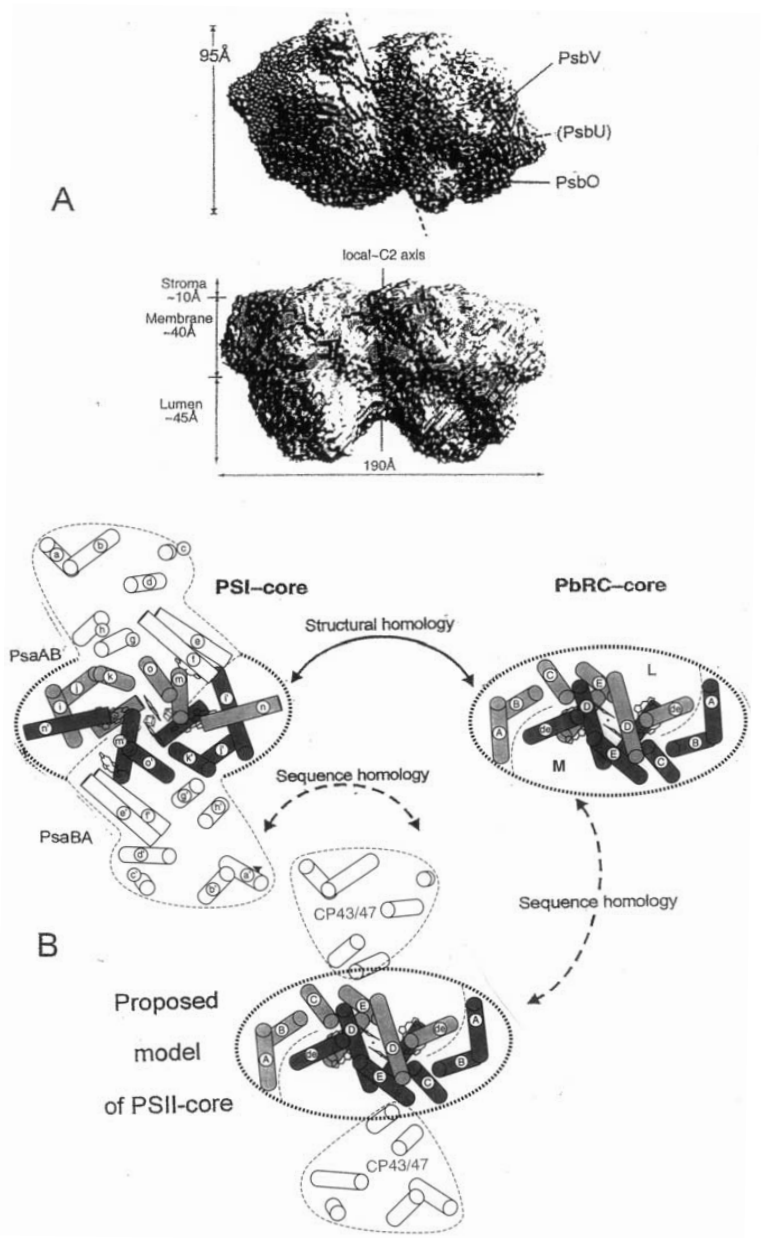

Fig. 2. A (Top): Surface of PS II homodimer drawn from the averaging mask generated during electron density modification followed by X-ray diffraction measurements at 3.8 Å resolution; view from the lumen onto the membrane plane (Witt et al., 2001). The extrinsic lumenal subunits PsbV (Cyt c_{550}), PsbU (12 kDa) and PsbO (33 kDa) are indicated. A (Bottom): The two monomers of the homodimer are related by the local c_2 axis perpendicular to the membrane plane: view along the membrane plane (Zouni et al., 2001a) B. Proposed helical structure of the RC core and antenna system of PS II monomer based on structural and sequential homologies with the known structure of PS I and purple bacteria. Modified from Schubert et al. (1998). For details, see text.

The multimers in Fig. 1B, obtained in 1987 at ~20 Å resolution, are compared in Fig. 1C with the overall arrangement of the helices and Chls within the interior of the supramolecular structure visualized later by X-ray structure analysis of PS I (Schubert et al., 1997) and PS II (Section X) at 4 and 3.8 Å resolution, respectively. These structures also reflect the presence of trimeric and dimeric complexes. Each of the monomeric subunits of these multimers is built from equal numbers of helices and Chls (Fig. 1C).

Figure 2A shows the surface structure of the homodimer of PS II along and perpendicular to the membrane plane elucidated by X-ray structure analysis at 3.8 Å resolution (Witt et al., 2001; Zouni et al. 2001a). The two monomers of the homodimer are related by a local c_2 axis. The characteristic bulges of the surface of the dimer in Fig. 2A (top) additionally indicate the position of the three extrinsic lumenal subunits PsbO, PsbU and PsbV discussed in Section X. The latter are also responsible for the ~55 Å extended lumenal region of PS II indicated in Fig. 2A (bottom).

IX. Homology of the Photosystem II Core Complex with Photosystem I and the Bacterial Reaction Center

Information on the arrangement of the helices in PS II follows from the observed structural and amino acid sequence homology between the complexes in question as shown in Fig. 2B. This is outlined here for the monomeric part of the dimer. The 2 × 5 transmembrane helices i, j, k, m and o of the C-terminal part form the electron transfer domain of the RC in PS I (subunit PsaA/B) and A, B, C, D and E in purple bacteria (subunit L/M). They are arranged in an 'interlocking C-shape.' The carboxyl (C)-terminal amino acid sequence homology between purple bacteria and PS II indicates that this helical structure must be also that of the RC of PS II (Trebst, 1985; Michel and Deisenhofer, 1988; Schubert et al., 1998). The 2 × 6 transmembrane helices a, b, c, d, g and h of the amino (N)-terminal parts form the two peripheral antenna domains in PS I. They are arranged in a 'trimer-of-dimer' structure. Based on the N-terminal sequence homology between PS I and PS II, it was expected that this helical structure is also found in the antenna system of PS II (Schubert et al., 1998). However, in PS I both considered domains are fused to a single protein but in PS II the antenna domains are located in two distinct subunits CP43/47 (see Fig. 2B) (Chapter 3, Eaton-Rye and Putnam-Evans); the latter is a result obtained by the X-ray structure analysis of PS II discussed in the next section. Based on homology the structures of the helio and green-sulfur bacterial photosystems were also predicted by Schubert et al. (1998), thereby establishing an evolutionary tree and a common ancestor for oxygenic and anoxygenic photosynthetic systems.

X. First 3-D Crystals of Photosystem II Capable of Water Oxidation and X-Ray Structure Analysis at 3.8–3.6 and 3.2 Å Resolution

PS II homodimers from the cyanobacterium *Thermosynechococcus elongatus* were isolated and prepared without the phycobilisome antenna (Rögner et al., 1987; Dekker et al. 1988). The PS II monomer is composed of at least 14 membrane intrinsic subunits, PsbA to PsbN and PsbX (Zouni et al., 2001b) (see also Chapters 20, Shen and Kamiya, and 21, Barber and Iwata). The six main subunits are the D1/D2 (PsbA/B) heterodimeric protein core that binds the cofactors of the electron transport chain (ETC), the antenna subunits CP43 (PsbC) and CP47(PsbB), and the α and β subunits of Cyt b_{559} (PsbE and PsbF). The remaining eight intrinsic subunits (PsbH to PsbN and PsbX) are small and contain together 12 helices. The three membrane-extrinsic subunits PsbO (33 kDa), PsbU (12 kDa) and PsbV (Cyt c_{550}, 17 kDa) are located at the lumenal side (see Section VIII). The dimeric core complex has a mass of ~700kDa. This was crystallized with polyethylene glycol as precipitating agent (Zouni et al., 2000) analogous to the conditions of the 'salting out' crystallization developed for PS I (Witt et al., 1988).

The crystals with a size up to 1 mm belong to the ortho-rhombic space group $P2_12_12_1$ with unit cell constants a = 134 Å, b = 227 Å and c = 310 Å. The unit cell accommodates 4 dimers. In light flash excitation the crystals show highly active water oxidation measured by O_2 evolution and the corresponding proton release (Zouni et al., 2000), yielding the expected stoichiometry of 4 H^+ per O_2. The crystals are very stable. After 10,000 flashes the activity only decreases by 30%, whereas with PS II in suspension by 70%.

The X-ray diffraction of these fully active crystals resulted in electron density maps at 3.8 Å and 3.6 Å

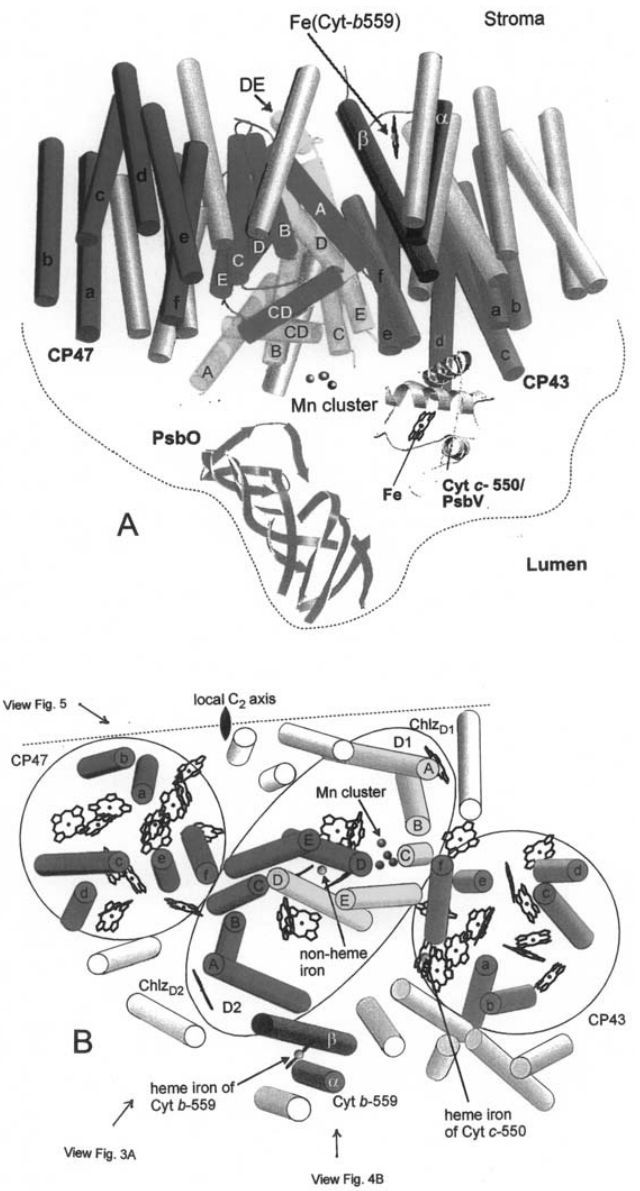

Fig. 3. Structure of the monomeric part of PS II with assignment of helices, cofactors and subunits at 3.8 Å resolution (Zouni et al., 2001a, modified). A. Side view of PS II monomer along the long axis of D2/D1 subunits with slightly tilted membrane plane. The five transmembrane helices of subunit D1/D2 and the six transmembrane helices of the antenna core subunit CP47/CP43 are shown. The twelve transmembrane helices of eight small subunits have not been assigned here. The α and β helices of Cyt b_{559} are shown. The extrinsic subunit PsbO (33 kDa) is shown as a β-sheet structure and Cyt c_{550} (17 kDa) as helical model. The Mn cluster within the membrane is located close to the domain of the extrinsic subunits. For clarity the Chl cofactors and others have been omitted. B. The structure in A with view direction from the stromal side onto the membrane plane. The local c_2-axis at the interface between the two monomeric parts of the dimer are indicated as well as the view direction of Figs. 3A, 4B and 5 (top). See Color Plate 5, Fig. 1.

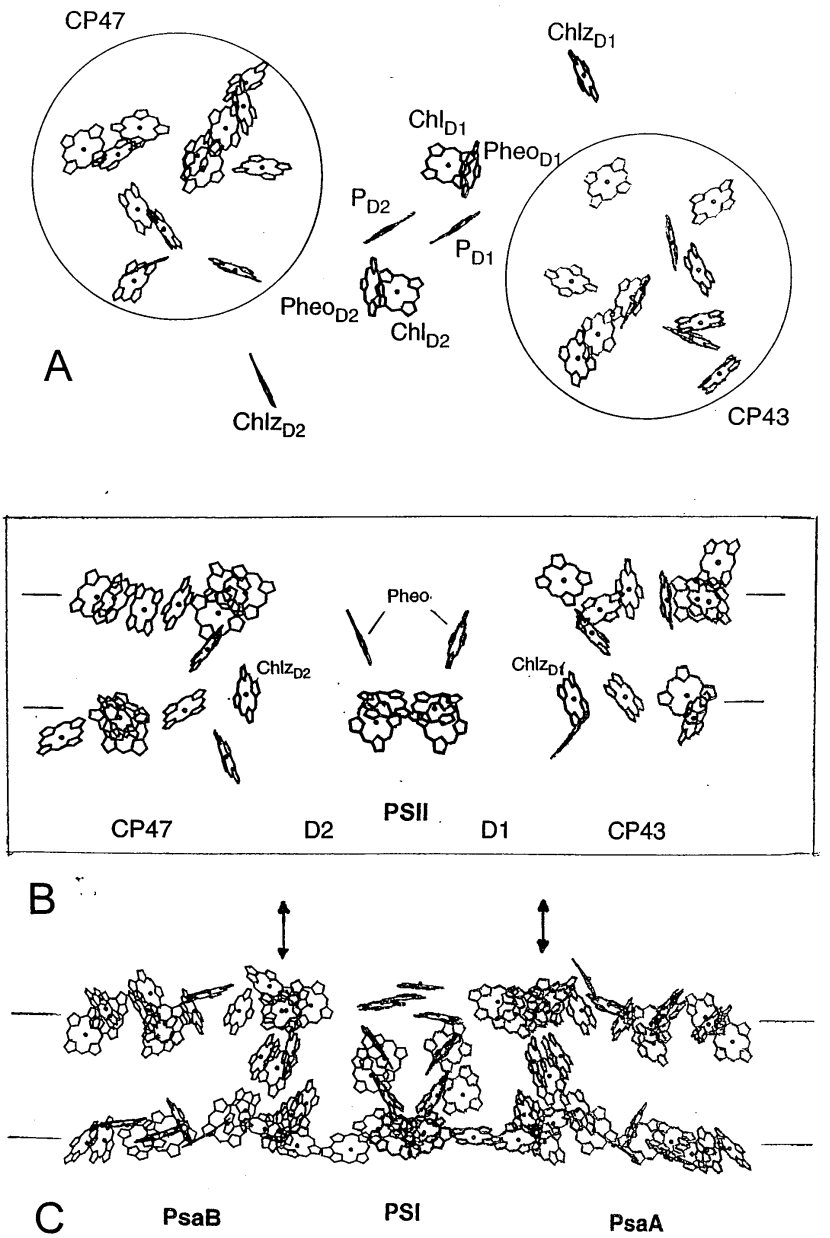

Fig. 4. (A) Arrangement of the cofactors in the electron transport chain (ETC) of subunit D1/D2 of PS II and the antenna chlorophylls of CP47/CP43; view from the stromal side perpendicular onto the membrane plane (Zouni et al., 2001a, modified). (B) View along the membrane plane indicating that the antenna chlorophylls are located in two layers close to the stromal and lumenal membrane side (Witt, 2004). (C) Arrangement of the antenna chlorophylls of subunit PsaB/A of PS I view along the membrane plane (Jordan et al., 2001). The structure of the peripheral domain corresponds to that of PS II shown in (B). The chlorophylls of the central domain surround the ETC forming a wall that reaches from the stromal to the lumenal membrane side (see arrows). In PS II in B this place is 'empty' (see text).

resolution (Zouni et al., 2001a,b) (Figs. 3–5) and recently with improved crystals at 3.2Å resolution (Biesiadka et al., 2004; Fig. 6). A total of 47 cofactors have been identified per PS II monomer: 35 Chls; 2 Pheos; 1 Q_A; 2 heme irons, 1 non-heme iron, 2 redox-active tyrosine residues and 4 manganese atoms. A field of 36 transmembrane α-helices has been localized per monomer. Recently about nine β-carotenes (Cars) were determined for each active PS II center (Kern et al., 2005). However, even at 3.2 Å resolution only one Car can be unambiguously identified in the ETC (Section X.B). Cars located near the Chls in the PS II RC are unlikely to be involved in preventing harmful singlet oxygen formation through the quenching of Chl triplet states since they would more likely be oxidized by the high oxidation potential of these Chls (see Section XII). Based on the observed very short-lived triplet states, it was suggested that this quenching occurs by the singly reduced plastoquinone Q_A (van Mieghem et al., 1995; Noguchi, 2002).

A. The Helical Framework and the Antenna System

Two helices α and β belong to the subunits of Cyt b_{559}. Five transmembrane helices A-E were assigned to each of the main subunits D1 and D2. These helices coordinate the cofactors of the ETC in two pseudo-symmetrical branches, similar to the helices in the L and M subunits of the BRC and the 5 innermost helices of the C-terminal domains of the PsaA and PsaB subunits of PS I. They are arranged in an interlocking C-shape and coordinate six chlorins (Fig. 3B) (see also Section IX and Fig. 2B).

In each of the two core antenna systems of PS II, located in the separate subunits CP43 and CP47, six transmembrane helices a–f are arranged as trimers of dimers (Fig. 3B). These helices coordinate ~29 Chls (Fig. 4A). CP43 harbors 13 Chl, CP47 16 Chl. (In the later model, three additional Chls have been found.) The nearest center-center distance between the antenna Chls is 8.5–13.5 Å. The Chls are arranged in two layers close to the lumenal and the stromal membrane sides (Fig. 4B). This is consistent with the observation that most of the conserved twenty histidines in CP43/CP47 are also located towards the lumenal and stromal membrane sides (Barry et al., 1994), possibly functioning as ligands for the Chls. The remaining 12 helices in Fig. 3 belong to the 8 small subunits PsbH to N and PsbX but could not unambiguously be assigned at that time.

At the lumenal side of the RC domain in cyanobacteria, the extrinsic 17 kDa subunit Cyt c_{550} (PbsV), required for O_2 evolution (Shen et al., 1998), and the main part of the Mn-stabilizing 33 kDa (PsbO) subunit with a tunnel-like β-barrel structure, were identified (Fig. 3A). Recently, the expected 12 kD (PsbU) subunit has been located between the other two at the 'bottom' of the extrinsic domain (Biesiadka et al., 2004)(see also Fig. 2A).

PS I contains, in the PsaA and PsaB unit, besides the two peripheral antenna region with 36 Chls arranged in two layers as in PS II (Fig. 4C), a central domain surrounding the ETC with a wall of 43 Chls functioning as an efficient path for excitation energy between the peripheral antenna region and the ETC. However, the corresponding central domain 'surrounding' the ETC in PS II is occupied only by two Chls, Chl Z_{D1} and Chl Z_{D2} (Fig. 4B). PS II completely lacks the central domain of the PS I antenna. This raises the question whether this 'empty' field in PS II is a necessary consequence of the 'photodamage and repair process' of the D1 protein. The damage-repair cycle (Chapter 27, Chow and Aro) gives PS II a safety net to overcome the threat of destruction by the high oxidizing power of $P680^+$, which produces toxic oxidative species in excessive light intensities. In the repair it is possible that a damaged D1 unit is disassembled and a newly synthesized D1 is reassembled. The cycle is optimized when repair keeps up with damage. Perhaps the absence of the antenna Chls in this domain is advantageous for an optimal balance and that PS II is optimized for regulation of safety rather than for efficiency. More information may become available when at higher structural resolution of additional cofactors, e.g., carotenoids become visible and their function understood.

B. The Electron Transfer Chain

The cofactors of the ETC form two branches symmetrically along the non-crystallographic pseudo-c_2 axis. It starts with two Chl *a* molecules, P_{D1} and P_{D2}, at the lumenal side; they have been assigned to P680 of PS II (see Fig. 5, top). Their head groups are parallel to each other and perpendicular to the plane of the membrane (Fig. 4A). Based on the homology between PS II and the BRC, P_{D1} and P_{D2} are believed to be coordinated by D1-His198 and D2-His197. Towards the stromal side, P680 is followed by a pair of Chl_{D1} and $Chl_{D2,}$ tilted by ~30° against the membrane plane,

corresponding to the 'accessory' BChls in purple bacteria (see also van Mieghem et al., 1991). However, the homologous histidines that coordinate these Chls in the BRC are missing in PS II. Further up a pair of pheophytins is located, $Pheo_{D1}$ and $Pheo_{D2}$, with their planes roughly perpendicular to the membrane plane. Two 'distant' Chls, Chl Z_{D1} and Chl Z_{D2}, not present in purple bacteria, are located at the periphery of the ETC ~34 Å apart from the local pseudo c_2 axis running through the non-heme iron, Fe, in the center of the core complex. They are coordinated with D1-His118 and D2-His117 (Biesiadka et al., 2004).The six chlorins in the RC of PS II correspond to the number determined biochemically by Eijekelhoff and Dekker (1995). The stable electron acceptor of P680, the tightly bound plastoquinone Q_A, is located on the stromal side of subunit D2. The putative docking site of the molecule Q_B (Sections III and VI) at a corresponding symmetrical position of subunit D1 was not occupied. The symmetry of the ETC is broken by the presence of one Cyt b_{559} identified with its heme iron located near the stromal side at the periphery of D2, and by the Mn cluster for the first time visible to be localized on the lumenal side close to the surface helix CD and the C-terminus of D1 (see below). Cyt b_{559} may be involved in electron-transfer around the RC. It has been shown that the electron transfer from the Cyt b_{559} occurs via a Car (Hanley et al., 1999). One Car connects Cyt b_{559} and Chl Z_{D2} via Chl_{D2} with the ETC (Biesiadka et al., 2004). Located between P680 and the Mn cluster in D1 is the redox-active tyrosine Y_Z; its counterpart in D2, Y_D, not essential for water oxidation, is placed symmetrically to Y_Z. When P680 is oxidized the unpaired electron of $P680^{+\bullet}$ must be located predominantly on P_{D1} because it is closest to Y_Z in D1, (edge-to-edge 7 Å) and because we have shown that Y_Z acts as the immediate electron donor to $P680^{+\bullet}$ (Gerken et al., 1987, 1988). Therefore the P_{D1}-Chl_{D1}-$Pheo_{D1}$-Q_A branch is the one active in electron transfer. This agrees also with the spin distribution of 80:20 for P_{D1} and P_{D2} when P680 is oxidized (Rigby et al., 1994). Oxidized tyrosine is a neutral radical because its phenolic proton has been shifted and bound to His 190 in its vicinity (Tommas and Babcock, 2000), i.e., $Y_Z^{\bullet}$... H^+His 190 acts as a positive charge and is therefore named $Y_Z^{\oplus}$ or $Y_Z^{\bullet}.H^+$ is rebound upon reduction of $Y_Z^{\bullet}$. Y_D is hydrogen bonded with His 189 of D2 is not involved in water oxidation (for details, see Chapter 9, Diner and Britt).

In a model for the mechanism of water oxidation developed by the late Jerry Babcock and colleagues (Tommos and Babcock, 2000) direct hydrogen atom abstraction from the two water bound to the Mn cluster is proposed and promoted by the Y_Z radical in each turnover. The edge-to-edge distance between the keto-oxygen of Y_Z and the Mn cluster is 7 Å (Fig. 5). This distance is too large for such a hydrogen abstraction. Hydrogen abstraction via a proton-coupled electron transfer or a water pipeline between the cluster and Y_Z may be possible. But, according to the Babcock model, the proton 'lost' upon formation of $Y_Z^{\bullet}$ (see above) must be released along an H-bonding network so that $Y_Z^{\bullet}$ can abstract an electron as well as a proton from the water substrate. The resulting stoichiometry of the proton release therefore must be 1:1:1:1 per O_2 evolution. However, this pattern has not been measured but 1:0:1:2 instead (Section XIB).

C. The Manganese Cluster

The Mn cluster is the 'inner sanctum' of photosynthesis. Information on the location, size and shape of the Mn cluster has now been obtained. The dimensions of its electron density, which bulges in three directions, are 6.8 × 4.9 × 3.3 Å (Fig. 5a,b). Three Mn atoms were assigned to the 3 bulges, the fourth Mn to the density near the center. The Mn-topography resembles a '3 + 1' model or a distorted Y shape with inter-atomic distances of ~3 Å. The indication that the density is predominantly due to the contribution of manganese was concluded from anomalous diffraction data collected at 3.8 Å resolution with the X-ray wavelength of the Mn-edge (but see below). The model with two separate Mn-dimers based on EPR analysis (Smith and Pace, 1996) as well as the well known C-shaped cluster based on EXAFS measurements (Yachandra et al., 1996) are not supported by the result obtained in Fig. 5. A stronger improvement of structural information about the Mn cluster by EXAFS measurements is expected from the collection of data sets on single crystals in dependence on their orientation; this work has been started.

Various Mn structures with motifs such as a funnel, triangle, distorted cubane or a '3 + 1' arrangement have been suggested as in vivo models (Carrell et al., 2002; Goussias et al., 2002; Chapters 10, Yachandra and 25, Hillier and Messinger). Ca^{++} is a cofactor of water oxidation and is located in the vicinity of, or as part of, the Mn cluster or even a member (Cineo et al., 2002). In vitro models have been described, e.g., as a Ca-capped funnel core, where a Ca bridges two Mn atoms with anions as ligands (Carrell et al.,

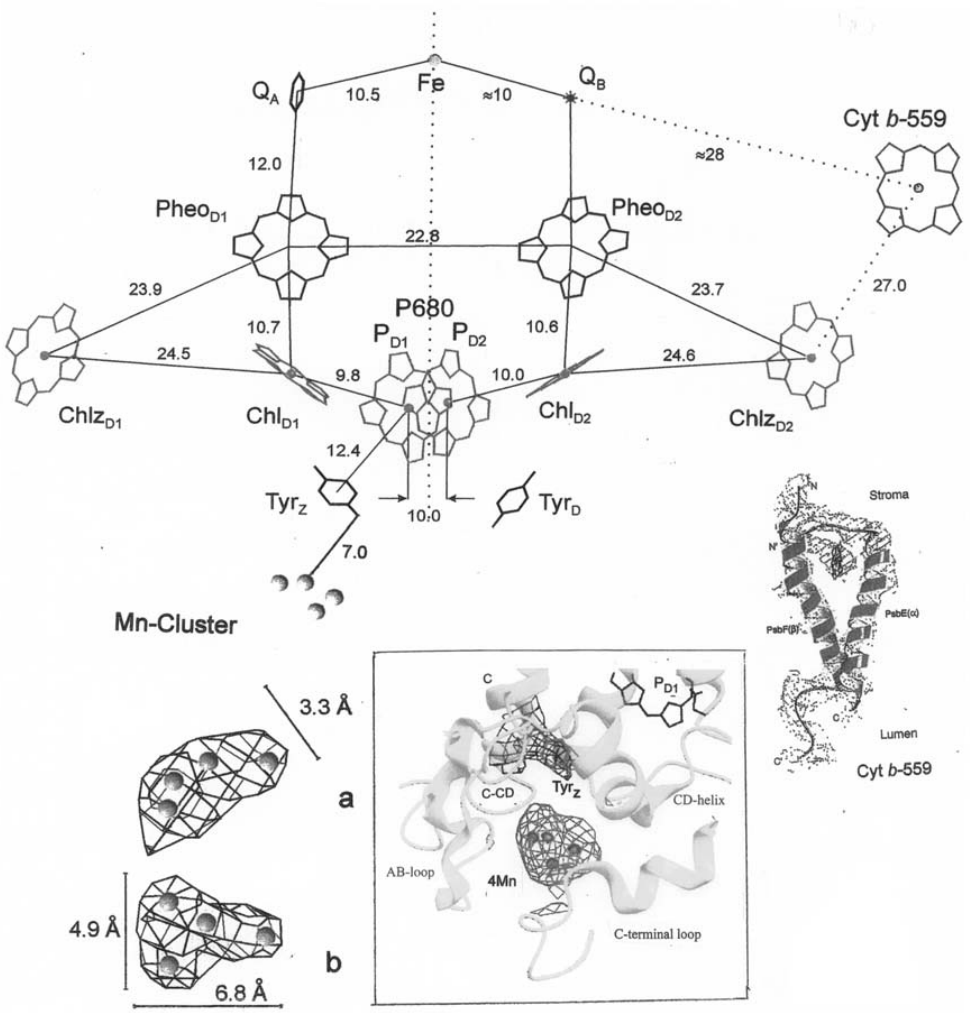

Fig. 5. Top: Arrangement of cofactors of the electron transport chain (ETC) located in subunit D1/D2 at 3.8 Å resolution (view direction as indicated in Fig. 3B and along the membrane plane). The center-center distances (Å) are indicated as well as the dotted pseudo-c_2 axis which is parallel to the local c_2 axis. The symmetry of the ETC is broken with the location of the Cyt b_{559} towards the stromal side and the Mn cluster towards the lumenal side. See also the close up view of Cyt b_{559} along the membrane plane (middle right). Bottom left: (a) Mn cluster with view along the membrane plane; its long axis points towards the lumen tilted ~23° against the plane; (b) view from the lumen onto the plane; Bottom right: Mn cluster surrounded by helices and loops of subunit D1 at 3.6 Å resolution. The position of P_{D1} of P680 and Y_Z of the ETC are indicated. Density of the Mn cluster contoured at 2.0 σ and of Tyr_z at 0.7 σ (Zouni et al., 2001a,b). Refined values at 3.2 Å resolution are discussed in Section XII. See Color Plate 6, Fig. 1.

2002). The volume of the electron density of the Mn cluster in Fig. 5a,b allows space for a Ca as shown in a model based on a combination of our density map with recent results of EXAFS analysis (Dau et al., 2003). However, at the resolution of the 3.8 Å model in Fig. 5, one cannot make an unambiguous statement on the internal arrangement of the metals in the cluster. A more detailed structure is needed to resolve these uncertainties (see below).

For the understanding of the function of the Mn

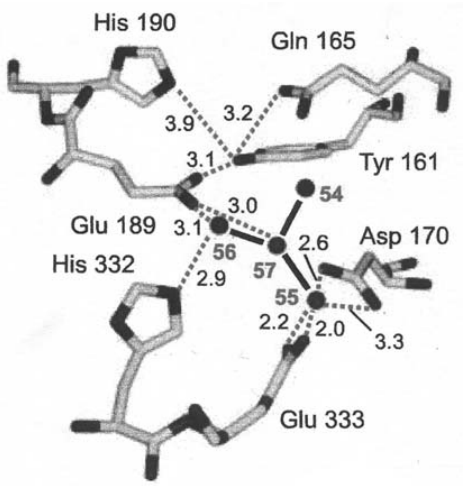

Fig. 6. Immediate environment of the Mn-Ca cluster at 3.2 Å resolution with view from the lumen onto the membrane (Biesiadka et al., 2004). Solid circles numbered 54–57 indicate four metal ions of the cluster and bold lines closest distance between them. Most probably the metal ions numbered 54–56 are three Mn ions and 57 a Ca^{2+} ion (see text). The identified side chains belong to the D1-transmembrane α-helix C (Tyr 161, Gln 165), loop C-CD (Asp 170), lumenal α-helix CD (Glu 189, His 190) and to the C-terminal region (His 332, Glu 333). Dotted lines show H bonding and coordinating interactions; distances are given in Å.

cluster, knowledge of its immediate environment is important. The Mn cluster is located outside the two-fold symmetry axis towards the lumenal surface at the end of the helices C and CD of the D1 subunit (Fig. 5). Regions of the D1 subunit which may provide coordination with the Mn cluster are shown by the X-ray structure analysis in Fig. 5 (bottom right). In this model these regions are the lumenal helix CD, the loop between the transmembrane helix C and CD, parts of the C-terminal loop and, finally, the loop between the transmembrane helix A and B. Thus, with the identification and location of amino acid side chains, the nature for the binding pocket of the Mn cluster can be realized.

According to site-directed mutagenesis studies (reviewed in Debus 2001; Chapter 11, Debus) different amino acid residues have been characterized which may provide ligands to the Mn cluster and the Ca^{2+} cofactor.

Based on the first excursion in the X-ray structural analysis at the improved resolution to 3.2 Å, the Berlin group has recently identified the side chains of D1-Asp 170, D1 Glu 333, D1-His 332, and D1-Glu 189 as ligands to the four metal ions of the cluster (Biesiadka et al., 2004) (see Fig. 6). This is in agreement with the conclusions by Debus (2001). In addition the identified location of D1-Tyr 161, D1-His 190 and D1-Gln 165 are shown in Fig. 6. Based on biochemical work, the residues of D1-His 337, D1-Asp 342 and D1-Ala 344 may be also Mn ligands (Debus, 2001). However, these are not clearly defined in the electron density map of Fig. 6.

The location of one Ca^{2+} ion as one of the four metal ions in Fig. 6, most probably no. 57, is based on X-ray diffraction data measured at and beyond the Mn edge. The remaining metal ions are three Mn ions. This may indicate that one Mn ion of the expected four Mn ions has not been identified. Subsequent research regarding this point has shown that part of the manganese has been reduced to Mn^{2+} by the X-ray radiation (J. Kern, personal communication). This observation strongly supports that there is Mn disorder or even depletion of one Mn ion. Thus, models of the Mn cluster so far published and based on X-ray structure analysis must be considered with reservation. With this finding it becomes clear that, henceforth, it will be necessary to make special experimental efforts to avoid the change of the electron density of the Mn cluster through long exposure of the crystal to X-ray radiation during the data collection (Biesiadka et al., 2004). The information on the location of the Ca^{2+} ion in the Mn cluster in Fig. 6 means that in Fig. 5b, where 4 Mns have been localized, the Ca^{2+} ion must be located in a position close to the central metal ion of the four ions indicated. On the other hand, chloride ions as potential ligands to the Mn cluster have not been localized in the crystal structures at the present resolution. For alternate interpretations of the Mn cluster, see Chapters 20 (Shen and Kamiya) and 21 (Barber and Iwata).

XI. Manganese Valences, Proton Releases and Water States of the Quaternary S-State Cycle of the Light Driven Engine

A. Manganese Oxidations up to the S_3 State and Intermediates in the $S_4 \rightarrow S_0$ Transition

After four turnovers of $P680^{*} \rightarrow P680^{+\cdot}$ by four single turnover flashes, one O_2 molecule per RC is released from the water substrate (Joliot and Kok, 1975). The water-oxidizing complex (WOC) and the Mn cluster

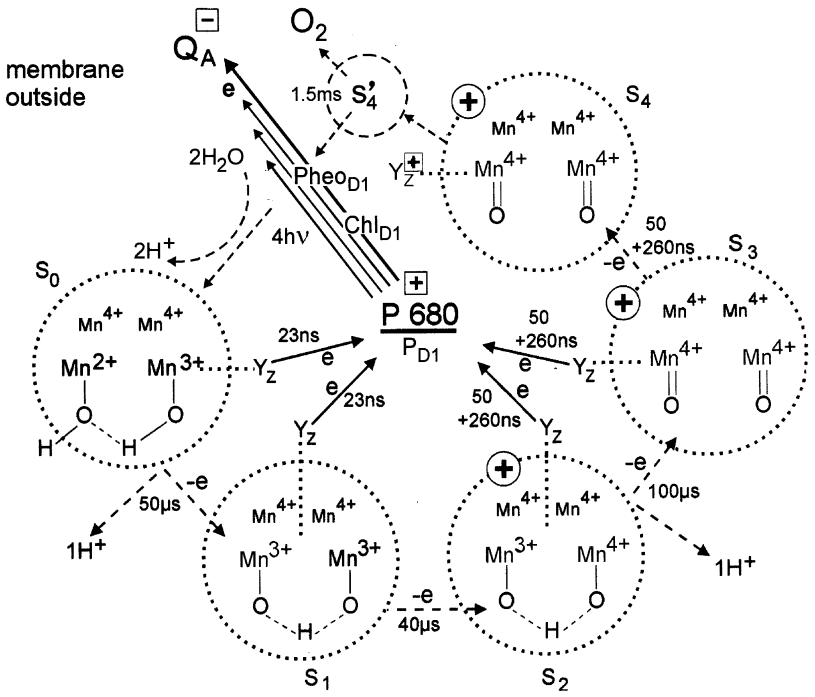

Fig. 7. Model for the period-four cycle of manganese oxidation and water deprotonation based on spectroscopic analysis (Sections I-IX). For clarity the charges of the water derivatives have been omitted. The S-state cycle $S_0 \rightarrow S_4$ is driven by transmembrane electron transfers induced by excited P_{D1} of P680 (or Phe_{D1} or Chl_{D1}, see Section XII) towards Q_A. Thereby, step by step via tyrosine Y_Z manganese is oxidized by $P680^+$ up to S_3. Oxidized tyrosine, $Y_Z^{\oplus}$, represents in S_4 the fourth oxidizing equivalent. Rate-limiting intermediate reactions in S_4' are followed by O_2 evolution and formation of S_0 coupled with uptake of 2 H_2O and release of $2H^+$ (see text). S states with a positive net charge relative to S_0 are indicated with a bold ⊕ (Saygin and Witt, 1987; Schlodder and Witt, 1999).

respectively thereby passes through four increased oxidized states, S_0-S_4, by electron abstraction through $P680^{+\bullet}$ via Y_Z (the S-state subscripts indicate the number of extracted electrons). Starting with S_0, O_2 evolution takes place after four flashes in the S_4-S_0 transition. Based on transient UV difference spectra observed during the quaternary S-state oscillation, the Mn-valence state changes have been elucidated (Saygin and Witt, 1987). They are shown in Fig. 7. For these measurements highly purified samples from *T. elongatus* were used. First the changes of the Mn valences were recorded in a 'window' open for a few ms at 0.5 s after the flash, i.e., after the absorption changes of P680, Q_A and Y_Z had relaxed, but before the newly created S state began to decay. Second, the initial heterogeneous S-state population normally present in the dark-adapted state, with S_1 as the predominant state, was changed to a condition so that the S_0 state predominates. To achieve this, the S states were exposed in the dark for several minues to the reductant NH_2OH which causes a delay in O_2 evolution by two flashes (Bouges, 1971). We have shown that this delay is due to the reduction of two Mn valence states by NH_2OH. This corresponds to a backward shift of two S states beyond S_1 creating an *overreduced* state, S_{-1}. After removal of NH_2OH in a train of single turnover light flashes the Mn ions are oxidized stepwise in each flash up to the fourth flash and are then reduced after the fifth flash releasing O_2 in 1.5 ms (Saygin and Witt, 1987; Kretschmann et al., 1991). Under these conditions, the weaker UV difference spectrum observed in the $S_0 \rightarrow S_1$ transition can be assigned in Fig. 7 to a Mn^{2+}-Mn^{3+} change and the stronger one in $S_1 \rightarrow S_2$ to a Mn^{3+}-Mn^{4+} change. These results are in agreement with the X-ray absorption Mn-K-edge data and EPR measurements (reviewed

in Goussiasa et al., 2002). Since we observed in the $S_2 \rightarrow S_3$ transition the same UV-difference spectrum as obtained in the preceding $S_1 \rightarrow S_2$ transition, which is due to a $Mn^{3+} \rightarrow Mn^{4+}$ change, it is likely that there is also such a Mn-oxidation event in $S_2 \rightarrow S_3$ as in $S_1 \rightarrow S_2$. This has been recently supported by new Mn-K-edge shift measurements (see below). Furthermore, the EPR signal observed upon formation of the S_2 state — a multiline signal with net spin ½ (Dismukes and Siderer, 1981) — disappears when S_3 is formed indicating that Mn oxidation has also taken place in $S_2 \rightarrow S_3$.

For the $S_3 \rightarrow S_4$ transition we observed no Mn changes. However, instead UV changes appear at 50 and 260 ns, which have been shown to be due to the oxidation of Y_Z (Gerken et al., 1987, 1988; Section X.B). This indicates that the fourth oxidizing equivalent created in $S_3 \rightarrow S_4$ is $Y_Z^{\oplus}$ itself, i.e., $S_4 \equiv S_3 Y_Z^{\oplus}$. In the last step from S_4 to S_0 the evolution of O_2 takes place in 1.5 ms (see above and Saygin and Witt, 1987). This step is rate limiting through reactions in an intermediate state S_4' (Fig. 7): We postulated in 1987 that the electric field of $Y_Z^{\oplus}$ is the promoter giving rise to a two-electron transfer from the two oxo-atoms in S_4 to the two active Mn^{4+} cations resulting in a peroxo-intermediate, Mn^{3+}-O-O-Mn^{3+} in state S_4'. Presumably, in a further two-electron oxidation of this intermediate, the formation of Y_Z, Mn^{2+}/Mn^{3+} and O_2 may be realized, followed by the uptake of 2 H_2O and the release of 2 H^+ to restore the state S_0 (see Fig. 7). The supposed start of this reaction sequence induced through the field of $Y_Z^{\oplus}$ may be supported by the recent structure at 3.2 Å resolution which identifies D1-Glu 189, as having its carboxylate bridge between the phenolic D1-Tyr 161 (Y_Z) and a Mn cation of the Mn-Ca cluster (see Fig. 6).

X-ray absorption Mn K-edge shifts — indicating Mn oxidation state changes —have been measured in $S_2 \rightarrow S_3$, with a shift of 0.3 eV. This shift is small compared with those of ~1 eV in $S_0 \rightarrow S_1$ and $S_1 \rightarrow S_2$ and was interpreted to indicate no Mn oxidation in $S_2 \rightarrow S_3$, but instead the formation of a bridging μ-oxo radical (Messinger et al., 2001). However, this is not a convincing argument because the size of the K-edge-shifts also strongly depends on accompanying changes of the structure and Mn coordination environments (Carroll et al., 2002; Goussias et al., 2002). Furthermore, the K-edge shifts were measured at cryogenic temperatures (10–80 K), i.e., in the absence of water oxidation and at temperatures where the equilibrium of the Mn-redox states may be different with regard to the state at physiological temperatures where the UV spectra have been measured. Recently, improved measurements of K-edge shifts have been made even at room temperature with results that can be explained by Mn oxidation $Mn^{3+} \rightarrow Mn^{4+}$ also in $S_2 \rightarrow S_3$ (H. Dau and M. Haumann, personal communication; Haumann et al., 2004). This supports our early results based on UV absorption spectroscopy (Saygin and Witt, 1987). Mn oxidation up to the S_3 state clearly indicates that water is oxidized not before but in the $S_4 \rightarrow S_0$ transition.

For completeness it should be mentioned that after long exposure of the S states to the reductant NH_2OH (hours instead of minutes), a three-flash delay of O_2 evolution is observed instead of a two-flash delay. This indicates a backward S-state transition ($S_{-2} \leftarrow S_{-1} \leftarrow S_0 \leftarrow S_1$) with the formation of a super-reduced state S_{-2}. This state can be reoxidized also in a light-induced forward reaction to S_0 and further on to O_2 evolution as shown above for the overreduced S_{-1} state. S_{-2} is the terminal state which is reversible, because its further reduction by treatment with NH_2OH shows no new *reversible* UV absorption changes of a further Mn reduction but increased deactivation ending with the depletion of the Mn^{2+} ions in the medium (Kretschmann and Witt, 1993).

B. Proton Stoichiometry of 1:0:1:2

With respect to the proton release during the S-state cycle, a *net charge* oscillation of 0:0:1:1 in the state S_0:S_1:S_2:S_3 has been observed. The net charge has been measured by an electrochromic band shift of membrane pigments (Section II) induced by the electric field of the net charges (Saygin and Witt, 1985a,b; Kretschmann et al., 1991, 1996; Schlodder and Witt, 1999). The net charge is positive relative to the overall charge of the S_0 state. The S states with a net charge are indicated in Fig. 7 by the bold symbol ⊕. The net charge formation is pH-*in*dependent between pH 5.5–7.0 and has been shown to be created as the charge difference between electron abstraction and H^+ release from the WOC and the Mn cluster, respectively. Thus, the measured net charge 0:0:1:1 observed for S_0:S_1:S_2:S_3 is explained if a H^+ release of 1:0:1:2 takes place from the WOC together with the four electron abstractions over the $S_0 \rightarrow S_1 \rightarrow S_2 \rightarrow S_{3,4} \rightarrow S_0$ transition. With the presence of a positive net charge in S_2 and S_3 it is expected that these should delay by Coulomb attraction the electron transfer times from Y_Z to $P680^{+\bullet}$. Indeed these transfers are

retarded in S_2 and S_3 more than ten times in contrast to the times in states S_0 and S_1 (see Fig. 7) (Brettel et al., 1984).

Direct proof of this proton release from the WOC by glass electrode measurements is not possible because a pH-dependent proton release from unknown amino acid residues of defective and unfolded protein domains takes place. However, proton measurements in the medium have been achieved by the use of crystallizable PS II core complexes from cyanobacteria (Schlodder and Witt, 1999). The observed pattern of protons between pH 5.5 and 7.2 measured with this optimal material is explained by a pH-*in*dependent proton release from the water-oxidizing center with a stoichiometry of 1:0:1:2 and a pH-dependent de- and re-protonation from an amino acid group (pK ≈ 5.7) induced by a shift of its pK value through the electrostatic interaction of this group with the electrical field of the oscillating net charge of 0:0:1:1 for S_0:S_1:S_2:S_3. At pH 7 the acid group is deprotonated. Therefore, at this pH the 1:0:1:2 stoichiometry has been measured with both methods.

C. The Water Derivatives in the S-States

Based on the above stoichiometry for proton release, the possible water derivatives in the S states have been predicted (Fig. 7). However, a 'calibration' can only be determined with the information of an additional proton event. The net charge indicating this event was observed in the overreduced S_{-1} state after the one-electron backward transition $S_{-1} \leftarrow S_0$ induced by the reductant NH_2OH in the dark (Section XI.A). This net charge disappears again in a light-induced forward S-state transition $S_{-1} \rightarrow S_0$. This is explained if, in the reducing backward transition two H^+ are taken up per electron and vice versa in the forward reaction, two H^+ are released from S_{-1}. In the subsequent $S_0 \rightarrow S_1 \rightarrow S_2 \rightarrow S_3$ transitions two H^+ are released also (Section XI.A), i.e., in total four H^+ are released between S_{-1} and S_3. This is consistent with the presence of 2 H_2O in state S_{-1} and two OH^- in S_0. With this 'calibration' the possible water derivatives in the S-state cycle are those depicted in Fig. 7 (Saygin and Witt, 1987; Kretschmann et al., 1991,1996; Schlodder and Witt, 1999).

XII. Functional Implications

The primary donor P680 of PS II is unique because of the high midpoint redox potential of $P680^{+\bullet}$ (≥1.2 V), which is capable of oxidizing water. However, the two Chls, P_{D1} and P_{D2}, of P680 show no unusual optical properties. Their Q_Y absorption maximum is only weakly red-shifted, by ~5–10 nm compared to the antenna absorption maximum and by ~15 nm compared to the Q_Y of Chl in organic solvents (~665 nm). The latter has an oxidation potential of only ~0.8 V. The exciton coupling between the two Chls, P_{D1} and P_{D2}, in P680 is weak with an interaction energy of 85–150 cm^{-1} (Tetenkin et al., 1989; Diner and Rappaport, 2002). This is about 2–3 time larger than the coupling between all other cofactors of the RC with their next neighbor. In the P870 'special pair' of purple bacteria, the BChls are red-shifted by as much as ~100 nm in *Rb. sphaeroides*, and coupled with an interaction energy of 500–1000 cm^{-1} (reviewed in Diner and Rappaport, 2002). The strong coupling between the two BChls in P870 leads to electron delocalization within the dimer, which may be one reason for the low oxidation potential of $P870^{+\bullet}$ (~0.45 V).

The center-center distances between the chlorins in the ETC of PS II has been measured to be ~10 Å (Fig. 5), indicating a weak coupling. This result has been used to explain that almost no spectral separation is induced among the chlorins and their absorption bands overlap, centered between ~670–680 nm. This effect contrasts with the well-separated bands in purple bacteria where maxima occur at 760 nm (BPheo), 800 nm (BChl), and 870 nm ('special pair'). Upon charge separation in PS II (see below), the cationic radical $P680^{+\bullet}$ is formed and localized predominantly on P_{D1}. The spin distribution is 80:20 for P_{D1}:P_{D2} (see Section X.B), while in $P870^{+\bullet}$, this ratio is 65:35 for P_L:P_M (Rautter et al., 1994).

The difference in properties between P680 of PS II and P870 of the BRC is not due to the inherent distances in the Chl pairs as previously supposed (monomeric character vs. dimeric character, respectively). The Berlin group measured the Mg-Mg distances between P_{D1} and P_{D2} and their interplanar separations as 10 Å/5 Å, respectively, at 3.8 Å resolution (Zouni et al., 2001a). Recently these distances were refined to 8.3 Å/3.6Å, respectively, at 3.2 Å (Biesidka et al., 2004). The London group published at 3.5 Å resolution similar values of 8.2 Å/3.4 Å (Ferreira et al., 2004). Thus the Mg^{2+}–Mg^{2+} distance in P680 is only 0.7 Å longer than that of P870 with 7.6 Å/3.6 Å. This reduces only slightly the coupling of the P_{D1} and P_{D2} of P680 connected with possibly only a small

change of its oxidation potential (positive charge delocalized over one Chl macrocycle instead of over two changes the oxidation potential by ~0.3 V) (Datta et al., 2001).

Obviously, other factors besides geometrical ones are more relevant to the different qualities of the primary electron donors of PS II compared with the BRC and to the formation of the high oxidation potential of $P680^{+\bullet}$. These may be the different oscillator strengths (Chl *a*: 23 debye²/BChl a 40 debye² in vitro), different immediate environments (hydrophobic/hydrophilic binding pockets) as well as several other features which have been suggested to play a part in the outstanding oxidation potential of $P680^{+}$: (i) strong hydrogen bonding of the chlorins (Allen and Williams, 1995; Chapter 32, Kálmán et al.)[2]; (ii) positively charged residues in the immediate vicinity of the oxidant (Mulkridjanian, 1999); (iii) protonation of the Chl (Maggiora et al., 1985); (iv) asymmetrical electron spin density established within the Chl *a* macroaromatic cycle of P_{D1} (Matysik et al., 2000). Thus, we have to wait for atomic resolution (~2.5 Å) of PS II to get insights as to how nature has set up the fine structure to understand the difference to the BRC and the oxidation potential capable of the cleavage of water. This high potential is not only a question with respect to the qualities of P_{D1} of P680 in order to keep the unpaired electron for oxidation of Y_Z on $P_{D1}^{+\bullet}$, which is the immediate electron acceptor of Y_Z (Gerken et al., 1987, 1988) but also with respect to the oxidation potential of Chl_{D1} and $Pheo_{D1}$ which must be even higher than that of P_{D1} to prevent their oxidation instead of Y_Z (Witt et al., 2001). Very recently, the redox-potentials of the cofactors of the ETC were calculated considering the protein environment available from the present 3.2 Å resolution of the crystal structure. The computed redox-potentials for P_{D1}, P_{D2}, Chl_{D1} and Chl_{D2} were 1.1–1.3 V relative to the hydrogen electrode at pH 7 (Rappaport et al., 2002; Ishikita et al., 2005).

The predicted high potentials of Chl_{D1} raise the question as to why Chl_{D1} does not act in its excited state as a primary electron donor besides P_{D1}, and whether excited $Pheo_{D1}$ does not function even as primary electron acceptor. In both cases the created positive charge on Chl_{D1} can move subsequently by fast migration to P_{D1} (see scheme of charge separation below). This view is supported by the following results.

[2] Crystal structure shows that P_{D1} and P_{D2} and Chl D1 are not involved in a hydrogen bond.

By mutation of the His 198 residue of P_{D1} it was shown by Diner et al. (2001) that at 5 K the Q_Y transition energy of Chl_{D1} is clearly lower (~684 nm) than that of P_{D1} (~675 nm) and $Pheo_{D1}$ (~680 nm). Therefore at 5 K, the excitation energy from the antenna system must be trapped exclusively on Chl_{D1}, which implies that Chl_{D1} is a primary electron donor and the only one at this temperature (Greenfield et al., 1997, 1999). Independent evidence for this conclusion is based on the observation that at 20K the Chl triplet state of the ETC, assumed to be on the same Chl as the primary donor, is located on a Chl tilted by ~30° with respect to the membrane plane (van Mieghem et al., 1991). But this is the orientation of Chl_{D1} determined by the X-ray structure analysis in Fig. 5. At higher temperature P_{D1} and P_{D2} are increasingly excited. This includes also $Pheo_{D1}$ and $Pheo_{D2}$ shown by their increase of fluorescence at > 70K (Konermann and Holzwarth, 1997). At 298 K the excitation energy is, according to the Boltzmann law and to the Q_y values cited above, distributed with different parts over all six chlorins on the two branches coupled with energy transfer between them (see also Diner and Rappaport, 2002). At 298 K the excited state population on Chl_{D1} over that of P_{D1} is favored by a factor ≥3. Thus charge separation could be initiated by all three excited chlorins on the active branch. In the first primary step the following two transient radical pair formations might be induced in < 1 ps:

$$P^{*}_{D1} \rightarrow (P^{+}_{D1} - Chl^{-}_{D1} - Phe_{D1}) \leftarrow Chl^{*}_{D1} \rightarrow (P_{D1} - Chl^{+}_{D1} - Phe^{-}_{D1}) \leftarrow Phe^{*}_{D1}$$

Phe represents pheophytin. The predicted two fast primary charge separations have not yet been measured. But these can extend spatially by charge migration into the unstable charged pair which has been observed (P^{+}_{D1}–Chl_{D1}–$Pheo^{-}_{D1}$) (Seibert and Wasielewski, 2003). This pair is followed by its stabilization in the well documented redox couple (P^{+}_{D1}–Chl_{D1}–$Pheo_{D1}$–Q^{-}_{A}) (Sections III and IV). The difference spectrum of $P680^{+\bullet}$–P680 is that measured in the latter stable state. This spectrum is not only the result of the bleaching at ~675 nm through the formation of the cationic radical state of P_{D1} and – to some extent – of P_{D2} (see above) but also of the electrochromic blue shift of the ~684 nm absorption band of Chl_{D1} predominantly induced by the charge of P^{+}_{D1}. This assignment to the spectral composition of P680 has recently been supplemented: the so-called 'multimer model' suggests that the charge transfer

in PS II occurs in a supramolecular complex. Based on this view, excitionic couplings between the six chlorins of the RC have been taken into account. For the coupling between P_{D1} and P_{D2} excitionic states centered at 675 nm and 660 nm have been calculated; the state at 660 nm has, however, a very small oscillator strength (for details see Barter et al., 2003; Raszewski et al., 2005; Chapter 22, Barter al.). This excitonic splitting characterizes the $P_{D1}P_{D2}$ dimer of P680 as a '*soft* special pair' in contrast to that of P870.

The contribution of the charge separations induced by the three excited chlorins would depend, however, not only on the excitation energy they are carrying, but also on the energy levels of the supposed radical pairs, the kinetics of pair formation and the exciton interaction of the cofactors between the inactive and active branch of the ETC (see Section X.B). This functional complexity remains to be solved as well as the open structural model at ≤ 2.5 Å resolution of the above cited cofactors and their environment. This is the challenge to research in the years to come for the final understanding of the water-oxidizing mechanism.

Acknowledgments

I would like to express my gratitude to my colleagues who worked with me in the previous years on the spectroscopic analysis of the functional and structural properties of the two photosystems, particularly G. Döring, H. Rüppel, B. Rumberg, W. Junge, H. Stiehl, Ch. Wolff, R. Reich, G.H. Schatz, K. Brettel, E. Schlodder, Ö. Saygin, M. Rögner, J.P. Dekker, E.J. Boekema, S. Gerken, and H. Kretschmann. I also acknowledge and thank my colleagues who continued the work with me on the crystallization and X-ray structure analysis of Photosystems I and II, I. Witt, N. Krauß, P. Jordan, W.D. Schubert, A. Zouni, P. Fromme, J. Kern, P. Orth, I. Biesiadka, B. Loll and W. Saenger. I am very grateful for the technical assistance of D. DiFiore and C. Lüneberg. I thank Eberhard Schlodder and Govindjee for reading the manuscript and their very helpful comments. The work was supported by the Deutsche Forschungsgemeinschaft in the Collaborative Research Centers 312 and 498 (Projects A3, C3) and by the Fonds der Chemischen Industrie. Beam times and support at ESRF (Grenoble) and DESY, Hamburg) are gratefully acknowledged. The article was written upon invitation by Tom Wydrzynski.

References

Allen JP and Williams JC (1995) Relationship between the oxidation potential of the bacteriochlorophyll dimer and electron transfer in photosynthetic reaction centers. J Bioenergetics and Biomembranes 27: 275–283

Barry BA, Boerner RJ and de Paula JC (1994) The use of cyanobacteria in the study of the structure and function of PS II. In: Bryant DA (ed) The Molecular Biology of Cyanobacteria, pp 217–257, Kluwer Academic Publishers, Dordrecht

Barter LMC, Durrant JR and Klug DR (2003) A quantitative structure-function relationship for the Photosystem II reaction center: Supermolecular behavior in natural photosynthesis. Proc Nat Acad Sci USA 100: 946–951

Biesiadka J, Loll B, Kern J, Irrgang KD and Zouni A (2004) Crystal structure of cyanobacterial Photosystem II at 3.2 Å resolution: A closer look at the Mn cluster. Phys Chem Chem Phys 6: 4733–4736

Boekema EJ, Dekker JP, van Heel MG, Rögner M, Saenger W, Witt I and Witt HT (1987) Evidence for a trimeric organization of the Photosystem I complex from the thermophilic cyanobacterium *Synechococcus sp.* FEBS Lett 217: 283–286

Bouges B (1971) Action of hydroxylamine on the O_2 evolution of *Chlorella* and chloroplasts of spinach. Biochim Biophys Acta 234, 103–112

Bouges-Bocquet B (1973) Electron transfer between two photosystems in spinach chloroplasts. Biochim Biophys Acta 314: 250–256

Brettel K, Schlodder E and Witt HT (1984) Nanosecond reduction kinetics of photooxidized chlorophyll a_{II}^{+} (P680) in single flashes as a probe for the electron pathway, H^+ release and charge accumulation in the O_2-evolving complex. Biochim Biophys Acta 766: 403–415

Brettel K, Sétif P and Mathis P (1986) Flash-induced absorption changes in Photosystem I at low temperature: Evidence that the electron acceptor A_1 is vitamin K_1. FEBS Lett 203: 220–224

Carrell TG, Tyryshin AM and Dismukes GC (2002) An evaluation of structural models for the photosynthetic water-oxidizing complex derived from spectroscopic and X-ray diffraction signatures. J Biol Inorg Chem 7: 2–22

Cinco RM, McFarlane Holman KL, Robblee JH, Yano J, Pizarro SA, Bellacchio E, Sauer K and Yachandra VK (2002) Calcium EXAFS establishes the Mn-Ca cluster in the oxygen-evolving complex of Photosystem II. Biochemistry 41: 12928–12933

Clayton RK and Straley SC (1970) An optical absorption change that could be due to reduction of the primary photochemical electron acceptor in photosynthetic reaction centers. Biochem Biophys Res Commun 39: 1114–1119

Datta SN, Parandekar PV and Lochan RC (2001) Identity of green plant reaction centers from quantum chemical determination of redox potentials of special pairs. J Phys Chem B 105: 1442–1451

Dau H, Liebisch P and Haumann M (2003) X-ray absorption spectroscopy to analyze nuclear geometry and electronic structure of biological metal centers — potential and questions examined with special focus on the tetra-nuclear manganese complex of oxygenic photosynthesis. Anal Bioanal Chem 376: 562–583

Debus R (2001) Amino acid residues that modulate the properties of tyrosine Y_Z and the manganese cluster in the water oxidizing complex of Photosystem II. Biochim Biophys Acta

1503: 164–186
Deisenhofer J, Epp O, Miki K, Huber R and Michel H (1985) Structure of the protein subunits in photosynthetic reaction centers of *Rhodopseudomonas viridis* at 3 Å resolution. Nature 318: 618–624
Dekker JP, Boekema EJ, Witt HT and Rögner M (1988) Refined purification and further characterization of oxygen evolving and Tris-treated Photosystem II particles from the thermophilic cyanobacterium *Synechococcus sp.* Biochim Biophys Acta 936: 307–318
Diner BA and Rappaport F (2002) Structure, dynamics, and energetics of the primary photochemistry of Photosystem II of oxygenic photosynthesis. Ann Rev Plant Physiol Plant Mol Biol 53: 551–580
Diner BA, Schlodder E, Nixon PJ, Coleman WJ, Rappaport F, Lavergne J, Vermaas WFJ and Chisholm DA (2001) Site-directed mutations at D1-His198 and D2-His197 of Photosystem II in *Synechocystis* PCC 6803: Sites of primary charge separation and cation and triplet stabilization. Biochemistry 40: 9265–9281
Dismukes G and Siderer Y (1981) Intermediates of a polynuclear manganese center involved in photosynthetic oxidation of water. Proc Natl Acad Sci USA 78: 274–278
Döring G, Stiehl HH and Witt HT (1967) A second chlorophyll reaction in the electron chain of photosynthesis — registration by the repetitive excitation technique. Z Naturforsch 22b: 639–644
Döring G, Bailey JL, Kreutz W and Witt HT (1968a) The active chlorophyll-a_{II} in light reaction II of photosynthesis. Naturwiss 55: 219–224
Döring G, Bailey JL, Kreutz W, Weikard and Witt HT (1968b) The action of two chlorophyll a_I molecules in light reaction I of photosynthesis. Naturwiss 55:219–200
Döring G, Renger G, Vater J and Witt HT (1969) Properties of the photoactive chlorophyll-a_{II} in photosynthesis. Z Naturforsch 24b: 1139–1143
Durrant JR, Klug DR, Kwa SLS, von Grondelle R, Porter G and Dekker JP (1995) A multimer model for P680, the primary electron donor of Photosystem II. Proc Natl Acad Sci USA 92: 4798–4802
Eijekelhoff E and Dekker JP (1995) Determination of the pigment stoichiometry of the photochemical reaction center of Photosystem II. Biochim Biophys Acta 1231: 21–28
Emrich HM, Junge W and Witt HT (1969) Further evidence for an optical response of chloroplast bulk pigments to a light-induced electrical field in photosynthesis. Z Naturforsch 24b: 1144–1146
Ferreira KN, Iverson TM, Maghlaoui K, Barber J and Iwata S (2004) Architecture of the photosynthetic oxygen-evolving center. Science 303: 1831–1838
Gerken S, Brettel K, Schlodder E and Witt HT (1987) Direct observation of the immediate electron donor to chlorophyll a_{II}^+ ($P680^+$) in oxygen-evolving Photosystem II complexes. Resolution of nanosecond kinetics in the UV. FEBS Lett 223: 376–380
Gerken S, Brettel K, Schlodder E and Witt HT (1988) Optical characterization of the immediate electron donor to Chl a_{II}^+ in O_2-evolving PS II complexes. Tyrosine as possible electron carrier between Chl a_{II} and the water-oxidizing manganese complex. FEBS Lett 237: 69–76
Gerken S, Dekker JP, Schlodder E and Witt HT (1989) Studies on the multiphasic charge recombination between chlorophyll a^+_{II} and plastoquinone Q_A^- in PS II complexes. UV difference spectrum of Chl a_{II}^+ /Chl a_{II}. Biochim Biophys Acta 977: 52–61
Goussias C, Boussac A and Rutherford AW (2002) Photosystem II and photosynthetic oxidation of water: An overview. Phil Trans R Soc Lond B 357: 1369–1381
Greenfield SR, Seibert M, Govindjee and Wasielewski MR (1997) Direct measurement of the effective rate constant for primary charge separation in isolated Photosystem II reaction centers. J Phys Chem B 101: 2251–2255
Greenfield SR, Seibert M and Wasielewski MR (1999) Direct measurement of the effective rate constant for primary charge separation in isolated Photosystem II reaction centers. J Phys Chem B 103: 8364–8374
Hanley J, Deligiannakis Y, Pascal A, Faller P and Rutherford AW (1999) Carotenoid oxidation in Photosystem II. Biochemistry 38: 8189–8195
Haumann M, Müller C, Liebisch P, Iuzzolino L, Dittmer J, Grabolle M, Neisius T, Meyer-Klaucke W and Dau H (2004) Structural and oxidation state changes of the Photosystem II manganese complex in four transitions of the water oxidation cycle ($S_0 \rightarrow S_1$, $S_1 \rightarrow S_2$, $S_2 \rightarrow S_{3,4} \Rightarrow S_0$) characterized by x-ray absorption spectroscopy at 20 K as well as at room temperature. Biochemistry 44: 1894–1908
Hauska G, Schütz M and Büttner M (1996) The Cyt b_6f complex-composition, structure and function. In: Ort DR and Yokum CF (eds) Oxygenic Photosynthesis: The Light Reactions, pp 377–398. Kluwer Academic Publishers, Dordrecht
Ishikita H, Loll B, Biesiadka J, Saenger W and Knapp E-W (2005) Redox potentials of chlorophylls in the Photosystem II reaction center. Biochemistry 44: 4118–4124
Jackson JB and Crofts AB (1969) The high energy state in chromatophores from *Rhodopseudomonas sphaeroides*. FEBS Lett 4: 185–189
Joliot P and Kok B (1975) Oxygen evolution in photosynthesis. In Govindjee (ed), Bioenergetics of Photosynthesis, Academic Press, New York, 387–412
Jordan P, Fromme P, Klukas O, Witt HT, Saenger W and Krauß N (2001) Three-dimensional structure of cyanobacterial Photosystem I at 2.5 Å Resolution. Nature 411: 909–917
Junge W and Witt HT (1968) On the ion transport system of photosynthesis — Investigations on a molecular level. Z Naturforsch 23b: 244–254
Käß H, Fromme P, Witt HT and Lubitz W (2001) Orientation and electronic structure of the oxidized primary donor P^+_{700} in Photosystem I: A single crystal EPR and ENDOR study. J Phys Chem 105: 1225–1239
Kamiya N and Shen JR (2003) Crystal structure of oxygen-evolving Photosystem II from *Thermosynechococcus vulcanus* at 3.7 Å resolution. Proc Nat Acad Sci USA 100: 98–103
Ke B (2001) Photosynthesis: Photobiochemistry and Photobiophysics. Kluwer Academic Publishers, Dordrecht
Kern J, Loll B, Lüneberg C, DiFiore D, Biesiadka J, Irrgang K-D and Zouni A (2005) Purification, characterization and crystallization of Photosystem II from *Thermosynechococcus elongatus* cultivated in a new type of photobioreactor. Biochim Biophys Acta 1706: 147–157
Klimov VV and Krasnovskii AA (1981) Pheophytin as the primary electron acceptor in Photosystem II reaction center. Photosynthetica 15: 592–609
Kok B (1956) On the reversible absorption change at 705 mμ

in photosynthetic organisms. Biochim Biophys Acta 22: 399–401

Kok B (1961) Partial purification and determination of oxidation reduction potential of the photosynthetic chlorophyll complex absorbing at 700 mμ. Biochim Biophys Acta 48: 527–533

Konermann L, Yruela I and Holzwarth AR (1997) Pigment assignment in the absorption spectrum of the Photosystem II reaction center by site-selection fluorescence spectroscopy. Biochemistry 36: 7498–7450

Krauß N, Hinrichs W, Witt I, Fromme P, Pritzkow W, Dauter Z, Betzel Ch, Wilson KS, Witt HT and Saenger W (1993) Three-dimensional structure of system I of photosynthesis at 6 Å resolution. Nature 361: 326–331

Kretschmann H and Witt HT (1993) Chemical reduction of the water splitting enzyme system of photosynthesis and its light-induced reoxidation characterized by optical and mass spectrometric measurements. Biochim Biophys Acta 1144: 331–345

Kretschmann H, Pauly S and Witt HT (1991) Evidence for a chemical reaction of hydroxylamine with the photosynthetic water splitting enzyme S in the dark — possible states of manganese and water in the S cycle. Biochim Biophys Acta 1059: 208–214

Kretschmann H, Schlodder E and Witt HT (1996) Net charge oscillation and proton release during water oxidation in photosynthesis. An electrochromic band shift study at pH 5.5–7.0. Biochim Biophys Acta 1274: 1–8

Kuhn H (1986) Electron transfer mechanism in the reaction center of photosynthetic bacteria. Physical Rev A 34: 3409–3425

Kuhl H, Rögner M, van Breemn JFL and Boekema EJ (1999) Location of cyanobacterial Photosystem II donor-side subunits by electron microscopy and supramolecular organization of Photosystem II in the thylakoid membrane. Eur J Biochem 266: 453–459

Maggiora LL, Petke JD, Gopal D, Iwamoto RT, Maggiora GM (1985) Experimental and theoretical studies of Schiff base chlorophylls. Photochem Photobiol 42: 69–75

Malkin R (1986) On the function of two vitamin K_1 molecules in the PS I-electron acceptor complex. FEBS Lett 208: 343–346

Matysik J, Gast P, van Gorkom HJ, Hoff AJ and de Groot HJM (2000) Photochemically induced nuclear spin polarization in reaction centers of Photosystem II observed by ^{13}C-solid-state NMR reveals a strongly asymmetric electronic structure of the P^{+}_{680} primary donor chlorophyll. Proc Natl Acad Sci USA 97: 9865–9870

Messinger J, Robblee JH, Bergmann U, Fernandez C, Glatzel P, Visser H, Cinco RM, McFarlane KL, Bellacchio E, Pizarro SA, Cramer SP, Sauer K, Klein MP and Yachandra VK (2001) Absence of Mn-centered oxidation in the $S_2 \rightarrow S_3$ transitions: Implication for the mechanism of photosynthetic water oxidation. J Am Chem Soc 123: 7804–7820

Michel H and Deisenhofer J (1988) Relevance of the photosynthetic reaction center from purple bacteria to the structure of Photosystem II. Biochemistry 27: 17

Mulkidjanian AY (1999) Photosystem II of green plants: On the possible role of retarded protonic relaxation in water oxidation. Biochim Biophys Acta 1410: 1–6

Nield J, Orlova EV, Morris EP, Gowen B, van Heel M and Barber J (2000) 3D map of the plant Photosystem II supercomplex obtained by cryoelectron microscopy and single particle analysis. Nature Struct Biol 7: 44–47

Noguchi (2002) Dual role of triplet localization on the accessory chlorophyll in the Photosystem II reaction center: Photoprotection and photodamage of the D1 protein. Plant Cell Physiol 43: 1112–1116

Norris JR, Uphaus RA, Crespi HL and Katz JJ (1971) Electron spin resonance of chlorophyll and the origin of signal I in photosynthesis. Proc Natl Acad Sci USA 68: 625–628

Rappaport F, Guergova-Kuras M, Nixon PJ, Diner BA and Lavergne J (2002) Kinetics and pathways of charge recombination in photosystems. Biochemistry 41: 8518–8527

Raszewski G, Saenger W and Renger Th (2005) Theory of optical spectra of Photosystem II reaction center: Location of the triplet state and the identity of the primary electron donor. Biophys J 88: 966–998

Rautter J, Lendzian F, Lubitz W, Wang S and Allen JP (1994) Comparative study of reaction centers from photosynthetic purple bacteria — electron-paramagnetic-resonance and electron-nuclear double-resonance spectroscopy. Biochemistry 33: 12077–12084

Rigby SEJ, Nugent JHA and O'Malley PJ (1994) ENDOR and special triple resonance studies of chlorophyll cation radicals in photosystem 2. Biochemistry 33: 10043–10050

Rögner M, Dekker JP, Boekema EJ and Witt HT (1987) Size, shape and mass of the oxygen-evolving Photosystem II complex from the thermophilic cyanobacterium *Synechococcus sp*. FEBS Lett 219: 207–211

Rögner M, Mühlenhoff U, Boekema EJ and Witt HT (1990) Mono, di- and trimeric PS I reaction center complexes isolated from the thermophilic cyanobacterium *Synechococcus sp*. Size, shape and activity. Biochim Biophys Acta 1015: 415–424

Rüppel H and Witt HT (1969) Measurements of fast reactions by single and repetitive excitation with pulses of electromagnetic radiation. In: Kustin K (ed) Methods in Enzymology, pp 317–379. Academic Press, New York

Saygin Ö and Witt HT (1985a) Evidence for the electrochromic identification of the change of charges in the four oxidation steps of the photoinduced water cleavage in photosynthesis. FEBS Lett 187: 224–226

Saygin Ö and Witt HT (1985b) Sequence of the redox changes of manganese and pattern of the changes of charges during water cleavage in photosynthesis. Photobiochem Photobiophys 10: 71–82

Saygin Ö and Witt HT (1987) Optical characterization of intermediates in the water splitting enzyme system of photosynthesis — possible states and configurations of manganese and water. Biochim Biophys Acta 893: 452–469

Schatz GH and Witt HT (1984a) Extraction and characterization of oxygen-evolving Photosystem II complexes from a thermophilic cyanobacterium *Synechococcus sp*. Photobiochem Photobiophys 7: 1–4

Schatz GH and Witt HT (1984b) Characterization of electron transport in oxygen-evolving Photosystem II complexes from a thermophilic cyanobacterium *Synechococcus sp*. Photobiochem Photobiophys 7: 77–89

Schliephake W, Junge W and Witt HT (1968) Correlation between field formation, proton translocation and the light reactions in photosynthesis. Z Naturforsch 23b: 1571–1578

Schlodder E and Witt HT (1999) Stoichiometry of proton release from the catalytic center in photosynthetic water oxidation. J Biol Chem 274: 30387–30392

Schmidt S, Reich R and Witt HT (1971) Electrochromism of chlorophylls and carotenoids in multilayers and in chloroplasts. Naturwiss 58: 414

Schmidt S, Reich R and Witt HT (1972) Electrochromic measurements in vitro as a test for the interpretation of field-indicating absorption changes in photosynthesis. In: Forti G, Avron M, Melandri A (eds) Proceedings Second International Congress on Photosynthesis Research, Stresa, 1971, pp 1087–1095. Dr. W. Junk NV Publishers, The Hague

Schubert WD, Klukas O, Krauß N, Saenger W, Fromme P and Witt HT (1997) Photosystem I of *Synechococcus elongatus* at 4 Å resolution: A comparative structure analysis. J Mol Biol 272: 741–769

Schubert WD, Klukas O, Saenger W, Witt HT, Fromme P and Krauß N (1998) A common ancestor for oxygenic and anoxygenic photosynthetic systems: A comparison based on the structural model of Photosystem I. J Mol Biol 280: 297–314

Seibert M and Wasielewski M (2003) The isolated Photosystem II reaction center: First attempts to directly measure the kinetics of primary charge separation. Photosynth Res 76: 263–268

Shen JR, Quian M, Inoue Y and Burnap RL (1998) Functional characterization of *Synechocystis sp.* PCC 6803 delta psbU and delta psbV mutants reveals important roles of Cyt c_{550} in cyanobacterial oxygen evolution. Biochemistry 37: 1551–1558

Shuvalov VA and Klimov VV (1976) The primary photoreaction in the complex cytochrome P890-P760 (bacteriopheophytin 760) of *Chromatium minutissimum* at low redox potentials. Biochim Biophys Acta 440: 587–599

Slooten L (1972) Electron acceptors in reaction center preparations from photosynthetic bacteria. Biochim Biophys Acta 275: 208–218

Smith PJ and Pace RJ (1996) Evidence for two forms of the g=4.1 signal in the S_2 state of Photosystem II. Two magnetically isolated manganese dimers. Biochim Biophys Acta 1275: 213–220

Stiehl HH and Witt HT (1968) Die kurzzeitigen ultravioletten Differenzspektren bei der Photosynthese. Z Naturforsch 23b: 220–224

Stiehl HH and Witt HT (1969) Quantitative treatment of the function of plastoquinone in photosynthesis. Z Naturforsch 24b: 1588–1598

Tetenkin VL, Gulayev BA, Seibert M and Rubin AB (1989) Spectral properties of stabilized D1/D2/cytochrome *b*-559 Photosystem II reaction center complex. Effects of Triton X-100, the redox state of pheophytin and β-carotene. FEBS Lett 250: 459–463

Tiemann R, Renger G, Gräber P and Witt HT (1979) The plastoquinone pool as possible hydrogen pump in photosynthesis. Biochim Biophys Acta 546: 498–519

Tommos C and Babcock GT (2000) Proton and hydrogen currents in photosynthetic water oxidation. Biochim Biophys Acta 1458: 199–219

Trebst A (1985) The topology of the plastoquinone and herbicide binding peptides of Photosystem II in the thylakoid membrane. Z Naturforsch 41c: 240–245

van Gorkom HJ (1974) Identification of the reduced primary electron acceptor of Photosystem II as a bound semiquinone anion. Biochim Biophys Acta 347: 439–442

van Mieghem FJE, Satoh K and Rutherford AW (1991) A chlorophyll tilted 30° relative to the membrane in the Photosystem II reaction center. Biochim Biophys Acta 1058: 379–385

van Mieghem F, Brettel K, Hillmann B, Kamlowski A, Rutherford AW and Schlodder E (1995) Charge recombination reactions in Photosystem II. 1. Yields, recombination pathways and kinetics of the primary pair. Biochemistry 34: 4789–4813

Vasmel H and Amesz J (1983) Photoreduction of manaquinone in reaction centers of green photosynthetic bacterium *Chloroflexus aurantiacus*. Biochim Biophys Acta 724: 118–121

Velthuys BR and Amesz J (1974) Charge accumulation and the reducing side of Photosystem 2 of photosynthesis. Biochim Biophys Acta 333: 85–94

Witt HT (1967) A. Direct measurements of reactions in the 10^{-1} to 10^{-8} second range by single and repetitive excitations with pulses of electromagnetic waves (flashes, microwaves, giant laser pulses). B. On the analysis of photosynthesis by pulse techniques in the 10^{-1} to 10^{-8} second range. In: Claesson S (ed) Fast Reactions and Primary Processes in Chemical Kinetics (Nobel Symposium V), (A) pp 81–97 and (B) pp 261–316. Almquist and Wiksell, Stockholm

Witt HT (1971) Coupling of quanta, electrons, field, ions, and phosphorylation in the functional membrane of photosynthesis. Results by pulse spectroscopic methods. Quart Rev Biophys 4: 365–477

Witt HT (1979) Energy conversion in the functional membrane of photosynthesis. Analysis by light pulse and electric pulse methods. The central role of the electric field. Biochim Biophys Acta 505: 355–427

Witt HT (1996) Primary reactions of oxygenic photosynthesis. Ber Bunsenges Phys Chem 100: 1923–1942

Witt HT (2004) Steps on the way to building blocks, topologies, crystals and X-ray structural analysis of Photosystem I and II of water-oxidizing photosynthesis. Photosynth Res 80: 85–107

Witt K and Wolff Ch (1970) Rise time of the absorption changes of chlorophyll-a_I and carotenoids in photosynthesis. Z Naturforsch 25b: 387

Witt HT, Müller A and Rumberg B (1961) Oxidized cytochrome and chlorophyll in photosynthesis. Nature 192: 194–195

Witt HT, Krauß N, Hinrichs W, Witt I, Fromme P and Saenger W (1992) Three-dimensional crystals of PS I from *Synechococcus sp.* and X-ray structure analysis at 6 Å resolution. In: Murata N (ed) Research in Photosynthesis, Vol I, pp 521–528. Kluwer Academic Publishers, Dordrecht

Witt HT, Zouni A, Kern J, Fromme P, Krauß N, Saenger W and Orth P (2001) Crystal structure of Photosystem II and aspects of its function. In: PS2001: Proceedings of the 12th International Congress on Photosynthesis, PL-1, pp 1–8. CSIRO, Melbourne, (CD-ROM)

Witt I, Witt HT, DiFiore D, Rögner M, Hinrichs W, Saenger W, Granzin J, Betzel CH and Dauter Z (1988) X-ray characterization of single crystals of the reaction center I of water-splitting photosynthesis. Ber Bunsenges Phys Chem 92: 1503–1506

Wolff Ch, Buchwalrd HE, Rüppel H, Witt K and Witt HT (1969) Risetime of the light-induced electrical field across the functional membrane of photosynthesis. Z Naturforsch 24b: 1038–1041

Yachandra VK, Sauer K and Klein MP (1996) Manganese cluster in photosynthesis: Where plants oxidize water to dioxygen. Chem Rev 96: 2927–2950

Zouni A, Jordan R, Schlodder E, Fromme P and Witt HT (2000) First Photosystem II crystals capable of water oxidation. Biochim Biophys Acta 1457: 103–105

Zouni A, Witt HT, Kern J, Fromme P, Krauß N, Saenger W and Orth

P (2001a) Crystal structure of Photosystem II from *Synechococcus elongatus* at 3.8 Å resolution. Nature 409: 739–743

Zouni A, Kern J, Loll B, Fromme P, Witt HT, Orth P, Krauß N, Saenger W, Biesiadka J (2001b) Biochemical characterization and crystal structure of water oxidizing Photosystem II from *Synechococcus elongatus*. In: PS2001: Proceedings of the 12th International Congress on Photosynthesis, S5-003. CSIRO, Melbourne, (CD-ROM)

Chapter 20

3D Crystal Structure of the Photosystem II Core

Jian-Ren Shen*
Department of Biology, Faculty of Science, Okayama University, Okayama 700-8530/PRESTO, JST, Japan

Nobuo Kamiya
RIKEN Harima Institute/Spring-8, Kouto 1-1-1, Mikazuki-cho, Sayou-gun, Hyogo 679-5148, Japan

Summary

The recent success in the crystallization and crystal structure analysis of the Photosystem II (PS II) core complex from thermophilic cyanobacteria has contributed greatly to our understanding of the structure and function of PS II. We describe here the crystallization and crystal structure of the PS II core from *Thermosynechococcus vulcanus*, with comparisons to the structures from *T. elongatus* and the photosynthetic bacterial reaction center. The crystal structure of *T. vulcanus* was analyzed at a 3.7 Å resolution and the structural model was built using sequences from the large subunits of PS II, while the structures of other subunits were represented either as polyalanines or alpha carbons (Cα). The crystal structure reveals a number of possible molecular interactions among different subunits on the lumenal side. The arrangement of the chlorophylls and other cofactors are also shown, including two β-carotene molecules not previously identified. The location of these β-carotenes has provided new insights into a possible secondary electron transport pathway involving a peripheral chlorophyll

*Author for correspondence, email: shen@cc.okayama-u.ac.jp

T. Wydrzynski and K. Satoh (eds): Photosystem II: The Light-Driven Water:Plastoquinone Oxidoreductase, pp. 449–467.

molecule bound to the D2 subunit and cytochrome b_{559}. In addition, the structure and environment surrounding the manganese cluster are described. In particular, the carboxyl-terminus of D1 polypeptide is shown to be connected to the manganese-cluster directly. The structural information obtained provides important insights into the mechanisms of the reactions taking place in PS II.

I. Introduction

Structural information is a prerequisite for complete understanding of Photosystem II (PS II) functions. PS II in its native form, however, contains nearly 30 polypeptides including the light-harvesting chlorophyll (Chl)-binding antenna proteins in higher plants and most eukaryotic algae or phycobilisomes in cyanobacteria and red algae (Chapter 2). Most of the protein subunits of PS II are intrinsic membrane proteins, and the total molecular mass of the native PS II complex exceeds 700 kDa. This complex is highly heterogeneous and liable to disintegration upon detergent solubilization of thylakoid membranes. The minimal oxygen-evolving complex (OEC) is depleted of light harvesting complex II (LHC II) proteins or phycobilisome proteins and consists of at least 17 polypeptides with a molecular mass of 320 kDa, among which 14 subunits are transmembrane and 3 are peripheral proteins. In addition to the protein components, the minimum PS II complex capable of O_2 evolution binds more than 40 cofactors including Chls, pheophytins (Pheos), Mn, Fe, carotenes (Cars), and possibly Ca^{2+} and Cl^- ions. Furthermore, the O_2-evolving activity of PS II from most mesophilic algae and higher plants is not stable for a long time at temperatures higher than 0 °C, e.g., from 20 °C to room temperature, which are often used for growing three-dimensional (3D) crystals. The complex nature and the instability of PS II presented a major challenge to obtaining good quality crystals for X-ray structural analysis. For this reason, structural analysis of PS II was first carried out using cryo-electron microscope of two-dimensional (2D) crystals obtained either from partially solubilized thylakoid membrane fragments or by reconstitution of the purified complexes into lipid bilayers (Nakazato et al., 1996; Morris et al., 1997; Rhee et al., 1998; Hankamer et al., 1999, 2001; Chapter 18). Recently, however, 3D crystals of PS II have been obtained from two closely related species of thermophilic cyanobacteria, *Thermosynecococcus elongatus* (formerly *Synechococcus elongatus*) (Zouni et al., 1998, 2000; Kuhl et al., 2000;) and *Thermosynechococcus vulcanus* (formerly *Syenchococcus vulcanus*) (Shen and Kamiya, 2000), largely owing to the use of the thermophilic cyanobacteria from which, highly purified, active, stable, intact and homogeneous PS II complexes could be obtained. These crystals retained a high activity of O_2 evolution, and have led to the structural analysis of PS II at reasonably high resolutions that allow identification of the positions of main subunits, and the determination of arrangements of transmembrane helices (TMHs) and most of the cofactors (Zouni et al., 2001b; Kamiya and Shen, 2003; Ferreira et al., 2004). We describe here the crystallization of PS II from various sources and the crystal structure of PS II from *T. vulcanus* in comparison with the structure of PS II from *T. elongatus* and the structure of bacterial reaction center (BRC).

Abbreviations: 2D – two-dimensional; 3D – three-dimensional; BRC – bacterial reaction center; Car – carotene; Chl – chlorophyll; Chl_{D1} and Chl_{D2} – two accessory Chl *a* molecules bound to D1 and D2 subunits, respectively; Chl Z_{D1} and Chl Z_{D2} – two peripheral Chl *a* molecules bound to D1 and D2 subunits, respectively; CP43 – Chl *a*-containing protein with apparent molecular mass of 43 kDa; CP47 – Chl *a*-containing protein with apparent molecular mass of 47 kDa; Cyt – cytochrome; DM – n-dodecyl-β-D-maltoside; OEC – oxygen evolving complex; P_{D1} and P_{D2} – PS II reaction center Chls bound to D1 and D2 subunits, respectively; PEG – polyethylene glycol; Pheo – pheophytin; PS II – Photosystem II; Q_A – primary plastoquinone acceptor; Q_B – secondary plastoquinone acceptor; RC – reaction center; TMH – transmembrane helix; Y_D – redox active tyrosine on D2; Y_Z – redox active tyrosine on D1

II. Crystallization

A. Two-Dimensional Crystallization

PS II exists mainly in stacked thylakoid membranes of green algae and higher plants in which, it is organized partly in a 2D crystal form naturally. In fact, PS II-enriched membrane fragments obtained by mild detergent solubilization of thylakoid membranes from higher plants have been found to contain partially ordered 2D crystals, which were used in the 2D crystal structure analysis by cryo-electron microscope (Morris et al., 1997; Hankamer et al., 1999, 2001). More highly ordered 2D crystals, however, have to be obtained by reconstitution of detergent-solubilized

PS II particles with exogenously supplemented lipids by the most commonly used methods for growing 2D crystals, namely, the dialysis method (Nakazato et al., 1996; Rhee et al., 1998; Chapter 18). So far, the best ordered 2D crystals were obtained for a so-called CP47-RC complex of spinach which has lost the CP43 subunit and all the three extrinsic proteins as well as O_2 evolution (Nakazato et al., 1996; Rhee et al., 1998; Chapter 18). Cryo-electron microscopy and 3D structure reconstitution have led to a PS II structure at 7-8 Å resolution from which, 23 transmembrane helices were resolved (Rhee et al., 1998; Chapter 18). Among these helices, 10 were assigned to the D1/D2 subunits by comparison with the BRC, and 6 to CP47. In addition, some of the helices were assigned to low-molecular mass subunits, and electron densities for reaction center (RC) Chls and some other antenna Chls were also assigned. The overall structure of this complex has been proved later by X-ray structural analysis of 3D crystals, although there are some apparent differences in the assignment of low molecular mass subunits as well as in the structure of the extrinsic 33 kDa protein (see below).

B. Three-Dimensional Crystallization

Due to the limited resolution of cryo-electron microscopy analysis of PS II 2D crystals and also the lack of CP43 and extrinsic proteins associated with the OEC in the preparations used for growing 2D crystals, more detailed structural information has to be obtained from X-ray crystallographic analysis of 3D crystals of PS II. Obtaining good-quality 3D crystals of PS II, however, presents a major challenge. Generally, purity, homogeneity and stability are among the most important factors for obtaining good quality 3D crystals of proteins. This is even more important for the PS II complex, since numerous factors affect the purity, homogeneity and stability of this very large and complicated membrane-protein complex. These include the source of organisms from which PS II is purified, detergents used for solubilization of the thylakoid membranes as well as for crystallization, purification procedures, the intactness of the complex obtained (especially with respect to the full attachment of the three extrinsic proteins required for O_2 evolution), pH and salts present in the final preparation, and the stability of the O_2-evolving activity at temperatures used for crystallization (which are often higher than 0 °C). The purity and homogeneity thus become very important for PS II, since it contains not only membrane-spanning subunits but also three peripheral components involved in O_2 evolution. The association between the three peripheral (extrinsic) proteins with the membrane proteins is much weaker than the association between membrane proteins. Thus, great care must be taken throughout the solubilization and purification procedures to maintain the intactness and homogeneity of purified PS II; in particular, every effort should be made in order not to lose even a small portion of the extrinsic proteins. This appears as a dilemma for purification: for the growth of good quality crystals the PS II complex needs to be as pure as possible, whereas for the full attachment of the extrinsic proteins and thus the retaining of high O_2-evolving activity an extensive purification procedure should be avoided. Practically, the balance between these is achieved from experience. The final step to obtain purified PS II from thermophilic cyanobacteria (as well as higher plants) is ion-exchange chromatography (Shen and Inoue, 1993; Zouni et al., 1998), during which the washing conditions (time and salt concentration) are controlled in order to remove the large amount of phycobiliproteins and other non-PS II components without any loss of the extrinsic proteins. PS II complexes thus prepared still contain some contaminating components but retain all of the three extrinsic proteins and a high O_2-evolving activity (Zouni et al., 1998, 2000; Kuhl et al., 2000; Shen and Kamiya, 2000); they were successfully used for crystallization (see below).

In addition to purity and homogeneity, stability is another important factor that needs to be considered. For membrane proteins and their complexes, finding a detergent with which the target membrane protein (complex) can be solubilized and exist stably is indispensable (Michel, 1990). For PS II, it has been found that n-dodecyl-β-D-maltoside (DM) is an efficient detergent that can solubilize and stabilize PS II complexes. Thus, successful crystallization of PS II has been performed in the presence of DM (Zouni et al., 1998, 2000; Kuhl et al., 2000; Shen and Kamiya, 2000). Another important factor that affects the stability is the temperature used for crystallization. Normally purified PS II is kept at around 0 °C for retaining the O_2-evolving activity but this temperature is not necessary optimum for growing membrane protein crystals (the PS II crystals so far obtained were grown at 20 °C, see below). This has been

overcome by using thermophilic cyanobacteria from which, PS II complexes stable enough at 20 °C could be obtained.

Initial trials for crystallization used PS II core complexes purified from higher plants (spinach, pea and rice) which retained the 33k Da extrinsic protein but were depleted of the 23 and 17 kDa extrinsic proteins (Fotinou et al., 1993; Adir, 1999; J. R. Shen, unpublished). The crystals were grown at 20 °C for 1–2 weeks with a hanging drop setup of the vapor diffusion method, with 6–10% polyethylene glycol (PEG) 4000 as precipitants and 0.4–1% DM as detergents in the sample (Adir, 1999; J. R. Shen, unpublished; Fig. 1A). PS II purified from higher plants exists in both dimeric and monomeric forms, both of which could be crystallized (Adir, 1999; J. R. Shen, unpublished). The resulting crystals typically had a hexagonal shape with sizes of 0.3 × 0.3 × 0.8 mm (Fig. 1A). While we have observed the crystal growth in the presence of only one detergent, e. g., DM, Adir has reported that well-shaped crystals could be obtained only by using a combination of two different detergents plus heptane-1,2,3-triol, which forms a three-components mixture. Ten different detergents were shown to promote crystal growth in nine different combinations. X-ray diffraction experiments showed that the crystals of higher plants diffracted to a maximum resolution of 5–6 Å, possibly with a hexagonal space group with unit-cell parameters a = 495, b = 495, c = 115 Å (Adir, 1999; J. R. Shen and N. Kamiya, unpublished). While Adir has shown that their crystals retained all of the subunits that were present in the samples before crystallization, we have found some degradation of PS II components after crystallization. The crystals from higher plants had a limited resolution and a very strong anisotropy in its diffraction pattern, which prevented further structural analysis with these crystals. This limited resolution and strong anisotropy may, at least partly, be attributable to the degradation of protein components observed during crystallization.

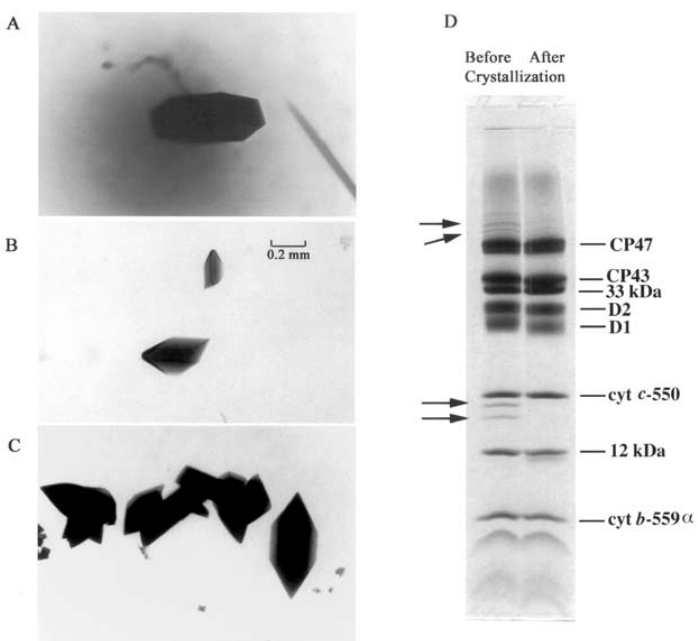

Fig. 1. A, PS II crystal from rice. B and C, Different sizes of PS II crystals from the thermophilic cyanobacterium *T. vulcanus*. Bar indicates 0.2 mm in all of the three panels. D, SDS-PAGE pattern of the cyanobacterial PS II core complex before and after crystallization. After crystallization, one single crystal was chosen and dissolved for SDS-PAGE analysis. Arrows indicate non-PS II components present in the sample before crystallization but were removed after crystallization.

Great progress was achieved when PS II preparations purified from thermophilic cyanobacteria were used for crystallization. These PS II core complexes are very stable at temperatures close to room temperature (Sugiura and Inoue, 1999), retained all of the three extrinsic proteins, namely the 33 kDa, 12 kDa proteins and Cyt c_{550}, and exhibited a very high O_2-evolving activity (Shen et al., 1992; Shen and Inoue, 1993; Sugiura and Inoue Y, 1999). Crystallization trials with these PS II preparations were performed with PS II from both *T. elongatus* and *T. vulcanus*. The first good-quality crystal was obtained with PS II from *T. elongatus* by Witt and his coworkers (Zouni et el., 1998; 2000). This was followed by success in crystallization of PS II from the same organism by Rogner's group (Kuhl et al., 2000), and that of PS II from *T. vulcanus* by the authors' group (Shen and Kamiya, 2000).

Crystals of *T. elongatus* were obtained with the batch method with PEG 2,000 as precipitant in the presence of DM at 20 °C (Zouni et al., 1998; 2000), or with the vapor diffusion method (Kuhl, 2000). Crystals of *T. vulcanus* were obtained with the micro-dialysis method, with 6–7% PEG1450 as precipitant in the presence of 0.02% DM at 20 °C (Shen and Kamiya, 2000). The crystals grew in 1–2 weeks to a typical size of 0.4 × 0.6 × 0.1 mm with a hexagonal shape, but larger sizes up to 0.8 × 1.2 × 0.3 mm could be obtained (Fig. 1B and C). SDS-PAGE analysis showed that the crystals retained all of the original PS II components presented in the preparation before crystallization (Fig. 1D). In addition, some contaminant bands presented in the preparations before crystallization were excluded in the crystals, indicating the successful incorporation of only PS II native components into the crystals. The crystals retained a high activity of O_2 evolution after crystallization measured either in the crystallized state under flash illumination (Zouni et al., 2000) or in solution after re-dissolving the crystals (Shen and Kamiya, 2000). Time-of-flight mass spectroscopic analysis has revealed that the crystal from *T. elongatus* contained at least 14 membrane-spanning subunits; they are: PsbA (D1), PsbB (CP47), PsbC (CP43), PsbD (D2), PsbE (α subunit of Cyt b_{559}), PsbF (β subunit of Cyt b_{559}), PsbH, PsbI, PsbJ, PsbK, PsbL, PsbM, PsbT, PsbX (Zouni et al., 2001a). In addition, three extrinsic proteins of 33 kDa (PsbO), Cyt c_{550} (PsbV), 12 kDa (PsbU) were included. These protein components together with Chls and other cofactors presented, give rise to a total molecular mass of 320 kDa for a PS II monomer.

PS II crystals from both *T. elongatus* and *T. vulcanus* are composed of PS II dimers with an apparent molecular mass of 580 kDa determined by gel filtration chromatography (Kuhl et al., 2000; Shen and Kamiya, 2000). They belong to the orthorhombic system with the space group of $P2_12_12_1$, and the unit cell dimensions a = 130 Å, b = 226 Å, c = 308 Å (Zouni et al., 1998; Kuhl et al., 2000; Shen and Kamiya, 2000). Four dimers existed in each unit cell; as a result, eight PS II monomers are included per unit cell. The V_M value, namely, the volume occupied by each standard molecular mass unit, was calculated to be 3.6 $Å^3$/Da, and the solvent content was estimated to be 66% in the crystals from *T. vulcanus* (Shen and Kamiya, 2000). The package of PS II dimers in the unit cell suggested that contacts between adjacent dimers are made mainly through interactions between two types of subunits: (i) Cyt c_{550} of one PS II dimer was found to be in close contact to the 12 kDa protein in an adjacent PS II dimer; (ii) The domain of extrinsic proteins (mainly the 33 kDa protein and 12 kDa protein) in one dimer is located in a position possibly in contact with loop regions extended from the TMHs of some small subunits in the adjacent dimers. These interactions are hydrophilic-hydrophilic interactions. In addition, the stromal side of one PS II dimer is faced to the stromal side of another PS II dimer; possible interactions in this region may also occur. The space between stromal sides of two adjacent PS II dimers, however, are rather large, and because not all of the hydrophilic loop regions in the stromal side have been identified, the interaction in this region cannot be determined unambiguously at present. In any case, the interaction between the stromal sides of two PS II dimers should also be hydrophilic, if it is to occur. These results indicate that hydrophilic interactions dominate the molecular contacts within the PS II crystal, and in particular, extrinsic proteins play an important role in crystallizing the cyanobacterial PS II. This may partially account for why good-quality crystals could not be obtained with higher plant PS II, since purified higher plant PS II contains only the 33 kDa protein but had lost the 23 kDa and 17 kDa proteins (Fotinou et al., 1993; Adir, 1999; J. R. Shen, unpublished). Thus, the PS II complex of higher plants has a relatively less hydrophilic area than the PS II complex from cyanobacteria. An effective approach to obtaining

good quality crystals from higher plant PS II would be to increase the hydrophilic surface area of the complex by means of binding the two lost extrinsic proteins or other hydrophilic molecules.

III. Crystal Structure of Photosystem II from Thermophilic Cyanobacteria

The first PS II crystal structure was solved by Witt and his co-workers at a 3.8 Å resolution with PS II from *T. elongatus* (Zouni et al., 2001b; Chapter 19, Witt). This was followed by the structural analysis of PS II from *T. vulcanus* at a 3.7 Å resolution (Kamiya and Shen, 2003). We describe here the crystal structure of PS II from *T. vulcanus* with comparisons with the structure of PS II from *T. elongatus* and that of the RC of photosynthetic purple bacteria.

A. Subunit Structure

The PS II structure from *T. vulcanus* was determined by the multiple heavy atom isomorphous replacement method. Real sequences of CP47, CP43, D1, D2, Cyt b_{559} α and β subunits, PsbK and extrinsic Cyt c_{550} were traced into the electron density map where applicable. The sequence tracing was performed with some of the large side chains of aromatic residues (His, Phe, Tyr and Trp) visible in the electron density map as markers (Kamiya and Shen, 2003). PsbI, PsbH, PsbX and the extrinsic 33 kDa, 12 kDa proteins were modeled as polyalanines for which, the direction of the polypeptides were determined but sequence alignment could not be achieved due to the lack of densities for side chains of appropriate aromatic residues as markers. Other low molecular mass subunits were represented as alpha carbon (Cα) structures for which, the identity and directions of the polypeptide chains could not be determined unambiguously. Gene-derived amino acid sequences of D1 and Cyt c_{550} used for structural construction were from *T. vulcanus*, whereas sequences of other subunits used were from *T. elongatus* (Nakamura et al., 2002), as the corresponding sequences from *T. vulcanus* are not available at present. Comparisons of the known sequences, however, have revealed that there are virtually no differences between sequences of the two organisms as far as photosynthetic proteins are concerned.

With the current structural model, a crystallographic *R*-value was calculated to be 0.53, and a root-mean-squares error was estimated to be 1.0 Å. These values indicate that shifts of one or two amino acid residues may frequently be included in the main-chain traces of the present structure.

1. Overall Structure

The overall structure of one PS II monomer from *T. vulcanus* consisted of 36 TMHs (Fig. 2A and B) and is similar to the structure reported for *T. elongatus* (Zouni et al., 2001b; Ferreira et al., 2004). This number of TMHs is more than what would be expected from the 14 transmembrane subunits identified by mass spectroscopic analysis of the PS II core complex: Each of the RC subunits D1 and D2 contains 5 TMHs; two large Chl-binding subunits CP47 and CP43 contain 6 TMHs each. These four large subunits account for 22 TMHs in total. In addition, there are 10 small subunits; each contains one TMH as expected from their sequences. Thus, PS II is predicted to contain 32 TMHs in total if we assume each of the small subunits is present in one copy per RC. The crystal structure of PS II showed 4 more TMHs than that were predicted. Two possibilities may account for this difference. First, there may be additional transmembrane, small subunits present in the PS II core complex that were failed to be identified by the mass spectroscopic analysis. Indeed, four more genes were found in the genome of *T. elongatus* which encode proteins with 1 TMH each and are homologous to subunits found in PS II of other organisms (Nakamura et al., 2002); the products of these genes were not identified in the PS II core complex used for crystallization by mass spectroscopy. These four genes were *psbN*, *psbY*, *psbW* and the gene encoding the PS II 11 kDa protein. These gene products may therefore be present in the PS II crystal. Second, some of the small subunits may be present in more than one copy in PS II. It is probable that both of these possibilities contributed to the difference in the number of TMHs between predicted and resolved.

2. Structure of the D1/D2 Subunits

In the PS II crystal structure, two monomers are arranged with a pseudo-two-fold symmetry to form a dimer. In the center of the PS II monomer, D1/D2 are arranged approximately symmetrically with respect to the transmembrane region (Fig. 2A, B and C), which is very similar to the structures of the L/M subunits in the BRC (Feher et al., 1989; Deisenhofer and Michel,

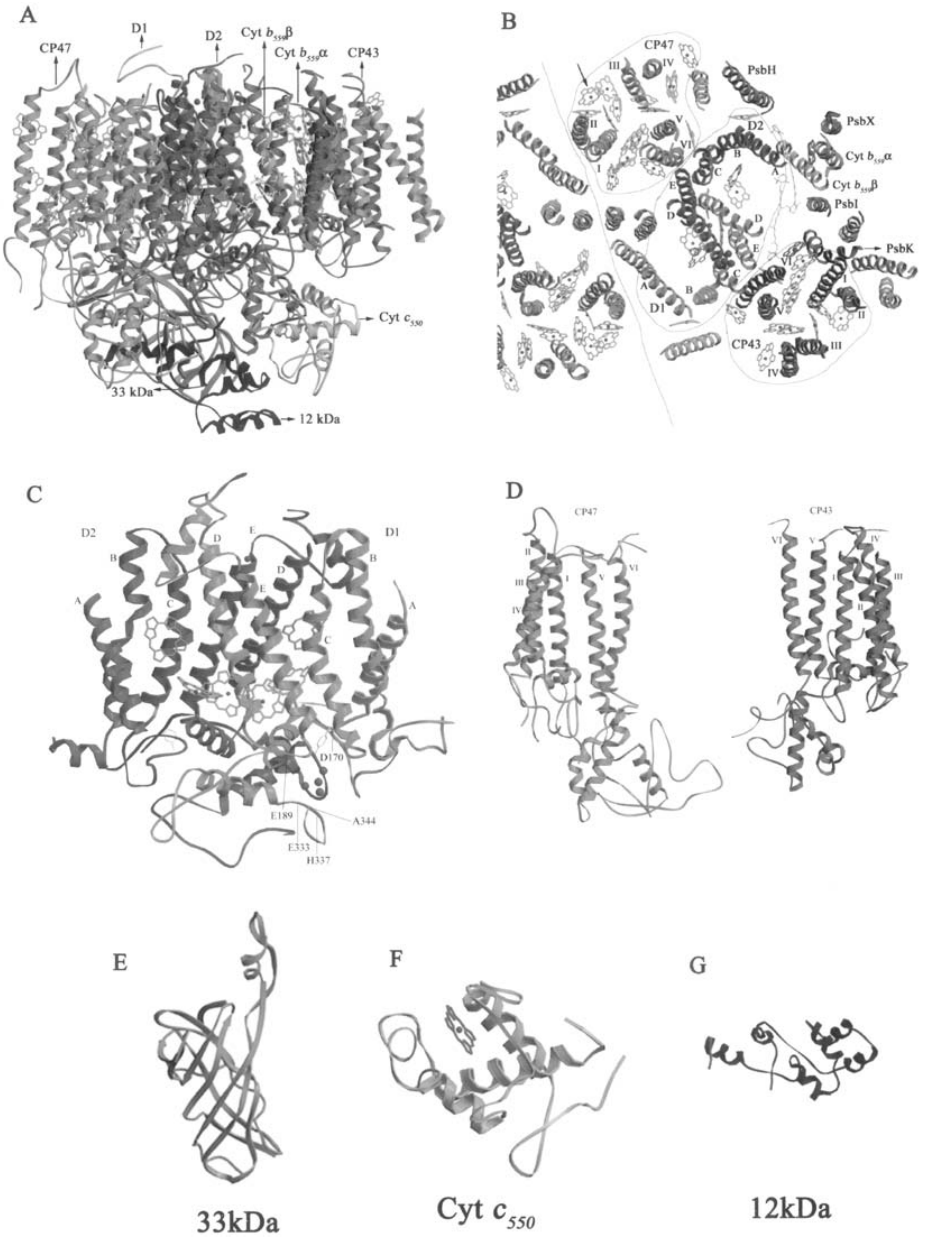

Fig. 2. Crystal structure of PS II from *T. vulcanus*. A, Side view of one PS II monomer. B, Top view of the transmembrane region from the lumenal side of one PS II monomer, together with part of a neighboring PS II monomer showing the formation of a PS II dimer in the crystal. TMHs of D1/D2 subunits are numbered A-E, and TMHs of CP47/CP43 are numbered I-VI. An arrow in B indicates one additional Chl found in CP47 of the structure of *T. vulcanus,* but not in the structure of *T. elongatus*. C, Structure of D1/D2 subunits. Four Chls and two Pheos are shown, together with Y_Z, Y_D and the Mn cluster. Residues possibly providing ligands to the Mn cluster were labeled. D, Structure of the CP47/CP43 subunits. E, Structure of the 33 kDa protein; F, Structure of Cyt c_{550}. G, Structure of the 12 kDa protein. See Color Plate 7, Fig. 1.

1991). The structure of D1, D2 subunits of *T. vulcanus* is also similar to that reported for *T. elongatus* (Zouni et al., 2001b; Ferriera et al., 2004). All five of the transmembrae helices (TMHs) of D1 and of D2 are tilted against the membrane plane, with the helix A and D of both D1 and D2 having the largest tilt angle (Fig. 2C). By analogy to the BRC and also from many mutational studies, D1-His198 and D2-His197 have been proposed to coordinate the two PS II RC Chls (Michel and Deisenhofer, 1988; Diner et al., 2001). This is indeed the case in our structure. D1-His215, D1-His272, D2-His214 and D2-His-268 are found to be close enough to provide coordination to the non-heme iron; this is consistent with predictions based on the sequence homology with the BRC (Michel and Deisenhofer, 1988; Svensson et al., 1996). Unlike the BRC structure, however, electron densities for residues close enough to serve as the fifth and sixth ligands to the non-heme iron are not found. Instead, nearby residues around the non-heme iron are found in the loop area immediately upstream from the DE helices of the D1 and D2 subunits on the stromal side; their distances to the non-heme iron are more than 3 Å longer than the distance from the fifth ligand, M-Glu232 (*Rp. virids* numbering) to the non-heme iron found in BRC (Deisenhofer and Michel, 1991). Thus, it is rather impossible for a direct ligation of the non-heme iron at its fifth and sixth coordinates by the nearby amino acid residues. Instead, our results support the well-documented notion that the non-heme iron in PS II is ligated by bicarbonate at the fifth and/or sixth coordinates (Diner and Petrouleas, 1990; Diner and Babcock, 1996; Chapters 8 and 14) as the electron density for the bicarbonate is not visible at the present resolution. The relatively close location of the loop region upstream of the DE helices of both D1 and D2 may imply that residues in this region may coordinate to the non-heme iron through the bicarbonate.

Another difference between the structures of PS II D1/D2 and BRC is the presence of two additional Chls (Chl Z_{D1} and Chl Z_{D2}, see below for a discussion of their function) in addition to the four closely related reaction center Chls in PS II. Mutagenesis studies have shown that these Chls are coordinated by D1-His118 and D2-His117, respectively (Lince and Vermaas, 1998; Stewart et al., 1998; Wang et al., 2002). The current structural model of *T. vulcanus* is consistent with this assignment.

In addition to TMHs, both D1 and D2 contain two α-helices in the lumenal side of the thylakoid membrane. One of them is the CD helix, and the other one is located close to the C-terminus of both subunits (Fig. 2C). The presence of the CD helix is similar to the structure of the BRC, but the presence of the C-terminal helix is different from that of the BRC (Deisenhofer and Michel, 1991). The structures of D1 and D2 are similar to each other and related by a local pseudo-two-fold symmetry; however, this symmetry is apparently broken in terms of the binding of the Mn cluster at the carboxyl (C)-terminal region of the D1 protein (see below).

3. Structure of the CP47/CP43 Subunits

The D1/D2 PS II RC is surrounded by CP47 and CP43, two large Chl-binding subunits serving as the inner antenna for the RC (Fig. 2A and B). Each of these subunits has six TMHs arranged approximately symmetrically (Fig. 2D). CP43 is located on the D1 side, and CP47 is on the D2 side (Fig. 2A and B). This is consistent with biochemical results which show that CP43 is more loosely bound to PS II than CP47 upon chaotropic or detergent treatments (Akabori et al., 1988; Yamaguchi et al., 1988). Since D1 undergoes rapid turnover in vivo, it requires a weaker association with other PS II components. The close location of D1 and CP43 is also consistent with results from photoinhibition studies in which D1 and CP43 were found to form cross-linking products under photoinhibition conditions (Ishikawa et al., 1999; Henmi et al., 2003).

The crystal structure shows that helix VI of CP47 is located close to helices E and C of D2; similarly, helix VI of CP43 is close to helices E and C of D1 (Fig. 2B). There are 11 and 10 conserved His residues in the transmembrane region of CP47 and CP43, respectively (Bricker and Frankel, 2002). All of these His residues are found to be close to a Chl molecule, suggesting that they are coordinated to the Chl molecules. There are, however, other Chl molecules that do not have a nearby His residue and are coordinated by other amino acid residues or inorganic ligands. The structures of CP47 and CP43 are similar to each other, especially in the transmembrane region (Fig. 2D) whose arrangement is also similar to that of PsaA and PsaB as noted previously (Rhee et al., 1998; Hankamer et al., 1999; Jordan et al., 2001). On the lumenal side, however, CP47 contains three helices, whereas CP43 has only two helices. Whether the lack of the third helix in the lumenal side of CP43 reflects its difference with

that of CP47 or is a result of the limited resolution currently available remains unclear. A clear difference does exist between CP47 and CP43 in their lumenal structures: CP47 has a large loop region between helix V and VI, the so-called E-loop, which has been proposed to be important for binding of the extrinsic 33 kDa protein and also for O_2 evolution (Bricker and Frankel, 2002), whereas CP43 has a shorter loop. The structure of the transmembrane region of CP47 and CP43 is similar to that reported for *T. elongatus* (Zouni et al., 2001b), but the latter structure was built as a Cα model with fewer residue numbers and also lacked the loop regions on the lumenal side.

4. Structure of the Low Molecular Mass Subunits

In addition to the four large subunits of PS II, several low molecular mass subunits have been assigned (Chapter 6, Thornton et al.). The α- and β-subunits of Cyt b_{559} are placed near the A helix of D2, based on the electron density of the heme moiety clearly visible in the electron density map (Fig. 2B). Only one heme is found in the transmembrane region of PS II, indicating that there is one Cyt b_{559} present per PS II in the crystal (Zouni et al., 2001b; Kamiya and Shen, 2003). This was confirmed by anomalous diffraction data collected at the peak and edge wavelengths of Fe atom from single PS II crystals (data not shown). We also determined that the number of Cyt b_{559} per PS II RC is close to one in our PS II preparations used for crystallization (K. Akabori and J. R. Shen, unpublished). These results suggest that the ratio of Cyt b_{559} per PS II is one, at least in the cyanobacterial PS II, and that no Cyt b_{559} is lost during crystallization. This is consistent with the fact that no significant loss of the O_2-evolving activity was observed in PS II after crystallization (Shen and Kamiya, 2000), as the loss of one Cyt b_{559} is expected to result in a significant decrease in O_2 evolution in view of the fact that deletion of Cyt b_{559} leads to a complete loss of O_2 evolution (Pakrasi et al., 1988, 1990, 1991).

In addition to Cyt b_{559}, four small subunits each bearing single TMH are assigned (Fig. 2B). PsbK was assigned to a significantly bended TMH based on the fact that it contains two Pro residues separated by two residues in the middle of its TMH (Nakamura et al., 2002), which is located in a position close to CP43. This is consistent with the result that PsbK is always co-purified with CP43 in a green algal PS II (Sugimoto and Takahashi, 2003). PsbX is assigned to a helix close to Cyt b_{559} α subunit since they were reported to cross-link with each other (Shi et al., 1999). Two helices surrounding Cyt b_{559} are assigned to PsbH and PsbI, respectively, based on the results that the former cross-links with PsbX (Büchel et al., 2001) and the latter cross-links with the Cyt b_{559} α subunit (Tomo et al., 1993). Among these two helices, PsbH is characterized by a longer TMH than PsbI, consistent with the results of secondary structure prediction (data not shown). The assignments of PsbH and PsbK in the *T. vulcanus* structure, however, are different from that in the *T. elongatus* structure (Zouni et al., 2001b). In the *T. elongatus* structure, these two subunits together with PsbL are placed in the central region of PS II dimer, e.g., a region joining two PS II monomers to form the PS II dimer. These assignments were based on the report that these subunits are found in PS II dimer but not in PS II monomer (Summer et al., 1997; Zheleva et al., 1998) in higher plant PS II and hence were proposed to be located in the region linking two PS II monomers. Different explanations, however, are possible for the loss of these subunits in the PS II monomer of higher plant PS II, e.g., they may be lost during the extensive detergent treatment to purify PS II monomer from dimer but not related to the PS II dimer formation. Alternatively, their location might be different between higher plant and cyanobacterial PS II. We should point out, however, that the assignments for these low molecular mass subunits in the crystal structure are tentative at present; conclusive assignments can only be attained when a higher resolution crystal structure is achieved.

Given the above small subunit assignments, there are four subunits whose positions remain to be resolved in the crystal structure but whose presence in PS II has been confirmed by mass spectroscopic analysis. They are PsbJ, PsbL, PsbM and PsbT, representing four TMHs assuming each contains one TMH. Considering that the number of TMHs resolved in the crystal structure is four more than predicted, there are eight TMHs in total that are not identified in the current crystal structure. As discussed above, these TMHs may be ascribed to some as yet unidentified low molecular mass subunits in the crystallized PS II or due to the presence of more than one copy of some known subunits.

5. Structure of the Extrinsic Proteins

On the lumenal side, three extrinsic proteins of 33 kDa, 12 kDa and Cyt c_{550} are assigned (Fig. 2A). They,

together with the large loop regions of D1, D2, CP47 and CP43 (some of which are still missing), form a large barrier which shields the Mn cluster from bulk solution. The 33 kDa manganese-stabilizing protein is characterized by an almost all β strand structure, with a very short helix located in a region close to the C-terminus (Fig. 2E). This large amount of β strand is consistent with the results of previous secondary structure predictions as well as spectroscopic measurements (Xu et al., 1994; Ahmed et al., 1995; Sonoyama et al., 1996; De Las Rivas and Heredia, 1999). The present model was built with polyalanines replacing real residues, and the number of alanines assigned represented 83.3% of the total residues of the 33 kDa protein (Kamiya and Shen, 2003). The protein has a cylindrical shape with dimensions of 20 Å in diameter and 45 Å in length (Fig. 2E). In addition, a 25-Å-long loop extends from one side of the cylinder. This structure of the 33 kDa protein is not compatible with the model constructed based on a combination of 3D structural prediction (Pazos et al., 2001) nor with the single-particle analysis by cryo-electron microscopy (Nield et al., 2002) of higher plant PS II. One of the possible causes for this difference may be that the 33 kDa protein has a different structure between higher plant and cyanobacterial PS II. Alternatively, the 33 kDa protein may adopt a different structure between solution and crystal, as the single-particle analysis was performed with PS II in solution and it was reported that the 33 kDa protein easily undergoes conformational changes in its isolated form (Lydakis-Simantiris et al., 1999; Shutova et al., 2000).

The overall shape of the 33 kDa protein, however, has some homology with those of the outer membrane proteins family OmpA (Pautsch and Schulz, 1998, 2000) and OmpX (Vogt and Schulz, 1999) in that both have a cylindrical shape. The structure of the outer membrane proteins is characterized by a general diffusion pore in its middle which allows the passage of small hydrophilic molecules with molecular weights up to 600 Da (Nakae and Nikaido, 1975; Benz and Bauer, 1988; Nikaido, 1992). The structure of the 33 kDa protein also reveals a pore inside the cylinder at this resolution. It is thus very attractive to assume that the 33 kDa protein functions by transporting small molecules in PS II; in particular water and O_2 which are the substrate and product respectively, for the water-splitting reaction that takes place at the Mn cluster located close to the 33 kDa protein. In fact, a hypothesis for the presence of a channel for water (Wydrzynski et al., 1996) and for O_2 (Anderson, 2001; Anderson and Chow, 2002) on the lumenal side has been proposed, taking into consideration that the Mn cluster is located close to the membrane surface but is largely shielded by the three extrinsic proteins and loop regions of D1, D2, CP47 and CP43. The transport of oxygen molecules immediately out of its generation site is especially important since the Mn cluster is very close to the RC Chls, which could very likely promote singlet oxygen generation via triplet Chl intermediates. This would result in an acceleration of photoinhibition of PS II (Chapter 27, Chow and Aro). Andersson (2001) proposed that water molecules may enter into the Mn cluster site via a specific pathway and O_2 may be directed out from the Mn cluster by a different hydrophobic channel, presumably formed in part by the 33 kDa protein and the required positioning of the large lumenal loop E of CP47. Whether CP47 has a role in transporting O_2 is not clear at present. Based on the crystal structure, a pore is located inside the 33 kDa protein and thus may not need CP47 for its formation and function. Since the 33 kDa protein is present in PS II from cyanobacteria to higher plants, a role of a channel for this protein would be universally consistent. Higher resolution structural analysis identifies a large pore (Ferriera et al., 2004; Chapter 21, Barber and Iwata). In this respect, it is interesting to note that the 33 kDa protein-deletion mutant of cyanobacterium *Synechocystis* sp. PCC 6803 shows a much faster dark-deactivation and a higher photoactivation efficiency with respect to flash numbers, than the wild-type cyanobacterium (Burnap et al., 1996). This has been interpreted to indicate that the 33 kDa protein shields the Mn cluster from access of bulk reductants which is the cause of dark-deactivation, and the access of Mn which is required for photoactivation. The loss of the 33 kDa protein caused easier access by both reductants and Mn to the Mn-binding site, resulting in a much faster dark-deactivation and higher photoactivation efficiency.

In addition to the extrinsic 33 kDa protein, the structures of two other extrinsic proteins, Cyt c_{550} and the 12 kDa protein were determined for *T. vulcanus* PS II (Fig. 2F and G). The structure of Cyt c_{550} represents 94.3% (129 out of the 137) residues of the protein, and contains 3 main α-helices. The overall structure of Cyt c_{550} associated with PS II of *T. vulcanus* is very similar to the structure of the same protein in an isolated form recently reported

for *Synechocystis* sp. PCC 6803 (Frazao et al., 2001), *Arthrospira maxima* (Sawaya et al., 2001), and *T. elongatus* (Kerfeld et al., 2003). Whether there are some structural differences in the protein between its free and PS II-associated forms, however, remains unclear at present due to the limited resolution of the PS II structure.

The structure of the 12 kDa protein was determined with *T. vulcanus* PS II. It shows an all-α-architecture consisting of 5 main α-helices (Fig. 2G). This structure has no homology with any known proteins when the currently available structural databases were searched and represents a new structure. The 12 kDa protein is located in between the 33 kDa protein and Cyt c_{550} but apart from the lumenal surface by approximately 30 Å. This is in agreement with results from in vitro release-reconstitution experiments, suggesting that this protein has no direct contact with the membrane and does not bind to PS II in the absence of the 33 kDa protein and Cyt c_{550} (Shen and Inoue, 1993). This location suggests that the 12 kDa protein helps to link the 33 kDa protein and Cyt c_{550} in the cyanobacterial PS II. As a result, the 33 kDa protein and Cyt c_{550} appears to interact not directly but through the 12 kDa protein. This is consistent with the independent roles of the 33 kDa protein and Cyt c_{550} have in cyanobacterial PS II, as revealed from comparisons of PS II function between the single deletion mutants (Burnap and Sherman, 1991; Burnap et al., 1992; Shen et al., 1995b) and double deletion mutants lacking both components (Shen et al., 1995a). The structural arrangement of these extrinsic proteins suggests a different organization of the extrinsic proteins i PS II of cyanobacteria and higher plants, since in higher plant PS IIs, 23 kDa protein cannot bind to PS II in the absence of the 33 kDa protein, and the 17 kDa protein cannot bind to PS II functionally in the absence of both the 33 kDa and 23 kDa proteins (Miyao and Murata, 1983, 1989). These results have been interpreted to indicate that the 33 kDa and 23 kDa proteins interact with each other directly, and the 17 kDa protein interacts with both the 33 kDa and 23 kDa proteins in higher plant PS II (Miyao and Murata, 1989).

6. Interactions Among the Different Subunits on the Lumenal Side

The three extrinsic proteins and the loop regions of CP47, CP43, D1 and D2 on the lumenal side form a large hydrophilic domain covering the membrane surface where the Mn cluster is located. Although not all of the loop regions are identified in the current structure, possible molecular interactions among different subunits may be pointed out. For example, CP47 is close to D2, the 33 kDa and 12 kDa proteins in some regions of their lumenal parts, suggesting possible interactions among these subunits. In particular, a close interaction between the large E-loop of CP47 and the extrinsic 33 kDa protein was found (Enami et al., 1987; Frankel and Bricker, 1989; Odom and Bricker, 1992). Similarly, part of the lumenal region of D2 was found to be close to those of D1, CP47, and the extrinsic 33 kDa protein; a part of D1 is close to CP43, D2, the 33 kDa protein and Cyt c_{550}; and a part of CP43 is close to D1 and all three extrinsic proteins in the lumenal side (Kamiya and Shen, 2003).

B. Arrangement of the Chlorophylls and Other Cofactors

1. Overall Arrangement of the Chlorophylls

Figures 3A and B show the overall arrangement of Chls and other cofactors in the PS II core complex. The Chls are located in three distinct regions occupied by CP47, CP43 and D1/D2, respectively. D1/D2 bind 6 Chls in total, which is the same in both the structure of *T. vulcanus* and *T. elongatus* (see below for a detailed functional discussion of these Chls). CP47 binds 17 Chls in the structure of *T. vulcanus*, which is one more than that found in the *T. elongatus* structure (Zouni et al., 2001b) (the density for the extra Chl found only in the *T. vulcanus* structure, however, was very weak). CP43 binds 12 Chls in *T. vulcanus* which is the same as that in the *T. elongatus*. We should point out that in the original structure reported for *T. vulcanus* PS II, there were 13 Chls assigned to CP43 (Kamiya and Shen, 2003). The extra Chl (Chl number 25) found only in the structure of *T. vulcanus* (for Chl numbering, see PDB file 1IZL) has a very weak electron density; upon improvement of electron density map by recalculations of reflection phases with the newly obtained molecular masks from the original structure, we found that the electron density for this extra Chl became much more weaker; thus we deleted this extra Chl in the modified structure (see below for the functional consequence of this modification).

An important feature of the overall arrangement of Chls in PS II is that most of the Chls in CP47 and CP43 are arranged as two clusters near the surface

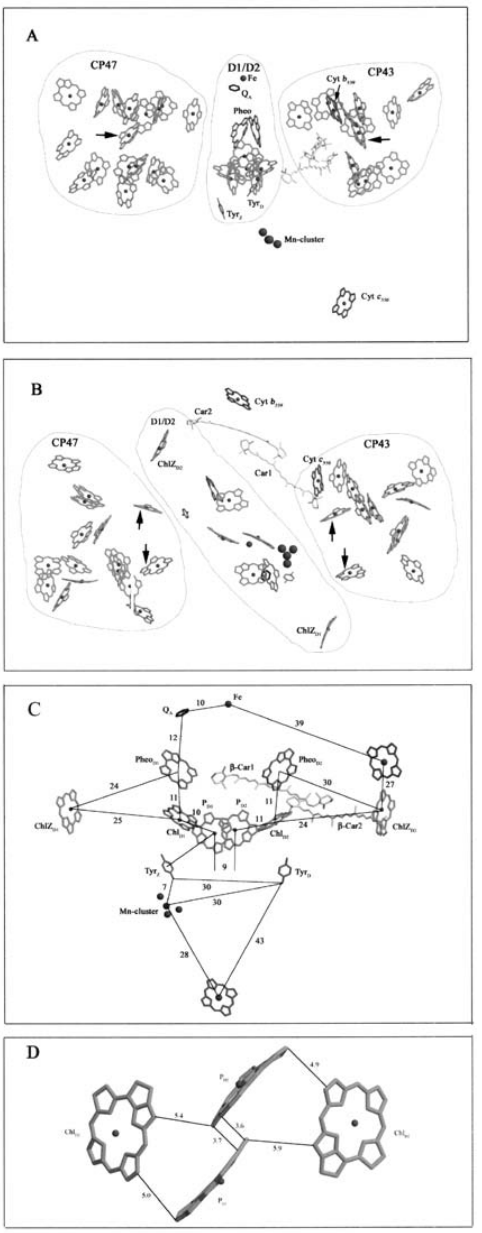

layers towards the stromal and lumenal sides of the membrane, whereas only one Chl is located in the middle of the membrane in both CP47 and CP43. The distances between adjacent Chls within the same surface layer are generally in the range of 8–12 Å, whereas the distances between Chls in the two surface layers are longer than 15–20 Å, except for the one Chl in the middle of the CP47 and the CP43 (marked with arrows in Fig. 3A), which have a distance of around 9–11 Å to the nearest Chl in either of the surface layers. This organization suggests that energy transfer within Chls in the same surface layer reaches equilibrium very fast, and that energy transfer between the different layers is mediated through the one middle Chl in both CP47 and CP43. Furthermore, two Chls in CP47 (arrows in Fig. 3B) and two in CP43 (arrows in Fig. 3B) are located most closely to the RC Chls. Thus, energy transfer from CP47 and CP43 to RC is most likely mediated by these four Chls (Vasil'ev et al., 2001). The distances between these Chls and the RC Chls, however, are in the range of 25-30 Å; this suggests that the energy transfer efficiency from CP47 and CP43 to the RC is not very high. These structural features of Chls are similar in PS II of *T. vulcanus* and *T. elongatus* (Chapter 19, Witt).

2. Reaction Center Chlorophylls and Other Cofactors

The arrangements of the RC Chls bound to the D1 and D2 subunits, together with other cofactors including two Pheos, two peripheral Chls Chl Z_{D1} and Chl Z_{D2}, the first bound quinone acceptor Q_A, non-heme iron, Y_Z and Y_D, Mn cluster, Cyt b_{559} and Cyt c_{550}, are shown in Fig. 3C. The second bound quinone accepter Q_B is not shown since it could not be identified in the present crystal structure either because of the limited resolution or the loss of the quinone in the core complex caused by the extended purification procedure. The arrangement of these cofactors determined for PS II of *T. vulcanus* (Kamiya and Shen, 2003) is largely

Fig. 3. Arrangement of Chls and other cofactors in *T. vulcanus* PS II. A, Side view. B, Top view from the stromal side. Chls bound to CP47, CP43 and D1/D2 subunits are separately circled. In addition, two Pheos, the first quinone acceptor Q_A, the non-heme Fe, Y_Z, Y_D, the Mn cluster, Cyt b_{559}, and Cyt c_{550} are shown. Arrows in panel A indicate one Chl in CP47 and one Chl in CP43 that are located in the middle between the two Chl layers near the stromal and lumenal surface, respectively. Arrows in panel B indicate two Chls in CP47 and two Chls in CP43, respectively, that are close to the RC and are thus possibly the mediators for energy transfer between bulk Chls bound to CP47, CP43 and the RC. C, Arrangement of functional components in the D1/D2 region of PS II and their relative distances (Å) from a side view along the membrane plane. D, An enlarged picture of the four Chls located in the center of PS II RC. Distances between the edges of each component are shown. See text for more details. See Color Plate 8, Fig. 1.

similar to those determined with PS II of *T. elongatus* (Zouni et al., 2001b; Ferreira et al., 2004; Chapters 19, Witt, and 21, Barber and Iwata).

On the oxidizing side, the distance between the center of the Mn cluster and Y_Z is 7 Å; this distance is consistent with spectroscopic measurements demonstrating a close proximity between Y_Z and the Mn cluster (Tang et al., 1996; Szalai et al., 1998). In the PS II RC, two Chls (P_{D1} and P_{D2}) are arranged parallel with each other; they are surrounded by two 'accessory Chls,' Chl_{D1} and Chl_{D2}, bound to the D1 and D2 subunits respectively. This arrangement is essentially the same as that of the BRC (Deisenhofer and Michel, 1991). The major difference between PS II RC and BRC is that the center-to-center distance between P_{D1} and P_{D2} in PS II RC is 9 Å; this distance is larger than the distance of 7.4–7.6 Å found for the BChl dimer in BRC (Deisenhofer and Michel, 1991; Feher et al., 1989). This suggests that the Chl dimer in PS II RC has a much weaker interaction than that in BRC; in other words, the two Chls in PS II RC have a stronger monomeric feature rather than dimeric. Moreover, the center-to-center distances between P_{D1} and the accessory Chl_{D1}, and between P_{D2} and Chl_{D2}, are 10 and 11 Å, respectively (Zouni et al., 2001b; Kamiya and Shen, 2003). These distances are only slightly longer than the distance between P_{D1} and P_{D2}; this has been taken as evidence suggesting a tetrameric organization of the four Chls in PS II RC (Durrant et al., 1995; Barber and Archer, 2001) rather than being a 'special' dimer surrounded by two 'accessory' Chls as in the BRC. A different situation, however, is found when the closest edge-to-edge distances among these Chls are examined. As Fig. 3D shows, the edge-to-edge distance between P_{D1} and P_{D2} is 3.6–3.7 Å, whereas those between P_{D1} and Chl_{D1}, and between P_{D2} and Chl_{D2}, are 5.0 Å and 4.9 Å, respectively. Thus, the distance between the two 'reaction center Chls' (P_{D1} and P_{D2}) is apparently shorter than those between the 'reaction center Chls' and 'accessory Chls' (Chl_{D1} and Chl_{D2}). Furthermore, the possible overlapping area between adjacent Chls appears larger for the two 'reaction center Chls' than those between 'reaction center Chls' and 'accessory Chls.' This suggests that the interaction between the two 'reaction center Chls' may be stronger than those between 'reaction center Chls' and 'accessory Chls'; in other words, PS II RC still has a dimeric feature. This dimeric feature, however, may be much weaker than the corresponding dimer in the BRC, and it is expected that the 'accessory Chls' may have a larger contribution to the energy and electron transfer in PS II than in the BRC, a notion implicated earlier from functional studies (Diner and Rappaport, 2002).

The center-to-center distances between Chl_{D1} and $Pheo_{D1}$, and between Chl_{D2} and $Pheo_{D2}$, are 11 Å and 12 Å, respectively. This is also close to the center-to-center distances between 'reaction center Chls' or between 'reaction center Chls' and 'accessory Chls.' The edge-to-edge distances between Chl_{D1} and $Pheo_{D1}$, and between Chl_{D2} and $Pheo_{D2}$, are 6.1 Å and 5.6 Å, respectively, which are longer than that between the two 'reaction center Chls'. In addition to these six pigments located in the center of PS II RC, two peripheral Chls Chl Z_{D1} and Chl Z_{D2} coordinated by D1-His118 and D2-His117 are identified; they are located 25 Å and 24 Å apart from Chl_{D1} and Chl_{D2} respectively. These distances are similar to the distances from Chl_{D1} and Chl_{D2} to the closest Chls in CP43 and CP47. This suggests that Chl Z_{D1} and Chl Z_{D2} are not efficient energy mediators to PS II RC.

Oxidation of Chl Z_{D1} or Chl Z_{D2} by PS II RC has been observed under some conditions where electron donation from Y_Z and/or the Mn cluster is limited or inhibited; e.g., under low temperature or with excess light illumination under which the rate of water-splitting reaction cannot compensate for the rate of primary charge separation (Visser et al., 1977; Faller et al., 2001; Tracewell et al., 2001a). Under these conditions, oxidation of β-Car (Schenck et al., 1982; Noguchi et al., 1994; Hanley et al., 1999; Tracewell et al., 2001b; Telfer et al., 2003; Tracewell and Brudvig, 2003) and Cyt b_{559} (Cramer, 1986; Stewart and Brudvig, 1998) are also observed. The electron donation from Chl Z_{D1} or Chl Z_{D2}, β-Car or Cyt b_{559}, to PS II RC, has been termed secondary, alternative or side electron transfer reactions (Hanley et al., 1999; Tracewell et al., 2001a; Chapter 15). In green algae and higher plants, Chl Z_{D2} has been identified to be the electron donor to PS II RC (Shigemori et al., 1998; Wang et al., 2002), whereas in cyanobacteria, Chl Z_{D1} rather than Chl Z_{D2} was reported to be oxidized by the RC (Stewart et al., 1998). The crystal structure revealed that the distances from Chl Z_{D1}, Chl Z_{D2} or Cyt b_{559} to the RC are rather far (the center-to-center distance between Cyt b_{559} and Chl_{D2} is 31 Å), making them difficult to donate electrons to the RC directly.

In the crystal structure of *T. vulcanus*, two β-Car molecules are identified. They are both located in the D2-side and in a space between Chl Z_{D2} and Chl_{D2}, and between Cyt b_{559} and Chl_{D2} (Fig. 3C). β-Car1 was an

all-*trans*-type, whereas β-Car2 was a *cis*-type in the initial structure (Kamiya and Shen, 2003). Similar to the situation found for the extra Chl (Chl No. 25) mentioned previously, however, the electron density for the cis-type β-Car2 has decreased in our recently improved electron density map. In contrast, a long, straight electron density distribution appeared in an adjacent area of the cis-type β-Car2. Based on the improved electron density map, we consider that β-Car2 is also a trans-type and its position should be slightly shifted toward Chl Z_{D2} than that was originally assigned. Based on this modified structure, the edge-to-edge distances between Chl Z_{D2} and β-Car2, and between Cyt b_{559} and β-Car2, are 5 Å and 14 Å, respectively. Furthermore, the distances between β-Car1 and β-Car2, between β-Car1 and Chl_{D2}, are 5 Å and 9 Å, respectively. These results suggest that the secondary or side electron transfer reactions may occur via two pathways; one is electron transfer from Chl Z_{D2} through β-Car2, β-Car1, to Chl_{D2} in RC, and the other one is electron transfer from Cyt b_{559} through β-Car2, β-Car1, to Chl_{D2}. A third pathway of electron transfer from Cyt b_{559} through Chl Z_{D2} to the RC has also been postulated (Tracewell et al., 2001a). The current crystal structure, however, indicates that the distance between Cyt b_{559} and Chl Z_{D2} is rather long (center-to-center distance of 27 Å, Fig. 3C). Thus, secondary electron transfer via this third pathway is rather unlikely.

It should be pointed out that in cyanobacteria, Chl Z_{D1} has been suggested to be the electron donor in the secondary electron transfer reactions from results of site-directed mutagenesis and resonance Raman spectroscopy (Stewart et al., 1998). Indeed, such an electron transfer pathway has been proposed involving Car1, Car2, and a chain of Chls bound to CP43 based on the published structure of *T. vulcanus* (Vasil'ev et al., 2003). This pathway depends critically on the presence of the 'extra' Chl (C25 in Kamiya and Shen, 2003) which is found in the *T. vulcanus* structure but not in the *T. elongatus* structure (Zouni et al., 2001b). The electron density for this 'extra' Chl, however, was very weak, and thus the assignment of this Chl in the original structure was tentative. Upon improvement of the electron density as described above, we found that the assignment of this 'extra' Chl is most probably incorrect. This 'extra' Chl should therefore be removed from the *T. vulcanus* structure. As a result, the secondary electron transfer pathway from Chl_{D1} through a chain of Chl on CP43 becomes less possible. This is in agreement with the above conclusion that Chl_{D2} is the donor in the secondary electron transfer reactions in the thermophilic cyanobacterial PS II, a situation similar to that has been reported for green algal and higher plant PS II (Shigemori et al., 1998; Wang et al., 2002). The experimental results reported with cyanobacterial PS II, however, is not consistent with this conclusion at present.

C. Structure of the Manganese Cluster and Its Environment

The Mn cluster consists of four Mn atoms and is the site of the water-splitting reaction. The shape of the Mn cluster is represented by a triangular shaped electron density contoured at 5.0 σ (Fig. 4). A most possible model fitting this electron density is that three Mn atoms are positioned in the large area of the density and one Mn atom positioned in the opposite, small area of the density (Fig. 4). This model is similar to that reported for *T. elongatus* (Zouni et al., 2001b), with the Mn-Mn distances ranging in 2.7-3.3 Å between immediately adjacent Mn atoms, agreeing with the results obtained from EXAFS spectra of various PS II preparations (Chapter 10). The four Mn atoms thus assigned are located roughly in a same plane tilted against the membrane surface plane by 36 degree in the lumenal side. A tilting of 24 degree has been reported for the *T. elongatus* structure (Zouni et al., 2001b).

From an electron density map contoured at 1.0 σ (Kamiya and Shen, 2003), residues that are possible to provide coordination to the Mn cluster were deduced. First of all, a strong density entering into the Mn cluster is found; this density is connected to a polypeptide main chain. Moreover, this density terminates just at the Mn cluster. According to the structural model, the polypeptide main chain assigned to this density was the C-terminal of the D1 subunit (Fig. 4). This suggests that the C-terminal carboxyl group of D1, namely D1-Ala344, provides ligands directly to the Mn cluster. This is in agreement with many mutagenesis studies suggesting the possible ligation of the Mn cluster by D1-C-terminus (Debus, 2000; 2001; Diner, 2001). Other residues possibly providing coordination to the Mn cluster are D1-Asp170 and D1-Glu333 (and/or D1-His332); connections from these residues to the Mn cluster are visible in the electron density map at a 1.0 σ level. In addition, D1-His337 and D1-Asp189 had weak connections to the Mn cluster with electron densities visible at a 0.2 σ level; these residues are therefore also possible to provide coordination to the Mn cluster. All these

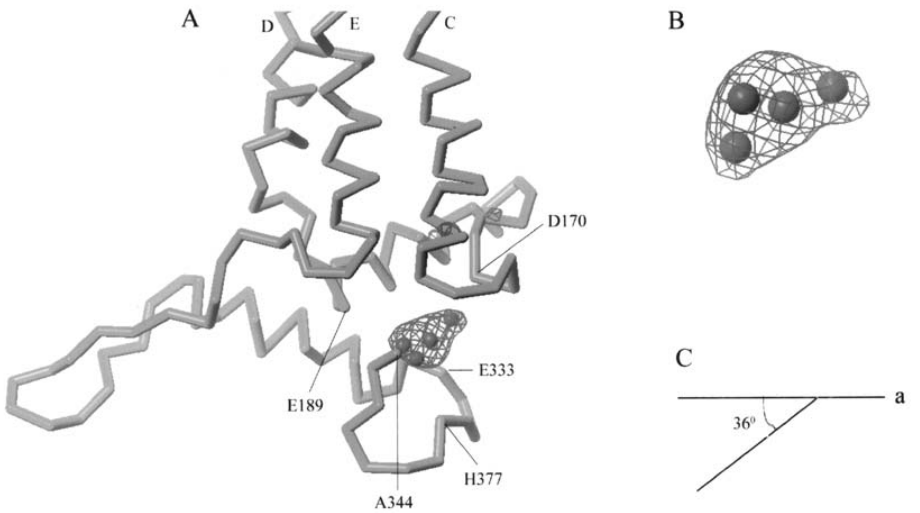

Fig. 4. Structure of the Mn cluster and its surrounding environment. A, Side view from the membrane plane. Electron density contoured at 5.0σ is shown, together with the polypeptide main chains in the region near the Mn cluster. TMHs labeled C, D and E were from the D1 polypeptide; residues located close to the Mn cluster are marked. B, Top view from the lumenal side of an enlarged picture of the electron density for the Mn cluster contoured at 5.0σ. C, The angle of the plane harboring the four Mn atoms against the membrane plane at the lumenal surface. Axis *a* represents a plane parallel to the membrane plane.

residues have been suggested as possible ligands to Mn from a number of mutagenesis studies (Debus, 2000, 2001; Diner, 2001) or chemical modification studies (Preston and Seibert, 1991). In addition to these residues, D1-Asa342 has been suggested as a possible ligand to Mn from mutagenesis studies (Debus, 2000, 2001). This possibility cannot be excluded unambiguously from the recently improved electron density map. The structural model also implies that no polypeptide carbonyl oxygen except the C-terminus of D1 is able to provide coordination to the Mn cluster, since no polypeptide main chain was found to be located close enough to the Mn cluster in order for their carbonyl oxygen to connect to the Mn cluster directly. We should point out here that these discussions on the possible ligands of the Mn cluster are based on the current resolution which is not high enough to give an unambiguous picture of the Mn cluster. (For a recent refined structure, see Ferreira et al., 2004; Chapter 21, Barber and Iwata.)

IV. Future Prospects and Concluding Remarks

Significant progress has been achieved on the understanding of reaction mechanisms of PS II based on the 3D crystallographic analysis of PS II from thermophilic cyanobacteria. The current resolution, however, is not high enough to give a full picture of the PS II structure at a real atomic level. Efforts toward improving the crystal resolution are underway, and it is expected that a real atomic resolution of PS II structure may be obtained in the near future. What remains challenging is that possible structural changes accompanying electron transfer at both the donor and acceptor sides need to be clarified at the atomic level; in particular, structural changes accompanying the oxidation of the Mn cluster are to be clarified. These may be achieved by time-resolved X-ray crystallography of high quality crystals combined with trapping of reaction intermediates at some specific temperatures using the crystal. In parallel, structural analysis of higher plant PS II is to be achieved. Since higher plant PS II has a different set of extrinsic proteins than that of cyanobacteria, structural differences in the hydrophilic, lumenal domain surrounding the Mn cluster are expected. Crystallization of higher plant PS II may be facilitated by binding of all of the three extrinsic proteins as is the case with the thermophilic cyanobacterial PS II, or by binding of some other hydrophilic molecules, for example, Fv fragments of some specific antibodies, to increase the hydrophilic surface of PS II. Finally, various mutants

of cyanobacteria are available; structural analysis of these mutants will significantly contribute to our understanding on the roles of individual subunits or residues in PS II. Information yielded from these lines of studies will ultimately lead to a complete elucidation of the structure and function of PS II.

Acknowledgments

We thank Drs. H. Ago, M. Miyano, M. Aoyama and Y. Shiro of RIKEN Harima Institute for their valuable suggestions to our original structure of PS II. Work performed in the authors' laboratories was supported in part by grants-in-aid for Scientific Research from the Ministry of Education, Science and Culture of Japan.

References

Adir N (1999) Crystallization of the oxygen-evolving reaction centre of Photosystem II in nine different detergent mixtures. Acta Crystallogr D Biol Crystallogr 55: 891–894

Ahmed A, Tajmir-Riahi HA and Carpentier R (1995) A quantitative secondary structure analysis of the 33 kDa extrinsic polypeptide of Photosystem II by FTIR spectroscopy. FEBS Lett 363: 65–68

Akabori K, Tsukamoto H, Tsukihara J, Nagatsuka T, Motokawa O and Toyoshima Y (1988) Disintegration and reconstitution of Photosystem II reaction center core complex. I. Preparation and characterization of three different types of subcomplexes. Biochim Biophys Acta 932: 345–357

Anderson JM (2001) Does functional Photosystem II complex have an oxygen channel? FEBS Lett 488: 1–4

Anderson JM and Chow WS (2002) Structural and functional dynamics of plant Photosystem II. Phil Trans R Soc London B 3072: 1421–1430

Barber J and Archer MD (2001) P680, the primary electron donor of Photosystem II. J Photochem Photobiol A 142: 97–106

Benz R and Bauer K (1988) Permeation of hydrophilic molecules through the outer membrane of Gram-negative bacteria. Review on Bacterial porins. Eur J Biochem 176: 1–19

Bricker TM and Frankel LK (2002) The structure and function of CP47 and CP43 in Photosystem II. Photosynth Res 72: 131–146

Büchel C, Morris E, Orlova E and Barber J (2001) Localisation of the PsbH subunit in Photosystem II: A new approach using labelling of His-tags with a Ni(2+)-NTA gold cluster and single particle analysis. J Mol Biol 312: 371–379

Burnap RL and Sherman L (1991) Deletion mutagenesis in *Synechocystis* sp. PCC6803 indicates that the Mn-stabilizing protein of Photosystem II is not essential for O_2 evolution. Biochemistry 30: 440–446

Burnap RL, Shen JR, Jursinic PA, Inoue Y and Sherman L (1992) Oxygen yield and thermoluminescence characteristics of a cyanobacterium lacking the manganese- stabilizing protein of Photosystem II. Biochemistry 31: 7404–7410

Burnap RL, Qian M and Pierce C (1996) The manganese stabilizing protein of Photosystem II modifies the in vivo deactivation and photoactivation kinetics of the H_2O oxidation complex in *Synechocystis* sp. PCC6803. Biochemistry 35: 874–882

Cramer WA, Theg SM and Widger WR (1986) On the structure and function of cytochrome b_{559}. Photosynth Res 10: 393–403

Debus RJ (2000) The polypeptides of Photosystem II and their influence on manganotyrosyl-based oxygen evolution. In: Sigel A and Sigel H (eds), Metal Ions in Biological Systems, pp 657–711. Marcel Dekker Inc, New York

Debus RJ (2001) Amino acid residues that modulate the properties of tyrosine Y_Z and the manganese cluster in the water oxidizing complex of Photosystem II. Biochim Biophys Acta 1503: 164–186

Deisenhofer J and Michel H (1991) High-resolution structures of photosynthetic reaction centers. Annu Rev Biophys Biophys Chem 20: 247–266

De Las Rivas J and Heredia P, (1999) Structural predictions on the 33 kDa extrinsic protein associated to the oxygen evolving complex of photosynthetic organisms. Photosynth Res 61: 11–21

Diner BA (2001) Amino acid residues involved in the coordination and assembly of the manganese cluster of Photosystem II. Proton-coupled electron transport of the redox-active tyrosines and its relationship to water oxidation. Biochim Biophys Acta 1503: 147–163

Diner BA and Babcock GT (1996) Structure, dynamics, and energy conversion efficiency in Photosystem II. In: Ort DR and Yocum CF (eds) Oxygenic Photosynthesis: The Light Reactions, pp 213–247. Kluwer Academic Publishers, Dordrecht

Diner BA and Petrouleas V (1990) Formation by NO of nitrosyl adducts of redox components of the Photosystem II reaction center. II. Evidence that HCO_3^-/CO_2 binds to the acceptor-side non-heme iron. Biochim Biophys Acta 1015: 141–149

Diner BA and Rappaport F (2002) Structure, dynamics, and energetics of the primary photochemistry of Photosystem II of oxygenic photosynthesis. Annu Rev Plant Biol 53: 551–580

Diner BA, Schlodder E, Nixon PJ, Coleman WJ, Rappaport F, Lavergne J, Vermaas WFJ and Chisholm DA (2001) Site-directed mutations at D1-His198 and D2-His197 of Photosystem II in *Synechocystis* PCC 6803: Site of primary charge separation and cation and triplet stabilization. Biochemistry 40: 9265–9281

Durrant JR, Klug D, Kwa SLS, Grondelle RV, Porter G and Dekker JP (1995) A multimer model for P680, the primary electron donor of Photosystem II. Proc Natl Acad Sci USA 92: 4798–4802

Enami I, Satoh K and Katoh S (1987) Crosslinking between the 33 kDa extrinsic protein and the 47 kDa chlorophyll-carrying protein of the PS II reaction center core complex. FEBS Lett 226: 161–165

Faller P, Maly T, Rutherford AW and MacMillan F (2001) Chlorophyll and carotenoid radicals in Photosystem II studied by pulsed ENDOR. Biochemistry 40: 320–326

Feher G, Allen JP, Okamura MY and Rees DC (1989) Primary processes in bacterial photosynthesis: Structure and function of reaction centers. Nature 339: 111–116

Ferreira K, Iverson T, Maghlaoui K, Barber J and Iwata S (2004) Architecture of the photosynthetic oxygen evolving center.

Science 303: 1831–1838
Fotinou C, Kokkinidis M, Fritzsch G, Haase W, Michel H and Ghanotakis DF (1993) Characterization of a photosystem-II core and its 3-D crystals. Photosynth Res 37: 41–48
Frankel LK and Bricker TM (1989) Epitope mapping of the monoclonal antibody FAC2 on the apoprotein of CPa-1 in Photosystem II. FEBS Lett 257: 279–282
Frazao C, Enguita FJ, Coelho R, Sheldrick GM, Navarro JA, Hervas M, De la Rosa MA and Carrondo MA (2001) Crystal structure of low-potential cytochrome c_{549} from *Synechocystis* sp PCC 6803 at 1.21 Ångstrom resolution. J Biol Inorg Chem 6: 324–332
Hankamer B, Morris EP and Barber J (1999) Revealing the structure of the oxygen-evolving core dimer of Photosystem II by cryoelectron crystallography. Nat Struct Biol 6: 560–564
Hankamer B, Morris E, Nield J, Gerle C and Barber J (2001) Three-dimensional structure of the Photosystem II core dimer of higher plants determined by electron microscopy. J Struct Biol 135: 262–269
Hanley J, Deligiannakis Y, Pascal A, Faller P and Rutherford AW (1999) Carotenoid oxidation in Photosystem II. Biochemistry 38: 8189–8195
Henmi T, Yamasaki H, Sakuma S, Tomokawa Y, Tamura N, Shen JR and Yamamoto Y (2003) Dynamic interaction between the D1 protein, CP43 and OEC33 at the lumenal side of Photosystem II in spinach chloroplasts: Evidence from light-induced cross-linking of the proteins in the donor-side photoinhibition. Plant Cell Physiol 44, 451–456
Ishikawa Y, Nakatani E, Henmi T, Ferjani A, Harada Y, Tamura N and Yamamoto Y (1999) Turnover of the aggregates and cross-linked products of the D1 protein generated by acceptor-side photoinhibition of Photosystem II. Biochim Biophys Acta 1413: 147–158
Jordan P, Fromme P, Witt HT, Klukas O, Saenger W and Krauß N (2001) Three-dimensional structure of cyanobacterial Photosystem I at 2.5 Å resolution. Nature 411: 909–916
Kamiya N and Shen JR (2003) Crystal structure of oxygen-evolving Photosystem II from *Thermosynechococcus vulcanus* at 3.7-Å resolution. Proc Natl Acad Sci USA 100: 98–103
Kerfeld CA, Sawaya MR, Bottin H, Tran KT, Sugiura M, Cascio D, Desbois A, Yeates TO, Kirilovsky D and Boussac A (2003) Structural and EPR characterization of the soluble form of cytochrome c_{550} and of the *psb*V2 gene product from the cyanobacterium *Thermosynechococcus elongatus*. Plant Cell Physiol 44: 697–706
Kuhl H, Kruip J, Seidler A, Krieger-Liszkay A, Bunker M, Bald D, Scheidig AJ and Rogner M (2000) Towards structural determination of the water-splitting enzyme. Purification, crystallization, and preliminary crystallographic studies of Photosystem II from a thermophilic cyanobacterium. J Biol Chem 275: 20652–20659
Lince MT and Vermaas WFJ (1998) Association of His117 in the D2 protein of Photosystem II with a chlorophyll that affects excitation-energy transfer efficiency to the reaction center. Eur J Biochem 256: 595–602
Lydakis-Simantiris N, Hutchison RS, Betts SD, Barry BA and Yocum CF (1999) Manganese stabilizing protein of Photosystem II is a thermostable, natively unfolded polypeptide. Biochemistry 38: 404–414
Michel H (1990) Crystallization of Membrane Proteins. CRS Press, Florida
Michel H and Deisenhofer J (1988) Relevance of the photosynthetic reaction center from purple bacteria to the structure of Photosystem II. Biochemistry 27: 1–7
Miyao M and Murata N (1983) Partial disintegration and reconstitution of the photosynthetic oxygen evolution system: Binding of 23 kilodalton and 18 kilodalton polypeptides. Biochim Biophys Acta 725: 87–93
Miyao M and Murata N (1989) The mode of binding of three extrinsic proteins of 33 kDa, 23 kDa, and 18 kDa in the Photosystem II complex of spinach. Biochim Biophys Acta 977: 315–321
Morris EP, Hankamer B, Zheleva D, Friso G and Barber J (1997) The three-dimensional structure of a Photosystem II core complex determined by electron crystallography. Structure 5: 837–849
Nakae T and Nikaido H (1975) Outer membrane as a diffusion barrier in *Salmonella typbimurium*. Penetration of oligo- and polysaccharides into isolated outer membrane vesicles and cells with degraded peptidoglycan layer. J Biol Chem 250: 7359–7365
Nakamura Y, Kaneko T, Sato S, Ikeuchi M, Katoh H, Sasamoto S, Watanabe A, Iriguchi M, Kawashima K, Kimura T, Kishida Y, Kiyokawa C, Kohara M, Matsumoto M, Matsuno A, Nakazaki N, Shimpo S, Sugimoto M, Takeuchi C, Yamada M and Tabata S (2002) Complete genome structure of the thermophilic cyanobacterium *Thermosynechococcus elongatus* BP-1. DNA Res 9: 123–30
Nakazato K, Toyoshima C, Enami I and Inoue Y (1996) Two-dimensional crystallization and cryo-electron microscopy of Photosystem II. J Mol Biol 257: 225–32
Nield J, Balsera M, De Las Rivas J and Barber J (2002) Three-dimensional electron cryo-microscopy study of the extrinsic domains of the oxygen-evolving complex of spinach: Assignment of the PsbO protein. J Biol Chem 277: 15006–15012
Nikaido H (1992) Porins and specific channels of bacterial outer membranes. Mol Microbiol 6: 435–442
Noguchi T, Mitsuka T and Inoue Y (1994) Fourier transform infrared spectrum of the radical cation of beta-carotene photoinduced in Photosystem II. FEBS Lett 356: 179-182
Odom WR and Bricker TM (1992) Interaction of CPa-I with the manganese-stabilizing protein of Photosystem II: Identification of domains crosslinked by 1-ethyl-3-[3-(dimethylamino)propyl]carbodiimide. Biochemistry 31: 5616–5620
Pakrasi HB, Williams JGK and Arntzen CJ (1988) Targeted mutagenesis of the *psb*E and *psb*F genes blocks photosynthetic electron transport: Evidence for a functional role of cytochrome b_{559} in Photosystem II. EMBO J 7: 325–332
Pakrasi HB, Nyhus KJ and Granok H (1990) Targeted deletion mutagenesis of the β-subunit of cytochrome b_{559} protein destabilizes the reaction center of Photosystem II. Z Naturforsch 45c: 423–429
Pakrasi HB, Ciechi PD and Whitmarsh J (1991) Site directed mutagenesis of the heme axial ligands of cytochrome b_{559} affects the stability of the Photosystem II complex. EMBO J 10: 1619–1627
Pautsch A and Schulz GE (1998) Structure of the outer membrane protein A transmembrane domain. Nat Struct Biol 5: 1013–1017
Pautsch A and Schulz GE (2000) High-resolution structure of the OmpA membrane domain. J Mol Biol. 298:273–282.

Pazos F, Heredia P, Valencia A and De Las Rivas J (2001) Threading structural model of the manganese-stabilizing protein PsbO reveals presence of two possible β-sandwich domains. Proteins Struct Funct Genet 45: 372–381

Preston C and Seibert M (1991) Protease treatments of Photosystem II membrane fragments reveal that there are four separate high-affinity Mn-binding sites. Biochemistry 30: 9625–9633

Rhee KH, Morris EP, Barber J and Kuhlbrandt W (1998) Three-dimensional structure of the plant Photosystem II reaction centre at 8 Å resolution. Nature 396: 283–286

Sawaya MR, Krogmann DW, Serag A, Ho KK, Yeates TO and Kerfeld CA (2001) Structures of cytochrome c_{549} and cytochrome c_6 from the cyanobacterium *Arthrospira maxima*. Biochemistry 40: 9215–9225

Schenck CC, Diner B, Mathis P and Satoh K (1982) Flash-induced carotenoid radical cation formation in Photosystem II. Biochim Biophys Acta 680: 216–227

Shen JR and Inoue Y (1993) Binding and functional properties of two new extrinsic components, cytochrome c_{550} and a 12 kDa protein, in cyanobacterial Photosystem II. Biochemistry 32: 1825–1832

Shen JR and Kamiya N (2000) Crystallization and the crystal properties of the oxygen-evolving Photosystem II from *Synechococcus vulcanus*. Biochemistry 39: 14739–14744

Shen JR, Ikeuchi M and Inoue Y (1992) Stoichiometric association of extrinsic cytochrome c_{550} and 12 kDa protein with a highly purified oxygen-evolving Photosystem II core complex from *Synechococcus vulcanus*. FEBS Lett 301: 145–149.

Shen JR, Burnap RL and Inoue Y (1995a) An independent role of cytochrome c_{550} in cyanobacterial Photosystem II as revealed by double-deletion mutagenesis of the *psb*O and *psb*V genes in *Synechocystis* sp. PCC 6803. Biochemistry 34: 12661–12668

Shen JR, Vermaas W and Inoue Y (1995b) The role of cytochrome c_{550} as studied through reverse genetics and mutant characterization in *Synechocystis* sp. PCC 6803. J Biol Chem 270: 6901–6907

Shi LX, Kim SJ, Marchant A, Robinson C and Schroder WP (1999) Characterisation of the PsbX protein from Photosystem II and light regulation of its gene expression in higher plants. Plant Mol Biol 40: 737–744

Shigemori K, Hara H, Kawamori A and Akabori K (1998) Determination of distances from tyrosine D to Q_A and chlorophyll$_Z$ in Photosystem II studied by 2′+1′ pulsed EPR. Biochim Biophys Acta 1363: 187–198

Shutova T, Irrgang K, Klimov VV and Renger G (2000) Is the manganese stabilizing 33 kDa protein of Photosystem II attaining a 'natively unfolded' or 'molten globule' structure in solution? FEBS Lett 467: 137–140

Sonoyama M, Motoki A, Okamoto G, Hirano M, Ishida H and Katoh S (1996) Secondary structure and thermostability of the Photosystem II manganese-stabilizing protein of the thermophilic cyanobacterium *Synechococcus elongatus*. Biochim Biophys Acta 1297: 167–170

Stewart DH and Brudvig GW (1998) Cytochrome b_{559} of Photosystem II. Biochim Biophys Acta 1367: 63–87

Stewart DH, Cua A, Chisholm DA, Diner BA, Bocian DF and Brudvig GW (1998) Identification of histidine 118 in the D1 polypeptide of Photosystem II as the axial ligand to chlorophyll Z. Biochemistry 37: 10040–10046

Sugiura M and Inoue Y (1999) Highly purified thermo-stable oxygen-evolving Photosystem II core complex from the thermophilic cyanobacterium *Synechococcus elongatus* having His-tagged CP43. Plant Cell Physiol 40: 1219–1231

Sugimoto I and Takahashi Y (2003) Evidence that the Psbk polypeptide is associated with the Photosystem II core antenna complex CP43. J Biol Chem 278: 45004–45010

Summer EJ, Schmid VH, Bruns BU and Schmidt GW (1997) Requirement for the H phosphoprotein in Photosystem II of *Chlamydomonas reinhardtii*. Plant Physiol 113: 1359–1368

Svensson B, Etchebest C, Tuffery P, Van Kan P, Smith J and Styring S (1996) A model for the Photosystem II reaction center core including the structure of the primary donor P680. Biochemistry 35: 14486–14502

Szalai VA, Kuhne H, Lakshmi KV and Brudvig GW (1998) Characterization of the interaction between manganese and tyrosine Z in acetate-inhibited Photosystem II. Biochemistry 37: 13594–13603

Tang XS, Randall DW, Force DA, Diner BA and Britt RD (1996) Manganese-tyrosine interaction in the Photosystem II oxygen-evolving complex. J Am Chem Soc 118: 7638–7639

Telfer A, Frolov D, Barber J, Robert B and Pascal A (2003) Oxidation of the two β-carotene molecules in the Photosystem II reaction center. Biochemistry 42: 1008–1015

Tomo T, Enami I and Satoh K (1993) Orientation and nearest neighbor analysis of *psb*I gene product in the Photosystem II reaction center complex using bifunctional cross-linkers. FEBS Lett 323: 15–18

Tracewell CA and Brudvig GW (2003) Two redox-active β-carotene molecules in Photosystem II. Biochemistry 42: 9127–9136

Tracewell CA, Cua A, Stewart DH, Bocian DF and Brudvig GW (2001a) Characterization of carotenoid and chlorophyll photooxidation in Photosystem II. Biochemistry. 40: 193–203

Tracewell CA, Vrettos JS, Bautista JA, Frank HA and Brudvig GW (2001b) Carotenoid photooxidation in Photosystem II. Arch Biochem Biophys 385: 61–69

Vasil'ev S, Orth P, Zouni A, Owens TG and Bruce D (2001) Excited-state dynamics in Photosystem II: Insights from the x-ray crystal structure. Proc Natl Acad Sci USA 98: 8602–8607

Vasil'ev S, Brudvig GW and Bruce D (2003) The X-ray structure of Photosystem II reveals a novel electron transport pathway between P680, cytochrome b_{559} and the energy-quenching cation, Chl_Z^+. FEBS Lett 543: 159–163

Visser JWM , Rijgersberg CP and Gast P (1977) Photooxidation of chlorophyll in spinach chloroplasts between 10 and 180 K. Biochim Biophys Acta 460: 36–40

Vogt J and Schulz GE (1999) The structure of the outer membrane protein OmpX from *Escherichia coli* reveals possible mechanisms of virulence. Structure Fold Des 7: 1301–1309

Wang J, Gosztola D, Ruffle SV, Hemann C, Seibert M, Wasielewski MR, Hille R, Gustafson TL and Sayre RT (2002) Functional asymmetry of Photosystem II D1 and D2 peripheral chlorophyll mutants of *Chlamydomonas reinhardtii*. Proc Natl Acad Sci USA 99: 4091–4096

Wydrzynski T, Hillier W and Messinger J (1996) On the functional significance of substrate accessibility in the photosynthetic water oxidation mechanism. Physiol Plant 96: 342–350

Xu Q, Nelson J and Bricker TM (1994) Secondary structure of the

33 kDa extrinsic protein of Photosystem II: a far-UV circular dichroism study. Biochim Biophys Acta 1188: 427–431

Yamaguchi N, Takahashi Y and Satoh K (1988) Isolation and characterization of a Photosystem II core complex depleted in the 43 kDa chlorophyll binding subunit. Plant Cell Physiol 29: 123–129

Zheleva D, Sharma J, Panico M, Morris HR and Barber J (1998) Isolation and characterization of monomeric and dimeric CP47-reaction center Photosystem II complexes. J Biol Chem 273: 16122–16127

Zouni A, Lüneberg C, Fromme P, Schubert WD, Saenger W and Witt HT (1998) Characterization of single crystals of Photosystem II from the thermophilic cyanobacterium *Synechococcus elongatus*. In: Garab G (ed) Photosynthesis: Mechanisms and Effects, Vol II, pp 925–928. Kluwer Academic Publishers, Dordrecht

Zouni A, Jordan R, Schlodder E, Fromme P and Witt HT (2000) First Photosystem II crystals capable of water oxidation. Biochim Biophys Acta 1457:103–105

Zouni A, Kern J, Loll B, Fromme P, Witt HT, Orth P, Krauss N, Saenger W and Biesiadka J (2001a) Biochemical characterization and crystal structure of water oxidizing Photosystem II from *Synechococcus elongatus*. In: PS2001 Proceedings: 12th International Congress of Photosynthesis Research, S5-003. CSIRO Publishers, Melbourne (CD-ROM)

Zouni A, Witt HT, Kern J, Fromme P, Krauss N, Saenger W and Orth P (2001b) Crystal structure of Photosystem II from *Synechococcus elongatus* at 3.8 Angstrom resolution. Nature 739–743

Chapter 21

Refined X-Ray Structure of Photosystem II and Its Implications

James Barber* and So Iwata*
Wolfson Laboratories, Department of Biological Sciences, Imperial College London, London SW7 2AZ, U.K.

Summary

We review the details and significance of the 3.5 Å refined X-ray structure of Photosystem II isolated from *Thermosynechococcus elongatus* (Ferreira NK, Iverson TM, Maghlaoui K, Barber J and Iwata S (2004) Science 303, 1831–1838) in the context of other studies. The complex contains 19 subunits and all but one have had their structures determined. Consequently the details of the protein environment of the 57 cofactors involved in light interception, energy transfer and charge separation have been revealed for the first time. Of particular importance are the details of the metal cluster of the oxygen evolving center (OEC). The X-ray analysis has shown the OEC to be composed of a cubane-like $Mn_3Ca^{2+}O_4$ cluster linked to a fourth Mn ion by one of the oxygens of the cubane. Six amino acid ligands have been identified for the four Mn ions and a number of other residues have been located close to the catalytic center. The organization of the OEC and its protein ligands suggest that only one Mn ion is involved directly in the binding of a substrate water molecule. This conclu-

*Authors for correspondence, email: j.barber@imperial.ac.uk and s.iwata@imperial.ac.uk

T. Wydrzynski and K. Satoh (eds): Photosystem II: The Light-Driven Water:Plastoquinone Oxidoreductase, pp. 469–489.

sion is compatible with a mechanism for O-O bond formation whereby a highly electrophilic Mn(V)=O or Mn(IV)-oxyl radical undergoes a nucleophilic reaction with the oxygen of a nearby water molecule located within the coordination sphere of Ca^{2+}.

I. Introduction

To elucidate fully the molecular mechanism of water oxidation by Photosystem (PS) II and possibly develop technologies from this understanding, we need to bring various disciplines and techniques to bear on the problem. Indeed the various chapters of this book emphasize the breadth and quality of studies that have been undertaken with this goal in mind. Clearly structural biology can play a major role in the overall challenge of fully understanding the functional properties of PS II and the water oxidation reaction in particular. As described in Chapter 18 (Hankamer et al.), freeze fracture and surface etch electron microscopy provided the first visual glimpse of PS II with some studies suggesting it was a dimeric complex (see also Hankamer et al., 1997). More recently, as discussed in detail in Chapter 18 (Hankamer et al.), electron microscopy has proven to be a powerful approach for obtaining intermediate resolution structures of PS II. Both single particle analyses and electron crystallography have contributed in different ways. Here we focus on X-ray crystallography as a technique and how it has provided a high resolution structure of PS II and its oxygen evolving center (OEC).

II. X-Ray Crystallography

A. Crystallization

Before an X-ray analysis of the structure of a protein can be undertaken, ordered (three dimensional) 3D crystals must be grown. In recent years considerable progress has been made in the crystallization of membrane proteins (Iwata, 2003). In most cases, membrane proteins are crystallized in the presence of detergent, with micelle covering the hydrophobic surfaces. Therefore the hydrophilic surfaces, which are exposed to the solvent, play a key role in crystal formation. There are, at least, six reports of 3D crystals of PS II, four with cyanobacterial PS II (Kuhl et al., 2000; Shen and Kamiya, 2000; Zouni et al., 2000, 2001; Ferreira et al., 2004) and two with higher plant PS II (Adir et al., 1992; Fontinou et al., 1993). The crystals of higher plant PS II were insufficiently ordered (diffracting to about 7 Å) for detailed X-ray analyses. However the cyanobacterial crystals diffracted from 3.8 Å to 3.5 Å and three independent structural analyses have been conducted (Zouni et al., 2001; Kamiya and Shen, 2003; Ferreira et al., 2004; Chapters 19, Witt, and 20, Shen and Kamiya). The structures were obtained for PS II complexes isolated from both *Thermosynechococcus elongatus* (Zouni et al., 2001; Ferreira et al., 2004) and *Thermosynechococcus vulcanus* (Kamiya and Shen, 2003).

In short, the sample preparation and crystallization procedures we used (Ferreira et al., 2004) are summarized as follows. *Thermosynechococcus* cells were grown in a 30 liter airlift fermenter at 57 °C using a standard culture medium (Castenholz, 1969). Thylakoid membranes were isolated and flash-frozen in liquid nitrogen using glycerol as a cryoprotectant. Isolation of PS II dimeric reaction center cores was based on the procedure described by Kuhl et al. (2000).

Crystallization was conducted using the hanging drop vapor diffusion method with polyethylene glycol as the precipitating agent. Crystals appeared within 2 days and grew to an average size of 0.5 mm × 0.5 mm × 0.1 mm in about 4 days. The crystals belonged to an orthorhombic space group $P2_12_12_1$ with cell dimensions of a = 135 Å, b = 228.9 Å and c = 309.9 Å. Each asymmetric unit contained two PS II dimeric reaction center cores.

Abbreviations: 2D – two-dimensional; 3D – three-dimensional; BChl – bacteriochlorophyll; BRC – bacterial reaction center; Chl Z_{D1}, Chl Z_{D2} – peripheral Chls of the PS II RC; Chl – chlorophyll; Chl_{D1}, Chl_{D2} – accessory Chls of the PS II RC; CP43, CP47 – antenna proteins of the PS II core; Cyt b_{559} – cytochrome b_{559}; EPR – electron paramagnetic resonance; ESEEM – electron spin echo envelope modulation; EXAFS – extended X-ray absorption fine structure; FTIR – Fourier transform infrared; LHCII – Chl *a/b* light harvesting complex; OEC – oxygen evolving center; P680 – primary electron donor; P_{D1}, P_{D2} – Chls of the PS II RC comparable with the special pair of the BRC; PS II – Photosystem II; Q_A – primary plastoquinone acceptor; Q_B – secondary plastoquinone acceptor; RC – reaction center; Y_D, Y_Z – redox active tyrosines of the PS II RC

B. Structure Determination

To complete an atomic model by X-ray crystallography, a native data set at around 3.5 Å resolution or better is usually required. However, for the transmembrane helices of membrane proteins, modeling at even a lower resolution is possible because of the regularity of alpha helices. For example, the first X-ray structure of the reaction center (RC) of purple photosynthetic bacterium, *Blastochloris* (*Rhodopseudomonas*) *viridis*, had a resolution of 3.8Å (Deisenhofer et al., 1985). Therefore at resolutions of the earlier X-ray structures of PS II at 3.8 Å (Zouni et al., 2001) and 3.7 Å (Kamiya and Shen, 2003), a complete atomic model could, in principle, have been built. Unfortunately, as clearly indicated by the R-factors of these structures (59% and 53%, respectively), the models derived from diffraction data were not sufficient to provide precise information for rigorous discussion of the many facets of PS II structure and function, including the molecular details of the water splitting mechanism. The R-factor and free R-factor of properly refined structures at these resolutions should be as low as 30–35% which was achieved in the case of Ferriera et al. (2004).

X-ray crystallography has the so-called 'phase problem.' To calculate electron density maps both amplitude and phase are required for each diffraction spot. However, only the amplitude information can be obtained from the diffraction data recorded on a detector. The lost phase information can be experimentally obtained by comparing the diffraction data from the native and the heavy atom derivative crystals. Because of non-isomorphism of heavy atom derivative crystals, the experimental phases usually contain large errors. Therefore, the quality of the electron density map is dependent on not only the resolution but also on the experimental phase quality; i.e., not all 3.5 Å electron density maps have the same quality.

If the experimental map is good enough to allow an initial reliable model to be built, the phases can be improved by refinement, where the phases calculated from the model are used to calculate the electron density map. Usually by repeating the cycles of model building and refinement, a structure, which is more accurate and complete than the model built for the experimental density map is obtained. However, if the initial model is not precise enough and there are not enough numbers of observations, the refinement process will never converge. This seems the case for earlier PS II structures (Zouni et al., 2001; Kamiya and Shen, 2003) as compared with that of our own (Ferreira et al., 2004).

Although X-ray crystallography on small soluble proteins has become routine, it is still very difficult to acquire high quality experimental phases for large membrane protein complexes. To obtain the refined structure of PS II reported by Ferreira et al. (2004) fine tuning of all the steps was required. First of all, we optimized the growing of the crystals and used the best available beam line for data collection. The beam line X06SA at the Swiss Light Source, which produces a finely focused beam (15 μ × 80 μ) with a very low background noise was essential for the data collection. This allowed us to collect a complete 3.5 Å resolution native data set and 6 high quality heavy atom data sets, four of them having a resolution of 3.8 Å. Initial phase calculation with high quality derivatives followed by careful phase extension to 3.5 Å using dodecyl maltoside (Cowtan, 1994) (three separate maps calculated with different phase extension strategies were averaged to improve the signal to noise ratio of the map) provided an experimental electron density map, where amino acid sequences were easily recognizable for most of the regions. The model was built using program O (Jones et al., 1991) with a matrix for the 'slider' command optimized for the modeling of cytochrome *c* oxidase (Iwata et al., 1995) and cytochrome bc_1 complex (Iwata et al., 1998). This was followed by refinement using the program CNS (Brunger et al., 1998); with amplitude and experimental phase probability distribution being critical for the refinement. The local scaling method, which is similar to the one used for the structural determination of cytochrome *c* oxidase (Iwata et al., 1995), was also applied during the refinement cycles to improve the scaling between observed and calculated structure factors. As a result, we succeeded in calculating a complete protein/pigment model of PS II except for uncertainty about one small subunit, which is putatively assigned as PsbN, but could be another subunit, such as PsbY.

III. Major Differences from Earlier Structures

In the case of the first reported structure of PS II at 3.8 Å (Zouni et al., 2001; Chapter 19, Witt), the model was confined mainly to transmembrane domains with some modeling of the extrinsic proteins.

Despite this limitation and the poor R-factor, the work was important because it provided information about cofactor positioning and gave the first electron density map of the metal cluster. Following on from this initial study, the X-ray structure of PS II isolated from *T. vulcanus* was obtained at 3.7 Å resolution (Kamiya and Shen, 2003; Chapter 20, Shen and Kamiya) providing a more extensive model with C_α-backbone assignment of extrinsic loops and a more extensive tracing of the extrinsic PsbO and PsbU proteins. Most of this structure was modeled as polyalanine and some bulky side chain assignments were made to densities within the map. These partial assignments were then used to propose the position of the intervening residues in several of the subunits. This modeling resulted in suggestions for possible protein ligands of the Mn cluster. More recently this model has been improved, as presented in Chapter 20 (Shen and Kamiya). Both studies interpreted the 'pear-shaped' density of the metal cluster to contain four Mn ions, one in each corner and one in the middle. Neither model suggested a position for the Ca^{2+} which is known to be located close to the Mn cluster based on EXAFS spectroscopy (Debus, 1992; Cinco et al., 2002; Yachandra, 2002). The PS II structure of *T. vulcanus* published by Kamiya and Shen (2003) did, however, identify density which was tentatively assigned to two β-carotenes, one all-*trans* and one *cis*, positioned between cytochrome b_{559} (Cyt b_{559}) and the primary electron donor (P680) Chls. This assignment has implications for the possible role of β-carotene in mediating electron flow from Cyt b_{559}, and also Chl Z, to P680 (Faller et al., 2001; Tracewell and Brudvig, 2003; Chapter 15, Faller et al.).

The structure of PS II discussed in this chapter and recently published (Ferreira et al., 2004) is fully refined at 3.5 Å with a R-factor of approximately 30% and provides the first model in which virtually all the side chains have been traced (2569 amino acids). Moreover it has provided the first real structural information of the Mn_4Ca-cluster of the OEC and identifies amino acids directly involved in ligating the metal ions. The refined electron density map, in combination with the simulated annealing omit-maps for each metal, clearly showed that the OEC is composed of five metals instead of the four modeled in the earlier structures. To identify the metal types, we collected two data sets using the X-rays of 1.89 and 2.25 Å wavelengths, respectively. At 1.89 Å, a Mn atom shows twice as much X-ray anomalous scattering than a Ca atom, whereas at 2.25 Å, anomalous scattering of a Ca atom is four times stronger than a Mn atom. Using these differences, we could calculate X-ray anomalous difference maps at 1.89 Å highlighting Mn atoms and at 2.25 Å highlighting Ca atoms (Ferreira et al., 2004). The Mn anomalous difference map clearly covered four metals in the OEC whereas the Ca anomalous difference map covered one metal. As a result, we could unambiguously assign the metal types in the OEC. Although this assignment is solely based on the X-ray diffraction experiments and independent of any other biochemical or biophysical results, our OEC model satisfies the majority of results from non-crystallographic analyses as discussed in later sections.

IV. Overall Structure

The PS II dimer has dimensions of 105 Å depth, 205 Å length and 110 Å width (Fig. 1). Within the dimer, the monomers are related by a non-crystallographic two-fold axis perpendicular to the membrane plane. Although these characterizations agree with those reported by Zouni et al. (2001) and Kamiya and Shen (2003), our model differs from these earlier studies in that we identify 35 rather than 36 transmembrane helices. The missing helix is designated PsbX in the model by Zouni et al. (2001). However all three models indicate that each PS II monomer binds a single copy of the three extrinsic proteins, PsbO, PsbV and PsbU, although the latter was not assigned by Zouni et al. (2001).

V. Protein Subunits

A. D1 and D2 Proteins

It has long been assumed that the D1 and D2 proteins were structurally homologous to the L and M subunits of the purple bacterial reaction center (Trebst, 1986; Barber, 1987; Michel and Deisenhofer, 1988). This analogy has provided the framework for genetic engineering strategies over the past one and half decades (Diner et al., 1991; Debus, 2001; Diner, 2001; Chapter 4, Nixon et al; Chapter 11, Debus.). The first direct evidence of this structural similarity came from electron crystallography (Rhee et al., 1997, 1998). All the X-ray crystallography studies have since confirmed and improved the structural models for the D1 and D2 proteins. The rms deviation between

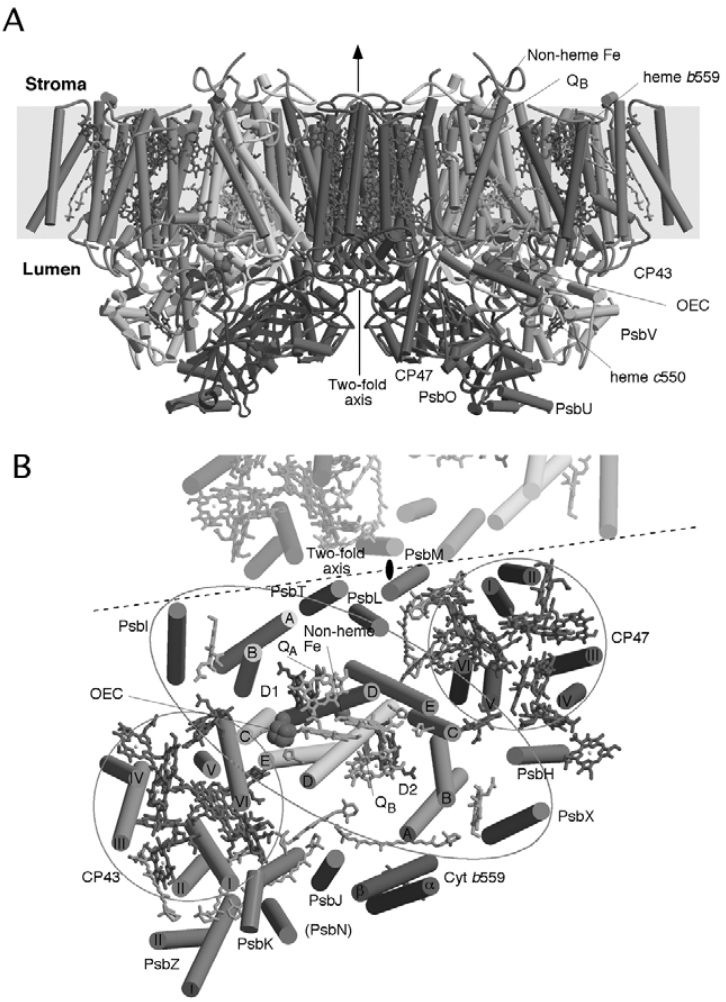

Fig. 1. Overall structure of PS II. (A) View of the PS II dimer perpendicular to the membrane normal. The 35 transmembrane helices present are represented as cylinders. The extrinsic proteins are PsbO, PsbU and PsbV. Also shown are chlorophylls of the D1/D2 reaction center and the antenna complexes CP43 and CP47. Pheophytins and β-carotenes are indicated as is the non-heme Fe and Q_A and Q_B acceptors. The oxygen evolving center (OEC), consisting of four Mn ions, one Ca^{2+} and four oxygen atoms is also shown. (B) View of the PS II monomer along the membrane normal from the lumenal side. A part of the other monomer in the dimer is shown to emphasise the region of monomer/monomer interaction along the dotted line. The pseudo-two-fold axis perpendicular to the membrane plane passing through the non-heme Fe relates the transmembrane helices of the D1/D2 heterodimer, the low molecular weight subunits, PsbI and PsbX and CP43 and CP47 as emphasised by the black lines encircling these subunits. See Color Plate 9, Fig. 1.

the transmembrane helices of these proteins in the structure by Ferreira et al. (2004) and those of the L and M subunits of *Blastochloris* (*Rhodopseudomonas*) *viridis* is 1.9 Å for 395 C_α atoms. However, the carboxyl-terminal (C-terminal) domains and loops joining the transmembrane helices are more extended in the case of the D1 and D2 subunits compared with their bacterial counterparts particularly on the lumenal side.

B. CP43 and CP47

Based on gene sequences, CP43 and CP47 were both predicted to have six transmembrane helices each (Bricker, 1990; Barber et al., 2000; Chapter 3, Eaton-Rye and Putnam-Evans). Moreover, these predictions indicated that the loops joining the lumenal ends of helices V and VI were very large, having about 150 and 200 amino acids for CP43 and CP47 respectively. They were also predicted to bind about 15 Chl *a* molecules each and contain several molecules of β-carotene (Barbato et al., 1991; Zheleva et al., 1998).

The first direct description of the CP43 and CP47 structures also came from electron crystallographic analyses (Rhee et al., 1998; Hankamer et al., 1999) which indicated that their transmembrane helices were arranged as three pairs around a pseudo-three fold axis. It was noted that this circular arrangement is remarkably similar to that of the six amino-terminal (N-terminal) transmembrane helices of the PS I reaction center proteins, PsaA and PsaB (Rhee et al., 1998). Moreover, the X-ray structure of the PS I reaction center (Krauss et al., 1996) had shown that the five C-terminal transmembrane helices of PsaA and PsaB were arranged in a 'hand-shake' motif rather like the L and M subunits of purple bacteria (Deisenhofer et al., 1985). Thus a structural homology was established between PS II and PS I indicative of a common evolutionary origin (Schubert et al., 1998). The electron crystallographic studies had been carried out on 2D crystals consisting of PS II complexes with and without CP43. Therefore it was concluded that CP47 was positioned adjacent to the D2 protein and CP43 adjacent to D1, with their transmembrane helices related to each other by the same pseudo-two-fold axis, which relates to those of the D1 and D2 proteins (Hankamer et al., 1999). The X-ray structure of Zouni et al. (2001) confirmed this arrangement while Kamiya and Shen (2003) made the first effort to trace the extrinsic loops of CP43 and CP47. We have now completely modeled these two proteins, assigning 421 amino acids to CP43 and 476 amino acids to CP47 (Fig. 1). The large loop joining transmembrane helices V and VI of CP43 is composed of 129 amino acids and contains two long and three short helices (Fig. 2A). In the case of CP47 the corresponding loop is bigger (188 amino acids) and contains two long and four short helices and three β-sheets (Fig. 2B). The importance of these large loops in making contact with the D1 and D2 proteins and with PsbO will be discussed below.

C. Low Molecular Weight Transmembrane Subunits

According to the biochemical analyses of Kashino et al. (2002a,b), the isolated PS II reaction center core complex of *T. vulcanus* contains 11 low molecular weight subunits; PsbE, F, H, I, L, M, T, X, Y, Z and Psb27. However, as shown in Fig. 1, using the genome sequence of *T. elongatus* (Nakamura et al., 2002), we have assigned 12 low molecular weight subunits into the electron density map (PsbE, F, H, I, J, K, L, M, N, T, X, Z); this is in contrast to earlier structures where the assignment of low molecular weight subunits was based mainly on biochemical evidence because of the lower quality of the map (Hankamer et al., 2001a,b; Zouni et al., 2001; Kamiya and Shen, 2003). As stated earlier, we did not find a density to accommodate the transmembrane helix assigned to PsbX in the X-ray model of Zouni et al. (2001). Perhaps this subunit is removed during our isolation procedure since it is located on the peripheral of the complex. PsbE and PsbF are the α- and β-subunits of Cyt b_{559} and their positions have been identified previously (Rhee, 1998; Zouni et al., 2001; Kamiya and Shen, 2003). PsbE has a long C-terminal extension containing an α-helix and lies close to the stromal surface. Its main interaction is with the AB-loop of the D2 protein in the vicinity of D2-Val55 to -Glu106, although it also lies close to the C-terminal D1 region from Ile307 to Ile314, the Asn49 toThr51 region of PsbH and the N-terminus of PsbV. There is no second copy of Cyt b_{559} as predicted for cyanobacterial PS II (Tang and Diner, 1994; Kashino et al., 2002a,b). The transmembrane helices of PsbI and PsbX are related by the same pseudo two-fold axis that relates the D1 and D2 proteins and CP43 and CP47 (ringed in Fig. 1). Their function seems to be to stabilize the Chl molecules ligated to D1-His118 and D2-His117 of the B-helices of the D1 and D2 proteins respectively. It has been known for some time that PsbI is closely associated with the D1/D2 heterodimer because of its presence in the isolated D1/D2/Cyt b_{559} complex (Ikeuchi and Inoue, 1988; Webber et al., 1989). When isolated from higher plants, this minimal RC complex has been reported to bind PsbW (Irrgang et al., 1995). However, the PsbW does not exist in cyanobacteria and could be replaced by PsbX in the cyanobacterial PS II structure.

The positioning of PsbH close to PsbX and Cyt b_{559} was predicted from cross-linking studies using His-tagging, Ni^{2+}-nitrilo triacetic acid (NTA)-gold labeling and single particle analyses (Buchel et al.,

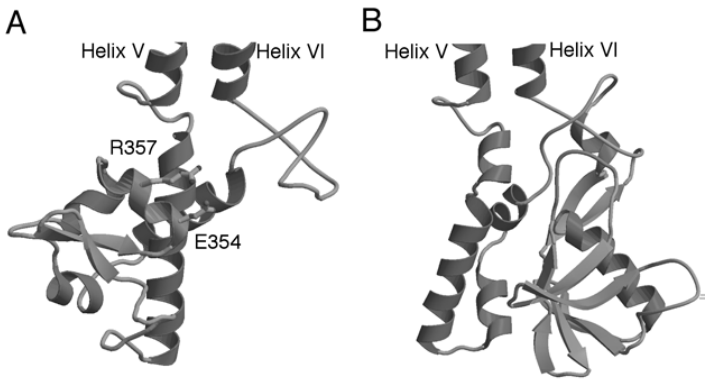

Fig. 2. Structure of the large extrinsic domains of (A) CP43 and (B) CP47. The membrane extrinsic domain of CP43 contains two long (residues 305 to 325; 385 to 399) and two short α-helices (residues 363 to 370; 376 to 383), a 2 strand β-sheet (residues 340 to 344; 348 to 352) and a 3/10 helix (residues 353 to 359). The 3/10 helix, composed of GGETMRFWD (residues 352 to 360) is fully conserved in all CP43 known sequences and contains residues involved in water oxidation at the OEC (Glu354 and Arg357). The lumenal domain of CP47 contains two long (residues 280 to 294; 413 to 427) and four short helices (residues 271 to 278; 297 to 305; 306 to 314; 328 to 335), and a four-stranded (residues 343 to 347; 352 to 354; 398 to 403; 407 to 412), a three-stranded (residues 355 to 357; 369 to 372; 376 to 381) and a two-stranded β-sheet (residues 336 to 338; 430 to 433). The conserved FFETFSVLV sequence (residue 362 to 370), which forms a hydrophobic environment around Y_D (D2-Tyr160). See Color Plate 10, Fig. 1.

2001). Zouni et al. (2001) misplaced PsbH in the dimerization domain between the two monomers while Kamiya and Shen correctly assigned PsbK based on a 'kink' in the transmembrane helix due to the presence of two prolines, Pro17 and Pro20. PsbJ and PsbZ were not previously assigned. The location of PsbK adjacent to CP43 is also supported by the recent biochemical studies of Sugimoto and Takahashi (2003). PsbZ is a recently discovered PS II subunit present in all types of oxygenic photosynthetic organisms (Shi and Schröder, 2004) and has been suggested to play a role in the binding of LHCII to PS II in plants and green algae (Swiatek et al., 2001). Cyanobacteria, however, do not have LHCII but use phycobilisomes as an outer light harvesting system for PS II (Chapter 2, Green and Gantt). Whether PsbZ helps in the binding of this extrinsic protein complex to the PS II stromal surface is an interesting idea worthy of further investigation (Barber et al., 2003). Together, PsbJ, PsbK, PsbZ and a transmembrane helix tentatively assigned to PsbN seems to form an interface with CP43 to aid the binding of carotenoids. The three remaining low molecular weight subunits, PsbL, PsbM and PsbT ($PsbT_c$ in plants and algae) are positively identified from the electron density and are located in the dimerization domain between the two monomers. Some of the genes for the low molecular weight subunits have been inactivated or deleted (Chapter 6, Thornton et al.).

D. Extrinsic Subunits

Although there have been suggestions that there may be two copies of the extrinsic proteins per monomer for higher plant PS II (Bricker and Frankel, 1998; Popelkova et al., 2003; Chapter 5, Bricker and Burnap), this clearly is not the case for cyanobacteria as demonstrated by our structure (Fig. 3) and the two other earlier X-ray diffraction studies (Zouni et al., 2001; Kamiya and Shen, 2003). The PsbO protein is ubiquitous for all oxygenic photosynthetic organisms although sequence differences can be as much as 70% (De Las Rivas and Barber, 2004; De Las Rivas et al., 2004). Ultraviolet circular dichroism (UVCD), Fourier transform infra red (FTIR) and molecular modeling (Bricker and Frankel, 1998; Pazos et al., 2001) indicated that PsbO is an all-beta protein. This was reinforced by the X-ray structures of Zouni et al. (2001) and Kamiya and Shen (2003). Our complete structure showed that this subunit is a β-barrel, about 40 Å long and 18 Å wide, composed of 8 antiparallel β-strands. Although the cylinder is 'porin-like', as noted by Kamiya and Shen (2003), it is not an open tube but is filled with bulky, hydrophobic residues, including 7 phenylalanines (Phe50, 95, 120, 142, 146, 215, 239). Three loops protrude from the cylinder: the N-terminal extension and loops extending from strands β1 and β2 and strands β5 and β6.

The long axis of the protein is oriented at about

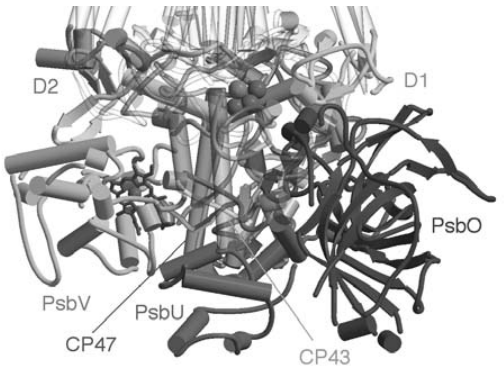

Fig. 3. A view of the lumenal surface showing the extrinsic proteins PsbO, PsbU and PsbV, the large extrinsic loops of CP47 and CP43 and the lumenal portions of the D1 and D2 proteins. Together these polypeptides form a 'protein-cap' over the OEC. See Color Plate 10, Fig. 2.

45° to the membrane plane with the C- and N-termini within 20 Å of each other and located at the lumenal end of the cylindrical domain. The N-terminal extension is stabilized by the sulfur bridge between Cys19 and Cys44 and interacts with the large extrinsic domain of CP43 while the loop between the strands β1 and β2 interacts with CP47 in the other monomer of the dimer. This interesting feature suggests that the PsbO protein may play a role in stabilizing the dimeric nature of the PS II complex. The main body of the cylindrical domain has no direct interaction with any other proteins and is exposed to the aqueous phase of the lumen. In contrast, the large loop joining β5-β6, is important for docking and stabilizing the metal cluster. It interacts with the large extrinsic domain of CP47 and importantly with the C-terminal regions of the D1 and D2 proteins as well as with the AB loop of the D1 protein. It seems that these interactions result in stabilization of the OEC and explains why the PsbO protein has earned the name 'Mn stabilizing protein' (MSP) (De Las Rivas and Barber, 2004; Chapter 5, Bricker and Burnap). Moreover, in stabilizing the Mn cluster by its multiple interactions with the lumenal surface, it might also optimize the local level of Cl^- necessary for the water oxidation reaction as well as facilitating the association of Ca^{2+} with the Mn cluster. In addition it seems to provide the latter part of a hydrophilic channel leading from the water splitting site of the OEC to the lumenal surface (see below).

The structure of the isolated PsbV protein has been determined by X-ray crystallography (Frazao et al., 2001; Sawaya et al., 2001; Kerfeld et al., 2003). In the PS II structure of Kamiya and Shen (2003), this subunit is placed correctly, although it lacks the C-terminal extension. It is a typical c-type cytochrome except for having two His as haem ligands instead of one His and one Met ligand. The PsbV protein interacts with the C-terminal extension of the D1, D2 and PsbU proteins (see Fig. 3) while its N-terminal extension interacts with the C-terminus of PsbE of Cyt b_{559}. There are no direct contacts with the PsbO protein.

The PsbU is an all-alpha protein as noted by Kamiya and Shen (2003), with its N-terminal extension interacting with the PsbO protein and C-terminal extension with PsbV and the C-terminal domain of the D2 protein. In this way, it bridges PsbV and PsbO while, at the same time, coming close to the metal-binding site of the OEC via its C-terminus (within ca. 15 Å).

VI. Pigments and Cofactors

Zouni et al. (2001) and Kamiya and Shen (2003) assigned the main cofactors involved in electron transport and we broadly agree with their conclusions (Fig. 4). In our structure, however, we have a shorter distance between the Mg ions of the P_{D1} and P_{D2} Chls of P680; 8.2 Å verses about 10 Å. We also found that the tetrapyrrole head groups of these two pigments have orientations slightly different from the special pair of the RC of purple bacteria (BRC). Together, these two features reduce the overlap between rings V of the two Chls and presumably give rise to the much reduced exciton interactions of P680 as compared with its bacterial counterpart (Diner and Babcock, 1996). In any event, as emphasized by Kamiya and Shen (2003), the P_{D1} and P_{D2} Chls are distinguished from the two accessory Chls (Chl_{D1} and Chl_{D2}) in being more closely interacting (Fig. 4B).

In the structure of Ferreira et al. (2004) (see Fig. 4A), we were able to assign density for plastoquinone molecules bound to the Q_A and Q_B sites and noted that Q_B-plastoquinone was in the proximal position (i.e., hydrogen bonded to Ser 264) unlike that found for ubiquinone in the BRC (Lancaster and Michel, 1997; Stowell et al., 1997; but see Breton, 2004). We confirm that the fifth ligand to the non-heme iron is not a glutamate as in the BRC (Deisenhofer et al., 1985) but a bicarbonate anion as suggested from other studies (Govindjee and van Rensen, 1993; Hie-

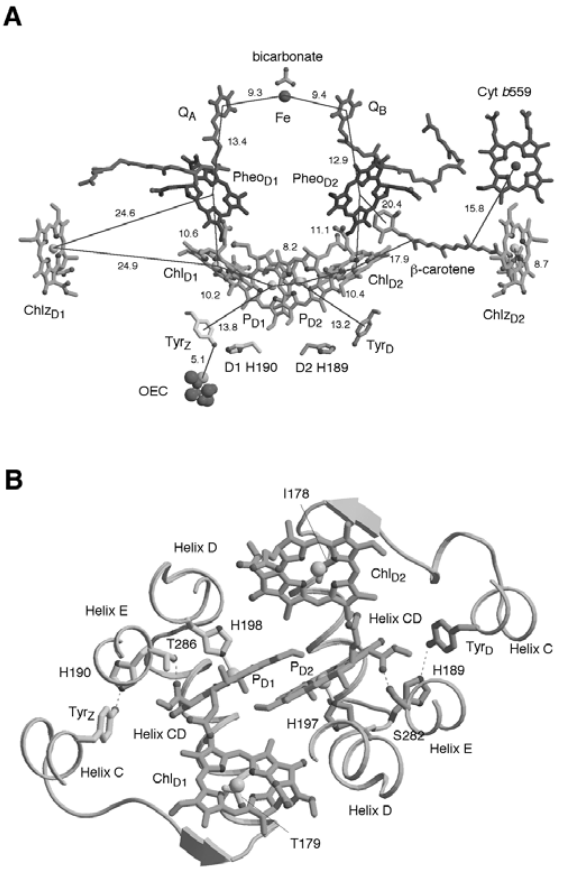

Fig. 4. Cofactors involved in electron transfer. (A) Electron transfer cofactors shown perpendicular to the internal pseudo-two-fold. The phytyl tails of the chlorophylls and pheophytins have been removed for clarity. Also shown are the side chains of Y_Z (D1-Tyr161), D1-His190, Y_D (D2-Tyr160) and D2-His189. The four chlorophylls comprising P680 are in direct van der Waals contact, and other electron transfer distances are given in Å. (B) The P680 dimer of chlorophylls (P_{D1} and P_{D2}) and accessory chlorophylls (Chl_{D1} and Chl_{D2}). The histidine ligands, D1-His 198 and D2-His 197, are shown as well as the redox active Y_Z - D1-His 190 and Y_D - D2-His 189 pairs. The view is down the pseudo-two-fold axis from the stromal side. See Color Plate 11, Fig. 1.

nerwadel and Berthomieu, 1995; Chapter 14). This anionic ligand is stabilized by hydrogen bonding to D1-Tyr246 and D2-Lys264.

According to previous X-ray studies, CP43 and CP47 bind 13 and 16 Chls (Zouni et al., 2001) or 13 and 17 Chls (Kamiya and Shen, 2003), respectively. We assign 14 Chls bound to CP43 and 16 Chls bound to CP47 (Fig. 5). As noted in the earlier X-ray structures and in an electron microscopy (EM) study (Rhee et al., 1998), the Chls are arranged on opposite sides of the membrane with the exception of one in each protein, which is located at almost equal distance from both surfaces (see Fig. 5B). There are some symmetrical relationships between the positions of the Chls in each protein (around a pseudo-three fold axis) and also between Chls of the two proteins (around the pseudo-two-fold axis which relates CP43 and CP47). Ten Chls of CP43 and 13 Chls of CP47 are ligated by histidines that are highly conserved. In CP43 another Chl has an asparagine ligand which is fully conserved in all known CP43 sequences while the remaining Chls of CP43 and CP47 do not have protein ligands. It should be noted that the two accessory Chls associated with the D1 and D2 proteins (Chl_{D1} and Chl_{D2}) also do not have direct protein ligands (see Fig. 4B) unlike the corresponding BChls

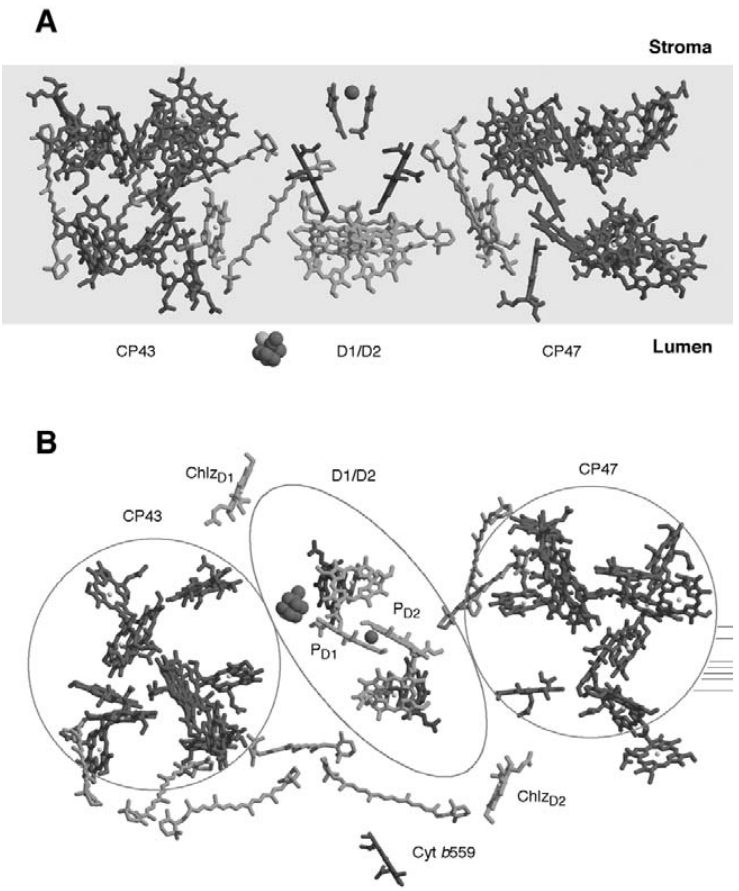

Fig. 5. Pigment organization in the PS II monomer complex. (A) View is perpendicular to the membrane normal. Chlorophylls have the phytyl tail omitted for clarity. Chlorophylls that are stacked with the planes of the porphyrin head group parallel and within van der Waals contact can be seen. β-Carotenes are shown as ball-and-stick models and tend to have one head group in direct van der Waals contact with a chlorophyll. (B) View of the pigments along the pseudo-two-fold axis, perpendicular to the view in Fig. 4A.

of the BRC. It is probable that water molecules act as the ligand for Mg of these Chls, as suggested for those Chls of PS I which also do not have protein ligands (Jordan et al., 2001).

Seven all-*trans* β-carotenes are assigned in our PS II structure (see Fig. 5), a number which is compatible with recent biochemical analyses (J. Duncan and J. Barber, unpublished). They seem to be located at the interface between the main subunits CP43, CP47, D2 and some of the low molecular weight subunits. One of the carotenoids lies approximately along the plane of the membrane with its head group close to Chl Z_{D2} and positioned about equidistant between P680 and Cyt b_{559}. It therefore seems that this is one of the two redox active carotenoids which facilitates electron flow from Cyt b_{559} and Chl Z_{D2} to P680 (Telfer et al., 1991, 2003; Hanley et al., 1999; Faller et al., 2001; Tracewell et al., 2001a,b; Tracewell and Brudvig, 2003; Chapter 15, Faller et al.). However there is evidence that there are two photooxidizable β-carotenes in PS II (Telfer et al., 2003; Tracewell et al., 2003a,b) and it is well established that the isolated D1/D2/Cyt b_{559} complex contains two β-carotenes (Kobayashi et al., 1990; Gounaris et al., 1990). Very close to the β-carotene positioned between Cyt b_{559} and P680 is another carotenoid that is approximately

perpendicular to the membrane plane. Since the distance between these two carotenoids is about 4 Å, this second β-carotene could rapidly donate an electron to the oxidized β-carotene closer to P680. This second carotenoid is also positioned such that it could co-purify with the D1/D2/Cyt b_{559} complex, although it may be less resistant to detergent treatment. The reported preferential removal of one β-carotene from the D1/D2/Cyt b_{559} complex (De Las Rivas et al., 1993) and the conclusion that the two carotenoids are orientated approximately at right angles to each other in this minimal isolated PS II complex (Breton et al., 1988) is, therefore, compatible with the X-ray structure of Ferreira et al. (2004).

Zouni et al. (2001) did not assign any carotenoids in their model but Kamiya and Shen (2003) proposed that there were two carotenoids between Cyt b_{559} and P680, one all-*trans* and one *cis*. Although these assignments have recently been modified to two all-*trans* carotenoids (Chapter 20, Shen and Kamiya) their precise positioning does not match with our assignment. It should be emphasized that at 3.7 Å to 3.5 Å resolution the assignment of carotenoids is problematic since it is difficult to distinguish a carotene from a lipid or a detergent molecule and could also be confused with the density of a phytol tail of a Chl. Our assignment of the carotenoid between Cyt b_{559} and P680 is reasonably rigorous but the positioning of some other carotenoids may be subject to modification as the quality of the electron density map improves.

VII. The Oxygen Evolving Center

The X-ray structure of Ferreira et al. (2004) has provided a structural model for the organization of the metal ions that make up the catalytic center of the water splitting reaction revealing the nature of the amino acid ligands and overall protein environment of the OEC. As reported previously (Zouni et al., 2001; Kamiya and Shen, 2003) the 'pear-shaped' electron density due to the metal ions of the OEC is located close to the lumenal surface of the D1 protein near to its CD surface helix and C-terminus. Associated with the density of the metal ions are densities of the protein ligands and other amino acids that are nearby. We will deal with each aspect of the new information in turn.

A. Structure of the Metal Cluster

The 'pear-shaped' density of the metal cluster was originally interpreted to contain three Mn ions in the larger domain and one in the extended region. However, in the electron density map of our 3.5 Å PS II structure, it is clear that four metal ions of the size of Mn can be accommodated at the corners of a tetrahedron in the large globular density whereas one metal ion is located in the center of the extended region (Fig. 6). This arrangement is strongly supported by the fact that the difference density map clearly shows the peak for the respective metal when each metal atom of the cluster is omitted from the model (Ferreira et al., 2004). As mentioned previously, we have identified the metals using wavelength dependent X-ray anomalous diffraction. The Mn anomalous map correlated with one metal in the small domain and three in the large globular domain whereas the Ca^{2+} absorption was restricted to the remaining one metal ion in the large domain (Fig. 6A).

The results clearly indicate that the OEC consists of a cubane-like Mn_3CaO_4 cluster with each metal ion in this cluster having three-μ-oxo bridges. The electron density is best explained by the model in which a fourth Mn, located at the narrow end of the pear-shaped density is linked to the cubic structure by one of its oxygen atoms. Thus, the structure consists of three Mn-di-μ-oxo-Mn bonds, three Mn-di-μ-oxo-Ca^{2+} bonds, two Mn-mono-μ-oxo-Mn bonds and a single Ca^{2+}-mono-μ-oxo-Mn bond. Distances for the bonds are refined to 2.7Å for Mn-di-μ-oxo-Mn, 3.3 Å for Mn-mono-μ-oxo-Mn and 3.4 Å for Mn-di-μ-oxo-Ca, which are compatible with values for μ-oxo bridges and with those measured for the OEC by X-ray absorption fine structure (EXAFS) (DeRose et al., 1994; Yachandra et al., 1996; Robblee et al., 2001; Yachandra, 2002; Chapter 10, Yachandra). The Ca^{2+} -mono-μ-oxo-Mn bond is approximately 4 Å. It should be emphasized, however, that these distances are approximate due to the resolution of the structure and may vary depending on the conformation of the cluster in various S-state intermediates.

Although the structure of the OEC derived from the X-ray work and shown in Fig. 6B has not been proposed before, there are many elements of it which have been suggested from EXAFS and electron paramagnetic resonance (EPR) studies (Robblee et al., 2002). EXAFS has provided substantial evidence for di-μ-oxy and mono-μ-oxy bridging and also for the close location of a bound Ca^{2+} to Mn (Cinco

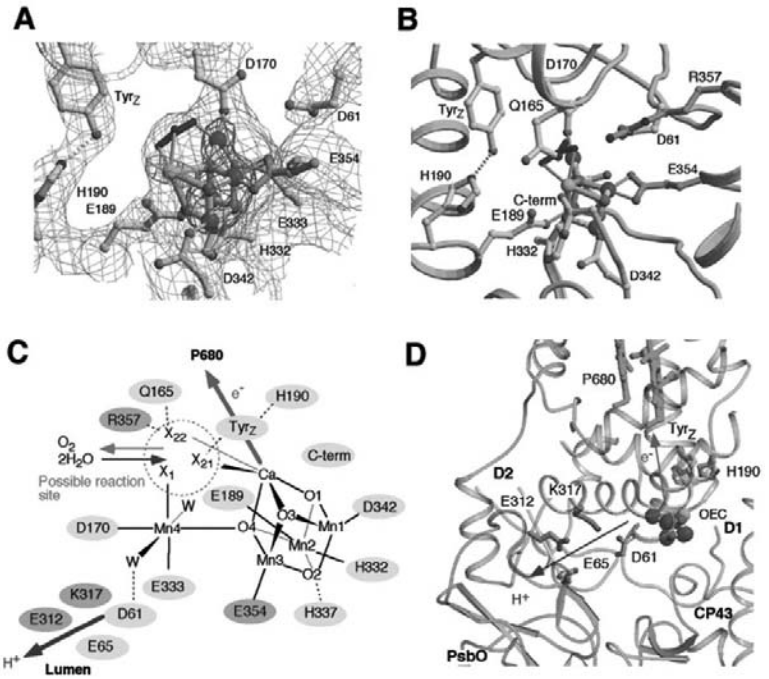

Fig. 6. The oxygen evolving center. (A) View of the OEC with side chain ligands and possible catalytically important side chain residues. An unidentified non-protein ligand to the OEC is modeled. $2|F_o| - |F_c|$ density is shown as a wire mesh contoured at 1.5σ. Anomalous difference Fourier maps at 1.89340 Å (Mn edge, contoured at 10σ.) and 2.25430 Å (highlights Ca^{2+}, contoured at 7σ) wavelengths are also shown. (B) The same as (A) but with a rotation around the y-axis of 40° and without electron density and anomalous difference maps. (C) Schematic view of the OEC. X_1, X_{21} and X_{22} are possible substrate water binding positions to Mn4 (X_{11}) and to Ca^{2+} (X_{21} and X_{22}) identified from the position of the non-protein ligand and coordination pattern of Mn and Ca^{2+} ions. Possible water molecules, which are not visible at the current resolution, are indicated as W. (D) Hydrophilic pathway between the active site and lumen (arrow). See Color Plate 12, Fig. 1.

et al., 2002; Yachandra, 2002). Both EXAFS and pulsed EPR studies concluded a '3 + 1' or 'dangler model' organization for the four Mn ions (Peloquin et al., 1998; Peloquin and Britt, 2001; Robblee et al., 2002). This '3 + 1' organization was also suggested by Zouni et al. (2001) and Kamiya and Shen (2003) as an interpretation for the pear-like density although the positioning of three of the Mn ions in their models is clearly different to that of Ferriera et al. (2004). The concept of a cubane-like organization with three oxo-ligands per Mn ion was suggested sometime ago by Brudvig and colleagues (De Paula et al., 1986) and, more recently, Dismukes and colleagues have also considered this idea (Dismukes et al., 1998; Masayuki et al., 2001; Carrell et al., 2002). In both cases it was suggested that the cubic structure was not maintained throughout the S-state cycle and that μ-oxo-bond breakage and conformational changes were necessary for dioxygen formation. The idea of a Mn_3CaO_4 cubane has not been considered before and at first sight seems surprising. However recent calculations by P. Siegbahn and M. Lundberg (personal communication) give theoretical credibility to such a structure with metal-metal distances consistent with our model derived from the X-ray diffraction analyses. The three μ-oxo-bridges provide structural stability to the cluster and ensure a certain degree of robustness for the OEC, possibly giving tolerance for ligand exchanges during the catalytic cycle or imposed artificially by site directed mutagenesis.

B. Protein Ligands

Depending on its valency state Mn has a coordination

number of five or six while for Ca^{2+} the anticipated coordination number is six or seven. Therefore in the cubane, the three μ-oxo ligands only partially satisfy the coordination requirement for the Mn and Ca ions it contains. The fourth Mn has just one μ-oxo ligand and it therefore will require even more additional ligating species. The structure of Ferreira et al. (2004) has revealed six, or possibly seven, direct protein ligands for the metals (see Fig. 6). This low number of protein ligands should have been anticipated since site directed mutagenesis studies had identified approximately the same number (Debus, 2001; Diner, 2001; Chapter 11, Debus). Therefore, there should be several solvent molecules serving as metal ligands to fulfill the coordination patterns of metals as discussed below. Almost all the protein ligands identified by X-ray analysis had been considered as potential ligands based on mutational studies which also clearly identified the D1 protein, especially its CD lumenal helix and C-terminal domain, as the binding site for OEC metals. Confirmation of this role of the D1 protein came from the X-ray structures of Zouni et al. (2001) and Kamiya and Shen (2003). As mentioned above, the latter study in particular identified four to five connections between the density of the metal cluster and the polypeptide backbone. Of those suggested, D1-Asp170, D1-His332 and D1-Glu333 are in agreement with our recently published refined X-ray model (Ferreira et al., 2004), although their positions are significantly different from our structure. In the new model six protein ligands have been assigned for the four Mn ions as well as identifying a number of other amino acids in the immediate vicinity (Fig. 6B). As shown in Fig. 6B, D1-Asp342 provides a ligand to Mn1 of the cubane while Mn2 seems to have two protein ligands, D1-Glu189 and D1-His332. The third Mn of the cubane (Mn3) is ligated by a Glu354 of CP43. Ca^{2+} does not seem to have a protein ligand although the carboxyl oxygen of the C-terminal residue of D1 protein, D1-Ala344, is very close (Fig. 6B) and may form a ligand during the catalytic cycle of water oxidation. The remaining two protein ligands are D1-Asp170 and D1-Glu333 and these link to Mn(4). In the immediate vicinity of the OEC (see Fig. 6C) are the side chains of other amino acids, D1-Asp61, D1-Gln165, CP43-Arg357, D1-His190, D1-His337 and D1-Tyr161, where the latter is the redox active tyrosine Y_Z providing the electron transfer pathway from the Mn cluster to P680. Our structure clearly shows that D1-Tyr161 is hydrogen bonded to D1-His190 in line with expectations (Diner and Babcock, 1996; Tommos and Babcock, 1998; 2000; Haumann and Junge, 1999) but contrary to the conclusions of Fromme et al. (2002). D1-His337 seems to be hydrogen bonded to one of the oxygen atoms of the cubane while D1-Asp61 may stabilize a water ligand to Mn4. The two CP43 residues, Glu354 and Arg357, are a part of a 3_{10}-helix which forms a 'lid' over the OEC and contained in fully conserved GGETMRFWD motif (see Fig. 2A).

The assignment of protein ligands of the metal cluster is consistent with mutational studies recently reviewed by Debus (2001) and Diner (2001) (Chapter 11, Debus). The idea that the C-terminal domain of D1 protein provides ligands for the Mn cluster stems back to the pioneering work of Diner and colleagues (1991) followed by several studies suggesting that D1-Asp342 and the D1-C-terminal carboxy group of D1-Ala344 could be possible metal ligands (Debus, 2001). Chu et al. (2004) have made a strong argument, based on FTIR measurements, for D1-Ala344 being a ligand to a Mn undergoing oxidation during the S_1 to S_2 transition (Chu et al., 2004). However according to the X-ray structure D1-Ala344 is not a direct ligand to Mn although it seems to be hydrogen bonded through its backbone nitrogen to D1-Asp342 which is a Mn ligand. Moreover, D1-Ala344 could be a ligand for Ca^{2+} as mentioned above. Whether the structural interpretation of the interactions of D1-Ala344 within the OEC can account for the FTIR data will require closer investigation. Recent 9.2 GHz electron spin echo envelope modulation (ESEEM) studies have given support to the likelihood that D1-His332 is a Mn-ligand (Debus, 2001) but less definitive for the same role for D1-Asp170 (Debus et al., 2003). Other studies however, have given strong support for D1-Asp170 providing a 'high affinity site' for the binding of the first Mn ion incorporated during the photoinduced assembly of the Mn_4-Ca^{2+} cluster (Nixon and Diner, 1992). The identification of CP43-Glu354 as a ligand was unexpected although a mutational study of this residue did hint that it may be involved in PS II activity (Rosenberg et al., 1999).

C. Other Ligands for the Metal Cluster

The Asp or Glu ligands can be either monodentate or bidentate thus providing one or two ligands. However, with the current resolution of the X-ray structure (3.5Å), it is difficult to distinguish between these two possibilities, the only clear candidate for providing two ligands is CP43-Glu354. This means therefore

that other ligands for the metals are possibly water, hydroxyls or anions, such as Cl^- or bicarbonate as suggested in biochemical studies (Stemler, 1987, 2002; Debus, 1992; Klimov and Baranov, 2001; Chapter 13, van Gorkom and Yocum). In this context, a non-protein density bridging to Mn4 and Ca^{2+} could be satisfactorily modeled into the density as a carbonate (Fig. 6A, B). Bearing in mind the coordination requirements of Ca^{2+}, it was suggested that this carbonate provides two ligands to this cation and one to Mn4. No density was detected to accommodate a Cl^- even though this anion is a cofactor for the water oxidation process (Debus, 1992). The relevance of the carbonate binding site in terms of the catalytic activity of the metal cluster will be discussed below.

D. Hydrophilic Channel

Assuming that the short fall in ligands for the metal cluster is satisfied mainly by water and hydroxyls, then clearly the $Mn_4Ca^{2+}O_4$-cluster is located in a hydrophilic environment. Leading from this environment is a hydrophilic channel with D1-Asp61 at its mouth (Gig. 6B). The channel proceeds approximately 10 to 15 Å to the lumenal surface through the interface of the D1/D2 proteins. It then continues for a further 20 Å across the PsbO protein, which could be filled with water molecule. The residues involved in this hydrophilic channel leading from the OEC to the lumenal surface are D1-Asp61, D1-Glu65, D2-Lys317 and D2-Glu312 (see Fig. 6D). The PsbO residues, Asp158, Asp222, Asp223, Asp224, His228 and Glu229 are also involved in the formation of the water-filled space. This hydrophilic channel may not only provide the exit pathway for protons derived from water oxidation but also facilitate a supply of water to the catalytic center.

E. Redox-Active Tyrosine Y_D and Its Environment

As expected the recent X-ray structure confirmed that the redox active D2-Tyr160 (Y_D) is related to D1-Tyr161 (Y_Z) by the pseudo-two-fold axis which relates the other cofactors of the PS II RC (Fig. 4). Moreover the structure indicates that it is hydrogen bonded to D2-His189 in agreement with several studies (Diner and Babcock, 1996; Diner, 2001; Chapter 9 Diner and Britt). However, unlike D1-Tyr161, this tyrosine is located in a hydrophobic environment. Indeed the 'cavity' equivalent to that containing the OEC on the D1 side of the RC is hydrophobic and filled with bulky side chains of the protein, Phe168, Phe184, Phe185 and Phe188 and of CP47-Phe362 and Phe363. The two CP47 residues are contained in the highly conserved motif FFETFSVLV of the large extrinsic domain, linking transmembrane helices V and VI (see Fig. 2B). This finding, together with the involvement of the large extrinsic domain of CP43 with the OEC, establishes the significance of CP43 and CP47 in PS II function over and above their roles as light harvesting systems.

VIII. General Implications of the Structure

The new X-ray structure (Ferreira et al., 2004) provides an enormous amount of information to discuss many aspects of PS II functioning, ranging from the physiological implications of the arrangement of its subunits (including the turnover of D1 protein; Barber and Andersson, 1992) to details about the protein environments of various cofactors. For example, revealing the structural properties of the Q_B site can now open up rigorous discussions about the protonation of the terminal plastoquinone acceptor and explore various features of this site in terms of herbicide binding with cross-referencing to the BRC. On the donor side (see Fig. 4), we now have structural information to investigate the possible factors that lead to the high redox potential properties of the four Chls, P_{D1}, P_{D2}, Chl_{D1} and Chl_{D2} and how they cooperate to provide the oxidizing potential of $P680^{\bullet+}$ (Barber and Archer, 2001; Barber, 2002; Diner and Rappaport, 2002; Chapters 4, Nixon et al., and 7, Renger and Holzwarth). For Chl_{D1} and Chl_{D2}, is the lack of His ligands a feature necessary for the high oxidation potential of these Chls as compared with their bacterial equivalents? Also, is it the more monomeric nature of P_{D1} and P_{D2} Chls compared with the special pairs of other types of RCs which underlies the high redox potential of P680? These and many other important questions can now be addressed in light of the new structural model of PS II. However, the main reason for determining the structure of PS II surely must be to provide a framework for the full elucidation of molecular processes of water oxidation.

IX. Water Oxidation Mechanism

The oxidation of water by PS II involves the five

different intermediates of the S-state cycle. In the dark, PS II relaxes mainly to the S_1-state due to the oxidation of S_0 by oxidized Y_D and charge recombination reactions bring about the reduction of S_3- and S_2-states (Goussias et al., 2002). The crystals used for obtaining the X-ray structure were kept as much as possible in the dark prior to their freezing for X-ray diffraction measurements (Ferriera et al., 2004). Thus, in the first approximation, we can assume that the structure is dominated by the S_1-state conformation. However X-rays can produce free electrons within the crystals which could reduce high valency Mn ions and cause radiation damage to metal clusters. Then there is the fact that a high level of $(NH_4)_2SO_4$ (100 mM) was used to generate the crystals (see online supporting materials of Ferreira et al., 2004) which may well have blocked PS II into a non-physiological conformational state. Therefore caution is needed in relating the present structural model for the OEC with the mechanism of water oxidation. Nevertheless our structure of the OEC elucidated by X-ray crystallography does seem to favor a particular type of mechanism which is discussed below.

Over the years, many different schemes for water oxidation chemistry have been formulated (Renger 2001; Goussias et al., 2002; Yachandra, 2002; Britt et al., 2004; Chapter 25, Hillier and Messinger). The new structure is compatible with those schemes which suggest that one of the substrate water molecules is bound to one Mn ion only, while the other is within the coordination sphere of a nearby Ca^{2+} (Messinger et al., 1995; Pecoraro et al., 1998; Siegbahn and Crabtree, 1999; Vrettos et al., 2001; Siegbahn, 2002). The organization of the Mn ions in our model of the OEC suggests that Mn4 is likely to be the site for a substrate water molecule since it is adjacent to the Ca^{2+} and bridged to it by a non-protein ligand, which could be a carbonate anion. It has been suggested that this 'active' Mn ion is oxidized to Mn(V) such that the ligated oxo group remaining after deprotonation of the substrate water molecule becomes highly electrophilic (Pecoraro et al., 1998; Vrettos et al., 2001). In so doing it is a candidate for nucleophilic attack by the oxygen of the second substrate water molecule bound to Ca^{2+} (see Fig. 7). Clearly the deprotonation of this second water molecule, its orientation to the electrophilic oxo ligand and the requirement for it to remain a nucleophile are key factors in facilitating the O-O bond formation. These requirements could be aided by the nucleophilic properties of Cl^- known to be an important cofactor for the water oxidation reaction (Debus, 1992; but see Olesen and Andreasson, 2003) and may become a ligand for Ca^{2+} in a higher S-state since it has not been detected in the present X-ray structure. The Lewis acidity of Ca^{2+} is also to be noted (Vrettos et al., 2001). Moreover, the deprotonation of the substrate water molecules and the stabilization of intermediates could be aided by the hydrogen bonding networks within the local environment of the OEC provided by protein side chains (Vrettos et al., 2001). Indeed, there are a number of candidate side chains identified in the X-ray model; CP43-Arg357 and D1-Gln165 (on the Mn4-side), and D1-Tyr161 and D1-Glu189 (on the Ca^{2+}-side) (see Fig. 7B, C).

The nucleophilic attack of the oxygen of the second water substrate molecule on the highly electrophilic oxo to bring about O-O bond formation is essentially the reverse of the first step in the reduction of oxygen to water in the binuclear center of cytochrome c oxidase. The first step of oxygen reduction involves the breaking of the O-O bond to form a ferryl-oxo and a cupric hydroxide. For this reaction to occur both Fe and Cu must be in their most reduced states; Fe^{2+} and Cu^+ and the O-O bond breakage is driven by their oxidation. This, therefore, creates a comparable species to those of the final step proposed for O-O bond formation in the mechanism suggested above except that intermediates are derived from oxidative rather than reductive chemistry.

Although it seems possible that O-O bond formation occurs as described above, there is the question of the detail of the other steps that lead to this terminal reaction step. It is often assumed that water substrate molecules bind at the S_0-state. However, thermodynamics tells us that to remove a hydrogen atom from water at pH 7.0 requires about 2.4 Volts and another 1.8 Volts is required to remove the second hydrogen to yield an oxygen atom (Radmer and Cheniae, 1977). Theoretically an oxygen atom (biradical) can react with a water molecule to produce dioxygen and release about 1 Volt of energy. Therefore overall about 3.2 Volts are required to oxidize two water molecules to dioxygen (~0.8 V per electron). Although an oxygen biradical cannot be created in PS II because of its extreme reactivity, electrophilic oxo (or possibly oxyl radical) is the nearest it can come to this situation. According to these thermodynamic considerations, the direct chemistry of water oxidation leading to O-O bond formation can only begin when about 3 Volts of oxidizing potential has been accumulated; that is when the energy of three

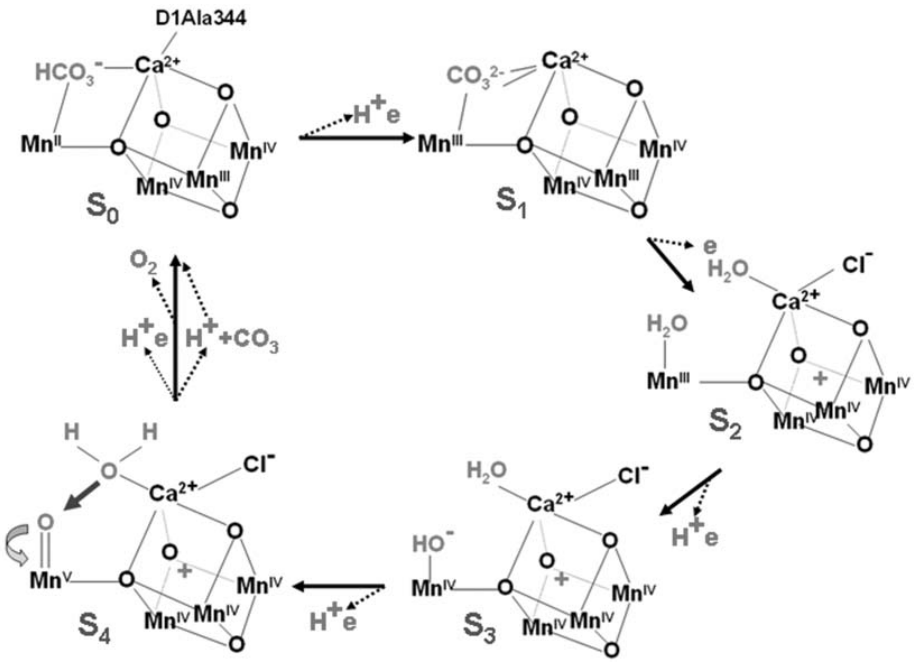

Fig. 7. A mechanism for water oxidation. A hypothetical scheme for water oxidation based on the X-ray structure whereby the O-O bond is formed by the nucleophilic attack of the oxygen of a substrate water molecule bound within the Ca^{2+}-coordination sphere of a highly electrophilic oxo attached to a high valency Mn (Mn(V)). It is postulated that bicarbonate/carbonate are bound to the active site during the early part of the S-state cycle. Deprotonation of the substrate water molecules is probably aided by the hydrogen-bonding network formed by the local protein environment (see text). No attempt has been made to adjust the geometry of the cluster during the S-state cycle although conformational changes may well occur in order to facilitate both protein and non-protein ligand reorganization. (From Barber, 2005.)

photons has been converted and stored. It follows, therefore, that the water substrate molecules need not bind into their catalytic orientations until higher S-states are attained. Indeed, this may be advantageous in terms of preventing any side reactions, such as generation of hydrogen peroxide. The concept that the water substrate molecules do not undergo oxidation until late in the S-state cycle is supported by isotopic exchange experiments (Messinger et al., 1995; Hillier and Wydrzynski, 2001) which also suggested that a substrate water molecule binds to Ca^{2+} (Hendry and Wydrzynski, 2003). With this in mind, could it be that the non-protein ligand attributed to carbonate in the X-ray structure is the physiological ligating species for the lower S-states? Indeed, there is evidence that bicarbonate is required both for the assembly of the Mn_4Ca^{2+} cluster (Baranov et al., 2000; Chapter 26, Dismukes et al.) and for the water oxidation processes (Stemler, 1980; Allakhverdiev et al., 1997; Klimov and Baranov, 2001; Chapter 14, van Rensen and Klimov). Bicarbonate is known to form complexes with Mn(II) (Dismukes et al., 2001) which is an anticipated valency for one of the Mn ions of the cluster in the S_0 state (according to the spin properties of S_0, the valencies for the four Mn ions are thought to be: Mn(II) Mn(III), Mn(IV) Mn(IV)) (see Robblee et al., 2001; Goussias et al., 2002; Yachandra, 2002). Therefore, in the S_0-state, bicarbonate could provide bridging ligands between Mn4 and Ca^{2+} where Mn4 has a valency of two. During the S_0 to S_1 transition, Mn4 is assumed to increase its valency to three and the conversion of bicarbonate to carbonate would provide an additional ligand to Ca^2. Bridging of bicarbonate/carbonate between Mn and Ca^{2+} in the OEC has also been suggested from FTIR studies (Yruela et al., 1998). Interestingly, in the lumen and close to the OEC, carbonic anhydrase exists which would facilitate bicarbonate availability (Stemler, 1987; Moskvin et al., 1998; Villarejo et al., 2002).

Structural changes in the upper S-state transition, perhaps induced by an oxidation of the Mn(III) of the cubane during the S_1 to S_2 transition, may break the carbonate cross-linkages and allow reorientation of water molecules into their 'substrate positions' for the subsequent deprotonation and oxidation reactions as outlined in Fig. 7. At this stage Cl^- may ligate to Ca^{2+}.

There is no doubt that each electron extracted from the metal-cluster is transferred to the neutral Y_Z radical but it remains uncertain whether the same route is used by the exiting protons derived from the oxidation of the water molecules as suggested by G. T. Babcock and colleagues (Hoganson and Babcock, 1997; Tommos and Babcock, 1998, 2000). The present X-ray structure is not particularly supportive of the 'hydrogen abstraction' model involving Y_Z. Although D1-His190 could act as an acceptor of the protons from Y_Z, there is no obvious pathway for subsequent proton transfer. D1-Glu189 has been suggested as a candidate residue involved in the proton translocation (Tommas and Babcock, 1998, 2000), but it is not close to D1-His190 but rather acts as a ligand for Mn3 of the cubane in the current structure. However Mn3 is unusual in that it also has D1-His332 as a protein ligand and it is not inconceivable that the weaker ligating properties of a glutamate, compared with a histidine, could mean that it undergoes a structural rearrangement, for example in higher S-states, and thus facilitate proton transfer from D1-His190 towards the hydrophilic channel with D1-Asp61 at its mouth. This possible readjustment of the position of D1-Glu189 could underlie the well established conformation change which occurs on the S_2 to S_3 transition (Messinger et al., 1991; Renger and Hanssum, 1992; Boussac et al., 1998).

X. Perspectives

The recent X-ray structure (Ferreira et al., 2004), together with previous structural works (Rhee et al., 1998; Hankamer et al., 2001a,b; Zouni et al., 2001; Kamiya and Shen, 2003) and outstanding contributions from EXAFS, EPR, FTIR and optical spectroscopy, from molecular biology and from a range of biochemical studies, have provided us with a substantial knowledge base to use to elucidate the many facets of PS II function, particularly the water splitting reaction. In the case of the latter, we can now home in on mechanisms which are compatible with the new structural information of the OEC. We have discussed one possibility here, which hopefully will provide a basis for new experiments and thinking. EXAFS, EPR and FTIR spectroscopy will remain important techniques together with appropriate biochemical and molecular biological backup to explore the chemistry of water oxidation. X-ray crystallography will, now, need to provide a higher resolution structure not only for the S_1-state but also for other intermediate states, whether they be induced by flashes of light (e.g., S_2 and S_3) or modified by the addition of inhibitors (e.g., acetate, formate) or by exclusion cofactors (Cl^-, HCO_3^- and Ca^{2+}). In any event we are now at the last stage of the challenge to reveal the molecular events of a reaction on which virtually all life depends and which makes our planet special.

Acknowledgments

We wish to thank the Biotechnology and Biological Research Council (BBSRC) for financial support. SI is a member of ATP System Project, ERATO, Japan Science and Technology Corporation. We acknowledge the significant contributions to our crystallographic studies of PS II by Kristina N. Ferreira, Tina M. Iverson and Karim Maghlaoui. For technical support we thank the Centre for Structural Biology and Bioinformatics Facility at Imperial College London and also Drs. Clemens Schulze-Briese and Takashi Tomizaki at PX06SA/SLS, Paul Scherrer Institute, Villigen, Switzerland and Dr. Bill Shepard at ID29, ESRF.

References

Adir N, Okamura MY and Feher G (1992) Crystallization of the PS II reaction center. In: Murata N (ed) Photosynthesis: From Light to Biosphere, Vol 2, pp 195–198. Kluwer Academic Publishers, Dordrecht

Allakhverdiev SI, Yruela I, Picorel R and Klimov VV (1997) Bicarbonate is an essential constituent of the water-oxidizing complex of Photosystem II. Proc Natl Acad Sci USA 94: 5050–5054

Baranov SV, Ananyev GM, Klimov VV and Dismukes GC (2000) Bicarbonate accelerates assembly of inorganic core of the water-oxidising complex in manganese-depleted Photosystem II: A proposed biogeochemical role for atmospheric carbon dioxide in oxygenic photosynthesis. Biochemistry 39: 6060–6065

Barbato R, Race HL, Friso G and Barber J (1991) Chlorophyll levels in the pigment binding proteins of PS II: A study based

on the chlorophyll to cytochrome ratio in different PS II preparations. FEBS Lett 286: 86–90
Barber J (1987) Photosynthetic reaction centres: A common link. Trends Biochem Sci 12: 321–326
Barber J (2002) P680: What is it and where is it? Bioelectrochem 55: 135–138
Barber J (2003) Photosystem II: The engine of life. Quart Revs Biophys 36: 71–89
Barber J (2005) Molecular architecture of photosynthetic systems: New developments and mechanisms. In: Phillips D and Barber J (eds) The Life and Scientific Legacy of George Porter. Imperial College Press, London, in press
Barber J and Andersson (1992) Too much of a good thing: Light can be bad for photosynthesis. Trends Biochem Sci 17: 61–66
Barber J and Archer MD (2001) P680, the primary electron donor of PS II. J Photochem Photobiol A142: 97–106
Barber J, Morris EP and Buchel C (2000) Revealing the structure of the photosystem two chlorophyll binding proteins, CP43 and CP47. Biochim Biophys Acta 1459: 239–247
Barber J, Morris EP and Da Fonseca PCA (2003) Interaction of the allophycocyanin core complex with PS II. Photochem Photobiol Sci 2: 536–541
Boussac A, Un S, Horner O and Rutherford AW (1998) High-spin states (S >/= 5/2) of the Photosystem II manganese complex. Biochemistry 24: 4001–4007
Breton J (2004) Absence of large-scale displacement of quinone Q_B in bacterial photosynthetic reaction centers. Biochemistry 43: 3318–3326
Breton J, Duranton J and Satoh K (1988) Orientation of pigments in the reaction centre and the core antenna of Photosystem II. In: Scheer H and Schneider S (eds) Photosynthetic Light-Harvesting Systems: Organisation and Function, pp 375–386. Walter de Gruyter, Berlin
Bricker TM (1990) The structure and function of CPa-1 and CPa-2 in Photosystem II. Photosynth Res 24: 1–13
Bricker TM and Frankel LK (1998) The structure and function of the 33 kDa extrinsic protein of Photosystem II: A critical assessment. Photosynth Res 56: 157–173
Britt RD, Campbell KA, Peloquin JM, Gilchrist ML, Aznar CP, Dicus MM, Robblee J and Messinger J (2004) Recent pulsed EPR studies of the Photosystem II oxygen-evolving complex: Implications as to water oxidation mechanisms. Biochim Biophys Acta 1655: 158–171
Brunger AT, Adams PD, Clore GM, DeLano WL, Gros P, Grosse-Kunstleve RW, Jiang JS, Kuszewski J, Nilges M, Pannu NS, Read RJ, Rice LM, Simonson T and Warren GL (1998) Crystallography & NMR system: A new software suite for macromolecular structure determination. Acta Cryst D54: 905–921
Buchel C, Morris E, Orlova E and Barber J (2001) Localisation of the PsbH subunit in Photosystem II: A new approach using labelling of His-tags with a $Ni2^{+}$-NTA gold cluster and single particle analysis. J Mol Biol 312: 371–379
Carrell TG, Tyryshkin AM and Dismukes GC (2002) An evaluation of structural models for the photosynthetic water-oxidizing complex derived from spectroscopic and X-ray diffraction signatures. J Biol Inorg Chem 7: 2–22
Castenholz RW (1969) Thermophilic blue-green algae and the thermal environment. Bacteriol Rev 33: 416–450
Chu H-A, Hillier W and Debus RJ (2004) Evidence that the C-terminus of the D1 polypeptide of Photosystem II is ligated to the manganese ion that undergoes oxidation during the S_1 to S_2 transition; An isotope-edited FTIR study. Biochemistry 43: 3152–3166
Cinco RM, McFarlane Holman KL, Robblee JH, Yano J, Pizarro SA, Bellacchio E, Sauer K and Yachandra VK (2002) Calcium EXAFS establishes the Mn-Ca cluster in the oxygen-evolving complex of Photosystem II. Biochemistry 41: 12928–12933
Cowtan K (1994) DM: An automated procedure for phase improvement by density modification. Joint CCP4 and ESF-EACBM Newsletter in Protein Crystallog 31: 34
Debus RJ (1992) The magnesium and calcium ions of photosynthetic oxygen evolution. Biochim Biophys Acta 1102: 269–352
Debus RJ (2000) The polypeptides of Photosystem II and their influence on manganese tyrosyl-based oxygen evolution. In: Sigel A and Sigel H (eds) Metal Ions in Biological Systems, Vol 37, 657–711. Marcel Dekker Inc, New York
Debus RJ (2001) Amino acid residues that modulate the properties of tyrosine Y_Z and the manganese cluster in the water oxidising complex of Photosystem II. Biochim Biophys Acta 1503: 164–186
Debus RJ, Aznar C, Campbell KA, Gregor W, Diner BA and Britt RD (2003) Does aspartate 170 of the D1 polypeptide ligate the manganese cluster in Photosystem II? An EPR and ESEEM study. Biochemistry 42: 10600–10608
Deisenhofer J, Epp O, Miki K, Huber R and Michel H (1985) Structure of the protein subunits in the photosynthetic reaction centre *Rhodopseudomonas viridis* at 3.8 Å resolution. Nature 318: 618–624
De Las Rivas J and Barber J (2004) Analysis of the structure of the PsbO protein and its implications. Photosynth Res 81: 329–343
De Las Rivas J, Telfer A, and Barber J (1993) Two coupled β-carotene molecules protect P680 from photodamage in isolated photosystem two reaction centres. Biochim Biophys Acta 1142, 155–164
De Las Rivas J, Balsera M and Barber J (2004) Evolution of oxygenic photosynthesis: Genome wide analysis of the OEC extrinsic proteins. Trends Plant Sci 9: 18–25
De Paula JC, Beck WF and Brudvig GW (1986) Magnetic properties of manganese in the photosynthetic O_2-evolving complex. 2. Evidence for a manganese tetramer. J Am Chem Soc 108: 4002–4009
DeRose VJ, Mukeriji I, Latimer MJ, Yachandra VK, Sauer K and Klein MP (1994) Comparison of the manganese oxygen-evolving complex in Photosystem II of spinach and *Synechococcus* sp. with multinuclear manganese model compounds by X-ray absorption spectroscopy. J Am Chem Soc 116: 5239–5249
Diner BA (2001) Amino acid residues involved in the coordination and assembly of the manganese cluster of Photosystem II. Proton-coupled electron transport of the redox-active tyrosines and its relationship to water oxidation. Biochim Biophys Acta 1503: 147–163
Diner BA and Babcock GT (1996) Structure, dynamics and energy conversion efficiency in Photosystem II. In: Ort DR and Yocum CF (eds) Oxygenic Photosynthesis: The Light Reactions, pp 213–247. Kluwer Academic Publishers, Dordrecht
Diner BA and Rappaport F (2002) Structure, dynamics and energetics of the primary photochemistry of Photosystem II of oxygenic photosynthesis. Annu Rev Plant Biol 53: 551–580

Diner BA, Nixon PJ and Farchaus JW (1991) Site-directed mutagenesis of photosynthetic reaction centers. Curr Opin Struct Biol 1: 546–554

Dismukes GC, Rüettinger W, Boelrijk AEM and Ho D (1998) Structure of the Mn_4Ca core of the PS II water oxidising complex and the Mn_4O_4-cubane/Mn_4O_2-butterfly model complexes. In: Garab G (ed) Photosynthesis: Mechanism and Effects, Vol II, pp 1259–1264. Kluwer Academic Publishers, Dordrecht

Dismukes GC, Klimov VV, Baranov SV, Kozlov YN, DasGupta J and Tyryshkin A (2001) The origin of atmospheric oxygen on earth: The innovation of oxygenic photosynthesis. Proc Natl Acad Sci USA 98: 2170–2175

Faller P, Pascal A and Rutherford AW (2001) Beta-carotene redox reactions in Photosystem II: Electron transfer pathway. Biochemistry 40: 6431–6440

Frazao C, Enguita FJ, Coelho R, Sheldrick GM, Navarro JA, Hervas M, De la Rosa MA and Carrondo MA (2001) Crystal structure of low-potential cytochrome *c*(549) from *Synechocystis* sp PCC6803 at 1.21 Å resolution. J Biol Inorg Chem 6: 324–332

Fromme P, Kern B, Loll J, Biesiadka J, Saenger W, Witt HT, Krauss N and Zouni A (2002) Functional implications on the mechanism of the function of Photosystem II including water oxidation based on the structure of Photosystem II. Phil Trans Roy Soc Lond B 357: 1337–1346

Ferreira K, Iverson T, Maghlaoui K, Barber J and Iwata S (2004) Architecture of the photosynthetic oxygen evolving center. Science 303: 1831–1838

Fontino C, Kokkinidis M, Fritzsch G, Haase W, Michel H and Ghanotakis DF (1993) Characterisation of a Photosystem II core and its three-dimensional crystals. Photosynth Res 37: 41–48

Gounaris K, Chapman DJ, Booth P, Crystall B, Giorgi LB, Klug DR, Porter G and Barber J (1990) Comparison of the D1/D2/cytochrome *b*559 reaction centre of photosystem two isolated by two different methods. FEBS Lett 265: 88–92

Goussias C, Boussac A and Rutherford AW (2002) Photosystem II and photosynthetic oxidation of water: An overview. Phil Trans Roy Soc Lond B 357: 1369–1381

Govindjee and van Rensen JJS (1993) Photosystem II reaction centre and bicarbonate. In: Deisenhofer and Norris J (eds) The Photosynthetic Reaction Center, pp 357–389. Acad Press, San Diego

Hankamer B, Barber J and Boekema E (1997) Structure and membrane organisation of Photosystem II in green plants. Annu Rev Plant Physiol Plant Mol Biol 48: 641–671

Hankamer B, Morris EP and Barber J (1999) Cryoelectron microscopy of photosystem two shows that CP43 and CP47 are located on opposite sides of the D1/D2 reaction centre proteins. Nat Struct Biol 6: 560–564

Hankamer B, Morris EP, Nield J, Gerle C and Barber J (2001a) Three-dimensional structure of Photosystem II core dimer of higher plants determined by electron microscopy. J Struct Biol 135: 262–269

Hankamer B, Morris EP, Nield J, Carne A and Barber J (2001b) Subunit positioning and transmembrane helix organisation in the core dimer of Photosystem II. FEBS Lett 504: 142–151

Hanley J, Deligiannakis Y, Pascal A, Faller P and Rutherford AW (1999) Carotenoid oxidation in Photosystem II. Biochemistry 38: 8189–8195

Haumann M and Junge W (1999) Photosynthetic water oxidation: A simplex-scheme of its partial reactions. Biochim Biophys Acta 1411: 86–91

Hendry G and Wydrzynski T(2003) ^{18}O isotope exchange measurements reveal that calcium is involved in the binding of one substrate-water molecule to the oxygen-evolving complex in Photosystem II. Biochemistry 42: 6209–6217

Hillier W and Wydrzynski T (2001) Oxygen ligand exchange at metal sites – implications for the O_2 evolving mechanism of Photosystem II. Biochim Biophys Acta 1503: 197–209

Hoganson CW and Babcock GT (1997) A metalloradical mechanism for the generation of oxygen from water in photosynthesis. Science 277: 1953–1956

Ikeuchi M and Inoue Y (1988) A new Photosystem II reaction centre component (4.8 kDa protein) encoded by the chloroplast genome. FEBS Lett 241: 99–104

Irrgang KD, Shi LX, Funk C and Schröder WP (1995) A nuclear encoded subunit of the Photosystem II reaction centre. J Biol Chem 270: 17588–17593

Iwata S (2003) Methods and results in crystallisation of membrane proteins. IUL Biotechnology Series, Pub International University Line, La Jolla

Iwata S, Ostermeier, C, Ludwig B and Michel H (1995) Structure at 2.8Å resolution of cytochrome *c* oxidase from *Paracoccus denitrificans*. Nature 376: 660–669

Iwata S, Lee JW, Okada K, Lee JK, Iwata M, Rasmussen B, Link TA, Ramaswamy S and Jap BK (1998) Complete structure of the bovine mitochondrial cytochrome bc_1 complex. Science 281: 64–71

Jones OTA, Zou JY, Cowan SW and Kjeldgaard M (1991) Improved methods for building protein models in electron density maps and location of errors in these models. Acta Cryst A47: 110–119

Jordan P, Fromme P, Witt HT, Klukas O, Saenger W and Kraus N (2001) Three-dimensional structure of cyanobacterial Photosystem I at 2.5 Å resolution. Nature 411: 909–916

Kamiya N and Shen JR (2003) Crystal structure of oxygen-evolving Photosystem II from *Thermosynechococcus vulcanus* at 3.7-Å resolution. Proc Natl Acad Sci USA 100: 98–103

Kashino Y, Koike H, Yoshio M, Egashira H, Ikeuchi M, Pakrasi HB and Satoh K (2002a) Low-molecular mass polypeptide components of a Photosystem II preparation from the thermophilic cyanobacterium *Thermosynechococcus vulcanus*. Plant Cell Physiol 43: 1366–1373

Kashino Y, Lauber WH, Carroll JA, Wang Q, Whitmarsh J, Satoh K and Pakrasi HB (2002b) Proteomic analysis of a highly active Photosystem II preparation from the cyanobacterium *Synechocystis* sp PCC6803 reveals the presence of novel polypeptides. Biochemistry 41: 8004–8012

Kerfeld CA, Sawaya MR, Bottin H, Tran KT, Sugiura M, Cascio D, Desbois A, Yeates TO, Kirilovsky D and Boussac A (2003) Structural and EPR characterisation of the soluble form of cytochrome *c*-550 and the *psb*V2 gene product from the cyanobacterium *Thermosynechoccus elongatus*. Plant Cell Physiol 44: 697–706

Klimov VV and Baranov SV (2001) Bicarbonate requirement for the water-oxidising complex of Photosystem II. Biochim Biophys Acta 1503: 187–196

Kobayashi M, Maeda H, Watanabe T, Nakane H and Satoh K (1990) Chlorophyll *a* and β-carotene content in the D1/D2/cytochrome *b*559 reaction centre complex from spinach. FEBS Lett 260: 138–140

Krauss N, Schubert WD, Klukas O, Fromme P, Witt HT and Saenger W (1996) Photosystem I at 4 Å resolution represents the first structural model of a joint photosynthetic reaction centre and core antenna system. Nature Struct Biol 3: 965–973

Kuhl H Kruip J, Seidler A, Krieger-Liszkay A, Bunker M, Bald D, Scheidig AJ and Rögner M (2000) Towards structural determination of the water-splitting enzyme — Purification, crystallization, and preliminary crystallographic studies of Photosystem II from a thermophilic bacterium. J Biol Chem 275: 20652–20659

Lancaster CRD and Michel H (1997) The coupling of light-induced electron transfer and proton uptake as derived from crystal structures of reaction centres from *Rhodopseudomonas viridis* modified at the binding site of the secondary quinone, Q_B. Structure 5: 1339–1359

Masayuki Y, Wolf KV, Baesjou PJ, Bernasek SL and Dismukes GC (2001) Selective photoproduction of O_2 from the Mn_4O_4 cubane core: A structural and functional model for the photosynthetic water-oxidising complex. Angew Chem, Int Ed 40: 2925–2928

Messinger J, Wacker U and Renger G (1991) Unusual low reactivity of the water oxidase in redox state S3 towards exogenous reductants. Analysis of NH_2OH- and NH_2NH_2-induced modification of flash-induced oxygen evolution in isolated spinach thylakoids. Biochemistry 30: 7852–7862

Messinger J, Badger M and Wydrzynski T (1995) Detection of one slowly exchanging substrate water molecule in the S_3 state of Photosystem II. Proc Natl Acad Sci USA 92: 3209–3213

Michel H and Deisenhofer J (1988) Relevance of the photosynthetic reaction center of purple bacteria to the structure of Photosystem II. Biochemistry 27: 1–7

Miyao M and Murata N (1986) Light-dependent inactivation of photosynthetic oxygen evolution during NaCl treatment of Photosystem II particles — The role of the 24 kDa protein. Photosynth Res 10: 489–496

Moskvin OV, Razguliayeva AY, Shutova TV, Kristin MS, Ivanov BN and Klimov VV (1998) Carbonic anhydrase activity In Garab G (ed) Photosynthesis: Mechanisms and Effects, Vol II, pp 1201–1204. Kluwer Academic Publishers, Dordrecht

Nakamura Y, Kaneko T, Sato S, Ikeuchi M, Katoh H, Sasamoto S, Watanabe A, Iriguchi M, Kawashima K, Kimura T, Kishida Y, Kiyokawa C, Kohara M, Matsumoto M, Matsuno A, Nakazaki N, Shimpo S, Sugimoto M, Takeuchi C, Yamada M, Tabata S. (2002) Complete genome structure of the thermophilic cyanobacterium *Thermosynechococus elongatus* BP-1. DNA Res 9: 123–130

Nixon PJ and Diner BA (1992) Aspartate 170 of the Photosystem II reaction center polypeptide D1 is involved in the assembly of the oxygen-evolving manganese cluster. Biochemistry 31: 942–948

Olesen K and Andreasson LE (2003) The function of the chloride ion in photosynthetic oxygen evolution. Biochemistry 42: 2025–2035

Pazos F, Heredia P, Valencia A and De Las Rivas J (2001) Threading structural model of the manganese-stabilizing protein PsbO reveals presence of two possible β-sandwich domains. Proteins 45: 2702–2711

Pecoraro VL, Baldwin MJ, Caudle MT, Hsieh WY and Law NA (1998) A proposal for water oxidation in Photosystem II. Pure Appl Chem 70: 925–929

Peloquin JM and Britt RD (2001) EPR/ENDOR characterisation of the physical and electronic structure of the OEC Mn cluster. Biochim Biophys Acta 1503: 96–111

Peloquin JM, Campbell KA, Randall DW, Evanchik MA, Pecoraro VL, Armstrong WH and Britt RD (1998) ^{55}Mn ENDOR of the S_2-state multiline EPR signal of Photosystem II: Implications on the structure of the tetranuclear Mn cluster. J Am Chem Soc 120: 6840–6841

Popelkova H, Wyman AJ and Yocum CF (2003) Amino acid sequences and solution structures of manganese stabilizing protein that affect reconstitution of Photosystem II activity. Photosynth Res 77: 21–34

Radmer R and Cheniae G (1977) Mechanisms of oxygen evolution In: Barber J (ed) Primary Processes of Photosynthesis, Topics in Photosynthesis, Vol 2, pp 303–348. Elsevier, Amsterdam

Renger G (2001) Photosynthetic water oxidation to molecular oxygen: Apparatus and mechanism. Biochim Biophys Acta 1503: 210–228

Renger G and Hanssum B (1992) Studies of the reaction-coordinates of the water oxidase in PS II membrane fragments from spinach. FEBS Lett 299: 28–32

Rhee KH (1998) Three-dimensional structure of Photosystem II reaction center by electron cryomicroscopy. PhD thesis. University of Heidelberg, Germany

Rhee KH, Morris EP, Zheleva D, Hankamer B, Kühlbrandt W and Barber J (1997) Two-dimensional structure of plant Photosystem II at 8Å resolution. Nature 389: 522–526

Rhee KH, Morris EP, Barber J and Kühlbrandt W (1998) Three dimensional structure of the plant Photosystem II reaction centre at 8Å resolution. Nature 396: 283–286.

Robblee JH, Cinco RM and Yachandra VK (2001) X-ray spectroscopy-based structure of the Mn cluster and mechanism of photosynthetic oxygen evolution. Biochim Biophys Acta 1503: 7–23

Robblee JH, Messinger J, Cinco RM, McFarlane KL, Fernandez C, Pizarro SA, Sauer K and Yachandra VK (2002) The Mn cluster in the S_0 State of the oxygen evolving complex of Photosystem II studied by EXAFS spectroscopy: Are there three di-μ-oxo-bridged Mn2 moieties in the tetranuclear Mn complex? J Am Chem Soc 124: 7459–7471

Rosenberg C, Christian J, Bricker TM and Putnam-Evans C (1999) Site-directed mutagenesis of glutamate residues in the large extrinsic loop of the Photosystem II protein CP43 affects oxygen-evolving activity and PS II assembly. Biochemistry 38: 15994–16000

Sawaya MR, Krogmann DW, Serag A, Ho KK, Yeates TO and Kerfeld CA (2001) Structures of cytochrome c-549 and cytochrome *c*-6 from the cyanobacterium *Arthrospira maxima*. Biochemistry 40: 9215–9225

Schubert WD, Klukas O, Saenger W, Witt HT, Fromme P and Krauss N (1998) A common ancestor for oxygenic and anoxygenic photosynthetic systems: a comparison based on the structural model of Photosystem I. J Mol Biol 280: 297–314

Shen JR and Kamiya N (2000) Crystallization and the crystal properties of the oxygen-evolving Photosystem II from *Synechococcus vulcanus*. Biochemistry 39: 14739–14744

Shi LX and Schröder WP (2004) The low molecular mass subunits of the photosynthetic supracomplex, Photosystem II. Biochim Biophys Acta 1608: 75–96

Siegbahn PEM (2002) Quantum chemical studies of manganese centers in biology. Curr Opin Chem Biol 6: 227–235

Siegbahn PEM and Crabtree RH (1999) Manganese oxyl radi-

cal intermediates and O-O bond formation in photosynthetic oxygen evolution and a proposed role for the calcium cofactor in Photosystem II. J Am Chem Soc 121: 117–127

Stemler AJ (1980) Inhibition of Photosystem II by formate: Possible evidence for a direct role of bicarbonate in photosynthetic oxygen evolution. Biochim Biophys Acta 593: 103–112

Stemler AJ (1987) The case for carbonic anydrase. Physiol Plant 99: 348–353

Stemler AJ (2002) The bicarbonate effect, oxygen evolution, and the shadow of Otto Warburg. Photosynth Res 73: 185–192

Stowell MHB, McPhillips TM, Rees DC, Soltis SM, Abresch E and Feher G (1997) Light-induced structural changes in photosynthetic reaction center: Implications for mechanism of electron-proton transfer. Science 276: 812–816

Sugimoto I and Takahashi Y (2003) Evidence that the PsbK polypeptide is associated with the Photosystem II core antenna complex CP43. J Biol Chem 278: 45004–45010

Swiatek M, Kuras R, Sokolenko A, Higgs D, Olive J, Cinque G, Muller B, Eichacker LA, Stern DB, Bassi R, Herrmann RG and Wollman FA (2001) The chloroplast gene *ycf9* encodes a Photosystem II (PS II) core subunit, PsbZ, that participates in PS II supramolecular architecture. Plant Cell 13: 1347–1367

Tang and Diner BA (1994) Biochemical and spectroscopic characterisation of a new oxygen-evolving Photosystem II core complex from the cyanobacterium *Synechocystis* PCC 6803. Biochemistry 33: 4594–4603

Telfer A, De Las Rivas and Barber J (1991) β-carotene within the isolated Photosystem II reaction centre: photooxidation and irreversible bleaching of this chromophore by oxidised P680. Biochim Biophys Acta 1060: 106–114

Telfer A, Frolov D, Barber J, Robert B and Pascal A (2003) Oxidation of the two β-carotene molecules in the PS II reaction center. Biochemistry 42: 1008–1015

Tommos C and Babcock GT (1998) Oxygen production in nature: A light driven metalloradical enzyme process. Acc Chem Res 31: 18–25

Tommos C and Babcock GT (2000) Proton and hydrogen currents in photosynthetic water oxidation. Biochim Biophys Acta 1458: 199–219

Tracewell CA and Brudvig GW (2003) Two redox-active β-carotene molecules in Photosystem II. Biochemistry 42: 9127–9136

Tracewell CA, Cua A, Stewart DH, Bocian DF and Brudvig GW (2001a) Characterization of carotenoid and chlorophyll photooxidation in Photosystem II. Biochemistry 40: 193–203

Tracewell CA, Vrettos JS, Bautista JA, Frank HA and Brudvig GW (2001b) Carotenoid photooxidation in Photosystem II. . Arch Biochem Biophys 385: 61–69

Trebst A (1986) The topology of the plastoquinone and herbicide binding peptides of Photosystem II — a model. Z Naturforsch 41c: 240–245

Villarejo A, Shutova T, Moskvin O, Forssen M, Klimov VV and Samuelsson G (2002) A Photosystem II-associated carbonic anhydrase regulates the efficiency of photosynthetic oxygen evolution. EMBO J 21: 1930–1938

Vrettos JS, Limburg J and Brudvig GW (2001) Coupling of electron and proton transfer in the photosynthetic water oxidase. Biochim Biophys Acta 1503: 246–259

Webber AN, Packman LC, Chapman DJ, Barber J and Gray JC (1989) A 5th chloroplast-encoded polypeptide is present in the PS II reaction centre complex. FEBS Lett 242: 259–262

Yachandra V K (2002) Structure of the Mn complex in Photosystem II: Insights from X-ray spectroscopy. Phil Trans Roy Soc Lond B 357: 1347–1358

Yachandra VK, Sauer K and Klein MP (1996) Manganese cluster in photosynthesis: where plants oxidise water to dioxygen. Chem Rev 96: 2927–2950

Yruela I, Allakhverdiev SI, Ibarra JV and Klimov VV (1998) Bicarbonate binding to the water-oxidising complex in the Photosystem II. A Fourier transform infrared spectroscopy study. FEBS Lett 425: 396–400

Zheleva D, Sharma J, Panico M, Morris HR and Barber J (1998) Isolation and characterisation of monomeric and dimeric CP47-reaction centre Photosystem II complexes. J Biol Chem 273: 16122–16127

Zouni A, Jordan R, Schlodder E, Fromme P and Witt HT (2000) First Photosystem II crystals capable of water oxidation. Biochim Biophys Acta 1457: 103–105

Zouni A, Witt HT, Kern J, Fromme P, Krauss N, Saenger W and Orth P (2001) Crystal structure of Photosystem II from *Synechococcus elongatus* at 3.8 Å resolution. Nature 409: 739–743

Chapter 22

Energy Trapping and Equilibration: A Balance of Regulation and Efficiency

Laura M. C. Barter* and David R. Klug
Molecular Dynamics Group, Department of Chemistry, Imperial College London SW7 2AY, U.K.

Rienk van Grondelle
Faculty of Sciences, Division of Physics and Astronomy, Department of Biophysics and Physics of Complex Systems, Vrije Universiteit and Institute of Molecular Biological Sciences (IMBW), Vrije Universiteit, de Boelaan 1081, 1081 HV Amsterdam, The Netherlands

*Author for correspondence, email: l.barter@ic.ac.uk

T. Wydrzynski and K. Satoh (eds): Photosystem II: The Light-Driven Water:Plastoquinone Oxidoreductase, pp. 491–514.

Summary

This chapter highlights some of the important, unresolved questions regarding the mechanism of energy transfer and trapping in Photosystem II (PS II), in particular, whether energy transfer is rate limiting and whether the primary acceptor pheophytin or the first bound plastoquinone Q_A traps the excitation energy in the reaction center. With these questions in mind, we review some of the results from spectroscopic studies made on isolated antenna, core, and reaction center complexes and discuss a number of models found in the literature that have been used to describe energy transfer and trapping. Although the rate-limiting step in PS II in vivo remains unknown, it is likely that the slow stabilization of the charge separation and consequent inefficiencies are related to the regulation of charge separation.

I. Introduction

In this chapter we address the question as to what is the rate-limiting step in the solar energy conversion by Photosystem II (PS II). PS II creates one of the strongest oxidants found in nature, capable of oxidizing water to form molecular oxygen (Diner and Babcock, 1996). It contains approximately 250 molecules of chlorophyll (Chl), most of which function as light harvesting antenna by absorbing photons of light and transferring the excitation energy to the redox active reaction center (RC). The PS II RC comprises the D1 and D2 proteins (Chapter 4), as well as the α and β subunits of cytochrome (Cyt) b_{559} (Chapters 6 and 15). In vivo the RC binds six Chl *a* molecules, two pheophytin (Pheo) *a* molecules, two β-carotenes (Chapters 7, 19-21), and contains the plastoquinones Q_A and Q_B (Chapter 8), the redox active tyrosines Y_Z and Y_D (Chapter 9), and one atom of non-heme iron. Following either direct absorption of a photon of light by the RC, or energy transfer from the antenna, a distribution of delocalized states is created in the RC (Durrant et al., 1995a). Charge transfer reactions follow, which result in the formation of a potential gradient across the thylakoid membrane, via the reduction of Pheo and oxidation of Chl (Danielus et al., 1987). Secondary electron transfer reactions first reduce the plastoquinone, Q_A and then Q_B (Diner and Babcock, 1996). This system is reset by the reduction of Chl cations by the oxygen evolving complex (OEC) via the tyrosine Y_Z (for reviews see Diner and Babcock, 1996; Nugent, 1996; Nugent et al., 2001). This allows further photons to drive subsequent charge separation. After two turnovers Q_B becomes doubly reduced, and takes up two protons. Q_BH_2 dissociates from the site into the membrane pool of PQ molecules and is replaced by a new molecule of Q_B.

The average oxidizing potential of the Chl cations in PS II have been estimated to be approximately 1.12V (Jursinic and Govindjee, 1977; Klimov et al., 1979; Rappaport et al., 2002), which is considerably greater than the typical values of 0.4–0.6 V observed for primary electron donors in Photosystem I (PS I) and purple bacterial reaction centers (RCs). It is this oxidizing strength, that ultimately enables PS II to extract electrons from water (Chapters 10, Yachandra, and 25, Hillier and Messinger) and it is important when considering the trapping of photon energy by PS II to set this process in context (for reviews, see Renger, 1992; van Grondelle et al., 1994; Diner and Babcock, 1996; Nugent, 1996; Dekker and van Grondelle, 2000; Nugent et al., 2001; Diner and Rappaport, 2002).

The mechanism of energy transfer and trapping in PS II has long been a subject of debate (Paillotin, 1976; Nairn et al., 1982; Butler et al., 1983; Berens et al., 1985a; van Gorkom, 1985; van Grondelle, 1985; Schatz et al., 1988; Bernarding et al., 1994; van Grondelle et al., 1994; Dau and Sauer, 1996; Konermann et al., 1997; Dekker and van Grondelle, 2000; Prokhorenko and Holzwarth, 2000; Vredenberg, 2000; Barter et al., 2001; Diner and Rappaport, 2002; Vassiliev et al., 2002; Yoder et al., 2002; Barter et al., 2003; Shiang et al., 2003). Although a consensual picture of the dynamics occurring within the PS II RC is now emerging (Barter et al., 2003; Shiang et al., 2003), there is still uncertainty regarding the rate limiting step of energy transfer and trapping in larger PS II particles and membrane fragments. It was initially proposed that there was a

Abbreviations: BChl – bacteriochlorophyll; BRC – bacterial reaction center; Chl – chlorophyll; CP43, CP47 – antenna proteins of the PS II core; Cyt – cytochrome; LHCII – light-harvesting complex II; NPQ – non-photochemical quenching; OEC – oxygen evolving complex; Pheo – pheophytin; PS I, PS II – Photosystem I, Photosystem II; Q_A – primary plastoquinone acceptor; Q_B – secondary plastoquinone acceptor; RC – reaction center; Y_D – redox-active tyrosine on D2; Y_Z – redox active tyrosine on D1

dynamic equilibrium between the singlet states of the antenna and the RC radical pair states (van Gorkom, 1985; van Grondelle, 1985; Schatz et al., 1988). Interspersed with this view has been the contradictory suggestion that the antenna singlet states are not in equilibrium with the RC antenna (Butler et al., 1983; Berens et al., 1985a,b). The correct identification of the rate limiting step in the first stages of solar energy conversion is important as this allows one to understand the causes of the relative inefficiency of solar energy trapping in PS II (demonstrated by its relatively high level of fluorescence), and some of the constraints imposed by the need to regulate the trapping mechanism.

One of the technical problems that must be overcome in establishing the mechanism of energy transfer and trapping in PS II is the identification of intermediate chemical species. This is hampered by spectral congestion, which is particularly problematic in large complexes. Nevertheless the analysis of smaller isolated complexes, such as isolated RCs or antenna complexes, has allowed the key states to be more easily identified. These observations however, have clearly to be integrated with those from PS II in vivo.

II. The Context for Solar Energy Conversion in Photosystem II

A. Photoinhibition and Photoprotection

PS II has an added complexity in that it is surprisingly sensitive to photoinduced damage (Barber and Andersson, 1992; Barber, 1994; Chapter 27). Photochemical damage to the pigments and proteins (primarily the D1 protein) occurs for example, as a result of the formation of the P680 triplet state (which can lead to singlet oxygen production), or from the high oxidizing power of the $P680^+$ cation (Barber and Andersson, 1992).

This vulnerability of PS II is linked to the stress induced condition of photoinhibition, which results in a decrease in the efficiency of the photosynthetic reactions. Although photochemical damage seems to be an inevitable consequence of the reactions in PS II, repair mechanisms are employed, which involve the disassembly, proteolysis and synthesis of new D1 protein. Indeed the D1 protein is one of the most rapidly turned over proteins found in nature (Mattoo et al., 1989; Barber and Andersson, 1992).

The overall goal of photoprotection is clearly to prevent photodamage from taking place. Thus, to cope with changing environmental conditions, such as variation in light levels, as well as with the presence of highly reactive intermediates, higher plants have employed a number of control and regulation mechanisms that are able to balance light utilization and dissipation, therefore protecting and regulating the unstable and damaging photochemistry with which the plant and in particular PS II is associated (Barber, 1994; Horton et al., 1996; Bassi et al., 1997; Niyogi, 1999). Long-term mechanisms include changes in pigment levels in the chloroplast, canopy and leaf rearrangements, while short-term mechanisms include state transitions (Bassi et al., 1997), cyclic electron transfer (Barber and Rivas, 1993; Stewart and Brudvig, 1998) and non-photochemical quenching (NPQ) (Horton et al., 1996, 2000; Bassi et al., 1997; Niyogi, 1999). See Chapter 27, Cho and Aro, for further details.

qE quenching is a pH dependent form of NPQ (Demmig-Adams, 1990; Horton et al., 1991; Ruban et al., 1996; Li et al., 2000; Chapter 23, Pogson et al.), which has to compete effectively with the forward charge separation mechanism. A balance must be achieved such that charge separation within the PS II RC is slow enough to allow the photoprotective mechanisms to be effective yet still allowing a reasonable quantum efficiency of charge separation to be attained when quenching is not required. Although the work that is discussed in this review focuses on the mechanism of energy transfer and trapping in systems where the photoprotective mechanisms are not switched on, it is important to realize that the slow charge separation of the isolated PS II RC, and the highly fluorescent nature of whole PS II, as well as isolated core particles and membrane fragments reflects an inefficiency which is not seen in any other RC in any other organism. This almost certainly reflects an efficiency versus protective quenching compromise.

B. Water Splitting

The sensitivity of PS II to photodamage is no doubt related to the constraints imposed by the system's role in water splitting. The high oxidizing potential of $P680^+$ is required to extract electrons from the OEC, via a tyrosine residue Y_Z located at the D1-161 site. The reduction of $P680^+$ is a multiphasic reaction with lifetimes over the timescale of ~20 ns to

~50 μs (Chapter 7). The P680 cation is reduced by Y_Z, and the neutral tyrosine radical $Y_Z^{\bullet}$ that forms, is reduced in turn by the OEC. The OEC contains four manganese atoms, and details of their arrangement are only recently emerging with the publication of the medium resolution X-ray crystal structure (Vasil'ev et al., 2001; Zouni et al., 2001; Kamiya and Shen, 2003; Ferreira et al., 2004; Chapters 19–21). The OEC passes through a series of redox states, which are known as S-states, and requires the accumulation of four charge equivalents to oxidize two molecules of water (Chapter 24). The kinetics of $P680^+$ reduction are dependent on the S-state of the complex. Electrons are removed on each step from S_0 to S_3 and O_2 is evolved at the transient S_4 state, before returning to the S_0 state, and allowing the cycle to be repeated.

In this chapter we discuss results from studies made on a range of different sized particles including isolated antenna complexes, D1/D2/ Cyt b_{559} RCs and core complexes. In light of these results we try to address some important questions. We ask whether energy transfer or charge separation is rate limiting in PS II. We also consider whether the excitation energy is trapped by Pheo, Q_A, or a combination of the two.

III. Rapid Energy Transfer and Equilibration within Isolated Complexes

Historically two energy equilibration mechanisms, called 'trap' and 'diffusion' limited, have been proposed to describe the energy transfer and trapping in PS II. The *trap limited* mechanism describes a rapid equilibration of the excitation energy between the antenna and the RC excited states followed by a relatively slow (rate limiting) charge separation. Thus, the differential equation for the overall process is such that the intrinsic rate constants $(k_+ + k_-) >> (k_{+1} + k_{-1})$; where k_+ and k_- are the forward and reverse rate constants, respectively, between the antenna and RC excited singlet states and k_{+1} and k_{-1} are the forward and reverse rate constants, respectively, between the RC excited singlet states and the primary radical pair states, i.e.,

$$\mathrm{Ant}^* \underset{k_-}{\overset{k_+}{\Leftrightarrow}} \mathrm{RC}^* \underset{k_{-1}}{\overset{k_{+1}}{\Leftrightarrow}} \mathrm{RP} \qquad (1)$$

A *diffusion limited* mechanism is where the rate-limiting step is the equilibration of the energy between the antenna and the RC, thus $(k_{+1} + k_{-1}) >> (k_+ + k_-)$, (Eq. 1). This mechanism has recently been elaborated, and it has been suggested that it is not the equilibration of the excitation energy within the antenna complexes that is rate limiting, but rather the rate limiting step is the slow transfer of energy from the antenna complexes to the RC. This mechanism is referred to as *transfer-to-the-trap-limited* energy transfer (Valkunas et al., 1995; Somsen et al., 1996; Dekker and van Grondelle, 2000; Vasil'ev et al., 2001; Diner and Rappaport, 2002).

A. Light Harvesting Antenna Complexes

In higher plants and green algae, PS II is associated with a number of light harvesting polypeptides, which bind Chl *a*, Chl *b* and carotenoids. Their main function is to absorb photons of light and transfer the excitation energy to the redox active RC. (For details about the photoprotective role of some of the light harvesting antenna see Horton et al., 1991, 1996, 2000; Ruban et al., 1996; Li et al., 2002).

1. Structural Issues

The light harvesting complexes may be divided into peripheral antenna and core antenna complexes. The peripheral light-harvesting antenna Chl *a*/*b* and xanthophyll binding proteins in higher plants and green algae consist of Lhcb1-3 (LHCII), Lhcb4 (CP29), Lhcb5 (CP26) and Lhcb6 (CP24) (Chapter 2, Green and Gantt). The crystal structure of LHCII is known to molecular resolution and forms a trimer with each monomer containing three membrane-spanning helices (Kühlbrandt et al., 1994). Each of the LHCII polypeptides consists of 232 amino acids and binds at least 12 Chl molecules, 2 luteins, 1 neoxanthin and sub-stoichiometric amounts of violaxanthin. Lhcb4, 5 and 6 bind less Chl *b* than LHCII and exist as monomers.

The core antenna complexes include the Chl *a* and β-carotene binding proteins CP43 and CP47 (encoded by the *psbC* and *psbB* genes, respectively). A number of structural studies have been carried out over the years with varying levels of resolution. For example, electron crystallography on two dimensional crystals from CP47/D1/D2 core complexes at 8 Å resolution (Rhee et al., 1998; Hankamer et al., 1999; Chapter 18, Hankamer et al.) and X-ray crystallography on crystals from the CP43/CP47/D1/D2 RC complex

isolated from the thermophilic cyanobacterium *Synechococcus elongatus* (Vasil'ev et al., 2001; Zouni et al., 2001; Chapter 19, Witt) and from *Synechococcus vulcanus* (Kamiya and Shen, 2003; Chapter 20, Shen and Kamiya) have been resolved to 3.8 Å and 3.7 Å resolutions, respectively. A 3.5 Å resolution structure has recently been published in a study of crystals obtained from *Synechococcus elongatus* (Ferreira et al., 2004); this is discussed in more detail in Chapter 21. These studies indicate that CP47 and CP43 each consist of six transmembrane helices, which are arranged as a trimer of dimers. It has been noted that the structure of both complexes has a strong resemblance to the six amino-terminal transmembrane α-helices of PsbA and PsbB protein in PS I (Rhee et al., 1998; Barber and Kühlbrandt, 1999; Zouni et al., 2001). The Chls in CP43 and CP47 seem to form in two layers near the stromal and lumenal sides of the membrane. Re-analysis of the X-ray crystal structure was able to locate some Chl molecules that were missing in the original publication (Zouni et al., 2001), and suggests that CP47 binds 16 Chl molecules and CP43 binds 13 (Vasil'ev et al., 2001). Kamiya and Shen (2003) however have located 17 Chl molecules that are associated with the CP47 complex in a study of crystals isolated from *Synechococcus vulcanus*. These numbers are all in agreement with previous estimates, obtained for example from low temperature absorption spectra, for example in CP47 (Chang et al., 1994b).

2. The Peripheral Light-Harvesting Complex (LHCII)

In LHCII most of the xanthophyll to Chl energy transfer takes place within several hundreds of femtoseconds, with possibly a small fraction occurring on a picosecond timescale (Connelly et al., 1997a,b; Peterman et al., 1997; Gradinaru et al., 2000; Walla et al., 2000; Croce et al., 2001). Indeed excitation at 500 nm (mainly exciting Chl *b* and lutein) showed rapid energy transfer (~220 fs) from xanthophyll to a Chl *a* spectral form peaking around 675 nm (Peterman et al., 1997). Similarly, one- and two-photon fluorescence excitation studies also concluded that the transfer mainly occurs from xanthophyll to Chl *a* (Walla et al., 2000). More specifically, in trimeric LHCII, isolated from spinach, lutein was found to

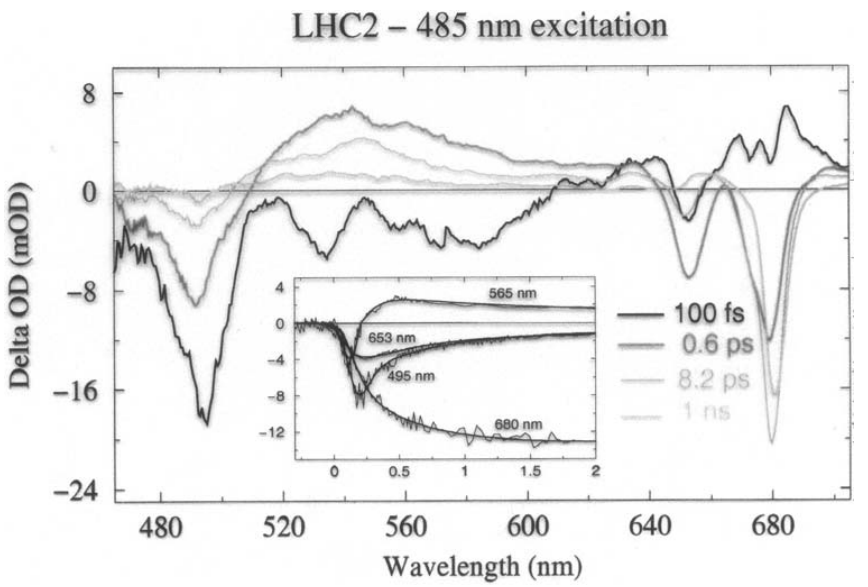

Fig. 1. Spectral evolution in LHCII at 77K following excitation with a 100fs laser pulse at 485nm. The experimental spectra as a function of delay time were analyzed with a linear scheme A→B→C→D→A with increasing decay times to visualize the spectral evolution in the system and the resulting species associated difference spectra (SADS) have been plotted. The insert shows the experimental kinetics at some selected wavelengths including the fits based on this model (from Gradinaru et al., 2000). See Color Plate 13, Fig. 1.

transfer excitations almost exclusively towards Chl *a*, whereas neoxanthin transfers to Chl *b* (Gradinaru et al., 2000). Figure 1 shows the time-resolved difference spectra obtained for trimeric LHCII following excitation at 485 nm. The species formed upon excitation is more or less a mixture of the 2nd singlet excited state of lutein and neoxanthin, with some excited Chl *b*. The structured negative spectrum between 520 and 600 nm is due to stimulated emission of the excited carotenoids. After ~100 fs, the ground → 2nd singlet excited energy state transition has recovered by about 60%, while at the same time the grow-in of the bleach in the Chl Q_y-region occurs. The replacement of the stimulated emission from the carotenoid excited states by 1st → nth singlet excited state absorption near 540 nm also occurs within this time window and reflects the fact that (part of) the carotenoids are now in the 1st singlet excited state. These dynamics are interpreted as the ultrafast energy transfer from the 2nd singlet excited state of neoxanthin to Chl *b*, from the 2nd singlet excited state of lutein to Chl *a* (mainly to Chl *a* absorbing around 679 nm), and the 2nd → 1st singlet excited state internal conversion in both excited lutein and neoxanthin. It is also likely that there is some ultrafast Chl *b* to Chl *a* energy transfer occurring on this timescale. This sequence of events was confirmed in a femtosecond transient absorption study on reconstituted LHCII monomers (Croce et al., 2001), and is consistent with the pigment assignments discussed above.

All of the observed transfer processes must occur within a monomeric subunit because the distances between pigments on different monomers are simply too large to explain the sub-picosecond transfer steps. Moreover the slowest transfer processes are observed in both LHCII monomers and trimers (Kleima et al., 1997). Energy transfer from Chl *b* to Chl *a* in LHCII is highly multi-exponential with time constants of ~200 fs (~40%), ~500 fs (~40%) and ~6 ps (~20%) (Kwa et al., 1992; Du et al., 1994; Visser et al., 1996; Connelly et al., 1997b; Kleima et al., 1997; Eads et al., 1998; Salverda et al., 2003). It has been interpreted that one of the five Chl *b* molecules transfers energy much more slowly than the others, with a time constant well above 1 ps. Recently, evidence was found for the occurrence of some fast Chl *b* to Chl *b* energy transfer, indicating some strongly coupled Chl *b* pairs, for instance the A3-B3 pair or a pair of Chl *b*'s in the A6-A7-B6 triplet (Agarwal et al., 2000; Salverda et al., 2003).

The Chl *a* to Chl *a* transfer kinetics in trimeric LHCII are also highly multiphasic, reflecting the variety of distances and orientations that are present in these complexes (Visser et al., 1996; Kleima et al., 1997; Gradinaru et al., 1998a; Agarwal et al., 2000; Novoderezhkin et al., 2003; Salverda et al., 2003). Excitation at 663 nm gave rise to a ~5 ps transfer time and it was argued that this slow transfer involved one (specific) Chl *a*. After excitation around 670 nm two downhill energy transfer time constants of 300 fs and 12 ps were observed, while excitation towards longer wavelengths revealed at least one other picosecond component. Thus, it is clear that even within a monomer some 'slow' processes are present. Recent 3PEPS (3-pulse photon echo peak-shift) measurements at room temperature identified both fast (150 fs), between 'blue' 670 nm absorbing Chl *a*'s and slow (~10 ps) Chl *a* equilibration times (Agarwal et al., 2000; Salverda et al., 2003).

Modeling of these experimental results (Novoderezhkin et al., 2003), using a disordered excitonic model based on the Kühlbrandt structure (Kühlbrandt et al., 1994), and allowing for relaxation between the excitonic levels showed that the Chl *a* to Chl *a* energy-transfer dynamics includes sub-ps (250–600 fs) exciton relaxation within dimeric or even more complicated Chl *a* clusters, sub-ps (600-800 fs) hopping between spatially separated clusters, and 'slow' (ps) migration between localized states. The interband (Chl *b* to Chl *a*) transfer is characterized by the presence of very fast decay channels, the fastest taking only 120 fs, which connects both localized and dimeric Chl *b*-states with the Chl *a*-band. The overall relaxation/migration dynamics can be directly viewed by means of the time-dependent density matrix site representation, which also allows the visualization of the degree of time-dependent delocalization. These dynamics are illustrated in (Fig. 2) for excitation in the Chl *b*-band and for a realization in which site A3 contains a Chl *b*, A6 is Chl *b*, A7 is Chl *a* and B3 is Chl *a*. Note that the multiphasic nature of the energy transfer kinetics, with the B3 Chl *a* is truly isolated and, furthermore, the complexity of the excited state remains after five picoseconds in LHCII.

CP29 is the only minor antenna complex that has been investigated with time-resolved spectroscopy, and it behaves qualitatively very similarly to LHCII. Following 640 nm excitation, energy transfer to a relatively 'red' Chl *a* occurs (with a time constant ~350 fs), whereas excitation at 650 nm results in transfer to a relatively 'blue' Chl *a* (with a time constant ~2.2 ps). Hole-burning measurements showed that transfer

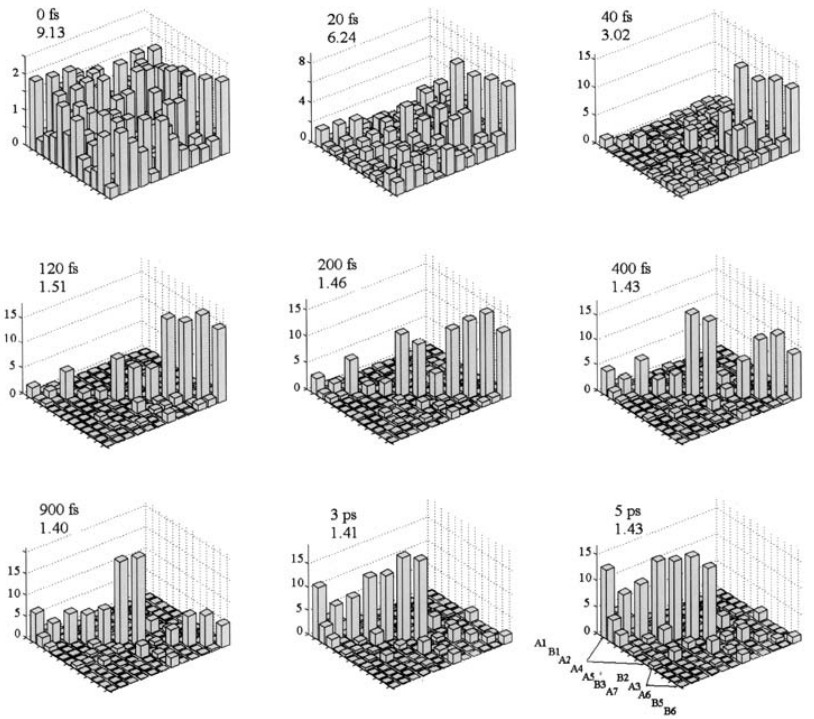

Fig. 2. Evolution of the one-exciton density matrix (in the site representation) upon blue side excitation (645 nm) with a 70 fs laser pulse. A configuration with A3 = Chl b, A6 = Chl b, A7 = Chl a and B3 = Chl a is used in this example. Time delays are 0, 20, 40, 120, 200, 400, 900, 3000, and 5000 fs as counted from the maximum of the excitation pulse. The numbers below the time delay values show the corresponding delocalization size of the exciton wavepacket determined as the inverse participation ratio of the density matrix. Note that we use a special order of the sites to highlight the transfer from b- to a sites (as shown in the 5ps panel). The density matrix amplitudes are shown in the same units for all delays (note the different scales for the first two panels).

from the 'red' Chl *b* is slower than transfer from the 'blue' Chl *b* (Pieper et al., 2000). Although following 640 nm excitation the dominant decay was fast, slower phases were also present, supporting the idea of mixed sites. Non-polarized sub-ps pump-probe spectroscopy has also been applied in the Chl *a* Q_y region (Gradinaru et al., 1998b). Due to the overlap of the absorption bands only two transfer processes could be observed, a very fast one of ~300 fs and a much slower process of 10–13 ps. In view of the rather isolated position of the Chl pair at sites A3-B3, it seems most likely that the latter process reflects transfer from the Chl *a* of this pair to the other Chl molecules.

To monitor spatial equilibration of excitations in trimeric and more complex aggregates of LHCII, singlet-singlet annihilation experiments have been performed, in which an intense (sub)-picosecond laser pulse creates several singlet excitations simultaneously in a photosynthetic complex. While migrating through the complex, these excitations can end up on the same molecule, which leads to the loss of one singlet excitation (annihilation) due to internal conversion. The annihilation kinetics provide information about the speed of excitation transfer throughout the domain (van Amerongen et al., 2000). As the excitation transfer from xanthophyll or Chl *b* to Chl *a* is extremely fast and essentially unidirectional (see above), only the transfer between Chl *a* molecules is important for the annihilation process. From such experiments a remarkably slow spatial equilibration time (first passage time or migration τ_{mig}) of 32 ps was estimated for one excitation in a trimeric LHCII complex (Barzda et al., 2001). For instance, in the PS I core complex τ_{mig} is less than 10 ps although the total number of Chl *a* molecules is ~4 times higher

than in trimeric LHCII. The difference in the average Chl *a* to Chl *a* transfer times in LHCII and PS I is probably caused by the different Chl *a* population densities in the two complexes. In fact, a calculation based on the LHCII structure and the pigment assignment yielded a reasonable agreement with the observed annihilation rate and the results from polarized and ultrafast experiments (van Amerongen and van Grondelle, 2001).

3. The Core Antenna Complex

Spectroscopic studies, using techniques such as spectral hole burning, fluorescence line narrowing, linear dichroism, transient absorption, transient fluorescence and time resolved triplet minus singlet absorption difference spectroscopy have been employed to investigate the rates, pathways and spectral distributions of the key states involved in energy transfer in isolated CP43 and CP47 antenna complexes (Chang et al., 1994b; den Hartog et al., 1998; Groot et al., 1999; Jankowiak et al., 2000; de Weerd et al., 2002a,b).

A model published by de Weerd et al. (2002a,b) employing parameters based on the 3.8 Å X-ray crystal structure of the CP43/CP47/RC complex (Zouni et al., 2001) has been used to interpret the results from these spectroscopic studies. At the current resolution of the structure it is not possible to determine the dipole orientations, although the planes of the chlorins are known. Orientations in the model calculations were therefore chosen to broadly agree with the results from linear dichroism studies on CP43 and CP47 proteins (van Dorssen et al., 1987; Groot et al., 1999). The energies of the all chlorins were taken as 14,925 cm^{-1} (670 nm) and inhomogeneous broadening of the site energies was included using a Monte Carlo simulation. Although as the authors note, the model in its current form is not able to reproduce all the states observed in, for example, the CP47 protein complex (e.g., the 690 nm state) (de Weerd et al., 2002b), a comparison between the experimental and calculated results obtained from isolated CP43 and CP47 antenna proteins with those from CP47-RC and CP43/CP47-RC complexes allows a greater understanding of the trapping dynamics in PS II.

a. The CP43 Protein

At physiological temperatures the average Chl Q_y transition peaks at ~670 nm (Groot et al., 1999). The low temperature absorption spectrum of the isolated CP43 protein, however, reveals more detail, and shows bands at ~660, ~669, ~679 and ~682.5 nm (Groot et al., 1999; Jankowiak et al., 2000; de Weerd et al., 2002b). Spectral hole burning and fluorescence line narrowing experiments have also identified two further states at 682.9 and 683.3 nm, which are monomer-like, quasi degenerate and only weakly coupled (Groot et al., 1999; Jankowiak et al., 2000).

Transient absorption experiments at 77 K have shown that the energy equilibration in the isolated CP43 protein occurs with lifetimes on the order of ~0.4 ps and ~3 ps (de Weerd et al., 2002b). The results from the structural based modeling suggest that the ~0.4 ps component results from energy transfer between Chls within the stromal layer. The ~3 ps component is ascribed to energy transfer from the lumenal to the stromal side (de Weerd et al., 2002b).

b. The CP47 Protein

The low temperature absorption spectrum from the isolated CP47 protein shows bands at ~661, ~670, ~677, ~683 and ~690 nm (van Dorssen et al., 1987; Chang et al., 1994b; Groot et al., 1995). Hole burning experiments have identified another state at 687 nm (Chang et al., 1994b).

Transient absorption studies probing the energy equilibration in the isolated CP47 protein following excitation at 660, 670 and 677 nm found lifetimes of the order ~0.2-0.3 ps and ~1.7-2.2 ps which resulted from the population of red-shifted states at 683 nm. A ~17-18 ps lifetime was also observed which was thought to result from an additional energy transfer to the 690 nm state (de Weerd et al., 2002b). A study that employed low burning fluence densities has shown that the 690 nm state dephases slowly in 4 ± 1 ns (den Hartog et al., 1998). A similar lifetime (5.8 ± 0.1 ns) has also been observed in 77 K time resolved fluorescence measurements (de Weerd et al., 2002b).

It seems unlikely that the 690 nm state is part of a dimer as suggested by Chang et al., (1994b), primarily because of the 3 nm splitting that is observed in the spectra and also the magnitude of the disorder. Indeed, de Weerd et al. (2002a,b) argue that the 690 nm state is a specific 'red' trap site, as they find that the 690 nm state has an oscillator strength corresponding to ~one Chl molecule. Indeed the observed red shift could be the result of strong hydrogen bonding interactions rather than the presence of a dimer.

The identity of the ~683 nm state has also not yet been clarified. Chang and co-workers suggest that it corresponds to a linker Chl *a* molecule located in the exterior region of the RC complex (Chang et al., 1994a), and that it relaxes to the 687 nm exciton state with a 10 ps relaxation time (Chang et al., 1994b). Following analysis of linear dichroism and absorption spectra, de Weerd et al. (2002a) found that the ~683 nm state carries an oscillator strength corresponding to approximately three chlorins and suggest that the state results from excitonic interactions between these pigments.

The results from calculations employing parameters based on the X-ray crystal structure of the CP47 complex suggest that the ~0.2-0.3 ps component results from excited state energy transfer within the stromal layer in a similar manner to the ultrafast component observed in CP43. The ~1.7-2.2 ps component is proposed to result from energy transfer to a specific lumenal or stromal excitonic state (de Weerd et al., 2002b).

In summary, equilibration of excitation energy within antenna complexes appears to be 80-90% complete within a few picoseconds. As the mean fluorescent lifetime in functional PS II is ~200 ps the dynamics within antenna systems do not appear to be rate limiting.

B. The Reaction Center Complex

1. Structural Issues

The smallest charge separating unit that can be isolated from PS II (Barber et al., 1987; Nanba and Satoh, 1987) is the D1/D2/Cyt b_{559}-RC, which loses its secondary electron acceptors (quinones) during the isolation procedure. The D1/D2/Cyt b_{559}-RC contains the proteins D1 (PsbA) and D2 (PsbD), and the α- and β-subunits of the Cyt b_{559} (PsbE and PsbF). The complex binds 6 Chl *a* molecules, 2 Pheo *a* molecules and 1-2 β-carotene molecules. As the isolated RC does not contain secondary electron acceptors or antenna complexes, the radical pairs formed by charge separation are more easily identified by transient absorption spectroscopy, as are the roles of the individual pigments and or states.

The X-ray crystal structures of the PS II RC assigns two clusters of five transmembrane helices, which are arranged in two interlocked semicircles, to the α-helices A-E of D1 and D2 (Vasil'ev et al., 2001; Zouni et al., 2001; Kamiya and Shen, 2003; Ferreira et al., 2004). The arrangement resembles that of the L and M subunits in the purple bacterial reaction center (BRC), as has long been suggested, thus supporting the evolutionary link between the two RCs, which has been the focus of much discussion in the literature, for example, (Barber, 1987; Hansson and Wydrzynski, 1990; Michel and Deisenhofer, 1998; Rhee et al., 1998; Schubert et al., 1998; Heathcote et al., 2002).

The elucidation of a high resolution structure of the BRC took place in the mid-1980s (*Rps. viridis* (Deisenhofer et al., 1985) and *Rb. sphaeroides* (Allen et al., 1987)), whereas medium resolution structural information about the PS II RC has only recently become available (Rhee et al., 1998; Vasil'ev et al., 2001; Zouni et al., 2001; Kamiya and Shen, 2003; Ferreira et al., 2004). As a consequence, the BRC has historically been used as a basis for the interpretation of spectroscopic results from the PS II RC. Indeed, the relatively high degree of sequence homology that is apparent on the acceptor side (Barber, 1987) has been utilized by many groups to propose structural models for the PS II RC (Svensson et al., 1990, 1996; Ruffle et al., 1992; Xiong et al., 1996, 1998). The recent structural data from crystals of the CP43/CP47/D1/D2/Cyt b_{559} complex from PS II (Vasil'ev et al., 2001; Zouni et al., 2001; Kamiya and Shen, 2003; Ferreira et al., 2004) of course provides a foundation for models investigating the dynamics of energy and electron transfer in PS II. However, although the planes of the chlorins can be determined at the current resolution, it is not possible to obtain information regarding the dipole orientation of the pigments from these published structures.

It is worth emphasizing that although structural studies can provide information about the pigment separations and orientations (depending on the resolution), they cannot provide information about the energies of states and species. State energies are a vital input when trying to understand reaction pathways and mechanisms.

Although the D1 and D2 proteins of PS II appear to be both functionally and structurally related to the L and M subunits of the BRC, there are a number of obvious differences between the two centers. For example, the PS II RC binds two more Chl molecules than the BRC, thought to be bound by the D1-His118 and D2-His118 residues, which are not present in the BRC. There are also differences on the donor side, for example the presence of Y_Z and the OEC, neither of which are present in the BRC, and which result from the ability to oxidize water to generate O_2 in PS II.

2. Spectroscopic Issues

A clear result of the differences between the isolated PS II and BRCs is apparent by comparison of the steady-state absorption spectra from both samples. Despite the D1/D2/Cyt b_{559}-RC being the smallest charge separating unit that can be isolated from PS II, the room temperature spectrum is dominated by a high degree of spectral congestion. Indeed, it only becomes possible to partially resolve the Q_y bands at low temperatures (<77 K) (van Kan et al., 1990; Konermann and Holzwarth, 1996). This contrasts the situation found in the BRC, and is most obvious for the (S_0–S_1) Q_y transitions in the room temperature spectra.

The differences between the steady-state absorption spectra from the PS II and BRCs result from differences between the coupling strengths in both systems. Approximately half of the splitting of the Q_y transitions in the BRC results from excitonic interactions between the special pair of bacteriochlorophylls (BChl) (P_{870} or P_{960}) (Knapp et al., 1985). The strong exciton coupling between these donor pigments (550 cm^{-1} for P_{870} and 905 cm^{-1} for P_{960}) causes a red shifted excited state, which forms an energetic trap within the RC. In contrast, studies such as triplet minus singlet absorption difference spectroscopy, transient absorption hole burning and circular dichroism measurements have demonstrated that the exciton coupling is much weaker in PS II (of the order of ~140 cm^{-1}) (Tetenkin et al., 1989; Braun et al., 1990; Durrant et al., 1990, 1992; Otte et al., 1992; Chang et al., 1994a; Kwa et al., 1994).

3. Supermolecular Nature of the Reaction Center

There has been much discussion in the literature about the degree of the excitonic coupling in PS II and therefore the nature of 'P680.' It was originally suggested that only the coupling between the Chl molecules, analogous to the special pair in the BRC, need to be considered, and that therefore P680 should be thought of as a weakly coupled dimer of Chl molecules, with all the other RC chlorins acting as monomers (Braun et al., 1990; Otte et al., 1992; Noguchi et al., 1993; Bosch et al., 1995; Konermann and Holzwarth, 1996; Mulkidjanian et al., 1996; Svensson et al., 1996; Konermann et al., 1997).

It has, however, been demonstrated that the similarity and magnitude of the coupling strengths between the six core RC chlorins (four Chl molecules and two Pheo molecules) means that the couplings between them all should not be ignored (Tetenkin et al., 1989; Kwa, 1993; Durrant et al., 1995a). Indeed, the multimer model calculations (Durrant et al., 1995a) have shown that the inhomogeneous broadening of the state energies (observed experimentally by Jankowiak et al., (1989) and by Groot et al., (1996)) and the magnitude of the coupling between the six core RC chlorin are all of the order of ~100-200 cm^{-1}, results in a significant degree of delocalization of the exciton states.

There is a debate regarding the interpretation of circular dichroism (CD) spectral data to determine the extent of excitonic coupling in the RC. Vácha et al. (2002) found that the Pheo reduction observed in a 5-Chl RC preparation results in only a small change in the CD spectra, suggesting that the Pheo on the active branch is not part of the RC multimer. In contrast, results from studies on RCs with modified Pheo composition, found that the replacement of the Pheo on the active branch caused large changes in the CD spectra (Germano et al., 2001). Germano et al. propose that these changes in the spectra result from the change in the excitonic interactions between the RC cofactors, therefore implying that the Pheo on the active branch is excitonically coupled.

Low temperature spectroscopic studies in the Pheo Q_x region of the spectra find that approximately two-thirds of the final amplitude of the Pheo bleach occurs instantaneously (within the pulse duration) which also suggests the involvement of the Pheo in the RC multimer (Greenfield et al., 1999).

The need to invoke a supermolecular description of the PS II RC has nevertheless been clearly demonstrated (Durrant et al., 1995b; Merry et al., 1996; Leegwater et al., 1997; Peterman et al., 1998; Barter et al., 2003). Indeed a supermolecular model, the multimer model provides a quantitative structure function relationship for the PS II RC that can be employed to consistently explain the primary function of PS II. A striking agreement has been found between experimental and calculated results, for example, rates of energy transfer (Durrant et al., 1992; Merry et al., 1996; Leegwater et al., 1997), relative orientation of red-most exciton states (Merry et al., 1996), relative oscillator strengths of red-most exciton states (Merry et al., 1996), absorption spectra (Durrant et al., 1995a), rates of electron transfer (Barter et al., 2003), effect of site directed mutagenesis (Barter et al., 2003), the similarity between the spectroscopic

features of both the emitting and charge separating states demonstrated by low temperature fluorescence line narrowing spectroscopy (Peterman et al., 1998). Moreover, this is the simplest description of the primary function of the PS II RC (Barter et al., 2003) that is also able to predict the presence of states with mixed exciton and charge transfer character shown in results from Stark spectroscopy experiments (Frese et al., 2003). Indeed multimer model calculations predict that 5–10% of radical pair states are formed directly on absorption of a photon by the RC (Barter et al., 2003). Recent measurements in the mid IR suggest however that up to 50% of radical pair states form within 500 fs (M.L. Groot, J. Breton and R. van Grondelle,unpublished). This discrepancy between the experimental and calculational results is likely to converge as the accuracy of the calculations and experimental data improves.

4. Energy Equilibration

The highly congested Q_y region of the optical spectra makes it difficult to separate the contribution of individual molecules or exciton states when trying to probe the dynamics of energy and electron transfer in PS II. There are however two small features in the spectra which are unambiguously assignable and have therefore been frequently employed in spectroscopic studies. These are the Pheo Q_x band, which is located at 545 nm and the stimulated emission vibrational side band, which is found in the emission spectrum between 725-735 nm.

Without an understanding of the supermolecular nature of the PS II RC the spectral congestion in the Q_y region makes the interpretation of spectroscopic data in this region difficult. Spectroscopic studies have however demonstrated that there is a rapid energy equilibrium within the six central core pigments in the PS II RC that takes place on a sub-picosecond timescale (Durrant et al., 1992; Merry et al., 1996). A 100 ± 50 fs component results from energy transfer between relatively high oscillator strength red states and relatively low oscillator strength blue states. A 400 ± 30 fs component results from energy transfer between two nearly orthogonal red state transitions (Durrant et al., 1992; Merry et al., 1996).

Multimer model calculations show that there is a relatively high probability that the red state transitions delocalize over opposite arms of the RC (Merry et al., 1996). In contrast, the probability distributions show that the blue states are able to co-exist with the red states on the same branch (Merry et al., 1996). The rates of energy transfer in the multimer model are dependent upon the spatial overlap of the states, as well as the extent of electron-phonon coupling at the site of overlap, and thus states that co-exist on the same chlorin sites are predicted to have a faster rate of energy transfer. Excellent quantitative agreement was found between the observed and the calculated rates of energy transfer. Multimer model calculations predicted ~250 fs time constant for energy transfer between the red and blue exciton states and 450 fs time constant between the two orthogonal red state transitions (Leegwater et al., 1997; Barter et al., 2003).

Slow energy transfer from the peripheral Chls has been shown to occur with a rate constant of approximately $(10–20 \text{ ps})^{-1}$ (Rech et al., 1994; Vacha et al., 1995), although it does not interfere with the rapid equilibration within the RC multimer states. The relatively slow energy transfer from the peripheral molecules does however raise the question as to whether they might provide a bottleneck for equilibration within the whole PS II complex, (this is discussed in more detail below). The energy transfer dynamics in isolated PS II RCs are summarized in the cartoon shown in Fig. 3.

IV. Conversion of Excited States into Charge Separated States

It is interesting to note that a rapid energy equilibration has been observed in both isolated antenna as well as within the isolated D1/D2/Cyt b_{559}-RC complex. What remains now is to consider the energy transfer step between the antenna and the reaction complex, and to discuss whether this energy transfer step or the trapping is the rate limiting process in PS II.

A. Trapping Dynamics in Isolated Reaction Center Complexes

The kinetics of primary electron transfer in PS II are multi-exponential, with lifetimes that range over approximately two orders of magnitude. Although there has until recently been a lack of agreement regarding the dominant time constant for primary charge separation, it is now generally accepted that the main components have lifetimes (and amplitudes) of 3 ps (0.19), 21 ps (0.57), 100 ps (0.14), >100 ps (0.10) (Hastings et al., 1992; Klug et al., 1995; Kumazaki

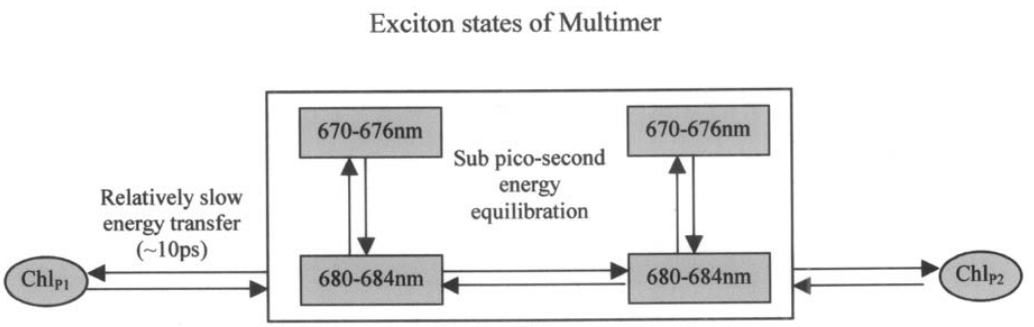

Fig. 3. Summary of the energy equilibration processes in the isolated PS II RC. Subpicosecond energy transfer within the P680 multimer and slower energy transfer from the peripheral chlorophylls (Chl_{p1} and Chl_{p2}) are shown. Both of the 670-676nm states that are shown are 2-fold degenerate.

et al., 1995). Similar data, though quantitatively different, were obtained by other groups, Donovan et al. (1996), Muller et al. (1996), Greenfield et al. (1997) and Groot et al. (1997).

As secondary electron transfer to the quinone acceptor cannot take place, due to the loss of Q_A in isolated RC particles, the primary radical pair either recombines to the ground state on the nanosecond time scale (Booth et al., 1990; Booth et al., 1991), or via the triplet state which has a lifetime of 1 ms under anaerobic conditions and 33 μs in the presence of O_2 (Durrant et al., 1990).

1. Slow Primary Charge Separation

It is striking that the primary trapping dynamics in the PS II RC are significantly slower (~21 ps dominant time constant) than those observed in the BRC, which has dominant charge separation dynamics with a lifetime of the order of 3 ps (Fleming et al., 1988; Holzapfel et al., 1990). Indeed, charge separation is also thought to be similarly fast in PS I (Owens et al., 1987; Gobets and van Grondelle, 2001), and the sequestration of PS II into granal stacks probably reflects the need to prevent PS I from competing too effectively with PS II for excitation energy. The slow trapping in PS II has been the subject of much discussion in the literature and a number of suggestions have been made to explain this observation.

Indeed, results from low temperature transient absorption measurements reported by Groot et al. (1994, 1996) indicated the presence of trap states in the RC, which underwent slow energy transfer to the multimer exciton states. It was suggested that these trap states could form an energy transfer bottleneck and therefore be responsible for the slow trapping dynamics observed in PS II (Groot et al., 1997).

Although sub-picosecond equilibration of excitation energy has been shown to take place within the core RC chlorins (Durrant et al., 1992; Merry et al., 1996), Rech et al. (1984) demonstrated that slow energy transfer from the peripheral Chls also occurs on a similar timescale to primary charge separation (~10–20 ps). However, following direct excitation of the RC multimer, it was shown that at least 75 ± 15% of primary radical pair formation occurred with a 21 ps time constant. This rate was shown to lengthen to 27 ps following blue excitation (Rech et al., 1994), demonstrating that the trapping rate is only slightly affected by slow energy transfer from the peripheral Chl molecules (Rech et al., 1994). This was also confirmed in studies of RCs where one of the peripheral Chl molecules was biochemically removed (Vacha et al., 1995). Indeed, transient absorption features at ~670 nm attributed to slow energy transfer from the peripheral Chls, showed a reduced amplitude in the 5-Chl RCs; however following direct excitation of the RC multimer states, identical spectra from both the 5 and 6 Chl RCs were reported (Vacha et al., 1995).

Studies on genetically engineered RCs isolated from the purple bacteria *Rb sphaeroides* found that mutating a specific tyrosine residue within the M subunit (at position 210) to a leucine, slowed the rate of charge separation to a similar magnitude found in PS II. Since the analogous amino acid residue in PS II is thought to be a leucine, it was suggested the difference between the trapping dynamics observed in the PS II and BRCs may be the result of differences between these specific residues (Hastings et al., 1992). Studies on *C, reinhardtii* showed, however,

that modifying the D2-205 residue to its homologue in the BRC, at the M-210 site, does not increase the rate of charge separation in PS II (Andronis et al., 1999), and is therefore not responsible for the slow trapping dynamics.

The observed dynamics of charge separation in the PS II RC emerge from a network of states, which are coupled together by individual rate constants. Although the rate constants are fast, the slow observed rate of charge separation in PS II is due to the fact that the singlet state populations are equally distributed over all the states with strong 'singlet' state character (Durrant et al., 1995a). Therefore as only ~1/6 of the excited states are associated with the electron donor of the major electron transfer pathway, the probability that charge separation can occur from that state is decreased, and the observed rate of charge separation in PS II will be slow. This is of course in contrast to the relatively fast charge separation dynamics observed in the BRC, where the entire population is localized on the special pair that forms a relatively deep energetic trap from which the majority of the charge separation results.

2. Reaction Center State Energies

At any given point in time, the time-dependent radical pair free energy gap between the excited singlet states and the primary radical pair states in the purple BRC is larger than in PS II. The isolated PS II RC (from *Pisum sativum*), for example, has a primary radical pair ($P680^+Pheo^-$) free energy which is ~100 meV below the singlet excited state energy (on nanosecond time scales at 277 K) (Booth et al., 1990; Volk et al., 1993), whereas in BRCs isolated from *Rb. sphaeroides* the free energy gap is ~250 meV in quinone depleted and reduced RCs on the same time scale (Hörber et al., 1986; Goldstein et al., 1988; Ogrodnik et al., 1988). The small energy gaps that drive the photochemistry in PS II RCs cause the RC kinetics to be highly sensitive to genetically modified changes in the redox potential of the anions and cations (Giorgi et al., 1996; Merry et al., 1998).

Spectroscopic studies on wild-type RCs can yield a vast amount of information on the dynamics in PS II; however, experiments on genetically modified RCs can add another dimension to this investigation. A number of spectroscopic studies have been made on mutants isolated from *Synechocystis* sp. PCC 6803 and *C. reinhardtii*, for example, Giorgi et al. (1996), Durrant et al. (1998), Merry et al. (1998), Andronis et al. (1999), Johnston et al. (2000), Stewart et al. (2000) and Diner et al. (2001).

In particular, studies have been reported on a range of genetically engineered RCs (Giorgi et al., 1996; Merry et al., 1998) and core complexes (Stewart et al., 2000; Diner et al., 2001) isolated from the cyanobacterium *Synechocystis* sp. PCC 6803, which have modified the environment of either the D1-Gln130 or D1-His198 sites. These mutations have allowed the energies of the terminal radical pair to be altered by changing the redox potential of either the Pheo anion on the active branch, or the D1-Chl *a* cation in the analogous position to one of the special pair Chls in the BRC.

On the basis of a fast decay component observed in the stimulated emission of PS II RCs, the presence of fast intermediate states in the charge separation reactions were postulated by Groot et al. (Groot et al., 1997), although such intermediates are not directly detectable in wild-type RCs. Modifying the energies of the radical pair states however allowed the presence of Chl anion states in PS II to be identified (Durrant et al., 1998). Spectra in the Q_x region were obtained from a range of mutants and were compared with simulations which summed the weighted contribution of $P680^*$ excited singlet states, $P680^+Pheo^-$ radical pair states, and $P680^+Chl^-$ chlorophyll anion states (Giorgi et al., 1996; Durrant et al., 1998; Merry et al., 1998; Barter et al., 2003). These simulations revealed the relative populations, and hence the relative energies of the key radical pair states in the PS II RC (Durrant et al., 1998; Barter et al., 2003). Knowledge of the state energies, which can only be obtained from studies such as these, is of course a requisite input when trying to understand the mechanisms and pathways of electron transfer in PS II.

3. Kinetic Modeling

There has been a focus on a multi-exponential lifetime analysis of the data from both isolated RC and core samples. While this type of analysis can be employed to provide a mathematical representation of the data, difficulties often arise when assigning the multi-exponential lifetimes to microscopic processes. Indeed, a multi-exponential decay can usually be decomposed into more than one set of exponentials depending on the fitting criteria. Thus, relating lifetimes and amplitudes directly to states can be somewhat misleading, particularly in a system such as PS II, which has a significant degree of inhomogeneous broadening of

the state energies. Inhomogeneous broadening has been observed in studies of both PS II (Booth et al., 1991; Groot et al., 1994) and BRCs (Wang et al., 1993; Ogrodnik et al., 1994).

There are many examples of macroscopic models of PS II which employ intrinsic rate constants as fitting parameters and which have used sample heterogeneity, static inhomogeneous broadening of the state energies, or dynamic protein coupled relaxations to account for the multi-exponential dynamics of energy and electron transfer (Freiberg et al., 1994; Gatzen et al., 1996; Konermann et al., 1997; Barter et al., 2001), but very few where the hypothesis has been controlled by the variation of parameters, for example, antenna size or modulation of radical pair free energy (Freiberg et al., 1994; Barter et al., 2001).

Macroscopic models cannot however provide information about the details of the states, and energy and electron transfer pathways within the PS II RC. To fully understand the dynamics and to probe these pathways a microscopic description is required which employs the energies of the key states and accounts for their inhomogeneous broadening.

Microscopic descriptions, such as the models published by Shiang et al. (2003), Prokhorenko and Holzwarth (2000) and the multimer model (Durrant et al., 1995b; Leegwater et al., 1997; Barter et al., 2003) have been employed to describe the dynamics of energy transfer and trapping in the PS II RC. In contrast to the models published by Shiang et al. (2003) and Prokhorenko et al. (2000), which employ fitting parameters, the multimer model is a fit free prediction. Indeed, all of the input parameters used in the multimer model calculations were determined experimentally (Durrant et al., 1995b; Leegwater et al., 1997; Barter et al., 2003).

There has been much discussion and speculation in the literature regarding the dominant pathway of electron transfer in PS II, (van Mieghem et al., 1991; Dekker and van Grondelle, 2000; Prokhorenko and Holzwarth, 2000; Diner et al., 2001; Barber, 2002; Diner and Rappaport, 2002; Yoder et al., 2002). It is however important to emphasize that the dominant pathway can only be determined if all possible charge separation pathways are considered and, more importantly, if the energies of all the radical pair states are known. These energies can only be determined from studies of genetically modified RCs such as those described in Giorgi et al. (1996), Durrant et al. (1998) and Merry et al. (1998).

Unlike the models published by Shiang et al. (2003) and Prokhorenko et al. (2000), the multimer model calculations, detailed in Durrant et al. (1995b), Leegwater et al. (1997) and Barter et al. (2003), employ the energies of all the radical pair states including Chl anion and cation states (Giorgi et al., 1996; Durrant et al., 1998; Merry et al., 1998), and therefore the multimer model calculations are directly predictive and have been able to show that the major charge separation pathway involves the formation of the radical pair state $Chl(1)^{+}Pheo(1)^{-}$ followed by electron transfer from Chl(2) to $Chl(1)^{+}$, producing the terminal radical pair $Chl(2)^{+}Pheo(1)^{-}$ (see Fig. 4). These results suggest that the majority of charge separation in PS II occurs in the reverse order to the dominant pathway found in wild-type BRCs. Interestingly, a similar reverse ordered charge separation pathway has been observed in genetically modified and wild type BRCs (van Brederode et al., 1997, 1999; van Brederode and van Grondelle, 1999).

It is also of note that low temperature studies of the triplet state formation in PS II have found that the triplet state is localized on a Chl molecule with its plane at a 30° orientation with respect to the membrane (van Mieghem et al., 1991). This result suggested that the triplet is likely to be located on the accessory Chl(1) (see Fig. 4 for labeling) and it was therefore proposed that the accessory Chl could be the primary donor in PS II (van Mieghem et al., 1991).

B. Rate Limiting Behavior: Explanation for High Levels of Fluorescence

The high levels of fluorescence observed in PS II compared to all other RCs (e.g., PS I and *Rb. sphaeroides*), highlights the relative inefficiency of PS II. While a 90-95% efficiency may seem high, it is still much lower that that seen in all other RCs complexes.

Experimental studies have concluded that energy transfer in isolated antenna complexes is fast. Likewise it has been shown that energy equilibration within the isolated RC is rapid, on a sub-picosecond time scale, with the charge separation that follows being the rate limiting step. We now discuss energy transfer and trapping in PS II core particles, and consider the rate limiting step in these functional systems. We question whether an energy transfer bottleneck exists in PS II, and also ask whether Pheo or Q_A traps the majority of the excitation energy.

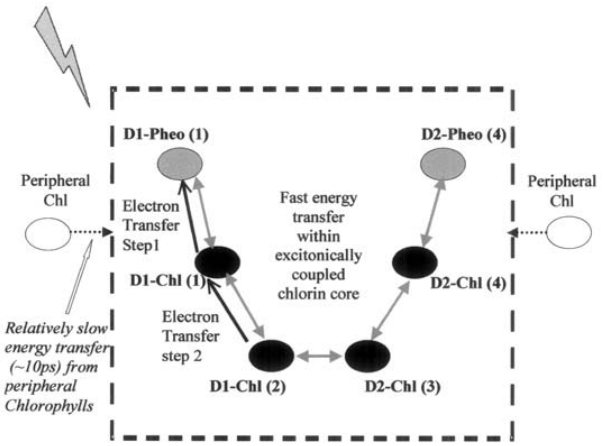

Fig. 4. Electron and energy transfer pathways in PS II RCs. Multimer model calculations, which employ the energies of the radical pair states, have shown that the major charge separation pathway involves the formation of the radical pair state $Chl(1)^{+}Pheo(1)^{-}$ followed by electron transfer from Chl(2) to $Chl(1)^{+}$, producing the terminal radical pair $Chl(2)^{+}Pheo(1)^{-}$.

1. Antenna Size Dependence of the Trapping Dynamics

There is a dilemma regarding whether the energy equilibration and/or charge separation dynamics observed in isolated complexes such as the D1/D2/Cyt b_{559}-RC complex and the isolated antenna complexes, can be related to those dynamics observed in larger particles. Indeed, some previous work (Renger, 1992; Hillmann et al., 1995; Vassiliev et al., 2002) has raised concerns regarding how far the photochemical properties of the remaining pigments in isolated D1/D2/Cyt b_{559} complexes have been altered in comparison to intact PS II. One way to resolve this issue is to monitor the antenna size dependence of the trapping dynamics in PS II.

Time resolved fluorescence measurements have been reported on a number of different sized core preparations with Q_A in fully open and closed states, and have proved a useful tool in investigating the trapping dynamics in PS II. As with the studies on isolated RCs, the majority of the results from core particles have focused on a multi-exponential lifetime analysis of the experimental data. A direct comparison of the lifetimes and amplitudes obtained from this type of analysis from different research groups is often misleading (as mentioned previously), particularly in the case of systems where the dynamics are multi-exponential, and the state energies inhomogeneous. The lifetimes and amplitudes are also strongly dependent on the data collection and analysis conditions. A few examples of the numerous spectroscopic studies on core particles are discussed below to provide a feel for the different samples that have been investigated in the literature.

Comparative picosecond time-resolved fluorescence studies, on isolated D1/D2/ Cyt b_{559} -RCs and monomeric CP47/D1/D2/Cyt b_{559} complexes (which do not contain the secondary electron acceptor Q_A), have allowed the impact of the CP47 antenna complex on the trapping dynamics to be investigated, (de Paula et al., 1994; Freiberg et al., 1994; Barter et al., 2001). Although the reported components obtained from the multi-exponential lifetime analysis differ in these examples, overlaying all the data shows reasonable agreement between the results, and the small differences in the lifetimes reported by Freiberg et al. (1994) are likely to result from the glycerol buffer used in these experiments.

Studies have also been reported on dimeric CP47/D1/D2/Cyt b_{559} (Barter et al., 2001) and CP43/CP47/D1/D2/Cyt b_{559} complexes (Schatz et al., 1987; Hodges and Moya, 1988; van Mieghem et al., 1992; Lui et al., 1993; Barter et al., 2001; Vasil'ev et al., 2001; Vassiliev et al., 2002). These complexes contain Q_A, and therefore not only allow the antenna size dependence of the trapping dynamics to be probed but also enable the secondary electron transfer dynamics to be studied in particles where Q_A is in a fully open state. There is however an inconsistency

that is apparent on comparison of the results from CP43/CP47/D1/D2/Cyt b_{559} complexes, which could be caused by the biochemistry of the samples or the experimental conditions used. It is clear that one of the major discrepancies arises from an uncertainty about the sample composition. The number of Chl molecules per complex in the samples studied varied from 40–80 in the examples detailed in Schatz et al. (1987), Hodges and Moya (1988), van Mieghem et al. (1992), Lui et al. (1993) and Barter et al. (2001). It is now generally accepted that the number of chlorins per RC in the CP43/CP47/D1/D2/Cyt b_{559} complex is ~40 (Hankamer et al., 1997), and it is therefore difficult to envisage the composition of some of the preparations reported (Schatz et al., 1987; Hodges and Moya, 1988; van Mieghem et al., 1992; Lui et al., 1993).

Studies on LHCII supercore complexes (Barter et al., 2001), PS II-enriched membranes (Hodges and Moya, 1986, 1987; van Mieghem et al., 1992; Vass et al., 1993; Barter et al., 2001), and thylakoid membranes (Gulotty et al., 1982; Haehnel et al., 1982, 1983; Berens et al., 1985a,b; Gulotty et al., 1985; Roelofs et al., 1992) have also been reported in the literature. Consistency is again not clear by comparison of the lifetimes and amplitudes from examples of decays from PS II enriched membranes with Q_A in both open and closed states. Overlaying the decays has, however, shown a much greater consistency. Interestingly the state of Q_A in the samples reported in only a few of the studies, is confirmed by either EPR measurements (van Mieghem et al., 1992) or power dependency studies (Barter et al., 2001).

2. Kinetic Modeling of the Trapping Dynamics in Core Preparations

Transient experiments allow the *observed* or *effective* rate constants and lifetimes to be recovered from data using, for example, multi-exponential fitting procedures. These experimental observables should not however be mistaken with *intrinsic* rate constants, which are model dependent. Many phenomenological models have been published in the literature on a variety of different sized core complexes isolated from PS II. The intrinsic rate constants in these studies are employed as fitting parameters to obtain agreement between the modeled and the experimental data. Models have been used to describe the transient data from chloroplasts (Butler et al., 1983; Berens et al., 1985a; Schatz and Holzwarth, 1986; Roelofs et al., 1992), PS II-enriched membranes (Vass et al., 1993; Renger et al., 1995; Dau and Sauer, 1996; Yruela et al., 1996; Vasil'ev and Bruce, 2000), CP43/CP47/D1/D2/Cyt b_{559} core complexes (Schatz et al., 1987; Schatz et al., 1988; Vasil'ev et al., 2001; Vassiliev et al., 2002) and CP47/D1/D2/Cyt b_{559} core complexes (Freiberg et al., 1994). These examples are just a sample of the many reports that can be found in the literature.

a. Trap Limited Energy Transfer Description

A trap limited description of the energy transfer and trapping dynamics in PS II core particles has frequently been discussed in the literature. Such a mechanism assumes a rapid equilibration of the excitation energy between the antenna and RC excited states followed by a relatively slow charge separation. It is interesting that a number of the trap limited models presented in the literature have included only one radical pair state and have not found it necessary to invoke inhomogeneous broadening of the state energies. For example, the reversible radical pair model, first introduced by Schatz et al. (1987), was employed to simulate the fluorescence decay kinetics from CP43/CP47/D1/D2/Cyt b_{559} core particles isolated from the cyanobacteria *Synechococcus* (Schatz et al., 1987, 1988). The model assumed a rapid equilibration of the excitation energy between the antenna and the RC, and an equilibrium between a primary radical pair state and the RC and antenna excited singlet states. Subsequent electron transfer from the primary radical pair state to the quinone electron acceptor was taken to be irreversible. Sample heterogeneity was employed to explain the multi-exponential experimentally observed kinetics from CP43/CP47/D1/D2/Cyt b_{559} core particles. Indeed, heterogeneous populations within samples have often been employed to explain the observed multi-exponential trapping dynamics (van Mieghem et al., 1992; Vass et al., 1993; Dau and Sauer, 1996). It is however hard to rationalize this type of model with the highly multi-exponential trapping dynamics observed in spectroscopic studies of isolated RCs.

Indeed, Freiberg et al. (1994) noted that it was not possible to reproduce the trapping dynamics in both isolated RCs and CP47/D1/D2/Cyt b_{559} core complexes, by employing such two state models (antenna/RC excited singlet states and a radical pair state), without the inclusion of, for example, sequential relaxations of the radical pair state (Freiberg et al., 1994).

It is therefore clear that to test this type of trap

limited macroscopic model, the controlled variation of parameters is required. An example of this is the study of the antenna size dependence of the trapping dynamics in PS II. As energy transfer is not rate limiting in the isolated RC, the consistency of the results from a range of different sized core particles showed that the energy equilibration is not rate limiting in larger core particles, and therefore, there is not an energy transfer bottleneck between the antenna and RC excited states in particles with Q_A in a fully closed state (Barter et al., 2001). Indeed, if such a bottleneck were to exist, the predicted time dependent singlet state populations would be larger than observed experimentally (Barter et al., 2001). Furthermore, this study showed that the key qualities of the shallow trap and slow kinetics of charge separation observed in isolated PS II RCs are not isolation artifacts but are intrinsic properties of PS II in particles with Q_A in a closed state.

b. Transfer-to-Trap Description

A 'transfer-to-trap' model has however recently been proposed to describe the energy transfer and trapping in PS II (Dekker and van Grondelle, 2000) and was primarily based on structural information available at that time (Rhee et al., 1998). The rationale behind the model came from the observation of a relatively large distance between the core antenna and the RC chlorins, which was suggested to act as a physical barrier that would slow the energy equilibration between the RC and the CP47 and CP43 antenna complexes. Interestingly, transfer-to-trap type energy equilibration mechanisms have been suggested to occur in *Rb. sphaeroides* (Beekman et al., 1994) and in PS I (Valkunas et al., 1995).

The advent of the 3.8 Å resolution crystal structure of the CP43/CP47/D1/D2 core complex, isolated from the thermophilic cyanobacterium *Synechococcus elongatus* (Zouni et al., 2001), also suggests that there is a relatively large gap between the Chls located on either CP43 or CP47 and the RC chlorins. It was concluded that there are only two antenna Chl molecules which can contribute significantly to the coupling between the antenna and the RC, therefore acting as linker molecules (one on CP47 and the other on CP43) (Vasil'ev et al., 2001; Zouni et al., 2001), with the closest center to center distance being ~21 Å (Vasil'ev et al., 2001; Zouni et al., 2001).

Vasil'ev et al. (2001) employed the cofactor separations from this structural data to model the energy transfer and trapping within the CP43/CP47/D1/D2 complex. A microscopic description of the energy transfer rates within the complex was employed, by considering the rates of pair-wise excited state energy transfer between chromophores, (whose separations were taken from the X-ray structural data). Two additional macroscopic states ($P680^+Pheo^-$ and $P680^+Q_A^-$) were included to account for the reversible charge separation and a unidirectional charge stabilization. The rate of Q_A reduction was taken as $(0.48\ ns)^{-1}$, and the intrinsic rate constants of the forward and reverse reactions between the RC excited states and the primary radical pair were used as fitting parameters. The model predicted a lower limit of $(0.7\ ps)^{-1}$ for the intrinsic rate constant of primary radical pair formation that was able to reproduce the time resolved fluorescence decay kinetics observed from CP43/CP47/D1/D2/Cyt b_{559} core complexes. This fast intrinsic rate constant was presumably found necessary to outweigh the slow rate of energy transfer between the antenna and the RC, estimated from the relatively large distance between the antenna and RC chlorins.

In a more recent publication, Vassiliev et al. (2002) question the origin of the multi-phasic fluorescence decay kinetics observed in PS II, by extending this initial transfer-to-trap model (Vasil'ev et al., 2001), and comparing the predicted decays with the results from time-resolved fluorescence data from His-tagged PS II core preparations, with Q_A in both open and closed states. The radical pair state invoked was characterized by either a single energy level, a static distribution of energy levels, or a dynamic energy level (Vassiliev et al., 2002). The best agreement with the experimental data was achieved by employing a dynamic relaxation of the radical pair with the inclusion of five sequential radical pair energy levels. Vasiliev et al. (2002) include such dynamic relaxations to reproduce the results from particles with Q_A in an open state, and suggest that a fast stabilization of the primary radical pair is required to reproduce the experimental data from particles with Q_A in an open state.

It is clearly hard to rationalize the transfer to trap model with the experimental observations from the study of the antenna size dependence on transfer and trapping (described briefly above and in Barter et al., 2001), which suggests that energy transfer is not rate limiting in particles with Q_A in a fully closed state.

This discrepancy could be rationalized if a 'linker Chl' between the antenna complexes and the RC were

missing in the structural information, which is plausible at the current resolution of the structure. Interestingly, the publication of the X-ray crystal structure of the CP43/CP47/D1/D2-RC complex isolated from the thermophilic cyanobacterium *Synechococcus vulcanus* locates another Chl molecule in the CP47 complex (Kamiya and Shen, 2003), compared to the results from *Synechococcus elongatus* (Vasil'ev et al., 2001; Zouni et al., 2001).

Förster theory has been shown to be inaccurate for certain specific energy transfer cases, such as the determination of the rates of energy transfer within LH2 of purple bacteria in *Rps. acidophila*, and *Rb. sphaeroides* (Scholes and Fleming, 2000). Methods that consider the electronic couplings, electron-phonon coupling and site energy distributions have been shown to have a significant impact on the calculated rate of energy transfer. In the case of energy transfer within LH2, disorder alone has been shown to increase the rate constant by a factor of 3, and when the variation in coupling is included the rate can vary by up to an order of magnitude (Scholes et al., 1999, 2001; Scholes and Fleming, 2000). When considering specific molecule to molecule steps Förster theory can be inaccurate, although it provides a good approximation for average behavior in ensembles. In light of this it would be interesting to recalculate the energy transfer rate between the antenna and the RC excited states using methods that consider the electronic couplings, electron-phonon coupling and site energy distribuions as they could have a significant impact on the rates and therefore on the interpretation of the model.

3. Does Pheo or Q_A Trap the Majority of Excitation Energy?

Historically the observed rate and the intrinsic rate constant of Q_A reduction have been considered as being identical, and of the order of a few hundred picoseconds. For example, flash induced absorption changes at 325 nm were used to probe the Q_A reduction kinetics from PS II O_2 evolving membrane fragments isolated from spinach, and found observed lifetimes of ~350 ± 100 ps (Eckert et al., 1988). Picosecond absorbance difference spectra following excitation at 532 nm (using 35 ps pulses) were employed to study PS II particles isolated from spinach (with 80 Chls per RC) and found observed rates of Q_A reduction of ~250-300 ps (Nuijs et al., 1986). Time resolved fluorescence studies on PS II particles from *Synechococcus* (with 80 Chl molecules per RC) found an observed rate of ~500 ps (Schatz et al., 1987). Interpretation of these results is nevertheless complicated because of the significant spectral overlap, and small absorption changes that result from reduction of Q_A. Uncertainty also arises because of the difficulty in unraveling the intrinsic rate constant for Q_A reduction in PS II from the observed lifetimes that are obtained from these experiments.

There is a discrepancy in the literature regarding whether Pheo or Q_A is the dominant trap of excitation energy in PS II. The quinone is commonly thought of as a deep stabilizing trap for the excitation energy (Nuijs et al., 1986; Schatz et al., 1987, 1988; Eckert et al., 1988; Bernarding et al., 1994). Experimental studies such as these have measured observed lifetimes, which are collective properties of the system. The lack of knowledge about the intrinsic rate constants of Q_A reduction and of the Q_A radical pair state energies, means that without tests of models based on calculations where the hypothesis is controlled by the variation of parameters, (such as antenna size or genetic modification), it is difficult to untangle the details of the trapping mechanism in core particles were secondary electron transfer to Q_A can occur.

V. Concluding Remarks

This chapter has reviewed current understanding about the nature of energy transfer and trapping in PS II. It has highlighted at least one of the unresolved questions regarding the mechanism of this process, by asking what is the rate-limiting step and questioning whether Pheo or Q_A traps the excitation energy in the reaction center. We have reviewed examples of spectroscopic data from isolated antenna, reaction center and core complexes and discussed these results in light of a number of kinetic models that have been proposed in the literature. We show that a consensual picture of the dynamics occurring within isolated antenna complexes and reaction centers is now emerging although there is still uncertainty regarding the rate limiting step of energy transfer and trapping in larger PS II particles and membrane fragments. It is clear that the identification of the rate limiting step of energy transfer and trapping in PS II is necessary, particularly if we are to understand the balance between efficiency and regulation that the plant has to maintain, as well as the causes of the relative inefficiencies of solar energy trapping in PS II. This

is all part of the move towards a more quantitative understanding of the structure function relationships of individual proteins, and the mesoscopic organization of the photosynthetic membranes.

Acknowledgments

We would like to thank the Biotechnology and Biological Sciences Research Council for supporting our photosynthesis research over many years.

References

Agarwal R, Krueger BP, Scholes GD, Yang M, Yom J, Mets L and Fleming GR (2000) Ultrafast energy transfer in LHC-II revealed by three-pulse photon echo peak shift measurements. J Phys Chem B 104: 2908–2918

Allen JP, Feher G, Yeates TO, Komiya H and Rees DC (1987) Structure of the reaction centre from *Rhodobacter sphaeroides* R-26: The co-factors. Proc Natl Acad Sci USA 84: 5730–5734

Andronis C, Merry SAP, Durrant JR, Klug DR, Barber J and Nixon PJ (1999) Mutation of the *Chlamydomonas reinhardtii* analogue of residue M210 of the *Rhodobacter sphaeroides* reaction centre slows primary electron transfer in Photosystem II. Photosynth Res 62: 205–217

Barber J (1987) Photosynthetic reaction centers: A common link. Trends Biol Sci 12: 321–326

Barber J (1994) Molecular basis of the vulnerability of Photosystem II to damage by light. Aust J Plant Physiol 22: 201–208

Barber J (2002) P680: What is it and where is it? Bioelectrochemistry 55: 135–138

Barber J and Andersson B (1992) Too much of a good thing: Light can be bad for photosynthesis. Trends Biol Sci 17: 61–66

Barber J and Kühlbrandt W (1999) Photosystem II. Curr Opin Struct Biol 9: 469–475

Barber J and Rivas JDL (1993) A functional role for the cytochrome *b*559 in the protection against donor and acceptor side photoinhibition. Proc Natl Acad Sci USA 90: 10942–10946

Barber J, Chapman DJ and Telfer A (1987) Characterisation of a PS II reaction centre isolated from the chloroplasts of *Pisum sativum*. FEBS Lett 220: 67–73

Barber J, Morris E and Büchel C (2000) Revealing the structure of the Photosystem II chlorophyll binding proteins, CP43 and CP47. Biochim Biophys Acta 1459: 239-247

Barter LMC, Bianchietti M, Jeans C, Schilstra MJ, B.Hankamer, Diner BA, Barber J, Durrant JR and Klug DR (2001) Relationship between excitation energy transfer, trapping and antenna size in Photosystem II. Biochemistry 40: 4026–4034

Barter LMC, Durrant JR and Klug DR (2003) A quantitative structure-function relationship for the Photosystem II reaction centre: Supermolecular behavior in natural photosynthesis. Proc Natl Acad Sci USA 100: 946–951

Barzda V, Gulbinas V, Kananavicius R, van Amerongen H, van Grondelle R and Valkunas L (2001) Singlet-singlet annihilation kinetics in aggregates and trimers of LHCII. Biophys J 80: 2409–2421

Bassi R, Sandonà D and Croce R (1997) Novel aspects of chlorophyll *a/b*-binding proteins. Physiologia Plantarum 100: 769–779

Beekman LMP, Mourik FV, Jones MR, Visser HM, Hunter CN and van Grondelle R (1994) Trapping kinetics in mutants of the photosynthetic purple *bacterium Rhodobacter sphaeroides*: Influence of charge separation rate and consequences for the rate limiting step in the light-harvesting process. Biochemistry 33: 3143–3147

Berens SJ, Scheele J, Butler WL and Madge D (1985a) Kinetic modelling of the time-resolved fluorescence in spinach chloroplasts. Photochem Photobiol 42: 59–68

Berens SJ, Scheele J, Butler WL and Madge D (1985b) Time Resolved Fluorescence studies of Spinach Chloroplasts — evidence for the heterogeneous bipartite model. Photochem Photobiol 42: 51–57

Bernarding J, Eckert H-J, Eichler HJ, Napiwotzki A and Renger G (1994) Kinetic studies on the stabilization of the primary radical pair $P680^{+}Pheo^{-}$ in different Photosystem II preparations from higher plants. Photochem Photobiol 59: 566–573

Booth PJ, Crystall B, Giorgi LB, Barber J, Klug DR and Porter G (1990) Thermodynamic properties of D1/D2/cytochrome *b*-559 reaction centers isolated by time-resolved fluorescence measurements. Biochim Biophys Acta 1016: 141–152

Booth PJ, Crystall B, Ahmad I, Barber J, Porter G and Klug DR (1991) Observation of multiple radical pair states in Photosystem 2 reaction centers. Biochemistry 30: 7573–7586

Bosch MK, Proskuryakov II, Gast P and Hoff AJ (1995) Relative orientation of the optical transition dipole and triplet axes of the Photosystem II primary donor. A magnetophotoselection study. J Phys Chem 99: 15310–15316

Braun P, Greenberg BM and Scherz A (1990) D1-D2-Cytochrome *b*559 complex from the aquatic plant *Spirodela oligorrhiza*: Correlation between complex integrity, spectroscopic properties, photochemical activity and pigment composition. Biochemistry 29: 10376–10387

Butler WL, Madge D and Berens SJ (1983) Fluorescence lifetimes in the bipartite model of the photosynthetic apparatus with α, β heterogeneity in Photosystem II. Proc Natl Acad Sci USA 80: 7510–7514

Chang H-C, Jankowiak R, Reddy RS, Yocum CF, Picorel R, Seibert M and Small GJ (1994a) On the question of the Chlorophyll *a* content of the Photosystem II reaction centre. J Phys Chem 98: 7725–7735

Chang H-C, Jankowiak R, Yocum CF, Picorel R, Alfonso M, Seibert M and Small GJ (1994b) Exciton level structure and dynamics in the CP47 antenna complex of Photosystem II. J Phys Chem 98: 7717–7724

Connelly JP, Müller MG, Bassi R, Croce R and Holzwarth AR (1997a) Femtosecond transient absorption study of carotenoid to chlorophyll energy transfer in the light-harvesting complex II of Photosystem II. Biochemistry 36: 281–287

Connelly JP, Müller MG, Hucke M, Gatzen G, Mullineaux CW, Ruban AV, Horton P and Holzwarth AR (1997b) Ultrafast spectroscopy of trimeric light-harvesting complex II from higher plants. J Phys Chem B 101: 1902–1909

Croce R, Müller MG, Bassi R and Holzwarth AR (2001) Carotenoid-to-chlorophyll energy transfer in recombinant major light-harvesting complex (LHCII) of higher plants. I. Femtosecond transient absorption measurements. Biophys J 80: 901–915

Danielus RV, Satoh K, van Kan PJM, Pliter J, Nuijs A and van Gorkom HJ (1987) The primary reaction of Photosystem II in the D1-D2-cytochrome *b*559 complex. FEBS Lett 213: 241–244

Dau H and Sauer K (1996) Exciton equilibration and Photosystem II exciton dynamics — a fluorescence study on Photosystem II membrane particles of spinach. Biochim Biophys Acta 1273: 175–190

Deisenhofer J, Epp O, Miki K, Huber R and Michel H (1985) Structure of the protein subunits in the photosynthetic reaction centre of *Rhodopseudomonas viridis* at 3Å resolution. Nature 318: 618–624

Dekker JP and van Grondelle R (2000) Primary charge separation in Photosystem II. Photosynth Res 63: 195–208

Demmig-Adams B (1990) Carotenoids and photoprotection in plants: A role for the xanthophyll zeaxanthin. Biochim Biophys Acta 1020: 1–24

den Hartog FTH, Dekker JP, van Grondelle R and Völker S (1998) Spectral distributions of 'trap' pigments in the RC, CP47 and CP47-RC complexes of Photosystem II at low temperature: A fluorescence line-narrowing and hole-burning study. J Phys Chem B 102: 11007–11016

de Paula JC, Liebshitz A, Hinsley S, Lin W, Chopra V, Long K, Williams SA, Betts S and Yocum CF (1994) Structure-function relationships in the 47kDa antenna protein and its complex the Photosystem II reaction centre core: Insights from picosecond fluorescence decay kinetics and resonance Raman spectroscopy. Biochemistry 33: 1455–1466

de Weerd FL, Palacios MA, Andrizhiyevskaya AG, Dekker JP and van Grondelle R (2002a) Identifying the lowest electronic states of the chlorophylls in the CP47 core antenna protein of Photosystem II. Biochem 41: 15224–15233

de Weerd FL, van Stokkum IHM, van Amerongen H, Dekker JP and van Grondelle R (2002b) Pathways from Energy transfer in the core light harvesting complexes CP43 and CP47 of Photosystem II. Biophys J 82: 1586–1597

Diner BA and Babcock GT (1996) Structure, dynamics and energy conversion in Photosystem II In: Ort DR and Yocum CF (eds) Oxygenic Photosynthesis: The Light Reactions, pp 213–247. Kluwer Academic Publishers, Dordrecht

Diner BA and Rappaport F (2002) Structure, dynamics, and energetics of the primary photochemistry of Photosystem II of oxygenic photosynthesis. Annu Rev Plant Biol 53: 551–580

Diner BA, Schlodder E, Nixon PJ, Coleman WJ, Rappaport F, Lavergne J, Vermaas WFJ and Chisholm DA (2001) Site directed mutations at D1-His198 and D2-His197 of Photosystem II in *Synechocystis* PCC 6803: Sites of primary charge separation and cation and triplet stabilization. Biochemistry 40: 9265–9281

Donovan B, II LAW, Yocum CF and Sension RJ (1996) Transient absorption studies of the primary charge separation in Photosystem II. J Phys Chem 100: 1945–1949

Du M, Xie X, Mets L and Fleming GR (1994) Direct observation of ultrafast energy-transfer processes in light-harvesting complex II. J Phys Chem 98: 4736–4741

Durrant JR, Giorgi LB, Barber J, Klug DR and Porter G (1990) Characterization of triplet-states in isolated Photosystem-II reaction centers—oxygen quenching as a mechanism for photodamage. Biochim Biophys Acta 1017: 167–175

Durrant JR, Hastings G, Joseph DM, Barber J, Porter G and Klug DR (1992) Sub-picosecond equilibration of excitation energy in isolated Photosystem II reaction centres. Proc Natl Acad Sci USA 89: 11632–11636

Durrant JR, Klug DR, Kwa SLS, van Grondelle R and Porter G (1995a) A multimer model for P680, the primary electron donor of Photosystem II. Proc Natl Acad Sci USA 92: 4798–4802

Durrant JR, Porter G, Barber J and Klug DR (1995b) The influence of energy level disorder on the charge separation / trapping kinetics in Photosystem II In: Mathis P (ed) Photosynthesis: from Light to the Biosphere, Vol 1, pp 611–614. Kluwer Academic Publishers, Dordrecht

Durrant JR, Nixon PJ, Barber J and Klug DR (1998) Identification of chlorophyll anion states during charge separation in mutant Photosystem II reaction centres In: Garab G (ed) Photosynthesis: Mechanisms and Effects, Vol II, pp1041–1044. Kluwer Academic Publishers, Dordrecht

Eads DD, Castner Jr. EW, Alberte R, Mets L and Fleming GR (1998) Direct observation of energy transfer in a photosynthetic membrane: Chlorophyll *b* to chlorophyll *a* transfer in LHC. J Phys Chem B 93: 8271–8275

Eckert H-J, Wiese N, Bernarding J, Eichler H-J and Renger G (1988) Analysis of electron transfer from Pheo- to Qa in PS II membrane fragments from spinach by time resolved 325nm absorbance changes in the picosecond domain. FEBS Lett 240: 153–158

Ferreira KN, Iverson TM, Maghlaoui K, Barber J and Iwata S (2004) Architecture of the photosynthetic oxygen-evolving centre. Science 303: 1831–1838

Fleming GR, Martin JL and Breton J (1988) Rates of primary electron transfer in photosynthetic reaction centres and their mechanistic implications. Nature 333: 190–192

Freiberg A, Timpmann K, Moskalenko AA and Kuznetsova NY (1994) Pico- and nanosecond fluorescence kinetics of Photosystem II reaction centre and its complex with the CP47 antenna. Biochim Biophys Acta 1184: 45–53

Frese RN, Germano M, de Weerd FL, van Stokkum IHM, Shkuropatov AY, Shuvalov VA, van Gorkom HJ, van Frondelle R and Dekker JP (2003) Electric field effects on the chlorophylls, pheophytins and β-Carotenes in the reaction centre of Photosystem II. Biochemistry 42: 9205–9213

Gatzen G, Müller MG, Griebenow K and Holzwarth AR (1996) Primary processes and structure of the Photosystem II reaction centre. 3. Kinetic analysis of picosecond energy transfer and charge separation processes in the D1-D2-cyt*b*559 complex measured by time resolved fluorescence. J Phys Chem 100: 7269–7278

Germano M, Shkuroptav AY, Permentier H, Wijn Rd, Hoff AJ, Shuvalov VA and van Gorkom HJ (2001) Pigment organization and their interactions in reaction centres of Photosystem II: Optical spectroscopy at 6 K of reaction centres with modified pheophytin composition. Biochemistry 40: 11472–11482

Giorgi LB, Nixon PJ, Merry SAP, Joseph DM, Durrant JR, de-las-Rivas J, Barber J, Porter G and Klug DR (1996) Comparison of primary charge separation in the Photosystem II reaction centre complex isolated from wild-type and D1-130 mutants of the cyanobacterium Synechocystis PCC 6803. J Biol Chem 271: 2093–2101

Gobets B and van Grondelle R (2001) Energy transfer and trapping in Photosystem I. Biochim Biophys Acta 1507: 80–99

Goldstein RA, Takiff L and Boxer SG (1988) Energetics of initial charge separation in bacterial photosynthesis: The triplet decay

rate in very high magnetic fields. Biochim Biophys Acta 934: 253–263

Gradinaru CC, Özdemir S, Gülen D, van Stokkum IHM, van Grondelle R and van Amerongen H (1998a) The flow of excitation in LHCII monomers. Implications for the structural model of the major plant antenna. Biophys J 75: 3064–3077

Gradinaru CC, Pascal AA, van Mourik F, Robert B, van Grondelle R and van Amerongen H (1998b) Ultrafast evolution of the excited states in the minor chlorophyll *a/b* complex CP29 from green plants studied by energy-selective pump-probe spectroscopy. Biochemistry 37: 1143–1149

Gradinaru CC, van Stokkum IHM, van Grondelle R and van Amerongen H (2000) Identifying the pathways of energy transfer between carotenoids and chlorophylls in LHCII and CP29. A multicolor, femtosecond pump-probe study. J Phys Chem B 104: 9330–9342

Greenfield SR, Seibert M, Govindjee and Wasielewski MR (1997) Direct measurement of the effective rate constant for primary charge separation in isolated Photosystem II reaction centres. J Phys Chem B 101: 2251–2255

Greenfield SR, Seibert M and Wasielewski MR (1999) Time-resolved absorption changes of the pheophytin Qx band in isolated Photosystem II reaction centres at 7K: Energy transfer and charge separation. J Phys Chem B 103: 8364–8374

Groot M-L, Petermann EJG, van Kan PJM, van Stokkum IHM, Dekker JP and van Grondelle R (1994) Temperature-dependent triplet and fluorescence quantum yields of the Photosystem II reaction centre described in a thermodynamic model. Biophys J 67: 318–330

Groot M-L, Petermann EJ, van Stokkum IHM, Dekker JP and van Grondelle R (1995) Triplet and Fluorescing states of the CP47 antenna complex of Photosystem II studied as a function of temperature. Biophys J 68: 281–290

Groot M-L, Dekker JP, van Grondelle R, den Hartog FTH and Volker S (1996) Energy transfer and trapping in isolated Photosystem II reaction centres of green plants at low temperature. A study by spectral hole burning. J Phys Chem 100: 11488–11495

Groot M-L, van Mourik F, Eijckelhoff C, van Stokkum IHM, Dekker JP and van Grondelle R (1997) Charge separation in the reaction centre of Photosystem II studied as a function of temperature. Proc Natl Acad Sci USA 94: 4389–4394

Groot M-L, Frese RN, de Weerd FL, Bromek K, Pettersson Å, Peterman EJG, van Stokkum IHM, van Grondelle R and Dekker JP (1999) Spectroscopic properties of the CP43 core antenna protein of Photosystem II. Biophys J 77: 3328–3340

Gulotty RJ, Fleming GR and Alberte RS (1982) Low intensity picosecond fluorescence kinetics and excitation dynamics in barley chloroplasts. Biochim Biophys Acta 682: 322–331

Gulotty RJ, Mets L, Alberte RS and Fleming GR (1985) Picosecond fluorescence study of photosynthetic mutants of *Chlamydomonas reinhardtii*: Origin of the fluorescence decay kinetics of chloroplasts. Photochem Photobiol 41: 487–496

Haehnel W, Nairn JA, Reisberg P and Sauer K (1982) Picosecond fluorescence decay kinetics and energy transfer in chloroplasts and algae. Biochim Biophys Acta 680: 161–173

Haehnel W, Holzwarth AR and Wendler J (1983) Picosecond fluorescence kinetics and energy transfer in the antenna chlorophylls of green algae. Photochem Photobiol 37: 435–443

Hankamer B, Nield J, Zhelva D, Boekema E, Jansson S and Barber J (1997) Isolation and biochemical characterisation of monomeric and dimer Photosystem II complexes from spinach and their relevance to the organisation of Photosystem II in vivo. Eur J Biochem 243: 422–429

Hankamer B, Morris EP and Barber J (1999) Revealing the structure of the oxygen-evolving core dimer of Photosystem II by crystallography. Nature Struct Biol 6: 560–564

Hansson O and Wydrzynski T (1990) Current perceptions of Photosystem II. Photosynth Res 23: 131–162

Hastings G, Durrant JR, Barber J, Porter G and Klug DR (1992) Observation of pheophytin reduction in Photosystem Two reaction centres using femtosecond transient absorption spectroscopy. Biochemistry 31: 7638–7647

Heathcote P, Fyfe PK and Jones MR (2002) Reaction centres: The structure and evolution of biological solar power. Trends Biol Sci 27: 79–87

Hillmann B, Brettel K, van Mieghem F, Kamlowski A, Rutherford AW and Schlodder E (1995) Charge recombination reactions in Photosystem II 2. Transient absorption difference spectra and their temperature dependence. Biochemistry 34: 4814–4827

Hodges M and Moya I (1986) Time Resolved chlorophyll fluorescence studies of Photosynthetic membranes: Resolution and characterisation of four kinetic components. Biochim Biophys Acta 849: 193–202

Hodges M and Moya I (1987) Modification of room temperature picosecond chlorophyll fluorescence kinetics in PS II enriched particles by photochemistry. Biochim Biophys Acta 892: 42–47

Hodges M and Moya I (1988) Time resolved chlorophyll fluorescence studies on pigment-protein complexes from photosynthetic membranes. Biochim Biophys Acta 935: 41–52

Holzapfel W, Finkele U, Kaiser W, Oesterhelt D, Scheer H, Stilz HU and Zinth W (1990) Initial electron-transfer in the reaction centre from *Rhodobacter sphaeroides*. Proc Natl Acad Sci USA 87: 5168–5172

Hörber JKH, Göbel W, Ogrodnik A, Michel-Beyerle ME and Cogdell RJ (1986) Time Resolved measurements of fluorescence from reaction centres of *Rhodopseudomonas Sphaeroides* R26.1. FEBS Lett 198: 273–278

Horton P, Ruban AV, Rees D, Pascal AA, Noctor G and Young AJ (1991) Control of the light-harvesting function of chloroplast membranes by aggregation of the LHCII chlorophyll-protein complex. FEBS Lett 292: 1–4

Horton P, Ruban AV and Walters RG (1996) Regulation of Light Harvesting in Green Plants. Annual Review of Plant Physiology and Plant Mol Biol 47: 655–684

Horton P, Ruban AV and Wentworth M (2000) Allosteric regulation of the light-harvesting system of Photosystem II. Phil Trans R Soc London B 355: 1361–1370

Jankowiak R, Tang D, Small GJ and Seibert M (1989) Transient and persistent hole burning of the reaction centre of Photosystem II. J Phys Chem 93: 1649–1654

Jankowiak R, Zazubovich V, Rätsep M, Matsuzaki S, Alfonso M, Picorel R, Seibert M and Small GJ (2000) The CP43 core antenna complex of Photosystem II possesses two quasi-degenerate and weakly coupled Qy-trap states. J Phys Chem B 104: 11805–11815

Johnston HG, Wang J, Ruffle SV, Sayre RT and Gustafson TL (2000) Fluorescence decay kinetics of wild type and D2-H117N mutant Photosystem II reaction centres isolated from *Chlam-*

ydomonas reinhardtii. J Phys Chem B 104: 4777–4781

Jursinic P and Govindjee (1977) Temperature dependence of delayed light emission in the 6 to 340 microsecond range after a single flash in chloroplasts. Photochem Photobiol 26: 617–628

Kamiya N and Shen J-R (2003) Crystal Structure of oxygen-evolving Photosystem II from Thermosynechococcus *vulcanus* at 3.7Å resolution. Proc Natl Acad Sci USA 100: 98–103

Kleima FJ, Gradinaru CC, Calkoen F, van Stokkum IHM, van Grondelle R and van Amerongen H (1997) Energy transfer in LHCII monomers at 77K studied by sub-picosecond transient absorption spectroscopy. Biochemistry 36: 15262–15268

Klimov VV, Allakhverdiev SI, Demeter S and Krasnovskii AA (1979) Pheophytin reduction in Photosystem II of chloroplasts in relation to oxidation-reduction potential of the medium. Dok Akad Nauk SSSR 249: 227–230

Klug DR, Rech T, Joseph DM, Barber J, Durrant JR and Porter G (1995) Primary processes in isolated Photosystem II reaction centres probed by magic angle transient absorption spectroscopy. Chem Phys 194: 433–442

Knapp EW, Fischer SF, Zinth W, Sander M, Kaiser W, Deisenhofer J and Michel H (1985) Analysis of optical spectra from single crystals of *Rhodopseudomonas viridis* reaction centres. Proc Natl Acad Sci USA 82: 8463–8467

Konermann L and Holzwarth AR (1996) Analysis of the absorption spectrum of Photosystem II reaction centres: Temperature dependence, pigment assignment and inhomogeneous broadening. Biochemistry 35: 829–842

Konermann L, Gatzen G and Holzwarth AR (1997) Primary processes and structure of the Photosystem II reaction centre. 5. Modelling the fluorescence kinetics of the D1/D2/cyt b559 complex at 77K. J Phys Chem B 101: 2933–2944

Kühlbrandt W, Wang DN and Fujioshi Y (1994) Atomic model of plant light-harvesting complex by electron crystallography. Nature 367: 614–621

Kumazaki S, Joseph DM, Crystall B, Tachibana Y, Durrant J, Barber J, Porter G, Yoshihara K and Klug DR (1995) Experimental observation of multiple trapping/charge separation steps in the isolated PS II reaction centre In: Mathis P (ed) Photosynthesis: From Light to Biosphere, 883–886. Kluwer Academic Publishers, Dordrecht

Kwa SLS, van Amerongen H, Lin S, Dekker JP, van Grondelle R and Struve WS (1992) Ultrafast energy transfer in LHC-II trimers from the Chl *a/b* light-harvesting antenna of Photosystem II. Biochim Biophys Acta 1102: 202–212

Kwa SLS, Eijckelhoff C, van Grondelle R and Dekker JP (1994) Site-selection spectroscopy of the reaction centre complex of Photosystem II. 1. Triplet-minus-Singlet absorption difference: Search for a second exciton band of P-680. J Phys Chem 98: 7702–7711

Leegwater JA, Durrant JR and Klug DR (1997) Exciton equilibria induced by phonons: Theory and application to PS II reaction centres. J Phys Chem B 101: 7205–7210

Li X-P, Björkman O, Shih C, Grossman AR, Rosenquist M, Jansson S and Niyogi KK (2000) A Pigment-binding protein essential for regulation of photosynthetic light harvesting. Nature 403: 391–395

Lui B, Napiwotzki A, Eckert H-J, Eichler HJ and Renger G (1993) Studies on the recombination kinetics of the radical pair P^{+}_{680} $Pheo^{-}$ in isolated PS II core complexes from spinach. Biochim Biophys Acta 1142: 129–138

Mattoo AK, Marder JB and Edelman M (1989) Dynamics of the Photosystem II reaction centre. Cell 56: 241–246

Merry SAP, Kumazaki S, Tachibana Y, Joseph DM, Porter G, Yoshihara K, Durrant JR and Klug DR (1996) Sub-picosecond equilibration of excitation energy in isolated Photosystem II reaction centres revisited: Time dependent anisotropy. J Phys Chem 100: 10469–10478

Merry SAP, Nixon PJ, Barter LMC, Schilstra M, Porter G, Barber J, Durrant JR and Klug DR (1998) Modulation of quantum yield of primary radical pair formation in Photosystem II by site directed mutagenesis affecting radical cations and anions. Biochemistry 37: 17439–17447

Michel H and Deisenhofer J (1998) Relevance of the photosynthetic reaction centre from Purple bacteria to the structure of Photosystem II. Biochemistry 27: 1–7

Mulkidjanian AY, Cherepanov DA, Haumann M and Junge W (1996) Photosystem II of green plants: Topology of core pigments and redox cofactors as inferred from electrochromic difference spectra. Biochemistry 35: 3093–3107

Muller MG, Hucke M, Reus M and Holzwarth AR (1996) Primary processes and structure of the Photosystem II reaction centre. 4. Low-intensity femtosecond transient absorption spectra of D1-D2-cyt-b559 reaction centres. J Phys Chem 100: 9527–9536

Nairn JA, Haehnel W, Reisberg P and Sauer K (1982) Picosecond fluorescence kinetics in spinach chloroplasts at room temperature: Effects of Mg^{2+}. Biochim Biophys Acta 682: 420–429

Nanba O and Satoh K (1987) Isolation of a Photosystem II reaction centre consisting of D-1 and D-2 polypeptides and cytochrome *b*-559. Proc Natl Acad Sci USA 84: 109–112

Niyogi KK (1999) Photoprotection revisited: Genetic and molecular approaches. Annu Rev Plant Physiol Plant Mol Biol 50: 333–359

Noguchi T, Inoue Y and Satoh K (1993) FT-IR studies of the triplet state of P680 in the Photosystem II reaction centre: Triplet equilibration within a chlorophyll dimer. Biochemistry 32: 7186–7195

Novoderezhkin V, Salverda JM, van Amerongen H and Grondelle RV (2003) Exciton modeling of energy-transfer dynamics in the LHCII complex of higher plants: A Redfield theory approach. J Phys Chem B 107: 1893–1912

Nugent JHA (1996) Oxygenic photosynthesis. Electron transfer in Photosystem I and Photosystem II. Eur J Biochem 237: 519–531

Nugent JHA, Rich AM and Evans MCW (2001) Photosynthetic water oxidation: Towards a mechanism. Biochim Biophys Acta 1503: 138–143

Nuijs AM, van Gorkom HJ, Plijter JJ and Duysens LNM (1986) Primary-charge separation and excitation of chlorophyll *a* in Photosystem II particles from spinach as studied by picosecond absorbance difference spectroscopy. Biochim Biophys Acta 848: 167–175

Ogrodnik A, Volk M, Letterer R, Feick R and Michel-Beyerle ME (1988) Determination of free energies in reaction centres of *Rb. sphaeroides*. Biochim Biophys Acta 936: 361–371

Ogrodnik A, Keupp W, Volk M, Aumeier G and Michel-Beyerle ME (1994) Inhomogeneity of radical pair energies in photosynthetic reaction centres revealed by differences in recombination dynamics of $P^{+}HA^{-}$ when detected in delayed emission and in absorption. J Phys Chem 98: 3432–3439

Otte SCM, van der Vos R and van Gorkom HJ (1992) Steady state spectroscopy at 6K of the isolated Photosystem II reac-

tion centre: Analysis of the red absorption band. J Photochem Photobiol B 15: 5–14

Owens TG, Webb SP, Mets L, Alberte RS and Fleming GR (1987) Antenna size dependence of fluorescence decay in the core antenna of Photosystem I: Estimates of charge separation and energy transfer rates. Proc Natl Acad Sci USA. 84: 1532–1536

Paillotin G (1976) Movement of excitons in the photosynthetic membrane. J Theor Biol 58: 219–235

Peterman EJG, Monshouwer R, van Stokkum IHM, van Grondelle R and van Amerongen H (1997) Ultrafast singlet excitation transfer from carotenoids to chlorophylls via different pathways in light-harvesting complex II of green plants. Chem Phys Lett 264: 279–284

Peterman EJG, van Amerongen H, van Grondelle R and Dekker JP (1998) The nature of the excited state of the reaction centre of Photosystem II of green plants: A high-resolution fluorescence spectroscopy study. Proc Natl Acad Sci USA 95: 6128–6133

Pieper J, Irrgang K-D, Rätsep M, Voigt J, Renger G and Small GJ (2000) Assignment of the lowest Qy-state and spectral dynamics of the CP29 chlorophyll *a/b* antenna complex of green plants: A hole-burning study. Photochem Photobiol 71: 574–581

Prokhorenko VI and Holzwarth AR (2000) Primary processes and structure of the Photosystem II reaction centre: A photon echo study. J Phys Chem B 104: 11563–11578

Rappaport F, Guergova-Kuras M, Nixon PJ, Diner BA and Lavergne J (2002) Kinetics and pathways of charge recombination in Photosystem II. Biochemistry 41: 8518–8527

Rech T, Durrant JR, Joseph DM, Barber J, Porter G and Klug DR (1994) Does slow energy transfer limit the observed time constant for radical pair formation in Photosystem II reaction centres? Biochemistry 33: 14678–14774

Renger G (1992) Energy Transfer and trapping in Photosystem II In: Barber J (ed) The Photosystems: Structure, Function and Molecular Biology, pp 45–99. Elsevier Science Publishers, Amsterdam

Renger G, Eckert H-J, Bergmann A, Bernarding J, Lui B, Napiwotzki A, Reifarth F and Eichler HJ (1995) Fluorescence and spectroscopic studies of exciton trapping and electron transfer in Photosystem II of higher plants. Aust J Plant Physiol 22: 167–81

Rhee KH, Morris EP, Barber J and Kühlbrandt W (1998) Three dimensional structure of the plant Photosystem II reaction centre at 8 Å resolution. Nature 396: 283–286

Roelofs TA, Lee C-H and Holzwarth AR (1992) Global target analysis of picosecond chlorophyll fluorescence kinetics from pea chloroplasts: A new approach to characterisation of the primary processes in Photosystem II alpha and beta subunits. Biophys J 61: 1147–1163

Ruban AV, Young AJ and Horton P (1996) Dynamic properties of the minor chlorophyll *a/b* binding proteins of Photosystem II, an in vitro model for photoprotective energy dissipation in the photosynthetic membrane of green plants. Biochemistry 35: 674–678

Ruffle SV, Donnelly D, Blundell TL and Nugent JHA (1992) A three-dimensional model of the Photosystem II reaction centre of *Pisum sativum*. Photosynth Res 34: 287–300

Salverda JM, Vengris M, Krueger BP, Scholes GD, Czarnoleski AR, Novoderezhkin V, van Amerongen H and van Grondelle R (2003) Energy transfer in light-harvesting complexes LHCII and CP29 of spinach studied with three-pulse echo peak shift and transient grating. Biophys J 84: 450–465

Schatz GH and Holzwarth AR (1986) Mechanisms of Chlorophyll fluorescence revisited: Prompt or delayed emission from Photosystem II with closed reaction centres? Photosynth Res 10: 309–318

Schatz GH, Brock H and Holzwarth AR (1987) Picosecond kinetics of fluorescence and absorbance changes in Photosystem II particles excited at low photon density. Proc Natl Acad Sci USA 84: 8414–8418

Schatz GH, Brock H and Holzwarth AR (1988) Kinetic and energetic model for the primary processes in Photosystem II. Biophys J 54: 397–405

Scholes GD and Fleming GR (2000) On the mechanism of light-harvesting in Photosynthetic Purple Bacteria: B800 to B850 energy transfer. J Phys Chem B 104: 1854–1868

Scholes GD, Gould IR, Cogdell RJ and Fleming GR (1999) *Ab Initio* molecular orbital calculations of electronic couplings in the LH2 bacterial light-harvesting complex of *Rps. Acidophila*. J Phys Chem B 103: 2543–2553

Scholes GD, Jordanides XJ and Fleming GR (2001) Adapting the Förster theory of energy transfer for modeling dynamics in aggregated molecular assemblies. J Phys Chem B 105: 1640–1651

Schubert W-D, Klukas O, Saenger W, Witt HT, Fromme P and Krauß N (1998) A common ancestor for oxygenic and anoxygenic photosynthetic systems: A comparison based on the structural model of Photosystem I. J Mol Biol 280: 297–314

Shiang JJ, Yoder LM and Sension RJ (2003) Structure and function in the isolated reaction centre complex of Photosystem II. 2. Models for energy relaxation and charge separation in a protein matrix. J Phys Chem B 107: 2162–2169

Somsen OJG, Valkunas L and van Grondelle R (1996) A perturbed two-level model for exciton trapping in small photosynthetic systems. Biophys J 70: 669–683

Stewart DH and Brudvig GW (1998) Cytochrome *b*559 of Photosystem II. Biochim Biophys Acta 1367: 63–87

Stewart DH, Nixon PJ, Diner BA and Brudvig GW (2000) Assignment of the Qy absorbance bands of Photosystem II chromophores by low-temperature optical spectroscopy of wild-type and mutant reaction centres. Biochemistry 39: 14583–14594

Svensson B, Vass I, Cedergren E and Styring S (1990) Structure of donor side components in Photosystem II predicted by computer modelling. EMBO J 9: 2051–2059

Svensson B, Etchebest C, Tuffery P, van Kan P, Smith J and Styring S (1996) A model for the Photosystem II reaction centre core including the structure of the primary donor P680. Biochemistry 35: 14486–14502

Tetenkin VL, Gulyaev BA, Seibert M and Rubin AB (1989) Spectral properties of stabilized D1/D2/cytochrome *b*-559 Photosystem II reaction centre complex. FEBS Lett 250: 459–463

Vacha F, Joseph DM, Durrant JR, Telfer A, Klug DR, Porter G and Barber J (1995) Photochemistry and spectroscopy of a five-chlorophyll reaction centre of Photosystem II isolated by using a Cu affinity column. Proc Natl Acad Sci USA 92: 2929–2933

Vácha F, Durchan M and Siffel P (2002) Excitonic interactions in the reaction centre of Photosystem II studied by using circular dichroism. Biochim Biophys Acta 1554: 147–152

Valkunas L, Liuolia V, Dekker JP and van Grondelle R (1995)

Description of energy migration and trapping in Photosystem I by a model with two distinct distance scaling parameters. Photosynth Res 43: 149–154

van Amerongen H, Valkunas L and van Grondelle R (2000) Photosynthetic Excitons. World Scientific, Singapore

van Amerongen H and van Grondelle R (2001) Understanding the energy transfer function of LHCII, the major light-harvesting complex of green plants. J Phys Chem B 105: 604–617

van Brederode ME and van Grondelle R (1999) New and unexpected routes for ultrafast electron transfer in photosynthetic reaction centres. FEBS Lett 455: 1–7

van Brederode ME, Jones MR, van Mourik F, van Stokkum IHM and van Grondelle R (1997) A new pathway for transmembrane electron transfer in photosynthetic reaction centres of Rhodobacter sphaeroides not involving the excited special pair. Biochemistry 36: 6855–6861

van Brederode ME, van Mourik F, van Stokkum IHM, Jones MR and van Grondelle R (1999) Multiple pathways of ultrafast transduction of light energy in the photosynthetic reaction centre of *Rhodobacter sphaeroides*. Proc Natl Acad Sci USA 96: 2054–2059

van Dorssen RJ, Breton J, Plijter JJ, Satoh K, van Gorkom HJ and Amesz J (1987) Spectroscopic properties of the reaction centre and of the 47 kDa chlorophyll protein of Photosystem II. Biochim Biophys Acta 893: 267–274

van Gorkom HJ (1985) Electron transfer in Photosystem II. Photosynth Res 6: 97–112

van Grondelle R (1985) Excitation energy transfer, trapping and annihilation in photosynthetic systems. Biochim Biophys Acta 811: 147–195

van Grondelle R, Dekker JP, Gillbro T and Sundstrom V (1994) Energy transfer and trapping in photosynthesis. Biochim Biophys Acta 1187: 1–65

van Kan PJM, Otte SCM, Kleinherenbrink FAM, Nieveen MC, Aartsma TJ and van Gorkom HJ (1990) Time-resolved spectroscopy at 10K of the Photosystem II reaction centre; Deconvolution of the red absorption band. Biochim Biophys Acta 1020: 146–152

van Mieghem FJE, Satoh K and Rutherford AW (1991) A chlorophyll tilted 30° relative to the membrane in the Photosystem II reaction centre. Biochim Biophys Acta 1058: 379–385

van Mieghem FJE, Searle GFW, Rutherford AW and Schaafsma TJ (1992) The influence of the double reduction of Q_A on the fluorescence decay kinetic of Photosystem II. Biochim Biophys Acta 1100: 198–206

Vasil'ev S and Bruce D (2000) Picosecond time resolved fluorescence studies on excitation energy transfer in a histidine 117 mutant of the D2 protein of Photosystem II in *Synechocystis* 6803. Biochemistry 39: 14211–14218

Vasil'ev S, Orth P, Zouni A, Owens TG and Bruce D (2001) Excited-state dynamics in Photosystem II: Insights from the X-ray crystal structure. Proc Natl Acad Sci USA 98: 8602–8607

Vassiliev S, Lee C-I, Brudvig GW and Bruce D (2002) Structure-based kinetic modelling of excited state transfer and trapping in histidine tagged Photosystem II core complexes from *Synechocystis*. Biochemistry 41: 12236–12243

Vass I, Gatzen G and Holzwarth A (1993) Picosecond time-resolved fluorescence studies on photoinhibition and double reduction of Q_A in Photosystem II. Biochim Biophys Acta 1183: 388–396

Visser HM, Kleima FJ, van Stokkum IHM, van Grondelle R and van Amerongen H (1996) Probing the many energy-transfer processes in the photosynthetic light-harvesting complex II at 77 K using energy-selective sub-picosecond transient absorption spectroscopy. Chem Phys 210: 297–312

Volk M, Gilbert M, Rousseau G, Richter M, Ogrodnik A and Michel-Beyerle M-E (1993) Similarity of Primary Radical Pair Recombination in Photosystem II and Bacterial Reaction Centres. FEBS Lett 336: 357–362

Vredenberg WJ (2000) A three-state model for energy trapping and chlorophyll fluorescence in Phostosystem II incorporating radical pair recombination. Biophys J 79: 26–38

Walla PJ, Yom J, Krueger BP and Fleming GR (2000) Two-photon excitation spectrum of light-harvesting complex II and fluorescence upconversion after one- and two-photon excitation of the carotenoids. J Phys Chem B 104: 4799–4806

Wang Z, Pearlstein RM, Jia Y, Fleming GR and Norris JR (1993) Inhomogeneous electron transfer kinetics in reaction centres of bacterial photosynthesis. Chem Phys 176: 421–425

Xiong J, Subramaniam S and Govindjee (1996) Modeling of the D1/D2 proteins and cofactors of the Photosystem II reaction centre: Implications for herbicide and bicarbonate binding. Protein Sci 5: 2054–2073

Xiong J, Subramaniam S and Govindjee (1998) A knowledge-based three dimensional model of the Photosystem II reaction centre of *Chlamydomonas reinhardtii*. Photosynth Res 56: 229–254

Yoder LM, Cole AG and Sension RJ (2002) Structure and function in the isolated reaction centre complex of Photosystem II: energy and charge transfer dynamics and mechanism. Photosynth Res 72: 147–158

Yruela I, Gatzen G, Picorel R and Holzwarth A (1996) Cu(II)-Inhibitory effect on Photosystem II from higher plants. A picosecond time resolved fluorescence study. Biochemistry 35: 9469–9474

Zouni A, Witt H-T, Kern J, Fromme P, Krauß N, Saenger W and Orth P (2001) Crystal structure of Photosystem II from Synechococcus elongatus at 3.8Å resolution. Nature 409: 739–743

Chapter 23

The Role of Carotenoids in Energy Quenching

Barry J. Pogson and Heather M. Rissler
School of Biochemistry and Molecular Biology, The Australian National University, Canberra, ACT 0200, Australia

Harry A. Frank*
Department of Chemistry, University of Connecticut, 55 North Eagleville Road, Storrs, CT 06269-3060, U.S.A.

Summary

Photoprotection remains one of the most challenging and complex areas for research in photosynthesis. Coping with a wide range of adverse environmental conditions, especially full sunlight, is central to plant survival in nature, and understanding mechanisms of light acclimation is increasingly important in crop improvement. Excess light and other environmental stresses can result in prolonged lifetimes of excited state chlorophylls and enhanced triplet state yields that, left unchecked, markedly increase the rate of formation of reactive oxygen species such as H_2O_2, singlet oxygen ($^1O_2^*$) and superoxide (O_2^-). Reactive oxygen species cause photo-oxidative damage such as bleaching and peroxidation to the photosystems and the whole plant. Carotenoids afford protection against photo-oxidative damage in complementary ways by stabilizing the pigment-protein complexes and quenching of excited state chlorophylls and reactive oxygen species.

*Author for correspondence, email: harry.frank@uconn.edu

T. Wydrzynski and K. Satoh (eds): Photosystem II: The Light-Driven Water:Plastoquinone Oxidoreductase, pp. 515–537.

I. Introduction

The first carotenoid was isolated in 1831 and in 1837 the xanthophylls received their name from the colours of autumn leaves (xanthos = yellow and phyll = leaf) (for a review, see Govindjee, 1999). In fact, for most of the last century the critical roles of carotenoids in photosystem assembly, light harvesting and photoprotection have been intensively researched in plants, alga and bacteria. Insights into carotenoid chemistry led to Nobel prizes for Paul Karrer and Richard Kuhn in 1937 and 1938, respectively. In 1943, excitation energy transfer from a carotenoid, fucoxanthin, to chlorophyll (Chl) *a* was first shown by Dutton and colleagues (Dutton et al., 1943). A decade later, the essential role of colored carotenoids in the protection from lethal photodamage was observed in the photosynthetic bacterium, *Rhodobacter sphaeroides*, by Roger Stanier and colleagues (Griffiths et al., 1955). In 1962, Harry Yamamoto identified the xanthophyll cycle that underpins an important aspect of photoprotection (Yamamoto, 1962). This brief snapshot of the history of carotenoids is covered in depth by Govindjee (1999) and has laid the foundation for most of the research underway in all of our laboratories today. The breadth of the topic necessitates a focus; to this end we will focus on aspects of current research in higher plants related to Photosystem II (PS II) and direct readers to the detailed coverage in many recent reviews (e.g., Demmig-Adams and Adams, 1996; F.J. Cunningham and Gantt, 1998; Frank et al., 1999; Gilmore and Govindjee, 1999; Niyogi, 1999; Hirschberg, 2001; Demmig-Adams, 2003; especially Vol 8, *The Photochemistry of Carotenoids,* of this series).

Abbreviations: APX – ascorbate peroxidase; Car – carotenoid; Chl – chlorophyll; ^{3}Chl* – triplet chlorophyll; CP – chlorophyll binding protein; CrtISO – carotenoid isomerase; Cyt c_{550} – cytochrome c_{550}; D1, D2 – reaction center core subunits ; FAD – flavin adenine dinucleotide; L – lutein; LHC – light harvesting complex; LHCIIb or Lhcb1-3 – major higher plant light-harvesting complex; N – neoxanthin; NPQ – nonphotochemical quenching; NXS – neoxanthin synthase; $^1O_2^*$ – singlet oxygen; O_2^- – superoxide; P680 – primary electron donor of PS II; PDS – phytoene desaturase; Pheo – pheophytin; PTOX – plastid terminal oxidase; PQ – plastoquinone; PsbS – CP22, protein associated with PS II; PS II – Photosystem II; PSY – phytoene synthase; qE – ΔpH-dependent energy dissipation; qI – quenching resulting from photoinhibition; qP – photochemical quenching; SOD – superoxide dismutase; V – violaxanthin; VDE – violaxanthin de-epoxidase; Z – zeaxanthin; ZDS – ζ-carotene desaturase; ZE – zeaxanthin epoxidase; βLCY – β-cyclase; βOH – β-hydroxylase; ΔpH – pH differential across the thylakoid membrane; εLCY – ε-cyclase; εOH – ε-hydroxylase

II. Biosynthesis and Photosystem Assembly

A. Carotenoid Biosynthesis

Seven primary photosynthetic pigments are found in chloroplasts of higher plants: Chl *a*, Chl *b* and four carotenoids (Fig.1). The four carotenoids: lutein, β-carotene, violaxanthin, and neoxanthin, are nearly ubiquitous amongst chloroplasts of higher plants (Young, 1993). Other commonly found carotenoids are zeaxanthin and antheraxanthin. A few species accumulate additional carotenoids, such as lactucaxanthin in lettuce or lutein-5,6 epoxide in some parasitic angiosperms (Siefermann-Harms et al., 1981; Bungard et al., 1999; Matsubara et al., 2001). Rarely are plants deficient in one of the primary carotenoids, with one of the few exceptions being the parasitic angiosperm, *Crustaca reflexa,* where lutein-5,6-epoxide accumulates in the absence of neoxanthin (Bungard et al., 1999). This is in stark contrast to algal, bacterial and fungal taxa where the vast majority of the over 600 naturally occurring carotenoids have been identified. The reason for the conservative carotenoid profile of higher plants is of considerable interest and indicates a strong selective pressure on the retention of each of the primary carotenoids (Pogson et al., 1998).

The carotenoids are all isoprenoids derived from phytoene, which is formed from two molecules of geranylgeranyl pyrophosphate (F.J. Cunningham and Gantt, 1998; Hirschberg, 2001). Phytoene is desaturated four times to form lycopene, carried out by the phytoene and ζ-carotene desaturases (PDS and ZDS, respectively) in higher plants (Fig. 2). Whereas the bacteria produce all-*trans*-lycopene with one enzyme, plants utilize 3 enzymes. There are two desaturases that produce tetra *cis*-lycopene, which is isomerized to all-*trans*-lycopene (Beyer and Kleinig, 1990) by the recently identified carotenoid isomerase (CrtISO) (Isaacson et al., 2002; Park et al., 2002).

The desaturation reactions require quinones and the plastid terminal oxidase (PTOX) (Carol and Kuntz, 2001), with the absence of either leading to phytoene-accumulating, photobleached tissue, albiet sectored in *immutans* (Wetzel et al., 1994; Norris et al., 1995). PTOX catalyzes the reduction of molecular

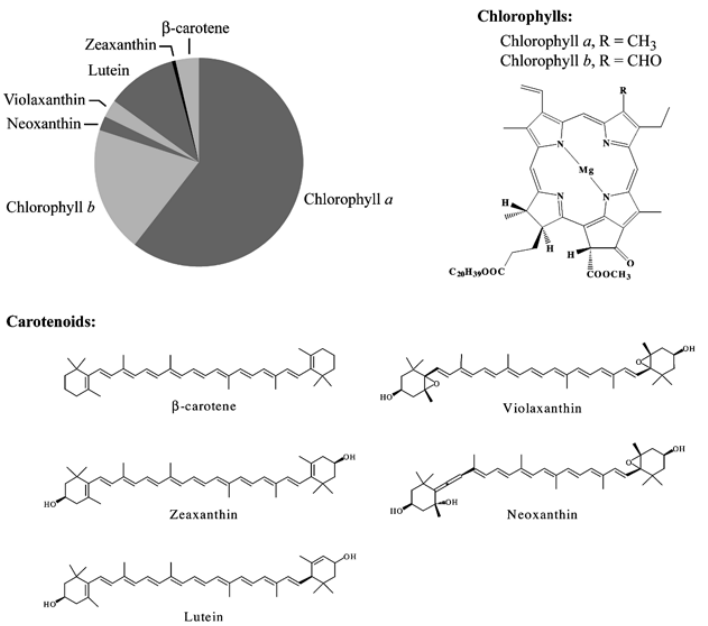

Fig. 1 Pigments of higher plant chloroplasts. Pie chart represents the typical pigment composition in weight of an higher plant chloroplast (*Arabidopsis*). Structures are shown for each pigment.

oxygen by quinones, and subsequently the oxidized quinones can accept electrons generated by the carotenoid desaturation reactions, possibly via a flavin adenine dinucleotide (FAD) redox intermediate that is proposed to bind to the desaturases (Al-Babili et al., 1996; Carol and Kuntz, 2001).

The ends of the lycopene molecule are cyclized to form β-carotene (β,β-carotene) or α-carotene (β,ε-carotene) by the β- and ε-cyclases (Chunaev et al., 1991; Bramley, 1993; F.X. Cunningham et al., 1994; Bishop, 1996; Pogson et al., 1996). Lesions in the β-cyclase are lethal and result in accumulation of the monocyclic ε,ψ-carotene in *Arabidopsis* (B.J. Pogson and D. DellaPenna, unpublished), indicating a requirement of bicyclic carotenoids for plant viability. The *lut2* mutation in the ε-cyclase blocks synthesis of β,ε-carotenoids, but result in a concomitant increase in xanthophylls derived from β-carotene, specifically violaxanthin and antheraxanthin, in place of lutein (Pogson et al., 1996).

The hydroxylation of α- and β-carotene are the first steps in the formation of the more polar xanthophylls (Milborrow et al., 1982; Pogson et al., 1996; Z.R. Sun et al., 1996; Bouvier et al., 1998; Tian and DellaPenna, 2001). α-Carotene rings are hydroxylated to form the most abundant carotenoid, lutein, by the recently identified ε-hydroxylase (*lut1*) (Pogson et al., 1996; Tian et al., 2004) and the β-hydroxylase. β-carotene is hydroxylated by the β-hydroxylase to form zeaxanthin, which usually only accumulates under high light-induced stress (Fig. 2). Zeaxanthin epoxidase catalyzes the expoxidation of zeaxanthin to form the intermediate antheraxanthin, with a subsequent epoxidation yielding violaxanthin (Fig. 2; Yamamoto, 1979). The identity of neoxanthin synthase is still a matter of conjecture with paralogues of the β-cyclase enzyme having limited neoxanthin synthase (NXS) capacity (Al-Babili et al., 2000; Bouvier et al., 2000), but there is no homologous gene in *Arabidopsis*, indicating an unrelated gene with NXS activity is yet to be identified. Further modification of neoxanthin leads to the synthesis of absicic acid (ABA) (Seo and Koshiba, 2002).

B. Environmental Factors That Alter Carotenoid Accumulation

In order to avoid extensive photo-oxidative damage, the synthesis of carotenoids and Chls and their subsequent binding to pigment-binding proteins

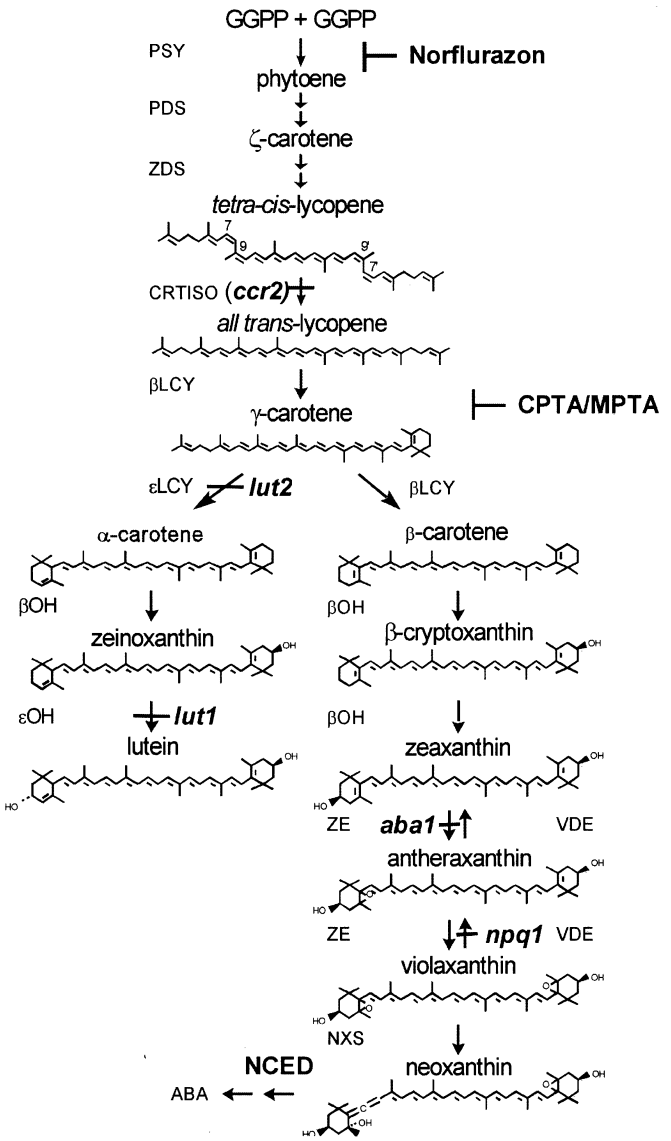

Fig. 2 Carotenoid biosynthetic pathway in higher plants. PSY, phytoene synthase; PDS, phytoene desaturase; ZDS, ζ-carotene desaturase; CRTISO, carotenoid isomerase; βLCY, β-cyclase; εLCY, ε-cyclase; βOH, β-hydroxylase; ZE, zeaxanthin epoxidase; VDE, violaxanthin de-epoxidase; NXS, neoxanthin synthase; NCED, 9-*cis*-epoxycarotenoid dioxygenase. *Arabidopsis* mutations are shown in italics and site of action of two classes of herbicides: norflurazon and CPTA (*N,N*-diethyl-*N*-[2-(4-chlorophenylthio)ethyl]amine) and MPTA (*N,N*-diethyl-*N*-[2-(4-methylphenoxy)ethyl]amine) are shown.

must be precisely balanced to meet the appropriate photosynthetic demands of the various growth conditions that plants are exposed to on a daily and seasonal basis (Herrin et al., 1992; Anderson et al., 1995). Phytoene synthase (PSY) expression, the first committed enzyme of carotenoid biosynthesis, is mediated by phytochrome and upregulated during photomorphogenesis (von Lintig et al., 1997; Welsch

et al., 2000), while PDS expression is unaffected in some species (von Lintig et al., 1997). Both red and far-red light treatments enhance accumulation of PSY mRNA, and this enhancement is abolished in the *phyA* phytochrome mutant of *Arabidopsis* (von Lintig et al., 1997; Welsch et al., 2000). However, the effect of light on PSY activity extends beyond transcriptional regulation. PSY is associated with the prolamellar body of etioplasts and is relatively inactive in dark grown seedlings (Welsch et al., 2000). White-light induction of photomorphogenesis results in induction of PSY activity and relocation of PSY to the newly developing thylakoid membranes (Welsch et al., 2000).

Light also plays a critical role in modulating xanthophyll biosynthesis and accumulation in mature leaves. Under normal light conditions, when the incident light can be safely utilized for photosynthetic electron transport, zeaxanthin epoxidase (ZE) converts zeaxanthin to violaxanthin (Fig. 2). However, under conditions of high light stress, when the incident light is in excess of the light utilized, then zeaxanthin biosynthesis is triggered. Violaxanthin de-epoxidase (VDE) becomes activated by an acidification of the thylakoid lumen, resulting in the de-epoxidation of violaxanthin to zeaxanthin (Pfündel and Bilger, 1994).

Light may also play an indirect role in regulating flux of lycopene through the carotenoid biosynthetic pathway. Mutations in the carotenoid isomerase (CrtISO) severly effect the accumulation of carotenoids in *Arabidopsis* etioplasts, with the wild-type violaxanthin and lutein being replaced by prolycopene, poly-*cis*-neurosperene (polyneurosperene) and ζ-carotene (Isaacson et al., 2002; Park et al., 2002). Most carotenoids accumulated to wild type levels in chloroplasts of CrtISO-deficient mutants, although lutein levels were substantially reduced, suggesting that light only partly compensated for the lack of CrtISO in vivo and that a deficiency of CrtISO or specific carotenoid isomers, influences partitioning of lycopene through the β,ε and β,β branches (Park et al., 2002). Interestingly, expression of the bacterial phytoene desaturase (crtI) in tobacco plants, which bypasses the isomerization steps that occur during phytoene desaturation in plants, also resulted in a reduction in lutein levels (Misawa et al., 1994). Combined, the two results indicate a level of regulation of β- and α-carotene synthesis that is dependent on light and CrtISO. Whether this reflects an isomer substrate preference by the enzymes or regulation of the enzymes remains an interesting question to be answered.

C. Carotenoids and Photosystem II

As discussed elsewhere in this volume, three-dimensional structures have been solved for the trimeric PS I and dimeric PS II reaction centers of *Thermosynechococcus elongatus* and *T. vulcanus* (Rhee et al., 1998; Jordan et al., 2001; Zouni et al., 2001; Kamiya and Shen 2003; Ferreira et al., 2004; Chapters 18–21). This, together with cryoelectron microscopy of single-particle PS II supercomplexes isolated from spinach chloroplasts, have provided a three-dimensional map of PS II resolving the reaction center core proteins, D1 and D2, associated with the cytochrome b_{559} (Cyt b_{559}), the inner antennae, Chl binding protein, CP43 and CP47, and the outer lying major and minor light harvesting complexes (LHCs) (Nield et al., 2000). The core complex of PS II binds β-carotene and Chl *a*, and possibly small amounts of lutein (Bassi et al., 1993; Satoh, 1993; Seibert, 1993; Alfonso et al., 1994; Chapters 20, Shen and Kamiya and 21, Barber and Iwata).

In the absence of cyclic carotenoids there is lethal photobleaching in plants and this was thought to reflect the critical role of β-carotene in the reaction center. This thesis was based on β-carotene's fundamental photoprotective role in triplet quenching in bacteria (Griffiths et al., 1955; Frank and Cogdell, 1993). The electron exchange mechanism of triplet quenching requires the carotenoid to be in van der Waals contact (approximately 4 Å) to enable efficient quenching of Chl triplets (Krinsky, 1971). In plants the oxidative potential of the Chl primary electron donor, P680, is such that it would oxidize any carotenoids in such close proximity and it is therefore unlikely that β-carotene contributes to Chl triplet quenching in the PS II reaction center (Telfer, 2002). However, the ubiquitous nature of β-carotene in the reaction centers of oxygenic photosynthetic organisms, suggests that it fulfils a fundamental role. Despite its inability to effectively quench Chl in the PS II core, β-carotene may afford photoprotection by several other mechanisms. In fact, instead of triplet quenching, a cationic β-carotene may donate an electron to the oxidized $P680^{+}$, and thereby provide a limited form of photoprotection perhaps via electron transport involving a redox active Chl (Chl Z) and Cyt b_{559} (Hanley et al., 1999; Vrettos et al., 1999; Chapter 15, Faller et al.). Other photoprotective roles

of β-carotene include singlet oxygen quenching and signalling of D1 degradation, which triggers repair of photoinhibited PS II complexes (Anderson and Chow, 2002; Telfer, 2002).

Carotenes are essential for quenching of Chl triplet states in purple bacterial reactions centers and their loss results in cell death (Griffiths et al., 1955; Frank and Cogdell, 1993). As β-carotene is not involved in quenching of singlet or triplet excited state Chls in the PS II reaction of oxygenic photosynthetic organisms (Telfer, 2002), these fundamental roles must be undertaken by the xanthophylls and/or β-carotene bound to CP43 and CP47 or the xanthophylls located in the antenna. The xanthophylls located in the LHCs and the inner antenna proteins, CP43 and CP47, act as light-harvesting pigments, absorbing in a region of the visible spectrum where Chl does not absorb and then transferring the energy to Chl. As yet, no-one has had access to an oxygenic photosynthetic organism lacking all xanthophylls and accumulating only β-carotene, so it has not been possible to define the respective functions of β-carotene and the xanthophylls within the PS II/LHCII supercomplex.

D. Carotenoids and Assembly of Light Harvesting Complexes

The light harvesting antenna that encircles the reaction center is composed of major and minor LHC apoproteins (Fig. 3) that are encoded by a large family of homologous genes (Bassi et al., 1993; Jansson, 1994, 1999; Green and Durnford, 1996). The minor LHCs (Lhcb4, 5, 6) comprise the inner antenna of PS II, which is encircled by trimeric LHCIIb complexes that comprise the outer antenna (Chapter 2). The LHCIIb trimers ($LHCII^3$) are comprised of 3 related proteins (Lhcb1, 2, or 3) aggregated in various combinations, which can be resolved by non-denaturing (native) gel electrophoresis (Jansson, 1994).

Carotenoids and Chls are both essential for folding and stability of LHC apoproteins and thus pigment biosynthesis is tightly co-ordinated with LHC synthesis (Plumley and Schmidt, 1995). Several studies have suggested that the chloroplast envelope is the

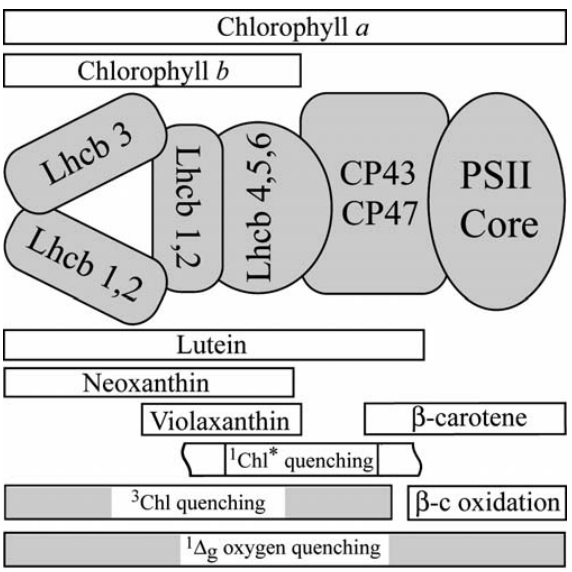

Fig. 3 Model showing pigment localization in PS II. The major LHC antennae (LHCIIb or Lhcb1-3) and the minor LHC antennae (Lhcb4-6) and PS II core antenna (CP43 and CP47) are shown. Bars indicate the distribution of each of the chlorophylls and carotenoids. Carotenoid binding to the L1, L2 and N1 sites of LHCIIb is described in Fig. 4. In the minor antennae, the L1 and L2 sites bind carotenoids (Lhcb4-6). L1 is occupied by lutein, whereas L2 is occupied by either violaxanthin, neoxanthin or zeaxanthin (Bassi et al., 1999; Croce et al., 1999). The V1 site may also peripherally bind violaxanthin or zeaxanthin (Bassi et al., 1999). Sites of the various types of photoprotection are shown by labelled bars. However, the location of some, such as $^1Chl^*$ quenching, are still being defined, indicated by jagged end of bar. Adapted from Gilmore and Govindjee (1999) and Bassi and Caffarri (2000).

site of LHC assembly (Hoober and Eggink, 1999) and free carotenoids in the chloroplast envelope have been suggested to facilitate folding of LHC apoproteins by modifying properties of the lipid bilayer (Paulsen, 1999).

The carotenoid binding sites have been elucidated by an elegant and thorough combination of structural studies, in vitro reconstitution of recombinant proteins and analyses of pigment binding to native LHCs (Bassi and Caffarri, 2000; Gastaldelli et al., 2003; Morosinotto et al., 2003; Havaux et al., 2004). The structure for LHCIIb, the major LHC of PS II, was resolved to 2.7–3 Å and it revealed 7 Chl *a* molecules, 5 Chl *b* molecules and 2 xanthophylls embedded in three transmembrane spanning helices (Kühlbrandt et al., 1994; Liu et al., 2004; Chapter 2). In vitro reconstitution studies have identified up to four distinct carotenoid binding sites in LHCs (L1, L2, N1, V1), although only three of these binding sites are occupied in plants grown at moderate light intensities (Fig. 4) (Bassi and Caffarri, 2000). The L1 and L2 sites bind lutein, although either violaxanthin or zeaxanthin can be accommodated, whereas the N1 site is specific for neoxanthin (Fig. 4). The V1 site is proposed to loosely bind violaxanthin under conditions of high light stress, aiding in accessibility for de-epoxidation to zeaxanthin, which subsequently fills the V1 site (Verhoeven et al., 1999; Bassi and Caffarri, 2000). Furthermore, pigments bound to the V1 site do not contribute to light harvesting and are presumably involved only in xanthophyll cycle activity, which is induced by high light stress (Yamamoto, 1979; Caffarri et al., 2001).

The minor LHC antennae proteins, Lhcb 4, 5, and 6 (also known as CP29, CP26 and CP24, respectively), typically bind 8 Chl *a* molecules, 2 Chl *b* molecules, and 2 xanthophyll molecules (Bassi and Caffarri, 2000; Chapter 2). In Lhcb4, the L1 site is occupied by lutein and the L2 site is occupied by either violaxanthin or neoxanthin (Bassi et al., 1999; Ruban et al., 1999). β-Carotene is typically excluded from LHCs, although β-carotene is found in Lhca1, the major LHC of PS I (Schmidt et al., 1997).

E. Plasticity of Xanthophyll Binding to Light Harvesting Complexes

Numerous in vitro reconstitution studies have shown that xanthophylls are required for folding and stability in a range of LHCs including: Lhcb1/2, Lhcb4 and

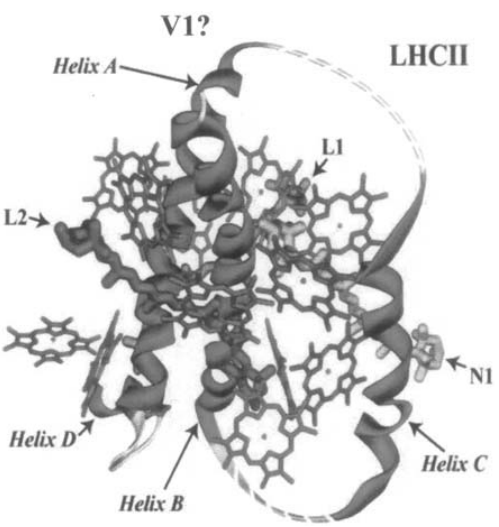

Fig. 4 Carotenoids and LHCIIb assembly. Specificity of each binding site is indicated (L, lutein; V, violaxanthin; N, neoxanthin; Z, zeaxanthin). An LHCIIb monomer binds approximately 7 Chl *a* molecules and 5 Chl *b* molecules (Kühlbrandt, et al., 1994; Bassi and Caffarri 2000). In an LHCIIb monomer, the L1 site is occupied by lutein, while the L2 site is typically occupied by either lutein or violaxanthin. The N1 site is specific for binding neoxanthin. Violaxanthin is proposed to bind loosely to the V1 site and is inter-exchangeable with zeaxanthin during the xanthophyll cycle (Caffarri et al., 2001). Adapted from Croce et al. (1999) and Bassi and Caffarri (2000). See Color Plate 13, Fig. 2.

Lhcb5 (Plumley and Schmidt, 1987; Giuffra et al., 1996; Ros et al., 1998). Maximal in vitro assembly of Lhcb1/2 and Lhcb4 requires Chl *a*, Chl *b* and at least 2 xanthophylls (Plumley and Schmidt, 1987; Giuffra et al., 1996). However, assembly can occur with just one xanthophyll and a range of 'non-native' xanthophylls, such as astaxanthin, capsanthin and fucoxanthin also support LHCII assembly with various degrees of efficiency (Kumagai et al., 1998; Phillip et al., 2002). A common structural feature of carotenoids that can support LHC assemly in vitro is the presence of a hydroxyl group at carbon 3 of a β-cyclohexane end group (Phillip et al., 2002).

A range of xanthophyll biosynthetic mutants have been identified and those that disrupt the synthesis of cyclic carotenoids and xanthophylls in *Arabidopsis*, *Scenedesmus* and *Chlamydomonas* are shown in Table 1 (Koornneef et al., 1982; Bishop et al., 1995; Marin et al., 1996; Pogson et al., 1996a; Niyogi et al., 1997a, 1998; Li et al., 2000). Investigations of LHC accumulation in carotenoid deficient mutants have both corroberated the in vitro reconstitution story and also demonstrated that a large degree of functional complementation occurs in vivo when carotenoid content and composition are altered.

In the green algae *Scenedesmus*, the absence of lutein results in reduced accumulation of LHCs and as a consequence, an increase in the Chl *a/b* ratio (Heinze et al., 1997). A similar, but less pronounced trend is observed in the *Chlamydomonas* orthologue, *lor1*, supporting a view that lutein has been evolutionarily conserved in all green plants due to a fundamental role in LHC assembly (Chunaev et al., 1991). Chlorophyll content and levels of LHC apoproteins are relatively unaltered in lutein deficient mutant, *lut2*, of *Arabidopsis* and there is little effect on growth and development compared to wild type plants (Pogson et al., 1998; Lokstein et al., 2002). This is despite a clear in vitro preference for lutein in reconstitution studies and its implied identification in the crystal structure of the LHC (Plumley and Schmidt, 1987; Kühlbrandt et al., 1994). This does not show that lutein is dispensable, rather that it is replaceable by xanthophylls with similar chemical composition and structure.

The fact that a complete loss of lutein still enables LHC assembly reveals a remarkable degree of functional plasticity for xanthophyll binding to LHCs in vivo. Violaxanthin is presumed to replace lutein in the LHCs of *lut1* and *lut2*, and may be accommodated because the angles of epoxidated rings of violaxanthin and the epsilon ring of lutein both bend away from plane of the carotene backbone to a similar degree (Pogson et al., 1998; Bassi and Caffarri, 2000; Lokstein et al., 2002).

There are limits to the flexibility of substitutions. Lactucaxanthin, a xanthophyll with two hydroxylated ε-ring endgroups, cannot support LHC assembly in vitro (Phillip et al., 2002). The *Arabidopsis lut2aba1* and *Chlamydomonas lor1npq1* mutants accumulating only zeaxanthin and β-carotene are viable (Polle et al., 2001), but *lut2aba1* plants exhibit delayed greening with about 1/3 of the seedlings dying in soil (Pogson et al., 1998). Of the seedlings that are viable, the mature leaves have photosynthetic rates and Chl *a/b* ratios approaching wild-type levels; presumably, zeaxanthin ultimately supports LHC formation as observed in *lor1npq1* (Pogson et al., 1998). The relative proportions

Table 1. Mutations affecting either carotenoid biosynthesis or nonphotochemical quenching (NPQ) of chlorophyll fluorescence for several different plant species

Mutation	Species	Protein	Reference
aba1	*Arabidopsis thaliana*	zeaxanthin epoxidase	Koornneef et al., 1982
npq2	*A. thaliana*	zeaxanthin epoxidase	Niyogi et al., 1998
aba2	*Nicotiana plumbaginifolia*	zeaxanthin epoxidase	Marin et al., 1996
npq1	*A. thaliana*	violaxanthin de-epoxidase	Niyogi et al., 1998
npq1	*Chlamydomonas reinhardtii*	violaxanthin de-epoxidase	Niyogi et al., 1997
lut1	*A. thaliana*	ε-hydroxylase	Pogson et al., 1996
lut2	*A. thaliana*	ε-cyclase	Pogson et al., 1996
lor1	*C. reinhardtii*	ε-cyclase**	Niyogi et al., 1997
C-2A´-34	*Scenedesmus obliquus*	ε-cyclase**	Bishop et al., 1995
npq4	*A. thaliana*	PsbS (CP22)	Li et al., 2000

**Indicates the enzyme most likely to be disrupted based on phenotype; however, its identification has not been confirmed by molecular genetics.

of different LHC apoproteins was altered in *lut2npq2,* which is equivalent to *lut2aba1* (Havaux et al., 2004). LHCII, CP26 accumulated to lower levels, in contrast CP29, CP24, LHCI proteins, and the PS I and PS II core complexes did not undergo major changes, while PS II-LHCII supercomplexes were not detectable (Havaux et al., 2004).

LHC accumulation was also relatively unaltered despite a 60% reduction in violaxanthin levels in transgenic plants with reduced expression of the β-carotene hydroxylase, anti-βOHase (Rissler and Pogson, 2001). However, levels of the major LHC apoproteins are significantly reduced in *lut2* anti-βOHase plants that lack lutein and have an overall reduction in the xanthophylls of nearly 50% (Rissler and Pogson, 2001). Xanthophylls that can occupy the L1, L2, or N1 binding sites (Fig. 4) are most significantly reduced in *lut2* anti-βOHase plants. It seems that the reduction in xanthophylls in the *lut2* anti-βOHase exceeded the critical number of pigment molecules required for complete LHC assembly.

F. How Do Xanthophylls Influence the Organization of the Antennae?

Although functional plasticity is observed for xanthophyll binding to LHC monomers, oligomerization of LHCs is strictly dependent upon lutein. Lutein deficient mutants of *Arabidopsis* and *Scenedesmus obliquus* lack LHCIIb trimers (Lokstein et al., 2002; Bishop, 1996; Rissler and Pogson, 2001). Conversely, the elevated ratio of lutein to violaxanthin in the anti-βOHase lines appears to favor formation of LHCIIb trimer over LHCIIb monomers (Rissler and Pogson, 2001). A similar phenomenon was observed in pigment biosynthetic mutants of pea, where high ratios of lutein to violaxanthin favoured a high ratio of LHCIIb trimers to monomers (Dobrikova et al., 2000). The mechanism by which lutein induces LHC trimerization is unclear. It has been proposed that replacement of lutein by violaxanthin in LHCs of *lut1* and *lut2* may deform the structure of LHC monomers and consequently inhibit trimerization (Lokstein et al., 2002). Alternatively, the position of lutein's polar hydroxyl groups within the LHC protein scaffold may act as a 'molecular glue' that promotes trimerization via hydrogen bonding to xanthophylls or amino acid residues of adjacent LHC monomers. Free lutein may also facilitate trimerization of LHCs by directly interacting with the lipid binding motif found in the amino-terminus of Lhcb1 (Nussberger et al., 1993; Hobe et al., 1994). The amino-terminus of Lhcb1 is important for trimerization (Nussberger et al., 1993; Hobe et al., 1994) and lutein may potentially bind the amino-terminus of Lhcb1 to facilitate or moderate the lipid dependent trimerization of LHCIIb.

III. Carotenoids and Photoprotection

Under full sunlight and other environmental stresses, light-harvesting and photoprotective mechanisms must be balanced to ensure optimal photoassimilate production to sustain plant growth while preventing lethal free radical damage to the plant. The energy and electron transfer reactions of photosynthesis occur in the light harvesting antennae and reaction centers, respectively. Factors that disrupt the balance between these reactions lead to the production of reactive oxygen species including singlet oxygen, superoxide anion radicals, hydroxyl radicals, and hydrogen peroxide (Noctor and Foyer, 1998; Niyogi, 1999) that cause photo-oxidative damage to the photosystems and the plant (Chow, 1994; Adir et al., 2003).

Therefore, effective acclimatory mechanisms at whole plant, cellular and molecular levels are essential to accommodate short and long-term exposure to potentially photodamaging full sunlight and environmental stresses that lead to plant death or greatly reduced crop yields due to free radical damage (Osmond et al., 1999). Consequently, there are complementary mechanisms that include: (i) the harmless dissipation of excess energy via nonphotochemical quenching (NPQ) that is mediated by certain xanthophylls; (ii) quenching of triplet Chls by carotenoids; (iii) antioxidants (ascorbate, tocopherols and carotenoids) and antioxidant enzymes, such as ascorbate peroxidase (APX) that de-toxify free radicals; (iv) a reduction in the amount of light harvested via regulation of the light-harvesting antenna size; and (v) repair of photoinhibition (Anderson et al., 1995; Niyogi, 1999; Chapter 27, Chow and Aro). This section will focus on the various mechanisms employed by carotenes and xanthophylls to prevent accumulation of reactive oxygen intermediates (Fig. 5). The white phenotype of mutants lacking cyclic carotenoids provides visual evidence for the importance of carotenoids in maintaining plant viability. In the absence of carotenoids, plastids photo-bleach due to the generation of reactive oxygen species that attack lipids and proteins (Knox and Dodge, 1995). Other mechanisms of photoprotection, involving antioxidants such as

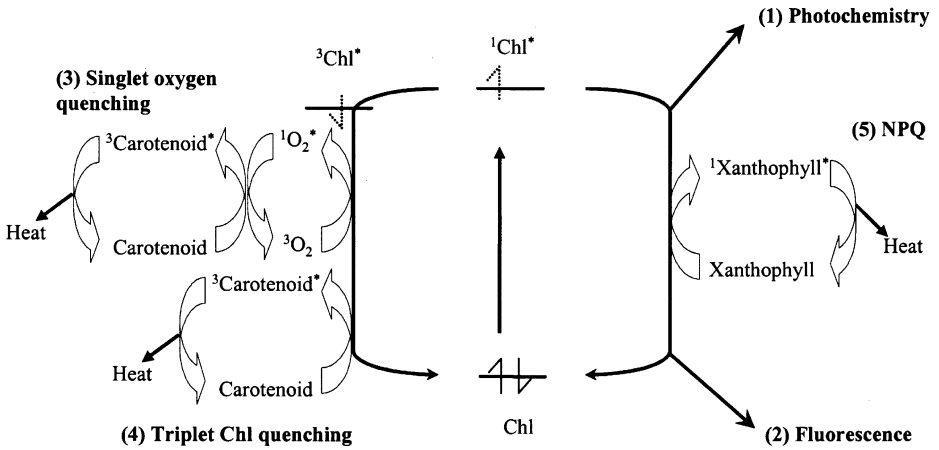

Fig. 5 Photoprotective roles of carotenoids. In addition to their role as light harvesters, carotenes and xanthophylls are essential for several photoprotective processes. When ground state Chl becomes excited (^{1}Chl*) photochemistry can occur in the reaction center (Reaction 1). If the number of photons is in excess of what can be utilized for the photochemical reactions of photosynthesis, ^{1}Chl* in the antennae and reaction center can fluoresce at a rate constant of 6×10^7 sec^{-1} resulting in a typical lifetime of about 15–20 ps (Reaction 2). A competing decay pathway of fluorescence is the formation of triplet state Chl (^{3}Chl*), which has a rate constant of 2×10^8 sec^{-1} resulting in a typical lifetime of about 5 ps ^{3}Chl* reacts with ground state oxygen ($^3O_2$) to form the phototoxic singlet oxygen species, $^1O_2^*$. Carotenoids can directly scavenge $^1O_2$* (Reaction 3). Alternatively, carotenoids can prevent the synthesis of $^1O_2^*$ by directly quenching ^{3}Chl* (Reaction 4) or certain xanthophylls can prevent formation of ^{3}Chl* by facilitating the quenching of chlorophyll fluorescence by nonphotochemical quenching (NPQ) (Reaction 5).

tocopherol and ascorbate and detoxifying enzymes such as APX and superoxide dismutase (SOD) are reviewed comprehensively elsewhere (Noctor and Foyer, 1998; Foyer, 2001).

Figure 5 illustrates the mechanisms by which carotenoids quench triplet and singlet state molecules, dissipating the excess energy as heat. Absorbed light energy results in the excitation of Chl from the ground state to its first and second excited singlet states, Q_y and Q_x, respectively and Soret transition. Herein the excited singlet state will be referred to as ^{1}Chl*. Under optimal conditions this energy is transferred to the PS II reaction center and initiates the photochemical reactions to catalyse the oxidation of water (Chapter 7). Because environmental conditions, such as full sunlight, low temperatures and drought often cause plants to absorb considerably more light than can be safely processed through the photochemistry in the reaction center, the excess light may persist in the excited electronic states of Chl molecules (Govindjee, 1995). Photosynthetic electron transfer results in photochemical quenching (qP) of Chl fluorescence. However, when the photosynthetic electron transfer reactions are saturated, the excited singlet state of Chl molecules will either deactivate radiatively emitting fluorescence or nonradiatively and return to ground state or undergo intersystem crossing to form excited triplet state Chl (^{3}Chl*). Typical rate constants for the two processes, given in Fig. 5, demonstrate that triplet Chl formation competes with singlet state decay. Left unchecked, triplet state formation may sensitize singlet oxygen formation, potentially resulting in oxidative damage to the cell.

A. Nonphotochemical Quenching and Thermal Dissipation

The first and critical strategy employed by all plants is to dissipate excess absorbed energy thereby preventing the formation of free radicals and oxidizing species. NPQ functions by non-radiative quenching of singlet Chl, which may limit the formation of Chl triplets, and prevent reactive oxygen species from being generated (Demmig-Adams and Adams III, 1992). Three mechanisms contribute to NPQ, including the ΔpH-dependent energy dissipation (qE); state transitions (qT); and quenching resulting from photoinhibition (qI) (Muller et al., 2001). qE is the only component of NPQ that is induced and reversed within tens of seconds in response to

changes in light intensity that alter lumenal pH. Under most environmental conditions, qE is the major component of NPQ, quenching up to 80% of $^1Chl^*$ (Demmig-Adams et al., 1996; Li et al., 2000), such that some authors use the terms interchangeably. The contribution of qI and qE to NPQ to the reduction in Chl fluorescence can be determined by measuring changes in Chl fluorescence in response to and during recovery from saturating pulses of light (Krause and Weis, 1991; Maxwell and Johnson, 2000).

As just mentioned, the primary mechanism for dissipation of excited singlet state Chls is NPQ. The xanthophylls contribute to NPQ in addition to their structural roles in photosystem assembly (Frank and Cogdell, 1993; Frank et al., 1994, 1995; Gruszecki et al., 1999). However, as opposed to the plasticity in LHC assembly, there are distinct roles for xanthophylls in NPQ, evidenced in the high light-induced accumulation of zeaxanthin and antheraxanthin via the xanthophyll cycle (Yamamoto, 1962). The effectiveness of NPQ depends on three main factors that result from exposure to high photon flux densities, namely, an acidification of the thylakoid lumen, which activates the violaxanthin deepoxidase enzyme of the xanthophyll cycle and also leads to the protonation of two glutamate residues of Lhcb1/2 (Walters et al., 1996; Gilmore et al., 1998; D.M. Kramer et al., 1999) and PsbS (Li et al., 2002a).

In PS II the lifetime of Chl *a* fluorescence increases from 0.3 ns (Genty et al., 1992) to 1.9 ns when PS II is reduced. The induction of NPQ results in a decreased in the number of Chl *a* molecules with a 1.9 ns lifetime and an increase in the short-lived, 0.3–0.4 ns lifetime (Gilmore et al., 1995). A series of elegant studies using isolated thylakoids, *npq* mutants, dithiothreitol as a reductant and nigericin as an uncoupler have correlated the shift in the lifetimes with zeaxanthin accumulation, thylakoid lumen acidification and binding of zeaxanthin to the site of NPQ, quite possibly PsbS, described by the binding constant k_b (Gilmore and Govindjee, 1999). A three state model was proposed to account for the contribution of ΔpH and xanthophylls to changes in Chl fluorescence lifetimes in isolated thylakoid membranes (Gilmore and Govindjee, 1999). The first state, W, reflects the reduction of the quinone pool (PS II traps closed) and the immediate thylakoid acidification; in this state the lifetime of Chl fluorescence ranges from ~1.7–2.2 ns. The second state, X, results in a minor decrease to ~1.6–1.8 ns. This is thought to reflect acidification of the thylakoid lumen and associated proton-induced conformational changes in antenna proteins and PsbS. This conformational change and decreased lifetime induces an absorbance change at 535 nm and requires PsbS (Li et al., 2000; Li et al., 2002b). The final state in the model, Y, is the binding of a 'quenching' xanthophyll, typically zeaxanthin, to site(s) within PS II to reduce the fluorescence lifetime to ~0.3–0.5 ns. Zeaxanthin does exchange with violaxanthin in the L2 site of the inner antenna proteins, Lhcb4 and Lhcb5 (Morosinotto et al., 2002) and may be able to interact with PsbS (Aspinall-O'Dea et al., 2002).

1. Photoprotection in Plants with Altered Carotenoid Composition

In addition to the insightful and detailed photophysical, physiological and mechanistic studies of NPQ by many researchers, significant advances regarding the mechanisms of NPQ have come from the analysis of carotenoid and NPQ mutants of *Chlamydomonas* and *Arabidopsis* (Table 2).

The *npq1* mutations of *Arabidopsis* and *Chlamydomonas* are mutations in the violaxanthin de-epoxidase (VDE) that prevent the high light-induced accumulation of antheraxanthin and zeaxanthin. The reduction in NPQ in these and antisense VDE lines confirmed decades of in vitro and physiological studies (Niyogi et al., 1997a, 1998; W.H. Sun et al., 2001; Verhoeven et al., 2001). Historically, two pools of violaxanthin have been observed, one available for de-epoxidation, and a second unavailable. The accessible pool has been estimated at about 67% of the total pool in intact leaves and 75% in isolated thylakoids (Siefermann and Yamamoto, 1975; Pfündel and Dilley, 1993). However, higher conversion rates of up to 90% were observed when the antenna size was reduced by intermittent light, high light or a disruption to Chl biosynthesis (Demmig et al., 1987; Thayer and Björkman, 1990; Falbel et al., 1994; Farber and Jahns, 1998). Antisense β-hydroxylase lines have a marked reduction in the violaxanthin pool while the antenna size and Chl content were maintained. Under high light similar amounts of violaxanthin remained in both wild type and antisense lines demonstrating the 'two pool' theory. Quite probably, these inaccessible primary sites promote LHC stability (Ros et al., 1998) and are preferentially filled if violaxanthin is limiting. The loosely bound molecules may be associated with the LHCs' secondary sites that bind xanthophylls, which are not required for assembly and stability in

Table 2. Summary of xanthophyll and nonphotochemical quenching (NPQ) levels in carotenoid biosynthetic mutants and transgenics*

	Mutant	Lutein (% WT)	V+A+Z (% WT)	NPQ at 30 Sec (% WT)	Max NPQ (% WT)	'qE' (% WT)
Chlamydomonas reinhardtii	*npq1*	100	102	100	80	60
	lor1	0	306	88	63	50
	npq1lor1	0	304	38	28	15
Arabidopsis thaliana	*npq1*	100	116	53	30	14
	lut2	0	262	24	67	62
	npq1lut2	0	350	13	24	6
	WT anti β-OHase	95	35	69	84	N.D.
	lut2 anti β-OHase	0	169	14	50	N.D.
	O/E ε-cyclase	130	69	130	104	N.D.
	npq4	N.D.	89	26	10	N.D.

*The measure for NPQ incorporates both the rapidly reversible ΔpH-dependent quenching (qE) and slowly reversible (qI) components. qE is estimated as maximum NPQ minus NPQ after 30 seconds of dark relaxation ('qE'). This illustrates that the rapidly reversible component is nearly eliminated in the double mutants, *npq1lut2* and *npq1lor1*. Data was derived from Niyogi et al. (1997a,b, 2001), Pogson et al. (1998), Li et al. (2000) and Rissler and Pogson (2001). Some values were not determined (N.D.).

vitro (Bassi et al., 1999; Croce et al., 1999). In fact, a fourth carotenoid binding site has been proposed in the LHC structure, V1, which may bind violaxanthin that could be rapidly converted to zeaxanthin (Verhoeven et al., 1999; Caffarri et al., 2001). However, the majority of the zeaxanthin accumulates in the L2 site of Lhcb4 and Lhcb5 (Morosinotto et al., 2002).

As stated above, *npq1* mutants still had some reversible NPQ or qE. In fact, whenever zeaxanthin has been eliminated either by dithiothreitol treatment or by mutation then reversible quenching is reduced, but never eliminated (Gilmore and Yamamoto, 1991; Niyogi et al., 1997b, 1998). This residual component is about 60% in *Chlamydomonas* and 14% in *Arabidopsis* (Table 2). The widely held view that zeaxanthin and antheraxanthin are the only carotenoids involved in NPQ has been challenged by the demonstration that lutein deficient plants and alga exhibit delayed induction of NPQ (Niyogi et al., 1997b; Pogson et al., 1998). Furthermore, the residual NPQ in zeaxanthin-deficient lines can be essentially eliminated by eliminating lutein (Table 2) (Niyogi et al., 1997b, 2001). The delayed induction of NPQ in *lut2* can be restored by constitutively accumulating zeaxanthin (Pogson et al., 1998). Furthermore, an increase in lutein with a corresponding decrease in the xanthophyll cycle pool in transgenic plants resulted in faster induction of NPQ during the first 30 s (Pogson and Rissler, 2000). In fact, no matter what the genetic background, when lutein levels have been either decreased or increased there has been an effect on NPQ consistent with lutein contributing to NPQ, particularly the early phase of induction.

However, these results are in contrast to observations in reconstituted LHC apoproteins, which showed that LHCs assembled with zeaxanthin as the only xanthophyll exhibit fluorescence quenching, while LHCs reconstituted with only lutein do not quench Chl fluorescence as efficiently as complexes reconstituted with zeaxanthin (Polivka et al., 2002). This contrast is not too surprising given the predominant role of lutein as a light-harvester and stabiliser of the folded LHC. Also, in vitro systems do not completely portray the entire in vivo apoprotein-pigment environment of thylakoid membranes, where LHC apoproteins form oligomeric complexes, interact with PsbS and the reaction center, are subject to pH, zeaxanthin, and possibly lutein-dependent conformational changes.

The role of lutein in NPQ may be to either directly quench Chl fluorescence, or simply to alter the conformation of the LHC antenna to 'facilitate' fluorescence quenching by zeaxanthin. Support for the latter has been noted by a correlation between

the decrease in NPQ and the reduced antenna size of the *lut* mutants (Lokstein et al., 2002). These authors suggest that loss of NPQ in lutein deficient mutants is due to the absence of LHCII trimers and the consequent alteration to the micro-organization of the antenna complex and demonstrated that NPQ could be restored in lutein deficient mutants following an initial light induction (Lokstein et al., 2002). These results suggest that a lutein dependent re-organization of the antenna structure may indeed be required for induction of NPQ. Whether lutein can replace zeaxanthin as a Chl fluorescence quencher or maximizing the macro-organization of the antennae to allow fewer zeaxanthin molecules to act as a 'fluorescence sink' remains unclear. Interestingly, *lut2* mutants have a much lower K_b value, meaning that for a given concentration of zeaxanthin molecules, fewer zeaxanthin molecules actually bind to the LHCs in *lut2* compared to wild type (Gilmore, 2001). Therefore the role of lutein in NPQ may be in the activation of zeaxanthin binding sites, possibly by mediating conformational changes within the antennae that promote formation of a PsbS 'quenching locus.' NPQ kinetics, Chl fluorescence lifetimes, and the integrity of the ΔA_{535} spectral feature should be further examined in ε-cyclase transgenic lines to determine whether lutein concentration directly correlates with induction rates for NPQ or K_b values and whether lutein is required for formation of a competent PsbS 'quenching locus.'

2. Nonphotochemical Quenching and PsbS

A key discovery demonstrating the necessity for the PsbS in NPQ has been published by Niyogi and coworkers (see Holt et al., 2004). The *npq4* mutation, which is a mutation in PsbS, has almost no NPQ and lacks a characteristic light-induced change in absorbance at 535nm (ΔA_{535}), which is associated with qE: yet *npq4* still accumulates antheraxanthin and zeaxanthin (Niyogi et al., 1998; Li et al., 2000). The fact that NPQ is abolished in mutants that lack PsbS, but have a wild-type complement of xanthophylls, suggests that an optimal protein environment is essential. Further insights have come from studies on the dosage effect of PsbS levels on NPQ (Li et al., 2002a), the functional domains of PsbS (Li et al., 2002a), characterization of the pigment binding properties of PsbS (Aspinall-O'Dea et al., 2002) and its localization with the PS II supercomplex (Dominici et al., 2002; Thidholm et al., 2002).

The level of NPQ correlates with PsbS titre (Li et al., 2002a). In plants that are heterozygous for the *npq4* mutation, a semi-dominant effect is observed as maximal levels of NPQ are reduced by approximately 40% (Li et al., 2000; 2002b) and qE can be increased by nearly two-fold by overexpression of PsbS (Li et al., 2002b). Clearly, changes in levels of the PsbS are proportional to the capacity for qE and this phenomenon may have consequences for modulation of NPQ levels in response to variations in environmental conditions during plant development and growth. However, while stress induces PsbS accumulation in some species, it does not in others (Savitch et al., 2002).

While PsbS is capable of binding PsbS in vitro (Aspinall-O'Dea et al., 2002), whether this occurs in vivo is debatable. PsbS has been isolated from spinach thylakoids with both Chls and carotenoids bound (Funk et al., 1995), although a similar study did not detect any pigments associated with PsbS (Dominici et al., 2002). In fact, PsbS is the only member of the light harvesting complex family that can form a stable tertiary structure in the absence of pigments (Funk, 1995; Aspinall-O'Dea et al., 2002; Dominici et al., 2002). Thus, the relationship between zeaxanthin and PsbS in mediating NPQ was unclear. Comparisons of carotenoid resonance Raman spectra in isolated thylakoids of wild type and *npq4* mutants led to the identification of a large red shift in the absorbance spectra of approximately 2 molecules of zeaxanthin in wild type that is absent in PsbS (Ruban et al., 2002). Therefore, the hypothesized binding of zeaxanthin to PsbS may activate a 'quenching-locus' that is characterized by the ΔA_{535} spectral feature (Aspinall-O'Dea et al., 2002). pH dependent protonation of PsbS is necessary for qE (Holt et al., 2004). Site directed mutagenesis of PsbS has shown that two conserved glutamic acid residues are also essential for the function of PsbS in qE (Li et al., 2002b). Finally, the monomer to dimer ratio of PsbS increases as the light intensity increases (Bergantino et al., 2003).

Where are qE and PsbS located? Several studies have suggested that qE is associated with the peripheral antenna (Horton et al., 1996) or inner antenna (Briantais et al., 1996; Gilmore et al., 1996a). An elegant recent study demonstrated that individual inner antenna proteins can be removed with minimal effect on NPQ (Andersson et al., 2001); however, other inner antenna proteins remain. Also barley Chl *b*-less mutants lacking the outer antenna LHCs can

still quench Chl fluorescence (Gilmore et al., 1996b). Conversely, qE is severely impaired in the *npq5* mutant of *Chlamydomonas*, which lacks a polypeptide of the major light harvesting complex, Lhcbm1 (Elrad et al., 2002). Given that differences exist with regards to the effect of the level of de-epoxidized xanthophylls on qE in *Chlamydomonas* and *Arabidopsis*, it is plausible that fundamental differences exist in the mechanism and location of thermal dissipation in algae and higher plants (Elrad et al., 2002). With respect to the location of PsbS, although it is not strongly associated with the PS II holocomplex on balance evidence suggests it is associated with the core of PS II (Thidholm et al., 2002; Dominici et al., 2002). Reports of an LHC association may be due to differing locations of the monomer and dimer. At pH 7 the dimer associates with the PS II core and at pH 4, resulting from thylakoid acidification, the dimer dissociates and the monomer associates with the antenna (Bergantino et al., 2003; Holt et al., 2004).

3. What is the Mechanism of qE?

While we know that antenna structure, a functional PsbS, and xanthophyll molecules all influence quenching kinetics, the mechanisms for these interactions, however, remain unclear. Is PsbS the site of NPQ or is it an allosteric effector of qE that acts in concert with LHC protonation and zeaxanthin to altering interactions amongs antenna and PS II complexes and the chromophores embedded within them? Is there a direct involvement of 'quenching' carotenoids with PsbS and does this include zeaxanthin, antheraxanthin or lutein? Is zeaxanthin the ultimate 'sink' for Chl fluorescence or is it merely an 'allosteric modulator' or signal molecule that induces structural changes within the antenna, enabling Chls to relax to the ground state by non-radiative mechanisms?

Although xanthophyll pigments are required for non-radiative dissipation of excess energy this does not prove that they directly quench Chl fluorescence. Some researchers have hypothesised that carotenoid- and ΔpH-dependent conformational changes within the antennae promote de-excitation of singlet excited state Chl molecules ($^1Chl^*$) by promoting excitonic coupling between Chls (Horton et al., 1996). At this time, there is no evidence that Chls can self-quench by nonradiative mechanisms in pigment-binding proteins.

Support for a direct xanthophyll quenching hypothesis seemingly appeared in the occurrence of the cycle in every higher plant examined, as well as ferns, mosses and green algae (Demmig-Adams and Adams, 1993) and mounting evidence that they are necessary for induction and maintenance of NPQ both in vitro and in vivo (Gilmore et al., 1998; Niyogi et al., 1998, 2001). The thesis is that carotenoids with low-lying excited states are the ultimate 'sinks' for Chl fluorescence. That is, the excited state energy levels of zeaxanthin (and lutein) and their proximity to Chls in the antennae would allow them to efficiently accept excitation energy from $^1Chl^*$ either via the coulomb or electron exchange mechanism of energy transfer (Frank et al., 1994; Kühlbrandt et al., 1994; Krueger et al., 1998). Alternatively, an electron transfer model is supported by some of the experiments on ß-carotene (Beddard and Tretheway, 1977) and synthetic carotenoporphyrins (Cardoso et al., 1996). The redox properties of carotenoids have recently been reviewed by Frank and Brudvig (2004). However, in the work by Cardoso et al., (1996) only some of the carotenoporphyrins quenched porphyrin fluorescence consistent with an electron transfer mechanism. Other carotenoporphyrins behaved in a manner more suggestive of an energy transfer mechanism.

It stands to reason that xanthophylls having an S_1 excited singlet state energy below that of Chl should be able to quench Chl fluorescence and the xanthophyll would then dissipate the absorbed energy as heat. In fact, quenching has been demonstrated, but the studies have focused almost exclusively on solutions or liquid crystal preparations of Chl *a* and ß-carotene (Frackowiak et al., 1995; Beddard and Tretheway, 1977; Frank et al., 1995). The lowest predicted excited singlet state energy levels (S_1) derived either from the energy gap law for radiative transitions or from fluorescence studies were consistent with zeaxanthin accepting excitation energy from adjacent Chl molecules (Young and Frank, 1996). The energies of the S_1 states of lutein and antheraxanthin would theoretically enable either light harvesting or quenching (Frank et al., 1994). If violaxanthin has an S_1 energy level higher than that of Chl, it should be able to effectively transfer excitation energy to Chl (Gruszecki et al., 1999). However, measurements of the S_1 energy states of xanthophylls by fluorescence showed substantial spectral overlap with the lowest excited singlet state of Chl, suggesting that either violaxanthin or zeaxanthin could effectively quench Chl fluorescence (Polivka et al., 1999; Frank et al., 2000; Josue and Frank, 2002). This does not

appear to be the case in vivo, where violaxanthin and zeaxanthin have defined roles in impeding and facilitating quenching respectively. Furthermore, it is unclear how relevant the studies of xanthophylls in solution are to the mechanism of energy transfer and quenching in vivo. This is because the distribution of distances and geometries of the xanthophylls and Chls randomly dispersed in solution bears little resemblance to the protein-bound, spatially-fixed, donor-acceptor, xanthophyll-Chl systems that exist in nature. More relevant are the studies on covalently-linked synthetic carotenoporphyrins where ß-carotene derivatives have been shown to quench porphyrin fluorescence (Gust et al., 1992; Cardoso et al., 1996). These studies suggest that xanthophylls could play a role in energy dissipation and in regulating the flow of energy among Chls in photosynthetic antenna. Recent evidence that zeaxanthin is directly excited and associated with qE changes in selective excitation of Chl utilised femtosecond spectroscopy to measure the rise in zeaxanthin excited states resulting from selective excitation of $^1Chl^*$ (Ma et al., 2003). Additional femtosecond transient absorption measurements by this same group on thylakoid membranes prepared from spinach and transgenic *Arabidopsis thaliana* revealed the formation of a zeaxanthin radical cation upon excitation of Chl under conditions of maximum qE (Holt et al., 2005). The results suggest that direct energy transfer from bulk Chl molecules to a special Chl-zeaxanthin radical pair, is the mechanism by which nonradiative deactivation of excess $^1Chl^*$ occurs. More work is still required to establish the precise mechanism by which xanthophylls, PsbS, and protonation of LHCs collaboratively interact to ensure energy dissipation.

B. Triplet Quenching and Scavenging of Free Radicals

There is a tendency in the literature to focus on the contribution of NPQ and the xanthophyll cycle to photoprotection. However, carotenoids have a range of 'constitutive' functions in preventing oxidative damage. Specifically, quenching of Chl triplets and scavenging free radicals.

In ethanoic solution fluorescence yield from singlet Chl is about half that of triplet formation (68% verses 32% of $^1Chl^*$) (Foyer and Harbinson, 1999). Similarly, triplet formation is double that of fluorescence decay in isolated thylakoids (H. Kramer and Mathis, 1980). Consistent with this is the observations of fluorescence quantum yield of 0.11 ± 0.03 at 4 K and the Chl triplet yield of 0.16 ± 0.03 from isolated CP47 core antenna complexes of PS II (Groot et al., 1995). Triplets cannot be measured in functioning, however the relative fluorescence lifetimes of $^1Chl^*$ enable estimations to be made (Foyer and Harbinson, 1999). Such estimates indicate the majority of triplet Chl formed will occur in PS II, rather than PS I (Foyer and Harbinson, 1999), which could be the reason why a singlet energy dissipation mechanism is located nearby and induced when PS II is reduced.

Triplet Chl itself is not deleterious to the cell as it can readily decay to ground state (Foyer and Harbinson, 1999). However, it can sensitize the production of the highly reactive and toxic (Foote, 1968) $^1\Delta_g$ singlet state of oxygen ($^1O_2^*$) from ground state oxygen ($^3O_2$). Singlet oxygen can rapidly oxidise any organic compound, including Chl. Given the rate of triplet formation is nearly an order of magnitude faster than singlet decay (Fig. 5), then the need for quenching of triplet states is apparent and essential for plant viability. Carotenoids function in a protective role in many ways (Fig. 5): By quenching Chl triplet states that prevent the Chl-sensitized formation of the $^1\Delta_g$ singlet state oxygen — a major oxidizing agent of Chl (Foote, 1968; Boucher and Gingras, 1977; Renger, 1977); by scavenging singlet oxygen directly (Foote and Denny, 1970; Krinsky, 1971); or, as described above, by dissipating excess excitation energy beyond that which is required for photosynthesis (Demmig-Adams, 1990).

Carotenoid triplets in higher plant antennas were shown to be formed by flash excitation of Chl in excess of levels required to saturate photosynthesis, confirming observations in organic solvents, reviewed in (Frank and Cogdell, 1993). Similar observations have also been made in isolated antenna from the bacterium, *Rhodobacter sphaeroides* (Cogdell et al., 1981). As noted in Figs. 3 and 5 any carotenoid in the outer, inner or core antenna that is proximal to a $^3Chl^*$ could theoretically quench triplet state Chl by an exchange mechanism. The notable exception being ß-carotene in the reaction center. In a recent study, Formaggio and colleagues reconstituted wild-type and site-directed mutated LHCIIb proteins with different xanthophyll combinations in the L1, L2 and N1 sites (Formaggio et al., 2001). The conclusion from this study was lutein bound to the L1 site in reconstituted LHCs is the main site of triplet quenching and this occurs via the Chls A1 and B1.

C. Physiological Relevance of Carotenoids in Photoprotection

The physiological relevance of xanthophylls is exemplified by the bleaching, delayed greening and semi-lethal phenotypes observed in several carotenoid and NPQ deficient mutants (Niyogi et al., 1997b; Pogson et al., 1998). Due to the overlapping and multiple functions of carotenoids in assembly, NPQ, triplet Chl quenching and free radical scavenging it is difficult to define the relative contributions of each carotenoid and the relative importance of each process in protecting from damage. For instance, to what extent is the delayed greening and semi-lethal phenotype of the zeaxanthin-accumulating *lut2aba1* due to impaired antenna assembly and stability, or photodamage induced by an altered carotenoid composition and antenna structure (Pogson et al., 1998). Systematic analysis of lipid peroxidation, photoinhibition and seed set are providing insight into the degree of complementarity and redundancy in photoprotection.

In the absence of zeaxanthin and lutein *Chlamydomonas* cultures photobleach and mature *Arabidopsis* leaves senesce and photobleach when they are exposed to high intensity light (Niyogi et al., 1997b, 2001). There is much less bleaching if only zeaxanthin is eliminated and residual NPQ is present. Zeaxanthin deficient mutants of *Arabidopsis*, *npq1*, exhibit enhanced lipid peroxidation and leaf necrosis upon exposure to light or chilling stress (Havaux and Niyogi, 1999). This effect can not be attributed to the lack of NPQ, since the *npq4* mutant that exhibits a loss of NPQ without a change in xanthophyll cycle pool sizes is more tolerant to lipid peroxidation than *npq1* (Havaux and Niyogi, 1999). Therefore, zeaxanthin appears to have a specific photo-protective role outside of the light harvesting antennae. These results are in agreement with studies on isolated thylakoids that suggested only a few zeaxanthin molecules are required for optimal Chl fluorescence quenching (Gilmore et al., 1998). The 'excess' zeaxanthin that is not directly involved in Chl fluorescence quenching may contribute to other processes such as protection against lipid peroxidation or protection of PS II from photoinhibition (Havaux and Niyogi, 1999; Jin et al., 2001).

In addition to binding directly to LHC apoproteins, carotenoids are also localized in the chloroplast envelope and thylakoid membranes, potentially spanning the lipid bilayer to afford photoprotection against lipid peroxidation (Havaux, 1998). Xanthophylls have also been implicated in photo-protection outside of the photosynthetic apparatus, including protection against lipid peroxidation and maintenance of membrane fluidity and thermostability (Gruszecki, 1999). The enhanced rates of zeaxanthin synthesis that occur during prolonged exposure to high intensity light do not correlate with levels of zeaxanthin found in the photosynthetic apparatus (Schindler and Lichtenthaler, 1994). Zeaxanthin and violaxanthin synthesis are also localized in the chloroplast envelope (Siefermann-Harms et al., 1978).

Is NPQ physiologically important if the *npq4* mutant of *Arabidopsis* is green and the aforementioned study of lipid peroxidation indicate a role for zeaxanthin in the lipid bilayer? Several recent manuscripts demonstrate that NPQ does indeed enhance plant fitness. The first is both elegant and simple in that the authors measured a very good indicator of plant fitness in *Arabidopsis*: the amount of seed formed under field conditions and in growth chambers that had fluctuating light regimes that mimicked field conditions (Kühlein et al., 2002). Seed set was reduced by 30–50% in the field experiments, which was due to both a reduction in the number of fruit (siliques) and the number of seed per fruit. A similar effect was observed for npq4 plants grown in the growth chamber under variable light. This reduction may reflect increased photoinhibition in *npq4* plants (Li et al., 2002c) and insightfully demonstrates the need to undertake appropriate and relevant physiological experiments to determine the effects of mutations and transgenic manipulations on plant development. As stated above a reduction of photoprotective pigments has generally compromised fitness. In the converse experiment Horton and colleagues increased the xanthophyll cycle pool by over-expression of the β-carotene hydroxylase (Davison et al., 2002). This resulted in increase tolerance of the plants to abiotic stress induced by high light and increased temperature.

Given the complexity of photoprotection it is important to remember that other photoprotective mechanisms contribute to viability and may be up-regulated or activated to provide a degree of compensation for a loss of xanthophylls and/or NPQ described above. These mechanisms may include state transitions of LHCs between PS I and PS II; alternative sinks for electrons including oxygen utilized by photorespiration; activation of antioxidants such as tocopherols and ascorbic acid; and the water-water

cycle of PS I which converts H_2O_2 to water in a reaction catalyzed by the ascorbate peroxidase (Niyogi, 1999b). The complex nature of pigment-protein complexes indicates structural protective mechanisms. That is, there is evidence for an oxygen barrier that surrounds the light harvesting antennae, which effectively reduces the production of reactive oxygen species (Siefermann-Harms and Angerhofer, 1998). It was argued that the trimeric nature of LHCII may provide an oxygen shield for internally localized Chls (Siefermann-Harms and Angerhofer, 1998). Rohmer et al. (1979) proposed that carotenoids in lipid bilayers of bacteria may play the same role as cholesterol in the biomembranes of eukaryotes. Cholesterol greatly decreases O_2 permeability of biomembranes (Subczynski et al., 1989). Similarly, free xanthophylls present in the thylakoid membrane may provide a shield that decreases O_2 permeability either by directly coating LHCs or by promoting LHC aggregation. It is quite possible that protective processes, such as tocopherol or ascorbate levels are up-regulated in carotenoid-deficient lines. There are data demonstrating the interaction between ascorbate pool size and zeaxanthin production (Müller-Moule et al., 2002). Global gene expression analyses in response to high light and mutant screens are identifying factors that may signal and coordinate the various photoprotective mechanisms employed by the chloroplast (Rossel et al., 2002; Ball et al., 2004). Unravelling the remaining fundamental questions about carotenoid function in PS II will require the coordinated and integrated physiological, biochemical, physical and molecular strategies that have been increasingly utilised in recent years.

Acknowledgments

Our thanks to the many colleagues, students and staff who provide many of the results and insights that form the basis of this chapter. Support from the Australian Research Council to BJP is gratefully acknowledged (DP0343160). Work in the laboratory of HAF is supported by grants from the National Science Foundation (MCB-0314380), the National Institutes of Health (GM30353), and the University of Connecticut Research Foundation.

References

Adir N, Zer H, Schochat S and Ohad I (2003) Photoinhibition. Photosynth Res 76: 343–370

Al-Babili S, Lintig JV, Haubruck H and Beyer P (1996) A novel, soluble form of phytoene desaturase from *Narcissus pseudonarcissus* chromoplasts is Hsp70-complexed and competent for flavinylation, membrane association and enzymatic activation. Plant J 9: 601–612

Al-Babili S, Hugueney P, Schledz M, Welsch R, Frohnmeyer H, Laule O and Beyer P (2000) Identification of a novel gene coding for neoxanthin synthase from *Solanum tuberosum*. FEBS Lett 485: 168–172

Alfonso M, Montoya G, Cases R, Rodriguez R and Picorel R (1994) Core antenna complexes, CP43 and CP47, of higher plant Photosystem II: Spectral properties, pigment stoichiometry, and amino acid composition. Biochemistry 33: 10494–10500

Anderson JM and Chow WS (2002) Structural and functional dynamics of plant Photosystem II. Philos Trans R Soc Lond Ser B-Biol Sci 357: 1421–1430

Anderson JM, Chow WS and Park YI (1995) The grand design of photosynthesis: Acclimation of the photosynthetic apparatus to environmental cues. Photosynth Res 46: 129–139

Andersson J, Walters RG, Horton P and Jansson S (2001) Antisense inhibition of the photosynthetic antenna proteins CP29 and CP26: Implications for the mechanism of protective energy dissipation. Plant Cell 13: 1193–1204

Aspinall-O'Dea M, Wentworth M, Pascal A, Robert B, Ruban A and Horton P (2002) In vitro reconstitution of the activated zeaxanthin state associated with energy dissipation in plants. Proc Natl Acad Sci USA 99: 16331–16335

Ball L, Accotto G-P, Bechtold U, Creissen G, Funck D, Jimenez A, Kular B, Leyland N, Mejia-Carranza J, Reynolds H, Karpinski S, Mullineaux P (2004) An *Arabidopsis* mutant with raised ASCORBATE PEROXIDASE2 expression reveals glutathione as a direct modulator of stress responsive gene expression. Plant Cell 16: 2448–2462

Bassi R and Caffarri S (2000) Lhc proteins and the regulation of photosynthetic light harvesting function by xanthophylls. Photosynth Res 64: 243–256

Bassi R, Pineau B, Dainese P and Marquardt J (1993) Carotenoid-binding proteins of Photosystem II. Eur J Biochem 212: 297–303

Bassi R, Croce R, Cugini D and Sandona D (1999) Mutational analysis of a higher plant antenna protein provides identification of chromophores bound into multiple sites. Proc Natl Acad Sci USA 96: 10056–10061

Beddard RS and Tretheway KR (1977) Quenching of chlorophyll fluorescence by β-carotene. Nature 267: 373–374

Bergantino E, Segalla A, Brunetta A, Teardo E, Rigoni F, Giacometti GM and Szabo I (2003) Light- and pH-dependent structural changes in the PsbS subunit of Photosystem II. Proc Natl Acad Sci USA 100: 15265–15270

Beyer P and Kleinig H (1990) On the desaturation and cyclization reactions of carotenes in chromoplast membranes. In: Krinksy N, Mathews-Roth M and Taylor R (eds) Carotenoids: Chemistry and Biology, pp 195–206. Plenum Press, New York

Bishop NI (1996) The beta,epsilon-carotenoid, lutein, is specifically required for the formation of the oligomeric forms of the light harvesting complex in the green alga, *Scenedesmus*

obliquus. J Photochem Photobiol B Biol 36: 279–283
Bishop NI, Urbig T and Senger H (1995) Complete separation of the beta,epsilon- and beta,beta-carotenoid biosynthetic pathways by a unique mutation of the lycopene cyclase in the green alga, *Scenedesmus obliquus*. FEBS Lett 367: 158–162
Boucher F, Vanderrest, M and Gingras, G (1977) Structure and function of carotenoids in the photoreaction center from *Rhodospirillum rubrum*. Biochim Biophys Acta 461: 339–357
Bouvier F, Keller Y, d'Harlingue A and Camara B (1998) Xanthophyll biosynthesis: molecular and functional characterization of carotenoid hydroxylases from pepper fruits (*Capsicum annuum L.*). Biochim Biophys Acta 1391: 320–328
Bouvier F, d'Harlingue A, Backhaus R, Kumagai M and Camara B (2000) Identification of a neoxanthin synthase as a carotenoid cyclase paralog. Eur J Biochem 267: 6346–6352
Bramley PM (1993) Inhibition of carotenoid biosynthesis. In: Young AJ and Britton G (eds) Carotenoids in Photosynthesis, pp 127–159. Chapman and Hall, London
Briantais JM, Dacosta J, Goulas Y, Ducruet JM and Moya I (1996) Heat stress induces in leaves an increase of the minimum level of chlorophyll fluorescence, F-o: A time-resolved analysis. Photosynth Res 48: 189–196
Bungard RA, Ruban AV, Hibberd JM, Press MC, Horton P and Scholes JD (1999) Unusual carotenoid composition and a new type of xanthophyll cycle in plants. Proc Natl Acad Sci USA 96: 1135–1139
Caffarri S, Croce R, Breton J and Bassi R (2001) The major antenna complex of Photosystem II has a xanthophyll binding site not involved in light harvesting. J Biol Chem 276: 35924–35933
Cardoso SLN, Nicodem, DE, Moore TA, Moore AL and Gust D (1996) Synthesis and fluorescence quenching studies of a series of carotenoporphyrins with carotenoids of various lengths. J Brazil Chem Soc 7: 19–30
Carol P and Kuntz M (2001) A plastid terminal oxidase comes to light: Implications for carotenoid biosynthesis and chlororespiration. Trends Plant Sci 6: 31–36
Chow WS (1994) Photoprotection and photoinhibitory damage. In: Bittar EE (ed) Molecular Processes of Photosynthesis, Vol 10, pp 151–196. JAI Press, Greenwich
Chunaev AS, Mirnaya ON, Maslov VG and Boschetti A (1991) Chlorophyll b- and loroxanthin-deficient mutants of *Chlamydomonas reinhardtii*. Photosynthetica 25: 291–301
Cogdell RJ, Hipkins MF, MacDonald W and Truscott TG (1981) Energy transfer between the carotenoid and bacteriochlorophyll within the B800-850 light-harvesting pigment-protein complex of *Rps. sphaeroides*. Biochim Biophys Acta 634: 191–202
Croce R, Remelli R, Varotto C, Breton J and Bassi R (1999) The neoxanthin binding site of the major light harvesting complex (LHCII) from higher plants. FEBS Lett 456: 1–6
Croce R, Canino G, Ros F and Bassi R (2002) Chromophore organization in the higher-plant Photosystem II antenna protein CP26. Biochemistry 41: 7334–7343
Cunningham FJ and Gantt E (1998) Genes and enzymes of carotenoid biosynthesis in plants. Ann Rev Plant Physiol Mol Biol 49: 557–583
Cunningham FX, Jr., Sun Z, Chamovitz D, Hirschberg J and Gantt E (1994) Molecular structure and enzymatic function of lycopene cyclase from the cyanobacterium *Synechococcus* sp strain PCC7942. Plant Cell 6: 1107–1121
Davison PA, Hunter CN and Horton P (2002) Overexpression of beta-carotene hydroxylase enhances stress tolerance in *Arabidopsis*. Nature 418: 203–206
Demmig B, Winter K, Kruger A and Czygan F-C (1987) Photoinhibition and zeaxanthin formation in intact leaves. Plant Physiol 84: 218–224
Demmig-Adams B (1990) Carotenoids and photoprotection in plants: A role for the xanthophyll zeaxanthin. Biochim Biophys Acta 1020: 1–24
Demmig-Adams B (2003) Linking the xanthophyll cycle with thermal energy dissipation. Photosynth Res 76: 73–80
Demmig-Adams B and Adams III WW (1992) Photoprotection and other responses of plants to high light stress. Ann Rev Plant Physiol Plant Mol Biol 43: 599–626
Demmig-Adams B and Adams III WW (1993) The xanthophyll cycle. In: Young AJ and Britton G (eds) Carotenoids in Photosynthesis, pp 206–252. Chapman and Hall, London
Demmig-Adams B and Adams III WW (1996) The role of xanthophyll cycle carotenoids in the protection of photosynthesis. Trends Plant Sci 1: 21–26
Demmig-Adams B, Adams III WW, Barker DH, Logan BA, Bowling DR and Verhoeven AS (1996) Using chlorophyll fluorescence to assess the fraction of absorbed light allocated to thermal dissipation of excess excitation. Physiol Plant 98: 253–264
Dobrikova A, Morgan RM, Ivanov AG, Apostolova E, Petkanchin I, Huner NPA and Taneva SG (2000) Electric properties of thylakoid membranes from pea mutants with modified carotenoid and chlorophyll-protein complex composition. Photosynth Res 65: 165–174
Dominici P, Caffarri S, Armenante F, Ceoldo S, Crimi M and Bassi R (2002) Biochemical properties of the PsbS subunit of Photosystem II either purified from chloroplast or recombinant. J Biol Chem 277: 22750–22758
Dutton HJ, Manning WM and Duggar BM (1943) Chl fluorescence and energy transfer in the diatom *Nitzscia closterium*. J Phys Chem 47: 308–317
Elrad D, Niyogi KK and Grossman AR (2002) A major light-harvesting polypeptide of Photosystem II functions in thermal dissipation. Plant Cell 14: 1801–1816
Falbel TG, Staehelin LA and Adams III WW (1994) Analysis of xanthophyll cycle carotenoids and chlorophyll fluorescence in light intensity-dependent chlorophyll-deficient mutants of wheat and barley. Photosynth Res 42: 191–202
Farber A and Jahns P (1998) The xanthophyll cycle of higher plants: Influence of antenna size and membrane organization. Biochim Biophys Acta 1363: 47–58
Ferreira KN, Iverson TM, Maghlaoui K, Barber J and Iwata S (2004) Architecture of the photosynthetic oxygen-evolving center. Science 303: 1831–1838
Foote CS (1968) Mechanisms of photosensitized oxidation. Science 162: 963
Foote CS and Denny RW (1970) Chemistry of singlet oxygen. X. Carotenoid quenching parallels biological protection. J Am Chem Soc 92: 5216
Formaggio E, Cinque G and Bassi R (2001) Functional architecture of the major light-harvesting complex from higher plants. J Mol Biol 314: 1157–1166
Foyer CH (2001) Prospects for enhancement of the soluble antioxidants, ascorbate and glutathione. Biofactors 15: 75–78

Foyer CH and Harbinson J (1999) Relationships between antioxidant metabolism and carotenoids in the regulation of photosynthesis. In: Frank HA, Young AJ, Britton G and Cogdell RJ (eds) The Photochemistry of Carotenoids, pp 305–325. Kluwer Academic Publishers, Dordrecht

Frackowiak D, Zelent B, Malak H, Cegielski R, Goc J, Niedbalska M, Ptak A. (1995) Interactions between chlorophyll-*a* and beta-carotene in nematic liquid-crystals. Biophys Chem 54: 95–107

Frank HA and Brudvig GW (2004) Redox function of carotenoids in photosynthesis. *Biochemistry* 43: 8607–8615

Frank HA and Cogdell RJ (1993) Photochemistry and function of carotenoids in photosynthesis. In: Young AJ and Britton G (eds) Carotenoids in Photosynthesis, pp 253–326. Chapman and Hall, London

Frank HA, Cua A, Chynwat V, Young A, Gosztola D and Wasielewski MR (1994) Photophysics of the carotenoids associated with the xanthophyll cycle in photosynthesis. Photosynth Res 41: 389–395

Frank HA, Cua A, Chynwat V, Young AJ, Zhu Y and Blankenship RE (1995) Quenching of chlorophyll excited states by carotenoids. In: Mathis P (ed) Photosynthesis: From Light to Biosphere, Vol. IV, pp 3–7. Kluwer Academic Publishers, Dordrecht

Frank HA, Kievit O, Brudvig GW, Kong J, Lu Z, Lvov YM, Bautista JA and Rusling JF (1999) Direct electrochemistry of redox sites in photosynthetic reaction centers. Biophys J 76: A256-A256

Frank HA, Bautista JA, Josue, JS, and Young, AJ (2000) Mechanism of nonphotochemical quenching in green plants: Energies of the lowest excited singlet states of violaxanthin and zeaxanthin. Biochemistry 39: 2831–2837

Funk C, Adamska I, Green BR, Andersson B and Renger G (1995) The nuclear-encoded chlorophyll-binding Photosystem II-S protein is stable in the absence of pigments. J Biol Chem 270: 30141–30147

Gastaldelli M, Canino G, Croce R and Bassi R (2003) Xanthophyll binding sites of the CP29 (Lhcb4) subunit of higher plant Photosystem II investigated by domain swapping and mutation analysis. J Biol Chem 278: 19190–19198

Genty B, Goulas Y, Dimon B, Peltier G, Briantais JM and Moya I (1992) Modulation of efficiency of primary conversion in leaves. Photosynth Res 34: 106–106

Gilmore A (2001) Xanthophyll cycle-dependent nonphotochemical quenching in Photosystem II: Mechanistic insights gained from *Arabidopsis thaliana* L. mutants that lack violaxanthin deepoxidase activity and/or lutein. Photosynth Res 67: 89–101

Gilmore AM and Yamamoto HY (1991) Zeaxanthin formation and energy-dependent fluorescence quenching in pea chloroplasts under artificially mediated linear and cyclic electron transport. Plant Physiol 96: 635–643

Gilmore A and Govindjee (1999) How higher plants respond to excess light: Energy dissipation in photosystem. In: Singhal G, Renger G, Sopory S, Irrgang K and Govindjee (eds) Concepts in Photobiology: Photosynthesis and Photomorphogenesis, pp 513–548. Narosa Publishing House, New Delhi

Gilmore AM, Hazlett TL and Govindjee (1995) Xanthophyll cycle-dependent quenching of Photosystem II chlorophyll a fluorescence: Formation of a quenching complex with a short fluorescence lifetime. Proc Natl Acad Sci USA 92: 2273–2277

Gilmore AM, Hazlett TL, Debrunner PG and Govindjee (1996a) Comparative time-resolved Photosystem II chlorophyll *a* fluorescence analyses reveal distinctive differences between photoinhibitory reaction center damage and xanthophyll cycle-dependent energy dissipation. Photochem Photobiol 64: 552–563

Gilmore AM, Hazlett TL, Debrunner PG, Govindjee (1996b) Photosystem II chlorophyll a fluorescence lifetimes and intensity are independent of the antenna size differences barley wild-type and chlorina mutants: Photochemical quenching and xanthophyll cycle-dependent nonphotochemical quenching of fluorescence. Photosynth Res 48: 171–187

Gilmore AM, Shinkarev VP, Hazlett TL and Govindjee (1998) Quantitative analysis of the effects of intrathylakoid pH and xanthophyll cycle pigments on chlorophyll *a* fluorescence lifetime distributions and intensity in thylakoids. Biochemistry 37: 13582–13593

Giuffra E, Cugini D, Croce R and Bassi R (1996) Reconstitution and pigment-binding properties of recombinant CP29. Eur J Biochem 238: 112–120

Govindjee (1995) Sixty-three years since Kautsky — Chlorophyll *a* fluorescence. Austr J Plant Physiol 22: 131–160

Govindjee (1999) On the requirement of minimum number of four versus eight quanta of light for the evolution of one molecule of oxygen in photosynthesis: A historical note. Photosynth Res 59: 249–254

Green BR and Durnford DG (1996) The chlorophyll-carotenoid proteins of oxygenic photosynthesis. Ann Rev Plant Physiol Mol Biol 47: 685–714

Griffiths M, Sistrom WR, Cohen-Bazire G and Stanier RY (1955) Function of carotenoids in photosynthesis. Nature 176: 1211–1214

Groot ML, Peterman EJG, Vanstokkum IHM, Dekker JP and van Grondelle R (1995) Triplet and fluorescing states of the Cp47 antenna complex of photosystem-II studied as a function of temperature. Biophys J 68: 281–290

Gruszecki W (1999) Carotenoid in membranes. In: Frank H, Young A, Britton G and Cogdell R (eds) The Photochemistry of Carotenoids, pp 363–379. Kluwer Academic Publishers, Dordrecht

Gruszecki WI, Grudzinski W, Banaszek-Glos A, Matula M, Kernen P, Krupa Z and Sielewiesiuk J (1999) Xanthophyll pigments in light-harvesting complex II in monomolecular layers: Localisation, energy transfer and orientation. Biochim Biophys Acta 1412: 173–183

Gust DM, Moore TA, Moore AL, Devadoss C, Liddell PA, Heman R, Nieman RA, Demanche LJ, Degraziano JM and Gouni I (1992) Triplet and singlet energy transfer in carotene-porphyrin dyads: Role of the linkage bonds. J Am Chem Soc 114: 3590–3603

Hanley J, Deligiannakis Y, Pascal A, Faller P and Rutherford AW (1999) Carotenoid oxidation in Photosystem II. Biochemistry 38: 8189–8195

Havaux M (1998) Carotenoids as membrane stabilizers in chloroplasts. Trends Plant Sci 3: 147–151

Havaux M and Niyogi KK (1999) The violaxanthin cycle protects plants from photooxidative damage by more than one mechanism. Proc Natl Acad Sci USA 96: 8762–8767

Havaux M, Dall'Osto L, Cuine S, Giuliano G and Bassi R (2004) The effect of zeaxanthin as the only xanthophyll on the structure and function of the photosynthetic apparatus in *Arabidopsis*

thaliana. J Biol Chem 279: 13878–13888
Heinze I, Pfuendel E, Huehn M and Dau H (1997) Assembly of light harvesting complexes II (LHC-II) in the absence of lutein. A study on the alpha-carotenoid-free mutant C-2A´–34 of the green alga *Scenedesmus obliquus*. Biochim Biophys Acta 1320: 188–194
Herrin DL, Battey JF, Greer K and Schmidt GW (1992) Regulation of chlorophyll apoprotein expression and accumulation. Requirements for carotenoids and chlorophyll. J Biol Chem 267: 8260–8269
Hirschberg J (2001) Carotenoid biosynthesis in flowering plants. Curr Opin Plant Biol 4: 210–218
Hobe S, Prytulla S, Kühlbrandt W and Paulsen H (1994) Trimerization and crystallization of reconstituted light-harvesting chlorophyll *a/b* complex. EMBO J 13: 3423–3429
Holt NE, Fleming GR and Niyogi KK (2004) Toward an understanding of the mechanism of nonphotochemical quenching in green plants. Biochemistry 43: 8281–8289
Holt NE, Zigmantas, Valkunas L, Li X-P, Niyogi KK and Fleming GR (2005) Carotenoid cation formation and the regulation of photosynthetic light harvesting. Science 307: 433–436
Hoober JK and Eggink LL (1999) Assembly of light-harvesting complex II and biogenesis of thylakoid membranes in chloroplasts. Photosynth Res 61: 197–215
Horton P, Ruban AV and Walters RG (1996) Regulation of light harvesting in green plants. Ann Rev Plant Physiol Plant Mol Biol 47: 655–684
Hughes DA (2001) Dietary carotenoids and human immune function. Nutrition 17: 823–827
Isaacson T, Ronen G, Zamir D and Hirschberg J (2002) Cloning of *tangerine* from tomato reveals a carotenoid isomerase essential for the production of β-carotene and xanthophylls in plants. Plant Cell 14: 333–342
Jansson S (1994) The light-harvesting chlorophyll *a/b*-binding proteins. Biochim Biophys Acta 1184: 1–19
Jansson S (1999) A guide to the Lhc genes and their relatives in *Arabidopsis*. Trends Plant Sci 4: 236–240
Jin ES, Polle JEW and Melis A (2001) Involvement of zeaxanthin and of the Cbr protein in the repair of Photosystem II from photoinhibition in the green alga *Dunaliella salina*. Biochim Biophys Acta 1506: 244–259
Jordan P, Fromme P, Witt H, Klukas O, Saenger W and Krauß BN (2001) Three-dimensional structure of cyanobacterial Photosystem I at 2.5 angstrom resolution. Nature 411: 909–917
Josue JS and Frank HA (2002) Direct determination of the S-1 excited-state energies of xanthophylls by low-temperature fluorescence spectroscopy. J Phys Chem A 106: 4815–4824
Kamiya N and Shen J-R (2003) Crystal structure of oxygen-evolving Photosystem II from *Thermosynechococcus vulcanus* at 3.7-Å resolution. Proc Natl Acad Sci USA 100: 98–103
Knox J and Dodge A (1985) Singlet oxygen and plants. Phytochemistry 24: 889–89
Koornneef M, Jorna ML, Brinkhorst van der Swan DLC and Karssen CM (1982) The isolation of abscisic acid (ABA) deficient mutants by selection of induced revertants in non-germinating gibberellin sensitive lines of *Arabidopsis thaliana* (L.) Heynh. Theor Appl Genet 61: 385–393
Kramer DM, Sacksteder CA and Cruz JA (1999) How acidic is the lumen? Photosynth Res 60: 151–163
Kramer H and Mathis P (1980) Quantum yield and rate of formation of the carotenoid triplet state in photosynthetic structures. Biochim Biophys Acta 593: 319–329
Krause GH and Weis E (1991) Chlorophyll fluorescence and photosynthesis: The basics. Ann Rev Plant Physiol Mol Biol 42: 313–349
Krinsky NI (1971) Function of carotenoids. In: Isler O, Guttman G and Solms U (eds) Carotenoids, pp 669–716. Birkhauser Verlag, Basel
Krueger BP, Scholes GD and Fleming GR (1998) Calculation of couplings and energy-transfer pathways between the pigments of LH2 by the ab initio transition density cube method. J Phys Chem B 102: 5378–5386
Kühlbrandt W, Wang DN and Fujiyoshi Y (1994) Atomic model of plant light-harvesting complex by electron crystallography. Nature 367: 614–621
Kühlein C, Agren J and Jansson S (2002) Rapid regulation of light harvesting and plant fitness in the field. Science 297: 91–93
Kumagai MH, Keller Y, Bouvier F, Clary D and Camara B (1998) Functional integration of non-native carotenoids into chloroplasts by viral-derived expression of capsanthin-capsorubin synthase in *Nicotiana benthamiana*. Plant J 14: 305–315
Landrum JT and Bone RA (2001) Lutein, zeaxanthin, and the macular pigment. Arch Biochem and Biophys 385: 28–40
Li X-P, Björkman O, Shih C, Grossman AR, Rosenquist M, Jansson S and Niyogi KK (2000) A pigment-binding protein essential for regulation of photosynthetic light harvesting. Nature 403: 391–395
Li X-P, Phippard A, Pasari J and Niyogi KK (2002a) Structure-function analysis of Photosystem II subunit S (PsbS) in vivo. Funct Plant Biol 29: 1131–1139
Li X-P, Gilmore AM and Niyogi KK (2002b) Molecular and global time-resolved analysis of a PsbS gene dosage effect on pH- and xanthophyll cycle-dependent nonphotochemical quenching in Photosystem II. J Biol Chem 277: 33590–33597
Li X-P, Muller-Moule P, Gilmore AM and Niyogi KK (2002c) PsbS-dependent enhancement of feedback de-excitation protects Photosystem II from photoinhibition. Proc Natl Acad Sci USA 99: 15222–15227
Liu Z, Yan H, Wang K, Kuang TY, Zhang J, Gul L, An X and Chang WR (2004) Crystal structure of spinach major light-harvesting complex at 2.72 Å resolution. Nature 428: 287–292
Lokstein H, Tian L, Polle JEW, DellaPenna D (2002) Xanthophyll biosynthetic mutants of *Arabidopsis thaliana*: Altered nonphotochemical quenching of chlorophyll fluorescence is due to changes in Photosystem II antenna size and stability. Biochim Biophys Acta 1553: 309–319
Ma YZ, Holt NE, Li X-P, Niyogi KK and Fleming GR (2003) Evidence for direct carotenoid involvement in the regulation of photosynthetic light harvesting. Proc Natl Acad Sci USA 100: 4377–4382
Marin E, Nussaume L, Quesada A, Gonneau M, Sotta B, Hugueney P, Frey A and Marion Poll A (1996) Molecular identification of zeaxanthin epoxidase of *Nictiana plumbaginifolia*, a gene involved in abscisic acid biosynthesis and corresponding to the ABA locus of *Arabidopsis thaliana*. EMBO J 15: 2331–2342
Matsubara S, Gilmore AM and Osmond CB (2001) Diurnal and acclimatory responses of violaxanthin and lutein epoxide in the Australian mistletoe *Amyema miquelii*. Aust J Plant Physiol 28: 793–800

Maxwell K and Johnson GN (2000) Chlorophyll fluorescence — a practical guide. J Exp Bot 51: 659–668

Milborrow BV, Swift IE and Netting AG (1982) The stereochemistry of hydroxylation of the carotenoid lutein in *Calendula officinalis*. Phytochemistry 21: 2853–2857

Misawa N, Masamoto K, Hori T, Ohtani T, Boger P and Sandmann G (1994) Expression of an *Erwinia* phytoene desaturase gene not only confers multiple resistance to herbicides interfering with carotenoid biosynthesis but also alters xanthophyll metabolism in transgenic plants. Plant J 6: 481–489

Morosinotto T, Baronio R and Bassi R (2002) Dynamics of chromophore binding to Lhc proteins in vivo and in vitro during operation of the xanthophyll cycle. J Biol Chem 277: 36913–36920

Morosinotto T, Caffarri S, Dall'Osto L and Bassi R (2003) Mechanistic aspects of the xanthophyll dynamics in higher plant thylakoids. Physiol Plant 119: 347–354

Müller P, Li X-P and Niyogi KK (2001) Non-photochemical quenching. A response to excess light energy. Plant Physiol 125: 1558–1566

Muller-Moule P, Conklin PL and Niyogi KK (2002) Ascorbate deficiency can limit violaxanthin de-epoxidase activity in vivo. Plant Physiol 128: 970–977

Nield J, Orlova EV, Morris EP, Gowen B, van Heel M and Barber J (2000) 3D map of the plant Photosystem II supercomplex obtained by cryoelectron microscopy and single particle analysis. Nature Structural Biol 7: 44–47

Niyogi KK (1999) Photoprotection revisited: Genetic and molecular approaches. Ann Rev Plant Physiol Mol Biol 50: 333–359

Niyogi KK, Björkman O and Grossman AR (1997a) *Chlamydomonas* xanthophyll cycle mutants identified by video imaging of chlorophyll fluorescence quenching. Plant Cell 9: 1369–1380

Niyogi KK, Björkman O and Grossman AR (1997b) The roles of specific xanthophylls in photoprotection. Proc Natl Acad Sci USA 94: 14162–14167

Niyogi KK, Grossman AR and Björkman O (1998) *Arabidopsis* mutants define a central role for the xanthophyll cycle in the regulation of photosynthetic energy conversion. Plant Cell 10: 1121–1134

Niyogi KK, Shih C, Chow WS, Pogson BJ, DellaPenna D and Björkman O (2001) Photoprotection in a zeaxanthin- and lutein-deficient double mutant of *Arabidopsis*. Photosynth Res 67: 139–145

Noctor G and Foyer CH (1998) Ascorbate and glutathione: Keeping active oxygen under control. Ann Rev Plant Physiol Mol Biol 49: 249–279

Norris SR, Barrette TR and DellaPenna D (1995) Genetic dissection of carotenoid synthesis in *Arabidopsis* defines plastoquinones as an essential component of phytoene desaturation. Plant Cell 7: 2139–2149

Nussberger S, Dorr K, Wang D and Kühlbrandt W (1993) Lipid-protein interactions in crystals of plant light-harvesting complex. J Mol Biol 234:

Osmond CB, Kramer D and Luttge U (1999) Reversible, water stress-induced non-uniform chlorophyll fluorescence quenching in wilting leaves of *Potentilla reptans* may not be due to patchy stomatal responses. Plant Biol 1: 618–624

Park H, Kreunen S, Cuttriss A, DellaPenna D and Pogson B (2002) Identification of the carotenoid isomerase provides insight into carotenoid biosynthesis, prolamellar body formation, and photomorphogenesis. Plant Cell 14: 321–332

Paulsen H (1999) Carotenoids and the assembly of light-harvesting complexes. In: Frank H, Young A, Britton G and Cogdell R (eds) The Photochemistry of Carotenoids, pp 123–135. Kluwer Academic Publishers, Dordrecht

Pearcy RW and Yang W (1998) The functional morphology of light capture and carbon gain in the Redwood forest understorey plant *Adenocaulon bicolor* Hook. Functional Ecology 12: 543–552

Peter GF and Thornber JP (1991a) Electrophoretic procedures for fractionation of photosystems I and II pigment-proteins of higher plants and for determination of their subunit composition. Meth Plant Biochem 5: 195–210

Peter GF and Thornber JP (1991b) Biochemical composition and organization of higher plant Photosystem II light-harvesting pigment-proteins. J Biol Chem 266: 16745–16754

Pfündel E and Bilger W (1994) Regulation and possible function of the violaxanthin cycle. Photosynth Res 42: 89–109

Pfündel E and Dilley RE (1993) The pH dependence of violaxanthin deepoxidation in isolated pea chloroplasts. Plant Physiol 101: 65–71

Phillip D, Hobe S, Paulsen H, Molnar P, Hashimoto H and Young AJ (2002) The binding of xanthophylls to the bulk light-harvesting complex of Photosystem II of higher plants — A specific requirement for carotenoids with a 3-hydroxy-beta-end group. J Biol Chem 277: 25160–25169

Plumley FG and Schmidt GW (1987) Reconstitution of chlorophyll *a/b* light-harvesting complexes: Xanthophyll-dependent assembly and energy transfer. Proc Natl Acad Sci USA 84: 146–150

Plumley F and Schmidt G (1995) Light-harvesting chlorophyll *a/b* complexes: Interdependent pigment synthesis and protein assembly. Plant Cell 7: 689–704

Pogson BJ and Rissler HM (2000) Genetic manipulation of carotenoid biosynthesis and photoprotection. Philos Trans Roy Soc Lond B 355: 1395–1403

Pogson B, McDonald K, Truong M, Britton G and DellaPenna D (1996) *Arabidopsis* carotenoid mutants demonstrate that lutein is not essential for photosynthesis in higher plants. Plant Cell 8: 1627–1639

Pogson BJ, Niyogi KK, Björkman O and DellaPenna D (1998) Altered xanthophyll compositions adversely affect chlorophyll accumulation and nonphotochemical quenching in *Arabidopsis* mutants. Proc Natl Acad Sci USA 95: 13324–13329

Polivka T, Herek J, Zigmantas D, Akerlund H and Sundström V (1999) Direct observation of the (forbidden) S1 state in carotenoids. Proc Natl Acad Sci USA 96: 4914–4917

Polivka T, Zigmantas D, Sundström V, Formaggio E, Cinque G and Bassi R (2002) Carotenoid S-1 state in a recombinant light-harvesting complex of Photosystem II. Biochemistry 41: 439–450

Polle JEW, Niyogi KK and Melis A (2001) Absence of lutein, violaxanthin and neoxanthin affects the functional chlorophyll antenna size of photosystem-II but not that of photosystem-I in the green alga *Chlamydomonas reinhardtii*. Plant Cell Physiol 42: 482–491

Redmond TM, Gentleman S, Duncan T, Yu S, Wiggert B, Gantt E and Cunningham FX (2001) Identification, expression, and substrate specificity of a mammalian beta-carotene 15,15′-dioxygenase. J Biol Chem 276: 6560–6565

Rhee K-H, Morris EP, Barber J and Kühlbrandt W (1998) Three-dimensional structure of Photosystem II reaction center at 8 angstrom resolution. Nature 396: 283–286

Rissler HM and Pogson BJ (2001) Antisense inhibition of the beta-carotene hydroxylase enzyme in *Arabidopsis* and the implications for carotenoid accumulation, photoprotection and antenna assembly. Photosynth Res 67: 127–137

Rohmer M, Bouvier P and Ourisson G (1979) Molecular evolution of biomembranes — structural equivalents and phylogenetic precursors of sterols. Proc Natl Acad Sci USA 76: 847–851

Ros F, Bassi R and Paulsen H (1998) Pigment-binding properties of the recombinant Photosystem II subunit CP26 reconstituted in vitro. Eur J Biochem 253: 653–658

Ruban AV, Phillip D, Young AJ and Horton P (1998) Excited-state energy level does not determine the differential effect of violaxanthin and zeaxanthin on chlorophyll fluorescence quenching in the isolated light-harvesting complex of Photosystem II. Photochem Photobiol 68: 829–834

Ruban AV, Lee PJ, Wentworth M, Young AJ and Horton P (1999) Determination of the stoichiometry and strength of binding of xanthophylls to the Photosystem II light harvesting complexes. J Biol Chem 274: 10458–10465

Ruban AV, Pascal AA, Robert B and Horton P (2002) Activation of zeaxanthin is an obligatory event in the regulation of photosynthetic light harvesting. J Biol Chem 277: 7785–7789

Satoh K (1993) Isolation and properties of the Photosystem II reaction center. In: Deisenhofer J and Norris J (eds) The Photosynthetic Reaction Center, Vol 1, pp 289–318. Academic Press, San Diego

Savitch LV, Leonardos ED, Krol M, Jansson S, Grodzinski B, Huner NPA and Öquist G (2002) Two different strategies for light utilization in photosynthesis in relation to growth and cold acclimation. Plant Cell Environ 25: 761–771

Schindler C and Lichtenthaler H (1994) Is there a correlation between light-induced zeaxanthin accumulation and quenching of variable chlorophyll *a* fluorescence. Plant Physiol Biochem 32: 813–823

Schmid VHR, Cammarata KV, Bruns BU and Schmidt GW (1997) In vitro reconstitution of the Photosystem I light-harvesting complex LHCI-730: Heterodimerization is required for antenna pigment organization. Proc Natl Acad Sci USA 94: 7667–7672

Seibert M (1993) Biochemical, biophysical, and structural characterization of the Photosystem II reaction center complex. In: Deisenhofer J and Norris J (eds) The Photosynthetic Reaction Center, Vol 1, pp 319–356. Academic Press, San Diego

Seo M and Koshiba T (2002) Complex regulation of ABA biosynthesis in plants. Trends Plant Sci 7: 41–48

Siefermann D and Yamamoto HY (1975) Light-induced de-epoxidation of violaxanthin in lettuce chloroplasts. Biochim Biophys Acta 387: 149–158

Siefermann-Harms D and Angerhofer A (1998) Evidence for an O_2-barrier in the light-harvesting chlorophyll-*a*/*b*-protein complex LHC II. Photosynth Res 55: 83–94

Siefermann-Harms D, Joyard J and Douce R (1978) Light-induced changes of the carotenoid levels in chloroplast envelopes. Plant Physiol 61: 530–533

Siefermann-Harms D, Borch G and Liaaen-Jensen S (1981) Lactucaxanthin, an e, e-carotene-3,3′-diol from Lactuca sativa. Phytochemistry 20: 85–88

Subczynski W, Hyde J and Kusumi A (1989) Oxygen permeability of phosphatidylcholine-cholesterol membranes. Proc Natl Acad Sci USA 86: 4474–4478

Sun WH, Verhoeven AS, Bugos RC and Yamamoto HY (2001) Suppression of zeaxanthin formation does not reduce photosynthesis and growth of transgenic tobacco under field conditions. Photosynth Res 67: 41–50

Sun ZR, Gantt E and Cunningham FX (1996) Cloning and functional analysis of the beta-carotene hydroxylase of *Arabidopsis thaliana*. J Biol Chem 271: 24349

Telfer A (2002) What is beta-carotene doing in the Photosystem II reaction centre? Phil Trans R Soc Lond B 357: 1431–1439

Thayer SS and Björkman O (1990) Leaf xanthophyll content and composition in sun and shade determined by HPLC. Photosynth Res 23: 331–343

Thidholm E, Lindstrom V, Tissier C, Robinson C, Schroder WP and Funk C (2002) Novel approach reveals localisation and assembly pathway of the PsbS and PsbW proteins into the Photosystem II dimer. FEBS Lett 513: 217–222

Tian L and DellaPenna D (2001) Characterization of a second carotenoid B-hydroxylase gene from Arabidopsis and its relationship to the *LUT1* locus. Plant Mol Biol 47: 379–388

Tian L, Musetti V, Kim J, Magallanes-Lundback M, DellaPenna D (2004) The *Arabidopsis* LUT1 locus encodes a member of the cytochrome P450 family that is required for carotenoid epsilon-ring hydroxylation activity. Proc Natl Acad Sci USA 101: 402–407

Tracewell CA, Vrettos JS, Bautista JA, Frank HA and Brudvig GW (2001) Carotenoid photooxidation in Photosystem II. Arch Biochem Biophys 385: 61–69

Verhoeven AS, Adams III WW, B. D-A, Croce R and Bassi R (1999) Xanthophyll cycle pigment localization and dynamics during exposure to low temperatures and light stress in *Vican major*. Plant Physiol 120: 727–738

Verhoeven AS, Bugos RC and Yamamoto HY (2001) Transgenic tobacco with suppressed zeaxanthin formation is susceptible to stress-induced photoinhibition. Photosynth Res 67: 27–39

von Lintig J, Welsch R, Bonk M, Giuliano G, Batschauer A and Kleinig H (1997) Light-dependent regulation of carotenoid biosynthesis occurs at the level of phytoene synthase expression and is mediated by phytochrome in *Sinapis alba* and *Arabidopsis thaliana* seedlings. Plant J 12: 625–634

Vrettos JS, Stewart DH, de Paula JC and Brudvig GW (1999) Low-temperature optical and resonance Raman spectra of a carotenoid cation radical in Photosystem II. J Phys Chem B 103: 6403–6406

Walters RG, Ruban AV and Horton P (1996) Identification of proton-active residues in a higher plant light-harvesting complex. Proc Natl Acad Sci USA 93: 14204–14209

Welsch R, Beyer P, Hugueney P, Kleinig H and von Lintig J (2000) Regulation and activation of phytoene synthase, a key enzyme in carotenoid biosynthesis, during photomorphogenesis. Planta 211: 846–854

Wetzel CM, Jiang CZ, Meehan LJ, Voytas DF and Rodermel SR (1994) Nuclear-organelle interactions: The immutans variegation mutant of *Arabidopsis* is plastid autonomous and impaired in carotenoid biosynthesis. Plant J 6: 161–175

Yamamoto H (1962) Studies on the light and dark interconversions of leaf xanthophylls. Biochim Biophys Acta 97: 168–173

Yamamoto HY (1979) Biochemistry of the xanthophyll cycle in higher plants. Pure Appl Chem 51: 639–648

Ye X, Al-Babili S, Kloti A, Zhang J, Lucca P, Beyer P and Potrykus I (2000) Engineering the provitamin A (β-carotene) biosynthetic pathway into (carotenoid-free) rice endosperm. Science 287: 303–305

Young AJ (1993) Occurrence and distribution of carotenoids in photosynthetic systems. In: Young AJ and Britton G (eds) Carotenoids in Photosynthesis, pp 16–71. Chapman and Hall, London

Young AJ and Frank HA (1996) Energy transfer reactions involving carotenoids: Quenching of chlorophyll fluorescence. J Photochem Photobiol B 36: 3–15

Zouni A, Witt HT, Kern J, Fromme P, Krauß N, Saenger W and Orth P (2001) Crystal structure of Photosystem II from *Synechococcus elongatus* at 3.8 angstrom resolution. Nature 409: 739–743

Chapter 24

Flash-Induced Oxygen Evolution and Other Oscillatory Processes

Vladimir Shinkarev*
Department of Biochemistry, 419 Roger Adams Lab, 600 S. Mathews Avenue, and Center for Biophysics and Computational Biology, University of Illinois at Urbana-Champaign, Urbana, IL 61801, U.S.A.

*Author for correspondence, email: vshinkar@uiuc.edu

T. Wydrzynski and K. Satoh (eds): Photosystem II: The Light-Driven Water:Plastoquinone Oxidoreductase, pp. 539–565.

Summary

The light-induced oxidation of water by Photosystem II (PS II) of higher plants, algae and cyanobacteria is the main source of atmospheric oxygen. The discovery of the flash-induced period-four oscillations in the O_2 evolution [Joliot P, Barbieri G and Chabaud R (1969) Photochem Photobiol 10: 309–329] has had a lasting impact on current photosynthesis research. Such oscillations were explained by introducing the *cycle* of flash-induced transitions of states of an oxygen evolving complex [Kok B, Forbush B and McGloin M (1970) Photochem Photobiol 11: 467–475]. In order to describe dampening of the oscillations in the O_2 evolution the Kok model introduces *misses*, which characterize the failure to advance the S-states, and *double hits*, which characterize the two-step advancement of S-states. While the Kok model has been successfully used for over 30 years for interpretation of experimental data in photosynthesis, until recently there was no simple analytical solution for it. A much overdue analytical solution is presented here. Correlation of S-states transitions at the donor side of the PS II and Q_B transitions at the acceptor side leads to the recognition of two different reaction sequence cycles of PS II, so called cycles *V* and *W* [Shinkarev VP and Wraight CA (1993a) Proc Natl Acad Sci USA 90: 1834–1838]. In each of these cycles the quantitative description of binary oscillations of the Q_B semiquinone can be obtained from the analytical solution for individual S-states. Standard application of the Kok model consists in finding misses and double hits from measured sequence of flash-induced O_2 evolution. In alternative approach known kinetic and thermodynamic data are used to reconstruct period-four oscillations of O_2 evolution. This general kinetic model allows calculation of all transition probabilities in the Kok model from first principles. The model predicts that misses in the *V* and *W* cycles are different. The general character of the model allows simultaneous consideration of different flash-induced oscillation phenomena at the donor and acceptor sides of PS II, without limitations on the number of states needed to be considered.

Abbreviations: Chl – chlorophyll; Cyt – cytochrome; D1 and D2 – polypeptides of the PS II reaction center; DCMU – 3-(3,4-dichlorophenyl)-1,1-dimethyl urea; K_{nY} – equilibrium constant of reaction $S_nY_Z^+P680 \leftrightarrow S_{n+1}Y_ZP680$; K_{YP}^n – equilibrium constant of reaction $S_nY_ZP680^+ \leftrightarrow S_{n+1}Y_Z^+P680$; L_{AB} – equilibrium constant of reaction $Q_A^-Q_B \leftrightarrow Q_AQ_B^-$; M_i – different redox states of OEC, where i = 0,1,2,3 represents the number of oxidizing equivalents; M_{AB}^1 – equilibrium constant of reaction $Q_AQ_B \leftrightarrow Q_AQ_BH_2$; M_{AB}^2 – equilibrium constant of quinol replacement $Q_AQ_BH_2 \leftrightarrow Q_AQ_B$; n – number of the flashes; OEC – oxygen evolving complex; $p_1,\ldots, p_n$ – probabilities of individual states of RC; **p**(n) – the *row* vector of probabilities of S-states after n-th flash, $p(n) = (p_0(n), p_1(n), p_2(n), p_3(n))$; **p**(0) – the row vector of initial conditions, $p(0) = (p_0(0), p_1(0), p_2(0), p_3(0))$; P or P680 – primary electron donor of the reaction center of PS II; Pheo – pheophytin; PQ – plastoquinone; PS II – Photosystem II; $Q = \{q_{ij}\}$ – matrix of transition probabilities, each element of which, q_{ij} (i, j = 1, 2, 3, 4) is the probability for flash-induced transfer of the OEC from state S_{i-1} to state S_{i-1}; Q_A – primary acceptor plastoquinone, bound to the D2 protein; Q_B – secondary acceptor plastoquinone located on the D1 protein; Q_B^- – Q_B semiquinone; QH_2 – plastoquinol; $r = [(\alpha - \beta)^2+\gamma^2]^{1/2}$; R – matrix transpose to Q, $R = Q^T$; RC – reaction center; S_n – redox states of the OEC, where n = 0,1,2,3 represents the number of oxidizing equivalents; Y_D – redox active tyrosine of the D2 polypeptide; Y_Z – redox active tyrosine of the D1 polypeptide, fast electron donor to P680; Y(n) – oxygen yield after n-th flash; λ – characteristic value (eigenvalue) of a matrix; s_i – initial conditions for i-th S-state, $s_0 = p_0(0)$, $s_1 = p_1(0)$, $s_2 = p_2(0)$, $s_3 = p_3(0)$; $z = s_0 - s_1 + s_2 - s_3$; s_{ij} – difference $s_i - s_j$, where i and j are congruent modulo *4* indexes; *V*- cycle – correlated cycle of transitions donor and acceptor sides of PS II having S_1Q_B state; U – unitary matrix, transforming matrix Q to diagonal form; *W*- cycle – correlated cycle of transitions donor and acceptor sides of PS II having $S_1Q_B^-$ state; α – traditionally used notation for the miss in the Kok model; β – traditionally used notation for the double hit in the Kok model; γ – traditionally used notation for the hit in the Kok model; λ_1, λ_2, λ_3, λ_4 – eigenvalues of matrix Q; Λ – the *diagonal* matrix with eigenvalues λ_1, λ_2, λ_3, λ_4 of matrix Q; φ – $\arcsin(\gamma/r)$; $\rho = (s_{02}^2 + s_{13}^2)^{1/2}$; $\mu = \alpha - \gamma + \beta = 1 - 2\gamma$; $\theta_k = \arcsin((s_k - s_{k+2})/\rho)$

I. Introduction

The light-driven oxidation of water by Photosystem II (PS II) of higher plants, algae and cyanobacteria, is the main source of atmospheric oxygen. The water oxidizing enzyme complex is coupled to the photosynthetic reaction center (RC) of PS II, a heterodimer of the D1 and D2 polypeptides with a general architecture similar to that of the reaction center of purple bacteria (reviewed in Debus 1992; Rutherford et al 1992; Diner and Babcock, 1996; Renger, 1997; Ke, 2001; Blankenship, 2002; Renger, 2003; Chapter 4, Nixon et al.).

Figure 1 shows the simplified scheme of kinetics of electron transfer in the PS II. Following light excitation of the RC, an electron is passed from the primary electron donor P680 (P) to pheophytin (Pheo), and subsequently to the primary quinone acceptor Q_A in 0.2–0.6 ns (Eckert et al., 1988), producing a plastoquinone anion-radical, and finally to the secondary quinone acceptor Q_B in 0.1–0.6 ms (Bowes and Crofts, 1980). The oxidized primary donor, $P680^+$, is re-reduced by a donor, Y_Z, which is a tyrosine residue of the D1 subunit (Tyr 161; Debus et al., 1988; Metz et al., 1989). Subsequent activation of P680 further reduces the secondary quinone, which unlike Q_A is a two-electron acceptor (Bouges-Bocquet, 1973; Velthuys and Amesz, 1974; Hangulov et al., 1974). After each two turnovers, quinol is replaced by quinone in the Q_B site, releasing pairs of reducing equivalents to the quinone pool for transfer to the cytochrome b_6f complex (Crofts and Wraight, 1983).

Figure 2 shows classic 'oscillation experiments' indicating that the activation of PS II by a series of short actinic flashes leads to O_2 evolution with a periodicity of four and to binary oscillations of the acceptor quinone. Several phenomenological models were proposed to explain period-four oscillations (see e.g., Joliot et al., 1969; Mar and Govindjee, 1972), but only the model suggested by Kok and co-authors (Kok et al., 1970; Forbush et al., 1971) withstood the test of time

II. The Kok Model of Oxygen Evolution

A. Basics

In order to describe period-four oscillations in the flash-induced O_2 evolution (Fig. 2A, B), Kok et al. (1970) introduced a phenomenological model (Fig.3), essential elements of which are summarized below:

- Oxygen evolution occurs in independent (non-cooperative) units, the so called oxygen evolving complexes (OEC), each of which is fully operational when activated by light;
- 4 light activation steps are needed for complete cycle of reactions leading to O_2 evolution;
- 4 oxidative equivalents are accumulated before

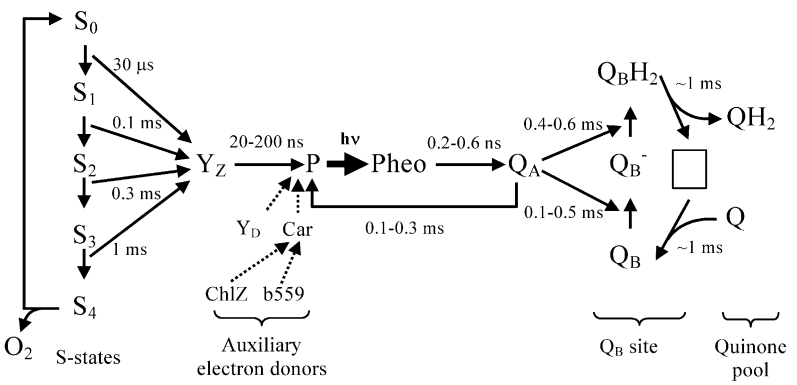

Fig. 1. The simplified scheme of kinetics of electron transfer in the reaction center of PS II. P is the primary electron donor of the reaction center of PS II (P680); Y_Z is tyrosine-161 on the D1 polypeptide (Debus et al., 1988; Metz et al., 1989), which serves as a donor of electrons to $P680^+$; Pheo, is pheophytin; Q_A, Q_B are the primary and secondary acceptor quinones; S_0,…, S_4 are different states of oxygen evolving complex (OEC); Y_D is the redox active tyrosine on the D2 polypeptide.

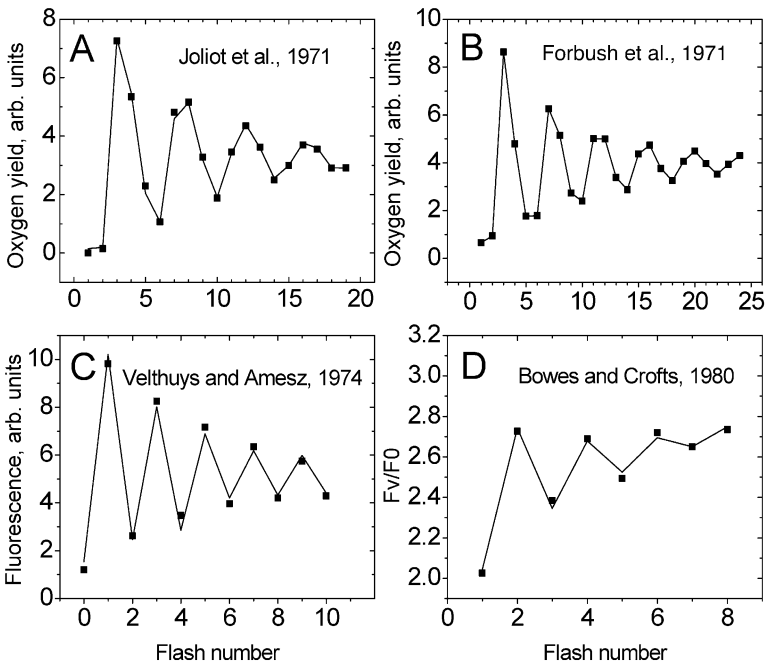

Fig. 2. Classic experiments describing flash-induced charge accumulation at the donor (A, B) and acceptor (C, D) sides of PS II. Panels C and D - Flash-induced binary oscillations of fluorescence measured by Velthuys and Amesz (1974) and by Bowes and Crofts (1980), respectively. The fit (solid lines) of the experimental points (squares) with Eq. 39 (plus trend) gave $\gamma = 0.91$ for panel C and $\gamma = 0.83$ for panel D.

O_2 evolution, and as a consequence, 2 water molecules are used for 1 molecule of O_2 evolved;

- 5 formal states of PS II with different number of oxidizing equivalents, S_0, S_1, S_2, S_3, and S_4 were introduced to describe observed oscillations of oxygen evolution (Kok et al., 1970);
- Oxygen evolution occurs during $S_4 \rightarrow S_0$ transition;
- Dampening of oscillations in O_2 yields is due to the presence of 'misses' (α) and 'double hits' (β). Observed O_2 evolution can be described by assuming that misses and double hits are the same for all transitions;
- Only states S_1 and S_0 are stable in the dark. All other states 'deactivated' back to S_1 and S_0 states. After prolong dark adaptation 25% of OECs are in the state S_0 and 75% in the S_1 state.

1. Interpretation of S-States

At least two different, although connected, descriptions of the 'S-states' have been widely used in the literature (Kok et al., 1970; Joliot and Kok, 1975; Vos et al., 1991; Witt, 1991; Debus 1992; Diner and Babcock, 1996).

According to the first approach, the S-states are formal states of PS II with different number of oxidizing equivalents needed to describe the observed flash-induced period-four oscillations of O_2 evolution (Kok et al., 1970). In this case, S-state is not single state of enzyme but fast equilibrating sets of states on the donor side with certain number of oxidizing equivalents. This approach takes into account that period-four oscillations in O_2 evolution are due to synchronous light activation of PS II. Because light activation of PS II depends on the state of the acceptor side of PS II, the description of O_2 evolution should take into account both donor and acceptor sides (Shinkarev and Wraight, 1993a,b).

According to the second approach, the S-states are

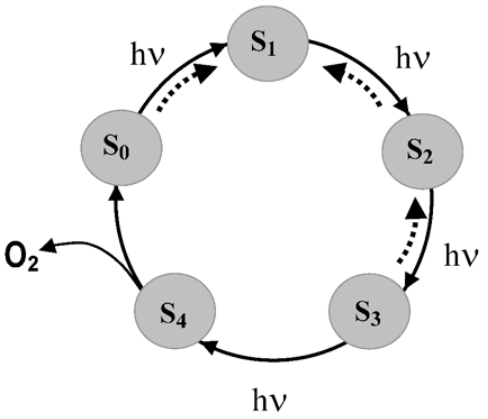

Fig. 3. The Kok model of O_2 evolution explaining period four in flash-induced O_2 evolution (Kok et al., 1970). The dashed arrows indicate processes of dark relaxation of S-states.

redox states of the Mn-containing OEC itself (sometimes denoted as M, M^+, M^{2+}, M^{3+}, see for example, Vos et al., 1991).

To illustrate the definition of S-states as the sum of the fast equilibrating states of the RC, consider the donor side of PS II only. The fast electron transfer between Y_Z and P680 (faster than 0.2 μs), as well as between S-states and Y_Z^+ (faster than 1–2 ms) leads to 'equilibration' of the 'hole' between OEC, Y_Z, and P680 within 1–2 ms. Thus, on a time scale >1–2 ms, oxidizing equivalents can be presented as a mixture of fast-equilibrating states of PS II donor side. For example, S_1 and S_2 can be written as follows:

$$S_1 = M_0 Y_Z P^+ \xleftrightarrow{K^0_{YP}} M_0 Y_Z^+ P \xleftrightarrow{K_{0Y}} M_1 Y_Z P$$

$$S_2 = M_1 Y_Z P^+ \xleftrightarrow{K^1_{YP}} M_1 Y_Z^+ P \xleftrightarrow{K_{1Y}} M_2 Y_Z P$$

where M_0, M_1 and M_2 are different redox states of OEC. K_{nY} is the equilibrium constant of reaction $M_n Y_Z^+ P680 \leftrightarrow M_{n+1} Y_Z P680$; K^n_{YP} is the equilibrium constant of reaction $M_n Y_Z P680^+ \leftrightarrow M_n Y_Z^+ P680$.

Figure 4 shows light-induced transitions between different states of the donor side of PS II, presented as sequence of fast equilibrating quasistates. One can see that, from kinetic point of view, the same S-state incorporates different redox states of oxygen evolving complex (here M).

2. Hypothesis of the Five Discrete States and Four Light Activations

The original Kok model explained the observed pattern of O_2 evolution by introducing five discrete states, S_0, S_1, S_2, S_3, and S_4, that could be accessed by four light activations of PS II (Figs. 3 and 4). The transient state S_4, is usually excluded from consideration in kinetic models of O_2 evolution (Joliot and Kok, 1975).

One of the reasons why the four-state Kok model frequently describes the observed flash-induced O_2 evolution is that this model incorporates apparent states (quasistates), which are the sums of quickly equilibrating states of the donor and acceptor sides (Fig. 4). This effectively diminishes the number of states and transitions that has to be taken into consideration. But in turn, it puts some limitations on the time frame of consideration, which should be long enough to allow such averaging, but short enough to avoid significant relaxation between flashes.

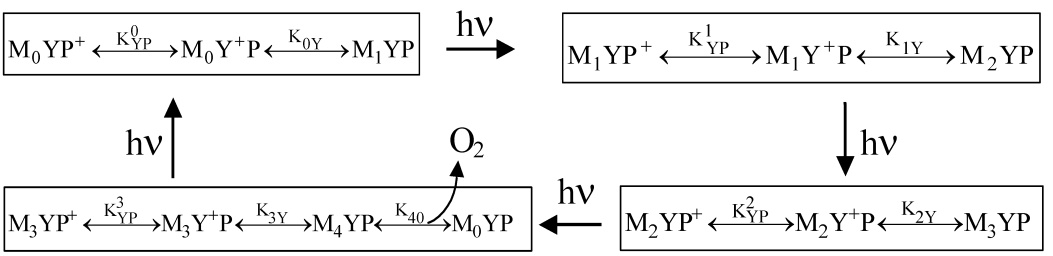

Fig. 4. Light-induced transitions on the donor side of PS II as sequence of fast equilibrating quasistates, extending the scheme presented in Fig. 3. Here M_i are different redox states of OEC, P is the primary electron donor of the reaction center of PS II (P680) and Y is redox active tyrosine serving as fast electron donor to $P680^+$. K_{YP}^n is the equilibrium constant of the transition $M_n YP^+ \leftrightarrow M_n Y^+ P$; K_{nY} is the equilibrium constant of the transition $M_n Y^+ P \leftrightarrow M_{n+1} YP$, and K_{40} is the equilibrium constant for the reaction: $M_4 YP \leftrightarrow M_0 YP$. Adapted from Shinkarev and Wraight (1993a).

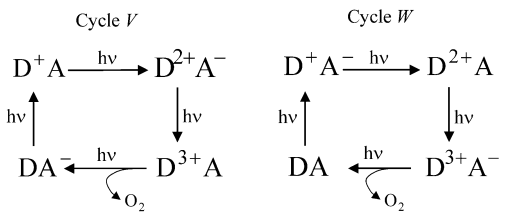

Fig. 5. Two cycles of O_2 evolution. The presence of two cycles is due to the difference in the initial state of quinone acceptors. Here D^{i+} indicates the state of the donor side of the RC of PS II in which i electrons have been extracted, and A^- means the acceptor side of the RC (Q_A+Q_B) containing one electron (Shinkarev and Wraight, 1993a,b). Here each state of PS II is viewed as fast-equilibrating states at its donor *and* acceptor sides. Simplified representation of *V* and *W* cycles in traditional notations is shown in Fig. 7.

Note that the Kok model introduces the lowest number of states, needed to describe oscillations of O_2 evolution yield. Generally, there may be more states, due to (i) incomplete dark relaxation of RCs after each flash; (ii) internal heterogeneity of PS II; (iii) different initial conditions; (iv) inactivation of RCs during the flash series; (v) nonhomogenous character of the transition probabilities, and others. In some cases, the introduction of extra states improves the fitting of experimental data (Engels et al., 1994).

3. Two Cycles

The light activation of PS II initiates simultaneous electron transfer at its donor and acceptor sides. This instant correlation of transitions at the donor and acceptor sides necessitates their simultaneous considerations. As a result, one should consider two distinct cycles of PS II turnover, arising from convolution of four long-living states of the donor side with two long-living states of the acceptor side (Fig. 5). In each cycle, single turnover of OEC is coupled with two turnovers of quinone acceptor complex. These two different internal cycles of PS II (so-called cycles *V* and *W*) are characterized by different transition probabilities (Shinkarev and Wraight, 1993a,b).

Each of the states in both cycles is a quasi-state obtained through equilibrium between many elementary states of the RC. As an example, Fig. 6 shows states D^+A^- and $D^{3+}A^-$ in cycle *W* (see Shinkarev and Wraight, 1993, for details). These quasistates are valid only during the time scale where equilibration between the elementary RC states has already been achieved. This occurs from about 1 ms. Fig. 7 shows the cycles *V* and *W* represented by most probable states in each quasi-state.

Using schemes above (Figs. 5 and 6) one can calculate the flash-induced transitions in PS II and estimate misses for each transition. Such approach allows one to estimate the dependence of O_2 evolution on values of respective rate and equilibrium constants governing donor and acceptor sides of PS II (Shinkarev and Wraight, 1993a,b).

4. States Accumulated After Dark Adaptation

To fit the observed O_2 evolution pattern, Kok et al. (1970) assumed that after prolonged dark adaptation only S_0 (≈20–30%) and S_1 (≈80–70%) states are ac-

$$
D^+A^- \equiv \begin{array}{ccccc}
S_0Y_ZP^+Q_A^-Q_B & \xleftrightarrow{K^0_{YP}} & S_0Y_Z^+PQ_A^-Q_B & \xleftrightarrow{K_{0Y}} & S_1Y_ZPQ_A^-Q_B \\
\updownarrow L_{AB} & & \updownarrow L_{AB} & & \updownarrow L_{AB} \\
S_0Y_ZP^+Q_AQ_B^- & \xleftrightarrow[K^0_{YP}]{} & S_0Y_Z^+PQ_AQ_B^- & \xleftrightarrow[K_{0Y}]{} & S_1Y_ZPQ_AQ_B^-
\end{array}
$$

$$
D^{3+}A^- \equiv \begin{array}{ccccc}
S_2Y_ZP^+Q_A^-Q_B & \xleftrightarrow{K^2_{YP}} & S_2Y_Z^+PQ_A^-Q_B & \xleftrightarrow{K_{2Y}} & S_3Y_ZPQ_A^-Q_B \\
\updownarrow L_{AB} & & \updownarrow L_{AB} & & \updownarrow L_{AB} \\
S_2Y_ZP^+Q_AQ_B^- & \xleftrightarrow[K^2_{YP}]{} & S_2Y_Z^+PQ_AQ_B^- & \xleftrightarrow[K_{2Y}]{} & S_3Y_ZPQ_AQ_B^-
\end{array}
$$

Fig. 6. Quasistates of cycle *W* as the set of fast equilibrating states of reaction center of PS II. K_{YP}^2, L_{AB}, K_{0Y}, K_{2Y} are respective equilibrium constants of electron transfer. Here vertical transitions correspond to electron transfer at the acceptor side and horizontal transitions correspond to electron transfer at the donor side of RC.

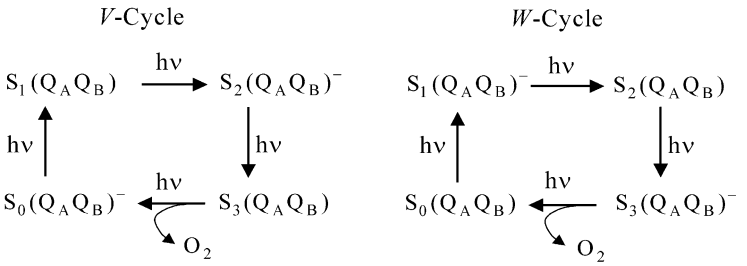

Fig. 7. Simplified schemes of flash-induced transitions in the PS II, indicating coexistence of S-state transitions at the donor side and Q_B transitions at the acceptor side (Shinkarev and Wraight, 1993a). Note that for each S-state, two cycles differ by the state of quinone acceptors only.

cumulated. There are at least two explanations for apparent ratio of S_0 and S_1 found in experiments. First explanation was originally suggested by Kok et al. (1970) and assumes equilibrium between S_0 and S_1. The second explanation (Velthuys and Visser, 1975; Vermaas et al. 1984) assumes that only the S_1 state is stable in the dark and the presence of the S_0 state is only apparent due to the presence of a donor of electrons, which reduces the S_2 to S_1 between flashes.

Using EPR Babcock and Sauer (1973) discovered an electron donor to the S-states (Y_D) with a time constant of about 1 s. The presence of this donor in the fraction of RCs after dark adaptation was used to explain the large 'miss' (Babcock and Sauer, 1973). From comparison of flash-induced oxygen evolution and kinetics of Y_D, Velthuys and Visser (1975) concluded that reduction of S-states by Y_D is responsible for the appearance of S_0 and that all centers revert to state S_1 in the dark. Vermaas et al. (1984) reported that changing the time between flashes leads to changes in the pattern of O_2 evolution corresponding to changes in the initial conditions. It was found that the amount of observed S_0 level is mainly due to the presence of a relatively slow ($t_{1/2}$ = 1–2 s) electron donor (Y_D) which reverses some light-induced transitions in about 25% of RCs as follows: $Y_D S_2 \rightarrow Y_D^+ S_1$; $Y_D S_3 \rightarrow Y_D^+ S_2$. Thus, the ratio $S_0/(S_0+S_1) \approx 0.25$ obtained at low flash frequencies after prolonged dark adaptation reflects the presence of reduced Y_D in a fraction of RCs (Velthuys and Visser, 1975; Vermaas et al., 1984; Styring and Rutherford, 1987; Naber, 1989; Isgandarova et al., 2003). An extension of the Kok model of oxygen evolution which takes into account the effect of fast electron donation from Y_D has been suggested by Vass et al. (1990) and by Isgandarova et al. (2003).

Because Y_D is very slowly re-reduced — slower than 5 min — the effect of this donor can be minimized by using one preflash to oxidize this donor. Therefore, the standard approach of removing Y_D from consideration is the use of one preflash with relatively short (5 min) dark-adaptation thereafter. The significant advantage of this preflash is the synchronization of all OECs in the S_1 state. Indeed, those OECs, which originally were in S_0 state, will transfer to the S_1 state, while those OECs, which originally were in the S_1 state will transfer to the S_2 state and relatively quickly return to the S_1 state. One should keep in mind that giving one preflash will also change the state of the acceptor side of PS II.

5. Initial Conditions

In most cases, only distribution between the S_0 and S_1 states before the flash series is taken into account (Lavergne, 1991; Messinger and Renger, 1993).

There are at least three reasons why other S-states can also exist in the dark before a flash series: (i) The time of dark adaptation may not be enough for complete relaxation; (ii) The reversibility of all reactions on the donor side can lead to the presence of some residual equilibrium concentrations of different S-states; (iii) the presence of reduced tyrosine Y_D after single preflash. Therefore, a reasonable approach of analyzing the flash-induced O_2 evolution pattern will be one which does not fix the initial conditions, but determines them directly from experimental data (Delrieu and Rosengard, 1987, 1991). For example, Delrieu and Rosengard (1988) found that in freshly-prepared thylakoids $[S_2(0)] \approx 5\%$.

It is important to note that initial conditions should be known not only for the donor, but also for the acceptor side of the RC.

B. Transition Probabilities

In order to describe dampening of the period-four oscillations in the flash-induced O_2 evolution Kok

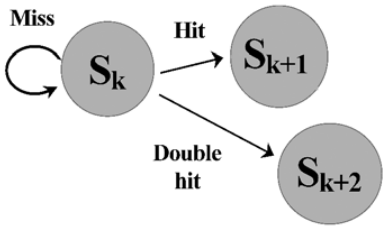

Fig. 8. Light-induced transition probabilities for each S-state in the standard Kok model.

et al. (1970) introduced misses, which characterize the probability of failure to advance the S-states, and double hits, which characterize the probability of advancement of S-states two at a time (Fig.8). The scheme of the transitions between S-states in the generalized Kok model (specific misses, double hits and zero step advances for each flash) is shown in Fig. 9.

The main goal of the kinetic analysis is finding transition probabilities from experimental flash-induced yields of O_2. In most cases, equal misses are assumed for all turnovers (Kok et al. 1970).

1. Misses

To explain dampening of the period-four oscillations in the flash-induced O_2 evolution, Kok et al. (1970) introduced the concept of a miss, which is the failure to proceed from one given S-state to the next S-state after light activation of the reaction center.

a. The Origin of Misses

Different physiological explanations have been proposed for reasons behind misses. Babcock and Sauer (1973) suggested that misses can be explained by the presence of a fast donor (Y_D), which reduces the S-states and reverses the effect of light. Joliot and Kok (1975) suggested that the misses are due to both the absence of photosensitivity of some centers and to

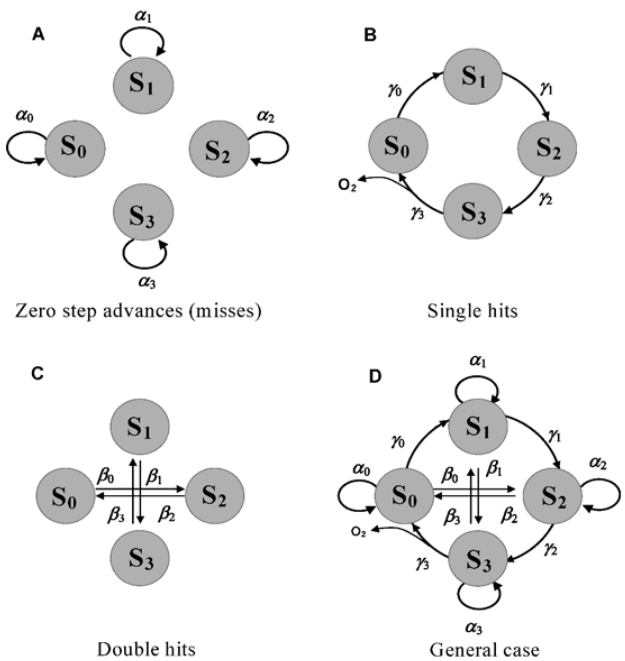

Fig. 9. The Kok model of flash-induced transitions in PS II. Scheme shows the four S-states, S_0, S_1, S_2 and S_3 (the transient state S_4 is excluded) - and transitions between them, presented as combinations of (A) zero-step advancements α_0, α_1, α_2 and α_3 (misses), (B) one-step advancements γ_0, γ_1, γ_2 and γ_3 (hits), (C) two-step advancements β_0, β_1, β_2 and β_3 (double hits) and (D) all transition probabilities together. Note that $\alpha_k + \gamma_k + \beta_k = 1$. O_2 evolution induced by double hits is not shown.

back reactions between flashes. Meunier and Popovic (1990) connected some misses with the reduction of the quinone pool between flashes. Shinkarev and Wraight (1993a,b) suggested that some misses can arise from to the presence of $P680^+$ or Q_A^- before the flash because of the reversibility of the reactions at the donor and acceptor sides. Misses may arise also from the rapid $P^+Q_A^-$ charge recombination, which can partially compete with the forward electron transfer reactions (Joliot and Kok, 1975; Shinkarev and Wraight, 1993b). Frequently the source of misses is more trivial and is due to the absence of light saturation for actinic flashes used.

Figure 10 illustrates the dependence of flash-induced O_2 evolution on misses, calculated from the Kok model. An increase of the miss value shows a drastic effect on the flash-induced O_2 evolution pattern. For a zero miss (panel A) one observes non-dampening oscillations with maximum after third, seventh, etc. flashes. Even a relatively small miss value of 0.1 leads to the significant dampening of oscillations. Further increase of the miss value to 0.4 leads to disappearance of the oscillations.

b. Are Misses the Same for Each Transition?

Kok et al. (1970) did not initially exclude the possibility that each miss and double hit could be different. However, they found that equal misses provide a satisfactory fitting of the experimental points. This conclusion was strongly supported by Thibault (1978), who found that the root mean square deviation between the Kok model with homogeneous transition probabilities and experimental sequences is better than 1%. He showed that excluding the first flash from the sequence decreases the deviation by two- to three-fold. As a result, the assumption of equal misses is predominantly used for the analysis of O_2 evolution (Engels et al., 1994; Messinger and Renger, 1994; Seeliger et al., 1997), absorbance changes of the OEC (Lavergne, 1991), proton release (Lavergne and Junge, 1993), electrochromic changes (Rappaport et al., 1994), and other quaternary processes in PS II.

Delrieu pioneered the explanation of different anomalies of O_2 evolution by introducing different values of misses. Using a least squares method for fitting experimental points, Delrieu (1974, 1983) found that fitting could be improved further if one of the misses is different from the others. Bouges-Bocquet (1980) suggested that all misses are different and estimated that largest misses should be observed for S_3 and S_2 states. Naber et al. (1993) stated that fitting could also be improved by assuming that two out of four misses are different.

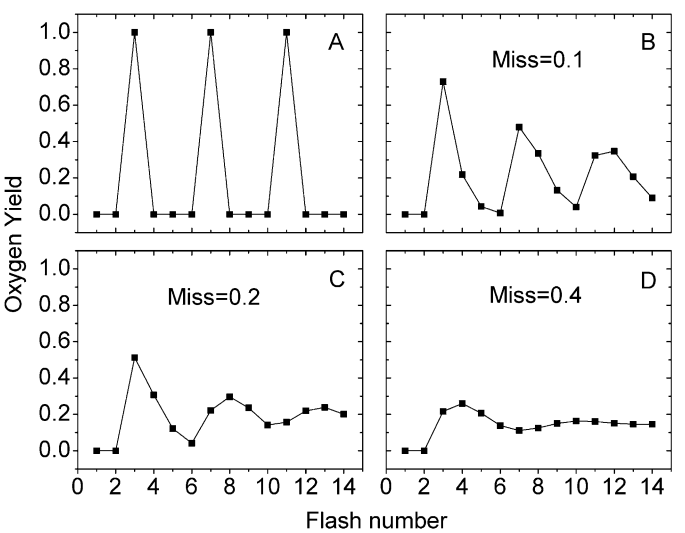

Fig. 10. Effect of miss value on the O_2 evolution yields, calculated from the Kok model for zero double hit and for (0, 1, 0, 0) initial conditions. O_2 evolution was estimated as (hit +double hit) × (fraction of S_3) + (double hit) × (fraction of S_2). Miss is equal to 0 (A), 0.1 (B), 0.2 (C) and 0.4 (D).

Different misses were used to explain absence of saturation of $S_2 \rightarrow S_3$ transition on light intensity (Delrieu, 1983). It is possible that this effect is due to the presence of the semiquinone Q_B^- before the second flash (Vermaas et al., 1984; Shinkarev and Wraight, 1993a,b).

We should stress here that the use of the O_2 evolution itself for localization of different misses during the cycle has principal uncertainty due to the fact that almost any permutation of misses gives the same O_2 evolution (see Fig. 15 for details), thus limiting the way of finding the position of different misses in the Kok model (Delrieu, 1974).

The inability of O_2 pattern to discriminate between equal and different misses does not mean that they are the same. Misses can originate from the equilibrium presence of part of P680 in the oxidized form and part of Q_A in reduced form, as well as from fast back reactions between Q_A^- and $P680^+$, both of which can be modulated by S-states. Using a general kinetic model, Shinkarev and Wraight (1993a,b) found that both sources of misses before establishing of the quasiequilibrium and during of the dark relaxation between flashes are responsible for the dependence of the miss on S-state. The main result of such calculations is that all misses are different and that the largest misses are for the $S_2 \rightarrow S_3$ and for $S_3 \rightarrow S_0$ transitions for neutral pH (arising from the small equilibrium constant of electron transfer between Y_Z and P680 for these transitions). Similar conclusion has been reached by de Wijn and van Gorkom (2002) who estimated the relative amplitudes of the misses from the kinetics of chlorophyll *a* fluorescence yield transients induced by a flash series. The authors suggested that misses are mostly due to failure of the reduction of the $P680^+$ by the Y_Z before the charge separation is lost by recombination.

2. Double Hits

Initially double hits were introduced to take into account double light activation of PS II due to the long duration of flash (Kok et al., 1970). Indeed, double hits are smaller if one uses laser flashes instead xenon flashes (Weiss and Sauer, 1970; Joliot and Kok, 1975). Effect of double hits on the flash-induced O_2 evolution is illustrated in Fig. 11.

Jursinic (1981) found that double hits induced by 3 μs xenon flashes increased 3-fold in chloroplasts, incubated with ferricyanide. This effect is possibly due to oxidation of non-heme iron. If the non-heme iron is oxidized before the flash, the first photomobilized electron quickly reduces none-heme iron (~7 μs, Diner and Petrouleas, 1987) and thus RC can be activated second time by the same flash. This source of

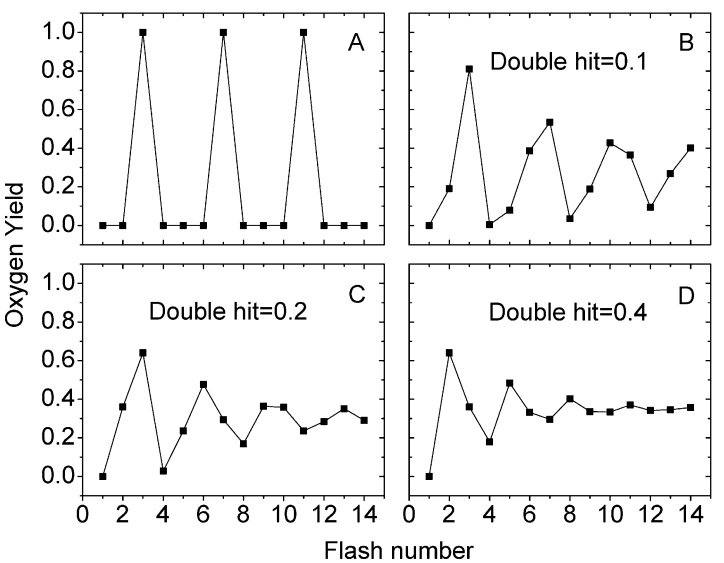

Fig. 11. Effect of double hit value on the O_2 evolution yields, calculated from the Kok model for zero miss and for (0, 1, 0, 0) initial conditions. Double hit is equal to 0 (A), 0.1 (B), 0.2 (C) and 0.4 (D).

double hit can be excluded by using a single preflash, which will reduce non-hem iron.

The other reason for the 'apparent' presence of double hits in the laser or short xenon flash-induced O_2 evolution can be the usage of the simple Kok model. Indeed, if one introduces extra parameters in the model such as initial conditions (Delrieu and Rosengard, 1991), or unequal misses (Delrieu, 1983; Naber, 1989), the double hit usually decreases. The artificial appearance of double hits during application of the simple Kok model can be illustrated by fitting theoretical curves generated with zero double hits (see Fig. 17 below).

C. Dark Relaxation of S-States

1. Different Pathways of S-State Relaxation

For a complete description of the kinetics of O_2 evolution it is necessary to incorporate changes of the OEC between individual flashes and between flash series.

The light activation of PS II populates S-states equally (Joliot and Kok, 1975). S_2 and S_3 can 'deactivate' in the dark to S_1 (Kok et al., 1970), resulting in approximately 3/1 ratio for S_1 and S_0 after 5 min dark adaptation. S_2 and S_3 states can be reduced by Y_D^{red} (Babcock and Sauer, 1973; Velthuys and Visser, 1975; Vermaas et al., 1984, Styring and Rutherford, 1987), acceptor quinones (Radmer and Kok, 1973; Diner, 1977; Rutherford et al., 1982; Robinson and Crofts 1983), or cytochrome b_{559} (Cyt b_{559}) (Buser et al., 1992).

It was also shown that Y_D^{ox} can oxidize S_0 to S_1 in pH-dependent manner (Vass and Styring, 1991). Such behavior of Y_D was explained by the value of redox potential of the Y_D^+/Y_D couple which is lower than that of S_2/S_1 and S_3/S_2 couples and higher than that of S_1/S_0 couple (Styring and Rutherford, 1987; Vass and Styring, 1991).

Some known processes of dark relaxation of the OEC between flashes are summarized in Fig.12. The formation of S_0 during the reaction of S_1 with reduced acceptors is feasible both kinetically and thermodynamically. However, the accumulation of S_1 after long dark adaptation creates the impression that S_0 state can be reached only during normal Kok cycle and is not attainable during backreaction of S_1 with photoreduced acceptors (Joliot and Kok, 1975). The puzzling apparent absence of this reaction is possibly due to the parallel S_0 oxidation by Y_D (Styring and Rutherford, 1987; Vass and Styring, 1991), or by other auxiliary high-potential component originating in PS II.

D. Hypothesis of Homogeneous Misses and Double Hits

The standard Kok model suggests that misses and double hits do not depend on the flash number. This means, for example, that the miss during transition $S_1 \rightarrow S_2$ is the same after the first, fifth, etc. flashes. Lavorel (1976) showed that the hypothesis of homogeneous transition probabilities is reasonably satisfied along the flash sequence. It can be seen independently from data shown in Fig. 2 A. One can find that misses determined from 2–11 and from 9–19 flashes are 10.6% and 11.7%, respectively.

It is evident from current understanding of PS II function that the suggestion of homogeneous transition probabilities is justified only for a relatively long time (> 20 ms) between flashes (the cytochrome b_6f complex and PS I can oxidize quinol pool only with limiting time of 5–50 ms). If the PQ pool is not oxidized between flashes, quinone exchange with PS II could diminish, which will lead to increase of Q_A^-, which, in turn, can lead to an increase of misses (see, however, Meunier and Popovic, 1990). Actually, any imbalance between donation and accepting electrons to the PQ pool can lead to flash-number dependence of transition probabilities.

In fact, it is easier to indicate the conditions that should lead to the violation of this hypothesis than to provide the right conditions to satisfy it. At least the following two conditions have to be satisfied to provide the homogeneity of transition probabilities: (i) the first flash of the trace should be excluded from the analysis. Usually after prolong dark adaptation Y_D is reduced and non-heme iron is oxidized. The first flash will oxidize former and reduce latter; (ii) only short sequences (as a rule, not more than 10–15 flashes) should be used for analysis. Otherwise one should expect the imbalance between reduction and oxidation of the PQ pool.

1. Heterogeneity Leads to Mixture of Different Oscillation Patterns

The original Kok model assumed the absence of any type of heterogeneity of PS II. However, many different types of heterogeneity of PS II have been demonstrated experimentally (Govindjee, 1990; Lavergne and Briantais, 1996). Heterogeneity in the state of Y_D

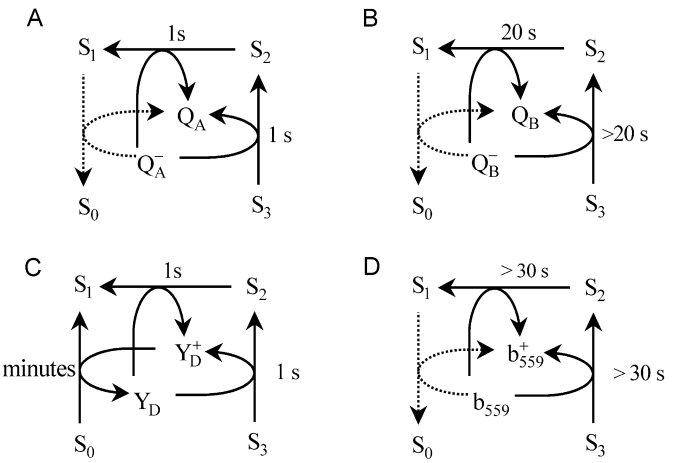

Fig. 12. Schemes of dark transitions of the S-states. (A) Dark relaxation of S-states due to interaction with Q_A (these reactions are significant when the reaction with Q_B is inhibited by herbicides such as DCMU). (B) Reaction of S-states with Q_B. (C) Interaction of S-states with Y_D. (D) Possible interaction of S-states with Cyt b_{559}. Note that S-states here are fast equilibrating states of donor side only. While thermodynamics allows S_0 formation via reduction of S_1 by Q_A^-, Q_B^-, and Cyt b_{559} (b_{559}^+), the stability of S_1 in the dark indicates that these reactions should be compensated by reaction(s) leading to S_0 oxidation (similar to that shown in panel C). All transitions leading to the formation of S_0 are indicated by dotted lines, to indicate their questionable nature.

(reduced or oxidized), non-heme iron, quinone acceptors, Cyt b_{559}, can easily produce deviations from the expectations of the Kok model. Table 1 shows some (definitely not all!) types of heterogeneity, which can complicate the observed pattern of O_2 evolution. In many cases the observed heterogeneity can be minimized, but it can't be eliminated completely.

E. The Kok Model as a Markov Chain

1. Definitions

The Kok model of O_2 evolution can be naturally formulated as a Markov chain (Delrieu 1974), i.e., a stochastic process with discrete states and discrete

Table 1. Different types of heterogeneity in PS II.

Source of heterogeneity	Possible different states before flash series	Consequences of heterogeneity
Redox state of tyrosine Y_D	$Y_D^+ \approx 70$ % $Y_D \approx 30$ %	Reduction of S-states in PS II with reduced Y_D increases apparent misses
Redox state of non-heme iron	Fe^{2+}/Fe^{3+}	Double hit is higher when Fe^{3+} is present, even if short xenon flash is used
Occupation of Q_B binding site	Q_B site can be vacant, occupied by quinone, semiquinone, or quinol. Different states of Q_B site could lead to observation of two cycles *V* and *W*	Can modify multiple turnovers of the RC
Size of quinone pool per PS II	Local quinone pool has different number of quinone molecules per PS II	Can modify multiple turnovers of the RC
Low/high potential forms of Cyt b_{559} (L/H)	Cyt b_{559}L oxidized Cyt b_{559}H reduced	Can modify the relaxation of S-states between flashes
Antenna heterogeneity	Different quantum yields	Can change the misses

times (reviewed in Feller, 1970). The Markov chain can be defined by introducing:

(i) The row vector of probabilities of S-states, $\mathbf{p}(n) = (p_0(n), p_1(n), p_2(n), p_3(n))$, where $p_i(n)$ is the probability to find the OEC of PS II in the S_i state (i = 0,1,2,3) after n-th flash (n = 0,1,2,…). For n = 0 row vector, $\mathbf{p}(0) = (p_0(0), p_1(0), p_2(0), p_3(0)) \equiv (s_0, s_1, s_2, s_3)$ describes initial (before the first flash) conditions.

(ii) The matrix $Q = \{q_{ij}\}$ of the transition probabilities:

$$Q = \{q_{ij}\} = \begin{pmatrix} \alpha_0 & \gamma_0 & \beta_0 & 0 \\ 0 & \alpha_1 & \gamma_1 & \beta_1 \\ \beta_2 & 0 & \alpha_2 & \gamma_2 \\ \gamma_3 & \beta_3 & 0 & \alpha_3 \end{pmatrix} \qquad (1)$$

where α_i (i = 0, 1, 2, 3) are the 'misses', γ_i (i = 0, 1, 2, 3) are the 'hits', and β_i (i = 0, 1, 2, 3) are the 'double hits'.

Each element q_{ij} (i, j = 1, 2, 3, 4) of this matrix is the transition probability for flash-induced transition of the OEC from state S_{i-1} to state S_{j-1}. The matrix in Eq. 1 can be presented in the 'text format' as follows:

$$Q = \{q_{ij}\} = \begin{pmatrix} \text{miss} & \text{hit} & \text{double hit} & 0 \\ 0 & \text{miss} & \text{hit} & \text{double hit} \\ \text{double hit} & 0 & \text{miss} & \text{hit} \\ \text{hit} & \text{double hit} & 0 & \text{miss} \end{pmatrix} \qquad (2)$$

This matrix of transition probabilities in graphic form is shown in Fig.9 D.

The transition probabilities, q_{ij} should satisfy to the following conditions:

$$\Sigma_j q_{ij} = 1,\ q_{ij} \geq 0 \qquad (3)$$

The probability for the OEC to be in the S_i state after the n-th flash is given by the respective component of the vector $\mathbf{p}(n) = (p_0(n), p_1(n), p_2(n), p_3(n))$, which, in turn, can be evaluated from the equation:

$$\mathbf{p}(n) = \mathbf{p}(n-1) \cdot Q \qquad (4)$$

This equation states that the probability of a certain state of the OEC after the n-th flash is determined by the probabilities of the state of the OEC at the n-1 flash, $\mathbf{p}(n-1)$, and by the matrix of one-step transition probabilities, Q. One can consider Eq. 4 as 'balance' equation, that shows how the probabilities of the S-states are redistributed after the n-th flash.

The general Eq. 4 in coordinate form can be written for the first flash (n = 1) as follows:

$$\begin{aligned} p_0(1) &= p_0(0) \cdot q_{00} + p_1(0) \cdot q_{10} + p_2(0) \cdot q_{20} + p_3(0) \cdot q_{30} \\ p_1(1) &= p_0(0) \cdot q_{01} + p_1(0) \cdot q_{11} + p_2(0) \cdot q_{21} + p_3(0) \cdot q_{31} \\ p_2(1) &= p_0(0) \cdot q_{02} + p_1(0) \cdot q_{12} + p_2(0) \cdot q_{22} + p_3(0) \cdot q_{32} \\ p_3(1) &= p_0(0) \cdot q_{03} + p_1(0) \cdot q_{13} + p_2(0) \cdot q_{23} + p_3(0) \cdot q_{33} \end{aligned} \qquad (5)$$

Here each line corresponds to all pathways leading to the respective state. For example, consider the second line. The S_1 state after the first flash, i.e., $p_1(1)$, can be observed only if before the first flash PS II was in the S_0 state and after the flash it transfers to the state S_1 (term $p_0(0) \cdot q_{01}$), or before the flash PS II was in the S_1 state and after the flash it stays in the state S_1 (term $p_1(0) \cdot q_{11}$), or before the first flash PS II was in the S_2 state and after the flash it transfers to the state S_1 (term $p_2(0) \cdot q_{21}$), or, finally, before the first flash PS II was in the S_3 state and after the flash it transfers to the state S_1 (term $p_3(0) \cdot q_{31}$). There are no other possibilities to arrive at the state S_1 after the first flash. Transition probability q_{11} to stay in the same S_1 state after the flash is miss α_1 in our notations. Transition probability q_{31} to transfer from state 3 to state 1 is hit γ_3 in our notation. Transition probability q_{21} to transfer from state 2 to state 1 is double hit β_2 in our notation.

For case of equal misses and double hits, Eq. 5 can be further simplified (using initial conditions s_i):

$$\begin{aligned} p_0(1) &= s_0 \cdot \alpha + s_1 \cdot 0 + s_2 \cdot \beta + s_3 \cdot \gamma \\ p_1(1) &= s_0 \cdot \gamma + s_1 \cdot \alpha + s_2 \cdot 0 + s_3 \cdot \beta \\ p_2(1) &= s_0 \cdot \beta + s_1 \cdot \gamma + s_2 \cdot \alpha + s_3 \cdot 0 \\ p_3(1) &= s_0 \cdot 0 + s_1 \cdot \beta + s_2 \cdot \gamma + s_3 \cdot \alpha \end{aligned} \qquad (6)$$

Iterating Eq. 4, we can obtain:

$$\mathbf{p}(n) = \mathbf{p}(0)Q^n \qquad (7)$$

In this equation, the probability of certain state of OEC after the n-th flash is determined by the vector of probabilities of the state of OEC at the initial time, $\mathbf{p}(0)$, and by matrix of one-step transition probabilities, Q.

In general form we can write for any integer $k \geq 0$, $m \geq 0$

$$\mathbf{p}(k + m) = \mathbf{p}(k)Q^m = \mathbf{p}(m)Q^k = \mathbf{p}(0)Q^{k+m} \qquad (8)$$

Thus, the state of the PS II after k+m flashes does not depend on the grouping of flashes; it can be obtained by applying first *k* flashes and then another *m* flashes, or vice versa by applying first *m* flashes and then another *k* flashes.

Equations (7–8) are written for the row vectors, because when written in this form they have clear probability interpretation. However, frequently one writes down equations using the column vectors instead. In this case equation 7 takes the form:

$$\mathbf{p}(n)^T = R \cdot \mathbf{p}(n-1)^T = R^n \cdot \mathbf{p}(0)^T \quad (9)$$

where $R = Q^T$ is matrix transpose to Q.

O_2 evolution by a single RC of PS II after the n-th flash is determined by the probability of PS II to be in the state S_3 before the n-th flash and by the probability to be in the S_2 state (assuming double hits are not zero):

$$\begin{aligned} Y(n) &= p_3(n-1) \cdot (\text{hit} + \text{double hit}) \\ &+ p_2(n-1) \cdot \text{double hit} = p_3(n-1) \cdot (1-\alpha_3) \\ &+ p_2(n-1) \cdot \beta_2 \end{aligned} \quad (10)$$

Thus, if one finds the probabilities of S_3 and S_2 states for each flash, one can determine the O_2 evolution by PS II.

Equation 7 shows that to find the probabilities $\mathbf{p}(n) = (p_0(n), p_1(n), p_2(n), p_3(n))$, one needs to calculate the n-th power of matrix Q of transition probabilities.

The characteristic equation for matrix Q is:

$$|Q - \lambda I| = 0 \quad (11)$$

where I is the identity matrix.

The characteristic equation is a polynomial of degree 4:

$$\lambda^4 + \sigma_1\lambda^3 + \sigma_2\lambda^2 + \sigma_3\lambda^1 + \sigma_4 = 0 \quad (12)$$

Let $\lambda_1, \lambda_2, \lambda_3, \lambda_4$ and $\mathbf{y}_1, \mathbf{y}_2, \mathbf{y}_3, \mathbf{y}_4$ be the eigenvalues and eigenvectors of matrix Q, respectively. Note that $\lambda = 1$ is always the solution of Eq.12 because of stochastic nature of matrix Q.

If matrix Q can be diagonalized

$$Q = U\Lambda U^{-1} \quad (13)$$

where Λ is the diagonal matrix of eigenvalues, $\Lambda = \text{diag}(\lambda_1, \lambda_2, \lambda_3, \lambda_4)$, then

$$\mathbf{p}(n) = \mathbf{p}(0)Q^n = \mathbf{p}(0)U\Lambda^n U^{-1} \quad (14)$$

This expression allows the calculation of the probabilities of states of OEC after the n-th flash via eigenvalues λ_i, and via initial condition $\mathbf{p}(0) = (s_1, s_2, s_3, s_4)$.

2. Relationships between Matrices, Vectors and Probabilities

According to the Hamilton-Cayley theorem (see, for example, Gilbert and Gilbert, 1995) a matrix always satisfies to its characteristic equation. Thus, matrix of transition probabilities Q satisfies to the following equation:

$$Q^4 + \sigma_1 Q^3 + \sigma_2 Q^2 + \sigma_3 Q^1 + \sigma_4 E = 0 \quad (15)$$

Multiplying both sides of this matrix equation by row vector $\mathbf{p}(k)$ yields:

$$\begin{aligned} &\mathbf{p}(k)Q^4 + \sigma_1\mathbf{p}(k)Q^3 + \sigma_2\mathbf{p}(k)Q^2 + \sigma_3\mathbf{p}(k)Q^1 \\ &+\sigma_4\mathbf{p}(k) = 0 \end{aligned} \quad (16)$$

Using Eq. 7 for each term, we have

$$\begin{aligned} &\mathbf{p}(k+4) + \sigma_1\mathbf{p}(k+3) + \sigma_2\mathbf{p}(k+2) \\ &+ \sigma_3\mathbf{p}(k+1) + \sigma_4\mathbf{p}(k) = 0 \end{aligned} \quad (17)$$

Again, multiplying both sides by the vector with only m-th non-zero component, $\mathbf{r}_m = (0, 0, 1, 0)$, we have for probability of m-th state:

$$\begin{aligned} &p_m(k+4) + \sigma_1 p_m(k+3) + \sigma_2 p_m(k+2) \\ &+ \sigma_3 p_m(k+1) + \sigma_4 p_m(k) = 0 \end{aligned} \quad (18)$$

Denoting O_2 yield induced by the k-th flash as Y(k) and assuming that O_2 yield after flash is a linear combination of the concentrations of the S_3 and S_2 states just before this flash, one could write the following equation including only O_2 evolution yield after respective flash:

$$\begin{aligned} &Y(k+4) + \sigma_1 Y(k+3) + \sigma_2 Y(k+2) \\ &+ \sigma_3 Y(k+1) + \sigma_4 Y(k) = 0 \end{aligned} \quad (19)$$

Thus, we see that the same coefficients $\sigma_1, \sigma_2, \sigma_3$, and σ_3 are used to write down:

- characteristic equation for matrix of transitional probabilities (Eq. 12);

- equation for matrices of the transition probabilities (Eq. 16);
- equation for vectors of probabilities of PS II states (Eq. 17);
- equation for probabilities of individual states of PS II (Eq. 18);
- expressions for O_2 evolution yields after respective flash (Eq. 19);
- any signal which can be presented as linear combination of S-state probabilities.

All this explains why Lavorel (1976) suggested using coefficients of characteristic equation (sigmas) instead of transition probabilities as was done in the initial Kok model to describe flash-induced O_2 evolution.

F. Simple Analytical Solution for the Kok Model

The Kok model has been used successfully over 30 years for interpretation of PS II experimental data in photosynthesis. From mathematical point of view, the Kok model is a difference equation with constant coefficients, the general solution for which is presented in standard textbooks of linear algebra. Many significant advances in adapting this general theory to O_2 evolution have been accomplished (Delrieu, 1974; Lavorel, 1976; Thibault, 1978; Jursinic 1981; Beckwith and Jursinic, 1982; Meunier and Popovic, 1991; Lavergne, 1991; Burda and Schmid, 1996; Meunier et al., 1996; Isgandarova et al., 2003). While the general form for the solution of the Kok model is known, the final analytical solution for any initial conditions has not yet been found, due to the tediousness of calculations. Recently Shinkarev (2003) was able to find surprisingly simple solution for the Kok model, thus solving this long overdue problem. While proper description of flash-induced O_2 evolution, require extension of the Kok model by incorporating additional states and dark relaxation processes (see, e.g., Isgandarova et al., 2003) this first approximation often provides quite accurate insights into the observed oxygen evolution.

1. Matrix of Transition Probabilities

The classic Kok model with 4 states can be completely characterized by only one miss, α, and one double hit, β. While value of hit, γ, is fully determined by value of miss and double hit, because, $\alpha + \gamma + \beta = 1$, the final solution can be simplified significantly and written in more symmetrical form if one consider hit in addition to miss and double hit. In this notation the matrix of transition probabilities (Eq. 1) takes the following simple form:

$$Q = \begin{pmatrix} \alpha & \gamma & \beta & 0 \\ 0 & \alpha & \gamma & \beta \\ \beta & 0 & \alpha & \gamma \\ \gamma & \beta & 0 & \alpha \end{pmatrix} \tag{20}$$

The probability for the OEC to be in the S_i state after the n-th flash is given by the (i+1)th component of the row vector $\mathbf{p}(n) = (p_0(n), p_1(n), p_2(n), p_3(n))$ which, in turn, can be evaluated from Eq. 7.

2. Eigenvalues of Matrix Q of Transition Probabilities

As can be checked directly, characteristic equation for matrix Q given by Eq. 20, has the following solution:

$$\lambda_1 = \alpha + \gamma + \beta = 1; \qquad \lambda_2 = \alpha - \gamma + \beta = 1 - 2\gamma$$
$$\lambda_3 = \alpha - \beta + i\gamma = re^{i\varphi}; \quad \lambda_4 = \alpha - \beta - i\gamma = re^{-i\varphi} \tag{21}$$

where α, γ and β are miss, hit and double hit, respectively, $r = [(\alpha-\beta)^2+\gamma^2]^{1/2}$, $\varphi = \arcsin(\gamma/r)$, $i^2 = -1$.

3. General Solution of the Kok Model

The matrix Q given by Eq. 20 can be diagonalized

$$Q = U\Lambda U^{-1} \tag{22}$$

where Λ is the diagonal matrix with eigenvalues of matrix Q given by Eq. 21, and U is unitary matrix ($U\bar{U}^T = 1$):

$$U = 0.5 \cdot \begin{pmatrix} 1 & -1 & i & -i \\ 1 & 1 & -1 & -1 \\ 1 & -1 & -i & i \\ 1 & 1 & 1 & 1 \end{pmatrix} \tag{23}$$

Thus, Eq. 7 can be written as

$$\mathbf{p}(n) = \mathbf{p}(0)Q^n = \mathbf{p}(0)U\Lambda^n\bar{U}^T \quad (24)$$

By multiplying all terms in Eq. 24, one can find the probabilities of individual S-states (Shinkarev, 2003):

$$\begin{aligned}
p_0(n) &= [1 + z\mu^n + 2r^n\left(s_{02}\cos(n\varphi) + s_{31}\sin(n\varphi)\right)]/4\\
p_1(n) &= [1 - z\mu^n + 2r^n\left(s_{13}\cos(n\varphi) + s_{02}\sin(n\varphi)\right)]/4\\
p_2(n) &= [1 + z\mu^n + 2r^n\left(s_{20}\cos(n\varphi) + s_{13}\sin(n\varphi)\right)]/4\\
p_3(n) &= [1 - z\mu^n + 2r^n\left(s_{31}\cos(n\varphi) + s_{20}\sin(n\varphi)\right)]/4
\end{aligned} \quad (25)$$

where $r = [(\alpha - \beta)^2 + \gamma^2]^{1/2}$, $\varphi = \arcsin(\gamma/r)$, $\mu = \alpha - \gamma + \beta = 1 - 2\gamma$, n – number of the flashes, $s_i = p_i(0)$ are initial conditions for S_i; $z = s_0 - s_1 + s_2 - s_3$, $s_{01} = s_0 - s_1$, $s_{23} = s_2 - s_3$, etc.

Equation 25 provides general solution of the classic Kok model and describes the flash-number dependence of individual S-states for arbitrary initial conditions. General solution is the sum of the term, $1 \pm (1-2\gamma)^n(s_{01} + s_{23})$, describing binary oscillations (see Fig. 18) and two quaternary oscillation terms with cos(nφ) and sin(nφ), the relative amplitude of which depends on initial conditions. While some quaternary terms have negative values, nevertheless after adding together they produce probability of individual state which is always positive or zero.

Figure 13 shows the flash-number dependence of individual S-states, calculated from Eq. 25 for particular value of parameters. Maxima and minima reached by respective S-state depend on the initial conditions.

O_2 evolution after n-th flash is determined in the Kok model by transition from S_3 to S_0. This transition occurs either when the system was originally in the S_3 state and flash induces single and double turnover of RC, or when the system was originally in the S_2 state and flash induces double turnover of the RC (double hit). Thus, one can use the following equation for O_2 yield induced by the n-th flash:

$$\begin{aligned}
Y(n) &= (\text{hit} + \text{double hit}) \times p_3(n-1)\\
&+ (\text{double hit}) \times p_2(n-1) \equiv (\gamma_3 + \beta_3) \times p_3(n-1)\\
&+ \beta_2 \times p_2(n-1)
\end{aligned} \quad (26)$$

where probabilities $p_2(n-1)$, $p_3(n-1)$ are given by Eq. 25.

There is a need to comment on the value of the

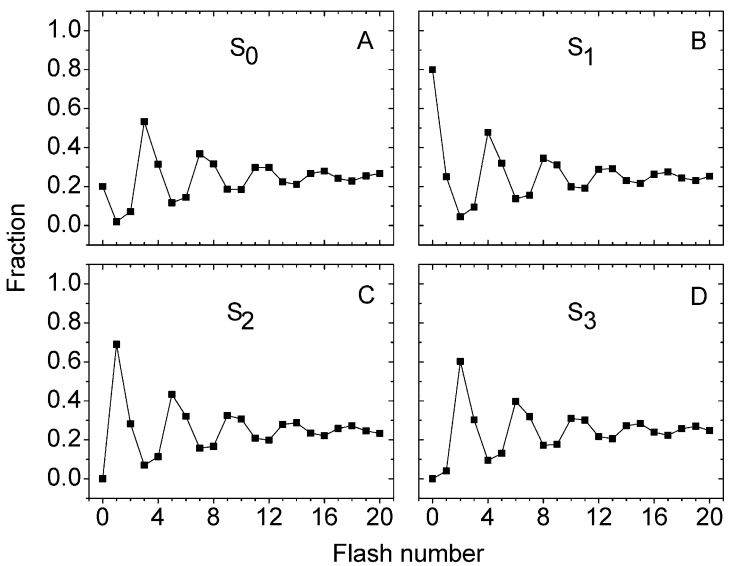

Fig. 13. Flash-number dependence of individual S-states, calculated from Eq. 25 using the following parameters: miss = 0.1, double hit = 0.05. Initial conditions: $s_0 = 0.2$; $s_1 = 0.8$; $s_2 = 0$; $s_3 = 0$.

double hit in Eq. 26. This double hit corresponds to the real double turnover of PS II during a long flash. In many cases double hit also appears during the fitting process as a consequence of application of the simple Kok model to cases with different misses, or non-standard initial conditions (see Section II.G.3). To avoid this source of double hit, one can use a compromise by calculating all S-states according to the Kok model with equal double hit for each transition and calculating oxygen evolution by ignoring double hit for S_3:

$$Y(n) = \gamma^{app} \times p_3(n-1) + \beta^{app} \times p_2(n-1) \qquad (27)$$

or even for S_2:

$$Y(n) = \gamma^{app} \times p_3(n-1) \qquad (28)$$

These modifications of the Kok model take into account double hit using averaged (over all S-states) value needed to fit flash-induced oxygen evolution profile with heterogeneous misses, but also take into account the absence of double turnovers of the RC in case of fast flashes.

Figure 14 shows flash-induced O_2 evolution calculated from Eq. 26 for different values of miss (A) and double hit (B). Increase of miss leads to significant reduction of the 'sharpness' of oscillation pattern. It also increases the apparent period of oscillations. The increase of double hit leads to disappearance of oscillations and to increase of the amplitude of O_2 yield after the second flash. Otherwise, the effects of miss and double hit on pattern of oscillations are similar.

General solution for the Kok model given by Eq. 25 can be rewritten as a single equation (Shinkarev, 2003):

$$p_k(n) = [1 + (1-2\gamma)^n(-1)^k(s_{01} + s_{23}) + 2\rho r^n \sin(n\varphi + \theta_k)]/4 \qquad (29)$$

where $\rho = [s_{02}^2 + s_{31}^2]^{1/2}$, $\rho\sin(\theta_k) = (s_k - s_{k+2})$, $\rho\cos(\theta_k) = (s_{k+3} - s_{k+1})$ and index k in s_k is congruent modulo *4* index taking only values 0, 1, 2 and 3, thus, for example, $s_4 = s_0$, $s_5 = s_1$, $s_6 = s_2$.

4. Period of Oscillations

Equation 27 shows that general solution includes the term $2\rho r^n \sin(n\varphi + \theta_k)$, describing damped oscillations with period

$$T = \frac{2\pi}{\varphi} \equiv 2\pi / \arcsin\left(\frac{\gamma}{\sqrt{(\alpha-\beta)^2 + \gamma^2}}\right) \qquad (30)$$

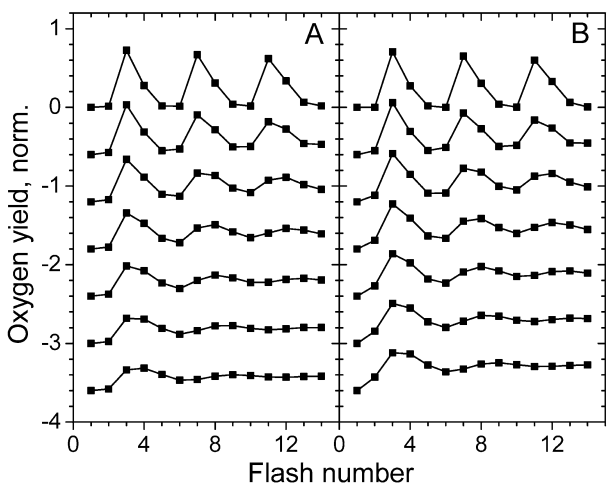

Fig. 14. Flash-induced O_2 evolution calculated from Eq. 26 for different miss (A) and double hit (B). In the panel A, the value of miss is increasing from 0 (top curve) to 0.3 (bottom curve) with 0.05 increment. Double hit is 0.02. In the panel B, the value of double hit is increasing from 0 for top curve to 0.3 for bottom curve with 0.05 increment. Miss is 0.02. The distribution of the states at the beginning of the flash series was assumed to be $s_0 = 0.25$ and $s_1 = 0.75$ for both panels. Traces are shifted vertically for clarity.

When miss is equal to double hit, $\varphi = \pi/2$ and the period of oscillations is exactly four: $T = 2\pi/(\pi/2) = 4$. In all other cases, the period is larger than 4. In particular case of zero double hit, the period is equal to about 4, 4.14, 4.30, 4.50, and 4.74 for misses 0, 0.05, 0.1, 0.15, and 0.2, respectively. Thus, increasing of miss value in this case leads to increase of the period. This can explain the deviation of maximum of oscillations of O_2 evolution from the classic pattern 3, 7, 11, etc. Such deviation can be seen in Fig. 2A, where maximum of O_2 evolution is observed after 8th flash (i.e. pattern 3, 8, 13 is observed). Fitting of data shown in Fig. 2 gave $T \approx 4.31$ for panel A and $T \approx 4.17$ for panel B.

5. Simplified Equations for Particular Cases

Above equations for individual S-states and O_2 evolution can be further simplified for particular cases of parameters or initial conditions.

a. Initial Conditions

For initial conditions $s_0 = 0$, $s_1 = 1$, $s_2 = 0$, $s_3 = 0$, frequently observed experimentally, Eq. 25 takes simpler form. For example, for $p_3(n)$ we have:

$$p3(n) = [1 + (1 - 2\gamma)^n - 2r^n \cos(n\varphi)]/4 \qquad (31)$$

b. Double Hits are Zero ($\beta = 0$)

When double hits are zero ($\beta = 0$), Eq. 26 for O_2 evolution takes the form:

$$Y(n) = \gamma \cdot p_3(n-1) = \gamma \cdot [1 - (1-2\gamma)^{n-1}(s_{01} + s_{23}) + 2r^{n-1}(s_{31}\cos((n-1)\varphi) + s_{20}\sin((n-1)\varphi))]/4 \qquad (32)$$

This is further simplified when only S_1 is present before the flash series:

$$Y(n) = \gamma[1 - (1-2\gamma)^{n-1} - 2r^{n-1}\cos((n-1)\varphi)]/4 \qquad (33)$$

G. Extracting Information from Flash-Induced Oxygen Evolution

The Kok model has a lot of surprises, which complicate extraction of information from observed O_2 pattern. Here we consider some of them.

1. Permutations of Transition Probabilities

Delrieu (1974) found that almost any permutation of misses gives the same flash-induced O_2 evolution profile. Figure 15 illustrates this point. Each flash profile was calculated with single miss of 0.4 for $S_0 \rightarrow S_1$ transition (A), for $S_1 \rightarrow S_2$ transition (B), for $S_2 \rightarrow S_3$ transition (C), or for $S_3 \rightarrow S_0$ transition (D). One could see that traces in panels B, C and D are identical.

Figure 16 show that some permutations of double hits can also give identical profiles of O_2 evolution.

2. Parameters Determining the Flash-Induced Oxygen Evolution

a. Number of Independent Parameters

General solution for individual S-states described by Eq. 25 allows specification of the number of independent parameters that govern observed period-four oscillations in the Kok model. Each solution depends on values of γ, r and φ, as well as on the values of initial conditions s_0, s_1, s_2 and s_3. However, one should take into account that r, γ and φ are interdependent, because $r \cdot \sin\varphi = \gamma$. The same is true for s_0, s_1, s_2 and s_3, because $s_0+s_1+s_2+s_3 = 1$. Thus, in the general case, only 5 independent parameters [e.g., γ, r, s_0, s_1, and s_2 (this work), or α (miss), β (double hit), s_0, s_1, and s_2 (the Kok model)] govern the pattern of oscillation for particular S-state.

b. Finding Parameters

Simple general solution found above provides basis for quantitative description of charge accumulation processes at the donor side of PS II. It also significantly simplifies finding of unknown parameters that govern observed oscillations.

Fitting experimental points of Fig. 2A with Eq. 26 gave the following parameters: $\alpha = 0.12$, $\gamma = 0.86$, $\beta = 0.02$, $s_0 = 0.32$, $s_1 = 0.68$, $s_2 = 0$. Fitting experimental points in Fig. 2B gave the following parameters: $\alpha = 0.08$, $\gamma = 0.89$, $\beta = 0.03$ $s_0 = 0.24$, $s_1 = 0.69$, $s_2 = 0.02$. Thus experiment shown in panel A of Fig.2 has less double hits and larger misses than experiment shown in panel B.

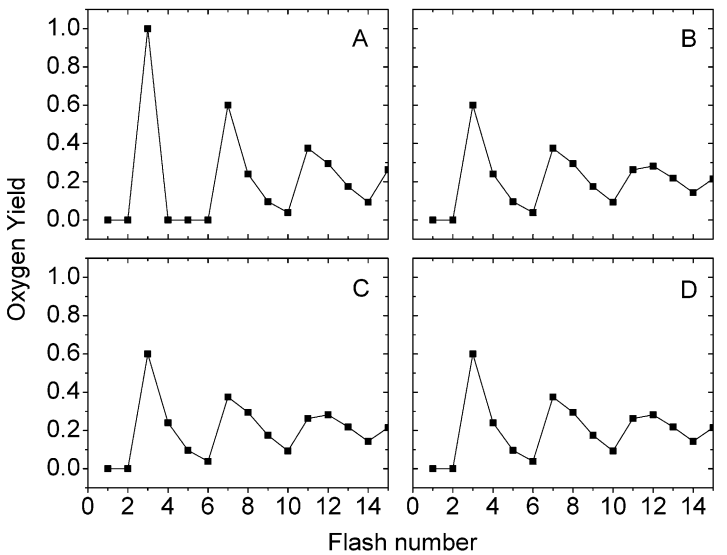

Fig. 15. Theoretical flash-induced O_2 evolution yields calculated for different position of misses in sequence leading to O_2 evolution. (A) Miss is 0.4 for $S_0 \rightarrow S_1$ transition and 0 for other transitions. (B) Miss is 0.4 for $S_1 \rightarrow S_2$ transition and 0 for other transitions. (C) Miss is 0.4 for $S_2 \rightarrow S_3$ transition and 0 for other transitions. (D) Miss is 0.4 for $S_3 \rightarrow S_0$ transition and 0 for other transitions. Initial conditions for all cases are identical ($[S_0] = 0$, $[S_1] = 1$) and double hits are zero for all transitions.

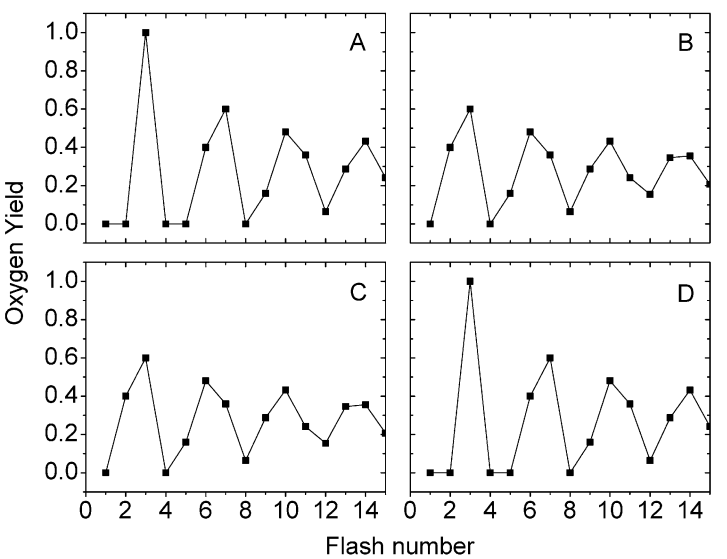

Fig. 16. Theoretical flash-induced O_2 evolution yields calculated for different position of double hit. (A) Double hit is 0.4 for $S_0 \rightarrow S_1$ transition and 0 for other transitions. (B) Double hit is 0.4 for $S_1 \rightarrow S_2$ transition and 0 for other transitions. (C) Double hit is 0.4 for $S_2 \rightarrow S_3$ transition and 0 for other transitions. (D) Double hit is 0.4 for $S_3 \rightarrow S_0$ transition and 0 for other transitions. Initial conditions for all cases are identical ($[S_0] = 0$, $[S_1] = 1$) and misses are zero for all transitions.

3. Fitting of Model Curves by the Kok Model

It should be clear from above that in reality misses are different. Nevertheless, simple Kok model with single miss and double hit frequently gives good approximation to the observed patterns of O_2 evolution. To better understand problems arising from approximation of different experimental data with the Kok model we examine here fitting of different model data.

a. Accuracy of the Fitting

To illustrate the accuracy of fitting of model data, theoretical points using the Kok model with α = 0.1, β = 0.05, s_0 = 0.25, s_1 = 0.75 were generated. Fitting these model points with the Kok model using non-linear regression analysis returns the following values: $\alpha = 0.1000 \pm 0.0002$, $\beta = 0.0495 \pm 0.0002$, $s_0 = 0.250 \pm 0.001$, $s_1 = 0.750 \pm 0.001$. Thus, such numerical analysis of model points gives parameters with accuracy better than 0.5 %.

b. Heterogeneous Misses

To test effect of miss heterogeneity, we generated model points with different misses ($\alpha_0 = 0$, $\alpha_1 = 0$, $\alpha_2 = 0.1$, $\alpha_3 = 0.3$), and zero double hits ($\beta_0 = \beta_1 = \beta_2 = \beta_3 = 0$) and then fitted these points with the Kok model with identical misses ($\alpha_0 = \alpha_1 = \alpha_2 = \alpha_3 = \alpha$) and double hits ($\beta_0 = \beta_1 = \beta_2 = \beta_3 = \beta$). The panel A of Fig. 17 shows results of fitting of the Kok model (lines) to the model points (squares). One can see that case with different misses could be reasonably fitted by the Kok model with apparent miss of ~0.11 and apparent double hit of ~0.006. While the Kok model with identical misses and double hits can fit the case with different misses, the apparent parameters of such fit deviate from the original parameters. It is important to note that during the fitting double hits were created for each transition, even though they were absent in the original model. In addition, apparent misses were assigned to each transition, while they were absent originally for some of them.

c. Heterogeneous Double Hits

To test the role of heterogeneous double hits we used the Kok model to fit generated model points with different double hits ($\beta_0 = 0.3$, $\beta_1 = 0.1$, $\beta_2 = 0$, $\beta_3 = 0$), but with single miss ($\alpha = 0.1$). The results of fitting are shown in panel B of Fig. 17. The Kok model fitted to the model points gave the following apparent parameters: $\alpha^{app} \sim 0.09$, $\beta^{app} \sim 0.08$. Thus, the case of heterogeneous double hits can be reasonably fitted in this example by the curve with a single double hit, $\beta^{app} \sim 0.08$. The application of a simplified model led to: (i) the small redistribution of initial probabilities of S states ($s_1^{app} \sim 0.78$ instead of $s_1 = 0.75$), (ii) the assigning slightly lower misses for each transition, and (iii) the creating apparent double hits for each transition, even though some of them were originally absent. The value for apparent double hit is close to the average value of $\beta^{av} = 0.1$ for the original data set.

From example above we can conclude, that good fit of the Kok model to experimental data does not prove that transition probabilities in the original curve of O_2 evolution are equal.

d. Role of Initial Conditions

In most cases the Kok model employs initial conditions only for S_0 and for S_1. To understand the role of initial conditions in the assigning of different values to the misses and double hits, we generated model points ($\alpha = 0.1$, $\beta = 0$) with extended set of initial conditions ($s_0 = 0.25$, $s_1 = 0.65$, $s_2 = 0.1$, $s_3 = 0$) and fitted this model points by the Kok model having a simplified set of initial conditions for S_0 and S_1 only. The results of fitting gave $\alpha^{app} = 0.097 \pm 0.008$, $\beta^{app} = 0.019 \pm 0.005$, $s_0^{app} = 0.29 \pm 0.04$, $s_1^{app} = 0.70 \pm 0.04$ (panel C of Fig. 17). In this example, the absence of variation of initial conditions for S_2 led to small change of miss (~0.097 instead of 0.1), to the appearance of double hit (~0.02 instead of 0), as well as to some redistribution of the initial conditions for S_0 (~0.29 instead of 0.25) and S_1 (~0.7 instead of 0.65).

Examples above illustrate that:

(1) In many cases simple Kok model with single miss and double hit can approximate nicely the case with different misses and double hits. Thus, the good fit to the observed experimental points does not indicate that all misses (or double hits) are the same.

(2) Double hits can appear (or increase) during the fit to compensate for heterogeneity of the misses or incomplete set of initial conditions. Thus, the presence of double hit in the fit can be caused by the application of the simplified Kok model, not only by the double turnover of PS II.

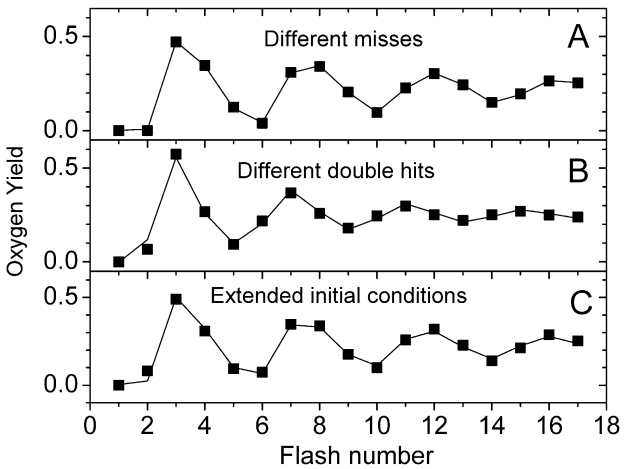

Fig. 17. Application of the simple Kok model to fitting theoretical points with different misses, double hits and non-standard set of initial conditions. (A) Model points (squares) were generated using different misses ($\alpha_0 = 0$, $\alpha_1 = 0$, $\alpha_2 = 0.1$, $\alpha_3 = 0.3$), zero double hits ($\beta_0 = \beta_1 = \beta_2 = \beta_3 = 0$), and 'standard' initial conditions $s_0 = 0.25$, $s_1 = 0.75$, $s_2 = 0$, $s_3 = 0$. Fitting the Kok model (line) to these model points gave the following apparent parameters: $\alpha^{app} = 0.109 \pm 0.002$, $\beta^{app} = 0.006 \pm 0.001$, $s_0^{app} = 0.31 \pm 0.01$, $s_1^{app} = 0.69 \pm 0.01$. (B) Model points (squares) were generated using single miss factor ($\alpha = 0.1$), different double hits ($\beta_0 = 0.3$, $\beta_1 = 0.1$, $\beta_2 = 0$, $\beta_3 = 0$) and regular initial conditions $s_0 = 0.25$, $s_1 = 0.75$, $s_2 = 0$, $s_3 = 0$. Fitting the Kok model (line) to model points gave the following apparent parameters: $\alpha^{app} = 0.088 \pm 0.012$, $\beta^{app} = 0.082 \pm 0.007$, $s_0^{app} = 0.22 \pm 0.05$, $s_1^{app} = 0.78 \pm 0.05$. (C) Model points (squares) were generated by the Kok model with $\alpha = 0.1$, $\beta = 0$ and with extended set of initial conditions, $s_0 = 0.25$, $s_1 = 0.65$, $s_2 = 0.1$, $s_3 = 0$. Fitting this model points with the Kok model assuming that only S_0 and S_1 should be reflected in initial conditions, gave the following apparent parameters: $\alpha^{app} = 0.097 \pm 0.008$, $\beta^{app} = 0.019 \pm 0.005$, $s_0^{app} = 0.29 \pm 0.04$, $s_1^{app} = 0.70 \pm 0.04$.

(3) Determined misses and double hits in the Kok model are close to the average values of misses ($\alpha^{av} = (\alpha_0+\alpha_1+\alpha_2+\alpha_3)/4$) and double hits ($\beta^{av} = (\beta_0+\beta_1+\beta_2+\beta_3)/4$), indicating that they, as a first approximation, can be treated as such.

e. Expression for Oxygen Evolution

As the examples above show, the double hit can appear in the fitting process, even though original curves were generated without the double hits. The presence of the double hit in this case has no clear meaning for O_2 evolution and can be treated as an additional fitting parameter. This additional meaning for the double hit (besides relating to the probability of true double turnover of PS II) raises the question of proper expression for oxygen evolution.

O_2 evolution after n-th flash is determined in the Kok model by the transition from S_3 to S_0. This transition can occur via single and double light activation of the S_3 state or via double light activation of S_2 state. Thus, in the Kok model one can use the following equation for oxygen yield induced by the n-th flash:

$$Y(n) = (\gamma_3 + \beta_3) \times p_3(n-1) + \beta_2 \times p_2(n-1) \qquad (34)$$

where $p_2(n-1)$, $p_3(n-1)$ are probabilities of S_2 and S_3 states after $n-1$ flash, γ_3 is the probability of single hit from S_3 state, β_2 is the probability of the double hit from S_2 state and β_3 is the probability of the double hit from S_3 state.

One should expect that in case of fast flashes the probability of double turnover of PS II is practically zero. In this case the presence of double hit in the fit can be caused by the application of the simplified Kok model, to the real case characterized by different misses, specific set of initial conditions, or by dark relaxation of S-states between flashes. This apparent double hit is not really responsible for the double turnover of the RC and should be ignored in the expression for O_2 evolution.

To illustrate the above point, let's consider the model points assuming zero double hits ($\beta_0 = \beta_1 = \beta_2 = \beta_3 = 0$), significant miss heterogeneity ($\alpha_0 = 0.35$,

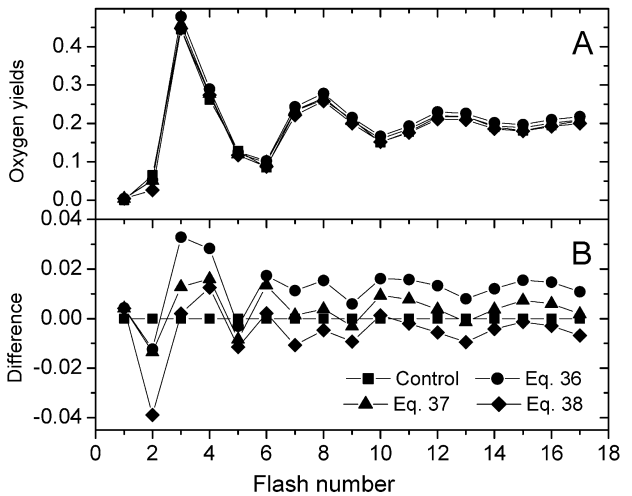

Fig. 18. Different approximations used for calculation of oxygen evolution form the Kok model (A) and differences between respective approximations and original data set (B). Original theoretical points (squares) were calculated assuming $\beta_0 = \beta_1 = \beta_2 = \beta_3 = 0$; $\alpha_0 = 0.35$, $\alpha_1 = 0$, $\alpha_2 = 0.35$, $\alpha_3 = 0$; $p_0 = 0.25$, $p_1 = 0.65$, $p_2 = 0.1$. These model points with different misses were approximated by the Kok model with single apparent miss and single apparent double hit. Using these apparent parameters, the oxygen evolution has been estimated from Eq. 36 (●), Eq. 37 (▲) and Eq. 38 (◆).

$\alpha_1 = 0$, $\alpha_2 = 0.35$, $\alpha_3 = 0$) and some particular initial conditions ($p_0 = 0.25$, $p_1 = 0.65$, $p_2 = 0.1$). Because double hits are zero and because there is no miss for S_3, the oxygen evolution for this model calculated according to Eq. 34 gives:

$$Y(n) = p_3(n - 1) \tag{35}$$

Approximation of this model curve with the simple Kok model gave the apparent miss (α^{app}) of ~0.2, the apparent hit (γ^{app}) of ~0.77, and the apparent double hit (β^{app}) of ~0.03. If we were to obtain this curve experimentally, we would try to calculate the oxygen evolution using Eq. 34:

$$\begin{aligned} Y(n) &= (\gamma^{app} + \beta^{app})\tilde{p}_3(n-1) + \beta^{app}\tilde{p}_2(n-1) \\ &\approx 0.8\tilde{p}_3(n-1) + 0.03\tilde{p}_2(n-1) \end{aligned} \tag{36}$$

Here the tilde above p indicates the new approximate solution according to the simplified Kok model with single miss and double hit. This expression is different from the correct expression (35). One can try to correct Eq. 36 by ignoring the double hits for S_3 (compare to Eq. 34):

$$Y(n) \approx \gamma^{app}\tilde{p}_3(n-1) + \beta^{app}\tilde{p}_2(n-1) \tag{37}$$

or even for S_2:

$$Y(n) \approx \gamma^{app}\tilde{p}_3(n-1) \tag{38}$$

These modifications of Kok model allow us to take into account the apparent double hit needed to fit flash-induced oxygen evolution profile with the heterogeneous misses, but ignore double turnovers of the RC induced by fast flashes.

Fig. 18 shows theoretical curves of O_2 evolution corresponding to the cases above. Panel A shows that all above approximations give close profiles of O_2 evolution. One can see from panel B that classic approximation given by Eq. 36 overestimates the O_2 evolution yields for most flashes, approximation given by Eq. 38 underestimates it for most flashes, and the approximation given by Eq. 37 is best. Despite the fact that this comparison has been done for particular numerical example, it, nevertheless, illustrates the problems that arise during application of the classic Kok model to the analysis of the O_2 evolution.

III. Binary Oscillations in the Kok Model

A. Binary Oscillations of Semiquinone in Photosystem II

By taking into account the fate of the electron on the acceptor side of PS II, one can see that the same scheme describes the accumulation of charges at the donor and acceptor sides (Fig. 7). Depending on initial conditions two different cycles are possible, so called V- and *W*- cycles (Shinkarev and Wraight, 1993a). Figure 7 shows that each single turnover of the OEC in each cycle is accompanied by two turnovers of the acceptor-quinone complex. As a result, the general equation for the acceptor side behavior can be obtained by summing the solutions for respective S-states in the Kok model. Let consider *V*-cycle only, for clarity. By adding p_0 and p_2 from Eq. 25 one can obtain the equation for binary oscillations of Q_B^- as function of flash number n:

$$Q_B^- = p_0(n) + p_2(n) = 0.5 \cdot [1 + (1 - 2\gamma)^n (s_0 - s_1 + s_2 - s_3)] \quad (39)$$

where, as before, $s_i = p_i(0)$, γ is the hit.

When the value of hit, γ, is close to 1, the term $(1\text{-}2\gamma)$ is negative. As a result, $(1\text{-}2\gamma)^n$ is positive for even n values, and is negative for odd n values. This alternating addition and subtraction of $(1\text{-}2\gamma)^n$ term in Eq. 39 is modulated by the initial conditions, $s_0 - s_1 + s_2 - s_3$. When PS II is in the state S_1Q_B before the first flash (i.e., $s_1 = 1$), dampening oscillations of semiquinone are described by a very simple equation:

$$Q_B^- = p_0(n) + p_2(n) = 0.5[1 - (1 - 2\gamma)^n] \quad (40)$$

Figure 19A (top curve) shows binary oscillations of Q_B^- described by Eq. 39, as well as probabilities for S_0 and S_2. This figure illustrates how two quaternary oscillations lead to binary oscillations. Similarly, by adding p_1 and p_3 one can obtain the equation for binary oscillations of oxidized form of Q_B in *V*-cycle or semiquinone Q_B^- in *W*-cycle.

Figure 20 shows Q_B^- binary oscillations for different value of misses (A) and for different initial conditions (B). Depending on initial conditions oscillations can change their direction. There are no oscillations when $s_1 = s_2 = 0.5$.

B. Conditions for Binary Oscillations

Let us consider the sum

$$\varepsilon_0 p_0(n,t) + \varepsilon_1 p_1(n,t) + \varepsilon_2 p_2(n,t) + \varepsilon_3 p_3(n,t) \quad (41)$$

This sum can be interpreted as absorbance of all

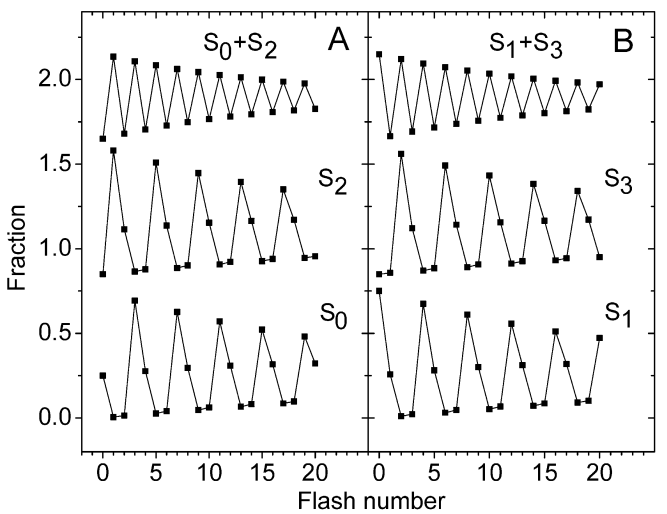

Fig. 19. (A) Flash-number dependence of the semiquinone $Q_B^- = p_0 + p_2$ (A), and $Q_B^- = p_1 + p_3$ (B) calculated using Eq. 25. Fractions of S_0 and S_2 states were calculated using Eq. 25. Miss = 0.02, double hit = 0.01. It is assumed that at the beginning of the flash series, 75% of PS II are in the S_1 state and 25% are in the S_0 state. Traces are shifted vertically to improve their visibility.

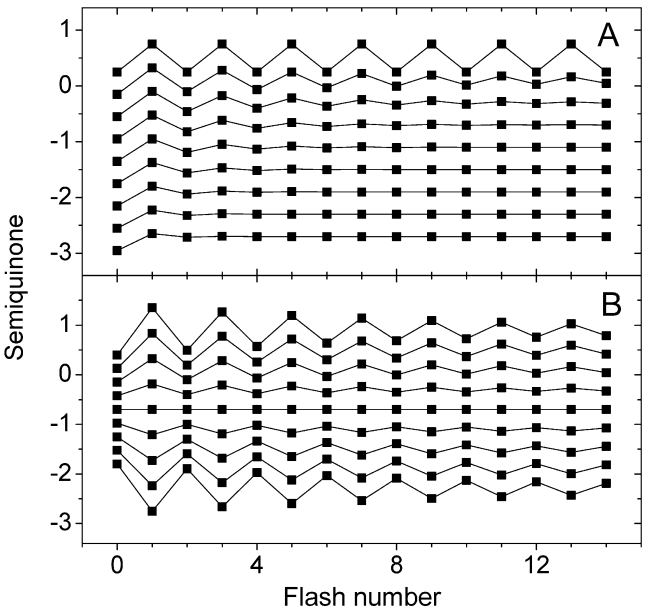

Fig. 20. Dependence of binary oscillations in PS II on different factors. (A) Effect of miss on the flash-number dependence of Q_B, calculated using Eq. 39. Miss is increasing from 0 (top curve) to 0.4 (bottom curve) with 0.05 increment. Initial conditions: $s_0 = 0.25$, $s_1 = 0.75$. Double hit is zero. (B) Effect of initial conditions on the flash-number dependence of the relative concentrations Q_B^-. Traces are calculated from Eq. 39. Initial conditions for S_0 are changing from 0 at the top to 1 at the bottom with 0.125 increment. It is assumed that $s_1 = 1 - s_0$, $s_2 = s_3 = 0$. The miss is 0.05. Double hit is zero. Traces are shifted vertically to improve their visibility.

S-states each of which has extinction coefficient ε_i. When, for example, $\varepsilon_0 = 1$, $\varepsilon_1 = 0$, $\varepsilon_2 = 1$, $\varepsilon_3 = 0$, this sum is just $p_0(n) + p_2(n)$, which oscillates with period of two (see Fig. 19). Binary oscillations in the Kok model even in case of *different* misses can be observed under surprisingly wide range of conditions. Let r be the right eigenvector corresponding to the negative eigenvalue of matrix Q given by Eq. 1. Then any vector $\varepsilon = (\varepsilon_0, \varepsilon_1, \varepsilon_2, \varepsilon_3)^T$ which linearly connected with vector r ($\varepsilon = c_1 r + c_2$), where c_1 is any number ($\neq 0$), and c_2 is any constant column vector, provides *binary* oscillations of the sum given by Eq. 41 (Shinkarev, 1996).

IV. Conclusions

Critical analysis of flash-induced O_2 evolution in photosynthesis, which is the main source of atmospheric O_2 on Earth, is presented. Measurements of O_2 evolution usually falls into one of the following three categories: (i) *kinetically resolved* measurements where one directly measures the kinetics of the oxygen-evolving step ($\tau \leq 1$ ms); (ii) measurements of the *flash-number dependence* of *amplitudes* of O_2 evolution (1 ms $\leq \tau \leq$ 100 ms); (iii) integrative measurements in which O_2 evolution is integrated over a series of flashes, or during steady-state illumination of certain duration (100 ms $\leq \tau$). The first kind of measurements is important when there is some expectation of changing the rate of O_2 evolution, for example, in some mutants. The second approach, which may not be resolved kinetically for each step, assumes that overall amplitudes (or surfaces under curves) are proportional to the amount of O_2 released after the respective flash. The third approach is only suitable for estimations of stoichiometry averaged over many flashes in a series. This chapter focused mostly on the second category, which allows extraction of information about the overall effectiveness of individual steps leading to the O_2 evolution. The discussion is limited to the Kok model (Kok et al., 1970). While this model has been successfully used for over 30 years for interpretation of experimental data in photosynthesis, till recently it lacked simple analytical

solution for it. Such solution is presented and discussed here. This solution allows determination of parameters of the Kok model via standard non-linear regression analysis implemented in widely used software packages such as Microcal Origin and many others. This simple analytical solution for O_2 evolution provides quite accurate insights into the observed oxygen evolution. For more detailed description of flash-induced oxygen evolution, one needs to extend the Kok model by incorporating additional states and dark relaxation processes (Isgandarova et al., 2003).

Correlation of S-states transitions at the donor side of the PS II and secondary acceptor quinone (Q_B) transitions at the acceptor side, leads to the recognition of two different reaction sequence cycles of Photosystem II, so called cycles *V* and *W* (Shinkarev and Wraight, 1993a). In each of these cycles the binary oscillations of the Q_B semiquinone can be obtained from the solution for individual S-states. Thus, the Kok model allows *simultaneous description* of individual S-states, Q_B^- and oxygen evolution with the same parameters.

Standard application of the Kok model consists in finding miss and double hit from measured sequence of flash-induced O_2 evolution. This method of analysis of observed flash-induced patterns is incomplete in the sense that it allows the extraction of only 5 independent parameters while, in reality, the general Kok model with different misses and double hits has 11 parameters. As a result, application of simple Kok model with single miss and double hit, leads to assigning artificial values to some parameters to compensate for the absence of others. Thus, flash-induced O_2 evolution profiles are limited in their suitability for testing different models of O_2 evolution.

In an alternative approach (Shinkarev and Wraight, 1993a,b) the known PS II kinetic and thermodynamic data are used to reconstruct period-four oscillations of O_2 evolution. We briefly described the general kinetic model of PS II, which allows calculation of all transition probabilities from first principles. Such approach shows that all misses are different for each transition. The general character of the model allows simultaneous consideration of different flash-induced oscillation phenomena at the donor and acceptor sides of PS II.

Acknowledgments

Author is grateful to Tony Crofts, Govindjee, Vince McNamara, Eiji Takahashi and Colin Wraight for useful comments. This work was partially supported by United States Department of Agriculture grant 9401725.

References

Babcock GT and Sauer K (1973) Electron paramagnetic resonance signal in spinach chloroplasts. I. Kinetic analysis for untreated chloroplasts. Biochim Biophys Acta 325: 483–503

Beckwith AC and Jursinic PA (1982) An alternative approach to the analysis of photosynthetic oxygen evolution. J Theor Biol 97: 251–265

Blankenship RE (2002) Molecular Mechanisms of Photosynthesis. Blackwell Science, Oxford

Bouges-Bocquet B (1973) Electron transfer between the two photosystems in spinach chloroplasts. Biochim Biophys Acta 314: 250–256

Bouges-Bocquet B (1980) Kinetic models for the electron donors of Photosystem II of photosynthesis. Biochim Biophys Acta 594: 85–103

Bowes JM and Crofts AR (1980) Binary oscillations in the rate of reoxidation of the primary acceptor of Photosystem II. Biochim Biophys Acta 590: 373–384

Burda K and Schmid GH (1996) On the determination of the S-state distribution in the Kok model. Z Naturforsch 51c: 329–341

Buser CA, Diner BA and Brudvig GW (1992) Photooxidation of cytochrome b_{559} in oxygen-evolving Photosystem II. Biochemistry 31: 11449–11459

Crofts AR and Wraight CA (1983) The electrochemical domain of photosynthesis. Biochim Biophys Acta 726: 149–185

de Wijn R and van Gorkom HJ (2002) S-state dependence of the miss probability in Photosystem II. Photosynth Res 72: 217–222

Debus RJ (1992) The manganese and calcium ions of photosynthetic oxygen evolution. Biochim Biophys Acta 1102: 269–352

Debus RJ, Barry BA, Babcock GT and McIntosh L (1988) Directed mutagenesis indicates that the donor to P in Photosystem II is tyrosine-161 of the D1 polypeptide. Biochemistry 27: 9071–9074

Delrieu MJ (1974) Simple explanation of the misses in the cooperation of charges in photosynthetic oxygen evolution. Photochem Photobiol 20: 441–454

Delrieu MJ (1983) Evidence for unequal misses in oxygen flash yield sequence in photosynthesis. Z Naturforsch 38c: 247–258

Delrieu MJ and Rosengard F (1987) Fundamental difference between period-4 oscillations of the oxygen and fluorescence yield induced by flash excitation in inside-out thylakoids. Biochim Biophys Acta 892: 163–171

Delrieu MJ and Rosengard F (1991) Changes in the S_0 and S_1 properties during dark adaptation in oxygen-evolving Photosystem-II-enriched thylakoid membranes. Biochim Biophys Acta 1057: 78–88

Diner BA (1977) Dependence of the deactivation reactions of Photosystem II on the redox state of plastoquinone pool a varied

under anaerobic conditions equilibria on the acceptor side of Photosystem II. Biochim Biophys Acta 460: 247–258
Diner BA and Babcock GT (1996) Structure, dynamics, and energy conversion efficiency in Photosystem II. In: Ort DR and Yocum CY (eds) Oxygenic Photosynthesis: The Light Reactions, pp 213–247. Kluwer Academic Publishers, Dordrecht
Diner BA and Petrouleas V (1987) Q400, the non-heme iron of the Photosystem II iron-quinone complex. A spectroscopic probe of quinone and inhibitor binding to the reaction center. Biochim Biophys Acta 895: 107–125
Eckert HJ, Wiese N, Bernarding J, Eichler HJ and Renger G (1988) Analysis of the electron transfer from $Pheo^-$ to Q_A in PS II membrane fragments from spinach by time resolved 325 nm absorption changes in the picosecond domain. FEBS Lett 240: 153–158
Engels DH, Lott A, Schmid GH and Pistorius EK (1994) Inactivation of the water-oxidizing enzyme in manganese stabilizing protein-free mutant cells of the cyanobacteria *Synechococcus* PCC7942 and *Synechocystis* PCC6803 during dark incubation and conditions leading to photoactivation. Photosynth Res 42: 227–244
Feller W (1970) An introduction to Probability Theory and Its Applications, Vol 1. Wiley, New York
Forbush B, Kok B and McGloin M (1971) Cooperation of charges in photosynthetic oxygen evolution. II. Damping of flash yield oscillation, deactivation. Photochem Photobiol 14: 307–321
Gilbert J and Gilbert L (1995) Linear Algebra and Matrix Theory. Academic Press, San Diego
Govindjee (1990) Photosystem-II heterogeneity — the acceptor side. Photosynth Res 25: 151–160
Hangulov SV, Golfeld MG and Blumenfeld LA (1974) To mechanism of phototransfer of electron in plant chloroplasts. Proc Acad Sci USSR 218: 726–730
Isgandarova S, Renger G and Messinger J (2003) Functional differences of Photosystem II from *Synechococcus elongatus* and spinach characterized by flash-induced oxygen evolution patterns. Biochemistry 42: 8929–8938
Joliot P and Kok B (1975) Oxygen evolution in photosynthesis. In: Govindjee (ed) Bioenergetics of Photosynthesis, pp 388–413. Academic Press, New York
Joliot P, Barbieri G and Chabaud R (1969) Un nouveau modèle des centers photochimiques du système II. Photochem Photobiol 10: 309–329
Joliot P, Joliot A, Bouges B and Barbieri G (1971) Studies of system II photocenters by comparative measurements of luminescence, fluorescence and oxygen emission. Photochem Photobiol 14: 287–305
Jursinic P (1981) Investigation of double turnovers in Photosystem II charge separation and oxygen evolution with excitation flashes of different duration. Biochim Biophys Acta 635: 38–52
Ke B (2001) Photosynthesis. Photobiochemistry and Photobiophysics. Kluwer Academic Publishers, Dordrecht
Kok B, Forbush B and McGloin M (1970) Cooperation of charges in photosynthetic O_2 evolution — I. A linear four step mechanism. Photochem Photobiol 11: 467–475
Lavergne J (1991) Improved UV-visible spectra of the S-transitions in the photosynthetic oxygen-evolving system. Biochim Biophys Acta 1060: 175–188
Lavergne J and Briantais JM (1996) Photosystem II heterogeneity. In: Ort DR and Yocum CY (eds) Oxygenic Photosynthesis: The Light Reactions, pp 265–287. Kluwer Academic Publishers, Dordrecht
Lavergne J and Junge W (1993) Proton release during the redox cycle of the water oxidase. Photosynth Res 38: 279–296
Lavorel J (1976) Matrix analysis of the oxygen evolving system of photosynthesis. J Theor Biol 57: 171–185
Mar T and Govindjee (1972) Kinetic models of oxygen evolution in photosynthesis. J Theor Biol 36: 427–446
Messinger J and Renger G (1994) Analyses of pH-induced modifications of the period four oscillation of flash-induced oxygen evolution reveal distinct structural changes of the Photosystem II donor side at characteristic pH values. Biochemistry 33: 10896–10905
Messinger J, Badger M and Wydrzynski T (1995) Detection of one slowly exchanging substrate water molecule in the S3 state of Photosystem II. Proc Natl Acad Sci USA 92: 3209–3213
Metz JG, Nixon PJ, Rogner M, Brudvig GW and Diner BA (1989) Directed alteration of the D1 polypeptide of Photosystem II: Evidence that tyrosine-161 is the redox component, Z, connecting the oxygen evolving complex to the primary electron donor, P680. Biochemistry 28: 6960–6969
Meunier PC and Popovic R (1990) Control of misses in oxygen evolution by the oxidoreduction state of plastoquinone in *Dunaliella Tertiolecta* Photosynth Res 23: 213–221
Meunier PC and Popovic R (1991) Improvement of 4 sigma-analysis for the investigation of oxygen evolution by Photosystem II. Photosynth Res 29: 113–115
Meunier PC, Burnap RL and Sherman LA (1996) Improved 5-step modeling of the Photosystem II S-state mechanism in cyanobacteria. Photosynth Res 47: 61–76
Naber JD (1989) Molecular aspects of herbicide binding in chloroplasts. PhD Thesis. Wageningen University, The Netherlands
Naber JD, van Rensen Jack JS and Govindjee (1993) High misses after odd flashes in oxygen evolution in thoroughly dark-adapted thylakoids from pea and *Chenopodium album.* Photosynth Res 38: 309–314
Radmer R and Kok B (1973) A kinetic analysis of the oxidizing and reducing sides of the oxygen evolving system of photosynthesis. Biochim Biophys Acta 314: 28–41
Rappaport F, Blanchard-Desce M and Lavergne J (1994) Kinetics of electron transfer and electrochromic change during the redox transitions of the photosynthetic oxygen evolving complex. Biochim Biophys Acta 1184: 178–192
Renger G (1997) Mechanistic and structural aspects of photosynthetic water oxidation. Physiologia Plantarum 100: 828–841
Renger G (2001) Photosynthetic water oxidation to molecular oxygen: apparatus and mechanism. Biochim Biophys Acta 1503: 210–228
Renger G (2003) Coupling of electron and proton transfer in oxidative water cleavage in photosynthesis. Biochim Biophys Acta 1655: 195–204
Robinson HH and Crofts AR (1983) Kinetics of the oxidation-reduction reactions of the Photosystem II quinone acceptor complex, and the pathway for deactivation. FEBS Lett 153: 221–226
Rutherford AW, Crofts AR and Inoue Y (1982) Thermoluminescence as a probe of Photosystem II photochemistry the origin of the flash-induced glow peaks. Biochim Biophys Acta 682: 457–465
Rutherford AW, Zimmerman JL and Boussac A (1992) Oxygen Evolution. Topics in Photosynthesis 11: 179–229

Seeliger A G, Kurreck J and Renger G (1997) Kinetics of S2 and S3 reduction by tyrosine Y_D and other endogenous donors as a function of temperature in spinach PS II membrane fragments with a reconstituted plastoquinone pool. Biochemistry 36: 2459–2464

Shinkarev V P (1996) Binary oscillations in the Kok model of oxygen evolution in oxygenic photosynthesis Photosynth Res 48: 411–417

Shinkarev VP (2003) Oxygen evolution in photosynthesis: Simple analytical solution for Kok model. Biophys J 85: 435–441

Shinkarev VP and Wraight CA (1993a) Oxygen evolution in photosynthesis: From unicycle to bicycle. Proc Natl Acad Sci USA 90: 1834–1838

Shinkarev VP and Wraight CA (1993b) Kinetic factors in the bicycle model of oxygen evolution by Photosystem II. Photosynth Res 38: 315–321

Shinkarev VP and Wraight CA (1993c) Electron and proton transfer in the acceptor quinone complex of reaction centers of phototrophic bacteria. In: Deisenhofer J and Norris J (eds) The Photosynthetic Reaction Center, Vol 1, pp 193–255. Academic Press, New York

Styring S and Rutherford AW (1987) In the oxygen evolving complex of Photosystem II the S_0 state is oxidized to the S_1 state by D^+ (signal II_{slow}). Biochemistry 26: 2401–2405

Thibault P (1978) A new attempt to study the oxygen evolving system of photosynthesis: Determination of transition probabilities of a state *i*. J Theor Biol 73: 271–284

Vass I and Styring S (1991) pH-dependent charge equilibria between tyrosine-D and the S-states in Photosystem II. Estimation of relative midpoint redox potentials. Biochemistry 30:830–839

Velthuys BR and Amesz J (1974) Charge accumulation at the reducing side of photosystem 2 of photosynthesis. Biochim Biophys Acta 333: 85–94

Velthuys BR and Visser JWM (1975) The reactivation of EPR signal I I in chloroplasts treated with reduced dichlorophenolindophenol: Evidence against a dark equilibrium between two oxidation states of the oxygen evolving system. FEBS Lett. 55: 109–112

Vermaas WFJ, Renger G and Dohnt G (1984) The reduction of the oxygen evolving system in chloroplasts by thylakoid components. Biochim Biophys Acta 764: 194–202

Vos MH, van Gorkom HJ and van Leeuwen PJ (1991) An electroluminescence study of stabilization reactions in the oxygen evolving complex of Photosystem II. Biochim Biophys Acta 1056: 27–39

Weiss C and Sauer K (1970) Activation kinetics of photosynthetic oxygen evolution under 20–40 nanosecond laser flashes. Photochem Photobiol 11: 495–501

Witt HT (1991) Functional mechanism of water splitting photosynthesis. Photosynth Res 29: 55–77

Chapter 25

Mechanism of Photosynthetic Oxygen Production

Warwick Hillier*
Photobioenergetics Group, Research School of Biological Sciences, The Australian National University, Canberra, ACT 0200, Australia

Johannes Messinger*
Max-Planck-Institut für Bioanorganische Chemie, Stiftstrasse 34 – 36, D-45470 Mülheim an der Ruhr, Germany

*Authors for correspondence, email: warwick.hillier@anu.edu.au and messinger@mpi-muelheim.mpg.de

T. Wydrzynski and K. Satoh (eds): Photosystem II: The Light-Driven Water:Plastoquinone Oxidoreductase, pp. 567–608.

Summary

This chapter deals with the mechanism of photosynthetic water oxidation that leads to O_2 formation in Photosystem II (PS II). After a brief introduction to the structure and function of the PS II complex, the S-state cycle (Kok model) is outlined and the structure and oxidation states of the catalytic Mn_4O_xCa complex are summarized. We then cover in detail the current information concerning substrate water binding and consider energetic and kinetic aspects of photosynthetic water oxidation. On that basis, we discuss several recent mechanistic proposals for O-O bond formation in PS II and summarize our current perceptions in a novel mechanistic proposal for photosynthetic water oxidation.

I. Introduction

Photosynthesis describes the complex biological processes by which solar energy is converted into chemical energy. This energy conversion is performed by so called photosystems. Photosystem II (PS II) is of pivotal importance to life on earth because it is the principle means by which molecular oxygen is generated. The light-induced formation of O_2 in PS II can be summarized as follows:

$$2\ H_2O + 4\ h\nu \rightarrow O_2\uparrow + 4\ H^+ + 4\ e^- \qquad (1)$$

PS II is distributed throughout all higher plants; the aquatic green, red and brown algae (*Chlorophyta, Rhodophyta, Phaeophyta*); cyanobacteria and diatoms (*Chrysophyta*). Common to all PS II complexes is the presence of chlorophyll (Chl) *a* pigments. Structurally, PS II is a multi-subunit Chl/protein complex that consists of close to 30 polypeptides (Hankamer et al., 2001; Shi and Schroder, 2004; Chapter 6, Thornton et al.; Chapter 18, Hankamer et al.). It is located within the thylakoid membrane. With the exception of the light-harvesting antenna system and a number of extrinsic proteins, only minor structural/functional differences have been reported between PS II complexes from these different species. The origin of PS II is unclear and extensive lateral gene transfer is likely involved between different reaction centers (Chapter 30, Dismukes and Blankenship).

Figure 1 presents a schematic overview of the arrangement of the co-factors in PS II (a more detailed picture is given in Chapters 19 (Witt), 20 (Shen and Kamiya), 21 (Barber and Iwata)). The catalytic center of water oxidation, the Mn_4O_xCa complex (see Fig. 1), is located on the lumenal side of PS II. However, due to large lumenal extensions of the inner antenna proteins CP43 and CP47 (Chapter 3, Eaton-Rye and Putnam-Evans) and the presence of three extrinsic proteins (Chapter 5, Bricker and Burnap), the Mn_4O_xCa complex is actually situated not far from the center of PS II, where it is apparently well shielded from the aqueous phase. In the case of higher plants, the extrinsic proteins have molecular weights of about 33 kDa, 23 kDa, and 17 kDa; while in cyanobacteria, the two smaller proteins are substituted by cytochrome c_{550} and a 12 kDa extrinsic protein (Shen et al., 1992; Seidler, 1996; Chapter 5, Bricker and Burnap).

The secluded position of the Mn_4O_xCa complex within the PS II structure suggests that the protein matrix is important for the proper function of the oxygen-evolving complex (OEC). In the absence of the extrinsic proteins, for example, nonphysiological

Abbreviations: Kβ XES – Kβ X-ray emission spectroscopy; Chl – chlorophyll; ENDOR – electron nuclear double resonance; EPR – electron paramagnetic resonance; ESEEM – electron spin echo envelope modulation; ET – electron transfer; EXAFS – extended X-ray absorption fine structure; NMR – nuclear magnetic resonance; OEC – oxygen-evolving complex; Pheo – pheophytin; PT – proton transfer; PCET – proton coupled electron transfer; PRE – proton-relaxation rate enhancement; P680 – the primary electron donor in PS II; S_n states (n = –5, …, 4) – formal notation for the oxidation states of the OEC; XANES – X-ray absorption near edge structure; Q_A, Q_B – plastoquinone molecules that act as one and two electron acceptors in PS II, respectively; Y_D – redox active tyrosine D2-Y160; Y_Z – redox-active tyrosine D1-Y161

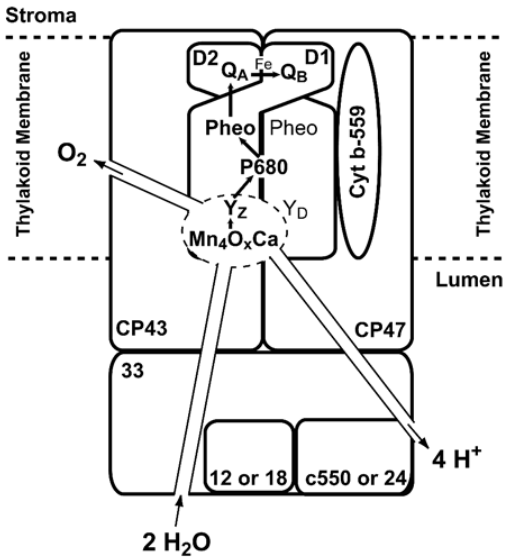

Fig. 1. Schematic view of PS II complex in plants (only core proteins are included). The central D1 and D2 polypeptides bind all the cofactors required for charge separation (P680, Pheo), charge stabilization (the redox-active tyrosine Y_Z, and the plastoquinones Q_A and Q_B), and also contains the oxygen evolving complex (OEC) sub domain (dashed circle). The OEC is comprised of the Mn_4O_xCa complex, Y_Z, substrate water and the Mn/Ca ligands. The function of the OEC is to oxidize substrate water releasing O_2 and protons (H^+). The OEC is located close to the center of the PS II complex, apparently sequestered from the aqueous phase and shielded by the extrinsic loops of the CP43 and CP 47 chlorophyll-*a* inner antenna and a number of extrinsic polypeptides of apparent molecular weights of 33 kDa, 24 kDa and 17 kDa in higher plants and 33 kDa, 12 kDa and the cytochrome c_{550} in case of cyanobacteria. The so-far-unidentified substrate and product channels are also indicated. Molecular oxygen is suggested to be channeled into the membrane where it is more soluble.

Ca^{2+} and Cl^- concentrations are required to restore O_2-evolution activity (Chapter 13, van Gorkom and Yocum). Similarly, small deletions in the extrinsic loop of CP47 can inactivate the OEC (Gleiter et al., 1995). Possible functions of the protein include: (i) prevention of unregulated access of water and other molecules to the Mn_4O_xCa complex by providing specific channels for substrate water entry and oxygen release (Wydrzynski et al., 1996); (ii) formation of specific H-bonding networks or proton release chains (proton wires) for effective release of protons into the lumen; (iii) support of structural changes of the Mn_4O_xCa complex during water oxidation; (iv) positioning and 'concentration' of the required co-factors (for review see Debus, 1992; Yocum, 1992); and (v) tuning of the energetics of the S state transitions. The possibility of channels for the entry of substrate water and for the release of the products O_2 and protons are schematically indicated in Fig. 1 (Chapter 21, Barber and Iwata).

The Mn_4O_xCa complex forms, together with its cofactors (possibly Cl^- and HCO_3^-; Chapter 13, van Gorkom and Yocum; Chapter 14; van Rensen and Klimov), ligands (Chapter 11, Debus) and tyrosine Z (Y_Z at D1-161) (Chapter 9, Diner and Britt) a functional unit within PS II that is referred to as the oxygen-evolving complex (OEC; also called the water-oxidizing complex, WOC, or water oxidase). On the basis of site-directed mutagenesis, possible direct ligands of the Mn_4O_xCa complex are Asp170, Glu 189, His190, His332, Glu333, His337, Asp342, and Ala344 of the D1 protein (Debus, 2001; Diner, 2001; Chu et al., 2004; Chapter 11, Debus). Many of these have been confirmed in the latest X-ray structure and in addition one ligand from CP43 was reported (Ferreira et al., 2004; Chapter 21, Barber and Iwata)

The OEC, symbolized by a dashed circle in Fig. 1, couples the light-induced one-electron chemistry of the primary charge separation in PS II (P680 Pheo $\rightarrow$ $P680^{+\bullet}$ $Pheo^{-}$; Chapter 7, Renger and Holzwarth) with the four-electron chemistry of water oxidation to molecular oxygen (Eq. 1). The OEC has, therefore, two functions: (i) it serves as a storage unit for four oxidizing equivalents; and (ii) it templates the O-O bond formation.

II. Photosynthetic O_2 Evolution Patterns and the Kok Model

The foundation for all proposed mechanisms of water oxidation in PS II is the Kok model and is summarized below (for further details refer to Chapter 24, Shinkarev). The storage capability of the OEC for oxidizing equivalents was first revealed when Joliot et al. (1969) illuminated dark-adapted algae and chloroplasts with a train of short, saturating flashes and found that the O_2 was evolved with a characteristic periodicity of four (Joliot et al., 1969). A typical 'oxygen oscillation pattern' of dark-adapted thylakoids is shown in Fig. 2A. The main features of such patterns are: (i) a pronounced first maximum after the 3rd flash, which repeats every fourth flash thereafter; (ii) the damping of the O_2 oscillation; and

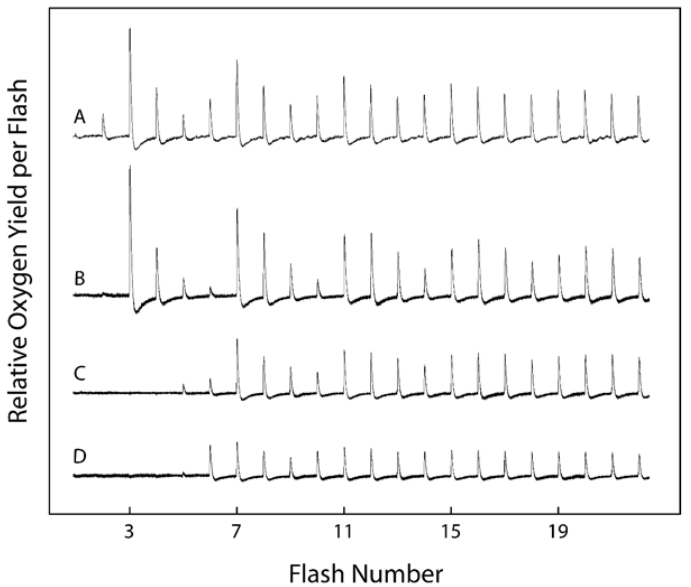

Fig. 2. Flash-induced O_2 yield patterns of *Thermosynechococcus elongatus* thylakoids showing the effects of flash length and sample pre-treatment. The double-hit phenomenon is illustrated in **A** with saturating xenon flashes (FWHM ~5 µs) and shown to be absent in **B** with saturating laser flashes (FWHM ~9 ns, 532 nm Nd:YAG). Both **A** and **B** were first subjected to single preflash/dark-adaptation regime to achieve a high (~100%) initial S_1 state population and to avoid back reactions with Y_D during the flash train. Super reduced S-states obtained by reduction with 10 mM NH_2NH_2: **C** 10 min incubation shifts about 60–70% of the centers from the dark-adapted S_1 state into the S_{-3} state, and **D** incubation starting from a sample enriched in the S_0 state by three preflashes results in about 40% S_{-2} and 40% S_{-3} state population. The fits of both C and D improve significantly if populations of 5% and 10% (C) or 20% and 5% (D) of S_{-4} and S_{-5} states are considered. Both C and D used laser illumination. All O_2 oscillation patterns were taken at pH 6.8 and 20ºC using, a 1 Hz flash frequency. For further details see (Messinger et al., 2001a).

(iii) a small O_2 yield after the 2nd flash. Kok et al. (1970) discovered that these characteristics remain essentially unchanged after inactivating about 90% of the PS II centers. Therefore, he proposed a model where each OEC works independently and cycles through five different oxidation states that he denoted as S_0, S_1, S_2, S_3 and S_4. The following scheme illustrates this sequence:

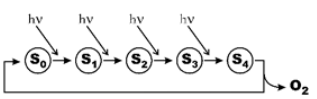

Scheme 1

In this nomenclature, the index (n = 0, .., 4) gives the number of stored oxidizing equivalents relative to the lowest redox state that the OEC attains during the water oxidation cycle.

After thorough dark-adaptation, almost all centers have relaxed to the 'dark-stable' S_1 state. This explains why the first maximum of O_2 evolution occurs after the 3rd flash. The S_0, S_2 and S_3 states are all meta-stable and convert to S_1 with half-times that strongly depend on temperature and pH (Vass et al., 1990; Vass and Styring, 1991; Messinger et al., 1993; Messinger and Renger, 1994). The time course for these reactions is generally in the seconds to minutes (S_2 and S_3) or tens of minutes (S_0) range. The main pathways for S_3 and S_2 decay are the recombination with electrons from the acceptor side ($Q_B^{-/2-}$ in Fig. 1; slow phase) (Diner, 1977; Rutherford et al., 1982; Robinson and Crofts, 1983; Rutherford and Inoue, 1984) and the reduction by the redox-active tyrosine Y_D of the D2 protein (see Fig. 1; fast phase) (Vermaas et al., 1984, 1988; Nugent et al., 1987; Rutherford and Styring, 1987. Deactivation of the S_3 state normally proceeds in one-electron steps via S_2 into the S_1 state. Because a very slow deactivation of S_2 is also observed in the presence of high levels of external quinone acceptors, other not-well-characterized pathways for S_2 and S_3 deactivations likely exist (Styring and Rutherford,

1988). The S_0 state is converted to S_1 by the oxidized form of Y_D, which is usually denoted as $Y_D^{\bullet}$ or Y_D^{ox} (Vermaas et al., 1984; Styring and Rutherford, 1987). Due to the long spatial separation of ~30 Å between Y_D and the Mn_4O_xCa complex, electron transfer probably involves charge equilibria with $P680/P680^{+\bullet}$ and $Y_Z/Y_Z^{\bullet}$ (Vass and Styring, 1991; Buser et al., 1992; Messinger et al., 1993).

To explain the damping in the O_2 oscillation patterns and the small O_2 yield after the second flash in well dark-adapted PS II samples, Kok and co-workers introduced the 'miss' (α) and the 'double-hit' (β) probabilities (Kok et al., 1970; Forbush et al., 1971). The miss probability gives the percentage of OECs that do not stably advance and therefore are in the same S_n-state before and after a flash. For any given flash the misses are statistically distributed over all PS II centers. Therefore, the miss event does not represent a permanent inhibition. It is believed that redox equilibria on the donor ($Y_ZP680^{+\bullet} \Leftrightarrow Y_Z^{\bullet}P680$) and the acceptor side ($Q_A^{-}Q_B \Leftrightarrow Q_AQ_B^{-}$) are responsible for the occurrence of misses (Renger and Hanssum, 1988; Shinkarev and Wraight, 1993). Similarly, the double-hit probability equals the percentage of centers that undergo a double advancement ($S_n \rightarrow S_{n+2}$) in a single flash. The double-hit probability depends on the flash profile, which, in the case of Xe-flashes, usually includes a 'tail' of residual intensity that extends over more than 100 μs (Kok et al., 1970; Forbush et al., 1971; Jursinic, 1981). As illustrated in Fig. 2B, double hits are essentially absent if 'tailless' ns laser flash illumination is employed. For spinach thylakoids, typical Kok parameters are $\alpha \cong 6$–10% and $\beta \cong 3$–5% with Xe-flashes, and when laser excitation is used, only the misses remain. However, the miss and double hit parameters are strongly temperature and pH dependent (Messinger et al., 1993; Messinger and Renger, 1994) and also affected by H/D exchange (Christen et al., 1999).

Normally it is assumed that the miss and double hit probabilities are S-state independent. However, also S state dependent miss parameters have been considered (Delrieu, 1983; Shinkarev and Wraight, 1993; de Wijn and van Gorkom, 2002; Noguchi and Sugiura, 2002a). On a theoretical basis, the concept of unequal misses is easy to accept, because the redox-equilibria between the cofactors in PS II are likely to shift in response to the redox state of the Mn_4O_xCa complex or of Q_B (Renger and Hanssum, 1988; Shinkarev and Wraight, 1993; Shinkarev, 1996). However, if, as with most techniques, only the population of one S-state is directly followed, then a unique deconvolution using an S-state dependent miss probability is impossible (see, however, de Wijn and van Gorkom, 2002; Noguchi and Sugiura, 2002a). It will be important to clarify the precise S-state dependents of the miss and double-hit parameters in future.

III. Structures and Oxidation States of the Mn_4O_xCa Complex

The geometric and electronic structures of the Mn_4O_xCa complex in its different S states form essential bench marks for the validity of any mechanistic proposal for photosynthetic water oxidation. Therefore, the most important facts are summarized below. For more detailed information and further references see Chapters 10 (Yachandra) and 12 (Åhrling et al.).

A. Possible Structures in the S_1 State

Until the recent crystal-structure determinations of PS II at 3.2–3.8 Å resolution (Zouni et al., 2001; Kamiya and Shen, 2003; Biesiadka et al., 2004; Ferreira et al., 2004; Chapters 19, Witt; 20, Shen and Kamiya; 21, Barber and Iwata), most of the information about the structure of the Mn_4O_xCa complex has come from studies using electron paramagnetic resonance (EPR) and X-ray absorption spectroscopy directed at the S_1 and S_2 states. Despite the very detailed model for the Mn_4O_xCa complex that was developed in one of the latest X-ray diffraction (XRD) studies (Ferreira et al., 2004; Chapter 21, Barber and Iwata) and is shown in Fig. 3H, other spectroscopic information is still highly valuable because it is presently unclear as to how much the XRD structures are affected by radiation damage. In contrast, photoreduction can be very well controlled in extended X-ray absorption fine structure (EXAFS) studies by using a significantly lower X-ray dose and by simultaneously recording the position of the Mn K-edge. In addition, EXAFS measurements have a much higher resolution (up to 0.03 Å) compared to XRD (now 3.2 Å).

EXAFS experiments firmly established that the OEC is comprised of 2–3 di-μ-oxo-bridged Mn_2 motifs, which show Mn–Mn scattering at distances of about 2.7 Å (Yachandra et al., 1993, 1996; Penner-Hahn, 1998; Dau et al., 2001; Robblee et al., 2001, 2002; Messinger, 2004). In addition, a single Mn–Mn, and 1–2 Mn–Ca interaction at 3.3–3.4 Å have been fit-

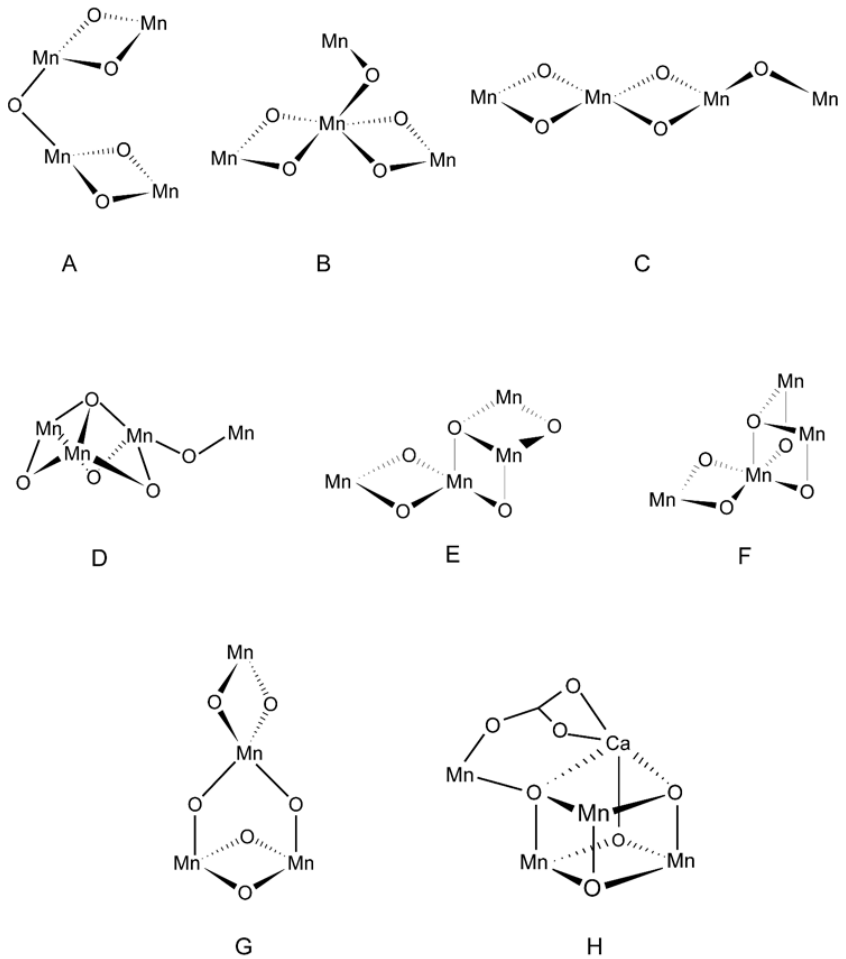

Fig. 3. **A-G**: Possible structures of the OEC based on EXAFS spectroscopy (Yachandra et al., 1996; Robblee et al., 2002). Structures **A, B** and **C** have two 2.7 Å Mn-Mn distances and one 3.3 Å Mn-Mn distance, while structures **D, E** and **F** have three 2.7 Å Mn-Mn and one 3.3 Å distances, and model G has two 2.7 Å and two 3.3 Å distances. To all models, one or two Mn-Ca distance(s) of about 3.4 Å should be added so that the average vector is close to the membrane normal (Cinco et al., 1998; Cinco et al., 2002; Cinco et al., 2004). **H**: Structural model for the Mn_4O_xCa complex on the basis of the 3.5 Å PS II crystal structure (Ferreira et al., 2004). It contains three '2.7 Å' Mn-Mn, two '3.3 Å' Mn-Mn and three '3.4 Å' Mn-Ca type distances.

ted to the data (Cinco et al., 1998, 2002, 2004; Latimer et al., 1998). With these EXAFS-derived structural building blocks, several different geometries can be proposed for the Mn_4O_xCa complex (Yachandra et al., 1996; Hasegawa et al., 1999; Robblee et al., 2001; Carell et al., 2002; Sauer and Yachandra, 2002), from which the most probable ones are displayed in Fig. 3. For clarity, Fig. 3 only shows possible arrangements of the four Mn ions. Ca should be incorporated into each of the proposed structures so that 1–2 Mn–Ca vectors exist with an average angle of about 20° to the membrane normal (Robblee et al., 2001; Cinco et al., 2004). The proximity of Ca to Mn has been confirmed by the latest XRD structures (Biesiadka et al., 2004; Ferreira et al., 2004).

The so-called 'dimer of dimers' model of the OEC (Fig. 3 A) was favored for a long time because of its simplicity and consistency with most EXAFS data (Yachandra et al., 1993, 1996). However, on the basis of simulations of EPR and ^{55}Mn-ENDOR spectra

from the S_2 state structures **B**, **C** or **D** have been supported, because they provide better rationales for the strong exchange coupling between two di-μ-oxo bridged Mn–Mn moieties (Hasegawa et al., 1999; Peloquin et al., 2000).

While models **A**, **B** and **C** contain two 2.7 Å distances and one 3.3 Å Mn-Mn distance, models **D, E** and **F** of Fig. 3 are among the few possible structures for the OEC that contain three di-μ-oxo type Mn–Mn moieties and one 3.3 Å Mn-Mn distance. These types of structures are now favored by the Berkeley group, based on a detailed analysis of EXAFS data of the S_0 state (Robblee et al., 2002). In contrast, Dau and co-workers prefer dimer of dimer models (Dau et al., 2003). Compact structures like **D**, **E** and **F** are in line with the small orientation dependence of the S_2 EPR multiline signal (Hasegawa et al., 1998), which contrasts the pronounced orientation dependence of the S_{-2} state EPR signal of the OEC (Goussias et al., 1997; Sarrou et al., 1998): in the former case, all four Mn ions are believed to contribute to the EPR signal (Zheng and Dismukes, 1996; Hasegawa et al., 1999; Peloquin et al., 2000), while in the latter case, for unknown reasons, only two of the four Mn ions participate (Sarrou et al., 1998). Interestingly, the S_{-2} EPR signal has striking similarities to the EPR signal of the Mn_2(II, III) form of di-Mn-catalase (Zheng et al., 1994; Sarrou et al., 1998). This may indicate structural analogies between parts of the Mn_4O_xCa complex of PS II and the dimeric catalytic site of Mn catalase (Sarrou et al., 1998; Sarrou et al., 2003).

Out of the structures displayed in Fig. 3, models **D**, **E** and **F** appear to offer the best geometry for containment within the electron-density envelope ascribed to the 3.2–3.8 Å XRD structures of the Mn_4O_xCa complex in PS II (Zouni et al., 2001; Kamiya and Shen, 2003; Biesiadka et al., 2004; Ferreira et al., 2004), although also dimer of dimer models (**A** and **G**) can be fit into the data (Carell et al., 2002; Dau et al., 2003). If Ca is added to structure **D** so that it is connected to the bis-μ-oxo bridges of the trimeric unit, then a heteronuclear cubane with a dangling Mn is formed that very closely resembles the structure proposed by Barber and co-workers (Ferreira et al., 2004).

B. S-State Dependent Structural Changes of the Mn_4O_xCa Complex

Although a unique structure determination of a multi-nuclear center like the Mn_4O_xCa complex is complicated using EXAFS alone, structural changes of the Mn_4O_xCa complex upon S-state transitions should be easily detectable. On the basis of EXAFS spectroscopy, the Mn_4O_xCa complex has essentially the same structure in the S_1 and S_2 states (for a recent review see Robblee et al., 2001). In contrast, in the S_0 state, one of the 2.7 Å distances is longer by ~ 0.15 Å (Robblee et al., 2002). This increase is consistent with the protonation of one μ-oxo bridge and/or the presence of one Mn(II) center in the S_0 state. A structural change of the Mn_4O_xCa complex is also seen during the $S_2 \rightarrow S_3$ transition. This was first proposed on the basis of the slow reactivity of the S_3 state towards hydrazine and ammonia (Boussac et al., 1990; Messinger et al., 1991), the lower binding affinity of Ca^{2+} in the S_3 state (Boussac and Rutherford, 1988), and because of the high reorganization energy of this transition (Koike et al., 1987; Renger and Hanssum, 1992). One older and two recent EXAFS studies provide direct evidence for a structural change in this S-state transition (Guiles et al., 1990; Liang et al., 2000; Dau et al., 2001). Unfortunately, not only the interpretation, but also the actual EXAFS data of the S_3 state are significantly different between the two new studies. One proposal calls for a lengthening of the 2.7 Å distances in the S_3 state to 2.8 Å and 3.0 Å (Liang et al., 2000); the other proposal invokes formation of an additional 2.7 Å Mn-Mn bis-μ-oxo bridge in S_3 (Dau et al., 2001). Obviously, these two opposing results lead to very different proposals for the mechanisms of water oxidation. It is, therefore, important to resolve this discrepancy in the near future.

Vibrational Fourier transform infrared (FTIR) spectroscopy also implicates structural change occurring within the OEC as a function of S-state. The recent studies of the $S_2 \rightarrow S_3$ transition by FTIR shows prominent carboxylic acid $\nu_{symm}(COO^-)$ band activity about 1430–1340cm^{-1} (Hillier and Babcock, 2001; Noguchi and Sugiura, 2001). Such strong changes are also features arising in the $S_1 \rightarrow S_2$ transition, which have been proposed to manifest from coordination changes involving the OEC (Noguchi et al., 1995a, b; Kimura and Ono, 2001). Currently only one amino acid residue has been assigned (Chu et al., 2004) and future FTIR spectral assignments will be necessary for understanding the dynamic aspects of the Mn_4O_xCa complex.

Moving beyond the precise structure of the Mn_4O_xCa complex, the observed structural changes during some S-state transitions suggest that the

Mn_4O_xCa complex actively participates in the chemistry of water oxidation.

C. Mn Oxidation States

The knowledge of the Mn oxidation states of each S-state is of great importance to the understanding of water oxidation in PS II. Many different techniques have been employed to address this question, for example, flash induced UV-absorption changes, EPR, X-ray absorption near edge structure (XANES), and Kβ X-ray emission spectroscopy (Kβ XES) (for reviews see Debus, 1992; Yachandra et al., 1996, 2002). The measurements and interpretations are complicated by the fact that: (i) on each S-state transition maximally one out of four Mn ions per OEC undergoes a change in redox state; and (ii) the S-states are not quantitatively advanced with light flashes due to misses and double hits (see above), thus necessitating careful deconvolution of the raw data into S-state spectra. Additionally, the interpretation of such measurements is potentially troubled by spectroscopic calibrations using 'comparative' inorganic Mn model compounds. The principle problem with this approach is that the OEC structure is unknown and that coordination by a protein matrix may create binding sites that deviate substantially from the currently used inorganic models. Such deviations may arise from: (i) lower symmetry; (ii) lower coordination number; and (iii) changes in coordination during S-state advancement. Until improvements in the structural resolution of PS II are achieved, the significance of these factors remains undetermined (see also Renger, 2001).

Nevertheless, rigorous experiments have been undertaken over the recent years to address the important question of Mn oxidation states in PS II. In the following, this question is split into two parts: (1) what are the Mn oxidation states in the S_1 and S_2 states, and (2) do Mn oxidation-state changes occur during all S-state transitions?

1. Mn Oxidation States of the S_1 and S_2 States

Because of the relative ease of preparing concentrated PS II samples with nearly 100% S_1 or S_2 state population, these two S-states have been studied in detail by EPR and XANES spectroscopy. A comparison of XANES Mn K-edges of PS II in the S_1 state and S_2 states with spectra of relevant Mn model compounds shows that: (i) a Mn-centered oxidation occurs on this transition; and (ii) that the Mn oxidation states of the S_1 state are best denoted as $Mn(III_2, IV_2)$ (Yachandra et al., 1993; Roelofs et al., 1996; Iuzzolino et al., 1998; Messinger et al., 2001b). This finding is corroborated by recent Kβ XES data of the S_1 and S_{-1} states (Bergmann et al., 1998; Messinger et al., 2001b) and by ^{55}Mn ENDOR spectra of the S_2 state (Peloquin et al., 2000). Most simulations of the S_2 EPR multiline signal are consistent with Mn_4(III, IV, IV, IV), which is in line with the above proposal for the S_1 state, but some groups argue for Mn_4(III, III, III, IV) in S_2, which would indicate Mn_4(III, III, III, III) in the S_1 state (Zheng and Dismukes, 1996; Kuzek and Pace, 2001; Carell et al., 2002; Chapter 12, Åhrling et al.).

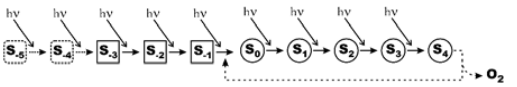

Scheme 2

In agreement with the relatively high Mn oxidation states in the above two proposals, several studies show that: (i) additional S-states exist below the S_0 state (see Scheme 2) that can be generated by reduction of the OEC with molecules like hydrazine, hydroxylamine, or $NO^{\bullet}$ (for review see Debus, 1992; Sarrou et al., 2003); and (ii) that light-induced oxidation of free Mn^{2+} by *apo*-PS II is required for the assembly of a functional Mn_4O_xCa complex in PS II (for reviews see Ananyev et al., 2001; Ono, 2001; Chapter 26, Dismukes, et al.; Chapter 26, Dismukes et al.). The reduction of the Mn_4O_xCa complex below the redox level of the S_0 state may be viewed as a reversal of the photoactivation process. Using hydrazine as a reductant, it has been clearly shown that relatively stable (hours) S_{-1}, S_{-2} and S_{-3} state populations of more than 60% can be generated in PS II (Messinger et al., 1997b; Messinger et al., 2001a). In addition, first indications for the existence of fragile S_{-4} and the S_{-5} states have been obtained from the analysis of the O_2-oscillation patterns such as that displayed in Fig. 2 C, D (Messinger et al., 1997b, 2001a; Sarrou et al., 2003). Photoactivation experiments have identified the first long-term stable intermediate as being Mn_4(II, II, III, III) (Tamura and Cheniae, 1987; Tamura et al., 1989). Taken together, these data indicate that the lowest long-term stable state of the OEC (S_{-3} state) has the same redox level as the first long-lived photoactivated state, i.e., Mn_4(II, II, III, III). Since the $NO^{\bullet}$ induced formation of the S_{-2} state

EPR multiline signal (Ioannidis et al., 1998; Sarrou et al., 1998, 2003; Schansker et al., 2002) and XAS measurements on reduced S-states (Riggs et al., 1992; Riggs-Gelasco et al., 1996) prove that Mn centered reductions occur down to at least the level of the S_{-2} state, these considerations strongly support the idea that the Mn oxidation states in the four steps more oxidized S_1 state are Mn_4(III, III, IV, IV) (Ono, 2001; Chapter 10, Yachandra).

2. Relative Changes During Water Oxidation

The EPR multiline spectra of the S_2 and S_0 states (Dismukes and Siderer, 1981; Åhrling et al., 1997; Messinger et al., 1997a,c) and the absence of an EPR signal in perpendicular mode for the S_1 state support the idea of Mn-centered oxidations on the $S_0 \rightarrow S_1$ and $S_1 \rightarrow S_2$ transitions (Chapter 12, Åhrling et al.). The same conclusion is reached independently, based on Mn K-edge shifts in XANES data and by Kβ XES (Iuzzolino et al., 1998; Messinger et al., 2001b). A Mn(II)→Mn(III) or a Mn(III)→Mn(IV) oxidation is consistent with the currently available data for the $S_0 \rightarrow S_1$ transition, with the former assignment being preferred by many researchers. Essentially all groups agree that a Mn(III)→Mn(IV) oxidation occurs during the $S_1 \rightarrow S_2$ transition, because of the striking similarities of the S_2 EPR multiline with EPR signals of synthetic Mn_2(III, IV) complexes. In contrast, the situation for the $S_2 \rightarrow S_3$ transition is still unclear despite the fact that recently agreement has been reached about the experimental XANES data and their primary interpretation (Messinger et al., 2001b; Dau et al., 2003): both groups agree now that the K edge difference spectra of the $S_1 \rightarrow S_2$ and $S_2 \rightarrow S_3$ transitions are significantly different and that therefore the nature of the $S_2 \rightarrow S_3$ transition cannot be identical to that of the $S_1 \rightarrow S_2$ transition, which is known to be a simple Mn(III) to Mn(IV) oxidation. However, due to different ways of quantifying edge shifts and due to a different bias with regard to the type of structural change that occurs during the $S_2 \rightarrow S_3$ transition either a ligand-centered oxidation (Messinger et al., 2001b; Chapter 10, Yachandra) or a Mn-centered oxidation plus a structural change from a 5-coordinated Mn(III) into a 6-coordinated Mn(IV) are proposed (Dau et al., 2003) to explain this finding. The lengthening of all Mn-Mn distances during the $S_2 \rightarrow S_3$ transition is considered to be best understood by the formation of a bridging radical (Liang et al., 2000; Chapter 10, Yachandra), while the formation of an additional 2.7 Å Mn-Mn distance (Dau et al., 2003) would favor the latter explanation. Independent experiments and a better theoretical understanding of XANES are now required to settle this question. In this regard Kβ XES experiments, which have been demonstrated to be less sensitive to structural changes (Visser et al., 2001), support a ligand centered oxidation (Messinger et al., 2001b).

Besides the ligand-centered and the Mn-centered oxidations discussed above, a third option involving partial substrate water oxidation in the form of a rapid redox equilibrium between Mn bound peroxide and two terminal hydroxo ligands was proposed as the electronic configuration for the S_3 state (Renger, 1987, 2001). In summary, further studies are required to uniquely identify the Mn redox states in PS II, especially for the S_0 and S_3 states. Possibly the newly developed RIXS spectroscopy, which allows the detection of L-edge like spectra, will help to remove the remaining uncertainties (Yachandra, 2002; Glatzel et al., 2004).

D. Cofactors

Ca^{2+}, Cl^- and possibly HCO_3^- have been found to be required for optimal O_2 evolution activity and photoactivation (for review see Yocum, 1992; van Rensen et al., 1999; Ananyev et al., 2001). Therefore, they are often inferred to bind at or close to the Mn ions. In functional studies, the natural co-factors are often substituted: Sr^{2+} (for Ca^{2+}), Br^- or F^- (for Cl^-), formate (for bicarbonate), to enable detection of functional and/or spectroscopic changes. Because other chapters in this book (Chapter 13, van Gorkom and Yocum; Chapter 14, van Rensen and Klimov) deal with the cofactors of the OEC in detail, only a very brief description of the mechanistically relevant details is given.

1. Calcium

In addition to the above (Section III.A.) reported evidence for the physical proximity of Ca^{2+} to Mn, there is also biochemical support for its functional relevance in water oxidation (for review see Debus, 1992; Yocum, 1992). Several metal ions, of different size and charge, are able to bind into the Ca^{2+} site in PS II, but the only one able to partially support O_2 evolution is Sr^{2+} (Ghanotakis et al., 1984). This finding was recently explained on the basis of a comparison of the ionic radii of a series of cations and the pK_a

values of their aqua ions: it was found that only Sr^{2+} has an approximate match in both of these parameters with Ca^{2+} (Vrettos et al., 2001a,b). It is interesting that even in Sr^{2+}-reconstituted PS II complexes all the S-state transitions are slowed (Westphal et al., 2000). These data support the idea that Ca may be involved in formation of the O-O bond, possibly via substrate water binding (Section IV.A.I) or by being an important part of the proton relay network of the OEC (Sections IV.C. and V.B.)

2. Chloride

Only one group has studied Cl^- binding directly by monitoring the release of radioactive $^{36}Cl^-$ from PS II membranes during dialysis against Cl^- free medium. These studies reveal that one slowly exchanging Cl^- exists per OEC (Lindberg et al., 1990, 1993). Oxygen measurements at various light intensities show that, after complete release of Cl^- by dialysis, all PS II centers are still active but evolve O_2 at reduced rate due to slower S-state turnover. Therefore, these authors conclude that Cl^- is not a cofactor for O_2 evolution (Lindberg and Andréasson, 1996) and that it does not bind directly to Mn (Olesen and Andréasson, 2003). They suggest that Cl^- is an important part in a proton-relay network that helps to shuttle protons from the OEC to the lumen.

However, removal of chloride by SO_4^{2-} or by low pH treatment and/or its replacement by F^- or N_3^- inhibits O_2 evolution, while Br^-, I^- or NO_3^- can functionally replace Cl^- (Hind et al., 1969; Kelley and Izawa, 1978; Critchley et al., 1982; Haddy et al., 1999). Recent studies have concluded that Cl^- is required in such samples for the $S_2 \rightarrow S_3$ and $S_3 \rightarrow S_0$, but not for the $S_0 \rightarrow S_1$ and $S_1 \rightarrow S_2$ transitions (Wincencjusz et al., 1998, 1999). Conclusive evidence for Cl^- binding to the Mn_4O_xCa complex has not yet been obtained. Preliminary Mn EXAFS data are consistent with Cl^- ligation to Mn in the S_3 state (Fernandez et al., 1998) and, in substituted samples, of Br^- in the S_2 state (Yachandra et al., 1996). However, the fact that the easily oxidizable I^- can functionally replace Cl^- has been used to argue against direct binding of Cl^- to Mn (Rashid and Homann, 1992; Olesen and Andréasson, 2003). Depletion of Cl^- also affects the magnetic properties of the Mn_4O_xCa complex by shifting the equilibrium between the EPR multiline and g = 4.1 form of the S_2 state (Ono et al., 1986, 1995; van Vliet and Rutherford, 1996). Interestingly, a similar effect of Cl^- can be observed in Ca^{2+}-depleted PS II preparations. This indicates that the Cl^- effect is independent of Ca^{2+} (van Vliet et al., 1994) and thus argues against the possibility that Cl^- is bound to Ca^{2+} in the S_2 state.

3. Bicarbonate

It was clearly shown that the main effect of bicarbonate on the electron transfer in PS II is through binding at the acceptor side of PS II, where it is involved in the protonation of Q_B^{2-}. This finding, together with mass-spectrometric results using $H_2{}^{18}O$, discounted earlier proposals in which bicarbonate was proposed to act as a mediator in photosynthetic water oxidation. In addition, no physical evidence for bicarbonate binding to Mn exists at present (for review see van Rensen et al., 1999). However, several recent reports conclude that bicarbonate also affects the PS II donor site. It was shown, for example, that bicarbonate promotes the assembly of the Mn_4O_xCa complex during photoactivation (Baranov et al., 2000, and references therein). For more details, see Chapters 14 (van Rensen and Klimov), 21 (Barber and Iwata) and 26 (Dismukes et al.).

IV. Substrate Interactions

A. Substrate Water Binding

The analysis of substrate binding within the OEC is a fundamental question for understanding the mechanism of water oxidation in PS II, yet it is a difficult problem to address. The principle reason for this is that an aqueous environment is required for all S-state turnovers (e.g., FTIR data by Noguchi and Sugiura, 2002a; Chapter 16, Noguchi and Berthomieu). As a consequence, the K_M for substrate water is undefined, and it was unknown until recently whether substrate water is bound to the catalytic site in all S-states or whether the OEC is dry up to the S_3 state and water binds only in the transient S_4 state. In addition, numerous intermediate situations between these two extremes can be proposed. Several techniques have been applied to analyze this question.

1. Mass Spectrometry

The most direct and unambiguous evidence for *substrate* water binding to the OEC is obtained mass spectrometrically by $H_2{}^{16}O/H_2{}^{18}O$ exchange measure-

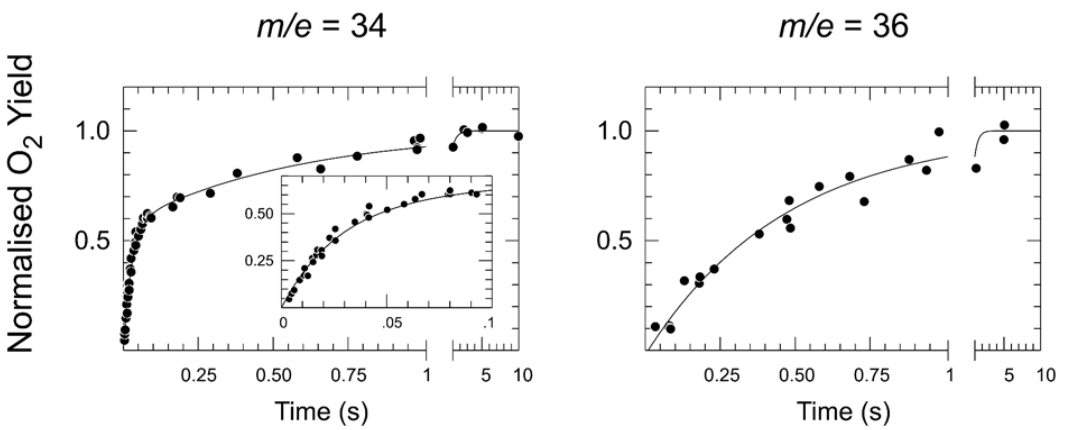

Fig. 4. The normalized yields of O_2 produced on the third flash by spinach thylakoid samples plotted as a function of $H_2{}^{18}O$ incubation time, in the S_3 state. Measurements were made at $m/e = 34$ (left) for the mixed labeled $^{16,18}O_2$ and at $m/e = 36$ (right) for the double labeled $^{18,18}O_2$ at 10 °C. Solid lines show first-order kinetic fits yielding rate constants of 38 ± 2 s^{-1} for the fast phase and 1.8 ± 0.2 s^{-1} for the slow phase. For further details see (Hillier et al., 1998).

ments with ms time resolution. Initial measurements with resolution limited by tens of seconds (Radmer and Ollinger, 1986; Bader et al., 1993) were unable to resolve this question. The current endeavors by Wydrzynski and colleagues are performed with PS II samples suspended in buffered $H_2{}^{16}O$ and pre-illuminated with 0, 1, 2, or 3 flashes to populate the S_1, S_2, S_3, or S_0 states, respectively (Messinger et al., 1995; Hillier and Wydrzynski, 2000). Then, $H_2{}^{18}O$ is injected at defined times before a detecting flash sequence, and the isotope distribution of the released oxygen is determined via a membrane inlet mass spectrometer (MIMS) system.

A typical measurement for the S_3 state is shown in Fig. 4. At mass 34 ($m/e = 34$), the $^{16,18}O_2$ product is measured to appear with a bi-exponential rise that has approximately equal amplitudes for the fast and the slow phase. These two phases can be shown (see below) to correspond to the two substrate water molecules required by each PS II center to produce O_2 (Messinger et al., 1995; Hillier et al., 1998). At mass 36, the $^{18,18}O_2$ signal increases mono-exponentially with a rate that equals that of the slow phase at mass 34. The biphasic rise of the 34 signal has been obtained with thylakoid membranes, spinach PS II membrane fragments and core particles from *Thermosynechococcus elongatus* (Table 1). Therefore, the two phases are not due to sample heterogeneity or sample type, but are an intrinsic property of PS II. The observed monophasic rise of the mass 36 peak provides an independent line of evidence for this conclusion, because in case of sample heterogeneity, this rise should also be biphasic. In contrast, a monophasic rise is expected for two inequivalent binding sites per OEC, since the appearance of this higher mass peak, for which both water molecules have to exchange, is naturally limited by the equilibration of the slowly exchanging binding site (Messinger et al., 1995). Similar biphasic responses have been observed for the S_0, S_1, and S_2 states, although with our current set up resolution of the fast phase is only possible for the S_2 and S_3 states (Hillier and Wydrzynski, 2004). Table 2 compares the temperature dependents of the substrate water exchange rates in the different S-states.

From these experiments (Tables 1 and 2), several conclusions can be drawn about the states of the Kok cycle in which substrate water binds to PS II: (i) Because both exchange rates in the S_2 and S_3 states are slower than the mixing of the water isotopes in the sample chamber ($k_{mix} = 175\ s^{-1}$), these data prove unambiguously that both substrate water molecules are bound to the OEC in the these states (Hillier et al., 1998; Hendry and Wydrzynski, 2002). (ii) Measurements of the S_0 and S_1 states resolve the slow phase of exchange showing that at least one substrate water molecule is present already in the beginning of the catalytic cycle (Hillier and Wydrzynski, 2000).

Due to the nature of the experiment (measuring O_2 yield via advancement to S_4), the *same* water binding site is for example monitored by $^{34}k_1$ in the S_0, S_1, S_2

Table 1. Rate constants for ^{18}O exchange in the S_3 state of different PS II samples at 10 °C

Sample	$^{34}k_1$ (s^{-1})	$^{34}k_2$ (s^{-1})
Thylakoid membranes (*Spinacia*)	1.8 ± 0.2	38.0 ± 2.0
Thylakoid membranes (*Synechocystis*)	3.8 ± 1.3	25.9 ± 6.7
PS II membrane fragments (*Spinacia*)	2.1 ± 0.1	37.3 ± 1.6
PS II core particles (*Spinacia*)	1.1 ± 0.4	18.0 ± 3.9
PS II core particles (*T. elongatus*)	0.5 ± 0.1	34.6 ± 2.3
PS II core particles (*Synechocystis*)	0.9 ± 0.2	15.2 ± 2.4

Table 2. ^{18}O Exchange rates from thylakoid membranes as a function of temperature and derived Arrhenius parameters

	S_0 state	S_1 state	S_2 state	S_2 state	S_3 state	S_3 state
Temperature °C	k_1 (s^{-1})	k_1 (s^{-1})	k_1 (s^{-1})	k_2 (s^{-1})	k_1 (s^{-1})	k_2 (s^{-1})
20	----	0.066 ±0.003	4.3 ± 0.3	----	5.0 ± 0.2	57 ± 4
15	----	----	----	----	2.93 ± 0.09	56 ± 4
10	13.6 ± 1.4	0.022 ± 0.001	1.96 ± 0.12	118.8 ± 3.6	2.02 ± 0.06	37.5 ± 1.6
5	----	----	----	----	1.23 ± 0.08	26.0 ± 5
0	----	0.0055 ± 0.0003	0.52 ± 0.14	98.8 ± 9.7	0.42 ± 0.02	18.7 ± 0.9
$A_O \times 10^{-12}$ (s^{-1})	----	38 ± 2	18 ± 2	----	360 ± 40	0.00091 ± 0.00009
E_a (kJ mol^{-1})	----	83 ± 4	71 ± 9	----	78 ± 9	40 ± 5

Data from Hillier and Wydrzynski (2004).

and S_3 states (Table 2). Therefore, the presence of two kinetically distinct phases in all S-states proves that PS II has two inequivalent water-binding sites throughout the reaction cycle. Furthermore, the S-state dependence of both exchange rates and their activation energies support the idea that the substrate water molecules bind at, or at least close to, the Mn_4O_xCa complex.

The nature of the substrate binding site is more difficult to judge, because the exchange rates depend on many factors, including: (i) the nature of binding site (Mn, Ca, protein); (ii) the protonation state of the substrate (i.e., whether water binds fully protonated or as hydroxo or oxo); (iii) the type and covalency of the bond (e.g., bridging vs. terminal); and (iv) possible hydrogen bonding interactions involving the bound substrate molecule. Due to this complexity of factors, a molecular interpretation of the exchange data is qualitative at present and relies on trends seen in relatively scarce model data. Such data indicate, for example, that a marked decrease in ligand-exchange rates (typically by 10^3–10^4) occurs when a metal ion is oxidized and/or the protonation state of the water ligand changes (Richens, 1997; Messinger, 2000; Hillier and Wydrzynski, 2001). When the magnitudes of the activation energies for the exchange reactions (40–80 kJ mol^{-1}) are also taken into account, one can, with the above precautions, suggest that: (i) terminal binding of substrate water in the hydroxo or even oxo form to Mn(III) and/or Mn(IV); and (ii) a bridge between Mn and Ca appear to be possible binding scenarios for the substrate molecules in PS II.

An important constraint for mechanistic proposals is that in the S_2 and S_3 states the slow phase of exchange is essentially identical in rate and activation energy (Table 2). This strongly suggests that this substrate water is bound to a site that does not feel the oxidation events and structural changes known to take place in this step of the reaction. In contrast, the fast-exchanging substrate molecule is clearly affected by this transition, because it is more tightly bound in the S_3 state than in the S_2 state. Similarly the slow exchange is significantly retarded during the $S_0 \rightarrow S_1$ transition. Puzzling findings are: (i) that the exchange rate for the slow phase increases during the $S_1 \rightarrow S_2$ transition; and (ii) that the slow exchange rate in the S_0 state is only 6-times faster than the slow exchange rate recorded in the S_2 and S_3 states.

The above discussion of possible water binding sites tacitly implies that the rates of substrate water exchange are not limited by its diffusion through the protein matrix. Assuming that both substrate water

molecules enter the catalytic site through the same path ('water channel'), a diffusion limitation can be clearly excluded for the slow-exchanging water molecule, but remains a possibility for the fast-exchanging water. Experiments with reductants of different size show (Section IV.B) that the main diffusional limitation from the lumen to the Mn_4O_xCa complex is formed by the three extrinsic proteins. Recent exchange measurements using PS II complexes from which these extrinsic proteins were removed by salt washing show that both rates of exchange do not increase after this treatment (actually a minor slowing of the fast phase by a factor of 2–3 was observed) (Hillier et al., 2001). Accordingly, a diffusional limitation is also very unlikely for the fast exchanging substrate water molecule. This result is important with regard to suggestions that the fast-exchanging substrate molecule might be bound as terminal water ligand to Ca or may even only be coordinated to the protein matrix via hydrogen bridges. Taking into account that the water exchange rate at Ca^{2+} in solution is many orders of magnitude faster than those found in PS II (Richens, 1997), these kind of binding modes appear to be very unlikely. To support Ca^{2+} as a substrate water binding site in S_3, one needs to slow down the exchange rate, perhaps via deprotonation or more likely via bridging the substrate oxygen between Ca^{2+} and Mn (Hendry and Wydrzynski, 2003). The latter assignment is supported for the slow exchanging substrate site by a recent study that shows that the slow phase of exchange is significantly affected, when the functional Ca of the Mn_4O_xCa complex is replaced by Sr (Hendry and Wydrzynski, 2003).

2. Magnetic Resonance

In PS II research continuous wave (cw) EPR, electron nuclear double resonance (ENDOR) and electron spin echo envelope modulation (ESEEM) spectroscopy can be employed to study substrate water binding via the coupling of nuclear spins of the substrate with paramagnetic states of the Mn_4O_xCa complex. In this regard exchangeable protons (I = ½), deuterons (I = 1) and ^{17}O (I = 5/2) are of special interest. One limitation of this technique is that at present only the paramagnetic S_2 state and, with more difficulties, the S_0 state can be directly studied. Despite some initial controversy, there is now agreement that, after H_2O/D_2O exchange, several deuterium couplings can be observed in the S_2 and S_0 states (Britt, 1996; Fiege et al., 1996; Messinger et al., 1998; Britt et al., 2000, 2004; Evans et al., 2000). The implication from these findings is that exchangeable protons exist ~3–6 Å from the Mn_4O_xCa complex in S_0 and S_2, therefore favoring at least partially protonated substrate intermediates up to the S_2 state. Furthermore, because deuterium modulations are also observed in the S_2 state following advancement from S_1 by low-temperature (200K) illumination, it was concluded that the exchangeable deuterons arising from water are bound also in the S_1 state close to the Mn_4O_xCa complex (Britt, 1996; Evans et al., 2000).

The Britt laboratory has extended these H/D exchange measurements by combining pulse ENDOR and ESEEM measurements (Aznar and Britt, 2002). The advantage of this approach is that ENDOR measurements give the dipolar hyperfine couplings and ESEEM measurements yield the number of couplings. The simulation parameters suggest that a number of exchangeable protons exist close to the Mn_4O_xCa complex of the OEC. One of these couplings in the S_2 state is isotropic and was interpreted to be suggestive of a strongly coupled Mn-aqua species. Similarly, deuterium modulations were also observed in ESEEM experiments of the S_0 state (Messinger et al., 1998; Britt et al., 2004), indicating that substrate water may already be bound in the beginning of the cycle. The simulation of ^1H and ^2H EPR and ENDOR spectra provide important insight into the organization of substrate intermediates (Fiege et al., 1996; Britt et al., 2000, 2004).

Measurements such as these provide the best insights into the solvation of the Mn centers in PS II, but are not necessarily specific for substrate molecules, because bound and unbound solvent molecules and even exchangeable protons of the protein matrix may contribute to the signal. In addition, some complexities have emerged as to the nature of the S_2 EPR signal (Åhrling et al., 2004), and one report indicates that the deuterium couplings decay much faster during low-temperature storage than the S_2 EPR multiline signal (Evans et al., 2000). A limitation with the H/D studies is also possible if the substrate molecule were to exist as unprotonated terminal or bridging oxo-species.

An alternative approach circumventing some uncertainties associated with protons is the use of $H_2{}^{17}O$. Spectroscopy of the ^{17}O nuclei is more difficult, because of the higher costs and the quadrupole moment of ^{17}O, which tends to broaden the signals. The first report of ^{17}O coupling to the OEC comes from a cw EPR study of the S_2 state (Hansson et al.,

1986). The minor changes were interpreted to show water binding to the Mn_4O_xCa complex. Recently the Evans laboratory has returned to this approach and reported ^{17}O modulation of the S_2 multiline signal using ESEEM spectroscopy (Evans et al., 2004). The obtained signals have been interpreted to favor of a Mn^{III}-aqua substrate species in the S_2 state.

A different magnetic resonance experiment using NMR to determine the T_1 relaxation rate of bulk water protons is referred to as NMR proton relaxation rate enhancement (PRE). This effect arises due to the magnetic coupling between the nuclear spin of the water protons with the unpaired electron spin of a metal. The relaxation enhancement effect is relevant to protons bound at or in vicinity of paramagnetic metal centers. It is translated to the bulk water via: (i) rapid exchange of ligated water molecules with free molecules from the bulk phase; (ii) by proton exchange from bound water with bulk-water molecules; or (iii) by spin diffusion. The resultant proton T_1 rates are, therefore, a function of the concentration of paramagnetic ions, the number of water binding sites, the exchange rates of the water ligands (protons) and the spin diffusion rate. The first application of this technique was by Wydrzynski et al. (1976), and a flash dependence of the relaxation enhancement effect was observed. Subsequent measurements and interpretations have involved some degree of controversy (Robinson et al., 1981; Wydrzynski and Renger, 1986), which have never been fully resolved. The most recent work with PS II membrane fragments reveals that PRE interactions leading up to the S_3 state are favored to invoke Mn^{IV} formation in the $S_1 \rightarrow S_2$ transition and no Mn oxidation state change during the $S_2 \rightarrow S_3$ transition (Sharp, 1992). Under the assumption that only substrate water binds to the Mn cluster, this result points to one substrate water molecule being still (partially) protonated up to the S_3 state and, thereby, disfavors mechanistic proposals in which both substrate water molecules are fully deprotonated in the S_3 state. The NMR-PRE results were furthermore interpreted in terms of only one water molecule bound to Mn throughout the cycle (Sharp, 1992).

3. Vibrational Spectroscopy

The vibrational characterization of water molecules within the OEC holds significant potential for the identification of the exact chemical nature of the two substrate water molecules within the catalytic site. The approach necessitates incorporation of stable isotopes (i.e., ^1H, ^2H, ^{16}O, ^{18}O) to characterize the O-H or Mn-O vibrations and can, in principle, establish protonation state, H-bonding interactions involving water, and changes associated with oxidation state (when compared with a subset of Mn - model compounds (Chu et al., 2001; Cua et al., 2003)). The technique is exquisitely sensitive, yet has the limitations that it requires a physical change to occur to enable resolution of a FTIR difference spectrum, and there also is the challenge to demonstrate that the signals originate from substrate water and not from spectator water molecules.

The FTIR approach has been employed to determine mid-frequency H-O stretching and bending modes and reveals the tantalizing vibrational signature of a single water molecule associated with a change during the S_1-S_2 transition (Noguchi and Sugiura, 2000). This mode exhibits a characteristic downshift upon ^{18}O and ^2H exchange and also exhibits a change in H-bonding with S-state advance. The water molecule is suggested to be asymmetric and strongly hydrogen bonded; factors perhaps indicative of metal coordination. A practical advantage with FTIR spectroscopy is the development of S-state dependent studies that allow to probe water binding in all S-states (Hillier and Babcock, 2001; Noguchi and Sugiura, 2001). This approach has now been employed to study the water bands and reveals a number of water vibrational bands that change with S-state (Noguchi and Sugiura, 2002b). Studies such as this, although not yet specifically able to pinpoint where and how the water binds, can be coupled with computational approaches (Fischer and Wydrzynski, 2001) to provide important molecular insight into the fate of protons and the bonding of water within the OEC.

Both FTIR and Raman spectroscopy have also been used to investigate the low-frequency metal-ligand modes. As FTIR and Raman techniques operate under different selection rules they will typically report mutually exclusive vibrational modes. The Raman approach utilizing NIR excitation and indicates a number of modes (~300–400 cm^{-1}) that downshift upon ^2H exchange, suggestive of the detection of two or more aqua or hydroxo species in the S_1 and S_2 states (Cua et al., 2000). FTIR revealed different modes, one of which (606 cm^{-1}) is sensitive to ^{18}O exchange and likely arises from a Mn-oxo bridging species (Chu et al., 2000). Several low frequency FTIR modes have recently been reported over the entire reaction cycle following ^{13}C and ^{15}N global

isotopic labeling (Yamanari et al., 2004). It will be particularly interesting, when similar results become available following ^{18}O labeling. As yet, no low frequency mode is conclusively attributable to substrate water.

4. XANES

Manganyl moieties, i.e., Mn(IV)=O and Mn(V)≡O, give large pre-edge peaks in XANES spectra. By comparing XANES spectra of model compounds with those of PS II it was recently concluded that Mn(IV)=O cannot be present in the S_0 to S_3 states (Weng et al., 2004).

B. Substrate Analogue Interactions

A variety of small molecules have been studied over the years as a means of providing information about substrate water binding to the OEC (Debus, 1992). The addition of such molecules, which include amines (R-NH_2; R = H, CH_3, OH), hydrazine (NH_2NH_2), hydrogen peroxide (H_2O_2), hydrogen sulfide H_2S, and primary alcohols (R-OH; R = CH_3, C_2H_5, ..) can be very insightful to the mechanism. In the strictest sense, these analogues have not been shown to displace substrate water, but Mn binding has been established for ammonia and methanol (Britt et al., 1989; Force et al., 1998). The substrate analogues can be grouped into three classes according to their reactivity.

The first class of molecules is formed by reductants like NH_2OH, N_2H_4, H_2O_2 and H_2S. These molecules have been shown to reduce the Mn_4O_xCa complex in the dark to levels below the S_0 state (Bouges, 1971; Kok and Velthuys, 1976; Velthuys and Kok, 1978; Sivaraja et al., 1988; Riggs-Gelasco et al., 1996; Messinger et al., 1997a,b). This property can be explored to gain information on the reactivity of the individual S-states and the Mn oxidation states (Section III.B and III.C). The pH dependence of the reduction rate of the Mn_4O_xCa cluster by NH_2OH and NH_2NH_2 shows that: (i) only the deprotonated forms are active (Beck and Brudvig, 1988a; Kebekus et al., 1995); and (ii) that structural changes with characteristic pH values between 5.3–5.6, 6.3–6.5, and of about 7.4 modulate the reactivity of these reductants with the Mn_4O_xCa complex (Kebekus et al., 1995). This indicates that substrate water also enters the catalytic site as H_2O, rather than as H_3O^+. In addition, organic derivatives of these reductants may be used to explore the size of possible water channels or binding sites, if molecules of different length and bulkiness are used. On that basis, Radmer and Ollinger (1983) estimated that the substrate-binding pocket (or channel) is about 2.5 Å × 4 Å; see also Sandusky and Yocum (1986). Nitric oxide (NO) is also able to reduce the Mn_4O_xCa complex down to the S_{-2} state (Schansker et al., 2002; Sarrou et al., 2003). However, NO may be better considered as a product (O_2) analogue. If separate product and substrate channels exist in PS II (Wydrzynski et al., 1996; Renger, 1999; Anderson, 2001), then it might be speculated that NO enters the catalytic site via an O_2 release channel, while the water analogues approach the site through the water channel. A significant change to the action and accessibility of these small molecules is conferred by the presence or absence of the extrinsic polypeptides (Debus, 1992). Such findings strongly support the notion that the OEC is sequestered.

The second class is formed by primary alcohols. Methanol and ethanol are known to shift the equilibrium between the EPR multiline signal and the g = 4.1 form of the S_2 state towards the multiline form (Zimmermann and Rutherford, 1986; Pace et al., 1991). They also affect the hyperfine structure of the S_2 multiline signal, and the S_0 multiline signal is only observed in the presence of a few percent methanol (Åhrling et al., 1997; Messinger et al., 1997a,c). Using ESEEM spectroscopy, interactions arising from methyl and ethyl alcohols with the Mn ions of the OEC can be revealed, but not for larger molecules. The interpretations of the S_2 spectra suggest either a direct coordination of methanol to the Mn ions (Force et al., 1998) or methanol in close proximity to the Mn_4O_xCa complex (Evans et al., 1999). One report also suggests that primary alcohols can be oxidized to aldehydes by the OEC (Frasch et al., 1988). However, since O_2 evolution rates do not decrease up to about 5% of alcohol, the efficiency for this reaction is for intact samples very low at best.

The third class is formed by ammonia and its organic derivatives. Addition of ammonia (isoelectronic with H_2O) to the OEC decreases water-oxidation activity (Hind and Whittingham, 1963), and two different binding sites are proposed to exist, one of which is said to be competitive with the binding of Cl^- ions. To the second, Cl^- insensitive site only NH_3 can bind, possibly for steric reasons (Sandusky and Yocum, 1984, 1986). Therefore, this latter site is favored to be a site associated with substrate water binding. Addition of ammonia results in a modification of the S_2

state EPR multiline signal and to an increase of the S_2 state g = 4.1 signal (Beck and Brudvig, 1986, 1988b; Beck et al., 1986), and nitrogen coupling can be seen with ESEEM measurements (Britt et al., 1989). Structural perturbations from NH_3 addition are also evident in EXAFS measurements, where a lengthening of one 2.7 Å Mn-Mn distance was observed (Dau et al., 1995). The mechanistic interpretation favored by EPR and EXAFS experiments is that ammonia binds in a bridging position and either generates a new μ_2-imido bridge or substitutes a Mn-Mn or Mn-Ca μ-oxo bridge. Together such data clearly indicate that NH_3 binds to the Mn_4O_xCa complex in the S_2 state and by inference also H_2O.

C. Proton Release

Understanding the S-state dependence of proton release stoichiometries and kinetics can in principle offer important insights into the protonation state changes of the substrate water molecules. However, the PS II protein matrix modulates the proton release pattern (Rappaport and Lavergne, 1991; Haumann and Junge, 1996; Junge et al., 2002). This observation becomes intuitively obvious, if the sequestered nature of the OEC is considered (Fig. 1). In line with this consideration, the measured proton release patterns have been found to depend on sample type and pH, while the intrinsic pattern may be expected to be largely independent from these conditions. This variability makes an interpretation of these data, with regard to deprotonation events of substrate water during the S-state cycle, nontrivial.

With intact samples, patterns are often observed that can be approximated by the release of 1:0:1:2 protons for the $S_0 \rightarrow S_1$, $S_1 \rightarrow S_2$, $S_2 \rightarrow S_3$ and $S_3 \rightarrow S_0$ transitions, respectively. These results are consistent with observed electrochromic band shifts that suggest 0:0:1:1 positive charges in the S_0, S_1, S_2 and S_3 states (for reviews, see Haumann and Junge, 1996; Witt, 1996). However, with spinach core particles, for example, H^+ patterns of 1:1:1:1 have been found and used to support the H-atom abstractor model for $Y_Z^{\bullet}$. The question remains if the fewer protein subunits containing core preparations are more (Tommos, 2002) or less likely (Junge et al., 2002) to reflect the true internal proton release pattern. In this regard, it is interesting that, if a glycerol-containing buffer is used, the 1:0:1:2 pattern is restored in core preparations of spinach. Similarly, in a study where the proton release pattern of highly active core particles from *T. elongatus* was measured using a glass electrode, the authors concluded that the internal proton release pattern of 1:0:1:2 was modulated by proton release from an amino acid group (pK_a 5.7), which protonation state is affected by the oscillating net charges (0:0:1:1) of the OEC (Schlodder and Witt, 1999). This finding is also supported by a detailed analysis of the kinetics of proton release (Junge et al., 2002) and a recent FTIR study (Noguchi and Sugiura, 2002b).

An internal proton release pattern of 1:0:1:2 can be realized in at least two ways: (i) two water molecules are bound in S_0, which become successively deprotonated up to the S_4 state and then two new water molecules bind upon S_0 formation; or (ii) two hydroxy are bound in S_0, which are fully deprotonated in the S_3 state, and then two hydroxy bind upon S_0 formation. This last step equals a net release of two protons. Witt and co-workers (Schlodder and Witt, 1999) attempted to distinguish between these options, and thereby, identify the bound water intermediates. They observed the disappearance of a net charge during the $S_{-1} \rightarrow S_0$ transition (Saygin and Witt, 1985; Kretschmann et al., 1991; Kretschmann and Witt, 1993), which requires the release of two protons on this step. This finding is consistent with direct proton release measurements of NH_2OH treated PS II samples by Junge and co-workers (Förster and Junge, 1985, 1986, 1988). By assuming that these two protons are derived from bound substrate water, Witt and co-workers favored option (ii). However, the reduction of the Mn cluster to the S_{-1} state by NH_2OH may well be coupled with the protonation of one or two μ-oxo bridges. These hydroxo-bridges may then be deprotonated during the $S_{-1} \rightarrow S_0$ transition and possibly offset the attempted calibration.

V. Energetic and Kinetic Considerations

A. Redox Potentials

The high, >1V midpoint potential of the $P680/P680^{+\bullet}$ couple is the remarkable feature of PS II that provides sufficient thermodynamic driving force for water oxidation. An accurate direct determination of its E_m value is impossible, since $P680^{+\bullet}$ never exists in a thermodynamic equilibrium state, but rapidly relaxes through a cascade of different energy states (Section V.C.1; Chapter 7, Renger and Holzwarth). Nevertheless, estimates of the $P680/P680^{+\bullet}$ poten-

tial relative to the experimentally determined redox potentials of Pheo/Pheo$^-$ and Q_A/Q_A^- are possible by: (i) taking 1830 mV as the singlet-singlet transition of P680; and (ii) by using measured equilibrium constants and electron transfer rates between these PS II cofactors. Jursinic and Govindjee estimated in this way that the P680/P680$^{+\bullet}$ potential lies between 1000 and 1300 mV (Jursinic and Govindjee, 1977). The large uncertainty in this estimate stems from the great range of potentials (–35 mV to –325 mV) reported for Q_A/Q_A^- at the time. Using the experimental value of –640 mV for Pheo/Pheo$^-$, Klimov et al. (1979) estimated that the P680/P680$^{+\bullet}$ potential is about 1100 mV. This number was recently revised upwards to 1260 mV (Rappaport et al., 2002) relying on a potential of –30 mV obtained in a very rigorous study of the Q_A/Q_A^- couple (Krieger et al., 1995) and detailed considerations on the charge recombination pathways in PS II. In Fig. 5 we use this latter estimate for P680/P680$^{+\bullet}$ to place other donor side components in a relative manner.

Estimates of the Y_Z potential relative to P680/P680$^{+\bullet}$ appear from a number of sources. Using Mn-depleted samples Metz et al. (1989) estimated Y_Z at 110 mV more negative than P680, i.e., $Y_Z/Y_Z^{\bullet}$ at 1150 mV, while a value of 40–90 mV more negative than that of P680, i.e., $Y_Z/Y_Z^{\bullet}$ at 1195 ± 25 mV, was obtained with intact samples (Brettel et al., 1984; Eckert and Renger, 1988). The midpoint potential of Y_Z appears to be almost S-state independent. This is reflected in the small changes in ΔG values associated with its oxidation kinetics (Section V.C.1 and Table 3).

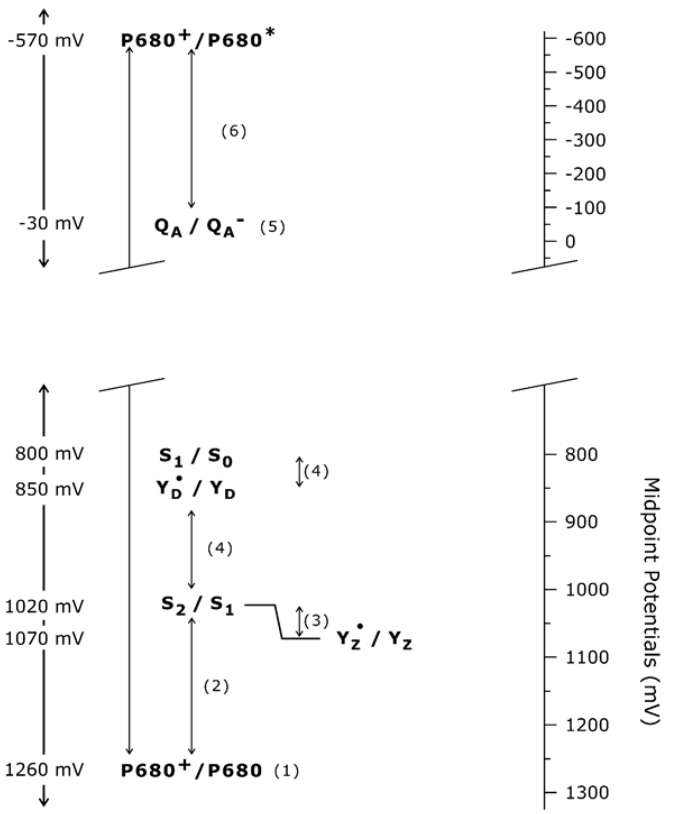

Fig. 5. Relative midpoint potentials for various PS II cofactors associated with water oxidation. The PS II reaction center chlorophyll P680 generates a 1.83 eV maximum free energy from a 680 nm photon and performs electron transfer to redox cofactors to kinetically stabilize and recover as much free energy as possible. Redox values for the PS II donor side have been revised downwards with the new E_m determination of P680. The data (1) 1260 mV, (2) 240 mV, (6) 540 mV (Rappaport et al., 2002), (3) 40–55 mV (Vos et al., 1991), (4) 170 mV (Vass and Styring, 1991), and (5) –30 mV (Krieger et al., 1995).

The midpoint potentials of the S_2/S_1 and S_3/S_2 couples have been estimated to reside 40–55 mV below that of $Y_Z/Y_Z^{\bullet}$ (Vos et al., 1991), i.e., $Y_Z/Y_Z^{\bullet}$ at 1145 ± 30 mV. However, on the basis that slower relaxation processes were not taken into account for those numbers, Rappaport et al. (2002) suggested that the S_2/S_1 couple has a potential of ~1020 mV. Regardless of the absolute value, these data show that only a relatively small driving force of 150–250 mV exists (relative to $P680/P680^{+\bullet}$) to drive the $S_1 \rightarrow S_2$ and $S_2 \rightarrow S_3$ transitions. On this basis it has been speculated that a special coupling between electron transfer and proton transfer is required for water oxidation in PS II (Rappaport and Lavergne, 2001).

The midpoint potentials of the S_0/S_1 couple can be estimated relative to S_2/S_1 through redox equilibria with Y_D. The redox potential of $Y_D/Y_D^{\bullet}$ has been reported to be 170 mV below the S_2/S_1 couple and 40 mV above the S_1/S_0 pair (Boussac and Etienne, 1982; Vass and Styring, 1991). This results in an estimated potential of about 800 mV for S_1/S_0. Therefore, in contrast to the $S_1 \rightarrow S_2$ and $S_2 \rightarrow S_3$ transitions, a higher driving force of about 400–500 mV is available for the $S_0 \rightarrow S_1$ transition (Fig. 5). Nevertheless, the OEC appears to perform significant redox leveling, maintaining almost constant potential during the incremental accumulation of oxidizing equivalents. This leveling is one of the arguments for charge neutrality within the OEC (Tommos and Babcock, 1998; Section V.B).

Using thermodynamic considerations mechanistic insights to water oxidation are possible, although one has to keep in mind that a reaction with the lowest thermodynamic barrier may proceed with a very slow rate and may therefore not take place in the enzyme. One such attempt from Krishtalik (1986, 1990) introduced the idea that the water oxidation reactions within the OEC are independent of the product (O_2, H^+) and starting material (H_2O) concentrations. Accordingly, he considered only the *configurational* component of both redox potential and free energy (i.e., E_c and ΔG_c respectively). Using Klimov's estimate of the $P680/P680^{+\bullet}$ potential as a bench mark he suggested that a concerted four-electron oxidation or two sequential two-electron oxidations of water (with bound peroxide as an intermediate) are thermodynamically more viable than the oxidation of water via four sequential one-electron abstractions (Krishtalik, 1986, 1990). This finding is supported experimentally by the fact that Mn centered oxidations are observed for at least three of the four S-state transitions (Section III.C).

In addition to studying the reaction coordinate for O-O bond formation several concepts were advanced from Krishtalik's analyses that continue to influence models today. These include optimizing the energy balance of the overall reaction by: (i) increasing the energy of the product by binding of substrate water as OH^- rather than H_2O; and (ii) lowering the energy of the products by participation of one or more bases X^- in the reaction sequence that accept water protons. This latter possibility is especially advantageous if the base(s) change(s) their pK_a-value(s) as a function of S-state. Another notion was that the reorganization energy of a four-electron reaction can be reduced significantly in proteins compared to solution chemistry by using several electron donors and/or acceptors. This, for example, might be a factor in why the OEC is comprised of four Mn ions instead of only two.

B. Electroneutrality vs. Charge Accumulation

Krishtalik's analysis as rigorous as it is does not take into account the long-range interactions in proteins caused, for example, by fixed polar groups and the low dielectric constant within the protein (Krishtalik, 1986). To implicitly include these kinds of effects, the structure of PS II at atomic resolution would have to be known. Nevertheless, some general considerations about the likelihood of creating positive charges within proteins have been made (Rich, 1996). Using the Born model of continuum electrostatics, it can be calculated that 130 $kJmol^{-1}$ of energy is required to transfer a net charge into a protein of low dielectric ($\varepsilon = 3.5$). This is a significant energy barrier, and a protein will try to minimize this energy cost by: (i) delocalization of the charge within the protein through movements of hydrogen bonds or local charges; and/or (ii) by delocalization of the charge within the cofactor; or (iii) by coupled proton or ion uptake/release to keep the reaction core electroneutral. This concept of electroneutrality has been extended to the reactions of the OEC and forms one of the cornerstones of the original H-atom abstraction mechanism (Hoganson et al., 1995; Hoganson and Babcock, 1997; Tommos and Babcock, 1998).

At variance with these theoretical considerations are literature data that suggest that a positive charge is accumulated in the OEC during the $S_1 \rightarrow S_2$ transition. These include the proton release patterns (Section IV.C.), the S-state dependent electrochromic band shifts (Schlodder and Witt, 1999), and information

obtained from $P680^{+\bullet}$ reduction kinetics (Section V.C.1). Alternative interpretations for these effects have been suggested by supporters of the H-atom abstractor model (Tommos et al., 1998; Tommos and Babcock, 2000; Tommos, 2002). However, the experimental results seem sufficiently compelling to suggest that: (i) there is indeed only during the $S_1 \rightarrow S_2$ transition a positive net charge increase; and (ii) that this net charge increase is coupled with protein conformational changes. Interestingly, this is also the only transition that does not involve a structural change of the Mn_4O_xCa complex itself. It might therefore be inferred that the OEC uses structural changes of the Mn_4O_xCa complex and charge accumulation (+ protein conformational changes) as alternative ways to maximize the use of the free energy available from $Y_Z^{\bullet}$ in accumulating oxidizing potential.

C. Kinetics

The kinetics of the electron transfer processes between the cofactors associated with the OEC have been measured using a variety of spectroscopic approaches. From such measurements, insights into electron-transfer and associated proton-transfer events have been gained, thereby providing information on the water oxidation reaction. An overview of the kinetics measured for the different electron transfer steps is given in Fig. 6 and Table 3.

1. $P680^{+\bullet}$ Reduction

The reduction of $P680^{+\bullet}$ by Y_Z is monitored by the ns-µs decay kinetics of a broad ~830 nm absorption increase that coincides with the formation of the

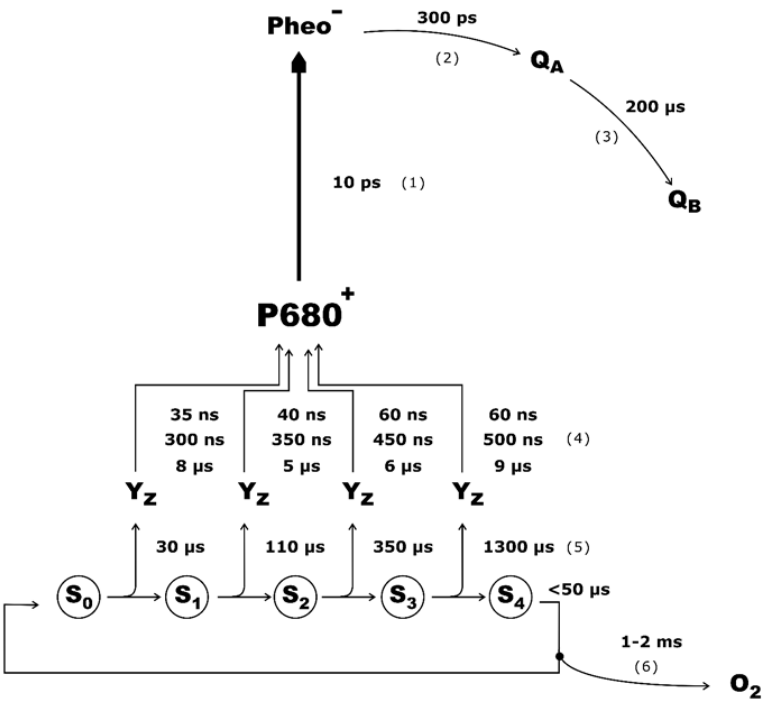

Fig. 6. A summary of electron transfer pathways with respective halftimes for reactions in PS II involved directly with water oxidation. The electron transfer reactions on the PS II donor side involving oxidation of Y_Z and Mn_4O_xCa complex are strongly S-state dependent and are discussed in detail in the text. The S_4 state is likely to be a transition state and recently first evidence for its existance has been reported (Clausen and Junge, 2004). All rates are experessed as $t_{½}$ halftimes (i.e., $\ln 2/k$). Kinetic data: (1) (Diner and Rappaport, 2002, Chapter 7, Renger and Holzworth; Chapter 22, Barter et al.); (2) (Bernarding et al., 1994; Chapter 7, Renger and Holzworth); (3) (Chapter 8, Petrouleas and Crofts); (4) (Jeans et al., 2002) (5); (Dekker et al., 1984); (6) rate intimately coupled to $Y_Z^{\bullet}$ decay (Razeghifard et al., 1997a; Clausen et al., 2004).

Table 3. Thermodynamic properties of donor side electron transfer reaction

	$S_0 \rightarrow S_1$	$S_1 \rightarrow S_2$	$S_2 \rightarrow S_3$	$S_3 \rightarrow S_0$	$S_3 \rightarrow S_4$	$S_4 \rightarrow S_0$
Y_Z oxidation, $t_{½}$ (ns phases) [A]	35, 300	40, 350	60, 450	60, 500		
H/D [B,C]	No	No	No	No		
*E*a (mV) [A]	60, 40	40, 70	250, 280	30, 240		
ΔG (mV) [A]	–35	–40	–30	–30		
λ (mV) [A]	270	300	1130	1025		
Y_Z oxidation, $t_{½}$ (μs phase) [A]	12†	7†	9†	12†		
H/D [D]	Pronounced isotope effect on amplitude and kinetic of oscillatory μs phase of $P680^{+\bullet}$ reduction					
*E*a (mV) [A]	270	300	210	220		
ΔG (mV) [A]	–15	–15	–20	–20		
λ (mV) [A]	1120	1230	880	920		
$Y_Z^{\bullet}$ reduction, $t_{½}$ (μs) [E]	30	110	350	1300		
H/D [B,C]	1.3	1.3	2.2	1.4		
*E*a (mV) [B,F]	50	130	370	210		
ΔG (mV) [G]	–250	–55	–40	–105		
λ (mV) [F]	430	410	1200	730		
O_2 release H/D [B,H]						1.4
ΔG (mV) [I]					18	–49

† Two μs phases are identified (3 μs, 35 μs) yet are approximated by a single term in this work. A (Jeans et al., 2002), B (Haumann et al., 1997), C (Karge et al., 1996, 1997), D (Schilstra et al., 1998; Christen and Renger, 1999), E (Dekker et al., 1984), F (Renger and Hanssum, 1992), G (Vass and Styring, 1991; Vos et al., 1991), H (Sinclair and Arnason, 1974), I (Clausen and Junge, 2004). ΔG conversion: 1 mV = 0.0965 kJ mol^{-1}.

$P680^{+\bullet}$ cation. In Mn-depleted *apo*-PS II centers, the kinetics are dominated by an ~100–200 μs phase governed by $P680^{+\bullet}/Q_A^-$ recombination (Havemann and Mathis, 1976; Renger and Wolff, 1976). More revealing, however, are the kinetics associated with PS II centers with a functional Mn complex. In these samples, Y_Z can effectively compete with Q_A^- in reducing $P680^{+\bullet}$, and multiphasic, S-state dependent $P680^{+\bullet}$ decay kinetics are observed for this process. The majority of centers in the S_0 and S_1 states decay with a $t_{½} = 20–60$ ns, although recent findings suggest that this phase is biphasic in nature (Table 3 and Fig. 6). The S_2 and S_3 states both decay with biphasic half times of $t_{½}$ = 60 ns and 400–500 ns (Brettel et al., 1984; Eckert and Renger, 1988; Meyer et al., 1989; Jeans et al., 2002). These fast ns kinetics are found to be largely H/D insensitive (Karge et al., 1996; Haumann et al., 1997; Schilstra et al., 1998) and can be correlated with a pure electron transfer reaction showing an ET rate consistent with the known distance and ΔG (Renger et al., 1998; Tommos and Babcock, 2000; Jeans et al., 2002). An additional, smaller contribution to the $P680^{+\bullet}$ reduction arises from 5–35 μs kinetic phases that oscillate with S-state and are significantly affected by replacement of exchangeable protons by deuterons (Christen et al., 1998; Schilstra et al., 1998; Christen and Renger, 1999). This H/D isotope effect suggests that protonic relaxation is required for the electron transfer reaction on longer time scales (Table 3). In summary, the initial fast ns events are attributed to electron donation from Y_Z and the deprotonation of Y_Z to a neighboring proton acceptor (Eckert and Renger, 1988), probably His190 (Hays et al., 1999). This fast reaction establishes a redox equilibrium involving $P680^{+\bullet}Y_Z \Leftrightarrow P680Y_Z^{\bullet}$, which lies far to the right. However, a measurable amount of $P680^{+\bullet}$ remains at times >1 μs. To completely shift the equilibrium toward $P680Y_Z^{\bullet}$, a protonic relaxation of the system is required, which occurs with the observed μs kinetics. In a recent paper, the competition between Q_A^- and Y_Z (μs components) in reducing $P680^{+\bullet}$ has been proposed to be the major source for S-state dependent misses in PS II (de Wijn and van Gorkom, 2002).

Initially, the slowing of the reduction rates in the S_2 and S_3 states was reconciled as being due to the formation of a positive charge created at or near the Mn_4O_xCa complex during the $S_1 \rightarrow S_2$ transition, while the $S_0 \rightarrow S_1$ transition and $S_2 \rightarrow S_3$ transition were to be electroneutral (Brettel et al., 1984; Meyer

et al., 1989). However, the more recent measurements of kinetic rates given in Table 3 indicate a rather more sequential decrease in rate with S-state advance (Jeans et al., 2002). Similarly, the small ΔG values for the $P680^{+\bullet}/Y_Z$ equilibria (Table 3) indicate that only subtle changes in the reaction coordinates take place during the $S_1 \rightarrow S_2$ transition (Brettel et al., 1984; Ahlbrink et al., 1998). In contrast a significant change in the reorganization energy (λ), with ~300 mV for S_0 and S_1 and 1000–1100 mV for the S_2 and S_3 states was found (Jeans et al., 2002). Such findings were used by these authors to argue in favor of the accumulation of a positive charge during the $S_1 \rightarrow S_2$ transition.

2. $Y_Z^{\bullet}$ Reduction

The $Y_Z^{\bullet}$ reduction rates have been determined via time-resolved optical spectroscopy and EPR techniques. In contrast to the multiphasic kinetics of $P680^{+\bullet}$ reduction by Y_Z, the process of $Y_Z^{\bullet}$ reduction by the Mn_4O_xCa complex is characterized by monophasic kinetics with rate constants that are 1000 times slower than in the former process. These S-state advancements are dependent on the redox state of the OEC and occur in spinach PS II membranes with rates that are characterized by the following half times ($t_{½}$): 30 μs, 110 μs, 350 μs and 1.3 ms for the $S_0 \rightarrow S_1$, $S_1 \rightarrow S_2$, $S_2 \rightarrow S_3$ and $S_3 \rightarrow S_0$ transitions, respectively (Dekker et al., 1984; Renger and Weiss, 1986; see Razeghifard et al., 1997b, for a summary of similar measurements). One report of a slower (250 μs) $S_0 \rightarrow S_1$ transition has been made and this divergence is unresolved (Rappaport et al., 1994).

The time scale of the $Y_Z^{\bullet}$ reduction reaction does not appear well correlated with a pure electron transfer reaction, when representative distances, λ, and ΔG values are substituted into the expression developed by Dutton and Moser (Page et al., 1999) for a non-adiabatic electron transfer reaction (Tommos and Babcock, 2000). This reaction is generally attributed as being an electron transfer reaction that is coupled with proton transfer. However, a number of studies have indicated that the rates of S-state advancements are associated only with small H/D isotope effects of ≤ 2 (Bögershausen et al., 1996; Karge et al., 1996, 1997; Lydakis-Simantiris et al., 1997).

Studies of temperature dependence of $Y_Z^{\bullet}$ reduction, summarized in Table 3, indicate that each S-state transition is coupled with a different activation energy (Koike et al., 1987; Renger and Hanssum, 1992; Bögershausen et al., 1996; Haumann et al., 1997; Karge et al., 1997). Also, the activation energies for the $S_2 \rightarrow S_3$ and $S_3 \rightarrow S_0$ transitions are greater than that of the first two transitions. These changes have unknown origin but may result from structural changes or the accumulation of a positive charge during the $S_1 \rightarrow S_2$ transition. The final $S_3 \rightarrow S_0$ transition was reported to exhibit non-linear Arrhenius behavior (Koike et al., 1987; Renger and Hanssum, 1992; Karge et al., 1997), yet this is not supported in recent papers by another group (Haumann et al., 1997; Clausen et al., 2004). Only one detailed study has examined the reaction coordinate for the reduction of $Y_Z^{\bullet}$ to derive reorganization energies (Renger and Hanssum, 1992). This work suggests that the largest reorganization energy is required for the $S_2 \rightarrow S_3$ transition. This finding has been used to support the idea of a structural change of the Mn_4O_xCa complex during the $S_2 \rightarrow S_3$ transition (Section III.B.).

3. O_2 Release

Employing polarography and EPR oximetry techniques, oxygen release times ($t_{½}$) on the order of 1–2 ms have been obtained for water oxidation chemistry (Jursinic and Dennenberg, 1990; Strzalka et al., 1990; Meunier and Popovic, 1991; van Gorkom and Gast, 1996; Razeghifard and Pace, 1999). The O_2 release times appear to have the propensity for slowing down, as the samples are refined from chloroplast/thylakoids to PS II membrane fragment and PS II core preparations; i.e., $t_{½}$ = 1.4 - 1.6 ms PS II membranes and $t_{½}$ = 5 ms for core preparations (Haumann et al., 1997; Razeghifard and Pace, 1999). The reason for this slowing is not known, but may relate to changes in electron and proton transfer during the $S_3 \rightarrow [S_4] \rightarrow S_0$ transition that are induced by the loss of the extrinsic 17 kDa and 23 kDa proteins or detergent exposure (see below). When also the extrinsic 33 kDa protein is removed, a further slowing of the O_2 release into the $t_{½}$ = 8–10 ms time regime is observed (Miyao et al., 1987; Burnap et al., 1992; Qian et al., 1999). Also, a number of point mutations to proteins of PS II polypeptides (D1, CP47) affect O_2 release kinetics (Putnam-Evans et al., 1996; Hundelt et al., 1998; Qian et al., 1999; Li and Burnap, 2001).

The O_2 release kinetics appear to closely follow those of the electron transfer in the $S_3 \rightarrow [S_4] \rightarrow S_0$ transition, indicating that the reduction of $Y_Z^{\bullet}$ is tightly coupled if not simultaneous with O_2 production (Babcock et al., 1976; van Leeuwen et al., 1993;

Haumann et al., 1997; Razeghifard and Pace, 1999). This finding also seems to hold for the above PS II samples with slowed O_2 release kinetics (Haumann et al., 1997; Razeghifard et al., 1997b). However, in recent experiments a short, temperature dependent lag-phase for O_2 release in the order of 450 μs (at 20 °C) was found that is not present in optical experiments that follow $Y_Z^{\bullet}$ reduction (Clausen et al., 2004). Therefore, this lag-phase corresponds to an intermediate after $Y_Z^{\bullet}$ reduction, i.e., one that occurs either at the level of the S_4-state or of freshly formed, bound O_2. The significance of this observation remains to be elucidated (Clausen et al., 2004).

Because of the close kinetic correlation between the $Y_Z^{\bullet}$ reduction and O_2 release, it has been questioned whether a distinct S_4 state intermediate exists or if this state is best denoted as $S_3Y_Z^{\bullet}$. In any case, S_4 is a highly reactive intermediate (or even a set of different intermediates) that appears to decay into the S_0 state (releasing O_2 and H^+) faster than it is formed. Until recently, all attempts to kinetically identify the S_4 intermediate have been unsuccessful (Rappaport et al., 1994; Haumann et al., 1997; Razeghifard and Pace, 1999; Clausen et al., 2004). Clausen and Junge (2004) have, however, made important progress on this question by using high partial O_2 pressure (up to 30 bar) to shift the equilibrium of O_2 release backwards (Clausen and Junge, 2004). From this work they have obtained the first evidence for the S_4 state intermediate. The electronic structure of this intermediate was tentatively assigned to be $S_2Y_ZH_2O_2$. Their analysis also included a kinetic model to derive the free energy for the formation of the intermediate and the release of the product. The intermediate is suggested to be mildly endergonic ($\Delta G = +1.7$ kJ/mol) relative to the S_4 state and that of product O_2 release mildly exergonic ($\Delta G = -4.7$ kJ/mol) (Clausen and Junge, 2004).

In high-resolution UV and EPR measurements, another kinetic lag phase of ~50–100 μs preceding reduction of $Y_Z^{\bullet}$ on the $S_3 \rightarrow S_0$ transition, is resolved (Koike et al., 1987; Rappaport et al., 1994; Haumann et al., 1997; Karge et al., 1997; Razeghifard and Pace, 1999), which may reflect the release of one proton prior to electron transfer. This latter lag-phase is therefore not directly connected to the process of O_2 release (Rappaport et al., 1994; see however Haumann et al., 1997).

D. Chemistry

In order to gain further insight into the mechanism of photosynthetic water oxidation, one needs to consider the following aspects: (i) how can triplet O_2 be formed from two singlet water molecules?; (ii) how much energy is required to break the four O-H bonds?; (iii) is H-atom abstraction feasible or even required for the oxidation of water in PS II?; and (iv) are changes in ligand coordination numbers or ligand binding strength associated with redox changes of the Mn ions? These four questions will be briefly addressed in the following sections.

1. Spin States

As outlined above (V.A), water oxidation most likely proceeds either in two two-electron steps or as a concerted four-electron reaction with a peroxidic transition state. Therefore, independent of the actual mechanism, the oxidation of water to molecular oxygen can conceptually be divided into two two-electron transfer steps.

The ground state of molecular oxygen (O_2) is a triplet, while those of the dioxo $(O^{2-})_2$ and peroxo (O_2^{2-}) species are singlet states. As a consequence, the initial O-O σ-bond formation requires the transfer of two electrons of opposite spin; while, for the final π-bond formation, two electrons of the same spin have to be transferred from the oxo and peroxo ligands to the Mn_4O_xCa complex, respectively (McGrady and Stranger, 1999). On the basis of DFT calculations on Mn_2-$(\mu\text{-}O)_2(\mu\text{-}O_2)(NH_3)_6^{2+}$, it was recently concluded that the σ-bond formation (or cleavage) is favored by antiferromagnetic coupling of the $Mn_2(\mu\text{-}O)_2$ core; while for π-bond formation, a ferromagnetic coupling with an $S = 3$ state appears to be favorable. Therefore, π-bond formation would be promoted by structural changes that reduce the exchange coupling between the Mn ions. Alternatively, it was suggested that σ-bond formation may occur on a bis-μ-oxo bridged part of the Mn_4O_xCa complex, while π-bond formation may occur at the mono-μ-oxo bridged Mn-Mn pair (McGrady and Stranger, 1999).

On the basis of spin considerations on a monomeric Mn model complex, Siegbahn and Crabtree concluded that the only species that is reactive enough to form the O-O bond is a high-spin Mn(IV)-O$^{\bullet}$ state (Siegbahn and Crabtree, 1999). In a more general sense, these results show that the formation of trip-

let O_2 from water is greatly facilitated by a radical intermediate.

2. O-H Bond Strength and H-Atom Abstraction

Another means of ascertaining the viability of mechanisms is to consider the bond dissociation energies (BDE) for the reaction. The strength of the O-H bonds from water has been determined, both experimentally (Caudle and Pecoraro, 1997), and theoretically using DFT approaches (Blomberg et al., 1997). The BDE for both O-H bonds of a water molecule is reduced significantly through binding to Mn(III) or Mn(IV), from about 500 $kJmol^{-1}$ to 350 $kJmol^{-1}$. The latter value is very close to that expected for the BDE of the tyrosine O-H (Tommos and Babcock, 1998). This shows that, in principle, H-atom abstraction from terminal water or hydroxo ligands of the Mn_4O_xCa complex is thermodynamically feasible and could proceed almost as a thermo-neutral reaction (Hoganson and Babcock, 1997). This is a prerequisite for the H-atom abstractor model discussed below.

Babcock and co-workers have suggested that the OEC in PS II could be viewed as a member of metallo-radical enzymes, related to O_2-dependent radical enzymes like galactose oxidase or ribonucleotide reductase, that perform concerted and coupled *electron transfer (ET)/proton transfer (PT)* reactions, i.e., H-atom transfer (Hoganson et al., 1995; Hoganson and Babcock, 1997; Tommos and Babcock, 1998). Britt and co-workers have also endorsed this mechanistic view (Gilchrist et al., 1995). The H-atom transfer proposal was founded on the following experimental constraints: (i) $Y_Z^{\bullet}$ is within 4.5 Å of the Mn_4O_xCa complex (Gilchrist et al., 1995); (ii) $Y_Z^{\bullet}$ has a larger mobility then expected for pure electron transport (Tommos et al., 1995) and a disordered H-bond within a hydrophobic environment (Tang et al., 1996); (iii) $Y_Z^{\bullet}$ reduction limits kinetically O_2 formation (Babcock et al., 1976); and (iv) H^+ release kinetics in core particles follow $Y_Z^{\bullet}$ formation, not its reduction kinetics (Haumann and Junge, 1994). From these notions, hydrogen abstraction was introduced as a mechanism whereby Y_Z is deprotonated upon oxidation by $P680^{+\bullet}$ and then $Y_Z^{\bullet}$ subsequently abstracts an H-atom on each S-state transition from the substrate that is coordinated to the Mn_4O_xCa complex as water or hydroxo (Gilchrist et al., 1995; Hoganson et al., 1995; Hoganson and Babcock, 1997).

The introduction of the H-atom abstraction mechanism for photosynthetic water oxidation by Babcock and co-workers has invoked intense interest in the field; cheekily it has been referred to as 'the H-atom bomb.' Mechanistically, it is not particularly dependent on the structure of the Mn_4O_xCa complex, it is thermodynamically viable within given constraints and it is currently one of the most detailed mechanism for water oxidation. However, as outlined in the previous sections, several lines of experimental evidence used to support the mechanism have controversial interpretations or are relevant only to Mn-depleted systems. One difficulty with hydrogen-atom transfer is that it only operates efficiently over distances of a few Å. Other challenges are: (i) the observed net charge accumulation from $S_1 \rightarrow S_2$ (Section V.B); (ii) the small H/D isotope effects for the S-state transitions using H_2O/D_2O as solvents and substrate (Table 3); and (iii) the discussion on the nature of tyrosine Z in its reduced, dark stable form: tyrosine (–OH) vs. tyrosinate ($–O^-$) (Nugent et al., 2002; Chapter 9, Diner and Britt). Such discussions have led to a number of alternate proposals for Y_Z that implicate in addition to the H-atom transfer, coupled (but not concerted) PCET or discrete ET and PT pathways. On that basis modified models have been developed, where H-atom abstraction or coupled electron and proton transfer only occurs on specific S-state transitions ($S_2 \rightarrow S_3$ and/or $S_3 \rightarrow S_0$) and may also involve an intermediate water molecule to bridge the distance of 7–9 Å between Y_Z and the Mn_4O_xCa complex (Haumann and Junge, 1999; Limburg et al., 1999; Renger, 2001; Vrettos et al., 2001a). A further proposal by Kuzek and Pace (2001) involves H-atom abstractions from a substrate water molecule coordinated to Ca^{2+} during the $S_2 \rightarrow S_3$ and $S_3 \rightarrow S_0$ transitions, which are thought to be mediated by two μ-oxo bridge radical intermediates. On the basis of a careful analysis of the phenomenology of the occurrence of $Y_Z^{\bullet}$ split signals after low temperature (10 K) illumination in the various S-states, it has also been suggested that the oxidation of Y_Z repels a proton from the OEC and then $Y_Z^{\bullet}$ accepts an electron (Ioannidis et al., 2002).

3. Mn Coordination Numbers

For the constructions of models of the Mn_4O_xCa complex and for understanding: (i) its structural changes; and (ii) the changes in water coordination during S-state advancement, it is important to know the preferred coordination numbers of Mn in its various redox states. In synthetic complexes and within

proteins, Mn ions (III, and IV) are often associated with a 6-coordinate environment (Wieghardt, 1989; Pecoraro, 1992; Dismukes, 1996; Sigel and Sigel, 2000). It is, therefore, usually assumed that the Mn ions in the Mn_4O_xCa complex of PS II are also 6-coordinated throughout the entire S-state cycle. However, Mn(III) ions are known to exhibit a pronounced Jan-Teller distortion, and quantum mechanical calculations show that this can result effectively in a 5-coordinate ligation sphere (Blomberg et al., 1997). Proposals suggesting 5-coordinate Mn exist within the Mn_4O_xCa complex of PS II have been based on S_2 EPR multiline simulations (Zheng and Dismukes, 1996) and DFT calculations (Blomberg et al., 1997). At present, it is not clear if 5-coordinated Mn(III) occurs within the OEC; however, it is a worthwhile consideration that during S-state cycling structural changes of the Mn_4O_xCa complex may be triggered by the formation of Mn(III) or its oxidation to Mn(IV).

VI. Mechanistic Overview of O-O Bond Formation Reactions

The structural, kinetic and thermodynamic properties outlined above have been used to develop mechanisms for photosynthetic water oxidation. Over the years, a raft of proposals have appeared in the literature offering solutions to this intriguing chemical reaction. A summary of mechanisms for photosynthetic water oxidation has been given in (Volkov, 1989). In the following, we discuss several more recent (1995–2004) proposals, which benefit from new experimental findings. Because of space limitations, our emphasis is placed mainly on the O-O bond formation; yet, we will also endeavor to point out novel features of the individual proposals and to discuss the validity of the proposed intermediates within the context of the experimental data outlined in the previous sections. O-O bond formation has been proposed to happen either through: (i) fusion of oxo or hydroxo groups terminally bound to Mn; (ii) nucleophilic attack of a water or hydroxo to a terminally bound oxo group; or (iii) fusion of two radicals. As we will see below, there are degrees to which these elements have been intermixed.

A. Oxo-/Hydroxo-Fusion

This class of mechanisms has been invoked in a number of publications. A prominent example is the mechanism of Witt and co-workers (Witt, 1996; Schlodder and Witt, 1999; Chapter 19, Witt), summarized in Fig. 7A. The reaction proposed is initiated in S_0 with two terminally bound hydroxo groups coordinated to Mn(II) and Mn(III), respectively. With proton release on $S_0 \rightarrow S_1$ and $S_2 \rightarrow S_3$ and Mn oxidations on each S-state transition, two terminal Mn(IV)=O groups and a net positive charge result in the S_3 state. Then $Y_Z^{\bullet}$ is formed in the transition to the S_4 state, which triggers the O-O bond formation and the O_2 release. O_2 formation is thought to occur via a transient Mn_2(III) peroxo intermediate. The S_0 state is reformed by the binding of two water molecules, coupled with the release of two protons. Only two Mn ions are involved in oxidation state changes and the binding of the substrate water molecules. This mechanism accounts for observed proton release patterns (1:0:1:2), electrochromic band shifts, P680 reduction kinetics, and assumes Mn oxidations on all S-state transitions leading to the S_4 state. It does not consider observed structural changes of the Mn_4O_xCa complex, discounts XANES data indicating a ligand centered oxidation for $S_2 \rightarrow S_3$, and does not fully account for information on substrate water binding. For example, the absence of any hydroxo group in the S_3 state is difficult to reconcile with NMR-PRE experiments, and the additional assumption of inequivalent hydrogen bridging is required to account for the observed heterogeneity of the substrate water exchange rates in S_3. In addition, the formation of Mn(IV)=O groups before the S_4 state have been recently excluded on the basis of the small area of the pre-edge XANES peaks of PS II samples (Weng et al., 2004).

With regard to the O-O bond formation, Mn oxidation state changes and the involvement of only two active Mn ions Hoganson and Babcock (1997) made similar proposals compared to that of Witt. However, the protonation state of the water molecules is offset by two protons, i.e., there are two fully protonated water molecules bound to Mn in the S_0 state. Furthermore, they invoke that on each S-state transition one $H^{\bullet}$ (e^- and H^+ via a concerted and coupled reaction) is removed from the water-Mn_4O_xCa complex to thereby arrive at a S_3 state that contains one terminal Mn(IV)=O and one terminal Mn(IV)-OH (Fig. 7 B). In the $S_3 \rightarrow S_4$ transition the remaining $H^{\bullet}$ is abstracted, but this time concerted with the formation of the O-O bond and the reduction of one Mn(IV) to Mn(III), conserving spin angular momentum and orbital symmetry (Hoganson and Babcock, 1997). The formed Mn-peroxo species is

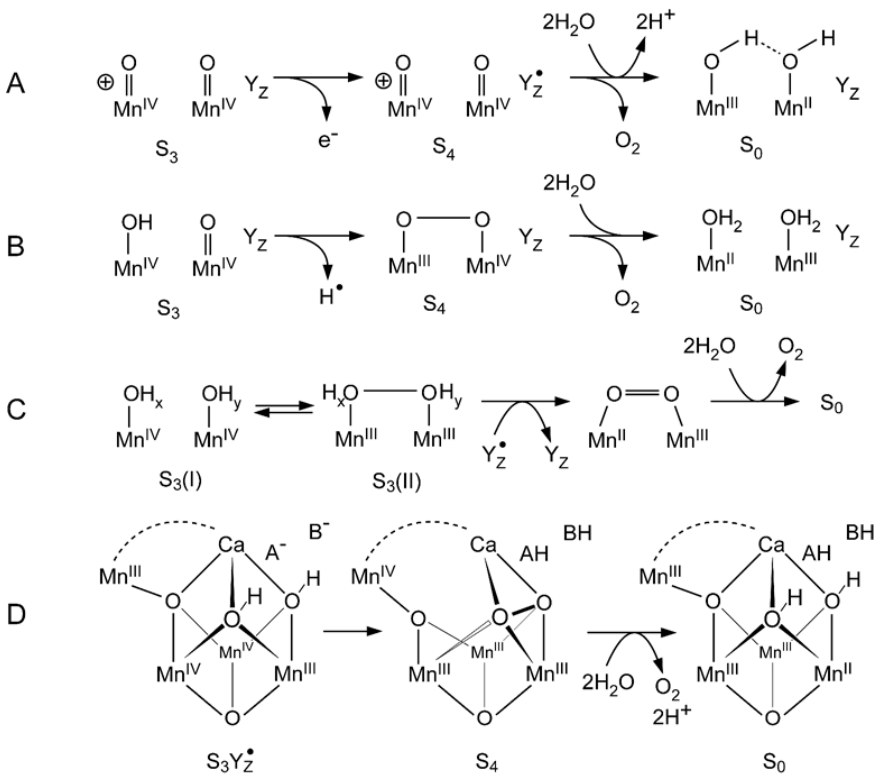

Fig. 7. Proposed mechanisms for O-O bond formation in photosynthetic water oxidation that involves the fusion of two Mn=O or two Mn-OH groups. A, B, C and D were redrawn after Witt (1996), Hoganson and Babcock (1997), Renger (1997) and Dasgupta et al. (2004), respectively. The dashed line in mechanism D represents a (bi)carboante ligand and A^- and B^- are carboxylic acids.

then assumed to rapidly decay into molecular oxygen and the free coordination sites are filled with water molecules. This mechanisms accounts well for the overall protonation state of the water molecules, but has problems to rationalize the observed S-state dependents of the water exchange rates. For example, the Mn(IV)=O of the S_3 state, which is likely to reflect the slow exchanging substrate molecule, is a Mn(III)-OH in the S_2 state. Such a model would predict a much faster exchange of H_2O_{slow} in S_2 than in S_3, which is counter to the observation that the exchange rate is practically identical in both states. Furthermore, this mechanism is in conflict with the generally accepted internal proton release pattern (1:0:1:2) and electrochromic bandshifts that predict the accumulation of a positive charge during the $S_1 \rightarrow S_2$ transition as discussed above.

The proposal by Renger (1997; 2001, Fig. 7 C) is the prototype for invoking that the formation of the O-O bond takes place already at the level of the S_3 state. To account for Mn oxidation states and water exchange rates, it is assumed that the S_3 state is undergoing a rapid redox equilibrium between two hydroxo groups and a bound peroxo species (i.e., S_3(I)-hydroxo $\Leftrightarrow$ S_3(II)-peroxo; Fig. 7C). The complexed peroxide in S_3(II) may additionally undergo an oxywater-hydrogenperoxide tautomerism. Upon formation of $Y_Z^\bullet$, the equilibrium shifts to favor the peroxo species, and further oxidation to O_2 proceeds concomitantly with $Y_Z^\bullet$ reduction. Two water molecules bind to displace the complexed molecular oxygen. Similar to the other mechanism described thus far, no effort is made to explain structural changes of the Mn_4O_xCa-complex. The precise protonation states of the water molecules are not specified; therefore, further discussions, with regard to water-exchange rates and proton release pat-

terns are not possible. The redox equilibrium of the S_3 state must also be expected to significantly favor the hydroxo species of the S_3(I) state to be in line with above discussed Mn oxidation state changes.

Recently a new suggestion was made by Dasgupta et al. (2004) that involves the fusion of two μ_3-oxo bridges. It is based on O_2 producing chemistry observed in a model complex with a Mn_4O_4 cubane core and the 3.5 Å PS II crystal structure (Ferreira et al., 2004), which proposes a Mn_3O_4Ca cubane core for the OEC. Only the $S_3Y_Z^{\bullet}$, S_4 and S_0 states are specified and those are reproduced in Fig. 7D. It is suggested that the oxidation of the monomeric Mn(III) to Mn(IV) opens up the cubane in the S_4 state by braking the μ_4-oxo-Ca bond. This then allows the formation of the O-O bond between two μ_3-hydroxo's under the reduction of the two Mn(IV) ions and the transfer of the two protons to two neighboring carboxylic acids (denoted as A^- and B^- in Fig. 7D). The O=O double bond is formed by reducing the monomeric Mn(IV) to Mn(III) and one of the Mn(III) in the opened cubane to Mn(II). Two water molecules bind and under the release of two protons the S_0 state is formed that contains two μ_3-OH bridges and a Mn(II) ion in the hetero-nuclear cubane. The dashed line in Fig. 7D represents a carbonate ion, which is suggested to stabilize the proposed structural rearrangement in the S_4-state. The strong point of this mechanism is that it takes into account chemistry that is observed in one of the few functional models of the OEC and that it gives functions to Ca and (bi)carbonate. The Mn oxidation states are not all indicated in the original scheme of Dismukes, but the low valence option (Section III.C), is a consequence of assigning a Mn(III) oxidation state to the monomeric Mn in the S_3 state and the absence of a radical. The model is not entirely compatible with the EXAFS data, because for example, the structure shown for S_0 would be most consistent with two 2.85 Å and one 2.7 Å distances, while the reverse is observed (Robblee et al., 2002). However, efforts have been made to make the model compatible with the water exchange rate measurements.

B. Nucleophilic Attack

On the basis of the discovery of the heterogeneity in substrate water binding in the S_3 state and by analogies to oxygenases, oxidases, and water oxidation chemistry of oxo-ruthenium complexes, Messinger et al. (1995) introduced the possibility that the O-O bond formation could be catalyzed via nucleophilic attack between a water molecule and a highly electrophilic terminal oxygen species. The species acting as the nucleophile was suggested to be a solvent water molecule either free or bound to a non Mn site like Ca^{2+} or a protein residue (component 'X' in Fig. 8 A), representing water in fast exchange (W_{fast}). The second, slow exchanging substrate water (W_{slow}) was denoted as Mn(V)=O, Mn(IV)-O$^{\bullet}$ or Mn(IV)$\equiv$O$^+$. The nucleophilic attack was suggested to be facilitated via a H-bond between W_{fast} and the μ-oxo bridge of the Mn_4O_xCa complex. Because only a partial cycle was presented, other features cannot be judged. Protonation of one μ-oxo bridge during this process is, however, consistent with the later reported presence of one 2.85 Å Mn-Mn distance in the S_0 state. As outlined above, the subsequent discovery that the fast exchange rate is only 20 times slower than the slow substrate water exchange rate puts some restrictions on all mechanisms involving Ca^{2+} or protein ligands as binding site for the fast-exchanging water molecule.

Another mechanism of nucleophilic attack was proposed by Pecoraro et al. (1998). In this case (Fig. 8 B), a Ca bound water molecule is assumed to deprotonate during the $S_2 \rightarrow S_3$ transition and a Mn(V)=O species is formed during the $S_3 \rightarrow S_4$ transition by abstracting an H-atom from Mn(IV)-OH. The Ca-bound OH^- then attacks the Mn(V)=O and forms a hydroperoxide. A special feature of this mechanism is the migration of the hydroperoxide to a second Mn_2(IV, IV) core, where it displaces Cl^- and is further reduced to O_2. Two water molecules then refill the empty coordination sites on Ca^{2+} and Mn, and the S_0 state is formed under rebinding of Cl^-. While it appears attractive to divide the four-electron water chemistry into two sequential, two-electron$^-$ processes on different parts of the Mn complex, the question may be raised whether such a transfer of hydroperoxide would not occur more slowly than the initial reduction of $Y_Z^{\bullet}$ by the Mn(IV)-OH unit and, thereby, violate the observation that O_2 release is rate limited by $Y_Z^{\bullet}$ reduction. In addition, although a deprotonation of the Ca-bound water is consistent with the slowing of the fast water exchange rate during the $S_2 \rightarrow S_3$ transition, it appears difficult to rationalize the changes of the slow water exchange rate, in part because the oxidation states of the individual Mn ions are not specified. Furthermore, no details are given concerning known structural changes associated with the Mn_4O_xCa complex or to account for the proposed

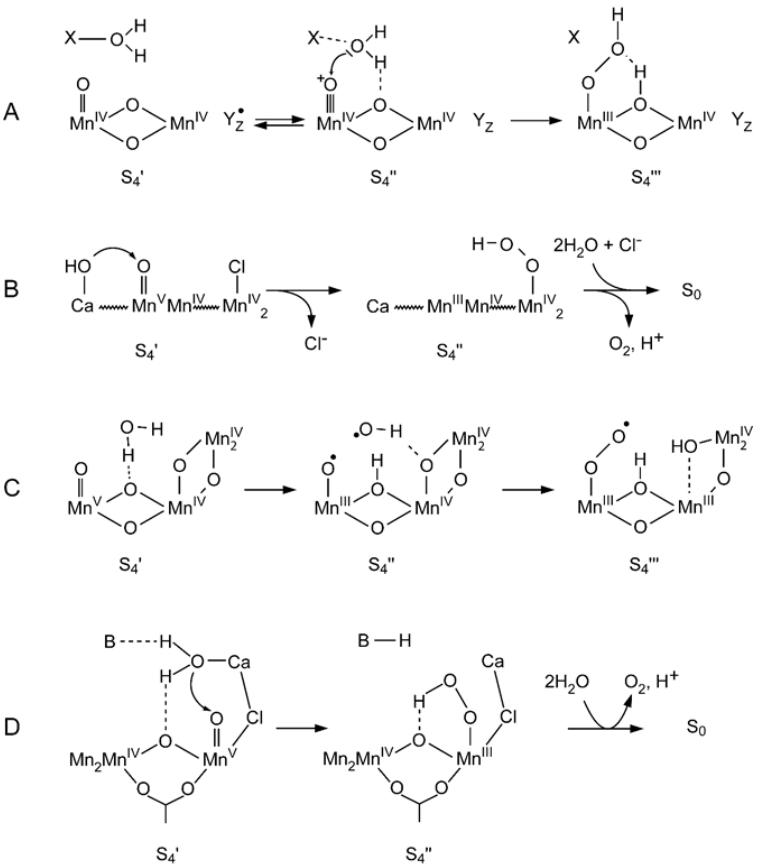

Fig. 8. Proposed mechanisms for O-O bond formation in photosynthetic water oxidation that involves the nucleophilic attack of a water or hydroxo onto a highly nucleophilic terminal Mn-oxo group. A, B, C and D were redrawn after Messinger et al. (1995), Pecoraro et al. (1998), Dau et al. (2001) and Vrettos et al. (2001a), respectively.

0:1:1:2 proton release pattern that conflicts with the above-discussed findings (Section IV.C.).

Dau et al. (2001) have presented a mechanistic proposal for water oxidation that involves O-O bond formation by nucleophilic attack, but also invokes radical intermediates (Fig. 8C). As a structural template, the Berkeley '**C** model' (Fig. 3) was adopted for the S_1 and S_2 states but, on the basis of their EXAFS measurements, they propose that the 3.3 Å Mn-Mn distance (mono μ-oxo bridge) transforms into a third 2.7 Å Mn-Mn distance (bis μ-oxo bridged) during the $S_2 \rightarrow S_3$ transition. This rearrangement of the Mn_4O_xCa complex is assumed to be triggered by an increase in Mn coordination from five to six due to Mn(III) to Mn(IV) oxidation. The S_4 state configuration is proposed to involve a Mn(V)=O species in equilibrium with Mn(IV)-O$^{\bullet}$ (W_{slow}) and a non-Mn-bound water molecule (W_{fast}) that forms a H-bridge to a neighboring μ-oxo bridge. For the initial O-O bond formation to occur, a H-atom transfer from the W_{fast} to the μ-oxo bridge under transient formation of an outer sphere hydroxyl radical is proposed, because the hydroxyl radical is thought to have a favorable orbital overlap with a singly occupied Mn-O$^{\bullet}$ π-orbital (Siegbahn and Crabtree, 1999). The decomposition of the formed hydroperoxide to molecular oxygen is assumed to involve a second H-atom transfer to the extra μ-oxo bridge created during the $S_2 \rightarrow S_3$ transition. The involvement of one or two μ-oxo bridges as H$^{\bullet}$ or proton acceptors is an attractive feature of

this mechanism (see also Messinger et al., 1995) because: (i) these bases change pK_a value during S-state transition, as required by Krishtalik's analysis, and can, thereby, lower the energy burden during O_2 formation; and (ii) the 2.85 Å Mn-Mn distance in the S_0 state can be easily rationalized. The model only specifies water binding in the S_3 and S_0 states, but reconstruction of required intermediates shows that the observed changes in the substrate water exchange rates cannot be understood on the basis of this model. For example, in the model of Dau et al. (2001) the slow water has to be bound to Mn(III) in S_1 and Mn(IV) in S_2, which would suggest a slowing of exchange instead of the observed slightly increased rate. Similarly, W_{slow} has to be deprotonated during the $S_2 \rightarrow S_3$ transition, while experimentally the exchange rate is identical in both S-states. No function for Ca^{2+} is specified and the kinetic coupling of $Y_Z^{\bullet}$ reduction and O_2 release kinetics is unclear. It is specifically assumed that the fast exchanging water is held in place by several protein-derived H-bridges, which is problematic if one takes into account the only 20 times faster exchange of W_{fast} compared to W_{slow} in the S_3 state.

Nucleophilic attack mechanisms have also been championed by Brudvig and co-workers (Fig. 8 D) and detailed mechanisms have appeared (Limburg et al., 1999; Vrettos et al., 2001a). On the basis of analogies to known biological and synthetic models, a structural proposal for the catalytic site was developed, which includes Ca^{2+}, Cl^-, and histidine. Two Mn ions are assumed to take part in redox changes, and a novel feature is that it is assumed that these two Mn form the 3.3 Å Mn-Mn distance observed with EXAFS spectroscopy and that the outer one is involved in binding W_{slow}, while the other Mn is part of a μ-oxo bridged trimer, possibly similar to structures **C** or **D** in Fig. 3. The fast exchanging water (W_{fast}) is suggested to bind to Ca^{2+}, which in variance to the EXAFS results, is postulated to be ~4.2 Å from Mn and connected via a bridging Cl^- ion. W_{fast} does not change protonation state up to the level of the S_4 state, but hydrogen bridging to the mono μ-oxo bridge of the 3.3 Å Mn-Mn distance is discussed to explain the slower water exchange in the S_3 state. However, the general problem with the probably far too fast exchange of a terminal water ligand of Ca, especially relative to W_{slow} (here proposed to be a Mn^{IV}=O), remains. An internal proton release pattern of 1:0:1:2 and a positive net charge in the S_2 and S_3 states is established by deprotonation of the mono μ-hydroxo bridge during the $S_0 \rightarrow S_1$ transition, and H-atom abstraction from the H_2O_{slow} by $Y_Z^{\bullet}$ during the $S_2 \rightarrow S_3$ and $S_3 \rightarrow S_4$ transitions. Because only Mn-centered oxidations are assumed to take place, a Mn(V)=O is formed in the S_4 state, which forms the O-O bond through nucleophilic attack by the Ca-bound water. To achieve the first deprotonation of W_{fast} and, thereby, hydroperoxide formation, an unspecified base B is involved, which temporarily binds one proton and releases it upon water binding and S_0 formation. The formed terminal hydroperoxide intermediate is H-bonded to the mono μ-oxo bridge, which accepts this proton, allowing for a very rapid decay of S_4'' into S_0 and O_2. Although many features of this mechanism are very attractive, a major shortcoming is that it does not give a rationale for S-state dependent structural changes of the Mn cluster. Indeed, the only redox state change of the Mn_3 unit occurs on the $S_1 \rightarrow S_2$ transition, which is not coupled to a structural change of the Mn_4O_xCa complex. Furthermore, all changes in substrate water exchange rates are explained via changes in H-bonding strength to the mono μ-oxo bridge. While this explanation cannot be fully discounted, it does appear unlikely that intermediates Mn(III)-OH_2 in the S_2 state, and Mn(IV)-OH in the S_3, exchange with the same rate and activation energy. This mechanism has recently been slightly modified (McEvoy and Brudvig, 2004) in light of the 3.5 Å PS II crystal structure (Ferreira et al., 2004), but this has not affected any of the above points.

A mechanistic feature of all the nucleophilic attack mechanisms is that they advocate the formation of Mn(V)=O intermediate (in the S_4 state) prior to the formation of the O-O bond. However, it is unknown if such a Mn oxidation state can be generated from the redox potential of $P680^{+\bullet}$ (Hoganson and Babcock, 1997). Currently there is no spectroscopic evidence for Mn(V) formation in PS II. Two mechanisms exist, where a Mn(IV)=O is assumed to be the electrophile. The mechanism by Hillier and Wydrzynski (2000; 2001) suggests that in the S_4 state Mn(III)-OH attacks Mn(IV)=O. This proposal is mainly an attempt to rationalize substrate water exchange rates. The oxidation states invoked throughout the S-state cycle are unconventionally low ($S_1 = Mn_4$(III, III, III, III)) and are not supported with the current calibration of XANES edge energy (Section III.C). Nugent and Evans (2001) postulate similarly to Dau et al. (2001) that a new bridge is formed during the $S_2 \rightarrow S_3$ transition, accounting for the significantly different biochemical properties of these two states.

This Mn(IV)-O(H)-Mn(IV) species is attacked by a Mn(IV)-OH group upon $Y_Z^{\bullet}$ formation in the S_4 state. Interestingly, in this mechanism $Y_Z^{\bullet}$ is proposed to stay oxidized until it is reduced by one of the two formed Mn(II) ions. Currently neither of the mechanisms makes consideration to account for structural changes of the Mn_4O_xCa complex.

Another variation of the nucleophilic attack mechanism was recently offered by Dismukes and colleagues (Dasgupta et al., 2004). In a modification of their above discussed mechanism (Section V.A. and Fig. 7D) they suggest that Ca bound bicarbonate (or carbonate) may attack either the monomeric Mn(IV)=O or the μ_4-oxo group. This suggestion is unique, since it involves bicarbonate (or carbonate) as one of the substrate molecules, or at least a trapped CO_2 molecule as binding site for W_{fast}. While this might be energetically favorable (Dasgupta et al., 2004), there is presently no strong experimental isotopic support for this suggestion from substrate labeling experiments.

C. Radical Mechanisms

The prototype for mechanisms involving a radical in the S_3 state was developed by Yachandra et al. (1996) and is shown in Fig. 9A. The basis for this mechanism is the observation that: (i) the Mn edge shift is significantly smaller on the $S_2 \rightarrow S_3$ transition than for other transitions; and (ii) in S_3, all Mn-Mn distances are longer than in the S_2 state. The latter finding suggests a weakening of the μ-oxo bridge bond strength, which is in line with oxidation of such a bridge. On the basis of a suggested mechanism for O-O bond formation in bis μ-oxo bridged Cu complexes, it was then suggested that, in the S_4 state, a second μ-oxo bridge radical is formed in the same Mn_2 unit (Fig. 9A). The two adjacent radicals then form the initial O-O bond, extract two electrons from the Mn_2 unit, and ligated O_2 is replaced by two μ-hydroxo bridges to form S_0. This mechanism gives elegant rationale for the contraction of one Mn-Mn distance on the $S_0 \rightarrow S_1$ transition and the elongation of distances during the $S_2 \rightarrow S_3$ transition. However, because the dimer of dimers model (Fig. 3 A) was used as a structural template, it is difficult to understand why the distance of the second Mn_2 unit should also increases during the latter transition. Furthermore, the proposed proton release pattern (2:0:0:2) and the protonation states of the substrate water molecules in the S_1, S_2 and S_3 states (always two oxo's) deviate from the above analysis (Sections IV.A and C). In addition, the different S-state dependencies of the exchange rates of W_{fast} and W_{slow} are very difficult to reconcile with this proposal. To better account for the heterogeneity of the substrate water exchange reactions it was alternatively suggested that in S_4 the μ-oxo bridge radical (W_{slow}) could be attacked by a free water molecule or hydroxide radical (W_{fast}), as illustrated in Fig. 9 B (Liang et al., 2000). The lengthening of all bis μ-oxo bridges was later explained (Robblee et al., 2002) by assuming that the radical is partly delocalized within a trimeric Mn_3 core, such as is illustrated in models **D**, **E** or **F** in Fig. 3.

An intentionally simplistic scheme involving radical-based chemistry (Fig. 9C), which contains only two Mn ions, Y_Z and a histidine, was developed by Haumann and Junge (1999). In this model, the first two S-state transitions are thought to occur by normal electron transfer from Mn to $Y_Z^{\bullet}$, while the $S_2 \rightarrow S_3$ transition is thought to involve $H^{\bullet}$ abstraction and the formation of a terminal hydroxyl radical. Similar to the above-discussed model of Renger (Fig. 7 C), it is assumed that this terminal radical is the majority component in equilibrium with a pre-peroxide that can be formed together with the neighboring hydroxyl anion. In the S_4 state, $Y_Z^{\bullet}$ is formed and it is assumed that it cannot oxidize the second terminal hydroxyl anion, but only the Mn(III)Mn(III)-peroxide entity. Since this is present only as a small fraction, it is proposed that the low probability of this peroxide state, rather than the rate of electron transfer, is rate limiting for O_2 evolution. This minimal model is mainly aimed to address the function of Y_Z in water oxidation and is therefore consistent with the proton release pattern, electrochromic band shifts, and Mn oxidation states as discussed above but, for example, cannot fully account for structural changes and substrate water exchange kinetics.

A more complex mechanistic proposal (Fig. 9D) that aims to account for structural changes of the Mn_4O_xCa complex, Mn redox states, proton release pattern, electrochromic band shifts, the idea of keeping the Mn_4O_xCa complex electroneutral throughout the cycle and for the substrate water exchange rates was developed by Messinger (2000). Structurally, the proposal is based on the Berkeley C motif (Fig. 3 **A**), and only one Mn_2 core undergoes redox changes. Similar to the proposal of Yachandra et al. Mn(II) → Mn(III) and Mn(III) → Mn(IV) oxidations take place during the $S_0 \rightarrow S_1$ and $S_1 \rightarrow S_2$ transition, while a μ-oxo bridge radical is formed in the S_3 state. The

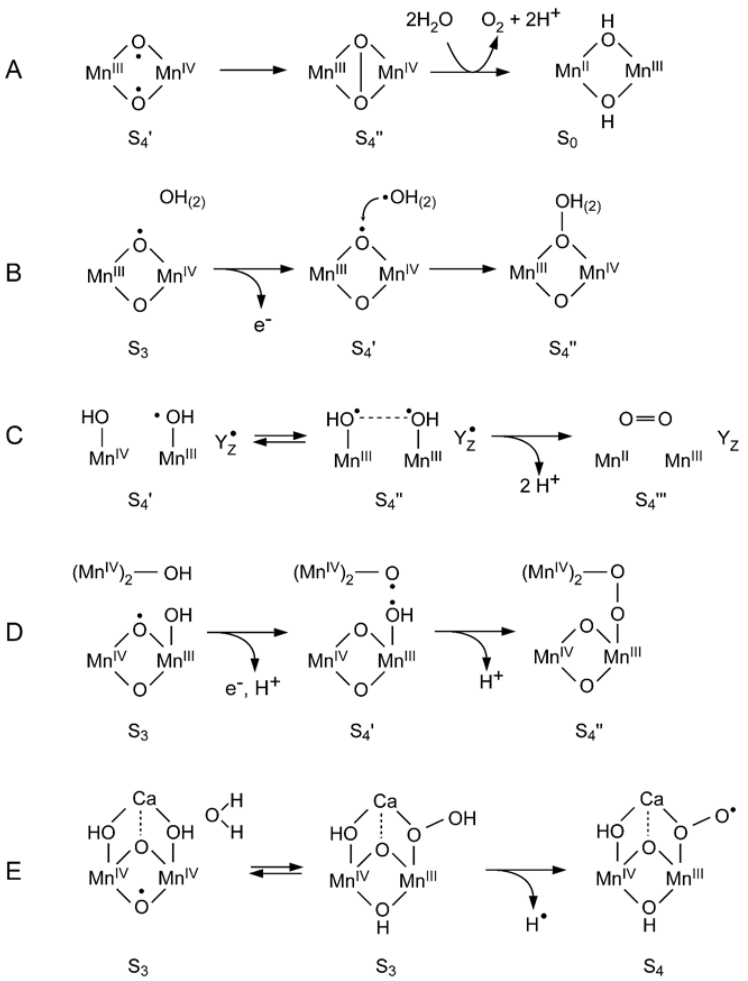

Fig. 9. Proposed mechanisms for O-O bond formation in photosynthetic water oxidation that involves the fusion of two radicals. A, B, C, D and E were redrawn after Yachandra et al. (1996), Liang et al. (2000), Haumann and Junge (1999), Messinger (2000) and Siegbahn (2000), respectively.

model (Fig. 9D), contains three interesting aspects: (i) it is discussed that this radical might be delocalized over several bridges, if more tightly coupled structures like those shown in Fig. 3 **B**, **C** and **D** were assumed; (ii) despite μ-oxo bridge oxidation during the $S_2 \rightarrow S_3$ transition, two terminal water molecules are assumed to form the O-O bond, which was thought to be facilitated by a certain probability that the μ-oxo bridge radical resides on one of the terminal water ligands; and (iii) Cl^- binding to the Mn cluster during the $S_2 \rightarrow S_3$ transition in a trans position to W_{slow} is suggested to explain the somewhat faster exchange in S_2, keep the Mn cluster electroneutral, and account for the electrochromic band shifts by having a positive charge at the original Cl^- binding site near the Mn_4O_xCa complex (see also Hoganson and Babcock, 1997). Therefore, in this proposal, radical formation in S_3 is used as a way to store an oxidizing equivalent in a form advantageous for the O-O bond formation. Shortcomings of this proposal are that it does not provide a function for Ca^{2+}, involves Cl^- binding to Mn and does not explain the tight kinetic coupling

between $Y_Z^{\bullet}$ reduction and O_2 release in the $S_3 \rightarrow S_0$ transition. Furthermore, on several steps, the proposed deprotonations occur on groups distant from the sites of oxidation. An extension of this model on the basis of two Mn_4O_xCa structures with geometries similar to that shown in Fig. 3D has recently been published (Messinger, 2004).

On the basis of DFT calculations, Siegbahn (2000) made an interesting proposal for water oxidation in the OEC (Fig. 9E). Structurally, the model derived from a bent version of model **C** in Fig. 3 and a Ca^{2+} ion was added such that an open cube structure is formed by the two central Mn ions and Ca^{2+}. The two bridges between Ca^{2+} and the Mn ions are formed by two water molecules in the S_0 state. Y_Z is thought to fill the fourth corner of the cube and to abstract $H^{\bullet}$-atoms from a Mn-Mn μ-hydroxo bridge in the $S_0 \rightarrow S_1$ transition and from the two bridging water molecules in the other S-state transitions. In this proposal, only one Mn ion is undergoing redox changes from Mn(II) in S_0 via Mn(III) in S_1 to Mn(IV) in S_2. Because general spin considerations and DFT calculations suggest that an oxyl radical should be formed prior to the step of O-O bond formation, a μ-oxo bridge oxidation is invoked for the $S_2 \rightarrow S_3$ transition. Confirming qualitative considerations by Yachandra adn co-workers, the DFT calculations for such complexes reproduce the observed structural changes discussed earlier. For a stabilization of the radical it is assumed that it can migrate from a bridge between Mn and Ca to another one between two Mn centers. Similar to suggestions of Renger and Junge, it is assumed that, in the S_3 state, this reactive oxyl radical is in an equilibrium with hydroperoxide (Mn-OOH), which is proposed to be formed by the reaction of a free water molecule with the oxyl radical (Siegbahn and Crabtree, 1999). In the S_4 state, $Y_Z^{\bullet}$ abstracts, in a rate-limiting reaction, an $H^{\bullet}$-atom from the hydroperoxide, molecular oxygen is released, and the S_0 state is reformed under water binding. An internal proton release pattern of 1:1:1:1 is suggested, which implies that no positive charge is accumulated during the $S_1 \rightarrow S_2$ transition. It is furthermore difficult to reconcile the S-state dependence of the substrate water exchange kinetics with this proposal.

VII. A New Mechanistic Rendition of Photosynthetic Oxidation Production

The above discussion has provided a mechanistic overview of many of the recent models for photosynthetic water oxidation. Each mechanism addresses some experimental findings very well, but has weaknesses with others. In the following, we will try to collate experimental findings and mechanistic features introduced in many of these proposals to formulate a working model (Fig. 10) that reflects our current ideas of photosynthetic water oxidation and provides rationale for as many experimental findings as possible.

As a structural model for our proposal, we invoke model **D** of Fig. 3 to rationalize the available structural data, although other models appear also viable. Addition of Ca^{2+} is made to this model such that there are 2 Mn-Ca vectors of about 3.4 Å, having an average angle of about 20° to the membrane normal. Within the chosen model, two options exist for placing Ca^{2+}: either as part of a bridge over the 3.3 Å Mn-Mn distance, or alongside one of the sites of the trimeric core. The latter structure is used here, because it better resembles the overall shape of the electron density of the Mn_4O_xCa cluster as determined in all current PS II crystal structure (Zouni et al., 2001; Kamiya and Shen, 2003; Biesiadka et al., 2004; Ferreira et al., 2004; Chapter 19, Witt; Chapter 20, Shen and Kamiya; Chapter 21, Barber and Iwata). The Mn oxidation states in the S_0 state are suggested to be Mn_4(III, III, III, IV) or, alternatively, Mn_4(II, III, IV, IV). The findings from EXAFS spectroscopy show that one Mn-Mn distance is shortened from 2.85 Å to 2.7 Å in the $S_0 \rightarrow S_1$ state transition. This is consistent with: (i) the presence of Mn(II) in a bis μ-oxo bridged unit, which is oxidized to Mn(III) in the $S_0 \rightarrow S_1$ transition; and/or (ii) a μ-hydroxo bridge in a μ-oxo-μ-hydroxo bridged Mn(II,III) or Mn(III,III) unit, which is deprotonated during its oxidation. Placing Mn(II) into the trimeric core would result in an elongation of two 2.7 Å Mn-Mn distances, while a 'monomeric' Mn_a(II) is not expected to affect the 2.7 Å distances. Therefore, within the chosen structure, one of the μ-oxo bridges of the trimeric core must be protonated in the S_0 state and the oxidation states have to be Mn_4(III, III, III, IV). It should be noted that, in all other structures of Fig. 3, a Mn(II) remains an option. The assignment of the oxidation states to the four Mn centers in the S_0 state (Fig. 10) is partly arbitrary, but two Mn(III) ions are likely to be next to the μ-hydroxo bridge. Deprotonation of this μ-OH bridge during the $S_0 \rightarrow S_1$ transition is then best explained by a Mn(III) to Mn(IV) oxidation of one of these two ions, i.e., either of Mn_b(III)

or Mn_c(III). The slow-exchanging substrate 'water' (W_{slow}) should also be bound to the Mn(III) that is oxidized in this transition, since this arrangement is consistent with the 600-fold slower exchange rate in the S_1 state. For simplicity it is tempting to identify the μ-hydroxo-bridge with W_{slow}, but in order to account for the described evidence that Ca is involved in binding W_{slow} we propose that the μ-oxo bridge between Mn_b and Ca is W_{slow}. Given this assignment for W_{slow}, the most logic binding site for W_{fast} appears to be Mn_a(III), since this offers a good geometry for O-O bond formation. Furthermore, the binding of W_{fast} to Mn gives the best rational for the finding that the slow and fast exchange rates are within a factor of 20 in the S_3 state. The Ca ion also coordinates a terminal water molecule in a substrate holding function. The fate of this water molecule is to reload a substrate site immediately after release of the O_2.

For the $S_1 \rightarrow S_2$ transition two possibilities can be discussed. The oxidation of the monomeric Mn_a(III) to Mn_a(IV) during the $S_1 \rightarrow S_2$ transition (option A) can nicely explain: (i) the slowing of the fast water exchange that renders this substrate molecule detectable for the first time in the cycle; and (ii) the fact that EXAFS does not detect any significant structural changes in the cluster. This situation is also in line with the NMR-PRE experiments which were interpreted as showing a Mn(III)-OH_2 in S_1 and Mn(IV)-OH_2 in S_2. A weak point of this assignment is that deprotonation of W_{fast} might be expected to occur when Mn_a is oxidized; while experimental data show that there is no proton release on this transition. Therefore, also the oxidation of the last Mn(III) of the trimer (Mn_c) is a viable option (option B). In this case the lack of a proton release might be explainable by the absence of: (i) a deprotonizable ligand at Mn_c; or (ii) of a suitable proton exit pathway. The presence of a Mn(III)-OH_2 would be in line with the interpretation of a recent ^{17}O-ESEEM study (Evans et al., 2004). However, in this scenario changes in the H-bonding situation of W_{fast} and W_{slow} have to be proposed to explain the slowing and 100-fold increase of their exchange rates, respectively. It is not unlikely that such changes are triggered by the accumulation of a positive charge in this transition, and FTIR measurements indicating such changes have been mentioned in section IV.A.3. It is difficult to judge at present which of these two options is more likely, but for the following we continue with option B. The changed H-bonding situation in the S_2 state is indicated in Fig. 10 by the formation of an H-bond between W_{fast} and W_{slow}.

The $S_2 \rightarrow S_3$ and $S_3 \rightarrow S_4$ transitions are believed to be rate limited by a tight coupling between proton and electron transfer steps or even by H-atom abstraction. As outlined before (Section III.C.2.) the nature of the $S_2 \rightarrow S_3$ transition remains unclear, but clearly more complex changes take place compared to the simple Mn(III) → Mn(IV) oxidation in the $S_1 \rightarrow S_2$ transition. In our model the required structural changes may be triggered by: (i) oxidation of the Mn_a(III) to Mn_a(IV) and the formation of an extra μ-oxo bridge; or (ii) by the oxidation of a μ-oxo bridge leading to the lengthening of all 2.7 Å Mn-Mn distances. To emphasize the different nature of this transition we decided to depict the latter option in Fig. 10. The reason why Mn_a(III) may have a higher oxidation potential than a μ-oxo bridge is not obvious from our simplistic model, and detailed calculations including the surrounding of the cluster are required to investigate this question. However, DFT calculations suggest that if a μ-oxo bridge radical is formed in the S_3 state, it should be located between two Mn(IV) centers and it should also be able to induce trans-effects (Siegbahn, 2000). In our model the most likely position is therefore the μ-oxo bridge between Mn_b and Mn_c. The trans-effects may also be the reason for the deprotonation of W_{fast}, which could account for the observation of a pH independent release of one proton in this transition. Because the exchange rate of W_{fast} slows only by a factor of 4–5 in this transition, one needs to postulate in this case, however, that protonation of W_{fast} is not rate limiting for its exchange rate, which seems at odds with the assumptions we made for the S_2-state. Therefore, also the deprotonation of a non-substrate ligand of the Mn_4O_xCa complex should be considered. An attractive option would be a water ligand to Ca, because this could explain: (i) why the $S_2 \rightarrow S_3$ transition is blocked by Ca removal; and (ii) why the similar pK_a of water ligands of Ca and Sr may be the reason why Sr is the only metal that is able to functionally replace Ca, yet leads to slower transfer rates. Because in our model the electron and proton originate from different places of the Mn_4O_xCa complex, PCET rather than H$^{\bullet}$-atom abstraction is assumed for this transition.

It has been suggested in several mechanisms that in the S_3 state the O-O bond may be preformed in a very small fraction of centers due to a redox equilibrium. This possibility is indicated in Fig. 10. It appears attractive (but is not required) to assume that the formation of this peroxide intermediate is

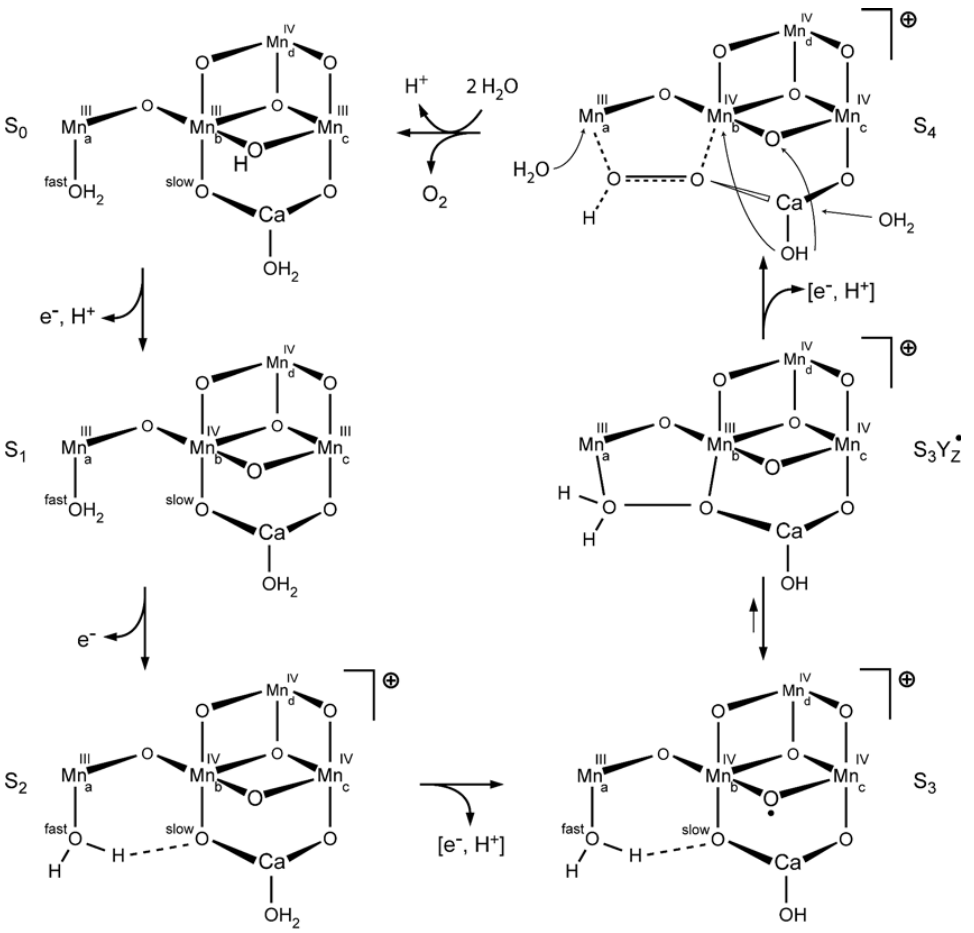

Fig. 10. Proposed mechanism for photosynthetic water oxidation. A structural framework for the catalytic Mn_4O_xCa complex is derived from EXAFS data, ^{55}Mn ENDOR and crystallographic information and rationalizes S-state dependent structural changes observed with EXAFS spectroscopy. Mn oxidation states were taken from XANES and Kβ XES experiments. Substrate water binding involves one terminal Mn and a bridging position between Ca and Mn. The overall features of this model are discussed in detail within the text and seek to rationalize kinetic and thermodynamic information at hand.

rate limiting for the $S_3Y_Z^{\bullet} \rightarrow S_4$ transition and subsequent O_2 release. Certainly the latest data by the Junge group indicates that PS II can be blocked in the S_4 state by an overpressure of only a few bar of O_2 (Clausen and Junge, 2004). A possible configuration of the S_4 intermediate is shown in Fig. 10, which also indicates the further changes required for O_2 release: concomitant with the reduction of Mn_b(IV) and Mn_c(IV) to Mn_b(III) and Mn_c(III) ground state triplet O_2 and a proton are released, and the Ca bound hydroxide takes the place of W_{slow} by transferring its proton to the μ-oxo bridge between Mn_b and Mn_c. These product/substrate exchange reactions are likely promoted by the Jan-Teller effect of Mn(III). Finally, the S_0 state is reformed by the binding of two new water molecules: one to Mn_a(III), and one to reload the substrate holding Ca.

The above mechanism invokes only small structural changes, because large structural rearrangements appear unlikely on the basis of the discussed thermodynamic, kinetic and structural (EXAFS) information. This comprehensive proposal qualitatively accounts for many experimental findings. However, at this point it appears not to be unique solution to an intricate

reaction. Unfortunately, Mother Nature has held many of her secrets tightly, and divergent lines of argument concerning the details exist that require further critical testing by experiments and calculations. Many of the open questions have been discussed above and we hope that this Chapter will help to inspire research that sets out to solve the remaining mysteries of this fascinating reaction.

Acknowledgments

The authors like to thank Dave Britt, Fabrice Rappaport, Gernot Renger and Tom Wydrzynski for helpful discussions and comments. WH acknowledges support by the Human Frontier Science Program Organization (RGP0029/2002) and JM support by the Max-Planck-Gesellschaft and Deutsche Forschungsgemeinschaft (Me 1629/2–3).

References

Ahlbrink R, Haumann M, Cherepanov D, Bögershausen O, Mulkidjanian A and Junge W (1998) Function of tyrosine Z in water oxidation by Photosystem II: Electrostatical promoter instead of hydrogen abstractor. Biochemistry 37: 1131–1142

Åhrling KA, Peterson S and Styring S (1997) An oscillating manganese electron paramagnetic resonance signal from the S_0 state of the oxygen evolving complex in Photosystem II. Biochemistry 36: 13148–13152

Åhrling KA, Evans MCW, Nugent JHA and Pace RJ (2004) The two forms of the S_2 state multiline signal in Photosystem II: effect of methanol and ethanol. Biochim Biophys Acta 1656: 66–77

Ananyev GM, Zaltsman L, Vasko C and Dismukes GC (2001) The inorganic biochemistry of photosynthetic oxygen evolution/water oxidation. Biochim Biophys Acta 1503: 52–68

Anderson JM (2001) Does functional Photosystem II complex have an oxygen channel? FEBS Lett 488: 1–4

Aznar CP and Britt RD (2002) Simulations of the ^{1}H electron spin echo-electron nuclear double resonance and ^{2}H electron spin echo envelope modulation spectra of exchangeable hydrogen nuclei coupled to the S_2 state Photosystem II manganese cluster. Philos Trans Roy Soc London B 357: 1359–1365

Babcock GT, Blankenship RE and Sauer K (1976) Reaction kinetics for positive charge accumulation on the water side of chloroplast Photosystem II. FEBS Lett 61: 286–289

Bader KP, Renger G and Schmid GH (1993) A mass-spectrometric analysis of the water splitting reaction. Photosynth Res 38: 355–361

Baranov SV, Ananyev GM, Klimov VV and Dismukes GC (2000) Bicarbonate accelerates assembly of the inorganic core of the water-oxidizing complex in manganese depleted Photosystem II: A proposed biogeochemical role for atmospheric carbon dioxide in oxygenic photosynthesis. Biochemistry 39: 6060 –6065

Beck WF and Brudvig GW (1986) Binding of amines to the O_2 evolving center of Photosystem II. Biochemistry 25: 6479–6486

Beck WF and Brudvig GW (1988a) Resolution of the paradox of ammonia and hydroxylamine as substrate analogs for the water-oxidation reaction catalyzed by Photosystem II. J Am Chem Soc 110: 1517–1523

Beck WF and Brudvig GW (1988b) Ligand substitution reactions of the oxygen evolving center of Photosystem II. Chem Script 28A: 93–98

Beck WF, Depaula JC and Brudvig GW (1986) Ammonia binds to the manganese site of the O_2evolving complex of Photosystem II in the S_2 state. J Am Chem Soc 108: 4018–4022

Bergmann U, Grush MM, Horne CR, DeMarois P, Penner-Hahn JE, Yocum CF, Wright DW, Dubé CE, Armstrong WH, Christou G, Eppley HJ and Cramer SP (1998) Characterization of the Mn oxidation states in Photosystem II by Kß X-ray fluorescence spectroscopy. J Phys Chem B 102: 8350–8352

Bernarding J, Eckert HJ, Eichler HJ, Napiwotzki A and Renger G (1994) Kinetic studies on the stabilization of the primary radical pair $P680^+$ $Pheo^-$ in different Photosystem II preparations from higher plants. Photochem Photobiol 59: 566–573

Biesiadka J, Loll B, Kern J, Irrgang K-D and Zouni A (2004) Crystal structure of cyanobacterial Photosystem II at 3.2 Å resolution: A closer look at the Mn-cluster. Phys Chem Chem Phys 6: 4733–4736

Blomberg MRA, Siegbahn PEM, Styring S, Babcock GT, Åkermark B and Korall P (1997) A quantum chemical study of hydrogen abstraction from manganese coordinated water by a tyrosyl radical: A model for water oxidation in Photosystem II. J Am Chem Soc 119: 8285–8292

Bögershausen O, Haumann M and Junge W (1996) Photosynthetic oxygen evolution: H/D isotope effects and the coupling between electron and proton transfer during transitions S_2 to S_3 and S_3 to S_4 to S_0. Ber Bunsen Phys Chem 100: 1987–1992

Bouges B (1971) Action de faibles concentrations d'hydroxylamine sur l'emission d'oxygene des algues chlorella et des chloroplastes d'epinards. Biochim Biophys Acta 936: 228–235

Boussac A and Etienne AL (1982) Oxido-reduction kinetics of Signal II_{slow} in Tris washed chloroplasts. Biochem Biophys Res Commun 109: 1200–1205

Boussac A and Rutherford AW (1988) Ca^{2+} binding to the oxygen evolving enzyme varies with the redox state of the Mn cluster. FEBS Lett 236: 432–436

Boussac A, Rutherford AW and Styring S (1990) Interaction of ammonia with the water splitting enzyme of Photosystem II. Biochemistry 29: 24–32

Brettel K, Schlodder E and Witt HT (1984) Nanosecond reduction kinetics of photooxidised chlorophyll a_{II} (P680) in single flashes as a probe for the electron pathway, H^+ release and charge accumulation in the O_2 evolving complex. Biochim Biophys Acta 766: 403–415

Britt RD (1996) Oxygen evolution. In: Ort DR and Yocum CF (eds) Oxygenic Photosynthesis: The Light Reactions, pp 137–164. Kluwer Academic Publishers, Dordrecht

Britt RD, Zimmermann J-L, Sauer K and Klein MP (1989) Ammonia binds to the catalytic Mn of the oxygen evolving complex of Photosystem II: Evidence by electron spin-echo envelope modulation spectroscopy. J Am Chem Soc 111: 3522–3532

Britt RD, Peloquin JM and Campbell KA (2000) Pulsed and parallel-polarization EPR characterization of the Photosystem II oxygen evolving complex. An Rev Biophys Biomol Struct

29: 463–495
Britt RD, Campbell KA, Peloquin JM, Gilchrist ML, Aznar CP, Dicus MM, Robblee J and Messinger J (2004) Recent pulsed EPR studies of the Photosystem II oxygen-evolving complex: Implications as to water oxidation mechanisms. Biochim Biophys Acta 1655: 158–171
Burnap RL, Shen J-R, Jursinic PA, Inoue Y and Sherman LA (1992) Oxygen yield and thermoluminescence characteristics of a cyanobacterium lacking the manganese stabilizing protein of Photosystem II. Biochemistry 31: 7404–7410
Buser CA, Diner BA and Brudvig GW (1992) Photooxidation of cytochrome b_{559} in oxygen evolving Photosystem II. Biochemistry 31: 11449–11459
Carell TG, Tyryshkin AM and Dismukes GC (2002) An evaluation of structural models for the photosynthetic water oxidizing complex derived from spectroscopic and X-ray diffraction signatures. J Biol Inorg Chem 7: 2–22
Caudle MT and Pecoraro VL (1997) Thermodynamic viability of hydrogen atom transfer from water coordinated to the oxygen evolving complex of Photosystem II. J Am Chem Soc 119: 3415–3416
Christen G and Renger G (1999) The role of hydrogen bonds for the multiphasic $P680^{+\cdot}$ reduction by Y_Z in Photosystem II with intact oxygen evolution capacity. Analysis of kinetic H/D isotope exchange effects. Biochemistry 38: 2068–2077
Christen G, Reifarth F and Renger G (1998) On the origin of the 35 μs kinetics of $P680^{+\cdot}$ reduction in Photosystem II with an intact water oxidising complex. FEBS Lett 429: 49–52
Christen G, Seeliger A and Renger G (1999) $P680^{+\cdot}$ reduction kinetics and redox transition probability of the water oxidizing complex as a function of pH and H D isotope exchange in spinach thylakoids. Biochemistry 38: 6082–6092
Chu H-A, Sackett H and Babcock GT (2000) Identification of a Mn-O-Mn cluster vibrational mode of the oxygen evolving complex in Photosystem II by low-frequency FTIR spectroscopy. Biochemistry 39: 14371–14376
Chu HA, Hillier W, Law NA and Babcock GT (2001) Vibrational spectroscopy of the oxygen-evolving complex and of manganese model compounds. Biochim Biophys Acta 1503: 69–82
Chu HA, Hillier W and Debus RJ (2004) Evidence that the C-terminus of the D1 polypeptide of Photosystem II is ligated to the manganese ion that undergoes oxidation during the S_1 to S_2 transition: An isotope-edited FTIR study. Biochemistry 43: 3152–3166
Cinco RM, Robblee JH, Rompel A, Fernandez C, Yachandra VK, Sauer K and Klein MP (1998) Strontium EXAFS reveals the proximity of calcium to the manganese cluster of oxygen evolving Photosystem II. J Phys Chem B 102: 8248–8256
Cinco RM, Holman KLM, Robblee JH, Yano J, Pizarro SA, Bellacchio E, Sauer K and Yachandra VK (2002) Calcium EXAFS establishes the Mn-Ca cluster in the oxygen evolving complex of Photosystem II. Biochemistry 41: 12928–12933
Cinco RM, Robblee JH, Messinger J, Fernandez C, Holman KLM, Sauer K and Yachandra VK (2004) Orientation of calcium in the Mn_4Ca cluster of the oxygen-evolving complex determined using polarized strontium EXAFS of Photosystem II membranes. Biochemistry 43: 13271–13282
Clausen J and Junge W (2004) Detection of an intermediate of photosynthetic water oxidation. Nature 430: 480–483
Clausen J, Debus RJ and Junge W (2004) Time-resolved oxygen production by PS II: Chasing chemical intermediates. Biochim Biophys Acta 1655: 184–194
Critchley C, Baianu IC, Govindjee and Gutowsky HS (1982) The role of chloride in O_2 evolution by thylakoids from salt tolerant higher plants. Biochim Biophys Acta 682: 436–445
Cua A, Stewart DH, Reifler MJ, Brudvig GW and Bocian DF (2000) Low-frequency resonance Raman characterization of the oxygen evolving complex of Photosystem II. J Am Chem Soc 122: 2069–2077
Cua A, Vrettos JS, de Paula JC, Brudvig GW and Bocian DF (2003) Raman spectra and normal coordinate analyses of low-frequency vibrations of oxo-bridged manganese complexes. J Biol Inorg Chem 8: 439–451
Dasgupta J, van Willigen RT and Dismukes GC (2004) Consequences of structural and biophysical studies for the molecular mechanism of photosynthetic oxygen evolution: Functional roles for calcium and bicarbonate. Phys Chem Chem Phys 6: 4793–4802
Dau H, Andrews JC, Roelofs TA, Latimer MJ, Liang W, Yachandra VK, Sauer K and Klein MP (1995) Structural consequences of ammonia binding to the manganese cluster of the photosynthetic oxygen evolving complex: An X-ray absorption study of isotropic and oriented Photosystem II particles. Biochemistry 34: 5274–5287
Dau H, Iuzzolino L and Dittmer J (2001) The tetra-manganese complex of Photosystem II during its redox cycle: X-ray absorption results and mechanistic implications. Biochim Biophys Acta 1503: 24–39
Dau H, Liebisch P and Haumann M (2003) X-ray absorption spectroscopy to analyze nuclear geometry and electronic structure of biological metal centers — Potential and questions examined with special focus on the tetra-nuclear manganese complex of oxygenic photosynthesis. Anal Bioanal Chem 376: 562–583
de Wijn R and van Gorkom HJ (2002) S-state dependence of the miss probability in Photosystem II. Photosynth Res 72: 217–222
Debus RJ (1992) The manganese and calcium ions of photosynthetic oxygen evolution. Biochim Biophys Acta 1102: 269–352
Debus RJ (2001) Amino acid residues that modulate the properties of tyrosine Y_Z and the manganese cluster in the water oxidizing complex of Photosystem II. Biochim Biophys Acta 1503: 164–186
Dekker JP, Plijter JJ, Ouwehand L and van Gorkom HJ (1984) Kinetics of manganese redox transitions in the oxygen evolving apparatus of photosynthesis. Biochim Biophys Acta 767: 176–179
Delrieu MJ (1983) Evidence for unequal misses in oxygen flash yield sequence in photosynthesis. Z Naturforsch 38c: 247–258
Diner BA (1977) Dependence of deactivation reactions of Photosystem II on redox state of plastoquinone pool-a varied under anaerobic conditions. Equilibria on the acceptor side of Photosystem II. Biochim Biophys Acta 460: 247–258
Diner BA (2001) Amino acid residues involved in the coordination and assembly of the manganese cluster of Photosystem II. Proton-coupled electron transport of the redox active tyrosines and its relationship to water oxidation. Biochim Biophys Acta 1503: 147–163
Diner BA and Rappaport F (2002) Structure, dynamics, and energetics of the primary photochemistry of Photosystem II of

oxygenic photosynthesis. An Rev Plant Biol 53: 551–580
Dismukes GC (1996) Manganese enzymes with binuclear active sites. Chem Rev 96: 2909–2926
Dismukes GC and Siderer Y (1981) Intermediates of a polynuclear manganese cluster involved in photosynthetic oxidation of water. Proc Natl Acad Sci USA 78: 274–278
Eckert HJ and Renger G (1988) Temperature dependence of $P680^+$ reduction in O_2 evolving PS II membrane fragments at different redox states S_i of the water oxidizing system. FEBS Lett 236: 425–431
Evans MCW, Gourovskaya K and Nugent JHA (1999) Investigation of the interaction of the water oxidizing manganese complex of Photosystem II with the aqueous solvent environment. FEBS Lett 450: 285–288
Evans MCW, Rich AM and Nugent JHA (2000) Evidence for the presence of a component of the Mn complex of the Photosystem II reaction centre which is exposed to water in the S_2 state of the water oxidation complex. FEBS Lett 477: 113–117
Evans MCW, Nugent JHA, Ball RJ, Muhiuddin I and Pace RJ (2004) Evidence for a direct manganese-oxygen ligand in water binding to the S_2 state of the photosynthetic water oxidation complex. Biochemistry 43: 989–994
Fernandez C, Cinco RM, Robblee JH, Messinger J, Pizarro SA, Sauer K, Yachandra VK and Klein MP (1998) Calcium and chloride cofactors of the oxygen evolving complex: X-ray absorption spectroscopy evidence for a Mn/Ca/Cl heteronuclear cluster. In: Garab G (ed) Photosynthesis: Mechanisms and Effects, pp 1399–1402. Kluwer Academic Publishers, Dordrecht
Ferreira KN, Iverson TM, Maghlaoui K, Barber J and Iwata S (2004) Architecture of the photosynthetic oxygen-evolving center. Science 303: 1831–1838
Fiege R, Zweygart W, Bittl R, Adir N, Renger G and Lubitz W (1996) EPR and ENDOR studies on the water oxidizing complex of Photosystem II. Photosynth Res 42: 227–244
Fischer G and Wydrzynski T (2001) Isotope effects in FTIR difference spectra of the photosynthetic oxygen evolving catalytic site determined by *ab initio* calculations on model compounds. J Phys Chem B 105: 12894–12901
Forbush B, Kok B and McGloin MP (1971) Cooperation of charges in photosynthetic oxygen evolution. II. Damping of flash yield oscillation, deactivation. Photochem Photobiol 14: 307–321
Force DA, Randall DW, Lorigan GA, Clemens KL and Britt RD (1998) ESEEM studies of alcohol binding to the manganese cluster of the oxygen evolving complex of Photosystem II. J Am Chem Soc 120: 13321–13333
Förster V and Junge W (1985) Interaction of hydroxylamine with the water-oxidizing enzyme investigated via proton release. Photochem Photobiol 41: 191–194
Förster V and Junge W (1986) On the action of hydroxylamine, hydrazine and their derivatives on the water oxidizing complex. Photosynth Res 9: 197–210
Förster V and Junge W (1988) Protolytic reactions of the photosynthetic water oxidase in the absence and in the presence of added ligands. Chem Script 28A: 111–116
Frasch WD, Mei R and Sanders MA (1988) Oxidation of alcohols catalyzed by the oxygen evolving complex. Biochemistry 27: 3715–3719
Ghanotakis DF, Babcock GT and Yocum CF (1984) Calcium reconstitutes high rates of oxygen evolution in polypeptide depleted Photosystem II preparations. FEBS Lett 167: 127–130
Gilchrist ML, Jr., Ball JA, Randall DW and Britt RD (1995) Proximity of the manganese cluster of Photosystem II to the redox-active tyrosine Y_Z. Proc Natl Acad Sci USA 92: 9545–9549
Glatzel P, Bergmann U, Yano J, Visser H, Robblee JH, Gu WW, de Groot FMF, Christou G, Pecoraro VL, Cramer SP and Yachandra VK (2004) The electronic structure of Mn in oxides, coordination complexes, and the oxygen-evolving complex of Photosystem II studied by resonant inelastic X-ray scattering. J Am Chem Soc 126: 9946–9959
Gleiter HM, Haag E, Shen J-R, Eaton-Rye JJ, Seeliger AG, Inoue Y, Vermaas WFJ and Renger G (1995) Involvement of the CP47 protein in stabilization and photoactivation of a functional water oxidizing complex in the cyanobacterium *Synechocystis sp* PCC 6803. Biochemistry 34: 6847–6856
Goussias C, Ioannidis N and Petrouleas V (1997) Low-temperature interactions of NO with the S_1 and S_2 states of the water oxidizing complex of Photosystem II. A novel Mn multiline EPR signal derived from the S_1 state. Biochemistry 36: 9261–9266
Guiles RD, Zimmermann J-L, McDermott AE, Yachandra VK, Cole JL, Dexheimer SL, Britt RD, Wieghardt K, Bossek U, Sauer K and Klein MP (1990) The S_3 state of Photosystem II: Differences between the structure of the manganese complex in the S_2 and S_3 states determined by X-ray absorption spectroscopy. Biochemistry 29: 471–485
Haddy A, Hatchell JA, Kimel RA and Thomas R (1999) Azide as a competitor of chloride in oxygen evolution by Photosystem II. Biochemistry 38: 6104–6110
Hankamer B, Morris E, Nield J, Carne A and Barber J (2001) Subunit positioning and transmembrane helix organization in the core dimer of Photosystem II. FEBS Lett 504: 142–151
Hansson Ö, Andréasson L-E and Vänngård T (1986) Oxygen from water is coordinated to manganese in the S_2 state of Photosystem II. FEBS Lett 195: 151–154
Hasegawa K, Kusunoki M, Inoue Y and Ono T-A (1998) Simulation of S_2-state multiline EPR signal in oriented Photosystem II membranes: Structural implications for the manganese cluster in an oxygen-evolving complex. Biochemistry 37: 9457–9465
Hasegawa K, Ono T-A, Inoue Y and Kusunoki M (1999) How to evaluate the structure of the tetranuclear Mn cluster from magnetic and EXAFS data: Case of the S_2 State Mn cluster in Photosystem II. Bull Chem Soc Jpn 72: 1013–1023
Haumann M and Junge W (1994) Extent and rate of proton release by photosynthetic water oxidation in thylakoids: Electrostatic relaxation versus chemical production. Biochemistry 33: 864–872
Haumann M and Junge W (1999) Photosynthetic water oxidation: A simplex scheme of its partial reactions. Biochim Biophys Acta 1411: 86–91
Haumann M and Junge W (1996) Protons and charge indicators in oxygen evolution. In: Ort DR and Yocum CF (eds) Oxygenic Photosynthesis: The Light Reactions, pp 165–192. Kluwer Academic Publishers, Dordrecht
Haumann M, Bögershausen O, Cherepanov D, Ahlbrink R and Junge W (1997) Photosynthetic oxygen evolution: H/D isotope effects and the coupling between electron and proton transfer during the redox reactions at the oxidizing side of Photosystem II. Photosynth Res 51: 193–208
Havemann J and Mathis P (1976) Flash-induced absorption changes of the primary donor of Photosystem II at 830 nm in

chloroplasts inhibited by low pH or Tris-treatment. Biochim Biophys Acta 440: 346–355

Hays A-MA, Vassiliev IR, Golbeck JH and Debus RJ (1999) Role of D1-His190 in the proton coupled oxidation of tyrosine Y_Z in manganese depleted Photosystem II. Biochemistry 38: 11851–11865

Hendry G and Wydrzynski T (2002) The two substrate water molecules are already bound to the oxygen evolving complex in the S_2 state of Photosystem II. Biochemistry 41: 13328–13334

Hendry G and Wydrzynski T (2003) ^{18}O isotope exchange measurements reveal that calcium is involved in the binding of one substrate-water molecule to the oxygen-evolving complex in Photosystem II. Biochemistry 42: 6209–6217

Hillier W and Babcock GT (2001) S-state dependent Fourier transform infrared difference spectra for the Photosystem II oxygen evolving complex. Biochemistry 40: 1503–1509

Hillier W and Wydrzynski T (2000) The affinities for the two substrate water binding sites in the O_2 evolving complex of Photosystem II vary independently during S-state turnover. Biochemistry 39: 4399–4405

Hillier W and Wydrzynski T (2001) Oxygen ligand exchange at metal sites: Implications for the O_2 evolving mechanism of Photosystem II. Biochim Biophys Acta 1503: 197–209

Hillier W and Wydrzynski T (2004) Aspects of Substrate Water Interactions within the Photosystem II Oxygen Evolving Complex. Phys Chem Chem Phys 6: 4882–4889

Hillier W, Messinger J and Wydrzynski T (1998) Kinetic determination of the fast exchanging substrate water molecule in the S_3 state of Photosystem II. Biochemistry 37: 16908–16914

Hillier W, Hendry G, Burnap RL and Wydrzynski T (2001) Substrate water exchange in Photosystem II depends on the peripheral proteins. J Biol Chem 276: 46917–46924

Hind G and Whittingham CP (1963) Reduction of ferricyanide by chloroplasts in the presence of nitrogenous bases. Biochim Biophys Acta 75: 194–202

Hind G, Nakatani HY and Izawa S (1969) The role of Cl^- in photosynthesis. The Cl^- requirement of electron transport. Biochim Biophys Acta 172: 277–289

Hoganson CW and Babcock GT (1997) A metalloradical mechanism for the generation of oxygen from water in photosynthesis. Science 277: 1953–1956

Hoganson CW, Lydakis-Simantiris N, Tang X-S, Tommos C, Warncke K, Babcock GT, Diner BA, McCracken J and Styring S (1995) A hydrogen-atom abstraction model for the function of Y_Z in photosynthetic oxygen evolution. Photosynth Res 46: 177–184

Hundelt M, Hays A-MA, Debus RJ and Junge W (1998) Oxygenic Photosystem II: The mutation D1-D61N in *Synechocystis sp.* PCC 6803 retards S-state transitions without affecting electron transfer from Y_Z to $P680^+$. Biochemistry 37: 14450–14456

Ioannidis N, Sarrou J, Schansker G and Petrouleas V (1998) NO reversibly reduces the water oxidizing complex of Photosystem II through S_0 and S_1 to the state characterized by the Mn(II)-Mn(III) multiline EPR signal. Biochemistry 37: 16445–16451

Ioannidis N, Nugent JHA and Petrouleas V (2002) Intermediates of the S_3 state of the oxygen evolving complex of Photosystem II. Biochemistry 41: 9589–9600

Iuzzolino L, Dittmer J, Dörner W, Meyer-Klaucke W and Dau H (1998) X-ray absorption spectroscopy on layered Photosystem II membrane particles suggests manganese centered oxidation of the oxygen evolving complex for the S_0-S_1, S_1-S_2, and S_2-S_3 transitions of the water oxidation cycle. Biochemistry 37: 17112–17119

Jeans C, Schilstra MJ and Klug DR (2002) The temperature dependence of $P680^+$ reduction in oxygen evolving photosystem. Biochemistry 41: 5015–5023

Joliot P, Barbieri G and Chabaud R (1969) Un nouveau modele des centres photochimiques du systém II. Photochem Photobiol 10: 309–329

Junge W, Haumann M, Ahlbrink R, Mulkidjanian A and Clausen J (2002) Electrostatics and proton transfer in photosynthetic water oxidation. Philos Trnas Roy Soc London B 357: 1407–1417

Jursinic P (1981) Investigation of double turnovers in Photosystem II charge separation and oxygen evolution with excitation flashes of different duration. Biochim Biophys Acta 635: 38–52

Jursinic PA and Dennenberg RJ (1990) Oxygen release time in leaf disks and thylakoids of peas and Photosystem II membrane fragments of spinach. Biochim Biophys Acta 1020: 195–206

Jursinic P and Govindjee (1977) Temperature dependence of delayed light emission in the 6 to 340 microsecond range after a single flash in chloroplasts. Photochem Photobiol 26: 617–628

Kamiya N and Shen J-R (2003) Crystal structure of oxygen-evolving Photosystem II from *Thermosynechococcus vulcanus* at 3.7 Å resolution. Proc Natl Acad Sci USA 100: 98–103

Karge M, Irrgang KD, Sellin S, Feinaugle R, Liu B, Eckert HJ, Eichler HJ and Renger G (1996) Effects of hydrogen deuterium exchange on photosynthetic water cleavage in PS II core complexes from spinach. FEBS Lett 378: 140–144

Karge M, Irrgang K-D and Renger G (1997) Analysis of the reaction coordinate of photosynthetic water oxidation by kinetic measurements of 355 nm absorption changes at different temperatures in Photosystem II preparations suspended in either H_2O or D_2O. Biochemistry 36: 8904–8913

Kebekus U, Messinger J and Renger G (1995) Structural changes in the water oxidizing complex monitored via the pH dependence of the reduction rate of redox state S_1 by hydrazine and hydroxylamine in isolated spinach thylakoids. Biochemistry 34: 6175–6182

Kelley PM and Izawa S (1978) The role of chloride ion in Photosystem II: Effects of chloride ion on Photosystem II electron transport and hydroxylamine inhibition. Biochim Biophys Acta 502: 198–210

Kimura Y and Ono TA (2001) Chelator induced disappearance of carboxylate stretching vibrational modes in S_2/S_1 FTIR spectrum in oxygen-evolving complex of Photosystem II. Biochemistry 40: 14061–14068

Klimov VV, Allakverdiev SI, Demeter S and Krasnovsky AA (1979) Photoreduction of pheophytin in Photosystem II of chloroplasts as a function of redox potential of the medium. Dokl Akad Nauk SSSR 249: 227–230

Koike H, Hanssum B, Inoue Y and Renger G (1987) Temperature dependence of the S-state transitions in a thermophilic cyanobacterium, *Synschococcus vulcanus* Copeland measured by absorption changes in the ultraviolet region. Biochim Biophys Acta 893: 524–533

Kok B and Velthuys BR (1976) Present status of the O_2 evolution model. In: Castellani A (ed) Research in Photobiology, pp 111–119. Plenum Press, New York

Kok B, Forbush B and McGloin M (1970) Cooperation of

charges in photosynthetic O_2 evolution. Photochem Photobiol 11: 457–476

Kretschmann H and Witt HT (1993) Chemical reduction of the water splitting enzyme system of photosynthesis and its light-induced reoxidation characterized by optical and mass spectrometric measurements: A basis for the estimation of the states of the redox active manganese and of water in the quaternary oxygen evolving S-state cycle. Biochim Biophys Acta 1144: 331–345

Kretschmann H, Pauly S and Witt HT (1991) Evidence for a chemical reaction of hydroxylamine with the photosynthetic water splitting enzyme S in the dark: Possible states of manganese and water in the S-cycle. Biochim Biophys Acta 1059: 208–214

Krieger A, Rutherford AW and Johnson GN (1995) On the determination of redox midpoint potential of the primary quinone electron acceptor Q_A in Photosystem II. Biochim Biophys Acta 1229: 193–201

Krishtalik LI (1986) Energetics of multielectron reactions. Photosynthetic oxygen evolution. Biochim Biophys Acta 849: 162–171

Krishtalik LI (1990) Activation energy of photosynthetic oxygen evolution: An attempt at theoretical analysis. Bioelectrochem Bioenerg 23: 249–263

Kuzek D and Pace RJ (2001) Probing the Mn oxidation states in the OEC. Insights from spectroscopic, computational and kinetic data. Biochim Biophys Acta 1503: 123–137

Latimer MJ, DeRose VJ, Yachandra VK, Sauer K and Klein MP (1998) Structural effects of calcium depletion on the manganese cluster of Photosystem II: Determination by X-ray absorption spectroscopy. J Phys Chem B 102: 8257–8265

Li ZL and Burnap RL (2001) Mutations of arginine 64 within the putative Ca^{2+} binding lumenal interhelical a-b loop of the Photosystem II D1 protein disrupt binding of the manganese stabilizing protein and cytochrome c_{550} in *Synechocystis sp* PCC6803. Biochemistry 40: 10350–10359

Liang W, Roelofs TA, Cinco RM, Rompel A, Latimer MJ, Yu WO, Sauer K, Klein MP and Yachandra VK (2000) Structural change of the Mn cluster during the S_2 to S_3 state transition of the oxygen evolving complex of Photosystem II. Does it reflect the onset of water/substrate oxidation? Determination by Mn x-ray absorption spectroscopy. J Am Chem Soc 122: 3399–3412

Limburg J, Vrettos JS, Liable-Sands LM, Rheingold AL, Crabtree RH and Brudvig GW (1999) A functional model for O–O bond formation by the O_2 evolving complex in Photosystem II. Science 283: 524–527

Lindberg K and Andréasson L-E (1996) A one-site, two-state model for the binding of anions in Photosystem II. Biochemistry 35: 14259–14267

Lindberg K, Wydrzynski T, Vänngård T and Andréasson L-E (1990) Slow release of chloride from ^{36}Cl-labeled Photosystem II membranes. FEBS Lett 264: 153–155

Lindberg K, Vänngård T and Andréasson L-E (1993) Studies of the slowly exchanging chloride in Photosystem II of higher plants. Photosynth Res 38: 401–408

Lydakis-Simantiris N, Ghanotakis DF and Babcock GT (1997) Kinetic isotope effects on the reduction of the Y_Z radical in oxygen evolving and Tris washed Photosystem II membranes by time resolved EPR. Biochim Biophys Acta 1322: 129–140

McEvoy JP and Brudvig GW (2004) Structure-based mechanism of photosynthetic water oxidation. Phys Chem Chem Phys 6: 4754–4763

McGrady JE and Stranger R (1999) Redox induced formation and cleavage of O–O σ and π bonds in a peroxo-bridged manganese dimer: a density functional study. Inorg Chem 38: 550–558

Messinger J (2000) Towards understanding the chemistry of photosynthetic oxygen evolution: Dynamic structural changes, redox states and substrate water binding of the Mn cluster in Photosystem II. Biochim Biophys Acta 1459: 481–488

Messinger J (2004) Evaluation of different mechanistic proposals for water oxidation in photosynthesis on the basis of Mn_4O_xCa structures for the catalytic site and spectroscopic data. Phys Chem Chem Phys 6: 4764 - 4771

Messinger J and Renger G (1994) Analysis of pH-induced modifications of the period four oscillation of the flash induced oxygen evolution reveal distinct structural changes of the Photosystem II donor side at characteristic pH values. Biochemistry 33: 10896–10905

Messinger J, Wacker U and Renger G (1991) Unusual low reactivity of the water oxidase in the redox state S_3 toward exogenous reductants. Analysis of the NH_2OH and NH_2NH_2 induced modifications of flash induced oxygen evolution in isolated spinach thylakoids. Biochemistry 30: 7852–7862

Messinger J, Schröder WP and Renger G (1993) Structure-function relations in Photosystem II. Effects of temperature and chaotropic agents on the period four oscillation of flash induced oxygen evolution. Biochemistry 32: 7658–7668

Messinger J, Badger M and Wydrzynski T (1995) Detection of *one* slowly exchanging substrate water molecule in the S_3 state of Photosystem II. Proc Natl Acad Sci USA 92: 3209–3213

Messinger J, Nugent JHA and Evans MCW (1997a) Detection of an EPR multiline signal for the S_0^* state in Photosystem II. Biochemistry 36: 11055–11060

Messinger J, Seaton G, Wydrzynski T, Wacker U and Renger G (1997b) S_{-3} state of the water oxidase in Photosystem II. Biochemistry 36: 6862–6873

Messinger J, Robblee JH, Yu WO, Sauer K, Yachandra VK and Klein MP (1997c) The S_0 state of the oxygen evolving complex in Photosystem II is paramagnetic: detection of an EPR multiline signal. J Am Chem Soc 119: 11349–11350

Messinger J, Robblee JH, Fernandez C, Cinco RM, Visser H, Bergmann U, Glatzel P, Cramer SP, Campbell KA, Peloquin JM, Britt RD, Sauer K, Klein MP and Yachandra VK (1998) Oxidation states and structure of the manganese cluster in the S_0 State of the oxygen evolving complex. In: Garab G (ed) Photosynthesis: Mechanisms and Effects, pp 1279–1282. Kluwer Academic Publishers, Dordrecht

Messinger J, Robblee J, Bergmann U, Fernandez C, Glatzel P, Isgandarova S, Hanssum B, Renger G, Cramer S, Sauer K and Yachandra V (2001a) Manganese oxidation states in Photosystem II. In: PS2001: Proceedings of the 12th International Congress on Photosynthesis, S10-019. CSIRO Publishing, Melbourne (CD-RO)

Messinger J, Robblee JH, Bergmann U, Fernandez C, Glatzel P, Visser H, Cinco RM, McFarlane KL, Bellacchio E, Pizarro SA, Cramer SP, Sauer K, Klein MP and Yachandra VK (2001b) Absence of Mn centered oxidation in the S_2 to S_3 transition: implications for the mechanism of photosynthetic water oxidation. J Am Chem Soc 123: 7804–7820

Metz JG, Nixon PJ, Rögner M, Brudvig GW and Diner BA (1989) Directed alteration of the D1 polypeptide of Photosystem II:

Evidence that tyrosine-161 is the redox component, Z, connecting the oxygen evolving complex to the primary electron donor, P680. Biochemistry 28: 6960–6969

Meunier PC and Popovic R (1991) The time for oxygen release in photosynthesis: Reconciliation of flash polarography with other measurement techniques. Photosynth Res 28: 33–39

Meyer B, Schlodder E, Dekker JP and Witt HT (1989) O_2 evolution and Chl *a* II^+ ($P680^+$) nanosecond reduction kinetics in single flashes as a function of pH. Biochim Biophys Acta 974: 36–43

Miyao M, Murata N, Lavorel J, Maisonpeteri B, Boussac A and Etienne AL (1987) Effect of the 33-kDa protein on the S-state transitions in photosynthetic oxygen evolution. Biochim Biophys Acta 890: 151–159

Noguchi T and Sugiura M (2000) Structure of an active water molecule in the water oxidizing complex of Photosystem II as studied by FTIR spectroscopy. Biochemistry 39: 10943–10949

Noguchi T and Sugiura M (2001) Flash induced Fourier transform infrared detection of the structural changes during the S-state cycle of the oxygen evolving complex in Photosystem II. Biochemistry 40: 1497–1502

Noguchi T and Sugiura M (2002a) Flash-induced FTIR difference spectra of the water oxidizing complex in moderately hydrated Photosystem II core films: Effect of hydration extent on S-state transitions. Biochemistry 41: 2322–2330

Noguchi T and Sugiura M (2002b) FTIR detection of water reactions during the flash-induced S-state cycle of the photosynthetic water oxidizing complex. Biochemistry 41: 15706–15712

Noguchi T, Ono T-A and Inoue Y (1995a) Direct detection of a carboxylate bridge between Mn and Ca^{2+} in the photosynthetic oxygen evolving center by means of Fourier transform infrared spectroscopy. Biochim Biophys Acta 1228: 189–200

Noguchi T, Ono T-A and Inoue Y (1995b) A carboxylate ligand interacting with water in the oxygen evolving center of Photosystem II as revealed by Fourier transform infrared spectroscopy. Biochim Biophys Acta 1232: 59–66

Nugent JHA, Demetriou C and Lockett CJ (1987) Electron donation in Photosystem II. Biochim Biophys Acta 894: 534–542

Nugent JHA, Rich AM and Evans MCW (2001) Photosynthetic water oxidation: Towards a mechanism. Biochim Biophys Acta 1503: 138–146

Nugent JHA, Muhiuddin IP and Evans MCW (2002) Electron transfer from the water oxidizing complex at cryogenic temperatures: The S_1 to S_2 step. Biochemistry 41: 4117–4126

Olesen K and Andréasson L-E (2003) The function of the chloride ion in photosynthetic oxygen evolution. Biochemistry 42: 2025–2035

Ono T-A (2001) Metallo-radical hypothesis for photoassembly of Mn_4 cluster of photosynthetic oxygen evolving complex. Biochim Biophys Acta 1503: 40–51

Ono T-A, Zimmermann J-L, Inoue Y and Rutherford AW (1986) EPR evidence for a modified S-state transition in chloride depleted Photosystem II. Biochim Biophys Acta 851: 193–201

Ono T-A, Noguchi T, Inoue Y, Kusunoki M, Yamaguchi H and Oyanagi H (1995) XANES spectroscopy for monitoring intermediate reaction states of Cl^- depleted Mn cluster in photosynthetic water oxidation enzyme. J Am Chem Soc 117: 6386–6387

Pace RJ, Smith P, Bramley R and Stehlik D (1991) EPR saturation and temperature dependence studies on signals from the oxygen evolving center of Photosystem II. Biochim Biophys Acta 1058: 161–170

Page CC, Moser CC, Chen XX and Dutton PL (1999) Natural engineering principles of electron tunnelling in biological oxidation-reduction. Nature 402: 47–52

Pecoraro VL (ed) (1992) Manganese Redox Enzymes. VCH Publishers, New York

Pecoraro VL, Baldwin MJ, Caudle MT, Hsieh W-Y and Law NA (1998) A proposal for water oxidation in Photosystem II. Pure Appl Chem 70: 925–929

Peloquin JM, Campbell KA, Randall DW, Evanchik MA, Pecoraro VL, Armstrong WH and Britt RD (2000) ^{55}Mn ENDOR of the S_2-State Multiline EPR Signal of Photosystem II: Implications on the Structure of the Tetranuclear Mn Cluster. J Am Chem Soc 122: 10926–10942

Penner-Hahn JE (1998) Structural characterization of the Mn site in the photosynthetic oxygen evolving complex. Struct Bond 90: 1–36

Putnam-Evans C, Burnap R, Wu J, Whitmarsh J and Bricker TM (1996) Site directed mutagenesis of the CP 47 protein of Photosystem II: Alteration of conserved charged residues in the domain ^{364}E-^{444}R. Biochemistry 35: 4046–4053

Qian M, Dao L, Debus RJ and Burnap RL (1999) Impact of mutations within the putative Ca^{2+}-binding lumenal Interhelical a-b loop of the Photosystem II D1 protein on the kinetics of photoactivation and H_2O oxidation in *Synechocystis sp.* PCC6803. Biochemistry 38: 6070–6081

Radmer R and Ollinger O (1983) Topography of the O_2 evolving site determined with water analogs. FEBS Letter 152: 39–43

Radmer R and Ollinger O (1986) Do the higher oxidation states of the photosynthetic O_2 evolving system contain bound water? FEBS Lett 195: 285–289

Rappaport F and Lavergne J (1991) Proton release during successive oxidation steps of the photosynthetic water oxidation process — Stoichiometries and pH-dependence. Biochemistry 30: 10004–10012

Rappaport F and Lavergne J (2001) Coupling of electron and proton transfer in the photosynthetic water oxidase. Biochim Biophys Acta 1503: 246–259

Rappaport F, Blanchard-Desce M and Lavergne J (1994) Kinetics of electron transfer and electrochromic change during the redox transitions of the photosynthetic oxygen evolving complex. Biochim Biophys Acta 1184: 178–192

Rappaport F, Guergova-Kuras M, Nixon PJ, Diner BA and Lavergne J (2002) Kinetics and pathways of charge recombination in Photosystem II. Biochemistry 41: 8518–8527

Rashid A and Homann PH (1992) Properties of iodide activated photosynthetic water oxidizing complexes. Biochim Biophys Acta 1101: 303–310

Razeghifard MR and Pace RJ (1999) EPR kinetic studies of oxygen release in thylakoids in PS II membranes: a kinetic intermediate in the S_3 to S_0 transition. Biochemistry 38: 1252–1257

Razeghifard MR, Klughammer C and Pace RJ (1997a) Electron paramagnetic resonance kinetic studies of the S states in spinach thylakoids. Biochemistry 36: 86–92

Razeghifard MR, Wydrzynski T, Pace RJ and Burnap RL (1997b) $Y_Z^{\bullet}$ reduction kinetics in the absence of the manganese stabilizing protein of Photosystem II. Biochemistry 36: 14474–14478

Renger G (1987) Mechanistic aspects of photosynthetic water cleavage. Photosynthetica 21: 203–224

Renger G (1997) Mechanistic and structural aspects of photosynthetic water oxidation. Physiol Plant 100: 828–841

Renger G (2001) Photosynthetic water oxidation to molecular oxygen: Apparatus and mechanism. Biochim Biophys Acta 1503: 210–228

Renger G (1999) Mechanism of photosynthetic water cleavage. In: Singhal GS, Renger G, Sopory SK, Irrgang K-D and Govindjee (eds) Concepts in Photobiology: Photosynthesis and Photomorphogenesis, pp 292–329. Narosa Publishing House, New Delhi, India

Renger G and Hanssum B (1988) Studies on the deconvolution of flash induced absorption changes into the difference spectra of individual redox steps within the water oxidizing enzyme system. Photosynth Res 16: 243–259

Renger G and Hanssum B (1992) Studies on the reaction coordinates of the water oxidase in PS II membrane fragments from spinach. FEBS Lett 299: 28–32

Renger G and Weiss W (1986) Functional and structural aspects of photosynthetic water oxidation. Biochem Soc Trans 14: 17–20

Renger G and Wolff C (1976) The existence of a high photochemical turnover rate at the reaction centers of system II in Tris-washed chloroplasts. Biochim Biophys Acta 423: 610–614

Renger G, Christen G, Karge M, Eckert H-J and Irrgang K-D (1998) Application of the Marcus theory for analysis of the temperature dependence of the reactions leading to photosynthetic water oxidation: results and implications. J Bioinorg Chem 3: 360–366

Rich PR (1996) Electron transfer complexes coupled to ion translocation. In: Bendall DS (ed) Protein Electron Transfer, pp 217–248. BIOS Scientific Publishers, Oxford

Richens DT (1997) The Chemistry of Aqua Ions. John Wiley & Sons, Chichester

Riggs PJ, Mei R, Yocum CF and Penner-Hahn JE (1992) Reduced derivatives of the manganese cluster in the photosynthetic oxygen evolving complex. J Am Chem Soc 114: 10650–10651

Riggs-Gelasco PJ, Mei R, Yocum CF and Penner-Hahn JE (1996) Reduced derivatives of the Mn cluster in the oxygen evolving complex of Photosystem II: an EXAFS study. J Am Chem Soc 118: 2387–2399

Robblee JH, Cinco RM and Yachandra VK (2001) X-ray spectroscopy based structure of the Mn cluster and mechanism of photosynthetic oxygen evolution. Biochim Biophys Acta 1503: 7–23

Robblee JH, Messinger J, Cinco RM, McFarlane KL, Fernandez C, Pizarro SA, Sauer K and Yachandra VK (2002) The Mn cluster in the S_0 state of the oxygen evolving complex of Photosystem II studied by EXAFS spectroscopy: Are there three di-μ-oxo-bridged Mn_2 moieties in the tetranuclear Mn complex? J Am Chem Soc 124: 7459–7471

Robinson HH and Crofts AR (1983) Kinetics of the oxidation reduction reactions of the Photosystem II quinone acceptor complex, and the pathway for deactivation. FEBS Lett 153: 221–226

Robinson HH, Sharp RR and Yocum CF (1981) On the origin of light induced changes in the proton magnetic relaxation rate of chloroplast thylakoid membrane suspensions. Arch Biochem Biophys 207: 1–8

Roelofs TA, Liang W, Latimer MJ, Cinco RM, Rompel A, Andrews JC, Sauer K, Yachandra VK and Klein MP (1996) Oxidation states of the manganese cluster during the flash-induced S-state cycle of the photosynthetic oxygen evolving complex. Proc Natl Acad Sci USA 93: 3335–3340

Rutherford AW and Inoue Y (1984) Oscillation of delayed luminescence from PS II: Recombination of $S_2Q_B^-$ and $S_3Q_B^-$. FEBS Lett 165: 163–170

Rutherford AW and Styring S (1987) EPR signal II in Photosystem II: Redox and paramagnetic interactions with the molecular oxygen evolving enzyme. Cytochrome Syst: Mol Biol Bioenerg, [Proc UNESCO Int Symp]: 541–547

Rutherford AW, Crofts AR and Inoue Y (1982) Thermoluminescence as a probe of Photosystem II photochemistry. The origin of the flash-induced glow peaks. Biochim Biophys Acta 682: 457–465

Sandusky PO and Yocum CF (1984) The chloride requirement for photosynthetic oxygen evolution: analysis of the effects of chloride and other anions on amine inhibition of the oxygen evolving complex. Biochim Biophys Acta 766: 603–611

Sandusky PO and Yocum CF (1986) The chloride requirement for photosynthetic oxygen evolution: Factors affecting nucleophilic displacement of chloride from the oxygen evolving complex. Biochim Biophys Acta 849: 85–93

Sarrou J, Ioannidis N, Deligiannakis Y and Petrouleas V (1998) A Mn(II)-Mn(III) EPR signal arises from the interaction of NO with the S_1 state of the water oxidizing complex of Photosystem II. Biochemistry 37: 3581–3587

Sarrou J, Isgandarova S, Kern J, Zouni A, Renger G, Lubitz W and Messinger J (2003) Nitric Oxide induced formation of the S_{-2} state in the oxygen evolving complex of Photosystem II from *Synechococcus elongatus*. Biochemistry 42: 1016–1023

Sauer K and Yachandra VK (2002) A possible evolutionary origin for the Mn_4 cluster of the photosynthetic water oxidation complex from natural MnO_2 precipitates in the early ocean. Proc Natl Acad Sci USA 99: 8631–8636

Saygin O and Witt HT (1985) Sequence of the redox changes of manganese and pattern of the changes of charges during water cleavage in photosynthesis. Optical events in the UV and the red region in the presence and absence of hydroxylamine. Photobiochem Photobiophys 10: 71–82

Schansker G, Goussias C, Petrouleas V and Rutherford AW (2002) Reduction of the Mn cluster of the water oxidizing enzyme by nitric oxide: formation of an S_{-2} state. Biochemistry 41: 3057–3064

Schilstra MJ, Rappaport F, Nugent JHA, Barnett CJ and Klug DR (1998) Proton/hydrogen transfer affects the S-state dependent microsecond phases of $P680^+$ reduction during water splitting. Biochemistry 37: 3974–3981

Schlodder E and Witt HT (1999) Stoichiometry of proton release from the catalytic center in photosynthetic water oxidation. J Biol Chem 274: 30387–30392

Seidler A (1996) The extrinsic polypeptides of Photosystem II. Biochim Biophys Acta 1277: 35–60

Sharp PR (1992) Proton NMR relaxation due to photosynthetic oxygen evolving center. In: Pecoraro VL (ed) Manganese Redox Enzymes, pp 177–196. VCH Publishers, New York

Shen J-R, Ikeuchi M and Inoue Y (1992) Stoichiometric association of extrinsic cytochrome c_{550} and 12 kDa protein with a highly purified oxygen evolving Photosystem II core complex from *Synechococcus vulcanus*. FEBS Lett 301: 145–149

Shi LX and Schroder WP (2004) The low molecular mass subunits of the photosynthetic supracomplex, Photosystem II. Biochim Biophys Acta 1608: 75–96

Shinkarev VP (1996) Binary oscillations in the Kok model of oxygen evolution in oxygenic photosynthesis. Photosynth

Res 48: 411–417
Shinkarev V and Wraight CA (1993) Oxygen evolution in photosynthesis: From unicycle to bicycle. Proc Natl Acad Sci USA 90: 1834–1838
Siegbahn PEM (2000) Theoretical models for the oxygen radical mechanism of water oxidation and the water oxidizing complex of Photosystem II. Inorg Chem 39: 2923–2935
Siegbahn PEM and Crabtree RH (1999) Manganese oxyl radical intermediates and O-O bond formation in photosynthetic oxygen evolution and a proposed role for the calcium cofactor in Photosystem II. J Am Chem Soc 121: 117–127
Sigel A and Sigel H (2000) Manganese and Its Role in Biological Processes. Marcel Dekker, Inc, New York
Sinclair J and Arnason T (1974) Studies on a thermal reaction associated with photosynthetic oxygen evolution. Biochim Biophys Acta 368: 393–400
Sivaraja M, Hunziker D and Dismukes GC (1988) The reaction of hydrogen sulfide with the photosynthetic water oxidizing complex and its lack of reaction with the primary electron acceptor in spinach. Biochim Biophys Acta 936: 228–235
Strzalka K, Walczak T, Sarna T and Swartz HM (1990) Measurement of time-resolved oxygen concentration changes in photosynthetic systems by nitroxide-based EPR oximetry. Arch Biochem Biophys 281: 312–318
Styring S and Rutherford AW (1987) In the oxygen evolving complex of Photosystem II the S_0 state is oxidized to the S_1 state by Y_D^+ (Signal II_{slow}). Biochemistry 26: 2401–2405
Styring S and Rutherford AW (1988) Deactivation kinetics and temperature dependence of the S-state transitions in the oxygen evolving system of Photosystem II measured by EPR spectroscopy. Biochim Biophys Acta 933: 378–387
Tamura N and Cheniae G (1987) Photoactivation of the water-oxidizing complex in Photosystem II membranes depleted of Mn and extrinsic proteins. I. Biochemical and kinetic characterization. Biochim Biophys Acta 890: 179–194
Tamura N, Inoue Y and Cheniae GM (1989) Photoactivation of the water oxidizing complex in Photosystem II membranes depleted of Mn, Ca and extrinsic proteins. II. Studies on the functions of Ca^{2+}. Biochim Biophys Acta 976: 173–181
Tang XS, Zheng M, Chisholm DA, Dismukes GC and Diner BA (1996) Investigation of the differences in the local protein environments surrounding tyrosine radicals $Y_Z^{\bullet}$ and $Y_D^{\bullet}$ in Photosystem II using wild type and the D2-Tyr160Phe mutant of *Synechocystis* 6803. Biochemistry 35: 1475–1484
Tommos C (2002) Electron, proton and hydrogen-atom transfers in photosynthetic water oxidation. Philos Trans Roy Soc London B 357: 1383–1394
Tommos C and Babcock GT (1998) Oxygen production in nature: A light-driven metalloradical enzyme process. Acc Chem Res 31: 18–25
Tommos C and Babcock GT (2000) Proton and hydrogen currents in photosynthetic water oxidation. Biochim Biophys Acta 1458: 199–219
Tommos C, Tang XS, Warncke K, Hoganson CW, Styring S, McCracken J, Diner BA and Babcock GT (1995) Spin-density distribution, conformation, and hydrogen bonding of the redox active tyrosine Y_Z in Photosystem II from multiple electron magnetic resonance spectroscopies: implications for photosynthetic oxygen evolution. J Am Chem Soc 117: 10325–10335
Tommos C, Hoganson CW, Di Valentin M, Lydakis-Simantiris N, Dorlet P, Westphal K, Chu H-A, McCracken J and Babcock GT (1998) Manganese and tyrosyl radical function in photosynthetic oxygen evolution. Curr Op Chem Biol 2: 244–252
van Gorkom HJ and Gast P (1996) Measurement of photosynthetic oxygen evolution. In: Amesz J and Hoff AJ (eds) Biophysical Techniques in Photosynthesis, pp 391–405. Kluwer Academic Publishers, Dordrecht
van Leeuwen PJ, Heimann C and van Gorkom HJ (1993) Absorbance difference spectra of the S-state transitions in Photosystem II core particles. Photosynth Res 38: 323–330
van Rensen JJS, Xu C and Govindjee (1999) Role of bicarbonate in Photosystem II, the water-plastoquinone oxido-reductase of plant photosynthesis. Physiol Plant 105: 585–592
van Vliet P and Rutherford AW (1996) Properties of the chloride depleted oxygen evolving complex of Photosystem II studied by electron paramagnetic resonance. Biochemistry 35: 1829–1839
van Vliet P, Boussac A and Rutherford AW (1994) Chloride depletion effects in the calcium deficient oxygen evolving complex of Photosystem II. Biochemistry 33: 12998–13004
Vass I and Styring S (1991) pH dependent charge equilibria between tyrosine-D and the S-states in Photosystem II. Estimation of relative midpoint potentials. Biochemistry 30: 830–839
Vass I, Deak Z and Hideg E (1990) Charge equilibrium between the water oxidizing complex and the electron donor tyrosine D in Photosystem II. Biochim Biophys Acta 1017: 63–69
Velthuys B and Kok B (1978) Photosynthetic oxygen evolution from hydrogen peroxide. Biochim Biophys Acta 502: 211–221
Vermaas WEJ, Renger G and Dohnt G (1984) The reduction of the oxygen evolving system in chloroplasts by thylakoid components. Biochim Biophys Acta 764: 194–202
Vermaas WFJ, Rutherford AW and Hansson O (1988) Site directed mutagenesis in Photosystem II of the cyanobacterium *Synechocystis sp.* PCC 6803: Donor D is a tyrosine residue in the D2 protein. Proc Natl Acad Sci USA 85: 8477–8481
Visser H, Anxolabéhère-Mallart E, Bergmann U, Glatzel P, Robblee JH, Cramer SP, Girerd J-J, Sauer K, Klein MP and Yachandra VK (2001) Mn K-edge XANES and Kβ XES studies of two Mn-Oxo Binuclear complexes: Investigation of three different oxidation states relevant to the oxygen-evolving complex of Photosystem II. J Am Chem Soc 123: 7031–7039
Volkov AG (1989) Oxygen evolution in the course of photosynthesis: Molecular mechanisms. Bioelectrochem Bioenerg 21: 3–24
Vos MH, van Gorkom HJ and van Leeuwen PJ (1991) An electroluminescence study of stabilization reactions in the oxygen evolving complex of Photosystem II. Biochim Biophys Acta 1056: 27–39
Vrettos JS, Limburg J and Brudvig GW (2001a) Mechanism of photosynthetic water oxidation: Combining biophysical studies of Photosystem II with inorganic model chemistry. Biochim Biophys Acta 1503: 229–245
Vrettos JS, Stone DA and Brudvig GW (2001b) Quantifying the ion selectivity of the Ca^{2+} site in Photosystem II: evidence for direct involvement of Ca^{2+} in O_2 formation. Biochemistry 40: 7937–7945
Weng TC, Hsieh WY, Uffelman ES, Gordon-Wylie SW, Collins TJ, Pecoraro VL and Penner-Hahn JE (2004) XANES evidence against a manganyl species in the S_3 state of the oxygen-evolving complex. J Am Chem Soc 126: 8070–8071
Westphal KL, Lydakis-Simantiris N, Cukier RI and Babcock GT

(2000) Effects of Sr^{2+} substitution on the reduction rates of $Y_Z^{\bullet}$ in PS II membranes: Evidence for concerted hydrogen atom transfer in oxygen evolution. Biochemistry 39: 16220–16229

Wieghardt K (1989) The active sites in manganese containing metalloproteins and inorganic model complexes. Angew Chem Int Ed Engl 28: 1153–1172

Wincencjusz H, Yocum CF and van Gorkom HJ (1998) S-state dependence of chloride binding affinities and exchange dynamics in the intact and polypeptide-depleted O_2 evolving complex of Photosystem II. Biochemistry 37: 8595–8604

Wincencjusz H, Yocum CF and van Gorkom HJ (1999) Activating anions that replace Cl^- in the O_2 evolving complex of Photosystem II slow the kinetics of the terminal step in water oxidation and destabilize the S_2 and S_3 states. Biochemistry 38: 3719–3725

Witt HT (1996) Primary reactions of oxygenic photosynthesis. Ber Bunsenges Phys Chem 100: 1923–1942

Wydrzynski T and Renger G (1986) On the interpretation of the NMR water-proton relaxivity of photosynthetic membrane samples: Ramifications in the use of EDTA. Biochim Biophys Acta 851: 65–74

Wydrzynski T, Zumbulyadis N, Schmidt PG, Gutowsky HS and Govindjee (1976) Proton relaxation and charge accumulation during oxygen evolution in photosynthesis. Proc Natl Acad Sci USA 73: 1196–1198.

Wydrzynski T, Hillier W and Messinger J (1996) On the functional significance of substrate accessibility in the photosynthetic water oxidation mechanism. Physiol Plant 96: 342–350

Yachandra VK (2002) Structure of the manganese complex in Photosystem II: Insights from X-ray spectroscopy. Philos T Roy Soc B 357: 1347–1358

Yachandra VK, DeRose VJ, Latimer MJ, Mukerji I, Sauer K and Klein MP (1993) Where plants make oxygen: A structural model for the photosynthetic oxygen evolving manganese cluster. Science 260: 675–679

Yachandra VK, Sauer K and Klein MP (1996) Manganese cluster in photosynthesis: Where plants oxidize water to dioxygen. Chem Rev 96: 2927–2950

Yamanari T, Kimura Y, Mizusawa N, Ishii A and Ono T-A (2004) Mid- to low-frequency Fourier transform infrared spectra of the S-state cycle for photosynthetic water oxidation in *Synechocystis* sp. PCC 6803. Biochemistry 43: 7479–7490

Yocum CF (1992) The calcium and chloride requirements for photosynthetic water oxidation. In: Pecoraro VL (ed) Manganese Redox Enzymes, pp 71–84. VCH Publishers, New York

Zheng M and Dismukes GC (1996) Orbital configuration of the valence electrons, ligand field symmetry, and manganese oxidation states of the photosynthetic water oxidizing complex: Analysis of the S_2 state multiline EPR signals. Inorg Chem 35: 3307–3319

Zheng M, Khangulov SV, Dismukes GC and Barynin VV (1994) Electronic structure of dimanganese(II,III) and dimanganese(III,IV) complexes and dimanganese catalase enzyme: A general EPR spectral simulation approach. Inorg Chem 33: 382–387

Zimmermann J-L and Rutherford AW (1986) Electron paramagnetic resonance properties of the S_2 state of the oxygen-evolving complex of Photosystem II. Biochemistry 25: 4609–4615

Zouni A, Witt HT, Kern J, Fromme P, Krauß N, Saenger W and Orth P (2001) Crystal Structure of Photosystem II from *Synechococcus elongatus* at 3.8 Å resolution. Nature 409: 739–743

Chapter 26

Photo-Assembly of the Catalytic Manganese Cluster

G. Charles Dismukes*[1,2] and Gennady M. Ananyev[1]
[1]Department of Chemistry and [2]Princeton Environmental Institute, Princeton University, Princeton, NJ 08544, U.S.A.

Richard Watt
Department of Chemistry, University of New Mexico, Albuquerque, NM 87131, U.S.A.

*Author for correspondence, email: dismukes@princeton.edu

T. Wydrzynski and K. Satoh (eds): Photosystem II: The Light-Driven Water:Plastoquinone Oxidoreductase, pp. 609–626.

Summary

The biogenesis of the Photosystem II (PS II) water oxidizing complex is reviewed with emphasis on the sequence and location of assembly of the subunits within the internal membrane systems of prokaryotes and chloroplasts. The uptake and distribution of manganese in cyanobacterial cells are discussed. The role of individual subunits in isolated PS II in light-induced assembly of the inorganic core of the water splitting complex is discussed (photoactivation process). The roles of the inorganic cofactors (Mn^{2+}, Ca^{2+}, Cl^- and bicarbonate) in water splitting are revealed by examining the effects of their reconstitution with non-native cofactors. Novel instrumentation for the measurement of O_2 concentration and the kinetics and mechanism of photoactivation are described.

I. Introduction

The photosynthetic water oxidizing comlex (WOC) located within Photosystem II (PS II) reaction center is responsible for nearly all biological O_2 production on Earth. It is remarkable in that, despite enormous diversification of the classes of oxygenic photoautotrophs, there is but one type of enzymatic core that performs this chemistry (Chapter 30, Dismukes and Blankenship**)**. The active site is a unique manganocalcium cluster comprised of five constituents plus water, $Mn_4Ca_1Cl_x(OH_n)_y(HCO_3)_z$, that is assembled *de novo* from elementary ions, water and bicarbonate by a light-driven photoassembly process within the cofactor-free apo-WOC-PS II complex. This process is called photoactivation, after the defining works of George Cheniae and coworkers (Frasch adn Sayre, 2001)

This chapter covers recent advances dealing with the uptake, distribution, photoassembly and function of the inorganic cofactors comprising the WOC-PS II from cyanobacteria and higher plants. It covers aspects of Mn transport, localization and photoassembly, both in vivo during biogenesis/repair and in vitro during reconstitution of the isolated WOC-PS II. This material examines processes from the cellular level down to the atomic level.

II. Function of Photosystem II Subunits in Water Splitting and Photo-Assembly

A summary of the subunit positioning derived from X-ray diffraction (XRD) analysis can be found in Chapters 19–21. Information derived from XRD is not considered in this review. We begin with an overview of the composition of the intact PS II protein complex and the associated inorganic core of the WOC.

A. The Photosystem II Core Complex

The detergent-solubilized isolated PS II protein core complex from the thermophillic cyanobacterium *Thermosynechococcus elongatus* is composed of 19 polypeptide subunits (Zouni et al., 2001; Ferreira et al., 2004), while 19 or more subunits are present in higher plants like spinach (Hankamer et al., 2001). However, these numbers may be underestimates of the composition in the native membrane based on more sensitive studies using mass spectrometry and amino (N)-terminal amino acid sequencing methods that have identified 31 unique subunits within an isolated PS II core complex from the cyanobacterium *Synechocystis* sp. PCC 6803 (Kashino et al., 2002) This large increase in the number of subunits within the PS II core complex may reflect both species differences and improvements in purification afforded by polyhistidine tagging of the CP47 subunit. The native PS II complex exists as a dimer with two-fold symmetry comprised of two sets of reaction centers and antenna complexes that operate more or less independently in terms of redox chemistry, but do exchange excitation energy. No reports have indicated any difference in the properties of the WOC in monomers and dimers, although PS II heterogeneity in the thermal activation parameters associated with water splitting is known (Burda et al., 2001)

The D1 (*psbA* gene product) and D2 (*psbD* gene product) proteins are homologous and form a heterodimeric reaction center (RC) within each monomeric unit. However, the smallest isolated RC complex that performs primary charge separation also contains the two subunits of cytochrome b_{559} (Cyt b_{559}), α (*psbE*

Abbreviations: CA – carbonic anhydrase; Chl – chlorophyll; EPR – electron paramagnetic resonance; MSP – manganese-stabilizing protein; RC – reaction center; WOC – water oxidizing complex; XAS – X-ray absorption spectroscopy; XRD – X-ray diffraction

gene product) and β (*psbF* gene product) (Nanba and Satoh, 1987; Seibert 1993). The D1, D2, CP47, CP43 and Cyt b_{559} subunits comprise what is called the PS II core, as no complex without these five subunits has been isolated that evolved O_2 (a number of small subunits that lack cofactors are also generally present in cores). A stable CP47RC subcore complex assembles within the thylakoid membrane of cyanobacteria in the deletion mutant lacking the *psbC* gene for CP43 (Rögner et al., 1991). These complexes can be isolated and are active in electron transport but inactive in O_2 evolution, presumably due to an incomplete Mn cluster. A stable CP47RC subcore complex has been prepared from spinach by removal of CP43 with detergents. Although the CP47RC subcore is devoid of Mn and inactive in O_2 evolution, it is capable of full activity after reconstitution of the Mn cluster by photoactivation in the presence of the free inorganic cofactors (Büchel et al., 1999) The successful reconstitution of the CP47RC subcore together with the subunit positioning data and XRD of the Mn binding site (see below) suggest that a RC subcore lacking CP47, might also be capable of O_2 evolution. However, to date no stable subcore complex lacking CP47 has been isolated to test this hypothesis.

The Mn-cluster is surrounded primarily by the lumenal surface of the D1 trans-membrane protein of the PS II reaction center, as predicted by previous mutational studies (Debus, 2001; Diner, 2001; Chapter 11, Debus) and model building (Svensson et al., 1996). Nixon et al. (1992) showed that Asp170 plays a critical role in the binding and oxidation of the first Mn^{2+} required for the formation of the Mn cluster. Further spectroscopic analysis confirmed that deletion of Asp170 significantly alters the EPR signal of the first photooxidized Mn^{3+} bound to PS II (Campbell et al., 2000). Chemical modification studies also confirmed that Asp170 is required for the binding of Mn^{2+} at the high affinity site and that D1-His337 may play a role in ligating the Mn cluster (Ghirardi et al., 1998).

The Y_D radical has been found to advance the lowest S-state of the Mn cluster from $S_0 \rightarrow S_1$ in the dark, while in its reduced form it shortens the lifetime of the S_2 and S_3 states (Babcock et al., 1975; Styring et al., 1987; Vass et al., 1991; Chapter 9, Diner and Britt). On this basis the Y_D radical was proposed to function in vivo to stabilize the Mn cluster against over-reduction and thus possible loss of reduced Mn^{2+} (Rova et al., 1998).

B. Extrinsic Proteins

In plants three water-soluble extrinsic proteins are attached non-covalently to the lumenal surface of the PS II complex. Their associated genes and molecular masses are used to identify these proteins as the 33 kDa (*psbO* gene product), 23 kDa (*psbP* gene product) and 19 kDa (*psbQ* gene product) (Debus, 1992, 2000; Chapter 5, Bricker and Burnap). The 33 kDa protein binds first at the interface of the D1/D2 dimer and the 23 kDa protein binding adjacent to the 33 kDa protein near to the CP43 protein with the 19 kDa protein binding last (Nield et al., 2002) The PsbO protein is found universally in all oxygenic photoautotrophs. The PsbP and PsbQ proteins were until recently not believed to be present in PS II core complexes from cyanobacteria and the role of these proteins appears to be substituted by the cytochrome c_{550} (*psbV* gene product) and to a lesser extent a 12 kDa protein (*psbU* gene product) (Shen et al., 1995a,b, 1998; Ohta et al., 1999; Katoh et al., 2001; Vrettos et al., 2001a). However, recently a smaller protein of 11 kDa with high homology to the *psbQ* gene product was found in a PS II core complex isolated from *Synechocystis,* suggesting a wider distribution than previously thought (Kashino et al., 2002; Chapters 5, Bricker and Burnap, and 6, Thronton et al.).

1. The Manganese Stabilizing Protein

The PsbO protein is also called the manganese stabilizing protein (MSP) because removal of this protein exposes the Mn cluster to exogenous reductants and competition for replacement of manganese by other metal ions. In vitro photoassembly of spinach apo-WOC-PS II is slowed by the binding of this protein. This protein is unfolded in solution and only assumes a folded structure when bound to the intrinsic proteins of PS II (Lydakis-Simantiris et al., 1999). The isolated spinach MSP was found not to bind Mn^{2+} or Ca^{2+} ions in solution based on low affinity (dissociation constant K_D ~3 mM) and low stoichiometry (0.14 Mn/MSP) (Hunziker et al., 1987). The MSP binds to PS II somewhat more tightly when the Mn cluster is present (Miyao et al., 1989; Kavelaki et al., 1991; Leuschner et al., 1996). Changes in the oxidation state of the Mn cluster in the PS II core complex alter the structure of the MSP making it susceptible to proteolysis (Hong et al., 2001). PS II does not require the MSP for O_2 evolution in vitro (Bricker, 1992) nor in vivo (Burnap et al., 1991), but in its absence, the

steady-state O_2 evolution rates are decreased (Miyao et al., 1987; Burnap et al., 1992). This decrease is attributed to deactivation of the Mn-cluster by endogenous reductants in the lumen. A deletion mutant of the MSP reveals that it acts as a diffusion barrier in vivo by suppressing electron donation from Mn^{2+} and decreasing the quantum yield of photoactivation in whole cells (Chu et al., 1994; Burnap et al., 1996). When reductants are added to PS II membranes in the presence of Ca^{2+} with the MSP, the Mn^{2+} ions are trapped and do not diffuse away, indicating they are trapped in a compartment for later photooxidation and reassembly of the Mn cluster (Mei et al., 1992; Riggs-Gelasco et al., 1996). The removal of the MSP results in the release of two Mn^{2+} ions from PS II membranes unless high concentrations of Cl^- and Ca^{2+} are used (Miyao et al., 1984; Ono et al., 1984). In the absence of the MSP, the $S_3 \rightarrow (S_4) \rightarrow S_0$ transition is slowed 5-fold (Miyao et al., 1987; Vass et al., 1987; Burnap et al., 1992), the S_2 state is abnormally stable against dark decay to S_1, the reduction kinetics of $Y_Z^{\bullet}$ are altered (Razeghifard et al., 1997), the substrate water exchange rates are slightly decreased (Hillier et al., 2001) and the susceptibility to photo-oxidative damage increases (Mayes et al., 1991; Philbrick et al., 1991).

PS II appears to possess its own mechanism and biochemical machinery for regulating the bicarbonate concentration within the lumenal space near the WOC. A low level of carbonic anhydrase (CA) activity has been found to be intrinsic to oxygen-evolving PS II membranes (Lu et al., 2002). Careful analysis showed that after washing the membranes with 1 M $CaCl_2$ to remove the extrinsic polypeptides, the CA activity could be found in both fractions, an intrinsic CA associated with the membranes that functions in the hydration direction and an extrinsic CA in the soluble fraction that functions in the dehydration direction. The soluble CA activity was found associated with a 33 kDa protein that comigrated with the 33-MSP extrinsic protein of PS II (PsbO). The authors proposed, and later confirmed that these are the same protein and have demonstrated that the 33 kDa protein of PS II possesses very low level CA activity (~ 60 s^{-1} vs. 10^5 s^{-1} of typical Zn^{2+}-CA) that is dependent on the concentration of Mn^{2+} and Cl^- (A. J. Stemler, personal communication). The latter results are at variance with earlier work showing that neither Mn^{2+} nor Ca^{2+} have specific binding sites on the spinach 33-MSP when studied as a free protein (Hunziker et al., 1987). The discrepancy may be resolved if the Mn-dependent CA activity represents non-specifically associated Mn^{2+} arising from electrostatic attraction. These results are provocative and should be tested further to judge whether this CA activity is found in vivo and how it may be linked, if at all, to the possible function of bicarbonate as an alternate substrate for O_2 evolution.

In cyanobacterial cells MSP binding to the PS II complex is weakened by genetic mutations to the lumenal E-loop of CP47 which introduce anionic residues (carboxylates) for positive residues (arginines). These same mutants also support the highest quantum yields for photoactivation of O_2 evolution. The data point to two consequences of the lumenal surface charges on the E-loop of CP47. In wild type, two arginine groups of the E-loop of CP47 help to maintain tight MSP binding which blocks achieving a high quantum yield of photoactivation (presumably under Mn-limiting conditions), while the anionic mutants bind less MSP and exhibit the highest yields of photoactivation. The latter result is consistent with photoactivation studies showing that absorption of anionic molecules (tetraphenylboron) but not cationic molecules (tetraphenylphosphonium) into isolated PS II membranes accelerates the rate and increases the quantum yield of photoactivation under conditions of low Mn^{2+} concentrations (Ananyev et al., 1996, 2001). Thus, surface-bound anionic groups in PS II, both native and exogenous in origin, are able to attract/steer Mn^{2+} ions from solution closer to the PS II complex. This role of surface anionic residues at the PS II protein/aqueous interface is analogous to that played by the surface carboxylates in cation transporter proteins (Sansom et al., 2000) This function should not be confused with catalytic residues involved in the direct coordination of Mn in the native complex (Ishikawa et al., 2002).

2. Other Extrinsic Proteins

The 23 kDa protein (*psbP* gene product) has been implicated in increasing the affinity for Ca^{2+} to the WOC, while the 19 kDa protein (*psbQ* gene product) enhances the Cl^- binding affinity (Yocum, 1991). As with the 33 kDa protein, when all 3 extrinsic proteins are bound, they form a diffusion barrier that keeps the intrinsic Mn^{2+}, Ca^{2+} and Cl^- ions sequestered so that the manganese cluster can be reassembled rapidly upon illumination (Adelroth et al., 1995; Wincencjusz et al., 1998). In the absence of the 23- and 19-kDa proteins, O_2 evolution requires higher concentrations

of Ca^{2+} and Cl^- ions, indicating these proteins mediate tighter binding of these ions.

C. Small Subunits

There are several other intrinsic proteins found in the PS II protein complex; however, their role in the photo-activation process is not yet clear. PsbI (*psbI* gene product), 4.2 kDa, $PsbT_c$ (*psbT*$_c$ gene product), 3.8 kDa, PsbW (*psbW* gene product) and 5.9 kDa are intimately associated with the D1/D2 dimer (Debus, 2000). The PsbL (*psbL* gene product), 4.3 kDa, and PsbK (*psbK* gene product), 4.3 kDa, proteins are also found with D1/D2. PsbL appears to aid in electron transfer ($Y_zP680^+ \rightarrow Y_z^+P680$)(Hoshida et al., 1997a,b), while both have been implicated in plastoquinone binding and are hypothesized to be positioned to play a role in forming dimeric core units composed of two D1/D2 dimers (Zheleva et al., 1998).

D. $[Mn]_4$ Core

The composition and structure of the inorganic core of the intact PS II-WOC has been examined by a number of techniques in higher plants and cyanobacteria (primarily *Synechocystis* and *Thermosynechococcus*). There is emerging consensus that the stoichiometry is $Mn_4Ca_1(OH_n)_xCl_y$ with as few as 1–2 high affinity chlorides in spinach (Debus, 1992; Ananyev et al., 2001; Vrettos et al., 2001b; Carrell et al., 2002). The number of tightly bound non-exchangeable $O^{2-}/OH^-/OH_2$ molecules has not been directly established and the proton ionization state depends on oxidation state.

E. The Calcium Effector Site

Calcium is essential for water oxidation in the native enzyme and can be functionally replaced by Sr^{2+} (Boussac et al., 1988). EPR reveals that removal of Ca^{2+} from the holoenzyme changes the distribution of unpaired spin density among the four Mn ions. Inhibition by lanthanides reveals that the affinity for the Ca site in the holoenzyme increases with charge density (Ono, 2000; Vrettos et al., 2001b). However, this finding differs from photoactivation studies showing that Sr^{2+}, a lower charge density ion, binds eight-fold tighter to the Ca effector site in PS II membranes depleted of the three extrinsic subunits (Ananyev et al., 2001). EPR reveals that Ca^{2+} binding to apo-WOC-PS II selectively templates the folding of the protein complex into a form that exhibits higher affinity for Mn^{2+} and binds two Mn^{2+} ions as a dimanganese(II,II) binuclear site (Ananyev et al., 1997). Strontium XAS of Ca-depleted/Sr-reconstituted PS II indicates a close positioning (~3.5 Å) between Sr and Mn (Cinco et al., 1998). Calcium XAS of Ca-sufficient PS II also suggests a heavy atom scatter in the second shell (Cinco et al., 2002). These and other data indicate that Ca^{2+} directly participates in the catalysis of water splitting as an integral cofactor. The reader is referred to Chapters 13 (van Gorkom and Yocum) and 14 (van Rensen and Klimov) on the roles of Cl^-, Ca^{2+} and bicarbonate in the holoenzyme.

III. Biogenesis of the Water Oxidizing Complex

A. Subunit Assembly

1. Prokaryotes

The site of oxygenic photosynthesis in cyanobacteria, green algae and chloroplasts is the specialized inner membrane called the thylakoid. Photoactivation of the inorganic cofactors of the WOC occurs within PS II complexes bound to the thylakoid membrane (Cheniae et al., 1971). Biochemical and electron micrographic studies of green algae and chloroplasts indicates that the chloroplast envelope is the major biogenic structure from which thylakoid membranes emerge (Hoober et al., 1994). This function also holds true for cyanobacteria. Analogous to other gram-negative bacteria, cyanobacteria have an envelope barrier consisting of an outer membrane, a peptidoglycan layer and an inner (plasma) membrane, which are physically and functionally distinct from the thylakoid membrane (Gantt, 1994). The two membrane systems exchange components via vesicle transport. The localization of photosystem proteins in cyanobacterial cells and chloroplasts has been studied by fractionation methods. Thylakoid and plasma membranes have been purified from *Anacystis nidulans* (Smith et al., 1993). A number of polypeptides from both photosystems were found in both membranes. In particular, the D1 and extrinsic 33 kDa proteins were localized in both membranes, but the latter formed functional complexes only in the thylakoid membrane. Both CP43 and CP47 were confined to the

thylakoid membrane. Two-dimensional fractionation methods combined with immunoblotting analysis has demonstrated that the purified plasma membrane from *Synechocystis* contains a number of protein components closely associated with the reaction centers of both photosystems (Zak et al., 2001). Localization of a functional PSI reaction center capable of primary charge separation was found, but not a functional PS II reaction center. However, evidence for localization of D1, D2 and Cyt b_{559} subunits in the plasma membrane was established, but not CP43 or CP47. The absence of CP47 and CP43 indicates that assembly of a functioning WOC is highly unlikely in the plasma membrane, based on observations that PS II subcomplexes from which both CP43 and CP47 have been dissociated do not assemble a functional inorganic core during photoactivation (Büchel et al., 1999).

The newly synthesized D1 protein contains an extension of the carboxyl (C) terminus that is cleaved by a protease in the mature PS II. The D1 C-terminal extension was shown not to be required for assembly of functional PS II complexes, nor for growth under optimal conditions in both *Synechocystis* (Nixon et al., 1992) and *Chlamydomonas reinhardtii* (Lers et al., 1992) However, the C-terminal extension must be cleaved beyond Ala344 by the soluble protease, called ctpA, prior to assembly of an active inorganic core (Nixon et al., 1992; Trost et al., 1997). In *Synechocystis* cultures which lack the C-terminal extension or have a genetically engineered two-fold longer extension no difference in growth rates or O_2 evolution rates versus wild type were detected (Ivleva et al., 2000). Thus, following cleavage, the C-terminal extension is not involved in the assembly of an active WOC. Nonetheless, the C-terminal extension in wild type does provide a selective advantage, albeit for reason that remain unclear. The timing and location of D1 processing in relation to the sequence of PS II biogenesis has been explored, although much remains to be understood (Zhang et al., 2000). Translation elongation of newly synthesized D1 is tightly regulated, as it occurs in vivo only if proper insertion into the thylakoid membrane pre-exists and a transmembrane potential is required. However, co- and post-translational assembly steps of D1 into PS II RC and core complexes occur without requirement for photosynthetic electron transfer or *trans*-thylakoid proton gradient.

In summary (Table 1), assembly of PS II subunits in prokaryotes begins in the plasma membrane where the components of the RC and the 33 kDa extrinsic subunit are found in a non-functional state. Final assembly, addition of the two inner antenna subunits of the PS II core complex, uptake of the inorganic cofactors and binding of a functional extrinsic 33 kDa protein all occur outside of the plasma membrane in the thylakoid system.

2. Chloroplasts

The thylakoid membrane system in chloroplasts has a more complex structure than the undifferentiated thylakoid membrane system of cyanobacteria. SDS-PAGE of the polypeptide distribution(Wollenberger et al., 1994) and biophysical studies (Wollenberger et al., 1995; Mamedov et al., 2000) of the light-harvesting antenna attachment and the localization and specific O_2 evolution activity of PS II-WOC

Table 1. Sequence and location of assembly of PS II core complex protein subunits and inorganic core cofactors in cyanobacteria and chloroplasts

Membrane:	Plasma	Stroma	Grana Margin	Core Grana
PS II-WOC Maturation	Unassembled reaction center	PS II-β, Inner antenna insertion, Labile inorganic core	PS II core-β, Completed polypeptide core Labile inorganic core	PS II core-α, Assembled polypeptide core, Stable inorganic core + LHC II
	→	→	→	
Major Subunits	RC[a], 33-MSP (nf)[b]	RC[a] + CP47 + partial CP43	RC[a] + CP43 + CP47	All major subunits + 33-MSP
Electron Transport	None	Slow $Q_A \rightarrow Q_B$	Slow $Q_A \rightarrow Q_B$	Normal PS II kinetics
WOC Photoactivation	None	~40% Photoactivatible, Labile $O_2\uparrow$	Photoactivation yield increases	Fully assembled, Stable $O_2\uparrow$

[a] RC subunits D1, D2, Cyt b_{559}; [b] (nf) non-functional

complexes found within different regions of the thylakoid membrane system in chloroplasts indicates that a gradient exists in the number of subunits and complexity of functional activity. PS II size and functional complexity increases in going from the individual stroma lamellae, to the periphery of the appressed multi-membrane grana lamellae (so-called margins) to the centers of the appressed grana lamellae (core grana), as summarized in Table 1. At least two sub-types of PS II, designated PS II-α and PS II-β, are known that are distinguished by the number of light-harvesting antenna Chl *a/b* binding proteins that funnel energy to the RC. PS II-α has more LHC II and a larger antenna size compared to PS II-β (Wollenberger et al., 1994). The Mn cluster is absent or inactive in the PS II found in the stroma membrane; a major fraction of the peripheral grana PS II-WOC are active but have slow $Q_A \rightarrow Q_B$ electron transfer kinetics; while greater than 80–90% of the core grana PS II-WOC are fully active in O_2 evolution and have normal acceptor side kinetics (Mamedov et al., 2000). The authors hypothesize that the 'photoactivation' process (here meaning both subunit assembly and inorganic core uptake) is initiated in the stroma lamellae, diffuses into the grana periphery, and is completed within the appressed regions of the inner grana core.

In summary, studies of PS II-WOC biogenesis in both cyanobacteria and chloroplasts support an 'assembly line' model for the manufacturing of functional PS II core complexes. Beginning with insertion into the plasma membrane of PS II reaction center subunits (D1, D2, Cyt b_{559}, association unknown) and a non-functional version of the 33-kDa MSP (likely pre-protease processing). This is followed by transport to stroma lamellae where acquisition of inefficient primary electron transport (slow $Q_A \rightarrow Q_B$) occurs. Some CP43 and CP47 are present (Mamedov et al., 2000), although gels reveal that CP43 is present at lower levels than the RC subunits (Wollenberger et al., 1994) Photoactivation of O_2 evolution occurs in some centers (≤ 40%) but the activity is unstable in the dark, suggesting that stable binding of the extrinsic 33 kDa protein has not been established in those centers that do photoactivate. PS II core assembly develops further in the grana margins where gels reveal more prominent staining from CP47 and CP43 and fluorescence reveals opening of $Q_A \rightarrow Q_B$ electron transfer. Lastly, diffusion to the core grana lamellae occurs where the most stable and active PS II core complex-WOC is found, also in association with additional LHC II subunits that create the light-efficient PS II-β core complex (Wollenberger et al., 1994; White et al., 1996). The high stability of the O_2 evolution activity in the latter complexes is associated with the binding of the extrinsic 33 kDa protein (Burnap et al., 1996). Not all of the details of the assembly steps needed to support this biogenesis model have been tested. However, we note that deletion of a single gene called *VIPP1* (vesicle-inducing protein in plastids 1) is deleterious to thylakoid membrane formation. *VIPP1* is a hydrophilic protein that is found in both the inner envelope and the thylakoid membranes and is a potential candidate for facilitating protein transport between the two membrane systems.

B. Mn^{2+} Uptake into the Cell

The Mn content of cyanobacterial cells is generally well in excess of that needed to supply all PS II complexes; however, intracellular distribution and transport are other determinants not as well known. The capsular peptidoglycan comprising the cyanobacterial envelope plays a major role in concentrating free Mn^{2+} from extracellular solution (Mohamed, 2001). Mature cells of *Synechocystis* take up or exchange free Mn^{2+} at a rate of about 2×10^6 Mn^{2+}/cell in a period of 30 minutes (Ogawa et al., 2002). There are two pools of intracellular Mn^{2+} which have been identified (Keren et al., 2002). The largest pool, A ~10^8 atoms/cell, is found closely associated with the outer membrane, possibly on either the outside or the inner leaflet (periplasm). This pool can be removed by EDTA, is electrogenically generated under light and can be prevented by electron transport inhibitors (DCMU) or abolished by proton uncouplers (CCCP). A tightly associated second pool, B ~1.5×10^6atoms/cell, is not affected by EDTA, light or proton uncouplers and has traversed the inner membrane. Under Mn^{2+} starvation conditions pool B contains about 10^5Mn/cell which is essential for photosynthesis, of which the majority is targeted to PS II. By comparison, the marine cyanobacterium *Synechococcus* sp. PCC7002 contains 1.5×10^6 Mn/cell in pool B, while the non-oxygenic purple bacterium *Rhodobacter capsulatus* contains 1% of this amount. A two-component regulatory machinery for sensing of extracellular Mn^{2+} concentrations and maintenance of intracellular Mn homeostasis in cyanobacteria and non-photosynthetic prokaryotes has begun to emerge (Ogawa et al., 2002).

C. Inorganic Core Assembly Involves No Protein Chaperones

Intracellular transport of transition metal ions used in the enzymatic machinery is typically under tight control by proteins or small molecule chelators that ensure proper targeting of the metal to its final destination and also protect the nascent system from unwanted reactions. These 'chaperone' proteins are widely distributed in the case of iron and copper regulator systems. The thermodynamic potentials for aqueous Fe^{2+}/Fe^{3+} and Cu^{+}/Cu^{2+} metals indicate that these metals are susceptible to redox changes within cells and thus will undergo major changes in speciation if not coordinated during transport. Thus it may seem curious that no essential chaperone protein has yet been identified for delivery of Mn^{2+} to the apo-WOC-PS II complex during biogenesis. The explanation is likely due to the inaccessibility of the Mn^{3+} oxidation state in aqueous media at neutral pH owing to the large thermodynamic barrier which prevents Mn^{2+} oxidation (standard reduction potential 1.2 V at pH 7 vs NHE). Moreover, divalent Mn^{2+} with its spherical electronic distribution and half-filled $3d^5$ electronic configuration (two sigma anti-bonding electrons) forms relatively weak coordination complexes with all monodentate O, N, S ligands (Smith et al., 1976). Thus, free Mn^{2+} does not generally associate tightly with the internal machinery of the cell unless there are preorganized chelation sites present with multiple ligand donors. Generally, the latter sites are specific for ions of a particular size, charge and dehydration energy so that biosynthetic discrimination is almost always ensured. Surface electrostatics plays a major role in guiding metal ions to their functional binding sites and this mechanism is important for steering Mn^{2+} to the apo-WOC-PS II site (Ananyev and Dismukes, 1996b). Binding of aquo-Mn^{2+} to the high affinity site in apo-WOC-PS II is influenced by three factors: alkaline pH, bicarbonate ions and Ca^{2+} are discussed in the next sections. Although no chaperone for Mn^{2+} insertion appears to exist, repair of the PS II protein complex caused by light absorption does involve chaperone-like proteins (Schroda et al., 2001).

A new and novel protein called Slr0286 was identified in *Synechocystis* which has no homologues in other organisms and is not known to be associated with PS II (Kufryk et al., 2001). Deletion of Slr0286 did not affect photoautotrophic capacity in wild type, but led to a marked decrease in the population of Ca^{2+} bound to the WOC of PS II. A chaperone role for Slr0286 in photoactivation was postulated. However, an alternate role in elevating the Ca^{2+} supply within the lumenal space of the thylakoid membrane would also be consistent with the data.

IV. Roles of the Inorganic Cofactors from Photo-Assembly

A. Assembly of the Inorganic Core

1. Instrumentation

In 1995–96 we constructed a modified Clark-type electrochemical cell for the detection of dissolved O_2 gas in photosynthetic samples (Ananyev, 1995; Ananyev and Dismukes, 1996a,b). It enabled measurements of O_2 concentration with exceptional sensitivity (50 femtomoles O_2), micro-volume sample volume (5 μL) and 10-fold faster time-resolution than the commercially available Clark electrodes. The electronic layout and novel material innovations have been described and circuit diagrams are available upon request. It features a platinum-iridium (Pt:Ir = 75:25) electrode which is 10 times harder than Pt and more chemically resistant to oxidation, reducing the formation of PtO_2 and the resulting photocurrents. By using a thin (1 μm) silicone membrane instead of Teflon, both rapid response (0.1 second rise time) and substantial reduction in the dark current and loss of membrane fatigue were achieved. The electrode assembly includes an integral preamplifier, further reducing susceptibility to transients. This cell is integrated with a versatile LED light source for both red and blue wavelength excitation, digital control of the pulse-shape and duration (0.5 ms to infinity), and digital data acquisition system and programming environment (Labview). This instrument permits measurement of the rate and yield of O_2 production in samples containing 1 μM PS II centers and exhibiting as little as 0.5% activity and, by integration, as little as 0.05% of the activity.

2. Kinetics and Mechanism

In the 1960s George Cheniae discovered the photoactivation process, and together with his coworkers established many of the fundamental properties of the WOC over the next three decades (Frasch and Sayre, 2001). This includes determination of the Mn

stoichiometry (3–5 Mn/PS II), cooperative nature of the Mn association, and two-step sequence of intermediates (light-dark-light) required for reconstitution of O_2 evolution. The insights provided by the pioneering results from his laboratory are an enduring legacy made more remarkable by the fact that they were performed using simple tools: a Petri dish, a commercial Clark electrode and a light bulb as the photoactivation reactor.

Application of the photoactivation instrument described in Section IV.A has enabled kinetic resolution of the first two steps prior to the rate-limiting step in the assembly of the inorganic cofactors (Ananyev and Dismukes, 1996b). The steps that follow the rate-limiting step are not individually resolved, but their Mn stoichiometry needed to restore O_2 evolution has been determined. Photoactivation follows a two-step sequence, as originally discovered by Cheniae and Tamura (1987) on the basis of steady-state O_2 yield measurements and confirmed by Miller and Brudvig (1989). Kinetic resolution of these steps revealed a reversible, light-dependent lag phase where no O_2 is produced, followed by a single exponential recovery phase (Zaltsman et al., 1997). The kinetic resolution provides values of the three rate constants shown in Fig. 1 (k_1, k_{-1} and k_2). The sensitivity of the cell permits measurement of these rate parameters using sub-stoichiometric concentrations and higher of Mn^{2+}. This permitted exceptionally accurate titrations of the Mn stoichiometry required for O_2 evolution, based on measuring both an extensive variable (O_2 flash yield) (Ananyev and Dismukes, 1996a) and an intensive variable (initial rate of recovery of O_2 evolution capacity) (Ananyev et al., 2001). The latter approach provided a particularly accurate assay of Mn stoichiometry (4.0) because it does not require determination of the number of apo-WOC centers. The photoactivation of PS II-WOC in whole cells

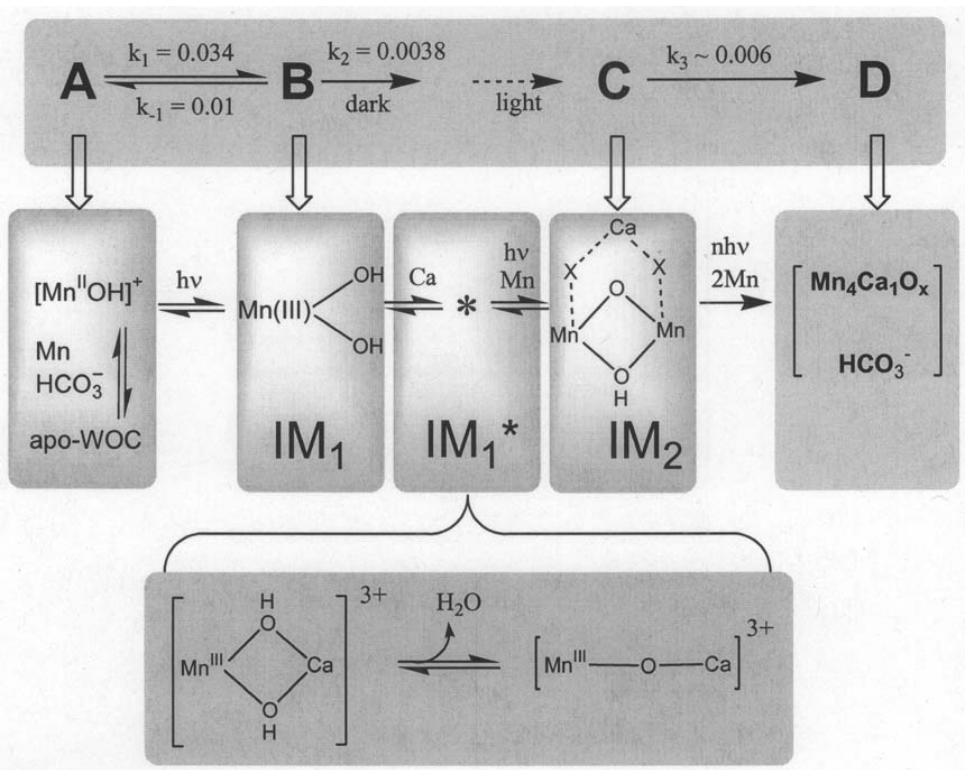

Fig. 1. The sequence of kinetic intermediates (top) formed during assembly of the inorganic core of the WOC by photoactivation (A, B, C) (Ananyev et al., 2001). Proposed structures of intermediates (bottom).

appears to occur similarly to the isolated PS II core complex. The ability to examine the role of accessory proteins in assembly of the inorganic core under native conditions is possible (Burnap et al., 1996; Qian et al., 1997).

Two mild methods have been described for removal of the inorganic cofactors and extrinsic proteins from PS II complexes (apo-WOC-PS II) that is essential for quantitative work and avoids the denaturation created by the alkaline TRIS method (Ananyev and Dismukes, 1996a; Ananyev et al., 1998; Baranov et al., 2004). Application of these methods has enabled measurement of the following characteristics of the photoactivation process, primarily using spinach PS II membranes and PS II core complexes(Ananyev et al., 1995; Ananyev and Dismukes, 1996a,b; Ananyev et al., 1998; Ananyev et al., 2001): (i) optimization of the total yield of reactivated holo-enzyme capable of O_2 production (70%–100%); (ii) a molecularity of 1.0 Mn^{2+}/PS II on the first photooxidation step; (iii) linear light intensity dependence of the first step reflecting a single turnover that forms Mn^{3+}; (iv) determination of the proton stoichiometry of the first two steps ($1H^+ + 1H^+$, as described in the next section); (v) determination of the rate constant of the subsequent rate-limiting dark step that is independent of Mn^{2+} concentration and exhibits a molecularity of approximately 1 Ca^{2+}/PS II (step IM1→ IM2*); (vi) the Ca^{2+} affinity of this site (denoted the Ca^{2+} effector site) increases following binding and photoxidation of the high affinity Mn^{2+}, reflecting mutual cooperativity in binding; (vii) subsequent rapid light and dark steps that are kinetically unresolved and involve the uptake of 3.0 Mn^{2+}/PS II; (viii) strong cooperativity in the uptake of the Mn ions is seen in Mn^{2+} titration of the final O_2 evolution flash yield (25, 50, 75 and > 90% with 1, 2, 3, and 4 Mn/PS II, respectively).

3. Proton Evolution

Alkaline pH accelerates the rate of Mn-dependent photoactivation by 10-fold between pH 5.5 and 7.5, while the final yield of O_2 per flash follows closely the known pH dependence of the holo-enzyme. The data indicate that protons are released during the first two steps of assembly (Ananyev and Dismukes, 1996b; Ananyev et al., 2001). Direct measurements of proton release during photoactivation have been described using a commercial ISFET (ion-selective field-effect transistor) detector (Ananyev et al., 2001). There are advantages to the ISFET detector that can help resolve ambiguities obtained with glass electrodes or pH dyes as detectors. Measurement of the proton concentration in bulk solution during photoactivation by flashes reveals that a single proton is released upon photooxidation of the initial dark precursor, attributed to $Mn^{II}(OH)^+$ based on studies of cesium inhibition (see below). Thus, the first light-induced assembly intermediate contains one fewer proton and is formulated as, $Mn^{III}(OH)_2^+$, in which ionization of a water ligand is postulated.

4. Oxo/Hydroxo/Bicarbonate Sites

Bicarbonate ions were shown to efficiently replace alkaline pH buffers in accelerating the rate of photoactivation, while increasing the yield of reactivated centers, quite contrary to the reduction seen upon alkalinization. Bicarbonate binds to two sites within apo-WOC complex as depicted in Fig. 2 and described next. A high affinity site operates at concentrations as low as 10 μM in the presence of stoichiometric Mn^{2+}/PS II concentrations where it accelerates the first step of Mn^{2+} binding and/or photooxidation (Baranov et al., 2000). The high affinity site is attributed to the ionization of carboxylate residues or neutralization of cationic residues on the surface of the WOC protein complex, possibly the D1 protein, which electrostatically attract Mn^{2+} from solution close to the WOC (Baranov et al., 2004). The effect is much like that seen with lipid soluble anions like tetraphenylboron(Ananyev and Dismukes, 1996b). In more extensive studies covering 10 and 100 fold higher concentrations of Mn^{2+} and Ca^{2+}, respectively, a second bicarbonate binding site to apo-WOC-PS II having lower affinity that depends upon the Mn^{2+} concentration has been identified (hence called the ternary site). Bicarbonate produces a much larger three-fold rate acceleration at the ternary site. The data suggest that bicarbonate may serve to deliver oxide/hydroxide needed for Mn-oxo/hydroxo assembly or, possibly, as an integral cofactor within the WOC (Baranov et al., 2004). Since its conjugate acid CO_2 is highly soluble in the membrane phase, there will be higher concentration of bicarbonate near the thylakoid membrane than in bulk solution at equilibrium in any system which gets all of its inorganic carbon from CO_2.

At higher (millimolar) concentrations of bicarbonate and Mn^{2+} the formation of free Mn^{2+}-bicarbonate complexes occurs in solution. The formation of these species coincides with a reduction in the O_2 yield and

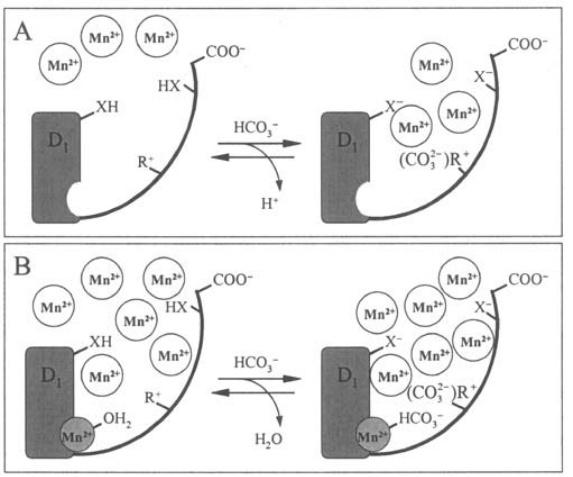

Fig. 2. The two proposed sites for bicarbonate stimulation of Mn^{2+} assembly during the photoactivation reaction (Baranov et al., 2004). (A) The high-affinity bicarbonate site: At low Mn^{2+} concentrations (<8 Mn^{2+}/PS II), bicarbonate anions electrostatically steer Mn^{2+} ions into the apo-WOC-PS II complex from solution by partitioning or ionization of protons or through ion-pairing with cationic side chains of arginines (R+). (B) The low-affinity bicarbonate site: At high Mn^{2+} concentrations (> 30 Mn^{2+}/PS II), bicarbonate binds to the photoactive high-affinity Mn^{2+} binding site.

slowing of the rate of photoactivation. These free complexes appear to serve as a competitive electron donors to the functional site for photoassembly (i.e., the ternary site, Fig. 2). EPR studies of the role of calcium have extended the model in Fig. 2 by establishing an electronic interaction between Mn^{III} and Ca^{2+} in the first photo-intermediate, IM_1 (Baranov et al., 2004).

5. Calcium

The kinetics of photoactivation reveal that the Ca^{2+} binding affinity increases following photooxidation of the high affinity Mn^{2+}. Ca^{2+} binding is coupled to a slow dark process that is postulated to represent a protein conformational change. This process leads to more rapid uptake and photooxidation of the remaining 3 Mn^{2+}(Zaltsman et al., 1997). EPR spectroscopy reveals that Ca^{2+} binding in the dark causes cooperative binding of a dimanganese(II,II) center to apo-WOC-PS II (Ananyev et al., 1997). The yield of this Ca-induced dimanganese signal is optimal at a ratio of 2 Mn/PS II, and saturates with increasing Ca^{2+} concentration. The calcium concentration for induction of the Mn_2(II,II) signal matches the value observed for both the activation of steady-state O_2 evolution and also the light-induced assembly of the functional WOC by photoactivation. Formation of the Mn_2(II,II) signal is specific for Ca^{2+} as it does not occur in the presence of Mg^{2+}. The spectral features of this signal are indicative of a variety of weakly interacting Mn_2(II,II) pairs that have Mn^{2+} ions coupled by magnetic dipolar forces in the range of inter-manganese separations of ca. 4.1 ± 0.4 Å (Khangulov et al., 1995). This Ca-induced Mn_2(II,II) center is a more efficient electron donor to the photooxidized tyrosine radical, Y_z, than is the mononuclear Mn^{2+} center present in the absence of Ca^{2+}, as measured by the $Y_z^{\cdot}$ radical yield. Formation of the Mn_2(II,II) EPR signal by addition of Ca^{2+} correlates with reduction of flash-induced catalase activity, indicating that calcium modulates the accessibility or reactivity of the Mn_2(II,II) core with added H_2O_2. These EPR studies indicates that Ca^{2+} organizes the binding site for higher affinity cooperative binding of the first two Mn^{2+} ion to the apo-WOC protein.

The photoactivation and spectroscopic data noted above provide a self-consistent picture locating the Ca-effector site as an integral part of the Mn_4 core, probably via shared bridging ligands to Mn (aqua/hydroxo/carboxylato/chloro) (Carrell et al., 2002). Binding of the calcium cofactor to Ca-depleted holoenzyme induces an increase in the energy of the Mn K-shell electron edge by 0.6-1.0 eV in three oxidation states (S_1, S_2 and S_3 states) where Ca-depletion/reconstitution has been measured by XANES

(reviewed in Carrell et al., 2002). Therefore, a reasonable interpretation of the role of Ca^{2+} is that it serves as an electrostatic promoter to raise the Mn oxidation potential. This increase could be achieved if Ca^{2+} were to increase the extent of electron transfer from shared (bridging) ligands (oxo, hydroxo, aquo) to the empty 4p valence orbitals on Mn. This interpretation suggests a possible direct role for Ca^{2+} in increasing the Mn-ligand covalency and thus activating the Mn-water (substrate) molecule(s) for easier oxidation. We have postulated that this role may involve Ca-induced ionization of protons from the substrate water molecules that are bound to the Mn_4 cluster (Carrell et al., 2002). This role is also consistent with the observed correlation between equilibrium binding affinity for divalent metals bound to the Ca-effector site and their pK_a (Vrettos et al., 2001b).

6. Protein Subunits Required for Photoactivation

Büchel et al. (1999) demonstrated that the smallest PS II protein complex that is capable of catalyzing water oxidation is the CP47RC subcore complex (Büchel et al., 1999). This complex is isolated from thylakoid membranes by fractionation of a detergent-solubilized complex. It is comprised of only four major subunits (D1, D2, Cyt b_{559} and CP47) and a number of small subunits, but lacks CP43 and all of the inorganic cofactors of the WOC. The isolated complex is inactive in O_2 evolution, but does photoactivate at slower rate (lower quantum efficiency) and produces centers having O_2 flash yield of 30% vs. PS II membranes. These studies established that CP43 is not an essential subunit for water splitting, but does provide a functional advantage for both assembly and O_2 evolution activity.

Y_D is the symmetry related photoactive tyrosine in the D2 subunit (Tyr160) that is homologous to the essential photoactive Tyr161 of the D1 subunit of PS II (Y_Z). It has been implicated in stabilizing the higher S-states and in photoactivation (Styring et al., 1987), but is not essential as mutants lacking Y_D grow photoautotrophically, although at much slower rates. Diner and coworkers investigated Y_D in both wild-type and a mutant strain (Tyr160Phe) in which phenylalanine replaces Y_D in the cyanobacterium *Synechocystis*. The quantum yield for O_2 in the intact holo-enzyme was found to be identical in the mutant and wild-type PS II cores using long (saturating) pulses or continuous illumination, confirming earlier work. However, the O_2 yield was shown to be appreciably reduced in the mutant using short non-saturating light pulses (< 50 ms). Evidence was presented that the positive charge associated with the presence of a hole on the Y_D-$HisH^+$ radical center may promote the higher quantum yield for O_2 production in wild-type centers via increasing the oxidation potential of $P680^+$, thereby accelerating the rate of electron transfer from Mn_4Y_Z to $P680^+$. It was also found that the mutant can assemble a functional WOC from the free inorganic cofactors, but at a three-fold slower rate and with reduced quantum efficiency vs wild type. The steps responsible for the slower photoactivation kinetics in the mutant were identified. These features indicate that the $Y_D^{\bullet}$ radical plays at least two important roles during assembly of a functional WOC, including increasing the probability of oxidation of Mn^{2+} in the dark and suppressing decay of the assembly intermediates by charge recombination at low light flux. They contribute a competitive advantage to organisms that retain the Y_D residue and therefore may account for its retention in the genome of all oxygenic photoautotrophs.

B. 'Inorganic Mutants' of the Manganese and Calcium Sites

Inhibitor binding at the high affinity Mn^{2+} site is characterized by slowing of the rate constant k_1 and is competitive with Mn^{2+}. Acceleration of the decay of the first photooxidized Mn^{III} intermediate is described by rate constant k_{-1}. Inhibition at the Ca-effector site is characterized by slowing of the rate constant k_2 and is competitive with Ca^{2+} concentration.

1. Manganese Mutants

Mn appears to be unique in catalyzing O_2 evolution in all oxygenic photoautotrophs. No other metals have been found to date that can replace it. We have examined several metal ions as potential surrogates for Mn^{2+} in the assembly process of spinach apo-WOC-PS II (Ananyev et al., 2001). These studies were conducted by replacing Mn^{2+}, while keeping all other components fixed at the optimal concentrations for Mn-dependent photoactivation (Cl^-, Ca^{2+} and the electron acceptor ferricyanide). The following metal ions were found to inhibit Mn-dependent photoactivation with varying affinities and none were found capable of supporting O_2 evolution in the absence of Mn^{2+} (Cs^+, Ba^{2+}, VO^{2+}, V^{3+}, Cr^{3+}, Fe^{2+}, Co^{3+}, Ni^{2+}, Cu^{2+},

Zn^{2+}, MoO_4^{2-},Ru^{3+}, Rh^{3+}, Re^{3+}, UO_2^{2+}). However, only a very limited range of conditions were studied: fixed pH 6 and concentrations of Ca^{2+}, Cl^- and electron acceptor. Other pH and concentrations conditions ought to be examined before it is known for sure whether Mn can be replaced.

Cesium (Cs^+) is the strongest, competitive, inhibitor of the high affinity Mn^{2+} site, while the smaller alkali metal ions bind with progressively weaker affinity ($Cs^+ > Rb^+ > K^+ > Na^+ > Li^+$). The equilibrium thermodynamic binding affinities were measured for all alkali metal ions and a clear correlation with charge density was seen. Cs^+ binding is highly selective for the Mn site, vs. $> 10^4$ weaker binding to the Ca effector site. These data indicate that Cs^+ mimics the size and charge of the functional Mn^{2+} species that binds to apo-WOC-PS II and initiates the assembly process. Assignment of this dark precursor to $Mn(OH)^+$ rather than Mn^{2+} is implied by these results. This conclusion is in full accord with the proton evolution results noted above and the bicarbonate dependence. This proposal is further supported by the observation that metal-oxo cations like UO_2^{2+} and VO^{2+} are among the strongest competitive inhibitors of the Mn site. These results enabled the Mn and hydroxide composition of the first two assembly intermediates to be determined (up to IM_1, Fig. 1).

2. Calcium Mutants

Boussac discovered that Sr^{2+} can functionally exchange Ca^{2+} in the intact holo-enzyme of PS II membranes by restoring O_2 evolution activity (Boussac et al., 1988). Later we found that there is a kinetic advantage for uptake of Sr^{2+} versus Ca^{2+} at the Ca-effector site during assembly of the apo-WOC enzyme and determined how each of the three rate constants measured by photoactivation are affected (Table 2) (Ananyev et al., 2001). Sr^{2+} was shown to be five times more effective than Ca^{2+} in accelerating the rate of the first two assembly steps (k_1 and k_2) and two times better in retarding the deactivation step (k_{-1}). Sr^{2+} competes with Ca^{2+} and thus occupies the Ca-effector site of the photoassembled PS II. A 65% lower O_2 evolution yield per flash is obtained for the Sr-photoactivated enzyme, which is very close to the decreased steady-state O_2 evolution rate in the Sr-exchanged holo-enzyme. This decrease in O_2 flash yield is known to reflect a retardation of the rate of the final step, $S_3 \rightarrow S_0 + O_2$ (Westphal et al., 2000). Thus, the data taken together indicate that Ca^{2+} is clearly involved in accelerating the final step in the S-state catalytic cycle. This step includes the O-O bond formation reaction. No other metal ion other than Sr^{2+} has been found to functionally replace Ca^{2+} in water splitting.

Another interesting probe of the Ca^{2+} site is the vanadyl ion. VO^{2+} stimulates Mn-dependent photoactivation by accelerating the first step (k_1) and increasing the yield of photoactivated centers when using stoichiometric Mn^{2+} concentrations or less (Table 2) (Ananyev et al., 2001). The apparent Michaelis constant at this site is 15 μM. By contrast, at higher concentrations vanadyl slows the first step and

Table 2. Activator/inhibitors at the Ca-effector site of Mn-dependent photoactivation of O_2 evolution in spinach apo-WOC-PS II (Ananyev et al., 2001)

Metal	Photoactivation step affected	O_2 yield at pH 6.5	Michaelis constant (k_M)
Ca^{2+}	k_1 no effect k_{-1} accelerated k_2 accelerated	70-100%	1.5mM
Sr^{2+}	k_1 no effect k_{-1} accelerated k_2 accelerated	30%	~30 mM
Mg^{2+}	Weak non-specific effect	<0.5%	>0.1 M (inhibition)
Ba^{2+}	k_1 slowed	<0.5%	Blocks Mn not Ca site
VO^{2+}	k_1 accelerated k_1 slowed	<0.5%	15 μM (k_1) 200 μM

reduces the overall yield of photoactivated centers (I_{50} ~200 μM) by serving as a competitive electron donor to Y_z. The location of the VO^{2+} binding site appears to be the Ca-effector site, since Ca^{2+} blocks the inhibition by VO^{2+}. Previous studies had observed stimulation of Mn-dependent O_2 evolution by VO^{2+} in the absence of Ca^{2+} (Lockett et al., 1990). However, by using the photoactivation method we were able to show that this result is likely due to mobilization of residual Ca^{2+} by vanadyl ions. The vanadyl stimulation of the rate constant k_1 (Mn site) through binding at the Ca^{2+} site suggests a cooperative interaction between the two sites, with binding of VO^{2+} at the Ca-effector site causing higher affinity binding of Mn^{2+} at the Mn site. This cooperativity suggests the possibility of either electrostatic or conformational coupling of the two sites. This interpretation is consistent with equilibrium binding studies showing that lanthanides of higher charge density bind more strongly to the Ca-depleted holo-enzyme (Ono, 2000). This cooperativity between the Mn and Ca sites provides a possible mechanism for the observed correlation in other physico-chemical properties, including XAS and EPR properties, noted previously. Alternatively, it is possible that the acceleration of the Mn-dependent k_1 step observed by the VO^{2+} ion is due to stimulation of proton evolution from Mn^{II} or Mn^{III}, since vanadyl is a weak base ($pK_1 = 4.3$, $pK_2 = 11.5$). In previous studies we found that organic bases stimulate the rate of the initial step of photoactivation (Ananyev et al., 2001). Evidence was presented that the mechanism involves stimulation of proton evolution from (or hydroxide binding to) Mn (assembly of $Mn^{II}(OH)^+$ and $Mn^{III}(OH)_2^+$). Distinction between these alternative proposals for the vanadyl effect on k_1 may be resolved by examination of the effect on photoactivation of lanthanides binding to the Ca-effector site.

3. Other Metal Ion Sites

Recently, Cu^{2+} was shown to bind to PS II complexes from tobacco at stoichiometric concentrations and produce stimulation of the electron transfer rate from water (Burda et al., 2002). The location of the Cu^{2+} binding site was not identified, but the authors speculated a possible site in the WOC. This finding is novel as there is no precedent for an endogenous functional Cu^{2+} site in any WOC. An alternative binding site for this novel Cu^{2+} may be the acceptor side, based on data showing that a binding site for exogenously added Ni^{2+} or Zn^{2+} has been identified near the Q_B acceptor in purple bacterial reaction centers and found to slow the rate of proton transfer into reduced Q_B^{2-} (Utschig et al., 1998; Keller et al., 2001).

V. Concluding Remarks

The universality of the inorganic core of the WOC among all oxygenic phototrophs, its high efficiency of assembly and the absence of protein chaperones during assembly indicates that the inorganic core can be assembled spontaneously from elementary ions, light and the apo-WOC protein. Kinetically, the process is simple. It can be resolved into two steps in which 1 Mn^{2+} and 1 Ca^{2+} are taken up in light and dark steps, respectively, followed by rapid light-dependent uptake of 3 Mn^{2+}. This kinetic simplicity indicates minimal control by the protein and thus implies the core structure may be intrinsically stable relative to other core topologies. Hence, we can expect it to be among the known Mn_4O_x core types previously prepared or accessible by self-assembly (Mukhopadhyay et al., 2002). This sequence of uptake of the cofactors during photoactivation, depicted in Fig. 1, the strong

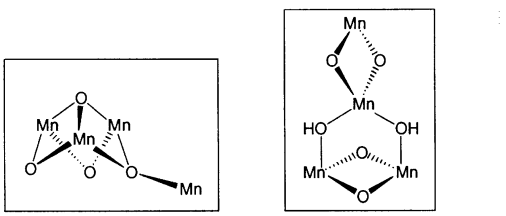

$(\mu_3\text{-oxo})_2(\mu_2\text{-oxo})_2$ $(\mu_2\text{-oxo})_4(\mu_2\text{-hydroxo})_2$

Fig. 3. Two of the manganese-oxo core types proposed for the PS II-WOC on the basis of EPR and EXAFS data (Carrell et al., 2002).

cooperativity in binding of the high affinity Mn^{3+} and Ca^{2+} ions, their coupling to proton release, and the rapid cooperative uptake of the remaining 3 Mn^{2+} ions provide support for two of the eight possible Mn_4O_x core types proposed on the basis of EPR/EXAFS spectroscopies (Carrell et al., 2002). The two Mn_4O_x core types deduced by EPR/EXAFS that are consistent with the photoactivation data are depicted in Fig. 3. The placement of a Ca^{2+} ion within each of these structures located along the pseudo three-fold axis produces core types that are structurally in good agreement with the Mn_4Ca_1 heterocubane core type proposed on the basis of XRD of a cyanobacterial PS II core complex (Ferreira et al., 2004). We may conclude that the Mn_4Ca heterocubane core topology is supported not only by the available spectroscopic data from various sources, including XRD, EPR, and EXAFS, but also by the photoactivation data on assembly.

Acknowledgments

We thank Drs. M. Seibert, H. Pakrasi and J. Barber for reprints. GCD appreciates helpful discussions with Drs. S. Baranov, A. Tyryshkin and A. Stemler. Financial support by the NIH (GM-39932) is gratefully acknowledged.

References

Adelroth P, Lindberg K and Andreasson L-E (1995) Studies of Ca^{2+} binding in spinach Photosystem II using $^{45}Ca^{2+}$. Biochemistry 34: 9021–9027

Ananyev GM and Dismukes GC (1995) Photoassembly of the tetra-Mn site of photosynthetic water oxidation: EPR evidence for dark ligation of a binuclear Mn intermediate. In: Mathis P (ed), Photosynthesis: From Light to Biosphere, pp 431–438. Kluwer Academic Publlishers, Dordrecht

Ananyev GM and Dismukes GC (1996a) Assembly of the tetra-mn site of photosynthetic water oxidation by photoactivation: Mn stoichiometry and detection of a new intermediate. Biochemistry 35: 4102–4109

Ananyev GM and Dismukes GC (1996b) High-resolution kinetic studies of the reassembly of the tetra- manganese cluster of photosynthetic water oxidation: Proton equilibrium, cations, and electrostatics. Biochemistry 35: 14608–14617

Ananyev GM and Dismukes GC (1997) Calcium induces binding and formation of a spin-coupled dimanganese(II,II) center in the apo-water oxidation complex of photosystem ii as precursor to the functional tetra-mn/ca cluster. Biochem 36: 11342–11350

Ananyev GM, Zaltsman L, McInturff RA and Dismukes GC (1998). Assembly intermediates and 'inorganic mutants' of the PS II oxygen evolving complex. In: Garab G (ed), Photosynthesis: Mechanisms and Effects, pp 1347–1350. Kluwer Academic Publishers, Dordrecht

Ananyev GM, Zaltsman L, Vasko C and Dismukes GC (2001) The inorganic biochemistry of photosynthetic oxygen evolution/water oxidation. Biochim Biophys Acta 1503: 52–68

Babcock GT and Sauer K (1975) A rapid, light-induced transient in electron paramagnetic resonance signal II activated upon inhibition of photosynthetic oxygen evolution. Biochim Biophys Acta 376: 315–28

Baranov SV, Ananyev GM, Klimov VV and Dismukes GC (2000) Bicarbonate accelerates assembly of the inorganic core of the water-oxidizing complex in manganese-depleted Photosystem II: A proposed biogeochemical role for atmospheric carbon dioxide in oxygenic photosynthesis. Biochemistry 39: 6060–6065

Baranov S, Tyryshkin A, Katz D, Dismukes G, Ananyev G and Klimov V (2004) Bicarbonate is a native cofactor for assembly of the manganese cluster of the photosynthetic water oxidizing complex: II. Kinetics of reconstitution of O_2 evolution by photoactivation. Biochemistry 43: 2070–2079

Boussac A and Rutherford AW (1988) The nature of the inhibition of the oxygen evolving enzyme of psII which is induced by NaCl washing and reversed by the addition of Ca^{2+} or Sr^{2+}. Biochemistry 27: 3476–3483

Boussac A, Rappaport F, Carrier P, Verbavatz J-M, Gobin R, Kirilovsky DL, Rutherford AW and Sugiura M (2004) Biosynthetic Ca^{2+}/Sr^{2+} exchange in the photosynthetic oxygen evolving enzyme of *Thermosynechoccocus elongatus*. J Biol Chem 279: 22809–22819

Bricker TM (1992) Oxygen evolution in the absence of the 33-kilodalton manganese-stabilizing protein. Biochemistry 31: 4623–4628

Büchel C, Barber J, Ananyev GM, Eshaghi S, Watt R and Dismukes GC (1999) Photoassembly of the manganese cluster and oxygen evolution from monomeric and dimeric CP47-reaction center Photosystem II complexes. Proc Nat Acad Sci USA 96: 14288–14293

Burda K and Schmid GH (2001) Heterogeneity of the mechanism of water splitting in Photosystem II. Biochim Biophys Acta 1506: 47–54

Burda K, Kruk J, Stralka K and Schmid GH (2002) Stimulation of oxygen evolution ins psii by copper(II) ions. Z Naturforsch 57: 853–857

Burnap RL and Sherman LA (1991) Deletion mutagenesis in synechocystis sp pcc6803 indicates that the Mn-stabilizing protein of Photosystem-II is not essential for O_2 evolution. Biochemistry 30: 440–446

Burnap RL, Shen JR, Jursinic PA, Inoue Y and Sherman LA (1992) Oxygen yield and thermoluminescence characteristics of a cyanobacterium lacking the manganese-stabilizing protein of photosystem-II. Biochemistry 31: 7404–7410

Burnap RL, Qian M and Pierce C (1996) The manganese-stabilizing protein of Photosystem II modifies in vivo deactivation and photoactivation kinetics of the H_2O oxidation complex in *Synechocystis* sp. PCC 6803. Biochemistry 35: 874–882

Campbell KA, Force DA, Nixon PJ, Dole F, Diner BA and Britt RD (2000) Dual-mode EPR detects the initial intermediate in the photoassembly of the PS II Mn cluster. J Am Chem Soc 122: 3754–3761

Carrell TG, Tyryshkin A and Dismukes GC (2002) An evaluation of structural model for the photosynthetic water-oxidizing complex derived from spectroscopic and X-Ray diffraction signatures. J Biol Inorg Chem 7: 2–22

Cheniae GM and Martin IF (1971) Photoactivation of manganese catalyst of O_2 evolution.1. Biochemical and kinetic aspects. Biochim Biophys Acta 253: 167–181

Chu H-A, Nguyen AP and Debus RJ (1994) Site-directed PS II mutants with perturbed oxygen evolving properties. 1. Instability or inefficient assembly of the Mn cluster in vivo. Biochemistry 33: 6137–6149

Cinco RM, Robblee JH, Rompel A, Fernandez C, Yachandra VK, Sauer K and Klein MP (1998) Strontium EXAFS reveals the proximity of calcium to the manganese cluster of OEC-PS II. J Phys Chem B 102: 8248–8256

Cinco RM, McFarlane Holman KL, Robblee JH, Yano J, Pizarro SA, Bellacchio E, Sauer K and Yachandra VK (2002) Calcium EXAFS establishes the Mn-Ca cluster in the oxygen-evolving complex of Photosystem II. Biochem 41: 12928–12933

Debus RJ (1992) The manganese and calcium ions of photosynthetic oxygen evolution. Biochim Biophys Acta 1102: 269–352

Debus RJ (2000). The polypeptides of Photosystem II and their influence on manganotyrosyl-based oxygen evolution. In: Sigel A (ed) Metal ions in Biological Systems: Manganese and Its Role in Biological Processes, pp 657–711. Marcel Dekker, Inc., New York

Diner BA (2001) Amino acid residues involved in the coordination and assembly of the manganese cluster of Photosystem II. Proton-coupled electron transport of the redox-active tyrosines and its relationship to water oxidation. Biochim Biophys Acta 1503: 147–163

Ferreira KN, Iverson TM, Maghlaoui K, Barber J and Iwata S (2004) Architecture of the photosynthetic oxygen-evolving center. Science 303: 1831–38

Frasch W and Sayre RT (2001) Remembering George Cheniae. Photosynth Res 70: 245–247

Gantt E (1994) Supramolecular membrane organization. In: Bryant D (ed) The Molecular Biology of Cyanobacteria, pp 119–138. Kluwer Academic Publishers, Dordrecht

Ghirardi ML, Lutton TW and Seibert M (1998) Effects of carboxyl amino acid modification on the properties of the high-affinity, manganese-binding site in Photosystem II. Biochemistry 37: 13559–13566

Hankamer B, Morris E, Nield J, Gerle C and Barber J (2001) Three-dimensional structure of the Photosystem II core dimer of higher plants determined by electron microscopy. J Struct Biol 135: 262–269

Hillier W, Hendry G, Burnap RL and Wydrzynski T (2001) Substrate water exchange in Photosystem II depends on the peripheral proteins. J Biol Chem 276: 46917–24

Hong SK, Pawlikowski SA, Vander Meulen KA and Yocum CF (2001) The oxidation state of the Photosystem II manganese cluster influences the structure of manganese stabilizing protein. Biochim Biophys Acta 1504: 262–74

Hoober JK, White RA, Marks DB and Gabriel JL (1994) Biogenesis of thylakoid membranes with emphasis on the process in *Chlamydomonas*. Photosynth Res 39: 15–31

Hoshida H, Nakano Y and Toyoshima Y (1997a) PS II-L is required in the electron transfer at the donor side of P-680 to generate Y(z)(+)P(680)Pheo(–)state in PS II. Plant Physiol 114: 1032–1032

Hoshida H, Sugiyama R, Nakano Y, Shiina T and Toyoshima Y (1997b) Electron paramagnetic resonance and mutational analyses revealed the involvement of Photosystem II-L subunit in the oxidation step of Tyr-Z by P-680(+) to form the Tyr- Z(+)P(680)Pheo(–) state in Photosystem II. Biochemistry 36: 12053–12061

Hunziker D, Abramowicz DA, Damoder R and Dismukes GC (1987). Manganese and calcium binding properties of the extrinsic 33 kDa protein and of Photosystem II membranes. In: Biggins J (ed) Progress in Photosynthesis Research, pp 5997–5600. Martinus-Nijhoff, Dordrecht

Ishikawa Y, Yamamoto Y, Otsubo M, Theg SM and Tamura N (2002) Chemical modification of amine groups on psII protein(s) retards photoassembly of the photosynthetic water-oxidizing complex. Biochemistry 41: 1972–1980

Ivleva NB, Shestakov SV and Pakrasi HB (2000) The carboxyl-terminal extension of the precursor D1 protein of Photosystem II is required for optimal photosynthetic performance of the cyanobacterium *Synechocystis* sp PCC 6803. Plant Physiol 124: 1403–1411

Kashino Y, Lauber WM, Carroll JA, Wang QJ, Whitmarsh J, Satoh K and Pakrasi HB (2002) Proteomic analysis of a highly active Photosystem II preparation from the cyanobacterium *Synechocystis* sp. PCC 6803 reveals the presence of novel polypeptides. Biochemistry 41: 8004–8012

Katoh H, Itoh S, Shen JR and Ikeuchi M (2001) Functional analysis of psbV and a novel c-type cytochrome gene *psbV2* of the thermophilic cyanobacterium *Thermosynechococcus elongatus* strain BP-1. Plant Cell Physiol 42: 599–607

Kavelaki K and Ghanotakis DF (1991) Effect of the manganese complex on the binding of the extrinsic proteins (17-kDa ; 23-kDa and 33-kDa) of Photosystem-II. Photosynth Res 29: 149–155

Keller S, Beatty JT, Paddock M, Breton J and Leibl W (2001) Effect of metal binding on electrogenic proton transfer associated with reduction of the secondary electron acceptor (Q(B)) in *Rhodobacter sphaeroides* chromatophores. Biochemisty 40: 429–439

Keren N, Kidd MJ, Penner-Hahn JE and Pakrasi HB (2002) A light-dependent mechanism for massive accumulation of manganese in the photosynthetic bacterium *Synechocystis* sp. PCC 6803. Biochemistry 41: 15085–15092

Khangulov SV, Pessiki PJ, Barynin VV, Ash DE and Dismukes GC (1995) Determination of the metal-ion separation and energies of the 3 lowest electronic states of dimanganese(Ii,Ii) complexes and enzymes—catalase and liver arginase. Biochemistry 34: 2015–2025

Kufryk GI and Vermaas WF (2001) A novel protein involved in the functional assembly of the oxygen-evolving complex of Photosystem II in *Synechocystis* sp. PCC 6803. Biochemistry 40: 9247–55

Lers A, Heifetz PB, Boynton JE, Gillham NW and Osmond CB (1992) The carboxyl-terminal extension of the D1 protein of Photosystem-II is not required for optimal photosynthetic performance under CO_2-saturated and light-saturated growth-conditions. J Biol Chem 267: 17494–17497

Leuschner C and Bricker TM (1996) Interaction of the 33 kDa extrinsic protein with Photosystem II: Rebinding of the 33 kDa

extrinsic protein to Photosystem II membranes which contain four, two, or zero manganese per Photosystem II reaction center. Biochemistry 35(14): 4551–4557

Lockett CJ, Demeriou C, Bowden SJ and Nugent JA (1990) Studies on calcium depletion of PS II by pH 8.3 treatment. Biochim Biophys Acta 1016: 213–218

Lu YK and Stemler AJ (2002) Extrinsic Photosystem II carbonic anhydrase in maize mesophyll chloroplasts. Plant Physiol 128: 643–9

Lydakis-Simantiris N, Hutchison RS, Betts SD, Barry BA and Yocum CF (1999) Manganese stabilizing protein of Photosystem II is a thermostable, natively unfolded polypeptide. Biochemistry 38: 404–14

Mamedov F, Stefansson H, Albertsson PA and Styring S (2000) Photosystem II in different parts of the thylakoid membrane: A functional comparison between different domains. Biochemistry 39: 10478–10486

Mayes SR, Cook KM, Self SJ, Zhang ZH and Barber J (1991) Deletion of the gene encoding the photosystem-II 33-kDa protein from *Synechocystis* sp. PCC 6803 does not inactivate water-splitting but increases vulnerability to photoinhibition. Biochim Biophys Acta 1060: 1–12

Mei R and Yocum CF (1992) Comparative properties of hydroquinone and hydroxylamine reduction of the Ca^{2+}-stabilized O_2-evolving complex of PS II: Reductant-dependent Mn^{2+} formation and activity inhibition. Biochemistry 31: 8449–8454

Miller A-F and Brudvig G (1989) Manganese and calcium requirement for reconstruction of oxygen-evolution activity in manganese-depleted Photosystem II membranes. Biochemistry 28: 8181–8190

Miyao M and Murata N (1984) Role of the 33-kDa polypeptide in preserving Mn in the photosynthetic oxygen-evolution system and its replacement by chloride-ions. FEBS Lett 170: 350–354

Miyao M and Murata N (1989) The mode of binding of 3 extrinsic proteins of 33-kDa; 23-kDa and 18-kDa in the photosystem-II complex of spinach. Biochem Biophys Acta 977: 315–321

Miyao M, Murata N, Lavorel J, Maison-Peteri B, Boussac A and Etienne AL (1987) Effect of the 33-kDa protein on the S-state transitions in photosynthetic oxygen evolution. Biochim Biophys Acta 890: 151–159

Mohamed ZA (2001) Removal of cadmium and manganese by a non-toxic strain of the freshwater cyanobacterium gloeothece magna. Water Res 35: 4405–4409

Mukhopadhyay S, Staples R and Armstrong W (2002) Toward synthetic models for high oxidation state forms of the Photosystem II active site metal cluster: The first tetranuclear manganese cluster containing a $[Mn4(mu\text{-}O)_5]^{6+}$ core. Chem Commun 8: 864–865

Nanba O and Satoh K (1987) Isolation of a Photosystem-II reaction center consisting of D-1 and D-2 polypeptides and cytochrome-B-559. Proc Natl Acad Sci U S A 84: 109–112

Nield J, Balsera M, De Las Rivas J and Barber J (2002) Three-dimensional electron cryo-microscopy study of the extrinsic domains of the oxygen-evolving complex of spinach: Assignment of the PsbO protein. J Biol Chem 277: 15006–15012

Nixon PJ and Diner BA (1992) Asp170 of the PS II reaction center polypeptide D1 is involved in the assembly of the oxygen-evolving mn cluster. Biochemistry 31: 942–948

Nixon P, Trost J and Diner B (1992) Role of the carboxy terminus of polypeptide D1 in the assembly of a functional water-oxidizing manganese cluster in Photosystem II of the cyanobacterium *Synechocystis* sp. PCC 6803: Assembly requires a free carboxyl group at C-terminal position 344. Biochemistry 31: 10859–10871

Ogawa T, Bao D, Katoh H, Shibata M, Pakrasi H and Bhattacharyya-Pakrasi M (2002) A two-component signal transduction pathway regulates manganese homeostasis in *Synechocystis* 6803, a photosynthetic organism. J Biol Chem 277: 28981–28986

Ohta H, Okumura A, Okuyama S, Akiyama A, Iwai M, Yoshihara S, Shen JR, Kamo M and Enami I (1999) Cloning, expression of the *psbU* gene, and functional studies of the recombinant 12-kda protein of Photosystem II from a red alga *Cyanidium caldarium*. Biochem Biophys Res Commun 260: 245–50

Ono T (2000) Effects of lanthanide substitution at Ca^{2+}-site on the properties of the oxygen evolving center of Photosystem II. J Bioinorg Chem 82: 85–91

Ono T and Inoue Y (1984) Ca^{2+}-dependent restoration of O_2-evolving activity in Cacl2-washed PS-II particles depleted of 33-dKa; 24-kDa and 16-kDa proteins. FEBS Lett 168: 281–286

Philbrick JB, Diner BA and Zilinskas BA (1991) Construction and characterization of cyanobacterial mutants lacking the manganese-stabilizing polypeptide of photosystem-II. J Biol Chem 266: 13370–13376

Qian M, Al-Khaldi SF, Putnam-Evans C, Bricker TM and Burnap RL (1997) Photoassembly of the PS II Mn_4 cluster in site-directed mutants impaired in the binding of the Mn-stabilizing protein. Biochemistry 36: 15244–15252

Razeghifard MR, Wydrzynski T, Pace RJ and Burnap RL (1997) Yz. Reduction kinetics in the absence of the manganese-stabilizing protein of Photosystem II. Biochemistry 36: 14474–14478

Riggs-Gelasco PJ, Mei R, Yocum CF and Penner-Hahn JE (1996) Reduced derivatives of the Mn cluster in the oxygen-evolving complex of Photosystem II: An EXAFS study. J Am Chem Soc 118: 2387–2399

Rögner M, Chisholm DA and Diner BA (1991) Site-directed mutagenesis of the psbC gene of Photosystem II: Isolation and functional characterization of CP43-less Photosystem II core complexes. Biochemistry 30: 5387–5395

Rova M, Mamedov F, Magnuson A, Fredriksson PO and Styring S (1998) Coupled activation of the donor and the acceptor side of Photosystem II during photoactivation of the oxygen evolving cluster. Biochemistry 37: 11039–11045

Sansom M, Shrivastava I, Ranatunga K and Smith G (2000) Simulations of ion channels — watching ions and water move. Trends Biochem Sci. 25: 368–374

Schroda M, Krpat J, Oster U, Rüdiger W, Vallon O, Wollman F-A and Beck CF (2001) Possible role for molecular chaperones in assembly and repair of PS II. Biochem Soc Trans 29: 413–418

Seibert M (1993) Biochemical, biophysical, and structural characterization of the isolated PS II reaction center complex. In: Deisenhofer J and Norris JR (eds) The Photosynthetic Reaction Center Vol. 1, pp 319–356. Academic Press, New York

Shen JR, Burnap RL and Inoue Y (1995a) An independent role of cytochrome *c*-550 in cyanobacterial photosystem II as revealed by double-deletion mutagenesis of the *psbO* and *psbV* genes in *Synechocystis* sp. PCC 6803. Biochemistry 34: 12661–12668

Shen JR, Vermaas W and Inoue Y (1995b) The role of cyto-

chrome c-550 as studied through reverse genetics and mutant characterization in synechocystis sp. PCC 6803. J Biol Chem 270(12): 6901–6907

Shen JR, Qian M, Inoue Y and Burnap RL (1998) Functional characterization of synechocystis sp. PCC 6803 delta psbu and delta psbv mutants reveals important roles of cytochrome *c*-550 in cyanobacterial oxygen evolution. Biochemistry 37: 1551–1558

Smith D and Howe CJ (1993) The distribution of photosystem-I and photosystem-II polypeptides between the cytoplasmic and thylakoid membranes of cyanobacteria. Fems Microbiol Lett 110: 341–347

Smith RM and Martell AE (1976) Critical Stability Constants. Plenum, New York

Styring S and Rutherford AW (1987) In the oxygen-evolving complex of PS II the S_0 state is oxidized to the S_1 state by D+. Biochemistry 26: 2401–2405

Svensson B, Etchebest C, Tuffery P, Van Kan P, Smith J and Styring S (1996) A model for the Photosystem II reaction center core including the structure of the primary donor P680. Biochemistry 35: 14486–14502

Tamura N and Cheniae GM (1987) Photoactivation of the water-oxidizing complex in Photosystem II membranes depleted of Mn and extrinsic proteins. I. Biochemical and kinetic characterization. Biochim Biophys Acta 890: 179–194

Trost JT, Chisholm DA, Jordan DB and Diner BA (1997) The D1 C-terminal processing protease of Photosystem II from *Scenedesmus obliquus* — protein purification and gene characterization in wild type and processing mutants. J Biol Chem 272: 20348–20356

Utschig LM, Ohigashi Y, Thurnauer MC and Tiede DM (1998) A new metal-binding site in photosynthetic bacterial reaction centers that modulates Q_A to Q_B electron transfer. Biochemistry 37: 8278–8281

Vass I and Styring S (1991) Ph-dependent charge equilibria between tyrosine-d and the s states in Photosystem II. Estimation of relative midpoint redox potentials. Biochemistry 30: 830–9

Vass I, Ono T and Inoue Y (1987) Removal of 33 kDa extrinsic protein specifically stabilizes the S2qa- charge pair in photosystem-II. FEBS Lett 211: 215–220

Vrettos JS, Reifler MJ, Kievit O, Lakshmi KV, de Paula JC and Brudvig GW (2001a) Factors that determine the unusually low reduction potential of cytochrome *c*(550) in cyanobacterial Photosystem II. J Biol Inorg Chem 6: 708–716

Vrettos JS, Stone DA and Brudvig GW (2001b) Quantifying the ion selectivity of the Ca^{2+} site in Photosystem II: Evidence for direct involvement of Ca^{2+} in O_2 formation. Biochemistry 40: 7937–7945

Westphal KL, Lydakis-Simantiris N, Cukier RI and Babcock GT (2000) Effects of Sr^{2+}-substitution on the reduction rates of Y_Z in PS II membranes — evidence for concerted hydrogen-atom transfer in oxygen evolution. Biochemistry 39: 16220–16229

White RA, Wolfe GR, Komine Y and Hoober JK (1996) Localization of light-harvesting complex apoproteins in the chloroplast and cytoplasm during greening of *Chlamydomonas reinhardtii* at 38 degrees C. Photosynth Res 47: 267–280

Wincencjusz H, Yocum CF and van Gorkom HJ (1998) S-state dependence of chloride binding affinities and exchange dynamics in the intact and polypeptide depleted O_2 evolving complex of PS II. Biochemistry 37: 8595–8604

Wollenberger L, Stefansson H, Yu SG and Albertsson PA (1994) Isolation and characterization of vesicles originating from the chloroplast grana margins. Biochim Biophys Acta 1184: 93–102

Wollenberger L, Weibull C and Albertsson PA (1995) Further characterization of the chloroplast grana margins — the non-detergent preparation of granal Photosystem-I cannot reduce ferredoxin in the absence of NADP(+)reduction. Biochim Biophys Acta 1230: 10–22

Yocum CF (1991) Calcium activation of photosynthetic water oxidation. Biochim Biophys Acta 1059: 1–15

Zak E, Norling B, Maitra R, Huang F, Andersson B and Pakrasi HB (2001) The initial steps of biogenesis of cyanobacterial photosystems occur in plasma membranes. Proc Nat Acad Sci USA 98: 13443–13448

Zaltsman L, Ananyev G, Bruntrager E and Dismukes GC (1997) A quantitative kinetic model for photo-assembly of the photosynthetic water oxidase from its inorganic constituents: Requirements for Mn and Ca in the kinetically resolved steps. Biochemistry 36: 8914–8922

Zhang L, Virpi Paakkarinen V, van Wijk K and Aro E-M (2000) Biogenesis of the chloroplast-encoded d1 protein: Regulation of translation elongation, insertion, and assembly into Photosystem II. Plant Cell 12: 1769–1781

Zheleva D, Sharma J, Panico M, Morris HR and Barber J (1998) Isolation and characterization of monomeric and dimeric CP47-reaction center Photosystem II complexes. J Biol Chem 273: 16122–16127

Zouni A, Kern J, Loll B, Fromme P, Witt H, Orth P, Krauß N, Saenger W and Biesiadka J (2001) Biochemical characterization and crystal structure of water oxidizing Photosystem II from *Synechococcus elongatus*. In: PS2001: Proceedings of the 12th International Congress on Photosynthesis, S05-003. CSIRO Publishing, Melbourne (CD-ROM)

Chapter 27

Photoinactivation and Mechanisms of Recovery

Wah Soon Chow*
Photobioenergetics Group, Research School of Biological Sciences, The Australian National University, Canberra, ACT 0200, Australia

Eva-Mari Aro
Department of Biology, University of Turku, FIN-20014 Turku, Finland

*Author for correspondence, email: chow@rsbs.anu.edu.au

T. Wydrzynski and K. Satoh (eds): Photosystem II: The Light-Driven Water:Plastoquinone Oxidoreductase, pp. 627–648.

Summary

Photoinactivation of Photosystem II (PS II) is unavoidable in oxygenic photosynthesis, but the photodamage is counteracted by an elaborate repair process without which the photosynthetic apparatus would soon perish. Photoinactivation of PS II depends on the light dosage; the quantum yield of photoinactivation is such that practically the entire population of PS II would be photoinactivated during the course of a sunny day if repair were inhibited. An agent predominantly and inadvertently responsible for the photoinactivation of PS II is likely to be $P680^+$, the strongest oxidant in photosynthesis needed for the oxidation of water molecules. Amelioration of photoinactivation of PS II occurs via many strategies, including one mechanism that appears to sustain activity in a small population of PS II during prolonged high-light stress. The majority of PS II complexes, however, have to be repaired following their photoinactivation. The repair process, culminating in the biosynthesis and insertion of a new copy of the D1 protein in a re-assembled PS II reaction center, consists of many steps. These include: (1) 'triggering' of the D1 protein, leading to monomerization and partial disassembly of the PS II dimer complex in granal appressed membranes in higher-plant chloroplasts; (2) migration of the PS II core monomer to stroma-exposed thylakoids; (3) D1 proteolysis catalyzed, for example, first by the proteases DegP2 followed by FtsH1, or directly by FtsH2; (4) targeting of the ribosome/nascent D1 chain complex to the thylakoid membrane; (5) translation elongation of D1 and insertion of new D1 into a D1-depleted PS II; (6) ligation of cofactors in the PS II reaction center; (7) termination of translation and carboxyl-terminal processing of D1; (8) post-translational assembly of PS II monomers; and (9) migration of re-assembled PS II monomers to granal membranes, where functional PS II dimers are formed. In this way, the functionality of PS II is maintained despite the inevitability of photoinactivation.

I. Introduction

> '*Photosynthetic oxygen evolution is intrinsically suicidal'* (van Gorkom and Schelvis, 1993).

Light is both necessary for photosynthesis and detrimental to the photosynthetic apparatus — a paradox recognized by Ewart more than a century ago. Ewart (1896) reported that, 'Leaves exposed, attached to the parent plant, to full sunlight till 4 P.M. show no assimilation though living, green, and with normal chlorophyll (Chl) grains.' The loss of the ability to evolve oxygen is nowadays known as the photoinactivation (or photoinhibition) of Photosystem (PS) II, the pigment-protein complex that is most susceptible to light-induced damage during photosynthesis.

Ewart (1896) also recognized that, 'Before the vitality of the plant is permanently affected, there appears to be an intermediate condition from which perfect recovery is possible, but during which the power of assimilation is in abeyance.' We now know that ongoing photoinactivation of PS II is counteracted by a repair process, both occurring simultaneously and continually during photosynthesis.

In oxygenic photosynthesis two photosystems, PS II and PS I, work in series in performing the reaction: $2H_2O \rightarrow O_2 + 4H^+ + 4e^-$. The electrons released from water are transferred along a chain consisting of: PS II complex → PQ pool → Cyt *b/f* complex → Plastocyanin → PS I complex → $NADP^+$. PS II, responsible for splitting water molecules, has to generate oxidants that are sufficiently strong to oxidize water. Because of its role in forming such strong oxidants, PS II is itself highly susceptible to damage by the strong oxidants. This is presumably a primary reason for photosynthetic oxygen evolution being 'suicidal'.

Once photoinactivated, PS II needs to be repaired by de novo synthesis of the D1 protein which is the primary site of damage in the PS II reaction center (Kyle et al, 1984; Prásil et al., 1992; Aro et al., 1993; Melis, 1999; Andersson and Aro, 2001). If repair of the photodamage occurs at a sufficient rate, little net

Abbreviations: ΔpH – transthylakoid pH difference; Car – carotenoid; Chl – chlorophyll; CP47, CP43 – Chl *a*-binding proteins of PS II with molecular masses approximately 47 and 43 kDa, respectively; Cyt – cytochrome; D1, D2 protein – *psbA*/*psbB* gene product in the PS II reaction center, respectively; DCMU – 3-(3,4-dichlorophenyl)-1,1-dimethylurea; DTT – dithiothreitol; IPQ – inactive PS II-mediated quenching; k_i and k_r – rate coefficient for photoinactivation and repair of PS II, respectively; LMW – low molecular weight; $NADP^+$ – oxidized nicotinamide adenine dinucleotide phosphate; P680 – the primary electron donor in the PS II reaction center; Pheo – pheophytin; PQ – plastoquinone; PS I, PS II – Photosystem I, Photosystem II; Q_A, Q_B – first and second quinone acceptor of an electron in PS II, respectively

loss of function occurs. But if repair is retarded or photoinactivation is accelerated by an environmental stress, PS II becomes dysfunctional. Any net loss of PS II function will decrease photosynthetic efficiency measured in low light (Powles, 1984), and when more than about 40% of PS II complexes are inactivated, will also limit the maximum photosynthetic rate in high light (Lee et al., 1999).

Here we review the inter-related partial processes of photoinactivation and repair, and examine the molecular mechanisms of these processes. It is hoped that the use of light as a stress factor will help us understand not only the physiological implications of PS II dysfunction but also functional mechanisms in PS II itself.

II. The Inevitability of Photoinactivation of Photosystem II

It is usually thought that photoinactivation of PS II only occurs when the absorbed light exceeds the capacity of chloroplasts to utilize the excitation energy. This view, however, conceals the fact that photoinactivation of PS II occurs even in low light, and that it is the continual repair of PS II in vivo that ensures little *net* loss of function in low light.

A. The Dependence of Photosystem II Photoinactivation on the Light Dose

Combinations of irradiance and duration of illumination that give the same photon exposure (i.e., total incident photons m^{-2}) will produce the same extent of photoinactivation of PS II, *other things being equal*. This is the law of reciprocity, found to hold in photosynthetic organisms subjected to light stress (Jones and Kok, 1966; Lee et al., 1999; Park et al., 1995, 1996a). In the decrease in functional PS II complexes m^{-2} as a function of photon exposure for pea leaf discs in 1.1 % CO_2 (Anderson et al., 1997), for example, varying the irradiance at constant duration of illumination gives the same curve as varying the duration at constant irradiance. Similarly, reciprocity also holds in leaf discs of high-light grown capsicum that are illuminated in the presence of lincomycin (an inhibitor of D1 repair; Aro et al., 1994) while being floated on water in normal air. Figure 1A plots the decline in the functional PS II content with photon exposure when capsicum leaf discs are illuminated at 460, 900 or 1800 μmol m^{-2} s^{-1} for various durations;

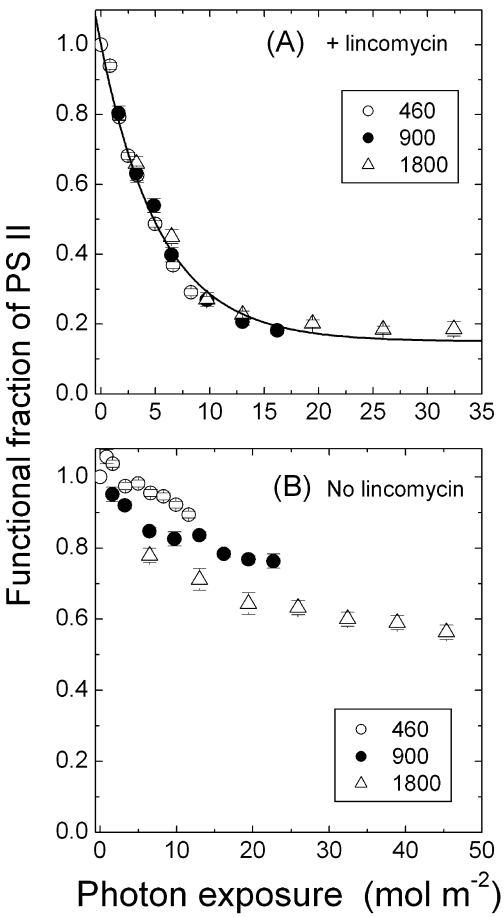

Fig. 1. The decrease in the content of functional PS II with photon exposure given to leaf discs of capsicum plants (grown under high light, 500 μmol photons m^{-2}) in the presence (A) or absence (B) of lincomycin. The irradiance was 460, 900 or 1800 μmol photons m^{-2}, applied for varied durations to give the photon exposures. Re-plotted from Lee et al. (2001).

the points essentially fall on the same curve. That is, the critical factor causing PS II photoinactivation is the number of incident photons, rather than the rate of their arrival per se.

However, reciprocity does not strictly hold when capsicum leaf discs are illuminated in normal air in the *absence* of lincomycin (Fig. 1B). It appears that the law of reciprocity is more likely to apply when D1 protein synthesis is inhibited, for example, by lincomycin. On the other hand, when repair via D1 protein synthesis is allowed to occur, the rate of repair

may be *irradiance dependent*, so that the extent of net photoinactivation for a given photon exposure may depend on the irradiance used (see Section IV.D). Similarly, when the rate of photosynthesis varies during photosynthetic induction, the rate of utilization of the excitation energy is *time-dependent*. Under such conditions, a long illumination at low irradiance does not have the same effect as a short illumination of high irradiance even if the photon exposure is the same, so reciprocity does not hold (Shen et al., 1996).

B. The Quantum Yield and Probability of Photosystem II Photoinactivation

In capsicum leaf discs, as is also true for pumpkin (Tyystjärvi et al., 1994) and *Tradescantia* (Park et al., 1996b), PS II is photoinactivated with an *approximately* single-exponential dependence on photon exposure (Lee et al., 1999, 2001). The steepest decline of functional PS II complexes occurs at low photon exposures. The magnitude of the steepest slope is the maximum quantum yield of photoinactivation of PS II. It is not constant, but varies, for example, with the light environment during growth and whether repair occurs. In PS II membrane fragments isolated from spinach, the quantum yield of photoinactivation is 0.1–0.3 μmol PS II per mol photons (Eckert et al., 1991), somewhat larger than the values for lincomycin-treated leaf discs of various plant species. Interestingly, the lowest maximum quantum yield of photoinactivation of PS II has been reported for grapevines leaves: 0.02 μmol PS II per mol photons even at 9 °C in the presences of lincomycin (Hendrickson et al., 2004).

A typical quantum yield of 0.1 μmol PS II per mol photons (as observed at low photon exposures in the absence of repair) means that, for every 10^7 incident photons, one member among a collection of PS II complexes is inactivated. This does not necessarily mean, however, that *each* PS II complex is inactivated after it has processed 10^7 photons). The value 0.1 μmol PS II per mol photons represents a small but significant cumulative photoinactivation of PS II because of the large number of photons incident on a leaf over a normal photoperiod. In the absence of repair, and at 25 % full sun (500 μmol photons m^{-2} s^{-1}) and assuming a typical initial concentration of 1 μmol functional PS II m^{-2}, the maximum rate of photoinactivation is calculated to be 18 percent of PS II inactivated per hour. In the presence of repair, the rate of D1 protein synthesis must also occur at a similar rate if there is to be little or no net loss of PS II activity. Thus, over a sunny day, practically the entire population of PS II complexes has to be repaired via de novo D1 protein synthesis.

To a certain extent, the photoinactivation of PS II complexes can be considered to be analogous to the decay of radioactive atoms. In the latter, identical atoms decay independently, with a probability that is directly proportional to an increment in time, resulting in an exponential decline in the population of radioactive atoms with time. Similarly, if it is assumed that (1) PS II complexes in a homogeneous population are photoinactivated independently, at least in the early to middle stages of the population decline (see Section IV.C), and (2) the probability of photoinactivation is directly proportional to an increment in photon exposure (Δx), i.e., $p = k\Delta x$, where k is a constant, then the number of functional PS II complexes (y) should decrease exponentially with photon exposure from an initial value y_o (Lee et al., 1999):

$$y = y_o \exp(-kx)$$

The quantum yield of photoinactivation at a given value of y is the slope at that point, while k ($= p/\Delta x$) is the probability per unit photon exposure. Further, since light treatments are usually carried out for different durations (t) at a fixed irradiance (I), y is usually plotted against t. Then the rate coefficient for the exponential decay is the product kI:

$$y = y_o \exp[-(kI)t]$$

Therefore, the rate coefficient (kI) is directly proportional to the irradiance, as observed (Tyystjärvi and Aro, 1996; Lee et al., 2001).

III. Potential Agents of Photosystem II Photoinactivation

A. Free Radicals Containing Oxygen

In an atmosphere containing oxygen, electron transfers inevitably lead to the formation of some superoxide anion radicals:

$$O_2 + e^- \rightarrow O_2^-$$

Superoxide anions are not very reactive radicals, not

much more reactive than oxygen itself, but superoxide dismutase catalyses a reaction to form H_2O_2 which is much more reactive:

$$2O_2^- + 2H^+ \rightarrow O_2 + H_2O_2$$

H_2O_2 can undergo one further reaction to form the hydroxyl radical, either by reaction with a reduced iron center or with another superoxide anion:

$$Fe^{2+} + H_2O_2 \rightarrow Fe^{3+} + OH^- + HO^\bullet \quad \text{or}$$

$$O_2^- + H_2O_2 \rightarrow O_2 + OH^- + HO^\bullet$$

$HO^\bullet$ is the most reactive of the three species, being able to render proteins susceptible to proteolytic attack; its formation must, therefore, be prevented. Leaves contain an enzyme system (ascorbate peroxidase, monodehydroascorbate peroxidase, dehydroascorbate peroxidase and glutathione reductase) which helps to convert H_2O_2 to H_2O, while regenerating the electron donors (Asada, 1996, 1999). Provided this enzyme system functions adequately, reactive oxygen species will not contribute to the photoinactivation of PS II. Indeed, when the concentration of oxygen is increased to 60%, photoinactivation of PS II in pea leaves is *ameliorated* (due to utilization of excess light by the Mehler reaction and photorespiration, and the dissipation of excitation energy via a pH gradient promoted by the Mehler reaction) despite the increased production of O_2^- (Park et al., 1996c).

Under normal circumstances, it seems reasonable to conclude that O_2^- and H_2O_2 are safely disposed of, thereby avoiding the formation of $HO^\bullet$. In adverse conditions, however, such as in the case of chilling-sensitive plants exposed to low temperatures, reactive oxygen species may constitute a problem. When that happens, PS I, the predominant site of production of O_2^-, may be photoinactivated more easily than PS II (Terashima et al., 1994; Sonoike 1996, 1998).

B. Singlet Excited Oxygen

The reaction center of PS II is a shallow trap: excitation energy trapped by the reaction center and inducing an electron transfer from a special Chl (P680) to pheophytin (Pheo), may re-emerge when charge recombination occurs in the radical pair, $P680^+$ $Pheo^-$. This is the basis of the exciton/radical pair equilibrium model (Schatz et al., 1988; Roelofs et al., 1992; Trissl and Lavergne, 1995; Chapters 7 and 22). If the radical pair is in a singlet state, $^1[P680^+ Pheo^-]$, where the two unpaired electrons have anti-parallel spin, charge recombination will produce (singlet excited) $^1P680^*$:

$$^1[P680^+ Pheo^-] \rightarrow {}^1P680^* + Pheo$$

On the other hand, a triplet state of the radical pair, in which the two unpaired electrons have parallel spin, will give triplet excited $^3P680^*$:

$$^3[P680^+ Pheo^-] \rightarrow {}^3P680^* + Pheo$$

Triplet P680, having a relatively long lifetime, may react with ordinary triplet oxygen to give singlet excited oxygen:

$$^3P680^* + {}^3O_2 \rightarrow P680 + {}^1O_2$$

Singlet oxygen is highly reactive, and has been suggested to trigger photoinactivation (e.g., Oxborough and Baker, 2000). Ideally, it should not be formed in the first place. Once formed, it should be removed quickly. Carotenoids play a role in de-activating singlet oxygen (van Gorkom and Schelvis, 1993; Telfer, 2002; Chapter 23):

$$^1O_2 + {}^1Car \rightarrow {}^3Car + {}^3O_2$$

$$^3Car \rightarrow {}^1Car + heat$$

The alternative possibility that carotenoids could prevent the formation of singlet oxygen by dissipating $^3P680^*$ does not seem to hold in practice because β-carotene in the reaction center must be located at a safe distance from $P680^+$, the strongest oxidant in photosynthesis (Barber, 1995; Telfer, 2002). Fortunately, under conditions where charge recombination is expected to be enhanced, namely, during continuous illumination when the primary quinone acceptor (Q_A) is chemically reduced and forward electron transfer from $Pheo^-$ to Q_A cannot occur, the decay of $^3P680^*$ may be hastened by a hundred fold, at least at the cryogenic temperatures of the experiments (van Mieghem et al., 1995). If this mechanism can operate under physiological conditions, singlet oxygen production is minimized, and the ever-occurring photoinactivation of PS II is less likely to be caused by singlet oxygen in vivo. Further, it has been proposed that the site of location of P680 in a *functional* PS II complex is

not freely accessible to oxygen molecules, and that there is a specific channel to direct O_2 liberated from water molecules out to the membrane surface, thereby restricting the formation of singlet oxygen (Anderson, 2001). A similar exclusion of oxygen from the site of production of triplet P700 has also been proposed for the PS I complex (Sétif et al., 1981).

In *photoinactivated* PS II complexes, however, there may have occurred some structural alteration which then allows oxygen to access ^{3}P680*, in which case singlet oxygen will be formed. Thus, it has been reported that singlet oxygen is produced in broad bean leaves, the rate of production being directly proportional to the concentration of *non-functional* PS II complexes (Hideg et al., 1998). Although structurally perturbed non-functional PS II complexes may allow singlet oxygen to be formed, *functional* PS II complexes are presumably not inactivated by singlet oxygen in the first place.

In a special case, the relative production of singlet oxygen can be maximized by infrequent excitation of PS II, e.g., by single-turnover flashes spaced many seconds apart (Keren et al., 1995, 1997). Under such conditions, Q_B^- free radicals are produced that have to wait for a considerable period before the next electron arrives at the two-electron gate (Chapter 8). The long waiting period presumably allows a conversion of ^{1}[P680$^+$ Pheo Q_A Q_B^-] to ^{3}[P680$^+$ Pheo Q_A Q_B^-], thence to ^{3}[P680$^+$ Pheo$^-$ Q_A Q_B], thereby increasing the likelihood of a charge recombination of the triplet radical pair ^{3}[P680$^+$ Pheo$^-$] (Keren et al., 1997). Recombination of the radical pair then produces ^{3}P680 from which $^1O_2$ is formed. In this way, a high quantum efficiency of photoinactivation of PS II can be achieved at a very low irradiance (~5 nmol photons m^{-2} s^{-1}; Keren et al., 1995).

C. P680$^+$

P680$^+$, the most powerful oxidant in photosynthesis, is formed when an electron is transferred from P680 to Pheo. P680$^+$ is ultimately required to extract electrons from otherwise stable water molecules. Anderson et al. (1998) concluded that P680$^+$ is most probably the chemical species that inadvertently inactivates PS II. Although direct evidence is difficult to obtain, there is indirect evidence for the case (Anderson et al., 1998), including:

(i) While Pheo$^-$ quickly transfers its electron to Q_A within about 0.4 ns after light is absorbed, P680$^+$ does not obtain its replacement electron for 20–200 ns. Therefore, P680$^+$ exists for a relatively long time during which it may react with its surroundings.

(ii) Illumination of PS II in which the donor side has been impaired leads to the accumulation of highly oxidizing radicals such as P680$^+$, which may cause photoinactivation (Theg et al., 1986; Thompson and Brudvig, 1988; Blubaugh and Cheniae, 1990; Jeggerschöld et al., 1990).

(iii) Photoinactivation occurs readily when leaf discs are illuminated in 100% N_2 in which there is no photosynthesis or oxygen generation and, therefore, no $^1O_2$ or O_2^- is produced (Park et al., 1997).

IV. The Variability of the Extent of Photosystem II Photoinactivation

A. Brief Overview of Ameliorating Factors

Plants have evolved numerous strategies to minimize the photoinactivation of PS II (for reviews, see Prásil et al., 1992; Aro et al., 1993; Chow, 1994; Osmond, 1994; Melis, 1999 and Niyogi, 1999; Adir et al., 2003). Briefly, these include adjustment of leaf orientation (Ludlow and Björkman, 1984; Öquist and Huner, 1991), chloroplast movement as a light-avoidance response (Chow et al., 1988; Park et al., 1996b), scavenging of reactive oxygen species (Asada, 1996, 1999), photorespiration as a safety valve (Powles and Osmond, 1979; Osmond, 1981), the Mehler reaction (Robinson, 1988; Park et al., 1996c), transthylakoid ΔpH-dependent quenching of excitation energy (Murata and Sugahara, 1969; Krause and Behrend, 1986; Oxborough and Horton, 1988; Horton et al., 1996), dissipation via zeaxanthin in the xanthophyll cycle (Demmig et al., 1987; Bilger and Björkman, 1990; Gilmore and Yamamoto, 1991; Gilmore, 1997; Gilmore and Govindjee, 1999; Ruban et al., 2002), adjustment to a smaller antenna (Park et al., 1997), adjustment of the redox potentials of Q_A and Q_B to enhance thermal dissipation in the functional reaction center (Sane et al., 2003) and photosynthetic acclimation to high light (see Chow, 1994 and references therein). The extent of PS II photoinactivation is thus modulated by the operation of various ameliorating factors.

B. Inactive Photosystem II-Mediated Quenching in Photoprotection

1. The Inactive Photosystem II-Mediated Quenching Phenomenon and Its Apparent Dependence on a ΔpH

Here, we consider one particular strategy of photoprotection, which operates when the majority of PS II complexes have been photoinactivated. Krause (1988) hypothesized that a photoinactivated PS II complex may dissipate excitation energy efficiently as heat, thereby preventing further damage to itself, e.g., destruction of antenna pigments. Giersch and Krasue (1991) and Öquist et al. (1992) extended this hypothesis by proposing that a photoinactivated PS II complex, by acting as an energy sink, may protect neighboring, connected functional PS II complexes from photoinactivation. Lee et al. (2001) extended the light treatment of capsicum leaf discs to large photon exposures which decreased the functional fraction of PS II to 30% or less, and observed a small, resilient population which survived large photon exposures despite the inhibition of D1 protein synthesis by lincomycin. The residual sub-population of PS II is depicted in Fig. 1A. A similar observation has also been reported for pea (Park et al., 1997) and *Arabidopsis* (Norén et al., 1999). This mechanism of photoprotection is termed inactive PS II-mediated quenching, IPQ, by Chow et al. (2002).

The above observation was analyzed by Lee et al. (2001) in terms of a hypothesis that a small sub-population of functional PS II is protected by photoinactivated and extensively-modified neighbors. They postulated that the 'intrinsic' rate coefficient (k_i) is significantly decreased by a certain numerical factor (which varies with the fraction of active PS II) only when more than about 70% of the PS II complexes have been photoinactivated; at a lesser extent of photoinactivation, the numerical factor has a negligible effect on k_i. This numerical factor, a purely formal description of an effect that comes into play only after a heavy loss of functional PS II complexes, is dependent, in this model, on the effectiveness with which the severely-photoinactivated PS II complexes are able to protect their functional neighbors. From the effects of the uncoupler, nigericin, the effectiveness with which photoinactivated PS II complexes protect their functional neighbours appears to depend on a ΔpH across the thylakoid membrane (Lee et al., 2002).

It is not clear how an acidic lumen or a transthylakoid ΔpH can regulate the IPQ photoprotective mechanism. However, protonation of proteins can certainly have profound effects on, for example, energy-dependent quenching (Horton et al., 1996; Gilmore, 1997) and calcium-binding to PS II (Krieger and Weis, 1993). Horton et al. (1996) have described four targets of protonation, each capable of regulating energy flow in PS II. In this context, it is interesting to note that grana formation allows a controlled dissipation of excitation energy (Horton, 1999): in low light, the presence of grana prevents a collapse of the dense array of proteins into a highly dissipative state; in high light, protonation of protein residues is prevalent, favoring closer packing and enhancing non-photochemical quenching. Given these various profound effects of protonation, perhaps the connectivity among PS II neighbors is itself promoted by protonation but impaired when nigericin is present.

2. Energy Dissipation in Photoinactivated Photosystem II Reaction Centers

How could a severely-photoinactivated PS II complex act as a strong sink for excitation energy? When the excitation energy reaches a PS II reaction center, a temporary charge separation occurs, leaving an electron on the acceptor side and an electron hole on the donor side of PS II. Since a photoinactivated reaction center is incapable of transferring an electron further down the chain, one possible dissipatory pathway is for a charge recombination to take place *directly to form the ground state*. In this way, the light energy could be safely dissipated as heat. Charge recombination directly to the ground state has been proposed for moderately photoinactivated pea thylakoids (Richter et al., 1999). It could conceivably occur to a much greater extent in severely-photoinactivated PS II reaction centers that have been subjected to extensive modification, for example, by oxygenation (Miyao, 1994; Barber, 1998). Indeed, two populations of photoinactivated PS II reaction centers in vivo have been observed. One is weakly-quenching with a chlorophyll fluorescence lifetime of 1.25 ns and the other strongly-quenching with a lifetime of 0.58 ns, the latter corresponding to severely-photoinactivated PS II reaction centers (Matsubara and Chow, 2004).

A specific mechanism has been proposed for reaction-center dissipation in over-wintering pine needles. On the acceptor side of PS II are two quinone accep-

tors, Q_A and Q_B (Chapter 8). The redox potential of the Q_B^-/Q_B couple is normally less negative than that of Q_A^-/Q_A, allowing further stabilization of charge separation. However, from thermoluminescence measurements of over-wintering pine needles, Ivanov et al. (2002) concluded that severe photoinactivation of PS II renders the redox potential of the Q_B^-/Q_B couple closer to that of Q_A^-/Q_A. This presumably favors the distribution of electrons on Q_A, increasing the population of Q_A^-. In turn, the increased $[Q_A^-]$ increases the probability of non-radiative charge recombination between Q_A^- and an electron hole on the donor side of PS II, including the special Chl cation, $P680^+$ (Krieger-Liszkay and Rutherford, 1998; Vavilin and Vermaas, 2000). Such a charge recombination, if resulting in a ground state directly and not an excited state, could allow the reaction center to act as an energy sink.

However, to enhance charge recombination of Q_A^- and $P680^+$ to the ground state directly probably requires closer proximity of the redox potentials of the couples Q_A/Q_A^- and $P680/P680^+$. A smaller redox potential difference between these two couples will enhance radiationless transition in a way that is analogous to an increased probability of radiationless transition at a smaller energy gap in large molecules (Englman and Jortner, 1970). A smaller redox potential difference could be achieved in two ways, each with additional photoprotective effects (Fig. 2). First, the redox potential of Q_A/Q_A^- could be rendered less negative following photoinactivation, as occurs when DCMU binds to PS II (Krieger-Laszkay and Rutherford, 1998). Then the redox potential difference between Q_A/Q_A^- and $Pheo/Pheo^-$ is increased, impairing a back electron transfer and inhibiting the formation of the $P680^+/Pheo^-$ state. In this way, the formation of triplet P680 is minimized, thereby minimizing the formation of highly-reactive singlet oxygen. Second, the redox potential of $P680/P680^+$ could be rendered less positive following photoinactivation, as proposed by Anderson and Chow (2002). The less oxidizing $P680^+$ implies less likelihood of further damage induced by light. At the same time, a smaller energy gap between Q_A/Q_A^- and $P680/P680^+$ favors charge recombination directly to the ground state.

C. Rate Coefficients of Photosystem II Photoinactivation

As Kok (1956) postulated, the rate of PS II photoinactivation is directly proportional to the concentration

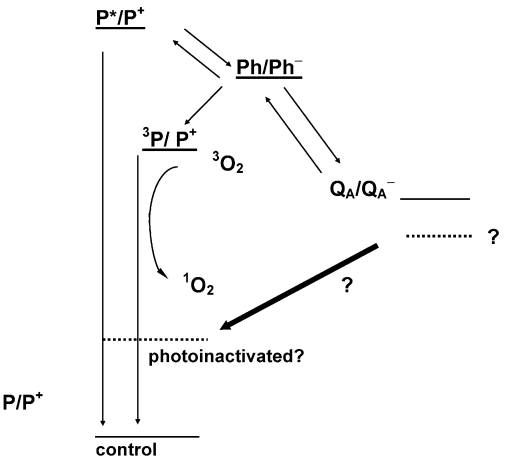

Fig. 2. A schematic diagram of the potentials of redox couples involved in the recombination of the radical pair P^+/Q_A^-. Negative potentials are at the top of the diagram, and positive potentials at the bottom. Back electron transfer from Q_A^- to Pheo (abbreviated as Ph) leads to either a singlet state of P680 (abbreviated as P) or a triplet state (^3P). ^3P may lead to the formation of reactive singlet oxygen $^1O_2$ if P is accessible to molecular oxygen. The generation of $^1O_2$ can be minimized by a less negative potential for Q_A/Q_A^- (greater energy gap between Ph/Ph^- and Q_A/Q_A^-). Alternatively, a less positive potential for P/P^+ could result from modification of PS II after photoinactivation, and would less readily cause further damage. In either case, a smaller energy gap between Q_A/Q_A^- and P/P^+ could enhance radiationless dissipation of the radical pair P^+/Q_A^- (see text) by a charge recombination directly to the ground state (thick arrow).

of active PS II (y) when no repair occurs:

$$dy/dt = -k_i\, y$$

where k_i is the rate coefficient of photoinactivation. The value of k_i increases linearly with irradiance (Tyystjärvi and Aro, 1996; Lee et al., 2001). Baroli and Melis (1996) also showed that the rate of loss of D1 protein increased linearly with the irradiance under which *Duniella salina* cells were grown and measured. The range of k_i values obtained by Lee et al. (2001) for capsicum was similar to that observed for *Dunaliella* (Baroli and Melis, 1966); it was understandably somewhat greater than that observed by Tyystjärvi and Aro (1996) for pumpkin because the pumpkin plants had been acclimated to very high growth irradiance and were consequently more resistant to high light stress.

Lee et al. (2001) showed that at a given test irradiance, k_i was slightly lower for capsicum plants

grown at a lower growth irradiance. They ascribed this decreased susceptibility of PS II to photoinactivation to the better connectivity of PS II complexes when plants are grown in low light. The better connectivity then allows better sharing of the excitation energy either for photochemical utilization or safe dissipation, as has been postulated by Anderson and Aro (1994). Interestingly, k_i was higher at 35 °C than at 25 °C or 15 °C (Lee et al., 2001), in agreement with the earlier finding of Tyystjärvi et al. (1994) using isolated thylakoids. The higher temperature might have caused instability in the water oxidation complex, such that electron donation to $P680^+$ was slow, and the longer-lived $P680^+$ could then damage PS II with an increased probability.

D. Rate Coefficients of Repair

The observed rate of PS II photoinactivation is the net result of simultaneous gross photoinactivation and repair of PS II. The two partial processes can be separated if the net rate of photoinactivation is measured in the presence and absence of repair and two equations are solved simultaneously. The solution yields the separate coefficients of photoinactivation and repair under a given irradiance. The value of k_r in *Capsicum* so obtained (Lee et al., 2001) is comparable to values observed for D1 protein synthesis using [^{35}S]methionine labeling in *Brassica* (Sundby et al., 1993), peas (Aro et al., 1994), and *Dunaliella* (Vasilikiotis and Melis, 1994).

As expected, k_r is highly dependent on temperature (Greer et al., 1986): it is very low at 15 °C but increased by an order of magnitude at 35 °C, both in low-light and high-light grown *Capsicum* plants (Lee et al., 2001). The acceleration of repair at a higher temperature could be attributed to increased enzymic activity and faster temperature-dependent lateral diffusion of photoinactivated PS II, or parts of the entity, from granal stacks to stroma-exposed membrane regions where chloroplast ribosomes are located (see Section V).

When measured over a wide range of irradiance, the repair rate coefficient is very low (but not zero) in darkness (He and Chow, 2003). Further, a low irradiance (e.g., 29 μmol m^{-2} s^{-1}) is sufficient to give nearly the maximum rate coefficient. Only a small further increase is achieved when the test irradiance is increased to the growth irradiance or slightly higher.

Another general trend is a decrease in k_r with further increase in treatment irradiance far beyond growth irradiance (Lee et al., 2001; He and Chow, 2003), implying slower rates of repair at higher irradiances. This is consistent with the results of Sundby et al. (1993) who reported that incorporation of radio-labeled methionine into D1 protein was already maximal at approximately the same irradiance as during growth, but that higher irradiances inhibited incorporation of radio-label.

It is curious that the rate coefficient of repair (Lee et al., 2001) and the gross rate of D1 protein synthesis (Sundby et al., 1993; see re-analysis by Chow, 2001) decrease at high irradiance just when repair is most needed. This trend with high irradiance is probably due to oxidative stress encountered by leaf discs floating on water while illuminated: the restriction of CO_2 entry into the tissue is likely to lead to O_2 playing a more prominent role as an electron acceptor, with consequent generation of H_2O_2 and potentially $^{\bullet}HO^{\bullet}$. It has been shown that oxidative stress induced by the presence of H_2O_2 (Nishiyama et al., 2001) or $^1O_2$ (Nishiyama et al., 2004) inhibits the repair of PS II rather than causing direct damage to PS II.

V. Molecular Rearrangements Preceding the Degradation of the D1 Protein

As described above, PS II photoinactivation and photodamage are determined by intrinsic light-induced chemical properties of the PS II reaction center. D1 protein is the primary target of photodamage, and the replacement of the damaged protein is a prerequisite for restoration of photosynthetic function. The light-induced damage to the D1 protein occurs in the appressed grana membranes (Cleland et al., 1986; Mäenpää et al., 1987; Adir et al., 1990), where functional PS II centers exist as dimers. It is, however, well established that the repair of PS II and replacement of the damaged D1 protein with a newly synthesized copy take place in the stroma-exposed thylakoid domains (Mattoo and Edelman, 1987) where PS II exists in the monomer configuration (Aro et al., 2005).

The D1 protein is located in the very heart of the PS II supercomplex, in which each of the two PS II monomers comprises up to 25 different protein subunits (Chapters 3–6) and are surrounded by a complex set of Lhcb antenna proteins (Chapter 2, Green and Gantt) in higher plants and green algae. Several lines of evidence suggest that damage to the D1 protein

leads to monomerization of the PS II complex (Prásil et al., 1992; Aro et al., 1993; Hankamer et al., 1997), which may facilitate the migration of damaged PS II to stroma-exposed thylakoid regions and subsequent degradation of the damaged copy of D1. Only a rather small and fixed number of PS II centers can undergo repair in stroma-exposed thylakoids at a time (Kettunen et al., 1997). Indeed, under conditions that induce severe photoinactivation of PS II, most of the damaged PS II centers remain in the grana (Aro et al., 2005), with their D1 protein in a phosphorylated state (Baena-Gonzalez et al., 1999). Phosphorylation of PS II core proteins in granal appressions is likely to prevent a premature disassembly of photodamaged PS II complexes. Only after the migration of the damaged PS II complex to stroma-exposed thylakoid domains and dephosphorylation of the PS II core proteins, both processes requiring light, does the damaged D1 protein become susceptible to proteolytic degradation (Rintamäki et al., 1996).

PS II complexes in cyanobacteria, which lack both the granal structures and core protein phosphorylation, have their reaction centers constantly exposed to the cytosol. In these organisms the inactivation of PS II and subsequent photodamage to the D1 protein are more directly followed by proteolytic degradation of the D1 protein than in higher-plant chloroplasts in which the photodamage and repair processes are segregated to grana and stroma thylakoids, respectively.

VI. Degradation of the Damaged D1 Protein

Prerequisites for degradation of the photodamaged D1 protein in all oxygenic photosynthetic organisms are a partial disassembly of the PS II complex and the presence of a membrane-associated proteolytic enzyme system. This might suggest that either the partial disassembly of the PS II complex could be enough to allow access of a proteolytic system to degrade D1 or, alternatively, an irreversible photodamage should induce some kind of 'triggering' of the D1 protein in the reaction center, making it a substrate for proteolysis.

There are several pieces of information suggesting an involvement of a conformational change (triggering) in the D1 protein before proteolytic degradation. This possibility is supported by the well-characterized protective effect of urea and triazine type herbicides on the D1 protein degradation (Kyle et al., 1984; Mattoo et al., 1984; Trebst et al., 1988; Jansen et al., 1993). These herbicides bind tightly to the Q_B site of the D1 protein and may thereby restrict a conformational change and thus a triggering of the protein for proteolysis. The fact that the D1 protein undergoes transient phosphorylation in higher-plant PS II complexes has sometimes been suggested to play a role in the triggering process. However, the phospho-D1 protein is a poor substrate for proteolytic degradation (Koivuniemi et al., 1995) and its phosphorylation appears to have more of a regulatory function during the turnover process (Rintamäki and Aro, 2001). Moreover, the triggering and subsequent degradation of the D1 protein in green algae as well as in cyanobacteria proceed in the absence of any post-translational phosphorylation process.

A. D1 Protein Degradation Patterns

The D1 protein is an integral membrane protein composed of five transmembrane helices (designated A–E) with connecting stromal and lumenal loops (Chapter 4, Nixon et al.). Its amino (N)-terminus and carboxyl (C)-terminus are exposed at the stromal and lumenal thylakoid surfaces, respectively (Hankamer et al., 1997). The D1 protein forms a heterodimer with the homologous D2 protein, surrounded by approximately 25 other subunits forming the PS II supercomplex. The proteolytic degradation of such a membrane spanning protein in a multisubunit pigment protein complex is apparently not a trivial process but requires special molecular arrangements in the thylakoid membrane, as briefly discussed above, as well as a coordinated proteolytic machinery.

Much experimental effort has been made in the past to identify the D1 protein degradation fragments in order to pinpoint where the protein is initially cleaved. Most data concerning D1 protein degradation fragments stem from in vitro photoinhibitory experiments on isolated thylakoids or purified PS II preparations. Typically, an N-terminal 23 kDa fragment and a C-terminal 10 kDa fragment are identified in vitro (Aro et al., 1993; Andersson and Barber, 1996) corroborating the primary cleavage in the stromal DE-loop. This fragmentation pattern is seen under conditions of acceptor side induced photoinhibition. Contrariwise, when the PS II particles were subjected to donor side photoinhibition, the primary D1 degradation fragments were identified as an N-terminal 9 kDa fragment and a C-terminal 24 kDa fragment (Barbato et al., 1991; De Las Rivas et al., 1992; Andersson and

Barber, 1996). This suggests that the primary cleavage under donor side photoinhibitory conditions is not the stromal DE-loop but rather the lumenal loop between helices A and B. It remains to be established whether the different fragmentation patterns associated with the two photoinhibitory mechanisms are due to triggering effects at the substrate level or the enzymatic action of different proteases. Importantly, it is still unclear whether the degradation of the D1 protein follows the same pattern in vitro and in vivo (see below).

B. Proteases Involved in D1 Protein Degradation

The identification of the protease or proteases responsible for the D1 protein degradation has been a central issue in the research field during the last decade (Aro et al., 1993; Andersson and Barber, 1996; Adam and Clarke, 2002; Silva et al., 2003). The number of candidate proteases is, however, increasing and no consensus on this field exists so far.

Although several in vitro experiments have suggested that the proteolytic activity is closely associated with the PS II complex, since at least a slow degradation could be induced in various isolated PS II particles (Shipton and Barber, 1991; De Las Rivas et al., 1992), the efficiency of D1 degradation clearly increases in preparations that also include stromal thylakoids. Biochemical approaches to identify and isolate a D1-specific protease, despite intense efforts for more than a decade, have not been successful, possibly due to the fact that the relevant enzymes are not very abundant. Consideration of the prokaryotic origin of the chloroplast and application of the results obtained by molecular and biochemical analysis of bacterial proteases to this organelle have been key features in the progress made during the last few years (Lindahl et al., 2000; Haussühl et al., 2001; Adam and Clarke, 2002; Bailey et al., 2002; Sakamoto et al., 2002; Silva et al., 2003). Moreover, recent computational and experimental analyses with *Arabidopsis thaliana* genome have revealed a complex and intriguing chloroplast degradation machinery with nearly 50 putative proteolytic enzymes (Adam et al., 2001; Sokolenko et al., 2002). So far, there is experimental evidence for two key chloroplast protease families being involved in D1 protein degradation, the DegP proteases and the FtsH proteases (Lindahl et al., 2000; Haussühl et al., 2001; Adam and Clarke, 2002; Bailey et al., 2002; Silva et al., 2003).

1. DegP Proteases

The *Arabidopsis* genome has up to 14 genes encoding the members of the DegP peptidase family (Adam et al., 2001; Sokolenko et al., 2002). Four of them are indisputably targeted to the chloroplast. A homologue of the cyanobacterial protease designated DegP (DegP1) was first found in chloroplasts of *Arabidopsis* and pea (Itzhaki et al., 1998). This protease is located in the lumenal space of the thylakoid membrane system. More recently two other DegP peptidases, DegP5 and DegP8, were localized to the lumenal compartment by a proteome approach (Schubert et al., 2002). Genomic analysis has further revealed the presence in *Arabidopsis* of a highly conserved homologue of these DegP proteases, which has been designated DegP2 and was suggested to be involved in D1 protein degradation (Haussühl et al., 2001). DegP2 is encoded as a precursor 66.8 kDa protein containing a transit peptide typical of chloroplast-targeted proteins. The mature protein has a molecular weight of 60 kDa and has no predicted membrane span but a short hydrophobic domain at its C-terminal region. It contains a catalytic triad (serine, histidine and aspartic acid) typical of serine proteases (Adam et al., 2001). Membrane topological experiments suggest that the protein is located at the outer thylakoid surface of the stroma-exposed thylakoid regions.

Overexpression of the DegP2 protein in *E. coli* followed by His-tag affinity purification was performed in order to experimentally test the potential role of DegP2 in D1 protein degradation (Haussühl et al., 2001). When added to photoinhibited thylakoid membranes where the endogenous enzyme had been removed by salt washing, DegP2 could induce a significant degradation of the D1 protein with a concomitant production of an N-terminal 23 kDa fragment. Under similar conditions no other proteins were degraded by the purified protease. DegP2 could also degrade the D1 protein in thylakoids subjected to elevated temperatures. The overexpressed enzyme itself, however, appeared to be more active at lower temperatures, in apparent contradiction to the previous in situ experiments demonstrating only limited D1 protein degradation at low temperatures (Aro et al., 1990). However, it is conceivable that the triggering of the D1 protein for degradation, i.e., the conformational change in the protein, is more susceptible to low temperature than the proteolysis itself. The DegP2 protease appears currently as one of the candidates for the elusive primary D1 protease.

2. FtsH Proteases

Members of the FtsH family of proteases are encoded by up to 16 homologous genes in *Arabidopsis*, and most of these proteins are localized or predicted to reside in chloroplasts (Adam and Clarke, 2002; Sokolenko et al., 2002). The FtsH protease is a membrane-integrated ATP-dependent peptidase, which also has chaperone activity, the protease existing in an oligomeric state when catalytically active. However, ATP has not been found to directly promote the light-induced D1 protein degradation when tested under in vitro conditions. The role of an FtsH family peptidase (FtsH1) in D1 protein degradation was first demonstrated using an in vitro biochemical approach to study the degradation of the D1 protein primary fragment. An enhanced proteolytic removal of the N-terminal 23 kDa primary fragment was observed in the presence of ATP, and the most efficient degradation of this fragment was obtained when the ATP was supplemented with zinc ions. These observations made a logical connection between the bacterial type of the FtsH protease in chloroplasts and the D1 protein secondary degradation, the enzyme having been earlier shown to be located in the stroma-exposed regions of plant thylakoid membranes (Lindahl et al., 1996). FtsH is a 78 kDa integral membrane protein with two predicted transmembrane regions. The C-terminus comprises a bulky hydrophilic region, which is exposed to the chloroplast stroma and contains the catalytic and nucleotide binding sites. The enzymatic activity of FtsH is dependent on ATP and Zn^{2+}. Over-expressed and affinity-purified *Arabidopsis* FtsH was shown to specifically degrade the accumulated N-terminal 23 kDa fragment both in isolated thylakoids and in PS II core complexes (Lindahl et al., 2000). In experiments involving thylakoids, and thus an endogeneous FtsH protease in the stroma exposed membranes, the catalytic domain of the endogenous FtsH was first removed by trypsin, a treatment that upon illumination resulted in the accumulation of the 23 kDa fragment of the D1 protein. Based upon these experiments, it was concluded (Lindahl et al., 2000) that the secondary proteolysis during D1 protein degradation is catalysed by FtsH in a process requiring ATP and Zn^{2+}. This member of the FtsH family has been assigned as FtsH1 (Adam et al., 2001).

Results discussed above suggest that the D1 protein is degraded in a two-step proteolytic event (Fig. 3), which is not unexpected considering its complicated folding with five membrane-spanning regions. It is conceivable that even proteases other than DegP2 and FtsH1 are involved in D1 degradation, considering the need for cleavages also in the loops exposed to the inner thylakoid surface. Possible candidates for such proteases could be the lumenal DegPs (now termed DegP1, DegP5 and DegP8) (Itzhaki et al., 1998; Schubert et al., 2002).

The two-step proteolytic degradation of the D1 protein is probably not the only mechanism to deplete PS II centers of the damaged D1 protein. Indeed, there is now compelling evidence that the members of the FtsH family are not only functioning in the secondary degradation of the D1 protein primary fragments but are also capable of chewing the whole D1 protein when damaged (Fig. 3). The *Arabidopsis* Var2 mutant, with inactivated FtsH2 protein, showed enhanced susceptibility to photoinhibition that was experimentally demonstrated to result from reduced capacity for D1 protein degradation (Bailey et al., 2002). Similarly, a FtsH2 inactivation mutant of *Synechocystis* sp. PCC 6803 resulted in severe retardation of D1 protein degradation (Bailey et al., 2001; Silva et al., 2003). Based on these in vivo experiments, it was suggested that the FtsH2 protease is capable of complete digestion of the damaged D1 protein and possibly no initial cleavage site in the D1 protein is necessary. In line with these observations it was recently reported that

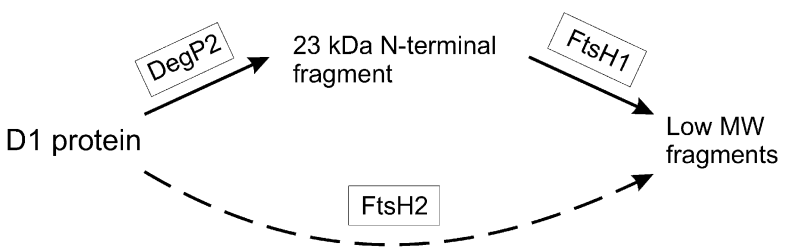

Fig. 3. Degradation of the D1 protein can occur in a two-step proteolytic process involving DegP2 and FtsH1 but there is also compelling evidence that the FtsH2 isomer can chew the D1 protein without a need for preceding primary cleavage.

FtsH in *E. coli* can initiate progressive proteolysis of membrane embedded substrates at the N-terminal cytosolic tail of a membrane protein, by recognizing its length but not the exact sequence (Chiba et al., 2002). The N-terminal end of the substrate protein should consist of at least 20 amino acids, which is well in accordance with the length of D1 protein N-terminus in various oxygenic organisms. Moreover, the absolute ATP dependence of FtsH proteolytic activity has recently been questioned. Experiments with bacterial systems have shown that the proteolytic and ATPase activities of FtsH can be uncoupled under conditions where the substrate is sufficiently unstructured (Cooper and Baneyx, 2001; Krzywda et al., 2002). Such a loss of structure apparently can occur in the D1 protein upon photodamage, possibly thereby making it susceptible to proteolysis by FtsH without an absolute requirement of ATP. It is also interesting to note that the transcript levels of both *ftsH1* and *ftsH2* genes increase in *Synechocystis* cells upon transfer of cyanobacteria to high light intensity (Hihara et al., 2001).

Considering the location of proteases so far known to be involved in D1 protein degradation, the degradation of the D1 protein in vivo apparently occurs on stroma exposed thylakoid regions where the FtsH proteases are located. Interestingly, a mass spectrometric analysis of the polypeptide composition of *Synechocystis* PS II complex, isolated by His-tag (in CP47) affinity purification, revealed more than 25 polypeptides including two FtsH proteases, one corresponding to FtsH1 and the other to FtsH2 protease (according to Sokolenko et al., 2002) as intrinsic PS II proteins (Kashino et al., 2002). It can be concluded that the redundancy of the proteolytic machinery in the chloroplast probably guarantees a safe degradation of the damaged D1 protein under a variety of environmental conditions. Indeed, the removal of the photodamaged D1 protein copy is essential for plant survival and during evolution the proteolytic system might have become more complex to guarantee the continuation of plant life on earth.

VII. Biogenesis and Assembly of the New D1 Copy into Photosystem II

A. PsbA Transcripts and Translation Initiation

The PS II reaction center protein D1 is encoded by the *psbA* gene (Zurawski et al., 1982). In chloroplasts a single *psbA* gene encodes the D1 protein. Cyanobacteria, on the other hand, generally have a small *psbA* gene family with three to four gene copies (Curtis and Haselkorn, 1984; Jansson et al., 1987). Not only the number of genes but also the regulation of cyanobacterial *psbA* genes differs from that in chloroplasts. In cyanobacteria the *psbA* gene transcription is strongly regulated by light (Mohamed and Jansson, 1989, Tyystjärvi et al., 1996) and the transcripts produced have a half-life of 10 to 20 min in light (Mulo et al., 1998; Herranen et al., 2001). In chloroplasts, on the other hand, the *psbA* transcripts are remarkably stable with the half-life ranging between 10 and 40 hours (Mullet and Klein, 1987; Klaff and Gruissem, 1991). Although some up-regulation in *psbA* gene transcription takes place at high irradiances, the diurnal fluctuations in *psbA* transcripts are relatively small as compared to those in cyanobacteria. Indeed, the main regulation of *psbA* gene expression resides at the level of transcription initiation in cyanobacteria (Golden et al., 1986; Mohamed and Jansson, 1989) whereas in higher plants the corresponding main regulatory level resides on translation initiation of *psbA* mRNAs (Chapter 28, Yamaguchi et al.).

Somanchi and Mayfield (2001) first demonstrated the connection between active photosynthesis and *psbA* mRNA translation initiation using *Chlamydomonas* as an experimental model. They elucidated a complicated light-driven activation of *psbA* mRNA translation initiation occurring upon increase in the ATP/ADP ratio and the generation of reduced thioredoxin (Chapter 28). Such conditions were shown to induce a binding of a nuclear-encoded protein complex to the 5′untranslated region of the *psbA* mRNA. This allows a proper association of ribosomes and the scanning of *psbA* mRNA to be initiated. Such highly regulated mechanism for translation initiation is apparently missing from cyanobacteria, and with *Synechocystis* it was demonstrated that the *psbA* transcripts are probably always attached to ribosomes (Tyystjärvi et al., 2001).

B. Targeting and Insertion of D1 Nascent Chains to the Thylakoid Membrane

Although only low light intensities are required to saturate the initiation of *psbA* mRNA translation in chloroplasts, and although all the *psbA* transcripts seem to be associated with ribosomes in cyanobacteria irrespective of light conditions, the D1 protein is not synthesized in uncontrolled amounts either

in cyanobacteria or in chloroplasts. It was recently shown with *Synechocystis* that the targeting of the ribosome/nascent D1 chain complexes to the thylakoid membrane is probably an important step in the regulation of D1 elongation in cyanobacterial cells (Tyystjärvi et al., 2001). In chloroplasts, the *psbA* mRNA ribosome complexes are efficiently targeted to the thylakoid membrane in light, most likely via binding of cpSRP54 (Nilsson et al., 1999), a chloroplast homologue of the signal recognition particle (SRP). In line with this observation, reverse genetics studies have revealed that *Arabidopsis* cpSRP54 mutants fail to accumulate the D1 protein early in development (Amin et al., 1999). After targeting of the *psbA* mRNA-ribosome-nascent D1 chain complex to the thylakoid membrane, the elongation and membrane insertion of the D1 protein are controlled by a variety of factors, including a translocon association and availability of assembly partners, as well as redox control and ligation of pigments (Zerges, 2002; Zhang and Aro, 2002). Despite an efficient association of the *psbA* mRNA ribosome complexes with the thylakoid membrane in light, they have, however, turned out to be under elongation arrest if the membranes, or rather the PS II complexes, are not in the need for new D1 copies (Kettunen et al., 1997; Zhang et al., 1999). It is conceivable that the synthesis of a new D1 copy can be accomplished only after the cleavage of the damaged D1 protein. Thus the synthesis process can only be completed when an assembly partner, a D1-depleted PS II composed of at least the D2 protein and the Cyt b_{559} subunits, is available.

Early pulse-labeling studies with intact isolated chloroplasts already revealed that ribosomes pause at discrete sites on *psbA* mRNA, presumably to facilitate the insertion of transmembrane domains of D1 into the thylakoid membrane, and the ligation of various factors to the D1 protein (Kim et al., 1991). More recently, we used the in vitro translation system in intact chloroplast to find novel proteins interacting with D1 nascent chains during early phases of membrane insertion (Zhang et al., 2001). The ribosome-nascent D1 chain complexes were isolated from intact chloroplasts after a short pulse labeling. Subsequently, an association of labeled nascent D1 chains with other interacting proteins was studied by immunoprecipitation, co-immunoprecipitation and cross-linking experiments. An intriguing discovery was a close interaction of ribosome-D1 nascent chain complexes with cpSecY (Zhang et al., 2001), a chloroplast homologue of the bacterial translocation channel protein SecY (Roy and Barkan, 1998). This strongly suggests that the cpSecY/E/G translocon in thylakoid membranes does not only function in post-translational translocation and insertion of a set of nuclear-encoded thylakoid proteins (Schnell, 1998; Keegstra and Cline, 1999; Chapter 29, Theg and Shi) but also guides the translocation and insertion of the chloroplast-encoded D1 protein. Strong interaction of ribosomes with cpSecY suggests that the ribosomes anchor at this translocon channel, which then starts guiding the membrane insertion of the elongating D1 protein (Zhang et al., 2001).

C. Regulation of D1 Protein Elongation and Co-translational Assembly Steps

As discussed above, the elongation of D1 protein is strictly dependent on the availability of assembly partners (Kettunen et al., 1997; Zhang et al., 1999; Zerges, 2002; Baena-Gonzales and Aro, 2002). Recently, this interpretation was further supported by studies with the *Arabidopsis var-2-2* mutant, which is not capable of efficient D1 protein degradation (Bailey et al., 2002). Interestingly, the translation of the D1 protein in this mutant is also severely retarded, as was revealed by pulse-chase experiments. This result is consistent with the hypothesis that D1 synthesis is strongly controlled by the availability of assembly partners, in this case a PSII subcomplex depleted of the D1 protein.

In vitro translation in intact chloroplasts and subsequent 'protective' fractionation of the thylakoid membrane has provided an excellent method for studies of the regulation of D1 protein elongation and assembly into PS II (Zhang et al., 1999, 2000). Applying as short pulses as possible (only a couple of minutes) to incorporate a sufficient amount of radiolabeled methionine into elongating D1 chains, it has been possible to chase the label into precursor D1 protein via different D1 elongation intermediates and finally to follow the maturation of the D1 protein through C-terminal processing. It was demonstrated that already during the elongation phase the D1 protein starts to interact with other PS II proteins.

Translation elongation has been noted to have a crucial regulatory role in the biogenesis of the D1 protein for a long time (Kim et al., 1991, 1994; Taniguchi et al., 1993; Kuroda et al., 1996; Edhofer et al., 1998). Labeling studies with intact chloroplasts have made it possible to get new insights into the regulation of D1 translation elongation without interference

from complicated regulation of translation initiation (Somanchi and Mayfield, 2001). Translation elongation of *psbA* mRNA was shown to be dependent on electron transport, which provides the system with essential reducing compounds via PS I electron flow (Kuroda et al., 1996; Zhang et al., 1999), and maintains a transmembrane proton gradient (Mühlbauer and Eichacker, 1998, Zhang et al., 2000). The former claim is supported by the ability of either PS I electron transfer or a reduced thiol reactant dithiothreitol (DTT) to restore D1 elongation under conditions where PS II electron transfer was blocked with DCMU. Dissipation of the proton gradient with nigericin or other uncouplers completely blocks the elongation process (Mühlbauer and Eichaker, 1998; Zhang et al., 2000). These observations are in accordance with several earlier experiments (Aro et al., 1994) indicating that the synthesis of the new D1 copy and repair of PS II centers are mostly prohibited in darkness.

Light, although obligatory for PS II repair, is required only in very low fluence rates to saturate the synthesis of the D1 protein and to allow maximal recovery of plants from photoinhibition (He and Chow, 2003). Besides being required for the initiation and elongation of the *psbA* mRNA translation, light is probably also essential for migration of the damaged PS II complexes from the grana membranes to the stroma-exposed membranes as well as for subsequent dephosphorylation and degradation of the D1 protein (Rintamäki and Aro, 2001).

Most of the cofactors in PS II are ligated to the reaction center proteins D1 and D2. Ligation of cofactors to the D1 protein during its turnover cycle has been suggested to occur upon pausing of ribosomes at specific sites on the *psbA* mRNA (Kim et al., 1991). This has been considered also to stabilize the nascent D1 chains against proteolytic degradation. Further information about the assembly of the D1 protein into PS II was obtained by searching for possible interactions between the ribosome-D1 nascent chain complexes and the other PS II core proteins and/or yet unknown proteins possibly involved in D1 protein biogenesis (Zhang et al., 1999, 2000).

Protein-protein interactions during D1 protein elongation were not limited to cpSecY. It was revealed that the 17 kDa D1 intermediate, composed of two transmembrane α-helices, with the third helix still in the ribosome tunnel, is already interacting with the D2 protein (Zhang et al., 1999). This association, however, is rather weak and easily disrupted, e.g., by detergents. When four transmembrane helices of D1 have been translated and inserted into the thylakoid membrane, a strong interaction between the elongating D1 and the D2 protein was evident. Ligation of most cofactors is probably accomplished at this stage (Kim et al., 1991), while the formation of a transient disulfide bridge between the nascent D1 chain and the D2 protein is likely to strengthen this interaction (Zhang et al., 2000). Indeed the elongation of the nascent D1 chain and its interaction with the D2 protein are strongly hampered if the thiol groups are chemically reduced by DTT or alkylated by N-ethylmaleimide (Zhang et al., 2000).

Further elongation and finally the termination of *psbA* mRNA translation result in a release of a precursor D1 protein (pD1) from ribosomes. This is followed by fast insertion of the fifth transmembrane helix into the membrane with concomitant traversal of the C-terminus with its cleavable extension into the thylakoid lumen.

D. Post-translational Assembly Steps in the Repair of Photosystem II

C-terminal processing of the precursor D1 protein is conducted by a lumenal protease (Anbudurai et al., 1994) soon after termination of translation (Chapter 29, Theg and Shi). This step in the repair of PS II is particularly temperature-dependent and completely inhibited at low temperatures (Kanervo et al., 1997). As described above, the newly synthesized D1 is co-translationally associated with a pre-existing PS II subcomplex (comprised at least of the D2 protein and the α and β subunits of Cyt b_{559}) during the repair of damaged PS II centers. This repair step is followed by the attachment of a pre-existing CP47 protein to the PS II subcomplex (Fig. 4). Many of the low molecular weight (LMW) subunits are also already present at this stage. Recent pulse-chase experiments showed relatively rapid turnover for the PsbH subunit, which associates with the PS II subcomplex in parallel with CP47 (Rokka et al., 2005). The possibility that CP47 and several LMW subunits do not dissociate from PS II during the repair process cannot, however, be completely excluded, as the biochemical isolation procedures employed include detergents that may destabilize the PS II subcomplexes undergoing repair. Finally, the CP43 protein is attached to the PS II complex (Zhang et al., 2000). It was recently shown that the PsbL subunit is particularly important in stabilizing the assembly of CP43 (Suorsa et al.,

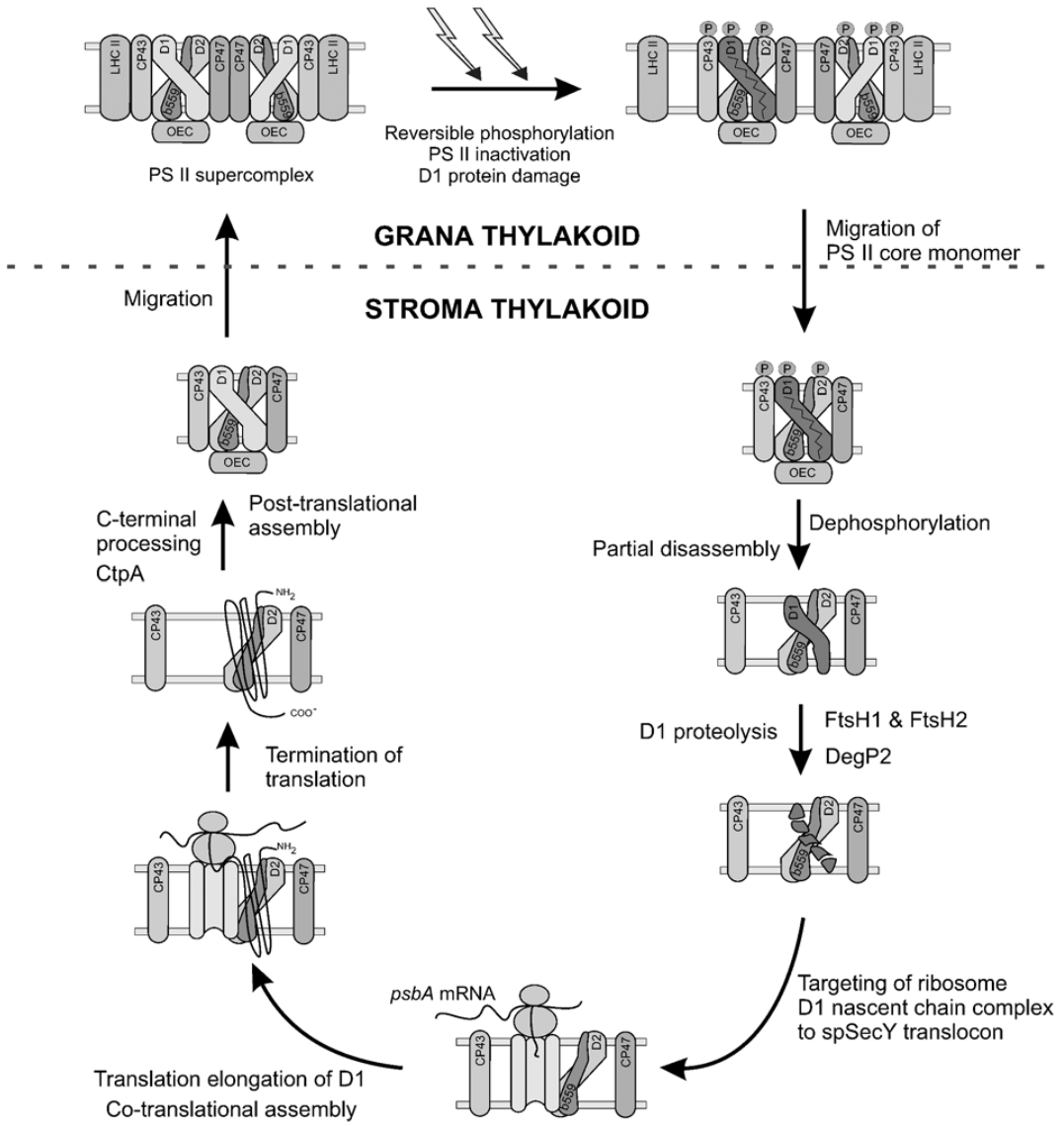

Fig. 4. Photoinhibition-repair cycle of the PS II complexes. See text for details. See Color Plate 14, Fig. 1.

2004). Reversible dissociation and re-association of CP43 with PS II during the repair process is indisputable, as opposed to the uncertainty concerning CP47. Labeling of intact chloroplasts show that either a nonlabeled, and thus pre-existing CP43, or a newly synthesized CP43 can associate with PS II after a replacement of the damaged D1 protein. Moreover, an antibody against CP47 (but not against the CP43 protein) is capable of co-immunoprecipitation with D1 elongation intermediates. All the PS II assembly steps discussed above require oxidizing conditions in the thylakoid membrane (Zhang et al., 2000).

Chase of the newly synthesized D1 protein into PS II assemblies revealed that either a precursor or a mature form of the D1 protein could be present in the assemblies that also include D2, Cyt b_{559}, CP47 and

presumably several LMW subunits. On the contrary, the CP43 protein was stably assembled only in those PS II complexes where the D1 protein had undergone maturation via C-terminal processing (Zhang et al., 2000). These subcomplexes were also shown to include the PsbJ subunit (Suorsa et al., 2004), which is known to be essential for proper association of the oxygen-evolving complex (Hager et al., 2002). Coordination between the processing of the C-terminal extension of the D1 protein and the assembly of CP43/PsbJ might be important for 'safe' ligation of the Mn cluster and subsequent photoactivation of the oxygen evolving complex. These processes have been shown to be extremely vulnerable to light-inactivation (Rova et al., 1998). Removal of the C-terminal extension has long been known to be a prerequisite for re-association of the oxygen evolving complex and restoration of the water splitting activity of PS II (Diner et al., 1988; Bowyer et al., 1992).

All the assembly steps discussed above probably take place on stroma-exposed thylakoid domains where the PS II monomers are assembled. Repair of PS II by such assembly steps is not directly dependent on de novo synthesis of Chl or carotenoid pigments, evidenced by efficient synthesis of D1 and its normal assembly into PS II despite the presence of inhibitors of Chl or carotenoid biosynthesis (Zhang et al., 2000). PS II monomers, properly assembled in stroma thylakoids, then migrate to the grana where PS II core dimerization and hierarchical association of various LHCII complexes are accomplished. Essential roles in the coordination of this higher organization of the PS II supercomplexes in the grana are probably played by two LMW subunits, the PsbW and PsbZ proteins (Shi et al., 2000; Swiatek et al., 2001; Aro et al., 2005).

In summary, although PS II performing oxygenic photosynthesis is intrinsically suicidal, there is an elaborate mechanism by which the inactivated photosystem is partially disassembled, damaged components synthesized, and a new functional complex assembled – a kind of 'death and resurrection' cycle.

Acknowledgments

WSC would like to thank Jan Anderson, Y-I Park, H-Y Lee, Y-M Park and Y-N Hong, for collaboration. He is very grateful to Barry Osmond for an opportunity, at a critical time, to work in his former laboratory and to continue with the fun of photosynthesis research. He thanks the Australian Research Council for funding support (DP0343160). E-MA would like to acknowledge her colleagues for stimulating discussions and Mika Keränen for preparing Figs. 3 and 4. Research in E-MA's laboratory has been supported by the Academy of Finland, Finnish Ministry of Agriculture and Forestry and Nordiskt Kontaktorgan för Jordbruksforskning.

References

Adam Z and Clarke AK (2002) Cutting edge of chloroplast proteolysis. Trends Plant Sci 7: 451–456

Adam Z, Adamska I, Nakabayashi K, Ostersetzer O, Haussuhl K, Manuell A, Zheng B, Vallon O, Rodermel SR, Shinozaki K and Clarke AK (2001) Chloroplast and mitochondrial proteases in *Arabidopsis*. A proposed nomenclature. Plant Physiol 125: 1912–1918

Adir N, Shochat S and Ohad I (1990) Light-dependent D1 protein synthesis and translocation is regulated by reaction center II. Reaction center II serves as an acceptor for the D1 precursor. J Biol Chem 265: 12563–12568

Adir N, Zer H, Shouchat S and Ohad I (2003) Photoinhibition — a historical perspective. Photosynth Res 73: 343–340

Amin P, Sy DA, Pilgrim ML, Parry DH, Nussaume L and Hoffman NE (1999) *Arabidopsis* mutants lacking the 43- and 54-kilodalton subunits of the chloroplast signal recognition particle have distinct phenotypes. Plant Physiol 121: 61–70

Anbudurai PR, Mor TS, Ohad I, Shestakov SV and Pakrasi HB (1994) The *ctpA* gene encodes the C-terminal processing protease for the D1 protein of the Photosystem II reaction center complex. Proc Natl Acad Sci USA 91: 8082–8086

Anderson JM (2001) Does functional Photosystem II complex have an oxygen channel? FEBS Lett 488: 1–4

Anderson JM and Aro E-M (1994) Grana stacking and protection of Photosystem II in thylakoid membranes of higher plant leaves under sustained high irradiance: An hypothesis. Photosynth Res 41: 315–326

Anderson JM and Chow WS (2002) Functional/structural dynamics of plant Photosystem II. Phil Trans Roy Soc London B, 357: 1441–1450

Anderson JM, Park Y-I and Chow WS (1997) Photoinactivation and photoprotection of Photosystem II in nature. Physiol Plant 100: 214–223

Anderson JM, Park YI and Chow WS (1998) Unifying model for the photoinactivation of Photosystem II in vivo under steady-state photosynthesis. Photosynth Res 56: 1–13

Andersson B and Aro E-M (2001) Photodamage and D1 protein turnover in Photosystem II. In: Aro E-M and Andersson B (eds) Regulation of Photosynthesis, pp 377–394. Kluwer Academic Publishers, Dordrecht

Andersson B and Barber J (1996) Mechanisms of photodamage and protein degradation during photoinhibition of Photosystem II. In: Baker NR (ed) Photosynthesis and the Environment, pp 101–121. Kluwer Academic Publishers, Dordrecht

Aro EM, Hundal T, Carlberg I and Andersson B (1990) In vitro studies on light-induced inhibition of Photosystem II and D1-

protein degradation at low temperatures. Biochim Biophys Acta 1019: 269–275
Aro EM, Virgin I and Andersson B (1993) Photoinhibition of Photosystem II. Inactivation, protein damage and turnover. Biochim Biophys Acta 1143: 113–134
Aro EM, McCaffery S and Anderson JM (1994) Recovery from photoinhibition in peas (*Pisum sativum L.*) acclimated to varying growth conditions. Plant Physiol 104: 1033–1041
Aro EM, Suorsa M, Rokka A, Allahverdiyeva Y, Paakkarinen V, Saleem A, Battchikova N and Rintamäki E. (2005) Dynamics of Photosystem II — a proteomic approach to thylakoid protein complexes. J Exp Bot 56: 347–356
Asada K (1996) Radical production and scavenging in the chloroplasts. In: Baker NR (ed) Photosynthesis and the Environment, pp 123–150. Kluwer Academic Publishers, Dordrecht
Asada K (1999) The water-water cycle in chloroplasts: Scavenging of active oxygens and dissipation of excess photons. Annu Rev Plant Physiol Plant Mol Biol 50: 601–639
Baena-Gonzalez E, Barbato R and Aro EM (1999) Role of PSII phosphorylation in the PSII repair cycle and oligomeric structure. Planta 208: 196–204
Bailey S, Silva P, Nixon P, Mullineux CW, Robinson C and Mann N (2001) Auxiliary functions in photosynthesis: The role of the FtsH protease. Biochem Soc Trans 29: 455–459
Bailey S, Thompson E, Nixon P, Horton P, Mullineux CW, Robinson C and Mann NH (2002) A critical role for the Var2 FtsH homologue of *Arabidopsis thaliana* in the Photosystem II repair cycle in vivo. J Biol Chem 277: 2066–2011
Barbato R, Shipton CA, Giacometti, GM and Barber J (1991) New evidence suggests that the initial photoinduced cleavage of the D1 protein may not occur near the PEST sequence. FEBS Lett 290: 162–166
Barber J (1995) Molecular basis of the vulnerability of Photosystem II to damage by light. Aust J Plant Physiol 22: 201–208
Barber J (1998) Photosystem two. Biochim Biophys Acta 1365: 269–277
Baroli I and Melis A (1996) Photoinhibition and repair in *Dunaliella salina* acclimated to different growth irradiance. Planta 198: 640–646
Bilger W and Björkman O (1990) Role of the xanthophyll cycle in photoprotection elucidated by measurements of light-induced absorbance changes, fluorescence and photosynthesis in leaves of *Hedera canariensis*. Photosynth Res 25: 173–185
Blubaugh DJ and Cheniae GM (1990) Kinetics of photoinhibition in hydroxylamine-extracted Photosystem II: Relevance to photoinactivation and sites of electron donation. Biochemistry 29: 5109–5118
Bowyer JR, Packer JCL, McCormack BA, Whitelegge JP, Robinson C and Taylor M (1992) Carboxyl-terminal processing of the D1 protein and photoactivation of water splitting in Photosystem II. J Biol Chem 267: 5424–5433
Chiba S, Akiyama Y and Ito K (2002) Membrane protein degradation by FtsH can be initiated from either end. J Bacteriol 184: 4775–4782
Chow WS (1994) Photoprotection and photoinhibitory damage. Adv Mol Cell Biol 10: 151–196
Chow WS (2001) The photoinactivation of Photosystem II in leaves: A personal perspective. J Photoscience 8: 43–53
Chow WS, Qian L, Goodchild DJ and Anderson JM (1988) Photosynthetic acclimation of *Alocasia macrorrhiza* (L.) G. Don to growth irradiance: Structure, function and composition of chloroplasts. Aust J Plant Physiol 15: 107–122
Chow WS, Lee H-Y, Park Y-I, Park Y-M, Hong Y-N and Anderson JM (2002) The role of inactive photosystem-II-mediated quenching in a last-ditch community defence against high light stress in vivo. Phil Trans R Soc Lond B 357: 1441–1450
Cleland RE, Melis A and Neale JP (1986) Mechanism of photoinhibition: Photochemical reaction center inactivation in system II of chloroplasts. Photosynth Res 9: 79–88
Cooper KW and Baneyx F (2001) *Escherichia coli* FtsH (HflB) degrades a membrane-associated TolAl-II-β-lactamase fusion protein under highly denaturating conditions. Protein Express Purif 21: 323–332
Curtis SE and Haselkorn R (1984) Isolation, sequence and expression of the two members of the 32 kd thylakoid membrane protein gene family from the cyanobacterium *Anabaena* 7120. Plant Mol Biol 3: 249–258
De Las Rivas J, Shipton CA, Ponticos M and Barber J (1992) Acceptor side mechanism of photo-induced proteolysis of the D1 protein in Photosystem II reaction centers. Biochemistry 32: 6944–6950
Demmig B, Winter K, Krüger A and Czygan F-C (1987) Photoinhibition and zeaxanthin formation in intact leaves. Plant Physiol 84: 218–224
Diner BA, Ries DF, Cohen BN and Metz JG (1988) COOH-terminal processing of polypeptide D1 of the Photosystem II reaction center of *Scenedesmus obliquus* is necessary for the assembly of oxygen evolving complex. J Biol Chem 263: 8972–8980
Eckert H-J, Geiken B, Bernading, Napiwotzki A, Eichler H-J and Renger G (1991) Two sites of photoinhibition of the electron transfer in oxygen evolving and Tris-treated PS II membrane fragments from spinach. Photosynth Res 27: 97–108
Edhofer I, Mühlbauer SK and Eichacker LA (1998) Light regulates the rate of translation elongation of chloroplast reaction center protein D1. Eur J Biochem 257: 78–84
Englman R and Jortner J (1970) The energy gap law for radiationless transition in large molecules. Mol Phys 18: 145–164
Ewart AJ (1896) On assimilatory inhibition in plants. J Linn Soc 31: 364–461
Giersch C and Krasue GH (1991) A simple model relating photoinhibitory fluorescence quenching in chloroplasts to a population of altered Photosystem II reaction centers. Photosynth Res 30: 115–121
Gilmore AM (1997) Mechanistic aspects of xanthophyll cycle-dependent photoprotection in higher plant chloroplasts and leaves. Physiol Plant 99: 197–209
Gilmore A and Govindjee (1999) How higher plants respond to excess light: Energy dissipation in Photosystem II. In: Singhar AS, Renger A, IIrrang K-D, Sopory S and Govindjee (eds) Concepts in Photobiology: Photosynthesis and Photomorphogenesis, pp 513–548. Narosa Publishers, New Dehli/Kluwer Academic Publishers, Dordrecht
Gilmore AM and Yamamoto HY (1991) Zeaxanthin formation and energy-dependent fluorescence quenching in pea chloroplasts under artificially mediated linear and cyclic electron transport. Plant Physiol 96: 635–643
Golden SS, Brusslan J and Haselkorn R (1986) Expression of a family of *psbA* genes encoding a Photosystem II polypeptide in the cyanobacterium *Anacystis nidulans* R2. EMBO J 5: 2789–2798
Greer DH, Berry JA and Björkman O (1986) Photoinhibition of photosynthesis in intact bean leaves: Role of light and tempera-

ture, and requirement for chloroplast-protein synthesis during recovery. Planta 168: 253–260

Hager M, Herrmann M, Biehler K, Krieger-Liszkay A and Bock R (2002) Lack of the small plastid-encoded PsbJ polypeptide results in a defective water-splitting apparatus of Photosystem II, reduced Photosystem I levels and hypersensitivity to light. J Biol Chem 277: 14031–14039

Hankamer B, Boekema EJ and Barber J (1997) Structure and membrane organization of Photosystem II in green plants. Annu Rev Plant Physiol Plant Mol Biol 48: 641–671

Haussühl K, Andersson B and Adamska I (2001) A chloroplast DegP2 protease performs the primary cleavage of the photodamaged D1 protein in plant Photosystem II. EMBO J 20: 1–10

He J and Chow WS (2003) The rate coefficient or repair of photosystem II after photoinactivation. Physiol Plant 118: 297–304

Hendrickson L, Förster B, Furbank RT and Chow WS (2004) Processes contributing to photoprotection of grapevine leaves illuminated at low temperature. Physiol Plant 121: 272–281

Herranen M, Aro EM and Tyystjärvi T (2001) Two distinct mechanisms regulate the transcription of Photosystem II genes in *Synechocystis* sp. PCC 6803. Physiol Plant 112: 531–539

Hideg E, Kálai T, Hideg K and Vass I (1998) Photoinhibition of photosynthesis in vivo results in singlet oxygen production. Detection via nitroxide-induced fluorescence quenching in broad bean leaves. Biochemistry 37: 11405–11411

Hihara Y, Kamei A, Kanehisa M, Kaplan A and Ikeuchi M (2001) DNA microarray analysis of cyanobacterial gene expression during acclimation to high light. Plant Cell 13: 793–806

Horton P (1999) Are grana necessary for regulating of light harvesting? Aust J Plant Physiol 26: 659–669

Horton P, Ruban AV and Walter RG (1996) Regulation of light harvesting in green plants. Annu Rev Plant Physiol Plant Mol Biol 47: 655–684

Itzhaki H, Naveh L, Lindahl M, Cook M and Adam Z (1998) Identification and characterization of DegP, a serine protease associated with the lumenal side of the thylakoid membrane. J Biol Chem 273: 7094–7098

Ivanov AG, Sane PV, Zeinalov Y, Simidjiev I, Huner NPA and Öquist G (2002) Seasonal responses of photosynthetic electron transport in Scots pine (*Pinus sylvestris* L.) studied by thermoluminescence. Planta 215: 457–465

Jansen MAK, Depka B, Trebst A and Edelman, M (1993) Engagement of specific sites in plastoquinone niche regulates degradation of D1 protein in Photosystem II. J Biol Chem 268: 21246–21252

Jansson C, Debus RJ, Osiewacz HD, Gurevitz M and McIntosh L (1987) Construction of an obligate photoheterotrophic mutant of the cyanobacterium *Synechocystis* 6803. Inactivation of the psbA family. Plant Physiol 85: 1021–1025

Jegerschöld C, Virgin I and Styring S (1990) Light-dependent degradation of the D1 protein in Photosystem II is accelerated after inhibition of the water splitting reaction. Biochemistry 29: 6179–6186

Jones LW and Kok B (1966) Photoinhibition of chloroplast reactions. Kinetics and action spectra. Plant Physiol 41: 1037–1043

Kanervo E, Murata N and Aro EM (1997) Membrane lipid unsaturation modulates processing of the Photosystem II reaction-center protein D1 at low temperatures. Plant Physiol 114: 841–849

Kashino Y, Lauber WM, Carroll JA, Wang Q, Whitmarsh J, Satoh K and Pakrasi HB (2002) Proteomic analysis of a highly active Photosystem II preparation from the cyanobacterium *Synechocystis* sp. PCC 6803 reveals the presence of novel polypeptides. Biochemistry 41: 8004–8012

Keegstra K and Cline K (1999) Protein import and routing system of chloroplasts. Plant Cell 11: 557–570

Keren N, Gong H and Ohad I. (1995) Oscillations of reaction center II-D1 protein degradation in vivo induced by repetitive light flashes. J Biol Chem 270: 806–814

Keren N, Berg A, van Kan PJM, Levanon H and Ohad I (1997) Mechanism of Photosystem II photoinactivation and D1 protein degradation at low light: The role of back electron flow. Proc Natl Acad Sci USA 94: 1579–1584

Kettunen R, Pursiheimo S, Rintamäki E, van Wijk KJ and Aro EM (1997) Transcriptional and translational adjustments of *psbA* gene expression in mature chloroplasts during photoinhibition and subsequent repair of Photosystem II. Eur J Biochem 247: 441–448

Kim J, Klein PG and Mullet JE (1991) Ribosomes pause at specific sites during synthesis of membrane-bound chloroplast reaction center protein D1. J Biol Chem 266: 14931–14938

Kim J, Eichaker LA, Rüdiger W and Mullet JE (1994) Chlorophyll regulates accumulation of the plastid-encoded chlorophyll-proteins P700 and D1 by increasing apoprotein stability. Plant Physiol 104: 907–916

Klaff P and Gruissem W (1991) Changes in chloroplast mRNA stability during leaf development. Plant Cell 3: 517–529

Koivuniemi A, Aro EM and Andersson B (1995) Degradation of D1 and D2 proteins of Photosystem II in higher plants is regulated by reversible phosphorylation. Biochemistry 34: 16022–16029

Kok B (1956) On the inhibition of photosynthesis by intense light. Biochim Biophys Acta 21: 234–244

Krause GH (1988) Photoinhibition of photosynthesis. An evaluation of damaging and protective mechanisms. Physiol Plant 74: 566–574

Krause GH and Behrend U (1986) ΔpH-dependent chlorophyll fluorescence quenching indicating a mechanism of protection against photoinhibition of chloroplasts. FEBS Lett 200: 298–302

Krieger A and Weis E (1993) The role of calcium in the pH-dependent control of Photosystem II. Photosynth Res 37: 117–130

Krieger-Liszkay A and Rutherford AW (1998) Influence of herbicide-binding on the redox potential of the quinone acceptor in Photosystem II: Relevance to photodamage and phototoxicity. Biochemistry 37: 17339–17344

Krzywda S, Brzozowski AM, Verma C, Karata K, Ogura T and Wilkinson AJ (2002) The crystal structure of the AAA domain of the ATP-dependent protease FtsH of *Escherichia coli* at 1.5 Å resolution. Structure 10: 1073–1083

Kuroda M, Kobashi K, Kaseyama H and Satoh K (1996) Possible involvement of a low redox potential component(s) downstream of Photosystem I in the translational regulation of the D1 subunit of the Photosystem II reaction center in isolated pea chloroplasts. Plant Cell Physiol 37: 754–761

Kyle DJ, Ohad I and Arntzen CJ (1984) Membrane protein damage and repair; selective loss of a quinone protein function in chloroplast membranes. Proc Natl Acad Sci USA 81: 4070–4074

Lee H-Y, Chow WS and Hong Y-N (1999) Photoinactivation of

Photosystem II in leaves of *Capsicum annuum*. Physiol Plant 105: 377–384

Lee H-Y, Hong Y-N and Chow WS (2001) Photoinactivation of Photosystem II complexes and photoprotection by non-functional neighbours in *Capsicum annuum* L leaves. Planta 212: 332–342

Lee H-Y, Hong Y-N and Chow WS (2002) Putative effects of pH in intra-chloroplast compartments on photoprotection of functional Photosystem II complexes by photoinactivated neighbours and on recovery from photoinactivation in *Capsicum annuum* leaves. Funct Plant Biol 29: 607–619

Lindahl M, Tabak S, Cseke L, Pickersky E, Andersson B and Adam Z (1996) Identification, characterization and molecular cloning of a homologue to the bacterial FtsH protease in chloroplasts of higher plants. J Biol Chem 271: 29329–29334

Lindahl M, Spetea C, Hundal T, Oppenheim AB, Adam Z and Andersson B (2000) The thylakoid FtsH plays a role in the light-induced turn-over of the Photosystem II D1 protein. Plant Cell 12: 419–432

Ludlow MM and Björkman O (1984) Paraheliotropic leaf movement in Siratro as a protective mechanism against drought-induced damage to primary photosynthetic reactions: Damage by excessive light and heat. Planta 161: 505–518

Mäenpää P, Andersson B and Sundby C (1987) Difference in sensitivity to photoinhibition between Photosystem II in the appressed and non-appressed thylakoid region. FEBS Lett 215: 31–36

Matsubara S and Chow WS (2004) Populations of photoinactivated Photosystem II reaction centers characterized by chlorophyll *a* fluorescence lifetime in vivo. Proc Natl Acad Sci USA 101: 18234–18239

Mattoo AK and Edelman M (1987) Intramembrane translocation and posttranslational palmitoylation of the chloroplast 32-kDa herbicide-binding protein. Proc Natl Acad Sci USA 84: 1497–1501

Mattoo AK, Hoffman-Falk H, Marder JB and Edelman M (1984) Regulation of protein metabolism: Coupling of photosynthetic electron transport to in vivo degradation of the rapidly metabolized 32-kilodalton protein of the chloroplast membranes. Proc Natl Acad Sci USA 81: 1380–1384

Melis A (1999) Photosystem-II damage and repair cycle in chloroplasts: What modulates the rate of photodamage in vivo? Trends Plant Sci 4: 130–135

Miyao M (1994) Involvement of active oxygen species in degradation of the D1 protein under strong illumination in isolated subcomplexes of Photosystem II. Biochemistry 33: 9722–9730

Mohamed A and Jansson C (1989) Influence of light on accumulation of photosynthesis-related transcripts in the cyanobacterium *Synechocystis* 6803. Plant Mol Biol 13: 693–700

Mühlbauer SK and Eichaker LA (1998) Light-dependent formation of the photosynthetic proton gradient regulates translation elongation in chloroplasts. J Biol Chem 273: 20935–20940

Mullet JE and Klein RR (1987) Transcription and mRNA stability are important determinants of higher plants chloroplast RNA levels. EMBO J 6: 1571–1579

Mulo P, Eloranta T, Aro EM and Mäenpää P (1998) Disruption of a spe-like open reading frame alters polyamine content and *psbA2* mRNA stability in the cyanobacterium *Synechocystis* sp. PCC 6803. Bot Acta 111: 71–76

Murata N and Sugahara K (1969) Control of excitation transfer in photosynthesis. III. Light-induced decrease of chlorophyll *a* fluorescence related to photophosphorylation system in spinach chloroplasts. Biochim Biophys Acta 189: 182–192

Nilsson R, Brunner J, Hoffman NE and van Wijk KJ (1999) Interactions of ribosome nascent chain complexes of the chloroplast-encoded D1 thylakoid membrane protein with cpSRP54. EMBO J 18: 733–742

Nishiyama Y, Yamamoto H, Allakhverdiev SI, Inaba M, Yokota A and Murata N (2001) Oxidative stress inhibits the repair of photodamage to the photosynthetic machinery. EMBO J 20: 5587–5594

Nishiyama Y, Allakhverdiev SI, Yamamoto H, Inaba M, Hayashi H and Murata N (2004) Singlet oxygen inhibits the repair of Photosystem II by suppressing translation elongation of the D1 protein in *Synechocystis* sp. PCC 6803. Biochemistry 43: 11321–11330

Niyogi K (1999) Photoprotection revisited: Genetic and molecular approaches. Annu Rev Plant Physiol Plant Mol Biol 50: 333–359

Norén H, Svensson P and Andersson B (1999) Auxiliary photosynthetic functions of *Arabidopsis thaliana* — Studies in vitro and in vivo. Biosci Reports 19: 499–509

Öquist G and Huner NPA (1991) Effects of cold acclimation on the susceptibility of photosynthesis to photoinhibition in Scots pine and in winter and spring cereals: A fluorescence analysis. Functional Ecol 5: 91–100

Öquist G, Chow WS and Anderson JM (1992) Photoinhibition of photosynthesis represents a mechanism for the long-term regulation of Photosystem II. Planta 186: 450–460

Osmond CB (1981) Photorespiration and photoinhibition. Some implications for the energetics of photosynthesis. Biochim Biophys Acta 639: 77–89

Osmond CB (1994) What is photoinhibition? Some insights from comparisons of shade and sun plants. In: Baker NR and Bowyer JR (eds) Photoinhibition of Photosynthesis: From Molecular Mechanisms to the Field, pp 1–24. BIOS Scientific Publishers, Oxford

Oxborough K and Baker B (2000) An evaluation of the potential triggers of photoinactivation of Photosystem II in the context of a Stern-Volmer model for the downregulation and the reversible radical pair equilibrium model. Phil Trans Roy Soc London B 355: 1489–1498

Oxborough K and Horton P (1988) A study of the regulation and function of energy-dependent quenching in pea chloroplasts. Biochim Biophys Acta 934: 135–143

Park Y-I, Chow WS and Anderson JM (1995) Light inactivation of functional Photosystem II in leaves of peas grown in moderate light depends on photon exposure. Planta 196: 401–411

Park Y-I, Anderson JM and Chow WS (1996a) Photoinactivation of Photosystem II and D1-protein synthesis in vivo are independent of the modulation of the photosynthetic apparatus by growth irradiance. Planta 198: 300–309

Park Y-I, Chow WS and Anderson JM (1996b) Chloroplast movement in the shade plant *Tradescantia albiflora* helps protect Photosystem II against light stress. Plant Physiol 111: 867–875

Park Y-I, Chow WS, Osmond CB and Anderson JM (1996c) Electron transport to oxygen mitigates against the photoinactivation of photosystem II in vivo. Photosynth Res 50: 23–32

Park Y-I, Chow, WS and Anderson JM (1997) Antenna size dependency of photoinactivation of Photosystem II in light-

acclimated pea leaves. Plant Physiol 115: 151–157
Powles SB (1984) Photoinhibition of photosynthesis induced by visible light. Annu Rev Plant Physiol 35: 15–44
Powles SB and Osmond CB (1979) Photoinhibition of intact attached leaves of C_3 plants illuminated in the absence of both carbon dioxide and of photorespiration. Plant Physiol 64: 982–988
Prásil O, Adir N and Ohad I (1992) Dynamics of Photosystem II: Mechanisms of photoinhibition and recovery process. In: Barber J (ed) The Photosystems: Structure, Function and Molecular Biology, Vol 11, pp 295–348. Elsevier Science Publishers, Amsterdam
Richter M, Goss R, Wagner B and Holzwarth AR (1999) Characterisation of the fast and slow reversible components of non-photochemical quenching in isolated pea thylakoids by picosecond time-resolved chlorophyll fluorescence analysis. Biochemistry 83: 12718–12726
Rintamäki E and Aro EM (2001) Phosphorylation of Photosystem II subunits. In: Aro EM and Andersson B (eds) Regulation of Photosynthesis, pp 395–418. Kluwer Academic Publishers, Dordrecht
Rintamäki E, Kettunen R and Aro EM (1996) Differential D1 dephosphorylation in functional and photodamaged Photosystem II centers. Dephosphorylation is a prerequisite for degradation of the damaged D1*. J Biol Chem 271: 14870–14875
Robinson JM (1988) Does O_2 photoreduction occur within chloroplasts in vivo? Physiol Plant 72: 666–680
Roelofs TA, Lee C-H and Holzwarth AR (1992) Global target analysis of picosecond chlorophyll fluorescence kinetics from pea chloroplasts. A new approach to the characterization of the primary processes in Photosystem II α- and β-units. Biophys J 61: 1147–1163
Rokka A, Suorsa M, Saleem A, Battchikova N and Aro EM (2005) Synthesis and assembly of thylakoid protein complexes. Multiple assembly steps of Photosystem II. Biochem J 386: 1–10
Rova M, Mamedov F, Magnuson A, Fredriksson PO and Styring S (1998) Coupled activation of the donor and the acceptor side of Photosystem II during photoactivation of the oxygen evolving cluster. Biochemistry 37: 11039–11045
Roy M and Barkan A (1998) A SecY homologue is required for the elaboration of the chloroplast thylakoid membrane and for normal chloroplast gene expression. J Biol Chem 141: 385–395
Ruban AV, Pascal AA, Robert B and Horton P (2002) Activation of zeaxanthin is an obligatory event in the regulation of photosynthetic light harvesting. J Biol Chem 277: 7785–7789.
Sakamoto W, Tamura T, Hanba-Tomita Y, Sodmergen and Murata M (2002) The *VAR1* locus of *Arabidopsis* encodes a chloroplastic FtsH and is responsible for leaf variegation in the mutant alleles. Genes Cells 7: 769–780
Sane PV, Ivanov AG, Hurry V, Huner and Öquist G (2003) Changes in the redox potential of primary and secondary electron-accepting quinones in Photosystem II confer increased resistance to photoinhibition in low-temperature-acclimated Arabidopsis. Plant Physiol 132: 2144–2151
Schatz GH, Brock H and Holzwarth AR (1988) Kinetic and energy model for the primary processes of Photosystem II. Biophys J 54: 397–405
Schnell DJ (1998) Protein targeting to the thylakoid membrane. Annu Rev Plant Physiol Plant Mol Biol 49: 97–106
Schubert M, Petersson UA, Haas BJ, Funk C, Schröder WP and Kieselbach T (2002) Proteome map of the chloroplast lumen of *Arabidopsis thaliana*. J Biol Chem 277: 8354–8365
Sétif P, Hervo G and Mathis P (1981) Flash-induced absorption changes in Photosystem I radical pair or triplet formation? Biochim Biophys Acta 638: 257–267
Shen Y-K, Chow WS, Park Y-I and Anderson JM (1996) Photoinactivation of Photosystem II by cumulative exposure to short light pulses during the induction period of photosynthesis. Photosynth Res 47: 51–59
Shi L-X, Lorkovic ZJ, Oelmüller R and Schröder WP (2000) The low molecular mass PsbW protein is involved in the stabilization of the dimeric Photosystem II complex in *Arabidopsis thaliana*. J Biol Chem 275: 37945–37950
Shipton CA and Barber J (1991) Photoinduced degradation of the D1 polypeptide in isolated reaction centers of Photosystem II: Evidence for an autoproteolytic process triggered by the oxidizing side. Proc Natl Acad Sci USA 88: 6691–6695
Silva P, Thompson E, Bailey S, Kruse O, Mullineaux CW, Robinson C, Mann NH and Nixon PJ (2003) FtsH is involved in the early stages of repair of Photosystem II in *Synechocystis* sp PCC 6803. Plant Cell 15: 2152–2164.
Sokolenko A, Pojidaeva E, Zinchenko V, Panichkin V, Glaser VM, Herrmann GR and Shestakov SV (2002) The gene complement for proteolysis in the cyanobacterium *Synechocystis* sp. PCC 6803 and *Arabidopsis thaliana* chloroplasts. Curr Genet 41: 291–310
Somanchi A and Mayfield SP (2001) Regulation of chloroplast translation. In: Aro EM and Andersson B (eds) Regulation of Photosynthesis, pp 137–151. Kluwer Academic Publishers, Dordrecht
Sonoike K (1996) Photoinhibition of Photosystem I: Its physiological significance in the chilling sensitivity of plants. Plant Cell Physiol 37: 239–247
Sonoike K (1998) Various aspects of inhibition of photosynthesis under light/chilling stress: 'Photoinhibition at chilling temperature' versus 'chilling damage in the light'. J Plant Res 111: 121–129
Sundby C, McCaffery S and Anderson JM (1993) Turnover of the Photosystem II D1 protein in higher plants under photoinhibitory and nonphotoinhibitory irradiance. J Biol Chem 268: 25476–25482
Suorsa M, Regel RE, Paakkarinen V, Battchikova N, Herrmann RG and Aro EM (2004) Protein assembly of Photosystem II and accumulation of subcomplexes in the absence of low molecular weight subunits PsbL and PsbJ. Eur J Biochem. 271: 96–107
Swiatek M, Kuras M, Sokolenko A, Higgs D, Olive J, Cinque G, Muller B, Eichaker LA, Stern DB, Bassi R, Herrmann RG and Wollman F-A (2001) The chloroplast gene *ycf 9* encodes a Photosystem II (PSII) core subunit, PsbZ, that participates in PSII supramolecular architecture. Plant Cell 13: 347–367
Taniguchi M, Kuroda H and Satoh K (1993) ATP-dependent protein synthesis in isolated pea chloroplasts. FEBS Lett 317: 57–61
Telfer A (2002) What is β-carotene doing in the Photosystem two reaction center? Phil Trans R Soc London B 357: 1431–1440
Terashima I, Funayama S and Sonoike K (1994) The site of photoinhibition in leaves of *Cucumis sativus* L. at low temperatures is Photosystem I, not Photosystem II. Planta 193: 300–306
Theg SM, Filar LJ and Dilley RA (1986) Photoinhibition of chloroplasts already inhibited on the oxidising site of Photosystem II. Biochim Biophys Acta 849: 104–111

Thompson LM and Brudvig GW (1988) Cytochrome *b*-559 may function to protect Photosystem II from photoinhibition. Biochemistry 27: 6653–6658

Trebst A, Depka B, Kraft B and Johanningmeier U (1988) The Q_B site modulates the conformation of the Photosystem II reaction center polypeptide. Photosynth Res, 18: 163–177

Trissl H-W and Lavergne J (1995) Fluorescence induction from Photosystem II: Analytical equations for the yields of photochemistry and fluorescence derived from analysis of a model including exciton-radical pair equilibrium and restricted energy transfer between photosynthetic units. Aust J Plant Physiol 22: 183–193

Tyystjärvi E and Aro E-M (1996) The rate constant of photoinhibition, measured in lincomycin-treated leaves, is directly proportional to light intensity. Proc Natl Acad Sci USA 93: 2213–2218

Tyystjärvi E, Kettunen R and Aro E-M (1994) The rate constant of photoinhibition in vitro is independent of the antenna size of Photosystem II but depends on temperature. Biochim Biophys Acta 1186: 177–185

Tyystjärvi T, Mulo P, Mäenpää P and Aro E-M (1996) D1 polypeptide degradation may regulate *psbA* gene expression at transcriptional and translational levels in *Synechocystis* sp. PCC 6803. Photosynth Res 47: 111–120

Tyystjärvi T, Herranen M and Aro E-M (2001) regulation of translation elongation in cyanobacteria: Membrane targeting of the ribosome nascent-chain complexes controls the synthesis of D1 protein. Mol Microbiol 40: 467–484

van Gorkom HJ and Schelvis JPM (1993) Kok's oxygen clock: What makes it tick? The structure of P680 and consequences of its oxidising power. Photosynth Res 38: 297–301

van Mieghem F, Brettel K, Hillmann B, Kamlowski A, Rutherford WA and Schlodder E (1995) Charge recombinations in Photosystem II. I. Yields, recombination pathways and kinetics of the primary pair. Biochemistry 34: 4798–4813

Vasilikiotis C and Melis A (1994) Photosystem II reaction center damage and repair cycle: Chloroplast acclimation strategy to irradiance stress. Proc Natl Acad Sci USA 91: 7222–7226

Vavilin DV and Vermaas WFJ (2000) Mutations in the CD-loop region of the D2 protein in *Synechocystis* sp. PCC 6803 modify charge recombination pathways in Photosystem II in vivo. Biochem 39: 14831–14838

Zerges W (2002) Does complexity constrain organelle evolution? Trends Plant Sci 7: 175–182

Zhang L and Aro E-M (2002) Synthesis, membrane insertion and assembly of the chloroplast-encoded D1 protein into Photosystem II. FEBS Lett 512: 13–18

Zhang L, Paakkarinen V, van Wijk KJ and Aro E-M (1999) Co-translational assembly of the D1 protein into Photosystem II. J Biol Chem 274: 16062–16067

Zhang L, Paakkarinen V, van Wijk KJ and Aro E-M (2000) Biogenesis of the chloroplast-encoded D1 protein: Regulation of translational elongation, insertion, and assembly into Photosystem II. Plant Cell 12: 1769–1781

Zhang L, Paakkarinen V, Suorsa M and Aro E-M (2001) A secY homologue is involved in chloroplast-encoded D1 protein biogenesis. J Biol Chem 276: 37809–37814

Zurawski G, Bohnert HJ, Whitfeld PR and Bottomley W (1982) Nucleotide sequence of the gene for M_r32,000 thylakoid membrane protein from *Spinacia oleracea* and *Nicotiana debneyi* predicts a totally conserved primary translation product of M_r 38,950. Proc Natl Acad Sci USA 79: 7699–7703

Chapter 28

Transcriptional and Translational Regulation of Photosystem II Gene Expression

Kenichi Yamaguchi and Stephen P. Mayfield*
Department of Cell Biology and Skaggs Institute for Chemical Biology, The Scripps Research Institute, 10550 N. Torrey Pines Road, La Jolla, CA 92037, U.S.A.

Mamoru Sugita*
Center for Gene Research, Nagoya University, Nagoya 464-8602, Japan

*Authors for correspondence, email: mayfield@scripps.edu, sugita@gene.nagoya-u.ac.jp

T. Wydrzynski and K. Satoh (eds): Photosystem II: The Light-Driven Water:Plastoquinone Oxidoreductase, pp. 649–668.

Summary

The plastid gene expression system employs a highly developed transcription and translation system that is an elaborated prokaryotic and eukaryotic chimera. Photosystem II (PS II) gene expression is regulated during transcription, post-transcriptionally, and translationally, and responds to environmental changes. Many regulatory factors and elements necessary for PS II biosynthesis and repair have been identified and characterized in the last decade. This chapter reviews recent progress on understanding PS II gene expression, introducing mechanisms common to algae and higher plants, as well as differences between these organisms. Transcriptional regulation is critical for chloroplast biogenesis and PS II accumulation. Unlike algae land plants have developed complex transcriptional regulatory systems for plastid differentiation, e.g., chloroplasts in leaves and amyloplasts in roots. Post-transcriptional RNA processing of primary transcripts is also an important step in the control of plastid gene expression, and is required for translation initiation of many plastid mRNAs. A set of chloroplast RNA-binding proteins and nucleases are involved in this process. Translational regulation is a key step for the rapid response to dark/light changes, and for PS II repair associated with photo-oxidation, in both algae and higher plants. Light-activated translation of several PS II encoding mRNAs requires *cis*-acting RNA elements, found in the 5′-untranslated region of the mRNA, as well as nuclear-encoded *trans*-acting protein factors. Genetic and biochemical analysis has identified a number of the components and mechanisms involved in regulating expression of PS II proteins.

I. Introduction

Chloroplasts are thought to have arisen by endocytobiosis of a photosynthetic unicellular prokaryote into an eukaryotic host, with a subsequent translocation of genes from the plastid to the host nucleus (Martin and Herrmann, 1998). In algae and higher plants the Photosystem II (PS II) complex is comprised of more than 20 proteins (Ruffle and Sayre, 1998; Rhee, 2001; Swiatek et al., 2001; Chapter 18, Hankamer et al.). Fifteen of these genes (*psbA-F*, *psbH-N*, *psbT*, and *psbZ*) are encoded in the chloroplast genome, while the others (*psbO-X*) are encoded in the nucleus (Ruffle and Sayre, 1998; Swiatek et al., 2001). Having genes encoded in two separate genomes requires novel regulatory interactions to maintain a coordinate expression of proteins involved in photosynthesis. It has been proposed (Race et al., 1999) that PS II core proteins have remain encoded in the plastid genome to ensure a rapid response in the synthesis of these proteins to counteract the adverse side effects of electron transport and O_2 evolution. Photosynthetic gene expression and plant development are also closely tied to environmental signals, especially light. Many mRNAs of the plastid-encoded PS II proteins accumulate to relatively high levels in dark-grown plants, and show little additional accumulation upon exposure to light (Malnoë et al., 1988). Exposure of dark-adapted plants to light results in a rapid increase in the translation of chloroplast mRNAs (Malnoë et al., 1988), whereas light modulation of nuclear gene expression is primarily a transcriptional response, mediated by photoreceptors such as the phytochromes and cryptochromes (Nagy and Schafer, 2002). Signaling networks that involve a mutual exchange of information between the nucleo-cytoplasmic and chloroplast compartments have also evolved to ensure stoichiometric accumulation of proteins derived from the two genomes. Finally, the PS II reaction center proteins are the main targets of oxidative damage (Vass et al., 1992; Telfer et al., 1994), hence degradation of damaged PS II proteins (Depka et al., 1998) and their replacement by a *de novo* synthesis (van Wijk et al., 1996; Melis, 1999; Chapter 27, Chow and Aro) represent an importance mechanism of PS II repair. In cyanobacteria, PS II protein expression is mainly regulated during transcription (Golden, 1994), whereas in chloroplasts of algae and higher plants, translation initiation has an important regulatory role and is controlled by nuclear-encoded translational activators (Sugita and Sugiura, 1996; Somanchi and

Abbreviations: IF – initiation factor; LRP – light responsive promoter; NEP – nuclear-encoded plastid RNA polymerase; PABP – poly(A) binding protein; PDI – protein disulfide isomerase; PEP – plastid-encoded plastid RNA polymerase; Poly(A) – polyadenylic acid; PNPase – polynucleotide phosphorylase; PPR – pentatricopeptide repeat; PRP – plastid ribosomal protein; PS II – Photosystem II; PSRP – plastid-specific ribosomal protein; PTK – plastid transcription kinase; RB – ribosome binding; SD – Shine-Dalgarno; SLF – sigma-like factor; UTR – untranslated region

Mayfield, 1999). Translational activators have yet to be identified in cyanobacteria. Regulation of PS II D1 protein synthesis during translation elongation has recently been reported in cyanobacteria (Tyystjarvi et al., 2001), but the mechanisms involved in translation initiation in cyanobacteria have not been characterized. Genetic and biochemical approaches in algae and land plants, mainly using *Chlamydomonas*, *Arabidopsis*, maize, tobacco, and spinach, has identified numerous nucleus-encoded factors that are involved in several post-transcriptional steps of chloroplast gene expression (Rochaix, 1996; Sugita and Sugiura, 1996; M. Sugiura et al., 1998; Barkan and Goldschmidt-Clermont, 2000; Somanchi and Mayfield, 2001). In this chapter we will discuss transcriptional and translational regulation of PS II protein expression, and will separately discuss data derived from algae from that of higher plants, because control of gene expression in algae and higher plants are often different mechanistically.

II. Regulation of Photosystem II Gene Expression in Algae

Expression of PS II proteins requires the interaction of the nuclear and chloroplast genomes and although the interactions between the two genomes are still not completely understood, a large number of nuclear factors required for expression of chloroplast genes have now been identified. Plastid development also has an effect on nuclear gene expression, and several potential signaling molecules involved in this chloroplast feedback have also been identified (reviewed in Hippler et al., 1998; Somanchi and Mayfield, 1999; Brown et al., 2001; Harris, 2001). In general, it appears that the nuclear genome sets a developmental program in which expression of specific nuclear-encoded factors is required for the synthesis and assembly of the photosynthetic apparatus. This overall program is fine tuned by environmental signals that affect both plastid and nuclear gene expression to establish a highly coordinate pattern of protein synthesis, assembly, turnover and repair.

A. Transcriptional Regulation of Plastid-Encoded Genes

Transcription in the chloroplast resembles that of prokaryotes, particularly in the use of consensus bacterial-type promoter sequences. In higher plants, plastid genomes are transcribed by two different RNA polymerases: a nuclear-encoded RNA polymerase (NEP) that transcribes genes required for transcription and translation, and a plastid-encoded RNA polymerase (PEP), that transcribes the photosynthetic genes (Hess and Börner, 1999; see Section III). Analysis of the chloroplast promoters from the green algae *Chlamydomonas reinhardtii* identified bacterial-type promoter elements (–10 and –35 elements) as being required for transcription in chloroplasts (U. Klein et al., 1992). Each of the PS II encoding genes contains –10 and –35 consensus elements that appear to function as authentic promoter sequences. Lilly et al., (2002) proposed that unlike higher plants, the *Chlamydomonas* chloroplasts lack a NEP, since a PEP inhibitor, tagetitoxin, appeared to inhibit transcription of all the chloroplast mRNAs.

The activity of plastid polymerases may be enhanced by sigma-like factors, and two nuclear-encoded sigma factors for plastid RNA polymerases (sigB and sigC) have been identified from the red algae *Cyanidium* (Oikawa et al., 1998). How these sigma factors may contribute to transcriptional regulation of plastid genes is not yet known, but presumably they act to enhance transcription of specific chloroplast genes. Transcription of chloroplast genes in *C. reinhardtii* has been shown to be regulated in a circadian manner, and this transcriptional activation requires cytoplasmic protein synthesis (Kawazoe et al., 2000), again suggesting that nuclear encoded factors function to regulate chloroplast transcription.

B. Post-transcriptional Regulation of Plastid-Encoded Genes

1. Stability of Plastid-Encoded mRNAs

While there is not a good correlation between activation of chloroplast transcription and activation of protein accumulation, a number of nuclear genes have been identified that impact accumulation of PS II mRNAs and proteins (Barkan and Goldschmidt-Clermont, 2000; reviewed in Somanchi and Mayfield, 2001). Nuclear mutants have been identified that affect accumulation of the *psbA* mRNA (Yohn et al., 1996, 1998a), the *psbB* mRNA (Monod et al., 1992), the *psbC* mRNA (Rochaix et al., 1989), and the *psbD* mRNA (Kuchka et al., 1989). Several of these nuclear mutants have been shown to affect the stability of specific RNA transcripts via interaction with the 5′ untranslated region (UTR) of the message (Nickelsen

et al., 1994; Zerges et al., 1997). Some of these genes have now been cloned (Rattanachaikunsopon et al., 1999; Boudreau et al., 2000; Vaistij et al., 2000), but the sequence of these gene products does not suggest how they might function in mRNA stability. A nuclear mutant of *C. reinhardtii* showing degradation of the *petD* mRNA by 5′ to 3′ exoribonuclease activity provides evidence that at least this nuclear gene product, MCD1, protects RNA from degradation as it interacts with the 5′ UTR (Drager et al., 1998). Similar mechanisms have been shown for the processing of the *psbD* and *psbB* mRNAs, respectively, by the nuclear factors Nac2 and Mbb1 (Boudreau et al., 2000; Vaistij et al., 2000). It is not yet clear whether this is a generic protective mechanism, or how many of the other nuclear gene products function in a similar manner, but it is clear that a number of nuclear encoded factors are required for the stability of all PS II encoding mRNAs in plastids.

The 3′ end of plastid mRNAs has also been shown to be involved in mRNA stability (Rott et al., 1998a; Komine et al., 2002), and translation (Rott et al., 1998b), and a number of 3′ interacting factors have been identified. How the 5′ and 3′ elements and factors interact to control mRNA stability and translation remains undefined, but likely involves direct interaction of these components (Katz and Danon, 2002).

Polyadenylation of plastid mRNAs is an important process for chloroplast mRNA turnover (see details in Section III.C.2). Although polyadenylation of algal PS II related genes has not been studied, polyadenylation of three classes of *Chlamydomonas* plastid RNA (*atpB* and *petD* mRNAs, Arg and Glu tRNAs, and 5S rRNA) has been observed in vitro and in vivo (Komine et al, 2000, 2002).

2. Processing of Plastid-Encoded mRNAs

Many chloroplast genes are transcribed as precursor mRNAs that require intra and intermolecular splicing and processing to form the mature transcript (reviewed in Barkan and Goldschmidt-Clermont, 2000). Introns belonging to both group I and group II have been characterized in plastid genes. While little is known about the splicing machinery of the plastid introns, nuclear mutants in *C. reinhardtii* have indicated a direct, or at least essential, role for nuclear factors in mRNA splicing (reviewed in Barkan and Goldschmidt-Clermont, 2000).

Deshpande et al. (1997) reported that light stimulates pre-RNA intron splicing in the *C. reinhardtii psbA* mRNA, and showed that this splicing is dependent upon photosynthetic electron transport. This light-induced increase in *psbA* pre-RNA splicing suggests that this processing event could function as a light responsive regulator of *psbA* gene expression. In addition, a PS I deficient mutant did not show light-activated pre-RNA splicing, and complementation of the mutant to restore photoautotrophy restored light-responsive pre-RNA processing, again suggesting a feed back between photosynthesis and PS II gene expression.

The 5′ UTR of the *psbA* mRNA is processed (Bruick and Mayfield, 1998) by the removal of 54 nucleotides upstream of a putative ribosome binding sequence. Chloroplast or nuclear mutations that block *psbA* translation block processing of the 5′ UTR. Interestingly, the correlation between processing and ribosome association shows that loss of translation blocks processing, and not that loss of processing blocks translation, suggesting that processing of the *psbA* mRNA occurs after the mRNA is loaded onto ribosomes. How this processing affects *psbA* translation is not yet understood, but the relationship between processing and PS II protein expression is quite strong, suggesting that this processing event is acting in a regulatory fashion.

C. Transcriptional Regulation of Nuclear-Encoded Genes

Regulation of nuclear PS II gene expression is primarily regulated during transcription. In algae, transcription of the *lhcII* genes is regulated in response to light, chlorophyll content, and circadian rhythms (Blankenship and Kindle, 1992; Hwang and Herrin, 1994; Jacobshagen et al., 1996; Hahn and Kuck, 1999). Phytochrome has not been identified as a photoreceptor for nuclear transcriptional activation in algae, but cryptochrome (blue light receptor) has been identified (G.D. Small et al., 1995), and likely acts in a similar manner as described for blue light receptors in higher plants. The process of nuclear gene transcription is much better characterized in higher plants than in algae.

D. Translational Regulation

Genetic analysis in *C. reinhardtii* and higher plants has identified translational regulation as a key component of plastid photosynthetic gene expression

(reviewed in Zerges, 2000). These analysis have identified a number of gene-specific factors that appear to bind to RNA elements contained within the 5′ UTR of chloroplast mRNAs to act as regulators of chloroplast gene expression (reviewed in Somanchi and Mayfield, 2001). In addition, the general components of chloroplast translational apparatus, and the mechanisms of interactions between these components, are being identified. The plastid translational machinery is similar to that of bacteria, but there are also large differences between plastids and bacteria in how the basic machine is regulated (reviewed in Gillham et al., 1994; Harris et al., 1994; Mayfield et al., 1995; Hauser et al., 1998; Zerges, 2000).

1. Translational Regulation by Cis-acting RNA Elements

Shine-Dalgarno (SD) sequences are located 5′ to the initiation codon of prokaryotic mRNAs and base pair to a complementary sequence, the anti-SD sequence, at the 3′ end of the 16 S rRNA (Shine and Dalgarno, 1974). It has been shown that the SD interaction plays a crucial role in the selection of the prokaryotic translation initiation start site and in the control of translation efficiency (reviewed in MacCarthy and Brimacombe, 1994). In chloroplasts, 3′-terminal regions of 16S rRNAs (potential anti-SD sequences) are highly conserved with those of photosynthetic bacteria and *E. coli*. Prokaryotic-like SD sequences have been identified in a number of chloroplast transcripts, but not in all (M. Sugiura et al., 1998). The 5′ UTR of many chloroplast messages do contain sequences capable of pairing with the 3′ end of the 16S rRNA, but most of these do not have a bacterial type location in relation to the initiation codon, which in *E. coli* must be within 10 nucleotides. Fargo et al. (1998) analyzed the function of bacterial-type SD sequences of four transcripts, *atpB*, *atpE*, *rps4* and *rps7*, by replacement mutagenesis and showed no effect on the expression of these genes, leading them to propose an SD independent mechanism for plastid translation. A bacterial consensus SD-like sequences was also shown to have little affect on translation of the *psbD* mRNA (Nickelsen et al., 1999). However, studies on SD-like sequences of tobacco *rps14* (Hirose et al., 1998) and *C. reinhardtii psbA* mRNA (Bruick and Mayfield, 1998) showed a requirement for these sequence for translation of the mRNAs. In *C. reinhardtii* the putative SD sequence required for translation is 27 nucleotides upstream of the *psbA* initiation codon, and deletion of this sequence results in a loss of ribosome association and also a decrease in message stability, both strongly suggestive of an authentic SD sequence. The structural changes wrought on the 5′ UTR by manipulation of any sequence, including the SD sequences, makes interpretation of the above results complicated. The existing evidence supports the presence of SD sequences, with non-prokaryotic spacing, for some chloroplast messages, while in others translation initiation may result from mechanism independent of SD sequences (Fig. 2; discussed below).

A number of other message specific RNA elements have been identified as required for translation of specific plastid mRNAs. Genetic analysis has revealed involvement of products of three nuclear loci *TBC1*, *TBC2*, and *TBC3* in the translation of the *C. reinhardtii* chloroplast *psbC* mRNA (Zerges and Rochaix, 1994; Zerges et al., 1997). A region of the *psbC* mRNA located 236 nucleotides 5′ of the initiation codon in the *C. reinhardtii* was shown to be required for activation of translation initiation of this message (Zerges et al., 1997). Recently, *cis*-acting elements in the 5′ leader interacting with TBC1, TBC2, and TBC3 were identified (Zerges et al., 2003), and the *TBC2* gene has been cloned and characterized (Auchincloss et al., 2002). Mutations leading to a loss of a potential secondary structure element in this region resulted in the loss of reporter gene expression. Analysis of chloroplast 5′ UTRs shows that many of these RNAs have extensive secondary structures that are predicted to form stem-loop structures directly upstream of the initiation codon (Hauser et al., 1998). Such secondary structures have also been detected in relatively short 5′ UTRs, such as in the chloroplast *atpH* mRNA of *Euglena gracilis* (Betts and Spremulli, 1994). Site-directed mutations affecting stem-loop elements found in the 5′ UTR of the *psbA* mRNA greatly reduced D1 protein synthesis (Mayfield et al., 1994). Additional RNA elements have been identified that impact plastid mRNA accumulation and stability, although the exact nature of these elements, as well as the factors that bind them, remain to be characterized (reviewed in Zerges, 2000).

2. Translational Regulation by Trans-acting Factors

Many factors required for translation of chloroplast mRNAs are nuclear encoded. Genetic analysis in *C. reinhardtii* has revealed a class of nuclear genes that

are required for translation of specific chloroplast mRNAs. Many of these nuclear factors are predicted to interact with the 5′ UTR of specific mRNAs. The 5′ UTRs of chloroplast mRNAs tend to be A/U-rich (Fig. 1) and often contain predicted stem-loop structures. Sequences upstream of the chloroplast initiation codon have been proposed to affect translation, containing binding sites for these nuclear encoded activators and repressors.

Studies on photosynthetic mutants of *Chlamydomonas*, suggest that many of the nuclear encoded factors are message specific. Using complementation rescue the gene disrupted in the mutant *ac115* has been identified (Rattanachaikunsopon et al., 1999), and shown to encode a novel protein that has been proposed to play a role in the localization of the *psbD* mRNA or perhaps act to stabilize intermediates of D2 translation product. Several proteins identified to recognize the 5′ UTR of chloroplast PS II transcripts, like *psbA*, *psbC*, and *psbD* have been shown to be at least partially membrane associated, indicating a role in the proper localization of these messages to the thylakoid membrane (reviewed in Zerges, 2000). Of the set of proteins that associate with *psbC*, the 46

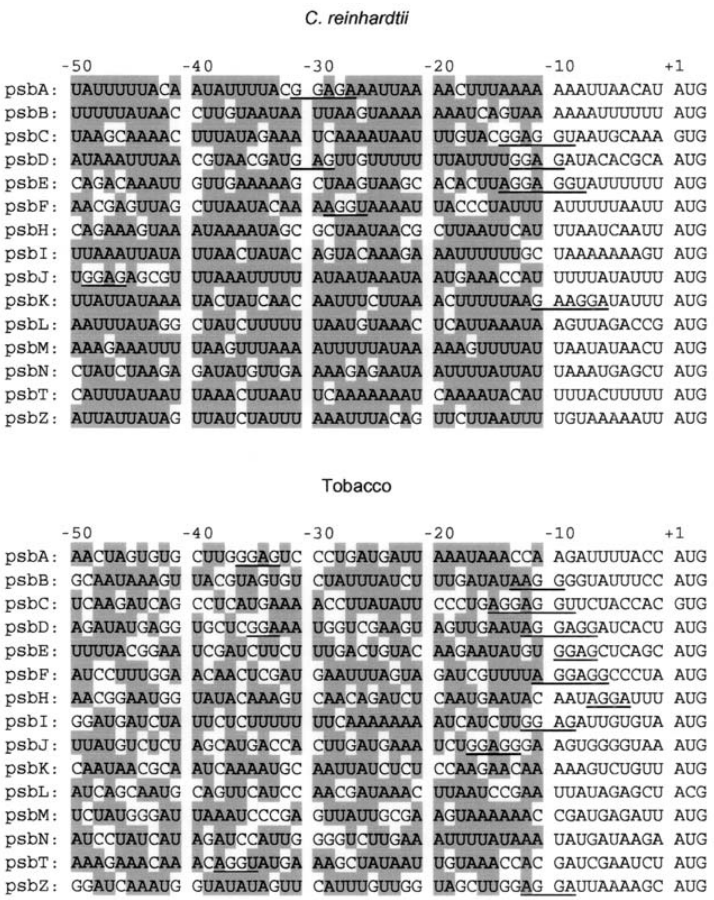

Fig. 1. 5′ Untranslated regions (UTRs) of plastid-encoded PS II gene transcripts from *C. reinhardtii* and tobacco. The region of the 5′ UTR immediately upstream of initiation codons of mRNAs are shown. Potential SD-sequences complementary to 3′-ends of 16S rRNAs (*C. reinhardtii*: 3′-cuUCCUCCAcucg-; tobacco: 3′-uuUCCUCCAcuag-) are underlined. A and U residues in the –50 to –11 regions are highlighted by gray. Nucleotide sequences were obtained from complete chloroplast genome sequence of *C. reinhardtii* (Maul et al., 2002) and that of tobacco (*Nicotiana tabacum*, accession number Z00044), respectively.

kDa protein has been shown to bind A/U-rich regions. The binding of this 46 kDa protein is light-dependent and binding can be inhibited by ADP (Zerges et al., 1997). Auchincloss et al. (2002) recently cloned and characterized TBC2, one of several nuclear factors that bind to the *C. reinhardtii psbC* 5′ UTR. The TBC2 protein is approximately 140 kDa protein and has some sequence homology with Crp1, a maize nuclear factor that is required for processing and translation of the *petA* and *petD* mRNAs. The TBC2 protein is localized in the stroma and is associated with a 400 kDa protein complex.

A biochemical approach used to identify factors potentially regulating translation of chloroplast messages has been to isolate specific proteins that bind the 5′ UTR of chloroplast messages. While a number of proteins have been identified by RNA affinity chromatography, little is known regarding their specificity and function (Danon and Mayfield, 1991; Zerges and Rochaix, 1994). A comparison of the 5′ UTRs, of *psbA, rps12, rbcL*, and *atpB,* led to the identification of at least seven proteins, of 15, 36, 38, 47, 56, 62, and 81 kDa, associated with the RNA (Hotchkiss and Hollingsworth, 1995, 1999; Hauser et al., 1996). Multiple forms of the 47 kDa and 81 kDa proteins have been identified (Hauser et al., 1996). The 38 kDa, 47 kDa, and 81 kDa proteins appear to associate with the 5′ UTRs of all the RNAs. The level of the 36 kDa protein was reduced in cells that translate chloroplast encoded ribosomal proteins at high rates, suggesting that this protein may be required for translation of the class of mRNAs encoding photosynthetic proteins (Hauser et al., 1996).

The 5′ UTR of the *C. reinhardtii psbD* mRNA has been shown to associate with a number of proteins. A nuclear mutation with reduced abundance of a 47 kDa protein showed decreased accumulation of the *psbD* mRNA and absence of D2 protein accumulation, suggesting that this protein might influence *psbD* message stability or translation (Nickelsen et al., 1994). Studies on the proteins associating with the 5′ UTR of *psbC* resolved three proteins of 95, 65 and 46 kDa. A 46kDa protein was detected binding to the 5′ UTR of *psbC* mRNA only in the nuclear mutant F64, which lacks translation of that mRNA, leading the authors to hypothesize that the binding of the 46kDa protein may inhibit translation of *psbC* (Zerges and Rochaix, 1994, 1998).

A protein complex consisting of four polypeptides of 38, 47, 55 and 60 kDa that bind the 5′ UTR of *psbA* mRNA has also been isolated (Danon and Mayfield, 1991). There is a strong correlation between the RNA binding activity of the complex and *psbA* mRNA translation under light and dark growth conditions (Danon and Mayfield, 1991, 1994). The binding activity of this complex is lower in the dark though there is little variation in accumulation of these proteins between the dark and light grown cells. This suggests that modulation of specific RNA binding activity is used to regulate mRNA translation (Danon and Mayfield, 1991, 1994; Yohn et al., 1998b). Two of these RNA binding (RB) proteins, RB47 and RB60, have been cloned and sequenced. The RB47 protein shows homology to polyadenylic acid (poly(A)) binding proteins (PABP, Yohn et al., 1998b) and RB60 shows homology to protein disulfide isomerases (PDI, Kim and Mayfield, 1997). Cross-linking studies of RB47 indicate that this protein is directly in contact with the *psbA* 5′ UTR (Danon and Mayfield, 1991). In vitro studies showed that this protein is imported into the chloroplasts (Yohn et al., 1998b), and associates with a low-density membrane fraction that may be part of the envelope membrane (Zerges and Rochaix, 1998). Nuclear mutants that affect the levels and activity of this chloroplast localized PABP (cPABP) affect light activated translation initiation of the *psbA* mRNA (Yohn et al., 1996). Finally, binding of RB47 has shown to be regulated by chloroplast redox potential (Danon and Mayfield, 1994, Kim and Mayfield, 1997, Yohn et al., 1998a, Fong et al., 2000). A model for redox regulated PS II translation is depicted in Fig. 2.

3. The Chloroplast Translational Apparatus

Recent proteomic analyses of spinach chloroplast ribosomes (Yamaguchi and Subramanian, 2000, 2003; Yamaguchi et al., 2000) and *C. reinhardtii* chloroplast ribosomes (Yamaguchi et al., 2002, 2003) have identified the set of ribosomal components that function in plastids. These studies have begun to identify differences between plastid and bacterial ribosome that may influence how photosynthetic mRNAs are translated. The spinach plastid ribosome has 6 plastid-specific ribosomal proteins (PSRP-1 to PSRP-6), in addition to 52 *E. coli* orthologues (S1-S21, L1-L36), but lacks the L25 and L30 orthologues. PSRP-1 to PSRP-4 are found in the 30S subunit and PSRP-5 and PSRP-6 are found in the 50S subunit. Two genes encoding PSRP-1 and PSRP-3 homologues are present in the complete genome sequence of the cyanobacterium *Synechocystis* sp. PCC6803 (Yamaguchi and Subramanian,

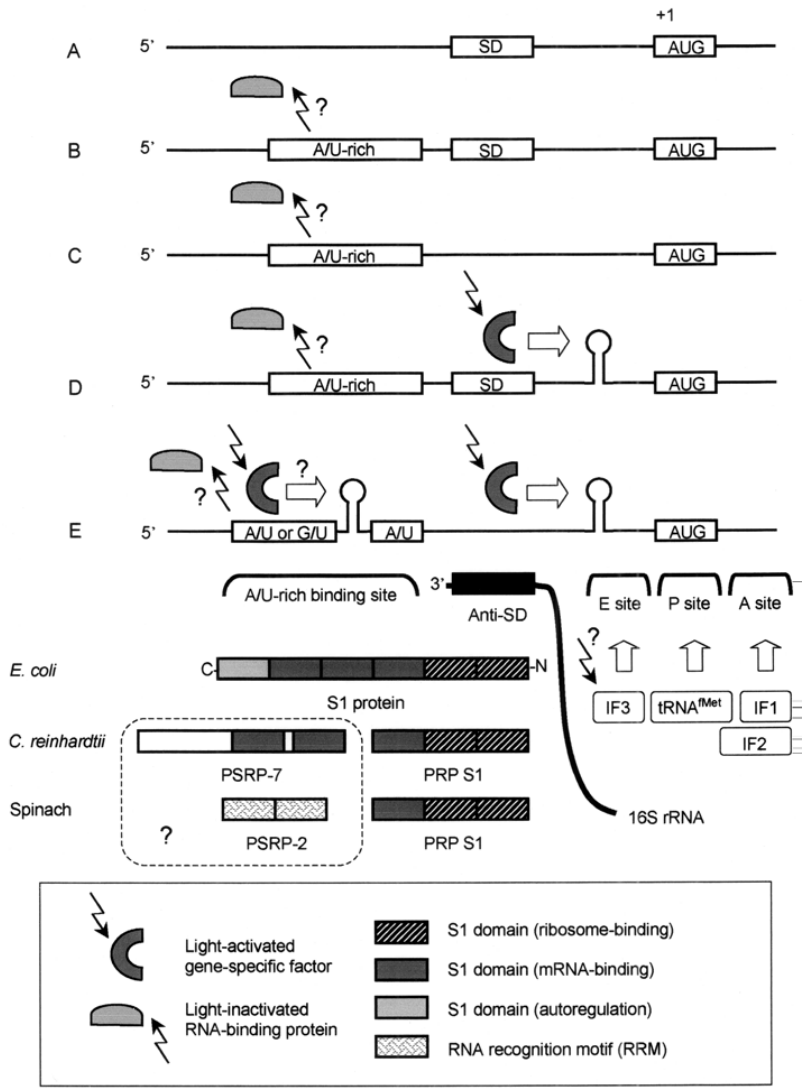

Fig. 2. A model of chloroplast translation regulation. Various 5′ UTRs of chloroplast mRNAs (A-E) are schematically shown, including A/U-rich sequence binding sites, anti-Shine-Delagarno (SD) sequence, and stem-loop elements. In eubacteria, IF1 binds in the A site, IF2 binds over the A site, the P site is occupied by $tRNA^{fMet}$, and IF3 occupies the E site (Ramakrishnan, 2002). Chloroplast IF3 activity can be modulated, probably via light-regulated factor association (Yu and Spremulli, 1998). The *E. coli* S1 protein has six S1 domains (Subramanian, 1983; Gribskov, 1992). The first two domains are involved in ribosome-binding, and the following three domains are involved in mRNA-binding (Subramanian, 1983), and the last domain is for autoregulation (Boni et al., 2001). In plastids, the *E. coli* S1 counterparts are called PRP S1 (plastid ribosomal protein S1). PRP S1 has similar functions in the N-terminal half on the *E. coli* S1 protein (Shteiman-Kotler and Schuster, 2000). Putative mRNA-binding proteins (PSRP-2 and PSRP-7) may be involved in A/U sequence binding to the plastid 30S subunit, to complement mRNA recognition of PRP S1. A: Prokaryotic-like SD-sequence dependent translation initiation. Most bacterial mRNAs utilize this interaction for translation initiation (Hager and Rabinowitz, 1985). B: An enhanced SD-sequence dependent translation initiation with interaction of A/U-rich sequence and S1 protein. A number of *E. coli* mRNAs encoding abundant proteins use this mode (Boni et al., 1991). Several PS II genes such as *psbC, psbD,* and *psbE* (Fig. 1) may utilize this mode. C: SD-sequence independent translation initiation by interaction of A/U-rich sequence and S1 protein. Several PS II genes such as *psbL*, *psbM*, and *psbN* (Fig. 1) may employ this mode. D: Factor-mediated translation initiation, which may adjust proper spacing between SD-sequence and AUG codon.

2003). It remains to be seen whether these proteins are associated with ribosomes in cyanobacteria. The *C. reinhardtii* chloroplast ribosome contains a similar set of proteins as those found in spinach, except that *C. reinhardtii* appears to lack the L29, PSRP-2 and PSRP-5 counterparts. In addition, the *C. reinhardtii* chloroplast 30S ribosome contains a novel protein of 66 kDa designated PSRP-7, which contains two S1 domains. Several of the plastid ribosomal proteins (PRPs) are larger than their *E. coli* counterparts, harboring N-terminal or C-terminal extensions. The *C. reinhardtii* PRPs S2, S3, and S5 are significantly larger than their *E. coli* counterparts with long N-terminal extensions (S2 and S5) or long insertion sequence (S3). Thus, chloroplast ribosomes share a bacteria-type 70S core, but contain additional PSRPs and extra domains mainly in their small subunits as compared to bacterial ribosomes. It seems likely that the plastid 70S core is responsible for fundamental translation processes, whereas the additional PSRPs and additional domains may function in translational regulation, perhaps for light-activated translational regulation.

a. Potential Role of Plastid Ribosomal Proteins

E. coli ribosomes are able to translate the *rpsA* gene (encoding S1 protein, Boni et al., 2001) or plant viral mRNAs (Tzareva et al., 1994), even though these mRNAs lack Shine-Dalgarno (ribosome binding) sequences in their 5′ UTRs. Boni et al. (1991) have proposed that the ribosomal protein S1 binds a U-rich sequence upstream of the SD region, thus serving as a determinant in recognition of bacterial mRNAs by the ribosome. It has been suggested that the S1 protein is dispensable when a strong SD interaction can be formed and the S1 protein is required when SD interactions are lacking (Farwell et al., 1992). In spinach and *C. reinhardtii* chloroplasts, and in cyanobacteria, the S1 proteins have truncated structures with only three S1 domains (Franzetti et al., 1992; Sugita et al., 1995; Sugita et al., 2000; Yamaguchi et al., 2002). The plastid and cyanobacterial S1 proteins have similar RNA binding functions as bacterial S1 and thus seem likely to facilitate mRNA ribosome interactions. In *C. reinhardtii* an additional S1 domain containing protein, PSRP-7, has been identified. As the S1 domains in PSRP-7 shows significant similarity with those of *E. coli* S1, RNA affinity to A/U-rich sequence can be expected. *C. reinhardtii* does not contain the putative RNA binding protein PSRP-2 as in spinach plastids, and thus PSRP-7 may be a functional counterpart of PSRP-2 (Fig. 2). C. Sugita et al. (2000) have recently identified an S1-like mRNA binding protein (Nbp1) from cyanobacteria. Perhaps PSRP-7 and Nbp1 are functional counterpart of PSRP-2 and cpRNP, respectively, acting to bind mRNA in a protective manner and to facilitate mRNA/ribosome association.

b. Control of Synthesis During Translation Elongation

Evidence is also mounting that other step in chloroplast gene expression are subjected to photosynthetic redox control, including translation elongation (Edhofer et al., 1998), RNA degradation (Monde et al., 2000), and RNA splicing (reviewed in Barkan and Goldschmidt-Clermont, 2000). Superimposed on modulation of translation initiation by redox-regulated factors is the light regulated elongation of nascent translation products. In barley, ribosomes were shown to pause at specific sites during elongation of the D1 polypeptide, which was attributed to a requirement for adding components to the newly synthesized apoprotein (Kim et al., 1991). Subsequent studies by Kuroda et al. (1996) in etiolated pea chloroplast identified the regulator of pausing as a redox-reactive factor that arises from photosynthetic electron transport. Electron transport uncouplers were used to release the proton gradient generated by photosynthetic electron transport, resulting in the inhibition of light dependent translation elongation (Mühlbauer and Eichacker, 1998). From these studies the authors propose that light-activated translation elongation in chloroplast is dependent on the formation of a proton gradient

Fig. 2. Continued. The *psbA* genes from *C. reinhardtii* and tobacco likely use this mode (Hirose and Sugiura, 1996; Bruick and Mayfield, 1999). E: Multiple factor-mediated translation initiation of –SD mRNA. A factor is required for proper spacing between A/U-rich sequence and AUG codon, thus the A/U-rich element is able to interact with PRP S1. Additional factors may be required for enhanced translation to adjust spacing between the first downstream A/U-rich sequence and second upstream A/U-rich sequence or G/U-rich sequence complementary to PSRP-7 (*C. reinhardtii*) or PSRP-2 (spinach), respectively. This hypothetical model has to be experimentally evaluated. General light-activated translation may also be present (B-E). Under dark conditions mRNAs are not translated, and are protected by RNA-binding proteins (e.g., cpRNPs; Nakamura et al., 2001), and this mRNA binding activity can be modulated by phosphorylation (Lisitsky and Schuster, 1995). Under light growth, general RNA-binding proteins may be displaced by specific RNA-binding proteins and/or by PSRP-7/PRP S1 or PSRP-2/PRP S1 to activate formation of a translation initiation complex.

across the thylakoid membrane. It will be interesting to see which component(s) function to couple elongation and electron transport in this process.

c. Control by Epistasy of Synthesis

In *Chlamydomonas*, the translation rate of some chloroplast-encoded proteins is regulated during their assembly into complexes. This process has been called control of epistasy of synthesis (CES) (reviewed in Choquet et al., 2001). The rate of synthesis of CES proteins is regulated by the availability of their assembly partners from the same complex. Cytochrome *f*, a major subunit of the cytochrome b_6f complex encoded by the *petA* gene is a model protein for the study of the CES process, and TCA1, a nuclear-encoded translation activator specific for *petA* mRNA appears to be an effector involved in the CES process (Wostrikoff et al., 2001). It remains to be elucidated whether this CES process is also used to coordinate expression of the D1 and D2 reaction center polypeptides of PS II.

III. Regulation of Photosystem II Gene Expression in Higher Plants

A. Complex Transcription Machinery in Higher Plant Plastids

Plastid genomes of most vascular plants contain approximately 100 genes that encode the components involved in photosynthesis, transcription/translation and biosynthesis of fatty acids and pigments (Wakasugi et al., 2001). Unlike unicellular green algae, higher plant plastids diverge, both functionally and morphologically, and include undifferentiated proplastids in the meristem, etioplasts in dark-grown seedlings, chloroplasts in leaves and amyloplasts in roots (Herrmann et al., 1992). Regulation of the expression of plastid genes is light dependent, and also depends on the tissue and the developmental stage of the plants.

Significant developments in the last decade were the discoveries of non-plastid (nuclear)-encoded RNA polymerases (Hess and Börner, 1999) and multiple sigma factors (Allison, 2000). Plastids of higher plants contain two distinct DNA-dependent RNA polymerases: the plastid-encoded plastid RNA polymerase (PEP), and the nuclear-encoded plastid RNA polymerase (NEP). PEP comprises a core complex $\alpha_2\beta\beta'\beta''$ encoded as *rpoA*, *rpoB*, *rpoC1* and *rpoC2*. Exceptionally, the PEP α subunit is encoded by the nuclear genome in mosses (C. Sugiura et al., 2003). The subunit composition coincides with the cyanobacterial enzyme (Curtis and Martin, 1994) and supports the theory that plastids originated from the ancestral cyanobacterium.

1. Nuclear-Encoded Plastid RNA Polymerase

The existence of NEP was initially found in the barley nuclear mutant, *albostrians*, which has no plastid ribosomes (Hess et al., 1993). Although plastid-encoded PEP is not produced within the plastids, several plastid gene transcripts accumulated in this mutant, a similar finding to the complete genome analysis of the parasitic angiosperm *Epifagus virginiana*, which has no plastid-encoded *rpo* genes (Wolfe et al., 1992). This was also proven by knockout mutagenesis of the *rpo* genes of tobacco (Hajdukiewicz et al., 1997; De Santis-Maciossek et al., 1999). The first biochemical evidence of NEP was obtained by Lerb-Mache (1993) who identified a monomeric enzyme of 110 kDa in spinach chloroplasts with all the characteristics of single subunit RNA polymerases of the T7 bacteriophage. Following this, the gene encoding bacteriophage T7/T3-like RNA polymerase was cloned and its gene product was demonstrated to localize in the chloroplasts (Hedtke et al., 1997). These results support the idea that phage-type RNA polymerase is one of the NEPs. A third plastid RNA polymerase, NEP-2, was recently found in spinach chloroplasts (Bligny et al., 2000). Interestingly, NEPs have never been identified in green algal chloroplasts, and it is possible that they were acquired after the appearance of land plants (Lilly et al., 2002). NEP preferentially transcribes housekeeping genes such as *accD*, *rpl23*, *rpoB* and *clpP* (Hübschmann and Börner 1998, Weihe and Börner, 1999) and operates one of the multiple promoters of *atpB* and 16S rDNA (Vera and Sugiura, 1995; Kapoor et al., 1997). In general, genes for non-photosynthetic components are transcribed by NEP during the early stage of plastid differentiation and development. Subsequent transcription of the genes for photosynthesis related components are directed by PEP (Mullet, 1993; Hess and Börner, 1999).

The NEP promoter resembles the plant mitochondrial gene promoter sequence (Tracy and Stern, 1995), which suggests that the origin of NEP is completely different to that of PEP (Gray and Lang, 1998).

2. Transcription by Plastid-Encoded Plastid RNA Polymerase

Upstream regions of many transcription initiation sites on plastid DNA contain DNA sequences similar to *E. coli* '–10' and '–35' consensus sequences (reviewed in Igloi and Kössel, 1992). The *psbA* gene, and several other photosynthesis-related plastid genes in higher plants, contain both prokaryotic-type promoter sequences and, between them, a sequence motif similar to the TATA box of nuclear genes. Prokaryotic –10 and –35 promoter regions are required for proper transcription (Gruissem and Tonkyn, 1993) and the TATA-like region is also critical for correct *psbA* transcription in vitro (Eisermann et al., 1990). Plastid sigma factors recognize the promoter sequence, –10 and –35 regions of the photosynthetic genes, and subsequently recruit PEP.

3. Multiple Plastid Sigma Factors

Plastid sigma factors are encoded by a gene family in the nuclear DNA (Allison, 2000) and six members have been identified in *Arabidopsis thaliana* (The Arabidopsis Genome Initiative, 2001). The expression of nuclear-encoded plastid σ factor genes is light dependent and leaf-specific. Interestingly, the wheat *sigA* mRNA level exhibited circadian oscillation with phase patterns similar to the patterns of *psbD* mRNA levels (Nakahira et al., 1998; Morikawa et al., 1999). Expression of Sig5, one of six *Arabidopsis* sigma factors, is extensively induced by blue light (Tsunoyama et al., 2002). These observations imply that each member of several sigma factors can recognize and discriminate specific promoter sequences of photosynthetic genes and respond to the developmental program or environmental conditions.

B. Light-Regulated Transcription

Most PS II genes are light-regulated and actively transcribed during illumination. The mRNA levels rise upon light illumination and fall during dark periods. Transcription/translation activity increases within non-photosynthetic plastids during plastid development, followed by an early build-up of the photosynthetic apparatus. Further accumulation and maintenance of photosynthetic apparatus requires light.

1. Light Responsive Promoter of the psbD Gene

The *psbD* gene encoding D2 of PS II is co-transcribed with *psbC* and *orf62* (*psbZ*) in dicots but with *psbK*, *psbI*, *psbC*, *psbZ* and *trnG* in monocots (Christopher et al., 1992). Interestingly, *psbD* is transcribed from four distinct sites in barley and wheat (Christopher et al., 1992; Satoh et al., 1997). One of the transcription initiation sites of *psbD* is directed by a light-responsive promoter (LRP) called *psbD* LRP, which is activated by high light, blue or UV-A light and is, therefore, alternatively called *psbD* BLRP. It is proposed that the high-irradiance activation of the *psbD* LRP serves to maintain D2 protein levels photodamaged under high-intensity light conditions (Christopher and Mullet, 1994). The level of *psbD* LRP mRNA is controlled not only by light but also by endogenous circadian rhythms (Chen et al., 1995; Kim et al., 1999; Nakahira et al., 1998). Blue-light-specific activation of the *psbD* LRP involves cryptochromes and phytochrome A in *Arabidopsis* (Thum et al., 2001a).

2. Cis-Elements and Trans-acting Factors for the Light Responsive Promoter of the psbD Gene

Sequences within 130 bp of the *psbD* LRP are highly conserved in higher plants (Christopher et al., 1992). The barley *psbD*-LRP introduced into the tobacco plastid genome is also activated in tobacco by blue or white light, confirming the importance of the *psbD*-LRP in light regulation (Thum et al., 2001b). A 53-bp DNA region of the *psbD* LRP, from –57 to –6, is sufficient for transcription and termed the AAF-box, while the sequence –36 to –57 is required for blue light-response transcription. A positive factor, AGF, binds to the AAG-box and interacts with PEP to promote transcription from the *psbD* LRP (Kim and Mullet, 1995). Thus, transcription from the *psbD* LRP is similar to type II bacterial promoters that use activating proteins to stimulate transcription. Furthermore, Kim et al. (1999) identified a second sequence-specific DNA-binding complex, PGTF, which binds upstream of AAG between –71 and –100 in barley *psbD* LRP. PGTF is ADP-dependently phosphorylated in darkness and functions as a negative regulator of light-dependent transcription. Therefore, ADP-dependent phosphorylation in chloroplasts may inactivate enzymes involved in carbon assimilation,

protein synthesis and transcription during diurnal light/dark cycles. The detailed protein structures of AGF and PGTF remain to be analyzed. Recently, Baba et al. (2001) used yeast one-hybrid screening of an *Arabidopsis* cDNA library to isolate PTF1, a possible DNA-binding protein of the *psbD* LRP upstream sequence. PTF1 has 355 amino acids and contains a basic helix-loop-helix DNA binding motif. The ACC repeat, located between the AAG-box and –35 regions, was shown to be essential for PTF1 binding. The rate of *psbD* LRP mRNA accumulation was significantly reduced in the T-DNA-inserted *Arabidopsis ptf1* mutant. PTF1 functions as one of the *trans*-acting factors of the *psbD* LRP. Several plastid DNA-binding proteins have been identified for spinach, tobacco and pea (reviewed in Sato, 2001). More than 100 DNA-binding proteins and transcription factors are predicted to be plastid-targeted in *Arabidopsis* (The Arabidopsis Genome Initiative, 2000).

3. Transcriptional Regulation of the psbA Gene

Extensive studies on the regulation of *Chlamydomonas psbA* expression indicate that chloroplast gene expression is controlled by mechanisms with key regulatory roles in photosynthesis, such as protein phosphorylation and redox poise (Mayfield et al., 1995). Likewise, with regard to plastid transcription in higher plants, evidence for concerted regulation by phosphorylation and redox poise has recently accumulated (Tullberg et al., 2000; Pfannschmidt et al., 2002).

The *psbA* encoding D1 is one of the most widely studied plastid genes and serves as a paradigm in understanding the regulatory mechanism of photosynthetic gene expression. The *psbA* promoter contains prokaryotic –10 and –35 sequence elements and the 'TATA' sequence between them. In contrast to *psbD* LRP, no *cis*-element for light-regulated expression of *psbA* were identified further upstream from the –35 region. In mustard plastids, there are two distinct PEP activities, the A and B enzymes (Pfannschmidt and Link, 1994, 1997), with the B enzyme predominating in etioplasts of dark-grown plants and the A enzyme being more abundant in the chloroplasts. During light-dependent differentiation from etioplasts to chloroplasts, the highly phosphorylated B enzyme is dephosphorylated and interacts with A-enzyme-specific subunits and associated protein factors to form the A enzyme (reviewed in Link, 1996). The etioplast sigma-like factors (SLFs), which are distinct from the sigma 70 (σ^{70})-type factor and are highly phosphorylated, could be converted into chloroplast-type SLFs. This conversion is achieved in the differential phosphorylation state and controls plastid-type specific *psbA* transcription (Tiller and Link, 1993).

RNA polymerase-associated plastid transcription kinase (PTK) from mustard catalyzes phosphorylation of SLFs in vitro and controls PEP activity (Baginsky et al., 1997). PTK activity is enhanced in vitro by reducing glutathione (Baginsky et al., 1999). Glutathione is thought to be important for enhancing the expression of the *psbA* gene after high light stress, i.e., under increased amounts of oxidized glutathione (Karpinski et al., 1997). Christopher et al. (1997) showed that plastid transcription activity in barley plants was enhanced in the presence of protein kinase inhibitors and decreased in the presence of phosphatase inhibitors. It was concluded that a plastid protein kinase was responsible for the down-regulation of chloroplast transcription and that protein phosphatases are required for the proper function of plastid transcription and chloroplast development. However, a protein kinase represses the *psbD* LRP in plants grown in the dark (Baena-González et al., 2001).

C. Post-transcriptional and Translational Control in Higher Plants

In higher plants, most plastid genes are co-transcribed dicistronically or polycistronically together with genes of either a related or an unrelated function (Sugita and Sugiura, 1996). Post-transcriptional RNA processing of primary transcripts is an important step in the control of plastid gene expression and is required for translation initiation of some processed and mature mRNAs (Sugiura et al., 1998).

1. Stability of psbA mRNA

The *psbA* mRNA accumulates at substantial levels in both light and dark periods. Most of the *psbA* mRNA is found in non-polysomal fractions from the stroma, and ~20% of the total *psbA* mRNA is associated with thylakoid membranes, mostly in the polysome fraction in dark-grown barley seedlings (R. R. Klein et al., 1988). Upon illumination, membrane-bound polysomal *psbA* mRNA levels rapidly increase (Kim and Mullet, 1994) and translation

initiation occurs on the associated membrane. *psbA* mRNA is quite stable and its half-life is over 40 h (Klaff and Gruissem, 1991). Most *psbA* mRNAs in the stroma are associated with RNA-binding proteins of 28–33 kDa and form the RNA-protein complexes (Nakamura et al., 2001). The mRNA in the complexes could be protected from cleavage by ribonucleases. Association of the RNA-binding proteins with *psbA* mRNA and their dissociation from the mRNA could be regulated by phosphorylation and dephosphorylation of the proteins (Lisitsky and Schuster, 1995). The UTRs of plastid RNAs act as regulatory elements for post-transcriptional and/or translational control of gene expression (Stern et al., 1997; Eibl et al., 1999; Shiina et al., 1998). The 5′ UTR of *psbA* mRNA associated with a 43 kDa protein (ribosomal protein S1), which is present in the stroma and in membrane fractions in spinach (Alexander et al., 1998). RNA binding-proteins of 43- and 30-kDa interact specifically with the *Arabidopsis psbA* mRNA 5′ UTR and its binding activity is controlled in a redox-dependent manner (Shen et al., 2001). Thus, redox-dependent interactions, between specific sequences in the 5′ UTR and these proteins, could be involved in the post-transcriptional regulation of *psbA* gene expression in chloroplasts of higher plants such as occurs in *Chlamydomons* (reviewed in Somanchi and Mayfield, 2001).

2. Polyadenylation and Degradation of Plastid mRNAs

The steady-state levels of many plastid mRNAs are determined by their transcription rate in comparison with its degradation rate. Like *E. coli*, plastid *psbA* mRNAs are endonucleolytically cleaved at several sites and poly(A)-rich tails are added to their 3′ end of the cleaved products of mRNA (Kudla et al., 1996, Lisitsky et al., 1996). Plastid poly(A) tails are very long, several tails of 270 nucleotides were detected, compared with only 40 to 60 nucleotides in bacteria (Sarkar, 1997). Such cleavage and polyadenylation of mRNAs also occur in *petD* and *rps14* (Kudla et al., 1996). The poly(A) moiety is not a ribohomopolymer of adenosine residues, but poly(A) tails usually contains 70% adenosines, 25% guanosines, and others. Once the initial endonucleolytic cleavage has occurred, cleaved mRNA will be rapidly polyadenylated and exonucleolytically degraded (Schuster et al., 1999). Therefore, the steady-state levels of polyadenylated RNAs are not detectable in the chloroplasts and they could be detected only by powerful detection method of RT-PCR. Unlike *E. coli*, polyadenylation and exonucleolytic degradation of RNA in chloroplasts are performed by one enzyme, polynucleotide phosphorylase (PNPase) (Yehudai-Resheff et al., 2001). Chloroplast PNPase exists as a homo-multimer complex of 600 kDa (Baginsky et al., 2001) and has poly(A) polymerase activity and 3′ → 5′ exonuclease activity. PNPase polyadenylation activity is strongly increased in plastids of dark-adapted plants and RNA degradation proceeds in the dark (Baginsky and Gruissem, 2002). This suggests that plastid mRNA stability is controlled by the regulation of a specific dark-induced RNA degradation pathway.

3. Processing of Pre-mRNAs

Many chloroplast genes in higher plants are transcribed as polycistronic pre-mRNAs, which are then endonucleolytically processed into mostly monocistronic mRNAs. The tobacco *psaC-ndhD* gene cluster is transcribed as a dicistronic pre-mRNA that is then cleaved into monocistronic mRNAs. In vitro translation assays showed that the dicistronic mRNA is not functional and that the intercistronic cleavage is a prerequisite for both *psaC* and *ndhD* translation (Hirose and Sugiura, 1997). Lack of the monocistronic forms of the *petB* and *petD* mRNAs, which instead accumulate in the dicistronic form, and loss of the cytochrome b_6f complex, was found in the maize nuclear mutant, *crp1* (Barkan et al., 1994). Thus, precise RNA processing is required for efficient translation in higher plants. The plastid RNA processing enzyme P54 is involved in cleavage at the intercistronic region of *trnK-psbA* pre-mRNA and the activity is influenced by reducing agents in vitro (Liere and Link, 1997). Spinach CSP41, a sequence-specific mRNA binding protein, has endoribonuclease activity (Yang et al., 1996). The maize *crp1* has been cloned and sequenced and the CRP1 protein shows weak homology to *Neurospora crassa* CYA5 and yeast PET309, which both function in mitochondrial gene expression (Fisk et al., 1999). Interestingly, CRP1 is a member of the pentatricopeptide repeat (PPR) protein superfamily (I. D. Small and Peeters, 2000). The nonphotosynthetic mutant, *hcf152*, of *Arabidopsis* is impaired in the processing of the chloroplast polycistronic transcript, *psbB-psbT-psbH-petB-petD*, resulting in nonproduction of the essential photosynthetic cytochrome b_6f complex (Meurer et

al., 1996). The nucleus-encoded HCF152 gene was identified to encode a PPR protein with 12 putative PPR motifs (Meierhoff et al., 2003). The HCF152 may be involved in the processing or stabilization of the *petB* transcript by binding to the exon-intron junctions (Nakamura et al., 2003). The chloroplast NDH complex, NAD(P)H dehydrogenase, reduces the plastoquinone pool non-photochemically and is involved in cyclic electron flow around Photosystem I (PS I). The *Arabidopsis* nuclear mutants, *crr2-1* and *crr2-2* (chlororespiratory reduction), are recessive mutant alleles in which accumulation of the NDH complex is impaired. CRR2 encodes a PPR protein with 9 putative PPR motifs and functions in the intergenic processing of chloroplast RNA between *rps7* and *ndhB*, which is possibly essential for *ndhB* translation (Hashimoto et al., 2003). Thus, PPR proteins involve in the maturation steps of plastid RNA.

4. Translational Regulation of psbA mRNA

SD-like and A/U-rich sequences at –24 to –14 of *psbA* mRNA are critical elements for in vitro translation initiation of the tobacco *psbA* mRNA (Hirose and Sugiura, 1996, see Fig. 1 for tobacco). The existence of the A/U-rich binding protein was identified by gel shift assay. The 5′ UTR of plastid mRNAs are an important determinant of translation initiation in algae and higher plants (Bruick and Mayfield, 1999; Sugiura et al., 1998). D1 has the highest turnover rate of all thylakoid proteins because of light-induced damage to D1 (Aro et al., 1993; Pfannschmidt et al., 2002; Zerges, 2002). The mechanisms of targeting, insertion and assembly of plastid-encoded thylakoid membrane proteins are not fully understood. The plastid signal recognition particle, cpSRP54, interacts with the D1 nascent chain attached to the ribosome (Nilsson et al., 1999), which implies a crucial role for cpSRP54 in D1 biogenesis.

The molecular mechanism of translation initiation mediated interaction of RNA-binding proteins with 5′ UTR of mRNA has been extensively characterized (reviewed in Bruick and Mayfield, 1999), which enabled us to easily illustrate a similar regulatory process operating in higher plants. Most of the evidence for the involvement of nuclear-encoded *trans*-factors in translation comes from genetic and molecular analyses of nuclear mutants of maize (Barkan et al., 1994; McCormac and Barkan, 1999; Till et al., 2001). The elucidation of the function involved in the regulation of plastid gene transcription and translation in higher plants requires further characterization by solid biochemical and powerful genetic approaches and by transgenic techniques.

Acknowledgments

Research in the Mayfield lab was supported by grants from the National Institutes of Health (GM54659) and the US Department of Energy (DE-FG03-93ER70116) to SPM. KY was supported by a Skaggs Institute postdoctoral fellowship. Research in the Sugita lab was supported by Grant-in-Aids from the Japan Society for the Promotion of Science (14340252) and from the Ministry of Agriculture, Forestry and Fisheries to MS.

References

Alexander C, Faber N and Klaff P (1998) Characterization of protein-binding to the spinach chloroplast *psbA* mRNA 5′ untranslated region. Nucleic Acids Res 26: 2265–2272

Allison LA (2000) The role of sigma factors in plastid transcription. Biochimie 82: 537–548

Aro EM, Virgin I and Andersson B (1993) Photoinhibition of Photosystem II: Inactivation, protein damage and turn-over. Biochim Biophys Acta 1143: 113–134

Auchincloss AH, Zerges W, Perron K, Girard-Bascou J and Rochaix JD (2002) Characterization of Tbc2, a nucleus-encoded factor specifically required for translation of the chloroplast *psbC* mRNA in *Chlamydomonas reinhardtii*. J Cell Biol 157: 953–962

Baba K, Nakano T, Yamagishi K and Yoshida S (2001) Involvement of a nuclear-encoded basic helix-loop-helix protein in transcription of the light-responsive promoter of *psbD*. Plant Physiol 125: 595–603

Baena-González E, Baginsky S, Mulo P, Summer H, Aro EM and Link G (2001) Chloroplast transcription at different light intensities. Glutathione-mediated phosphorylation of the major RNA polymerase involved in redox-regulated organellar gene expression. Plant Physiol 127: 1044–1052

Baginsky S, Gruissem W (2002) Endonucleolytic activation directs dark-induced chloroplast mRNA degradation. Nucleic Acids Res 30: 4527–4533

Baginsky S, Tiller K and Link G (1997) Transcription factor phosphorylation by a protein kinase associated with chloroplast RNA polymerase from mustard (*Sinapis alba*). Plant Mol Biol 34: 181–189

Baginsky S, Tiller K, Pfannschmidt and Link G (1999) PTK, the chloroplast RNA polymerase-associated protein kinase from mustard (*Sinapis alba*), mediates redox control of plastid in vitro transcription. Plant Mol Biol 39: 1013–1023

Baginsky S, Shteiman-Kotler A, Liveanu V, Yehudai-Resheff S, Bellaoui M, Settlage RE, Shabanowitz J, Hunt DF, Schuster G, Gruissem W (2001) Chloroplast PNPase exists as a homomultimer enzyme complex that is distinct from the *Escherichia*

coli degradosome. RNA 7: 1464–1475

Barkan A and Goldschmidt-Clermont M (2000) Participation of nuclear genes in chloroplast gene expression. Biochimie 82: 559–572

Barkan A, Walker M, Nolasco M and Johnson D (1994) A nuclear mutation in maize blocks the processing and translation of several chloroplast mRNAs and provides evidence for the differential translation of alternative mRNA forms. EMBO J 13: 3170–3181

Betts L and Spremulli LL (1994) Analysis of the role of the Shine-Dalgarno sequence and mRNA secondary structure on the efficiency of translational initiation in the *Euglena gracilis* chloroplast *atpH* mRNA. J Biol Chem 269: 26456–26463

Blankenship JE and Kindle KL (1992) Expression of chimeric genes by the light-regulated cabII-1 promoter in *Chlamydomonas reinhardtii*: A cabII-1/nit1 gene functions as a dominant selectable marker in a nit1$^-$ nit2$^-$ strain. Mol Cell Biol 12: 5268–52679

Bligny M, Courtois F, Thaminy S, Chang CC, Lagrange T, Baruah-Wolff, Stern D and Lerbs-Mache S (2000) Regulation of plastid rDNA transcription by interaction of CDF2 with two different RNA polymerases. EMBO J 19: 1851–1860

Boni IV, Isaeva DM, Musychenko ML and Tzareva NV (1991) Ribosome-messenger recognition: mRNA target sites for ribosomal protein S1. Nucleic Acids Res 19:155–162

Boni IV, Artamonova VS, Tzareva NV and Dreyfus M (2001) Non-canonical mechanism for translational control in bacteria: Synthesis of ribosomal protein S1. EMBO J 20: 4222–4232

Boudreau E, Nickelsen J, Lemaire SD, Ossenbuhl F and Rochaix JD (2000) The *Nac2* gene of *Chlamydomonas* encodes a chloroplast TPR-like protein involved in *psbD* mRNA stability. EMBO J 19: 3366–3376

Brown EC, Somanchi A and Mayfield SP (2001) Interorganellar crosstalk: New perspectives on signaling from the chloroplast to the nucleus. Genome Biol 2: 1021–1024

Bruick RK and Mayfield SP (1998) Processing of the *psbA* 5′ untranslated region in *Chlamydomonas reinhardtii* depends upon factors mediating ribosome association. J Cell Biol 143: 1145–1153

Bruick RK and Mayfield SP (1999) Light-activated translation of chloroplast mRNAs. Trends Plant Sci 4: 190–195

Chen SCG, Wu SP, Lo PK, Mon DP and Chen LFO (1995) Regulation of plastid photosynthetic *psbK-I-D-C* gene expression by light in rice plants. Physiol Plant 93: 617–623

Choquet Y, Wostrikoff K, Rimbault B, Zito F, Girard-Bascou J, Drapier D and Wollman FA (2001) Assembly-controlled regulation of chloroplast gene translation. Biochem Soc Trans 29: 421–426

Christopher DA and Mullet JE (1994) Separate photosensory pathways co-regulate blue light/ultraviolet-A-activated *psbD-psbC* transcription and light-induced D2 and CP43 degradation in barley (*Hordeum vulgare*) chloroplasts. Plant Physiol 104: 1119–1129

Christopher DA, Kim M and Mullet JE (1992) A novel light-regulated promoter is conserved in cereal and dicot chloroplasts. Plant Cell 4: 785–798

Christopher DA, Li X, Kim M and Mullet JE (1997) Involvement of protein kinase and extraplastidic serine/threonine protein phosphatases in signaling pathways regulating plastid transcription and the *psbD* blue light-responsive promoter in barley. Plant Physiol 113: 1273–1282

Curtis SE and Martin JA (1994) The transcription apparatus and the regulation of transcription initiation. In: Bryant DA (ed) The Molecular Biology of Cyanobacteria, pp 614–639. Kluwer Academic Publishers, Dordrecht

Danon A and Mayfield SP (1991) Light regulated translational activators: Identification of chloroplast gene specific mRNA binding proteins. EMBO J 10: 3993–4001

Danon A and Mayfield SP (1994) ADP-dependent phosphorylation regulates RNA-binding in vitro: Implications in light-modulated translation. EMBO J 13: 2227–2235

Depka B, Jahns P and Trebst A (1998) Beta-carotene to zeaxanthin conversion in the rapid turnover of the D1 protein of Photosystem II. FEBS Lett 424: 267–270

De Santis-Maciossek G, Kofer W, Bocj A, Schoch S, Maier RM, Wanner G, Rudiger W, Koop HU and Herrmann RG (1999) Targeted disruption of the plastid RNA polymerase genes *rpoA*, *B* and *C1*: molecular biology, biochemistry and ultrastructure. Plant J 18: 477–489

Deshpande NN, Bao Y and Herrin DL (1997) Evidence for light/redox-regulated splicing of *psbA* pre-RNAs in *Chlamydomonas* chloroplasts. RNA 3: 37–48

Drager RG, Girard-Bascou J, Choquet Y, Kindle KL and Stern DB (1998) In vivo evidence for 5′ → 3′ exoribonuclease degradation of an unstable chloroplast mRNA. Plant J 13: 85–96

Edhofer I, Muhlbauer SK and Eichacker LA (1998) Light regulates the rate of translation elongation of chloroplast reaction center protein D1. Eur J Biochem 257: 78–84

Eibl C, Zou Z, Beck A, Kim M, Mullet J and Koop HU (1999) In vivo analysis of plastid *psbA*, *rbcL* and *rpl32* UTR elements by chloroplast transformation: Tobacco plastid gene expression is controlled by modulation of transcript levels and translation efficiency. Plant J 19: 333–345

Eisermann A, Tiller K and Link G (1990) In vitro transcription and DNA binding characteristics of chloroplast and etioplast extracts from mustard (*Sinapsis alba*) indicate differential usage of the *psbA* promoter. EMBO J 9: 3981–3987

Fargo DC, Zhang M, Gillham NW and Boynton JE (1998) Shine-Dalgarno-like sequences are not required for translation of chloroplast mRNAs in *Chlamydomonas reinhardtii* chloroplasts or in *Escherichia coli*. Mol Gen Genet 257: 271–282

Farwell MA, Roberts MW and Rabinowitz JC (1992) *Escherichia coli* and *Micrococcus luteus* on protein synthesis in vitro by *E. coli* and *Bacillus subtilis*. Mol Microbiol 6: 3375–3383

Fisk DG, Walker MB and Barkan A (1999) Molecular cloning of the maize gene *crp1* reveals similarity between regulators of mitochondrial and chloroplast gene expression. EMBO J 18: 2621–2630

Fong CL, Lentz A and Mayfield SP (2000) Disulfide bond formation between RNA binding domains is used to regulate mRNA binding activity of the chloroplast poly(A)-binding protein. J Biol Chem 275: 8275–8278

Franzetti B, Carol P and Mache R (1992) Characterization and RNA-binding properties of a chloroplast S1-like ribosomal protein. J Biol Chem 267: 19075–19081

Gillham NW, Boynton JE and Hauser CR (1994) Translational regulation of gene expression in chloroplasts and mitochondria. Annu Rev Genet 28: 71–93

Golden S (1994) Light-responsive gene expression and the biochemistry of Photosystem II reaction center. In: Bryant DA (ed) The Molecular Biology of Cyanobacteria, pp 91–118. Kluwer Academic Publishers, Dordrecht

Gray MW and Lang BF (1998) Transcription in chloroplasts and mitochondria: A tale of two polymerases. Trends Microbiol 6: 1–3

Gribskov M (1992) Translational initiation factors IF-1 and eIF-2 alpha share an RNA-binding motif with prokaryotic ribosomal protein S1 and polynucleotide phosphorylase. Gene 119: 107–111

Gruissem W and Tonkyn JC (1993) Control mechanisms of plastid gene expression. Crit Rev Plant Sci 12: 19–55

Hager PW and Rabinowitz JC (1985) Translational specificity in *Bacillus subtilis*. In: Dubnau D (ed) The Molecular Biology of the *Bacilli*, pp 1–29. Academic Press, New York

Hahn D and Kuck U (1999) Identification of DNA sequences controlling light- and chloroplast-dependent expression of the *lhcb1* gene from *Chlamydomonas reinhardtii*. Curr Genet 34: 459–466

Hajdukiewicz PTJ, Allison LA and Maliga P (1997) The two RNA polymerases encoded by the nuclear and the plastid compartments transcribe distinct groups of genes in tobacco plastids. EMBO J 16: 4041–4048

Harris EH (2001) *Chlamydomonas* as a model organism. Annu Rev Plant Physiol Plant Mol Biol 52: 363–406

Harris EH, Boynton JE and Gillham NW (1994) Chloroplast ribosomes and protein synthesis. Microbiol Rev 58: 700–754

Hashimoto M, Endo T, Peltier G, Tasaka M, Shikanai T (2003) A nucleus-encoded factor, CRR2, is essential for the expression of chloroplast *ndhB* in *Arabidopsis*. Plant J 36: 541–549

Hauser CR, Gillham NW and Boynton JE (1996) Translational regulation of chloroplast genes. Proteins binding to the 5′-untranslated regions of chloroplast mRNAs in *Chlamydomonas reinhardtii*. J Biol Chem 271: 1486–1497

Hauser CR, Gillham NW and Boynton JE (1998) Regulation of Chloroplast Translation. In: Rochaix JD, Goldschmidt-Clermont M and Merchant S (eds) The Molecular Biology of Chloroplasts and Mitochondria in *Chlamydomonas*, pp 197–217. Kluwer Academic Publishers, Dordrecht

Hedtke B, Börner T and Weihe A (1997) Mitochondrial and chloroplast phage-type RNA polymerases in *Arabidopsis*. Science 277: 809–811

Herrmann RG, Westhoff P and Link G (1992) Biogenesis of plastids in higher plants. In: Herrmann RG (ed) Cell Organelles, pp 276-349. Springer-Verlag, Wien/New York

Hess WR and Börner T (1999) Organellar RNA polymerases of higher plants. Int Rev Cytol 190: 1–59

Hess WR, Probona A, Fieder B, Subramanian AR and Börner T (1993) Chloroplast *rps15* and the *rpoB/C1/C2* gene cluster are strongly transcribed in ribosome-deficient plastids: Evidence for a functioning non-chloroplast-encoded RNA polymerase. EMBO J 12: 563–571

Hippler M, Redding K and Rochaix JD (1998) *Chlamydomonas* genetics, a tool for the study of bioenergetic pathways. Biochim Biophys Acta 1367: 1–62

Hirose T and Sugiura M (1996) *Cis*-acting elements and *trans*-acting factors for accurate translation of chloroplast *psbA* mRNAs: Development of an in vitro translation system from tobacco chloroplasts. EMBO J 15: 1687–1695

Hirose T and Sugiura M (1997) Both RNA editing and RNA cleavage are required for translation of tobacco chloroplast *ndhD* mRNA: A possible regulatory mechanism for the expression of a chloroplast operon consisting of functionally unrelated genes. EMBO J 16: 6804–6811

Hirose T, Kusumegi T and Sugiura M (1998) Translation of tobacco chloroplast *rps14* mRNA depends on a Shine-Dalgarno-like sequence in the 5′-untranslated region but not on internal RNA editing in the coding region. FEBS Lett 430: 257–260

Hotchkiss TL and Hollingsworth MJ (1995) Factors in a chloroplast extract specifically bind to the 5′ untranslated regions of chloroplast mRNAs. Nucleic Acids Symp Ser 33: 207–208

Hotchkiss TL and Hollingsworth MJ (1999) ATP synthase 5′ untranslated regions are specifically bound by chloroplast polypeptides. Curr Genet 35: 512–520

Hübschmann T and Börner T (1998) Characterization of transcript initiation sites in ribosome-deficient barley plastids. Plant Mol Biol 36: 493–496

Hwang S and Herrin DL (1994) Control of *lhc* gene transcription by the circadian clock in *Chlamydomonas reinhardtii*. Plant Mol Biol 26: 557–569

Igloi GL and Kössel H (1992) The transcriptional apparatus of chloroplasts. Crit Rev Plant Sci 10: 525–558

Jacobshagen S, Kindle KL and Johnson CH (1996) Transcription of CABII is regulated by the biological clock in *Chlamydomonas reinhardtii*. Plant Mol Biol 31: 1173–1184

Kapoor S, Suzuki J and Sugiura M (1997) Identification and functional significance of a new class of non-consensus-type plastid promoters. Plant J 11: 327–337

Karpinski S, Escobar C, Karpinska B, Creissen G and Mullineaux PM (1997) Photosynthetic electron transport regulates the expression of cytosolic ascorbate peroxidase genes in *Arabidopsis* during excess light stress. Plant Cell 9: 627–640

Katz YS and Danon A (2002) The 3′-untranslated region of chloroplast *psbA* mRNA stabilizes binding of regulatory proteins to the leader of the message. J Biol Chem 277: 18665–18669

Kawazoe R, Hwang S and Herrin DL (2000) Requirement for cytoplasmic protein synthesis during circadian peaks of transcription of chloroplast-encoded genes in *Chlamydomonas*. Plant Mol Biol 44: 699–709

Kim J and Mayfield SP (1997) Protein disulfide isomerase as a regulator of chloroplast translational activation. Science 278: 1954–1957

Kim J and Mullet JE (1994) Ribosome-binding sites on chloroplast *rbcL* and *psbA* mRNAs and light-induced initiation of D1 translation. Plant Mol Biol 25: 437–448

Kim J and Mullet JE (1995) Identification of a sequence-specific DNA binding factor required for transcription of the barley chloroplast blue light-responsive *psbD-psbC* promoter. Plant Cell 7: 1445–1457

Kim J, Klein PG and Mullet JE (1991) Ribosomes pause at specific sites during synthesis of membrane-bound chloroplast reaction center protein D1. J Biol Chem 266: 14931–14938

Kim M, Klein PG and Mullet JE (1994) Synthesis and turnover of Photosystem II reaction center protein D1. J Biol Chem 269: 17918–17923

Kim M, Christopher DA and Mullet JE (1999) ADP-dependent phosphorylation regulates association of a DNA-binding complex with the barley chloroplast *psbD* blue-light-responsive promoter. Plant Physiol 119: 663–670

Klaff P and Gruissem W (1991) Changes in chloroplast mRNA stability during leaf development. Plant Cell 3: 517–529

Klein RR, Mason HS and Mullet JE (1988) Light-regulated translation of chloroplast proteins. I. Transcripts of *psaA-psaB*, *psbA*, and *rbcL* are associated with polysomes in dark-grown

and illuminated barley seedlings. J Cell Biol 106: 289–301

Klein U, De Camp JD and Bogorad L (1992) Two types of chloroplast gene promoters in *Chlamydomonas reinhardtii*. Proc Natl Acad Sci USA 89: 3453–3457

Komine Y, Kwong L, Anguera MC, Schuster G, Stern DB (2000) Polyadenylation of three classes of chloroplast RNA in *Chlamydomonas reinhardtii*. RNA 6: 598–607

Komine Y, Kikis E, Schuster G and Stern D (2002) Evidence for in vivo modulation of chloroplast RNA stability by 3′-UTR homopolymeric tails in *Chlamydomonas reinhardtii*. Proc Natl Acad Sci USA 99: 4085–4090

Kuchka MR, Goldschmidt-Clermont M, van Dillewijn J and Rochaix JD (1989) Mutation at the *Chlamydomonas* nuclear *NAC2* locus specifically affects stability of the chloroplast *psbD* transcript encoding polypeptide D2 of PS II. Cell 58: 869–876

Kudla J, Hayes R, Gruissem W (1996) Polyadenylation accelerates degradation of chloroplast mRNA. EMBO J 15: 7137-7146.

Kuroda H, Kobashi K, Kaseyama H and Satoh K (1996) Possible involvement of a low redox potential component(s) downstream of Photosystem I in the translational regulation of the D1 subunit of the Photosystem II reaction center in isolated pea chloroplasts. Plant Cell Physiol 37: 754–761

Lerbs-Mache S (1993) The 110-kDa polypeptide of spinach plastid DNA-dependent RNA polymerase: Single-subunit enzyme or catalytic core of multimeric enzyme complexes? Proc Natl Acad Sci USA 90: 5509–5513

Liere K and Link G (1997) Chloroplast endoribonuclease p54 involved in RNA 3′-end processing is regulated by phosphorylation and redox state. Nucleic Acids Res 25: 2403–2408

Lilly JW, Maul JE and Stern DB (2002) The *Chlamydomonas reinhardtii* organellar genomes respond transcriptionally and post-transcriptionally to abiotic stimuli. Plant Cell 14: 2681–2706 (Retracted in Plant Cell 16: 785 (2004))

Link G (1996) Green life: Control of chloroplast gene transcription. BioEssays 18: 465–471

Lisitsky I and Schuster G (1995) Phosphorylation of a chloroplast RNA-binding protein changes its affinity to RNA. Nucleic Acids Res 23: 2506–2511

Lisitsky I, Klaff P, Schuster G (1996) Addition of poly(A)-rich sequences to endonucleolytic cleavage sites in the degradation of spinach chloroplast mRNA. Proc Natl Acad Sci USA 93: 13398-13403.

MacCarthy JEG and Brimacombe R (1994) Prokaryotic translation: The interactive pathway leading to initiation. Trends Genet 10: 402–407

Malnoë P, Mayfield SP and Rochaix JD (1988) Comparative analysis of the biogenesis of Photosystem II in the wild-type and Y-1 mutant of *Chlamydomonas reinhardtii*. J Cell Biol 106: 609–616

Martin W and Herrmann RG (1998) Gene transfer from organelles to the nucleus: How much, what happens, and why? Plant Physiol 118: 9–17

Maul JE, Lilly JW, Cui L, DePamphilis CW, Miller W, Harris EH and Stern DB (2002) The *Chlamydomonas reinhardtii* plastid chromosome: Islands of genes in a sea of repeats. Plant Cell 14: 2659–2679

Mayfield SP, Cohen A, Danon A and Yohn CB (1994) Translation of the *psbA* mRNA of *Chlamydomonas reinhardtii* requires a structured RNA element contained within the 5′ untranslated region. J Cell Biol 127: 1537–1545

Mayfield SP, Yohn CB, Cohen A and Danon A (1995) Regulation of chloroplast gene expression. Annu Rev Plant Physiol Plant Mol Biol 46: 147–166

McCormac DJ and Barkan A (1999) A nuclear gene in maize required for the translation of the chloroplast *atpA/E* mRNA. Plant Cell 11: 1709–1716

Meierhoff K, Felder S, Nakamura, Bechtold N and Schuster G (2003) HCF152, an *Arabidopsis* RNA binding pentatricopeptide repeat protein involved in the processing of chloroplast *psbB-psbT-psbH-petB-petD* RNAs. Plant Cell 15: 1480–1495

Melis A (1999) Photosystem-II damage and repair cycle in chloroplasts: What modulates the rate of photodamage? Trends Plant Sci 4: 130–135

Meurer J, Meierhoff K and Westhoff P (1996) Isolation of high-chlorophyll-fluorescence mutants of *Arabidopsis thaliana* and their characterization by spectroscopy, immunoblotting and Northern hybridization. Planta 198: 385–396

Monde RA, Schuster G and Stern DB (2000) Processing and degradation of chloroplast mRNA. Biochimie 82: 573–582

Monod C, Goldschmidt-Clermont M and Rochaix JD (1992) Accumulation of chloroplast *psbB* RNA requires a nuclear factor in *Chlamydomonas reinhardtii*. Mol Gen Genet 231: 449–459

Morikawa K, Ito S, Tsunoyama Y, Nakahira Y, Shiina T and Toyoshima Y (1999) Circadian-regulation expression of a nuclear-encoded plastid σ factor gene (*sigA*) in wheat seedlings. FEBS Lett 451: 275–278

Mühlbauer SK and Eichacker LA (1998) Light-dependent formation of the photosynthetic proton gradient regulates translation elongation in chloroplasts. J Biol Chem 273: 20935–20940

Mullet JE (1993) Dynamic regulation of chloroplast transcription. Plant Physiol 103: 309–313

Nagy F and Schafer E (2002) Phytochromes control photomorphogenesis by differentially regulated, interacting signaling pathways in higher plants. Annu Rev Plant Physiol Plant Mol Biol 53: 329–355

Nakahira Y, Baba K, Yoneda A, Shiina T and Toyoshima Y (1998) Circadian-regulated transcription of the *psbD* light-responsive promoter in wheat chloroplasts. Plant Physiol 118: 1079–1088

Nakamura T, Ohta M, Sugiura M and Sugita M (2001) Chloroplast ribonucleoproteins function as a stabilizing factor of ribosome-free mRNAs in the stroma. J Biol Chem 276: 147–152

Nakamura T, P Meierhoff K, Westhoff, Schuster G. (2003) RNA-binding properties of HCF152, an *Arabidopsis* PPR protein involved in the processing of chloroplast RNA. Eur J Biochem 270: 4070–4081

Nickelsen J, van Dillewijn J, Rahire M and Rochaix JD (1994) Determinants for stability of the chloroplast *psbD* RNA are located within its short leader region in *Chlamydomonas reinhardtii*. EMBO 13: 3182–3191

Nickelsen J, Fleischmann M, Boudreau E, Rahire M and Rochaix JD (1999) Identification of *cis*-acting RNA leader elements required for chloroplast *psbD* gene expression in *Chlamydomonas*. Plant Cell 11: 957–970

Nilsson R, Brunner J, Hoffmann NE and van Wijk KJ (1999) Interactions of ribosome nascent chain complexes of the chloroplast-encoded D1 thylakoid membrane protein with cpSRP54. EMBO J 18: 733–742

Oikawa K, Tanaka K and Takahashi H (1998) Two types of

differentially photo-regulated nuclear genes that encode sigma factors for chloroplast RNA polymerase in the red alga *Cyanidium caldarium* strain RK-1. Gene 210: 277–285

Pfannschmidt T and Link G (1994) Separation of two classes of plastid DNA-dependent RNA polymerases that are differentially expressed in mustard (*Sinapis alba* L.) seedlings. Plant Mol Biol 25: 69–81

Pfannschmidt T and Link G (1997) The A and B forms of plastid DNA-dependent RNA polymerase from mustard (*Sinapis alba* L.) transcribe the same genes in a different developmental context. Mol Gen Genet 257: 35–44

Pfannschmidt T, Allen JF and Oelmuller R (2002) Principles of redox control in photosynthesis gene expression. Physiol Plant 112: 1–9

Race HL, Herrmann RG and Martin W (1999) Why have organelles retained genomes? Trends Genet 15: 364–370

Ramakrishnan V (2002) Ribosome structure and the mechanism of translation. Cell 108: 557–572

Rattanachaikunsopon P, Rosch C and Kuchka MR (1999) Cloning and characterization of the nuclear AC115 gene of *Chlamydomonas reinhardtii*. Plant Mol Biol 39: 1–10

Rhee KH (2001) Photosystem II: The solid structural era. Annu Rev Biophys Biomol Struct 30: 307–328

Rochaix JD (1996) Post-transcriptional regulation of chloroplast gene expression in *Chlamydomonas reinhardtii*. Plant Mol Biol 32: 327–341

Rochaix JD, Kuchka M, Mayfield S, Schirmer-Rahire M, Girard-Bascou J and Bennoun P (1989) Nuclear and chloroplast mutations affect the synthesis or stability of the chloroplast *psbC* gene product in *Chlamydomonas reinhardtii*. EMBO J 8: 1013–1021

Rott R, Liveanu V, Drager RG, Stern DB and Schuster G (1998a) The sequence and structure of the 3′-untranslated regions of chloroplast transcripts are important determinants of mRNA accumulation and stability. Plant Mol Biol 36: 307–314

Rott R, Levy H, Drager RG, Stern DB and Schuster G (1998b) 3′-Processed mRNA is preferentially translated in *Chlamydomonas reinhardtii* chloroplasts. Mol Cell Biol 18: 4605–4611

Ruffle S and Sayre RT (1998) Functional analysis of Photosystem II. In: Rochaix JD, Goldschmidt-Clermont M and Merchant S (eds) The Molecular Biology of Chloroplasts and Mitochondria in *Chlamydomonas*, pp 287–322. Kluwer Academic Publishers, Dordrecht

Sarkar N (1997) Polyadenylation of mRNA in prokaryotes. Annu Rev Biochem 66: 173-197

Sato N (2001) Was the evolution of plastid genetic machinery discontinuous? Trends Plant Sci 6: 151–155

Satoh J, Baba K, Nakahira Y, Shiina T and Toyoshima Y (1997) Characterization of dynamics of the *psbD* light-induced transcription in mature wheat chloroplast. Plant Mol Biol 33: 267–278

Schuster G, Lisitsky I, Klaff P (1999) Polyadenylation and degradation of mRNA in the chloroplast. Plant Physiol 120: 937–944 (1999)

Shen Y, Danon A and Christopher DA (2001) RNA binding-proteins interact specifically with the *Arabidopsis* chloroplast *psbA* mRNA 5′ untranslated region in a redox-dependent manner. Plant Cell Physiol 42: 1071–1078

Shiina T, Allison L and Maliga P (1998) *rbcL* transcript levels in tobacco plastids are independent of light: Reduced dark transcription rate is compensated by increased mRNA stability. Plant Cell 10: 1713–1722

Shine J and Dalgarno L (1974) The 3′-terminal sequence of *Escherichia coli* 16S ribosomal RNA: Complementarity to nonsense triplets and ribosome binding sites. Proc Natl Acad Sci USA 71: 1342–1346

Shteiman-Kotler A and Schuster G (2000) RNA-binding characteristics of the chloroplast S1-like ribosomal protein CS1. Nucleic Acids Res 28: 3310–3315

Small GD, Min B and Lefebvre PA (1995) Characterization of a *Chlamydomonas reinhardtii* gene encoding a protein of the DNA photolyase/blue light photoreceptor family. Plant Mol Biol 28: 443–454

Small ID and Peeters N (2000) The PPR motif — a TPR-related motif prevalent in plant organellar proteins. Trends Biochem Sci 25: 46–47

Somanchi A and Mayfield SP (1999) Nuclear-chloroplast signalling. Curr Opin Plant Biol 2: 404–409

Somanchi A and Mayfield SP (2001) Regulation of chloroplast translation. In: Aro E-M and Andersson B (eds) Regulation of Photosynthesis, pp 137–151. Kluwer Academic Publishers, Dordrecht

Stern D, Higgs DC and Yang J (1997) Transcription and translation in chloroplasts. Trends Plant Sci 2: 308–315

Subramanian AR (1983) Structure and functions of ribosomal protein S1. Prog Nucleic Acids Res Mol Biol 28:101–142

Sugita M and Sugiura M (1996) Regulation of gene expression of chloroplasts of higher plants. Plant Mol Biol 32: 315–326

Sugita M, Sugita C and Sugiura M (1995) Structure and expression of the gene encoding ribosomal protein S1 from the cyanobacterium *Synechococcus* sp. strain PCC 6301: Striking sequence similarity to the chloroplast ribosomal protein CS1. Mol Gen Genet 246: 142–147

Sugita C, Sugiura M and Sugita M (2000) A novel nucleic acid-binding protein in the cyanobacterium *Synechococcus* sp. PCC 6301: A soluble 33-kDa polypeptide with high sequence similarity to ribosomal protein S1. Mol Gen Genet 263: 655–663

Sugiura C, Kobayashi Y, Aoki S, Sugita C and Sugita M. (2003) Complete chloroplast DNA sequence of the moss *Physcomitrella patens*: Evidence for the loss and relocation of *rpoA* from the chloroplast to the nucleus. Nucleic Acids Res 31:5324–5331

Sugiura M, Hirose T and Sugita M (1998) Evolution and mechanism of translation in chloroplasts. Annu Rev Genet 32: 437–459

Swiatek M, Kuras R, Sokolenko A, Higgs D, Olive J, Cinque G, Muller B, Eichacker LA, Stern DB, Bassi R, Herrmann RG and Wollman FA (2001) The chloroplast gene *ycf9* encodes a Photosystem II (PS II) core subunit, PsbZ, that participates in PS II supramolecular architecture. Plant Cell 13: 1347–1367

Telfer A, Bishop SM, Phillips D and Barber J (1994) Isolated photosynthetic reaction center of Photosystem II as a sensitizer for the formation of singlet oxygen. Detection and quantum yield determination using a chemical trapping technique. J Biol Chem 269: 13244–13253

The Arabidopsis Genome Initiative (2000) Analysis of the genome sequence of the flowering plant *Arabidopsis thaliana*. Nature 408: 796–815

Thum KE, Kim M, Christopher DA and Mullet JE (2001a) Cryp-

tochrome 1, cryptochrome 2, and phytochrome A co-activate the chloroplast *psbD* blue light-responsive promoter. Plant Cell 13: 2747–2760

Thum KE, Kim M, Morishige DT, Eibl C, Koop HU and Mullet JE (2001b) Analysis of barley chloroplast *psbD* light-responsive promoter elements in transplastomic tobacco. Plant Mol Biol. 47: 353–366

Tiller K and Link G (1993) Phosphorylation and dephosphorylation affect functional characteristics of chloroplast and etioplast transcription systems from mustard (*Sinapis alba* L.). EMBO J 12: 1745–1753

Till B, Schmitz-Linneweber C, Williams-Carrier R and Barkan A (2001) Crs1 is a novel group II intron splicing factor that was derived from a domain of ancient origin. RNA 7: 1227–1238

Tracy and Stern D (1995) Mitochondrial transcription initiation: Promoter structures and RNA polymerases. Curr Genet 28: 205–216

Tsunoyama Y, Morikawa K, Shiina T and Toyoshima Y (2002) Blue light specific and differential expression of a plastid σ factor, Sig5 in *Arabidopsis thaliana*. FEBS Lett 516: 225–228

Tullberg A, Alexciev K, Pfannschmidt T and Allen JF (2000) Photosynthetic electron flow regulates transcription of the *psaB* gene in pea (*Pisum sativum* L.) chloroplasts through the redox state of the plastoquinone pool. Plant Cell Physiol 41: 1045–1054

Tyystjarvi T, Herranen M and Aro EM (2001) Regulation of translation elongation in cyanobacteria: Membrane targeting of the ribosome nascent-chain complexes controls the synthesis of D1 protein. Mol Microbiol 40: 476–484

Tzareva NV, Makhno VI and Boni IV (1994) Ribosome-messenger recognition in the absence of the Shine-Dalgarno interactions. FEBS Lett 337: 189–194

Vaistij FE, Boudreau E, Lemaire SD, Goldschmidt-Clermont M and Rochaix JD (2000) Characterization of Mbb1, a nucleus-encoded tetratricopeptide-like repeat protein required for expression of the chloroplast *psbB*/*psbT*/*psbH* gene cluster in *Chlamydomonas reinhardtii*. Proc Natl Acad Sci USA 97: 14813–14818

van Wijk KJ, Andersson B and Aro EM (1996) Kinetic resolution of the incorporation of the D1 protein into Photosystem II and localization of assembly intermediates in thylakoid membranes of spinach chloroplasts. J Biol Chem 271: 9627–9636

Vass I, Styring S, Hundal T, Koivuniemi A, Aro EM and Andersson B (1992) Reversible and irreversible intermediates during photoinhibition of Photosystem II: Stable reduced Q_A species promote chlorophyll triplet formation. Proc Natl Acad Sci USA 89: 1408–1412

Vera A and Sugiura M (1995) Chloroplast rRNA transcription from structurally different tandem promoters: An additional novel-type promoter. Curr Genet 27: 280–284

Wakasugi T, Tsudzuki T and Sugiura M (2001) The genomics of land plant chloroplasts: Gene content and alteration of genomic information. Photosynth Res 70: 107–118

Weihe A and Börner T (1999) Transcription and the architecture of promoters in chloroplasts. Trends Plant Sci 4: 169–170

Wolfe KH, Morden CW and Palmer JD (1992) Function and evolution of a minimal plastid genome from a nonphotosynthetic parasitic plant. Proc Natl Acad Sci USA 89: 10648–10652

Wostrikoff K, Choquet Y, Wollman FA and Girard-Bascou J (2001) TCA1, a single nuclear-encoded translational activator specific for *petA* mRNA in *Chlamydomonas reinhardtii* chloroplast. Genetics 159: 119–132

Yamaguchi K and Subramanian AR (2000) The plastid ribosomal proteins: Identification of all the proteins in the 50S subunit of an organelle ribosome (chloroplast). J Biol Chem 275: 28466–28482

Yamaguchi K and Subramanian AR (2003) Proteomic identification of all plastid-specific ribosomal proteins in higher plant chloroplast 30S ribosomal subunit: PSRP-2 (U1A-type domains), PSRP-3α/β (ycf65 homologue) and PSRP-4 (Thx homologue). Eur J Biochem 270: 190–205

Yamaguchi K, von Knoblauch K and Subramanian AR (2000) The plastid ribosomal proteins: Identification of all the proteins in the 30S subunit of an organelle ribosome (chloroplast). J Biol Chem 275: 28455–28465

Yamaguchi K, Prieto S, Beligni MV, Haynes PA, McDonald WH, Yates JR III and Mayfield SP (2002) Proteomic characterization of the small subunit of *Chlamydomonas reinhardtii* chloroplast ribosome: Identification of a novel S1 domain-containing protein and unusually large orthologues of bacterial S2, S3, and S5. Plant Cell 14: 2957–2974

Yamaguchi K, Beligni MV, Prieto S, Haynes PA, McDonald, WH, Yates, JR III and Mayfield SP (2003) Proteomic characterization of the *Chlamydomonas reinhardtii* chloroplast ribosome: Identification of proteins unique to the 70 S ribosome. J Biol Chem 278: 33774–33785

Yang J, Schuster G and Stern DB (1996) CSP41, a sequence-specific chloroplast mRNA binding protein, is an endoribonuclease. Plant Cell 8: 1409–1420

Yehudai-Resheff S, Hirsh M, Schuster G (2001) Polynucleotide phosphorylase functions as both an exonuclease and a poly(A) polymerase in spinach chloroplasts. Mol Cell Biol 21: 5408–5416

Yohn CB, Cohen A, Danon A and Mayfield SP (1996) Altered mRNA binding activity and decreased translational initiation in a nuclear mutant lacking translation of the chloroplast *psbA* mRNA. Mol Cell Biol 16: 3560–3566

Yohn CB, Cohen A, Rosch C, Kuchka MR and Mayfield SP (1998a) Translation of the chloroplast *psbA* mRNA requires the nuclear-encoded poly(A)-binding protein, RB47. J Cell Biol 142: 435–442

Yohn CB, Cohen A, Danon A and Mayfield SP (1998b) A poly(A) binding protein functions in the chloroplast as a message-specific translation factor. Proc Natl Acad Sci USA 95: 2238–2243

Yu NJ and Spremulli LL (1998) Regulation of the activity of chloroplast translational initiation factor 3 by NH_2- and COOH-terminal extensions. J Biol Chem 273: 3871–3877

Zerges W (2000) Translation in chloroplasts. Biochimie 82: 583–601

Zerges W (2002) Does complexity constrain organelle evolution? Trends Plant Sci 7: 175–182

Zerges W and Rochaix JD (1994) The 5′ leader of a chloroplast mRNA mediates the translational requirements for two nucleus-encoded functions in *Chlamydomonas reinhardtii*. Mol Cell Biol 14: 5268–5277

Zerges W and Rochaix JD (1998) Low density membranes are associated with RNA-binding proteins and thylakoids in the chloroplast of *Chlamydomonas reinhardtii*. J Cell Biol 140: 101–110

Zerges W, Girard-Bascou J and Rochaix JD (1997) Translation of the chloroplast *psbC* mRNA is controlled by interactions between its 5′ leader and the nuclear loci *TBC1* and *TBC3* in *Chlamydomonas reinhardtii*. Mol Cell Biol 17: 3440–3448

Zerges W, Auchincloss AH and Rochaix JD (2003) Multiple translational control sequences in the 5′ leader of the chloroplast *psbC* mRNA interact with nuclear gene products in *Chlamydomonas reinhardtii*. Genetics 163: 89–904

Chapter 29

Protein Transport and Post-translational Processing in Photosystem II Biosynthesis and Homeostasis

Steven M. Theg* and Lan-Xin Shi
Division of Biological Sciences, Section of Plant Biology, University of California at Davis, Davis, CA 95616, U.S.A.

Summary

The biogenesis, repair and homeostasis of Photosystem II (PS II) requires both protein targeting and post-translational modification. The various chloroplast targeting pathways for both nuclear-encoded and chloroplast-encoded proteins are described, with emphasis on the subunits of PS II. Also discussed are three post-translational processing events required for the development of PS II activity — removal of the stromal-targeting transit peptides from nuclear-encoded proteins by the stromal processing protease, removal of the thylakoid lumen-targeting signal peptides by the thylakoid processing protease, and trimming of the carboxyl-terminus of the precursor D1 protein by the protease CtpA. Where appropriate, similarities and differences in PS II biogenesis and homeostasis between cyanobacteria and green plants are discussed.

*Author for correspondence, email: smtheg@ucdavis.edu

T. Wydrzynski and K. Satoh (eds): Photosystem II: The Light-Driven Water:Plastoquinone Oxidoreductase, pp. 669–682.

I. Introduction

Photosystem II (PS II) constitutes one of four large multisubunit protein complexes present in the thylakoid membrane. It can be defined at many levels of organization, from the smallest unit capable of carrying out the light-triggered charge separation in the PS II reaction center, to a large unit consisting of many more accessory proteins involved in oxygen evolution and light harvesting. The latter definition is used in this article, as the targeting of some of these accessory proteins points to some interesting aspects of chloroplast biogenesis and homeostasis.

It is well known that PS II is a protein complex with a bigenomic origin (Wollman et al., 1999). Many of the proteins of the core reaction center are encoded in the chloroplast DNA, and are synthesized within the plastid on 70 S ribosomes. Other proteins associated with PS II are encoded in the nucleus, translated in the cytoplasm on 80 S ribosomes and are post-translationally imported into the chloroplast. Since the thylakoid membrane appears not to be attached to the envelope membranes, proteins destined for PS II association must cross the two envelope membranes and traverse the aqueous chloroplast stroma before encountering the thylakoid membrane. Indeed, some proteins are destined to a location on the inner surface of the thylakoid membrane, and so must cross three membranes completely before being incorporated into PS II.

In addition to the complexity of coordinately regulating subunits derived from two genomes, PS II proteins act primarily in the granal region of the heterogeneous thylakoid membrane system. Many aspects of the manner through which PS II, the assembly of which starts in the stromal exposed membranes, finds its functional location in the grana remain unexplained.

Moreover, a number of PS II-associated proteins undergo post-translational modifications during their targeting. Related to this is the lack of proteolytic targeting of unassembled subunits of the oxygen-evolving complex (OEC). These issues are discussed below. Additional post-translational processing events that effect function, rather than biogenesis (i.e., as phosphorylation) are not addressed herein.

Cyanobacteria are a large group of prokaryotic organisms that are capable of oxygenic photosynthesis. It is broadly accepted that cyanobacteria are the progenitors of chloroplasts in green plants. The major components and overall structure and function of PS II complexes in chloroplasts and cyanobacteria show high degrees of similarity (Rhee et al., 1998; Zouni et al., 2001; Chapter 18, Hankamer et al.). On the other hand, some differences do exist between them. For example, neither phosphorylation of PS II core proteins (Pursiheimo et al., 1998) nor lateral migration of the PS II complex along the thylakoid membrane (Mullineaux et al., 1997) occurs during PS II damage-repair cycle in cyanobacteria. In addition, PsbP, PsbR, PsbS, PsbTn and PsbW proteins are unique to higher plants and green algae, whereas PsbU and PsbV proteins, two extrinsic proteins located on the lumenal side of the thylakoid membrane, are found exclusively in cyanobacteria. The PsbP protein which had until recently been regarded as subunit uique to higher plants and green algae, has recently been found to have homologs in cyanobacteria (De Las Rivas et al., 2004; Thornton et al., 2004) and a red alga (Ohta et al., 2003).

II. Targeting Pathways Utilized by Different Photosystem II Subunits

Photosystem II in higher plants contains over 20 polypeptides, many of which have molecular masses of 10 kDa or less (Wollman et al., 1999; Shi and Schroeder, 2004, Chapters 2–6). In contrast to the total chloroplast protein compliment in which just 2% are encoded in the plastid genome (in *Arabidopsis*, Arabidopsis_Genome_Initiative, 2000), over 60% of the proteins in PS II are derived from plastid DNA. This perhaps speaks to the difficulty of retrieving hydrophobic proteins from the cytoplasm, although numerous examples of nuclear-encoded membrane proteins do exist and so hydrophobicity cannot provide the entire explanation.

Although most of the PS II subunits in higher plants are encoded in the chloroplast, the various targeting pathways for proteins in the chloroplast are better

Abbreviations: LHCP – light harvesting chlorophyll-binding protein; LTD – lumen targeting domain; OEC – oxygen-evolving complex; prOE17 – precursor to the 17 kDa, PsbQ protein; prOE23 – precursor to the 23 kDa, PsbP protein; prOE33 – precursor to the 33 kDa, PsbO protein; Sec – secretory pathway, with suffix 'cp' indicating pathway in chloroplasts; SPP – stromal processing protease; SRP – signal recognition particle-dependent pathway, with suffix 'cp' indicating pathway in chloroplasts; Tat – twin arginine translocon targeting pathway, with suffix 'cp' indicating pathway in chloroplasts; Toc/Tic – translocon of the outer and inner envelope membranes, respectively; TPP – thylakoid processing protease

known for nuclear-encoded imported proteins. Accordingly, the discussion of targeting will start with the latter group.

A. Targeting of Nuclear-Encoded Subunits

Chloroplast proteins encoded by nuclear DNA are imported from the cytoplasm to the stroma under the direction of information encoded in amino (N)-terminal extensions called transit peptides (reviewed in Keegstra and Cline, 1999; Jarvis and Soll, 2001). With the possible exception of the precursor to photochlorophyllide reductase A (Reinbothe et al., 2000; Kim and Apel, 2004; however, see Aronsson et al., 2000; Dahlin et al., 2000), all precursors examined appear to use the same pathway through a pair of translocons called the Toc and Tic machineries present in the outer and inner envelope membranes, respectively (Fig. 1). This is evidenced not only by the interchangeability of transit peptides on different precursors to effect the same import reaction (for a review, see Bruce, 2001), but more convincingly, by the ability of different precursors to compete with one another for transit across the envelope membranes (Row and Gray, 2001). PS II subunits that have been examined in this manner are the precursors to the three extrinsic subunits of the OEC, i.e., prOE33, prOE23 and prOE17 (Cline et al., 1993; Row and Gray, 2001), and in each instance competition for import sites was observed either with one another or with the precursor of the small subunit of Rubisco, the prototypical Toc/Tic import substrate (Cline et al., 1985).

Proteins destined for compartments other than the stroma, including PS II subunits, must contain additional targeting information. For some proteins, including PS II subunits PsbO, PsbP, PsbQ and PsbTn (Kapazoglou et al., 1995), PsbX, PsbW and PsbY proteins, the precursor form possesses a bipartite transit peptide in which the amino (N)-terminal stromal targeting domain is followed immediately by a cleavable lumen-targeting domain (LTD) (Keegstra and Cline, 1999). Such LTDs are homologous to signal peptides that direct proteins into the endomembrane system through the endoplasmic reticulum, or to traverse the plasma membrane in bacteria or the inner membrane in mitochondria (Paetzel et al., 2002). The homology between LTDs and these other signal peptides extends from their common domain structure (Paetzel et al., 2002) to a nearly identical cleavage motif at their carboxyl (C)-termini (Halpin et al., 1989) to the ability to functionally replace one another in the homologous systems (Lingappa et al., 1984; Mori and Cline, 1998; Wexler et al., 1998). Nonetheless, as described below, the presence of a bipartite transit peptide alone does not place all such proteins on the same thylakoid targeting pathway. Other nuclear-encoded thylakoid proteins, including the major PS II light harvesting chlorophyll-binding protein complex (LHCP) and the PsbS protein, contain subchloroplast targeting information within their mature sequences. The inability of many researchers (Auchincloss et al., 1992; L. Huang et al., 1992) to identify specific regions of the mature LHCP responsible for membrane integration suggests that targeting 'patches' rather than 'sequences' may be persent in these, and perhaps other, polypeptides. Such proteins do not undergo additional cleavage upon reaching the thylakoid.

In contrast to the single pathway for proteins across the envelope membranes, proteins travel at least four routes from the stroma to the thylakoids, either for integration into the membrane or for transport completely across the membrane into the lumen (Fig. 1) (for reviews, see Keegstra and Cline, 1999; Mori and Cline, 2001; Robinson et al., 2001). The cpSec pathway is used by a subset of proteins containing bipartite transit peptides, with PsbO among those best studied. This pathway is homologous to the Sec secretion pathway of bacteria, and contains counterparts to the subunits SecA, SecY and SecE. Protein transport on the cpSec pathway is driven by ATP hydrolysis, presumably in the stroma by SecA, and is assisted by but does not strictly require the transmembrane pH gradient. A different pathway for proteins entering the thylakoid lumen is used by the PS II subunits PsbP, PabQ and the PsbTn protein (Kapazoglou et al., 1995). These proteins, whose signal peptides contain a pathway-signature double arginine motif (Chaddock et al., 1995; Henry et al., 1997), utilize the ΔpH-dependent or cpTat pathway. This remains the only energy-dependent protein transport pathway known that does not derive its driving force from the hydrolysis of NTPs and instead relies solely on the ΔpH across the thylakoid membrane. The targeting of these proteins does not rely on the action of any additional factors in the stroma (Cline et al., 1992).

Two additional routes appear to be available for proteins that are integrated into the thylakoid membrane, as are most PS II subunits. LHCP is transferred into the thylakoid membrane via a pathway that utilizes a homolog of the 54 kDa subunit of the signal recognition particle (SRP) involved in targeting secretory

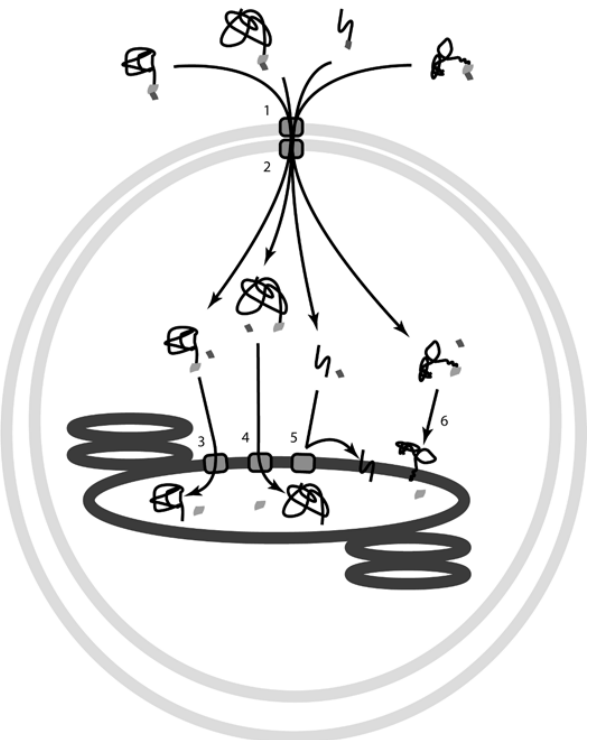

Fig. 1 Thylakoid protein targeting pathways for nuclear-encoded proteins. The proteins at the top represent, from left to right, proteins on the cpSec, cpTat, cpSRP and spontaneous pathways, respectively. 1, Toc translocon; 2, Tic translocon. These translocons probably operate in concert at sites where the envelope membranes are closely appressed in 'contact sites.' 3, the cpSec pathway, utilizing soluble cSecA and integral cpSecY and cpSecE. 4, the cpTat pathway, utilizing integral Tha4 protein, Hcf106 protein and cpTatC. 5, the cpSRP pathway, utilizing soluble cpSRP54, soluble cpSRP43, membrane cycling cpFtsY, and integral Alb3. 6, the spontaneous insertion pathway. Considering just the nuclear-encoded PS II proteins: all utilize the Toc/Tic machinery; OE33 and likely the PsbS protein follow the cpSec pathway; PsbP, PsbQ and the PsbTn protein follow the cpTat pathway; LHCP and other accessory LH proteins utilize the cpSRP pathway; PsbW, PsbX and PsbY use the spontaneous insertion pathway. Thick light and dark gray ovals represent the envelope and thylakoid membranes, respectively; the dark thicker line at the end of the represented proteins represents the stromal targeting transit peptide; the light gray line following represents lumen targeting signal peptides.

proteins to the endoplasmic reticulum (Eichacker and Henry, 2001). Proteins on this pathway are integrated through the action of stromal proteins cpSRP54 and cpSRP43, the receptor cpFtsY, and Alb3, a putative translocation pore homologous to YidC in bacteria and Oxa1 in mitochondria. The cpSRP pathway is powered by GTP hydrolysis and is assisted by the ΔpH. A fourth thylakoid protein targeting pathway is followed by three PS II subunits, the PsbW, PsbX and PsbY proteins (Robinson et al., 2001). These proteins, which possess bipartite transit peptides, take up residence in the membrane apparently without any exogenous energy input or the involvement of stromal or thylakoid membrane surface factors, placing them on the so-called spontaneous insertion pathway.

The details of the discovery and characterization of these various pathways are the subject of a number of excellent recent reviews (Keegstra and Cline, 1999; Eichacker and Henry, 2001; Jarvis and Soll, 2001; Mori and Cline, 2001; Robinson et al., 2001) to which interested readers are directed for further details.

B. Targeting of Chloroplast-Encoded Subunits

Compared to the targeting of nuclear-encoded proteins, the manner in which chloroplast-encoded

proteins are directed to thylakoids has received much less attention. This is due in part to difficulties in the isolation of a functional chloroplast translation system. Such a system was finally described in 1996 (Hirose and Sugiura, 1996), and has now been used in a few studies to examine targeting of proteins encoded in the chloroplast genome (Houben et al., 1999; Nilsson et al., 1999; Rohl and van Wijk, 2001; Nilsson and van Wijk, 2002).

Among the chloroplast-encoded proteins, the majority of the research regarding targeting has centered on D1, with cytochrome *f* also drawing some (much less) attention. This is likely due to the high rate of synthesis of D1 compared to the other chloroplast-encoded proteins, making it easy to identify in pulse-chase experiments.

One question often asked with respect to the targeting of chloroplast-encoded proteins is the identification of the translocation components used by these polypetides for integration into the thylakoid membrane – are they the same as those transporting nuclear-encoded substrates? This led to the examination of chloroplast-encoded proteins in mutants defective in the different pathways. Unfortunately, many such mutants are pleotropic and gave ambiguous results. For instance, both D1 and D2 levels were reduced to 10 to 20% of wild type levels in both *tha1* and *hcf106*, maize mutants in cpSecA and cpTatB, respectively (Voelker and Barkan, 1995). A SecY mutant accumulated no detectable D1, with a more severe phenotype than the *tha1*/*hcf106* double mutant (Roy and Barkan, 1998). In contrast, a cytochrome *f* signal sequence mutant in *Chlamydomonas* showed pleotropic loss of D1 and LCHP (Smith and Kohorn, 1994), the latter of which is not effected by knocking out the cpSec or cpTat pathways. It seems likely that the loss of D1 and other PS II proteins in these mutants is the result of destabilization of the PS II complex rather than of specific loss of the targeting pathway for D1.

The first biochemical study addressing this question sought to examine the effects of pathway inhibitors on the targeting of D1 (van Wijk et al., 1995). The requirement for the ΔpH for protein transport on the cpTat pathway makes the protonophore nigericin a potent inhibitor of this pathway (Cline et al., 1992), and azide is a non-specific inhibitor of SecA (Knott and Robinson, 1994; Yuan et al., 1994). Curiously, neither inhibitor was found to have much effect on the integration of D1, leading the authors of that study to suggest that D1 insertion did not proceed through either the cpSec of cpTat pathways.

More recent studies making use of nascent chain crosslinking and immunoprecipitation have led to a somewhat different conclusion. As described above, the cpSRP pathway mediates LHCP integration into the thylakoid membrane utilizing the stromal proteins cpSRP54 and cpSRP43. van Wijk and his colleagues demonstrated that nascent D1 polypeptides are contacted by cpSRP54 during their elongation, and that this contact is lost upon release of the protein from the ribosome (Nilsson et al., 1999; Nilsson and van Wijk, 2002). This contrasts with the integration of cytochrome *f*, in which interaction with cpSecA but not with cpSRP54 (or cpSRP43) was detected (Rohl and van Wijk, 2001). Interestingly, D1 integration was recently shown to proceed through a contact with cpSecY (Zhang et al., 2001), which is thought to be the translocation channel of the cpSec pathway. As with cpSRP54, this contact was not detectable after completion of translation.

These results lead to the intriguing conclusion that the thylakoid translocation machineries are more flexible than was previously appreciated (Table 1). Without considering D1, it would appear that different translocon components are reserved for specific targeting pathways. For instance, localization of the LHCP proceeds through contact with a cpSRP54/cpSPR43 complex in the stroma, docking with the membrane/soluble cycling receptor cpFtsY, and then integrating through a possible translocation channel formed by Alb3. No evidence for an involvement of cpSec pathway components has been obtained (Cline et al., 1993; Eichacker and Henry, 2001). Proteins targeted by the cpSec pathway are similarly not effected by disruptions in the cpSRP pathway (Hutin et al., 2002). Among the chloroplast-encoded proteins, cytochrome *f* interacts with cpSecA, but not with cpSRP54. However, it is observed with D1 that short nascent chains are in contact with cpSRP54, and not SecA or cpSRP43. Yet, it is also co-translationally associated with cpSecY. This might be interpreted as pathway cross-over, wherein D1 starts on the cpSRP pathway and finishes on the cpSec pathway. Alternatively, a distinct pathway built from stable association of cpSRP54 and the cpSecY translocon might govern D1 integration.

C. Targeting of Cyanobacterial Subunits

Much less is known about protein targeting in cyanobacteria than in higher plants. As pointed by

Table 1. Utilization of components of both the chloroplast secretory (Sec) and signal recognition particle-dependent (SRP) pathways for D1 integration

Protein	cpSecA	cpSecY	cpSRP54	cpSRP43
LHCP	no	no	yes	yes
Cytochrome *f*	yes	assumed	no	n.d.
Leader Peptidase	yes	assumed	n.d.	n.d.
D1	no	yes	yes	no

n.d., not determined.

Spence et al. (2003), this limited knowledge may be a reflection of the fact that an in vitro assay for studying protein targeting has not been established, and that subfractionation of the fragile thylakoids into membranes and lumen is particularly tricky in cyanobacteria. In addition, mutants defective in protein translocation have not been generated for in vivo studies. Nevertheless, other approaches such as genomic sequence comparison (Reumann and Keegstra, 1999; Fulda et al., 2000), proteomics analyses (F. Huang et al., 2002), and development of a GFP-based protein targeting assay (Spence et al., 2003) all point to the fact that many components of the various chloroplast protein targeting pathways have counterparts in cyanobacteria. Genes encoding *Synechocystis* homologs to envelope (Toc75, Tic55, Tic20, Tic22 and Toc34) and stromal translocation components (Hsp93, Hsp70 and SPP) were identified by sequence analysis (Reumann and Keegstra, 1999; Fulda et al., 2000). It was demonstrated that Toc75 is localized in the outer membrane (Reumann et al., 1999), and Tic22 is mainly localized in the thylakoid lumen, instead of expected cytoplasmic membrane (Fulda et al., 2002). In addition, SecY was shown to be present in both thylakoid and cytoplasmic membranes in *Synechococcus* sp. PCC 7942 (Nakai et al., 1993).

Experiments with a fusion protein consisting of the TorA (a typical Tat substrate in *E. coli*) targeting signal and GFP convincingly demonstrated the presence of a functional Tat pathway in *Synechocystis* (Spence et al., 2003). Interestingly, the GFP so targeted was exclusively localized in the periplasm, indicating that the Tat translocon may be present only in the cytoplasmic membrane, and/or that the TorA-GFP might be transported into the lumen by the thylakoid-located Tat and the GFP may be sorted subsequently to the periplasm. This latter proposal is reminiscent of the *Synechococcus* SecY which also has a dual location and which has been suggested to be involved in both protein export to the periplasm and in protein translocation into the thylakoid lumen (Nakai et al., 1993). Proteomic methodology has identified numerous proteins that are predicted to bear Tat- or Sec-determinant transit peptides. For example, the *Synechocystis* PsbO precursor was predicted to contain a Sec-specific transit peptide (Huang et al., 2002). In aggregate, these findings suggest that multiple translocation pathways exist in cyanobacteria; however, it remains to be experimentally established which ones are involved in the targeting of PS II subunits.

III. Assembly of Subunits into Photosystem II

The assembly of chloroplast-encoded PS II subunits has been the subject of numerous excellent reviews in recent years (Wollman et al., 1999; Zhang and Aro, 2002), while that of the nuclear-encoded subunits has received less attention. Accordingly, the former topic is only outlined herein, with more emphasis falling on the latter.

It has been known for many years that the membrane integration of numerous chloroplast-encoded PS II subunits takes place co-translationally. Similarly, assembly of at least some subunits into the PS II complex occurs during translation. Thus, the targeting, synthesis and assembly of PS II subunits are inextricably linked. For the reasons mentioned above, the assembly of D1 into PS II has been studied extensively, whereas that of the other subunits has received considerably less attention. This protein is synthesized by ribosomes bound to stromal-exposed membranes, and so must migrate from the site of synthesis to its final location in the grana (Herrin and Michaels, 1985; Adir et al., 1990). Elongation of the nascent chain is subject to a number of translational pauses at defined locations (Kim et al., 1991), perhaps giving the nascent protein time to interact with pigments and other PS II components, and/or to slip from the translocon into the membrane. During translation D1 can be crosslinked to its D2 partner already incorporated into PS II cores likely containing CP47, PsbI and cytochrome b_{559} (Zhang et al., 1999; Zhang et al., 2000; Zhang and Aro, 2002). The point at which CP43 joins the newly assembled PS II complex is unclear, and may be just after incorporation of the completed D1 protein (Zhang et al., 2000; Zhang and Aro, 2002). Since D1 also undergoes processing

at its C-terminus (see below), this post-translational modification must occur after assembly into the new reaction center

Less information is available regarding the assembly of the nuclear-encoded proteins of PS II. It has been shown that upon photoinhibitory illumination the extrinsic subunits of PS II are released and migrate from the grana to the stromal membranes, from where they are retrieved for assembly into new PS II units (Hundall et al., 1990; Barbato et al., 1992). Thus, assembly of these proteins into PS II in developing plastids likely occurs by the same mechanism as in photodamaged chloroplasts.

The three nuclear-encoded subunits of the OEC, PsbO, PsbP and PsbQ, are present in two locations within mature chloroplasts; approximately half are assembled into the OEC attached to PS II and the other half are present in soluble pools within the thylakoid lumen (Ettinger and Theg, 1991). This finding was unexpected given that subunits of protein complexes that do not assemble immediately are generally quickly degraded, as are apoproteins that fail to pick up their prosthetic groups. This is true throughout the cell (Luzikov, 1986), and has been documented many times in plastids (Schmidt and Mishkind, 1983; Biekmann and Feierabend, 1985; Merchant and Bogorad, 1986; Rochaix and Erickson, 1988; Mullet et al., 1990; Nilsson et al., 1990). Thus it is surprising that the OEC subunits should be present in long-lived soluble pools within the lumen. This is even more striking considering that a mutated version of PsbP in which ten amino acids were removed from the C-terminus was subjected to rapid proteolysis in the lumen (Roffey and Theg, 1996), indicating that proteases that can recognized aberrant OEC subunits are present in this compartment (Adam and Ostersetzer, 2001).

The proteins present in the soluble pool of nuclear-encoded OEC subunits are fully competent for assembly into the membrane-bound enzyme. This was demonstrated by the ability of subunits isolated from this pool to reconstitute PS II particles that had been stripped of the extrinsic OEC subunits by washing in high salts (Hashimoto et al., 1996). Curiously, the assembly competence of PsbO was extremely sensitive to the presence of trace amounts of Triton X-100 applied to the soluble protein. That is, even though high concentrations of Triton X-100 are routinely used to isolate PS II particles, and PsbO subsequently isolated from them can be used in reconstitutions, any Triton X-100 exposure of the soluble PsbO renders it incompetent for reconstitution, even after extensive purification. This result suggests that PsbO possesses a surface-exposed hydrophobic patch(es) that is important for assembly. The presence of a hydrophobic patch on the surface of PsbO is unusual for a soluble protein, and may be consistent with its designation as a 'natively unfolded' protein (Lydakis-Simantiris et al., 1999).

Newly imported OEC subunits partition between the lumen pool of unassembled subunits and those assembled into the PS II-bound OEC (Hashimoto et al., 1997). Since they partition in the same ratio as do the endogenously present subunits, it can be inferred that they join the assembled OEC from their position in the pools. It is interesting that these subunits should assemble into the OEC in mature and undamaged chloroplasts, as this is known to be a stable complex. On the one hand, the incorporation of newly imported subunits suggests that the assembled subunits should be in rapid equilibrium with those in the soluble pools. On the other hand, the OEC is stable in opened thylakoid membranes or PS II particles, and does not fall apart as might be expected if the subunits are in rapid equilibrium with the bathing medium. To reconcile these seeming disparate facts it was postulated that swapping of individual subunits was mediated by a displacement mechanism wherein the incoming subunit bound first to the OEC and caused the displacement of the original subunit (Hashimoto et al., 1997). Such a mechanism is consistent with both the ability of newly arriving subunits to enter the OEC and the stability of those already present in the absence of a competing population of soluble subunits. This hypothesis suggests that under normal operating conditions, the assembled OEC subunits continually exchange with those in the lumen pool.

As is the case with the co-translational integration apparatus of chloroplast-encoded membrane proteins, the protein translocation machineries of the cpSec and cpTat pathways are located in the stromal-exposed thylakoid membranes (Mori et al., 1999). Since PS II operates in the grana, this dictates that the nuclear-encoded OEC subunits must migrate from their site of transport to their site of action. One can ask then where are these subunits assembled?

This issue has been addressed for PsbO and PsbP (Hashimoto et al., 1997). Specifically, the location of the assembled proteins was probed by performing in vitro import experiments for specific times, followed by fractionation of the thylakoids into granal and

stromal membranes. Interestingly, PsbO was seen to assemble directly into the stromal membranes, and then migrate to the grana over the next 40 to 60 minutes. This is consistent with PsbO binding to PS II reaction centers during their synthesis in the stromal-exposed membranes and then migrating to the grana in the PS II supercomplex. In contrast to this, PsbP did not bind to membranes and migrate subsequently, but displayed a strong preference for granal binding locations from the start. The nature of the differences between PS II units in the stromal and granal membranes that prohibit PsbP from binding to the former but not the latter have not been elucidated. An idealized scheme depicting the assembly of PS II and including both chloroplast-encoded and nuclear-encoded subunits is shown in Fig. 2.

A new twist to the assembly (or recovery) of PS II was recently provided by the recognition that the nuclear-encoded PsbW protein undergoes extremely rapid turnover, rivaling that of D1 (Hagman et al., 1997). This discovery makes sense of the observation that mature chloroplasts continue to maintain active protein import machineries, albeit at somewhat reduced capacities (Dahlin and Cline, 1991). While the mechanism of turnover of the PsbW protein is not known, it is tempting to speculate that it is related to D1 turnover, suggesting that it sits close to D1 in the reaction center. If so, one would predict that the PsbW protein would be assembled in newly forming PS II reaction centers with D1 in the stromal membranes. Alternatively, given the small size of this protein and the fact that it's membrane insertion appears to occur spontaneously, its assembly in the grana remains a possibility. The same comments would also apply to the PsbX and PsbY proteins, which are also membrane integrated spontaneously, but which are not subject to the rapid turnover seen with PsbW protein. This issue remains to be decided by future experiments.

The pioneering work with respect to the PS II biogenesis in cyanobacteria was reported in the paper by Zak et al. (2001). Building on their previous work (Norling et al., 1998), in which a method was developed to yield pure cyanobacterial plasma and thylakoid membranes by combining two-phase partition and density centrifugation techniques, Zak et al. (2001) showed that a small amount of some PS II core proteins, including D1, D2, cytochrome b_{559} and PsbO, is present in the plasma membrane. Interestingly, the D1 C-terminal processing protease CtpA is exclusively located in the plasma membrane. The authors excluded the possibility that their data could be explained as contamination of the plasma membrane fraction with thylakoid proteins, and proposed that the initial steps of cyanobacterial PS II biogenesis take place in the plasma membranes. The PS II core complexes are then translocated to the thylakoid membrane either via vesicle transport or by lateral migration through regions where the two membranes are joined. Eventually, other protein subunits join the PS II core to form a fully functional complex in the thylakoid membrane (Zak et al., 2001). This hypothesis was bolstered by the recent finding that the partially assembled PS II core in the plasma membrane is competent for photochemical activity (Keren et al., 2005).

IV. Post-Translational Modifications

As with all proteins, those in PS II have finite lifetimes and are turned over by specific proteases. The turnover of D1 that accompanies photoinhibition is well studied, and is addressed in Chapter 27 of this book. Two main post-translational processing events of PS II proteins that are not related to turnover concern the removal of transit and signal peptides from the N-termini of nuclear-encoded proteins, and trimming of the D1 protein at its C-terminus. The importance of the former processing event is underscored when one considers that over 3,000 chloroplast proteins are encoded in the nucleus (Arabidopsis_Genome_Initiative, 2000), and that at least some require removal of their transit peptides to gain activity (Li et al., 1990; Archer and Keegstra, 1993; Levy and Adam, 1995). Similarly, C-terminal trimming of D1 in higher plants is also required for the development of PS II with water-splitting capability (Diner et al., 1988; Bowyer et al., 1992; Nixon et al., 1992).

A. Transit Peptide Cleavage

Precursor proteins cross the envelope membranes into the stroma under the direction of a cleavable transit peptide. Thus, each nuclear-encoded thylakoid protein undergoes at least one post-translational modification when the peptide specifying the stromal targeting domain is removed by the stromal processing peptidase (SPP). SPP is itself a nuclear-encoded metalloprotease possessing a number of activities (Richter and Lamppa, 1999). Using immobilized SPP it was determined that it binds the precursor with high affinity and cleaves the transit peptide in an endoproteolytic

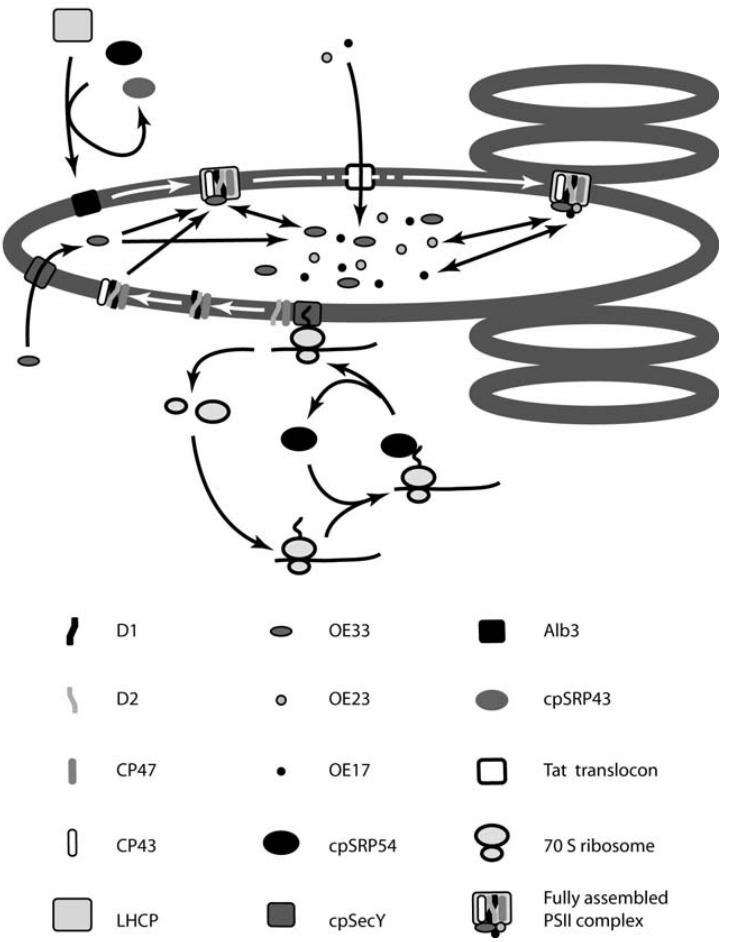

Fig. 2. Schematic representation of the assembly of the oxygen-evolving PS II. The binding of cpSRP54 to nascent D1 in the stroma and subsequent docking to cpSecY are speculative, as is the delivery of LHCP to the Alb3 translocon by cpSRP54 and cpSRP43. The order of assembly of CP43, LHCP and OE33 is not known, and the assembly of OE17 in the granal membranes has not been experimentally verified. Drawn after Hashimoto et al. (1997) and Baena-Gonzalez and Aro (2002). OE33, OE23 and OE17 are the PsbO, PsbP and PsbQ proteins, respectively.

reaction, releasing the mature protein. After cleavage at the transit peptide/mature protein junction, the SPP further trims and then releases the transit peptide. A different, as yet undefined metalloprotease appears to be responsible for complete degradation of the trimmed transit peptide. A number of questions remain concerning these protease activities, including the exact nature of the cleavage site determinants, and whether more than one SPP acts in processing all chloroplast precursors (Bruce, 2001).

B. Signal Peptide Cleavage

Some nuclear-encoded thylakoid proteins such as LHCP and PsbS possess internal targeting information, and therefore undergo the single post-translational modification by the SPP just described. Other thylakoid proteins, including some within PS II, possess a second targeting peptide specifying a lumenal location. This lumen targeting domain peptide is removed during or immediately after transport across the thylakoid membrane by the thylakoid processing

peptidase (TPP). TPP is homologous to the bacterial leader peptidase functioning in the Sec pathway, to the signal peptidases of the endoplasmic reticulum and the mitochondrial Imp2 (Paetzel et al., 2002). All these enzymes recognize identical motifs consisting of short aliphatic amino acids in the –3 and –1 positions relative to the cleavage site. In analogy to its counterparts in bacteria and the ER, TPP is likely to be an endopeptidase; the cleaved signal peptide is not generally observed, suggesting that it is rapidly degraded upon removal from its passenger protein.

A number of interesting questions remain to be answered concerning the TPP. Only one such protein has been reported in thylakoids (Chaal et al., 1998), which suggests its involvement in cleaving the signal peptides from both cpSec and cpTat pathway precursors. Its location in the stromal membranes (Kirwin et al., 1988) is consistent with the similar location of the two translocases. Evidence for co-translocational processing has been presented for substrates on both pathways (Hashimoto et al., 1997; Berghofer and Klosgen, 1999), yet the TPP has not been isolated in contact with either translocation complex (Mori and Cline, 2001). In addition, the complete nature of the cleavage site motif remains a question, as the canonical Ala-X-Ala sequence is present but not recognized in the mature sequences of a number of thylakoid proteins, including PsbO and PsbP.

C. Carboxy-Terminal Processing of the D1 Protein

In addition to removal of the targeting sequences from nuclear-encoded thylakoid proteins, another proteolytic processing event takes place during PS II assembly with the removal of 8–16 amino acids from the C-terminus of D1 precursor by the endoprotease CtpA. This occurs during or just after the assembly of D1 into PS II, and is required for the development of full activity of the O_2-evolving reaction center complex (Zhang and Aro, 2002). One of the last integral subunits to join the PS II reaction center complex is CP43 (Zhang et al., 2000). While the normal order of CP43 assembly and D1 processing has not been determined with certainty, the former can occur before the latter, leading Zhang and Aro to speculate that the binding of CP43 to the growing PS II reaction center might stimulate D1 processing (Baena-Gonzalez and Aro, 2002). Studies with the LF-1 mutant in *Scenedesmus obliquus* (Diner et al., 1988; Bowyer et al., 1992), as well as directed knockout, in *Synechocystis* (Nixon et al., 1992; Roose and Pakrasi, 2004), demonstrated that D1 processing is required for assembly of the Mn cluster into the OEC. the crystal strucure of PS II from *Thermosynechococcus vulcanus* (Kamiya and Shen, 2003) indicates that the C-terminal carboyyl group of Ala-344 from processed D1protein can provide a direct ligand tothe Mn cluster, although this was not seen in the PS II structure from *Thermosynechococcus elongatus* (Ferriera et al., 2004).

CtpA is a member of a newly recognized group of C-terminal processing proteases that includes the tail-specific protease Tsp in *E. coli* (Inagaki et al., 2001a). Using sequences conserved between proteases from higher plants, cyanobacteria and *E. coli*, Inagaki et al. (2001a) undertook a site-directed mutagenesis approach to identify those amino acids required for CtpA activity. They found that five of the 14 conserved amino acids examined were critical for photoautotrophic growth, a capacity that is lost when CtpA is inactive (Anbudurai et al., 1994). Among the critical residues invariantly conserved are a Ser and Lys pair (S-313 and K-338 in *Synechocystis* 6803) that has been postulated to act in a catalytic dyad mechanism as a nucleophile and base, respectively. In addition, a glutamic acid residue (E-316) was found to be critical for CtpA activity, raising the possibility that CtpA operates by a more classic catalytic triad mechanism known for serine proteases.

The structure of CtpA has been determined at 1.8Å resolution from the green alga *Scenedesmus obliquus* (Liao et al., 2000). The conserved and required Ser and Lys residues noted above were found to reside in a catalytic grove along the surface of the protease. Interestingly, the required Glu residue (E-375 in *Scenedesmus*) was seen to be hydrogen bonded to main chain amide nitrogens in two residues nearby in the crystallized protein, making it impossible for it to operate in as part of a catalytic triad. This raises the possibility that the enzyme undergoes a significant conformational change upon substrate binding, thereby bringing this Glu residue within the proper orientation for a charge relay through the catalytic site. Alternately, it was suggested that perhaps an invariant Asp residue on all D1 proteins located near the cleavage site acts as the third member of the putative catalytic triad (Liao et al., 2000). Confirmation of this interesting postulate, namely that that the substrate contributes a critical member of the active site triad, awaits further experimentation.

As is the case with many of the small PS II subunits, CtpA homologs appear to have slightly different activities in cyanobacteria and in green plants. The C-terminal extension on D1 is 9 amino acids in the higher plants examined to date, whereas it is 16 amino acids in *Synechocystis*. In spinach, D1 is cleaved in a single step, while evidence points to two-step processing in *Synechocystis* (Inagaki et al., 2001b). The reasons underlying these differences between green plants and cyanobacteria are presently obscured.

V. Concluding Remarks

The assembly of PS II during chloroplast biogenesis or repair is a complex processes requiring the coordination of the appearance of products of two genomes, the integration of membrane proteins both co- and post-translationally and through four different thylakoid targeting pathways, post-translational processing, and stepwise progress in different regions of the thylakoid. Despite significant gains in knowledge in the recent past, much remains to be learned before a detailed understanding of this complex process will emerge. Developments in new techniques, such as the ability to perform in vitro experiments with chloroplast translation systems (Houben et al., 1999), as well as an ever improving understanding of PS II structure (Zouni et al., 2001; Kamiya and Shen, 2003; Ferreira et al., 2004), will play an important role in elucidating the mechanism of assembly of this multimeric protein complex.

Acknowledgments

The authors thank Samantha Barling-Silva for her assistance in preparing the drawings in Figs. 1 and 2. Support from the Department of Energy and The National Science Foundation during the preparation of this chapter is gratefully acknowledged.

References

Adam Z and Ostersetzer O (2001) Degradation of unassembled and damaged thylakoid proteins. Biochem Soc Trans 29: 427–430

Adir N, Shochat S and Ohad I (1990) Light-dependent D1 protein synthesis and translocation is regulated by reaction center II. Reaction center II serves as an acceptor for the D1 precursor. J Biol Chem 265: 12563–12568

Anbudurai PR, Mor TS, Ohad I, Shestakov SV and Pakrasi HB (1994) The ctpA gene encodes the C-terminal processing protease for the D1 protein of the Photosystem II reaction center complex. Proc Natl Acad Sci USA 91: 8082–8086

Arabidopsis_Genome_Initiative (2000) Nature 408: 796–815

Archer EK and Keegstra K (1993) Analysis of chloroplast transit peptide function using mutations in the carboxyl-terminal region. Plant Mol Biol 23: 1105–1115

Aronsson H, Sohrt K and Soll J (2000) NADPH:Protochlorophyllide oxidoreductase uses the general import route into chloroplasts. Biol Chem 381: 1263–1267

Auchincloss AH, Alexander A and Kohorn BD (1992) Requirement for three membrane-spanning alpha-helices in the post-translational insertion of a thylakoid membrane protein. J Biol Chem 267: 10439–10446

Baena-Gonzalez E and Aro EM (2002) Biogenesis, assembly and turnover of Photosystem II units. Philos Trans R Soc Lond B Biol Sci 357: 1451–1459

Barbato R, Friso G, Rigoni F, Dalla Vecchia F and Giacometti GM (1992) Structural changes and lateral redistribution of Photosystem II during donor side photoinhibition of thylakoids. J Cell Biol 119: 325–335

Berghofer J and Klosgen RB (1999) Two distinct translocation intermediates can be distinguished during protein transport by the TAT (delta pH) pathway across the thylakoid membrane. FEBS Lett 460: 328–332

Biekmann S and Feierabend J (1985) Synthesis and degradation of unassembled polypeptides of the coupling factor of photophosphorylation CF1 in 70S ribosome-deficient rye leaves. Eur J Biochem 152: 529–535

Bowyer JR, Packer JC, McCormack BA, Whitelegge JP, Robinson C and Taylor MA (1992) Carboxyl-terminal processing of the D1 protein and photoactivation of water-splitting in Photosystem II. Partial purification and characterization of the processing enzyme from *Scenedesmus obliquus* and *Pisum sativum*. J Biol Chem 267: 5424–5433

Bruce BD (2001) The paradox of plastid transit peptides: Conservation of function despite divergence in primary structure. Biochim Biophys Acta 1541: 2–21

Chaal BK, Mould RM, Barbrook AC, Gray JC and Howe CJ (1998) Characterization of a cDNA encoding the thylakoidal processing peptidase from *Arabidopsis thaliana*. Implications for the origin and catalytic mechanism of the enzyme. J Biol Chem 273: 689–692

Chaddock AM, Mant A, Karnauchov I, Brink S, Herrmann RG, Klosgen RB and Robinson C (1995) A new type of signal peptide: central role of a twin-arginine motif in transfer signals for the delta pH-dependent thylakoidal protein translocase. EMBO J 14: 2715–2722

Cline K, Werner-Washburne M, Lubben TH and Keegstra K (1985) Precursors to two nuclear-encoded chloroplast proteins bind to the outer envelope membrane before being imported into chloroplasts. J Biol Chem 260: 3691–3696

Cline K, Ettinger WF and Theg SM (1992) Protein-specific energy requirements for protein transport across or into thylakoid membranes. Two lumenal proteins are transported in the absence of ATP. J Biol Chem 267: 2688–2696

Cline K, Henry R, Li C and Yuan J (1993) Multiple pathways for protein transport into or across the thylakoid membrane. EMBO J 12: 4105–4114

Dahlin C and Cline K (1991) Developmental regulation of the

plastid protein import apparatus. Plant Cell 3: 1131–1140
Dahlin C, Aronsson H, Almkvist J and Sundqvist C (2000) Protochlorophyllide-independent import of two NADPH:Pchlide oxidoreductase proteins (PORA and PORB) from barley into isolated plastids. Physiol Plant 109: 298–303
De Las Rivas J, Balsera M and Barber J (2004) Evolution of oxygenic photosynthesis: Genome-wide analysis of the OEC extrinsic proteins. Trends Plant Sci 9: 18–25
Diner BA, Ries DF, Cohen BN and Metz JG (1988) COOH-terminal processing of polypeptide D1 of the Photosystem II reaction center of *Scenedesmus obliquus* is necessary for the assembly of the oxygen-evolving complex. J Biol Chem 263: 8972–8980
Eichacker LA and Henry R (2001) Function of a chloroplast SRP in thylakoid protein export. Biochim Biophys Acta 1541: 120–134
Ettinger WF and Theg SM (1991) Physiologically active chloroplasts contain pools of unassembled extrinsic proteins of the photosynthetic oxygen-evolving enzyme complex in the thylakoid lumen. J Cell Biol 115: 321–328
Ferreira KN, Iverson TM, Maghlaoui K, Barber J and Iwata S (2004) Architecture of the photosynthetic oxygen-evolving center. Science 303: 1831–1838
Fulda S, Huang F, Nilsson F, Hagemann M and Norling B (2000) Proteomics of *Synechocystis* sp. strain PCC 6803. Identification of periplasmic proteins in cells grown at low and high salt concentrations. Eur J Biochem 267: 5900–5907
Fulda S, Norling B, Schoor A and Hagemann M (2002) The Slr0924 protein of *Synechocystis* sp. strain PCC 6803 resembles a subunit of the chloroplast protein import complex and is mainly localized in the thylakoid lumen. Plant Mol Biol 49: 107–118
Hagman A, Shi LX, Rintamaki E, Andersson B and Schroder WP (1997) The nuclear-encoded PsbW protein subunit of Photosystem II undergoes light-induced proteolysis. Biochemistry 36: 12666–12671
Halpin C, Elderfield PD, James HE, Zimmermann R, Dunbar B and Robinson C (1989) The reaction specificities of the thylakoidal processing peptidase and *Escherichia coli* leader peptidase are identical. EMBO J 8: 3917–3921
Hashimoto A, Yamamoto Y and Theg SM (1996) Unassembled subunits of the photosynthetic oxygen-evolving complex present in the thylakoid lumen are long-lived and assembly-competent. FEBS Lett 391: 29–34
Hashimoto A, Ettinger W, Yamamoto Y and Theg SM (1997) Assembly of newly imported oxygen-evolving complex subunits in isolated chloroplasts: Sites of assembly and mechanism of binding. Plant Cell 9: 441–452
Henry R, Carrigan M, McCaffrey M, Ma X and Cline K (1997) Targeting determinants and proposed evolutionary basis for the Sec and the delta pH protein transport systems in chloroplast thylakoid membranes. J Cell Biol 136: 823–832
Herrin D and Michaels A (1985) The chloroplast 32 kDa protein is synthesized on thylakoid-bound ribosomes in *Chlamydomonas reinhardtii*. FEBS Lett 184: 90–95
Hirose T and Sugiura M (1996) *Cis*-acting elements and *trans*-acting factors for accurate translation of chloroplast psba mrnas — development of an in vitro translation system from tobacco chloroplasts. EMBO J 15: 1687–1695
Houben E, de Gier JW and van Wijk KJ (1999) Insertion of leader peptidase into the thylakoid membrane during synthesis in a chloroplast translation system. Plant Cell 11: 1553–1564
Huang F, Parmryd I, Nilsson F, Persson AL, Pakrasi HB, Andersson B and Norling B (2002) Proteomics of *Synechocystis* sp. strain PCC 6803: Identification of plasma membrane proteins. Mol Cell Proteomics 1: 956–966
Huang L, Adam Z and Hoffman NE (1992) Deletion mutants of chlorophyll *a/b* binding proteins are efficiently imported into chloroplasts but do not integrate into thylakoid membranes. Plant Physiol 99: 247–255
Hundall T, Aro E-M, Carlberg I and Andersson B (1990) Restoration of light induced Photosystem II inhibition without de novo protein synthesis. FEBS Lett 267: 203–206
Hutin C, Havaux M, Carde JP, Kloppstech K, Meiherhoff K, Hoffman N and Nussaume L (2002) Double mutation cpSRP43 -- /cpSRP54 -- is necessary to abolish the cpSRP pathway required for thylakoid targeting of the light-harvesting chlorophyll proteins. Plant J 29: 531–543
Inagaki N, Maitra R, Satoh K and Pakrasi HB (2001a) Amino acid residues that are critical for in vivo catalytic activity of CPa, the carboxyl-terminal processing protease for the D1 protein of Photosystem II. J Biol Chem 276: 30099–30105
Inagaki N, Yamamoto Y and Satoh K (2001b) A sequential two-step proteolytic process in the carboxyl-terminal truncation of precursor D1 protein in *Synechocystis* sp. PCC6803. FEBS Lett 509: 197–201
Jarvis P and Soll J (2001) Toc, Tic, and chloroplast protein import. Biochim Biophys Acta 1541: 64–79
Kamiya N and Shen JR (2003) Crystal structure of oxygen-evolving Photosystem II from *Thermosynechococcus vulcanus* at 3.7-A resolution. Proc Natl Acad Sci USA 100: 98–103
Kapazoglou A, Sagliocco F and Dure L III (1995) PS II-T, a new nuclear encoded lumenal protein from Photosystem II. Targeting and processing in isolated chloroplasts. J Biol Chem 270: 12197–12202
Keegstra K and Cline K (1999) Protein import and routing systems of chloroplasts. Plant Cell 11: 557–570
Keren N, Liberton M and Pakrasi HB (2005) Photochemical competence of assembled Photosystem II core complex in cyanobacterial plasma membrane. J Biol Chem 280: 6548–6553
Kim C and Apel K (2004) Substrate-dependent and organ-specific chloroplast protein import in planta. Plant Cell 16: 88–98
Kim J, Klein PG and Mullet JE (1991) Ribosomes pause at specific sites during synthesis of membrane-bound chloroplast reaction center protein D1. J Biol Chem 266: 14931–14938
Kirwin PM, Elderfield PD, Williams RS and Robinson C (1988) Transport of proteins into chloroplasts. Organization, orientation, and lateral distribution of the plastocyanin processing peptidase in the thylakoid network. J Biol Chem 263: 18128–18132
Knott TG and Robinson C (1994) The secA inhibitor, azide, reversibly blocks the translocation of a subset of proteins across the chloroplast thylakoid membrane. J Biol Chem 269: 7843–7846
Levy M and Adam Z (1995) Mutations in the processing site of the precursor of ribulose-1,5-bisphosphate carboxylase/oxygenase small subunit: Effects on import, processing, assembly and stability. Plant Mol Biol 29: 53–61
Li HM, Theg SM, Bauerle CM and Keegstra K (1990) Metal-ion-center assembly of ferredoxin and plastocyanin in isolated chloroplasts. Proc Natl Acad Sci USA 87: 6748–6752
Liao DI, Qian J, Chisholm DA, Jordan DB and Diner BA (2000)

Crystal structures of the Photosystem II D1 C-terminal processing protease. Nat Struct Biol 7: 749–753

Lingappa VR, Chaidez J, Yost CS and Hedgpeth J (1984) Determinants for protein localization: Beta-lactamase signal sequence directs globin across microsomal membranes. Proc Natl Acad Sci USA 81: 456–460

Luzikov VN (1986) Proteolytic control over topgenesis of membrane proteins. FEBS Lett 200: 259–264

Lydakis-Simantiris N, Hutchison RS, Betts SD, Barry BA and Yocum CF (1999) Manganese stabilizing protein of Photosystem II is a thermostable, natively unfolded polypeptide. Biochemistry 38: 404–414

Merchant S and Bogorad L (1986) Regulation by copper of the expression of plastocyanin and cytochrome c(552) in *Chlamydomonas reinhardii*. Mol Cell Biol 6: 462–469

Mori H and Cline K (1998) A signal peptide that directs non-Sec transport in bacteria also directs efficient and exclusive transport on the thylakoid Delta pH pathway. J Biol Chem 273: 11405–11408

Mori H and Cline K (2001) Post-translational protein translocation into thylakoids by the Sec and Delta pH-dependent pathways. Biochim Biophys Acta 1541: 80–90

Mori H, Summer EJ, Ma X and Cline K (1999) Component specificity for the thylakoidal Sec and Delta pH-dependent protein transport pathways. J Cell Biol 146: 45–56

Mullet JE, Klein PG and Klein RR (1990) Chlorophyll regulates accumulation of the plastid-encoded chlorophyll apoproteins CP43 and D1 by increasing apoprotein stability. Proc Natl Acad Sci USA 87: 4038–4042

Mullineaux CW, Tobin MJ and Jones GR (1997) Mobility of photosynthetic complexes in photosynthetic membranes. Nature 390: 421–424

Nakai M, Sugita D, Omata T and Endo T (1993) Sec-Y protein is localized in both the cytoplasmic and thylakoid membranes in the cyanobacterium *Synechococcus* PCC7942. Biochem Biophys Res Commun 193: 228–234

Nilsson R and van Wijk KJ (2002) Transient interaction of cpSRP54 with elongating nascent chains of the chloroplast-encoded D1 protein; 'cpSRP54 caught in the act'. FEBS Lett 524: 127–133

Nilsson F, Andersson B and Jansson C (1990) Photosystem II characteristics of a constructed Synechocystis 6803 mutant lacking synthesis of the D1 polypeptide. Plant Mol Biol 14: 1051–1054

Nilsson R, Brunner J, Hoffman NE and van Wijk KJ (1999) Interactions of ribosome nascent chain complexes of the chloroplast-encoded D1 thylakoid membrane protein with cpSRP54. EMBO J 18: 733–742

Nixon PJ, Trost JT and Diner BA (1992) Role of the carboxy terminus of polypeptide D1 in the assembly of a functional water-oxidizing manganese cluster in Photosystem II of the cyanobacterium *Synechocystis* sp. PCC 6803: Assembly requires a free carboxyl group at C-terminal position 344. Biochemistry 31: 10859–10871

Norling B, Zak E, Andersson B and Pakrasi H (1998) 2D-isolation of pure plasma and thylakoid membranes from the cyanobacterium *Synechocystis* sp. PCC 6803. FEBS Lett 436: 189–192

Ohta H, Suzuki T, Ueno M, Okumura A, Yoshihara S, Shen JR and Enami, I (2003) Extrinsic proteins of Photosystem II: An intermediate member of PsbQ protein family in red algal PS II. Eur J Biochem 270: 4156–4163

Paetzel M, Karla A, Strynadka NC and Dalbey RE (2002) Signal peptidases. Chem Rev 102: 4549–4580

Pursiheimo S, Rintamaki E, Baena-Gonzalez E and Aro EM (1998) Thylakoid protein phosphorylation in evolutionally divergent species with oxygenic photosynthesis. FEBS Lett 423: 178–182

Reinbothe S, Mache R and Reinbothe C (2000) A second, substrate-dependent site of protein import into chloroplasts. Proc Natl Acad Sci USA 97: 9795–9800

Reumann S and Keegstra K (1999) The endosymbiotic origin of the protein import machinery of chloroplastic envelope membranes. Trends Plant Sci 4: 302–307

Reumann S, Davila-Aponte J and Keegstra K (1999) The evolutionary origin of the protein-translocating channel of chloroplastic envelope membranes: Identification of a cyanobacterial homolog. Proc Natl Acad Sci USA 96: 784–789

Rhee KH, Morris EP, Barber J and Kühlbrandt W (1998) Three-dimensional structure of the plant Photosystem II reaction centre at 8 Å resolution. Nature 396: 283–286

Richter S and Lamppa GK (1999) Stromal processing peptidase binds transit peptides and initiates their ATP-dependent turnover in chloroplasts. J Cell Biol 147: 33–44

Robinson C, Thompson SJ and Woolhead C (2001) Multiple pathways used for the targeting of thylakoid proteins in chloroplasts. Traffic 2: 245–251

Rochaix J-D and Erickson J (1988) Function and assembly of Photosystem II: Genetic and molecular analysis. Trends Biochem Sci 13: 56–59

Roffey RA and Theg SM (1996) Analysis of the import of the carboxyl-terminal truncations of the 23-kilodalton subunit of the oxygen-evolving complex suggests that its structure is an important determinant for thylakoid transport. Plant Physiol 111: 1329–1338

Rohl T and van Wijk KJ (2001) In vitro reconstitution of insertion and processing of cytochrome *f* in a homologous chloroplast translation system. J Biol Chem 276: 35465–35472

Roose JL and Pakrasi HB (2004) Evidence that D1 processing is required for manganese binding and extrinsic protein assembly into Photosystem II. J Biol Chem 279: 45417–45422

Row PE and Gray JC (2001) Chloroplast precursor proteins compete to form early import intermediates in isolated pea chloroplasts. J Exp Bot 52: 47–56

Roy LM and Barkan A (1998) A SecY homologue is required for the elaboration of the chloroplast thylakoid membrane and for normal chloroplast gene expression. J Cell Biol 141: 385–395

Schmidt GW and Mishkind ML (1983) Rapid degradation of unassembled ribulose 1,5-bisphosphate carboxylase small subunits in chloroplasts. Proc Natl Acad Sci USA 80: 2632–2636

Shi L-X and Schroeder W (2004) The low molecular mass subunits of the photosynthetic supracomplex, Photosystem II. Biochim Biophys Acta 1608: 75–96

Smith TA and Kohorn BD (1994) Mutations in a signal sequence for the thylakoid membrane identify multiple protein transport pathways and nuclear suppressors. J Cell Biol 126: 365–374

Spence E, Sarcina M, Ray N, Moller SG, Mullineaux CW and Robinson C (2003) Membrane-specific targeting of green fluorescent protein by the Tat pathway in the cyanobacterium *Synechocystis* PCC6803. Mol Microbiol 48: 1481–1489

Thornton LE, Ohkawa H, Roose JL, Kashino Y, Keren N and Pakrasi HB (2004) Homologs of plant PsbP and PsbQ pro-

teins are necessary for regulation of Photosystem II activity in the cyanobacterium *Synechocystis* 6803. Plant Cell 16: 2164–2175

van Wijk KJ, Knott TG and Robinson C (1995) Evidence for SecA- and deltapH-independent insertion of D1 into thylakoids. FEBS Lett 368: 263–266

Voelker R and Barkan A (1995) Two nuclear mutations disrupt distinct pathways for targeting proteins to the chloroplast thylakoid. EMBO J 14: 3905–3914

Wexler M, Bogsch EG, Klosgen RB, Palmer T, Robinson C and Berks BC (1998) Targeting signals for a bacterial Sec-independent export system direct plant thylakoid import by the delta pH pathway. FEBS Lett 431: 339–342

Wollman FA, Minai L and Nechushtai R (1999) The biogenesis and assembly of photosynthetic proteins in thylakoid membranes. Biochim Biophys Acta 1411: 21–85

Yuan J, Henry R, McCaffery M and Cline K (1994) SecA homolog in protein transport within chloroplasts: evidence for endosymbiont derived sorting. Science 266: 796–798

Zak E, Norling B, Maitra R, Huang F, Andersson B and Pakrasi HB (2001) The initial steps of biogenesis of cyanobacterial photosystems occur in plasma membranes. Proc Natl Acad Sci USA 98: 13443–13448

Zhang L and Aro EM (2002) Synthesis, membrane insertion and assembly of the chloroplast-encoded D1 protein into Photosystem II. FEBS Lett 512: 13–18

Zhang L, Paakkarinen V, van Wijk KJ and Aro EM (1999) Co-translational assembly of the D1 protein into Photosystem II. J Biol Chem 274: 16062–16067

Zhang L, Paakkarinen V, van Wijk KJ and Aro EM (2000) Biogenesis of the chloroplast-encoded D1 protein: Regulation of translation elongation, insertion, and assembly into Photosystem II. Plant Cell 12: 1769–1782

Zhang L, Paakkarinen V, Suorsa M and Aro EM (2001) A SecY homologue is involved in chloroplast-encoded D1 protein biogenesis. J Biol Chem 276: 37809–37814

Zouni A, Witt HT, Kern J, Fromme P, Krauss N, Saenger W and Orth P (2001) Crystal structure of Photosystem II from *Synechococcus elongatus* at 3.8 A resolution. Nature 409: 739–743

Chapter 30

The Origin and Evolution of Photosynthetic Oxygen Production

G. Charles Dismukes*
Department of Chemistry and Princeton Environmental Institute, Princeton University, Princeton, NJ 08544, U.S.A.

Robert E. Blankenship
Department of Chemistry and Biochemistry, Arizona State University, Tempe, AZ 85287-1604, U.S.A.

Summary

This chapter reviews some of the evidence and the postulated proposals for how oxygenic photosynthesis first emerged as a distinct form of photoautotrophic metabolism using water as an electron donor. This form of photosynthesis is the most successful photoautotrophic metabolism in the contemporary biosphere and is found in all higher plants, green and red algae and both cyano- and oxyphoto-bacteria. We summarize the timetable for emergence and the biogeochemical consequences of oxygenic photosynthesis. Particular attention is paid to evolution of the inorganic core of the enzyme that catalyzes water oxidation, chemical speciation of the

*Author for correspondence, email: dismukes@princeton.edu

T. Wydrzynski and K. Satoh (eds): Photosystem II: The Light-Driven Water:Plastoquinone Oxidoreductase, pp. 683–695.

inorganic cofactors and possible alterative substrates. We discuss possible mineral remnants of early oxygenic photosynthesis and the emerging role of bicarbonate in assembly of the inorganic core and as an hypothesized evolutionary cofactor.

I. The Timetable and Biogeochemical Consequences of Oxygenic Photosynthesis

The history of life on Earth since the beginning of the Universe following the 'big bang,' can be traced through a number of biological 'innovations' that, like the geochemical beginning, had profound global impact. The innovation of anoxygenic photosynthetic metabolism probably occurred at an early stage following the beginning of chemosynthetic metabolism (Des Marais, 2000). It enabled light energy to be utilized to drive unfavorable oxidation-reduction reactions using easily oxidizable reductants that yielded electrons of higher potential energy and chemiosmotic energy derived from proton gradients. Photosynthetic metabolism thrived in the early Archean era as reduced substrates (e.g., Fe^{2+}, S^{2-}, reduced carbohydrates) and CO_2 were in great abundance. Geochemical evidence shows that these sources waned throughout the Archean era (Holland et al., 1998), resulting in global depletion of the soluble electron donors and CO_2 in the regions where anoxygenic photosynthesis once ruled.

This consumption/loss of easily oxidizable substrates set the stage for the innovation of oxygenic photosynthesis in which water became the source of electrons and protons and oxygen gas formed as by-product. During the late Archean era, the concentration of atmospheric O_2 rose dramatically circa 2.3 billion years ago (BYA) based on evidence from multiple chemical markers and microfossils (Holland, 1984; Holland et al., 1998). This rise is almost universally attributed to photosynthetic O_2 production from water (Cloud, 1972; Holland et al., 1998; Farquhar et al., 2000; Kasting et al., 2002), although alternative theoretical hypotheses exist (Catling et al., 2001). There is also a minority view that the concentration of O_2 in the atmosphere has been substantial throughout all or most of the Earth's history (Towe, 1994; Ohmoto, 1997; Lasaga et al., 2002).

Cyanobacteria are the generally accepted source of the rise in atmospheric O_2. This view is consistent with evidence from biomarkers that date to 2.7 BYA (Summons, 1999). Although photosynthesis is the accepted metabolic source of the Archean atmospheric O_2 flux, the pioneer oxyphotobacteria that invented water splitting chemistry have never been identified. However, it is also not clear that the 2.7 BYA organisms that produced the biomarkers that today are specific for cyanobacteria were themselves cyanobacteria with true oxygenic photosynthesis, or were rather the ancestors of these organisms that had not yet developed the capacity for water splitting, or possibly another bacterial line that has since gone extinct. So the precise date for the invention of oxygenic photosynthesis is not known from geological data, but a reasonable estimate is sometime between 2.7 and 2.3 BYA. An estimate based on molecular phylogeny is consistent with this, at 2.6 BYA (Hedges, 2001).

The innovation of oxygenic photosynthesis set in motion a biological 'big green bang' that profoundly and forever transformed the Earth's atmosphere and surface. The capacity to split water in the pioneer oxyphotobacteria freed photosynthesis to invade new environments. For the first time, photosynthesis had an unlimited source of electrons and protons by using water as reductant. Because water was distributed everywhere, oxygenic photosynthesis could now emerge on terrestrial habitats. This transformed the face of the Earth from a drab inorganic aluminosilicate surface to a luscious organic green carpet of chlorophyll and other pigments. Oxygenic photosynthesis breathed copious amounts of O_2 gas into Earth's anaerobic atmosphere, transforming it into one suitable for the emergence of aerobic metabolism. As gaseous O_2 accumulated in the atmosphere, new opportunities opened for heterotrophic organisms to evolve mechanisms that make direct use of O_2 via non-photosynthetic respiratory metabolism. Because aerobic metabolism has a much higher energy efficiency per substrate oxidized, the engine of life became *supercharged*. Photosynthetic oxygenation of the Earth's atmosphere provided the metabolic oxidant that powered this biological explosion and permitted the evolution of all complex organisms, including humans.

So, how did oxygenic photosynthesis emerge and

Abbreviations: EPR – electron paramagnetic resonance; EXAFS – extended x-ray absorption spectroscopy; OEC – oxygen evolving complex; PS II – Photosystem II; WOC – water oxidizing complex; XRD – X-ray diffraction

are there multiple classes of photocatalysts for splitting water, much like there are numerous examples of anoxygenic photoautotrophism? Surprisingly, the available species of oxygenic photoautotrophs examined to date (cyanobacteria, green algae and higher plants) contain an inorganic catalyst having identical composition ($Mn_4Ca_1O_xCl_y$), despite having evolved for circa 2.7 billion years. The water splitting reaction catalyzed by the contemporary water oxidizing complex (WOC) is a concerted (all-or-nothing) four-electron step mechanism that is thermodynamically efficient. No other 'molecular blueprint' for this catalyst has been identified and no firm evidence for transitional Photosystem II water-oxidizing complexes (PS II-WOC) yet exists that can use other substrates for O_2 production (Blankenship, 2002). It thus seems that the invention of oxygenic photosynthesis was a 'singular event.'

The invariance of the inorganic catalyst in all contemporary oxygenic photoautotrophs indicates either an exceptionally rare example of biological non-adaptation over this vast geological period, or, more likely, the evidence for alternative catalysts has not yet been uncovered. Identification of the 'missing links' that served as transitional organisms in the evolution of the O_2-producing photoautotrophs (cyano- and oxyphotobacteria) is based largely upon scant genomic and geochemical evidence which we review herein. Lastly, we consider how the geochemical composition of the early Earth's atmosphere and oceans could have had a major influence in the emergence of oxygenic photosynthesis via adoption of bicarbonate as the transitional electron donor prior to water.

Several essential questions need to be answered concerning the evolutionary process that led to water oxidation in photosynthesis. First, were transitional electron donors used by the first O_2-producing phototrophs before water was adopted as the universal reductant (Olson, 1970, 2001; Blankenship et al., 1998). Second, how did the PS II photochemical apparatus evolve to generate a sufficiently strong one-electron photooxidant as precursor to chlorophyll *a* found in all contemporary PS II organisms? Third, while the current day mechanism of O_2 evolution from water produces no free, partially oxidized, intermediates (i.e., is a concerted four-electron process), this may well not have been the case initially. How did the early system survive, as it was probably producing compounds, including the O_2 final product, that it or any other life forms were not equipped to deal with? Finally, did the linkage of the two types of reaction centers to form the tandem arrangement found today in all oxygenic photosynthetic organisms come before or after the development of the ability to make O_2? We currently do not have adequate answers for any of these questions, so this entire area of research is still in its infancy.

II. Minimal Cofactor Diversity in Water Oxidizing Complexes

A. Polypeptide Binding Site

The X-ray diffraction map of the PS II-WOC from two strains of *Thermosynechococcus* reveals 36 transmembrane α-helices assigned to 17 protein subunits (Zouni et al., 2001; Kamiya et al., 2003; Ferriera et al., 2004; Chapters 19–21). The map reveals the location of the major reaction center subunits D1 and D2 (Chapter 4, Nixon et al.), the two inner antennas CP47 and CP43 (Chapter 3, Eaton-Rye and Putnam-Evans), the two subunits of cytochrome b_{559}, four unassigned transmembrane α-helices (PsbJ, K L and X) and the two extrinsic subunits (the manganese-stabilizing protein or PsbO and cytochrome c_{550}) (Chapter 5, Bricker and Burnap).

The Mn-cluster is surrounded primarily by the lumenal surface of the D1 protein, as predicted by previous mutational studies (Diner, 1998, 2001; Debus, 2000, 2001; Chapter 11, Debus) and model building (Dismukes, 1988; Svensson et al., 1996; Xiong et al., 1998). The side chains of the specific residues involved in Mn coordination have not been fully resolved or modeled yet, but the location of the peptide backbones of the five trans-membrane α-helices of D1 were located and the extensions of these backbones into the lumenal aqueous space surrounding the Mn cluster could be discerned. In both structures the location of the Mn cluster is within 10 Å to four or five lumenal domains of the D1 protein. The complexity of the emerging protein structure indicates that no single domain of the D1 protein comprises the binding site for the inorganic core.

B. The Inorganic Cofactors

1. Manganese and Calcium

The inorganic components of the catalyst responsible for O_2 evolution are $Mn_4O_xCa_1Cl_y$ in all photosynthetic organisms studied to date, including higher

plants, green algae and cyanobacteria (Debus, 1992; Raven et al., 1999; Ananyev et al., 2001; Vrettos et al., 2001). A range of ten allowed core structures has been inferred from XRD, EXAFS and EPR studies (Robblee et al., 2001; Zouni et al., 2001; Carrell et al., 2002; Kamiya et al., 2003; Ferriera et al., 2004). All of these structures formulate the catalyst as having a tetramanganese core, while the EXAFS and EPR data further indicate oxo/hydroxo-bridges between the Mn ions that enable intermanganese electronic coupling essential for the multi-electron catalysis (Chapters 10, Yachandra, and 12, Åhrling et al.). Several core geometries are compatible with the available electron density and magnetic resonance data for the reduced core, including a funnel-shaped-$Mn_4O_4(OH_x)_2$ core and a $Mn_4O_2(OH_x)_2$-butterfly/cubane core (Carrell et al., 2002). EPR, EXAFS and XRD studies further indicate that Ca^{2+} is an integral cofactor of the core. The EPR and EXAFS data indicate a possible location that is juxtaposed to the Mn_4 cluster, possibly as a capping $Ca(OX)_2$ unit bridging between a pair of Mn atoms. Removal of Ca^{2+} lowers the Mn ionization potential and alters the strength of the intermanganese coupling to a degree that water splitting activity is lost. Strontium is the only other element that can replace Ca^{2+} in water splitting, albeit with 35% lower steady-state rate of O_2 evolution (Boussac et al., 1988) No naturally occurring inorganic mutants have yet been observed in the environment. Several proposals exist for how these physico-chemical properties are important for catalysis (Chapter 25, Hillier and Messinger).

2. Role of Bicarbonate in the Water Oxidizing Complex

Biogenesis of the inorganic core of the WOC occurs in vivo by ligation and photo-oxidation of Mn^{2+} to apo-PS II-WOC in the presence of the other elementary inorganic ions: Ca^{2+}, Cl^-, H_2O or HCO_3^-. This process, called photoactivation by George Cheniae, creates a functional catalyst (reviewed in Chapter 26, Dismukes et al.). Bicarbonate was found to stimulate the rate and yield of the first step of photoassembly involving photooxidation of Mn^{2+} in spinach (Baranov et al., 2000, 2004). The data clearly establish that the high affinity Mn^{2+} site in PS II has a specific interaction with bicarbonate with a binding constant that is orders of magnitude larger than is the affinity between Mn^{2+} and bicarbonate alone. Bicarbonate/carbonate is also a weak chelating ligand that leads to the formation of Mn^{2+}-bicarbonate/carbonate complexes in solution (Dismukes et al., 2001). Paradoxically, formation of these free complexes in solution (> 1 mM) does not stimulate the photoassembly process in spinach apo-PS II-WOC, but rather actually slows the assembly rate and lowers the yield of active centers (Baranov et al., 2004). This decrease is attributed to electron donation to PS II by free Mn-bicarbonate complexes in solution that compete with the native site.

The photoassembly data suggest a possible evolutionary role for bicarbonate in promoting selectivity for Mn^{2+} binding and photooxidation by apo-PS II-WOC over other divalent metals. Geochemical evidence indicates that the ferrous ion was considerably more concentrated in the anaerobic Archean seas than it is today in O_2-rich seas. So how does PS II discriminate between Mn^{2+} and Fe^{2+}, particularly since the Fe^{2+} concentration is likely to have been higher than Mn^{2+} in an anaerobic world? The answer appears to be that the high affinity Mn^{2+} site in the apo-PS II-WOC is tailored to bind $[Mn^{2+}(OH^-)]^+$ or $[Mn^{2+}(HCO_3^-)]^+$ instead of Mn^{2+}_{aq} ions. This is seen in the size and charge density selectivity for inhibition of photoassembly (Ananyev et al., 1999). For example, the alkali metal ions inhibit the first step in photoassembly according to their size ($Cs^+ > Rb^+ > K^+ > Na^+ > Li^+$) with Cs^+ affinity being comparable to Mn^{2+} affinity and 3000-fold higher affinity constant than Li^+. Similarly, large metal-oxo cations (VO^{2+}, UO_2^{2+}) are among the most potent inhibitors of photoassembly (Ananyev et al., 2001). Fe^{2+} inhibits photoassembly and when used in mixed ratios with Mn^{2+} blocks photoassembly of active WOC centers without added bicarbonate (Ananyev et al., 2001). The dissociation constants for Mn^{2+} and Fe^{2+} as steady-state electron donors (i.e., multi-electron turnover) to apo-PS II-WOC are about 1 and 2 μM, respectively, without added bicarbonate (Semin et al., 2002). Atmospheric dissolved CO_2 gives about 10 μM bicarbonate at pH 6, which is already enough to partially stimulate electron donation by Mn^{2+} (bicarbonate K_D = 20–34 μM) (Klimov et al., 2001). Upon increasing the bicarbonate concentration to saturating value the Mn^{2+} affinity increases, as seen by a decrease in the Michaelis constant. This increase in Mn^{2+} affinity is also seen in photoassembly kinetics and yield. Thus, the ternary complex of Mn^{2+}-bicarbonate-apo-PS II-WOC is recognized rather than the free ion. Studies of the bicarbonate effect on electron donation by Fe^{2+} have not yet been done to see whether bicarbonate can aid discrimination between Mn^{2+} and Fe^{2+}. The

mechanism of Fe^{2+} inhibition of Mn^{2+} photoassembly is due to competitive photooxidation of Fe^{2+} which binds tightly to the apo-PS II-WOC complex but can be removed by use of excess reducing agents (Semin et al., 2002).

Bicarbonate also enhances the thermal stability of the holo-WOC-enzyme isolated as detergent extracted PS II membranes possibly by preventing protein denaturation (Klimov et al., 2001). The rate of thermoinactivation at 40 °C was shown to decrease by three-fold in the presence of bicarbonate. This greater thermal stability could have been important for the emergence of the first WOC in the Archean era when the average temperature was predicted to have been considerably warmer than the mean temperature over the last 20,000 years.

III. Transitional Electron Donors and 'Missing Links'

A. Was There a Transitional Electron Donor Before Water?

An appealing idea that was first advanced by John Olson (Olson, 1970) is that transitional electron donors may have existed in early organisms, and that a series of donors of increasing redox potential may have existed. In this view, the system slowly gained the ability to oxidize weaker and weaker reductants until it eventually was able to use water as an electron donor (Olson, 1970). This author proposed a series of nitrogen compounds, including hydrazine and hydroxylamine as transitional donors. Other authors have proposed other compounds, including hydrogen peroxide (Blankenship et al., 1998) and Mn bicarbonate complexes (Dismukes et al., 2001).

The driving force for all these proposals is that the jump in capabilities of the reaction center is so huge to permit it to use water as an electron donor that it is difficult to imagine how this process might have taken place while preserving a functional system. This is analogous to the classic problem of the evolution of the eye, addressed by Charles Darwin and countless others. How can such a complex organ as an eye ever evolve if selection can only work to improve a system that functions already? The eye of a complex animal like a human is such that all the parts are required to make it functional, so how could it possibly have arisen and evolved? Darwin himself advanced the answer to this question, which is still valid today. The complex eye of humans did not appear in one jump from nothingness. Rather, a whole series of light-sensitive organs can be identified in simpler organisms, each of which is of immense benefit to the organisms that possess them. The old saying, '*In the land of the blind, the one-eyed man is king*,' describes graphically how much benefit even a primitive light sensing system will be to the only organism that possesses it. The evolution of the eye can thereby easily be traced from the most rudimentary light sensitive spot in microorganisms through nonfocusing eyes of invertebrates all the way to the incredibly sophisticated human eye. The same logic applies so that an organism that has even a rudimentary system to oxidize water or other ubiquitous substrates will be at a huge selective advantage, provided that it doesn't kill itself with the toxic products of this newly acquired activity.

B. Electron Donors in Anoxygenic Bacteria

We will now examine the sorts of substrate oxidation systems that can be identified in known photosynthetic organisms, and consider whether any of these could possibly be intermediates in the development of the WOC. Unfortunately, none of these systems turn out to be very helpful in understanding the origin of the WOC.

Anoxygenic bacterial phototrophs use a variety of substrates that donate electrons to the photooxidized reaction center. These include Fe^{2+}, H_2S, S_x, numerous reduced carbon sources and others. Even some cyanobacteria can use H_2S as an electron donor, thereby carrying out a form of anoxygenic photosynthesis driven by Photosystem I (Cohen, 1986). However, these organisms also still retain the complete mechanism for carrying out water oxidation, so are probably best considered as more recent adaptations to sulfide rich environments rather than transitional forms.

The nature of the catalysts that mediate all these substrate oxidations in anoxygenic bacterial photosynthesis is relatively poorly understood. The best understood of these donor capabilities is the system that uses sulfur compounds as electron donors (Brune, 1995), while the specific proteins and cofactors that are involved in Fe^{2+} oxidation are completely unknown. In some cases, such as sulfur oxidation, donation appears to occur at the level of the quinone pool, so that reducing equivalents do not directly interact with the oxidized reaction center.

Nothing that is known about any of these donation systems suggests that they may have been adapted by evolution to form the WOC. Sulfur oxidation in these organisms is mediated by soluble enzymes that have no apparent cofactor or mechanistic similarity to how O_2 is produced from water oxidation in the integral membrane reaction center protein of PS II. At the current level of knowledge of these systems, there are no clues to how the PS II-WOC originated or evolved.

C. Existing Organisms that May Be Transitional Forms

One type of organism has recently been discovered that may possibly be a transitional form between anoxygenic and oxygenic photosynthesis, although it too might in the end turn out to be an adaptation to a particular environmental niche. The Chl-*d* containing cyanobacterium *Acaryochloris marina* was discovered as a symbiont in a marine ascidian (Miyashita et al., 1996). It contains Chl *d* as its principal photopigment, although it also contains minor amounts of Chl *a*. Chl *d* has been suggested as a possible transitional pigment between bacteriochlorophyll (BChl) *a* and Chl *a* (Blankenship et al., 1998), because it is both structurally and energetically intermediate between these two pigments. For this reason, this organism or others like it may be critical in understanding the transitional forms that almost certainly had to have existed. The absorbance maximum of Chl *d* is intermediate between those of BChl *a* and Chl *a,* with the major in vivo maximum at 710 nm. Biochemical and spectroscopic studies by Hu et al. (1998) have clearly shown that the PS I complex contains only Chl *d*, including as the photoactive special pair, which absorbs at 740 nm in this organism. It is not yet certain whether the PS II complex also utilizes Chl *d*, which is the more important point for the purposes of this discussion. There is conflicting evidence on this point (Mimuro et al., 1999; Itoh et al., 2001).

IV. Possible Evolution Pathways for the Photosystem II Water Oxidizing Complex

All evidence to date indicates that the biogenesis of the inorganic core of the WOC in extant phototrophs does not require the binding of 'ready-made' Mn clusters from solution, but rather occurs by photoassembly from the free inorganic constituents. Additionally, there is no evidence for chemical extraction of a whole or partial Mn cluster from the intact WOC from any organism. Extraction of the inorganic core from PS II leads to cluster fragmentation, suggesting it may be an intrinsically unstable core in the absence of suitable ligands. Hence, efforts to identify novel manganese minerals as natural building blocks for biosynthesis of the core or as remnants of a decomposed photosynthetic core have not been essential, based on the currently available evidence. In Sections V.D and V.E we examine a few novel proposals that have been postulated for how natural Mn minerals or soluble Mn clusters could have 'jump-started' the evolution of oxyphotobacteria in the early geochemistry of the Earth. We begin by discussing the question of availability and speciation of Mn in the Archean seas and relate this to the redox chemistry of Mn, bicarbonate and water.

A. Chemical Speciation in the Archean Ocean: Mn^{2+} and HCO_3^-

The inorganic composition of 'Darwin's little pond' that spawned the first oxygenic phototroph in the Archean era is not likely to ever be known accurately. Hence, we focus on the average composition of the early oceans and ask: did these constitute a permissive habitat for oxygenic photosynthesis to emerge?

Geochemical markers indicate that the Archean seas had different chemical composition, pH and temperature than the contemporary seas that foster photosynthetic life (Dismukes et al., 2001; Table 1) The pH of the Archean oceans is predicted to have been 1–4 pH units lower than the contemporary oceans, based on evidence from Archean ferruginous cherts (Sugisaki et al., 1995) and model calculations (Grotzinger et al., 1993; Morse, 1998).

It is generally accepted that the CO_2 partial pressure in the atmosphere has fallen by many orders of magnitude since the formation of the atmosphere. Models predict that the partial pressure of CO_2 fell continuously throughout the Hadeon Era (4.3–3.8 BYA) from a maximum value of 10 atm to about 0.5 atm (Morse, 1998). Biogeochemical evidence indicates that the partial pressure of CO_2 in the Archean era was drawn down by photosynthetic carbon fixation, yet was 30 to 3×10^4-fold greater than the contemporary atmosphere. This greatly elevated CO_2 level is consistent with the predicted lower Archean pH, owing to formation of carbonic acid. The predicted concentrations of dissolved car-

Table 1. Composition of the Archean ocean and atmosphere

Component	Contemporary	Archean (>2.2 BYA)
CO_2, atmosphere (kPa)	0.03	0.9[a], 9[b], 900[c]
HCO_3, seawater (mM)	2	10-200 (5–100×)[e]
Mn^{2+}, seawater (mean) (ng/kg)	20[d]	40-100 (2–5×)[f]
Mn^{2+}, speciation in seawater	Mn^{2+}_{aq}	$[Mn(HCO_3)_2]_n$ [g]
pH	8.1	4~7 [a,h]

[a] Holland (1984), [b] Kasting (1993), [c] Walker (1985), [d] Bruhland (1983), [e] estimation from atmospheric CO_2 using equilibrium data, [f] Precambrian vs Phanerozoic limestones (Holland et al., 1998), [g] predicted Archaean speciation based on binding constant data in Table 2:

$$\frac{Mn(HCO_3)^+}{Mn^{2+}} = 0.6 - 12; \quad \frac{\left[Mn(HCO_3)_2\right]_n}{Mn^{2+}} = 0.1 - 48,$$

[h] Archean ferruginous cherts (Sugisaki et al., 1995) and CO_2 dissolution (Grotzinger et al., 1993).

bonic acid and bicarbonate in the Archean seas were proportionately higher (Table 1) based on estimates from the Henry's law constant for CO_2 dissolution in water and the proton equilibrium constants.

A key consequence of the elevated bicarbonate concentration is that certain metal ions will speciate in solution as the metal-bicarbonate complex in preference to the metal-aquo complex. As a result of the lower Archean pH, precipitation of the insoluble metal-carbonate/hydroxide minerals is suppressed, thus leading to increased concentration of the metal-bicarbonate complexes in solution. The favorable oxidation potentials of the resulting Mn-bicarbonate species enables them to serve as electron donors to photosynthetic prokaryotes.

This shift in Mn-bicarbonate speciation with pH can be calculated using the thermodynamic phase equilibria for the ternary water/Mn/CO_2 system at the CO_2 fugacity of both the current atmospheric (approximately equal to the mean fugacity since the last ice age) and the estimated Archean fugacity (3000-fold higher at 10^5 Pascal) (see for example Fig. 24 in Russell et al., 2003). In this calculation the association constant for the formation of the 1:1 $Mn^{2+}(HCO_3^-)$ complex reported in the literature was used (Table 2). Two features emerge from this analysis. As a result of the lower pH, the boundary between aquo-Mn^{2+} and rhodochrosite, $MnCO_3$(s), drops by two pH units to 6.5, corresponding to the lower limit imposed by the buffering due to carbonic acid/bicarbonate equilibrium ($pK_a = 6.3$). As a result of the elevated bicarbonate concentration in solution, thermodynamic equilibrium predicts that a window of 1 pH unit now supports the existence of $Mn^{2+}(HCO_3^-)$ as the major soluble Mn^{2+} species at the phase boundary between aquo-Mn^{2+} and rhodochrosite. Using a concentration of 1 μM for the total dissolved Mn^{2+}, the equilibrium calculation predicts that the concentration of $[Mn^{2+}(HCO_3^-)]^+$ exceeds that of aquo-Mn^{2+} between pH 6.5 and 7. Thus, it can be concluded from elementary thermodynamic considerations that the Archean oceans would have provided more favorable conditions than the contemporary oceans for the speciation of soluble $(Mn^{2+})_x$(bicarbonate)$_y$ complexes as the dominant forms of soluble Mn^{2+}.

Electrochemical data for the reduction of aqueous Mn^{2+} solutions to Mn^0 as a function of ligand concentration further suggest that bicarbonate is capable of forming two Mn-bicarbonate species with stoichiometries 2:1 and 1:2, corresponding to complexes with empirical formulas, $Mn^{II}_2(HCO_3)^{3+}$ and $[Mn^{II}(HCO_3)_2]_n$ (Dismukes et al., 2001). Thus, oligomeric Mn-bicarbonate complexes may also have existed in the Archean seas in sufficient abundance at pH values close to the rhodochrosite precipitation boundary.

The two component system of CO_2/water has a much higher buffer capacity than pure water and as a result can serve as an abundant source of bicarbonate ions within the pK_a range of bicarbonate (6.3–10.3). For each mole of CO_2 that is dissolved in water only 8.6 kcal/mol are required for dissociation into bicarbonate and proton, whereas dissociation of one mole of water to hydroxide and protons requires 21.4 kcal/mol. Hence, any system that can use bicarbonate as a source for generation of hydroxide will need to input only 8.9 kcal/mol to release it from CO_2 versus 21.4 kcal/mol to ionize pure water. Moreover, if the system can use bicarbonate as a direct surrogate for hydroxide than no further energy input is needed in

Table 2. Manganese-bicarbonate physico-chemical data

Mn(II) species	K_B HCO_3 binding, M^{-1}	E^0 (V, NHE) for oxidation [b]	Catalase activity[c]
$Mn^{2+}_{aq.}$	–	1.20	zero
$[Mn^{2+}(HCO_3^-)]^+$	11–60[a,b]	0.92. irreversible	?
$[Mn^{2+}(HCO_3^-)_2]_n$	4[b]–20	0.52–0.61 irreversible	active

[a] Smith et al. (1976), [b] Kozlov et al. (1997) and Dismukes et al. (2001), [c] catalysis of peroxide dismutation: $2\ H_2O_2 \rightarrow 2\ H_2O + O_2$, [d] Stadtman et al. (1990).

the two component system! This energetic advantage of bicarbonate as a source for hydroxide can be equivalently expressed in terms of the dissociation constants:

$$H_2O \leftrightarrow H^+ + HO^- \ (K = 2 \times 10^{-15})$$

$$HCO_3^- \leftrightarrow CO_2 + HO^- \ (K = 2.8 \times 10^{-7})$$

In other words, at neutral pH a solution containing 0.1M bicarbonate ion will contain 10^6-fold more bicarbonate ion than the concentration of hydroxide ion in pure water.

The measured stability constants for the formation of Mn-bicarbonate complexes (Table 2) together with estimates for the Mn^{2+}_{aq} concentration in the Archean ocean (Table 1) indicate that these Mn-bicarbonate complexes would have represented the dominant form of soluble Mn^{2+} present in the Archean ocean, unlike today where the speciation favors the monomeric aquo ion Mn^{2+}_{aq}. The pK_a of Mn^{2+}_{aq} is 10.5. Hence, at the pH of the contemporary ocean (~ 8) the fractional concentration of $Mn(OH)^+$ would be vanishingly small ($10^{-2.5} \times Mn^{2+}_{aq}$) if there was no bicarbonate to serve as hydroxide source. In the Archean ocean (pH ~4-7) it would have been even smaller. Thus, bicarbonate, not free hydroxide, is the major source of hydrolytic species formed from Mn^{2+}_{aq}, including $Mn(OH)^+$, in both the contemporary and Archean oceans.

B. Redox Properties of Mn-Bicarbonate

Electrochemical oxidation of these Mn^{II}-bicarbonate complexes in the presence of excess bicarbonate leads to formation of Mn^{III}-bicarbonate complexes at much more favorable potentials (Table 2) than for Mn^{2+}_{aq} (E_0 = 1.18 V) (Kozlov et al., 1997). Importantly, other coordinating ligands (Cl^-, NO_3^-, formate, acetate) form only 1:1 complexes with Mn^{2+} and these do not exhibit such favorable oxidation potentials. The electrochemical data do not reveal whether bicarbonate binds to manganese or delivers hydroxide to form the corresponding Mn-hydroxo/oxo species. These potential shifts are sufficiently large that they would enable Mn-bicarbonate clusters to function as electron donors to reaction centers from anoxygenic phototrophs utilizing BChl *a* as their primary photooxidant (Dismukes et al., 2001).

Evidence in the literature shows that solutions of Mn^{2+} and bicarbonate catalyze the two-electron dismutation of hydrogen peroxide ($2H_2O_2 \rightarrow O_2 + 2H_2O$), or the so-called catalase activity (Stadtman et al., 1990; Sychev et al., 1993). The rate of Mn-dependent dismutation depends on the bicarbonate concentration to the third power, suggesting the formation of an active species with 1:3 Mn:bicarbonate stoichiometry. Electrochemical evidence suggests the active species could be dimanganese-bicarbonate complexes or oligomers (Dismukes et al., 2001). It is also known that all manganese catalases, which are found exclusively in prokaryotes, contain dimanganese centers. Similarly, all efficient abiotic manganese catalase model complexes contain di- or multi-manganese centers. In summary, coupled proton-electron transfer chemistry of H_2O_2 occurs most efficiently via dimanganese centers than mono-manganese centers and the former use the Mn_2(II,II) → (III,III) redox transition. Bicarbonate further enhances this activity, possibly by serving as a proton transfer catalyst.

C. Thermodynamics of Oxygen Production from Bicarbonate versus Water

This brings us to the key issue relevant to the thermodynamics of water oxidation. By use of a thermodynamic cycle one can calculate the experimentally unmeasured free energy change for the oxidation of bicarbonate ion to form O_2 (Dismukes et al., 2001). Table 3 lists some possible overall reactions leading to O_2 production. Formation of one mole O_2 from bicarbonate costs 49.6 versus 74.6 kcal/mol from

Table 3. Oxidation of bicarbonate is thermodynamically favored over water oxidation

	Reaction	E° *(V), pH 7*	ΔG^{0}, *kcal/mol*
a	$2\ H_2O \leftrightarrow O_2 + 4\ e^- + 4\ H^+$	–0.81	74.6
b	$2\ HCO_3^- \leftrightarrow O_2 + 4\ e^- + 2\ CO_2 + 2\ H^+$	–0.54	49.6

water. In other words, it is 25 kcal/mol easier (34% lower free energy) to produce one mole O_2 from bicarbonate than water at pH 7. Thus, thermodynamic considerations reveal that bicarbonate is a better electron donor than from water for O_2 evolution. An additional energy advantage is realized if bicarbonate were to serve as a base to neutralize the protons released by bicarbonate or water oxidation. This very substantial energetic advantage together with the predicted abundance of bicarbonate in the Archean seas raises the possibility that bicarbonate could have been the transitional electron donor prior to water that enabled the evolution of simpler anoxygenic photosynthetic metabolism to oxygenic phototrophism. This possibility remains untested. Alternatively, bicarbonate may have merely served as a cofactor within the early WOC that stimulates the enzyme to oxidize water more efficiently.

A key aspect of this chemistry is that the enzyme needs to provide only sufficient free energy to convert substrate to product and not to form the substrate by hydration of CO_2. The latter free energy is extracted from the system (not the enzyme) upon dissolution of atmospheric CO_2. Because reaction (b) in Table 3 serves as a pump to drive CO_2 back into the atmosphere, bicarbonate oxidation by photosynthesis in the early Earth would have been a powerful throttle for movement of CO_2 out of the ocean and into longer term terrestrial deposits via acid rain.

D. Mineral Building Blocks/Remnants of Oxygenic Photosynthesis?

Russell and Hall (2002) have postulated that colloidal clusters of a precursor to the mineral rancieite, $[CaMn_4O_9{\cdot}3H_2O]$, might have been produced by abiotic photochemistry and subsequently taken up by an anoxygenic phototroph for incorporation into a type II reaction center protein (Russell et al., 2002, 2003). Following subsequent mutations of the protein to form a binding site this sequence of event was proposed as a possible route to a precursor of the WOC. There are two novel aspects to this proposal related to the structure of the minerals and their hypothesized photochemical origin.

Powder XRD data indicate that rancieite $[(CaO)Mn_4O_8{\cdot}3H_2O]$ and birnessite $[MnO_2{\cdot}nH_2O]$ are both mainly comprised of $Mn^{(IV)}O_2$ units forming two-dimensional layered sheets separated by water molecules (Sauer et al., 2002). The layered structure provides open access to water and mobile cations. In rancieite the interlayer sites contain Ca^{2+} ions with charge neutralization by an additional O^{2-}, while birnessite contains a variety of minor cations that adsorb together with hydroxide or oxide counterions $[(Na,Ca,K)(Mg,Mn)Mn_6O_{14}{\cdot}5H_2O]$ (Russell et al., 2003). These MnO_2 lattices are generally imperfect such that loss of $(Mn^{IV}O)^{2+}$ sites can occur by exchange with cations (Ca^{2+} in the case of rancieite). Because the local structure of these defects is not fully revealed, there is incomplete structural information known about the most interesting local sites in these minerals. In the bulk structure, each Mn^{IV} ion is octahedrally coordinated to O^{2-} or H_2O ligands. All oxides are sp^3 hybridized and occupy apical bridging sites between Mn_3 units. Sauer and Yachandra (2002) note that both structures contain the characteristic 2.7–2.8 Å Mn-Mn scattering vector of the PS II-WOC, but lack the 3.3–3.4 Å Mn-Mn scattering vector and thus are not accurate structural models (of the partially reduced S_0, S_1, S_2 and S_3 states). However, the latter shortcoming may not invalidate this proposal, as the rancieite core structure was postulated as a model for the reactive O_2 producing WOC, e.g., the S_4 state. There are no structural data for the S_4 state. Moreover, this state is believed to be structurally different from the partially reduced S states on the basis of the substantial activation energy for the reaction $S_3 \rightarrow S_4 \rightarrow S_0 + O_2$. Russell and Hall (2002) hypothesize that placement of a Ca^{2+} at an $(MnO)^{2+}$ vacancy in rancieite could prevent the insertion of Mn^{2+} or other cations and provide a geometry suitable for water binding and activation that enables O_2 production. The rancieite hypothesis is intuitively appealing and should be examined further. Sauer et al (2002) have extended the structural comparison to include other classes of MnO_2 minerals.

It may be significant that the sp^3 hybridized

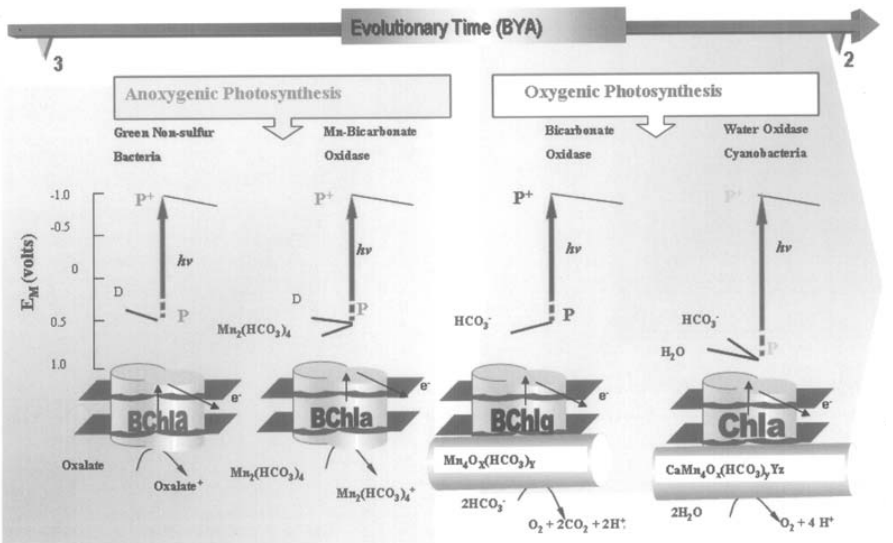

Fig. 1. Possible evolution of the inorganic core of the PS II-WOC from an anoxygenic phototroph to cyanobacterium via two intermediate forms not known to exist or not yet identified in contemporary relics. From Dismukes et al. (2001).

O^{2-} bridges present in rancieite (the only type of bulk O^{2-} ions) are structurally analogous to the O^{2-} bridges found in the corners of the 'cubane' cores $[Mn_4O_4]^{6+}$ and $[Mn_4O_4]^{7+}$ present in the molecular complexes $[Mn_4O_4(O_2PPh_2)_6]^{0/+}$, respectively. The Mn_4O_4-cubane topology of these complexes has been shown to be key to their unique ability to release O_2 following removal of a capping chelate ($Ph_2PO_2^-$, diphenylphosphinate) from its bridging position on one of the faces of the cube (Ruettinger et al., 2000; Yagi et al., 2001). The resulting reduced $[Mn_4O_2]^{6+}$ core has a bent butterfly geometry with wingtip Mn^{2+} ions. The critical requirements for O_2 release in the cubanes are the presence of unusually long (e.g., weak) Mn-O bonds (~2.0 Å), the corner bridging location of the sp^3 hybridized O^{2-}, and the $Mn_2^{III}Mn_2^{IV}$ oxidation state. It has been hypothesized that the role of $Ca^{2+}(OH_x)$ in such a mechanism might be to occupy a bridging position on the face of the cube for substrate activation and for preventing access to the open butterfly core in the reduced S states (Dismukes et al., 1998). This idea is echoed in the rancieite postulate.

One element of the mineral theory origin of the WOC that has not been addressed is that it is not clear what sorts of biological processes could take place that could encode the structural information necessary to carry out the synthesis and assembly of the WOC. How the transition could have taken place from organisms that simply incorporated the preformed cores to the modern situation in which the WOC is assembled stepwise from soluble cofactors is difficult to envision.

E. Bicarbonate as Evolutionary Substrate and Cofactor for Mn Core Assembly

Figure 1 summarizes an hypothesis by Dismukes et al. (2001) for the origin and sequence of evolution of the PS II-WOC based on the proposition that Mn-bicarbonate complexes were the building blocks for constructing the inorganic core (Dismukes et al., 2001). It is postulated that preformed Mn^{II}-bicarbonate clusters that were widely distributed as described above, served initially as terminal substrates to anoxygenic phototrophs containing type II reaction centers, such as the green non-sulfur bacteria or purple bacteria (Mn-Bicarbonate Oxidase, Stage 1). Mn-bicarbonate clusters would have been feasible, although inefficient, electron donors to these bacteria owing to the mismatch in electrochemical potentials for the primary BChl-a pigment found in the reaction center. In the next evolutionary step, two features may have been adopted in the Archean period which characterize the 'missing link' in evolutionary development (Bicarbonate Oxidase, Stage 2): (1) mutations in the L/M type II reaction center proteins occurred

which favored binding of a tetramanganese-bicarbonate cluster, $Mn_4O_x(HCO_3)_y$, and (2) evolution of a higher potential photooxidant, such as BChl *g*, the suggested evolutionary precursor pigment to Chl *a* (Xiong et al., 2000). These developments could have been sufficient to enable bicarbonate to serve as an inefficient substrate for the concerted four-electron oxidation to O_2.

The most recent proposed stage of development represents the emergence of cyano- and oxyphotobacteria and thus is denoted the Water Oxidase, Stage 3. This stage was brought on by the enormous reduction of atmospheric CO_2 in the post Archean period. Although it is unclear how this transition occurred, it would have required the evolution of a stronger inorganic catalyst and a stronger photooxidant in order to split water efficiently. It was postulated that this developmental stage may correspond to the incorporation of Ca^{2+} as integral cofactor within the Mn cluster (Dismukes et al., 2001). The Ca^{2+} cofactor boosts the electrochemical potential of the Mn cluster in the contemporary PS II-WOC by 0.6 to 1 eV, thus permitting weaker reductants such as water to serve as terminal substrates. Importantly, the adoption of a stronger photooxidant such as Chl *a* or Chl *d* would have greatly increased the quantum efficiency of water oxidation, owing to its considerably higher potential (Blankenship et al., 1998). This final stage of development is postulated to include the incorporation of two catalytically essential classes of amino acid residues in the reaction center protein environment. Tyrosine-Z, Y_z, of the D1 subunit (homolog of L/M) is conserved in all oxygenic phototrophs (Diner et al., 2002) and may have been introduced as this stage. Placement of Y_Z in between the photooxidant and the Mn cluster could serve two developmental functions. First, it suppresses the rate of charge recombination reactions in the proto-enzyme between Q_A^- and $[Mn_4]^+$ by increasing the distance by another 8-12 Å. Second, it reduces the yield of excited state quenching of the primary photoexcited pigment that is essential for forming a high yield of the primary photooxidant (Abrahamsson et al., 2002). Direct evidence for tyrosine oxidation by BChl *a* has been demonstrated in a 'Y_z mutant' of *Rhodobacter sphaeroides* (Kálmán et al., 1999). Also, the introduction of basic amino acid residues within the D1 subunit to serve as proton acceptor/transfer cofactors in water splitting and assembly of the inorganic core is an essential developmental step in evolution. This step could have been triggered by the disappearance of the copious bicarbonate buffer from the oceans following the Archean period.

V. Concluding Remarks

Partial answers to the four questions posed in the introduction of this chapter are beginning to trickle in. Recent evidence has been published describing the electron donation and electrochemical properties of aqueous bicarbonate solutions of Mn^{2+} which demonstrates large shifts in oxidation potential ($E_0 = 0.55$ to 0.62 V) and unique speciation, possibly oligomeric clusters, compared to other counter anions (Kozlov et al., 2004). Although the current day mechanism of O_2 evolution from water is a concerted four-electron process, there are several examples showing that the two-electron oxidation of water to hydrogen peroxide occurs in modified PS II complexes that are defective in proton evolution (reviewed by Dasgupta et al., 2004). These authors hypothesized that the formation of H_2O_2 by the two-electron donation employed by early oxygenic phototrophs. Additional evidence has recently pointed to the unusually faster rate of O_2 evolution (×5) and high efficiency of the Kok cycle in high-carbonate requiring strains of the cyanobacterium *Arthrospira maxima* that originate from alkaline soda lakes (Ananyev and Dismukes, 2005). Future studies are needed to address the question of a specific role for bicarbonate in the PS II-WOC in these strains. Lastly, we refer readers to a recent historical perspective of the evolution of PS I and PS II reaction center complexes that has brought into clearer focus the debated models for evolution of the proteome (Olson and Blankenship, 2004).

Acknowledgments

We thank Michael Russell, Ken Sauer and Vittal Yachandra for stimulating discussions.

References

Abrahamsson MLA, Baudin HB, Tran A, Philouze C, Berg KE, Raymond-Johansson MK, Sun LC, Akermark B, Styring S and Hammarstrom L (2002) Ruthenium-manganese complexes for artificial photosynthesis: Factors controlling intramolecular electron transfer and excited-state quenching reactions. Inorg Chem 41: 1534–1544

Ananyev GM and Dismukes GC (2005) How fast can Photo-

system II split water? Kinetic performance at high and low frequencies. Photosynth Res, in press
Ananyev GM, Murphy A, Abe Y and Dismukes GC (1999) Remarkable affinity and selectivity for Cs^+ and uranyl ($UO22^+$) binding to the manganese site of the apo-water oxidation complex of Photosystem II. Biochemistry 38: 7200–7209
Ananyev GM, Zaltsman L, Vasko C and Dismukes GC (2001) The inorganic biochemistry of photosynthetic oxygen evolution/water oxidation. Biochim Biophys Acta 1503: 52–68
Baranov SV, Ananyev GM, Klimov VV and Dismukes GC (2000) Bicarbonate accelerates assembly of the inorganic core of the water-oxidizing complex in manganese-depleted Photosystem II: A proposed biogeochemical role for atmospheric carbon dioxide in oxygenic photosynthesis. Biochemistry 39: 6060–6065
Baranov S, Tyryshkin A, Katz D, Ananyev G, Klimov V and Dismukes G (2004) Bicarbonate is a native cofactor for assembly of the manganese cluster of the photosynthetic water oxidizing complex: II. Kinetics of reconstitution of O_2 evolution by photoactivation. Biochemistry 43: 2070–2079
Blankenship RE (2002) Molecular mechanisms of photosynthesis. Oxford, Blackwell Science
Blankenship RE and Hartman H (1998) The origin and evolution of oxygenic photosynthesis. Trends Biochem Sci 23: 94–97
Boussac A and Rutherford AW (1988) The nature of the inhibition of the oxygen evolving enzyme of PS II which is induced by NaCl washing and reversed by the addition of Ca2+ or Sr2+. Biochemistry 27: 3476–3483
Bruhland K (1983). Trace elements in seawater. In: Riley JP and Chester R (eds) Chemical Oceanography, pp 147–220. Academic Press, London
Brune D (1995) Sulfur compounds as photosynthetic electron donors. In: Blankenship RE, Madigan MT and Bauer CE (eds) Anoxygenic Photosynthetic Bacteria, pp 847–870, Kluwer Academic Publishers, Dordrecht
Carrell TG, Tyryshkin A and Dismukes GC (2002) An evaluation of structural model for the photosynthetic water-oxidizing complex derived from spectroscopic and X-ray diffraction signatures. J Biol Inorg Chem 7: 2–22
Catling DC, Zahlne KJ and McKay CP (2001) Biogenic methane, hydrogen escape and the irreversible oxidation of early Earth. Science 293(5531): 839–842
Cloud PE (1972) Atmospheric and hydrospheric evolution on the primitive Earth. Science 160: 729–736
Cohen Y, Jorgensen, BB, Revsbech, NP and Poplawski R (1986) Adaptation to hydrogen-sulfide of oxygenic and anoxygenic photosynthesis among cyanobacteria. Appl Environ Microbiol 51: 398–407
Dasgupta J, van Willigen RT and Dismukes GC (2004) Consequences of structural and biophysical studies for the molecular mechanism of photosynthetic oxygen evolution: Functional roles for calcium and bicarbonate. Phys Chem Chem Phys 6: 4793–4802
Debus RJ (1992) The manganese and calcium ions of photosynthetic oxygen evolution. Biochim Biophys Acta 1102: 269–352
Debus RJ (2000) The polypeptides of Photosystem II and their influence on manganotyrosyl-based oxygen evolution. In: Sigel A and Sigel H (eds) Metal Ions in Biological Systems: Manganese and Its Role in Biological Processes, pp 657–711. Marcel Dekker Inc, New York
Debus RJ (2001) Amino acid residues that modulate the properties of tyrosine Y_z and the manganese cluster in the water oxidizing complex of PS II. Biochim Biophys Acta 1503: 164–186
Des Marais DJ (2000) When did photosynthesis emerge on Earth? Science 289: 1703–1704
Diner BA (1998) Application of spectroscopic techniques to the study of PS II mutations engineered in *Synechocystis* and *Chlamydomonas*. Meth Enzymol 297: 337–360
Diner BA (2001) Amino acid residues involved in the coordination and assembly of the manganese cluster of Photosystem II. Proton-coupled electron transport of the redox-active tyrosines and its relationship to water oxidation. Biochim Biophys Acta 1503: 147–163
Diner BA and Rappaport F (2002) Structure, dynamics and energetics of the primary photochemistry of PS II on oxygenic photosynthesis. Annu Rev Plant Biol: 551–580
Dismukes GC (1988) The spectroscopically derived structure of the manganese site for photosynthetic water oxidization and a proposal for the protein-binding sites for calcium and manganese. Chemica Scripta 28A: 99–104
Dismukes GC, Ruettinger W, Boelrijk AEM and Ho D (1998) Structure of the mn_4cal core of the PS II water oxidizing complex and the Mn_4O_4-cubane/Mn_4O_2-butterfly model complexes. In: Garab G (ed) Photosynthesis: Mechanisms and Effects, Vol II, pp 1259–1264. Kluwer Academic Publishers, Dordrecht
Dismukes GC, Klimov VV, Baranov SV, Kozlov YN, Dasgupta J and Tyryshkin A (2001) The origin of atmospheric oxygen on Earth: The innovation of oxygenic photosynthesis. Proc Nat Acad Sci USA 98: 2170–2175
Farquhar J, Bao HN and Thiemans M (2000) Atmospheric influence of Earth's earliest sulfur cycle. Science 289: 756
Ferreira KN, Iverson TM, Maghlaoui K, Barber Jand Iwata S (2004) Architecture of the photosynthetic oxygen-evolving center. Science 303: 1831–1838
Grotzinger JP and Kasting JF (1993) New constraints on precambrian ocean composition. J Geol 101(2): 235–243
Hedges S, Chen H, Kumar H, Wang D Y-C, Thomson AS and Watanabe H (2001) A genomic timescale for the origin of eukaryotes. BMC Evol Biol 1: 4
Holland HD (1984) Chemical Evolution of the Atmosphere and Oceans. Princeton University Press, Princeton
Holland H and Rye R (1998) Paleo-reconstruction of early O_2 evolution. Amer J Science 298: 621–672
Hu QM, Miyashita H, Iwasaki I, Kurano N, Miyachi S, Iwaki M and Itoh S (1998) A Photosystem I reaction center driven by chlorophyll *d* in oxygenic photosynthesis. Proc Natl Acad Sci USA 95: 13319–13323
Itoh S, Iwaki M, Noguti T, Kawamori A and Mino H (2001) In: PS2001 Proceedings: 12th International Congress on Photosynthesis, S6-028. CSIRO Publishing, Melbourne (CD-ROM)
Kálmán L, LoBrutto, Allen JP and Williams JC (1999) Modified reaction centers oxidize tyrosine in reactions that mirror PS II. Nature 402: 696–699
Kamiya N and Shen J-R (2003) Crystal structure of oxygen-evolving Photosystem II from *Thermosynechococcus vulcanus* at 3.7-Å resolution. Proc Nat Acad Sci USA 100: 98–103
Kasting J (1993) Earth's early atmosphere. Science 259: 920–926
Kasting JF and Seifert JL (2002) Life and the evolution of Earth's atmosphere. Science 296: 1066–1068
Klimov VV and Baranov SV (2001) Bicarbonate requirement

for the water-oxidizing complex of Photosystem II. Biochim Biophys Acta 1503: 187–196

Kozlov YN, Kazakova AA and Klimov VV (1997) Changes in the redox-potential and catalase activity of Mn^{2+} ions during formation of Mn-bicarbonate complexes. Biologicheskie Membrany (Russian) 14: 93–97

Kozlov YN, Zharmukhamedov SK, Tikhonov KG, Dasgupta J, Kazakova AA, Dismukes GC and Klimov VV (2004) Oxidation potentials and electron donation to Photosystem II of manganese complexes containing bicarbonate and carboxylate ligands. Phys Chem Chem Phys 6: 4905–4911

Lasaga A and Ohmoto H (2002) The oxygen geochemical cycle: Dynamics and stability. Geochim Cosmochim Acta 66: 361–381

Mimuro M, Akimoto S, Yamazaki I, Miyashita H and Miyachi S (1999) Fluorescence properties of chlorophyll *d*-dominating prokaryotic alga *Acaryochloris marina*: Studies using time-resolved fluorescence spectroscopy on intact cells. Biochim Biophys Acta 1412: 37–46

Miyashita H, Ikemoto H, Kurano N, Adachi K, Chihara M and Miyachi S (1996) Chlorophyll *d* as a major pigment. Nature 383: 402

Morse JW and Mackenzie FT (1998) Hadean ocean carbonate geochemistry. Aquatic Geochem 4: 301–319

Ohmoto H (1997) When did the Earth's atmosphere become oxic? Geochem News 97: 26–27

Olson JM (1970) The evolution of photosynthesis. Science 168: 438–446

Olson JM (2001) 'Evolution of photosynthesis' (1970) re-examined thirty years later. Photosynth Res 68: 95–112

Olson JM and Blankenship RE (2004) Thinking about the evolution of photosynthesis. Photosynth Res 80: 373–386

Raven JA, Evans MCW and Korb RE (1999) The role of trace metals in photosynthetic electron transport in O_2-evolving organisms. Photosynth Res 60: 111–149

Robblee JH, Cinco RM and Yachandra VK (2001) X-ray spectroscopy-based structure of the Mn cluster and mechanism of photosynthetic oxygen evolution. Biochim Biophys Acta 1503: 7–23

Ruettinger W, Yagi M, Wolf K, Bernasek S and Dismukes GC (2000) O_2 evolution from the manganese-oxo cubane core $[Mn_4O_4]6^+$: A molecular mimic of the photosynthetic water oxidation enzyme? J Am Chem Soc 122: 10353–10357

Russell MJ and Hall AJ (2002) From geochemistry to biochemistry: Chemiosmotic coupling and transition element clusters in the onset of life and photosynthesis. Geochem News 113: 6–12

Russell MJ, Hall AJ and Mellersh AR (2003) On the dissipation of thermal and chemical energies on the early Earth: The onsets of hydrothermal convection, chemiosmosis, genetically regulated metabolism and oxygenic photosynthesis. In: Ikan R (ed) Natural and Laboratory-Simulated Thermal Geochemical Processes. Kluwer Academic Publishers, Dordrecht

Sauer K and Yachandra VK (2002) A possible evolutionary origin for the Mn_4 cluster of the photosynthetic water oxidation complex from natural MnO_2 precipitates in the early ocean. Proc Nat Acad Sci USA 99: 8631–8636

Semin BK, Ghirardi ML and Seibert M (2002) Blocking of electron donation my Mn(II) to Yz following incubation of Mn-depleted PS II membranes with Fe(II) in the light. Biochemistry 41: 5854–5864

Smith RM and Martell AE (1976) Critical Stability Constants. Plenum, New York

Stadtman ER, Berlett PB and Chock PB (1990) Manganese-dependent disproportionation of hydrogen peroxide in bicarbonate buffer. Proc Nat Acad Sci USA 87: 384–388

Sugisaki R, Horiuchi Y, Sugitani K and Adachi M (1995) Acid character of archean ocean waters revealed by 3.3-Ga-old ferruginous chart compositions, Western-Australia. Proc Japan Acad: B-Phys Biol Sci 71: 170–174

Summons RE, Jahnke LL, Hope JM and Logan GA (1999) 2-methylhopanoids as biomarkers for cyanobacteria oxygenic photosynthesis. Nature 400: 554–557

Svensson B, Etchebest C, Tuffery P, Van Kan P, Smith J and Styring S (1996) A model for the Photosystem II reaction center core including the structure of the primary donor P680. Biochemistry 35: 14486–14502

Sychev AY and Isac VG (1993) The catalase, peroxidase, and oxidase properties of the coordination compounds of manganese. Russ Chem Rev 62: 279–290

Towe KM (1994) Earth's early atmosphere: Constraints and opportunities for early evolution. In: Early Life on Earth, Nobel Symposium No 84, Columbia University Press, New York

Vrettos JS, Stone DA and Brudvig GW (2001) Quantifying the ion selectivity of the Ca^{2+} site in Photosystem II: Evidence for direct involvement of Ca^{2+} in O_2 formation. Biochemistry 40: 7937–7945

Walker JCG (1985) Carbon dioxide on the early Earth. Orig Life Evol Biosph 16: 117–127

Xiong J, Subramanium S and Govindjee (1998) A knowledge-based three dimensional model of the Photosystem II reaction center of *Chlamydomonas reinhardtii*. Photosynth Res 56: 229–254

Xiong J, Fisher WM, Inoue K, Narakhara M and Bauer CE (2000) Molecular evidence for the early evolution of photosynthesis. Science 289: 1724–1730

Yagi M, Wolf KV, Baesjou PJ, Bernasek SL and Dismukes GC (2001) Selective photoproduction of O_2 from the Mn_4O_4 cubane core: A structural and functional model for the photosynthetic water oxidizing complex. Angew Chem Int Ed 40: 2925–2928

Zouni A, Witt HT, Kern J, Fromme P, Krauss N, Saenger W and Orth P (2001) Crystal structure of Photosystem II from *Synechococcus elongatus* at 3.8 Å resolution. Nature 409: 739–743

Chapter 31

Mechanistic Comparisons Between Photosystem II and Cytochrome *c* Oxidase

Gary W. Brudvig*
Department of Chemistry, Yale University, P.O. Box 208107, New Haven, CT, 06520-8107, U.S.A.

Mårten Wikström
Institute of Biotechnology, Helsinki Bioenergetics Group, University of Helsinki, PB 65 Biocenter 3 (Viikinkaari 1), FIN-00014 Helsinki, Finland

Summary

Photosystem II (PS II) uses light to split water and form O_2, protons and electrons. Cytochrome *c* oxidase (CcO) is the respiratory enzyme found in mitochondria that catalyzes the reverse reaction: the four-electron reduction of molecular oxygen to water. Because these two enzymes catalyze the opposite directions of the same chemical reaction, they share mechanistic similarities. For example, in both systems, the four-electron oxygen/water reaction occurs in essentially a single reaction step, without requirement of electron or proton transfer from a source outside the active site. In this chapter, the chemistry of water oxidation/oxygen reduction by PS II/CcO is discussed with a consideration of the thermodynamics of the reactions, the roles of protons, and the analogies in the reaction mechanisms of the two systems.

*Author for correspondence, email: gary.brudvig@yale.edu

T. Wydrzynski and K. Satoh (eds): Photosystem II: The Light-Driven Water:Plastoquinone Oxidoreductase, pp. 697–713.

I. Introduction

The O_2 produced in oxygenic photosynthesis serves as the terminal electron acceptor in aerobic respiration. The resulting water-oxygen cycle is of fundamental importance in biological energy transduction. Key to these processes is the four-electron/four-proton oxido-reduction chemistry that occurs in the interconversion of water and oxygen (Eq. 1). As described in detail in previous chapters in this volume, Photosystem II (PS II) uses light to split water and form O_2, protons and electrons. Cytochrome *c* oxidase (CcO) is the respiratory enzyme found in mitochondria that catalyzes the reverse reaction: the four-electron reduction of molecular oxygen to water. Because these two enzymes catalyze the opposite directions of the same chemical reaction, it has long been thought that they may share mechanistic similarities. In the expectation that an exchange of ideas between the groups researching the structure and function of CcO and PS II would be productive, a Nobel Conference on 'The Biophysical Chemistry of Dioxygen Reactions in Respiration and Photosynthesis' was held on the west coast of Sweden in July 1987. However, the early work did not indicate a close mechanistic relation between the two systems and the two communities of researchers did not find much common ground. The proceedings of this conference were published and provide a good record of the status of research at the time (Vänngård, 1988).

$$2H_2O \underset{\text{Cytochrome Oxidase}}{\overset{\text{Photosystem II}}{\rightleftharpoons}} O_2 + 4H^+ + 4e^- \quad (1)$$

One of the people attending the Nobel Conference in 1987 was Gerald Babcock (Jerry). Jerry was one of the few researchers who had studied both PS II and CcO; he was the only attendee with an active program of research on both systems. With his knowledge of both fields, Jerry helped to facilitate the exchange of ideas between the two largely independent groups of researchers. Nonetheless, the two communities remained separate throughout the 1980s and 1990s. Jerry continued his programs of research on both systems because of his conviction that there would be synergism in studies of the dioxygen chemistry. In the mid-1990s, emerging structural information, together with the recognition of the key roles played by protons in the two systems, focused attention on the mechanistic similarities of the reactions catalyzed by CcO and PS II. Indeed, when the reverse direction of reaction of PS II is compared to the reactions of CcO (or vise versa), we may have very analogous water/oxygen chemistry for these two enzymes.

In this chapter, we will focus on the chemistry of water oxidation/oxygen reduction by PS II/CcO with a consideration of the thermodynamics of the reactions, the roles of protons, and the analogies in the reaction mechanisms of the two systems. Additional information can be found in a number of excellent reviews that have been published on PS II (Debus, 1992; Britt, 1996; Diner and Babcock, 1996; Yachandra et al., 1996; Tommos and Babcock, 1998; Limburg et al., 1999; Britt et al., 2000; Vrettos and Brudvig, 2004) and CcO (Babcock and Wikström, 1992; Ferguson-Miller and Babcock, 1996; Wikström, 2000; Yoshikawa et al., 2000; Zaslavsky and Gennis, 2000; Schultz and Chan, 2001) as well as three recent special issues of journals devoted to PS II (Nugent et al., 2001; Barber and Anderson, 2002; Messinger and Lubitz, 2004).

Gerald Babcock played a central role in the development of mechanistic ideas on the dioxygen chemistry in both systems. It is highly fitting that this volume is a tribute to Jerry. We would like to dedicate this chapter, in particular, to his memory and to the many contributions he made to our current understanding of the dioxygen chemistry of CcO and PS II.

II. Protein Structure and Cofactors

A. Photosystem II and the Oxygen-Evolving Complex

Photosystem II is a transmembrane complex of proteins found in the thylakoid membrane of plants and cyanobacteria. It functions to utilize solar energy to oxidize water and reduce plastoquinone. The PS II complex contains more than twenty polypeptide subunits (for review, see Debus, 2000). These include light-harvesting complexes (Chapters 2, Green and Gantt, and 3, Eaton-Rye and Putnam-Evans), several extrinsic membrane-associated proteins that stabilize the oxygen-evolving complex (OEC) (Chapter 5,

Abbreviations: CcO – cytochrome *c* oxidase; Cyt *c* – cytochrome *c*; OEC – oxygen-evolving complex; P680 – primary electron donor in PS II; PCET – proton-coupled electron transfer; Pheo – pheophytin; PS II – Photosystem II; Q_A – primary quinone electron acceptor in PS II; Q_B – secondary quinone electron acceptor in PS II; Y_D – redox-active tyrosine in the D2 subunit of PS II; Y_Z – redox-active tyrosine in the D1 subunit of PS II

Bricker and Burnap), cytochrome b_{559} that appears to play a role in a photoprotection mechanism (Chapter 15, Faller et al.), and a number of small subunits whose functions are not clear (Chapter 6, Thornton et al.). The core D1 and D2 subunits of PS II form a heterodimer that contains the redox centers that couple the oxidation of water to the reduction of plastoquinone (Chapter 4, Nixon et al.). An exciting recent advance is that crystal structures of the PS II complex have been solved at 3.8 Å (Zouni et al., 2001), 3.7 Å (Kamiya and Shen, 2003) and 3.5 Å (Ferreira et al., 2004) resolution (Chapters 19–21).

The energy required to oxidize water to O_2 is provided by visible photons, which produce a charge separation in the PS II reaction center (Chapter 7, Renger and Holzwarth). Photons are collected by an array of chlorophylls in light-harvesting proteins (Chapter 2, Green and Gantt) and funneled by energy-transfer mechanisms to the PS II reaction center chlorophylls (Chapter 22, Barter et al.) shown in Fig. 1. The excited state of these chlorophylls is a strong reductant and rapidly transfers an electron to a pheophytin molecule ($Pheo_A$), which in turn reduces a protein-bound plastoquinone (Q_A). The final electron acceptor is a diffusible plastoquinone, Q_B (Chapter 8, Petrouleas and Crofts). Following its reduction to hydroquinone, Q_BH_2 dissociates from PS II and carries its reducing equivalents on to the next step in the electron-transport chain.

The charge-separated state $P680^{+\bullet}/Q_A^{-\bullet}$ is stabilized through reduction of $P680^{+\bullet}$ by a redox-active tyrosine residue, Tyr161 (Y_Z) (Chapter 9, Diner and Britt); the $P680^{+\bullet}$ radical cation is localized on P_A (see Fig. 1) at 5 K (Diner et al., 2001; Rappaport et al., 2002). The tyrosyl radical thus formed, $Y_Z^{\bullet}$, oxidizes a tetranuclear manganese-oxo (Mn_4) cluster, which is the active site of water oxidation (Chapters 10, 12 and 25). Each oxidation state of the Mn_4 cluster is referred to as an S_n-state (n = 0–4) (Chapter 24, Shinkarev), i.e.,

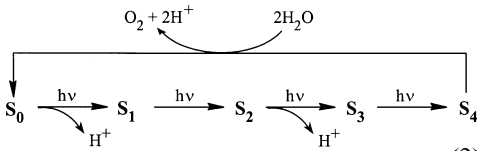

(2)

S_0 is the most reduced and S_4 is the most oxidized of the S states formed during the four-electron cycle leading to O_2 evolution (Joliot and Kok, 1975). Upon

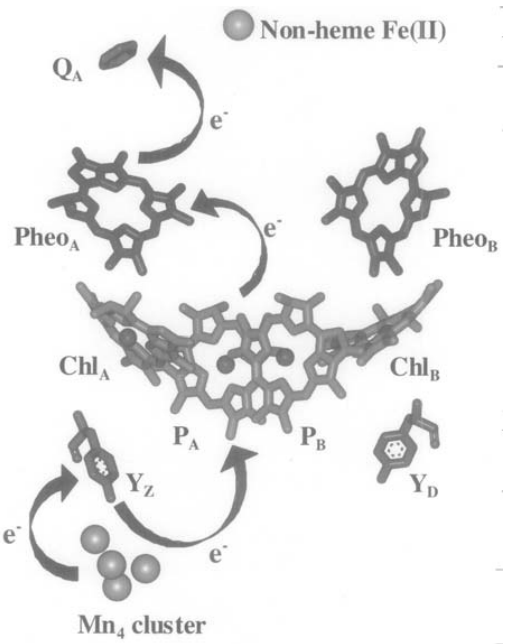

Fig. 1. Redox cofactors of PS II: Mn_4 cluster, redox-active tyrosines Y_Z and Y_D, chlorophylls (Chl_A, Chl_B, P_A and P_B), pheophytins ($Pheo_A$ and $Pheo_B$), Q_A and non-heme iron. The sequence of light-induced electron transfer from the Mn_4 cluster to Q_A is shown with arrows.

oxidation to the S_4 state, the Mn_4 cluster is spontaneously reduced to S_0 by oxidizing water to form O_2 and protons (reviewed in Debus, 1992). Calcium and chloride are required for advancement beyond the S_2 state (Yocum, 1991; Andréasson et al., 1995; Wincencjusz et al., 1997; Chapter 13, van Gorkom and Yocum). Together, Y_Z, the Mn_4 cluster, Ca^{2+} and Cl^- constitute the OEC.

The Mn_4 cluster is bound to the D1 protein adjacent to Y_Z. The distance from the nearest Mn ion to the phenoxyl oxygen of Y_Z is approximately 7 Å. The OEC is shielded from the aqueous phase by several extrinsic membrane-associated proteins, as well as large loop regions of the transmembrane proteins. This buried position of the OEC is no doubt essential to prevent reaction of molecules in the aqueous phase with the highly oxidizing intermediates formed in the water oxidation process. However, it requires specific channels for substrate water molecules to access the OEC and for product protons and O_2 to be released. In the X-ray structure of Ferreira et al. (2004; Chapter

21, Barber and Iwata), a channel of hydrophilic residues is identified that extends from the Mn_4 cluster to the lumenal surface of PS II and is proposed to be the pathway for conduction of protons from the OEC to the lumen. Ferreira et al. (2004) also reported the first atomic-resolution model for the structure of the OEC. The four Mn and one Ca^{2+} ions are modeled as a Mn_3CaO_4 'cubane'-like cluster that is connected to the fourth 'dangler' Mn via a mono-μ-oxo bridge involving one of the corners of the 'cubane'. This structure is generally consistent with the information that has been obtained by spectroscopic and biochemical methods on the structure of the OEC, its redox states and its coordination environment. For example, the Mn_3CaO_4-Mn structure fits with X-ray spectroscopic studies that identify 2–3 Mn-Mn scatterers at 2.7 Å, a distance that is diagnostic of a di-μ-oxo-bridged dimanganese structure, and 1 Mn-Mn scatterer at 3.3 Å, a distance that is observed for mono-μ-oxo- and/or carboxylate-bridged dimanganese centers (Yachandra, 2002; Chapter 10, Yachandra). It also appears that chloride is closely associated with the Mn_3CaO_4-Mn cluster and may be a ligand to Ca^{2+} (McEvoy et al., 2005). Other current proposals for the active site in the OEC include a variety of topologies for an oxo-bridged Mn_4/Ca/Cl structure (reviewed in Vrettos and Brudvig, 2004).

Several amino acids in the D1 protein have been shown to affect the functionality of the OEC (reviewed in Diner et al., 1991; Debus, 2000; Chapter 11, Debus). Many of these residues are either ligands to the Mn_4 cluster, such as Asp170 (Nixon and Diner, 1992; Chu et al., 1995a) and His332 (Chu et al., 1995b; Debus et al., 2000), or participants in proton-coupled electron-transfer reactions, such as His190 (Chu et al., 1995a; Hays et al., 1998, 1999; Mamedov et al., 1998).

B. Cytochrome c Oxidase

The Cyt *c* oxidases (CcOs) are members of a large family of heme-copper oxidases that serve as catalysts of O_2 reduction to water in cell respiration of all aerobic organisms. X-ray structures of CcOs from four organisms are known (Iwata et al., 1995; Tsukihara et al., 1995; Soulimane et al., 2000; Svensson-Ek et al., 2002). In addition, the structure of the related quinol oxidase from *E. coli* has been published (Abramson et al., 2000). The variation in protein primary structure among the heme-copper oxidases is extensive; the only structure common to all is that of the largest subunit, subunit I (Fig. 2), which always encompasses two heme groups and one copper center. One heme (usually heme a_3 in the CcOs) and the copper (Cu_B) form a binuclear site that binds O_2 and catalyzes its reduction to water. A second low spin heme (heme *a* in most CcOs) is closely opposed, and functions as the electron donor to the binuclear site. Both heme groups are arranged with their porphyrin planes perpendicular to the membrane, almost at a right angle to one another, and at the same depth in the membrane, approximately 1/3 from the positively charged *P*-side (Fig. 2). Subunit I has a unique structure with 12–15 transmembrane helices arranged in a three-blade propeller-like fashion, best seen when viewed orthogonally to the membrane (Fig. 3). In this structure, helices II, VI and X have

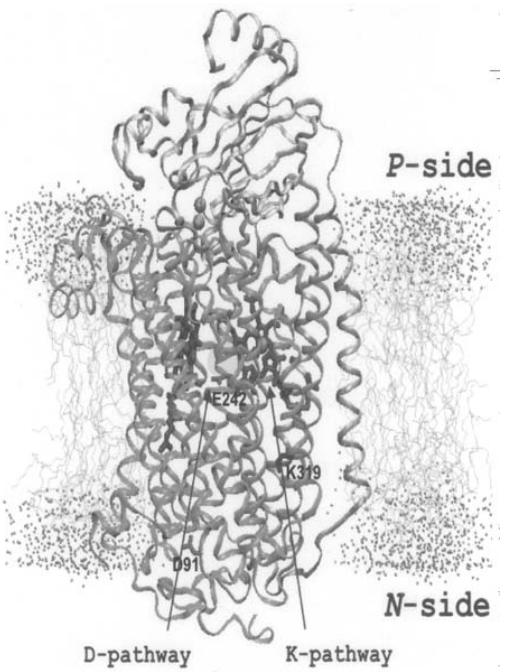

Fig. 2. Rhodobacter sphaeroides CcO (Svensson-Ek et al., 2002) in a model membrane. Subunits I and II are shown, as are the hemes and coppers. The structure is drawn from 1M56.pdb and a model membrane, by the program MOLSCRIPT (Kraulis, 1991). The proton transfer pathways D and K are roughly outlined, as are the key proton transfer residues Asp91, Glu242 and K319 (numbering according to the bovine heart enzyme). A hydrophobic cavity between Glu242 and heme a_3 may transiently contain a number of water molecules (see text). See Color Plate 15, Fig. 1.

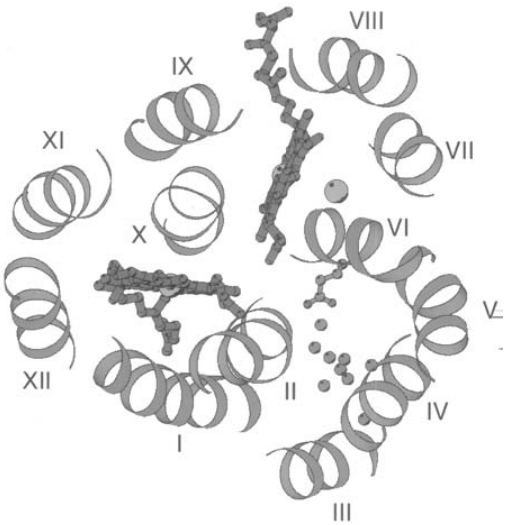

Fig. 3. Top view of the *Rhodobacter* enzyme perpendicular to the membrane. Helices are numbered from I to XII, and only the center parts of them are shown, for clarity. Heme a_3 and the Cu_B site (large sphere) are shown in the upper, and heme *a* in the lower, part of the figure. The residue Glu242 in helix VI is also shown, as well as crystallographically detectable water molecules (small sphers) in the D-pathway (See text). The structure is rotated by 90 degrees relative to Fig. 2.

central positions relative to the others, and provide the axial histidine ligands for the heme groups as well as one of the three histidine ligands of Cu_B (the two other histidine ligands of Cu_B are adjacent residues in helix VII). The helices form three 'channels', two of which are occupied by the binuclear site and the low spin heme, respectively. The third 'channel' contains the so-called D-pathway of proton transfer and includes a well-conserved glutamic acid residue (Glu242) that is essential for function (Verkhovskaya et al., 1997; Brzezinski and Adelroth, 1998) (Fig. 2). In some aberrant heme-copper oxidases this is replaced, however, and the proton transfer function of the D-pathway is modified (Soulimane et al., 2000; Gomes et al., 2001).

A second proton transfer pathway from the *N*-side of the membrane to the binuclear site (the K-pathway shown in Fig. 2; Brzezinski and Adelroth, 1998) is apparently engaged for transfer of two of the four 'substrate protons', that is those that are taken up during reduction of the ferric/cupric binuclear site to the ferrous/cuprous form. This pathway is named after a conserved lysine residue, and its structure is thus very different from that of the D-pathway.

In most CcOs, the electron donor to the low spin heme is a bimetallic copper center (Cu_A) that resides outside the membrane dielectric in an externally exposed domain of subunit II that is anchored to the membrane by two transmembrane helices (Fig. 2). This domain also contains the binding site for Cyt *c*, the electron donor to Cu_A. Interestingly, subunit II is retained in the quinol oxidase subfamily of heme-copper oxidases, which uses a hydroquinone as the electron donor in place of Cyt *c*, although Cu_A and its ligands are missing (Abramson et al., 2000).

Subunit III is also usually found in the heme-copper oxidases, albeit not in some very distant relatives. It is a highly hydrophobic protein with 5–7 transmembrane helices and lacks redox-active metal centers. Its function is enigmatic, although it has been suggested to be involved in the assembly of subunits I and II (Haltia et al., 1989), as an oxygen reservoir (Riistama et al., 1996), and to prevent the enzyme from undergoing suicide inhibition during activity (Bratton et al., 1999).

Bacterial Cyt *c* and quinol oxidases contain an additional subunit (IV) with a single transmembrane helix, the function of which is unknown and which can be deleted with a phenotype indistinguishable from wild type (Witt and Ludwig, 1997). The mitochondrial CcOs contain up to ten subunits (Tsukihara et al., 1996), in addition to subunits I-III which are homologous to the bacterial counterparts. In contrast to subunits I-III, which are coded for in mtDNA, these auxiliary subunits are coded for by nuclear DNA and imported into the mitochondrion. Their function is still largely unknown, although regulatory properties have been proposed (Ludwig et al., 2001). In any case, it is clear from the examples of bacteria that subunits I–III suffice for the main functions of O_2 activation and reduction, as well as for proton translocation, by which these enzymes function as primary energy transformers in biology.

III. Energetics of Water Oxidation and Oxygen Reduction

The four-electron reduction of O_2 to water is a highly exergonic reaction ($E_{m,7} = 0.815$ V). In respiration, the free energy of O_2 reduction is utilized to translocate protons across the mitochondrial membrane. On the other hand, light is used to drive the endergonic formation of O_2 from water. Thus, although the wa-

ter/oxygen chemistry is analogous in PS II and CcO, the two systems are fundamentally different with regard to the energy transduction processes. PS II functions on the principle of 'directed chemistry' (Mitchell, 1966), in which electrons are extracted from water and transferred across the membrane to reduce quinone on the other side. Protonmotive force is generated by PS II as the result of production of protons on the lumenal side of the membrane and consumption of protons in quinone reduction on the stromal side. Analogously, CcO also catalyzes 'directed chemistry' with uptake of the electrons and protons required for reduction of O_2 to water from opposite sides of the membrane (Fig. 4). However, it adds a proton-pumping function on top of this, yielding an overall membrane translocation of two electrical charge equivalents per transferred electron, thus doubling the efficiency of energy transduction. This does not take place in PS II.

The thermodynamics of O_2 reduction/water oxidation in aqueous solution are characterized by different standard reduction potentials at pH 7 for the one-electron transfer steps: O_2/O_2^- (–0.33 V), O_2^-/H_2O_2 (0.94 V), $H_2O_2/OH^\bullet$ (0.305 V) and $OH^\bullet/H_2O$ (2.33 V) (Babcock and Wikström, 1992). The conversion of O_2 to superoxide is unfavorable at the operating redox potential of Cyt *c*, but two of the three subsequent reductions are very favorable, especially the reduction of hydroxyl radical to water. The potentials of these downhill reactions must provide the driving force for the proton-pumping reactions of CcO. Conversely, the water-splitting reactions in PS II are uphill. Here, it is essential that the reduction potentials of the individual steps do not exceed the potential of $P680^+$ that is generated photochemically.

In order to maintain efficient biological catalysis, the potentials of the individual one-electron reactions should be optimized in the proteins. This is done by 'redox leveling' in which the reduction potentials of the steps in the O_2 reduction/water oxidation chemistry are adjusted within the protein active site relative to the solution values. The mechanisms by which 'redox leveling' is achieved remain to be established, but proton management and binding of intermediates to metal sites are likely to play key roles. For example, it is known that sequential oxidations of oxo-manganese complexes can occur at nearly the same potential if each electron-transfer step is coupled to ligand deprotonation; in contrast, the potential of each oxidation increases by hundreds of millivolts when the redox reaction is not accompanied by proton transfer (Thorp and Brudvig, 1991).

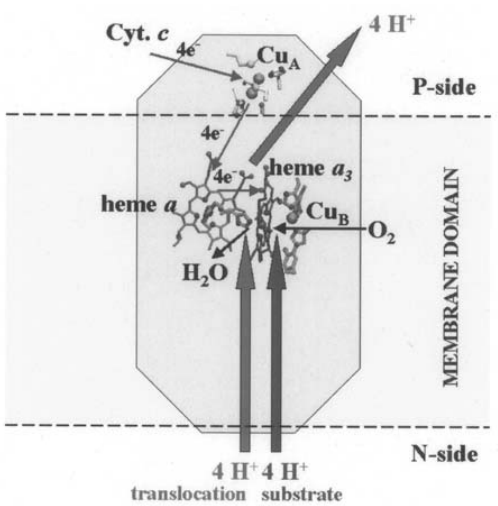

Fig. 4. Overall function of CcO. Heme group and copper ions are shown. The histidine ligands of the heme groups and of Cu_B are shown, as is the tyrosine residue in the binuclear site that is covalently bonded to one of the histidine ligands of Cu_B. The lower right arrows depict how the chemistry of O_2 reduction to water (by electron and proton transfer) is oriented with respect to the positively charged *P*-side and negatively charged *N*-side of the membrane. The upper and lower left arrows depict proton translocation. The program VMD was used for the molecular graphics (Humphrey et al., 1996). See Color Plate 15, Fig. 2.

IV. Catalytic Mechanisms

A. Photosystem II

The S-state cycle defines the five intermediate oxidation states of the OEC that are sequentially formed by the photochemistry of PS II (Eq. 2). X-ray absorption spectroscopy has provided information on the oxidation states of the Mn_4 cluster (Yachandra et al., 1996). Application of the bond valence sum method predicts an oxidation state of (3/3/4/4) for the S_1 state (Thorp, 1992). It is generally agreed that Mn is oxidized in each step up through the S_2 state. However, it is unclear whether the $S_2 \rightarrow S_3$ transition involves a Mn-centered oxidation or ligand oxidation, giving either (4/4/4/4) or (3/4/4/4)L$^\bullet$ as the S_3 oxidation states. Interestingly, two of the four Mn ions appear to remain in the Mn(IV) oxidation state throughout the S-state cycle. Based on a consideration of biophysical studies of PS II and inorganic manganese model chemistry, we have argued that all of the S-state transitions involve Mn-centered oxidation, yielding a Mn(V) species in the S_4 state that is essential to

activate a water molecule for O-O bond formation (Vrettos et al., 2001). We will focus on this mechanism in this chapter as it has the closest analogy to mechanisms proposed for CcO; other proposals are reviewed in Vrettos and Brudvig (2004).

1. The Role of Tyrosine Z

The oxidation of Y_Z by $P680^{+\bullet}$ forms $Y_Z^{\bullet}$, a neutral tyrosyl radical (Tommos et al., 1995). Based on evidence that the pK_a of the hydroxyl group of Y_Z is above 9 (Hays et al., 1999), the reduced form of Y_Z is expected to be protonated over the physiological range of pH (Berthomieu et al., 1998). Consequently, a proton must be transferred from Y_Z to a nearby basic protein residue during the photooxidation of Y_Z and from a nearby acidic residue to $Y_Z^{\bullet}$ during the reduction of $Y_Z^{\bullet}$. From a consideration of proton-coupled electron-transfer (PCET) reactions involved in tyrosine redox reactions and EPR data indicating that Y_Z is close to the Mn cluster (Gilchrist et al., 1995), Hoganson and Babcock (1997) proposed a landmark metalloradical mechanism for the OEC (Hoganson and Babcock, 1997). The ideas outlined by Hoganson and Babcock have transformed our view of the mechanism of the water splitting chemistry in PS II and form the framework for our discussion of the mechanism of O_2 evolution by PS II in this chapter.

A substantial body of data provides evidence that both the photooxidation of Y_Z and the reduction of $Y^{\bullet}_Z$ involve the coupled transfer of an electron and a proton (Vrettos et al., 2001 and references therein). Mutagenesis studies identify D1-His190 as a key proton-accepting residue in the photooxidation of Y_Z (Hays et al., 1998), and the recent X-ray crystal structure (Ferreira et al., 2004) substantiates this conclusion. The proton-accepting residue subsequently must deprotonate to dissipate the positive charge. In this regard, it has been found that rate of proton release into the lumenal aqueous phase following photoexcitation of PS II correlates with the rate of oxidation of Y_Z (Renger and Völker, 1982; Bögershausen and Junge, 1995). Therefore, it appears that an efficient pathway for proton transfer from the OEC to the lumen must exist and that the proton-release reactions are coupled to the redox state of Y_Z.

The reduction of $Y_Z^{\bullet}$, on the other hand, can proceed via two pathways. In the first case, $Y_Z^{\bullet}$ is reduced by the Mn_4 cluster and protonated by D1-His190, the protein residue that is the hydrogen-bonding partner of $Y_Z^{\bullet}$. The net result is oxidation of the Mn_4 cluster by one electron. Alternately, $Y_Z^{\bullet}$ may be both reduced and protonated by the Mn_4 cluster, as proposed by Hoganson and Babcock (1997). In this case, an O-H bond of water ligated to Mn is broken and the tyrosyl O-H bond is formed by proton transfer from a Mn-bound water to Y_Z. Such a proton transfer could proceed via a direct hydrogen bond between water bound to Mn and Y_Z, although the distance of 7 Å between the Mn_4 cluster and Y_Z seems too long for a direct hydrogen bond. Alternatively, proton transfer could proceed via a hydrogen-bonded chain that connects a substrate water molecule bound to Mn and Y_Z. The net result is oxidation of the Mn_4 cluster by one electron and deprotonation of a manganese-bound water molecule via a concerted PCET reaction. Such a concerted electron/proton transfer could provide a favorable contribution to the free energy of the reaction if the bond-dissociation energy of the tyrosyl O-H bond is higher than that of a substrate O-H bond, as is indicated by both experimental and computational results (Blomberg et al., 1997; Caudle and Pecoraro, 1997).

A variety of measurements, including H/D isotope effects and temperature studies, indicate that the $S_2 \rightarrow S_3$ and $S_3 \rightarrow S_4$ transitions proceed via a different mechanism than the $S_0 \rightarrow S_1$ and $S_1 \rightarrow S_2$ transitions (reviewed in Vrettos et al., 2001). Of particular significance is the observation that a variety of inhibitory treatments, including Ca^{2+} or Cl^- depletion and acetate or ammonia addition, cause a block beyond the $S_2Y_Z^{\bullet}$ state. We have argued that these seemingly disparate treatments could have a common effect of disrupting a hydrogen-bonding connection between $Y_Z^{\bullet}$ and water bound to Mn (Szalai and Brudvig, 1996). This would prevent a concerted PCET mechanism for oxidation of the Mn_4 cluster by $Y_Z^{\bullet}$. It is expected that progressive oxidations of a single tetrameric manganese cluster will occur at increasingly higher potentials, ultimately reaching a point where the thermodynamic driving force for oxidation of the Mn_4 cluster by $Y_Z^{\bullet}$ is unfavorable. We have argued that the S-state transitions beyond the S_2 state are unfavorable unless the additional driving force provided by a concerted PCET mechanism is contributed. This explains why inhibitory treatments all cause a block beyond the $S_2Y^{\bullet}_Z$ state. Additionally, these observations provide evidence that only the last two S-state transitions proceed by a concerted PCET mechanism.

The $S_1 \rightarrow S_2$ transition is exceptional in that this step can occur at much lower temperatures than the other S-state transitions. It has been found that this

is the only S-state transition for which no proton is released (Lavergne and Junge, 1993). The $S_1 \rightarrow S_2$ transition may occur via a simple outer-sphere electron transfer from the Mn_4 cluster to $Y_Z^{\bullet}$ together with the low-barrier movement of a proton to/from $Y_Z^{\bullet}/Y_Z$ from/to its hydrogen-bonding partner along a strong hydrogen bond. Owing to the lack of proton release in the $S_1 \rightarrow S_2$ transition, this step results in a net increase in positive charge in the OEC. Consistent with this conclusion is the observation of chlorophyll absorbance band shifts that have been attributed to an electrochromic effect of the charge accumulated in the S_2 and S_3 states (Kretschmann et al., 1996). We previously hypothesized that this charge increase is the molecular switch that causes a change from consecutive proton and electron transfer to a concerted PCET mechanism in the S-state cycle (Vrettos et al., 2001; McEvoy and Brudvig, 2004).

2. Mechanism of O-O Bond Formation

Two sequential concerted PCET steps in the $S_2 \rightarrow S_3$ and $S_3 \rightarrow S_4$ transitions will convert a Mn(III)-OH_2 moiety in the S_2 state into a Mn(V)=O species in the S_4 state (see Fig. 5); a Mn(V)=O species has been proposed to be the key reactive species in O-O bond formation (reviewed in Vrettos et al., 2001). Based on previous studies of metal terminal-oxo species in inorganic systems (Groves et al., 1997), it is expected that the oxo ligand of a Mn(V)=O species will be an electrophilic center. We have proposed that O-O bond formation occurs in the S_4 state via nucleophilic attack on an electron-deficient Mn(V)=O species by a calcium-bound water molecule (Limburg et al., 1999), as shown in Fig. 5. A related mechanism has been proposed by Pecoraro and coworkers (1998).

In our proposed mechanism, O-O bond formation begins by bringing the calcium-bound substrate water closer to the Mn(V)=O moiety in an S_N2-like reaction (S_4 state in Fig. 5). This movement could be initiated when the ligand that bridges Mn and Ca moves closer to Mn upon formation of the high-valent Mn(V)=O center (the single-atom bridging ligand was suggested to be chloride by Limburg et al. (1999), as shown in Fig. 5, and is modeled as a μ–oxo by Ferreira et al. (2004)). Such a movement of the bridging ligand toward the Mn(V) center would also increase the Lewis acidity of Ca(II) because the bond between the bridging ligand and Ca(II) would be a lengthened. This would have the effect of enhancing the nucleophilicity of the calcium-bound water concomitant with formation of an electrophilic Mn(V)-bound oxo. In this way, a requirement for a single-atom bridge between Mn and Ca is explained in terms of both a structural role to position the calcium-bound water properly for nucleophilic attack and as a bridge that couples the electrophilic and nucleophilic centers for reaction. In order for the O-O bond to form, there must be overlap between the oxygen lone pair of the water molecule with an empty (non- or anti-bonding) Mn=O orbital, in accordance with Woodward-Hoffman rules of symmetry. The orientation of the calcium-bound water should be optimized for nucleophilic attack by hydrogen bonding to the μ-oxo bridge and possibly to a Lewis base (B in Fig. 5). This base would also aid the deprotonation of water, as the pK_a of calcium-bound water (12.7 for the aqua ion) is likely too high for the calcium-bound water in PS II to be deprotonated at physiological pH.

Nucleophilic attack by the Ca-bound water on the Mn(V)=O moiety, concomitant with its deprotonation, would result in a transiently formed hydroperoxide species (denoted S_4' in Fig. 5), in which the OOH moiety is suggested to be hydrogen bonded to the bridging oxo. This structure is analogous to that of the reversibly bound O_2 in the O_2-carrying diiron protein hemerythrin. By analogy to the release of O_2 from hemerythrin, release of O_2 from the OEC is proposed to proceed by transfer of the proton to a bridging oxo concomitant with a two-electron reduction of the Mn cluster.

B. Cytochrome c Oxidase

1. Protonmotive Function of Cytochrome c Oxidase

Figure 4 summarizes the protonmotive function of CcO. It is especially noteworthy that the chemistry of reduction of O_2 is vectorially oriented such that electrons arrive at the binuclear center from the *P*-side of the membrane, whereas the protons required for water formation derive from the opposite *N*-side. This arrangement in space generates separation of four charges across the membrane per catalytic cycle. In addition, the enzyme functions as a proton pump in which four additional charges (protons) are translocated per cycle (Wikström, 1977). It has been shown that all four pumped protons, and two of the four substrate protons, are transferred via the D-pathway that starts at a conserved aspartate (Asp91) near the *N*-side of the membrane, and continues into subunit I

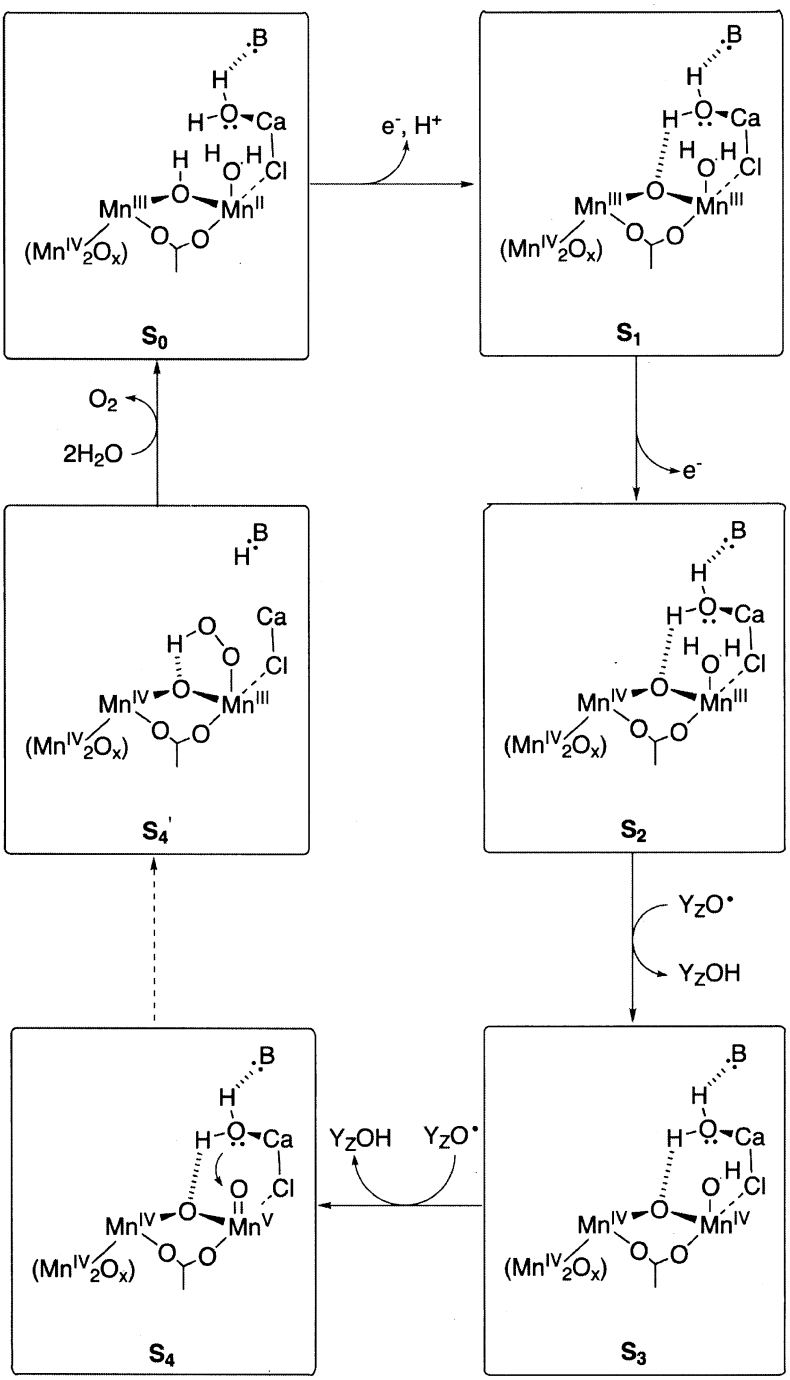

Fig. 5. Proposed catalytic cycle for the OEC. Adapted from Vrettos and Brudvig (2002).

along bound water molecules and hydrophilic amino acid side chains, to reach the conserved Glu242 about 10 Å from the binuclear center (Brzezinski and Adelroth, 1998) (Fig. 2). While the X-ray structures show no further protonic connections beyond Glu242, calculations have suggested the presence of water molecules, at least transiently, in the hydrophobic cavity on the *P*-side of this residue (Riistama et al., 1997; Hofacker and Schulten, 1998; Zheng et al., 2003) that may provide such a proton 'wire' connectivity (Nagle and Tristram-Nagle, 1983) via a Grotthuss-type proton transfer mechanism. A key problem, then, is to understand how protons destined to be pumped across the membrane, and protons destined for consumption at the binuclear center, could utilize the same proton transfer pathway. It would also be necessary to understand the means by which the redox reaction is coupled to proton pumping. A very recent proposal addresses these points (Wikström et al., 2003). Water molecules in the hydrophobic cavity were suggested to function as a redox-state-dependent protonic 'switch' due to orientating the water dipoles as a function of a redox-state-dependent electric field between heme *a* and the binuclear site. In this way, a water array would conduct protons to be pumped via the Δ-propionate group of heme a_3 (Iwata et al., 1995; Hofacker and Schulten, 1998; Puustinen and Wikström, 1999), but not to the binuclear site when the electron is at heme *a*. Transfer of this proton allows electron transfer from heme *a* to the binuclear site, which in turn switches the water array to conduct protons from Glu242 to this latter site. Finally, uptake of the substrate proton into the binuclear site causes ejection of the 'pre-pumped' proton towards the *P*-side of the membrane by electrostatic repulsion (Wikström et al., 2003).

2. Mechanism of O-O Bond Activation and Intermediates

Binding of O_2 to the ferrous heme iron of heme a_3 in the binuclear site (Fig. 6) takes place in approximately 10 μs at room temperature (for reviews, see Babcock and Wikström, 1992; Ferguson-Miller and Babcock, 1996). This generates an O_2 adduct (Compound A), analogous to oxymyoglobin, that was first described at low temperatures by optical spectroscopy by Chance et al. (1975), and subsequently by time-resolved resonance Raman (Babcock and Wikström, 1992; Ferguson-Miller and Babcock, 1996) and optical (Verkhovsky et al., 1996a) spectroscopy at room temperature. The reaction with O_2 has usually been studied in two different conditions. In the 'mixed valence' enzyme, the binuclear site is reduced (Fe_{a3}(II); Cu_B(I)), but the two other metal centers are oxidized. In this case, the reaction is relatively simple as Compound A is converted in approximately 200 μs to a relatively stable final state, originally called Compound C (Chance et al., 1975). This state of the binuclear center was originally thought to have a ferric-peroxide structure and was called P_M (derived from 'mixed-valence' enzyme). However, there is now strong evidence for the notion that the O-O bond is already broken in the P_M state, and that heme a_3 has a ferryl structure (Fe_{a3}(IV)=O) in that state (Proshlyakov et al., 1996; Fabian and Palmer, 1999; Fabian et al., 1999). The two other reducing equivalents have been proposed to stem from Cu_B (leaving Cu_B(II) in the P_M state), and from a conserved tyrosine residue in the site that is covalently bonded to one of the Cu_B histidine imidazole ligands (Yoshikawa et al., 1998; Buse et al., 1999; Proshlyakov et al., 2000), thus forming a neutral tyrosine radical. However, the evidence for a tyrosine radical in P_M is still not very strong. The radical has not been observed by EPR spectroscopy, presumably due to spin coupling to Cu_B. The tyrosine is possibly also the donor of the proton that is required in O-O bond scission, and which ends up as a hydroxide ligand of Cu_B (Fann et al., 1995) in the P_M state.

The mechanism of O-O bond splitting has been modeled using hybrid density functional theory calculations (Blomberg et al., 2000), and this has indicated an unstable ferric peroxide intermediate state in the reaction, the formation of which is rate-limiting. One key feature of O-O bond splitting in cell respiration is the scission of this bond and a formally full four-electron reduction of the bound dioxygen essentially in a single reaction step, without requirement of electron or proton donation from a source outside the binuclear site. Thus, in this single reaction step the high oxidizing power of O_2 is transferred to the active site of the enzyme, thereby producing the strongly oxidizing P_M intermediate. It is especially noteworthy that this reaction is not associated with uptake of protons from either side of the membrane; this proton uptake — eventually to form the product water — is delayed to later steps in the mechanism, and is intimately linked to the proton-translocating function of the enzyme.

In the second often studied case, fully reduced CcO is allowed to react with dioxygen in which case the

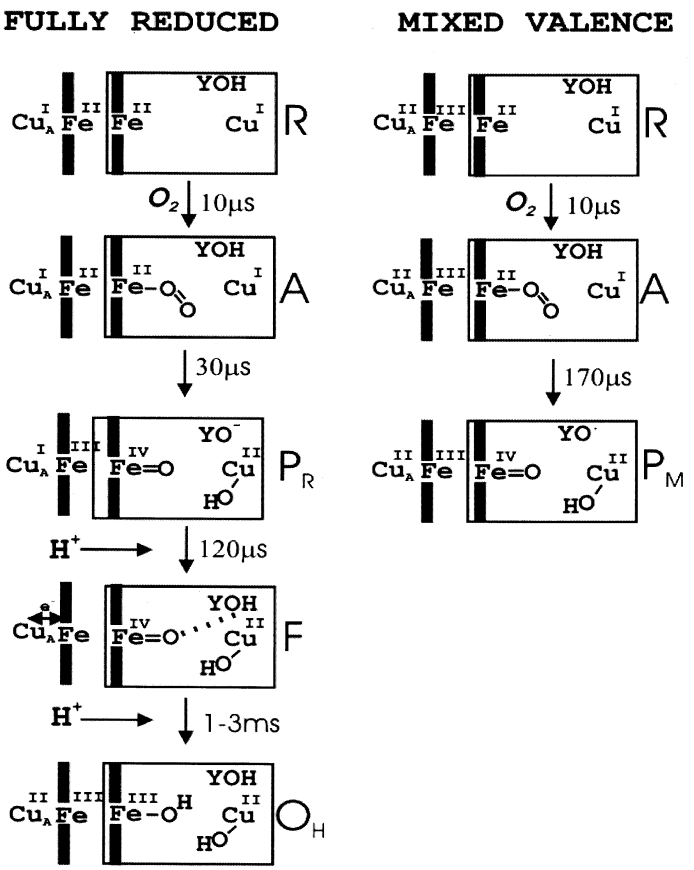

Fig. 6. Tentative structures of the metal centers during the reaction of fully reduced and 'mixed valence' CcO with O_2. Y depicts the conserved tyrosine in the binuclear site.

enzyme undergoes the complete 'oxidative phase' of the catalytic cycle (Fig. 6). Here, too, Compound A is formed first with the same kinetics as for the 'mixed-valence' enzyme, but the subsequent reactions are different and more complicated. First, the oxygen adduct (Compound A) is converted into a species called P_R (to distinguish it from P_M), which has an optical spectrum that is similar to P_M. However, this reaction takes only about 30 μs at room temperature and it is accompanied by oxidation of heme *a* (Verkhovsky et al., 1994; Sucheta et al., 1998; Karpefors et al., 2000). Thus, P_R has one more electron than P_M within the binuclear site, presumably reducing the putative tyrosine radical. In contrast to P_M, which is EPR-silent, the P_R state exhibits a very unusual EPR spectrum stemming from Cu_B(II) that shows magnetic interaction with the ferryl iron (Morgan et al., 2001).

Subsequently in approximately 0.1 ms, P_R decomposes into the ferryl F state that has a very different optical absorption spectrum. This reaction is accompanied by uptake of a proton from the medium; in vesicular systems, it is accompanied by proton uptake from the negatively charged *N*-side of the membrane, and with translocation of a proton across the membrane (Verkhovsky et al., 1999). Finally, the F state of the binuclear site turns into the ferric/cupric O_H state in a millisecond event. As in the P_R to F transition, this is also accompanied by uptake of a proton from the *N*-side as well as with translocation of another proton from the *N*- to the *P*-side of the membrane.

To complete the catalytic cycle, the O_H state of the binuclear center is reduced by two electrons back to the ferrous/cuprous R state before a new O_2 molecule is bound to initiate the next cycle. Reduction of state O_H to state R is associated with net uptake of two protons, and this reaction is also linked to translocation of the last two protons across the membrane (Bloch et al., 2004).

3. Proton Translocation and a Departure from the Main Catalytic Cycle

A few years ago it was shown, quite unexpectedly, that the reductive part of the catalytic cycle (intermediates O_H through R) was coupled to translocation of two protons across the membrane, but only if the reduced enzyme had previously been oxidized by O_2 (Verkhovsky et al., 1999). This prompted the postulate that the ferric/cupric state O_H would tend to decay into another oxidized form of the binuclear center (O), the reduction of which is no longer linked to proton translocation. However, at present, the structural difference between states O_H and O is not known, although it seems likely that the redox potential of Cu_B is much higher in the O_H state than in O. In fact, the redox potentials of both Cu_B and Fe_{a3} have been known for years for the one-electron transitions O/E and E/R (Fig. 7), being ≤ 0.4 V, as determined from anaerobic redox potential titrations (Wilson and Dutton, 1970; Wikström et al., 1981). At such low acceptor potentials, it would not be possible for an electron transfer from the donor (Cyt *c* at approximately 0.3 V) to the binuclear site to be coupled both to the electron and proton uptake from the opposite sides of the membrane (translocation of a single charge equivalent), and to additional translocation of a proton, against a typical protonmotive force of 0.2 V. It seems, therefore, that the reaction of O_2 with the binuclear center not only confers high redox potentials to the ferryl iron and putative tyrosine radical sites of the P_M intermediate, but that the redox potential of Cu_B is also elevated in this reaction, although there is no direct evidence for this at present.

A current view of proton translocation by CcO during the catalytic cycle is shown in Fig. 7 (but, see Michel, 1999). According to this, translocation of one proton is linked to each transfer of an electron to the binuclear center, as long as the enzyme cycles through the main catalytic cycle. If deprived of reductant, the binuclear site in state O_H will decay into the O state, which may be re-reduced into R, but this is not coupled to proton-pumping. The departure from the main cycle in the absence of electron donors could be an artifact of the isolated enzyme, but it is also possible that it is a regulatory feature of physiological importance where the efficiency of the proton pump may be modulated.

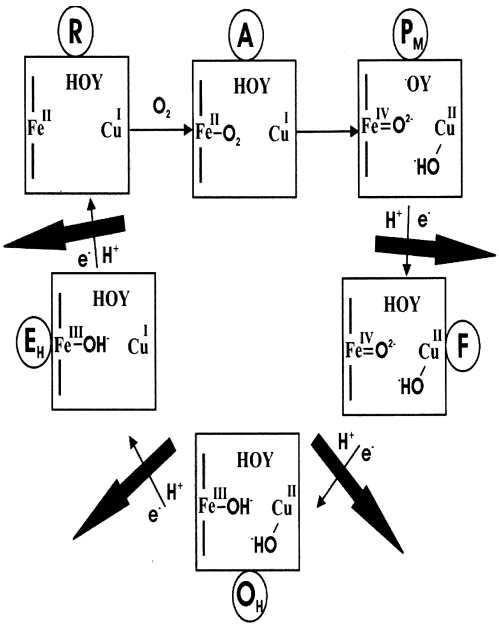

Fig. 7. Catalytic cycle of CcO. Labeled states of the binuclear center are equivalent to those in Fig. 6. Intermediate O (not shown, see text) is in the same redox state as intermediate O_H. Note that the main cycle shown here can be interrupted at intermediate O_H which may decay into the O state in the absence of electron donors. Recovery is obtained only by reducing the O state back to R, which is not associated with proton translocation (see text).

V. Analogies between the Oxygen Chemistry of Photosystem II and Cytochrome *c* Oxidase

As discussed above, the detailed mechanisms of O_2 evolution by PS II and O_2 reduction by CcO remain uncertain. However, in both systems, the four-electron oxygen/water reaction occurs in essentially a single reaction step, without requirement of electron or proton transfer from a source outside the active site. A further similarity in the chemistry is that a high-valent metal ion-terminal oxo species appears

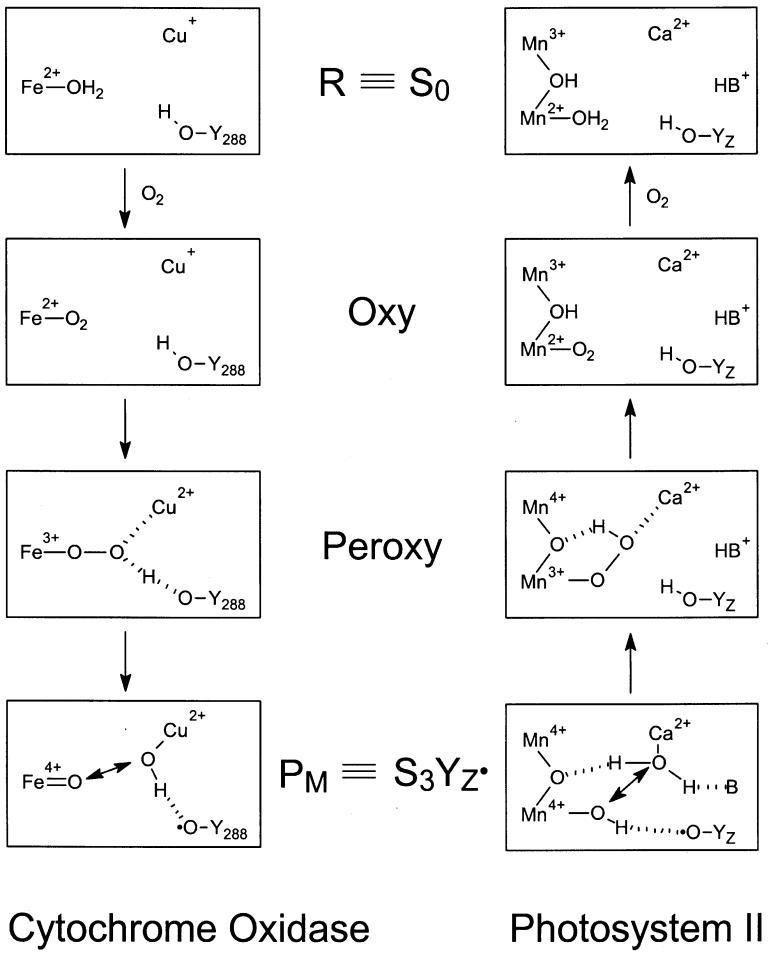

Fig. 8. Analogy between the oxygen chemistry of PS II and CcO.

to be formed immediately prior/subsequent to O-O bond formation/cleavage. In addition, evidence is emerging for a redox role of tyrosine in the P_M state of CcO (Proshlyakov et al., 2000), which parallels the involvement of Y_Z in the water-oxidation chemistry of the OEC. Taken together, these results point to a much closer analogy between the oxygen chemistry of PS II and CcO than was evident at the Nobel Conference on 'The Biophysical Chemistry of Dioxygen Reactions in Respiration and Photosynthesis' that was held in 1987 (Vänngård, 1988).

In Fig. 8, possible mechanisms for the O-O bond-formation/cleavage reactions of PS II and CcO are compared. Only the steps involving O-O bond formation/cleavage are shown and several hypothetical states are included to facilitate the comparison. For example, the Oxy state has not been observed for PS II and the Peroxy states are not known for either system. Sequential one-electron reductions of the $P_M/S_3Y_Z^{\bullet}$ states would generate a series of lower redox states that are not shown but are analogous in the two systems: $F \equiv S_3$, $O_H/O \equiv S_2$, and $E_H/E \equiv S_1$ (see Figs. 5, 6 and 7). While these mechanisms are speculative, it is interesting to compare the intermediates that are formed in the two enzymes. Knowledge of the intermediates in one system may provide insights into the chemistry of the other.

The question immediately is raised as to why each

enzyme catalyzes a specific direction of reaction. Of course, for CcO, the formation of O_2 from water is an uphill reaction and would require an input of energy, such as a membrane potential, to proceed. In the presence of a large membrane potential, the CcO reaction has been shown to be reversed from the O_H/O state to P_M (Wikström, 1981; Wikström and Morgan, 1992), but it has not been found to evolve O_2. Based on a comparison to the OEC, it may be that the reduction potential of the cross-linked tyrosyl radical in CcO is not sufficiently high to initiate formation of the O-O bond. In addition, the oxo moiety in the Fe(IV)=O species may not be sufficiently electrophilic for the reaction. However, the major thermodynamic reason for the failure of CcO to evolve O_2 is that the crucial O-O bond-breaking step is not coupled to translocation of charge across the membrane (Fig. 7), and is, therefore, not driven in the reverse direction by a membrane potential. In the case of the OEC, there is no energetic barrier for the reverse reaction. In fact, it has been reported that the OEC can catalyze O_2 uptake, but only in the 'active' state that is formed during light-driven turnover of the system. Upon dark adaptation, the OEC converts into a 'resting' state that is inactive (Beck et al., 1985). This may reflect a change in the coordination chemistry of the manganese cluster in the OEC, and is in some ways reminiscent of the reversion of CcO to a 'resting' oxidized state in the absence of electron donors (see above). Another factor for the low rate of O_2 reduction by the OEC may be that the affinity of the OEC for O_2 is very low in the S_0 state, as is expected for a Mn(II) ion. On the other hand, the binding affinity of the binuclear heme/copper site for O_2 in CcO ($K_D \sim$ 0.3 mM) is also low and the high operational oxygen affinity ($K_M < 1\ \mu M$) stems from kinetic trapping of the oxygen-bound state by fast electron transfer (Chance et al., 1975; Verkhovsky et al., 1996a).

Acknowledgments

MW acknowledges Dr. Liisa Laakkonen for help with the figures and the Academy of Finland for financial support (programme 44895). GWB acknowledges Dr. K. V. Lakshmi for help with the figures. Work at Yale University was supported by the National Institutes of Health (GM32715).

References

Abramson J, Riistama S, Larsson G, Jasaitis A, Svensson Ek M, Laakkonen L, Puustinen A and Wikström M (2000) The structure of the ubiquinol oxidase from *Escherichia coli* and its ubiquinone binding site. Nature Struct Biol 7: 910–917

Andréasson L-E, Vass I and Styring S (1995) Ca^{2+} depletion modifies the electron transfer on both donor and acceptor sides in Photosystem II from spinach. Biochim Biophys Acta 1230: 155–164

Babcock GT and Wikström M (1992) Oxygen activation and the conservation of energy in cell respiration. Nature 356: 301–309

Barber J and Anderson JM (eds) (2002) Photosystem II: Molecular structure and function. Phil Trans R Soc Lond B 357: 1325–1512

Beck WF, de Paula JC and Brudvig GW (1985) Active and resting states of the O_2-evolving complex of Photosystem II. Biochemistry 24: 3035–3043

Berthomieu C, Hienerwadel R, Boussac A, Breton J and Diner BA (1998) Hydrogen bonding of redox-active tyrosine Z of Photosystem II probed by FTIR difference spectroscopy. Biochemistry 37: 10547–10554

Bloch D, Belevich I, Jasaitis A, Ribacka C, Puustinen A, Verkhovsky MI and Wikström M (2004) The catalytic cycle of cytochrome *c* oxidase is not the sum of its two halves. Proc Natl Acad Sci USA 101: 529–533

Blomberg MRA, Siegbahn PEM, Styring S, Babcock GT, Åkermark B and Korall P (1997) A quantum chemical study of hydrogen abstraction from manganese-coordinated water by a tyrosyl radical: A model for water oxidation in Photosystem II. J Am Chem Soc 119: 8285–8292

Blomberg MRA, Siegbahn PEM, Babcock GT and Wikström M (2000) Modeling cytochrome oxidase: A quantum chemical study of the O-O bond cleavage mechanism. J Am Chem Soc 122: 12848–12858

Bögershausen O and Junge W (1995) Rapid proton-transfer under flashing light at both functional sides of dark-adapted Photosystem II particles. Biochim Biophys Acta 1230: 177–185

Bratton MR, Pressler MA and Hosler JP (1999) Suicide inactivation of cytochrome *c* oxidase: Catalytic turnover in the absence of subunit III alters the active site. Biochemistry 38: 16236–16245

Britt RD (1996) Oxygen evolution. In: Ort DR and Yocum CF (eds) Oxygenic Photosynthesis: The Light Reactions, pp 137–159. Kluwer Academic Publishers, Dordrecht

Britt RD, Peloquin JM and Campbell KA (2000) Pulsed and parallel-polarization EPR characterization of the Photosystem II oxygen-evolving complex. Annu Rev Biophys Biomol Structure 29: 463–495

Brzezinski P and Adelroth P (1998) Pathways of proton transfer in cytochrome *c* oxidase. J Bioenerg Biomemb 30: 99–107

Buse G, Soulimane T, Dewor M, Meyer HE and Bluggel M (1999) Evidence for a copper-coordinated histidine-tyrosine cross-link in the active site of cytochrome oxidase. Protein Sci 8: 985–990

Caudle MT and Pecoraro VL (1997) Thermodynamic viability of hydrogen atom transfer from water coordinated to the oxygen-evolving complex of Photosystem II. J Am Chem Soc 119: 3415–3416

Chance B, Saronio C and Leigh JS (1975) Functional intermediates in the reaction of membrane-bound cytochrome oxidase with oxygen. J Biol Chem 250: 9226–9237

Chu H-A, Nguyen A-P and Debus RJ (1995a) Amino acid residues that influence the binding of manganese or calcium to Photosystem II. 1. The lumenal interhelical domains of the D1 polypeptide. Biochemistry 34: 5839–5858

Chu H-A, Nguyen A-P and Debus RJ (1995b) Amino acid residues that influence the binding of manganese or calcium to Photosystem II. 2. The carboxy-terminal domain of the D1 polypeptide. Biochemistry 34: 5859–5882

Debus RJ (1992) The manganese and calcium ions of photosynthetic oxygen evolution. Biochim Biophys Acta 1102: 269–352

Debus RJ (2000) The polypeptides of Photosystem II and their influence on mangano-tyrosyl based oxygen evolution. In: Sigel A and Sigel H (eds) Manganese and Its Role in Biological Processes, pp 657–711. Marcel Dekker, New York

Debus RJ, Campbell KA, Peloquin JM, Pham DP and Britt RD (2000) Histidine 332 of the D1 polypeptide modulates the magnetic and redox properties of the manganese cluster and tyrosine Y_Z in Photosystem II. Biochemistry 39: 470–478

Diner BA and Babcock GT (1996) Structure, dynamics, and energy conversion efficiency in Photosystem II. In: Ort DR and Yocum CF (eds) Oxygenic Photosynthesis: The Light Reactions, pp 213–247. Kluwer Academic Publishers, Dordrecht

Diner BA, Nixon PJ and Farchaus JW (1991) Site-directed mutagenesis of photosynthetic reaction centers. Curr Opin Struct Biol 1: 546–554

Diner BA, Schlodder E, Nixon PJ, Coleman WJ, Rappaport F, Lavergne J, Vermaas WFJ and Chisholm DA (2001) Site-directed mutations at D1-His198 and D2-His197 of Photosystem II in *Synechocystis* PCC 6803: Sites of primary charge separation and cation and triplet stabilization. Biochemistry 40: 9265–9281

Fabian M and Palmer G (1999) Redox state of peroxy and ferryl intermediates in cytochrome *c* oxidase catalysis. Biochemistry 38: 6270–6275

Fabian M, Wong WW, Gennis RB and Palmer G (1999) Mass spectrometric determination of dioxygen bond splitting in the 'peroxy' intermediate of cytochrome *c* oxidase. Proc Natl Acad Sci USA 96: 13114–13117

Fann YC, Ahmed I, Blackburn NJ, Boswell JS, Verkhovskaya ML, Hoffman BM and Wikström M (1995) Structure of Cu_B in the binuclear heme-copper center of the cytochrome aa_3-type quinol oxidase from *Bacillus subtilis*: An ENDOR and EXAFS study. Biochemistry 34: 10245–10255

Ferguson-Miller S and Babcock GT (1996) Heme/copper terminal oxidases. Chem Rev 96: 2889–2907

Ferreira KN, Iverson TM, Maghlaoui K, Barber J and Iwata S (2004) Architecture of the photosynthetic oxygen-evolving center. Science 303: 1831–1838

Gilchrist ML, Jr, Ball JA, Randall DW and Britt RD (1995) Proximity of the manganese cluster of Photosystem II to the redox-active tyrosine Y_Z. Proc Natl Acad Sci USA 92: 9545–9549

Gomes CM, Backgren C, Teixeira M, Puustinen A, Verkhovskaya ML, Wikström M and Verkhovsky MI (2001) Heme-copper oxidases with modified D- and K-pathways are yet efficient proton pumps. FEBS Lett 497: 159–164

Groves JT, Lee J and Marla SS (1997) Detection and characterization of an oxomanganese(V) porphyrin complex by rapid-mixing stopped-flow spectrophotometry. J Am Chem Soc 119: 6269–6273

Haltia T, Finel M, Harms N, Nakari T, Raitio M, Wikström M and Saraste M (1989) Deletion of the gene for subunit III leads to defective assembly of bacterial cytochrome oxidase. EMBO J 8: 3571–3579

Hays A-MA, Vassiliev IR, Golbeck JH and Debus RJ (1998) Role of D1-His190 in proton-coupled electron transfer reactions in Photosystem II: A chemical complementation study. Biochemistry 37: 11352–11365

Hays A-MA, Vassiliev IR, Golbeck JH and Debus RJ (1999) Role of D1-His190 in the proton-coupled oxidation of tyrosine Y_Z in manganese-depleted Photosystem II. Biochemistry 38: 11851–11864

Hofacker I and Schulten K (1998) Oxygen and proton pathways in cytochrome *c* oxidase. Prot Struc Func Gene 30: 100–107

Hoganson CW and Babcock GT (1997) A metalloradical mechanism for the generation of oxygen from water in photosynthesis. Science 277: 1953–1956

Humphrey W, Dalke K and Schulten K (1996) VMD — visual molecular dynamics. J Mol Graph 14: 33–38

Iwata S, Ostermeier C, Ludwig B and Michel H (1995) Structure at 2.8 Å resolution of cytochrome *c* oxidase from *Paracoccus denitrificans*. Nature 376: 660–669

Joliot P and Kok B (1975) Oxygen evolution in photosynthesis. In: Govindjee (ed) Bioenergetics of Photosynthesis, pp 387–412. Academic Press, New York

Kamiya N and Shen J-R (2003) Crystal structure of oxygen-evolving Photosystem II from *Thermosynechococcus vulcanus* at 3.7 Å resolution. Proc Natl Acad Sci USA 100: 98–103

Karpefors M, Ädelroth P, Namslauer A, Zhen Y and Brzezinski P (2000) Formation of the 'peroxy' intermediate in cytochrome *c* oxidase is associated with internal proton/hydrogen transfer. Biochemistry 39: 14664–14669

Kraulis PJ (1991) MOLSCRIPT a program to produce both detailed and schematic plots of protein structures. J Applied Crystallogr 24: 946–950

Kretschmann H, Schlodder E and Witt HT (1996) Net charge oscillation and proton release during water oxidation in photosynthesis. An electrochromic band shift study at pH 5.5–7.0. Biochim Biophys Acta 1274: 1–8

Lavergne J and Junge W (1993) Proton release during the redox cycle of the water oxidase. Photosynth Res 38: 279–296

Limburg J, Szalai VA and Brudvig GW (1999) A mechanistic and structural model for the formation and reactivity of a Mn^V=O species in photosynthetic water oxidation. J Chem Soc, Dalton Trans: 1353–1363

Ludwig B, Bender E, Arnold S, Huttemann M, Lee I and Kadenbach B (2001) Cytochrome *c* oxidase and the regulation of oxidative phosphorylation. Chembiochem 2: 392–403

Mamedov F, Sayre RT and Styring S (1998) Involvement of histidine 190 on the D1 protein in electron/proton transfer reactions on the donor side of Photosystem II. Biochemistry 37: 14245–14256

McEvoy JP and Brudvig GW (2004) Structure-based mechanism of photosynthetic water oxidation. Phys Chem Chem Phys 6: 4754–4763

McEvoy JP, Gascon JA, Sproviero EM, Batista VS and Brudvig GW (2005) Computational structural model of the oxygen evolving complex in Photosystem II: Complete ligation by protein, water and chloride. In: Bruce D and van der Est A (eds)

Photosynthesis: Fundamental Aspects to Global Perspectives, Vol 1, pp 278–280. Allen Press, Lawrence

Messinger J and Lubitz W (eds) (2004). Biophysical studies of Photosystem II and related model systems. Phys Chem Chem Phys 6: 4733–4912

Michel H (1999) Cytochrome *c* oxidase: Catalytic cycle and mechanisms of proton pumping — A discussion. Biochemistry 38: 15129–15140

Mitchell P (1966) Chemiosmotic coupling in oxidative and photosynthetic phosphorylation. Biol Rev 41: 445–502

Morgan JE, Verkhovsky MI, Palmer G and Wikström M (2001) The role of the P_R intermediate in the reaction of cytochrome *c* oxidase with O_2. Biochemistry 40: 6882–6892

Nagle JF and Tristram-Nagle S (1983) Hydrogen bonded chain mechanisms for proton conduction and proton pumping. J Memb Biol 74: 1–14

Nixon PJ and Diner BA (1992) Aspartate 170 of the Photosystem II reaction center polypeptide D1 is involved in the assembly of the oxygen-evolving manganese cluster. Biochemistry 31: 942–948

Nugent J (ed) (2001) Photosynthetic water oxidation. Biochim Biophys Acta 1503: 1–259

Pecoraro VL, Baldwin MJ, Caudle MT, Hsieh W and Law NA (1998) A proposal for water oxidation in Photosystem II. Pure Appl Chem 70: 925–929

Proshlyakov DA, Ogura T, Shinzawa-Itoh K, Yoshikawa S and Kitagawa T (1996) Resonance Raman/absorption characterization of the oxo intermediates of cytochrome *c* oxidase generated in its reaction with hydrogen peroxide: pH and H_2O_2 concentration dependence. Biochemistry 35: 8580–8586

Proshlyakov DA, Pressler MA, DeMaso C, Leykam JF, DeWitt DL and Babcock GT (2000) Oxygen activation and reduction in respiration: Involvement of redox-active tyrosine 244. Science 290: 1588–1591

Puustinen A and Wikström M (1999) Proton exit from the heme-copper oxidase of *Escherichia coli*. Proc Natl Acad Sci USA 96: 35–37

Rappaport F, Guergova-Kuras M, Nixon PJ, Diner BA and Lavergne J (2002) Kinetics and pathways of charge recombination in Photosystem II. Biochemistry 41: 8518–8527

Renger G and Völker M (1982) Studies on the proton release pattern of the donor side of system 2. Correlation between oxidation and deprotonization of donor D1 in tris-washed inside-out thylakoids. FEBS Lett 149: 203–207

Riistama S, Hummer G, Puustinen A, Dyer RB, Woodruff WH and Wikström M (1997) Bound water in the proton translocation mechanism of the haem-copper oxidases. FEBS Lett 414: 275–280

Riistama S, Puustinen A, Garcia-Horsman A, Iwata S, Michel H and Wikström M (1996) Channelling of dioxygen into the respiratory enzyme. Biochim Biophys Acta 1275: 1–4

Schultz BE and Chan SI (2001) Structures and proton-pumping strategies of mitochondrial respiratory enzymes. Annu Rev Biophys Biomol Struct 30: 23–65

Soulimane T, Buse G, Bourenkov GP, Bartunik HD, Huber R and Than ME (2000) Structure and mechanism of the aberrant ba(3)-cytochrome *c* oxidase from *Thermus thermophilus*. EMBO J 19: 1766–1776

Sucheta A, Szundi I and Einarsdóttir Ó (1998) Intermediates in the reaction of fully reduced cytochrome *c* oxidase with dioxygen. Biochemistry 37: 17905–17914

Svensson-Ek M, Abramson J, Larsson G, Tornroth S, Brzezinski P and Iwata S (2002) The X-ray crystal structures of wild-type and EQ(I–286) mutant cytochrome *c* oxidases from *Rhodobacter sphaeroides*. J Mol Biol 321: 329–339

Szalai VA and Brudvig GW (1996) Reversible binding of nitric oxide to the tyrosyl radicals of Photosystem II. Biochemistry 35: 15080–15087

Thorp HH (1992) Bond valence sum analysis of metal-ligand bond lengths in metalloenzymes and model complexes. Inorg Chem 31: 1585–1588

Thorp HH and Brudvig GW (1991) The physical inorganic chemistry of manganese relevant to photosynthetic oxygen evolution. New J Chem 15: 479–490

Tommos C and Babcock GT (1998) Oxygen production in Nature: A light-driven metalloradical enzyme process. Acc Chem Res 31: 18–25

Tommos C, Tang X-S, Warncke K, Hoganson CW, Styring S, McCracken J, Diner BA and Babcock GT (1995) Spin-density distribution, conformation, and hydrogen bonding of the redox-active tyrosine Y_Z in Photosystem II from multiple electron paramagnetic-resonance spectroscopies: Implications for photosynthetic oxygen evolution. J Am Chem Soc 117: 10325–10335

Tsukihara T, Aoyama H, Yamashita E, Tomizaki T, Yamaguchi H, Shinzawa-Itoh K, Nakashima R, Yaono R and Yoshikawa S (1995) Structures of metal sites of oxidized bovine heart cytochrome *c* oxidase at 2.8 Å. Science 269: 1069–1074

Tsukihara T, Aoyama H, Yamashita E, Tomizaki T, Yamaguchi H, Shinzawa-Itoh K, Nakashima R, Yaono R and Yoshikawa S (1996) The whole structure of the 13-subunit oxidized cytochrome *c* oxidase at 2.8 Å. Science 272: 1136–1144

Vänngård T (ed) (1988) Biophysical chemistry of dioxygen reactions in respiration and photosynthesis. Chem Scripta 28A: 1–131

Verkhovsky MI, Morgan JE and Wikström M (1994) Oxygen binding and activation: Early steps in the reaction of oxygen with cytochrome *c* oxidase. Biochemistry 33: 3079–3086

Verkhovsky MI, Morgan JE, Puustinen A and Wikström M (1996a) The 'ferrous-oxy' intermediate in the reaction of dioxygen with fully reduced cytochromes aa_3 and bo_3. Biochemistry 35: 16241–16246

Verkhovsky MI, Morgan JE, Puustinen A and Wikström M (1996b) Kinetic trapping of O_2 in cell respiration. Nature 380: 268–270

Verkhovskaya ML, Garcìa-Horsman A, Puustinen A, Rigaud J-L, Morgan JE, Verkhovsky MI and Wikström M (1997) Glutamic acid 286 in subunit I of cytochrome bo_3 is involved in proton translocation. Proc Natl Acad Sci USA 94: 10128–10131

Verkhovsky MI, Jasaitis A, Verkhovskaya ML, Morgan JE and Wikström M (1999) Proton translocation by cytochrome *c* oxidase. Nature 400: 480–483

Vrettos JS and Brudvig GW (2002) Water oxidation chemistry of Photosystem II. Phil Trans R Soc Lond B 357: 1395–1405

Vrettos JS and Brudvig GW (2004) Oxygen evolution. In: Que L Jr and Tolman WB (eds) Comprehensive Coordination Chemistry II: From Biology to Nanotechnology, Vol 8, pp 507–547. Elsevier, Amsterdam

Vrettos JS, Limburg J and Brudvig GW (2001) Mechanism of photosynthetic water oxidation: combining biophysical studies of Photosystem II with inorganic model chemistry. Biochim Biophys Acta 1503: 229–245

Wikström M (1977) Proton pump coupled to cytochrome *c* oxidase in mitochondria. Nature 266: 271–273

Wikström M (1981) Energy dependent reversal of the cytochrome oxidase reaction. Proc Natl Acad Sci USA 78: 4051–4054

Wikström M and Morgan JE (1992) The dioxygen cycle — spectral, kinetic, and thermodynamic characteristics of ferryl and peroxy intermediates observed by reversal of the cytochrome oxidase reaction. J Biol Chem 267: 10266–10273

Wikström M (2000) Mechanism of proton translocation by cytochrome oxidase: A new four-stroke histidine cycle. Biochim Biophys Acta 1458: 188–198

Wikström M, Krab K and Saraste M (1981) Cytochrome Oxidase *a* Synthesis. Academic Press, London

Wikström M, Verkhovsky MI and Hummer G (2003) Water-gated mechanism of proton translocation by cytochrome *c* oxidase. Biochim Biophys Acta 1604: 61–65

Wilson DF and Dutton PL (1970) The oxidation-reduction potentials of cytochromes *a* and a_3 in intact rat liver mitochondria. Arch Biochem Biophys 136: 583–584

Wincencjusz H, van Gorkom HJ and Yocum CF (1997) The photosynthetic oxygen-evolving complex requires chloride for its redox state $S_2 \rightarrow S_3$ and $S_3 \rightarrow S_0$ transitions but not for $S_0 \rightarrow S_1$ or $S_1 \rightarrow S_2$ transitions. Biochemistry 36: 3663–3670

Witt H and Ludwig B (1997) Isolation, analysis, and deletion of the gene coding for subunit IV of cytochrome *c* oxidase in *Paracoccus denitrificans*. J Biol Chem 272: 5514–5517

Yachandra VK (2002) Structure of the manganese complex in Photosystem II: insights from X-ray spectroscopy. Philos Trans R Soc Lond B 357: 1347–1357

Yachandra VK, Sauer K and Klein MP (1996) Manganese cluster in photosynthesis: Where plants oxidize water to dioxygen. Chem Rev 96: 2927–2950

Yocum CF (1991) Calcium activation of photosynthetic water oxidation. Biochim Biophys Acta 1059: 1–15

Yoshikawa S, Shinzawa-Itoh K, Nakashima R, Yaono R, Yamashita E, Inoue N, Yao M, Fei MJ, Libeu CP, Mizushima T, Yamaguchi H, Tomizaki T and Tsukihara T (1998) Redox-coupled crystal structural changes in bovine heart cytochrome *c* oxidase. Science 280: 1723–1729

Yoshikawa S, Shinzawa-Itoh K and Tsukihara T (2000) X-ray structure and the reaction mechanism of bovine cytochrome *c* oxidase. J Inorg Biochem 82: 1–7

Zaslavsky D and Gennis RB (2000) Proton pumping by cytochrome oxidase: Progress, problems and postulates. Biochim Biophys Acta 1458: 164–179

Zheng X, Medvedev DM, Swanson J and Stuchebrukhov AA (2003) Computer simulation of water in cytochrome *c* oxidase. Biochim Biophys Acta 1557: 99–107

Zouni A, Witt HT, Kern J, Fromme P, Krauß N, Saenger W and Orth P (2001) Crystal structure of Photosystem II from *Synechococcus elongatus* at 3.8 Å resolution. Nature 409: 739–743

Chapter 32

Mimicking the Properties of Photosystem II in Bacterial Reaction Centers

László Kálmán[1], JoAnn C. Williams and James P. Allen*
Department of Chemistry and Biochemistry and Center for the Study of Early Events in Photosynthesis, Arizona State University, Tempe, AZ 85287-1604, U.S.A.

Summary

The core structural motif of the photosynthetic pigment-protein complexes that generate a charge-separated state by the absorption of light is remarkably conserved between reaction centers from purple bacteria and Photosystem II (PS II). These systems differ in the functional ability of PS II to make use of much higher energies to oxidize water through electron transfer events involving a tyrosine residue and manganese complex. In this chapter we present models of the evolutionary developments of photosynthesis from the standpoint of the alterations of the pigment-protein complexes needed to perform increasingly complex photochemical reactions. We also describe experimental efforts that are designed to mimic these evolutionary developments by altering the bacterial reaction center such that it gains specific functional features of the oxygen-evolving complex.

*Author for correspondence, email: jallen@asu.edu
[1]Permanent address: Department of Physics, Concordia University, 7141 Sherbrooke West, SP-365.10, Montréal, QC, H4V 2B1, Canada

T. Wydrzynski and K. Satoh (eds): Photosystem II: The Light-Driven Water:Plastoquinone Oxidoreductase, pp. 715–727.

I. Evolutionary Developments

Conditions on the early earth would have been significantly different than those found today. The anaerobic environment supported only primitive life forms, including the first photosynthetic organisms (Schopf, 1983; Woese, 1987; Olson and Pierson, 1987; Blankenship and Hartman, 1998). The nature of the earliest phototrophs is unknown, but these organisms presumably contained a simple photosystem that was capable of absorbing light and creating a charge-separated state that could be used for the production of energy-rich chemicals such as ATP and NADPH. One of the most critical events in the development of the earth was the emergence of organisms capable of water oxidation and thus having an essentially unlimited source of electrons. Although the details surrounding this event remain controversial (Des Marais, 2001), it is generally thought to have occurred approximately 3 billion years ago and to have led to significant changes in the composition of the earth. The tremendous increase in molecular oxygen in the atmosphere provided an opportunity for the evolutionary development of organisms that could perform energy conversion using aerobic respiration. Emerging from this picture of the development of the earth is the idea that primitive anaerobic phototrophs evolved into cyanobacteria, algae and plants.

A new understanding of the evolutionary relationships among photosynthetic organisms resulted from the sequencing of the bacterial reaction center (BRC) and Photosystem II (PS II) genes and the structure determination of the BRC in the 1980s. The genes encoding the L and M subunits of the BRC were found to be homologous to those encoding the D1 and D2 subunits of PS II (Williams et al., 1983, 1986; Youvan et al., 1984; Michel et al., 1986; Belanger et al., 1988). The structure of the BRC from *Blastochloris viridis* (formerly *Rhodopseudomonas viridis*) and *Rhodobacter sphaeroides* showed that the L and M subunits each possess five transmembrane helices that are related to each other by an approximate two-fold symmetry axis (Deisenhofer et al., 1985; Allen et al., 1987). These two subunits envelop the cofactors, which are also related by the same two-fold symmetry. Although the overall similarity of the L and M sequences to those of D1 and D2 is fairly low, many of the key residues observed in the structure of the BRC were found to be conserved in PS II (Rochaix et al., 1984; Trebst, 1986; Komiya et al., 1988; Deisenhofer and Michel, 1989). The homology between the L and M subunits of the BRC and the D1 and D2 subunits of PS II has been born out by the determination of the three-dimensional structure of PS II (Zouni et al., 2001; Kamiya and Shen, 2003; Ferreira et al., 2004; Chapters 19-21). These studies have established the presence of a common structural motif of the BRC and the oxygen-evolving complex (OEC), namely a central core with two-fold symmetry formed by subunits each containing five transmembrane helices and two branches of cofactors.

The shared structural and functional features provide a basis for experiments in the BRC that are designed to investigate three key attributes required for water oxidation by PS II. First, the primary electron donor is highly oxidizing. Second, the electron transfer process is coupled to proton transfer through the tyrosyl radical $Y_Z^{\bullet}$. Third, the four electron equivalents are collected in the manganese cluster. Reproduction of each of these features by modification of the BRC will be addressed in this chapter. We first discuss the factors that influence the oxidation/reduction midpoint potential of tetrapyrroles and their application to the BRC in order to achieve a highly oxidizing donor as found in PS II, with an examination of the consequences in terms of the energetics of electron transfer. The subsequent incorporation of a tyrosine residue that can serve as a secondary electron donor followed by experimental characterization of such an amino acid radical is presented. The additional ability of modified BRCs to oxidize manganese is then shown. In the last section, ideas are presented that could lead to the design of a modified BRC possessing a manganese cluster that can store electron equivalents. For each of these steps, it should be emphasized that the goal is not to directly copy specific structural components of PS II or to duplicate an evolutionary pathway but rather to modify the BRC such that it gains functional features similar to those found in PS II.

Abbreviations: BChl – bacteriochlorophyll; BPheo – bacteriopheophytin; BRC – bacterial reaction center; Chl – chlorophyll; Cyt – cytochrome; FTIR – Fourier transform infrared; HP – High midpoint potential (highly oxidizing) bacterial reaction centers; OEC – oxygen evolving complex; PS II – Photosystem II; Y_D – redox-active tyrosine on the D2 subunit; Y_L – mutant containing reaction centers with redox-active tyrosine on the L subunit; Y_M – mutant containing reaction centers with redox active tyrosine on the M subunit; Y_Z – redox-active tyrosine on the D1 subunit

II. Achieving a Highly Oxidizing Electron Donor

The electron donor of BRCs is a bacteriochlorophyll (BChl) *a* dimer (Fig. 1). The spectroscopic properties of the two well-coupled BChls can be approximated using simple Hückel theory, assuming the two BChls are slightly different energetically due to asymmetry in their interactions with the surrounding protein (Breton et al., 1992; Lendzian et al., 1993). A pair of Chls is found at a similar position in PS II (Chapters 19–21). The electronic properties of the electron donors of BRCs and PS II are discussed elsewhere (Feher et al., 1989; Blankenship et al., 1995; Chapter 7). Here, we focus on the oxidation/reduction midpoint potential, the critical parameter describing the oxidation ability of an electron donor. The mechanisms by which the protein environment can alter the potentials of tetrapyrroles are discussed below with an emphasis on those amino acid mutations that can make the electron donor of the BRC highly oxidizing.

A. Effects of Protein Interactions on Midpoint Potential

1. Magnesium Coordination

Each of the central magnesium atoms of the BChl molecules forming the electron donor of the BRC is coordinated with a histidine residue. Mutation of either of these two ligands to leucine results in significant changes in the properties of the donor due to formation of a BChl-bacteriopheophytin (BPheo) 'heterodimer' (Bylina and Youvan, 1988; McDowell et al., 1991; Allen et al., 1996; Laporte et al., 1996; van Brederode et al., 1999; King et al., 2001). Because BPheo molecules are more difficult to oxidize than BChl molecules, the midpoint potential of the donor is increased by approximately 130 mV (Allen et al., 1996). Correspondingly the unpaired electron of the oxidized state is localized largely on the BChl com-

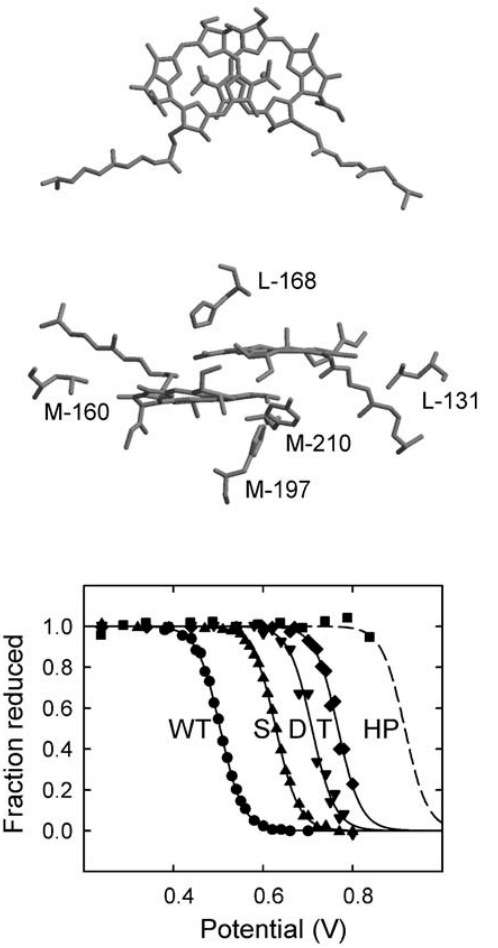

Fig. 1. The bacteriochlorophyll (BChl) dimer comprising the electron donor of bacterial reaction centers and nearby residues whose modification results in increases in the oxidation/reduction midpoint potential. *(top)* In the three-dimensional structure of the BChl dimer from *Rhodobacter sphaeroides*, the two BChl *a* molecules overlap at ring A and are separated by approximately 3.5 Å. The two tetrapyrroles are related by a C_2 symmetry axis that lies approximately vertically in the plane of the paper. *(middle)* Wild-type (WT) reaction centers have one hydrogen bond to the dimer involving L-His168. Substitutions at three positions, L-Leu131His, M-Leu160His, and M-Phe197His, introduce hydrogen bonds to the dimer. A fourth mutation, M-Tyr210Trp, was also characterized. The view is approximately down the C_2 symmetry axis. *(bottom)* Redox titration curves show the additive effect of changes in midpoint potential for WT, the M-Phe197His mutant with a single hydrogen bond added (S), the L-Leu131His+M-Phe197His mutant with two hydrogen bonds added (D), the L-Leu131His+M-Leu160His+M-Phe197His mutant with three hydrogen bonds added (T), and the HP mutant that contains the three added hydrogen bonds and the M-Tyr210Trp mutation. The HP mutant has a highly oxidizing electron donor with a midpoint potential of over 800 mV, or at least 300 mV higher than WT, but determination of the exact midpoint potential of this mutant was not possible due to the rapid degradation of the protein at ambient potentials over 800 mV. The solid lines correspond to fits of the data to the Nernst equation, and the dashed line represents an approximate fit using the available data.

ponent (Huber et al., 1996). The functional changes of the heterodimer can be attributed to the change in cofactor composition rather than the change of the histidine ligand, since replacement of a histidine ligand with glycine results in a dimer with essentially the same properties, including the midpoint potential, as wild type (Goldsmith et al., 1996). The behavior of the heterodimer is significantly different than that of the BChl dimer, and it is not as amenable to the generation of very high potential electron donors.

2. Hydrogen Bonds

Each BChl *a* molecule has two substituents that are part of the conjugated π electronic system and are possible proton acceptors for hydrogen bonds, resulting in a total of four such positions in the dimer. In the wild-type *R. sphaeroides* structure, only one of the four possible hydrogen bond interactions is observed (Fig. 1). To investigate how hydrogen bonds influence the electronic structure of the dimer, mutants were constructed in which the number of hydrogen bonds to the donor ranged from zero to four (Lin et al., 1994). Fourier transform infrared (FTIR) and Raman spectroscopy measurements on these mutants are consistent with well-defined, local changes of the structure due to the alteration of hydrogen bonding. The FTIR difference spectra exhibit large frequency downshifts that support the conclusion that hydrogen bonds have been introduced to the dimer (Nabedryk et al., 1993). Well-resolved infrared spectra of the primary donor obtained by using Fourier transform Raman spectroscopy provide direct evidence for the hydrogen bonding states of the conjugated carbonyls, confirming the presence of the designed hydrogen bonds in BRCs with single site and multiple mutations (Mattioli et al., 1994). When mutations that alter the hydrogen bonding are combined with additional mutations of surrounding residues, the effect of the change in hydrogen bonding on the properties of the BChl dimer dominates over the effects of nonspecific interactions (Stocker et al., 1992; Coleman et al., 1997).

The midpoint potential of the electron donor in BRCs with hydrogen bonds added was found to be increased for each mutant compared to the wild-type value of ~500 mV (Fig. 1). A striking feature of these results is the additive nature of the changes in the midpoint potential. The midpoint potential increased by 60 to 125 mV for each addition of a hydrogen bond from a histidine residue in every mutant. Due to this additive effect, a high midpoint potential of 765 mV was observed for the mutant that has three hydrogen bonds added. Changes at residue M-Tyr210 have also been found to result in increases in the midpoint potential of up to 50 mV (Jia et al., 1993; Nagarajan et al., 1993). A very high midpoint potential of at least 800 mV was achieved in a mutant (HP mutant) with the change M-Tyr210Trp and the addition of three hydrogen bonds (Fig. 1).

3. Electrostatic Interactions

The energy of the oxidized donor can also be affected by charge-charge interactions with ionizable amino acid residues. For example, the midpoint potential of the electron donor would be expected to increase as positive charges are added nearby. Several mutations have been made in which ionizable residues have been placed near the electron donor of the BRC (Williams et al., 2001; Haffa et al., 2002; Johnson and Parson, 2002; Johnson et al., 2002). These types of mutations raise or lower the midpoint potential by up to 50 mV at pH 8. The pH dependence of the change in the midpoint potential was determined for BRCs with the mutation M-Asn199Asp (Williams et al., 2001). The midpoint potential of the donor was found to follow a well-defined pH dependence with a 60 mV decrease in midpoint potential as the pH was increased. The pH dependence could be attributed to the introduction of a negative charge located approximately 10 Å from the donor. As was found for the hydrogen bonds, the effect of multiple changes on the midpoint potential due to electrostatic interactions was additive. Thus although these changes were in general smaller than those associated with the hydrogen bonds, in principal large shifts in the midpoint potential could be accumulated by altering the charge distribution in the protein environment around the donor.

B. Characterization of Electron Donors with Altered Midpoint Potentials

The ability to systematically alter the midpoint potential of the primary electron donor was demonstrated in several sets of mutants made at residues L-131 and M-160, near the conjugated carbonyl groups of the dimer, and at residue L-168, which forms a hydrogen bond to one of the acetyl groups (Fig. 1). Measurements were made on several key properties of the dimer, including the midpoint potential, the spin density distribution of the unpaired electron in the

cation radical state, the three-dimensional structure, and the formation and strength of hydrogen bonds (Müh et al., 2002; Spiedel et al., 2002). In general, higher midpoint potentials were correlated with stronger hydrogen bonds.

The relationship between the midpoint potential and the spin density distribution can be represented by a simple molecular orbital model. The oxidation of the dimer corresponds to removing an electron from the highest occupied molecular orbital of the dimer. The energy level of this orbital is determined by the energy levels of the two halves of the dimer and by the coupling between them. In the wild type, the energy levels of the two halves are asymmetric. Changes such as hydrogen bonds to M-160 stabilize the M side of the dimer, making it more asymmetric, whereas changes at L-131 stabilize the L side, making it more symmetric. In both cases, stabilization results in a higher midpoint potential, that is, a larger amount of energy required to remove an electron. This model can be formalized into a relationship between the unpaired electron spin density and the midpoint potential that can be used to understand other spectroscopic features, such as the different optical transitions of the mutants (Reimers et al., 2000; Johnson and Parson, 2002; Johnson et al., 2002; Müh et al., 2002; Reimers and Hush, 2004).

The resulting model serves as a foundation for understanding the altered electron transfer rates of the mutants. The changes in the dimer midpoint potential in the mutants are assumed to cause parallel changes in the energy levels of each of the charge-separated states. Thus, the free energy difference for each of the electron transfer rates is altered in the mutants, and correspondingly the rates are observed to change by up to two orders of magnitude, in some cases altering the path of electron transfer. These results were analyzed using theoretical Marcus models for the dependence of the rate on the reorganization energy and the free energy difference (Allen and Williams, 1995).

C. Chlorophylls

Electron transfer in BRCs proceeds from the excited state of the donor to the BPheo and the two quinones (Fig. 2). The high potential mutants have an increase in the energy of the charge-separated state but no appreciable change in the energy of the excited state of the primary donor. Because the initial electron transfer proceeds from the excited state, the free energy difference for this step is lower in the mutants than in the wild type, and consequently the quantum yield is decreased to approximately 5 to 10% in the HP mutant. The conversion of light energy in strains with donors having high midpoint potentials is therefore not very efficient.

PS II also has high-potential charge-separated states but can efficiently drive electron transfer processes in part because the excited state has much more energy due to having a chlorophyll (Chl) *a* donor that absorbs at 680 nm compared to the BChl *a* donor that absorbs at 865 nm. Evolutionarily, this would have required the conversion from use of BChl to Chl. Production of Chl precedes BChl in the biosynthetic pathway (Scheer, 1991), and the loss of the enzymes driving the last steps of rings B and D reduction could have led to the first Chl-containing photosystem (Blankenship and Hartman, 1998).

The midpoint potential of the primary donor of PS II is estimated to be substantially higher than that of Chl *a* in solution, probably due to protein interactions similar to those shown to contribute to the midpoint potential of the BChl dimer. However, Chl *a* has a vinyl group on ring A rather than the acetyl found for BChl *a*, and so a Chl *a* dimer can form at most two possible hydrogen bonds. While the presence of hydrogen bonds may be involved in the elevation of the midpoint potential of the Chl dimer, it is likely that electrostatic interactions with a number of nearby positively charged or polar residues constitute the major mechanism that produces the high midpoint potential of the donor in PS II.

To increase the yield of the light-driven reactions of the high potential BRC mutants, it would be advantageous to substitute Chl for BChl. However, despite success in creating the heterodimer mutant and chemically inserting different cofactors into the other tetrapyrrole positions (Scheer and Hartwich, 1995), BRCs with a Chl donor remain an elusive goal, and the work described below is all based upon highly oxidizing mutants that have a BChl dimer and hence a low quantum yield.

III. Oxidation of Tyrosine Residues and Metals

For both BRCs and PS II, light excitation drives the transfer of an electron from an excited donor to quinone acceptors. In the BRC, the donor is excited by relatively low energy near-infrared light, and after

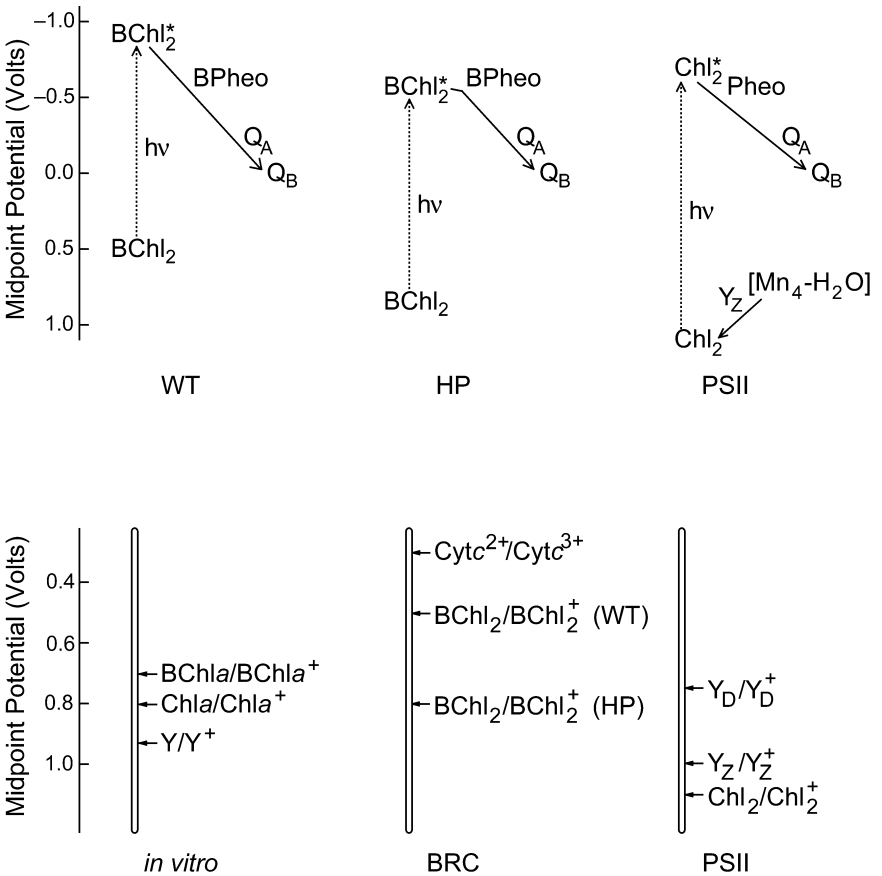

Fig. 2. Comparison of the midpoint potentials and energetics of cofactors of the bacterial reaction center (BRC) and Photosystem II (PS II). (*top*) The increase in the midpoint potential of the bacteriochlorophyll dimer ($BChl_2$) in the high midpoint potential mutant (HP) compared to wild type (WT) changes the relative free energy difference between the ($BChl_2$) and the bacteriopheophytin (Bpheo) and quinone (Q_A and Q_B) acceptors, but not the energy difference between the ground state and the excited state from which electron transfer is initiated. (*bottom)* The midpoint potentials for isolated tetrapyrroles in vitro (Scheer, 1991) differ from those in BRCs and PS II. Midpoint potentials have been estimated for tyrosine in vitro (Y), for Y_D and Y_Z in PS II, and measured for cytochrome c_2 (Cyt *c*). Unlike the $BChl_2$ in WT, the chlorophyll dimer (Chl_2) in PS II is able to oxidize the tyrosines Y_D and Y_Z. In order to achieve the ability to oxidize tyrosines, it is necessary to increase the oxidation potential of the $BChl_2$ from the WT value to the highly oxidizing HP potential by altering the protein environment.

the initial electron transfer the donor is subsequently reduced by fairly low potential secondary electron donors, such as cytochrome (Cyt) c_2. In contrast, PS II operates at energies sufficiently high enough to oxidize water through the manganese complex, using Y_Z as an intermediary (Chapter 9). Unlike wild type, modified BRCs with a highly oxidizing donor have a sufficient midpoint potential for tyrosine and manganese oxidation (Fig. 2), providing the opportunity to create new light-induced electron and proton pathways.

A. Creating Tyrosyl Radicals in Reaction Centers

1. Design of Tyrosine Mutants

The involvement of a tyrosine residue would have had many advantages in the development of the water-oxidizing complex. Tyrosyl radicals can contribute in both electron and proton transfer reactions, both of which are used in the water-oxidizing process. Aromatic residues are commonly found near tetra-

pyrroles, and tyrosine participation would allow the creation of a new pathway without the incorporation of a new molecule into the protein. Other amino acid residues could also serve as electron donors, but their midpoint potentials are all higher than that of tyrosine (Stubbe and van der Dork, 1998), and their use would have necessitated an even stronger oxidant than the electron donor of PS II, potentially creating unfavorable secondary reactions.

The construction of a BRC that is capable of oxidizing tyrosine residues involves careful consideration of many factors, such as electron transfer theory, models of tyrosines in other systems such as PS II, and the inclusion of proton acceptors. Theoretical treatments of electron transfer have sought to define the parameters that control the rates of such reactions. These models can in principle be applied to biological electron transfer, and several different specific parameters can be identified as being key determinants of electron transfer rates (Marcus and Sutin, 1985; Moser et al., 1992). Of these factors, the most amenable to manipulation in the design of tyrosine residues as secondary electron donors to the dimer are the free energy difference and the distance from the tyrosine to the dimer. The free energy difference for tyrosine oxidation is determined by the relative midpoint potentials of the tyrosine and dimer. For a midpoint potential of approximately 800 mV, the reaction will be energetically favorable if the engineered tyrosine residue has a potential at the lower end of the 700 to 1000 mV range estimated for tyrosine residues in proteins (Fig. 2).

The location of tyrosyl radicals in other proteins provides a means of evaluating favorable locations of engineered tyrosines in the HP mutant. In PS II, the two tyrosyl radicals generated by photochemically initiated electron transfer reactions, $Y_Z^{\bullet}$ and $Y_D^{\bullet}$, have been identified as D1-Tyr161 and D2-Tyr160 (Chapter 9). The residues in BRCs that correspond to the positions of the Y_Z and Y_D tyrosine residues of PS II are L-Arg135 and M-Arg164 (Fig. 3). These residues are each approximately 10 Å from the dimer (Fig. 3). Substitution of tyrosine at the L-135 and M-164 positions in the HP mutant resulted in the Y_L and the Y_M mutants, respectively.

2. Identification and Characterization of Tyrosyl Radicals

The introduction of a tyrosine residue as a secondary donor is expected to result in specific changes in the optical and electron paramagnetic resonance (EPR) spectra of the BRC (Fig. 4). In the wild-type BRC, the bleaching of the dimer band at 865 nm and the electrochromic shift of the 800 nm band are characteristic of the charge-separated state involving the oxidized dimer and reduced quinone. Reaction centers from the HP mutant have the same spectral features as wild type. In the Y_L and the Y_M mutants distinct changes in the features are observed, in particular a loss of bleaching of the band at 865 nm, that are consistent with the presence of a secondary electron donor (Kálmán et al., 1999). New spectral features are found in the 300 nm to 450 nm region, with an absorption increase near 300 nm, an increase at 410 nm, and a decrease centered at 420 nm. In PS II, $Y^{\bullet}/Y$ difference spectra of both Y_Z and Y_D obtained from analysis of kinetic data show absorption bands near 250 nm and 300 nm, and exhibit a derivative shape with absorption increases near 390 nm and 440 nm with a minimum near 430 nm (Diner et al., 1995). The derivative shape is attributed to a localized electrochromic effect on nearby Chls associated with tyrosine oxidation. Since the spectral features of Y_Z and Y_D are similar to those observed in the new state evident for the Y_L and the Y_M mutants, the most likely explanation for the new spectral features is that the tyrosine residue introduced in each mutant is serving as a secondary electron donor. The technique of EPR spectroscopy has been key in the identification of tyrosine radicals in PS II as well as other proteins. Tyrosyl radicals are expected to have g values of 2.0040 to 2.0045 as found for both Y_D and Y_Z (Chapter 9). For the Y_L and the Y_M mutants, EPR measurements show a $g = 2.0042$ signal while the signal of the HP mutant was at $g = 2.0025$ as is found for wild-type BRCs.

3. Influence of Protein Environment on Tyrosyl Formation

An emerging picture is that amino acid radicals are controlled energetically by coupling of the electron and proton transfers through a hydrogen abstraction process. Briefly, in these models of PS II, the oxidized tyrosyl Y_Z abstracts both an electron and a proton from the manganese cluster during each of the S state transitions by which water is oxidized (Chapter 9). The proton-electron coupling is postulated to provide the necessary driving force required for the oxidization of the manganese cluster in its higher S states. Subsequent to the development of these models for

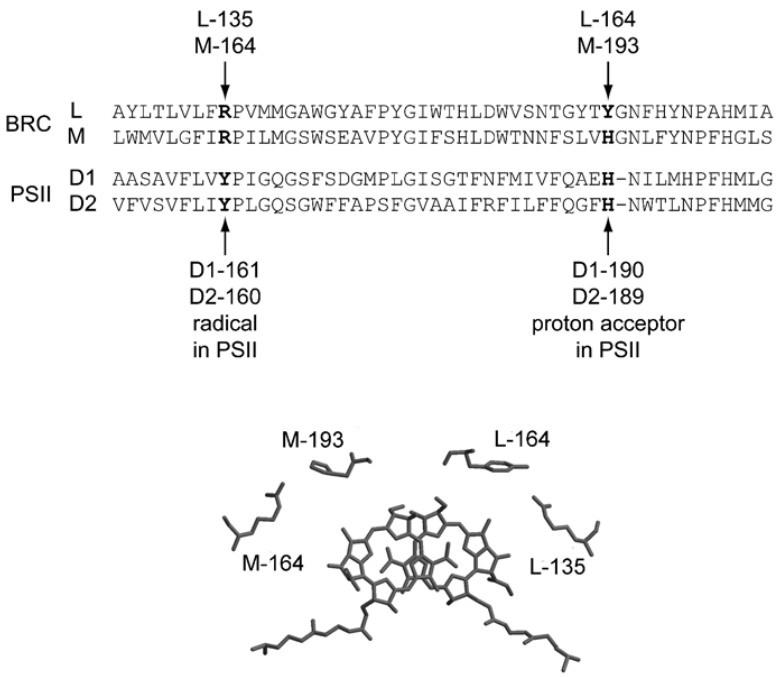

Fig. 3. Correspondence between amino acid residues L-Arg135 and M-Arg164 of the bacterial reaction center (BRC) and D1-Tyr161 and D2-Tyr160 of Photosystem II (PS II). (*top*) The positions of the tyrosine radicals Y_Z at D1-Tyr161 and Y_D at D2-Tyr160 and the histidine residues that act as proton acceptors for the radicals are indicated in a portion of the sequences of the D1 and D2 subunits of PS II from *Chlamydomonas reinhardtii*, along with the corresponding residues in the sequences of the L and M subunits of the BRC from *R. sphaeroides*. (*bottom*) The amino acid residues L-Arg135, L-Tyr164, M-Arg164, and M-His193 are near the bacteriochlorophyll (BChl) dimer in the three-dimensional structure of wild-type BRCs. In the Y_M and Y_L mutants, a tyrosine residue is introduced at either M-164 or L-135, respectively, in BRCs that also contain the changes found in the high midpoint potential HP mutant (Fig. 1). Residues M-His193 and L-Tyr164 are putative proton acceptors for the phenolic protons of M-Tyr164 and L-Tyr135 in the Y_M and Y_L mutants, respectively. The C_2 symmetry axis lies approximately vertically in the plane of the paper.

the water oxidation in PS II (Tommos and Babcock, 2000), they have been extended to other enzymes such as cytochrome oxidase (Proshlyakov et al., 2000).

The availability of proton acceptors is a critical factor for the generation of tyrosyl radicals, as oxidation of tyrosine is energetically unfavorable unless the phenolic proton is released to a proximal base (Tommos and Babcock, 2000). In PS II it is thought that the Y_Z and Y_D tyrosine residues form hydrogen bonds with D1-His190 and D2-His189, respectively, and that these histidine residues act as proton acceptors (Chapter 9). The residues in BRCs that are equivalent to these histidine residues are L-Tyr164 and M-His193 (Fig. 3), and modeling of the structure of the BRC indicates that these residues would be within hydrogen bonding distance to tyrosine residues at L-135 and M-164, respectively.

The influence of the local environment is demonstrated by the pH dependences of the Y_M and Y_L mutants (Fig. 4). The formation of the tyrosyl radical in the Y_M mutant has a distinctive pH dependence that is well described using a pK_a value of 6.9. This pH dependence is explained by assuming that formation of the radical is coupled to release of the phenolic proton to a nearby proton acceptor, resulting in a neutral tyrosyl radical. The pK_a value of 6.9 for the Y_M mutant is consistent with M-His193 serving as a proton acceptor, similar to the role proposed for the analogous histidine residue in PS II. Substitution of other amino acids for M-His193 results in shifts of the pK_a value (Narvaez et al., 2002). A higher value of 8.3 is found for the pK_a for the Y_L mutant, in which a tyrosine is the position of the proton acceptor.

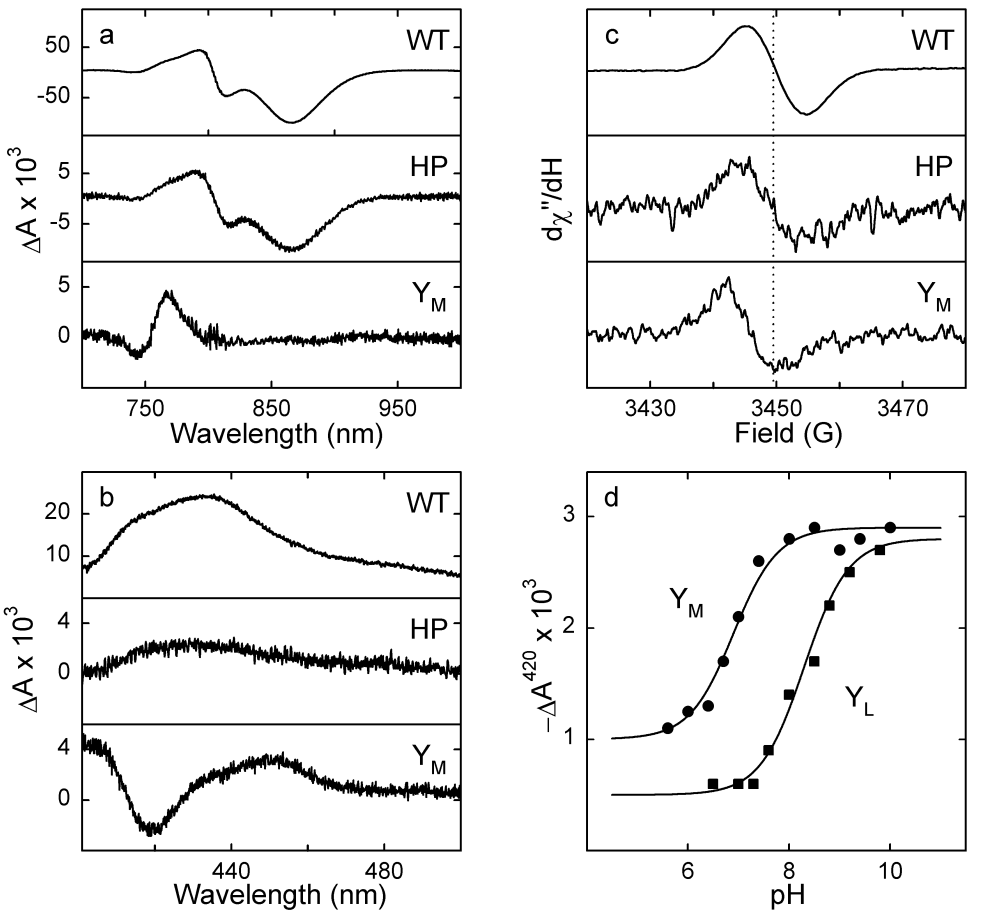

Fig. 4. Characterization of bacterial reaction centers (BRCs) from the wild type (WT), the high midpoint potential mutant (HP), and the Y_M and Y_L mutants. (*a*) In light-minus-dark optical spectra in the near-infrared region of 700 to 1000 nm at pH 8, the spectral features of the HP mutant are similar to those of WT, while the significant differences in the spectra of the Y_M mutant provide evidence for electron transfer from M-Tyr164 to the dimer. The smaller amplitude of the signals is due to the lower quantum yield in mutants with high midpoint potentials. (*b*) The same pattern of the relative spectral features in the different BRCs is seen in light-minus-dark optical spectra in the visible region of 400 to 500 nm region. (*c*) Light-minus-dark electron paramagnetic resonance spectra at pH 8 show corrobative evidence for the formation of a tyrosyl radical in the Y_M mutant. (*d*) The light-induced absorption changes at 420 nm that are indicative of tyrosyl formation are highly pH dependent. Fits using the Henderson-Hasselbalch equation result in pK_a values of 6.9 and 8.3 for the Y_M and the Y_L mutants respectively, consistent with titration of proton-accepting residues near the tyrosyl radicals (Fig. 3). Modified from Kálmán et al. (1999).

B. Manganese Oxidation

The involvement of manganese as an electron donor would have been a logical possible development for photosynthetic organisms and may have been an intermediate step in the evolution of water oxidation at a manganese complex (Pierson, 1994; Anayev et al., 2001; Sauer and Yachandra, 2002; Chapter 30) (Fig. 5). Manganese is often found in surface layers of sediments, and its widescale availability would have provided primitive photosynthetic organisms with an electron source and a special ecological niche. Many different microorganisms, including bacteria, cyanobacteria, algae, yeast, and fungi can either oxidize or reduce manganese, and such activity plays a major role throughout natural environments ranging

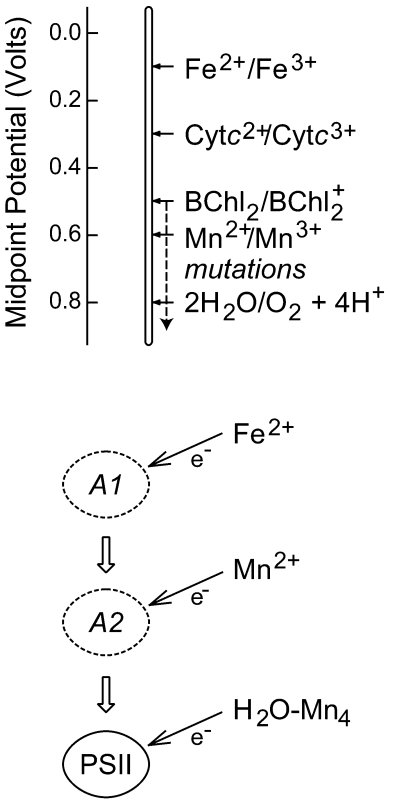

Fig. 5. Considerations for the oxidation of manganese by photosynthetic complexes. (*top*) The bacteriochlorophyll dimer ($BChl_2$) from wild-type bacterial reaction centers (BRCs) has a midpoint potential of 0.5 V, and so reduced iron can be used during photosynthetic growth, but the use of manganese is energetically unfavorable. The dashed line indicates the change in midpoint potential of BRCs containing mutations that produce highly oxidizing dimers, with potentials of 0.7 V and above, that are energetically capable of oxidizing manganese, as is true for Photosystem II (PS II), which has a potential of approximately 1.1 V. (*bottom*) One possible scheme for the evolution of photosynthetic complexes is that an ancestral photosystem (*A1*) that could oxidize Fe evolved into PS II by way of an intermediate photosystem (*A2*) that could bind and oxidize Mn.

from fresh and marine waters to deep sea vents and desert climates (Gounot, 1994). Manganese oxidation pathways in biological systems are diverse, and some are indirect, for example manganese oxidation occurs due to the production of hydrogen peroxide in some bacteria. To date the capability of manganese oxidation has not been demonstrated in anoxygenic photosynthetic bacteria. The midpoint potential of the Mn^{2+}/Mn^{3+} couple is about 0.6 V (Anayev et al., 2001) and hence higher than the usual midpoint potential of approximately 0.5 V for the electron donor in purple bacteria. The availability of the highly oxidizing reaction centers provides the opportunity to investigate oxidation of manganese by BRCs.

The manganese serving as the secondary donor in primitive bacteria could have been provided by either metalloproteins or free metal complexes. One possibility is that a manganese-containing enzyme, such as manganese catalase, may have been recruited to serve the role of secondary donor (Blankenship and Hartman, 1998). This would have required that the proposed manganese catalase develop a positively charged region of the surface, as found for Cyt *c*, that would provide electrostatically favorable interactions for binding to the BRC. Another possibility is for direct oxidation of metal complexes in solution. At low pH values, metals possess very high midpoint potentials of approximately 1.0 V, however, under biologically relevant conditions metal complexes can have significantly lower potentials. For example, under very acidic conditions (pH < 2.5), a simple Fe^{2+} to Fe^{3+} transition exists with a midpoint potential of 0.77 V, but iron can also undergo a $FeCO_3$ to $Fe(OH)_3$ transition that has a midpoint potential of approximately 0.1 V at pH 8 (Ehrenreich and Widdel, 1994). This potential of 0.1 V is comparable to other known secondary electron donors such as Cyt *c*, which has a midpoint potential of approximately 0.3 V (Fig. 5). Since the BRC has a potential of 0.5 V, the reaction involving iron is energetically feasible. Support for the concept of direct metal oxidation is provided by the ability of a wide range of bacteria to oxidize iron under photosynthetic conditions (Widdel et al., 1993).

Reaction centers with elevated midpoint potentials have been found to directly oxidize manganese in solution (Kálmán et al., 2003). The presence of manganese does not change the light-induced electron transfer events in wild-type BRCs, as expected from the unfavorable energetics of the reaction. In striking contrast, mutants with increased midpoint potentials readily oxidize manganese as evident by the loss of the absorption changes associated with the oxidized electron donor when manganese is present (Fig. 6). Measurements of mutants with different dimer midpoint potentials show that the electron transfer from manganese to the oxidized dimer is a well-defined reaction that is dependent upon the driving force. The dependence of the rate on the manganese concentration indicates that the manganese is not tightly

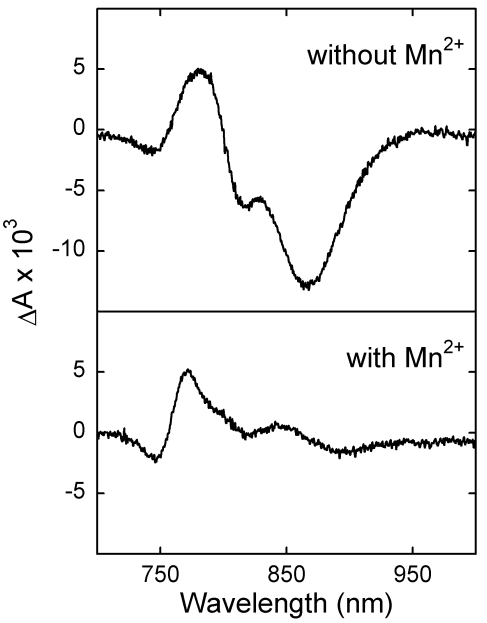

Fig. 6. Light-minus-dark optical spectra of a highly oxidizing mutant in the near-infrared region of 700 to 1000 nm demonstrating manganese oxidation. (*top*) Without manganese, the spectral changes indicate the presence of both the oxidized dimer and reduced quinone. (*bottom*) When manganese is present the bleaching at 865 nm is lost but the changes at 760 nm are still observed indicating that only the reduced quinone is present and the dimer is reduced by the manganese. Modified from Kálmán et al. (2003).

bound but only weakly associated with the BRC. Thus, manganese can be oxidized but achieving a tight binding site requires additional modification of the BRC.

IV. Designing a Manganese Cluster

The achievement of a highly oxidizing donor provides the BRC with a sufficient oxidation potential for water oxidation; however, the conversion of H_2O to O_2 requires the ability to collect four electron equivalents. In the water-oxidizing complex these equivalents are collected at the manganese cluster (Chapters 10–12). In order to mimic this functional ability of the water-oxidation complex, it would be necessary to bind a metal cluster near the dimer such that it can serve as a secondary donor. Because many properties of the manganese cluster in PS II remain elusive, the development of a metal cluster that can perform this new electron transfer process is a challenge.

Insight into the design of a binding site on the BRC is provided by studies of the water oxidation complex with the manganese biochemically depleted or altered through mutagenesis. Considerable evidence exists for a high affinity manganese-binding site that is associated with the assembly of the cluster in PS II (Chapters 10–12). Extensive measurements of mutants with changes at D1-Asp170 have indicated that this residue has considerable influence on the manganese binding and assembly, leading to the hypothesis that manganese binding is initiated at D1-Asp170, and that the cluster assembly occurs by a proton abstraction pathway involving Y_Z. This photoactivation model suggests a structural plan for a possible manganese-binding site on the BRC. Based upon a comparison of the sequences, three residues in the Y_M mutant, M-Tyr164, M-His193 and M-Glu173, correspond to key amino acid residues of PS II (Fig. 3). The addition of several carboxylic acid groups to this area of the Y_M mutant may provide a site suitable for manganese binding. Once a binding site is developed on the BRC near M-Tyr164, then it may be possible to build a di-μ-oxo-bridged or a di-μ-hydroxo-bridged manganese dimer core as proposed for PS II. The availability of a highly oxidizing BRC with a bound manganese complex would open the doors for probing the mechanism of photoactivation, the properties of manganese complexes required for water oxidation, and the influence of metal complexes on the properties of amino acid radicals.

Acknowledgments

The work described is supported by a grant from the National Science Foundation, MCB 0131764.

References

Allen JP and Williams JC (1995) Relationship between the oxidation potential of the bacteriochlorophyll dimer and electron transfer in photosynthetic reaction centers. J Bioenerg Biomemb 27: 275–283

Allen JP, Feher G, Yeates TO, Komiya H and Rees DC (1987) Structure of the reaction center from *Rhodobacter sphaeroides* R-26: the cofactors. Proc Natl Acad Sci USA 84: 5730–5734

Allen JP, Artz K, Lin X, Williams JC, Ivancich A, Albouy D, Mattioli TA, Fetsch A, Kuhn M and Lubitz W (1996) Effects

of hydrogen bonding to a bacteriochlorophyll-bacteriopheophytin dimer in reaction centers from *Rhodobacter sphaeroides*. Biochemistry 35: 6612–6619

Ananyev GM, Zaltsman L, Vasko C and Dismukes GC (2001) The inorganic biochemistry of photosynthetic oxygen evolution/water oxidation. Biochim Biophys Acta 1503: 52–68

Belanger G, Berand J, Corriveau P and Gingras G (1988) The structural genes coding for the L and M subunit of *Rhodospirillum rubrum* photoreaction center. J Biol Chem 263: 7632–7638

Blankenship RE and Hartman H (1998) The origin and evolution of oxygenic photosynthesis. Trends Biol Sci 23: 94–97

Blankenship RE, Madigan MT and Bauer CE (eds) (1995) Anoxygenic Photosynthetic Bacteria. Kluwer Academic Publishers, Dordrecht

Breton J, Nabedryk E and Parson WW (1992) A new infrared electronic transition of the oxidized primary electron donor in bacterial reaction centers: a way to assess resonance interactions between the bacteriochlorophylls. Biochemistry 31: 7503–7510

Bylina EJ and Youvan DC (1988) Directed mutations affecting spectroscopic and electron transfer properties of the primary donor in the photosynthetic reaction center. Proc Natl Acad Sci USA 85: 7226–7230

Coleman WJ, Mattioli TA, Youvan DC and Rutherford AW (1997) Site-directed mutations near the L-subunit D-helix of the purple bacterial reaction center: A partial model for the primary donor of Photosystem II. Biochemistry 36: 2178–2187

Deisenhofer J and Michel H (1989) The photosynthetic reaction center from the purple bacterium *Rhodopseudomonas viridis*. Science 245: 1463–1473

Deisenhofer J, Epp O, Miki K, Huber R and Michel H (1985) Structure of the protein subunits in the photosynthetic reaction centre of *Rhodopseudomonas viridis* at 3 Å resolution. Nature 318: 618–624

Des Marais DJ (2001) When did photosynthesis emerge on earth? Science 289: 1703–1705

Diner BA, Tang X-S, Zheng M, Dismukes C, Force DA, Randall DW and Britt RD (1995) Environment and function of the redox active tyrosines of Photosystem II. In: Mathis P (ed) Photosynthesis: From Light to Biosphere, pp 229–234. Kluwer Academic Publishers, Dordrecht

Ehrenreich A and Widdel F (1994) Anaerobic oxidation of ferrous iron by purple bacteria, a new type of phototropic metabolism. Appl Environ Microbiol 60: 4517–4526

Feher G, Allen JP, Okamura MY and Rees DC (1989) Structure and function of bacterial photosynthetic reaction centres. Nature 339: 111–116

Ferreira KN, Iverson TM, Maghlaoui K, Barber J and Iwata S (2004) Architecture of the photosynthetic oxygen-evolving center. Science 303: 1831–1838

Goldsmith JO, King B and Boxer SG (1996) Mg coordination by amino acid side chains is not required for assembly and function of the special pair in bacterial photosynthetic reaction centers. Biochemistry 35: 2421–2428

Gounot A-M (1994) Microbial oxidation and reduction of manganese: Consequences in groundwater and applications. FEMS Microbiol Rev 14: 339–349

Haffa ALM, Lin S, Katilius E, Williams JC, Taguchi AKW, Allen JP and Woodbury NW (2002) The dependence of the initial electron transfer rate on driving force in *Rhodobacter sphaeroides* reaction centers. J Phys Chem B 106: 7376–7384

Huber M, Isaacson RA, Abresch EC, Gaul D, Schenck CC and Feher G (1996) Electronic structure of the oxidized primary electron donor of the HL(M202) and HL(L173) heterodimer mutants of the photosynthetic bacterium *Rhodobacter sphaeroides*: ENDOR on single crystals of reaction centers. Biochim Biophys Acta 1273: 108–128

Jia Y, DiMagno TJ, Chan C-K, Wang Z, Du M, Hanson DK, Schiffer M, Norris JR, Popov MS and Fleming GR (1993) Primary charge separation in mutant reaction centers of *Rhodobacter capsulatus.* J Phys Chem 97: 13180–13191

Johnson ET and Parson WW (2002) Electrostatic interactions in an integral membrane protein. Biochemistry 41: 6483–6494

Johnson ET, Müh F, Nabedryk E, Williams JC, Allen JP, Lubitz W, Breton J and Parson WW (2002) Electronic and vibronic coupling of the special pair of bacteriochlorophylls in photosynthetic reaction centers from wild-type and mutant strains of *Rhodobacter sphaeroides.* J Phys Chem B 106: 11859–11869

Kálmán L, LoBrutto R, Allen JP and Williams JP (1999) Modified reaction centres oxidize tyrosine in reactions that mirror Photosystem II. Nature 402: 696–699

Kálmán L, LoBrutto R, Williams JC and Allen JP (2003) Manganese oxidation by modified reaction centers from *Rhodobacter sphaeroides*. Biochemistry 42: 11016–11022

Kamiya N and Shen JR (2003) Crystal structure of oxygen-evolving Photosystem II from *Thermosynechococcus vulcanus* at 3.7-Å resolution. Proc Natl Acad Sci USA 100: 98–103

King BA, de Winter A, McAnaney TB and Boxer SG (2001) Excited state energy transfer pathways in photosynthetic reaction centers. 4. Asymmetric energy transfer in the heterodimer mutant. J Phys Chem B 105: 1856–1862

Komiya H, Yeates TO, Rees DC, Allen JP and Feher G (1988) Structure of the reaction center from *Rhodobacter sphaeroides* R26 and 2.4.1: Symmetry relations and sequence comparisons between different species. Proc Natl Acad Sci USA 85: 9012–9016

Laporte LL, Palaniappan V, Kirmaier C, Davis DG, Schenck CC, Holten D and Bocian DF (1996) Influence of electronic asymmetry on the spectroscopic and photodynamic properties of the primary electron donor in the photosynthetic reaction center. J Phys Chem 100: 17696–17707

Lendzian F, Huber M, Isaacson RA, Endeward B, Plato M, Bonigk B, Mobius K, Lubitz W and Feher G (1993) The electronic structure of the primary donor cation radical in *Rhodobacter sphaeroides* R-26: ENDOR and TRIPLE resonance studies in single crystals of reaction centers. Biochim Biophys Acta 1183: 139–160

Lin X, Murchison HA, Nagarajan V, Parson WW, Allen JP and Williams JC (1994) Specific alteration of the oxidation potential of the electron donor in reaction centers from *Rhodobacter sphaeroides*. Proc Natl Acad Sci USA 91: 10265–10269

Marcus RA and Sutin N (1985) Electron transfers in chemistry and biology. Biochim Biophys Acta 811: 265–322

Mattioli TA, Williams JC, Allen JP and Robert B (1994) Changes in primary donor hydrogen-bonding interactions in mutant reaction centers from *Rhodobacter sphaeroides*: Identification of the vibrational frequencies of all the conjugated carbonyl groups. Biochemistry 33: 1636–1643

McDowell LM, Gaul D, Kirmaier C, Holten D and Schenck CC (1991) Investigation into the source of electron transfer asymmetry in bacterial reaction centers. Biochemistry 30: 8315–8322

Michel H, Weyer KA, Gruenberg H, Dunger I, Oesterhelt D and Lottspeich F (1986) The 'light' and 'medium' subunits of the photosynthetic reaction centers from *Rhodopseudomonas viridis*: Isolation of the genes, nucleotide and amino acid sequence. EMBO J 5: 1149–1158

Moser CC, Keske JM, Warncke K, Farid RS and Dutton PL (1992) Nature of biological electron transfer. Nature 355: 796–802

Müh F, Lendzian F, Roy M, Williams JC, Allen JP and Lubitz W (2002) Pigment-protein interactions in bacterial reaction centers and their influence on oxidation potential and spin density distribution of the primary donor. J Phys Chem B 106: 3226–3236

Nabedryk E, Allen JP, Taguchi AKW, Williams JC, Woodbury NW and Breton J (1993) Fourier transform infrared study of the primary electron donor in chromatophores of *Rhodobacter sphaeroides* with reaction centers genetically modified at residues M160 and L131. Biochemistry 32: 13879–13885

Nagarajan V, Parson WW, Davis D and Schenck CC (1993) Kinetics and free energy gaps of electron transfer reactions in *Rhodobacter sphaeroides* reaction centers. Biochemistry 32: 12324–12336

Narváez AJ, Kálmán L, LoBrutto R, Allen JP and Williams JC (2002) Influence of the protein environment on the properties of a tyrosyl radical in reaction centers from *Rhodobacter sphaeroides,* Biochemistry 41: 15253–15258

Olson JM and Pierson BK (1987) Origin and evolution of photosynthetic reaction centers. Origins Life Evol B 17: 419–430

Pierson BK (1994) The emergence, diversification, and role of photosynthetic eubacteria. In: Bengtson S (ed) Early Life on Earth (Nobel Symposium, No 84), pp 161–180. Columbia University Press, New York

Proshlyakov DA, Pressler MA, DeMaso C, Leykam JF, DeWitt DL and Babcock GT (2000) Oxygen activation and reduction in respiration: involvement of redox-active tyrosine 244. Science 290: 1588–1591

Reimers JR, Hughes JM and Hush NS (2000) Modeling the bacterial photosynthetic reaction center 3: Interpretation of effects of site-directed mutagenesis on the special-pair midpoint potential. Biochemistry 39: 16185–16189

Reimers JR and Hush NS (2004) A unified descripton of the electrochemical, charge distribution, and spectroscopic properties of the special-pair radical cation in bacterial photosynthesis. J Am Chem Soc 126: 4132–4144

Rochaix JD, Dron M, Rahire M and Malnoe P (1984) Sequence homology between the 32K dalton and the D2 chloroplast membrane polypeptides of *Chlamydomonas reinhardtii.* Plant Mol Biol 3: 363–370

Sauer K and Yachandra VK (2002) A possible evolutionary origin for the Mn_4 cluster of the photosynthetic water oxidation complex from natural MnO_2 precipitates in the early ocean. Proc Natl Acad Sci USA 99: 8631–8636

Scheer H (ed) (1991) Chlorophylls. CRC Press, Boca Raton

Scheer H and Hartwich G (1995) Bacterial reaction centers with modified tetrapyrrole chromophores. In: Blankenship RE, Madigan MT and Bauer CE (eds) Anoxygenic Photosynthetic Bacteria, pp 649–663. Kluwer Academic Publishers, Dordrecht

Schopf JW (ed) (1983) Earth's Earliest Biosphere: Its Origin and Evolution. Princeton University Press, Princeton

Spiedel D, Roszak AW, McKendrick K, McAuley KE, Fyfe PK, Nabedryk E, Breton J, Robert B, Cogdell RJ, Isaacs NW and Jones MR (2002) Tuning of the optical and electrochemical properties of the primary electron donor bacteriochlorophylls in the reaction centre from *Rhodobacter sphaeroides*: spectroscopy and structure. Biochim Biophys Acta 1554: 75–93

Stocker JW, Taguchi AKW, Murchison HA, Woodbury NW and Boxer SG (1992) Spectroscopic and redox properties of sym1 and (M)F195H: *Rhodobacter sphaeroides* reaction center symmetry mutants which affect the initial electron donor. Biochemistry 31: 10356–10362

Stubbe J and van der Donk WA (1998) Protein radicals in enzyme catalysis. Chem Rev 98: 705–762

Tommos C and Babcock GT (2000) Proton and hydrogen currents in photosynthetic water oxidation. Biochim Biophys Acta 1458: 199–219

Trebst A (1986) The topology of the plastoquinone and herbicide binding peptides of Photosystem II in the thylakoid membrane. Z Naturforsch 41c: 240–245

van Brederode ME, van Stokkum IHM, Katilius E, van Mourik F, Jones MR and van Grondelle R (1999) Primary charge separation routes in the BChl:BPhe heterodimer reaction centers of *Rhodobacter sphaeroides*. Biochemistry 38: 7545–7555

Widdel F, Schnell S, Heising S, Ehrenreich A, Assmus B and Schink B (1993) Ferrous iron oxidation by anoxygenic phototropic bacteria. Nature 362: 834–836

Williams JC, Steiner LA, Ogden RC, Simon MI and Feher G (1983) Primary structure of the M subunit of the reaction center from *Rhodopseudomonas sphaeroides*. Proc Natl Acad Sci USA 80: 6505–6509

Williams JC, Steiner LA and Feher G (1986) Primary structure of the reaction center from *Rhodopseudomonas sphaeroides*. Proteins 1: 312–325

Williams JC, Haffa ALM, McCulley JL, Woodbury NW and Allen JP (2001) Electrostatic interactions between charged amino acid residues and the bacteriochlorophyll dimer in reaction centers from *Rhodobacter sphaeroides*. Biochemistry 40: 15403–15407

Woese CR (1987) Bacterial evolution. Microbiol Rev 51: 221–271

Youvan DC, Bylina EJ, Alberti M, Begusch H and Hearst JE (1984) Nucleotide and deduced polypeptide sequences of the photosynthetic reaction-center, B870 antenna, and flanking polypeptides from *R. capsulata*. Cell 37: 949–957

Zouni A, Witt HT, Kern J, Fromme P, Krauss N, Saenger W and Orth P (2001) Crystal structure of Photosystem II from *Synechococcus elongatus* at 3.8 Å resolution. Nature 409: 739–743

Chapter 33

De Novo Protein Design in Respiration and Photosynthesis

Brian R. Gibney
Department of Chemistry, Columbia University, New York, NY 10027, U.S.A.

Cecilia Tommos*
Department of Biochemistry and Biophysics, Arrhenius Laboratories for Natural Sciences, Stockholm University, SE-106 91 Stockholm, Sweden

Summary

An emerging biomimetic approach to exploring protein structure/function relationships has grown out of the creation of proteins from first principles, i.e., *de novo* design. Over the past two decades, *de novo* protein design has progressed from demonstrating the feasibility of designing simple secondary structures such as monomeric α-helices to synthesizing holoproteins containing a variety of different metals, light-absorbing pigments and redox cofactors. A range of prosthetic groups are involved in energy transfer, electron transfer and proton-coupled electron transfer in biological energy transduction and, by using rational design, computational and combinatorial approaches, many of these have been introduced into designed proteins. In this chapter we review synthetic work aimed at revealing the engineering specifications and tolerances for the protein/cofactor

*Author for correspondence, email: cecilia@dbb.su.se

T. Wydrzynski and K. Satoh (eds): Photosystem II: The Light-Driven Water:Plastoquinone Oxidoreductase, pp. 729–751.

interactions as well as the influence by the protein matrix on the chemical and redox properties of the six most prominent groups of cofactors involved in the respiratory and photosynthetic processes. Redesign strategies and *de novo* design of heme proteins, (bacterio)chlorophyll proteins, flavoproteins, amino-acid radical proteins, iron-sulfur proteins, and copper-containing proteins are described. In addition, the structural and functional properties of more complex *de novo* designed proteins containing multiple cofactors are summarized. The overall engineering principles can then be applied to the understanding of Photosystem II structure and function.

I. Introduction

To capture the design principles underlying biological energy transduction and reproduce them in man-made constructions is compelling. This will give a deeper understanding of the natural systems on a fundamental level and, in addition, provides the opportunity to make molecular machines useful for energy and medical research and for biotechnology in general. The scope of this chapter is to describe the structural and functional characteristics of model proteins whose designs were inspired by respiratory and photosynthetic enzymes. The main focus is on *de novo* designed proteins rather than related work on engineered natural proteins. To provide a background to the synthetic work, we first summarize the protein/cofactor complexes catalyzing the respiratory and photosynthetic energy-converting reactions and then review early work and recent progress made in the research area of *de novo* protein design.

A. Energy Conversion in Biological Systems

Electron and proton transfers within and between protein complexes located in an insulating membrane form the basis for biological energy conversion, as embodied in the chemiosmotic model (Mitchell, 1961). In aerobic respiration, high-energy electrons derived from food oxidation are transported to O_2 via a series of redox proteins located in the inner mitochondrial membrane of eukaryotic organisms or in the plasma membrane of bacteria. The free energy made available in the exergonic redox reactions drives endergonic transport of protons across the membrane. The electrochemical potential stored in the trans-membrane proton gradient is subsequently used to drive ATP synthesis and active transport of a variety of ions and metabolites. In photosynthesis, sunlight provides the ultimate energy source for ATP generation. The capture and absorption of a photon produces a charge-separated state, which is stabilized via a series of secondary electron-transfer reactions. These light driven electron-transfer steps are coupled to active proton translocation and the formation of a proton gradient. Proteins associated with the thylakoid membranes of chloroplasts and cyanobacteria catalyze the light-harvesting events, the photochemistry and the secondary redox reactions.

Abbreviations: (B)Chl – (bacterio)chlorophyll; (B)Pheo – (bacterio)pheophytin; Cyt – cytochrome; ETF – electron-transferring flavoprotein; LH – light harvesting; PQ – plastoquinone; PS II – Photosystem II; RC – reaction center; TASP – Template-assembled synthetic protein; UQ – ubiquinone

1. Electron and Proton Transfers in Respiration

The enzymes and redox cofactors involved in the respiratory electron-transport chain are schematically illustrated in Fig. 1 (Ohnishi, 1998; Saraste, 1999; Schultz and Chan, 2001). Three trans-membrane protein complexes couple the redox chemistry to active proton transport. The first enzyme in the respiratory chain is complex I (NADH:UQ oxidoreductase). This enzyme transfers two electrons from NADH to ubiquinone (UQ) and couples this redox process to the translocation of up to four protons from the negative (N) to the positive (P) side of the membrane. The catalytic core of bacterial complex I contains 14 subunits and the bovine enzyme contains as many as 43 polypeptides (Friedrich and Scheide, 2000). Electron microscopy studies have produced a low-resolution structural model of complex I showing an L-shape complex with one arm embedded in the membrane and the second arm extending into the matrix (Sazanov and Walker, 2000). The electron-transfer chain contains a number of redox cofactors most of which lack distinct optical signals. This feature has hampered detailed spectroscopic characterization of the reaction mechanism. Complex I comprises one flavin mononucleotide, eight or nine $[Fe_2S_2]$ and $[Fe_4S_4]$ clusters and at least two sites for UQ binding (Ohnishi, 1998; Schultz and Chan, 2001). The flavin and the iron-sulfur clusters are associated mainly, if not exclusively, with the soluble subunits of the

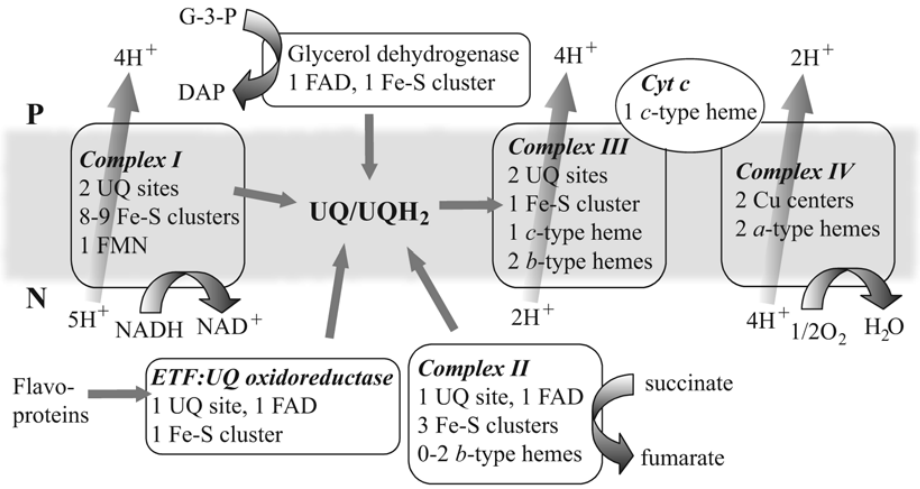

Fig. 1. Schematic illustration of the protein complexes and redox cofactors involved in aerobic respiration. The solid grey arrows show the electron flow while the shaded arrows indicate sites of proton translocation across the membrane. The figure is described in detail in the main text.

enzyme while the UQ-binding pockets are found in the membrane-bound part.

At least three other enzymes donate electrons to the UQ/UQH_2 pool in addition to complex I (Fig. 1). These include complex II (succinate:UQ oxidoreductase), which is a membrane-anchored enzyme containing a covalently linked flavin dinucleotide, a $[Fe_2S_2]$, a $[Fe_3S_4]$ and a $[Fe_4S_4]$ type iron-sulfur cluster, and at least one UQ-binding site (Hederstedt, 2003). Depending on the organism, the enzyme may also contain one or two *b*-type hemes. This enzyme fuels the respiratory chain by transferring electrons from succinate generated in the Krebs cycle to ubiquinone. Also connecting to the respiratory chain at the level of the UQ/UQH_2 pool is the electron-transferring flavoprotein:ubiquinone (ETF:UQ) oxidoreductase. This soluble protein contains one flavin dinucleotide, one iron-sulfur cluster and a Q-binding pocket. Finally, the flavin and iron-sulfur cluster containing glycerol-3-phosphate dehydrogenase is capable of binding and reducing UQ to UQH_2. Of the enzymes described above, only complex I contributes to the formation and maintenance of the chemiosmotic proton gradient used for ATP synthesis.

Complex I and II, ETF:UQ oxidoreductase and glycerol-3-phosphate dehydrogenase provide the UQ/UQH_2 pool with reducing equivalents. Its subsequent oxidation is catalyzed by complex III (UQH_2:cytochrome *c* oxidoreductase) also denoted cytochrome (Cyt) bc_1 complex. The structure of the mitochondrial enzyme has been determined to atomic resolution (Berry et al., 2000). Complex III contains 3-11 subunits, depending on the organism. The functional core consists of the Rieske subunit, Cyt c_1 and Cyt *b*. The Rieske protein ligates a high-potential $[Fe_2S_2]$ cluster and a *c*-type heme is covalently attached to Cyt c_1. Cyt *b* contains the b_H and b_L hemes and two UQ-binding pockets denoted Q_o and Q_i. The Q_o site is located towards the P-side of the membrane and the Q_i site is close to the N-side.

The net reaction catalyzed by complex III is the reduction of two ferriCyt *c* to their Fe(II) state and the oxidation of one UQH_2 to UQ. This redox process is coupled to a translocation of four protons across the membrane. The structural basis for the capability of complex III to translocate two protons per single electron transferred from UQH_2 to ferriCyt *c* arises from the spatial organization of its redox centers into a bifurcated electron-transfer chain containing one high-potential branch and one low-potential branch. A complete cycle of the enzyme contains the following steps. A fully reduced and protonated ubiquinol binds to the Q_o pocket and transfers one electron via the high-potential route, consisting of the Rieske iron-sulfur center and Cyt c_1, to the water-soluble Cyt *c* protein. A second electron is delivered from the semiquinone $QH^{\bullet}$ radical formed in the Q_o site via the low-potential branch *b*-type hemes to a ubi-

quinone bound to the Q_i pocket. The fully oxidized ubiquinone in the Q_o pocket is replaced by a ubiquinol and the two separate electron transfers are repeated generating a second ferroCyt *c* molecule and a fully reduced ubiquinol in the Q_i site. The Q_o and Q_i sites are located on opposite side of the membrane and the protonic reactions coupled to the Q/QH_2 redox processes give rise to the net translocation of protons across the membrane bilayer.

Cyt *c* shuttles electrons from complex III to complex IV (cytochrome *c* oxidase), which catalyzes the final step in aerobic respiration by oxidizing ferroCyt *c* and reducing O_2 to H_2O (Ferguson-Miller and Babcock, 1996; Babcock, 1999). This reaction requires a total of four electrons and four protons and, importantly, the substrate protons are taken up exclusively from the N-side of the membrane. In addition, four protons are pumped vectorially from the N-side to the P-side. Both the substrate and the pumped protons are transported in a unidirectional manner, although the mechanism for this is unknown. In contrast to complex III, which uses free diffusion of lipid-soluble quinones for the physical transport of protons across the membrane, complex IV transports the protons through protein-mediated channels.

High-resolution structures of complex IV have been obtained from several species (Schultz and Chan, 2001). The mammalian enzyme contains 13 subunits of which, interestingly, three are encoded by the mitochondrial DNA. These three proteins carry the redox-active centers and form the electron and proton-transfer unit of the enzyme. Bacterial complex IV has three or four subunits most of which are homologous to the three major proteins of the mammalian enzyme. The binuclear copper Cu_A center receives electrons from Cyt *c* and transfers them one at the time to heme *a*, which, in turn, reduces the binuclear heme a_3/Cu_B active site. In addition to heme a_3 and the mononuclear Cu_B center, the active site contains a tyrosine that has been proposed to form a radical during catalysis. Tyrosine redox chemistry is also essential for photosynthetic water oxidation, as will be described below.

2. Electron and Proton Transfers in Photosynthesis

Many of the processes that occur in photosynthetic energy conversion are analogous to the respiratory reactions. The unique events catalyzed by the photosynthetic organisms are the capture of light quanta and the photochemical reactions in which the photon energies are converted into chemical energy in the form of charge-separated states. Green plants, algae and photosynthetic bacteria contain (bacterio)chlorophylls ((B)Chl), carotenoids and bilin molecules to collect the solar energy. The exact pigment composition depends on the organism and the growth conditions. The light-harvesting (LH) pigments have in general high extinction coefficients and absorbance maxima at a variety of different wavelengths, which allow the photosynthetic organisms to efficiently collect light over a broad spectral range. The pigments are bound to proteins that form antenna complexes, which are highly organized and dynamic structures constructed to efficiently capture light quanta and funnel the excitation energy to the reaction center (RC). Atomic models have been obtained for several antenna systems including the external LH complex associated with Photosystem II (PS II) (Kühlbrandt et al., 1994; Chapter 2, Green and Gantt; Chapter 18, Hankamer et al.) and the antenna of purple bacteria (Cogdell et al., 1999).

A photosynthetic RC is a trans-membrane protein/pigment complex in which the light energy to chemical energy conversion occurs. RCs contain electronically coupled (B)Chl molecules, which trap the excitation energy delivered by the antenna. Upon excitation, the photochemically active pigments transfer an electron to a nearby acceptor. A charge-separated state is formed, which is subsequently stabilized via a series of electron-transfer reactions. These exergonic redox reactions are coupled to proton transfers and the creation of a proton gradient across the thylakoid membrane. The photochemically reduced acceptor molecule and the redox cofactors that participate in the secondary electron-transfer reactions vary between different species. The composition of the redox cofactors divides the RC into two major groups: Photosystem I (PS I) and the RCs found in green-sulfur bacteria and heliobacteria use iron-sulfur clusters as the terminal electron acceptors. In contrast, PS II and the RCs of purple bacteria and green filamentous bacteria employ (bacterio)pheophytin ((B)Pheo) and quinones as electron acceptors (Chapter 7, Renger and Holwartz; Chapter 8, Petrouleas and Crofts).

Spectroscopic and X-ray crystallographic studies have provided detailed kinetic and structural information on RCs from several different organisms (Allen and Williams, 1998; Hillier and Babcock, 2001; Heathcote et al., 2002). Figure 2 summarizes the proteins and prosthetic groups involved in the

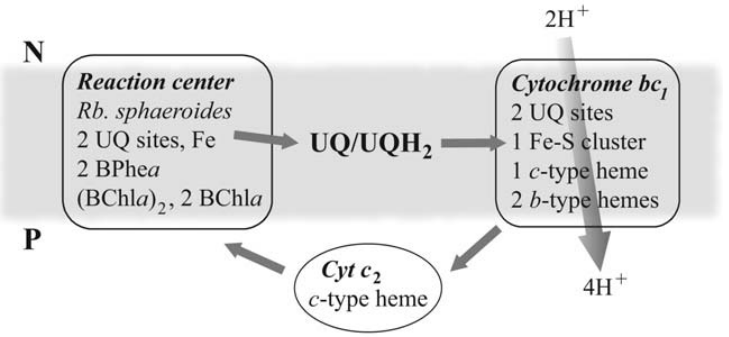

Fig. 2. Schematic summery of the protein complexes, pigments and redox cofactors involved in photosynthetic energy conversion in the purple bacterium *Rhodobacter sphaeroides*. The solid grey arrows show the electron flow while the shaded arrow indicates the site of trans-membrane proton transport. The figure is described in detail in the main text.

light-driven generation of a chemiosmotic proton gradient in the purple bacterium *Rhodobacter sphaeroides*. The RC contains three subunits, which together binds four BChl *a*, two BPheo *a*, two UQ and a single non-heme iron. These cofactors are positioned symmetrically around a central two-fold axis, which is a structural theme common to all RCs. The RC also contains a carotenoid that is believed to have a photoprotective function and a large number of BChls and carotenoids are bound to the surrounding antenna systems (Cogdell et al., 1999). Two of the RC chromophores form a BChl dimer, called the special pair, which serves as the photochemically active electron donor in this organism. Following absorption of an 870 nm photon by the special pair, an electron is transferred to the accessory BChl, to the BPheo, on to the first UQ acceptor Q_A and further to the second UQ denoted Q_B. The latter is reduced twice, protonated and then replaced by an oxidized UQ from the membrane pool. The UQH_2 molecules are re-oxidized by a Cyt bc_1 complex homologous to the respiratory complex III. The flow of electrons through the bifurcated electron-transfer pathway of the bc_1 complex generates the trans-membrane proton gradient. A soluble *c*-type Cyt closes the cyclic electron flow by reducing the RC $(BChla)_2^+$ radical with electrons from the bc_1 complex (Fig. 2).

In chloroplasts and cyanobacteria, PS I and PS II operate in series to drive the reduction of $NADP^+$ with electrons from water (Fig. 3). Research on oxygenic photosynthesis has recently advanced significantly with the availability of high and medium-resolution structures for cyanobacterial PS I and PS II, respectively (Fromme et al., 2001, 2002; Jordan et al., 2001; Rutherford and Faller, 2001; Zouni et al., 2001; Kamiya and Shen, 2003; Ferreira et al., 2004; Chapters 19–21). PS II is a Pheo/quinone type RC and the redox reactions that occur on the reducing side of this enzyme are very similar to those described above for the RC in *Rb. sphaeroides.* The redox cofactors and reactions that take place on the oxidizing side of PS II are, however, unique. The primary electron donor is a multimeric Chl *a* complex with absorption maximum at 680 nm (Chapter 7). Following photooxidation, $P680^+$ is rapidly reduced by a tyrosine denoted Y_Z (Chapter 9). This residue is in turn reduced by a $(Mn)_4$ cluster, which binds substrate water (Chapters 10–12, 25). Calcium and chloride are required for catalysis and are most likely directly associated with the active site (Chapter 13). A second redox-active tyrosine, Y_D, and Cyt b_{559} serve as auxiliary electron donors in PS II (Chapter 15). The multimeric PS II complex also contains a large number of LH pigments that are associated with its integral and external antenna systems (Chapters 2 and 3). The electron-transfer chain in PS II is linked to Cyt b_6f via the plastoquinone/plastoquinol (PQ/PQH_2) pool in the thylakoid membrane (Fig. 3). Cyt b_6f is structurally less well characterized as compared to the respiratory bc_1 enzyme. Nonetheless, the electron-transfer chain and the catalytic cycle of Cyt b_6f are most likely very similar to those described above for Cyt bc_1 (Berry et al., 2000). Cyt b_6f reduces the primary electron donor in PS I via plastocyanin. This small, soluble protein contains a single copper ion and is in some organisms replaced by a cytochrome.

The crystal structure of PS I is a trimer with each monomer containing 12 subunits and 127 cofactors

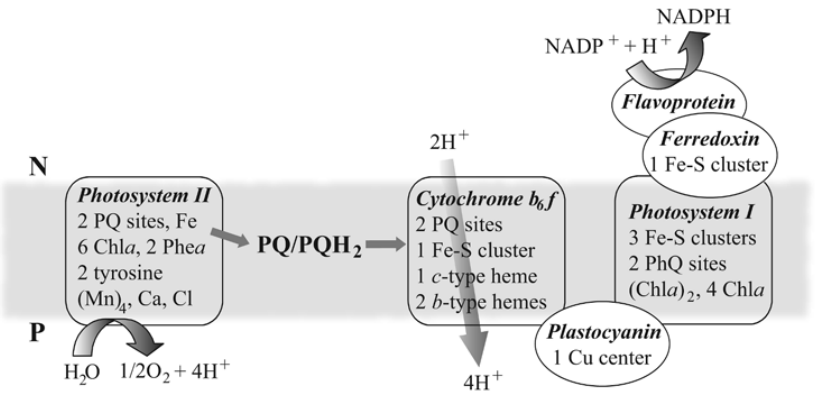

Fig. 3. Schematic overview of the protein complexes, pigments and redox cofactors involved in photosynthetic energy conversion in plants, green algae and cyanobacteria. The solid grey arrows show the electron flow while the shaded arrow indicates the site of transmembrane proton transport. The figure is described in detail in the main text.

(Fromme et al., 2001; Jordan et al., 2001; Chapter 19, Witt). The integral antenna of each monomer contains about 90 Chl *a* and 22 carotenoids. The RC core contains six Chl *a*, two phylloquinones (PhQ) and three $[Fe_4S_4]$ clusters. The primary donor in PS I is a Chl *a* pair with absorption maximum at 700 nm denoted P700. Upon photooxidation, P700 delivers an electron to a second Chl *a* species denoted A_0 and further to one of the phylloquinones. The electron-transport chain ends with the iron-sulfur clusters denoted F_X, F_A and F_B. The electrons are finally transferred from PS I to $NADP^+$ via ferredoxin and a flavoprotein.

3. Cofactor Properties and the Function of the Protein Matrix

In summary, the respiratory and photosynthetic enzymes contain several groups of cofactors. Prosthetic groups containing tetrapyrrolic macrocycles are functionally prominent. Hemes are involved in a variety of different reactions. Chl and BChl are the major LH pigments in photosynthetic organisms and the primary photochemistry involves (B)Chl and (B)Pheo molecules. A third group of common organic cofactors is the flavin nucleotides. For example, a number of flavoproteins donate electrons to the UQ/UQH_2 pool of the inner mitochondrial membrane (Fig. 1). Lipid-soluble quinones represent a fourth group of important organic redox cofactors. Plastoquinone, phylloquinone and ubiquinone, which in some organisms are replaced by menaquinone, are key players in the redox driven proton-translocation processes occurring in respiration and photosynthesis. Furthermore, amino acids are being used as endogenous redox cofactors. Tyrosines are involved in photosynthetic water oxidation and this residue has also been proposed to participate in the catalytic cycle of complex IV. In addition to heme iron, a number of redox-active metals are involved in biological energy transduction. Iron-sulfur clusters are essential for the electron-transfer chains in complex I, II and III of the respiratory chain, they serve as electron acceptors in photosynthetic RCs and in ferredoxins. Copper centers are found in complex IV and in plastocyanin and a $(Mn)_4$ cluster is essential for the activity of PS II.

Despite the range of chemical functionality represented by these prosthetic groups, the protein matrix has been recruited by evolution to further control chemical reactivity. A clear example of this is provided by (B)Chl *a* which performs energy transfer when located in the LH complexes and electron transfer when serving as a RC pigment. Proteins have the capability to modulate the kinetic and thermodynamic redox properties of their cofactors substantially. For example, tyrosine oxidation is an irreversible process in solution (Tommos et al., 1999). In contrast, the redox cycles of Y_Z and Y_D are reversible with the former being oxidized and reduced about 200 times per second in saturating light. The reduction potentials of Y_Z and Y_D differ by about 250 mV, with the former being the most oxidizing and having a potential close to tyrosine in water (Tommos and Babcock, 2000). Thus, PS II stabilizes $Y_Z^{\bullet}$ kinetically rather than thermodynamically to prevent

deleterious side reactions. Kinetic stabilization is required since a lowering of the $Y_Z^{\bullet}/Y_Z$ potential to suppress side reactions would result in a loss of the free energy necessary for catalysis. Redox proteins organize their cofactors spatially to form electron-transfer chains that are able to rapidly move electrons tens of Ångströms (Gray and Winkler, 1996; Page et al., 1999; Balabin and Onuchic, 2000). The core pigments in the RCs are arranged as to promote forward electron transfer and prevent energetically wasteful charge-recombination reactions. The quantum yield for the light driven charge-separation reactions approaches unity (Allen and Williams, 1998), which clearly shows the efficiency of the natural design. Moreover, enzymes contain catalytic clusters of cofactors to efficiently handle difficult chemistry, such as the breaking of strong chemical bonds or the accumulation of highly oxidizing potentials, without the formation of reactive, potentially toxic reaction intermediates (Tommos and Babcock, 1998; Babcock, 1999; Page et al., 1999).

B. Natural Protein Design

Biochemical function is determined by chemical structure. Indeed, the seemingly simple albeit lengthy amino-acid sequences of the respiratory and photosynthetic enzymes provide the entire information content for proper biological function (Anfinsen, 1973). A multiplicity of information is encoded within these sequences which are used to establish the protein fold and stability (Anfinsen and Sheraga, 1975), localize the protein in the cell (Muller and Blobel, 1984), assemble cofactors and subunits into functional complexes, bind substrates and perform catalysis, and even degrade (Narula et al.,1999). Natural protein sequences are engineered to satisfy all of these overlapping and sometimes competing requirements for function. The inherent complexity of the engineering requirements of the respiratory and photosynthetic enzymes coupled with their immense size present a daunting challenge to understanding the structure/function relationships in these proteins. Indeed, attempts to study catalytic action in much smaller and simpler natural protein structures are often complicated by interference from other parallel biological functions.

C. De Novo Protein Design

An emerging biomimetic approach to exploring protein structure/function relationships has grown out of the creation of proteins from first principles, i.e., *de novo* design (Richardson et al., 1984). As an inherently constructive approach, *de novo* design starts with simplicity and builds toward biological complexity (DeGrado et al., 1999). This approach provides for the rigorous testing of our understanding of fundamental biochemical structure and function relationships in natural proteins and enzymes. Over the past two decades, *de novo* protein design has progressed from demonstrating the feasibility of designing simple secondary structures such as monomeric α-helices (Marqusee et al., 1989) to synthesizing proteins with incipient enzymatic activity (D.E. Benson et al., 2000; Moffet et al., 2000; Baltzer et al., 2001; Bolon and Mayo, 2001).

The robust literature on natural proteins provides critical spectroscopic, electrochemical, structural and functional benchmarks for the success of *de novo* designed proteins. *De novo* design is not, however, solely restricted to biological mimicry as it is not limited by biological constraints. Virtually all peptide sequences can be studied since designed proteins need not be biologically competent. This allows for a fuller understanding of the design as well as the topology of sequence space (Maynard Smith, 1970). Additionally, protein folds not observed within the context of genomic biology may be possible within *de novo* protein design. Lastly, the ever-increasing variety of non-natural amino acids and synthetic cofactors provides designers with an augmented ability to adapt their designs.

The initial studies in protein design were aimed at constructing α-helices, the most common protein secondary structure. The engineering requirements for α-helix formation in aqueous solution have been delineated. Stable monomeric α-helices can be designed from short peptides composed mostly of alanines (Marqusee et al., 1989). Oligomeric α-helical designs utilize larger hydrophobic residues to drive association. The observed seven amino-acid, or heptad, pattern of hydrophobic and hydrophilic residues in coiled coils such as tropomyosin provided a critical insight for *de novo* design of associated α-helices (Hodges et al., 1972, 1981). The typical heptad repeat, denoted $(abcdefg)_n$ (McLachlan and Stewart, 1975), was composed of hydrophobic residues at positions *a* and *d* with charged residues at *e* and *g* and polar side chains at *b*, *c* and *f*. In either a two-, three- or four-stranded coiled coil, the residues in the heptad *a* and *d* positions form the hydrophobic core shrouded by

the interfacial *e* and *g* side chains with the *b*, *c* and *f* positions exposed to solvent. Hodges and co-workers demonstrated that the observed heptad repeat could be used as a design concept for the fabrication of two stranded coiled-coil proteins (Lau et al., 1984).

These simple α-helical peptides and their successors have helped to delineate the role of various factors in α-helix protein folding (Hill et al., 2000) and stabilization (Bryson et al., 1995). These designs allowed for the measurement of the intrinsic helical propensities of the individual amino acids. The observed preference for certain amino acids at α-helical termini due to terminal hydrogen bonding (N- and C-capping) was demonstrated to parallel the helix-capping propensities of the amino acids (Chakrabartty et al., 1993). Additionally, the role of electrostatic interactions (side chain/side chain and side chain/helix dipole) in stabilizing the α-helix was delineated.

The assembly of α-helices into more complex folds, the helical bundles and related coiled coils, progressed from these early studies on α-helices. Several general approaches to control oligomerization of *de novo* α-helical proteins have emerged. The minimalist approach utilizes leucines at heptad positions *a* and *d* to form the hydrophobic core (DeGrado et al., 1989). Peptides (α) composed of two heptads were shown to fold into $(\alpha)_4$ tetramers, or four-helix bundles. These sequences were shown to be modular in that they could be linked with loop regions to form dimeric $(\alpha_2)_2$ and monomeric (α_4) four-helix bundles (Ho and DeGrado, 1987). This family of highly stable *de novo* proteins is the ancestor of many designs relevant to respiration and photosynthesis.

A combinatorial approach demonstrated that a binary pattern of hydrophobic and hydrophilic residues was sufficient to generate stable four-helix bundles (Kamtekar et al., 1993). Synthetic genes were constructed from degenerate codons, NTN and NAN, containing a mixture of all four nucleotides (N). Hydrophobic positions, containing Phe, Leu, Ile, Met or Val, were engineered using the NTN codons while hydrophilic positions were composed of Glu, Asp, Lys, Asn, Gln or His from NAN codons. From the resultant library, 108 clones were selected, 48 possessed sequences consistent with the H/P binary-pattern design, and 29 could be expressed. Thus, the identity of the amino acid in each of the heptad positions was not critical for α-helix formation, but may play roles in generating a well-packed hydrophobic core (see below).

Aside from hydrophobic core design, metal ions can also be used to overcome the entropic barrier to helix association and provide for specificity of oligomerization of designed peptides. Simple poly-alanine based sequences elaborated with ligands provide for the metal-induced folding of helical bundles (Ghadiri et al., 1992). Unstructured, monomeric peptides with N-termini containing bipyridine (bpy) derivatives trimerize and fold into α-helices upon incorporation of the exchange inert transition metals Co(II) and Ru(II). Furthermore, the photophysics of the pendant $Ru(bpy)_3$ provides a convenient trigger for light induced electron-transfer events.

De novo design has progressed to the design of more complex protein folds using rational, computational and combinatorial methods. Mixed α/β secondary structures have been achieved using iterative rational and computational methods (Struthers et al., 1996; Dahiyat and Mayo, 1997). Impressive results have been obtained with the Zif268 zinc-finger domain ββα fold. While the natural zinc-finger requires Zn(II) to fold, removal of the metal ligands and iterative redesign of the hydrophobic core and critical turn regions provided a 23 amino acid ββα peptide whose structure matched the design. Successful design of the ββα fold was also achieved *de novo* by automated amino-acid selection using the backbone coordinates of Zif268. The selection of suitable amino acids from rotamer libraries was accelerated by use of a dead-end elimination algorithm. The design of β-sheet proteins has also progressed with simple β-sheet designs emerging (Kortemme et al., 1998; Wang and Hecht, 2002). Lastly, computational methods are being applied to globular proteins (Isogai et al., 1999, 2000) and $(\beta/\alpha)_8$ folds (Silverman et al., 2001). Thus, *de novo* protein design continues to mature.

The construction of simple protein scaffolds whether by rational design, computational means, recursive iteration or randomized combinatorial libraries has provided keen insight into protein folding and structure (DeGrado et al., 1999; Baltzer et al., 2001; Moffet and Hecht, 2001). In the helical bundles, the role of inter-helical interactions in protein oligomerization, stabilization and specificity have been delineated. The heptad repeat and the choice of hydrophobic residues are critical to conformational specificity and oligomerization state (Harbury et al., 1993). The nobs-into-holes packing of natural coiled coils is best reproduced using a combination of small and large side chains at each core layer (Munson et al., 1994,

1996). The judicious use of aromatic and β-branched residues provides for uniquely structured cores since these amino acids have few allowed rotamers on the α-helix (Dolphin et al., 1996; Gibney et al., 1997). The conformational specificity of a designed protein has even been mapped on sequence space (Gibney et al., 1999; Skalicky et al., 1999). Surface salt-bridges increase stability and provide a mechanism by which to avoid competing folds or topologies, i.e., negative design (Hecht et al., 1990). In addition, internal salt-bridges may lower the stability but can provide specificity (Schneider et al., 1997).

More than 30% of natural proteins contain metal cofactors and protein designers have incorporated metal ions into designed proteins to access their unique structural, Lewis acid, redox and catalytic activities (Holm et al., 1996). *De novo* metalloprotein design requires not only the selection of a sequence that folds into the designed structure but that also provides the correct ligands in an appropriate geometry for the metal. A variety of designed protein scaffolds have been explored for the incorporation of metals including hemes, iron-sulfur clusters, copper, zinc, nickel, mercury, arsenic and lanthanides (DeGrado et al., 1999). In addition to heme, iron-sulfur and copper designs, peptide/protein systems containing other prosthetic groups common in respiration and photosynthesis have been synthesized and characterized.

II. Construction of Proteins Containing Cofactors Involved in Energy Conversion

Just as simple helical peptides elucidated the governors of helix stability (Chakrabartty and Baldwin, 1995), designed cofactor/protein complexes are beginning to unveil the fundamental properties of their natural counterparts. As described in the introduction, a range of prosthetic groups are involved in the transfer of excitation energy, electron transfer and proton-coupled electron transfer in biological energy transduction. Members of the six most prominent cofactor groups are shown in Fig. 4. Below we review synthetic work aimed at revealing the engineering specifications and tolerances for the protein/cofactor interactions as well as the influence by the protein matrix on the chemical and redox properties of the type of cofactors shown in Fig. 4. Thus, redesign strategies and *de novo* design of heme proteins, (B)Chl proteins, flavoproteins, amino-acid radical proteins, iron-sulfur proteins, and copper-containing proteins are described. We end by summarizing the structural and functional properties of designs containing multiple cofactors.

A. Heme Protein Design

Hemes are used for a variety of functions including electron transfer, oxygen transport (Antonini and Brunori, 1971) and reduction (Babcock, 1999), substrate oxidation (Sono et al., 1996) and gene regulation (Brusslan and Peterson, 2002). In light of this, *de novo* heme protein design has seen a flurry of activity following the construction of the first synthetic heme protein (Sasaki and Kaiser, 1990). Since the focus of this review is on protein designs most pertinent to respiration and photosynthesis, we refer interested readers to two recent and comprehensive overviews of heme protein design (Gibney and Dutton, 2001; Lombardi et al., 2001).

The scaffolds chosen for heme protein design span from small, unfolded peptides to structured proteins with hydrophobic cores capable of sequestering the cofactors from solvent (Gibney and Dutton, 2001). Heme-peptide complexes, whose assembly is driven by the coordination chemistry of the metal, offer the ability to explore fundamental issues of heme-protein assembly and stabilization. Using spontaneous self-assembly reactions, metalloporphyrins have been incorporated into monomeric, disulfide-bridged dimeric and cyclic peptides via histidine coordination (Huffman et al., 1998; Rosenblatt et al., 2002). The covalent attachment of short His-containing peptides to the porphyrin propionate groups has provided minimal models. Due to their covalent nature, these complexes bear some relationship to the cysteine ligated *c*-type hemes. The peptide sequences can be either based on natural heme proteins, the mimochromes (Nastri et al., 1997), or *de novo* designed as in the peptide-sandwiched mesohemes (D. R. Benson et al., 1995). The spectral properties of these complexes are typical of *b*-type cytochromes and evince bis-His ligation as designed. Since the peptides fold into α-helices upon metal ligation, heme-peptide complexes have been used to study metal-based protein folding and oligomerization (D.R. Benson et al., 1995).

Larger proteins which are folded prior to metal incorporation provide the opportunity to utlize the protein matrix to direct metal ion coordination. As noted earlier, these designs require a primary sequence that codes for a proper ligand constella-

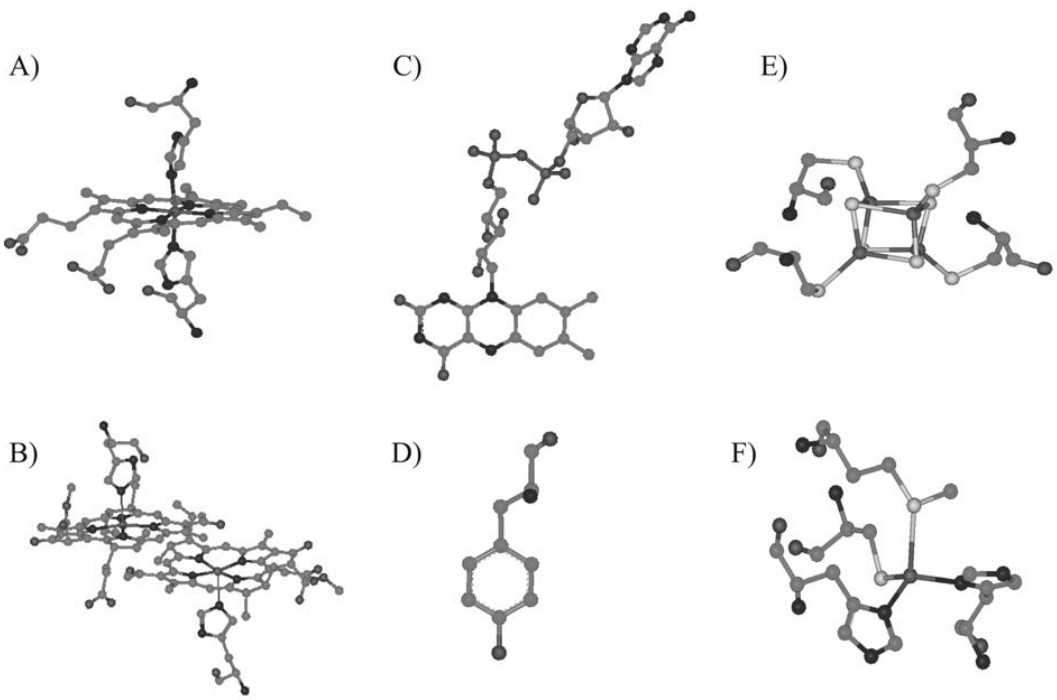

Fig. 4. The photosynthetic and respiratory complexes contain several different types of redox cofactors including hemes, (B)Chls, flavins, amino acids, iron-sulfur clusters and copper ions. (A) The b_L heme in the cytochrome bc_1 complex (Berry et al., 2000) contains a protoporphrin IX macrocycle and is axially ligated by His84 and His183. (B) The magnesium ions of the BChl special pair in the *Rb. sphaeroides* RC are ligated to the protein by histidines in a cofacial arrangement. The Chl phytyl chains have been deleted in the figure for clarity. (C) Flavin cofactors like flavin adenine dinucleotide (FAD) often perform $2e^-/2H^+$ chemistry and are required for function in complex I and complex II. (D) The $1e^-/1H^+$ redox chemistry of a tyrosine residue is essential for the catalytic cycle of PS II. (E) The $[Fe_4S_4]$ cluster from *E. coli* complex II is affixed to the protein by four cysteines, Cys148, Cys151, Cys154 and Cys214. (F) Representation of the blue-copper active site from plastocyanin (Guss and Freeman, 1983) in which the copper ion is ligated to the protein by His37, Cys84, His87 and Met92.

tion within a desired structure. Four-helix bundles are clearly most prevalent in *de novo* heme protein design and, in addition, serveral globular designs are known. Helical-bundle designs are aided by the structural predictability of this scaffold which allows for precise placement of the His ligands. Proper ligand placement and designed heme pockets allow for the efficient self-assembly of the heme-protein complexes. Additionally, the stable hydrophobic cores characteristic of helical bundles allow for structural alterations modulating the properties of the bound hemes. Notably, while the folds of these proteins are not determined by the metal, heme incorporation may alter the final holoprotein structures.

A disulfide bridged four-helix bundle represents one of the earliest successful *de novo* heme protein designs (Choma et al., 1994). The symmetric retro(S-S) construct contains two histidines disposed diagonally across the hydrophobic core in a designed, high-affinity heme pocket ($K_D \approx 10$ nM). The UV-visible spectra (Soret λ_{max} 414 nm (oxidized) and 426 nm (reduced)) and the EPR spectrum of the ferric species (g = 2.97, 2.25, 1.51) are typical of bis-His ligated *b*-type cytochromes. Additionally, its reduction potential (E_m value) of –220 mV *vs.* SHE is in the range observed for natural cytochromes. Control designs of retro(S-S) provided critical insight into the engineering of *b*-type cytochromes. First, the hydrophobic core can bind heme in the absence of His ligands. Second, the inclusion of histidines does not necessarily results in heme coordination. Lastly, a fully folded and highly stable scaffold may not be optimal for heme incorporation.

Dutton and co-workers combined the *de novo*

approach with insight from the respiratory and photosynthetic systems to construct cofactor/protein designs denoted maquettes (Robertson et al., 1994). The prototype heme-binding H10H24 maquette was designed using insight from complex III. First, the helical regions (28 amino acids) are longer than typical *de novo* designed proteins since the Cyt *b* subunit spans the membrane. Second, His ligands were placed in heptad *a* positions 10 and 24 by analogy to the spacing in complex III. Third, a Phe was placed in between the heme-binding His residues as observed in the natural system. Fourth, an Arg was placed at position 27, one helical turn below His24, to raise the heme midpoint potential as observed for Cyt b_H. Lastly, a Cys was placed at the N-terminus for the purposes of disulfide formation limiting the di-α-helical monomer, (α-SS-α), to a parallel orientation. The (α-SS-α) monomers self-assemble in solution as C_2 symmetric dimers, $(\alpha\text{-SS-}\alpha)_2$. The resulting 124-residue four-helix bundle H10H24 binds four hemes via bis-His ligation, two at 10, 10′ and two at 24, 24′. Furthermore, substitution of the His ligands with Ala, H10A24 or A10H24, resulted in loss of heme affinity as expected. The E_m value of a single heme *b* in H10A24 is –156 mV *vs.* SHE, which is fairly close to that of b_L (Fig. 4A) on which its design was based. The electrochemical properties of the four bound hemes are all slightly different. First, the designed heme-Arg27 electrostatic interaction raises the 24,24′ heme midpoint potential relative to the 10,10′ hemes. Second, electrostatic interactions between adjacent hemes, those at 10 vs. 10′ or 24 vs. 24′, result in a splitting of the midpoint potentials. Similar electrostatic effects on heme potentials have been observed for natural cytochromes.

Template-assembled synthetic protein (TASP) design has been utilized for the construction of modular protein 1, MOP1, a diheme Cyt *b* model (Rau and Haehnel, 1998). A pair of bis-His ligated hemes has been designed into a 122 amino acid four-helix bundle composed of four different helices, ABCD. Helices B and D, diagonal across the core, provide the His ligands while A and C aid in heme burial. Similar to H10H24, the hemes in MOP1 display distinct midpoint potentials, –106 and –170 mV *vs.* SHE, due to their local microenvironments with slightly more positive potentials than H10A24 due to greater heme burial. Thus, the TASP approach offers a synthetic route to heme protein designs with designed asymmetry.

A combinatorial approach has been applied to heme protein design both genetically and chemically. Within the library of four-helix bundles designed to test the H/P binary-pattern approach to protein design, fully half of the selected proteins bind heme (Rojas et al., 1997). His and Met residues provide ample ligands to heme binding in these proteins and, as observed previously, the presence of histidine does not guarantee heme affinity. Using the TASP approach, a 400-member combinatorial library was constructed to modulate the redox properties of the bound hemes. The resulting E_m values of the heme proteins could be varied by 60 mV (Rau et al., 2000) a value consistent with that later observed in hydrophobic variants of H10H24 (Gibney et al., 2001).

Computational methods have been applied to heme protein design. A tetraheme four-helix bundle has been designed using the CORE algorithm (Xu and Farid, 2001). The repacking algorithm designed a hydrophobic core around hemes ligated to a His-His motif analogous to the His-Phe-His motif utilized in complex IV to bind hemes *a* and a_3. The resulting 6H7H protein bound four *b*-type hemes perpendicular to each other in close proximity via bis-His ligation as designed. In a second computational study using a 3D-1D compatibility function, a globular heme protein has been designed. The designed globin 1 shares 26% sequence identity with myoglobin and binds a single heme via bis-His ligation (Isogai et al., 1999).

While most of the designed proteins are based on heme *b*, models for Cyt *a* have been fabricated as well. Heme *a* was isolated from beef heart and incorporated into H10A24 via a self-assembly reaction (Gibney et al., 2000). The spectroscopic hallmarks of the resulting bis-His ligated heme *a* maquette are similar to the bis-His ligated a_3 center. The E_m value of the soluble heme *a* protein, –45 mV *vs.* SHE, is substantially lower than the membrane-bound Cyt a_3.

Delineating the role of various factors in setting and modulating heme midpoint potentials is an area where *de novo* designed heme proteins have impressively demonstrated their utility (Gibney and Dutton, 2001). Indeed, the E_m of H10A24 was tuned over a 435 mV range without changing the axial ligands (Shifman et al., 2000). Aside from the axial ligands, the two most significant factors in modulating the potential of heme *b*-H10A24 are the type of porphyrin and the solution pH. The type of ligands and porphyrin can modulate the heme E_m over roughly a 300 mV range (Privett et al., 2002). Redox-Bohr effects modulate the E_m values of hemes in H10A24 by 200 mV between

pH 4 and 11. The combination of this redox-Bohr effect with different porphyrin types appears additive and results in the 435 mV range observed for H10A24. This 435 mV range spans nearly half that observed for natural heme proteins and covers the majority of *de novo* heme protein designs. Several other factors that also combine with the previous effects are involved in tuning heme potentials in designed proteins. First, the burial of the heme within a hydrophobic core can elevate the E_m value by 50–80 mV in larger heme protein systems (Shifman et al., 2000). Notably, this results in simple heme-peptide complexes being slightly more reducing than their corresponding designed heme protein counterparts. Second, the presence of charges local to the heme can modulate the potential by ± 50 mV (Shifman et al., 2000). Third, the interaction of aromatic amino acids with the porphyrin macrocycle can enhance the histidine to iron coordination equilibrium in designed heme proteins and alter the E_m by 50–80 mV (Kennedy et al., 2001). The results of these stepwise studies of heme potentials correlate well with the results from natural proteins and further validate using *de novo* design to study protein structure/function relationships.

B. (Bacterio)chlorophyll Protein Design

Chl and BChl represent the primary LH pigments in photosynthesis and, in addition, they serve as the photochemically active RC chromophores. In this section we focus on the former function by describing redesigns of natural proteins and *de novo* peptide/pigment model systems aimed at investigating assembly of (B)Chl-binding proteins. Efforts made to redesign or model properties of RC pigments are summarized in the Sections II.D. and G.

To promote efficient light absorption and energy transfer, the antenna tunes the electronic properties of its light-absorbing pigments and organizes the chromophores spatially with respect to each other and to the RC core. Antenna complexes exist in many different shapes and forms some of which are water-soluble while others are membrane associated (Chapter 2, Green and Gantt). Of the latter class, structural information is available for light-harvesting complex 1 (LH1) and 2 (LH2) of purple bacteria (Cogdell et al., 1999), the integral antenna of PS I (Fromme et al., 2001; Jordan et al., 2001) and the external and integral antenna of PS II (Kühlbrandt et al., 1994; Zouni et al., 2001; Kamiya and Shen, 2003; Ferreira et al., 2004; Chapters 18–21). The structural data show that (B)Chl binding is intricate and involves a number of pigment-protein and pigment-pigment interactions including coordination of the central Mg(II) ion to polar amino acids or to main-chain carbonyl groups, hydrophobic interactions of the phytyl tail with the protein matrix and/or other pigments, hydrogen bonds between the tetrapyrrole ring and the protein, and π-π interactions between pigments. Redesigns of natural antenna proteins in combination with reconstitution techniques have been employed to reduce the complexity of the (B)Chl-protein interactions and identify structurally and functionally important amino-acid sequences. The circular structures of LH1 and LH2 are constructed by a repeating building block containing a peptide pair. These two subunits are named α and β and the central 20–24 residue region of each peptide forms a single trans-membrane α-helix. The β-peptides of LH1 isolated from *Rb. sphaeroides* and *Rhodospirillum rubrum* contain 48 and 54 residues, respectively. Loach and co-workers chemically synthesized truncated versions of these β-subunits to identify residues required for subunit formation and for assembly of LH1. A peptide containing the last 16 residues of the C-terminus of the *Rb. sphaeroides* β-peptide did not fold with or without the native α-peptide. Expanding the sequence to a 31-mer, which included the whole central trans-membrane part, induced folding but neither of the *Rb. sphaeroides* and *Rs. rubrum* 31-residue β-peptides associated with their native α-peptides to assemble LH1-type complexes (Meadows et al., 1998). Expanding the β-sequences even further induced antenna assembly (Kehoe et al., 1998). Similar approaches to study (B)Chl binding and antenna assembly have been used by other research groups. Nango and co-workers studied assembly of Zn-BChl *a* (Kashiwada et al., 2000) and BChl *a* (Nango et al., 2002) with abridged variants of the LH1 β-peptide in lipid bilayers and n-octyl-β-D-glucopyranoside micelles. Braun et al. (2002) redesigned the sequence of the LH2 α-subunit from *Rb. sphaeroides* and showed that eight residues in the 25-residue trans-membrane helix part could be replaced by three Ala and five Leu without major effects on the biochemical and spectroscopic features of LH2. Interestingly, an additional insertion of four residues on the outside of the C-terminus of the redesigned helix abolished functional complex formation. Redesign studies have also been made on antennas of green plants including a recent demonstration of Chl binding to 16-residue

peptide segments of light-harvesting complex II (Eggink and Hoober, 2000).

Considering the complexity of natural (B)Chl-binding proteins, it is not surprising that *de novo* work in this research area are scarce. Nango and co-workers synthesized two polypeptides intended to assemble into BChl-binding four-helix bundles in n-octyl-β-D-glucopyranoside micelles (Kashiwada et al., 1999). Although the α-helical content of the synthetic peptides was low, ≤ 25% in the presence of BChl *a*, some indications of pigment/peptide interactions were detected. In a recent report by Haehnel and co-workers, preliminary data on a stepwise methodology to control binding of one or two Chl derivatives to specific sites in TASP four-helix bundles are described (Rau et al., 2001). The strategy used by these authors was to delete the phytyl tail of the tetrapyrrole macrocycle, replace the central Mg(II) ion with Zn(II) to increase the binding strength to side-chain ligands, and attach the macrocycle covalently to the protein. This method could prove to be a valuable tool in the further development of novel (B)Chl-binding proteins.

C. Flavoprotein Design

Flavoproteins contain tightly bound flavin nucleotides, which participate in two proton coupled electron-transfer reactions when converting from the fully reduced form to the semiquinone radical to the fully oxidized state. Flavins are key cofactors in several respiratory and photosynthetic redox enzymes and in a number of other oxidoreductases (Massey, 1995). In early work by Kaiser and co-workers, the catalytic versatility of flavins was utilized by the construction of semisynthetic flavoenzymes. These proteins were made by covalently attaching flavin analogs to side chains at or near the active sites of natural enzymes such as papain (Levine and Kaiser, 1978) and hemoglobin (Kokubo et al., 1987). This method, coined 'chemical mutation' by the authors, produced enzymes with catalytic activities significantly different to those of the native systems (Kaiser and Lawrence, 1984). Flavin redox chemistry has also been explored in more elaborate redesign of natural proteins. Mihara et al. (1996) attached 21-residue segments of trans-membrane α-helices from bacteriorhodopsin onto a manganese porphyrin template. The template-assisted construction contained three peptides of identical sequence and a fourth peptide with a different amino-acid sequence containing a unique Cys. The flavin analog 7-acetyl-10-methyl-isoalloxazine was attached to the Cys with the aim of constructing an electron-transfer system in which the flavin serves as a mediator between externally added N-alkyl-1,4-dihydronicotinamide compounds and the Mn(III) porphyrin template. The rate of Mn(III) reduction was measured in lipid vesicle samples containing the template-assisted protein construct with and without the covalently attached flavin. The reduction rate was accelerated about six times in samples containing the flavin. The rate enhancement was about twofold when comparing samples with covalently bound *vs*. externally added flavin. Similar work in which one or two isoalloxazine rings were attached to a single polypeptide chain designed to fold into a four-helix bundle structure have been reported more recently (Tomizaki et al., 2000). In one study, the oxidation rate of N-benzyl-1,4-dihydronicotinamides was measured in micelles containing surfactants with different length of their hydrocarbon tails. The authors noted that the oxidation rate increased about six times when surfactants containing chains longer than twelve carbons were used. This result was interpreted that the flavin-containing bundle and the long-chain surfactants formed an expanded hydrophobic core that was more easily accessible for the substrate. In a second study, the oxidation rate of N-alkyl-1,4-dihydronicotineamide was investigated as a function of the length of the substrate alkyl chain. The oxidation rate was sensitive to the substrate size suggesting that the interior of the bundle was involved in positioning the substrate relative to the attached flavin unit(s) (Tomizaki et al., 2000).

Although RCs are driven by (B)Chl-based photochemistry, flavins can be used to study the major functional theme in photosynthesis — light-induced electron transfer. Mauk and co-workers made a semi-synthetic flavoCyt *c* by attaching 7-acetyl-10-methylisoalloxazine covalently to the surface of the protein (Twitchett et al., 1997). Electron transfer from the fully reduced flavin to the ferric heme group was achieved by laser flash photolysis of the flavin moiety. The electron-transfer rate was measured as a function of driving force and temperature. From these experiments, the nuclear reorganization energy associated with the intramolecular electron-transfer process could be estimated and, by comparing with data in the literature, the contribution of the solvent-exposed flavin moiety derived. This work demonstrated the feasibility of using a covalently

attached flavin as a light-induced initiator to trigger and characterize intramolecular electron-transfer reactions in proteins. Dutton and co-workers took advantage of the photochemical activity of flavins in the construction of a photoactivatable flavo-heme four-helix bundle (Sharp et al., 1998). The H10H24 heme-binding protein described in Section II.A was redesigned into a dimeric helix-loop-helix protein. Covalent attachment of 7-acetyl-10-methylisoalloxazine to a single Cys present on each 62-residue monomer followed by heme ligation provided the fully assembled flavoCyt. The designed protein exhibited the characteristics of a stable, water-soluble four-helix bundle with two tightly bound heme groups and two flavins incorporated into the hydrophobic core. Following the structural characterization, Sharp et al. (1998) investigated the functional properties of the *de novo* designed protein. The singly reduced flavosemiquinone radical state was produced by illuminating samples containing the fully oxidized flavoCyt with white light in the presence of a sacrificial electron donor. Electron transfer between the photogenerated semiquinone radical and the ferric heme cofactors was monitored optically by following the accumulation of reduced heme. By using two hemes with different midpoint potentials as electron acceptors, the rate of electron transfer between the semiquinone groups and the ferric hemes was investigated in both a thermodynamically downhill and uphill reaction. With a driving force of ~ –100 mV, the laser-induced electron transfer from the semiquinone state to a ferric 1-methyl-2-oxomesoheme XIII occurred on the 100 ns time scale. The energetically unfavorable reduction of ferric protoheme IX by the semiquinone radical was substantially more sluggish. This work provides an example of using design proteins to investigate reactions that occur in biology, in this case light-induced electron transfer between cofactors residing in a hydrophobic protein environment.

D. Amino-Acid Radical Protein Design

Above we have described redesign and *de novo* design strategies aimed at exploring the interactions between peptide/protein systems and cofactors containing tetrapyrrole macrocycles (Figs. 4A and B) or an isoalloxazine ring (Fig. 4C). In addition to these exogenous cofactors, amino acids are involved in catalytic redox reactions. Studies performed in the Babcock laboratory have shown that tyrosine redox chemistry is key to both H_2O oxidation in PS II (Tommos, 2002) and O_2 reduction in complex IV (Babcock, 1999; Schultz and Chan, 2001). In addition to Tyr (Fig. 4D), Trp, Cys and Gly serve as redox cofactors in a number of enzymes (Stubbe and van der Donk, 1998). Amino-acid radicals are typically highly oxidizing and this property, combined with the inherent reactivity of the radical state, suggests the existence of structural motifs to promote the reversible and controlled radical chemistry occurring in proteins. Protein engineering studies, work on short non-structured peptides and *de novo* protein design have been performed to relate structural themes to the functional characteristics of amino-acid radical enzymes.

Allen, Williams and their co-workers performed a careful investigation on how hydrogen-bonding interactions between side chains and the macrocycles of the *Rb. sphaeroides* special pair influence its E_m value (Lin et al., 1994; Chapter 32). The wild-type $(BChl)_2$ species (Fig. 4B) is H-bonded to a His and, upon removal of this interaction, the E_m drops from 505 to 410 mV. The addition of a single H-bond at various ring positions raises the potential and, interestingly, the effects of the single-site mutations are additive. By using various combinations of single, double and triple mutants, the $(BChl)_2$ E_m value could be tuned within the range of 410–765 mV. In a later study, this observation was used to engineer a quadruple mutant in which the $(BChl)_2$ potential was elevated to > 800 mV (Kálmán et al., 1999). Tyrosine was introduced at positions analogous to the Y_Z or Y_D site in PS II. Following light excitation, the optical and EPR spectra of the engineered RC samples changed in a manner consistent with Tyr radical formation. The spectra represent a mixture of BChl and Tyr radicals whose relative contributions were sensitive to the bulk pH with alkaline conditions favoring the latter. Remarkably, the alterations made in the bacterial RC did not duplicate PS II pigments or protein sequences but strictly used a design concept to create a dramatic change in its functional properties.

Light-induced oxidation of aromatic residues was recently demonstrated in another redesigned system and, in this case, the template protein was not of photosynthetic origin (Di Bilio et al., 2001). Gray and co-workers have combined synthetic methods with laser flash/quench techniques to characterize electron-tunneling reactions in a range of natural proteins (Gray and Winkler, 1996). In addition to the well-established method of using ruthenium as a photo-triggered reductant or oxidant, the Gray laboratory more recently introduced the use of rhenium to

create a light-induced highly oxidizing electron acceptor. A rhenium complex was attached to either of two histidines, H83 or H107, on the surface of azurin from *Pseudomonas aeruginosa* and the structures of the two metal-modified proteins were determined to high resolution by X-ray crystallography. Following light excitation, irreversible oxidation of residue W48 was observed in the H83 protein and of Y108 in the H107 metal-modified system. Notably, radical migration to Y108 following $W48^{\bullet}$ formation was not observed in the H83 protein, as would be predicted from comparing the solution potentials of the aromatic residues. The authors concluded that the protein matrix influences the thermodynamic and/or kinetic properties of the amino-acid radicals.

To investigate the redox properties of Trp and Tyr residing in a structurally well-determined protein milieu was also the goal with the construction of a *de novo* designed radical maquette (Tommos et al., 1999). Radical formation and migration have been studied by pulse radiolysis on non-structured peptides of various length spanning from simple Trp–Tyr dimers (Prütz and Land, 1979) to Trp/Tyr-containing poly-proline linkers (Bobrowski et al., 1999). As noted earlier, the characteristics of radical chemistry in solution are very different to the properties of functional amino-acid redox cofactor. Consequently, a buried radical site represents a key design feature of the radical maquette. This protein is based on a three-helix bundle scaffold (Johansson et al., 1998) and has either a unique Trp or Tyr in a heptade *a* position. The remaining 64 residues of the monomeric protein sequence were chosen to be redox inert in order to isolate the radical chemistry to a single site in this initial design. The Trp or Tyr containing three-helix bundles, denoted α_3W and α_3Y respectively, were chemically synthesized and an initial characterization provided data consistent with two stable, helical structures each containing a single aromatic side chain residing in a hydrophobic environment (Tommos et al., 1999). This conclusion was confirmed in a structural analysis of the recombinantly expressed α_3W protein using multidimensional NMR techniques (Dai et al., 2002). The derived structural model shows that α_3W is a three-helix bundle with its Trp located in the core, as shown in Fig. 5. Calculation of the accessible surface area shows that the Trp is buried except a ~ 30 % solvent exposure of its indole hydrogen. The NMR work also revealed that the Trp is involved in a cation-π interaction with a nearby lysine. The effect of this interaction on the Trp reduction potential was investigated using density-functional theory (Dai et al., 2002). The calculations predict an increase in the potential, which is consistent with electrochemical data on α_3W relative to Trp free in solution. Cation-π interactions are common in natural proteins and may represent one mechanism by which redox proteins control the thermodynamic properties of its aromatic residues. Thus, the combination of *de novo* design with detailed structural, electrochemical and quantum mechanical analyses identified a structural motif of interest for understanding amino-acid redox chemistry in proteins.

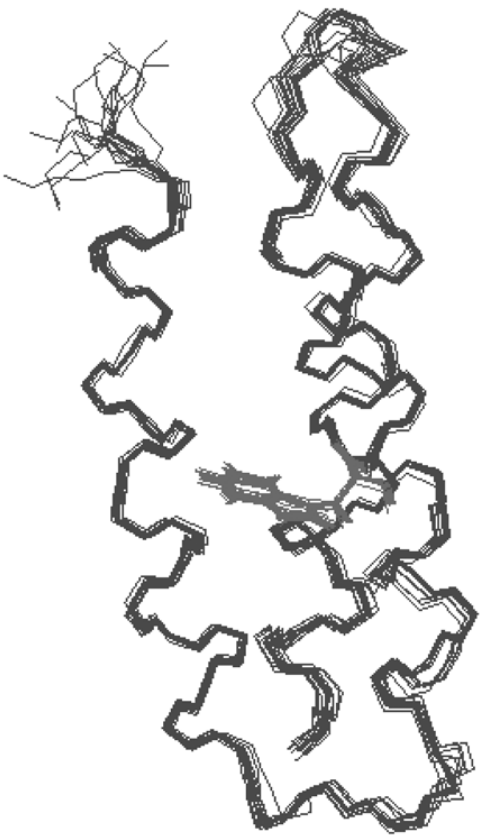

Fig. 5. Superposition of the family of 16 refined structures of the *de novo* design radical protein α_3W (Dai et al., 2002). The figure represents a back-bone trace of the monomeric three-helix bundle protein with its unique tryptophan shown as a line drawing. The PDB accession number is 1LQ7.

E. Iron-Sulfur Protein Design

While most recognized for their electron-transfer roles in the energy-converting enzymes, iron-sulfur proteins are involved in a number of biochemical processes including regulatory roles in iron homeostasis and catalytic roles in RNA, β-branched amino acid and vitamin syntheses (Beinert et al., 1997). Most iron-sulfur proteins utilize Cys residues to ligate mono-, bi-, tri- or tetra-nuclear clusters, while occasionally His, Asp or exogenous ligands are observed (Johnson, 1994). Although respiratory and photosynthetic proteins contain a variety of these clusters, the high potential iron protein (HiPIP) and ferredoxin-type clusters, $[Fe_4S_4]^{3+/2+}$ and $[Fe_4S_4]^{2+/+}$, respectively, have been the major focus of iron-sulfur protein design efforts to date.

Using a minimalist approach, Gibney et al. (1996) utilized the consensus sequence -Cys-X_{aa}-X_{aa}-Cys-X_{aa}-X_{aa}-Cys- from *Clostridial* ferredoxins to design a 16-residue $[Fe_4S_4]^{2+/+}$ binding peptide. The resulting ferredoxin maquette (FdM) binds a single $[Fe_4S_4]^{2+/+}$ cluster using four Cys ligands in a fashion similar to that of complex II (Fig. 4E). The UV-visible (λ_{max} at 385 nm and $\varepsilon = 16{,}100\ M^{-1}\ cm^{-1}$) and EPR (resonances at $g = 2.05$, 1.93 and 1.89) spectroscopic signatures are reminiscent of natural $[Fe_4S_4]^{2+/+}$ ferredoxins. Furthermore, the measured E_m value for the $[Fe_4S_4]^{2+/+}$ couple at –350 mV *vs.* SHE is typical of a natural tetranuclear ferredoxin. Scott and Biggins (1997) used a similar concept designing a helical bundle to bind a single $[Fe_4S_4]^{2+/+}$ cluster. The $[Fe_4S_4]^{2+/+}$ binding loop regions from the F_X cluster of PS I were placed into a designed four-helix bundle. The UV-visible (λ_{max} at 408 nm) and EPR (resonances at $g = 2.053$, 1.936 and 1.910) spectroscopic features of the resulting α_4-FeS construct indicate that it is a $[Fe_4S_4]^{2+/+}$ ferredoxin. The E_m value of α_4-FeS is –422 mV *vs.* SHE, which is significantly higher than the –670 mV potential measured for F_X (Vassiliev et al., 2001), but close to the value observed for the FdM. Using the computational redesign algorithm DEZYMER, Coldren et al. (1997) created a HiPIP $[Fe_4S_4]^{3+/2+}$ binding site within the core of thioredoxin. The resulting construct denoted Trx-Fe_4S_4 binds a single $[Fe_4S_4]^{3+/2+}$ cluster. The electrochemical ($E_m > 300$ mV) and EPR (resonances at $g = 2.06$, 2.03 and 2.01) properties of Trx-Fe_4S_4 are consistent with a HiPIP character and distinct from the two ferredoxin designs, FdM and α_4-FeS. Thus, three different design concepts have all provided successful iron-sulfur proteins relevant to photosynthesis and respiration.

The construction of ferredoxin maquettes has aided efforts to probe the engineering tolerances of $[Fe_4S_4]^{2+/+}$ cluster assembly and stability within a minimal peptide scaffold. Mulholland et al. (1998, 1999) found that the initial FdM design based on *Clostridial* ferredoxins stabilized the cluster to a greater extent than designs based on other iron-sulfur proteins including the Rieske protein. Additionally, both the liganding and non-liganding amino acids of the FdM have been found to be critical to $[Fe_4S_4]^{2+/+}$ assembly and stability. Indeed, the non-ligand amino acid requirements of the FdM correlated well with bioinformatic analysis of natural ferredoxins. Recently, the FdM has been used to investigate electrochemical function relevant to proton pumping at the $[Fe_4S_4]^{2+/+}$ cluster N2 of complex I (Kennedy and Gibney, 2002). The E_m value of the $[Fe_4S_4]^{2+/+}$ couple in IGA (related to the FdM by a single Ala to Gly change at position 9) demonstrates a 60 mV/pH unit dependence between pH 7 and 11. This redox-Bohr effect is indicative of a single proton - single electron coupled reaction. The observed reduced state pK_{red} value is 9.3 and the oxidized state pK_{ox} value is 6.35. The observed shift in pK_{red} upon metal incorporation suggests that the proton-coupling site is localized either on the metal cluster or its ligands, and not on a remote residue. This initial study shows the utility of simple designed metalloproteins in revealing the engineering specifications of important biological phenomena like proton-coupled electron transfer.

F. Copper Protein Design

Since the discovery of copper at the active site of the type 1 or blue copper protein azurin (Broman et al., 1963), the copper centers in respiration and photosynthesis have intrigued biochemists and bioinorganic chemists alike. The flattened tetrahedral ligand geometry about the Cu(II) ion in plastocyanin (Fig. 4F; Guss and Freeman, 1983), composed of two His and one Cys^- ligand in a trigonal plane with a axial Met sulfur, suggests a rack or enatatic state in which the coordination geometry is determined by the protein fold rather than by the metal (Malmström, 1994; Williams, 1995). The coordination of the Cu(II) imparts unique spectroscopic and electrochemical properties on the metal center including an intense blue color (λ_{max} at 600 nm; $\varepsilon = 2500 - 6000\ M^{-1}\ cm^{-1}$), a small Cu(II) parallel hyperfine coupling constant ($A_{||}$ of $60 - 90 \times 10^{-4}\ cm^{-1}$) and relatively oxidizing potentials

(+150 mV to +800 mV vs. SHE) (Solomon et al., 1998). These represent the critical hallmarks of a successful blue copper protein design.

Several attempts to design a blue copper protein *de novo* have been made using concepts similar to those that proved successful in iron-sulfur protein design. In a minimalist approach, DeRose and co-workers designed and characterized a pair of copper-binding peptides denoted BCP-A and BCP-B (Daugherty et al., 2002). The 22 amino-acid BCP-A peptide contained the Cu(II)-binding loop of plastocyanin with the fourth ligand, a His, modeled at an appropriate position in a design analogous to that of the ferredoxin maquette. In BCP-B the metal ligands were modeled on either side of a designed β-turn. Working at pH 9.8 to minimize Cu(II)-thiol redox chemistry, stable Cu(II) complexes of BCP-A and BCP-B were formed in 50% and 65% yield, respectively. The EPR and ENDOR spectra of BCP-A and BCP-B indicate that the peptide ligands provide His_2Cys_1 coordination to the Cu(II) in a Jahn-Teller distorted octahedral environment with additional exogenous ligands. Notably, BCP-A evinces a tetrahedral twist in the square plane that elevates its E_m value by 76 mV relative to BCP-B (–11 mV *vs.* SHE). Both designs indicate that these minimal peptides are not sufficient to enforce Met ligation nor protect the metal from solvent coordination.

Haehnel and coworkers have used the TASP strategy together with a combinatorial library approach to design a His_2Cys_1 copper center within a four-helix bundle (Schnepf et al., 2001). Of the 96 proteins synthesized, about one third bound Cu(II) as evinced by the presence of a S to Cu(II) charge-transfer absorption band near 400 nm at pH 7.5. Notably, the LMCT bands bleached within 15 minutes presumably due to oxidation of the cysteines by Cu(II). The three protein constructs most stable to Cys oxidation, MOP5, MOP6 and MOP7, were selected for more detailed studies. The placement of the MOP5 ligands at the center of the helix and the presence of two local Leu residues serve to protect the Cu(II)-Cys from solvent and redox chemistry which leads to the enhanced stability of the Cu(II)-MOP5 complex. The spectroscopic properties of these three copper proteins indicate that they possess coordination geometries between planar (type 2) and tetrahedrally distorted (type 1.5) Cu(II)-binding sites. In concert with the entatic or rack state hypothesis, it was concluded that the stability of the folded apoprotein is essential to enforce the weak metal-ligand bonds observed in blue copper proteins.

Using DEZYMER, Hellinga (1998) designed a series of $His_2Cys_1Met_1$ centers into thioredoxin. The algorithm was improved via an iterative redesign process based on the results from the initial designs. Two significant design concepts were employed in later designs. First, the site was buried within the protein core to limit water access and Cu(II)-thiol redox chemistry. Second, negative protein design was implemented to destabilize other competing Cu(II) coordination geometries. Spectroscopic characterization of the final copper(II) complexes demonstrate $His_2Cys_2(H_2O)_1$ coordination within the thioredoxin mutants. While attempts at replacing a H_2O ligand with a Met proved unsuccessful, azide addition resulted in formation of a $His_2Cys_2(N_3)_1$ site consistent with the azide complex of the type 1.5 Met121 mutants of azurin. Thus, while a design that provides all the hallmarks of a blue copper protein remains elusive, these designs provide basis for further optimization and illustrate several key engineering requirements of blue copper proteins.

G. Multicofactor Protein Design

Respiratory and photosynthetic protein complexes invariably contain a combination of redox-active cofactors organized for electron/proton transfer and catalysis (Figs. 1–3). Remarkably, complex I sequesters more than ten individual redox cofactors including a flavin mononucleotide, quinones and a host of $[Fe_2S_2]$ and $[Fe_4S_4]$ clusters. Thus, protein biomimetics for energy-transducing enzymes requires design concepts and construction methodologies for the assembly of multicofactor proteins. Below we describe designs that begin to reveal the engineering specifications requisite for the construction of these biomimetics.

Kálmán et al. (1999) redesigned the hydrogen bonding to the $(BChl)_2$ electron donor in *Rb. sphaeroides* (Fig. 4B) to construct a PS II-like RC capable of Tyr oxidation (Chapter 32). Attempts have also been made to reproduce the structural and functional properties of this remarkably complex light-activated cofactor in *de novo* designed systems. In an early study from the Dutton laboratory, coproporphyrin I (CP) was selected as a model for the $(BChl)_2$ species (Rabanal et al., 1996). The CP was attached to the N-terminus of a H10H24 peptide and this construct was

connected via an unsymmetric disulfide bond to a second H10H24 peptide with an acetylated N-terminus. When dissolved in aqueous solution, the CP-H10H24$_2$ heterodimer assembles into a four-helix bundle. The monomeric and dimeric forms of CP have distinct optical spectra that were used to characterize the properties of the appended chromophore. The dimer-monomer K_D value for the CP attached to H10H24 is considerably lower, $< 10^{-8}$ M, than the value of about 2×10^{-5} M for CP free in solution. The dimer spectrum remained unchanged upon heme ligation, consistent with an external, solvent-exposed location of the CP pair. Thus, the structural characterization of [CP-H10H24$_2$]$_2$ showed that it assembles into a parallel four-helix bundle with four hemes bound in the core and a cofacial CP pair at the N-terminus as designed. In a more recent study, pyrene was used to model a (B)Chl special pair (Jones et al., 2000). A pyrene chromophore was attached to the N-terminus of a 24-residue peptide containing Leu and Ile residues in heptad *a* and *d* positions and residues with high helical propensities in the majority of the remaining positions. The peptide also contained a Trp in a solvent-exposed heptad *f* position. In aqueous buffer the pyrene-peptide has ~ 60% secondary structure and exists in a concentration-dependent monomer-dimer-octamer equilibrium. Laser flash photolysis experiments were performed using peptide samples in the μM range at which the octamer state dominates. Photo-oxidation of the pyrene resulted in the reduction of the externally added electron acceptor methyl viologen followed by formation of a species assigned to a tryptophan cation radical. Although the pyrene/peptide assembly describe above does not represent a well-defined system, it shows promise with respect to introducing function into photosynthetic RC inspired designs.

The covalent attachment of cofactors at the peptide termini provides one method to construct mixed-cofactor proteins. In addition, Lys, Cys and His residues can be used for covalent linkage of various cofactors. To study Chl/protein-binding interactions, Rau et al. (2001) formed covalent oxime bonds between modified lysines and aldehyde groups on the tetrapyrrole rings of Zn-Chl derivatives. Flavins can be attached to Cys via alkylation, as originally described by Levine and Kaiser (1978). A novel flavoCyt was constructed by redesigning the prototype disulfide-bridged H10H24 into a helix-loop-helix protein with a unique Cys in each monomer. Flavin attachment followed by heme self-assembly provided the photoactivatable heme-flavin maquette described in more detail above (Sharp et al. 1998).

The methodologies developed by Gray, Millett and their respective co-workers to attach photoactive ruthenium complexes to His (Gray and Winkler, 1996) and Cys (Geren et al., 1991) residues, have been of ample use in the construction of functional *de novo* designed proteins. The TASP four-helix bundles MOP2 and MOP3 were synthesized by covalent attachment of a Ru(bpy)$_3$ complex (Rau et al., 1998). These designs contain an interior bis-His heme-binding site as well as a unique Cys to which he Ru(bpy)$_3$ analogue was coupled. Flash-induced electron transfer between the solvent exposed Ru(II)(bpy)$_3$ complex to the ferric heme in the protein core was studied as a function of distance between the two metal centers. By changing the position of the Cys, the through-helix electron donor/acceptor distance was increased by about 4 Å in MOP2 relative to MOP3. The measured drop in the electron-transfer rate was in reasonable agreement with predictions made using literature values for electron-tunneling rates.

The Ru(II)(bpy-peptide)$_3$ complex used to explore metal-induced protein folding (Ghadiri et al., 1992) has been redesigned into a mixed cofactor three-helix bundle to study electron transfer (Mutz et al., 1999). The Ru(II)(α*p*)3 bundle contains two 20-residue peptides of identical sequence and a third peptide in which an exterior His has been introduced to coordinate a Ru(III)(NH$_3$)$_5$ complex. Photo-oxidation of the Ru(II)(bpy)$_3$ electron donor results in electron transfer along the α-helix to the Ru(III)(NH$_3$)$_5$ acceptor. By changing the position of the metal-coordinating His, the electron donor/acceptor distance was increased by 4.2 Å and 6.3 Å in a stepwise manner. Electron-transfer rates were measured for the Ru(II)(α*p*)3 series using laser-flash photolysis and pulse-radiolysis methods. A β value, reflecting the electronic coupling between the electron donor and acceptor, of 1.2 ± 0.1 Å^{-1} was derived from the kinetic data. The authors concluded that this value is within the 0.9–1.4 Å^{-1} range typically observed for natural proteins and consistent with predictions made using theoretical pathway models of through-helix electron tunneling. This work further validates the use of *de novo* proteins to study biochemical function.

Ogawa and co-workers have constructed ruthenium modified two-stranded coiled coils to study electron transfer across a non-covalent interface and, more recently, directionally along helices. Kozlov and Ogawa (1997) designed and synthesized an amphiphatic

31-residue peptide with a single His in a heptad *f* position, to which Ru(II)$(bpy)_3$ or Ru(III)$(NH_3)_5$ were attached. Dissolving the metallopeptides in buffer gives a statistical mixture of homo- and heterodimers but, as noted by the authors, only the latter species is capable of intramolecular electron transfer across the helix-helix interface. Using the laser-flash quench method (Chang et al., 1991), a first-order rate constant that was independent of the peptide concentration was derived. This rate constant was assigned to the Ru(II)$(NH_3)_5$ to Ru(III)$(bpy)_3$ electron-transfer reaction across the hydrophobic core of coiled-coil dimer. This initial study was followed by more detailed characterizations of the metallopeptides (Kornilova et al., 2000) and an investigation of the influence of surface charge on the interhelical electron-transfer process (Kornilova et al., 2001).

Gibney et al. (1996) used a modular approach to synthesize simple analogues for the respiratory complexes II and III, which contain both hemes and iron-sulfur clusters (Fig. 1). The helix-loop-helix ferredoxin-heme maquette (HLH-FdM) bridged the heme-binding helical regions of H10H24 with the $[Fe_4S_4]$-binding FdM as a loop region. The resulting 67 amino-acid peptide self-associates as a dimeric four-helix bundle and binds four hemes and two iron-sulfur clusters. Notably, constraining the FdM within the HLH-FdM scaffold did not alter the spectroscopic or electrochemical properties of the bound $[Fe_4S_4]$ centers. The requisite specificity was designed using different ligand sets arranged in different coordination geometries, linear bis-His *vs.* tetrahedral Cys_4, to provide selectivity for heme and $[Fe_4S_4]$. Additionally, the order of cofactor incorporation was important for assembly. The $[Fe_4S_4]$ cluster was inserted first followed by the hemes because the incorporation of heme first leads to a kinetic Cys-ligated heme product, which slowly converts to the thermodynamically favored bis-His ligated heme. Other researchers have used a similar methodology to generate *de novo* designed protein containing a bridged nickel-$[Fe_4S_4]$ site analogous to that proposed for the A-cluster of carbon monoxide dehydrogenase (Laplaza and Holm, 2001). The HC_4H_2-$[Fe_4S_4]$-Ni peptide complex utilizes a His_3Cys_1 tetrahedral site to provide selectivity for the Ni(II) and a tetrahedral Cys_4 site for the $[Fe_4S_4]$ cluster. As designed, the Ni(II) and iron-sulfur cluster are bridged by the shared Cys ligand (Musgrave et al., 2002). Thus, by employing the inherent coordination preferences of the metal ion cofactors and the geometric constraints imposed by the protein fold multicofactor sites can be assembled.

The order of cofactor addition can be used to generate mixed-cofactor proteins when the ligand type and geometrical arrangement are similar. H10H24 was designed to bind four *b* hemes but it has also been used as a scaffold to simultaneously bind two heme *a* and two heme *b* cofactors (Gibney et al. 2000). Stoichiometric addition of two equivalents of heme *b* followed by two equivalents of heme *a* results in the formation of the mixed cofactor [heme *a*-heme *b*-H10H24]$_2$. Spectroscopic measurements demonstrate that the construct is similar to the bacterial oxidase Cyt ba_3. Detailed electrochemical analysis indicates that the heme *b* cofactors bind to the H10 positions while the heme *a* cofactors bind to the H24 sites. The stability of the mixed-cofactor complex has been attributed to the tight binding of heme *a* and *b* and the correspondingly slow off kinetics.

III. Perspective

Marked progress continues to be made towards the ultimate goal of designing functional photosynthetic and respiratory biomimetics from scratch. A number of lines of chemical and biochemical research are synergistically merging to provide the necessary fundamental concepts for construction of such systems. Several distinct approaches to each of several critical areas in the design of biomimetics have proven successful. Designed protein scaffolds whose structures match the intended design are known and future progress promises to provide even more with cofactors bound. Rational, computational and combinatorial approaches have provided protein designs containing most of the cofactors relevant to photosynthesis and respiration. Heme, photoactive Zn-BChl *a*, flavin, amino-acid protein radical, iron-sulfur cluster and copper sites have all been assembled in *de novo* designed protein scaffolds. In fact, designs containing combinations of these cofactors are demonstrating novel design concepts as well as functional photoactivated electron transfer reactions. All of these are necessary steps in the constructive progression of the *de novo* design of photosynthetic and respiratory biomimetics. Starting from the simplicity of a folded helical peptide sequence, *de novo* design has a strong start towards the ultimate biological complexity of the photosynthetic and respiratory complexes. The future challenge lies in fulfilling the promise of *de*

novo design to delineate and expand biochemical function.

Acknowledgments

This work was funded by the National Science Foundation (Grant CHE 02-12884 to BRG) and by the Swedish Research Council (CT).

References

Allen JP and Williams JC (1998) Photosynthetic reaction centers. FEBS Lett 438: 5–9

Anfinsen CB (1973) Principles that govern the folding of protein chains. Science 181: 223–230

Anfinsen CB and Scheraga HA (1975) Experimental and theoretical aspects of protein folding. Adv Prot Chem 29: 205–300

Antonini E and Brunori M (1971) Hemoglobin and Myoglobin in their reactions with ligands. In: Frontiers in Biology, Vol 21, North-Holland Publishing Co., Amsterdam

Babcock GT (1999) How oxygen is activated and reduced in respiration. Proc Natl Acad Sci USA 96: 12971–12973

Balabin IA and Onuchic JN (2000) Dynamically controlled protein tunneling paths in photosynthetic reaction centers. Science 290: 114–117

Balzter L, Nilsson H and Nilsson J (2001) *De novo* design of proteins—What are the rules? Chem Rev 101: 3153–3163

Beinert H, Holm RH and Münck E (1997) Iron-sulfur clusters: Nature's modular, multipurpose structures. Science 277: 653–659

Benson DE, Wisz MS and Hellinga HW (2000) Rational design of nascent metalloenzymes. Proc Natl Acad Sci USA 97: 6292–6297

Benson DR, Hart BR, Zhu X and Doughty MB (1995) Design, synthesis, and circular dichroism investigation of a peptide-sandwiched mesoheme. J Am Chem Soc 117: 8502–8510

Berry EA, Guergova-Kuras M, Huang L and Crofts AR (2000) Structure and function of cytochrome *bc* complexes. Annu Rev Biochem 69: 1005–1075

Bobrowski K, Poznanski J, Holcman J and Wierzchowski KL (1999) Pulse radiolysis studies of intramolecular electron transfer in model peptides and proteins. 8. Trp[$NH^{\bullet+}$] –> Tyr[$O^{\bullet}$] radical transformation in H-Trp-$(Pro)_n$-Tyr-OH, n = 3–5, series of peptides. J Phys Chem B 103: 10316–10324

Bolon DN and Mayo SL (2001) Enzyme-like proteins by computational design. Proc Natl Acad Sci USA 98: 14274–14279

Braun P, Olsen JD, Strohmann B, Hunter CN and Scheer H (2002) Assembly of light-harvesting bacteriochlorophyll in a model transmembrane helix in its natural environment. J Mol Biol 318: 1085–1095

Broman L, Malmström BG, Aasa R and Vänngård T (1963) The role of copper in the catalytic action of laccase and ceruloplasmin. Biochim Biophys Acta 75: 365–376

Brusslan JA and Peterson MP (2002) Tetrapyrrole regulation of nuclear gene expression. Photosynth Res 71: 185–194

Bryson JW, Betz SF, Lu HS, Suich DJ, Zhou H, O'Neil KT and DeGrado WF (1995) Protein design: A hierarchic approach. Science 270: 935–941

Chakrabartty A and Baldwin RL (1995) Stability of alpha-helices. Adv Prot Chem 46: 141–176

Chakrabartty A, Doig AJ and Baldwin RL (1993) Helix capping propensities in peptides parallel those in proteins. Proc Natl Acad Sci USA 90: 11332–11336

Chang I-J, Gray HB and Winkler JR (1991) High-driving-force electron transfer in metalloproteins: Intramolecular oxidation of ferrocytochrome *c* by $Ru(2,2'\text{-bby})_2(im)(His\text{-}33)^{3+}$. J Am Chem Soc 113: 7056–7057

Choma CT, Lear JD, Nelson MJ, Dutton PL, Robertson DE and DeGrado WF (1994) Design of a heme-binding four-helix bundle. J Am Chem Soc 116: 856–865

Cogdell RJ, Isaacs NW, Howard TD, McLuskey K, Fraser NJ and Prince SM (1999) How photosynthetic bacteria harvest solar energy. J Bacteriol 181: 3869–3879

Coldren CD, Hellinga HW and Caradonna JP (1997) The rational design and construction of a cuboidal iron-sulfur protein. Proc Natl Acad Sci USA 94: 6635–6640

Dahiyat BI and Mayo SL (1997) *De novo* protein design: Fully automated sequence selection. Science 278: 82–87

Dai Q-H, Tommos C, Fuentes EJ, Blomberg MRA, Dutton PL and Wand AJ (2002) Structure of a *de novo* designed protein model of radical enzymes. J Am Chem Soc 124: 10952–10953

Daugherty RG, Wasowicz T, Gibney BR and DeRose VJ (2002) Design and spectroscopic characterization of peptide models for the plastocyanin copper-binding loop. Inorg Chem 41: 2623–2632

DeGrado WF, Wasserman ZR and Lear JD (1989) Protein design, a minimalist approach. Science 243: 622–628

DeGrado WF, Summa CM, Pavone V, Nastri F and Lombardi A (1999) *De novo* design and structural characterization of proteins and metalloproteins. Annu Rev Biochem 68: 779–819

Di Bilio AJ, Crane BR, Wehbi WA, Kiser CN, Abu-Omar MM, Carlos RM, Richards JH, Winkler JR and Gray HB (2001) Properties of photogenerated tryptophan and tyrosyl radicals in structurally characterized proteins containing rhenium (I) tricarbonyl diimines. J Am Chem Soc 123: 3181–3182

Dolphin GT, Brive L, Johansson G and Baltzer L (1996) Use of aromatic amino acid residues to restrict the dynamics in the hydrophobic core of a designed helix-loop-helix dimer. J Am Chem Soc 118: 11297–11298

Eggink LL and Hoober JK (2000) Chlorophyll binding to peptide maquettes containing a retention motif. J Biol Chem 275: 9087–9090

Ferguson-Miller S and Babcock GT (1996) Heme/copper terminal oxidases. Chem Rev 96: 2889–2907

Ferreira K, Iverson TM, Maghlaoui K, Barber J and Iwata S (2004) Architecture of the photosynthetic oxygen-evolving center. Science 303: 1831–1838

Friedrich T and Scheide D (2000) The respiratory complex I of bacteria, archaea and eukarya and its module common with membrane-bound multisubunit hydrogenases. FEBS Lett 479: 1–5

Fromme P, Jordan P and Krauß N (2001) Structure of Photosystem I. Biochim Biophys Acta 1507: 5–31

Fromme P, Kern J, Loll B, Biesiadka J, Saenger W, Witt HT, Krauß N and Zouni A (2002) Functional implications on the mechanism of the function of Photosystem II including water oxidation based on the structure of Photosystem II. Philos Trans Royal Soc London B 357: 1337–1345

Geren L, Hahm S, Durham B and Millett F (1991) Photoinduced

electron transfer between cytochrome *c* peroxidase and yeast cytochrome *c* labeled at Cys 102 with (4-bromomethyl-4′-methylbipyridine[bis(bipyridine)]ruthenium^{2+}. Biochemistry 30: 9450–9457

Ghadiri MR, Soares C and Choi C (1992) A convergent approach to protein design. Metal ion-assisted spontaneous self-assembly of a polypeptide into a triple-helix bundle protein. J Am Chem Soc 114: 825–831

Gibney BR and Dutton PL (2001) *De novo* design and synthesis of heme proteins. In: Mauk AG and Sykes AG (eds) Advanced Inorganic Chemistry, pp 409–455. Academic Press, New York

Gibney BR, Mulholland SE, Rabanal F and Dutton PL (1996) Ferredoxin and ferredoxin-heme maquettes. Proc Natl Acad Sci USA 93: 15041–15046

Gibney BR, Rabanal F, Skalicky JJ, Wand AJ and Dutton PL (1997) Design of a unique protein scaffold for maquettes. J Am Chem Soc 119: 2323–2324

Gibney BR, Rabanal F, Skalicky JJ, Wand AJ and Dutton PL (1999) Iterative protein redesign. J Am Chem Soc 121: 4952–4960

Gibney BR, Isogai Y, Rabanal F, Reddy KS, Grosset AM, Moser CC and Dutton PL (2000) Self-assembly of heme A and heme B in a designed four-helix bundle: Implications for a cytochrome *c* oxidase maquette. Biochemistry 39: 11041–11049

Gibney BR, Huang SS, Skalicky JJ, Fuentes EJ, Wand AJ and Dutton PL (2001) Hydrophobic modulation of heme properties in heme protein maquettes. Biochemistry 40: 10550–10561

Gray HB and Winkler JR (1996) Electron transfer in proteins. Annu Rev Biochem 65: 537–561

Guss JM and Freeman HC (1983) Structure of oxidized poplar plastocyanin at 1.6 Å resolution. J Mol Biol 169: 521–563

Harbury PB, Zhang T, Kim PS and Alber T (1993) A switch between two-, three-, and four- stranded coiled coils in GCN4 leucine zipper mutants. Science 262: 1401–1407

Heathcote P, Fyfe PK and Jones MR (2002) Reaction centres: The structure and evolution of biological solar power. Trends Biochem Sci 27: 79–87

Hecht MH, Richardson JS, Richardson DC and Ogden RC (1990) *De novo* design, expression, and characterization of Felix: a four-helix bundle protein of native-like sequence. Science 249: 884–891

Hederstedt L (2003) Complex II is complex too. Science 299: 671–672

Hellinga HW (1998) Construction of a blue copper analogue through iterative rational protein design cycles demonstrates principles of molecular recognition in metal center formation. J Am Chem Soc 120: 10055–10066

Hill RB, Raleigh DP, Lombardi A and DeGrado WF (2000) *De Novo* design of helical bundles as models for understanding protein folding and function. Acc Chem Res 33: 745–754

Hillier W and Babcock GT (2001) Photosynthetic reaction centers. Plant Physiol 125: 33–37

Ho SP and DeGrado WF (1987) Design of a 4-helix bundle protein: Synthesis of peptides which self-associate into a helical protein. J Am Chem Soc 109: 6751–6758

Hodges RS, Sodek J, Smillie LB and Jurasek L (1972) Tropomyosin: Amino acid sequence and coiled-coil structure. Cold Spring Harbor Symp Quant Biol 37: 299–310

Hodges RS, Saund AK and Chong PCS, St.-Pierre SA, Reid RE (1981) Synthetic model for two-stranded α-helical coiled-coils. Design, synthesis, and characterization of an 86-residue analog of tropomyosin. J Biol Chem 256: 1214–1224

Holm RH, Kennepohl P and Solomon EI (1996) Structural and functional aspects of metal sites in biology. Chem Rev 96: 2239–2314

Huffman DL, Rosenblatt MM and Suslick KS (1998) Synthetic heme-peptide complexes. J Am Chem Soc 120: 6183–6184

Isogai Y, Ota M, Fujisawa T, Izuno H, Mukai M, Nakamura H, Iizuka T and Nishikawa K (1999) Design and synthesis of a globin fold. Biochemistry 38: 7431–7443

Isogai Y, Ishii A, Fujisawa T, Ota M and Nishikawa K (2000) Redesign of artificial globins: Effects of residue replacements at hydrophobic sites on the structural properties. Biochemistry 39: 5683–5690

Johansson JS, Gibney BR, Skalicky JJ, Wand AJ and Dutton PL (1998) A native-like three-α-helix bundle protein from structure-based redesign: A novel maquette scaffold. J Am Chem Soc 120: 3881–3886

Johnson MK (1994) Iron-sulfur proteins. In: King RB (ed) Encyclopedia of Inorganic Chemistry, Vol 4, pp 1896–1915. Wiley, Chichester

Jones G, Vullev V, Braswell EH and Zhu D (2000) Multistep photoinduced electron transfer in a *de novo* helix bundle: Multimer self-assembly of peptide chains including a chromophore special pair. J Am Chem Soc 122: 388–389

Jordan P, Fromme P, Witt HT, Klukas O, Saenger W and Krauß N (2001) Three-dimensional structure of cyanobacterial Photosystem I at 2.5 Å resolution. Nature 411: 909–917

Kaiser ET and Lawrence DS (1984) Chemical mutation of enzyme active sites. Science 226: 505–511

Kálmán L, LoBrutto R, Allen JP and Williams JC (1999) Modified reaction centres oxidize tyrosine in reactions that mirror Photosystem II. Nature 402: 696—699

Kamiya N and Shen J-R (2003) Crystal structure of oxygen-evolving Photosystem II from *Thermosynechococcus vulcanus* at 3.7-Å resolution. Proc Natl Acad Sci USA 100: 98–103

Kamtekar S, Schiffer JM, Xiong H, Babik J and Hecht MH (1993) Protein design by binary pattering of polar and nonpolar amino acids. Science 262: 1680–1685

Kashiwada A, Nishino N, Wang Z-Y, Nozawa T, Kobayashi M and Nango M (1999) Molecular assembly of bacteriochlorophyll *a* and its analogues by synthetic 4α-helix polypeptides. Chem Lett 2: 1301–1302

Kashiwada A, Watanabe H, Tanaka T and Nango M (2000) Molecular assembly of zinc bacteriochlorophyll *a* by synthetic hydrophobic 1α-helix polypeptides. Chem Lett 5: 24–25

Kehoe JW, Meadows KA, Parkes-Loach PS and Loach PA (1998) Reconstitution of core light-harvesting complexes of photosynthetic bacteria using chemically synthesized polypeptides. 2. Determination of structural features that stabilize complex formation and their implications for the structure of the subunit complex. Biochemistry 37: 3418–3428

Kennedy ML and Gibney BR (2002) Proton coupling to [4Fe-4S]$^{2+/+}$ and [4Fe-4Se]$^{2+/+}$ oxidation and reduction in a designed protein. J Am Chem Soc 124: 6826–6827

Kennedy ML, Silchenko S, Houndonougbo N, Gibney BR, Dutton PL, Rodgers KR and Benson DR (2001) Model hemoprotein reduction potentials: The effects of histidine-to-iron coordination equilibrium. J Am Chem Soc 123: 4635–4636

Kokubo T, Sassa S and Kaiser ET (1987) Flavohemoglobin: A semisynthetic hydroxylase acting in the absence of reductase. J Am Chem Soc 109: 606–607

Kornilova AY, Wishart JF, Xiao W, Lasey RC, Fedorova A, Shin

Y-K and Ogawa MY (2000) Design and characterization of a synthetic electron-transfer protein. J Am Chem Soc 122: 7999–8006

Kornilova AY, Wishart JF and Ogawa MY (2001) Effect of surface charges on the rates of intermolecular electron-transfer between *de novo* designed metalloproteins. Biochemistry 40: 12186–12192

Kortemme T, Ramirez-Alvarado M and Serrano L (1998) Design of a 20-amino acid, three-stranded β-sheet protein. Science 281: 253–256

Kozlow GV and Ogawa MY (1997) Electron transfer across a peptide-peptide interface within a designed metalloprotein. J Am Chem Soc 119: 8377–8378

Kühlbrandt W, Wang DN and Fujiyoshi Y (1994) Atomic model of plant light-harvesting complex by electron crystallography. Nature 367: 614–621

Laplaza CE and Holm RH (2001) Helix-loop-helix peptides as scaffolds for the construction of bridged metal assemblies in proteins: The spectroscopic A-cluster structure in carbon monoxide dehydrogenase. J Am Chem Soc 123: 10255–10264

Lau SYM, Taneja AK and Hodges RS (1984) Synthesis of a model protein of defined secondary and quaternary structure. Effect of chain length on the stabilization and formation of two-stranded α-helical coiled-coils. J Biol Chem 259: 13253–13261

Levine HL and Kaiser ET (1978) Oxidation of dihydronicotinamides by flavopapain. J Am Chem Soc 100: 7670–7677

Lin X, Murchison HA, Nagarajan V, Parson WW, Allen JP and Williams JC (1994) Specific alteration of the oxidation potential of the electron donor in reaction centers from *Rhodobacter sphaeroides*. Proc Natl Acad Sci USA 91: 10265–10269

Lombardi A, Nastri F and Pavone V (2001) Peptide-based heme-protein models. Chem Rev 101: 3165–3190

Malmström BG (1994) Rack-induced bonding in blue-copper proteins. Eur J Biochem 223: 711–718.

Marqusee S, Robbins VH and Baldwin RL (1989) Unusually stable helix formation in short alanine-based peptides. Proc Natl Acad Sci USA 86: 5286–90

Massey V (1995) Introduction: Flavoprotein structure and mechanism. FASEB J 9: 473–475

Maynard Smith J (1970) Natural selection and the concept of a protein space. Nature 225: 563–564

McLachlan AD and Stewart M (1975) Tropomyosin coiled-coil interactions: Evidence for an unstaggered structure. J Mol Biol 98: 293–304

Meadows KA, Parkes-Loach PS, Kehoe JW and Loach PA (1998) Reconstitution of core light-harvesting complexes of photosynthetic bacteria using chemically synthesized polypeptides. 1. Minimal requirements for subunit formation. Biochemistry 37: 3411–3417

Mihara H, Tomizaki K, Fujimoto T, Sakamoto S, Aoyagi H and Nishino N (1996) Artificial membrane protein functionalized with electron transfer system. Chem Lett 3: 187–188

Mitchell P (1961) Coupling of phosphorylation to electron and hydrogen transfer by a chemi-osmotic type of mechanism. Nature 191: 144–148

Moffet DA and Hecht MH (2001) *De novo* proteins from combinatorial libraries. Chem Rev 101: 3191–3203

Moffet DA, Certain LK, Smith AJ, Kessel AJ, Beckwith KA and Hecht MH (2000) Peroxidase activity in heme proteins derived from a designed combinatorial library. J Am Chem Soc 122: 7612–7613

Mulholland SE, Gibney BR, Rabanal F and Dutton PL (1998) Characterization of the fundamental protein ligand requirements of $[4Fe\text{-}4S]^{2+/+}$ clusters using sixteen amino acid maquettes. J Am Chem Soc 120: 10296–10302

Mulholland SE, Gibney BR, Rabanal F and Dutton PL (1999) Determination of nonligand amino acids critical to $[4Fe\text{-}4S]^{2+/+}$ assembly in ferredoxin maquettes. Biochemistry 38: 10442–10448

Muller M and Blobel G (1984) In vitro translocation of bacterial proteins across the plasma membrane of *Escherichia coli*. Proc Natl Acad Sci USA 81: 7421–7425

Munson M, O'Brien R, Sturtevant JM and Regan L (1994) Redesigning the hydrophobic core of a four-helix-bundle protein. Protein Sci 3: 2015–2022

Munson M, Balasubramanian S, Fleming KG, Nagi AD, O'Brien R, Sturtevant JM and Regan L (1996) What makes a protein a protein? Hydrophobic core designs that specify stability and structural properties. Protein Sci 5: 1584–1593

Musgrave KB, Laplaza CE, Holm RH, Hedman B and Hodgson KO (2002) Structural characterization of metallopeptides designed as scaffolds for the stabilization of nickel(II)-Fe_4S_4 bridged assemblies by X-ray absorption spectroscopy. J Am Chem Soc 124: 3083–3092

Mutz MW, Case MA, Wishart JF, Ghadiri MR and McLendon GL (1999) *De novo* design of protein function: Predictable structure-function relationships in synthetic redox proteins. J Am Chem Soc 121: 858–859

Nango M, Kashiwada A, Watanabe H, Yamada S, Yamada T, Ogawa M, Tanaka T and Iida K (2002) Molecular assembly of bacteriochlorophyll *a* using light-harvesting model 1α-helix polypeptides and 2α-helix polypeptides with disulfide-linkage. Chem Lett 3: 312–313.

Narula J, Pandey P, Arbustini E, Haider N, Narula N, Kolodgie FD, Dal Bello B, Semigran MJ, Bielsa-Masdeu A, Dec GW, Israels S, Ballester M, Virmani R, Saxena S and Kharbanda S (1999) Apoptosis in heart failure: Release of cytochrome *c* from mitochondria and activation of caspase-3 in human cardiomyopathy. Proc Natl Acad Sci USA 96: 8144–8149

Nastri F, Lombardi A, Morelli G, Maglio O, D'Auria G, Pedone C and Pavone V (1997) Hemoprotein models based on covalent helix-heme-helix sandwich. 1. Design, Synthesis, and Characterization. Chem Eur J 3: 340–349

Ohnishi T (1998) Iron-sulfur clusters/semiquinones in complex I. Biochim Biophys Acta 1364: 186–206

Page CC, Moser CC, Chen X and Dutton PL (1999) Natural engineering principles of electron tunneling in biological oxidation-reduction. Nature 402: 47–52

Privett HK, Reedy CJ, Kennedy ML and Gibney BR (2002) Nonnatural amino acid ligands in heme protein design. J Am Chem Soc 124: 6828–6829

Prütz WA and Land EJ (1979) Charge transfer in peptides. Pulse radiolysis investigation of one-electron reactions in dipeptides of tryptophan and tyrosine. Int J Radiat Biol 36: 513–520

Rabanal F, DeGrado WF and Dutton PL (1996) Toward the synthesis of a photosynthetic reaction center maquette: A cofacial porphyrin pair assembled between two subunits of a synthetic four-helix bundle multiheme protein. J Am Chem Soc 118: 473–474

Rau HK and Haehnel W (1998) Design, synthesis, and properties of a novel cytochrome *b* model. J Am Chem Soc 120: 468–476

Rau HK, DeJonge N and Haehnel W (1998) Modular synthesis of *de novo*-designed metalloproteins for light-induced electron transfer. Proc Natl Acad Sci USA 95: 11526–11531

Rau HK, DeJonge N and Haehnel W (2000) Combinatorial synthesis of four-helix bundle hemoproteins for tuning of cofactor properties. Angew Chem Int Ed 39: 250–253

Rau HK, Snigula H, Struck A, Robert B, Scheer H and Haehnel W (2001) Design, synthesis and properties of synthetic chlorophyll proteins. Eur J Biochem 268: 3284–3295

Richardson JS, Richardson DC and Erickson BW (1984) *De Novo* design and synthesis of a protein. Biophys J 45: A25

Robertson DE, Farid RS, Moser CC, Urbauer JL, Mulholland SE, Pidikiti R, Lear JD, Wand AJ, DeGrado WF and Dutton PL (1994) Design and synthesis of multi-haem proteins. Nature 368: 425–432

Rojas NRL, Kamtekar S, Simons CT, Mclean JE, Vogel KM, Spiro TG, Farid RS and Hecht MH (1997) *De novo* heme proteins from designed combinatorial libraries. Protein Sci 6: 2512–2524

Rosenblatt MM, Huffman DL, Wang XT, Remmer HA and Suslick KS (2002) Cyclic and hairpin peptide complexes of heme. J Am Chem Soc 124: 12394–12395

Rutherford AW and Faller P (2001) The heart of photosynthesis in glorious 3D. Trends Biochem Sci 26: 341–344

Saraste M (1999) Oxidative phosphorylation at the *fin de siècle*. Science 283: 1488–1493

Sasaki T and Kaiser ET (1990) Helichrome: Synthesis and enzymatic activity of a designed hemeprotein. J Am Chem Soc 111: 380–381

Sazanov LA and Walker JE (2000) Cryo-electron crystallography of two sub-complexes of bovine complex I reveals the relationship between the membrane and peripheral arms. J Mol Biol 302: 455–464

Schneider JP, Lear JD and DeGrado WF (1997) A designed buries salt-bridge in a heterodimeric coiled coil. J Am Chem Soc 119: 5742–5743

Schnepf R, Hörth P, Bill E, Wieghardt K, Hildebrandt P and Haehnel W (2001) *De novo* design and characterization of copper centers in synthetic four-helix-bundle proteins. J Am Chem Soc 123: 2186–2195

Schultz BE and Chan SI (2001) Structures and proton-pumping strategies of mitochondrial respiratory enzymes. Annu Rev Biophys Biomol Struct 30: 23–65

Scott MP and Biggins J (1997) Introduction of a [4Fe-4S (S-cys)$_4$]$^{1+/2+}$ iron-sulfur center into a four-α helix protein using design parameters from the domain of the Fx cluster in the Photosystem I reaction center. Protein Sci 6: 340–346

Sharp RE, Moser CC, Rabanal F and Dutton PL (1998) Design, synthesis, and characterization of a photoactivatable flavocytochrome molecular maquette. Proc Natl Acad Sci USA 95: 10465–10470

Shifman JM, Gibney BR, Sharp RE and Dutton PL (2000) Heme redox potential control in *de novo* designed four-α-helix bundle proteins. Biochemistry 39: 14813–14821

Silverman JA, Balakrishnan R and Harbury PB (2001) Reverse engineering the $(\beta/\alpha)_8$ barrel fold. Proc Natl Acad Sci USA 98: 3092–3097

Skalicky JJ, Gibney BR, Rabanal F, Bieber Urbauer RJ, Dutton PL and Wand AJ (1999) Solution structure of a designed four-α-helix bundle maquette scaffold. J Am Chem Soc 121: 4941–4951

Solomon EI, LaCroix LB and Randall DW (1998) Electronic structure contributions to function in bioorganic chemistry: The blue copper active site. Pure Appl Chem 70: 799–808

Sono M, Roach MP, Coulter ED and Dawson JH (1996) Heme-containing oxygenases. Chem Rev 96: 2841–2887

Struthers MD, Cheng RP and Imperiali B (1996) Design of a monomeric 23-residue polypeptide with defined tertiary structure. Science 271: 342–345

Stubbe J and van der Donk WA (1998) Protein radical in enzyme catalysis. Chem Rev 98: 705–762

Tomizaki K, Tsunekawa Y, Akisada H, Mihara H and Nishino N (2000) Design and characterization of flavoenzyme models in the course of chemical evolution of four-a-helix bundle polypeptides. J Chem Soc Perkin Trans 2: 813–822

Tommos C (2002) Electron, proton and hydrogen-atom transfers in photosynthetic water oxidation. Philos Trans Royal Soc London B 357: 1383–1394

Tommos C and Babcock GT (1998) Oxygen production in nature: A light-driven metalloradical enzyme process. Acc Chem Res 31: 18–25

Tommos C and Babcock GT (2000) Proton and hydrogen currents in photosynthetic water oxidation. Biochim Biophys Acta 1458: 199–219

Tommos C, Skalicky JJ, Pilloud DL, Wand AJ and Dutton PL (1999) *De novo* proteins as models of radical enzymes. Biochemistry 38: 9495–9507

Twitchett MB, Ferrer JC, Siddarth P and Mauk AG (1997) Intramolecular electron transfer kinetics of a synthetic flavocytochrome *c*. J Am Chem Soc 119: 435–436

Vassiliev IR, Antonkine ML and Golbeck JH (2001) Iron-sulfur clusters in type I reaction centers. Biochim Biophys Acta 1507: 139–160

Wang W and Hecht MH (2002) Rationally designed mutations convert *de novo* amyloid-like fibrils into monomeric β-sheet proteins. Proc Natl Acad Sci USA 99: 2760–2765

Williams RJP (1995) Energized (entatic) states of groups and of secondary structures in proteins and metalloproteins. Eur J Biochem 234: 363–381

Xu Z and Farid RS (2001) Design, synthesis, and characterization of a novel hemoprotein. Protein Sci 10: 236–249

Zouni A, Witt HT, Kern J, Fromme P, Krauß N, Saenger W and Orth P (2001) Crystal structure of Photosystem II from *Synechococcus elongatus* at 3.8 Å resolution. Nature 409: 739–743

Chapter 34

Understanding Photosystem II Function by Artificial Photosynthesis

Ann Magnuson and Stenbjörn Styring*
Molecular Biomimetics, Uppsala University, Villavagen 6, S-752 36 Uppsala, Sweden

Leif Hammarström
Department of Physical Chemistry, Uppsala University, Box 579, S-751 23 Uppsala, Sweden

Summary

Inspired by the Photosystem II reaction center and the water oxidation chemistry that it performs, we aim to develop artificial photosynthesis for fuel production. Besides the original work we do in this direction, we also acquire knowledge feedback from our novel compounds. Our man-made systems create new perspectives on electron and proton transfer, bioinorganic chemistry, excitation energy transfer and other issues that are central to photosynthesis research. In this chapter we describe some of the highlights in our research and the conclusions they have generated.

*Author for correspondence, email: stenbjorn.styring@fki.uu.se

T. Wydrzynski and K. Satoh (eds): Photosystem II: The Light-Driven Water:Plastoquinone Oxidoreductase, pp. 753–775.

I. Introduction

Of all the processes of life on earth, photosynthesis is the one that provides a net increase of energy to the biosphere by absorbing and converting solar energy into chemical energy. The most successful photosynthetic organisms today are the O_2 forming green plants, algae and cyanobacteria. The key reaction in these organisms is catalyzed by the Photosystem II (PS II) reaction center. PS II is able to drive electron transfer, using solar energy, from water to plastoquinone. Two water molecules are oxidized to molecular oxygen while the four electrons that are abstracted are transferred to plastoquinone. The reduced plastoquinol is a versatile reductant, which is used in a variety of processes depending on the organism and ambient conditions.

PS II reactions thus provide the biosphere with a sustainable source of reduced compounds from the endless resources of sunlight and water. In particular the components involved in the water oxidizing reactions are unique to PS II. The chemical reactions that they catalyze are complex and offer a vast spectrum of fascinating chemical, physical and biological challenges for the scientific researcher. We will not discuss in depth here the details of the water oxidizing center of PS II (but refer to many of the specialized papers in this, and other volumes). After a short introduction to the PS II reaction center, we will turn the focus to some lessons that we can learn from our ongoing research on artificial photosynthesis.

A. Why Artificial Photosynthesis?

When light reaches PS II, the primary electron donor complex P680 is excited (Chapter 22, Barter et al.) and an electron is transferred from P680* to pheophytin, and further on to the quinones Q_A and Q_B (Chapter 8, Petrouleas and Crofts), creating a charge-separated state (Chapter 7, Renger and Holzwarth). The charge separation needs to be stabilized towards charge recombination, for which PS II heavily relies on the electron donor capacity of the components on the donor side, the redox-active tyrosine (Y_Z) (Chapter 9, Diner and Britt) and the manganese cluster (Chapters 10–12). The photo-oxidized P680* is re-reduced by Y_Z within tens of nanoseconds in the oxygen-evolving complex (OEC), and on the microsecond time scale in manganese-depleted or photoinhibited PS II centers (Britt, 1996, and references therein). $Y_Z^{\bullet}$ then extracts an electron, or an electron and a proton, from the manganese cluster, forwarding the oxidation state of the manganese cluster by one step.

There are so far no conclusive arguments of why four manganese ions should be needed for water oxidation. However, there are indications that the manganese cluster undergoes structural changes during the catalytic cycle, possibly involving exchange of terminal and/or bridging manganese ligands. Since protons are one of the products of water oxidation, it is reasonable to assume that pH effects are central to the mechanism. Indeed, the rate for electron extraction from the manganese cluster varies with pH and the oxidation state for the manganese cluster, between ca 50 μs and 1 ms (Lavergne and Junge, 1993; Britt, 1996; Diner and Babcock, 1996; Rappaport and Lavergne, 2001; Bernat et al., 2002). In the following sections we shall discuss both proton transfer and structural rearrangements in electron transfer reactions in biomimetic complexes.

During catalysis, the manganese cluster cycles through the four oxidation states of the S-cycle (Chapter 24, Shinkarev) which are characterized by specific EPR signals (Britt 1996; Chapters 10, Yachandra; and 12, Åhrling et al.), the S_0 state being the most reduced. The S_0 state gives rise to a recently discovered EPR signal, (Åhrling et al., 1997; Messinger et al., 1997) that suggests that the manganese cluster in the S_0-state includes at least one Mn(II) ion. In S_1, EPR signals have only been detected by parallel mode EPR, indicating an even number of unpaired electrons (Peloquin and Britt, 2001), while the S_2 state again gives rise to a wide EPR signal of the 'multiline' type (Dismukes and Siderer, 1981; Yamauchi et al., 1997). This EPR signal has been intensely investigated during the past two decades, with the hope that it could shed some light on the structure and valence of the manganese cluster. It has become clear, however, that EPR spectroscopy alone will not answer the fundamental questions about e.g., the valences of the manganese ions. By combining EPR and X-ray absorption spectroscopy, two models for the manganese cluster and its valence in the S_2-state have emerged as being the most probable description. In the most favored model, the valence is

Abbreviations: bpy – bipyridine; EPR – electron paramagnetic resonance; MV^{2+} – oxidized methyl viologen; NHE – natural hydrogen electrode; OEC – oxygen evolving complex ; P680 – primary electron donor of PS II; PS II – Photosystem II; Q_A – primary plastoquinone acceptor of PS II; Q_B – secondary plastoquinone acceptor of PS II; SCE – saturated calomel electrode; Y_Z – redox active tyrosine on D1 of PS II

$Mn(III)Mn_3(IV)$ (Carrell et al, 2002; Chapter 10).

The consensus for our understanding of the manganese chemistry of the water oxidation mechanism, is that the S_0 to S_1, and the S_1 to S_2 transitions involve pure, manganese centered oxidation (Kuzek and Pace, 2001). In contrast, for the S_2 to S_3 transition, there is no consensus about whether the transition involves manganese, ligand, oxo-bridge or substrate centered oxidation. Spectroscopic handles for the S_3-state have recently been discovered by parallel mode EPR (Mino et al., 1998; Matsukawa et al., 1999; Ioannidis and Petrouleas, 2000). The S_3 state in active centers might also give rise to split radical signals (Geijer et al., 2001), due to the close and pH dependent equilibrium between manganese and $Y_Z^{\bullet}$. The equilibrium $S_3Y_Z \leftrightarrow S_2Y_Z^{\bullet}$ can be driven to the right by raising the pH of the bulk medium (Geijer et al., 2001), or under certain conditions by illumination with near-infra red light (Ioannidis and Petrouleas, 2000).

An important issue in this field is how the oxygen-oxygen bond is formed during the $S_3 \rightarrow [S_4] \rightarrow S_0$ transition, when molecular oxygen is evolved. This is beyond the scope of this text, and it is sufficient to say that there are numerous suggestions on this mechanism (Nugent, 2001; Chapter 25, Hillier and Messinger). We do appreciate however that this is a problem that urgently needs to be solved, perhaps via the development of new experimental approaches.

The reactions in the natural photosynthetic reaction centers seem very complex at first. However, they follow a small number of physical and chemical principles and can be described as variations on a common theme. To develop artificial photosynthesis is to design, synthesize and physically characterize man-made systems that mimic the principles of natural photosynthesis, and possibly even to improve on the efficiency of the natural systems. Artificial photosynthesis in this respect has been developed during the past few decades, and substantial progress has been made in creating light-induced charge separation and charge stabilization, coupling of pigments for light harvesting and energy transfer amongst other things, in artificial systems. It has even been possible to achieve photo-induced buildup of a proton gradient coupled to ATP production, using entirely synthetic light absorbers and proton translocators in synthetic vesicles (Steinberg-Yfrach et al., 1998).

There is another, entirely different reason for developing artificial photosynthesis. In 1994 we founded the Swedish Consortium for Artificial Photosynthesis, based on the need in modern society for sustainable, environmentally friendly energy sources. Our research initiative was founded in the fast advancing research field of natural photosynthesis, where we continuously seek inspiration in our work. The aim is fuel production using artificial photosynthesis, in particular by oxidizing water in a controlled catalytic way, and forming H_2 from the extracted electrons and protons (Hammarström et al., 1999, 2001; Sun et al., 2001). In Fig. 1 we show the basic principles of how an artificial photosynthetic system should work. The aim in our research is to resolve the details of this 'machine,' the structure of its parts, and what properties and functions it has to exhibit. In the present chapter we will first briefly describe our idea and where this research stands today. Then we will proceed to draw conclusions from our 'simple' man-made molecules, which will have bearing on our understanding of how natural photosynthesis works.

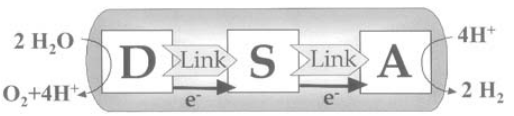

Fig. 1. Design of a multifunctional molecular system able to harvest solar energy. The excited sensitizer (S) transfers an electron to a catalytic acceptor system (A). The acceptor system is able to reduce protons to molecular hydrogen. The photo-oxidized sensitizer extracts electrons from the donor moiety (D). This is also catalytic and is able to oxidize two water molecules to molecular oxygen and protons. The sensitizer is covalently linked to both the acceptor and the donor via redox active links that rectify the electron transfer. All of the different parts (S, D, A and the links) have counterparts in the natural systems that inspire us in the bio-mimetic approach we have taken.

B. Ruthenium-Manganese Super Complexes

The principle of artificial photosynthesis for H_2 production, is presented in Fig. 1. A molecular photosensitizer (S) should be linked to both a donor (D) and an acceptor (A) system. Upon excitation with light, the sensitizer should transfer an electron to the acceptor. The electron transfer will occur via a redox active link. The photo-oxidized sensitizer should have a high oxidation potential, and retrieve an electron from the donor. Also in this step the electron transfer should proceed via a redox active link, in order to prevent back reactions. The donor system should also be able to perform multiple electron transfers. In addition, both the donor and acceptor systems will be active chemical catalysts. The donor will do

oxidative chemistry involving water as substrate, and the acceptor will catalyze the reduction of protons to molecular hydrogen.

The greatest difficulty in this reaction scheme, is to accomplish catalytic water oxidation. We seek inspiration and ideas from the water-oxidizing center in PS II, which is the only molecular catalyst we know of, capable of oxidizing water completely to O_2 by using photochemistry. As a photosensitizer we use ruthenium(II)-*tris*bipyridine complexes. The photochemistry and photophysics of these complexes are well known, and provide an abundance of various approaches to link different functional groups to the ruthenium center (Juris et al., 1988). The Ru center can be linked with a donor complex that contains Mn ions in different ligands. Figure 2 shows a number of linked dinuclear Ru-Mn supercomplexes, that were the first generation of such molecules (Sun et al., 1997). In a later development, we created complexes that included two Mn ions, forming a coupled Mn dimer, that was connected to the Ru moiety via a redox active link (see below, and Fig. 5). The Ru center corresponds to P680 in PS II. When it is photo-excited, the Ru(II)* becomes a powerful reductant which transfers an electron to an electron acceptor. Like $P680^+$, Ru(III)-*tris*bipyridine is a strong oxidant, with an oxidation potential of E_m=1.32 V, which is even more positive than that of $P680^+$ ($E_m \approx 1.2$ V).

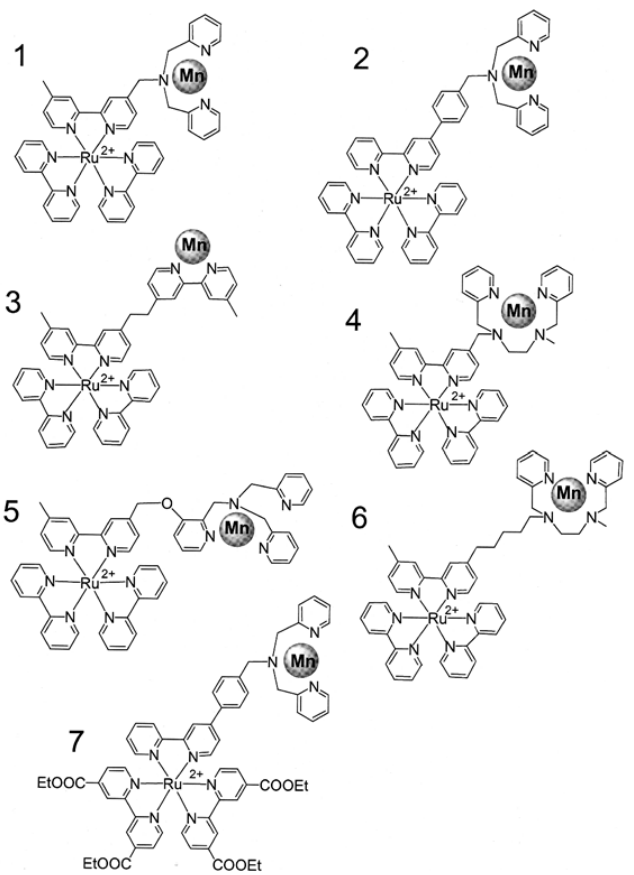

Fig. 2. The first generation of supramolecular Ru(II)-Mn(II) complexes. 1–7, referred to as 1b–7b in the text are the same moleucles as depicted and referred to as 1a–7a in the text but without Mn in the Mn-binding moiety.The difference between them is mainly in the manganese-binding moiety of the molecule. When the ruthenium absorbs light, in the presence of an exogenous electron acceptor, the complexes all undergo intramolecular electron transfer from the Mn(II) to Ru(III). Excitation lifetimes and electron transfer properties are depicted in Tables 1 and 2.

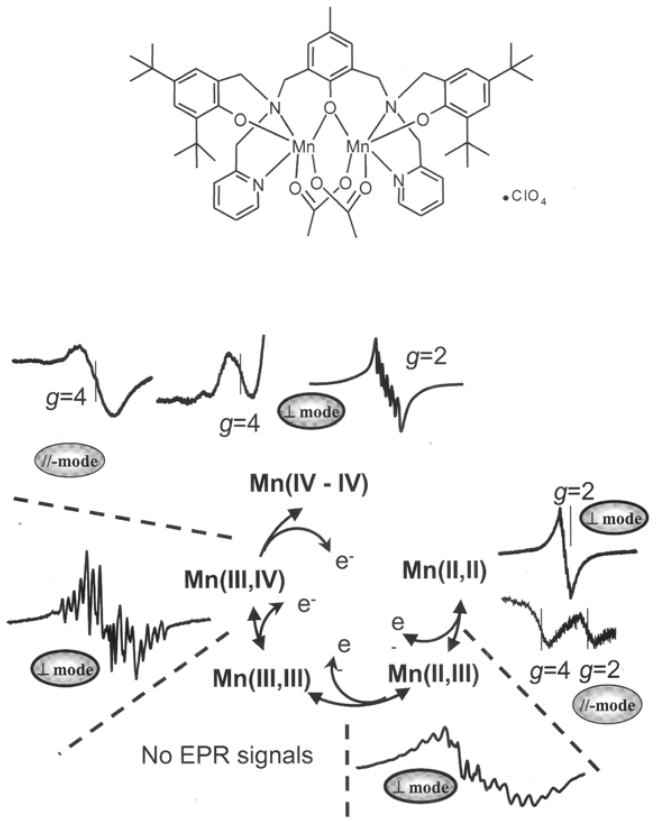

Fig. 3. (Top) A synthetic dinuclear manganese complex that has the ability of forming up to four or five different oxidation states. (Bottom) The different EPR spectra in different oxidation states of the manganese dimer. The EPR signals of the most reduced state of the complex are depicted to the right.

Our Ru-Mn complexes are built in analogy with the components of the donor side in PS II. At present they include, not four Mn ions, but two (Hammarström et al., 2001; Sun et al., 2001). In this system the Mn ions are coordinated by a well-known ligand with a N_3O ligand set (Diril et al., 1987). This is different from the situation in PS II where oxygen atoms are dominating the coordination sphere of the manganese cluster (Yachandra et al., 1996; Dau et al., 2001; Kuzek and Pace, 2001; Robblee et al., 2001; Chapter 10). In the recently prepared Mn_2(III/III) dimer shown in Fig. 3 (Lomoth et al., 2002), we have introduced more oxygen ligands so that the ligand set is N_2O_2. This molecule has very rich redox chemistry and is stabilized in the higher oxidation states.

The emphasis on EPR spectroscopy throughout our work is warranted by the rich redox chemistry that these complexes perform. As is the case with PS II, we need to follow the complex toggling between EPR-visible and –invisible states. EPR is most useful for this purpose as it is 'blind' to everything but the paramagnetic species — in our case it is the manganese complex, which is the point of our interest. By coupling EPR studies to electrochemistry (Fig. 3), we have seen that this novel molecule can occupy five distinct redox states. It is synthesized in the Mn(III/III) state, which is EPR silent under our instrumental conditions. It can be both oxidized and reduced photolytically or electrochemically, resulting in paramagnetic states with recognizable EPR signals in both the Mn_2(III,IV) and Mn_2(II,III) states. The Mn_2(II,III) state can also be further reduced to what

probably is the Mn_2(II,II) state, and the Mn_2(III,IV) state can be oxidized further to a state which at present is less well understood.

In the early development of our project, we made a series of dinuclear Ru-Mn compounds, i.e., with only one Mn ion bound to the complex (Fig. 2). In all these complexes it proved possible to oxidize the Mn moiety via intra-molecular electron transfer to the photo-oxidized Ru center (Sun et al., 1997; Abrahamsson et al., 2002). Later on we also performed a more detailed study of the electronic interactions between the Ru and Mn centers in the compounds (see below). It was clear however, that these simple compounds will never be able to oxidize water, which is why we turned to systems including dimeric Mn complexes of the type discussed above. In these compounds we coupled together a Mn dimer and a Ru complex via a peptide bond and a tyrosine derivative. When the system in Fig. 5 (bottom) was exposed to a series of laser flashes in the presence of an irreversible electron acceptor such as Co(III) pentaamine (Magnuson et al, 1997, 1999), the Mn dimer underwent sequential oxidation to the Mn_2(III,IV) state (Huang et al., 2002). Thus, the Mn moiety was able to deliver three electrons, one at a time, to the photo oxidized Ru center. This represents an important step towards a truly biomimetic system. In a future, fully biomimetic molecular system, water oxidation will demand extraction of four electrons from the Mn moiety. We are seemingly not far away from reaching this goal in our compounds. However, the Ru-Mn complex described above has one drawback: the Mn dimer operates at too low redox potentials, and is also rather unstable in water containing environments (Huang et al., 2002). A choice of a ligand molecule that contains more oxygen atoms that directly bind the Mn ions, may help to stabilize the complex in higher oxidation states, but it is not clear if a dimeric Mn complex will ever be mechanistically able to oxidize water. In Section III, we will explore further the reason why four manganese ions are needed for water oxidation.

II. Mimicking Photosystem II Reactions

A. Distance Dependence of Electron Transfer Rates in Ruthenium-Manganese Complexes

Our work has been focused on mimicking the donor side of PS II by synthesizing supramolecular systems containing both a manganese moiety, and a ruthenum(II)*tris*bipyridyl moiety as the photo-oxidizable sensitizer (Sun et al., 1997; Berglund-Baudin et al., 1998; Berg et al., 2001). In this line of work, we first produced a series of dinuclear Ru(II)-Mn(II) complexes with slightly different Mn binding ligands and also varying links between the

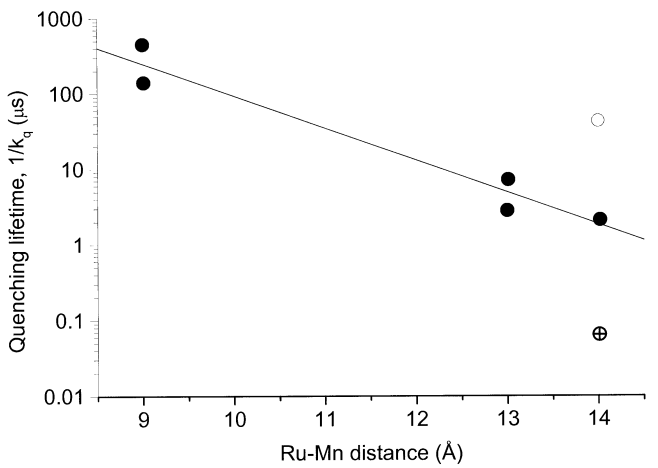

Fig. 4. Life time of the ruthenium excited state in complexes 1b-7b, as a function of distance between the Ru and the Mn moieties (closed circles). The open circle depicts the lifetime of complex 2b, and the crossed circle that of complex 7b. The values for the quenching rate constants are also given in Table 2.

metal centers (Fig. 2). When the Ru(II)$(bpy)_3$ moiety is photo-oxidized by an external electron acceptor, the Ru(III) state which is generated is reduced back to Ru(II) via intramolecular electron transfer from the Mn(II) moiety (Sun et al., 1997; Abrahamsson et al., 2002). These simple systems cannot perform the complex redox reactions necessary to accomplish water oxidation. However, they provide an important knowledge platform in the incremental development towards artificial photosynthesis, and as we move on towards the construction of systems containing several Mn ions that are capable of multi-electron transfer, we need to incorporate the basic principles which we can establish in simpler systems.

According to Marcus theory for electron transfer (Marcus and Sutin, 1985), in all electron transfer processes, the efficiency depends on the distance between the interacting cofactors, the driving force, reorganization energies, and electronic coupling. The rate, k_{ET}, is given by:

$$\ln k_{ET} = \ln A - \frac{(\Delta G^\circ + \lambda)^2}{4\lambda k_B T} \quad (1)$$

where

$$A = \frac{4\pi^2}{h} H_{rp}^2 \frac{1}{\sqrt{4\pi\lambda k_B T}} \quad (2)$$

and λ is the reorganization energy, H_{rp} is the electronic coupling matrix, and k_B is the Boltzmann constant.

The redistribution of electrons is associated with or followed by nuclear rearrangements, leading to a reorganization energy λ. In a low dielectric environment such as a protein, electron transfer generates charges and the nuclei have to rearrange in order to balance these charges. The longer distance the nuclei have to distort from the equilibrium position of the reactants, the larger the reorganization energy, λ.

Recently we investigated different components that govern electron transfer rate in the dinuclear Ru(II)-Mn(II) complexes 1–7 (Fig. 2) (Sun et al., 1997; Berglund-Baudin et al., 1998; Abrahamsson et al., 2002). The $E_{½}$ (midpoint potential) values for the Mn(II) oxidation in these compounds vary from 0.79 to 0.90 V vs. SCE, whereas the $E_{½}$ for Ru(II) oxidation is 1.29 V vs. in all cases, except for 7b (Table 1). Electron transfer from Mn(II) to the oxidized Ru(III) is therefore consistent with the electrochemical potentials for the Ru(III/II) and Mn(III/II) couples. The rate constants for intramolecular electron transfer from Mn(II) to photo-oxidized Ru(III), vary in the different complexes from $1 \times 10^5 - 2 \times 10^7$ s^{-1}. It was also found that the Mn(II) moiety quenches the Ru(II) excited state in some complexes, presumably by intramolecular energy transfer (Table 2; Berglund-Baudin et al., 1998; Berg et al., 2001; Abrahamsson et al., 2002). In the following section we will discuss the mechanism of both electron transfer and energy transfer in the Ru-Mn complexes, and how these properties can shed new light on the complex photochemistry of PS II.

1. Excited State Quenching

We first look at the lifetime of the excited state of the Ru moiety in the synthetic Ru-Mn complexes. The lifetime of the Ru(II) excited state is crucial for a successful electron transfer from Ru(II)* to the external acceptor (in this case, oxidized methyl viologen MV^{2+}). A complicating factor, which we have found in these complexes, is that Mn(II) quenches the excited state, and therefore competes with the intermolecular electron transfer to MV^{2+}. In some of the Ru(II)-Mn(II)complexes the excited state lifetime became so short that it was difficult to obtain any electron transfer even with very high concentrations of MV^{2+}. In order to control the efficiency of the complexes, it was important to understand through which mechanism the quenching occurs. The emission lifetimes for the Ru(II) complexes without manganese (1a – 7a) were all between 800–1300 ns (Table 2). In the Ru(II)- Mn(II) complexes 1b – 6b, the lifetime was reduced to 2 ns – 300 ns (Table 3). For 7b on the other hand, the obtained lifetime was ca.1200 ns, i.e. almost the same as in the absence of the manganese.

The rate of the excited state quenching was found to decrease with the metal-to-metal distance (Fig. 4). There are several possible mechanisms that can affect quenching efficiency. Coordination of manganese in the complex could cause changes in the electronic properties of the $Ru(bpy)_3^{2+}$ moiety. This possibility was excluded from close inspection of optical spectra that were all very similar. Two other plausible mechanisms are: (i) energy transfer from Ru(II)* to the Mn(II); and (ii) electron transfer from Mn(II) to Ru(II)*. One way to discriminate between electron and energy transfer, is to measure the emission lifetimes at low temperature. In an electron transfer reaction, the solvent molecules around the complex need to reorganize in response to the new

Table 1. Electron transfer data for the ruthenium(II)-manganese(II) complexes (Abrahamsson et al., 2002)

	D [a] Å	$E_{1/2}$ ($Mn^{III/II}$) V vs. SCE	$E_{1/2}$ ($Ru^{III/II}$) V vs. SCE	ΔG° eV	k_{ET} s^{-1} [b]	λ eV	H_{rp} meV
1b	9	(0.90)[c]	1.28	(–0.38)[c]	1.1×10^6	–	–
2b	14	0.90	1.29	–0.39	1.7×10^6	2.0	12
3b	13	0.85	1.28	–0.43	1.8×10^5	1.8	1.7
4b	9	0.85	1.30	–0.45	$>2 \times 10^7$	–	–
5b	13	0.79	1.28	–0.49	1.4×10^5	1.5	0.27
6b	14	(0.85)[d]	–	–	1×10^5	–	–
7b	14	(0.90)[e]	1.49	(–0.59)[e]	1.4×10^7	–	–
$Ru(bpy)_3^{2+}$	–	–	1.32	–	–	–	–

[a] The distance between the ruthenium(II) and the coordinated manganese(II). These are the maximum distances estimated by molecular mechanics starting from the most extended conformations using constrained metal-ligand distances. [b] Determined with an excess of $MnCl_2$ in acetonitrile, in order to obtain a larger fraction of coordinated manganese(II) and thus a more reliable value. [c] The $Mn^{III/II}$-couple was not observed due to instability of the complex towards dissociation of the manganese(II). The redox potential for the manganese is assumed to be the same as for 2b, since the manganese ligand is the same. [d] The redox potential for the metals are assumed to be the same as for 4b. [e] The redox potential for the manganese is assumed to be the same as for 2b.

Table 2. Luminescence data for the mono-nuclear ruthenium complexes 1a – 7a at 293 K

	λ_{max} (nm)	τ (ns) [a]
1a	636	880 [a]
2a	631	1400 [a]
3a	631	919 [a]
4a	638	1050 [a]
5a	631	900
6a	630	800
7a	669	1300

[a] From Berglund et al. (1998); Abrahamsson et al. (2002)

Table 3. Luminescence data for the dinuclear Ru-Mn complexes 1b – 7b at 293 K

	λ_{max} (nm)	τ_1 (ns)	k_q (s^{-1})
1b	636	2.2 [a]	4.5×10^8
2b	632	23 [a]	4.3×10^7
3b	631	255 [a]	2.8×10^6
4b	639	7 [a]	1.4×10^8
5b	631	120 [a]	7.2×10^6
6b	[b]	300	2.1×10^6
7b	669	1200	6.4×10^4

[a] From Berglund et al. (1998); Abrahamsson et al. (2002); [b] not measured.

charge distribution. When the reaction occurs in a frozen medium the reorganization cannot take place, resulting in a decreased driving force (Chen and Meyer, 1996; Wasielewski et al., 1988; Gaines et al., 1991). As a consequence the electron transfer would be unfavorable, and this type of quenching would not occur at all. However, in an energy transfer reaction, the effect of the frozen solution would be much less dramatic because the solvent reorganization then is relatively small (Sutin, 1982). Thus, because of the strong reduction of the emission lifetimes also at 77 K, it was concluded that quenching of the excited state of Ru(II) does not occur through an electron transfer mechanism, but through energy transfer to a short-lived excited state of the Mn(II) moiety.

Energy transfer (Dexter type) is possible since Mn(II) complexes have excited states that are below the energy of the Ru(II) excited state (Porter and Schäfer, 1964; Balzani and Carassiti, 1970). The rate constant for the energy transfer decreases exponentially with distance, and this correlation in the different complexes indicates that although the ligand that coordinates the Mn(II) is different for the different complexes, the energy of the Mn(II)-based excited state is constant (Fig. 4). Thus, a change in the Mn(II) ligands does not affect the excited state quenching. The only way to do that is to increase the distance between the two metals.

A deviation from this behavior was observed in complexes 2b and 7b. In spite of the relatively long metal-to-metal distance (14 Å), the excited state lifetime of 2b is only 23 ns, while the lifetime of 7b is much longer. The reason is the difference in the ligands around the Ru(II)-metal center. In 2b the Mn

ligand was linked to the Ru moiety via a phenyl group. It is known that the electron in a metal-to-ligand charge transfer excited state of $Ru(bpy)_3$ complexes, can be delocalized over a conjugated ligand, leading to a decrease in the excited state energy (Hammarström et al., 1997; Treadway et al., 1996; Damrauer et al., 1997). This means that the lowest excited state involves the bridging ligand, which brings the excited state of 2b much closer to the Mn moiety compared to the other complexes. The result is that its excited state lifetime is shorter, even though the metal-to-metal distance is the same. Complex 7 on the other hand, was designed to have the same structure and Ru(II) to Mn(II) distance as 2, except that four ester groups have been introduced in the bipyridine ligands. This localizes the excited state on the ester-substituted bipyridines, as we could show by the spectral properties of 7a (Abrahamsson et al., 2002). Therefore we concluded that the ester groups move the excited state away from the Mn(II), increasing the excited state lifetime from 23 ns to ~1200 ns. This dramatic improvement shows that it is possible to control the quenching without changing the metal-to-metal distance per se. Instead it is achieved by controlling the localization of the excited state.

Thus, for complexes with similar ligands around the Ru(II), the quenching rate constant decreases exponentially with the metal-to-metal distance. This tells us that an efficient photo-oxidation of the photosensitizer requires that the distance to the Mn is not too short. We also found it interesting that manipulation of the excited state energy can increase the efficiency of the complex, by leading the excited state energy away from the Mn onto the remote ligands. In this way the probability of the Mn moiety performing oxidative chemistry, is greatly increased.

One can imagine analogies in PS II, where Mn(II) is believed to be involved in the lowest oxidation state (S_0) of the manganese cluster (Åhrling et al., 1997; Iuzzolino et al., 1998; Carrell et al., 2002). Quenching of the P680* by Mn(II) in the S_0 state, may be a potential problem that nature has solved by keeping these units at ca 20 Å distance (Zouni et al., 2001; Kamiya and Shen, 2003; Ferreira et al., 2004; Chapters 19–21). In spite of this distance, reduction of $P680^+$ is still fast, thanks to that the photosensitizer and the manganese cluster are interfaced by Y_Z. Thus, the risk of quenching of P680* is minimized, while the electron donation from Y_Z to $P680^+$ can still be efficient and ensure charge stabilization.

2. Manganese as Electron Donor

We now move our focus to the electron transfer reactions. With flash photolysis we could observe intramolecular electron transfer from the coordinated Mn(II) to the photo-oxidized Ru(III). The rate constants for this reaction varies, from $1 \times 10^5 - 2 \times 10^7$ s^{-1} in 1b – 7b (Table 1). In contrast to the excited state quenching, the electron transfer rate did not follow a simple dependence on the metal-to-metal distance. For example, the rate constant for k_{ET} in 1b and 4b are 1.1×10^6 s^{-1} and $> 2 \times 10^7$ s^{-1} respectively, although the metal-to-metal distance is 9 Å in both complexes.

From Eqs. 1 and 2, it can be seen that there are three factors that affect the k_{ET} and could cause this variation: the reaction driving force ($\Delta G°$), the electronic coupling constant between the reactant and product state (H_{rp}) and the reorganization energy (λ). The $\Delta G°$ values for the different complexes were calculated from the electrochemical $E_{½}$ values. The free energy in these compounds vary, but the difference is too small to explain the large variation in k_{ET}. The reorganization energies for 2b and 5b are 2.0 and 1.5 eV respectively. This is larger than expected for the solvent reorganization energy alone in a polar solvent (Marcus and Sutin, 1985), and indicates an important contribution from inner reorganizations from the Mn complex. Although 2b was found to have the largest λ value (2.0 eV), it displayed a larger electron transfer rate than 3b and 5b. The explanation is that a relatively large electronic coupling between the metal centers is obtained due to the extended π-system of the bridging ligand. However, despite the high coupling constant in 2b, the electron transfer is still relatively slow compared to what would be expected in a complex of this size. The explanation is that the activation energy for the electron transfer reaction becomes high, due to the large reorganization energies.

The unexpectedly large values for λ are due to internal rearrangements of the Mn moiety, as the Mn(II) complex is oxidized to the Mn(III) state. This can be understood by the high-spin d^4-electron configuration of the Mn(III) ion, which due to the degeneracy of the e_g orbitals, adopts varying tetragonally distorted geometries. In contrast to Mn(II), Mn(III) does not assume a pure octahedral symmetry (Pecoraro, 1992, and references therein). The tetragonal distortion of Mn(III) complexes, away from the octahedral symmetry of the Mn(II) ion, gives an important contribution to the reorganization energies. On the

other hand, complexes containing more than one Mn ion are much more stable in the Mn(III) and Mn(IV) state, as compared to Mn(II) complexes which tend to decompose in favor to forming hexaquo-Mn(II). In the last section of this chapter we will discuss the necessity of having four Mn ions in a water oxidizing complex.

Another, and most important result, was that the observed k_{ET} for 7b, is much higher than that for 2b although their Mn-binding sites are identical. This is because the modified bipyridine ligands in 7b improves the electron transfer properties. Complex 7b displayed a ten-fold increase in electron transfer rate constant as compared to 2b, which can only be explained by a larger driving force. Thus, in the Ru-Mn compounds, it is variations in reorganization energy and electronic coupling that are the important factors that determine the electron transfer rates, rather than simply the metal-to-metal distance. Internal reorganization of the Mn-ligand bonds is one major component. This suggests that Mn complexes containing the divalent Mn(II) ion may never be fast electron donors, because they will always have large reorganization energy going from the Mn(II) to the Mn(III) state.

In PS II, the electron transfer from the manganese cluster to Y_Z is on the μs to ms time scale. In analogy to what we observed in the Ru(II)-Mn(II) complexes above, this probably reflects a high reorganization energy for the S-state transitions. However, the dominating Mn oxidation state in the water oxidizing complex is Mn(III) and Mn(IV), possibly keeping the reorganization energy due to shifts in ligand sphere symmetry to a minimum. Instead, the S-state transition reactions involve mechanistically crucial proton- or hydrogen atom movements that contribute significantly to the reorganization energy for the overall reaction (see next section). Thus, keeping the pure Mn-ligand rearrangements to a minimum, may be a prerequisite to minimize the activation barrier for S-state transitions.

A rapid regeneration of the photo-oxidized sensitizer is necessary in order to avoid costly recombination reactions, in natural as well as artificial photosynthesis. We have learnt from the dinuclear Ru-Mn-complexes 1b-7b that Mn(II) is an efficient quencher of excited states, and that this is distance dependent. From this perspective it seems important to keep a sizeable distance between the manganese cluster and the P680 in PS II, as we noted above. The fast (ns time scale) electron transfer from Y_Z to $P680^+$ therefore secures charge stabilization and allows the water chemistry to take place, although this involves much slower electron transfer from the manganese cluster.

B. Tyrosyl Radical Chemistry

Electron transfer in proteins is often coupled to the transfer of protons. This also holds for PS II, when $P680^+$ is re-reduced by electron transfer from Y_Z, the Y_Z radical oxidizes the O_2-evolving manganese cluster in a subsequent step. Without deprotonation, the oxidized Y_Z would have a positive charge, and the high redox potential of the $TyrOH^+$/TyrOH couple makes that reaction endoergonic. However, tyrosine deprotonates readily upon oxidation, which increases the driving force. The resulting reaction free energy depends on the deprotonation reaction, and in the OEC the overall reaction is slightly exoergonic. When Y_Z subsequently is reduced by the manganese cluster, the reaction is coupled to re-protonation of Y_Z.

It is much debated in what way the proton transfer and electron transfer reactions of Y_Z are coupled: if one is a prerequisite for the other, if Y_Z is hydrogen bonded to one or more bases and under all conditions, where the proton goes to and from where it comes back, or if Y_Z is even deprotonated before oxidation (Ahlbrink et al., 1998; Diner et al., 1998; Hays et al., 1998, 1999; Diner, 2001; Rappaport and Lavergne, 2001; Renger, 2001; Tommos and Babcock, 2000, Nugent et al., 2001). This discussion was fuelled by a proposal that Y_Z is not just an electron transfer intermediate, but is intimately involved in the water oxidation mechanism by abstracting hydrogen atoms from water bound to the manganese cluster (Hoganson et al., 1995; Tommos et al., 1995; Hogansson and Babcock, 1997). The necessity of maintaining charge neutrality was emphasized (Tommos and Babcock, 2000), because of the energy penalty for creating a charge in a protein.

In order to gain new understanding of the electron/proton transfer mechanism of Y_Z, we have investigated the photo-induced proton coupled electron transfer from a tyrosine in a simple ruthenium-tyrosine model compound (Fig. 5, top). In electron transfer reactions, the positions of the nuclei have to distort before electron transfer can occur. When dissociative nuclear motions are involved as in deprotonation reactions, the reorganization energy λ is often large. The reorganization energy is consequently an important parameter in proton coupled electron

transfer reactions, which can help in elucidating the mechanism.

Proton motion can be coupled to the electronic motion in two limiting ways. In one case, the proton has to dissociate prior to electron transfer, a consecutive proton-first reaction, and in the other case the proton dissociates as a consequence of the electron transfer, giving a consecutive electron-first reaction. The proton motion is not involved in the electron transfer event in either case, so the reorganization energy is unaffected by the proton movement. Between these two extremes is the concerted mechanism, where electron-transfer and deprotonation are simultaneous, with a single transition state. The reorganization energy for such a reaction may be high due to reorganizations associated with the proton coordinate (solvent polarization and internal reorganization). Concerted electron transfer is a charge neutral reaction that avoids high-energy intermediates, in contrast to the consecutive mechanisms. Thus the concerted reaction is an energy-conservative mechanism, that allows for reactions with a low driving force to occur, but at the

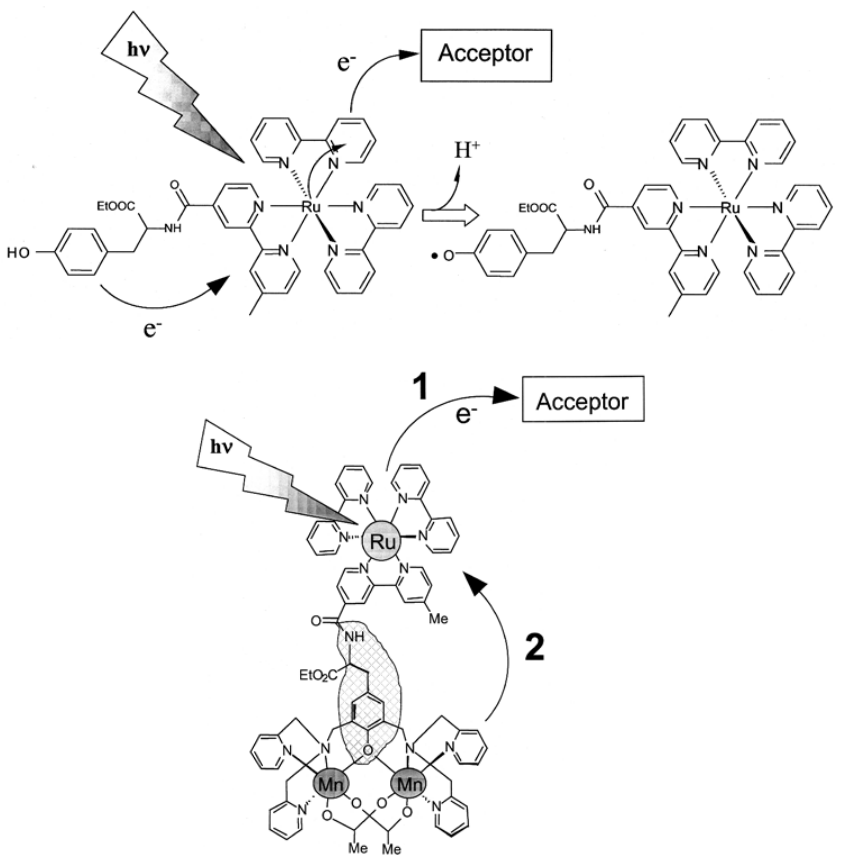

Fig. 5. Light-induced electron transfer in biomimetic complexes. (Top) A synthetic Ru-TyrOH complex, linked via a peptide bond. On illumination in the presence of an electron acceptor, the tyrosine moiety gives an electron to the photooxidized Ru-center, generating a neutral tyrosyl radical. For transient optical absorption measurements, methyl viologen was used as external electron acceptor. The neutral tyrosine radical could be detected by EPR at room temperature, using Co^{III}-pentaaminechloride as sacrificial electron acceptor. (Bottom) A supramolecular Ru-tyr-Mn_2 molecule, where the Mn moiety is coordinated to the BPMP-ligand (see text). When this complex is exposed to a laser flash an electron is given off to the external acceptor (reaction 1). The electron is then retrieved by intramolecular electron transfer from the Mn-dimer which is oxidized, probably via the tyrosine derivative link (reaction 2). This can be repeated three times. In this particular compound we have achieved oxidation from the Mn(II/II) level to the Mn_2(III/IV) level.

cost of a relatively large reorganization energy.

Figure 5 (Top), shows the structure of a synthetic Ru-TyrOH complex, in which a tyrosine is covalently linked to a Ru(II)-polypyridine photosensitizer. The Ru(II) complex can be photo-oxidized to Ru(III) in the presence of an external acceptor. In aqueous media, the tyrosine then reduces the Ru(III) by intramolecular electron transfer on the μs-time scale, forming a neutral tyrosine radical in the process (Magnuson et al., 1997). The electron transfer is coupled to deprotonation of the tyrosine (Sjödin et al., 2000) and can be measured by following the absorption changes of Ru(II). The rate constant is highly dependent on pH (Fig. 6A). At pH-values below the pKa of the tyrosine proton (pKa~10) the rate constant increases with pH. Above the pKa the rate constant is much larger, and independent of pH. Around the pKa value both kinetic phases are found. At low pH, the activation energy is high (E_a = 0.32 eV at pH = 7), but at pH>10 it is much lower (E_a = 0.05 eV at pH >10). These data cannot be explained by any of the consecutive mechanisms. In the electron-first mechanism, none of the reaction steps is pH-dependent, so the overall reaction would not show the experimentally found pH-dependence. In the proton-first mechanism, the reaction rate will be limited by the rate for tyrosine deprotonation, k_d. However, the pKa = 10 for tyrosine implies that the deprotonation with water as proton acceptor is very slow, $k_d \leq 10\ s^{-1}$, which is much too slow to account for the observed reaction rates. Also deprotonation to OH- or buffer species prior to electron transfer could be excluded (Sjödin et al., 2004).

Instead the electron transfer from tyrosine to $Ru(bpy)_3$, must be a concerted reaction where electron transfer and deprotonation of the tyrosine occur simultaneously in a single transition state. This means that the reorganizational components associated with electron transfer (mainly solvent polarization) and deprotonation (both solvent and internal motion) are both contributing to reaching the transition state, through a relatively large reorganization energy.

With a concerted mechanism, one can explain why the electron transfer rate is pH dependent. The redox potential for tyrosine decreases by 59 mV per pH-unit, until the pKa value is reached at pH = 10, above which the potential is constant. Thus, the free energy of the products decreases with pH giving rise to a pH dependent driving force in the reaction. This also leads to a decrease in activation energy with pH, and a faster reaction. We could fit our data for Ru-TyrOH electron transfer at pH <10 to the standard Marcus equation (Eqs. 1 and 2) by incorporating a pH-dependent driving force obtained from the redox potential for tyrosine (Fig. 6A). Since the reaction is in a region where $-\Delta G^0 << \lambda$, the fit follows a nearly linear dependence. The observed reaction rate thus follows the change in driving force for the overall reaction and it is important to note that only a concerted mechanism can explain this behavior.

By fitting temperature dependent data to Eqs. 1 and 2, the reorganization energy λ for a concerted reaction can be calculated to λ=2.0 eV at neutral pH. In this calculation the entropy increase, due to the mixing of the released proton, is ignored. If a correction is made for the ΔS^0, the value becomes lower, λ=1.4 eV. This entropy increase is pH dependent, and is actually the reason for the pH dependence of the tyrosine redox potential. We could estimate the entropy change to 1.4×10^{-3} J mol^{-1} K^{-1} at pH = 7 (Sjödin et al., 2004). Since $\Delta S^0 > 0$, the driving force increases with temperature, and the entropic contribution would decrease ΔG^0 by 0.41 eV at 25°C. A recalculation of the reorganization energy gives λ = 1.4 eV, which is much lower. However, the reorganization energy is still higher than for a simple electron transfer reaction, due to the concerted deprotonation.

It is important to emphasize here that a large entropy change may lead to large errors in the calculation of reorganization energies from activation energy data, if the entropy change is not taken into account. In biological systems it is usually difficult to evaluate the reaction entropy. Therefore our investigations might clarify to what extent entropy changes connected to proton release are involved in biological electron transfer reactions (Sjödin et al., 2002).

We now compare kinetic data for our Ru-TyrOH complex with that in manganese-depleted PS II (Fig. 6B). At pH<10 the proton-coupled electron transfer in Ru-TyrOH is a concerted reaction, with a large reorganization energy (λ = 1.4 eV). At pH >10 the reaction is much faster and pH-independent, corresponding to electron transfer from the deprotonated tyrosine in Ru^{III}-$TyrO^-$. The reorganization energy (λ = 0.9 eV at high pH) is then more typical for a simple electron transfer reaction in water. Close to the pKa of reduced tyrosine the tyrosine oxidation rate is bi-exponential, with the fast phase a hundred times faster than the slow phase.

The proton-coupled electron transfer reactions in PS II show strong similarities in the behavior for electron transfer from Y_Z to $P680^+$ in manganese-depleted PS II (Ahlbrink et al., 1998, Fig. 6B). At pH <7, Y_Z

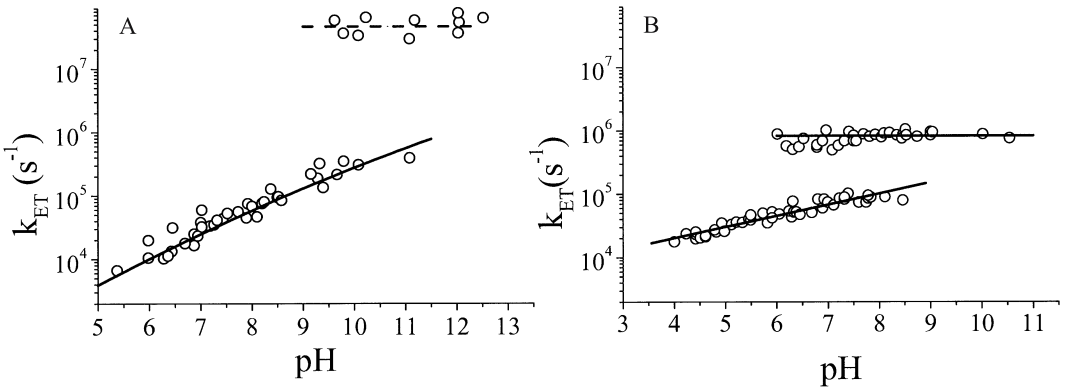

Fig. 6. pH-dependence of the rate constant for the light-induced electron transfer from tyrosine to the oxidized photosensitizer. (A) In the RuTyrOH complex (Fig. 2), and (B) in Mn-depleted Photosystem II-particles (Ahlbrink et al., 1998). The solid line in (A) is a theoretical linear fit to a Marcus type function. See text for discussion.

shows a pH dependence similar to that in Ru-TyrOH. The activation energy (E_a=0.30 eV) and the isotope effect ($k_H/k_D \approx 2.2$) in PS II, are also very similar to those in Ru-TyrOH (k_H/k_D = 2.0–2.5). At pH>7 in PS II, the rate was much higher and pH-independent, and the activation energy was lower (E_a = 0.15 eV). At pH around 7 both kinetic phases were present, differing in rate by one order of magnitude. Because of the similarity in the kinetics at low pH, we think that Y_Z oxidation at pH <7 in manganese-depleted PS II also is a concerted reaction, involving proton release to the bulk. The reorganization energy at neutral pH can be estimated to λ = 1.4 eV (Sjödin et al., 2004; not corrected for entropy changes) from the data in Ahlbrink et al. (1998). The kinetics at higher pH are also very similar, but show important differences. The activation energy in PS II at high pH is E_a = 0.15 eV, while it is 0.05 eV for Ru-TyrOH. Moreover, the switch to a faster kinetic phase occurred at pH = 10 in Ru-TyrOH but at pH = 7 for PS II. Finally, the difference in rate between the slower and faster phases is one order of magnitude in PS II, but two orders of magnitude in Ru-TyrOH.

In one of their mechanistic models, Ahlbrink et al. (1998) explained the results by hydrogen bonding of Y_Z to a base (presumably His190, compare Hays et al., 1998, 1999; Mamedov et al., 1998) that was titrated with an apparent pKa of 7. Below pH = 7, the base is protonated and the tyrosine releases the proton to the bulk. Above pH = 7, the proton is instead transferred to His190. The hydrogen bond would thus increase the rate by a factor of ten, and decrease the activation energy from 0.30 to 0.15 eV (Ahlbrink et al., 1998). If the reaction in PS II still follows a concerted mechanism, when the Y_Z is hydrogen bonded, this could explain why the rate becomes pH independent. Since the proton is no longer released to the bulk, the reaction driving force is no longer dependent on pH.

Our results from the Ru-TyrOH complex shed more light on the fundamental question: In what way does hydrogen-bonding increase the rate of tyrosine oxidation? Different factors may cause rate enhancement when tyrosine is hydrogen bonded, the most likely being either a change in the reaction driving force ($-\Delta G^0$) or the reorganization energy (λ). When tyrosine is hydrogen bonded to a base, the driving force for a concerted reaction is not dependent on bulk pH, because the proton moves to the base instead of being released to the water. A higher driving force in the hydrogen-bonded case could then explain the higher electron transfer rate. We therefore estimated the driving force for the concerted reaction with a hydrogen bonded tyrosyl residue, from a thermodynamic cycle, in which data for Ru-TyrOH is used for the pure electron transfer steps. We found that $\Delta G^0 = -0.27 \pm 0.05$ eV for the concerted reaction in a hydrogen bonded system.

In PS II, the $P680^+$ potential has been estimated to ca. +1.12 V (vs. SCE) (Tommos and Babcock, 2000; Diner, 2001), that is, ca. 0.14 V below that for $Ru(bpy)_3^{3+}$. We can predict that the driving force for a concerted reaction in PS II when tyrosine is hydrogen bonded to a histidine, is $\Delta G^0 \approx -0.13$ eV. However,

the rate constant for oxidation of a hydrogen bonded Y_Z in manganese depleted PS II is about ten times higher than in the absence of hydrogen bonds. Thus, the hydrogen bond does not induce a sufficient change in ΔG^0 to explain the higher rate.

The increased rate may be explained by a decrease in reorganization energy λ of the tyrosine O-H bond. By using the reported activation energy for PS II at pH >7 which is 0.15 eV (Ahlbrink et al., 1998), and our estimated $\Delta G^0 = -0.13$ eV, we can obtain a value of $\lambda = 0.85$ eV. This is almost equal to the reorganization energy for Ru-TyrOH at pH >10, when tyrosine is deprotonated: $\lambda = 0.90$ eV. This indicates that the hydrogen bond removes most of the reorganization of the O-H coordinate! This explanation is supported by recent experiments where Y_Z seems to be efficiently oxidized even at extremely low temperatures (ca. 5K), in the S_0 and S_1 states of intact oxygen evolving complexes (Zhang and Styring, 2002; Nugent et al., 2002).

We suggest that the reorganization energy of Y_Z in PS II without the manganese cluster goes from high to intermediate to low when the tyrosine goes from non-hydrogen bonded to hydrogen bonded to deprotonated. The pH dependence for the rate constant in a general system can now be described with a 'rate ladder': Step 1. At low pH values, tyrosine is deprotonated to the bulk, which gives a pH-dependent rate due to an increasing reaction entropy, and a high value for λ. Step 2. At intermediate pH and in the presence of a hydrogen bond, the proton doesn't see the bulk, and the rate is then independent of pH, and λ is at intermediate values. Step 3. Finally, at pH>10 when the reduced tyrosine is initially deprotonated, the rate is pH-independent and λ is small.

Other mechanisms for tyrosine oxidation in manganese depleted PS II have been suggested, e.g., a consecutive proton transfer-first mechanism (Ahlbrink et al., 1998; Diner et al., 1998; Haumann et al., 1999; Rappaport and Lavergne, 2001), or a gated mechanism where the hydrogen bond network would have to settle before the electron transfer could become fast (Diner et al., 1998; Diner, 2001). However, comparing the results from PS II with the data presented from the Ru-TyrOH complex, neither of these models fit with the observed micro-second rates and the pH dependence (Sjödin et al., 2002). Therefore, we favor the concerted mechanism in both the presence and absence of a hydrogen bond.

C. Donor Side Photoinhibition Revisited

During turnover, the PS II reaction center is constantly inhibited and damaged due to the formation of oxidizing species formed as a consequence of the complex photochemistry. These photo-induced, deleterious reactions are collectively called photoinhibition of PS II, and are an important phenomenon in vivo and in vitro (for reviews, see Barber and Andersson, 1992; Prasil et al., 1992; Aro et al., 1993; Styring and Jegerschöld, 1994). The reactions leading to photoinhibition involve side reactions due to the physical limitations of both the acceptor and donor side of PS II. These lead, first to inhibition of the overall electron transfer through PS II, then to damage to the D1 reaction center protein, and ultimately to complete degradation of this important protein. In repair after photoinhibition, new copies of the D1 protein are re-assembled with the other subunits of PS II (Aro et al., 1993; van Wijk et al., 1994; Chapter 23, Pogson et al.).

In our investigations of the Ru-TyrOH complex (Fig. 5) we observed side reactions that were remarkably similar to early events in photoinhibition of the PS II donor side. The results are summarized in Fig. 8. When the Ru-Tyr complex is exposed to light in the presence of an irreversible electron acceptor, it forms a neutral tyrosyl radical at high yield (see above). The half time of the decay of the tyrosyl radical formed on a flash (Fig. 7), was concentration dependent and about 50–100 ms for a 1 mM solution of Ru-TyrOH compound (Magnuson et al., 1997). When we continued to illuminate the complex, the amount of tyrosyl radicals that can be observed on each flash decreased linearly with the amount of light given (Fig. 8); Magnuson et al. 1997, 1999). The decreased radical yield is a result of deleterious reactions such as crosslinking between tyrosine radicals in different molecules, which lead to a decrease in the number of active Ru-TyrOH molecules capable of forming tyrosyl radicals (Magnuson et al., 1997).

In contrast, when methyl viologen was used as external electron acceptor, the yield of tyrosine radicals did not decrease even during prolonged laser flashing (Sjödin et al., 2000). This is because electron recombination between the reduced methyl viologen and the tyrosyl radical prevented the irreversible reactions between tyrosyl radicals. This situation is very similar to the situation in newly assembled PS II complexes (Rova et al., 1993, 1996, 1998). Before the manganese cluster has been inserted and

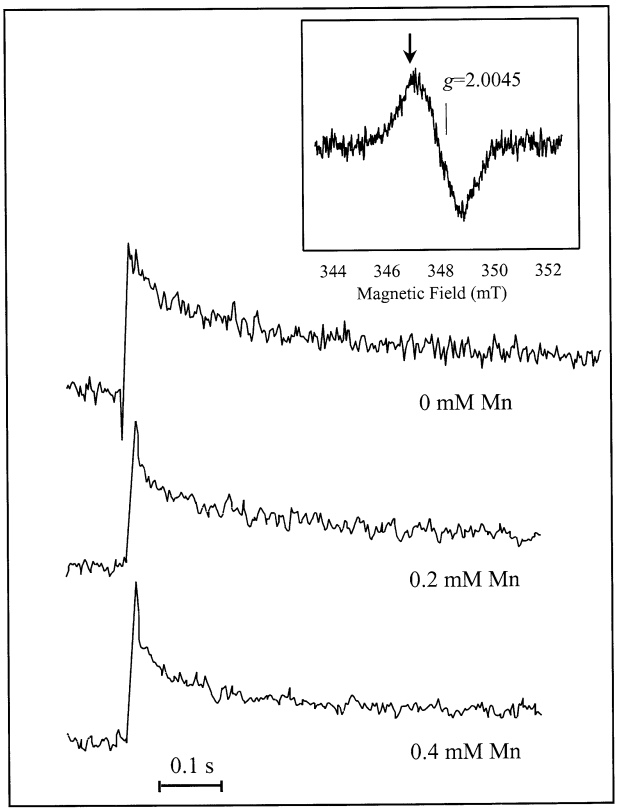

Fig. 7. Flash photolysis experiment with a synthetic 'triad' consisting of the RuTyrOH complex and a linear μ-oxo-$Mn(III)_2$ complex (see text). The ruthenium is photooxidized and recaptures an electron from the tyrosyl moiety which forms a neutral radical (insert: EPR spectrum). The tyrosine radical then oxidizes the Mn complex to the mixed-valence Mn(III)-Mn(IV) state. By following the transient tyrosyl radical formation and decay, after adding different concentrations of Mn-complexes, it is clear that the Mn complex donates electrons directly to the tyrosine radical. We found that the Mn-complex not only functions as electron donor, but also protects the tyrosine against deleterious side reactions.

activated, PS II is very vulnerable to light and uses several defense systems to protect itself. The most important protection mechanism is that the forward electron transfer form Q_A to Q_B is slowed down in the absence of a functional manganese cluster (Rova et al., 1998; Krieger et al., 1995) promoting efficient and fast electron recombination reactions between Q_A^- and $Y_Z^\bullet$. Deleterious reactions of the tyrosine radical are thereby prevented.

These early reactions during assembly of PS II were mimicked in an experiment where we investigated the possibility to use a manganese compound as exogenous electron donor to the tyrosyl moiety in Ru-TyrOH when this was photo-oxidized, in analogy with the reactions on the PS II donor side. For this purpose we used a Mn_2(III,III) dimer, in which the two Mn ions are linked by a single μ-oxo bridge, and each Mn ion has a terminal phenoxyl ligand (Horner et al., 1999). This complex can be reversibly oxidized in two steps. The first step, at 0.58V (vs. NHE and at pH=7), involves the formation of the Mn_2(III,IV) state. We showed that the photo-generated tyrosyl radical indeed could extract electrons from the Mn dimer (Magnuson et al., 1999). As a result, we could observe light driven formation of the Mn_2(III,IV) state by EPR. The second oxidation could not be achieved under our conditions, as the oxidation potential of the tyrosyl radical at neutral pH values is below that of the ligand oxidation (Magnuson et al., 1999).

Using transient EPR measurements (Fig. 7), we

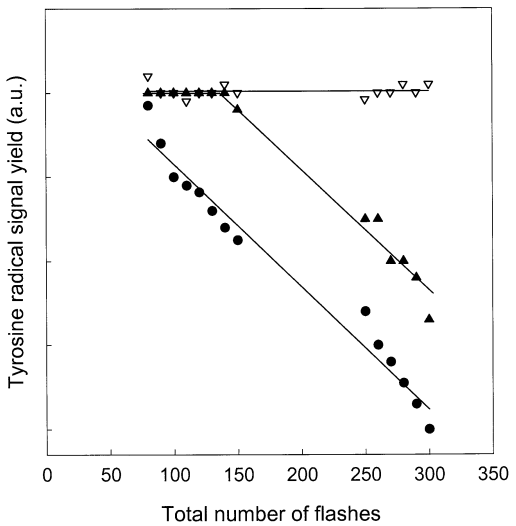

Fig. 8. Decrease in tyrosyl radical signal in the Ru-TyrOH complex due to deleterious reactions as an effect of light-induced electron transfer. The filled circles depict the radical signal amplitude in the absence of Mn, the filled triangles in the presence of 0.2mM Mn and the open triangles after adding 0.8 mM Mn. The concentration of Ru-TyrOH was 1mM.

also observed that when the Ru-TyrOH-complex was illuminated with single laser flashes in the presence of the Mn_2(III,III) dimer, the initial concentration of tyrosyl radicals was high and independent of Mn concentration. The radical lifetime, however, was considerably shorter in the presence of the Mn dimer. This showed that the Mn complex indeed reduced the radical back to Ru-TyrOH (Fig. 7). The yield of tyrosine radicals remained high even after repetitive flashing, and it took many flashes before the radical yield started to decrease (Fig. 8). The more Mn dimer that was present, the more flashes were needed to observe a decrease in the photochemical yield of the tyrosyl radical. Apparently, electron donation from the Mn dimer efficiently prevented side reactions of the tyrosyl radicals. However, when all the Mn dimer molecules had been oxidized, the tyrosines became inactivated just as we observed after a few flashes in the absence of Mn.

These reactions show strong similarity to a situation that arises in PS II when the manganese cluster is absent or inhibited for some reason (for example in experiments when PS II is devoid of the necessary cofactors Cl^- or Ca^{2+}, or in presence of other inhibitory agents). The capacity of Y_Z to function as electron donor is then rapidly inhibited if PS II is illuminated (Jegerschöld et al., 1990; Jegerschöld and Styring, 1992, 1996). In the reactions that follow, the charge separation involving P680 is first inactivated and then the D1 protein becomes damaged and triggered for degradation (Jegerschöld et al., 1990; Jegerschöld and Styring, 1996). In contrast, when the same system is illuminated in the presence of the herbicide DCMU, which blocks the forward electron transfer from Q_A, the function of both Y_Z and P680 are kept stable much longer. This is because the electron recombination from Q_A^- to the oxidized $Y_Z^{\bullet}$ is fast enough to prevent side reactions between the Y_Z radical and its environment.

In a fully functional, water oxidizing PS II center, forward electron transfer from the manganese cluster rapidly reduces Y_Z. However, even in the presence of the manganese cluster, the electrons may arrive too slowly from the manganese cluster. This is for example the situation in Cl^- depleted PS II, where the manganese cluster can only deliver one electron to the oxidized Y_Z before the S-cycle stalls in the S_2-state. The next photon gives rise to a long-lived Y_Z radical in presence of a modified S_2-state, a situation where side reactions efficiently and quickly inactivate and destroy Y_Z. The stability of the Y_Z radical has not been studied in detail, but the $S_2 - Y_Z^{\bullet}$ radical pair has been found, in other situations, to be stable for minutes (Geijer et al., 2001). These reactions manifest themselves as a high light sensitivity, of both the function and the protein structure of PS II lacking the Cl^- cofactor.

Y_Z is spatially completely surrounded by amino acid side chains of the D1 protein (Svensson et al., 1991, 1996). It is therefore likely that an abnormally long lived Y_Z radical reacts with amino acid side chains in its vicinity, leading to D1-protein damage. This donor-side triggered photodamage of the D1 protein is independent of the presence of oxygen and is therefore not the result of singlet O_2 formation (Jegerschöld and Styring, 1991). Instead it involves Y_Z or $P680^+$ triggered radical side reactions between the redox cofactors and amino acids side-chains in their neighborhood. Interestingly, there are reports of cross-linking reactions between amino acids in the D1 protein and a tyrosine (presumably Y_Z itself) (Prasil et al., 1992), and even to chemical modifications of the tyrosine itself, during illumination of PS II mutants without the manganese cluster (Boerner and Barry, 1994; Ma and Barry, 1996).

The environment of Y_Z contains mainly inert side chains (Svensson et al., 1991, 1996) that might

explain why the radical can prevail for seconds to minutes in manganese containing PS II (Geijer et al., 2001; Andreasson et al., 1995). In manganese depleted PS II, the Y_Z radical never exists for longer than a few hundred milliseconds, suggesting that the environment is less well protected against exogenous reductants in the absence of the active manganese cluster. This is a beneficial situation in newly synthesized PS II centers. The protein complexes in PS II are assembled without the manganese cluster, which only becomes assembled in the very last step (van Wijk et al., 1994; Rova et al., 1998). In this process, the Y_Z radical is thought to oxidize diffusible Mn(II) ions in the lumen space, in stepwise and light-dependent reactions. However, the molecular details of photoactivation are not completely known and it remains an open question how Mn ions located more remotely from Y_Z are oxidized and incorporated into the cluster. One obvious explanation would be that Mn(II) ions reversibly form bridges to other Mn ions in the growing cluster, before becoming oxidized via electron transfer through the manganese complex itself. An interesting and conceivable alternative is that the Y_Z radical could trigger a radical chain reaction, via close lying side chains, ultimately oxidizing more distantly located manganese ions.

III. Redox Properties in Natural and Artificial Photosynthetic Systems

The redox chemistry in our synthetic Mn-containing systems is well-defined in comparison to what we know about the manganese cluster in PS II. Therefore, there are probably lessons that can be learnt from these more simple systems that apply when we try to understand the chemistry in PS II and which should be incorporated during the development and synthesis of more sophisticated structural and mechanistic mimics of the donor side in PS II. We (and others) have concentrated our synthetic efforts to construct Mn-systems with high flexibility in their redox properties. We have also chosen to study many of our compounds in aqueous solution. Most often one tries to stay away from water in studies of synthetic Mn compounds, as water tends to destabilize the Mn-complex and complicate the chemical reactions. Mn is a metal that easily undergoes ligand exchange and becomes dislodged from most chelators. We have found this to be common in our Mn complexes too, and in many cases our compounds are unstable during prolonged exposure to water-containing solutions. However, since we want to accomplish water oxidation, it is necessary to learn to control the stability of the complexes.

In order to increase the charge storing capacity of our Mn complexes, and get closer to an actual mimic of the water oxidizing complex, we have constructed several systems involving dimeric Mn complexes. Here we will describe the redox chemistry in two of them (Figs. 3 and 5, Bottom). The first complex is a Mn_2(II,II) dimer, with a well-known N_3O ligand sphere (Diril et al., 1987), which we linked covalently to a Ru(II)-trisbipyridyl moiety (Fig. 5, Bottom). The Mn ions are bridged via a phenoxy group and two terminal acetate molecules. It was known from earlier electrochemical studies that this Mn dimer could form the Mn_2(II,II), the Mn_2(II,III) and the Mn_2(III,III) oxidation states in organic solvent (Diril et al., 1987). In contrast we were able to accomplish stepwise oxidation of this Mn dimer by flash photolysis, from the Mn_2(II,II) state, via Mn_2(II,III) and Mn_2(III,III), up to the Mn_2(III,IV) oxidation state in presence of a small amount of water (Huang et al., 2002). Interestingly, we also found that all three oxidation steps are within the range of the Ru(III)$(bpy)_3$ oxidation potential only when water is present in the reaction mixture. On the other hand the Mn_2(III/IV) state could not be reached in the absence of water at the potential of Ru(III)$(bpy)_3$. We have therefore hypothesized that a water-induced bridging mode change is a necessary prerequisite to form the higher oxidation states. This proposition has recently been supported by EXAFS measurements on this Mn dimer in the different oxidation states. In the Mn_2(II,III) state the Mn-Mn distance was 3.42 Å, while in the Mn_2(III,III) state more than half of the complexes showed a Mn-Mn-distance of ca. 2.9 Å. The sample contained small amounts of water, suggesting that formation of a di-μ-oxo bridge takes place in that oxidation state (A. Magnuson et al., unpublished).

The other complex is a similar Mn-dimer, but with a N_2O_4 ligand set where two of the pyridine groups have been exchanged for oxygen-containing phenol groups, thereby enhancing the electron donating properties of the ligand (Fig. 3, Top) (Lomoth et al., 2002). The importance of oxygen ligands is implicit from PS II, where predominantly carboxylic acid side chains of aspartate and glutamate, and the carboxyl-terminal of the D1 protein, coordinate the manganese cluster. In constructing this Mn-dimer, we hoped that the ligand system would stabilize the higher oxidation

states that are thought to be a prerequisite for water oxidation. The redox chemistry in this compound is very rich, and recent studies show that, in the presence of water, it is possible to accommodate at least five separate oxidation states in this molecule (Lomoth et al., 2002; Huang et al., 2004). All of these states are not formed reversibly, with irreversible steps probably involving bridging mode changes in the higher oxidation states. In flash photolysis experiments using a $Ru(II)(bpy)_3$ complex as photosensitizer, we could observe oxidation to Mn_2(III,IV) after limited illumination. With prolonged photolysis the EPR spectra revealed that also Mn_2(IV) could be reached in this Mn complex, which supports our hypothesis that this ligand can accommodate higher oxidation states. We have also studied the different oxidation states in the molecule with EXAFS. Our data show that the distance between the Mn ions also in this complex decrease in the higher oxidation states, but in this case it takes place in the Mn_2(III,IV) state, suggesting that a change in bridging mode takes place prior to, or concomitantly with oxidation (A. Magnuson et al., unpublished). We have also synthesized a series of complexes that are analogous to this Mn-dimer (Fig. 3), where the only difference is different substituent groups on the peripheral parts of the ligand. These groups have small, but significant influence on the redox properties of the Mn-dimer, so that with the different substituents we now have a range of similar Mn-dimers with slightly different redox properties.

Theoretical accounts for the possible reactions involved do not foresee why more than two (or even more than one) Mn ions are necessary to accomplish water oxidation in PS II (Vrettos et al., 2001; Siegbahn and Crabtree, 1999; Pecoraro et al., 1998). In the manganese compounds discussed above, the redox reactions involving the Mn(II) to Mn(III) transition (i.e., Mn_2(II,II) to Mn_2(II,III), and Mn_2(II,III) to Mn_2(III,III)) occur several hundred millivolts lower than oxidation from the Mn(III) to the Mn(IV) level. In all the Mn complexes that we have investigated, there is a rather wide interval in the redox potential scale (about 500–600 mV), where the manganese oxidation state (the $Mn(III)_2$ state in our present molecules) is stable both against oxidation and reduction. Seemingly, the ability to have all the oxidation states of a complex accessible within a narrow potential range, breaks down when the complex has to support more than two redox transitions. Very interestingly, we found that the potentials for oxidizing the Mn dimer to the Mn_2(III,III) and the Mn_2(III,IV) states in the complex shown in Fig. 5, were lower in the presence of 10% water. This suggests that water-induced bridging mode changes will stabilize the higher oxidation states by accommodating the increased charge. Thus, a manganese complex that can accommodate three oxidation states, can be constructed such that the potential difference between the states is less than 100 mV.

We hypothesize that a similar situation holds also for the manganese cluster in PS II (Fig. 9). The driving force for oxidizing the manganese cluster is provided by Y_Z. The operating potential at normal pH (pH 5–7) of the Tyr/Tyr$^\bullet$ couple is ca +0.95 V (vs. NHE). This potential is available to drive each S-state transition (Vass and Styring, 1991). Over the entire cycle a driving force of about $4 \times 0.95 = 3.8$ V is available, which should be compared to the 3.2 V necessary to oxidize two water molecules to molecular oxygen. After four turnovers of the enzyme, enough oxidizing equivalents have been stored to drive the overall reaction thermodynamically downhill. Suppose that the S-state transitions involve the oxidation of only one and the same manganese ion, while the others act as 'voyeur' manganese ions. The 'active' manganese would then have to pass through four or five different oxidation states. This would certainly involve structural changes that are energetically costly and too much of the free energy available in each transition would be lost, so that a higher driving force than available from Y_Z would be necessary to drive the whole reaction. This is not possible in PS II which can not change the potential available from Y_Z very much. Instead, it is likely that nature has circumvented this problem by dividing the oxidation state changes between several manganese ions (in the case of PS II, four Mn are used). Then, the structure of the complex can remain relatively the same despite it going through many oxidation state changes, thus lowering the reorganization energy and minimizing energy losses. Interestingly, the bridging mode between Mn ions seems to change upon at least two of these redox transitions, which could account for the compression of redox potentials in the OEC of PS II (Liang et al., 2000; Dau et al., 2001; Robblee et al., 2001).

Two hypotheses for the Mn valence states in the different S-states dominate the literature. The two models originate from simulations of the EPR signals in the S_2 state, and from X-ray absorption data in the different S-states. One model is that the S_2 state

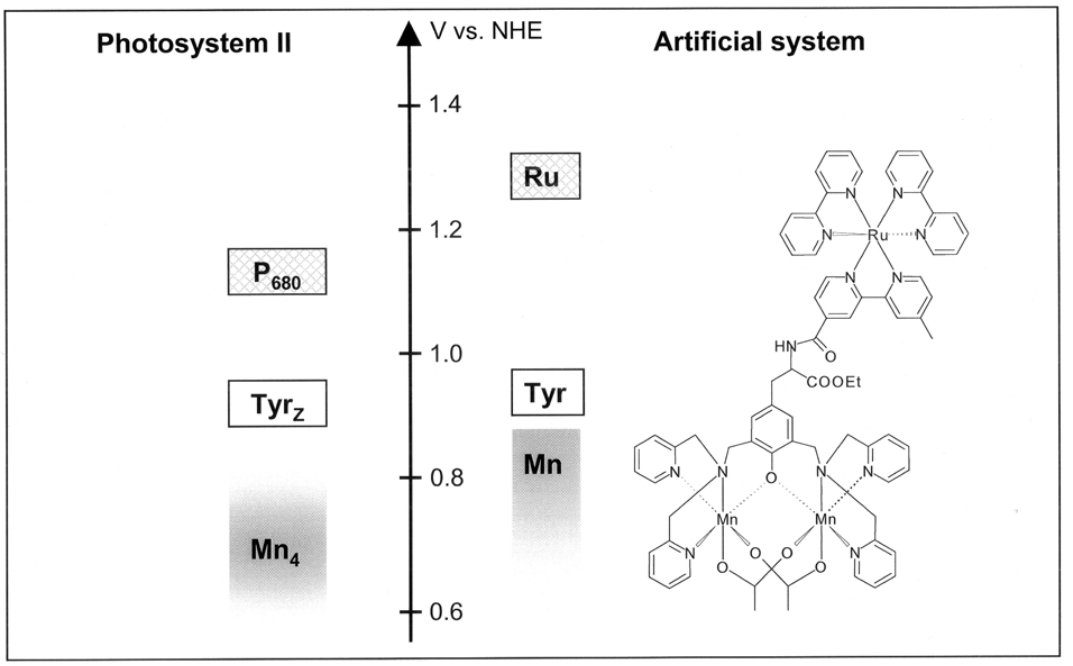

Fig. 9. Redox potential diagram showing the similarities between the components on the donor side of Photosystem II (left), and the synthetic ruthenium-, tyrosine-, and manganese complexes designed for artificial photosynthesis (right).

contains Mn_4(III,III,III,IV) and in this model the S_0 state would be at the Mn_4(II,III,III,III) level since the presence of Mn(II) in the S_0 state is probably necessary to explain the wide multiline EPR signal from the manganese cluster in that state (Åhrling et al., 1997; Messinger et al., 1997). Another, and presently the most favored model, is that the manganese cluster in the S_2 state is best represented by Mn_4(III,IV,IV,IV) state (Yachandra et al., 1996; Dau et al., 2001; Carrell et al., 2002). In the S_0 state, the same model predicts that Mn_4(II,III,IV,IV) oxidation number distribution to best describe available data.

From our photochemical work with the Mn-dimers we favor the idea that the manganese cluster operates in the higher of the two redox potential regimes available. In our synthetic complexes, we have so far never been able to observe oxidation states higher than the Mn(IV) level in compounds that contain phenol type ligands. At higher potential regimes, as that of the Ru(II)/Ru(III) couple (ca. +1.32V vs. NHE), we often observe oxidation of the ligand molecule when the limit of manganese oxidation has been reached. It therefore seems that only the Mn(III)/Mn(IV) redox couple is available for storage of oxidizing equivalents as long as we use phenol containing ligand molecules. This holds for nature that actually uses a phenol (Y_Z) to oxidize the manganese cluster. In contrast, the Mn(II)/Mn(III) couple lies too low on the redox scale to be useful in our multimeric manganese complexes, while the Mn(IV)/Mn(V) couple is not available at these potentials. Within the potential range of tyrosine radicals (ca. +0.9 V at pH=7) the Mn(III)/Mn(IV) state seems to be the optimum and the limit in our systems. In PS II, the first ligand sphere around the manganese is dominated by oxygen ligands, which tends to lower the potential for the Mn(III) to Mn(IV) oxidation (Lomoth et al., 2002). By analogy, we therefore believe that oxidations from Mn(III) to Mn(IV) are likely to dominate the S-state cycle in steps where Mn oxidation is involved but that the oxidation sometimes can be spread over several of the Mn ions. In addition, to accommodate 4 oxidative steps more than 2 Mn-ions must be involved.

Presently, we have limited our attempts to mimic the complicated manganese cluster in PS II, to mono- or dinuclear Mn complexes. Perhaps these will never be able to store four oxidizing equivalents at suffi-

ciently high potential to accomplish water oxidation. Instead, it will probably become necessary to drive our biomimetic approach even further, and synthesize all-Mn(III) trimers or tetramers, to reach the level of complexity that is necessary. We are presently attempting to develop such systems that will be linked to a photoactive ruthenium center.

IV. Future Outlook

In this chapter, we have described results from a project of artificial photosynthesis. We have still more lessons to learn about the natural photosynthetic systems. Hopefully also the future man made complexes will prove an important source of new knowledge, in this learning process. If we ever shall be able to accomplish light-induced H_2 production from water, our Ru-Mn systems should be coupled to reductive catalysts capable of reduction of protons to hydrogen, with electrons derived from water. Also in this case can we find inspiration in nature, and start to design biomimetic complexes. In nature, H_2 is produced by hydrogenases of different types. The active sites of hydrogenases contain metal centers, and are comprised of either a di-iron complex (in the so-called iron-only hydrogenases) or an iron-nickel complex (Frey, 2002, and references therein). Several X-ray structures are known from this class of enzymes, and a quite well developed biomimetic chemistry already exists.

In the future, an important goal is to link synthetic iron-iron molecules of this type to the ruthenium photosensitizers, in order to accomplish light-driven H_2 production. Potential candidates for a chemical link between the ruthenium moiety and the acceptor-catalyst, are quinone derivatives, similar to the quinone acceptors in the photosynthetic reaction centers. There are also several entirely man-made candidates available that have a suitable redox potential and have been shown to work in donor-acceptor systems. These latter acceptor molecules may be more forgiving synthetically, than the quinones. The chemistry of these new types of donor-photosensitizer-acceptor assemblies, need to be tested and developed, but hopefully there will be progress also in this area in the future.

Our aim in this project is to accomplish H_2 production with water as raw material, and using solar energy as driving force. We will continue our efforts in this field by further developments of our Ru-Tyr-Mn systems. In the future we hope to develop compounds where the number of Mn ions are increased to four, and where all of the Mn ions are at the Mn(III) or higher oxidation level.

Acknowledgments

Most of this work was carried out through our collaboration within the Swedish Consortium for Artificial Photosynthesis. We gratefully acknowledge the continuous and rewarding collaborations and discussions with all our earlier and present colleagues in the Consortium. In particular we are deeply indebted to Prof Em. Björn Åkermark and Dr Licheng Sun (Stockholm University, Sweden) for their endless supply of the wonderful synthetic Ru-Tyr-Manganese containing super-molecules. This project was supported by grants from the Swedish National Energy Administration, the Knut and Alice Wallenberg Foundation, the European TMR program (TMR network CT96-0031), the Swedish Research Council for Engineering Sciences (TFR), the Swedish Natural Science Council (NFR), the Swedish Science Council (VR), the Nordic Energy Program and the Delegation for Energy Supply in South Sweden (DESS).

References

Abrahamsson MLA, Baudin HB, Tran A, Philouze C, Berg KE, Raymond-Johansson MK, Sun L, Åkermark B, Styring S and Hammarström L (2002) Ruthenium-manganese complexes for artificial photosynthesis: Factors controlling intramolecular electron transfer and excited-state quenching reactions. Inorg Chem 41: 1534–1544

Ahlbrink R, Haumann M, Cherepanov D, Bögershausen O, Mulkidjanian A and Junge W (1998) Function of TyrosineZ in water oxidation by Photosystem II: Electrostatical promoter instead of hydrogen abstractor. Biochemistry 37: 1131–1142

Åhrling KA, Peterson S and Styring S (1997) An oscillating manganese electron paramagnetic resonance signal from the S_0 state of the oxygen evolving complex in Photosystem II. Biochemistry 36: 13148–13152

Andréasson L-E, Vass I and Styring S (1995) Ca^{2+} depletion modifies the electron transfer on both the donor and acceptor side of Photosystem II from spinach. Biochim Biophys Acta 1230: 155–164

Aro E-M, Virgin I and Andersson B (1993) Photoinhibition of Photosystem II. Inactivation, protein damage and turnover. Biochim Biophys Acta 1143: 113–134

Babcock GT, Espe M, Hoganson C, Lydakis-Simantiris N, McCracken J, Shi W, Styring S, Tommos C and Warncke K

(1997) Tyrosyl radicals in enzyme catalysis: Some properties and a focus on photosynthetic water oxidation. Acta Chemica Scandinavica 51: 533–540

Balzani V and Carassiti V (1970) Photochemistry of Coordination Compounds. Academic Press, London

Barber J and Andersson B (1992) Light can be both good and bad to photosynthesis. Trends Biochem Sci 17: 61–66

Berg KE, Tran A, Raymond MK, Abrahamsson M, Wolny J, Redon S, Andersson M, Sun L, Styring S, Hammarström L, Toftlund H and Åkermark B (2001) Covalently linked Ruthenium(II)-Manganese (II) complexes: Distance dependence of quenching and electron transfer. Eur J Inorg Chem 4: 1019–1029

Berglund-Baudin H, Sun L, Davydov R, Sundahl M, Styring S, Åkermark B, Almgren M and Hammarström L (1998) Intramolecular electron transfer from manganese (II) coordinatively linked to a photogenerated Ru(III)-polypyridine complex: A kinetic analysis. J Phys Chem A 102: 2512–2518

Bernat G, Morvaridi F, Feyziyev Y and Styring S (2002) pH-dependence of the four individual transitions in the catalytic S-cycle during photosynthetic oxygen evolution. Biochemistry 41: 5830–5843

Boerner RJ and Barry BAB (1994) EPR evidence that the M^+ radical which is observed in three site directed mutants of Photosystem II is a tyrosine radical. J Biol Chem 269: 134–137

Britt RD (1996) Oxygen evolution. In: Ort D and Yocum C (eds) Oxygenic Photosynthesis: The Light Reactions, pp 137–164. Kluwer Academic Publishers, Dordrecht

Carrell, TG, Tyryshkin AM and Dismukes GC (2002) An evaluation of structural models for the photosynthetic water-oxidizing complex derived from spectroscopic and X-ray diffraction signatures. J Biol Inorg Chem 7: 2–22

Chen P and Meyer TJ (1996) Electron transfer in frozen media. Inorg Chem 35: 5520–5524

Damrauer NH, Boussie TR, Devenney M and McCusker JK (1997) Effects of intraligand electron delocalization, steric tuning, and excited-state vibronic coupling on the photophysics of aryl-substituted bipyridyl complexes of Ru(II). J Am Chem Soc 119: 8253–8268

Dau H, Iuzzolino L and Dittmer J (2001) The tetra-manganese complex of Photosystem II during its redox cycle — X-ray absorption results and mechanistic implications. Biochim Biophys Acta 1503: 24–39

Diner BA (2001) Amino acid residues involved in the coordination and assembly of the manganese cluster of Photosystem II. Proton-coupled electron transfer of the redox-active tyrosines and its relationship to water oxidation. Biochim Biophys Acta 1503: 147–163

Diner BA and Babcock GT (1996) Structure, dynamics and energy conversion efficiency in Photosystem II. In: Ort D and Yocum C (eds) Oxygenic Photosynthesis: The Light Reactions, pp 213–247. Kluwer Academic Publishers, Dordrecht

Diner BA, Force DA, Randall DW and Britt RD (1998) Hydrogen bonding, solvent exchange, and coupled proton and electron transfer in the oxidation and reduction of redox-active tyrosine Y_Z in Mn-depleted core complexes of Photosystem II. Biochemistry 37: 17931–17943

Diril H, Chang H-R, Zhang X, Larsen SK, Potenza JA, Pierpont CG, Schugar HJ, Isied SS and Hendrickson DN (1987) Binuclear mixed-valence MnIIMnIII complexes: Insight about the resolution of hyperfine structure in the EPR spectrum. J Am Chem Soc 109: 6207–6208

Dismukes GC and Siderer Y (1981) Intermediates of a polynuclear manganese center involved in the photosynthetic oxidation of water. Proc Natl Acad Sci USA 78: 274–178

Ferreira KN, Iverson TM, Maghlaoui K, Barber J and Iwata S (2004) Architecture of the photosynthetic oxygen-evolving center. Science 303: 1831–1838

Frey M (2002) Hydrogenases: Hydrogen-activating enzymes. Chem Bio Chem 3: 153–160

Gaines GL, O'Neil MP, Svec WA, Niemczyk MP and Wasielewski MR (1991) Photo-induced electron transfer in the solid state—Rate vs. free energy dependence in fixed-distance porphyrin acceptor molecules. J Am Chem Soc 113: 719–721

Geijer P, Morvaridi F and Styring S (2001) The S_3 state of the oxygen evolving system in Photosystem II is converted to the $S_2Y_Z^{\bullet}$ state at alkaline pH. Biochemistry 40: 10881–10891

Hammarström L, Barigelletti F, Flamigni L, Indelli MT, Armaroli N, Calogero G, Guardigli M, Sour A, Collin J-P and Sauvage J-P (1997) A study on delocalization of MLCT excited states by rigid bridging ligands in homometallic binuclear complexes of Ruthenium. J Phys Chem A 101: 9061–9069

Hammarström L, Sun L, Magnuson A, Frapart Y, Berglund-Baudin H, Åkermark B and Styring S (1999) Mimicking Photosystem II reactions in artificial photosynthesis. Zeitschrift Phys Chem 123: 157–163

Hammarström L, Sun L, Åkermark B and Styring S (2001) A biomimetic approach to artificial photosynthesis: Ru(II)-polypyridine photosensitisers linked to tyrosine and manganese electron donors. Spectrochimica Acta A 37: 2145–2160

Haumann M, Mulkidjanian A and Junge W (1999) Tyrosine-Z in oxygen-evolving Photosystem II: A hydrogen-bonded tyrosinate. Biochemistry 38: 1258–1267

Hays A-MA, Vassiliev IR, Golbeck JH and Debus RJ (1998) Role of D1-His190 in proton-coupled electron transfer reactions in Photosystem II: A chemical complementation study. Biochemistry 37: 11352–11365

Hays A-MA, Vassiliev IR, Golbeck JH and Debus RJ (1999) Role of D1-His190 in the proton-coupled oxidation of tyrosine Y_Z in manganese-depleted Photosystem II. Biochemistry 38: 11851–11865

Hogansson CW and Babcock GT (1997) A metalloradical mechanism for the generation of oxygen from water in photosynthesis. Science 277: 1953–1956

Hoganson CW, Lydakis-Simantiris N, Tang X-S, Tommos C, Warncke K, Babcock GT, Diner BA, McCracken J and Styring S (1995) A hydrogen-atom abstraction model for the function of Y_Z in photosynthetic oxygen evolution. Photosynth Res 46: 177–184

Horner O, Anxolabehere-Mallart E, Charlot MF, Tchertanov L, Guilhem J, Mattioli TA, Boussac A and Girerd JJ (1999) A new manganese dinuclear complex with phenolate ligands and a single unsupported oxo bridge. Storage of two positive charges within less than 500 mV. Relevance to photosynthesis. Inorganic Chemistry 38: 1222–1232

Huang P, Magnuson A, Lomoth R, Abrahamsson M, Tamm M, Sun L, van Rotterdam B, Park J, Hammarström L, Åkermark B and Styring S (2002) Three-step oxidation of a $Mn^{II,II}$dimer to $Mn^{III,IV}$ by photogenerated Ru^{III}: Towards a functional mimic of the water oxidizing center in Photosystem II. J Inorg Biochemistry 91: 159–172

Huang P, Högblom J, Anderlund MF, Sun L, Magnuson A and Styring S (2004) Light-induced multistep oxidation of dinuclear

manganese complexes for artificial photosynthesis. J Inorg Biochemistry 98: 733–745

Ioannidis N and Petrouleas V (2000) Electron paramagnetic resonance signals from the S3 state of the oxygen evolving complex: A broadened radical signal induced by low-temperature near-infrared light illumination. Biochemistry 39: 5246–5254

Iuzzolino L, Dittmer J, Dorner W, Meyer-Kaucke W and Dau H (1998) X-ray absorption spectroscopy on layered Photosystem II membrane particles suggests manganese-centered oxidation of the oxygen-evolving complex for the S_0-S_1, S_1-S_2, and S_2-S_3 transitions of the water oxidation cycle. Biochemistry 37: 17112–17119

Jegerschöld C and Styring S (1991) Fast oxygen-independent degradation of the D1 reaction center protein in Photosystem II. FEBS Lett 280: 87–90

Jegerschöld C and Styring S (1992) Photoinhibition of Cl-depleted thylakoid membranes. Effects of illumination under anaerobic conditions. In: Barber J, Medrane H and Guerrero MG (eds) Trends in Photosynthesis Research, pp 59–69. Intercept Ltd, Andover

Jegerschöld C and Styring S (1996) Spectroscopic characterization of intermediate steps involved in donor-side photoinhibition of Photosystem II. Biochemistry 35: 7794–7801

Jegerschöld C, Virgin I and Styring S (1990) Light-dependent degradation of the D1 protein in Photosystem-II is accelerated after inhibition of the water splitting reaction. Biochemistry 29: 6179–6186

Juris A, Balzani V, Barigelletti F, Campagna S, Belser P and von Zelewsky A (1988) Ru(II) polypyridine complexes: Photophysics, photochemistry, electrochemistry and chemiluminescence. Coord Chem Rev 84: 85–277

Kamiya N and Shen J-R (2003) Crystal structure of oxygen-evolving Photosystem II from *Thermosynechococcus vulcanus* at 3.7-Å resolution. Proc Natl Acad Sci USA 100: 98–103

Krieger A, Rutherford AW and Johnson GN (1995) On the determination of redox midpoint potential of the primary quinone electron acceptor, Q_A, in Photosystem II. Biochim Biophys Acta 1229: 193–201

Kuzek D and Pace RJ (2001) Probing the Mn oxidation states in the OEC. Insights from spectroscopic, computational and kinetic data. Biochim Biophys Acta 1503: 123–137

Lavergne J and Junge W (1993) Proton release during the redox cycle of the water oxidase Photosynth Res 38: 279–296

Liang WC, Roelofs TA, Cinco RM, Rompel A, Latimer MJ, Yu WO, Sauer K, Klein MP and Yachandra VK (2000) Structural change of the Mn cluster during the $S_2 \rightarrow S_3$ state transition of the oxygen-evolving complex of Photosystem II. Does it reflect the onset of water/substrate oxidation? Determination by Mn X-ray absorption spectroscopy. J Am Chem Soc 122: 3399–3412

Lomoth R, Huang P, Zheng J, Sun L, Hammarström L, Åkermark B and Styring S (2002) Synthesis and characterization of a dinuclear manganese(III,III) complex with three phenolate ligands. Eur J Inorg Chem 2965–2974

Ma C and Barry BAB (1996) Electron paramagnetic resonance characterization of tyrosine radical M^+, in site-directed mutants of Photosystem II. Biophys J 71: 1961–1972

Magnuson A, Berglund H, Korall P, Hammarström L, Åkermark B, Styring S and Sun L (1997) Mimicking electron transfer reactions in Photosystem II: Synthesis and photochemical characterization of a ruthenium(II) tris-bipyridyl complex with a covalently linked tyrosine. J Am Chem Soc 119: 10720–10725

Magnuson A, Frapart Y, Abrahamsson M, Horner O, Åkermark B, Sun L, Girerd J-J, Hammarström L and Styring S (1999) A biomimetic model system for the water oxidizing triad in Photosystem II. J Am Chem Soc 121: 89–96

Mamedov F, Sayre RT and Styring S (1998) Involvement of histidine 190 on the D1 protein in electron/proton transfer reactions on the donor side of Photosystem II. Biochemistry 37: 14245–14256

Marcus RA and Sutin N (1985) Electron transfers in chemistry and biology. Biochim Biophys Acta 811: 265–322

Matsukawa T, Mino H, Yoneda D and Kawamori A (1999) Dual-mode EPR study of new signals from the S_3-state of oxygen-evolving complex in Photosystem II. Biochemistry 38: 4072–4077

Messinger J, Robblee JH, Yu WO, Sauer K, Yachandra VK and Klein MP (1997) The S_0 state of the oxygen-evolving complex in Photosystem II is paramagnetic: Detection of an EPR multiline signal. J Am Chem Soc 119: 11349–11350

Mino H, Kawamori A, Matsukawa T and Ono T (1998) Light-induced high-spin signals from the oxygen evolving center in Ca^{2+}-depleted Photosystem II studied by dual mode electron paramagnetic resonance spectroscopy. Biochemistry 37: 2794–2799

Nugent JH (ed) (2001) Special Issue: Photosynthetic Water Oxidation. Biochim Biophys Acta 1503: 1–259

Nugent JHA, Rich AM and Evans MCW (2001) Photosynthetic water oxidation: Towards a mechanism. Biochim Biophys Acta 1503: 138–146

Nugent JHA, Muhiuddin IP and Evans MCW (2002) Electron transfer from the water oxidizing complex at cryogenic temperatures: The S_1 to S_2 Step. Biochemistry 41: 4117–4126

Pecoraro V (ed) (1992) Manganese Redox Systems. Wiley, New York

Pecoraro VL, Baldwin MJ, Caudle MT, Hsieh W-Y and Law NA (1998) A proposal for water oxidation in Photosystem II. Pure Appl Chem 70: 925–929

Peloquin JM and Britt RD (2001) EPR/ENDOR characterization of the physical and electronic structure of the OEC Mn cluster. Biochim Biophys Acta 1503: 96–110

Porter GB and Schäfer HL (1964) Zur Frage der Lumineszenz bei Ubergangsmetallverbindungen. Ber Bunsen-Ges Phys Chem 68: 316–331

Prasil O, Adir N and Ohad I (1992) Dynamics of Photosystem II: Mechanism of photoinhibition and recovery process. In: Barber J (ed) Current Topics in Photosynthesis Vol 11, pp 220–250. Elsevier Science Publishers, Amsterdam

Rappaport F and Lavergne J (2001) Coupling of electron and proton transfer in the photosynthetic water oxidase. Biochim Biophys Acta 1503: 246–259

Renger G (2001) Photosynthetic water oxidation to molecular oxygen: Apparatus and mechanism. Biochim Biophys Acta 1503: 210–228

Robblee JH, Cinco RM and Yachandra VK (2001) X-ray spectroscopy-based structure of the Mn cluster and mechanism of photosynthetic oxygen evolution. Biochim Biophys Acta 1503: 7–23

Rova M, Franzén L-G, Fredriksson P-O and Styring S (1993) Photosystem II in a mutant of *Chlamydomonas reinhardtii I* lacking the 23 kDa psbP protein is sensitive to photoinhibition

in the absence of chloride. Photosynth Res 39: 75–83
Rova M, MacEwen B, Fredriksson PO and Styring S (1996) Photoactivation and photoinhibition are competing in a mutant of *Chlamydomonas reinhardtii* lacking the 23kDa subunit of Photosystem II. J Biol Chem 271: 28918–28924
Rova M, Mamedov F, Magnuson A, Fredriksson P-O and Styring S (1998) Coupled activation of the donor and the acceptor Side of Photosystem II during photoactivation of the oxygen evolving cluster. Biochemistry 37: 11039–11045
Siegbahn PEM and Crabtree RH (1999) Manganese oxyl radical intermediates and O-O bond formation in photosynthetic oxygen evolution and a proposed role for the calcium cofactor in Photosystem II. J Am Chem Soc 121: 117–127
Sjödin M, Styring S, Åkermark B, Sun L and Hammarström L (2000) Proton coupled electron transfer from tyrosine in a tyrosine-ruthenium-tris-bipyridine complex: Comparison with tyrosine$_Z$ oxidation in Photosystem II. J Am Chem Soc 122: 3932–3936
Sjödin M, Styring S, Åkermark B, Sun L and Hammarström L (2002) The mechanism for proton coupled electron transfer from tyrosine in a model complex and comparisons with tyrosine Z oxidation in Photosystem II. Phil Trans B 357: 1471–1478
Sjödin M, Ghanem R, Polivka T, Pan J, Styring S, Sun L, Sundström V and Hammarström L (2004) Tuning proton coupled electron transfer from tyrosine: A competition between concerted and step-wise mechanisms. Phys Chem Chem Phys 6: 4851–4858
Steinberg-Yfrach G, Rigaud J-L, Durantini EN, Moore AL, Gust D and Moore TA (1998) Light-driven production of ATP catalysed by F_0F_1-ATP synthase in an artificial photosynthetic membrane. Nature 392: 479 – 482
Styring S and Jegerschöld C (1994) Light induced reactions impairing the electron transfer through Photosystem II. In: Baker NR and Bowyer JR (eds) Photoinhibition of Photosynthesis, pp 51–73. BIOS Scientific, Oxford
Styring S, Virgin I, Ehrenberg A and Andersson B (1990) Strong light photoinhibition of electron transport in Photosystem II. Impairment of the function of the first quinone acceptor QA. Biochim Biophys Acta 1015: 269–278
Sun L, Berglund H, Davydov R, Norrby T, Hammarström L, Korall P, Börje A, Philouze C, Berg K, Tran A, Andersson M, Stenhagen G, Mårtensson J, Almgren M, Styring S and Åkermark B (1997) Binucelar ruthenium-manganese complexes as simple artificial models for Photosystem II in green plants J Am Chem Soc 119: 6996–7004
Sun L, Åkermark B, Hammarström L and Styring S (1999) Intramolecular electron transfer from manganese to photogenerated $Ru(bpy)_3^{3+}$. A functional mimic of the photoevents on the donor side of Photosystem II. Trends Inorg Chem 6: 151–155
Sun L, Raymond MK, Magnuson A, LeGourriérec D, Tamm M, Abrahamsson M, Kenéz PH, Mårtensson J, Stenhagen G, Hammarström L, Styring S and Åkermark B (2000) Towards an artificial model for Photosystem II: A manganese (II,II) dimer covalently linked to ruthenium(II)tris-bipyridine via a tyrosine derivative. J Inorg Biochemistry 78: 15–22
Sun L, Hammarström L, Åkermark B and Styring S (2001) Towards artificial photosynthesis: Ruthenium-manganese chemistry for energy production. Chem Soc Rev 30: 36–49
Sutin N (1982) Nuclear, electronic, and frequency factors in electron-transfer reactions. Acc Chem Res 15: 275–282
Svensson B, Vass I and Styring S (1991) Sequence analysis of the D1 and D2 reaction center proteins of Photosystem II. Z Naturforsch 46c: 62–73
Svensson B, Etchebest C, Tuffery P, van Kan P, Smith J and Styring S (1996) A model for the Photosystem II reaction centre core including the structure of the primary donor P680. Biochemistry 35: 14486–14502
Tommos CT and Babcock GT (2000) Proton and hydrogen currents in photosynthetic water oxidation. Biochim Biophys Acta 1458: 199–219
Tommos C, Tang X-S, Warncke K, Hoganson CW, Styring S, McCracken J, Diner BA and Babcock GT (1995) Spin-density distribution, and hydrogen bonding of the redox-active tyrosine Yz in Photosystem II from multiple electron magnetic-resonance spectroscopies: Implications for photosynthetic oxygen evolution. J Am Chem Soc 117: 10325–10335
Treadway JA, Loeb B, Lopez R, Anderson PA, Keene FR and Meyer TJ (1996) Effect of delocalization and rigidity in the acceptor ligand on MLCT excited-state decay. Inorg Chem 35: 2242–2246
van Wijk KJ, Nilsson LO and Styring S (1994) Synthesis of reaction center proteins and reactivation of redox components during repair of Photosystem II after light induced inactivation. J Biol Chem 269: 28382–28392
Vass I and Styring S (1991) pH-dependent charge-equilibria between tyrosine D and the S-states in Photosystem II. Estimation of relative midpoint potentials. Biochemistry 30: 830–839
Vrettos JS, Limburg J and Brudvig GW (2001) Mechanism of photosynthetic water oxidation: combining biophysical studies of Photosystem II with inorganic model chemistry. Biochim Biophys Acta 1503: 229–245
Wasielewski MR, Johnson DG, Svec WA, Kersey KM and Minjsek DW (1988) Achieving high quantum yield charge separation in porphyrin-containing donor-acceptor molecules at 10 K. J Am Chem Soc 110: 7219–7221
Yachandra VK, Sauer K and Klein MP (1996) Manganese cluster in Photosystem II: Where plants oxidize water to dioxygen. Chem Rev 96: 2927–2950
Yamauchi T, Mino H, Matsukawa T, Kawamori A and Ono T (1997) Parallel polarization electron paramagnetic resonance studies of the S-1-state manganese cluster in the photosynthetic oxygen-evolving system. Biochemistry 36: 7520–7526
Zhang C and Styring S (2003) Formation of split electron paramagnetic resonance signals in Photosystem II suggests that Tyrosine$_Z$ can by photooxidized at 5 K in the S_0 and S_1 states of the oxygen-evolving complex. Biochemistry 42: 8066–8076
Zouni A, Witt H-T, Kern J, Fromme P, Krauss N, Saenger W and Orth P (2001) Crystal structure of Photosystem II from *Synechococcus elongatus* at 3.8Å resolution. Nature 409: 739–743

Index

Numerical

A

B

C

D

E

F

G

H

I

J

K

L

M

N

O

P

Q

R

S

T

U

V

W

X

Y

Z

Advances in Photosynthesis and Respiration

Series editor: Govindjee, University of Illinois, Urbana, Illinois, U.S.A.

1. D.A. Bryant (ed.): *The Molecular Biology of Cyanobacteria.* 1994 ISBN Hb: 0-7923-3222-9; Pb: 0-7923-3273-3
2. R.E. Blankenship, M.T. Madigan and C.E. Bauer (eds.): *Anoxygenic Photosynthetic Bacteria.* 1995 ISBN Hb: 0-7923-3681-X; Pb: 0-7923-3682-8
3. J. Amesz and A.J. Hoff (eds.): *Biophysical Techniques in Photosynthesis*. 1996 ISBN 0-7923-3642-9
4. D.R. Ort and C.F. Yocum (eds.): *Oxygenic Photosynthesis: The Light Reactions.* 1996 ISBN Hb: 0-7923-3683-6; Pb: 0-7923-3684-4
5. N.R. Baker (ed.): *Photosynthesis and the Environment.* 1996 ISBN 0-7923-4316-6
6. P.-A. Siegenthaler and N. Murata (eds.): *Lipids in Photosynthesis: Structure, Function and Genetics.* 1998 ISBN 0-7923-5173-8
7. J.-D. Rochaix, M. Goldschmidt-Clermont and S. Merchant (eds.): *The Molecular Biology of Chloroplasts and Mitochondria in Chlamydomonas.* 1998 ISBN 0-7923-5174-6
8. H.A. Frank, A.J. Young, G. Britton and R.J. Cogdell (eds.): *The Photochemistry of Carotenoids.* 1999 ISBN 0-7923-5942-9
9. R.C. Leegood, T.D. Sharkey and S. von Caemmerer (eds.): *Photosynthesis: Physiology and Metabolism*. 2000 ISBN 0-7923-6143-1
10. B. Ke: *Photosynthesis: Photobiochemistry and Photobiophysics.* 2001 ISBN 0-7923-6334-5
11. E.-M. Aro and B. Andersson (eds.): *Regulation of Photosynthesis.* 2001 ISBN 0-7923-6332-9
12. C.H. Foyer and G. Noctor (eds.): *Photosynthetic Nitrogen Assimilation and Associated Carbon and Respiratory Metabolism.* 2002 ISBN 0-7923-6336-1
13. B.R. Green and W.W. Parson (eds.): *Light-Harvesting Antennas in Photosynthesis.* 2003 ISBN 0-7923-6335-3
14. A.W.D. Larkum, S.E. Douglas and J.A. Raven (eds.): *Photosynthesis in Algae*. 2003 ISBN 0-7923-6333-7
15. D. Zannoni (ed.): *Respiration in Archaea and Bacteria.* Diversity of Prokaryotic Electron Transport Carriers. 2004 ISBN 1-4020-2001-5
16. D. Zannoni (ed.): *Respiration in Archaea and Bacteria.* Diversity of Prokaryotic Respiratory Systems. 2004 ISBN 1-4020-2002-3
17. D. Day, A.H. Millar and J. Whelan (eds.): *Plant Mitochondria*. From Genome to Function. 2004 ISBN 1-4020-2399-5
18. H. Lambers and M. Ribas-Carbo (eds.): *Plant Respiration.* From Cell to Ecosystem. 2005 ISBN 1-4020-3588-8

Advances in Photosynthesis and Respiration

19. G. Papageorgiou and Govindjee (eds.): *Chlorophyll a Fluorescence*. A Signature of Photosynthesis. 2004 ISBN 1-4020-3217-X
20. Govindjee, J.T. Beatty, H. Gest and J.F. Allen (eds.): *Discoveries in Photosynthesis*. 2005 ISBN 1-4020-3323-0
21. B. Demmig-Adams, W.W. Adams III and A. Mattoo (eds.): *Photoprotection, Photoinhibition, Gene Regulation, and Environment*. 2005 ISBN 1-4020-3564-0
22. T.J. Wydrzynski and K. Satoh (eds.): *Photosystem II*. The Light-Driven Water: Plastoquinone Oxidoreductase. 2005 ISBN 1-4020-4249-3

For further information about the series and how to order please visit our Website
http://www.springeronline.com